Digitized by Arya Samaj Foundation Chennai and eGangotri

Digitized by Arya Samaj Foundation Chennai and eGangotri

गुरुकुल कांगड़ी विश्वविद्यालय, हरिद्वार
पुस्तकालय

R
530.5
AM3R
V.25

विषय संख्या
पुस्तक संख्या
आगत पञ्जिका संख्या 3900

पुस्तक पर किसी प्रकार का निशान लगाना वर्जित है। कृपया १५ दिन से अधिक समय तक पुस्तक अपने पास न रखें।

यह पुस्तक वितरित न की जाय
NOT TO BE ISSUED

112446

CC-0. In Public Domain. Gurukul Kangri Collection, Haridwar.

Digitized by Arya Samaj Foundation Chennai and eGangotri

सन्दर्भ ग्रन्थ
REFRENCE BOOK

यह पुस्तक वितरित न की जाय
NOT TO BE ISSUED

अ० नाथीकस्य १२७२-१२८५

CC-0. In Public Domain. Gurukul Kangri Collection, Haridwar

Digitized by Arya Samaj Foundation Chennai and eGangotri

CC-0. In Public Domain. Gurukul Kangri Collection, Haridwar

Digitized by Arya Samaj Foundation Chennai and eGangotri

REVIEWS OF MODERN PHYSICS

CHECKED 1973
Initial

BOARD OF EDITORS

S. A. GOUDSMIT, *Managing Editor*

J. W. BUCHTA, *Editor*

Associate Editors

H. H. BARSCHALL
L. I. SCHIFF
S. K. ALLISON
N. F. RAMSAY
R. C. HERMAN
E. R. PIORE

R 530.5
5 AM 5
v.25

VOLUME 25
1953

पुस्तकालय
पुस्तक संख्या .....
आगत सं० .....
तिथि .....
गुरुकुल कांगड़ी विश्वविद्यालय

Published for the

AMERICAN PHYSICAL SOCIETY

by the

AMERICAN INSTITUTE OF PHYSICS
Incorporated

CC-0. In Public Domain. Gurukul Kangri Collection, Haridwar

Digitized by Arya Samaj Foundation Chennai and eGangotri

REVIEWS OF MODERN PHYSICS

Reviews of Modern Physics is published quarterly to provide those interested in developments in physics with comprehensive and timely discussions of the problems which are of especial interest and importance.

It is hoped that the studies in this journal will give to the specialist the benefit of the viewpoint of other specialists; to the student, a background of critical knowledge and an adequate bibliography of source material; to those whose time is absorbed in the teaching of physics, a stimulating account of the forward movement of their science.

Published by the American Institute of Physics
for the
AMERICAN PHYSICAL SOCIETY

OFFICERS

President

ENRICO FERMI
Institute for Nuclear Studies
University of Chicago
Chicago 37, Illinois

Vice President

H. A. BETHE
Cornell University
Ithaca, New York

Secretary

K. K. DARROW
Bell Telephone Laboratories
Office:
Columbia University
New York, New York

Treasurer

G. B. PEGRAM
Columbia University
New York, New York

Local Secretary for the Pacific Coast

J. KAPLAN
University of California at Los Angeles
Los Angeles, California

Managing Editor

S. A. GOUDSMIT
Brookhaven National Laboratory
Upton, Long Island,
New York

BOARD OF EDITORS

Managing Editor

S. A. GOUDSMIT

Editor

J. W. BUCHTA

Associate Editors

H. H. BARSCHALL
L. I. SCHIFF
S. K. ALLISON
N. F. RAMSAY
R. C. HERMAN
E. R. PIORE

Manuscripts for publication should be submitted to J. W. Buchta, University of Minnesota, Minneapolis 14, Minnesota.

Proof and all correspondence concerning papers in the process of publication should be addressed to the Publication Manager, American Institute of Physics, 57 East 55 Street, New York 22, New York.

Subscription Price

	U. S. and Canada	Elsewhere
To members of the American Physical Society	$3.00	$3.40
To all others	4.00	4.40

Back Numbers

Yearly rate when complete year is available: **$8.00**
Single copies: **$2.25** each.
Combined issues: **$4.50**

Subscriptions, renewals, and orders for back numbers should be addressed to the American Institute of Physics, 57 East 55 Street, New York 22, New York.

Changes of address should be addressed to the American Institute of Physics.

Reviews of Modern Physics is published quarterly in January, April, July, and October at Prince and Lemon Streets, Lancaster, Pennsylvania.

Entered as second-class matter December 27, 1945, at the post office at Lancaster, Pennsylvania, under the Act of March 3, 1879.

Acceptance for mailing at the special rate of postage provided for in paragraph (d-2), section 34.40, P. L. & R. of 1948, authorized December 27, 1945.

CC-0. In Public Domain. Gurukul Kangri Collection, Haridwar

Digitized by Arya Samaj Foundation Chennai and eGangotri

112446

112446

CONTENTS

JANUARY, 1953

Introduction . . . . . R. Smoluchowski 1
Analysis of Magnetization Curves . . . . . Edmund C. Stoner 2
Heat Effects in the Magnetization of Silicon Iron . . . . . L. F. Bates and G. Marshall 17
Discussion . . . . . G. Rathenau, L. F. Bates, C. A. Fowler, and E. M. Fryer 33
Spontaneous Magnetization—Techniques and Measurements . . . . . W. Sucksmith, C. A. Clark, D. J. Oliver, and J. E. Thompson 34
Discussion . . . . . C. J. Gorter and A. Arrott 41
Permalloy Problem . . . . . R. M. Bozorth 42
Uniaxial Anisotropy of a Permalloy Crystal . . . . . Seiji Kaya 49
Discussion . J. E. Goldman, J. M. Hastings, E. B. Stoner, L. R. Aronin, and G. W. Rathenau 53
Experimental Study of Barkhausen Noise in Nickel-Iron Alloys . . . . . D. I. Gordon 56
Some New Results on Antiferromagnetism and Ferromagnetism . . . . . Louis Néel 58
Elementary Mechanisms of Magnetization in Mixed Oxides of Iron and Cobalt . . . . . Charles Guillaud 64
Discussion . . . . . A. H. Geisler 74
Low Temperature Transformation in Ferrites . . . . . L. R. Bickford, Jr. 75
Magnetic Study of Low Temperature Transformation in Magnetite . . . . . H. J. Williams and R. M. Bozorth 79
Magnetic Spectra of Ferrites . . . . . George T. Rado 81
Resonance Phenomena in Ferrites . . . . . D. Polder and J. Smit 89
Discussion . . . . . G. T. Rado 90
Note on the High Frequency Dispersion in Nickel Zinc Ferrites . . . . . H. P. J. Wijn, M. Gevers, and C. M. van der Burgt 91
Discussion . . . . . G. T. Rado 92
Motion of Domain Walls in Ferrite Crystals . . . . J. K. Galt, J. Andrus, and H. G. Hopper 93
Richter Type After-Effect in Ferrites Containing Ferrous and Ferric Ions . . . . . H. P. J. Wijn and H. van der Heide 98
Neutron Diffraction Studies of Various Transition Elements . . . . . C. G. Shull and M. K. Wilkinson 100
Discussion . . . . . W. J. Carr, Jr., and H. Eckstein 107
Atomic Moments in Alloys . . . . . J. E. Goldman 108
Discussion . . . . . C. J. Gorter and J. E. Goldman 113
Neutron Diffraction Studies of Zinc Ferrite and Nickel Ferrite . . . . . J. M. Hastings and L. M. Corliss 114
Discussion . . . C. Kittel, C. P. Guillaud, R. Smoluchowski, J. C. Slater, and L. M. Corliss 119
High Temperature Magnetic Susceptibility of V, Nb, Ta, W, and Mo . . . . C. J. Kreissman 122
Magnetic Moment Orientation and Thermal Expansion of Antiferromagnetic CrSb . A. I. Snow 127
Paramagnetic Scattering of Neutrons by Trivalent Ions of Nd and Er . . . . . W. C. Koehler and E. O. Wollan 128
Discussion . . . . . H. Grayson-Smith 128
Some Magnetic and Electrical Properties of Gadolinium, Dysprosium, and Erbium Metals . . . . . S. Legvold, F. H. Spedding, F. Barson, and J. F. Elliott 129
Magnetic Energy Formulas and their Relation to Magnetization Theory . . . . . William Fuller Brown, Jr. 131
Rotational Relaxation in Nickel at High Frequencies . . . . . W. P. Mason 136
Ultrasonic Attenuation in Magnetic Single Crystals . . . . . Sheldon Levy and Rohn Truell 140
Domain Pattern in Silicon-Iron under Stress . . . . . L. J. Dijkstra and U. M. Martius 146
Hall Effect in Ferromagnetic Materials . . . . . Emerson M. Pugh and Norman Rostoker 151
Magnetomechanical Effects in an Antiferromagnet, CoO . . . . . M. E. Fine 158
On the Theory of the Ising Model of Ferromagnetism . . . . . Gordon F. Newell and Elliott W. Montroll 159
Discussion . . . . . W. Opechowski, G. H. Wannier, and M. Lax 159
Anomalous Paramagnetism of Copper Acetate . . . . . B. Bleaney 161

CC-0. In Public Domain. Gurukul Kangri Collection, Haridwar

Digitized by Arya Samaj Foundation Chennai and eGangotri

CONTENTS

Some Magnetization Studies of Cr^{+++}, Fe^{+++}, Gd^{+++}, and Cu^{++} at Low Temperatures and in Strong Magnetic Fields . . . . . Warren E. Henry 163

Exchange Coupling between Three Iron Ions in Two Organic Molecules . . . . . J. Yvon, J. Horowitz, and A. Abragam 165

Discussion . . . . . C. J. Gorter 165

Note on Exchange Interactions . . . . . K. W. H. Stevens 166

Crystal Field Theory in the Rare Earths . . . . . R. J. Elliott 167

Measurement of the Nuclear and Electronic Contributions to the Specific Heat of Neodymium Ethyl Sulfate near 1°K . . . . . L. D. Roberts, C. C. Sartain, and B. Borie 170

Optically Induced Nuclear Magnetization. A Progress Report . . . . . F. Bitter, R. F. Lacey, and B. Richter 174

Discussion . . . . . B. Bleaney and F. Bitter 177

Magnetic Susceptibility of Bromine-Graphite . . . . . R. Smoluchowski 178

Discussion . . . . . S. Mrozowski and W. P. Eatherly 180

Helmholtz Coils for Production of Powerful and Uniform Fields and Gradients . . . . . S. T. Lin and A. R. Kaufmann 182

Symposium on Exchange—Introduction . . . . . C. Kittel 191

Exchange Interactions . . . . . C. Zener and R. R. Heikes 191

Ferromagnetism and the Band Theory . . . . . J. C. Slater 199

Theoretical and Experimental Status of the Collective Electron Theory of Ferromagnetism . . . . . E. P. Wohlfarth 211

Models of Exchange Coupling in Ferromagnetic Media . . . . . J. H. Van Vleck 220

Summary of the Discussion . . . . . R. Smoluchowski 227

Microwave Resonance Absorption in Gadolinium Metal . . . . . Arthur F. Kip 229

Discussion . . . . . B. Bleaney 232

Relaxation Processes in Ferromagnetism . . . . . C. Kittel and Elihu Abrahams 233

Discussion . . . . . G. T. Rado and C. Kittel 238

Relaxation Effects in the Ferromagnetic Resonance . . . . . R. W. Damon 239

New Variation of the Rotation-by-Magnetization Method of Measuring Gyromagnetic Ratios . . . . . C. J. Davisson and J. W. Beams 246

Ferromagnetic Faraday Effect at Microwave Frequencies and its Applications . . C. L. Hogan 253

Discussion . . . . . A. G. Fox and M. T. Weiss 262

Magneto-Optical Effects and Paramagnetic Resonance . . . . . W. Opechowski 264

Discussion . . . . . A. Abragam 268

Exchange Narrowing in Paramagnetic Resonance . . . . . P. W. Anderson and P. R. Weiss 269

Antiferromagnetism and Antiferromagnetic Resonance in a Rhombic Crystal at $T=0$ . . . . . C. J. Gorter 277

Antiferromagnetic Resonance . . . . . L. R. Maxwell and T. R. McGuire 279

Discussion . . . . . A. I. Snow 284

Paramagnetic Resonance Absorption in Solutions of K in Liquid NH_3 . . . . . Clyde A. Hutchison, Jr., and Ricardo C. Pastor 285

Paramagnetic Resonance in Phosphors at Microwave Frequencies . . . . . W. D. Hershberger and H. N. Leifer 291

New Adiabatic Demagnetization Apparatus at the National Bureau of Standards . . . . . D. de Klerk and R. P. Hudson 292

Thermoremanent Magnetization of Fine Powders . . . . . Louis Néel 293

Discussion . . . . . John W. Graham and Clarence Zener 295

Saturation and Magnetization of Hexagonal Iron Oxide Compounds . . . . G. W. Rathenau 297

Discussion . . . . . G. W. Rathenau, C. L. Hogan, and M. T. Weiss 301

Experimental Study of the Coercive Force of Fine Particles . . . . . W. H. Meiklejohn 302

New Permanent Magnet from Powdered Manganese Bismuthide . . . . . Edmond Adams 306

Discussion . . . . . C. Guillaud, W. Sucksmith, L. F. Bates, C. Kittel, and E. C. Stoner 308

Thin Films of Ferromagnetic Materials . . . . . E. C. Crittenden, Jr., and R. W. Hoffman 310

Discussion . . . . . T. L. Gilbert, C. J. Gorter, R. W. Hoffman, and C. Guillaud 315

Coercive Force of Precipitation Alloys . . . . . A. H. Geisler 316

Physical and Magnetic Structure of the Mishima Alloys . E. A. Nesbitt and R. D. Heidenreich 322

Texture of Fine Ferromagnetic Powders . . . . . L. Weil 324

Molecular Field Treatment of Antiferromagnetism . . . . . J. Samuel Smart 327

Observations on Antiferromagnetic $CuCl_2 \cdot 2H_2O$ Crystals . . . . . C. J. Gorter 332

Discussion . . . . . M. Lax and F. Keffer 337

CC-0. In Public Domain. Gurukul Kangri Collection, Haridwar

Digitized by Arya Samaj Foundation Chennai and eGangotri

Magnetic Anisotropy of the Iron-Group Fluorides . . . . J. W. Stout and L. M. Matarrese 338
Spin-Wave Theory as a Variational Method and Its Application to Antiferromagnetism . . . . . Ryogo Kubo 344

April, 1953

On the Theory of the Ising Model of Ferromagnetism . . . . . Gordon F. Newell and Elliott W. Montroll 353
Energy Levels and the Structure of Light Nuclei . . . . . D. R. Inglis 390
Gravitational Motion . . . . . A. E. Scheidegger 451
Table of Isotopes . . . . . J. M. Hollander, I. Perlman, and G. T. Seaborg 469

July, 1953

Acoustic Radiation Pressure of Plane Compressional Waves . . . . . F. E. Borgnis 653
Thermal Expansion of Anisotropic Metals . . . . . B. G. Childs 665
Fourier Inversion of Diffraction Data . . . . . Jürg Waser and Verner Schomaker 671
Least-Squares Adjustment of the Atomic Constants, 1952 . . . . . Jesse W. M. DuMond and E. Richard Cohen 691
Basis for the Criterion of Least Squares . . . . . E. Richard Cohen 709
Introduction to Spinors . . . . . W. L. Bade and Herbert Jehle 714
Theory of Angular Correlation of Nuclear Radiations . . . L. C. Biedenharn and M. E. Rose 729

October, 1953

Passage of Heavy Particles through Matter . . . . . S. K. Allison and S. D. Warshaw 779
On Statistical Estimation in Physics . . . . . M. Annis, W. Cheston, and H. Primakoff 818
Virial Coefficients and Models of Molecules in Gases . . . . . Taro Kihara 831
Mathematical Theory of Electrical Discharges in Gases. B. Velocity-Distribution of Positive Ions in a Static Field . . . . . Taro Kihara 844
Interpretation of the Virtual Level of the Deuteron . . . . . S. T. Ma 853

CC-0. In Public Domain. Gurukul Kangri Collection, Haridwar

Digitized by Arya Samaj Foundation Chennai and eGangotri

CC-0. In Public Domain. Gurukul Kangri Collection, Haridwar

Digitized by Arya Samaj Foundation Chennai and eGangotri

CC-0. In Public Domain. Gurukul Kangri Collection, Haridwar

Digitized by Arya Samaj Foundation Chennai and eGangotri

CC-0. In Public Domain. Gurukul Kangri Collection, Haridwar

Digitized by Arya Samaj Foundation Chennai and eGangotri

REVIEWS OF
MODERN PHYSICS

VOLUME 25, NUMBER 1 JANUARY, 1953

Introduction

The present issue of the *Reviews of Modern Physics* contains the papers and the pertinent discussions presented at the Washington Conference on Magnetism which was held at the University of Maryland on September 2–6, 1952. The conference, first of its kind in this country, was sponsored by the U. S. Office of Naval Research through its Advisory Committee on Magnetism in keeping with the increasing interest shown in recent years by the ONR in supporting and in promoting fundamental magnetic research. The purpose of the conference was not only to bring together most of the American scientists and a representative group of foreign scientists who are interested in magnetism, but also to review the present status of the many important and active problems in this field. Although the Washington conference was held only two years after the international conference on magnetism in Grenoble, the amount of new experimental and theoretical developments fully justified its scope and size.

It is interesting to note that papers and discussions stemming from academic, industrial, and governmental institutions were fairly evenly divided among the various branches of experimental and theoretical magnetism: Industrial and governmental institutions contributed each about a fifth of the total.

It is a great pleasure to express in the name of the Advisory Committee on Magnetism our appreciation to the Office of Naval Research and in particular to Messrs. L. M. McKenzie and J. A. Osborn of its Physics Branch for their generous and efficient support of the conference. Our thanks are also due President Harry C. Byrd for making available the excellent facilities of the University of Maryland. Finally, the undersigned wishes to express his appreciation to his colleagues on the Advisory Committee on Magnetism: Drs. F. Bitter, R. M. Bozorth, W. F. Brown, Jr., J. E. Goldman, C. Kittel, E. Montroll, G. T. Rado, J. H. Van Vleck, and V. C. Wilson for their unsparing efforts and cooperation.

R. SMOLUCHOWSKI

CC-0. In Public Domain. Gurukul Kangri Collection, Haridwar

Digitized by Arya Samaj Foundation Chennai and eGangotri

REVIEWS OF MODERN PHYSICS VOLUME 25, NUMBER 1 JANUARY, 1953

The Analysis of Magnetization Curves

EDMUND C. STONER

Physics Department, University of Leeds, Leeds, England

By an analysis of a magnetization curve is meant the determination of the character and extent of the various elementary changes occurring over any part of the curve. Even if the quantitative characteristics of the various elementary processes are known, an analysis cannot in general be made simply on the basis of the information provided by a given magnetization curve, owing to the varied and complicated way in which the different processes are superposed with an ordinary polycrystalline specimen. Further information is obtainable from measurements such as those of Bates on the thermal changes accompanying adiabatic magnetization, but little progress can be made in the analysis of curves in the hysteresis range unless the magnetic and thermal effects due to the reversible and irreversible changes separately can be unambiguously determined.

A broad survey of the general problem is given with particular reference to recent theoretical and experimental work at Leeds. The theoretical approach and the methods of analysis are along the same lines as in the treatment of the magnetocaloric effect by Stoner and Rhodes (1949). The experimental work reviewed includes studies of the reversible susceptibility, the Barkhausen effect, and the reversible change of magnetization with temperature at constant field (Tebble, with Corner; Newhouse, Skidmore, Wood, and others, 1948 onwards).

Through this work, it is now possible to determine not only the relative contributions from reversible and irreversible processes to the change of magnetization over any range but also the thermal changes associated with each. The part of the reversible change due to change in intrinsic magnetization can be determined, and in many cases analysis will show whether the remainder of the reversible change is mainly due to rotation of the magnetization against the crystalline and strain anisotropy forces, or to other processes such as boundary movements. Much detailed information about irreversible processes is obtained from determinations of the number-size relations of Barkhausen discontinuities, which in general correspond not to spontaneous movements of primary domain walls as wholes, but to smaller scale sectional irregularities in the motion. The thermal effect associated with these irreversible processes may be a heating or a cooling.

Partial analyses are presented for annealed nickel, hard-drawn iron, and other materials. These show clearly the potentiality of the general method for obtaining detailed quantitative information about the elementary processes contributing to the change of magnetization along a magnetization curve.

I. INTRODUCTION

THE magnetization curves of ordinary polycrystalline ferromagnetic materials present a complicated problem, or group of problems, and it is still far from possible to give a complete detailed explanation of their forms and quantitative characteristics, although during the past twenty-five years great progress has been made. On the one hand, the essential characteristics of ferromagnetic materials have received a satisfying explanation within the general framework provided by quantum-mechanical principles. On the other, the various secondary effects which determine the form of a magnetization curve have been intensively studied, and a better knowledge, if not always understanding, has been gained of the various types of elementary process by which change of magnetization may occur.

Three main types of elementary process contribute to the change in apparent magnetization: change of intrinsic magnetization, that is, of the orientational distribution of the elementary carriers of the magnetic moment, within each uni-directionally magnetized region, or domain; rotation of the magnetization vector in such a region as a whole against anisotropy forces; and movement of the boundaries of these regions. Elementary changes of the last two types may be reversible or irreversible.

With the wealth of information now available about elementary processes it might seem that a careful consideration of the quantitative characteristics of a given magnetization curve of a particular material could result in fairly definite conclusions about the nature, sequence, and relative proportions of the elementary changes contributing to the observed changes in magnetization. In fact, except for very restricted ranges of a magnetization curve, little more than a rough guess can be made as to the relative contributions from the different types of elementary process. This paper is concerned with the general problem of the "analysis" of magnetization curves with a view to obtaining more definite and more complete information about the elementary processes taking place. Without further information than is provided by the magnetization curve itself (together with a knowledge of the essential magnetic constants of the material) it is not possible to determine with any certainty which elementary processes are mainly contributory to the observed changes in magnetization. The subject matter is therefore in part experimental, in that a brief account is given of some of the recent and current experimental investigations which provide additional material which can contribute to such analyses; and, in part, in a broad sense, theoretical, in that the methods by which the experimental material may be utilized in analyses are indicated, and the thermodynamic and other arguments involved are outlined.

It will be obvious that a very wide range of work is potentially relevant to the general theme. In a contribution to a symposium, however, it is proper that the writer should present primarily an account of work with which he has been immediately associated, and this paper is accordingly largely concerned with recent work at Leeds, published and unpublished, to which

CC-0. In Public Domain. Gurukul Kangri Collection, Haridwar

Digitized by Arya Samaj Foundation Chennai and eGangotri

specific references will be restricted. This, however, is not intended to ignore other work, much of which has been fully surveyed in a recent comprehensive review article[1] on magnetization curves. That article makes it unnecessary to refer, except incidentally, to the general background or the wider bearing of the work here considered.

The information additional to that given directly by magnetic measurements which is thought to be of the greatest value in analyzing magnetization curves is that which can be provided by studies of the thermal changes accompanying magnetization. Hysteresis losses and the magnetocaloric effect in high fields are special examples of these thermal effects, but they have usually been considered in isolation. The determination of the temperature changes accompanying adiabatic magnetization in low and moderate fields presents a difficult experimental problem which has been successfully attacked only in fairly recent years, notably by Bates and his collaborators at Nottingham. The extraction of information in the most convenient form from the experimental results, and the planning of these and related experiments, call for careful consideration of the thermodynamics of magnetization, which, as the general problem is approached here, is of central importance in the analysis of magnetization curves.

After this introduction, a few of the more important of the relevant thermodynamic relations are stated, with a short commentary (II), and a summary is given of the characteristics of the main elementary magnetization processes (III). Some recent experimental investigations on magnetization curves are then outlined, first the more purely magnetic (IV), and next the magnetothermal investigations (V). The combination of the results of different experiments in analyzing magnetization curves is considered, and some illustrative results are presented (VI). Finally, the requirements, possibilities, and limitations of the general method are considered in a summarizing discussion (VII).

II. THE THERMODYNAMICS OF MAGNETIZATION

The thermodynamics of magnetization has been developed in a number of papers[2] in a form which is convenient when the "system of interest" is a particular magnetizable body in an external field. The most useful relations for the present purpose are given in a recent paper[3] on magnetothermal effects in ferromagnetics. Here only a few essential equations will be given with a brief commentary.

A starting point is the equation for the increase of total energy E_t associated with a magnetizable body, with increase in the external field H_e, namely,

$$dE_t = dQ - I dH_e, \tag{1}$$

where I is the volume intensity of magnetization, dQ the heat transferred to the body, and E and Q refer to unit volume. The total energy includes the potential energy of the body in the external field $-IH_e$, and also the demagnetizing field energy $+\frac{1}{2}N_D I^2$, where N_D is the demagnetization coefficient. When these are subtracted from E_t, remembering that the demagnetizing field H_i is equal to $-N_D I$ and that the "corrected" field H is equal to $H_e + H_i$, the following defining equation is obtained for an internal energy function E:

$$dE = dQ + H dI. \tag{2}$$

This equation is in a form convenient for further development. It has the obvious advantage that the energy E and the I, H relations are characteristic of the material, and are not, like the I, H_e relations, dependent on the shape of the specimen. (It may be noted that it is by no means always possible to allow for shape effects by a simple "correction" of the external field, but it is not necessary to consider this particular complication here.)

Equation (2) is applicable whether or not the changes are reversible. A change of energy ΔE may be divided into two parts, a "thermal" part ΔE_T associated with change of temperature, and a magnetic part ΔE_M, associated with change of magnetization. For an adiabatic change ($\Delta Q = 0$), it follows that

$$\Delta E = \Delta E_T + \Delta E_M = \int H dI. \tag{3}$$

It is often convenient to consider, instead of the change of temperature ΔT, with adiabatic change of field, the corresponding "heat developed," $\Delta Q'$ (not to be confused with ΔQ), related to ΔT by

$$\Delta Q' = C\rho \Delta T, \tag{4}$$

where C is the specific heat and ρ the density. Thus, in an adiabatic change,

$$\Delta E_M = \int H dI - \Delta Q'. \tag{5}$$

The change of internal energy associated with a change of magnetization along a magnetization curve can therefore be determined if measurements are also made of the thermal effect accompanying adiabatic magnetization.

For reversible changes, (2) may be written as

$$dE = T dS + H dI, \tag{6}$$

where S is the entropy. Over a reversible range the state is determined uniquely by T or S and H or I, and three other thermodynamic functions may be formed in the usual way. One of these, $E' = E - HI$, is of the energy type, and two, $F = E - TS$ and $F' = E' - TS$, are of the free energy type. From (6) and the corresponding equations for E', F, and F', four reciprocal relations of the

[1] E. C. Stoner, Repts. Prog. Phys. 13, 83 (1950).
[2] E. C. Stoner, Phil. Mag. 19, 565 (1935); 23, 833 (1937); Trans. Roy. Soc. (London) A235, 165 (1936).
[3] E. C. Stoner and P. Rhodes, Phil. Mag. 40, 481 (1949).

CC-0. In Public Domain. Gurukul Kangri Collection, Haridwar

Digitized by Arya Samaj Foundation Chennai and eGangotri

Maxwell type are at once obtainable. Among the many relations which may be derived, the following are the most useful in the present connection:

$$\left(\frac{\partial T}{\partial H}\right)_S = -\left(\frac{\partial I}{\partial S}\right)_H = -\frac{T}{\rho C_H}\left(\frac{\partial I}{\partial T}\right)_H = -\frac{T}{\rho C_H}\left(\frac{\partial S}{\partial H}\right)_T; \quad (7)$$

$$\left(\frac{\partial T}{\partial I}\right)_S = \left(\frac{\partial H}{\partial S}\right)_I = \frac{T}{\rho C_I}\left(\frac{\partial H}{\partial T}\right)_I = -\frac{T}{\rho C_I}\left(\frac{\partial S}{\partial I}\right)_T. \quad (8)$$

In the applications to be made, the specific heats at constant field C_H and at constant magnetization C_I may both be taken, with negligible error, as equal to the specific heat C, as ordinarily measured in zero field.

The value of these relations will only become apparent in subsequent sections, but it will be clear at once that over ranges in which the changes of magnetization are reversible, there is full scope for the application of thermodynamic reasoning. Over ranges in which irreversible changes occur, that is, for ferromagnetics, in low and moderate fields, the information which can be derived from thermodynamic considerations is much more limited. Broadly speaking, conclusions can be drawn about energy changes but not about entropy changes.

The difficulties in the application of thermodynamics to the magnetic behavior of ferromagnetics do not arise simply because of the occurrence of irreversible processes. For many systems which pass irreversibly from an initial to a final state (e.g., a gas expanding into a vacuum) it is possible to find the change of entropy by devising a reversible path for the passage from one state to the other. For ferromagnetics the alternative reversible path may indeed be difficult to devise, but this is connected with an even more fundamental difficulty. This is that the state of the system is not uniquely specified by the parameters, say H and I, giving the position of the representative point on the magnetization curve. The state so specified is not in general an equilibrium state, nor is it a metastable state of a simple kind, and it is compatible with a vast number of different small scale "patterns." The macroscopic state of the system (a particular ferromagnetic specimen) corresponds to the aggregate of the stable and metastable states of the constituent groups of units, that is, domains large and small, which form a pattern ever changing as the magnetization changes. The scale of this pattern falls in an awkward range. If it were larger, the methods of thermodynamics would be more readily applicable; if it were smaller, those of statistical mechanics would apply.

III. ELEMENTARY MAGNETIZATION PROCESSES

A ferromagnetic may be regarded as made up of domains 1, 2, $\cdots j, \cdots$, of volumes $v_1, v_2 \cdots v_j \cdots$, each of which, at temperatures well below the Curie point θ, has an intrinsic magnetization I_m approximating closely to the quasi-saturation magnetization. The value of I_m varies with temperature and field. It may be well to note at once that though the change with field may be small (e.g., for nickel at room temperature the difference between I_m for $H=10^4$, and I_m for $H=0$ is less than 1 in 200) the associated energy change may be of predominant importance. The apparent magnetization, as ordinarily measured, may be written

$$I = \sum_j v_j (I_m)_j \cos\phi_j, \quad (9)$$

where ϕ_j is the angle between $(I_m)_j$ and I, and the summation is over the domains in unit volume ($\sum v_j = 1$). Change of I may therefore be expressed as a resultant effect of changes in I_m, ϕ, and v:

$$dI = \sum_j \{v_j \cos\phi_j d(I_m)_j - v_j (I_m)_j \sin\phi_j d\phi_j + (I_m)_j \cos\phi_j dv_j\}. \quad (10)$$

The three terms correspond to the following three elementary processes: (a) change of intrinsic magnetization, (b) rotation of the domain magnetization vector, and (c) boundary movement. The relative magnitudes of the contributions to the change of I in passing from the demagnetized state to quasi saturation are ordinarily in the order c, b, a, while the associated energetic changes are in the order a, b, c. The effective utilization of the results of magnetothermal measurements in the analysis of magnetization curves is largely dependent on the extent to which this qualitative statement can be made quantitative and precise. A full discussion of the various elementary processes would require a book, and the points mentioned here are limited to those which have a direct bearing on the problem of analysis. It will be sufficient for the present purpose to make the statements in a form applicable to ferromagnetics well below the Curie point (e.g., iron, nickel, or cobalt at room temperature).

Change in Intrinsic Magnetization

It is not commonly appreciated that there is no precise knowledge of the variation of intrinsic magnetization with field even in high fields. In the quasi-saturation range the variation of the apparent magnetization may be represented empirically by

$$I = I_0\left(1 - \frac{a}{H} - \frac{b}{H^2}\right) + cH, \quad (11)$$

but it is fair to say that there are at present no experimental results from which the value of c in the term in H, corresponding to increase in intrinsic magnetization, can be determined with any certainty. Indirect methods are therefore necessary to determine the effects associated with changes in intrinsic magnetization.

CC-0. In Public Domain. Gurukul Kangri Collection, Haridwar

Digitized by Arya Samaj Foundation Chennai and eGangotri

The most promising procedure is to make use of (7), which in conjunction with (4) gives for the heat developed in a reversible adiabatic magnetization process

$$\left(\frac{\partial Q'}{\partial H}\right)_S = -T\left(\frac{\partial I}{\partial T}\right)_H. \tag{12}$$

As the variation of the intrinsic magnetization I_m over the field range from 0 to several thousand oersteds is small, the variation with temperature is given nearly enough over the whole range by $(\partial I_0/\partial T)$, where I_0 is the spontaneous magnetization in zero field. This quantity is known, or determinable, with considerable accuracy. The sorting out of the contribution $(\Delta Q')_i$ from the change in intrinsic magnetization to the aggregate heat developed, $\Delta Q'$, along a section of a magnetization curve involves a rather tricky argument. Except in high fields the local directions of I_m are not in general parallel to H, but are distributed in a manner which gives the resultant bulk magnetization I; further, there are changes of the local I_m accompanying the changes of local directions with H. The final result of the argument[3] is, however, simple. The contribution is given by

$$(\Delta Q')_i = a\int d(IH), \tag{13}$$

where $a=-(T/I_0)(\partial I_0/\partial T)$. The relation (13) is believed to hold generally, whether or not the changes along the magnetization curve are reversible; for the changes in intrinsic magnetization themselves are, unlike rotational changes and boundary movements, always reversible. Since $(\partial I_0/\partial T)$ is negative, increase of intrinsic magnetization in an adiabatic change of field is accompanied by heating. In terms of entropy, this arises from the decrease in magnetic entropy.

The situation is somewhat peculiar in that although only the roughest estimate may be made of the change of intrinsic magnetization with field, the corresponding heat developed in an adiabatic change of field may be accurately determined. It has long been known that the magnetocaloric effect in high fields is almost entirely due to change in intrinsic magnetization. From a quantitative application of (13) it turns out that even in low fields $(\Delta Q')_i$ may account for the greater part of the observed $\Delta Q'$. The relation (13) is therefore of central importance in the effective utilization of magnetothermal results in the analysis of magnetization curves.

Rotational Processes

Change of magnetization due to rotation of the domain magnetization vectors may occur to some extent over any part of a magnetization curve, but it is usually predominant between the knee of the curve and technical saturation (or between saturation and remanence). As the field increases rotation takes place from "easy" directions determined by the local anisotropy towards the direction of the field. Extensive experimental and theoretical investigations, fully reviewed elsewhere,[1] have been made of natural crystalline anisotropy, of anisotropy due to strain and, with particular reference to single-domain particles, of anisotropy due to shape. To avoid complication of detail in dealing with principles it will be convenient to fix attention on crystalline anisotropy, and to suppose that the main anisotropy characteristics are determined by a single coefficient whose modulus is symbolized by k (e.g., for nickel, $k=|K_4|$, $K_4\simeq -4.9\times 10^4$ erg cm^{-3}). When k is constant throughout a specimen, the magnetization curve is, in principle, calculable if the orientational distribution of the constituent crystals is known. Whether it is or not, however, a straightforward argument[3] gives as an expression for the heat developed from rotational changes $(\Delta Q')_k$ in an adiabatic change of field over a reversible rotational range,

$$(\Delta Q')_k = b\int HdI, \tag{14}$$

where $b=(T/k)(dk/dT)$. Since (dk/dT) is usually, if not invariably, negative, increase of magnetization by rotations in an adiabatic change of field is accompanied by cooling. This corresponds to an increase in the magnetic entropy. The range of validity of (14) is much more restricted than that of (13). It holds only over a range in which the change of magnetization is reversible, and due entirely (apart from the small change in intrinsic magnetization) to rotations of the local magnetization vectors. The value of b which can be calculated from the single crystal data (when these are available) can be expected to apply closely to a polycrystalline specimen only if this is made as free as possible from internal strains by a thorough annealing treatment.

In general the value of k and of dk/dT will be modified by local strains and possibly other irregularities. Owing to the complexity of the internal stress distribution problem, and also, incidentally, to the paucity of fundamental data on crystal magnetostriction coefficients and their temperature variation, it is virtually impossible at present to make even rough *a priori* estimates of the effective value of b (and of its possible variation with field) for unannealed specimens.

Under certain conditions rotational changes may take place irreversibly. Irreversible rotational changes have been very fully studied in relation to the interpretation of the properties of certain types of high coercivity material in terms of the behavior of single domain particles.[4] It is interesting to note that precise thermodynamical calculations for a complex irreversible magnetization process can be made, when, as here, the mechanism of the process is known.[5] In "ordinary"

[4] E. C. Stoner and E. P. Wohlfarth, Trans. Roy. Soc. (London) A240, 599 (1948).

[5] P. Rhodes, Proc. Leeds Phil. Soc. 5, 116 (1948).

CC-0. In Public Domain. Gurukul Kangri Collection, Haridwar

Digitized by Arya Samaj Foundation Chennai and eGangotri

materials, however, irreversible processes of this kind are unlikely to be important, and they will not therefore be discussed in this paper.

Boundary Movement

There is now no doubt that in ordinary unstrained polycrystalline material nearly the whole of the change of magnetization in the lower field range may be attributed to reversible or irreversible movements of domain boundaries. In recent years extensive investigations have been made on domain structure by the powder pattern method (Williams, Bozorth, Bates, and others), and the general character of the beautiful patterns obtained is now well known. In one simple (though experimentally very difficult) case, with a "picture-frame" crystal, the change of magnetization has been quantitatively correlated with the observed boundary movement (Williams and Shockley). On the theoretical side, boundary energies and widths have been studied (Néel, and more recently Lilley[6]) and also the dynamics of the boundary movements (Néel, Kittel, and others). Most of this work has been fully reviewed elsewhere.[1] Although so much more is now known than, say, ten years ago, there are still many gaps and uncertainties. For example, fundamental difficulties are encountered in attempting to make any but the roughest theoretical estimates of the absolute value of boundary energies, and experimental estimates are indirect and uncertain; and even for simple domain patterns, whose form is in accordance with theoretical calculations, the spacings as measured often differ by a factor of two or more from those given by the unavoidably somewhat idealized theory.

The complexity in detail of the powder patterns obtained when the conditions are other than the very simplest (i.e., with single-crystal specimens and with the surfaces examined close to well-defined crystallographic planes containing at least one easy axis) suggests that theoretical treatments of ordinary magnetization curves, in the boundary movement ranges, must at present, to be useful, be of a somewhat general type rather than of a type which takes cognizance, explicitly, of the details of the elementary processes involved.

Usually, over the initial part of a magnetization curve, the magnetization is reversible over a limited range, and

$$I=\kappa_0 H.$$

It follows at once from (4) and (7) that over this range

$$\Delta Q'=a'\int d(IH)=b'\int H dI, \qquad (15)$$

where $a'=-\frac{1}{2}(T/\kappa_0)(d\kappa_0/dT)$, $b'=2a'$. Since $(d\kappa_0/dT)$ is usually positive, adiabatic increase of field is accompanied by cooling, as for rotational changes. In low fields boundary movement results in a change of direction of magnetization vectors from one easy direction to another, more favorably orientated with respect to the field. The effects indicated by (15) may be in part attributed to slight differences in the energy associated with orientations along different ideally equivalent easy axes (so that the atomic interpretation of the effects would be the same as for ordinary rotational changes), and in part to the hindrances to boundary movement due to local irregularities. There is no generally applicable method of making *a priori* calculations of the coefficients in (15).

Beyond the very limited initial reversible range, reversible and irreversible boundary movements are superposed. Recent experimental work on the determination of the reversible susceptibility over the whole of the magnetization curve will be described in the next section. From such a determination, in conjunction with the magnetization curve, it is possible to find the irreversible contribution to the change of magnetization, that is, in ordinary materials, the contribution from irreversible boundary movements. Information about the character of the elementary irreversible changes can be obtained from experiments on the Barkhausen effect, which are also described. It will be convenient, therefore, to give further consideration to reversible and irreversible boundary movements in the next section rather than here.

IV. EXPERIMENTAL INVESTIGATIONS: MAGNETIC

With a view to illustrating the kind of "supplementary" magnetic investigations which are of value in the analysis of magnetization curves, a brief outline will be given in this section of some recent experimental work at Leeds by Tebble and others on reversible susceptibility and the Barkhausen effect. When it became possible to include experimental work on ferromagnetism in the research program of the Physics Department at the University of Leeds some few years ago, the study of the Barkhausen effect was an almost obvious choice, for little work was being done on it elsewhere, and indeed comparatively little had been done on the ordinary effect since the classical investigations of Bozorth and Dillinger (1929–32), which left many questions unanswered. In connection with this work, it became necessary to measure reversible susceptibilities, for which improved methods were developed. For the kind of analysis in view here, reversible susceptibility measurements are of more direct importance than those on the Barkhausen effect, and they will therefore be considered first.

Reversible Susceptibility

It is well known that the differential suceptibility, as measured by the slope of the magnetization curve at a particular point, may be separated into reversible

[6] B. A. Lilley, Phil. Mag. 41, 792 (1950).

CC-0. In Public Domain. Gurukul Kangri Collection, Haridwar

Digitized by Arya Samaj Foundation Chennai and eGangotri

and irreversible components such that

$$\kappa_d = \kappa_r + \kappa_{irr}. \tag{16}$$

The conventional definition of κ_r corresponds to

$$\kappa_r = \lim_{\Delta H \to 0} (\Delta I / \Delta H), \tag{17}$$

where the field increment ΔH is in the *opposite* direction to the last increment of the field bringing the specimen to the point (I, H). Experimental methods for measuring κ_r based directly on (17) are tedious and inaccurate. It is usually supposed that the same reversible susceptibility is measured by the use of alternating fields. The methods developed by Tebble and his collaborators (1950 onwards) involve essentially the measurement of the mutual inductance of two coaxial coils with and without the specimen under test as a core. Measurements were made with various amplitudes of the alternating field. Over most of the steady field range the limiting value of κ_r for the materials examined did not differ significantly from that for an amplitude of the order 10^{-3} oersted, which was ordinarily used in the work.

In the first method the mutual inductance was measured by an inductometer bridge arrangement, which, with amplification of the out-of-balance current, gave an over-all accuracy in measurements of κ_r of about 1 in 1000. Some typical results are shown in Fig. 1. With results of this kind, the fractional part of the total change which is due to reversible processes may readily be found. An incidental result of the experiments was a demonstration that κ_r is not a unique function of the magnetization I, as has sometimes been suggested. This is shown by Figs. 1(a) and 1(b), and that the suggested relation is not even a rough approximation was shown conclusively by measurements of κ_r at points within the main hysteresis loop; κ_r is, in fact, not a unique function of I except in the higher field range where I is a unique function of H.

The method of measuring κ_r which has been outlined is capable of high accuracy, but the time required for a complete set of measurements is considerable. For many purposes a somewhat lower accuracy is adequate, and in making measurements at temperatures other than room temperature a method of recording (κ_r, H) curves rapidly while the temperature of the specimen is held constant and measured accurately is particularly desirable. In a semi-automatic method which has been developed,[7,8] a κ_r, H curve is traced out on an oscilloscope screen, and is recorded photographically. After applying the usual corrections, the measurements give κ_r values to an over-all accuracy of about 1 percent. For measurements above and below room temperature

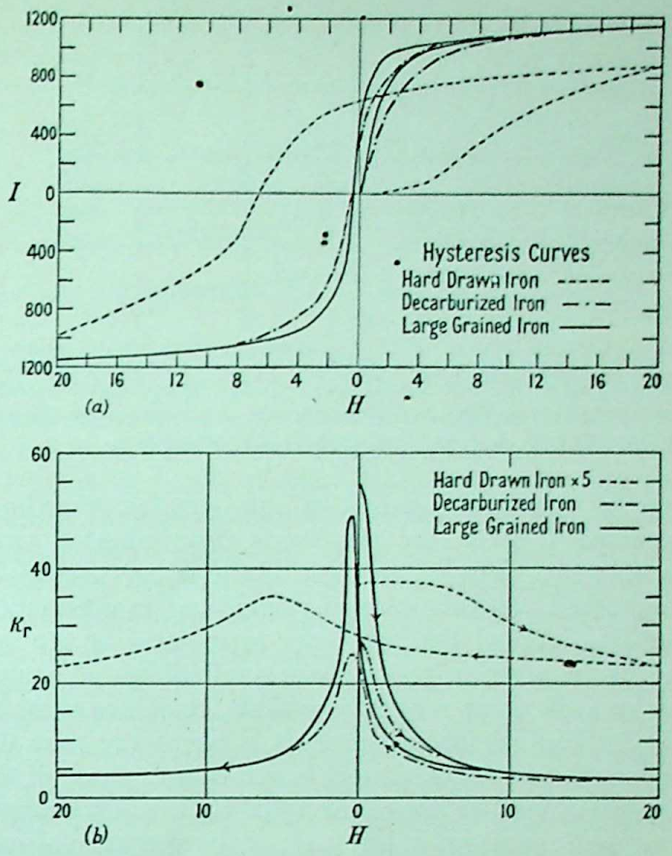


FIG. 1. (a) Hysteresis curves for hard-drawn iron, decarburized iron, and large grained iron. (b) Variation of reversible susceptibility κ_r with polarizing field H.

suitable heated and cooled liquids are pumped through the specimen tube.

The forms of the curves obtained photographically by this arrangement are the same as those in Fig. 1(b). Measurements have been made over a temperature range from $-50°C$ to $+200°C$ for annealed nickel and nickel under tension, with a maximum field of 100 oersteds. The details of the κ_r, H and also the κ_r, I curves at different temperatures present many interesting features, which are of obvious importance in connection with the question of the contributions to the reversible changes from rotational and boundary movement processes. These details cannot, however, be usefully discussed in this paper.

The Barkhausen Effect

In the experimental work started by Bush and Tebble[9] and carried further by Tebble and others, the aim has been to develop a method for determining the number, size distribution of Barkhausen discontinuities over the whole, or any part of a magnetization curve between specified field limits. A slowly changing field is applied to the specimen, and the discontinuous changes in magnetization are detected as voltage pulses induced in a search coil wound round the specimen. These pulses are amplified and can be displayed on an oscillo-

[7] R. S. Tebble and W. D. Corner, Proc. Phys. Soc. (London) **B53**, 1005 (1950).

[8] Tebble, Corner, and Wood, Proc. Phys. Soc. (London) **B54**, 753 (1951).

[9] H. D. Bush and R. S. Tebble, Proc. Phys. Soc. (London) **60**, 370 (1948).

CC-0. In Public Domain. Gurukul Kangri Collection, Haridwar

Digitized by Arya Samaj Foundation Chennai and eGangotri

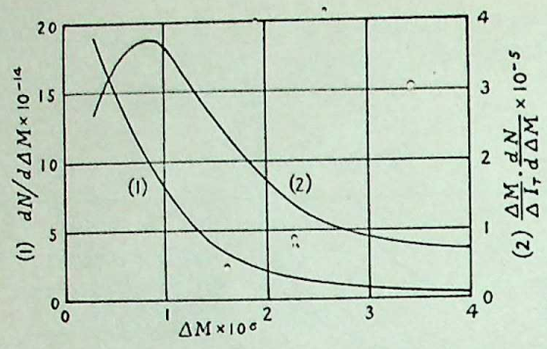


FIG. 2. Distribution and contribution curves for Barkhausen discontinuities in hard-drawn iron. ΔM, change in magnetic moment corresponding to discontinuity. N, number of discontinuities per cm³. ΔI_T, total change in magnetization.

scope for visual observation or photographic recording, or passed through an amplitude discriminator to a counting unit. For an account of the many subsidiary experiments and calculations carried out in connection with the detailed design of the later form of the apparatus in attempting to insure reliability of counts over as wide a size range as possible, reference must be made to the original paper.[10] It is necessary that the dimensions of the search coil in relation to those of the specimen should be such that equal elementary changes of magnetic moment in any part of the specimen should induce equal voltage pulses in the coil. In connection with this (and also with the process of calibration by the use of a small current-carrying coil placed axially in the search coil) a rigorous theoretical investigation has been made of the flux distribution of a magnetic dipole in a cylindrical specimen.[11]

In the experiments under review the minimum discontinuous changes of magnetic moment which could be detected with reasonable certainty above the noise level were about 0.3×10^{-6} emu (corresponding to about 0.74×10^{13} atoms or a volume of 0.87×10^{-10} cm³ in iron, and to 2.6×10^{13} atoms or 3.1×10^{-10} cm³ in nickel). It should be mentioned that the time required for anything approaching a complete investigation of a single specimen may be several months. This is because the number of countable discontinuities in a half-cycle is very large (of the order of 10^7 for the specimens of iron used), and to minimize overlap effects the rate of change of field must be very small (of the order of 10^{-4} oersted sec^{-1} in these experiments).

The primary results give the number of discontinuities over the chosen H range above a minimum size fixed by the discriminator setting. From the results for different settings, corresponding to different minimum values of ΔM, the change in magnetic moment, curves giving the number, size distribution ($dN/d\Delta M$ against ΔM) may be obtained; multiplication of the ordinates of these curves by ΔM then gives contribution, size curves (i.e., curves giving the contribution to the discontinuous change of magnetization per unit ΔM range against ΔM). Examples of these curves are shown in Fig. 2. The distribution curves are all quasi-exponential in character, and their general form appears to be much the same for particular sections of the magnetization curve as for the whole range examined. The noise level sets a lower limit to the value of ΔM for which the counts may be regarded as reliable. With a contribution curve such as that for hard-drawn iron, a plausible extrapolation may be made to zero ΔM, but for most of the materials examined the contribution curves, like the distribution curves, are quasi-exponential over the experimental range, and there is no soundly based method for extrapolating the curves to lower values of ΔM. It is, however, a simple matter to estimate the contribution $(dI/dH)_B$ from Barkhausen discontinuities above the minimum ΔM for which reliable counts may be made to the total change of magnetization with field $(dI/dH)_T$. As an illustrative example, the results obtained for hard-drawn iron (for which other curves are given in Figs. 1 and 2) are shown in Fig. 3, and some numerical details for this material and for annealed nickel are given in Table I.

Curves such as those of Fig. 3 provide a very searching test of the experimental methods. Too much attention should not be paid to the $(dI/dH)_B$ curve lying in part above the $(dI/dH)_T$ curve; this obvious but not serious discrepancy is attributed in the main to the relatively large errors which may arise in the differentiation of experimental curves even when the errors in the experimental points are relatively small. The figure is believed to give a fair impression of the order of magnitude of the incidental uncertainties which arise in comparisons of this kind. The numbers in Table I indicate that for hard-drawn iron nearly the whole of the directly measured change of magnetization is accounted for as the sum of the reversible changes (as determined from the reversible susceptibility) and the Barkhausen discontinuities actually counted (with

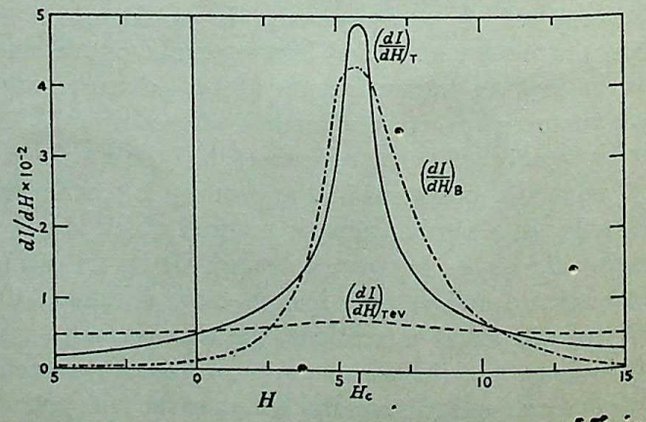


FIG. 3. dI/dH curves for hard-drawn iron: ——— $(dI/dH)_T$; — — — — $(dI/dH)_B$; ——— $(dI/dH)_{rev}$. The curves for $(dI/dH)_B$ and $(dI/dH)_{rev}$ give the contributions from the Barkhausen discontinuities and from the reversible changes, respectively, to the total change of magnetization with field $(dI/dH)_T$.

[10] Tebble, Skidmore, and Corner, Proc. Phys. Soc. (London) A63, 739 (1950).
[11] E. W. Elcock, Proc. Leeds Phil. Soc. 6, 1 (1952).

CC-0. In Public Domain. Gurukul Kangri Collection, Haridwar

Digitized by Arya Samaj Foundation Chennai and eGangotri

$\Delta M > 0.3\times10^{-6}$). The deficit of some 6 percent may plausibly be attributed to the smaller discontinuities.

For annealed nickel (see Table I) the difference of nearly 40 percent between ΔI_T and the sum of the actually "observed" ΔI_B and ΔI_{rev} is much greater than for hard-drawn iron, and for a single crystal iron specimen, subsequently investigated,[12] a still greater difference has been found. At least part of the difference may be accounted for by the contribution from the uncounted small discontinuities, but in addition to this errors may arise in the counts for some of the materials owing to the occurrence of discontinuities in "bursts." One discontinuous change may trigger a number of others, so that a succession of discontinuities occurs in a very short time interval which is independent of the rate of change of field. In the design of the apparatus particular attention is given to the optimum relations between the time constants of the coil, amplifier, and discriminator systems and the decay time of the eddy currents in the specimen associated with a discontinuity, and the arrangement is such that reliable counts can be made at a rate of the order of 1000 per sec for regular or randomly distributed single discontinuities. It seems inherently impossible to obtain accurate counts of the individual components in a burst. Fortunately the occurrence of bursts is manifested visually and audibly in the scaling unit and recorder with slow rates of field change, and is also obvious on oscillographic records. It was, for example, not apparent for hard-drawn iron, but very noticeable for large-grained and single-crystal iron. For the first material, the curves derived from the experimental counts show quantitatively that practically the whole of the difference between the total and reversible changes in magnetization, ΔI_T and ΔI_{rev}, is due to the irreversible changes associated with Barkhausen discontinuities. There can be little doubt that this is so in all cases, but that in materials for which the burst phenomena are prominent the actual number of discontinuities may be significantly greater than the number counted in the experiments. Even then the distribution and contribution curves are believed to be substantially accurate for the larger values of ΔM (say, $\Delta M > 10^{-6}$), for in a burst it will be mainly the smaller discontinuous changes initiated by a larger one which are missed.

The mean, or weighted average value of ΔM can perhaps best be taken as the value above which the discontinuities account for half the total discontinuous magnetization (i.e., $\frac{1}{2}(\Delta I_T - \Delta I_{rev})$). For hard-drawn iron this mean value is $\Delta M = 1.6\times10^{-6}$ (corresponding to a minimum of 6.5×10^{11} atoms or a volume of 4.6×10^{-10} cm^3). For large-grained iron the mean value is about half as great, for annealed nickel about a quarter (through the corresponding volume here is about the same as for hard-drawn iron). The volumes corresponding to these discontinuities in magnetization are very much smaller (by a factor of the order of 10^5) than the volumes of the primary domains, as revealed by powder patterns, in single-crystal and large-grained material, though they are comparable in size with the smaller of the secondary domains (of the closure type, or associated with inclusions). Since the Barkhausen discontinuities may account for the greater part of the change of magnetization where boundary movement is predominant, they cannot be due solely to changes in the secondary domains, but must be associated mainly with the movement of the primary domain boundaries, in particular of the 180° boundaries. The usual minimum energy conditions do not preclude wrinkles or corrugations in these boundaries (as distinct from 90° boundaries), provided that the corrugations run parallel to the direction of magnetization.[12] The state of minimum energy may therefore be attained by small scale variations of curvature conditioned by the localized strains, inclusions, or irregularities of composition and the associated disperse fields without seriously affecting a large-scale planeness. It is suggested that the Barkhausen discontinuities arise mainly from the continuous localized readjustments or jerks accompanying (and indeed constituting) the movement of the 180° boundary as a whole. The details of the individual processes involved have been worked out in certain idealized cases, and the usual formal theory of irreversible boundary movements can be taken over at once, though the detailed picture is different.

TABLE I. Contribution of Barkhausen discontinuities and reversible processes (ΔI_B and ΔI_{rev}) to the total change in magnetization.

Material	H range	Limits of ΔM (10^{-6} emu)	ΔI_T	Contributions (and percentage of ΔI_T) ΔI_B	ΔI_{rev}	$\Delta I_B + \Delta I_{rev}$
Hard-drawn iron	±18.6	0.3–35	2150	1844 (86)	180 (8.4)	2024 (94)
Annealed nickel	±14.9	0.3–12	700	326 (47)	115 (16.4)	441 (63)

With small-grained materials the Barkhausen volumes may be comparable in size with the individual grains, and considerable caution would be necessary in extending the interpretation just outlined to these materials. A discussion of this particular aspect of the general problem cannot, however, usefully be taken up here.

Whether or not the general type of interpretation suggested is correct, these studies of the Barkhausen effect have provided quantitative knowledge about elementary irreversible processes which will be invaluable as a background to constructive thinking about the individual processes, and also about the aggregate effects as manifested in the over-all irreversible changes along a magnetization curve.

[12] V. L. Newhouse, thesis, Leeds, 1952. A paper on this work is in preparation.

CC-0. In Public Domain. Gurukul Kangri Collection, Haridwar

Digitized by Arya Samaj Foundation Chennai and eGangotri

V. EXPERIMENTAL INVESTIGATIONS: MAGNETOTHERMAL

Change of Temperature with Change of Field

The importance of studies of the magnetocaloric effect (the change of temperature accompanying adiabatic change of field) in low and moderate as well as in high fields has already been indicated. The experimental work, which has been surveyed elsewhere,[1,3] will not be considered here, as it will be dealt with in the paper contributed by Bates, who is responsible for most of the recent work and whose papers may be consulted for full details. It will be sufficient to recall that, if accurate estimates of dT/dH are to be made from the observed values of $\Delta T/\Delta H$ in the lower field ranges, where I and dI/dH may change rapidly with H, the increments ΔH must be small; a lower limit is set by the many difficulties in measuring small temperature changes. It seems unlikely that there will be any substantial and useful increase over the highest sensitivity which has been attained, of 1 scale division for a temperature change of about 5×10^{-6} degree (corresponding to a heat developed of about 200 erg cm^{-3}). This in itself is a remarkable achievement. The minimum field change necessary to give a reliably measurable temperature change varies with the material and field range, but inspection of the curves given in the next section shows that it is seldom likely to be less than 5 or 10 oersteds. The Q' curves in Figs. 5–8 show the general character of the results that have been obtained.

Change of Magnetization with Temperature

The magnetocaloric measurements give the temperature change (or the heat developed) in all the superposed processes contributing to the change of magnetization, and one of the main obstacles to a more detailed interpretation of the results in the lower field range is the difficulty of estimating separately the contributions from reversible and irreversible processes. This was emphasized in the course of a discussion of magnetothermal effects,[3] where it was shown that in the extensive series of magnetocaloric measurements of Okamura (1936) the method used for estimating separately the reversible and irreversible heat developed was unsound, and that it could lead at best to only a very rough qualitative indication of the general trend of the separate heat changes. It was suggested that the required information might be obtainable from measurements of κ_r, H curves over a range of temperatures, but further consideration has shown that this argument too was defective. A solution of the problem has been found, in principle, in the direct application of the thermodynamic relation (7), or (12), namely,

$$\left(\frac{\partial Q'}{\partial H}\right)_S = C\rho\left(\frac{\partial T}{\partial H}\right)_S = -T\left(\frac{\partial I}{\partial T}\right)_H . \qquad (18)$$

This equation relates the reversible part of the heat change accompanying adiabatic change of field with the reversible change of magnetization with temperature at constant field. Thus if $(\Delta I/\Delta T)_H$ can be determined with increments of T sufficiently small that the change is reversible, the corresponding value of $(\partial Q'/\partial H)_{rev}$ can be derived. By measurements at different values of H, the value of $(\Delta Q')_r$ over any part of the range can be obtained, and if magnetocaloric measurements of $\Delta Q'$ have been made, the reversible and irreversible contributions in

$$\Delta Q' = \Delta Q_r' + \Delta Q'_{irr} \qquad (19)$$

are separately determined.

Suitable experimental methods for making the necessary measurements have recently been developed and applied in a detailed investigation of annealed nickel.[13] There is, of course, no difficulty in principle in determining $(\partial I/\partial T)_H$ in the higher fields (i.e., well above the hysteresis range), as it is merely necessary to determine the ordinary magnetization curve with sufficient accuracy at a number of different temperatures. In the lower fields, where I is not a unique function of H and T, this procedure does not give the required results. It is necessary to start at the point on a magnetization curve at which $(\partial I/\partial T)_H$ is required, and to measure the change of I as the temperature is changed. A magnetometer method is clearly indicated. Some curves obtained with the standard type of arrangement are shown in Fig. 4. With the change of temperature of the order of 20°C at a field of 1.40, well above the coercive field for this particular specimen (about 0.2) it is apparent from the large temperature hysteresis that most of the change of magnetization is irreversible. Experiments on the Barkhausen effect accompanying change of temperature have given similar indications,[14] even qualitative observations enabling a useful estimate to be made of the relative degrees of irreversibility in different changes. From the work on reversible

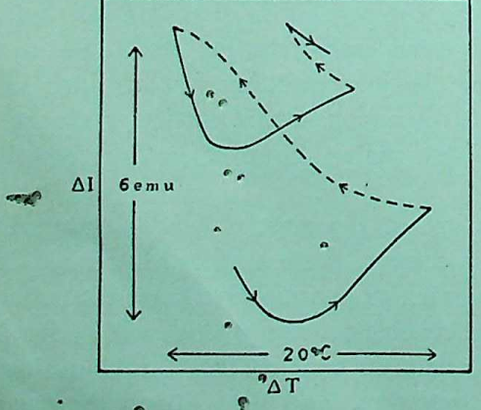


FIG. 4.—Typical results of magnetometer experiments showing variation of intensity of magnetization with temperature. Annealed nickel, $H=1.40$ oersteds. $(\Delta T)_{max}=20°C$.

[13] Tebble, Wood, and Florentin, Proc. Phys. Soc. (London), to be published (1952).

[14] V. L. Newhouse, Proc. Phys. Soc. (London) A65, 325 (1952).

CC-0. In Public Domain. Gurukul Kangri Collection, Haridwar

Digitized by Arya Samaj Foundation Chennai and eGangotri

susceptibility,[7] the magnitude of ΔI within which the change is effectively reversible can be found; from this and a rough knowledge of $(\partial I/\partial T)_H$ the corresponding magnitude of ΔT can be estimated. In the range of special interest it is of the order of 1°C, and the experimental problem is therefore that of devising a method of measuring the corresponding small changes of intensity. With the standard arrangement used in obtaining the curves of Fig. 4, the over-all sensitivity was 1-mm magnetometer scale deflection for a change ΔI of 0.38 emu. An increase in sensitivity by about 20 is required to enable reliable measurements to be made of $(\partial I/\partial T)$ in the range 0.4 to 0.04.

The essentials of the arrangement finally adopted are as follows. Two "identical" specimens were mounted within identical magnetizing solenoids, connected in series opposition, and placed equidistant from the magnetometer. The temperature of one specimen was kept constant by a flow of water, that of the other raised or lowered by a controlled flow of butyl alcohol, heated or cooled. The specimens, about 40 cm long, were accurately prolate spheroidal in shape, with an equatorial diameter of about 0.4 cm. (This has the double advantage that the intensity is uniform, and that, as the field at an external point can be exactly calculated, the magnetometer may be close to the specimen.) The magnetometer was an astatic modification of the Sucksmith horizontal suspension type. An over-all sensitivity of up to 1-mm scale deflection for a change ΔI of 0.020 emu could be used. With the specimen at the same I, H point as in Fig. 4, the change of I with T was found to be reversible and linear over the maximum range of 1.3°C, with $(\Delta I)_{\max}$ about 0.16, and reliable readings could be taken at intervals of about a tenth of this range.

The above details are very incomplete, but they are given to show that while it is quite practicable to make measurements of $(\partial I/\partial T)_{\text{rev}}$ over the low field range of a magnetization curve, considerable care is necessary if reliable results are to be obtained. A presentation and discussion of some of these results will be included in the next section.

VI. THE ANALYSIS OF MAGNETIZATION CURVES: ILLUSTRATIVE RESULTS

The low field magnetic properties of ferromagnetics are strongly structure sensitive. Ideally, therefore, if the results of different types of experiment are to be utilized in the analysis of the magnetization curves of a particular material, the experiments should all be made with the same specimen. This is not entirely practicable, as specimens differing in dimensions are required for the different investigations, but with cooperation between the different experimentalists, it can be sufficiently nearly attained by the use of the same material subjected to the same thermal and mechanical treatments; the most sensitive criterion of similarity being the magnetization curve itself. Most of the work so far has been carried out without having clearly in mind the requirements to be fulfilled if the different results are to be satisfactorily linked together, and usually only one or two sets of data are available for each particular material. For this reason it is not possible to illustrate the full scope of the type of analysis envisaged.

In the different investigations, however, the materials used have often been sufficiently similar magnetically (sometimes by deliberate choice) that useful cross comparisons can be made. Following the historical course of development of the general scheme, an account will first be given of the partial analysis which can be effected by utilizing magnetization curve and magnetocaloric data, and the manner in which this analysis can be made more complete by utilizing other data will then be outlined.

Magnetization Curves and Magnetocaloric Data

In the method of analysis introduced by Stoner and Rhodes,[3] the heat developed in an adiabatic change of field from an appropriate initial value H_0 to H is expressed by

$$Q'=a\int d(IH)+\int b''HdI, \tag{20}$$

where the lower and upper limits of the integrals correspond to H_0 and H. The first term corresponds to change in intrinsic magnetization (see Eq. (13)), and the coefficient a can be calculated from I_0 and dI_0/dT (see Eqs. (12) and (13)). Since a is known, or determinable, with considerable accuracy, it is convenient to subtract this part of the contribution to the experimental Q' and to consider the remainder, Q'', where

$$Q''=Q'-a\int d(IH)=\int b''HdI. \tag{21}$$

The coefficient b'' is essentially experimental and is to be determined from the I, H and Q'', H curves from the relation

$$b''=(I/H)(dQ''/dI)\simeq\Delta Q''/\Delta\int HdI, \tag{22}$$

using increments as small as is consistent with the avoidance of nonsignificant irregularities due to the inevitable scatter of the experimental points. If the change in magnetization corresponding to Q'' were entirely due to reversible rotations in the natural anisotropy fields of the crystals, b'' would be constant and equal to b as calculated from the crystal anisotropy constants (see Eq. (14)). In general, b'' will differ from b owing to internal strains and other irregularities, and also it will vary with H, particularly over ranges where irreversible changes are predominant. A comparison of b'' with b may then give some indication of the state of the material and the nature of the elementary mag-

CC-0. In Public Domain. Gurukul Kangri Collection, Haridwar

Digitized by Arya Samaj Foundation Chennai and eGangotri

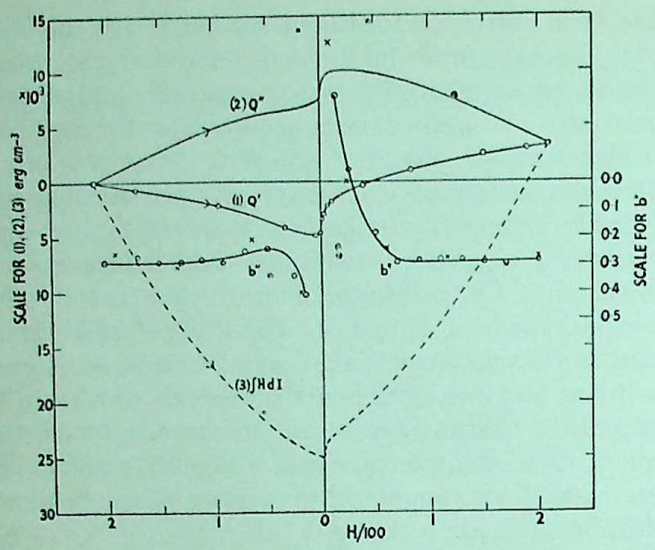


FIG. 5. Magnetocaloric effect in annealed Armco iron. Data for curves (1) and (3) from Hardy and Quimby (1938). Q', heat developed. Q'', heat developed less that due to change in intrinsic magnetization. $b''=\Delta Q''/\Delta\int HdI$. Circles, values derived from smoothed curves. Crosses, values from experimental points.

netization processes occurring. The "ideal" values of a and b and some other data for the ferromagnetic elements are given in Table II, and the results of representative analyses are shown graphically in Figs. 5–8.

As the curves of Figs. 5, 6, and 7 have been fully discussed elsewhere,[3] mention will be made here of only a few of the main points. It becomes evident on considering the curves that the greater part of the adiabatic temperature change accompanying magnetization can be accounted for by a superposition of two effects: the reversible heating (on increase of field) associated with increase of intrinsic magnetization, and the reversible cooling (on increase of field) associated with rotations of the domain magnetization vectors in the local anisotropic field. (It should be noted that over a half-cycle, starting from $|H_{\max}|$ as H_0, a "cooling" effect gives a positive Q', or Q'', in the low field region and conversely.) In cobalt the rotational effect is predominant. The other extreme, in which the intrinsic

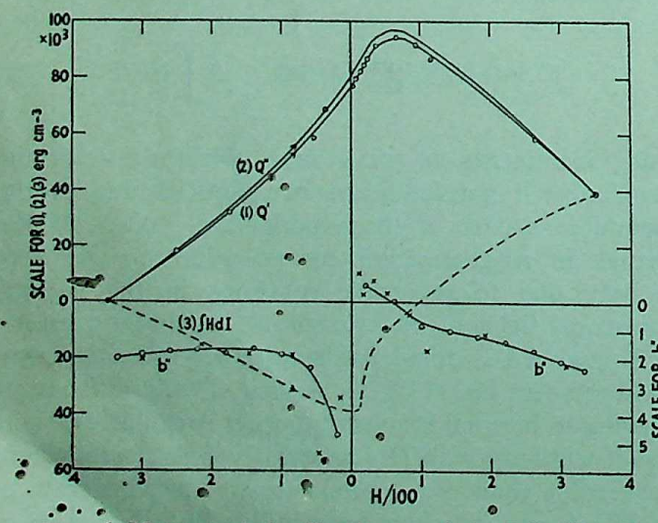


FIG. 6. Magnetocaloric effect in annealed cobalt. Data for curves (1) and (3) from Bates and Edmondson (1947).

effect is predominant is represented by certain alloys, in which, particularly when the Curie point is not far above the temperature of the experiments, relatively enormous heating effects have been obtained (e.g., for Monel metal, 70 Ni, 30 Cu in a half-cycle with $|H_{\max}|$ about 360, $-Q'$ exceeds 100×10^3). For iron and nickel the component heating and cooling effects are of the same order of magnitude, the resultant effects are small (and hence difficult to measure), and the experimental Q' curves show an extraordinary diversity for closely similar materials, and also for the same material taken over half-cycles with different limits.

The values of b'' obtained from the experimental results are in many cases reasonably constant over a field range in which the change of magnetization would ordinarily be assumed to be due to reversible and primarily rotational processes. The mean values of $-b''$ from the initial $I_{\max}$ to I_{rem} for Fe, Co, and Ni (Figs. 5–7) are about 0.30, 2.0, and 3.7 as compared with calculated values of b (at the temperatures of the experiments) of 0.63, 1.3, and 5.9. (It should be noted that the temperature of the specimens was about 41°C in the experiments of Hardy and Quimby, and about 20°C in those of Bates.) Over the constant b'' range be-

TABLE II. Data for ferromagnetic elements at 290°K. $a=-(T/I_0)(dI_0/dT)$. $b=(T/k)(dk/dT)$. $\Delta Q'$, energy change, erg cm^{-3}, corresponding to temperature change ΔT.

	$I_0\times10^{-3}$	$a\times10^2$	$-b$	$(\Delta T/\Delta Q')\times10^8$
Fe	1.72	3.4	0.58	2.8_3
Ni	0.48_5	14.3	4.5	2.5_6
Co	1.42	0.8_8	1.3	2.6_2

tween about 50 and 200 oersteds in Fig. 8, the value of b'' of about 4.7 agrees almost exactly with the calculated value of 4.5 for b. When it is borne in mind that by the method of treatment of the results experimental uncertainties are all concentrated in b'', and that owing to the uncertainties in the values of the crystal constants[1] the calculated values of b may be in error by 20 percent or more, the agreement as to order of magnitude of b'' and b must be considered satisfactory. The differences, however, even in the quasi-constant ranges, are probably significant and may be tentatively attributed to residual strains even in annealed materials. It has been shown[3] that the effect of such strains is to reduce the effective numerical value of b in nickel, but in general not even a rough estimate of the effect can be made owing to the absence of reliable data on the crystal magnetostriction coefficients.

In low fields the striking variations of b'' may be taken as an indication of the occurrence of irreversible processes, and little progress can be made in analyzing this part of the magnetization curve unless the reversible and irreversible heating effects can be separated (see below). The decrease in the numerical value of b'' in high fields, apparent in Figs. 7 and 8 for nickel, occurs in

CC-0. In Public Domain. Gurukul Kangri Collection, Haridwar

Digitized by Arya Samaj Foundation Chennai and eGangotri

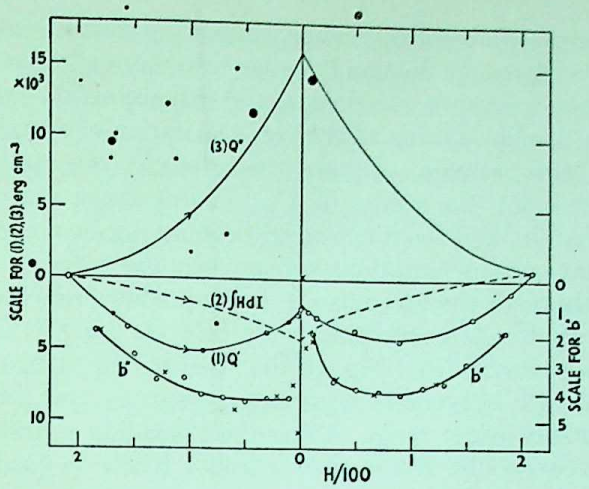


FIG. 7. Magnetocaloric effect in annealed nickel. Data for curves (1) and (3) from Hardy and Quimby (1938).

a reversible range, and raises an entirely new problem. Although accurate estimates of b'' cannot be made in the higher fields without precision measurements of the magnetization curves, the systematic decrease in $|b''|$ cannot be attributed to uncertainties arising for this reason. In connection with Fig. 7, it was suggested[3] that the decrease might be due to a relative increase in higher fields in the contribution from crystal grains with higher strain anisotropy and numerically smaller b. It does not seem possible, however, to account for very small values of b'' in this way (an estimated lower limit[15] to $-b''$ is 0.27), and it is still less possible to account for a change of sign, such as is shown in the highest fields in Fig. 8. The basic fact is that in the higher fields the rate at which heat is developed with change of field dQ'/dH approaches and eventually exceeds the calculated rate due to change in intrinsic magnetization dQ_i'/dH. In other words, unless the calculated dQ_i'/dH is much in error, which there is no reason to suppose, there is an additional heating effect other than those so far considered which may exceed, numerically, the coiling effect associated with rotational processes. Two possible processes have been suggested. One is the quasi-paramagnetic re-orientation of the moments of "small domains," which provides a possible explanation of an otherwise unexplained excess in the value of dI/dH in very high fields.[16] The other is the gradual "fading-out" of domain boundaries as the directions of magnetization on either side become more nearly parallel. Either of these processes would lead to an increase in the effective value of the coefficient a, which preliminary calculations show could be of the required order of magnitude over the relevant ranges of magnetization curves. Much more theoretical and experimental work will, however, be required before definite conclusions can be reached.

Variation of Magnetization with Temperature

From suitable measurements on the change of magnetization with temperature in constant field it is possible, as described in Sec. V, to derive values of $(\partial Q'/\partial H)_S$ [see Eq. (18)], so that in principle the thermal changes associated with reversible and irreversible processes can be separated. Some results obtained by Tebble *et al.*[13] for annealed nickel are shown in Fig. 9.

That the curves 1a and 1b do not join smoothly is probably attributable mainly to incomplete reversi-

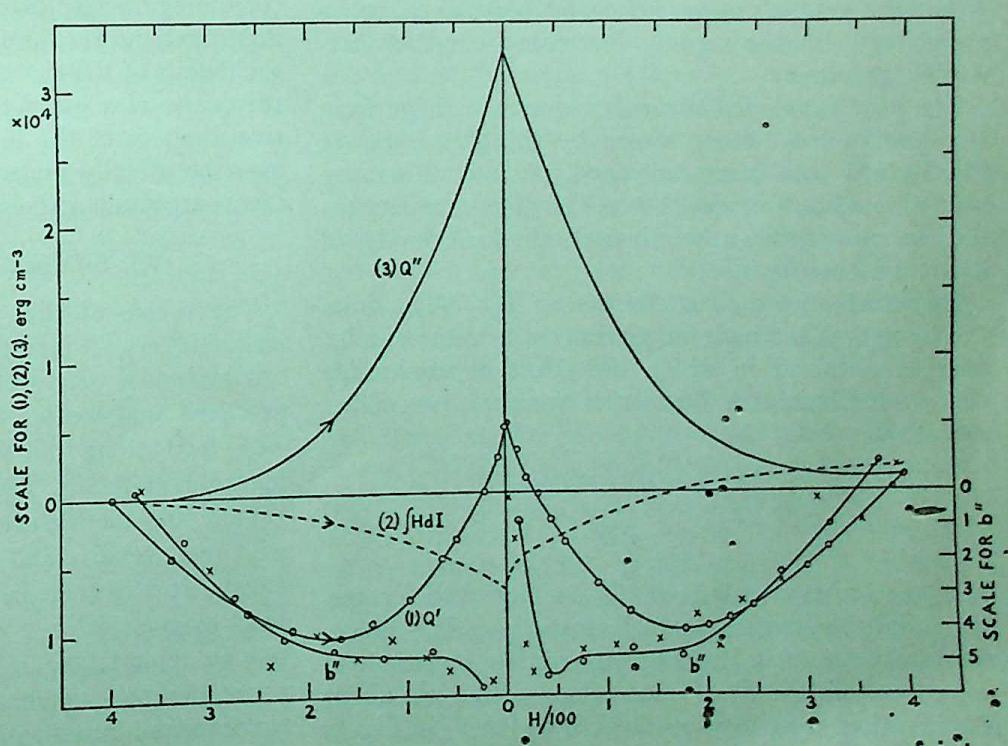


FIG. 8. Magnetocaloric effect in annealed nickel. Data for curves (1) and (3) from Bates and Davis (1950).

[15] P. Rhodes, unpublished.
[16] K. L. Hunt (to be published, 1952).

CC-0. In Public Domain. Gurukul Kangri Collection, Haridwar

Digitized by Arya Samaj Foundation Chennai and eGangotri

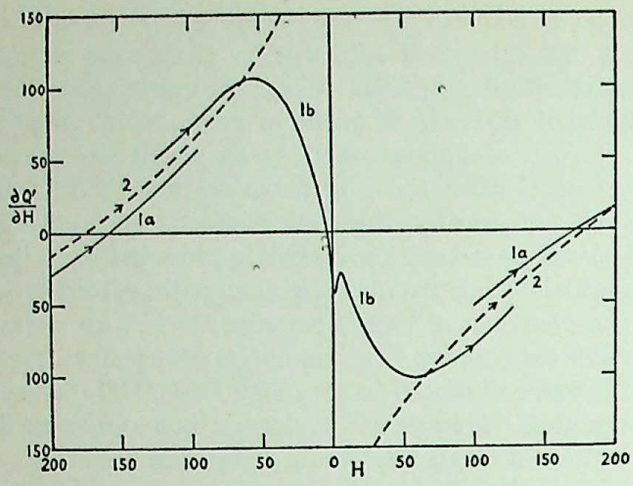


FIG. 9. Reversible and total magnetocaloric effect in annealed nickel. $(\partial Q'/\partial H)$, erg cm^{-3} oersted^{-1}. 1. $(\partial Q'/\partial H)_S$ (isentropic) derived from $(I/T)_H$ for nickel 2. 1a. $(T)_{max}=20°C$. 1b. $(T)_{max}=1.3°C$. Data from Tebble, Wood, and Florentin (1952). 2. $(\partial Q'/\partial H)_Q$ (adiabatic) from direct measurements for nickel 1. Data from Bates and Davis (1950) (for I, H curves see Fig. 10).

bility of the change of I with T with a maximum value of ΔT of 20°C even in fields greater than 100 oersteds. The "annealed nickel" of Tebble was sufficiently similar (see Fig. 10) to that of Bates, for which the magnetocaloric results are shown in Fig. 8, for a comparison of the two sets of results to be significant at fields well above the coercive fields (about 0.4 and 2.0, respectively). The close agreement between the curves (1) and (2), obtained by totally different methods, for fields greater than about 60 oersteds, where the changes are predominantly reversible, confirms the general theoretical treatment, and indicates, in a striking way, the general reliability of the experimental results. The divergence of the curves below 60 oersteds is to be associated with the rapidly increasing effect of irreversible processes.

The heat developed reversibly over the range from $H=-50$ to $H=+50$ is shown by the Q'_{rev} curve in Fig. 10. The total heat developed, Q', over this range (taken from Fig. 8) is also shown. The difference between the two curves gives approximately the heat developed in irreversible processes.

By allowing for the contribution to $(\partial Q'/\partial H)_{rev}$ from the changes in intrinsic magnetization, a value of b''_{rev} may be obtained in which the effect of irreversible changes is eliminated. When κ_r is known, a convenient formula is

$$b''_{rev}=\frac{(dQ'_{rev}/dH)-a(I+\kappa_r H)}{\kappa_r H}. \qquad (23)$$

The so calculated values of b''_{rev}, which should correspond only to reversible rotations and boundary movements, are shown in Fig. 10. Approximate constancy of this "reversible" b'' is maintained down to about $H=5$, rather than to about $H=70$ as for b'' in Fig. 9. The actual value of b''_{rev} is very close to the ideal value of b calculated from the crystal anisotropy (Table I) over the whole of this range, suggesting that reversible movements of a domain boundary are thermally equivalent to reversible rotations of the magnetization vector in a domain. Owing to the rapid variation of I with H for fields between -2 and $+2$ oersteds for this material ($H_c\simeq 0.36$), the values of b''_{rev} in this range are very uncertain, and too much weight should not be attached to the curious variations indicated by the curve.

Although the ascending and descending branches of the hysteresis curve practically coincide for $|H|>20$, it is apparent from Fig. 10 that thermal effects associated with irreversible processes are spread over a considerably wider range. Along the ascending branch of the curve, the irreversible changes result in heating (positive gradient of the Q'_{irrev} curve) up to the region of the coercive field, and thereafter in cooling. (The net irreversible effect over a complete ascending curve is a heating corresponding to half the "hysteresis loss," but for this particular material the maximum value of Q' greatly exceeds the net heating over the half-cycle.) There is, of course, no general thermodynamic reason for expecting an irreversible change to be accompanied by heating rather than cooling, and these experiments show quite clearly that the thermal changes associated with irreversible magnetization processes are neither necessarily positive nor wholly irreversible. In fact, the major part of the thermal change associated with irreversible processes for annealed nickel is reversible, and the sign and magnitude of the effect indicate that the associated change of internal magnetic energy [see Eq. (5)] is mainly due to the change of direction of the magnetization vectors in the local anisotropic fields.

The above short discussion shows that potentially by combining the results of magnetic and magnetothermal investigations much information can be obtained about the details of the elementary processes occurring along the course of a magnetization curve. A fully quantitative analysis of the lower field regions cannot, however, be usefully undertaken until the various experiments are made with essentially the "same" material.

VII. SUMMARIZING DISCUSSION

The theme of this paper has been magnetic and magnetothermal investigations, the results of which can be linked together to give information about the processes contributing to the change of magnetization with field along the magnetization curves of ferromagnetic materials. The basic question being asked is, "What are the elementary processes occurring, and with what relative and absolute magnetic and thermal effects, at each stage in the course of the change of the bulk magnetization?" An inquiry of this kind could not be undertaken unless much was already known about the main elementary processes from more direct experimental investigations and theoretical studies; for a quantitative treatment, moreover, the spontaneous magnetization I_0 and the crystal anisotropy and

CC-0. In Public Domain. Gurukul Kangri Collection, Haridwar

Digitized by Arya Samaj Foundation Chennai and eGangotri

magnetostriction coefficients must be known, and also the variation with temperature of each of these.

Reference has been made to five types of experimental investigation, the results of which have been utilized in such partial analyses as have been presented:

(1) The variation of I with H at constant temperature, i.e., the ordinary magnetization curves.

(2) The reversible susceptibility κ_r.

(3) The magnetocaloric effect, that is, the change of temperature accompanying adiabatic magnetization. The experimental results give effectively $(\partial T/\partial H)_Q$, or the corresponding heat developed $(\partial Q'/\partial H)_Q$.

(4) The reversible change of magnetization with temperature, $(\partial I/\partial T)_H$, which gives the reversible change of temperature, or the heat developed reversibly with change of field, that is, $(\partial Q'/\partial H)_S$.

(5) The Barkhausen effect. The experiments give the size distribution of the discontinuities in magnetization above a certain minimum size, and the contribution of these essentially irreversible changes to the total change of magnetization over the whole or any part of the field range examined.

In connection with (1) and the frequent use of the phrase "the magnetization curve" in this paper, it may be prudent to state explicitly that there is not a unique magnetization curve for any material showing hysteresis effects, but that it has not seemed necessary to enter here into either the subtleties of the defining conditions or the difficulties of accurate measurement. The curves mainly considered in illustration have been the ascending branches of hysteresis loops taken after the establishment of cyclic conditions by the standard methods; but the general scheme of analysis would apply equally well to any reproducible type of curve.

Measurements of κ_r (2) in conjunction with (1) will give the reversible component of the change of magnetization over any part of the field range.

The magnetocaloric measurements (3) give the thermal effects associated with the total change of magnetization. Over reversible ranges conclusions can be drawn, from the sign and magnitude of the effect, about the contributions from the change in intrinsic magnetization and from other reversible changes, by far the most important of these, in the cases so far examined, being the rotations of the domain magnetization vectors. The thermal effects associated with change in magnetization by change in intrinsic magnetization and by rotational change are of opposite sign, and the remarkable diversity in the magnetocaloric curves for different materials is largely due to the different magnitudes and relative proportions of these two effects. The presence of strain is qualitatively indicated by a deviation in the values of a characteristic coefficient b'', calculable from the experimental results, from the value of a coefficient b, which may be derived from the crystal anisotropy data. The possibility of giving a more quantitative interpretation of the experimental results is dependent on further, or more accurate data becoming available for crystal anisotropy and magnetostriction.

Little progress can be made in interpreting the mag-

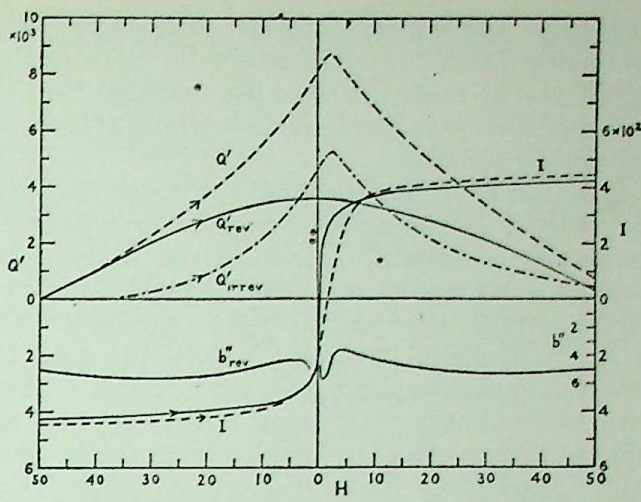


FIG. 10. Magnetocaloric effect in annealed nickel. Q', total heat developed from magneto-caloric measurements for nickel 1 (I, H curve broken) (Bates and Davis). Q'_{rev}, heat developed in reversible changes, from measurements of $(\partial I/\partial T)_H$ for nickel 2 (I, H curve full) (Tebble, Wood, and Florentin). $Q'_{irrev} = Q' - Q'_{rev}$. b''_{rev}, effective thermal change coefficient, derived from Q'_{rev}.

netocaloric results in the lower field ranges unless the thermal effects associated with reversible and irreversible processes can be separately estimated. This is made possible by measurements on the reversible change of magnetization with temperature (4), from which the thermal contribution from reversible processes to the magnetocaloric effect can be derived, and hence also, if measurements of type (3) and (4) are made on the same material, that from irreversible processes. The reversible thermal effects even well into the hysteresis region are mainly associated with rotation of the domain magnetization vectors. The thermal effects associated with irreversible processes may be of either sign and are not wholly irreversible. In the material which has been most carefully examined, annealed nickel, the main part of the thermal change, is that associated with the change in state, corresponding to the change in direction of the domain magnetization vectors or the magnitude of the intrinsic magnetization, and the strictly irreversible heating effect associated with the irreversible processes by which the change of state is attained is comparatively small. It is this residual effect which contributes to the net heating over a complete cycle, or half-cycle.

The work on the Barkhausen effect (5) has shown that the discontinuities in magnetization are not in general due to spontaneous movements of primary domain boundaries as wholes, but to irregularities on a smaller scale in the movement, particularly of 180° boundaries. It seems probable that as the field changes the boundary adjusts itself to its changing quasi-equilibrium position and maintains an approximate planeness by a sequence of sudden localized jumps of sections of the boundary, of magnitudes conditioned by localized irregularities. It seems certain that almost the whole of the irreversible change of magnetization is due to these Barkhausen jumps but that in all materials part of the

CC-0. In Public Domain. Gurukul Kangri Collection, Haridwar

Digitized by Arya Samaj Foundation Chennai and eGangotri

irreversible contribution must be attributed to discontinuities below the minimum size for which reliable counts can be made, and in some materials the discontinuities occur in part in rapid bursts and cannot be individually recorded.

It can hardly be suggested that a thorough investigation of the Barkhausen effect should be made for every ferromagnetic material. This is, indeed, unnecessary, for, although there are many special problems in connection with it which call for fuller examination, the recent work which has been outlined has gone far towards showing the character of the processes to which irreversible changes in magnetization may be attributed. The over-all irreversible change can be most readily obtained by the more direct determinations of the I, H curves (1) and the κ_r, H curves (2). The two types of magnetothermal investigation ((3) and (4)) are, however, indispensable if an adequate analysis is to be made. As investigations of this kind make considerable demands on experimental skill and on time, it is particularly desirable that there should be the closest cooperation between those engaged in such work in the choice of materials for examination.

The information that can be obtained by combining the results of different investigations has been exemplified in Sec. VI. The analyses are, however, partial, and it will not be possible to assess fully the value of the general method until more complete sets of results are available for one and the same material. It would be unwise to base general conclusions on the partial analyses for a limited number of materials which have so far been made. These partial analyses do, however, show that by making measurements on the macroscopic behavior of ferromagnetic materials in two or more types of experiment, and combining the results in some such manner as that outlined, extensive information may be obtained about the microscopic processes taking place. An analysis of this kind does not, of course, provide a theoretical "explanation" of the form and quantitative characteristics of a given magnetization curve; but the prospects of a satisfying explanation will become much brighter when what is happening becomes clearer—when it is known, in short, what it is that has to be explained.

ACKNOWLEDGMENTS

My indebtedness to all those whose work has been referred to will be apparent. I wish to thank specifically Dr. Rhodes and Dr. Tebble for valuable help in connection with this paper. I also gratefully acknowledge permission from the Physical Society to reproduce Figs. 1 and 3 and from the Editors of the *Philosophical Magazine*, Figs. 5, 6, and 7.

CC-0. In Public Domain. Gurukul Kangri Collection, Haridwar

Digitized by Arya Samaj Foundation Chennai and eGangotri

REVIEWS OF MODERN PHYSICS VOLUME 25, NUMBER 1 JANUARY, 1953

Heat Effects in the Magnetization of Silicon Iron

L. F. BATES AND G. MARSHALL

University of Nottingham, Nottingham, England

A brief description is given of the method used by Bates and his co-workers which permits the measurement of the thermal changes which accompany the step-by-step magnetization of ferromagnetic metals. The method has now been used to examine the behavior of 0.5 and 4 percent silicon iron in the untreated and annealed states when magnetized along the virgin curve and in cycles with fields up to 380 oersteds. In this work, some twenty copper-constantan thermocouples generate currents when a magnetic field acting on the ferromagnetic specimen is changed, and these are transmitted ballistically via a toroidal Mu Metal transformer to a highly sensitive moving coil galvanometer of long period. As the thermal changes in the present work were very small, a new technique had to be developed to deal with them. The measured thermal changes are plotted as functions both of the intensity of magnetization and of the effective magnetic field. The several errors and experimental difficulties, including asymmetry in thermal readings, stray induction effects, heating due to eddy currents, and thermal and electromagnetic disturbances experienced during the measurements are briefly discussed, and the methods used to overcome them are briefly outlined.

The results are examined in the light of current domain theory and a theoretical procedure developed by Stoner and Rhodes, in which the thermal contributions resulting from change in intrinsic magnetization, often described as the magnetocaloric effect, is subtracted from the recorded thermal change, and the residue is considered in detail. Another procedure recently applied to results for nickel was also examined, but it was found inapplicable to the silicon iron data. An unusual depression or dip is found in the curves of thermal change plotted as a function of the applied field when the region of low field values is reached upon reducing the field from the maximum used in describing a hysteresis cycle. This observation provides evidence in support of Kittel's theory of flux closure which Bozorth has used to explain the low remanence of such alloys which exhibit little magnetostriction and magnetic anisotropy and small internal strain. It is suggested that the strange depression may be correlated with some peculiar domain boundaries recorded by the Bitter powder technique on the (100) surface of a single crystal of silicon iron when it is demagnetized either thermally or in the above manner. These boundaries "wriggle" in an extraordinary manner which suggests that they separate regions either of flux closure in opposite directions or domains whose magnetization vectors meet head-on.

I. INTRODUCTION

IN a series of papers,[1–7] experiments on the thermal changes which accompany the magnetization of some ferromagnetic metals on making step-by-step changes in an applied magnetic field have been reported. The study has so far been confined to low and moderate fields, and the purpose of the investigations is to gain insight into the complicated hysteresis phenomena which exist in these regions. The behavior of iron, nickel, and cobalt and of many of their alloys have been described, and a resumé of the more important results was given at the Grenoble Colloquium (1950).[7] In the present communication are reported experiments made with specimens of silicon iron containing approximately 0.5 and 4 percent silicon, both in the untreated and in the annealed states.

Ewing was the first to emphasize the smallness of the temperature changes which result on taking a specimen of iron of reasonable purity through a single hysteresis cycle, and it is now well known that if temperature changes are to be measured as a cycle is described with step-by-step changes in magnetic field, the recording system must be capable of detecting changes of the order of 10^{-6} °C. The method used in the present work follows that described by Bates and Weston in 1941 and will be only briefly outlined here.

The specimen under investigation is usually in the form of a rod or stout wire, some 40 cm long and about 0.5 cm or less in diameter. It is mounted symmetrically inside a vertical water-cooled solenoid which supplies the magnetizing field, while the vertical component of the earth's magnetic field is separately compensated. The magnetizing current can be varied in steps by connecting or cutting out resistances in parallel with the magnetizing solenoid, a choke of high inductance and low resistance being permanently in series with the supply from the mains, to avoid too rapid field changes with consequent serious eddy-current heating of the specimen.

Attached to the specimen are the "hot" junctions of some 20 copper-constantan thermocouples, the "cold" junctions being close to, but not in contact with, the specimen. Each thermocouple has its own primary winding on a Mu Metal spiral core or transformer, the secondary winding of which is connected to a sensitive galvanometer of long period. The galvanometer scale distance is of the order of 8 meters, and the ballistic deflections are observed with a large telescope. When the field is changed, the temperature of the specimen changes by about 10^{-5} °C, and a current flows in each thermocouple circuit; the flux through the secondary winding of the transformer changes and then remains constant for a short time so that the galvanometer gives a ballistic deflection, after which the galvanometer spot returns to its zero position.

[1] L. F. Bates, J. phys. et radium **10**, 353 (1949).
[2] L. F. Bates, J. phys. et radium **12**, 459 (1951).
[3] L. F. Bates and J. C. Weston, Proc. Phys. Soc. (London) **53**, 5 (1941).
[4] L. F. Bates and A. S. Edmondson, Proc. Phys. Soc. (London) **59**, 329 (1947).
[5] L. F. Bates and E. G. Harrison, Proc. Phys. Soc. (London) **60**, 213 (1948).
[6] L. F. Bates and D. R. Healey, Proc. Phys. Soc. (London) **55**, 188 (1943).
[7] L. F. Bates and J. H. Davis, Proc. Phys. Soc. (London) **63A**, 1265 (1950).

CC-0. In Public Domain. Gurukul Kangri Collection, Haridwar

Digitized by Arya Samaj Foundation Chennai and eGangotri

These deflections are calibrated by producing a calculated adiabatic cooling of the specimen by suddenly hanging a weight from its lower end, in accordance with the Joule expression

$$\Delta T = -\alpha TF/J\rho SA \quad \text{or} \quad \Delta Q = -\alpha TF/A,$$

where ΔT is the change in temperature which occurs when a tension F dynes is applied to a rod of coefficient of expansion α; specific heat is S, density ρ, and area of the cross section A, at the absolute temperature T. It is usually more convenient to calculate the corresponding quantity of heat ΔQ expressed in ergs per cc.

The magnetizing solenoid, 70 cm long, consisted of some 10 000 turns of No. 21 S.W.G. glass-covered wire wound in 15 layers on the outside of two concentric brass cylinders through which cooling water circulates at a maximum rate of over a liter per minute. The solenoid is energized from the 220-volt dc mains.

II. PREPARATION AND MOUNTING OF SPECIMENS

The silicon iron specimens were supplied as long bars, one inch in diameter, which were cut into four quadrants. From these quadrants specimens were ground to shape by hand because of the brittle nature of the material. The final surface was not as satisfactory as those of specimens normally used in such work, and, since the specimens were not of strictly uniform diameter, the average diameter for use in the calculation of intensities of magnetization was therefore found by measuring the length of fine wire in a search coil of known number of turns wound tightly upon a specimen.

The prepared specimen was attached by sockets and grub screws to a brass extension piece supported from the top of the solenoid housing; a second brass extension piece carrying a link to support the calibration load was similarly attached to the lower end of the specimen. The constantan portions of the thermocouples were made as short as possible, and the thermojunctions were filed thin to give minimum thermal capacity. The thermocouples were made of strips of copper and constantan, 3 mm wide, rolled from No. 20 S.W.G. wire, and were shaped in a jig to fit the specimens. The thermocouple leads were made as thick as possible and as long as necessary to give a good distance between the solenoid and Mu Metal core.

The thermojunctions were bound to the middle third of the specimen with waxed thread, for it is important that the specimen shall be able to expand and contract as freely as possible. When the junction was covered with a small quantity of paraffin wax, the disturbing effects of galvanometer drift resulting from convection currents within the solenoid were very greatly reduced, although of course the thermal capacity of the thermocouple system was thereby increased and the sensitivity of the arrangement reduced.

When a change is made in the solenoid current, it is found that a sudden, "inductive" motion is in general superimposed upon the true, leisurely, "thermal" deflection of the galvanometer. This inductive effect is produced by magnetic pick-up in the thermocouple leads. It is eliminated by placing in the stray field of the solenoid a small coil which is connected to its own primary winding on the Mu Metal core, the total resistance of the coil circuit being the same as that of a thermocouple circuit. If the coil is suitably placed with respect to the specimen, a pick-up effect equal and opposite to that induced in the thermocouple leads is supplied, and only the "thermal" deflection of the galvanometer remains. Incidentally, the galvanometer was a commercial Tinsley Type 4789 with its control magnet shunted.

III. DETAILS OF SPECIMENS

Five specimens were investigated and details of their composition and relevant physical constants are given below.

Specimen I: 4 Percent Si-Fe Unannealed (Stalloy)

Length, 37.20 cm at 18°C. Volume, 8.32 cc. Mean area of cross section, 0.224 sq cm. Coefficient of expansion between 18 and 100°C, 12.8×10^{-6} *per* °C. Demagnetizing factor, 0.0085.

Specimen IA: 4 Percent Si-Fe Annealed

This was specimen I after annealing. The actual treatment as carried out by G.K.N. Research Laboratories staff was the normal works anneal, i.e., approximately 15 hours heating up to 830°C, 20 hours at 830°C "in own atmosphere," followed by approximately 48 hours in the town's gas supply.

Specimen II: 4 Percent Si-Fe Annealed

This was a specimen cut from the same bar as specimen I and annealed by G.K.N. as follows: 16–20 hours at 830°C, the total time occupied including heating-up time at high temperature, and cooling-down extending over 34 hours. Some oxidation of the surface took place. Length, 37.69 cm. Volume, 7.16 cc. Mean area of cross section, 0.230 sq cm. Coefficient of expansion between 18 and 100°C, 13.3×10^{-6} *per* °C. Demagnetizing factor, 0.0085.

Specimen III: 0.5 Percent Si-Fe Untreated (Lohys)

Length, 37.95 cm. Volume, 7.16 cc. Mean area of cross section, 0.189 sq cm. Coefficient of expansion between 18° and 100°C, 12.7×10^{-6} *per* °C. Demagnetizing factor, 0.0071.

Specimen IIIA: 0.5 Percent Si-Fe Annealed

This was specimen III after annealing. The treatment received was the same as specimen IA. Both these specimens oxidized slightly, with some scaling of the surface, and had to be cleaned with emery cloth.

CC-0. In Public Domain. Gurukul Kangri Collection, Haridwar

Digitized by Arya Samaj Foundation Chennai and eGangotri

IV. EXPERIMENTAL MEASUREMENTS

The magnetic hysteresis curves of the specimens were found by the usual ballistic method, correction being made for demagnetization effects, using the following expression for the demagnetization factor:[8]

$$(N/4\pi)_{\mu=\infty} = (4.02 \log_{10} m - 0.92)/2m^2 \quad \text{for} \quad m \geqslant 10,$$

where m is the ratio of the length to the diameter of the rod specimen.

The thermal readings were difficult to obtain, because of their smallness, and the number of steps for a given hysteresis cycle of chosen maximum field was naturally somewhat less than the number used in describing the magnetic cycles. Reference has already been made to the elimination of the "inductive" effect by means of a compensating coil. In most of the previous work the position of this coil did not have to be determined with great accuracy, but in the present work the coil settings for certain field changes were relatively widely spaced and frequently very critical, a displacement of 0.5 mm often giving appreciable "inductive" deflections. The position of the coil had also to be predetermined before the final thermal measurements could be made. The position was considered correct when the galvanometer deflection was the same whether one made a field change from, say, $+H_1$ to $+H_2$ in one sense or the other, i.e., with the north-seeking end of the specimen upwards or with the south-seeking end upwards. (The technique of using the compensating coil for virgin curve measurements was slightly different and need not be described here.)

But a new technique had to be developed for making accurate thermal measurements when the galvanometer deflections were about 1 mm; incidentally, the deflection could easily be read to at least 0.1 mm. The inductive effect, which had hitherto been regarded as a spurious and unnecessary evil, was now used to estimate the true thermal deflection. For a number of positions of the compensating coil in the vicinity of the true compensation setting, the successive deflections accompanying a given field change made in each of the two senses were recorded and plotted against the corresponding position of the coil as read from a graduated bar. In this way two lines were obtained, one on each side of the true compensation position, each corresponding to a true thermal effect upon which was superimposed an increasing inductive effect in the same direction. Consequently, if the inductive effect is a continuous function of the distance of the coil from the solenoid, the intersection of the lines gives the true thermal deflection and also, incidentally, the true compensating position. This method proved to be very effective with small deflections. The sensitivity of the galvanometer was frequently checked by reversing a standard current in a control circuit.

In spite of precautions such as the use of a shunted solenoid circuit and the use of a large choke in the supply from the mains, thermal effects produced by eddy currents remained surprisingly large, particularly in view of the high resistivity of silicon iron, and the over-all heating for a complete cycle depended on the number of steps in its description. Correction for eddy current heating was made by assuming that the difference between the sum of the thermal deflections recorded in describing one-half of a cycle and the corresponding $\int HdI$ was the result of eddy current heating. Then this difference D was assumed to be proportional to ΣdB_n^2, where dB_n is the change of magnetic induction associated with the nth step, and therefore the eddy current heating in any particular step dB_1 could be calculated from the ratio $D \cdot dB_1^2/\Sigma dB_n^2$. It is realized that this procedure is not entirely satisfactory, as it presupposes that the time constant of the circuit remains constant throughout the cycle and that Warburg's law holds.

Asymmetry in readings, i.e., in the values for the deflections obtained on describing a half-cycle in the two possible directions, which had been noted by previous workers, was at first extremely pronounced in the present work. It was finally traced to an interaction between the transformer core and the combined stray field of the solenoid and specimen, which gave rise to slow galvanometer deflections very like those caused by true thermal changes. But it was interesting to note that even when the asymmetry was great, the mean of the two deflections in the two directions was undoubtedly correct, and therefore it is not necessary to balance out the asymmetry exactly. It was greatly reduced by raising the transformer and rotating it in a horizontal plane, and it is certain that with an ideally wound transformer it could be avoided altogether, a remark which also applied to spurious deflections produced by stray fields arising from sources outside the laboratory.

For the Joule calibration a load of 1500 g was generally employed. This produced a temperature change of about 5.3×10^{-4} °C, with a corresponding galvanometer deflection of about 250 tenths of 1 mm. Consequently, 0.1 mm corresponded to about 2.1×10^{-6} °C. Several workers have enjoyed a greater sensitivity, but in the present case some sensitivity was sacrificed to obtain improved stability. For the first time on record, the Joule calibration was found in the present work to depend on the state of magnetization of the specimen. Actually, this was traced to a slight movement of thermocouple leads when the calibrating load was applied; this gave rise to a disturbing inductive effect which caused a galvanometer deflection. The effect was, of course, avoided by always attaching the calibration load to a demagnetized specimen.

It was convenient to express the galvanometer deflections in units of 0.1 mm, and the greatest deflections were seldom more than 100 units. For example, in the 40-oersted cycle with the specimen of 0.5 percent silicon

[8] H. Neumann and K. Warmuth, Wiss. Veröffentl. Siemens-Konzern 11, 25 (1930).

CC-0. In Public Domain. Gurukul Kangri Collection, Haridwar

Digitized by Arya Samaj Foundation Chennai and eGangotri

iron in the untreated state, the sum of all the deflections in the half-cycle was only 45 units. Naturally, when the number of very small deflections in a cycle is large, the over-all accuracy of the measurements suffers, apart from the much increased experimental difficulties, and readings were recorded only when there was no doubt that they were taken when the galvanometer was free of drift, etc.

Since the hysteresis loops were so narrow, the value of $\oint HdI$ was found as follows. A graph of H was plotted against ΔI, where ΔI is the difference in the values of I for the same value of H, and the area under this graph was measured.

V. EXPERIMENTAL RESULTS

It will readily be appreciated that the results described below are characteristic of the particular specimens investigated, and that other specimens, nominally of the same composition and heat treatment, might give different results; in particular, structure-sensitive properties such as coercivity, remanence, and hysteresis loss might be greatly different.

We turn first to the magnetic I, H data for 4 percent silicon iron, specimens I and II. We were surprised to find that the values of I for maximum fields of 40, 200, and 400 oersteds, respectively, were consistently less for the annealed specimen. The measurements on both specimens were repeated with substantially the same results. These observations were rather disturbing, as one would expect annealing to relieve strain and increase permeability. Measurements by Smith and Shermann[9] on the effects of compression and tension on the permeability of silicon steel indicate that at low inductions compression reduces permeability, while at high inductions the reverse is found. But it seems difficult to explain our observations on these lines.

The untreated specimen was then annealed according to the given specification. On repeating the I, H measurements, we now found values of I, as expected, to be everywhere greater over the whole field range than with the same specimen before heat treatment. The values of I at 400 oersteds were practically the same, and the slopes of the curves showed that the difference between them was less as the field was increased, finally becoming zero at saturation. The forms of the curves for the two annealed specimens were not the same, the initial slope of the virgin curve of specimen II being slightly greater with the knee of the curve occurring at a lower value of the induction. The curve for specimen I after annealing, referred to as IA, was more rounded, and at fields greater than 2.3 oersteds it was above that for specimen II.

The following explanation of these observations is suggested. Sixtus,[10] by using torque measurements, x-ray analysis, and a method involving reflection from crystal surfaces, showed that preferred orientation exists in cold- and hot-rolled silicon iron both before and after annealing. He concluded that in hot-rolled silicon iron the highest permeability was to be found in directions at 45° to the rolling direction, with smaller values in directions at 0° and 90°, in that order. The reason therefore was the preferred orientation of the crystals set with their [100] axes at 45° to the rolling direction.

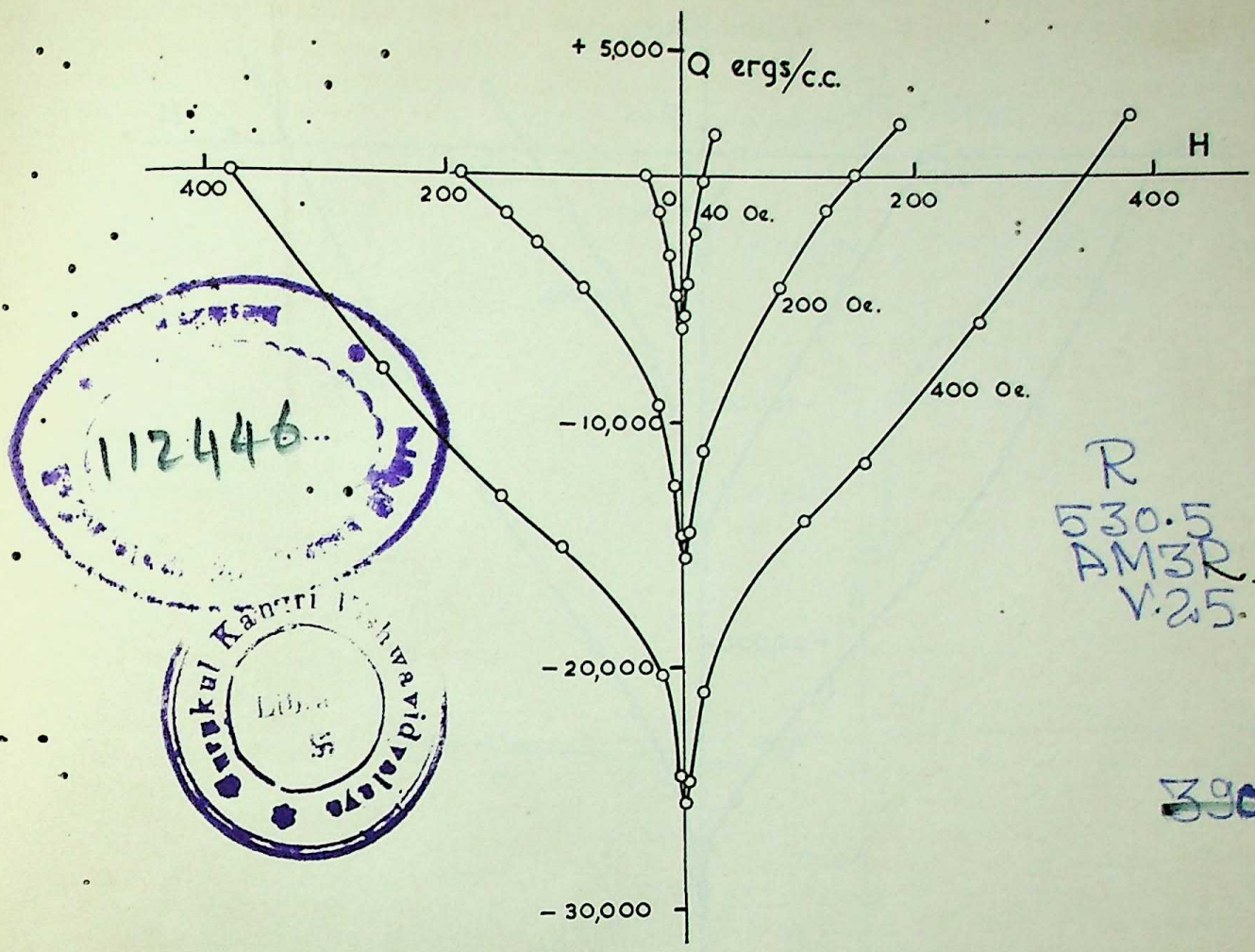
Now, although specimens I and IA were cut from the same bar, it is possible either that they were not cut exactly along the same direction or that the crystal orientation was different in different parts of the bar. Some evidence of this is found in the values of the coefficient of expansion, that of specimen I being less than that of specimen II. If the orientation was assumed to be more favorable in specimen I, this would explain the higher values of the induction found for this specimen in high fields. In low fields, below the knee of the I, H curve, where boundary movements predominate, the effect of annealing would be to facilitate such movements and to outweigh the effects of less favorable crystal orientations. Above the knee, where boundary movements are much less frequent, the effects of crystal orientation would predominate and therefore the induction should be greater in specimen I. At very high field values, both specimens should have the same induction, and this was indicated in the I, H curves. We therefore conclude that very close comparison of the I, H or thermal curves for specimens I and II is unwarranted, and that if we wish to make detailed comparison of such curves they must always be obtained with one single specimen, first in the untreated state and secondly after it has been annealed. The same specimen of the 0.5 percent silicon iron was so used in the untreated and annealed states. We may record that annealing in the case of specimen I increased I_R from 265 to 385 gauss and reduced H_c from 0.65 to 0.33 oersted for the 40-oersted cycle, the corresponding values for the annealed specimen II being 170 gauss and 0.176 oersted. In the case of the 0.5 percent silicon iron specimen, annealing increased I_R from 605 to 980 gauss and reduced H_c from 1.92 to 0.278 oersted. When the I, H curves were plotted on a very large scale to obtain $\oint HdI$, a peduliar 'waist' was found for the 40- and 400- oersted cycles. This phenomenon seems also to have been observed by MacLaren[11] in hysteresis loops for low content silicon steels.

We shall now review a few of the thermal curves obtained in the course of the work. The virgin curves will not be reproduced here as most of their main features are to be seen in the curves for the closed cycles of magnetization, which are usually much more informative and more satisfactory for making comparison between experiment and theory. Following the general procedure of earlier work, we save space by plotting only one-half of the $\int dQ$, I or $\int dQ$, H curves, since the

[9] C. M. Smith and G. W. Shermann, Phys. Rev. 4, 267 (1914).
[10] K. J. Sixtus, Physics 6, 105 (1935).
[11] M. MacLaren, Trans. Am. Inst. Elec. Engrs. 31, 2025 (1912).

CC-0. In Public Domain. Gurukul Kangri Collection, Haridwar

Digitized by Arya Samaj Foundation Chennai and eGangotri



112446
Gurukul Kangri Vishwavidyalaya
Library
R
530.5
AM3R
V.2.5.
3900

FIG. 1. Four percent silicon iron, untreated (specimen I). Q, H curve for $H_{max}=40$, 200, and 400 oersteds, approximately.

remaining portion may be obtained from the plotted portion by suitable displacement and rotation. For convenience, we always start demagnetization from the left-hand side of the figure.

In Fig. 1 are reproduced a series of Q, H curves for the untreated 4 percent silicon iron. The 400-oersted curve shows an initial cooling which is more or less linear with H, but this becomes less rapid as H is reduced to about -40 oersteds, when a pronounced cooling sets in, and this continues until H reaches a small positive value. The same features are reproduced in the opposite direction, i.e., heating instead of cooling, to give a curve which is moderately symmetrical about the Q axis. The over-all heating, corresponding to one-half the area of the appropriate hysteresis loop, is given by the position of the final point above the H axis on the right-hand side of the curve. The central portions of this curve are also seen in the 200- and 40-oersted cycles. The virgin Q, H curve, not reproduced here, follows closely that part of the Q, H curve of Fig. 1 for which H is positive, and lies entirely above the H axis.

In the case of the annealed 4 percent silicon iron specimen, Fig. 2, the curves for all three cycles show remarkably well how the cycles with the lower field ranges correspond with the central portions of the 400-oersted cycle. Once again the curves are fairly symmetrical about the Q axis, with a pronounced minimum in their central portions. It is interesting that if one superimposes Fig. 1 on Fig. 2, the curves of the former lie inside the latter.

The Q, H curves for the 0.5 percent silicon iron warrant rather more detailed treatment. The curve for the 40-oersted cycle for the annealed specimen, Fig. 3, shows an initial steady cooling with decrease in field, and this continues down to a field of -1 oersted, after which there is a rapid heating. The curve becomes less steep at about $+0.4$ oersted and is thereafter practically linear up to the final value of Q equal to the ordinary hysteresis loss. There appears to be a slight discontinuity at about $+0.2$ oersted. The same discontinuity is found in the Q, H curve for the untreated specimen, Fig. 4. Figures 3 and 4 are indeed in marked contrast.

The 400-oersted cycle Q, H curve for the annealed 0.5 percent specimen may be seen in Fig. 10, where it is labelled Q'. It is linear when H is large and has a dip at a small positive field; the virgin curve shows a slight cooling followed by a sharp heating, thus agreeing with the 400-oersted cycle at a positive value of the field. The 400-oersted cycle curve for the untreated 0.5 percent specimen gives the usual initial cooling with, in

CC-0. In Public Domain. Gurukul Kangri Collection, Haridwar

Digitized by Arya Samaj Foundation Chennai and eGangotri

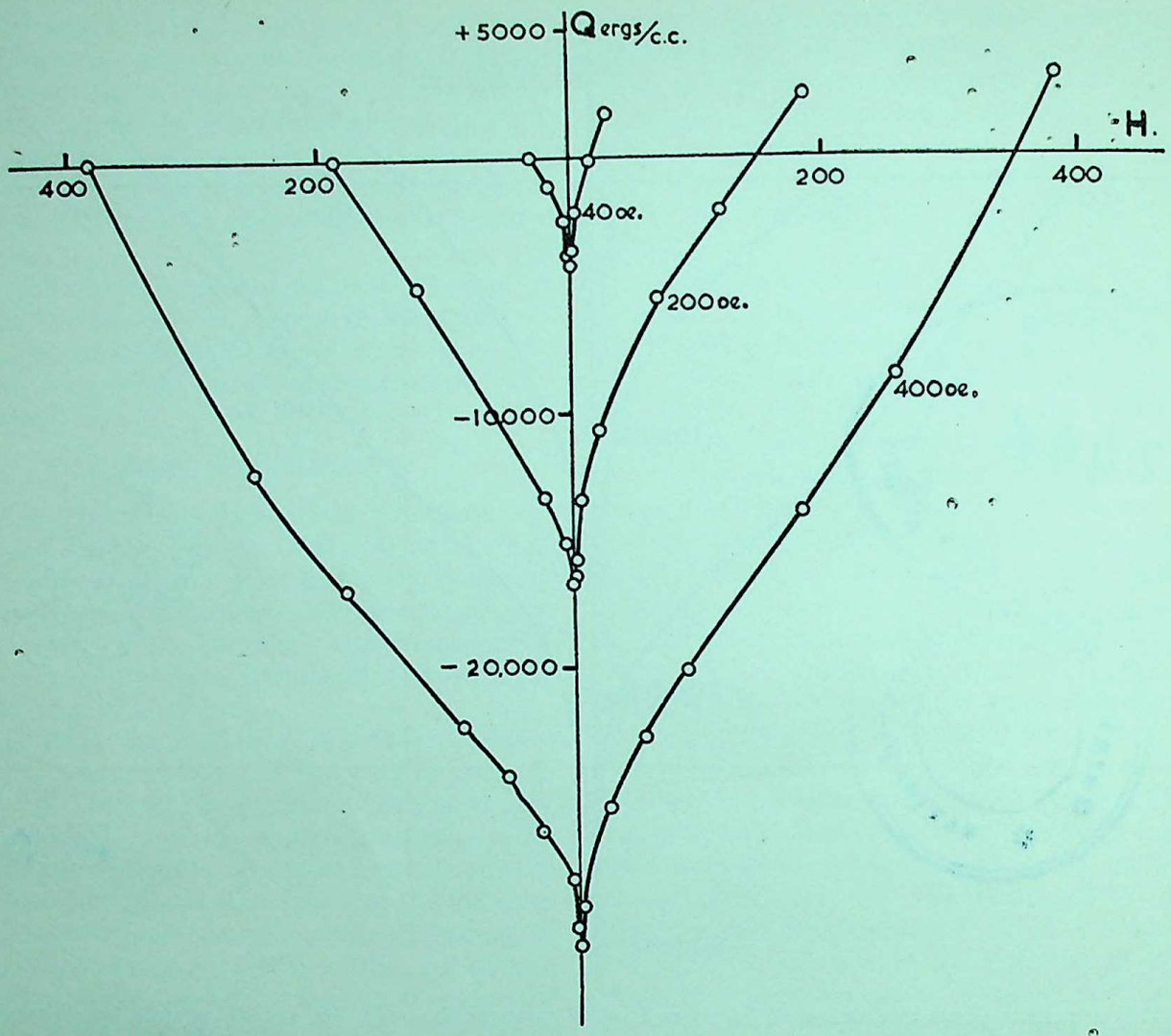


FIG. 2. Four percent silicon iron, annealed (specimen II). Q, H curves for $H_{max}=40$, 200, and 400 oersteds, approximately.

this case, a minimum at about -20 oersteds, as shown in Fig. 9. Thereafter there is a rapid heating, with a discontinuity at about $+1$ oersted, and then the heating becomes less rapid and increases linearly with H to the maximum value of the field.

Now, although the Q, H and the Q, I curves both

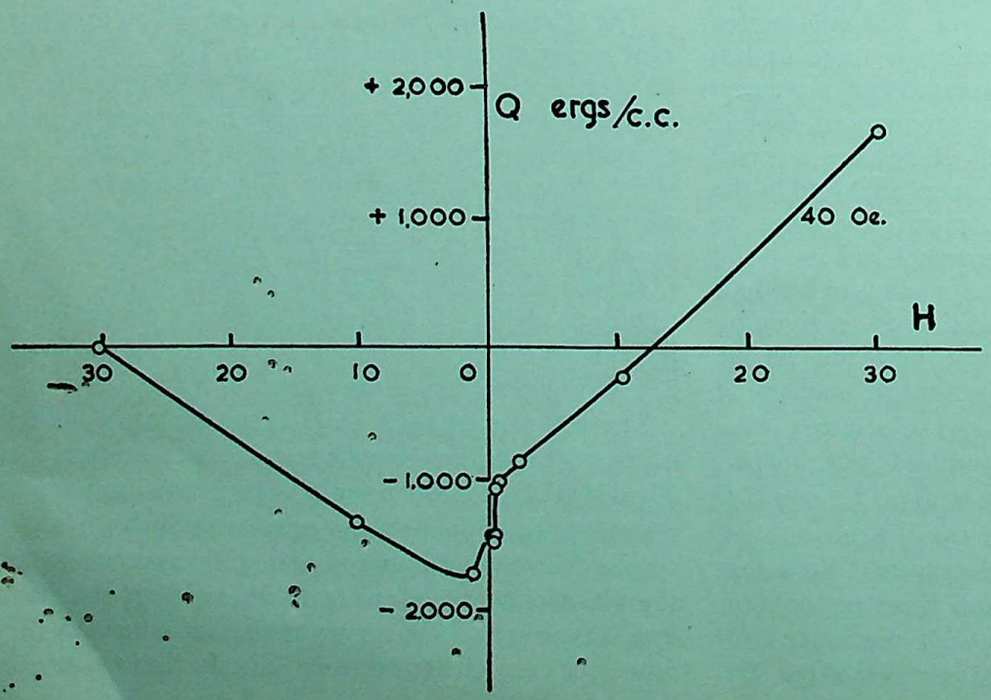


FIG. 3. 0.5 percent silicon iron, annealed (specimen IIIA). Q, H curve for $H_{max}=40$ oersteds, approximately.

CC-0. In Public Domain. Gurukul Kangri Collection, Haridwar

Digitized by Arya Samaj Foundation Chennai and eGangotri

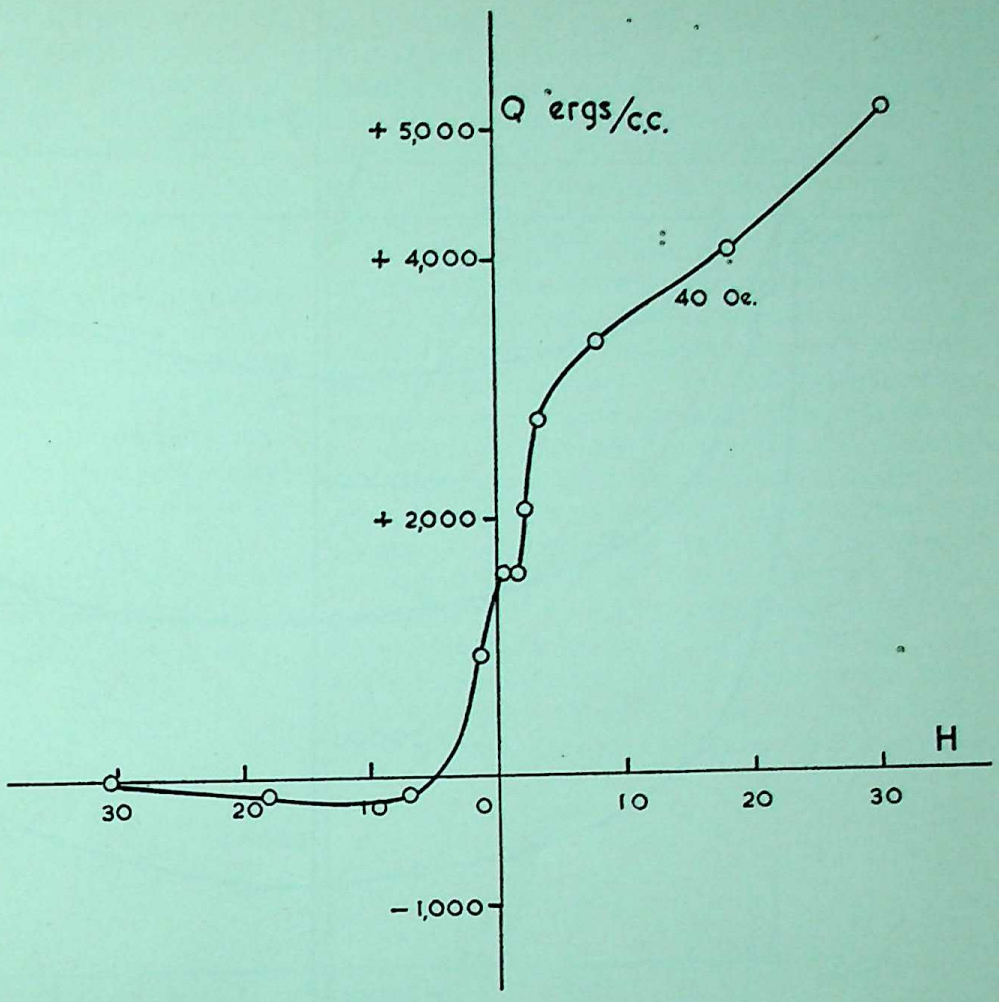


FIG. 4. 0.5 percent silicon iron, untreated (specimen III). Q, H curve for $H_{max}=40$ oersteds, approximately.

give the same information, the former are not as well suited for the illustration of energy changes occurring in the region of low field values, because I then changes rapidly with very small changes in field. Consequently, some of our results plotted as functions of I are reproduced in Figs. 5, 6, 7, and 8. All the Q, I curves for the larger cycles show a very pronounced initial cooling and corresponding final heating in the half-cycle, since large changes in field are needed to produce an appreciable change in I, except over a small field range near the origin of the hysteresis curve. Again, the curves for the 40- and 200-oersted cycles show remarkably well how the effects recorded in describing a cycle with a low maximum field are reproduced in the appropriate regions of the Q, I curve for the larger 400-oersted cycle.

In the case of untreated 4 percent silicon iron the curves for the three cycles have a rounded, symmetrical form with a minimum in the region of $I=0$, while in contrast, the corresponding cycles for the annealed material are much steeper at the outer extremities with their central portions more flat. The results for the 0.5 percent specimens also show the distinction between the rounded type of curve characteristic of unannealed material and the angular type of curve for annealed material. The 40-oersted cycle curve (not reproduced here) for the annealed 0.5 percent specimen has two peaks around $I=-700$ gauss and $I=+300$ gauss, respectively. Our records show that these are also present in the 400-cycle curves although they are not visible on the latter graphs because of the coarse energy scale. Two marked changes in slope are also found both in the 40- and 400-oersted cycle curves for untreated 0.5 percent material, but actual peaks are not found.

VI. DISCUSSION OF RESULTS

In many of the earlier papers the equation

$$\sum \Delta E_M = \int H dI - \sum \Delta Q, \qquad (1)$$

which is valid whether the thermal changes are reversible or irreversible, was used as a basis for the examination of results. In this equation, ΔE_M is the finite change in the magnetic as distinct from the change in thermal energy associated with a change ΔI in the magnetization. Accordingly, E_M was usually plotted against I in order to make clear those parts of a cycle in which the internal energy is changing and the extent of the changes.

We have examined the present results in this form, although the graphs are not reproduced here. It may be mentioned that the graphs of E_M for the 40- and 200-oersted cycles in all cases show the same features as the central portions of 400-oersted cycles. In the case of the

CC-0. In Public Domain. Gurukul Kangri Collection, Haridwar

Digitized by Arya Samaj Foundation Chennai and eGangotri

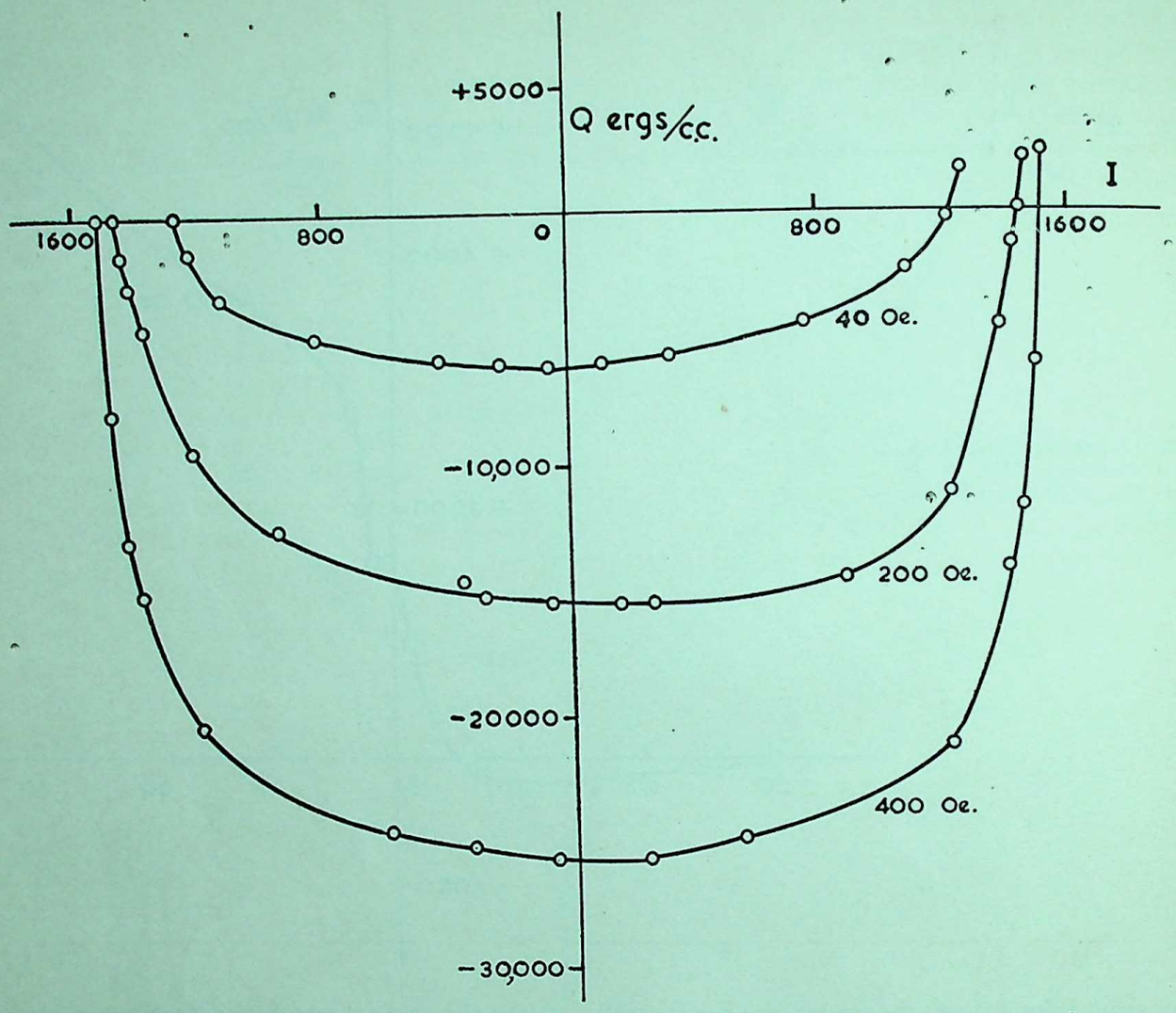


FIG. 5. 4 percent silicon iron, untreated (specimen I). Q, I curves for $H_{max}=40$, 200, and 400 oersteds, approximately.

larger cycles, at high field values $\int HdI$ is nearly always numerically larger than $\Sigma\Delta Q$, although both are negative, so that the E_M curves show a steep initial fall and a final rise. In most cases, the central portions of these curves are flat, although there are some interesting kinks well brought out when the 40-oersted cycle curves are plotted on a large scale. The E_M curves for the annealed 4 percent silicon iron specimen show a pronounced hump in the central portions which extends from $I=-1200$ to $I=+1200$ gauss.

In two papers[2,7] attempts were made to interpret the form of the thermal curves from the I, H curves of the specimen and certain other magnetic and thermoelastic data, etc. In particular, it was suggested that there was evidence that the energy supplied to each cm³ of a specimen when its magnetization increases by dI is not HdI but $HdB/4\pi$. The same treatment was applied to the present results, and although the application is not easy, it can definitely be stated that it is of little or no value in the case of 4 percent silicon iron. The separate energy changes recorded by experiment were very much smaller than—less than half of—those predicted. In particular, the treatment did not lead to a prediction of the sharp cooling and subsequent heating which is found as the field is reduced to a small value and increased again; on the contrary, arising from a magnetostriction term, there was a very pronounced peak of about 250 00 ergs per cm³ in the calculated curve, precisely in the field region where the dip is observed experimentally. Consequently, we do not reproduce the calculations here.

Probably the most important theoretical study of the thermal changes which accompany magnetization is that of Stoner and Rhodes,[12] who have attempted to interpret Q, H curves in terms of fundamental theoretical concepts, in particular those of intrinsic magnetization, rotation of domain magnetization vectors, and domain boundary movements. They were at pains to emphasize that Weiss and Forrer magnetocaloric phenomena could occur in weak as well as in strong fields and that they could be especially pronounced in the cases of alloys with low Curie points.

Following Stoner and Rhodes, we write

$$\Delta Q'=a\int d(IH)+b\int HdI, \qquad (2)$$

[12] E. C. Stoner and P. Rhodes, Phil. Mag. 40, 481 (1949).

CC-0. In Public Domain. Gurukul Kangri Collection, Haridwar

Digitized by Arya Samaj Foundation Chennai and eGangotri

where $\Delta Q'$ is the heat liberated per cm³, $a=-T/I_0 \times (dI_0/dT)$, and $b=T/K(dK/dT)$; here K is an anisotropy constant which measures the variation of the potential energy of the system as a function of the orientation of the intrinsic magnetization I_0 with respect to the crystalline axis. The first term on the right-hand side of Eq. (2) represents the contribution arising from changes in the intrinsic magnetization of the domains, while the second term represents the contribution resulting from domain vector rotations. Thus, for the adequate testing of this theory we must have data for I_0, dI_0/dT, K, and dK/dT. Stoner and Rhodes showed that effects due to internal stresses and reversible boundary movements could be taken into account by modifying the coefficient b, and those due to the formation of new boundaries by modifying a.

If we now subtract from the observed heat changes those which may reasonably be attributed to changes in spontaneous magnetization, we have

$$Q''=\sum dQ'-a\int d(IH)=\int b''HdI. \qquad (3)$$

In this equation, b'' formally corresponds to b, but we place it within the integral sign in case it should be found to be a variable coefficient which has to be calculated from the experimental results. Hence, $b''=1/H\,(dQ''/dI)$ or, if we wish to make perfectly clear what we do with the experimental results, we may write $b''=\Delta Q''/\Delta\int HdI$.

We thus see that the quantity b'' is of considerable interest, and it should be possible to find how it varies over a hysteresis cycle, always bearing in mind that it is expected to be equal to the calculated value b. Naturally, exact agreement between b'' and b cannot be expected, because we do not know the exact value of b, we have no means as yet of separating reversible and irreversible heat changes, and we do not know how to allow for the effects of internal stresses. The latter would require an accurate knowledge of the variation of the magnetostriction of the material with temperature. But, we would expect b'' to exhibit discontinuities in regions where irreversible processes are prevalent, as, for example, in the hysteresis region between coercive points.

Representative values of b and b'' now available, many of them calculated by Stoner and Rhodes, are

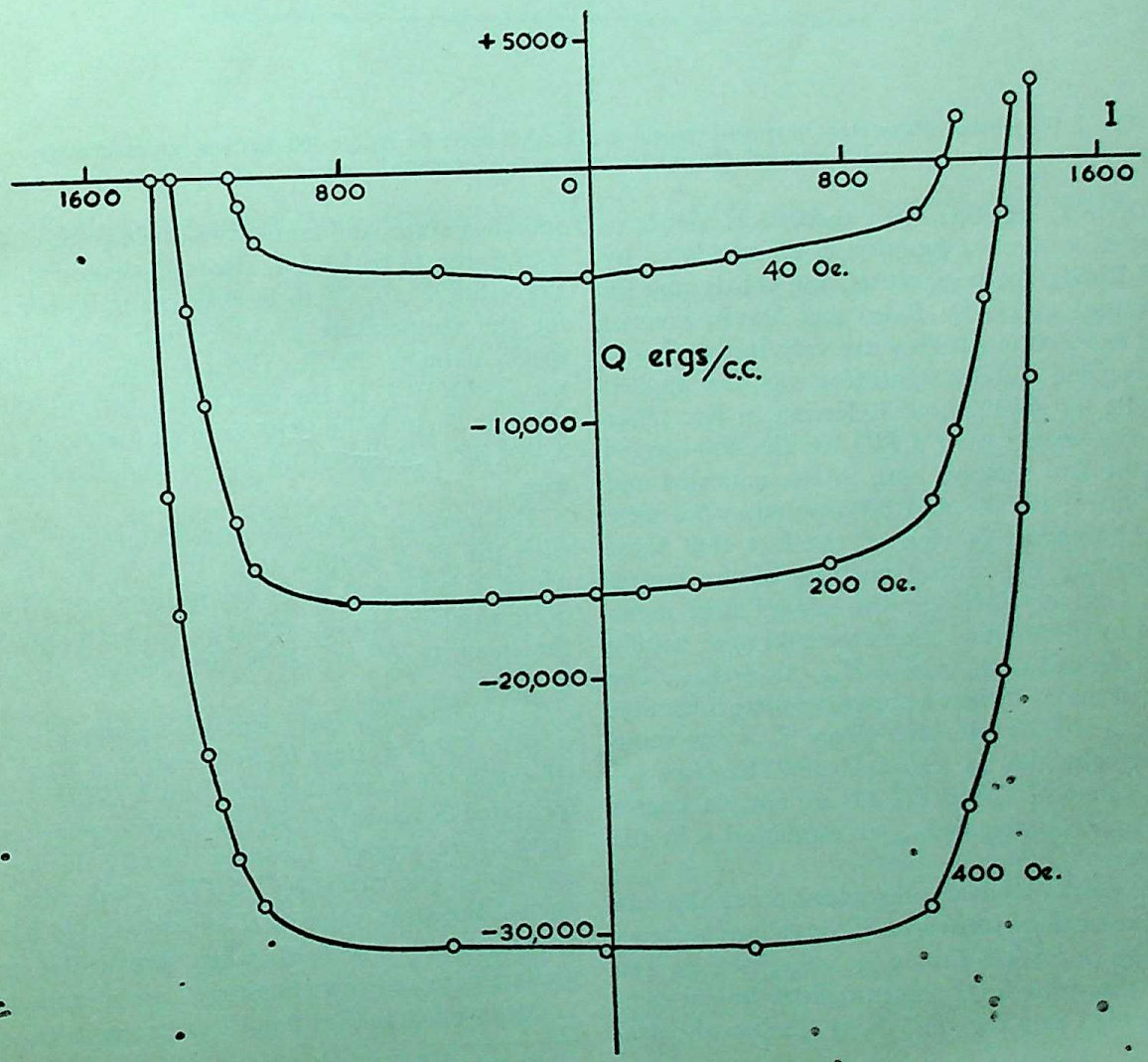


FIG. 6. Four percent silicon iron, annealed (specimen II). Q, I curves for $H_{max}=40$, 200, and 400 oersteds, approximately.

CC-0. In Public Domain. Gurukul Kangri Collection, Haridwar

Digitized by Arya Samaj Foundation Chennai and eGangotri

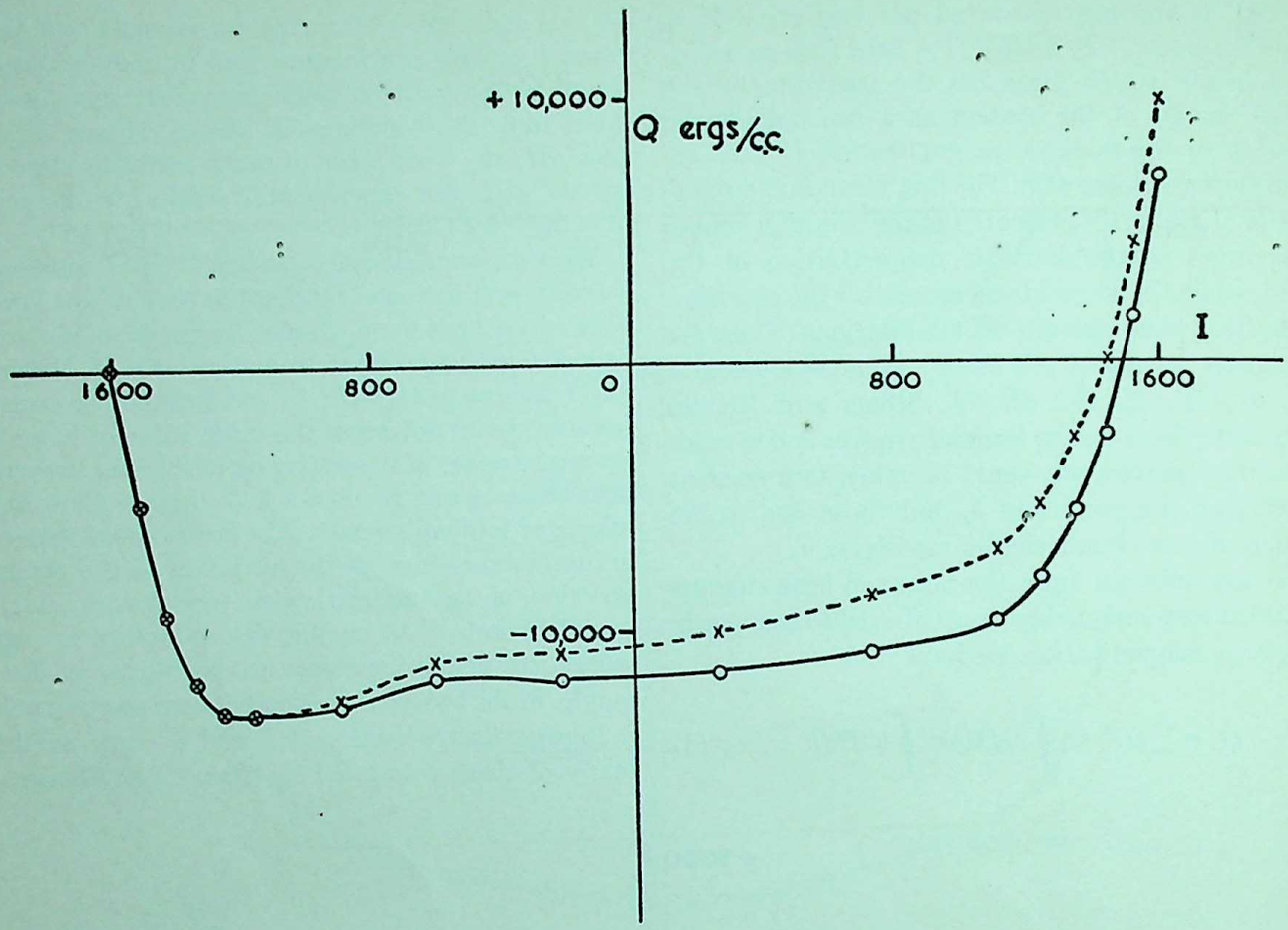


FIG. 7. 0.5 percent silicon iron, untreated (specimen III). Q, I curve for $H_{max}=400$ oersteds, approximately. Uncorrected for eddy currents – – – –; corrected ———.

given in Table I, together with theoretical values of b. The curves of b'' as a function of H calculated by Stoner and Rhodes for iron, nickel, and cobalt, and for heavily strained nickel by Bates and Davis, are not reproduced here, although they are very instructive.

The Stoner and Rhodes treatment was now applied to our results for silicon iron. Referring to Eq. (3)we calculated the quantity $a\int d(IH)$ for the 400-oersted cycles for the two samples both in the annealed and untreated states; the 40- and 200-oersted cycles were not further examined in view of the fact that these merely reproduce the central portions of the largest cycle. The products (IH) for the several field increments used in the thermal measurements were readily found over the half-cycle from $-H_{max}$ to $+H_{max}$. The calculation of the coefficient a presented some difficulty. It is equal to $-T/I_0\ (dI_0/dT)$ where I_0 is the spontaneous magnetization in zero field at T°K. Now experimental values of I_0 and dI_0/dT are not yet known for silicon iron. Consequently, we estimated a in the following way.

The effect on the intrinsic magnetization at absolute zero of adding small quantities of silicon to iron is shown graphically by Bozorth.[13] Taking the value for pure iron to be 1740, the value for 4 percent silicon iron is computed to be 1583 emu per cm³. Using the law of corresponding states and taking the Curie point of 4 percent silicon iron to be 1008°K (from Brailsford[14]), we found the value of dI_0/dT to be 0.19 cgs units per degree C for the temperature at which our experiments were made, namely, 290°K. Consequently, the value of a was 3.51×10^{-2}. In the case of 0.5 percent silicon iron there is likely to be little error in assuming the value 3.40×10^{-2} calculated by Stoner and Rhodes for pure iron.

The quantity $a\int d(IH)$ was then plotted against H with the Q', H graphs as in Figs. 9, 10, 11, and 12, where it is labeled M.C. (magnetocaloric effect). The difference between the ordinates of the two graphs gives the quantity Q'' which is also plotted on the same graphs.

To calculate the coefficient b'', we found it necessary to plot $\int HdI$ against H, and from this graph and the Q'' graph the increments $\Delta Q''$ and $\Delta\int HdI$ were found for stated increments of H, the latter increments usually being those actually recorded directly during the experiment. The ratio $\Delta Q''/\Delta\int HdI$ was then plotted against the mean value of H for each stated increment, except at very low fields where irreversible processes predominate and the values of b'' are meaningless.

Turning now to Figs. 9 to 12, we first note the shape of

[13] R. M. Bozorth, *Ferromagnetism* (1951), p. 79.

[14] H. D. Brailsford, *Magnetic Materials* (Methuen and Company, Ltd., London, 1951), p. 90.

CC-0. In Public Domain. Gurukul Kangri Collection, Haridwar

Digitized by Arya Samaj Foundation Chennai and eGangotri

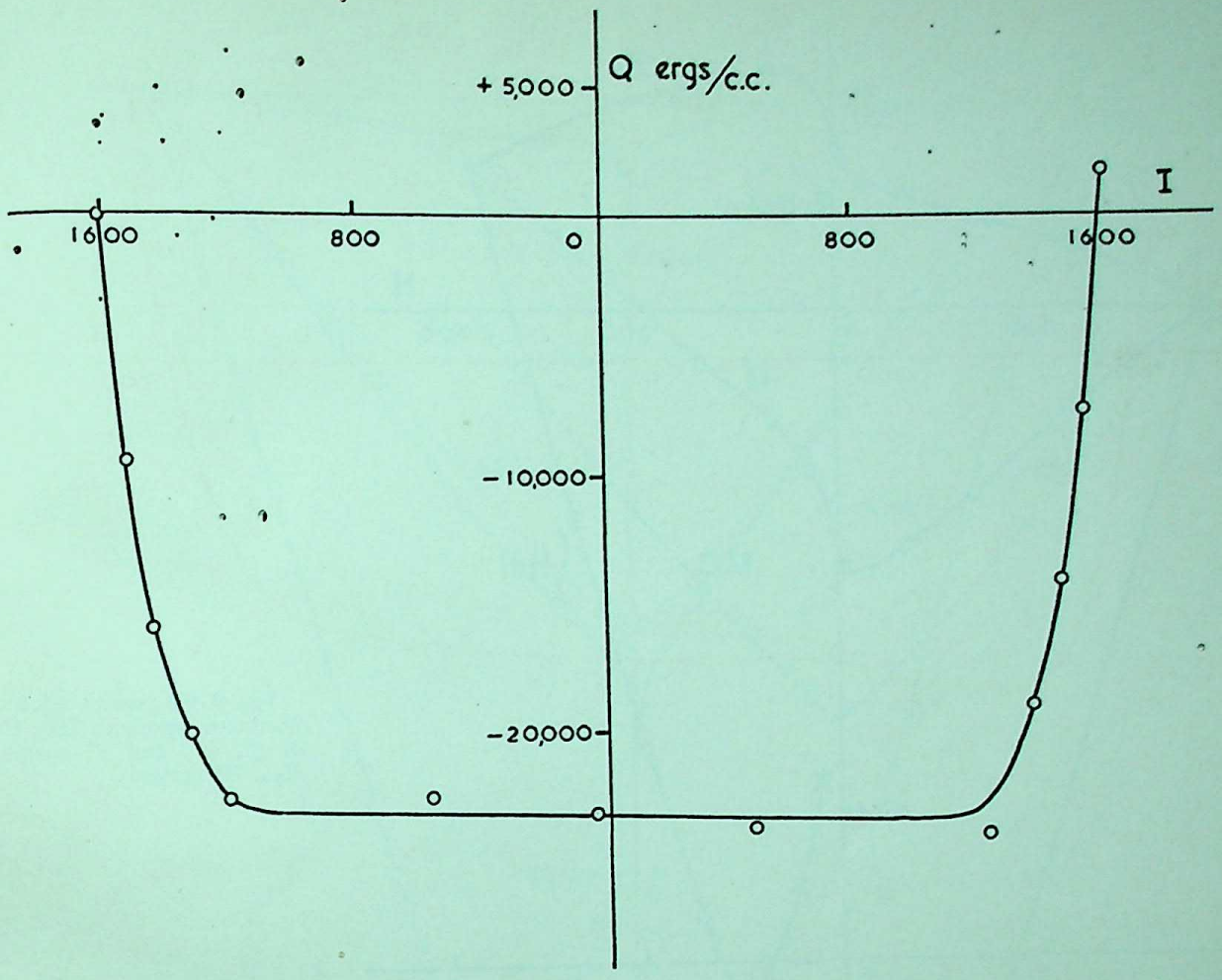


FIG. 8. 0.5 percent silicon iron, annealed (specimen IIIA). Q, I curve for $H_{max}=400$ oersteds, approximately.

the $a\int d(IH)$, H curve with the symmetrical heating and cooling effects associated with the negative value of dI_0/dT which are characteristic of the magnetocaloric effect. In the case of 0.5 percent silicon iron, both annealed and untreated, $\int HdI$ is considerably greater in magnitude than Q'; while for 4 percent silicon iron at the higher fields, $\int HdI$ is smaller in magnitude than Q', but is greater at low fields. The relative magnitudes of Q' and the magnetocaloric effect for the untreated material (Fig. 9) are such that the Q'' curve shows a steady heating as H is reduced from $-H_{max}$, corresponding to reversible rotations of domain vectors or reversible boundary movements. This persists until a field of -10 oersteds is reached, when the rate of heating changes sharply with the marked onset of irreversible changes. When H exceeds $+50$ oersteds, cooling from reversible processes predominates and continues almost linearly to $+H_{max}$. This is precisely what one would expect, and is very similar to the curve calculated by Stoner and Rhodes from the results of Hardy and Quimby on annealed Armco iron. Our untreated silicon iron specimen had a comparatively high coercivity (approximately 1.9 oersteds) and the irreversible heating, of some 7000 ergs per cm^3, is much greater than is found for the other specimens. The reversible heat change which occurs between $\pm H_{max}=377$ oersteds

TABLE I. Values of b and b''.

	b	b''	Remarks	Author
Fe	0.58	−0.30	Armco, annealed	a
	(−0.63 ideal)	−0.26	Armco, annealed	b
		−0.20	Hilger H.S.	b
		−0.36	Armco, unannealed	b
		−0.38	Armco, unannealed	a
		−0.22	Armco, annealed	c
Ni	−4.5	−3.70	Annealed, H_m 200 oersteds	a
	(−5.9 ideal)	−4.20, −4.30, −3.70	Annealed specimens with H_m 200 oersteds	d
		−4.80		
		−1.40	$H_m>200<400$ oersteds	d
		−4.00	H_m 400 oersteds	e
		−0.65, −0.84	Hard-drawn	d
		−0.40		f
		+0.37?	Unannealed	a
Co	−1.3	−2.0, −2.0, −2.4	Annealed	g
		−2.9, −3.3, −2.6	Unannealed	g
Silicon iron		−0.11	Untreated 0.5 percent	h
		+0.04	Annealed 0.5 percent	
		−0.05	Untreated 4 percent	
		+0.10	Annealed 4 percent	

[a] Hardy and Quimby.
[b] Bates and Harrison.
[c] Bates and Healey.
[d] Bates and Weston.
[e] Bates and Davis.
[f] Davis.
[g] Bates and Edmondson.
[h] Bates and Marshall.

CC-0. In Public Domain. Gurukul Kangri Collection, Haridwar

Digitized by Arya Samaj Foundation Chennai and eGangotri

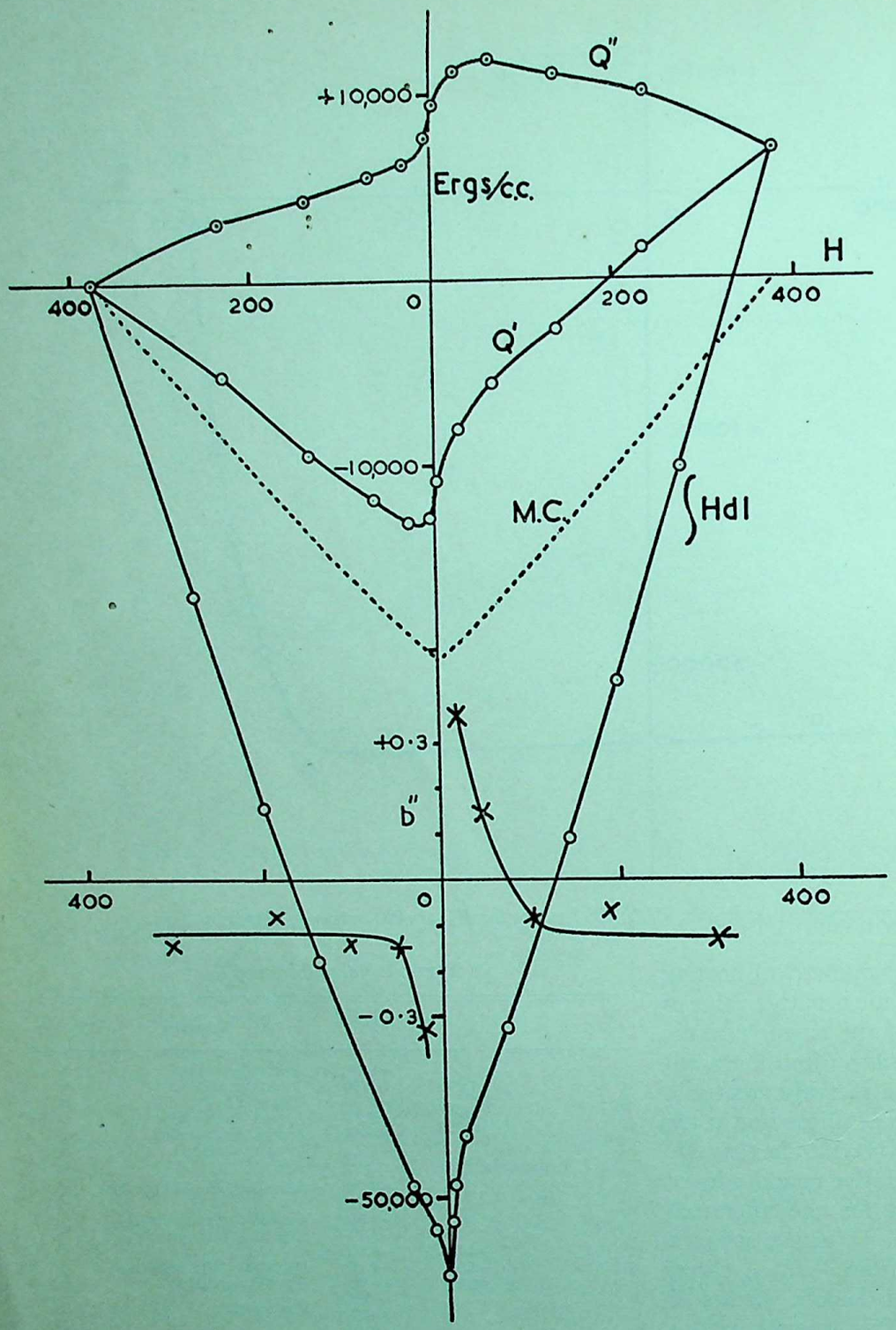


FIG. 9. 0.5 percent silicon iron, untreated (specimen III). Curves of Q', Q'', and b'' against H; H_{max} 400 oersteds.

and $H=0$ corresponds also to about 6 to 7000 ergs per cm^3.

The values of b'' obtained as described above show some degree of scatter about the lines drawn through them since they are calculated directly from experimental points. As H is decreased from $-H_{max}$ towards zero, b'' remains fairly constant until the region of irreversible processes is reached, when it rapidly assumes a large negative value. When H is subsequently increased to a positive value, b'' first takes a large positive value at low fields to fall to the same fairly constant value of -0.11 in high positive fields. This value may be compared with the values -0.26 and -0.22 given for Armco iron and Hilger iron, respectively (from Bates and Harrison[5]), and the value -0.30 for the Armco iron (from Hardy and Quimby[15]). (The estimated value for polycrystalline iron free from internal strains is -0.58; values for alloys of silicon and iron are not yet known.)

We consider next the results for the annealed specimen of 0.5 percent silicon iron. The curve of Q'' against H in Fig. 10, does not show the initial heating found with the untreated specimen when the field is decreased

[15] T. C. Hardy and L. Quimby, Phys. Rev. 54, 217 (1938).

CC-0. In Public Domain. Gurukul Kangri Collection, Haridwar

Digitized by Arya Samaj Foundation Chennai and eGangotri

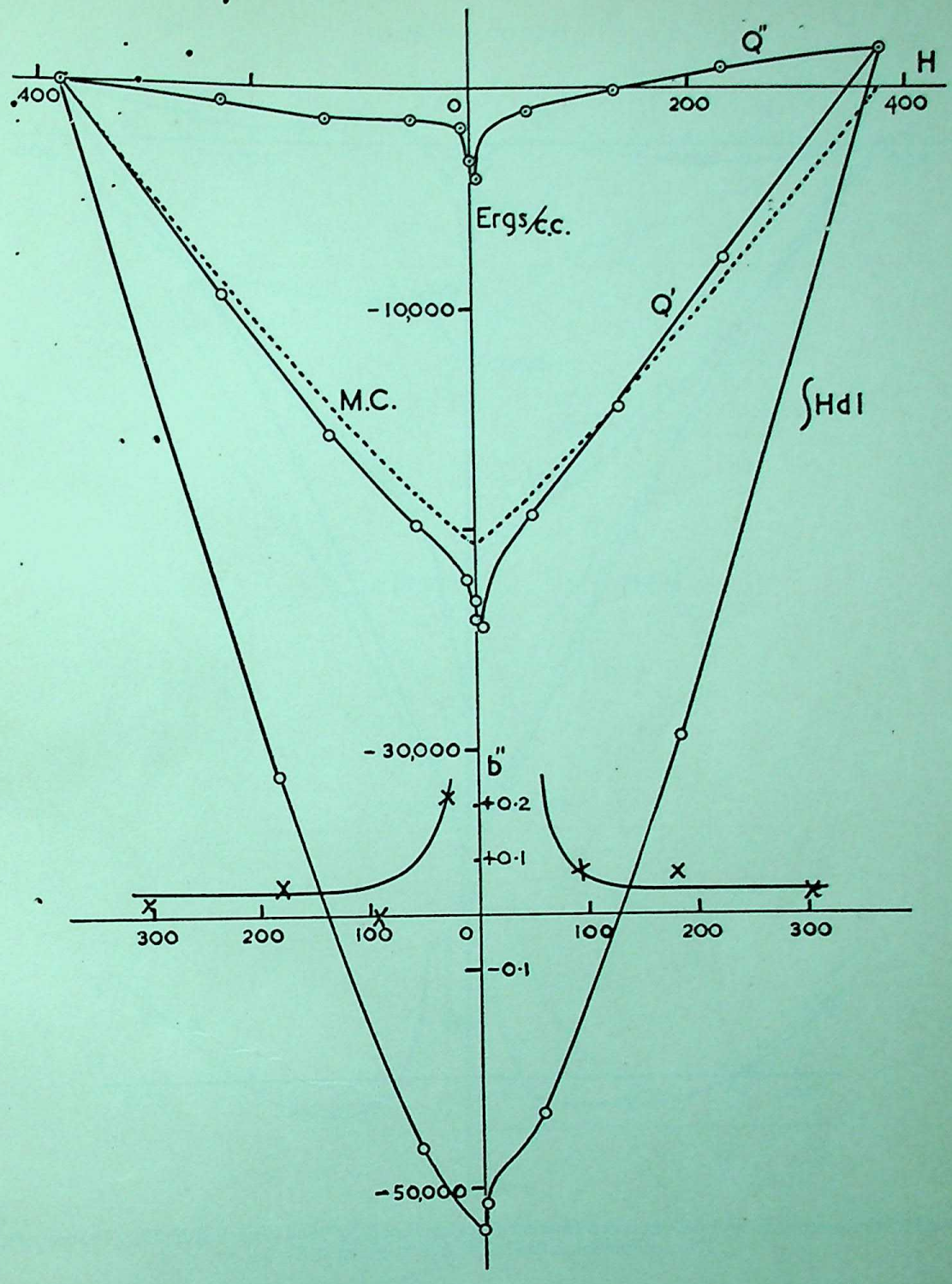


FIG. 10. 0.5 percent silicon iron, annealed (specimen IIA).
Curves of Q', Q'', and b'' against H; H_{max} 400 oersteds.

from $-H_{max}$ towards zero. In contrast, there is a slight and almost linear cooling which persists until the field has a small negative value, whereupon there is a sharp dip or trough in the curve, some 2500 ergs per cm³ in magnitude, which is followed by a more pronounced rise succeeded by linear heating up to $+H_{max}$. This behavior is remarkable, because the sharp dip in the curve occurs in a region where we would anticipate an irreversible heating effect. Since the Q'', H and $\int HdI$, H curves slope in the same direction, the values of b'' are now positive, and b'' has the value +0.04 in high fields. and remains fairly constant until the region of the dip, where it takes a large positive value.

The Q'', H curve for untreated 4 percent silicon iron in Fig. 11 shows little energy change in the higher fields after allowance has been made for the magnetocaloric effect. There is actually a small cooling near $-H_{max}$, and one near $+H_{max}$, which gives way to a slight heating

CC-0. In Public Domain. Gurukul Kangri Collection, Haridwar

Digitized by Arya Samaj Foundation Chennai and eGangotri

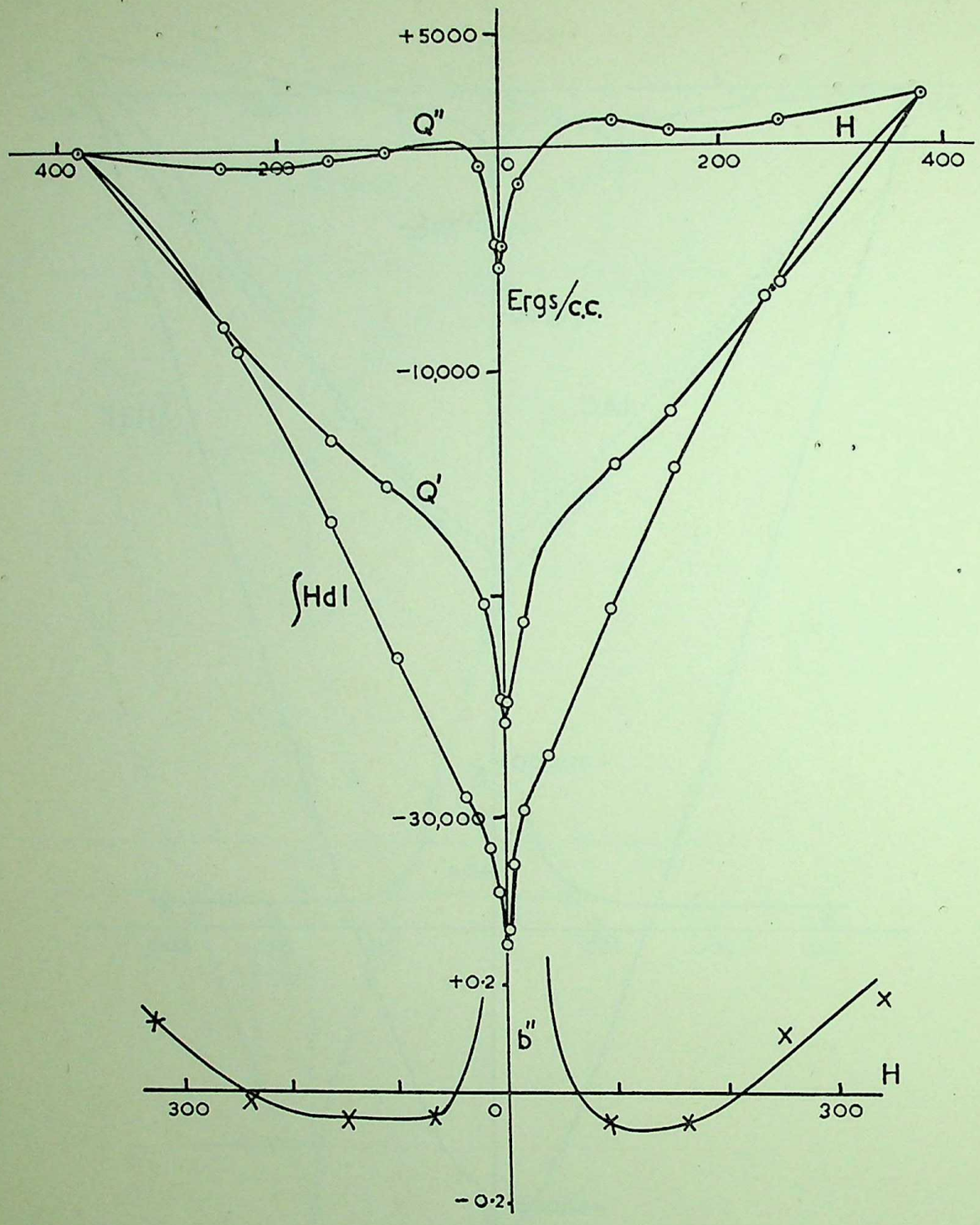


FIG. 11. Four percent silicon iron, untreated (specimen I). Curves of Q', Q'', and b'' against H; H_{max} 400 oersteds. (Note pronounced dip in Q'', H curve around $H=0$.)

which persists except in the field region between -50 and $+50$ oersteds approximately. In the latter region there is again a pronounced dip, of magnitude about 6000 ergs per cm^3, even greater than that with the annealed specimen. We note that b'' is initially positive near $-H_{max}$, but, as H is decreased, b'' falls to a negative value of -0.05, to remain constant until the region of irreversible processes is reached when it again becomes positive.

The curves for annealed 4 percent silicon iron in Fig. 12 are somewhat similar to those for the untreated specimen, but the magnitudes of the changes in the two cases are very different. In Fig. 12 the minimum values of Q' and of the magnetocaloric effect are about $-31\,000$ and $-19\,000$ ergs per cm^3, respectively, and the Q' curve is always below the other. Therefore as H is first reduced the Q'' curve shows a sharp initial cooling which becomes less pronounced until a field of -50 oersteds is reached, when we find the sudden dip recorded for the two previous specimens. When we increase the field to $+H_{max}$, the phenomena are repeated in the reverse order with an irreversible heating superimposed. The b'' curve has the same form as that for the untreated 4 percent silicon iron specimen, but b'' is

CC-0. In Public Domain. Gurukul Kangri Collection, Haridwar

Digitized by Arya Samaj Foundation Chennai and eGangotri

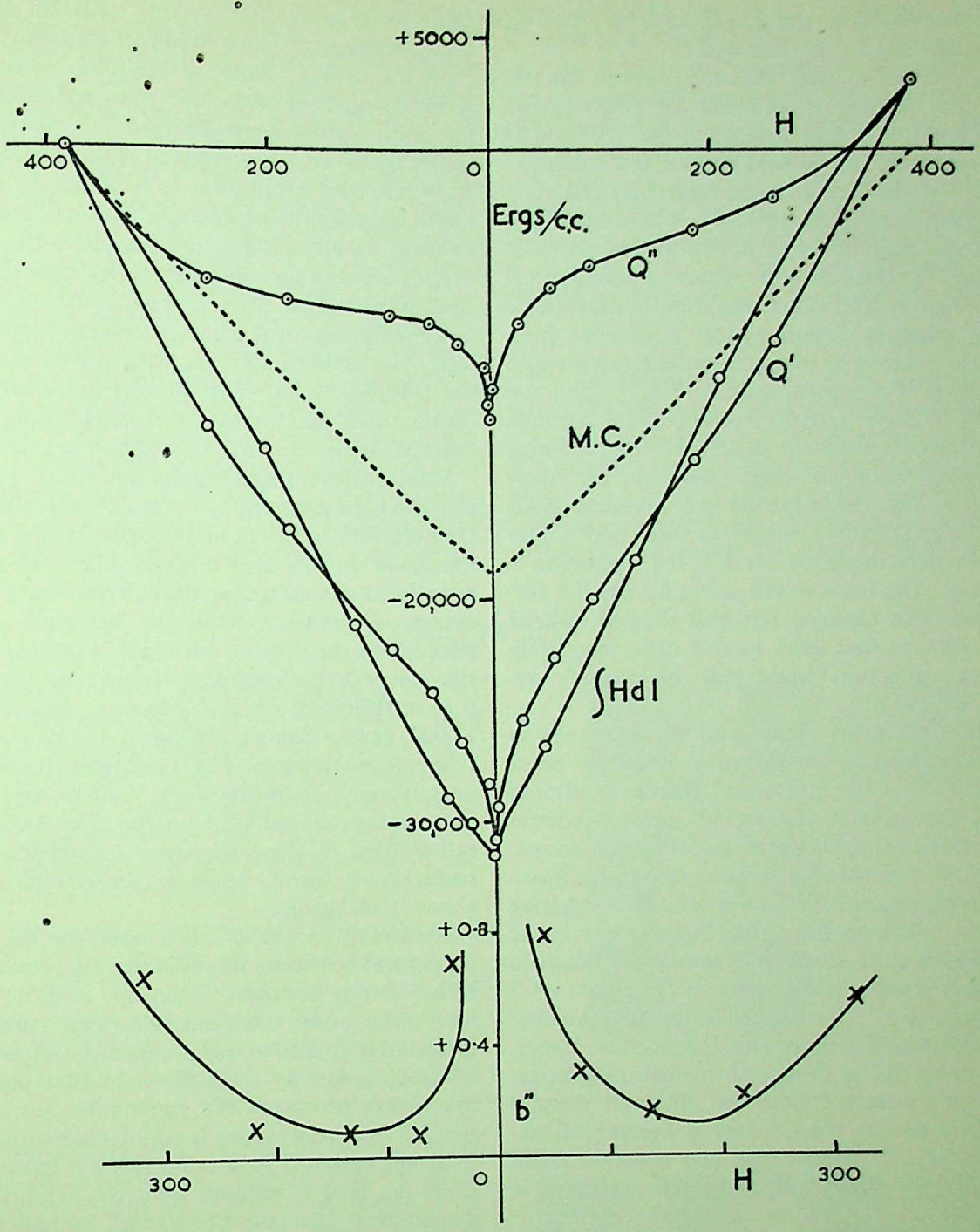


FIG. 12. Four percent silicon iron, annealed (specimen II). Curves of Q', Q'', and b'' against H; H_{max} 400 oersteds. (Note pronounced dip in Q'', H curve.)

now always positive with small regions round about $H=-150$ oersteds and $H=+150$ oersteds where it has a fairly constant value of 0.1.

Perhaps the most striking feature of the Q'', H curves for the last three specimens, the 0.5 percent annealed and the two 4 percent specimens, is the dip or trough described above. It should be mentioned that it was, of course, present in the 40- and 200-oersted cycles, although very different field increments from those employed in the largest cycle were used in these cases. This dip is most unusual, but Bates and Healey[6] made somewhat similar observations in a 100-oersted cycle for annealed Armco iron. They considered that the dip was a spurious effect, possibly the result of the effects of vibrations upon the measurements, and they avoided its appearance by changing the field in one operation from a small negative value to a small positive value, so that in their view the specimen did not remain in magnetostrictive contraction for an appreciable interval of time. It seems clear, however, that as the effect appears in the present curves in all the cycles whatever field steps were employed, it must be a real effect and characteristic of the material. Incidentally, the dips are clearly visible only on the Q'', H and not on Q'', I

CC-0. In Public Domain. Gurukul Kangri Collection, Haridwar

Digitized by Arya Samaj Foundation Chennai and eGangotri

curves, so emphasizing the importance of plotting thermal changes against both H and I.

A priori, one might think that the cause of the dip resided in the method of allowing for eddy-current heating. The latter is proportional to $(dB/dt)^2$ and is therefore very large in low field regions and comparatively small elsewhere, so that the correction described above is applied mainly in the region where the dip is found. Suppose now that the method of correction is unsound and that the actual correction applied in that region is too large. The effect would be to accentuate the cooling which is expected as H is reduced from $-H_{max}$ towards zero and to decrease the apparent rate of heating as H is increased again, in fact, to give the form of Q'', H curve actually recorded. To test this suggestion, the curves for the three specimens showing the effect were plotted without correction for eddy-current effects. The curves for the two 4 percent specimens were only slightly changed in form and a pronounced minimum remained, so that the suggestion is here ruled out. The uncorrected curve for the 0.5 percent specimen was changed but still showed distinct traces of a dip, so that even in this case, inaccurate eddy-current correction could not be entirely responsible.

Again, the dip cannot be a result of inaccuracy in applying the correction for the magnetocaloric effect on the grounds that the Stoner and Rhodes treatment can only be approximate at low fields, for the order of magnitude of the correction rules out this explanation.

Now, the saturation magnetization of iron decreases with increase in temperature, so that dI_s/dT is negative and there is a cooling on decreasing the field. But, in the hysteresis region where reversible rotations of domain vectors and reversible movements of boundary walls are important, dI/dT is normally positive because magnetic anisotropy decreases with temperature. Hence, when the cooling due to change of intrinsic magnetization has been subtracted from the observed thermal changes, there should remain only a heating on decreasing the field. Consequently, the question arises as to whether the sign of dI/dT can be negative in low fields.

A mechanism by which the sign of dI/dT could be rendered negative in low fields was suggested by the work of Dr. E. W. Lee. It is based on some work by Bozorth[16] who tried to account on the domain theory for the very low remanence exhibited by certain alloys, which may be as low as 0.07 I_s for a certain Permalloy after heat treatment. Bozorth put forward several ways in which such low values might arise.

The most likely explanation takes into account a possible departure from normal domain structure in materials of low crystal anisotropy. On such crystal surfaces, Bitter powder patterns are not successfully formed, because the Bloch walls between domains must be so wide, if they exist, that the stray fields above them must be too weak to act upon the colloid particles used to form the pattern deposits. Now, Kittel[17] suggested that under these conditions the flux in comparatively large regions of the material forms closed paths when the material is in the demagnetized state. On the application of a magnetic field these closed lines will be broken, but they will reform on its removal. In other words, the material tends to demagnetize itself and the remanence falls to less than the old theoretical value. This process is clearly the more favored the less the magnetostriction and crystal anisotropy, and as both decrease with rise in temperature, the field remaining constant, the flux-closing process occurs more easily and the magnetization is further reduced. In other words, $(dI/dT)_H$ is negative.

Some evidence regarding the sign of dI/dT for silicon iron has been provided by Spooner,[18] who measured the temperature coefficient of permeability of a number of specimens of low and medium silicon electric sheet material at various temperatures from $-20°C$ to $+46°C$ over a wide range of induction. The main conclusions relevant to the present discussion were that 4 percent silicon iron on the average has a large negative temperature coefficient of permeability at all inductions up to 15 000 gauss, though individual samples show considerable variations. The coefficient becomes more negative with increasing silicon content, and the shape of the curves also seems to be a function of the induction rather than of the field, since a maximum negative coefficient is found, whatever the silicon content, at about 10 000 gauss.

Returning to the Q'', H curves for the annealed 0.5 percent specimen, shown in Fig. 10, there appears to be no heating between $-H_{max}$ and zero, but simply a faint cooling over the whole field range. Again, as H is increased from zero to $+H_{max}$, we find a slight evolution of heat apparently in addition to that produced by irreversible processes. We might take this to indicate that boundary formation is taking place at high as well as at low values of field as the latter is reduced.

As the field is reduced from the saturation value, domain boundaries must be formed. Initially they are of low energy per unit area of boundary surface, since they then separate domains in which the domain vectors are almost parallel. The boundary pattern becomes more and more complex as the field is further reduced, and since its formation requires energy, there will be a cooling associated therewith.

The very slight cooling observed at high field values with the untreated 4 percent specimen as the field is reduced, and the slight heating on increase to $+H_{max}$, is probably to be explained on the same lines as for the annealed 0.5 percent specimen. The cooling is much more pronounced in the case of the annealed 4 percent specimen and extends over the whole range from $-H_{max}$

[16] R. M. Bozorth, Z. Physik **124**, 519 (1945).

[17] C. Kittel, Revs. Modern Phys. **21**, 541 (1949).

[18] T. Spooner, Phys. Rev. **30**, 136 (1927).

CC-0. In Public Domain. Gurukul Kangri Collection, Haridwar

Digitized by Arya Samaj Foundation Chennai and eGangotri

to zero field. It seems difficult to account for these large thermal changes in the opposite direction to what one would normally expect purely on the basis of Bozorth's flux-closure hypothesis. But some Bitter patterns recently recorded on the surface of a single crystal of some 3 percent silicon iron by D. H. Martin may throw some light on the problem. The crystal was exposed to a high field which was subsequently reduced to zero, and during the course of the experiment it was noted that closure domain daggers shot across the surface and that strange domain boundaries were formed in a perfectly regular sequence. Some of these boundaries separated domains whose vectors appeared to meet head-on, just as if the page before us was divided into two portions by a boundary running across it more or less parallel to the lower edge of the page. In the upper portion we may imagine the domain vectors to be parallel to the long edge of the page and directed downwards, and in the lower portion to be likewise parallel and directed upwards. But the boundary is not now the normal straight and clear-cut boundary as frequently recorded in Bitter figure work. It twists and wriggles in an extraordinary way as if it were trying to counteract the formation of free poles on its surfaces. If we have here the type of flux closure postulated by Bozorth and Kittel, then at the boundary the flux must turn either upwards or downwards into the surface of the page on both sides of the boundary. The latter is, however, so serrated and so narrow that considerable energy must be associated with it, and one feels that here is the most likely explanation of the observed cooling.

VII. ACKNOWLEDGMENTS

We are indebted to Mr. A. E. De Barr (now at Elliott Brothers), and Dr. R. J. Wakelin of Guest, Keen, and Nettlefolds Research Department for the provision and treatment of the silicon iron samples used in this work; one of us (G.M.) thanks the Department of Scientific and Industrial Research for a maintenance allowance which made the work possible.

DISCUSSION

G. RATHENAU, *N. V. Philips Gloeilampen Fabrieken, The Netherlands:* The number of domain walls formed by thermal demagnetization may be much larger than the number formed by demagnetization in an alternating current field of decreasing amplitude at room temperature. These additional walls may be in metastable equilibrium at room temperature and give rise to nonequilibrium configurations.

L. F. BATES, *University of Nottingham, England:* The results of measurements of Bitter figures have shown very little change in magnetization patterns with the temperature ranges from solid CO_2 to about 150°C. We have found that "wriggly" boundaries appear on specimens which have been demagnetized by heating.

C. A. FOWLER, JR. (with E. M. FRYER), *Pomona College, Claremont, California:* By employing the longitudinal Kerr magneto-optic effect, photographs of domains in the (100) surface of a large crystal of silicon iron have been obtained. A series of such pictures clearly shows the characteristic movement of domain walls as the sample is carried through an initial magnetization curve to saturation. A second series of photographs, taken as the originally saturated sample has its magnetization gradually reversed to saturation in the opposite direction, reveals the sudden appearance of a single narrow antiparallel domain which proceeds to grow, with increasing reverse field, until it covers the entire crystal surface. Preliminary results have been described[1] and photographs of these effects are attached (see Figs. 1 and 2).

[1] C. A. Fowler, Jr., and E. M. Fryer, Phys. Rev. 86, 426 (1952).

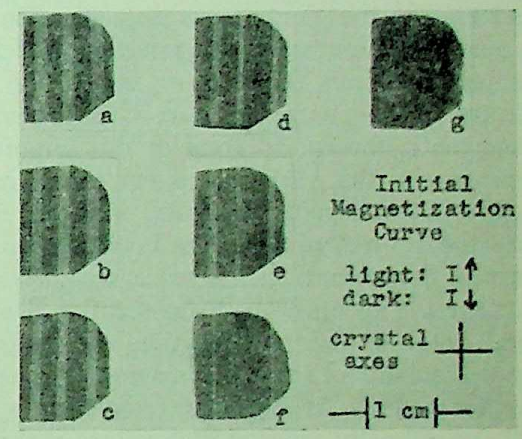


FIG. 1.

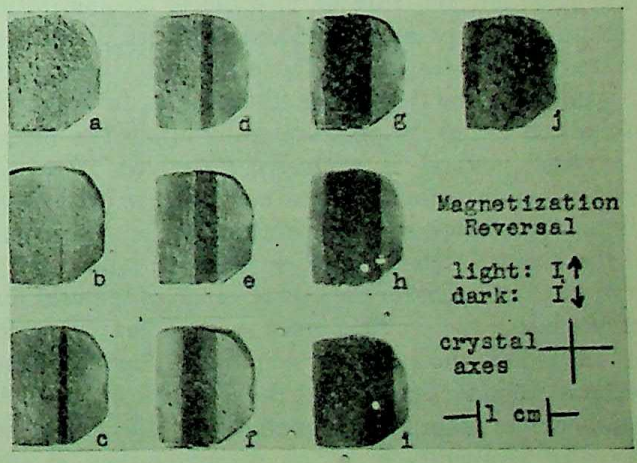


FIG. 2.

CC-0. In Public Domain. Gurukul Kangri Collection, Haridwar

Digitized by Arya Samaj Foundation Chennai and eGangotri

Spontaneous Magnetization—Techniques and Measurements

W. Sucksmith, C. A. Clark, D. J. Oliver, and J. E. Thompson

University of Sheffield, Sheffield, England

Measurements on the temperature variation of spontaneous magnetization by both the magnetothermal and magnetic methods have hitherto been confined to nickel; the extension of these measurements, calling for greater sensitivity, is discussed. To the direct method devised by Weiss and Forrer has been added a direct current amplifier, which allows a small magnetocaloric rise of temperature to be measured accurately. The original ferromagnetic balance devised by Sucksmith has been improved and now is capable of wider application to measurements of magnetic intensity in fields which are due to either air core coils or electromagnets. The method is not complicated by the presence of any image effect so that measurements of $d\sigma/dH$ in high fields can be made with considerable precision.

Measurements on a copper-nickel alloy (27.5 percent Cu) have been made, and it is shown that the two methods give identical results except in the immediate neighborhood of the Curie temperature, where the thermal measurements give a steeper descent to the temperature axis with little "tail," while the magnetic data indicate a higher Curie temperature with a significant tail. Below the Curie temperature the linear relationship between the magnetocaloric rise of temperature and the square of the intensity magnetization is found as in nickel and iron; above this temperature there is pronounced curvature.

Measurements have also been carried out on a mixed ferrite ($MgO\ ZnO\ 2Fe_2O_3$). Satisfactory agreement between the results by the two methods are obtained, both curves differing markedly from the law of corresponding states for the ferromagnetic elements.

INTRODUCTION

THE magnetization of a domain in zero applied field is known as the spontaneous magnetization (σ_{0T}) and is a quantity of fundamental significance. Its change with temperature, from the absolute zero to the Curie temperature, plays an important part in the formulation of ferromagnetic theory. In spite of this importance, our knowledge of this variation, is extremely limited. Of the three ferromagnetic elements, only one, nickel, has been the subject of adequate investigation. The experimental determinations are not a straightforward matter, since the spontaneous magnetization does not, in general, admit of direct observation, and it can only be obtained by indirect use of the magnetic isothermals in high external fields. At the lowest temperatures, there is usually no difficulty, since at high values of the field, the magnetization increases so slowly and linearly that simple extrapolation of this to the axis of zero field can be carried out with accuracy. With increasing temperature, however, the rate of increase of magnetization with field becomes more rapid and nonlinear, so that the accuracy decreases as the Curie point is approached. It is in this region that two methods, both developed by Weiss and Forrer,[1] were successfully applied to nickel. The first method is exclusively derived from the magnetization isothermals, and curves are plotted giving the field as a function of temperature for constant values of the magnetization. These curves were found by the authors to be linear for the higher values of the field, and extrapolation to zero field gives the temperature which corresponds to the value of σ employed. The second and better method for determining the spontaneous magnetization comes from the magnetocaloric effect. The increase of temperature ΔT on magnetization, at first increases only very slowly until "saturation" is reached, after which it increases linearly with the square of the observed magnetization. Theoretical considerations show that extrapolation to the axis $\Delta T=0$ gives the spontaneous magnetization and Weiss and Forrer considered that the two methods gave identical results, the Curie temperatures obtained differing by not more than 1°C. It is necessary to draw attention to the fact that the former, purely magnetic method, becomes less accurate as the Curie point is approached, while the magnetocaloric determinations increase to a maximum accuracy at this temperature. This consideration, therefore, offsets in some degree the significance of the agreement between the two methods.

Unfortunately, this complete investigation has not been reproduced for any other ferromagnetic material, probably owing to the severe experimental difficulties which confront accurate measurements by both methods Potter,[2] succeeded in making simultaneous magnetic and magnetothermal measurements on iron in the elevated temperature range from 523°C to 826°C (Curie temperature about 770°C). Up to the present, this work is the only attempt to make measurements on the magnetocaloric effect other than that of the originators, Weiss and Forrer.

Recently, Myers and Sucksmith[3] made magnetic observations on cobalt (earlier investigations by Bloch[4]), where the high Curie temperature (1120°C) makes magnetocaloric measurements virtually impossible. In this case, there are difficulties attributable mainly to the abnormally high crystalline anisotropy which makes the approach to saturation of the polycrystalline material very slow. In addition, at ordinary tempera-

[1] P. Weiss and R. Forrer, Ann. phys. 5, 153 (1926).

[2] H. H. Potter, Proc. Roy. Soc. (London) A146, 362 (1934).

[3] H. P. Myers and W. Sucksmith, Proc. Roy. Soc. (London) A207, 427 (1951).

[4] O. Bloch, Vierteljahrsschrift naturforschende Ges. Zürich. 56, 415 (1911).

CC-0. In Public Domain. Gurukul Kangri Collection, Haridwar

Digitized by Arya Samaj Foundation Chennai and eGangotri

tures, polycrystalline cobalt exists as a mixture of hexagonal and face-centered cubic structures, which at about 370°C becomes wholly cubic. For accurate measurements it was necessary to use single crystals and utilize the properties in the direction of easy magnetization in the low temperature hexagonal state, while above the transition range, this breaks down to the ordinary polycrystalline cubic material and, therefore, suffices.

These three researches constitute the total information on spontaneous magnetization available on the three ferromagnetic elements. It now is necessary to review briefly the comparison of these results with existing theory. The simple quantum modification of the Weiss theory predicts that the variation of the ratio σ_{0T}/σ_{00} (the latter being the spontaneous magnetization at absolute zero, i.e., the absolute saturation moment) with T/θ (where θ is the Curie temperature in degrees absolute) is dependent only on the quantum number j. For the ferromagnetics we put $j=\frac{1}{2}$, and thence it follows that the variation of spontaneous magnetization with temperature should be the same for all ferromagnetics, i.e., the quantum version of the Weiss' Law of corresponding states. For the case of nickel, when the reduced magnetization (σ_{0T}/σ_{00}) is plotted against the reduced temperature (T/θ), there are slight but definite divergences from the theoretical curve. For small values of T/θ the experimental values are slightly below, and for T/θ approaching unity, more markedly above the calculated curve. Potter's results for iron in the lower temperature range agree approximately with those of Weiss and Forrer for nickel, his results cutting the theoretical curve at $T/\theta \cong 0.6$, but above this temperature, the values are in excess of the nickel data, thus showing greater divergence from the theoretical $j=\frac{1}{2}$ curve. It should be noted that Potter used only the magnetothermal method of determining the law for iron. The purely magnetic results obtained by Myers and Sucksmith fall naturally into two parts, the portion below the phase change, in which the structure is close-packed hexagonal, and the range above this temperature where the structure is face-centered cubic. The former portion, extending to $T/\theta=0.5$ where σ_{0T}/σ_{00} falls only to 0.94, is too short to admit of accurate comparison with theory, although the experimental accuracy in this range is high. In the face-centered cubic phase, the range is adequate for comparison with the previous results, and the trend is identical with that of nickel. In other words, both face-centered cubic structures agree within experimental error, yet differ from the quantum modification of the law of corresponding states. It would appear that, at least to some extent, the law is structure sensitive.

Although a considerable amount of work on magnetic alloys has been carried out, there is comparatively little which admits of spontaneous magnetization data being extracted from the experimental results. Two exceptions are the early papers of Bloch[4] on cobalt-nickel alloys and papers of Alder,[5] who carried out measurements on copper-nickel. The reduced magnetization-temperature curves for the former system are almost coincident over the range extending from pure nickel to the cobalt rich alloys, and an extrapolation to 100 percent cobalt is employed rather than the interpretation of the slow approach to saturation of the mixed hexagonal and face-centered cubic polycrystalline material. While this is a somewhat hazardous procedure, the later results of Myers and Sucksmith discussed above provide justification. When we come to the results of Alder on the copper-nickel alloys, it is evident that with increasing dilution, the departure from the trend both for theory and for pure nickel becomes very marked in that the curves become less concave towards the origin. The method of determination of the spontaneous magnetization is of an arbitrary type, and as such open to criticism. The intensity values at 10 000 and 5000 oe are extrapolated linearly to $H=0$. Many other cases of experiments on alloys assume that the saturation intensity is an adequate measure of the spontaneous magnetization.

It will be appreciated from the foregoing discussion that the determinations on nickel are the only ones which can be regarded as satisfactory, and in view of the importance of the quantities involved, it seems desirable to extend the field of reliable determinations, particularly for ferromagnetic materials other than the three elements. Furthermore, the assumption that both the methods are equally valid rests only on the observations on nickel, and verification of this assumption for a selection of other ferromagnetics is called for. For these reasons it was decided to initiate measurements by both methods on representative materials. The copper-nickel series, which has played an important role in the development of the theory of ferromagnetic solid solutions is an obvious subject for investigation, and an alloy, chosen so as to afford the maximum range for profitable measurements, has been used. The ferrites have recently become prominent in ferromagnetic researches, and there are drastic differences from ordinary ferromagnetics in the intensity-temperature relationships of some of these substances. Experiments have also been carried out on a suitable ferrite. The present paper gives an account of the measurements which have been already carried out on one each of these types of ferromagnetics.

The experimental problem consists of the measurement of the magnetization in high fields together with the small reversible rise of temperature (ΔT) owing to the magnetization. In previous work these determinations have been made in a single apparatus, but in the work described here this has not been attempted and two distinct pieces of apparatus have been used. The resulting freedom in the design of the experimental arrangements renders a high degree of accuracy at-

[5] M. Alder, thesis, Zürich (1916).

CC-0. In Public Domain. Gurukul Kangri Collection, Haridwar

Digitized by Arya Samaj Foundation Chennai and eGangotri

tainable in the separate determinations. The magnetocaloric technique has been sufficiently improved to enable measurements of the rise of temperature, which is much smaller than in previous investigations, to be made accurately over an adequate range of reduced temperature. The ferromagnetic balance designed and used earlier by one of us[6] was originally employed for the intensity measurements and was, indeed, used for the earlier observations, but during the course of the work an improved form was developed which possesses considerable advantages over the original, particularly for measurements such as where the greatest possible accuracy is required for the rate of increase of magnetization with field.

THE MEASUREMENT OF THE MAGNETOCALORIC EFFECT

In principle, the method is simple and consists in measuring the temperature change in a specimen placed between the poles of an electromagnet of which the field is switched on or off.

The specimen was spherical in shape and 0.6–0.7 cm in diameter. The thermocouple was inserted in a small hole of diameter about 0.05 cm and held firmly in position in good thermal contact with the specimen.

THE THERMOCOUPLE

A thermocouple of high thermoelectric power is required for the experiment. The conflicting requirements are for low electrical resistance in order to secure high sensitivity and low thermal conductivity to minimize the heat losses. Since the thermal conductivity of copper-nickel is very much greater than that of the non-metallic ferrite, the couple appropriate to the specimen has to be selected with some care. This feature will be dealt with in connection with the appropriate materials below.

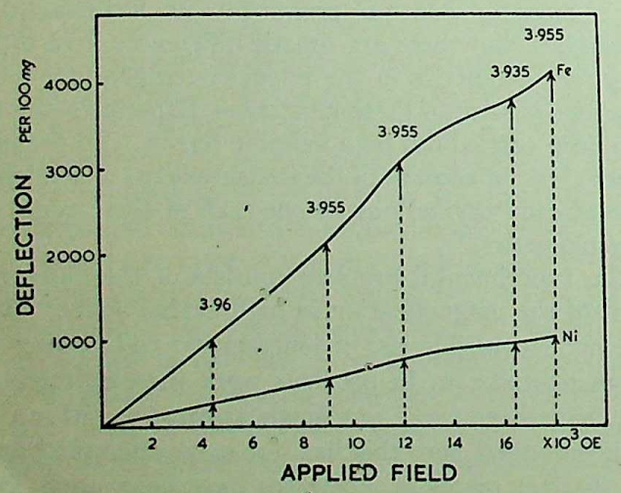


FIG. 1. Graph showing the relationship between the deflection per 100 mg of iron or nickel to the applied magnetic field in the original Sucksmith ring balance for ferromagnetics.

THE GALVANOMETER SYSTEM

The maximum magnetocaloric effect, even at the Curie point, is only about 0.35°C, and with even the sensitive thermoelements described above, together with a suitable low resistance galvanometer of short period to give adequate quickness of response, it is clear that some form of amplification must be employed in order to measure the effect accurately over a wide range of both magnetic field and temperature. A galvanometer amplifier employing a high degree of negative feedback similar to that of Preston[7] was constructed. This employs two photovoltaic cells connected in parallel with the input signal in order to secure a low input resistance. The primary galvanometer had resistance 15 ohms, period 4.5 seconds, and current sensitivity 193 mm/μA. In the secondary circuit, a short period galvanometer of period 2 seconds, resistance 26 ohms, and current sensitivity 150 mm/μA was used. The over-all sensitivity of the arrangement using maximum feedback was about 30 mm/μv corresponding to about 1100 mm/°C for the copper-constantan thermocouple. If necessary, this could easily be increased by reducing the feedback.

THE POTENTIOMETER

It was essential to reduce extraneous thermoelectric emf's as far as possible. The commercial potentiometers which were used in the initial stages exhibited these spurious emf's to such an extent as to make accurate measurements impracticable. It was found necessary to construct a special potentiometer in which the electrical circuit was composed entirely of copper and a special resistance alloy "minalpha" which has a low thermal emf against copper, i.e., 0.9μv/°C. The potentiometer itself was completely immersed in an insulating oil in order to minimize changes of ambient temperature. These precautions proved to be highly successful.

THE ELECTROMAGNET

A Weiss type electromagnet with 10-cm diameter poles was employed. The pole pieces were conical truncated to a plane pole face diameter of 2.0 cm, with a gap of 1.72 cm. With an excitation of 55 000 ampere-turns a maximum field of 20 000 oe was produced.

EXPERIMENTAL PROCEDURE

The potentiometer described above was used to balance the main emf of the thermocouple and thus gave the mean temperature at which observations were being taken. After recording the general slow drift of the galvanometer at 10-second intervals, the magnet was switched on, the magnetocaloric rise of temperature being shown by the out of balance deflection. The heat produced is dissipated in various ways, and a cooling curve is observed, observations still being taken at 10-second intervals; after about a minute the magnet field is switched off, and the same procedure followed

[6] W. Sucksmith, Proc. Roy. Soc. (London) **A170**, 551 (1939).

[7] J. S. Preston, J. Sci. Instr. **23**, 173 (1946).

CC-0. In Public Domain. Gurukul Kangri Collection, Haridwar

Digitized by Arya Samaj Foundation Chennai and eGangotri

during the cooling. Immediately after this, a calibrating emf producing the same order of deflection is injected into the circuit, and a similar procedure followed during the switching on and later during the switching off. These four readings insure adequate accuracy in determining the magnetocaloric ΔT.

Eddy current effects due to the magnetic field can be shown to be too small to be observable. Radiation loss is kept as low as possible by carrying out the experiments in vacuum. The chief source of error is probably that owing to thermal conduction down the thermocouple leads; and by deliberately increasing the extrapolation time, it was shown satisfactorily that this source of error must be less than 10^{-3}°C for the nickel-copper specimens. The procedure for the points is dealt with below, along with the measurements on that material.

THE MEASUREMENT OF THE INTENSITY OF MAGNETIZATION AT VARIOUS VALUES OF THE MAGNETIZING FIELD

The intensities of magnetization were, in the initial stages, obtained by the method developed by Sucksmith.[6] During the coarse of the work, an improved apparatus was developed, and since the method is particularly suitable for this type of measurement, it is described in some detail. In order to appreciate the significance of the modifications, some reference to the original method is necessary.

THE ORIGINAL BALANCE METHOD

This is a traction method, and the principle is that a ferromagnetic material placed in a inhomogeneous magnetic field experiences a force according to the equation

$$F_x = \sigma m dH_y/dx. \quad (1)$$

The magnetic field H can have any direction, but by far the majority of applications find it most convenient to employ a field whose direction is perpendicular to the direction of the force.

This force is measured by the ring balance, in which the displacement of the small specimen, very highly magnetized, is linearly proportional to the force which amounts to a few grams weight. The field must be sufficiently large for the requirements of the investigation, while the gradient must be constant over the working volume and involving only a small change in the absolute value of the field. To achieve this, stepped pole faces were employed such that a region of constant (and maximum) gradient existed. The balance is only intended for fields of some thousands of oersteds and upwards, and calibration is effected by comparison with a standard iron specimen, whose moment is assumed constant in fields above about 5000 oe at liquid air temperature. This assumption is fully justifiable for the maximum absolute accuracy claimed ($\frac{1}{4}$ percent). Comparison results for nickel and iron, together with sample ratios obtained at different fields, are given in Fig. 1. The field gradient which varies between 140 oe/cm to 600 oe/cm at the maximum magnetizing field of 18 000 oe was, of course, not separately controlled, and efforts were made to replace this with a coil system, a problem in which the suitable disposition and sensitivity of which presents the chief difficulty. Finally, the following improved arrangement for the field and field gradient was found satisfactory and adopted.

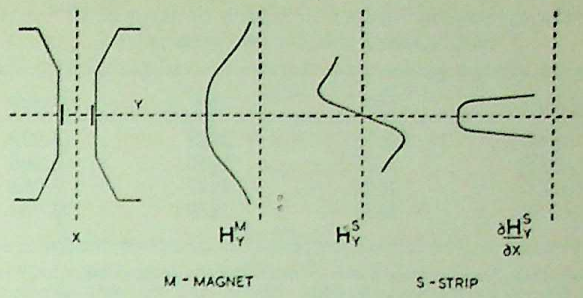


FIG. 2. Variation of magnetic fields and field gradient in gap of magnet.

A uniform field is employed throughout, and an electromagnet of similar type to that previously employed is used. The 10-cm pole pieces are truncated with a pole face diameter of 5.0 cm, and the gap width is 2.2 cm. To produce the field gradient, two horizontal copper strips 1.0×0.15 cm mounted symmetrically along, but insulated from, the face of the magnet poles (see Fig. 2) carry currents in the same direction being mounted in series so that the field due to these currents at the midpoint is zero. The variation of this field along the x axis together with the gradient is also shown in Fig. 2. The gradient at the center is shown as a flat maximum with variation less than 1 part in 2000 over the central 1.0 mm. Perpendicular to this, the gradient is a minimum the the center, so that in so far as horizontal displacement is concerned, the specimen will be in a position of unstable equilibrium. On the other hand, the flat spirals, preventing motion other than in the x direction, easily make this equilibrium quite stable. The gradient is directly proportional to the current, and for the dimensions employed the constant of proportionality is close to 0.5 when the current is measured in amperes. This means that since currents up to about 60 amperes were used the forces vary between 5 percent and 20 percent of those for the original balance. As stated above, the earlier form was concerned with forces up to a few grams weight so that no serious difficulty is presented by this change. Since the deflection produced is directly proportional to the current in the gradient strips, this must be measured accurately, and accordingly the usual potentiometer method is employed.

If measurements are restricted to high fields, i.e., those appreciably in excess of likely demagnetizing fields, accurate shaping of the specimens is unimportant, but for reasons which will be discussed below, ellipsoids of revolution were used for most measurements. The length was fixed at 5.0 mm, the diameter ranging from 1.25 to 2.50 mm, according to the intensity of magnetization.

Any nonuniformity of the field will be shown by a

CC-0. In Public Domain. Gurukul Kangri Collection, Haridwar

Digitized by Arya Samaj Foundation Chennai and eGangotri

TABLE I. Relation between deflection (in units of 10^{-2} mm) and applied field for two specimens.

H in oe	Fe[a]	Ni[b]	Ratio[c]
4600	2678	2483	3.972
8600	2677	2486	3.966
10 900	2678	2487	3.966
14 150	2679	2489	3.964

[a] Deflection for specimen of iron, weight 64.8 mg, strip current 36.00 amp.
[b] Deflection for specimen of nickel, weight 143.2 mg, strip current 60.00 amp.
[c] Ratio of the deflection per unit mass of iron to that of nickel.

deflection when the field is switched on, even in the absence of current through the gradient strips. Even with the utmost care in choice of material and machining of the pole tips, it was impossible to reduce this to a negligible magnitude. This residual effect, however, is not difficult to eliminate. The double deflection when the current through the gradient strips is reversed is always used. This procedure eliminates the error due to magnet field nonuniformity, the actual "zero" being unimportant and not figuring explicitly in the observations.

Table I shows a sample set of measurements on a nickel and an iron specimen. It will be seen that the ratios per unit mass of iron to nickel are in good agreement with the generally accepted ratio (Weiss and Forrer[8]). There is no correction for the image effect, and deflections expressed per unit mass have only to be multiplied by an instrumental constant for conversion to mass intensity. The double deflection is accurately proportional to force up to about 5000 scale divisions (1 division=0.01 mm), which represents ± 0.15 mm movement of the specimen, over which the gradient does not change perceptibly. This feature promises a high relative accuracy in estimating dH_y/dx, a precise knowledge of which is particularly important in determinations of the spontaneous magnetization. In order to test this, high field measurements were carried out on ellipsoidal single crystals of nickle cut with their easy directions of magnetization along the long axis of revolution of the specimen. In no case was there any determinable increase in σ between 5000 and 15 000 oe, i.e., $d\sigma/dH \geqslant 0.04\times10^{-4}$. On the other hand, a specimen of polycrystalline nickel increased from 2483 ± 1 at 4600 oe to 2489 ± 1 at 14 100 oe, (see Table I). This gives $d\sigma/dH$ as 0.14×10^{-4}, whereas the value given by the results of Weiss and Forrer[8] for room temperature is 0.2×10^{-4}.

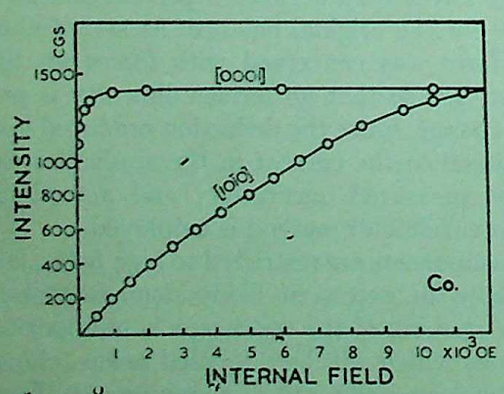


FIG. 3. Anisotropy of cobalt as measured in new ring balance (high fields).

While it is not strictly within the purview of spontaneous magnetization to deal with measurements in the low fields below saturation, it would seem not out of place in a Congress on Magnetism, in which experimental techniques are included in the program, and this extension is, therefore, included. There is no *a priori* reason why a pair of air core coils should not replace the electromagnet, while the same strips are employed to produce the field gradient. Two coils were, therefore, disposed Helmholtz fashion to give calculable uniform fields at their mid-point. These coils cover the range up to about 2000 oe, and the measurement procedure does not differ from that employed for high fields. (There are no complications due to stray nonhomogeneity of magnetizing field.) Both electromagnet and air core coils are disposed so as to be capable of horizontal translatory

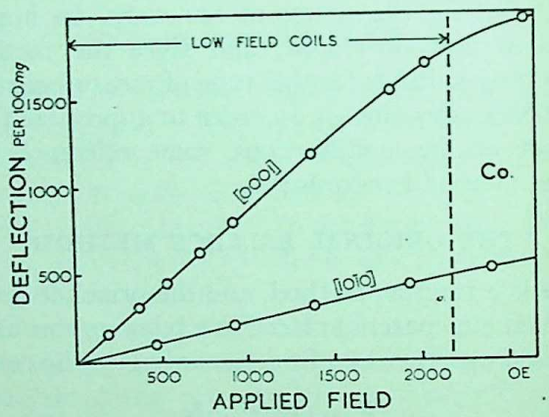


FIG. 4. Air core field measurement on single crystals of cobalt.

motion in a direction perpendicular to their fields, so that a continuous series of measurements from the lowest fields to the highest can be carried out. Calibration is effected by one measurement only at a selected high field. The standard calibration material was an ellipsoid of pure iron, whose intensity of magnetization at 15 000 oe and 15°C is taken as 217.7 per unit mass. This single calibration is in contrast with the previous balance where comparison at all the high field values employed was necessary.

To illustrate the adequacy of the method for the complete range of fields, the measurements on two single crystal ellipsoids of cobalt cut along the easy and difficult directions of magnetization are included. Figure 3 gives the results of measurements (corrected for demagnetizing field), while Fig. 4 on a larger scale shows the data as obtained for the lower range of magnetizing fields. As with the earlier form of the balance, measurements can be carried out at all temperatures up to about 1600°C without any modification or disturbance of the moving system.

[8] P. Weiss and R. Forrer, Ann. phys. 12, 279 (1929).

CC-0. In Public Domain. Gurukul Kangri Collection, Haridwar

Digitized by Arya Samaj Foundation Chennai and eGangotri

THE SPONTANEOUS MAGNETIZATION OF A COPPER-NICKEL ALLOY

The alloy, chosen so as to afford the maximum range over which both methods could be applied with accuracy contained 27.5 atomic percent copper. From magnetic measurements below room temperature, σ_{00}, the spontaneous magnetization at absolute zero, was found to be 31.0 units, in satisfactory agreement with the results of Alder (see reference 5). The magnetic intensity-temperature measurements were carried out for small temperature intervals up to 150°C (Curie temperature ~100°C) and exhibit the characteristic that the linearity at high fields persists to much higher (reduced) temperatures than is the case for pure nickel. Even above the Curie temperature there is marked linearity. This property allowed linear extrapolation to zero field, as well as the employment of the curves of constant intensity, to determine the spontaneous magnetization; and there is little if any difference between the two methods of extrapolation.

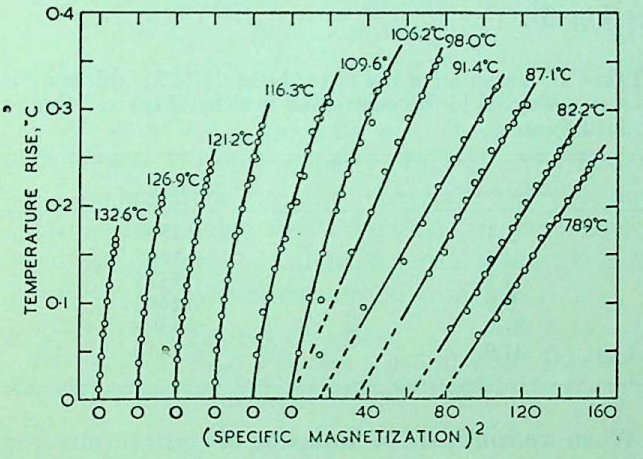


FIG. 5. Variation of magnetocaloric rise of temperature for 27.5 percent Cu-Ni alloy with square of intensity of magnetization per unit mass.

The magnetocaloric rise of temperature plotted against field shows the same features as those previously noted by Weiss and Forrer, i.e., linearity for low temperature with concavity towards the temperature axis developing with increasing temperature. The maximum ΔT is 0.35°C as compared with about 1.25°C for nickel and about twice this value for iron, while the variation with temperature is very similar to the previous results, though the half-width of the peak extends over a larger temperature range than in these cases. When we examine the variation of ΔT against the square of the magnetization (see Fig. 5), there are new features. Below the Curie point the linearity previously observed is reproduced, but above this temperature there is pronounced curvature, i.e., the relationship $\Delta T = A\sigma^2$ is not followed, and to express the variation a term involving a higher power of σ is required.

It is now necessary to compare the values of the spontaneous magnetization obtained by the two methods, and this is summarized in Fig. 6. For values of T/θ between zero and about 0.9, there is satisfactory agreement between the purely magnetic and the magnetothermal methods. Above this temperature, however, the curves diverge, and the Curie temperature deduced from the magnetothermal data is some 5.5°C below that determined from magnetic data alone.* Furthermore, the "tail" is much less pronounced in the case of the magnetocaloric effect, with a corresponding decrease in the uncertainty of extrapolation.

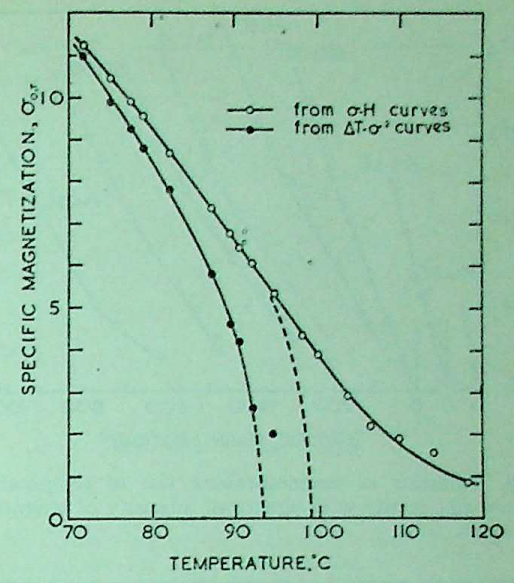


FIG. 6. Comparison of spontaneous magnetization for a 27.5 percent Cu-Ni alloy determined from the magnetic measurements and from the magnetocaloric effect.

Finally there is the comparison of these curves with the shapes previously obtained, and with the theoretical $j=\frac{1}{2}$ curve. This is shown in Fig. 7. It is quite evident that the departure from the theoretical curve is quite firmly established.

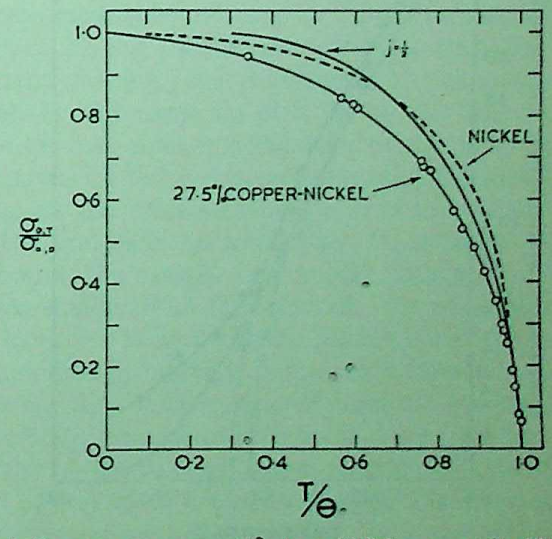


FIG. 7. Spontaneous magnetization of 27.5 percent Cu-Ni alloy compared with nickel and with theory.

* The Curie point determined from paramagnetic measurements was 111°C, i.e., about 12°C higher than the ferromagnetic Curie temperature.

CC-0. In Public Domain. Gurukul Kangri Collection, Haridwar

Digitized by Arya Samaj Foundation Chennai and eGangotri

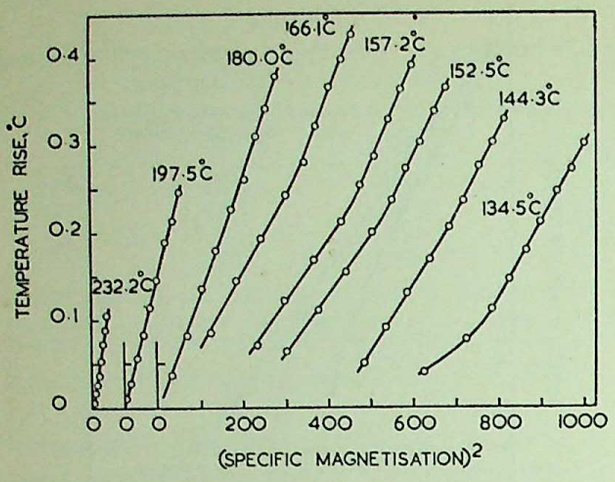


FIG. 8. Variation of magnetocaloric rise of temperature for magnesium zinc ferrite with square of intensity of magnetization per unit mass.

THE SPONTANEOUS MAGNETIZATION OF A FERRITE

As previously stated, the ferrite chosen was $MgO \cdot ZnO \cdot 2Fe_2O_3$. The reason for the employment of this particular material was twofold: the low Curie temperature combined with the departure of the saturation intensity-temperature curve from the conventional type [see Snoek, *New Developments in Ferromagnetic Materials* (Elsevier Publishing Company, Inc., Houston, 1947), pp. 87–90]. No further difficulty was presented in the magnetic determinations, but serious reconsideration of the thermal measurements was necessary on account of the low thermal conductivity. In this connection Stoner[9] has drawn attention to the error in the results of Weiss and Forrer owing to neglect of the thermal capacity of the thermocouple. In order to minimize this, various thermo-elements of different thermal conductivities and appropriate cross sections were employed for test experiments. Any heat loss will be proportional to the product KA for each element, where K is the thermal conductivity and A the cross-sectional area of the element of the couple. Table II gives the observed value of ΔT for a particular set of conditions plotted against ΣKA. It can be seen that such error as remains for materials of low conductivity can be easily corrected for.

The intensity-field relationships are quite similar to those already obtained for other substances, though with increasing temperature, the linear portions in the curves of constant intensity become shorter, until at $\sigma=5$ there is virtually no linear portion, whereas even at $\sigma=1$ the copper-nickel alloy displays linearity. On the other hand, the magnetocaloric rise of temperature, in general, follows the same trend as the ferromagnetic elements and is shown in Fig. 8. It is noteworthy that above the Curie temperature there is no evidence of the curvature characteristic of the copper-nickel alloy (see Fig. 5).

TABLE II. Variation of rise of temperature (ΔT) with material of thermoelements for different cross-sectional areas and thermal conductivities.

$\Sigma KA \times 10^5$	ΔT(deg C)
1.4	0.1590
2.1	0.1593
4.3	0.1573
9.9	0.1493
31.9	0.1399
31.9	0.1416

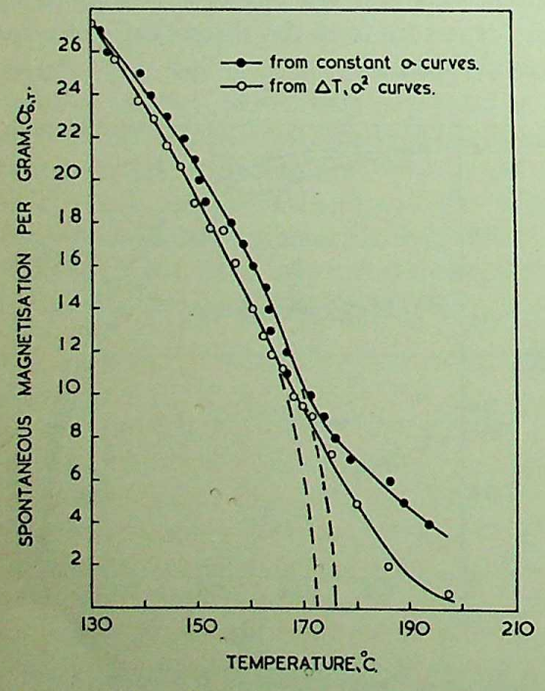


FIG. 9. Comparison of spontaneous magnetization for a magnesium zinc ferrite determined from magnetic measurements with that from the magnetocaloric effect.

When we consider the variation of spontaneous magnetization with temperature, we find satisfactory agreement by the two methods until the immediate neighborhood of the Curie temperature is reached. Above 130°C ($T/\theta>0.9$) there is a slight but definite divergence, the curve derived from the magnetocaloric rise of temperature being lower as is the case with the copper-nickel alloy (Fig. 9). The difference is, however, quite small, being only about 3°C, and the "tail" is markedly less than for other ferromagnetics. Finally in Fig. 10, σ_{0T}/σ_{00} is shown, together with the magnetocaloric ΔT for comparison. (The difference between the two curves of Fig. 9 is too small to be indicated in the figure.) It is quite evident that the variation of the reduced magnetization with temperature lies well inside the quantum-theory modifications of the law of corresponding states even for the largest values of j. The lowest temperatures employed were around 90°K, and the figure shows linear extrapolation to zero temperature. Guillaud (*Grenoble Conference on Ferromagnetism and Antiferromagnetism*, pp. 91–103) has shown that this linearity in ferrites may persist at least to the neighborhood of 20°K, so that probably little error is involved in this extrapolation. Measurements of the paramag-

[9] E. C. Stoner, Trans. Roy. Soc. (London) A235, 165 (1936).

CC-0. In Public Domain. Gurukul Kangri Collection, Haridwar

Digitized by Arya Samaj Foundation Chennai and eGangotri

netism above the Curie temperature are in progress, so that the method devised by Néel[10] for the law of variation of intensity with temperature can be calculated. Comparison with existing data for other ferrites indicates that there is likely to be substantial agreement between the theoretical and experimental curves.

CONCLUSIONS

It is clear that the two methods hitherto employed for the determination of the spontaneous magnetization are justified over a wide range from the lowest temperature to within the neighborhood of the Curie point. In this region the two methods diverge at the point where T/θ is greater than about 0.9. The tail is not so extensive as had been expected and is smaller for both materials when deduced from the magnetocaloric measurements. This feature prompts a re-examination of the results for nickel; and this suggests that the absence of tail is not so certain as these writers have supposed (e.g., see Potter, reference 2, for comments on this point).

The magnetocaloric experiments on the nickel-copper alloy show that there is substantial deviation from the $j=\frac{1}{2}$ curve, and it may be that the explanation is to be found in Stoner's collective electron theory,[11] but the values do not correspond with those suggested by Wohlfarth.[12] The new property of nonlinearity between the magnetocaloric rise of temperature and the square of the magnetization above the Curie temperature may be a characteristic of a diluted ferromagnetic, but this point calls for experiments on other alloys.

[10] L. Néel, Ann. phys. 3, 137 (1948).
[11] E. C. Stoner, Proc. Roy. Soc. (London), A165, 372 (1938).
[12] E. P. Wohlfarth, Phil. Mag. 40, 703 (1949).

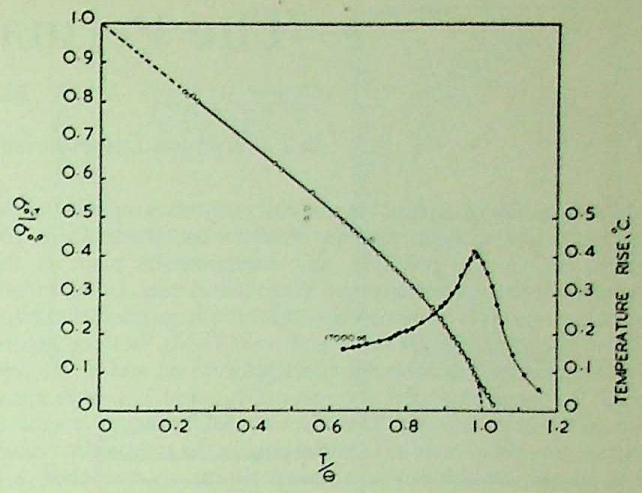


FIG. 10. Curve showing variation of spontaneous magnetization with temperature for a magnesium zinc ferrite. The magnetocaloric effect for a high value of the magnetic field is also shown.

The most marked feature of the experiments on the ferrite is the very close agreement between the magnetic and magnetothermal measurements. This is all the more striking in the mixed ferrite where deviations could reasonably be attributed to the nature of the material. When paramagnetic data is available, it is to be expected that a satisfactory correlation between theory and experiment will be available.

It should be emphasized that the results presented do not represent a completed work, and, therefore, detailed discussion would be premature. Further experiments, both on diluted ferromagnetics and on ferrites are planned or in progress.

DISCUSSION

C. J. GORTER, *Leiden University, The Netherlands:* Does not the fact that in the Cu-Ni alloy the ΔT is not proportional to σ^2 above the Curie temperature indicate that there the susceptibility must depend on the field? Then we would not have to do with paramagnetism proper. In view of the inhomogenity to be expected, a tail of ferromagnetism in the paramagnetic region is no wonder.

A. ARROTT, *Carnegie Institute of Technology, Pittsburgh, Pennsylvania:* We have used for the measuring of paramagnetic susceptibilities a method similar to that of Shoenberg which we think could be used with several modifications to measure saturation magnetization of ferromagnets. The motion of a paramagnetic cylinder in a uniform magnetic field may be picked up by a pair of detector coils connected in opposition in order to cancel out signals induced by fluctuations of the field. A zero pitch solenoid may be wound on the cylindrical surface of the paramagnet so that, with the proper current flowing, the movement of the sample plus solenoid will cause no pick up by the detector coils. The current then is a measure of the magnetization. This works for weak paramagnets, but with ferromagnets the solenoid's field affects the magnetization of the sample in no small way. If, as suggested by J. Osborne, the sample is a needle with a cross section much smaller than the solenoid, it is possible for both to have the same magnetic moment without the solenoid's field being large enough to influence the sample. The equality of the magnetic moments can be detected by placing pick-up coils some distance from the sample where both the needle-like sample and the solenoid will approximate extended dipoles. The advantages of the measurement are in the use of a uniform field and negligible demagnetizing effect and in the absence of image effects.

CC-0. In Public Domain. Gurukul Kangri Collection, Haridwar

Digitized by Arya Samaj Foundation Chennai and eGangotri

REVIEWS OF MODERN PHYSICS VOLUME 25, NUMBER 1 JANUARY, 1953

The Permalloy Problem

R. M. Bozorth

Bell Telephone Laboratories, Inc., Murray Hill, New Jersey

In attempting to explain the unusual magnetic properties of the iron-nickel alloys, single crystals of alloys containing 35 to 100 percent nickel were prepared, and measurements made of the magnetic crystal anisotropy and magnetostriction as dependent on cooling rate. It is confirmed that there is a large effect of cooling rate on the anisotropy in the region near $FeNi_3$, but the experiments show also a substantial effect between 50 and 85 percent nickel. Two magnetostriction constants, λ_{100} and λ_{111}, were measured on the same crystals. The effect of cooling rate on magnetostriction was found to be substantial only in the composition range 70 to 80 percent nickel. When the specimens are quenched, λ_{111} goes through zero for a nickel content just below 80 percent nickel, a composition very close to that for highest permeability. This is understandable because the magnetostrictive strain caused by movement of the boundary between two domains, each magnetized spontaneously in a [111] direction, depends on λ_{111} alone. The same physical picture predicts that near 45 percent nickel, where [100] is the direction of easiest magnetization and λ_{100} goes through zero, the permeability *vs* composition curve should again have a maximum. Such a maximum is known to exist, and initial permeabilities as high as 15 000 have been observed.

Although simple theory suggests that domain-rotation should occur in very weak fields when the crystal anisotropy is very small (75 percent nickel in quenched alloys), nevertheless, rotation involves magnetostrictive strains which prevent μ_0 from becoming infinite. Internal poles are also likely to be formed. In slowly cooled alloys the anisotropy is zero at about 63 percent nickel; here there are random strains caused by magnetostriction and possibly also by atomic ordering.

The principal changes in magnetic properties with composition are explained in terms of the crystal anisotropy and magnetostriction, and their change with heat treatment.

INTRODUCTION

THE "Permalloy problem" is to explain the characteristic magnetic properties possessed by the binary iron-nickel alloys containing 35 to 100 percent nickel. They have unusually high permeabilities which are a maximum at about 79 percent nickel, the permeabilities are influenced markedly by heat treatment and specifically are increased by cooling rapidly, and a magnetic anneal (cooling in the presence of a magnetic field) causes drastic changes in various magnetic properties, particularly the maximum permeability and the form of the hysteresis loop. The present investigation of the magnetic crystal anisotropy, and of the magnetostriction of single crystals of these alloys, is a contribution to the explanation of the behavior of these alloys as dependent on composition and heat treatment.

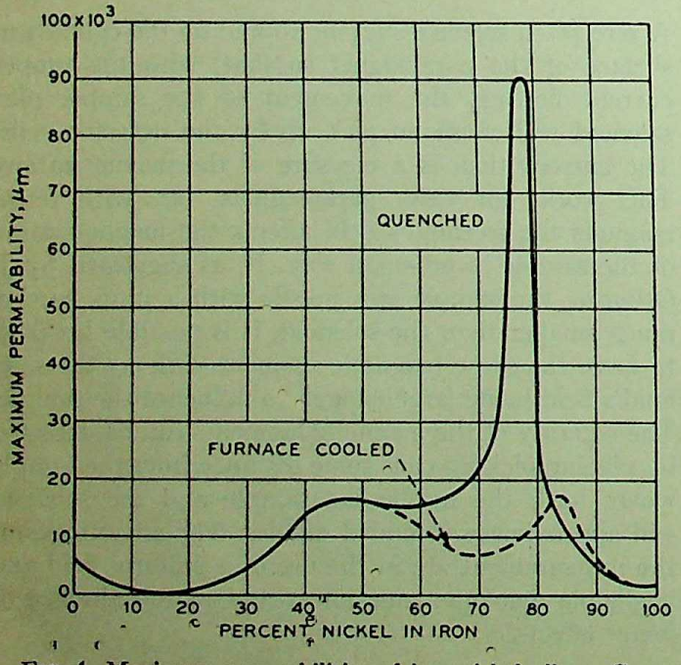


FIG. 1. Maximum permeabilities of iron-nickel alloys. Curves show mean values of many measurements taken over a period of years.

These properties are illustrated in Figs. 1–3, which were drawn some time ago and represent mean values of many data.[1] In addition to the maxima of the permeabilities at about 79 percent nickel (Figs. 1 and 2), one should note the secondary maxima at about 45 percent nickel, which we will refer to later, and the shift of the 79 percent maximum with heat treatment. The change in the form of the loop with heat treatment in a magnetic field, and the associated change in maximum permeability, are drastic; there is practically no corresponding change in initial permeability.

In previous attempts to explain these phenomena, McKeehan[2] first stated a qualitative relation between the high permeability and the low magnetostriction. Kersten[3] derived an expression for the highest initial permeability attainable in a material which has residual magnetostrictive strains. Both McKeehan and Kersten used the magnetostriction of the polycrystalline material, which passes through zero at 81 to 83 percent nickel. Lichtenberger[4] found that the composition for zero magnetostriction is different for the [100], [110], and [111] directions. Also, he noted that the permeability maximum at 79 percent lies between the composition for zero polycrystalline magnetostriction and the composition for zero crystal anisotropy.

Using the ideas of domain theory which have been developed during recent years, we expect that when the crystal anisotropy is zero and imperfections are absent,

[1] See, for example, R. M. Bozorth, *Ferromagnetism* (D. Van Nostrand Company, Inc., New York, 1951).
[2] L. W. McKeehan, Phys. Rev. 28, 158 (1926).
[3] M. Kersten, Z. tech. Physik 12, 665 (1931). See also R. Becker and Döring, *Ferromagnetismus* (Springer Verlag, Berlin, 1939).
[4] R. Lichtenberger, Ann. Physik 15, 45 (1932).

CC-0. In Public Domain. Gurukul Kangri Collection, Haridwar

Digitized by Arya Samaj Foundation Chennai and eGangotri

domain rotation will occur with great ease and the permeability will be very high. Also, when the magnetostriction is zero, displacement of domain boundaries will occur with negligible resistance, and the permeability will also be high. The work summarized below was carried out in order to subject this physical picture to a quantitative test and to find out if possible the separate roles of anisotropy and magnetostriction. This necessitated determination of the crystal anisotropy constants, and of the magnetostriction at saturation in the principal crystal directions, in single crystals subjected to various heat treatments, that is, various rates of cooling.

A qualitative theory of heat treatment in a magnetic field was suggested by the author some years ago.[5] This dealt with the relief of magnetostrictive strains by diffusion, in material of low crystal anisotropy. Further consideration can now be given to this theory, using the results of the present investigation as a background.

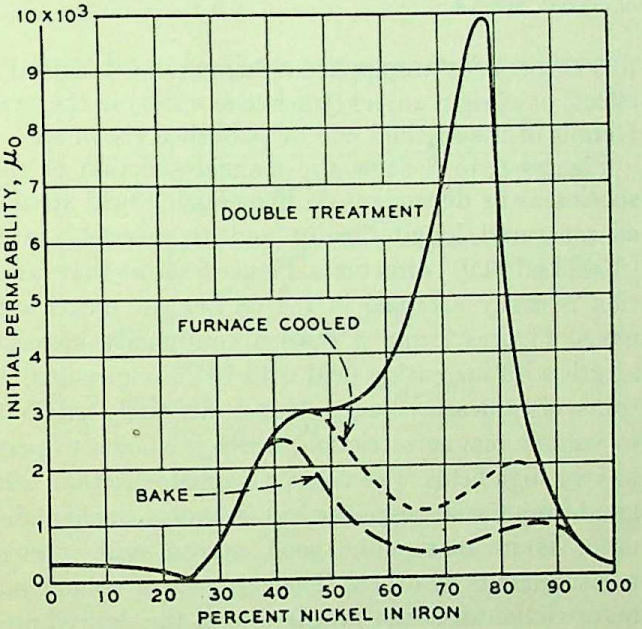


FIG. 2. Initial permeabilities of iron-nickel alloys, averaged over many measurements.

Determinations of crystal anisotropy and saturation magnetostriction in various crystal directions will now be described.

CRYSTAL ANISOTROPY

Single crystals were prepared by slow cooling of the melt, as described by Walker, Williams, and Bozorth.[6] Specimens were cut in the form of disks, usually in the (100) plane, and were normally about 1 cm in diameter and 2 mm thick. Accuracy of orientation was a few tenths of a degree. After annealing, all specimens were cooled at two standard rates: (1) they were withdrawn from the furnace at about 700°C and placed quickly on a cold copper plate (quenched), or (2) they were automatically cooled from above 600° to below 300°C at 2°C/hr (baked). The known order-disorder transformation of $FeNi_3$ is at 506°C. Presumably (1) gives a high degree of disorder, (2) a high degree of order, but some of our experiments indicate that a definitely higher degree of order is obtained by cooling at 1°C/hr.

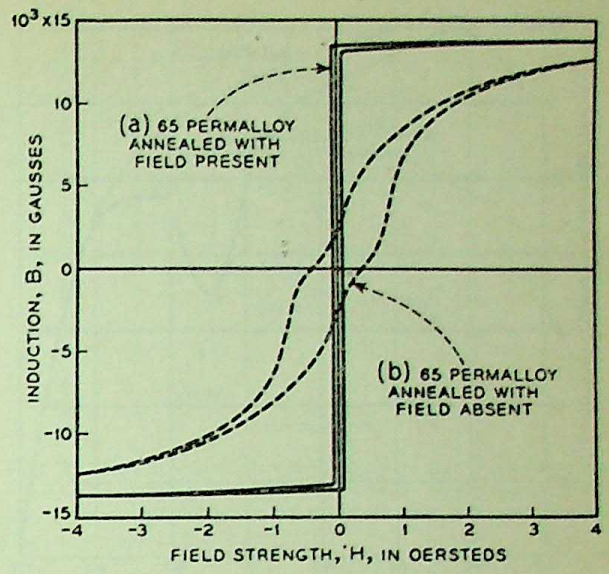


FIG. 3. Hysteresis loops of 65 Permalloy, showing effect of heat treatment in a magnetic field.

Measurements, already reported briefly,[7] were made by the use of a sensitive torsion magnetometer designed by Mr. H. J. Williams, with which a torque of 6 dyne-cm could be readily detected. Details of the measurements will be reported elsewhere.

The results are shown in Fig. 4. It is noted at once that the slowly cooled alloys have lower (more negative) anisotropy constants, especially in the composition range near $FeNi_3$ (76 percent nickel), at which a deep minimum occurs. This confirms measurements previously reported by Grabbe.[8] Atomic ordering was detected by x-rays and by neutron diffraction in the slowly cooled alloys containing 74 and 68 percent nickel but not in the quenched alloys or in a slowly cooled specimen containing 90 percent nickel. It seems probable that some ordering occurs in alloys containing as little as 40 percent nickel but not in those containing 90 percent or over.

The alloy containing 74 percent nickel was cooled at various rates, with the results shown in Fig. 5. This shows that the degree of ordering is still increasing as the cooling rate falls below 2°C/hr.

The composition for zero anisotropy varies from 63 to 75 percent nickel, depending on the cooling rate. It has previously been pointed out that a low anisotropy is related to other magnetic phenomena, for example, low

[5] K. M. Bozorth and J. F. Dillinger, Physics 6, 285 (1935); see also J. S. Marsh, *Alloys of Iron and Nickel* (McGraw-Hill Book Company, Inc., New York, 1938), pp. 214–219.

[6] Walker, Williams, and Bozorth, Rev. Sci. Instr. 20, 947 (1949).

[7] R. M. Bozorth and J. G. Walker, Phys. Rev. 83, 871 (1951).

[8] E. M. Grabbe, Phys. Rev. 57, 728 (1940).

CC-0. In Public Domain. Gurukul Kangri Collection, Haridwar

Digitized by Arya Samaj Foundation Chennai and eGangotri

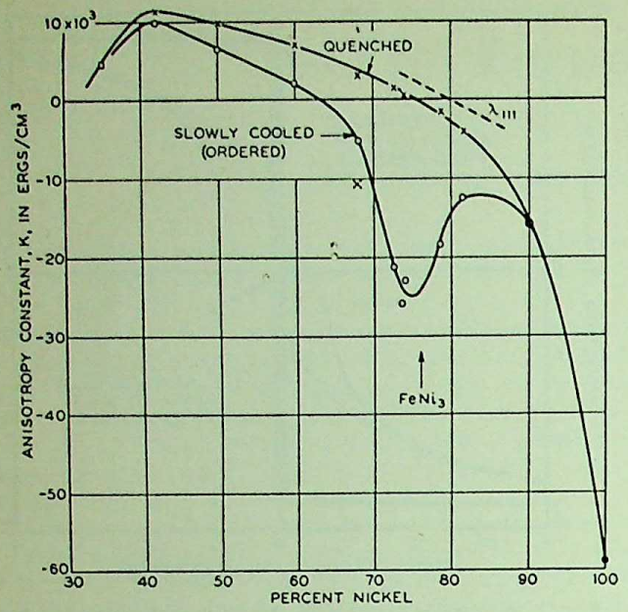


FIG. 4. Crystal anisotropy constants of quenched and of slowly cooled alloys. Broken line λ_{111} indicates the composition at which the magnetostriction in the [111] direction goes through zero.

remanence,[9] high strain sensitivity,[10] and susceptibility to magnetic anneal.[11] More quantitative tests of these relations can now be made.

MAGNETOSTRICTION

Magnetostriction was determined on the same disks that were used for anisotropy measurements, using strain gauges according to the method described by Goldman.[12] Gauges, usually of $\frac{1}{8}$-in. size, were oriented in the [100] and [110] directions in the (001) plane. A magnetic field of high uniformity and of strength up

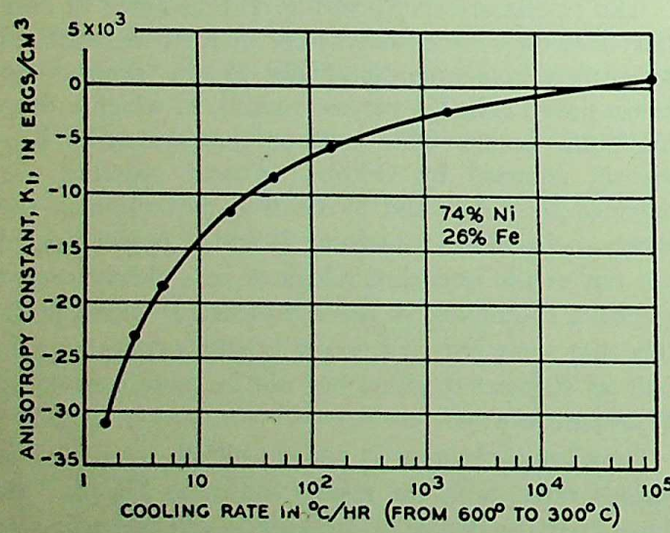


FIG. 5. Anisotropy constants of 74 percent nickel alloy as dependent on rate of cooling from 600° to 300°C. Highest cooling rate is a rough estimate only.

[9] R. M. Bozorth, Z. Physik 124, 519 (1948).
[10] R. M. Bozorth and H. J. Williams, Revs. Modern Physics 17, 72 (1945).
[11] J. F. Dillinger and R. M. Bozorth, Physics 6, 279 (1935); see also reference 4.
[12] J. E. Goldman and R. Smoluchowski, Phys. Rev. 75, 140 (1949).

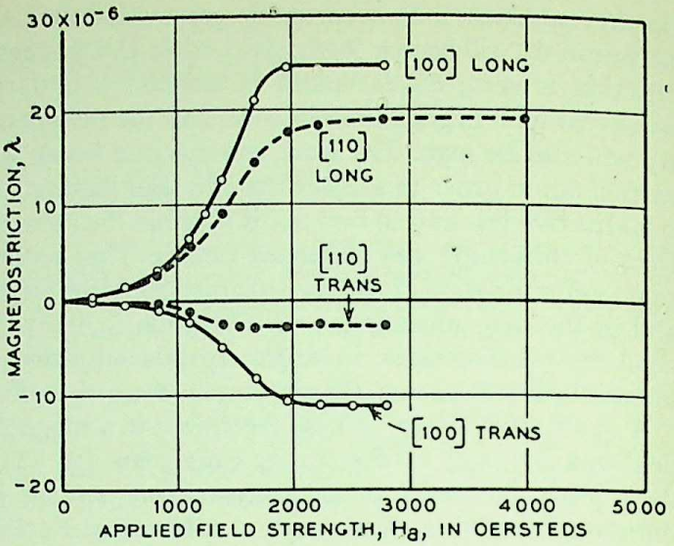


FIG. 6. Longitudinal and transverse magnetostriction of 68 percent nickel crystal, measured in [100] and [110] directions, as dependent on external applied field. Ratio of diameter to thickness of crystal, $m=4.4$.

to 5000 oersteds was applied either parallel (longitudinal effect) or at right angles (transverse effect) to the gauge. Details of the method will be published elsewhere.

Figures 6 to 8 show the magnetostriction of three specimens as dependent on magnetizing field strength, as measured longitudinally and transversely in the [100] and [110] directions. Figure 6 shows that saturation is easily attained in the 68 percent nickel specimens. Figures 7 and 8 show a continually increasing length with increasing field with both longitudinal and transverse measurements. This is definitely attributed to volume magnetostriction, which is known to persist to very high fields. The volume magnetostriction, calculated from the slopes of the λ *vs* H lines in the high fields used, is in reasonably good accord with previous measurements by others. The existence of volume magnetostriction does not interfere with the desired measurement of λ_{100} and λ_{111} for reasons indicated below.

Using the 2-constant formula[1] for magnetostrictive

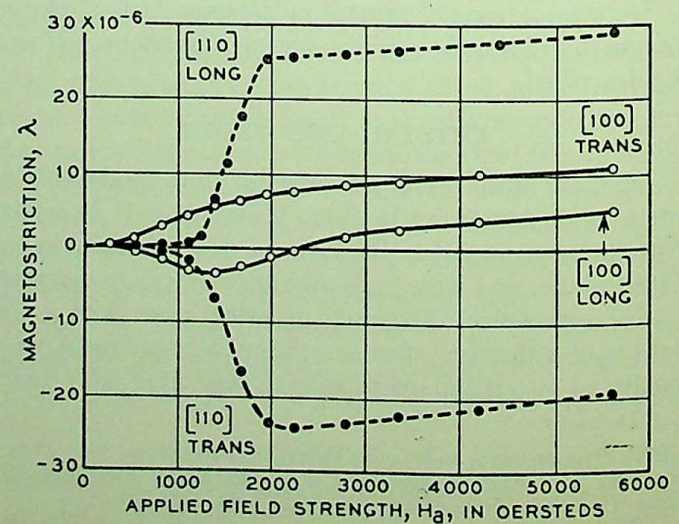


FIG. 7. Magnetostriction of 42 percent nickel crystal, $m=5.5$.

CC-0. In Public Domain. Gurukul Kangri Collection, Haridwar

Digitized by Arya Samaj Foundation Chennai and eGangotri

change in length at saturation, we have

$$\lambda=(3/2)\lambda_{100}(\alpha_1^2\beta_1^2+\alpha_2^2\beta_2^2+\alpha_3^2\beta_3^2-1/3)$$
$$+3\lambda_{111}(\alpha_1\alpha_2\beta_1\beta_2+\alpha_2\alpha_3\beta_2\beta_3+\alpha_3\alpha_1\beta_3\beta_1),$$

in which the α's are the direction cosines of the magnetization with respect to the crystal ones, and the β's are the direction cosines of the measured change in length; and it is apparent that the difference between the longitudinal (λ_l) and the transverse (λ_t) changes in length in the [100] direction gives λ_{100}:

$$\lambda_l-\lambda_t=(3/2)\lambda_{100}, \quad \text{for [100]}.$$

Here $\beta_1=1$, $\beta_2=\beta_3=0$; $\alpha_1=1$, $\alpha_2=\alpha_3=0$ or $\alpha_2=1$, $\alpha_1=\alpha_3=0$. Not quite so obviously, the corresponding changes in length in the [110] direction give λ_{111}:

$$\lambda_l-\lambda_t=(3/2)\lambda_{111}, \quad \text{for [110]}.$$

Here $\beta_1=\beta_2=1/\sqrt{2}$, $\beta_3=0$; $\alpha_1=\alpha_2=1/\sqrt{2}$, $\alpha_3=0$ or $\alpha_1=-1/\sqrt{2}$, $\alpha_2=1/\sqrt{2}$, $\alpha_3=0$.

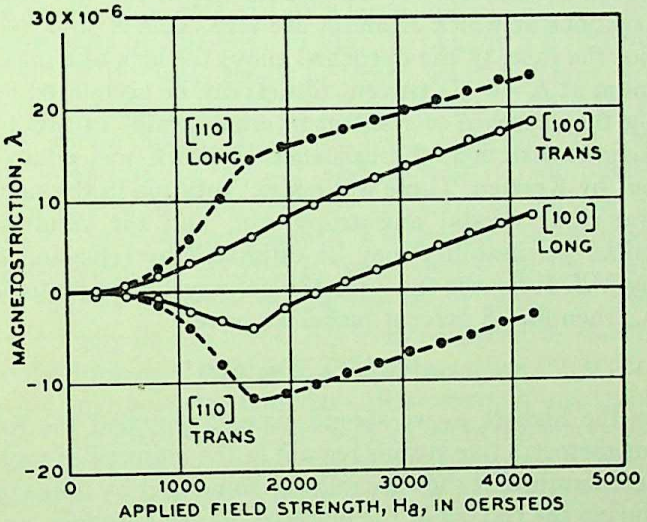


FIG. 8. Magnetostriction of 35 percent nickel crystal, showing large volume effect; $m=3.9$.

Values of λ_{100} and λ_{111} for crystals heat treated in the two ways (quenched on a cold copper plate or cooled at 2°C/hr) are shown in Fig. 9. It is apparent that the magnetostriction varies with heat treatment in a narrower composition range than was observed for the anisotropy, namely, from about 68 to 81 percent nickel. The measurements for the quenched alloys agree tolerably well with the results of Lichtenberger,[4] but the new measurements are somewhat higher in the range 40 to 50 percent nickel. The ordered alloys are more nearly isotropic than the disordered alloys, and at about 73 percent nickel λ_{100} and λ_{111} are almost equal. Data for the range 60 to 90 percent nickel are shown on a larger scale in Fig. 10.

It will be shown later that the composition at which λ_{111} equals zero is of special importance for the theory of Permalloy. According to the data just presented, this composition is slightly greater than 80 percent nickel for the quenched alloys. However, consideration

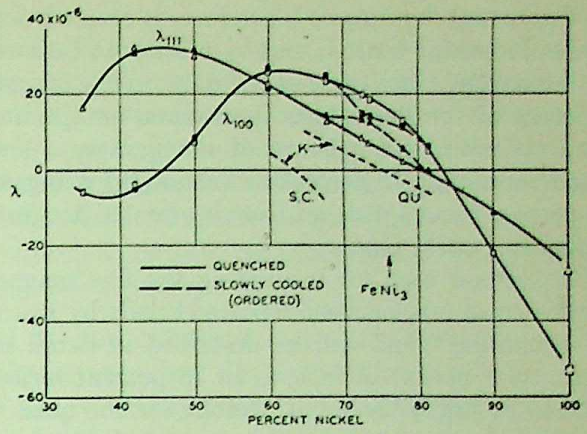


FIG. 9. Magnetostriction constants λ_{100} and λ_{111}, showing dependence on cooling rate. Broken curves show compositions at which crystal anisotropy goes through zero, for quenched (QU) and slowly cooled (S.C.) alloys.

of the 5-constant formula[1] for magnetostriction:

$$\lambda_s=h_1(\alpha_1^2\beta_1^2+\alpha_2^2\beta_2^2+\alpha_3^2\beta_3^2-1/3)$$
$$+2h_2(\alpha_1\alpha_2\beta_1\beta_2+\alpha_2\alpha_3\beta_2\beta_3+\alpha_3\alpha_1\beta_3\beta_1)$$
$$+h_4(\alpha_1^4\beta_1^2+\alpha_2^4\beta_2^2+\alpha_3^4\beta_3^2+2s/3-1/3)$$
$$+2h_5(\alpha_1\alpha_2\alpha_3^2\beta_1\beta_2+\alpha_2\alpha_3\alpha_1^2\beta_2\beta_3+\alpha_3\alpha_1\alpha_2^2\beta_3\beta_1$$
$$+h_3(s-1/3) \text{ for nickel, } +h_3 s \text{ for iron,}$$
$$s=\alpha_1^2\alpha_2^2+\alpha_2^2\alpha_3^2+\alpha_3^2\alpha_1^2,$$

shows that

$$\lambda_{111}=2h_2/3+2h_5/9,$$

whereas the last term is neglected in the 2-constant formula. Obviously the constant h_5 might possibly make an important contribution. (If we take the five constants determined[1] by Döring from the data of Masiyama for nickel, we have

$$2h_2/3=-31\times10^{-6},$$
$$2h_2/3+2h_5/9=-20\times10^{-6},$$

a large discrepancy between the results of the 2-constant

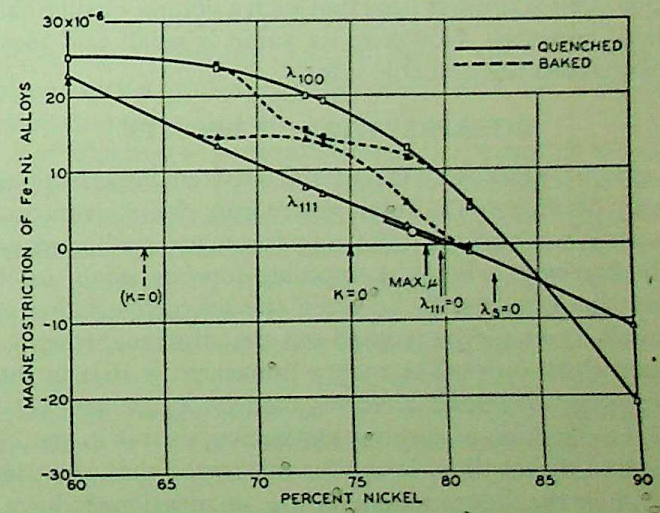


FIG. 10 Magnetostriction constants for range 60 to 90 percent nickel. Single point shows λ_{111} as determined with greater accuracy for a specimen containing 0.5 percent manganese.

CC-0. In Public Domain. Gurukul Kangri Collection, Haridwar

Digitized by Arya Samaj Foundation Chennai and eGangotri

and 5-constant formulas.) Therefore, it seemed necessary to determine both h_2 and h_5 in order to be sure of λ_{111}. Moreover, since most of the data on the magnetic properties of the Permalloys were taken for specimens which contained 0.5 percent of manganese, a single crystal containing 78 percent nickel and 0.5 manganese was prepared and a disk cut from it oriented accurately parallel to a (011) plane.

The method used for evaluating the five magnetostriction constants has been reported briefly by Bozorth and Hamming,[13] and will be described in detail elsewhere. As a matter of fact, h_5 in 78 percent nickel is found to be negligibly small. Results for the quenched specimens are $h_1=13$, $h_2=2.6$, $h_3=-0.3$, $h_4=-0.1$, all $\times 10^{-6}$. Therefore,

$$\lambda_{111}=1.7\times 10^{-6}.$$

This point is plotted with a large circle in Fig. 10. It lies close to the λ_{111} curve previously drawn, and a new line drawn parallel to the old crosses the axis at about 79.5 percent nickel. This is very close to the composition for highest permeability.

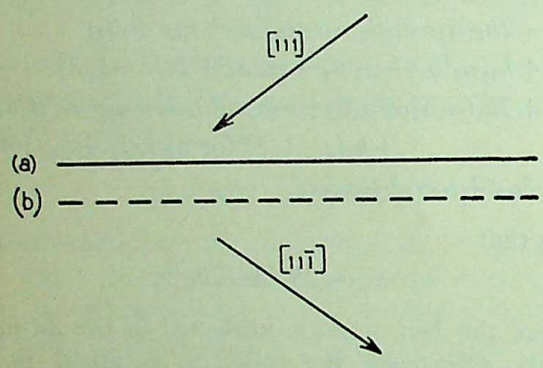


FIG. 11. Ideal domain boundary separating [111] and [11$\bar{1}$] domains. No poles are formed at boundary since the normal component is constant across the boundary. The strain produced by boundary movement depends only on λ_{111}.

Incidentally, it may be pointed out that h_3 is a measure of the volume change associated with domain rotation. This is the first time that such a volume change has been measured. However, its value is small and may not exceed the probable error.

INTERPRETATION OF RESULTS

High permeability in material free from imperfections may be expected to result either from domain rotation against weak crystal anisotropy forces or from boundary displacement when the opposing force is small, as it may be expected to be when the magnetostriction is small. It should be pointed out that the magnetostriction which opposes boundary movement is that in the *easy crystallographic direction*, namely, λ_{111} when [111] is the direction of easy magnetization, as it is in the 79 percent nickel alloy. It was for this reason that care was taken in the determination of λ_{111}, as mentioned above.

[13] R. M. Bozorth and R. W. Hamming, Phys. Rev. 87, 209 (1952).

According to domain theory,[1] as developed by Becker and others, the rotation of magnetization by the field, against the forces of crystal anisotropy, gives the following formula for the initial permeability:

$$\mu_0-1=2\pi\overline{\sin^2\theta}(I_s^2/K),$$

θ being the smallest angle between the magnetization and a crystal axis, or

$$\mu_0\approx 2I_s^2/K.$$

A formula for μ_0 for the moving boundary process has been given by Becker and Döring[3] in terms of internal strains σ_i. Putting $\sigma_i=\lambda E$, as Kersten has proposed, we have

$$\mu_0\approx 5I_s^2/(\lambda^2 E),$$

E being Young's modulus and λ being the saturation magnetostriction in the direction of easy magnetization.

According to simple theory one might expect the initial permeability to become infinite at the two compositions at which K and λ are zero. This is obviously not the case. In the quenched alloys the lack of a maximum at $K=0$ (75 percent nickel) can be accounted for by the presence of residual internal strains caused by magnetostriction, the existence of which was pointed out by Kersten. These will restrict rotation in the same way that crystal anisotropy will, and the resulting initial permeability may be estimated by replacing K by $\lambda^2 E$. If we use the λ for the polycrystalline material λ_s, then for 75 percent nickel we have

$$\mu_0\approx 2I_s^2/\lambda_s^2 E\approx 9000$$

as the highest μ_0 we should expect, provided the full magnetostrictive strains remain in the material at room temperature. If they are relieved somewhat by diffusion during the cooling of the material, μ_0 can be larger, and if imperfections are present μ_0 is less.

In a similar way the calculated limit of the initial permeability of the slowly cooled alloy having $K=0$ (63 percent nickel) is 2000 or more. This fits rather well with a measured value[11] of 3000 in 65 percent nickel that had been carefully purified in hydrogen, a treatment that increases the permeability of 45 percent nickel from 3000 to 15 000, according to measurements of Williams.[14] It is not necessary to invoke any strains of atomic ordering in order to account for the permeability observed.

Therefore, reduction of the anisotropy to zero does not lead to high permeabilities (rotation process) unless the magnetostriction also approaches zero. However, disappearance of the magnetostriction in the direction of easy magnetization can cause high permeability (moving boundary) even though the anisotropy is not zero. The importance of λ_{111} in a material for which [111] is the direction of easy magnetization is illustrated in Fig. 11, which is particularly applicable to

[14] H. J. Williams, reference 1, pp. 122–123.

CC-0. In Public Domain. Gurukul Kangri Collection, Haridwar

Digitized by Arya Samaj Foundation Chennai and eGangotri

the understanding of maximum permeability (see below). The magnetostriction strain in the material caused by movement of the boundary from (a) to (b) is found by calculation, using either the 2-constant or the 5-constant formula, to be a shear strain determined entirely by λ_{111}. A similar calculation shows that only λ_{100} is involved when [100] is the direction of easy magnetization. Becker and Döring[3] have already proposed that the initial permeability is controlled by the magnetostriction in the direction of easy magnetization (λ_{100} or λ_{111}).

Some suggestions regarding the effect of annealing in a magnetic field were proposed by the author at an earlier date,[5] and it appears at the present time[15] that the proposed explanation, of the "freezing in" of magnetostrictive strains, is basically correct. However, one of the features of the phenomenon that has not been explained is that the initial permeability remains unchanged by the treatment while the maximum permeability is increased by a large factor. This may be understood by reference to Fig. 12. Let the solid curve represent the local strain (σ) from point to point (x) in the material, and let P represent the position of a wall before application of a field, according to the representation of Becker and Döring.[3] The initial permeability is determined by the form of the σ *vs* x curve near P. When the field is increased toward that corresponding to maximum permeability, so that the wall moves over the top of the strain "hill," it will move freely until a higher hill is encountered, as shown by the horizontal solid line. This occurs when the strain is not increased by boundary movement, a situation that takes place with a 180° wall, or when the magnetostriction in the direction of easy magnetization is zero. Ordinarily materials contain walls of both kinds, but in materials that have responded to heat treatment in a magnetic field only 180° walls are present.[16] However, when walls of both kinds occur, movement of the 90° walls (or 70° or 110° when $K<0$) builds up a strain, as shown in Fig. 11 and as represented in Fig. 12 by the line S. When this strain is added to the local strain we obtain the dotted curve. In this case the wall movement is limited by strains of random amplitude more severely than it is when only 180° walls exist, and in the latter case corresponding to the material heat-treated in a field, the maximum permeability is therefore higher.

A different explanation of the increase in maximum permeability of material heat treated in a magnetic field can be based on the existence of Néel "spikes."[17] Williams and Shockley[18] have shown that in silicon-iron, where there are six directions of easy magnetization, these spikes exert a pull on neighboring domain walls and so contribute to the coercive force. However, in magnetically annealed material in which there are only two directions of easy magnetization[16] the geometry does not permit the existence of spikes of this kind, and so the retarding action is absent and the coercive force is smaller and the maximum permeability larger.

Let us now compare the experimental results with the predictions of theory:

(1) In the quenched alloys the permeability is a maximum very near the composition at which $\lambda_{111}=0$. The theory also requires that near 45 percent nickel, when [100] is the direction of easy magnetization and λ_{100} is zero, we should expect another maximum in the μ_0 *vs* composition curve. Such maxima are apparent in Figs. 1 and 2, though they are not as pronounced as they are near 79 percent nickel. This may be because K is larger at 45 than at 79 percent nickel, and consequently, domain rotation will not contribute as much toward the permeability. In alloys purified by treatment in hydrogen, however, Williams[14] has observed an initial permeability of 15 000.

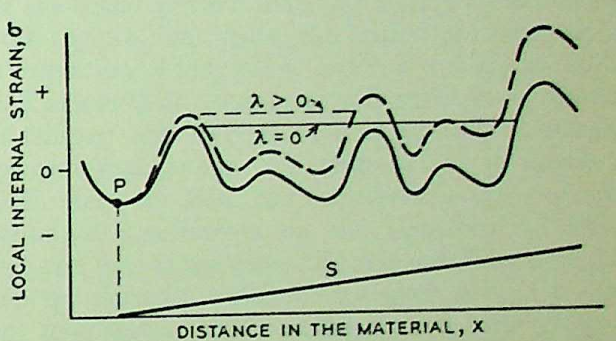


FIG. 12. Diagram of internal strains in material having zero magentostriction or having only 180° boundaries (solid curve), or in material in which stress is developed by boundary movement (dotted curve), showing different magnitudes of maximum permeability expected.

(2) In slowly cooled alloys as compared with quenched alloys, the optimum composition is shifted toward higher nickel content, in agreement with the shift in composition for $\lambda_{111}=0$.

(3) The higher permeabilities of the quenched alloys appear to result from the smaller anisotropy of the latter (about 10 times smaller) at the composition at which $\lambda_{111}=0$. The same reason appears to exist for the lower permeability at 45 percent nickel than at 79 percent nickel, as mentioned above under (1). In slowly cooled alloys the maximum (and initial) permeabilities of the 45 and 80 percent nickel alloys are comparable. Also, the magnitudes of the anisotropy constants are about the same (positive in the one case, negative in the other).

(4) Two mechanisms have been suggested, both of which are probably applicable, for the increase of the maximum permeability of iron-nickel alloys by heat treating in a magnetic field.

[15] E. C. Stoner, Repts. Prog. Phys. 13, 83–183 (1950), especially pp. 167–8.
[16] H. J. Williams and M. Goertz, J. Appl. Phys. 23, 316 (1952).
[17] Williams, Bozorth, and Shockley, Phys. Rev. 75, 155 (1949).
[18] H. J. Williams and W. Shockley, Phys. Rev. 75, 178 (1949).

CC-0. In Public Domain. Gurukul Kangri Collection, Haridwar

Digitized by Arya Samaj Foundation Chennai and eGangotri

The general course of the permeability *vs* composition curves of the Permalloys, and their changes with heat treatment, can be understood in a qualitative way in terms of the magnetostriction and crystal anisotropy, when we note the importance of the magnetostriction in the direction of easy magnetization, and of the internal fields associated with the rotation process.

This work was carried out with the able assistance of J. G. Walker in the preparation of the crystals. The author is also indebted to Mrs. M. H. Read for the detection of atomic ordering by x-rays, and more recently to Dr. L. Corliss, Dr. J. M. Hastings, and Dr. R. J. Weiss of the Brookhaven National Laboratory for observation of atomic ordering in one of the crystals by neutron diffraction. Finally, the benefit of discussions with H. J. Williams, J. K. Galt, and E. A. Nesbitt is gratefully acknowledged.

CC-0. In Public Domain. Gurukul Kangri Collection, Haridwar

Digitized by Arya Samaj Foundation Chennai and eGangotri

REVIEWS OF MODERN PHYSICS VOLUME 25, NUMBER 1 JANUARY, 1953

Uniaxial Anisotropy of a Permalloy Crystal

SEIJI KAYA

Physics Department, Tokyo University, Tokyo, Japan

If Permalloy (76 percent Ni—24 percent Fe) which has been previously quenched from 600°C is annealed at 490°C, its energy content decreases with time of annealing, not monotonically but in two steps. By direct measurement of the time-rate of energy decrease, it was concluded that the first step is connected with formation of short-range order and the second with that of long-range order.

The effect of a magnetic field applied during the course of cooling on the maximum permeability is associated mainly with formation of short-range order. Taking into consideration the fact that the saturation of the ordered state is about 4 percent higher than that of the disordered one, one would expect the short-range order to develop in the form of prolate ellipsoids elongated in the direction of spontaneous magnetization. Torque curves, measured on a disk cut from a Permalloy crystal parallel to the (110) plane and heat treated in a magnetic field showed uniaxial anisotropy, superposed on the ordinary cubic one. This uniaxial anisotropy increases with the formation of short-range order, but the formation of long-range order, followed after that of short-range one, has a tendency to annihilate it. The constricted hysteresis loop, which is characteristic of the Perminvar property, becomes most eminent at the end of short-range order formation.

If we assume two neighboring uniaxial domains, whose axes intersect perpendicularly with each other, and whose boundary bisects the angle between them, we can easily calculate the hysteresis loop of constricted form. The main characteristic of this model is that the displacement of the boundary cannot take place even in a strong field.

I. EFFECTIVE TEMPERATURE RANGE FOR MAGNETIC FIELD COOLING

SINCE the discovery of Kelsal[1] in 1934, it has been well known that, in some nickel-iron alloys, application of a magnetic field during cooling from a high temperature strongly influences their ferromagnetic properties, e.g., a large increase in maximum permeability and a large decrease in saturation magnetostriction are observable in the direction of the previously applied field, and conversely for the perpendicular direction. This phenomenon indicates that magnetic domains within the specimen are held firmly parallel or antiparallel to the direction in which the field was applied during cooling. Later experiments[2] have shown that this tendency is closely related to the formation of superlattice of Ni_3Fe type, which is known to take place in the temperature range from 600°C to 400°C in the course of cooling.

In an experiment made to determine more definitely the effective temperature range for field cooling, Tomono[3] applied a magnetic field of 50 oersteds only in a limited temperature interval of 30°C while the specimen was cooling and measured the dependence of saturation magnetostriction on the temperature at which the field was applied. Figure 1 illustrates the results thus obtained for 76 Permalloy. As shown in the figure, the temperature range between 540°C and 510°C is most effective for field cooling.

When the specimen is cooled in this temperature range without the presence of an external magnetic field, magnetic domains, orientations of which are distributed at random, will show the tendency to retain the same randomness which characterized this distribution at high temperature. This is why slowly cooled Permalloy has a low permeability.

[1] G. A. Kelsal, Physics 5, 169 (1934).
[2] S. Kaya, J. Faculty of Science, Hokkaido University 2, 29 (1938).
[3] Y. Tomono, J. Phys. Soc. Japan 4, 298 (1948).

II. ANNEALING AT THE CRITICAL TEMPERATURE

It has been reported[2] that, in the alloy corresponding to the composition Ni_3Fe, the critical temperature for the formation of long-range order on cooling is 490°C. Small amounts of manganese will result in increase of this temperature. For instance, in an alloy containing 1 percent manganese, this temperature is raised to 500°C. Recently Iida[4] has completed a series of very instructive experiments on the formation of short-range and long-range order. He measured the time rate of energy decrease while the specimen is kept at constant temperature, after cooling from a high temperature as rapidly as possible. This was carried out by measuring the necessary temperature difference between specimen and the surrounding container in order to maintain the temperature of the specimen constant. Figures 2 and 3 illustrate how the rate of energy decrease $-dU/dt$ varies with time of annealing, when specimen is kept at 510°C and 500°C, respectively, after having been cooled rapidly from 600°C. At 510°C,

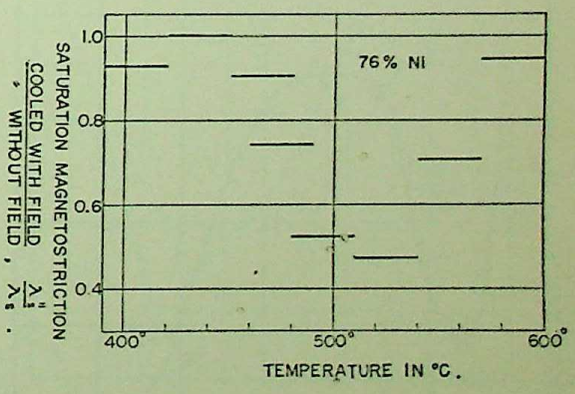


FIG. 1. Dependence of saturation magnetostriction of 76 Permalloy on the temperature at which an external magnetic field of 50 oersteds is applied during cooling. Magnetic field is kept on for a temperature interval of 30°C. Cooling velocity is about 1°C/min.

[4] S. Iida, J. Phys. Soc. Japan 7, 373 (1952).

CC-0. In Public Domain. Gurukul Kangri Collection, Haridwar

Digitized by Arya Samaj Foundation Chennai and eGangotri

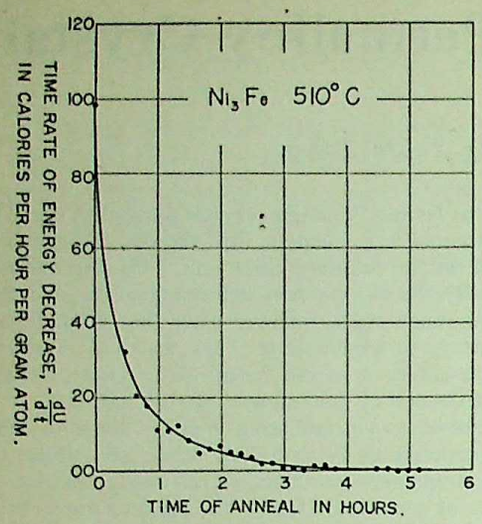


FIG. 2. Dependence of time rate of energy decrease $-(dU/dT)$ on the time of annealing, when 76 Permalloy is kept at 510°C, after cooling rapidly from high temperature.

$-dU/dt$ decreases monotonically and tends to zero after 3 or 4 hours. At 500°C quite some change takes place at the beginning, but after several hours it begins to increase, attains its maximum at 20 to 30 hours and again decreases to zero after about 50 hours.

These results differ somewhat in numerical details from those previously obtained[2] by measuring electric resistance changes; but this can probably be attributed to the difference in manganese content. It can be concluded that the first step of the energy decrease corresponds to the formation of short-range order and the second step to that of so-called long-range one. Special emphasis must be laid on the essential difference between the curve form of the first and second energy

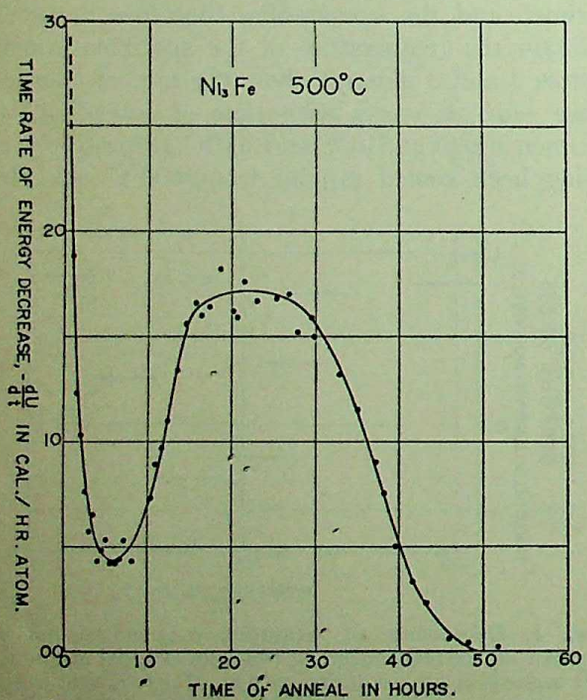


FIG. 3. Dependence of time rate of energy decrease $-(dU/dt)$ on the time of annealing, when 76 Permalloy is kept at 500°C, after cooled rapidly from high temperature.

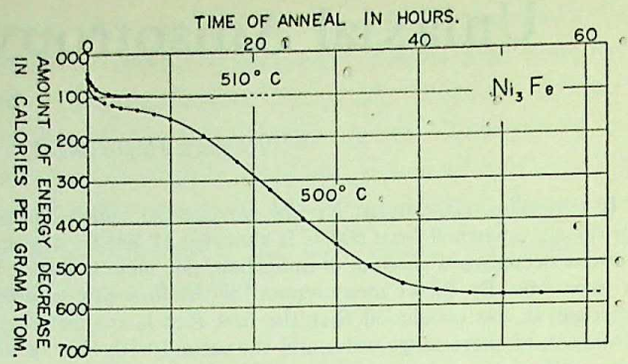


FIG. 4. Dependence of energy decrease on the annealing time. Annealing temperatures are 510°C and 500°C.

decrease. The first simple decrease can be associated with the formation of short-range order, or the increase of the number of pairs of near neighbors with unlike atoms, while the second decrease shows the characteristics of a cooperative rate process or the formation of long-range order. Figure 4 illustrates how the energy decreases with time of annealing, when the specimen is maintained at the respective temperature after cooling from 600°C.

III. CHANGE OF MAGNETIC CHARACTERISTICS WITH TIME OF ANNEALING

As to the dependence of magnetic characteristics of 76 Permalloy on the time of annealing, Nagashima[5] has carried out a comprehensive study. The specimens of 0.3 mm in diameter and 140 cm in length were quenched from 600°C, and then were annealed at 490°C for a few hours and quenched to room temperature again. Figure 5 illustrates how the hysteresis loop of 76 Permalloy, thus heat treated, varies in its form with time of annealing. This shows that hysteresis loops of constricted form are absent in both the quenched and fully annealed states. In contrast to this, hysteresis loops of the specimen in which the composition deviates from Ni_3Fe (for instance, 81.5 Permalloy) show well-developed

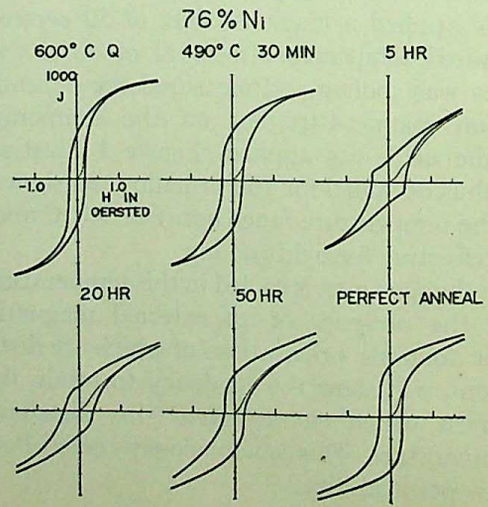


FIG. 5. Variation of the form of hysteresis loop for 76 Permalloy with time of annealing. (Annealing temperature=490°C.)

[5] T. Nagashima, J. Appl. Phys. Japan 19, 53 (1950).

CC-0. In Public Domain. Gurukul Kangri Collection, Haridwar

Digitized by Arya Samaj Foundation Chennai and eGangotri

constricted form even in the fully annealed state, as will be seen in Fig. 6. Such a difference is to be attributed to the lack of perfectness of atomic ordering even in the fully annealed state. Figure 7 shows the dependence of coercive force and remanence of 76 Permalloy on the time of annealing.

If we examine the corresponding change shown in Fig. 2 and Fig. 7, it can be concluded that the properties of Perminvar or of constricted hysteresis loops are mainly related to the formation of short-range order, and further that the uniform formation of long-range order has a tendency to annihilate them.

IV. TORQUE CURVES TAKEN ON A DISK OF 76 PERMALLOY CRYSTAL

In order to obtain a better understanding of the mechanism of magnetic field cooling, Chikazumi[6] prepared a disk of 76 Permalloy crystal, which was cut parallel to the (110) plane, and measured torque curves

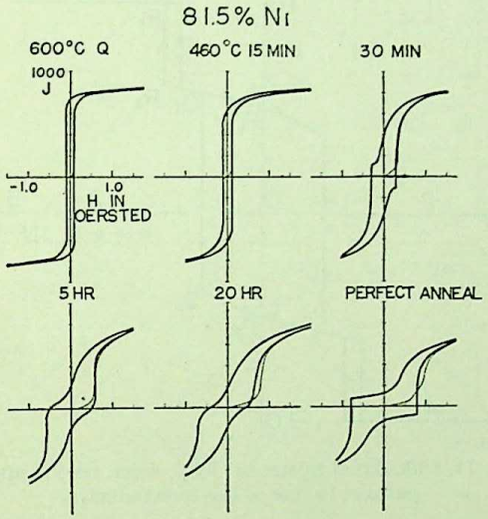


FIG. 6. Variation of the form of hysteresis loop for 81.5 Permalloy with time of annealing. (Annealing temperature=490°C.)

for this crystal disk, after it was cooled in a magnetic field, applied parallel to $[1\bar{1}1]$, $[1\bar{1}0]$, and $[001]$ directions, respectively. Since the torque is the negative rate of change of energy with crystal orientation, the energy necessary to bring the crystal to saturation can be obtained by integrating the torque curve with angle. Figure 8 illustrates the dependence of this energy, thus obtained, on the crystal orientation in the (110) plane. The energy E_t can be separated easily into two parts, E_c and E_u. E_c is the ordinary anisotropy energy with cubic symmetry, and E_u is an anisotropy energy with uniaxial symmetry. They can be expressed in most simplified form:

$$E_t = E_c + E_u = K_c(\alpha_2^2\alpha_3^2 + \alpha_3^2\alpha_1^2 + \alpha_1^2\alpha_2^2) + K_u(\alpha_1\beta_1 + \alpha_2\beta_2 + \alpha_3\beta_3)^2,$$

where α_i, β_i represent the direction cosines of spin and field, respectively, referred to the cubic axes.

[6] S. Chikazumi (unpublished data).

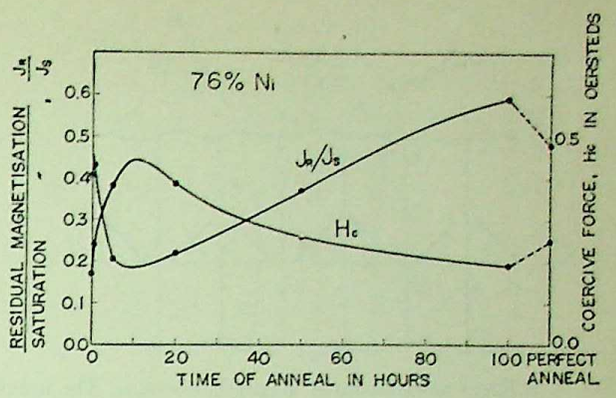


FIG. 7. Dependence of coercive force H_c and remanence J_r of 76 Permalloy on the time of annealing. (Annealing temperature=490°C.)

As can be seen in Fig. 8, both K_c and K_u are negative in this experiment. The absolute magnitude of K_c has

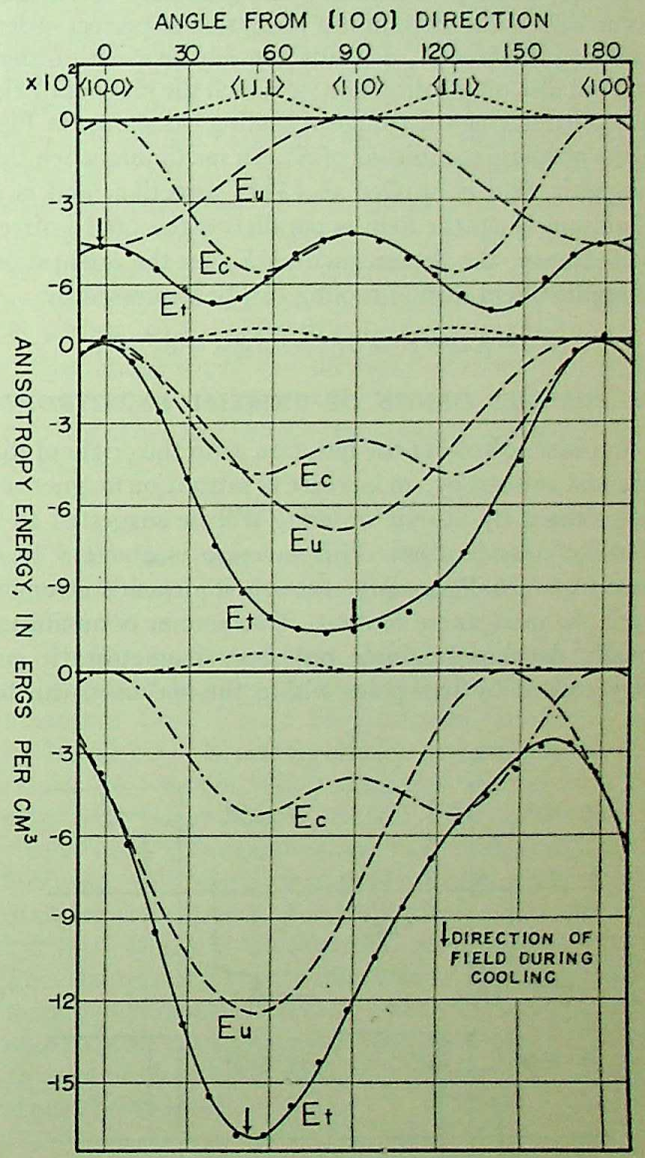


FIG. 8. Dependence of anisotropy energy of a 76 Permalloy crystal on the orientation in the (110) plane. Arrows indicate the orientations in which an external magnetic field is applied during cooling. (Cooling velocity=22°C/min.) Total energy E_t is analyzed into E_c and E_u; the former has cubic symmetry and the latter uniaxial symmetry.

CC-0. In Public Domain. Gurukul Kangri Collection, Haridwar

Digitized by Arya Samaj Foundation Chennai and eGangotri

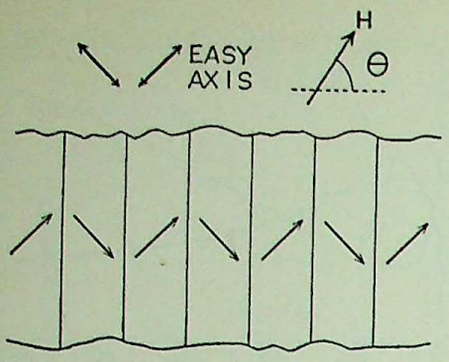


FIG. 9. A linear assemblage of magnetic domains. The uniaxial axes of neighboring domains intersect perpendicularly with each other, and their boundary bisects the angle between them.

been known to increase with the atomic ordering, whereas that of K_u is expected to increase rapidly with ordering, attain its maximum, and gradually decrease in accordance with the uniform formation of perfect order. The magnitude of K_u depends not only on atomic ordering, but also on the direction, to which the magnetic field is applied during the course of cooling. As shown in Fig. 8, the absolute magnitude of K_u is a maximum when the magnetic field is applied to [111] direction, and is a minimum when the field is parallel to the [001] direction. Hence, the dependence of K_u on the orientation of applied field during cooling can be expressed by

$$K_u = K_{u1} + K_{u2}(\beta_2^2\beta_3^2 + \beta_3^2\beta_1^2 + \beta_1^2\beta_2^2).$$

V. POSSIBLE ORIGIN OF UNIAXIAL ANISOTROPY

In order to answer the question as to the origin of the uniaxial anisotropy, an increase in saturation magnetization caused by atomic ordering will be suggested as a possible consideration. This increase is about 3 to 4 percent in 76 Permalloy, though it depends strongly upon the manganese content. If we assume nonuniform, locally developed atomic ordering, magnetostatic energy caused by free poles within the specimen can be

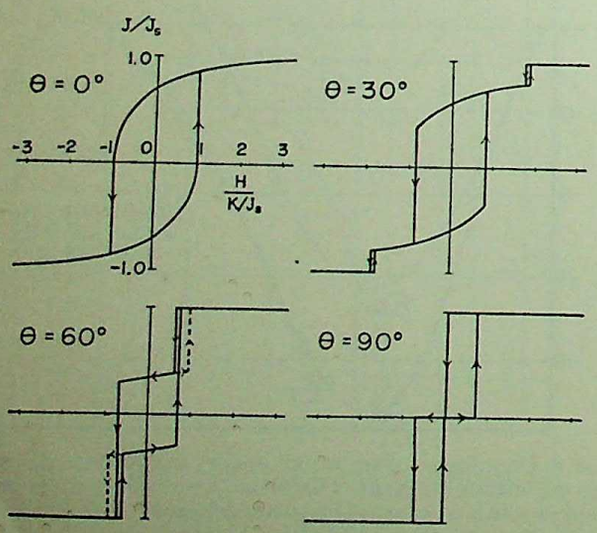


FIG. 10. Dependence of the form of hysteresis loop on the orientation of applied field.

expressed as follows:

$$E_m = \tfrac{1}{2}N(\Delta J_s)^2 V(1-V),$$

where N is the demagnetization factor of the ordered phase, ΔJ_s is the increased amount in saturation magnetization caused by atomic ordering, and V is the volume proportion of ordered phase. If atomic ordering develops in needle shape, N varies from zero to 2π, according to the orientation of magnetization.

If the values $\Delta J_s = 40$, $V = 0.5$ are substituted in this expression, we obtain an anisotropy energy of about 1000 erg/cc, which is in accord with the experimental data hitherto observed. The suggested mechanism of the origin of uniaxial anisotropy would become more comprehensible if attention is drawn to the fact that the Curie point is higher in the ordered phase than in disordered one.

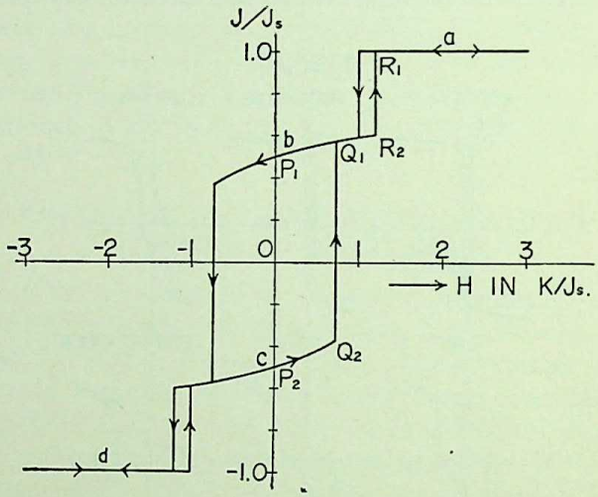


FIG. 11. Calculated hysteresis loop, when field is applied parallel to one of the uniaxial axes.

VI. DEDUCTION OF CONSTRICTED HYSTERESIS LOOP FROM UNIAXIAL ANISOTROPY

Hitherto the constricted hysteresis loop and the properties of Perminvar were believed to be the consequence of strong interaction between two constituent phases, which show quite different magnetic characteristics with each other. Quite recently Iida[7] has succeeded in deducing mathematically the Perminvar properties using the simple model shown in Fig. 9. This model is, as shown in the figure, a linear assemblage of magnetic domains with uniaxial anisotropy only. The orientations of adjacent domains are at right angle to each other, and their boundary bisects the angle between them. (In the actual case the angle subtended between the adjacent domains is 70° or 110°.)

The action of the external field will be calculated in the ordinary way by minimizing the total energy, composed of the crystal anisotropy energy and the energy of interaction of the magnetization and the external field. It must be borne in mind, that in every case the condi-

[7] S. Iida (unpublished data).

CC-0. In Public Domain. Gurukul Kangri Collection, Haridwar

Digitized by Arya Samaj Foundation Chennai and eGangotri

tion of the continuity of normal component of magnetization at the boundary should be satisfied. Mathematical deduction of the hysteresis loop and of the initial curve can be carried out in quite an elementary way. Figure 10 shows the dependence of the shape of the hysteresis loop thus calculated on the orientation of applied field, where θ denotes the angle between the field and the wall normal. Explanation will be given here only in one typical case, where the magnetic field is applied parallel to one of the uniaxial axes ($\theta=\frac{1}{4}\pi$). As shown in Fig. 11, the descending branch of the loop is divided into four sections *a*, *b*, *c*, and *d*, and three abrupt decreases of magnetization (*ab*), (*bc*), and (*cd*) exist between them. The change of domains in each

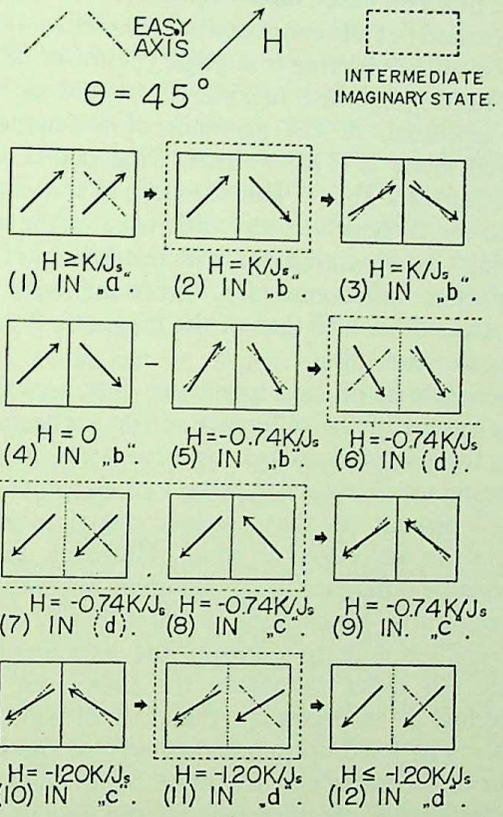


FIG. 12. Schematic diagram of the transitions of neighboring domains, when magnetization varies along the descending hysteresis curve.

stage is illustrated in Fig. 12. Following the decreasing applied field, an abrupt change (*ab*) will be initiated, if the energy of configuration (2) becomes smaller than that of configuration (1), and this will be carried out by the creation of a new boundary. Since the energy of configuration (3) is smaller than that of configuration (2), the transition (2) and (3) will be completed simultaneously.

At the abrupt change (*bc*), the transition is (5) to (9), and this will be analyzed into four intermediate transitions, of which (5) to (6) means annihilation of boundary and (7) to (8) means its creation. In the actual case of an abrupt change, creation or annihilation of a domain boundary would be accompanied with some difficulties associated with nucleation, but we have neglected this effect in this calculation. The field intensity, at which the abrupt change (*bc*) occurs, can be interpreted as the coercive force H_c and this amounts in this case to $0.73\ K_u/J_s$. If we substitute $K_u=1000$, H_c becomes 0.73 oersteds.

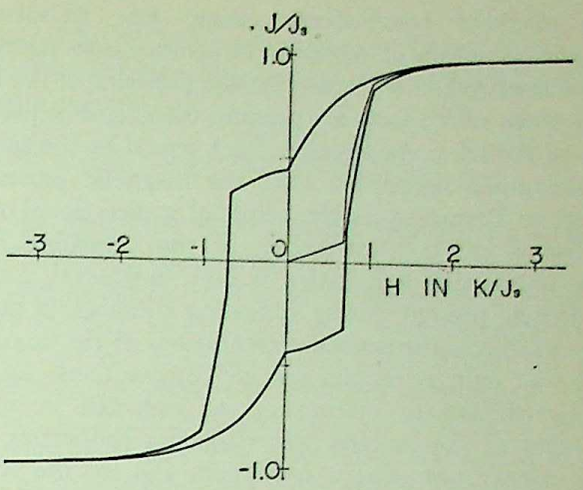


FIG. 13. Calculated hysteresis loop of polycrystalline material.

The initial curve can be easily obtained, by superposing the two branches of hysteresis loop, $P_1Q_1R_2R_1$ and $P_2Q_2Q_1R_2R_1$. Initial permeability μ_0 is expressed in this case:

$$\mu_0=1+\tfrac{1}{2}\pi(J_s^2/K_u),$$

and this furnishes us: $\mu_0=1500$, with $K_u=1000$, $J_s=1000$. Both H_c and μ_0 accord well with the experimental values.

It will be emphasized here, that, in some orientations of applied field, the initial curve extends out of the hysteresis loop. Figure 13 illustrates the initial and hysteresis curve of polycrystalline material, deduced by taking the average value, when the orientation of applied field varies from 0° to 90°. This agrees qualitatively with the experimental one shown in Fig. 5. Quantitatively some discrepancies exist between theories and experiment. For instance, the remanence J_r is $0.45\ J_s$, while the experimental value is much smaller. This discrepancy is probably due to the simplicity of the adopted model. In a more complete theory, a three-dimensional assemblage of domains, which, in the absence of an external field, would permit flux closure, should be adopted.

DISCUSSION

J. E. GOLDMAN, *Carnegie Institute of Technology, Pittsburgh, Pennsylvania:* There are two alternative possibilities in approaching an explanation of the effect of the magnetic anneal on the properties of Permalloy in certain specific composition ranges. One of these is to suppose that the certain characteristic properties of

CC-0. In Public Domain. Gurukul Kangri Collection, Haridwar

Digitized by Arya Samaj Foundation Chennai and eGangotri

the effective composition range, e.g., anisotropy, magnetostriction or presence of order, cause the alloy to be sensitive in some way to the presence of the field and, when such effects are present, the magnetic properties of the alloy are affected. Such would be the case in Chikazumi's suggestion that the magnetic annealing effect in Permalloy is the result of a directional order governed by the orientation of the annealing field. The alternative supposition is that, in general, a magnetic field present during annealing and cooling nearly always affects the possible orientations of the domains, but that only at certain specific compositions can this preferred domain orientation be reflected in major changes of the macroscopic magnetic properties.

Evidence obtained a few years ago by the writer and A. I. Schindler tends to support the latter alternative. Strips of $4\frac{1}{2}$ percent silicon iron were annealed at 650°C in a magnetic field directed along the long axis of the strip in this field. No significant changes were observed in the permeability at various inductions or in the coercive force. But the magnetostriction as measured along the axis showed a radical change on annealing in a field. The magnetostriction curves obtained on samples treated in an identical manner but with the field not present were virtually parabolic with a magnetostriction at saturation of the order of $5\text{–}7\times10^{-6}$. In the case of the samples annealed in a field, at low inductions the magnetostriction was very small and negative and increased slowly becoming positive at approximately 11 000 gauss and reaching a maximum value of the order of 1×10^{-6} at saturation. This effect is readily understood if one assumes that the field present during annealing and cooling brings about a preferred domain orientation in which all domains tend to be oriented in the direction of easy magnetization nearest that of the field. Thus the process of magnetization takes place almost exclusively by 180° boundary displacements. Since these do not contribute to the magnetostriction, the net effect is to decrease the magnetostriction.

Whether this can result in a significant change in other magnetic properties depends on the energy required to move such a 180° boundary. In the theory of Becker and Kersten, this would depend principally upon the magnetostriction. Miss Goetz of the Bell Telephone Laboratories does, in fact, observe a large effect of a magnetic anneal on the properties of an alloy containing 6–7 percent silicon where the magnetostriction tends toward zero. We believe that this is probably the case in Permalloy as well. Thus it appears on the basis of the foregoing that the effect of the field present during annealing and cooling in determining the domain distribution is not limited to the specific compositions at which large magnetic effects are observed but is rather there at other compositions as well. Where large effects of the macroscopic magnetic properties are observed, these must be because of the fact that, where only 180° boundaries exist, the magnetoelastic energy is the principal cause of resistance to domain motion and this is minimized when the magnetostriction is zero. Such an explanation is also consistent with the sensitivity of the alloys in the Permalloy range to rate of cooling, for, as first shown by the writer,[1] the magnetostriction is very sensitive to cooling rate near the composition Ni_3Fe owing to its strong dependence on the state of the order.

[1] J. E. Goldman, Phys. Rev. **76**, 471 (1949).

J. M. HASTINGS, *Brookhaven National Laboratory, Upton, Long Island, New York:* Following a suggestion of Dr. Bozorth, based on a proposal of S. Chikazumi, we have carried out a preliminary neutron diffraction investigation of the ordering in a single crystal of 68 Permalloy. The sample, which he kindly furnished us, was carefully annealed, in the presence of a magnetic field directed along a (110) normal, from 600°C to 200°C at the rate of 2°/hour. The objective of this experiment was to see if there was any difference in the degree of ordering, as measured by the relative intensities of superlattice reflections, for directions both parallel and perpendicular to that of the magnetic field applied during the annealing.

The intensity of the superlattice lines is proportional to the square of the difference of the scattering amplitudes for iron and nickel. Unfortunately, the nuclear scattering amplitudes for these two elements differ by only 7 percent so that nuclear contribution to the superlattice reflections is small. However, there is an appreciable difference in the coherent magnetic scattering amplitudes which adds to the intensity and, therefore, enables one to perform the experiment rather readily. In order to obtain the maximum magnetic scattering, it is necessary that the atomic magnetic moments be lined up perpendicularly to the scattering vector of the particular reflection being observed. This is an important consideration for the case at hand, for the domains are all spontaneously magnetized along the (110) normal parallel to the magnetic field used in the annealing.

The integrated intensity, nuclear plus magnetic, from the set of (110) planes whose normals were along the direction of magnetic anneal was measured by applying an external field to orient the moments perpendicular to their spontaneously aligned direction. Then the external field was removed and the integrated intensity from a set of (110) planes having normals perpendicular to the direction of magnetic anneal was measured. After making an absorption correction, these two intensities were the same, and hence, to within the precision of our measurement, approximately 10 percent, there is no difference in the degree of long range order in these two directions.

CC-0. In Public Domain. Gurukul Kangri Collection, Haridwar

Digitized by Arya Samaj Foundation Chennai and eGangotri

E. B. STONER, *University of Leeds, England:* There are many difficulties in the way of making *a priori* calculations of the magnetization curves of polycrystalline materials. This may be illustrated by considering the three main types of elementary change in turn. (1) The change of intrinsic magnetization with field is small, but where it is usually assumed that after-effects are negligible (i.e., in high fields), the experimental variation of I with H does not agree satisfactorily with that given by any of the current theoretical treatments. This means that other factors are involved possibly connected with the effect of "small domains" or with the "fading out" of domain walls. (2) For a random aggregate of crystals free from strain, the change of magnetization with field in a reversible rotational region can in principle be calculated if the single crystal anisotropy coefficients are known. The result should apply most closely for well-annealed material. There is, however, no completely satisfactory method of taking into account the interaction between the crystal grains; the forms and the orientation distribution of the crystals are in general unknown; and the degree and character strain distortion is not known and, even if it were, the effect on the magnetic properties could not be estimated with any accuracy. It is not surprising that the agreement between calculated and observed curves is very poor except under special conditions. (3) The detailed character of the boundary movement processes depends in a complex way, via the localized disperse fields, on the detailed localized structural irregularities, caused by inclusions, holes, and strains. The detailed character of these is again not known and, even if it were, calculation of their effect would present prohibitive difficulties.

The above three types of process are superposed and since the extent to which each has taken place is determinative of the subsequent course of the changes with further change of field, it is virtually impossible to calculate magnetization curves *a priori* except over particular ranges of field for materials in a well-defined state or under special conditions (e.g., under strong tension).

It is because of these difficulties that the carrying out of supplementary measurements, magnetic and magnetothermal, and the consideration of the combined sets of results have been put forward in the paper as the only sound means at present of obtaining definite information about the character and proportions of the elementary changes occurring along any part of a magnetization curve. When the magnetization curves of a number of representative materials have been satisfactorily analyzed, it may be hoped that the general course of the changes will become much clearer quantitatively as well as qualitatively, and that the way will be opened for a more fruitful attack on the complex groups of theoretical problems involved. Reasonably accurate prediction as well as interpretation of the forms of magnetization curves may then gradually become possible.

---

[1] L. R. Aronin, J. Appl. Phys. 23, 642 (1952).

L. R. ARONIN, *Massachusetts Institute of Technology, Cambridge, Massachusetts:* Dr. Kaya has shown a two-step behavior in the order-annealing kinetics of Ni_3Fe at 580°C as compared with a simple behavior at 510°C. In this connection I should like to point out that we have recently observed,[1] through resistivity and saturation induction measurements, an anomalous kinetic behavior in Ni_3Mn which we have interpreted as indicating changes in local order accompanied by somewhat slower growth of order domain size.

Reheating at 425°C an alloy, previously cooled through the ordering range and held isothermally at 400°C and 375°C, resulted in a dip in saturation induction followed by a subsequent increase. The dip may be considered as a decrease in local order with the subsequent rise indicating antiphase domain growth. The magnitude of this reversal appears dependent on the relative extents of local order and domain size. In low temperature treatment for ordering, the value of saturation induction attainable exhibits dependence on domain growth previously obtained at higher temperatures.

G. W. RATHENAU, *N. V. Philips' Gloeilampenfabrieken, The Netherlands:* Experiments which are related to those of Dr. Kaya have been performed at Eindhoven by the late Dr. Snoek, and lately by Mr. Smit.

We have found that an alloy of the composition Ni_3Fe does not show an energy of anisotropy ($E_{\text{perpendicular}} - E_{\text{parallel}}$) to field, if, before performing the cooling in a magnetic field, the alloy has been ordered.

Some difficulties remain if one assumes that the effect of cooling in a field is to form, only along the field direction, cigar-shaped particles of ordered phase within the disordered matrix, the anisotropy of shape being the only cause of ($E_{\text{perpendicular}} - E_{\text{parallel}}$).

(1) The anisotropy of shape calculated in the extreme case that the alloy as a whole has been transformed into the cigar shaped bodies is 1000 ergs/cm$_3$. Experimentally more than 2000 ergs/cm$_3$ are found.

(2) The high initial permeability found for alloys which have been field cooled is astonishing. Why are the 180° walls not hampered in their movement by the inclusions? Is it because the diameter of these ordered particles is so small compared to the wall thickness?

(3) Anisotropy resulting from field cooling has been found to occur also with NiCo binary alloys and very strongly in FeNiCo+alloys; yet no ordering has been reported as yet for the NiCo alloys.

CC-0. In Public Domain. Gurukul Kangri Collection, Haridwar

Digitized by Arya Samaj Foundation Chennai and eGangotri

REVIEWS OF MODERN PHYSICS VOLUME 25, NUMBER 1 JANUARY, 1953

An Experimental Study of Barkhausen Noise in Nickel-Iron Alloys

D. I. GORDON

U. S. Naval Ordnance Laboratory, White Oak, Maryland

INTRODUCTION

THIS experimental study of the Barkhausen effect in nickel-iron alloys was undertaken in the Magnetics Division of the Naval Ordnance Laboratory as a part of its program of developing improved magnetic materials for military and industrial applications. This particular study has yielded practical results in the form of a high permeability magnetic core material with minimum Barkhausen noise. As a by-product of this development, experimental data were obtained showing the dependence of Barkhausen noise on alloy composition and heat treatment and showing a correlation with initial permeability.

MEASUREMENT TECHNIQUE AND APPARATUS

Figure 1 is a schematic drawing of the apparatus used. The samples under test were 0.014-inch strips, $\frac{1}{8}$ inch wide and 4 inches long. They were cyclicly magnetized by means of a magnet rotating at approximately 33 rpm. This system was used because of its convenience, although it is realized that the direction of the applied field continually changes. The shielded search coils were connected to an amplifier with low input noise level followed by a high pass filter and then a Ballantine electronic voltmeter as the output meter. The average between the maximum and minimum deflections of the voltmeter during a cycle of magnetization was taken as the average noise per cycle.

MEASUREMENT RESULTS

By use of the method described above, measurements were taken on samples of binary nickel-iron alloys ranging in composition from 35–99.5 percent Ni. The samples were prepared from materials melted, processed, and heat treated in the Magnetics Division of the Naval Ordnance Laboratory. Samples of molybdenum nickel-iron alloys were also measured.

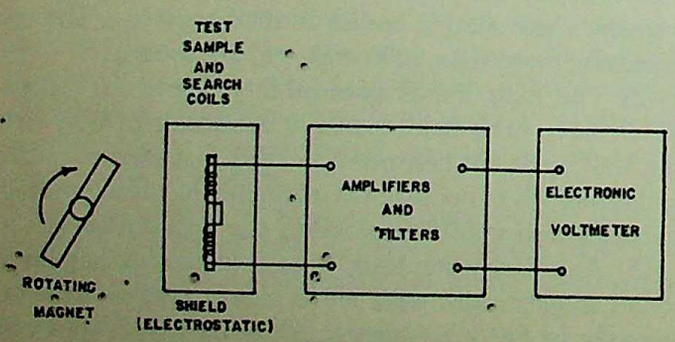


FIG. 1. Block diagram of Barkhausen comparator.

Figure 2 shows average noise per cycle as a function of composition for three conditions of heat treatment; namely, bake, anneal, and quench. This figure clearly shows the dependence of noise on composition and heat treatment for the binary-nickel-iron series.

Figure 3 was obtained from measurements on ternary molybdenum nickel-iron samples (79 percent Ni, 4 and 5 percent Mo), heat treated so as to obtain various

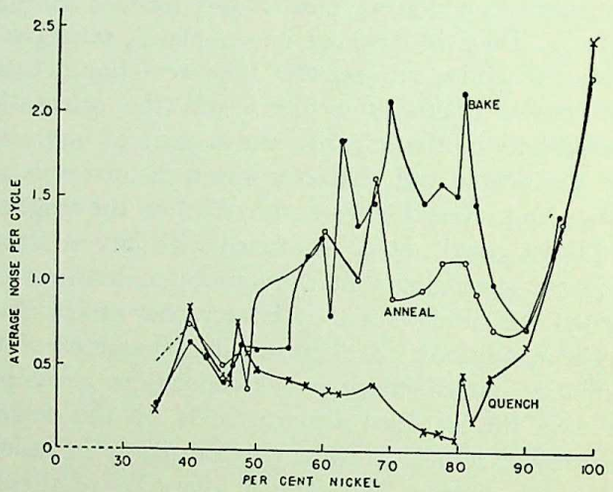


FIG. 2. Variation of magnetic noise with composition and heat treatment of binary nickel-iron alloys.

values of initial permeability. It is a plot of average noise per cycle *versus* initial permeability. The values of initial permeability were obtained from ballistic measurements at $B=20$ gauss on ring laminated samples cut from the same sheets and processed and heat treated simultaneously with the strips used in

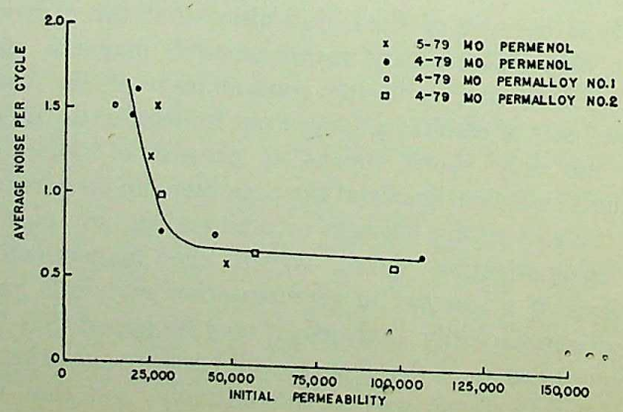


FIG. 3. Magnetic noise *vs* initial permeability of ternary Mo-Ni-Fe alloys.

CC-0. In Public Domain. Gurukul Kangri Collection, Haridwar

Digitized by Arya Samaj Foundation Chennai and eGangotri

obtaining the noise data. This figure shows a definite dependence of noise on initial permeability.

CONCLUSION

The results of this brief experimental study summarized in Fig. 2 and Fig. 3 have been presented here with the hope that they may be useful in further development of the theories relating to the Barkhausen effect and the magnetization curve.

It is planned to extend this study further, with (1) improved measurement techniques, (2) different sample configurations, and (3) other alloys.

CC-0. In Public Domain. Gurukul Kangri Collection, Haridwar

Digitized by Arya Samaj Foundation Chennai and eGangotri

REVIEWS OF MODERN PHYSICS VOLUME 25, NUMBER 1 JANUARY, 1953

Some New Results on Antiferromagnetism and Ferromagnetism

LOUIS NÉEL

Institut Fourier, Grenoble, France

1. The study of the thermomagnetic properties of a natural single crystal of rhomobohedral iron sesquioxide, Fe_2O_3, by Pauthenet, confirms the hypothesis of the superposition of a fundamental antiferromagnetism and a parasitic ferromagnetism. Below 260°K the direction of antiferromagnetism coincides with the ternary axis; above 260°K this direction is situated in the plane perpendicular to the ternary axis, with complete freedom of orientation in this plane. The parasitic ferromagnetism seems to be formed of two parts, one isotropic, the other anisotropic. The latter, tightly coupled with the direction of antiferromagnetism, can be observed only above 260°K and in a direction perpendicular to the ternary axis. The corresponding spontaneous magnetization may arise from the local imperfections in the compensation of the two constituent sublattices of the antiferromagnetism, and it is the freedom of orientation of the antiferromagnetism in the basic plane which permits observation of this spontaneous magnetization.

2. Pyrrhotite corresponds closely to the molecular formula Fe_7S_8. The crystal structure contains holes: one of the eight sites which could be occupied by iron ions is vacant. Bertaut showed that at room temperature these holes form an ordered lattice such that the crystal unit of Fe_7S_8 does not have the NiAs unit but one much more complicated, pseudohexagonal and slightly monoclinic, containing 8 Fe_7S_8. This unit is such that the successive planes of iron perpendicular to the pseudo-hexagonal axis are not identical: only the odd-numbered planes contain holes. Because the two sublattices are crystallographically different, we have imperfect antiferromagnetism or ferrimagnetism, analogous to that of ferrites. A magnetic study by Benoit, at temperatures above the Curie point, seems to show that the ordered distribution of the holes disappears at 560°K. Finally, a thermomagnetic study by Pauthenet shows that the pseudo-hexagonal axis, which at ordinary temperature is a direction of very difficult magnetization, becomes progressively, at lower temperatures, a direction of easy magnetization.

I. RHOMBOHEDRAL Fe_2O_3

As it was foreseen in the early theory,[1] we know that in antiferromagnetic substances there exists a coupling between the direction of antiferromagnetism and the directions of the axes of the crystal, analogous to the magnetocrystalline coupling which, in ferromagnetics, ties the direction of spontaneous magnetization to the axes of the crystal. Unfortunately, the properties connected with the orientation of the direction of antiferromagnetism are much more difficult to demonstrate than those which are connected with the orientation of spontaneous magnetization. In particular, while several thousands of oersteds are usually sufficient to align the spontaneous magnetization of a ferromagnetic body in the direction of an applied magnetic field, several hundreds of thousands of oersteds are probably necessary in most cases to orient the direction of antiferromagnetism in the plane perpendicular to the preferred direction (see reference 2, p. 161). To study these couplings, which are of great theoretical interest, it is almost indispensable to prepare single crystals and to study them magnetically in different directions. Up to now two examples are known: Bizette and Tsai on the one hand, Stout and Griffel on the other, have studied ferrous flouride FeF_2, which is an antiferromagnetic of the classic type, while C. J. Gorter and his colleagues have studied copper chloride, $CuCl_2, 2H_2O$, which becomes antiferromagnetic at the temperature of liquid helium.

Thus it is particularly interesting to study from this point of view rhombohedral iron sesquioxide, α Fe_2O_3, which is found in nature in the form of large, almost pure crystals (hematite). Unfortunately, as is shown in the works of Townsend Smith[2] and especially of Chevallier,[3] the magnetic properties of this substance are extremely complex. However, as we noted several years ago,[4] it seems that these properties are the result of the presence of a fundamental antiferromagnetism superimposed on a weak parasitic ferromagnetism, one hundred to a thousand times smaller than that of ordinary ferromagnetics. This ferromagnetism could arise from a defect of stoichiometry or of defects of crystallization, and we will discuss this later.

As to the fundamental antiferromagnetism, it is probably caused by strong negative interactions of superexchange of the type Fe-O-Fe, produced by the intermediary of oxygen ions. Iron atoms are arranged in almost-plane layers, perpendicular to the ternary axis. Each layer is spontaneously magnetized to saturation in a definite direction, and the successive layers are magnetized alternately in opposite directions. This structure, deduced from the study of magnetic properties[4,5] was subsequently confirmed by Shull and his colleagues[6] by means of neutron diffraction.

At my request, Mr. Pauthenet has studied[7] a natural single crystal of α Fe_2O_3 which came from the island of Elbe and appeared quite pure. The separation of the

[1] L. Néel, Ann. phys. 5, 232 (1936).

[2] T. Townsend Smith, Phys. Rev. 8, 721 (1916).

[3] R. Chevallier and S. Mathieu, Ann. phys. 18, 258 (1943); R. Chevallier, Rapport à la Réunion Int. Ferromagnétisme et Antiferromagnétisme, Grenoble, 1950.

[4] L. Néel, Ann. phys. 4, 249 (1949).

[5] L. Néel, Ann. phys. 3, 137 (1948).

[6] Shull, Strauser, and Wollan, Phys. Rev. 83, 333 (1951).

[7] L. Néel and R. Pauthenet, Compt. rend. 234, 2172 (1952).

CC-0. In Public Domain. Gurukul Kangri Collection, Haridwar

Digitized by Arya Samaj Foundation Chennai and eGangotri

ferro- and antiferromagnetism is obtained by determining the variation of the specific magnetization σ in a magnetic field H which is relatively high, 5000 to 20 000 oersteds. One obtains approximately for 1 g of substance

$$\sigma = \sigma + \chi H,$$

where σ_0 may be considered as the spontaneous magnetization of the ferromagnetic part while χ is the antiferromagnetic susceptibility. Measurements have been made along the ternary axis and along different directions in the basic plane, perpendicular to the ternary axis. Orientation of the crystal was controlled by x-rays.

Figure 1 gives the thermal variation of the antiferromagnetic susceptibility χ, measured along the ternary axis (curve 2) and along a perpendicular direction (curve 1). These curves are rather complicated, but as a first approximation, taking into account the inevitable imperfections inherent in a natural crystal and the difficulties of separation of superimposed ferromagnetism, they can be described schematically in the following way. In the first place, in curve 2, in the neighborhood of 260°K, there is a discontinuity of susceptibility which corresponds to that which was previously observed in the polycrystalline powder by Morin[8] and by Guillaud.[9] Above this temperature of 260°K the susceptibility along the axis has a value independent of the temperature, in the neighborhood of $20 \cdot 10^{-6}$. Below 260°K the susceptibility is reduced to a relatively small value which seems to approach zero at absolute zero. On the contrary, in a direction in the basal plane, the susceptibility maintains a constant value, also in the neighborhood of $20 \cdot 10^{-6}$, and independent of the temperature up to 950°K, that is up to the antiferromagnectic transition point (948°K).

The properties which we have just described correspond exactly to those of an antiferromagnetic body in which the direction of antiferromagnetism is parallel to the ternary axis below 260°K and perpendicular to this axis above This result agrees with the conclusions of a former[4,5] study and with the experimental results of Shull, given by neutron diffraction.[6] This thermal variation of orientation of the direction of antiferromagnetism is obviously to be compared with the analogous phenomena observed in a great number of uniaxial ferromagnetic materials. Cobalt and manganese-bismuth also possess a temperature of transition at which the direction of spontaneous magnetization changes from one orientation to another. Finally, this interesting thermal change of the orientation of the direction of antiferromagnetism shows, in agreement with theoretical considerations and contrary to the opinions of certain authors, that the direction of antiferromagnetism is not determined by the orientation of antiferromagnetic coupling of the type Fe-O-Fe.

[8] F. J. Morin, Phys. Rev. 78, 819 (1950).
[9] C. Guillaud, J. phys. et radium 12, 489 (1951).

We have also investigated whether a small anisotropy subsists in the basic plane above 260°K, but we have verified that, within one percent, the susceptibility did not depend on direction. The result is that, under the conditions of the experiment, the direction of antiferromagnetism turns freely in the basic plane and aligns itself always in a direction perpendicular to the applied field, while the susceptibility remains independent of the temperature. Thus it appears that here is an example where the original theory of antiferromagnetism[10] can be applied rigorously. It appears that the fundamental antiferromagnetic properties of α Fe_2O_3 can be interpreted in a fairly simple manner.

This is not true of the parasitic ferromagnetism. Figure 2 gives the results of Pauthenet. Everything happens as though there were present an *isotropic* parasitic ferromagnetism which disappears in the classical manner at the Curie point, about 1000°K, and on which is superimposed, above 260°K, another parasitic ferromagnetism essentially *anisotropic* and dependent

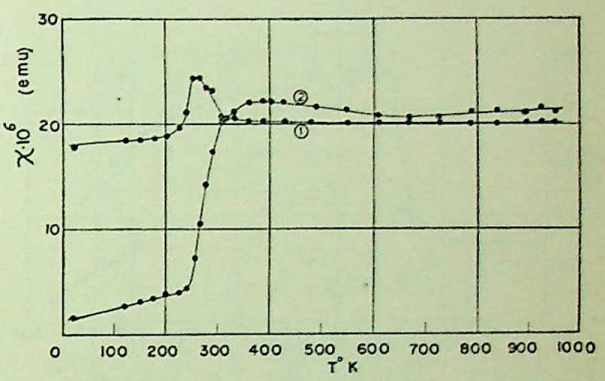


FIG. 1. Thermal variation of antiferromagnetic susceptibility of α Fe_2O_3, along a direction in the basal plane perpendicular to ternary axis (curve 1) and along the ternary axis (curve 2), (*after Pauthenet*).

on direction in the basic plane. This ferromagnetism disappears also around 1000°K. These results are in accord with former observations of Towsend Smith. What is new here is the disappearance of the anisotropic parasitic ferromagnetism below the transition temperature of 260°K.

This curious phenomenon can be interpreted if we suppose that the direction of the spontaneous magnetization of the anisotropic parasitic ferromagnetism is parallel to the direction of fundamental antiferromagnetism, or, more precisely, that it is parallel to the direction of spontaneous magnetization of one of the two constituent sublattices of the antiferromagnetism. Above 260°K, this parasitic ferromagnetism is easily observed in some directions in the basic plane, since the direction of antiferromagnetism can orient itself freely in this plane, which is really an exceptional fact. On the contrary, below 260°K the direction of antiferromagnetism coincides with the ternary axis; the parasitic spon-

[10] L. Néel, Compt. rend. 203, 304 (1936).

CC-0. In Public Domain. Gurukul Kangri Collection, Haridwar

Digitized by Arya Samaj Foundation Chennai and eGangotri

taneous magnetization is, then, also oriented along the ternary axis, but there is an equal probability that this is in one direction or in the opposite direction and there is no possibility of returning from one direction to the other since the direction of antiferromagnetism is practically fixed. The anisotropic parasitic ferromagnetism should, then, disappear, or more precisely, the magnetic fields used are much too weak to produce saturation.

One problem now remains: that of the origin of parasitic ferromagnetism and of the nature of the relation between the direction of its spontaneous magnetization and the direction of antiferromagnetism. The simplest interpretation is to suppose that the fundamental antiferromagnetism of iron sesquioxide is not perfect and that for some reason the two sublattices are not exactly identical, and that there remains a residual spontaneous magnetization due to the imperfect compensation of the two sublattices. This is a case analogous to that which we encountered in pyrrhotite and which we will take up later, but with much less dissymmetry between the two sublattices.

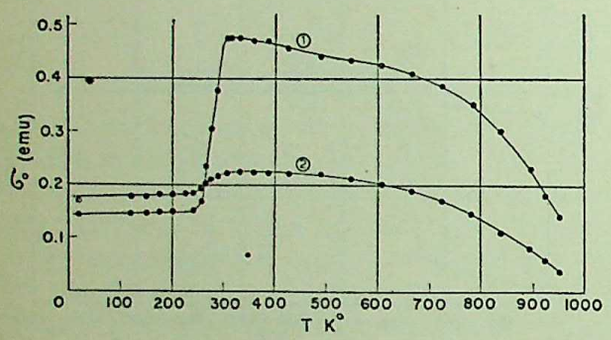


FIG. 2. Thermal variation of the parasitic ferromagnetic magnetization of α Fe_2O_3, along a direction in the basal plane, perpendicular to ternary axis (curve 1) and along the ternary axis (curve 2).

This dissymmetry could arise, as in pyrrhotite, from a defect of stoichiometry, the exact formula of the compound studied being $Fe_{2+x}O_3$, with x small; the excess iron atoms distributing themselves on only one of the two sublattices. According to this hypothesis, one should find a relation between the magnitude of the parasitic ferromagnetism and the excess of iron or oxygen, but so far the experiments have not been conclusive. This kind of explanation, subject to the same objection, is related to the explanation that we proposed previously[4,11] and which supposes the formation of very small magnetic particles more or less deformed, oriented by epitaxy on one of the principal faces of the crystal.

A different kind of explanation is to suppose that locally, inside of a kind of elementary domain, the two sublattices are not equivalent, either for geometrical reasons or on account of local fluctuations of composition, the average composition corresponding to Fe_3O_3. Each elementary domain would thus possess a resulting spontaneous magnetization parallel in one direction or the opposite to the direction of antiferromagnetism. This interpretation could also be extended to other antiferromagnetic substances than rhombohedral sesquioxide of iron, and would possibly permit explanation of the hysteresis of certain antiferromagnetic substances at low temperatures. This parasitic ferromagnetism could be checked experimentally only if the direction of antiferromagnetism, to which it is associated, had a freedom of orientation sufficient to be modified by the applied magnetic fields.

[11] L. Néel, Compt. rend. 228, 64 (1949).

II. THE FERRIMAGNETISM OF PYRRHOTITE

Pyrrhotite is an iron sulfide in which the sulfur content is slightly greater than in FeS, which is an antiferromagnet of the classic type.[12,13] Pyrrhotite is ferromagnetic and has been studied in detail for a long time by Weiss and his colleages.[14] The hexagonal axis is a direction of very difficult magnetization; in this direction the crystal is practically paramagnetic. In the basic plane the magnetic symmetry is less than the crystallographic symmetry; in the direction of the easiest magnetization one finds a magnetization at saturation which is remarkably small, of the order of a quarter of Bohr magnetron per iron atom. The smallness of this value suggests immediately, by analogy with the ferrites, the consideration of pyrrhotite as a ferrimagnetic substance.

The study of the magnetic properties of the iron sulfides FeS_{1+x} as a function of the composition throws some light on the question. According to Haraldsen,[12] these sulfides have a crystal structure of the NiAs type, in the range $0<x<0.20$. However, from the point of view of magnetics they are antiferromagnetic in the interval $0<x<0.08$ and ferromagnetic beyond. According to Benoit,[13,15] magnetization at saturation, at first very weak, passes through a maximum at about $x=0.14$, that is, for a formula of a type Fe_7S_8 in the neighborhood of natural pyrrhotite.

By analogy with FeO, it is likely to suppose that the successive plane layers of iron atoms, perpendicular to the hexagonal axis are, in FeS and the neighboring alloys ($x<0.08$), magnetized alternately to saturation in opposite directions: one of the sublattices is composed of odd-numbered planes of iron atoms, the other even-numbered planes. The two sublattices are essentially and crystallographically identical, so that their spontaneous magnetizations compensate each other exactly; here we have antiferromagnetism of the classical type. On the contrary, when x is greater than 0.08 the two sublattices become different and so there is a resulting

[12] V. H. Haraldsen, Z. anorg. u. allgem. Chem. 231, 78 (1937).
[13] R. Benoit, Compt. rend. 234, 2175 (1952).
[14] P. Weiss, J. phys. et radium 8, 542 (1899); 4, 469 (1905); 4, 829 (1905); P. Weiss and J. Kuntz, J. phys. et radium 4, 847 (1905); P. Weiss and R. Forrer, Ann. phys. et radium 12, 279 (1929).
[15] R. Benoit (unpublished, private communication).

CC-0. In Public Domain. Gurukul Kangri Collection, Haridwar

Digitized by Arya Samaj Foundation Chennai and eGangotri

net spontaneous magnetization. The problem consists in illucidating the nature of this difference.

A first solution, proposed by several Japanese authors and in particular by Yosida, consists in noting that as a result of the bivalence of the sulfur, a composite of formula FeS_{1+x} contains necessarily $(1-2x)Fe^{++}$ ions and $(2x)Fe^{+++}$ ions. These ions possess different atomic moments, so that it is sufficient for example to suppose that the ferric ions assemble on the odd-numbered iron planes, in order to obtain the necessary dissymmetry between the two sublattices. However, serious objections may be raised against this conception. In the first place, it appears that the electrostatic forces of exchange would bring about electrical equilibrium between the successive planes of iron and consequently the two sublattices would be identical. In the second place, this conception does not take into account an important phenomenon which we are going to analyze.

The lattice of the composition FeS_{1+x} necessarily contains holes because the structure of the crystal is determined by the size of the sulfur ions, which are much larger than the iron ions. In a molecule FeS_{1+x}, there exists $1+x$ sites which may be occupied by the iron ions, and there remain x vacancies or holes. The properties of the crystal will thus depend on the actual positions of these holes. In particular the composition Fe_7S_8 may be written Fe_7S_8L where L represents a hole. It seems hardly probable that at low temperature these holes will be distributed at random in the crystalline network; it is much more likely to suppose that they are ordered in a regular manner. It is tempting to wonder if the regular order of these holes would not be at the origin of the dissymmetry between the two sublattices. *A priori*, it must be relatively easy to find out with the help of x-rays if there is a regular distribution of the holes, because the reflecting power of a hole is very different from that of a ferrous or a ferric ion.

While the previous experiments have been in accord in attributing to pyrrhotite the simple NiAs structure, we asked Mr. Bertaut to take up the study again. In fact, this author in studying a natural crystal with prolonged exposures, discovered[16] in the diffraction pattern several hundred spots incompatible with the NiAs structure, and he showed that pyrrhotite possessed in reality a pseudohexagonal unit, slightly monoclinic, with parameters $A=11.9A$, $B=6.865A\approx 4a$, $C=22.72A\approx 4c$, $\beta=89°33'$, where a and c are the parameters of the unit usually used. Figure 3 represents the positions of the atoms in the unit cell; this contains 64 sulfur atoms and 56 iron atoms, therefore 8 molecules of Fe_7S_8. The black circles represent the iron atoms, the white circles the holes. In order to simplify the figure, only the iron planes containing holes are shown, that is, the odd-numbered iron planes. The even-numbered planes, which contain no holes are not represented, nor the intermediate sulfur planes.

[16] F. Bertaut, Compt. rend. 234, 1295 (1952).

The apparently complicated structure results from the tendancy of the holes to place themselves as far as possible from each other. Their minimum distance in the planes, and in neighboring planes, is always about $2a$. Let us note that the symmetry of the unit, represented by Fig. 3, is consistent with the magnetic symmetry: the two directions A and B in the basic plane are different.

Thus, as we predicted, the two sublattices of iron atoms are crystallographically different on account of the regular distribution of the holes. To finish defining the structure and to deduce from it the molecular moment, it is necessary to know also the distribution of the ferrous and ferric ions between the different available sites. This is practically impossible with x-rays. Theoretically, the problem can perhaps be solved without too much calculations. In distributing the ferric ions equally on all the planes of iron, one finds that the magnetic moment of a molecule Fe_7S_8 reduces itself

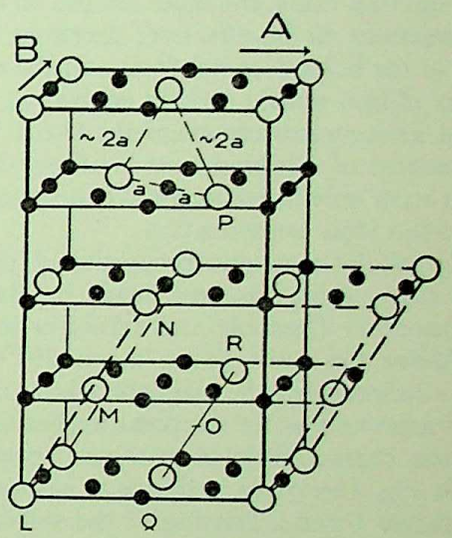


FIG. 3. Crystal lattice of pyrrhotite (*after Bertaut*).

to the atomic moment of the Fe^{++} ion or four Bohr magnetons, μ_B, if we neglect the orbital moment, while the experiment gives scarcely more than $2\mu_B$. Of course this value can be criticized and we can find a distribution of ions giving the correct experimental value of the saturation moment, but this has little purpose because we expect the orbital moment of the ferrous ion to play an important role. Study of the gyromagnetic ratio by Coeterier yielded the extraordinary value $g=0.67$, impossible to justify *a priori*.

Thus there remains much to be done before we have a complete quantitative interpretation of the saturation moment of pyrrhotite. However, the general interpretation that we propose here nevertheless permits coordination of a certain number of experimental facts. In particular, it easily explains why ferromagnetism does not appear as soon as the composition is no longer stoichiometric, and why a minimum value of x, in the vicinity of $x=0.08$, is necessary. In fact, when x is less

CC-0. In Public Domain. Gurukul Kangri Collection, Haridwar

Digitized by Arya Samaj Foundation Chennai and eGangotri

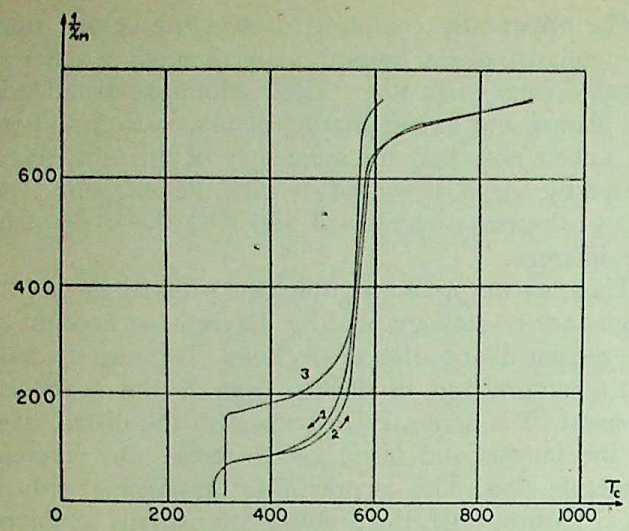


FIG. 4. Thermal variation of the reciprocal, $1/\chi_m$, of the magnetic susceptibility of a single crystal of pyrrhotite. Curves 1 and 2, artificial pyrrhotite; curve 3, natural pyrrhotite (*after Benoit*).

than this limiting value, the holes are too far apart for their interactions to be effective; therefore a superstructure of the holes does not form and the even and odd planes of iron remain strictly equivalent, and the compound is simply antiferromagnetic. Also, it is known that phenomena of this kind exist in alloys, the superstructures occur only in relatively narrow range around the theoretical ideal concentration.

A study of the magnetic properties of pyrrhotite above its Curie point has been made by Benoit[13] at the laboratory in Grenoble and furnishes interesting results. Above the Curie point, about 292°C, up to 450°C, the reciprocal of the magnetic susceptibility χ_m, plotted as a function of the temperature, has the hyperbolical form characteristic of antiferrimagnetism,[5] as is shown in Fig. 4 by curve 3 relating to natural pyrrhotite and curves 1 and 2 relating to the sulfide $FeS_{1.14}$. Around 560°C a new phenomenon appears; the susceptibility undergoes a sudden discontinuity and becomes 5 or 6 times smaller. At higher temperatures, both in general behavior and in magnitude, the thermal variation of susceptibility is much like that of FeS. It is tempting to consider this temperature of 560°C as the temperature of the disappearance of the ordered structure of the holes; beyond that, the holes are distributed at random on all sites of the sublattices in such a way that the magnetic properties of the substance become like those of FeS.

In order to prove this hypothesis, Benoit tried to quench the pyrrhotite from a temperature above 560°C, in order to preserve the disordered arrangement of the holes. The ferromagnetism should than disappear and we should have antiferromagnetism of the classic type. As a matter of fact, the samples have always remained antiferromagnetic. This negative result is explained well enough if one notes that the holes should diffuse from one place to another more easily than the atoms of binary alloys; the states in unstable equilibrium should then be more difficult to preserve than in metallic alloys. Thus it is not yet proved definitely that the ordering of the holes disappears at 560°C, but it is magnetically very probable.

Pauthenet[17] has studied the thermal variation of magnetization along different crystallographic directions in a natural pyrrhotite crystal below room temperature. The measurements have confirmed the results obtained by Weiss and Forrer[14] in the basic plane, which alone had been studied up to now. But, in the direction of the axis, as shown in Fig. 5 which summarizes the experiments, Pauthenet obtained unexpected results.

In the basic plane (upper part of the figure) the curves do not show any remarkable particularities, and they resemble those of any ferromagnet, except that the magnetization at saturation seems to pass through a maximum around 150°K and diminish when the temperature is lowered further. This phenomenon has already been observed by Weiss and Forrer.

Along the axis (lower part of the figure) the magnetization at room temperature is apparently proportional to the applied field, but it still remains less than one-fourth of the magnetization at saturation in the basic plane in a field of 20 000 oersteds. Thus there is a strong magnetocrystalline anisotropy which holds the spontaneous magnetization in the basic plane. When the temperature drops below 250°K, there appears a new phenomenon: a ferromagnetism superposes itself progressively on the preceding paramagnetism, the susceptibility of which varies little with the temperature. Actually, a spontaneous magnetization, parallel to the *C* axis (see Fig. 3), gradually increases. This spontaneous magnetization seems to pass through a maximum, around 50°K, of about one-fourth of the magnetization at saturation in the basic plane, and then to diminish slightly when the temperature is further reduced. One has the impression that the magnetizations at saturation, in the basic plane *AB* and along the axis *C*, vary in

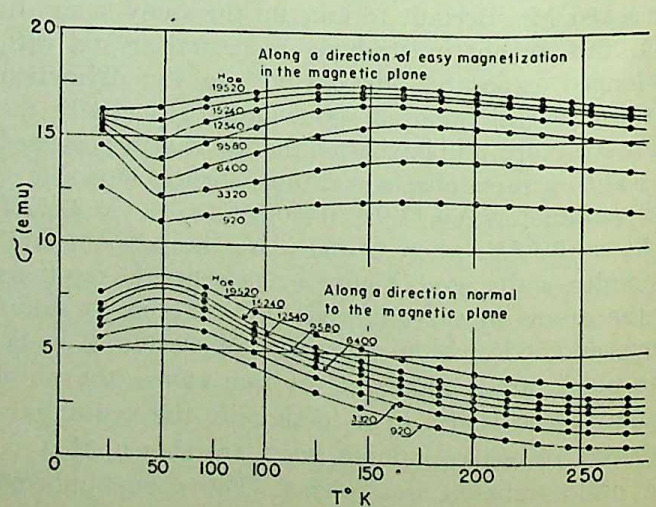


FIG. 5. Thermomagnetic study of a crystal of pyrrhotite (*after Pauthenet*).

[17] R. Pauthenet, Compt. rend. 234, 2261 (1952).

CC-0. In Public Domain. Gurukul Kangri Collection, Haridwar

Digitized by Arya Samaj Foundation Chennai and eGangotri

complimentary fashion: when one grows, the other shrinks, and vice versa. This all happens as if, in a portion of the substance that is larger, at lower temperatures, there is a change in the direction of easy magnetization. In itself, a change with the temperature of easy magnetization is a common phenomenon, but generally it is produced suddenly and completely at a definite temperature. Here, on the contrary, there is a progressive change as if the substance were heterogeneous. As the examples studied are of natural substances, likely to contain many impurities, it is possible that local inhomogeneities are at the origin of the observed phenomenon.

Thus it is not certain whether we are concerned with a special property of pyrrhotite, Fe_7S_8 or with a chemical effect. Experiments are in process to clarify this point. From a practical point of view, these curious phenomena complicate greatly the problem of the magnetization of pyrrhotite at saturation: is it necessary, in order to obtain the absolute value, to add the magnetization along the axis C to the spontaneous magnetization of the basic plane? It seems that one must reply in the affirmative, but the practical application of this principle is difficult. One can estimate that in the example studied the magnetization at saturation is from 21 to 22 cgs units/g.

CC-0. In Public Domain. Gurukul Kangri Collection, Haridwar

Digitized by Arya Samaj Foundation Chennai and eGangotri

REVIEWS OF MODERN PHYSICS VOLUME 25, NUMBER 1 JANUARY, 1953

Elementary Mechanisms of Magnetization in Mixed Oxides of Iron and Cobalt

CHARLES GUILLAUD

Centre National de la Recherche Scientifique, Bellevue, France

The magnetic properties of mixed ferrites of iron and cobalt of the general class, $[x\mathrm{Fe_2O_3}, (1-x)\mathrm{CoO}]$, where x is the molar fraction, varying from 0.5 to 0.6, are studied. Depending on the conditions of preparation, a small amount of the trivalent iron may also transform into the bivalent form. These materials not only possess remarkable magnetic properties but are particularly amenable to a theoretical as well as experimental study of the fundamental mechanisms involved in orientation in a magnetic field, coercive force, remanence, initial susceptibility, law of approach to saturation, and the energies of magnetization. An attempt has been made to correlate all these factors for these materials.

An x-ray examination shows that these materials consist of only a single phase. Direct evidence concerning the mechanism of orientation by annealing in a magnetic field has been obtained. A study of the magnetostriction as a function of composition, density, and temperature—both on oriented and non-oriented materials—permits us to investigate the important factors affecting the fundamental mechanism of magnetization. These materials reveal an unusual characteristic in that the values for magnetostriction are very high ($\lambda\sim3\times10^{-4}$) and their dependence on temperature is very great ($\lambda\sim10^{-4}$ at 20°C and 3×10^{-4} at −196°C). The basic phenomena can thus be readily characterized.

As for the coercive force, we place emphasis on the fact that the value of H_c depends on the density. When the density, δ, of the materials is less than 2.9 (theoretical density is 5.1), the value of H_c for a given temperature is independent of δ which strongly suggests rotations as the only elementary mechanism. Between −80°C and room temperature, we have shown that H_c is effectively only a function of the magnetoelastic energy. At temperatures lower than this, the phenomena are more complicated and one must consider as well the magnetocrystalline energy in order to account for the values of H_c encountered. If the density is between 2.9 and 5.1, H_c depends on δ and, therefore, on the relative volume of voids. Accordingly, it is probable that, in this case, wall displacements also contribute to the properties and we have shown that H_c is approximately proportional to the square of the volume of voids.

We next give a theoretical study of the remanent magnetization. The value of the ratio I_r/I_s, with a mechanism of orientation which places the magnetic vectors along cubic axes nearest the direction of the field, is in good agreement with our experimental results, at least to −80°C. Below this temperature, other phenomena intervene which we shall discuss.

A theoretical and experimental study of the initial susceptibility both on oriented and non-oriented materials has made it possible for us to discern the particular mechanisms which affect the orientation, the coercive force, and the remanence. The ratio $\chi_{\text{oriented}}/\chi_{\text{non-oriented}}$ has been confirmed.

An investigation of the law of approach has proved that in all cases Weiss's law, $\sigma_H=\sigma_\infty[1-(a/H)]$, is confirmed. The value of "a" depends on the relative volume of voids and on λ.

A study of the energy of magnetization as a function of temperature on both oriented and non-oriented materials has afforded a supplementary proof of the interconnection between the different mechanisms.

Finally, we give a résumé of the principal magnetic characteristics of these mixed oxides.

I. GENERAL CONSIDERATIONS

MIXED oxides of iron and cobalt, the magnetic properties of which are the subject of this paper, can be represented by the formula

$$x\mathrm{Fe_2O_3}, (1-x)\mathrm{CoO}, \qquad (1)$$

x being the molecular content of $\mathrm{Fe_2O_3}$, which varies from 50 to 60 percent. The conditions of preparation were such that several percent of trivalent iron are transformed to bivalent iron.

These mixed oxides possess remarkable magnetic properties, which will be discussed throughout the paper. Technical literature has already pointed out their properties as magnets of iron and cobalt oxides, particularly of vectolites,[1] but these materials differ in composition and properties from those represented by reference 1. We have made this study because it was very interesting to explore the main magnetic properties in general. In the present study the principal magnetic properties are explored, and a study is made of the mechanism of treatment in a magnetic field, of coercive force, of remanent magnetization, of initial magnetization, of approach to saturation, and of energy of magnetization. The results are not complete, but it is believed that the principal magnetic properties already observed can be profitably discussed. The research is being continued.

We shall not describe here the different methods of preparation and measurement used, except as they are necessary for understanding the text. We have made many preparations of these oxides and we have studied their properties. In this study, they cannot be published in the whole, but our results established with any samples are general. By varying the conditions of preparation, it is possible, for example, to obtain very different coercive forces, but the laws of variation on account of different parameters remain valid.

This study is the result of group work in which the following research men of the Laboratory have collaborated: Bertrand, Medvedieff, Vautier, Gary, Martinet, and Barbezat. Detailed publications will be made later on the various separate problems.

[1] Magnets of "vectolite" were pointed out for the first time in Japanese publications and patents (for instance: Y. Kato and T. Takei, J. Inst. Elec. Engrs. (Japan) 53, 408 (1933)). United States patent No. 1 977 193, April 9, 1935.

II. X-RAY STUDIES

Studies with x-rays have been undertaken on non-oriented samples and on samples oriented by heating in

CC-0. In Public Domain. Gurukul Kangri Collection, Haridwar

Digitized by Arya Samaj Foundation Chennai and eGangotri

TABLE I. Dependence of magnetostriction and coercive force on density.

Density	3.75	3.50	3.25	2.90
$\lambda \cdot 10^6$	−110	−110	−110	−110
H_c	1260	1490	1720	2050

the presence of a magnetic field. These were in the form of flat disks or of cubes. We have used the back reflection method with a camera 240 mm in circumference, with radiation from an iron tube, monochromated by reflection from a curved quartz crystal and focused on the camera slit. The camera used a system of baffles such that the lower half and the upper half of the film could be exposed successively. In this way one obtained on the film two diagrams centered in the same manner. From this it was possible to measure very small differences.

Results

1. In spite of an excess of Fe_2O_3 above the stoichiometric content for cobalt ferrite (50 percent mole), the samples showed a single phase. The diagrams, after

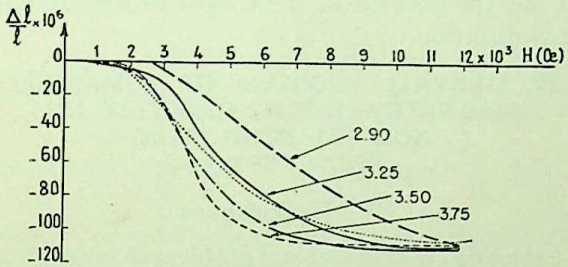


FIG. 1.

exposures reaching 48 hours, did not allow us to find a second phase. But we intend to perform longer exposures to ascertain the nonexistence of a second phase.

Though the consequences of orientation are similar to those for Alnico permanent magnets, we believe that the conditions are much better here, since in our samples we have no second phase, which was believed till now to play an important part in the orientation process.

2. When studying the oriented material, we used a cube cut in this material, in such a way that the direction of orientation be along a cube edge, and we recorded two diagrams on the same film: one for a face perpendicular to the direction of orientation, the other one for a face parallel to this direction. In the former case, we find $a' = 8.379$A); in the latter, $a = 8.380$A.

TABLE II. Dependence of magnetostriction and coercive force on temperature.

Temperature, °C	$\lambda \times 10^6$	H_c
20°C	−110	2050
−80°C	−190	3100
−196°	−270	6500

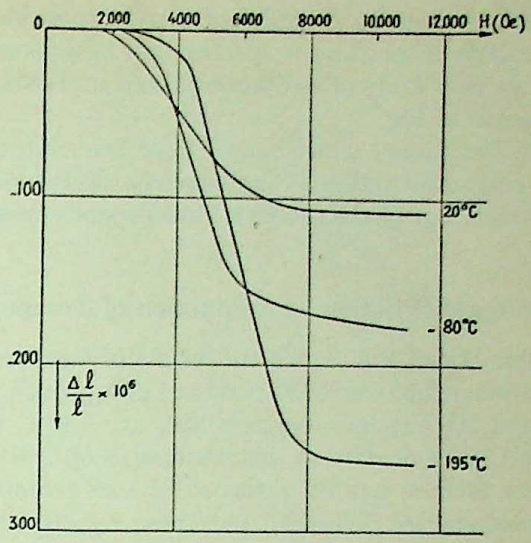


FIG. 2.

We shall give of these results the following interpretation: under the effect of heating in a magnetic field, the direction of spontaneous magnetization becomes this of the cube edge next to the direction of the magnetizing field. Under the effect of this spontaneous magnetization, the cube edge bearing the magnetization is contracted by about 0.001A. This deformation (magnetostriction) is shown by x-rays—when the face tested is perpendicular to the easy direction, it is nearly perpendicular to the contracted edges, and we obtain reflections on planes perpendicular to these axes (and thus have a').

Where the surface is parallel to the direction of easy magnetization, it is the axis a which one obtains. This interpretation based on our present results must still be supported by other research which we are doing for confirmation.

We have thus a direct measure of magnetostriction:

$$\lambda_{100} \approx 1.2 \times 10^{-4}.$$

III. MAGNETOSTRICTION

Knowledge of magnetostriction is indespensable to this study. We have measured it as a function of composition and temperature and density, in both isotropic and oriented materials.

(1) Magnetostriction as a Function of Density

Because the coercive field depends on the density, we have studied magnetostriction as a function of density for mixed oxides of the same chemical composition (56 mole percent Fe_2O_3), which have had the same

TABLE III. Effect of composition.

Content of Fe_2O_3(%)	52	56	59	62	65
$\lambda \cdot 10^6$	−110	−110	−90	−80	−60
H_c	1500	2050	2000	1800	1600

CC-0. In Public Domain. Gurukul Kangri Collection, Haridwar

Digitized by Arya Samaj Foundation Chennai and eGangotri

thermal treatments. Samples of this composition have particularly interesting properties and have been used often in this study. Results are shown in Table I and the curves of Fig. 1.

The conclusion, which might have been foreseen, is that magnetostriction is independent of the density. Thus the value of the coercive force depends on density alone.

(2) Magnetostriction as a Function of Temperature

Table II and Fig. 2 give the results of measurements made on a mixed oxide (56 percent Fe_2O_3) which is non-oriented, at ordinary temperature, at $-80°C$ and at $-196°C$. The density of this material is of 2.90.

Here there is a rapid variation of λ as a function of the temperature. We shall use these results when we study the mechanism of the coercive force and its dependance on magnetostriction.

(3) Magnetostriction as a Function of the Composition

We have varied the composition of mixed oxides from 50 to 60 molar percent of Fe_2O_3. The results are given in Table III. Later we will draw conclusions from these data regarding the mechanism of coercive force.

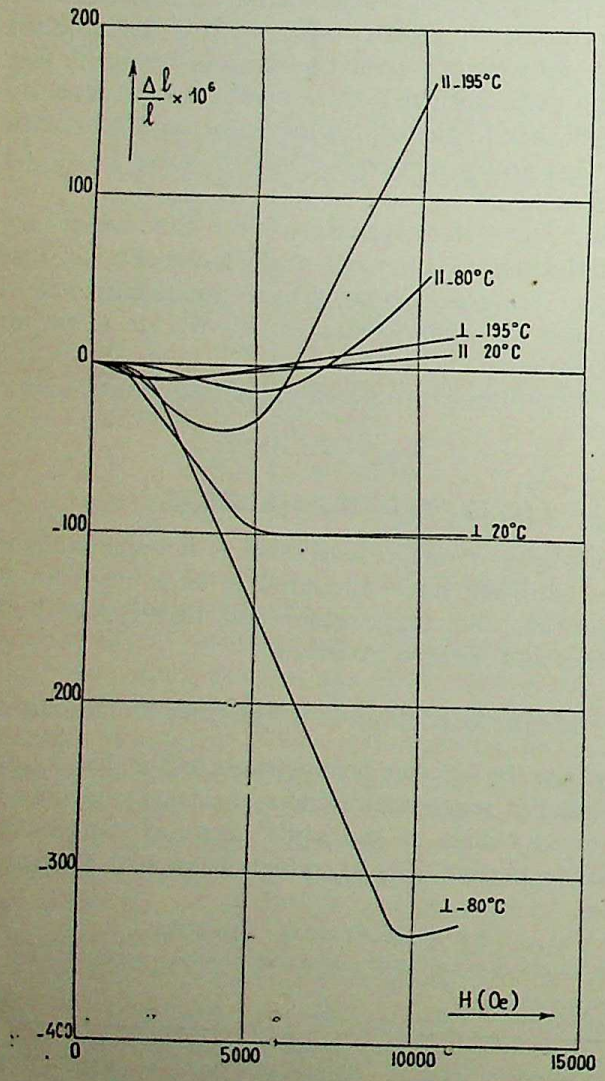


FIG. 3.

(4) Magnetostriction of the Oriented Sample as a Function of Temperature

At temperatures of 20° and $-80°C$ the behavior of the curves is normal (Fig. 3); that is, in the direction of orientation the magnetostriction is small and in the perpendicular direction it is negative and large. In addition, the curves obtained seem compatible with those of non-oriented oxides. One will note, however, the particularly high value of λ at $-80°C$ for the perpendicular direction.

At $-196°C$ the phenomena become complicated; the measurements become very difficult because the curve for the direction of easy magnetization bends over at its end in function of the measures and shows a contraction of $-145 \cdot 10^{-6}$. For magnetostriction perpendicular to the direction of orientation there is a well-defined curve.

At the temperature of liquid nitrogen we find ourselves in the presence of a new phenomenon. All occurs as if the spontaneous magnetization prefers to be oriented in a perpendicular direction. Below we will also point out the relation of these data to the mechanism of magnetization.

IV. GENERAL PROBLEM OF REMANENT MAGNETIZATION OF ORIENTED OR NON-ORIENTED CUBIC POLYCRYSTALS

(1) Hypotheses

We shall discuss the general problem of magnetization in a cubic polycrystal starting with the following hypotheses, which are in accordance with our experimental results:

(1) The microcrystalline structure prevents wall displacements.
(2) Definite magnetocrystalline energy and magnetoelastic energy caused by internal stresses of mean value σ, distributed in a statistical manner, are present.
(3) After orientation the vectors of magnetization place themselves preferentially on the crystallographic axes of easy magnetization oriented nearest to the directing field.

(2) Determination of the Ratio I_r/I_s for Anisotropic Material

Isotropic material is composed of crystals having axes distributed in a statistical manner. The directions of the magnetization vector are restricted according to our third hypothesis. Everything occurs as if, after orientation by the field, H, during treatment, the material considered as the sum of grains possessed a unique axis of magnetization lying inside of a well-defined area on the sphere unit.

To solve this problem it is simplest to fix the position of magnetization and to consider the area in which the field vector H is distributed. This field describes in the limits a cone in which the generator is the intersection of the unit sphere with planes bisecting $x \pm z = 0$ and $y \pm z = 0$ (Fig. 4).

CC-0. In Public Domain. Gurukul Kangri Collection, Haridwar

Digitized by Arya Samaj Foundation Chennai and eGangotri

The probability of the presence of the field H in a given area, inside the limiting area, is proportional to the area. Let us calculate the expression $\int\int \mathbf{k}\cdot\mathbf{n}d\sigma$ by designating by S the area of zone $ABCD$ cut out on the unit sphere by planes $x-z=0$, $y-z=0$, $x=0$, $y=0$, and by $\mathbf{k}$ the unit vector along the axis $0z$; then $\mathbf{n}d\sigma$ is the oriented element of area in the zone.

To simplify the limits of integration, let us choose a system of coordinates u, v, such that the direction of field H is defined by planes

$$x-z\tan u=y-z\tan v=0.$$

The integral is then

$$\int\int\left(\mathbf{k}\frac{\partial\mathbf{M}}{\partial u}\cdot\frac{\partial\mathbf{M}}{\partial v}\right)dudv,$$

which reduces to

$$\int\int\begin{vmatrix} x_u' & y_u' \\ x_v' & y_v' \end{vmatrix}dudv.$$

The calculation of the derivatives gives as the final value of the integration

$$I=\int_0^{\pi/4}\int_0^{\pi/4}\frac{dudv}{\cos^2u\cos^2v(1+\tan^2u+\tan^2v)^2}.$$

The value of the ratio I_r/I_s is equal to I/S; but

TABLE IV. Remanence along the axis of easy magnetization.

Temp. in °K	77	110	140	200	230	290
I_r/I_s	0.90	0.88	0.87	0.85	0.84	0.84

$S=\pi/6$, as one may easily verify. The integration of I gives

$$I=(\sqrt{2}/2)\csc\tan(\sqrt{2}/2),\quad I=0.439.$$

The corresponding value of I_r/I_s is thus equal to 0.839.[2]

(3) Ratio I_r/I_s for $K<0$

The preceding hypothesis corresponds to a positive value of K. A negative value leads on the contrary to eight directions of easy magnetization parallel to the body diagonals of the cube. It is easy to see that the limiting area for H is a spherical triangle with 3 right angles. The corresponding value of I_r/I_s is 0.86.

One could also consider a more arbitrary direction of magnetization, that along the cube face diagonals. In this case the area is limited by a spherical rectangle of area $\pi/3$, since there are 12 possible directions, and the calculation of the product I_r/I_s gives 0.91.

[2] Mention should be made of Gans and of Hoselitz and McCaig on the values of this ratio.

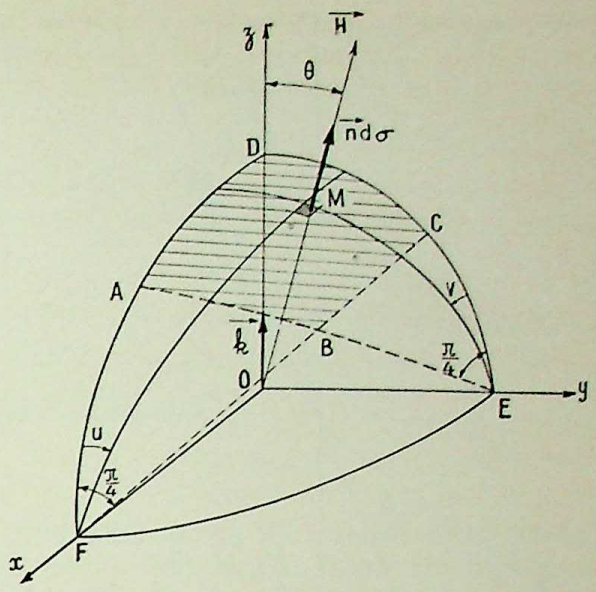


FIG. 4.

(4) Determination of I_r/I_s for Anisotropic Material Magnetized Perpendicular to the Axis

This calculation is complemental to the preceding one, the integral $I=\int\int\mathbf{k}\cdot\mathbf{n}d\sigma$ being the complement of the preceding zone with respect to the eighth of the sphere. The calculation can be simplified by noting that

$$I=\int\int_{FDE}\mathbf{k}\cdot\mathbf{n}d\sigma-\int\int_{ABCD}\mathbf{k}\cdot\mathbf{n}d\sigma.$$

The first integral is $\pi/4$ and the second $(\pi/2)\csc\tan(\sqrt{2}/2)$, whence comes the desired value of the ratio:

$$I_r/I_s=0.330.$$

(5) Comparison with the Experimental Results

(a) *Along the Axis of Easy Magnetization*

Our experimental results are shown in Table IV. Above 200°K we find a value equal to 0.84, while for low temperatures the ratio increases. But it is necessary to give more weight to our results obtained above 200°K because at low temperatures it is difficult to realize saturation. Thus at 77°K the maximum value of H_c is not yet attained for the very high magnetizing field of 30 000 oe.

To determine the limiting values of H_c we have used laws of approach. In the case of oriented material a law in $1/H$, analogous to that of magnetization at saturation, was satisfactorily used, while for non-oriented material the law in $1/H^2$ was best for interpreting our results.[3] We will have the chance to refer in a future publication to the theoretical interpretation of the laws of approach.

However, taking into account the values of magnetostriction at 77°K, we may say that the mechanism of

[3] Medvedieff, thesis (Paris, 1952).

CC-0. In Public Domain. Gurukul Kangri Collection, Haridwar

Digitized by Arya Samaj Foundation Chennai and eGangotri

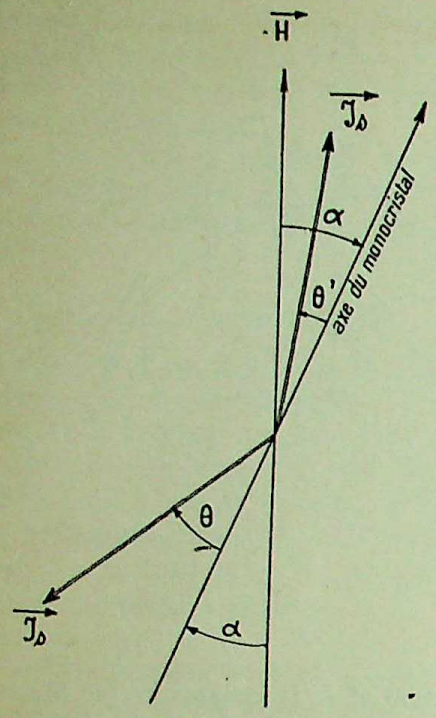


FIG. 5.

orientation at low temperatures is not simple as assumed in our hypothesis.

(b) Along a Perpendicular Direction

We find that the values of the ratio at 290°C and at 77°C are, respectively, 0.29 and 0.46.

(c) Case of Non-Oriented Material

Our results are given in Table V.

(6) Conclusions

In material that is oriented along the axis of easy magnetization there is agreement between calculation and experiment, from ordinary temperature down to about 200°K. But below this temperature the value of the ratio increases, while if the magnetization vectors were always distributed along cubic axes, this ratio should remain constant.

Along the axis of difficult magnetization we find a result slightly too small at the ordinary temperature but still acceptable, and much too high at 77°K. The values of the ratio I_r/I_s with non-oriented material are also too high below 200°K.

If we bring these results together with those obtained by the study of magnetostriction, it is necessary to admit that at low temperature the cubic symmetry no longer exists and that there is a possibility of permutation of easy and difficult axis of magnetization. We will go no further for the moment toward the analysis of this phenomenon. Studies at low temperatures must still be continued and also research with x-rays. Thus we admit our elementary mechanisms to be correct only to a temperature of 200°K.

V. COERCIVE FORCE

We have shown that coercive force depends on the density of the material, other things being constant. The theoretical density obtained with x-rays is about 5. By varying the conditions of pressing we have been able to obtain densities which rise gradually from about 2 to 4.8. In these samples the coercive force increases until the density attains 2.9, that is, until the relative volume of the holes is about 0.43. Materials at density lower than 2.9 have practically constant coercive force which is the maximum.

In order to interpret these results we distinguish two regions for the coercive force. From a density of 2.9, below which the coercive force is constant, we imagine that only rotations occur. The walls which bisect the greatest number of holes occupy a position of lowest energy and have no effect on the coercive force. Also the interactions between crystallites are not effective. The coercive force then depends only on K, on $\lambda\sigma$, and on I_s.

The mechanism of rotation here is similar to that observed in single domains.[4] Physically we do not have isolated domains here; but the elementary mechanism is the same. After considering the coercive force under these conditions we shall study it as dependent on the volume and the number of holes, when both irreversible wall displacements and rotation are supposed to take place, and when interactions among crystallites are no longer negligible.

(1) Coercive Force of a Domain Having Uniaxial Symmetry

The study of x-rays of this oriented material, having the large value of λ, justifies the assumption of uniaxial symmetry. The presence of elastic strains tends to destroy the cubic symmetry by establishing a preferred direction. In this way the problem goes back to the simple calculation of coercive force for a uniaxial crystal, the magnetocrystalline energy of which can be written

$$F = K_1 \sin^2\theta$$

if we neglect higher terms.

Adding the magnetoelastic energy to the magnetocrystalline energy, we have

$$F = (K_1 + 3\lambda\sigma/2) \sin^2\theta = K \sin^2\theta.$$

Under the action of an inducing field H, making the angle α with the axis (see Fig. 5), we have

$$F = K \sin^2\theta + HI_s \cos(\theta - \alpha).$$

TABLE V. Ratio I_r/I_s at different temperatures.

Temp. in °K	77	140	200	290
I_r/I_s	0.64	0.55	0.51	0.46

[4] This elementary mechanism of coercive force was pointed out first by the author as follows: (1) thesis, Strasbourg (1943), (2) sealed letter given March 8, 1943, to Compt. rend. 229, 992 (1949), (3) Comm. Soc. franc. de Physique Strasbourg (May 31, 1947); J. phys. et radium 8, 34S (1947), (4) J. Recherches CNRS, No. 9, (1949), (5) Compt. rend. 229, 818 (1949).

CC-0. In Public Domain. Gurukul Kangri Collection, Haridwar

Digitized by Arya Samaj Foundation Chennai and eGangotri

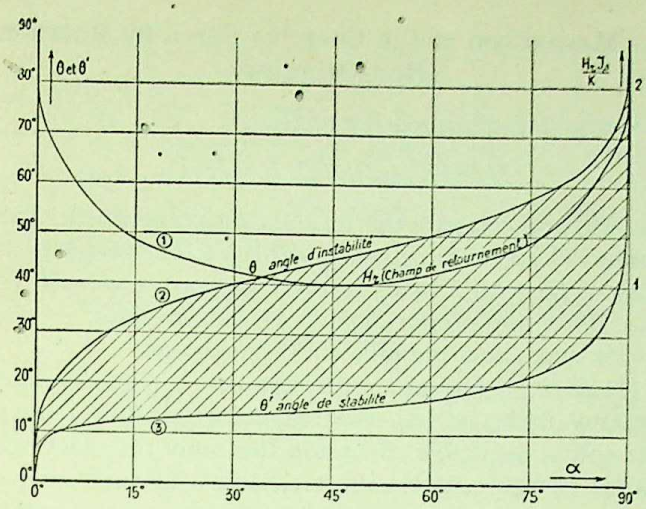


FIG. 6.

The conditions for equilibrium and for stability are obtained by putting $\partial F/\partial\theta=0$ and $\partial^2F/\partial\theta^2=0$. Elimination of α from the resulting equations gives

$$H=H_r=(K/I_s)(1+3\cos^2 2\theta)^{\frac{1}{2}}, \qquad (1)$$

the field strength for reversal of the domain.

The coercive force is thus a maximum for $\theta=0$, $H_r=2K/I_s$. There is also an apparent maximum for $\theta=\pi/2$, but its value is purely fictitious because there is no corresponding reversal.

Calculation of the angle θ corresponding to the position of instability, as a function of the parameter α, gives

$$\tan\alpha=\tan^3\theta. \qquad (2)$$

Now one can trace directly the curve of the coercive force of each domain as a function of α by combining Eqs. (1) and (2). One obtains finally for each position of a domain characterised by the angle α which its axis makes with the field, a definite value of $H_r=H_r(\alpha)$. In the following we shall use the reduced field H_rI_s/K. The curves H_rI_s/K, θ, and θ' may be traced as a function of α, θ, and θ' being, respectively, the position of equilibrium corresponding to the loss of stability, and the position of stability corresponding to the same critical value H_r of the inducing field (Fig. 6).

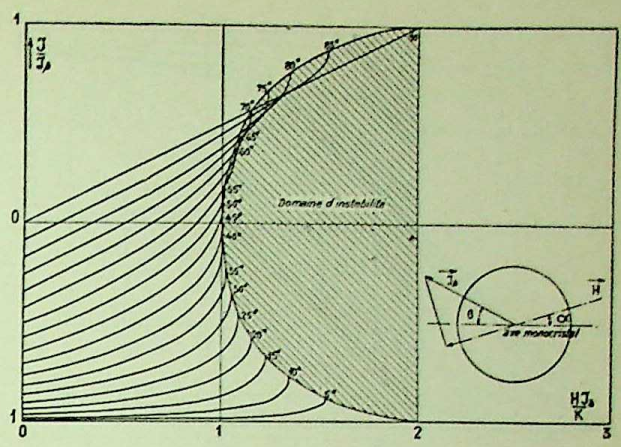


FIG. 8.

Let us calculate now the moment of the particle in terms of the field HI_s/K. There are two cases to consider. The domains being distributed statistically in the nonmagnetized state, one may represent the group by two domains having the same axis but antiparallel magnetization. When the spontaneous magnetization is parallel to the field there is no instability and the angle θ' is a continuous function of HI_s/K and the component of the magnetization in the direction of H has the value $I_s\cos(\alpha-\theta')$ (see Fig. 7).

Where the spontaneous magnetization is antiparallel to H, there is a continuous increase with θ up to a predetermined value which corresponds to the coercive force for the direction α; then the return of the I_s vector to the stable position θ, brings us back to the preceding case (Fig. 8). The magnetization curves of the two grains are represented in Fig. 9.

Giving each curve the probability $\sin\alpha d\alpha$, and integrating the expressions

$$\int\cos(\alpha-\theta')\sin\alpha d\alpha, \quad \int\cos(\alpha+\theta)\sin\alpha d\alpha,$$

one obtains the lower and upper branches of the hysteresis loop. The algebraic sum of these two curves gives the initial magnetization curve (Fig. 10). The experimental curves are given in Fig. 11. The value of the coercive force is

$$H_c\approx K/I_s.$$

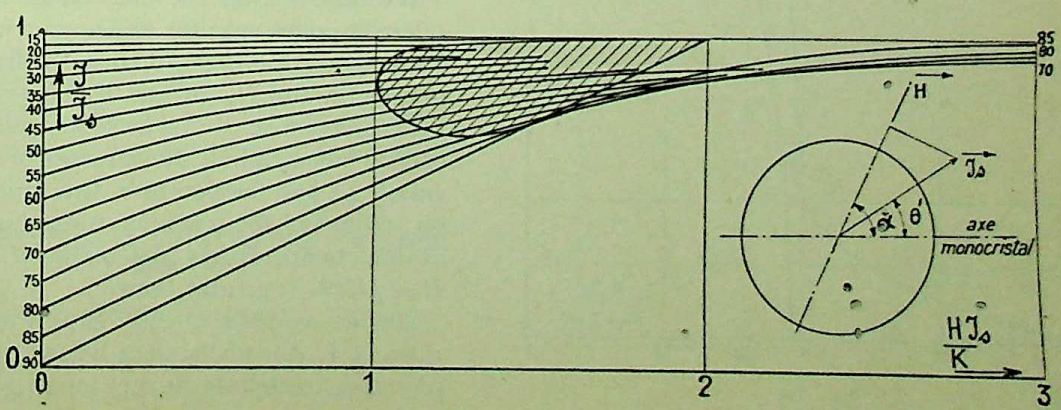


FIG. 7.

CC-0. In Public Domain. Gurukul Kangri Collection, Haridwar

Digitized by Arya Samaj Foundation Chennai and eGangotri

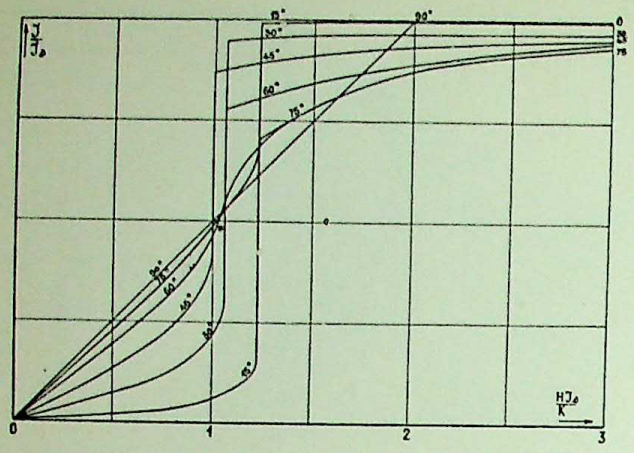


FIG. 9.

(2) Conclusions on the Magnetization Curve

This curve shows the results of our knowledge of the material, using the original hypotheses. It gives the initial susceptibility (tangent at origin) and also the ratio I_r/I_s that we have calculated by another method. Finally it gives directly the coercive force which could have been obtained only by graphical integration of the equation

$$\int_0^{\alpha} \{\cos[\alpha+\theta(\alpha, H_c)]-\cos[\alpha-\theta'(\alpha, H_c)]\} \sin\alpha d\alpha=0.$$

On the other side, the curve of first magnetization must be the mean value of the two parts of the loop of hysteresis, the lower and upper branches; it is easy to confirm with the results of experimentation.

For the oriented and non-oriented material one obtains a value of H_cI_s/K between 1 and 1.1. A perfect orientation would make this approach the value 2, but this can be realized only by a truly uniaxial polycrystal.

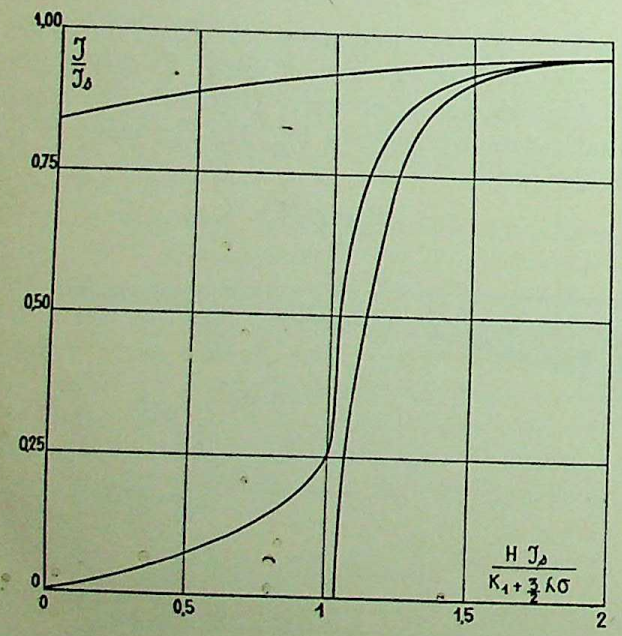


FIG. 10.

(3) Mechanism of the Coercive Force by Rotation (Non-Oriented)

We have established the relation

$$H_c \approx (K_1+3\lambda\sigma/2)/I_s \approx K/I_s,$$

and will now compare this formula with experiment. The numerical values are given in Table VI. The proportionality of H_c with λ holds to the temperature of $-80°C$. At $-196°C$ the proportionality no longer exists.

One may draw the following conclusions:

(1) at 20°C and at $-80°C$ the first hypothesis that we may make is that the magnetocrystalline energy has only a negligible effect and that only the magnetoelastic energy controls the mechanism of the coercive force.

(2) If we have a magnetocrystalline energy K it is necessary that the variation of this energy be such that the ratio H_c/H_c' is equal to λ_1/λ_2, which is not very probable. To solve this question definitely it would be necessary to determine σ by independent means.

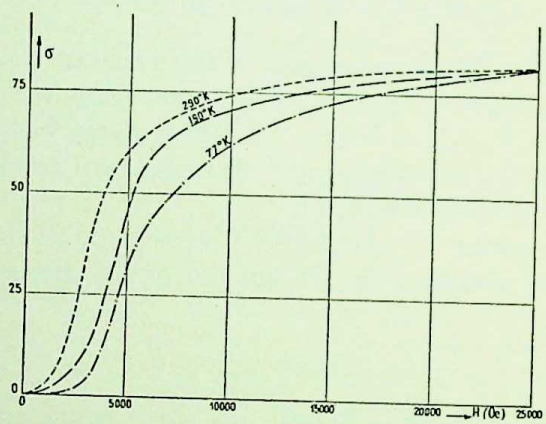


FIG. 11.

If we go back to Table V giving λ and H_c as a function of the composition, we see that the variations of H_c cannot be explained by variations of λ. We then make the hypothesis that as the iron atoms go into solid solution the value of σ increases—it is the product $\lambda\sigma$ which determines the value of H_c. For a molecular content of Fe_2O_3 higher than 59 percent the mechanism is less simple because above this percentage there are two phases.

We believe that the mechanism that we have considered applies only for Fe_2O_3 contents between 50 and 60 percent. At $-196°C$ there is no longer proportionality between λ and H_c; in fact if this proportionality held, the coercive force would be 4850, while experiment gives 6500. Thus we admit the influence of magnetocrystalline energy at low temperature. One can also imagine that on account of the tendancy toward uniaxial orientation at low temperatures the value of p in the formula $H_c=pK/I_s$ is greater than 1.

But as we have already shown in discussion of the ratio I_r/I_s, the phenomena below 200°K are more complex and necessitate further investigation.

CC-0. In Public Domain. Gurukul Kangri Collection, Haridwar

Digitized by Arya Samaj Foundation Chennai and eGangotri

As to the influence of orientation above 200°K, we have shown that in two chemically identical samples, which are very difficult to produce, the coercive force of the oriented material is slightly greater than the coercive force of the non-oriented material. The statistical study which we have made has shown that this must be so.

(4) Coercive Force when H_c Depends on the Holes

The coercive forces of material having a density, d, higher than about 2.9 are given in Table VII and Figs.

TABLE VI. Coercive force and magnetostriction.

t°C	H_c	$\lambda \times 10^6$	$H_{c,20}\lambda_t/\lambda_{20}$
20°C	2050	−110	2050
−80°C	3100	−180	3200
−196°C	6500	−270	4850
−253°C	15000		

12 and 13. Values of H_c are shown as a function of d and of the relative volume, v, of holes. The upper curve (1) is the envelope of all the points corresponding to the measurements which we have made on a great number of samples. Above the curve are all the experimental points, because the absolute value of the coercive force depends greatly on the conditions of preparation and it is difficult to reproduce these extreme values with any certainty. This is why we give another curve (2) which corresponds to the samples which we have studied in this investigation.

We have looked for the law which would give H_c as a function of v and we find that the most probable one is

$$H_c - H_{c0} \approx (K/I_s)(v/v_0)^2,$$

H_{c0} being the value of the coercive force of the bulk material and v_0 the volume of the holes for which the value of H_c becomes constant. I_s is the intensity of magnetization of the basic material.

TABLE VII. H_c as dependent on the volume of holes.

v	0	0.05	0.1	0.15	0.20	0.25	0.30	0.35	0.40	0.43
H_{c1}	750	790	900	1060	1270	1580	1930	2380	2870	3200
H_{c2}	750	770	820	920	1050	1220	1420	1650	1900	2100

The values of the exponent of v that we find generally in the various series which we have studied, rise gradually between 1.9 to 2.2.

VI. INITIAL SUSCEPTIBILITY OF POLYCRYSTALLINE MATERIAL

(1) Non-Oriented Material

The total energy is composed of magnetocrystalline energy, $K_1 \sin^2\theta$, of strain energy, $(\frac{3}{2})\lambda\sigma \sin^2\theta$, and of the energy of the field, $HI_s \cos(\theta' - \theta)$, as illustrated in Fig. 14.

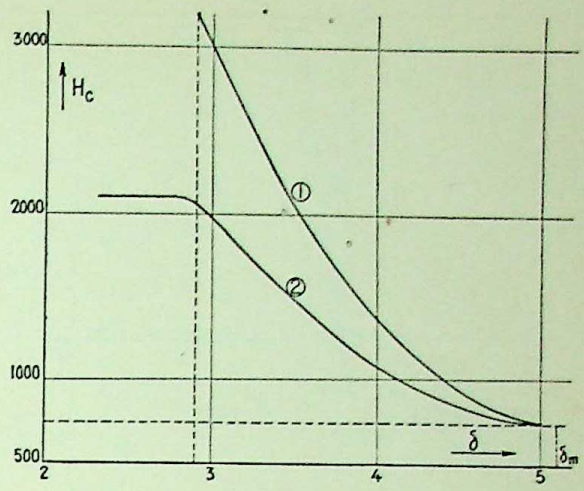


FIG. 12.

Introducing the reduced field, $h = HI_s/K$, we have

$$F = K[\sin^2\theta - h\cos(\theta' - \theta)].$$

The condition for equilibrium is

$$\partial F/\partial\theta = K[\sin 2\theta - h\sin(\theta' - \theta)] = 0,$$

and the expression for initial magnetization is

$$\chi_0 = (I_s^2/2K)\sin^2\theta'.$$

The average of this expression over the unit sphere is

$$\chi = (I_s^2/4K)\int_0^\pi \sin^3\theta' d\theta' = I_s^2/3K.$$

(2) Susceptibility of Material Oriented Along the Easy Axis

In oriented material, the limits of integration are changed so that

$$\chi = (I_s^2/2K)\int_0^\alpha \sin^3\theta' d\theta' \Big/ \int_0^\alpha \sin\theta' d\theta',$$

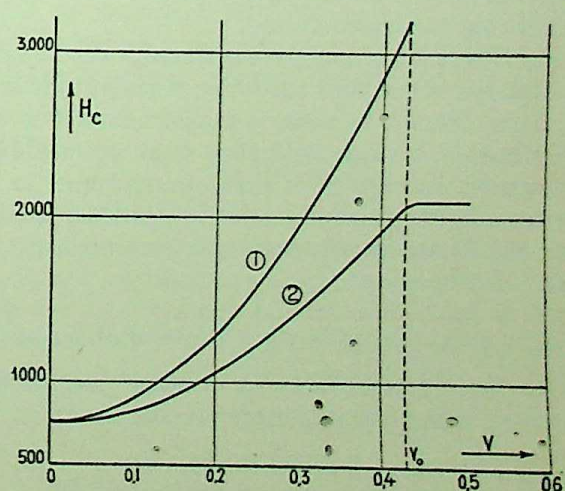


FIG. 13.

CC-0. In Public Domain. Gurukul Kangri Collection, Haridwar

Digitized by Arya Samaj Foundation Chennai and eGangotri

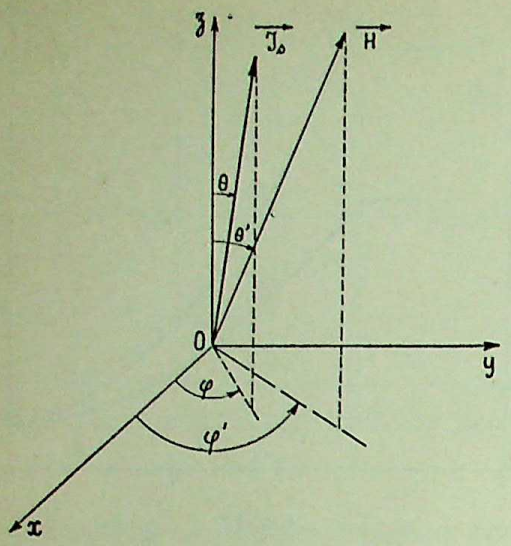


FIG. 14.

which gives for the susceptibility along the easy axis of a polycrystal

$$\chi=(I_s^2/6K)(3\cos\alpha-\cos 3\alpha-2)/(\cos\alpha-1),$$

or, when $\alpha=47°20'$,

$$\chi=0.435I_s^2/3K.$$

The susceptibility of oriented material is thus about half of the susceptibility of a non-oriented material.

(3) Susceptibility of Material Oriented Perpendicular to the Axis

Here we have

$$\chi=(I_s^2/2K)\int_{\pi/2}^{\alpha}\sin^3\theta'd\theta'\Big/\int_{\pi/2}^{\alpha}\sin\theta'd\theta'=1.17I_s^2/3K.$$

(4) Comparison with Experiment

(a) *Susceptibility Deduced from Coercive Force*

Using formula (1) we can deduce K from the coercive force and so obtain the calculated values of χ shown in the 5th column of Table VIII, and we can then compare these with the measured values.

The values of measured χ are systematically less than the calculated values, but the order of magnitude is the same. It is difficult to make measurements of χ with much precision, because with such weak permeabilities the magnetic leakage is of great importance. In the measurements there may be relative errors as much as 20 percent. However, the results appear to justify the mechanism assumed.

(b) *Initial Susceptibility of Oriented Material*

There is a further way of testing the assumed mechanism, using oriented material. We have

$$\frac{\chi_1,\text{ measured parallel to the axis}}{\chi_2,\text{ in non-oriented material}}=0.44.$$

Measurements give $\chi_1/\chi_2=0.50$. In this case also the agreement is not exact, but we were not able to orient the material in the form of a torus so have used a circuit of square form having sides of oriented material. By taking into account the experimental difficulties these results may be considered satisfactory.

We have not made measurements in a direction perpendicular to the direction of orientation. The value 1.17 has not been tested.

VIII. LAW OF APPROACH TO SATURATION

(1) Variation of a as a Function of Temperature and λ

(a) *Case of Non-oriented Material*

Measurements have been made on numerous samples; the law of approach $\sigma_H=\sigma_\infty(1-a/H)$ is verified without exception up to fields as high as 25 000 oe. Our results are summarized in Table IX.

One looks for the relation between a and λ; in column 5 are given the values of

$$a_t'=a_{20}\lambda_t/\lambda_{20}.$$

Although the variation of λ and of a with temperature is nearly the same, the proportionality is not rigorous.

TABLE VIII. Susceptibility and coercive force.

t°C	H_c	$K\cdot10^{-5}$	χ(calculated)	χ(measured)
20°C	2000	8.5	0.023	0.020
−80°C	3050	12.8	0.016	0.013
−196°C	6500	27.1	0.009	0.007

This applies to all the samples we have studied. The small variation of spontaneous magnetization at low temperature cannot account for the deviation.

(b) *The Case of Oriented Material*

The law in $1/H$ is also verified in oriented material. The 6th column in Table IX gives the values of a determined from magnetization curves for the easy direction. Here there is greater lack of proportionality between λ and a. But the magnetostriction in this case is not isotropic, and the results are much more difficult to interpret; the magnetostriction should be measured in different directions. We have also determined a as a function of the relative volumes of the holes, but our results are still too scanty to be published.

VIII. THE WORK OF MAGNETIZATION

The work of reversible magnetization measured on the curve $I=f(H)$ is equal to $\lambda\sigma$, if we consider only the magnetoelastic energy; if we include the magnetocrystalline energy this becomes $F=\lambda\sigma+2K_1/3$.

In the case of non-oriented material we find $F=6\times10^5$ ergs/cm³ at 20°C. If the effect of magnetoelastic energy is dominant, we have according to the

CC-0. In Public Domain. Gurukul Kangri Collection, Haridwar

Digitized by Arya Samaj Foundation Chennai and eGangotri

measurements,

$$(\tfrac{3}{2})\lambda\sigma = 9\times 10^5 \text{ ergs/cm}^3.$$

If we take into account the various errors, this value agrees with the value K deduced from the coercive force, 8.5×10^5.

At the temperature of solid carbon dioxide

$$F = 8.5\times 10^5, \quad (\tfrac{3}{2})\lambda\sigma = 12.7\times 10^5.$$

This agrees with the value of K deduced from the coercive force at this temperature.

In the case of oriented material, the mean value according to the calculation already made is 0.44. The reversible work corresponding to the oriented state is then $0.44\lambda\sigma$. We thus have a check on the theory by testing the constancy of the ratio of these values of F as a function of temperature. The experiment shows that the ratio is constant to -80°C, but not below.

Thus all the properties that we observe lead to the same conclusion: at low temperatures we have a more perfect uniaxial symmetry.

IX. THE MECHANISM OF ORIENTATION

First we eliminate the influence of a second phase, which up to now has been considered to be of great importance, because the evidence does not support it. Also, we will not consider the idea that the lattice is oriented so that the cubic axes have a common direction, that of the field, because the x-ray evidence is against it. We will not consider the effect of a demagnetizing field of form, the thermal variations of H_c invalidating it. Similarly, the orientation of crystallites, not supported by x-ray study, is not believed to exist.

TABLE IX. Values of a at various fields.

t°C	H_c	$\lambda\times 10^6$	a(measured)	a_t'	a(measured oriented)
20°C	2050	−110	1560	1560	1000
−80°C	3100	−180	2200	2500	2250
−196°C	6500	−270	3200	3800	5300

The whole interpretation of the mechanism of orientation rests on our results with x-rays which show that the cube axes are different in the directions parallel and perpendicular to the direction of the field present during the treatment. Although the interpretation of our results are not definitive, we believe that the magnetization vectors have the directions of the axes nearest to the direction of the field. Because the effect of magnetostriction is considerable, we observe a real deformation of the crystal lattice. At temperatures below 200°K the deformation is still more marked and a really uniaxial system approximated:

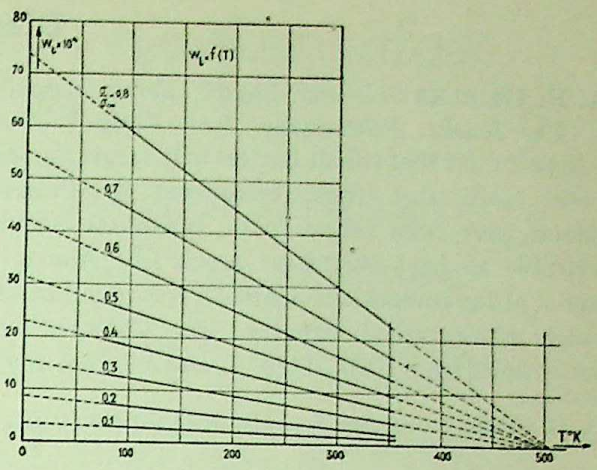


FIG. 15.

It is easy to understand why the orientation is established at a temperature near to 300°C, by referring to Fig. 15 by Medvedieff. Here curves are traced giving the energy of magnetization as a function of the temperature for different values of the ratio σ/σ_0. All of these energies approach zero for a temperature close to 300°C, when the magnetization vectors are oriented with great ease. In the phenomena of orientation this temperature of 300°C plays a part analogous to that of the Curie point. We add finally some results on electric anisotropy—the ratio of the resistance along the direction of orientation to the resistance along a perpendicular direction is equal to 1.2.

X. PROPERTIES AS MAGNETS

These mixed oxides possess very interesting magnetic properties. Remanent magnetism is of the order of 2500, and can attain 3000. The coercive force (for zero induction) is about 1500 and can exceed 2000. Finally the product $(BH)_{max}$ is about 1.5×10^6. It is not difficult to imagine a new type of magnet which would use these elementary mechanisms,—they would be magnets with holes, and would be complementary to fine-powder magnets. For example, it would be of the greatest interest to form holes in metals and alloys possessing large values of magnetocrystalline energy or of magnetoelastic energy. Cobalt, for example, because of its large magnetocrystalline energy, seems to be especially interesting.

CONCLUSION

Mixed oxides of iron and cobalt permit us to relate several of the most important ferromagnetic properties. We do not consider this study to be finished, but already we can better understand certain elementary mechanisms of magnetization. It also opens horizons interesting from a practical point of view.

CC-0. In Public Domain. Gurukul Kangri Collection, Haridwar

Digitized by Arya Samaj Foundation Chennai and eGangotri

DISCUSSION

A. H. GEISLER: *General Electric Research Laboratory, The Knolls, Schenectady, New York:* I should like to point out that cobalt ferrites with larger amounts of iron oxide that those considered by Professor Guillaud have been found to be two-phase material susceptible to heat treatment much like Alnico.[1] A material of the composition $CoFe_5O_8$ was found to have a single phase spinel structure like $CoFe_2O_4$ when rapidly cooled from 1050°–1150° C, and on reheating for ten hours at 800°C or less a second phase precipitated with a rhombohedral structure like α-Fe_2O_3. The suggestion was made that the Fe_2O_3 type phase when it first formed also had a spinel structure characteristic of the γ-Fe_2O_3 modification so that the response to heat treatment and magnetic properties could depend upon a miscibility gap in the solid solution field much like that in the Fe-Ni-Al system. Sensitivity limitations of the x-ray diffraction technique might prohibit the detection of the precipitate that could be responsible for the high coercive force of other cobalt ferrites.

[1] A. H. Geisler, Trans. Am. Soc. Metals 43, 70–104 (1951).

CC-0. In Public Domain. Gurukul Kangri Collection, Haridwar

Digitized by Arya Samaj Foundation Chennai and eGangotri

REVIEWS OF MODERN PHYSICS VOLUME 25, NUMBER 1 JANUARY, 1953

The Low Temperature Transformation in Ferrites

L. R. BICKFORD, JR.

State University of New York, College of Ceramics, at Alfred University, Alfred, New York

The general behavior of magnetite (iron ferrite) at its low temperature transformation (*ca* 118°K) is reviewed. One of the properties which undergoes a large change is the magnetocrystalline anisotropy, which is larger in magnitude and has a lower symmetry below the transformation. The magnetic symmetry axis below the transition temperature can be predetermined by cooling a single crystal through the transition in a magnetic field, and can be changed from one cube edge to another below the transformation by means of a strong magnetic field.

Directional pressure also appears to be effective in establishing the axis. Hysteresis loop measurements show that if a compressive stress is applied along the length of a rod-shaped specimen cut parallel to [100] as it cools through the transition, the specimen is more easily magnetized in this direction. No such effect was observed along [110] or [111] directions.

Changes in dimension occurring at the transition have been measured by means of resistance strain gages cemented along the principal crystallographic directions. Data were obtained as the crystal warmed through the transition in the demagnetized state after having been cooled in various conditions of biasing magnetic field and pressure. It is concluded that the large changes in magnetic symmetry accompany small changes in crystal structure. The low temperature form appears to be orthorhombic, the maximum distortion from cubic symmetry, along [110], amounting to *ca* 0.07 percent. All three orthorhombic axes can be established unambiguously by cooling the crystal through the transformation in a magnetic field along [100] with pressure applied simultaneously along [011]. The change in direction of easy magnetization above the transition from [111] to [100] is accompanied by a small dimension change (*ca* 0.002 percent).

Similarities with the behavior of barium titanate at its ferroelectric Curie temperature are pointed out. Evidence for the existence of similar transformations in the other ferrites is discussed briefly.

I. INTRODUCTION

NUMEROUS investigations over the past twenty-five years have brought to light many interesting changes occurring in magnetite (iron ferrite) at its low temperature transformation (*ca* 118°K). Three of the more significant changes are illustrated in Fig. 1. Weiss and Forrer[1] found that the magnetization decreases abruptly at the transition, as shown in Fig. 1(a). The magnitude of the discontinuity is smaller for larger magnetic fields, the saturation magnetization remaining unchanged through the transformation. The specific heat curve[2] shows an anomalous peak (Fig. 1(b)), and the electrical resistivity[3] changes rapidly with temperature (Fig. 1(c)). Li[4] found that the magnetocrystalline symmetry decreases from cubic to uniaxial, with a large increase in anisotropy energy. He also demonstrated that a magnetic memory effect exists; that is, the direction of easy magnetization, or magnetic axis, below the transformation temperature can be predetermined by cooling the crystal in a magnetic field. It has been established that the magnetic axis becomes the cube edge most nearly parallel to the direction of this biasing magnetic field and that it can be shifted from [100] to [010] or [001] below the transformation by means of a strong magnetic field.[5]

Verwey[6] has proposed that the transformation is an electronic ordering phenomenon, in which the random distribution of ferrous and ferric ions on the octahedral sites of the cubic inverse spinel lattice changes, on cooling, to an ordered arrangement. If one makes use of this picture, some of the physical changes characteristic of the transition can be attributed directly to the ordering (specific heat and resistivity), and others to a small crystallographic change accompanying the ordering (magnetic properties).

The crystalline structure change must be very small, since a large single crystal will withstand numerous traversals through the transformation without shattering. Several attempts[3,4,7] to detect a crystal structure change by means of x-ray diffraction ended in failure.

Experimental investigation of magnetite below its transformation temperature is somewhat unsatisfactory because the physical properties depend on the condition in which the crystal was cooled through the transition. Exact reproducibility in the measurements is difficult to obtain even when these conditions are controlled as closely as possible.

II. HYSTERESIS LOOP MEASUREMENTS

Directional pressure has been found to be effective in selecting the magnetic symmetry axis, but to a lesser extent than magnetic field. The ease of magnetization

* This work was supported in part by the U. S. Office of Naval Research.

[1] P. Weiss and R. Forrer, Ann. phys. 12, 279 (1929).
[2] R. W. Millar, J. Am. Chem. Soc. 51, 215 (1929).
[3] T. Okamura, Sci. Repts. Tôhoku Imp. Univ. 21, 231 (1932).
[4] C. H. Li, Phys. Rev. 40, 1002 (1932).
[5] L. R. Bickford, Jr., Phys. Rev. 78, 449 (1950).
[6] Verwey, Haayman, and Romeijn, J. Chem. Phys. 15, 181 (1947).
[7] H. Shôji, Sci. Repts. Tôhoku Imp. Univ. 24, 250 (1935).

CC-0. In Public Domain. Gurukul Kangri Collection, Haridwar

Digitized by Arya Samaj Foundation Chennai and eGangotri

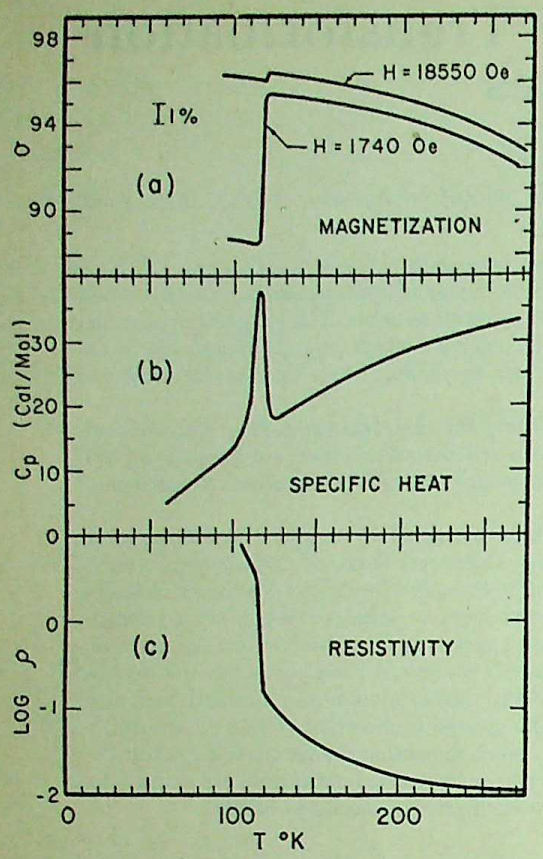


FIG. 1. Anomalies in magnetization, specific heat, and electrical resistivity at the magnetite low temperature transformation.

of a rod-shaped specimen with its axis parallel to [100] is increased below the transformation by cooling under compressive stress along the axis. This effect is not observed in specimens cut parallel to [110] or [111].

Figure 2 shows a photographic sequence of oscilloscope traces representing hysteresis loops obtained below the transformation with a 60-cycle magnetic field parallel to the axis of a [100] specimen cut from a natural single crystal. Curves (b) through (e) were obtained under identical conditions during measurement, as indicated in (a). The differences arise entirely from the different conditions under which the crystal was cooled through the transformation, as shown schematically by each inset.

Curve (b) was obtained after the crystal had been cooled with a magnetic field applied along the specimen axis and corresponds to a measurement along the magnetic axis. The crystal was cooled in a magnetic field along [010] (perpendicular to the specimen axis) prior to obtaining curve (c). As a result of this treatment the specimen axis is the direction of most difficult magnetization. The measuring field was much too weak to saturate the crystal. A comparison of curves (b) and (c) will serve to illustrate the large magnetic anisotropy.

Curve (d) was photographed after the crystal had been cooled in the absence of a magnetic field and is intermediate in appearance between (b) and (c). Curve (e) was obtained after the crystal had been cooled in a compressive stress of 4 kg/mm² parallel to the specimen axis. It shows the effect of a directional pressure. The behavior of the crystal in the transformation region is illustrated in Fig. 2(f), in which is superimposed a number of hysteresis loops photographed as the crystal warmed slowly through the transformation.

III. STRAIN GAUGE MEASUREMENTS AT THE TRANSFORMATION

Although dilatometric measurements[3,8] had shown that an anisotropy exists in linear thermal expansion along different crystal directions, Tombs and Rooksby[9] reported the first concrete evidence of a change in crystalline structure, obtained through an x-ray analysis of powder samples. They concluded that the low temperature modification is rhombohedral, with the maximum distortion from cubic symmetry amounting to 0.1 percent along the body diagonal at 95°K.

Rhombohedral symmetry, however, does not seem to fit in with the magnetic behavior, which indicates that the magnetic symmetry axis is one of the cube edges. The magnetic symmetry should be related to the crystalline symmetry. Moreover, it is of fundamental importance to know just how intimately magnetic symmetry is related to crystalline symmetry; whether for example, the switching of the magnetic axis is accompanied by a corresponding change in crystalline structure.

Our approach to these questions has been to measure macroscopically the changes in length of magnetite single crystals in the transformation region. Resistance strain gauges were cemented along the principal crystallographic directions of disk-shaped specimens cut from

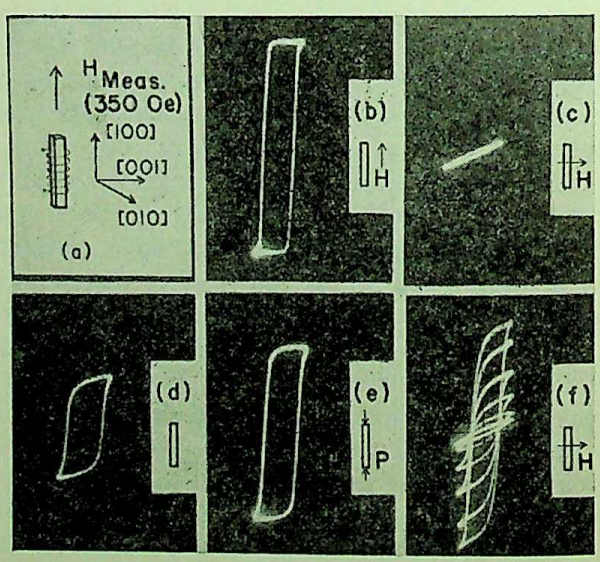


FIG. 2. Sixty-cycle hysteresis loops at 88°K for natural single crystal of magnetite after different conditions of cooling through transformation (schematically represented by each inset). In (f) are superimposed loops obtained as crystal warmed through transformation.

[8] C. A. Domenicali, Phys. Rev. 78, 458 (1950).
[9] N. C. Tombs and H. P. Rooksby, Acta Cryst. 4, 474 (1951).

CC-0. In Public Domain. Gurukul Kangri Collection, Haridwar

Digitized by Arya Samaj Foundation Chennai and eGangotri

a synthetic single crystal.† The strain was measured as the sample warmed slowly through the transition, after having been cooled under various conditions of magnetic field and stress. This method has two distinct advantages over x-ray analysis: one, greater sensitivity ($\Delta l/l = 10^{-6}$ or better); and two, ability to observe the changes taking place. The structure cannot be determined directly in a single measurement but can be deduced by measuring total dimension changes occurring along the different directions as the crystal transforms from the unknown state to one in which its symmetry and lattice constant are known. For the known state, we chose a point 12° above the transition (130°K). The magnetocrystalline anisotropy energy is extremely low at this temperature, and therefore the symmetry most nearly cubic.

The first significant observation from the strain gauge measurements was that the cube edge which becomes the magnetic axis contracts by *ca* 0.027 percent with respect to the others, which actually expand on cooling through the transition. Warming curves corresponding to these two conditions are shown in Fig. 3, along with a curve for [111].

The magnetic axis transfer from one cube edge to another below the transformation is also accompanied by a dimension change. Figure 4 shows the relative dimensional change along [100] as the direction of a strong magnetic field oscillates slowly in the (001) plane between [100] and [010]. An abrupt contraction occurs as the magnetic axis transfers to [100] and an elongation, as it transfers to [010]. The amount of angular hysteresis depends upon the temperature and magnitude of the magnetic field.

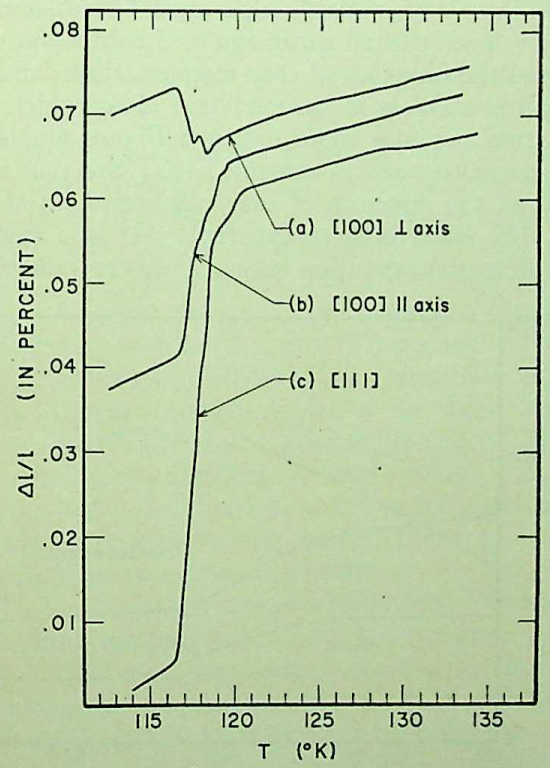


FIG. 3. Thermal expanison behavior of magnetite single crystal along [100] and [111] in the transformation region.

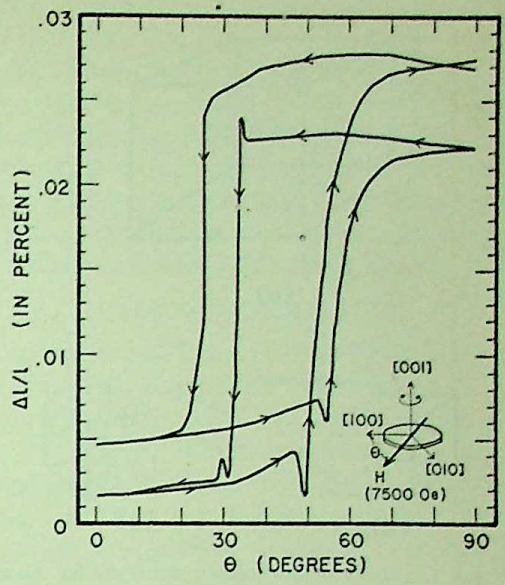


FIG. 4. Dimensional change along [100] accompanying switching of magnetic axis in magnetite single crystal between [100] and [010] at 98°K.

1. Structure of the Low Temperature Modification

The orthorhombic structure shown in Fig. 5(a) has been worked out tentatively for magnetite at 115°K (just below the transformation), on the basis of strain gauge measurements completed to date. The numbers on the diagram refer to measured percentage changes relative to the dimensions of the cubic crystal at 130°K (indicated by the dotted lines). The relatively large changes for the face diagonals in the plane perpendicular to the *c* axis (i.e., along *a* and *b* axes) were measured only after the crystal had been cooled through the transformation under the simultaneous influence of a magnetic field and a directional pressure (*ca* 3 kg/mm²), orineted as shown in Fig. 5(b). Without pressure, both diagonals displayed roughly the same expansion behavior. All other measurements were made without pressure.

The volume change at the transformation, calculated on the basis of this model, only amounts to 0.025 percent. Figure 5(c) shows the ordered arrangement of ferrous and ferric ions on the octahedral sites, as proposed by Verwey. Our tentative structure is compatible with this arrangement.

2. Crystallographic Interpretation of the Transformation

The interpretation which suggests itself is that the large change in magnetocrystalline anisotropy occurring at the transformation is intimately associated with a

† Kindly furnished by Professor A. R. von Hippel, Laboratory for Insulation Research, MIT; see J. Smiltens, Tech. Rept. 49, Lab. Ins. Res., MIT (December, 1951).

CC-0. In Public Domain. Gurukul Kangri Collection, Haridwar

Digitized by Arya Samaj Foundation Chennai and eGangotri

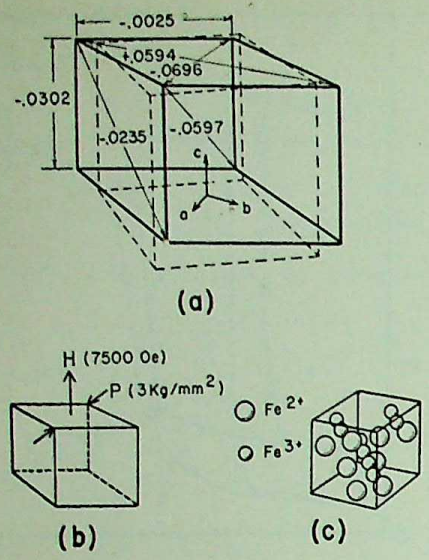


FIG. 5. (a) Tentative orthorhombic structure for magnetite at 115°K, with measured percentage changes in dimension relative to the cubic crystal at 130°K. (b) Experimental cooling conditions prior to obtaining data for plane perpendicular to *c* axis. (c) Verwey model of low temperature form.

very small orthorhombic distortion of the cubic crystal structure, the magnetic axis coinciding with the orthorhombic *c* axis. If a single crystal is cooled through the transformation in a demagnetized condition and in the absence of external stress, the resultant state is determined by the internal stress pattern and magnetic domain pattern. The domain pattern predominates because the large crystal anisotropy discourages any arrangement not resulting in the alignment of the magnetization with the magnetic axis. As a result, the crystal is no longer a single crystal below the transition temperature, but is rather a "hybrid" in which the orthorhombic *c* axis coincides with different original cubical axes in different regions. In this condition, the crystal is not easily magnetized in any direction.

Cooling the crystal in a magnetic field partially removes the hybridization by establishing the *c* axis along the same [100] (most nearly parallel to the magnetic field) throughout the crystal. Some twinning remains, however, in that the *a* and *b* axes are interchanged in different regions. This partial twinning is probably determined by the internal stresses, which appear to be especially significant in the synthetic crystals. Calhoun[10] has already suggested the existence of such a situation as an explanation for the double absorption peaks below the transition observed in microwave resonance experiments.[5]

It is suggested that the hybridization can be completely removed by cooling the crystal in a strong magnetic field along one of the cube axes [100] and at the same time applying pressure along one of the body diagonals [011] in the plane perpendicular to this axis.

[10] B. A. Calhoun, Prog. Rept. IX, Lab. for Ins. Res., MIT, p. 50 (May, 1951).

3. Comparison with the Titanates

The phenomenon of hybridization is known to exist in titanates. Megaw[11] has found direct x-ray evidence for its occurrence in a titanate cooled through the Curie region in the absence of an electric field. Certain other similarities with the behavior of barium titanate at its ferroelectric Curie point are suggestive. It is perhaps unusual to point this out, since comparisons are usually made the other way around; that is, ferroelectric behavior is usually described by analogy with ferromagnetic behavior. Moreover, the magnetite transformation is not a Curie point transformation. However, the intimate association of domain structure with crystalline structure displayed by magnetite below the transformation is more characteristic of ferroelectrics than of ferromagnetics. Barium titanate shows the effects of predetermination of the crystallographic *c* axis by an electric field applied as the crystal cools through the transformation and of the switching of the axis below the Curie point by an electric field. Ferroelectric barium titanate has a tetragonal structure, however, so there is no ambiguity regarding *a* and *b* axes.

IV. DIMENSIONAL CHANGES ABOVE THE TRANSFORMATION

The direction of easy magnetization in cubic magnetite changes, on cooling, from [111] to [100] above the transformation at *ca* 130°K. We have found by strain gauge measurements that this change is accompanied in a demagnetized single crystal by dimensional changes: one, a small shrinkage in the direction which becomes the direction of easy magnetization; and two, a small elongation in the direction along which magnetization becomes more difficult. Figure 6(a) shows the thermal expansion along a [100] direction in the region of the direction of easy magnetization change-over. The effect is most apparent when one measures the differential expansion between two crystallographic

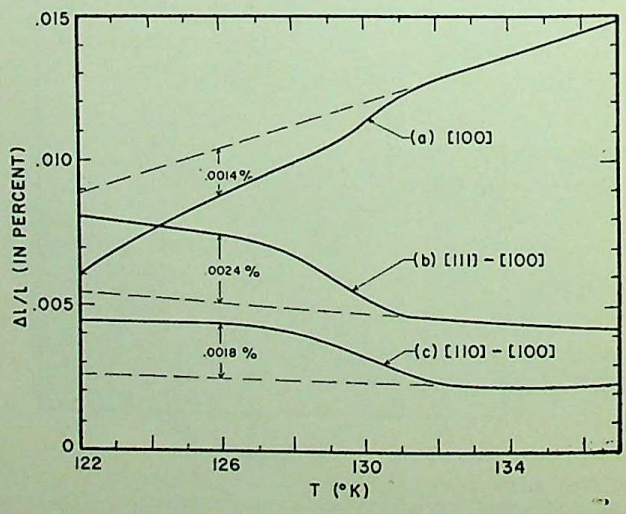


FIG. 6. Dimensional changes accompanying change-over of direction of easy magnetization in magnetite from [111] to [100] above transformation temperature.

[11] H. D. Megaw, Nature 157, 20 (1946).

CC-0. In Public Domain. Gurukul Kangri Collection, Haridwar

Digitized by Arya Samaj Foundation Chennai and eGangotri

directions. Strain gauges are particularly suitable for making this type of measurement directly. Figure 6(b) shows differential expansion between [111] and [100], and (c), between [110] and [100]. The shape of these curves, obtained as the crystal warmed, was found to be independent of the condition of the crystal below the transformation.

V. TRANSFORMATION IN THE OTHER FERRITES

Several references have been made in the literature to a low temperature transformation in other ferrites, including those of cobalt,[12] nickel,[13] and manganese.[13] The most convincing evidence is the magnetization data of Guillaud for cobalt ferrite, which show discontinuities similar to those displayed by magnetite. However, present evidence is insufficient to determine whether any of the reported anomalies can be classified along with the magnetite transformation. Healy's microwave resonance absorption study[14] of nickel ferrite has shown that no sudden change in magnetic symmetry occurs between the Curie temperature and 78°K, although the anisotropy constants change in a manner somewhat similar to those of magnetite. If the interpretation of the magnetite transformation as an ordering phenomenon is correct, it is difficult to understand how a similar transformation could occur in other ferrites in the same temperature region, since ordering in any other ferrite would necessitate ionic motion.

ACKNOWLEDGMENTS

The writer would like to acknowledge his indebtedness to Dr. C. A. Domenicali of the Franklin Institute, who was associated with this work during its early stages; to Mr. M. Nerenstone, for assistance in the strain gauge measurements; to Dr. J. E. Goldman of Carnegie Institute, for having suggested the use of strain gauges in studies of magnetite; and to Dr. E. A. Wood, of Bell Telephone Laboratories, for an illuminating discussion of low temperature structure possibilities, during which the idea for the experiment of Fig. 5(b) was evolved.

[12] C. Guillaud and H. Creveaux, Comp. rend. 230, 1256 (1950).
[13] T. Okamura and J. Simoizaka, Phys. Rev. 83, 664 (1951).
[14] D. W. Healy, Jr., Phys. Rev. 86, 1009 (1952).

REVIEWS OF MODERN PHYSICS VOLUME 25, NUMBER 1 JANUARY, 1953

Magnetic Study of Low Temperature Transformation in Magnetite

H. J. WILLIAMS AND R. M. BOZORTH

Bell Telephone Laboratories, Murray Hill, New Jersey

THE magnetic crystal anisotropy of magnetite has been investigated with special reference to the effect of cooling through the transformation at about −160°C in the presence of a magnetic field. In a natural crystal we have found an anisotropy such that the difference in energy between the directions of easy and of hard magnetization is 1.07×10^6 ergs/cm^3. When the field is applied in a (100) plane parallel to a [001] direction, this direction becomes the easy direction whereas [010] becomes the hard direction. This confirms the observation first reported by Li.[1]

When fields are applied along other directions in this plane, the relation between the direction of applied field and the consequent direction of easy magnetization is shown in Fig. 1, and similar data for the (011) plane are given in Fig. 2. A set of torque curves for the (100) plane are shown in Fig. 3.

The results for the (100) plane can be explained as follows: When the field used during cooling was applied within about 40 degrees of a [001] direction, that direction becomes the direction of easy magnetization for all of the crystal; the directions [010] and [001] being hard directions. When the field during cooling is near a [011] direction, some portions of the crystal

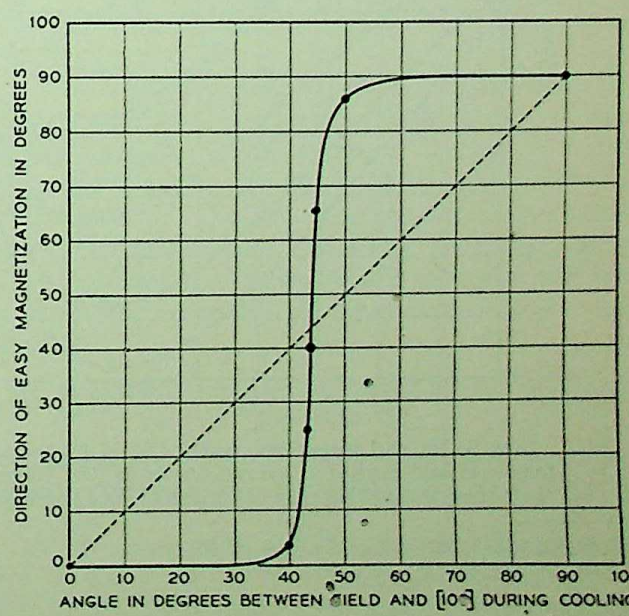


FIG. 1. Natural magnetite crystal, liquid N_2 tempefature. Relation between direction of magnetic field present during cooling, and resultant direction of easy magnetization, in (100) plane.

[1] C. H. Li, Phys. Rev. 40, 1002 (1932); see also Domenicali, Phys. Rev. 78, 458 (1950).

CC-0. In Public Domain. Gurukul Kangri Collection, Haridwar

Digitized by Arya Samaj Foundation Chennai and eGangotri

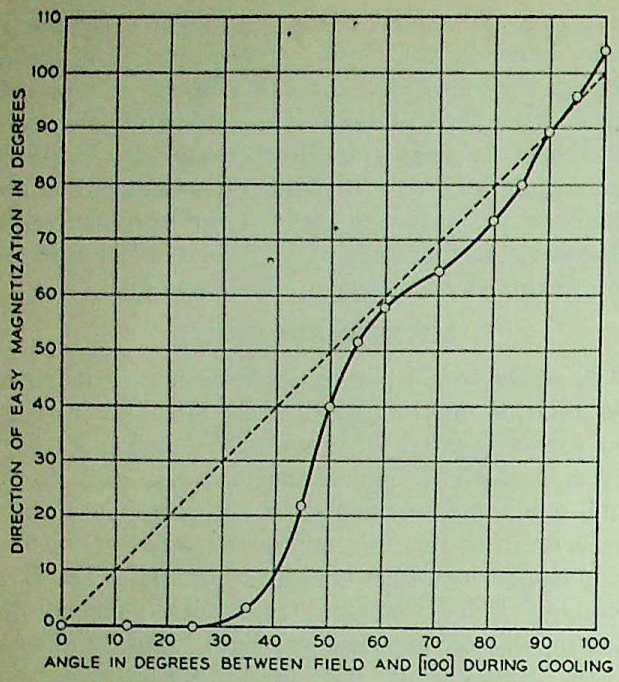


FIG. 2. Same as Fig. 1, except for (110) plane.

have easy directions parallel to [001] and some parallel to [010]. One can always explain the form of a torque curve for the (100) plane by assuming a distribution between these two directions, and torque curves so determined are given as dotted lines in Fig. 3 where they show agreement with the observed curves. However, a more complicated mechanism is necessary to explain the data for the (110) plane.

An artificial crystal cut parallel to a (110) plane showed a behavior different from that of the natural crystal just described. The direction of easy magnetization was always the [001] direction, and could not be influenced by cooling in a field using field strengths up to 9000 oersteds. Higher fields have not yet been tried.

At room temperature the crystal anisotropy constant was observed to be $-144\,000$ for the natural crystal, and $-122\,000$ for the artificial crystal. These may be compared with the value, $-112\,000$, observed by Bickford[2] in his experiments on ferromagnetic resonance.

We gratefully acknowledge the assistance of Miss M. Goertz throughout the course of the work.

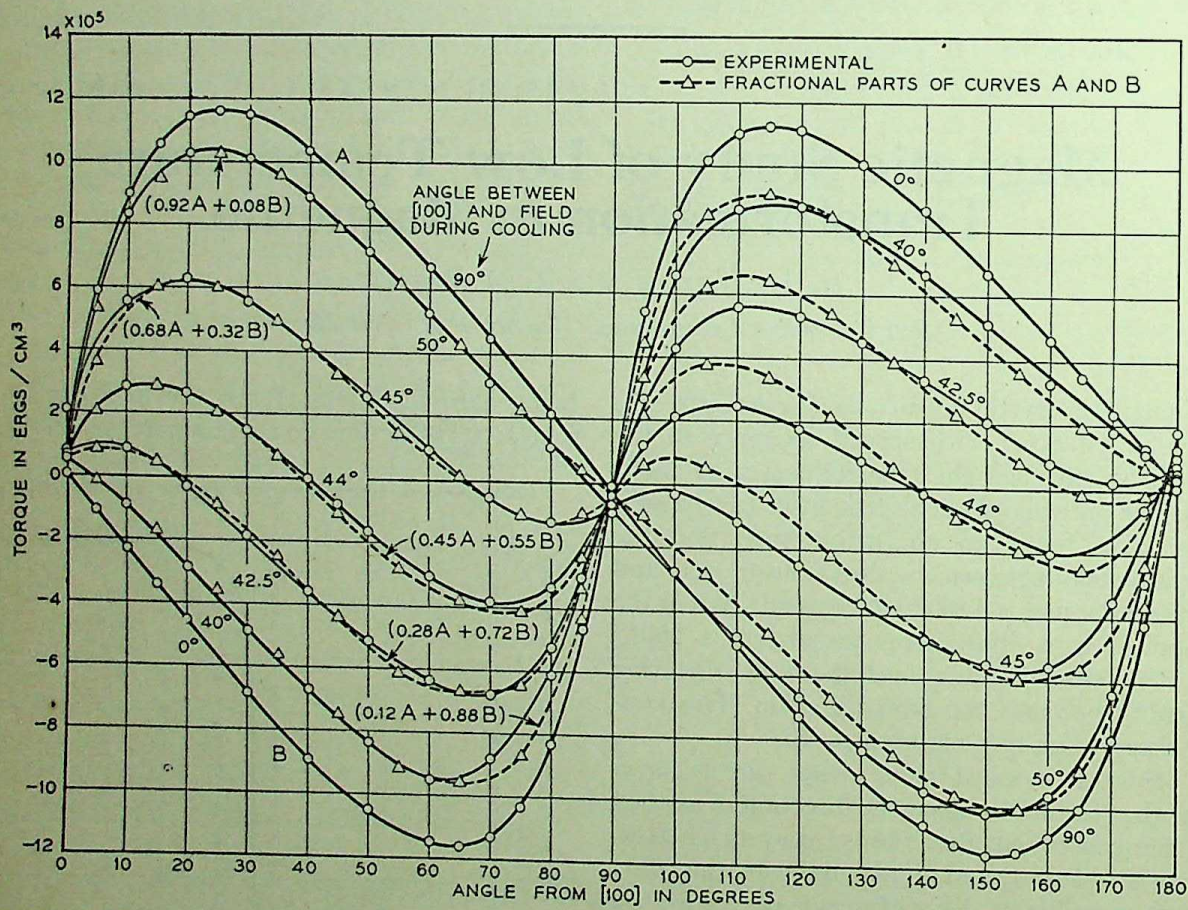


FIG. 3. Natural magnetite crystal. Liquid N_2 temperature. Torque curves in (100) plane, crystal cooled with magnetic field applied at various angles to [001] direction. Broken curves are calculated assuming various fractions of crystal having easy directions of [001] and [010].

[2] L. R. Bickford, Phys. Rev. 78, 449 (1950).

CC-0. In Public Domain. Gurukul Kangri Collection, Haridwar

Digitized by Arya Samaj Foundation Chennai and eGangotri

REVIEWS OF MODERN PHYSICS VOLUME 25, NUMBER 1 JANUARY, 1953

Magnetic Spectra of Ferrites

GEORGE T. RADO

Naval Research Laboratory, Washington, D. C.

A brief discussion is given of the meaning of initial permeability, the principles of its measurement, and the nature of "dimensional resonance." In considering magnetic spectra containing only a single resonance, typical data on sintered ferrites and on finely divided ferrite powders are reviewed, and some of the theoretical interpretations previously advanced are criticized. The investigations involving the two natural resonances found at this laboratory in a commercial Mg-ferrite are then summarized, including resonance in single-domain particles as a method for identifying dispersion mechanisms, experimental evidence for the inertia of domain walls, the nature of internal fields, and the temperature dependence of the natural resonances and of the spectroscopic splitting factor. Using the information obtained from these special studies, the following general hypothesis is advanced: In principle, two natural resonances are present in the magnetic spectrum of any sintered ferrite, and the single resonance sometimes observed represents the coalescence of two resonances. Reasons are given for expecting this coalescence to occur in some materials only, as in certain sintered mixed ferrites containing Zn-ferrite. The new hypothesis is consistent with all presently available data, including new spectra, some containing two resonances, that were recently obtained on pure ferrites at this laboratory. Additional confirmatory experiments are described which provide methods for separating or coalescing two resonances, and permit distinguishing between internal fields due to anisotropy and magnetic interactions. The limitations and possibilities of ferrites for obtaining useful microwave permeabilities are discussed from the new viewpoint, the criteria involved in this problem being shown to differ from those used at radiofrequencies.

I. INTRODUCTION

IT is the purpose of this paper to review the magnetic spectra of special ferrites and to propose a hypothesis, supported by new experiments, with regard to the magnetic spectrum of an arbitrary ferrite.

In order to avoid ambiguities, several definitions are stated below and adhered to throughout the paper. The term "magnetic spectrum" will denote the frequency dependence of the complex *initial* permeability, the frequency range of interest extending, in general, from zero to about 10^4 megacycles per second (Mc/sec). For the sake of brevity, the word "ferrite" will include any ferromagnetic oxide, as well as the (ferromagnetic or nonferromagnetic) ferrites customarily defined by means of the formula MFe_2O_4, where M represents a bivalent metallic ion. The expression "natural resonance" will refer to any resonance contained in the magnetic spectrum. This kind of resonance differs from ordinary ferromagnetic resonance, which is sometimes called "induced resonance," because the latter requires the application of a suitable static magnetic field to the material in question. Finally, the adjective "ferromagnetic" will include "ferrimagnetic" unless the need for this distinction is specifically noted.

Apart from their theoretical interest, magnetic spectra are important because it is usually the initial permeability that expresses the effect of the magnetic properties of a medium on the propagation of electromagnetic waves. In some particular situations, of course, this is not the case, and these situations will not be discussed here. However, it should be kept in mind that permeabilities other than the initial permeability play a role in the microwave Faraday effect,[1] or any other arrangement in which a static magnetization exists in a ferromagnetic material, as well as in experiments involving alternating fields possessing amplitudes sufficiently large to produce nonlinear effects.[2]

Although the magnetic properties of solids are, in general, most advantageously studied on monocyrstalline specimens, there are two reasons for investigating the magnetic spectra of polycrystalline ferrites. First, satisfactory monocrystals of ferrites are difficult to grow, and so far only a few such crystals of convenient size have been produced. It seems probable, in fact, that for some time to come the major applications of ferrites will involve sintered polycrystals. Second, the very perfection and regularity of monocrystals makes it difficult, as shown later on, to observe the important phenomenon of resonance due to domain walls, and to appreciate the strong influence of irregular internal demagnetizing fields on resonance due to domain rotations.

Accordingly, the present paper deals primarily with polycrystals,[3] and it represents a first attempt at ascertaining the factors that determine the types of natural resonance contained in the magnetic spectrum of an arbitrary ferrite. The discussion is confined to resonance frequencies and related line width problems, and no attempt is made to elucidate the nature of the basic absorption processes beyond the phenomenology usually employed.

II. MEANING AND MEASUREMENT OF INITIAL PERMEABILITY

The initial permeability of a polycrystal represents an average value of a certain position-dependent quantity.

[1] F. F. Roberts, J. phys. et radium 12, 305 (1951); C. L. Hogan, Bell System Tech. J. 31, 1 (1952).

[2] J. J. Went and H. P. J. Wijn, Phys. Rev. 82, 269 (1951); H. P. J. Wijn and J. J. Went, Physica 17, 976 (1951). See also comments in reference 18.

[3] For the magnetic spectrum of *mono*crystals of Fe_3O_4 and $NiFe_2O_4$ see, respectively, J. K. Galt, Phys. Rev. 85, 664 (1952), and Galt, Matthias, and Remeika, Phys. Rev. 79, 391 (1950).

CC-0. In Public Domain. Gurukul Kangri Collection, Haridwar

Digitized by Arya Samaj Foundation Chennai and eGangotri

If the magnetization proceeds solely by domain rotations, rather than by domain wall displacements, then this quantity is clearly a special case of the permeability tensor derived by Polder;[4] the effective field H_e, occurring in his analysis, is now due to anisotropy and internal magnetic fields. Whatever magnetization processes prevail in any given material, the average value mentioned here is only meaningful if the material is *macroscopically* isotropic and homogeneous. This condition obviously requires, in the case of alternating fields, that the variations in local properties of a sample be on a scale which is small compared to λ_m, the wavelength in the material. In the permeability measurements performed at this laboratory, the experimental method used prescribes that the thickness of each sample be much smaller than this wavelength, so that the requirement stated above was necessarily fulfilled.

On the basis of these remarks, the initial permeability of a macroscopically isotropic and homogeneous material, possessing no static magnetization, may be defined as the ratio

$$B/H=\mu=\mu_1-i\mu_2, \tag{1}$$

where B and H, representing the magnitudes of the parallel vectors **B** and **H**, respectively, are proportional to $\exp i\omega t$, and H is supposed to be sufficiently small to insure μ being independent of H. Here ω is the circular frequency, and H represents the field inside the specimen, rather than the applied field. The corresponding initial susceptibility χ is given by

$$M/H=(\mu-1)/4\pi=\chi=\chi_1-i\chi_2, \tag{2}$$

where M is the magnitude of the magnetization, **M**.

In principle, the two components of μ are determined by measuring the reactive and resistive parts of the "impedance" (or related property) of a circuit containing the material in question. To determine μ uniquely, two sets of impedance measurements must be made unless the dielectric constant, $\epsilon=\epsilon_1-i\epsilon_2$, is known, or the magnetic material is located in a region of the electromagnetic field where the electric intensity is negligibly small. The latter condition is easily fulfilled at sufficiently low frequencies, and at these frequencies it is customary to obtain μ from the impedance of a coil wound around a ring-shaped core of the ferromagnetic material. If the conductivity of the core material is negligibly small, the well-known formulas

$$\mu_1=L_f/L_0 \tag{3a}$$

and

$$\mu_2=\Delta R/\omega L_0 \tag{3b}$$

apply in this simple case. Here L_f and L_0 are, respectively, the inductance of the coil with and without the core, and ΔR is the additional resistance of the coil due to the presence of the core. Appropriate details on bridge circuits and resonance methods for measuring L_f, L_0, and ΔR may be found in summary articles.[5]

[4] D. Polder, Phil. Mag. 40, 99 (1949).
[5] D. Polder, Proc. Inst. Elec. Engrs. (II) 97, 246 (1950).

At sufficiently high radiofrequencies and in the microwave range, on the other hand, the reactive and resistive measurements involve, respectively, the imaginary and real parts of the input impedance of a transmission line, or the resonance frequency and quality factor of a cavity resonator. The input impedance can be determined by standing wave techniques. At this laboratory, measurements have been made over a large frequency range ($\sim$10 to 10^4 Mc/sec) by a method[6,7] which uses a thin toroidal ferrite specimen of rectangular cross section, the specimen being inserted into a coaxial line at a position of large H (and small E) adjacent to the short-circuited termination. By solving the appropriate boundary value problem, it can be shown that for *TEM*-type propagation

$$\mu_1=1+(s/L) \tag{4a}$$

and

$$\mu_2=\left(\frac{1}{\xi}-\frac{1}{\xi'}\right)\frac{\lambda_0}{2\pi L}, \tag{4b}$$

where L is the thickness of the sample, λ_0 is the free-space wavelength, and s is the displacement of the voltage minimum from its (previously observed) location in the shorted empty line. The quantities ξ and ξ' denote the voltage standing wave ratio of the actual line and the empty line, respectively. Equations (4) apply only if the relation

$$|\epsilon\mu|^{\frac{1}{2}}(2\pi L/\lambda_0)\ll 1 \tag{5}$$

is satisfied, and if the coaxial conductors are highly conducting. These requirements mean, in effect, that the sample is thin compared to a quarter-wavelength in the material, and that the perturbation of the *TEM* mode is small. The "thin-sample method" outlined above, as well as the corresponding method[6] for measuring ϵ, was originated by Halpern[8] in 1942, and the ξ' correction was developed later.[7] In addition to the conceptual simplicity resulting from the "separation" of electric and magnetic effects, the thin-sample method possesses some practical advantages over certain frequently used "thin-sample methods" which require additional data and involve reference to transmission line charts or hyperbolic function tables. A general survey of permeabilities at microwave frequencies, including concepts, methods, and results pertaining to metals, was given by the writer.[9]

For many years it has been known that resonance effects are obtained if the relation $L=\lambda_m/4$ is satisfied in the type of set-up described above, and that these effects are of practical interest. Such a "dimensional resonance" could exist, of course, even if μ were independent of ω in the vicinity of the observed resonance,

[6] Rado, Wright, and Emerson, Phys. Rev. 80, 273 (1950).
[7] Rado, Wright, Emerson, and Terris, Phys. Rev. 88, 909 (1952).
[8] O. Halpern and M. H. Johnson, unpublished work, M.I.T. Radiation Laboratory, 1942.
[9] G. T. Rado, *Advances in Electronics* (Academic Press, Inc., New York, 1950), Vol. II, p. 251.

CC-0. In Public Domain. Gurukul Kangri Collection, Haridwar

Digitized by Arya Samaj Foundation Chennai and eGangotri

and thus it should not be regarded as a natural resonance or any other purely magnetic phenomenon. Dimensional effects may be expected to occur in any arrangement where L is comparable to the wavelength in the material. Brockman *et al.*[10] found, in fact, that dimensional resonances can exist at frequencies near the remarkably low value of 2 Mc/sec, the most surprising result of their experiments being the discovery of enormously large apparent dielectric constants in certain ferrites studied at these frequencies.

III. SPECTRA CONTAINING A SINGLE RESONANCE

A. Sintered Ferrites

In experiments on several sintered Ni-Zn and Mn-Zn ferrites, Snoek[11] observed a broad natural ferromagnetic resonance at radio frequencies. The typical data reproduced in Fig. 1 appear to be the most complete results published by him and his collaborators. Except for the broad peak in each μ_1 curve, the resonance behavior looks almost like a relaxation because no values of $\mu_1<1$(i.e., $\chi_1<0$) were observed.

Snoek's explanation of the resonance is based on the idea, contained in the basic paper of Landau and Lifshitz,[12] that crystalline anisotropy is equivalent to an effective static magnetic field H_i, acting inside each crystallite, and that H_i produces a Larmor precession of the appropriate electron spins. Since the rotation of the spins is subject to damping, it is apparent that resonance absorption occurs in any given crystallite if a small magnetic field, oscillating near the Larmor frequency, is applied to that crystallite along a direction differing from that of H_i. Using the simplifying assumptions mentioned below, Snoek found by means of an averaging calculation that the (circular) resonance frequency due to domain rotations, ω'_0, is given by

$$\omega_0'=\gamma(M_s/\chi_0')(2/3), \tag{6}$$

for a polycrystal containing randomly oriented crystallites. Here M_s is the saturation magnetization, χ_0' is the static initial susceptibility due to domain rotations, and γ, equal to $ge/2mc$, is the magnetomechanical ratio corresponding to the spectroscopic splitting factor, g. For an electron spin, the relevant numerical values are $\gamma/2\pi=2.80$ Mc/(sec oersted), and $g=2$. As pointed out elsewhere[6] (see also Sec. IV), χ_0' is not necessarily identical with χ_0, the total static initial susceptibility. In deriving Eq. (6), Snoek neglected all magnetic interactions and attributed H_i solely to crystalline (and later to stress-induced) anisotropy. The (first-order) anisotropy constant K does not appear in Eq. (6) because the relations

$$H_i=2K/M_s \tag{7}$$

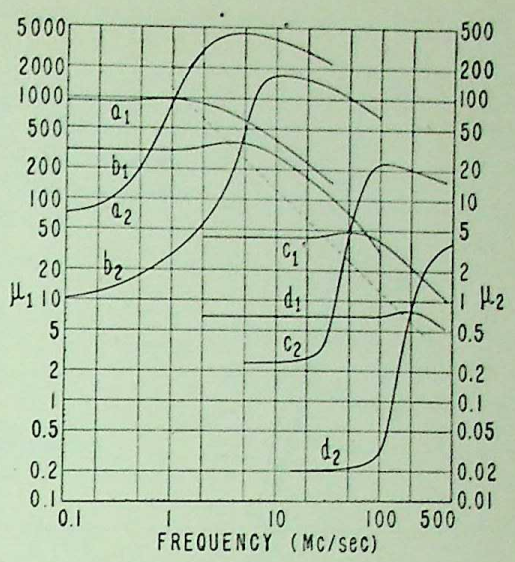


FIG. 1. Magnetic spectrum, at room temperature, of Mn−Zn ferrite (a) and of a number of Ni−Zn ferrites of different composition (b)–(d). The subscripts 1 and 2 for a given material (e.g., a) refer to μ_1 and μ_2, respectively. The dashed line indicates the mean relation between the low frequency value of μ_1 (i.e., essentially μ_0) of a certain ferrite and the critical frequency setting a limit to the range within which that ferrite can be used in filter coils [$\tan(\mu_2/\mu_1)\leq 0.06$]. (Reproduced, with minor alterations of the labeling, from the paper of H. G. Beljers and J. L. Snoek, Philips Tech. Rev. 11, 313 (1949)).

and

$$\chi_0'=M_s^2/3K, \tag{8}$$

which apply if K is positive, express H_i in terms of χ_0'. It should be noted that the right-hand sides of Eqs. (6) and (8) would have to be multiplied by $[1-(3^{\frac{1}{2}}/\pi)]$ if domain wall displacements were permitted in the theory, because in that case the magnetization vectors at the onset of domain rotations would not be oriented at random but in accordance with the distribution envisaged by Gans.[13] Using Snoek's model, and thus neglecting magnetic interactions, Kittel[14] extended the theory of domain rotations in a polycrystal by deriving an expression for the complex χ. His result is

$$\frac{\chi}{\chi_0'}=\frac{\omega_0'^2+(\lambda/\chi_{00}')[i\omega+(\lambda/\chi_{00}')]}{\omega_0'^2+[i\omega+(\lambda/\chi_{00}')]^2}, \tag{9}$$

where χ_{00}' is an average rotational susceptibility approximately equal to χ_0' and λ is the relaxation frequency (or damping factor) defined by the last term in the Landau-Lifshitz equation of motion

$$\frac{d\mathbf{M}_s}{dt}=\gamma\mathbf{M}_s\times\mathbf{H}_i-\lambda\left[\frac{(\mathbf{H}_i\cdot\mathbf{M}_s)\mathbf{M}_s}{M_s^2}-\mathbf{H}_i\right], \tag{10}$$

which describes the response of $\mathbf{M}_s$ to the total field $\mathbf{H}_i$. As noted previously,[6,7] it seems probable that Eq. (6), and equations similar to (9), cannot be used for reliably interpreting observed spectra (even when these are

[10] Brockman, Dowling, and Steneck, Phys. Rev. 77, 85 (1950).
[11] J. L. Snoek, Philips Tech. Rev. 8, 353 (1946); Nature 160, 90 (1947); Physica 14, 207 (1948); H. G. Beljers and J. L. Snoek, Philips Tech. Rev. 11, 313 (1949).
[12] L. Landau and E. Lifshitz, Physik. Z. Sowjetunion 8, 153 (1935).
[13] R. Gans, Ann. Physik V 15, 28 (1932).
[14] C. Kittel, J. phys. et radium 12, 332 (1951).

CC-0. In Public Domain. Gurukul Kangri Collection, Haridwar

Digitized by Arya Samaj Foundation Chennai and eGangotri

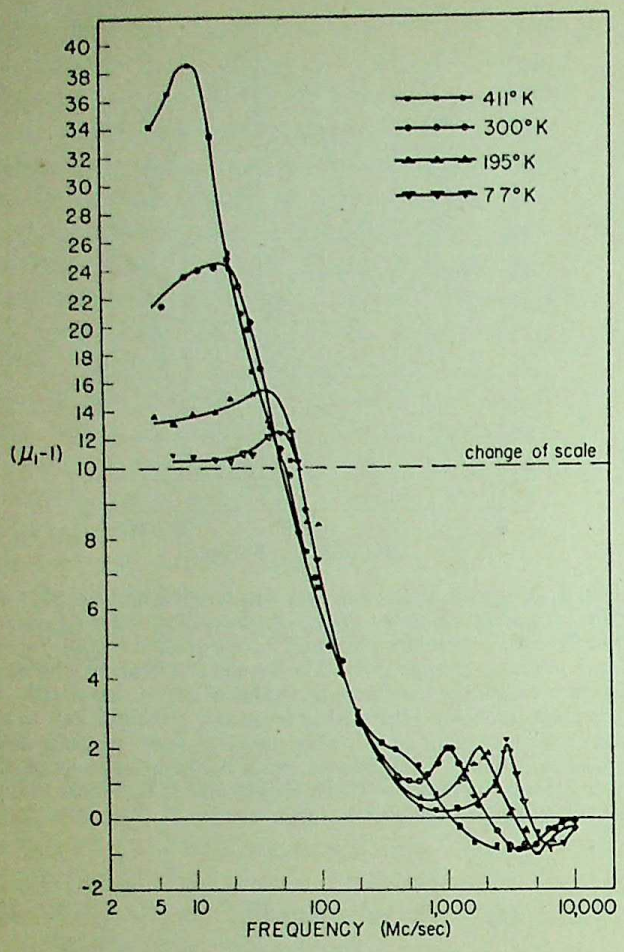


FIG. 2. μ_1-1 *versus* frequency in the magnetic spectrum of solid ferramic *A* at various temperatures (see reference 7).

solely due to rotations), because the equations not only neglect the effect of magnetic interactions on the mean ω_0' but ascribe the over-all line width to damping only, i.e., they do not include the line width caused by a distribution in ω_0' values.

Snoek assumes that domain wall displacements do not contribute to the linear magnetization at radio frequencies. Although some of Snoek's data agree reasonably well with Eq. (6) and are, therefore, not incompatible with his assumption, it was shown elsewhere[6] (see also Sec. IV) that this approximate agreement does not prove the absence of wall displacements in his experiments or later[2] studies. As shown in Secs. IV and V, moreover, in some ferrites there are actually two resonances, and one of these is due to domain walls. In Sec. V it will be suggested that the apparently single resonance observed by Snoek is due to the presence of Zn-ferrite in his mixed ferrites, and it will be argued that this very presence, which is advantageous in the low radiofrequency region, leads to unsatisfactory magnetic properties at microwave frequencies.

B. Powdered Ferrites

Shortly after Snoek's first paper appeared, Birks published a note on natural resonance at microwave frequencies in magnetite and gamma-ferric oxide. In these experiments, as in his later work on Ni-Zn ferrite and Mn-Zn ferrite, all of which he summarized in his last paper, Birks[15] used oxides that had not been sintered but consisted of fine powers embedded in wax. Unfortunately, the results given represent derived magnetic properties obtained by extrapolations of observed data on the concentration dependence of oxide-wax mixtures. As shown by unpublished experiments performed at this laboratory, the logarithmic relations used for these extrapolations, being adaptations of Lichtenecker's relations for dielectric mixtures, appear to be of rather limited validity. It seems doubtful, in fact, whether the permeability of a ferromagnetic solid can be obtained by any extrapolation whatsoever. Subsequent work (Sec. IV) has shown that the resonances in single-domain particles, at least, are fundamentally different from those in "solid" substances.

As to the mechanism of microwave magnetization, Birks ascribed it to domain rotations in a manner similar to that used by Snoek in his work on sintered ferrites at radio frequencies. In this connection, mention should be made of experiments at this laboratory which have shown that even in (commercial) mixed ferrites which contain Zn-ferrite, where the single observed dispersion region in sintered samples is at radio frequencies, the location of this region in fine powders is

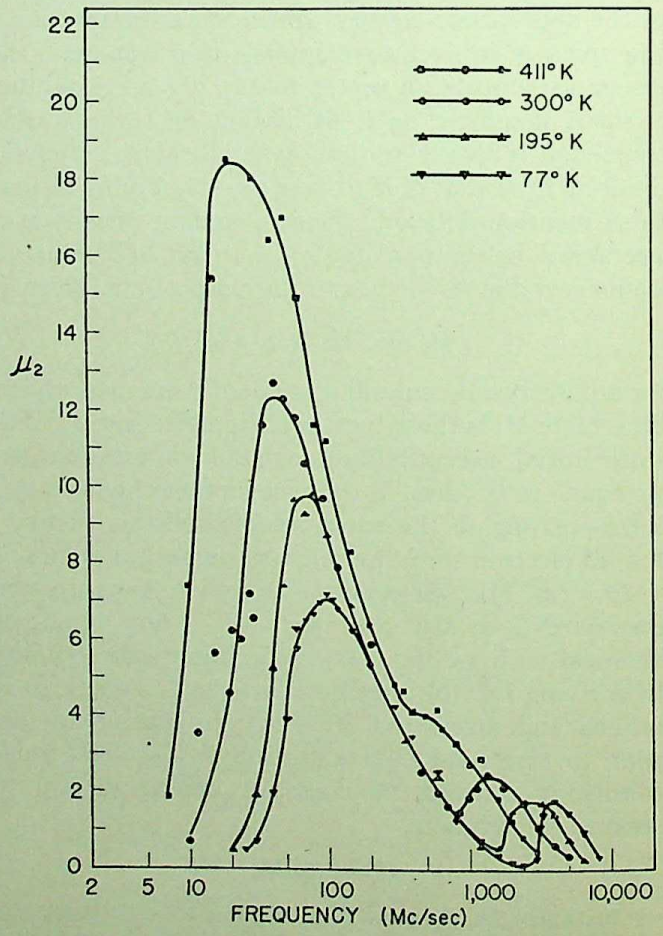


FIG. 3. μ_2 *versus* frequency in the magnetic spectrum of solid ferramic *A* at various temperatures (see reference 7).

[15] J. B. Birks, Proc. Phys. Soc. (London) **B63**, 65 (1950).

CC-0. In Public Domain. Gurukul Kangri Collection, Haridwar

Digitized by Arya Samaj Foundation Chennai and eGangotri

at microwave frequencies. In some cases this behavior may be due to the pronounced stiffness, and hence high resonance frequency, of domain walls in sufficiently small particles; more often, however, this behavior is probably due to the particles being sufficiently small to approach single-domain characteristics so that only rotations can occur (Sec. IV).

IV. A SPECTRUM CONTAINING TWO RESONANCES

A. Dispersion Mechanisms

Measurements performed at this laboratory on commercial ferrites of the "ferroxcube" and "ferramic" class have shown that in most of these materials the magnetic spectrum contains only a single natural resonance in the large frequency range investigated. It was particularly interesting to find, therefore, that the magnetic spectrum of "ferramic *A*," a sintered substance composed of several oxides[16] but consisting primarily of magnesium ferrite, contains two natural resonances at room temperature. These are shown by the curves representing the values, at 300°K, of μ_1-1 (Fig. 2) and μ_2 (Fig. 3).

Previous studies[17] conducted at this laboratory had demonstrated for the first time that domain rotations and wall displacements depend on frequency differently, and that at high frequencies ($\geq$200 Mc/sec, or even lower) the μ of iron is primarily due to domain rotations and not, as at zero frequency, due to wall displacements. In view of these findings it seemed tempting to conjecture that the two resonances in ferramic *A* arise, respectively, from the two magnetization processes mentioned. To verify this surmise, it was necessary, as in the case of iron, to originate a method for identifying dispersion mechanisms experimentally. In the case of ferramic *A*, the identification was based on the following idea.[6] Domain wall motion is obviously suppressed if the walls are eliminated, and this can be achieved by dividing the material into sufficiently small particles to insure that they are essentially single domains; any resonance observed after this suppression must then necessarily be due to domain rotations, the only other kind of basic magnetization process that is possible if the conventional concept of domain structure is at all meaningful in the material (and at the temperature) in question. This idea proved practicable, and the details of the experiments were described elsewhere.[6,7] Briefly, it was shown that relatively large particles (~0.5 micron) of ferramic *A* exhibit essentially single-domain behavior, and that the measured spectrum of a mixture of these particles and wax clearly indicates (Fig. 4) the *absence* of the radiofrequency resonance (occurring at 43 Mc/sec in the sintered samples) as well as the *presence* of the microwave resonance, the latter occurring, however, at a somewhat higher frequency (2300 Mc/sec) than in the sintered samples (1400 Mc/sec). This result means that in ferramic *A* the rf resonance is due to domain walls, thus providing the first experimental support for the concept of domain wall inertia, and that the microwave resonance is due to domain rotations; these conclusions are not affected by the existence of impurities in the material. When combined with other evidence, the data show that in ferramic *A* the rotational resonance is due not only to crystalline anisotropy but also to internal demagnetizing fields,[6,7] that the effect of internal stresses is probably negligible[6,7] in both resonances, and that the damping is not due to microscopic eddy currents.[6] Furthermore, a measurement of the effective anisotropy[18] indicated, as expected, that the total static initial permeability μ_0 is too small to be accounted for on the basis of rotations only. Finally, the above identification of the dispersion mechanisms is supported by the nature of the observed spectrum at remanence even though this particular argument cannot be regarded as being independent.[6] In this connection, it should be mentioned that the theoretical value of the relative remanence, M_r/M_s, might have been based on the "Gans" distribution," but for reasons which are, perhaps, connected with the occurrence of 180° wall displacements, the data seem to favor the distribution assumed in reference 6.

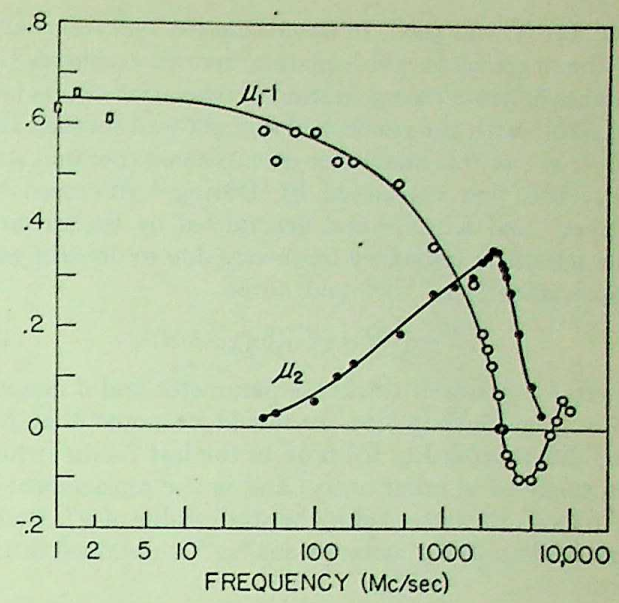


FIG. 4. Magnetic spectrum of 70 percent (by weight) mixture of ferramic *A* powder and wax at room temperature. The powder particles are essentially single-domains (see reference 6).

It was pointed out[6] in analyzing the data that, in general,

$$\chi=\chi'+\chi'', \qquad (11)$$

where χ'' is the initial susceptibility resulting from wall displacements. In describing the rotational resonance at room temperature, the method of Snoek

[16] Ferramic *A*, Type A-34, Batch No. 165, is referred to. In a later shipment, the "ferramic *A*" contained no Mg but more Zn, and the spectrum showed only one pronounced resonance.

[17] Johnson, Rado, and Maloof, Phys. Rev. 71, 322 (1947); M. H. Johnson and G. T. Rado, Phys. Rev. 75, 841 (1949); Rado, Johnson, and Maloof, Rev. Sci. Instr. 20, 927 (1949).

[18] G. T. Rado and A. Terris, Phys. Rev. 83, 177 (1951).

CC-0. In Public Domain. Gurukul Kangri Collection, Haridwar

Digitized by Arya Samaj Foundation Chennai and eGangotri

(Sec. III A) was used. In describing the wall resonance, on the other hand, the equation derived combines the Landau-Lifshitz representation of relaxation effects (see Eq. (10)) with the concept of domain wall inertia. The value, m_w, of this inertia (or effective mass per unit wall area) was first calculated by Döring,[19] discussed by Becker[20] and Kittel,[21] and generalized by the writer.[22] The (circular) resonance frequency due to domain wall displacements, ω_0'', is found[6] to be

$$\omega_0''=\gamma(M_s/\chi_0'')(8\pi\chi_0''\delta/d)^{\frac{1}{2}}, \tag{12}$$

where δ is the wall thickness parameter and d denotes an average domain size. It should be noted that Eq. (12) differs from Eq. (6) only in the last factor (which can easily be of order unity) and in the replacement of χ_0' by χ_0'', the latter being the static value of χ''. Under certain simplifying assumptions,[6] χ'' is obtained in the form

$$\chi''=\frac{\chi_0''}{1-(\omega/\omega_0'')^2+i(\omega/\omega_c'')}, \tag{13}$$

where the various quantities are given by

$$\omega_0''=(\alpha/m_w)^{\frac{1}{2}}, \quad \omega_c''=\alpha/\beta \tag{14}$$

and

$$\alpha=M_s^2/\chi_0''d, \quad \beta=\lambda/\gamma^2\delta, \quad m_w=1/8\pi\gamma^2\delta. \tag{15}$$

The approximate condition for a wall resonance (rather than a relaxation) to occur is formally expressed by[6]

$$\lambda<\gamma M_s(\delta/2\pi\chi_0''d)^{\frac{1}{2}}. \tag{16}$$

In a monocrystal the perturbing effect of internal demagnetizing fields, and hence the value of α, the "stiffness parameter" of the walls, is expected to be relatively small, and $\chi_0''d$ relatively large. The inequality (16) is, therefore, difficult to satisfy (other quantities being assumed the same as in a polycrystal) so that the dispersion in a monocrystal is usually a relaxation, as observed by Galt.[3] Finally, Eqs. (12) through (16) do not include the line width due to a distribution in ω_0'' values, a limitation that is also present in the Eqs. (6) and (9) for rotations.

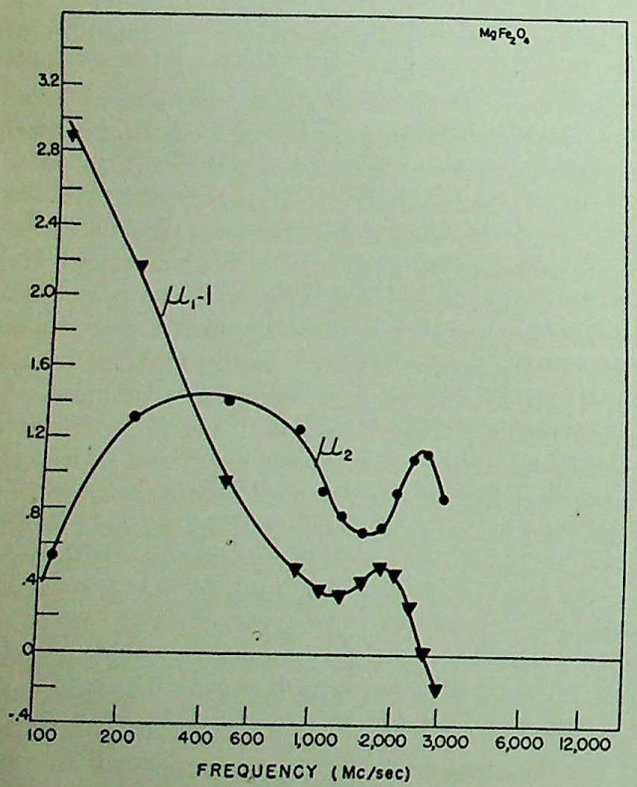


FIG. 5. Magnetic spectrum of sintered $MgFe_2O_4$ sample at room temperature.

B. Temperature Dependence

The measured magnetic spectrum of the sintered samples of ferramic A at various temperatures, represented by curves of μ_1-1 (Fig. 2) and μ_2 (Fig. 3), shows that two resonances were observed at 77°K, 195°K, 300°K, and 411°K. However, the two resonances begin to merge at the highest temperature investigated, a fact which is probably related to the nature of the spectrum, at room temperature, of mixed ferrites containing Zn-ferrite (Sec. V). For a detailed discussion of the temperature effects the original paper[7] should be consulted. Here it will only be noted that μ is much more temperature dependent in the low rf range, where it is ascribed primarily to domain walls, than at microwave frequencies, where it is ascribed primarily to rotations; this fact clearly substantiates that two magnetization processes play a role in the spectrum. It is also noteworthy that the spectrum of the single-domain particles at various temperatures, which is not reproduced here, shows that the (single) observed resonance frequency, denoted by Ω_0' (rather than ω_0'), depends on temperature in a similar way as ω_0' and ω_0''.

Although it is not yet possible to predict theoretically the widths and shapes of the absorption "lines" in a polycrystal, it is possible, as outlined below, to account for the following two simple experimental facts concerning the temperature dependence of the *mean* resonance frequencies (ω_0'', ω_0', and Ω_0') in this material. (a) As the temperature is decreased from 300°K to 77°K, the three frequencies ω_0'', ω_0', and Ω_0' increase by approximately the same fractional amount. (b) This common fractional increase is somewhat larger than that of M_s in the range stated.

Assuming, as indicated by various data, that the role of internal stresses is negligible in ferramic A, and that, as in the molecular field theory of ferrimagnetism[23] for substances possessing only one kind of magnetic ion, the exchange energy varies with temperature as M_s^2, it can be shown[7] that the temperature dependence of each of the three resonance frequencies is given by $gM_s\Psi(K/M_s^2)$, where the function Ψ of K/M_s^2 is

[19] W. Döring, Z. Naturforsch. 3a, 374 (1948).
[20] R. Becker, J. phys. et radium 12, 332 (1951).
[21] C. Kittel, Phys. Rev. 80, 918 (1950).
[22] G. T. Rado, Phys. Rev. 83, 821 (1951).
[23] L. Néel, Ann. phys. 3, 137 (1948).

CC-0. In Public Domain. Gurukul Kangri Collection, Haridwar

Digitized by Arya Samaj Foundation Chennai and eGangotri

different in the three cases and is, moreover, calculable for special situations[7] only. The temperature dependence stated above neglects damping but takes into account anisotropy, exchange forces, and magnetic interactions. If one assumes that, in the range under consideration, the proportionality $K \propto M_s^2$ is valid as a rough approximation, and neither the atomic order nor the sign of K changes, then one obtains

$$\omega_0'' \propto \omega_0' \propto \Omega_0' \propto gM_s, \tag{17}$$

which explains "fact (a)" *quantitatively*. However, "fact (b)" is only *qualitatively* accounted for by (17) because measurements[7] on ferramic A show that the product gM_s does not increase quite as rapidly in the range from 300°K to 77°K as the natural resonance frequencies. It is of independent interest, in fact, that studies[7] of induced resonance indicate that the excess of the apparent g over the value $g=2$, as well as its temperature dependence, decreases in ferramic A with increasing resonance field. The possible reasons for the residual discrepancy between (17) and "fact (b)" were discussed elsewhere.[7]

V. ON THE SPECTRUM IN THE GENERAL CASE

It may seem pertinent to inquire into the causes responsible for the apparently unique "double resonance" property of ferramic A. However, there are two reasons for approaching the problem from a different viewpoint. (1) As shown by the experiments discussed below, ferramic A is not the only substance possessing the double resonance property. (2) There is, at present, no acceptable theoretical argument which indicates that the spectrum of an arbitrary sintered ferrite should not, in principle, contain a wall resonance as well as a rotational resonance; it is only in single-domain particles and in suitably oriented monocrystals that domain theory excludes the possibility of both resonance mechanisms playing a role. The general validity of this statement is not influenced by effects due to internal stresses or cavities in a given material.

For these reasons, it seems natural to propose the hypothesis that the spectrum of any sintered ferrite contains both types of natural resonance and that in some cases these resonances coalesce to give the appearance of a single broad resonance. The phenomenon of relaxation is, of course, considered to be a special case of resonance. On the basis of the new viewpoint, and apart from the question of the physical origin of the "damping" (i.e., relaxation) mechanism described by the phenomenological λ—term in Eq. (10), the principal problem of magnetic spectra consists in accounting for the coalescence that leads to the apparently single resonance discussed in Sec. IIIA. Before suggesting a solution to this problem, it is appropriate to present some recent data, obtained at this laboratory, on magnetic spectra of pure ferrites exhibiting the double resonance effect.

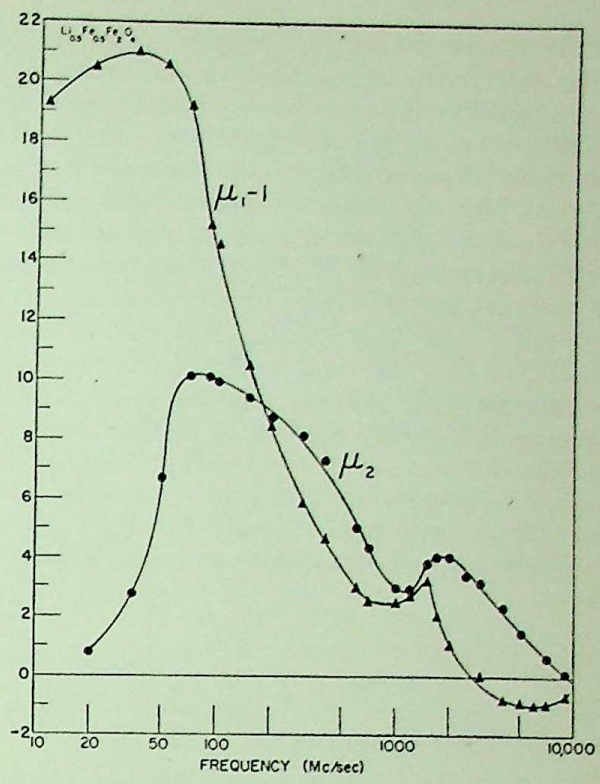


FIG. 6. Magnetic spectrum of sintered $Li_{0.5}Fe_{0.5}Fe_2O_4$ sample at room temperature. The over-all M_s and density are, respectively, 258 and 4.15.

Figures (5) and (6) show the magnetic spectrum, at room temperature, of Mg-ferrite ($MgFe_2O_4$) and Li-ferrite ($Li_{0.5}\,Fe_{0.5}\,Fe_2O_4$), respectively. Similar spectra were obtained on Mg-ferrites deviating by ± 5 mole percent from the stoichiometric composition and possessing different densities. In all these cases the *general* form of the spectrum is seen to resemble that of ferramic A. It should be noted, of course, that these results, as well as those mentioned later, are not necessarily intrinsic characteristics of the materials investigated, and they do not yet cover the whole spectrum; the data represent, instead, limited measurements on samples described by a certain chemical composition, saturation magnetization, density, and sintering treatment. At present, the crucial point is simply the fact, indicated by the figures, that two resonances occur in the spectrum of a pure Mg-ferrite and a pure Li-ferrite. A theoretical explanation for this behavior of these particular substances is not now possible because the anisotropy constant K is not known. The value of K is known,[24] however, for Ni-ferrite ($NiFe_2O_4$), and Eqs. (6) to (8) predict a rotational resonance frequency (ω_0') of about 840 Mc/sec at 298°K. This frequency is considerably lower than 3000 Mc/sec, the approximate location of the barely resolved microwave resonance in this material at room temperature (Fig. 7). It seems possible, therefore, that this "peak" of μ_2 at 3000 Mc/sec arises from a rotational resonance caused, in part, by internal

[24] D. W. Healy, Jr., Phys. Rev. 86, 1009 (1952); Yager, Galt, Merritt, and Wood, Phys. Rev. 80, 744 (1950).

CC-0. In Public Domain. Gurukul Kangri Collection, Haridwar

Digitized by Arya Samaj Foundation Chennai and eGangotri

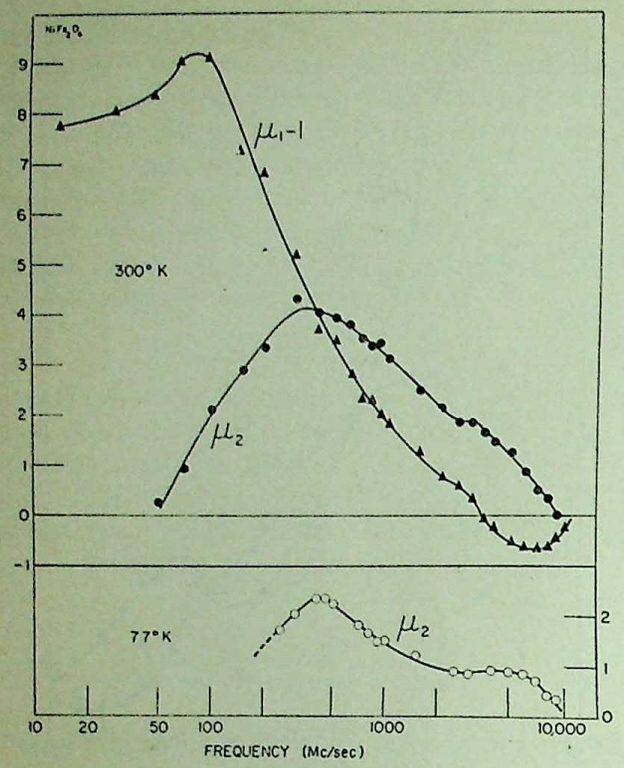


FIG. 7. Upper part: magnetic spectrum of sintered $NiFe_2O_4$ sample at room temperature. Lower part: μ_2 *versus* frequency in the magnetic spectrum of same sample at 77°K. The over-all M_s and density at room temperature are, respectively, 163 and 3.56.

fields due to magnetic interactions. As seen by the lower part of Fig. 7, the separation of the two resonances in Ni-ferrite can be enhanced by cooling the material to 77°K; unlike in the case of ferramic *A*, however, the simple theory[7] of the temperature dependence of ω_0' and ω_0'' (Sec. IVB) is not applicable here.

The mixed ferrites investigated by Snoek (Sec. IIIA), as well as most commercial ferrites, contain Zn-ferrite as an essential component. According to Snoek's important discovery, which was interpreted by Néel[23] in his theory of ferrimagnetism, the presence of Zn-ferrite in a mixture decreases the Curie temperature, thus decreasing *K* at toom temperature and increasing μ_1 at frequencies below the resonance region. The decrease of *K* results, moreover, in the (single) resonance region occurring at relatively low frequencies (see Eqs. (6) to (8)). As implied near the beginning of this section, however, neither this fact nor the evidence discussed in Sec. IIIA requires that the resonance in question be necessarily due to rotations only. It seems more reasonable to suppose that the lowering of the anisotropy field causes not only a decrease of the mean ω_0', but also a relative enhancement of magnetic interactions compared to anisotropy (i.e., a decrease of K/M_s^2), and thus brings about a broadening of both resonances. Since the mean wall resonance frequency (ω_0'') is not,[7] in general, expected to depend more strongly on *K* than the mean ω_0', the two resonances should coalesce if the Zn-ferrite content of the mixtures is sufficiently high. An alternative explanation of Snoek's single resonance is incoherent, of course, in the lack of microwave data in his published results.

The above suggestion concerning the role of Zn-ferrite was confirmed at this laboratory by showing that the addition of enough Zn-ferrite to Mg-ferrite causes a coalescence of the two resonances. An analogous but more informative experiment was performed on a mixture containing 40 mole percent Li-ferrite and 60 mole percent Zn-ferrite. Not only do the two resonances almost coalesce (Fig. 8), but the large decrease of the mean ω_0' is, in this case, probably due to a decrease of anisotropy rather than magnetic interaction fields. This interpretation is based on the fact that, by the choice of composition, M_s was kept roughly constant (226 compared to 258 in Li-ferrite) while the Curie point was lowered substantially. Similar experiments, in which Gorter's[25] data for obtaining compositions of different Zn-ferrite content but equal M_s are used, should make it possible to distinguish in many other cases between the contribution of K/M_s and M_s to ω_0'. Whenever the change in ω_0' is small, of course, then the suggested identification is not unique unless the crystallite and inclusion sizes and the density (and hence the coefficient of M_s) are about the same in the two compositions under consideration.

To summarize, the hypothesis proposed in this paper is consistent with all presently available data. These include the facts presented in Secs. III to V, the single-

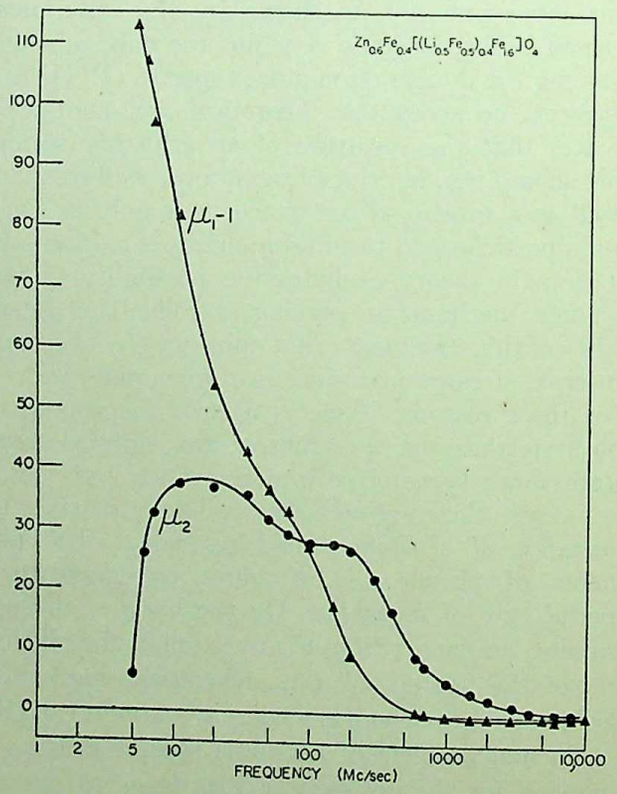


FIG. 8. Magnetic spectrum of sintered $Zn_{0.6}Fe_{0.4}[(Li_{0.5}Fe_{0.5})_{0.4}Fe_{1.6}]O_4$ sample at room temperature. The over-all M_s and density are, respectively, 226 and 4.72.

[25] E. W. Gorter, Compt. rend. 230, 192 (1950).

CC-0. In Public Domain. Gurukul Kangri Collection, Haridwar

Digitized by Arya Samaj Foundation Chennai and eGangotri

resonance spectra observed at this laboratory on a suitably prepared Mn-ferrite and Cu-ferrite, as well as other results.[26] While the interpretations proposed here may even apply to magnetic semiconductors other than ferrites, it must be anticipated that, in substances possessing a small M_s value, the role of Kittel's ferrimagnetic effects[27] may have to be considered in the resonance problem. A more detailed understanding of magnetic spectra will probably depend on additional measurements of the magnetic constants (K, M_s, λ, etc.) of various materials, and on further studies of relaxation processes and magnetic interactions.

On the basis of the above discussion it appears that high μ_1 values will be difficult to obtain at microwave frequencies. To obtain even $\mu_1=2$ (with $\mu_2 \ll 2$) at 10^4 Mc/sec, for example, Eqs. (6) to (8) show that a substance characterized by $M_s \gg 430$ (and hence $K \gg 7.5 \times 10^5$ ergs/cc) would be required. Nevertheless, $\mu_1=2$ is clearly more useful than $\mu_1=1$, and, in addition, interesting wave propagation effects can be achieved by operating within a (narrow) resonance region. It is also noteworthy that, contrary to Snoek's theory, the total low frequency μ_1 may still be large even if the microwave μ_1 is small (see Eq. (11)). Furthermore, materials with a low Curie point, such as mixed ferrites containing a large amount of Zn-ferrite, are clearly not satisfactory for ordinary microwave use, but may sometimes be suitable for obtaining low insertion loss in devices based on the Faraday effect.

In conclusion, the writer wishes to thank R. W. Wright, W. H. Emerson, A. Terris, and M. Maloof for their invaluable contributions to the experiments discussed in this paper.

[26] Welch, Nicks, Fairweather, and Roberts, Phys. Rev. 77, 403 (1950).
[27] C. Kittel, Phys. Rev. 82, 565 (1951).

REVIEWS OF MODERN PHYSICS VOLUME 25, NUMBER 1 JANUARY, 1953

Resonance Phenomena in Ferrites

D. POLDER* AND J. SMIT

Philips Research Laboratories, N. V. Philips Gloeilampenfabrieken, Eindhoven, Netherlands

ABOVE a certain frequency, of the order of 5–100 Mc/sec, losses of ferrites in an alternating magnetic field are very high. Snoek[1] has ascribed this absorption to rotational resonance of the spins in the internal anisotropy fields, and has related the resonance frequency f_0 with the static initial permeability μ_0 by means of the equation

$$f_0(\mu_0-1)=(4/3)\gamma M, \qquad (1)$$

with γ the gyromagnetic ratio and M the saturation magnetization. Experimentally considerable losses are found at the predicted f_0, but the absorption region is very broad and extends to frequencies above 1000 Mc/sec. In this connection one of us[2] has pointed out that in the resonating unmagnetized material magnetic poles will be created and annihilated on a Bloch wall, if the alternating field has a component parallel to it. In some regular arrangements of Weiss domains this effect can, together with demagnetization at the grain boundaries, give rise to high resonance frequencies. This, and also the occurrence of losses near f_0, will be illustrated with the following model.

Consider an ellipsoid divided into thin Weiss domains separated by 180° walls perpendicular to one of its principal axes. The ellipsoid is embedded in a medium with the average permeability $\mu(f)$ of the material. For ac fields perpendicular to the walls only the external demagnetization in the field direction plays a role (Fig. 1). The effect is reduced by the presence of the medium by a factor of the order of μ, which is large at relatively low frequencies. The influence of demagnetization and the formation of poles on the walls

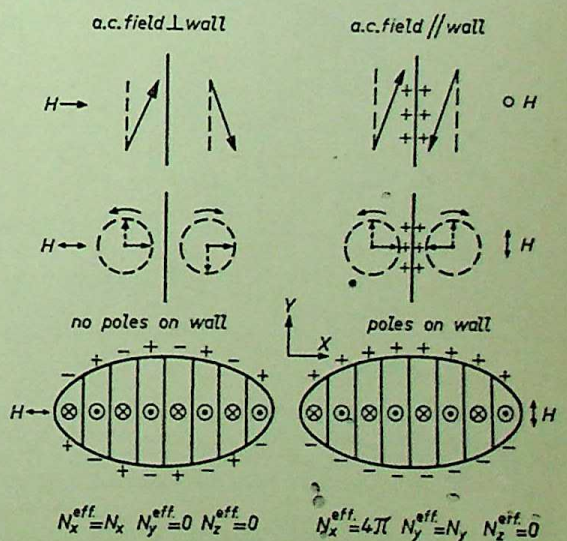


FIG. 1. Effect of Weiss domain structure on ferromagnetic resonance conditions.

* At present at H. H. Wills Laboratory University of Bristol, England.
[1] J. L. Snoek, Nature 160, 60 (1947) and Physica 14, 207 (1948).
[2] D. Polder, J. phys. et radium 12, 337 (1951).

CC-0. In Public Domain. Gurukul Kangri Collection, Haridwar

Digitized by Arya Samaj Foundation Chennai and eGangotri

can be shown to be small also for less regular configurations. From this it may be inferred that a considerable part of the resonances in the actual material occurs at frequencies mainly determined by the internal anisotropy fields giving an absorption peak at f_0 from Eq. (1).

For ac fields parallel to the walls we have, besides the external demagnetization of the ellipsoid, the poles at the walls. The resonance frequency is now given by

$$2\pi f = \gamma M(4\pi N)^{\frac{1}{2}},$$

N being the demagnetization coefficient in the field direction (Fig. 1). Here we ignore anisotropy and the effect of the medium because of the low μ at this high high f. The maximum resonance frequency is accordingly given by $2\pi f_{\max} = \gamma 0.4\pi M$, as to be compared with $\gamma 0.2\pi M$ for an isolated homogeneously magnetized ellipsoid. With this mechanism one can explain the high frequency losses in unmagnetized ferrites as observed by Beljers, v.d. Lindt, and Went.[3] In these experiments strong absorption occurred only if $\gamma 0.4\pi M$ exceeded $2\pi f$, as was found by temperature variation.

For the explanation of the losses near f_0 the ratio of the wall thickness and the domain thickness has been assumed to be small. The relative influence on the resonance frequency is then of the order of this ratio.

In grains of the ferrite materials with dimensions of 10^{-5} or 10^{-4} cm especially when they are isolated some type of flux closure configuration[4] will exist, or the whole grain will be one Bloch wall. It is seen that in these cases losses near f_0 will be far less pronounced, since the resonance condition will largely be determined by demagnetization effects giving a peak at some thousands Mc/sec this being a fraction of $\gamma/2\pi 0.4\pi M$. We believe that these effects apply to the resonance phenomena observed by Wijn and van der Burgt,[5] and may contribute to the two dispersion mechanisms found by Rado, Wright, and Emerson.[6]

[3] Beljers, v. d. Lindt, and Went, J. Appl. Phys. **22**, 1506 (1951).

[4] C. Kittel, Revs. Modern Phys. **21**, 541 (1949).
[5] H. P. J. Wijn and C. M. v. d. Burgt (to be published).
[6] Rado, Wright, and Emerson, Phys. Rev. **80**, 273 (1950).

DISCUSSION

G. T. RADO, *Naval Research Laboratory, Washington, D. C.:* As stated in my paper, as well as in previous publications, the experimental evidence obtained by our group indicates clearly that internal demagnetizing fields have an important effect on wall resonance frequencies and on rotational resonance frequencies. The model suggested by Polder and Smit describes some detailed manifestations of such demagnetizing effects in particular situations.

CC-0. In Public Domain. Gurukul Kangri Collection, Haridwar

Digitized by Arya Samaj Foundation Chennai and eGangotri

Note on the High Frequency Dispersion in Nickel Zinc Ferrites

H. P. J. WIJN, M. GEVERS, AND C. M. VAN DER BURGT

Philips Research Laboratories, N. V. Philips' Gloeilampenfabrieken, Eindhoven, Netherlands

AS is known,[1] ferrites show a dispersion of the initial permeability μ_0 at a frequency which is intimately related to the low frequency value of the initial permeability. Snoek[2] explained his phenomenon as a gyromagnetic resonance of the electron spins. Rado, Wright, and Emerson[3] found two regions of dispersion in a ferrite material, "Ferramic *A*." The lower frequency of dispersion which according to Snoek's formula corresponds to the value of the initial permeability, has been described by these authors as a resonance of the domain boundaries, whereas the resonance at 1300 Mc/sec has been ascribed to spin rotation.

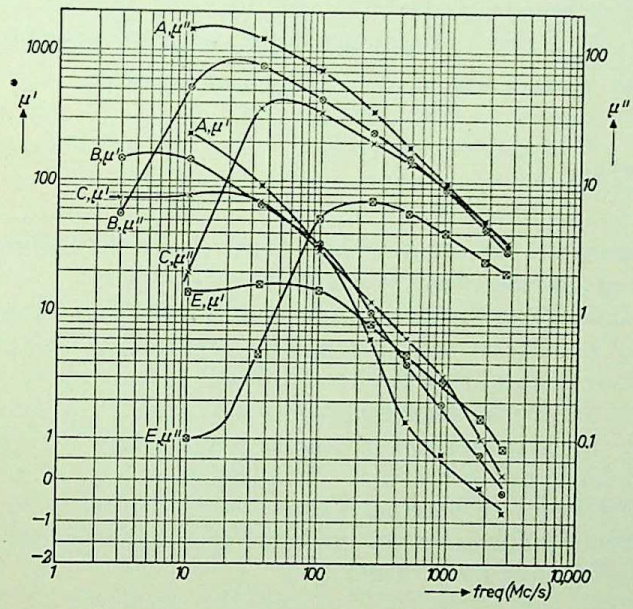


FIG. 1. The real and imaginary part of the initial permeability, μ' and μ'', respectively, as a function of frequency f for samples of NiZn ferrite with varying Ni−Zn ratio

	Chemical composition in mole percent		
Ferrite	NiO	ZnO	Fe_2O_3
A	18	32	50
B	25	25	50
C	32	18	50
E	50	—	50

In order to investigate whether two regions of dispersion occur in NiZn ferrites (Ferroxcube IV), we have measured the complex initial permeability ($\mu_0=\mu_1-j\mu''$) from low frequencies up to about 3000 Mc/sec. The measurements have been carried out on ring cores in a coaxial line resonator as described elsewhere,[4] and care has been taken to avoid dimensional resonance effects.[5] Figure 1 gives the results of the measurements

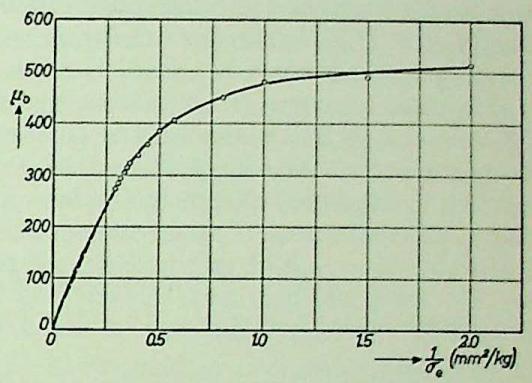


FIG. 2. The initial permeability μ_0 of a rod of NiZn ferrite (chemical composition in mole percent 18 NiO, 32 ZnO, and 50 Fe_2O_3) as a function of externally applied tension σ_e.

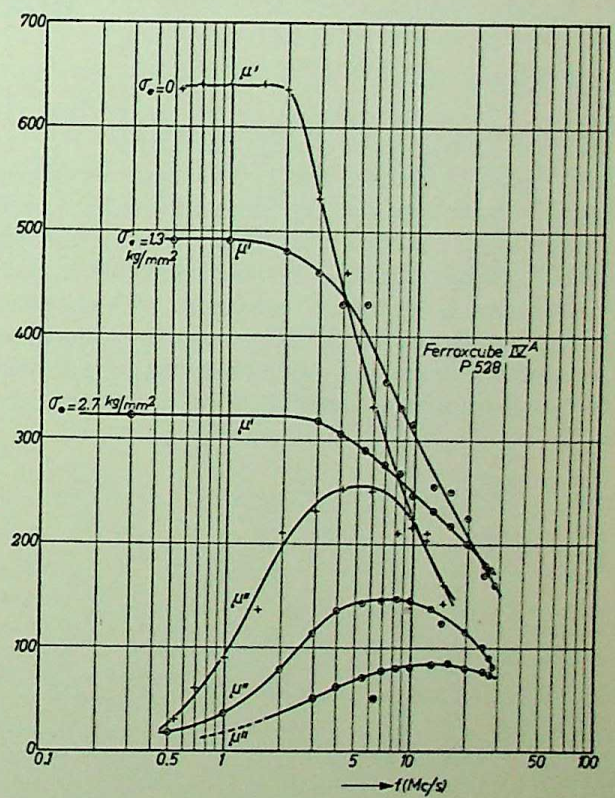


FIG. 3. The real and imaginary part of the initial permeability, μ' and μ'', respectively, plotted against frequency for different values of externally applied tension σ_e. Chemical composition of the ferrite is that of ferrite *A* of Fig. 1.

[1] J. L. Snoek, *New Developments in Ferromagnetic Materials* (Elsevier Publishing Company, Inc., New York, 1947).
[2] J. L. Snoek, Physica 14, 207 (1948).
[3] Rado, Wright, and Emerson, Phys. Rev. 80, 273 (1950).
[4] van der Burgt, Gevers, and Wijn, Philips Tech. Rev. 14, 206 (1952).
[5] Brockman, Dowling, and Steneck, Phys. Rev. 75, 1298 (1949).

CC-0. In Public Domain. Gurukul Kangri Collection, Haridwar

Digitized by Arya Samaj Foundation Chennai and eGangotri

for NiZn ferrites with varying Ni—Zn ratios on a logarithmic scale, so that all the results can be compiled in one figure. For each ferrite only one region of dispersion is found, *viz.*, that which has been reported previously.[6] Moreover, the negative values of $\mu'-1$ at high frequency must be due to a resonance phenomenon.

If this resonance is related to the simultaneous rotation of the electron spins in a Weiss domain, it must still occur in ferrites in which boundary displacements cannot contribute to the initial permeability. This condition is fulfilled for NiZn ferrites under external tensile stress, if the direction of the stress coincides with that of the magnetic field. For the NiZn ferrite with chemical composition in mole percent 18 NiO, 32 ZnO, and 50 Fe_2O_3, the internal anisotropy is sufficiently small that the energy $\frac{3}{2}\lambda_s \cdot \sigma_e$ can be made predominant. λ_s denotes the magnetostriction constnat and σ_e the external stress. This becomes clear from Fig. 2 in which for a rod of this ferrite, μ_0 is plotted against $1/\sigma_e$, from which it may be seen that above $\sigma_e = 2.5$ kg/mm^2 the relation between μ_0 and $1/\sigma_e$ becomes a straight line, as is to be expected.[7] We have measured μ' and μ'' *vs* frequency at different values of the tension (Fig. 3). For $\sigma_e = 0$ the same magnetic spectrum should be expected as that found for a ring-shaped specimen of the same chemical composition (Fig. 1). It must, however, be borne in mind that the rod has been formed by an extrusion process whereas the ring was formed by pressing. The permeability μ_0 decreases when stress is applied, and at the same time the frequency f_{res} at which the μ'' curve has a maximum shifts to a higher value, according to Snoek's relation:

$$\tfrac{1}{2} \cdot f_{res}(\mu_0 - 1) = (2/3) \cdot \gamma I_s.$$

Since under a tension of $\sigma_e = 2.7$ kg/mm^2 the greater part of the spins can be assumed to be oriented perpendicular to the direction in which μ_0 is measured, the factor 2/3 in Snoek's formula must be omitted. This experiment on a NiZn ferrite is in agreement with the view that the dispersion in these ferrites is related to a rotation process.

We wish to thank Dr. G. W. Rathenau for suggesting the experiment and Mr. A. van der Grijp and Mr. H. van der Heide for assistance during the measurements.

[6] J. J. Went and E. W. Gorter, Philips Tech. Rev. 13, 181 (1951).

[7] R. Becker and M. Kersten, Z. Physik 64, 644 (1930).

DISCUSSION

G. T. RADO, *Naval Research Laboratory, Washington, D. C.:* It was suggested in my paper that the addition of Zn-ferrite to a magnetic ferrite (e.g., Li-ferrite) tends to coalesce the two natural resonances, and it was shown that our experimental results support this suggestion. The fact that Wijn, Gevers, and van der Burgt (WGv) found only one resonance in some Ni—Zn ferrites is, therefore, consistent with the views presented in my paper. It is noteworthy, moreover, that in pure Ni-ferrite our group observed an indication of a second resonance (see Fig. 7 of my paper) at a microwave frequency which is just above the highest frequency shown in the results of WGv.

Concerning the mechanisms of magnetization, it may well be that at certain relatively low frequencies the initial permeability due to rotations predominate over that due to wall displacements in the special case of some Ni—Zn ferrites. However, the method used by WGv to establish this point may be questioned because the presence of an external stress obviously modifies the magnetization processes and hence changes the physical conditions of the problem.

CC-0. In Public Domain. Gurukul Kangri Collection, Haridwar

Digitized by Arya Samaj Foundation Chennai and eGangotri

REVIEWS OF MODERN PHYSICS VOLUME 25, NUMBER 1 JANUARY, 1953

Motion of Domain Walls in Ferrite Crystals

J. K. GALT, J. ANDRUS, AND H. G. HOPPER

Bell Telephone Laboratories, Murray Hill, New Jersey

I. INTRODUCTION

THE experience of Williams[1] and his collaborators has shown that it is possible to cut a sample from a single crystal of a magnetic material in such a way that the domain pattern includes only one movable wall. This wall moves as the sample is magnetized, and a linear relation exists between the magnetization of the sample and the distance between the wall and a fixed plane parallel to it.

We have used similar samples to study the motion of domain walls in ferrites, where eddy currents are a relatively unimportant source of damping. These samples are polygonal rings with each leg along an easy direction of magnetization. Since the (111) direction is the easy direction in ferrites, the rings are diamond shaped with their faces in the (110) plane as shown schematically by the solid lines in Fig. 1. The expected domain pattern consists of four stationary walls, one at each corner, and one movable wall all around the ring. This pattern is indicated by dotted lines in Fig. 1.

The results of our experiments can be understood very satisfactorily in terms of the theory of domain walls and their motion developed in the last few years. In fact, these results may be used to evaluate many of the parameters used in that theoretical development.

II. EXPERIMENTAL

A. Descriptive

The first experiment performed on these samples is designed to measure, by means of pulse techniques, domain wall velocity as a function of the field causing the wall to move. The sample is wound with a primary and a secondary winding. A square pulse of positive voltage is applied to the primary winding in series with a resistor which is large enough to keep the pulse rise time short. The rise time must be short compared to the time required for the field produced by the pulse to reverse the magnetization of the sample. On the other hand, since the pulse is applied for the purpose of reversing the magnetization of the sample, the length of the pulse must be longer than the time required for the reversal to occur. It must, therefore, be longer than the time required for the mobile wall to move from one side of the sample to the other under the field produced by the pulse. A second pulse of negative voltage is applied to the primary during each duty cycle in order to bring the wall back to its original position, so that the phenomenon may be observed repetitively. By synchronizing an oscilloscope sweep with the pulser, the signal induced in the secondary winding is observed while the applied pulse is on the primary. Since this signal is proportional to the velocity of the wall, it is constant during the application of a constant field. Irregularities in the crystal may cause this value to vary somewhat during the motion of the wall, as we shall see later, but the observer reads an average value.

The applied field due to the primary pulse is deduced from the current in the primary winding (measured by observing the voltage across the series resistor) using the solenoid formula $H_{app}=4\pi NI$. To obtain the relation between wall velocity and induced voltage per secondary turn we have

$$\text{Volts/turn}=d\Phi/dt\times10^{-8}$$
$$=8\pi M_s(\Delta z/\Delta t)w_{wall}\times10^{-8}, \quad (1)$$

where $\Delta z/\Delta t$ is equal to domain wall velocity v, and w_{wall} is the width of the wall between the boundaries of the sample in the direction perpendicular to the direction of magnetization. The result of the experiment is thus a plot of ferromagnetic domain wall velocity *versus* the applied field. The slope of this plot measures a viscous damping coefficient for the motion of the domain wall.

The second experiment is the measurement of the complex initial permeability *versus* frequency. Standard bridge measurements are made of the impedance of a coil wound on the sample.

The interpretation of these experiments is, of course,

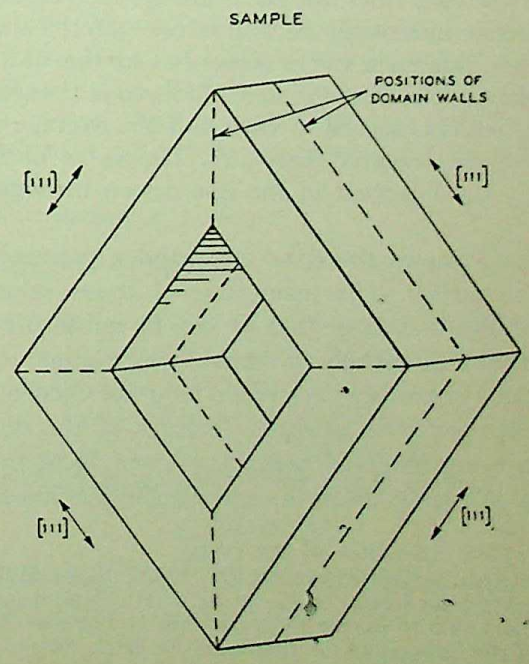


FIG. 1.

[1] H. J. Williams and W. Shockley, Phys. Rev. 75, 178 (1949).

CC-0. In Public Domain. Gurukul Kangri Collection, Haridwar

Digitized by Arya Samaj Foundation Chennai and eGangotri

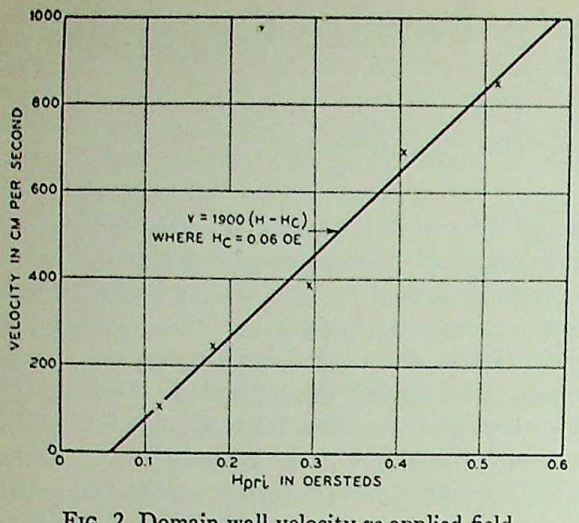


FIG. 2. Domain wall velocity *vs* applied field.

based on the domain pattern indicated by the dotted lines in Fig. 1. Observations on the actual domain pattern of each sample are, therefore, desirable. These observations have thus far proved the most difficult part of the experiments, but the essential features of the ideal domain pattern have been observed.

As a further check to indicate how freely the movable wall actually can move in the sample, a hysteresis loop is also obtained on the recording fluxmeter.[2] If the wall does move freely, the loop should have sides which are almost vertical, of course.

B. Results

The first experiments were done on a sample cut from a crystal of Fe_3O_4.[3] These data are shown in the accompanying figures which indicate the nature of the results.

Figure 2 shows the result of the velocity *versus* applied field experiment. We see that, since the line through the data does not pass through the origin, the field effective in moving the wall is less than the applied field. This difference varies somewhat as the wall traverses the sample, since the signal induced in the secondary winding is observed to vary, but the average is by definition the coercive force, H_c. The value of H_c is given by the intercept of the line drawn through the data.

Figure 3 shows the data on complex permeability *versus* frequency. The magnitude of these values of permeability is so large that we can be quite sure that it is due almost entirely to domain wall motion.

Figure 4 shows the hysteresis loop obtained on the Fe_3O_4 sample. The essential features of the domain pattern were observed using the same technique as that of Williams, Bozorth, and Shockley.[4] These observations are discussed in more detail in a previous publication.[5]

The nickel ferrite results are broadly similar, but they are not as good, and must be regarded as preliminary. $NiFe_2O_4$ is, of course, a more complicated substance chemically, and the crystals available thus far are not as perfect as the Fe_3O_4 crystal. Under chemical attack they show some signs of a variation in chemical composition with position in the crystal, and the composition of the crystal from which the best sample was cut corresponded to the formula $(NiO)_{0.91}$-$(FeO)_{0.09}Fe_2O_3$. As a result of these inhomogeneities, the hysteresis loop was not as square as is desirable, and as a result of the differential chemical attack, the domain pattern on this sample could not be observed.

The data on domain wall velocity *versus* applied field seem reasonably satisfactory, however. The signal in the secondary winding had a sharp peak at the start of the applied pulse which we attribute to the motion of walls around inhomogeneities, but a fairly constant signal of the sort expected followed the peak, and the observations were therefore made in this flat region. The data followed a straight line of the form $v = 20\,000\,(H - 1.5)$ where v is in centimeters/sec, and H is in oersteds. Data on other samples indicate that the 20 000 is accurate to something like 25–50 percent. Since this value is considerably higher than the value for magnetite given in Fig. 2, we see that the damping of wall motion in nickel ferrite is considerably less than that in magnetite.

The data on permeability *versus* frequency show indications that only part of the movable pattern has been observed. There is a substantial contribution which shows no frequency dependence up to 20 mc/sec, which was the highest frequency at which data could be taken. There is a contribution, however which fits a relaxation curve much like Fig. 2. This contribution gives a permeability at zero frequency of 32, and its relaxation frequency is approximately 7 mc/sec. This is consistent with the smaller damping in nickel ferrite indicated by the domain wall velocity *versus* applied

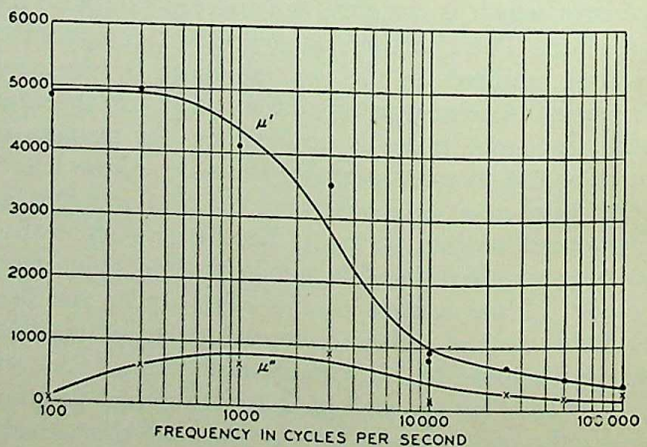


FIG. 3. μ', μ'' *vs* frequency.

[2] P. P. Cioffi, Phys. Rev. **67**, 200 (1945).

[3] J. Smiltens, J. Chem. Phys. **20**, 990 (1952); Technical Report 49. Laboratory for Insulation Research, M.I.T., December, 1951. The authors wish to express their gratitude to Professor A. von Hippel of the Laboratory for Insulation Research for providing a crystal of Fe_3O_4.

[4] Williams, Bozorth, and Shockley, Phys. Rev. **75**, 155 (1949).

[5] J. K. Galt, Phys. Rev. **85**, 664 (1952).

CC-0. In Public Domain. Gurukul Kangri Collection, Haridwar

Digitized by Arya Samaj Foundation Chennai and eGangotri

field experiment and with the high coercive force of this sample (1.5 oersteds) which leads us to expect a high α. These data are probably somewhat less accurate than those on wall velocity *versus* applied field.

III. THEORY

A theoretical treatment of the data divides itself rather naturally into two parts. First, we may correlate the data in terms of an equation of motion for unit area of domain wall. In doing this we determine the constants of motion (mass, viscous resistance, and stiffness) of unit area of wall. Secondly, we can show the relation between the mass and viscous resistance of unit area of domain wall and the constants which characterize the ferromagnetic material in general. This last step is essentially an application of the recent work of Becker,[6] Döring,[7] and Kittel.[8]

Consider unit area of a 180° domain wall between two regions of saturated material. Such a system has an equation of motion for small amplitudes of the applied applied magnetic field H which may be written

$$m\ddot{z}'+\beta\dot{z}'+\alpha z=2M_sH, \tag{2}$$

where z is the displacement of the domain wall along its normal, m is its mass per unit area, β is a parameter measuring viscous resistance, and α is a stiffness parameter, which has meaning only for small fields such as those used in initial permeability measurements. When fields larger than the coercive force are applied, as in the experiment on wall velocity *versus* applied field, the term containing α disappears and the effective field inside the material is less than the applied field by an amount equal to the coercive force; this is shown by the data given in Sec. II. These results are quite reasonable when one remembers the spikes which pull back on the wall, in the experiments of Williams and Shockley for small wall motions, and snap off entirely if the wall moves a large distance.

As these remarks indicate, under the conditions of the experiment in wall velocity, Eq. (2) takes the form

$$\beta\dot{z}'=2M_s(H_{\text{app}}-H_c). \tag{3}$$

This relation obviously fits the data given in Sec. II.

Let us now consider the initial permeability data. We have for the relation between z and μ,

$$\mu=\Delta B/\Delta H=\Delta\Phi/A_{\text{coil}}\Delta H=8\pi M_szw_{\text{wall}}/A_{\text{coil}}H, \tag{4}$$

where w_{wall} is the width of the domain wall between the boundaries of the sample in a direction perpendicular to the magnetization and A_{coil} is the cross-sectional area of the coil around the sample. The general solutions of Eq. (2) for a sinusoidal applied field will not be reproduced here, because we note that Eq. (2) can be further simplified since we observe a relaxation mechanism

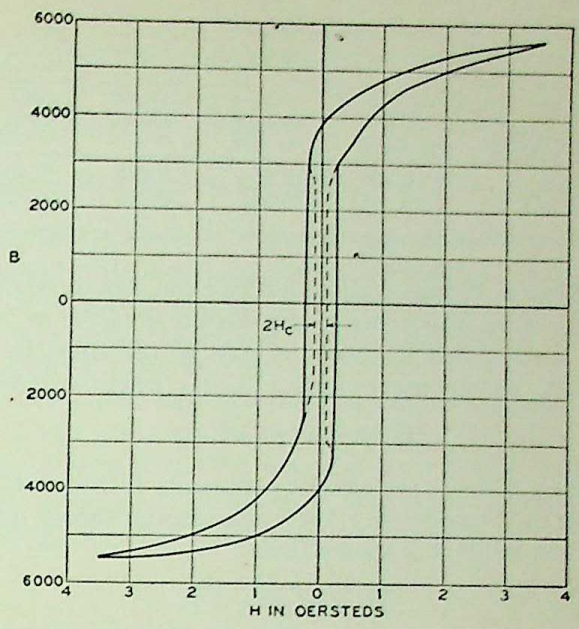


FIG. 4. Hysteresis loop.

(see Sec. II). The values of α, β, and m will be calculated later; suffice it to say here that the order of magnitude of m is such that the first term on the left in Eq. (2) is negligible, and we may write

$$\beta\dot{z}'+\alpha z=2M_sH, \tag{5}$$

which we may solve to give, if $H=H_0e^{j\omega t}$,

$$z=\frac{2M_sH_0}{\alpha}\left[\frac{1}{1+\omega^2\beta^2/\alpha^2}-\frac{j\omega\beta/\alpha}{1+\omega^2\beta^2/\alpha^2}\right]e^{j\omega t}. \tag{6}$$

We shall derive values of α and β later by fitting Eqs. (3) and (6) to the data.

We now come to the second part of the theoretical problem. Starting with the now familiar equation of motion for the magnetization M in a small volume first used by Landau and Lifshitz[9] and taking advantage of the recent work of Kittel,[8] Becker,[6] and Döring,[7] we derive the relations between β and m and the fundamental constants which characterize the ferromagnetic material.

The equation of motion is

$$d\mathbf{M}/dt=\gamma[\mathbf{M}\times\mathbf{H}]-(\lambda/M^2)[\mathbf{M}\times(\mathbf{M}\times\mathbf{H})], \tag{7}$$

where γ is the gyromagnetic ratio, and λ is a parameter characteristic of a given ferromagnetic material which is determined by the magnitude of the damping effects in the motion of M and thus determines the magnitude of the last term on the right in (7). The power dissipated per unit volume is $\mathbf{H}\cdot(d\mathbf{M}/dt)$, which is

$$\mathbf{H}\cdot d\mathbf{M}/dt\cong\lambda H_e^2, \tag{8}$$

where $\mathbf{H}=\mathbf{H}_0+\mathbf{H}_e$, $\mathbf{H}_0$ is the applied field and $\mathbf{H}_e$ is a field associated with the motion of the wall as Becker[6]

[6] R. Becker, J. phys. et radium 12, 332 (1951).
[7] W. Döring, Z. Naturforsch. 3a, 374 (1948).
[8] C. Kittel, Phys. Rev. 80, 918 (1950); J. phys. et radium 12, 291 (1951).
[9] L. Landau and E. Lifshitz, Physik. Z. Sowjetunion 8, 153 (1935).

CC-0. In Public Domain. Gurukul Kangri Collection, Haridwar

Digitized by Arya Samaj Foundation Chennai and eGangotri

TABLE I. Values of β.

Substance	α	β (from $\mu_{initial}$)	β (from wall vel vs H)	β (corrected for eddy current effects)
Fe_3O_4	9.1×10^3	0.5	0.484	0.406
$NiFe_2O_4$	7.2×10^5	0.016	0.026	0.026

has shown. It exists only in the wall and is perpendicular to the wall. The value of this field is determined from the precessional angular velocity of the spins in the moving wall by means of the Larmor relation. It is

$$\mathbf{H}_e=-(\mathrm{v}/\gamma)(\partial\theta/\partial z), \tag{9}$$

where γ is the gyromagnetic ratio and θ is the rotational angle of the spins in a 180° wall. In the theory of the domain wall[10] it is shown that

$$\partial\theta/\partial z=[g(\theta)/A]^{\frac{1}{2}}, \tag{10}$$

where A is a measure of the exchange energy per unit volume due to gradients in the direction of the magnetization as given by Eq. (11):

$$\text{Exchange energy/unit vol.}=A[(\nabla\alpha_1)^2+(\nabla\alpha_2)^2+(\nabla\alpha_3)^2]. \tag{11}$$

Here α_1, α_2, α_3 are the direction cosines of the magnetization. $g(\theta)$ is the anistropy energy density:

$$g(\theta)=K_1(\alpha_1^2\alpha_2^2+\alpha_2^2\alpha_3^2+\alpha_3^2\alpha_1^2), \tag{12}$$

expressed in terms of θ. K_1 is the first-order anistropy constant.

If we use Eqs. (9) and (10) in Eq. (8) and integrate over z to get the power dissipated for unit area of wall, we have

$$\int_{-\infty}^{\infty}H\cdot\frac{dM}{dt}dz=2H_0M_s v=(\lambda v^2/\gamma^2A^{\frac{1}{2}})\int_0^{\pi}[g(\theta)]^{\frac{1}{2}}d\theta, \tag{13}$$

where we have used Eq. (10) to transform from integration over z to integration over θ as well as to evaluate Eq. (9). We may now write

$$v=\frac{2M_s\gamma^2A^{\frac{1}{2}}}{\lambda\int_0^{\pi}[g(\theta)]^{\frac{1}{2}}d\theta}H_0. \tag{14}$$

This is the desired relation between v and H_0 which is to be compared with Eq. (3). In this way we find

$$\beta=(\lambda/\gamma^2A^{\frac{1}{2}})\int_0^{\pi}[g(\theta)]^{\frac{1}{2}}d\theta. \tag{15}$$

We derive m from the energy of motion of the wall, which we equate to $\frac{1}{2}mv^2$. This was first done by Becker.[6] He pointed out that this energy was equal to $(1/8\pi)\int H_e^2dV$, and by means of Eq. (9) he was able to write

$$m=(1/4\pi\gamma^2)\int_{-\infty}^{\infty}\left(\frac{\partial\theta}{\partial z}\right)^2dz. \tag{16}$$

If we use Eqs (10), (11), and (12), this becomes

$$m=(1/4\pi\gamma^2A^{\frac{1}{2}})\int_0^{\pi}[g(\theta)]^{\frac{1}{2}}d\theta. \tag{17}$$

It will be noted that the above analysis neglects the effect of eddy currents. If this effect is not negligible (it is not negligible in Fe_3O_4), Williams, Shockley, and Kittel[11] have shown that it will contribute part of the measured value of β. The equations of Williams, Shockley, and Kittel may be used to correct for this effect when necessary.

IV. DISCUSSION

It is clear that Eq. (3) fits data of the type shown in Fig. 2, and we therefore obtain a value of β in this way. A value for α, and a second, independent, value for β are determined by fitting the data on initial permeability to Eqs. (4) and (6). As mentioned in Sec. II, we use only the frequency dependent part of the permeability for this calculation in the case of nickel ferrite. The consistency of the two values of β provides a useful internal check on the validity of the data of course, but the value obtained from the initial permeability involves an estimate of the cross-sectional area of the winding, and is therefore not as accurate as the other.[5]

The values of α and β are given in Table I. In the case of Fe_3O_4, eddy currents make a small but not negligible contribution. This has been taken account of by means of the low field theory of Willimas, Shockley and Kittel,[11] and the corrected value is given in the last column.

Some remarks on the significance of α and β are in order here. As Eq. (2) shows, α measures the rate of which magnetostatic energy is built up when the position of the wall changes. This energy is built up as the wall passes crystal imperfections, impurity inclusions, and other impediments to its motion. α is thus a measure of the magnetic imperfection of the sample. It is characteristic of a particular sample, and may differ widely among different samples of the same material. As Eqs. (4) and (6) show, the factor $(2M_s^2/\alpha)$ determines the value of the initial permeability at low frequency.

β, on the other hand, is a fundamental property of the material, as Eq. (15) shows. It is determined by the relaxation time of the spin system, and therefore is a measure of the damping of the wall.

It will be noted that these samples are not expected to show the natural ferromagnetic resonance[12] in the

[10] C. Kittel, Revs. Modern Phys. 21, 541 (1950); see Eq. (3.3.9).

[11] Williams, Shockley, and Kittel, Phys. Rev. 80, 1090 (1950).

[12] Rado, Wright, and Emerson, Phys. Rev. 80, 273 (1950).

CC-0. In Public Domain. Gurukul Kangri Collection, Haridwar

Digitized by Arya Samaj Foundation Chennai and eGangotri

anisotropy field, since the alternating field and the anisotropy field are parallel. Equations (4) and (6) therefore, are a rather complete description of initial permeability *versus* frequency for these samples over the whole frequency range. Another characteristic of these samples is the freedom of the moving wall from interaction with other domain walls. This removes one impediment to wall motion which must be present ordinarily and tends to give them a lower α than might be expected in other samples.

The second part of our theoretical discussion, and Eq. (15) in particular, makes it possible to determine a value for λ from our measured β. It should be emphasized that this value is determined independently of the value deduced from ferromagnetic resonance line width; it is therefore of interest to compare them. The availability of a second independent determination of λ is especially desirable since the damping mechanism in ferromagnetics is not understood.

In order to evaluate λ using Eq. (15) we proceed as follows. Since the wall is in a 110 plane we have

$$g(\theta)=\tfrac{1}{4}K_1[\cos^4(\theta+35°16')+\sin^2 2(\theta+35°16')], \quad (18)$$

where $\theta=0$ on one side of the wall and π on the other. Then,

$$\int_0^{\pi}[g(\theta)]^{\frac{1}{2}}d\theta=1.38|K_1|^{\frac{1}{2}}. \quad (19)$$

In performing this integration, care must be taken to use the positive value of the square root over the whole interval. A is best evaluated from a fundamental relation recently derived by Herring and Kittel[13] between A and the Bloch constant:

$$A=[S_0/\Omega]^{\frac{1}{3}}[k/13.3C^{\frac{1}{2}}], \quad (20)$$

where k is Boltzmann's constant, C is Bloch's constant as used in the relation $M_s=M_0(1-CT^{3/2})$, S_0 is the atomic spin, and Ω is the atomic volume. (S_0/Ω) is equal to the saturation magnetization at 0°K divided by the Bohr magneton.

For Fe_3O_4, we find $C=4\times10^{-6}$ by fitting the Bloch $T^{\frac{3}{2}}$ law to the saturation magnetization measurements of Weiss and Forrer.[14] From Eq. (20), we then find $A=1.53\times10^{-6}$. $K_1=-1.1\times10^5$ as given by Bickford.[15] $\gamma=1.76\times10^7$. Now from Eq. (15), we find $\lambda=3.5\times10^8$ in Fe_3O_4.

[13] C. Herring and C. Kittel, Phys. Rev. 81, 869 (1951); see Eq. (5).
[14] P. Weiss and R. Forrer, Ann. Phys., Series 10, 12, 279 (1929).
[15] L. R. Bickford, Jr., Phys. Rev. 78, 449 (1950).

TABLE II.

Substance	λ wall motion	λ ferromag. res.
Fe_3O_4	3.5×10^8	9×10^8 (24,000 mc)
$NiFe_2O_4$	2.2×10^7	2.1×10^7 (24,000 mc)
		7.2×10^7 (9000 mc)

For nickel ferrite in the same way, using the data of Guillaud and Roux[16] for saturation magnetization we find $C=7\times10^{-6}$ and $A=9.0\times10^{-7}$. $K_1=-6.2\times10^4$.[17] Using these figures and our measured value for β, we find $\lambda=2.2\times10^7$ in nickel ferrite.

The relation between ferromagnetic resonance line width and λ has been given elsewhere.[18] Sample shape enters this relation, but not in a critical way, and we therefore ignore it except as it affects the value of the dc magnetic field at resonance, H_{res}. The relation is

$$\lambda=\Delta H\gamma M_s/H_{res}, \quad (21)$$

where the line width is $2\Delta H$.

Data taken at 24,000 mc[16] lead by means of Eq. (21) to $\lambda=2.1\times10^7$ for nickel ferrite. Data taken at 9000 mc,[19] however, lead to $\lambda=7.2\times10^7$ for the same material. If we use Bickford's data on Fe_3O_4 taken at 24,000 mc,[15] Eq. (21) leads to $\lambda=9\times10^8$ for Fe_3O_4.

The various values of λ are compared in Table II.

In view of some of the as yet unresolved experimental difficulties in the wall motion experiments and the inaccuracy they may have caused, it seems wise to emphasize the agreement in order of magnitude between the values determined in the two different ways. The value of λ determined from ferromagnetic resonance, in Fe_3O_4, however, is probably somewhat too high because of experimental problems which arise when samples are not small compared to the skin depth.[20] Also, further ferromagnetic resonance work is desirable to determine the variation of λ with frequency,

All the factors in Eq. (17) have now been evaluated. We find for Fe_3O_4, $m=9.5\times10^{-11}$ g/cm^2, and for $NiOFe_2O_3$, $m=9.4\times10^{-11}$. These values are so small that we can neglect the first term in Eq. (2) in both cases. It is possible, however, that with better crystals the value of m in nickel ferrite could be measured from the shape of the signal induced in the secondary winding in the wall velocity *versus* applied field experiment.

[16] C. Guillaud and M. Roux, Compt. rend. 229, 1133 (1949).
[17] Yager, Galt, Merritt, and Wood, Phys. Rev. 80, 744 (1950).
[18] See Eq. (A-6) of reference 16. The λ of the present paper is equal to $\gamma\alpha M_s$ in the notation of reference 16.
[19] D. W. Healy, Jr., Phys. Rev. 86, 1009 (1952).
[20] Yager, Merritt, and Guillaud, Phys. Rev. 81, 477 (1951).

CC-0. In Public Domain. Gurukul Kangri Collection, Haridwar

Digitized by Arya Samaj Foundation Chennai and eGangotri

A Richter Type After-Effect in Ferrites Containing Ferrous and Ferric Ions

H. P. J. WIJN AND H. VAN DER HEIDE

Philips Research Laboratories, N. V. Philips' Gloeilampenfabrieken, Eindhoven, Netherlands

IN magnetic materials the losses in low fields can be divided into three kinds, e.g., hysteresis, eddy-current, and residual losses.[1] In ferrites the eddy-current losses generally are negligible, and for very small amplitudes of the magnetic field strength, the residual losses are predominant. Snoek[2] found that in this case the loss factor tanδ remains constant up to a certain frequency and from here on rises suddenly to high values. He ascribes[2,3] this rise to a gyromagnetic resonance of the electron spins.

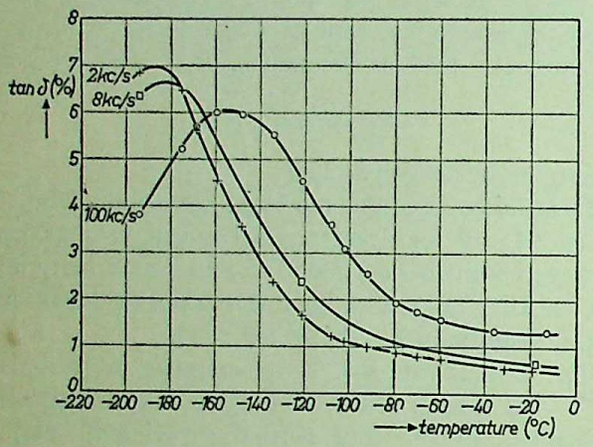


FIG. 1. The loss factor tanδ of a MnZn ferrite with chemical composition in mole percent about 28 MnO, 19 ZnO, 3 FeO, and 50 Fe_2O_3 as a function of temperature, measured for various frequencies at a field strength of 2.5 mθ.

We have measured the complex permeability of ring-shaped ferrite cores in a Maxwell bridge[4] as a function of temperature and frequency, and we found that for some ferrites still another region of dispersion of the initial permeability exists. Figure 1 shows the results of these measurements for a MnZn ferrite having a chemical composition in mole percent of about 28 MnO, 19 ZnO, 3 FeO, and 50 Fe_2O_3. These results are typical for a relaxation phenomenon, and look quite similar to those found by Schulze[5] for carbonyl iron having a high Richter type after-effect, which has been explained by Snoek.[6] In Fig. 2 is shown the relation between the logarithm of the frequency and the inverse of the temperature at which the tanδ-curves of Fig. 1 have a maximum. This relation can be described by the general relaxation formula

$$\tau = \tau_\infty \exp(E/kT),$$

where τ is the reciprocal of the angular frequency, T is the absolute temperature, and E an activation energy determining the relaxation process. The slope of the straight line in Fig. 2 corresponds to an activation energy $E = 0.11$ ev. As this small activation energy points to an electron diffusion process, the same kind of measurements has been carried out for a NiZn ferrite (chemical composition in mole percent approximately 25 NiO, 25 ZnO, and 50 Fe_2O_3) with a high resistivity, e.g., about $10^7\Omega$ cm, while the MnZn ferrite has a resistivity of about 100Ω cm at room temperature. The

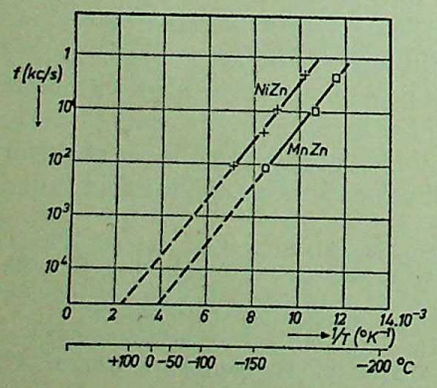


FIG. 2. The relation between the frequency and the temperature at which the tanδ curves of the figures 1 and 3 have a maximum.

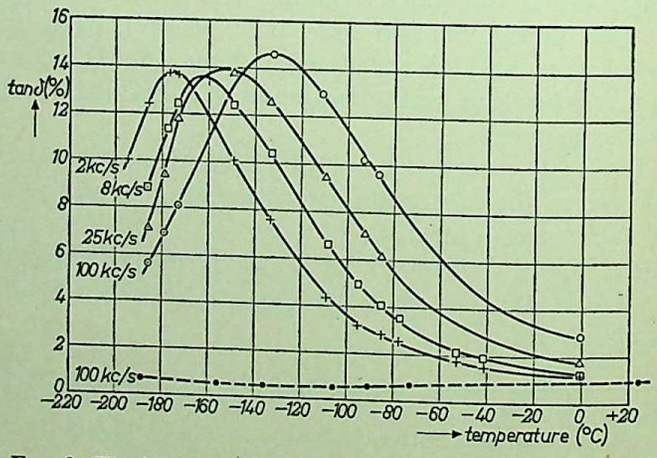


FIG. 3. The loss factor tanδ at a field strength of 2.5 $m\theta$ as a function of temperature for two NiZn ferrites with chemical composition in mole percent about 25 NiO, 25 ZnO, and 50 Fe_2O_3. – – – – ferrite fired at 1250°C, and having a resistivity of $10^7\Omega$ cm. ——— ferrite fired at 1525°C. and having a resistivity of $10^4\Omega$ cm.

[1] R. M. Bozorth, *Ferromagnetism* (D. Van Nostrand Company, Inc., New York, 1951), p. 780.
[2] J. L. Snoek, Physica 14, 207 (1948).
[3] J. L. Snoek, Nature 160, 90 (1947).
[4] This Maxwell bridge was constructed by J. W. L. Köhler and C. G. Koops of this laboratory.
[5] H. Schulze *Probleme der Technischen Magnetisierungskurven* (Julius Springer, Berlin, 1938), p. 114.
[6] J. L. Snoek, Physica 8, 711 (1941).

CC-0. In Public Domain. Gurukul Kangri Collection, Haridwar

Digitized by Arya Samaj Foundation Chennai and eGangotri

dotted curve in Fig. 3 gives for this NiZn ferrite the loss factor tanδ, measured at 100 kc/sec as a function of temperature. Though in the temperature range covered, tanδ is not wholly constant, the large relaxation effects which have been found in the MnZn ferrite are now absent. This NiZn ferrite with a high resistivity was fired at 1250°C in an atmosphere of oxygen and we must assume that the iron ions are in the trivalent state. Therefore we have refired this kind of ferrite in the same atmosphere but at a higher temperature (1525°C), thereby introducing the order of 0.5 percent of ferrous ions in the ferrite. The influence of this refiring upon the loss factor tanδ is also shown in Fig. 3. It can be seen that similar results are obtained as for the MnZn ferrite which also contains both ferric and ferrous ions. Also the activation energies of the relaxation processes in both ferrites are the same (Fig. 2). An activation energy of the order of 0.1 ev was found earlier by Verwey and Haayman[7] from the temperature dependence of the resistivity of Fe_3O_4 above the transition point. For a NiZn ferrite the same activation energy has been found for the mechanism which governs the residual losses and for the temperature dependence of the direct current resistance of this ferrite.

These results are quite similar to the relaxation found by Galt, Matthias, and Remeika[8] in the permeability of a single crystal of Ni ferrite, and also to the relaxation found by Kamiyoshi[9] for the dielectric constants of Ni and Co ferrite. They warrant the conclusion that the after-effect found in ferrites containing iron ions in two valencies is due to a diffusion process of electrons.

[7] E. J. W. Verwey and P. W. Haayman, Physica 8, 979 (1941).
[8] Galt, Matthias, and Remeika, Phys. Rev. 79, 391 (1950).
[9] K. Kamiyoshi, Phys. Rev. 84, 374 (1951).

CC-0. In Public Domain. Gurukul Kangri Collection, Haridwar

Digitized by Arya Samaj Foundation Chennai and eGangotri

REVIEWS OF MODERN PHYSICS VOLUME 25, NUMBER 1 JANUARY, 1953

Neutron Diffraction Studies of Various Transition Elements

C. G. SHULL AND M. K. WILKINSON

Oak Ridge National Laboratory, Oak Ridge, Tennessee

Neutron diffraction measurements are reported on a series of transition elements as an investigation into their magnetic structures. Scattering data have been taken for W, Mo, Nb, V, Cr, Mn, and Fe at various temperatures as low as 4.2°K, and these data are interpreted in terms of the magnetic structure existing in the pure metals. For the first four-named elements, no magnetic scattering either coherent or incoherent is found. Cr and α-Mn are established as being antiferromagnetic with Néel temperatures of 475°K and 100°K, respectively. Paramagnetic scattering has been observed in manganese at room temperature, and the atomic moments determined for Cr and Mn follow the general trend of the Slater-Pauling curve. Magnetic superstructure effects and magnetic disorder scattering were looked for in iron and neither was found.

INTRODUCTION

IN striking contrast to the situation in crystals containing ions of the transition elements or the rare-earth elements, the magnetic structures existing in the transition elements can be considered as being very poorly understood. Aside from the relatively few cases of ferromagnetism for which an average, effective magnetic moment per atom can be ascertained from magnetic measurements, the magnetic susceptibility data are not too informative. Temperature-independent susceptibility values are the rule for the transition elements and the interpretation of this is certainly not straightforward. Recent researches by Zener and coworkers have followed the atomistic viewpoint in which the electronic structure of a given atom in the metal lattice is considered to be much the same as the configuration in a free atom. These considerations have suggested the presence of strong localized atomic moments arranged in an antiferromagnetic manner, and hence their presence is not easily evidenced in macroscopic magnetic properties. Since neutron diffraction measurements are able in principal to determine the strength and relative orientation of atomic moments in a scattering lattice, it was to be hoped that such measurements would offer illuminating information on the magnetic structures.

The transition elements which have been investigated in the present study are listed in Table I along with the characteristic configuration of the outer electron assembly in the atom as determined from spectroscopic data on the free atoms. If these configurations were representative of the metallic atoms, we should expect large atomic moments in the metals, for example $5\mu_B$ for chromium, since the five $3d$ electrons are arrayed with parallel spin according to usual spectroscopic rules. Such atomic moments should contribute (a) pronounced coherent scattering to the neutron diffraction pattern if there is any alignment correlation between neighboring moments or (b) measurable diffuse scattering in the pattern if the moments are uncorrelated in orientation. Powder diffraction data were obtained for these elements both at room temperature and when held at very low temperature in a double-jacketed vacuum cryostat. All were examined at liquid hydrogen temperature (20.4°K), some were cooled to liquid helium temperature (4.2°K), and others were studied at various intermediate temperatures including examination at elevated temperatures up to 500°C in a furnace. Temperature gradients within the sample container were studied by superconductivity observations at the very lowest temperatures and with calibrated thermocouples at higher temperatures.

TABLE I. Electronic configuration existing in isolated atoms of the various transition elements for which neutron diffraction studies are reported.

	3d	4s	4d	5s	5d	6s
V	3	2				
Cr	5	1				
Mn	5	2				
Fe	6	2				
Nb			4	1		
Mo			5	1		
W					4	2

EXPERIMENTAL RESULTS

V, Nb, Mo, and W

The data for these elements are discussed collectively since they indicate the complete absence of any measurable coherent or incoherent magnetic scattering in the powder diffraction patterns for these materials. All of these materials were of the highest purity available (spectroscopically 99.9 percent or higher) and were examined in the form of filings or fine powder. The samples were sealed in a thin-walled aluminum specimen capsule which in turn was placed in a double-jacketed Dewar cryostat. The cryostat construction was such that a minimum of neutron scattering occurred from the vacuum walls and thermal radiation shields, and corrections were made for this scattering in the neutron

CC-0. In Public Domain. Gurukul Kangri Collection, Haridwar

Digitized by Arya Samaj Foundation Chennai and eGangotri

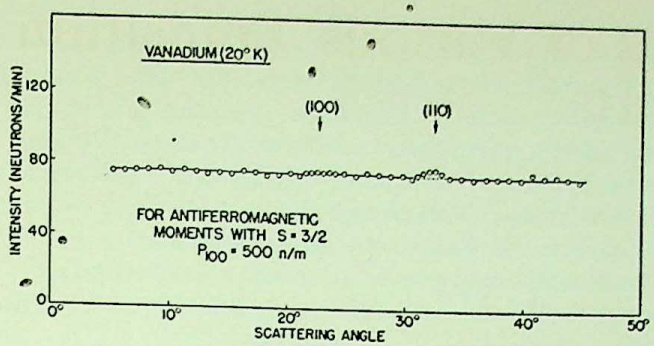


FIG. 1. Neutron diffraction pattern for V taken at 20°K. No antiferromagnetic reflection at the (100) position is to be noted.

diffraction patterns. Typical patterns taken at liquid hydrogen temperature (20.4°K) are shown for V and for Mo in Figs. 1 and 2.

The pattern for V in Fig. 1 shows the presence of a very weak (110) reflection and this is a regular body-centered cubic lattice reflection. It is very weak because the coherent nuclear scattering cross section for vanadium is very small, amounting to only 0.035 barn as determined in the reflection. Practically all of the vanadium nuclear scattering is nuclear spin disorder scattering, and this appears as a completely isotropic diffuse scattering in the pattern. Of interest here is the absence of any measurable (100) intensity. If an antiferromagnetic body-centered cubic lattice existed in vanadium, magnetic reflection should be observable at the (100) position with an intensity commensurate with the strength of the vanadium magnetic moment. Calculating the expected intensity on the basis of a magnetic moment of 3 Bohr magnetons (for the three electrons in Table I) leads to an expected (100) peak intensity of 500 neutrons/minute whereas nothing like this is observed. An upper limit on the possible (100) intensity can be estimated, and this implies that any *aligned* moments in vanadium must be smaller than about 0.1 Bohr magneton. Likewise, the diffraction data can be used to evaluate the strength of any *unaligned* moments in vanadium from the appearance of the diffuse scattering. If unaligned moments are present, then incoherent diffuse scattering should be observable and this should be recognizable by its form factor angular variation. In Fig. 3 is shown the observed diffuse scattering for vanadium after correction for the isotropic nuclear spin incoherent scattering of 5.1 barns and for comparison the calculated scattering for unaligned moments of 3 Bohr magnetons. Again the data do not support such a large moment and from the sensitivity of observation an upper limit of about 0.1 Bohr magneton for the possible *unaligned* moments is the most that would be consistent with the data.

Unlike the vanadium pattern, the pattern for Mo given in Fig. 2 contains strong nuclear reflections at the regular b.c.c. positions. In addition to the principal reflections at the (110), (200), etc., positions produced with the primary neutron wavelength of 1.212A, there exists a series of weak reflections produced by a beam of second-order neutron wavelength (0.606A) which is obtained from the monochromating crystal in the neutron diffraction spectrometer. The relative intensity of second-order neutrons to primary neutrons has been determined accurately, and the observed intensities of the secondary peaks in Fig. 2 are such as to be explained entirely by this contaminant wavelength. Thus, there is no observable (100) intensity in the pattern, and this indicates the absence of an antiferromagnetic lattice in Mo. Arguments similar to those used for vanadium would place an upper limit of about 0.3 Bohr magneton for the possible aligned moments and about 0.2 Bohr magneton for the possible

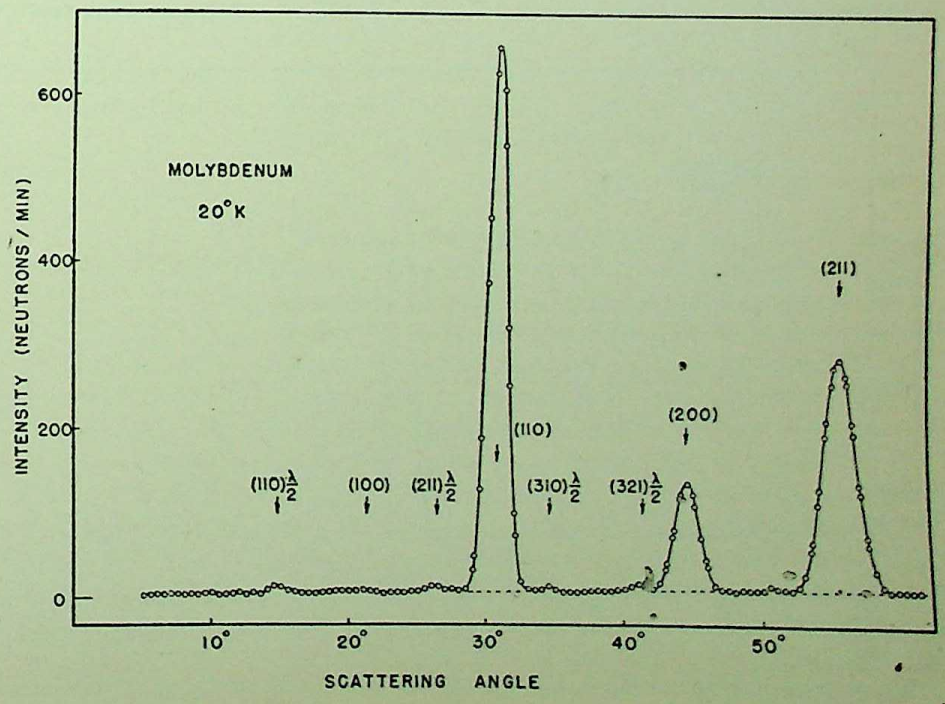


FIG. 2. Neutron diffraction pattern for Mo taken at 20°K. Large nuclear reflections are seen along with secondary weak reflections of half-wavelength origin.

CC-0. In Public Domain. Gurukul Kangri Collection, Haridwar

Digitized by Arya Samaj Foundation Chennai and eGangotri

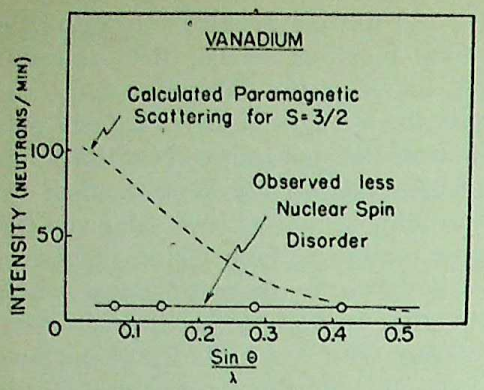


FIG. 3. Diffuse scattering observed for V after correction for nuclear spin disorder scattering. The expected paramagnetic scattering for $S=3/2$ is shown.

unaligned moment strength. The room temperature pattern for Mo, which is not shown, was completely similar to the low temperature pattern except for a slight decrease in the intensities of the lines (the normal Debye-Waller temperature effect) and a noticeable change in the amount of thermal diffuse scattering from the lattice.

A study of the patterns for Nb and W gave results completely analogous to those of V and Mo. There was no observable (100) intensity in any of the patterns, either at 20°K or 295°K, and no suggestion of an angularly dependent diffuse scattering. Thus no localized atomic moment, either aligned or unaligned, could be attributed to the metallic lattice.

In addition to the patterns taken at liquid hydrogen temperature, two of the elements, V and Nb, were also studied at liquid helium temperature (4.2°K) below their superconducting transition. This produced no change in their patterns so that the magnetic structure conclusions are unaltered. Further details of these last-mentioned measurements will be given in a separate publication.

Cr

A sample of electrolytic chromium flake was the principal source of diffraction specimens. This flake was given a quantitative spectroscopic assay and found to be 99.98+ percent pure with less than 0.01 percent Fe and less than 0.01 percent Mn as the only detectable impurities. The flakes were ground in a mortar and the examination was carried out on a fine powder. A typical pattern obtained at 20°K is shown in Fig. 4. Normal nuclear reflections are seen at the (110), (200), and (211) positions, along with secondary peaks of second-order wavelength contribution. In this case, however, the intensity at the (100) position is about five times what it should be if there were only $\lambda/2$ contribution from the (200) reflection. Thus, there appears to be a weak but perfectly measurable (100) reflection for Cr which suggests an antiferromagnetic lattice.

This reflection has been studied in detail to see if it really were of magnetic origin. It was found to be temperature sensitive, much more so than the other nuclear reflections, either the large normal reflections or the weak secondary ones. Figure 5 summarizes this temperature dependence, and it is seen that the (100) reflection disappears at temperatures above 200°C. The temperature dependence is strongly suggestive of a magnetic reflection since it follows a Brillouin function variation with a suggested Néel temperature of 200°C. It was found to be perfectly reversible. The possibility that this might be an impurity reflection and not a true Cr lattice reflection was studied in a variety of ways. An x-ray diffraction pattern of the sample showed no lines other than for the pure metal, and a very careful study* of the x-ray pattern in the region of the (100) reflection showed the complete absence of a (100) reflection. Moreover, the angular position and temperature dependence of this reflection were such as to rule out it being a magnetic reflection

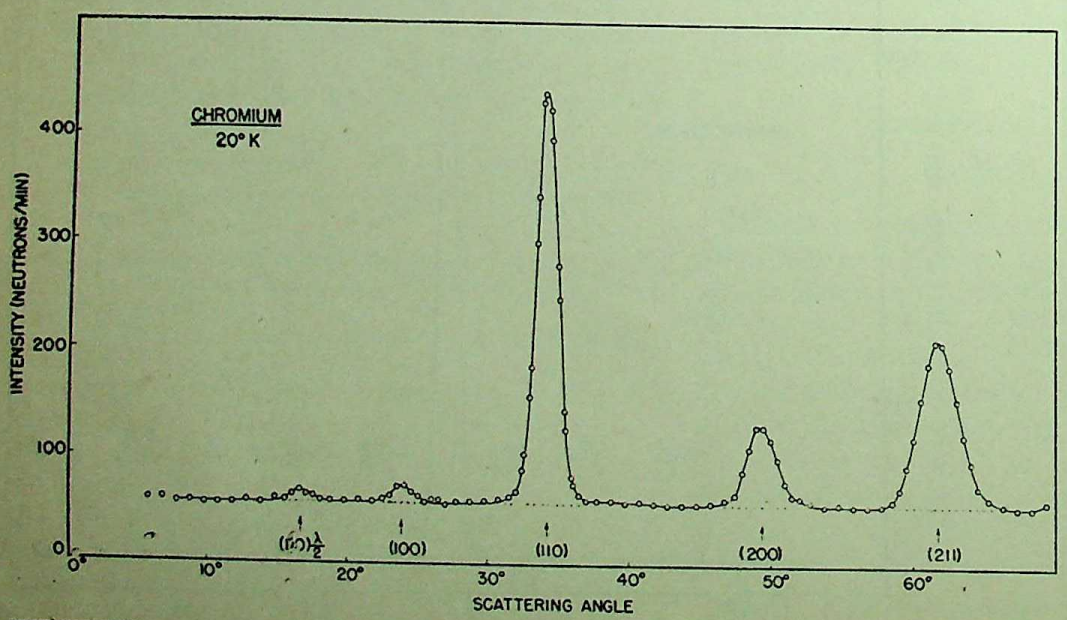


FIG. 4. Neutron diffraction pattern for Cr taken at 20°K. Extra antiferromagnetic intensity exists in the (100) reflection over and above a weak $\lambda/2$ contribution (compare with Fig. 2).

* We are much indebted to Mr. B. S. Borie and Mr. R. S. Steele for these x-ray measurements.

CC-0. In Public Domain. Gurukul Kangri Collection, Haridwar

Digitized by Arya Samaj Foundation Chennai and eGangotri

(and hence not measurable with x-rays) of the two stable chromium oxides, Cr_2O_3 and CrO_2. Additionally, several samples which were obtained from different sources or had been subjected to different treatment were examined. These included (1) a sample of very fine electrolytic chromium powder from a different source than the chips, (2) a sample of the electrolytic flakes which had been crushed only to 30<40 mesh rather than a fine powder, (3) a sample of relatively impure chromium (containing 0.96 percent Fe and 0.2 percent Mn) manufactured by an aluminum reduction method, (4) a sample of electrolytic flake which had been degassed by high vacuum heat treatment at 500°C, and (5) a sample of electrolytic flake which had been heat treated in air at 500°C until noticeable oxide had been formed. Examination of all of these samples showed the same anomalous neutron intensity at the (100) position relative to the large (110) intensity or the (110) ($\lambda/2$) intensity.

The intensity in the (100) reflection has been placed on an absolute scale in terms of differential scattering cross section, and this has been plotted in Fig. 5. It is seen to saturate at a value of 0.0038 barn/steradian per Cr atom, and this can be used to evaluate the magnetic moment of the Cr atoms arranged in a simple antiferromagnetic array. This results in an effective magnetic moment of 0.40 Bohr magnetons per atom, a value which is still very much smaller than that predicted on the atomistic viewpoint expressed in Table I.

Again it is instructive to look at the diffuse scattering in the Cr pattern to see if there might be any unaligned moment contribution. Figure 6 shows the observed diffuse scattering obtained for Cr at a temperature of 20°K and for comparison purposes the calculated magnetic diffuse scattering for unaligned moments of strength 5 Bohr magnetons. From the apparent isotropy in the observed intensity an upper limit on the possible magnetic diffuse scattering places the maximum strength of the unaligned moments at about 0.1 magneton. Thus the large difference between the predicted atomistic moment and the $0.40\mu_B$ which is observed in antiferromagnetic alignment can by no means be accounted for by an unaligned component.

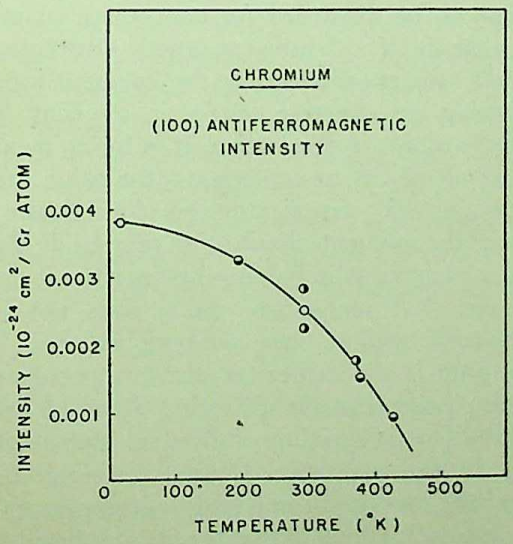


FIG. 5. Temperature dependence of the Cr (100) antiferromagnetic intensity in absolute units of differential scattering cross section.

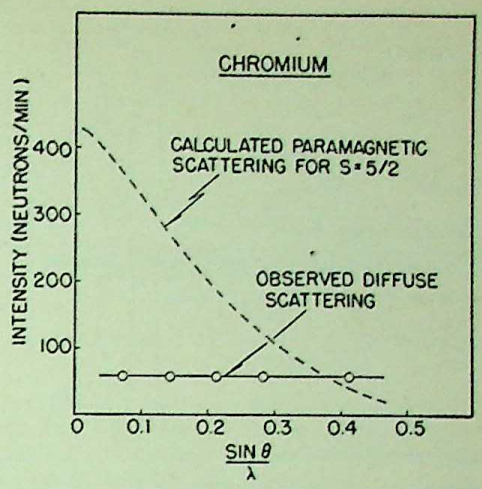


FIG. 6. Diffuse scattering observed in the neutron diffraction pattern for Cr showing the absence of any appreciable component of paramagnetic scattering.

It has been suggested that the low value for the observed Cr moment might be associated with a rapidly changing polarity of the moment in the lattice. The observed small value of $0.4\mu_B$ would then represent a residual moment which the neutron would see during its passage time ($\sim 10^{-13}$ sec) in the vicinity of an atomic moment. If such were the case, the residual moment should be quite sensitive to the neutron's velocity or wavelength. As a test on this, a pattern was taken with a neutron wavelength of 0.900A rather than the usual 1.212A, and this showed no significant change in the intensity of the (100) reflection relative to that of the (110) nuclear reflection. Changing the passage time by 25 percent should have changed the residual magnetic moment by several hundred percent if there had been a coincidental phase relationship between the neutron's speed and the polarity flipping of the magnetic moments, and nothing like this was observed.

Mn

This material was examined in the form of α-manganese, which possesses a cubic unit cell of size 8.894A containing 58 atoms. The sample first examined was of electrolytic origin in the form of a very fine powder. This was found to show oxide impurity in the diffraction pattern and was discarded in favor of treated electrolytic chips. As obtained from the commercial vendor the electrolytic manganese flakes possessed a characteristic surface layer of brownish oxide. This oxide layer was removed by dipping the electrolytic flakes into dilute hydrochloric acid followed by rinsing and drying. The flakes, of bright metallic appearance, were then fragmented in a mortar and placed in a high vacuum furnace for degassing at about 300°C. Following this, the

CC-0. In Public Domain. Gurukul Kangri Collection, Haridwar

Digitized by Arya Samaj Foundation Chennai and eGangotri

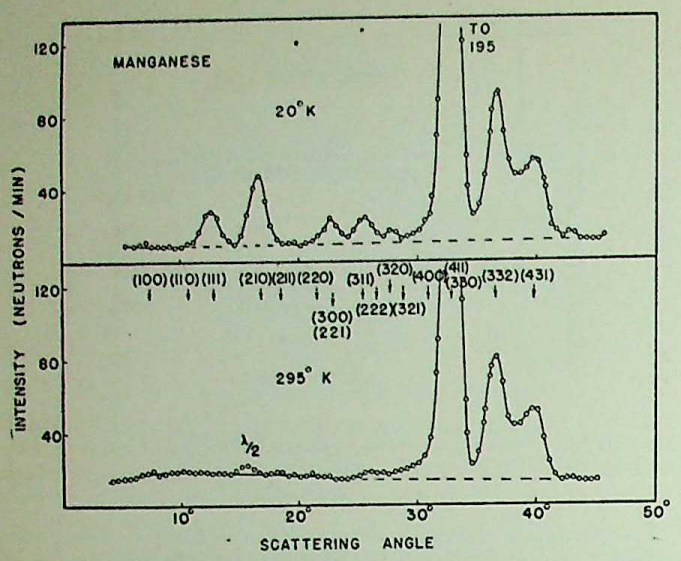


FIG. 7. Neutron diffraction patterns for α-Mn taken at 20° and 295°K. Extra antiferromagnetic reflections are to be seen in the low temperature pattern which transform into paramagnetic scattering with short-range order characteristics at room temperature.

small chips were sealed into an aluminum capsule for examination in the neutron diffraction spectrometer. This procedure of specimen preparation was found to show no measurable oxide impurity in the diffraction pattern. Spectroscopic analysis indicated a purity of 99.98+ percent with Ca and Cu as the primary impurities.

Figure 7 shows diffraction patterns for α-Mn taken at room temperature and at 20.4°K. In the room temperature pattern are observed the normal lattice reflections caused by nuclear scattering, as well as an angularly dependent diffuse scattering which is attributed to paramagnetic scattering. At the low temperature there is noticed a decrease in the paramagnetic diffuse scattering and a pronounced build-up of extra coherent scattering. The new reflections are at the (111), (210), (300)–(221), and (311) positions. Since these reflections have zero structure factors for a lattice in which

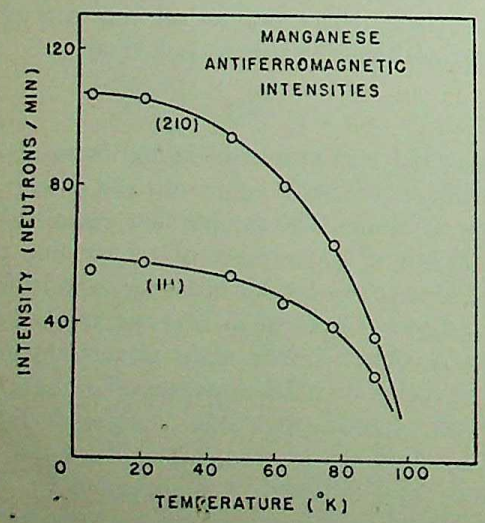


FIG. 8. Temperature dependence of the (111) and (210) antiferromagnetic reflections in α-Mn. The Néel temperature is at 100°K.

every Mn atom is the same, their appearance in the low temperature neutron pattern immediately suggests an antiferromagnetic lattice. The nuclear reflections are unaltered in intensity or location, aside from a normal temperature dependence, and this can be taken as evidence that there has not occurred any gross crystallographic transformation on cooling.

A careful study of the temperature dependence of the extra low temperature reflections at temperatures as low as 4.2°K has been made, and Fig. 8 summarizes this for the two reflections, (111) and (210). Again as with the extra reflection in Cr, a Brillouin-type temperature dependence is indicated with a Néel temperature of 100°K. The intensities are reversible and within the significance of the measurements show no hysteresis effects.

Because of the lattice complexity and the limited number of magnetic reflections which were measurable, it has not been possible to describe the antiferromagnetic structure which sets in below 100°K. A number of possible models were studied† which led to finite and

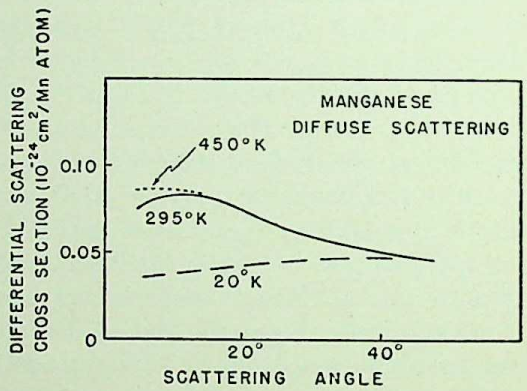


FIG. 9. Diffuse scattering observed in the neutron diffraction pattern for α-Mn at various temperatures. The paramagnetic scattering in the forward direction amounts to $0.060 \cdot 10^{-24}$ cm^2/steradian per Mn atom.

reasonable intensities for the magnetic reflections, but these had to be discarded for one reason or another. In the absence of a detailed magnetic structure model it has not been possible to use the coherent intensities in assigning an effective magnetic moment for the manganese atoms in the lattice. It is by no means certain that all of the atoms possess the same magnetic moment and this complicates the picture even more. Whatever the moment distribution may be, it is certain that they must exist in balanced pairs since it has been established that manganese metal does not become ferromagnetic even at these low temperatures.

Of interest in the higher temperature patterns is the observable paramagnetic scattering. At room temperature there is a suggestion of residual short range coherence in the magnetic diffuse scattering and this short-range order has been found to disappear at higher temperatures. Figure 9 illustrates the absolute intensity

† We wish to thank Dr. B. W. Roberts for investigating some of these models.

CC-0. In Public Domain. Gurukul Kangri Collection, Haridwar

Digitized by Arya Samaj Foundation Chennai and eGangotri

of the diffuse scattering expressed in units of differential scattering cross section for temperatures of 20°, 295°, and 450°K. These curves have been corrected for a small amount of thermal diffuse scattering, and the differences from one temperature to another represent changes in magnetic diffuse scattering. The characteristic form factor variation of the scattered intensity with scattering angle is to be noticed in the higher temperature curves. From the absolute intensity of the magnetic scattering (that portion associated with the form factor), which is seen to amount to about 0.060 barn/steradian per Mn atom in the forward direction, it is possible to determine an average or effective magnetic moment for manganese in the paramagnetic state. Halpern and Johnson[1] have given a theoretical evaluation of the paramagnetic cross section as

$$d\sigma\ (\text{para}) = 0.194 \cdot 10^{-24} S(S+1)\ \text{cm}^2$$

in the forward direction. Here S represents the spin quantum number of the magnetic atom. A straightforward application of the above experimental cross

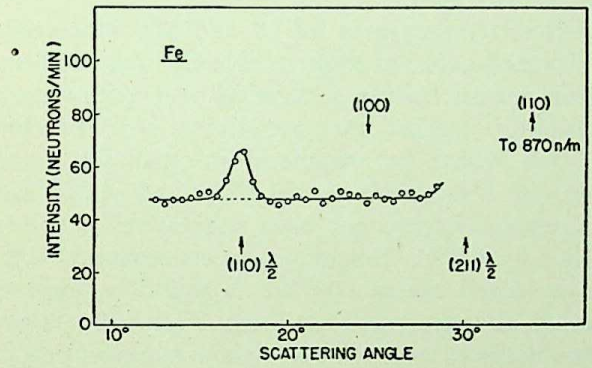


FIG. 10. Portion of the neutron diffraction pattern for Fe showing the region around the (100) reflection.

section leads to $S = 0.25$ and hence a magnetic moment of 0.5 Bohr magneton per Mn atom. However, it is rather doubtful that the above formulation can be significantly used with such a small cross section corresponding to less than one electronic magnetic moment. Perhaps a more significant interpretation of the cross section is in terms of the fraction of the atoms which possess say one Bohr magneton with the rest exhibiting no magnetic moment. In this way a distribution of 40 percent of the atoms having $1\mu_B$ and 60 percent having no moment would be in agreement with the observation.

Fe

Neutron diffraction measurements on unmagnetized and magnetized Fe have been reported earlier,[2] and these have shown the presence of ferromagnetic scattering superimposed on strong nuclear reflections. The

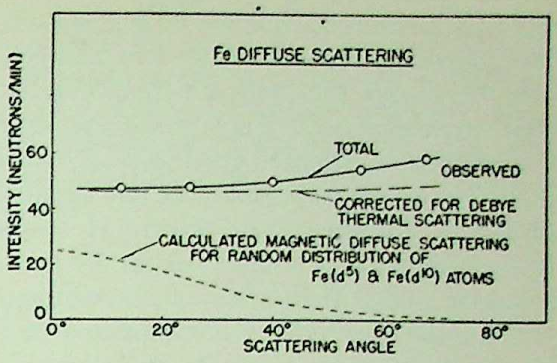


FIG. 11. Diffuse scattering observed in the neutron diffraction pattern for Fe. Magnetized sample studies permit a quantitative determination of the amount of magnetic disorder scattering which might be present in the diffuse scattering.

strength of the magnetic scattering was found to be in agreement with the Fe moment of $2.22\mu_B$ and the angular variation of the magnetic scattering was in satisfactory agreement with theoretical estimates of the magnetic form factor. Since that time, additional measurements have been made on the intensity at the possible superstructure line position (100) and on the diffuse scattering in order to establish limits on the possible difference between local atomic moments.

A concentrated study of the intensity at the (100) position for iron was carried out for two neutron wavelengths, 1.212A and 0.900A. The sample was in the form of filings from pure Armco iron which were given a vacuum heat treatment at 500°C. Figure 10 illustrates the intensity in the region of the (100) reflection, and it has been established that all of the observed reflection here can be accounted for satisfactorily by the second-order contaminant of known amount. From the sensitivity of observation it has been established that the differential scattering cross section F^2_{100} for magnetic scattering in the (100) superstructure line must be less than $0.0010 \cdot 10^{-24}$ cm² per Fe atom. This can then be used to set an upper limit on the difference between the magnetic moments μ_1 and μ_2 which might exist for the two unique atoms of the body-centered cubic unit cell. Such considerations show that $\mu_1 - \mu_2$ must be less than $0.4\mu_B$. In other words, if an ordered array of iron atoms existed with a unit cell containing an iron atom of moment μ_1 at the corner position and an iron atom of moment μ_2 at the body-centered position, then these two atomic moments could not differ *algebraically* by more than $0.4\mu_B$. This upper limit for the difference is very much smaller than the $6.0\mu_B$ suggested by Zener's model[3] or the $5.0\mu_B$ suggested by Hume-Rothery, Irving, and Williams.[4]

In addition to the investigation of the coherent scattering effects produced by a possible ordered distribution of magnetic moments in metallic iron, a study of the diffuse scattering should yield information on the

[1] O. Halpern and M. H. Johnson, Phys. Rev. 55, 898 (1939). See also Shull, Strauser and Wollan, Phys. Rev. 83, 333 (1951) for experimental results.
[2] Shull, Wollan, and Koehler, Phys. Rev. 84, 912 (1951).
[3] C. Zener, Phys. Rev. 85, 324 (1952).
[4] Hume-Rothery, Irving, and Williams, Proc. Roy. Soc. (London) 208, 431 (1951).

CC-0. In Public Domain. Gurukul Kangri Collection, Haridwar

Digitized by Arya Samaj Foundation Chennai and eGangotri

presence of a random distribution of moments. If two magnetic ions of moments μ_1 and μ_2 were randomly distributed throughout the body-centered cubic lattice, magnetic incoherent scattering would be expected whose intensity would depend upon $(\mu_1-\mu_2)$ and which would exhibit a magnetic form factor variation of intensity with scattering angle. Figure 11 shows the diffuse scattering which is observed for Fe and after correction for normal Debye thermal scattering, this is seen to be closely isotropic. For comparison purposes there is also shown on the graph the expected magnetic disorder scattering for a randomly distributed arrangement of Fe(d^5) and Fe(d^{10}) ions. Since all of the known components in the diffuse scattering are isotropic or very nearly so, it is not considered possible that the observed scattering could contain very much of the form factor magnetic scattering.

A more quantitative estimate of the magnetic portion can be obtained if the diffuse scattering is studied

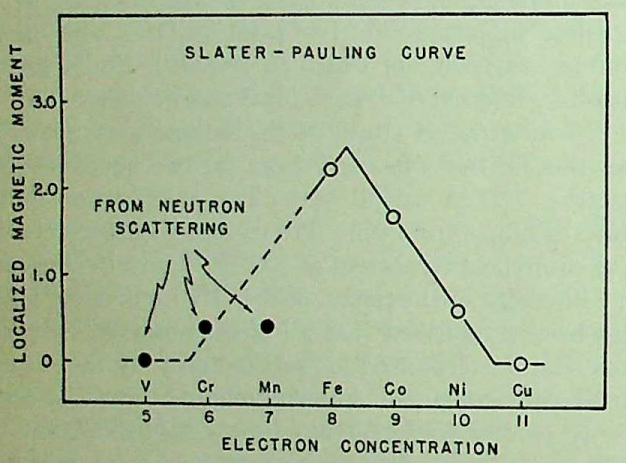


FIG. 12. Comparison between the observed atomic moments as determined by neutron scattering and the Slater-Pauling curve.

with a magnetized scattering sample. By magnetizing the sample in a direction parallel to the scattering vector, thereby directing all of the atomic moments in this sense, all of the magnetic scattering should disappear according to the theory of magnetic scattering for neutrons. This has been tested experimentally by placing the sample between the pole pieces of an electromagnet capable of applying a field of about 8000 oersteds. The diffuse scattering was studied at a scattering angle of 8°, and it was found not to change by more than 1 percent upon magnetization. This upper limit on the change of intensity has been converted to absolute units and places the magnetic disorder scattering at less than $0.0035\cdot10^{-24}$ cm²/Fe atom. In turn this implies that the difference $(\mu_1-\mu_2)$ must be less than $0.6\mu_B$, or there would have been a noticeably larger magnetic diffuse scattering in the neutron pattern. This difference is again very much smaller than those mentioned in the above references.

DISCUSSION

Most of the present observations on the magnetic structures existing in the transition elements can be summarized by reference to the Slater-Pauling curve shown in Fig. 12. In attempting to explain the variation of saturation magnetization among the ferromagnetic elements and some of their alloys, Slater has offered band theory arguments to account for the almost linear variation of moment with outer electron concentration. A simplified picture was independently developed by Pauling in terms of a distribution of the outer electron system among stable atomic orbitals (which contribute to the macroscopic magnetic properties) and molecular bonding orbitals (which serve valence purposes), and Pauling extended the treatment to include other nonferromagnetic elements. It is seen that the experimental data for vanadium, chromium, and manganese do indeed follow the general trend of their predictions. The manganese crystal structure is so complicated and so different from all of the other simple structures that the apparent numerical disagreement for this case may not be troublesome.

The Néel temperatures for Cr and Mn which have been reported here have not received strong confirmation from measurements of physical properties such as susceptibility, specific heat, resistivity, etc. For chromium, the recent paramagnetic susceptibility measurements of Fine, Greiner, and Ellis[5] and of McGuire and Kriessman[6] have not been suggestive of a Néel transition at 200°C. This may be a consequence of the relatively small moment which is found by neutron scattering and the relatively high Néel temperature. The anomalies in resistivity and other physical properties found by Fine *et al.* at 40°C for chromium do not correlate with the Néel temperature of 200°C. The early work of Serres[7] on the susceptibility of manganese did indeed suggest a low temperature antiferromagnetic transition, but this was open to suspicion because of possible oxide presence (both MnO and MnO_2 possess Néel temperatures in this region) as Serres has pointed out. A noticeable specific heat anomaly in manganese at 95°K has been reported by Shomate,[8] and recent unpublished measurements by Patrick have also indicated an abrupt change in resistivity at about 83°K. Both of these latter measurements may very well be associated with an antiferromagnetic transition.

The observations on iron have indicated the lack of either an ordered or disordered distribution of sizeably different magnetic ions at least as seen by neutrons in a scattering experiment. Of course, if such a distribution of ionic strength did occur and there were very rapid transitions for any one ion from one state to

[5] Fine, Greiner, and Ellis, J. Metals **189**, 56 (1951).
[6] T. R. McGuire and C. J. Kriessman, Phys. Rev. **85**, 452 (1952).
[7] A. Serres, J. phys. et radium **9**, 377 (1938).
[8] C. H. Shomate, J. Chem. Phys. **13**, 326 (1945).

CC-0. In Public Domain. Gurukul Kangri Collection, Haridwar

Digitized by Arya Samaj Foundation Chennai and eGangotri

another in a time which is much shorter than the neutron passage time of 10^{-3} seconds, then the neutron would see just the average of the different states and all iron atoms would appear identical, in agreement with experiment. Since it appears necessary to admit of a mixture of states to account for the odd moment, this may very well be a reasonable picture.

ACKNOWLEDGMENT

We wish to thank Mr. L. A. Rayburn for considerable assistance in the preparation of suitable samples and in some of the later data accumulation. Very helpful conversations and correspondence with Dr. J. E. Goldman, Dr. J. C. Slater, and Dr. C. Zener have been appreciated.

DISCUSSION

W. J. CARR, JR., *Westinghouse Research Laboratory, East Pittsburgh, Pennsylvania:* In connection with the data on Ni_3Mn and Ni_3Fe it seems worth pointing out that, since the alloys did not have perfect order, one would expect a number of Mn or Fe nearest neighbors to exist. If such Mn or Fe nearest neighbors exhibit an antiferromagnetic behavior, it would require a reinterpretation of Dr. Shull's data and lead to different calculated moments for the Fe, Mn, and Ni atoms.

H. ECKSTEIN, *Armour Research Foundation, Chicago, Illinois:* Have you assumed purely elastic scattering? Is it possible that the spin coupling is only of the order of a fraction of an ev? Then the elastic scattering should be considered.

CC-0. In Public Domain. Gurukul Kangri Collection, Haridwar

Digitized by Arya Samaj Foundation Chennai and eGangotri

REVIEWS OF MODERN PHYSICS VOLUME 25, NUMBER 1 JANUARY, 1953

Atomic Moments in Alloys

J. E. GOLDMAN

*Carnegie Institute of Technology, Pittsburgh, Pennsylvania**

The saturation moment of ferromagnetic alloys has been considered from the point of view of the collective electron theory. Perturbations in band shape due to the fluctuating lattice potential are considered and are found to be more important in some cases than the simple effects of changing electron density characteristic of the usual treatment of alloys. The influence of order on the moment is treated on the basis of Slater's theory of the relation between the long range order and the energy bands in an alloy. Results of measurements of electronic specific heat and Hall effect are presented which make possible a model capable of explaining the unique effects of the order-disorder transformation in Ni_3Mn on this basis. In other alloys, particularly those which do not follow the Slater-Pauling curve or the classical band model, the saturation properties are attributed to the perturbations in the band resulting from the presence in the lattice of ions with different potentials as seen by the itinerant electrons. The screening of the positive Coulombic charge on these ions is accomplished by fluctuations in local electron density of the Fermi gas in some cases and by localized bound states in other cases. The effect on the magnetic properties in these two alternative cases can be explained and correlated with changes in electrical resistivity on alloying. Atomic moments of the constituent atoms for some ordered alloys have been calculated and are in good agreement with the experimental values found by Shull in neutron diffraction experiments.

I. INTRODUCTION

THE inadequacy of the treatment of the 3*d* electrons in transition metals using localized atomic wave functions as in the unmodified Heitler-London-Heisenberg and the Zener theories of ferromagnetism has been emphasized from a theoretical point of view by Slater[1] and recently mentioned by Anderson.[2] On the other hand, several empirical factors support the itinerant electron model for these electrons. In particular, the high electronic specific heat in transition metals, and the large effective number of conduction electrons as evidenced by the Hall effect measurements[3] strongly suggest that a reasonable fraction of the 3*d* electrons are not localized. Moreover, this model is particularly successful in explaining many of the properties of ferromagnetic alloys in a very natural way as summarized by Stoner[4] and by Wohlfarth in a paper presented at this conference.

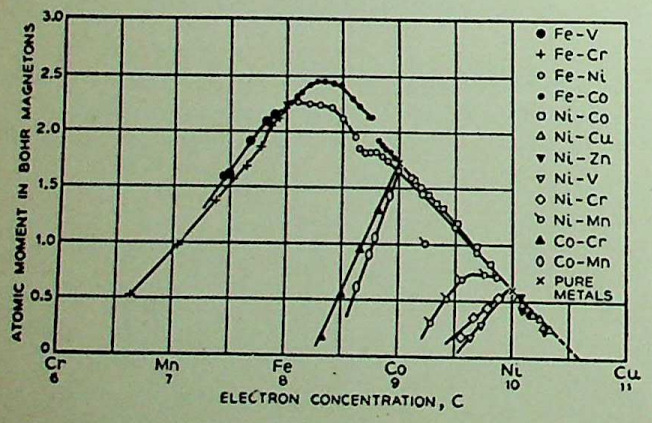


FIG. 1. Atomic moments of the ferromagnetic elements and their alloys (after Slater, Pauling, Bozorth).

Several important magnetic phenomena—particularly those pertaining to alloys—are not readily explained in terms of the simplified collective electron theory of Slater and Stoner. We shall consider four of these properties in some detail and attempt to interpret these properties in terms of a modified collective treatment in which alloying is shown to have an effect upon more than just the electron concentration in the unfilled bands. We are concerned specifically with the following apparent anomalies.

(A) Alloys of Iron with such Elements as Aluminum and Silicon

Additions of small amounts of the latter elements to iron appear to decrease the moment by precisely 2.2 Bohr magnetons per atom of solute added. Thus Al and Si act as simple diluents. At first sight this is more consistent with an atomic viewpoint than with the collective electron theory, for in the latter case we would expect at least some of the valence electrons of the solute atom to go into available 3*d* states; the effect on the magnetization would thus be more than a simple atomic dilution.

(B) The Great Sensitivity of the Magnetic Properties to the State of Order in the Lattice

This is particularly evident in such cases as Ni_3Mn which is ferromagnetic in the ordered state with a moment greater than that of pure nickel but is only paramagnetic when disordered. In a smaller measure

* Supported by the U. S. Office of Naval Research.

[1] J. C. Slater: Paper presented at this U. S. Office of Naval Research Conference on Magnetism. The author is indebted to Professor Slater for the privilege of seeing the manuscript of this paper in advance of publication.

[2] P. W. Anderson, Phys. Rev. 86, 694 (1952).

[3] See, for example, the review article by E. M. Pugh and N. Rostocker, Revs. Modern Phys. 25, 151 (1953).

[4] E. C. Stoner, J. phys. radium 12, 373 (1951). (*Proceedings of the Grenoble Conference on Ferro- and Antiferromagnetism*, p. 224, references to other papers by Stoner are included therein.)

CC-0. In Public Domain. Gurukul Kangri Collection, Haridwar

Digitized by Arya Samaj Foundation Chennai and eGangotri

such effects are present in many binary ferromagnetic alloys which go through order-disorder transformations.[5] Some of these effects have been interpreted by Goldman and Smoluchowski[6] on the basis of assumed fluctuations in local electron concentration the statistics of which depend on the state of order. This interpretation, which agrees remarkably well with the observed phenomena in many cases,[7] effectively localizes the electrons and hence is more closely related to an atomic model.

(C) Saturation Moments of Transition Alloys

Most of the alloys of the ferromagnetic metals with other members of the first transition series have characteristic magnetic moments which fall neatly into a single curve. Slater, Pauling, and others have made use of this curve to interpret various theoretical problems pertaining to energy bands in these materials. This curve is reproduced in Fig. 1. The right-hand portion of the curve is readily understood from the point of view of the band theory. The assumption that the only effect of alloying is to change the Fermi level in an otherwise undistorted $3d$ band appears tenable. Thus, the addition of copper to nickel tends to fill up the nearly full $3d$ band, and the addition of cobalt or iron tends to deplete it which would cause an increase in the net magnetic moment. However, several alloys of nickel and cobalt with transition metals do not follow this curve. For example, the addition of manganese to cobalt or of chromium to nickel has an effect on the moment opposite to that which would be expected by assuming a simple depletion of the electron concentration of the d band. In fact, the decrease in moment per atom of diluent is particularly large—of the order of four to six Bohr magnetons per atom depending on the particular alloy. As pointed out by the author,[8] following a suggestion by Neel, this is not inconsistent with an atomic approach in which the magnetic interaction is a purely local one and is more likely to be antiferromagnetic in the case of the transition metals in question when interacting with their nearest neighbors in the ferromagnetic matrix. Such a mechanism is also consistent with Zener's theory as demonstrated by Carr.[9]

(D) Properties of the Copper-Rich Nickel-Copper Alloys

The band theory offers a very direct explanation of the linear decrease of the saturation moment and Curie point of nickel-copper alloys and the fact that both quantities tend to disappear at 60-atomic percent copper since the 0.6 hole in the nickel d band would be filled at that composition if one assumes that the s electrons of higher energy donated by the copper would tend to occupy available vacant d states. The electronic specific heat in alloys containing more than 60 percent copper does not, however, support this oversimplified view. The data of Keesom and Kurrelmeyer[10] are reproduced in Fig. 2. We note that in the region of interest, the γ-values, which are a measure of the density of states at the Fermi surface and are high in the case of transition metals with unfilled d bands, are still anomalously high in the composition range of interest. Moreover, the magnetic susceptibility of these alloys[11] also reflects a complication not anticipated in the straightforward application of the band theory.

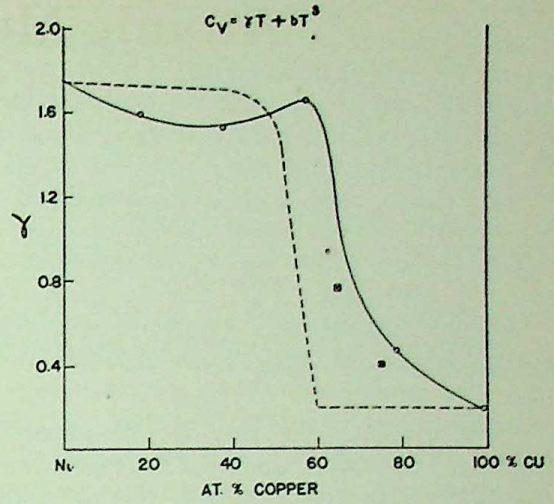


FIG. 2. The electronic specific heat of nickel-copper alloys plotted against composition. The dashed curve is that which one would expect from a straightforward application of band theory. The solid curve is the experimental curve of Keesom and Kurrelmeyer. The two points marked by an x are theoretical points based on the author's theory [J. E. Goldman, Phys. Rev. 82, 339 (1951)].

II. NATURE OF THE ENERGY BANDS IN TRANSITION METALS

Any attempt to interpret the magnetic properties mentioned above on the basis of the band theory requires a more complete consideration of the influence of alloying elements on the energy bands apart from changes in electron concentration. We first consider the nature of the unfilled bands in transition metals. Several calculations have been made of the bands in such metals. The first of these is due to Slater and Krutter[12] who carried out calculations for copper using the cellular method and one electron Bloch wave functions. Manning and his collaborators[13] carried out a similar calculation for both allotropic

[5] These are summarized in two review papers: J. E. Goldman, J. Appl. Phys. 20, 1131 (1949); R. Smoluchowski, J. phys. et radium 12, 389 (1951).
[6] J. E. Goldman and R. Smoluchowski, Phys. Rev. 75, 140 (1949); also reference 5.
[7] R. Smoluchowski, Phys. Rev. 84, 511 (1951).
[8] J. E. Goldman, Phys. Rev. 85, 375 (1952).
[9] W. J. Carr, Jr., Phys. Rev. 85, 590 (1952).
[10] W. H. Keesom and B. Kurrelmeyer, Physica 7, 1003 (1940).
[11] A. R. Kaufmann and C. Starr, Phys. Rev. 63, 445 (1943).
[12] H. M. Krutter, Phys. Rev. 48, 664 (1935); J. C. Slater, Phys. Rev. 49, 537, 931 (1936).
[13] M. F. Manning, Phys. Rev. 63, 190 (1943); J. B. Greene and M. F. Manning, Phys. Rev. 63, 203 (1943).

CC-0. In Public Domain. Gurukul Kangri Collection, Haridwar

Digitized by Arya Samaj Foundation Chennai and eGangotri

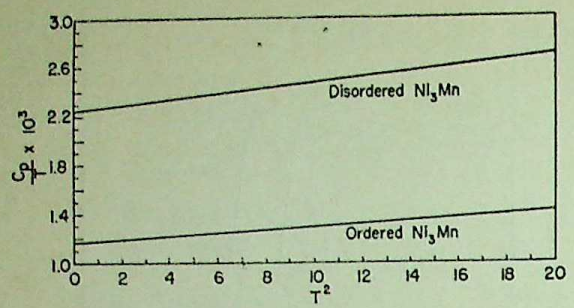


FIG. 3. C_p/T plotted against T^2 for ordered and disordered Ni_3Mn. The intercept on the ordinate is the coefficient of the electronic term in the specific heat.

forms of iron. Recently, Fletcher and Wohlfarth[14] and Fletcher[15] have calculated the band structure of nickel from the alternative approximation of tight binding. All the calculations show a fine structure in the density of states *vs* energy curve in the 3*d* band with two peaks separated by a minimum. Thus, the basic features of Slater and Krutter's curve for the density of states in the *d* band for copper may be extrapolated back to other elements of the transition series. That this type of structure can be carried as far back as titanium is suggested by the experimental measurements of the electronic specific heat in Ti and Cr by Friedberg, Estermann, and Goldman.[16] The very low value obtained for the density of states at the Fermi level in chromium suggests that the Fermi level in this case lies at the minimum of the curve. That the extrapolation is reasonable is also suggested by the fact that effects on the band due to the changing lattice constant and ion-core potential (both of which are very small) will tend to oppose each other.

The absolute energy values at the Fermi level and at the top of the band present a slightly different picture. In this case the only evidence available is that obtained from soft x-ray absorption and emission data. Comparison of the energies corresponding to the peak in the $K\beta_5$ emission line in copper and in nickel from the work of Beeman and Friedmann[17] shows the energy level at the maximum density in copper to lie somewhat below that of nickel. This result although small is not unexpected in view of the greater positive ionic potential of the copper ions. We shall return to this question later.

III. INFLUENCE OF ORDER ON THE BANDS: Ni_3Mn

As first pointed out by Slater,[18] there is a very direct effect on the energy band in an ordered alloy. The superposed double periodicity of the lattice potential splits the band in two and effectively alters the density of states-energy curve. We have investigated the effect of ordering on the bands in Ni_3Mn. Measurements have been carried out by the author and D. Burk on the electronic specific heat of ordered and disordered Ni_3Mn. The cryogenic technique is identical with that used in the earlier investigation of the specific heat of transition metals by Friedberg *et al.*[16] The presence and absence of order in the two samples used in the investigation was confirmed by means of neutron diffraction at the Brookhaven pile. On the basis of approximate measurements of the integrated intensity of the (100) superlattice line, it is estimated that the long range order parameter in the ordered sample is of the order of 0.75. The results of the specific heat measurement are given in Fig. 3, where C_p/T is plotted against T^2. The intercept on the ordinate is γ which is directly proportional to the density of states at the Fermi surface. The values of γ are 11.7 and 22.4×10^{-4} for the ordered and disordered samples, respectively. Since the ordered sample is ferromagnetic, it is probable that the half-band of one spin is full or nearly full and hence only *d* electrons of one spin contribute to the electronic specific heat. Thus, the difference of a factor of approximately 2 in the values of γ is not unexpected. The observed difference does, however, substantiate the Mott-Slater approach to the band theory of the *d* electrons in transition metals and emphasizes all the more the validity of the itinerant electron model.

The measured electronic specific heat coupled with the disappearance of ferromagnetism in the disordered state has made it possible for us to put together a qualitative picture of the *d* band in ordered and disordered Ni_3Mn. This schematic representation of the density function in these two cases is presented in Fig. 4. The fine structure in the *d* band for the disordered alloy has been smeared out in this case. As will be shown below, this is not unexpected when the two alloying constituents differ in atomic number by more than one or two. The electron "sees" only the average potential of the nickel and manganese ion core. The resulting band should be not very different from that in γ-iron both as regards shape and band spread. The fact that this alloy is not ferromagnetic agrees with this and further suggests that at the Fermi level the density must be decreasing as a function of energy so that a possible gain in exchange energy would be more than offset by the additional Fermi energy that would be required to achieve such a spontaneous magnetization.

The situation is altered in the ordered alloy. Following Slater[18] we suppose that the band is now split although the energy limits are unchanged. Thus, the Fermi level is at a point in the density-energy curve where the former is increasing which would be conducive to ferromagnetism on the collective electron theory. This representation is confirmed by recent unpublished results obtained in our laboratory by Foner on the Hall effect in ordered and disordered Ni_3Mn.[19] These

[14] G. C. Fletcher and E. P. Wohlfarth, Phil. Mag. 42, 106 (1951).
[15] G. C. Fletcher, Proc. Phys. Soc. (London) 65, 192 (1952).
[16] S. A. Friedberg, I. Estermann, and J. E. Goldman, Phys. Rev. 85, 375 (1952).
[17] W. W. Beeman and H. Friedmann, Phys. Rev. 56, 392 (1939).
[18] J. C. Slater, Phys. Rev. 84, 179 (1951).

[19] S. Foner (to be published). We are indebted to Dr. Foner for permission to quote his results prior to publication. In the

CC-0. In Public Domain. Gurukul Kangri Collection, Haridwar

Digitized by Arya Samaj Foundation Chennai and eGangotri

measurements were made on samples of the same material treated in the same manner. The results show a change of sign in the Hall effect; the disordered sample has a positive Hall coefficient suggesting hole conduction and the ordered sample has a negative Hall coefficient, indicating conduction by electrons. This is consistent with our picture since in the ordered case, $N(E)$ is increasing with E which implies that $\partial^2 E/\partial k^2$ will be positive for most directions and conduction will be by electrons and conversely for the disordered alloy.

IV. SPATIAL CORRELATION OF THE *d* ELECTRONS; THE MOMENT IN Ni_3Mn

Thus far, we have considered only the distribution of electron states in energy space which corresponds to the usual treatment of energy bands in pure metals. The determinantal wave functions for the crystal are eigenfunctions appropriate to each of the energy eigenvalues in the band and would consist of linear combinations of atomic wave functions normalized to unity in the volume comprising the crystal. One cannot think of individual localized electrons but rather of the probability amplitude of the distribution of electronic charge in the crystal which for any small volume is given by $\sum_i \int e\psi_i^2 d\tau$ integrated over that volume and clearly would have maxima near the lattice positions, since near the nucleus the wave functions are essentially atomic in character. This spatial distribution of the charge associated with the electrons in the Fermi distribution is of particular importance in considering alloys. In an alloy, the potential attributed to an ion at a lattice point must be a screened Coulomb field in order to avoid an anomaly inelectrical resistance.[20] Since, in this model, the *d* as well as the *s* electrons are assumed to constitute the Fermi gas, the screening must be done by the positional correlation of these various electrons. (The argument is not at all altered if one assumes that some fraction of these electrons are in localized bound states as was done by Freedel.[21])

Consider now the specific case of an alloy such as Ni_3Mn which we shall use as an example. The total number of "valence" electrons contributed by the nickel and manganese atoms to the Fermi distribution is 10 and 7, respectively. An atomic cell containing a Ni^{+10} ion must also contain a net distribution of charge due to a probability concentration of "*s*" and "*d*" states equal to 10, i.e., $\sum_i \int e\psi_{si}^2 d\tau + \sum_j \int e\psi_{dj}^2 d\tau = 10$, where, as before, the integration is over the volume of the atomic polyhedron. We shall assume that the overlap between the 4*s* and 3*d* bands is not very much different from the case of the pure ferromagnetic elements and therefore, the number of Fermi electrons in the *s* band is the same. Suppose we take for the number of *s* electrons in the case under consideration 0.3 (a value half that of nickel is justifiable both on theoretical grounds and on the basis of the Hall effect data). The remaining +9.7 ionic charge must be screened by a local concentration of states of primarily *d* character. Of these, at most five can be occupied by electrons of given spin but we should expect all states of positive spin to be occupied if the *d* band satisfies the criteria for ferromagnetism. There will thus be 5 occupied states of +spin and 4.7 of −spin or a net moment per nickel atom of 0.3 Bohr magneton. No coherent polarization of electrons in *s* states can take place without requiring the expenditure of too much kinetic and correlation energy. Similarly, near the manganese atoms there will be a build-up of charge to shield the ionic charge of +7 with 0.3 electron in *s* states, 5 in *d* states of positive spin or a net moment of 3.3 Bohr magnetons. This gives good agreement with the macroscopic moment as well as with the local moments observed by Shull in neutron diffraction experiments on ordered Ni_3Mn.[22] In this representation we have assumed that distribution in space of charge density associated with *s* states does not vary for the two types of constituent atom. Although this is a reasonable assumption, the general result will not be changed very much if the local concentration of charge owing to *s* states is allowed to vary slightly.

A similar analysis carried out for the case of Ni_3Fe gives for the moments of the Ni and Fe atoms 0.4 and 2.4 magnetons, respectively, which again gives the proper macroscopic moment and agrees very well with Shull's results and is reasonably close to those of Weiss, Corliss, and Hastings. This treatment contrasts, however, with the local electron density model of Goldman and Smoluchowski based on statistical fluctuations in atomic concentration. The moment and the influence of order is interpreted quite differently in these two models. In particular, the discussions of Ni_3Mn and $FeNi_3$ by the author[5] are based on a quasi-atomic model of the ferromagnetic interaction and, therefore, may not be expected to hold. On the other hand, the correlations discussed by Smoluchowski[5] for some of the other properties probably fit into the band scheme quite readily if one considers the adjustable range of the screened Coulomb potential and assumes that this is

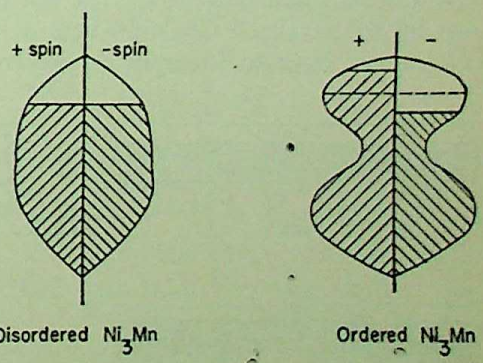


FIG. 4. Schematic representation of the probable distribution of states in energy space for ordered and disordered Ni_3Mn based on the electronic specific heat and Hall effect measurements.

case of the ferromagnetic ordered alloy, the results quoted are for the Hall coefficient above saturation (see E. M. Pugh and N. Rostocker, reference 3).

[20] N. F. Mott, Proc. Cambridge Phil. Soc. 32, 381 (1936).

[21] J. Freedel, Phil Mag. 43, 153 (1952).

[22] C. G. Shull (private communication).

CC-0. In Public Domain. Gurukul Kangri Collection, Haridwar

Digitized by Arya Samaj Foundation Chennai and eGangotri

the quantity that varies depending upon the local fluctuations in concentration.

V. THE SATURATION MOMENT OF TRANSITION ALLOYS

We have considered above the atomic moments in alloys with ordered structures. In this qualitative treatment, it has been implicitly assumed that the distribution of states in the band is not appreciably altered on alloying. This is a reasonable assumption in the case of the ordered state when the disturbance in the perfect periodicity of the lattice potential is itself periodic and would, therefore, have an effect on the density of states in the band as noted. Consider, however, small additions of an alloying element which differs greatly in atomic number, e.g., chromium in nickel or vanadium in cobalt. These will presumably be randomly disposed in the lattice. As in the previously discussed case, the boundary condition requiring the crystal wave functions to approach the atomic wave functions near any nucleus leads us to the conclusion that certain energy eigenvalues allowed where all sites have the same potential will now no longer be possible if the potential at one or more lattice points is changed. If the "impurity" ion has a less positive potential, the states of lower energy are those which are affected. The density of states at the bottom of the band is thus decreased and additional allowed states would be added at the top of the band. In a ferromagnetic alloy, the states of lowest energy are all of one sign of spin due to exchange. This is represented schematically in Fig. 5. It is seen that on this model the role of the impurity is to decrease the density and to cause electrons, which would have occupied states of + spin if the band had been unperturbed, to distribute themselves among the available states of both spin at the top of the Fermi distribution. The number of states so affected and, therefore, the net decrease in moment, is to be determined by the relative difference in ionic potential of the two constituent types of atom. An alternative mechanism for demonstrating quantitatively the proposed effect of alloying on the band is that proposed by Friedel and employing scattering theory. Friedel's calculations for the scattering of s electrons by the screened Coulomb field of a solute ion can be carried over to itinerant $3d$ electrons and the same effect on the distribution in energy space of allowed states is noted.

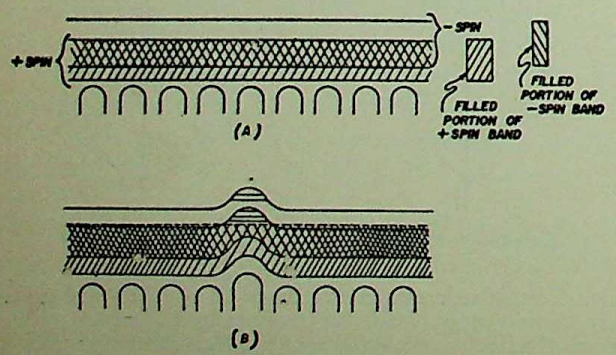


FIG. 5. Schematic representation of the effect of a perturbation in the periodic potential of the lattice on a ferromagnetic alloy.

An interesting case that may be explained on this basis is that of the nickel-copper alloys. The variation of the saturation moment with composition in the nickel-rich region of alloys is usually interpreted on the basis of the filling of the available states in the $3d$ band by the additional electrons contributed by the copper atoms which at 60 percent copper would be sufficient to fill the $3d$ band completely. If this were in fact the case, one would expect the electronic specific heat in these alloys to decrease to approximately that of copper at a composition of 60 percent Cu as shown in the dashed curve of Fig. 2. Actually, we see that this is not the case and that at even higher copper concentrations the electronic specific heat remains large. That the alloys in this composition range do, in fact, behave anomalously is further supported by the peculiar temperature dependence of the *paramagnetic* susceptibility of these alloys as shown in Fig. 6 and the unusual behavior of the Hall effect in this same region.[23] Clearly, the peculiar temperature dependence of the susceptibility precludes the association of the anomaly with either clustering of the nickel atoms or an atomic shell character with unfilled levels for the nickel atoms, for, in such cases one would expect normal paramagnetic behavior.

It has been suggested[24] by the author that these anomalous properties can in fact be at least qualitatively understood on the basis of the band perturbations discussed above. The effect of copper atoms in the lattice is again to cause some of the states at the bottom of the d band to become less probable and new, somewhat localized, states added at the top of the band. These are the states that are not normally occupied but to which electrons can ordinarily be excited so that there would be an additional contribution to the electronic specific heat. This implies, too, that a collective treatment for the electrons is appropriate and that some form of peculiar temperature dependence of the susceptibility is to be anticipated. This is being investigated from both a theoretical and experimental point of view in the author's laboratory by A. Arrott and the writer.†

VI. ALLOYS OF IRON WITH SILICON AND ALUMINUM

Several of the alloys of iron behave quite differently from those of nickel. For example, alloys of nickel with aluminum are explainable in terms of the simple band considerations previously applied to copper but with appropriate correction for the different valence state

[23] A. I. Schindler and E. M. Pugh (to be published).
[24] J. E. Goldman, Phys. Rev. 82, 339 (1951).
† *Note added in proof*.—The author has recently suggested that such states may, in fact, also explain the anomalous resistance of copper at low temperatures when small amounts of impurities are present (see Bull. Am. Phys. Soc. 28, No. 1 (1953)). The possibility of segregation in the Cu-Ni alloy and the ensuing paramagnetic behavior of the subdomain nickel particles with interactions as being responsible for the effects in Cu-Ni are being further investigated.

CC-0. In Public Domain. Gurukul Kangri Collection, Haridwar

Digitized by Arya Samaj Foundation Chennai and eGangotri

of the aluminum atoms. The decrease of the moment with added aluminum is readily understood if one assumes that the three valence electrons contributed by each aluminum atom occupy available d states. On the other hand, addition of Al to iron merely decreases the moment by the effective moment of the single iron atom it replaces. The same is true in the case of silicon-iron alloys.

A reasonable explanation may be given of this on the basis of the band theory. One would suspect that the energy spread of the d band in iron is somewhat greater than in the elements which follow it in the periodic table. This is consistent with observations of the relative interatomic spacing, the soft x-ray spectra and the theoretical calculations of Manning *et al.* Although the ground state of the system is a ferromagnetic one, the greater spread means that the Fermi energy of the electrons is greater for a ferromagnetic case. The state of minimum energy need not necessarily be one in which the half-band of positive spin is completely filled. One may suppose, therefore, that the number of s electrons is the same as in the other ferromagnetic elements, and that for small additions of Al or Si, the valence electrons contributed by the solute occupy states of either spin with equal probability. However, if all such valence electrons were to thus go into available d states, the half-band of + spin would be filled up all too rapidly, and the change of shape in the moment *vs* composition curve would be appreciable at a much lower Al or Si concentration than is actually observed. We suspect, however, that some of these electrons do in fact remain in p states and, therefore, do not affect the magnetic moment other than by simple dilution. This is supported by the empirical observations that the addition of silicon or aluminum to iron has a much greater effect on the electrical resistivity than other alloying constituents. Preliminary calculations by Rostocker and the author show that this is just what one would be led to expect if the screening electrons surrounding the "impurity" ion are in p states rather than d states. Such an explanation is admittedly very qualitative but there is good reason to expect that further calculations on this problem will make possible a clearer picture of the band structure in such alloys.

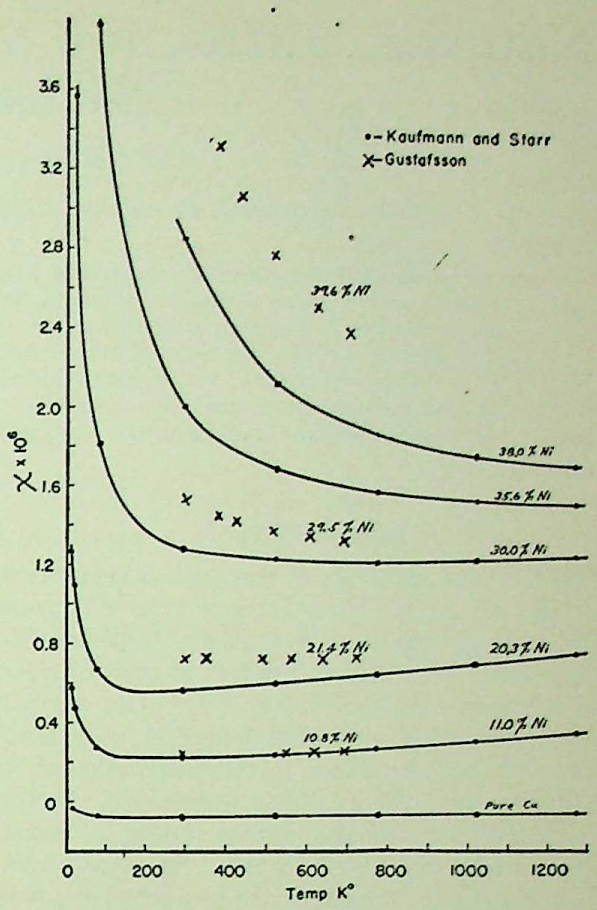


FIG. 6. Temperature-susceptibility curves of nickel-copper alloys of various compositions (after Kaufmann and Starr).

VII. ACKNOWLEDGMENT

Part of this paper was written while the author was a visiting scientist and consultant at the Brookhaven National Laboratory. The author would like to express his gratitude to the laboratory for its hospitality during this period and, in particular, to Professor J. C. Slater Dr. D. Kleinman, and the neutron diffraction group (Dr. R. J. Weiss, Dr. L. Corliss, and Dr. J. Hastings) for many stimulating discussions and very helpful cooperation. He is also indebted to Dr. N. Rostocker for his helpful criticism of the manuscript and his collaboration on some of the theoretical problems contained therein; and to Dr. C. G. Shull for discussions of the results of his neutron diffraction experiments in advance of publication.

DISCUSSION

C. J. GORTER, *University of Leiden, Holland:* According to the Heisenberg model a specific heat anomaly should be expected below the temperatures where in Cr and Mn antiferromagnetism disappears, and an entropy of at least $R\ln 2$ should be connected with this anomaly. In the band model this anomaly might be much smaller, as would seem in better agreement with the data on specific heats.

J. E. GOLDMAN, *Carnegie Institute of Technology, Pittsburgh, Pennsylvania:* We have investigated the specific heat of chromium not only in the liquid helium temperature range but at higher temperatures as well in order to see if there is any evidence of a second-order phase transformation as first suggested by Néel and recently re-echoed by Zener. We have found that the curve is continuous from 2°K to a little under room temperature and merges very well with the curve of Armstrong and Grayson-Smith. There is no evidence of an anomaly either in the low or high temperature range other than the appearance of a significant electronic contribution to the specific heat at temperatures low compared to the probable degeneracy temperature.

CC-0. In Public Domain. Gurukul Kangri Collection, Haridwar

Digitized by Arya Samaj Foundation Chennai and eGangotri

REVIEWS OF MODERN PHYSICS VOLUME 25, NUMBER 1 JANUARY, 1953

Neutron Diffraction Studies of Zinc Ferrite and Nickel Ferrite*

J. M. HASTINGS AND L. M. CORLISS

Chemistry Department, Brookhaven National Laboratory, Upton, Long Island, New York

The chemical and magnetic structures of zinc ferrite and nickel ferrite have been investigated at room temperature by means of neutron diffraction. In agreement with previous x-ray investigations zinc ferrite has been found to possess a completely regular spinel structure with an oxygen parameter of 0.385 ± 0.002. The diffraction peaks show no evidence of coherent magnetic scattering, whereas the background exhibits normal paramagnetic diffuse scattering. This eliminates the possibility of an antiferromagnetic structure at room temperature. In the case of nickel ferrite, calculated intensities based upon an inverted structure and the Néel model of ferrimagnetism are in good agreement with the observed intensities.

INTRODUCTION

THE crystal structure of ferrites has been the subject of several investigations in recent years.[1,2] Aside from questions of technology, considerable interest derives from the explanation of their interesting magnetic properties given by Néel.[3] The saturation moment, according to the theory of Néel, is related in a simple and elegant manner to the distribution of magnetic ions among the available lattice sites. However, the precise location of the various cations by means of x-rays presents a difficult problem in many cases of interest because of the similarity in scattering power of the iron group elements. Neutron diffraction as a tool for studying the ferrite problem offers not only the means of distinguishing between the various members of the iron group but also a means of determining the location, magnitude, and relative orientation of atomic moments.

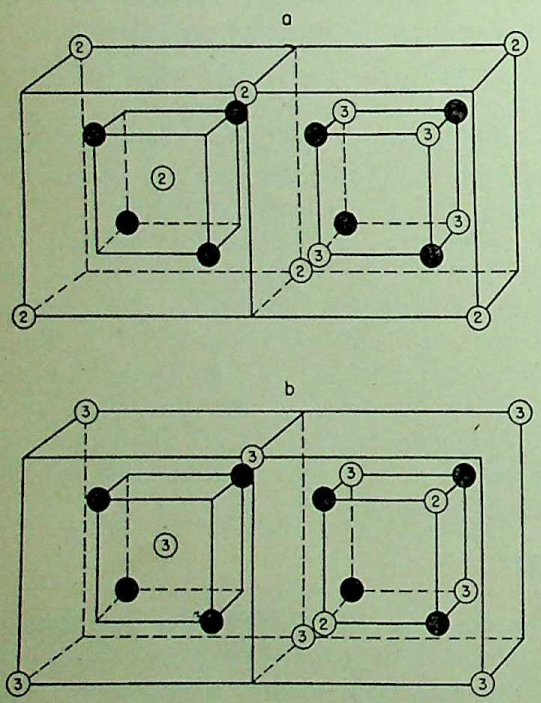


FIG. 1. (a) Two octants of the regular spinel structure. Open circles with numbers refer to di- and tri-valent cations. Solid circles refer to oxygen anions. (b) Same for inverted spinel.

CRYSTAL STRUCTURE

Nickel and zinc ferrite belong to a large class of compounds having the general formula $X^{+2}Y_2^{+3}O_4$ and crystallizing with the spinel structure. The unit cell is cubic with a cell edge of approximately 8.4A and contains eight molecules. The structure can be described as a close-packed assemblage of oxygen atoms with metal atoms occupying positions in some of the interstices. The metal positions are of two types: those in which the oxygen atoms are tetrahedrally coordinated

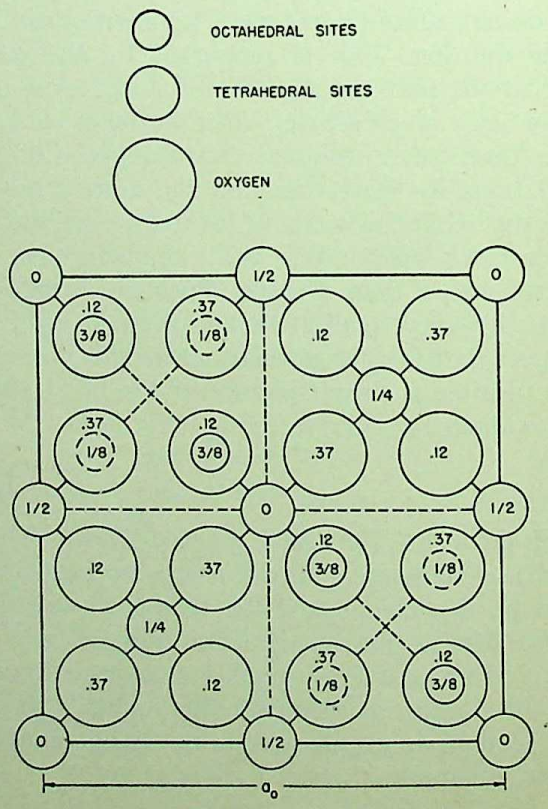


FIG. 2. Projection on a cube face of lower half of spinel unit cell (after Wyckoff).

* Research carried out under the auspices of the U. S. Atomic Energy Commission.

[1] E. J. W. Verwey and E. L. Heilmann, J. Chem. Phys. 15, 174 (1947).
[2] E. F. Bertaut, J. phys. et radium 12, 252 (1951).
[3] L. Néel, Ann. phys. 3, 139 (1948).

CC-0. In Public Domain. Gurukul Kangri Collection, Haridwar

Digitized by Arya Samaj Foundation Chennai and eGangotri

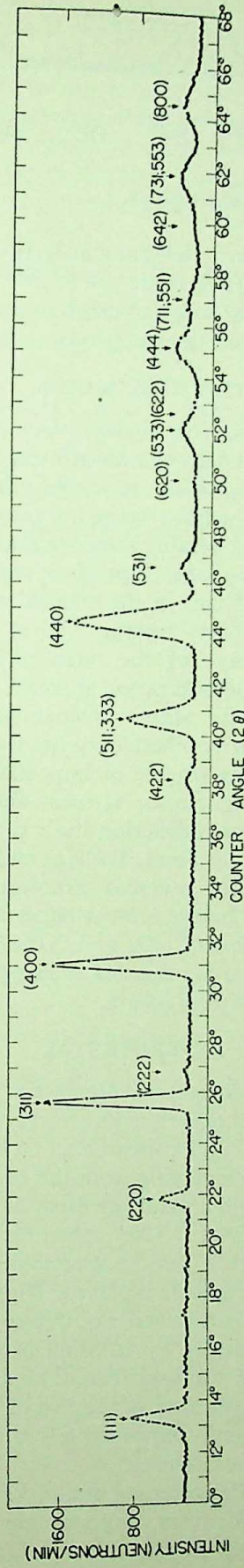


FIG. 3. Neutron diffraction pattern of $ZnFe_2O_4$.

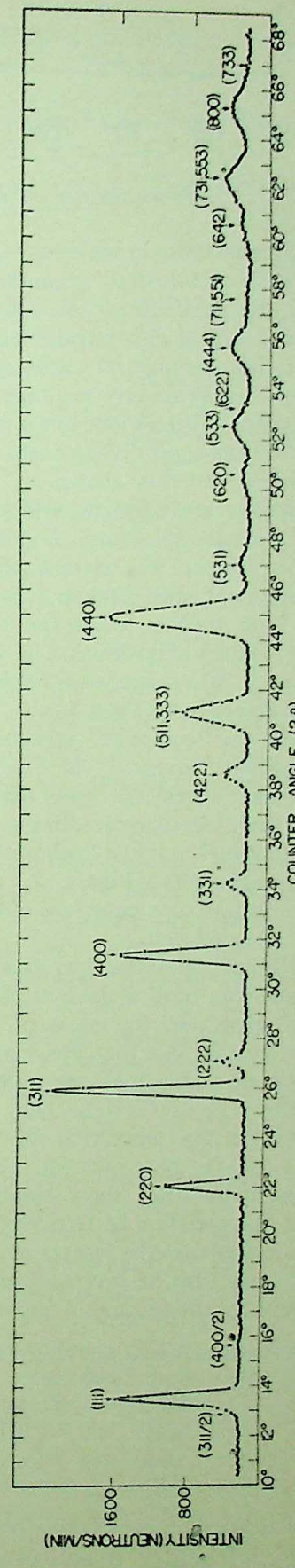


FIG. 4. Neutron diffraction pattern of $NiFe_4O_2$.

CC-0. In Public Domain. Gurukul Kangri Collection, Haridwar

Digitized by Arya Samaj Foundation Chennai and eGangotri

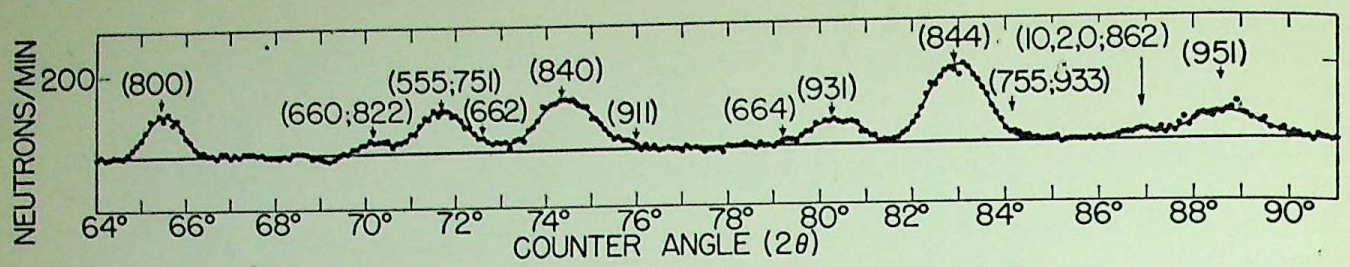


FIG. 5. Neutron diffraction pattern of $NiFe_2O_4$ with improved resolution.

to the metal atom, and those in which the surrounding oxygen atoms have octahedral symmetry. Of the twenty-four positions available to the metal atoms in the unit cell, eight are of the tetrahedral type and sixteen belong to the octahedral category. One obvious way to meet the symmetry requirements would be to place the sixteen trivalent ions in the sixteen octahedral positions and the eight divalent ions in the eight tetrahedral positions. It was shown by Barth and Posnjak[4] that another arrangement, which they have termed an "equipoint" structure, is also possible. According to this scheme, the sixteen trivalent ions occupy all of the tetrahedral sites and half the octahedral sites taken at random, while the divalent ions fill the remaining octahedral positions. The first arrangement in which each cation species occupies only one type of site is commonly referred to as "regular" or "normal," whereas the "equipoint" structure has been given the designation "inverted" or "inverse." It is also conceivable that cases will arise that are intermediate between these two extremes. In Fig. 1 are shown two octants of the spinel unit cell for both the inverted and regular arrangements. Figure 2, taken from Wyckoff,[5] is a projection on a cube face of the atoms in the lower half of the unit cell.

Verwey and Heilmann[1] have investigated a large number of spinels from both a theoretical and experimental point of view. On the basis of electrostatic considerations, they conclude that the regular arrangement should be more stable than the inverted one, in compounds of the type $X^{+2}Y_2^{+3}O_4$. They report that x-ray studies confirm the prediction for the cases of $ZnFe_2O_4$ and $CdFe_2O_4$ but not for $CuFe_2O_4$ and $MgFe_2O_4$. Furthermore, they show empirically by a consideration of the variation of lattice constant with the divalent ion radius that the ferrites of Mn^{++}, Fe^{++}, Co^{++}, and Ni^{++} may also be inverted. More recently Bertaut,[2] working in the region of anomalous x-ray dispersion, has concluded that zinc ferrite is regular and nickel ferrite inverted, while the ferrites of magnesium and copper are partially inverted to an extent which depends on the conditions of preparation.

TABLE I. Coherent scattering amplitude$\times 10^{12}$ cm.

	Nuclear	Magnetic
O^{-2}	0.58	...
Fe^{+3}	0.96	$1.35f$
Ni^{+2}	1.03	$0.54f$
Zn^{+2}	0.59	...

[4] T. F. W. Barth and E. Posnjak, Z. Krist. 82, 325 (1932).
[5] R. W. G. Wyckoff, *Crystal Structures* (Interscience Publishers, Inc., New York, 1951).

THE NÉEL MODEL

According to the Néel model of ferrimagnetism,[3] the exchange integrals between an arbitrary pair of metal ions is such as to produce an antiparallel alignment of the two. The octahedral-tetrahedral coupling, however, is taken to be considerably stronger than that between ions located on the same type of crystallographic site. Thus, the spins of ions in the octahedral positions are coupled parallel to one another and at the same time antiparallel to those of the tetrahedral ions. In an inverted spinel the saturation moment is then determined solely by the atomic moment of the divalent cation. In zinc ferrite where only the weak octahedral-octahedral coupling can be of importance, one would anticipate paramagnetic or at most antiferromagnetic behavior. A neutron diffraction study of Fe_3O_4 has been recently reported by Shull, Wollan, and Koehler,[6] and it confirms both the inverted structure and the Néel coupling scheme. In the present paper neutron diffraction data on both $ZnFe_2O_4$ and $NiFe_2O_4$ will be presented. Work on other ferrites is in progress and will be reported in the near future.

EXPERIMENTAL

The neutron diffraction apparatus and technique used in the present experiments are very similar to those of Shull, Wollan, and co-workers.[7] A heterochromatic beam of neutrons emerging from the reactor is made to strike a lead single crystal oriented on a spectrometer table set to diffract 1.125A neutrons. The reflected beam passes over a second spectrometer table upon which the powder sample is placed. The monochromatic beam is diffracted into a series of Debye halos which are scanned automatically by rotation of a BF_3 detector about the axis of the specimen. The chief innovation of the present apparatus is the use of Soller slits and wide beams to obtain improved resolution without too great a sacrifice in intensity.

The samples of zinc ferrite and nickel ferrite used in the present investigation were very kindly prepared by Dr. V. C. Wilson at the General Electric Research

[6] Shull, Wollan, and Koehler, Phys. Rev. 84, 912 (1951).
[7] E. O. Wollan and C. G. Shull, Phys. Rev. 73, 822 (1948).

CC-0. In Public Domain. Gurukul Kangri Collection, Haridwar

Digitized by Arya Samaj Foundation Chennai and eGangotri

Laboratory. The specimens were examined in the form of 325 mesh powders, contained in flat cells $\frac{1}{2}$ in.$\times 2\frac{1}{2}$ in. $\times 4$ in. in size, and as sintered blocks having about the same dimensions and about 0.9 the theoretical density. Different preparations were found to agree to within the precision of measurement on any one sample.

Diffraction patterns obtained with these materials are shown in Figs. 3, 4, and 5. The last of these patterns was taken under conditions of somewhat improved resolution.

METHOD OF CALCULATION

The integrated power P_{hkl} of a diffraction peak obtained in transmission through a flat cell is computed from the expression

$$P_{hkl}=(P_0\lambda^3 l/4\pi r)(N^2 h\rho'/\rho)(e^{-\mu h\sec\theta}/\sin^2 2\theta)J_{hkl}F_{hkl}^2. \quad (1)$$

The first term is an instrumental constant in which P_0 is the number of neutrons striking the sample in unit time, λ the wavelength, l the counter slit height, and r the distance from the counter slit to the sample. The second term, which is a constant for a given specimen contains N the number of unit cells per unit volume, h the nominal thickness of the sample, ρ' the apparent density of the powder, and ρ the density of the solid. In the third term, θ is the Bragg angle, and μ is the effective linear absorption coefficient determined by measurement of the actual transmission of the sample $e^{-\mu h}$. J_{hkl} is the multiplicity, and F_{hkl} is the structure factor for the (hkl) reflection. In the case of scattering of unpolarized neutrons both by nuclei and by aligned atomic spins, Halpern and Johnson[8] have shown that the structure factor is given by

$$F^2=F_{\text{nuc}}^2+q^2F_{\text{mag}}^2, \quad (2)$$

where F_{nuc}^2 is the structure factor for nuclear scattering alone and F_{mag}^2 is the structure factor for magnetic scattering. If $\mathbf{e}$ is a unit vector parallel to the scattering vector (in this case, the normal to the set of diffracting planes) and $\boldsymbol{\kappa}$ is a unit vector in the direction of magnetization, then the quantity q^2 is given by

$$q^2=1-(\mathbf{e}\cdot\boldsymbol{\kappa})^2=\sin^2(\mathbf{e},\boldsymbol{\kappa}). \quad (3)$$

The magnetic atomic scattering amplitude to be used in the computation of F_{mag}^2 is given by the expression

$$D=\frac{e^2}{mc^2}\gamma Sf=0.539\times 10^{-12}Sf \text{ cm}, \quad (4)$$

where S is the electronic spin quantum number of the scattering atom, e and m are the charge and mass of the electron, γ is the magnetic moment of the neutron in nuclear magnetons, and f is the form factor for the magnetic electrons. Halpern and Johnson have also shown that for the case of an ideal paramagnetic substance the magnetic scattering will be entirely incoherent. The differential cross section for magnetic scattering into solid angle $d\Omega$ is given by

$$d\sigma_m=\tfrac{2}{3}S(S+1)(e^2\gamma/mc^2)^2f^2d\Omega, \quad (5)$$

where all the symbols have the same meaning as in (4). The above equations and their experimental implications have been discussed at length by Shull and coworkers[6,9] in connection with their extensive investigations of the scattering of neutrons by magnetic materials. The coherent scattering amplitudes used in the present calculations are listed in Table I. The nuclear amplitudes are taken from the tabulation of Shull and Wollan,[10] and the magnetic amplitudes are computed from Eq. (4).

The diffraction pattern of $ZnFe_2O_4$ shown in Fig. 3 can be interpreted quantitatively in terms of a regular spinel structure, with no coherent magnetic contribution. Table II lists the calculated integrated intensities

TABLE II. A comparison of observed intensities with those calculated for a regular structure for $ZnFe_2O_4$. Absolute units (neutrons/min) are used, based upon nickel as a standard.

hkl	Calculated	Observed
(111)	1900	1900
(220)	727	757
(311)	4820	4840
(222)	166	144
(400)	5890	6320
(331)	52	0
(422)	375	325
(511); (333)	3940	4100
(440)	9820	10300
(531)	900	1035
(620)	172	100
(533) } (622)	1210	1190
(444)	2340	2300
(711); (551)	1030	1205
(642) } (731); (553)	2620	2720
(800)	2260	2360

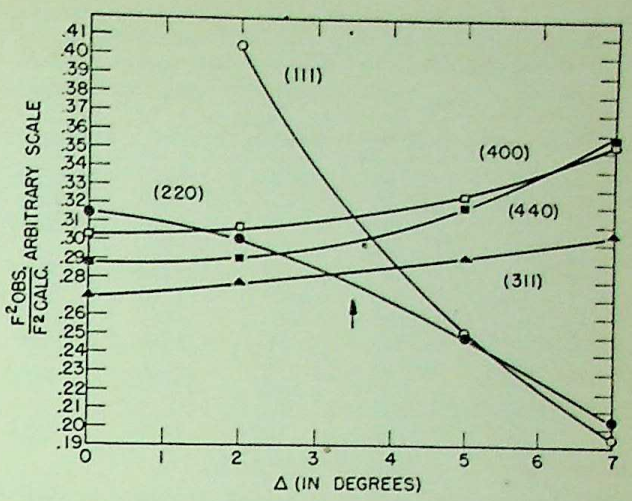


FIG. 6. The ratio $F_{\text{obs}}^2/F_{\text{calc}}^2$ for $ZnFe_2O_4$ plotted as a function of the parameter Δ, which describes the oxygen positions in the lattice.

[8] O. Halpern and M. H. Johnson, Phys. Rev. 55, 898 (1939).

[9] Shull, Strauser, and Wollan, Phys. Rev. 83, 333 (1951).

[10] C. G. Shull and E. O. Wollan, Phys. Rev. 81, 527 (1951).

CC-0. In Public Domain. Gurukul Kangri Collection, Haridwar

Digitized by Arya Samaj Foundation Chennai and eGangotri

TABLE III. Comparison of calculated and observed integrated intensities for $NiFe_2O_4$ for inverted form using Néel scheme of magnetic coupling. Absolute units (neutrons/minute) are used.

hkl	Nuclear	Calculated magnetic	Total	Observed
(111)	730	6020	6750	6470
(220)	2010	1270	3280	3270
(311)	8490	0	8490	8550
(222)	93	893	986	1110
(400)	5880	1210	7090	7270
(331)	2	1207	1210	1170
(422)	1280	380	1660	1700
(511); (333)	5530	0	5530	5790
(440)	14450	15	15440	15620
(531)	370	600		
(620)	730	105		
(533)	2115	0	3150	3280
(622)	55	145		
(444)	2530	105	3180	3040
(711); (551)	385	155		
(642)	1195	45	5390	5280
(731); (553)	4150	0		
(800)	3530	0	3550	3390
(733)	20	0		
(660); (822)	705	0		
(751); (555)	3170	0	3920	4120
(662)	40	0		
(840)	4420	0	4650	4710
(911)	230	0		

based on this structure together with the corresponding observed intensities. The data have been put on an absolute basis by comparison with a nickel standard having a coherent scattering cross section of 13.4 barns. The Debye-Waller temperature factor was obtained in the usual way from a plot of F_{calc}^2/F_{obs}^2 against $\sin^2\theta/\lambda^2$. The positions of the oxygen atoms in the spinel structure are fixed by a parameter u, which is in the neighborhood of $\frac{3}{8}$. If u is exactly $\frac{3}{8}$, the oxygen atoms form a cubic close-packed array. A u parameter greater than this value implies a contraction of the oxygen lattice about the octahedrally coordinated metal atoms and a corresponding expansion about the tetrahedrally coordinated ones. Figure 6 shows a plot of F_{calc}^2/F_{obs}^2 *versus* the deviation Δ of this parameter, expressed in angular measure from the value $\frac{3}{8}$ [$u=(135°+\Delta)/360°$]. A value of $\Delta=3.5°$ or $u=0.385$ was used. The calculated intensities are sufficiently sensitive to this parameter, as well as to partial inversion, to permit a determination of Δ to $\pm 0.7°$ or u to ± 0.002. An upper limit of 5 percent can be set on the amount of possible inversion.

An examination of the diffraction pattern of $ZnFe_2O_4$ shows a sloping background at low angles characteristic of paramagnetic diffuse scattering. The diffuse scattering cross section has been measured as a function of angle, and the extrapolated value for unit form factor is equal to 3.5 ± 0.3 barns/steradian/molecule. The calculated cross section for a paramagnetic arrangement of the ferric ions in the octahedral positions is 3.39 barns/steradian/molecule. This agreement together with the fit obtained in the absolute intensities of the Bragg reflections in which only nuclear scattering was considered leads to the conclusion that there is no octahedral-octahedral magnetic coupling at room temperature. It should be emphasized that antiferromagnetic coupling of the Fe^{+3} ions on the octahedral sites would lead to a coherent magnetic contribution to the diffraction pattern comparable in magnitude with that of the nuclear scattering, thereby completely spoiling the agreement in Table II.

The interpretation of the $NiFe_2O_4$ data involves an additional consideration, namely, the coherent magnetic scattering. The "chemical" structure, as distinct from the "magnetic" structure, can in principle be determined from the outer Bragg peaks which have no magnetic contributions because of the form factor falloff. However, the nuclear scattering amplitudes of nickel and iron differ by only seven percent, so that these peaks are insensitive to the degree of inversion. The magnetic contributions, on the other hand, are strongly dependent on the model. If one assumes a completely inverted structure and the Néel scheme of antiferromagnetic coupling between octahedral and tetrahedral sites, satisfactory agreement with experiment is obtained as is shown in Table III. The magnetic scattering has been corrected assuming a g factor[11] for Ni^{++} of 2.3

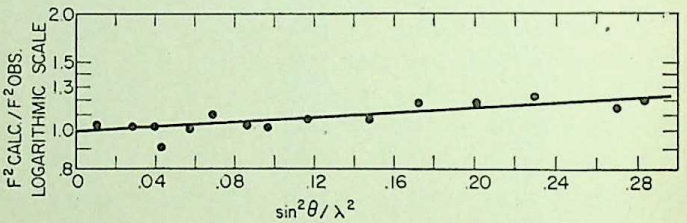


FIG. 7. Ratio of calculated to observed structure factors for diffraction peaks of $NiFe_2O_4$ plotted against $\sin^2\theta/\lambda^2$.

and a saturation magnetization[12] at room temperature equal to 0.9 times the value at absolute zero. As in the case of $ZnFe_2O_4$, a Debye-Waller temperature correction and a u parameter were determined. Figure 7 shows a plot of F_{calc}^2/F_{obs}^2 *versus* $\sin^2\theta/\lambda^2$ which was used to obtain the effective Debye temperature of $NiFe_2O_4$. The u parameter was determined in the same manner as for the zinc compound and has the value 0.381 ± 0.003.

In order to fit the calculated intensities to the observed, it is necessary to assume a form factor, shown in Fig. 8, describing the angular dependence of the magnetic scattering amplitude. In the case of $NiFe_2O_4$ the form factor cannot be obtained by independent means but can be justified by the following considerations. The curve shown in Fig. 8 is smooth and can be made to extrapolate, as it should, to unity at zero scattering angle. The use of an incorrect model to calculate not only the relative peak intensities but also the absolute intensities of Table III would, in general, require a form factor curve of irregular shape. The curve of Fig. 8 is similar to that obtained by Shull, Strauser, and Wollan[9] for Mn^{++} in the compounds MnF_2 and MnO.

[11] H. G. Beljers and D. Polder, Nature **165**, 800 (1950).
[12] R. Pauthenet and L. Bochirol, J. phys. et radium **12**, 249 (1951).

CC-0. In Public Domain. Gurukul Kangri Collection, Haridwar

Digitized by Arya Samaj Foundation Chennai and eGangotri

In fact, the intensities computed using the Mn^{++} form factor agree moderately well with those observed for $NiFe_2O_4$. While it is not unreasonable to expect the form factor to resemble that for Mn^{++}, it should be remembered that the curve for nickel ferrite is a rather complicated average involving two ionic species and two different crystallographic sites. A radial distribution of the magnetic electrons is obtained in a formal way by inverting the form factor curve. Such a distribution, which of course can have only qualitative theoretical significance, is shown in Fig. 9.

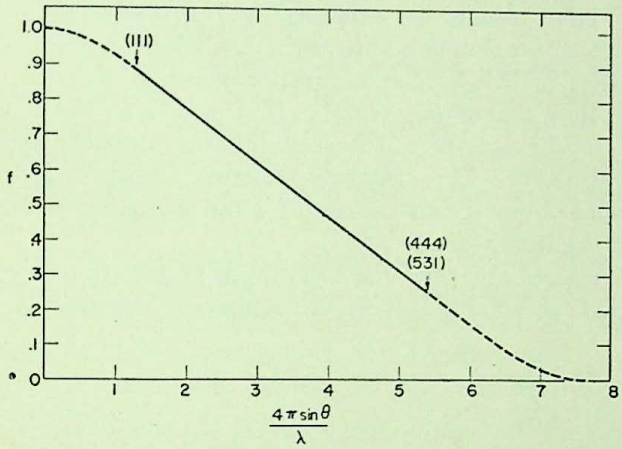


FIG. 8. Magnetic amplitude form factor for $NiFe_2O_4$ obtained from Bragg reflections.

Although the fit obtained using the Néel model is not necessarily unique, certain other structures consistent with the saturation moment can be unambiguously eliminated by the diffraction data. For example, a completely regular structure containing ferromagnetically coupled Ni^{++} ions on tetrahedral sites, and either paramagnetic or antiferromagnetically coupled Fe^{+++} ions on octahedral sites would result in a (111) intensity which is lower than the observed by a factor of about 20. An inverted arrangement in which the Fe^{+++} ions are paramagnetic is likewise eliminated by the data. On the other hand, assuming the Néel model, the computed intensities are not sensitive to incomplete inversion. The data require nickel ferrite to be at least 80 percent inverted, i.e., 80 percent of the nickel ions must occupy tetrahedral sites. If, however, the departure from the ideally inverted structure were as great as this, the saturation moment as calculated by Néel's method would be grossly in error. The possibility of ordering the Fe^{+++} and Ni^{++} ions on octahedral sites according to the scheme proposed by Verwey, Haayman, and Romeijn[13] for Fe_3O_4 at low temperatures has also been considered. Calculations show the effect to be too small to be observable with a powdered sample.

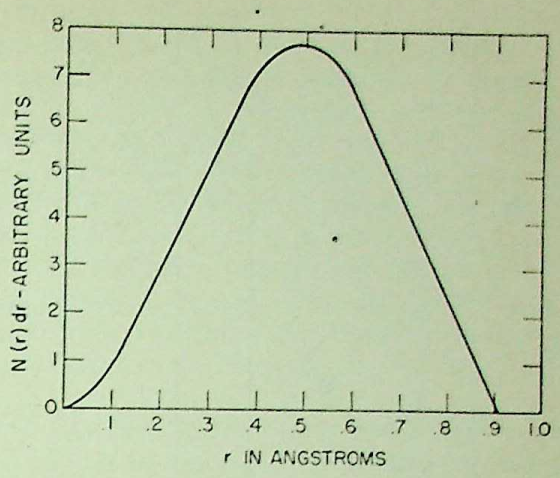


FIG. 9. Radial distribution of "3d" electrons in $NiFe_2O_4$ obtained from inversion of form factor in Fig. 8.

[13] Verwey, Haayman, and Romeijn, J. Chem. Phys. 15, 181 (1947).

DISCUSSION

C. KITTEL, *University of California, Berkeley, California:* We can estimate the Néel temperature for zinc ferrite by extrapolating experimental measurements of the Curie temperatures of Mn-Zn and Ni-Zn ferrites. In this way we find $T_c = 150 \pm 50°K$, so that Hastings and Corliss should not have expected order in zinc ferrite at room temperature. Neutron work at liquid air temperature is indicated.

C. P. GUILLAUD, *Centre National de la Recherche Scientifique, Bellevue, France:* We pointed out for the first time that atoms located in different crystallographic planes could give rise to a kind of antiferromagnetism, which afterward Néel called ferrimagnetism. In the definite compound Mn_2Sb,[1] we distinguished between manganese Mn_I atoms located in the (001) planes and manganese Mn_{II} atoms not located in the basic planes (Fig. 1). In order to interpret the saturation moment, we advanced the hypothesis that the Mn_I atoms are in the $3d^5, 4s^2$ state and the Mn_{II} atoms in the $3d^7$ state, the moments of spin of these two groups of atoms being antiparallel. In support of this hypothesis, we had considered the paramagnetic properties, the curvature of the curve $1/\chi = f(T)$ being explained by the existence of two different values of the molecular field. This hypothesis was likewise supported by the spontaneous magnetization curve $\sigma/\sigma_0 = f(T/\theta)$, by the empirical laws of Hume-Rothery and by the distance of 2.70A between Mn_I and Mn_{II} which gives rise to negative interactions.

In the course of our work, other substances have exhibited these properties in our opinion. We mention in particular the definite compound Mn_4N, which was

[1] C. Guillaud, thesis, Strasbourg (1943).

CC-0. In Public Domain. Gurukul Kangri Collection, Haridwar

Digitized by Arya Samaj Foundation Chennai and eGangotri

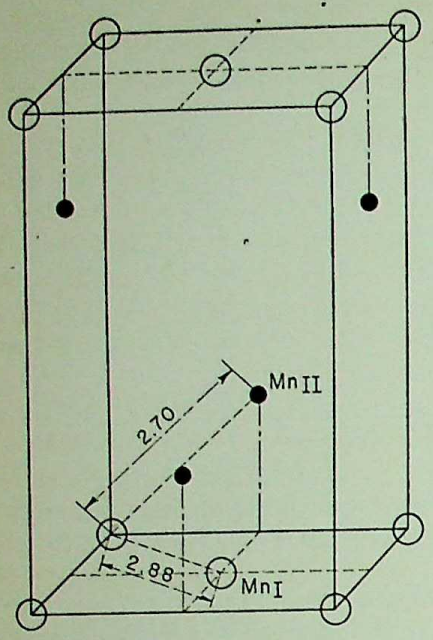


FIG. 1.

studied with Wyart[2] as co-worker, the saturation moment of which can be explained by an analogous mechanism.

In the diagrams of alloys of composition close to Mn_4N, superstructure lines appear with lattice spacings of 3.8A and 2.71A corresponding to the planes (100) and (110), respectively; they are caused only by the diffraction of the nitrogen atoms. In the close-packed cubic lattice which contains 8 tetrahedral holes located at the centers of the cubes and 4 octahedral holes located at the middle of the edges, the nitrogen atoms could be imagined to be distributed at random in the octahedral holes which are the largest. The x-ray diagrams show that the nitrogen atoms are regularly arranged in the centers of the cubes (Fig. 2).

In order to explain the resultant moment, which we find is very close to one Bohr magneton, we have considered two different states of the manganese atoms: $3d^5 4s^2$ for the atom at the corner of the cube and $3d^8$ for the three atoms at the centers of the faces. With an antiparallel arrangement of the spins of the two groups of manganese atoms we then obtain a resultant moment equal to $3\times 2-5=1$ Bohr magneton in agreement with the experimental moment. The distinction between the Mn atoms is supported by the difference in the distances to the nitrogen atom; this should result in the ionization of the manganese atoms which are nearest to the nitrogen atom. We have likewise proved this mechanism by the spontaneous magnetization curve (Fig. 3). The distance of 2.72A which we found between manganese atoms of the two groups therefore would give rise to negative interactions.

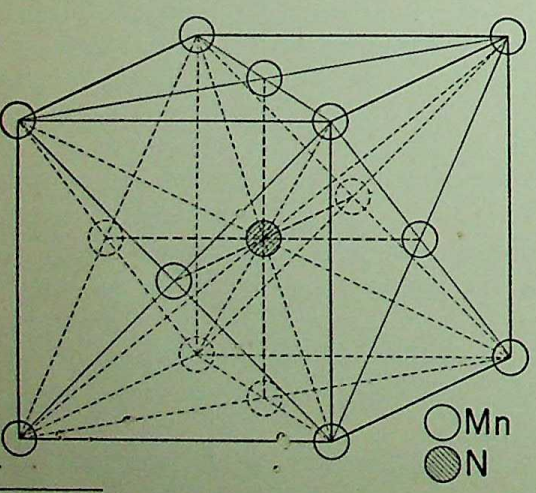


FIG. 2.

We shall compare the properties of Mn_4N with those of Fe_4N,[3] which we prepared and investigated and which also exhibits a superstructure which is identical to that of Mn_4N. The saturation moment of Fe_4N is 2.20 Bohr magnetons, equal to that of iron. In this case, the mechanism of antiferromagnetism probably does not operate. The distances causing negative interactions obviously are different for the manganese atoms and the iron atoms.

We also advanced the hypothesis of negative interactions in solid solutions of manganese arsenides and antimonides.[1] In the manganese antimonides, the variation of the saturation moments with composition leads us to believe that the Mn atom which enters into solution is in the $3d^5$, $4s^2$ state, the other manganese atoms being in the $3d^7$ state, as we demonstrated. The solid solution limit ends when an Sb atom is replaced by a Mn atom and the experimental saturation moment which is found for this limit is in good agreement with the discussed mechanism of antiferromagnetism.

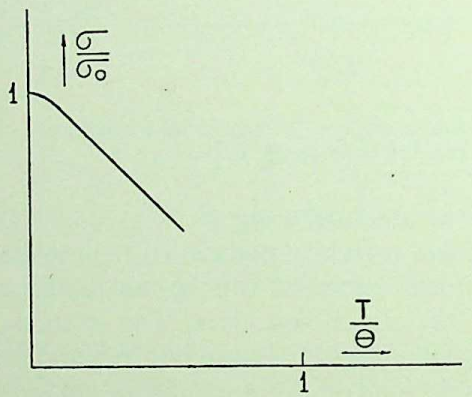


FIG. 3.

An additional factor is supplied by this study. The distance 2.78A should also give rise to negative interactions.

We shall probably find this same mechanism in the manganese arsenides,[1] although our investigations in this field are less accurate. The manganese atom which replaces for the arsenic atom should be in the $3d^5$, $4s^2$ state, with an antiparallel arrangement of the manganese atoms in the basic planes.

We supplement these results with results relating to the definite compound Mn_2As. We prepared a single crystal of the Mn_2As compound, which denotes the

[2] C. Guillaud and J. Wyart, Recherches du Centre National de la Recherche Scientifique No. 123 (1947).

[3] C. Guillaud and H. Creveaux, Compt. rend. 222, 1170 (1946)

CC-0. In Public Domain. Gurukul Kangri Collection, Haridwar

Digitized by Arya Samaj Foundation Chennai and eGangotri

limit of ferromagnetism of manganese-arsenic alloys. The results obtained until now enable us to consider the Mn atoms as arranged in alternate planes. We advance the hypothesis of a mechanism of antiferromagnetism between two adjacent planes. Thus Mn_2As would have a perfectly compensated antiferromagnetism.

We assume that this mechanism of antiferromagnetism likewise operates in the compound MnP,[4] the consecutive planes being occupied by atoms in the $3d^5$, $4s^2$, and $3d^7$ states. This hypothesis is supported by the small moment which we found experimentally and which is slightly higher than 1 Bohr magneton, We also call attention to the very great variation of the Curie point with field strength for MnP.

This mechanism which we observed in manganese alloys, however, is not peculiar to manganese. We investigated in particular the compound CrTe[5] and the small moment which is found, 2.40 Bohr magnetons, seems to be explicable by a mechanism of antiferromagnetism.

We shall supplement these data on the distances causing negative interactions in manganese alloys by data on the lower limit of positive interactions which result in ferromagnetism. If the Curie points of the definite compounds, MnBi, MnSb, and MnAs are plotted against the effective distances between manganese atoms, the lower limit of the distances giving rise to positive interactions is found to be about 2.81A.

[4] C. Guillaud and H. Creveaux, Compt. rend. 224, 266 (1947).
[5] C. Guillaud and S. Barbezat, Compt. rend. 222, 1224 (1946).

R. SMOLUCHOWSKI, *Carnegie Institute of Technology, Pittsburgh, Pennsylvania:* From your experimentally determined form factor you calculated the radial density distribution of the $3d$ electrons. How does this distribution compare with the results of theoretical calculations based either on the Fermi or the Hartree method? Would this indicate the location of the unpaired spins in the $3d$ shell?

J. C. SLATER, *Massachusetts Institute of Technology, Cambridge, Massachusetts:* In answer to this question I may say that the radius of the $3d$ shell as obtained from these neutron diffraction data is smaller than the theoretical radius. We really do not understand why it is so and what this signifies.

L. M. CORLISS, *Brookhaven National Laboratory, Upton, Lond Islang, New York:* One should add also that the results are average values for the $3d$ shells of nickel and of iron atoms in the nickel ferrite. Also the atoms do not occupy equivalent sites in the lattice so that a direct interpretation of our radial density distribution is not simple.

CC-0. In Public Domain. Gurukul Kangri Collection, Haridwar

Digitized by Arya Samaj Foundation Chennai and eGangotri

The High Temperature Magnetic Susceptibility of V, Nb, Ta, W, and Mo†‡

C. J. KRIESSMAN

U. S. Naval Ordnance Laboratory, White Oak, Maryland, and
The Catholic University of America, Washington, D. C.

The temperature range of magnetic susceptibility measurements has been extended from 1450°C to 1850°C. In the range from 25°C to the highest temperature measured, the susceptibilities of V, Nb, and Ta decrease with increasing temperature, while the susceptibilities of Mo and W increase. A periodicity in the sign of the temperature coefficient of the magnetic susceptibility of the transition elements is discussed in relation to various theories of metals.

INTRODUCTION

THE paramagnetism of the nonferromagnetic transition elements might be explained on the basis of several theoretical approaches which should give at least general predictions about the variation of magnetic susceptibility with temperature. These approaches are the collective electron picture suggested by Stoner[1] and extended by Wohlfarth[2] and the antiferromagnetic model advanced by Néel[3] and Zener.[4,5] However, comparison with experiment, especially at high temperatures, has not been possible because of the lack of data. The only data over an appreciable high temperature range were those on Ti and Zr,[6] Cr,[7] and Mn.[8–10] Much of the classic work of Honda[11] on almost all of the transition elements up to 1100°C is considered unreliable because of impurities in the samples used. The present work extends the temperature range of magnetic susceptibility measurements from 1450°C to 1850°C and furnishes data on the susceptibilities of V, Nb, Ta, Mo, and W from 25°C to about 1850°C.

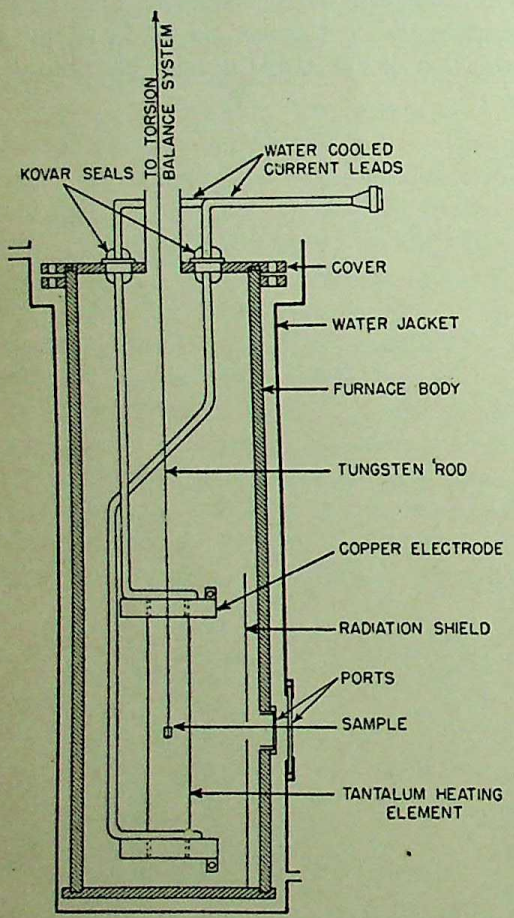


FIG. 1. Schematic drawing of the high temperature furnace.

EXPERIMENTAL METHOD

The susceptibility was measured with apparatus similar to that described by McGuire and Lane.[12] A small sample is suspended in an inhomogeneous magnetic field from one end of a torsion balance arm. The force, which is directly proportional to the suscep-

TABLE I. Purities and susceptibilities of the metals measured.

Metal	Purity, %	$\chi \cdot 10^6$ Literature	$\chi \cdot 10^6$ Present work	$\frac{10^{10}}{\chi_{Av}} \cdot \frac{\Delta\chi}{\Delta T}$
V	99.8	4.5[12]	5.00	−0.52
Nb	99.9	2.28[a]	2.20	−1.3
Ta	99.9	0.8490[b]	0.827	−1.2
W	99.99	0.284[a]	0.32	+0.87
Mo	99.95	0.949[a]	0.93	+0.88

[a] W. J. deHaas and P. M. Van Alphen, Proc. Acad. Sci. Amsterdam, 36, 263 (1933).
[b] F. E. Hoare and J. C. Walling, Proc. Phys. Soc. (London) 64B, 337 (1951).

† A dissertation presented to the faculty of the Graduate School of the Catholic University of America in partial fulfillment of the requirements for the degree of Doctor of Philosophy.
‡ Supported in part by the U. S. Office of Naval Research.
[1] E. C. Stoner, Proc. Roy. Soc. (London) 154A, 656 (1936).
[2] E. P. Wohlfarth, Phil. Mag. 40, 1095 (1949); Proc. Roy. Soc. (London) 195A, 434 (1949).
[3] L. Néel, Ann. Phys. 5, 232 (1936).
[4] C. Zener, Phys. Rev. 81, 440 (1951).
[5] C. Zener, Phys. Rev. 85, 324 (1952).
[6] C. F. Squire and A. R. Kaufmann, J. Chem. Phys. 9, 673 (1941).
[7] T. R. McGuire and C. J. Kriessman, Phys. Rev. 85, 452 (1952).
[8] G. Grube and O. Winkler, Z. Electrochem. 42, 815 (1936).
[9] A. Serres, J. phys. et radium 9, 377 (1938).
[10] M. Isobe, Sci. Rept. Tohoku University A3, 78 (1951).
[11] K. Honda, Ann. Physik 32, 1027 (1910).
[12] T. R. McGuire and C. T. Lane, Rev. Sci. Instr. 20, 489 (1949).

CC-0. In Public Domain. Gurukul Kangri Collection, Haridwar

Digitized by Arya Samaj Foundation Chennai and eGangotri

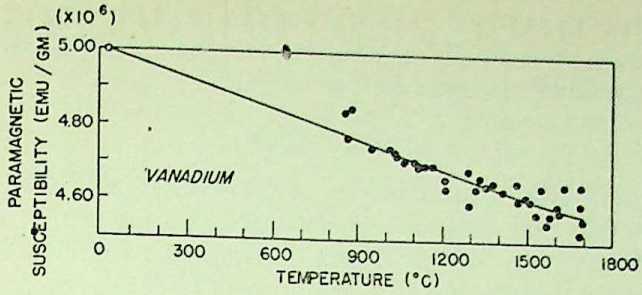


FIG. 2. The magnetic susceptibility of vanadium.

tibility according to the equation

$$F_z = m\chi H_x \frac{dH_x}{dz},$$

where χ is the magnetic susceptibility per gram, is balanced electrodynamically by passing a small current through a coil on the other end of the torsion balance arm. The balance condition is determined by a split cathode photocell method.

The high temperature furnace is shown in Fig. 1. The heating element is a cylinder of 0.003-inch sheet tantalum which is firmly clamped in heavy copper electrodes. Water-cooled copper tubes which are brought through the demountable brass furnace cover by glass-to-metal Kovar seals both support the electrodes and carry the heating current. The cover is sealed to the brass furnace body by a Neoprene gasket, and the furnace is evacuated and then filled with helium to protect the sample and heating element. The furnace body is cooled by water flowing in the outer jacket.

At 1900°C the heating current is about 500 amperes at 10 volts, which is supplied by a 208-volt step-down transformer. These large alternating currents cause vibrations in the heating element which restrict its life time to an average of three runs from 25°C to 1900°C. However, it is a relatively simple matter to remove the heating element assembly and replace the tantalum cylinder.

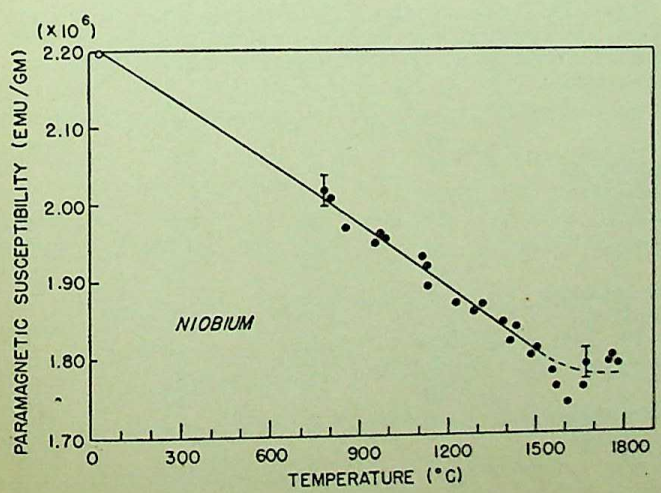


FIG. 3. The magnetic susceptibility of niobium.

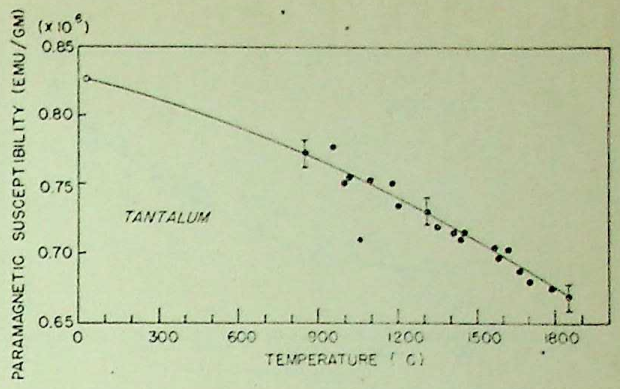


FIG. 4. The magnetic susceptibility of tantalum.

The metal to be measured, usually in the form of a small cylinder, is suspended from the torsion balance by a thin tungsten rod which passes through an axial hole in the sample. This eliminates the use of a container which might react with the metal. The small force introduced by the tungsten rod is eliminated by calibration.

The temperature is measured with a Leeds and Northrup optical pyrometer, which is sighted on the inside of the furnace through a small hole in the heating element. There are glass ports in the furnace body and the water jacket. A radiation shield protects the inner port. The optical path is calibrated for absorption by placing a standard tungsten filament blackbody source inside the furnace.

RESULTS

The Nb, Ta, Mo, and W samples were obtained in the form of spectroscopically pure rods from Johnson, Mathey, and Company, while the V sample came from the Electro Metallurgical Company. The purities of the samples as reported by the suppliers are shown in Table I. Field-dependence data at room temperature indicate that the spectroscopic samples contain only small ferromagnetic impurities requiring corrections of 0.01 to 0.02×10^{-6} susceptibility unit at 2600 gauss, the field used in the high temperature measurements.

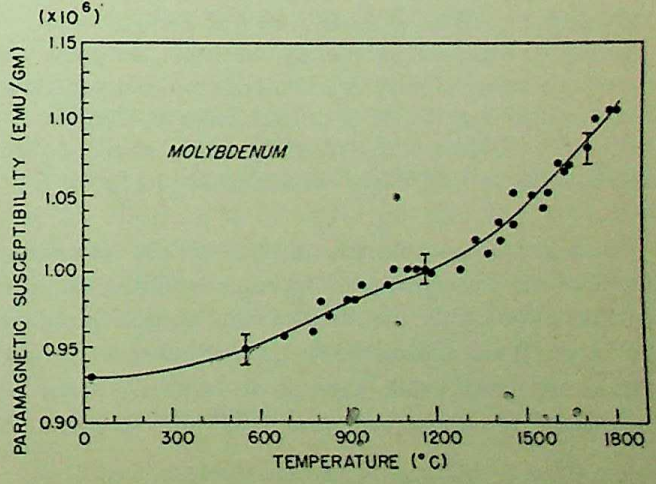


FIG. 5. The magnetic susceptibility of molybdenum.

CC-0. In Public Domain. Gurukul Kangri Collection, Haridwar

Digitized by Arya Samaj Foundation Chennai and eGangotri

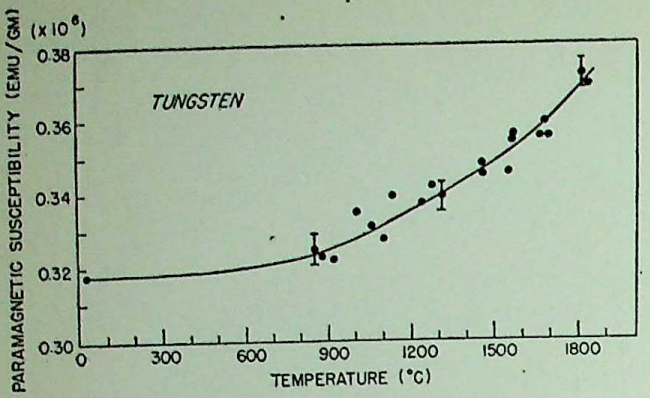


FIG. 6. The magnetic susceptibility of tungsten.

The same type of correction for V amounts to 0.25×10^{-6} unit. The experimental results are shown in Figs. 2 to 6. Data have also been taken between room temperature and 800°C with another furnace,[7] and these results are indicated by solid lines.

The susceptibility of V decreases from 5.00×10^{-6} at 25°C to 4.57×10^{-6} at 1700°C, although this high temperature value is in doubt because there is a large scattering of the data as the melting point is approached. The temperature dependence observed here for V is different from that of Honda,[11] who reported that the susceptibility of V increased with temperature. However, the data of Klemm[13] from −195°C to room temperature indicate a slight decrease in susceptibility with increasing temperature, and Klemm's room temperature value of 4.5×10^{-6} is much closer to the present value than Honda's 1.50×10^{-6}. Klemm suggests that the temperature dependence he observed for V is due to a small amount of iron present in a paramagnetic form, but this would not account for the continued decrease in susceptibility at high temperatures.

The susceptibility of Nb decreases from 2.20×10^{-6} at 25°C to 1.79×10^{-6} at 1575°C, at which point it appears to level off. A crystal structure change might explain this behavior, but recent x-ray studies[14] reveal no such transition in Nb.

The susceptibility of Ta decreases uniformly from 0.827×10^{-6} at 25°C to 0.668×10^{-6} at 1850°C.

Unlike the preceding metals, W and Mo show an increasing susceptibility with increasing temperature. The susceptibility of W increases from 0.32×10^{-6} at 25°C to 0.37×10^{-6} at 1850°C, while that of Mo increases from 0.93×10^{-6} at 25°C to 1.11×10^{-6} at 1825°C.

Table I shows a comparison between the best room temperature susceptibility values available in the literature for these metals and the values found in this work. If the difficulties in the preparation of these metals are considered, agreement is good except in the case of W, where the value 0.32×10^{-6} is closer to Honda's old data. The last column in Table I gives a rough measure of the relative change in susceptibility over the entire temperature range.

[13] L. Klemm, Z. Electrochem. 45, 354 (1939).
[14] Edwards, Speiser, and Johnston, J. Appl. Phys. 22, 424 (1951).

DISCUSSION

The most notable feature of the experimental results is that the temperature coefficient of the magnetic susceptibility of the transition elements alternates in sign with the columns in the periodic table. V, Nb, and Ta, all in the fifth column of the periodic table, have a negative temperature coefficient, while W and Mo, in the sixth column of the periodic table, have a positive temperature coefficient. When the data on Ti, Zr, Cr, and Mn are added, as shown in Table II, this periodicity becomes more evident. The ability of existing theories to qualitatively account for this effect will be discussed.

Stoner[1] has investigated the temperature coefficient of the magnetic susceptibility by using

$$\chi=\chi_0(1+c\gamma T^2);\quad \gamma=\left[\frac{\partial^2 \ln N(E)}{\partial E^2}\right]_{E_0},$$

where $N(E)$ is the number of energy states per energy interval and χ_0 and c are constants. The sign of the temperature coefficient γ depends critically on the shape of the curve for the distribution of energy states at E_0, the Fermi limit. For the usual forms assumed for $N(E)$ at E_0, e.g., $E^{\frac{1}{2}}$ or E^n, γ is negative. However, if E_0 is very close to a minimum in the $N(E)$ curve as shown in Fig. 7(a) then γ can be positive and the magnetic susceptibility can increase with temperature. Now if we assume that the main contribution to the paramagnetism of the transition elements is from electrons in the d band, then the Fermi limit of an element like Cr, which has a positive γ, should occur at a minimum in the $N(E)$ curve for the $3d$ band. No actual calculation for the curve of the distribution of states for Cr has been made, but it should qualitatively resemble the $N(E)$ curves for Ni and Cu. The $N(E)$

TABLE II. The temperature coefficient of the magnetic susceptibility, the electronic specific heat constant, and the antiferromagnetic ordering μ_n (in Bohr magnetons) found by neutron diffraction.

	Ti	V	Cr	Mn
Temperature coefficient	+	−	+	−
$a\cdot10^4$	8.3	14	3.7	42
μ_n		0	0.4	(≃0.3)
	Zr	Nb	Mo	Tc
Temperature coefficient	+	−	+	
$a\cdot10^4$	6.9	60		
μ_n		0		
	Hf	Ta	W	Re
Temperature coefficient		−	+	
$a\cdot10^4$		19.4	5.1	
μ_n			0	

CC-0. In Public Domain. Gurukul Kangri Collection, Haridwar

Digitized by Arya Samaj Foundation Chennai and eGangotri

curve for the 3*d* band in Cu given by Krutter and Slater[15] and a more exact calculation for the 3*d* band in Ni by Fletcher[16] are shown in Fig. 7(b) on arbitrary scales. Although these curves differ in some important details, both indicate a minimum where the 3*d* band would be approximately half filled with electrons. This minimum occurs, then, about where one would expect the Fermi limit of Cr with its five to six 3*d* electrons.

Another property which depends on the distribution of states at E_0 is the electronic specific heat. Recently, Friedberg, Estermann, and Goldman[17] have suggested that the surprisingly low electronic specific heat of Cr may be explained by a minimum in the 3*d* $N(E)$ curve for Cr. Values for the constant a (often called γ in the literature), which is a measure of the magnitude of the electronic specific heat, are shown in Table II. Here too, a periodicity is evident. Elements in the Ti and Cr columns have lower electronic specific heats than their neighbors. Therefore, reasoning as in the Cr case, one might expect minima in the *d* band $N(E)$ curves of Ti, Zr, Mo, and W, and a resulting increase of susceptibility with temperature, just the behavior which is observed. The basic feature, then, of the *d* band in the transition metals would be its division into two parts, the upper part having a very high density of states. In the case of the Ti and Cr type of elements an increase in temperature will cause a movement of electrons to the high density portion of the band, resulting in an increase in susceptibility. The $N(E)$ curve and Fermi limit calculated for W by Manning and Chodorow[18] is shown in Fig. 7(c). Here again the Fermi limit occurs at a minimum in the $N(E)$ curve, and here again the susceptibility increases with temperature as in the case of Cr.

Another approach which may also give a qualitative explanation of the periodicity in the sign of γ is the assumption of Néel and Zener that the *d* shells of the transition elements are antiferromagnetic. The metals with a positive γ would have a high antiferromagnetic Curie point, i.e., the observed susceptibility curve is rising toward a maximum while the metals with a negative γ would have a low antiferromagnetic Curie point, i.e., the observed susceptibility curve is decreasing from a maximum. No Curie point in the susceptibility of the transition metals has been observed except the apparent one found at low temperatures in crystalline Mn by Serres[9] and more recently by McGuire and Kriessman;[19] however, in the same temperature range Bates and Pantalu[20] have observed no such Curie

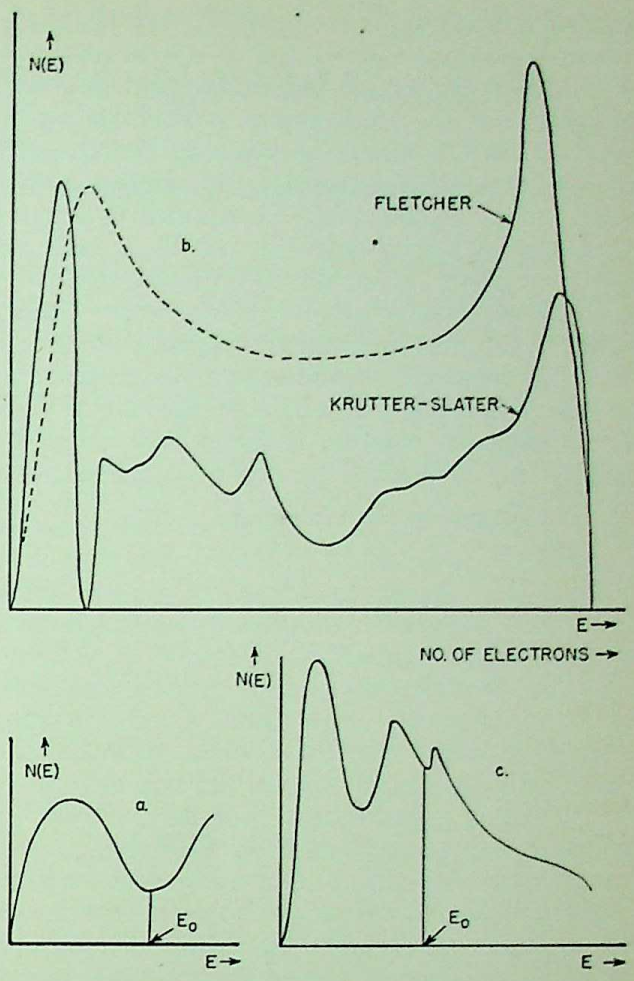


FIG. 7. (a) Idealized $N(E)$ curve with a minimum occurring at E_0. (b) Two calculations for the 3d band distribution of states curve. The Krutter-Slater curve for Cu is based on the cellular approximation. The Fletcher curve for Ni is based on a tight binding approximation. Both curves are qualitatively reproduced here, and only the solid portion of the Fletcher curve represents the actual calculation. The dotted portion has been added according to a suggestion in the original paper by Fletcher. (c) The $N(E)$ curve and Fermi limit for W calculated by Manning and Chodorow.

point in amorphous Mn. This would seem to indicate that the maximum observed depends on the crystalline ordering, and this is consistent with the requirements for antiferromagnetism. The absence of Curie points in the other metals is not contradictory at the present time since their susceptibilities have not yet been measured at the highest or the lowest temperatures.

Antiferromagnetism can be detected directly by neutron diffraction.[21] Therefore, one should find a high temperature antiferromagnetic ordering for the positive γ-metals like Ti and Cr and a low temperature antiferromagnetic ordering for the negative γ-metals like V and Mn. The data of Shull[22] on some of the transition metals are shown in Table II. Antiferromagnetic ordering is found in Cr corresponding to about 0.4 of a Bohr magneton with a Curie point of about 150°C. However, it is difficult to see how this antiferro-

[15] H. M. Krutter, Phys. Rev. 48, 664 (1935); J. C. Slater, Phys. Rev. 49, 537 (1936).
[16] G. C. Fletcher, Proc. Phys. Soc. (London) 65, 192 (1952).
[17] Friedberg, Estermann, and Goldman, Phys. Rev. 85, 375 (1952).
[18] M. F. Manning and M. I. Chodorow, Phys. Rev. 56, 787 (1939).
[19] T. R. McGuire and C. J. Kriessman (unpublished results).
[20] L. F. Bates and D. V. Pantalu, Proc. Phys. Soc. (London) 47, 197 (1935).
[21] C. G. Shull and J. S. Smart, Phys. Rev. 76, 1256 (1949).
[22] C. G. Shull, Phys. Rev. 86, 599 (1952).

CC-0. In Public Domain. Gurukul Kangri Collection, Haridwar

Digitized by Arya Samaj Foundation Chennai and eGangotri

magnetism which disappears at 150°C can account for the susceptibility which is still slowly increasing at 1400°C, unless in keeping with a suggestion by Zener,[5] the polarity of the atoms begins to fluctuate rapidly enough at 150°C to make detection of antiferromagnetic ordering by neutrons impossible. No ordering in W is found, but its moment might be expected to be undetectable since the susceptibility of W is only one tenth that of Cr. Now Mn, which has a negative γ, should show antiferromagnetic ordering at low temperatures. Shull[23] does find antiferromagnetic ordering in Mn at low temperatures, although at the present time the type of ordering is uncertain. In the case of V and Nb no magnetic ordering is found, and unless the moments are too small to detect or fluctuate too rapidly, this weakens the argument that antiferromagnetism is responsible for the periodicity in γ. Neutron diffraction data on Ti would be enlightening, since they should show antiferromagnetic ordering similar to that in Cr if antiferromagnetism actually is responsible for the periodicity in γ.

[23] C. G. Shull (private communication).

ACKNOWLEDGMENT

I wish to thank Dr. T. R. McGuire and Dr. L. R. Maxwell for many valuable suggestions and discussions during the course of this work, Dr. J. Samuel Smart for suggesting the problem, and the Naval Ordnance Laboratory for making this research possible. I would also like to thank Dr. Richard L. Petritz and Professors Karl F. Herzfeld and Francis E. Fox for their help and encouragement.

CC-0. In Public Domain. Gurukul Kangri Collection, Haridwar

Digitized by Arya Samaj Foundation Chennai and eGangotri

REVIEWS OF MODERN PHYSICS VOLUME 25, NUMBER 1 JANUARY, 1953

Magnetic Moment Orientation and Thermal Expansion of Antiferromagnetic CrSb

A. I. SNOW*

Institute for the Study of Metals, University of Chicago, Chicago, Illinois

THE magnetic moment orientation and the thermal expansion of the antiferromagnetic compound CrSb have been investigated by neutron and x-ray diffraction techniques. The crystal structure and magnetic properties of this compound previously have been investigated by Haraldsen, Rosenqvist, and Grønvold.[1] They confirmed that this compound has the nickel-arsenide crystal structure and found that the magnetic susceptibility showed the typical behavior of an antiferromagnetic compound with an antiferromagnetic Curie point of 450°C.

Neutron diffraction data, obtained by the author[2] at the Argonne National Laboratory, led to the relative atomic magnetic moment orientations shown in Fig. 1. The atomic magnetic moments are aligned perpendicular to [001] planes, i.e., along the *c* axis, in such a manner that they are aligned in the same direction (ferromagnetically) in any [001] plane but oppositely directed (antiferromagnetically) in adjacent [001] planes. The nearest neighbor chromium atoms are thus aligned antiferromagnetically whereas second nearest neighbors are aligned antiferromagnetically.

The thermal expansion of CrSb has been investigated from room temperature to 800°C with the results shown in Fig. 2. There are several interesting correlations among the thermal expansion data, the magnetic data, and the neutron diffraction results, but only a fragmentary discussion can be given here.

The axis which expands on heating is the *c* axis which is the axis along which the magnetic moments are aligned. The break in the *a* axis *vs* temperature curve and the upper break in the *a* axis *vs* temperature curve both occur at 450°C which is the antiferromagnetic Curie point. There is no change in lattice type observable at any temperature from room temperature to 800°C. A 19-cm x-ray diffraction camera was used which had a high enough resolution to make any appreciable line splitting easily visible. A plot of unit cell volume *vs* temperature also shows a break at 450°C. The unit cell volume undergoes an increase of 2.9 percent from room temperature to 450°C. The question of whether the interactions between chromium atoms are direct or whether the interactions are through the antimony atoms or the extent to which each mode of interaction contributes is of interest, and some light can be shed on these points by consideration of the various types of data available. Experimental details and a fuller discussion of the experimental results will be given elsewhere.

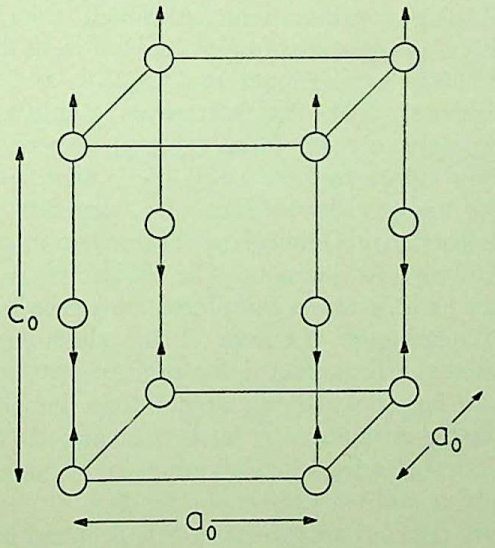


FIG. 1. Unit cell of CrSb. Arrows indicate the relative alignments of atomic magnetic moments. Only chromium atoms are shown.

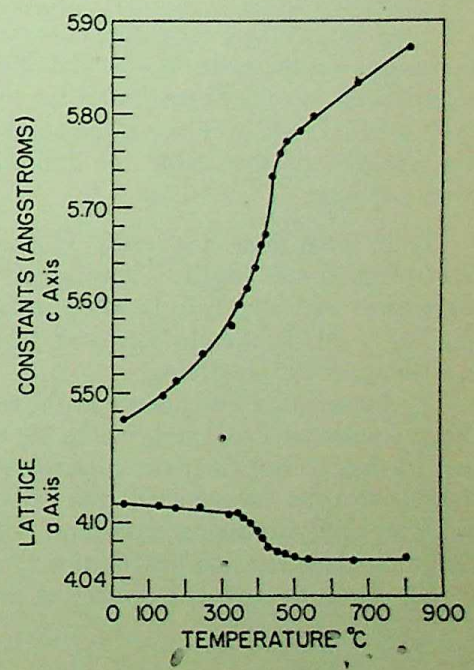


FIG. 2. Thermal expansion of CrSb.

* Present address: Sinclair Research Laboratories, Inc., Harvey, Illinois.

[1] Haraldsen, Rosenqvist, and Grønvold, Arch. Math. Naturvidensk, B. L. Nr. 4.

[2] A. I. Snow, Phys. Rev. 85 365 (1952).

CC-0. In Public Domain. Gurukul Kangri Collection, Haridwar

Digitized by Arya Samaj Foundation Chennai and eGangotri

Paramagnetic Scattering of Neutrons by Trivalent Ions of Nd and Er

W. C. KOEHLER AND E. O. WOLLAN

Oak Ridge National Laboratory, Oak Ridge, Tennessee

NEUTRON diffraction measurements have been made on the oxides of the rare earths in order to study the paramagnetic scattering by ions of the $4f$ series. Up to the present, magnetic scattering studies have been confined primarily to members of the $3d$ transition group for which the orbital moments are in general strongly quenched and the scattering arises in most cases from spin moments only. This is the case for which the magnetic scattering theory of Halpern and Johnson has been worked out. For many rare earth ions, however, magnetic susceptibility data show the orbital moments to be wholly operative, and it was one of the objects of this study to obtain information on the nature of the magnetic scattering for such cases.

Not all of the rare earths are amenable to study by neutron diffraction methods, either because of the excessive thermal neutron capture cross sections of some of them, or because of the extreme rarity of others. Fortunately, as a result of the development of column extraction techniques, we were able to obtain sizeable quantities (several grams) of Nd_2O_3 and Pr_2O_3 from Dr. F. Spedding at Ames, and of Er_2O_3 from Dr. G. Boyd of Oak Ridge. The pair $Nd^{+++}-Er^{+++}$ is particularly interesting because these ions are complementary; Nd^{+++} with three $4f$ electrons is in a ${}^4J_{9/2}$ state, and Er^{+++} with three vacancies in the $4f$ shell is in a ${}^4J_{15/2}$ state.

Room temperature measurements were made on the hexagonal sesquioxides of Pr and Nd for scattering angles from 3 to 90 degrees, and for the cubic form of Nd_2O_3 and Er_2O_3 over the same angular range. From the analysis of the data, the following conclusions were reached:

(1) In each case the cross section for magnetic scattering in the forward direction is in satisfactory agreement with that calculated by replacing $g^2{}_sS(S+1)$ by $g^2{}_JJ(J+1)$ in the Halpern and Johnson expression for the magnetic scattering.

(2) The angular dependence of the magnetic scattering is similar for Pr_2O_3 and Nd_2O_3, but markedly different for Er_2O_3. For comparison purposes the amplitude form factor for the $4f$ shell was calculated from the semiempirical screening constants of Pauling and Sherman. This electron distribution form factor, which would apply to magnetic scattering arising from spin moments only, falls essentially to zero for $k=4\pi \sin\theta/\lambda = 5.0$. For Er_2O_3, the observed magnetic scattering amplitude has the same general character but it persists to considerably higher k values. In Nd_2O_3 and Pr_2O_3, the scattering amplitude is essentially angularly independent from $k=0$ to $k=3.5$ after which it fails off slowly to zero in the neighborhood of $k=6.5$.

(3) The cubic form of Nd_2O_3 was prepared to change the electrostatic field acting on the Nd ion. Within an estimated experimental error of less than 10 percent no change in the magnetic scattering was observed.

Measurements were also made on these salts at temperatures down to 20.4°K. No coherent scattering effects suggestive of strong exchange coupling were observed, and the diffuse scattering remained constant within experimental error.

The theory of magnetic scattering of neutrons has, as we have mentioned, been worked out for the case of spin moments. In those cases where there are also orbital contributions the theory becomes much more difficult.

The difference in the angular dependence of the scattering by the neodymium and erbium ions, however, can be approximately accounted for on the basis of the following considerations. Although the forward scattering is proportional to $g^2J(J+1)$, it is, in this case, approximately proportional to $(L\pm 2S)^2$, and it may be considered that the scattering amplitudes are approximately of the form $(f_L \pm f_s)$, where the $+$ sign would apply to Er^{+++} and the $-$ sign to Nd^{+++}. Now the angular dependence of f_s depends on the electron distribution and can be obtained approximately from Pauling and Sherman. The orbital moments, on the other hand, may be considered, on a classical basis, as distributed over the area of the electronic orbit, and hence the form factor for orbital scattering will persist to larger scattering angles than for the spin. A reasonable estimate of f_L leads to an angular dependence of the scattering by neodymium and erbium which is in good accord with the experiments.

A more rigorous treatment of this problem has been made by G. Trammel of the Oak Ridge National Laboratory who calculated the first two terms in a series expansion of the magnetic form factor for Nd^{+++} and Er^{+++}, and, over the range of validity of the expansion, the calculation agrees with experiment.

DISCUSSION

H. GRAYSON-SMITH, *University of Alberta, Canada:* Concerning the specific heat of chromium, as Dr. Shull has mentioned, Armstrong and myself observed no anomaly in the neighborhood of 475°K,

CC-0. In Public Domain. Gurukul Kangri Collection, Haridwar

Digitized by Arya Samaj Foundation Chennai and eGangotri

where the neutron diffraction experiment indicates an antiferromagnetic Curie point. However, at the highest temperatures reached, around 1150°K, the specific heat was observed to be rising rapidly, in a manner to suggest an anomaly at some still higher temperature.

REVIEWS OF MODERN PHYSICS VOLUME 25, NUMBER 1 JANUARY, 1953

Some Magnetic and Electrical Properties of Gadolinium, Dysprosium, and Erbium Metals*

S. Legvold, F. H. Spedding, F. Barson, and J. F. Elliott

Institute for Atomic Research and Department of Physics, Iowa State College, Ames, Iowa

Measurements of the ferromagnetic properties of the rare earth transition metals have been reported by Trombe[1,2] and Klemm and Bommer.[3] Further measurements on these metals are currently under way at the Ames Laboratory and this report presents results of some of the preliminary work.

In the case of gadolinium metal, which has the h.c.p. structure, a ring wound torus has been used for determining the Curie point and the magnetization as a function of field intensity for low fields. The torus was machined from a vacuum-cast cylinder of metal and had a rectangular cross section with an outer diameter of 2.58 cm, an inner diameter of 2.00 cm, and a thickness of 3.3 mm. The Curie point data are shown in Fig. 1, where the value indicated for the Curie point is 16±1°C in good agreement with the 16±2°C reported by Trombe.[1]

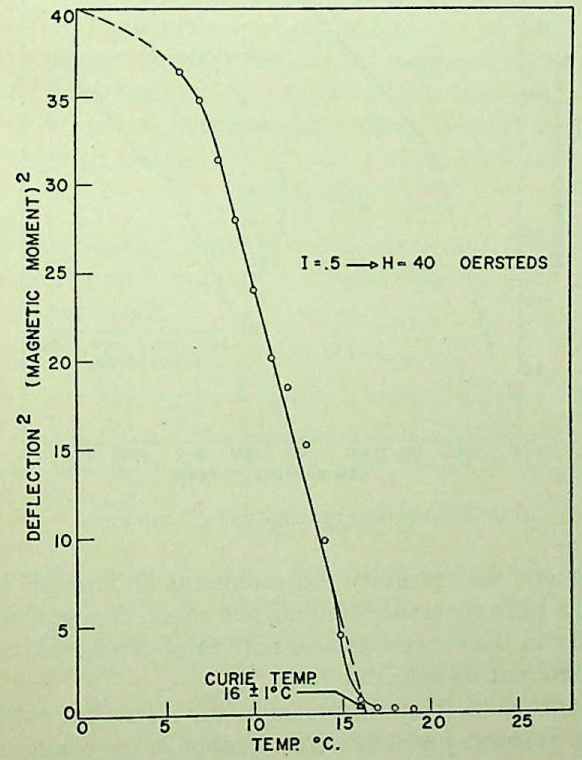


Fig. 1. Curie temperature of gadolinium.

Magnetization curves obtained with the torus are shown in Fig. 2. The data have been corrected for leakage through the pick-up coil. For the 77°K data, it is believed that an additional small correction should be made because of the oxygen content of the nitrogen bath, but it is difficult to estimate the magnitude of the correction. The results reported here indicate much higher magnetizations at low fields than those indicated by Trombe's[1] data. His lowest field intensity measurement was at 3000 oersteds at which the specific magnetization σ was about 195 cgs units. In the data of Fig. 2 this value of σ is obtained at the same temperature with an applied field of the order of 500 oersteds.

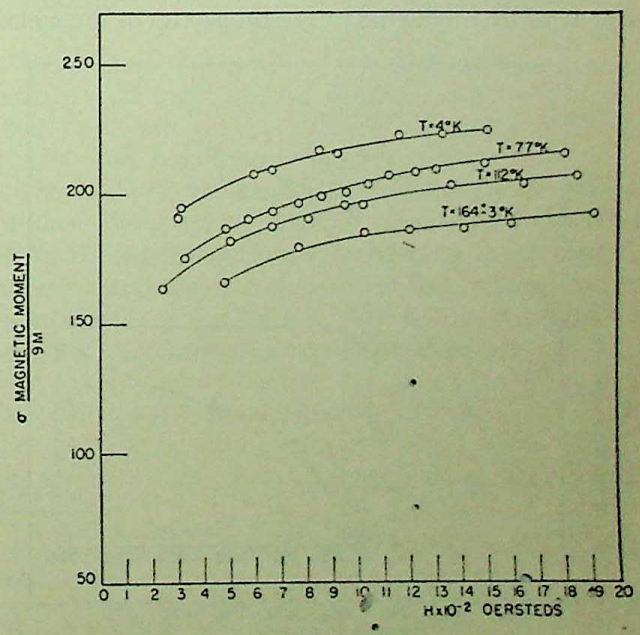


Fig. 2. Magnetization data for gadolinium. (Ordinate values are in cgs units.)

* Work was performed in the Ames Laboratory of the U. S. Atomic Energy Commission.

[1] M. F. Trombe, Ann. phys. 7, 383 (1937).

[2] M. F. Trombe, Compt. rend. 221, 19 (1945).

[3] W. Klemm and H. Bommer, Z. anorg. u. allgem. Chem. 231, 138 (1937).

CC-0. In Public Domain. Gurukul Kangri Collection, Haridwar

Digitized by Arya Samaj Foundation Chennai and eGangotri

TABLE I. Data on samples (spectrographic analysis).

	Mg	Ca	Tb	Fe	Sm	Ho	Y	Ta
Gadolinium[a]	<0.02%	<0.03%	Faint trace	~0.02%	<0.15%			
Dysprosium[b]	Weak line (No quant. methods)	Strong line		Faint trace		~0.1%	~0.07%	Faint trace
Erbium[c,d]		<200 ppm		<300 ppm				Faint trace

[a] Cast under vacuum, rolled to shape, and annealed 7 hours at 550°C.
[b] Cast under argon atmosphere, turned to size, and annealed at 500°C for 66 hours.
[c] Free of all other rare earth metals.
[d] Cast under vacuum, filed to shape, unannealed.

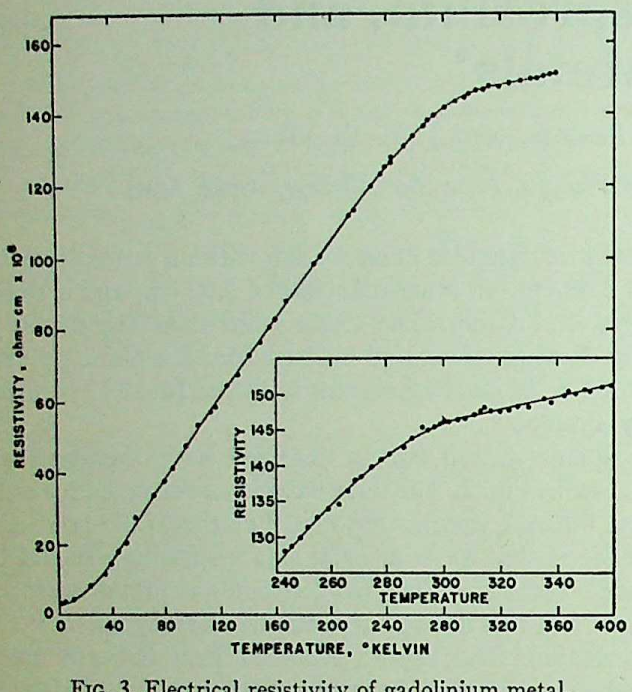


FIG. 3. Electrical resistivity of gadolinium metal.

Further measurements at higher field intensities are under way.

The electrical resistivities of gadolinium, dysprosium, and erbium rods have been determined from room temperature down to 2.2°K to ascertain the temperatures at which anomalies in the properties of the metals occur. The purities and methods of preparation of the rods are shown in Table I.

In Fig. 3 it is seen that there is an abrupt change in the slope of the resistivity curve for gadolinium at about 300°K. This we consider evidence of the influence of the magnetic properties of the metal on the conduction process at this temperature. The break occurs some ten degrees above the Curie point reported above.

For dysprosium a behavior similar to that for gadolinium is observed in the neighborhood of 155°K. See Fig. 4. Here, however, there is a long temperature interval over which the resistivity is nearly constant.

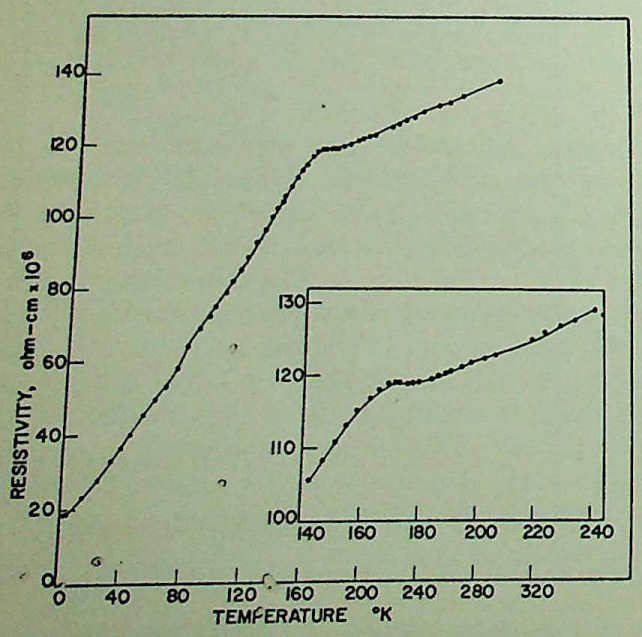


FIG. 4. Electrical resistivity of dysprosium metal.

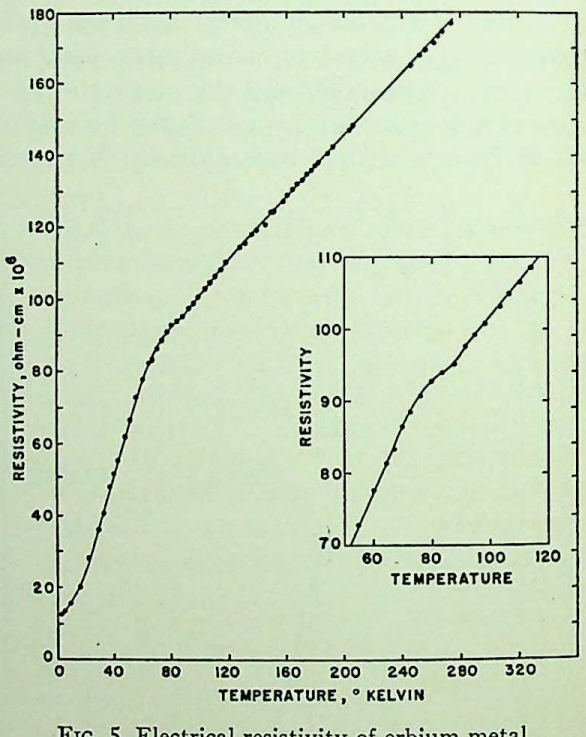


FIG. 5. Electrical resistivity of erbium metal.

Magnetic susceptibility measurements of Trombe[2] suggest a basis for understanding the effect. A slight peculiarity in the curve was also noticeable (and repeatable on different samples) at 73°K.

Contrasted with dysprosium, the curve for erbium (Fig. 5) shows just a moderate change in the conduction process at about 80°K. Magnetic susceptibility measurements of Klemm and Bommer[3] indicate that the magnetic properties of this metal may be associated with this resistivity anomaly. It may be noted that erbium has an extremely high resistivity for a pure metal at room temperature.

CC-0. In Public Domain. Gurukul Kangri Collection, Haridwar

Digitized by Arya Samaj Foundation Chennai and eGangotri

REVIEWS OF MODERN PHYSICS VOLUME 25, NUMBER 1 . JANUARY, 1953

Magnetic Energy Formulas and their Relation to Magnetization Theory

WILLIAM FULLER BROWN, JR.

Sun Physical Laboratory, Newtown Square, Pennsylvania

Present theories of magnetization are based largely on energy formulas. These are incomplete because they rely on a calculation of magnetization work in the absence of strain and of strain work in the absence of magnetization. The present paper summarizes and relates to magnetization theory a calculation, already published elsewhere, in which magnetization and strain are assumed from the start to be present simultaneously; furthermore forces are calculated directly, without use of energy arguments until the properties special materials are considered. An important result is that the separation of the force on part of a body into a "magnetic" force and a force derivable from "stresses" can be accomplished in more than one way. The theory confirms the traditional results for fluids; but for elastic solids, it yields terms not present in the formulas of the traditional theory. These terms may be important in the magnetization process. For a uniformly magnetized ellipsoid they lead to a nonuniform magnetostriction "form effect" with a mean strain equal to the strain calculated by Becker.

THE theory of domain formation, magnetization, and magnetostriction is based on the concept of spontaneous magnetization, on symmetry requirements, and on energy formulas. The energy formulas are usually quoted as if they were a part of everybody's background of knowledge. Unfortunately this knowledge is not in a very satisfactory state. Many of the textbook treatments assume a constant permeability; the results are therefore useless for ferromagnetic purposes. Other treatments introduce other restrictive assumptions, which are often not stated explicitly.

The basic formulas used in magnetization and magnetostriction theory may be summarized as follows. The work of magnetizing unit volume is calculated for a body with no strains:

$$dw_m = \mathbf{H}\cdot d\mathbf{M} \tag{1}$$

($\mathbf{H}$ = magnetizing force, $\mathbf{M}$ = magnetization). The work of straining unit volume is calculated for a body with no magnetization:

$$dw_s = X_x de_{xx} + \cdots + Y_z de_{yz} + \cdots \tag{2}$$

(the stress and strain notation is that of Love[1]). These two expressions are added to get a formula for the change of free energy density when magnetization and strain both occur:

$$dF = dw_m + dw_s. \tag{3}$$

The free energy density is expressed as a series in the magnetization and strain components, in conformity with symmetry requirements and to as many terms as seem necessary. Other formulas are derived from this one by simple applications of differential calculus:

$$\partial F/\partial M_x = H_x, \quad \partial F/\partial e_{xx} = X_x, \quad \partial F/\partial e_{yz} = Y_z = Z_y. \tag{4}$$

Occasionally a magnetician becomes uneasy about the effect of strains on magnetic formulas. Stoner[2] in 1937 recognized that his formulas applied strictly only to a rigid body; but he found no way of improving on them. Becker[3] in 1933 took account of magnetization and strain simultaneously, in his calculation of the magnetostriction of an ellipsoid. He concluded that the magnetostriction is shape-dependent, and he verified this conclusion experimentally. Nevertheless this "form effect" is scarcely mentioned in Becker and Döring's book;[4] and it has been ignored by recent authors. Furthermore, Becker's calculation does not tell us what happens to the form effect when the specimen is not an ellipsoid or the magnetization is not uniform.

Occasionally, also, an elastician becomes uneasy about the effect of magnetization on elastic formulas. Brillouin,[5] in his book on tensors, remarks that in a polarized body the stress tensor is no longer symmetrical: that is, Y_z, the y component of force across unit area perpendicular to z, is no longer equal to Z_y, the z component of force across unit area perpendicular to y. Sokolnikoff[6] makes a similar statement in his book on elasticity. If Brillouin and Sokolnikoff are right, then what does one get by differentiating a free energy density with respect to a shearing strain?

The traditional formula for magnetization work has various "derivations." One of them is the following. When the magnetization is changed by controlling the current I through a coil, work is done against the induced electromotive force E_c. The rate at which work is done can be expressed as a volume integral:

$$dW/dt = -IE_c = -\int \mathbf{J}\cdot\mathbf{E}\,d\tau, \tag{5}$$

where $\mathbf{J}$ is the current density and $\mathbf{E}$ the electric field

[1] A. E. H. Love, *A Treatise on the Mathematical Theory of Elasticity* (Cambridge University Press, New York, 1934), fourth edition.

[2] Edmund C. Stoner, Phil Mag. 23, 833 (1937).

[3] R. Becker, Z. Physik 87, 547 (1933).

[4] R. Becker and W. Döring, *Ferromagnetismus* (Julius Springer, Berlin, 1939).

[5] L. Brillouin, *Les Tenseurs en Mécanique et en Elasticité* (Dover Publications, New York, 1946), pp. 11, 216–217.

[6] I. S. Sokolnikoff, *Mathematical Theory of Elasticity* (McGraw-Hill Book Company, Inc., New York, 1946), p. 43.

CC-0. In Public Domain. Gurukul Kangri Collection, Haridwar

Digitized by Arya Samaj Foundation Chennai and eGangotri

intensity. The integral can be transformed by use of Maxwell's equations. The result is

$$\frac{dW}{dt}=\frac{d}{dt}\left[\frac{1}{2\gamma}\int \mathbf{H}^2 d\tau\right]+\int \mathbf{H}\cdot\frac{\partial \mathbf{M}}{\partial t}d\tau \qquad (6)$$

plus terms that are unimportant in magnetostatics. The constant γ is 4π in Gaussian units. Up to this point the derivation is completely general. In the next step the quantity $(\partial\mathbf{M}/\partial t)dt$, the change of magnetization at a fixed point of space, is identified with the change $d\mathbf{M}$ of magnetization at a definite point in a body:

$$dW=\text{perfect differential}+\int \mathbf{H}\cdot d\mathbf{M}d\tau. \qquad (7)$$

This step is valid only for rigid bodies and, under special conditions, for fluids. In the final step a transition is made from a whole body to a volume element, by re-

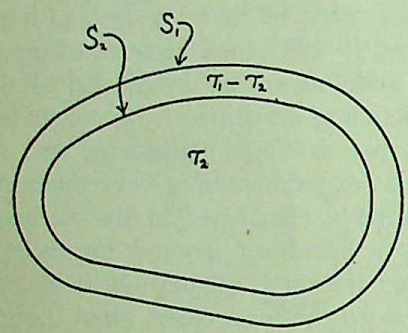


FIG. 1. Definition of the *magnetic* or *long-range* force on an arbitrary part of a magnetized body. First calculate, by macroscopic methods, the force exerted on the matter inside S_2 by the matter outside S_1; then let $S_1 \rightarrow S_2$. Deviations of the actual force from the force thus calculated are interpretable in terms of *stresses*. Such deviations are due partly to the presence of nonmagnetic short-range forces and partly to inaccuracy of the macroscopic magnetic formulas at molecular distances. In a macroscopic theory, the two terms cannot be distinguished, and even the separation of the total force into a long-range term and a stress term can be made in several ways.

moving the integral sign (Eq. (1)). This step has no mathematical justification, for the preceding formula has been established only when the integral is extended over all space. The final formula is therefore not a logical consequence of the preceding argument; it is an additional postulate suggested by it.

Other derivations use other postulates. Some of these postulates concern the nature of the "effective field" inside a magnetized body. Some concern the localization of energy in the electromagnetic field, or the derivability of forces from tensors. The literature in this field is full of speculations and controversy. Livens[7] at his death in 1950 was still publishing polemics on the subject. Sommerfeld[8] shortly before his death published a paper on the subject, and Diesselhorst,[9] Gans,[10] and Döring[11] promptly rushed into print to refute it.

Are such postulates necessary, or can the general problem of magnetic forces and energies be handled by using only the laws of mechanics and the formula for the forces between dipoles? I once thought that additional postulates were necessary, because the dipole formula does not lead to any unique expression for the "effective field intensity" inside a magnetized body. Several years ago, however, I decided that despite this fact, the dipole formula should be sufficient, without additional postulates. My reasoning is illustrated by Fig. 1.

The basic problem is to calculate the magnetic force and torque on an arbitrary part of a magnetized body. To do this, let us first calculate the force and torque exerted on the matter inside a surface S_2 by the matter outside a slightly larger surface S_1; and then let us find the limit as the surfaces come together. For this calculation we do not need to know anything about an effective field inside S_2; all we need to know is the part of the field inside S_2 that is due to magnetized matter outside S_1, and this we know how to calculate.

The result can be written in several equivalent forms; here is one of them:

$$\mathbf{F}=\int \mathbf{M}\cdot\nabla\mathbf{H}d\tau+\tfrac{1}{2}\gamma\int \mathbf{n}M_n^2 dS, \qquad (8)$$

$$\mathbf{L}=\int \mathbf{r}\times[\mathbf{M}\cdot\nabla\mathbf{H}]d\tau +\tfrac{1}{2}\gamma\int \mathbf{r}\times[\mathbf{n}M_n^2]dS+\int \mathbf{M}\times\mathbf{H}d\tau. \qquad (9)$$

These formulas are rather distressing because each contains a surface integral that cannot be transformed into a volume integral. The force is not just so much per unit volume; it also contains a term that depends on the shape of the volume considered. Such forces are quite different from the "body forces" allowed in the standard theory of elasticity. Therefore, how can we justify applying the elasticity formulas to a magnetized body?

In the end I decided that there was only one way out of this difficulty: to abandon the standard theory of elasticity, and to develop, instead, a theory that would take account of the peculiar nature of magnetic forces.

It turned out that the modifications needed were rather minor. One is the asymmetry of the stress tensor mentioned by Brillouin and Sokolnikoff:

$$Y_z-Z_y=(\mathbf{M}\times\mathbf{H})_x; \qquad (10)$$

this comes from the existence of a couple per unit

[7] G. H. Livens, Phil. Mag. 36, 1 (1945) and 38, 453–479 (1947); Phys. Rev. 71, 58–63 (1947); Proc. Cambridge Phil. Soc. 44, 534–545 (1948). Editorial note, Proc. Cambridge Phil. Soc. 47, 450 (1951).

[8] A. Sommerfeld and F. Bopp, Ann. Physik 8, 41–45 (1950).

[9] H. Diesselhorst, Ann. Physik 9, 316–324 (1951).

[10] Richard Gans, Ann. Physik 9, 337–340 (1951).

[11] W. Döring, Ann. Physik 9, 363–372 (1951).

CC-0. In Public Domain. Gurukul Kangri Collection, Haridwar

Digitized by Arya Samaj Foundation Chennai and eGangotri

volume, $\mathbf{M}\times\mathbf{H}$. Then there are some extra terms in the surface traction formula:

$$X_\nu=[X_x+\tfrac{1}{2}\gamma(M_x^2-M_n^2)]l+X_y m+X_z n. \quad (11)$$

Finally, there are extra terms in the equations of motion:

$$(\partial/\partial x)(X_x+\tfrac{1}{2}\gamma M_x^2)+(\partial X_y/\partial y)+(\partial X_z/\partial z)+\mathbf{M}\cdot\nabla H_x+\rho X=\rho f_x. \quad (12)$$

Once these formulas were derived, the special case of a fluid was easy to treat. All the electrostrictive or magnetostrictive properties of a fluid in equilibrium came out of the theory directly, without introduction of thermodynamic arguments as such. But the results were very perplexing. All the final formulas for observable quantities were identical with those derived by the energy method and given, for instance, in Abraham-Becker.[12] Yet some of the intermediate formulas were incompatible with those of Becker. For instance, according to Becker a fluid is a substance in which "there is only one kind of elastic stress, namely equal pressure in all directions"; but according to my formulas the pressure in a polarized fluid depends on the orientation of the surface element across which the pressure is being computed. This same anisotropy of of pressure had been found earlier by Guggenheim.[13]

Eventually it became clear that these differences were differences only of definition: my "pressure" and Becker's "pressure" were different quantities. The principle involved here is the following. There is no unique way of separating the total force into a long-range or "magnetic" force and a short-range force described in terms of "stresses." The reason is that "long-range" forces, such as magnetic forces, do not act exclusively over large distances; they are also effective at small distances. The expression for the magnetic force can always be changed by adding a term that affects only the short-range behavior; for the change can be neutralized by making a corresponding change in the definition of the stresses. Whether such a term is to be considered part of the magnetic force or part of the stress system is purely a matter of definition, and it happens that my definition is different from Becker's. The reason that this nonuniqueness has escaped attention so long is that most of the calculations have been done by energy methods, rather than by direct calculation of the forces. In an energy method, it is difficult to determine what definition of magnetic force is implied by the equations.

Once this nonuniqueness principle has been grasped, most of the controversy in the literature becomes pointless. The question is not "Which of these formulas is right?" It is "What definition of magnetic force and stress is implied by each of these formulas?" It is not important which definitions are used, but it is essential that the stress formulas used be the ones appropriate to the force definition adopted.

With this apparent discrepancy explained, the next step was to calculate the work done, in an arbitrary change of magnetization and deformation, upon an arbitrary mass m. One form of the result is the following. The work done can be separated into two terms:

$$dW=dU_m+\int_m dF dm. \quad (13)$$

The first term is the differential of

$$U_m=-\frac{1}{2}\int_\tau \mathbf{M}\cdot\mathbf{H}_1 d\tau; \quad (14)$$

here τ is the volume instantaneously occupied by the mass m, and $\mathbf{H}_1$ is the contribution to $\mathbf{H}$ from magnetization in τ. The value of U_m for two parts of a body combined is not the sum of its values for the separate parts. The other term of dW does have this additivity property but is not in general a perfect differential:

$$dF=\mathbf{H}\cdot D\mathbf{M}+V[(X_x+\tfrac{1}{2}\gamma M_x^2)de_{xx}+\cdots+\tfrac{1}{2}(Y_z+Z_y)de_{yz}+\cdots]. \quad (15)$$

Here $\mathbf{M}$ is the moment and V the volume of unit mass, and the symbol D is used for a change computed with respect to axes attached to the mass element. In this formula the strains are not necessarily infinitesimal: de_{xx} etc. are defined not as differentials of strains but as products of dt by velocity strains.

The separation into two terms is not unique; it can be made in various ways, corresponding to choice of $\mathbf{H}$, of $\mathbf{B}$, or of something else as independent field variable. The ultimate formulas for observable quantities will be independent of this choice.

For reversible isothermal processes, the term with the additivity property becomes the differential of a free energy. Since the formula holds for an arbitrary part of a material body, and not just for all space, the integrand is the differential of a free energy per unit mass. This differential is given by an expression (Eq. (15)) more complicated than that of the traditional theory.

For elastic strains, the free energy per unit mass can be expressed as a series in the strains, through degree 2, with coefficients that are functions of the components of specific magnetization $\mathbf{M}$ in axes fixed in the mass element. Symmetry can be used, high order terms neglected, and so on, as in the traditional theory. In this way the theory of magnetization and magnetostriction can be put on a sound basis. If the quantity being calculated in shape-dependent, that fact will emerge automatically from the calculation, because everything relevant has been put into the basic equations. No restrictive assumptions have been made, and no arbitrary postulates have been introduced.

[12] Max Abraham, *The Classical Theory of Electricity and Magnetism*, revised by Richard Becker, translated by John Dougall (G. E. Stechert and Company, New York, 1932), Chapter V.

[13] E. A. Guggenheim, Proc. Roy. Soc. (London) A155, 49–70 and 70–101 (1936).

CC-0. In Public Domain. Gurukul Kangri Collection, Haridwar

Digitized by Arya Samaj Foundation Chennai and eGangotri

I have worked out the details of such a calculation for an ellipsoidal specimen of isotropic material, in a state of uniform magnetization and strain. The problem is to find the applied tractions necessary to maintain such a strain, and in particular to find whether the assumed uniform strain is compatible with zero surface traction. It turns out that it is not. The magnetostriction is therefore not uniform, as was assumed by Becker in his form effect calculation. The actual strain can be calculated approximately by the following method: first find the surface tractions necessary to maintain zero strain; then imagnine the negative of these tractions applied to an ordinary elastic, nonmagnetic body, and calculate the resulting strains. The second step is difficult to carry out completely, except for a sphere; but the *average* strain is easy to compute. It turns out to be equal to the strain that Becker computed by assuming uniform strain and minimizing the energy.

The details of this special calculation are given in an appendix to this paper. The general theory appeared in the *American Journal of Physics* in 1951.[14,15] I hope that it will prove useful in other problems in magnetization and magnetostriction.

APPENDIX. MAGNETOSTRICTION OF AN ELLIPSOID

In Voigt's[16] notation ($x_1=e_{xx},\cdots$, $x_4=e_{yz},\cdots$), for small elastic strains

$$F=A+\sum_i B_i x_i+\tfrac{1}{2}\sum_i\sum_j C_{ij}x_i x_j, \tag{A1}$$

where A, B_i, and $C_{ij}=C_{ji}$ are functions of $\mathcal{M}_x$, $\mathcal{M}_y$, and $\mathcal{M}_z$. The strain and specific magnetization components are referred to axes that rotate with the mass element (reference 14, Sec. 4.4).

Suppose first that $\mathbf{M}$ is everywhere along the local z axis: then for isotropic material, by symmetry, $B_1=B_2$, $B_4=B_5=B_6=0$, and the nonvanishing C's are $C_{11}=C_{22}$, C_{33}, $C_{44}=C_{55}$, C_{66}, $C_{12}=C_{11}-2C_{66}$, and C_{13} (reference 1, p. 160, Sect. 110, (2)). Since $M_x=M_y=0$, the conditions that dF in Eq. (15) be a perfect differential give

$$\begin{aligned} VX_x&=\partial F/\partial x_1=B_1+C_{11}x_1+C_{12}x_2+C_{13}x_3,\\ VY_y&=\partial F/\partial x_2=B_1+C_{12}x_1+C_{11}x_2+C_{13}x_3,\\ V(Z_z+\tfrac{1}{2}\gamma M^2)&=\partial F/\partial x_3=B_3+C_{13}(x_1+x_2)+C_{33}x_3; \end{aligned} \tag{A2}$$

$$\begin{aligned} V\cdot\tfrac{1}{2}(Y_z+Z_y)&=\partial F/\partial x_4=C_{44}x_4,\\ V\cdot\tfrac{1}{2}(Z_x+X_z)&=\partial F/\partial x_5=C_{44}x_5,\\ V\cdot\tfrac{1}{2}(X_y+Y_x)&=\partial F/\partial x_6=C_{66}x_6. \end{aligned} \tag{A3}$$

Now suppose further that the rotation vanishes; that the only nonvanishing strains are an extension x_1 along the fixed x and y axes and an extension x_3 along the fixed z axis; and that x_1, x_3, and $\mathcal{M}=\mathcal{M}_z$ are all independent of (x, y, z). Then since the magnetization is along and the strain symmetric about the z axis, $H_x(=\partial F/\partial\mathcal{M}_x)$ and $H_y(=\partial F/\partial\mathcal{M}_y)$ must vanish; and the relation $H_z=\partial F/\partial\mathcal{M}_z$ requires that H_z be independent of (x, y, z). Since $\mathcal{M}$ and the dilatation are independent of (x, y, z), so too is M. If, therefore, the specimen is an ellipsoid, the assumed state of magnetization and strain can be maintained by a uniform applied field and by suitable surface tractions, which will now be determined.

Under the assumed conditions $\mathbf{M}\times\mathbf{H}=0$, so that $Y_z-Z_y=0$, etc., by Eq. (10); and since $x_4=x_5=x_6=0$, $Y_z+Z_y=0$, etc. by Eqs., (A3). Therefore $Y_z=Z_y=0$, etc. The remaining stress components are given by Eqs. (A2). To the first order in the strains,

$$1/V=(1/V_0)(1-2x_1-x_3), \tag{A4}$$

where V_0 is the specific volume in the unstrained state, and therefore

$$\begin{aligned} X_x=Y_y&=b_1+(c_{11}+c_{12})x_1+c_{13}x_3,\\ Z_z+\tfrac{1}{2}\gamma M^2&=b_3+2c_{31}x_1+c_{33}x_3, \end{aligned} \tag{A5}$$

with

$$b_i=B_i/V_0,\quad c_{ij}=(C_{ij}-B_i)/V_0. \tag{A6}$$

(Note that if $B_3\neq B_1$, then $c_{13}\neq c_{31}$.)

The tractions on the surface of the ellipsoid are, by Eqs. (11),

$$\begin{aligned} X_\nu&=(X_x-\tfrac{1}{2}\gamma M_n^2)l,\quad Y_\nu=(Y_y-\tfrac{1}{2}\gamma M_n^2)m,\\ Z_\nu&=[Z_z+\tfrac{1}{2}\gamma(M^2-M_n^2)]n. \end{aligned} \tag{A7}$$

Substitution of Eqs. (A5) in Eqs. (A7) gives

$$\begin{aligned} X_\nu/l=Y_\nu/m&=(c_{11}+c_{12})x_1+c_{13}x_3+b_1-\tfrac{1}{2}\gamma M^2n^2,\\ Z_\nu/n&=2c_{31}x_1+c_{33}x_3+b_3-\tfrac{1}{2}\gamma M^2n^2. \end{aligned} \tag{A8}$$

Consistently with the symmetry already assumed, suppose the ellipsoid to be one of revolution about the z axis. Then if the ellipsoid is finite, the quantities on the right vary with position on the surface because of the term $-\frac{1}{2}\gamma M^2n^2$. Consequently, no values of x_1 and x_3 will make X_ν, Y_ν, and Z_ν vanish at all points of the surface. The assumed uniform state is not a possible one for an ellipsoid with its surface free; such a state can be maintained only by applying forces to the surface.

The tractions required to maintain zero strain are

$$\begin{aligned} X_{\nu 0}&=(b_1-\tfrac{1}{2}\gamma M^2n^2)l,\\ Y_{\nu 0}&=(b_1-\tfrac{1}{2}\gamma M^2n^2)m,\\ Z_{\nu 0}&=(b_3-\tfrac{1}{2}M^2n^2)n. \end{aligned} \tag{A9}$$

The actual magnetostrictive strains can be calculated approximately by finding the strains produced in a

---

[14] William Fuller Brown, Jr., Am. J. Phys. 19, 290–304 and 333–350 (1951).

[15] The work reported here grew out of the author's activities as a member of the Coulomb's Law Committee of the American Association of Physics Teachers. The Committee, under the chairmanship of Professor E. C. Kemble, was appointed in 1944 and presented its report in Am. J. Phys. 18, 1–25 and 69–88 (1950).

[16] Woldemar Voigt, *Lehrbuch der Kristallphysik* (B. G. Teubner, Leipzig, 1910 and 1928), p. 563.

CC-0. In Public Domain. Gurukul Kangri Collection, Haridwar

Digitized by Arya Samaj Foundation Chennai and eGangotri

nonmagnetic elastic ellipsoid by the tractions $(-X_{\nu 0}, -Y_{\nu 0}, -Z_{\nu 0})$. In the limiting case of a long needle-ellipsoid, the term $-\frac{1}{2}\gamma M^2 n^2$ becomes negligible except near the ends, and the strains are those due to tractions $(-b_1 l, -b_1 m, -b_3 n)$. This part of the strain is independent of position and corresponds to uniform stresses $X_x = Y_y = -b_1$, $Z_z = -b_3$ in the nonmagnetic ellipsoid. With respect to it as standard, the "form effect" strain is that produced by normal tension $\frac{1}{2}\gamma M^2 n^2$.

The strains produced by such a normal tension can be computed for a sphere by methods described in reference 1, Chapter XI. For a nonspherical ellipsoid of revolution, the complete solution would require an extension of methods at present available.[17] However, the *volume average* strains can be computed by formula (13) of reference 1, p. 175:

$$\bar{x}_1 = (\gamma M^2/2EV)\int [lx - \sigma(my+nz)]n^2 dS,$$
$$\bar{x}_3 = (\gamma M^2/2EV)\int [nz - \sigma(lx+my)]n^2 dS. \quad \text{(A10)}$$

Here E is Young's modulus, σ is Poisson's ratio, and V is the ellipsoid volume. For a prolate spheroid, the parametric equation of the surface in cylindrical coordinates is

$$z = a\cos\theta, \quad \rho = b\sin\theta, \quad \text{(A11)}$$

and the volume is $\pi ab^2/3$. By integration over ϕ and introduction of the eccentricity $e = (1-b^2/a^2)^{\frac{1}{2}}$, the problem can be reduced to the evaluation of the two integrals

$$J_1 = \int_0^1 u^2(1-e^2u^2)^{-1}du = e^{-3}\{\tfrac{1}{2}\ln[(1+e)/(1-e)] - e\}$$
$$= N/[4\pi(1-e^2)], \quad \text{(A12)}$$
$$J_2 = \int_0^1 u^4(1-e^2u^2)^{-1}du = e^{-2}(J_1 - \tfrac{1}{3}). \quad \text{(A13)}$$

Here N is the longitudinal demagnetizing factor.

The strains given by Eq. (A10) consist of a pure dilatation

$$x_1' = x_3' = \gamma M^2(1-e^2)J_1/6k = (\gamma/4\pi)NM^2/6k \quad \text{(A14)}$$

(k = bulk modulus) and an equivoluminal strain

$$-2x_1'' = x_3'' = \gamma M^2(1-e^2)(3J_2 - J_1)/4G$$
$$= (\gamma/4\pi)[(3-e^2)N - 4\pi(1-e^2)]M^2/4e^2G \quad \text{(A15)}$$

(G = rigidity). These agree with Becker's formulas for the form effect, which he assumed to be uniform.

This method of evaluating the strains is an approximation, not merely because it neglects the variation of "elastic constants" (c_{ij}) with magnetization, but also because it neglects in all the equations some terms that no longer vanish when the strain varies with position. A rigorous calculation would require simultaneous solution of the equations of elastic equilibrium and of Poisson's equation and would probably show that the magnetization as well as the strain varies with position.

My crystal calculation of 1945,[18] which led to a paradox, was valid for a rigid crystal; but for a crystal capable of deformation, the derivation holds only if the approximations of the traditional theory are accepted. The theory outlined here provides a method of carrying out a rigorous calculation for a deformable crystal.

[17] M. A. Sadowsky and E. Sternberg, J. Appl. Mech. 14, A191–A201 (1947).

[18] William F. Brown, Jr., Revs. Modern Phys. 17, 15–19 (1945).

CC-0. In Public Domain. Gurukul Kangri Collection, Haridwar

Digitized by Arya Samaj Foundation Chennai and eGangotri

REVIEWS OF MODERN PHYSICS VOLUME 25, NUMBER 1 JANUARY, 1953

Rotational Relaxation in Nickel at High Frequencies

W. P. MASON

Bell Telephone Laboratories, Murray Hill, New Jersey

Measurements of the ΔE effect and the decrement made by Bozorth, Mason, and McSkimin and by Johnson and Rogers are compared with that expected from a calculation of domain wall relaxations for a distribution of domain sizes as determined by the optical measurements of Williams and Walker. At low frequencies the agreement is good but at high frequencies a second relaxation region is indicated. It is shown that this region is consistent with a domain rotation relaxation and introducing this effect, a good agreement is obtained between theory and experiment for the entire frequency range.

I. INTRODUCTION

IF one wishes to measure relaxation effects connected with single domains in a ferromagnetic material, he finds that it is difficult to do this by purely magnetic methods since a magnetic field causes all domains to grow in the direction of the field and hence they are essentially coupled. Any relaxation effects, such as those connected with eddy currents, are characteristic of the specimen size rather than the domain size. However, if one applies a compressive stress to a nickel specimen, it is well known that domain wall motion and domain rotation occur in such a way that the domains tend to line up along the direction of the applied stress. On the average, half of them line up with their magnetic vector pointing along one direction parallel to the applied stress and the other half in the opposite direction and hence no over-all flux is generated by the applied stress. As a result of this the effects of magnetic changes in surrounding domains cancel out on the average in any given domain and hence relaxation effects connected with mechanical properties are determined by domain sizes.

The two mechanical properties affected by domain wall motions and domain rotation are the elastic constants and the decrement. In an annealed specimen it is well known that the elastic modulus is lower in the demagnetized state than in the magnetized state, since an applied stress generates not only an elastic strain but also a strain due to the magnetostriction effect caused by the shift in the direction of the domain to directions parallel to the applied stress, and these effects are additive. This difference in the elastic modulus for saturated and demagnetized states is called the ΔE effect. If the stress alternation is so rapid that the domain wall motion or the domain rotation cannot follow the applied stress, this effect disappears. The other mechanical property affected by domain wall motion or domain rotation is the decrement of the material which is determined by the eddy current loss in the regions for which the direction of magnetization is changing. When these regions are connected with domain sizes this loss is known as the microeddy current loss. As long as the motions can follow the applied stress this loss should be proportional to the frequency but when the wall motion or domain rotation can no longer follow the applied stress, the decrement should rise to a maximum value and decrease to zero for very high frequencies.

II. EXPERIMENTS AND THEORETICAL CALCULATIONS

Previous measurements[1] of the ΔE effect in polycrystalline nickel rods have shown the presence of a

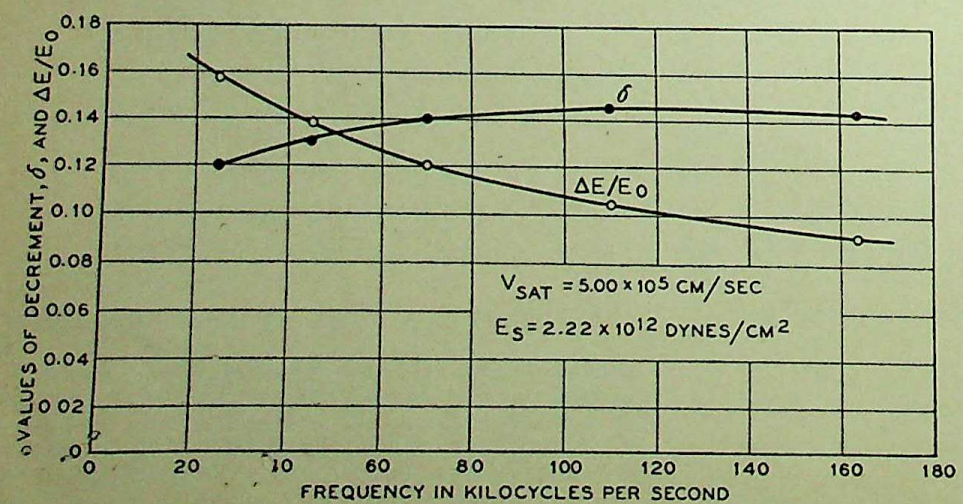


FIG. 1. Fractional change in Young's modulus, and the decrement, plotted as a function of frequency for rod No. 1.

[1] Bozorth, Mason, and McSkimin, Bell System Tech. J. Part I, XXX, No. 4, (October, 1951).

CC-0. In Public Domain. Gurukul Kangri Collection, Haridwar

Digitized by Arya Samaj Foundation Chennai and eGangotri

domain wall relaxation in nickel which causes the effective domain susceptibility and hence also the ΔE effect to decrease with increasing frequency. For a single domain size it was shown that the ΔE effect and the associated decrement are given by the formulas

$$\frac{\Delta E}{E_D}=\frac{4}{5}\left[\lambda_{111}\left(\frac{5C_{44}}{C_{11}-C_{12}+3C_{44}}\right)\right]^2\frac{\chi_0 E_s}{I_s^2}\times\frac{1}{1+f^2/f_0^2},$$

$$\delta=\frac{4\pi}{5}\left[\lambda_{111}\left(\frac{5C_{44}}{C_{11}-C_{12}+3C_{44}}\right)\right]^2\frac{\chi_0 E_s}{I_s^2}\left(\frac{f/f_0}{1+(f/f_0)^2}\right), \tag{1}$$

where λ_{111} is the magnetostrictive constant for nickel along the [111] direction (-25×10^{-6}); $5C_{44}/(C_{11}-C_{12}+3C_{44})$ is a ratio of elastic constants equal to 1.33; χ_0 is the initial susceptibility; E_s the saturated value of Young's modulus (2.22×10^{12} dynes/cm^2); I_s

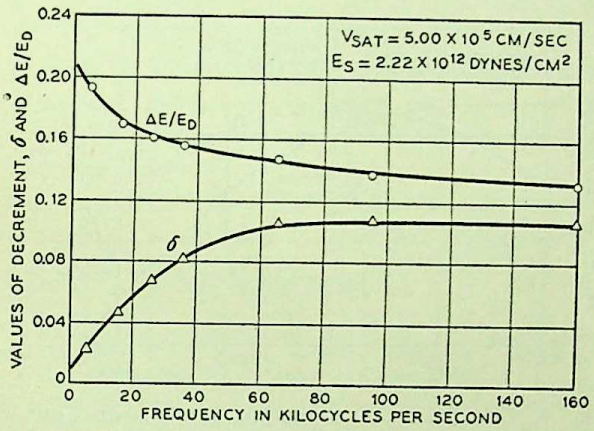


FIG. 2. Fractional change in Young's modulus, and the decrement, plotted as a function of frequency for rod No. 2.

the saturation magnetic intensity (485 for nickel) and f_0 the relaxation frequency for domain motion given by the equation

$$f_0=R/96\chi_0 D^2, \tag{2}$$

where R is the resistivity in cgs electromagnetic units (8000 for nickel) and D is the domain thickness in the direction of domain wall motion.

The measured values for two nickel rods are shown by Fig. 1 and Fig. 2. The rods had a measured permeability of about 340—$\chi_0=27.1$—and the measured value of $\Delta E/E_D$ and the measured decrement do not indicate a single domain size; this is confirmed by optical domain size measurements made by Willimas[2] and Walker of which a typical photograph is shown by Fig. 3. The photograph indicates a domain size range from 0.02 mm to 0.2 mm. To take account of the domain size range, Eqs. (1) should be replaced by equations

[2] H. J. Williams and J. G. Walker, Phys. Rev. 83, 634 (1951).

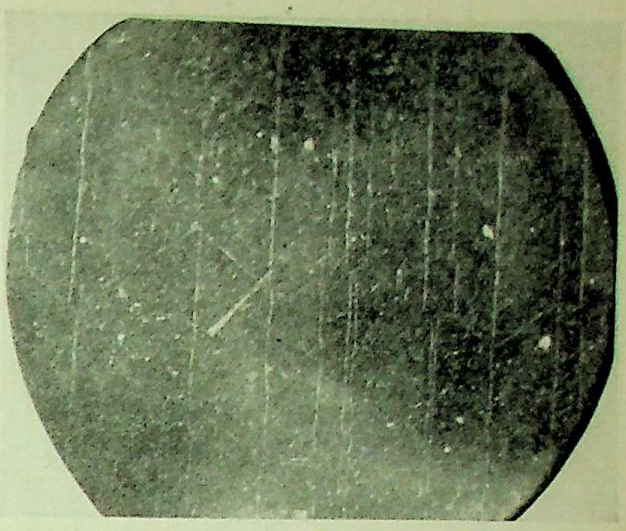


FIG. 3. Photograph of domains in a single nickel crystal (after Williams and Walker). Field of view, 0.5 mm.

$$\frac{\Delta E}{E_D}=\frac{4}{5}\left[\lambda_{111}\left(\frac{5C_{44}}{C_{11}-C_{12}+3C_{44}}\right)\right]^2\frac{\chi_0 E_s}{I_s^2}\sum_{i=1}^{n}\frac{V_i/V}{1+f^2/f_i^2},$$

$$\delta=\frac{4\pi}{5}\left[\lambda_{111}\left(\frac{5C_{44}}{C_{11}-C_{12}+3C_{44}}\right)\right]^2 \tag{3}$$

$$\times\frac{\chi_0 E_s}{I_s^2}\sum_{i=1}^{n}\frac{(V_i/V)(f/f_i)}{1+f^2/f_i^2},$$

where V_i/V is the ratio of the volume of domains of size D_i to the total volume and f_i is the relaxation frequency for a domain size D_i. The measured values of rod No. 1 which was carefully annealed at 1100°C for an hour are quite well matched by taking 5 relaxation frequencies ranging from 8 kilocycles to 800 kilocycles equally distributed on a logarithmic scale and all with equal weights. As shown by Fig. 4, the calculated values from Eqs. (3) are shown by the lines marked theoretical ΔE effect and theoretical decrement while the measured values are shown by the dashed lines. The second rod which was annealed at 1050°C for a shorter time indicates a smaller number of the large size

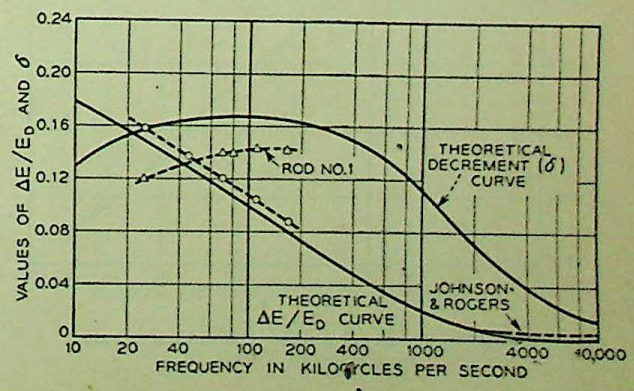


FIG. 4. Calculated values of $\Delta E/E_D$ and the decrement for a distribution of relaxation frequencies determined by the optical measurements of domain size range.

CC-0. In Public Domain. Gurukul Kangri Collection, Haridwar

Digitized by Arya Samaj Foundation Chennai and eGangotri

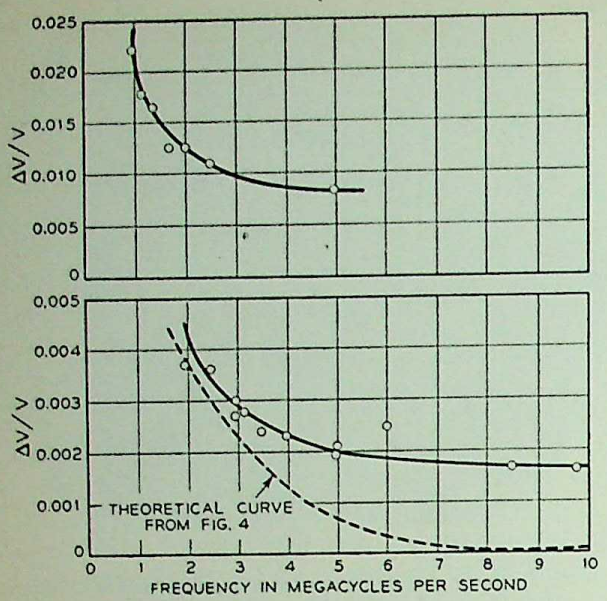


FIG. 5. Measurements of Johnson and Rogers for the change in elastic shear modulus and Young's modulus in a high frequency range.

domains. From the assumed relaxation frequencies the domain sizes vary from 0.02 mm to 0.2 mm, in agreement with the optical measurements.

Recent measurements of the change in velocity of shear and longitudinal waves in a polycrystalline nickel rod made by S. J. Johnson and T. F. Rogers,[3] show that the change in velocity divided by the velocity, in going from the demagnetized state to the saturated state, decreases rapidly with increase in frequency up to a frequency of about 5 megacycles but then levels off to a value of 0.008 for shear waves and 0.002 for longitudinal waves as shown by Fig. 5. The longitudinal points multiplied by 2 to give the ΔE change are plotted on Fig. 4 and agree reasonably well with the theoretical curve up to 3 megacycles but show a larger effect for higher frequencies. The higher frequencies correspond to the conditions that domain wall motion can no longer occur but domain rotation can still occur. For shear waves Döring[4] has shown that the change in elastic constant divided by the shear elastic constant is equal to

$$\frac{\Delta\mu}{\mu}=\frac{4\mu\lambda_{111}^2\chi_0}{I_s^2}, \tag{4}$$

where $\Delta\mu$ and μ are, respectively, the change and the value of the shear elastic constant. From the measured value of $\Delta\mu/\mu$ equal to 0.016 (twice the $\Delta v/v$ value) and the shear modulus of 0.8×10^{12} dynes/cm^2, the indicated value of initial susceptibility is 1.87. The value indicated by the longitidinal wave measurement is less than this but is less reliable since the elastic constant controlling the longitudinal wave is no longer the Young's modulus for these high frequencies but is approaching the average C_{11} value for which the calculated ΔE effect is zero.[4]

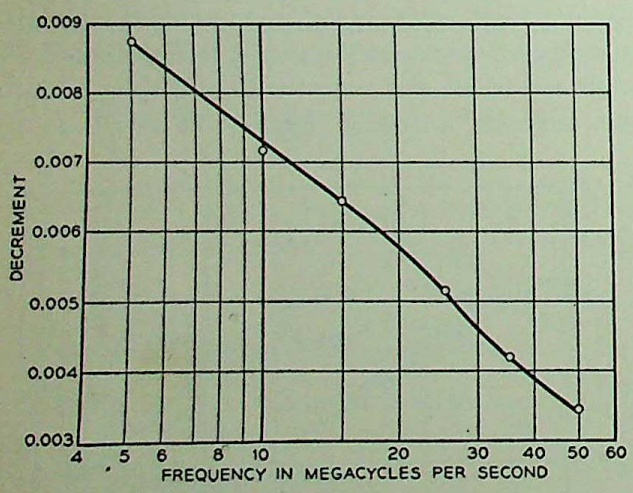


FIG. 6. Decrement for single crystal as measured by Levy and Truell.

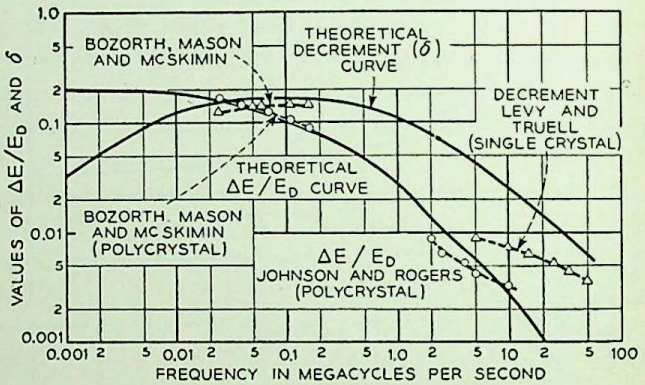


FIG. 7. Comparison of theoretical curves with experiment taking account of both domain boundary motion and domain rotation.

The value of initial susceptibility of 1.87 is not far from what one would calculate for rotational effects. If there are no stored internal stresses the initial susceptibility is

$$\chi_0=\frac{1}{2}\frac{I_s^2}{K_1}=\frac{235\,000}{2\times59\,000}=1.99, \tag{5}$$

where K_1 is the anisotropy constant which for nickel is 59,000 ergs per cubic centimeter.

From the data on the initial permeability and loss, due to rotations, given in Becker and Döring,[5] it can be shown that the relaxation frequency for rotational processes is given by the formula

$$f_c=R/25\pi\chi_R D^2, \tag{6}$$

where χ_R is the susceptibility due to domain rotations, and hence is not much different from the domain wall

[3] S. J. Johnson and T. F. Rogers, J. Appl. Phys. 23, 574–578 (1952). Thanks are due T. F. Rogers who furnished an advance copy of his curves shown by Fig. 5.

[4] W. Döring, Z. Physik, 114, 597 (1939).

[5] R. Becker and W. Döring, *Ferromagnetismus* (Julius Springer, Berlin 1939), pp. 380–381.

CC-0. In Public Domain. Gurukul Kangri Collection, Haridwar

Digitized by Arya Samaj Foundation Chennai and eGangotri

relaxation formula of Eq. (2). Hence one would not expect the ΔE effect due to rotation to fall markedly before a frequcndy of 10 megacycles with an average domain size of 0.03 mm found above.

The only measurement of decrement due to the microeddy current effect in the high frequency range are those on single nickel crystals made by Levy and Truell.[6] In this paper the difference in attenuation between a demagnetized and a saturated crystal is measured for a longitudinal wave whose direction is approximately 12° from the [111] direction of the crystal. The path length per trip is 1.62 centimeters and the decrement of the crystal can be calculated from the equation

$$\delta = A_0 v/f, \tag{7}$$

where A_0 is the attenuation in nepers per centimeter (1 neper equals 8.68 db) v is the wave velocity and f the frequency. From their measurements the decrement for this crystal *versus* frequency is shown by Fig. 6. While the absolute values are not comparable with those calculated for the decrement since a different elastic constant is operative, the shape of the curve is indicative of a relaxation in the rotational effect[7] with an average domain size of about 0.03 mm, which is consistent with the average size measured for domain wall relaxations.

For both domain wall motion and domain rotation, the formulas for the $\Delta E/E_D$ effect and the decrement become

$$\frac{\Delta E}{E_D} = \frac{4}{5}\left[\lambda_{111}\left(\frac{5C_{44}}{C_{11}-C_{12}+3C_{44}}\right)\right]^2 \times\left[\sum_{i=1}^{n}\frac{\chi_T E_s}{I_s^2}\left(\frac{V_i/V}{1+f^2/f_{iT}^2}\right)+\sum_{i=1}^{n}\frac{\chi_R E_s}{I_s^2}\left(\frac{V_i/V}{1+f^2/f_{iR}^2}\right)\right],$$

$$\delta = \frac{4\pi}{5}\left[\lambda_{111}\left(\frac{5C_{44}}{C_{11}-C_{12}+3C_{44}}\right)\right]^2 \times\left[\sum_{i=1}^{n}\frac{\chi_T E_s}{I_s^2}\left(\frac{(V_i/V)(f/f_{iT})}{1+f^2/f_{iT}^2}\right)+\sum_{i=1}^{n}\frac{\chi_R E_s}{I_s^2}\left(\frac{(V_i/V)(f/f_{iR})}{1+f^2/f_{iR}^2}\right)\right], \tag{8}$$

where χ_T and χ_R are, respectively, the initial susceptibility due to domain wall translations and domain rotations. If one takes these to be 25 and 2, respectively, Fig. 7 shows a comparison of the theoretical curves with experiment and it is evident that a good agreement is obtained.

Note added in proof.—In a recent Air Force report, Johnson and Rogers have ascribed the high frequency ΔE effect of Fig. 5 to a frequency-independent microhysteresis effect. However, at low inductions when Rayleigh's law applies, the expression for ΔE depends on the initial permeability (Eq. (3) above) which is not affected by a hysteresis loss. Thus, it is hard to understand how the microhysteresis loss can affect ΔE. It can, of course, affect δ, the expression for which involves the hysteresis loss when the usual term for this loss is added to Eq. (3) above.

[6] Sheldon Levy and Rohn Truell, Phys. Rev. 83, 668–669 (1951).

[7] According to the second half of Eq. (8) with the distribution in domain sizes from 0.02 mm to 0.2 mm, 80 percent of the decrement is due to domain wall motion and 20 percent to domain rotation at 10 megacycles. At 60 megacycles, 46 percent is due to domain wall motion and 54 percent to domain rotation.

CC-0. In Public Domain. Gurukul Kangri Collection, Haridwar

Digitized by Arya Samaj Foundation Chennai and eGangotri

REVIEWS OF MODERN PHYSICS VOLUME 25, NUMBER 1 JANUARY, 1953

Ultrasonic Attenuation in Magnetic Single Crystals*

SHELDON LEVY AND ROHN TRUELL

Brown University, Providence, Rhode Island

A striking connection has been found between the magnetic properties and the ultrasonic attenuation properties of a nickel single crystal. The magnetic anisotropy has been detected by measuring the attenuation as a function of applied field intensity. Information about the vibrations of Bloch walls and the number of vibrating walls per unit length has also been obtained. The dependence of the attenuation on magnetic induction for 5–100 mc shear and longitudinal waves propagated in the [1$\bar{1}$0] direction was the same for B parallel to both the [111] and [001] directions. The shear modes induce much greater losses than the longitudinal mode.

Similar measurements on a 3.8 percent Si-Fe crystal showed that the walls in this alloy are not as easily vibrated, i.e., there is a small difference in attenuation between the magnetized and unmagnetized states. At these frequencies this indicates that there is a direct connection between the magnetostrictive constants and the dynamic behavior of Bloch walls.

The elastic constants were computed from velocity measurements, but no ΔE effect was observed.

Pulsed ultrasonic techniques as described by Roderick and Truell (see reference 4) were used in taking the measurements. The single crystals used were grown from the melt in a hydrogen atmosphere and then oriented so that pure modes of vibration could be propagated.

I. INTRODUCTION

IT is well known that internal strain is coupled to Bloch wall movement in a ferromagnetic material; however, no law governing the interaction has been established. This coupling is responsible for the magnetomechanical loss which occurs when an elastic wave traverses a ferromagnetic material.

Recently there has been a great deal of interest in the magnetomechanical losses[1–3] as well as the absorption of ultrasound in the saturated crystal. This last interest is due to the possibility of using such measurements to determine ferromagnetic resonance.

It is about the magnetomechanical losses associated with the transmission of 5–100 mc ultrasound through Ni and 3.8 percent Si-Fe crystals that this paper is written.

II. EXPERIMENTAL METHODS

1. Ultrasound Equipment and Techniques

The pulsed ultrasound technique for determining attenuation and velocity in solids requires the production of a short pulse of mechanical energy and the ability to accurately measure the ratio of the amplitudes of successive echoes and the time-delays between them. At megacycle frequencies this can be done with radar type circuits and piezoelectric transducers which convert the electrical energy into mechanical energy and vice versa. Such equipment has been built in the Metals Research Laboratory at Brown University and has been described elsewhere.[4,5] The transducers, X and AC—cut quartz, were cemented to the specimens with salol.

2. Specimen Preparation

The large single crystals of nickel and 3.8 weight percent silicon-iron used were grown from the melt in a hydrogen atmosphere and then accurately oriented by means of x-rays. The stock metals from which they were grown had the following trade names and percent purities: Mond nickel pellets, 99.90; Plast-Iron, 99.91; silicon (Electrometallurgical Corporation), 99.8+.

Surfaces parallel to the (100), (010), and (011) planes were cut and accurately ground on both Si-Fe crystals while the nickel crystal was prepared with its surfaces parallel to the (111), (1$\bar{1}$0), and (001) planes, as in Fig. 1. These planes were chosen to satisfy the requirements for propagating longitudinal and shear elastic waves in the crystal (see Appendix I) and permitted the external magnetic field to be applied in the easy, medium, and hard directions of magnetization in the nickel sample.

Great care was exercised in surface grinding the crystals so that the strained layer caused by this operation would be as shallow as possible. The depth of the layer in the nickel crystal was less than 0.1 mm as was determined by taking back reflection Laue photographs after successive acid etches until all strained material was shown to be removed. The sharply defined Laue spots on the last of the above photographs indicated that the crystal was well annealed and possessed a high degree of perfection.

The dimensions of the nickel crystal Ni-I are $l_{[1\bar{1}0]}=1.28$ cm, $l_{[001]}=1.76$ cm, and $l_{[111]}=1.67$ cm. The Fe-Si crystals will be referred to as Fe-Si I and Fe-Si II,

* Supported by the United States Air Force Contract AF 33(038)—15602.

[1] J. De Klerk, Nature (London) 168, 963 (1951).

[2] Bozorth, Mason, and McSkimin, Bell Syst. Tech. J. 30, 970 (1951).

[3] T. F. Rogers and S. J. Johnson, J. Appl. Phys. 21, 1067 (1950).

[4] R. L. Roderick and R. Truell, J. Appl. Phys. 23, 267–279 (1952).

[5] R. Roderick, Ph.D. thesis, "On the measurements of ultrasonic attenuation in solids by the pulse technique," Brown University (1951).

CC-0. In Public Domain. Gurukul Kangri Collection, Haridwar

Digitized by Arya Samaj Foundation Chennai and eGangotri

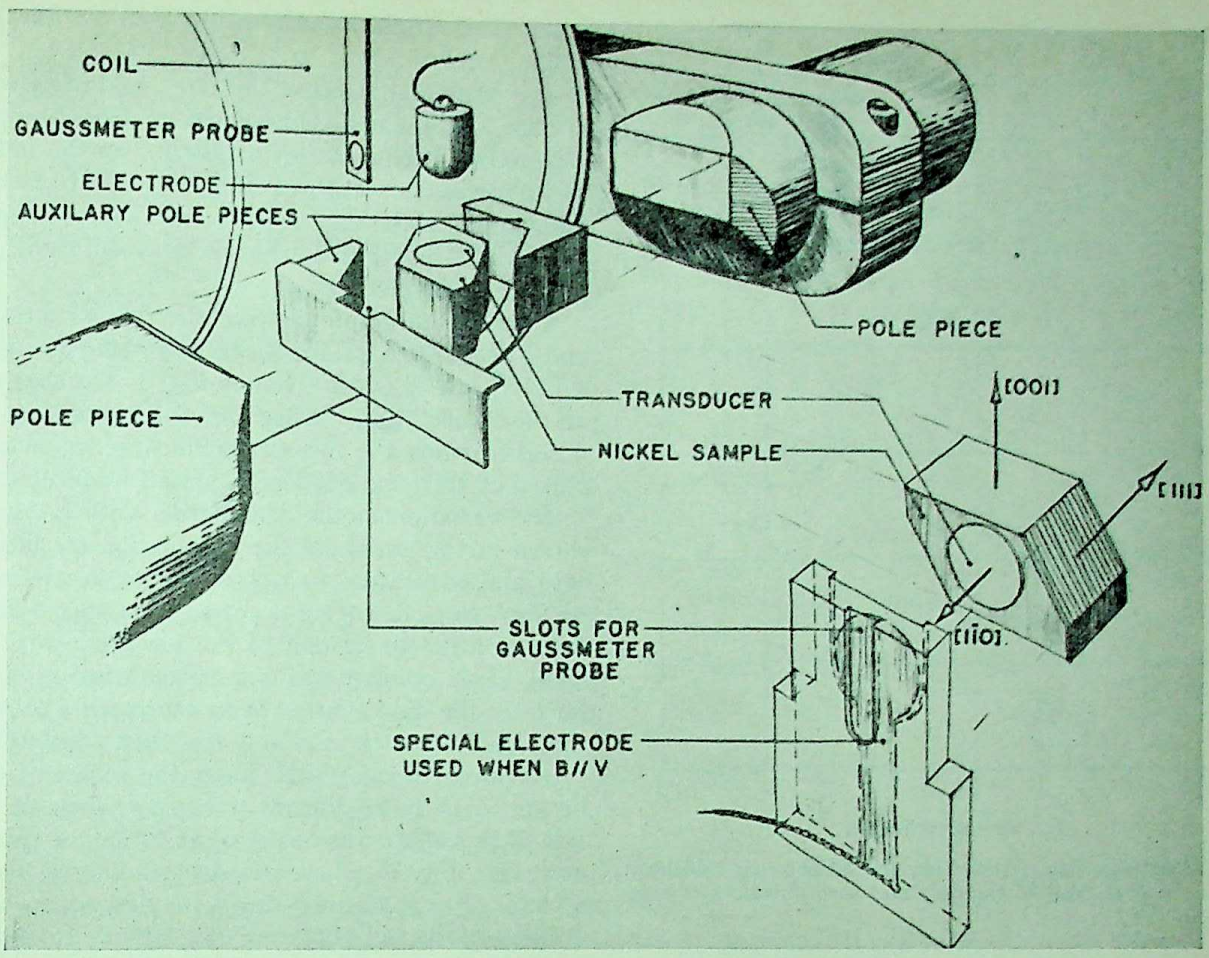


FIG. 1. Exploded view of experimental arrangement.

whose respective dimensions are $l_{[100]}=2.35$ cm, $l_{[011]}=1.29$ cm, and $l_{[100]}=2.28$ cm, $l_{[011]}=2.07$ cm.

3. Magnetic Considerations and Measurements

The magnetic field was supplied by an electromagnet with a cold-rolled steel core of 16 cm² mean area, wound with 5550 turns of No. 22 wire. The cylindrical poles of the magnet were tapered to a rectangular shape 1.6 cm $\times$3.2 cm, which permitted a uniform field of 19 kilogauss to be obtained with an air gap of 0.1 cm.

Because of the irregular shape of the nickel crystal and its large anisotropy energy, auxiliary soft iron pole pieces (accurately ground to match the crystal surfaces) were inserted when the magnetic field was applied in the [001] and [111] directions. These were essential when the field was applied in the hard direction of magnetization because of the large anisotropy energy.

The magnetic field was measured with a Dyna-Labs Gaussmeter (probe size 1.75 in.$\times$0.200 in.$\times$ 0.025 in.), which measures the component of magnetic induction normal to a germanium crystal whose cross-sectional area is 0.01 in.². The probe was inserted in the air gap between the auxiliary pole pieces and the specimen, and it was assumed that the field measured was the same as the field in the specimen. This assumption was made because the normal component of the induction must be continuous across a boundary. The accuracy of the gaussmeter was within 3 percent as determined by measuring the field of a solenoid and was frequently checked with a 1000-gauss standard.

When the field was applied parallel to the direction of propagation, a special electrode was used.

Figure 1 shows the arrangement employed for applying and measuring the magnetic field.

III. EXPERIMENTAL RESULTS

1. Velocity Measurements

The velocity of propagation of ultrasound in nickel was measured at 27 mc for a longitudinal wave propagated in the [001] direction and at 30 mc for the longitudinal and the two transverse waves propagated in the $[1\bar{1}0]$ direction. The mean time delay between echoes was obtained by least square computations, and the effect of the transducer on the length of the sound path was not taken into account. These velocities and the elastic parameters as computed from (11) and (13) of the Appendix I and $\rho=8.90$ g/cm³ are listed below:

$$V_{[100]}=5.27\times10^5 \text{ cm/sec},$$
$$V_{[110]}=5.96\times10^5 \text{ cm/sec},$$
$$V_{T_2[110]}=3.69\times10^5 \text{ cm/sec},$$
$$V_{T_2[110]}=2.31\times10^5 \text{ cm/sec},$$
$$C_{11}=2.47\times10^{12} \text{ dynes/cm}^2,$$
$$C_{44}=1.21\times10^{12} \text{ dynes/cm}^2,$$
$$C_{12}=1.52\times10^{12} \text{ dynes/cm}^2.$$

CC-0. In Public Domain. Gurukul Kangri Collection, Haridwar

Digitized by Arya Samaj Foundation Chennai and eGangotri

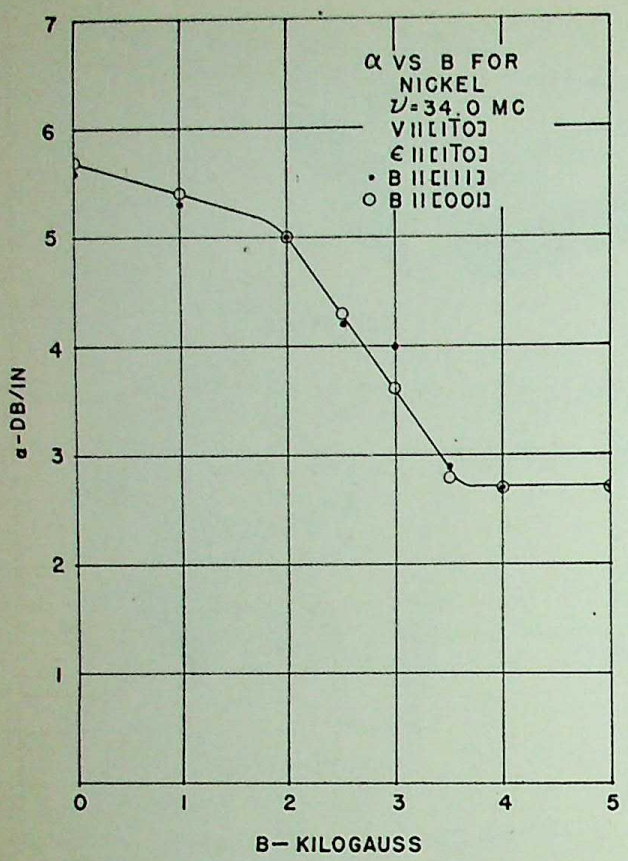


FIG. 2. Attenuation *vs* induction for Ni showing coincident behavior for B parallel to the easy and hard directions of magnetizations.

The ΔE effect was not observed at any frequency covered, i.e., no change in velocity with the application of a magnetic field was detected.

The velocities of propagation of ultrasound in 3.8 percent Si-Fe, and the corresponding elastic parameters were found to be

$$V_{[100]}=5.30\times10^5 \text{ cm/sec},$$
$$V_{[110]}=6.20\times10^5 \text{ cm/sec},$$
$$V_{T[100]}=4.01\times10^5 \text{ cm/sec},$$
$$C_{11}=2.15\times10^{12} \text{ dynes/cm}^2,$$
$$C_{12}=1.27\times10^{12} \text{ dynes/cm}^2,$$
$$C_{44}=1.23\times10^{12} \text{ dynes/cm}^2.$$

In computing the above we used $\rho=7.65$ g/cm^3.

2. Dependence of the Attenuation of Ultrasound in Nickel on the Magnetic Induction

The attenuation per unit length was computed using the method of least squares from measurements taken with the techniques described in Part II. In all cases only readings taken within the plane wave region were used.[4] Except for frequencies adjacent to 50 mc the measurements were highly reproducible if care was taken in cementing the transducer to the sample. In fact, measurements taken at the same frequency obtained by using different harmonics of separate transducers (e.g., ninth of 5.5 mc and seventh of 7.0 mc) gave attenuation measurements well within experimental error.

The results for the case $V\|[1\bar{1}0]$, $\epsilon\|[1\bar{1}0]$ are shown in Figs. 2, 3, 4, and 5. The coincident dependence of the attenuation coefficient α, in DB/in., on the induction for an ultrasonic wave with $V\|[1\bar{1}0]$, $\epsilon\|[1\bar{1}0]$ when the induction is in the easy or hard directions of magnetization, is shown by Fig. 2, which is representative of these plots at all frequencies.

A composite graph showing the relation between α and B at 5.8, 16.5, 21, 27, 30, 52, and 90 mc for $V\|[1\bar{1}0]$, $\epsilon\|[1\bar{1}0]$, and $B\perp V$ is given by Fig. 3. The sharp break at the "knee" and "instep" of the curves was easily observed when the measurements were made and occurred at 1800 and 3800 gauss for all frequencies.

The variation of the attenuation with frequency is shown in Fig. 4, where the attenuation coefficient for zero and saturation values of induction are plotted. A "dip" in both curves occurred near 49 mc and was first throught to be due to the low frequency equipment. This opinion was not substantiated, however, for later the dip occurred in measurements made with the high frequency gear and was then attributed to a "resonance" in the nickel. Later the source of the dip become even more difficult to explain when an indication of this effect was observed at 49 mc for transverse waves (cf. Fig. 7), whose wavelength differed by nearly a factor of two. Figure 5 shows the dependence of α on B for $v\|[1\bar{1}0]$, $\epsilon\|[1\bar{1}0]$, and $B\|[1\bar{1}0]$ at 15, 19.5, and 34.5 mc. Here the sharpness of the "knee" and "instep"

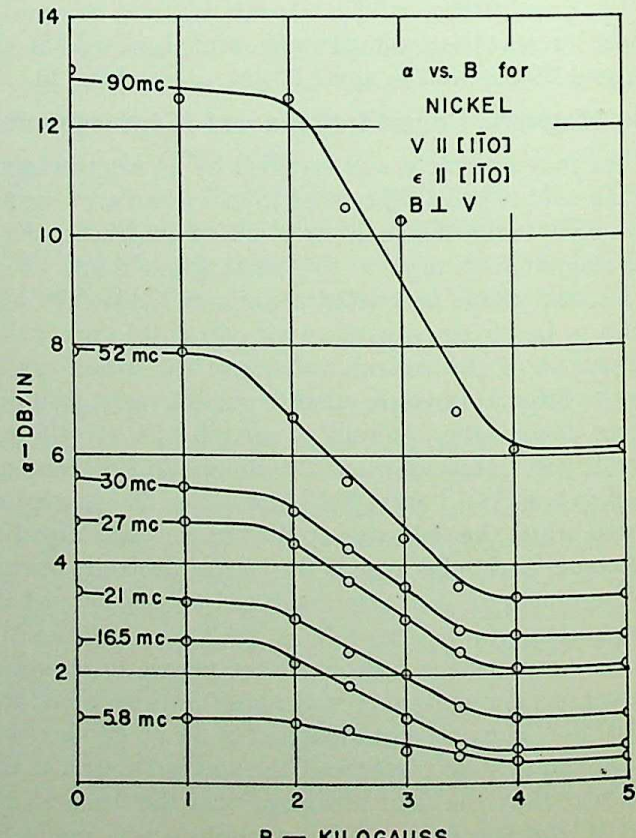


FIG. 3. Attentuation *vs* induction for Ni with $V\|[1\bar{1}0]$. $\epsilon\|[1\bar{1}0]$, and $B\perp V$ at 5.8, 16.5, 21, 27, 30, 52, and 90 mc.

CC-0. In Public Domain. Gurukul Kangri Collection, Haridwar

Digitized by Arya Samaj Foundation Chennai and eGangotri

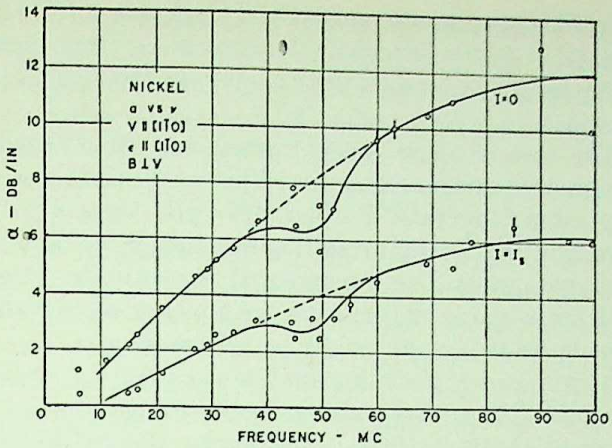


FIG. 4. Attenuation *vs* frequency for Ni in the unmagnetized state ($I=0$) and saturated state ($I=I_s$) with $V\|[1\bar{1}0]$, $\epsilon\|[1\bar{1}0]$, and $B\perp V$.

breaks is absent, but the value of α for zero and saturation induction is in agreement with the values obtained for $B\perp V$.

The coincident behavior of α *vs* B for the two possible cases of $B\perp V$ was observed at all frequencies used for $V\|[1\bar{1}0]$ and $\epsilon\|[001]$.

A composite plot of α *vs* B for $V\|[1\bar{1}0]$, $\epsilon\|[001]$, and $B\perp V$ is shown in Fig. 6, while Fig. 7 reveals the dependence of α (saturation) and α (no field) on frequency for these conditions.

Only one set of measurements was taken with $V\|[1\bar{1}0]$, $\epsilon\|[110]$, and $B\perp V$. The response of α to the induction for this case at 10 mc is shown in Fig. 8.

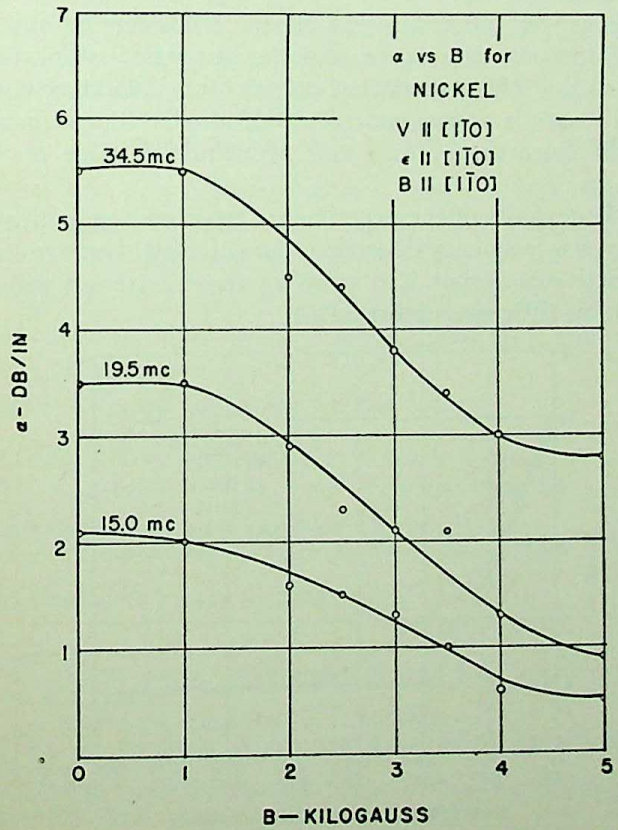


FIG. 5. Attenuation *vs* induction for Ni with $V\|[1\bar{1}0]$ $\epsilon\|[1\bar{1}0]$, and $B\|V$ at 15, 19.5, and 34.5 mc.

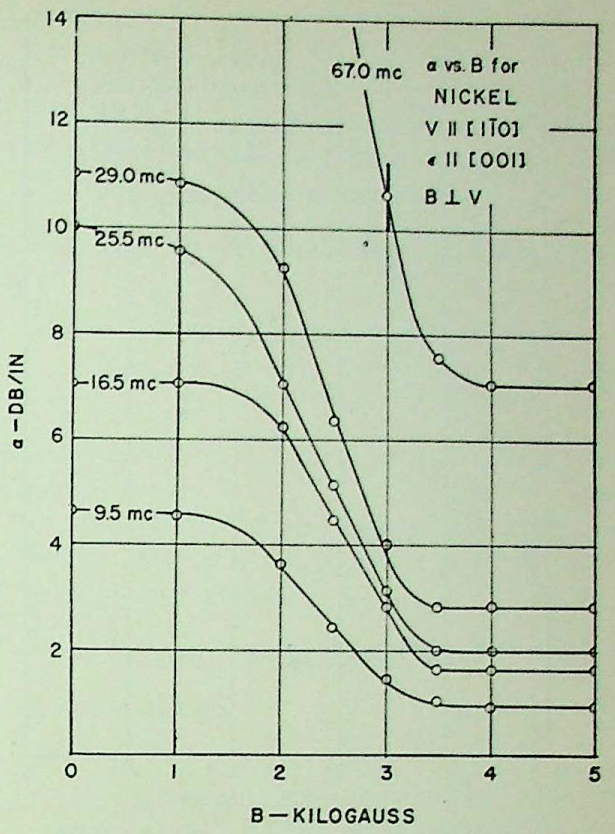


FIG. 6. Attenuation *vs* induction for Ni with $V\|[1\bar{1}0]$, $\epsilon\|[001]$, and $B\perp V$ at 9.5, 16.5, 25.5, and 29 mc.

The coincident dependence of α and B for $B\perp V$ in the foregoing results is further exemplified by Fig. 9 where the attenuation coefficient for a transverse wave is plotted against the magnetization current. This current is essentially proportional to the magnetic field intensity H. These measurements show the behavior one would expect from the foregoing results on the dependence of α on B and the B–H curves for the easy and hard directions of magnetization of nickel.

The attenuation coefficient of 3.8 percent Si-Fe was found to be small at all frequencies, less than 1 *DB*/in. at 50 mc for longitudinal vibrations in the [110] direction. The change in this value as a saturation

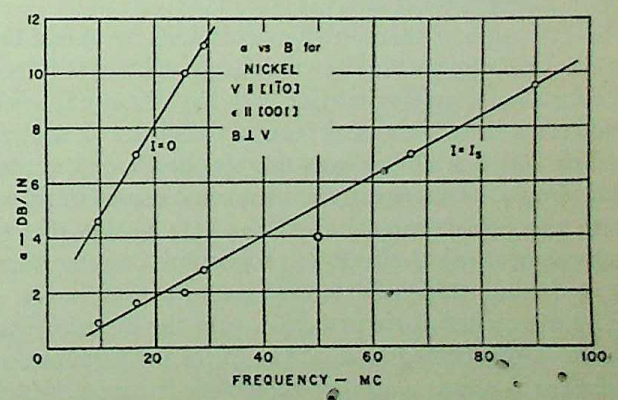


FIG. 7. Attenuation *vs* frequency for Ni in the unmagnetized state ($I=0$) and saturated state ($I=I_s$) with $V\|[110]$, $\epsilon\|[001]$, and $B\perp V$.

CC-0. In Public Domain. Gurukul Kangri Collection, Haridwar

Digitized by Arya Samaj Foundation Chennai and eGangotri

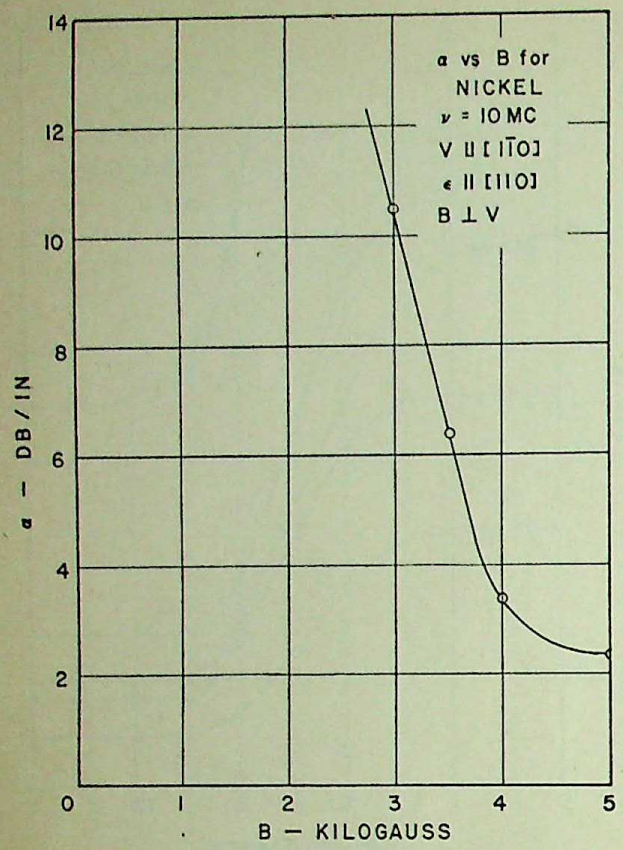


FIG. 8. Attenuation *vs* frequency for Ni with $V\|[1\bar{1}0]$, $\epsilon\|[110]$, and $B \perp V$ at 10 mc.

magnetic field was applied, and although present, was not measurable with the present equipment.

IV. CONCLUSION

The magnetomechanical losses associated with the propagation of ultrasound through a nonsaturated ferromagnetic crystal arise from the fact that the spins of the lattice are affected by the energy in the sonic wave. While the law governing the behavior of the spins as the elastic wave traverses them has not been established, it is plausible to consider the Bloch wall as being "driven" by the harmonic elastic wave. Two effects probably occur: (1) a vibration of the center plane of the wall, and (2) a periodic variation in the width of the wall. A combination of these two effects include domain rotations.

An extension of theoretical calculations by one of the authors† has shown that the magnetomechanical losses, to a first-order approximation, are the result of "rigid wall" vibrations. This work lead to defining a "coupling coefficient," k, which relates the amplitude of the wall vibration to the energy in the ultrasonic beam. Furthermore, the calculations showed the attenuation due to magnetomechanical effects is proportional to the number of domain walls affected by the ultrasonic wave.

The theory agrees, in principle, with the experimental results as interpreted from the shape of the attenuation coefficient α *versus* magnetic induction B curves, which exhibit no magnetic anisotropy.

† S. L. Levy, Ph.D. thesis, Brown University, 1952.

In the approximate ranges $0<B<\frac{1}{3}B_s$, $\frac{1}{3}B_s<B<\frac{2}{3}B_s$, and $\frac{2}{3}B_s<B$ one has small decrease in α, large linear decreases in α and constant α, respectively, as B increases.

The first of these ranges corresponds to reversible wall movements and show that k decreases slightly with increasing induction. For $\frac{1}{3}B_s<B<\frac{2}{3}B_s$ there are reversals of the domains resulting in a loss of the number of domain walls. The experimental results in this range indicate a linear decrease in the number of movable domain walls per unit length with increasing B.

A proposed explanation for the constant value of α when $B>\frac{2}{3}B_s$ is that walls with some orientations, because of the anisotropy, may not be affected by the ultrasonic wave. Hence, after $B\approx\frac{2}{3}B_s$ all of the walls which can be vibrated by the wave have been eliminated in the magnetization process. We speak here of wall motion in the general sense which includes partial rotation of the domain.

The smoothing out of the curves (Fig. 5) as compared with Fig. 3) showing the response of α *vs* B for $B\|V\|\epsilon\|[1\bar{1}0]$ may have been caused by the larger air gap required in the magnetic circuit in order that the special electrode (Fig. 1) could be inserted. This effect warrants further investigation.

As expected, greater sensitivity occurred when transverse waves were used. The anisotropy or the large difference of attenuation between the two polarizations of transverse waves propagated in the $[1\bar{1}0]$ direction is interesting. The attenuation was so great in the unmagnetized state for $V\|[1\bar{1}0]$ and $\epsilon\|[110]$ that no echoes were observable at 10 mc. However, by extrapolating the data taken near the saturation region one finds that the attenuation caused by magnetomechanical losses is approximately 30–35 db/in. which agrees with Bozorth, Mason, and McSkimin's[2] value of 32 db/in.

The results of the experiments reported here indicate that k is frequency dependent, large for highly magnetostrictive materials, and small for those materials which exhibit little magnetostriction.

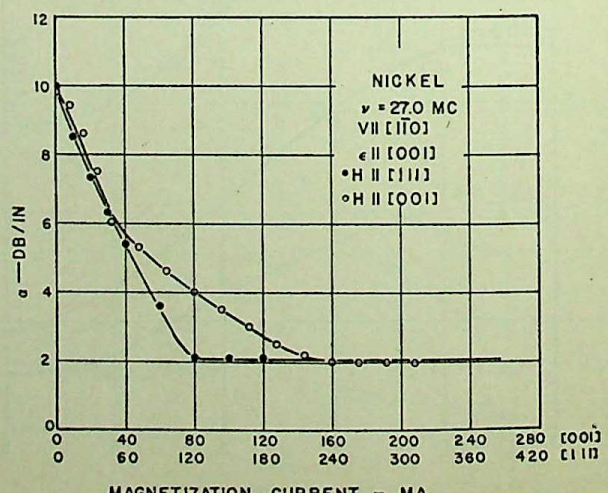


FIG. 9. Anisotropy of attenuation in Ni at 27 mc with $V\|[1\bar{1}0]$, $\epsilon\|[001]$.

CC-0. In Public Domain. Gurukul Kangri Collection, Haridwar

Digitized by Arya Samaj Foundation Chennai and eGangotri

The ease with which the elastic parameters can be determined with pulsed ultrasound is apparent from (11) and (13) of Appendix I. The values obtained for the elastic parameters of nickel agree with those reported in the literature.[2,3,5–7]

ACKNOWLEDGMENT

The suggestions of Mr. H. J. Williams of the Bell Telephone Laboratories on the processing of single crystals are gratefully acknowledged as are the contributions of the staff of the Metals Research Laboratory at Brown University. Accurate orientation of the crystals was made possible by the generous loan of a 90° Norelco Geiger Counter Spectrometer by the M. W. Kellogg Corporation.

APPENDIX I. ON THE PROPAGATION OF LONGITUDINAL AND TRANSVERSE WAVES IN AN ANISOTROPIC ELASTIC SOLID

In an anisotropic elastic solid the stress-strain relations are

$$\sigma_{ij}=c_{ijkl}e_{kl} \quad i,j=1,2,3, \tag{A1}$$

where the c_{ijkl} are the elastic parameters. In the absence of body forces the equations of equilibrium read

$$\sigma_{ij,i}=\rho\ddot{u}_j, \quad j=1,2,3. \tag{A2}$$

Here ρ is the density of the solid. Using the definition of the strain $\epsilon_{ij}=\frac{1}{2}(u_{i,j}+u_{j,i})$, one gets from (A1) and (A2)

$$\tfrac{1}{2}c_{ijkl}(u_{k,li}+u_{l,ki})=\rho\ddot{u}_j, \quad j=1,2,3. \tag{A3}$$

If a plane wave is traveling in the (l_1, l_2, l_3) direction with the velocity v and the displacement is in the (d_1, d_2, d_3) direction, one has the displacements given by

$$u_j=Ad_je^{i\kappa(vt-l\cdot r)} \quad j=1,2,3, \tag{A4}$$

where κ is propagation constant. The l_i's, d_i's, and v must satisfy

$$c_{ijkl}l_il_ld_k=\rho v^2d_j, \quad j=1,2,3. \tag{A5}$$

For any direction of propagation (A5) gives three real velocities (see Love[9]), which have mutually orthogonal displacements.

For cubic symmetry (1) has the form

$$\begin{aligned}
&(c_{11}-c_{44})l_1^2d_1+(c_{12}+c_{44})l_1l_2d_2+(c_{12}+c_{44})l_1l_3d_3 &&=(\rho v^2-c_{44})d_1,\\
&(c_{12}+c_{44})l_2l_1d_1+(c_{11}-c_{44})l_2^2d_2+(c_{12}+c_{44})l_2l_3d_3 &&=(\rho v^2-c_{44})d_2,\\
&(c_{12}+c_{44})l_3l_1d_1+(c_{12}+c_{44})l_3l_2d_2+(c_{11}-c_{44})l_3^2d_3 &&=(\rho v^2-c_{44})d_3,
\end{aligned} \tag{A6}$$

where

$$\begin{aligned}
&c_{11}=c_{1111}=c_{2222}=c_{3333},\\
&c_{12}=c_{1122}=c_{2211}=c_{1133}=c_{3311}=c_{2233}=c_{3322},\\
&c_{44}=c_{1212}=c_{2121}=c_{1313}=c_{3131}=c_{2323}=c_{3232}.\\
&0=c_{ijkl} \text{ for all other parameters.}
\end{aligned} \tag{A7}$$

Solving (A6) for the displacement direction, one obtains

$$(d_1, d_2, d_3)=\left(\frac{l_1}{\lambda+cl_1^2}, \frac{l_2}{\lambda+cl_2^2}, \frac{l_3}{\lambda+cl_3^2}\right). \tag{A8}$$

Here $\lambda=\rho v^2c_{44}^{-1}-1$ and $c=(c_{12}+2c_{44}-c_{11})c_{44}^{-1}$ is the anisotropy factor.

In ultrasonic testing one usually uses either longitudinal or transverse waves; hence we shall consider these modes of vibrations.

Case I. Longitudinal Waves

Equation (A8) gives

$$d_1:d_2:d_3=\frac{l_1}{\lambda+cl_1^2}:\frac{l_2}{\lambda+cl_2^2}:\frac{l_3}{\lambda+cl_3^2}. \tag{A9}$$

If $c\neq 0$, clearly

$$\begin{aligned}
&l_1=l_2=l_3,\\
&l_1=l_2, \quad l_3=0,\\
&l_1\neq 0, \quad l_2=l_3=0,
\end{aligned} \tag{A10}$$

and their equivalents are the only directions in which longitudinal waves can be propagated. From (A6) one finds the corresponding ρv's are

$$\begin{aligned}
&\rho v^2_{[100]}=c_{11}, \quad \rho v^2_{[110]}=\tfrac{1}{2}(c_{11}+c_{12}+2c_{44}),\\
&\rho v^2_{[111]}=\tfrac{1}{3}(c_{11}+2c_{12}+4c_{44}).
\end{aligned} \tag{A11}$$

Case II. Transverse Waves

From (A8) and $d_il_i=0$ one gets

$$\lambda^2+2\lambda c(l_1^2l_2^2+l_2^2l_3^2+l_3^2l_1^2)+c^2l_1^2l_2^2l_3^2=0. \tag{A12}$$

If the solutions for λ of (A12) are substituted into (A6), one finds that the only directions which satisfy the conditions for transverse waves are those which satisfy the conditions for longitudinal waves. Furthermore, it is only necessary to polarize the vibration for propagation in the [110] direction. The ρv^2's are

$$\begin{aligned}
&\rho v^2_{T[100]}=c_{44},\\
&\rho v^2_{T1[110]}=c_{44},\\
&\rho v^2_{T2[110]}=\tfrac{1}{2}(c_{11}-c_{12}),\\
&\rho v^2_{T[111]}=\tfrac{1}{3}(c_{11}+c_{44}-c_{12}).
\end{aligned} \tag{A13}$$

[6] K. Honda, and Y. Shirakawa, Sci. Rep. Res. Inst. Tohoku Univ. 1, 9 (1949).
[7] M. Yamamoto, Phys. Rev. 77, 566 (1950).
[8] Bozorth, Mason, McSkimin, and Walker, Phys. Rev. 75, 1954 (1949).
[9] A. E. H. Love, *Mathematical Theory of Elasticity* (Cambridge University Press, 1934), fourth edition, p. 298.

CC-0. In Public Domain. Gurukul Kangri Collection, Haridwar

Digitized by Arya Samaj Foundation Chennai and eGangotri

REVIEWS OF MODERN PHYSICS VOLUME 25, NUMBER 1 JANUARY, 1953

Domain Pattern in Silicon-Iron under Stress

L. J. DIJKSTRA AND U. M. MARTIUS*

Ontario Research Foundation, Toronto, Ontario, Canada

This paper discusses investigations into the detailed changes in domain structure of ferromagnetic material under externally applied stress. The changes in the domain pattern of grain-oriented silicon steel with large grain size were observed and photographed while the specimen was stressed in tension.

Experiments in which the grain under observation had the {110} plane in the surface of the specimen and the ⟨110⟩ direction parallel to the specimen axis, along which tension was applied, are discussed in detail. At a load of approximately 0.2 kg/mm² the original domain pattern vanishes. After a transition stage in which, over a certain range of loads, no pattern is visible at all, a new stress-induced domain pattern appears. The behavior of these patterns in horizontal and vertical magnetic fields was studied, and an interpretation of both the transition stage and the stress-induced pattern is given. In these experiments the applied stresses are all within the elastic range of the material. In the plastic range, the knowledge of the stress-induced pattern permits the detection of residual lattice strains in suitably oriented materials.

IT has long been known that a direct relationship exists between the ferromagnetic properties of a crystal and its state of stress. The ferromagnetic domain pattern of a crystal which is a manifestation of its magnetic properties changes with suitable change in state of strain of the crystal. Williams, Bozorth, and Shockley[1] and others observed changes in domain pattern of samples which were subjected to external stresses.

On the other hand, it must be possible to develop the relation between stress and domain pattern to such an extent that some conclusions can be drawn from a given pattern as to the stage of strain of the specimen.[2]

It was the purpose of this investigation to study the detailed changes in the domain structure of grain-oriented silicon steel under externally applied stress.

Some work along these lines has been done before.

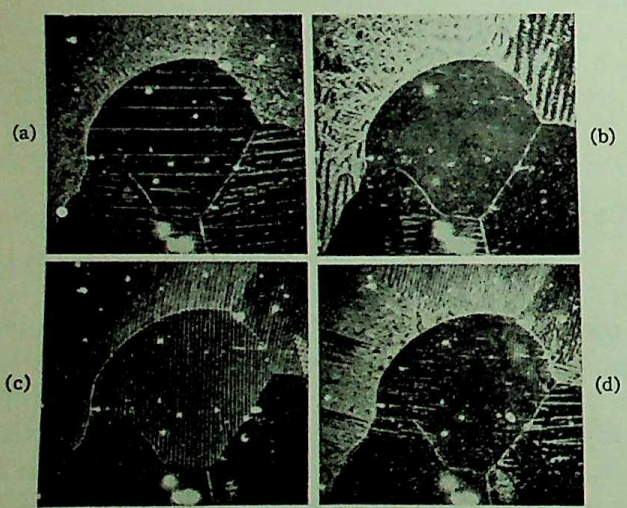


FIG. 1. Domain pattern under stress (25×); ↕=direction of stress; →[001]; ↑[1$\bar{1}$0]. (a)=original pattern; (b)=transition stage; (c)=stress pattern *I*; (d)=residual stresses after plastic deformation.

Williams, Bozorth, and Shockley[1] showed how slip lines in Permalloy were made visible by colloid-technique, and Akulov and Myriasov[3] studied the domain pattern of plastically deformed crystals. These latter, however, did not electropolish their specimens and hence observed the maze pattern.

I. EXPERIMENTAL TECHNIQUE

The investigations were conducted on grain-oriented silicon steel. The rolling texture of this material is such that the {110} plane is the preferred surface plane and the ⟨001⟩ direction is close to the rolling direction. Small specimens of tensile test piece shape were chosen so that the center of the specimen contained a large single grain with the {110} plane close to the plane of the specimen. The grain diameter is approximately 1 mm, and the specimen thickness is 0.1 mm. The direction of the applied load made a known angle with ⟨001⟩ direction. These specimens were etched out or cut out of the sheet and subsequently annealed, polished, and electropolished. They were tested in a micro tensile test machine. The tension was applied by means of a calibrated spring and the whole set-up could be placed on the stage of a Bausch and Lomb metallographic microscope. During the test the specimen was kept between two microscope cover glasses under liquid colloid. The changes in domain pattern with increasing stress were observed, and photographs were taken at all stages of the experiment.

II. EXPERIMENTAL RESULTS

A. Pattern Under Stress

As long as the applied stresses were within the elastic range of the material, the original pattern returned after unloading. Figures 1(a), (b), (c), and (d) show a sequence of changes in domain pattern with increasing load. The tension is applied along the [1$\bar{1}$0] direction in the plane of the specimen. Although the details of

* Mrs. F. Franklin.

[1] Williams, Bozorth, and Shockley, Phys. Rev. 75, 155 (1949).

[2] Dijkstra, Cavanagh, and Martius, Proceedings of the Detroit Congress of the American Society for Metals, 1951.

[3] N. S. Akulov and N. Z. Mirygsov, J. Tech. Phys. U.S.S.R. 18, 389 (1948).

CC-0. In Public Domain. Gurukul Kangri Collection, Haridwar

Digitized by Arya Samaj Foundation Chennai and eGangotri

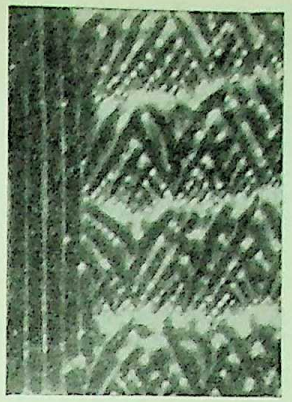


FIG. 2. Stress pattern *II* (100×); ↑[1$\bar{1}$0]; ↕ = direction of stress.

these changes in domain structure may vary from sample to sample, the general picture is always the same. Figure 1(a) shows the domain pattern with no applied load. The grain is divided into large domains magnetized along [001]; the direction of the domain walls in the picture is also [001]. In the silicon steel, used in these investigations, the plane of the surface of most grains is close to (110). In this case the domain walls are generally continuous across the grain boundary, because in such arrangement magnetic charges at the grain boundary are kept to a minimum. With increasing load the domain walls along [001] get less and less pronounced. They break up and disappear gradually. This breaking up is followed by a transition stage (Fig. 1(b)) where, within a certain range of load, no pattern is visible at all. Further increase in load causes the appearance of a set of parallel lines perpendicular to the original domain structure and more narrowly spaced, the stress induced pattern *I* (Fig. 1(c)). It is faint at its first appearance, but becomes more distinct and narrower in spacing as the load increases. Figure 1(d) shows the residual stress pattern after plastic deformation, as discussed in Sec. IV.

There is, however, a second type of stress induced pattern (stress pattern *II*), which can be seen in Fig. 2. It is characterized by wavy boundaries approximately parallel to ⟨001⟩ and a very fine division in the surface with its main direction close to ⟨111⟩. The two patterns can exist side by side within one grain. The first pattern to appear is usually pattern *I*, but pattern *II* once started at any point within a given grain grows on the expense of pattern *I*. Apparently there is complete flux closure between the two types of pattern. Both patterns occur within the elastic range and disappear when the stress is relieved.

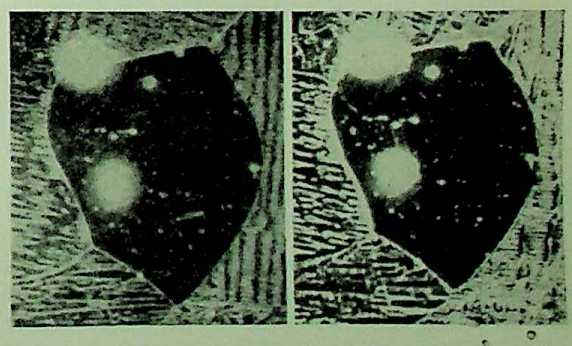
B. Stress Pattern in a Field

In order to determine the change in basic domain arrangement, the behavior of the stress induced pattern and the transition stage were studied in horizontal and vertical magnetic fields. The field strengths ranged from 25 to 75 oersteds. First a weak magnetic field was applied normally to the surface of a grain in the "transition stage." This normal field causes the stress induced pattern *I* to appear under loads which were not sufficient to cause its appearance in the absence of the field. Figure 3(a) shows the transition stage in one of the specimens. Figure 3(b) gives the same spot in a field normal to the surface. Figures 4(a), (b), and (c) show the action of a normal field of opposite directions on pattern *I*. The load was sufficiently high to cause the clear appearance of the stress patterns in the absence of a field. If pattern *I* is subjected to a horizontal field, the pattern changes in such a manner that adjacent domains shrink and grow, respectively. Figures 5(a), (b), (c), and (d) show the same pattern in a field of identical strength but varying direction. Observing a specific domain it can be seen that this domain grows when the field makes an angle between 0° and 90° with [001], reaching its maximum width at 90°. It then shrinks within the range of 90° to 180°. At 180° the pattern is identical with the original. After 180° the domain shrinks further, reaches minimum width at 270°, and starts to grow after that until the original configuration comes back at 360°. In addition to the change in spacing, there is a change in the intensity of the lines. Adjacent lines change their intensity in the opposite sense. For 0° and 180° spacing and intensity are identical over the whole pattern.

If the same experiments are carried out with pattern *II* the basic domains shrink and grow in the same way as in pattern *I*. The above described behavior in a horizontal magnetic field shows that the wall between the basic domains of both pattern *I* and *II* is a 180° wall, because when the direction of the field changes with respect to the direction of the specimen axis, the same pattern occurs after rotation of 360°. Ninety-degree walls would show a 180° symmetry.

III. INTERPRETATION OF THE STRESS INDUCED DOMAIN STRUCTURES

The observations, described above, led to the following interpretation of the stress induced domain patterns. The basic domain configuration of the unstressed grain consists of large domains magnetized along [001] or [00$\bar{1}$]. In the majority of the grains the angle θ between the [001] axis and the surface does not exceed a few



(a) (b)

FIG. 3. Transition stage in normal field (50×); [1$\bar{1}$0]↑. (a) = no field; (b) = magnetic field normal to the surface.

CC-0. In Public Domain. Gurukul Kangri Collection, Haridwar

Digitized by Arya Samaj Foundation Chennai and eGangotri

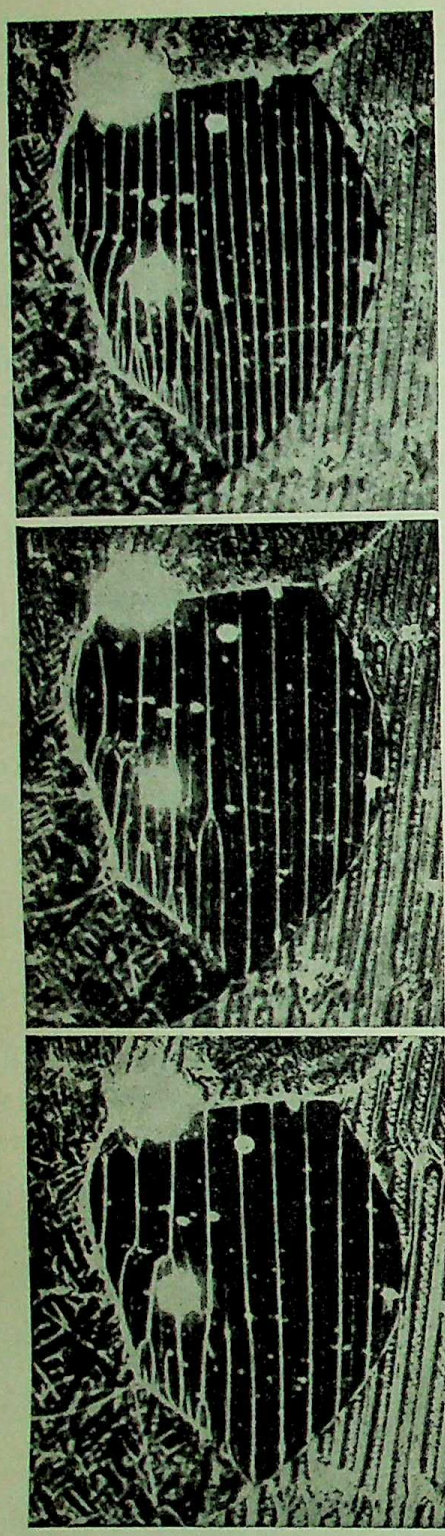


FIG. 4. Pattern I in a normal field (80×); [110]↑. (a)=no field; (b) and (c)=normal fields of equal strength and opposite directions.

degrees. The observed spacing of the walls of the domain pattern in these grains is always of the order of 0.01 cm.

This magnitude can be understood as follows: The spacing is determined by the minimum value of the sum of the magnetostatic energy E_M, owing to magnetic pole distributions and the wall energy E_γ. Because of the interaction between the grains, the observed spacing is an average value to which more than one grain contributes. As a basis for an estimate of the spacing we take the domain pattern of the center grain of Fig. 1(a). X-ray determination showed that a value for θ of about 1° is generally representative for this type of pattern. (If θ is a few degrees, E_M increases, but is greatly reduced by the formation of more or less complicated patterns on the surface of the basic domains, also visible in Fig. 1(a). This effect, which means that the higher magnetostatic energy is reduced by the substructure and not by a decrease in spacing, tends to justify our estimate on the basis of the simple pattern). Then (see Kittel[4]) the magnetostatic energy per cm² of the surface equals

$$E_M = 1.7 I_s^2 \sin^2 \frac{2d}{1-\mu^*} = Ad;$$

d=domain spacing, $\mu^* = 4I_s^2/2K$, K=crystal energy constant. The wall energy per cm² of the surface is equal to

$$E_\gamma = \frac{a \cdot \gamma_{180°}}{d} = \frac{B}{d};$$

a=specimen thickness. The equilibrium spacing $d_0 = (B/A)^{\frac{1}{2}}$. If we take $\theta = 1°$, $I_s = 1580$ gauss, $K = 2.8 \times 10^5$ ergs/cm³, $\gamma_{180°} = 1.5$ ergs/cm², then $d_0 = 2a$ cm. This is the observed order of magnitude since "a" is approximately 0.01 cm.

A few remarks have to be made. In the first place we have neglected, in the energy term E_M, the magnetostatic interaction between the magnetic poles on top and bottom face of the specimen. Further calculation shows that this is not serious for an estimate of the order of magnitude of the spacing d as long as d is not larger than a, as is indeed the case. In the second place we have neglected the contribution to E_M by the magnetic pole distributions at the grain boundaries. But usually the angle between the [001] axis in adjacent grains does not exceed 5°, and very often the magnetostatic energy located at the grain boundaries is reduced by the formation of spikes. An upper limit of this energy term can be obtained by using the above formula

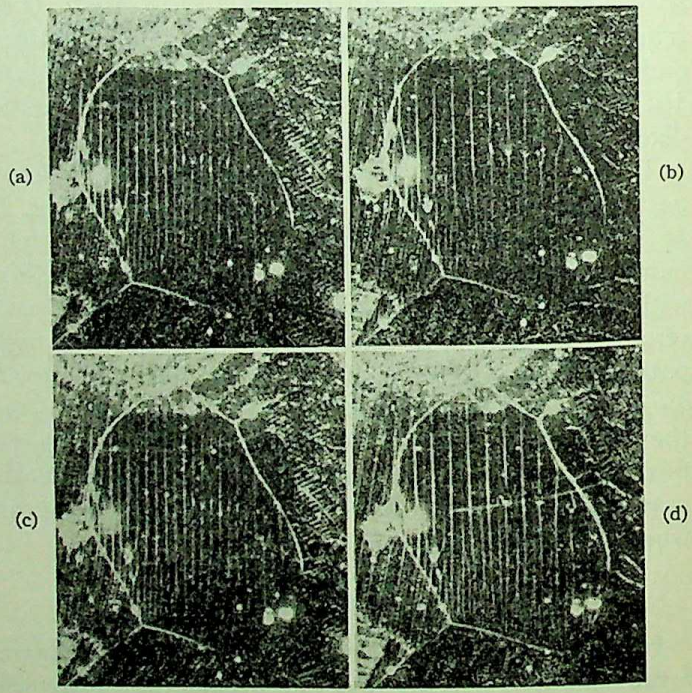


FIG. 5. Pattern I in horizontal field. (α=angle between $\vec{H}$ and [001]) (50×); [110]↑. (a) $\alpha=0$. The pattern for $\alpha=0$ is identical with the pattern for $H=0$; (b) $\alpha=90°$; (c) $\alpha=180°$; (d) $\alpha=270°$.

[4] C. Kittel, Revs. Modern Phys. 21, 541 (1949).

CC-0. In Public Domain. Gurukul Kangri Collection, Haridwar

Digitized by Arya Samaj Foundation Chennai and eGangotri

for E_M, which is, strictly speaking, only valid if the spacing is very small compared with the dimensions of the plane. [One has to take $1/\mu^*$ instead of $2/(1+\mu^*)$, since the ferromagnetic medium is on both sides of the boundary.] In our case where the grain diameter is about $10a$, this limit turns out to be of the same order as the term Ad. Hence, it will not be too serious to neglect this energy term. The grain diameter will only enter in the calculation for values of this diameter much smaller than $10a$.

The plane of the specimen is a (110) plane; hence, [001] is the only direction of easy magnetization that lies in the surface. Under the conditions of our experiments the magnetostriction of Si-Fe is always positive;[5] when the external stress is applied along [1$\bar{1}$0], then the two other directions of easy magnetization become more favorable because they form angles of 45° with the direction of stress. This results in a rearrangement of the basic domains. They will now be magnetized along [010] or [100]. It should be emphasized here that this change in domain structure is not a continuous transition from the original pattern by growth or shrinkage of domain under stress (as pictured in most of the earlier work on ferromagnetism); it is the formation of a new configuration which requires nucleation of new domains. Details of this nucleation process are not known. There is, however, experimental evidence on how the new domains within pattern *I* nucleate and spread. The spacing of the domains in pattern *I* decreases with increasing stress. That means that new domains must nucleate and propagate through the grain. This process starts, as shown in Fig. 6, at the grain boundaries. Here conditions seem to be favorable for the formation of a stable nucleus, because of two factors that come into the picture. There are, first of all, magnetic charges at the grain boundaries which have opposite charges in neighboring domains. The spacing of these opposite charges, and hence the magnetic energy, is reduced by the formation of new domains. Secondly, stress concentrations can occur at grain boundaries, which may also facilitate the nucleation of new domains. Figure 6(b) and (c) show this process of nucleation and propagation of new domains. Because of the coherence of the domain pattern within a group of grains these new domains propagate across grain boundaries across which the domain configuration is continuous.

When the original pattern changes then there are important differences between the possible configuration of the basic domains magnetized along [010] or [100]. If they are separated by walls parallel to (011), the flux through the specimen can be closed by surface domains magnetized along [001]. This is not possible if the basic domain walls are parallel to (100).

The stress induced pattern *I* corresponds to the flux closure configuration with surface domains magnetized along [001] [Fig. 7(a)], while pattern *II* is interpreted as a configuration with basic domain walls parallel to (001) and with a complicated surface pattern due to the free charges.

[5] W. J. Carr, Jr., dissertation, Carnegie Institute of Technology, (1950).

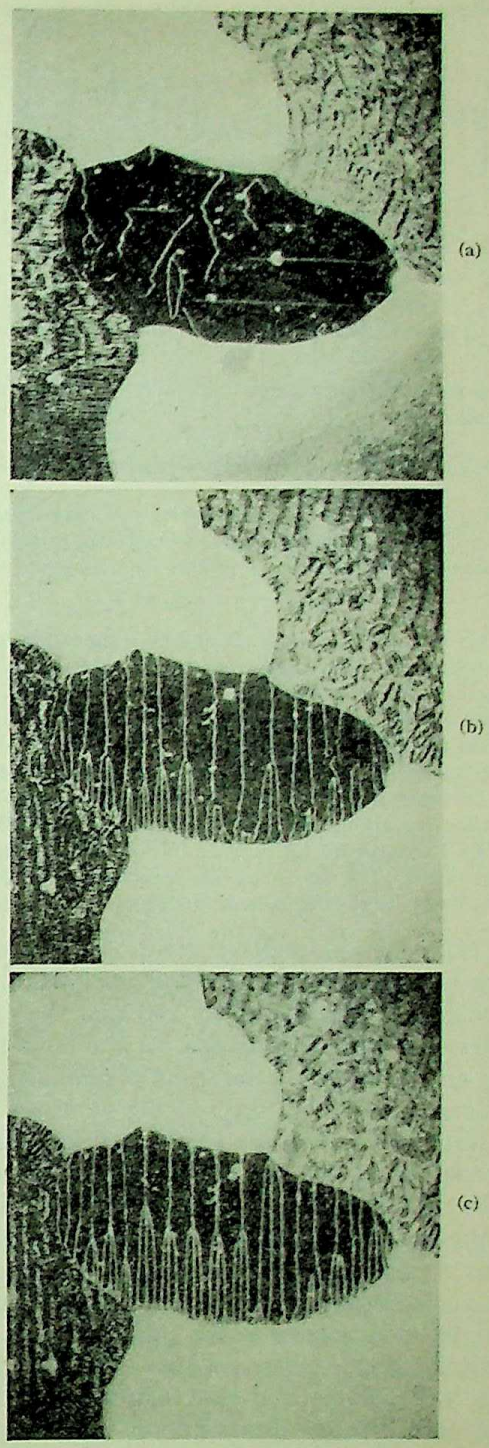


FIG. 6. Nucleation and propagation of new domains (40×); ↑ [110]; ↕ direction of stress. (a) = initial state (no applied stress but residual stresses); (b) and (c) = increasing applied stress.

In order to obtain a rough value of the critical stress σ, at which the original pattern switches over to pattern *I* and of the spacing for which the secondary pattern appears, the following estimate can be made. We shall neglect the strain energy caused by the elastic interaction between the superficial and interior domains. Taking the state of the primary pattern, spacing d_0 and stress σ, as the

CC-0. In Public Domain. Gurukul Kangri Collection, Haridwar

Digitized by Arya Samaj Foundation Chennai and eGangotri

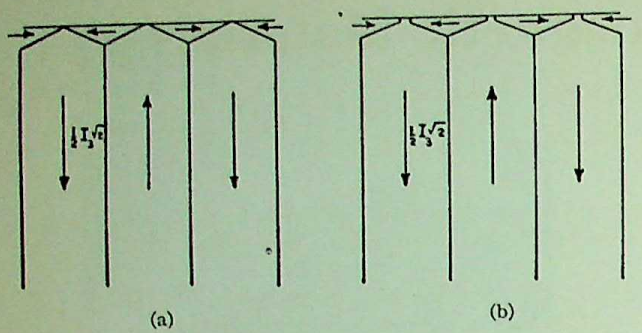


FIG. 7. Configuration of pattern I (schematic).

reference state, the thermodynamic potential of the secondary configuration is

$$\phi = A(d-d_0) + \left(\frac{a}{d} - \frac{a}{d_0} - \tfrac{1}{2}\sqrt{2} + \sqrt{6}\right)\gamma_{180°} - \sigma\Delta l(a - \tfrac{1}{4}d\sqrt{2});$$

d = spacing of secondary pattern, $\gamma_{90°} = \frac{1}{2}\gamma_{180°}$, Δl = magnetostriction along [011] axis on turning I_s from [001] into [010]. The equilibrium spacing for given σ follows from $(\partial\phi/\partial d)_\sigma = 0$ and is

$$d = [a\gamma_{180°}/(A + \tfrac{1}{4}\sqrt{2}\sigma\Delta l)]^{\frac{1}{2}}. \quad (1)$$

[To obtain the actual dependence of d on σ the strain interaction and the opening-up effect, discussed later, had to be considered.] For a qualitative comparison Fig. 8 shows the observed values of d^2 against σ for increasing stress. The solid line represents the slope of the theoretical curve, based on formula (1). The crosses are experimental data measured for increasing stress. The secondary pattern becomes more stable than the primary for $\phi < 0$. This yields, using the above value for d and taking $\Delta l = 10^{-5}$, $a = 0.01$ cm and $\theta = 1°$, $\sigma_{crit} = 0.2$ kg/mm^2 and $d_{crit} = a$ in agreement with the observation. The foregoing are equilibrium considerations which do not take the kinetics of the process into account.

The experimental evidence mentioned earlier shows that the lines in pattern I become more and more pronounced with increasing stress and that the originally fine lines widen out into bands. At the same time the spacing decreases. When the stress is gradually released the process is reversed, the spacing increases and the bands form back into lines, get fainter, and disappear. This behavior can be explained qualitatively as follows: In the closed flux configuration which is formed when the original pattern switches over, the surface domains which are magnetized along [001] still constitute a considerable portion of the total volume of the crystal. With increasing stress these domains become energetically less and less favorable. The tendency to decrease this volume will lead first to a decrease in spacing through the formation of new domains as described above [see also formula (1)], and secondly there will be an "opening up" of the closed flux structure as pictured in Fig. 7(b). In this case there is an increase in energy due to the free charges from the basic domains on the surface but also a decrease in energy due to the decrease in wall area, in addition to the decrease in energy due to the increased volume of the basic domains.

This picture leads to a possible explanation of the "transition stage." At very low loads the opening up effect is very small, and consequently, the close proximity of the opposite charges of the domain walls and the basic domains localize the stray field at the surface so that no distinct pattern can be observed.

The observed behavior of the domain pattern in a field substantiates this interpretation. The magnetic field in these experiments is weak, so as not to upset the basic domain structure. The basic domains grow and shrink depending on their orientation with respect to the field, but the surface domains remain practically unchanged. The change in volume of the basic domains leads to the "opening up" effect of the growing domains and an increase in intensity of the corresponding lines on the surface. The effect is reversed in the case of the shrinking domains.

In the transition range the normal field causes the appearance of the pattern, but, as shown in Fig. 5(c) and (d), only every second line appears in a normal field of a given direction. In addition to any action of the "opening up" effect, there is of course the well-known effect of an applied field on the line intensity.[4] This effect, however, cannot explain the observed behavior of the pattern in a horizontal field.

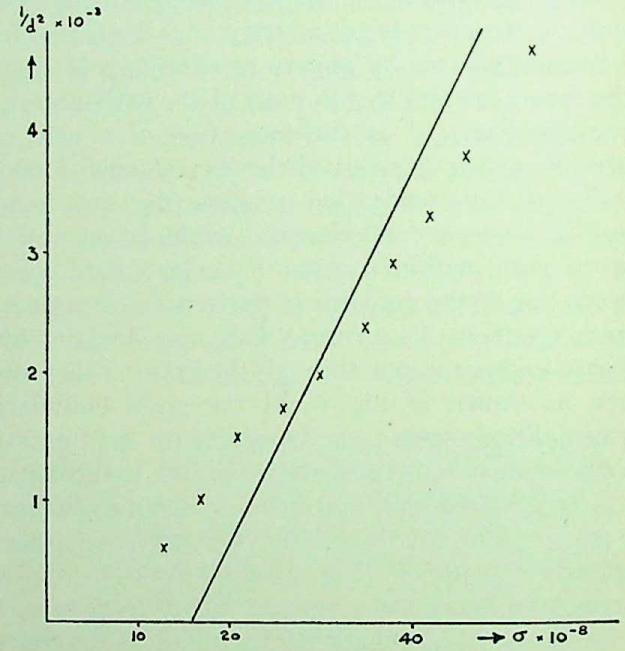


FIG. 8. Change in line spacing of pattern I with increasing stress.

IV. PLASTIC DEFORMATION

As soon as the applied load is increased beyond the elastic limit of the material, permanent changes occur in the mechanical state of the specimen.

After unloading the original pattern does not return completely. In some parts of the grain stress induced patterns are still visible, which means that these parts of the grain are under residual strains. Figure 1(d) and 6(a) show two examples. Figure 1(d) is the picture of the center grain of Fig. 1(a) after the specimen had been deformed plastically and the load had been released. This picture shows the residual strains in the interior of the grain as well as the residual strains between neighboring grains.

The authors are indebted to Dr. O. W. Ellis, Director, Department of Engineering and Metallurgy, Ontario Research Foundation, for his continued interest in this work.

CC-0. In Public Domain. Gurukul Kangri Collection, Haridwar

Digitized by Arya Samaj Foundation Chennai and eGangotri

REVIEWS OF MODERN PHYSICS VOLUME 25, NUMBER 1 JANUARY, 1953

Hall Effect in Ferromagnetic Materials

EMERSON M. PUGH AND NORMAN ROSTOKER

Carnegie Institute of Technology, Pittsburgh, Pennsylvania

Experimental results are reviewed for Fe, Co, Ni, the Co—Ni and Ni—Cu alloy series. Most of the measurements were made at room temperature. In the case of Ni, data are available from about 10°K to 800°K.

In every case studied, the Hall emf consists of a sum of two terms. The first term is proportional to the magnetizing field and has been called the ordinary Hall effect. Its order of magnitude and sensitivity to variations in temperature and in composition are comparable with the Hall effect in nonferromagnetic metals. The second term is proportional to the magnetization and has been called the extraordinary Hall effect.

At room temperature, the extraordinary effect is usually much larger than the ordinary effect. Large changes in the extraordinary effect may be produced by variations in temperature or composition.

In the theory of the ordinary effect, a representation is employed in which conduction may take place in both the *s*- and *d*-bands. This theory appears to be moderately successful in interpreting the experimental data.

Various proposals that have been advanced to account for the extraordinary effect are considered briefly. We consider that a satisfactory physical basis for this phenomenon has not yet been established.

1. INTRODUCTION

As early as 1893,[1] it was known that the Hall effect in the ferromagnetic elements Fe, Co, and Ni is determined mainly by the magnetization. In subsequent experiments by one of us,[2] it was established that the Hall voltage is proportional to the magnetization at fields up to magnetic saturation and has all of the inherent irreversibilities of magnetization curves. These experiments were made with polycrystalline materials. Webster[3] measured the Hall effect in single crystals of iron and obtained similar results. Webster's measurements were made with the primary current and Hall potential along the simple crystallographic axes [100], [110], and [111]. His results showed that the Hall effect due to magnetization is practically isotropic.

Most of the early measurements were made for fields below saturation. The Hall constant was defined as it is in nonferromagnetic materials. That is

$$R=E_y/H_0 j_x, \tag{1}$$

where R=Hall constant, E_y=Hall electric field, j_x =primary current density, and H_0=applied magnetic field in the z direction. Usually a sample was measured that was sufficiently thin in the z direction relative to the dimensions in the x and y directions so that the demagnetizing factor would be very nearly 4π and $H_0 \cong B$, the magnetic induction of the sample.

In Fig. 1 the measurements made by Smith[4] for Ni are reproduced. We have plotted the Hall electric field per unit current density $e_y=E_y/j_x$, against the applied field or magnetic induction of the sample. The Hall constant according to Eq. (1) would be the slope of the initial steep portion of each curve. The temperature dependence of R, as shown in Fig. 2, is particularly striking because the Hall constant does not usually vary significantly with temperature in metals. More recent measurements for Ni by Kikoin[5] confirm the essential features of Smith's data. Smith[4] also made measurements for Co and Fe which show similarly anomalous behavior.

The Hall effect in ferromagnetic metals appears to be a fundamentally different phenomenon from the Hall effect in other metals according to the experimental data for fields below saturation. When magnetic saturation is achieved, or the domains have been oriented in the direction of the applied field, the magnetization is almost constant. The Hall effect continues to increase with increasing applied field, but much more slowly as can be seen in Fig. 1. Accordingly the following empirical formula has been suggested for the Hall effect in ferromagnetic metals[2,6]:

$$e_y=R_0 H+R_1 M, \tag{2}$$

where e_y=Hall electric field per unit current density, H=magnetizing force in the z direction, and M=magnetization in the z direction. R_0 and R_1 have been designated the ordinary and extraordinary Hall constants, respectively. The data of Smith for Ni have been

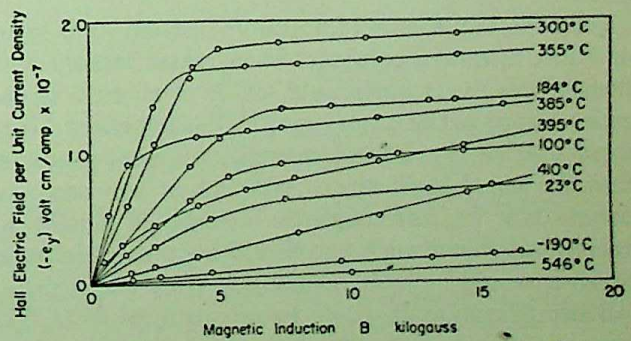


FIG. 1. Hall effect in nickel from the data of A. W. Smith.

[1] A. Kundt, Wied. Ann. 49, 257 (1893).
[2] E. M. Pugh, Phys. Rev. 36, 1503 (1930); E. M. Pugh and T. W. Lippert, Phys. Rev. 42, 709 (1932).
[3] W. L. Webster, Proc. Cambridge Phil. Soc. 23, 800 (1925).
[4] A. W. Smith, Phys. Rev. 30, 1 (1910).
[5] I. K. Kikoin, Physik. Z. Sowjetunion 9, 1 (1936).
[6] A. W. Smith and R. W. Sears, Phys. Rev. 34, 1466 (1929).

CC-0. In Public Domain. Gurukul Kangri Collection, Haridwar

Digitized by Arya Samaj Foundation Chennai and eGangotri

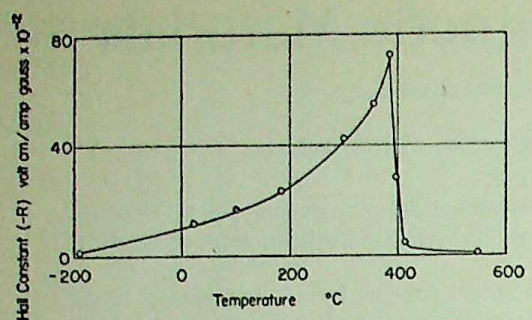


FIG. 2. Hall constants for nickel determined from the slopes of the initial steep portions of the plots of Hall electric field per unit current density *versus* magnetic induction.

reconsidered[7] on the basis of Eq. (2). Although Smith's data above saturation are not very accurate it was possible to determine approximate values of R_1 and R_0 over the entire temperature range studied by Smith.

The constant $R_0 = -0.61 \times 10^{-12}$ volt cm/amp gauss at room temperature, was of the same order of magnitude as the Hall constants for the nearest neighbor nonferromagnetic elements in the periodic table ($R = -0.93 \times 10^{-12}$ volt cm/amp gauss for Mn and $R = -0.55 \times 10^{-12}$ volt cm/amp gauss for Cu). The Hall constant defined in the usual way for ferromagnetic metals by Eq. (1) is about a factor of 20 larger. Of particular significance was the fact that the values of R_0 determined from Smith's data were approximately independent of temperature over the entire temperature range.[8] Recently Jan and Gijsman[9] have obtained more accurate data at low temperatures which show that R_0 decreases significantly in magnitude between room temperature and 14°K. With the possible exception of this fact, the order of magnitude and temperature dependence of R_0 is about the same as for the Hall constant of nonferromagnetic metals. (Above the Debye characteristic temperature of the lattice the Hall constant is almost independent of temperature in most metals. Low temperature behavior is rather varied. According to Alterthum,[10] when the temperature is decreased from room temperature to very low temperatures, the Hall constant increases to a maximum in diamagnetic metals such as Au, Cu, Cd, and decreases to a minimum in paramagnetic metals such as Al, Pt.)

The constant $R_1 = -74.9 \times 10^{-12}$ volt cm/amp gauss for Ni at room temperature. It increases rapidly with temperature by as much as a factor of about 5 in the neighborhood of the Curie point.[7] The Hall effect due to magnetization is of a fundamentally different character from the usual Hall effect. Although it has been observed only in ferromagnetic metals, it should be pointed out that if such an effect were present in other metals it would be indistinguishable from the ordinary Hall effect because M would be proportional to H. The existence of this effect above the ferromagnetic Curie point when Ni is still strongly paramagnetic suggests the possibility that it may occur in nonferromagnetic materials.[2,5,8]

In most of the earlier measurements found in the literature, investigators have studied the Hall effect below saturation. The main reason for this is that a very high magnetic field is required to study most ferromagnetic materials above saturation. The only data above saturation that has been available is for Ni. The recent acquisition of an A.D.L. magnet at Carnegie Institute of Technology has made fields up to 40 kilogauss available. The group at C.I.T. has undertaken the study of a variety of ferromagnetic metals with the primary objective of measuring the ordinary Hall constant R_0 for which no data have been available. The results to date will be reported herein, and the interpretation of the measured values in terms of the usual theory of the Hall effect will be discussed. These data help to fill an existing gap in the knowledge of the electrical properties of ferromagnetic metals and when completely understood may considerably enhance our presently inadequate understanding of the behavior of the d-shell electrons.

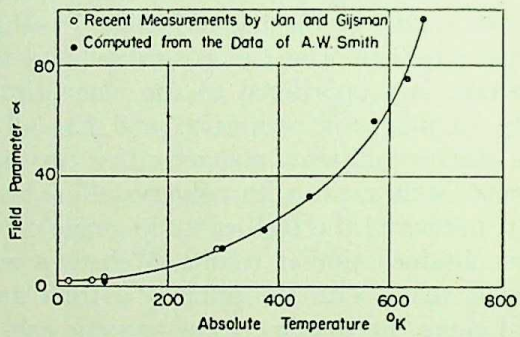


FIG. 3. Temperature dependence of the field parameter α, for nickel.

The origin of the Hall effect due to magnetization must be of a fairly general character since similar effects due to magnetization are present in an entire class of conduction phenomena. For example, the Ettinghausen, Nernst, and Righi-Leduc effects are also proportional to the magnetization below saturation and increase linearly with H after all of the domains have been oriented.[11,12]

Considerable thought has been given to the possibility that an effective magnetic field deflects[7,13] the conduction electrons. That is,

$$\mathbf{H}_{\text{eff}} = \mathbf{H} + 4\pi\alpha\mathbf{M}_s, \qquad (3)$$

where $\mathbf{H}$ = magnetizing force, $\mathbf{M}_s$ = saturation magnetization in a domain, α = a parameter which would usually be much greater than unity.

[7] Pugh, Rostoker, and Schindler, Phys. Rev. 80, 688 (1950).
[8] N. Rostoker and E. M. Pugh, Phys. Rev. 82, 125 (1951).
[9] J. P. Jan and H. M. Gijsman, Physica 5, 277 (1952).
[10] H. Alterthum, Ann. phys. 39, 933 (1912); 40, 391 (1913).
[11] L. L. Campbell, *Galvanomagnetic and Thermomagnetic Effects* (Longmans Green and Company, New York, 1932).
[12] G. S. Nielson, Phil. Mag. 18, 575 (1934).
[13] K. Kondo, Rep. Inst. of Sc. and Tech., Tokyo 4, 79 (1950) (in Japanese).

CC-0. In Public Domain. Gurukul Kangri Collection, Haridwar

Digitized by Arya Samaj Foundation Chennai and eGangotri

Below saturation when the domains are only partially aligned, the effective field given by Eq. (3) would produce a Hall electric field whose magnitude and direction would be different for each domain. However, it has been proved[7] that the resultant observable Hall emf would depend on the macroscopic magnetization $\mathbf{M}$ or the average domain orientation and the Hall constants for the sample would be the same as the Hall constants for the domains. Therefore without loss of generality we can forget about the domains and replace the $4\pi\alpha\mathbf{M}_s$ term of Eq. (3) by the uniform field $4\pi\alpha\mathbf{M}$. Then Eqs. (2) and (3) imply the following expression for Hall effect:

$$e_y = R_0 H_{\text{eff}}, \tag{4}$$

where $H_{\text{eff}} = H + 4\pi\alpha M$ is the effective field in the z direction, and $\alpha = R_1/4\pi R_0$.

In the case of Ni it has been possible to estimate the values of α over a wide range of temperatures from Smith's data. In Fig. 3, α has been plotted against temperature. It is not possible to estimate α satisfactorily for low temperatures from these data. This gap has recently been filled by the measurements of Jan and Gijsman[9] which are also shown in Fig. 3. It appears quite definite that α approaches 2 at very low temperatures.

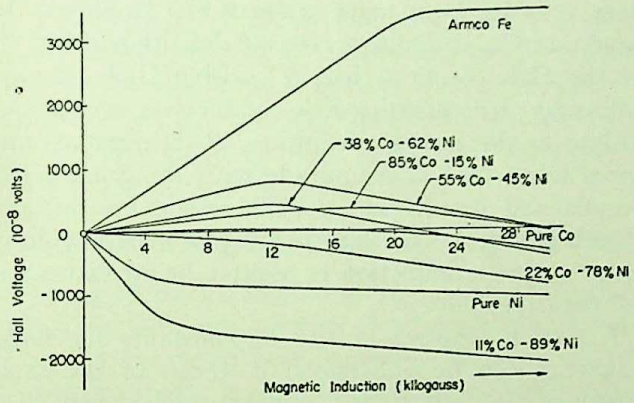


FIG. 4. Comparison of Hall effects for a number of materials investigated by S. Foner. (The Hall voltages refer to samples which are 1 mm thick in the direction of the field and carry a current of 25 amperes.)

This is in good agreement with the recent work on the magnetoresistance of Ni carried out by Smit.[14] According to Smit the magnetoresistance produced by the influence of the Lorentz magnetic force on the electron orbits is obscured by the much larger magnetoresistance due to the influence of changes in intrinsic magnetization on the scattering probability of electrons, except at low temperatures. He has studied the "orbital" magnetoresistance at liquid nitrogen temperature and finds that an effective field with $\alpha \cong 2$ is consistent with his data.

Several attempts have been made to give a physical basis for the effective field.[7,13,15,16] These attempts have all started from the one-electron approximation in a perfect lattice corresponding to 0°K and might be considered as possible explanations for the low temperature behavior of the Hall effect due to magnetization. However, no success has been achieved in explaining the increase of α from about 2 to almost 100 in Ni when the temperature is increased up to the Curie point. These attempts also fail to clarify the experimental data for Fe, Co, the Co—Ni and Ni—Cu alloy series presented herein.

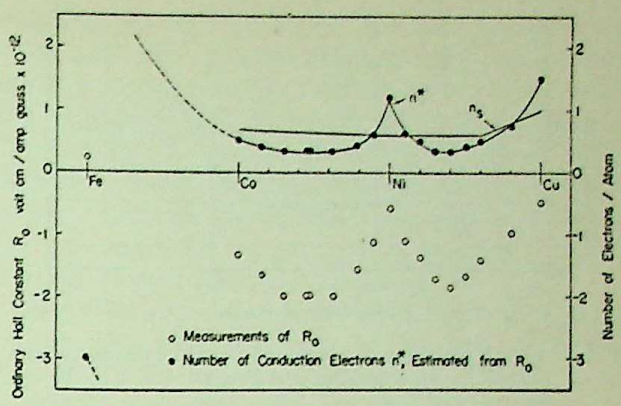


FIG. 5. Ordinary Hall constant *versus* composition from the measurements of Hall emf above saturation by Schindler and Foner. (n^* is the number of conduction electrons according to elementary theory for the Hall effect. n_s is the number of s-band electrons according to the simple band picture.)

2. RECENT MEASUREMENTS OF HALL EFFECT AT ROOM TEMPERATURE

Hall effects in the Cu—Ni and Co—Ni systems have recently been measured by Schindler[17] and Foner.[18] In Fig. 4 the Hall voltage is plotted against the applied magnetic field for a number of materials investigated by Foner. From such curves, the values of R_0 and α in Eq. (4) were determined. In Fig. 5 the values of R_0 are shown for all of the elements and alloys measured to date. In Fig. 6 the corresponding values of α are shown.

3. INTERPRETATION OF THE ORDINARY HALL EFFECT IN FERROMAGNETIC MATERIALS

According to the Sommerfeld theory the Hall constant R is related to the number of conduction electrons by the formula[19]

$$R = -1/(nNec), \tag{5}$$

where n = number of conduction electrons/atom, N = number of atoms/unit volume, e = magnitude of elec-

[14] J. Smit, Physica 17, 612 (1951).
[15] V. Rudnitsky, J. Exp. Theoret. Phys. USSR 9, 262 (1939).
[16] A. G. Samolovich and B. L. Konkov, J. Exp. Theoret. Phys. USSR 20, 783 (1950).
[17] A. I. Schindler and E. M. Pugh, Phys. Rev. 83, 208 (1951).
[18] S. Foner and E. M. Pugh, Phys. Rev. 87, 210 (1952). References 17 and 18 refer to abstracts of papers presented to the American Physical Society. The experimental results have not yet been published at the time of writing this paper and are reproduced here with the kind permission of Dr. A. I. Schindler and Dr. Simon Foner.
[19] A. Sommerfeld and N. H. Frank, Revs. Modern Phys. 3, 1 (1931).

CC-0. In Public Domain. Gurukul Kangri Collection, Haridwar

Digitized by Arya Samaj Foundation Chennai and eGangotri

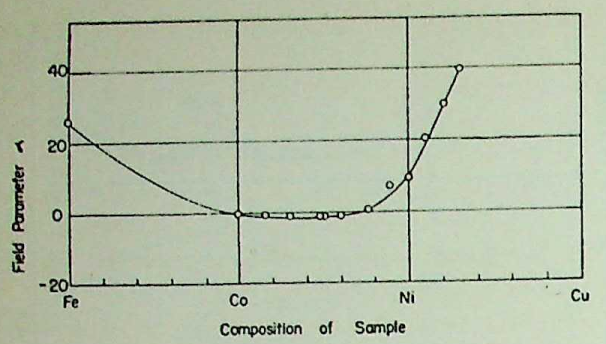


FIG. 6. Field parameter α, estimated from the measurements of Schindler and Foner.

tronic charge, and c=velocity of light. Equation (5) is applicable to a case where conduction occurs in a single band which is nearly empty. In this case the energy levels are approximately given by

$$\epsilon=(\hbar^2/2m_s)k^2, \tag{6}$$

where ϵ=electron energy relative to the lowest energy level of the band, k=magnitude of electron wave vector, and m_s=effective mass of electrons in for example an s-band.

An effective number of electrons n^* can be calculated from Eq. (5) and the experimentally determined values for R_0. Making use of Eq. (5),

$$n^*=-(1/R_0Nec) \tag{7}$$

has been calculated and plotted in Fig. 5. The numbers of s-band electrons/atom indicated by magnetization measurements, are also shown in Fig. 5 for each material. Excluding the case of Fe, n^* does not differ from n_s by more than a factor of 2 in any case. This is about the extent of agreement usually obtained between the number of conduction electrons expected and the number calculated by means of Eq. (5) and Hall effect measurements for nonferromagnetic metals. For example the agreement in the case of Cu shown in Fig. 5 is within a factor of 1.5.

In the case of nonferromagnetic metals the discrepancies between the measured Hall coefficients and Eq. (5) can often be resolved by replacing Eq. (6) with a more realistic assumption for the band structure. For metals that conduct in a single band such as Cu, a more general formula for R such as Jones and Zener[20] have given indicates that the discrepancies may be accounted for by departures of the Fermi surfaces from spheres. For metals that can be expected to conduct in more than one band a representation has been employed where one band is nearly empty and the other nearly filled. In the nearly empty band (s-band) the energy levels are assumed to be given by Eq. (6) and in the nearly filled band (d-band) by

$$\epsilon=\epsilon_m-(\hbar^2/2m_d)l^2, \tag{8}$$

where ϵ_m=maximum energy of the band, $-m_d$=effective mass of d-electrons, $\mathbf{l}$=wave vector measured from the highest level ϵ_m. With this representation Sondheimer[21] gives for the Hall constant,

$$R=-\frac{1}{Nec}\left[\frac{1}{n_s}\left(\frac{\sigma_s}{\sigma}\right)^2-\frac{1}{n_d}\left(\frac{\sigma_d}{\sigma}\right)^2\right], \tag{9}$$

where n_s=number of s-band electrons, n_d=number of d-band holes, σ_s=s-band conductivity, σ_d=d-band conductivity, $\sigma=\sigma_s+\sigma_d$=total conductivity. Equation (9) has been moderately successful in explaining departures from the Sommerfeld formula[22] and the occurrence of positive Hall coefficients in many metals where conduction can be expected from more than one band.

It appears to be both reasonable and necessary to assume for the ferromagnetic materials that the d-electrons are itinerant and contribute to conduction. We can for example account for the measured Hall coefficient of Ni by means of Eq. (9) with $n_s=n_d=0.6$/atom and $\sigma_d/\sigma=0.23$.[7] Similarly the measured Hall coefficient for Fe can be accounted for with $n_s=0.6$ atom, $n_d=2.2$/atom, and $\sigma_d/\sigma=0.87$. It should be noted that Co, according to the old definition of Eq. (1) for the Hall constant, had a positive Hall constant indicating predominating hole conduction, whereas according to the present definition, R_0 is negative and agrees fairly well in magnitude with the Sommerfeld formula and $n_s=0.7$/atom. (The reason for this can be seen in Fig. 4. The slope of the plot of Hall voltage *versus* magnetic induction is positive below saturation and negative above.)

The main features of the R_0 constants for ferromagnetics can be understood in terms of the usual theory of Hall effect for a uniform applied field. The degree to which measured values of the Hall constants agree with predictions by theory is about the same as for nonferromagnetic metals. Close agreement with formulas based on spherical Fermi surfaces such as Eqs. (5) and (9) usually cannot be expected since most attempts at calculating wave functions and energy levels for ferromagnetics indicate that the Fermi surfaces are not spherical to a good approximation except in limiting cases.[23]

4. SPECULATIONS ON THE ORIGIN OF THE HALL EFFECT DUE TO MAGNETIZATION

There are usually transverse voltages present which are not due to the Hall effect. Transverse temperature gradients produced, for example, by the Ettingshausen effect, result in a transverse voltage due to the thermocouple action of the sample and potential leads. Magnetoresistance effects which are particularly large in ferromagnetic materials may also result in a transverse voltage. In the data reported herein, particular

[20] H. Jones and C. Zener, Proc. Roy. Soc. (London) **A145**, 269 (1934).

[21] E. H. Sondheimer, Proc. Roy. Soc. (London) **A193**, 484 (1948).

[22] For example, see E. Justi and M. Kohler, Abh. Braunschweig Wiss. Ges. 3, 44 (1951).

[23] For example, see H. M. Krutter, Phys. Rev. 48, 664 (1935); G. C. Fletcher, Proc. Phys. Soc. (London) **A65**, 192 (1952).

CC-0. In Public Domain. Gurukul Kangri Collection, Haridwar

Digitized by Arya Samaj Foundation Chennai and eGangotri

care has been exercised to correct for these voltages so that the corrected measurements may be properly regarded as Hall effect.

In order to describe the Hall effect in ferromagnetic materials within the framework of existing theory, an effective Lorentz force has been introduced. We assume effective magnetic fields for the Lorentz force,

$$H_s = H + 4\pi\alpha_s M \tag{10}$$

for electrons that are mainly in s-states and

$$H_d = H + 4\pi\alpha_d M \tag{11}$$

for electrons that are mainly in d-states. This leads to the Hall effect expression of Eq. (4) where R_0 is given by Eq. (9) and

$$\alpha = \frac{1}{R_0 N e c}\left[\left(\frac{\sigma_s}{\sigma}\right)^2 \frac{\alpha_s}{n_s} - \left(\frac{\sigma_d}{\sigma}\right)^2 \frac{\alpha_d}{n_d}\right]. \tag{12}$$

In order to explain the observed values of α for Ni, it is necessary to give a physical basis for values of α_s and α_d that are much greater than unity and to account for the rapid increase of α with temperature from about 2 to almost 100 mainly through a temperature dependence of α_s, α_d. A correct explanation must also suggest the changes in α with changes in composition shown in Fig. 6.

a. Lorentz Force due to Internal Magnetic Fields

The magnetization arises from the electron spin which produces dipoles that are very small even on an atomic scale. The magnetic field produced by these dipoles varies over a wide range of values in extremely short distances. The resultant effect on an electron which traverses many interatomic distances can be described in terms of an effective magnetic field such that

$$\langle \mathbf{f} \rangle_{Av} = -(e/c)\langle \mathbf{v} \times \mathbf{h} \rangle_{Av} = -(e/c)(\langle \mathbf{v} \rangle_{Av} \times \mathbf{H}_{eff}), \tag{13}$$

where $\mathbf{f}$ = Lorentz force; the $\langle\ \rangle_{Av}$ denotes an average for the electron being deflected, $\mathbf{h}$ = actual magnetic field at the location of the electron under consideration, $\mathbf{v}$ = electron velocity, $\mathbf{H}_{eff}$ = effective magnetic field. For a beam of Dirac electrons with extremely high velocity, so that $\mathbf{v}$ may be considered a constant of the motion, Weizsäcker[24] has shown that $\mathbf{H}_{eff} = \mathbf{H} + 4\pi\mathbf{M}$. According to Lorentz the spatial average of $\mathbf{h}$ is $\langle \mathbf{h} \rangle_{Av} = \mathbf{H} + 4\pi\mathbf{M}$ so that in this case the beam electrons simply report the average field. Wannier's[25] calculations for high energy cosmic ray particles consider the effect of the beam particle on the local distribution of magnetization. He finds small deviations from the limiting case treated by Weizsäcker which are produced by Coulomb interaction between the beam particle and the d-electrons.

These calculations do not apply to the relatively slow conduction electron for which the crystalline field cannot be neglected and for which $\mathbf{v}$ could not be considered a constant of the motion. Nevertheless, it has been considered by Webster[26] that on the basis of Wannier's calculations the effective field for conduction electrons would be less than $\langle \mathbf{h} \rangle_{Av}$ because the Coulomb repulsion between conduction and d-electrons would prevent conduction electrons from reaching the high field regions near the d-electrons.

Kondo[27] has recently made a calculation appropriate to the conduction electrons of Ni and finds that $H_{eff} = H + 4\pi\alpha M$ where $\alpha_s = 0.34$ for s-electrons and $\alpha_d = 2.5$ for d-electrons. He has also found a linear increase with temperature of α_s, α_d due to the influence of the lattice vibrations on the microscopic distribution of magnetization, but it is much too small to explain the Hall effect.

There does not seem to be any possibility of accounting for values of α very different from unity on the basis of the magnetic field due to the polarized d-electrons.

b. Effective Field due to Spin-Orbit Interaction

Rudnitsky[15] first suggested the possibility of a Hall effect due to the action of the inhomogeneous field from the primary current on the spins of the d-electrons. The magnetic field due to the current is illustrated in Fig. 7. For simplicity we consider a model where there are N electrons per unit volume of magnetic moment μ and charge $-e$. These electrons are assumed to produce the primary current and to have their spins aligned in the z direction so as to produce a magnetization $M = N\mu$. Due to the inhomogeneous field from the primary current, the force on an electron in the y

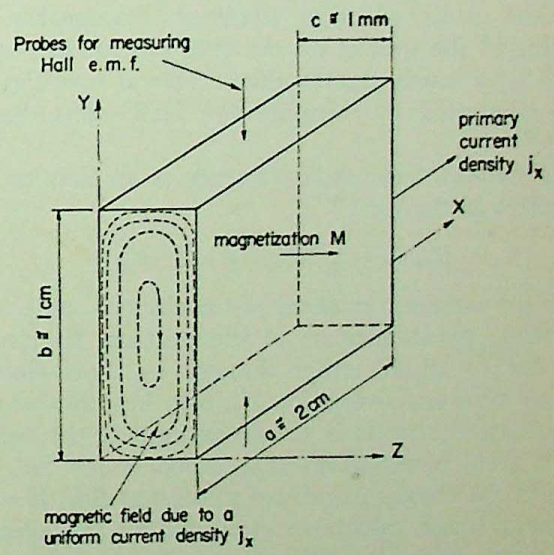


FIG. 7. A typical Hall effect sample. The directions of magnetization, primary current, and Hall voltage are shown. The magnetic field due to the primary current density is indicated roughly by field lines.

[24] C. F. v. Weizsäcker, Ann. Physik 17, 869 (1933).
[25] G. H. Wannier, Phys. Rev. 72, 304 (1947).
[26] D. L. Webster, Am. J. Phys. 14, 360 (1946).
[27] K. Kondo, Saitama University, Tokiwacho, Urawa, Japan. We wish to thank Professor Kondo for showing us his calculations prior to publication.

CC-0. In Public Domain. Gurukul Kangri Collection, Haridwar

Digitized by Arya Samaj Foundation Chennai and eGangotri

direction would be

$$f_y=\mu(\partial H_y/\partial z), \tag{14}$$

where H_y=magnetic field due to the primary current density j_x. According to Maxwell's theory,

$$\partial H_y/\partial z=(\partial H_z/\partial y)-(4\pi/c)j_x. \tag{15}$$

H_y, H_z may be calculated from the Biot-Savart law with the assumption that j_x is constant. For a sample of the dimensions ordinarily employed in Hall effect studies

$$\partial H_y/\partial z\cong-(4\pi/c)j_x,$$

and

$$f_y\cong-(4\pi\mu/c)j_x. \tag{16}$$

In order to satisfy the condition that $j_y=0$, there must be a transverse electric field such that $f_y-eE_y=0$. Making use of Eq. (16) and writing $M=N\mu$, we obtain the following rough estimate of the Hall effect,

$$E_y=-(4\pi M/Nec)j_x. \tag{17}$$

Equation (17) has the required symmetry and form of a Hall effect expression. Aside from the questionable formulation, the main objection is that the estimated effect is too small to explain the Hall effect except perhaps at very low temperatures. If we take into consideration the fact that the d-electrons carry only a small fraction of the primary current in most ferromagnetic materials, the predicted Hall effect would be still smaller than the right-hand side of Eq. (17) by a factor of (σ_d/σ). Furthermore, there is no suggestion of the observed temperature dependence in this theory.

Rudnitsky's theory can be interpreted as a classical calculation of the interaction of the spin of an electron with the orbits of other electrons. Presumably the coupling of the spin of an electron with its own orbit should be a much greater effect. Several investigators have attempted to calculate the Hall effect due to this.[14,17]

The spin-orbit interaction energy of an electron can be written in the form[28]

$$U_{so}=-(1/2\mathrm{mc})[(\boldsymbol{\mu}\times\mathbf{E})\cdot\mathbf{p}], \tag{18}$$

where $\boldsymbol{\mu}$=magnetic moment of the electron under consideration, $\mathbf{p}$=momentum of the electron, $\mathbf{E}$=electric field due to all the other charges. In a one-electron Hartree type approximation U_{so} may be regarded as a perturbation term. It is similar in form to the perturbation term $(e/\mathrm{mc})(\mathbf{A}\cdot\mathbf{p})$ that accounts for the Hall effect in the usual theory[29] for a constant field $\mathbf{H}=\mathrm{curl}\,\mathbf{A}$. For a rough calculation we consider the effective field due to spin-orbit interaction to be

$$\mathbf{H}_{so}=\mathrm{curl}-(\boldsymbol{\mu}\times\mathbf{E})/2e$$
$$=(1/2e)[(\boldsymbol{\mu}\cdot\nabla)\mathbf{E}-\boldsymbol{\mu}(\nabla\cdot\mathbf{E})]. \tag{19}$$

An order of magnitude estimate is obtained by regarding the magnetic moment and velocity of the electron under consideration as constants of the motion and $\mathbf{H}_{so}$ as an operator for which the average value is

$$\mathbf{H}_{\mathrm{eff}}=\int\varphi_k^*\mathbf{H}_{so}\varphi_k d\tau. \tag{20}$$

φ_k is the unperturbed Bloch wave function for the electron under consideration in a crystal lattice. We shall consider a unit volume over which φ_k is normalized.

For a perfect lattice $|\varphi_k|^2$ and $\mathbf{E}$ should have crystal periodicity making possible the reduction of Eq. (20) to an integral over a single atomic polyhedron. Any polyhedron may be approximated by an inscribed sphere of radius r_0 and volume $\tau_0=1/N$ where N is the number of atoms per unit volume. In the atomic polyhedron we assume that φ_k has the symmetry of an s- or d-function and $\mathbf{E}\cong E(r)\mathbf{r}/r$ is approximately spherically symmetric. With these assumptions Eq. (20) can be reduced to

$$\mathbf{H}_{\mathrm{eff}}=-(4\pi N\boldsymbol{\mu}/3e)\int|\varphi_k|^2\rho d\tau_0, \tag{21}$$

where ρ is the charge density define by $\nabla\cdot E=4\pi\rho$, which is due to the nuclei and all other electrons except the one under consideration. Equation (21) is essentially the same as the result obtained by Konkov and Samolovich.[16]

In the limiting case where the electron under consideration is free, $|\varphi_k|^2=1$, $N\int\rho d\tau_0=e$, so that the result due only to the missing charge under consideration is $H_{\mathrm{eff}}\cong-(4\pi/3)\mu$ which is vanishingly small.

A very much larger result can be obtained when the electron under consideration is not free. We shall consider the case of a d-electron and assume that near the center of the polyhedron the wave function approaches the atomic wave function which vanishes at the center. This is a characteristic property of the d-state. Accordingly, the charge density ρ to be considered in evaluating Eq. (21) is only that due to the Z electrons outside the nucleus. For any polyhedron $\int\rho d\tau_0=-Ze$, omitting the nuclear charge and neglecting the charge of the electron under consideration. Therefore

$$\int|\varphi_k|^2\rho d\tau_0=-Ze|R_k(r_1)|^2,$$

where $R_k(r)$ is the radial part of φ_k and r_1 is some value of r between 0 and r_0, the radius of the inscribed sphere of the polyhedron. Since $N\boldsymbol{\mu}$ is of the order of magnitude of the magnetization $\mathbf{M}$, the effective field is of the form

$$\mathbf{H}_{\mathrm{eff}}=4\pi\alpha\mathbf{M},$$

with

$$\alpha=\tfrac{1}{3}Z|R_k(r_1)|^2. \tag{22}$$

For the ferromagnetic elements Z is about 26, and it is

[28] L. I. Schiff, *Quantum Mechanics* (McGraw-Hill Book Company, Inc., New York, 1949), Chapter XII.

[29] H. Jones and C. Zener, Proc. Roy. Soc. (London) A144, 101 (1934).

CC-0. In Public Domain. Gurukul Kangri Collection, Haridwar

Digitized by Arya Samaj Foundation Chennai and eGangotri

reasonable to suppose that $|R_k(r_1)|^2$ would be greater than the free electron value of unity so that a value of α might be obtained that is much greater than unity. According to this rough calculation, the direction of effective field for an electron depends on the spin orientation. Therefore a net effect would only be expected if there is a net polarization of the conduction electrons.

A Hartree type calculation such as we have outlined would give too large a result for the effective field because it neglects correlations of the electrons. The probability of finding any other electron close to the electron under consideration should be very small. It is especially improbable to find an electron of the same spin close to the electron under consideration. Kondo[14] attempted to correct for correlation of electrons by introducing "Fermi holes" around electrons where it would be improbable to find any other electron. From a numerical calculation he estimated $\alpha_d \cong 14$ and $\alpha_d \cong 28$ for d-electrons in Fe and Ni, respectively. His calculations show that these results are extremely sensitive to the choice of wave functions and therefore should not be taken too seriously except perhaps as order of magnitude estimates.

Calculations to date have only been attempted for a perfect lattice with all spins oriented consistent with the Pauli principle and the observed magnetization. The temperature dependence observed for α has not yet been explained. It does not seem likely that the influence of lattice vibrations on charge distribution can account for this. A possible explanation of the temperature dependence may be in the spin dependence of the correlations of electrons. The correlation of electrons when there is a net polarization of electron spins at low temperatures should be substantially different from the correlation near the Curie point when the net polarization becomes very small. It will be necessary to improve considerably the semiclassical calculations made to date in order to investigate such effects.

5. CONCLUSIONS

The ordinary process for Hall effect accounts for only a small part of the observed Hall voltage in ferromagnetic materials. A satisfactory physical basis has not yet been established for the large Hall effect produced by the magnetization. Of the proposals advanced to account for this, only the spin-orbit coupling of conduction electrons appears to offer any possibility.

Since the situation is simpler at low temperatures from a theoretical point of view, we are of the opinion that at present, the most profitable approach to the problem is to study Hall effect in ferromagnetic materials at low temperatures where experimental data is nonexistent except in the case of Ni.

We wish to express our appreciation to Dr. A. I. Schindler and Dr. Simon Foner for permission to present their measurements and to Dr. J. E. Goldman for discussions and criticism of this paper.

CC-0. In Public Domain. Gurukul Kangri Collection, Haridwar

Digitized by Arya Samaj Foundation Chennai and eGangotri

Magnetomechanical Effects in an Antiferromagnet, CoO

M. E. FINE

Bell Telephone Laboratories, Murray Hill, New Jersey

THE formation of antiferromagnetic order in CoO, Street and Lewis[1] report, causes a large decrease in Young's modulus. We have made a detailed study of Young's modulus and internal friction in a sample of CoO. The experimental facts are as follows: On cooling, Young's modulus decreases rapidly near the Néel temperature, −2°C in our sample, reaching a minimum value at approximately −17°C. The modulus drops from 17 to 6.4×10^{11} dynes cm^{-2}, a change of 60 percent. The effects of antiferromagnetism on the modulus persist to at least −196°C, for at −196°C the modulus is half of its room temperature value. The internal friction, on cooling from room temperature, rapidly increases near the Néel temperature reaching a maximum value of $1/Q=9\times10^{-3}$ at approximately the same temperature as the minimum in modulus. At room temperature and at −20°C increasing the maximum strain amplitude from 10^{-8} to 10^{-5} has little effect on E or $1/Q$, but at −190°C E decreases 1 percent and $1/Q$ increases from 5 to 25 $\times10^{-4}$.

The large decrease in E implies that an applied stress causes strains in addition to the normal elastic strain. The additional strains are comparatively large approximately equalling the normal elastic strain. In trying to deduce the origin of these strains one can get ideas from the sources of anelastic strains in ferromagnets. For example, in CoO at low temperatures where E and $1/Q$ are functions of strain amplitude, a mechanism, predicted by Bozorth,[2] analogous to the stress-induced change in domain structure in ferromagnets[3] (the so-called ΔE effect) is plausible. In annealed nickel[4] the ΔE effect lowers the modulus some 30 percent. In CoO Shull, Strausser, and Wollin[5] have found the atomic magnetic moments to be aligned antiferromagnetically parallel to a ⟨100⟩ direction. The antiferromagnetism distorts CoO from cubic (NaCl structure) to tetragonal. This has been reported by Tombs and Rooksby[6] and Greenwald and Smart.[7] The c/a ratio becomes increasingly less than one as the temperature is lowered below the Néel point. Now suppose we have a single crystal at room temperature. As it becomes antiferromagnetic on cooling there are 3⟨100⟩ type directions which may become the magnetization direction and the direction of the shortened c axis. Thus the crystal when it becomes antiferromagnetic may become divided into 3 types of domains differing as to which of the original ⟨100⟩ directions is the c axis. If a tensile stress is applied, the area of that domain whose c axis is most nearly perpendicular to the stress axis would increase thus increasing the length of the sample. The converse would occur on compression. Hence there is a lowering in modulus. The tetragonality at −180 is approximately 100 times the magnetostriction in nickel and is ample to yield strains of the same order of magnitude as the normal elastic strain. Since the tetragonality increases on cooling, one might expect the modulus to continually decrease, contrary to our observation. But as the temperature is lowered domain boundary movement becomes more difficult because it generates larger internal strains.

Near the Néel temperature where the magnetic moments are loosely coupled and any domain structure would be diffuse and where E and $1/Q$ are independent of strain amplitude, another mechanism may be the source of the additional strain. Analogous to the stress induced volume magnetostriction in ferromagnets,[8] in CoO near the Néel temperature an applied stress may change the degree of antiferromagnetic order. The strain would come from the tetragonality and volume change. The volume increases 10×10^{-3} cm^3/cm^3 on cooling. E and $1/Q$ are more conceivably independent of strain amplitude by this mechanism.

Thus in these measurements of elasticity and internal friction in an antiferromagnet we find evidence for mechanical effects similar to magnetomechanical effects in ferromagnets and also experimental evidence for a domain structure.

[1] R. Street and B. Lewis, Nature 168, 1036 (1951).
[2] R. M. Bozorth, *Ferromagnetism* (D. Van Nostrand Company, Inc., New York, 1951), pp. 472, 595.
[3] M. Kersten, Z. Physik 85, 708 (1933).
[4] S. Siegel and S. L. Quimby, Phys. Rev. 49, 663 (1936).
[5] Shull, Strausser, and Wollin, Phys. Rev. 83, 333 (1951).
[6] N. C. Tombs and H. P. Rooksby, Nature 165, 442 (1950).
[7] S. Greenwald and J. S. Smart, Nature 166, 523 (1950).
[8] R. Becker and W. Döring, *Ferromagnetismus* (Julius Springer, Berlin, 1939), p. 337.

CC-0. In Public Domain. Gurukul Kangri Collection, Haridwar

Digitized by Arya Samaj Foundation Chennai and eGangotri

REVIEWS OF MODERN PHYSICS VOLUME 25, NUMBER 1 JANUARY, 1953

On the Theory of the Ising Model of Ferromagnetism*

GORDON F. NEWELL AND ELLIOTT W. MONTROLL

Institute for Fluid Dynamics and Applied Mathematics, University of Maryland, College Park, Maryland

IN the Ising model of ferromagnetism a scalar "spin" variable, σ, is associated with each lattice point. The possible values of σ are chosen to be ± 1, and the interaction between the jth and kth lattice points is postulated to be

$$E_{jk}=\begin{cases}-J\sigma_j\sigma_k & \text{if } j \text{ and } k \text{ are nearest neighbors,}\\ 0 & \text{otherwise.}\end{cases}$$

A magnetic moment μ is assigned to each spin so that the interaction energy of the jth particle with an external field H is chosen to be

$$E_j=-\mu H\sigma_j.$$

Although the Ising model lacks several important characteristics of a real ferromagnet, it is of considerable interest because it is one of the simplest examples of a system of interacting particles which still has some features of physical reality left in it. Also, it is equivalent to a very good model of a binary substitutional alloy and an interesting model of a gas or liquid.

The partition function of the Ising model can be expressed conveniently in terms of either of the following two quantities

(a) the largest characteristic value of a matrix whose elements $P(\Sigma, \Sigma')$ are

$$\exp-\{V(\Sigma)+V(\Sigma, \Sigma')\}/kT=P(\Sigma, \Sigma'),$$

where Σ and Σ' represent spin configurations on two adjacent layers of a crystal (or two adjacent rows in a two dimensional lattice), $V(\Sigma)$ is the potential energy of interaction between nearest neighbors on a layer in the Σth configuration, and $V(\Sigma, \Sigma')$ is the potential energy of interaction between spins in neighboring layers.

(b) The number of ways a closed path of a given length can be constructed on a lattice of interest.

Both of these formulations of the partition function have been successfully applied in the investigation of two-dimensional lattices. The first was used by Onsager in his derivation of the thermodynamic properties of a square lattice, and the second has been examined recently by Kac and Ward. Both formulations are discussed in our review.

The specific heat of a two-dimensional Ising model has a logarithmic infinity at the temperature at which long range order disappears. The spontaneous magnetization, which has been calculated exactly by Yang, drops very rapidly to zero at the Curie point. To date no one has found exact expressions for thermodynamic and magnetic properties of the two-dimensional Ising model in the presence of an external magnetic field, or in a lattice in which interactions between next nearest neighbors contribute to the interaction energy. The effect of lattice vibrations on spin interactions has not been determined.

No exact formulas for the partition function of a three-dimensional Ising model have been discovered. However, a rather large number of terms have been calculated in series expansions which are valid at very high or very low temperatures. These are discussed in the review.

* This is an abstract of an extensive review (with the same title) of recent developments in the theory of the Ising model of ferromagnetism. Because of its length, the publication of the full text will be postponed until the next issue of the *Reviews of Modern Physics*.

DISCUSSION

W. OPECHOWSKI, *University of British Columbia, Vancouver, Canada:* All calculations on the two-dimensional Ising crystal involve the assumption that $N\to\infty$ (N is the number of atoms composing the crystal). The results so obtained will, in general, give an excellent approximation to the actual physical situation, for which N is very large but necessarily finite. However, it may not be so for a range of temperatures that includes the Curie point. The range would certainly be very narrow, but perhaps not so narrow as one might think at first sight. The reason for these doubts is as follows. In the one-dimensional case rigorous formulas can be obtained easily for any finite N. The Curie point is, in this case, of course identical with the absolute zero. It turns out that, for the susceptibility *vs* temperature curve, deviations of the kind mentioned above occur for temperatures T for which $T<J/k\log N$, where J is the interaction constant (note the logarithmic dependence on N).[1]

[1] For more details, see Opechowski and Bryan, Can. J. Phys. **29**, 236 (1951).

CC-0. In Public Domain. Gurukul Kangri Collection, Haridwar

Digitized by Arya Samaj Foundation Chennai and eGangotri

G. H. WANNIER, *Bell Telephone Laboratories, Murray Hill, New Jersey:* The formulas found in the literature, to which Dr. Opechowski objects, I believe represent the correct answer, because the range of the alternative formula which he proposes gets probably smaller and smaller as the number of particles is increased. However, it should be possible to investigate this point explicitly because the results for finite N are published as sums, and the assumption of infinite N makes integrals out of them. Opechowski's problem arises therefore in this passage to the limit.

M. LAX, *Syracuse University, Syracuse, New York:* For the study of the statistical mechanics of a magnetic system, the scalar Ising model discussed by Dr. Montroll can be improved upon by using instead a lattice of dipole vectors, i.e., the Heisenberg model. The partition function in the vector case has been evaluated in the spherical approximation,[1] as a generalization of the Berlin-Kac treatment of the scalar case.

An improvement of the spherical model in either the scalar or vector cases can be made by treating exactly one atom or cluster of atoms. For the case of a single atom, this leads to an expression for the molecular field acting on that atom. The molecular field has the usual form of the external field plus a term linear in the magnetization: H_0+WM. The molecular field constant W of the Weiss-Van Vleck theory is independent of temperature. Our constant W varies slowly with temperature above the Curie temperature T_c. The effect of this variation is to make the "paramagnetic temperature" of the high temperature susceptibility larger than the actual transition temperature T_c.

The Curie temperature for a simple cubic lattice with exchange constant J is found in dimensionless units kTc/J to be given by 1.98. The corresponding result by the Bethe-Peierls-Weiss method is 1.85. The most reliable Zehler-Opechowski result is 1.93. The seemingly high accuracy of the spherical model at this stage of approximation is probably fortuitous.

For the case of a negative exchange integral, antiferromagnetic order occurs, and the molecular field is found to contain a part that changes sign from one sublattice to another. Results similar to those of Van Vleck (1941) are obtained.

As usual in the spherical approximation, phase transitions are found to occur in three dimensions but not in one or two. The method discussed here can be applied to a variety of crystal structures, spins, and types of interaction; e.g., it can be used to handle long range dipole-dipole coupling that may be important in some of the paramagnetic salts.

Improvements in accuracy can be obtained by treating exactly a cluster of atoms, i.e., by combining the spherical and Bethe-Peierls-Weiss techniques. Results will be reported in detail elsewhere.

[1] Melvin Lax, J. Chem. Phys. 20, 1351 (1952).

CC-0. In Public Domain. Gurukul Kangri Collection, Haridwar

Digitized by Arya Samaj Foundation Chennai and eGangotri

REVIEWS OF MODERN PHYSICS VOLUME 25, NUMBER 1 JANUARY, 1953

Anomalous Paramagnetism of Copper Acetate*

B. BLEANEY

Clarendon Laboratory, Oxford, England

THE paramagnetic behavior of most salts of divalent copper is relatively simple. The free copper ion is in a ^2D state, but in the solid the orbital angular momentum is largely quenched, and the ion is effectively in an ^2S state. Residual coupling to the orbit causes the spectroscopic splitting factor g to be anisotropic, with values ranging from about 2.05 to 2.4, but the susceptibility follows Curie's law rather accurately. Thus for Tutton salts of copper (ionic volume about 200 cc), deviations from Curie's law become appreciable only well below 1°K. In the less dilute salt, $CuCl_2\ 2H_2O$, whose ionic volume is 70 cc, antiferromagnetism sets in only below 4.3°K, according to the work of Gorter and his colleagues at Leiden.

The ionic volume of copper acetate monohydrate, $Cu(CH_3COO)_2\ H_2O$, is 106 cc, and one would not therefore expect any serious deviations from Curie's law above helium temperatures. Guha,[1] however, found that the susceptibility of this salt passes through a maximum at about room temperature, and then decreases so rapidly that it would apparently fall to zero at about 50°K. No sharp transition is observed, which suggests that if this is due to a cooperative phenomenon, only a few atoms are involved.

On investigating the paramagnetic resonance spectrum (mostly at 90°K) of single crystals of copper acetate, it was observed immediately that the spectrum was quite different from that of normal copper salts. At 3-cm wavelength a line was observed in zero magnetic field, which is quite incompatible with a spin $\frac{1}{2}$. At 300°K, the lines were stronger and broader, but at 20°K they vanished. This intensity variation is, of course, related to that of the susceptibility. At shorter wavelengths the spectrum showed a triplet structure, which was very similar to that of the nickel Tutton salts (Griffiths and Owen[2]) where the divalent nickel ion has spin 1.

The hypothesis which we have put forward to explain these anomalies is as follows: Isolated pairs of copper ions are coupled together strongly by exchange forces. The two electron spins then interact to form a triplet state, in which the spins are parallel, and a singlet state with the spins antiparallel. The former would be paramagnetic and would give a spectrum corresponding to $S=1$, while the latter is diamagnetic, with $S=0$. If the former lies higher in energy by about 450°K, the drop in the susceptibility at low temperatures can be accounted for by the ions (or rather pairs of ions) draining out of the paramagnetic state into the diamagnetic state. The vanishing of the spectrum at 20°K follows, since only the diamagnetic level is occupied at this temperature.

Copper acetate grows in monoclinic prismatic form, but the detailed crystallographic arrangement has not yet been established by x-ray methods. The paramagnetic resonance spectrum corresponds to there being two paramagnetic units in the crystal cell, one derived from the other by a reflection in the crystallographic ac plane. The spectrum of each pair can be fitted to the spin Hamiltonian

$$\mathcal{H}_1=D\{S_z^2-\tfrac{1}{3}S(S+1)\}+E(S_x^2-S_y^2)+\beta[g_zS_zH_z+g_xS_xH_x+g_yS_yH_y] \quad (1)$$

with $S=1$. The values of the constants are found to be as follows:

$$|D|=0.34\pm0.03\ \text{cm}^{-1}, \qquad g_z=g_{\parallel}=2.42\pm0.03,$$
$$E=0.01\pm0.005\ \text{cm}^{-1}, \quad g_x=g_y=g_{\perp}=2.08\pm0.03.$$

Apart from the small term in E, the Hamiltonian reflects axial symmetry, with the axis of the splitting term D being the same as that of the g values. The latter are very close to those found in many other copper salts.

To explain these results, we have assumed a Hamiltonian in which two copper ions with the usual types of crystal field are coupled together by an exchange term. We have then

$$\mathcal{H}_2=X_1+X_2-J\mathbf{S}_1\cdot\mathbf{S}_2+\lambda[\mathbf{L}_1\cdot\mathbf{S}_1+\mathbf{L}_2\cdot\mathbf{S}_2]+\beta\mathbf{H}\cdot[(\mathbf{L}_1+2\mathbf{S}_1)+(\mathbf{L}_2+2\mathbf{S}_2)]+N_1+N_2. \quad (2)$$

Here subscripts 1,2 refer to the two ions. X is the crystal field, of predominantly cubic symmetry, with a component of axial symmetry; the axes of the crystal fields are assumed to be identical for the two ions. J is the exchange integral, λ the spin-orbit coupling coefficient, and N the interaction with the nucleus of the copper ion.

When this Hamiltonian is evaluated as far as terms of the order $(\lambda/\Delta)^2$, (J/Δ) in the energy (when Δ is the crystal field splitting of the orbital levels), it is found that it gives a singlet state which has only a quadratic Zeeman effect, together with a triplet state which lies higher in energy by $-J$. The quadratic Zeeman effect gives rise to a small temperature-independent susceptibility. The behavior of the triplet state in a magnetic field is equivalent to that given by the spin Hamiltonian

* The following is a résumé of work by B. Bleaney and K. D. Bowers, which has been briefly reported in Phil. Mag. 43, 372 (1952), and of which a full account will appear shortly in the *Proceedings of The Royal Society*.

[1] B. C. Guha, Proc. Roy. Soc. (London) A206, 353 (1951).

[2] J. H. E. Griffiths and J. Owen, Proc. Roy. Soc. (London) A213, 459 (1952).

CC-0. In Public Domain. Gurukul Kangri Collection, Haridwar

Digitized by Arya Samaj Foundation Chennai and eGangotri

(1) with

$$D=-\tfrac{1}{8}J\{\tfrac{1}{4}(g_{\parallel}-2)^2-(g_{\perp}-2)^2\}, \qquad (3)$$

and expressions for the g values which are similar to those for ordinary copper salts, involving λ and Δ. Thus the splitting of the triplet state due to the term in D arises from the combination of the exchange coupling and the crystal field interaction.

The susceptibility may readily be evaluated, and by choosing a value of about 450°K=315 cm^{-1} for $(-J)$, a reasonable fit with the experimental results of Guha is obtained. The calculated values lie a little too high at the low temperature end, but this could be corrected if J is assumed to vary slightly with temperature. This may well be the case, since the overlap of the wave functions which determines J varies rapidly with the inter-ionic distance, which may change slightly with temperature owing to thermal expansion. A reduction in J of 20 percent at 90°K would fit both the susceptibility measurements and the variation in intensity of the spectrum between 60°K and 90°K, which gives $-J=370\pm50$°K. The sign of J corresponds to antiferromagnetism.

The hypothesis of two interacting ions receives further support from the peculiar hyperfine structure. This shows seven equally spaced lines, with intensities in the ratios 1:2:3:4:3:2:1. This would be expected from the known nuclear spin $\frac{3}{2}$ for copper, since two ions would then give seven components shifted by $A(m_1+m_2)$ from the center, where A is the hfs coupling coefficient, and m_1 and m_2 the nuclear magnetic quantum numbers. The various ways in which these can combine to give a particular value of the sum accounts for the intensity ratios. A is anisotropic and varies from about 0.008 cm^{-1} parallel to the z axis, to less than 0.001 cm^{-1} perpendicular to this axis. These values are roughly the same as those observed for the copper Tutton salts.[3]

Insertion of the values of J, $g_{\parallel}$, and $g_{\perp}$ into (3) gives a value for D of 1.1 ± 0.4 cm^{-1}. This is rather larger than that observed experimentally, but the discrepancy is probably due to the assumption that J is the same for all the orbital levels. The value of J which has been deduced from the susceptibility measurements is that for the ground orbital level, but in fact in (3) the values of J involved are those for two excited orbital levels. We may conclude from the results that J is probably not greatly different for these levels from that found for the ground state.

Finally, we should add that preliminary x-ray analysis of the crystal structure by Dr. Davies at Oxford supports our hypothesis of isolated pairs of copper ions. Though the analysis is not complete, it seems likely that the distance between the two ions of a pair is about 2.5A and the line joining them is parallel to the z axis of our measurements. With this small distance there will also be a magnetic dipole interaction between the ions which gives a splitting of about 0.2 cm^{-1}, and its sign is such that it would reduce the value of D found from (3).

[3] Bleaney, Bowers, and Ingram, Proc. Phys. Soc. (London) **A64**, 758 (1951).

CC-0. In Public Domain. Gurukul Kangri Collection, Haridwar

Digitized by Arya Samaj Foundation Chennai and eGangotri

REVIEWS OF MODERN PHYSICS VOLUME 25, NUMBER 1 JANUARY, 1953

Some Magnetization Studies of Cr^{+++}, Fe^{+++}, Gd^{+++}, and Cu^{++} at Low Temperatures and in Strong Magnetic Fields

WARREN E. HENRY

Naval Research Laboratory, Washington, D. C.

WE have undertaken a study of magnetic properties of paramagnetic coolants at well-known temperatures in as low a range as possible. First, we studied moderately "well-behaved" paramagnetic substances in the liquid helium range. As is shown in Fig. 1, these substances, containing Cr^{+++} ($^4F_{3/2}$ state for the free ion, but quenched to a free spin system by the crystalline electric field), Fe^{+++} ($^6S_{5/2}$ state for free ion), and Gd^{+++} ($^8S_{7/2}$ state for the free ion), all follow free spin Brillouin functions (except for almost negligible deviations) up to over 99.5 percent saturation[1] for 50 000 gauss and 1.30°K.

In order to extend our knowledge of the possible causes and consequences of small departures which may become important in some paramagnetic coolants at extremely low temperatures, we carried out similar magnetization experiments on copper sulfate pentahydrate[2] in which the departure from a Brillouin function was very pronounced in the helium range. That is, a plot of magnetic moment against H/T gives magnetic isotherms which do not superimpose. In Fig. 2 we note that this dispersion is in qualitative agreement with calculated moment isentropes of Geballe[3] since isothermal and adiabatic moments should approach each other in the limit of zero field. It has been suggested by Geballe that this anomalous behavior may be associated with antiferromagnetism.[4] Since it is inconvenient to work under the Néel (antiferromagnetic) temperature for $CuSO_4 \cdot 5H_2O$ which is considerably under 1°K, we have also started a study of $CuCl_2 \cdot 2H_2O$ for sub-Néel magnetization studies as its Néel temperature[5] is ~4.3°K. We used the same technique for copper chloride dihydrate as for the other salts. This consisted in moving a spherical sample (a powder in this case) from the center of one coil to the center of a duplicate, oppositely wound coil. The deflection of a ballistic galvanometer in series with the coil system was proportional to the moment of the sample. The experimental results which we obtained indicated constant moments for fixed fields in the sub-Néel range studied as is indicated by sample values in Fig. 3 and symbolized by

$$(\partial M(H)/\partial T)_H = 0 \qquad (1)$$

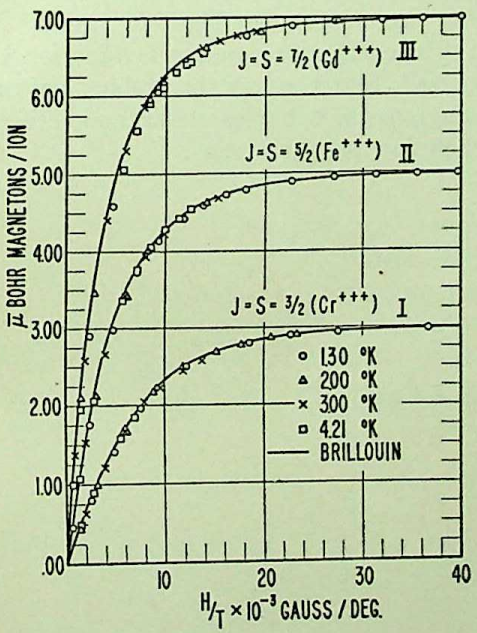


FIG. 1. Plot of magnetic moment *vs* H/T for (I) potassium chromium alum, (II) ferric ammonium alum, and (III) gadolinium sulphate octahydrate.

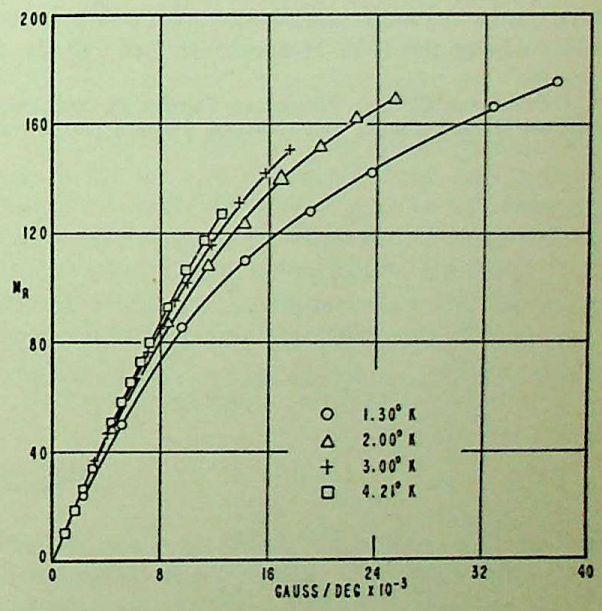


FIG. 2. Plot of relative moment *vs* H/T for copper sulfate pentahydrate.

[1] W. E. Henry, Phys. Rev. 85, 487 (1952); Phys. Rev. 88, 559 (1952).
[2] W. E. Henry, Phys. Rev. 87, 1133 (1952).
[3] T. H. Geballe and W. Giauque, J. Am. Chem. Soc. 74, 3513 (1952).
[4] L. Néel, Ann. Physik X 18, 5 (1932); XI 5, 232 (1936); J. H. Van Vleck, J. Chem. Phys. 9, 85 (1941).
[5] C. J. Gorter and J. Haantjes, Physica 18, 285 (1952).

CC-0. In Public Domain. Gurukul Kangri Collection, Haridwar

Digitized by Arya Samaj Foundation Chennai and eGangotri

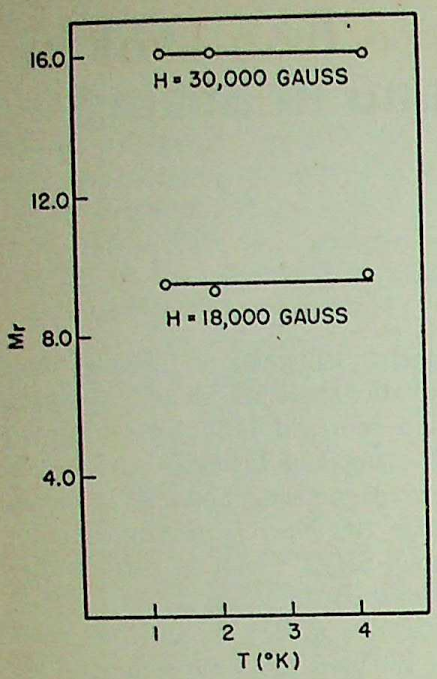


FIG. 3. Plot of relative moment *vs* T for two values of magnetic field for copper chloride dihydrate.

in the moderately high field range at liquid helium temperatures. Our experimental results may be compared qualitatively with announced[6] results of van den Handel, Poulis, and Gijsman[7] in the moderately high field range. According to our results, if one now plots M against H/T (see Fig. 4) as was done for the very closely paramagnetic salts, one obtains, for a given H/T, a moment which decreases linearly with temperature. If the assumption is made that the transition from paramagnetic to antiferromagnetic behavior is not necessarily abrupt, but perhaps gradual for some structures, then for these structures one may expect a departure from a Brillouin function even for a sample considerably above the Néel temperature (see Fig. 2). In

[6] N. J. Poulis and G. E. G. Hardeman, Physica **18**, 201 (1952).
[7] van den Handel, Poulis, and Gijsman, Physica (to be published).

the linear range (no saturation effects), the magnetic moment may be represented by

$$M = F(T)H, \tag{2}$$

where $F(T)$ goes from a T^{-1} dependence in the paramagnetic case to a constant in the antiferromagnetic case. $F(T)$ depends, at least in part, on the distance

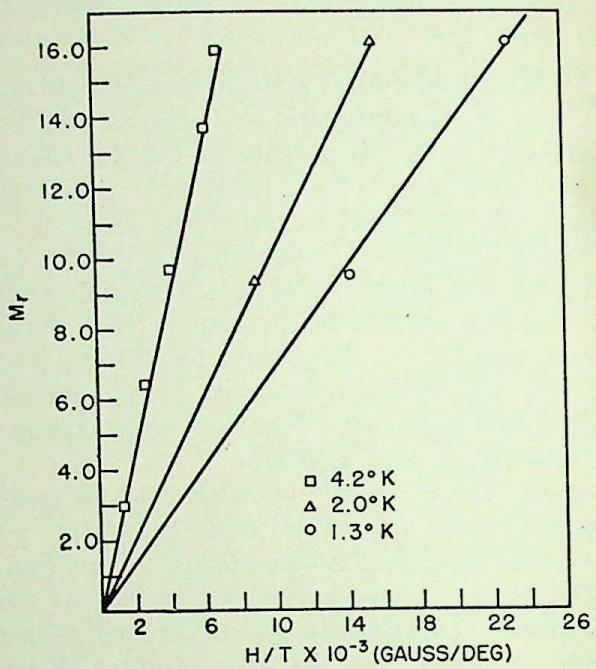


FIG. 4. Plot of relative moment *vs* H/T for copper chloride dihydrate.

above the Néel temperature and the strength of the forces contributing to the manifestations of antiferromagnetism, as was shown by Van Vleck.[4] Further study on this dependence would be helpful, for, knowing $F(T)$, one could better attack the problems of magnetic and thermodynamic behavior of paramagnetic coolants at extremely low temperatures.

CC-0. In Public Domain. Gurukul Kangri Collection, Haridwar

Digitized by Arya Samaj Foundation Chennai and eGangotri

Exchange Coupling Between Three Iron Ions in Two Organic Molecules

J. YVON, J. HOROWITZ, AND A. ABRAGAM

Laboratoire de Chatillon, Seine, France

FOEX, Tsai, and Wucher[1] have studied the variation of susceptibility with temperature of two organic molecules:

$[Fe_3(CH_3COO)_6(OH)_2]NO_3+6H^2O$ acetate,

$[Fe_3(C_6H_5COO)_6(OH)]\times(C_6H^5COO)(ClO^4)+H^2O$ benzoate,

between the temperatures of 2°K and 293°K. Between 73°K and 293°K the two complexes follow Weiss law with

acetate $\mu_B=5.19$ per atom $\theta=-443°$,
benzoate $\mu_B=5.5$ per atom $\theta=-572°$.

Below 20° they follow another Weiss law:

acetate $\mu_B=1.2$ per molecule $\theta=-2°$,
benzoate $\mu_B=1.26$ per molecule $\theta=-6.°5$.

As suggested by Foex *et al.*, the three spins of the ferric ions must be coupled in such a way as to give a smaller magnetic moment at low temperatures.

The experimental value of χ at high temperatures demand $S=5/2$ for each ion, in accordance with the electronic structure of Fe^{+++}.

The simplest possible interaction between the 3 spins is

$$\mathcal{H}=J(\mathbf{s}_1\cdot\mathbf{s}_2+\mathbf{s}_2\cdot\mathbf{s}_3+\mathbf{s}_3\cdot\mathbf{s}_1)=\tfrac{1}{2}JS(S+1)+\text{const},$$

where S is the total spin. S can take all values between 1/2 and 15/2. Each value, except 15/2, can be obtained in several ways (2 for the ground state $S=\frac{1}{2}$).

The theoretical curve $1/\chi$ against T, obtained with this hypothesis is not unlike the experimental one, except for an important bump which does not actually occur. In order to improve the model, we assume that the interaction between two of the ionic spins $\mathbf{s}_2$ and $\mathbf{s}_3$ is different from the other interactions. The Hamiltonian can be written:

$$\mathcal{H}=J(\mathbf{s}_1\cdot\mathbf{s}_2+\mathbf{s}_1\cdot\mathbf{s}_3)+J(1+\tfrac{1}{2}m)\mathbf{s}_2\cdot\mathbf{s}_3,$$

where m is a parameter

$$\mathcal{H}=\tfrac{1}{2}JS(S+1)+\tfrac{1}{4}mJS'(S'+1),$$

and S' is the resulting spin of $\mathbf{s}_2$ and $\mathbf{s}_3$. The additional interaction $\frac{1}{4}mJS'(S'+1)$ lifts all the degeneracies except those due to orientation. Reduced curves $(1/\chi)/J=f(kT/J)$ can be plotted for different values of m. Some of these curves (particularly $m=0,5$) have shapes similar to those of the experimental curves.

To obtain agreement between the experimental and theoretical curves, a value of J/k of the order of magnitude 60, is required. There remains, however, a serious discrepancy at very low temperatures. The existence of a small negative Curie temperature could be explained by assuming a negative intermolecular field.

However, the slope of the low temperature part of the curve, which corresponds to $\mu_B=1.2$ or 1.26, instead of $\mu_B=1$ as demanded by the hypothesis $S=\frac{1}{2}$ for the ground state, is not understood.

It has been thought preferable to wait for more experimental evidence (in particular in replacing of the ferric ions by other ions), before trying a more complicated model.

Note added in proof.—After this work was completed we learned that Dr. Kenjiro Kambe[2] had already proposed this model in 1949 to explain the susceptibility measurements made by Welo[3] in 1928. Welo's measurements did not extend below 200°K, which led Kambe to assume that equal interactions between the three ions gave satisfactory agreement with experiment.

[1] Foex, Tsai, and Wucher, Compt. rend. 233, 1432 (1951).

[2] Kenjiro Kambe, J. Phys. Soc. of Japan, 5, 48 (1950).

[3] L. A. Welo, Phil. Mag. 6, 481 (1928).

DISCUSSION

C. J. GORTER, *University of Leiden, The Netherlands:* Dr. J. van den Handel has found susceptibility curves for a substance containing organic radicals which are somewhat similar to those mentioned by the preceding speakers (papers of B. Bleaney, and of Yvon, Horowitz, and Abragam).

It seems to be quite frequent that negative exchange interaction does not lead to antiferromagnetism but to saturation within small groups of ions.

CC-0. In Public Domain. Gurukul Kangri Collection, Haridwar

Digitized by Arya Samaj Foundation Chennai and eGangotri

REVIEWS OF MODERN PHYSICS VOLUME 25, NUMBER 1 JANUARY, 1953

A Note on Exchange Interactions

K. W. H. STEVENS

Clarendon Laboratory, Oxford, England

THE purpose of this note is to give a brief account of some theoretical work which was done some time ago and which has a bearing on the resonance phenomena in copper acetate.

The problem considered was that of investigating the exchange interactions between two paramagnetic ions in a crystal field and allowing for the spin-orbit couplings. Two approaches can be used. First it can be assumed that the exchange interactions between the ions are large compared with spin-orbit forces within the ions. This is the method used by Bleaney and Bowers,[1] except that they do not use the Coulomb interaction as the coupling between the ions but replace it by an interaction $J\mathbf{S}_1\cdot\mathbf{S}_2$. This is not strictly correct, but it has the advantage that their theory contains only one unknown, J, apart from the g values. The other approach is to assume that the exchange forces are small compared with the spin-orbit forces and use as unperturbed wave functions the states of the copper ion in its crystal field. We shall give a short account of the results of this in a form suitable for certain other problems as well (e.g., the ceric ion).

Neglecting the interactions the wave functions are

$$A\begin{cases} f^{+}+g^{-} \\ f^{-*}-g^{+*} \end{cases} \qquad B\begin{cases} p^{+}+q^{-} \\ p^{-*}-q^{+*}, \end{cases}$$

where f and g denote orbital wave functions centered on nucleus A, and p and q denote orbital wave functions centered on nucleus B. The above states are the most general possible for a single electron system. The Hamiltonian is written as a 4×4 matrix and expressed in terms of Pauli spin matrices along the lines of the usual spin-Hamiltonian formulation. The result is that the interaction becomes

$$\begin{aligned} u=&\tfrac{1}{2}(A+B)1+\tfrac{1}{2}(A-B)\sigma_z^1\sigma_z^2+\tfrac{1}{4}(E+\bar{E}+F+\bar{F})\sigma_x^1\sigma_x^2 \\ &-\tfrac{1}{4}i(F+\bar{F}-E-\bar{E})\sigma_y^1\sigma_y^2-\tfrac{1}{4}i(E-\bar{E}-F+\bar{F})\sigma_x^1\sigma_y^2 \\ &-\tfrac{1}{4}i(E-\bar{E}+F-\bar{F})\sigma_x^2\sigma_y^1+\tfrac{1}{2}(C+\bar{C})\sigma_z^1\sigma_x^2 \\ &-\tfrac{1}{2}i(C-\bar{C})\sigma_z^1\sigma_y^2 \\ &+\tfrac{1}{2}(D+\bar{D})\sigma_z^2\sigma_x^1-\tfrac{1}{2}i(D-\bar{D})\sigma_z^2\sigma_y^1, \end{aligned}$$

where

$$A=-2\int u_1 V u_2^* d\tau, \quad B=-2\int v_1^* V v_2 d\tau,$$

$$C=2\int v_1^* V u_2^* d\tau, \qquad D=-2\int u_1 V v_2^* d\tau,$$

$$E=2\int v_1^* V v_2 d\tau, \qquad F=-2\int u_1 V u_2 d\tau,$$

where $u_1=(f^*p+g^*q)$ for electron 1,
$u_2=(f^*p+g^*q)$ for electron 2,
$v_1=(fq-gp)$ for electron 1,
$v_2=(fq-gp)$ for electron 2,

and V is the Hamiltonian of the combined system.

The wave functions for copper have been given by Polder,[2] so that

$$f=\frac{\phi_2+\phi_{-2}}{\sqrt{2}}-\frac{\lambda}{F_4-F_3}\frac{\phi_2-\phi_{-2}}{\sqrt{2}},$$

$$g=\frac{-\lambda}{F_5-F_3}\frac{\phi_{-1}}{\sqrt{2}},$$

and p and q are similar but with possibly a different direction for the axis of quantization. It does not seem possible to evaluate the coefficients A, B, etc., without prohibitive labor and the only thing to do is to consider their orders of magnitude. Thus

$$\begin{aligned} &A\sim F, \\ &C,D\sim(\lambda/\Delta)A, \\ &B,E\sim(\lambda/\Delta)^2A, \end{aligned}$$

assuming that the exchange integrals for different orbital states are of the same orders of magnitude. By using these relative magnitudes in the interaction Hamiltonian, one finds that it approximates very closely to that used by Bleaney and Bowers.

It may be noted, in conclusion, that in ions like cerium where there is a strong spin-orbit coupling, similar arguments suggest that exchange interactions may be considerably anisotropic.

[1] B. Bleaney and K. D. Bowers, Phil. Mag. 43, 372 (1952).

[2] D. Polder, Physica 9, 709 (1942).

CC-0. In Public Domain. Gurukul Kangri Collection, Haridwar

Digitized by Arya Samaj Foundation Chennai and eGangotri

REVIEWS OF MODERN PHYSICS VOLUME 25, NUMBER 1 JANUARY, 1953

Crystal Field Theory in the Rare Earths

R. J. ELLIOTT

Clarendon Laboratory, Oxford, England

The paramagnetic properties (in particular the resonance data) of the rare earth ethyl sulfates are considered in the light of a theory in which each ion is assumed to be in a static electric field of C_{3h} symmetry. It is found that this is consistent with the observations in cerium ethyl sulfate, and it is possible to solve that problem to find the magnitude of the interaction of this field with an ion. It is then shown that similar fields give good agreement with the observations in other salts.

THIS work on the theoretical interpretation of the paramagnetic properties of some rare earth salts has been done in association with Dr. K. W. H. Stevens and will be published elsewhere in a more complete form.[1] It has been stimulated by recent measurements on these salts by Bleaney and others[2,3] using resonance methods, which have added important new information to the older measurements of susceptibility, Faraday effect, and absorption spectra. It is found that it is now possible to treat the problem more extensively and completely than was possible in the earlier work of Penney *et al.*[4] The basic approximation is essentially the same one as they used and has been used by other workers on the iron group salts (Abragam and Pryce,[5] Van Vleck,[6] etc.), namely, that the rare earth ions in the crystal are free except for the interaction between an ion and its surrounding lattice, which is replaced by a static electric field (the crystal field). The problem is then reduced to finding the eigenvalues of an ion in such a field. The energy of interaction of the field with the electron cloud is found to be smaller than the spin-orbit interaction (this is opposite to the state of affairs which holds in iron group salts). Thus, the field can be considered as causing a Stark splitting of the lowest energy level of the free ion. This level is given to a good approximation by Russel-Saunders coupling and the Hund rule, which means that it is characterized by values of L, S, and J, the orbital, spin, and total angular momenta. This was shown to be consistent with susceptibility measurements at room temperature by Van Vleck.[6]

The crystal field will have a certain symmetry related to the crystal structure. The work here reported has been carried out on the ethyl sulfates, where each ion has identical surroundings which have a threefold symmetry axis with a plane of reflexion symmetry perpendicular to this; i.e., C_{3h} symmetry (Ketelaar[7]). This is rather different from the predominantly cubic fields which usually hold in iron group salts; and it is not improbable that fields with a threefold axis occur in a number of rare earth salts. The interaction of the field and the electron cloud adds a term to the Hamiltonian which may be expanded in spherical harmonics. Only electrons not in closed shells give a nonzero contribution to this term, and since in this instance these are f electrons, only spherical harmonics of order not greater than 6 are required. Terms of odd order also give a zero contribution, so that the term has the form

$$V=\Sigma(A_2^0(3z^2-r^2)+A_4^0(35z^4-30z^2r^2+3r^4)+A_6^0(231z^6-315z^4r^2+105z^2r^4-5r^6)+A_6^6(x^6-15x^4y^2+15x^2y^4-y^6)), \quad (1)$$

where (x, y, z) are the coordinates of an electron and the summation is taken over all f electrons. The A_e^m are constants related to the complex of charges surrounding the ion, but they are difficult to determine from the crystal structure.

Most of the work has been carried out on those ions with an odd number of electrons. In this case by Kramers'[8] theorem all the energy levels must have an even degeneracy, and in fact, the above type of field always reduces these to doublets. (In ions with an even number of electrons the problem is complicated by Jahn-Teller[9] effects. The above theory does, however, provide a starting point for these calculations which will not be considered here.) It is in the lowest of these doublets that resonance transitions are observed when the doublet is resolved by applying a constant magnetic field H to give a Zeeman splitting. The resonance is often complicated by hyperfine structure caused by the magnetic and electric fields set up by the electron cloud, interacting with the magnetic and quadrupole moments of the nucleus. It is always found that the resonance pattern can be described by a "spin Hamilto-

[1] R. J. Elliott and K. W. H. Stevens, Proc. Roy. Soc. (London) (to be published).
[2] B. Bleaney and H. E. D. Scovil, Proc. Phys. Soc. (London) A63, 1369 (1950), ibid. A64, 204 (1951).
[3] G. S. Bogle and H. E. D. Scovil, Proc. Phys. Soc. (London) A65, 368, (1952).
[4] W. G. Penney and R. Schlapp, Phys. Rev. 41, 194 (1932); W. G. Penney and G. J. Kynch, Proc. Roy. Soc. (London) 170, 112(1939).
[5] A. Abragam and M. H. L. Pryce, Proc. Roy. Soc. (London) 205, 135 (1951); 206, 164, 173 (1951).
[6] J. H. Van Vleck, *The Theory of Electric and Magnetic Susceptibilities* (Oxford University Press, London, 1932).
[7] J. A. A. Ketelaar, Physica 4, 619 (1937).
[8] H. A. Kramers, Proc. Amsterdam Acad. Sci. 33, 959 (1930).
[9] H. O. Jahn and E. Teller, Proc. Roy. Soc. (London) 161, 220 (1937).

CC-0. In Public Domain. Gurukul Kangri Collection, Haridwar

Digitized by Arya Samaj Foundation Chennai and eGangotri

TABLE I. Comparison of experimental and theoretical results. Parameters and energies given are in cm^{-1}. For experimental results see references 2, 3, and 11.

Ion		$Ce^{+++}4f^2F_{5/2}$		$Nd^{+++}4f^3\,{}^4I_{9/2}$	$Sm^{+++}4f^5\,{}^6H_{5/2}$	$Er^{+++}4f^{11}\,{}^4I_{15/2}$
Energy		3	0	0	0	0
Experimental values	$g_\parallel$	0.955±.005	3.725±0.01	3.535±0.002	0.596±0.002	1.47±0.03
	$g_\perp$	2.185±.005	0.20 ±0.05	2.073±0.002	0.604±0.002	8.85±0.2
	A/B	—	—	1.92	0.24	0.166
First-order states		$\|\pm1/2\rangle$	$\|\pm5/2\rangle$	$\cos\theta\|\pm7/2\rangle+\sin\theta\|\pm5/2\rangle$ $\theta\simeq25°$	$\|\pm1/2\rangle$	$\cos\theta\|\pm7/2\rangle+\sin\theta\|\mp5/2\rangle$ $\theta=43°42'$
Parameters	$A_2^0\langle r^2\rangle_{Av}$	−15±10		−10	0	0
	$A_4^0\langle r^4\rangle_{Av}$	−40±12		−34	−36	−40
	$A_6^0\langle r^6\rangle_{Av}$	−92±2		−60	−54	−30
	$A_6^6\langle r^6\rangle_{Av}$	1150±30		660	590	330
Theoretical values	$g_\perp$	0.955	3.72	3.57	0.635	1.47
	$g_\parallel$	2.185	0.22	2.11	0.645	8.85
	A/B	—	—	1.94	0.24	0.166

nian" (Abragam and Pryce):[4]

$$\mathcal{H}=g_\parallel\beta H_zS_z+g_\perp\beta(H_xS_x+H_yS_y)+AS_zI_z +B(S_xI_x+S_yI_y)+P[I_z^2-\tfrac{1}{3}I(I+1)], \quad (2)$$

where S is a spin operator corresponding to a spin of $\frac{1}{2}$ and I is the angular momentum vector of the nuclear spin. The terms in g represent the Zeeman effect, those in A and B the nuclear magnetic effect, and P the nuclear quadrupole effect. The resonance data give these constants. It is the task of the theory to find a crystal field (since this must be of the form (1), from the crystal structure this involves finding the A_e^m) that will give a ground doublet which has $g_\parallel$, $g_\perp$ and A/B like the experimental values. The theory can then be used to find the nuclear magnetic and quadrupole moments from the magnitudes of A and P. The values of A_e^m chosen must of course also account for the positions and properties of the other doublets. These can in principle be found experimentally from susceptibility and spectral measurements, although there are often difficulties of interpretation.

As a first approximation the terms in (1) are considered to be sufficiently small to ensure that the lowest doublets arise entirely from the Hund level. The first three terms in (1) are of purely axial symmetry, so that these cause a splitting into doublets which have eigenstates $|\pm J_z\rangle$ where z is the symmetry axis. The fourth term of (1) admixes states in which J_z differs by 6, so that the doublets are in fact described by states of the form

$$a|L,S,J,\pm J_z\rangle+b|L,S,J,\pm(J_z-6)\rangle +c|L,S,J,\pm(J_z+6)\rangle. \quad (3)$$

The matrix elements of (1), and hence the separation of the doublets is found in terms of parameters $A_e^m\langle r^e\rangle_{Av}$ ($\langle r^e\rangle_{Av}$ is the average of r^e over the $4f$ wave functions) by using operator equivalents (Stevens[10]). Cerium ethyl sulfate is in some ways a simple example. The lowest level of a Ce^{+++} ion is $^2F_{\frac{5}{2}}$, and here the fourth term of (1) is zero and the doublets are simply characterized by $|\pm J_z\rangle$. Two doublets are observed in resonance (Bogle *et al.*[11]) with $g_\parallel=0.955\pm.005$, $g_\perp=2.185\pm0.005$ and $g_\parallel=3.72\pm0.01$, $g_\perp=0.20\pm0.05$, respectively. Doublets with $J_z=\frac{1}{2}$ and $\frac{5}{2}$ have theoretically $g_\parallel=0.86$, $g_\perp=2.57$, and $g_\parallel=4.29$, $g_\perp=0$. Although these values are near to the experimental ones, more refined calculations are clearly needed.

It can be deduced that one of the approximations has broken down by considering the results on an ion with a hyperfine structure in the light of the following theorem. Both the magnetic moment of the electron cloud and the magnetic field set up by the electrons at the nucleus are vector quantities. Within a manifold of constant angular momentum (i.e., where J is a good quantum number), these will transform in the same way, and in particular,

$$Ag_\perp/Bg_\parallel=1. \quad (4)$$

In the measurements of those ethyl sulfates that display a hyperfine structure this quantity has the following values: 1.12, in neodymium, 0.24 in samarium, and 1.0 in erbium. In the first two cases it is clear that J is no longer a good quantum number, and this can only have been destroyed by the crystal field terms (1) admixing states of other J levels into the lowest doublets. This is borne out by the fact that in samarium where the discrepancies are largest the first excited J multiplet is close (Van Vleck[6]), while in erbium where they are smallest the excited level is more distant and the terms of (1) smaller. These arguments are independent of any assumption of Russel-Saunders coupling. In fact, it is known from spectral work[12] that this assumption is also inadequate, but it can be shown that the correction to the magnetic properties is negligible. The calculation of the higher order perturbation effects involving the crystal field are straightforward

[10] K. W. H. Stevens, Proc. Phys. Soc. (London) A65, 209 (1952).

[11] Bogle, Cooke, and Whitley, Proc. Phys. Soc. (London) A64, 931 (1951).

[12] H. A. Bethe and F. H. Spedding, Phys. Rev. 52, 454 (1937); F. H. Spedding, Phys. Rev. 58, 253 (1940).

CC-0. In Public Domain. Gurukul Kangri Collection, Haridwar

Digitized by Arya Samaj Foundation Chennai and eGangotri

and have, in general, been done by perturbation methods; but the numerical work is very heavy, and no details will be given here. The matrix elements of (1) between the manifolds of different J are found to be related to the Wigner coefficients (Stevens[10]).

When detailed calculations are made, it is found that cerium ethyl sulfate proves to be a special case. Since Ce^{3+++} has only one electron outside closed shells the theory is fairly simple, and the problem of a cerium ion in the crystal field can be solved without using perturbation theory. It is assumed that the electron is in a $4f$ state, and the spin-orbit interaction and (1) are considered together. In cerium ethyl sulfate it was found necessary to add small terms of trigonal symmetry to (1) in order to obtain agreement with experiment. Such terms are not incompatible with the crystal structure, for it is possible that the internal structure of the waters and the ethyl groups may destroy the reflection symmetry. With this added term and using the accurate g values of the two levels observed in resonance, it is possible to work back and determine unique values of the parameters $A_e{}^m\langle r^e\rangle_{Av}$ for the dilute salt. Unfortunately, however, the $g_\perp{}^{(5/2)}=0.20\pm0.05$ is too inaccurate for this, so instead we assume the third doublet is situated 125 ± 25 cm^{-1} above the ground ones, which is compatible with susceptibiltiy measurements. The parameters so obtained are

$$A_2{}^0\langle r^2\rangle_{Av}=-15\pm10,\quad A_4{}^0\langle r^4\rangle_{Av}=-40\pm12,$$
$$A_6{}^0\langle r^6\rangle_{Av}=-92\pm2,\quad A_6{}^6\langle r^6\rangle_{Av}=1150\pm30 \text{(all in cm}^{-1}\text{)}.$$

These give, with a suitable trigonal term, $g_\perp{}^{(5/2)}=0.22$ which is within the experimental error. Slightly different values of the parameters also give agreement with the susceptibility and rotation measurements in the concentrated salt where the g values and level scheme are a little different. It is hoped that more information will become available to provide a more exact check.

It has not proved possible to determine the parameters uniquely in any of the other ethyl sulfates, because there is less information available and because susceptibilities are difficult to interpret. Instead an extrapolation of the above parameters has been used in a perturbation calculation. For example, in the Nd salt the extrapolated parameters give as lowest doublet

$$\cos\theta|{}^4I_{9/2},\quad J_z=\pm7/2\rangle+\sin\theta|{}^4I_{9/2},\quad J_z=\mp5/2\rangle,$$

where $\theta\simeq25°$ and $g_{11}=3.52$, $g_\perp=2.24$, which agrees quite well with the experimental $g_{11}=3.545$, $g_\perp=2.072$ (Bleaney and Scovil[2]). The agreement is improved by higher order calculations and slight adjustments of the parameters, and those giving best agreement with experiment are given in Table I. By use of these parameters the calculated susceptibility is found to be in good agreement with the experimental determination of Van den Handel and Hupse[13] (see Fig. 1).

Further along the series the information is scantier and sometimes contradictory. We have confined ourselves to choosing rather arbitrarily values of the parameters not unlike those of cerium which predict a lowest doublet with properties like those observed in resonance. The best values of the parameters and the theoretical results they give are compared with experiment in Table I.

It has been shown that a type of crystal field has been found which gives a good agreement with the experimentally observed results. It is then possible to use this theory to obtain values of the nuclear magnetic and quadrupole moments; these are given in Table II. The large errors arise almost entirely from an uncertainty in $\langle 1/r^3\rangle_{Av}$.

TABLE II. Nuclear data. μ_N is the nuclear magnetic moment in nuclear magnetons; Q is the nuclear quadrupole moment in units of $e\times10^{-24}$ cm^2; $\langle 1/r^3\rangle_{Av}$ is used throughout in A^{-3}. For experimental results see references 2 and 3.

Isotope	^{143}Nd	^{145}Nd	^{147}Sm	^{149}Sm	^{167}Er
$\lvert A\rvert$ $\times10^{-4}$ cm^{-1}	380.4	236.4	60	49	52
$\lvert B\rvert$ $\times10^{-4}$ cm^{-1}	198.9	123.7	251	205	314
$\lvert P\rvert$ $\times10^{-4}$ cm^{-1}	<1	<1	<4	<4	30
$\mu_N\lvert\langle 1/r^3\rangle_{Av}\rvert$	40.7	25.3	38.1	31.0	39.6
$\lvert Q\rvert\langle 1/r^3\rangle_{Av}$	<40	<40	<29	<29	795
$\langle 1/r^3\rangle_{Av}$	40±10	40±10	46±10	46±10	78±20
$\lvert\mu_N\rvert$	1.0±0.25	0.62±0.15	0.82±0.2	0.67±0.2	0.50±0.12
$\lvert Q\rvert$	<1	<1	<0.9	<0.9	10±3

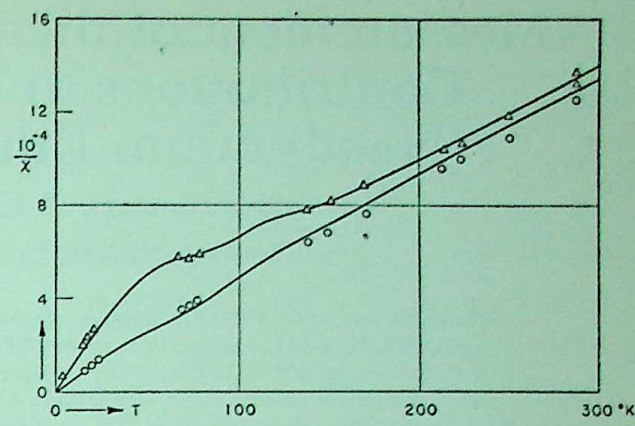


FIG. 1. The theoretical susceptibility of neodymium ethyl sulfate compared with experimental points. Upper curve, perpendicular to axis; lower curve parallel to axis (χ in emu/g).

[13] J. H. Van den Handel and J. C. Hupse, Physica 9, 225 (1942).

CC-0. In Public Domain. Gurukul Kangri Collection, Haridwar

Digitized by Arya Samaj Foundation Chennai and eGangotri

REVIEWS OF MODERN PHYSICS VOLUME 25, NUMBER 1 JANUARY, 1953

Measurement of the Nuclear and Electronic Contributions to the Specific Heat of Neodymium Ethyl Sulfate near 1°K

L. D. ROBERTS, C. C. SARTAIN,* AND B. BORIE

Oak Ridge National Laboratory, Oak Ridge, Tennessee

The molar specific heat C_I of neodymium ethyl sulfate has been measured on three samples of separated neodymium isotopes in the temperature range 0.95°K–2.15°K by the magnetic method of Benzie and Cooke at frequencies from 300 to 1200 cps. The measured C_I may be described within 1 percent by $C_I=b/T^2$, where T is the temperature and b is the constant. All three samples were shown by x-ray diffraction measurements to have the same structure as that given for neodymium ethyl sulfate by Ketelaar. For the electron contribution to the specific heat we obtained $b_e=0.146\pm0.004\times10^5$, and for the hyperfine splitting contributions we obtained $b_{143}=5.08\pm0.05\times10^5$ and $b_{145}=1.7\pm0.2\times10^5$ erg degree. These values of b_{143} and b_{145} agree within experimental error with the corresponding values computed from the microwave measurements of Scovil. Thus, the hyperfine splitting contribution to the specific heat for $Nd^{143}(C_2H_5SO_4)_3\cdot9H_2O$ is some 35 times larger than the electron contribution which makes this material of interest for the study of nuclear effects below 1°K.

INTRODUCTION

IT has been suggested by H. B. G. Casimir[1] and by C. J. Gorter[2] that the properties of magnetically dilute paramagnetic salts (excluding lattice effects) can be described in terms of a paramater b/C the ratio of the specific heat constant b to the Curie constant C. Here, b is given by the equation $C_I=b/T^2$, with C_I the molar specific heat at constant magnetization and T the absolute temperature.

In this paper, we show that $b=b_e+b_n$, where b_e is produced by the electron dipole-dipole and exchange interaction contribution to the specific heat, and b_n arises from the electron nuclear interaction. Because of this linear contribution of b_n to b, it is possible to measure b for several samples of different isotopic composition and separate the nuclear contribution. This new procedure differs from the dilution technique[3] of measuring the nuclear contribution to the specific heat in that extrapolation to infinite dilution is unnecessary and assumptions regarding the linearity of b_e as a function of dilution do not enter. Thus it is possible to measure a small b_e in the presence of a large b_n.

The parameter b/C has been measured for three samples of neodymium ethyl sulfate $Nd(C_2H_5SO_4)_3\cdot9H_2O$ in the temperature region near 1°K. Sample I was prepared from neodymium of normal isotopic composition, sample II was prepared from neodymium highly enriched in Nd^{142}, and in sample III the neodymium was highly enriched in Nd^{143}. When the measured values of b/C for each of the three samples were multiplied by the Curie constant C, the respective specific heat constants b were obtained. Collecting these values of b in three simultaneous equations, we have calculated the electron spin interaction contribution to the specific heat b_e/T^2 and the hyperfine splitting contribution to the specific heat b_n/T^2, for both Nd^{143} and Nd^{145}.

THEORY

Following Casimir[1], Gorter,[2] and Benzie and Cooke[4] we may obtain the specific heat from purely magnetic measurements. It is given by

$$C_I=\frac{CT}{(T-\theta)^3}\frac{\chi_s}{\chi_T-\chi_s}H^2, \qquad (1)$$

where θ is the Weiss constant, χ_T and χ_s are the isothermal and adiabatic differential magnetic susceptibilities, respectively, and H is an applied constant magnetic field. The above H is applied parallel to the relatively small alternating field used to measure the susceptibilities. At zero magnetic field, $\chi_T=\chi_s$; and when a field is applied, χ_T remains constant within a small saturation correction.[4] On the other hand, χ_s is, in general, a function of the magnetic field, the specific heat resulting from electron-spin interactions, the electron spin-lattice relaxation time, the specific heat of the lattice along with the sample surroundings, and their thermal conductivities.[5] When χ_s is measured at sufficiently high frequencies, relaxation time and thermal conductivity effects can be made negligible. In these experiments, the reactive component of the susceptibility χ_s' was shown experimentally to be independent of the frequency within approximately one percent in the range from 300 to 1200 cycles per second. This is taken as sufficient evidence that χ_s' varies with H, T, and C_I only, in this frequency range, and that the

* Summer research participant from the University of Alabama.

[1] H. B. G. Casimir, *Magnetism and Very Low Temperatures* (Cambridge University Press, Cambridge, 1940).

[2] C. J. Gorter, *Paramagnetic Relaxation* (Elsevier Publishing Company, Amsterdam, Netherlands, 1947).

[3] R. J. Benzie and A. H. Cooke, Nature 164, 837 (1949).

[4] R. J. Benzie and A. H. Cooke, Proc. Phys. Soc. (London) A63, 213 (1950).

[5] J. Eisenstein, Phys. Rev. 84, 548 (1951).

CC-0. In Public Domain. Gurukul Kangri Collection, Haridwar

Digitized by Arya Samaj Foundation Chennai and eGangotri

measured χ_s' is the χ_s of Eq. (1). Assuming that the specific heat from about 1°K to 2°K may be described by

$$C_I = b/T^2, \tag{2}$$

we find that Eq. (1) reduces to

$$\frac{b}{C} = \frac{T^3}{(T-\theta)^3} \frac{\chi_s}{\chi_T - \chi_s} H^2. \tag{3}$$

Equation (3) was used to calculate θ and b/C from our measured values of H, T, χ_s, and χ_T.

To demonstrate that $b = b_e + b_n$, we begin with the partition function z

$$z = Tre^{-\mathcal{H}/kT},$$

where $\mathcal{H}$ is the Hamiltonian describing the salt and k is the Boltzmann constant. The specific heat is then given by

$$C_I = T\frac{\partial S}{\partial T} = NkT\frac{\partial^2 T \ln z}{\partial T^2},$$

where N is Avogadro's number. Expanding z to second order in $Tr\mathcal{H}/kT$, we find

$$C_I = Nk \cdot \frac{1}{k^2T^2} \frac{Tr\mathcal{H}^2}{(2S+1)(2I+1)}. \tag{4}$$

Here S and I are the electron and nuclear spins.

The Hamiltonian for $Nd(C_2H_5SO_4)_3 \cdot 9H_2O$ at liquid He temperatures is

$$\mathcal{H} = AI_xS_x + B(I_yS_y + I_zS_z) + P(S). \tag{5}$$

The first two terms on the right are the contribution to the Hamiltonian produced by the asymmetrical hyperfine coupling as given by Bleaney and Scovil,[6] and the third term $P(S)$ corresponds to the electron dipole-dipole and exchange interactions as discussed by Van Vleck.[7]

Since $TrI = 0$, there are no cross terms, and $Tr\mathcal{H}^2$ reduces to

$$Tr\mathcal{H}^2 = Tr[AI_xS_x + B(I_yS_y + I_zS_z)]^2 + TrP^2(S). \tag{6}$$

TABLE I. Isotopic composition of the neodymium used to prepare the samples.

Isotope	Percent abundance Sample I	Sample II	Sample III
142	27.13	93.00	4.04
143	12.20	3.18	83.93
144	23.87	2.89	8.83
145	8.30	0.368	1.78
146	17.18	0.414	1.16
148	5.72	0.084	0.149
150	5.60	0.066	0.108

[6] B. Bleaney and H. E. D. Scovil, Proc. Phys. Soc. (London) A63, 1369 (1950).
[7] J. H. Van Vleck, J. Chem. Phys. 5, 320 (1937).

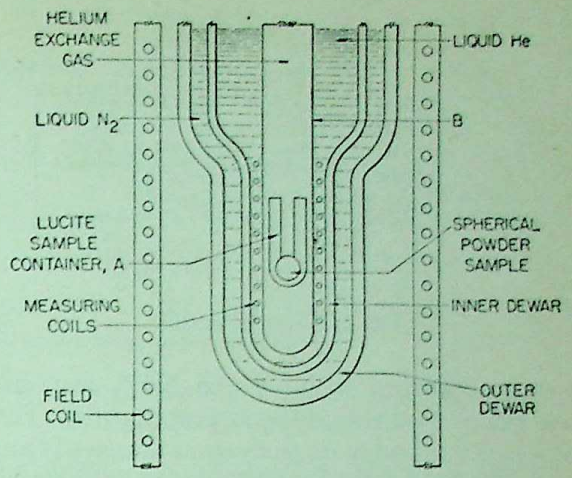


FIG. 1. Apparatus.

Thus, the specific heat is

$$C_I = \frac{b}{T^2} = \frac{(b_n + b_e)}{T^2}, \tag{7}$$

where

$$b_e = \frac{N}{k} \frac{TrP^2(S)}{(2S+1)(2I+1)}, \tag{8}$$

$$b_n = \frac{N}{k} \frac{Tr[AI_xS_x + B(I_yS_y + I_zS_z)]^2}{(2S+1)(2I+1)}. \tag{9}$$

The latter trace from Bleaney,[8] gives

$$b_n = [\tfrac{1}{9}](A^2 + 2B^2) \cdot S(S+1)I(I+1)Nk.$$

Thus, since there are no cross terms, the traces Eqs. (8) and (9) and, hence, b_e and b_n are independent of the isotopic composition of the paramagnetic salt. For a given isotopic composition of paramagnetic ions, one may write the equation

$$b = b_e + \sum_i F_i b_{ni}, \tag{10}$$

where F_i is the fraction of the ith paramagnetic isotope present and b_{ni} is the corresponding nuclear specific heat constant. By measuring b for a series of salts having different isotopic compositions, one may solve the corresponding set of simultaneous equations for b_e and for the b_{ni} of each isotope.

EXPERIMENTAL PROCEDURE

The normal neodymium ethyl sulfate, sample I, was prepared by D. E. LaValle of this laboratory from neodymium oxide which was spectrosocopically pure. The neodymium isotopic composition of this sample was assumed to be that given by J. Mattauch[9] and coworkers.

The neodymium ethyl sulfate samples II and III were prepared by R. H. Sampley of this laboratory using

[8] B. Bleaney, Phys. Rev. 78, 214 (1950).
[9] J. Mattauch and V. Hauk, Naturwiss. 25, 781 (1937).

CC-0. In Public Domain. Gurukul Kangri Collection, Haridwar

Digitized by Arya Samaj Foundation Chennai and eGangotri

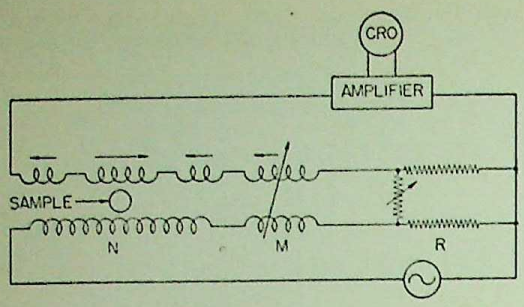


FIG. 2. Electrical circuit.

the oxides enriched in Nd^{142} and Nd^{143}, respectively. These oxides were also of spectroscopic purity. The isotope separation and mass analyses of samples II and III were performed by the Stable Isotopes Division of this laboratory. Their results for the mass analyses are tabulated in Table I.

Each of the three samples of the salt was identified by x-ray diffraction methods. A single crystal (approximately 0.1 mm in diameter) was mounted by means of grease on a glass fiber. A Weissenberg goniometer was used to take a rotation photograph and zero and first-layer Weissenberg photographs. From these data the three samples were found to be identical and to be hexagonal, with $a=14.02$ A, $c=7.12$ A, and $c/a=0.5078$. This compares favorably with the optical measurements of Singh,[10] who reported $Nd(C_2H_5SO_4)_3\cdot 9H_2O$ to be hexagonal with $c/a=0.5075$, and with the x-ray measurements of Ketelaar,[11] who reported $a=13.992$, $c=7.07$, and $c/a=0.505$.

Each of the three samples was recrystallized three times. The last recrystallization in each case was performed immediately before the low temperature measurements were made.

Each sample contained approximately one gram of small crystals of the salt (about 0.1 mm^3 average size) which were compressed into a spherical Lucite container A (Fig. 1) of 12.7 mm internal diameter. The compression was to about 80 percent of the crystal density. Container A was inserted into a glass tube B. This tube was immersed in liquid helium which was in turn contained in a Dewar flask jacketed in liquid nitrogen. Thermal contact between the sample in A and the liquid helium which surrounded tube B was maintained by helium gas at a pressure of about 50 microns Hg.

The susceptibilities χ_s and χ_T of the sample salt were measured by a compensated mutual-inductance (Hartshorn) bridge as described by de Klerk.[12] The electrical circuit is shown schematically in Fig. 2. The sample was placed in a mutual inductance N (Fig. 2) in the cryostat. Its susceptibility in arbitrary units was given in terms of the setting of the variable mutual inductance M required to balance the contribution of the sample to the mutual inductance. The loss component of the susceptibility was balanced by the resistance net R.

The secondary winding of the mutual inductance N was divided into three sections. The central section of 2441 turns was opposed by two end sections of $1220\frac{1}{2}$ turns each. The sample was carefully positioned at the center of the middle section. The primary coil of N, of 298 turns per cm, produced an alternating field of approximately seven gauss at the sample.

To obtain the adiabatic susceptibility, a steady magnetic field ($0<H<1000$ gauss) was applied to the sample by an iron-free oil-cooled solenoid fed by storage batteries. The field current was measured by a standard shunt and a type K potentiometer. The field was calibrated by both the standard mutual inductance and the proton resonance methods with good agreement. The accuracy of every field measurement was to within $\frac{1}{2}$ percent.

Above 1.1°K the temperature of the sample was determined by measuring the vapor pressure over the surrounding liquid-helium bath and converting to temperature by the Royal Society Mond Laboratory Tables of June, 1949. This pressure was regulated by adjusting a suitable valve in the pumping line. Below 1.1°K the temperature was obtained from the sample susceptibility.

RESULTS

Measurements of the parameter b/C were made at 300, 600, 900, and 1200 cycles per sec at a number of temperatures (Table II), and the value listed for a given temperature is the average result for these four frequencies with an average deviation of less than 1 percent.

The value for the specific heat constant b for each of the three samples was obtained by multiplying the average value of b/C for the several temperatures by the Curie constant per mole. The latter constant $C=0.663$ for the powder sample was calculated both from microwave measurements by Scovil[13] and from the suscepti-

TABLE II. Measurements of b/C on three neodymium samples.

T (°K)	$b/C\times10^{-5}$ [a] Sample I	Sample II	Sample III
2.155			6.81
2.150		0.481	
2.145	1.363		
1.640		0.476	
1.630			6.62
1.450			6.64
1.390		0.466	
1.122	1.361		
1.121			6.70
1.103		0.477	
1.000	1.377		
0.970		0.472	
0.950			6.72
Average	1.367	0.474	6.70

Weiss $\theta=0.013\pm0.005$°K

[a] Average value for 300, 600, 900, and 1200 cps.

[10] Von Sohan Singh, Z. Krist. 105, 384 (1944).
[11] J. A. A. Ketelaar, Physica 4, 619 (1937).
[12] D. de Klerk, thesis, Leiden, 1948.
[13] H. E. D. Scovil, *Proceedings of the International Conference on Low Temperature Physics*, R. Bowers, editor (Clarendon Laboratory, Oxford, 1951), p. 150.

CC-0. In Public Domain. Gurukul Kangri Collection, Haridwar

Digitized by Arya Samaj Foundation Chennai and eGangotri

bility measurements of Van den Handel and Hupse[14] with excellent agreement. For sample I, the normal neodymium sample, $b_I = 0.906 \times 10^5$ erg deg; for sample II, $b_{II} = 0.314 \times 10^5$ erg deg; and for sample III, $b_{III} = 4.44 \times 10^5$ erg deg. Collecting these values of b in the corresponding simultaneous equations, we then found it possible to solve for the three contributions of the specific heat: b_e, the specific heat constant b_{143} corresponding to the Nd^{143} hyperfine splitting, and the specific heat constant b_{145} corresponding to the Nd^{145} hyperfine splitting. These equations and the values of b_e, b_{143}, and b_{145} are given in Table III.

The values of b given in Table III are to be compared with the values $b_{143} = 5.17 \times 10^5$ erg deg and $b_{145} = 2.00 \times 10^5$ erg deg computed from the microwave measurements of Scovil.[13] Because of the small percentage of Nd^{145} in the three samples, the experimental error of our b_{145} measurement is relatively large. This value of $b_e = 0.146 \pm 0.004 \times 10^5$ is one of the smallest electron-electron interactions that has been observed, and this smallness is consistent with the fact that in his microwave measurements Bleaney[6] was able to resolve the hyperfine structure on the undiluted salt. This results in the unusual circumstance that for $Nd^{143}(C_2H_5SO_4)_3 \cdot 9H_2O$ the hyperfine splitting contribution to the specific heat is some 35 times larger than the electron-electron interaction contribution, which makes this material of interest in the study of nuclear effects below 1°K.

In Table II a Weiss constant of 0.013 ± 0.005°K was used in calculating the specific heat. This value is smaller than can be obtained precisely from susceptibility measurements. Our value of b_{143} without a Weiss constant correction was approximately 4 percent lower than the corresponding microwave value. In that the precision of our susceptibility and magnetic field measurements was considerably better than 1 percent, it is reasonable to assume that the above 4 percent discrepancy is produced by a small Weiss constant, and the above value of θ is that which is necessary to bring our b_{143} value into agreement with the microwave results within our experimental error. Since θ can be shown to be independent of the isotopic composition, the value determined above applies to all three samples.

This comparison provides a very sensitive technique for observing a Weiss constant in that the Weiss constant enters into the specific heat measurement to the third power, whereas it only enters linearly in susceptibility measurements.

This θ of 0.013°K leads to a b (exchange) which is small compared to our measured value for b_e. This suggests that b_e for these salts is predominantly the result of dipole-dipole interaction.

[14] J. Van den Handel and J. C. Hupse, Physica 9, 223 (1942).

TABLE III. Simultaneous equations for specific heats of neodymium samples.

$$4.44 \times 10^5 = b_e + 0.8393 b_{143} + 0.0178 b_{145}$$
$$0.906 \times 10^5 = b_e + 0.1220 b_3 + 0.0830 b_5$$
$$0.314 \times 10^5 = b_e + 0.0318 b_3 + 0.0037 b_5$$
$$b_{143} = 5.08 \pm 0.05 \times 10^5 \text{ erg deg}$$
$$b_{145} = 1.7 \pm 0.2 \times 10^5 \text{ erg deg}$$
$$b_e = 0.146 \pm 0.004 \times 10^5 \text{ erg deg}$$

APPLICATION OF THIS TECHNIQUE TO TRIVALENT URANIUM

Experiments are in progress applying the above separated isotope technique to the measurement of the nuclear specific heat of trivalent uranium. The only stable compounds of trivalent uranium are the halides; and, as these become antiferromagnetic at about 350°K, according to Dawson,[15] they are unsuitable for these measurements. Since the uranium trihalides are isomorphous with the lanthanum trihalides, it is possible to prepare solid solutions of these. Because of the low symmetry of the crystal, and because UX_3 has an odd number of electrons, solid solutions dilute in uranium may be expected to have a Kramers doublet as the ground state and thus be paramagnetic in the liquid helium temperature region. We have prepared a number of UF_3-$LaCl_3$ and UCl_3-$LaCl_3$ samples with uranium molar volumes in the range from 600 cc to 3000 cc. All of these, when freshly prepared, are found to follow a Curie law in the temperature region from 1°K–4°K. The Curie constant for the powder is of the order of magnitude to be expected for a Kramers doublet and an average spectroscopic splitting factor g of the order of 2. This g is probably anisotropic, so single crystal measurements would be necessary to obtain complete information about it. The more dilute of these normal uranium solid solutions have been cooled by adiabatic demagnetization from 1.17° to about 0.7° using initial magnetic fields of about 5000 gauss.

Note added in proof.—Professor R. J. Elliott has calculated the b_e to be expected from dipole-dipole interaction for $Nd(C_2H_5SO_4)_3 \cdot 9H_2O$ and obtains the value $b_e = 0.144 \times 10^5$ erg degree. This is to be compared with our experimental value, $b_e = 0.146 \times 10^5$. The good agreement between these values indicates that the electronic contribution to the specific heat is almost entirely due to dipole-dipole interaction.

[15] J. K. Dawson, Harwell, AERE Report C/R 578, September, 1950.

CC-0. In Public Domain. Gurukul Kangri Collection, Haridwar

Digitized by Arya Samaj Foundation Chennai and eGangotri

REVIEWS OF MODERN PHYSICS VOLUME 25, NUMBER 1 JANUARY, 1953

Optically Induced Nuclear Magnetization. A Progress Report*

F. BITTER, R. F. LACEY, AND B. RICHTER

Research Laboratory of Electronics, Massachusetts Institute of Technology, Cambridge, Massachusetts

Following a suggestion by A. Kastler, an attempt has been made to produce a high degree of nuclear orientation in Hg^{199} vapor by the absorption of circularly polarized resonance radiation. A method is described for detecting the nuclear orientation by observing the intensity of the π-component of the resonance radiation. No indication of orientation was found. The probable cause for this failure is considered to be the imprisonment and consequent depolarization of the effective component of the resonance radiation.

THE parallel orientation of a substantial fraction of an assembly of atomic nuclei would be of great help in experimental investigations of nuclear structure. The following is a progress report concerning an attempt to produce a preferred orientation of Hg^{199} nuclei in mercury vapor, following a suggestion by Kastler.[1] The method should produce nuclear orientation with respect to a magnetic field, and does not depend on making the Boltzmann factor approach unity. The "Maxwell demons," used to produce order out of disorder, are circularly polarized electromagnetic quanta whose angular momentum is imparted to the nuclei being oriented. These quanta must, of course, have an atomic resonance frequency in order to be effective. After absorbing a quantum, an excited atom can in general re-emit the same radiation it has absorbed. In this case, the system is left unchanged. If, however, the excited atom has open to it some means of losing its energy without also losing its newly acquired angular momentum, the cycle may produce a change in orientation, or in mangetization. Under suitable circumstances this magnetization may be specifically nuclear, as in the case of Hg^{199}, further discussed below.

The m sublevels of the diamganetic $^1S_0$ ground state and of the $^3P_1$ excited state of Hg^{199} are shown in Fig.1. The transition probabilities for the various Zeeman components of the 2536A resonance line are also shown. Transitions in which the magnetic quantum number does not change involve the emission or absorption of plane-polarized light when the electric vector is parallel to the magnetic field. This is generally called the π-component of the radiation. Transitions involving a change in the magnetic quantum number by ± 1 give rise to the σ-component of the resonance radiation. When observed in the direction of the magnetic field, the resonance radiation is then circularly polarized; the sense depends on the sign of the change in m. If Hg^{199} vapor is illuminated with circularly polarized resonance radiation of such a sense that it produces an increase in m by 1, the absorption and re-emission of a quantum may increase the number of nuclei in the magnetic sublevel of the ground state with $m=+\frac{1}{2}$. To see this, observe that nuclei in this sublevel at the start will not be reoriented by the absorption and emission of a quantum. However, those initially in the sublevel with $m=-\frac{1}{2}$ may return to either of the ground-state sublevels with comparable probability. The net effect of an absorption and emission cycle will be to pump some of the nuclei from the sublevel with $m=-\frac{1}{2}$ into the sublevel with $m=+\frac{1}{2}$. In order to be effective, three conditions must be fulfilled: (a) the incident radiation must be sufficiently intense to produce orientation at a greater rate than the thermal rate of disorientation, (b) changes of state of excited atoms due to collisions must be negligible, and (c) the radiation which excites the Hg^{199} atoms must be circularly polarized.

The apparatus used was essentially that described in a previous publication,[2] and shown schematically in

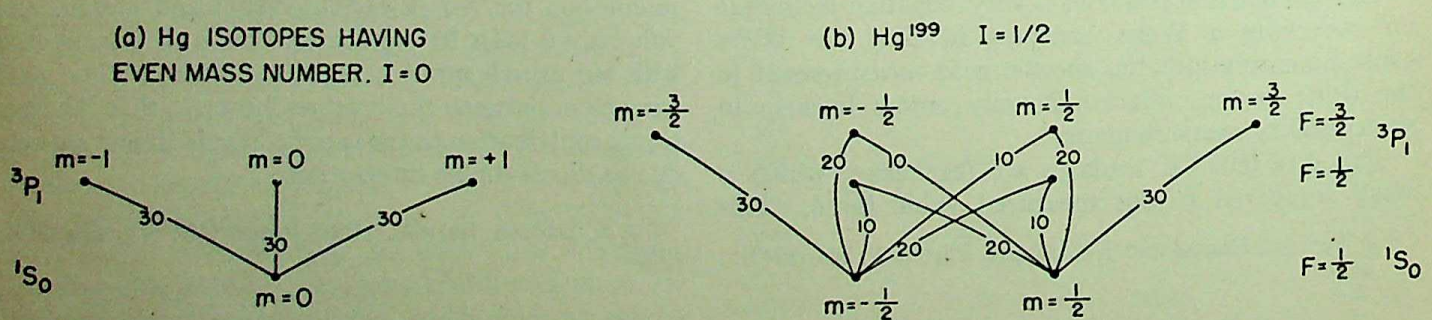


FIG. 1. Transition probabilities for some of the components of the resonance line of mercury.

* This work has been supported in part by the Signal Corps, the Air Materiel Command, and the U. S. Office of Naval Research.

[1] A. Kastler, J. phys. 11, 255. 1950.

[2] F. Bitter and J. Brossel, Phys. Rev. 85, 1051 (1952). See also J. Brossel and F. Bitter, Phys. Rev. 86, 308 ,1952, for further details concerning the apparatus used.

CC-0. In Public Domain. Gurukul Kangri Collection, Haridwar

Digitized by Arya Samaj Foundation Chennai and eGangotri

Fig. 2. Circularly polarized light moving in the direction of a constant magnetic field is used to illuminate mercury vapor. The intensities of the π- and σ-components of the resonance radiation are measured with an IP28 phototube and galvanometer. In some of the experiments an optical bridge, described in the publications mentioned above, was used to reduce disturbing effects due to fluctuations of the intensity of the light source.

The experiment performed may be described as follows. The vapor is illuminated with circularly polarized light, which we shall call σ_+, to pump atoms from the ground state a, in which $m=-\frac{1}{2}$, into state b, in which $m=+\frac{1}{2}$. Let the number in ground state a when a steady state is established be $N_a=f_aN$, where f_a lies between 0 and $\frac{1}{2}$. If we produce complete orientation, $f_a=0$. For complete disorientation, $f_a=\frac{1}{2}$. Neglecting depolarizing effects caused by collisions, which assumption we shall justify further on, we notice that the intensity of the π-component in the resonance radiation must be proportional to N_a, the number of atoms in ground state a. The proportionality factor will involve the intensity of the light of just the frequency required to produce the transitions involved. We shall call this factor k_+. We have then, if π_+ is the intensity of the π-component under these conditions,

$$\pi_+=k_+f_aN. \tag{1}$$

Similarly, if we use incident circularly polarized light of the opposite sense, we shall find some different intensity of the π-component of the resonance radiation,

$$\pi_-=k_-f_bN. \tag{2}$$

The difference arises from the fact that different absorption frequencies will be involved, and since the incident line has an irregular complicated shape as a result of its hyperfine structure, right- and left-circular polarized light will in general produce different effects. If, by rotating the quarter-wave plate by 45° we use one-half of the σ_+ and one-half of the σ_- intensity, we shall surely produce no nuclear orientation, and the factor f will be just $\frac{1}{2}$. We have

$$\pi_\pm=(k_+\tfrac{1}{2}N+k_-\tfrac{1}{2}N)\tfrac{1}{2}, \tag{3}$$

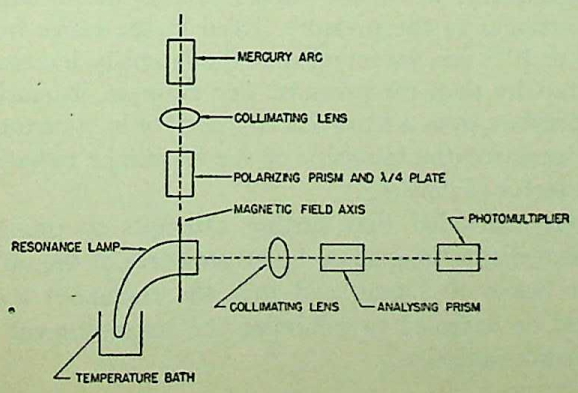


FIG. 2. Diagram of the apparatus.

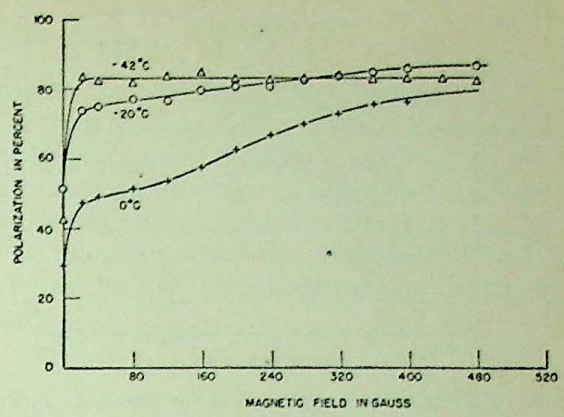


FIG. 3. Polarization *vs* magnetic field for resonance radiation from even isotopes of mercury using umpolarized σ-exciting light parallel to the applied field.

or, on combining the above results,

$$\frac{1}{4}\frac{\pi_++\pi_-}{\pi_\pm}=\frac{k_+f_a+k_-f_b}{k_++k_-}. \tag{4}$$

For our present purposes it suffices to put $f_a=f_b$. We then get as our final result

$$\frac{1}{4}\frac{\pi_++\pi_-}{\pi_\pm}=f. \tag{5}$$

This experiment was performed in fields of the order of 500 gauss at vapor pressures in the vicinity of a few times 10^{-4} mm. At no time was any indication of nuclear orientation observed. For the best of the runs an orientation of a few percent of the nuclei would have been observable.

We are now confronted with the problem of accounting for this negative result. This will presumably involve our finding wherein we have failed to satisfy the three fundamental conditions laid down above. The first point is related to the intensity of the light used. From the observed galvanometer deflections, the known sensitivity of the instrument, the photocell characteristics, and the geometry of the optical system, we estimate that, if every atom in the cell is excited by the incident light, it is excited about once a second. This estimate may be off by a factor of ten, or possibly even one hundred, but not much more. The nuclear thermal relaxation time of a diamagnetic gas is known to be extremely long. Assuming that the agency responsible is the transient magnetic field produced by the nuclei of colliding atoms, and assuming that in the range of pressures involved in our experiments only collisions with atoms magnetically equivalent to Hg^{199} atoms in the wall of the container are effective, we estimate[3] thermal relaxation times of the order of 10^{12} sec. Even if we make the drastic assumption that every collision

[3] The expression used in making these estimates is given, for example, in N. Bloembergen's thesis, Leiden, 1948, on page 108. $1/T=2\gamma_1^2\gamma_2^2\hbar^2d^{-4}v^{-2}\tau_c^{-1}$, where γ_1 and γ_2 are the gyromagnetic ratios of the colliding atoms, d is the atomic diameter, v the velocity, and τ_c the collision time.

CC-0. In Public Domain. Gurukul Kangri Collection, Haridwar

Digitized by Arya Samaj Foundation Chennai and eGangotri

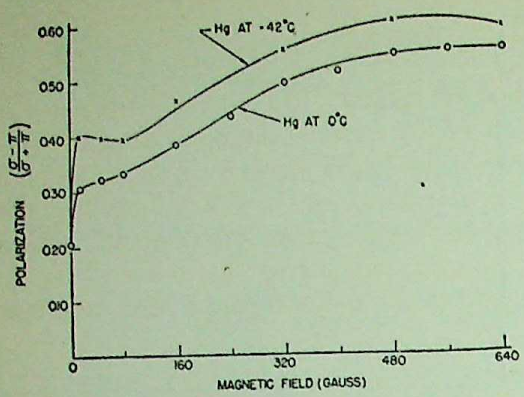


FIG. 4. Polarization *vs* magnetic field for resonance radiation from sample of mercury enriched in isotope of mass number 199, using unpolarized σ-exciting light parallel to the applied field.

is with the magnetic equivalent of a paramagnetic atom, we get relaxation times of the order of 10^5 sec. It seems unlikely, therefore, that if nuclear reorientation is the result of collision processes, these are sufficient to overcome the orienting tendency of the light used in the experiments. The possibility that mercury is adsorbed on the quartz cell, and that thermal equilibrium is produced in the adsorbed state, is here neglected.

The effect of collisions in producing depolarization was investigated on a sample of mercury supplied by the U. S. Atomic Energy Commission containing chiefly isotopes of even mass number and zero nuclear angular momentum. The composition reported was as follows:

Isotope	Atom percent
Hg 196	0.017
Hg 198	0.483
Hg 199	0.499
Hg 200	1.56
Hg 201	0.626
Hg 202	7.65
Hg 204	89.17

The even isotopes with no nuclear spin have a single nondegenerate ground state to which excited atoms can decay. It follows that apart from effects produced by collisions, every optically excited atom can emit only light having the same polarization as that involved in the excitation process. Any observed depolarization will consequently be the result of a transfer of excited atoms from one to another of the magnetic sublevels of the excited $^3P_1$ state.

The results obtained are shown in Fig. 3. With no current through the magnet the resonance radiation is considerably depolarized, but in a few gauss this depolarization is diminished by an amount depending on the vapor pressure. This initial change is presumably caused by the removal of the degeneracy of levels having the observed[2] mean life of 1.5×10^{-7} sec, which would require some three or four gauss. However, the pressure dependence of the degree of polarization persists in fields up to 500 gauss for pressures in the range from 10^{-4} to 10^{-6} mm Hg. In this range the mean free path of an atom is large compared to the dimensions of our cell, so that we conclude that the depolarizing cross section is very much larger than the kinetic-theory collision cross section. A further point concerns the reasons for the maximum observed degree of polarization, defined as $(\sigma-\pi)/(\sigma+\pi)$, of only approximately 85 percent. In view of the experimental difficulties encountered, further work is required to ascertain whether, in this range of pressures, the true value is not considerably nearer 100 percent. The result given above is in qualitative agreement with the finding of von Keussler[4] that in natural mercury in a field of 7900 gauss, sufficient to produce a Paschen-Back effect of the hyperfine structure, and at pressures below 10^{-3} mm, resonance radiation approaches a degree of polarization of 100 percent. In these strong fields the nuclei are completely uncoupled from the atoms, and natural mercury consequently radiates just as do the even isotopes in our experiment. We conclude that in fields sufficient to remove the degeneracy, collisions are ineffective in depolarizing the resonance radiation.

The results for the odd isotope are quite different. A sample containing 62 percent of the isotope of mass number 199 and 5.23 percent of the isotope of mass number 201 (also supplied by the U. S. Atomic Energy Commission) gave the results shown in Fig. 4. The much greater depolarization is due to the fact that atoms in excited sublevels with $m=\pm\frac{1}{2}$ can radiate with either π- or σ-polarization. This brings us to the third condition to be satisfied, namely, that the effective component of the radiation must be circularly polarized. If the resonance radiation does not leave the vapor without being reabsorbed, we see that there is a considerable depolarization to be expected at precisely the frequency which does the optical pumping. It is well known that even at low pressures the cross section for absorption of resonance radiation is very large, of the order of $(\lambda/2\pi)^2$, and that this leads to the "imprisonment" of the resonance radiation. We must therefore expect to work at very low pressures, presumably in the vicinity of 10^{-6} mm.

The present apparatus is inadequate for precise polarization experiments in this range. However, an attempt was made to determine the intensity of the resonance radiation as a function of vapor pressure. If there is no imprisonment, we should expect to find the intensity proportional to the pressure. Even in the range from 10^{-6} to 10^{-5} mm we found that the intensity increased less rapidly than the pressure. For example, increasing the pressure from 3.6 to 9.7×10^{-5} mm, or by a factor of 2.7, increased the intensity of the resonance radiation by a factor of only 2.2.

It is concluded that further attempts to produce nuclear orientation should be at pressures of the order of or below 10^{-6} mm, and that the resonance lamp should be designed to minimize the imprisonment of resonance radiation.

[4] V. von Keussler, Ann. Physik 82, 793, 1927.

CC-0. In Public Domain. Gurukul Kangri Collection, Haridwar

Digitized by Arya Samaj Foundation Chennai and eGangotri

DISCUSSION

B. BLEANEY, *Oxford University, England:* What degree of polarization of nuclei may be expected with this method, and what types of experiment can be performed when it is perfected?

F. BITTER, *Massachusetts Institute of Technology, Cambridge, Massachusetts:* Essentially complete orientation of Hg^{199} nuclei may be expected if our present conception of the difficulties to be overcome are correct.

If substantially unequal populations of the sublevels of the ground state of atoms in a vapor can be achieved, we can hope to measure the separations of these sublevels by magnetic resonance experiments. The method may be especially significant in studies of the nuclear moments of radioactive isotopes of zinc, cadmium, and mercury.

CC-0. In Public Domain. Gurukul Kangri Collection, Haridwar

Digitized by Arya Samaj Foundation Chennai and eGangotri

REVIEWS OF MODERN PHYSICS VOLUME 25, NUMBER 1 JANUARY, 1953

Magnetic Susceptibility of Bromine-Graphite*

R. SMOLUCHOWSKI

Carnegie Institute of Technology, Pittsburgh, Pennsylvania

Bromine, even in small quantities, is known to alter very radically properties of graphite such as conductivity, Hall effect, and others. In particular, the relatively large diamagnetic susceptibility of graphite is rapidly decreased by addition of bromine and the effect cannot be explained by assuming presence of bromine in either molecular or atomic form. It appears that this effect can be interpreted in terms of the Brillouin zone structure of graphite. Using Peierls' theory of diamagnetism of free electrons in a solid and Wallace's results concerning the band structure of graphite an expression is derived which relates the change in the magnetic susceptibility to the change in the number of electrons in the Brillouin zones. The theory is in good agreement with experiment if the effectiveness of bromine in accepting electrons is assumed to be that obtained from Hall effect and conductivity data. The probable influence of lattice imperfections is briefly considered.

1. THEORY

IT has been shown by Goldsmith[1] that addition of bromine to graphite lowers its diamagnetic susceptibility rapidly and also that this effect cannot be explained assuming presence of atomic or molecular bromine in the graphite lattice. The present paper is an attempt to explain these observations on the basis of an analysis of the band structure of graphite. Graphite is strongly diamagnetic and shows a strong anisotropy of its susceptibility:[2] $\chi_\perp \gg \chi_\parallel$ where $\chi_\parallel$ is measured in the plane of the hexagonal layers while $\chi_\perp$ is measured in a direction perpendicular to it. It seems natural to conclude that the unusual magnetic properties are closely related to the crystalline structure and thus to the quasi-free electrons responsible for conductivity. The behavior of the latter is best described in terms of Brillouin zones as it has been done for graphite for the first time by Wallace.[3] Peierls[4] has shown that the susceptibility of such quasi-bound electrons for a field in the z direction is proportional to

$$\int\left[\frac{\partial^2\epsilon}{\partial k_x^2}\frac{\partial^2\epsilon}{\partial k_y^2}-\left(\frac{\partial^2\epsilon}{\partial k_x\partial k_y}\right)^2\right]\frac{\partial f}{\partial\epsilon}dk, \qquad (1)$$

in which ϵ is the energy of the electrons with respect to the bottom of the first zone, k_x, k_y, k_z are components of the momentum vector k, f is the Fermi distribution function and the integration extends over the k space. In the following considerations only the $\chi_\perp$, in the z direction, will be taken into account since it is representative of the contribution due to electrons in the bands while $\chi_\parallel$ is well accounted for by the closed-shell diamagnetism.

For our theory the following properties of the Brillouin zone structure of graphite are important: the first zone is a section of a hexagonal prism; the second zone is obtained by extending the sides of the first zone so as to form a hexagonal star as shown in Fig. 1. At absolute zero the first zone is full, the second empty and with increasing temperature some electrons are excited from the first to the second zone. This excitation occurs across a gap of zero width which occurs at the corners of the first zone. It follows from the above that in evaluating expression (1) it is enough to consider only the proximity of the corners of the first zone since only there the factor $\partial f/\partial\epsilon$ will be different from zero (see Fig. 2). The derivatives of the energy ϵ with respect to the vector k are easily computed[3] from

$$\epsilon-\epsilon_0=-\gamma_1\Gamma\pm[\gamma_1^2\Gamma^2+\gamma_0^2|S|^2]^{\frac{1}{2}}, \qquad (2)$$

where ϵ_0 is the maximum possible energy in the first

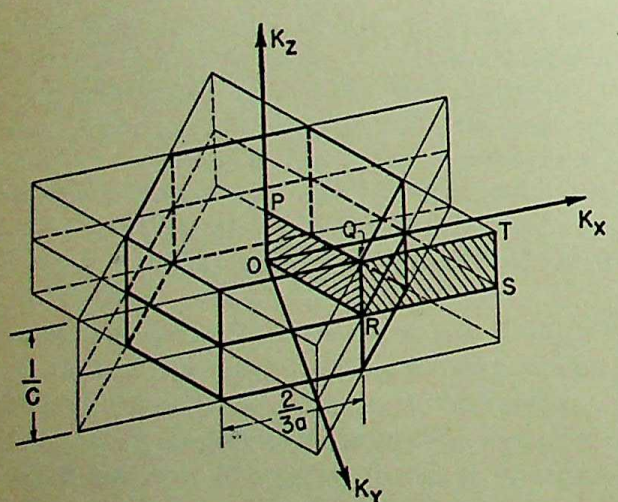


FIG. 1. Brillouin zones of graphite.

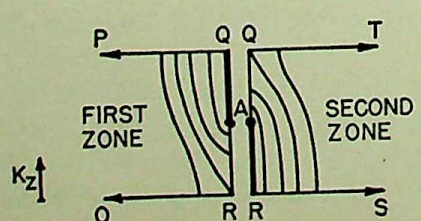


FIG. 2. Lines of constant energy and the point of continuity A.

LINES OF CONSTANT ENERGY AND THE POINT OF CONTINUITY, A.

* Supported by the U. S. Office of Naval Research.

[1] M. Goldsmith, J. Chem. Phys. 18, 523 (1950).

[2] See, for instance, W. Ganguli and K. S. Krishnan, Proc. Roy. Soc. (London) 177, 168 (1941).

[3] P. R. Wallace, Phys. Rev. 71, 622 (1947).

[4] R. Peierls, Z. Physik 80, 763 (1933).

CC-0. In Public Domain. Gurukul Kangri Collection, Haridwar

Digitized by Arya Samaj Foundation Chennai and eGangotri

zone,

$$\Gamma=\cos\pi k_z C$$

$$S=\exp\left[-2\pi i k_x\frac{a}{\sqrt{3}}\right]+2\cos\pi k_y a\cdot\exp\left[\pi i k_x\frac{a}{\sqrt{3}}\right],$$

in which a and c are the lattice constants of graphite and γ_0 and γ_1 are exchange integrals between nearest neighbors in a layer and in neighboring layers, respectively. These integrals have been evaluated by Coulson:[5]

$$\gamma_0\cong 0.9eV,\quad \gamma_1\cong 0.09eV.$$

At the corners of the hexagon S vanishes and thus approximately

$$|S|^2\cong 3\pi^2a^2\lambda^2=B\lambda^2,$$

where λ is a momentum vector measured from the corner of the first zone. The minus sign in (2) applies to the first zone, the plus sign to the second zone and the function $\epsilon(k)$ is thus discontinuous at the zone boundary except for two points on each short edge of the zone. One of such points and its neighborhood is shown in Fig. 2.

For graphite, at absolute zero, the parameter ϵ' (free energy per electron) in the Fermi distribution

$$f(\epsilon)=\frac{1}{\exp[(\epsilon-\epsilon')/kT]+1}$$

is equal to ϵ_0, the highest energy of the electrons in the filled first zone i.e., the energy at the corner of the hexagon. By changing the dimensions of the unit cell or by adding impurities which add or subtract electrons from the first zone, one can alter ϵ'. This in turn effects the quantity

$$\frac{\partial f}{\partial\epsilon}=-(kT)^{-1}\left(\cosh\frac{\epsilon-\epsilon'}{2kT}\right)^{-2} \tag{3}$$

in (1) and thus changes the magnetic susceptibility of graphite.

Substituting (2) into (1) one obtains for the expression in the square brackets under the integral

$$\gamma_0^4\gamma_1^2B^2\Gamma^2(\gamma_1^2\Gamma^2+\gamma_0^2B\lambda^2)^{-2}$$
$$=\gamma_0^4\gamma_1^2B^2\Gamma^2(\epsilon-\epsilon_0+\gamma_1\Gamma)^{-4}. \tag{4}$$

For the purpose of simplifying the change of the integration variable from k to ϵ we put $\gamma_1=0$ in (2) and in the denominator of (4). In this way after an integration over k_z we are left with an integral in the k_xk_y plane which leads to an expression proportional to

$$\int_0^\infty(\epsilon_0-\epsilon)^{-3}\left(\cosh\frac{\epsilon-\epsilon'}{2kT}\right)^{-2}d\epsilon \tag{5}$$

which is divergent at $\epsilon=\epsilon_0$. It seems that this divergence is due to the simplifying assumptions made in integration† and that the first term in (5) instead of becoming infinite at $\epsilon=\epsilon_0$ is actually large but finite. This appears plausible since as mentioned before ϵ is continuous between the first and second zone only at two points instead of being continuous for all $\lambda=0$ as our simplifying assumption would indicate. We obtain thus the approximate result

$$\chi\sim\left(\cosh\frac{\epsilon_0-\epsilon'}{2kT}\right)^{-2}. \tag{6}$$

To estimate the change of ϵ' with changing concentration of free electrons we need the total number of electrons contained between ϵ' and ϵ_0. From Wallace's formula (5.4) we obtain for the density of electrons per unit volume near the zone corner approximately,

$$n(\epsilon)=16(\epsilon_0-\epsilon)/3\pi a^2c\gamma_0^2,$$

or, since the atomic volume is $\sqrt{3}a^2c/8$, we have for the density of electrons per atom

$$n(\epsilon)=2(\epsilon_0-\epsilon)/\sqrt{3}\pi\gamma_0^2. \tag{7}$$

By integrating (7) from ϵ' to ϵ_0 we obtain for the total number of electrons within these limits:

$$N(\epsilon')=(\epsilon_0-\epsilon')^2/\sqrt{3}\pi\gamma_0^2. \tag{8}$$

Knowing the number of electrons removed from the first zone per added bromine atom we can now calculate, from Eqs. (6) and (8), the relative change of the magnetic susceptibility.

2. COMPARISON WITH EXPERIMENT

Formula (6) indicates that, with increasing deviation from a full first and an empty second zone, the diamagnetic susceptibility of graphite will decrease. In order to make this comparison quantative we should know how many electrons are taken away by each bromine atom. Certain recent measurements[6] of conductivity and of Hall effect on artificial graphite containing bromine indicate, using free-electron formulas, that about 0.038 of an electron is taken away per added atom of bromine. This can be interpreted in two ways: either that only 3.8 percent bromine atoms actually go into solution and each accepts one electron while the remainder is adsorbed in some way on the particles of artificial graphite and in the imperfect intercrystalline material or that actually 0.038 electron are taken out per "dissolved" bromine atom.

Goldsmith's data[1] indicate that gram susceptibility of graphite at room temperature drops from -5.3×10^{-6} to -4.2×10^{-6} at a concentration corresponding to 7.6×10^{-3} bromine atoms per atom of carbon and it drops further to -0.30×10^{-6} at a concentration of 0.10. Since the susceptibility of graphite is a sum of the

[5] Bradburn, Coulson, and Rushbrooke, Proc. Roy. Soc. (Edinburgh) 62, 336 (1947).

† See note added in proof.

[6] Unpublished data obtained at the National Carbon Company Research Laboratory.

CC-0. In Public Domain. Gurukul Kangri Collection, Haridwar

Digitized by Arya Samaj Foundation Chennai and eGangotri

TABLE I. Susceptibility of graphite at various bromine concentrations.

Br atoms / C atoms	0	0.0076	0.100
$-\chi\times10^6$(obs)	5.3	4.2	0.3
$-\chi\times10^6$(calc)	(5.3)	3.5	0.15

Peierls diamagnetism and the usual, small, closed-shell diamagnetism it is advisable to calculate the relative, rather than the absolute, change of the susceptibility in which the constant term plays only a small role in the denominator: From (6) we have

$$(\chi_0-\chi_{Br})\chi_0^{-1}=\left(tgh\frac{\epsilon_0-\epsilon'}{2kT}\right)^2, \qquad (9)$$

where χ_0 and χ_{Br} are susceptibilities of graphite without and with bromine. By combining Eqs. (8) and (9) we obtain for $N(\epsilon')$ the values 0.146×10^{-3} and 2.8×10^{-3} electron at the two concentrations, respectively. The value of $N(\epsilon')$ at the higher bromine content is comparable to the effective number of free electrons n_{eff} in graphite[3] which indicates that the change of the various properties is indeed drastic. This number of electrons missing from the first zone is respectively about 2 and 3 percent of the concentration of added bromine, which is close to 3.8 percent obtained from Hall effect and conductivity measurements. Conversely putting $N(\epsilon')$ equal 3.8 percent of the added bromine atoms leads to the calculated susceptibilities shown in Table I. The agreement is satisfactory.

It should be pointed out that the theory has been developed assuming tacitly that the influence of bromine is due exclusively to the change in the number of electrons in the Brillouin zones, that is, without taking into account any other changes which the presence of bromine may bring about. It is known[7] that at very high bromine content the spacing between graphite layers increases appreciably. This increase of c decreases the thickness of the zones and it may affect the conditions at the zone corners. There is no x-ray evidence of a change in the lattice at the lower bromine content here considered (although there may be some distortion at the higher concentration) and thus no correction for this effect is made. For similar reasons a consideration of an influence of the presence of bromine on the value of the exchange integral γ_1 in Eq. (4), through an increase of the c spacing, seems unnecessary at the present time.

The formulas derived above can be also applied to imperfect (pure) graphite in which either the lattice spacing c, in small crystallites, is abnormally large[8] or the otherwise perfect layers are displaced (or rotated) with respect to each other.[9] These kinds of defects can produce traps for electrons[10] and thus lower the "free electron" concentration or they can increase the c dimension of the Brillouin zone or finally they can change the quantity γ_1. Also, the gap between the first and second zone in such imperfect graphite is very likely[11] different from zero. It is well known that with increasing deviation from the ideal graphite structure the magnetic susceptibility drops[10,12,13] down to values corresponding to almost pure closed-shell diamagnetism. In view of the incompleteness of the x-ray data a quantitative analysis is not yet possible although qualitatively the decrease of the susceptibility is in agreement with the theory here outlined.

The author is indebted to the staff of the National Carbon Company Research Laboratory for permission to use their unpublished data and for stimulating discussion.

Note added in proof:—Dr. W. P. Eatherly of the North American Aviation informed me privately that he made similar calculations (to appear in *The Physical Review*) and was able to demonstrate that the integral in (1), which in a two-dimensional integration leads to (5), is indeed convergent in an approximate three-dimensional treatment.

A recent report by G. Hennig (ANL-4723) indicates that electrical resistivity of halogen compounds of graphite is accounted for by assuming that about 18 percent of bromine atoms are ionized rather than about 4 percent as concluded in this paper. If the higher percentage is correct and if the experimental data on susceptibility here quoted are reliable then γ_0 should be about three times smaller than indicated by Coulson—this seems rather doubtful. Recent data kindly supplied by Dr. Eatherly indicate 10 percent ionized Br atoms.

[7] W. Rüdorff, Z. anorg. u. allgem. Chem. 245, 383 (1941).

[8] G. E. Bacon, Acta Cryst. 3, 137 (1950); 4, 558 (1951).
[9] J. Biscoe and B. E. Warren, J. Appl. Phys. 13, 364 (1942).
[10] S. Mrozowski, Phys. Rev. 85, 609 (1952) and private communication.
[11] E. A. Kmetko, Phys. Rev. 82, 456 (1951).
[12] M. Miwa, Sci. Rep. Tohoku Univ. 23, 242 (1934).
[13] S. R. Rao, Indian J. Phys. 6, 241 (1931).

DISCUSSION

S. MROZOWSKI, *University of Buffalo, Buffalo, New York:* In a paper which I submitted recently to the *Journal of Chemical Physics* for publication, the influence of the shape of the energy-momentum relation at the Brillouin zone corners and of the position of the Fermi level on the properties of graphite compounds is discussed in a semiquantitative manner. The commonly adopted viewpoint, that the changes in properties like electric resistivity and magnetic susceptibility are mainly the result of the variation in the position of the Fermi level, is substantiated by these considerations. It is shown, however, that no simple relation of the type $E\sim k_1^n$ can reasonably well explain changes in both these properties at the same time and that presumably agreement would be reached only when the energy surfaces are considered in their full complexity. Furthermore it is concluded on basis of experimental evidence

CC-0. In Public Domain. Gurukul Kangri Collection, Haridwar

Digitized by Arya Samaj Foundation Chennai and eGangotri

that a large crystal of graphite has slightly overlapping bands and is therefore a semimetal and not a semiconductor with a zero energy gap. Dr. D. Polder (Bristol) has kindly informed me that calculations, in which he takes more interactions between neighbors into consideration than Wallace, lead to the same conclusion.

It was pointed out in my recent paper on the diamagnetism of carbons[1] that the decrease of the susceptibility of graphite with decrease in crystallite size can be caused by two effects: a depression of the Fermi level and/or a decrease of the curvature of the energy surfaces at the Brillouin zone corners. In our laboratory Mr. H. T. Pinnick is engaged at present in a study of susceptibilities of carbons and graphites. The number of samples investigated until now is small. The results, however, show clearly that the large drop in susceptibility occurs for carbons in the range of crystallite diameters from 150 to 50A. This drop must be the result, at least partly, of the rounding off of the energy peaks, since samples with widely different thermoelectric powers show approximately the same susceptibilities.

Mr. E. A. Kmetko has thoroughly investigated the resistivity and the thermoelectric and Hall effects in graphite and carbon bisulfate compounds (lammellar and residual ones). The paper will be sent for publication in a matter of a few weeks. His results furnish a good evidence of the progressing depression of the Fermi level in the regular carbons with decreasing crystallite sizes. We have not determined the susceptibilities of such compounds yet. I should like to point out at this time, however, that in the course of Mr. Kmetko's work we realized that in experimenting with carbons and its compounds we study cases where the Fermi level drops down as far as, and even below, the inflection curve on the energy surface. Graphite is the only substance for which the inflection is located close enough to the Brillouin zone boundaries, so that the transition from hole to electron conduction can be observed experimentally. Naturally, since the notion of the effective mass loses its meaning in this region, the quantitative estimates given in my former paper[1] have to be revised (the N_{eff} estimated there is too low).

[1] S. Mrozowski, Phys. Rev. 85, 609 (1952).

W. P. EATHERLY, *North American Aviation, Inc., Downey, California:* The properties of graphite have been examined in considerable detail both experimentally and theoretically[1] by the U. S. Atomic Energy Commission laboratory at North American Aviation. I should like to add a few qualitative remarks concerning our results.

The three-dimensional expression for the susceptibility must be integrated numerically, and is extremely sensitive to the energies γ_0 and γ_1. It appears, however, that the calculated susceptibility is too small by a factor somewhat larger than ten, but that the temperature dependence, at least above 100° K, is correct. This amount of agreement is probably as much as one can expect, because of the sensitivity to the parameter appearing in the band calculation.

It is a well-known fact that the sum of three susceptibilities measured in orthogonal directions is an invariant property of single crystals, but it does not seem to be so widely realized that the same invariance applies to polycrystalline materials. That is to say, the sum of the susceptibilities of a polycrystal is the same as that for a single crystal, independent of the degree of preferred orientation, provided that the individual crystallites are sufficiently large to have developed crystalline fields typical of "infinite" crystals. This is essentially the case in artificial graphite, in that the summed susceptibilities range from -21.5 to -22.5 $\times 10^{-6}$ emu/g, as compared to the single-crystal value -23.5×10^{-6}. The remaining discrepancy is undoubtedly the result of particles too small to be considered crystals. Our observations range over graphites manufactured from lampblack, petroleum cokes, and natural flake or block.

The band structure computed by Wallace[2] is usually criticized on the basis that it yields the wrong anisotropy ratio for the resistivities, and that overlap integrals are ignored. One can show easily that including overlap does not affect the band structure near the zone boundary. The problem of electronic scattering resulting from collisions is an extremely difficult one, but there is no doubt that the scattering is anisotropic and energy dependent. These factors are ignored in Wallace's calculation of the conductivity. Hence neither objection is valid as a criticism of the band calculation itself. However, one is left with the magnetic susceptibility as the only electronic property which can give, in a fairly direct way, experimental verification of the band structure.

[1] W. P. Eatherly, Phys. Rev. 85, 768 (1952).
[2] P. R. Wallace, Phys. Rev. 71, 622 (1947).

CC-0. In Public Domain. Gurukul Kangri Collection, Haridwar

Digitized by Arya Samaj Foundation Chennai and eGangotri

REVIEWS OF MODERN PHYSICS VOLUME 25, NUMBER 1 JANUARY, 1953

Helmholtz Coils for Production of Powerful and Uniform Fields and Gradients*

S. T. Lin† and A. R. Kaufmann‡

Massachusetts Institute of Technology, Cambridge, Massachusetts

The magnet is an air core and water-cooled massive Helmholtz type with rectangular cross section. It consists of a field coil 10 cm in mean radius which can produce 35 000 oersteds at a power of 1700 kw with a uniformity of about 10 ppm at the center within a region of 10 percent of the mean radius, and a gradient coil 5.2 cm in mean radius which can produce a gradient of 100 oersteds per cm at a power of 2.5 kw with a uniformity of about 140 ppm within the same region. The fields and gradients are separately controlled.

INTRODUCTION

THE solenoid which is described below was designed for precise magnetic susceptibility determinations on metals and alloys over a wide range of temperature. For this purpose it is desirable to have a strong and uniform field of at least 30 000 oersteds and an accurately known and separately controllable uniform gradient. Another requisite is that there be enough room in the region of high field to accommodate Dewar flasks and more especially furnaces for high temperature observations. It has been our experience that one cannot achieve a high temperature accuracy of 1°C in tiny furnaces in a severely restricted region. A secondary objective was to achieve a field uniformity of 10 parts per million or better over the sample volume so that the apparatus might be used for magnetic resonance studies. The equipment we have constructed meets all of these requirements.

GENERAL DESCRIPTION OF APPARATUS

The field is produced by massive water-cooled Helmholtz coils. With 1700 kw, it is possible to obtain about 35 000 oersteds with a field uniformity of 10 ppm over a distance of about 13 mm along the axis. The internal working space is about 4.4 inches in diameter. We have used part of this region to install a pair of water-cooled coils which can produce a gradient of 100 oersteds per cm with a uniformity of about 0.2 percent over 2 cm. The gradient is produced independently of the field so that it is possible to vary the gradient both in magnitude and direction as desired. It is thus possible to obtain the force on the specimen due to this known gradient, regardless of whether the main field is producing a small gradient or not. The gradient coils can also be used to compensate for variations in the main field, thus achieving a greater uniformity than is produced by the field coils alone. Inside the gradient coils, there is a space of about $3\frac{1}{8}$ inches diameter for working equipment. The coils have a vertical axis and are open at each end.

MAGNETIC DESIGN

Many workers have designed different types of coil systems for homogeneous fields but some of them, such as spherical harmonic current sheets, have just theoretical interest because they are too complicated to put into practice and others, such as Maxwell's three-loop combination[1] and McKeehan's four-loop system[2] are not suitable for high powered design because of the difficulty of obtaining homogeneous cooling and of eliminating the lead effects. On the other hand, the very simple and efficient single solenoids which are most suitable for high power construction fail to produce very homogeneous fields. It was decided to choose a system for our field coil which is a compromise between the highest possible uniformity and the highest engineering efficiency.

A. Field Coil

Our main objective was to obtain high uniformity of the magnetic field without sacrificing efficiency too much and, at the same time, to simplify the difficulties of construction. We decided to use a massive Helmholtz pair with rectangular cross section, as this system is simple to construct and requires only a single adjustable parameter to achieve a great uniformity.

Since the work of Maxwell and Grey, it has been well known that for an axially symmetric system the uniformity of the field along and off the axis is almost the same order of magnitude. The problem is how to obtain the correct separation of the Helmholtz pair to insure that the field along the axis is uniform. Many workers have calculated the best separation for a Helmholtz pair by different expansion series with different approximations.

It seemed that the most direct way to obtain this result was to use the exact formula for the field and

* This work was carried out at the M.I.T. Metallurgical Project under Contract No. AT(30–1)–981 with the U. S. Atomic Energy Commission.

† Staff Member, Division of Industrial Cooperation, Massachusetts Institute of Technology, Cambridge, Massachusetts.

‡ Associate Professor, Department of Metallurgy, Massachusetts Institute of Technology, Cambridge, Massachusetts.

[1] J. C. Maxwell, *A Treatise on Electricity and Magnetism*, Volume II. (Clarendon Press, Oxford, 1892).

[2] L. W. McKeehan, Rev. Sci. Instr. 7, 178 (1936).

CC-0. In Public Domain. Gurukul Kangri Collection, Haridwar

Digitized by Arya Samaj Foundation Chennai and eGangotri

TABLE I. Uniformity of the magnetic field in parts per million of the central field. The values in the first column were calculated from Eq. (A3) and the rest values from Eqs. (1), (2), and (3).

Distance	$\theta=0°$	$\theta=0°$	15°	30°	45°	60°	75°	90°
$r=0.025r_0=2.5$ mm	+2.4	+2.4	+2.2	+1.7	+0.9	−0.2	−1.2	−1.5
$0.05r_0=5$ mm	+4.5	+4.5	+5.5	+6.8	+5.5	+0.5	−5.4	−8.0
$0.075r_0=7.5$ mm	−8.1	−8.4	−0.4	+15	+20	+6.5	−15	−25
$0.10r_0=10$ mm	−60	−61	−32	+25	+54	+25	−33	−62
$0.15r_0=15$ mm	−417	−435	−277	+50	+243	+142	−117	−251

by adjusting the separation to achieve the maximum uniformity in the region in which we are interested. With the exact formula there is no question of convergency and order of approximation as when series are used.

We desired, also, to detect the effect of inhomogeneous coil heating on the uniformity, so we derived in the Appendix the general formula including this effect.

Substituting in Eq. (A3) a set of values of coil dimensions r_0, b, d, or the corresponding values of k and y, and choosing a few appropriate values of x, one can find the proper S which determines the best separation. Usually only a few adjustments need be made until the desired uniformity of H at the chosen positions is obtained. For an ordinary Helmholtz pair the correct separation is about a few percent larger than for the Helmholtz filament of the same mean radius. With a good initial guess the proper S can be obtained by one or two interpolations after two trial values have been used.

Taking values for $k=0.961$ and $y=0.383$, we find the proper S to be 0.5286. The coil dimensions we used were as follows:

mean radius $=r_0=10$ cm,
radial thickness $=2d=2yr_0=7.66$ cm,
axial breadth $=2b=2kyr_0=7.36126$ cm (each coil),
mean separation between tow coils $=2Sr_0=10.572$ cm.

The calculated uniformity for these dimensions is tabulated in the first column of Table I.

Alternative Calculation

We are deeply grateful to Professor M. W. Garrett[3] of Swarthmore College for showing us his elegant series method for calculating the field around coils. By using his method we had a chance to check our calculations.

For an axially symmetric system with a plane of symmetry the magnetic field can be expressed as zonal harmonics of even powers.

$$H_x=H_{x0}\left[1+k_2\left(\frac{r}{r_0}\right)^2P_2(\cos\theta)+k_4\left(\frac{r}{r_0}\right)^4P_4(\cos\theta)+\cdots\right], \quad (1)$$

where H_{x0} is the x component of the field at the origin, r_0 an arbitrary numerical value, and $k_2(r/r_0)^2P_2$ and $k_4(r/r_0)^4P_4$ are second- and fourth-order errors, respectively. According to Garrett, for thick solenoids k_2 and k_4 can be expressed as follows:

$$k_2=\frac{r_0^2}{2}\sum\frac{1}{x}(1-\sin^3\alpha)/\sum x\log_e(a+R), \quad (2)$$

$$k_4=\frac{r_0^4}{24}\sum\frac{1}{x^3}[2-\sin^3\alpha(15u^4+3u^2+2)]/\sum x\log_e(a+R), \quad (3)$$

where u denotes $\cos\alpha$ and $\sum$ denotes the summation over the four corners of the coil with alternate signs on adjacent corners, giving plus sign to the corner nearest the origin (see Fig. 1).

Substituting the above coil dimensions and the separation, we have found k_2 and k_4 to be 0.00445045 and −1.057581. The uniformity is indicated in Table I. The sixth-order error is negligibly small at the small distances in which we are interested. From the first and second columns of Table I is is clear that the calculated values from the series methods agree almost entirely with that from the exact formula. The other columns of the table give the field uniformity at points off the axis.

Effect of Coil Heating

In order to observe the heating effect, substitute the above coil dimensions in Eq. (A2) and take c equal to 0.004. This means the current density varies along the axis by 0.4 percent/cm of the central value of each coil, or the temperature varies by about 1°C/cm along the axis assuming that the temperature coefficient of re-

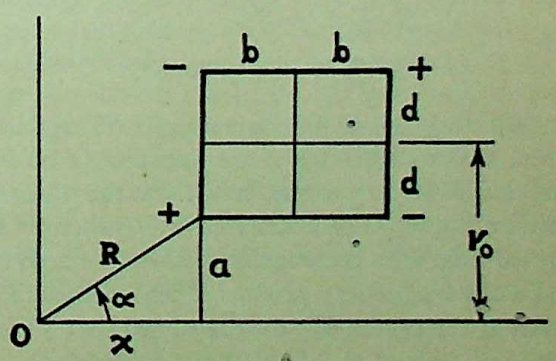


FIG. 1. Rule of signs on corners of coil to be used in calculation [Eq. (3)].

[3] Part of M. W. Garrett's work has been published in J. Appl. Phys. 82, 109 (1951).

CC-0. In Public Domain. Gurukul Kangri Collection, Haridwar

Digitized by Arya Samaj Foundation Chennai and eGangotri

TABLE II. Effect of water cooling on the uniformity of magnetic field. It is assumed that the temperature varies by 1°C per cm along the axis. The last column is compensated by a slope of 0.0055 percent per cm.

Distance from the center of the two coils	Uniformity in parts per million of the central field: Without compensation	With compensation
$0.15r_0$=15 mm	−356	−439
$0.1r_0$=10 mm	−7	−62
$0.075r_0$=7.5 mm	35	−7
$0.05r_0$=5 mm	35	8
$0.025r_0$=2.5 mm	18	4
0	0	0
$-0.025r_0$=−2.5 mm	−13	0.6
$-0.05r_0$=−5 mm	−25	2
$-0.075r_0$=−7.5 mm	−51	−10
$-0.1r_0$=−10 mm	−112	−57
$-0.15r_0$=−15 mm	−477	−395

sistivity is equal to 0.004. With these conditions the uniformity near the center of the system has been calculated and tabulated in Table II. It is interesting that in the neighborhood of the center the field varies almost linearly along the axis: the larger the c, the more prominent is the linearity. If we use the gradient from our gradient coil to compensate this small variation, a great uniformity can be obtained. The column 3 of Table II is the result of compensating the values of column 2 by a gradient of 0.0055 percent of the central field per cm, which is about 2 oersteds per cm at full power.

Power Requirement

If the specific resistance of the conductor of which the coil is made is ρ ohms/cc and if only a fraction λ of the volume of the coil is occupied by the conductor, the total power required to maintain the current density I_0 in the Helmholtz pair is

$$\omega=4\pi\rho I_0^2\lambda\int_{r_1}^{r_2}rdr\int_{-b}^{b}dx=4\pi\rho I_0^2\lambda b(r_1^2-r_2^2), \quad (4)$$

where r_1 and r_2 are the inside and outside radius of the coil and the other notations are the same as before. Eliminating I_0 between Eq. (4) and (A4) multiplied by λ, we have

$$H=[\omega\lambda/\rho r_1]^{\frac{1}{2}}G,$$

where

$$G=[\pi(1-y)]^{\frac{1}{2}}g/20yK^{\frac{1}{2}}. \quad (5)$$

Substituting the coil dimensions in Eq. (5) and letting x equal to zero in factor g, we found G to be 0.144, which is about 20 percent less than the theoretical maximum value 0.179 calculated by Cockcroft[4] for a single solenoid with rectangular section. For a power of 1700 kw the magnet can produce a field of about 35 000 oersteds at the center. We have assumed that λ is equal to 0.57 and ρ equal to $2.5\frac{1}{2}\times10^{-6}$ at full power.

[4] J. D. Cockcroft, Trans. Roy. Soc. (London) 227, 325 (1928).

B. Gradient Coil

As gradient power increases with r_0^3, the gradient coil was designed to be put inside the field coil. For the sake of obtaining great uniformity, we decided to use a long and a thin wall Helmholtz pair connected in opposition. The dimensions of the coils are as follows:

mean radius $=r_0=5.2$ cm,
axial breadth $=2b=5.3$ cm,
radial thickness $=2d=0.4191$ cm.

The properties of Helmholtz gradient coils are just like those of field coils. The greatest uniformity of gradient can be obtained by proper separation of the pair of coils. For axially symmetric systems with a plane of antisymmetry the gradient can be expressed as follows:

$$\frac{dH_x}{dx}=\left(\frac{dH_x}{dx}\right)_0\left[1+k_2'\left(\frac{r}{r_0}\right)^2P_2(\cos\theta)+k_4'\left(\frac{r}{r_0}\right)^4P_4(\cos\theta)+\cdots\right], \quad (6)$$

where $(dH_x/dx)_0$ is the gradient at the origin, r_0 an arbitrary numerical value, and $k_2'(r/r_0)^2P_2$ and $k_4'(r/r_0)^4P_4$ are second- and fourth-order errors, respectively. According to Garrett, for thick solenoids

$$k_2'=\frac{r_0^2}{2}\sum\frac{1}{x^2}[1-\sin^3\alpha(3u^2+1)]/D, \quad (7)$$

$$k_4'=\frac{r_0^4}{8}\sum\frac{1}{x^4}[2-\sin^3\alpha(35u^6+0+3u^2+2)]/D, \quad (8)$$

where

$$D=\sum[\sin\alpha-\log_e(a+R)-1].$$

The notations and the processes of taking the summation are the same as in Eqs. (2) and (3). The proper separation of the Helmholtz pair in terms of the x coordinate of the center of the solenoid can be found by adjusting its value until the k_2' in Eq. (7) vanishes.

Substituting the above coil dimensions we found the separation to be 11.21 cm, which made the k_2' to be a small positive number instead of zero in order to produce a prolate gradient. The values of k_2', k_4' and the uniformity along the axis are shown in Table III.

TABLE III. Uniformity of the gradient along the axis. $k_2'=0.0047208$; $k_4'=-1.70989$.

Distance from the center of the gradient coil	Uniformity in parts per million of the central gradient
$0.025r_0$=1.3 mm	−0.4
$0.05r_0$=2.6 mm	−10
$0.075r_0$=3.9 mm	−51
$0.1r_0$=5.2 mm	−165
$0.15r_0$=7.8 mm	−841[a]
$0.1923r_0$=10 mm	−2262[a]

[a] These two values are corrected for sixth-order errors.

CC-0. In Public Domain. Gurukul Kangri Collection, Haridwar

Digitized by Arya Samaj Foundation Chennai and eGangotri

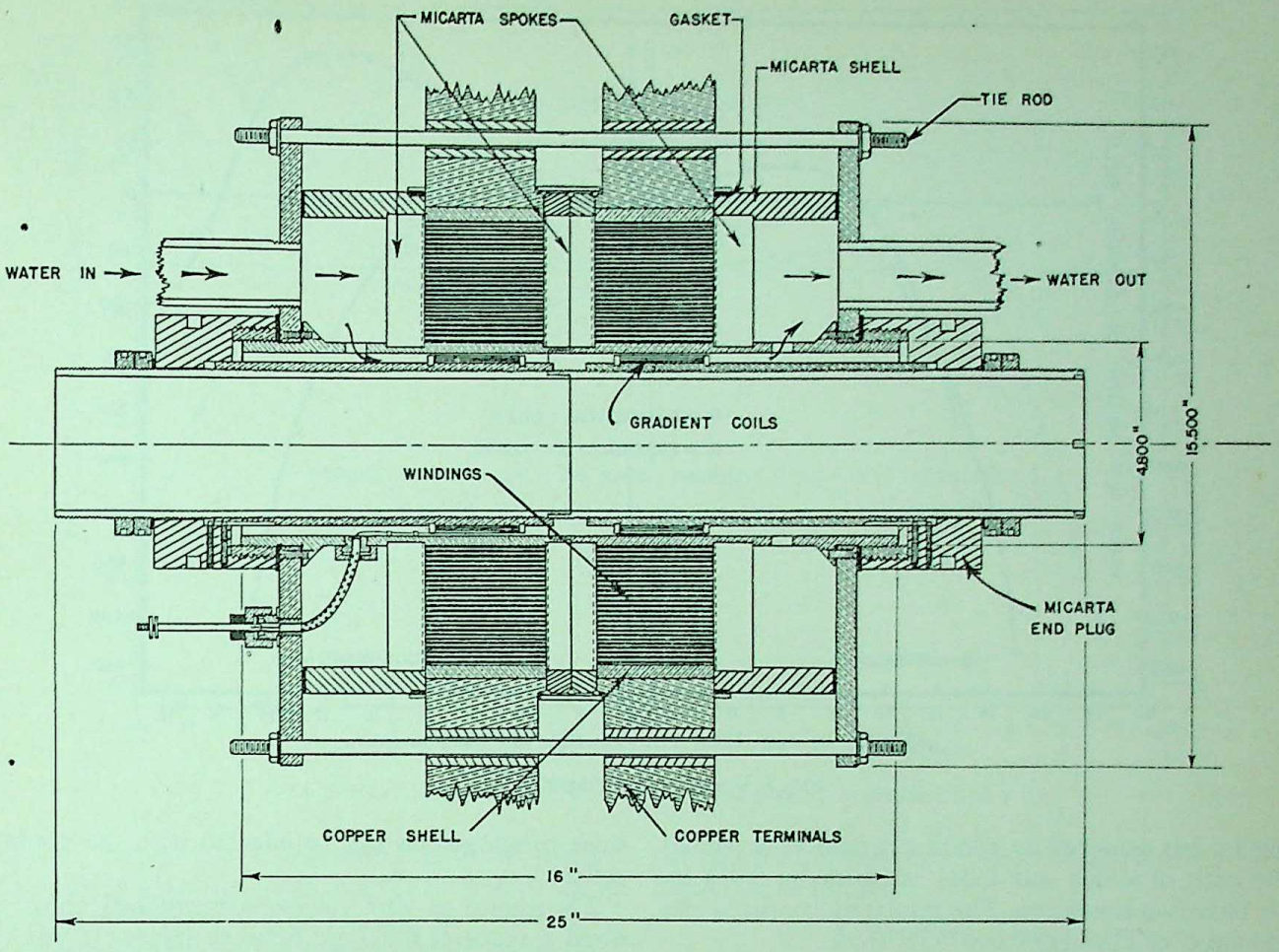


FIG. 2. Cross-sectional view of magnet.

The present coil with a power of about 2.5 kw will produce a gradient at the center of the coil of about 100 oersteds/cm. Another thick coil is under design which is more efficient and can produce a gradient of about 550 with a power of 6 kw and 1000 with 20 kw.

The gradient coil was designed to serve double purposes. First, it could be used for compensating the very small variation of the main field near the center of the magnet. This variation usually happens either due to inaccuracy of construction or the inhomogeneous temperature. Secondly, it could be used as a separate gradient in conjunction with the main field for accurate determination of magnetic susceptibilities. The separation of the two solenoids of the gradient coil can be adjusted to the correct value, and the whole coil can move along its axis in order to let its center coincide with that of the field coil.

ENGINEERING DESIGN

A. Field Coil

The available laboratory facilities provide 10 000 amperes at 170 volts and a heat exchanger system for water cooling. To best meet these conditions it was decided to wind the Helmholtz coil in layers with one turn per layer, as in a roller bandage, and with water flowing between each layer. In an effort to minimize leakage currents it was decided to use enamel insulation over the copper. With these basic conditions prescribed, the detailed design was worked out as follows:

1. Over-All Dimensions

An internal diameter of about 5 in. was selected as giving a satisfactory compromise between large internal working space and stronger field. The choice of this diameter also makes the heat removal conditions less severe than with a smaller coil. The cross section of the windings is almost square and was determined largely by the dimensions of commercially available flat wire and the necessary heat removal area. The spacing to give maximum uniformity over a distance of about one centimeter was then calculated as previously described.

The two coils of the Helmholtz pair were wound on two sections of heavy walled brass pipe as shown in Fig. 2. The two pieces of pipe were then threaded in the region between the coils and screwed onto each other. This construction was used in order that the distance between coils might be varied after testing in order to obtain the best spacing.

2. Current Conductors

It was decided to use commercially available enamel coated copper wire for the winding. The axial width of

CC-0. In Public Domain. Gurukul Kangri Collection, Haridwar

Digitized by Arya Samaj Foundation Chennai and eGangotri

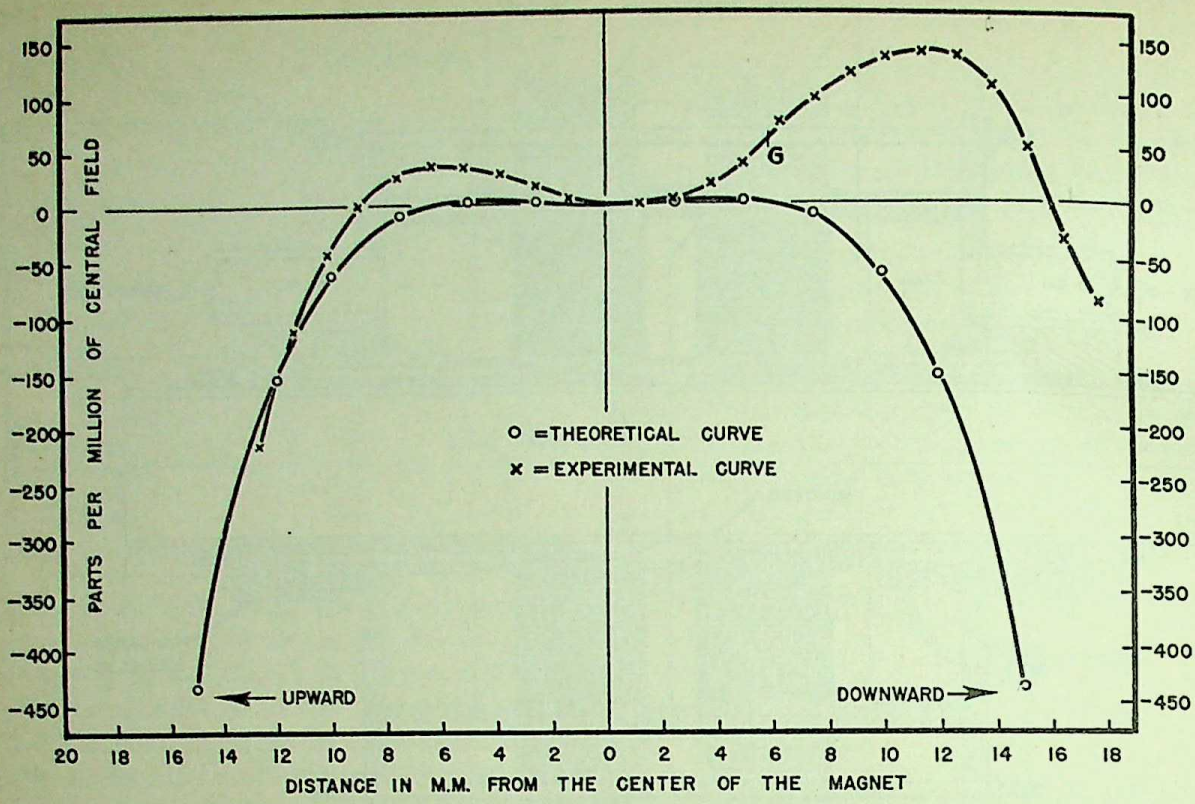


FIG. 3. Uniformity of magnetic field.

2.898 in. was achieved by winding in parallel seven flat wires each of which was 0.044 in. thick by 0.414 in. wide including insulation. The insulation consisted of a single layer of Formex§ 0.00075 in. thick.

The flat wire was carefully wound under tension into helical coils of 40 layers each with space between each layer as described below. Current enters the outermost layer of one coil, flows across the brass tube on which the coils are wound, and then leaves from the outer layer of the second coil. It is conceivable that the flow of current through the brass tube at the center might lead to a distortion of the field on the axis. Measurement of this effect on a model indicated the least distortion of field when the coil connections were made along the same axial line.

3. *Cooling*

Heat is removed by water flowing axially between each layer of the coils as shown in Fig. 2. Water is brought into and out of the coils by means of eight $1\frac{1}{4}$-in. pipes fitted into each end plate. With this arrangement the downstream coil will be hotter than the other but will not affect the current flow since the two coils are in series. Each coil will also experience an axial variation in temperature within each layer due to heating of the water. Because of the temperature coefficient of resistivity this effect will lead to a non-uniform current density within each coil. It is calculated, as mentioned before, that this will cause a field gradient of about 2 oersteds per cm at full power. This distortion of the field was not considered intolerable since compensation can be effected with the gradient coils.

The choice of wire thickness mentioned above alowed a space of 0.027 in. between layers. It was determined experimentally that the available water pressure (100 psi) would allow ample cooling water to flow through the coils with this spacing. The heat removal rate at 1700 kw is about 25 watts per sq cm. This was considered a conservative figure since other solenoids designed by Professor F. Bitter[5] have operated at 200 watts per cm^2. We hope that the moderate heat removal rate will allow us to get away with poor heat transfer conditions at the points where the windings are supported.

The layer of insulation causes the copper to operate at a higher temperature than if water were in direct contact with the metal. This problem was studied by passing current through water-cooled wires having various thicknesses of Formex insulation. By a combination of measurements and calculations it was found that with a single layer (0.00075 in. thick) the copper would be about 40°C hotter than the water at full power. It was felt that the insulating value of the Formex more than offset the disadvantage of operating the copper at this temperature.

4. *Support of the Windings*

An accurate space of 0.027 in. between layers was achieved by inserting axially oriented micarta strips between each layer. These strips were obtained by milling slices 0.027 in. thick from a sheet of 0.050-in.

§ Sold by the General Electric Company.

[5] F. Bitter, Rev. Sci. Instr. 7, 482 (1936).

CC-0. In Public Domain. Gurukul Kangri Collection, Haridwar

Digitized by Arya Samaj Foundation Chennai and eGangotri

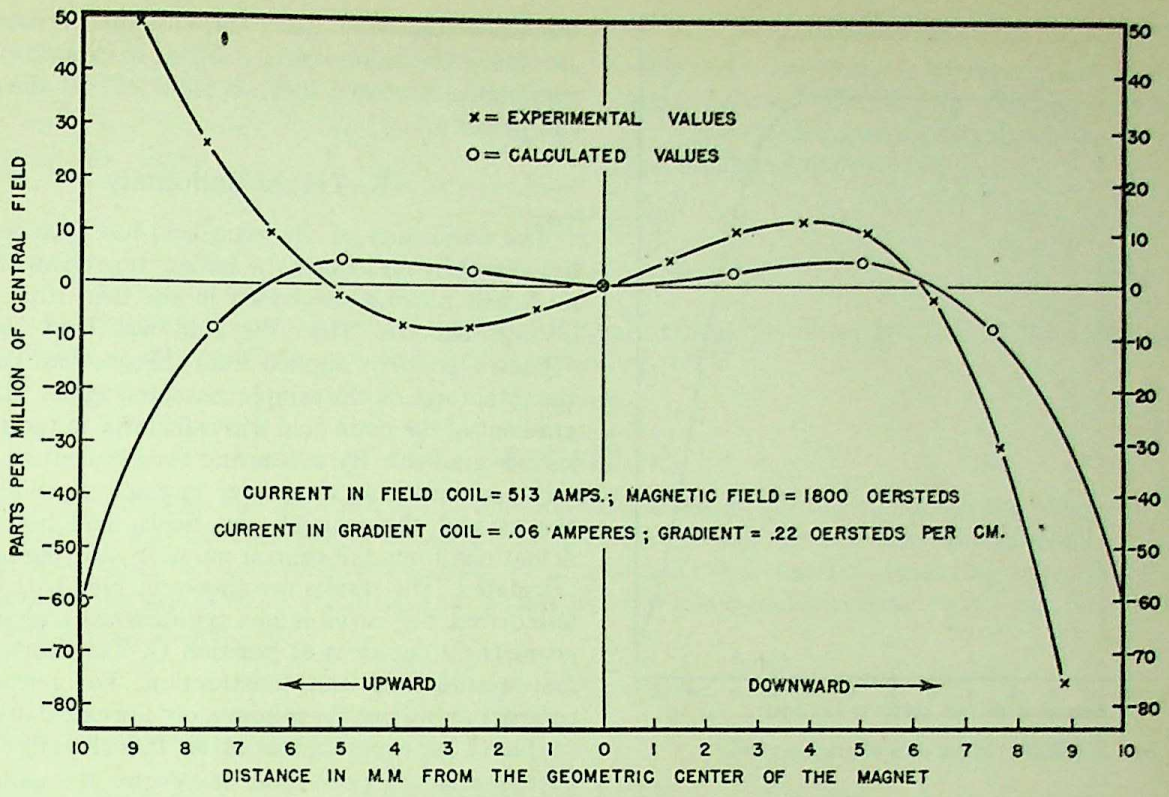


FIG. 4. Uniformity of magnetic field when compensated by gradient coil.

thickness. There are 42 equally positioned spacers around each turn of the helix, and the successive layers of spacers lie over each other exactly. This positioning was achieved by having the spacers slightly longer than the coil width and then having the projecting ends fit into radial slits which were cut into radial micarta spokes. There are 42 spokes and these are in contact with the side of the coils as shown in Fig. 2. The ends of the spokes are inserted into slots which are recessed into the brass pipe at the center and the micarta casing at the outside. In order to achieve a perfect helix for the innermost layer to avoid a hump at every layer and a perfect circle for the outermost spacers which must make good contact everywhere with the 5/16 in. thick copper ring for terminal connection, the micarta spacers at these layers were machined to a series of increasing thicknesses.

The windings are not in contact with flowing water over the 0.050-in. width of each spacing strip. It is believed that conduction of heat through the copper will avoid overheating at these points. The faces of the spokes in contact with the sides of the winding are 3/16 in. wide. These faces were not tapered since support of the coil against axial forces was considered more important than avoidance of eddys in the water flow.

The radial forces acting on the conductors were given some consideration. These forces are transmitted through the spacers, and at the outermost turn the force per spacer is estimated to be about 1500 lb at 10 000 amperes. It was determined by means of compression tests that the flat spacers described above did not appreciably indent the copper or damage the Formex insulation at this load.

5. *Terminal Connections*

Slabs of copper 5/16 in. thick and of coil width were shaped into rings which were placed around the outer turn of each coil in good contact against the outer layer of spacers. The ends of the slabs were tapered and then overlapped to form a passage which was a continuation of the coil helix. The flat wires were brought out through this passage and were then soldered and riveted to the copper ring over a distance of about two inches in the region of overlapping ends. The ring was attached to the micarta casing by means of brass keys in order that there could be no unwinding of the coil, especially when the winding tension on the wires was released. The final step was to cut the wires and then carefully machine the outside of the copper ring to a perfect surface. The wires of both coils were terminated in about the same angular position with respect to the coil axis.

Electrical contact was made by clamping massive slabs of copper around each of the coils. The slabs were accurately machined to make a light mechanical contact with the copper rings when the bolts were tightened in order not to crush the coil. These bolts were calculated to be strong enough to resist the bursting forces of the coil at full current.

6. *Miscellaneous*

The outer casing of the apparatus consists of micarta shells in order to minimize insulation and leakage cur-

CC-0. In Public Domain. Gurukul Kangri Collection, Haridwar

Digitized by Arya Samaj Foundation Chennai and eGangotri

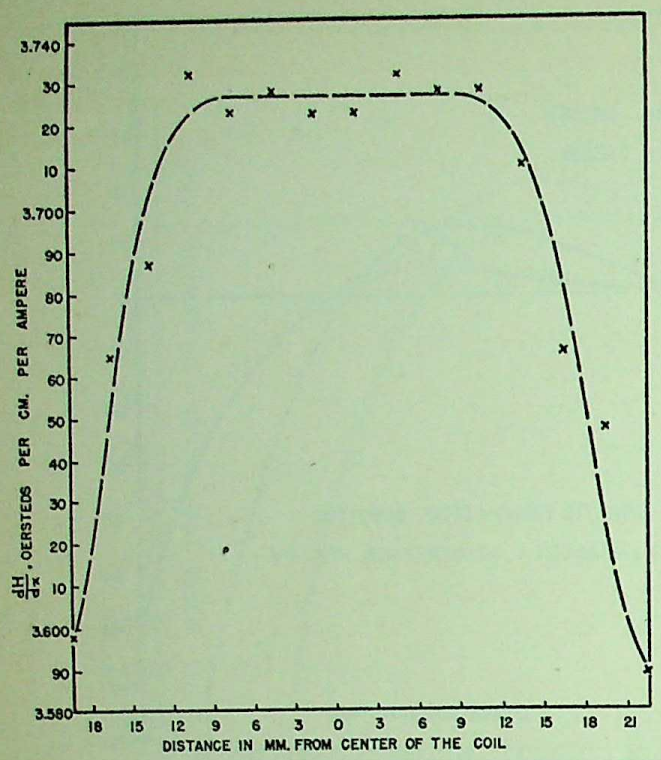


FIG. 5. (dH/dx) along axis of gradient coil.

rent problems. The end plates consist of brass which are bolted to a flange on the central pipe as shown in Fig. 2 and are held together with axial tie rods on the outside.

Water leakage is prevented with an assortment of rubber gaskets and O rings at various points. These gaskets were located in such a way that dead water does not occur at any place across an electrical potential.

The assembled magnet is supported along the length of the heavy copper terminals. Thus the solenoid casing hangs from these terminals and is free to expand or contract without pulling apart at the gasketed joints.

B. Gradient Coils

The gradient coils were located and dimensioned as shown in Fig. 2.

There are three layers with 55 turns per layer of No. 19 Formex-covered wire with a 0.026-in. space between layers. A stream of water in parallel with the main circuit effects cooling. The coils are wound on threaded brass bushings in order that the distance of separation may be accurately varied. Likewise, the two gradient coils together may be moved axially by means of the threaded end caps. The No. 19 wire is fastened to heavier copper rod inside the end plates and this rod comes out through insulated Wilson seals.

EXPERIMENTAL RESULTS

A. Test of Magnet

The apparatus was connected up to the water and power source on a temporary basis and operated at 5000 amperes for several hours. At this current which corresponds to about 300 kw the field strength was measured to be 18 000 oersteds, which agrees well with our calculated value using the measured resistivity of the coil. Everything went according to expectation, and therefore we believe that no troubles will develop at full power.

B. Test of Uniformity

The uniformity of the main field has been tested at low power by measuring the force acting on an annealed steel ball bearing suspended in the field from an analytical balance. Then the field was kept constant, a known gradient applied from the gradient coil, and the total force on the sample measured again. The small gradient of the main field was calculated in terms of the known gradient. By measuring the gradient at successive positions near the center in small intervals along the axis of the magnet, the fields, and hence their deviations from the central value in this region, were calculated. The results are shown in Fig. 3. It is to be noted that the curve is not symmetrical and that the geometrical center is at position G. This imperfection may result from the construction. For purposes of comparison we put the minimum of the calculated curve at that of the experimental curve. It is clear from Fig. 3 that in a small region near the center the actual uniformity is a little worse, but in larger regions better than the calculated values, and that the field near the geometrical center is almost linear making a small slope with the axis. If the small slope is compensated by means of the gradient coil, an almost entirely flat region of about 5 mm can be obtained. For a little under compensation a uniformity of about 10 parts per million in a distance of 13 mm can be reached, as shown in Fig. 4.

The uniformity of the gradient has been roughly tested by quickly shifting a search coil successively along the axis in definite, small intervals and observing

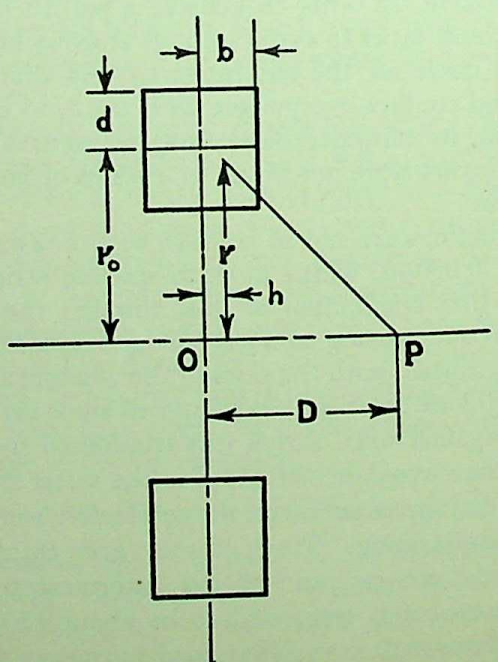


FIG. 6. Current element of radius r.

CC-0. In Public Domain. Gurukul Kangri Collection, Haridwar

Digitized by Arya Samaj Foundation Chennai and eGangotri

the change of field by means of a ballistic galvanometer. Figure 5 shows this rough determination. The scattered points showing the experimental error are not a measure of the true uniformity since this is beyond the sensitivity of the apparatus.

ACKNOWLEDGMENTS

We wish to express our appreciation of the assistance of Mr. Francis Vidito and Mr. Oscar James Van Sant, Jr., who supplied many valuable ideas for the actual construction of the solenoid.

APPENDIX

Derivation of Field Equation

If I is the current density in amp/cm^2 of a circular current element of radius r (see Fig. 6), the field at a point P on the axis at a distance D from the center of the cylindrical coil is

$$\frac{2\pi I r^2 dr dh}{10\{(D-h)^2+r^2\}^{\frac{3}{2}}}.$$

If the cooling water comes in from one end of the coil and goes out at the other, the heating effect and hence the current density I may be, assumed linear along the axis of the coil and can be expressed as $I=I_0(1-ch)$, where I_0 is the current density at the middle cross section of the coil and c is a constant depending upon the temperature gradient along the axis. The total field at point P, due to the whole cylinder of mean radius r_0, axial width $2b$, and radial thickness $2d$, is given by

$$H=\frac{2\pi}{10}\int_{-b}^{b}\int_{r_0-d}^{r_0+d} I_0(1-hc)\frac{r^2 dr dh}{\{(D-h)^2+r^2\}^{\frac{3}{2}}}.$$

Evaluating the integrals we obtain

$$H=\frac{2\pi I_0}{10}\left[\left\{1-\frac{c(D-b)}{2}\right\}(D+b)\log_e\frac{r_0+d+[(D+b)^2+(r_0+d)^2]^{\frac{1}{2}}}{r_0-d+[(D+b)^2+(r_0-d)^2]^{\frac{1}{2}}}-\left\{1-\frac{c(D+b)}{2}\right\}(D-b)\right.$$
$$\left.\times\log_e\frac{r_0+d+[(D-b)^2+(r_0+d)^2]^{\frac{1}{2}}}{r_0-d+[(D-b)^2+(r_0-d)^2]^{\frac{1}{2}}}\right]+\frac{2\pi I_0 c}{10}\left[\frac{r_0+d}{2}[(D-b)^2+(r_0+d)^2]^{\frac{1}{2}}+\frac{r_0-d}{2}[(D+b)^2+(r_0-d)^2]^{\frac{1}{2}}\right.$$
$$\left.-\frac{r_0+d}{2}[(D+b)^2+(r_0+d)^2]^{\frac{1}{2}}-\frac{r_0-d}{2}[(D-b)^2+(r_0-d)^2]^{\frac{1}{2}}\right]. \quad \text{(A1)}$$

Taking account of the two identical coils separated at a distance $2Sr_0$ and substituting the coil dimensions in terms of the mean radius r_0, i.e., $d=yr_0$, $b=kd=kyr_0$, and $D=Sr_0$, we find the field on the common axis at a distance xr_0 from the center of the Helmholtz pair to be

$$H=\frac{2\pi I_0 r_0}{10}\left[\left\{1-\frac{cr_0(S+x-ky)}{2}\right\}\left\{(S+x+ky)\log_e\frac{1+y+[(S+x+ky)^2+(1+y)^2]^{\frac{1}{2}}}{1-y+[(S+x+ky)^2+(1-y)^2]^{\frac{1}{2}}}\right\}\right.$$
$$-\left\{1-\frac{cr_0(S+x+ky)}{2}\right\}\left\{(S+x-ky)\log_e\frac{1+y+[(S+x-ky)^2+(1+y)^2]^{\frac{1}{2}}}{1-y+[(S+x-ky)^2+(1-y)^2]^{\frac{1}{2}}}\right\}$$
$$+\left\{1+\frac{cr_0(S-x-ky)}{2}\right\}\left\{(S-x+ky)\log_e\frac{1+y+[(S-x+ky)^2+(1+y)^2]^{\frac{1}{2}}}{1-y+[(S-x+ky)^2+(1-y)^2]^{\frac{1}{2}}}\right\}$$
$$\left.-\left\{1+\frac{cr_0(S-x+ky)}{2}\right\}\left\{(S-x-ky)\log_e\frac{1+y+[(S-x-ky)^2+(1+y)^2]^{\frac{1}{2}}}{1-y+[(S-x-ky)^2+(1-y)^2]^{\frac{1}{2}}}\right\}\right]$$
$$+\frac{\pi c I_0 r_0^2}{10}[(1+y)\{[(S+x-ky)^2+(1+y)^2]^{\frac{1}{2}}-[(S-x-ky)^2+(1+y)^2]^{\frac{1}{2}}\}$$
$$+(1-y)\{[(S+x+ky)^2+(1-y)^2]^{\frac{1}{2}}-[(S-x+ky)^2+(1-y)^2]^{\frac{1}{2}}\}$$
$$-(1+y)\{[(S+x+ky)^2+(1+y)^2]^{\frac{1}{2}}-[(S-x+ky)^2+(1+y)^2]^{\frac{1}{2}}\}$$
$$-(1-y)\{[(S+x-ky)^2+(1-y)^2]^{\frac{1}{2}}-[(S-x-ky)^2+(1-y)^2]^{\frac{1}{2}}\}]. \quad \text{(A2)}$$

CC-0. In Public Domain. Gurukul Kangri Collection, Haridwar

Digitized by Arya Samaj Foundation Chennai and eGangotri

It is expected that the main field is superimposed by an auxiliary field which is proportional to the parameter c.

If c is zero, which means the coil temperature is uniform and the current density is constant throughout the Helmholtz pair, the above formula is reduced to the following simple form:

$$H=\frac{2\pi I_0 r_0}{10}\left[\left\{(S+x+ky)\log_e\frac{1+y+[(S+x+ky)^2+(1+y)^2]^{\frac{1}{2}}}{1-y+[(S+x+ky)^2+(1-y)^2]^{\frac{1}{2}}}\right\}\right.$$

$$-\left\{(S+x-ky)\log_e\frac{1+y+[(S+x-ky)^2+(1+y)^2]^{\frac{1}{2}}}{1-y+[(S+x-ky)^2+(1-y)^2]^{\frac{1}{2}}}\right\}$$

$$+\left\{(S-x+ky)\log_e\frac{1+y+[(S-x+ky)^2+(1+y)^2]^{\frac{1}{2}}}{1-y+[(S-x+ky)^2+(1-y)^2]^{\frac{1}{2}}}\right\}$$

$$\left.-\left\{(S-x-ky)\log_e\frac{1+y+[(S-x-ky)^2+(1+y)^2]^{\frac{1}{2}}}{1-y+[(S-x-ky)^2+(1-y)^2]^{\frac{1}{2}}}\right\}\right] \tag{A3}$$

$$=2\pi I_0 r_0 g/10, \tag{A4}$$

where g is the square bracket of Eq. (A3).

CC-0. In Public Domain. Gurukul Kangri Collection, Haridwar

Digitized by Arya Samaj Foundation Chennai and eGangotri

REVIEWS OF MODERN PHYSICS VOLUME 25, NUMBER 1 JANUARY, 1953

Symposium on Exchange—Introduction

C. KITTEL

University of California, Berkeley, California

THIS symposium consisted of a round-table discussion on exchange forces in ferromagnetics, and began with the presentation of invited papers by C. Zener, J. C. Slater, E. P. Wohlfarth (read by E. C. Stoner), and J. H. Van Vleck. A lengthy but lively discussion period, partly with the audience participating, followed the invited papers. It is unfortunately not possible to reproduce here the discussions, but R. Smoluchowski has been kind enough to prepare a brief summary and reconciliation of the invited papers: his discussion follows here after the papers.

REVIEWS OF MODERN PHYSICS VOLUME 25, NUMBER 1 JANUARY, 1953

Exchange Interactions

C. ZENER AND R. R. HEIKES

Westinghouse Research Laboratories, East Pittsburgh, Pennsylvania

I. INTRODUCTION

EXCHANGE interaction represents a characteristic quantum effect having no analog in classical mechanics. Before defining exchange interaction, we shall give a simple example of a two-electron system. Let A and B represent two quantum states, and let suffixes α and β represent electron spins pointing parallel and antiparallel, respectively, to some preferred direction. Then the two states $A_\alpha B_\beta$ and $A_\beta B_\alpha$ are degenerate, i.e., have the same energy. Since these two states combine, more appropriate wave functions are

$$\psi_S = A_\alpha B_\beta + A_\beta B_\alpha,$$
$$\psi_A = A_\alpha B_\beta - A_\beta B_\alpha.$$

These states are no longer degenerate. The energy values will be denoted by E_S and E_A, respectively. The energy difference $E_S - E_A$ is called the exchange energy. The quantity $(E_S - E_A)/h$ is called the exchange frequency, and may be given the following vivid interpretation. Suppose that, through the appropriate linear combination of $\psi_S \exp(-iE_S t/\hbar)$ and of $\psi_A \exp(-iE_A t/\hbar)$, we construct an approximate solution to the time dependent wave equation which reduces to $A_\alpha B_\beta$ at $t=0$. We then have a wave function which oscillates between $A_\alpha B_\beta$ and $A_\beta B_\alpha$ with the exchange frequency.

Exchange energy is of particular importance to magnetism since the two states ψ_S and ψ_A represent different spin configurations. In the first state the two electron spins are parallel, in the second state they are antiparallel. This difference in relative spin orientation is necessarily associated with a difference in electron configuration. Thus, in the first state ψ_S, the two electrons have a tendency to avoid one another, while in the second state ψ_A, the contrary is the case. It is, in fact, just this difference in electron configuration which gives rise to the exchange energy. In general, we define as the exchange energy that part of the total energy of a system which is dependent upon relative spin orientation, this energy excluding the pure magnetic energy arising from dipole-dipole interaction.

Since an exchange interaction has a meaning only in reference to the approximate wave functions with which we choose to describe our system, it is necessary in discussing such interactions to clearly describe the approximate wave functions from which one starts. A considerable difference of opinion exists as to the most appropriate type of approximate wave functions for solids. The most appropriate approximate wave functions for a particular investigation will depend to some extent upon the objective of the investigation. If this objective is to understand the basis for the various types of crystal structure, it is conceivable that the most appropriate starting wave functions for all the electrons will be the localized atomic wave functions. If this objective is to make a precise calculation of the binding energy, it is probable that the most appropriate approximate wave function for all electrons will be the band functions, i.e., solutions of a periodic potential. If, as in the present case, the objective is to understand the magnetic properties, the authors believe that for the inner incomplete d shell electrons the localized atomic wave functions are the most appropriate, while for the outer s electrons the band wave functions are the most appropriate. The last type of description will therefore be used in the present paper.

CC-0. In Public Domain. Gurukul Kangri Collection, Haridwar

Digitized by Arya Samaj Foundation Chennai and eGangotri

II. DOMINANT EXCHANGE INTERACTIONS

Once having decided on our initial approximation to describe d electrons by localized atomic wave functions, outer s electrons by band wave functions, we find the following types of exchange interactions to be of dominant importance for magnetic properties.

A. Arising from an Exchange of Electrons within the d Shell of the Same Atom

This exchange interaction has been found by Slater[1] to provide the physical basis for Hund's rule[2] of highest multiplicity. Applied to the transition metal atoms or ions, this rule states that when a d shell first begins to be filled, all the electron spins point in the same direction. When the d shell is half-filled, five electrons have spins pointing in the same direction. Thereafter, further added electrons have spins pointing in the opposite direction. Hund's rule may be unambiguously tested for those transition metal ions in which the orbital angular momentum is completely quenched, as manifested by g being equal to 2. Such quenching appears to be complete in cubic lattices, examples of which are the ferrites[3] and the manganese perovskites.[4,5] In all these examples the saturation magnetic moment is just that which is predicted by application of Hund's rule. Since the consequences of the exchange interaction between electrons within the d shell of the same atom have been known for many years, and since there appears to be no difference of opinion regarding this exchange interaction, it will not be further discussed in this paper.

B. Arising from an Exchange of Electrons between the d Shells of Adjacent Atoms

This interaction, which we shall henceforth call *direct-exchange*, has been, and still is, the subject of considerable controversy. The controversy is over the sign of the exchange integral J. A positive J corresponds to a ferromagnetic coupling, a negative J to an antiferromagnetic coupling. Now the usual sign of J is negative, as is necessary in order that a chemical bond may be formed. In his classic paper on ferromagnetism Heisenberg[6] assumed that the direct exchange furnished the ferromagnetic coupling in Fe, Co, and Ni. In explaining the positive sign of J which such a coupling demanded, he pointed out that for a sufficiently large value of principal quantum number one would indeed anticipate a change in J from a negative to a positive sign. Heisenberg's explanation was rather unsatisfactory in that it left uninterpreted the absence of ferromagnetism in the second and third transition periods, which according to his reasoning should be stronger than in the first transition period.

A way out of this dilemma was found by Slater,[7] who emphasized the importance of the degree of overlap of the d shells. He postulated that as the degree of overlap decreased from a large to a small value, J changed from a negative to a positive quantity. Since the degree of overlap is a continuously decreasing function of the ratio (internuclear distance)/(radius of d shell), Slater assumed that J varied in the general manner as indicated in Fig. 1. This single postulate explained not only why the ferromagnetism does not occur in the second- and third-row transition period, where the ratio (internuclear distance)/(radius of d shell) is smaller than in the first period, but also why only the last elements in the first transition row are ferromagnetic.

Slater's postulate was sufficiently satisfying so that it was accepted until 1951 by all those workers in the field who used the localized atomic model for the d electrons. In 1951 one of the present authors[8] pointed out that an important exchange interaction (see Sec. D) had heretofore been neglected, and that, when it was taken into account, the necessity for a positive J disappeared. It therefore appeared more logical to assume that the magnitude of J decreases as the ratio (internuclear distance)/(radius of d shell) increases. In view of the current interest in this subject, detailed arguments, of both theoretical and empirical character, are now presented in support of the thesis that J varies as represented in Fig. 2 rather than as in Fig. 1.

The exchange integral corresponding to the exchange of a single pair of electrons between two atoms contains two dominant terms,

$$J=A+B.$$

Here A is the mutual energy of the two exchange charge distributions, while B is the sum of the energies of the

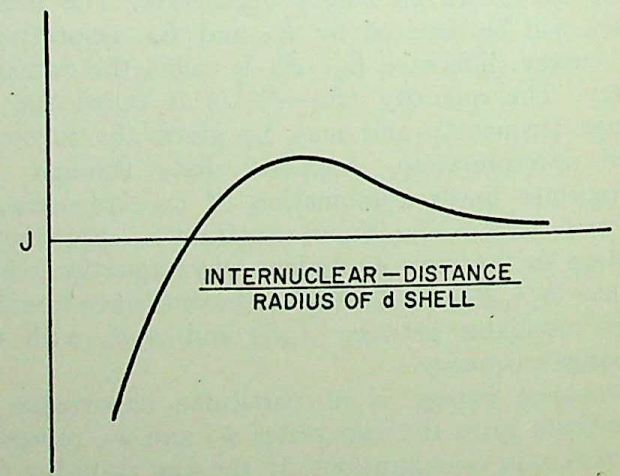


FIG. 1. Variation of exchange integral postulated by Slater (see reference 7).

[1] J. C. Slater, Phys. Rev. 34, 1243 (1929).
[2] F. Hund, *Linienspektren und Periodisches System der Elemente* (Verlag Julius Springer, Berlin, 1927) p. 124.
[3] L. Neel, Ann. phys. 3, 137 (1948).
[4] G. H. Jonker and J. H. Van Santen, Physica 16, 337 (1950).
[5] J. Volger, *Semi-Conducting Materials* (Butterworths Scientific Publications, Ltd., London, 1951), p. 162.
[6] W. Heisenberg, Z. Physik 49, 619 (1928).
[7] J. C. Slater, Phys. Rev. 36, 57 (1930).
[8] C. Zener, Phys. Rev. 81, 440 (1951); 83, 299 (1951).

CC-0. In Public Domain. Gurukul Kangri Collection, Haridwar

Digitized by Arya Samaj Foundation Chennai and eGangotri

two exchange charges in the "reduced" potential of the two atoms. In obtaining the reduced potential, we first take the actual potential of the two atoms, the two electrons which are exchanging being considered as absent. This potential is then multiplied by the total exchange charge of one of the exchanging electrons. The first term A is always positive, while the second term B is always negative. The sign of J therefore depends upon which of the two terms dominates.

Under certain conditions A dominates. This occurs when the pertinent wave function on the two atoms are orthogonal to one another, thereby leading to a zero total exchange charge, and hence to a zero B. This condition is satisfied in a diatomic molecule when the exchanging electrons are in two states having angular momental with different projections on the axis of the molecule. Under this condition, J is positive for all distances of separation.

Another set of conditions favors the dominance of B. This condition is that the atoms between which the two electrons are exchanging have several electrons in the same shell as the exchanging electrons. Since these additional electrons shield the nuclei only partially, they increase the magnitude of the reduced potential of the two atoms, and hence increase the magnitude of the negative B.

When we are having an exchange of electrons between two closed shells, the situation is rather ambiguous from the strictly theoretical viewpoint. On the one hand, we have many exchanges between states which are mutually orthogonal. Thus the exchange integral between two filled d shells involves 40 exchanges between mutually orthogonal states, only 10 between states which are not mutually orthogonal. On the other hand, the large number of electrons in the closed shells insures a relatively large reduced potential, and therefore favors the dominance of B. The situation is perfectly clear, however, from the experimental viewpoint. Under all cases which have been observed, the exchange interaction between closed shells is a repulsive interaction. Thus in the interaction between inert gas atoms, between ions in ionic crystals, and between the inner cores in Cu, Ag, and An, the overlapping of the charge distributions leads to a repulsion at all those distances of separation at which interactions have been observed. Since the transition metals Fe, Co, and Ni have a large number of electrons in the d shell, larger than the number of electrons in the outer closed shell of the inert gases, it appears likely that they will also have a repulsive exchange interaction, and that the repulsion will be greater the larger the number of exchanges. Since exchange occurs only between parallel spins, we conclude that the repulsive exchange interaction between incomplete d shells will be greater when the spins are aligned parallel than when aligned antiparallel.

We shall now review some of the consequences of the antiferromagnetic coupling of direct exchange.

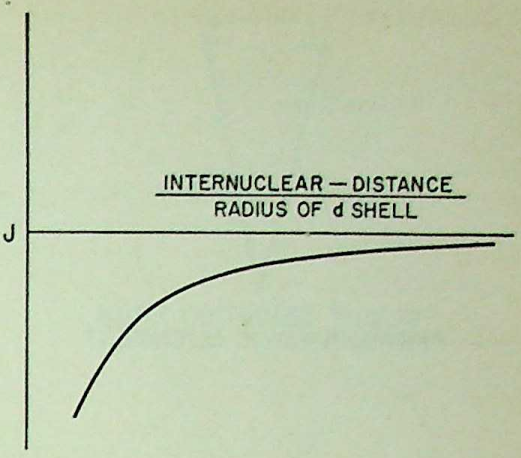


FIG. 2. Variation of exchange integral postulated by Zener.

We anticipate that metals will crystallize in a close-packed structure provided no counteracting tendency is present. One counteracting tendency, operating at high temperature, is the increased entropy associated with the larger amplitudes of vibration of loose-packed structures. This entropy effect is probably responsible for the close packed→body centered cubic (b.c.c.) transition at high temperatures in Ti, Zr, and Fe. Another counteracting tendency must, however, be operating in the case of the transition metals of the V and Cr columns (V, Cb, Ta; Cr, Mo, Ta). These metals retain their loose b.c.c. lattice down to the lowest temperatures. One of the authors[3] has ascribed this b.c.c. structure to the direct exchange between adjacent d shells. In this structure it is possible for nearest neighbors to have an antiparallel alignment of spin, whereas in a close-packed lattice such an antiparallel arrangement is not possible. After this interpretation of the b.c.c. structure in the V and Cr columns was proposed, several investigations have appeared which corroborate this interpretation. These are discussed below.

(1) The above interpretation leads to the prediction of an ordered arrangement of spins in the V and Cr columns of the transition metals. An extensive search for such an ordered arrangement has been made by Shull. As we discussed in this conference, he has found negative results in all cases except Cr. Here he finds an ordered arrangement which disappears at 500°K. The experimental magnitude of the magnetic moments is, however, an order of magnitude less than the theoretical. The inconsistencies between theory and experiment can possibly be interpreted in terms of the intrinsic instability associated with an antiferromagnetic arrangement. As indicated in Fig. 3, when two spins which are coupled ferromagnetically become slightly uncoupled, they suffer a slight precession, whereas in the case of an antiferromagnetic coupling they undergo a large precession. This interpretation of Shull's negative results can be taken seriously only if the period of precession is comparable to or less than

CC-0. In Public Domain. Gurukul Kangri Collection, Haridwar

Digitized by Arya Samaj Foundation Chennai and eGangotri

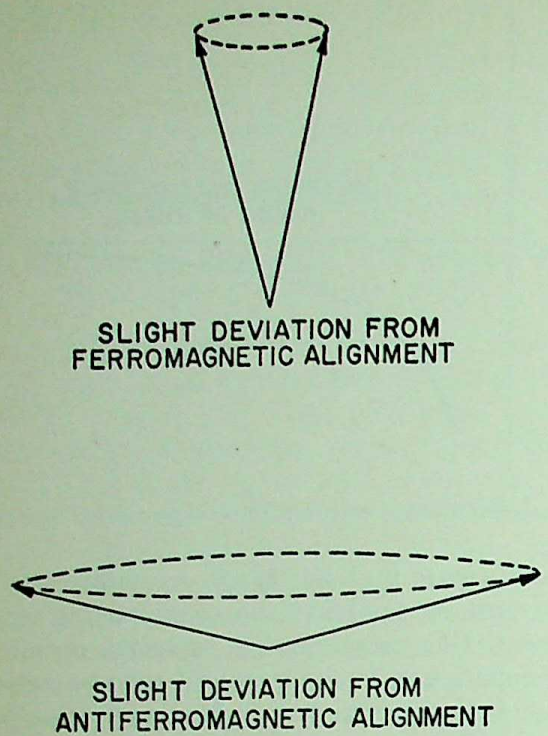


FIG. 3. Comparison of precession in cases of ferromagnetic and antiferromagnetic coupling.

the time of flight of a neutron through a single atom. In order to estimate the precessional frequency, we shall consider two spins of mechanical moment of momentum nh each, the energy J being required to change the relative orientation from an antiparallel to a parallel alignment. We then find that if the uncoupling energy is kT, and if kT is small compared to J, the precessional frequency ν is given by

$$nh\nu \simeq 2(JkT)^{\frac{1}{2}}.$$

Upon taking T as 300°K, J as $2kT$, n as 5/2 appropriate to the Cr d shell, we obtain the period of precession as 1.4×10^{-13} second. This period is of the same order as the time of transit of a neutron through a Cr atom, the neutron having a velocity suitable for diffraction studies. We thus see that the negative results of Shull may arise from the comparatively long time of transit of the neutrons through the individual atoms.

(2) An antiferromagnetic arrangement of spins should be accompanied by a rise in magnetic susceptibility with increasing temperature until the Curie temperature is reached. Such an increase has in fact been found by McGuire and Kriessman[9] in the case of Cr. In this metal the magnetic susceptibility continues to rise up to the highest temperature investigated, namely, 1400°C. At the upper part of this range the susceptibility rises at an accelerated rate as if a Curie temperature were not far above 1400°C.

(3) The metal Cr has been found by Friedberg[10] to have an anomalously low electronic specific heat at low temperatures. The electronic specific heat is linear in T, the coefficient of T being commonly denoted by γ, and is expressed in units of 10^{-4} calorie/mole-°C. The γ of Cr is only 3, as compared to the value of 15 for V, to the left of Cr, and to the value of 42 for Mn, the metal to the right of Cr. This anomalously low value of γ for Cr is just what our model would predict. Whereas in the band description of metals it is commonly assumed that the potential for an electron is the same in every atom, it is of course only necessary to assume that the potential has the periodicity of the lattice. In particular, in our model, an electron with a positive spin (α) sees a lower potential on that simple cubic lattice occupied by atoms whose d electrons all have positive spins (α). Our model requires that the energy band is thereby split into two parts, the lower band for an α-electron corresponding to the electron spending most of its time on α-type atoms, the upper band corresponding to the electron spending most of its time on β-type atoms. The lower band is thus precisely filled by the 5 electrons in the d shell of the Cr atoms. The d electrons thus contribute essentially nothing to the specific heat. The only other metal in the Cr column whose electronic specific heat has been measured is W. Whereas in all other metals the γ measured at high and at low temperatures agree, they are here in marked disagreement.[11] The high temperature measurement yields a low value of 5, in accord with our ideas, while the low temperature measurement yields a high value of 51, in discord with our ideas. This discrepancy in γ as measured at high and at low temperature is in fact in discord with any current theory of the electronic structure of the metals.

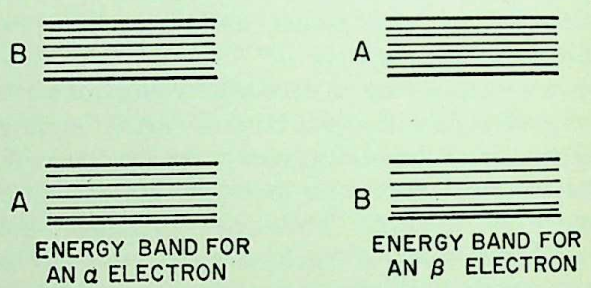


FIG. 4. Energy bands in chromium metal. Wave functions of A bands are concentrated on the A simple cubic lattice, those of the B bands on the B simple cubic lattice.

(4) One of the most convincing arguments for the intrinsic antiferromagnetic nature of the b.c.c. lattices of the V or Cr columns has been presented by Isenberg[12] through a theoretical analysis of elastic constants. Two independent elastic shear coefficients of cubic metals are C_{44} and $(C_{11}-C_{12})/2$. We shall define the elastic anisotropy factor by

$$A = 2C_{44}/(C_{11}-C_{12}).$$

[9] T. R. McGuire and C. J. Kriessman, Phys. Rev. 82, 774 (1951); 85, 452 (1952).
[10] Friedberg, Estermann, and Goldman, Phys. Rev. 85, 375 (1952).
[11] A. A. Silvidi and J. G. Daunt, Phys. Rev. 77, 125 (1950).
[12] I. Isenberg, Phys. Rev. 83, 637 (1951).

CC-0. In Public Domain. Gurukul Kangri Collection, Haridwar

Digitized by Arya Samaj Foundation Chennai and eGangotri

Isenberg has shown that, with neglect of very small terms, this factor may be written as

$$A=(8/9)[r^2W'']_1/\{(8/3)[rW']_1+[r^2W'']_2\}.$$

Here W refers to the mutual potential energy of the cores of two atoms at a distance r apart. The subscripts 1 and 2 indicate that the bracketed expressions are to be taken for first nearest and for second nearest neighbors, respectively. If now W represented a repulsive potential energy which decreased monotonically with r, we would conclude that the anisotropy factor A would be quite large. This conclusion would be reached by observing that rW'' would be considerably larger for first nearest than for second nearest neighbors, and that rW' would be negative. Actually, such is indeed the case for the b.c.c. lattice of β-brass, where A is 8.8. It is quite impossible to make A unity by a reasonable repulsive W. A natural interpretation for the low values of A observed for tungsten and for molybdenum,[25] namely, 1.0 and 0.71, is to assume, that W is attractive for nearest neighbors, repulsive for next nearest neighbors, as indicated in Fig. 5. Such an interpretation makes sense only if an antiferromagnetic structure is postulated for W, nearest neighbors thereby having no direct exchange between their d shells, but next nearest neighbors having such exchange. Hsu[13] has found that the high binding energy for tungsten is given by such an antiferromagnetic structure, the binding energy coming primarily from the classical attraction of two interpenetrating diffuse negative charges in each of which is imbedded concentrated positive charges of like magnitude.

C. Arising from an Exchange of Electrons within the Conduction Band

The sign of this exchange interaction is the same as of the exchange interaction discussed in Sec. A above, and hence tends towards a parallel alignment of the spins of all the conduction electrons. In contrast to the case of the exchange interaction of Sec. A this aligning tendency is opposed by the anti-aligning tendency of the kinetic energy. Thus the kinetic energy is a minimum when half the spins point in one direction, the other half in the other direction. Under ordinary conditions the anti-aligning tendency of the kinetic energy is dominant, resulting in a zero net spin. Bloch[14] has pointed out, however, that for a sufficiently low concentration of conduction electrons the aligning tendency of the exchange interaction is dominant, resulting in the magnetization of the conduction electrons. The critical electron density which separates the region where the kinetic energy dominates from the region where the exchange energy dominates is in the vicinity of the density of the conduction electrons in cesium. Wigner[15] has, however, pointed out that such a magnetization of the conduction electrons would probably not take place, since at just about the same electron density the conduction electrons automatically become localized about lattice positions. Nonetheless, the exchange interaction arising from an exchange of electrons within the conduction band is of importance in helping to align the incomplete d shells of the transition metals, as is discussed later in this section.

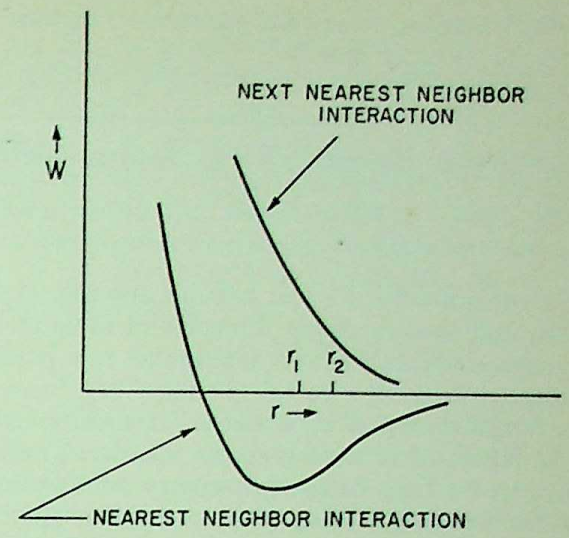


FIG. 5. Interactions postulated by Isenberg for tungsten.

D. Arising from an Exchange of Electrons between the Conduction Band and the Incomplete d Shells

Hund's rule of highest multiplicity applies to the coupling of the spin of an outer s electron to the spin of an incomplete d shell of isolated atoms, as well as to the coupling of the spins of the d electrons among themselves. When the outer s shell contains only one electron, the state of lowest energy will thus be that in which the spin of this s electron is aligned parallel with the spin of the inner incomplete d shell (see Table I). In Table I we consider the lowest configuration in which the outer s shell contains only one electron, and compare the two energies where the spin of this electron is parallel and antiparallel to that of the inner d shell.

In the model which we have adopted, the outer s electrons of the isolated atoms become conduction electrons in the condensed metallic state. The exchange interaction between a conduction electron and an inner incomplete d shell will therefore be ferromagnetic in nature. Each individual conduction electron tends to align the spins of the incomplete d shells in a direction parallel to its own spin. In the usual model of conduction electrons, equal numbers have spins pointing in one direction as in the opposite direction, and hence the net influence upon the spin of the incomplete d shells is zero. As soon as we relax the condition of equal numbers of conduction electron spins pointing in opposite directions, we find that the total energy of

[13] Yee-Chuang Hsu, Phys. Rev. 83, 975 (1951).
[14] F. Bloch, Z. Physik 57, 545 (1929).
[15] E. Wigner, Trans. Faraday Soc. 34, 678 (1938).

CC-0. In Public Domain. Gurukul Kangri Collection, Haridwar

Digitized by Arya Samaj Foundation Chennai and eGangotri

TABLE I. Coupling energy ΔE of spin of outer s electron to that of inner d shell.

	Cr	Mn	Fe	Co	Ni
Metal configuration	$3d^5(^7S)4s$	$3d^6(^5D)4s$	$3d^7(^4F)4s$	$3d^8(^4F)4s$	$3d^9(^2F)4s$
ΔE, in ev	0.92	0.77	0.62	0.50	0.30

the system is lowered by first aligning the spin of the d shells, and then reversing the spins of some of the conduction electrons from an antiparallel to a parallel alignment.

The formal theory[8] of the above exchange interaction may be presented in a very simple manner. Towards this end we let E_{spin} be the spin energy per atom of a metal, the zero energy being taken as the unmagnetized state; S_d be the mean component per atom of the d shell spin along the magnetization direction, the unit of spin being a Bohr magneton; and finally S_c be the mean component per atom of the conduction electron spin along the magnetization direction. The spin energy may then be written as

$$E_{\text{spin}}=(\tfrac{1}{2})\alpha S_d^2-\beta S_d S_c+(\tfrac{1}{2})\gamma S_c^2. \quad (1)$$

A minimization of this spin energy with respect to S_c leads to

$$E_{\text{spin}}=(\tfrac{1}{2})(\alpha-\beta^2/\gamma)S_d^2 \quad (2)$$

for

$$S_c=(\beta/\gamma)S_d. \quad (3)$$

The present theory becomes formally identical to the Heisenberg-Slater theory through the following correspondence

$$J=(\beta^2/\gamma)-\alpha. \quad (4)$$

The reason for the success of Slater's theory now becomes evident. The "exchange integral" J is really the difference of two terms. One term β^2/γ arises from the indirect coupling via the conduction electrons. This term is always positive, and is independent of the amount of overlap of adjacent d shells. The second term $-\alpha$ arises from the direct exchange between adjacent d shells. We assume this term to be always negative, and its magnitude decreases rapidly with decreasing overlap of adjacent d shells. The change in sign of the "exchange integral" J with decreasing amount of overlap thus arises naturally as a transition from the dominance of the direct exchange at a large overlap to the dominance of the indirect exchange via the conduction electron at a small overlap.

Whereas in the older theory the ferromagnetic coupling arose from the short-range direct exchange between adjacent d shells, in the present theory the ferromagnetic coupling via the conduction electrons is intrinsically a long-range type. We thus find a natural interpretation of the ferromagnetism of the Heusler alloys and of alloys of the type $CrPt_3$, materials in which the separation of the magnetic atoms is too large to allow an appreciable direct coupling. A quantitative comparison of the predictions of the two theories for different Heusler alloys has been given by one of the authors.[16] The 16 percent difference in volume between the two Heusler alloys Cu_2MnIn and Cu_2MnAl would lead to an increase in 100 percent of the Curie temperature (in °K) of the latter over that of the former alloy according to the Heisenberg-Slater theory, an increase of only 20 percent according to the present theory. The observed increase is in fact just 20 percent. The success of the present theory in providing a qualitative interpretation of ferromagnetism in metals is paralleled by a corresponding success in providing a quantitative estimate of the magnetic coupling. Of the three coupling coefficients in Eq. (1), the last two may be readily estimated. The exchange coupling between the outer s and inner d electrons for isolated atoms is obtained from spectroscopic data. A comparison of the Hartree wave function for the s electrons with the cellular wave function for the metal shows how this exchange coupling is modified in the metal. The estimate of β for Ni is 0.48 ev per atom. The model of a free electron gas for the conduction electrons leads at once to an estimate for γ. This is 2.9 ev per atom for Ni. An estimate is thereby obtained for J by negiect of the direct exchange coefficient α. The estimate so obtained for Ni is 25 percent higher than the observed value, thereby allowing for a small direct coupling.

E. Arising from an Exchange of Valence States between Two Cations of the Same Transition Element

Because of their preoccupation with ionic solids of the NaCl type, physicists customarily think of the cations of ionic crystals as having a fixed degree of ionization, i.e., a fixed valency. Now ionic crystals can usefully be divided into two groups: one in which the cations have closed shells, of which NaCl is a typical example, the other in which the cation does not have a closed shell, a typical example of which is FeO. Crystals of the first class have an extremely small range of composition, and may, for most purposes, be thought of as existing only at the stoichiometric ratio. This narrowness in composition range arises from the fact that in order to create a deficiency in the cation lattice, one or more cations must become further ionized, and large energies are required to ionize a closed shell. Crystals of the second class have, on the whole, a comparatively wide range of composition, corresponding to a variable cation deficiency. This variable cation deficiency is possible only because of the comparative ease with which the cations in the ionic lattice may become further ionized. Common examples of the second group are found in the oxides, sulfides, selenides, and tellurides of the transition metals lying to the right of the Ti column in the periodic

[16] R. Heikes, Phys. Rev. 84, 376 (1951).

CC-0. In Public Domain. Gurukul Kangri Collection, Haridwar

Digitized by Arya Samaj Foundation Chennai and eGangotri

table. A mixture of the cation valency of the same transition element may also be produced by admixing a second cation of restricted valency. For example, if one replaces a small fraction of the Ni atoms in NiO by Li, one Ni^{++} ion is forced to change to Ni^{+++} for each Li atom introduced.

We are currently interested in the second group of crystals since, as has recently been pointed out by one of the authors,[17] the exchange of valence states between two cations of the same transition element leads to a ferromagnetic coupling of the cation spins. That this coupling is of a ferromagnetic nature may be seen from the following argument. Let ψ_1 and ψ_2 represent the two states indicated below,

$$\psi_1: \quad C^{++} \quad C^{+++},$$
$$\psi_2: \quad C^{+++} \quad C^{++}.$$

We shall suppose that each cation is in its lowest energy state, and hence in its state of highest multiplicity. Whereas each state ψ_1 and ψ_2 has the same energy, a state with still lower energy may be obtained by taking one of the linear combinations $\psi_1+\psi_2$ or $\psi_1-\psi_2$, the appropriate linear combination depending upon the sign of the exchange integral. This energy will be lower the greater the exchange integral between these two states. Now the exchange integral will be greatest when the spins of the two cations are aligned parallel. The state of lowest energy therefore represents a ferromagnetic alignment of spins.

In actual ionic crystals, the distances between adjacent cations are usually too large to admit of an appreciable direct interaction. However, this exchange interaction is aided greatly by the intervening anions by a process which is called *double exchange*. In this process an electron jumps from the C^{++} ion to the intervening anion, simultaneous with the jump of a second electron from the anion to the C^{+++} ion.

An interesting feature of double exchange is that it promotes a mechanism not only for ferromagnetic coupling but also for electrical conductivity. If the concentration of C^{++} and C^{+++} ions is comparable, and if the temperature is sufficiently high, an electron leaving a particular C^{++} ion by double exchange has an essentially equal probability of jumping to any of the C^{+++} ions which are its immediate neighbors. Two features of the resulting electrical conductivity deserve special comment. (1) Since under the above conditions the frequency of jumping of an electron from a particular C^{++} ion to a neighboring C^{+++} ion is independent of temperature, the diffusion coefficient D of the d electron is likewise independent of temperature. Since now the electrical conductivity σ is related to D by the Einstein relation

$$\sigma \sim D/T,$$

we see that σ varies inversely as T. Any substance with such a temperature dependence we commonly call a metallic conductor. (2) In the absence of other pertinent exchange interactions, the magnitude of the double exchange determines both the Curie temperature T_c and the exchange frequency ν, and hence ν is determined uniquely by T_c. When use is made of this relation, one finds that the electrical conductivity at the Curie temperature for the case where the C^{++} and C^{+++} ions are of comparable concentration is essentially independent of the particular system, and has the order of magnitude given by

$$\sigma \sim e^2/ah,$$

where e is the electronic charge, a the lattice parameter. If one takes for the lattice parameter a typical value of 3A, one obtains for e^2/ah the value $1.2\times10^{+3}$ ohm^{-1} cm^{-1}. This is the order of magnitude of the conductivity of mixed valency crystals, such as magnetite,[18] manganese perovskites,[4,5] and chromium chalkogenides.[19]

F. Arising from an Exchange of Excited Valence States of Cations of the Same Transition Element

Our final exchange interaction, commonly known as super exchange, was first discussed by Kramers,[20] and later analyzed in detail by Anderson[21] and Van Vleck.[22] One of the authors[19] has recently given a detailed discussion of the physical significance of this exchange interaction, and discussed its application to a variety of systems.

In order to understand the physical basis of super exchange, it is wise to first review the proper description of a typical polar molecule such as NaCl. A perfectly polar molecule would be represented by Na^+Cl^-, and would have the ideal dipole moment of er, where r is the internuclear distance. Now most polar molecules have a dipole moment considerably less than the ideal value, indicating that the average charge on the anion and cation is considerably less than e. A possible method of representing the molecule, a method used extensively by Pauling,[23] is to define a polar and a nonpolar wave function as follows:

$$\psi_p: \quad Na^+ \quad Cl^-,$$
$$\psi_{np}: \quad Na \quad Cl.$$

The appropriate wave function is then written as $\psi_p+\beta\psi_{np}$.

We now consider a slightly more complicated molecule of the type COC where C will denote a cation. The pure polar state would be represented by

$$\psi_p: \quad C^+O^=C^+.$$

A wave function more appropriate than ψ_p can be

[17] C. Zener, Phys. Rev. 82, 403 (1951).

[18] C. A. Domenicali, Phys. Rev. 76, 460 (1949).
[19] R. Heikes (to be published in Acta Metallurgica).
[20] H. A. Kramers, Physica 1, 182 (1934).
[21] P. Anderson, Phys. Rev. 79, 350 (1950).
[22] J. H. Van Vleck, Grenoble Conference, 114 (1951).
[23] L. Pauling, *The Nature of the Chemical Bond* (Cornell University Press, Ithaca, New York, 1940).

CC-0. In Public Domain. Gurukul Kangri Collection, Haridwar

Digitized by Arya Samaj Foundation Chennai and eGangotri

obtained by allowing for an admixture of the somewhat less polar states

$$\psi_1: \ C\ O^-C^+,$$
$$\psi_2: \ C^+O^-C.$$

We now consider the further complication of letting C^+ be a transition metal cation having a nonzero electronic spin. The pure polar state will then be highly degenerate, the energy being independent of the relative orientation of the spins of the two cations. We shall consider in particular the two extreme states represented below:

$$\psi_{p,F}{}^5 \quad \underset{\uparrow\ \Updownarrow\ \uparrow}{C^+O^=C^+} \quad \text{and} \quad \psi_{p,A}: \quad \underset{\uparrow\ \Updownarrow\ \downarrow}{C^+O^=C^+}.$$

The arrows beneath $O^=$ denote the spins of those two dumb-bell type p wave functions whose axes are parallel to the axis of the molecule. We shall now attempt to describe those semipolar states of the type ψ_2 which combine with the above. Since we are concerned only with those states of lowest energy, we shall consider Hund's rule to apply to the spin configuration of both C^+ and of C. Then if the d shell of C^+ is less than half filled, the combining states of the type ψ_2 are

$$\psi_{2,F}: \quad \underset{\uparrow\ \downarrow\ \updownarrow}{C^+O^-C} \quad \text{and} \quad \psi_{2,A}: \quad \underset{\uparrow\ \uparrow\ \downarrow\!\!\uparrow}{C^+O^-C}.$$

We now make the important observation that these two states are not degenerate. The direct exchange interaction of the left-hand C^+ with O^- will lower the energy of ψ_{2F} with respect to that of ψ_{2A}. The energy of the appropriate linear combination of $\psi_{p,F}$ and $\psi_{2,F}$ will therefore be lower in energy than that of the appropriate linear combination of $\psi_{p,A}$ and $\psi_{2,A}$. We therefore conclude that when the d shell of C^+ is less than half filled, a ferromagnetic coupling exists between the cations. A similar analysis leads to the conclusion that when the d shell of C^+ is half-filled or more than half filled, an antiferromagnetic coupling exists.

The first application of superexchange to particular systems was made by Nèel.[24] He showed that the ferromagnetism of the ferrites could be interpreted in terms of this exchange.

III. SUMMARY

The above-described six types of exchange interactions, taken in conjunction with our model of localized d electrons and lattice wave functions for the outer s electrons, are able to interpret the main features of magnetic coupling. The magnetic coupling giving rise to the magnetic moment of the isolated transition metal ions comes from the type of exchange described in Sec. A. The exchange coupling which aligns these isolated ionic moments is of type described in Sec. B in metals, of types in Sec. E and/or F in ionic lattices. The last type of exchange tends to align the d shell spins only in the case of less than half filled d shells, as in the case of CrTe. In case the d shells are half filled or more than half filled, as in the case of the ferrites, this exchange type is antiferromagnetic. The exchange type in Sec. B is also antiferromagnetic in nature. In any particular material several of these exchange interactions may be in simultaneous operation and may be comparable in magnitude. Such is the case, for example, in the chromium chalkogenides (Cr-S, Cr-Se, Cr-Te). An interpretation of the complex magnetic behavior found in these substances has been given by one of the authors.[19]

[21] L. Nèel, Ann. phys. 3, 137 (1948).

CC-0. In Public Domain. Gurukul Kangri Collection, Haridwar

Digitized by Arya Samaj Foundation Chennai and eGangotri

REVIEWS OF MODERN PHYSICS VOLUME 25, NUMBER 1 JANUARY, 1953

Ferromagnetism and the Band Theory

J. C. SLATER

Massachusetts Institute of Technology, Cambridge, Massachusetts

Two rival methods of handling molecular problems, the Heitler-London and the molecular orbital methods, have been used for many years, and they have their counterparts in magnetism in the Heisenberg and the energy-band methods. The first part of this paper shows that the Heitler-London and Heisenberg methods, as usually applied, are not appropriate for problems containing more than a few electrons. The reason is the lack of orthogonality of the one-electron orbitals of atomic type. This involves the presence of overlap integrals which, if included in the calculation, make the method essentially divergent and unsuitable for numerical calculation if the product of the number of electrons in the system, times an overlap integral between nearest neighbors, is large compared to unity, which in practice confines the application to problems of a few electrons. Most applications of the method, including all applications of the Heisenberg method to ferromagnetism and antiferromagnetism, disregard many integrals which are not as a matter of fact negligible, and for this reason cannot be regarded as valid.

Van Vleck many years ago tried to overcome this difficulty, but his results are only partially satisfactory on account of lack of generality. The straightforward way to overcome it is to use really orthogonal one-electron orbitals, either molecular orbitals or Wannier functions, and the remainder of the paper considers how the familiar facts of ferromagnetism are to be explained on this basis. If we use a single determinantal wave function composed of energy-band orbitals, we have the familiar energy-band or collective electron theory of ferromagnetism. This simple method may well be fairly accurate at small internuclear distances; it predicts correctly that ferromagnetism must be impossible when the atoms are close enough together to broaden the energy bands greatly. For large internuclear distances, however, it leads to quite wrong limiting behavior, since it gives a wave function involving a considerable contribution of ionic states. To eliminate these ionic states, at large internuclear distances, we must make linear combinations of different determinantal functions, corresponding to different assignments of electrons to orbitals. The results of such a calculation are sketched.

To treat magnetic problems properly, we must make such calculations for different total spins, calculate the energy of the states of different magnetizations as a function of internuclear distance, and see which states lie lower, the magnetic or nonmagnetic. At infinite separation, the energy will be independent of total magnetization, since in this limit the spins of different atoms can be oriented in any arbitrary way without affecting the energy. At very small distances, the elementary band theory shows that the nonmagnetic state must lie below the magnetized state, so that ferromagnetism is impossible. At intermediate distances, the elementary theory can show only that ferromagnetism is possible, not that it is necessary; to find whether it actually exists, we should really have to carry out a calculation of the type described. If we find ferromagnetism, we shall necessarily find that the energy difference between nonferromagnetic and ferromagnetic states was zero at infinite internuclear distance, increased as the internuclear distance decreased, went through a maximum, and then went to zero and changed sign. This behavior is often postulated for the Heisenberg exchange integral, although we do not feel that this integral has the direct theoretical meaning often ascribed to it.

These problems are closely related to the correlation energy, which is discussed. We do not feel that the familiar Wigner-Seitz calculation of correlation energy is very accurate; the correlation energy is in fact a function of magnetization, decreasing numerically with decreasing internuclear distance, and its interpretation cannot be given properly except by considering its intimate connection with magnetization. The net result of the present discussion is that to give a proper account of ferromagnetism, we are forced to use orthogonal orbitals and, therefore, must make close connection with the band theory. We must, however, carry our theory further than has usually been done, though the prediction of the elementary band theory, i.e., that ferromagnetism is impossible for broad bands and can exist only for narrow bands and electronic wave functions which overlap only slightly, is verified by the present more accurate approach.

As an illustration of the general method of calculating magnetic energies described in this paper, we may mention the recent calculation of Meckler, not yet published, on the oxygen molecule. This has been carried out by setting up many determinantal wave functions formed from orthogonal atomic orbitals made out of the original nonorthogonal orbitals. The secular equations involving these determinantal functions were solved by use of a digital computer. The resulting energy levels and wave functions reduce to the proper type to represent the ^3P ground state of the oxygen atom at infinite internuclear distance. Meckler's energy for the triplet ground state is very accurate; that for the next singlet excited state is quite good. The energy separation between singlet and triplet shows the behavior expected for the energy difference between a ferromagnetic and nonferromagnetic state, being zero at infinite distance, then increasing, going to a maximum, then decreasing again. As far as the writer is aware, this is the first time when such a behavior has been found as a result of straightforward calculation from quantum mechanics.

FOR many years, there have been two competing approaches to problems in molecules and solids. First there is the Heitler-London method for molecules, with the related Heisenberg method for magnetism; second, there is the molecular orbital method for molecules, with the energy-band method for solids. Many students of molecular structure, following Pauling, have based their work on the Heitler-London method, and many students of magnetism, following Van Vleck, have used the Heisenberg theory as fundamental. Another school of molecular theory, following Lennard-Jones and Mulliken, has used the molecular orbital method; and other workers in magnetism, as for instance Stoner, have used the energy-band or collective electron method. It has often been shown that for simple systems, in particular the hydrogen molecule, the two methods as properly amplified are equivalent, and this has been regarded as a justification for the use of either method for complicated molecules and solids. For a very long time the present writer has believed otherwise: He believes that the Heitler-London and Heisenberg methods are by their nature incapable of being rigorously applied to systems containing more than a very few electrons, except in special cases like ionic

CC-0. In Public Domain. Gurukul Kangri Collection, Haridwar

Digitized by Arya Samaj Foundation Chennai and eGangotri

crystals, and feels, therefore, that they are unsuited for most problems in the structure of molecules and solids and for almost all problems in magnetism. It is the purpose of the present paper to give the reasons for this belief and then to outline how the energy-band method can be adapted to problems of solids, particularly in the limit of large internuclear distance where difficulties in its application are sometimes pointed out.

I. THE OBJECTIONS TO THE HEITLER-LONDON AND HEISENBERG METHODS

All methods under discussion work with one-electron orbitals; the characteristic of the Heitler-London and Heisenberg methods to which we object is that in these methods the orbitals represent atomic functions on different atoms, and hence necessarily are not orthogonal to each other. In the present section we shall make two points: first, that for systems of more than a few electrons, the use of nonorthogonal orbitals involves us in practically insuperable computational difficulties; secondly, that the use of nonorthogonal orbitals is inherent in the Heitler-London and Heisenberg methods. Before making these points we must note that there are three general methods which have been proposed for using one-electron orbitals for many-electron problems. Before 1929, the group theory was generally used. This method involved a great deal of superfluous mathematical machinery, and it was supplanted in 1929 by the determinantal method suggested by the present writer[1] and by the spin operator method proposed by Dirac.[2] The determinantal method is completely general and will be made the basis of the discussion of the present section. The spin operator method, which has been widely used by Van Vleck[3] and his school for magnetic problems, is less general. It will be shown in Sec. II that this lack of generality makes it inadequate as a foundation for a theory of magnetism.

We now take up our first point: that the use of nonorthogonal orbitals involves practically insuperable difficulties in many-electron problems. The writer[4] has discussed in principle the application of the Heitler-London method, using nonorthogonal orbitals, to such problems and has carried through illustrative cases involving a small number of electrons. The characteristic step in this application is the calculation of matrix components of the energy of the n-electron system, and of unity, between determinantal n-electron functions formed from nonorthogonal one-electron orbitals $u_1(x)$, $u_2(x)$, etc., where the orbitals, and the coordinates, x, involve both spacial coordinates and spin. Once these matrix components are calculated, we can set up a secular equation for finding the energy levels, and the combinations of determinantal functions which best represent the correct wave function. The difficulties arise in the calculation of these matrix components, and can be illustrated by the very simplest example, the calculation of the diagonal component of the matrix of unity with respect to a determinantal function $\det|u_i(x_j)|$, which is required in order to normalize the determinant, provided the u_i's are normalized but not orthogonal. We wish in other words to compute $\int \det|u_i^*(x_j)|\det|u_i(x_j)|\,dx_1\cdots dx_n$. We can at once reduce this to the form

$$n!\sum(\text{permutations } P)\int u_1^*(x_1)\cdot u_n^*(x_n)(\pm P)u_1(x_1)\cdot u_n(x_n)dx_1\cdots dx_n, \quad (1)$$

where P represents a permutation of the subscripts of the u's. The term of this summation for which P represents the identity is unity, by the normalization of the u's; and if the u's were orthogonal, all other terms would give zero, so that the result would be simply $n!$, and the normalized determinant would be $(n!)^{-\frac{1}{2}}\times\det|u_i(x_j)|$. If the u's are not orthogonal, however, we shall next have $n(n-1)/2$ terms involving single interchanges of two subscripts. If the kth and lth are interchanged, the integral in (1) will be

$$-\int u_k^*(x_k)u_l^*(x_l)u_l(x_k)u_k(x_l)dx_k dx_l = -\left[\int u_k^*(x_k)u_l(x_k)dx_k\right]^2, \quad (2)$$

the square of the overlap integral between the kth and lth atomic orbitals. We know that these integrals fall off rapidly with internuclear distance, so that only those terms of (1), involving interchange of two subscripts, will be appreciable in which k and l represent near neighbors. There will be of the order of magnitude of $zn/2$ pairs of near neighbors in the system, if z is the number of near neighbors which a given atomic orbital has. Thus, from interchange of pairs of subscripts we shall have of the order of $zn/2$ terms in the summation (1), each of the order of magnitude of the square of the overlap integral between neighboring atoms. Since these squares can well be of the order of 0.01 or larger in practical cases, it is clear that the sum of the terms of (1) coming from simple interchange can be of the order of n, as compared to unity for the leading term. Similarly, by considering more complicated permutations we see that next we have sets of terms adding to something of the order of n^2, then something of the order of n^3, and so on. If n is more than a very small integer, it is clear that this sum involves terms each of which

[1] J. C. Slater, Phys. Rev. 34, 1293 (1929).
[2] P. A. M. Dirac, Proc. Roy. Soc. (London) A123, 714 (1929); or *The Principles of Quantum Mechanics* (Oxford University Press, London, 1947), third edition, Chap. IX.
[3] J. H. Van Vleck, *The Theory of Electric and Magnetic Susceptibilities* (Oxford University Press, London, 1932); Phys. Rev. 45, 405 (1934); J. H. Van Vleck and A. Sherman, Revs. Modern Phys. 7, 167 (1935); J. H. Van Vleck, Physica 15, 197 (1949); J. phys. et radium 12, 262 (1951); P. W. Anderson, Phys. Rev. 79, 350, 705 (1950); and many other references by Van Vleck and students.
[4] J. C. Slater, Phys. Rev. 38, 1109 (1931).

CC-0. In Public Domain. Gurukul Kangri Collection, Haridwar

Digitized by Arya Samaj Foundation Chennai and eGangotri

is enormously larger than the preceding one. Closer examination shows that the signs of the terms alternate, so that the sum can be finite; but it will be found as the difference of very large positive and negative quantities and, hence, is entirely unsuited for computation. We shall point out later how to get around this difficulty, but the present point is that it cannot be avoided by direct and straightforward methods.

Closely related to the difficulty just mentioned is that encountered when we start calculating the matrix components of the energy and the exchange integrals which are involved in the calculation. The energy operator H is a sum of quantities $f_1 \cdots f_n$, each involving the coordinates of one electron only (the kinetic energy operator, plus the potential energy in the field of all the nuclei), and of quantities g_{ij}, the Coulomb repulsive energy between the ith and jth electrons. The resulting integral is just like (1), but with the operator H inserted after the factor $u_n^*(x_n)$. The integral coming from the identity permutation is the Coulomb integral, which will not concern us further; it is easy to compute. The only remaining term in the two-particle case is the ordinary Heitler-London or Heisenberg exchange integral,

$$J_{12}=\int u_1^*(x_1)u_2^*(x_2)(f_1+f_2+g_{12}) \\ u_2(x_1)u_1(x_2)dx_1dx_2. \quad (3)$$

In the general case of n particles, if the u's are orthogonal, two things happen. First, the exchange integral (3) reduces to the form

$$J_{12}=\int u_1^*(x_1)u_2^*(x_2)g_{12}u_2(x_1)u_1(x_2)dx_1dx_2. \quad (4)$$

Second, the sum in the expression similar to (1) reduces to the Coulomb term, minus the sum of the exchange integrals, of form (4), for all pairs of orbitals. If the u's are not orthogonal, however, there is no comparable simplification. We have a very great variety of types of exchange integrals, involving permutations of many electrons, which by no means vanish. The whole problem of computing the diagonal or nondiagonal matrix component of energy between two determinantal functions becomes even more formidable than that of computing the normalization integrals.

Thus, we see the computational difficulties involved in the use of nonorthogonal orbitals. Unless some simplification can be made, they are quite insuperable for anything but very simple problems, and no one has tried to carry through all the terms in a complicated case. Much work has been done, in both molecular and magnetic problems, by making the following assumptions: We assume that the diagonal matrix component of energy can be written as the Coulomb integral, minus the sum of the J_{kl}'s, as we should have for orthogonal u's, but use the form of J_{kl} given in (3), appropriate only for nonorthogonal u's: and we disregard all overlap integrals in the matrix component of unity. These assumptions are completely unjustified. The molecular orbital or energy-band methods can be used to make accurate calculations of molecular energy levels, as Mulliken and Lennard-Jones and Coulson and others of their school[5] have shown; and the energy-band method can be used for accurate calculations of the structure of solids, as Löwdin[6] and others have shown. These calculations, though made with a different starting point, eventually encounter the same exchange and overlap integrals which are met in the Heitler-London and Heisenberg methods. It is very clear from these accurate calculations that the terms which are disregarded in the approximate methods described above are by no means negligible, and that if they are omitted from a correct calculation, agreement with experiment is completely vitiated.

We reject completely, then, that large body of work which has simply neglected the nonorthogonality or overlap of one-electron orbitals, as representing an unjustified oversimplification which forms no valid approximation to the real predictions of wave mechanics. To be taken more seriously, however, is Van Vleck's[7] attempt to justify the procedure outlined in the paragraph above. This attempt was made as an answer to the criticism of Inglis[8] regarding the catastrophe produced by nonorthogonality in a many-electron system. This criticism was equivalent to that made in the preceding paragraphs of this section; the same difficulty had been pointed out earlier by the present writer.[9] Van Vleck showed essentially that the matrix components of unity and of energy between two determinantal functions, which we have been considering above, could be factored, if we neglect certain terms. The final answer in every case will be a ratio of two integrals, one coming from the energy in the numerator and one from the matrix of unity in the denominator. Most factors in numerator and denominator are identical and can be canceled. The remaining ratio then proves, as Van Vleck showed, to be of the sort described in the preceding paragraph, and to involve sums in which the number of integrals coming from simple exchange was only proportional to z, the number of near neighbors, rather than to $nz/2$.

If Van Vleck's treatment had been really general, it would have provided the complete answer to the difficulties. Unfortunately, it was not; we have mentioned that certain terms had to be omitted, and the

[5] R. S. Mulliken and R. G. Parr, J. Chem. Phys. 19, 1271 (1951), and many other references given there; numerous papers in Proc. Roy. Soc. (London) A207, 1–136 (1951), and many references given there.

[6] P.-O. Löwdin, *A Theoretical Investigation into Some Properties of Ionic Crystals*, thesis, Uppsala, 1948; J. Chem. Phys. 18, 365 (1950); 19, 1570, 1579 (1951).

[7] J. H. Van Vleck, Phys. Rev. 49, 232 (1936).

[8] D. R. Inglis, Phys. Rev. 46, 135 (1934).

[9] J. C. Slater, Phys. Rev. 35, 509 (1930); see particularly pp. 526–527.

CC-0. In Public Domain. Gurukul Kangri Collection, Haridwar

Digitized by Arya Samaj Foundation Chennai and eGangotri

results were worked out only for special cases. We can give an idea of how it works, however, from our simple example of the normalization integral $\int \det|u_i^*(x_j)| \times \det|u_i(x_j)|\, dx_1 \cdots dx_n$. At the same time our example will show how Van Vleck's method can be extended so as to be perfectly general. Suppose we have a particularly simple case, in which the n functions u_i represent atomic functions, all corresponding to electrons of the same spin, on the n lattice sites of a regular lattice. In other words, our determinantal function represents a state in which we have a completely filled set of wave functions, one per atom, corresponding to one spin. Then we know that we can make from the u's a set of n normalized, orthogonal Block functions, which can easily be shown to be

$$b_i(r) = d_i n^{-\frac{1}{2}} \sum(\mu) \exp(ik_i \cdot R_\mu) u(r - R_\mu), \qquad (5)$$

where

$$d_i = \left\{ \sum(R_m) \exp(ik_i \cdot R_m) \int u^*(r) u(r - R_m) dv \right\}^{-\frac{1}{2}}. \qquad (6)$$

Here r is the vector position of an electron, and $u(r-R_\mu)$ is an atomic function located on the lattice point at R_μ and corresponding to a + spin. If the u's on different lattice sites were orthogonal, the quantity d_i would be unity; if they are not orthogonal, we have an additional term which involves only a summation over the z near neighbors of an atom. There are n functions $b_i(r)$, corresponding to the n values of the propagation vector k_i consistent with the boundary conditions in the crystal (for instance, periodic boundary conditions). Now we know that if we form the determinant $(n!)^{-\frac{1}{2}} \times \det|b_i(r_j)|$, this function will be normalized, since the b's are normalized and orthogonal. However, we also know by general properties of determinants that this determinant is proportional to $(n!)^{-\frac{1}{2}} \det|u_i(x_j)|$. In fact, it is not hard to find the relation between these two determinants and to show that the function $(n!)^{-\frac{1}{2}} \{\Pi(i) d_i\}^{\frac{1}{2}} \det|u_i(x_j)|$ is normalized. In other words we have found our difficult normalization integral, for this special case, and we have shown that it factors into a product of d_i's. This is the simplest example of the factoring procedure that Van Vleck used in the reference quoted above, although he did not use the Bloch functions directly. It is clear that the product of all the d_i's, as defined in (6), will have the form described earlier: It will have unity for the leading term, then something like zn terms each of the order of an overlap integral between neighboring atoms, then $(zn)^2$ terms involving products of overlap integrals, and so on. But its factorization has simplified the situation. We can carry out a similar factorization in the energy integral, and the ratio of the two, giving the diagonal energy of this state, has most of the factors canceling in numerator and denominator, reducing to a simple final result, in accordance with the findings of Van Vleck.

We thus see how Van Vleck's result can come about: that the catastrophe of nonorthogonality in a many-electron system really follows from the method of calculation, and is not inherent in the problem. We may well believe that if we could really set up a Heitler-London approximation for a problem of many electrons, and carry through the calculations exactly, the results would be quite reasonable and might well form as good an approximation as with hydrogen. Nevertheless, the computational difficulties remain. We may ask, then, can we not extend Van Vleck's method to the general case, without making the approximations which he was forced to make in reference 7? The answer is obvious from the discussion we have just given: We can rewrite our problem in terms of really orthogonal one-electron orbitals, and then everything goes through simply. We have just pointed out that we can use Bloch combinations of atomic orbitals, so as to get orthogonal functions; this was pointed out in reference 9. We can also use Wannier functions,[10] orthogonalized one-electron orbitals, as the writer has done for magnetic problems,[11] and as Löwdin[6] has done for problems in cohesive energy in crystals. Either of these methods gets away from the nonorthogonality catastrophe; and it is doubtful whether any essentially independent method would accomplish the same purpose.

By introducing orthogonal orbitals, either of the Bloch or the Wannier type, then, we escape the nonorthogonality difficulty. But at the same time we find that we no longer have the Heitler-London method; we have instead the energy-band method, which is the one which the writer is advocating. We might think that all we had to do was to introduce orthogonal orbitals, and then proceed exactly according to the pattern of the Heitler-London and Heisenberg methods; but this is not true, and those methods depend essentially on the use of nonorthogonal orbitals. Thus, we come the second principal point of the present section, the fact that nonorthogonal orbitals are essential to the Heitler-London and Heisenberg methods. The writer has already pointed this out[12] with reference to problems in molecular structure. Let us state the argument in somewhat different language, appropriate for the magnetic problem. Let us suppose specifically that we set up Wannier functions, which in many ways resemble atomic functions, and that we set up a theory analogous to the Heisenberg theory of ferromagnetism, using these functions. They are orthogonal, and hence the exchange integrals J_{kl} take the form (4), which is necessarily positive, since it represents the electrostatic interaction of a charge distribution with itself. But we remember that a positive exchange integral, in Heisenberg's theory, corresponds to ferromagnetism. We should therefore conclude, if we used the Heisenberg method naively, that all substances were ferromagnetic, an obviously absurd conclusion. To get a negative exchange integral, as in the Heitler-London method, we

[10] G. Wannier, Phys. Rev. 52, 191 (1937).
[11] J. C. Slater, Phys. Rev. 52, 198 (1937).
[12] J. C. Slater, J. Chem. Phys. 19, 220 (1951).

CC-0. In Public Domain. Gurukul Kangri Collection, Haridwar

Digitized by Arya Samaj Foundation Chennai and eGangotri

must have the interaction term between electrons and nuclei in f_1 and f_2 in the expression (3); these are the only negative terms in the exchange integral, and in the case of the hydrogen molecule they outweigh the positive terms. But they are missing with orthogonal orbitals. Since most substances are not ferromagnetic, it is clear that we must carry a calculation, starting with Wannier functions, through a further step than we are used to in the Heitler-London or Heisenberg methods, to get results of any reliability.

We can easily see what this additional step is, by considering the familiar case of the hydrogen molecule. If a and b represent (nonorthogonal) atomic functions on atoms a and b, we can set up orthogonalized atomic orbitals, as in reference 12, by the relations $A=c_1a+c_2b$, $B=c_2a+c_1b$, where c_1 and c_2 are determined to make A and B orthogonal and normalized. We can set up the spin degeneracy problem corresponding to one electron being in orbital A, one in B, either electron having either spin. The resulting spin degeneracy problem is carried through exactly as in the Heitler-London calculations for H_2, and it results in a singlet and a triplet. The orbital part of the triplet wave function (disregarding normalization) is $A(1)B(2)-B(1)A(2)$, where 1, 2 symbolize the electronic coordinates; substitution shows that this is the same as $a(1)b(2)-b(1)a(2)$, so that this method gives the same result for the triplet as the Heitler-London method, and hence the energy of this state must be the same. For the singlet, the wave function is $A(1)B(2)+B(1)A(2)$. This singlet state must lie above the triplet since as we have seen the exchange integral is always a positive for orthogonal wave functions. Thus, the singlet state as given by this method is not attractive; this fact was pointed out in reference 12, but this is a more direct proof than is given in that reference. Since we know that the Heitler-London singlet state lies below the triplet, and has an energy low enough to lead to the molecular binding in H_2, it is clear that the wave function for the singlet given by the orthogonal atomic orbitals is very incorrect. Let us see why this is true, by writing A and B in terms of a and b. When we do this, we find the wave function to be equivalent to

$$(c_1^2+c_2^2)[a(1)b(2)+b(1)a(2)] + 2c_1c_2[a(1)a(2)+b(1)b(2)]. \quad (7)$$

The first term is the ordinary Heitler-London function for the singlet, which gives an energy below the triplet; but the second is the Heitler-London function for the ionic state where both electrons are on the same atom. Since this state has a much higher energy, it is the admixture of this ionic state which spoils the singlet wave function as calculated by the Wannier function method.

We know, of course, that the Heitler-London calculation for H_2 is surprisingly good, so that to get a good wave function for the singlet state, we must modify (7) to restore it very nearly to the Heitler-London form $a(1)b(2)+b(1)a(2)$. To do this, starting with the Wannier functions, we must consider a configurational interaction between the state already described, in which one electron is in a state A, one in state B, and the state where both electrons are in orbital A, or both in B. The singlet function of proper symmetry which can be formed from this configuration is $A(1)A(2)+B(1)B(2)$. Writing this in terms of a and b, it is

$$(c_1^2+c_2^2)[a(1)a(2)+b(1)b(2)] + 2c_1c_2[a(1)b(2)+b(1)a(2)]. \quad (8)$$

The result of a configurational interaction between this wave function and that given in (7) will yield two final functions, one of which will be close to the function $a(1)b(2)+b(1)a(2)$, or the Heitler-London ground state, the other close to the Heitler-London ionic function $a(1)a(2)+b(1)b(2)$. In other words, the use of Wannier functions artificially introduces an ionic character into the wave functions, and a configurational interaction with the configuration in which a Wannier function is occupied by two electrons, one of each spin, is absolutely necessary in order to counteract this ionic effect and get a description of covalent binding, or of a negative Heisenberg exchange integral or a nonferromagnetic state. It is the absolute necessity of this configurational interaction which distinguishes this calculation from the ordinary Heitler-London or Heisenberg approach, where the interaction with ionic configurations is regarded as a refinement, which is generally disregarded.

The net result of this section, then, is that a direct calculation of any molecular problem except the very simplest by the Heitler-London method is impossible. If the calculation could be made, the answer might be quite a good representation of the true wave function. The only practical way to get at it, however, is to start with orthogonal orbitals, either of the energy-band Bloch type or of the localized Wannier type. When we do this, the calculation becomes practicable. But all exchange integrals become positive, which puts us on our guard against using a naive form of the Heitler-London or Heisenberg method. Rather, to get correct results, it is essential to consider configuration interaction with ionic states, in which one Wannier function is occupied by two electrons. When this is done, the method may be expected to give good results; but it is now so far from the original Heitler-London or Heisenberg method that it should no longer be described in terms of those methods.

II. OBJECTIONS TO THE DIRAC SPIN OPERATOR FOR MAGNETIC PRABLEMS

Before we go on to the applications of the energy-band method, we should consider one additional point, the validity of the expression

$$-\tfrac{1}{2}\sum(\text{pairs } k, l)J_{kl}(1+4s_k\cdot s_l), \quad (9)$$

where J_{kl} is an exchange integral, and s_k and s_l are the spin matrices of the kth and lth electrons. This expression was introduced by Dirac,[2] and it gives the impres-

CC-0. In Public Domain. Gurukul Kangri Collection, Haridwar

Digitized by Arya Samaj Foundation Chennai and eGangotri

sion of being a justification of the Heisenberg method, and the use of exchange integrals, on a sufficiently general basis so that we are led to ask if it avoids the difficulties with the Heisenberg method, pointed out in the preceding section. We shall see when we examine it that it does not avoid these difficulties, and that it does not in fact form a valid starting point for a complete theory of magnetism.

If we examine Dirac's derivation of the expression (9), we see that it was set up for problems of spin degeneracy. That is, for a problem of n electrons, we start with a set of orbitals $u_1 \cdots u_n$ involving coordinates only, not necessarily all different, and consider the various functions of coordinates and spin which can be made up from them by assigning spins in all possible ways to these orbitals. In such a set of functions of coordinates, it is clear that any function, on account of the exclusion principle, can be identical with at most one other function. Each pair of identical functions must be occupied with an electron of each spin. If there are n' remaining functions, each appearing once, each one can appear with either spin, so that there are $2^{n'}$ ways of arranging spins. The problem of spin degeneracy then involves the $2^{n'}$ determinantal wave functions arising in this way. Dirac's operator is set up so as to give the same matrix components of energy between these $2^{n'}$ states as the correct Hamiltonian operator used with the determinantal method, provided the orbitals $u_1 \cdots u_n$ are orthogonal. It does not give matrix components between different configurations, that is, between two determinantal functions corresponding to different sets of u's, and it does not give correct values if the u's are not orthogonal.

These limitations, though clearly pointed out by Van Vleck,[3] are generally glossed over. It is clear, however, that the method based on (9) is more specialized than the determinantal method. In the first place, it cannot rigorously be used for the Heitler-London or Heisenberg methods, for we have pointed out that the nonorthogonality of wave functions is essential to these methods. The approximation, often made, of assuming that it can be used in these cases, with an exchange integral J_{kl} given by (3), which can have either sign, is on exactly the same basis as the approximation which we have already dismissed as invalid in Sec. I, of writing the diagonal energy as the Coulomb energy minus the sum of all exchange integrals J_{kl}, of computing these by Eq. (3), and of disregarding overlap integrals. If we use really orthogonal orbitals, it is a correct starting point for discussing spin degeneracy; but we have just seen that in this case we must also consider configurational interaction with ionic states in which the Wannier functions are occupied by two electrons, and the Hamiltonian (9) is not able to describe these configurational interactions. Our feeling about this Hamiltonian (9) is thus very definite, and very adverse, as far as its application to magnetic problems is concerned: We believe that it has given a false and unjustifiable feeling of security to those who wished to use the Heisenberg method, and that in fact the uses which have been made of it are unjustifiable and incorrect. We do not feel that it is correct, in any way which has been justified from wave mechanics, to speak of exchange integrals between electrons in a crystal, in the Heisenberg sense, or to decide whether a substance should be ferromagnetic, or nonferromagnetic, or antiferromagnetic, on account of a positive or negative sign for such a hypothetical exchange integral. This criticism extends to the use of the term superexchange[13] in its relation to theories of antiferromagnetism; the derivation of this quantity, by Kramers, neglects orthogonality in just the same sort of way which we are objecting to in the present paper, and the writer sees nothing in the work on the subject which overcomes this difficulty in the use of the method. Before leaving the expression (9), we should point out that Serber[14] has shown how to remove the limitations which we have mentioned, i.e., that (9) demands orthogonal orbitals, and does not apply to configuration interaction; Anderson[13] uses some of these methods in his paper on superexchange, though he disregards nonorthogonality.

III. THE ENERGY-BAND THEORY OF FERROMAGNETISM

In the two preceding sections, we have endeavored to show that treatments of magnetism by the Heisenberg method are unjustified, and that if we try to overcome the difficulties of that method, we are led inevitably to the use of the determinantal method, with orthogonal one-electron functions or orbitals. If we have a complete orthogonal set of one-electron functions $u_i(x)$, involving coordinates and spin, we can pick n functions out of such a complete orthogonal set and form a determinantal function $(n!)^{-\frac{1}{2}} \det|u_i(x_j)|$. If we take all possible ways of picking out n one-electron functions from the complete orthogonal set, and set up all such determinantal functions, this will form a complete orthogonal set of antisymmetric functions of n electronic coordinates and spins, so that the correct wave function of the problem can be rigorously expanded in terms of them. For the one-electron functions, in a problem of a crystal, we may use the solutions of a periodic potential problem, which have the characteristics of Bloch waves; or we may use the Wannier functions arising from them. Since either type of function forms a complete orthogonal set, either one forms a proper starting point for a rigorous calculation. If we do not have exact solutions of the periodic potential problem, we can proceed as Mulliken[5] and others have done in the molecular problem, or as Löwdin[6] has done in discussing crystals: We can start with atomic orbitals and make orthogonal linear com-

[13] H. A. Kramers, Physica 1, 182 (1934); P. W. Anderson, Phys. Rev. 79, 350 (1950); J. H. Van Vleck, J. phys. et radium 12, 262 (1951).

[14] R. Serber, Phys. Rev. 45, 461 (1934).

CC-0. In Public Domain. Gurukul Kangri Collection, Haridwar

Digitized by Arya Samaj Foundation Chennai and eGangotri

binations of these atomic orbitals, either of the Bloch-like or Wannier-like type. The results of these calculations show that good results can be obtained in this way. The writer feels that our best hope at present of obtaining quantitative results for magnetic problems is to proceed in this way, using linear combinations of atomic orbitals, of an orthogonal nature, and calculating the energy of the crystal as Löwdin has done, but for both magnetized and unmagnetized states, comparing the energies of the two states.

The calculations of Mulliken and Löwdin mentioned above, and the usual applications of the molecular-orbital or energy-band method, are more specialized than we have indicated above. They are based on the use of a single determinantal wave function, formed from the n Bloch-like energy-band functions whose one-electron energies are lowest. The details of how to specify these one-electron energies involve a certain amount of subtlety, relating to problems of the Hartree-Fock equation, which we shall not go into here. We expect theoretically, and we find in practice, that a single such determinant gives a good description of an actual molecule or crystal at its observed internuclear distance. However, as the interatomic distances increase to infinity, it is well known that this single determinantal solution does not behave properly and that its asymptotic energy, at infinite internuclear distance, is too high. We have a situation shown schematically in Fig. 1, where the full curve shows the diagonal energy of the state represented as a single determinant, as a function of internuclear distance. The horizontal line is supposed to represent the correct energy of the system at infinite internuclear distance, and the dotted line represents the energy of the correct ground state, as determined by making linear combinations of determinants, as will be described later. It can then very well be that the single determinant forms quite a good approximation to the ground state near the minimum of the curve. It can also well be that we can independently determine the energy at infinite distance. Thus, the dissociation energy D can be well calculated from this single determinant, even though its energy at infinity is too high by the amount A. A solution like that shown in Fig. 1 is found in the simplest molecular problem, the H_2 molecule; a very similar situation is shown in Löwdin's[15] calculation of the sodium crystal, where he has been able to make a very good calculation of cohesive energy, even though his energy curve, like the full curve of Fig. 1, goes to much too high a value at infinity. Similar justification for this method of using a single determinant is provided by the calculations of Mulliken[5] and others mentioned earlier: they get good values for binding energies, from wave functions which would behave incorrectly at infinite distance.

For magnetic problems, however, this failing of the simple energy-band method using a single determinant,

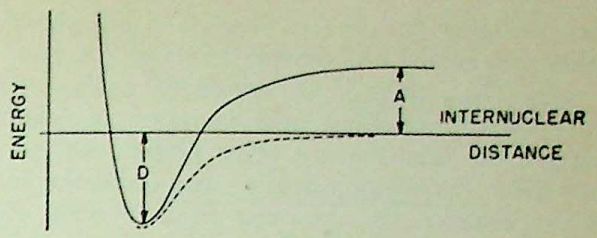


FIG. 1. Energy of single determinantal state formed from molecular orbitals (full curve), and correct energy of ground state (dotted curve).

at large internuclear distances, can be serious; for it is well known that the $3d$ orbitals concerned in magnetism are far apart in relation to their size, in ferromagnetic and more particularly in paramagnetic substances. Thus, we must look at the sort of situation described in Fig. 1, particularly at large distances, in a good deal more detail. First let us remind ourselves why the energy of the single energy-band determinantal function, given by the full curve in Fig. 1, is too high at infinite internuclear distance by the amount A. It is well known that this results because there is nothing in the wave function to keep electrons of opposite spin out of each other's way, and we are quite likely to find ionic states, in which positive or negative ions are found on some lattice sites rather than neutral atoms. Thus, in the H_2 problem, where the molecular orbital functions are $a \pm b$, the determinantal wave function corresponding to this state, as far as its orbital dependence is concerned, is $[a(1)+b(1)][a(2)+b(2)]=[a(1)b(2)+b(1)a(2)]+[a(1)a(2)+b(1)b(2)]$, a combination of the Heitler-London ground state, and of the Heitler-London ionic state, with equal coefficients. At infinite separation, there is a fifty percent chance that the wave function represents an ionic state. In computing the diagonal energy of the state, as shown in the full curve of Fig. 1, we then find terms representing the interaction of two electrons on the same atom, required to calculate the energy of the H^- ion. The energy A represents the energy required to form H^+ and H^- ions from the neutral H atoms, in the fifty percent of the cases where the ions are found, according to the determinantal wave function.

The situation described in Fig. 1 is for a state with no net magnetic moment. For investigating ferromagnetism, however, we must compare the energies of states of different magnetic moments; in a ferromagnetic problem, the lowest state will have a magnetic moment, and in a nonmagnetic case it will not. We next ask, therefore, how the energy of a single determinant, as a function of internuclear distance, depends on whether it represents a magnetic state or not. First, at small internuclear distances, where the energy band is broad, increase of magnetic moment will increase the energy, for in the nonmagnetized state each of the lowest one-electron energy levels will be occupied by two electrons, one of each spin, whereas in the magnetized state electrons of one spin (say $-$) are removed

[15] P.-O. Löwdin, J. Chem. Phys. 19, 1570, 1579 (1951).

CC-0. In Public Domain. Gurukul Kangri Collection, Haridwar

Digitized by Arya Samaj Foundation Chennai and eGangotri

from low-lying one-electron levels and are placed in higher unoccupied one-electron levels of the band of + spin. Thus, there is an increase of energy of the whole system, resulting from increased one-electron energies, the total amount being proportional to the band width, and hence increasing with decreasing internuclear distance. On the other hand, another effect works in the opposite direction, and persists to infinite separation, tending to lower the energy of the state of maximum magnetization below the unmagnetized state. This is the effect of exchange. The diagonal energy of a single determinantal state formed from orthogonal orbitals is the sum of the one-electron and Coulomb energies (these terms take care of the result of broadened energy bands just mentioned) minus the sum of exchange integrals J_{kl} of type given in Eq. (4), for all pairs of electrons with parallel spin. These exchange integrals are always positive; and when the orbitals u_i are Bloch functions, we find that at large nuclear separations they do not go to zero in the limit, but become interaction integrals between different electrons in the same atom. Thus, we have a set of such terms, coming in with negative sign, one for each pair of electrons with parallel spin. Now there are more such pairs for a magnetized state than for an unmagnetized state; thus, this exchange energy is lower for the magnetized state than the unmagnetized one.

The net result of these two effects, then, is that the energies of determinantal functions representing nonmagnetized and magnetized states formed from energy-band orbitals will look as shown schematically in Fig. 2. We can easily see why the energy of the magnetized state lies below that of the unmagnetized state, at infinite separation. This is on account of the incorrect tendency for electrons of opposite spin to get close together and form ions, in the determinantal wave function, as mentioned earlier. But electrons of the same spin are prevented from getting too close together by the exclusion principle. Thus, the greater the magnetization the fewer are the pairs of electrons which can improperly get together, and the smaller is the error. If the completely magnetized state happens to be one in which a band is just filled with electrons of + spin, with no electrons of − spin, then the exclusion principle by itself will entirely prevent ionic states,

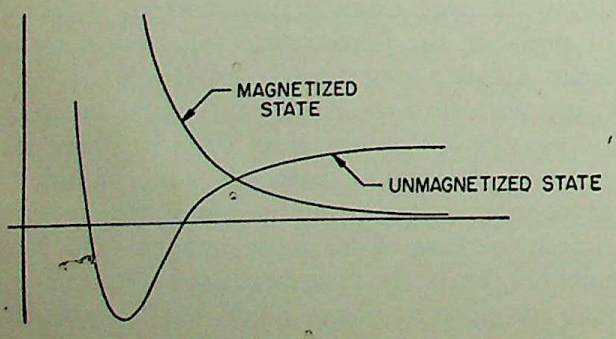


FIG. 2. Energy of single determinantal state formed from molecular orbitals for magnetized and unmagnetized states.

and the state of maximum magnetization will go to the correct energy at infinity. This is the case in H_2. It is also the case taken up by the writer[11] in a more detailed study of the present problem; this case is simple enough so that quantitative results can be obtained in computing the energy as a function of internuclear distance. A consideration of the exchange terms coming into the energy of the determinantal state, which as we have seen involve interaction between electrons on the same atom, shows that these are just the correct terms to describe this tendency of electrons of opposite spins in the unmagnetized state to form positive and negative ions.

Now that we have considered the behavior of the energy of a single determinantal wave function formed from Bloch orbitals, both for magnetized and unmagnetized states, we can ask how the energies of the correct wave functions are related to them, for example, as indicated in the dotted curve of Fig. 1. From the case of H_2, and the magnetic case worked out by the writer in reference 11, we can tell the general lines which the discussion must take. To get good results, we must use many determinantal functions and solve a perturbation problem between them. If we are using Bloch functions as one-electron orbitals, we must use not only the determinant composed of the n lowest orbitals in the energy band concerned, but rather all determinants which can be formed from the orbitals in the whole band. We shall find an equal number of determinants formed from the Wannier functions of the band, provided we consider all the ionic Wannier states, which we have seen to be necessary from our discussion of Sec. I. The determinants formed from Bloch functions, or from Wannier functions, are found from each other by a unitary transformation, so that the same final result will be obtained by starting with either set. We must then solve the perturbation problem between these states, finding the set of resulting energy levels for each total spin. The lowest such energy level, for each total magnetization, will of course have to lie lower than the diagonal energy of the single determinantal function of the same magnetization indicated in Fig. 2. We can go further than this, however. At infinite internuclear distance, we shall of course have a paramagnetic sort of behavior, and the correct solution will have a very high degeneracy: The energy will be independent of the orientation of the magnetic moments of the separated atoms, so that the energy of the lowest state corresponding to each total magnetization, from the maximum to zero, will be the same. If, for instance, we have the simple case mentioned in the preceding paragraph, in which the state of maximum magnetization corresponds to no electrons of − spin, so that the energy of the single determinant is the correct energy value at infinite distance, we can be sure that the lowest energy level of zero magnetization will come at the same value at infinite distance. This situa-

CC-0. In Public Domain. Gurukul Kangri Collection, Haridwar

Digitized by Arya Samaj Foundation Chennai and eGangotri

tion is clearly shown in the calculation carried out in reference 11.

Let us now ask what the correct energy levels must look like, resulting from this calculation. For simplicity, we take the case just mentioned, where the wave function of the state of maximum magnetization is correctly given by a single determinant, though the general situation is not changed in any essential feature if we do not have this simplification. Then the correct energy of the unmagnetized states, as a function of internuclear distance, must have a form somewhat like that given by the dotted curve in Figs. 3(a) and 3(b). In both cases shown there, we have indicated that the dotted curve lies below the diagonal energy of the single determinant representing an unmagnetized state, but reduces to the same energy at infinity as the magnetized state. In the case of Fig. 3(a), the unmagnetized state everywhere has a lower energy than the magnetized, and the system must be nonmagnetic. In Fig. 3(b), on the other hand, the unmagnetized energy lies above the magnetized value at large internuclear distances and there is a region of distances over which the substance will be ferromagnetic.

There are many conclusions which can be drawn from these instructive figures. First, perhaps, is the nature of the energy difference between magnetized and unmagnetized states in the ferromagnetic problem, shown in Fig. 3(b). This energy difference is zero at infinity, increases as the internuclear distance decreases, goes through a maximum, then decreases to zero and changes sign at smaller internuclear distances. It is well known that there is much experimental evidence for this sort of behavior. In the language of the Heisenberg exchange integral, it has often been described by saying that one integral, for a ferromagnetic material, is positive for large internuclear distances, negative for smaller distances, just like the energy difference just described. We have already given reasons for feeling that the Heisenberg method is invalid, and that no exchange integral, of the Heisenberg or Heitler-London type, can be found which correctly represents the problem and shows the dependence on internuclear distance just described. It is clear, however, that the energy-band theory, when examined carefully, must necessarily lead to just the type of behavior which we have just described.

As a second point, if Fig. 3(b) represents the true state of affairs with any reasonable approximation, we see that the correct energy of the unmagnetized state will cross the energy of the magnetized state at an internuclear distance not far from that where the diagonal energy of the unmagnetized state crosses the energy of the magnetized state. In other words, the internuclear distance where the ferromagnetic interaction (a notation which might well replace "exchange integral") changes sign is given to a fair approximation by finding where the diagonal energies of the magnetized

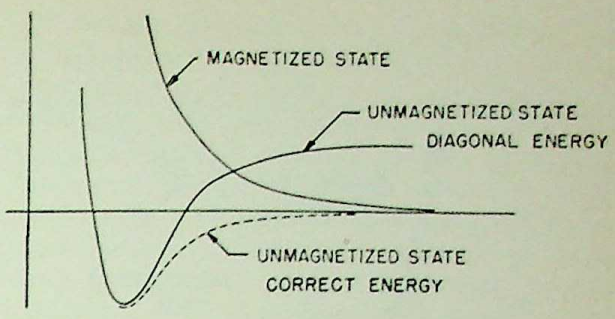


FIG. 3(a). Energy of single determinantal function, for magnetized and unmagnetized states, compared with correct energy of unmagnetized state (dotted curve), for nonmagnetic case.

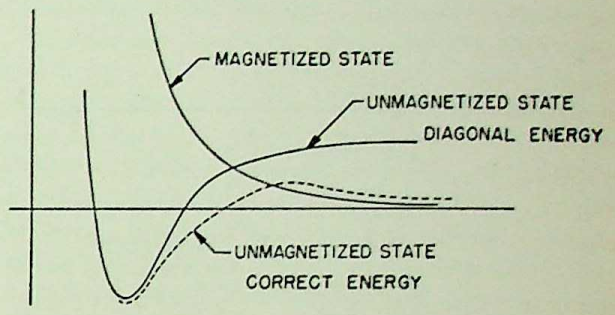


FIG. 3(b). Same as Fig. 3(a), for ferromagnetic case.

and unmagnetized energy-band functions cross. This is the reason, as pointed out in reference 11, why the estimates made by the energy-band method by the writer[16] as to which elements should be ferromagnetic were approximately correct, even though these estimates were based on a naive picture like that of Fig. 2.

We may assume that the diagrams of Fig. 3 represent the energies of the *3d* electrons. Superposed on this, of course, is the energy of the *4s* electrons (which presumably have no significant magnetic effect). Since the *4s* band is much broader than the *3d*, and its radius is much larger, this will result in a much deeper minimum of the energy curve than shown in Fig. 3(b), and at larger internuclear distances. Thus, we may expect curves like Fig. 4(a) and 4(b) to represent actual energy of the iron group elements as functions of internuclear distance. If the ferromagnetic interaction is positive at the minimum of the curve, as in Fig. 4(a), the substance will be ferromagnetic. If, however, the *3d* orbital is of larger size, as in the earlier elements of the transition group, like Ti and V, then the ferromagnetic interaction will change sign at a larger internuclear distance and will be negative at the minimum of the curve, as in Fig. 4(b), so that the substance will be nonmagnetic, even though the interaction of *3d* electrons is as shown in Fig. 3(b).

From Fig. 3(a) or Fig. 3(b), we may conclude that when the internuclear distance is small enough so that the diagonal energy of the unmagnetized state, as computed by the energy-band method, lies below that of the magnetized state, we cannot possibly have ferro-

[16] J. C. Slater, Phys. Rev. 49, 537, 931 (1936).

CC-0. In Public Domain. Gurukul Kangri Collection, Haridwar

Digitized by Arya Samaj Foundation Chennai and eGangotri

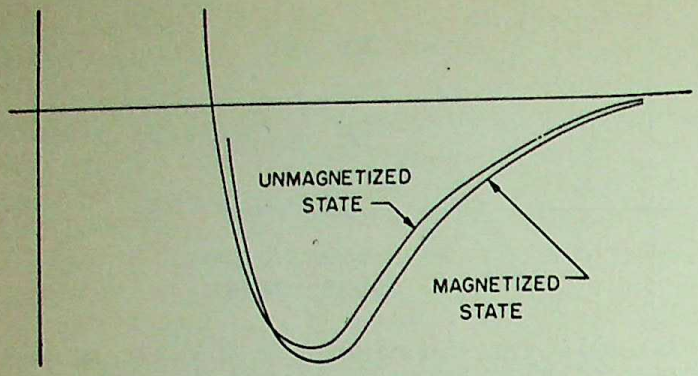


FIG. 4(a). Combined effect of 3*d* and 4*s* electrons, ferromagnetic case.

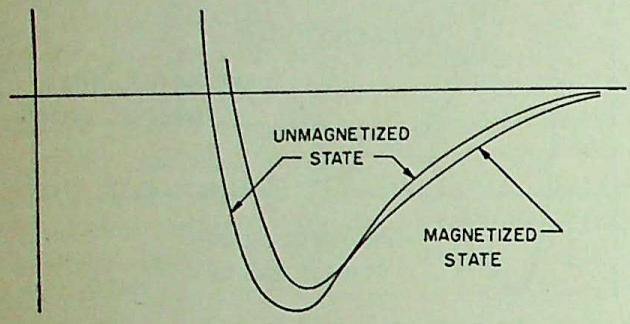


FIG. 4(b). Same as Fig. 4(a), nonmagnetic case.

magnetism. Furthermore, in this limit the true wave function of the unmagnetized state cannot lie far from the single determinantal wave function of the energy-band method. Thus, in such elements as Ti and V, we expect each individual atom to have zero magnetic moment, completely in contrast to the behavior of individual ions, but in agreement with the experimental results of Shull[17] and his collaborators. For cases where the 3*d* shell is smaller, however, we can say from the energy-band theory only that we can have either the case of Fig. 3(a) or Fig. 3(b). That is, the energy-band theory can show unequivocally that for substances with wide bands, ferromagnetism is impossible. For narrow energy bands, it can only show that it is possible; but it cannot distinguish, without more accurate calculations than have yet been made, whether ferromagnetism actually exists in these cases, or nonferromagnetism, or antiferromagnetism.

Let us finally take up the relation between our energy-band treatment of the problem and correlation energy. This term has been used to describe the decrease of energy when we go from an incorrect model of a metal, formed from a single determinant of Bloch-like functions, in which electrons of opposite spin can be found too close together, to a correct model in which the electrons of opposite spin are kept apart. Wigner and Seitz,[18] as is well known, have made estimates of the correlation energy for the alkali metals and have included a correction for this effect, which amounts to a large fraction of the cohesive energy. Löwdin,[6] on the other hand, has got very good numerical results for the cohesive energy of sodium, without using such a correction for correlation energy. Wohlfarth,[19] in private correspondence with the writer, takes essentially the position that at infinite internuclear distance the correlation energy represents just the difference between the full curve and the dotted curve of Fig. 1. That is, at infinite internuclear distance, it is the amount A indicated in Fig. 1. The writer agrees with this point of view; though the term "correlation energy" has meant so many things to different people that he feels it perhaps better not to use the word at all. If the correlation energy does in fact represent the difference between the two curves of Fig. 1, and if these curves really have something like the form shown there, then we should expect it to be a very small correction at the internuclear distance corresponding to the minimum of the curve of Fig. 1. This would be in accordance with the result of Löwdin, who got a very good result for a single determinantal wave function for sodium. It would not agree with the calculation of correlation energy of Wigner and Seitz, as given in reference 18. The writer is inclined to believe that this calculation of Wigner and Seitz represents a poor approximation, inapplicable at the minimum of the energy curve, and feels that the true correlation energy at the energy minimum is much smaller. The numerical accuracy of Wigner and Seitz's calculation of cohesive energy of sodium, using their correlation correction, is probably fortuitous.

Now let us consider the relation between correlation energy and the ferromagnetic interaction. The point of view of Wohlfarth[19] is that at finite internuclear distance there are two different effects: a correlation energy, and an exchange interaction which is responsible merely for the separation of the final magnetized and unmagnetized states, like the hypothetical Heisenberg exchange interaction. The writer disagrees with this point of view. From the general argument of the present paper, he feels that there can be no doubt as to the actual state of affairs. We must make our correlation correction, like that described with reference to Fig. 1, to reduce the energy of the unmagnetized state from the diagonal value coming from a single determinantal wave function, to the correct final value; that is, from the curve marked "unmagnetized state-diagonal energy" to that marked "unmagnetized state-correct value" in Fig. 3(a) or 3(b). We must make a similar but independent calculation for the magnetized state. In the particular case shown in Fig. 3, this correction is zero, but in general, where the completely magnetized state still has electrons of both spins, there will still be some correlation correction, though not as much as

[17] C. G. Shull and M. K. Wilkinson, Phys. Rev. 86, 509 (1952).

[18] E. Wigner and F. Seitz, Phys. Rev. 43, 804 (1933); 46, 509 (1934); E. Wigner, Phys. Rev. 46, 1002 (1934); Trans. Faraday Soc. 34, 678 (1938).

[19] E. P. Wohlfarth, private correspondence.

CC-0. In Public Domain. Gurukul Kangri Collection, Haridwar

Digitized by Arya Samaj Foundation Chennai and eGangotri

for the unmagnetized states. Having carried out these calculations for both magnetized and unmagnetized states, we must then compare these final corrected energies; their difference will be the ferromagnetic interaction energy whose sign determines whether the metal is ferromagnetic or not. With this point of view, the correlation energy is inextricably tied up with the ferromagnetic interaction, and no independent calculation of the ferromagnetic interaction can be made; but it can be found only through the correlation energy calculation just described.

The detailed method of carrying out these calculalations at large internuclear distance will not be described here. We have already mentioned one case[11] in which the writer has carried through such a calculation. A description of that calculation will illustrate the type of problems which will be encountered. The case taken up in reference 11 is that in which the magnetized state has a band entirely filled with electrons of + spin, with no electrons of − spin, so that it is expressed by a single determinant, as in the case illustrated in Fig. 3(a) and 3(b). The energy of this state was compared with that of a state which had just one electron of reversed spin. Effectively this consists of an electron in the otherwise empty band corresponding to − spin, and a hole in the otherwise filled band of + spin. The lowest diagonal energy of a single determinantal function representing this state is that in which the electron is at the bottom of the band of − spin and the hole is at the top of that of + spin; this corresponds to the energy marked "unmagnetized state-diagonal energy" in Fig. 3(a) or 3(b). The calculation corresponding to setting up the exact energy of the unmagnetized state involves setting up the lowest bound stationary state, in which the electron and hole are executing an oribt about their center of mass, similar to an exciton. This type of level has a lower energy, on account of the binding energy of the electron and hole. It was set up in detail in reference 11, and it was found that it led to an energy level of the correct sort. At infinite internuclear distance, it corresponded to the electron and hole being on the same atom; that is, to a state in which each atom of the crystal is neutral. As the internuclear distance decreased, the dimension of the "exciton" formed from the electron and hole increased, and its binding energy became less and less, until for a wide energy band the binding energy, which represents teh correlation energy, was negligible.

Under other circumstances the correlation energy comes, not from the attractive interaction of an electron and a hole, but from the repulsive interaction of two charges of like sign. Thus, a band almost filled with electrons of both spins (like the *d* band in Ni) will have a few vacancies, and they will tend to repel each other and stay out of each other's way. The calculation of either of these types of cases will remind us of the calculation of the behavior of electrons or holes near impurity atoms in a lattice of a semiconductor,[20] and like that problem, it is most easily handled in terms of Wannier functions. We shall not try to go further with these matters here; but it is the belief of the writer that it is only through such methods that we shall get a correct understanding not only of correlation energy, but also of the ferromagnetic interaction which in a satisfactory theory of magnetism will replace the inadequate concept of the Heisenberg exchange integral.

A beginning in the direction of such calculations has been made by Dr. A. Meckler,[21] who has calculated the structure of the O_2 molecule. He has set up atomic 1*s*, 2*s*, and 2*p* orbitals, for each atom, and has made orthogonal linear combinations of them. Then he has set up the $(12!)/(8!)(4!)=495$ determinants formed by assuming the 1*s* and 2*s* orbitals to be all occupied, but by assigning the remaining eight electrons, with both possible spins, in all possible ways to the remaining 12 orbitals (including spin). Of these 495 determinants, 9 have the symmetry characteristic of the $^3\sum$ ground state, and 12 of the next higher $^1\sum$ state. He has computed the matrix components of the Hamiltonian function between these determinants and has solved the resulting secular equations numerically on the Whirlwind digital computer at the Massachusetts Institute of Technology. This yields energy and wave functions for the ground state and the next excited state, as functions of the internuclear distance. Since all possible determinants are considered, the resulting energies and wave functions go into the best approximations to the ^3P ground state of the oxygen atoms at infinite separation. Meckler finds, as was to be expected, that the triplet state lies below the singlet. His calculated dissociation energy and internuclear distance for the ground state agree with experiment to about a percent, and the vibration frequency to a few percent. The values for the next excited state are not as accurate,

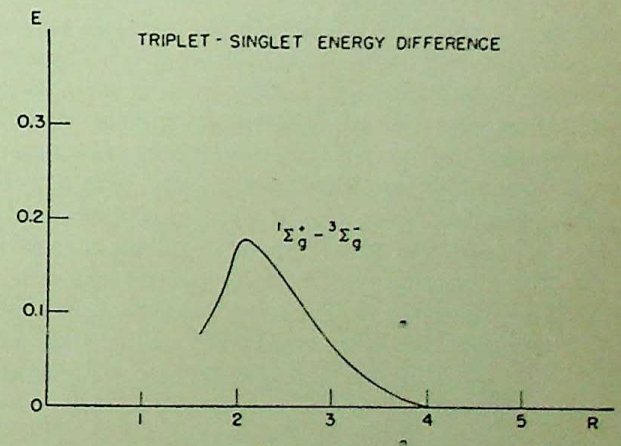


FIG. 5. Energy difference between magnetic and nonmagnetic state, for oxygen molecule, from calculation of Meckler.

[20] J. C. Slater, Phys. Rev. **76**, 1592 (1949).

[21] A. Meckler, Quarterly Progress Report on the Solid-State and Molecular Theory Group, M.I.T., July 15, 1952, and October 15, 1952.

CC-0. In Public Domain. Gurukul Kangri Collection, Haridwar

Digitized by Arya Samaj Foundation Chennai and eGangotri

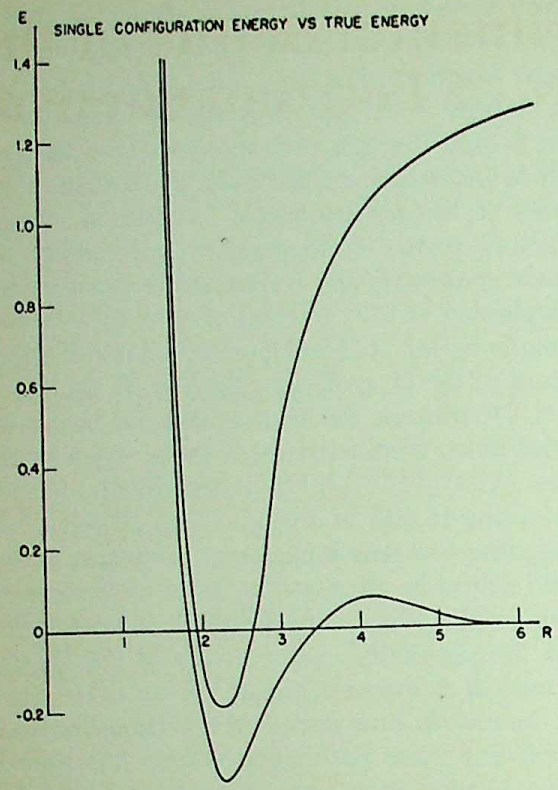


FIG. 6. Diagonal energy of molecular orbital state, compared with correct energy of ground state, for oxygen molecule, from calculation of Meckler.

but still are good approximations. The separation between singlet and triplet energies is shown in Fig. 5. It has the form which we have learned to expect of a ferromagnetic interaction energy, being zero at infinite distance, rising to a maximum, and then decreasing again at small distances, presumably changing sign at somewhat smaller distances than those for which the calculations are made. This, as far as the writer knows, is the first case where such a magnetic interaction has been directly calculated from Schrödinger's equation, using a correct molecular model.

It is interesting to compare the correct energy level of the ground state, as calculated by Meckler, and the corresponding diagonal energy of the molecular orbital state. This is shown in Fig. 6, and it is the specific application to this case of the general argument illustrated in Fig. 1. We see that the molecular orbital state, though it gives binding at internuclear distances of the right order of magnitude, is very inaccurate, and its energy rises much too high at large distances, as in Fig. 1. The diagonal energy of the triplet molecular orbital state, shown in Fig. 6, lies below that of the singlet molecular orbital state. This is in accordance with the prediction of Lennard-Jones,[22] one of the first deductions from the molecular orbital point of view. From Fig. 6, however, we see that the molecular orbital approximation is really quite bad here, and that it is very necessary to take linear combinations of a number of determinantal functions, as Mecker has done, and as we are advocating for the magnetic problem, in order to get good agreement with experiment.

[22] J. E. Lennard-Jones, Trans. Faraday Soc. **25**, 668 (1929); see particularly p. 684.

CC-0. In Public Domain. Gurukul Kangri Collection, Haridwar

Digitized by Arya Samaj Foundation Chennai and eGangotri

REVIEWS OF MODERN PHYSICS VOLUME 25, NUMBER 1 JANUARY, 1953

The Theoretical and Experimental Status of the Collective Electron Theory of Ferromagnetism

E. P. WOHLFARTH

Department of Mathematics, Imperial College, London, England

This paper is intended to supplement the review articles published by Stoner in 1948 and 1951, firstly by considering in greater detail the quantum-mechanical and statistical-mechanical foundations of the collective electron theory and secondly by considering briefly a wider range of relevant experimental results.

In Sec. 1 previous theoretical work is recalled. In Sec. 2 the difficulties of a rigorous quantum mechanical derivation of the internal energy of a ferromagnetic metal at absolute zero are outlined. In order to determine at least the form of the expressions, a calculation based on the tight binding approximation is described for a crystal containing N singly charged ions, which are fairly widely separated, and N electrons. The forms of the Coulomb and exchange contributions to the energy are discussed in the two instances of maximum and minimum multiplicity. The need for a correlation correction is stressed, and the effects of this correction are discussed with special reference to the state of affairs at infinite ionic separation. The fundamental difficulties involved in calculating the energy as function of magnetization are considered below; it is shown that they are probably less serious for tightly bound than for free electrons, so that the approximation of neglecting them in the first instance is not too unreasonable. The dependence of the exchange energy on the relative magnetization ζ is then of the form $\Sigma_n A_n \zeta^{2n}/2n$, and the relative orders of magnitude of A_1 and A_2 are considered. A previous calculation by Slater is critically reviewed.

In an application of statistical mechanics the difficulty arises that only if $\zeta=1$ or 0 will the zero-order wave function be in general a single Slater determinant. A calculation by Lidiard on this problem, that of spin degeneracy, is referred to. The relevance of the dependence of the interaction energies on wave vector is stressed. If these energy contributions are constant, then the free energy expression is that derived by Stoner, based on Fermi-Dirac statistics, even if spin degeneracy is taken into account. Several related difficulties are exemplified by a discussion of the properties of the free-electron gas, for which the exchange energy varies rapidly with wave vector $\mathbf{k}_i$, $\mathbf{k}_j$ when $|\mathbf{k}_i-\mathbf{k}_j|\to 0$. For tightly bound electrons the dependence on wave vector is much less rapid, and it is suggested that spin degeneracy effects are here less serious. A simple calculation of the low temperature electronic heat of tightly bound electrons, including exchange and correlation, is referred to in exemplification.

In Sec. 3 several experimental results are briefly discussed, including the following: (1) The variation with composition of the Curie temperature and saturation magnetization, and the variation with temperature of the susceptibility of nickel alloys; (2) the variation with temperature of the magnetization, electronic heat, and magnetocaloric effect of cubic cobalt, nickel, and nickel alloys below the Curie point; (3) the high temperature electronic heat of nickel and palladium; (4) the electronic properties of chromium and some other transition metals; (5) the electronic properties of palladium and its alloys.

1. PREVIOUS THEORETICAL WORK

SINCE many aspects of the collective electron treatment of ferromagnetism have recently been reviewed by Stoner,[1,2] there appears little justification for writing yet another review. Perhaps the main apology for, nevertheless, doing so is that the present paper is intended to supplement the earlier reviews, rather than to present their main substance again, by covering more fully the quantum-mechanical and statistical-mechanical foundations of the treatment and considering a wider range of relevant experimental results.

In this section a brief outline of the historical development of the subject is given. The earliest analysis of the ferromagnetic properties of collective electrons was made by Bloch,[3] who considered the effects of introducing exchange terms into the Sommerfeld description of a free-electron gas. Bloch predicted that the lowest energy state at 0°K is the ferromagnetic state if the electron density is small enough. The problem was later taken up by Brillouin.[4] The introduction and discussion of correlation effects by Wigner[5,6] left little doubt, however, that the conditions for ferromagnetism of free electrons are so stringent as to be practically never satisfied. The first attempt at analyzing the properties of a real ferromagnetic metal, nickel, was made by Slater.[7,8] Basing his discussion on the energy band calculation by Krutter,[9] Slater recognized the essential features of a satisfactory theory of ferromagnetism and attempted to calculate the exchange energy for the 3*d* electrons. The main results of this calculation[7] are: (1) The main contribution to the exchange energy is provided by the atomic exchange integral for electrons within one cell; (2) the contribution arising from nearest neighbor interaction is only about half a percent of the total exchange energy. These conclusions are critically discussed in Sec. 2. Slater also discusses temperature effects:[8] He calculates the magnetization, temperature curve of nickel below the Curie point, using Fermi-Dirac statistics and representing the exchange energy by a Weiss term, notes that magnetic saturation is not necessarily complete at 0°K, and attains good agreement with the observed low temperature electronic heat coefficient of nickel. In a further paper Slater[10] discusses ferromagnetism by

[1] E. C. Stoner, Phys. Soc. Rept. Progress Phys. 11, 43 (1948).
[2] E. C. Stoner, J. phys. et radium 12, 372 (1951).
[3] F. Bloch, Z. Physik 57, 545 (1929).
[4] L. Brillouin, J. phys. et radium 3, 565 (1932).
[5] E. P. Wigner, Phys. Rev. 46, 1002 (1934).
[6] E. P. Wigner, Trans. Faraday Soc. 34, 678 (1938).
[7] J. C. Slater, Phys. Rev. 49, 537 (1936).
[8] J. C. Slater, Phys. Rev. 49, 931 (1936).
[9] H. M. Krutter, Phys. Rev. 48, 664 (1935).
[10] J. C. Slater, Phys. Rev. 52, 198 (1937).

CC-0. In Public Domain. Gurukul Kangri Collection, Haridwar

Digitized by Arya Samaj Foundation Chennai and eGangotri

interpolating between band theory and spin wave theory. He concludes again that the occurrence of ferromagnetism is determined in the main by the magnitude of the interaction energy for electrons close to one atom and by the band width, but also that the low temperature variation of magnetization follows the $T^{\frac{3}{2}}$ law. In a progress report Slater[11] has recently discussed these problems again, and the writer is indebted to him for much fruitful correspondence.

In the meantime Stoner had published two papers on collective electron ferromagnetism.[12,13] The main assumptions underlying Stoner's calculations are: (1) the ferromagnetism of a metal results from the holes in the so-called $3d$ band, taken to be parabolic in the neighborhood of the Fermi limit; (2) the exchange energy $J(\zeta)$ is proportional to the square of the relative magnetization ζ, as in the Weiss theory—specifically, $J(\zeta)=\frac{1}{2}N_e k\theta'\zeta^2$, where N_e is the number of holes and θ' a constant parameter; (3) the particles obey Fermi-Dirac statistics. The results of the deductive treatment based on these assumptions were discussed in the earlier reviews.[1,2] Later Wohlfarth[14–16] was able to make some extensions of the treatment and to apply the results in an analysis of experimental data (see Sec. 3). By extending Stoner's work to rectangular energy bands Wohlfarth[17] showed that band shape is less decisive in determining many of the properties of ferromagnetic substances than the form of $J(\zeta)$ (see Sec. 2). The success of Stoner's treatment in correlating experimental results emphasizes the need for a satisfactory fundamental theoretical treatment to justify the assumptions underlying it and to provide an estimate of the parameters inherent in the treatment, particularly the parameter θ'. A preliminary discussion has already been given.[18] Recently, Lidiard has considered several of the outstanding fundamental problems of the collective electron treatment. He discusses[19] the properties of the free-electron gas, including exchange, and stresses the need for a correlation correction. He also discusses[20] the fundamental problem of spin degeneracy (see Sec. 2). This work is valuable in indicating the conditions under which Stoner's equations are valid or approximately valid. Some discussion of relevant problems has also been given by Bell[21] and Smith.[22]

2. QUANTUM-MECHANICAL AND STATISTICAL-MECHANICAL FOUNDATIONS

In this section a quantum-mechanical derivation of the absolute zero internal energy expression, applicable to a simple model of a ferromagnetic metal, is first outlined. Then the problems of statistical mechanics are briefly discussed.

(a) The Internal Energy of a Ferromagnetic Metal at Absolute Zero

In calculating the internal energy of a ferromagnetic metal many of the hitherto unresolved difficulties in the theory become immediately apparent. It is particularly difficult to treat what is almost an experimental fact, that the electrons outside closed shells may be divided, apparently, into those responsible for a large part of the conduction properties and those responsible for ferromagnetism. The usual description of this state of affairs, first given by Mott,[23] regards the loosely bound electrons, originating largely in the $4s$ shell of the isolated atoms, as principally the conduction electrons and ascribes ferromagnetism to the more tightly bound electrons originating largely in the $3d$ shell. Although Mott's hypothesis finds some confirmation in the band calculation of Krutter[9] and Slater,[7] there is little evidence that the conduction electrons are entirely s electrons or the ferromagnetic electrons entirely d electrons. Because of band overlap, there is, doubtless, some very strong mixing between them, and a fully satisfying theory would have to be based on wave functions including this effect.

It is proposed in this paper to consider the collective electrons responsible for ferromagnetism by the tight binding approximation. A first attempt at a quantitative treatment is the energy band calculation of Fletcher and Wohlfarth.[24,25] In this work the tightly bound electrons in nickel were ascribed pure d character solely so as to keep the computational labor within manageable limits. Even so, an extension to calculate the exchange energy is at present quite impracticable, again owing to computational difficulties. In order to determine at least the form of the energy expression, a calculation is outlined below for a crystal containing N singly charged ions which are widely separated, and $N_e=N$ electrons described by Bloch type wave functions. The Hamiltonian operator for this assembly is

$$\mathbf{H}=-(h^2/8\pi^2\mu)\sum_i \nabla_i^2+\sum_i\sum_l V_l(\mathbf{r}_i)$$

$$+\frac{e^2}{2}\sum_i\sum_j r_{ij}^{-1}+\frac{e^2}{2}\sum_l\sum_m R_{lm}^{-1}, \quad (1)$$

where i, j refer to the positions of the electrons, l, m the positions of the ions, and $V_l(\mathbf{r}_i)$ is the potential energy operator for electron i in the field of ion l. For maximum and minimum multiplicity (the relative magnetization $\zeta=1$ or 0), the zero-order wave function may

[11] J. C. Slater, Quart. Progress Rept. M.I.T. No. 2, 4 (1951).
[12] E. C. Stoner, Proc. Roy. Soc. (London) **A165**, 372 (1938).
[13] E. C. Stoner, Proc. Roy. Soc. (London) **A169**, 339 (1939).
[14] E. P. Wohlfarth, Proc. Roy. Soc. (London) **A195**, 434 (1949).
[15] E. P. Wohlfarth, Phil. Mag. **40**, 1095 (1949).
[16] E. P. Wohlfarth, Proc. Leeds Phil. Soc. **5**, 89 (1949).
[17] E. P. Wohlfarth, Phil. Mag. **42**, 374 (1951).
[18] E. P. Wohlfarth, Phil. Mag. **40**, 703 (1949).
[19] A. B. Lidiard, Proc. Phys. Soc. (London) **A64**, 814 (1951).
[20] A. B. Lidiard, Proc. Phys Soc. (London) **A65**, 885 (1952).
[21] G. M. Bell, Phil. Mag. **43**, 127 (1952).
[22] R. S. Smith, thesis, Case Institute of Technology (1951).
[23] N. F. Mott, Proc. Phys. Soc. (London) **47**, 571 (1935).
[24] G. C. Fletcher and E. P. Wohlfarth, Phil. Mag. **42**, 106 (1951).
[25] G. C. Fletcher, Proc. Phys. Soc. (London) **A65**, 192 (1952).

CC-0. In Public Domain. Gurukul Kangri Collection, Haridwar

Digitized by Arya Samaj Foundation Chennai and eGangotri

be written, in general, as a single Slater determinant and as the product of two such determinants, respectively,

$$\Psi(\zeta=1)=(N!)^{-\frac{1}{2}}\Delta|\psi_i(\mathbf{r}_j)|, \tag{2}$$

$$\Psi(\zeta=0)=[(N/2)!]^{-1}\Delta^+|\psi_i(\mathbf{r}_j)|\cdot\Delta^-|\psi_i(\mathbf{r}_j)|, \tag{3}$$

where Δ^+ contains wave functions for electrons with $+$ spin and Δ^- with $-$ spin. The total energy is

$$E=\int\cdots(N)\cdots\int\Psi^*\mathbf{H}\Psi d\tau(\mathbf{r}_1,\cdots\mathbf{r}_N). \tag{4}$$

The one-electron wave functions in (2), (3) take the form

$$\psi_i(\mathbf{r}_j)=N^{-\frac{1}{2}}\sum_l\exp(i\mathbf{k}_i\cdot\mathbf{R}_l)\phi(\mathbf{r}_j-\mathbf{R}_l), \tag{5}$$

where $\mathbf{k}_i$ is the wave vector of electron i and ϕ the atomic wave function. If the atomic level generating the energy bands is degenerate, e.g. a $3d$ level, then (5) is replaced by a more complicated function.[25] The evaluation of (4) is straightforward,[26] giving

$$E=(F'+2K)+(C'-K)-J, \tag{6}$$

where

$$\left.\begin{aligned}
F'&=\sum_i F_i=\sum_i\int\psi_i^*(\mathbf{r})[-(h^2/8\pi^2\mu)\nabla^2\\
&\qquad+\sum_l V_l(\mathbf{r})]\psi_i(\mathbf{r})d\tau(\mathbf{r}),\\
C'&=\frac{e^2}{2}\sum_i\sum_j C_{ij}\\
&=\frac{e^2}{2}\sum_i\sum_j\int\int\frac{1}{r_{12}}|\psi_i(\mathbf{r}_1)|^2|\psi_j(\mathbf{r}_2)|^2d\tau(\mathbf{r}_1,\mathbf{r}_2),\\
J&=\frac{e^2}{2}\sum_i\sum_j\delta_{ij}J_{ij}=\frac{e^2}{2}\sum_i\sum_j\delta_{ij}\\
&\qquad\times\int\int\frac{1}{r_{12}}\psi_i^*(\mathbf{r}_1)\psi_i(\mathbf{r}_2)\psi_j^*(\mathbf{r}_2)\psi_j(\mathbf{r}_1)d\tau(\mathbf{r}_1,\mathbf{r}_2),\\
K&=\frac{e^2}{2}\sum_l\sum_m\frac{1}{R_{lm}}=\frac{Ne^2}{2}\sum_l\frac{1}{R_l},
\end{aligned}\right\} \tag{7}$$

and where $\delta_{ij}=1$ for i, j representing electrons with parallel spins and 0 for antiparallel spins. The energy is written in the particular form (6) since then each of the three terms converges, although F', C', K separately diverge for an infinite crystal. Each of the terms in (7) may be simplified using (5). Thus

$$\left.\begin{aligned}
F_i&=E_0+\sum_l\int|\phi(\mathbf{r})|^2[V_l(\mathbf{r})-U(\mathbf{r})]d\tau(\mathbf{r})\\
&\qquad+\sum_l\int\phi^*(\mathbf{r}-\mathbf{R}_l)[V_l(\mathbf{r})\\
&\qquad-U(\mathbf{r})]\phi(\mathbf{r})d\tau(\mathbf{r})\exp(i\mathbf{k}_i\cdot\mathbf{R}_l),
\end{aligned}\right\} \tag{8}$$

where NE_0 is the energy of the isolated atoms, $U(\mathbf{r})$ the potential energy of an electron in the field of an isolated ion, and the summation means that the potential whose mean value is required is that of the electron in the field of all the ions except the central ion. The second term in (8) thus diverges after summation like $-2K$ (see Eq. 7) so that $F'+2K$ in (6) converges. The third term in (8) converges since the overlap integral de-decreases exponentially and is here to be taken negligible beyond nearest neighbors at distance R. The overlap integral is called $A(R)$. This term is the one of interest in energy band calculations and its exact form depends on the lattice structure.[25] The dependence of F' on relative magnetization ζ is found by summing F_i over the occupied volume of $\mathbf{k}$ space and this contribution to the total energy, the Fermi energy, is in general least when $\zeta=0$. The second term in (6) is the Coulomb energy, and

$$\begin{aligned}
C_{ij}=N^{-1}\sum_m\sum_n\sum_p\int\int\frac{1}{r_{12}}&\phi^*(\mathbf{r}_1)\phi(\mathbf{r}_1-\mathbf{R}_m)\\
&\times\phi^*(\mathbf{r}_2-\mathbf{R}_n)\phi(\mathbf{r}_2-\mathbf{R}_p)d\tau(\mathbf{r}_1,\mathbf{r}_2)\\
&\times\exp i\{\mathbf{k}_i\cdot\mathbf{R}_m-\mathbf{k}_j\cdot(\mathbf{R}_n-\mathbf{R}_p)\}.
\end{aligned} \tag{9}$$

For simplicity neglect all 3- and 4-center integrals,[27] although these as well as nonorthogonality integrals could in principle be included. Also, the exponentially decreasing integrals in (9) are assumed to be negligible for all but nearest neighbors. Then

$$\left.\begin{aligned}
C_{ij}&=N^{-1}\{I_0+\sum_l I_1(\mathbf{R}_l)\}+zN^{-1}\{4I_2(R)\cos\mathbf{k}_i\cdot\mathbf{R}\\
&\qquad+2I_3(R)\cos\mathbf{k}_i\cdot\mathbf{R}\cos\mathbf{k}_j\cdot\mathbf{R}\},
\end{aligned}\right\} \tag{10}$$

where

$$\left.\begin{aligned}
I_0&=\int\int\frac{1}{r_{12}}|\phi(\mathbf{r}_1)|^2|\phi(\mathbf{r}_2)|^2d\tau(\mathbf{r}_1,\mathbf{r}_2),\\
I_1(\mathbf{R}_l)&=\int\int\frac{1}{r_{12}}|\phi(\mathbf{r}_1)|^2|\phi(\mathbf{r}_2-\mathbf{R}_l)|^2d\tau(\mathbf{r}_1,\mathbf{r}_2),\\
I_2(R)&=\int\int\frac{1}{r_{12}}|\phi(\mathbf{r}_1)|^2\phi(\mathbf{r}_2)\phi^*(\mathbf{r}_2-\mathbf{R})d\tau(\mathbf{r}_1,\mathbf{r}_2),\\
I_3(R)&=\int\int\frac{1}{r_{12}}\phi^*(\mathbf{r}_1)\phi(\mathbf{r}_1-\mathbf{R})\\
&\qquad\times\phi^*(\mathbf{r}_2-\mathbf{R})\phi(\mathbf{r}_2)d\tau(\mathbf{r}_1,\mathbf{r}_2),
\end{aligned}\right\} \tag{11}$$

[26] F. Seitz, *Modern Theory of Solids* (McGraw-Hill Book Company, Inc., New York, 1940).

[27] S. O. Lundqvist and P. O. Löwdin, Arkiv Fys. 3, 147 (1951).

CC-0. In Public Domain. Gurukul Kangri Collection, Haridwar

Digitized by Arya Samaj Foundation Chennai and eGangotri

where $z(R)$ is the number of nearest neighbors. Relation (10) for C_{ij} contains overlap integrals independent of interatomic distance, I_0, integrals varying as R^{-1}, I_1, and integrals decreasing exponentially, I_2 and I_3. For an infinite crystal the sum involving I_1 diverges after summation over i, j, canceling then exactly with $-K$ in (6), so that $C'-K$ in (6) converges. The final term in (6) is the exchange energy and

$$J_{ij}=N^{-1}\sum_m\sum_n\sum_p\int\int\frac{1}{r_{12}}\phi^*(\mathbf{r}_1)\phi^*(\mathbf{r}_2-\mathbf{R}_m)\times\phi(\mathbf{r}_1-\mathbf{R}_n)\phi(\mathbf{r}_2-\mathbf{R}_p)d\tau(\mathbf{r}_1,\mathbf{r}_2)\times\exp i\{\mathbf{k}_i\cdot\mathbf{R}_p-\mathbf{k}_j\cdot(\mathbf{R}_m-\mathbf{R}_n)\},\quad(12)$$

and with the same simplifications as before

$$\left.\begin{aligned}J_{ij}=N^{-1}[I_0+\sum_l I_1(\mathbf{R}_l)\cos\mathbf{k}_i\cdot\mathbf{R}_l\cos\mathbf{k}_j\cdot\mathbf{R}_l]\\+zN^{-1}[4I_2(R)\cos\mathbf{k}_i\cdot\mathbf{R}\\+I_3(R)(1+\cos\mathbf{k}_i\cdot\mathbf{R}\cos\mathbf{k}_j\cdot\mathbf{R})].\end{aligned}\right\}\quad(13)$$

Here the sum involving I_1 converges rapidly after summation over i, j, as shown below, and may be replaced by its leading term involving $I_1(R)$, corresponding to nearest neighbor interaction, as for I_2 and I_3.

With C_{ij} and J_{ij} given by (10) and (13) the last two terms in the total energy expression (6) may be calculated by summation over $\mathbf{k}_i$, $\mathbf{k}_j$. It is convenient to discuss separately the two cases $\zeta=1$ and 0.

(i) $\zeta=1$. Here the electron spins are all parallel and every state in the Brillouin zone is singly occupied. In summing over the zone it may be noted that, if $\mathbf{R}_l$ is a lattice vector,

$$\sum_{\text{zone}}\cos(\mathbf{k}\cdot\mathbf{R}_l)=\left.\begin{aligned}0\quad&\text{when}\quad\mathbf{R}_l\neq0,\\N_e\quad&\text{when}\quad\mathbf{R}_l=0,\end{aligned}\right\}\quad(14)$$

where N_e is the number of electrons. Hence the total energy is easily seen to be identical with that calculable with the Heitler-London approximation, a well known theorem[26] relating to full zones which has applicability in discussing nonconducting solids like diamond.[28] It may be specially noted that the term $\sum_i\sum_j I_0$ in C' is here canceled exactly by the term $\sum_i\sum_j I_0\delta_{ij}$ in J.

(ii) $\zeta=0$. Here (14) no longer holds and the total energy differs from that calculable with the Heitler-London treatment. Consider first the terms in (6) which do not vanish as $R\to\infty$. In this limit

$$E-NE_0=\frac{e^2I_0}{2N}\sum_i\sum_j(1-\delta_{ij})=\frac{e^2N_e^2}{4N}I_0=\frac{Ne^2I_0}{4},\quad(15)$$

when $N_e=N$. Hence as $R\to\infty$ the total energy is larger for $\zeta=0$, by an amount given by (15), than for $\zeta=1$, so that the crystal is apparently ferromagnetic at infinite separation of the atoms. This "catastrophe" was noted by Seitz.[26] Now as $R\to\infty$ $E-NE_0$ must vanish whether $\zeta=1$ or 0, and this result is given correctly by the Heitler-London treatment. The form of the integral I_0 in (11) shows that the anomalous molecular field arises from the interaction of electrons close to one atom. Hence the anomaly results from the overemphasis in the Bloch approximation of ionized states. In this limit the anomalous term is in fact canceled exactly by the correlation correction, equal to $-Ne^2I_0/4$ when $\zeta=0$ and zero when $\zeta=1$, when $E-NE_0=0$ on both approximations [see (i) above].

For finite values of R the total energy of the demagnetized crystal includes all the terms given in (10) and (13). The problem of calculating the correlation energy in this general case is perhaps the most difficult one in the electron theory of metals. A similar problem, that of calculating configurational interactions, arises in the quantum theory of molecules.[29] For H_2, Coulson and Fischer[30] have given a very clear exposition of the nature of the problem and have gone a long way towards its solution. A similar calculation for the present case is, however, quite impracticable. Since, as already noted, the correlation energy in the limit $R\to\infty$ is known, and in the absence of a rigorous treatment, it will be assumed that for *finite, though still large* values of R, the correlation energy remains equal to the value $-Ne^2I_0/4$ for infinite separation, thus canceling exactly the anomalous terms in the Coulomb and exchange energy involving I_0. Although it is clear that the R dependent terms must also be modified, it is probable, though impossible to prove, that these modifications are slight, since the bulk of the correlation correction must be included in the large term required to cancel the anomalous terms in C' and J. On the basis of this approximation the parameter θ' varies with R via overlap integrals of the type $I(R)$ given in (11). At the same time the degeneracy temperature, which depends on the band width, varies with R via overlap integrals of the type $A(R)$ given in (8). Hence θ' and the degeneracy temperature are expected to be both very much of the same order of magnitude and, as pointed out below, this result is also indicated by the experimental results for real ferromagnetic metals.

In order to calculate the Coulomb and exchange energies arising from the R dependent terms in C_{ij} and J_{ij} for the demagnetized crystal, it is strictly necessary to calculate first the shape of the occupied part of the Brillouin zone. For simplicity this may be assumed to be spherical with radius k_0. Now

$$\sum_{\text{sphere}}\cos(\mathbf{k}\cdot\mathbf{R})=\frac{V}{8\pi^3}\int\cos(\mathbf{k}\cdot\mathbf{R})d\tau(\mathbf{k})=\frac{N_e}{2}f(k_0R),\quad(16)$$

[28] K. Ganzhorn, Naturwiss. 39, 62 (1952).

[29] Coulson, Craig, and Jacobs, Proc. Roy. Soc. (London) A206, 297 (1951).

[30] C. A. Coulson and I. Fischer, Phil. Mag. 40, 386 (1949).

CC-0. In Public Domain. Gurukul Kangri Collection, Haridwar

Digitized by Arya Samaj Foundation Chennai and eGangotri

where

$$f(x)=3(\sin x-x\cos x)/x^3=3(\pi/2)^{\frac{1}{2}}x^{-\frac{3}{2}}J_{3/2}(x), \quad (17)$$

V is the volume and N_e the number of electrons. The function $f(x)$ tends to 1 as $x\to 0$ and converges rapidly as x increases. Hence the R dependent terms in C' and J have the general form

$$ne^2N_e^2I(R)f^p(k_0R)/N, \quad (18)$$

where n is a numerical factor of order unity, $I(R)$ one of the overlap integrals in (11), and $p=0$, 1, or 2 depending on whether the term which has been integrated is constant, depends on either $\mathbf{k}_i$ or $\mathbf{k}_j$ only or on both. In particular, $p=2$ for the term in J_{ij} in (13) which involves I_1. Hence this contribution to the exchange energy converges very rapidly beyond nearest neighbors through the convergence of $f^2(k_0R)$ and will at most be of the same order of magnitude as the other contributions to J involving I_2 and I_3, for some of which $p=0$. For these latter terms the convergence occurs only through the exponential dependence on R of the integrals which may not be as rapid as the dependence on R of $f(k_0R)$. In an early calculation by Brillouin[31] integrals of the form I_2, I_3 were not considered, the exchange energy being taken to be proportional to $I_1(R)$ only. The above discussion shows that Brillouin's calculation may be at fault (see also below). In the same paper[31] Brillouin also considers the Coulomb contribution to the total energy. The present discussion shows that, whereas terms in C_{ij} which are independent of $\mathbf{k}_i$, $\mathbf{k}_j$ reduce after summation to the same value whether $\zeta=1$ or 0, those terms which depend on $\mathbf{k}$ give differing contributions depending on ζ. Hence the Coulomb as well as the exchange energy contributes towards the molecular field energy. It is only for free electrons, where C_{ij} is constant, that C' is strictly independent of magnetization.

The discussion so far has been limited to the two extreme cases $\zeta=1$ or 0, since only then can the total wave function be represented by a single Slater determinant. As shown below, however, the approximation of using the above expressions in calculating the total energy as a function of magnetization $E(\zeta)$ is probably less serious for tightly bound than for perfectly free electrons. Then, considering the expression (13) giving J_{ij}, a term, involving the integral $I_3(R)$, is independent of $\mathbf{k}_i$, $\mathbf{k}_j$. The corresponding contribution to the exchange energy $J(\zeta)$ is $(ze^2/2N)I_3(R)\times(N_1^2+N_2^2)$, where N_1, $N_2=\frac{1}{2}N_e(1\pm\zeta)$. Hence the contribution to $E(\zeta)$ is $-(ze^2/4N)N_e^2I_3(R)\zeta^2$, equivalent to a constant value of the parameter θ', given by $k\theta'=\frac{1}{2}zqe^2I_3(R)$, where $q=N_e/N$ is the number of electrons per atom. Again (13) contains a term, involving $I_2(R)$, which depends on $\mathbf{k}_i$ but not on $\mathbf{k}_j$. This contributes to $E(\zeta)$ a term equal to

$$-(ze^2/2N)I_2(R)\{N_1^2f(k_{01}R)+N_2^2f(k_{02}R)\}, \quad (19)$$

where $k_{01}^3=(6\pi^2N_1/V)$, $k_{02}^3=(6\pi^2N_2/V)$. Now $f(x)$ may be expanded in the form $f(x)=1-x^2/10+0(x^4)$. Hence (19) becomes

$$\left.\begin{aligned} &-\tfrac{1}{2}N_ek\theta'\zeta^2(1+\tfrac{1}{2}A\zeta^2+0(\zeta^4)),\\ \text{where}\quad &k\theta'=\tfrac{1}{2}zqe^2I_2(R), \quad A\doteqdot(2/243)(3\pi^2qNR^3/V)^{\frac{1}{3}},\end{aligned}\right\}(20)$$

corresponding to an effective θ' which increases with magnetization. For nickel, $q=0.6$, $A\doteqdot 0.07$. Finally, (13) contains terms, involving $I_1(R)$ and $I_3(R)$, which depend on both $\mathbf{k}_i$ and $\mathbf{k}_j$. These again give a contribution to $E(\zeta)$ of the form (20) but with A twice as large as before. In general, with the approximation that $E(\zeta)$ is calculable from the above formulas, the dependence of energy on magnetization has the form $\sum_n A_n\zeta^{2n}/2n$; the rough calculation just outlined shows that $A=A_2/A_1$ may be of order 0.1 (see Sec. 3).

This subsection will be concluded by a critical discussion of Slater's paper.[7] It seems to the writer (1) that in taking the main contribution to the exchange energy to be the atomic integral he calls J, Slater has taken no account of correlation, thus obtaining anomalous ferromagnetism at large interatomic separation as discussed above. Slater has recently reconsidered this problem[11] and also concludes that the result of the earlier paper is due to the neglect of correlation. His method of overcoming the difficulty, however, is to postulate that beyond some large value of R ionized states must be completely excluded from the treatment and the Heitler-London treatment used in describing the metallic state. This view is also held by Mott.[32] The work of Coulson and Fischer[30] suggests to the writer, however, that the Bloch approximation, duly corrected for correlation as suggested above, is applicable over the whole range of R. In both cases the correct energy is obtained as $R\to\infty$. (2) With the atomic integral J virtually cancelled by the correlation correction Slater's expression (3) is reduced to the R dependent second term. The reason why this gives only half a percent of the total calculated exchange energy (which, incidentally, leads to roughly the correct value of the Curie temperature) seems to be the following. Slater, like Brillouin,[31] reduces this term to

$$(ze^2/2N)I_1(R)\sum_i\sum_j\cos\mathbf{k}_i\cdot\mathbf{R}\cos\mathbf{k}_j\cdot\mathbf{R} \quad (21)$$

(see Eq. 13), and states that "the quantities $\mathbf{k}_i$ and $\mathbf{k}_j$ should be allowed to range over a polyhedral cell in $\mathbf{k}$ space." Now (14) shows that then the above contribution vanishes identically. A small nonvanishing contribution was in fact obtained only because Slater replaced the zone by a sphere of equal volume and radius k_0, which, understandably, makes the value of (k_0R) lie close to a zero of $f(k_0R)$ (see Eq. 17). The above discussion suggests that the exchange energy is given by summing the *full* expression for $J_{ij}(R)$ given by (13) over the *occupied* part of the zone, while Brillouin and

[31] L. Brillouin, J. phys. et radium 4, 333 (1933).

[32] N. F. Mott, Proc. Phys. Soc. (London) A62, 416 (1949).

CC-0. In Public Domain. Gurukul Kangri Collection, Haridwar

Digitized by Arya Samaj Foundation Chennai and eGangotri

Slater consider only the term (21) involving I_1. Further, the occupied volume in $\mathbf{k}$ space only corresponds to a full zone, and summation only reduces the contribution to zero, when $\zeta=1$. For the unmagnetized state the zone is half-full and the contribution does not vanish.

Although the formulas derived above are applicable to a very simple model of a ferromagnetic, it seems clear empirically that many features of a satisfactory theory of ferromagnetism, applicable to real metals, are given by considering the magnetic carriers (holes in the d band) much in the same way as were the tightly bound electrons to which these formulas apply. In summing expressions like (13) over effectively the unoccupied part of the d band, the volume of integration for holes with + and − spin depends on ζ and does not in general correspond to a full zone. Consequently, the nearest neighbor contribution to the exchange energy, here suggested to be the most important contribution, does not vanish after summation.

(b) Statistical Mechanics—Spin Degeneracy

For an arbitrary value of the relative magnetization ζ, a Slater determinant including spin functions may be constructed to give the total wave function for the metal. The spin functions may, however, be permuted in a large number of ways, so that the energy state is very highly degenerate. The correct zero-order wave function is thus a linear combination of a large number of Slater determinants. If this problem could be correctly formulated,[33] the final energy expression would be accurate even in as far as it would include some correlation terms. In analyzing this problem, that of spin degeneracy, Lidiard[20] shows that the more accurate free energy expression is identical with that derived by Stoner, if the sum of the Coulomb and exchange energies, $C_{ij}+J_{ij}$, is independent of $\mathbf{k}_i$, $\mathbf{k}_j$. Now, as shown above (see also Lidiard[19]), if C_{ij} were constant summation over i, j gives C' independent of ζ, and if J_{ij} were constant $J(\zeta)\propto\zeta^2$, corresponding to a constant molecular field coefficient. For this simple case, it is permissible to consider the electrons (or holes) with + spin to be distributed in a sub-band whose lowest state is displaced relative to that of the sub-band for electrons with − spin by an amount proportional to ζ and to the (constant) value of J_{ij}. On the other hand, if J_{ij} is not constant, this familiar description of the ferromagnetic state, on which Stoner's equations are based, is no longer applicable. This situation arises in its most serious form in discussing the free-electron gas. Here C_{ij} is constant but J_{ij} is not, being given by

$$J_{ij}=(4\pi/V)|\mathbf{k}_i-\mathbf{k}_j|^{-2}. \tag{22}$$

It is thus easy to understand why use of (22) in calculating many of the properties of the free-electron gas leads to absurd results: (1) The low temperature electronic heat varies anomalously with temperature;[34–36] (2) the magnetization, temperature curve drops suddenly at a critical temperature;[19] (3) the low energy tail of the soft x-ray emission curve has infinite width.[37] It was suggested[35,37] that results in better agreement with observation could be obtained if allowance were made for correlation by the use of a screened Coulomb potential in the Hamiltonian operator [Eq. (1)], giving a less rapid variation of J_{ij}. The fundamental validity of this procedure is, however, very doubtful (Wohlfarth[35] pointed out that the total energy could not now be calculated correctly); the problem has been reconsidered by Macke,[38] and Bohm and Pines.[39]

Relation (13) for tightly bound electrons shows that here the variation of J_{ij} is much less rapid than the variation (22) for free electrons. It is, therefore, suggested that here spin degeneracy effects are much less serious and that Stoner's equations, based on Fermi-Dirac statistics, give a very good approximation to the accurate statistical equations which would be obtained by inclusion of spin degeneracy effects. Apart from the general consistency of the above argument, two further supporting arguments for the general viewpoint may be given: (1) As already noted, constant J_{ij} implies a constant value of the parameter θ'. For tightly bound electrons it was shown earlier that the effective θ' varies with ζ, the molecular field energy being given by $-\frac{1}{2}N_e k\theta'\zeta^2(1+\frac{1}{2}A\zeta^2+\cdots)$. Both theory and experiment (see Sec. 3) show, however, that the variation is very gradual, since A is only about 0.1. (2) A calculation has been carried out [40] of the temperature variation of the electronic heat C_e of tightly bound electrons including that contribution to J_{ij} which depends most strongly on $\mathbf{k}$, *viz.* the term in (13) involving I_1. The method of calculation used was that suggested by Koppe,[34] giving $C_e=\gamma T$, where γ is related to the corresponding coefficient neglecting exchange, γ_0, by

$$\gamma_0/\gamma=1+\frac{z}{24}e^2f^2(k_0R)I_1(R)/A(R). \tag{23}$$

Here R is the interatomic distance, z the number of nearest neighbors, f is given by (17), and $A(R)$ is the overlap integral determining band width, given in (8). In deriving (23) the electrons are taken to be distributed in a sphere with radius k_0 in $\mathbf{k}$ space. The other contributions to J_{ij} have similar but less pronounced effects. It appears, therefore, that, contrary to the behavior of the free-electron gas,[35] the electronic heat of tightly bound electrons is strictly proportional to T, with γ only slightly less than the value derivable by

[33] S. F. Boys, Proc. Roy. Soc. (London) **A200**, 542 (1950).

[34] H. Koppe, Z. Naturforsch. **2A**, 429 (1947).
[35] E. P. Wohlfarth, Phil. Mag. **41**, 534 (1950).
[36] A. B. Lidiard, Phil. Mag. **42**, 1325 (1951).
[37] P. T. Landsberg, Proc. Phys. Soc. (London) **A62**, 806 (1949).
[38] W. Macke, Z. Naturforsch. **5A**, 192 (1950).
[39] D. Bohm and D. Pines, Phys. Rev. **80**, 903 (1950); **82**, 625 (1951); **85**, 338 (1952).
[40] E. P. Wohlfarth (unpublished).

CC-0. In Public Domain. Gurukul Kangri Collection, Haridwar

Digitized by Arya Samaj Foundation Chennai and eGangotri

neglecting exchange. It may be recalled, however, that unless a correction is made for correlation, the assembly exhibits anomalous ferromagnetism at large R and hence an anomalous magnetic specific heat. As for free electrons,[35] reasonable results are only obtained after allowing for correlation.

(c) Summary

The results obtained in this section may be conveniently summarized by relating them directly to the premises underlying Stoner's treatment,[12,13] recalled in Sec. 1. (1) "The ferromagnetism of a metal results from the holes in the so-called 3d band." It is suggested that the magnetic carriers are best described by tight binding wave functions. These allow in principle the calculation of band shape and width, determined by overlap integrals of the form $A(R)$ given in (8). (2) "The exchange energy $J(\zeta)$ is proportional to the square of the relative magnetization—specifically $J(\zeta)=\frac{1}{2}N_e k\theta'\zeta^2$." It is shown that this assumption is not strictly true, $J(\zeta)$ being more generally given by relations of the form (20), involving overlap integrals $I(R)$ of the type given in (11). The fundamental requirement of correcting for correlation has been discussed. It is shown how, in the absence of a rigorous treatment, this requirement may be approximately satisfied. The condition for ferromagnetism in Stoner's treatment, that the ratio of the parameter θ' to the degeneracy temperature be larger than a critical value, may be formulated in principle in the form that the ratio of certain overlap integrals be large enough. The appearance of ferromagnetism is thus closely related to the structure of the metal and to the magnitude of the interatomic distance. (3) "The particles obey Fermi-Dirac statistics." The fundamental problem of spin degeneracy is outlined and the relevance of the dependence of J_{ij} on $\mathbf{k}_i$, $\mathbf{k}_j$ pointed out. It is suggested that for particles described by tight binding wave functions the variation is slow enough for Stoner's statistical equations to be good approximations to the exact equations.

3. SOME EXPERIMENTAL RESULTS

In this section certain experimental results are briefly discussed, including some having a bearing on the theoretical results obtained in Sec. 2 and others having some topicality in view of recent developments in the theory of the properties of transition metals.

(a) The Variation with Composition of the Curie Temperature and Saturation Magnetization, and the Variation with Temperature of the Susceptibility of the Alloys Ni-Cu, Ni-Co, and Ni-Pd

(i) Ni—Cu.[14] Analysis of the susceptibility results leads to an estimated variation with concentration c of $k\theta'/\epsilon_0$ and ζ_0, where ϵ_0/k is the degeneracy temperature and ζ_0 the relative magnetization at 0°K. The observed variation with c of the Curie temperature θ may be used to estimate the variation of ζ_0, in good agreement with the values derived from the susceptibility results, and of θ' (reference 14, Fig. 4). Now the working formula for θ' derived in Sec. 2 is $k\theta'=\frac{1}{2}zqe^2I(R)$. For Ni-Cu the overlap integrals $I(R)$ probably do not vary appreciably with c, since the atomic functions ϕ of Ni and Cu are probably not very different, and the interatomic distance R is almost constant. The practically linear variation of θ' with c derived from the θ values is thus in qualitative agreement with this formula, since $q\doteqdot 0.6-c$. Using the estimated values of ζ_0 the variation with c of σ_0, the saturation magnetization, may be obtained (reference 14, Fig. 5), in good agreement with the observed linear variation. Values of $k\theta'/\epsilon_0$ estimated from the data are of order 1, confirming that the molecular field arises from overlap forces of the same origin and order of magnitude as those causing band spread (see Sec. 2).

(ii) Ni-Co.[15] Analysis of the susceptibility results indicates that $k\theta'/\epsilon_0$ and ζ_0 are practically independent of c. Since for this alloy system both q and $I(R)$ must vary appreciably with c, the analysis is less conclusive. Using the experimental values of σ_0 the variation with c of the Curie temperature θ may be estimated, in fair agreement with experiment (reference 15, Fig. 5).

(iii) Ni-Pd.[16] Analysis shows that θ' varies only slowly with c (with particular approximations $\theta'=1.23\times10^3$°K for Ni, 1.02×10^3°K for Pd). For Ni-Pd, q is probably constant (remaining equal to about 0.6), and the above formula for θ' shows that the slight variation of θ' results from small changes of $I(R)$ with Pd concentration c. The observed values of σ_0 may be used to estimate the variation of θ with c, in excellent agreement with experiment (reference 16, Fig. 2).

(b) The Variation with Temperature of the Magnetization, Specific Heat, and Magnetocaloric Effect of Co, Ni, and Ni Alloys below the Curie Point

The curve for Ni relating the reduced magnetization σ/σ_0 with the reduced temperature T/θ differs considerably from the theoretical curve deduced from Stoner's calculations.[12] It was suggested [17,18] that better agreement should be obtained by using the more general expression for the exchange energy (20) in carrying out the calculation. A full analysis by Hunt,[41] based on this suggestion, indicates that excellent agreement may be obtained for Ni and Co[42] with the parameter A in (20) equal to about 0.1. Hunt also considers the data for Ni-Cu alloys[14] and finds that A decreases with increasing Cu concentration, in qualitative agreement with the expression (20). A similar modification of Stoner's equations is necessary in analyzing the specific heat data. For Ni, for example, the calculated reduced spe-

[41] K. L. Hunt, Proc. Roy. Soc. (London) A (to be published).
[42] H. P. Myers and W. Sucksmith, Proc. Roy. Soc. (London) A207, 427 (1951).

CC-0. In Public Domain. Gurukul Kangri Collection, Haridwar

Digitized by Arya Samaj Foundation Chennai and eGangotri

cific heat discontinuity at the Curie point, $\Delta C/N_e k$, is about 0.6,[13,17] the observed value being 1.5. Hunt shows that the excellent agreement over the whole temperature range may again be attained with $A \doteqdot 0.1$; a value of this order is also required in interpreting the magnetocaloric data for Ni, but here difficulties arise from domain effects.[43]

Went[44] has recently found that the σ/σ_0, T/θ curves for many Ni alloys are all, to a varying extent, less concave to the T/θ axis than the curve for pure Ni. He interprets this finding by postulating the presence of small isolated nickel-rich particles in the alloys, giving rise to rapid density fluctuations.[45] It seems to the writer that this interpretation is strictly inadmissible for the more dilute alloys, where the deviations are probably mainly the result of the above mentioned effect, a variation of the parameter A with composition. For the less dilute alloys the deviations may be the result of density fluctuations, the alloy consisting of regions of differing compositions and Curie temperatures, giving rise to pronounced tailing of the curves in

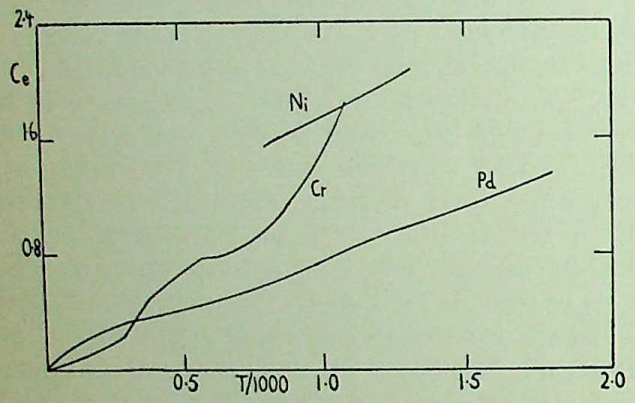


FIG. 1. The electronic heat of Ni above the Curie point, Pd and Cr. C_e, electronic heat, cal mole^{-1} deg^{-1}; T, absolute temperature.

the "Curie point" region: Went's curve for Ni-Si for example is suggested to be "all tail." This situation has been very fully investigated by Marian.[46] Both the above effects are the more pronounced the higher the valency of the solute metal, in qualitative agreement with Went's results.[44]

(c) The High Temperature Specific Heat of Ni and Pd

(i) Ni. Very reliable data were obtained by Persoz[47] (800°–1300°K). The variation of the derived electronic heat C_e ($C_p - C_v$, Stoner;[48] $\theta_D = 400$°K) is shown in Fig. 1. Contrary to earlier theoretical treatments[13] C_e does not approach a constant value at high temperatures. The observed variation is, in fact, that given by Wohlfarth,[14] who showed that an approximately linear variation, as observed, is calculable by inclusion of the "transfer effect" (reference 14, Fig. 14). With the overlap parameter r_0[14] equal to 10 and $q = 0.6$, the theoretical and experimental curves may be brought into coincidence taking the degeneracy temperature to equal 2.3×10^3°K, in agreement with independent estimates. (ii) Pd. Experimental data are available covering the temperature range 0°–1800°K.[49–51] The variation of C_e ($C_p - C_v$, Jaeger and Rosenbohm;[52] $\theta_D = 275$°K) is shown in Fig. 1. The low and medium temperature values of C_e are anomalously low; at higher temperatures C_e is approximately proportional to T as for Ni, but the Pd values are consistently smaller. The deviations are difficult to explain on the assumption[16] that the band structures of the two metals are closely similar [see (e) below].

(d) Magnetic and Thermal Properties of Cr

Recent investigations give the following results: (i) The linear low temperature electronic heat coefficient γ is equal[53] to only 3.74×10^{-4} cal mol^{-1} deg^{-2}, (ii) the high temperature variation of electronic heat C_e is anomalous, the observed values[54] being many times larger than γT (see Fig. 1, curve drawn from published data), (iii) the paramagnetic susceptibility increases quite markedly at high temperatures.[55] In metallic Cr the overlap of d as well as s wave functions must be much stronger than in nickel, and the electrons outside closed shells will then behave much more nearly as if they were free.[15] The supposition that the d-s band in Cr is relatively wide has recently been supported by the results of soft x-ray measurements.[55a] If the Fermi limit of the electron distribution lies close to a minimum in the density of states curve, the γ value would be lower than for neighboring metals in the periodic table,[53] the susceptibility would increase with temperature[56,14] and, as for Ni, owing to the transfer effect, C_e would be anomalously large at high temperatures, as observed. Measurements on some other transition metals[57–59] indicate that an increase of susceptibility with temperature is at least as common as a decrease. The interpretation put forward above to account for the properties

[43] E. C. Stoner, Trans. Roy. Soc. (London) A235, 165 (1936).
[44] J. J. Went, Physica 17, 98, 596 (1951).
[45] A. D. Fokker, Physica 8, 109, 159 (1941).
[46] V. Marian, Ann. phys. 7, 459 (1937).
[47] B. Persoz, Ann. phys. 14, 237 (1940).
[48] E. C. Stoner, Phil. Mag. 22, 81 (1936).
[49] G. L. Pickard and F. E. Simon, Proc. Phys. Soc. (London) 61, 1 (1948).
[50] K. Clusius and L. Schachinger, Z. Naturforsch. 2A, 90 (1947).
[51] F. M. Jaeger and W. A. Veenstra, Proc. Koninkl. Nederland. Akad. Wetenschap. 37, 280 (1934).
[52] F. M. Jaeger and E. Rosenbohm, Rec. trav. chim. 51, 13 (1932).
[53] Friedberg, Estermann, and Goldman, Phys. Rev. 85, 375 (1952).
[54] L. D. Armstrong and H. Grayson-Smith, Can. J. Research A28, 51 (1950).
[55] T. R. McGuire and C. J. Kriessman, Phys. Rev. 85, 452 (1952).
[55a] E. M. Gyorgy and G. G. Harvey, Phys. Rev. 87, 861 (1952).
[56] E. C. Stoner, Proc. Roy. Soc. (London) A154, 656 (1936).
[57] C. J. Kriessman, Bull. Am. Phys. Soc. 27(3), 33 (1952).
[58] F. E. Hoare and J. C. Matthews, Proc. Roy. Soc. (London) A212, 137 (1952).
[59] C. F. Squire and A. R. Kaufmann, J. Chem. Phys. 9, 673 (1941).

CC-0. In Public Domain. Gurukul Kangri Collection, Haridwar

Digitized by Arya Samaj Foundation Chennai and eGangotri

of Cr may have wider applicability, although for some of the other transition metals the γ values are large, an extreme case being W.[60]

(e) Magnetic Properties of Pd and its Alloys

The electronic properties of Pd had been discussed earlier.[16] Recent very careful low temperature measurements[58] show that the paramagnetic susceptibility χ varies anomalously with temperature at about 80°K, where the curve passes through a slight maximum. No immediate interpretation of this behavior can be given, but, as stated,[58] it cannot result from the metal being antiferromagnetic since there is no corresponding anomaly in the specific heat curve at this temperature.[59] Also, recently, magnetic measurements have been reported by Wucher[61] on alloys of Pd with diamagnetic metals and on Pd-H. Although the susceptibility measurements were not extended to low temperatures, some attempt may be made to extrapolate the $1/\chi$, T curves to 0°K. Figure 2 shows the variation of χ_0, the extrapolated paramagnetic susceptibility, with the *electronic* concentration (H/Pd for the Pd-H system). The points for the alloys lie approximately on a single curve A, showing that, as for the variation of σ_0 in nickel alloys, the decrease must be primarily an electronic effect. The points on B for Pd-H are higher than those for the alloys; the difference may result from the more complicated phase diagram of this system. Both curves A and B tend to zero at a value of c close to 0.6. Figure 2 also contains a "theoretical curve" C, calculated on the assumption of parabolic band shape and taking the parameter θ' to be proportional to q, the number of holes

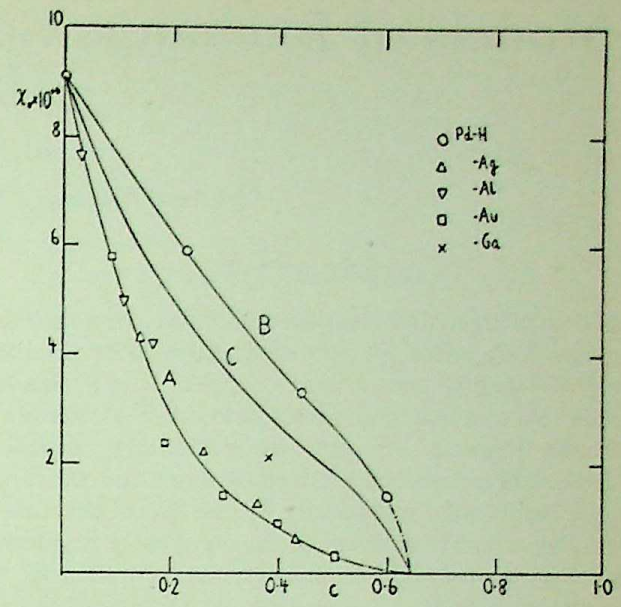


FIG. 2. Paramagnetic susceptibility of Pd alloys and Pd-H. χ_0, mass susceptibility at 0°K (see reference 61) (Pd-Au, 90°K (E. Vogt, Ann. Physik 14, 1 (1932)); c, electronic concentration or H/Pd. A, Pd alloys; B, Pd-H; C, theoretical (see text).

per atom (see Sec. 2). The difference between A and C may result from a variation of θ' which c more complicated than that assumed, since, owing to an appreciable variation of interatomic separation with concentration, the overlap integrals $I(R)$ discussed above may also vary appreciably on alloying.

I wish to acknowledge the help and advice I have had from Professor E. C. Stoner ever since he first introduced me to the study of magnetism. In preparing this paper I have benefited by discussions with Professor J. C. Slater, Dr. A. B. Lidiard, Dr. B. R. Coles, Dr. R. S. Leigh, Dr. F. E. Hoare, and Dr. K. L. Hunt.

[60] A. A. Silvidi and J. G. Daunt, Phys. Rev. 77, 125 (1950).
[61] J. Wucher, Ann. phys. 7, 317 (1952).

CC-0. In Public Domain. Gurukul Kangri Collection, Haridwar

Digitized by Arya Samaj Foundation Chennai and eGangotri

REVIEWS OF MODERN PHYSICS VOLUME 25, NUMBER 1 JANUARY, 1953

Models of Exchange Coupling in Ferromagnetic Media

J. H. Van Vleck

Harvard University, Cambridge, Massachusetts

INTRODUCTION

In contradistinction to superconductivity, the mechanism responsible for ferromagnetism is at present fairly well understood in broad outline. It is generally agreed that the exchange forces between electrons provide the coupling between the elementary magnets which is a prerequisite to ferromagnetism and which is so well represented empirically by the Weiss molecular field. The accurate solution of the eigenvalue problems for a complicated solid is, however, so complex that it is necessary to resort to some kind of simplifying model, for which at least approximate calculations can be made. Some of the more important models, each of which has its own fervent supporters, are as follows:

(a) the original Heisenberg theory.[1]

(b) the collective electron ferromagnetism of Stoner and Wohlfarth.[2]

(c) the generalized Heisenberg model, wherein there is a nonintegral number of spins per atom, and the spins are continually being redistributed among the different lattice sites. Model (c) differs from (b) in that the motions of the electrons instead of being uncorrelated, are so constrained that states corresponding to higher degrees of ionization are excluded. Hence we shall sometimes refer to this model as that of minimum polarity. For large interatomic distances or very narrow bands, (c) is approximately the correct physical picture, while for close spacings or wide bands, (b) is more suitable.

(d) Zener's theory.[3]

We shall not attempt to describe the details of (b) and (d), as they are the subject of other papers in this conference, and we shall assume that the reader is familiar with the rudiments of (a), which are presented in practically any book on magnetism. On the other hand, no elaboration of (c) is, as far as we know, published in the literature; the fullest description appears in an unpublished doctor's thesis of H. Hurwitz;[4] it has also been more briefly mentioned in articles by the writer.[5]

[1] W. Heisenberg, Z. Physik 49, 619 (1928).

[2] E. C. Stoner, Phil. Mag. 21, 145 (1936); Proc. Roy. Soc. (London) A165, 372 (1938); 169, 339 (1939); J. Phys. et radium 12, 372 (1951); E. P. Wohlfarth, Proc. Roy. Soc. (London) A195, 434 (1951); Phil. Mag. 42, 374 (1951); G. C. Fletcher and E. P. Wohlfarth, Phil. Mag. 42, 106 (1951).

[3] C. Zener, Phys. Rev. 81, 440; 82, 403; 83, 299 (1951); 85, 324 (1952).

[4] H. Hurwitz, thesis, Harvard University, 1941.

[5] J. H. Van Vleck, Revs. Modern Phys. 17, 42 (1945); Physica 15, 204 (1949).

Zener's Theory

In Zener's model the exchange effects responsible for ferromagnetism are to be found mainly in the interaction between $3d$ and $4s$ electrons rather than between $3d$ electrons as ordinarily assumed. According to Zener, the $3d-4s$ coupling is so strongly ferromagnetic that it dominates the $4s-4s$ and $3d-3d$ interactions, which he assumes are antiferromagnetic. There are two difficulties which the Zener theory must surmount in order to be acceptable. One is that the $4s$ conduction band may be so wide that the promotion energy required to make $4s$ electrons parallel inhibits ferromagnetism. The other difficulty is a more subtle but less serious one. It can be shown that if the s band is half-full (one conduction electron per atom), it is possible to construct linear combinations of $4s$ wave functions such that the spin of the $4s$ band alternately points north and south, as one passes from one atom to another, and such that the translational kinetic energy is no higher than for the Zener model.[6] With this scheme one can make the spins of the $3d$ and $4s$ electrons parallel when they are on the same atom, and the spins of neighboring $3d$ electrons antiparallel. The implication of this possibility is that with the Zener hypothesis and a half-filled conduction band, the configuration of lowest

[6] We shall indicate here briefly how the waves of spin reversal are constructed in two simple cases, *viz.*, the one-dimensional free electron model with periodic boundary conditions, and the Bloch approximation of tight binding. Consider first free electrons in a strip long enough to include $2n+1$ nuclei spaced distances d from each other. Then the $2n+1$ wave functions of lowest energy satisfying the boundary conditions are usually taken as $e^{-in\alpha x}$, $\cdots$, 1, $\cdots$, $e^{in\alpha x}$, with $\alpha=2\pi/(2n+1)d$. However, equivalent linear combinations are (neglecting normalization factors)

$$e^{-in\alpha x}+\cdots+1\cdots+e^{in\alpha x}=\sin[(n+\tfrac{1}{2})\alpha x]/\sin\tfrac{1}{2}\alpha x$$

and $2n$ other functions differing by integral multiples of d in origin. Each of these functions has a maximum at one particular nucleus and nodes at the others. The waves of spin reversal are constructed by assigning alternatively north and south spins to these functions, and, of course, antisymmetricizing. With the tight-binding approximation the construction is even easier, for if each state in the band is occupied once, the energy is the same as for individual atomic functions, and one simply alternates in the spin assignment to successive atoms.

The equivalence of the band energy with these rather unorthodox systems of wave functions with alternating spins to that with a conventional system is contingent on there being one electron for each orbital state or in other words on the s band being half-full. The writer unfortunately did not realize this limitation when he presented his paper at the Washington conference. It should also be mentioned that the alternating arrangement gives as favorable $s-d$ exchange energy as when the s-spins are all parallel only if the radius of the d shell can be regarded as small compared with the atomic volume, for in the staggered model the expectation value of the spin moment varies sinusoidally with position, and is zero mid-way between two atoms.

CC-0. In Public Domain. Gurukul Kangri Collection, Haridwar

Digitized by Arya Samaj Foundation Chennai and eGangotri

energy is antiferromagnetic rather than ferromagnetic. However, this difficulty is probably rather academic, as the s band is about 30 to 40 percent rather than 50 percent full in most ferromagnetic materials, and then the translational kinetic energy of the s electrons is lower for the parallel rather than the alternating arrangement.

The Difference in Polarity between Models (b) and (c)

We shall not pursue these questions further, and shall henceforth discuss the more orthodox theories (a-b-c) in which it is assumed that ferromagnetism results because of, rather than in spite of, the interaction of $3d$ electrons with each other. Some $3d-4s$ exchange, however, doubtless enters, and Zener can well claim that we should not overlook $3d-4s$ exchange completely. I think it can be regarded as agreed that the simple Heisenberg theory is too crude, since the experimental values of the saturation magnetization show clearly that there is not an integral number of spins per atom. We shall center our discussion on nickel, as it is probably the most important and typical case. It is generally recognized that it has 0.6 electrons per atom in the $4s$ band, and 9.4 in $3d$ states, so that symbolically the atomic configuration is $3d^{9.4}\,4s^{0.6}$. The $4s$ conduction band is so wide that the $4s$ electrons are pretty well represented by the band theory based on itinerant, uncorrelated electrons. The question is how the $3d$ electrons are to be treated. In the Stoner-Wohlfarth model of collective electron ferromagnetism, the motions of the $3d$ electrons through the lattice are completely uncorrelated except for the constraints imposed by the Pauli exclusion principle, or in other words, no allowance is made for the fact that the Coulomb repulsions tend to keep electrons apart. Thus, although in nickel the average configuration of the d electrons on an atom is $d^{9.4}$ it is a mixture of configurations

$$d^{10},\ d^{9},\ d^{8},\ d^{7},\ \cdots.$$

The work required to tear off an electron increases rapidly with the degree of ionization. Hence the energy is appreciably lower if, for instance, two atoms with eighteen d electrons all told, are each in $3d^9$ states rather than one in $3d^8$ and the other in $3d^{10}$.

In the "forgotten model" (c), the states of higher ionization are arbitrarily ruled out completely, and the configuration $3d^{9.4}$ is considered to be

40 percent $3d^{10}$ 60 percent $3d^{9}$ (model c).

The lattice sites occupied by $3d^9$ and $3d^{10}$ are continually redistributing themselves. As a result there is a band structure and an excess specific heat, though neither is as large as with model (b). It should be particularly emphasized that the results of neutron diffraction show that the redistribution of the ions among the different lattice sites takes place in a time shorter than the time of passage of a neutron through an atom, so that the scattering pattern is the same as though each atom carried the same mean charge. Otherwise there would be a diffuseness in pattern due to fluctuation effects. Dr. Shull and Dr. Kittel point out to the writer that the passage time is of the order 10^{-13} sec, and consequently the band width cannot be much smaller than about 0.1 volt and still be consistent with the experiments on neutron diffraction.

The true state of affairs is in between (b) and (c). To investigate which of the two is closer to reality we must probe a little more quantitatively and examine the extent to which the collective electron model (b) involves different degrees of ionization. Here the estimates can be made only with certain limiting approximations, but fortunately even at the extremes the results are not widely different. The limiting approximations are obtained by assuming (1) that one particular d state or (2) that all five d states participate in the "effective band structure," i.e., the portion of the band over which electrons are redistributed in passing from the nonferromagnetic to the ferromagnetic condition or vice versa. According to G. C. Fletcher,[7] for instance, the d band has an over-all width of 2.7 volts, of which only the upper part is shown in our Fig. 1, reproduced from his paper. In the nonferromagnetic condition, the band is doubly populated (i.e., each direction of spin represented) out to the line labeled "Paramagnetic Ni," and is vacant thereafter. In the ferromagnetic condition the band is doubly populated out to the line labeled "Ferromagnetic Ni," and the balance of the band is singly populated. What we call the effective structure or width is essentially the interval to the right

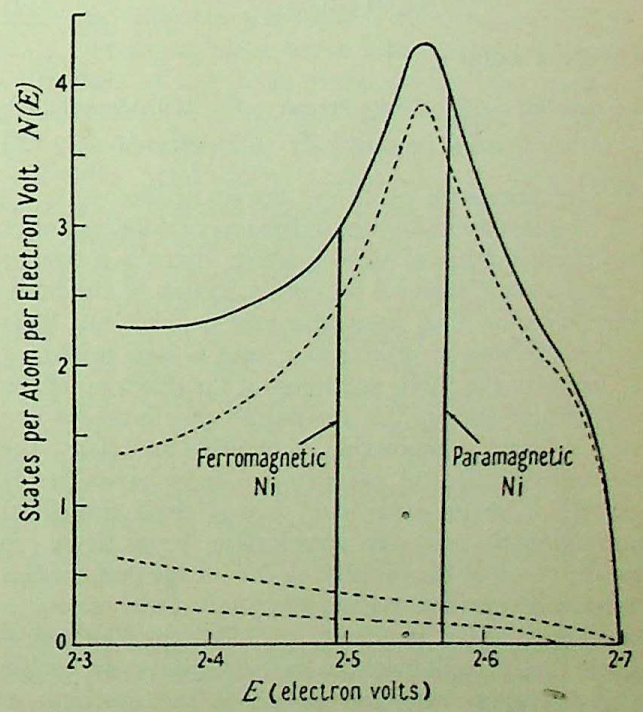


FIG. 1. Density curve for the upper part of the $3d$ band of nickel, according to Fletcher.

[7] G. C. Fletcher, Proc. Phys. Soc. (London) A65, 192 (1952).

CC-0. In Public Domain. Gurukul Kangri Collection, Haridwar

Digitized by Arya Samaj Foundation Chennai and eGangotri

of the line labeled "Ferromagnetic Ni" in Fig. 1. It is obviously much less than the over-all band width. If all the different energy levels in this interval are based on a single d state, than the highest degree of ionization which is obtainable is d^8, as all the four d states other than the given d state are completely filled and are effectively *hors de combat* as far as spin reversals are concerned. On the other hand, the substates of north and south pointing spins for the given d state can be regarded as completely uncorrelated in the unmagnetized condition, and from this fact it is readily shown that the fractions of the time that a nickel atom is in the configurations d^{10}, d^9, d^8 are, respectively, the coefficients of x^0, x, x^2 in

$$(0.7+0.3x)^2. \tag{1}$$

The numbers 0.7 and 0.3 owe their existence to the fact that in nickel the number of d electrons per atom is 9.4, and so for each spin direction the fifth d state, corresponding to the most loosely bound electron, is occupied 70 percent of the time. From (1) we find that the percentages work out as follows:

49 percent d^{10}, 42 percent d^9, 9 percent d^8. (1′)

The other limiting case is obtained by assuming that all five d states participate in the effective band structure. The exclusion principle involves restrictions only on electrons in the same d state. Consequently the fractional percentages of atoms in the configurations d^{10}, d^9, d^8 $\cdots$ are, respectively, the coefficients of x^0, x $\cdots$ in the expression

$$(0.94+0.06x)^{10}, \tag{2}$$

or in other words

53.8 percent d^{10}, 34.4 percent d^9, 9.9 percent d^8, 1.7 percent d^7, 0.2 percent d^6. (2′)

The percentages for d^5, d^4, $\cdots$ are negligible.

If, as Fletcher and other writers have done, one uses the approximation of tight binding, there is a secular determinant of degree 5 for each direction of the propagation vector. One particular root depends but little on the direction of propagation, and is responsible for the hump in Fig. 1. If, regardless of the direction of the propagation vector, the significant root involves one and the same combination of d wave functions, the relevant estimates of polarity are those given in (1) and (1′). If, on the other hand, five different orthogonal linear combinations are appropriate, respectively, to one-fifth each of the possible choices of the propagation vector in the critical region, then the correct estimates are those involved in (2) and (2′). Actually, the appropriate linear combinations vary continuously rather than discretely with the choice of the propagation vector, and the actual amount of polarity with the collective electron model is doubtless intermediate between (1) and (2), but somewhat closer to (2) than (1).

Comparison of Energies of Models (b) and (c)

If assumption (1) is used the excess in polar or correlation energy (i.e., energy of interelectronic repulsion) of model (b) over model (c) is

$$0.09[E(d^8)-E(d^9)]-0.09[E(d^9)-E(d^{10})], \tag{3}$$

as is seen in subtracting from (1′) the percentages of polarity (40 percent, d^{10}, 60 percent d^9) for model (c). Here $E(d^8)$ denotes the energy for the configuration d^8 (really $3d^84s^{0.6}$), etc. If (2′) is appropriate, we have instead for the excess

$$+0.099[E(d^8)-(d^9)]+0.017[E(d^7)-E(d^9)] \\ +0.0018[E(d^6)-E(d^9)]-0.140[E(d^9)-E(d^{10})]. \tag{4}$$

We have, for convenience, grouped terms in such a way as to use $E(d^9)$ as essentially an origin of energy. The energies of the higher ionized configurations d^7, d^6, etc., are not known spectroscopically (except for d^7), but surely

$$E(d^{9-n})-E(d^9)>n[E(d^8)-E(d^9)], \quad n=2, 3. \tag{5}$$

We will be underestimating the excess energy, i.e., favoring model (b), if we replace the inequality by an equality sign in (5). Then (4) becomes simply[8]

$$0.138[E(d^9)-E(d^9)]-0.138[E(d^9)-E(d^{10})]. \tag{6}$$

To evaluate (4) or (6) numerically it is not fair to use the spectroscopic energies of the ordinary nickel atom or ion in the configuration $Ni(d^{10})$, $Ni^+(d^9)$, $Ni^{++}(d^8)$, $\cdots$ since the d electrons are partially screened by the 0.6 s electrons. The screening influence of an s electron in the solid state is somewhat greater than in the free ion, as the mean charge per electron is, on the average, compressed into the atomic volume. It is for orders of magnitude, sufficient to assume that in the solid state, the 0.6 s electrons per atom have the same screening action as 1.0 s electrons do in the gas. The relevant energies for our sequence d^{10}, d^9, d^8 are then

$$Ni^-(3d^{10}4s), \quad Ni(3d^94s), \quad Ni^+(3d^84s).$$

Even so, the energy of the negative nickel ion is not known spectroscopically, but can be obtained, though only very crudely, by extrapolation by means of the irregular doublet law, i.e., the assumption that the square root of the binding energy is a linear function of the screening constant. In this fashion one finds that

$$[E(d^8)-E(d^9)]-[E(d^9)-E(d^{10})]=7.6 \text{ volts}. \tag{7}$$

The expressions (3) and (6) are then, respectively, 0.7 and 1.1 volts. Fortunately, for our purposes an error of a volt or two in the estimation of $E(d^{10})$ is of little consequence. If one made no allowance at all for the

[8] With the assumptions made, both coefficients in (6) are exactly equal in numerical value, and equal to the excess of the fraction of d^{10} in (2′) over 0.40. This statement is readily shown to be a consequence of the fact that the mean deficit in charge per atom is $0.60e$.

CC-0. In Public Domain. Gurukul Kangri Collection, Haridwar

Digitized by Arya Samaj Foundation Chennai and eGangotri

screening effect of the 0.6s electron, the value of the expression (7) would instead be 12.5 volts.[8a]

We must now evaluate for comparison how much increase in energy model (c) involves in comparison with (b) because (c) does not have as wide a band structure. If a single d state is assumed to enter it is easy to obtain an approximate estimate for the loss in banding energy. Namely, the degree of polarity of the collective electron model in the ferromagnetically saturated state is then the same as that of model (c), regardless of the degree of magnetization in the latter. Furthermore, the mean square energy dispersion can be shown to be the same in the model (c) as in the ferromagnetic state of model (b). It is therefore natural to assume that model (c) in any state of magnetization has the same band width as model (b) in the ferromagnetic state. This is all on the assumption (1) of a single effective d state, so that the exclusion principle prohibits two co-directed spin-holes on the same atom. From inspection of Fig. 1 one seens that the difference in band energy between the paramagnetic and ferromagnetic states in the collective electron model is about 1.4×0.05 or 0.07 electron volts, only one tenth of the difference (7) in correlation energy.

If instead the assumption involved in (2′) concerning the occupancy of d states is made, the ferromagnetic state in the collective electron model still involves more polarity than the generalized Heitler-London model. The various degrees of polarity correspond to the different coefficients of x in $(0.88+0.12x)^5$, whence the percentages are found to be

52.7 percent d^{10}, 36.0 percent d^9, 9.8 percent d^8,
1.3 percent d^7, 0.1 percent d.[6]

With the approximation of using the equality sign in (5), the excess of polar energy in the paramagnetic as compared with the ferromagnetic collective electron model is

$$[0.138-0.127][\{E(d^8)-E(d^9)\}-\{E(d^9)-E(d^{10})\}]=0.08 \text{ volt.}$$

On the other hand, the decrease in band energy in the paramagnetic as compared with the ferromagnetic state is only 0.07 volt. Thus elimination of excess polarity still pays off, though not as much as with the assumptions (1−1′). Extrapolation to zero excess polarity indicates that model (c) as compared with model (b) has 1.0 volt higher band energy, but 1.1 volts lower energy of interelectronic repulsion, and so wins out, though by a slim margin.

This method of extrapolation is none too reliable, but another approach is available. Let us, for rough purposes of estimation, assume the band shape is rectangular. If one assumed that model (c) had no band energy at all, the decrease in energy, due to band effects, in passing from model (c) to model (b) would be $\frac{1}{2}\times0.06\times2.7\times9.4=0.75$ volt. This figure is obtained by noting that the lowest 94 percent of the band is filled in the paramagnetic state by the 9.4 d electrons, and that in first approximation the center of the band coincides with where it would be in the absence of any banding. We have used Fletcher's value 2.7 volts of the over-all band width. However, these estimates based on the assumption that the generalized Heisenberg model (c), has no band structure at all are unduly unfavorable to this model. Actually this model has an appreciable band structure, because of the fact that the positions of the d^9 and d^{10} sites are continually being interchanged. Unfortunately, the detailed band structure cannot be feasibly calculated, but estimates of orders of magnitude can be made from examination of the root-mean-square dispersion in energy, which can be readily computed, thanks to the invariance of the diagonal sum. One finds that with the assumption of a single effective d state, the r.m.s. band width with model (c) is about 70 percent as wide with model (c) as with model (b). (More precisely, the percentage is 75 with assumption (1′) and 66 with (2′).[9] If the rectangular assumption concerning band shape is applicable to both models (b) and (c), the difference in band energy between the two models amounts to 0.3×0.75 or only 0.2 volt, about a fifth of the difference (7) in correlation energy.

With any of our various ways of estimation, the improvement in correlation energy in (c) *vis-a-vis* (b) more than offsets the contrary change in band energy. Using the Ritz variational principle, we see that the true state of affairs, while undoubtedly intermediate between (b) and (c), is probably closer to (c) than (b). Without relying on detailed numerical estimates, one can see qualitatively that model (b) is more or less between Scylla and Charybdis. If the band width is too

[8a] *Note added in proof.*—Dr. C. Herring points out to the writer that in reality the screening by the 4s electrons is progressively greater for the configurations d^{10}, d^9, d^8, since more negative charge is sucked in, the greater the positive charge of the lattice site. This effect tends to diminish the difference (7). A limiting case, doubtless too extreme, is one in which each unit cell is neutral, and there is simply a redistribution of configurations $3d^{10}$, $3d^94s$, $3d^84s^2$ among the different lattice sites. Instead of (7), the relevant energy difference in determining the occurrence of the d^{10}, d^9, d^8 configurations is then $E(3d^84s^2)+E(3d^{10})-2E(3d^94s)$, which in nickel amounts to about 3 volts when one averages over the different multiplets belonging to each configuration. Such a model, wherein the d and s migrations compensate so as to preserve neutrality, cannot be considered as either (b) or (c). It goes even further than our generalized Heitler-London model in ironing out fluctuations in polarity, but may not suppress the d^8 states as completely are in our model (c). Possibilities such as Herring suggests show that too much significance should not be attached to quantitative comparisons of models (b) and (c), as the actual situation is even more complicated, but at the same time essentially support our main contention that in dealing with d shells correlation effects are far more important than in ordinary conductors, and that the ordinary band picture is at best a crude approximation.

[9] The rms band width is proportional to the square root of the probability that an electron on an adjacent lattice-site makes a transition to a hole on some given atom. With assumption 1 (one effective d-state), this probability is proportional to 2×0.40 with model (c) and to $2\times0.49+0.42$ with model (b) (cf. Eq. (1′)). With assumption 2 (five effective d-states), the probability is proportional to 10×0.40 with model (c) and to $10\times0.538+9\times0.344+8\times0.099\cdots$ with model (b) (cf. Eq. (2′)). In model (c) an electron cannot jump away from a d^9 site, and hence only the d^{10} sites contribute to the transition probability.

CC-0. In Public Domain. Gurukul Kangri Collection, Haridwar

Digitized by Arya Samaj Foundation Chennai and eGangotri

wide, ferromagnetism will be suppressed, and the model as actually used is close to this limit. On the other hand, if the band is narrowed, the correlation effects will be so large compared to the band structure that (c) will be closer to reality than (b).

Computational Difficulties with Model (c)

There is, however, one practical difficulty with model (c), and that is the fact that there is apparently, at least as yet, no feasible way of making good numerical calculations with it, and in this respect model (b) is undoubtedly superior. Even the original over-simplified Heisenberg model has computational difficulties, as Slater has pointed out in an earlier paper in this conference. From a practical standpoint, if the overlap integrals are small, a fairly good answer, at least qualitatively, appears to be obtainable by neglecting the nonorthogonality except in the primary exchange integrals, but a rigorist can well find all sorts of objection to this procedure. A long time ago, I pointed out in a semiquantitative way that it was plausible[10] that the nonorthogonality corrections largely canceled out. The following example shows, I think, that the nonorthogonality effects cannot be as bad as the pessimist would make them out. Consider, for example, two hydrogen atoms banded together to form a hydrogen molecule in a large box full of widely separated hydrogen atoms. We know that the binding energy of this molecule can be computed as a two-atom problem. However, the nonorthogonality corrections coming from the remote hydrogen atoms, though infinitesimal, can be made, by taking the box sufficiently large, to spoil the convergence and hence the apparent rigor of the calculation made in the standard way—a rather absurd state of affairs. Consequently, it appears to us probable that the convergence can be greatly improved by using a different grouping of terms or iteration procedure.

Even if one adopts an optimistic point of view as regards the effects of nonorthogonality, calculations with model (c) are apparently not feasible at low or even ordinary temperatures. At very high temperatures, large compared to the Curie point, a series development of the partition function may be utilized. This development has been studied by H. Hurwitz.[4] Model (c), like model (b), involves besides the two-electron exchange integral J, the one-electron "transfer" or "hopping" integral K associated with the transfer of an electron from one lattice site to another:

$$J=\int\cdots\int\psi_A(1)\psi_B(2)H\psi_A(2)\psi_B(1)dv_1dv_2,$$

$$K=\int\cdots\int\psi_A(1)H\psi_B(1)dv_1.$$

Hurwitz shows that K first affects the molecular field in the approximation K^3, whereas J enters already in the first power. Unfortunately, K is doubtless much larger than J, so that development in powers of K/kT has even worse convergence than that in J/kT, which, though slow, is better than once supposed.[11]

One thing stands out clearly. That is that such phenomena as curvature of the $1/\chi-T$ graph above the Curie point, excess specific heat linear in T at low temperatures, nonintegral numbers of magnetons per atom, different magneton numbers deduced from saturation and from the susceptibility at high temperatures, cannot be construed as evidence favoring model (b) over (c), as is often done. It is true that except perhaps for the curvature effect these phenomena are not present with the oversimplified model (a), but they all can exist in (c), because the mean configuration is $3d^{9.4}4s^{0.6}$, and there are continual fluctuations in the way the d^{10} and d^9 states are distributed among the different lattice sites. Hurwitz shows that the specific heat already enters in the approximation K^2/k^2T^2, but, of course, a series development of this character is irrelevant at low temperatures.

Origin of the Exchange Integral

We now turn to the mooted question of the origin of the positive[12] exchange integral necessary for ferromagnetism. Two possible mechanisms can be debated. One is the original Heisenberg hypothesis that the integral has an inter-atomic origin, i.e., arises from the exchange of electrons on different atoms, but neighbors of each other. The other mechanism, suggested by Slater[13] in 1936, is that the positive integral has an intra-atomic origin, and is a reflection of the fact that in the configuration d^8 the triplets are deeper than the singlets. We might, incidentally, mention that in general our views are not so very different from those of Slater in his 1936[13] and 1937[14] papers. In particular, his 1937 article[14] had a calculation of the energies for the states of a crystal of one reversed spin that indicated that the deepest state is essentially one of type (c) rather than (b), but Slater has not pushed this viewpoint subsequently.

Whether interatomic exchange really gives a positive integral, rather than a negative one such as serves as the common basis of valence theory, is a question which has been argued pro and con in the literature and is one into which we do not propose to enter. The numerical calculations necessary to yield a definitive answer are exceedingly difficult. The most recent effort is that of Kaplan,[15] who comes out with a positive integral, but even so the results, though definitely en-

[10] J. H. Van Vleck, Phys. Rev. 49, 232 (1936).

[11] V. Zehler, Z. Naturforsch. 5a, 349 (1950).

[12] The interatomic exchange integrals of which we speak are those computed with ordinary atomic orbitals. The integrals computed with the orthogonal Wannier functions are always positive, but are not germane to our discussion.

[13] J. C. Slater, Phys. Rev. 49, 537, 931 (1936).

[14] J. C. Slater, Phys. Rev. 52, 198 (1937).

[15] H. Kaplan, Phys. Rev. 85, 1038 (1952).

CC-0. In Public Domain. Gurukul Kangri Collection, Haridwar

Digitized by Arya Samaj Foundation Chennai and eGangotri

couraging, are inconclusive because the accurate computations were not made at the internuclear distance appropriate to actual ferromagnetic material.

The idea that the exchange responsible for ferromagnetism has an intra-atomic origin has many elements of attractiveness. In the first place, if correct it makes it unnecessary to invoke interatomic effects unlike those in standard valence theory. In the second place, it provides an easy explanation as to why the transition elements are ferromagnetic, whereas the alkalis and alkaline earths are not. Namely, the intra-atomic mechanism requires degenerate orbital states, as we will explain in more detail, and this degeneracy is missing in s bands. (On the other hand, an explanation of why conductors with p bands are not ferromagnetic is provided only after more detailed quantitative examination, inasmuch as p levels have spatial degeneracy.) We should mention that Zener's theory also has an intra-atomic origin of the exchange integral, but with the exchange between s and d rather than between degenerate d states, such as we are discussing here.

It is not difficult to estimate the size of the molecular field constant (the manifestation of the exchange integral) which is to be expected from the collective electron model if one uses approximations similar to those employed in (1) or (2). With (1) the answer is particularly simple: there can be no ferromagnetic coupling at all due to interatomic exchange, as two electrons can never be in a triplet state on an atom, if only one state is relevant. With (2), the molecular field constant θ' has a value approximately 1750 cm^{-1} or 2500°. (We follow the usage of Stoner and Wohlfarth in denoting the field constant by θ' and in evaluating it in degrees rather than cm^{-1} or volts; $2\theta'$ is the work required to reverse an individual spin against this field.) This estimate is reached as follows: In the collective electron model, the difference ΔE in exchange energy between the unmagnetized state and that of maximum magnetization is $\Delta E = -\frac{1}{2}\eta\theta'$, where $\eta = 0.6N$ is the number of holes. On the other hand, if ΔE arises solely from intra-atomic effects, the value of ΔE must also be $\Delta E = -\frac{1}{2}JNp$, inasmuch as two electrons have exchange energy $-J$ if their spins are parallel, and on the average $-\frac{1}{2}J$ if their spins are uncorrelated. Here p denotes the fraction of lattice sites which are in the configuration d^8. The numerical value of θ' follows from comparison of the two expressions for ΔE on taking $p = 0.14$ as in Eq. (6), and $J = 7500$ cm^{-1}. This value of p is one obtained by making assumptions for the correction of the influence of states of higher polarity d^7, d^6, etc., analogous to those used in reducing (4) to (6). For the effective exchange integral J, Slater obtained the value 7430 cm^{-1} on averaging over the various d states in the configuration $3d^84s^2$. As noted earlier in the paper, we assume that the screening effect of the 0.6 $4s$ electron in the solid state is approximately the same as in the gaseous configuration $3d^94s$. However, the electrostatic intervals separating the various states of $3d^84s$ are little greater than those of $3d^84s^2$, and so we use the round value 7500 cm^{-1} for J. We should mention that Slater long ago[13] estimated the molecular field constant by using considerations somewhat similar to those of the present paragraph, but we believe that our value is a somewhat more refined one, and we are unable to agree with certain quantitative details of his calculation.

A molecular field constant of 2500° which we deduced above for the collective model is more than adequate to give the proper ferromagnetic behavior. It is larger than the value 1230° obtained by Wohlfarth from observed susceptibility data on the assumption of a parabolic band, or the value 1760° deduced by Wohlfarth and Fletcher[2] with rectangular bands. In our opinion, it is probable that the actual molecular field constant is somewhat smaller than either of these estimates. In the first place, the actual band shape in the collective electron model apparently has a sharp peak near the upper end, as shown in Fig. 1, narrowing the effective band width and hence reducing the molecular field necessary to produce ferromagnetism. In the second place, and probably more important, the correlation effects arising from interelectronic repulsion alter the band structure, as we will amplify below.

If the correlation effects are so large that the model (c) of minimum polarity is relevant, then clearly the molecular field should be calculated with this model. At first glance, any attempt to provide an intra-atomic mechanism for this field with (c) appears hopeless, as the essence of (c) is that states of higher polarity are absent. Hence, in the model in its purest form, there are no states at all of structure d^8, d^7, etc., and hence no possibility of favorable intra-atomic exchange energy as a result of electron spins being parallel in unclosed shells. However, model (c) is an ideal limit, and the true wave function, which is a linear combination of everything in sight, doubtless contains some terms of structure d^8, d^7, etc. In other words, model (c) is never completely pure and is always contaminated by some states of higher polarity as, so to speak, a concession to model (b). It is only this contamination which is responsible for intra-atomic exchange. At first one wolud guess that any such contamination would be inadequate, since we have seen that even in model (b) the molecular fields calculated with the intra-atomic mechanism are not a great deal larger than those required by the observed ferromagnetism, and so it would seem that any second-order effect would be insufficient. This is not really the case, for with model (b) there is the familiar band structure which tends to inhibit parallel aligning of the spins and so makes the molecular field constant much larger than it would be otherwise, for it must be sufficient to overpower the unfavorable band structure. We have emphasized that with model (c) there is also a band structure, and, in fact, the so-called excess specific heat is probably of almost the same order of magnitude with (c) as with (b). However, the band structure is of a basically different type with (c)

CC-0. In Public Domain. Gurukul Kangri Collection, Haridwar

Digitized by Arya Samaj Foundation Chennai and eGangotri

than with (b), being no longer an uncorrelated one-electron affair, and the band energy (i.e., the energy including the transfer integral K but not the exchange integral J) depends much less drastically on spin alignment than in (b). The spin first begins to enter when third powers of K are included, and it is not even clear whether the band structure tends to favor states of high or low spin, though probably the latter in a weak way. Since in (c) the inhibiting effect of the band structure on the spin is to a large extent removed, it is probably a better approximation with (c) to calculate the molecular field as though the band structure were completely absent (essentially the simple Heisenberg theory with $0.6N$ atoms having $s=\frac{1}{2}$) than to try and take over calculations based on model (b). The molecular field constant is then the same as the Curie constant, and hence only 630° in nickel.

It appears likely that the contamination by states of higher polarity can give a molecular field of this order of magnitude in model (c). This is indicated by a skeleton perturbation calculation which we present in the next paragraphs.

Rough Calculation of Perturbation by Higher Polar States in Model (c)

Consider a pair of neighboring atoms in the configuration d^9+d^9. We wish to examine the effect of perturbations by d^8+d^{10} or $d^{10}+d^8$. For brevity, we do not include the s conduction electrons in our notation, and write d^8, d^9, d^{10} for d^8s, d^9s, $d^{10}s$. In dealing with the spatial degeneracy we shall assume that the transfer integral K associated with the transition of an electron from a d state of one atom to the d state of its neighbor is unaffected by which particular spatial substate one selects. In other words we assume that transitions are equally probable from any given substate of atom A to all five substates of B. This is an extreme form of the assumption (2) explained earlier in the paper, but is sufficient for estimating orders of magnitude. A straightforward application of second-order perturbation theory shows that when the disturbing influence of the excited states d^8+d^{10} and $d^{10}+d^8$ is considered, the excess of the energy of singlet ground state over the triplet is

$$ {}^1E-{}^3E=2K^2\left[\frac{4}{h\nu}-\frac{6}{h\nu+\Delta}\right]. \qquad (8) $$

Here $h\nu$ denotes the mean excess of energy of the triplet states of d^8+d^{10} over the energy of d^9+d^9 and Δ is the mean separation of the singlet and triplet states of the d^8 ion (including screening correction for the $4s$ electron). The multiplicity of the configuration d^8+d^{10} is, of course, the same as that of the d^8 ion. The coefficient of the term in $1/h\nu$ is 4 rather than 5 (the degree of spatial degeneracy) because the d^8 ion can be only in a singlet when the two "holes" are in the same spatial substate, and then is incapable of perturbing the triplet ground level. The coefficient of $1/(h\nu+\Delta)$ is 6 because the perturbation of the singlet ground level is correspondingly augmented. (If there were one rather than five effective d substates, the coefficients would be 0, 2 rather than 4, 6, and the expression (8) would necessarily be negative, showing that if assumption (1) rather than (2) were used, the coupling resulting from intra-atomic exchange is antiferromagnetic as we saw was also the case in model (b).) For the coupling to be ferromagnetic it is necessary that the expression (8) be positive. The fact that (8) is negative if the exchange separation Δ in the upper state is zero or small is a manifestation of the fact that the perturbation by polar states is making an incipient collective electron band theory out of the original model starting with "frozen" d^9 lattice sites; and, of course, in a collective electron scheme without exchange, the states of lowest multiplicity are lowest because the band need not be filled so high. Our perturbation calculation does not include correction for the fact that the d^9 lattice sites are migratory even in model (c); this gives a fine structure in the ground state in addition to the one we are computing here. The superposition of the interchange of d^9 and d^{10} sites in model (c) would make a rigorous calculation of the perturbing influence of the upper polar states exceedingly difficult, but for estimating orders of magnitude the present procedure appears adequate.

To evaluate (8), we take $K=0.1$ volt, as this is the order of magnitude indicated, for instance, by Fletcher's paper.[7] The separation Δ is twice the exchange integral for the upper state, which we previously estimated as 7500 $\text{cm}^{-1}=0.9$ volt. Assumptions similar to those used in connection with (6) suggest[16] that $h\nu=7.6$ volts, but there is a correction arising from the fact that the configuration d^9+d^9 has an extra electrostatic energy e^2/r, where r is the separation of neighboring ions. As a result $h\nu$ is reduced to about 1.7 volts and the expression (8) is approximately 0.01 volt.

The existence of a nonvanishing expression (8) is equivalent to the existence of a coupling $-\alpha \mathbf{s}_A\cdot\mathbf{s}_B$ between the two d^9 ions under consideration The expression (8) is in fact, identical with the coefficient α in the vector model. Thus ferromagnetism will result if α is positive. The coefficient θ' of the molecular field is $\theta'=\frac{1}{4}z\alpha$. The number z of neighbors we must not take as 12, the number of nearest neighbors in a face-centered lattice, but rather as $0.6\times12=7.2$ inasmuch as only 60 percent of the lattice sites have the d^9 holes. The value of the constant θ' according to our rough perturbation calculation is thus 200°, almost the right order of magnitude. So the traces of higher polarity in model (c) may be able to yield an adequate molecular

[16] The energy interval computed in (7) relates to $h\nu$, and not say $h\nu+\frac{1}{2}\Delta$, for in computing (7) we "lumped" all the states of the configuration d^8 at the ${}^3F$ level, the lowest state. This approximation, incidentally, slightly favors model (b) in the comparison of the energies of models (b) and (c) earlier in the paper.

CC-0. In Public Domain. Gurukul Kangri Collection, Haridwar

Digitized by Arya Samaj Foundation Chennai and eGangotri

field purely on the basis of intra-atomic exchange coupling. It should, however, be cautioned that this calculation of the molecular field is only a rough one, and should be taken *cum grano salis*. It is much more sensitive to the precise values selected for the energy intervals[17] than the computations earlier in the paper of the relative correlation energies of model (b) and (c), which are much more reliable. The only reason that we came out with a positive field was the drastic lowering of the frequency denominators in (8) because of the corrections to the energy because d^9+d^9 had a higher ionic energy e^2/r than d^8+d^{10}. One at first wonders whether there should not be similar corrections in our comparisons earlier in the paper of the relative energies of models (b) and (c). This, however, is not the case, for the essence of model (b) is that there is no correlation between the motion of the various electrons, so that a positive ion has no extra probability of having a closed shell on neighboring sites even though the electrostatic energy is thereby lowered. Actually there is doubtless some correlation, but this is not pure model (b), but rather a tendency in the direction of (c).

It should also be noted that any comparison of molecular fields calculated on the basis of an intra-atomic mechanism with those found empirically in ferromagnetic media is uncertain, because actually the intra-atomic and interatomic exchange effects are additive. The corrections for interatomic contributions cannot be reliably made for, as we have already emphasized, neither the order of magnitude of the interatomic exchange integrals, nor even their sign, is really known at present.

In summary, it may be said that the results of the present paper are rather discouraging, as the essence of what we have said is that the truth is somewhere between the collective electron model (b) and the generalized Heisenberg (c), probably closer to (c) than (b). Unfortunately, it is much more feasible to make detailed calculations with (b) than with (c). The calculations with the collective electron model have an elegance and clear-cut character which stand in sharp contrast to the crude qualitative estimates which are the best which can be done at present with (c). The gist of this paper is that it would be highly desirable if good methods of computation with (c) could be developed, including some means of circumventing the convergence difficulties associated with nonorthogonality. At present, for definite numerical answers it is certainly necessary to use model (b) rather than (c). However, this fact does not imply that (c) is physically unsound, as some writers seem to have done, and computational difficulties, important as they are, should not obscure the recognition in principle of the situation which conforms closest to physical reality.

[17] The configuration d^8 actually has two different triplet and three different singlet levels. In (8), the two triplets were assumed to coincide, with a similar approximation for the singlets, but a calculation as gross as the present one does not warrant the use of additional frequency denominators.

SUMMARY OF THE DISCUSSION

R. SMOLUCHOWSKI, *Carnegie Institute of Technology, Pittsburgh, Pennsylvania:* It is perhaps advisable to make a brief appraisal of the relative position of the various theories presented in the preceding four papers and to summarize the main points brought up in the discussion. As it often happens in theoretical physics the differences between the theories stem not from basically different concepts of the phenomenon of ferromagnetism. but rather from a different "taste" or philosophy of theoretical approximation.

Slater's method of attacking the full problem with all necessary wave functions orthogonalized and solving it by means of numerical methods such as a digital computer is probably the most complete and quantum-mechanically exact procedure. The difficulties in handling an actual ferromagnetic material in that manner seem, at the present time, to be enormous. On the other hand, the success in the treatment of the paramagnetic oxygen molecule is most promising and it provides strong arguments in favor of the molecular orbitals method. It supports, also, the well-known dependence of the balance between kinetic and exchange energies upon the distances between the 3-*d* shells. The estimate of this dependence was until now based on rather qualitative arguments.

It is natural that the difficulties of the direct procedure make all approximate methods, which use intuitive concepts, of paramount interest and importance. Van Vleck considers the excited states of atoms in the crystal lattice and allows in this way for nonintegral number of spins per atom. In first approximation, the nonorthogonality corrections are considered to be negligible. This generalized form of the Heisenberg approximation appears capable of explaining many facts which were not understandable in terms of the classical Heisenberg model. If successful, it will be a very useful method, and at the same time it will allow the application of intuitive physical reasoning and will give insight into the physical significance of the mathematical procedures.

The collective electron theory developed by Stoner and Wohlfarth is based on a set of assumptions and parameters, one of them being the exchange energy. The calculations are relatively simple and the success in correlating various ferromagnetic and other properties is indeed striking. The effort is now directed towards analyzing the assumptions and the important quantities in terms of other more basic properties. This is particularly true of the exchange energy and of

CC-0. In Public Domain. Gurukul Kangri Collection, Haridwar

Digitized by Arya Samaj Foundation Chennai and eGangotri

its relation to the structure of metals and the interatomic distances.

Zener's suggestion to consider the interaction between the conduction electrons and the *d* shells as mainly responsible for ferromagnetism has many very attractive features although certain assumptions do not seem to be borne out by Slater's results on oxygen. The theory appears to be especially suitable in handling Heusler alloys, ferrites, and others, but at present it seems not to be in agreement with certain neutron diffraction data on atomic moments in alloys below and above Curie temperature. These experiments are rather recent and their interpretation is not quite certain, and thus a definite conclusion has to await further results.

It should be pointed out that neutron diffraction data have a central role in helping to make the proper choice between the various approximations and theoretical models. They indicate the existence of energy bands, they allow an estimate of their width, they can give information about the existence and magnitude of atomic moments, etc. It seems certain that on the basis of a further improvement of present theories, and with new experimental data, approximations will be perfected which will be applicable to metals or to ionic crystals or to ferrites, etc., and which, in each of these cases, will give us concepts that are suitable for intuitive handling. The quantitative results of the numerical calculations based on Slater's method will yield theoretical criteria for the various conceptually simpler models.

CC-0. In Public Domain. Gurukul Kangri Collection, Haridwar

Digitized by Arya Samaj Foundation Chennai and eGangotri

REVIEWS OF MODERN PHYSICS VOLUME 25, NUMBER 1 JANUARY, 1953

Microwave Resonance Absorption in Gadolinium Metal*

ARTHUR F. KIP

Department of Physics, University of California, Berkeley, California

The microwave resonance absorption in gadolinium metal has been measured at 9000 and 24 000 Mc/sec. The g value in the paramagnetic region is found to be 1.95 ± 0.03. In the ferromagnetic region extreme line breadth prevents accurate determination of the g value. Calculations neglecting effects of line breadth give a ferromagnetic g value of 1.94.

I. INTRODUCTION

MICROWAVE resonance absorption in gadolinium metal has been measured in the 9000 and 24 000 Mc/sec ranges. This investigation was prompted by interesting properties of gadolinium metal, as emphasized by Van Vleck.[1] Gd is known to exhibit a saturation magnetization[2] corresponding closely to the value expected for an ^8S state, where the magnetic moment of each atom is due to the seven electrons in the $4f$ shell. It is therefore likely that Gd is a good representative of the atomic model of a ferromagnet, in great contrast to other ferromagnetic metals, all of which show saturation magnetizations which cannot be explained on such a simple basis. From this point of view, we wished to determine how closely the g value corresponds to the value for free electron spin, as expected for a half-filled shell. A further useful characteristic of Gd metal is that its ferromagnetic Curie point is 16°C.[2] This allows measurements to be made conveniently in both ferromagnetic and paramagnetic regions.

In the paramagnetic region we find that the g value is 1.95 ± 0.03. In the ferromagnetic region the extreme breadth of the absorption curve prevents accurate determination of the g value. However, we have made calculations of the ferromagnetic g value, ignoring possible shifts in peak positions arising from relaxation effects. These calculations lead to a ferromagnetic g value of 1.94. A limit of uncertainty cannot be assigned to this value because of the extreme and unknown breadth of the absorption curves, but it may be significant that the g value is not inconsistent with that in the paramagnetic range.

II. MEASUREMENTS

A circular disk 2.3 cm in diameter and 0.04 cm thick was used in these experiments. The sample had been annealed and contained no more than 0.1 percent of other rare earths. Absorption measurements were made by clamping the sample behind a hole of area 0.049 cm^2 drilled into the end wall of a resonant cavity. Thus the sample effectively forms a small part of this wall. Variations in the microwave power reflected from the cavity because of absorption in the sample were measured as a function of the externally applied magnetic field. The geometry was such that the external and microwave magnetic fields were in the plane of the sample and perpendicular to each other.

The measurements were made by sweeping the external magnetic field slowly through a suitable range while simultaneously measuring the microwave power reflected from the cavity. Data were obtained by placing a signal proportional to the magnetic field on the horizontal axis of a CRO and a signal proportional to the reflected power on the vertical axis. An electronic switch superimposed arbitrary field markers on the absorption pattern. Data were recorded by photographing the CRO traces.

Details of microwave and electronic circuits will not be presented here, since the techniques are relatively standard, but a few aspects of the apparatus which affect the accuracy of the results will be mentioned. The microwave power incident on the resonant cavity is amplitude—modulated at 6 kc/sec. This allows the use of a narrow band ac amplifier in the detection circuit. In the 9000 Mc/sec apparatus the 6 kc/sec modulation is imposed by the use of a microwave gyrator;[3] in the 24 000 Mc/sec apparatus modulation is imposed by a crystal placed in the microwave transmission line.

In all resonance effects there are both real and imaginary components in the absorption. The real part changes the Q of the resonant cavity and the imaginary part shifts its resonant frequency. In these experiments we measure only the real part of the absorption. Complete separation of the two aspects of magnetic absorption has been obtained by a slight modification of the technique suggested by Weidner and Whitmer.[4] The klystron is frequency modulated at a few cycles per second through a frequency range greater than any shift in the resonant frequency of the cavity. Thus at

* A brief account of the material presented in this paper will appear in *The Physical Review* under the authorship of R. Barton, A. F. Kip, C. Kittel, A. M. Portis, and F. H. Spedding.

[1] J. H. Van Vleck, Physica **15**, 197 (1949).

[2] F. Trombe, Ann. phys. **7**, 385 (1937).

[3] C. L. Hogan, Bell System Tech. J. **31**, 1 (1952).

[4] R. T. Weidner and C. A. Whitmer, Rev. Sci. Instr. **23**, 75 (1952).

CC-0. In Public Domain. Gurukul Kangri Collection, Haridwar

Digitized by Arya Samaj Foundation Chennai and eGangotri

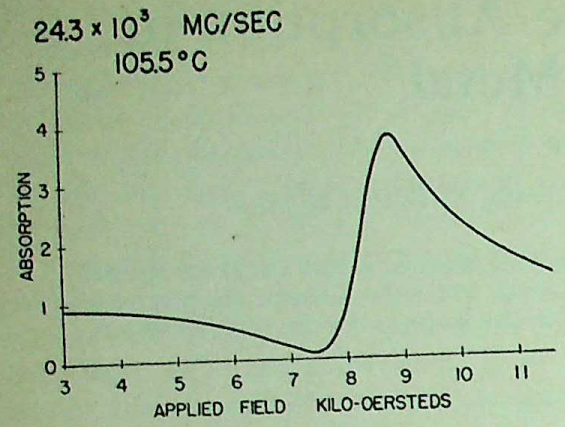


FIG. 1. Absorption curve of gadolinium metal.

some part of the FM cycle, the klystron frequency will be equal to the resonant frequency of the cavity. Since the reflection from the cavity is a minimum at resonance, it is possible to identify in the traces those points in each FM cycle for which the klystron is at the resonant frequency of the cavity. This method corresponds exactly to the "point-by-point" technique in which each point is obtained after retuning the klystron to the cavity resonant frequency.

The external magnetic field is measured by a technique similar to that used by Lamb and Retherford.[5] The emf from a rotating coil inserted in the external field is compared with the emf from a second rotating coil mounted on the same shaft. The second coil is in the field of a permanent magnet. Comparison is made in a bridge circuit in such a way that the two emf's may be made to cancel at any desired value of the applied field. By changing the bridge constants during the sweep of the external field, a series of field markers are superimposed on the trace. Absolute calibration of the field is obtained from proton resonance or from a small amount of diphenyl-trinitro phenyl hydrazyl[6] placed in the cavity. The field can be determined with an accuracy of ± 10 oersteds by this technique.

III. EXPERIMENTAL RESULTS

Figure 1 shows the experimental absorption curve of Gd taken at 105.5°C at a frequency of 24.3×10^3 Mc/sec. This temperature is in the paramagnetic region, well above the Curie point of 16°C. This curve exhibits the typical shape of resonance curves expected for metals, as found by Yager[7] and Bloembergen[8] in the case of Supermalloy and nickel. All curves taken in the paramagnetic range are similar, showing very little change in width for temperatures well above the Curie temperature.

Figure 2 summarizes the results at 24.3×10^3 Mc/sec for the positions of maximum absorption. The principal cause of the shift of the peak position in going from the paramagnetic to the ferromagnetic region is the increase in magnetization of the sample.

Figure 3 shows the variation in the width of the resonance curve as a function of temperature. The data plotted show the width of the absorption curve in oersteds, measured from the lower half-power point to the peak. The power absorbed is measured relative to the absorption of zero field. Below 0°C, in the ferromagnetic region half-widths are unobtainable because of the extreme breadth of the absorption curve.

No data are given for the 9000 Mc/sec experiments. The results at this frequency are consistent with the 24 000 Mc/sec results, but do not provide the accuracy available at the higher frequency.

IV. CALCULATIONS OF g VALUES

In order to determine the g values, it is necessary to compare our experimental curves with theoretical curves which take into account the various causes of shift in the absorption maxima. Causes of shift include demagnetizing factors due to the geometry of the sample, and relaxation effects. Furthermore, the "effective field" for the resonance condition[9] must be used. In addition, account must be taken of the effect of variation of eddy current losses in the sample, affecting the shape and position of the absorption curve.[7]

In obtaining our theoretical curves we used essentially the method of Yager, Galt, Merritt, and Wood.[10]

We assume an equation of motion of the form

$$\frac{d\mathbf{M}}{dt}=\gamma(\mathbf{M}\times\mathbf{H})-\frac{\gamma\alpha}{M}\mathbf{M}\times(\mathbf{M}\times\mathbf{H}). \qquad (1)$$

Here $\mathbf{M}$ = magnetization; $\mathbf{H}$ = internal field; $\gamma = ge/2mc$, the magnetomechanical ratio; and α = relaxation parameter.

From this equation one can calculate μ_1 and μ_2, the

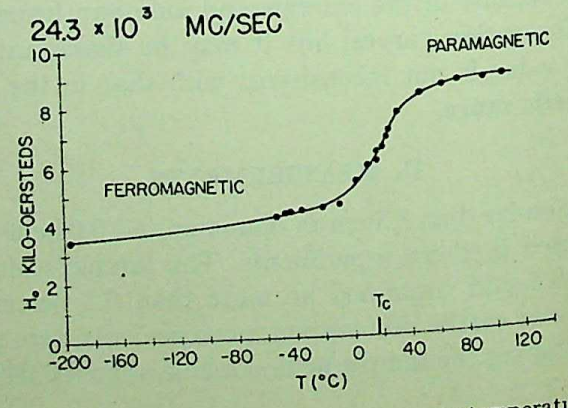


FIG. 2. Peak position of absorption curves *vs* temperature. Gadolinium metal.

[5] W. E. Lamb, Jr., and R. C. Retherford, Phys. Rev. 81, 222 (1951).
[6] Holden, Kittel, Merritt, and Yager, Phys. Rev. 77, 147 (1950).
[7] W. A. Yager, Phys. Rev. 75, 316 (1949).
[8] N. Bloembergen, Phys. Rev. 78, 572 (1950).
[9] C. Kittel, Phys. Rev. 73, 155 (1948).
[10] Yager, Galt, Merritt, and Wood, Phys. Rev. 80, 744 (1950).

CC-0. In Public Domain. Gurukul Kangri Collection, Haridwar

Digitized by Arya Samaj Foundation Chennai and eGangotri

real and imaginary parts of the permeability:

$$(\mu_1-1)/4\pi\chi_0=(\omega_0/\omega)^2\frac{(\omega_0/\omega)^2-1+4\delta^2/(1+\eta^2)}{[(\omega_0/\omega)^2-1]^2+4(\omega_0/\omega)^2\delta^2},$$

$$\mu_2/4\pi\chi_0=[2\delta/(1+\eta^2)](\omega_0/\omega)\times\frac{1+(\omega_0/\omega)^2\eta^2}{[(\omega_0/\omega)^2-1]^2+4(\omega_0/\omega)^2\delta^2},$$

where

$$\omega_0=\frac{\eta}{\zeta}\gamma(1+\alpha^2)^{\frac{1}{2}}H_0,$$

$$\delta=\frac{\alpha}{(1+\alpha^2)^{\frac{1}{2}}}\frac{1+\eta^2}{2\eta},$$

$$\eta=(1+N_y\chi_0),$$

$$\zeta=(1+N_z\chi_0),$$

and ω = angular frequency of microwave source, H_0 = applied external field, N_z = demagnetizing factor in plane of sample, $N_y\cong 4\pi$ = demagnetizing factor perpendicular to plane of sample, and χ_0 = static susceptibility per unit volume.

Because of the effect of varying eddy current losses, and changes in skin depth, the quantity which we observe experimentally is $\mu_R^{\frac{1}{2}}$, where $\mu_R=(\mu_1^2+\mu_2^2)^{\frac{1}{2}}+\mu_2$. The theoretical curves were fitted to our experimental curves by finding the values of the relaxation parameter α which gave the best fit. This procedure is perhaps somewhat unjustified since it is not clear that all of the width of our curves is due to relaxation effects. However, this form of equation involving a relaxation parameter as given in Eq. (1), allows a good fit between experiment and theory, and presumably leads to correct g values.

Table I shows the result of these calculations at a number of temperatures in the paramagnetic region. The values of χ_0 at the various temperatures were obtained from data given by Trombe.[2]

As stated above, the large and unknown widths of the absorption curves in the ferromagnetic region preclude calculation of possible shifts due to line width. We have therefore obtained the ferromagnetic g factor by using the equation of Kittel[9] for calculating the "effective field." The g factor is then calculated from the relation $\omega=\gamma H_{\text{eff}}$. The value of the magnetization was obtained from unpublished data of Elliott, Legvold and Spedding.[11] The g value obtained at -196°C is 1.94.

TABLE I. Calculated g values of gadolinium metal in the paramagnetic region.

Temp. °C	Freq. Mc/sec	H_0 max oersteds	$4\pi\chi_0$	g
48.7	24 300	8270	0.196	1.96
64.0	24 290	8510	0.130	1.96
75.5	24 280	8690	0.103	1.95
93.7	24 280	8730	0.079	1.96
105.5	24 275	8850	0.065	1.95

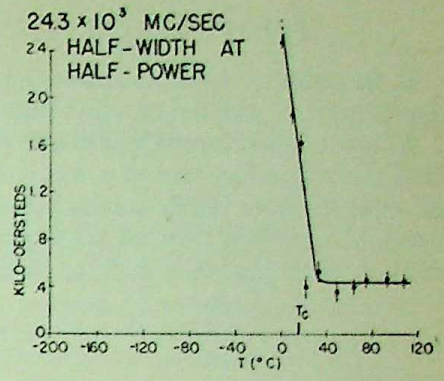


Fig. 3 Variation of absorption curve width with temperature.

V. SUMMARY

Resonance absorption curves in gadolinium taken over a wide temperature range show the expected shift due to the increase in magnetization as the sample is cooled from the paramagnetic to the ferromagnetic region. Only in the paramagnetic region can accurate g values be obtained; the extreme breadth of the absorption in the ferromagnetic region precludes accurate assignment of a g value below the Curie point. Our value, $g=1.95$, is to be compared with values available from other experiments. From the results of Trombe[2] on the value of the saturation magnetization, extrapolated to 0°K and infinite applied field, one obtains a g value of 2.03. This value may be in some doubt in view of the fact that extrapolation is necessary from 77°K to 0°K. Also the purity of Trombe's material is not accurately known. On the other hand, measurements similar to those of Trombe have been made on much purer gadolinium metal[11] down to 4°K. These measurements yield a g value of 1.96. Another value for g may be obtained from the determination of the Curie constant. Using Trombe's[2] data, we calculate $g=1.99$.

Although it seems that our value for g in the paramagnetic region is open to little question, it would be desirable to obtain and test a single crystal of gadolinium, in order to determine the g-value in the ferromagnetic region.

The author wishes to emphasize the fact that this was a cooperative project with very important contributions from R. Barton, C. Kittel, A. M. Portis, and F. H. Spedding. In addition, thanks are due to T. W. Griswold, who assisted in making many of the measurements. The research was assisted in part by the U. S. Office of Naval Research and the U. S. Atomic Energy Commission.

[11] Elliott, Legvold, and Spedding (unpublished data).

CC-0. In Public Domain. Gurukul Kangri Collection, Haridwar

Digitized by Arya Samaj Foundation Chennai and eGangotri

DISCUSSION

B. BLEANEY, *Clarendon Laboratory, Oxford, England:* The g value of gadolinium ethyl sulfate is 1.992.

At low temperatures Pippard and others have shown that the rf conductivity of a metal is less than would be expected from the dc conductivity because the skin depth becomes less than the mean free path of the conduction electrons. In a ferromagnetic metal the skin depth varies with the permeability, and so will change as one goes through the resonance. As the permeability increases the skin depth decreases and the anomalous skin effect becomes more serious. This may cause a distortion of the resonance curve, particularly at low temperatures.

CC-0. In Public Domain. Gurukul Kangri Collection, Haridwar

Digitized by Arya Samaj Foundation Chennai and eGangotri

REVIEWS OF MODERN PHYSICS VOLUME 25, NUMBER 1 JANUARY, 1953

Relaxation Processes in Ferromagnetism

C. KITTEL AND ELIHU ABRAHAMS

Department of Physics, University of California, Berkeley, California

(Received September 25, 1952)

This paper surveys current theoretical work on spin-spin and spin-lattice relaxation in ferromagnetic substances with reference to ferromagnetic resonance. It is shown that it is possible to give a reasonable explanation of the principal features of the experimental results. The calculations, carried out for nickel in particular, make use of a macroscopic spin-lattice interaction determined by the observed magnetostriction and a pseudo-dipolar spin-spin interaction determined by the observed anisotropy. It is not sufficient to use magnetic dipole coupling alone for either of the two relaxation processes. The zero-point fluctuations in the pseudo-dipolar field play a central role in the development of the theory.

THIS paper is concerned with the problem of relaxation processes in ferromagnetic substances. The ferromagnetic phenomena in which relaxation effects are exhibited include the following:

(1) Line width in ferromagnetic spin resonance absorption.

(2) Power saturation with intense rf magnetic fields in ferromagnetic resonance.

(3) Velocity of propagation of the Bloch wall separating domains in ferromagnetic insulators.

(4) Lag and elevation angles of magnetization with respect to the direction of a rotating magnetic field.

(5) Time delay in the establishment of a new equilibrium position for the magnetic moment of a specimen after a sudden change in the external magnetic field.

(6) Time delay in heat transfer between lattice and spin systems.

We shall review below the current experimental and theoretical positions with regard to spin-spin and spin-lattice relaxation times. The review will draw heavily on work recently completed at Berkeley by F. Keffer, and also on unpublished work done in collaboration with J. M. Luttinger at the Institute for Advanced Study.

When a spin-resonance absorption experiment[1] is performed on a ferromagnetic single crystal at the usual microwave frequencies it is observed that the resonance line has a half-width ΔH of the order of 50 to 500 oersteds, corresponding to over-all relaxation times of 10^8 to 10^9 sec. We believe that the principal contribution to the line width at room temperature and below comes from spin-spin relaxation.

By the half-width of the line we mean one-half of the width on a plot of the effective permeability μ_R (or, with ferrites, μ'') against the static magnetic field intensity H between the points at which $\mu_R=\frac{1}{2}\mu_R(\max)$. Typical values of the half-width are given in Table I. Measurements on polycrystalline specimens must be interpreted with considerable caution because the crystalline anisotropy energy causes an apparent line width as a result of the scatter in the resonance frequencies of the individual crystal grains.[2]

It has always been the occasion of some astonishment that the line widths are as broad as they are observed to be, and it is only recently, as discussed below, that we have recognized what seem to be the real mechanisms causing the widths. A number of somewhat superficial mechanisms were explored without success in the early phases of research on ferromagnetic resonance, as discussed in the reviews cited above.

If we were to neglect all mutual interactions among the electron spins in an atomic model of a ferromagnet, other than the isotropic exchange interaction, then the resonance line would be exceedingly sharp, the width being determined by magnetic field inhomogeneities, saturation effects or radiation damping. The energy levels in the static magnetic field H are given by

$$W=g\mu_B HM, \tag{1}$$

where M is the magnetic quantum number associated with the total spin $\mathcal{S}\hbar$ of the entire specimen, and g is the spectroscopic splitting factor. The selection rules for magnetic dipole transitions are $\Delta\mathcal{S}=0$, $\Delta M=\pm 1$, so that only the single frequency

$$\omega=g(e/2mc)H \tag{2}$$

will be observed. We should, strictly, write $H_{\text{effective}}$

TABLE I. Half-width of ferromagnetic resonance lines (near 24 000 Mc/sec and at room temperature).

Substance	Approximate half-width in oersteds
Silicon iron (single crystal)	several hundred
Nickel	400
Supermalloy (annealed)	100
Supermalloy (cold rolled)	300
Nickel ferrite (single crystal)	75
Nickel zinc ferrite	150
Manganese zinc ferrite	50–400[a]
Heusler alloy	100

[a] Appears to vary from sample to sample.

[1] Ferromagnetic resonance is reviewed by J. H. Van Vleck, Physica 17, 234–252 (1951); C. Kittel, J. phys. et radium 12, 291–302 (1951).

[2] The half-width in unoriented polycrystalline specimens from this effect alone is expected to be roughly of the order of $\frac{1}{4}$ of the anisotropy field $H_a=2K/M_s$, provided that $H_a \ll H_{res}$.

CC-0. In Public Domain. Gurukul Kangri Collection, Haridwar

Digitized by Arya Samaj Foundation Chennai and eGangotri

instead of H, to allow for sample shape and crystal anisotropy. The exchange energy $-2J\sum \mathbf{S}_i\cdot\mathbf{S}_j$ does not change during the transition. The resonance line width in this case will be determined by the secondary effects mentioned above, and we may expect a very narrow line.

The identical model may be considered from the viewpoint of the spin wave approximation[3] to the low-lying states of a ferromagnet. The energy in the external magnetic field is now, for low k,

$$W=\sum_k (n_k+\tfrac{1}{2})(Ck^2+g\mu_B H), \tag{3}$$

where n_k is the excitation quantum number of the spin wave of wave vector $\mathbf{k}$ and C is a constant proportional to the exchange energy. The former selection rules go over to the rule that transitions in a uniform rf field will occur only among the $k=0$ levels, and we have $\Delta n_0=\pm 1$; $\Delta n_k(k\neq 0)=0$. The resonance frequency is thus identical with Eq. (2). We have introduced the spin wave viewpoint because it is used in the recent developments in relaxation problems.

Our model considering only the exchange and Zeeman interactions is thus too idealized to yield a description of the line width. It is known however that there are other interactions among ferromagnetic electrons, including magnetic dipole interactions and also interactions of a spin-orbit-exchange-lattice character, which contribute to the important phenomena of magnetocrystalline anisotropy and magnetostriction. It is essential to include these interactions in the theory. We first consider the calculation of the spin-lattice relaxation time characterizing the exchange of energy between the system of spin waves and the system of lattice vibrations (phonons). What shall we use as the interaction between the spin system and the phonon system? We recall that the observed magnetostriction of ferromagnets results from the magnetoelastic interaction of the magnetization or spin direction and the crystal lattice. We know that we can account approximately for the observed magnetostriction by postulating a coupling term in the free energy density of the form[4]

$$f_1=B_1(\alpha_1^2e_{xx}+\alpha_2^2e_{yy}+\alpha_3^2e_{zz}) +B_2(\alpha_1\alpha_2e_{xy}+\alpha_2\alpha_3e_{yz}+\alpha_3\alpha_1e_{zx}); \tag{4}$$

here the α's are direction cosines of the magnetization, and the e's are elastic strain components. Terms of this form may be thought of as representing the dependence of the anisotropy energy on the state of strain of the crystal. Values of the constants B_1, B_2 are readily deduced from the observed magnetostriction.

Starting from the macroscopic interaction represented by Eq. (4), we may calculate the spin-lattice relaxation time using some of the standard methods of quantum field theory. We set up a macroscopic spin-wave field and a macroscopic phonon field. The magnetoelastic interaction given by Eq. (4) is treated as a perturbation which causes collisions between the spin waves and the phonons. The kinetic equation for the collision process leads us directly to the spin-lattice relaxation frequency.

The Hamiltonian of the exchange and Zeeman energies is, writing $\mathbf{M}$ as the magnetization,

$$\mathcal{H}_{\rm spin}=\int\{(A/M_s^2)[(\nabla M_x)^2+(\nabla M_y)^2+(\nabla M_z)^2] -\mathbf{H}\cdot\mathbf{M}\}dV, \tag{5}$$

where A is the usual macroscopic exchange constant[5] and on the atomic model is related to the exchange integral J by

$$A=ZS^2R^2J/6\Omega, \tag{6}$$

where Z is the number of nearest neighbors of any given atom, R their distance and Ω the atomic volume. Near saturation we may assume that the magnetization $\mathbf{M}$ is oriented very nearly in the z direction, so that

$$\mathcal{H}_{\rm spin}\cong\int\{(A/M_s^2)[(\nabla M_x)^2+(\nabla M_y)^2] +(H/2M_s)(M_x^2+M_y^2)\}dV, \tag{7}$$

apart from a constant term.

We consider $\mathbf{M}_x$, $\mathbf{M}_y$ as amplitudes of a vector field. The field is quantized[6] by use of the commutation relation

$$\mathbf{S}_j\times\mathbf{S}_k=i\mathbf{S}_j\delta_{jk}. \tag{8}$$

We express the magnetization in terms of a spin density

$$\mathbf{M}(\mathbf{r})=(g\mu_B\nu/a^3)\sum\mathbf{S}_j\delta(\mathbf{r}-\mathbf{r}_j), \tag{9}$$

where ν is the number of atoms per unit cell of volume a^3. We find, using Eq. (8),

$$[M_x(\mathbf{r}),M_y(\mathbf{r})]=ig\mu_BM_s\delta(\mathbf{r}-\mathbf{r}'). \tag{10}$$

It is convenient to introduce the usual creation and destruction operations a_k^* and a_k into the Fourier analysis of the transverse components of magnetization:

$$M_x(\mathbf{r})=(g\mu_BM_s/2V)^{\frac{1}{2}}\sum(a_k+a_{-k}^*)e^{i\mathbf{k}\cdot\mathbf{r}};$$
$$M_y(\mathbf{r})=i(g\mu_BM_s/2V)^{\frac{1}{2}}\sum(a_{-k}^*-a_k)e^{i\mathbf{k}\cdot\mathbf{r}}, \tag{11}$$

where V is the volume of the sample. The commutation relation becomes

$$[a_k,\ a_{k'}^*]=\delta_{kk'}. \tag{12}$$

On substituting Eq. (11) back in to Eq. (7) and carrying out the volume integration using Eq. (12), we find for the eigenvalues of the unperturbed Hamiltonian

$$W_{\rm spin}=\sum_k (n_k+\tfrac{1}{2})[(2g\mu_BA/M_s)k^2+g\mu_BH], \tag{13}$$

[3] An elementary semiclassical treatment of the Bloch theory of spin waves is given in the forthcoming book, *Introduction to Solid State Physics* by C. Kittel (John Wiley and Sons, Inc. New York, 1953), Appendix J.

[4] See, for example, Sec. 2.3 in C. Kittel, Revs. Modern Phys. 21, 541 (1949); the equation above is the "two constant" form for cubic crystals; more general forms are given in the standard literature.

[5] Reference 4, Eq. (2.1.11).

[6] The field theory of spin waves is treated by C. Herring and C. Kittel, Phys. Rev. 81, 869 (1951); a simple introduction to quantum field theory is given in L. I. Schiff, *Quantum Mechanics* (McGraw-Hill Book Company, Inc., New York, 1949).

CC-0. In Public Domain. Gurukul Kangri Collection, Haridwar

Digitized by Arya Samaj Foundation Chennai and eGangotri

where n_k is the eigenvalue of the operator $a_k^* a_k$ and is a positive integer. We gain insight into Eq. (13) on recognizing that n_k is the number of reversed spins in the spin wave of wave vector $\mathbf{k}$; the term in k^2 is the familiar spin wave term arising from exchange energy, while the term in H is the Zeeman energy.

We treat the lattice vibrations as a macroscopic field in a crystal which is elastically isotropic. On expressing the elastic energy in terms of the phonon creation and destruction operators b_K^*, b_K we find for the unperturbed elastic energy, using $b_K^* b_K = N_K$,

$$W = \sum [\hbar c_L K (N_K^{(1)} + \tfrac{1}{2}) + \hbar c_T K (N_K^{(2)} + N_K^{(3)} + 1)], \quad (14)$$

where the superscripts 1, 2, 3 refer to orthogonal polarization directions; c_L and c_T are the longitudinal and transverse sound velocities, respectively. This expression becomes more familiar on recognizing that $\omega_L = c_L K$, etc. The operator for the lattice displacement vector used in deriving Eq. (14) is

$$\mathbf{u} = V^{-\frac{1}{2}} \sum \mathbf{q}_K e^{i\mathbf{K}\cdot\mathbf{r}}, \quad (15)$$

where

$$\mathbf{q}_K = \sum_{s=1}^{3} \boldsymbol{\varepsilon}_K^{(s)} q_K^{(s)} = (\hbar/2\rho K)^{\frac{1}{2}} \sum_{s=1}^{3} c_s^{-\frac{1}{2}} \boldsymbol{\varepsilon}_K^{(s)} [b_K^{(s)} + b_{-K}^{(s)*}]; \quad (16)$$

here the $\boldsymbol{\varepsilon}_K^{(s)}$ are an orthonormal set of unit polarization vectors such that $\boldsymbol{\varepsilon}_K^{(1)}$ is parallel to $\mathbf{K}$; ρ is the density; $c_1 = c_L$; and $c_2, c_3 = c_T$. The strains e_{ij} are readily derived from Eq. (15) by differentiating with respect to the spatial coordinates.

We next treat the collisions between the spin waves and phonons caused by the magnetoelastic coupling term given in Eq. (4). The interaction Hamiltonian in the present approximation is

$$\mathcal{H}_{\text{int}} = \int \{(B_1/M_s^2)[M_x^2(e_{xx} - e_{zz}) + M_y^2(e_{yy} - e_{zz})] + (B_2/M_s^2)[M_x M_y e_{xy} + M_x M_s e_{xz} + M_y M_s e_{yz}]\} dV. \quad (17)$$

This may be written in terms of phonon and spin wave creation and destruction operators using the transformations in Eqs. (11), (15), and (16). The form resulting from the transformations may be interpreted directly in terms of various types of collision processes. For example, a term $a_{k'}^* a_k b_K^*$ represents a process in which the spin wave $\mathbf{k}$ decays into a spin wave $\mathbf{k}'$ and a phonon $\mathbf{K}$.

The machinery above was set up in 1950 by Luttinger and Kittel in work which has remained unpublished. They went on from Eq. (17) to calculate the relaxation time characterizing a spin wave state with $k = 0$ in the presence of a distribution of spin waves and phonons in thermal equilibrium at room temperature. Under the conditions prevailing in microwave resonance experiments the rf magnetic field excites spin waves with wave numbers in the range 1 to 10^5 cm^{-1}, the higher values occurring in metals where the eddy current skin depth rather than the radiation wavelength is decisive. The thermally excited spin waves have k's for the most part much higher, near 10^7 cm^{-1}, so that for all practical purposes we may regard the spin waves excited by the rf field as having $k = 0$.

The calculations of Luttinger and Kittel gave, for typical values of the ferromagnetic constants and using the interaction (17) which is linear in the strains, a spin-lattice relaxation time of the order of 10^{-1} sec. The experimental data suggest a spin-lattice relaxation time of the order of 10^{-7} sec at room temperature, so that the disagreement is very serious. The interpretation of the experiments is not, however, unambiguous. It is also possible to consider an interaction quadratic in the strains: for a cubic crystal one adds to Eq. (4) terms of the form

$$B_3(\alpha_1^2 e_{xx}^2 + \alpha_2^2 e_{yy}^2 + \alpha_3^2 e_{zz}^2),$$

plus other terms quadratic in the strains. These quadratic terms are responsible for the dependence of the velocity of a given elastic wave on the direction of magnetization in the crystal.[7] For nickel it is found experimentally that $B_3 \sim 6 \times 10^9$ cgs. By use of only the coupling $(B_3/M_s^2) M_x^2 e_{xx}^2$, the relaxation was calculated to be approximately 10^{-2} sec, still much too long.

We are faced then with the problem of accounting for a factor of 10^5 to 10^6 discrepancy between the experimental and calculated values of the spin-lattice relaxation times. On studying the calculation above and comparing it with a related calculation by Akhieser[8] we are able to see where the trouble lies. Akhieser calculated the lifetime averaged over all $\mathbf{k}$ of a spin wave state with respect to interactions with other spin waves (spin-spin relaxation) and with the lattice vibrations (spin-lattice relaxation). Akhieser's spin-lattice relaxation times are shorter by a factor of the order of 10^{-5} than those calculated by Luttinger and Kittel for their problem, even though Akhieser used only the magnetic dipole interaction which is known to be too weak to account for the observed magnetostrictive properties of ferromagnets. The reason Akhieser gets short times is that he is interested in thermal problems and is therefore dealing with an average over all spin wave states, thus weighting states of high $k (\approx 10^7$ cm$^{-1})$ heavily, whereas Luttinger and Kittel deal with a state of low $k (\approx 0)$ excited by the microwave field.

Now if the $k = 0$ spin waves were to come into equilibrium with other spin-waves in a time short in comparison with the time for equilibrization with the lattice vibrations, then the microwave spin-lattice problem would take on a form very close to Akhieser's problem, and we might expect to come up with reasonable theo-

[7] W. P. Mason, Phys. Rev. 82, 715 (1951).
[8] A. Akhieser, J. Phys. (U.S.S.R.) 10, 217 (1946).

CC-0. In Public Domain. Gurukul Kangri Collection, Haridwar

Digitized by Arya Samaj Foundation Chennai and eGangotri

retical values of the spin-lattice relaxation time in ferromagnetic resonance. Fortunately there are in fact good reasons for believing that the spin-spin relaxation time is usually shorter than the spin-lattice relaxation time, at least at not too high temperatures.

We note first that if we neglect spin-lattice relaxation the width of the resonance line is a measure of the spin-spin relaxation time. Our earlier result that resonance occurs only at a discrete field strength resulted directly from the selection rules $\Delta n_0=\pm 1$, $\Delta n_k(k\neq 0)=0$ applied to Eq. (3). However, in the presence of magnetic dipolar and pseudo-dipolar interactions between the spin waves the states of a single k will no longer be eigenstates. The correct eigenstates are mixtures of the unperturbed states of various k's. The mixing may be thought of as caused by the action of the fluctuating demagnetizing or pseudo-dipolar fields of the spin waves on each other. For temperatures of the order of half the Curie temperature or less the zero-point demagnetizing fields associated with the zero-point motion of the transverse components of the spin waves are expected to be more important than the magnetic fields associated with thermally excited spin waves. The transverse magnetization components go as $S_t=(S_x^2+S_y^2)^{\frac{1}{2}}=[S(S+1)-S^2]^{\frac{1}{2}}=S^{\frac{1}{2}}$. In the classical limit $S\rightarrow\infty$, the zero-point transverse components of the magnetization become relatively insignificant, and the mixing effect vanishes: The interaction energy per spin is of the order $\mu H_t\sim\mu M_s/S^{\frac{1}{2}}$, where M_s is the saturation magnetization,[9] or $\mu H_t\sim C/S^{\frac{1}{2}}$, where C is the pseudo-dipolar interaction energy of two adjacent spins.

As a result of the mixing of the originally unperturbed states caused by the dipolar-type interaction, admixtures of the $k=0$ state will be found in other states, especially in those within μH_t of the original state. This means that magnetic dipole transitions may now be expected to take place over a broad group of states, instead of only between the equi-spaced $k=0$ levels. For T less than, say, half of the Curie temperature the mixing arises almost entirely from the zero point motion and in this way we can account for a temperature independent line width (within an order of magnitude) from room temperature to absolute zero, although the experimental evidence for such an extrapolation is at present incomplete. Yager in preliminary unpublished measurements finds that the line width in Supermalloy is roughly constant between room temperature and liquid air temperature. The constancy of the line widths measured by Bloembergen[10] in nickel below 100°C and in Supermalloy below 300°C is very suggestive, although he did not continue the measurements below room temperature. Healy[11] finds an increase of width in a nickel ferrite single crystal by a factor of two on going from 600°C to −200°C.

We now suggest that ordinary ferromagnetic substances are characterized, at temperatures substantially below the Curie point, by a spin-spin relaxation time of the order of 10^{-8} to 10^{-9} second. We have not made a direct calculation of the spin-spin time, but our estimate follows plausibly on introducing the pseudo-dipolar interaction into Akhieser's results; it also follows from the argument below. An apparent objection to our point of view is based on Van Vleck's calculations[12] of the second and fourth moments of magnetic resonance frequencies in paramagnetic and ferromagnetic crystals. The result of Van Vleck which is apparently the strongest contradiction of our arguments is that at 0°K in a ferromagnetic crystal

$$\langle\Delta\omega^2\rangle_{\text{Av}}=0. \tag{18}$$

This would require unambiguously that the line be of zero width. However, we believe that the argument by which Van Vleck derived Eq. (18) is incomplete, as shown by Keffer.[13] The essential point is that Van Vleck has worked throughout with a truncated Hamiltonian, omitting entirely those parts of the dipolar Hamiltonian corresponding to transitions with $\Delta M=0,\ \pm 2,\ \pm 3$, while the part he retains allows only $\Delta M=\pm 1$. The other transitions are omitted in paramagnetic problems because they are associated with weak satellite lines distinct from the principal line. However, when the dipolar energy is comparable with the Zeeman energy the satellites can spread out over the main line and the classification of transitions by ΔM changes is no longer applicable. For the $\Delta M=2$ transition Keffer finds that the second moment about its center contains terms of the order J^2, indicating that the satellite has spread out. The part of the Hamiltonian Van Vleck retains gives no mixing of spin wave states, while the part he drops does give mixing. Keffer's argument is that in the ferromagnetic problem ($J,C\gg\mu H$), because of the overlap of the satellites with the main line, we should work with the whole Hamiltonian. The second moment at absolute zero as calculated by Keffer comes out to be, for a fcc lattice,

$$\hbar^2\langle\Delta\omega^2\rangle_{\text{Av}}\cong(3g\mu_B M_s/S^{\frac{1}{2}})^2. \tag{19}$$

We note that the second moment vanishes if we let $S\rightarrow\infty$ while keeping M_s constant. The nonvanishing of the second moment is therefore a quantum effect, as

[9] In reality we have to deal with a pseudo-dipolar interaction C (arising from spin-orbit effects) which may be 10 to 100 times stronger than the magnetic dipolar interaction; the mixing is increased in the same ratio. For estimates of the magnitude of the pseudo-dipolar interaction, see J. H. Van Vleck, Ann. inst. Henri Poincaré 10, 57 (1947); see also reference 4, Appendix B. For nickel Van Vleck finds that the pseudo-dipolar interaction must be about 50 times greater than the magnetic dipolar interaction in order to account for the anisotropy. For the superexchange interaction a relation due to Van Vleck and Kittel gives $C\approx J(g-2)^2$.

[10] N. Bloembergen, Phys. Rev. 78, 572 (1950).
[11] D. W. Healy, Jr., Phys. Rev. 86, 1009 (1952).
[12] J. H. Van Vleck, Phys. Rev. 74, 1168 (1948); 78, 266 (1950).
[13] F. Keffer, thesis, University of California, Berkeley, 1952, pp. 40–59; Phys. Rev. 88, 686 (1952). Keffer has also shown that the width in the paramagnetic region ($T>T_c$) under the same conditions is increased by the factor 10/3, a result later obtained by P. W. Anderson independently.

CC-0. In Public Domain. Gurukul Kangri Collection, Haridwar

Digitized by Arya Samaj Foundation Chennai and eGangotri

expected from our earlier discussion of the fluctuating transverse demagnetizing fields associated with the zero-point spin waves.

Except for the numerical constant and the dependence on the spin quantum number S, Eq. (19) has the same form as the usual Van Vleck expression for the second moment of the resonance line in a paramagnetic salt, and we may expect just as in the paramagnetic case to find that Eq. (19) is not by itself a good index to the apparent width of the resonance, as the fourth moments in both the paramagnetic and the absolute-zero ferromagnetic calculations involve J^2. The general effect of the exchange interaction may be interpreted qualitatively following Van Vleck and Gorter as leading to a motional narrowing of the resonance line. The concept is useful, but probably not rigorous. The apparent line width due to spin-spin relaxation is given qualitatively on this empirical analogy by

$$\hbar\Delta\omega \approx \hbar(\Delta\omega)_d[\hbar(\Delta\omega)_d/J], \tag{20}$$

where $(\Delta\omega)_d$ is the dipolar width which would obtain in the absence of the exchange interaction. The effect of exchange is to reduce the width in the ratio $\hbar(\Delta\omega)_d/J$. Writing the pseudo-dipolar interaction energy between two atoms as C we have

$$\hbar\Delta\omega \approx C^2/JS. \tag{21}$$

Estimating $C \approx 3\text{cm}^{-1}$ and $J \approx 100\ \text{cm}^{-1}$, we see that the line width may very reasonably be of the order of 0.1 cm^{-1}, corresponding to a spin-spin relaxation time of the order of 10^{-9} second at 0°K. This is the proper order of magnitude.

We have thus made our basic assumption $\tau_{\text{spin-spin}} < \tau_{\text{spin-lattice}}$ for $T/T_c < \frac{1}{2}$ seem plausible. We can account for a spin-spin relaxation time of the order of 10^{-9} second, which is shorter than the room temperature spin-lattice time ($\approx 10^{-7}$ sec). We suppose then in what follows that for the purpose of calculating spin-lattice relaxation times we may assume the spin system to be effectively in thermal equilibrium.

The calculation of spin-lattice relaxation times at various temperatures under the assumption that the spins are in thermal equilibrium has carried out by Abrahams.[14] The calculation is not too unlike one which Akhieser carried out for another purpose, but Abrahams uses the realistic interaction given in Eqs. (4) and (17), while Akhieser used the magnetic dipolar interaction which is known to be 10 to 100 times too small. Abrahams applied the general method discussed above as it lends itself easily to the use of the phenomenological interaction, while Akhieser used an extension of the Holstein-Primakoff method.[15] It would be quite possible, however, to apply the Holstein-Primakoff method with a pseudo-dipolar interaction.

It turns out from the calculations of Abrahams that the terms of greatest importance in Eq. (17) are those describing the scattering of a spin-wave with the emission or absorption of a phonon. The effective part of the interaction Hamiltonian then consists of a phonon emission term

$$\mathcal{H}_{\text{int}}{}^e \propto \sum_{K,k} b_K{}^* a_k a_{k'}{}^* f(\mathbf{K}), \tag{22}$$

plus a phonon absorption term

$$\mathcal{H}_{\text{int}}{}^a \propto \sum_{K,k} b_K a_k a_{k'}{}^* f(\mathbf{K}), \tag{23}$$

with the condition

$$\mathbf{k}' = \mathbf{k} + \mathbf{K} \tag{24}$$

applying in both cases. Here $f(\mathbf{K})$ denotes a function of $\mathbf{K}$.

The net number of collisions for unit time which transfer energy to the lattice is given by the kinetic equation, where ϵ denotes the energy,

$$w_{\text{coll}} = \frac{2\pi}{\hbar} \sum_{K,k} [|H_{\text{int}}{}^e|^2 - |H_{\text{int}}{}^a|^2] \delta(\epsilon_K + \epsilon_k - \epsilon_{k'}). \tag{25}$$

Now the matrix elements of the creation and destruction operators are simply expressible in terms of the occupation numbers N_K, n_k, $n_{k'}$, so that Eq. (25) assumes the form

$$w_{\text{coll}} = \frac{2\pi}{\hbar} \sum_{K,k} |f(K)|^2 [N_K n_k (n_{k'}+1) - (N_K+1)(n_k+1) n_{k'}] \delta(\epsilon_K + \epsilon_k - \epsilon_{k'}). \tag{26}$$

We now define a spin temperature T_s and a lattice temperature T_l. This permits us to express the occupation numbers in terms of the Bose-Einstein factors appropriate to the two temperatures. We proceed from Eq. (26) to calculate the net rate of energy transfer $\dot{Q}$ between the two systems. The result of the calculation is that

$$\dot{Q} \cong \frac{V\Delta T}{T^2} \cdot \frac{1}{(2\pi)^3} \cdot \frac{\hbar B_1{}^2}{2\rho k} \cdot \left(\frac{\hbar c}{2A}\right)^8 \cdot \left(\frac{M_s}{g\mu_B}\right)^6 \cdot \frac{1}{2\gamma} \cdot I(\gamma, \xi), \tag{27}$$

where, writing c for the sound velocity,

$$\gamma = (\hbar c)^2 M_s / 2g\mu_B AkT,$$
$$\xi = 2(g\mu_B/\hbar c)^2 (AH/M_s), \tag{28}$$

and

$$I(\gamma, \xi) = \int_0^\infty \frac{x^4 dx}{\cosh \gamma x - 1} \left[\log \frac{e^{\alpha+\gamma\xi} - e^{-\gamma x}}{e^{\alpha+\gamma\xi} - 1}\right],$$

where $\alpha = \gamma(x-1)^2/4$. The integral must be evaluated numerically.

[14] Elihu Abrahams, thesis, University of California, Berkeley, 1952; E. Abrahams and C. Kittel, Phys. Rev. 88, 1200 (1952).
[15] T. Holstein and H. Primakoff, Phys. Rev. 58, 12 (1940).

CC-0. In Public Domain. Gurukul Kangri Collection, Haridwar

Digitized by Arya Samaj Foundation Chennai and eGangotri

Assuming that the temperature difference $\Delta T = T_s - T_l$ decays exponentially, the spin-lattice relaxation time τ is defined by

$$\frac{d}{dt}\Delta T = -\frac{1}{\tau}\Delta T. \tag{29}$$

In terms of the rate of energy transfer $\dot{Q}$ and the heat capacities C_s, C_l of the spin and lattice system, we find

$$\tau = \frac{\Delta T}{\dot{Q}[(1/C_s)+(1/C_l)]}. \tag{30}$$

We can estimate both C_s and C_l as a function of temperature, so that with Eq. (27) for $\dot{Q}$ we can determine τ.

In this way Abrahams calculates for nickel, at 300°K, $\tau = 6\times10^{-7}$ sec; at 3 K, $\tau = 5\times10^{-4}$ sec; at 1°K, $\tau \approx 1$ sec. The spin-lattice estimates reported here do not include the effect of relaxation by coupling with the conduction electrons. At low temperatures in metals we might expect this process to be important, and the relevant calculations are underway. In ferrites, however, the present estimates should be valid. There are at present no direct experimental measurements available for the spin-lattice relaxation time, although the line width measurements by Bloembergen[10] may be interpreted as suggesting that at high temperatures spin-lattice relaxation makes an appreciable contribution to the line width, so that the spin-lattice time well above room temperature may perhaps drop to 10^{-8} to 10^{-9} sec.

An important question not yet fully solved is the interpretation of several reorientation experiments which it had originally been thought measured the spin-lattice relaxation time. Galt[16] has deduced a spin-lattice relaxation frequency of 3×10^{8} sec^{-1} in magnetite at room temperature from measurements of the velocity of propagation of a domain wall.[17] Bloembergen and Damon[18] deduce a spin-lattice time of 3×10^{-8} sec for nickel ferrite at room temperature, while a similar value is found in manganese zinc ferrite. These values are obtained from ingenious microwave saturation measurements using intense rf fields, of the order of 40 oersteds. It has been suggested to the authors by M. H. Cohen and independently by P. W. Anderson that, as in Waller's calculations, experiments of these types measure essentially (to within a numerical factor) the same relaxation time as determines the line width. In brief, one argues that when the spins have come into equilibrium with each other in the time τ_s they will also have come into equilibrium in the external field. The processes which mix the spin wave states must give rise to angular momentum exchange with the specimen as a whole, thereby allowing the spin system to change its orientation with respect to an external field in a time of the order of τ_s. It may be expected that this question will shortly be resolved experimentally by low temperature measurements. At room temperature the reorientation time appears experimentally to be quite close to the time associated with the line width, in approximate agreement with the "one time" viewpoint.

The over-all picture given here of relaxation processes in common ferromagnetic substances suggests that, to within an order of magnitude at least, line widths (in single crystals) at 0°K will be roughly equal to line widths at temperatures as high as one-half the Curie temperature,[19] the spin-spin relaxation process being dominant and having values in the range 10^{-8} to 10^{-10} sec. At higher temperatures the spin-spin time may decrease, and the spin-lattice time will also decrease, perhaps in some cases sufficiently to dominate the line width near the Curie point, although calculations valid in this region have not been carried out. The reorientation time is thought to be approximately equivalent to the time associated with the line width. The spin-lattice time in ferrites is expected to become very long at low temperatures, of the order of one sec at 1°K, but will appear directly only in thermal measurements.

In conclusion we wish to express our thanks to Professor J. M. Luttinger and Professor F. Keffer for their collaboration on this problem, and for permission to refer to work of theirs unpublished at the time of writing. We are indebted to Professor J. H. Van Vleck for discussions of various aspects of the problem. This work has been supported in part by the U. S. Office of Naval Research.

[16] J. K. Galt, Phys. Rev. 85, 664 (1952).

[17] The connection is derived by L. Landau and E. Lifshitz, Physik. Z. Sowjetunion 8, 153 (1935); C. Kittel, Phys. Rev. 80, 918 (1950).

[18] N. Bloembergen and R. W. Damon, Phys. Rev. 85, 699 (1952); N. Bloembergen and Shyh Wang, Phys. Rev. 87, 392 (1952). According to a private communication from Bloembergen, this time should be reduced by a facter of 4π.

[19] There is no reason to exclude width changes by a factor of two or so such as are reported in a nickel ferrite single crystal by D. W. Healy, Jr., Phys. Rev. 86, 1009 (1952).

DISCUSSION

G. T. RADO, *Naval Research Laboratory, Washington, D. C.:* Did you consider in your calculations the effect of crystalline imperfections on the line width?

C. KITTEL, *University of California, Berkeley, California:* One can produce situations in which imperfections control the line width. Yager has, for example, broadened the line in Supermalloy by deliberate cold working. In the rather carefully selected specimens usually employed in resonance experiments I do not think that the width is caused by imperfections. The general agreement of the order of magnitude of the line widths over a wide range of substances is perhaps evidence for this statement.

CC-0. In Public Domain. Gurukul Kangri Collection, Haridwar

Digitized by Arya Samaj Foundation Chennai and eGangotri

REVIEWS OF MODERN PHYSICS VOLUME 25, NUMBER 1 JANUARY, 1953

Relaxation Effects in the Ferromagnetic Resonance*

R. W. DAMON†

Cruft Laboratory, Harvard University, Cambridge, Massachusetts

The spin-lattice relaxation time, T_1, has been determined in single crystals of nickel ferrite, by using the ferromagnetic resonance effect at a frequency of 9000 Mc/sec. At high levels of microwave power, the saturation effect is observed both in the resonance absorption and in the component of magnetization along the static field. T_1 is computed from these data.

The experimental method is described, and the results presented. Some of the results have not been encountered before in magnetic resonance, and are not predicted by available theories. Because of this, the relaxation time cannot be calculated from the classical theory of the magnetic resonance. By equating the energy absorbed to the energy transferred to the lattice, we obtain a value $T_1 \sim 3\times10^{-5}$ sec. This is longer than the decay time observed directly, which is less than a few tenths of a microsecond. The results are compared with available theories of the magnetic resonance and spin-lattice interaction.

I. INTRODUCTION

IN understanding the magnetic properties of solids, it is important to have information concerning the interaction between the system of spins, to which the magnetic properties are attributed, and the crystal lattice. In nuclear and paramagnetic systems, the spin-lattice coupling has been investigated by means of the magnetic resonance phenomenon.[1,2] According to Bloch's theory,[3] the transfer of energy from the electronic spin system to the crystal lattice can be described by the spin-lattice relaxation time, T_1, which is the characteristic time in which the spin system, when disturbed, returns to equilibrium with the lattice. We have observed the saturation effect in the ferromagnetic resonance absorption, analogous to measurements by which T_1 has been determined in other systems.[1,2] In addition, the change in the component of magnetization along the static field has been observed.[4] Both methods are applied to determining the spin-lattice relaxation time in a crystal of nickel ferrite.

For a ferromagnetic material in an externally applied field $H_x^{\text{ext}}=H_1e^{i\omega t}$, $H_y^{\text{ext}}=0$, $H_z^{\text{ext}}=H_0$, the classical steady-state solution for the x and y components of magnetization is[5,6]

$$M_x=\frac{\gamma^2M_z[H_0+(N_y-N_z)M_z]H_1}{\omega_0^2-\omega^2+i2\omega/T_2}, \tag{1a}$$

$$M_y=\frac{\gamma M_z[i\omega+1/T_2]H_1}{\omega_0^2-\omega^2+i2\omega/T_2}, \tag{1b}$$

$$\omega_0^2=\gamma^2[H_0+(N_x-N_z)M_z]\times[H_0+(N_y-N_z)M_z]+1/T_2^2. \tag{1c}$$

The quantities N_x, N_y, and N_z are demagnetizing factors for an ellipsoidal sample, and γ is the gyromagnetic ratio. The width of the resonance is described by T_2. We have neglected anisotropy effects and terms due to the inhomogeneous distribution of magnetization. In the low power resonance experiment, the former changes the value of ω_0,[5] and may have other effects in the saturation region. Neglecting high frequency components, and assuming a spherical sample ($N_x=N_y=N_z$), we find the time-average value of the z component of magnetization is[6]

$$M_z=M_0\left[1+\tfrac{1}{2}\gamma^2H_1^2T_1T_2\frac{\omega_0^2+\omega^2}{4\omega^2+T_2^2(\omega_0^2-\omega^2)^2}\right]^{-1}. \tag{2}$$

The ferromagnetic resonance experiment is usually performed at low levels of microwave power with $\gamma^2H_1^2T_1T_2\ll1$, so $M_z\approx M_0$ in (1) and (2). From measurements under these conditions T_2 can be determined from the relation $T_2=1/\gamma\Delta H$, where ΔH is the half-linewidth of the resonance line. In the present experiment, we utilize the saturation effect resulting from the term in H_1^2 as a means of determining T_1, and this approximation will not be made.

From (1) and (2), two methods of determining T_1 are apparent. The first utilizes the variation in M_z as a function of H_1^2, measured by observing the decrease in relative power absorbed as the microwave field-strength is increased. The quantity measured is the imaginary part of the complex permeability, μ'', defined by

$$\mu=\mu'-i\mu''=1+4\pi M_z/H_1. \tag{3}$$

Combining (1a), (2), and (3), and assuming a spherical sample, we obtain

$$\mu''=\frac{8\pi\omega T_2\gamma^2H_0M_0}{4\omega^2+T_2^2(\omega_0^2-\omega^2)^2+\frac{1}{2}\gamma^2H_1^2T_1T_2(\omega_0^2+\omega^2)}. \tag{4}$$

* This work was supported jointly by the Navy Department (U. S. Office of Naval Research), the Signal Corps of the U. S. Army, and the U. S. Air Force, under U. S. Office of Naval Research Contract N5ori-76, T.O. 1.

† Now at General Electric Research Laboratory, The Knolls, Schenectady, New York.

[1] Bloembergen, Purcell, and Pound, Phys. Rev. 73, 679 (1948).
[2] E. M. Purcell and C. P. Slichter, Phys. Rev. 76, 466 (1949).
[3] F. Bloch, Phys. Rev. 70, 460 (1946).
[4] N. Bloembergen and R. W. Damon, Phys. Rev. 85, 699 (1952).
[5] C. Kittel, Phys. Rev. 71, 270 (1947); 73, 155 (1948).
[6] N. Bloembergen, Phys. Rev. 78, 572 (1950).

CC-0. In Public Domain. Gurukul Kangri Collection, Haridwar

Digitized by Arya Samaj Foundation Chennai and eGangotri

At resonance,

$$(\mu''/\mu_0'')_{res}=(1+\tfrac{1}{4}\gamma^2H_1^2T_1T_2)^{-1}, \quad (5)$$

where $\mu_0''=2\pi T_2\gamma^2H_0M_0/\omega$ is the value of μ'' at resonance with no saturation. From measurements of $(\mu''/\mu_0'')_{res}$ *vs* H_1^2, with a knowledge of T_2 from line-width data, T_1 can be determined.

The second method is the more direct one of measuring M_z/M_0 as a function of H_1^2. This satisfies the same relation

$$(M_z/M_0)_{res}=(1+\tfrac{1}{4}\gamma^2H_1^2T_1T_2)^{-1}, \quad (6)$$

and T_1 should be obtainable alternatively in this way.

To interpret the experiment, the transient solutions of the equation of motion are also of interest. In the case when the microwave field is suddenly turned off the definition of T_1 implies an exponential return of magnetization to equilibrium, $M_z=M_0$; the time constant for the process is T_1. The case when the microwave field is suddenly turned on is more difficult to interpret because of induced transitions. The anisotropy and demagnetizing terms lead to a nonlinear equation of motion, but in spherical samples, the demagnetizing terms cancel. Some possible effects of anisotropy in ferromagnetic saturation have recently been discussed by Bloembergen and Wang.[7]

II. EXPERIMENTAL METHOD

Measurement of μ''

To determine T_1 by measurements of μ'' as a function of H_1^2 the sample is placed in a microwave cavity at a point of high microwave magnetic field, and μ'' is calculated from the change in the power dissipated in the cavity. By use of the perturbation theory for cavities, the relation

$$\mu''=\frac{8\pi u_1}{v}\left(\frac{1}{Q_u'}-\frac{1}{Q_u}\right), \quad (7a)$$

is obtained.[8] Here v is the volume of the sample, Q_u is the unloaded Q of the empty cavity, and Q_u' that under the conditions for which μ'' is to be measured. The quantity u_1 is a geometrical factor defined as

$$u_1=\frac{1}{8\pi}\int_{V_c}(H/H_1)^2d\tau, \quad (8)$$

where V_c is the cavity volume, H is the rf magnetic field amplitude in the cavity, and H_1 is the value of H at the sample position. In the rectangular cavities used, operated in a TE_{10n} mode, $u_1=(V_c/32\pi)(\lambda_g/\lambda)^2$.

The various Q's for the empty cavity were determined by measurements of band width[9] and the cavity conductance at resonance.[10] With this information, μ'' can be determined from the cavity reflection coefficient, Γ, which was measured in terms of incident and reflected power for the cavity, $|\Gamma|=(P_r/P_i)^{\frac{1}{2}}$. The result, in the case of an undercoupled cavity,[10] follows from (7) as

$$\mu''=\frac{8\pi u_1}{Q_ev}\left[\frac{1+|\Gamma|}{1-|\Gamma|}-G\right], \quad (9)$$

where $Q_e=Q_uG$ is the external Q, and G is the resonant conductance of the empty cavity.

The microwave field strength is determined from the cavity parameters and a power measurement as

$$H_1^2=(Q_eP_r/\omega u_1)[(1/|\Gamma|)-1]^2. \quad (10)$$

Measurement of M_z

The other method used to determine the spin-lattice relaxation time involves a measurement of the z component of magnetization as a function of the microwave magnetic field strength. The principle of this novel method is as follows. If the sample is in a static field only, the magnetization is M_0. Applying a microwave field of resonant frequency will change the z component of magnetization to M_z, given by (6). This change will occur in a time determined by the relaxation processes, and the changing induction will induce a voltage proportional to M_0-M_z in a coil of wire near the sample. By measuring the induced voltage, M_z is determined as a function of microwave magnetic field strength. With knowledge of T_2 from line-width data, the spin-lattice relaxation time can be calculated from (6).

The induced voltage will also depend on the rate at which the magnetization approaches equilibrium. Since induced transitions complicate the response when the microwave field is turned on, the pulse obtained when the field is turned off appears to be most suitable for the measurements. It must be remembered, however, that the build-up and decay of H_1^2 has the time constant Q_L/ω, where Q_L is the loaded Q of the cavity. If this time is long, it will be the controlling factor for either the magnetization build-up or decay. The loaded Q also depends on μ'', and thus on H_1^2, so this will not yield a constant decay time. No attempt was made to correct for this effect.

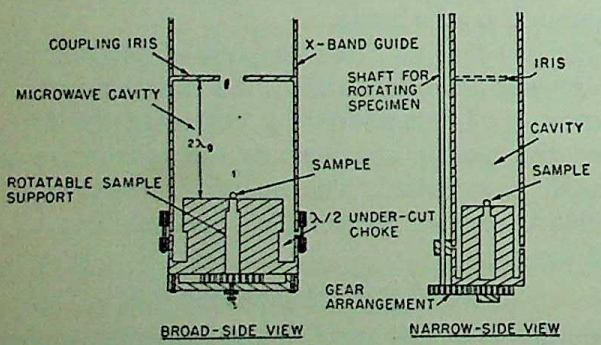


FIG. 1. Schematic cavity construction for measurement of μ'' along different crystal axes.

[7] N. Bloembergen and Shyh Wang, Phys. Rev. 87, 392 (1952).
[8] D. W. Healy, Jr., Phys. Rev. 86, 1009 (1952).
[9] C. G. Montgomery, *Technique of Microwave Measurements* (McGraw-Hill Book Company, Inc., New York, 1947), p. 396.
[10] See reference 9, Chapter 5.

CC-0. In Public Domain. Gurukul Kangri Collection, Haridwar

Digitized by Arya Samaj Foundation Chennai and eGangotri

Experimental Equipment

Two microwave cavities were used in the experiments. The first was the rectangular cavity shown in Fig. 1, used only for measurements of μ''.‡ This cavity was two wavelengths long, coupled to the wave guide by an inductive iris. The sample is located in the center of the cavity end-wall, which is a region of maximum microwave magnetic field and of zero electric field. It is mounted on a cylindrical post, which can be rotated to change the orientation of the crystallographic axes of the sample with respect to the static field.

To observe the change in z component of magnetization, the sample is placed in another microwave cavity, shown in Fig. 2. This second cavity is also rectangular. The sample is located on the top of the cavity, one-half wavelength from the cavity end-wall, at a point of high microwave magnetic field. The pick-up coil is placed outside the cavity, behind a wall of the cavity which is a metalized sheet, thin enough to transmit the signal due to the change in magnetization. In order to maintain a high cavity Q, the wall must also be thick compared to the skin depth at microwave frequencies. Both requirements can be met by using wall thicknesses of a few microns.

A block diagram of the equipment is shown in Fig. 3. The cavity is connected to one side-arm of a magic-tee, and a matched load to the other side-arm. The output of the magic-tee is then $\frac{1}{2}P_r$. The input power to the magic-tee is from a 9000-Mc/sec magnetron oscillator, which delivers one-microsecond pulses with a peak power of 50 kilowatts.

Because of transient effects, due to ringing of the cavity and frequency variations of the magnetron at the start and end of the pulse, the reflected power is not constant throughout the pulse. This makes it inaccurate to use any of the standard power-measuring techniques that measure average power. To measure the steady-state reflected power, the output of the magic-tee is detected with a crystal and the envelope observed on an oscilloscope. In this way the center of the pulse, where steady-state conditions exist, can be observed.

The crystal and oscilloscope are calibrated for power measurements by replacing the cavity by a shorting plunger and measuring the power incident on the magic-tee with the calibrated directional coupler and thermistor bridge. The steady-state power reflected from the cavity can henceforth be determined from the attenuation required to reduce the reflected power to a reference scope deflection.

A measurement of the cavity reflection coefficient, $|\Gamma|$, is necessary in the determination of both the microwave field strength and the sample permeability, according to (9) and (10). To make this measurement, attenuator No. 3 was set to give roughly the desired value of H_1^2 according to (10), and attenuator No. 1

‡ The author is indebted to D. W. Healy, Jr., for the use of this cavity.

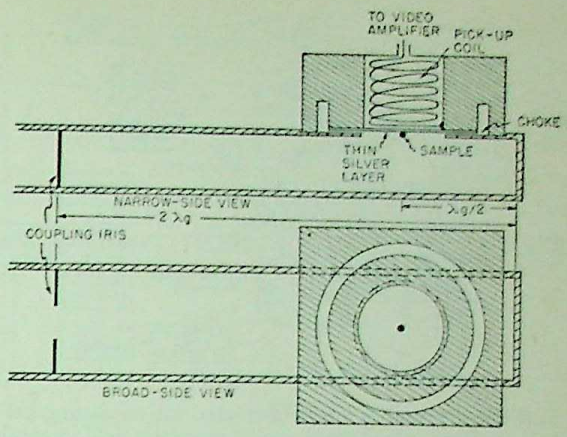


FIG. 2. Schematic cavity construction for measurement of change in z component of magnetization.

was used to set the incident power to the value which brings the scope deflection to the reference level, with the static field off. At the desired value of static field, attenuator No. 2 was adjusted to bring the crystal output back to the reference level, thus measuring only an increment in power, and from the three attenuator settings and the crystal calibration the quantities $|\Gamma|$, P_r, H_1^2, and μ'' were calculated. In plotting the μ'' data, all values were normalized by dividing by μ_0'', the permeability at resonance with no saturation.

For resonance-curve measurements, with varying static field, it would be desirable to maintain constant values of H_1^2 over a particular run. Owing to the complex dependence of H_1^2 on μ'', this was not possible by the method used. Instead, the resonance curves were taken at constant reflected power, and μ'' and H_1^2 were calculated for each point. By use of the saturation curves of μ'' *vs* H_1^2 at the resonant value of static field, these were then corrected to a constant value of H_1^2, chosen as the value of H_1^2 obtained at resonance. This procedure probably leads to a slight broadening of the curves, since H_1^2 varied by as much as a factor of two over some resonance curves, but this is probably not within the limits of accuracy of the experiment.

For measurements of M_z, the output voltage of the pick-up coil is connected through a video attenuator to the video amplifier[11] and pulse-stretcher.[12] The approximate wave shape at various points in the detecting system is shown in Fig. 4.

The output of the pulse-stretcher is fed through a cathode-follower into the lock-in detector. The lock-in reference signal is the sine-wave output of the synchroscope oscillator. Thus the lock-in detector is sensitive only to the fundamental frequency of the voltage induced in the pick-up coil. Because of the rectifier in the pulse-stretcher, the detecting system is nonlinear. For

[11] W. C. Elmore and M. L. Sands, *Electronics, Experimental Techniques* (McGraw-Hill Book Company, Inc., New York, 1949), pp. 3–49.

[12] Radio Research Laboratory Staff, *Very-High-Frequency Techniques* (McGraw-Hill Book Company, Inc., New York, 1947), p. 981.

CC-0. In Public Domain. Gurukul Kangri Collection, Haridwar

Digitized by Arya Samaj Foundation Chennai and eGangotri

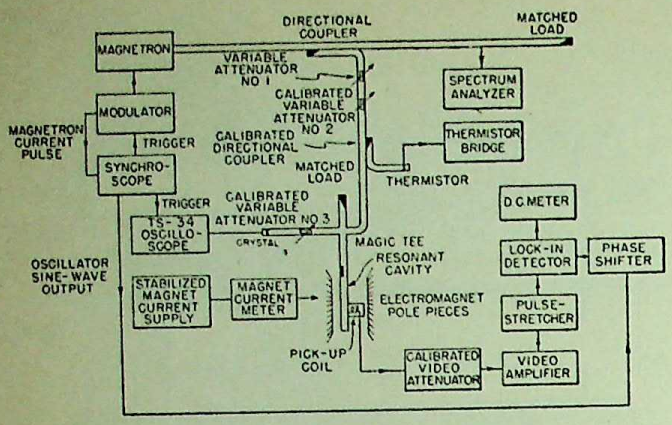


FIG. 3. Block diagram of equipment used for measuring both μ'' and M_z as functions of static and rf magnetic field strengths.

very small signals, the system was calibrated with the video attenuator. For larger signals, the signal was attenuated to a reference level, and measured by the amount of video attenuation required. The saturation curves for M_z were normalized by fitting the output of the lock-in as a function of H_1^2 at constant static field to (6).§

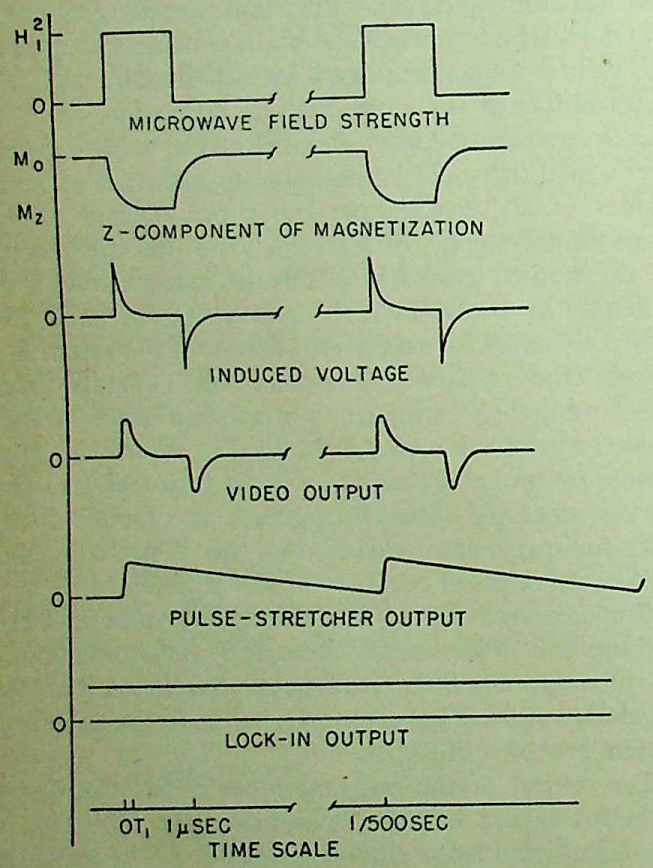


FIG. 4. Signal due to change in z component of magnetization at various points in the detecting system.

§ This is a somewhat questionable procedure of normalizing M_z, since it will be seen from the data to be presented that the classical theory does not explain the experimental results at all well. Dr. Shyh Wang has recently obtained a normalizing constant for the system by essentially the same method, but using a sample of paramagnetic $MnSO_4 \cdot 4H_2O$, for which the classical theory is apparently valid, and he finds that the actual change of magnetization is only about one-tenth as large as we calculate. This changes the calculated value of T_1, but leaves the results otherwise unchanged.

In choosing a material to be studied, it was felt that the ferrites would be particularly well suited to this experiment because of their low conductivity and the concomitantly large skin depth. Thus, samples of reasonable size could be used, with the field remaining uniform over the sample. Another advantage is that use of these materials practically eliminates the conduction electrons from consideration as a mechanism for the relaxation process, and so simplifies the theoretical problem.[6]

Single crystals of nickel ferrite were used.[11] These were made spherical in shape in order to have the demagnetizing field cancel the Lorentz local field. In this case the local field acting on a spin is equal to the field with no sample present. The samples had a diameter of about 0.5 mm, and were oriented by x-ray back-reflection techniques.

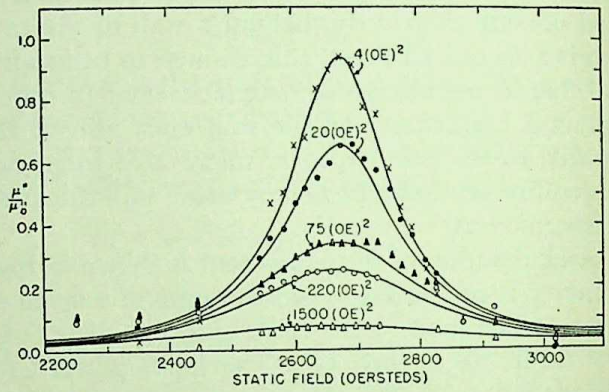


FIG. 5. Dependence of μ'' on static field, with H_1^2 as parameter. Sample 6, oriented with static field along [111] axis.

III. EXPERIMENTAL RESULTS

Results for Sample 6

Sample 6 was a good single crystal of $NiO \cdot Fe_2O_3$ as determined by x-ray techniques. All data on this sample were taken with the static field along the [111] axis, which is the direction of easy magnetization.[8,13] In Fig. 5, a set of resonance curves is shown. As previously discussed, each curve was taken with constant reflected power, and corrected to the given value of H_1^2. The curves drawn were calculated from (4) by obtaining T_2 from the width of the lowest power resonance curve and using the peak height to determine the value of $\frac{1}{2}\gamma^2 T_1 T_2$.

Figure 6 shows the z component of magnetization as a function of static field strength. According to the classical theory, M_z should show the same resonant behavior as μ''. It is found that although M_z increases rapidly above the resonant value of static field, there is a wide low field region where the change in magnetization is even larger than that at resonance.

It may be remarked here that there was some indication in the experiments of an increase in μ'' over this

[11] These were supplied through the courtesy of the Bell Telephone Laboratories, Inc.

[13] Yager, Galt, Merritt, and Wood, Phys. Rev. 80, 744 (1950).

CC-0. In Public Domain. Gurukul Kangri Collection, Haridwar

Digitized by Arya Samaj Foundation Chennai and eGangotri

region of low static field at intermediate levels of microwave field strength; at higher power levels, this appeared to decrease again. This is noticeable in Figs. 5 and 8, and such an energy absorption is of course necessary to change M_z, but no quantitative measurements were obtained.

The most significant result of these measurements is that the values of microwave field required to change the z component of magnetization are considerably greater than the field strength which saturates the absorption line. Figure 7 shows the maximum absorption and the minimum z component of magnetization as a function of the microwave field strength. The values of H_1^2 required for half-saturation in the two cases are seen to differ by about a factor of 100.¶

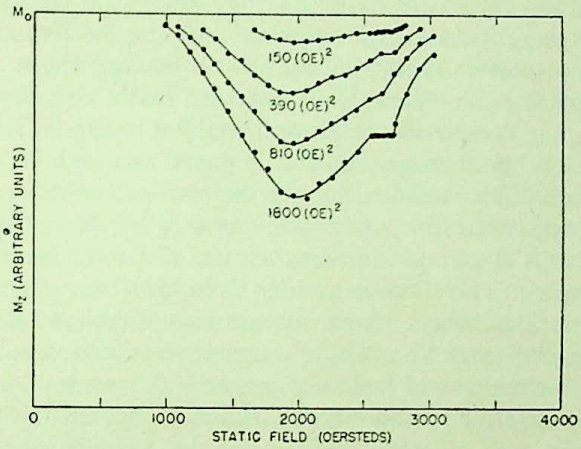


FIG. 6. Dependence of M_z on static field, with H_1^2 as parameter. Sample 6, with static field along [111] axis.

Experiments to Prove that Pick-Up Signal is Due to M_z

In view of the unexpected results obtained for the z component of magnetization, several simple experiments were performed to prove that the signal obtained is really due to the sample, and not to some spurious effect. The most convincing of these is that the output of the video amplifier as observed on the oscilloscope has the form shown in Fig. 4, and when the static field is reversed, thereby changing the sign of M_z, these pulses also change sign.

There is still some question as to whether the change in magnetization is due to true saturation of the spin system, the lattice remaining at constant temperature, or is simply due to heating the sample to the Curie point. Rough calculations indicate that during each pulse the temperature rise would be small, causing no appreciable change in magnetization; the time constant of the observed signal also is too short to be caused by thermal effects. This was further checked by setting H_1^2 to the region where μ'' or M_z changes most rapidly and varying the repetition rate of the magnetron modulator from 50 to 2000 pps. No measurable change in either μ'' or M_z was observed.

¶ This factor is even larger on the basis of Wang's calibration.

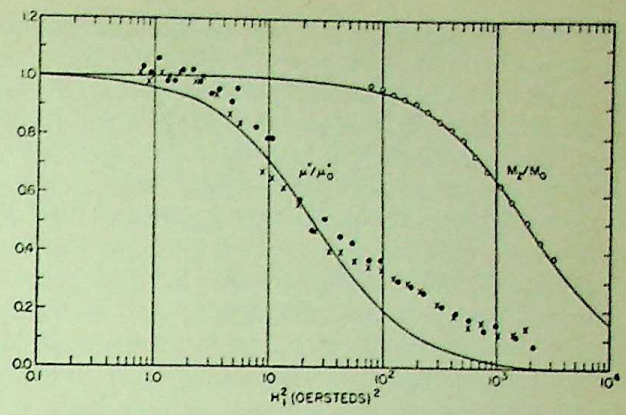


FIG. 7. μ'' and M_z as functions of H_1^2, at a fixed value of static field strength. Sample 6, with static field along [111] axis. Two successive runs for μ'' are shown. The curves are calculated from (5) and (6), and may be moved along the abscissa for best fit. (See reference §.)

Results for Sample 7

Since sample 6 did not behave at all as expected, data were taken on a second sample. The width of the absorption line for sample 6 indicated that it was not a very good sample. Sample 7 had been extensively investigated by Healy in the low power resonance and appeared to be satisfactory.[8] The results are shown in Figs. 8–10. For this sample there is a very definite minimum in the magnetization at about the resonant value of static field, but a large change also occurs at lower fields, just as for the first sample. The great difference between μ'' and M_z in the microwave field required for saturation also persists. The saturation values of H_1^2 are about the same as for sample 6.

Up to this point, all data on the z component of magnetization are observations of the rear peak, occurring when the microwave field is turned off at the end of a pulse. As discussed before, the relaxation time for this decay should be T_1, whereas the apparent relaxation time for the front peak depends on the microwave field strength. Data were also taken on the front peak, but no appreciable difference was observed in either the spectrum or the field required for saturation.

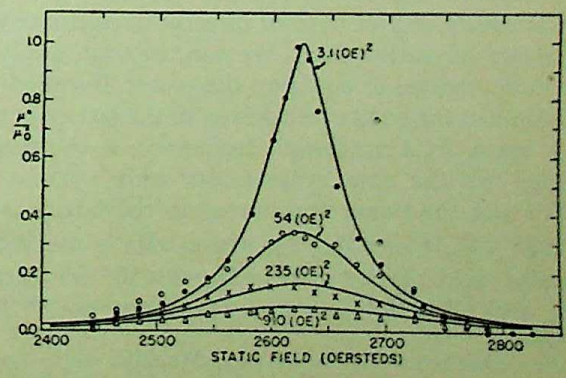


FIG. 8. Dependence of μ'' on static field, with H_1^2 as parameter. Sample 7, with static field along [111] axis.

CC-0. In Public Domain. Gurukul Kangri Collection, Haridwar

Digitized by Arya Samaj Foundation Chennai and eGangotri

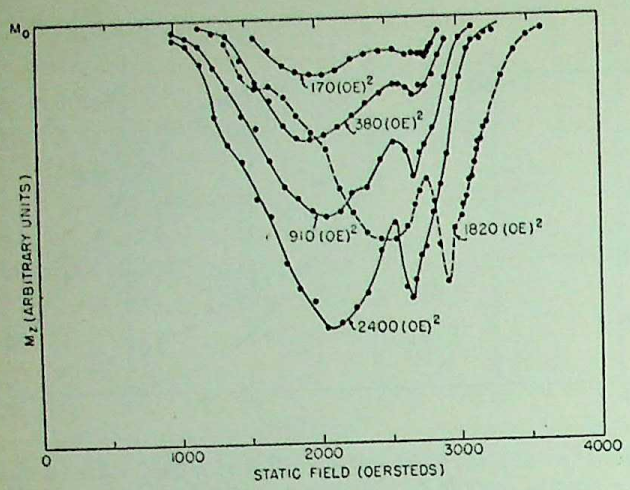


FIG. 9. Dependence of M_z on static field, with H_1^2 as parameter. Sample 7 —— static field along [110] axis; – – – static field along [100] axis.

Rotating the sample indicated that there is no basic dependence of the relaxation effects on crystallographic orientation. An example is shown in Fig. 9, for M_z *vs* static field. Note that the difference in static field between the two M_z minima is essentially constant, while the field required for resonance has changed by more than 300 oersteds. The orientation of the sample also had no effect on the dependence on microwave field strength, as shown in Fig. 10, and the absorption line, except for a shift of resonance field strength, was unchanged.

To find the effect of crystalline imperfections, sample 7 was heated to about 1000°C in air for five minutes and quenched in water. Subsequent measurements showed that the absorption line was broadened considerably. The unsaturated peak value was also reduced in about the same proportion, so the area under the curve remained approximately unchanged. The change in M_z at the resonant field was decreased, but the microwave field strength required for saturation was unchanged. This indicates that the wide absorption line and the large low field change in M_z are both due at least in part to sample imperfections.

Calculation of T_1

The experimental results make it apparent that the classical theory cannot be used directly to calculate the spin-lattice relaxation time. We can, instead, apply a more basic method of equating the power absorbed by the sample to the power transferred to the lattice in the steady state. At a microwave frequency, ν, the power absorbed by the spin system, per unit volume, is $\frac{1}{4}\mu''H_1^2\nu$ and the power transferred to the lattice is of the order $\Delta M_z(H_0+\alpha M_0)/T_1$, where αM_0 is the Weiss molecular field. If we take $\alpha M_0 \sim 3\times10^6$ for nickel ferrite, and $\mu_0''=35$,[8,13] we find $T_1\sim3\times10^{-5}$sec.** The decay time observed on an oscilloscope, as in Fig. 4, sets an upper limit to the value of T_1. This time was only a few tenths of a microsecond, most of which is attributable to the time constants of the apparatus. It thus appears that use of the Weiss molecular field is unjustified in this calculation, and the effective local field, during the times involved in the spin-lattice relaxation, is only a small fraction of the Weiss field.

IV. DISCUSSION

The experimental results obtained are not expected on the basis of the classical equations presented, and it does not appear that a more exact solution of the equation of motion would lead to significantly different results. Other classical equations of motion have been proposed,[5] differing in the form of damping used. These damping terms are based on the assumption that the total magnetization is a constant of the motion, and at low power levels give an absorption line-shape indistinguishable from that obtained with the Bloch damping terms.[8] However, our results strongly indicate that the total magnetization is not a constant of the motion. This is shown by the expression for the total magnetization at resonance, $M^2=(\mu''H_1/4\pi)^2+M_z^2$, which is found to decrease as the rf power level is increased. The classical results have also been derived in various ways from quantum-mechanical principles,[14–17] and Van Vleck[17] suggests contributions to the line-width which do not preserve the constancy of magnetization. These results, however, are all limited to the case of small changes in the z component of magnetization, and thus are probably not applicable to the present experiment.

The M_z spectrum observed can perhaps be explained by a breakdown of the selection rules for the transitions induced by the microwave magnetic field. This effect is

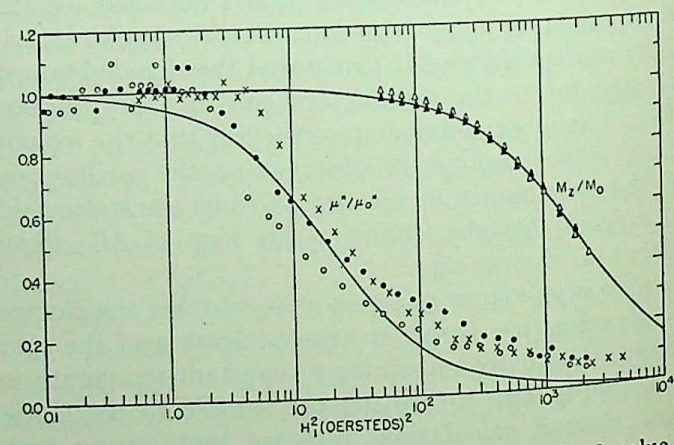


FIG. 10. μ'' and M_z as functions of H_1^2, at a fixed value of static field strength. Sample 7. ●▲ static field along [100] axis. ○△ static field along [110] axis. × static field along [111] axis. The curves are calculated from (5) and (6), and may be moved along the abscissa for best fit. (See reference §.)

** The author is indebted to Dr. Shyh Wang for discussion on the calculation of T_1. It should also be noted that on the basis of Wang's new calibration, $T_1\sim3\times10^{-6}$ sec, and is still longer than the time obtained by direct observation of the decay.

[14] J. M. Luttinger and C. Kittel, Helv. Phys. Acta 21, 480 (1948).
[15] J. M. Richardson, Phys. Rev. 75, 1630 (1949).
[16] D. Polder, Phil. Mag. 11, 99 (1949).
[17] J. H. Van Vleck, Phys. Rev. 78, 266 (1950).

CC-0. In Public Domain. Gurukul Kangri Collection, Haridwar

Digitized by Arya Samaj Foundation Chennai and eGangotri

apparently dependent on the microwave power level, since a corresponding energy absorption has not been observed in measurements at low power. Van Vleck[17] has suggested a mechanism for the breakdown of the selection rule for the x component of magnetization, based on dipolar coupling when the atoms are not all similarly situated. He suggests that some transitions, involving relatively small changes in exchange energy, will appear as wings on the resonance curve, and points out that anisotropic exchange coupling may be strong enough to make this effect significant. The effect of quenching lends support to this idea.

In the classical equations of motion, the relaxation times, T_1 and T_2, were introduced phenomenologically, with no attempt to estimate their magnitude or to inquire into their causes. The theory of the relaxation times in ferromagnetic materials has been treated by Van Vleck[17] and by Akhieser.[18] Van Vleck considers the contributions to the line-width due to spin-spin interaction. This is restricted to the case of small excitation, and will not be considered further.

Akhieser has treated relaxation times by making use of the spin-wave model, with the annihilation and creation of spin waves as the mechanism for the spin-spin and spin-lattice interactions. This occurs through the interaction of the spin waves with one another or with the normal modes of the lattice. Akhieser's results, unfortunately, are valid only at low temperatures, and cannot rigorously be applied to our room temperature data. Polder[16] has criticized Akhieser's calculation, stating that because of the selection rule for spin waves, one should consider only spin waves of long wavelength, rather than the entire spin-wave band. He finds that this leads to much longer spin-lattice relaxation times.

Akhieser's value of spin-spin relaxation time agrees quite well with the measured line-width, giving a time of 10^{-9} sec, but it must be emphasized that the temperature dependence of the line-width[8] is not explained. Extrapolation of Akhieser's results for the spin-lattice relaxation time to room temperature gives a time much shorter than we obtain. The extrapolation is so large, however, that the comparison is probably of little use. Akhieser's remark that the spin system reaches equilibrium in a time short compared to the spin-lattice relaxation time only at very low temperatures is a possible explanation of the discrepancy between the relaxation times obtained by energy absorption methods and by direct observation.

[18] A. Akhieser, J. Phys. USSR **10**, 217 (1948).

V. ACKNOWLEDGMENTS

The author is greatly indebted to Professor N. Bloembergen for suggesting this topic, and for many interesting and helpful discussions on both the experimental and theoretical aspects of this work. Thanks are also due Dr. D. W. Healy, Jr., for the loan of some of the equipment and samples used in the experiment. The interest and help of Professors E. L. Chaffee and Harvey Brooks, and of the staff of the Electronics Research Laboratory, Harvard University, are gratefully acknowledged.

CC-0. In Public Domain. Gurukul Kangri Collection, Haridwar

Digitized by Arya Samaj Foundation Chennai and eGangotri

REVIEWS OF MODERN PHYSICS VOLUME 25, NUMBER 1 JANUARY, 1953

A New Variation of the Rotation-by-Magnetization Method of Measuring Gyromagnetic Ratios*

C. J. DAVISSON AND J. W. BEAMS

University of Virginia, Charlottesville, Virginia

I. INTRODUCTION

ALL of the experimental arrangements which have so far been used to measure gyromagnetic ratios by the rotation-by-magnetization method have had certain features in common. The specimen has in all cases been a delicately suspended rod mounted on the common axis of one or more vertical solenoids. The experimental procedures, on the other hand, have been various. The first to be tried, though not the first to yield publishable results, was the ballistic, that in which the reaction of the rod to the change in internal angular momentum, consequent to a sudden change in its magnetization, is measured by the angular throw of the rod against the tortion of its suspension. An investigation of this kind was started by Richardson[1] at Princeton in 1908, the same year in which he predicted, on the basis of the electron theory, the existence of the gyromagnetic effect and derived a value for the gyromagnetic ratio. This line of work was continued at Princeton for ten years and culminated in the accurate measurements of gyromagnetic ratios made by J. Q. Stewart[2] in 1918. This was five years after Richardson had returned to England. The work had been continued under the direction of the late H. L. Cooke.

In the meantime (1915) Einstein and de Haas[3] had verified Richardson's prediction and had measured gyromagnetic ratios. (The same feat was performed in the same year by S. J. Barnett by the converse magnetization-by-rotation method with which we are not here concerned.) Einstein and de Haas employed a resonance method in which the magnetizing field was periodic and tuned to the natural frequency of the rod and its suspension. Values of the ratio were deduced from the amplitude of the vibration and other relevant dimensions of the system.

A third experimental procedure has been devised and perfected more recently by Chattock, Sucksmith and Bates.[4,5] As in the Einstein-de Haas method the magnetizing field is periodic, but the torque on the rod resulting from the gyromagnetic effect is countered by an equal and opposite torque derived from the varying field of the magnetized rod. It is a beautiful and ingeneous technique capable of precise measurements as its inventors have amply demonstrated.

There have, thus, been three ways in which the rod and filament experiment has been carried out—the ballistic method used by Stewart; the Einstein and de Haas resonance method; and the null method of Chattock, Sucksmith, and Bates. It is probable that variations on the rod and fiber theme have been exhausted, but by making some rather drastic alterations in the experimental arrangement, yet another way of measuring gyromagnetic ratios emerges. It is this new variation which is the subject of this communication.

II. THE NEW EXPERIMENTAL ARRANGEMENT

In the new arrangement the rod is replaced by a sphere, mechanical suspension is replaced by tortionless magnetic suspension, and solenoids of the usual kind are replaced by a pair of air-cored electromagnets mounted on a common vertical axis. The point of suspension, which is in vacuum, is at the center of symmetry of this pair of coils, as shown schematically in Fig. 1. Lateral stability is provided over a wide range of operating conditions by the form of the field. Longitudinal quasi stability is achieved by automatic control of the current in the upper coil. This is the rectified output of a rather elaborate vacuum tube circuit (Fig. 4) which operates at radio frequency. The control is in accordance with signals received in the circuit from a small pick-up coil located a short distance below the sphere with which it has a loose variable inductive coupling. This servomechanism was devised some years ago by one of us and his students[6] and has been developed to a high degree of dependability.

The weight mg of the magnetically suspended sphere is balanced by the upward force exerted on it by the field. This, to an exceedingly close approximation, is $M(dH/dz)=MH'$, the dipole magnetic moment of the sphere multiplied by the gradient of the magnetic field intensity H at its center:

$$MH'=mg. \tag{1}$$

The coil system is symmetrical with respect to a horizontal plane through the point of support. Consequently, the intensity H and all even derivatives of H are proportional to the sum of the currents in the two

* This work was supported by the Bureau of Ordnance, U. S. Navy, Contract NOrd-7873 at the University of Virginia.

[1] O. W. Richardson, Phys. Rev. 26, 248 (1908).

[2] J. Q. Stewart, Phys. Rev. 11, 100 (1918).

[3] A. Einstein and W. J. de Haas, Verhandl. deut. physik. Ges. 17, 152 (1915).

[4] A. P. Chattock and L. F. Bates, Trans. Roy. Soc. (London) A223, 257 (1923).

[5] W. Sucksmith and L. F. Bates, Proc. Roy. Soc. (London) 104A, 499 (1923).

[6] Beams, Young, and Moore, J. Appl. Phys. 17, 887 (1946); J. W. Beams, Wash. Acad. Sci. 37, 221 (1947); J. W. Beams, Rev. Sci. Instr. 21, 182 (1950).

CC-0. In Public Domain. Gurukul Kangri Collection, Haridwar

Digitized by Arya Samaj Foundation Chennai and eGangotri

coils, and all odd derivatives are proportional to the difference of these currents,

$$H=k_0(J_1+J_2),$$
$$H'=k_1(J_1-J_2), \qquad (2)$$
$$H''=k_2(J_1+J_2), \quad \text{etc.},$$

where J_1 and J_2 represent the current densities in the upper and lower coils, respectively. The constants k can be calculated from the dimensions of the coils and their separation.

By virtue of relations (2) H and H' are capable of independent variation. A change in M produced by a change in H can be coordinated with a change in H' which preserves the relation (1) and so leaves the position of the sphere unaltered. The sphere can be taken from a state 1 in which its magnetic moment is $M_1=mg/H_1'$ to a state 2 in which its moment is $M_2=mg/H_2'$ while it is held constantly at or near the center. The change in magnetic moment,

$$(M_2-M_1)=mg/(1/H_2'-1/H_1'), \qquad (3)$$

is accompanied, through the gyromagnetic effect, by a proportionate observable change in the angular momentum of the sphere about its vertical axis. The angular momentum is changed from some initial value Iw_1 to some final value Iw_2, where $I(=(2/5)mr^2)$ is the moment of inertia of the sphere and w is its angular velocity. The change in angular momentum is

$$(2/5)mr^2(w_2-w_1), \qquad (4)$$

and this divided by the change in magnetic moment (3) is, by definition, the gyromagnetic ratio ρ of the substance of the sphere, so that

$$\rho=[2r^2(w_2-w_1)]/[5g(1/H_2'-1/H_1')]. \qquad (5)$$

This is the fundamental equation of the new scheme of measurement.

The evaluation of (5) presents no great experimental difficulty. All that need be known about the sphere is its radius. Means must be provided for measuring accurately the uniform angular velocities w_1 and w_2, and for measuring the currents in the coils at the beginning and at the end of the transition. The values of H' are computed from the second of Eqs. (2) rewritten in the form

$$H'=k_1N(i_1-i_2), \qquad (6)$$

where i_1 and i_2 are the currents corresponding to J_1 and J_2, and N is the number of turns per unit area in the windings.

III. BEHAVIOR IN DETAIL

To examine the behavior of the system more closely we consider the special case in which the permeability of the sphere is infinite. The magnetic moment acquired by such a sphere in a field of intensity H is

$$M=r^3H. \qquad (7)$$

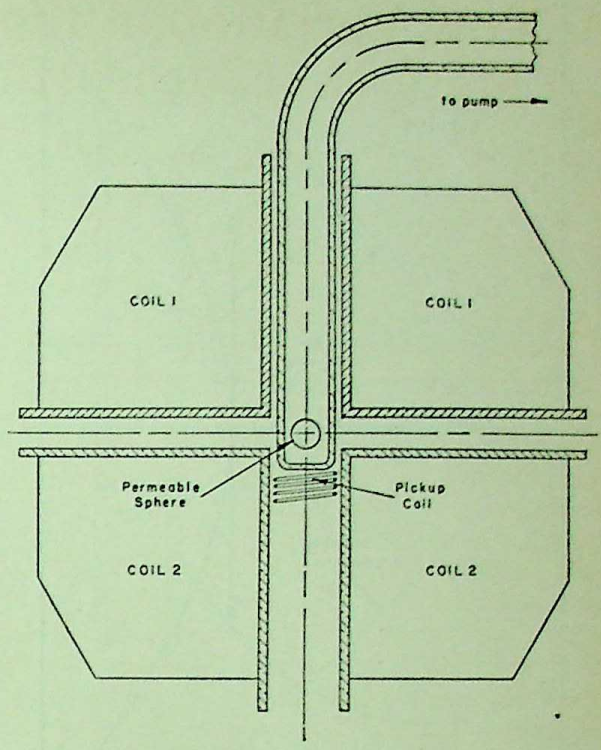


FIG. 1. Schematic diagram of experimental apparatus.

This is only slightly greater than the moment the sphere would acquire if its permeability instead of being infinite were merely high, say 10^4 or as low even as 10^3. The assumption is not, therefore, so very unrealistic.

Substituting this expression for M into (1) one obtains

$$HH'=(m/r^3)g=(4\pi/3)dg, \text{ a constant}, \qquad (8)$$

as the field condition for the magnetic suspension of a highly permeable sphere of density d. HH' is a constant proportional to the density of the sphere but independent of its size. For iron the constant is 3.23×10^4.

Substituting for H and H' the expressions for these quantities given in Eqs. (2) the condition for magnetic suspension in terms of the current densities in the two coils is found to be

$$J_1^2-J_2^2=\frac{4\pi dg}{3k_0k_1}=J_0^2, \text{ a constant}. \qquad (9)$$

J_0 is the current density in the upper coil when the sphere is supported by this coil alone. It is the same for spheres of all sizes. Of the two branches of the hyberbolic relationship (9) only one need be considered, the natural choice being that for which J_1 is positive. A central portion of this characteristic is plotted in Fig. 2. The part available for experimental observations is limited, in the first place, by the current-carrying capacity of the coils. If $\bar{J}$ represents the highest current density at which either of the coils can be safely operated, then the observations are restricted to the

CC-0. In Public Domain. Gurukul Kangri Collection, Haridwar

Digitized by Arya Samaj Foundation Chennai and eGangotri

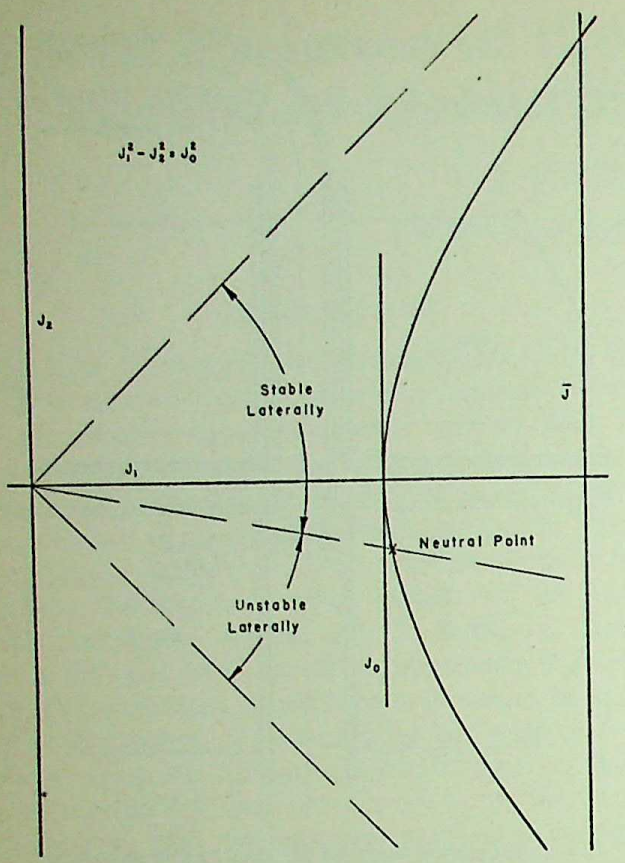


FIG. 2. J_1, J_2 characteristic of magnetically suspended sphere of high permeability.

range in which J_1 is not greater than $\bar{J}$. The coils must, of course, be so designed that J_0 is definitely less than $\bar{J}$.

When $J_1=\bar{J}$, $J_2=\pm(\bar{J}^2-J_0^2)^{\frac{1}{2}}$, and by the first of Eqs. (2),

$$H=k_0[\bar{J}\pm(\bar{J}^2-J_0^2)^{\frac{1}{2}}]. \tag{10}$$

The larger of these values of H is the magnetizing intensity to which the sphere is exposed when at the upper end of the observational range, and the smaller that to which it is exposed when at the lower end. Designating these H_2 and H_1, respectively, the range of values of H allowed by the current-carrying capacity is

$$H_2-H_1=2k_0(\bar{J}^2-J_0^2)^{\frac{1}{2}}. \tag{11}$$

By (7) the corresponding range of magnetic moment is

$$M_2-M_1=2k_0r^3(\bar{J}^2-J_0^2)^{\frac{1}{2}}. \tag{12}$$

The change in angular velocity is

$$w_2-w_1=\rho(M_2-M_1)/I, \tag{13}$$

where ρ represents the gyromagnetic ratio of the sphere and I its moment of inertia. Writing $I=(8\pi/15)dr^5$ and using (12), the expression for the change in velocity becomes

$$w_2-w_1=\frac{15k_0\rho}{4\pi d}\frac{1}{r^2}(\bar{J}^2-J_0^2)^{\frac{1}{2}}. \tag{14}$$

Other circumstances being the same, the change in angular velocity is inversely proportional to the square of the radius which, as it turns out, puts a premium on using as small a sphere as possible.

Equation (14) is an expression for the change in angular velocity which could be produced in an infinitely permeable sphere if the range of observation were limited by the current-carrying capacity of the coils alone. There is, however, another limitation.

A necessary condition for observing changes in velocity is, naturally, that the sphere remain on the axis—that it have lateral stability. There is always some part of the characteristic hyperbola (Fig. 2) over which this condition is not met. This may overlap the otherwise available range of observation, or even engulf it completely, depending on the design of the coils. The condition for lateral stability is that the quantity

$$F=(H'^2-2HH''), \tag{15}$$

which is a factor in the lateral force constant, be negative. In terms of the current densities

$$F=k_1^2(J_1-J_2)^2-2k_0k_2(J_1+J_2)^2. \tag{16}$$

When F is equal to zero the equilibrium is neutral. In this case (16) can be reduced to read

$$\frac{J_2}{J_1}=\frac{k_1\pm(2k_0k_2)^{\frac{1}{2}}}{k_1\mp(2k_0k_2)^{\frac{1}{2}}}. \tag{17}$$

There will be no real ratio J_2/J_1 for which the equilibrium is neutral, and, consequently, no part of the hyperbola over which the equilibrium is stable, unless $(2k_0k_2)$ is positive, and this is not necessarily the case. We assume that the coil has been so designed that the condition is satisfied. Equation (17) then represents two straight lines through the origin of the J_1, J_2 diagram, Fig. 2. One, and only one, of these intersects the hyperbole. There is, thus, only one pair of values J_1 and J_2, for which the sphere is stable longitudinally and neutral laterally. The part of the hyperbola on one side of this unique point is the region in which the lateral equilibrium is stable; the part on the other side is that in which the equilibrium is unstable. It can be argued from (9) and (16) that the stable region is that *above* the neutral point. The part of the hyperbola available for observations is, thus, that portion of the range allowed by current-carrying capacity which lies above the neutral point. This may be all, a part only, or none of this latter range, depending on the design of the coils and their separation.

The case here examined is that in which the permeability of the sphere is 10^3 or greater for all available values of H. If the permeability is low, but independent of H, the characteristics are the same as in the case of high permeability except for an increase in the value of J_0. As the permeability decreases J_0 approaches $\bar{J}$, the observational range becomes shorter, and at some permeability greater than 1 vanishes. The increase in J_0 with lowering permeability is not, however, as marked as might be expected. J_0 for permeability 10, for

CC-0. In Public Domain. Gurukul Kangri Collection, Haridwar

Digitized by Arya Samaj Foundation Chennai and eGangotri

example, is only 15 percent greater than for permeability infinite. If the permeability is not high and not independent of H, the characteristic is no longer a rectangular hyperbola, and if the specimen is hysteretic the characteristic is no longer single valued in J_1. But neither of these circumstances, nor the presence of residual magnetization, have any effect on the validity of Eq. (5) on which the measurement of gyromagnetic ratios is based.

IV. APPARATUS

(1) The Coil System

Parts of the coil system which have been built to try the new method of measuring gyromagnetic ratios are shown in cross section in Fig. 3. Described in polar coordinates with the center of the system as origin, the outer boundary of the coil is the surface

$$r=(27/4)^{\frac{1}{4}}\bar{r}\sin\theta\cos^{\frac{1}{2}}\theta, \tag{18}$$

where $\bar{r}$ = maximum extension = 15.75 cm.

The inner boundaries are

(a) a cylinder, $r=a/\sin\theta$, where $a=1.27$ cm, (19)

and

(b) a plane, $r=(1/2)^{\frac{1}{4}}a/\cos\theta$. (20)

The constant k_1 of the second of the Eqs. (2) is greater for this coil than for any other having the same inner boundaries and the same cross-sectional area. It was thought, erroneously, that coils of this form would produce the greatest change in the angular velocity of a given sphere. The error was recognized while the coils were being built, but the work was carried on to completion nevertheless.

The frame on which the coils are wound is of brass and is accurately machined. The central member is a 1-inch tube with $\frac{1}{8}$-inch walls. The plates which maintain the plane boundaries are $\frac{1}{8}$ inch thick and are separated by spacers—a central ring spacer integral with the tube and others further out. Ports cut through the ring spacer and tube afford views of the sphere from four directions. Fixed and temporary forms were used to give the coils the prescribed form. The wire is No. 25 (USG) plain enamel copper. The winding was done on a lathe with a counter to keep track of the turns. The finished structure, including end-plates not previously mentioned, is bolted together on four $\frac{1}{2}$-inch rods. Thin outer cylinders attached to the appropriate plates complete a reservoir about each of the coils, and these, when the structure is mounted, are filled with transformer oil—otherwise there is sparking.

The constants of the first three of the Eqs. (2), found by appropriate integrations over the cross section, are

$$k_0=4.54,\quad k_1=1.10,\quad k_2=0.313.$$

The number of turns per cm², N, is 408.

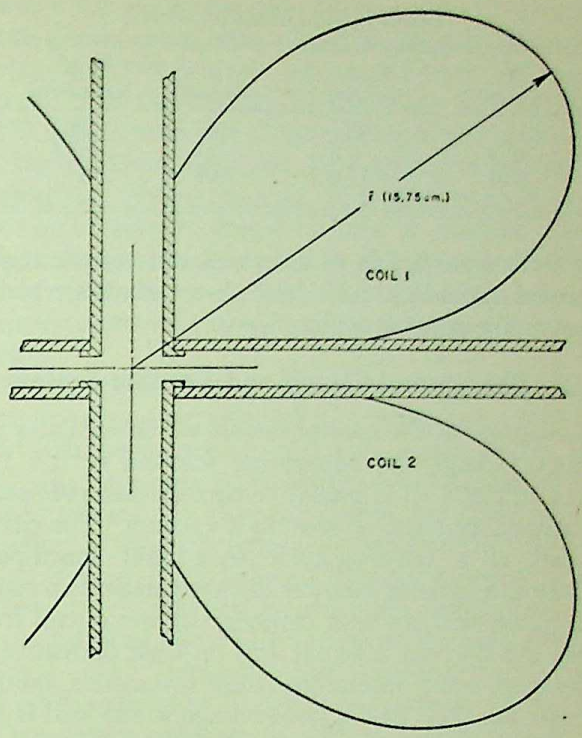


FIG. 3. Cross section of experimental coil system.

Substituting these values of the k constants into (17) one finds that the lateral equilibrium should be neutral when

$$J_2/J_1=-0.19.$$

The line which this equation represents in Fig. 1 intersects the hyperbole at the point marked X. The part of the hyperbola available for observation is from this point upward to the limit set by the current-carrying capacity of the coils. The range includes the point J_0, 0 at which the sphere is supported by the upper coil alone. Substituting in Eq. (9) one finds for iron

$$J_0=80.4 \text{ amp/cm}^2.$$

For this value of J_0 the coordinates of the neutral point are

$$J_1=\ \ 81.2 \text{ amp/cm}^2,$$
$$J_2=-15.6 \text{ amp/cm}^2.$$

Assuming the current-carrying capacity to be 125 amp/cm (it is known to be somewhat higher than this) the coordinates of the upper limit of the range of observations are

$$\bar{J}=J_1=125 \text{ amp/cm}^2,$$
$$J_2=(\bar{J}^2-J_0^2)^{\frac{1}{2}}=95.7 \text{ amp/cm}^2.$$

Equations (2) for H and H' can now be evaluated for the three J_1, J_2 points just considered. The results are given in the following table.

The total available change in H is 694 oersteds. Less than 10 percent of this change occurs in the part of the observational range in which J_2 is negative. Not much is gained by entering this part of the range, particu-

CC-0. In Public Domain. Gurukul Kangri Collection, Haridwar

Digitized by Arya Samaj Foundation Chennai and eGangotri

TABLE I. Field characteristics.

J_1 amp/cm²	J_2 amp/cm²	H oersteds	H' oersteds/cm
125	95.7	1002	32.2
80.4	0.0	365	88.4
83.4	−15.8	308	107

larly as it is advisable to keep well clear of the region of lateral instability. As a rule, observations are terminated at the point at which $J_2=0$.

(2) The Control Circuit and Vacuum System

A diagram of the control circuit which regulates the current through the supporting solenoid or coil 1 is shown in Fig. 4. It is similar to circuits used previously for supporting small spheres in a vacuum.[6] The circuit consists of a ten-megacycle tuned-grid tuned-plate oscillator, a cathode follower detector stage, two stages of amplification, another cathode follower circuit from which are derived a signal and its time derivative, a mixer stage which recombines these two signals, another cathode follower, and a power stage whose load is the support coil 1. The impedance of the pick-up coil L_1 is increased or decreased as the sphere moves down or up, and hence the tuning and amplitude of the oscillator depends upon the vertical position of the sphere. As a result, the circuit may be adjusted in such a way that the current in coil 1 is increased if the sphere moves downward and decreased if it rises. These current changes are adjusted so that the sphere is maintained accurately in the desired vertical position without "hunting." It will be observed from Fig. 4 that this is accomplished by introducing a derivative or "anti-hunt" along with the signal from L_1. When the circuit is properly adjusted, the vertical and horizontal stability of the freely suspended sphere is such that no motion can be observed with a 50-power microscope focused on scratches on the sphere. Coil 1 and coil 2 each consisted of 40,308 turns of no. 25 copper wire. The remaining values of the components of the circuit are given in Fig. 4.

The vacuum system is of glass except for a sealing wax joint and a black Bakelite support for the coil L_1. It is evacuated with a standard forepump, diffusion pump cold trap combination. The system contains both a McLeod and an ionization gauge. The drag on the rotating sphere resulting from air friction is given[6] by

$$\log_e N/N_0 = -5p/rd(M/2\pi RT)^{\frac{1}{2}}(t-t_0),$$

where N_0 is the number of rps at the time t_0, N is the number of rps at time t, p is the pressure in dynes/cm², d is the density of the sphere, T is the absolute temperature, M is the molecular weight of the gas, r is the radius of the spherical rotor, and R the gas constant. The working pressure is 10^{-6} mm of mercury or less, so for a 0.5 mm diameter sphere $N/N_0 = \exp[-4.8\times10^{-7}(t-t_0)]$, which is a very small correction.

V. THE CHANGE IN ANGULAR VELOCITY

To arrive at an estimate of the change in angular velocity that can be produced with the present coil system we rewrite Eq. (5) in the form

$$(w_2-w_1)=5g/2r^2(1/H_2'-1/H_1')$$

and evaluate for the case of a highly permeable sphere taken from state 1 in which $J_1=J_0$ to state 2 in which $J_1=\bar{J}$. As gyromagnetic ratio we take the base value

$$\rho=m/e=1/(1.76\times10^7).$$

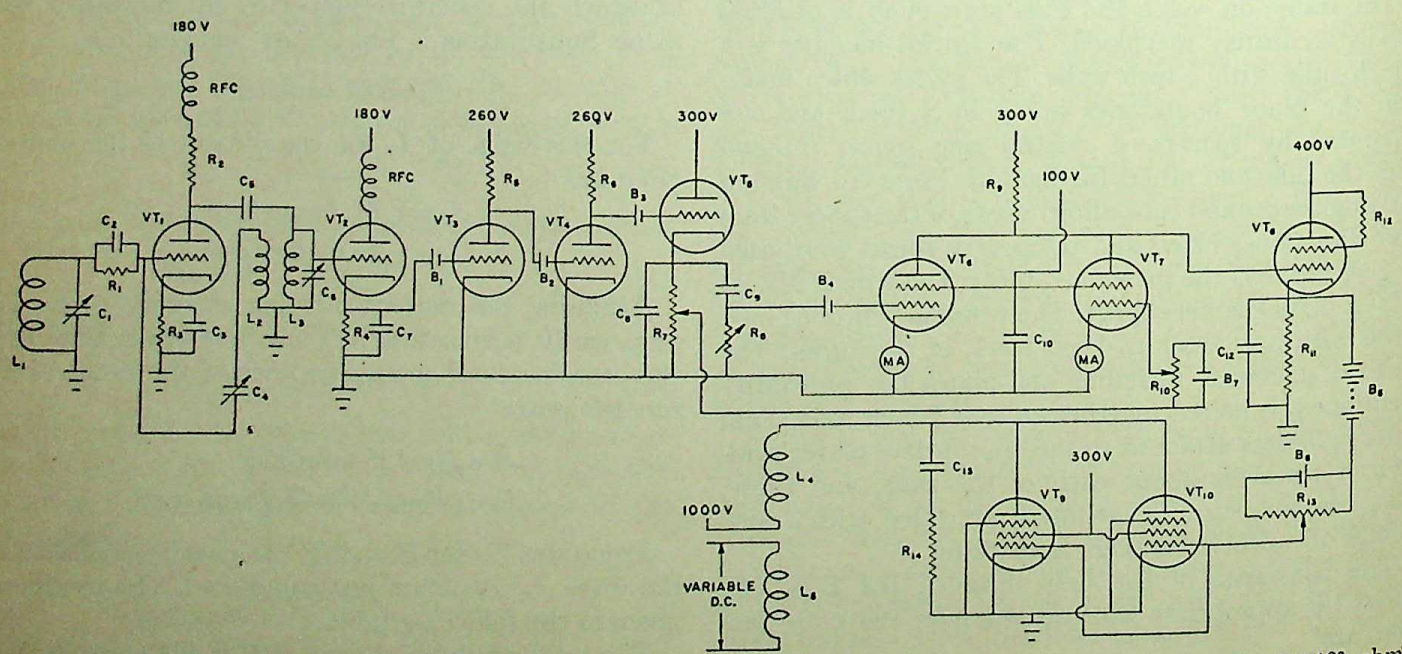


FIG. 4. Control circuit. $R_4=R_5=R_6=R_7=10^5$ ohms; $R_9=R_{10}=R_{13}=5\times10^4$ ohms; $R_{12}=R_{14}=2\times10^4$ ohms; $R_3=2\times10^2$ ohms; $R_1=8\times10^3$ ohms; $R_2=7.5\times10^4$ ohms; $R_{11}=5\times10^3$ ohms. $C_5=C_7=C_8=0.004$ mf; $C_{10}=C_{13}=0.5$ mf; $C_2=0.0025$ mf; $C_3=0.01$ mf; $C_9=0.1$ mf max (variable); $C_{12}=0.05$ mf. $VT_1-VT_2-VT_3-VT_4-VT_5-6J5$; VT_6-VT_7-6SJ7; VT_8-6L6; $VT_9-VT_{10}-813$. $B_1=28$ v; $B_2=157.5$ v; $B_3=90$ v: $B_4=9.5$ v; $B_7=45$ v; $B_5=45$ V; $B_6=180$ v.

CC-0. In Public Domain. Gurukul Kangri Collection, Haridwar

Digitized by Arya Samaj Foundation Chennai and eGangotri

Using the values of H' given in Table I we find that for

$2r = 1.0\text{ mm} = 0.1\text{ cm}$ $(w_2 - w_1) = 1.08 \times 10^{-3}\text{ rad/sec} = 3.89\text{ rad/hr}$,

$2r = 0.5\text{ mm}$ $(w_2 - w_1) = 15.6\text{ rad/hr} = 2.48\text{ rphr}$,

$2r = 0.25$ $(w_2 - w_1) = 9.90\text{ rphr}$.

VI. THE EXPERIMENTAL PROCEDURE

The experiment is begun with the sphere resting on a small platform several mm below the center of the system. The current in the lower coil is raised to about 100 amp/cm². The effect of this is to press the sphere more tightly against the platform. The current in the upper coil is then raised to 100 amp/cm². The sphere is now strongly magnetized but no force is exerted on it by the field, since H' is zero. It rests on the platform only under its weight. Next the current in the upper coil is raised to 110 or 115 amp/cm² and then increased slowly beyond this point. As this is done the point on the axis at which the sphere would be in quasi equilibrium longitudinally approaches the sphere from above. When the distance between the sphere and its equilibrium position has been reduced to about 1 mm the sphere springs upward and is locked in position by the servomechanism which controls the upper coil current. The sphere can now be raised by decreasing J_1 or lowered by increasing J_1. It may be touched back gently onto the platform to arrest any rotation it may have acquired at take-off, if it is desired to measure the increase of angular velocity from the zero value. Brought to the center, the sphere is in state 1 with w_1, zero or negligibly small. Measurements are made of the currents in the two coils to be used later in calculating H_1'.

The sphere is now brought by steps into state 2, that in which $J_2 = 0$. Decreasing J_1 raises the sphere, as has been mentioned, but decreasing J_2 lowers it. By decreasing first one and then the other of these currents by small amounts, the system is brought into state 2 with the sphere having been held constantly in suspension at or near the center. The current in the upper coil is measured for use in calculating H_2', and measurement is made of the angular velocity of the sphere. So far the velocity measurement has been based on visual observations and timing with a well regulated watch. The sphere is viewed through a low power microscope at magnification $\times 10$. It has not been found necessary to supply the sphere with fiducial marks. There have always been enough tiny specks and fine scratches on the spheres to serve this purpose.

VII. PRELIMINARY EXPERIMENTAL RESULTS

The present apparatus was constructed for the purpose of testing the method and ferreting out the various sources of error rather than for obtaining ultimate accuracy of measurement. As a result, only order of magnitude values have been obtained. Ball bearing steel spheres 0.75 mm, 0.55 mm, and 0.50 mm have been used in the experiment because they are commercially available and are supposed to be spherical and homogeneous. The spheres were stably suspended when the current in the upper coil was varied from 195 milliamperes with the current in the lower coil at zero, to 370 milliamperes when the current in the lower coil was about 300 milliamperes. This current range can be extended by cooling the coils. It is clear from Table I that smaller spheres should be used in order to obtain higher angular velocities, but it is only recently that we have perfected a method similar to that of Bond[7] for making accurate metal spheres down to 0.2 mm in diameter.

Two principal sources of trouble have developed which have greatly retarded the work but which no doubt can be overcome in future experiments. The first is the development of electrostatic charges on the walls of the vacuum chamber and on the small sphere. The effect of these charges while small on the 0.75-mm sphere is very disturbing on smaller spheres. These electrostatic charges are probably the result of several causes including the photoelectric effect produced by the light which illuminates the rotor and walls of the vacuum chamber, the friction of the rotor on the bottom of the vacuum chamber, as well as the friction of air currents around the vacuum chamber generated by heating of the coils. The effect has been markedly reduced by light filters (including water), but it may be necessary to use new materials for the vacuum chamber in order to completely eliminate it. The second trouble arises from the fact that a hard steel sphere, usually, is not magnetically homogeneous. This gives rise to a small oscillation about the axis of rotation of a suspended sphere rather than a uniform rotation when an extremely small torque is applied and of course reduces the accuracy of the angular velocity measurements and, if conducting material is very close by, perhaps introduces some drag. Two methods of correcting this difficulty have been found effective. The first consists in spinning the rotor to a high rotational speed and then bringing it to rest before the measurements are made. This reduces the effect, but is difficult to carry out with the present experimental arrangement. The second method consists in heat treating the metal sphere until it is as magnetically "soft" as possible. However, the final solution to this problem will probably be best secured by making the spheres of magnetically soft homogeneous material followed by heat treatment.

Spherical samples have been used in the present experiments because the calculations are greatly simplified. However, suspended long ellipsoids of revolution or rods should give rise to greater angular velocities than spheres with comparable radii. Also, the magnetism can more easily be made homogeneous. These favorable factors no doubt will more than compensate for the more detailed calculations necessary. As pointed

[7] W. L. Bond, Rev. Sci. Instr. 22, 344 (1951).

CC-0. In Public Domain. Gurukul Kangri Collection, Haridwar

Digitized by Arya Samaj Foundation Chennai and eGangotri

out previously, results to date are not as reliable as those obtained by other methods referred to above, but they show that the method ultimately should give a precision limited only by the accuracy with which the coils can be wound.

VIII. THEORY AND PRACTICE

In theory, the present scheme of measuring gyromagnetic ratios is simpler and less subject to disturbances than those previously used. The field acts to bring the magnetic axis of the sphere into coincidence with its own axis and, since all diameters of the sphere are mechanical axes, the magnetic and mechanical axes coincide, no matter in what diameter the magnetic axis happens to lie. Thus the ideal experimental conditions, which are realized only at the cost of much time and effort in the rod and fiber experiments, are set up automatically. There is a certain advantage also in having the measurement based on the determination of a uniform angular velocity rather than on the determination of the amplitude of a swing or a vibration.

However, in practice, as has been noted above, the behavior of the system is less simple than was anticipated. The fact that the sphere occasionally flies from the axis to the wall of the enclosure or sticks to the bottom of the vacuum chamber is a serious disturbance which must be eliminated, but it is extraneous and not chargeable to the theory of the measurements. The other unexpected behavior, which has been mentioned—that the angular velocity is not uniform, and may in certain circumstances degenerate to an oscillation—is more fundamental. It is natural to surmise that this is the result of the sphere acting as a compass in the horizontal component of the earth's field. This component has not as yet been compensated, so that this explanation has not been definitely ruled out. It is thought, however, that the trouble lies elsewhere. It is assumed in the theory that the sphere is magnetically homogeneous, that it contains a uniform distribution of permeability. If this condition does not obtain, a disturbance of the kind that is observed may be expected. The sphere may be thought of as having "a center of permeability." In the ideal specimen this is at the center of the sphere, but whether it is at the center of the sphere or not, it is the "center of permeability," and not the center of gravity, that the field holds to its axis. It can be seen, by considering an extreme case of non-uniformly distributed permeability, that, owing to a distorted demagnetizing field, the magnetic axis will make an angle with the axis of the field. The gyromagnetic torque acts about the magnetic axis which remains fixed. A consequence is that as the sphere rotates about its magnetic axis, its center of gravity is displaced vertically. It is this that gives rise to the oscillations. It is an essential condition for the success of the measurements that the specimen be both accurately spherical and magnetically homogeneous. Efforts are being made, as described above, to meet this condition.

CC-0. In Public Domain. Gurukul Kangri Collection, Haridwar

Digitized by Arya Samaj Foundation Chennai and eGangotri

REVIEWS OF MODERN PHYSICS VOLUME 25, NUMBER 1 JANUARY, 1953

The Ferromagnetic Faraday Effect at Microwave Frequencies and its Applications

C. L. HOGAN

Bell Telephone Laboratories, Murray Hill, New Jersey

INTRODUCTION

IN his analysis of the ferromagnetic resonance phenomenon, Polder[1] showed that the rf permeability of an infinite saturated ferromagnetic material is not a scalar quantity as it has been ordinarily assumed. He showed, in fact, that the alternating flux density in a saturated ferromagnetic medium is related to the alternating field by a tensor permeability. If the medium is saturated in the z direction, this relation can be written as

$$\mathbf{b}=T_{ij}\mathbf{h}, \tag{1}$$

where $\mathbf{b}$ = alternating component of the flux density, $\mathbf{h}$ = alternating component of the magnetic field, and the tensor T_{ij} has the following form:

$$T_{ij}=\begin{vmatrix} \mu & -j\kappa & 0 \\ +j\kappa & \mu & 0 \\ 0 & 0 & 1 \end{vmatrix}. \tag{2}$$

This solution can be derived from the equation of motion of magnetization,

$$\frac{d\mathbf{M}}{dt}=\gamma(\mathbf{M}\times\mathbf{H})-\lambda\left[\frac{(\mathbf{H}\cdot\mathbf{M})\mathbf{M}}{M^2}-\mathbf{H}\right], \tag{3}$$

where $4\pi\mathbf{M}$ = magnetization of medium (gauss); $\mathbf{H}$ = internal magnetic field (oersteds); λ = parameter which measures magnitude of damping force on the precessing dipole moment of ferromagnet; and γ = gyromagnetic ratio of the electron ($\gamma=ge/2mc$ where g is the Landé factor for the electrons concerned).

If a harmonic time dependence, $\exp[j\omega t]$, is assumed for the alternating magnetic field and magnetization, and if it is assumed that the alternating components of the magnetic field are small compared to the dc field applied along the z axis, it can be shown that Eqs. (1) and (2) follow directly from Eq. (3), where

$$\mu=\mu'-j\mu'' \tag{4}$$

$$\kappa=\kappa'-j\kappa'' \tag{5}$$

and

$$\mu'=1+\frac{[\gamma^2H_0^2-\omega^2][4\pi M_z\gamma^2H_0\chi_0^2]+8\pi\omega^2\lambda^2\chi_0}{\chi_0^2[\gamma^2H_0^2-\omega^2]^2+4\omega^2\lambda^2} \tag{6}$$

$$\kappa'=\frac{4\pi M_z\gamma\omega\chi_0^2[\gamma^2H_0^2-\omega^2]}{\chi_0^2[\gamma^2H_0^2-\omega^2]^2+4\omega^2\lambda^2}, \tag{7}$$

$$\mu''=\frac{4\pi\lambda\omega\chi_0^2[\gamma^2H_0^2+\omega^2]}{\chi_0^2[\gamma^2H_0^2-\omega^2]^2+4\omega^2\lambda^2}, \tag{8}$$

$$\kappa''=\frac{8\pi\omega^2\gamma\lambda H_z\chi_0^2}{\chi_0^2[\gamma^2H_0^2-\omega^2]^2+4\omega^2\lambda^2}, \tag{9}$$

where $H_0=H_z[1+(\lambda^2/\gamma^2M^2)]^{\frac{1}{2}}$ (oersteds), H_z = internal magnetic field in z direction (oersteds), and χ_0 = static susceptibility $(M_z)/(H_z)$.

If an infinite plane electromagnetic wave is propagated through a ferromagnetic medium which is saturated in the z direction, it is necessary, in order to describe this wave, to find a solution to Maxwell's equations which is compatible with Eq. (1), and in which b, h, E, and D are all proportional to $\exp[j\omega t-\Gamma(\mathbf{n}\cdot\mathbf{r})]$, where $\mathbf{n}$ is a unit vector in the direction of propagation of the wave and Γ is the propagation constant of the wave. It can be shown that for any given value of the angle θ between $\mathbf{n}$ and the z axis there are two values for the propagation constant which are given by

$$\Gamma_{\pm}=\frac{j\omega(\epsilon)^{\frac{1}{2}}}{c}\left[\frac{(\mu^2-\mu-\kappa^2)\sin^2\theta+2\mu\pm[(\mu^2-\mu-\kappa^2)^2\sin^4\theta+4\kappa^2\cos^2\theta]^{\frac{1}{2}}}{2[(\mu-1)\sin^2\theta+1]}\right]^{\frac{1}{2}}, \tag{10}$$

where $\epsilon=\epsilon'-j\epsilon''$ = complex dielectric constant of medium, c = velocity of light in free space, and ω = angular frequency of wave. The propagation constant of an infinite plane wave through a medium described by a scalar permeability and dielectric constant is

$$\Gamma=j\omega/c(\epsilon\mu)^{\frac{1}{2}}. \tag{11}$$

Hence it is possible to define the quantity which appears in the second radical of Eq. (10) as the effective permeability which the ferromagnetic medium exhibits to the particular wave whose direction of propagation is given by the angle θ and whose polarization is determined by the choice of the signs in Eq. (10). It is convenient to define this quantity as an effective wave permeability since it also occurs in the equations for intrinsic impedance, skin depth, etc., in the place usually occupied by the permeability. It is important at this point to stress that the permeability of a ferromagnetic medium does not have a unique meaning

[1] D. Polder, Phil. Mag. 40, 99–115 (1949).

CC-0. In Public Domain. Gurukul Kangri Collection, Haridwar

Digitized by Arya Samaj Foundation Chennai and eGangotri

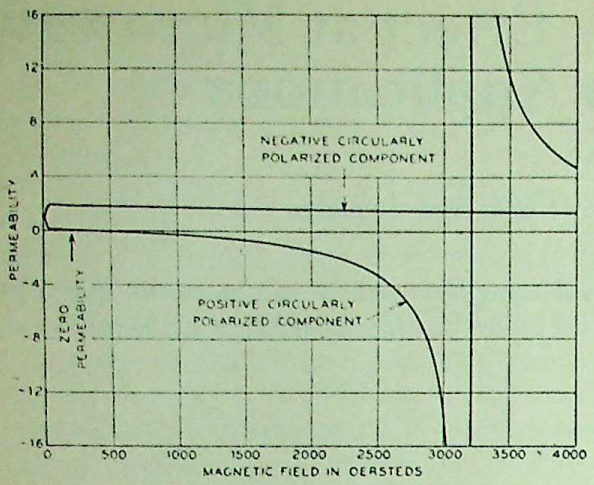


FIG. 1. Real part of the effective permeability of a ferromagnetic medium which is magnetized parallel to the direction of propagation of an infinite plane wave. The curves are computed for a medium whose saturation moment $4\pi M_s = 3000$ gauss and for a wave whose frequency is 9000 megacycles. $\mu_{DC} = 100$.

unless it is carefully defined. When permeabilities of ferromagnetic materials are determined by wave guide or coaxial techniques, the quantity that is determined is an effective wave permeability such as that which occurs in Eq. (10). In a demagnetized sample one actually obtains an average of this quantity over the various domains which constitute the sample in question. Hence at frequencies at which the tensor permeability as defined in Eq. (1) is important, it is obvious that experiments which are designed to measure the tensor components have much more significance than experiments which give some statistical average of the effective wave permeabilities exhibited by the individual domains of a demagnetized sample.

There are two cases of special interest with respect to wave propagation through a saturated ferromagnetic material. The first case is propagation along the z axis. It can be easily shown[2] that for this case the wave decomposes into positive and negative* circularly polarized components. The propagation constants for these two circularly polarized components follow from Eq. (10):

$$\Gamma_{\pm} = j\omega/c[\epsilon(\mu \mp \kappa)]^{\frac{1}{2}}. \tag{12}$$

The effective wave permeabilities for these circularly polarized components can be thus defined as

$$\begin{aligned} \mu_{\text{eff}}^{+} &= \mu - \kappa \\ \mu_{\text{eff}}^{-} &= \mu + \kappa. \end{aligned} \tag{13}$$

The complete expression for these effective permeabilities can be obtained by inserting Eqs. (4), (5), (6), (7), (8) and (9) into Eq. (13). If the effect of damping is neglected in the real part of the permeabilities given by (13), and if the small difference which exists between H_0 and H_z is neglected, these expressions can be written as

$$\mu' \pm \kappa' = 1 + (4\pi M_z \gamma / \gamma H_z \mp \omega), \tag{14}$$

and

$$\mu'' \pm \kappa'' = \frac{4\pi\lambda\omega\chi_0^2[\gamma H_z \pm \omega]^2}{\chi_0^2[\gamma^2 H_z^2 - \omega^2]^2 + 4\omega^2\lambda^2}. \tag{15}$$

Equation (14) describes the real part of the permeability for positive or negative circularly polarized waves, and Eq. (15) gives the imagninary part of the permeability for these two waves. The permeabilities given in Eqs. (14) and (15) are plotted in Figs. 1 and 2 as a function of the magnetic field H_z. The graphs pertain to a wave whose frequency is 9000 Mc, and the constants chosen for the medium are typical of many ferrites. From Figs. 1 and 2 it is quite easy to predict the behavior of an infinite plane wave which is being propagated through a saturated ferromagnetic material in the direction of the applied magnetic field. In the first place, the wave will decompose into circularly polarized components which encounter different permeabilities and hence travel at different velocities. This will result in a rotation of the plane of polarization of the wave which will be directly proportional to the difference between the square roots of the two permeabilities. Thus, the rotation of the plane of polarization as a function of the applied field can be easily predicted from Fig. 1.

Figure 2 indicates that both circular components are only very slightly attenuated by the phenomenon of ferromagnetic resonance except in the vicinity of the absorption line which exists for the positive circularly polarized component only. When the frequency of the wave corresponds to the resonance frequency for the electrons, the positive circularly polarized wave should be very highly attenuated. If the path length through the ferromagnetic material is long enough, this component will be substantially completely absorbed and only the negative circularly polarized component will be propagated. An approximate formula for the absorption

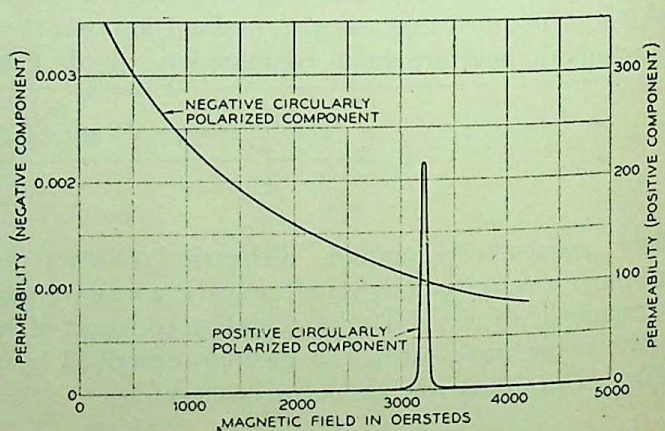


FIG. 2. Imaginary part of the effective permeability of a ferromagnetic medium which is magnetized parallel to the direction of propagation of an infinite plane wave. The constants chosen to compute the curves were the same as those in Fig. 1. In addition the relaxation frequency, λ, was arbitrarily taken as 1.9×10^7 for the curves.

[2] C. L. Hogan, Bell System Tech. J. 31, 1–31 (1952).

* The usual notation is used here, where the positive component is the component which is rotating in the direction of the positive electric current which creates the steady longitudinal field.

CC-0. In Public Domain. Gurukul Kangri Collection, Haridwar

Digitized by Arya Samaj Foundation Chennai and eGangotri

of the circularly polarized components by ferromagnetic resonance can be derived which is valid for the negative circularly polarized component at all field strengths and is valid for the positive circularly polarized component only in very weak fields. For a wave whose frequency is 9000 Mc and for a medium described by the constants given in Figs. 1 and 2 this formula reduces to

$$A=8.2(\epsilon')^{\frac{1}{2}}\frac{\mu''\pm\kappa''}{(\mu'\pm\kappa')^{\frac{1}{2}}}\text{db/cm}$$

(dielectric loss neglected). (16)

If it is assumed that the dielectric constant of the medium is 10, then this formula predicts a loss of approximately 0.4 db per cm for the positive component and 0.07 db per cm for the negative component when the applied field is just large enough to saturate the above sample (30 oersteds).

Figures 3 and 4 give experimentally measured values of the rotation of the plane of polarization and the absorption of the positive and negative circularly polarized components as a function of the applied magnetic field for the TE_{11} mode in a circular wave guide when a small cylinder of ferrite was placed along the axis of the wave guide and subjected to a longitudinal magnetic field. It is readily seen that these data agree qualitatively with the behavior predicted by Eqs. (14) and (15).

The angle of rotation of the plane of polarization is given by

$$\theta=\frac{l\omega}{2}\left[\frac{1}{v^-}-\frac{1}{v^+}\right], \tag{17}$$

where l=path length through ferromagnetic medium (cm); and $v_\pm$=velocity of propagation of positive and negative circularly polarized components, respectively. For the ferromagnetic medium discussed above this equation becomes

$$\frac{\theta}{l}=\frac{\omega}{2c}\left(\frac{|\epsilon|+\epsilon'}{2}\right)^{\frac{1}{2}}\times\left[\left(1+\frac{4\pi M_z\gamma}{\gamma H_z+\omega}\right)^{\frac{1}{2}}-\left(1+\frac{4\pi M_z\gamma}{\gamma H_z-\omega}\right)^{\frac{1}{2}}\right], \tag{18}$$

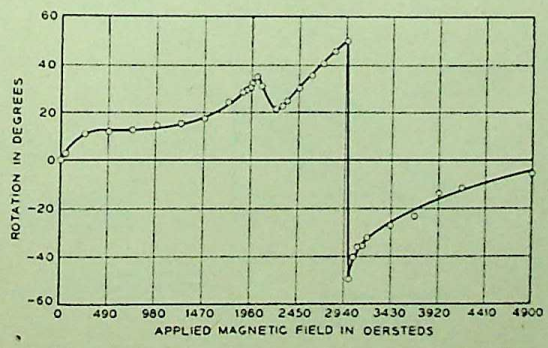


FIG. 3. Faraday rotation *versus* applied magnetic field for a thin "pencil" of nickel zinc ferrite supported along the axis of the wave guide. The minor resonance is believed to be a shape effect. The sample was a cylinder 0.123 in. diameter and 0.815 in. long. The data were taken at 9455 Mc.

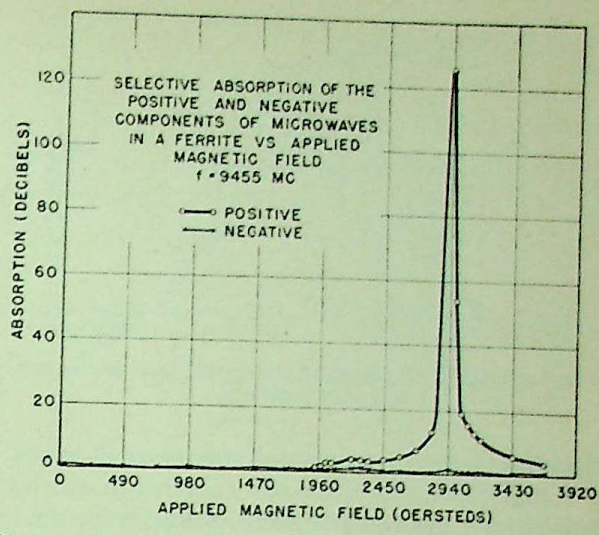


FIG. 4. Selective absorption of positive and negative circularly polarized waves when propagated over same sample as that of Fig. 3.

where $|\epsilon|=(|\epsilon'|^2+|\epsilon''|^2)^{\frac{1}{2}}$=absolute value of dielectric constant. Equation (18) will be valid only when the damping of the electrons in precessional motion can be neglected since it was derived from Eq. (14) where the damping parameter was set to zero. For ferromagnetic materials with absorption lines as narrow as that shown in Fig. 4 it is to be expected that Eq. 18 would be quantitatively valid everywhere except in the near vicinity of the absorption line.

Equation (18) can be reduced to a particularly simple form when the following approximations are valid:

$$\gamma H_z\ll\omega, \tag{19}$$

$$\frac{4\pi M_z\gamma}{\omega}\ll 1. \tag{20}$$

Under these conditions Eq. (18) can be written as

$$\frac{\theta}{l}=\frac{1}{2c}\left(\frac{|\epsilon|+\epsilon'}{2}\right)^{\frac{1}{2}}[4\pi M_z\gamma]. \tag{21}$$

Equation (21) is quite remarkable. It predicts large rotations in the presence of very small applied magnetic fields ($\gamma H_z\ll\omega$); it indicates that the rotation is directly proportional to the magnetization of the medium; and, when Eqs. (19) and (20) are valid, it predicts that the rotation will not depend upon the frequency of the incident radiation.

For the assumed values, $\epsilon'=10$, $\epsilon''=0$, $4\pi M_z=3000$ gauss, $\gamma=17.6\times10^6$ radians/sec/oersted.

Equation (21) predicts rotations of

$$\theta/l=160°/\text{cm}.$$

DESCRIPTION OF EQUIPMENT AND MEASURING TECHNIQUES

The Faraday rotation has been measured in a large number of ferrites in order to verify the above theory.

CC-0. In Public Domain. Gurukul Kangri Collection, Haridwar

Digitized by Arya Samaj Foundation Chennai and eGangotri

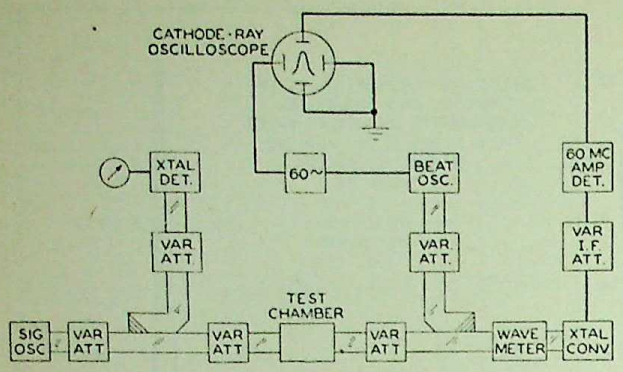


FIG. 5. Set-up of experimental equipment used to measure Faraday rotations.

A diagram of the experimental equipment is given in Fig. 5, and a diagram of the test chamber in which the rotations were measured is given in Fig. 6. In the test chamber, two rectangular wave guides are separated by a circular wave guide, the proper nonreflective transitions being made at each end of the circular section, which is about twelve inches long. One rectangular guide is supported so that it can be rotated about the longitudinal axis of the system. The dominant TE_{10} mode is excited in one rectangular guide, and by means of the smooth transition this goes over into the dominant TE_{11} mode in the circular guide. The rectangular guide on the opposite end will accept only that component of the polarization which coincides with the TE_{10} mode in that guide, the other component being reflected at the transition. Absorbing vanes, inserted in the circular section, absorb this reflected component. The circular guide is placed in a solenoid to establish an axial magnetic field along its length.

The ferrite cylinders to be measured were placed at the mid-section of the circular guide. When a cylinder was used which did not fill the cross section of the guide, it was supported along the axis of the guide by means of a hollow polystyrene cylinder which did fill the guide.

In addition to the Faraday rotation, measurements of insertion loss were made by determining the power transmitted under identical conditions with the ferrite cylinder removed, and the ellipticity of the transmitted wave was determined by measuring the power transmitted when the rectangular guide on the detector side was rotated both to positions of maximum and minimum transmission. Power transmission measurements could be repeated within 0.2 db. Measurements of the angle of rotation of the plane of polarization could be repeated within 0.5° except in the region close to the gyromagnetic resonance where rotations were large and ellipticity so great that it was difficult to determine the positions of maximum and minimum transmission. These errors increased up to the point where the transmitted wave was circularly polarized where it was impossible to measure the angle of rotation.

EXPERIMENTAL RESULTS

Equation (21) indicates that, in weak fields at least, the rotation per unit path length through the ferromagnetic material is proportional to the magnetization of the sample and is independent of the frequency of the wave. It is experimentally very difficult to obtain data to check the predictions of Eq. (21). In the first place, Eq. (21) was derived for an infinite plane wave and it is not to be expected that it will hold quantitatively for a guided wave. In fact, Suhl and Walker[3] have shown that in the case of small rotations (i.e., small rotation per wavelength) the rotation in a circular wave guide would be only about 86 percent of the rotation which would occur for an infinite plane wave. More recent work by Suhl and Walker,[4] has, however, indicated that large rotations in a circular wave guide would probably more nearly approach the rotation predicted by Eq. (21) for an infinite plane wave. In reality however, if the rotations are measured in a circular wave guide, the rotation to be expected will lie somewhere between the value predicted by Eq. (21) and 86 percent of that value. Hence, it is meaningless to claim a quantitative verification of Eq. (21) closer than these limits until a more complete analysis has been made.

The analysis of Suhl and Walker applies only to a circular wave guide whose entire cross section is filled with ferrite. If a cylinder of ferrite is used which completely fills the cross section of the wave guide, however, internal reflections within the sample produce an effective rotation, and an ellipticity which is different from that which would result if the wave passed through the ferrite only once. This effect is obviously frequency dependent since the electrical length of the sample changes with frequency. The effect of internal reflections can be reduced by using a ferrite which has a large dielectric loss. Some ferrites have such an extremely high dielectric loss that attenuations of the order of 50 db per centimeter path length can be obtained. Hence, in this type of ferrite, multiple reflections within the sample can be completely neglected even though the cross section of the wave guide is filled with the

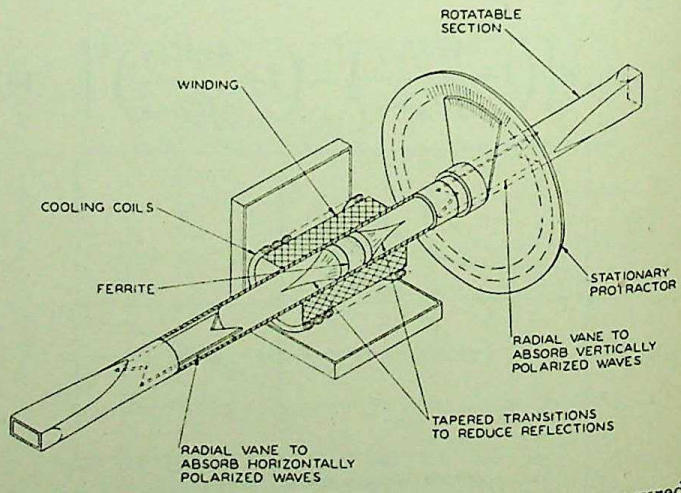


FIG. 6. Detail of test chamber in which rotations were measured.

[3] H. Suhl and L. R. Walker, Phys. Rev. 86, 122–3 (1952).
[4] H. Suhl and L. R. Walker, unpublished memoranda, Bell Telephone Laboratories.

CC-0. In Public Domain. Gurukul Kangri Collection, Haridwar

Digitized by Arya Samaj Foundation Chennai and eGangotri

ferrite and tapered transitions at the faces of the sample are eliminated.

Thus in order to obtain a quantitative check of Eq. (21), it is necessary that a ferrite have a high dielectric loss so that internal reflections can be avoided; it must have a relatively low magnetic anisotropy since anisotropy has been neglected in this analysis; and it must have a relatively low saturation moment so that the approximation expressed in Eq. (20) will be valid. It has been found possible to satisfy all these requirements in a particular manganese zinc ferrite which contained a small excess of iron over that required for perfect stoichiometry. This particular sample had the following measured properties:

$$\epsilon' = 17, \quad \epsilon'' = 24, \quad 4\pi M_{\text{sat}} = 1500 \text{ gauss}.$$

The rotation induced by this sample as a function of the applied magnetic field was measured, and the results are shown graphically in Fig. 7. The physical dimensions of the sample are given in Table I (sample No. 1). Figure 7 quite clearly shows the dependence of rotation upon the magnetization of the sample and indicates that, after the sample is saturated the rotation is sensibly independent of the applied magnetic field. This result verifies the work of Roberts[5] who has previously shown that the Faraday rotation induced in a round wave guide is proportional to the magnetization of the sample. In addition for this particular sample, Eq. (21) predicts

$$\theta/l = 121 \text{ degrees/cm}$$

for an infinite plane wave. As previously stated, Suhl and Walker have shown that the measured rotation in a round wave guide should be less than this and should probably lie somewhere between 104 degrees per centimeter and 121 degrees per centimeter for this particular sample. It is seen from Fig. 7 that the measured rotation at saturation is approximately 123 degrees per centimeter. It is felt that this agreement is good.

The above data seem to bear out Polder's theory of ferromagnetic resonance. A more complete check of his

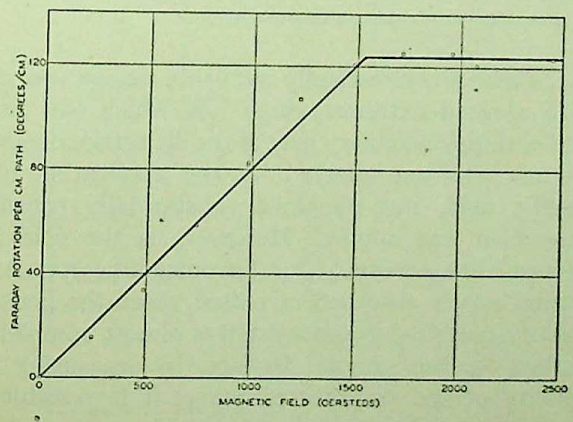


FIG. 7. Faraday rotation versus applied magnetic field for a thin disk of manganese zinc ferrite which completely filled cross section of wave guide.

[5] F. F. Roberts, J. phys. et radium 12, 305 (1951).

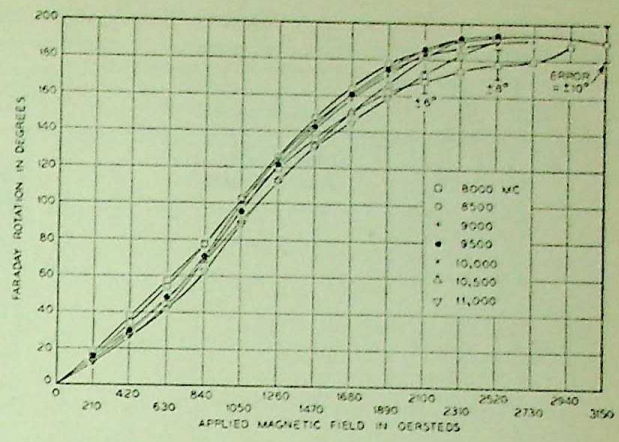


FIG. 8. Dependence of Faraday rotation upon frequency.

theory could, however, be obtained by measuring the rotation of the plane of polarization as a function of field up through the field required for resonance. Again, however, the wave guide introduces complications which are difficult to unravel. In the vicinity of ferromagnetic resonance the mode which exists in a wave guide completely filled with ferrite differs quite radically from the ordinary dominant mode in an empty guide. In addition, even if a wave guide is only partially filled with ferrite, it is possible for higher modes to exist to further complicate the picture. In order to overcome these difficulties it is necessary to place the ferrite along the axis of the wave guide in the form of an extremely thin pencil. If pencils of ferrite which are approximately 0.125 inch in diameter are placed in an ordinary X-band round wave guide (approximately one inch in diameter) results are obtained which are qualitatively in agreement with the theory developed for an infinite plane wave. If the diameter of the ferrite is increased to 0.250 inch the results are often not in accord with the above theory. Sometimes such samples show sudden increases in rotation soon after the magnetic field is raised above that required for saturation, as in the data Roberts has published. It has even been observed that a magnetized ferrite will not propagate the negative circularly polarized component although this ferrite might cause a relatively low loss to this particular wave when it is in a demagnetized state. There certainly is nothing in the above developed theory which will explain this phenomenon and this behavior must arise from the characteristics of the guided wave.

Since all ferrites which have been tested to date give data which are in complete agreement with the above theory when the ferrite is placed along the axis of the guide in the form of an extremely thin pencil and since quantitative agreement has been obtained for one carefully selected ferrite, it is believed that Polder's theory of ferromagnetic resonance is adequate to describe this phenomenon but considerably more work is necessary in order to understand the properties of wave guide modes in magnetized ferrites. A typical set of

CC-0. In Public Domain. Gurukul Kangri Collection, Haridwar

Digitized by Arya Samaj Foundation Chennai and eGangotri

TABLE I. Faraday effect for ferrites. Frequency = 9000 Mc.

Sample No.	Dimension (cm)	Applied magnetic field (oersteds)	Rotation/cm path	Insertion loss (db)	Ellipticity[a] db
No. 1	0.447×2.28 (length×diam.)	0	0	10.0	>50
		245	15.6	10.3	>50
		490	33.5	10.0	23.2
		735	58.2	9.2	15.0
		980	81.6	9.1	12.1
		1225	107	9.2	10.9
		1470	120	10.0	10.4
		1715	125	11.0	9.3
		1960	123	11.2	9.0
		2205	121	11.3	7.7
		2450	123	11.4	6.6
		2695	...	12.4	5.0
		2940	...	13.0	3.7
		3185	...	...	3.0
		3675	...	...	1.4
2	1.77×2.28	0	0	23.2	≫30.
		245	38	21.4	23.0
		490	77	16.7	7.6
		735	124	12.4	2.1
		980	157	9.9	1.4
		1225	170	7.7	0.7
		1470	180	6.0	0.7
		3430	183	7.1	0.0
3	5.08×0.32 (ends of cylinder tapered to a point)	0	0	<0.1	>50.
		215	4.0	0.1	50.
		430	5.0	0.1	50.
		645	5.1	0.1	50.
		860	5.6	0.1	50.
		1075	6.0	0.1	50.
		1290	7.0	0.1	50.
		1505	8.6		50.
		1720	10.8		50.
		1935	14.0		50.
		2150	20.4		27
		2365	16.8		10
		2580	4.0		9
		2795	−7.6		10
		3010	−12.0		
		3115	−12.8		
		3225	−13.2		26
		3440	−11.2		49
		3655	−9.2		>50
		3870	−7.6		>50
		4085	−6.0		>50
		4300	−5.0		>50
		4515	−4.2		>50
		4730	−3.8		>50

[a] Data given show the difference in db between the major and minor components of the elliptically polarized transmitted wave.

data taken on a thin pencil of ferrite is given in Figs. 3 and 4. Another set is given in Table I for a magnesium ferrite sample.

Figure 8 shows the rotation of the plane of polarization *versus* magnetic field for a cylinder of ferrite measured at several frequencies from 8000 to 11 000 megacycles per second. The rotation does not change appreciably for this change in frequency and it is believed that a large portion of this variation is associated with the properties of the guided wave and hence this particular data should not be applied too strictly as a check of Eq. (21) which was derived for an infinite plane wave.

The loss characteristics of different ferrites as a function of the applied magnetic field varied widely. Some, such as commercially available manganese zinc ferrite, showed extremely high loss which was associated with the imaginary part of the dielectric constant. This loss was not affected by the application of a magnetic field, but remained substantially constant as the field was applied. However, as the field approached that necessary for ferromagnetic resonance the total power absorbed increased, since the positive circularly polarized component was almost completely absorbed by the sample. In fact, by measuring the ellipticity of the transmitted wave, it is possible to compute the difference between the absorption of the positive and negative circularly polarized components. This has been done for the sample of nickel zinc ferrite which was discussed in connection with Figs. 3 and 4.

CC-0. In Public Domain. Gurukul Kangri Collection, Haridwar

Digitized by Arya Samaj Foundation Chennai and eGangotri

Figure 9 gives the ellipticity of the wave propagated through this sample as a function of the applied field and indicates how the wave becomes circularly polarized when the applied field is equal to that necessary for resonance. Figure 10 shows the total power absorbed by this material as a function of the applied field. It is to be noticed that the loss decreases as the sample is magnetized. For this particular sample this original loss is believed to be due to domain walls. Experiments are under way to verify this.

If, instead of propagating along the z axis, an infinite plane wave is propagated along the y axis, the propagation constant can be obtained by setting θ equal to $\pi/2$ in Eq. (10). This again gives two propagation constants:

$$\Gamma_- = j\omega(\epsilon)^{\frac{1}{2}}/c, \tag{22}$$

$$\Gamma_+ = \frac{j\omega}{c}\left[\epsilon\left(\frac{\mu^2-\kappa^2}{\mu}\right)\right]^{\frac{1}{2}}. \tag{23}$$

The first propagation constant refers to a wave which is polarized with its magnetic vector along the z axis and the other propagation constant is for a wave which is polarized with its magnetic vector along the x axis. Two very interesting results are apparent with respect to this second wave. In the first place, it is no longer completely transverse since there is a magnetic field along the y axis. The other interesting result is that the medium presents an effective permeability to this wave which is dependent upon the applied magnetic field in the z direction. The effective permeability is given by

$$\mu_{eff} = \frac{\mu^2-\kappa^2}{\mu} = \mu_{eff}' - j\mu_{eff}''. \tag{24}$$

Again, if damping is neglected, the real part of the above equation becomes

$$\mu_{eff}' = \frac{\gamma^2 B_z^2 - \omega^2}{\gamma^2 H_z B_z - \omega^2}, \tag{25}$$

where B_z = flux density in z direction ($B_z = H_z + 4\pi M_z$).

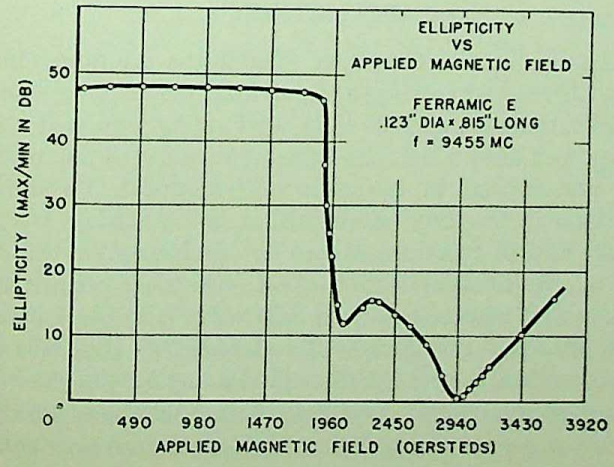


FIG. 9. Ellipticity of wave propagated through wave guide containing sample discussed in Figs. 3 and 4.

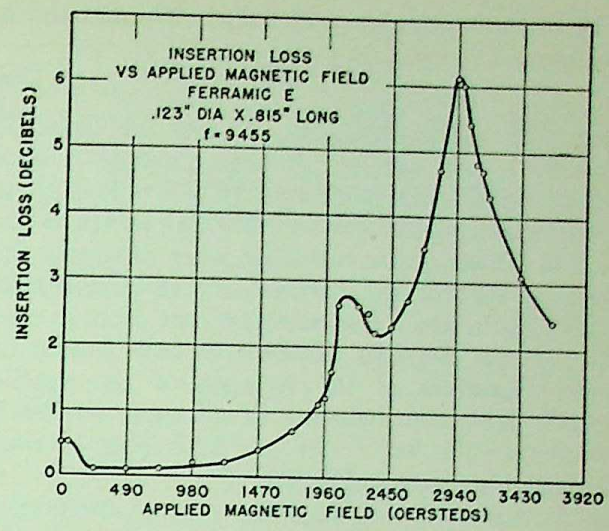


FIG. 10. Total insertion loss of wave under conditions referred to in Fig. 9.

Equation (25) is plotted as a function of the magnetic field, H_z, in Fig. 11 for a ferrite with the particular properties given. The curve applies to a wave whose frequency is 9000 Mc.

It will be noticed that at zero field the permeability is unity that it decreases rather rapidly toward zero in small fields. This part of the curve is actually a mirror image of the magnetization curve of the ferromagnet. The shape of this portion depends upon the dc permeability of the material. After the material saturates, the effective permeability curve levels out somewhat and is much less field dependent until the region of the resonance is approached. As indicated in Eq. (25) above, the effective permeability has a zero when $B_z = 3210$ gauss; this point may or may not come before saturation of the sample, depending upon whether the saturation magnetization is more or less than 3210 gauss. For the example taken, the zero occurs after the sample is saturated.

It is quite easy to preduct, from Fig. 11, the behavior of the dominant mode being propagated in a wave guide through a ferromagnetic medium under the above conditions.

At zero applied field, the wave sees a dielectric material with a permeability of unity and with an ordinary dielectric constant ($\epsilon = 6$ to 20 for ferrites at 9000 mc). As the field is gradually increased, the permeability of the medium approaches zero very rapidly. As the permeability approaches zero, the wavelength in the medium becomes longer and longer and obviously before a zero permeability is reached a phenomenon analogous to cutoff appears. However, since the propagation is in a lossy dielectric, the cutoff is not as sharp as in a lossless guide. Nevertheless, there should be a region when the permeability is close to zero where large reflections take place and very little power is propagated through a slug of ferrite which fills the guide.

CC-0. In Public Domain. Gurukul Kangri Collection, Haridwar

Digitized by Arya Samaj Foundation Chennai and eGangotri

The intrinsic impedance of a dielectric material is given by

$$Z=(\mu/\epsilon)^{\frac{1}{2}}, \tag{26}$$

where both the permeability, μ, and the dielectric constant, ϵ, are usually complex quantities. Some ferrites exist in which the imaginary part of both these quantities is negligibly small at 9000 Mc except in the region of ferromagnetic resonance when obviously the imaginary part of the permeability is large. Other ferrites exist in which the imaginary part of the permeability or the dielectric constant or both cannot be ignored regardless of the strength of the applied magnetic field. The behavior of all these ferrites is qualitatively the same and the differences between them are only matters of degree.

In particular, if the imaginary part of the permeability is negligible when the real part is zero, then the impedance of the ferromagnetic medium will be truly zero at this point regardless of the dielectric loss; and the medium will then have properties analogous to a material with infinite conductivity. A slug of ferrite should, under these conditions, completely reflect an incident wave. Ferramic I is a ferrite which satisfies the condition of having a negligible magnetic loss component at the point where the real part of the permeability is zero and this material can be made to almost completely reflect a microwave at this point. Other ferrites, such as Ferramic G, which have appreciable magnetic loss at all magnetic field strengths up to and beyond the field required for resonance, can never have a truly zero impedance and this should be evidenced by the fact that Ferramic G never can be made to be a perfect reflector. These predictions are substantiated by experiment.

When the field is increased beyond the resonance, it is possible to produce high effective positive permeabilities in the medium, and under some conditions it has been possible to make the effective permeability of the medium equal to the dielectric constant. Thus the intrinsic impedance of the ferrite was made equal to the intrinsic impedance of air. Under these conditions, no reflection from the ferrite slugs occurred and in fact some ferrite slugs have been made essentially completely transparent by this technique.

Data taken on a sample of Ferramic I are given in Table II. The data were taken at 9000 Mc by placing a cylinder of ferrite in a round wave guide.

It is interesting to compare this effect with that which leads to the Faraday rotation (longitudinal field). In the case of the longitudinal field, the wave splits into two circularly polarized components. The permeability of the negative circularly polarized component has no interesting behavior as a function of field. The permeability of the positive circularly polarized component, however, is qualitatively the same as the permeability shown in Fig. 11. Hence any effect which can be obtained in the transverse magnetic field can also be obtained with a longitudinal field if a positive circularly polarized wave is propagated rather than a linearly polarized wave. Thus it should be possible to produce circularly polarized waves by reflecting the positive component at the region of zero permeability rather than absorbing it in the region of ferromagnetic resonance. This prediction has been experimentally verified.

TABLE II. Data from sample of Ferramic I.

Applied magnetic field (oersteds)	Reflection coefficient E_r/E_i	Insertion loss (db)
Ferramic I (powdered cylinder—0.895-in. diam. ×0.38 in. long)		
0	···	7.4
1600	0.418	3.9
1700	0.335	4.1
2100	0.90	31.4—cutoff
2400	0.57	51.1—resonance absorption
3000	0.496	29.4
3800	0.571	7.7
4400	0.183	0.3—impedance match
Empty guide looking into matched load	0.170	···

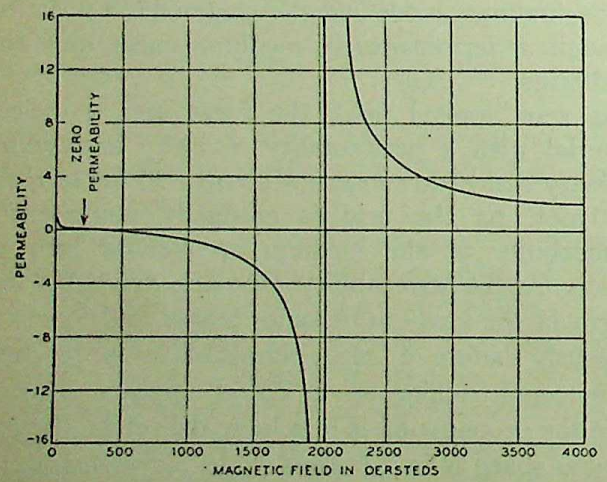


FIG. 11. Real part of the effective permeability of a ferromagnetic medium in which a magnetic field is applied parallel to the electric vector of an infinite plane wave. The curve applies to a wave frequency is 9000 megacycles being propagated through a medium whose saturation moment $4\pi M_s=3000$ gauss. $\mu_{DC}=100$.

APPLICATIONS

Applications of the above phenomena are numerous but the most interesting and potentially most important applications are derived from the Faraday effect. It has long been known that the Faraday rotation of the plane of polarization in optics is antireciprocal. Its antireciprocal property distinguishes the Faraday effect from optical rotations caused by birefringent crystals, or by the Cotton-Mouton effect, which are reciprocal. That is, if a plane polarized light wave is incident upon a birefringent crystal in such a manner that the plane of polarization is rotated through an angle θ in passing through the crystal then this rotation will be cancelled if the wave is reflected back through the crystal to its source. In the Faraday rotation, however, the angle of rotation is doubled if the wave is reflected back along

CC-0. In Public Domain. Gurukul Kangri Collection, Haridwar

Digitized by Arya Samaj Foundation Chennai and eGangotri

its path. Hence, if the length of path through the "active" material is adjusted so as to give a 90° original rotation, the beam on being reflected will have its plane of polarization rotated a total of 180° in passing in both directions through the material.

Lord Rayleigh[5] described a one-way transmission system in optics which makes use of the Faraday rotation. Lord Rayleigh's "one-way" system consisted of two polarizing Nicol prisms (oriented so that their planes of acceptance made an angle of 45° with each other), with the material causing the Faraday rotation placed between them. Thus, light which was passed by the first crystal and whose plane of polarization was rotated 45° would be passed by the second crystal also. But, in the reverse direction, the rotation would be in such a sense that light which was admitted to the system by the second crystal would not be passed by the first.

The antireciprocal property of the Faraday effect affords a means of realizing a microwave circuit element which is analogous to Tellegen's[6] gyrator. Such a gyrator is illustrated in Fig. 12 along with diagrams which help explain its action. Beneath the gyrator are construction lines which indicate the plane of polarization of a wave as it travels through the gyrator in either direction. On each diagram is a dotted sine wave for reference only which indicates the constant plane of polarization of an unrotated wave. It is noticed that for propagation from left to right in Fig. 12, the screw rotation introduced by the twisted rectangular guide adds to the 90° rotation given to the wave by the ferrite element making a total rotation of 180°. For a wave traveling in the reverse direction these two rotations cancel each other, producing a net zero rotation through the complete element. The unique property of the Faraday rotation becomes immediately apparent from this diagram. In the case of the rotation induced by the twisted rectangular guide, the wave rotates in one direction in going from left to right through the twisted section, and rotates in the opposite direction when it transverses the section from right to left. For the case of the rotation induced by the ferrite element, the direction of rotation is indicated by the arrow in the upper figure for either direction of propagation. The important characteristic of the element is the time phase relation between two points such as A and B in the upper diagram. It is seen with the help of the diagrams illustrating the rotating waves that the field variations are in phase at points A and B for propagation from left to right and they are 180° out of phase for propagation from right to left. In other words the transmission line is an integral number of wavelengths long between A and B for propagation from left to right and is an odd integral number of half-wavelengths long for propagation from right to left.

[5] Lord Rayleigh, Nature 64, 577 (1901).
[6] B. D. H. Tellegen, Philips Research Reports, 3, 81–101 (1948).

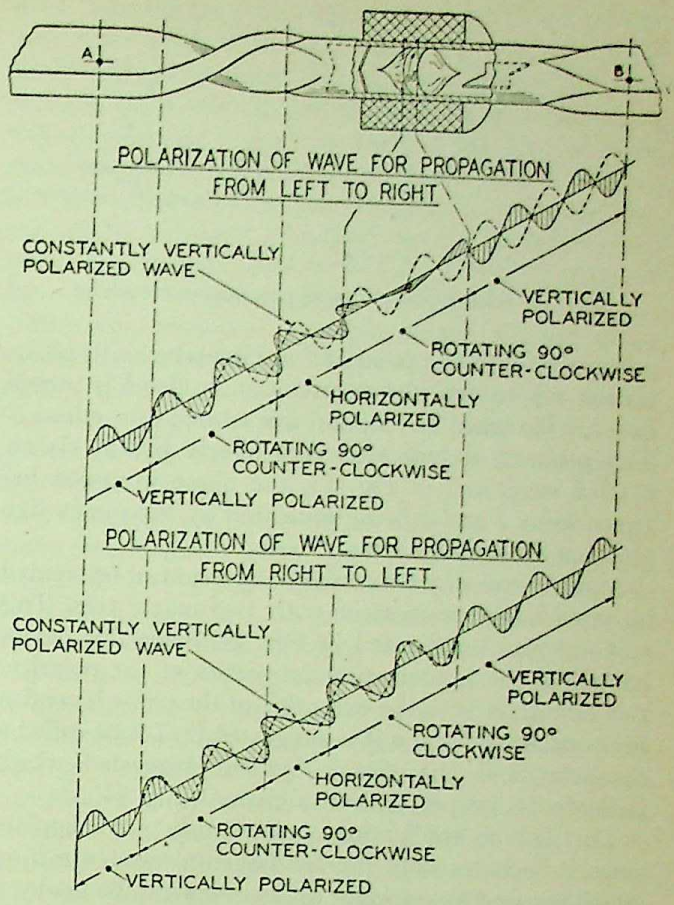


FIG. 12. The microwave gyrator with diagrams which help to explain its action.

If the rectangular wave guides on each side of the ferrite are rotated about their common axis so as to make an angle of 45° with each other, then a one-way transmission system can be created which is similar to Lord Rayleigh's one-way transmission system of optics. It is, however, probably more useful, for within the validity of the above analysis, this one-way transmission system does not depend upon frequency but is broad band. This one-way transmission system can be used, for example, to isolate the generator or detector from the wave guide in microwave systems. In this application it has the great advantage over the attenuators which are presently used for this purpose in that it can be made practically lossless for the direction of propagation which is desired but the reflected wave will be completely absorbed and hence more complete isolation can be effected.

It is suggested that this device which makes use of the 45° rotation be called a *polarization circulator* since it is essentially a more complex and more useful circuit element than its simple one-way transmission property would at first indicate. The polarization circulator actually has four output branches corresponding to the two different polarizations at each end of the device. The polarizations of the four output branches are indicated schematically in Fig. 13. It is noticed that

CC-0. In Public Domain. Gurukul Kangri Collection, Haridwar

Digitized by Arya Samaj Foundation Chennai and eGangotri

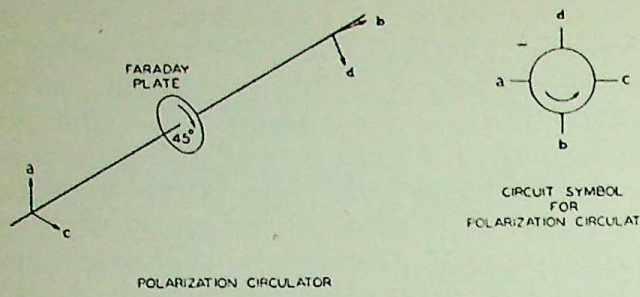


FIG. 13. Schematic diagram of polarization circulator.

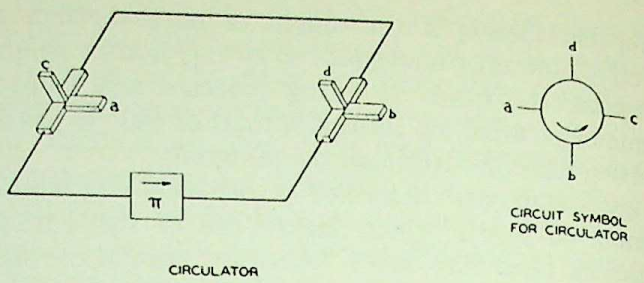


FIG. 14. Schematic diagram of circulator.

power sent into the polarization circulator with polarization *a* is turned into polarization *b*, also *b* is turned into *c*, *c* is turned into *d*, and *d* is turned into *minus a*. This property is indicated very clearly by the circuit symbol suggested in Fig. 13, the phase inversion between arms *d* and *a* being indicated by the minus sign between the *d* and *a* arms.

Another one-way transmission system can be created by combining the gyrator with two magic tees. This combination is indicated in Fig. 14. Since this device has all of the fundamental properties of the polarization circulator with the exception of the phase inversion between arms *d* and *a* it is suggested that it be called a *circulator* and the circuit symbol suggested which indicates its properties is also given in Fig. 14.

This list of applications is obviously not complete since it includes only the fundamental elements from which innumerable specific applications can be made.

In addition to the applications discussed above, which depend upon the antireciprocal property of the element for their operation there are several simple applications which are based only upon the fact that the amount of rotation can be controlled externally by adjusting the magnetic field. Among these uses are electrically controlled attenuators, modulators, and microwave switches.

If a circularly polarized wave is propagated in a circular guide or if the dominant mode is propagated in a rectangular wave guide with the magnetic field being applied along the electric vector of the wave, the above phenomenon allows one to realize externally controlled microwave phase shifters, attenuators, modulators, and microwave windows.

ACKNOWLEDGMENTS

The author is indebted to a number of persons for aid in performing the above work. In particular he wishes to thank J. K. Galt and W. A. Yaeger for the many enlightening discussions during the progress of the work. The author is also indebted to S. E. Miller, A. G. Fox, and several other members of the Bell Telephone Laboratories at Holmdel, New Jersey, whose contributions have been so extensive that it is impossible to completely enumerate them here.

DISCUSSION

A. G. FOX AND M. T. WEISS, *Bell Telephone Laboratories, Holmdel, New Jersey:* As Dr. Hogan has stated, one can apply the plane wave analysis of Faraday rotation, ferromagnetic resonance, and other phenomena in ferrites, only with very great caution to the interpretation of measurements made in ferrite filled wave guides. We would like to describe some of our own experiences in this matter.

1. Mode conversion problem.—Because of the relatively high index of refraction of most ferrites, a dominant mode hollow metal guide, when completely or even partially loaded with a ferrite rod, may be capable of propagating higher order modes. Furthermore, experiments have shown that a pencil of high index of refraction placed in the center of a circular wave guide will have a tendency to convert the dominant TE_{11} mode to the TM_{11} mode.

This mode conversion problem became apparent to us while making measurements in circular guide of loss and ellipticity of large diameter ferrite rods, properly tapered, as a function of magnetic field. The results showed peculiar large variations of these quantitites. We now believe that these variations can be attributed to a partial conversion of the dominant TE_{11} mode to the TM_{11} mode by the ferrite pencil which was of sufficient diameter to permit the propagation of both modes. Thus, as the magnetic field is varied, the permeability changes, causing the electrical length of the line to change, so that the interference between the TM_{11} and TE_{11} modes can vary also.

In order to check the foregoing hypothesis, experiments were performed using circularly polarized waves. As is well known, theory predicts that, for a positively rotating circularly polarized wave, the permeability, μ, of the ferrite starts at unity for zero magnetic field, and then decreases, passes through zero, and goes through resonance as the applied longitudinal magnetic field is increased. For a negatively rotating circularly polarized wave, on the other hand, μ starts at unity, increases until saturation is reached, and finally approaches unity again at very high magnetic fields.

CC-0. In Public Domain. Gurukul Kangri Collection, Haridwar

Digitized by Arya Samaj Foundation Chennai and eGangotri

From these considerations it is evident that the negatively rotating component should be more readily subject to mode conversion than the positively rotating component since the former has a higher index of refraction while the latter has an index of refraction which drops sharply with applied magnetic field. Our experiments with circularly polarized waves confirm the foregoing ideas and indicate that the negative component may have many loss peaks and valleys in a plot of loss *vs* applied field, while the positively rotating component has a smooth loss curve at fields below the resonance field value. For small diameter ferrite pencils, which cannot support the higher order modes, no peculiar loss peaks are observed.

2. Ferromagnetic resonance for negatively rotating wave guide mode.—When making circularly polarized wave measurements in wave guides on ferrite pencils thin enough to reduce though not eliminate mode conversion, the usual loss peak for positively rotating waves occurred at a high field value corresponding to ferromagnetic resonance. Surprisingly enough, however, we also observed a loss peak for the negatively rotating waves at magnetic fields very nearly the same as that required to produce ferromagnetic resonance for the positive wave. The magnitude of this negative peak depends on the size of ferrite used, being very small for very thin pencils and reaching values above the loss peak for the positive wave for some larger diameter samples.

It is believed that this effect is connected with the fact that for a wave guide propagating a circularly polarized wave of a given mode, the electric and magnetic field vectors are in general circularly polarized only at the center of the wave guide cross section. Thus, by reference to a field pattern for the TE_{11} mode, it can be seen that near the walls of the guide the transverse component of the rf electric and magnetic vectors is linearly polarized. Therefore, one would expect a small loss peak for negative circularly polarized waves at resonance field values, but this alone would not appear to account for the high loss peak obtained with the larger diameter ferrites.

The high negative wave loss observed in the larger diameter samples can perhaps be attributed to TM_{11} mode propagation. In this mode, when the rf magnetic field vector is circularly polarized in the positive sense in the center of the guide, it is polarized in the opposite sense near the periphery. This is substantiated by the theoretical work of H. Suhl and L. R. Walker (to be published) which shows that the propagation constant of both positively and negatively circular polarized waves are nearly equal in a ferrite filled circular wave guide propagating the TM_{11} mode. For this mode, the ferrite cannot distinguish between a positively or negatively circularly polarized wave. Therefore, one would expect equal loss for the positive and negative wave at the resonance magnetic field value.

However, when one has a mixture of TE_{11} and TM_{11} modes in the ferrite, the negative wave loss may be greater than, equal to, or less than the positive wave loss, depending upon the relative phasing of the two waves. Further work is planned to confirm the above hypothesis.

3. Loss near zero field.—It has long been known that many ferrites have rather large loss at low magnetic fields. With the application of moderate magnetic fields in any direction, longitudinal or transverse, this loss disappears. This strongly suggests that this low field loss may be the result of domain wall motion which disappears upon the application of magnetic field.

If domain wall motion were the cause of this low field loss, one would expect the loss to be independent of the direction of rotation of the circularly polarized wave propagating through the ferrite. However, our experiments on small diameter pencils of ferrite have shown that the loss has a peak for the negatively polarized wave. This rather puzzling asymmetry can be explained by examining the variation of μ with applied field as previously described. It is seen that μ increases for the negatively polarized wave and decreases for the positively polarized wave. Therefore, just as in the case of a dielectric wave guide, there will be a higher concentration of energy in the ferrite when $(\mu\epsilon)^{\frac{1}{2}}$ is larger, that is, on the negatively polarized side rather than on the positively polarized side. Therefore, if the loss peak at zero field in an infinite medium were symetrical with respect to the direction of circular polarization, one would still expect the loss to be higher for negatively rotating waves for a partially filled wave guide. For a fully filled wave guide, the asymmetry should again disappear, but experiments to check this are difficult to interpret because of mode conversion and cavity resonance effects.

CC-0. In Public Domain. Gurukul Kangri Collection, Haridwar

Digitized by Arya Samaj Foundation Chennai and eGangotri

Magneto-Optical Effects and Paramagnetic Resonance

W. OPECHOWSKI

Department of Physics, The University of British Columbia, Vancouver, Canada

INTRODUCTION

LET us consider a material medium in which electromagnetic radiation of two widely different frequencies, for instance, visible radiation and microwave radiation, both approximately monochromatic, is propagated. Concerning the medium, let us assume (as is usual in the dispersion theory) that it may be regarded as an assembly of a very large number of identical "unit systems," such as gas molecules or paramagnetic ions subjected to crystalline electric fields. The medium may or may not be placed in a constant, homogeneous magnetic field, although the former case will usually correspond to actual experimental situations.

In general, the properties of the medium as they show themselves in some observations on either radiation (e.g., observations of the state of polarization or of the Faraday rotation of the plane of polarization) will not be influenced appreciably by the presence of the other. Such an influence may, however, very well occur if the other radiation happens to be in resonance with the unit systems constituting the medium, as has repeatedly been emphasized in recent years.[1] For, in this case, the occupation numbers of the energy levels of the unit systems will, in general, be changed, which, in turn, may lead to modifications of those properties of the medium which determine the results of the observations. Obviously, the occurrence of such modifications implies that the initial energy level for the resonance transition, which may correspond to absorption or induced emission, is occupied, at least intermittently.

The initial level may be occupied for two different reasons, corresponding to two very different kinds of experimental situations. On the one hand, the initial level is occupied because it is, at the same time, the final level for a transition involving the other radiation. Such a "double resonance" case has recently been investigated, experimentally and theoretically, by Bitter and Brossel.[2] They have studied the change in the degree of polarization of the ultraviolet resonance radiation of mercury occurring when mercury vapor placed in a constant magnetic field is subjected to a radiofrequency radiation satisfying the magnetic resonance condition. Double resonance experiments in which the medium is an atomic beam, are also in progress, as reported very recently by Rabi.[3] In this case the changes in the properties of the "medium" are, of course, observed directly.[4]

On the other hand, the initial level is occupied because the temperature of the medium is such that the corresponding Boltzmann factor is not negligible. An experiment involving this kind of situation has recently been proposed by Kastler.[5] He pointed out that the paramagnetic Faraday rotation of visible light will, in general, change considerably under the influence of paramagnetic resonance; in other words, the rotation angle will change if the paramagnetic salt in question is subjected to microwave radiation the frequency of which corresponds to an allowed magnetic dipole transition between the energy levels of paramagnetic ions responsible for the Faraday rotation. Kastler restricted himself to a brief qualitative discussion of this effect. It is the purpose of the present paper to supplement his discussion with a formal quantum-mechanical theory.

Strictly speaking, the initial level may be occupied for both the above stated reasons simultaneously. This case will not, however, be considered here.

GENERAL THEORY

As is well known, the magneto-optical effects depend on the average polarizability tensor of unit atomic systems of which the medium consists ("average" in the sense of statistical mechanics). The average polarizability tensor is, in general, complex, and it can be regarded as composed of a Hermitian part and an anti-Hermitian part. The imaginary and real part of the Hermitian part determine the Faraday rotation and the birefringence, respectively; the anti-Hermitian part determines the absorption. If, besides light, microwave radiation is propagated in the medium, additional terms will appear in the expression for the average polariz-

[1] In particular, F. Bitter, Phys. Rev. 76, 833 (1949); J. Brossel and A. Kastler, Compt. rend. 229, 1213 (1949); A. Kastler, Compt. rend. 232, 953 (1952); See also a review article by A. Kastler, Experientia 8, 1 (1952).

[2] F. Bitter and J. Brossel, Phys. Rev. 86, 308 (1952).

[3] I. I. Rabi, Phys. Rev. 87, 379 (1952).

[4] If unit systems are atomic nuclei rather than atoms, still other experiments very similar in nature to those mentioned above, although involving quite different experimental techniques, become possible. Consider, for instance, an atomic nucleus which emits two gamma-photons in cascade, in the presence of a homogeneous magnetic field. Such a property of the emitted photons as the correlation between their directions of motion will, in general, be modified if a radiofrequency field is switched on, provided its frequency is in resonance with the possible transition frequency between the magnetic sublevels of the intermediate energy level. For these sublevels are final levels for the emission of the first gamma-photon, and initial levels for the emission of the second gamma-photon. *Note added in proof.*—A theory for this case has been developed by B. A. Jacobsohn (University of Washington) and will be published shortly.

[5] A. Kastler, Compt. rend. 232, 953 (1951).

CC-0. In Public Domain. Gurukul Kangri Collection, Haridwar

Digitized by Arya Samaj Foundation Chennai and eGangotri

ability tensor for light, provided the frequency of the microwave radiation is such as to give rise to resonance. It is just these additional terms which are to be calculated.

It should be emphasized that, in the theory here given, "light" means a radiation which induces only electric dipole transitions in the medium, and "microwave radiation" means a radiation which induces only magnetic dipole transitions.[6] The values of the frequencies of the two radiations play only a minor role in the theory. If the formulas are, in a rather early stage of theoretical derivations, specialized to the case that the frequencies are those of visible light and microwave radiation, in the usual sense of these terms, it is only because in such a case the effects described by the formulas will, under normal experimental conditions, most easily be observed.

According to the general principles of quantum statistical mechanics, the average $\langle \mathbf{p} \rangle_{Av}$ of the electric dipole moment $\mathbf{p}$ of a unit system is, at time t,

$$\langle \mathbf{p}(t) \rangle_{Av} = \text{trace}\,[\mathbf{p}\rho(t)], \tag{1}$$

where ρ is the density matrix of the system. If some system of representation is chosen, Eq. (1) becomes

$$\langle \mathbf{p}(t) \rangle_{Av} = \sum_m \sum_n \mathbf{p}_{nm}\rho_{mn}(t), \tag{2}$$

where $\mathbf{p}_{mn}$ and ρ_{mn} are the matrix elements of $\mathbf{p}$ and ρ.

The matrix ρ will be, in the approximation here considered, a linear function of the components of the electric vector of the light wave propagated in the medium. Hence, in view of Eq. (2), each component of the average electric dipole moment will be also a linear function of the components of electric vector of the light wave. In other words, Eq. (2) implicitly represents a tensor relation between $\langle \mathbf{p}(t) \rangle_{Av}$ and the electric vector of the light wave, the tensor in question being by definition, the polarizability tensor, which, as stated before, determines the magneto-optical effects. The problem is thus reduced to that of calculating ρ in the presence of light, microwave radiation and a constant homogeneous magnetic field.

It will be assumed that ρ satisfies the equation

$$\frac{\partial \rho}{\partial t} = -\frac{i}{\hbar}(\mathcal{H}\rho - \rho\mathcal{H}) - a(\rho - \rho_0). \tag{3}$$

Here $\mathcal{H}$ is the Hamiltonian of a unit system in the presence of both radiations; ρ_0 is the density matrix for the case in which the thermodynamic equilibrium of the assembly of unit systems would be determined by the instantaneous energy values of the levels of a unit system. In other words, ρ_0 is the solution of the equation

$$\frac{\partial \rho_0}{\partial t} = -\frac{i}{\hbar}(\mathcal{H}\rho_0 - \rho_0\mathcal{H}) \tag{4}$$

for the case in which the frequency of the perturbing radiation tends to zero, the assembly being supposed to be in thermodynamic equilibrium in the absence of radiation. The actual density matrix ρ must clearly satisfy an equation which takes into account the fact that the instantaneous equilibrium cannot be reached. The simplest way of taking this fact into account is embodied in the second term on the right-hand side of Eq. (3), where the constant a can be interpreted, in the case of a gas, as the number of collisions per unit time, and, in the case of a paramagnetic salt, as the reciprocal value of the spin-lattice relaxation time. Equation (3) has been used by Karplus and Schwinger[7] and, before them, by Fröhlich,[8] in its classical form, as the starting point for a computation of the shape of microwave absorption lines in a gas, a problem treated previously in a different way by Van Vleck and Weisskopf.[9] Later, Bijl[10] used Eq. (3) in connection with the paramagnetic resonance absorption. These problems are very closely related to the one treated in the present paper.

More explicitly, $\mathcal{H}$, which is a time-dependent operator, is given by

$$\mathcal{H}(t) = \mathcal{H}_0 + P\cos\omega_P t + M\cos\omega_M t, \tag{5}$$

$$P = -\mathbf{p}\cdot\mathbf{E}, \quad M = -\mathbf{m}\cdot\mathbf{H}; \tag{6}$$

here $\mathbf{p}$ and $\mathbf{m}$ are the electric and the magnetic dipole moment operators; $\mathbf{E}$ and ω_P are the amplitude of the electric vector, and the angular frequency of light; $\mathbf{H}$ and ω_M are, similarly, the amplitude of the magnetic vector and the angular frequency of the microwave radiation. Consequently, $\mathcal{H}_0$ is the Hamiltonian in the absence of both radiations. It is time-independent, and is supposed to include a term that takes into account the presence of the constant homogeneous magnetic field, and also of possible internal perturbations, such as a crystalline field in a paramagnetic salt. Eigenvalues of $\mathcal{H}_0$, which are assumed to be nondegenerate, will be denoted by E_k.

If in the absence of both radiations the medium is in thermal equilibrium, as is assumed here, the density matrix of a unit system will be

$$\rho^0 = \exp(-\mathcal{H}_0/kT)/\text{trace}\,\exp(-\mathcal{H}_0/kT), \tag{7}$$

where k is the Boltzmann constant and T the absolute temperature. In other words, ρ^0 is a diagonal matrix in the system of representation in which $\mathcal{H}_0$ is diagonal, and its matrix elements $\rho_{mn}{}^0$ are the familiar Boltzmann factors

$$\rho_{mn}{}^0 = \delta_{mn}\rho_m{}^0, \qquad \rho_m{}^0 = \exp(-E_m/kT)/\sum_l \exp(-E_l/kT). \tag{8}$$

[6] An analogous theory, with merely some minor formal modifications, could easily be developed for the case in which changes in the Faraday effect of microwave radiation are calculated arising from resonance of a radiation inducing electric dipole or quadrupole transitions.

[7] R. Karplus and J. Schwinger, Phys. Rev. 73, 1020 (1948).
[8] H. Fröhlich, Nature 157, 148 (1946).
[9] J. H. Van Vleck and V. F. Weisskopf, Revs. Modern Phys. 17, 227 (1945).
[10] D. Bijl, thesis, Leiden, 1950, p. 77.

CC-0. In Public Domain. Gurukul Kangri Collection, Haridwar

Digitized by Arya Samaj Foundation Chennai and eGangotri

We now introduce two auxiliary matrices σ_0 and σ,

$$\sigma_0=\rho_0-\rho^0, \quad \sigma=\rho-\rho^0. \tag{9}$$

If use is made of Eq. (5), Eq. (3) becomes, in terms of these matrices,

$$\frac{\partial\sigma}{\partial t}+\frac{i}{h}(\mathcal{H}_0\sigma-\sigma\mathcal{H}_0)=-a(\sigma-\sigma_0)$$
$$-\frac{i}{h}[M(\rho^0+\sigma)-(\rho^0+\sigma)M]\cos\omega_M t$$
$$+[P(\rho^0+\sigma)-(\rho^0+\sigma)P]\cos\omega_P t, \tag{10}$$

or, in the system of representation in which $\mathcal{H}_0$ is diagonal,

$$\left(\frac{\partial}{\partial t}+i\omega_{mn}+a\right)\sigma_{mn}=a(\sigma_0)_{mn}$$
$$+\frac{i}{h}(\rho_m{}^0-\rho_n{}^0)(M_{mn}\cos\omega_M t+P_{mn}\cos\omega_P t)$$
$$-\frac{i}{h}\sum_k[(M_{mk}\sigma_{kn}-\sigma_{mk}M_{kn})\cos\omega_M t$$
$$+(P_{mk}\sigma_{kn}-\sigma_{mk}P_{kn})\cos\omega_P t], \tag{11}$$

where

$$h\omega_{mn}=E_m-E_n. \tag{12}$$

A glance at Eqs. (3) and (4) shows that $(\sigma_0)_{mn}$ satisfies the equation which arises from Eq. (11) by setting $a=0$. If the intensity of radiation is not too high, the terms containing the matrix elements of σ_0 on the right-hand side of the equation so obtained may be neglected. In accordance with the above discussed meaning of ρ_0, the appropriate solution of this equation is readily found to be

$$h(\sigma_0)_{mn}=(\rho_m{}^0-\rho_n{}^0)[(M_{mn}/\omega_{mn})\cos\omega_M t$$
$$+(P_{mn}/\omega_{mn})\cos\omega_P t]. \tag{13}$$

For paramagnetic ions in crystals, the matrix elements P_{mn} usually vanish if the corresponding transition frequencies belong to microwave or radio regions. For high transition frequencies, $(\sigma_0)_{mn}\approx 0$, because ω_{mn} is then large.

Taking this into account and eliminating $(\sigma_0)_{mn}$ from Eq. (11), by means of Eq. (13), we obtain

$$h\left(\frac{\partial}{\partial t}+i\omega_{mn}+a\right)\sigma_{mn}$$
$$=i(\rho_m{}^0-\rho_n{}^0)[(1-ia/\omega_{mn})M_{mn}\cos\omega_M t$$
$$+P_{mn}\cos\omega_P t]-i\sum_k[(M_{mk}\sigma_{kn}-\sigma_{mk}M_{kn})\cos\omega_M t$$
$$+(P_{mk}\sigma_{kn}-\sigma_{mk}P_{kn})\cos\omega_P t]. \tag{14}$$

If one disregards those terms in σ_{mn} which do not vary with time like $e^{\pm i\omega_M t}$ or $e^{\pm i\omega_P t}$, an approximate solution of Eq. (14) will be of the form[11]

$$\sigma_{mn}=R_{mn}+A_{mn}e^{i\omega_M t}+B_{mn}e^{-i\omega_M t}$$
$$+C_{mn}e^{i\omega_P t}+D_{mn}e^{-i\omega_P t}. \tag{15}$$

To determine the constants in Eq. (15), we substitute this expression for σ_{mn} in Eq. (14), and so obtain the equations (we neglect $a/(\omega_P-|\omega_{mn}|)$, as the frequency of the visible radiation is supposed not be in the vicinity of resonance)

$$2haR=-\sum_k[M_{mk}(A_{kn}+B_{kn})-(A_{mk}+B_{mk})M_{kn}$$
$$+P_{mk}(C_{kn}+D_{kn})-(C_{mk}+D_{mk})P_{kn}], \tag{16}$$
$$(\omega_M+\omega_{mn}-ia)A_{mn}=S_{mn}{}^M, \tag{17}$$
$$(-\omega_M+\omega_{mn}-ia)B_{mn}=S_{mn}{}^M, \tag{18}$$
$$(\omega_P+\omega_{mn})C_{mn}=S_{mn}{}^P, \tag{19}$$
$$(-\omega_P+\omega_{mn})D_{mn}=S_{mn}{}^P, \tag{20}$$
$$2\hbar S_{mn}{}^M=(\rho_m{}^0-\rho_n{}^0)(1-ia/\omega_{mn})M_{mn}$$
$$-\sum_k(M_{mk}R_{kn}-R_{mk}M_{kn}), \tag{21}$$
$$2\hbar S_{mn}{}^P=(\rho_m{}^0-\rho_n{}^0)P_{mn}-\sum_k(P_{mk}R_{kn}-R_{mk}P_{kn}). \tag{22}$$

If both radiations are weak and neither frequency is nearly equal to any ω_{mn}, the matrix R may be put equal to zero. The constants C_{mn} and D_{mn} lead then, using Eqs. (2), (9), (15), to the usual expression for the average polarizability tensor for the frequency ω_P (the Kramers-Heisenberg dispersion formula). The terms in σ_{mn} containing A_{mn} and B_{mn} give no contribution to this tensor. They are proportional to $M_{mn}=-(\mathbf{m}_{mn}\cdot\mathbf{H})$, so that the corresponding terms in Eq. (2) are proportional to $\mathbf{p}_{mn}(\mathbf{m}_{mn}\cdot\mathbf{H})$, which all vanish, because the electric and the magnetic dipole matrix elements are never both different from zero for the same transition (at least, if the two states involved in the transition have definite parities).

Similarly, the constants A_{mn} and B_{mn} lead to an analogous expression for the magnetic susceptibility tensor for the frequency ω_M. The expression is slightly more complicated, owing to the presence of terms containing a, which are responsible for absorption.

If, however, ω_M is nearly equal to one of the ω_{mn}'s and the corresponding magnetic dipole transition is not forbidden, i.e., in the case of magnetic resonance, the sums on the right-hand side of Eqs. (16)–(22) cannot entirely be neglected. For, if $\omega_M\approx(E_u-E_l)/\hbar$ (subscript u refers to the upper level, subscript l to the lower level), A_{lu} and B_{ul} will be much larger than the remaining matrix elements of A and B. Hence, even in the lowest approximation, two of the matrix elements of R, namely, R_{uu} and R_{ll}, will be different from zero.

[11] The calculations which follow are a straightforward generalization of Karplus and Schwinger's calculations, reference 7.

CC-0. In Public Domain. Gurukul Kangri Collection, Haridwar

Digitized by Arya Samaj Foundation Chennai and eGangotri

Equations (16)–(22) then reduce to

$$2hiaR_{uu}=M_{ul}A_{lu}-B_{ul}M_{lu}, \tag{23}$$

$$R_{ll}=-R_{uu}, \tag{24}$$

$$2h(\omega_M-\omega_{ul}-ia)A_{lu}$$
$$=[(\rho_l{}^0-\rho_u{}^0)(1-ia/\omega_{lu})-(R_{uu}-R_{ll})]M_{lu}, \tag{25}$$

$$B_{ul}=A_{lu}{}^*, \tag{26}$$

$$2h(\omega_P+\omega_{mn})C_{mn}$$
$$=(\rho_m{}^0-\rho_n{}^0)P_{mn}-(\delta_{nl}P_{ml}-\delta_{ml}P_{ln})R_{ll}$$
$$-(\delta_{nu}P_{mu}-\delta_{mu}P_{un})R_{uu}, \tag{27}$$

$$D_{mn}-C_{nm}{}^* \tag{28}$$

Changes in the magneto-optical effects arising from paramagnetic resonance are derived from the terms containing R_{uu} and R_{ll} in Eqs. (27) and (28).

From Eqs. (23)–(26), one finds

$$R_{uu}=-R_{ll}=(\rho_l{}^0-\rho_u{}^0)W_{ul},$$
$$W_{ul}=-\frac{1}{2}\frac{\omega_M}{\omega_{ul}}\frac{|M_{ul}|^2}{\hbar^2(\omega_{ul}-\omega_M)^2+|M_{ul}|^2+\hbar^2a^2}. \tag{29}$$

This expression for R_{uu} is identical with Karplus and Schwinger's corresponding result if the meaning of symbols is appropriately reinterpreted [see reference 7, Eq. (30)]. Equations (27) and (28) together with Eq. (29) give explicit expressions for C_{mn} and D_{mn}. If one substitutes these expressions in Eq. (15), and uses the expression for σ_{mn} so obtained to calculate, by means of Eqs. (2) and (9), the terms of $\langle\mathbf{p}(t)\rangle_{Av}$ containing $e^{\pm i\omega_P t}$, which will be denoted by $\langle\mathbf{p}_{\omega_P}(t)\rangle_{Av}$, one finds after some straightforward but rather lengthy rearrangements

$$\langle\mathbf{p}_{\omega_P}(t)\rangle_{Av}=\mathrm{Re}[\langle\mathbf{p}(\omega_P)\rangle_{Av}e^{i\omega_P t}], \tag{30}$$

where

$$\mathrm{Re}\langle\mathbf{p}(\omega_P)\rangle_{Av}=\frac{1}{\hbar}\sum_n\rho_n{}^0\sum_m\frac{2\omega_{nm}\mathbf{P}_{nm}{}^+}{\omega_P{}^2-\omega_{mn}{}^2}$$
$$-(\rho_u{}^0-\rho_l{}^0)\frac{W_{ul}}{\hbar}\sum_m\left[\frac{2\omega_{um}\mathbf{P}_{um}{}^+}{\omega_P{}^2-\omega_{um}{}^2}-\frac{2\omega_{lm}\mathbf{P}_{lm}{}^+}{\omega_P{}^2-\omega_{lm}{}^2}\right], \tag{31}$$

$$\mathrm{Im}\langle\mathbf{p}(\omega_P)\rangle_{Av}=\frac{1}{\hbar}\sum_n\rho_n{}^0\sum_m\frac{2\omega_P\mathbf{P}_{nm}{}^-}{\omega_P{}^2-\omega_{mn}{}^2}$$
$$-(\rho_u{}^0-\rho_l{}^0)\frac{W_{ul}}{\hbar}\sum_m\left[\frac{2\omega_P\mathbf{P}_{um}{}^-}{\omega_P{}^2-\omega_{um}{}^2}-\frac{2\omega_P\mathbf{P}_{lm}{}^-}{\omega_P{}^2-\omega_{ln}{}^2}\right]. \tag{32}$$

The vectors $\mathbf{P}_{mn}{}^+$ and $\mathbf{P}_{mn}{}^-$ occurring in Eqs. (32) and (33) are defined by

$$\mathbf{P}_{mn}{}^+=\mathrm{Re}[\mathbf{p}_{mn}(\mathbf{p}_{nm}\cdot\mathbf{E})], \tag{33}$$

$$\mathbf{P}_{mn}{}^-=\mathrm{Im}[\mathbf{p}_{mn}(\mathbf{p}_{nm}\cdot\mathbf{E})]. \tag{34}$$

The tensor relationship between $\langle\mathbf{p}(\omega_P)\rangle_{Av}$ and $\mathbf{E}$, as given by Eqs. (31)–(34), determines the average polarizability tensor of a unit system. In particular, Eq. (31) determines the real part of this tensor, i.e., the part on which the magnetic birefringence depends. Similarly, Eq. (32) determines its imaginary part, which describes the Faraday effect, as will be discussed below in more detail. The tensor is Hermitian, as may be seen from Eqs. (31)–(34), and from the Hermitian character of the $\mathbf{p}_{mn}$'s. This corresponds to the fact that the absorption of the light wave is here neglected.

THE FARADAY EFFECT

Owing to the Hermitian character of the electric dipole moment matrix $\mathbf{p}_{mn}$, Eq. (34) can be written as follows:

$$\mathbf{P}_{mn}{}^-=\tfrac{1}{2}(\mathbf{p}_{mn}\times\mathbf{p}_{nm})\times\mathbf{E}. \tag{35}$$

Making use of this equation and introducing the abbreviation

$$\mathbf{\Omega}_n=\frac{\omega_P}{\hbar}\sum_m\frac{\mathbf{p}_{mn}\times\mathbf{p}_{nm}}{\omega_P{}^2-\omega_{mn}{}^2}, \tag{36}$$

one obtains from Eq. (32)

$$\mathrm{Im}\langle\mathbf{p}(\omega_P)\rangle_{Av}=\mathbf{\Omega}_{ul}\times\mathbf{E}, \tag{37}$$

where

$$\mathbf{\Omega}_{ul}=\textstyle\sum_n\rho_n{}^0\mathbf{\Omega}_n+W_{ul}(\mathbf{\Omega}_l-\mathbf{\Omega}_u)(\rho_u{}^0-\rho_l{}^0). \tag{38}$$

As is well known from the theory of the Faraday effect,[12] the rotation of the plane of polarization θ per centimeter is related to $\mathbf{\Omega}_{ul}$ in a simple way. If the direction of the constant homogeneous magnetic field and that of propagation of the light wave are parallel, θ is proportional to the component of $\mathbf{\Omega}_{ul}$ along the direction of the field. The proportionality constant is

$$G=8\pi^2\omega_P Ni/c\sqrt{\epsilon}, \tag{39}$$

where N is the number of unit systems per cc, and ϵ is the dielectric constant of the medium (it is assumed that the birefringence is small). Hence the term proportional to W_{ul} in Eq. (38) when multiplied by G represents the contribution of the paramagnetic resonance to the Faraday rotation.

It should be emphasized that the theory has been developed here for the case in which the shape of the paramagnetic resonance line is mainly determined by the spin-lattice relaxation time. If the predominant effects in determining the shape are the dipole-dipole and exchange interactions, the exact calculation of the contribution of the paramagnetic resonance to the Faraday rotation is a problem more or less equivalent to that of computing that shape, so that no straight-

[12] H. A. Kramers, Proc. Acad. Amsterdam 33, 959 (1930); see also L. Rosenfeld, Z. Physik 57, 835 (1930); R. Serber, Phys. Rev. 41, 489 (1932); J. H. Van Vleck and M. H. Hebb, Phys. Rev. 46, 17 (1934).

CC-0. In Public Domain. Gurukul Kangri Collection, Haridwar

Digitized by Arya Samaj Foundation Chennai and eGangotri

forward approach seems to be possible. Of course, the changes in the Faraday effect resulting from the paramagnetic resonance would remain roughly proportional to $(\Omega_u - \Omega_l)(\rho_l^0 - \rho_u^0)$.

When one applies the general formula (38) to the case of nickel fluosilicate, which has been considered by Kastler,[5] one easily confirms his qualitative conclusions.

DISCUSSION

A. ABRAGAM, *University of Paris, France:* It might be interesting to generalize slightly this calculation so as to include the dipole magnetic or quadrupole electric transitions for visible light, which may occur in crystals.

CC-0. In Public Domain. Gurukul Kangri Collection, Haridwar

Digitized by Arya Samaj Foundation Chennai and eGangotri

REVIEWS OF MODERN PHYSICS VOLUME 25, NUMBER 1 JANUARY, 1953

Exchange Narrowing in Paramagnetic Resonance

P. W. ANDERSON

Bell Telephone Laboratories, Inc., Murray Hill, New Jersey

AND

P. R. WEISS

Rutgers University, New Brunswick, New Jersey

In this paper the problem of the line shape in paramagnetic resonance when large exchange interaction is present is discussed from the standpoint of a simplified mathematical model. The mathematical model can be called the model of "random frequency modulation": It is assumed that the atom absorbs a single frequency, which varies over a distribution determined by the dipolar local fields, but that this frequency varies randomly in time at a rate determined by the exchange interactions.

The predicted line shape in the case in which exchange is large is of resonance type in the observable center of the line, but falls off more rapidly in the wings. This line shape has been verified experimentally in a number of cases. This conclusion seems quite independent of any assumption about the type of random frequency modulation, etc. The quantitative conclusions are reached in the following way: It is suspected, since the exchange motion is the superposition of the effects of a number of neighbors which is not particularly small, that a good approximation to the modulation function is Gaussian noise with a Gaussian spectrum. This, of course, is what would result from the superposition of a large number of rather small effects. Under this assumption both the second moment (which is independent of exchange) and the fourth moment of the line shape can be calculated. This kind of modulation is the simplest one which does give a finite fourth moment; a Markoffian, or "jump," type of modulation, which might seem more reasonable at first, does not. These moments are then compared with the moments computed by Van Vleck [Phys. Rev. 74, 1168 (1948)] to fix the two adjustable parameters, mean square frequency, and average rate of change of frequency, of the theory.

The result as to line breadth, which is essentially

$$\Delta \simeq \frac{\langle(\Delta\omega^2)\rangle_{Av}\ \text{dipole-dipole}}{J/\hbar},$$

if J is the exchange integral, can be compared with observed line breadths by estimating J from Curie-Weiss constants for a number of materials. The results are quite satisfactory if the theory is extended in two ways: (a) When the exchange frequency is larger than the resonance frequency, it can be shown that the off-diagonal elements of the dipolar interaction must be included, leading to a line-width larger by a factor of roughly 10/3; (b) in a number of cases hyperfine and Stark splitting is contributing importantly to the width.

The good agreement with experiment in the cases we have investigated leads us to believe that a quantitative approach to the paramagnetic resonance line breadth problem, using only the already known concepts of dipolar interaction, exchange narrowing, and fine structure splitting, will probably explain all the observed phenomena.

I. INTRODUCTION

THE phenomenon of exchange narrowing was first suggested as a possibility by Gorter and Van Vleck[1] and was demonstrated mathematically by Van Vleck.[2] These authors pointed out that in most pure salts the exchange interaction cannot broaden the paramagnetic resonance line because it commutes with the components of the total magnetic moment and, therefore, has no direct effect on either the Zeeman energy ($\sim S_z$) or the radiating dipole moment (S_z). On the other hand, exchange can cause rapid motion in the spin system, which can result in averaging out the effects of the broadening interactions such as magnetic dipolar interactions, thus narrowing the line.

At nearly the same time Bloembergen, Purcell, and Pound[3] observed that temperature motion of atoms in liquids and some solids had much the same kind of narrowing effect on nuclear magnetic resonance lines. These authors considered these narrowing phenomena in a way roughly similar to our present theory, but with a somewhat less schematized and therefore less quantitative model. With their considerations they deduced that narrowing occurred if the rate of motion (which we shall call ω_e) is rapid compared to the amplitude in frequency of the perturbations, which we call ω_p; and that then the line breadth is roughly

$$\Delta\omega \simeq \omega_p^2/\omega_e. \tag{1}$$

We have applied a similar model to the problem of narrowing by motion in the spin system because of exchange. In our model we assume the system to be absorbing a single frequency, which varies in a random way over a certain range determined only by the magnitude of the perturbations (primarily because of the magnetic interactions) but at a rate controlled by the motions. This is not an entirely new concept (see, for example, reference 1), but we have tried to carry the work through in a consistent, at least semiquantitative way, and to give the model as good a justification as possible.*

With this model it becomes possible to compute the actual line shape and line width, in contrast to the method of Van Vleck in which only the second and fourth moments of the line shape can be practically

[1] C. J. Gorter and J. H. Van Vleck, Phys. Rev. 72, 1128 (1947).
[2] J. H. Van Vleck, Phys. Rev. 74, 1168 (1948).
[3] Bloembergen, Purcell, and Pound, Phys. Rev. 73, 679 (1948).

* This justification, as well as some of the other more mathematical parts of the theory, will not be given fully here; we hope to cover these points more completely in a later publication.

CC-0. In Public Domain. Gurukul Kangri Collection, Haridwar

Digitized by Arya Samaj Foundation Chennai and eGangotri

calculated. This is important because these moments fail to describe the line shape with any accuracy just when exchange narrowing becomes important. In all the possible forms of the model the line shape is of resonance type in the center when the narrowing is large, falling off more rapidly on the wings near the frequency ω_e. This agrees with the results of a number of experiments.[4,5]

We have also found it possible, picking the "Gaussian" form of the model which is most suited to the exchange problem, to compute second and fourth moments and, comparing these with those of Van Vleck, to fit the adjustable constants ω_p and ω_e of the theory. That the forms of these moments are such as to make this possible in the first place is confirmation of the essential physical correctness of the model. When certain corrections are made, also suggested by the model, we find quite excellent agreement with measured line widths, using exchange integrals computed from paramagnetic Curie-Weiss constants.

In this quantitative aspect we feel that our theory, in spite of its apparent arbitrariness, is valuable both as an aid to understanding, particularly in regard to the corrections which have to be made, and as an extrapolation method encouraging one to try to use the rough relation (1) quantitatively. We feel that the success we have had indicates that the concepts already available are completely adequate to explain most of the observed phenomena; there seem to be no important mysteries left.

II. THE MODEL OF RANDOM FREQUENCY MODULATION

It is true in general[6] that the spectrum of the radiation or absorption of any quantum-mechanical system is given by the Fourier integral of the Heisenberg operator for the dipole moment S_x:

$$I(\omega)=\text{Trace}\left|\int S_x(t)e^{i\omega t}dt\right|^2, \tag{2}$$

where

$$ih\frac{dS_x}{dt}=HS_x-S_xH. \tag{3}$$

In our problem the Hamiltonian consists of three parts:

$$H=H_0+H_p+H_{ex}. \tag{4}$$

H_0 is the unperturbed Hamiltonian,

$$H_0=g\beta H\sum_j S_{zj}, \tag{5}$$

which causes the energy-splittings leading to the lines we are investigating. H_p is the "perturbing" Hamiltonian, for the time being assumed to be due to the dipolar interactions, which causes the broadening of these lines (Van Vleck, reference 2, has written it out in full); and H_{ex} is the exchange Hamiltonian,

$$H_{ex}=\sum_{j,k} J_{jk}\mathbf{S}_j\cdot\mathbf{S}_k. \tag{6}$$

We now calculate the spectral intensity (2) for a given absorption line (state $i\rightarrow$state j) under the following assumptions:

$$\text{(a)}\quad ih\dot{H}_p=[H_0+H_{ex}, H_p]\simeq[H_{ex}, H_p]. \tag{7}$$

This is not really an assumption, but merely the expression of the fact that the perturbation of the dipolar interactions varies in time because of the exchange Hamiltonian, according to the standard commutator law. Since very many states are available to the system, and since thermal energy is large compared with all the Hamiltonians of (4), this time variation will be a random one, the order of magnitude of the rate being given by H_{ex}/h. We write down (7) as an assumption to emphasize two facts: first, that H_{ex} does not commute with H_p, and thus it does cause a time variation of H_p; and second, that we leave out, at least for the time being, the time variation due to H_0; this is only justifiable on the basis of the later assumption (d), by which we throw away all the parts of H_p which are off-diagonal in H_0 as being, in the language of reference 3, nonsecular perturbations. In a later section we will consider the case in which $H_0\ll H_{ex}$; then, of course, no part of H_p is any more "secular" than any other part, and we retain assumption (a) but leave in all parts of H_p.

$$\begin{aligned}&\text{(b)}\quad [H_{ex}, H_0]=0.\\ &\text{(c)}\quad [H_{ex}, S_z]=0.\end{aligned} \tag{8}$$

These two easily verified assumptions express the fact that H_{ex} causes narrowing rather than broadening, since it cannot directly change the unperturbed energies (by b) or interrupt the radiation in any way (by c).

(d) Finally, the assumption is made that H_p is so small as to have no important matrix elements connecting different unperturbed states of H_0. This is the assumption which is most vital to the model, since it expresses the assumption that H_p changes only the frequency of the radiation from the system, without causing transitions or changing the amplitude.

This assumption is obviously not a rigorous one, since H_0 has many states of the same energy (e.g., all states of given S_z, no matter what S^2 is, have the same energy). Thus obviously H_p will have important off-diagonal elements. However, the assumption is very far from being as bad as this reasoning would make it appear. In the first place, it always turns out that we need not leave out of our calculation the off-diagonal elements of H_p; we need only treat them as if they were

[4] Unpublished work by R. T. Weidner on diphenyl picryl hydrazyl.

[5] Kumagai, Ono, Hayashi, Abe, Shimada, Shôno, and Ibamoto, Phys. Rev. 83, 1077 (1951).

[6] P. W. Anderson, Phys. Rev. 76, 647 (1949).

CC-0. In Public Domain. Gurukul Kangri Collection, Haridwar

Digitized by Arya Samaj Foundation Chennai and eGangotri

diagonal† For instance, in the present theory, we use Van Vleck's full mean square value of H_p, including both diagonal and off-diagonal effects.

A second way of thinking of assumption (d) is as an "isolated-atom" assumption; for the isolated atom H_p will not have important off-diagonal elements, so that we get qualitatively right answers; and then we renormalize by using the full perturbation as mentioned above.

It now becomes possible to compute the spectral intensity (2) for a given spectral line, which we pick out by using only the $i\rightarrow j$ matrix element of $S_x(t)$ in (2). This matrix element, from Eq. (3) and assumption (c), satisfies the equation

$$ih(\dot{S}_x)_{ij}=[H_0+H_p, S_x]_{ij}$$
$$=[H0_{ii}+H_{pii}(t)]S_{xij}-[H0_{jj}+H_{pjj}(t)]S_{xij}. \quad (9)$$

Here assumption (d) has eliminated all off-diagonal elements, and assumption (b) shows that

$$H0_{ii}-H0_{jj}=\hbar\omega_0, \quad (10)$$

the unperturbed resonant frequency, is not a function of time. The solution of (9) is obvious:

$$(S_x(t))_{ij}=(S_{xij})_0 \exp\left[-i\omega_0 t-i\int_0^t \Delta\omega_{ij}(t')dt'\right], \quad (11)$$

where

$$\Delta\omega_{ij}(t)=\frac{1}{\hbar}[H_{pii}(t)-H_{pjj}(t)] \quad (12)$$

is the randomly varying frequency introduced by the perturbation H_p, which in turn varies in time due to Eq. (7).

Equation (11) introduced into (2) gives

$$I_{ij}(\omega)\sim\left|\exp\left[-i(\omega-\omega_0)t-i\int_0^t \Delta\omega_{ij}(t')dt'\right]\right|^2. \quad (13)$$

Equation (13) is the basic equation of the random frequency-modulation model; it states that the spectrum is that which one would obtain from a frequency which varies about the mean frequency ω_0 in a random way, with amplitude controlled by the size of H_p but rate determined by H_{ex} through Eq. (7).

Before going on to the actual exchange narrowing problem let us introduce some transformations. First, we shall always think in terms of frequency differences from the line center, so that instead of $\omega-\omega_0$ we write simply ω; ω_0 enters nowhere else in the problem except in assumption (a). Second, we transform to the correlation-function form of the Fourier integral by the well-known process of Wiener and Khinchin:

$$I_{ij}(\omega)=\int_{-\infty}^{\infty} e^{i\omega\tau}\varphi(\tau)d\tau, \quad (14)$$

$$\varphi(\tau)=\langle S_{xij}(t)S_{xij}^*(t+\tau)\rangle_{Av} \text{ over } t$$
$$=\left\langle \exp\left[i\int_t^{t+\tau}\Delta\omega_{ij}(t')dt'\right]\right\rangle_{Av}. \quad (15)$$

Equation (15) forms the basis for our mathematical manipulations. It should also be noted that Eq. (15) is a very simple way of understanding the phenomena of exchange and motional narrowing. Namely, since I and φ are Fourier transforms of each other, if φ has a "breadth" T in time, i.e., falls off appreciably in time T, then the breadth of I is $1/T$.

Now, first suppose $\Delta\omega_{ij}(t')$ varies quite slowly in time. Then the integral in (15) will become appreciable when $\Delta\omega_{ij}\tau\simeq 1$, so that if ω_p is some average of $\Delta\omega_{ij}$ we have $\omega_p T\simeq 1$, and thus the line breadth $\simeq\omega_p$, as in the case of no narrowing; the rate of change is unimportant.

But now suppose ω_e, the rate of change of $\Delta\omega_{ij}$, is much faster than its average ω_p. Then before $\int\Delta\omega_{ij}$ can have reached any large value the integrand $\Delta\omega_{ij}$ will have changed sign, and the whole integral will roughly average out. Thus $\varphi(\tau)$ becomes very much broader, and $I_{ij}(\omega)$ correspondingly narrower.

III. THE SPECTRUM FOR GAUSSIAN RANDOM MODULATION; EXCHANGE NARROWING

Before any progress can be made in finding the correlation function, we must make a decision as to what the amplitude and random properties of the function $\Delta\omega_{ij}(t)$ are. This decision must be made, in the present state of the theory of random functions,[7] more on the basis of mathematical convenience than anything else; fortunately, in the exchange narrowing case physical realism is probably also satisfied fairly well.

The most easily handled type of random function is the Gaussian type. This may be defined in a number of ways: The physical way is to appeal to the law of large numbers and say that the superposition of the small effects of a large number of random causes is always a Gaussian random function, e.g., Brownian motion or the voltage due to motion of electrons in a resistor. A way of producing a Gaussian random function is to put "white" Gaussian noise—that is, Gaussian noise with an equal amount of energy in every frequency range, such as is produced by electrons in a resistor—through an arbitrary electrical filter. All the probability distributions, for instance the probability of finding a given amplitude in a given frequency range, are Gaussian. On the other hand, it must be emphasized that the ac-

† Thus we follow the procedure—remarkably successful quantitatively—of the "adiabatic approximation" in pressure broadening, replacing the transition effects of off-diagonal elements by equivalent energy perturbations.

[7] For a reference on random theory see M. C. Wang and C. E. Uhlenbeck, Revs. Modern Phys. 17, 323 (1945). The authors are indebted to Dr. Shannon and Dr. McMillan of Bell Laboratories for helpful discussions of this subject.

CC-0. In Public Domain. Gurukul Kangri Collection, Haridwar

Digitized by Arya Samaj Foundation Chennai and eGangotri

tual spectrum, corresponding to the type of filter in the above example, is still completely arbitrary.

In exchange narrowing the frequency $\Delta\omega_{ij}(t)$ is due to the random perturbing effects on the frequency of a number of neighbors, 6–10 or more, which is not large in the usual sense but from experience with random theory seems to be fairly large in the sense we need. In addition, Van Vleck has shown that the mean fourth moment of the value of $\Delta\omega_{ij}$ is near to that expected from the Gaussian shape. Measured shapes, when narrowing is small, are indeed roughly Gaussian. This, of course, does not insure that all distributions are Gaussian, as is required for the true Gaussian random function, but it does verify our reasoning that the function should be Gaussian. One can be sure that this assumption is by far the least drastic of this theory.

Once one has picked the Gaussian type of random function one still has the freedom, as pointed out above, of choosing either the spectrum or the correlation function of the random modulation in a completely arbitrary way. This spectrum characterizes the properties of the motion due to exchange, in contrast to the amplitude of the random function $\Delta\omega_{ij}$, which is a consequence of the dipolar interactions alone. We should emphasize that now we speak of the spectrum of $\Delta\omega_{ij}(t)$, which we call $I_{\Delta\omega}(\nu)$; the corresponding correlation function, related by (14) to $I_{\Delta\omega}$, we call $\varphi_{\Delta\omega}(t)$. Fortunately, Van Vleck's computations again furnish us a very useful condition: The mean fourth moment even with exchange is finite, which one can show requires that the spectrum not have an anomalously long "tail"; it must fall off at large ν more rapidly than ν^{-3}. In particular, this excludes the Markoffian type of random modulation in which the motion proceeds in jumps, such as one might expect from the oversimplified picture of electrons jumping back and forth due to exchange. It is more realistic to think of exchange causing fields which cause the electrons to precess at rates not much greater than $J/\hbar$.

Again we appeal to the fact that the exchange effect is also the superposition of the effects of a number of neighbors which is not particularly small, to assume that $I_{\Delta\omega}(\nu)$ is Gaussian. Here our assumption is not really quite so sound, but we can be sure that with the condition that the fourth moment is finite, and assuming a reasonably smooth spectrum, the final results will be quite typical of those we would obtain with other spectra.

The assumptions then are:

$\Delta\omega_{ij}(t)$ is a Gaussian random function

$$\varphi_{\Delta\omega}(t)=\frac{\langle\Delta\omega_{ij}(t')\Delta\omega_{ij}(t'+t)\rangle_{\text{Av}}}{\langle\Delta\omega_{ij}{}^2\rangle_{\text{Av}}}=\exp\left[-\frac{\pi}{4}\omega_e{}^2t^2\right]. \quad (16)$$

[Equation (16) is equivalent to assuming $I_{\Delta\omega}$ Gaussian; ω_e is an average exchange frequency, of order $J/\hbar$.]

We now find that these assumptions make it possible to compute (15). First we use a well-known theorem relating to Gaussian random functions: The distribution of any linear combination of values of a Gaussian random function is itself Gaussian. Now the integral in the exponent of (15),

$$X=\int_t^{t+\tau}\Delta\omega_{ij}(t')dt', \quad (17)$$

is itself just such a linear combination, so that we know the distribution of X,

$$P(X)dX=\frac{1}{[2\pi\langle X^2\rangle_{\text{Av}}]^{\frac{1}{2}}}\exp\left(-\frac{X^2}{2\langle X^2\rangle_{\text{Av}}}\right)dX,$$

where $\langle X^2\rangle_{\text{Av}}$ is the average value of X^2,

$$\langle X^2\rangle_{\text{Av}}=\left\langle\int_0^\tau dt\int_0^\tau dt'\Delta\omega_{ij}(t)\Delta\omega_{ij}(t')\right\rangle_{\text{Av}}.$$

This, after manipulation, can be shown to be

$$\langle X^2\rangle_{\text{Av}}=2\omega_p{}^2\int_0^\tau dt(\tau-t)\varphi_{\Delta\omega}(t). \quad (18)$$

Here we have defined $\omega_p{}^2$ as the mean square of $\Delta\omega_{ij}$:

$$\omega_p{}^2=\langle\Delta\omega_{ij}{}^2\rangle_{\text{Av}}. \quad (19)$$

With the distribution of X, $P(X)$, known, we can immediately take the average of (15)

$$\varphi(\tau)=\int_{-\infty}^{\infty}dXP(X)e^{iX},$$

$$\varphi(\tau)=\exp\left[-\frac{\langle X^2\rangle_{\text{Av}}}{2}\right]$$

$$=\exp\left[-\omega_p{}^2\int_0^\tau dt(\tau-t)\varphi_{\Delta\omega}(t)\right]. \quad (20)$$

Thus we see that with the Gaussian assumption, we can relate the correlation function for the spectral line to a rather easily performed integral (18) of the correlation function $\varphi_{\Delta\omega}$ of the random modulation, together with the second moment $\omega_p{}^2$ (19) of the original distribution.

Before going on to discuss the Gaussian form for $\varphi_{\Delta\omega}$ (16) which is of most interest to us, we shall obtain a few rather general conclusions which are valid in the limiting cases.

Case I: $\omega_p\gg\omega_e$ so that $\varphi_{\Delta\omega}(t)$ is constant at its value for $t=0$, unity, throughout the region in which the exponent of (20) takes on appreciable values. Then we have

$$\varphi(\tau)_{\text{case I}}\simeq\exp\left[-\omega_p{}^2\int_0^\tau dt(\tau-t)\right]$$

$$=\exp\left(-\frac{\omega_p{}^2\tau^2}{2}\right). \quad (21a)$$

CC-0. In Public Domain. Gurukul Kangri Collection, Haridwar

Digitized by Arya Samaj Foundation Chennai and eGangotri

This can easily be shown, through Eq. (14), to give a Gaussian line of mean width ω_p^2. This is, of course, exactly what we started out with; other forms of modulation function have been tried, but the general conclusion can always be drawn that in case I the modulation has no effect whatever.

Case II: $\omega_e \gg \omega_p$. In this case $\varphi_{\Delta\omega}$ will have caused the integrand in (20) to vanish long before t can take on a value comparable to τ. Then

$$\varphi(\tau)_{\text{case II}} \cong \exp\left[(-\omega_p^2)\tau \int_0^\infty \varphi_{\Delta\omega}(t)dt\right] \tag{21b}$$

$$= \exp\left(-\frac{\omega_p^2 \tau}{\omega_e}\right). \tag{21b}$$

Here ω_e can be defined by the equation (consistent with 16)

$$\frac{1}{\omega_e} = \int_0^\infty \varphi_{\Delta\omega}(t)dt,$$

and it is clearly a good measure of the inverse of the total width of $\varphi_{\Delta\omega}$, and thus of the true width of the spectrum $I_{\Delta\omega}(\nu)$. This Eq. (21b) is also remarkably general, holding as well for other types of random modulation. The line shape resulting from (21b) is the resonance shape:

$$I_{ij}(\omega) = \frac{2}{\pi} \frac{(\omega_p^2/\omega_e)}{\omega^2 + (\omega_p^2/\omega_e)^2}. \tag{22}$$

Clearly, if $I(\omega)$ is to have a finite second moment, as it must if $\Delta\omega_{ij}$ is Gaussian, (22) cannot hold throughout the frequency spectrum. It can be shown that the wings of the spectrum, which are determined primarily by $\varphi(\tau)$ at very small τ, where (21b) is no longer valid, fall off more rapidly than (22) indicates. In fact, (22) is a good approximation out to the frequency ω_e, beyond which the wings fall off quite rapidly.

As mentioned in the introduction, in a number of experimental cases of extreme narrowing[4,5] the resonance shape (22) has been found to be correct. We feel that the shape (22) is probably the most accurate conclusion of the theory.

Some of the moments of the distribution can also be found from Eq. (20) directly. The theorem which is most convenient to use is easily proved from Eq. (14), and is

$$\langle \omega^n \rangle_{Av} = i^n \left.\frac{d^n \varphi}{d\tau^n}\right|_{\tau=0}. \tag{23}$$

For the second moment this gives

$$\langle \omega^2 \rangle_{Av} = -\left.\frac{d^2}{dt^2}\left\{\exp\left[-\omega_p^2 \int_0^\tau dt(\tau - t)\varphi_{\Delta\omega}(t)\right]\right\}\right|_{\tau=0}, \tag{24}$$

$$\langle \omega^2 \rangle_{Av} = \omega_p^2.$$

We see that the second moment is completely independent of the effect of exchange, a fact which Van Vleck derived for the rigorously correct model.

The fourth moment is somewhat more complicated to derive from (23), but we shall write it down:

$$\langle \omega^4 \rangle_{Av} = 3\omega_p^4 - \omega_p^2 \left.\frac{d^2}{d\tau^2}\varphi_{\Delta\omega}(\tau)\right|_{\tau=0}. \tag{25}$$

Note that this will not be finite unless the spectrum of $\Delta\omega_{ij}(t)$ has a finite second moment, as stated previously.

With the specific Gaussian form (16) for the correlation function of $\Delta\omega_{ij}$, we can immediately write down the correlation function for this case. It is

$$\varphi(\tau) = \exp\left(-\frac{\omega_p^2 \tau}{\omega_e}\int_0^{\omega_e \tau} e^{-(\pi/4)x^2}dx + \frac{2\omega_p^2}{\pi\omega_e^2}\left[1 - \exp\left(-\frac{\pi}{4}\omega_e^2\tau^2\right)\right]\right). \tag{20a}$$

The actual spectral line shape is not of much interest except in the limiting cases, in which (22) and (21a) are quite satisfactory. It is of interest to go ahead and compute the fourth moment in this special case [(24) of course being quite satisfactory for the second moment]. One can do this quickly with (25) and obtain

$$\langle \omega^4 \rangle_{Av} = 3\omega_p^4 + \frac{\pi}{2}\omega_p^2\omega_e^2. \tag{25a}$$

IV. COMPARISON WITH EXPERIMENT

These general formulas, containing ω_p and ω_e as adjustable parameters, represent the extent of this model's ability to give quantitative information. We know only that

$$\omega_p \sim H_p/\hbar \cong (g^2\beta^2/\hbar a^3)$$

and $\omega_e \sim J/\hbar$ as to order of magnitude.

Fortunately, there is a way to make the method quantitative. We can use Van Vleck's values for the second and fourth moments and compare these with our values (24) and (25a). This gives two relations for our two parameters, ω_e and ω_p, so that then we can use (22) (at least in the extreme narrowing case) to predict the breadth. Thus we plan to use our model to "extrapolate" Van Vleck's numbers to get the entire line shape. Naturally no accurate limits of error may be set on such a procedure; nonetheless, one would be quite surprised if our assumptions combined to give an error of more than a factor of two, and less than this would be far more likely. For example, the two most extreme spectra $I_{\Delta\omega}(\nu)$ one could expect, the square spectrum and the simple exponential ($e^{-\tau/\omega_e}$), lead to errors of only about 1.5 in our extrapolation procedure, one in one direction and one in the other. The true deviation from the Gaussian is probably far less than these.

CC-0. In Public Domain. Gurukul Kangri Collection, Haridwar

Digitized by Arya Samaj Foundation Chennai and eGangotri

TABLE I. Exchange narrowing in Fe^{+++} and Mn^{++} salts.

Salt	θ	H_p	H_e	ΔHcalc(1)	ΔHobs	(10/3)ΔHcalc(1)
A. Extreme narrowing, $H_e \gg H_0$						
$FeNH_4(SO_4)_2$	13°K	840 oe	13 800 oe	51 oe	290 oe	170 oe
$Fe_2(SO_4)_3$	70	1200	74 100	19	90	64
$MnCl_2$	16	1750	17 000	175	625	585
$MnSO_4$	24	1600	25 400	100	330	330
B. $\theta \simeq 0$, weak narrowing						
$MnCl_2 \cdot 4H_2O$	3	750	<3000	>175	670	Upper limit ~1000
$MnSO_4 \cdot 4H_2O$	2	730	<2000	>250	570	
$MnSO_4 \cdot 5H_2O$	3	630	<3000	>125	625	
$MnSiF_6 \cdot 6H_2O$	~0	460	(0)		800	

The moments as given by Van Vleck are, for a simple cubic lattice structure,

$$\hbar^2\langle\omega^2\rangle_{Av} = 36.8\left(\frac{g^2\beta^2}{a^3}\right)^2 \frac{S(S+1)}{3} \times(\lambda_1^4+\lambda_2^4+\lambda_3^4-0.187), \quad (26a)$$

$$\hbar^4\langle\omega^4\rangle_{Av} = 3(\hbar^2\langle\omega^2\rangle_{Av})^2+490\left(\frac{g^2\beta^2}{a^3}\right)^2 J^2\left(\frac{S(S+1)}{3}\right)^2 \times(\lambda_1^4+\lambda_2^4+\lambda_3^4-0.187). \quad (26b)$$

The notation is: g = g-factor, β = Bohr magneton, a = lattice constant, $\lambda_{1,2,3}$ are direction cosines of the external field with respect to crystal axes, S = spin quantum number per atom, and J = exchange integral.

We should point out that the remarkable similarity between (26b) and (25a) in general form is not a necessary result of either theory; for instance, terms of form $(g^2\beta^2/a^3)^3$ can and do occur, but are extremely small, according to Van Vleck, and he drops them; while the coefficient of $\langle(\omega^2)\rangle_{Av}^2$ is not exactly, but approximately 3. The angular dependence is also an "accident." It seems to us that this agreement is good evidence for the physical sense of our model.

The uncertainties we already have seem bad enough that we need not worry about either crystal structure or directional properties very much, so we shall use the isotropic averages of (26). We then find for the two parameters

$$\omega_p^2 = \frac{15.2}{3}\left(\frac{g^2\beta^2}{\hbar}\right)^2 n^2 S(S+1), \quad (27)$$

$$\omega_e^2 = \frac{8.48}{3}\left(\frac{J}{\hbar}\right)^2 S(S+1). \quad (28)$$

n is the density of spins per cubic centimeter. The line breadth is then (half-width at half-power)

$$\Delta\omega = \omega_p^2/\omega_e. \quad (29)$$

In terms of magnetic field, as most measurements are made, this gives us the following fields corresponding to ω_e and ω_p:

$$H_p^2 = 5.1(g\beta n)^2 S(S+1), \quad (27a)$$

$$H_e = 2.83\frac{J}{g\beta}[S(S+1)]^{\frac{1}{2}}, \quad (28a)$$

and

$$\Delta H = H_p^2/H_e \quad (29a)$$

is the predicted half-width at half-power.

Kumugai and co-workers[8] have measured or compiled the line breadths for a number of salts of Mn^{++} and Fe^{+++}, where crystal anisotropy broadening is minor and thus powder data are reliable. For most of these salts an estimate of the exchange integral can be made from the Curie-Weiss law $\chi = C/(T+\theta)$, with θ obtained from the Weiss molecular field equations as

$$3k\theta = 2JZS(S+1). \quad (30)$$

Z is the number of nearest neighbors, which we always set equal to six for consistency with our previous assumption of simple cubic lattices. These salts are also advantageous in that crystal splittings do not contribute importantly to θ.

In Table I we make a comparison of our predicted line breadths from Eq. (29a) (column labeled $\Delta H_{calc}^{(1)}$) with the observed breadths (under ΔH_{obs}). The comparison is valid only for those salts with large θ which are collected in Table IA, both because the θ measurements are in most cases not valid to more than ±2°K, even if nothing but exchange is important, and because for the other salts the H_e values are not extreme enough to make our limiting formulas correct.

We see that in spite of the belief that our calculations should be good within a factor 2 at most, the comparison is bad, since errors as large as a factor 6 appear. This discrepancy is the same as that noticed by Kumugai *et al*,[8] using the simple order-of-magnitude formula (1). Fortunately, we can show that two very important sources of broadening have been so far neglected, and that their inclusion leads to good agreement with experiment.

The first source is the following. In Van Vleck's computation of the mean square broadening he leaves

[8] Kumugai, Ono, and Hayashi, Phys. Rev. 85, 925 (1952).

CC-0. In Public Domain. Gurukul Kangri Collection, Haridwar

Digitized by Arya Samaj Foundation Chennai and eGangotri

out terms in H_p which connect different Zeeman energy levels. (These are terms mixing $S_z \pm 1$ and $S_z \pm 2$ with S_z.) Van Vleck is perfectly correct in doing so, since when $H_p \ll H_0$, as in all resonance experiments, and when exchange is not too large, these terms contribute only in second order to the main line. On the other hand, because they mix up the S_z states they can lead to satellites at frequencies 0, $2\omega_0$, and $3\omega_0$, which are so far from the main line that in spite of their weakness their mean square breadth contribution is large.

In the present exchange narrowing cases, on the other hand, H_{ex} is not small compared to H_0, which introduces a new effect. One can show in a number of ways, by quantum-mechanical thinking or by the reasoning of reference 3, for instance, that these terms should no longer be omitted. Namely, the rapid variation of these terms due to exchange makes the fact that their "natural" unperturbed frequency is not zero immaterial.‡

One can demonstrate this on our model by assuming that these terms have a Gaussian spectrum centered not about zero but about ω_0. Van Vleck points out that the total mean square amplitude of these terms is 7/3 of that contributed by the zero-frequency terms, so that we may write

$$\langle \Delta\omega_{ij}^2 \rangle_{Av} \varphi_{\Delta\omega}(t) = \exp\left(-\frac{\pi}{4}\omega_e^2 t^2\right) \left[\omega_p^2 + 7/3\omega_p^2 \cos\omega_0 t\right]. \quad (31)$$

This equation embodies the assumption that the frequency ω_e of exchange motion is the same for the two types of terms, but otherwise is the only simple way to represent the situation. Using (31) one immediately sees that, if $\omega_e \gg \omega_0$, $\varphi_{\Delta\omega}$ will be zero long before $\cos\omega_0 t$ can vary much from unity, so that we can for practical purposes use (16), just multiplying ω_p^2 by 10/3 in obtaining the breadth. On the other hand, if $\omega_e \ll \omega_0$ the cosine term will be rapidly varying and will eventually average to zero in its contribution to the main line. In the last column of Table IA we see that the factor 10/3 greatly improves the agreement with experiment, bringing the ratio of theory and experiment within the factor of two we have allowed ourselves.

We can still improve this agreement, however, as is suggested by a glance at Table I. Those cases in which H_p is least still seem to have too great an observed breadth. Can there be still another source of broadening? A number of authors[9–11] have measured very appreciable fine structures, of order 1000 to 2000 gauss in total width, in dilute salts of Mn^{++} and Fe^{+++}. These fine structures are due both to the nuclear hyperfine splitting and to crystal field splittings. Naturally, the latter, major, source of splitting varies from crystal to crystal, but the order of magnitude is roughly constant; and there is no reason whatever to believe that the forces causing these splittings are not operative in the more concentrated salts. It is known (see, e.g., reference 2) that such splittings will be narrowed out by exchange just like dipolar interactions; but nonetheless they represent an extra interaction which must be added in with the dipolar interactions to compute the full width.

This extra contribution is taken into account in the following rough manner: we assume the fine structure fields to be roughly constant, of mean square magnitude H_H^2, in all salts. H_H^2 will represent only in order of magnitude the true mean square width of the fine structure since we know only to order of magnitude how to compute the corresponding exchange narrowing; even given the mean fourth moment we certainly could not use the Gaussian assumptions. The introduction of H_H^2 has been done graphically in Fig. 1 as follows. We assume, for extreme narrowing,

$$\Delta H = [(10/3)H_p^2 + H_H^2)]/H_e,$$

which may be written $H_e \Delta H = (10/3)H_p^2 + H_H^2$. Thus if, as in Fig. 1, we plot $H_e\Delta H$ against $(10/3)H_p^2$ for various salts we should get points which cluster around a line of slope unity with a positive intercept on the $H_e\Delta H$ axis, of order of magnitude $H_H^2 \simeq 10^6$. The figure shows that this is the case; the slope of the line is 1 ± 20 percent or so, the intercept $1 \pm 1 \times 10^6$. The agreement is excellent considering the variations of crystal structure effects from salt to salt which are to be expected.

In the second half of Table I we list those salts with small θ. We can certainly make no definite predictions

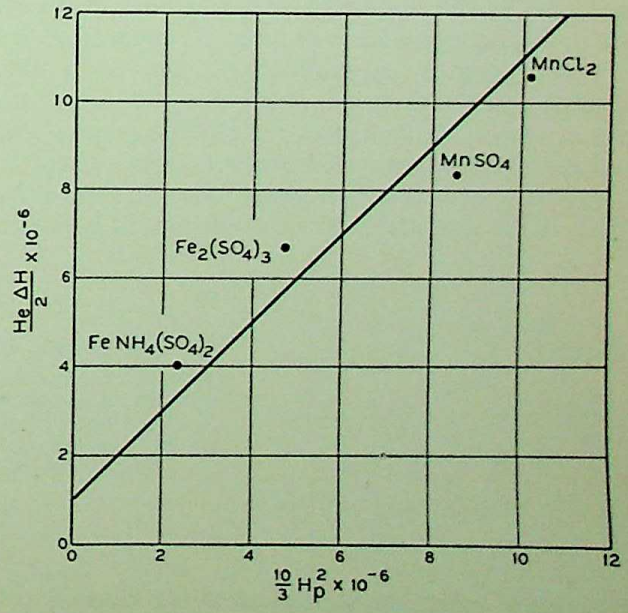


FIG. 1.

‡ F. Keffer has arrived independently at the same conclusion (thesis, University of California, Berkeley, 1951).

[9] Bragguley, Bleaney, Griffiths, Penrose, and Plumpton, Proc. Phys. Soc. (London) 61, 551 (1948).

[10] B. Bleaney, Physica 17, 175 (1951).

[11] Ubbink, Poulis, and Gorter, Physica 17, 213 (1951).

CC-0. In Public Domain. Gurukul Kangri Collection, Haridwar

Digitized by Arya Samaj Foundation Chennai and eGangotri

about these salts, in view of the experimental and theoretical uncertainties, but we have listed, first (H_p^2/H_e) taking H_e the maximum possible as a lower limit, and second $\sim(H_p^2+H_H^2)^{\frac{1}{2}}$ as an upper limit, to the predicted breadths. All cases lie within the limits.

The first three salts seem on the face of it to agree excellently with H_p, i.e., the Van Vleck theory, and to need no exchange narrowing correction. However, it is a little hard to believe that the authors who measured θ could be in such great error as to mistake $\theta=0$ for $\theta=2$ or 3, as would be required to explain this fact. The fourth salt, the fluosilicate,[12] is included to show that the agreement with Van Vleck can be illusory; we see that this salt has a breadth considerably larger than H_p, so that certainly there is a considerable H_H contribution. Thus we believe that the other three salts do indeed have exchange narrowing effects, with H_e of order 10^3 gauss, compensating the extra width owing to fine structure.

It is worth mentioning one other substance we have considered, $CuSO_4 \cdot 5H_2O$. Bagguley and Griffiths[13] have measured single crystal lines at a number of frequencies and in a number of directions. Cu^{++}, under conditions of roughly axial symmetry as in this salt, shows a fairly large anisotropy both of g and of hyperfine structure, with the width of the hyperfine structure being usually fairly negligible perpendicular to the axis. In this direction the half-width is about 25 oersted at their highest frequency, which leads one to estimate an exchange field of $\sim$1600 oe. The Curie point is about 0.7°K,[14] which corresponds to 2400 oe exchange field, in quite good agreement; while Bagguley and Griffiths were themselves able to estimate an exchange field, from the frequency at which they could resolve certain lines owing to the two molecules per unit cell, of around 2000 oe. In addition, at their lowest frequency ($\sim$3 cm) these authors found a slight increase in line widths, as would be predicted because here the "10/3 effect" should be beginning to appear.

It would be of interest to measure more directly the "10/3 effect" in a salt in which the exchange frequency can be bracketed by two measuring frequencies. It is extremely important, however, to avoid difficulties which are due to anisotropy broadening by using either single crystals or salts with $L=0$, and to be sure that spin lattice broadening is not present (i.e., that the spin-spin interactions make the lines reasonably broad).

Thus we find that in no cases we have considered are the data in appreciable disagreement with values predicted from our theory, if the corrections for off-diagonal elements of the dipolar interactions and for fine and hyperfine structure are taken into account. We feel that the theory and the concepts it uses are thus essentially correct. There seem in paramagnetic substances to be no unexplained sources of broadening such as are present in ferromagnetic materials and in antiferromagnetic materials near their Curie points.

[12] The measurement here is an unpublished one by W. A. Yager.

[13] D. M. S. Bagguley and J. H. E. Griffiths, Proc. Roy. Soc. (London) **A201**, 366 (1950).

[14] This value comes from de Haas and C. J. Gorter, Leiden Comm. 210d. K. S. Krishnan and A. Mookerji, Phys. Rev. **54**, 841 (1938) find a considerable anisotropy of θ, with only the roughest agreement with the above value found for the powder. Both sets of measurements are at 14°K or higher. T. H. Gaballe and W. F. Giauque, J. Am. Chem. Soc. **74**, 3513 (1952), working along a single axis, agree somewhat better at liquid helium temperatures with the earlier 0.7°K value than with the 1.8°K value found for this axis by Krishnan and Mookerji. In view of the uncertainties in the susceptibility work it is best to regard our agreement above as somewhat fortuitous.

CC-0. In Public Domain. Gurukul Kangri Collection, Haridwar

Digitized by Arya Samaj Foundation Chennai and eGangotri

REVIEWS OF MODERN PHYSICS VOLUME 25, NUMBER 1 JANUARY, 1953

Antiferromagnetism and Antiferromagnetic Resonance in a Rhombic Crystal at $T=0$

C. J. GORTER

Kamerlingh Onnes Laboratorium, Leiden, The Netherlands

Neél's phenomenological theory of antiferromagnetism at zero temperature has been worked out for a three-dimensional case. When the external magnetic field comes near to a certain hyperbola in the field space lying in the plane through the favored and the least favored direction of magnetization, an anomaly occurs. This anomaly consists of a rapid turn-over of the two opposed directions of magnetization into the direction perpendicular to the plane just mentioned. At much higher fields the two opposed directions of magnetization will deviate towards the field, and finally antiferromagnetism will go over into paramagnetic saturation.

Following the general method of Kittel, Ubbink has investigated antiferromagnetic resonance. At not too high frequencies two resonance fields will be flanking the hyperbola in field space. At higher frequencies one resonance field will decrease and vanish, while the other one will approach the field of paramagnetic resonance.

IN Neél's phenomenological description of antiferromagnetism[1] the magnetic ions are divided over two sublattices, which we shall indicate, respectively, by a single and by a double dash.

In addition to the external field H, the spins in the first sublattice experience a virtual magnetic field $-\alpha\sigma''$, while the spins in the double dashed sublattice experience a virtual field $-\alpha\sigma'$, where the σ's represent the average magnetization in the sublattice indicated.

Now the virtual fields tend to keep the magnetizations of the two sublattices exactly opposite to each other. As long as the external field is small compared to the virtual fields it tends to orientate the opposite magnetizations perpendicularly to itself, since then the magnetic decrease of energy is largest. On the other hand, crystalline anisotropy may favor certain orientations of the opposite magnetizations. When the external field becomes of the same order as the virtual fields, it forces the magnetizations into its own direction. In the investigation discussed the interplay of these different tendencies is analyzed.

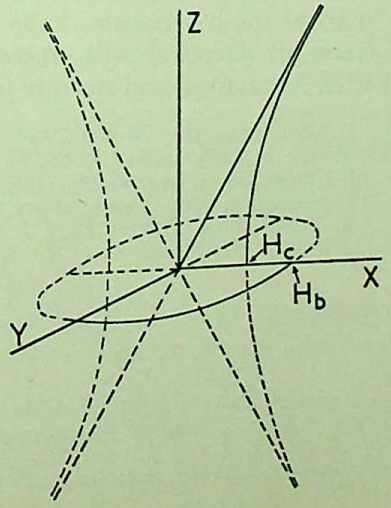


FIG. 1. Hyperbola and ellipse in the H space.

Let us suppose that α as well as μ differ in the direction of the three rhombic axes x, y, and z. Considering ionic levels with a twofold degeneration we get

$$H_x'=H_x-(\alpha_x\mu_xH_x''/W'')\tanh(W''/kT)(+\text{perm}),$$
$$H_x''=H_x-(\alpha_x\mu_xH_x'/W')\tanh(W'/kT)(+\text{perm}),$$

where

$$W'=+(\mu_x^2H_x'^2+\mu_y^2H_y'^2+\mu_z^2H_z'^2)^{\frac{1}{2}},$$
$$W''=+(\mu_x^2H_x''^2+\mu_y^2H_y''^2+\mu_z^2H_z''^2)^{\frac{1}{2}}.$$

In cooperation with Dr. J. Haantjes, professor of geometry in Leiden, the solutions of these eight equations have been analyzed for $T=0$, in which case the hyperbolic tangents are equal to one.[2]

Four different solutions are found which will be indicated by A, B, C, and D. At zero external field the A, B, and C solutions give saturated sublattices magnetized in the $\pm x$, $\pm y$, and $\pm z$ directions, respectively. The D solution has an identical magnetization of the sublattices, and this represents the case of paramagnetic saturation. Up to an external magnetic field of the order of $\alpha\mu$ only the solutions A, B, and C exist. If $\alpha_x\mu_x^2>\alpha_y\mu_y^2>\alpha_z\mu_z^2$, which means that the $\pm x$ directions are energetically the most favorable ones and the $\pm z$ directions the least favorable ones, the A solution has and keeps the lower energy and will thus be realized. Between a field of the order of $\alpha\mu$ and one of the order

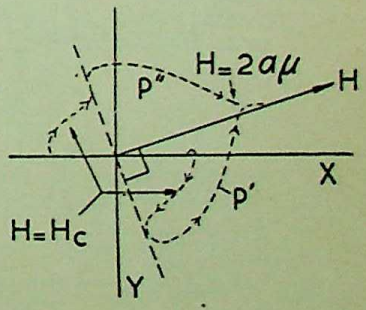


FIG. 2. The directions p' and p'' of the magnetizations of the sublattices when a field H, orientated in the xy plane, is increased.

[1] L. Neél, Ann. phys. 18, 5 (1932); 5, 232 (1936); 3, 137 (1948). J. H. Van Vleck, J. Chem. Phys. 9, 85 (1941).

[2] C. J. Gorter and J. Haantjes, Leiden Comm. Suppl. 104b, Physica 18, 285 (1952).

CC-0. In Public Domain. Gurukul Kangri Collection, Haridwar

Digitized by Arya Samaj Foundation Chennai and eGangotri

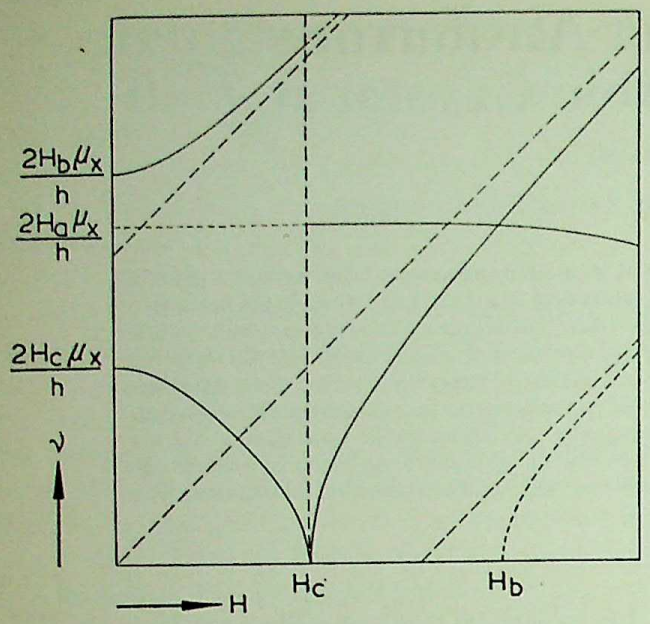


FIG. 3. Antiferromagnetic resonance frequencies drawn as a function of a field H in the x direction of the crystal. H_c is the turn-over field, and the dotted line through (0,0) gives the frequencies of paramagnetic resonance.

of $2\alpha\mu$ the magnetizations are strongly bent towards the field. In this region A, B, and D exist, while A remains the stable solution. Finally, the directions of the magnetizations in the three solutions merge, and the D solution is the only one that remains.

However, in the low field region certain very remarkable anomalies are to be expected. These anomalies occur when the field comes near to a certain hyperbola in the xz plane or to a certain ellipse in the xy plane. See Fig. 1. The anomaly then consists in a rapid exchange of place between the A and B solutions and the B and C solutions, respectively. In the neighborhood of the hyperbola we thus have, in the realized A solution, a rapid turn-over from directions near to $\pm x$ to directions near to $\pm y$. In this way the crystalline preference for magnetization in the $\pm x$ directions is checked by the magnetic field favoring directions perpendicular to itself. The turn-over field in the x direction is

$$H_c=(\alpha_x^2\mu_x^4-\alpha_y^2\mu_y^4)^{\frac{1}{2}}/\mu_x.$$

If the anisotropies are relatively small, we may say that the turn-over field

$$H_c=[2\alpha(\alpha_z\mu_x^2-\alpha_y\mu_y^2)]^{\frac{1}{2}}.$$

If the field lies in the xy plane, the turn-over takes place gradually in the same field region. If it lies in the xz plane, the magnetizations move gradually towards the $\pm c$ direction; but if the angle between field and x axis is smaller than $\arctan[\mu_x^2(\alpha_y^2\mu_y^4-\alpha_z^2\mu_z^4)/\mu^2(\alpha_x^2\mu_x^4-\alpha_y^2\mu_y^4)]^{\frac{1}{2}}$, a turn-over into the b direction occurs when the hyperbola in the field space is reached.

Figure 2 indicates how, as a result of all this, the two directions of magnetization move when a field, orientated in the xy plane, is gradually increased.

Following the general method of Bloch and Kittel,[3] Mr. J. Ubbink has extended the treatment given above to the antiferromagnetic resonance occurring when an alternating field is added.[4] If an external field is orientated in the x direction, resonance is, in general, to be expected at two frequencies (Fig. 3). In a very small field one of these is equal to $2H_c\mu_x/h$ and the other one is equal to $2H_b\mu_x/h$, where H_b is the field where the x axis cuts the ellipse in the xy plane. The lower one of these frequencies decreases with increasing field and becomes zero at $H=H_c$.

The larger frequency increases at the same time. At $H=H_c$ the turn-over takes place and the resonance frequencies are replaced by two others, one of which starts at zero and increases rapidly with increasing field, approaching the frequency of paramagnetic resonance $2H\mu_x/h$.

In practice the resonances are studied at constant frequency and varying field. As long as the frequency is relatively low we expect one resonance field slightly below and one slightly above H_c. The interval between the two will increase with increasing ν, and the low resonance field will become zero at $\nu=2H_c\mu_x/h$.

If H is having another position in the xz plane the hyperbola in field space will be flanked by two resonance curves, while in the xy plane the two resonances will merge and disappear when the angle with the x direction increases.

We shall not discuss now Ubbink's conclusions on the resonances in the higher fields of the order of $2\alpha\mu$.

Part of the conclusions of the calculations made in Leiden are identical with those obtained by Neél, Kittel, Nagamiya,[5] and recently by Yosida.[6]

[3] F. Bloch, Phys. Rev. **70**, 460 (1946); C. Kittel, Phys. Rev. **71**, 270 (1947); F. Keffer and C. Kittel, Phys. Rev. **85**, 329 (1952).
[4] J. Ubbink, Phys. Rev. **86**, 567 (1952).
[5] T. Nagamiya, Prog. Theoret. Phys. **6**, 350 (1951).
[6] K. Yosida, Prog. Theoret. Phys. **7**, 25 (1952).

CC-0. In Public Domain. Gurukul Kangri Collection, Haridwar

Digitized by Arya Samaj Foundation Chennai and eGangotri

REVIEWS OF MODERN PHYSICS VOLUME 25, NUMBER 1 JANUARY, 1953

Antiferromagnetic Resonance*

L. R. MAXWELL AND T. R. MCGUIRE

U. S. Naval Ordnance Laboratory, White Oak, Maryland

The frequencies at which electronic resonance will occur apparently lie beyond the region now available with conventional microwave equipment for those materials having Curie temperatures well above 0°K. Cr_2O_3, MnO, MnTe, and MnSe show a large decrease in the amount of resonance absorption as the material (powdered) is lowered through its Curie temperature, with only a small residual absorption remaining in the antiferromagnetic region. MnSe has an absorption *vs* temperature hysteresis loop that is correlated with a magnetic susceptibility loop previously reported for this material. The g values remain constant as the absorption decreases. Considerable absorption is found at zero static magnetic field for MnO, MnS, and MnTe. The line widths increase sharply as the temperature of the material approaches the Curie temperature. CoO and VO_2 give no detectable absorption either above or below their Curie temperatures. NiO and CuO show no absorption in the antiferromagnetic region.

I. INTRODUCTION

THE problem of predicting electronic resonance in the antiferromagnetic state is essentially a problem of understanding the behavior of the normal frequencies of precession of two sublattices of magnetization having oppositely directed spins. Once the normal frequencies are determined, then one can expect with certainty that magnetic resonance absorption will occur when the frequency of the applied transverse rf field is equal to a normal frequency. Although in actual experiments there may exist more than one sublattice in one direction, the experiment deals, in effect, with only two groups of spins; within each group each spin feels the same anisotropy and exchange fields.

The initial investigation[1] studied experimentally the change in absorption at 9300 Mc in going from the paramagnetic to the antiferromagnetic region for Cr_2O_3 by our group at the Naval Ordnance Laboratory. Similar work[2] was carried out on MnF_2 by Hutchison at the University of Chicago. These investigations showed a sharp break in the absorption as the material was cooled through its Curie temperature (T_c) with either no measurable absorption or only a small residual existing below T_c. As a result of this work, we believed that the normal frequencies of these materials lay beyond the region obtainable by our equipment. However, Okamura, Torizuka, and Kojima[3] reported appreciable amounts of absorption for MnO, MnS, and MnSe below the Curie temperature, with no sudden drop as had been found for Cr_2O_3 and MnF_2. The reason for this difference in response of these materials was not apparent.

Kittel[4] and Nagamiya[5] have calculated the equations of motion of the antiferromagnetic system where the exchange forces are treated as molecular fields and where, similar to the ferromagnetic case, an anisotropy term is introduced to take into account the turning of both spin systems together and relative to a cubic crystal lattice at 0°K. From this one obtains the resonance frequency as

$$\omega_0/\gamma = H_0 \pm [H_a(H_a+2H_e)]^{\frac{1}{2}}, \qquad (1)$$

where H_0 is the static applied magnetic field, H_a and H_e internal fields describing the anisotropy and exchange fields. Physically this means that there should exist two different directions of circular polarization both of which are capable of being excited by the rf field. For the materials mentioned above, which have relatively high Curie temperatures, H_e is of the order of 10^6 oersteds and much larger than either H_0 or H_a, in which case Eq. (1) reduces to a single frequency

$$\omega_0/\gamma = (2H_aH_e)^{\frac{1}{2}}, \qquad (2)$$

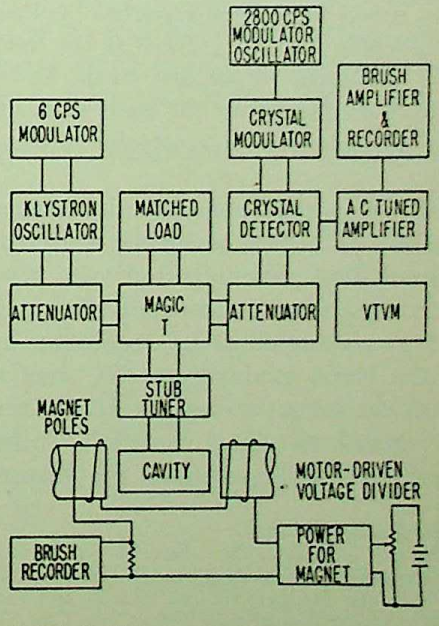


FIG. 1. Block diagram of microwave apparatus for recording magnetic resonance absorption.

* Supported in part by the U. S. Office of Naval Research.

[1] Trounson, Bleil, Wangsness, and Maxwell, Phys. Rev. 79, 542 (1950); L. R. Maxwell, Am. J. Phys. 20, 80 (1952).

[2] Reported by private communication (see also second paper reference 1).

[3] Okamura, Torizuka, and Kojima, Phys. Rev. 82, 285 (1951).

[4] C. Kittel, Phys. Rev. 82, 565 (1951).

[5] T. Nagamiya, Prog. Theoret. Phys. 6, 350 (1951).

CC-0. In Public Domain. Gurukul Kangri Collection, Haridwar

Digitized by Arya Samaj Foundation Chennai and eGangotri

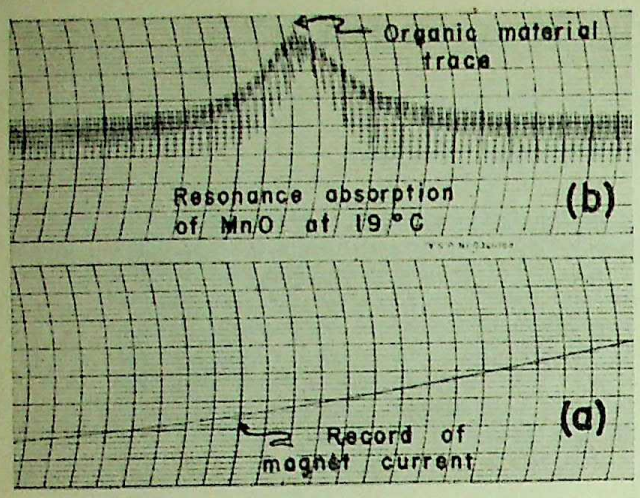


FIG. 2. Photograph of a recorded record showing a resonance curve for MnO.

From Eq. (2) we estimate that for no external static magnetic field the resonance frequency is beyond the range available with conventional microwave equipment. For MnF_2 Keffer[6] predicts resonance at a wavelength of 1.1 mm at 0°K.

The classical calculations have been extended by Keffer and Kittel[7] to cover ellipsoidal shapes, orthorhombic symmetry, and a generalized two lattice anisotropy; they also included a quantum-mechanical derivation of the resonance equations which agreed essentially with the classical treatment. Wangsness[8] has shown that both antiferromagnetic and ferromagnetic resonance conditions are special cases of a more general system of two interpenetrating magnetic sublattices.

The theory calls for the appearance of a doublet as the material is cooled through the Curie temperature, once the frequency and static magnetic field are within proper values. The existence of two electronic resonance absorption bands have been reported by Poulis *et al.*[9] at 9400-Mc region for $CuCl_2 \cdot 2H_2O$ at low temperatures where the exchange forces are weak. Ubbink[10] has interpreted their results on the basis of antiferromagnetism at absolute zero in a crystal having rhombic symmetry.

We wish now to confine our attention to experimental investigations of antiferromagnetic materials having Curie temperatures above liquid nitrogen temperature, using 3-cm equipment, and to study the change in the nature of the absorption as one approaches and passes through the Curie temperature. We shall report on recent work carried out at the Naval Ordnance Laboratory on various powdered materials, including the manganese compounds studied by the Japanese.

[6] F. Keffer (to be published).
[7] F. Keffer and C. Kittel, Phys. Rev. 85, 329 (1952).
[8] R. K. Wangsness, Phys. Rev. 86, 146 (1952).
[9] Poulis, van den Handel, Ubbink, Poulis, and Gorter, Phys. Rev. 82, 552 (1951); J. Ubbink, Proc. Conf. Low Temp. Phys. Oxford (1951), p. 163.
[10] J. Ubbink, Phys. Rev. 86, 567 (1952).

II. EXPERIMENTAL PROCEDURE

A. Experimental Method

We use the procedures developed by other investigators for paramagnetic resonance. The sample is located at the bottom of an iris coupled resonant cavity, placed in the presence of an external steady magnetic field in a direction perpendicular to the rf magnetic field. The absorption is detected as a change in intensity of reflection from the cavity. At resonance we have[11]

$$\frac{P_r}{P_i}=\left[\frac{(Q_e/Q_0)-1}{(Q_e/Q_0)+1}\right]^2, \tag{3}$$

where P_i = power incident upon the cavity; P_r = power reflected from the cavity; Q_e (external Q) = $\pi\times$energy stored in cavity/energy lost per $\frac{1}{2}$ cycle external to the cavity; Q_0 (unloaded Q) = $\pi\times$energy stored in cavity/energy lost per $\frac{1}{2}$ cycle in the cavity. We define Γ by

$$|\Gamma|=(P_r/P_i)^{\frac{1}{2}},$$

express

$$1/Q_0=(1/Q_w)+(1/Q_M),$$

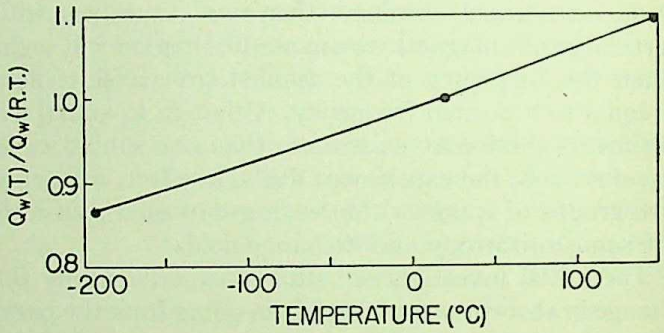


FIG. 3. Variation of $Q_w(T)/Q_w$(R.T.) with temperature.

and define Q_L by

$$1/Q_L=(1/Q_w)+(1/Q_e),$$

where $1/Q_w$ and $1/Q_M$ are proportional to the losses in the walls of the cavity and to magnetic absorption of the material within the cavity, respectively. Then one can formulate Eq. (3) as

$$\frac{Q_L}{Q_M}=\frac{|\Gamma|-|\Gamma_0|}{1-|\Gamma|}, \tag{4}$$

which is the expression given by Whitmer and Weidner,[12] where

$$|\Gamma_0|=(P_{r_0}/P_i)^{\frac{1}{2}} \tag{5}$$

is the reflection for $H=0$. Upon application of the magnetic field, P_r may decrease in a manner defined as

$$P_r=P_{r_0}(1-S). \tag{6}$$

[11] R. D. Arnold and A. F. Kip, Phys. Rev. 75, 1199 (1949).
[12] C. A. Whitmer and R. T. Weidner, Fifth Annual Progress Report on Nuclear and Electronic Paramagnetism and Low Temperature Studies (1951), p. 24; R. T. Weidner and C. A. Whitmer, Rev. Sci. Instr. 23, 75 (1952).

CC-0. In Public Domain. Gurukul Kangri Collection, Haridwar

Digitized by Arya Samaj Foundation Chennai and eGangotri

Substituting Eqs. (5) and (6) in Eq. (4) we have, for $S^2<1$ neglecting terms of S^3 and higher powers,

$$\frac{Q_L}{Q_M}=\frac{\frac{1}{2}S+\frac{1}{8}S^2}{1-\frac{1}{2}S-\frac{1}{8}S^2-(P_i/P_{r_0})^{\frac{1}{2}}}. \tag{7}$$

The magnetic loss is approximately linear with S provided that

$$(P_i/P_{r_0})^{\frac{1}{2}}\geqq 3.$$

B. Experimental Arrangement

Figure 1 indicates, by means of a block diagram, the essential units required for measuring the electronic resonance. The microwave power is furnished by a klystron oscillator operating at a frequency of approximately 9300 Mc under the influence of a low frequency modulator arranged to vary the reflector voltage. By this method the energy incident upon the magic tee is frequency modulated about 6 times each second. The material under examination is placed in a rectangular cavity located between the pole pices of an electromagnet with the static and alternating magnetic fields arranged orthogonally. Detection of the unbalance is made through the combination of a crystal modulator and detector; the latter is connected to an amplifier and recorded (I). The current through the windings of the electromagnet is recorded by a second brush recorder (II).

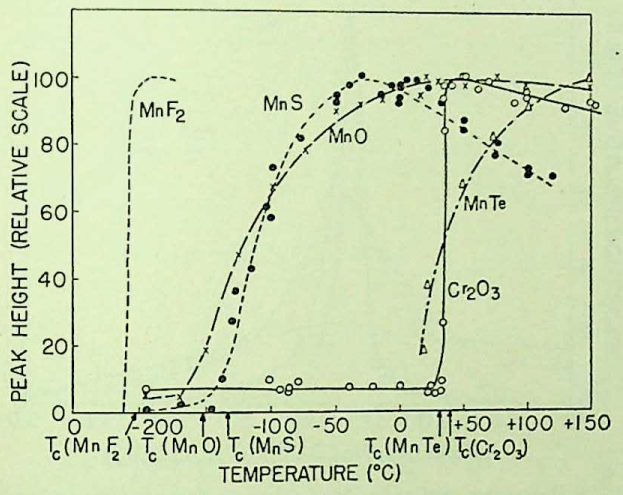


FIG. 4 Variation of the height of the resonance absorption with temperature.

Figure 2 illustrates a typical record made with the apparatus described above. A typical record of II is shown in Fig. 2(a) which gives an approximate linear variation in current with time. Power for this current is provided by an electronic power supply whose output is grid controlled through a motor driven voltage divider. The output from the detector is shown in Fig. (2b) as a trace oscillating at the frequency of the modulator. By varying the frequency of the klystron in this manner it is possible always to pass through the resonance frequency of the cavity. This procedure is somewhat similar to the method used by Whitmer and Weidner.[12] A specimen of diphenyl trinitrophenyl hydrazyl was usually added to the cavity to be used in determining the g values. This material produces a narrow pip superimposed upon the absorption record [see Fig. 2(b)].

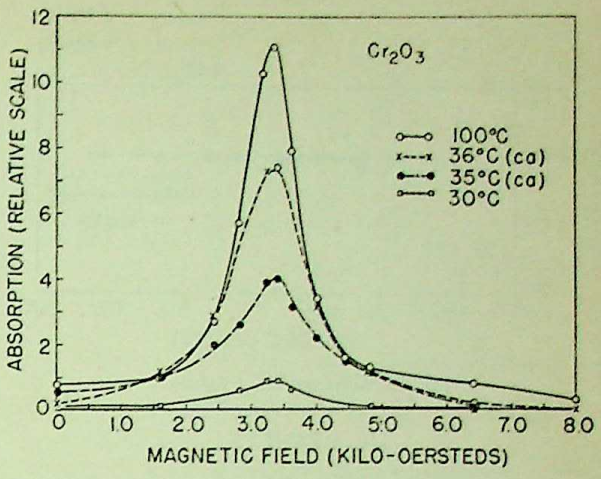


FIG. 5. Resonance curves for Cr_2O_3 taken at various temperatures.

The zero absorption has been arbitrarily defined as the amount of absorption existing at the maximum magnetic field used (approximately 8000 oersteds). The envelope formed by the upper portion of the trace shown in Fig. 2(b) gives the absorption of the material as a function of the applied static magnetic field and is a measure of the quantity S which is proportional to the magnetic absorption.

We have considered above that Q_w is temperature independent. Measurements made at various temperatures with the cavity empty gave a variation of $Q_w(T)/Q_w$ (room temperature) as illustrated by Fig. 3. These changes due to temperature variation were small compared to the changes in the magnetic losses which were found to occur in the neighborhood of the Curie temperatures and were therefore neglected.

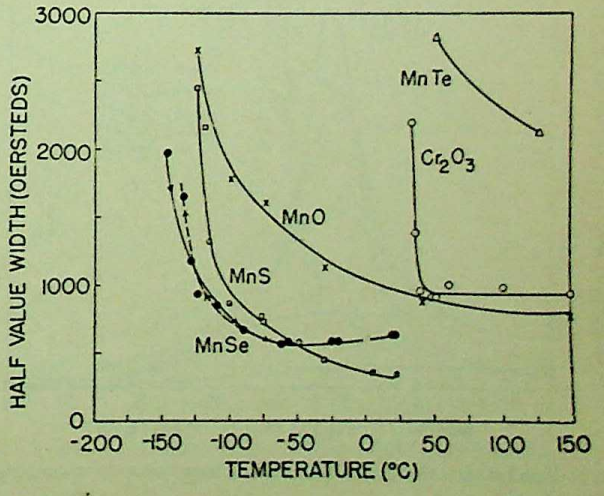


FIG. 6. Variation of half-value widths with temperature.

CC-0. In Public Domain. Gurukul Kangri Collection, Haridwar

Digitized by Arya Samaj Foundation Chennai and eGangotri

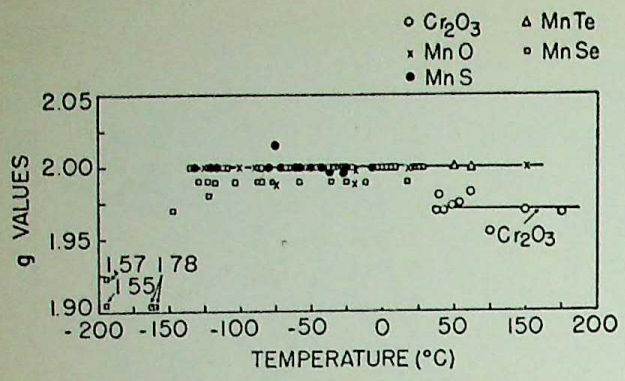


FIG. 7. Summary of g values.

III. RESULTS

Except for certain of the compounds given below, we have obtained as a function of the temperature the height of the peak absorption (normalized to 100 at the maximum), the absorption as a function of the applied static magnetic field, half-value widths, and g values. The g values have been determined with reference to the value of 2.004 reported[13] for diphenyl-trinitrophenyl hydrazyl. This value is temperature independent.[12] All data are for powdered material.

1. Cr_2O_3

Recent data have been obtained with a sample of high purity (Johnson, Matthey, and Company) which gives a variation of peak height *vs* temperature as shown in Fig. 4. This is essentially the same type of curve reported previously by us[1] but with a lesser slope above the Curie temperature. We find, for this material, that the temperature-dependent peak reported previously[1] is absent. As seen in Fig. 5 the absorption decreases to a small residual below the Curie temperature. The half-value width increases abruptly at the Curie temperature (Fig. 6). The g values, except for some scatter, are temperature independent at about 1.97, as seen in Fig. 7, and are significantly less than 2.00.

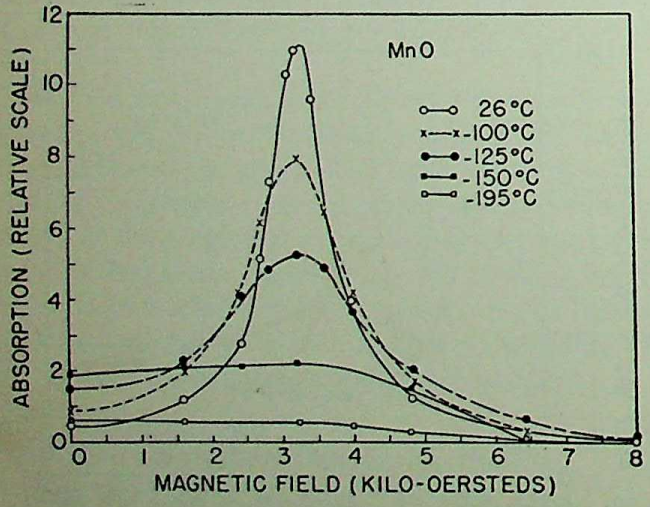


FIG. 8. Resonance curves for MnO taken at various temperatures.

[13] Holden, Kittel, Merritt, and Yager, Phys. Rev. 77, 147 (1950).

2. MnO

As contrasted to Cr_2O_3, the peak absorption decreases more gradually as the Curie temperature is reached and then levels off to a small residual (Fig. 4). The absorption diminishes and broadens as the Curie temperature is reached, losing its resonance characteristic (as shown in Fig. 8). It shows considerable absorption at zero magnetic field at −150°C. This fact was not evident in the preliminary measurements[1] made on this material because of insufficient data at the higher magnetic fields where zero absorption is fixed. The g values are independent of temperature and close to 2.00 (Fig. 7).

3. MnS

The peak absorption goes through a maximum at about −50°, dropping to a small residual below its Curie temperature. Similar to MnO, we find a broad

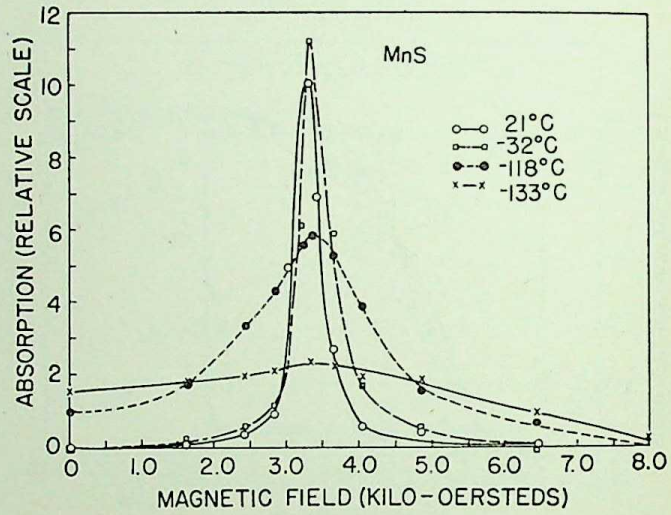


FIG. 9. Resonance curves for MnS taken at various temperatures.

absorption near the Curie temperature (Fig. 9) with appreciable absorption at zero magnetic field at −133°C. The half-value widths increase rapidly near the Curie temperature as seen in Fig. 6. The g values are close to 2.00 (Fig. 7).

4. MnTe

The magnetic absorption was considerably weaker for MnTe than for the materials mentioned above. This fact is not apparent from Fig. 4 because of the normalization. It was observed, however, that the peak absorption decreased to a small value below the Curie temperature. Again broad absorption was found below the Curie temperature (Fig. 10). Large half-value widths were found (Fig. 6) and g values are 2.00.

5. MnSe

Above the Curie temperature the peak absorption shows a temperature hysteresis loop as illustrated in Fig. 11. The loop opens at about room temperature and

CC-0. In Public Domain. Gurukul Kangri Collection, Haridwar

Digitized by Arya Samaj Foundation Chennai and eGangotri

closes at approximately −150°C, and then the absorption drops to a small residual at liquid air temperature. The upper portion of the loop is formed during the cooling part of the cycle. Figure 12 gives the variation of absorption with external static magnetic field as the temperature of the material is decreasing. The absorption broadens as the temperature approaches −150°C, showing definite absorption at zero field at −134°C. The half-value width, for both decreasing and increasing temperature, are given in Fig. 6; a slight hysteresis loop is present. At temperatures from about −150°C to liquid nitrogen there was a small residual peak, not illustrated in Fig. 12, that moved off the resonance condition to give low g values as shown in Fig. 7. At −130°C and above, the g values were temperature independent and scattered between 2.00 and 1.99.

6. CoO

With a Curie temperature of 12°C it was possible to investigate CoO both in the paramagnetic and antiferromagnetic region. Throughout the region studied, from −195°C to 25°C, no measurable absorption was detectable.

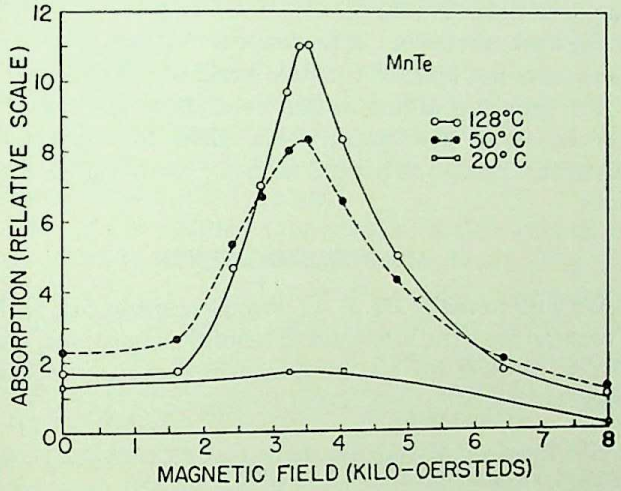


FIG. 10. Resonance curves for MnTe taken at various temperatures.

7. NiO

Only measurements below the Curie temperature (378°C) were made which gave no absorption.

8. CuO

No magnetic absorption was detectable in the antiferromagnetic region. The Curie temperature was approximately 250°C.

9. VO_2

Over the temperature region 25°C to 100°C no magnetic absorption was observed. The Curie temperature of VO_2 is about 60°C.

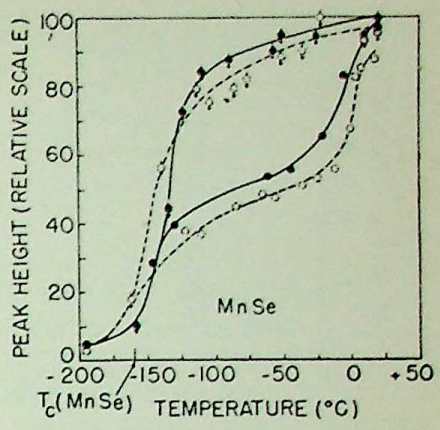


FIG. 11. Variation of peak height with temperature for MnSe for two sets of data.

IV. DISCUSSION

For all of these materials that exhibit paramagnetic resonance, we find that as the temperature is lowered through the Curie temperature, the amount of absorption decreases, the peaks broaden, and at a few degrees below the Curie temperature the absorption either disappears or remains as a low residual. In many instances, there is an appreciable amount of absorption at zero magnetic field. The abruptness of the decrease in absorption is greater for Cr_2O_3 and MnF_2 than for MnS, MnSe, MnTe, and MnO; the latter shows the slowest decent. This is illustrated in Fig. 13, where both temperature and peak heights are normalized.

Our data do not agree with the work reported by Okamura *et al.*[3] for MnO, MnS, and MnSe except in certain general features. We have no explanation for this difference. Our results not only conform to what one would expect from the theory, but, together with the response shown by Cr_2O_3 and MnF_2, they give a consistent picture of this phenomena at the temperatures investigated.

The hysteresis loop found for MnSe (Fig. 11) follows approximately a similar loop reported by Lindsay[14] for the variation of the magnetic susceptibility with temperature. He suggested that there exists three

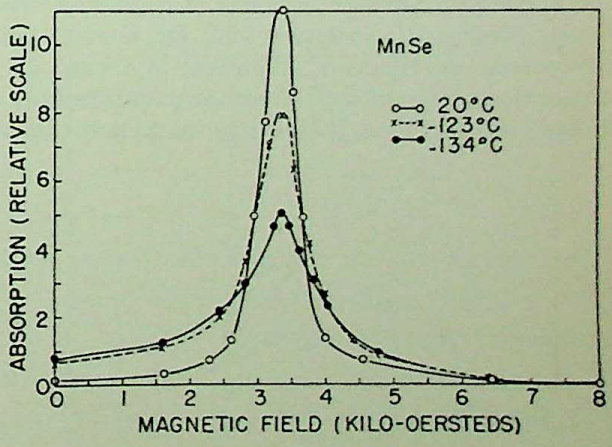


FIG. 12. Resonance curves for MnSe taken during decreasing temperature cycle.

[14] R. Lindsay, Phys. Rev. 84, 569 (1951).

CC-0. In Public Domain. Gurukul Kangri Collection, Haridwar

Digitized by Arya Samaj Foundation Chennai and eGangotri

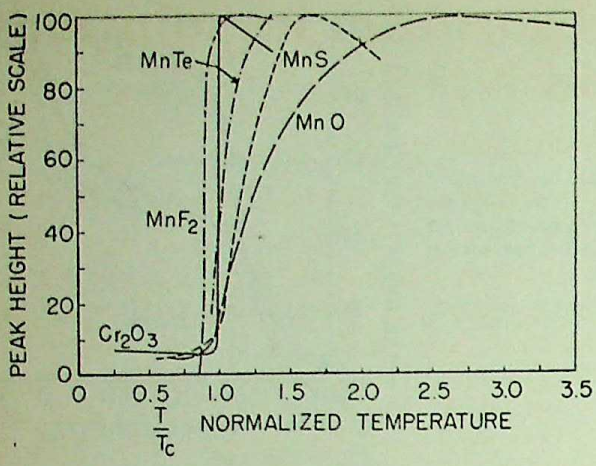


FIG. 13. Variation of the height of the resonance absorption with temperature normalized to the Curie temperature.

separate phases of MnSe. The presence of the loop is taken as a measure of the amount of the various phases present, which depends upon whether the material has been heated or cooled prior to the time of the measurement.

Within the paramagnetic region one finds for Cr_2O_3, MnS, and to a lesser degree for MnO, an increase in absorption with decreasing temperature similar to the magnetic susceptibility relationship. The departure from this similarity occurs as the antiferromagnetic alignment sets in. If, in the antiferromagnetic state, the frequency of the field could be tuned to the normal frequencies of the magnetic lattice, one might find new correlations between resonance absorption and magnetic susceptibility.

The origin of the low residual absorption found for certain materials below the Curie temperature cannot be definitely determined. They may be due to traces of ferromagnetic impurities. In the case of Cr_2O_3, magnetic susceptibility measurements showed the presence of a ferromagnetic impurity, although spectroscopic measurements showed no trace of Fe, Co, or Ni.

Line broadening with reduction in absorption as the Curie temperature is reached is characteristic of all of the materials for which paramagnetic resonance absorption was found. This is the trend indicated by Tsuya and Ichikawa,[15] who have calculated the line width as a function of temperature but without including crystal anisotropy.

V. CONCLUSION

The experiments made at liquid nitrogen and higher temperatures, where the exchange forces are strong, show no appreciable resonance absorption in the antiferromagnetic state. The theory has been concerned with determining the frequency requirement for resonance and has indicated the experimental condition necessary to obtain resonance. These conditions can be met by studying materials that have low Curie temperatures, going to considerably higher frequency (millimeters or less), and by using intense external static magnetic fields. At the present time, with the exception of the work carried out in Leiden, the theory and experiment have not reached common ground in this respect.

The problems of line widths, relaxation times, and a calculation of the quantitative yield for resonance absorption remain as fruitful fields for further investigations.

VI. ACKNOWLEDGMENTS

We wish to thank Dr. R. K. Wangsness and Mr. E. P. Trounson for their interest and helpful suggestions, and Mr. E. Wenzel for his assistance in the experimental work carried out at the Naval Ordnance Laboratory.

[15] N. Tsuya and Y. Ichikawa, Phys. Rev. 83, 1065 (1951); Sc. Reports, Tohoku University 35, 74 (1951).

DISCUSSION

A. I. SNOW, *Sinclair Research Laboratories, Inc., Harvey, Illinois:* In connection with Dr. Gorter's comments about the effects of differences in crystal structure on comparison of the Leiden work and the work of Maxwell and McGuire, it is interesting to note that the peak height and half-width curves for MnO, MnS, and MnTe obtained by Maxwell and McGuire show no abnormal changes although the crystal structures change from face-centered cubic (NaCl type) to hexagonal (probably NiAs type) as one goes from MnO to MnTe.

CC-0. In Public Domain. Gurukul Kangri Collection, Haridwar

Digitized by Arya Samaj Foundation Chennai and eGangotri

REVIEWS OF MODERN PHYSICS VOLUME 25, NUMBER 1 JANUARY, 1953

Paramagnetic Resonance Absorption in Solutions of K in Liquid NH_3*

CLYDE A. HUTCHISON, JR., AND RICARDO C. PASTOR

Institute for Nuclear Studies and Department of Chemistry, University of Chicago, Chicago, Illinois

SOLUTIONS OF METALS IN NH_3

THE alkali metals and the alkaline earth metals dissolve readily in liquid NH_3.[1–5] The solubilities[4] of Na and K at the boiling point of NH_3, −33.4°C, are about 5.4 and 4.9 mol l^{-1}, respectively, and the solubility changes very little with temperature. The concentrated solutions have the color of bronze and a metallic luster. The more dilute solutions are blue, the absorption spectrum of the dilute solutions of all the alkali metals being identical.[6] When the solvent is evaporated, the pure alkali metals remain as residues. (Reaction of the metal with the solvent will occur at varying rates depending upon temperature, impurities, etc., but in the absence of impurities the solutions contained in Pyrex glass at room temperature are quite stable enough to make possible a variety of measurements of physical properties.) A study of the vapor pressure[7] as a function of concentration shows the nonexistence of compounds in the freshly prepared solutions of the alkali metals.

One of the striking properties of such solutions is their electrical conductivity.[8–11] The conductivity is shown in Fig. 1. At all concentrations the equivalent conductivity is greater than that of any known salt in any known solvent. In the most dilute solutions the equivalent conductance reaches a limiting value of approximately 1000 ohm^{-1} cm^2 mol^{-1} which is three times that of the best conducting salts in liquid NH_3. Even more remarkable is the behavior of the conductivity at the higher concentrations. A saturated solution of K in NH_3 has a conductivity of approximately 4500 ohm^{-1} cm^{-1}. This may be compared with the conductance of Hg at 20°C, which is 10 400, and it is seen that these solutions have a conductivity of the same order as that of metals. The conductances of the solutions of the various alkali metals in liquid NH_3 agree very closely at all concentrations. Both electromotive force and conductance studies lead to the conclusion that in the most dilute solutions of sodium the speed of the negative charge carrier is about 7 times that of the positive charge carrier. When the concentration is increased, the equivalent conductance decreases, passes through a minimum at about 0.04 *M*, and then increases to the enormous values already mentioned. In the concentrated solutions the speeds of the negative carriers approach those of the electrons in metals.

One is led to the conclusion that when any of the alkali metals is dissolved in NH_3 there is a dissociation into positive alkali metal ions and electrons. The negative charge carrier is apparently the electron in each case. In the dilute solutions the electrons are evidently bound not too tightly in some way to the solvent molecules. In the concentrated solutions the electrons are much less tightly bound and move in much the same manner as in metals. In such solutions we have the possibility of examining the properties of electrons over a range of concentrations varying by a factor of 10^4 to 10^5.

The behavior of the conductivity with concentration was interpreted by Kraus and his co-workers in terms of equilibria between sodium atoms, sodium ions, free electrons, and solvated electrons. Several lines of evidence lead to the discarding of such models. One of the clearest reasons for rejecting models involving the existence of large concentrations of alkali metal atoms or solvated electrons is a consideration of the results of studies of the static magnetic susceptibilities of such

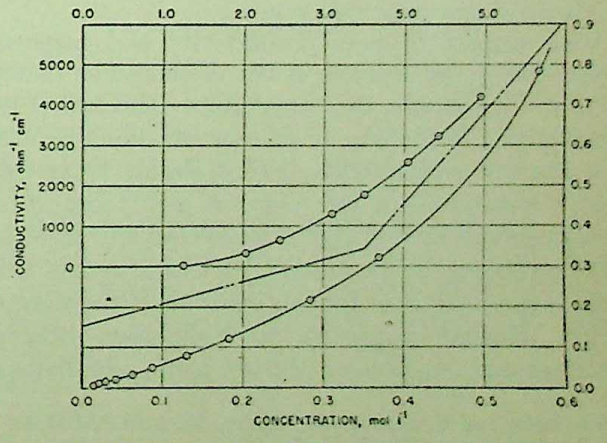


FIG. 1. Conductivity of K in NH_3 at NH_3 B. P. [C. A. Kraus, J. Am. Chem. Soc. 43, 755 (1921)].

* This research was assisted by the U.S. Office of Naval Research.

[1] C. A. Kraus, J. Franklin Inst. 212, 537 (1931).

[2] C. A. Kraus, *The Properties of Electrically Conducting Systems* (Chemical Catalog Company, New York, 1922.)

[3] D. M. Yost and H. Russell, *Systematic Inorganic Chemistry* (Prentice-Hall, Inc., New York, 1944), p. 136.

[4] W. C. Johnson and A. W. Meyer, Chem. Rev. 8, 273 (1931).

[5] W. C. Fernelius and G. W. Watt, Chem. Rev. 20, 195 (1931).

[6] Gibson and Argo, J. Am. Chem. Soc. 40, 1327 (1918).

[7] Kraus, Carney, and Johnson, J. Am. Chem. Soc. 49, 2206 (1927).

[8] C. A. Kraus, J. Am. Chem. Soc. 437, 49 (1921).

[9] C. A. Kraus and W. W. Lucasse, J. Am. Chem. Soc. 43, 2529 (1921).

[10] C. A. Kraus and W. W. Lucasse, J. Am. Chem. Soc. 45, 2551 (1923).

[11] G. E. Gibson and T. E. Phipps, J. Am. Chem. Soc. 48, 312 (1926).

CC-0. In Public Domain. Gurukul Kangri Collection, Haridwar

Digitized by Arya Samaj Foundation Chennai and eGangotri

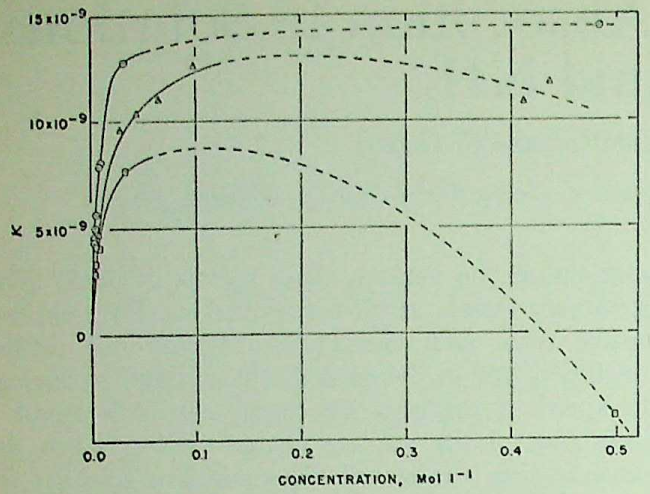


FIG. 2. Magnetic susceptibilities of solutions of alkali metals in liquid NH_3 (see reference 12). ⊙ K at 240°K. ⊡ K at 220°K (see reference 13). △ Na at 238°K.

solutions.[12,13] If such species existed in large numbers, the solutions would be paramagnetic and their susceptibilities would obey Curie's law with respect to variation of temperature and concentration. This type of behavior is not observed. The experimental measurements of the static susceptibilities are shown in Figs. 2, 3, and 4. In the very concentrated solutions and down to a few tenths normal, the susceptibiltiy is quite small of the order found in the metal and has a very small temperature coefficient. As the concentration is lowered, the molar susceptibility increases rapidly and approaches in the most dilute solutions the value for one mol of spins. This is the general qualitative type of behavior to be expected if the electrons are free or in a periodic potential as in a metal. Under such conditions they would at high concentrations form a degenerate Fermi gas with most of the electrons paired and not contributing to the paramagnetism. At the lower concentrations, however, the degeneracy would be removed and the susceptibility would be of the order of that of a mol of spins. Hence, in this particular respect the solutions behave much as would be expected for a metal in which the concentration of electrons could be varied over a very wide range.

With respect to both conductivity and magnetic susceptibility the behavior is not in detail like that of metals. For example, the temperature coefficient of the conductivity is positive at all concentrations.[10,11] Also the magnetic susceptibility is considerably lower than that calculated for a free electron gas,[13a] and at all concentrations investigated the susceptibility increases with increasing temperature.[12] Various attempts have been made to account for this behavior of the susceptibility. Huster[13] suggested an equilibrium between electrons and Na ions, on the one hand, and diatomic molecules on the other. The necessary molecular concentrations are, however, in disagreement with the apparent molecular weight measurements of Kraus.[14] Freed and Sugarman[12] have proposed a decrease of density of energy levels near the top of the Fermi distribution because of the binding of the electron in a variety of resonance structures involving NH_3 molecules and solvated metal ions. This would result in a reduction of the magnitude of the susceptibility. They also proposed that there are pairwise interactions between electrons similar to those which lead to the F' centers in crystals in which two electrons are trapped in a single vacancy.[15] These pairs would be expected to be diamagnetic and would thus lead to lowered susceptibilities. In particular they might be responsible for the increase of susceptibility with increasing temperature. Ogg[16–18] has discussed in some detail the formation of F'-like centers. He proposes that individual electrons are trapped in cavities which they create in the solution and are in equilibrium with pairs of electrons similarly trapped. He believes that he can account for the behavior of several physical properties, including the magnetic susceptibility on the basis of such an equilibrium. Moreover, he believes that the cavities are very large, and that as a consequence of this there is an extraordinarily large diamagnetic contribution to the susceptibility.

EXPERIMENTAL METHODS

Some time ago we observed paramagnetic resonance absorption in solutions of K in liquid NH_3 at microwave frequencies.[19] Observations of the resonance have also been made by Garstens and Ryan[20] and by Levinthal,

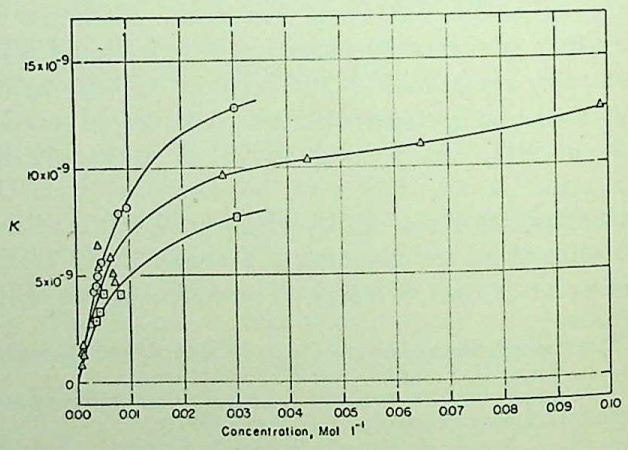


FIG. 3. Magnetic susceptibilities of solutions of alkali metals in liquid NH_3 (see reference 12). ⊙ K at 240°K. ⊡ K at 220°K (see reference 13). △ Na at 238°K.

[12] S. Freed and N. Sugarman, J. Chem. Phys. 11, 354 (1943).
[13] E. Huster, Ann. Physik 33, 477 (1938).
[13a] N. F. Mott and H. Jones, *Theory of Properties of Metals and Alloys* (The Clarendon Press, Oxford, 1936), p. 184.
[14] C. A. Kraus, J. Am. Chem. Soc. 30, 1197 (1908).
[15] F. Seitz, Revs. Modern Phys. 18, 384 (1946).
[16] R. A. Ogg, J. Chem. Phys. 14, 114 (1946).
[17] R. A. Ogg, J. Chem. Phys. 14, 295 (1946).
[18] R. A. Ogg, J. Am. Chem. Soc. 68, 155 (1946).
[19] C. A. Hutchison, Jr., and R. C. Pastor, Phys. Rev. 81, 282 (1951).
[20] Martin A. Garstens and Alden H. Ryan, Phys. Rev. 81, 888 (1951).

CC-0. In Public Domain. Gurukul Kangri Collection, Haridwar

Digitized by Arya Samaj Foundation Chennai and eGangotri

Rogers, and Ogg.[21] The width of 0.1 gauss, which we initially reported, turned out to be caused largely by magnetic field inhomogeneities. Whereas the resonances in paramagnetic salts are generally several thousands of times this broad and must be studied at microwave frequencies, we have investigated this extremely sharp and consequently enormously intense resonance at low frequencies and field strengths where it was much simpler for us to produce a homogeneous field and measure the actual widths.

We have studied the paramagnetic resonance absorption in solutions of K in liquid NH_3 at frequencies in the range 5.5 to 8.2 mc sec^{-1} corresponding to field strengths of 2.0 to 2.9 gauss. The static magnetic field was supplied by a solenoid which could be accurately aligned with the earth's field. The sample of K in liquid NH_3 was placed at the center of the solenoid in the coil of a regenerative oscillator-detector circuit. The magnetic field was modulated at 40 cycle sec^{-1} by means of a small auxiliary coil. A phase sensitive detector was employed and its output was recorded on a recording potentiometer. The modulation amplitude was sufficiently small to insure a signal proportional to the first derivative of the absorption. The static magnetic field was varied linearly with time by means of a motor-driven potentiometer in the current supply circuit. The current through the solenoid was recorded on the same chart as the magnetic signal. A Watkins-Pound calibrator[22] circuit was employed for determining signal intensities. With this device one may simulate the change in coil resistance produced by the magnetic signal by means of a changing plate resistance of a thermionic tube. One then employs the regenerative oscillator-detector-amplifier-recorder system to compare the magnetic signal with the calibrator signal produced when a 40 cycle sec^{-1} signal of known magnitude is placed on the grid of the calibrator tube at known fixed plate current. The recorder chart was

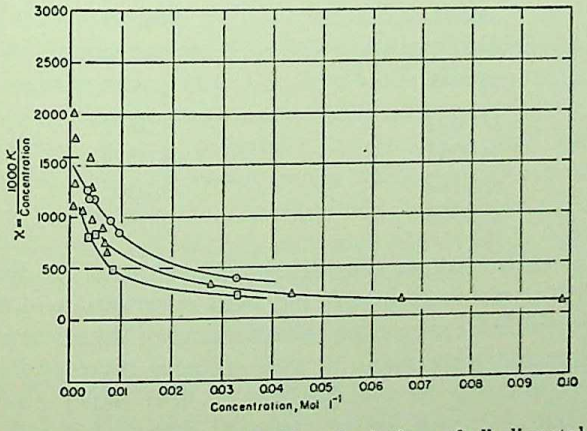


FIG. 4. Magnetic susceptibilities of solutions of alkali metals in liquid NH_3 (see reference 12). ⊙ K at 240°K. ⊡ K at 220°K (see reference 13). △ Na at 238°K. The bar at 1564×10^{-6} denotes the value of the susceptibility of a mol of electron spins at 240°K.

[21] Levinthal, Rogers, and Ogg, Phys. Rev. 83, 182 (1951).
[22] G. D. Watkins and R. V. Pound, Phys. Rev. 82, 343 (1951).

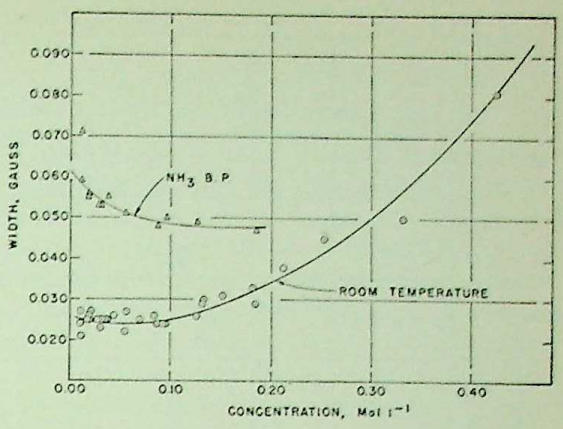


FIG. 5. Width of resonance at maximum slope *vs* concentration.

calibrated in terms of calibrator grid voltage immediately after each scanning of the magnetic resonance signal.

The samples of K in liquid NH_3 were prepared by distilling K several times in high vacuum and finally distilling it into Pyrex glass capsules. Then NH_3 dried by addition of K and subsequent distillation was added and the capsule sealed. The amount of K in these solutions was determined after completion of magnetic investigation by dissolving in H_2O and boiling to remove the NH_3. The resulting solution was titrated with standard acid. The weight of NH_3+K was determined by weighing the capsule before and after opening it.

Measurements were made at a room temperature of 28°C and at the boiling point of liquid NH_3 which is −33°C. For the low temperature runs the sample was immersed in a Dewar filled with liquid NH_3.

SPECTROSCOPIC SPLITTING FACTOR

The spectroscopic splitting factor for the solutions of K in liquid NH_3 was compared with the factor for 2,2-diphenyl-1-picrylhydrazyl[19,23] at approximately 8.2 mc sec^{-1}. In the case of the solution of K in NH_3 the rf coil field strength was 0.0023 gauss rms. The shift of the center of the resonance under these conditions due to the Bloch-Siegert[24] effect is by the factor

$$1-[(2H_1)^2/16H_0^2]=1-1.6\times10^{-7},$$

and is consequently small enough to be neglected. Assuming the splitting factor for 2,2-diphenyl-1-picrylhydrazyl to be 2.0037[19,23] (the microwave value), we find the factor at room temperature for K in NH_3 to be 2.0010±0.0002 at 0.425 mol l^{-1}, and 2.0011 ±0.0002 at 0.0365 mol l^{-1}. This is the same as the value 2.0012±0.0002 found at 23 500 mc sec^{-1}.[19] This factor is considerably lower than the value of the *g* factor, 2.0023, for a free electron spin. However, it is not nearly so low as the value 1.995,[25] which we have observed for additively colored crystals of KCl.

[23] Holden, Kittel, Merritt, and Yager, Phys. Rev. 77, 147 (1950).
[24] F. Bloch and A. Siegert, Phys. Rev. 57, 522 (1940).
[25] C. A. Hutchison, Jr., and G. A. Noble, Phys. Rev. 87, 1125 (1952).

CC-0. In Public Domain. Gurukul Kangri Collection, Haridwar

Digitized by Arya Samaj Foundation Chennai and eGangotri

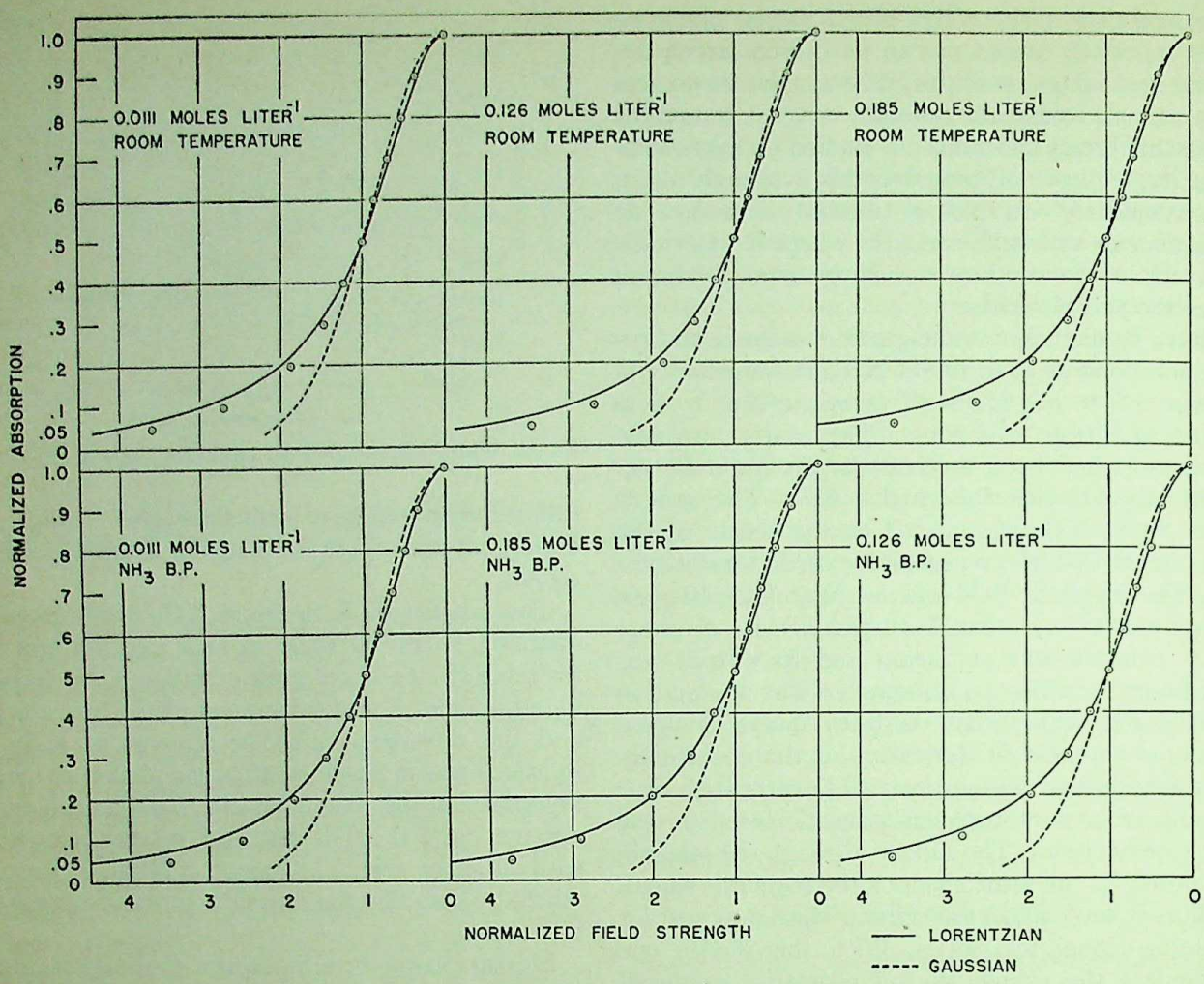


FIG. 6. Line shape.

WIDTH

The width of the resonance between the points of maximum slope was determined by measuring the distance between the maximum and minimum on the recorder chart which, when combined with the current record on the same chart, gave the width. The results are shown in Fig. 5. The width was measured at room temperature from a concentration of 0.425 down to 0.011 mol l^{-1}, and at the boiling point of NH_3 from 0.185 to 0.011 mol l^{-1}. It is clear that this resonance is by far the sharpest electronic resonance so far observed in a condensed phase. In the case of a resonance as sharp as this, one must consider the Rabi[26] width associated with the flipping of the spin by the perturbing rf magnetic field. This is approximated by

$$\Delta H/H = 4\sin(\theta/2),$$

where ΔH is the width at half-height and where θ is given by

$$\theta = \tan^{-1}\frac{\text{rf field strength}}{\sqrt{2}\text{H}}.\dagger$$

When θ is very small, as in our case,

$$\Delta H = \sqrt{2}\ \text{rf field strength}.$$

For a sample whose concentration was 0.152 mol l^{-1} the variation of width with rf field strength was investigated with the following results:

$\sqrt{2}$ rf field strength gauss	width at max slope gauss
0.0032	0.0311
0.0081	0.0327
0.0163	0.0335
0.0324	0.0388

It is clear that at the higher coil voltages the Rabi width is seriously interfering with observation of the true width. Consequently, all scannings of the resonance absorption were made at coil voltages corresponding approximately to the smallest rf field listed above, or about 0.05 volt. In the case of an organic free radical which is much wider than the K resonance there is, of course, no observable change of width with coil voltage.

The width of this resonance is several orders of magnitude less than that observed in aqueous solution

[26] I. I. Rabi, Phys. Rev. 51, 652 (1937).
† This is the rms field strength.

CC-0. In Public Domain. Gurukul Kangri Collection, Haridwar

Digitized by Arya Samaj Foundation Chennai and eGangotri

of paramagnetic salts of about the same concentrations. There is evidently an extraordinarily large exchange narrowing associated with the great mobility of the electrons in these solutions. The average value of β/r^3 (r is the distance between electrons) ranges from 0.06 to 2.6 gauss. The broadening by magnetic nuclei would be expected to be several gauss. At room temperature there is perhaps a slight increase in the width at the lowest concentrations, and the increase is marked at the lower temperature. This increase becomes pronounced in the vicinity of the region in which the susceptibility begins to rise rapidly with dilution. The room temperature measurements were extended to considerably higher concentrations than at the lower temperature, and there is apparently quite a large increase of width at the higher concentrations.

LINE SHAPES

The areas under the curves drawn by the recording potentiometer were obtained by numerical integration. The scale on the field strength axis was quite linear as determined from the current recording. The scale on the magnetic signal axis was quite linear in calibrator grid voltage. Moreover, it was found that the grid voltage at constant plate current was very close to being proportional to magnetic signal over the range employed in the experiments. This last was determined by comparing calibrator signals with magnetic signals of various sizes produced with an organic free radical by field modulation amplitudes of various sizes. It was consequently a simple matter to obtain the absorption curves with errors not greater than probably 5 percent. Some absorption curves were also determined using the Watkins-Pound RF Spectrometer.[22] The results were indistinguishable from those obtained with the regenerative oscillator-detector. The regenerative oscillator-detector was employed in our investigations because of its much more favorable signal-to-noise ratio. The results of the investigation of the line shapes are shown in Fig. 6. The points are taken from the experimental curves. The line shapes of three samples over a range of concentrations and at both room temperature and the boiling point of NH_3 were compared with Gaussians and Lorentzians. It is clear that these absorptions correspond much more closely to the Lorentzian than to the Gaussian over most of the range of the absorption, but drop considerably below the Lorentzian in the wings of the curve.

INTENSITIES

A second numerical integration yielded the areas under the absorption curves. By means of the current and signal calibrations the relative areas under the absorption curves for the various samples could be obtained.

Since the static susceptibilities of the samples are related to the rf susceptibilities by the Kronig-Kramers relation,

$$\chi=\frac{2}{\pi}\int_0^\infty \frac{\chi''(\nu)}{\nu}d\nu,$$

these second integrals afford a means of comparing the static susceptibilities of the spin systems. Our experiments are carried out at constant frequency and varying field strength. We may, however, for a sharp symmetrical absorption make the transformation of the above relation from the one type of experiment to the other and hence obtain static susceptibilities from our measurements of the rf susceptibilities. We must, of course, consider the changes in Q of the coil and the filling factors from sample to sample. We determined Q, ω, and C during each run. Filling factors were determined for each sample. The desired relationship is

$$\chi=\frac{2\beta}{\pi\xi\omega^2 Ch}\int_0^\infty \frac{\Delta R}{R^2}dH,$$

where χ is the static susceptibility, β is the Bohr magneton, ξ is the filling factor, ω is the angular frequency, C is the capacity across the coil, h is Planck's constant, R is the rf resistance of the coil, and H is the field strength. The grid voltage of the calibrator is proportional to $\Delta R/R^2$. We replaced $\int_0^\infty(\Delta R/R^2)dH$ with the second integral of the recorder curves and employed a standard substance to eliminate the proportionality constant. The standard substance employed was tris-*p*-nitrophenylmethyl, a completely dissociated free radical in which resonance was first observed by Pake, Weissman, and Townsend.[27] A sample of this material was prepared and later assayed for us by Professor Weissman. We carried out scannings of the resonance of this material. The comparison of the second integrals of the curves so obtained with the similar ones for the K in liquid NH_3 enabled us to

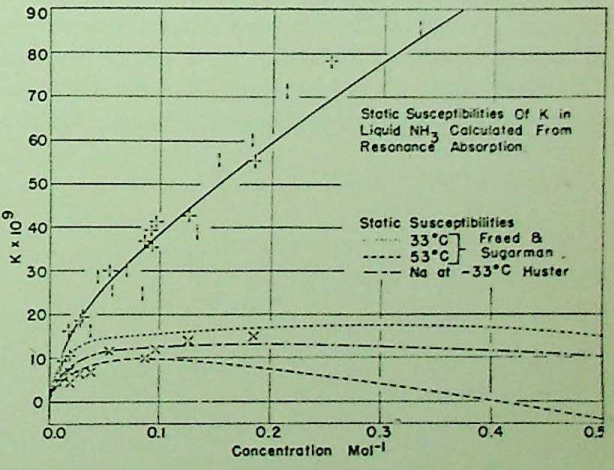


FIG. 7. Static susceptibilities of K in liquid NH_3 calculated from resonance absorption. + Room T. Series I, 28°C; | Room T. Series II, 26°C; × bp of NH_3 −33°C.

[27] Pake, Weissman, and Townsend, personal communication.

CC-0. In Public Domain. Gurukul Kangri Collection, Haridwar

Digitized by Arya Samaj Foundation Chennai and eGangotri

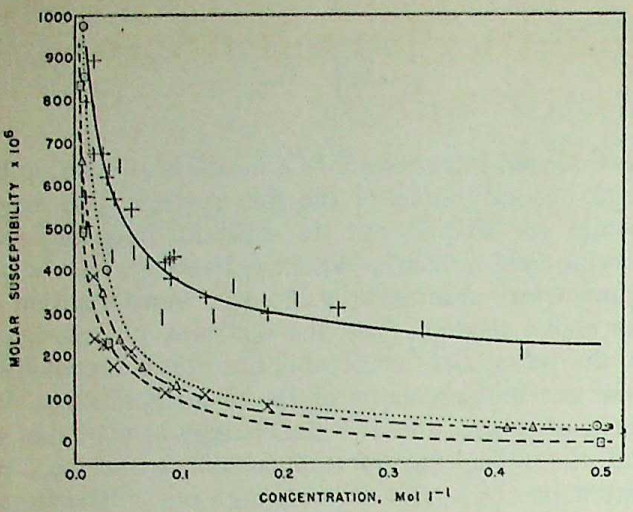


FIG. 8. Static susceptibilities of K in liquid NH_3 calculated from resonance absorption. + Room T. Series I, 28°C. | Room T. Series II, 26°C. × B.P. of NH_3 −33°C. ·····−33°C.; - - - - - −53°C, Freed and Sugarman; −·−·− Na at −33°C, Huster.

calculate static susceptibilities of the solutions relative to that of the organic compound. The free radical was assumed to have the static susceptibility of 1 mol of spins per mol of free radical at 28°C. The number of mols in the sample of organic free radical was known to approximately 5 percent.

The results of the susceptibility determinations are shown in Figs. 7 and 8. At room temperature the calculated static susceptibility is seen to follow the same sort of pattern as determined in static field experiments at low temperatures. The susceptibilities are considerably higher than those of the static experiments at the boiling point. Like the latter, they rise sharply with dilution at about the same concentration. The low temperature runs were made some time subsequent to the high temperature runs, and two points have been omitted for the two lowest concentrations where some decomposition is known to have occurred. These two samples also give obviously low results at the higher temperatures. Some of the other points at the lower concentrations are probably suspect for the same reason. The points for the molar susceptibility at the higher concentrations at the lower temperature are in reasonably good agreement with the static field measurements. The resonance phenomenon is peculiar to the paramagnetic spins and is relatively unaffected by the diamagnetism. Consequently, such a comparison of static field measurements with static susceptibilities calculated from rf measurements enables one to detect the presence of any abnormal diamagnetic susceptibilities. It is clear that no abnormally large diamagnetism exists in these solutions at the boiling point of NH_3 at the concentrations investigated by both methods. Such determinations of static susceptibilities from rf measurements afford a powerful tool for a number of problems of chemical and physical interest where large amounts of diamagnetic material or abnormally large diamagnetisms of the paramagnetic species itself may obscure the primary effect. We have discussed this problem recently for the case of the detection of organic free radicals in solution.[28]

ACKNOWLEDGMENT

We wish to thank Clarence Arnow for the design and construction of the electronic equipment used in these experiments; Jack Boardman for the numerical integrations and other computations; and Edward Bartal for the construction of the solenoid, low temperature apparatus, and other machine work.

[28] Hutchison, Kowalsky, Pastor, and Wheland, J. Chem. Phys. 20, 1485 (1952).

CC-0. In Public Domain. Gurukul Kangri Collection, Haridwar

Digitized by Arya Samaj Foundation Chennai and eGangotri

REVIEWS OF MODERN PHYSICS VOLUME 25, NUMBER 1 JANUARY, 1953

Paramagnetic Resonance in Phosphors at Microwave Frequencies

W. D. Hershberger and H. N. Leifer

University of California, Los Angeles, California

THIRTY-TWO inorganic phosphors containing paramagnetic activators have been examined. The phosphors are luminescent under ultraviolet irradiation and their paramagnetic resonance spectra have been investigated both when unirradiated and irradiated. Because the mechanisms of luminescence and paramagnetism both depend upon unpaired electrons, it has been anticipated that a change in paramagnetism would occur upon excitation to luminescence. The emphasis has been placed on phosphors containing dilute concentrations of doubly ionized manganese as activator. Mn^{++} is in an S state and, in dilute concentrations, should act very nearly as an ideal paramagnetic substance.

The unirradiated spectra may be classified into five groups. The first four groups contain all the manganese activated phosphors and the fifth group contains all nonmanganese activated phosphors. The spectrum for all members of group one consists of a single broad absorption curve from 750 to 1000 gauss wide. Group two contains four phosphors each of whose spectrum consists of six clearly defined peaks interpreted as hyperfine structure. The spacings between peaks vary from 68 to 88 gauss depending upon the host crystal. Group three contains two phosphors whose complex spectra contain thirty lines attributed to a combined fine and hyperfine structure. No spectrum could be resolved for the members of group four. Likewise, the phosphors of group five yielded no resolvable spectra.

The most striking features of the Mn^{++} spectra are the isotropic hyperfine structure and the fine structure resulting from crystal field splitting. These spectra have been shown to fit, qualitatively, the theory and mechanism proposed by Abragam and Pryce while quantitative discrepancies between theory and experiment have been indicated. Arguments have been offered based upon line broadening as a function of crystal field symmetry to account for the large line widths in group one and the lack of spectra in groups four and five. The arguments fit the existence of highly resolved spectra in groups two and three. The spectroscopic splitting factor, g, of all spectra was two (the free spin value) as expected for an S state. The hyperfine spectra verify the spin of the manganese nucleus as being 5/2.

The results of investigating the irradiated spectra have been negative with the exception of indications of photoconductivity. The negative results may well arise from inadequate volume illumination of the phosphor sample. Further research into illumination techniques and cavity design may rectify the situation and provide a critical, experimental test of the anticipated change in paramagnetism.

The experimental method utilized X-band microwave equipment and static magnetic fields of the order of 3350 gauss. The unique character of the technique consists in superposing a 2–5 gauss ac magnetic field sweep upon the static field while traversing the field range of interest in approximately four minutes. At each value of static magnetic field, the ac information signal is proportional to the slope of the absorption spectrum at that value. A phase detector is used to convert the information signal into a phase and amplitude dependent signal. In this manner the sign of the slope is conserved, permitting reconstruction of the original absorption curve. The irradiation technique consists in the removal of the ac magnetic sweep and square-wave-ultraviolet illumination of the sample. The resultant signal, upon traversal of the magnetic field range, should be proportional to the difference in spectra of the unirradiated and irradiated sample.

CC-0. In Public Domain. Gurukul Kangri Collection, Haridwar

Digitized by Arya Samaj Foundation Chennai and eGangotri

The New Adiabatic Demagnetization Apparatus at the National Bureau of Standards

D. de Klerk and R. P. Hudson

National Bureau of Standards, Washington, D. C.

SEVERAL years ago Dr. Brickwedde, Chief of the Division of Heat and Power of the National Bureau of Standards, proposed to start a project in the low temperature section on "magnetism at very low temperatures." His intention was to set up an apparatus with which it would be possible to produce and maintain temperatures well below 1°K by means of the adiabatic demagnetization method. The general purpose was to continue the work of the thermometry section in the region below 1°K as well as to study the magnetic properties of the paramagnetic salts used in the cooling process. Moreover, other projects of the low temperature group could be extended to lower temperatures.

The project was started in July, 1951. Dr. Hudson, who did the work for his doctor's thesis in the field of adiabatic demagnetization at the Clarendon Laboratory of the University of Oxford, England, joined the staff of the Bureau in July, 1951. Dr. de Klerk, leader of the demagnetization investigations at the Kamerlingh Onnes Laboratory of the University of Leiden, Holland, came to Washington as a consultant for one year in September, 1951.

Since the project was started, most of the time was devoted to building the apparatus and only recently some experimental results were obtained.

The magnetic fields used in the demagnetization process are produced by a commercial A. D. Little magnet, giving fields up to 23 kilooersteds in a pole gap of $2\frac{1}{4}$ in., using 25 kw. The cooling system for the magnet and the motor generator are located in the basement of the building. The panels for the motor generator are in the magnet room. The liquid helium Dewar is suspended from a horizontal wooden arm, approximately 2 meters long, which can be rotated around a vertical steel pillar. After the demagnetization, the poles of the magnet are separated and the cryostat is removed from the magnet, so that the measurements at the low temperature are not influenced by the iron of the magnet. The vapor pressure of the liquid helium bath is pumped down with the help of a large Kinney pump, located in the basement of the building, and it is connected to the Dewar by a copper tube, partly 5 in. in diameter, partly 3 in. The connection to the rotating arm is made by means of a flexible rubber hose, also 3 in. in diameter. Pressures below 0.5 mm can be obtained easily with this pumping arrangement. The high vacuum system, consisting of a VMF 20 oil diffusion pump and a glass valve system, is located on the wooden arm; hence, it turns with the cryostat, and no flexible connections or swivel joints are needed in the high vacuum line. The magnetic properties of the salt after the demagnetization are measured with the help of a Hartshorn mutual inductance bridge. Apart from a few minor details it is a copy of the bridge used in the demagnetization work at Leiden. The bridge can be used both for ac and ballistic measurements and by reversing some switches the transition from one to the other can be made in a few seconds. Mutual inductances up to 3 millihenries can be measured with an accuracy better than 10^{-8} henry. Small phase angles can be measured with an accuracy of 0.3 percent. For measurements in external fields an iron-free Helmholtz coil was wound giving fields up to 600 ϕ, using 1.5 kw. It is surrounded by three mutually orthogonal Helmholtz coils used for compensating the earth's magnetic field. The whole assembly is mounted in a brass frame and is counterweighted. Though the total weight is 170 pounds it can be raised and lowered easily around the cryostat.

Until now two experiments have been made with the new apparatus. We shall review them very briefly.

In cooperation with Dr. Pellam we measured the second sound velocity of liquid helium II in the region between 0.05 and 1°K. Above 0.9° the results are in excellent agreement with those of Herlin, but at the lower temperatures we have much higher values than those found by Atkins and Osborne. At 0.5°K the difference is a factor of 2.5. If we extrapolate our values to absolute zero, we find 190 m/sec instead of 152 m/sec, the value given by Atkins and Osborne.

Recently we performed some investigations on the magnetic behavior of chromium methylamine alum. The measurements are still in progress and I shall not go into many details, but it seems that this salt obeys the theoretical predictions better than the ordinary chromium potassium alum; for instance, it was found that the flat part in the entropy *versus* temperature curve occurs at $S=R\ln 2$, which is much more reasonable than the value $S=0.4R$ which was found for chromium potassium alum.

CC-0. In Public Domain. Gurukul Kangri Collection, Haridwar

Digitized by Arya Samaj Foundation Chennai and eGangotri

REVIEWS OF MODERN PHYSICS VOLUME 25, NUMBER 1 JANUARY, 1953

Thermoremanent Magnetization of Fine Powders

LOUIS NÉEL

Institut Fourier, Grenoble, France

This is a brief explanation of the magnetic properties of fine ferromagnetic grains of single elementary domains, especially in reference to the influence of time on the magnetization at a given temperature. Application is made to the interpretation of the thermoremanent magnetization of lavas and clays and to the determination of the direction and intensity of the terrestrial magnetic field in the past. It is shown that, when the substance contains two kinds of fine ferromagnetic grains with clearly different Curie points, it is possible, under certain conditions explained in the text, that the constituent having the lowest Curie point becomes magnetized in a direction opposite to the exterior field: there arise, by this phenomenon, interactions between the grains and the demagnetizing field created by the constituent having the highest Curie point. Also, in certain cases, the total thermoremanent magnetization is directed inversely to the acting field. Recently Nagata found samples of lava in which the thermo-remanent magnetization obeys the mechanism thus described. In the geophysical interpretation, there will be, then, reason to keep in mind the possibility of this curious phenomenon, in considering the possible inversions of the terrestrial magnetic field.

WE designate here under the name of fine powders the powders in which the grains are small enough for each one to contain only a single elementary Weiss domain. For this it is necessary that the diameter of the grains be less than a certain critical value d_s. This can be evaluated by determining the diameter of a single domain of uniform spontaneous magnetization that possesses the same free energy as a *closed* configuration having a resultant spontaneous magnetization equal to zero. One obtains thus[1] a critical value given by

$$d_s^2=\frac{3Na^2}{2\pi}\left(\log\frac{d_s}{a}-0.307\right), \qquad (1)$$

where N is the coefficient of the molecular field (5890 for iron) and a the distance between magnetically active neighbors (2.86A for iron). Thus one finds that the grains of iron of a diameter less than $d_s=320$A should contain only a single elementary domain. The variations of magnetization of a group of such fine grains arise then only from the rotations of the magnetic moments resulting from the individual grains.

In the theory of their magnetic properties[2–4] one takes account usually only of the rotations imposed by the magnetic field applied against the different forces of anisotropy: anisotropy of form, magnetocrystalline anisotropy, etc. . . , but in reality the grains are already so small that it is necessary to consider the spontaneous rotations due to the thermal fluctuations which provoke a kind of magnetic Brownian movement.[4,5] In a group of identical grains one can define the time of relaxation τ_0 such that, J_0 being the remanent magnetization of the group of grains at the initial instant, the magnetization at the instant t is spontaneously reduced in zero exterior field to the value $J=J_0e^{-t/\tau_0}$.

Approximate evaluation of this type of relaxation gives the result[4,5]

$$\frac{1}{\tau_0}=\frac{eH_c}{m}\left|3G\lambda_s+DJ_s^2\right|\left[\frac{2v}{\pi GkT}\right]^{\frac{1}{2}}\exp-\frac{vH_cJ_s}{2kT}, \qquad (2)$$

where e and m are the charge and the mass of electron, k the Boltzmann constant, v the volume of the grain, G its modulus of elasticity in shear, J_s its spontaneous magnetization, λ_s its longitudinal magnetostriction at saturation, and D a numerical coefficient which depends a little on the form of the grain and which is around 3. Finally H_c is the coercive force of the group of grains in question if the phenomenon of spontaneous demagnetization did not exist. Table I gives the variations of the times of relaxation as a function of v/T, for iron.

This table shows at what point the time of relaxation varies rapidly with the diameter of the grains. In order that the remanent magnetization of a group of grains remain perfectly stable, it is necessary that their time of relaxation be at least equal to 10^9 sec. Equation (1) shows that the diameter of the supposed spherical grain must then be at least equal to a certain critical diameter $d_i=160$A. This discussion shows that the diameter of the grains of iron powder, used in the manufacture of permanent magnets, must lie within well determined limits. Experimental results of Bertaut confirm this point of view.[6]

Let us suppose now that we are concerned with a group of grains that are perfectly stable at ordinary temperature, that is, such that their time of relaxation τ_0 is practically infinite. In order to produce a substan-

TABLE I.

τ_0	10^{-1}	10	10^3	10^5	10^7	10^9	sec
v/T	3.2	3.9	4.7	5.4	6.2	7.0	10^{-21} cm³/degree

[1] L. Néel, Compt. rend. 224, 1488 (1947).
[2] L. Néel, Compt. rend. 224, 1550 (1947).
[3] L. Weil, J. phys. et radium 12, 437 (1951).
[4] L. Néel, Ann. Géophys. 5, 99 (1949).
[5] L. Néel, Compt. rend. 228, 664 (1949).
[6] F. Bertaut, Compt. rend. 229, 417 (1949).

CC-0. In Public Domain. Gurukul Kangri Collection, Haridwar

Digitized by Arya Samaj Foundation Chennai and eGangotri

tial remanent magnetization in this group, it is necessary to apply a magnetic field of the same magnitude as the coercive force H_c. As shown in Eq. (2) it is the exponential term which determines the variations of τ_0. This time of relaxation diminishes at the same time as the factor H_cJ_s/T which appears in the exponential: this factor tends toward zero at the Curie point because J_s approaches zero and H_c diminishes when the temperature rises. Thus there exists a certain temperature T_b, lower than the Curie point called the *blocking temperature*, at which the time of relaxation has the order of magnitude of the duration of an experiment, several seconds to several minutes. Above this temperature, magnetization of a group of grains follows in a reversible and practically instantaneous manner the variations of the applied field and there is no more hysteresis. This blocking temperature depends on the nature and the dimensions of the grains.

At the blocking temperature and in the magnetic field H_b the magnetic moment resulting from a group of N identical grains is

$$M_b = NvJ_b \tanh(vJ_bH_b/kT_b), \tag{3}$$

where J_b represents the value of the spontaneous magnetization of the grain at the blocking temperature. This expression results from an equilibrium, according to Lenz's law, between two possible orientations, antiparallel to each other, of the magnetic moment vJ_b of the grain. This equilibrium is defined by the value of the hyperbolic tangent, $\tanh(J_bH_b/kT_b)$.

Now if one lowers the temperature below T_b while keeping the magnetic field, at least at the beginning, at the same value H_b, the time of relaxation becomes rapidly very big and the passage from one orientation of equilibrium to another becomes practically impossible. The magnetic moment of each grain preserves the orientation that it had at the temperature T_b. In other words the hyperbolic tangent maintains the same value. The magnetic moment resulting from the N grains continues meanwhile to vary because of the thermal variation of the spontaneous magnetization. At the temperature T_0, lower than T_b, at which the spontaneous magnetization possesses the value J_0, this resulting moment M_0 will be given by

$$M_0 = NvJ_0 \tanh(vJ_bH_b/kT_b). \tag{4}$$

The discussion of this formula shows that if v is big enough, it is possible to communicate in this manner to the grains a resulting moment which is of the order of size of the saturation moment NvJ_0, using a field H_b much lower than the coercive field H_c. The magnetization thus communicated is known under the name of *thermo-remanent magnetization*, in order to distinguish it from the remanent magnetization measured ordinarily at ordinary temperature and called isothermic remanent magnetization. Thermo-remanent magnetization has a large stability because, in order to modify its value, it is necessary to apply magnetic fields of the order of magnitude of H_c, that is, much larger than the field H_b which gave rise to it at the temperature T_b. Finally, as long as the acting magnetic fields remain small compared with the coercive field H_c, the magnetization of the group of grains remains completely fixed in magnitude and in orientation by the field H_b, which acts on it at the moment when, for the last time, its temperature passes through the value T_b of blocking. In order to modify the magnetization of this group in a weak field, it is necessary to heat it to the temperature T_b.

These considerations have permitted us to explain[4] theoretically why the clays and lavas preserve for an indefinite time a remanent magnetization parallel to the direction of the terrestrial magnetic field that acted on them during cooling.

In a group of heterogeneous grains there exists a whole series of blocking temperatures extending from ordinary temperatures to the highest Curie point of constituents. The result is that if the magnetic field has varied during cooling the group of grains is able to register the history of this variation in a sensitive manner and to preserve it indefinitely at ordinary temperatures. One can later find it again by a series of progressive reheatings. In an analogous fashion the curious phenomena discovered by Thellier[7] and Nagata[8] have been explained.

The theory of these phenomena is relatively simple when one neglects the interactions between the grains, that is, when the grains are largely separated from each other. In particular, let us consider a group of identical ferromagnetic grains which have the form of an elongated ellipsoid of revolution and of which the anisotropy is only an anisotropy of form. Their demagnetizing coefficient along the major axis can be put equal to $4\pi/3 - n$, where n varies from 0 for a sphere to $4\pi/3$ for a cylinder. Let us suppose also that the grains are dispersed in a *cluster* limited exteriorly by a sphere and oriented at random along the three mutually perpendicular directions. We will designate by c the fraction of the total volume of the cluster in each one of these categories; this is a measure of the density of the grouping of the grains and varies between 0 and $\frac{1}{3}$. Let us suppose now that the field H_b, applied at the blocking temperature T_b of the grains in question, is sufficiently weak so that the argument vJ_bH_b/kT_b of the hyperbolical tangent of Eq. (4) is small compared with one. One finds then that the average remanent magnetization of the cluster at the temperature T_0 is given by the formula

$$\bar{J} = cRs_bH_b, \tag{5}$$

if one neglects the interactions between the grains and if one puts

$$R = J_0/J_b \text{ and } s_b = vJ_b^2/kT_b.$$

[7] E. Thellier, thesis, Paris, 1938; Ann. Inst. Phys. Globe **16**, 157 (1938); see also bibliography in reference 4.

[8] T. Nagata, Bull. Earthquake Research Inst. **21** (March, p. 1) (1943).

CC-0. In Public Domain. Gurukul Kangri Collection, Haridwar

Digitized by Arya Samaj Foundation Chennai and eGangotri

When one considers these interactions, one must write

$$\bar{J} = cRS_b H_b, \tag{6}$$

with

$$S_b = \frac{1-2c}{(1-2c/3)/s_b + cn}.$$

In the lavas to which the preceding formulas are applicable, one finds that R is about 4, s_b of the order of 6 to 8, n about 1.7 (corresponding to an ellipsoid of elongation 1.8) while c lies between 0.03 and 0.20. Practically S_b differs generally little from s_b; the effect of the interaction is not very important.

The formulas (5) and (6) show also that the thermoremanent magnetization is proportional to H_b when H_b is small. One can also show that it is parallel to the field H_b and in the *same direction*, which has *a priori* appeared perfectly obvious.

The phenomena become complicated and can become extremely interesting if the cluster considered above contains two kinds A and B of ferromagnetic grains possessing clearly different Curie points such that the blocking temperature T_a of the constituent A having the highest Curie point is above the Curie point of the constituent B. Under these conditions, at the instant in the course of cooling when the temperature has attained the Curie point of B, the constituent A has already assumed, under the action of the applied field H_b, a thermo-remanent magnetization which is henceforth quenched and which will increase automatically during the subsequent cooling without letting itself be influenced by the variations of the existing field. The thermo-remanent magnetization of B develops then under the action of a field equal to the geometric sum of the applied field H_b and of the demagnetizing field created by the grains of A. It may well happen that the demagnetizing field created by A is larger than H_b so that the total field acting on B is *directed in the direction opposite to* H_b. The constituent B is then magnetized in a direction opposite to that of the applied field. It can happen also that the thermo-remanent magnetization of B is greater than that of A in absolute value; under these conditions the total thermo-remanent magnetization resulting from the cluster is directed in the direction opposite to the field which originated it.

If the constituents A and B are formed of grains of the same volume and shape, with the same value of R, and with the individual concentrations each one equal to $3c$, the theory shows[9] that the thermo-remanent magnetization of the group is certainly negative when the following inequality is satisfied:

$$cnRs_b > \frac{2[1-4c+(8c^2/3)]}{(1-2c)-(2/R)(1-3c)}.$$

With the values of R, n, and s_b indicated above, it is only necessary that the concentration $3c$ of each of the constituents is greater than 0.28 for this condition to fulfilled. In order that negative thermo-remanence appear, it is absolutely necessary that the grains be elongated. For spherical grains ($n=0$), the preceding inequality cannot be satisfied.

Experiment shows that the concentrations of the ferromagnetic constituents of lavas are generally less than the limiting value of 0.28 given above. But it is not necessary, in order to obtain a negative thermo-remanent magnetization, that this be the average concentration of the ferromagnetic constituents. It is sufficient that it be obtained within the complex clusters of grains. For example, one can imagine grains formed by the segregation in two phases, having different Curie points, of a solid homogeneous solution stable at a high temperature; here the necessary large concentration is automatically realized.

To summarize, the theory shows that it is possible for certain lavas to acquire a thermo-remanent magnetization directed inversely to the field which produced it. It is thus possible that certain inversions of the terrestrial magnetic field, supposed to occur in the course of geological ages and deduced from the remanent magnetization of the lavas, is in reality due simply to the specific properties of said lavas. Recently the Japanese geophysicist Nagata discovered,[10] among the discharge products of the Haruna volcano, samples of lava which assumed negative thermoremanent magnetization in the laboratory. These samples contain two ferromagnetic constituents. This discovery constitutes a good experimental verification of the proposed theory.[11]

[9] L. Néel, Ann. Géophys. 7, 90 (1951).
[10] T. Nagata, Nature (London) 169, 704 (1952).
[11] L. Néel, Compt rend. 234, 1991 (1952).

DISCUSSION

JOHN W. GRAHAM, *Carnegie Institution of Washington, Department of Terrestrial Magnetism, Washington, D. C.*: For a number of years at the Department of Terrestrial Magnetism we have been studying the extent to which it may be possible to trace the history of the earth's magnetic field in geologic time by observations of the magnetic properties of rocks. As early as 1949 we found it necessary from our observations to propose that the so-called inverse magnetizations of some rocks should be explained by factors other than a reversal of the sense of the earth's magnetic field or shifting of continental masses relative to the earth's magnetic axis. Professor Néel's subsequent treatment of this problem is thus of considerable interest and importance to us.

This summer we made extensive field samplings and observations in some remarkably well preserved and unweathered late pre-Cambrian diabase dikes in north-

CC-0. In Public Domain. Gurukul Kangri Collection, Haridwar

Digitized by Arya Samaj Foundation Chennai and eGangotri

ern Michigan. We were optimistic that we could provide, by direct field observations, a verification of the theory for self-reversal. Our premise[1] was that on the quickly cooled margins of the igneous intrusives, the ferromagnetic ingredient might cool as a single metastable phase and acquire a normal polarization, whereas in the central portion of the intrusive, with slower cooling, two interacting phases and inverse polarizations could develop. Dikes 200 ft, 70 ft, and 2 ft wide were all observed to have inverse magnetizations, essentially uniform in direction and intensity, prevailing to within at least $\frac{1}{8}$ in. of the contact with the enclosing rocks.

A simple experiment suggests that this fact cannot be explained by supposing that before the melt was injected, the ferromagnetic ingredient had already exsolved into two phases: samples of these rocks when cooled from above the Curie point in the earth's field acquire only normal polarizations of intensity comparable to those observed in the natural samples. Since the temperature of injection of diabase is generally held to be well above the Curie point, then it follows that heating briefly in this experiment to the neighborhood of 600°C should not have caused a recombination of the two phases. Therefore, presumably, they did not exist at the time the dike material was injected, but did, according to the theory, develop during the cooling of the dike.

The time interval of the magnetically important cooling of a 2-ft dike can be estimated to be of the order of a few days. In the first laboratory heating experiments, the samples were cooled in about an hour, and the question follows whether a longer interval than this is required for the phase splitting to take place in order to get inverse magnetizations. Accordingly, samples were cooled from 600°C to 100°C over an interval of several days. Once again normal polarizations were obtained.

It thus seems clear that we are not dealing here with material that today has the interesting self-reversal property that Néel has treated. From these observations alone, however, it cannot be determined whether the earth's field actually was reversed at the time these rocks were emplaced, or whether the magnetic properties today are reflecting the influence of chemical changes that may have taken place in these rocks during the many hundreds of million years of their past history.

These experiences provide a good example of the fact that there still remain a number of interesting facets to the problems of rock magnetism and tracing the history of the earth's magnetic field.

[1] John W. Graham, J. Geophys. Research **57**, 429 (1952).

CLARENCE ZENER, *Westinghouse Research Laboratory, East Pittsburgh, Pennsylvania:* Iron sulfide and chromium sulfide have similar crystal structure and similar dependence of magnetic properties upon x; optimum ferromagnetism occurs at $x \cong 1.14$. R. Heikes's very satisfying interpretation of the magnetic properties of chromium sulfide is also applicable to iron sulfide. As x increases beyond 1, the Cr lattice acquires vacancies; simultaneously, some Cr ions become Cr^{+++}. The interchange of Cr^{++} and Cr^{+++} ions, called double exchange, gives rise to ferromagnetic coupling, which is greatest when the product of the concentrations of Cr^{++} and Cr^{+++} ions is greatest, namely at $x = 1.14$. It also gives rise to metallic electrical conductivity; the conductivity is likewise greatest at $x = 1.14$. Whereas Heikes's interpretation predicts intimate association of electrical conductivity with ferromagnetism, Néel's does not. Thus a study of the electrical conductivity of FeS_x *vs* x will furnish a criterion for choice between the two interpretations.

CC-0. In Public Domain. Gurukul Kangri Collection, Haridwar

Digitized by Arya Samaj Foundation Chennai and eGangotri

REVIEWS OF MODERN PHYSICS VOLUME 25, NUMBER 1 JANUARY, 1953

Saturation and Magnetization of Hexagonal Iron Oxide Compounds

G. W. RATHENAU

Philips Research Laboratories, N. V. Philips Gloeilampenfabrieken, Eindhoven, The Netherlands

The value of the saturation magnetization at absolute zero of $BaO \cdot 6Fe_2O_3$ and related compounds can be explained as due to noncompensated antiferromagnetism.

The Bloch wall formation in small particles is discussed. One is led to the assumption that in these materials Bloch walls are nucleated at imperfections. In specimens containing randomly oriented large crystals, Bloch wall formation becomes appreciable at a positive field strength of the order of $4\pi I_s$.

By orienting the crystals in a magnetic field $(BH)_{max}$-values of 3×10^6 gauss oersted have been obtained.

The critical diameter for wall formation changes with temperature. An excess of walls formed at a different temperature from the temperature of measurement may persist in a metastable equilibrium.

I. SATURATION MAGNETIZATION

A CLASS of hexagonal iron-oxide compounds, of which $BaO \cdot 6Fe_2O_3$ is the prototype, has been dealt with in an earlier publication.[1] Figure 1 shows the saturation magnetization of $BaO \cdot 6Fe_2O_3$ as a function of temperature, as measured for single crystals along the hexagonal axis, which is the direction of easy magnetization. Figure 2(a) schematically shows the crystal structure.[2] In this hexagonal structure oxygen ions form a close packed lattice, some sites of which are occupied by Ba ions. The ferric ions are found on five nonequivalent sites in the interstices of the oxygen lattice.

The value of the saturation magnetization and the dependence of the paramagnetic susceptibility on temperature indicate that the magnetization of the materials under consideration is due to noncompensated antiferromagnetism. The value of the saturation magnetization at low temperatures could be estimated for this compound and related materials. In this estimation, based on Anderson's theory,[3] it is assumed that an angle $Me^{(1)}-O-Me^{(2)}$, where Me stands for two magnetic ions and O for the oxygen ion giving rise to superexchange between them, causes strong negative interaction if near 180°, while interactions between two magnetic ions can be neglected when this angle is near 90°. The dependence of the superexchange on distance is taken into account by neglecting all interactions which involve $Me-O$ distances in excess of 3A. Proceeding along these lines, one finds 40 Bohr magnetons as saturation moment of $BaO \cdot 6Fe_2O_3$ at absolute zero temperature, while an extrapolation of the measurements gives about 44 Bohr magnetons.

It has already[1] been shown that very slight alterations of the structure can change the noncompensated antiferromagnetism into compensated antiferromagnetism. The compound $K_2O \cdot 11Fe_2O_3$, the structure of which[2,4] is schematically represented in Fig. 2(b), is nonferromagnetic. This can be explained by the small change in ionic arrangement near the layer which contains the large Ba or K ion. The three O ions in the Ba layer are replaced by one O ion in the K layer so that again a strong interaction results. Because of this interaction the K layer now will be a mirror plane for the direction of the magnetic moments.

II. CRYSTAL ANISOTROPY AND COERCIVE FORCE

The energy of crystalline anisotropy K, which is shown as a function of temperature in Fig. 3, determines the coercive force. The strain energy can be neglected, since the magnetostriction constant measured normal to the direction of preferential magnetization is only about $2\cdot10^{-5}$, at room temperature, while the shape anisotropy may be ignored because of the relatively low value of the saturation magnetization. In Fig. 4 the temperature dependence of $2K/I_s$ is compared with that of the coercive force for fine-grained material oriented at random. For pure rotation the coercive force ${}_IH_c$ should equal $0.96K/I_s$. The difference between the curves shown in Fig. 4 indicates that wall formation and wall movement must be taken into account.

The critical diameter for wall formation in isolated

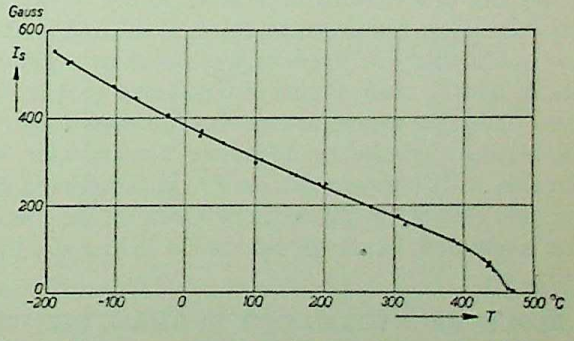


FIG. 1. The saturation magnetization of dense $BaO \cdot 6Fe_2O_3$ as a function of temperature.

[1] Went, Rathenau, Gorter, and van Oosterhout, Philips Tech. Rev. 13, 194 (1952).
[2] V. Adelsköld, Arkiv för Kemi, Mineralogi och Geologi 12A, No. 29, 1 (1938).
[3] P. W. Anderson, Phys. Rev. 79, 705 (1950).
[4] C. A. Beevers and M. A. S. Ross, Z. Krist. 97, 57 (1937).

CC-0. In Public Domain. Gurukul Kangri Collection, Haridwar

Digitized by Arya Samaj Foundation Chennai and eGangotri

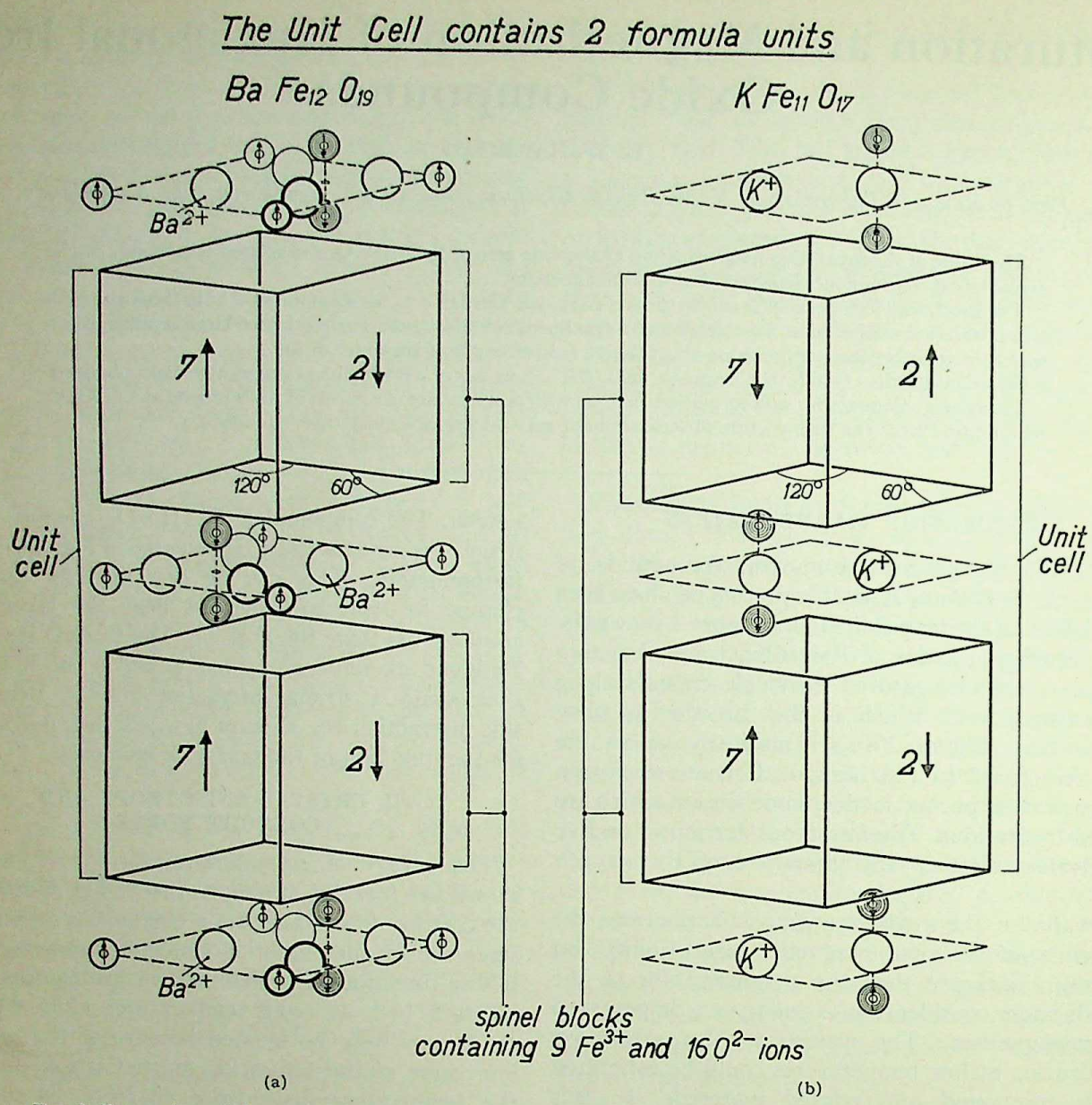


FIG. 2. Comparison of the crystal structures of $BaO \cdot 6Fe_2O_3$, which shows noncompensated antiferromagnetism, and $K\ Fe_{11}O_{17}$, which shows compensated antiferromagnetism; schematic. Large circles represent oxygen (or Ba or K) ions. Small circles represent ferric ion in different crystallographic sites.

spheres of the material can be estimated to be as large as one micron. It varies with temperature as $K^{\frac{1}{2}}/I_s$, a quantity which is plotted in Fig. 5. For a given grain the number of walls can thus be expected to decrease with increasing temperature below 430°C. Especially those walls that are fixed at inclusions or regions of suitable strain, and therefore are least mobile, will persist at higher temperatures. On the other hand, the field strength necessary to move a particular wall decreases with temperature as $K^{\frac{1}{2}}$. It is believed that these two effects, the influence of which on the coercive force is opposed, cause the maximum in the ${}_rH_c$ curve of Fig. 4.

III. BLOCH WALL FORMATION IN SMALL PARTICLES

Kittel[5] has stated that Bloch walls will be created spontaneously if the crystal size surpasses a critical diameter, while for smaller dimensions an external field has to be applied which increases with decreasing particle size. On treating again[6] his model of a single domain sphere, we arrive at the conclusion that the field strength at which a wall is formed should be independent of particle size, in case the thickness of the wall is small compared with the crystal size. It has been found experimentally that the coercive force of large particles of $BaO \cdot 6Fe_2O_3$ is much smaller than that of small particles and also than the critical field strength which has been calculated, just as in the case of MnBi.[7] Thus we are forced to assume that walls are nucleated at imperfections of the crystals such as, e.g., grain boundaries.

The calculation runs as follows. The largest field is needed in the initial stages of wall formation; therefore

[5] C. Kittel, Phys. Rev. 73, 810 (1948).

[6] Rathenau, Smit, and Stuyts, Z. Physik (to be published).

[7] C. Guillaud, thesis, Strasbourg, 1943.

CC-0. In Public Domain. Gurukul Kangri Collection, Haridwar

Digitized by Arya Samaj Foundation Chennai and eGangotri

only small angles θ have to be considered. If v is the disturbed region at the surface of the crystal and E_{ex} the increase in exchange energy, the energy balance reads

$$K\langle\theta^2\rangle_{Av}v+E_{ex}=[H_c+4\pi I_s/3]I_s\cdot\tfrac{1}{2}\langle\theta^2\rangle_{Av}v.$$

By taking the disturbed region sufficiently broad in the beginning, the exchange energy can be decreased. When it is neglected, one arrives at

$$H_c=2K/I_s-4\pi I_s/3.$$

The gain in demagnetization energy increases if the wall starts in the middle of the sphere. The coefficient of $4\pi I_s$ then becomes -0.86. In a thin plate magnetized along its normal, as is encountered in the hexagonal compounds, one arrives at the coefficients -1.01 and -2.02, respectively.

IV. THE MAGNETIZATION CURVE

While the stiffness with respect to rotation as given by $2K/I_s$ is very large, wall formation and wall displacement can be made difficult or easy at will by sintering the material at a low or a high temperature, respectively. The magnetization processes of rotation and wall displacement can therefore be separated.

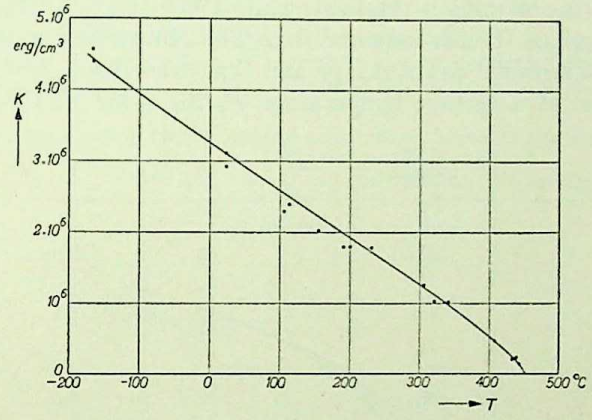


FIG. 3. Constant of crystal anisotropy K of $BaO\cdot 6Fe_2O_3$ as a function of temperature. (From $E_c=K\sin^2\theta+\cdots$.)

Let us consider the case that a wall can be created even in a small demagnetizing field, say zero. Owing to the random orientation of the crystals combined with a high resistance to rotation, large internal demagnetizing fields and, accordingly, wall displacements occur in positive external fields.

The problem can be approached[6] by ignoring rotations for the present, thus for $2K/I_s \gg H$. Let a crystal be represented as a small ellipsoid of revolution, with the easy direction along the axis. Let the demagnetization coefficient along the axis be n. The crystal is imbedded in a matrix which is thought to have the homogeneous magnetization I along a direction which makes an angle θ with the axis of the ellipsoid. The total internal field along the axis of the ellipsoid vanishes when an external field $H_0(\theta)$ parallel to the

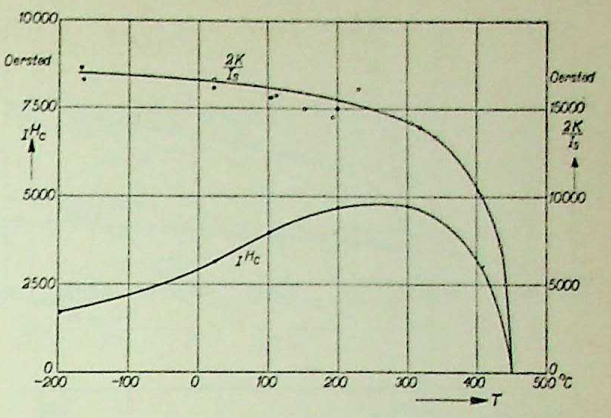


FIG. 4. The quantity $2K/I_s$ and the intrinsic coercive force ${}_iH_c$ as measured for fine-grained material as a function of temperature ($BaO\cdot 6Fe_2O_3$).

magnetization of the matrix is applied:

$$H_0(\theta)=(nI_s/\cos\theta)-nI.$$

If the external field exceeds $H_0(\theta)$, the ellipsoid is saturated, while for smaller external fields the magnetization of the ellipsoid decreases by wall formation

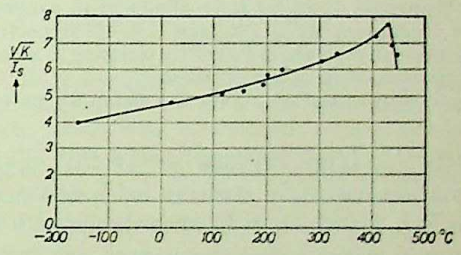


FIG. 5. The quantity $K^{\frac{1}{2}}/I_s$ as a function of temperature. ($BaO\cdot 6Fe_2O_3$.)

so as to render the total internal field zero. By averaging over θ, Fig. 6 is obtained.

Figure 7 gives magnetization curves measured at a low and a high temperature. Figure 7(a) applies to small crystals and shows that at positive field strengths the upper branch of the loops can be represented by Stoner and Wohlfarth's[8] calculations for pure rotation.*

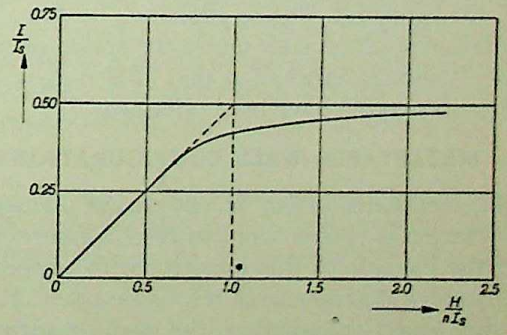


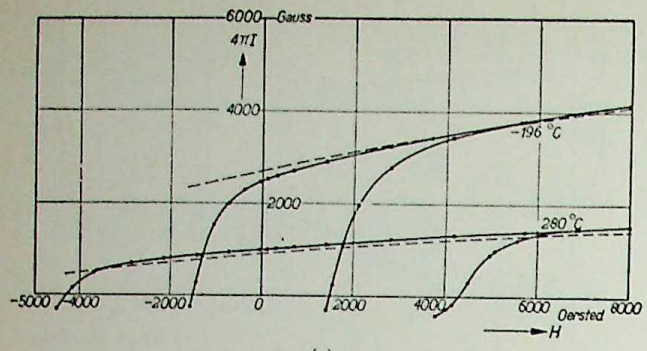
FIG. 6. Demagnetization by wall formation in positive fields as calculated for a model with $2K/I_s \gg nI_s$.

[8] E. C. Stoner and E. P. Wohlfarth, Phil. Trans. Roy. Soc. (London) 240, 599 (1948).

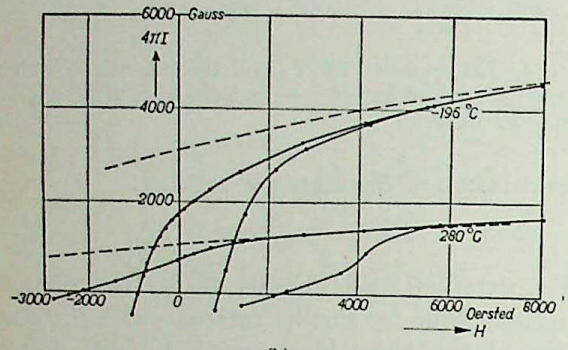
* The values for I_s and K used for the calculation of Stoner and Wohlfarth's curve were measured on single crystals.

CC-0. In Public Domain. Gurukul Kangri Collection, Haridwar

Digitized by Arya Samaj Foundation Chennai and eGangotri



(a)



(b)

FIG. 7. Hysteresis loops for $BaO \cdot 6Fe_2O_3$ with random crystal orientation, measured at −196 and 280°C, respectively: (a) material with small crystals, obtained by sintering at a low temperature; (b) material with larger crystals.
Dashed: Demagnetization curves calculated for pure rotation.

Figure 7(b) for large crystals shows that appreciable wall formation occurs in positive fields of the order of $4\pi I_s$ (see Fig. 1), which is in accordance with Fig. 6 if one takes into account that the crystals are small plates with the hexagonal axis as normal.

In Figs. 8(a) and (b) the magnetization curves at room temperature are compared for coarse-grained material oriented, respectively, at random and in such a way that the easy direction of magnetization coincides with the direction of the external field. As is to be expected there is almost no demagnetization in positive fields in the oriented material.

In a forthcoming paper[6] it will be shown that the texture of the oriented material is improved by firing at high temperatures. This is explained by the absorption of misoriented crystals under the action of surface tensions. It suffices here to say that (BH)max-values of 3×10^6 gauss oersted have been obtained.

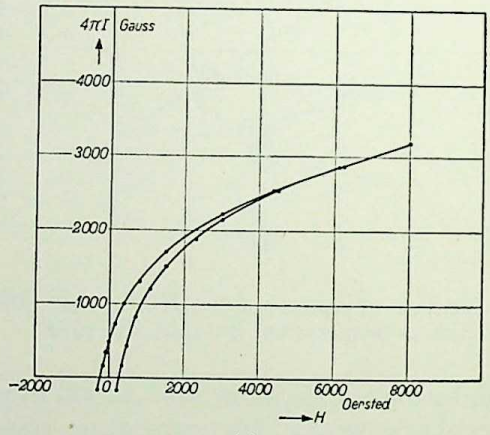
V. METASTABLE WALL CONFIGURATIONS

As was mentioned in Sec. II, the critical diameter for wall formation is proportional to $K^{\frac{1}{2}}/I_s$. Figures 5 and 9 show the increase of this quantity with temperature and its sudden decrease near the Curie point. It is an interesting question whether the wall configuration changes with a change in temperature in such a way that a stable equilibrium is maintained. The following experiment has been performed to answer this question.

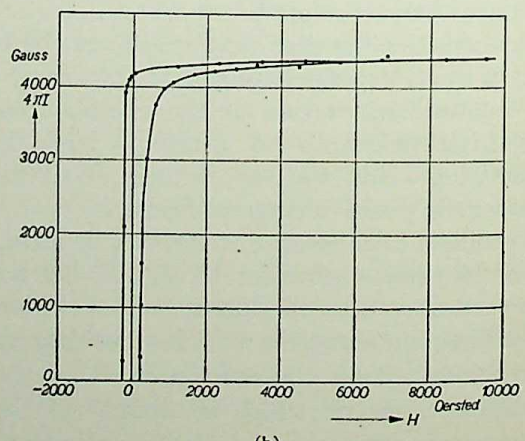
The "initial" permeability in a "small" field of 500 oersteds has been measured at 15°C after establishing the equilibrium configuration of the walls at various temperatures T_d by demagnetization at these temperatures in an ac field. Figure 9 shows that the susceptibility after demagnetization either at low temperatures or at temperatures very near the Curie point, where $K^{\frac{1}{2}}/I_s$ is smaller than at room temperature, greatly exceeds the value obtained by demagnetization at room temperature. An excess of walls apparently remains in a metastable state within the material. On the other hand, demagnetization at temperatures where $K^{\frac{1}{2}}/I_s$ exceeds its room temperature value only leads to a slightly reduced susceptibility at room temperature, indicating that walls enter.

It is interesting to note that the minimum in the (μ_0-1)-curve of Fig. 9 does not occur at 280°C, where ${}_IH_c$ is maximum, but near 400°C, where $K^{\frac{1}{2}}/I_s$ is maximum. For the fine-grained sample the permeability after demagnetization at elevated temperatures approaches the value calculated for rotation only.

Table I, in which (μ_0-1) after subtraction of the rotational part is given, reveals more clearly that an excess of walls is retained, while a deficiency is nearly supplied. If it is assumed that the stiffness of a wall is proportional to its energy and that after demagnetization at a certain temperature T_d the same wall con-



(a)



(b)

FIG. 8. Hysteresis loops for $BaO \cdot 6Fe_2O_3$ measured at room temperature for coarse grained material of small coercive force: (a) crystal orientation at random; (b) texture, the direction of easy magnetization being in the direction of the applied field.

CC-0. In Public Domain. Gurukul Kangri Collection, Haridwar

Digitized by Arya Samaj Foundation Chennai and eGangotri

figuration exists at different temperatures of measurement T_{m1}, T_{m2}, one expects

$$[(\mu_0-1)_{Td,\,Tm1}(K^{\frac{1}{2}}/I_s)_{Tm1}]/[(\mu_0-1)_{Td,\,Tm2}\cdot(K^{\frac{1}{2}}/I_s)_{Tm2}]=1.$$

Table I shows that this relation holds well if after demagnetization the change of temperature is such as to produce an excess of walls. The results are qualitatively summarized in the undermost part of Fig. 9.

The high degree of stability of an excess of walls might be due to some coupling of these walls during the demagnetization process by which they were formed. An additional experiment, in which no ac field was applied at the low temperature, points in this direction.

The specimens of Table I were demagnetized at 15° and, before being measured at 15°, cooled to −196°C. The (μ_0-1)-values obtained were 0.57 (specimen *A*) and 0.35 (specimen *B*). Comparison with (c) and (d) in Table I shows that an excess of walls is once more metastable. But not all walls formed at low temperatures are now retained.

TABLE I. Contribution of wall movement to (μ_0-1). T_m: temperature of measurement. T_d: temperature of demagnetization. Letters (a), (b), (c), and (d) as in the schematic representation of Fig. 9.

	T_m −196°	15°C	$\left[\frac{(\mu_0-1)_{-196}}{(\mu_0-1)_{15}}\cdot\frac{(K^{\frac{1}{2}}/I_s)_{-196}}{(K^{\frac{1}{2}}/I_s)_{15}}\right]_{Td=\text{const}}$
(A) large crystals			
T_d −196°C	1.31 (a)	1.12 (b)	0.96
15°C	0.97 (c)	0.41 (d)	1.94
(B) small crystals			
T_d −196°C	1.25 (a)	1.09 (b)	0.94
15°C	0.72 (c)	0.21 (d)	2.8

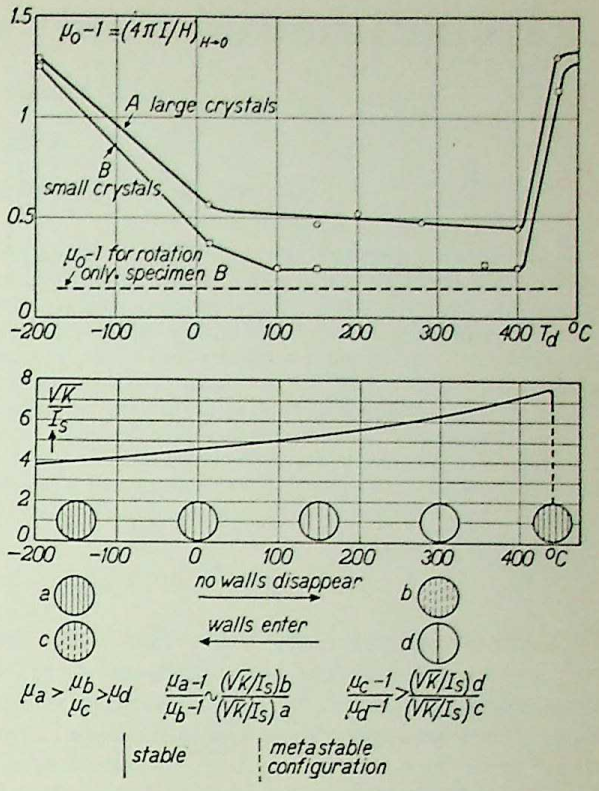


FIG. 9. Initial permeability μ_0 measured for $BaO\cdot 6Fe_2O_3$ with random crystal orientation at room temperature. Before the measurement the material was cooled down from above the Curie point in a field-free space, then demagnetized at the temperature T in an alternating-current field decreasing in amplitude from 4250 oersteds. It was then brought to 15°C and measured.
Curve A: large grains; curve B: small grains.

As is to be expected, demagnetization and measurement at −196°C, with an intermediate heating to 15°C, lead exactly to the values (a) of Table I.

The author wants to thank his colleagues Mr. J. Smit, Mr. E. W. Gorter, and Mr. A. L. Stuyts for help and discussions.

DISCUSSION

G. W. RATHENAU, *N. V. Philips Gloeilampen Fabrieken, The Netherlands* (in answer to questions): Near room temperature, magnetoelastic energy and shape energy are negligible compared with crystalline energy: λ (perpendicular to axis) $\cong 20\times 10^{-6}$. The results are consistent with the idea that this is true also at higher and lower temperatures.

The texture can be made very perfect, as is shown by the curve for the low coercivity oriented sample.

Saturation of nonoriented material requires very high fields.

C. L. HOGAN, *Bell Telephone Laboratories, Murray Hill, New Jersey:* According to data recently taken at the Bell Telephone Laboratories, Ferroxdure at 9000 Mc induces a Faraday rotation of less than 0.1 degree/cm in a round wave guide, in applied magnetic fields up to 6000 oersteds. Compared with ferrites, it shows a very low loss at 9000 Mc, but high loss at 48 000 Mc.

M. T. WEISS, *Bell Telephone Laboratories, Murray Hill, New Jersey:* Have any ferromagnetic resonance experiments been made on these $BaO\cdot 6Fe_2O_3$ materials?

G. W. RATHENAU, *N. V. Philips Gloeilampen Fabrieken, The Netherlands:* Such experiments are being conducted, but no final results can yet be reported.

CC-0. In Public Domain. Gurukul Kangri Collection, Haridwar

Digitized by Arya Samaj Foundation Chennai and eGangotri

REVIEWS OF MODERN PHYSICS VOLUME 25, NUMBER 1 JANUARY, 1953

Experimental Study of the Coercive Force of Fine Particles

W. H. MEIKLEJOHN

General Electric Research Laboratory, Schenectady, New York

The experiments described test the theory of fine-particle magnets. Particles of Fe, Co, and Ni, of size 100–2000A, were prepared by electrodeposition into a mercury cathode. Their sizes and shapes were determined with an electron microscope. Experiments on coercive force *vs* particle size show, in general agreement with theory, that the maximum coercive force of Fe particles occurs at about 150A and is about 1000 oersteds, for very small packing factors. The coercive force decreases rapidly for smaller particles, slowly for larger particles. The rapid decrease for particles smaller than 150A is attributed to thermal fluctuations; this is borne out by measurements at low temperatures.

Addition of 25 percent by weight of 20-oersted Fe particles to 1250-oersted Fe particles decreases the coercive force to 500 oersteds: thus any experiment designed to check the predicted 10 000 oersteds for particles of 10-to-1 shape anisotropy requires an extremely high percentage of such particles. For both Fe and Co, the temperature variation of coercive force closely follows that of crystalline anisotropy and not that predicted for particles with shape anisotropy. Electron micrographs show that many of these particles are bean-shaped, with axis ratio 1.5. The extent of the present work is not sufficient for evaluation of the contribution of shape anisotropy to the coercive force of Fe.

DURING the past fifty years there have been several independent investigations[1–5] of the ferromagnetic properties of small particles of iron, nickel, cobalt, and manganese bismuth. These investigations have shown extremely high coercive forces, of the order of 1000 oersteds for iron; and theoretical investigations have predicted coercive forces of ten times these experimental values.

What seems to be lacking is (1) the experimental relationship between the coercive force and particle size for iron, cobalt, and nickel, and (2) the exact shape of the particles that have a coercive force more than twice the value predicted by theory.

In order to obtain these relationships, fine particles of iron, cobalt, and nickel were prepared by the electrodeposition of these materials in a mercury cathode by use of standard electrolytes. The coercive force of the freshly deposited iron and cobalt could be made as low as 20 oersteds and subsequently increased to a maximum of 1000 oersteds by heating at a convenient temperature for a period of time. Further heat treatment would decrease the coercive force to as low as 40 oersteds. Figure 1 shows the relationship between the coercive force at liquid nitrogen temperature and time of heat treatment at 200°C.

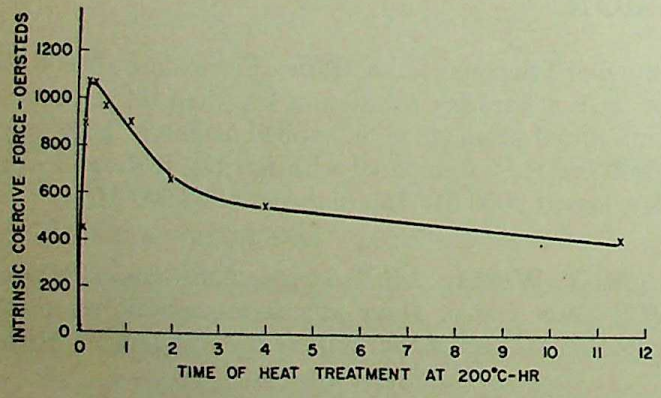


FIG. 1. Effect of heat treatment on the intrinsic coercive force of iron electrodeposited in mercury.

In order to measure the coercive force of the iron particles in the mercury it was necessary to prevent their movement or rotation by solidifying the matrix. This could be done by adding an alloying element such as silver to the mercury to obtain a solid matrix, or simply by freezing the mercury. Since experiment showed that the same coercive force was obtained by both methods, the latter method was used because it proved to be more expedient. The mercury was frozen by placing it in liquid nitrogen, and the coercive force was measured at this temperature.

In all cases, the coercive force listed is the intrinsic coercive force, measured by placing a magnetized sample in a coil immersed in a magnetic field which is directed opposite to that of the sample. The coil is connected to a galvanometer, which is caused to deflect by moving the sample in and out of the coil, yet keeping the sample in the reverse field. The reverse field is increased until no deflection is obtained, and therefore the intrinsic induction in the sample has been reduced to zero. The reverse field is then measured to obtain the intrinsic coercive force.

The above process gave excellent control of the coercive force, and as it happened also the particle size, so that a material was available for coercive-force and particle-size measurements. The measurements of the particle size, while the particles were still wetted by the mercury, proved to be both extremely difficult and unreliable. To remove the mercury from the particle by evaporation always resulted in a large particle size, as discussed in connection with Fig. 1. The best method of removing the particles and having the desired size was

[1] H. Nagaoka, Wiedemann Ann. Physik 59, 66 (1896).
[2] K. Honda, Japan Nickel Rev. 5, 517 (1937).
[3] R. S. Dean and C. W. Davis, U. S. Patent 2,239,144.
[4] F. Pawlek, Metall. 1950, 58.
[5] B. Kopelman, Elec. Eng. 71, 447 (1952).

CC-0. In Public Domain. Gurukul Kangri Collection, Haridwar

Digitized by Arya Samaj Foundation Chennai and eGangotri

to dewet the particles by diffusing oxygen through the mercury, to form an oxide shell around the particles, and collect them after they floated out of the mercury. The use of a "Mercury Oxifier" has proved very efficient in this respect. Since this removal takes place at essentially room temperature, the particles do not grow in size except for the volume increase due to the oxygen taken on by the surface to form FeO. One might expect that the particles would be completely oxidized, but this does not happen except for the very small sizes below 50 A. If the powder is pressed in a die it has an extremely metallic appearence, and both electron diffraction and x-ray diffraction data have shown that the material is not completely oxidized.

A comparison of the coercive force of the particles in the mercury and after removal by the introduction of an oxide shell on the particles is shown in Table I for iron. The room temperature value of the coercive force is also shown along with the percent change due to the temperature difference. One might expect a shift in the maximum coercive force of the oxide-coated material toward the apparent larger particle sizes. Any such shift might easily be offset by having a particle-size distribution in the mercury, in which case the larger particle would be the first to come out owing to the greater buoyancy force. Because of these opposing factors, a correction has not been made in the particle size to account for the oxide shell on the particle.

TABLE I. Intrinsic coercive force of iron.

Hci in mercury −196°C	Hci out of mercury −196°C	Hci out of mercury 20°C	Percent change in Hci 20°C to −196°C
450	590	35	1600
900	1025	670	53
1075	1100	880	25
1050	1050	850	23
975	1000	870	22
900	850	750	14
350	350	300	17

The percentage difference in the coercive force shown in Table I is in good agreement with what one would expect from crystalline anisotropy. The one exception is the case of the particle of 35 oersteds at room temperature (75 A diameter), in which case one must turn to some explanation such as that proposed by Néel. The critical particle diameter for thermal instability decreases as the temperature is decreased, and hence a judiciously chosen particle would have a tremendous increase in coercive force as the temperature is lowered. This condition was found to exist also in the iron particles in a mercury matrix, where the coercive force of particles smaller than the optimum size increased from 400 oersteds at liquid nitrogen temperature to 550 oersteds at liquid hydrogen temperature and 700 oersteds at liquid helium temperature.

The oxide-coated particles were prepared for measurement in an electron microscope, the first major problem being to show the effect of these small permanent magnets on the electron beam. It seemed very likely that the magnetic field of the particle would deflect the electron beam and cause the image not to be

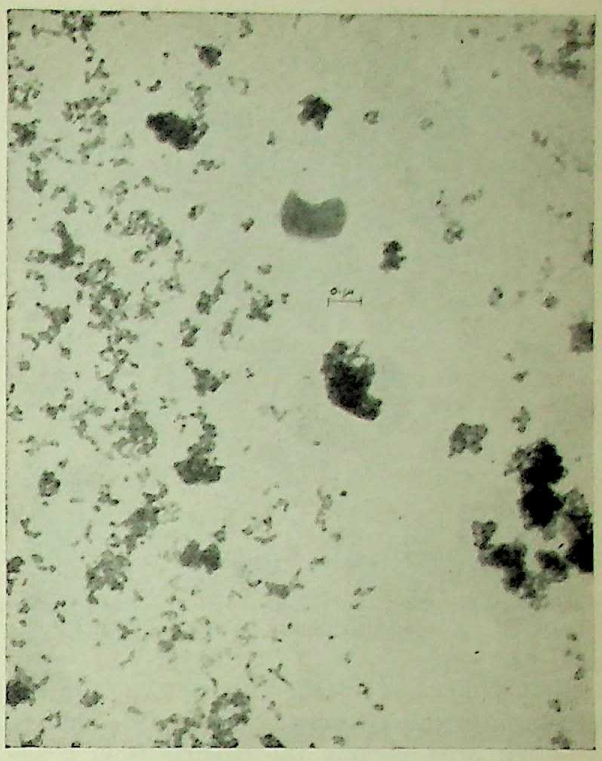


FIG. 2. Electron micrograph of iron particles in silicon monoxide.



FIG. 3. Electron micrograph of same area as Fig. 2 after dissolving the iron particles to form a cavity. Some particles that have not been dissolved can be used as size reference.

CC-0. In Public Domain. Gurukul Kangri Collection, Haridwar

Digitized by Arya Samaj Foundation Chennai and eGangotri

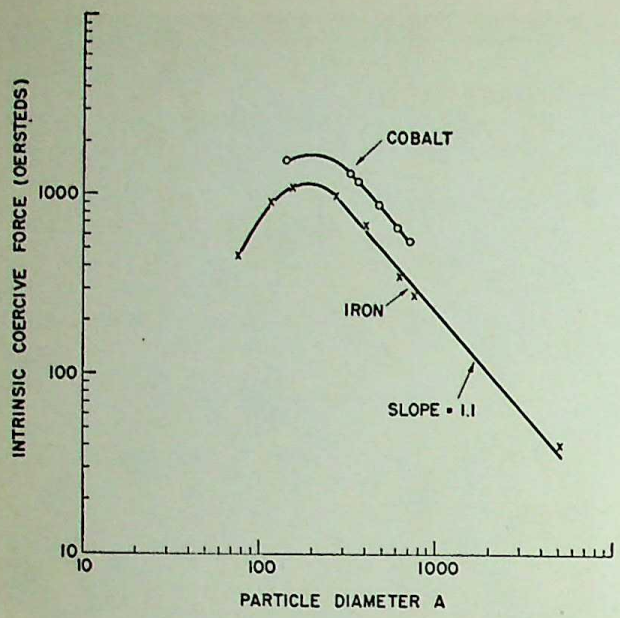


FIG. 4. Intrinsic coercive force at liquid nitrogen temperature of iron and cobalt particles as a function of particle size.

in direct proportion to the particle size and shape. Electron micrographs taken of the particle and of the cavity left after etching the particle from a silicon monoxide matrix show that the image does faithfully reproduce the size and shape of the particle. This is shown in Fig. 2 and Fig. 3.

The results of the measurement of particle size were plotted against coercive force and are shown in Fig. 4. It is apparent here that in the region from 5000A particles to 200A, where thermal fluctuations take over, the product of the coercive force and particle diameter is a constant and the curve is that of an equilateral hyperbola. This is in agreement with the relationship that Guillaud found for manganese bismuth particles. The present theoretical relationships of the simple theory of coercive force do not show this dependence of coercive force on particle size.[6]

The straight-line portions of the curves shown in Fig. 4 will probably extend to particles smaller than 200A and then become horizontal if the measurement is made at a sufficiently low temperature to eliminate the drop due to thermal fluctuations in the particles.

The curve for particle size *vs* coercive force for cobalt shown in Fig. 4 gives a value of the critical particle size for single domain behavior which is of the same order of magnitude as for iron, and not ten times the size of iron as has been predicted by theoretical calculations.[6]



FIG. 5. Electron micrograph of 115A iron particles.

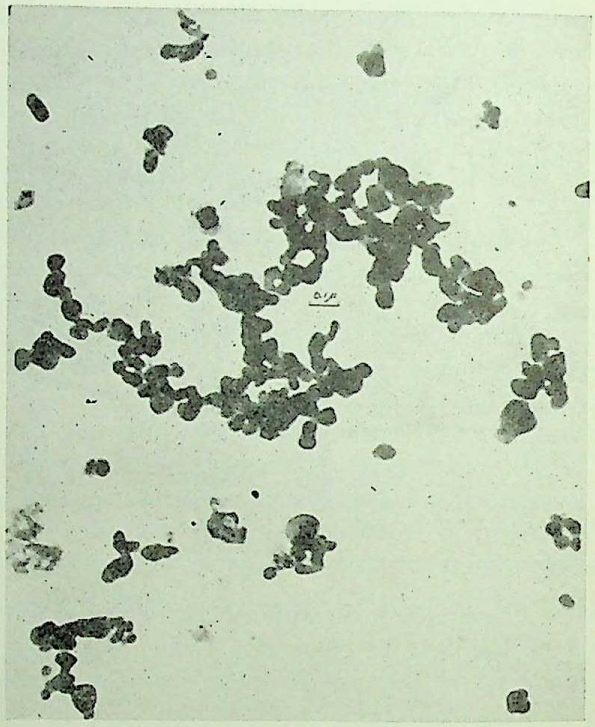


FIG. 6. Electron micrograph of 560A iron particles.

There is also disagreement, as has been known for some time, between the experimental values of the coercive force for cobalt and the value obtained from consideration of the crystalline anisotropy energy. Theoretical calculations[6] predict a value of 6000 oersteds for cobalt on the basis of its crystalline anisotropy, while the experimental value is of the order of 1000 oersteds.

The shapes of the particles are shown in Figs. 5, 6, and 7. An examination of these electron micrographs shows that many of the particles have a shape anisotropy of 11/2 to 1. Of course, this is only a two-dimensional view of the particles, but a lack of any plate-like particles leads to the belief that these particles are nearly prolate ellipsoids of an axial ratio of 11/2 to 1. Since

[6] C. Kittel, Revs. Modern Phys. 21, 541 (1949).

CC-0. In Public Domain. Gurukul Kangri Collection, Haridwar

Digitized by Arya Samaj Foundation Chennai and eGangotri

theory [6–8] predicts a value of nearly 3000 oersteds for this ratio of major to minor axis of the particles, there again seems to be disagreement with the theory. Since there is certainly a size and shape distribution of particles shown in the electron micrographs, an experiment was conducted to determine the effect of this on the measured coercive force. The results are shown by Fig. 8.

To determine this relationship, iron was electrodeposited into mercury so as to have a coercive force of 12 oersteds. Since the suspension of iron in mercury is very homogeneous for this particle size, volumetric ratios were taken as a measure of the amount of iron in the mercury. Eight different samples were taken. Four of these samples were heat treated to have a coercive force of approximately 1000 oersteds at liquid-nitrogen temperature. These samples were then mixed with the untreated samples to form the required percentage of low- and high-coercive-force material (0, 25, 50, 75, and 100 percent of the former). The results of this procedure are given by curve 1 of Fig. 8. Essentially the same procedure was used to mix the untreated iron with cobalt heat-treated to near the maximum coercive force, and the result is shown in Fig. 8, curve 2. In both cases there is a rapid decrease in the coercive force with a small percent admixture of the low-coercive-force material. On the other hand, if iron of near-maximum coercive force is mixed with iron particles heat treated beyond the maximum to 150 oersteds and approximately 1000A particle size, the effect on the coercive force is greatly reduced. This result is shown in Fig. 8, curve 3. The decrease in coercive force is linear with the weight percent of low-coercive-force material, instead of having the shape of an equilateral hyperbola as in the case of very small particles of low-coercive-force material.

To explain the 1000 oersteds coercive force obtained for iron on the basis that there is a mixture of low-coercive-force particles (that is, some that are round and of 500 oersteds coercive force) with 3000-oersted particles of $1\frac{1}{2}$ to 1 shape anisotropy would actually require data similar to those shown in Fig. 8 for particles of similar size but of about 10 to 1 ratio of coercive force. However, if it is assumed that this relationship would be the same as for curve 1 of Fig. 8, which is more favorable to the theory, then the electron micrographs must show approximately 25 percent by weight of the particles to be round, smaller than 75A, or larger than 500A. The electron micrographs cannot be evaluated very well to show that there is not a 25 percent by weight of round particles. Also it is extremely difficult to evaluate the percent by weight of particles less than 75A because this size approaches the resolution of the electron microscope.

[7] E. C. Stoner and E. P. Wohlfarth, Trans. Roy. Soc. (London) **A240**, 599 (1948).
[8] E. Kondorskii, Doklady Akad. Nauk SSSR (N.S.) **70**, 215 (1950).



FIG. 7. Electron micrograph of 620A iron particles.

It is hoped that stereographic electron micrographs can be taken that will allow an evaluation of the true coercive force of the particles having shape anisotropy.

There is still another evaluation to be made, and this is the effect of clustering of the particles. In spite of the measurements being made at 0.004 packing factor (the weight of iron per cubic centimeter divided by the density of iron), the particles have not been separated any better than is shown in these electron micrographs, where it is obvious that there is considerable clustering of the particles into groups as great as 100 particles.

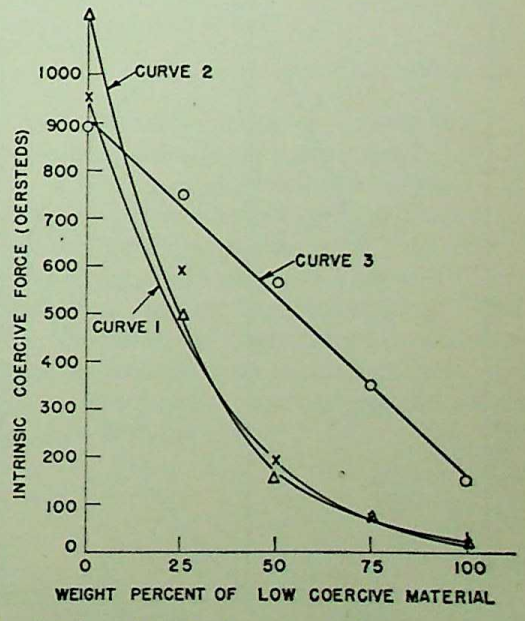


FIG. 8. Effect of mixing low coercive force particles with high coercive force particles.

CC-0. In Public Domain. Gurukul Kangri Collection, Haridwar

Digitized by Arya Samaj Foundation Chennai and eGangotri

One can probably assume a packing factor of the order of 50 percent for these clusters, whereupon Weil[9] has shown that the coercive force will be cut in half. In addition, this clustering makes it extremely difficult to line up the particles. If we assume that Néel's[10] calculation for randomly oriented cubic crystallites applies to both hexagonal cobalt and iron with shape anisotropy, then the theoretical value for iron particles of $1\frac{1}{2}$ to 1 shape anisotropy is reduced from 3000 oersteds for widely separated particles to approximately 500, and that for cobalt particles from 6000 oersteds to 1000 oersteds.

[9] L. Weil and S. Marfoure, Compt. rend. 225, 229 (1947).
[10] L. Néel, Compt. rend. 224, 1488 (1947).

It is apparent that in spite of having particles of $1\frac{1}{2}$ to 1 shape anisotropy, steps must still be taken (1) to better evaluate the effect of shape and size distribution, (2) to evaluate the effect of clustering on lining up of the particles, and (3) to evaluate the "apparent" packing factor due to clustering.

It is hoped that further work along these lines will lead to an experimental evaluation of the contribution of shape anisotropy to coercive force.

ACKNOWLEDGMENT

I wish to thank T. O. Paine for his many helpful suggestions and E. F. Fullam for his generous contribution to the taking of the electron micrographs.

REVIEWS OF MODERN PHYSICS VOLUME 25, NUMBER 1 JANUARY, 1953

A New Permanent Magnet from Powdered Manganese Bismuthide

EDMOND ADAMS

U. S. Naval Ordnance Laboratory, White Oak, Silver Spring 19, Maryland

BECAUSE the present demand for cobalt and nickel greatly exceeds their availability, there has been an increasing interest, both in this country and abroad, in the development of permanent magnets not containing these elements. The Magnetics Division of the Naval Ordnance Laboratory, as part of its program of developing improved and nonstrategic magnetic materials for military and industrial use, has developed bismanol, a new high energy product permanent magnet. This magnet was prepared by hot-pressing the finely pulverized anisotropic intermetallic compound, manganese bismuthide (MnBi). A typical demagnetization curve for bismanol is illustrated in Fig. 1, which shows a maximum energy product $(BH)_{max}$ of 4.3×10^6 gauss-oersteds, a coercive force (H_c) of 3400 oersteds, and a residual flux density (B_r) of 4300 gauss. That this was possible was first predicted by Guillaud[1] as early as 1939. Guillaud, in

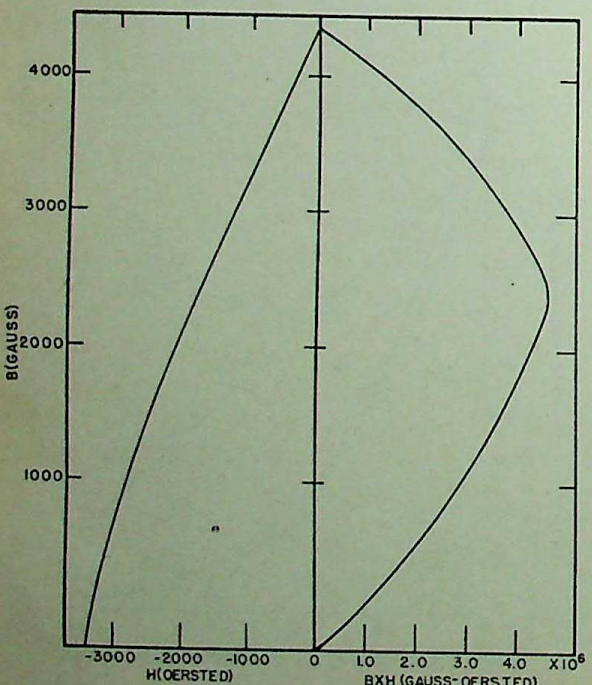


FIG. 1. Demagnetization and energy product curves—bismanol.

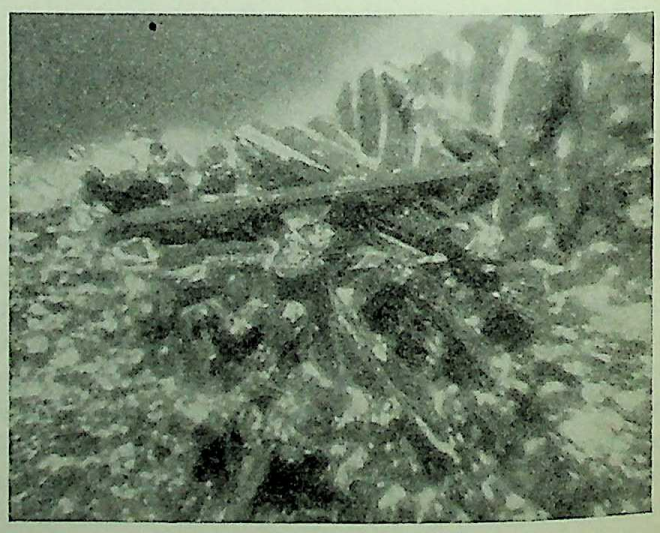


FIG. 2. Hexagonal crystals of MnBi.

[1] C. Guillaud, thesis, University of Strasbourg (Strasbourg, France), 1943.

CC-0. In Public Domain. Gurukul Kangri Collection, Haridwar

Digitized by Arya Samaj Foundation Chennai and eGangotri

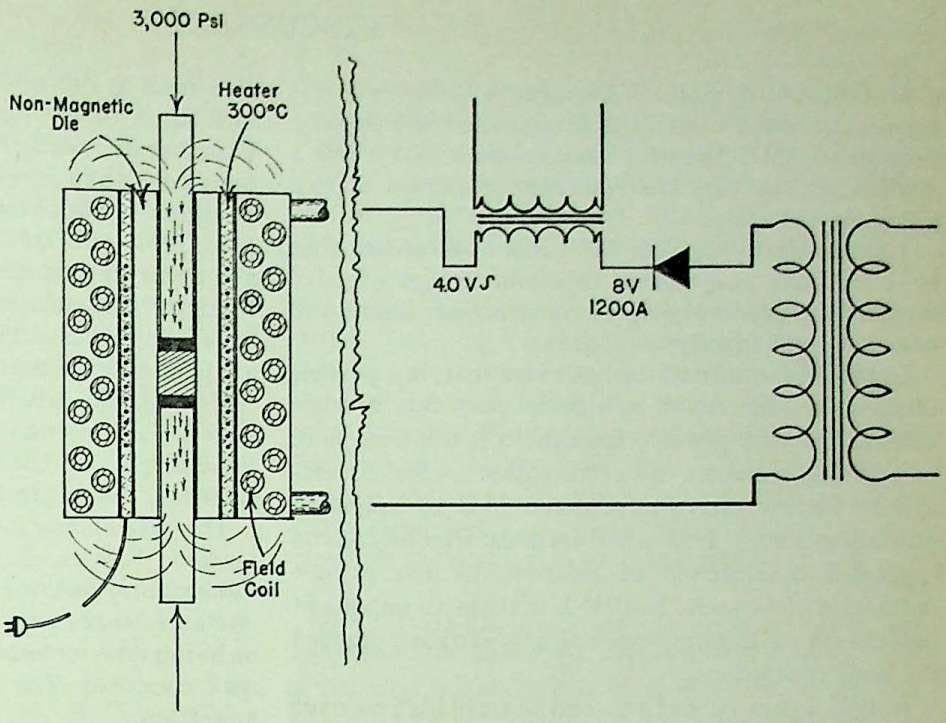


Fig. 3. Hot-pressing oriented MnBi powder into bismanol magnets.

addition to measuring the saturation moment, magnetic crystal anisotropy, and Curie temperature, established the dependence of the high coercive force of manganese bismuthide on its high crystal anisotropy and reduced particle size. Because of these considerations, MnBi was chosen for this investigation in spite of the practical difficulties involved.

Manganese and bismuth powders were heated in a rotating furnace to 700°C for the reaction to take place and aged at 450°C for MnBi crystals to increase in size. At this stage bismuth was allowed to diffuse through a MgO crucible. This exposed some almost perfect hexagonal crystals of MnBi as shown in Fig. 2. They were identified as the compound MnBi by x-ray diffraction as shown in Table I. Normally, in the preparation of a melt, visible crystals of MnBi are not exposed.

The melt of MnBi and unreacted manganese and bismuth was then pulverized in a high speed hammer mill, yielding irregular particles of approximately 8 microns in diameter. The magnetic MnBi was then separated from unreacted manganese and bismuth by use of a magnetic separator.

The enriched MnBi powder was then hot-pressed at comparatively low pressure (up to 3000 psi) at 300°C in a nonmagnetic cylindrical die with double-acting magnetic rams. The purpose of the field (up to 20 000 oersteds) was to align the particles with their easy direction of magnetization parallel to the direction of testing.

The compacting was performed in a heated die to provide a maximum density at low pressures. In this respect, it is probably desirable to have a small amount of free bismuth present in the powder. This provides a fluid medium at 300°C to facilitate particle alignment and after solidification, upon cooling, effectively separates and immobilizes the particles. Figure 3 illustrates schematically the compaction of the magnets.

TABLE I. X-ray data for MnBi crystals.

Sample	Unit cell length
NOL (quenched from 320°C)	5.87±0.02A
Guillaud (quenched from 400°C)	5.83A
Guillaud (slow cool)	6.11A

Thus, a new class of permanent magnets has been prepared by powder-metallurgy techniques. These magnets exhibit a coercive force (H_c) exceeded by no other known practical magnets. They can be used for practically all present applications of permanent magnets; however, in short lengths, where a high resistance to demagnetization is important, bismanol magnets exceed most commercial permanent magnets in available flux density.

CC-0. In Public Domain. Gurukul Kangri Collection, Haridwar

Digitized by Arya Samaj Foundation Chennai and eGangotri

DISCUSSION

C. GUILLAUD, *Centre National de la Recherche Scientifique, Bellevue, France:* The manganese-bismuth alloy prepared by Mr. Adams is identical with that which I studied; in fact the characteristic properties of this phase are the same.

I am going to mention the various researches that have led to a new method of attaining high coercive force and to practical magnet construction; then I will summarize the future possibilities.

In 1943[1] I formulated the basic idea that, in a particle of metal or alloy small enough to constitute a single domain, the only possible mechanism is rotation, since no wall displacements can occur without walls. Specifically,[1,2] for a coercive force determined by magnetocrystalline energy I gave the formula $H_c = pK/I_0$ and suggested construction of magnets by use of fine particles with large K. In 1946 Kittel,[3] in an important publication on the properties of fine particles, reached the same conclusions.

In 1947 I pointed[4] out a second cause of high coercive force in fine particles, the magnetoelastic energy, and gave the formula $H_c = p'\lambda\sigma/I_0$ based on a formula of R. Becker. Later Stoner and Wohlfarth[5] arrived at this same mechanism.

Finally, also in 1947, first Néel[6] and then Stoner and Wohlfarth[5] and I[4] gave a third cause of high coercive force, shape anisotropy, which leads to the formula $H_c = p''(N-N')I_0$.

Because of the energy necessary for wall formation and for existence of multidomain grains, the coercive force depends on the grain size; a general study was made in 1946 by Kittel.[3] Furthermore, in aggregates of grains the values of p, p', and p'' depend on the degree of orientation of the domains and on interactions between crystallites. The study of MnBi first gave experimental values of p; later Néel, followed by Stoner and Wohlfarth, perfected the theory and obtained values in good accord with experiment.

The experimental study of these elementary mechanisms is very difficult because it is necessary to separate the effects of the three types of energy. It was our work on MnBi and Mn_2Sb and L. Weil's work on nickel that made possible the clear separation of these effects, by study of the temperature variation of coercive force.

From consideration of rotation in fine particles, the application to magnets follows directly. The high coercive force is determined by one of the three factors mentioned or by several operating simultaneously. Experiments based on magnetocrystalline energy require metals and alloys with large K. Cobalt is of particular interest but so far has yielded unsatisfactory coercive forces—probably because (as L. Weil pointed out and as we have verified) lamellar grains are obtained. Manganese-bismuth magnets based on this mechanism have found industrial application. The possibilities here are far from exhausted.

Use of magnetoelastic energy requires materials with large λ; the internal stresses can then be controlled, for example, by hardening or by formation of solid solutions. Here a great field of research is open.

The possibilities for shape anisotropy are also important. Besides obtaining needle-shaped grains one can seek, for instance, to obtain a ferromagnetic precipitate in needle form within a nonferromagnetic phase, or to improve the usual massive magnets by producing ones composed of oriented crystals with large shape anisotropy.

Rotations against magnetocrystalline and magnetoelastic energy can be produced, not only in aggregates of fine particles, but also by use of holes (as we showed in the study of cobalt ferrites) or of nonmagnetic inclusions in massive materials. These elementary mechanisms have been studied by Kersten and by Néel.

Here is a new path of research on magnets. Practical results have already been obtained, and important progress can be foreseen.

W. SUCKSMITH: *University of Sheffield, England:* We have been investigating the magnetic properties of small iron and cobalt aggregates by utilizing the weakly ferromagnetic copper-rich binary alloys with iron or cobalt. When bulk specimens of these alloys, containing 1–2 percent of cobalt or iron, are quenched from high temperatures, they are paramagnetic, and the curve of intensity against field resembles that of a normal paramagnetic. By heating the alloy at a suitable temperature dependent on constitution, and interrupting this process at appropriate times, the transition from the solid solution to the ferromagnetic two-phase state can be followed in detail. In the initial stages the paramagnetism increases with a decrease in Δ. Later a small but gradually increasing coercivity develops, the I-H curves being quite linear up to $H = 500$ oersteds. At the same time the slope of the curve increases progressively, until the coercivity reaches a maximum value at about 450 oersteds. At this stage it is evident that a harder component is concealed. The remanence, and to a lesser extent the coercivity, increases with the maximum value of the magnetizing field used, even until the latter reaches more than 5000 oersteds. At the same time the reverse field required to decrease the remanence assumes a value considerably

---

[1] Charles Guillaud, *pli cacheté* deposited March 8, 1943; Compt. rend. 229, 992 (1949).
[2] Charles Guillaud, thesis (Strasbourg, 1943).
[3] C. Kittel, Phys. Rev. 70, 965 (1946).
[4] Charles Guillaud, Comm. Soc. franc. de Physique (Strasbourg, May 31, 1947); J. phys. et radium 8, 347 (1947).
[5] E. C. Stoner and E. P. Wohlfarth, Trans. Roy. Soc. (London) A240, 599–642 (1948).
[6] L. Néel, Compt. rend. 224, 1550 (1947).

CC-0. In Public Domain. Gurukul Kangri Collection, Haridwar

Digitized by Arya Samaj Foundation Chennai and eGangotri

in excess of that required to produce a similar effect in a normal ferromagnetic. For example, to reduce the remanence to zero required about 1500 oersteds; to reverse it completely required considerably greater values. At this stage the coercivity begins to fall off; the intensity continues to increase, but with increasing curvature of the *I-H* curve of the familiar shape concave to the field axis. Finally the coercivity falls to a value less than 100 oersteds with the completion of the precipitation process at the temperature employed. It seems evident, not only from the trend of the coercivity-time relationship, but also from the evidence for the concealed harder component of the magnetization, that with continued heat treatment single domain particles increase in size until the appearance of domain walls causes a decrease in coercive force.

L. F. BATES, *University of Nottingham, England:* I would like to draw the authors' attention to some experiments on the ferromagnetic properties of amalgams of iron, nickel, and cobalt in mercury; and in particular to the fact that amalgams of nickel are not ferromagnetic unless they are heated to about 260°C. They may find that experiments on fine particles obtained from the nickel amalgams will be of particular interest.

I should like to mention some experiments which Dr. E. W. Lee made in my department to test the theory of Stoner and Wohlfarth with Alnico. In their paper they assume that single domain particles are embedded in a nonmagnetic matrix, that they are prolate spheroids, and that their magnetic anisotropy is determined solely by their shape. If we assume further that the magnetostriction is isotropic, which is a good approximation as long as there is no regular connection between the crystal axes of the domain material and the axis of the spheroid, we find enough data in Stoner and Wohlfarth's paper to allow us to calculate the magnetostriction of Alnico. This Dr. Lee did.

Dr. Lee's calculation show that the initial magnetostriction should be negative and that there should be no residual magnetostriction. The experimental results for an Alnico with $H_c=133$ oersteds were chosen as most appropriate for comparison with the Stoner and Wohlfarth theory. The negative magnetostriction predicted by that theory was not found, although some Russian workers have recorded it, I understand, with magnetically isotropic Alcomax and Vicalloy.

We feel that if the observed positive magnetostriction is solely caused by islands, then these cannot be of pure iron or of pure cobalt, but might be of iron-cobalt alloy as suggested by Goldman and Smoluchowski.

C. KITTEL, *University of California, Berkeley, California:* The x-ray work of Lipson suggests that fine particles of cobalt have randomly stacked atomic planes. This would have the effect of reducing the crystalline anisotropy energy and therefore the coercive force of a single domain particle. If future x-ray work on fine cobalt particles should bear out this picture, it might be profitable to look for alloying elements which could act as "hexagonalizers" for cobalt.

E. C. STONER, *University of Leeds, England:* The idea that the very high coercivity of certain types of material might be explained in terms of the characteristics of single domain particles occurred to a number of physicists independently at much the same period. In 1939 I made the first calculations with a view to explaining the coercivity of the Alnico type of alloy on the basis of the shape anisotropy of single-domain precipitates of the more strongly ferromagnetic constituent of the alloy. Detailed calculations, equally applicable to shape, crystalline, and strain anisotropy, were resumed and full details published much later.[1] This paper contains the results of the very lengthy analytical and numerical work which is necessary even in the simplest case. Since it is in one of the relatively less accessible journals, attention is directed to it as being of considerable potential usefulness to all those concerned with the relevant alloys and micropowder materials. The extensive and beautiful recent work reported illustrates at once the range of applicability of the basic theoretical treatment and the many additional factors which must be taken into account in actual ferromagnetic materials.

---

[1] E. C. Stoner and E. P. Wohlfarth, Trans. Roy. Soc. (London) A240, 599–642 (1948).

CC-0. In Public Domain. Gurukul Kangri Collection, Haridwar

Digitized by Arya Samaj Foundation Chennai and eGangotri

Thin Films of Ferromagnetic Materials*

E. C. CRITTENDEN, JR., † AND R. W. HOFFMAN

Case Institute of Technology, Cleveland, Ohio

Experimental observations are reported on the magnetic properties of thin evaporated films of nickel. The saturation magnetization follows the general prediction of Klein and Smith after somewhat arbitrary modifications on the basis of fitting the Weiss curve for bulk specimens, as suggested by Drigo. Qualitatively observed properties due to domain structure follow the predictions of Kittle. The surface roughness of the specimens has been carefully controlled. Measurements of temperature coefficient of resistance have led to modification of the theory of electron mean free path in thin films. The mean free path is found to vary at small thicknesses, rather than remaining constant as assumed by Fuchs and Sondheimer. The surface roughness has been estimated with the help of this theory. The films of nickel behave as if surface variations extend into the film approximately 3 angstroms from each surface.

THERE are several theories of ferromagnetism which agree well with experimental evidence for bulk samples.[1] It appears, however, that if a magnetic specimen is made thin in one dimension while remaining large in the others, important differences develop between the theories.[2] In this respect investigation of the ferromagnetic properties of thin films has the nature of a critical experiment with regard to the theory of ferromagnetic behavior.

The Bloch spin-wave theory predicts that a three-dimensional lattice is ferromagnetic, but a two-dimensional one is not. Klein and Smith have extended the spin-wave method to obtain a quantitative prediction of the manner in which the magnetization should vary with thickness and with temperature. The temperature dependence of magnetization varies from a $T^{\frac{3}{2}}$ law for thick films to a linear dependence for very thin films. The Bloch theory is not considered to be valid except in the region where the magnetization is near its maximum value, I_0. This rather naturally persists in the extension to thin films. This is unfortunate since the interesting region for a thin film is the region where its magnetization falls decidedly below I_0. For lack of quantitative extension into this region based on any other model, an empirical modification of the Klein-Smith theory has been made for comparison with the experimental results.

The observations reported here have been made on evaporated films of nickel, extending down to a thickness of 10.2 angstroms. Experimentally the most serious problems have been those of being certain that the films were pure metallic nickel and of controlling and measuring the flatness. A number of details concerned with the experimental techniques of preparation will be discussed to dispel doubts concerning the nature of such extremely thin films.

Magnetic measurements have also been made by Drigo[3] on thin films of electroplated nickel, iron, and cobalt. These are shown later for comparison. However, it seems difficult to avoid the presence of impurities in the electroplated nickel and to control and determine the magnitude of surface roughness in the very thin films.

It is recognized that evaporated metal films have acquired a bad reputation as far as being specimens of metal which may be directly compared with pure bulk specimens of the same material. A number of effects have contributed to this reputation. Ordinarily the pressures used in evaporation are not low enough to avoid contamination. Connected with this is the lack of true protection offered by vacuum of the order of 10^{-5} mm of mercury, for which each surface atom is hit approximately once every half-second by a residual gas molecule. Evaporated films also tend to form in lumps or to agglomerate when the temperature is increased. In addition, they are formed with a high density of crystal imperfections, especially if the condensing surface is cold and the condensation rate high. On heating, these imperfections disappear and their loss leads to the development of a high tensile stress in the film which may cause rupture of the film. Evaporated films are polycrystalline with a small crystal size. Preferred orientation or oriented overgrowth may be present under some conditions. However, with due attention to these effects, evaporated films can be well behaved specimens of normal metal.

Nickel was chosen as the material for study because the energy of magnetization is not highly anisotropic and strain induced anisotropy is not strongly dependent on crystal orientation relative to the strain. This allows a polycrystalline thin specimen to act as one domain.

Specimens are prepared in the equipment shown diagramatically in Fig. 1. The substrate material is fire polished glass cut from microscope slides. Williams and Backus[4] have shown such glass to be smooth to less than 5 angstroms as regards sudden discontinuities. The glass substrate strips are approximately $\frac{1}{4}$ inch

* Work supported in part by the U. S. Office of Naval Research.

† On leave of absence at Atomic Energy Research Department, North American Aviation, Inc., Downey, California.

[1] J. H. Van Vleck, Revs. Modern Phys. 17, 27 (1945).

[2] M. J. Klein and R. S. Smith, Phys. Rev. 81, 378 (1951).

[3] A. Drigo, Nuovo cimento 8, 498 (1951).

[4] R. C. Williams and R. C. Backus, J. Appl. Phys. 20, 98 (1949).

CC-0. In Public Domain. Gurukul Kangri Collection, Haridwar

Digitized by Arya Samaj Foundation Chennai and eGangotri

by 3 inches. Silver current and potential contacts are fired on in advance to allow measurement of electrical conductivity. The conductance of the specimen in the "rate furnace" is recorded continuously and used to control the filament source of nickel vapor so that the film grows at a uniform rate of 60 angstroms per second. The rate furnace is kept at 250°C. This high a temperature for nickel leads to deposition of a polycrystalline film in which the microcrystals are essentially free of imperfections. This temperature is, however, not so high as to produce grain growth. The shutters are not opened until a thick layer is already present on the rate furnace specimen. This avoids trouble with electron surface scattering effects in the rate specimen. Timing of the shutters determines the thickness deposited on the specimen. Immediately after deposition of the nickel, a third shutter, not shown, is opened and a layer of about 200 angstroms of SiO evaporated over the specimen to prevent oxidation. The two filament sources are so arranged that no cross transfer occurs between them.

The source of nickel vapor is a tungsten filament electroplated with nickel. The entire system is outgassed for about 12 hours before evaporation takes place. The filament is operated at a temperature where very slow evaporation takes place during this 12 hours to remove dissolved hydrogen present in the electroplated nickel. Evaporation takes place in vacuum ranging between 5×10^{-7} and 3×10^{-6}. This gives a maximum possible gas contamination of 0.15 percent, taking the residual gas to be N_2.

The film thickness is determined from the rate of change of conductance of the monitor specimen in the rate furnace and from the time interval between opening and closing of the specimen shutters. Absolute calibration was obtained by chemical means. The specimen was dissolved and the mass of nickel determined by quantitative colorimetry using a spectrophotometer. The thickness agreed well with multiple beam interferometry results for thick films (2000A) where that technique is valid.

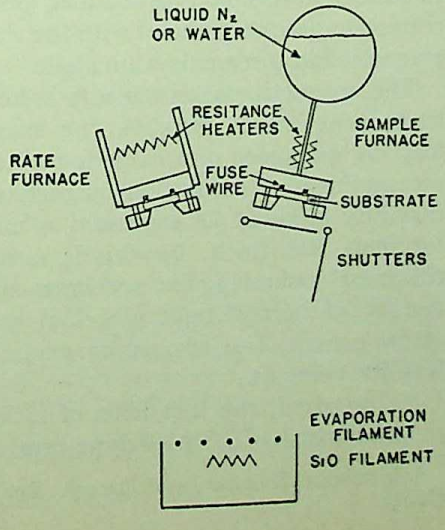


FIG. 1. Diagram of evaporation system.

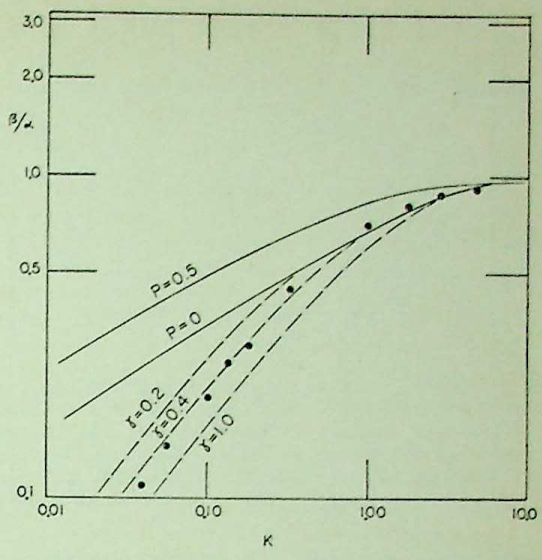


FIG. 2. Graph of temperature coefficient of resistance *vs* k, the ratio of thickness to electron mean free path. The solid curves result from the theory of Fuchs and Sondheimer for total inelastic scattering ($P=0$) and 50 percent inelastic scattering ($P=0.5$). The dotted curves are the result of introducing a variable mean free path for various values of the parameter γ.

The specimen temperature during deposit is held at 75°C. Temperatures somewhat lower than this (about 10°C) lead to cracking of the films because of very high tensile stress in the film. In general, the lowest temperature possible is desirable in order to reduce surface migration of the first arriving atoms. A high surface mobility leads to nucleation of a small number of crystals and a consequent increase in "lumpiness" of the initial deposit. For nickel 75°C was found to be satisfactory. Such films, however, have a high density of crystal imperfections. On heating, the resistivity falls irreversibly. Annealing at 275°C for four hours brings the specimens to a reproducible state.

An interesting point is illustrated by annealing very thin films. An intact, though rough, slab of metal should flatten out on annealing if the temperature is high enough to give some surface mobility. By flattening, the surface energy is reduced. However, a specimen consisting of isolated islands of metal or a cracked slab should tend to pull into spheres to reduce its surface energy. A film of apparent thickness, 5A, was deposited and coated with SiO. This film was just on the threshold of being an electrical conductor, i.e., "thinner" films consist of isolated crystals which do not touch. On annealing, the resistance of this film increased, indicating that it was pulling into isolated spheres. On the other hand, slightly thicker films became decidedly better conductors on annealing, indicating that they are becoming flatter. This effect is in addition to the loss of internal crystal imperfections which is occurring simultaneously. The thinnest specimen used for magnetic measurements was 10.2A, well above the thickness, 5A, at which agglomeration set in.

As a quantitative means of observing roughness, the electrical resistivity of these films was studied as

CC-0. In Public Domain. Gurukul Kangri Collection, Haridwar

Digitized by Arya Samaj Foundation Chennai and eGangotri

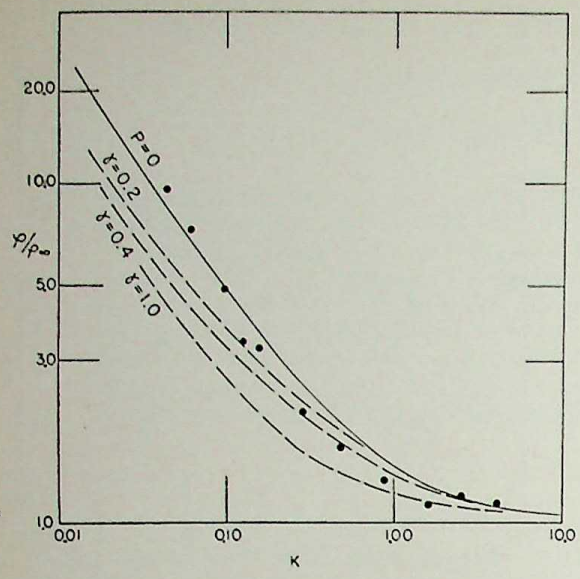


FIG. 3. Graph of resistivity *vs* k. The solid curve is that given by Fuchs and Sondheimer. The dotted curves result from introducing a variable mean free path.

a function of thickness. Surface scattering of the conduction electrons causes the resistivity to rise as thickness decreases. Experimentally the resistivity is difficult to observe with precision because the observed resistance must be divided by the thickness to obtain resistivity. On the other hand, the temperature coefficient of resistivity is a quantity which is independent of specimen geometry. Both quantities were determined on all specimens. Theoretical calculations of resistivity *vs* thickness have been made by Fuchs[5] and later by Sondheimer.[6] Both authors assumed a constant mean free path for conduction electrons. Their results can be readily extended to predict the temperature coefficient of resistance. However, the experimental data fails to fit their theoretical predictions for very small thickness. This is especially apparent for the temperature coefficient of resistance which falls far too fast as thickness decreases. Invoking elastic scattering at the surface for some fraction of the electrons, as suggested as a possibility by Fuchs, gives a poorer fit. In attempting to explain this, it was realized that the surfaces should have still another effect on the electrons besides scattering.[7] Since one must satisfy the boundary condition that the electron density falls to zero for any appreciable distance outside the specimen, one is forced to a standing wave pattern for ψ inside the metal. This limits the possible values of electron momentum normal to the specimen surface. The Brillouin zone structure, which for a large specimen of simple material has its filled region in the form of a sphere, is now crossed by a system of planes representing allowed momenta. This reduces the scattering probability for electrons moving in the film. The resistivity of the "material of the film" thus decreases as the film becomes thinner. The surface scattering is of course still present and is a large effect, so that the observed resistivity still rises as thickness falls. The temperature coefficient of resistivity is affected more markedly than the resistivity. Figure 2 shows the temperature coefficient as a function of thickness as observed and as predicted by both theories. The corresponding values of resistivity are shown in Fig. 3. An adjustable parameter γ enters which represents, in effect, the width of the "planes" crossing the Brillouin zone structure.

It will be noticed in Fig. 2 that the points for the smallest thickness begin to fall below the new theoretical curve. It seems reasonable to interpret this as an effect of specimen roughness. The point plotted at a thickness $\kappa=0.04$ (22.0A) would fall on the curve if displaced approximately 6 angstroms toward smaller thicknesses. The same displacement also places other points on the curve, although the importance of displacement rapidly disappears at higher thickness because of the logarithmic scale. The values of the resistivity plotted in Fig. 3 have not been corrected for the roughness. Adjustment for the roughness not only changes the thickness at which the points are plotted but also the value of the resistivity. If a 6-angstrom correction is made, the experimental points fall on the theoretical curve for $\gamma=0.4$. The 6A displacement possibly means that scattering points protrude frequently to the order of 3A into the film from each surface. It seems likely that this is nearly as flat a film as is possible, since the atomic diameter of nickel is 2.5A. It should also be noted that the height of the nickel unit cell is 3.5A, so that a detailed model of the roughness seems risky.

The magnetic measurements have been made in air whereas the electrical resistivity and temperature coefficients have been measured in vacuum. Although the films are coated with about 200A of SiO, some slight oxidation occurs on admitting air to the system. Each individual specimen was separately corrected for its oxidation on the basis of resistivity changes, the correction varying from 0.1A to 20A. The film continued to oxidize at a slow rate for long periods so that the correction necessary varied with the elapsed time before magnetic measurements were made.

The magnetic measurements were made with an instrument which displays the magnetic hysteresis loop on the screen of a cathode-ray oscillograph.[8] The measurement of saturation magnetization has an uncertainty of about 1A expressed as magnetic thickness for films 50A thick. By this is meant the apparent thickness assuming the specimen to have the flux density of normal bulk nickel at room temperature (6050 gauss). The applied magnetic field attainable is ± 400 oersteds.

As prepared, the thin films of nickel are in a state of tensile stress of 2.5×10^9 dynes/cm^2 at room tempera-

[5] K. Fuchs, Proc. Cambridge Phil. Soc. 34, 100 (1938).
[6] E. H. Sondheimer, Phys. Rev. 80, 401 (1950).
[7] Crittenden, Hoffman, and Layer, Phys. Rev. 86, 657 (1952).
[8] Crittenden, Hudimac, and Strough, Rev. Sci. Instr. 22, 872 (1951).

CC-0. In Public Domain. Gurukul Kangri Collection, Haridwar

Digitized by Arya Samaj Foundation Chennai and eGangotri

ture.[9] This stress is isotropic in the plane of the film. A small part of this stress results from simple differential expansion in cooling from deposition temperature to room temperature, but the principal part results from loss of crystal imperfections during deposition and during the annealing cycle. In the case of measurements made at much lower temperature than room temperature, differential expansion appreciably increases the stress. The associated strain causes uniaxial anisotropy of the energy of magnetization with an axis of easy magnetization perpendicular to the surface of the film. Since the film is polycrystalline, the strain induced anisotropy developed by each individual crystal is not truly uniaxial, but for all orientations the anisotropy figure has the general nature of uniaxial anisotropy. Under these conditions the films would be expected to behave as predicted by Kittel.[10] The general features of the predictions are born out. The hysteresis loop is rectangular for thin films, becoming more sharply rectangular as the films become thinner. This is consistent with the existence of a single domain magnetized parallel to the film surface for the thin films. Addition of a small static cross field in the plane of the film but at right angles to the oscillating large magnetizing field of the instrument drastically reduces the coercive force. The same small cross field applied perpendicular to the film has no effect. These observations also indicate the existence of a single domain magnetized in the plane of the film. Thicker films possess hysteresis loops that are more rounded and less sensitive to small cross fields. Presumably here the domain structure in zero applied field has the nature of that discussed by Kittel, in which domains are magnetized perpendicular to the plane of the film. On cooling a film of intermediate thickness, its hysteresis loop shifts from a sharp rectangular loop to a rounded loop. This indicates transition from a single domain parallel to the film to a domain system containing domains magnetized at right angles to the film, in zero field. Cooling the film increases the uniaxial anisotropy by virtue of increased tension due to differential expansion.

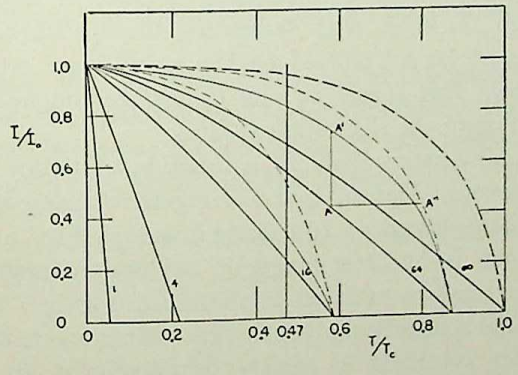


FIG. 4. Graph of intensity of magnetization *vs* temperature. The heavy dotted curve is the Weiss curve. The heavy solid curves are the theoretical results of Klein and Smith, setting $T_B = T_C$. The light solid curves result by adjusting magnetization at constant temperature. The light dotted curves are the result of adjusting the temperature at constant magnetization.

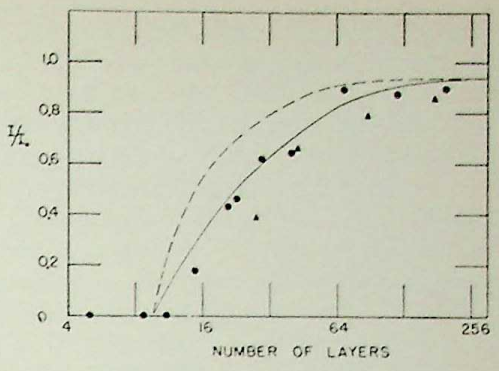


FIG. 5. Graph of magnetization *vs* thickness. The curves are the modified results of Klein and Smith. The solid curve corresponds to adjusting the magnetization at constant temperature. The dotted curve results from adjusting the temperature at constant magnetization. The points in triangles are the results of Drigo on electroplated films.

It is fortunate that thin films have rectangular hysteresis loops, as this simplifies the measurement of saturation magnetization. In case of the data to be reported, very thick films presented a problem because of lack of saturation at 400 oersteds.

Before presentation of the experimental data, the necessary modification of the theory of Klein and Smith[2] should be presented. Their theoretical results are reported in Fig. 4 as a plot of I/I_0 *versus* T/T_B, where T_B is the characteristic Bloch temperature. A family of curves for various values of the number of layers is shown. Since the Bloch $T^{\frac{3}{2}}$ law is not followed experimentally for bulk specimens, a modification of either the theoretical or experimental results must be found so that both can be compared on a common ground. One method would be to plot the experimental results as a function of T/T_B using the experimentally determined value of 2210°K for T_B.[11,12] However, it was felt that a more advantageous method would be to modify the theory to fit the Weiss curve, which agrees well with experiment for bulk specimens. Results can then be quoted in terms of T/T_C where T_C is the Curie temperature. One can set $T_B = T_C$ and plot both the theoretical curve and the Weiss curve on the same temperature scale T/T_C. Two simple, but arbitrary, methods for adjusting the theoretical curves to the Weiss curve for the case of an infinite number of layers will be illustrated. The first method, that used by Drigo,[3] is to adjust the magnetization of the infinite thickness curve at constant temperature to fit the Weiss curve. The magnetization of all the curves for smaller thickness was adjusted by the ratio of the Weiss magnetization to the Bloch curve at a given temperature. The second method is to adjust the temperature at constant

[9] R. W. Hoffman and E. C. Crittenden, Jr., Phys. Rev. **78**, 349 (1950).
[10] C. Kittel, Phys. Rev. **70**, 965 (1946).
[11] P. Weiss and R. Forrer, Ann. phys. **12**, 279 (1929).
[12] P. Weiss, Compt. rend. **198**, 1893 (1934).

CC-0. In Public Domain. Gurukul Kangri Collection, Haridwar

Digitized by Arya Samaj Foundation Chennai and eGangotri

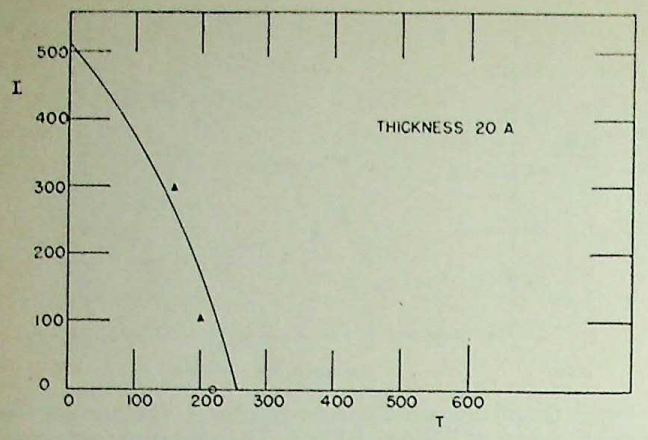


FIG. 6. Graph of intensity of magnetization in gauss *vs* temperature in degrees Kelvin for a 20A nickel film. The solid curve is the theoretical result of Klein and Smith modified by adjusting the magnetization.

magnetization. In this case each curve is adjusted by the ratio of the temperature of the Weiss curve to the Bloch curve at a given magnetization. The two methods of adjustment yield somewhat different results for the adjusted I/I_0 *versus* T/T_C curves. Figure 4 shows the Klein and Smith theoretical curves, and the two sets of adjusted curves, all plotted against T/T_C. The solid heavy curves are the theoretical curves obtained by Klein and Smith for different numbers of layers. The number with each family of curves corresponds to the number of atomic layers in a simple cubic lattice for which this theory was developed. The heavy dotted curve is the Weiss curve. The light solid line is the result of adjusting the magnetization at constant temperature. The light dotted lines are the result of adjusting the temperature at constant magnetization.

To illustrate the two methods of adjusting the theoretical curves, point A in Fig. 4 is transformed in both ways. Point A moves to A' if the magnetization is adjusted at a given value of the temperature. Point A is translated to A'' if the temperature is adjusted at a given magnetization.

Measurements of the saturation magnetization have been made with two models of the magnetic instrument

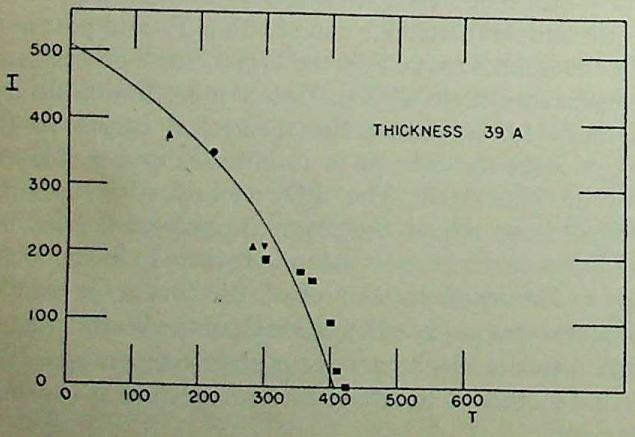


FIG. 7. Graph of intensity of magnetization in gauss *vs* temperature in degrees Kelvin for a 39A film.

mentioned earlier. One model was specifically designed for precision measurements at room temperature, the other was designed to provide measurements over the temperature range −190°C to +200°C. The results obtained with the two instruments will be described separately as the latter is subject to some additional uncertainties.

Measurements made at 25°C are plotted in Fig. 5. The theoretical curves are taken from Fig. 4 for $T/T_C=0.47$, the ratio for nickel at room temperature. The number of atomic layers has been obtained by dividing the thickness by 2A, the approximate distance between the 111 planes in the face-centered cubic nickel crystal. The points seem to fall rather close to the solid line representing the theoretical results of Klein and Smith after adjusting the magnetization by the Weiss curve at constant temperature. The thickness at which magnetization ceases at this temperature is in surprising agreement with the theoretical prediction.

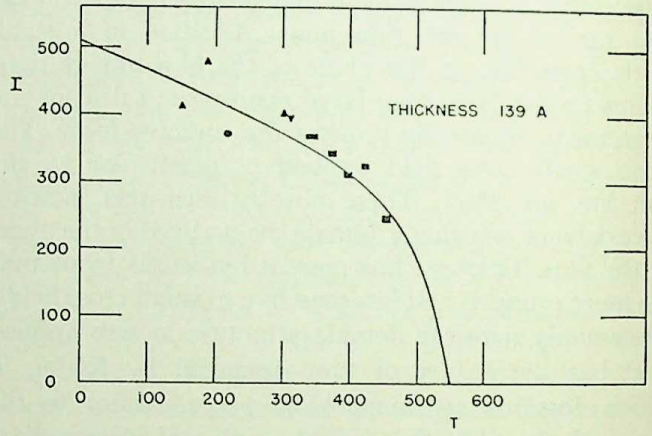


FIG. 8. Graph of intensity of magnetization in gauss *vs* temperature in degrees Kelvin for a 139A film.

The points for small thickness have less uncertainty than for the higher thicknesses because of difficulty at high thickness with saturating the specimen. The results of Drigo[3] plotted on the same figure seem to fall low. This might be due to surface roughness or oxidation of the electroplated films.

Measurements made as a function of temperature are shown in Figs. 6, 7, and 8. Figure 6 represents the specimen plotted at 10 atomic layers in Fig. 5. This specimen is not ferromagnetic at room temperature but becomes so at lower temperature. Figure 7 represents the specimen plotted at 19.5 atomic layers in Fig. 5. This specimen is weakly ferromagnetic at room temperature, and it has been possible to follow it to its Curie temperature. Figure 8 is a much thicker specimen, 69.5 atomic layers, for which the Curie temperature is nearly that of bulk nickel, but the curve still shows a definite flattening compared to the Weiss curve for bulk nickel.

A new instrument is under construction with which it

CC-0. In Public Domain. Gurukul Kangri Collection, Haridwar

Digitized by Arya Samaj Foundation Chennai and eGangotri

is hoped that curves such as Figs. 6–8 can be obtained with much better precision.

The general agreement between the observations and the modified theory of Klein and Smith is quite surprising. This may be largely fortuitous, as the modifications based on the Weiss curve are quite arbitrary. In addition, the theory was developed for the case of a simple cubic crystal whereas nickel is face-centered cubic. This has required the rather arbitrary guess that the distance between the 111 planes in the face-centered cubic crystal should be substituted for the distance between 100 planes in the simple cubic crystal. Nevertheless, the general features of the behavior appear to be well described by the theory of Klein and Smith.

It is hoped that the availability of experimental observations in this field will stimulate further theoretical work, particularly in the extension of other models of ferromagnetic behavior into this range.

The authors wish to thank Mr. Edwin H. Layer and Mr. John D. Groselle of this laboratory for their contributions to the experimental data reported. The work has been assisted by a fellowship provided by the Standard Oil Company of Ohio which was held by one of the authors (RWH).

DISCUSSION

T. L. GILBERT, *Armour Research Foundation, Chicago, Illinois:* It is commonly accepted that the Bloch spin wave method, which is based on the Heitler-London-Heisenberg model of a ferromagnet, predicts that two-dimensional arrays of atoms are always nonferromagnetic. This prediction is inferred from the fact that an integral which appears in the constant A in the theoretical magnetization-temperature curve, $M(T)/M(O)=1-AT^{3/2}$, is divergent.[1]

This inference is unjustified, for the divergence may be the result of entirely extraneous reasons. It is in disagreement with predictions based on the Ising model of a ferromagnet. This disagreement is, by itself, not too significant because the Ising model is, admittedly, a poor one. However, it has been shown by Ekstein[2] that, if one refines the spin-wave method by taking into account the interaction between reversed spins, using a perturbation approach, the integral appearing in the constant A may converge to a finite value for certain two-dimensional arrays. One infers from this that two-dimensional arrays can be ferromagnetic if the Heitler-London-Heisenberg model is valid.

Recent developments, as reported at this conference, indicate that the Heitler-London-Heisenberg model is inadequate, and so the matter is not fully settled; but this result does show that the present theory of thin films, in so far as it is based on the spin-wave method as used by Bloch, is open to serious question.

[1] Sommerfeld and Bethe, *Handbuch der Physik* (Julius Springer, Berlin, 1926), Vol. 24/2.
[2] H. Ekstein, Phys. Rev. **80**, 122 (1950).

C. J. GORTER, *Leiden University, The Netherlands:* At the Grenoble Conference, two years ago, I pointed out that according to Nernst's law the spontaneous magnetization should have a horizontal tangent with respect to T at $T=0$. I was not able then to extract a satisfactory explanation from Professor Stoner and Professor Néel, who presented curves in disagreement with this requirement.

I am now getting really worried about Nernst's law, since the theoretical curves shown by Dr. Crittenden also seem to violate it.

R. W. HOFFMAN, *Case Institute of Technology, Cleveland, Ohio:* (in answer to questions) No line broadening determinations were made with x-rays. However, electron diffraction line width measurements have been made by E. K. Halteman at this laboratory. Since the stress broadening and the broadening caused by particle size depend in different ways on the angle of reflection, the two parts may be separated experimentally.

C. GUILLAUD, *Centre National de la Recherche Scientifique, Bellevue, France:* In very thin films it is possible to obtain nonferromagnetic hexagonal nickel, which can be transformed to ferromagnetic cubic nickel by annealing.[1]

[1] A. Colombani, Ann. phys. **19**, 272–326 (1944).

CC-0. In Public Domain. Gurukul Kangri Collection, Haridwar

Digitized by Arya Samaj Foundation Chennai and eGangotri

REVIEWS OF MODERN PHYSICS VOLUME 25, NUMBER 1 JANUARY, 1953

Coercive Force of Precipitation Alloys

A. H. GEISLER

General Electric Research Laboratory, The Knolls, Schenectady, New York

Cunico, Cunife, and the various types of Alnico are structurally analogous in that at the state of high coercive force the crystal structure of the precipitate is distorted from a cubic lattice to a tetragonal lattice. A single empirical relation has been derived from the data for these types of materials in which maximum coercive force is directly related to degree of tetragonality and saturation induction of the precipitate. On the basis of the fine particle theory this result suggests that not only shape anisotropy but also crystal anistropy, as affected by strain, contributes to the coercive force. This work represents the first successful attempt to correlate the coercive force of the various commercial permanent magnet alloys with more fundamental characteristics.

THE energy of a magnetic material, as exhibited by the area under the demagnetization curve, increases directly with the three properties: residual induction, squareness of the loop, and coercive force. It would be desirable to relate these properties to more fundamental characteristics of the material. Although it seems that residual induction and squareness of the loop depend upon characteristics such as saturation induction, packing factor (ratio of ferromagnetic phase to total value), and orientation, the origin of coercive force has been somewhat more elusive. The coercive force of all permanent magnet alloys originates in a solid state transformation which is promoted by the heat treatment of these materials. The transformation proceeds by the nucleation and growth of a new phase within the parent matrix. The particles of the new phase are usually anisotropic in shape, frequently plate-like as in Fig. 1. Since the particles start from embryos of a few unit cells in size, they would be expected to grow during heat treatment through the size range where magnetic behavior is based on single domain particles. Thus, one would immediately expect that the fine particle theory derived for shape anisotropy would be applicable. In order to test this possibility, the coercive force of a variety of permanent magnet alloys is plotted in Fig. 2 against the saturation intensity estimated for the precipitates in these alloys. Both the packing factor and shape anisotropy are about the same for the alloys listed, and consequently, a direct proportionality would be expected between coercive force and saturation intensity. Since no simple relation is apparent in Fig. 2, an examination of the structural features of these alloys is essential in order to develop a good correlation with coercive force.

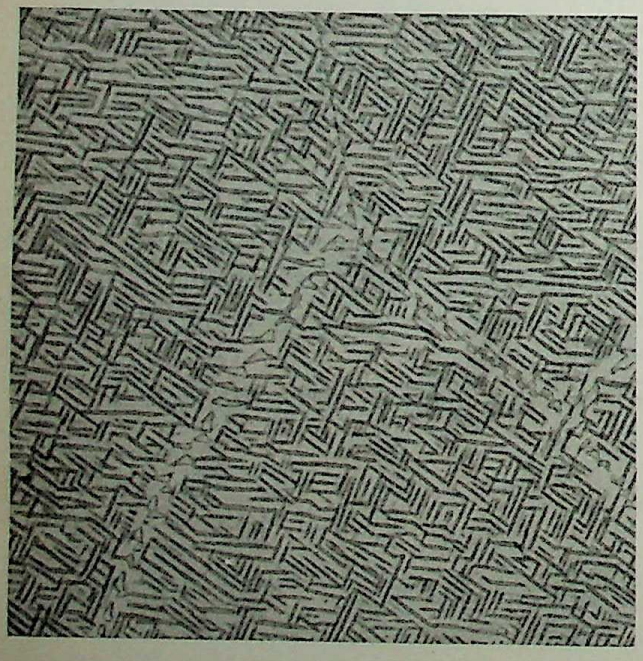


FIG. 1. Microstructure of Alnico 2 showing plate-like precipitate of resolvable particles larger than those responsible for high coercive force. 1000×.

Three of the commercial permanent magnet alloys, namely, Alnico, Cunico, and Cunife, are cubic solid solutions which decompose into two cubic phases of slightly different lattice parameters during the aging heat treatment. This behavior occurs over a specific range of compositions in the Fe-Ni-Al, Cu-Ni-Co, and Cu-Ni-Fe systems upon which the alloys are based, respectively. The prototype of these alloys is the Ni-Au system, which will be used for simplicity in describing the characteristics of this class of materials. During the precipitation heat treatment the properties change as shown in Fig. 3. Saturation magnetization and remanence increase as the ferromagnetic nickel precipitate forms. On the other hand, the coercive force first increases and than decreases. At the condition of high coercive force the decomposition products are coherent with each other and thus have tetragonal crystal structures instead of cubic.[1] A possible role of the tetragonal structure will be developed subsequently.

An interpretation for the composition dependence of properties of diverse series of alloys will be more extensive than a postulate of high coercive force that is based upon a single alloy. Thus in the present work the principal concern will be given to explaining the variation in properties across the composition scale as in Fig. 4; the magnetic annealing of Alnico 5, which has adequately been explained as an orientation effect of the

[1] A. H. Geisler, Trans. Am. Soc. Metals 43, 70 (1951).

CC-0. In Public Domain. Gurukul Kangri Collection, Haridwar

Digitized by Arya Samaj Foundation Chennai and eGangotri

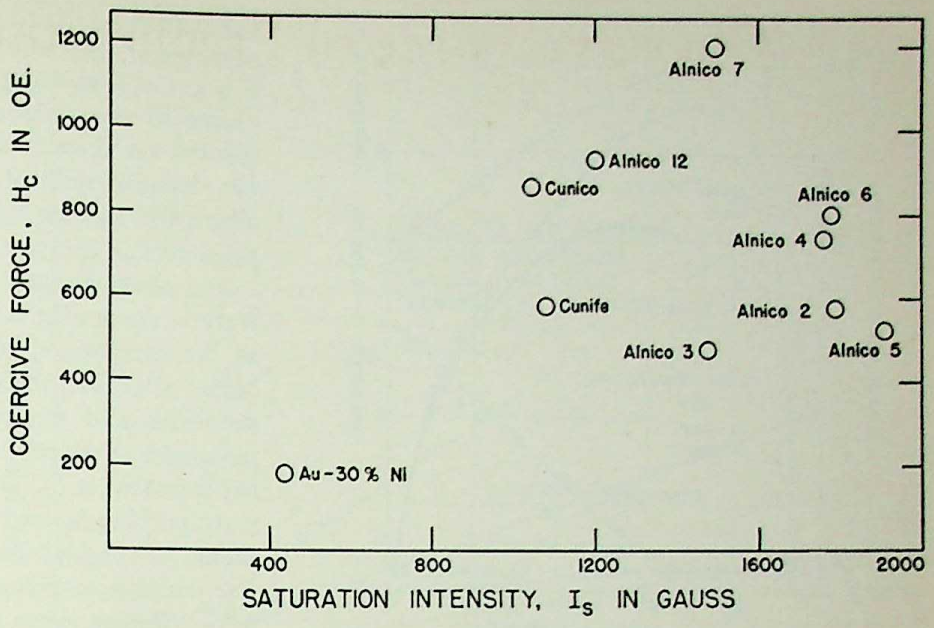


FIG. 2. Coercive force of various commercial alloys as related to intensity of magnetization at saturation of precipitate.

precipitate, will be neglected, and only properties for treatment without field will be considered. The variation in remanence in Fig. 4 is to be expected, since the induction increases as the amount of nickel in the alloy increases. On the other hand, the maximum coercive force from a curve such as in Fig. 3, when plotted against composition as in Fig. 4, increases continuously as the amount of nickel *decreases* when field strength is sufficient to saturate the alloy ($H_{max}=1500$ oersteds or greater).* The relationship appears to be general for the various alloy systems of the type considered here, in that the coercive force continuously increases as the ferromagnetic components of the alloy decrease within the composition range for heat-treatable alloys. The simplicity of the precipitation process in these alloy systems and the prototype Ni-Au permits an evaluation of the coherent state, relative to the fine particle theory, in explaining the variation of coercive force with alloy composition. Theoretical relationships for the coercive force of fine precipitates have been derived from fundamental properties such as saturation magnetization, magnetostriction, and magnetic anisotropy constant.[2] It would be in order now to seek empirical relationships expressing the composition dependence of coercive force in the precipitation alloys, in order to evaluate the theoretical relationships.

The usual theorist has not had a very deep appreciation of the heterogeneous state of matter. This conclusion is evident by past treatments of order-disorder phenomena, in which little recognition has been provided for a two-phase equilibrium at temperatures between that for disorder and that for long-range order. Likewise, a heterogeneous mechanism of nucleation and growth of the ordered phase from the disordered, which has been identified and found useful in explaining the transient maximum in the coercive force during order-

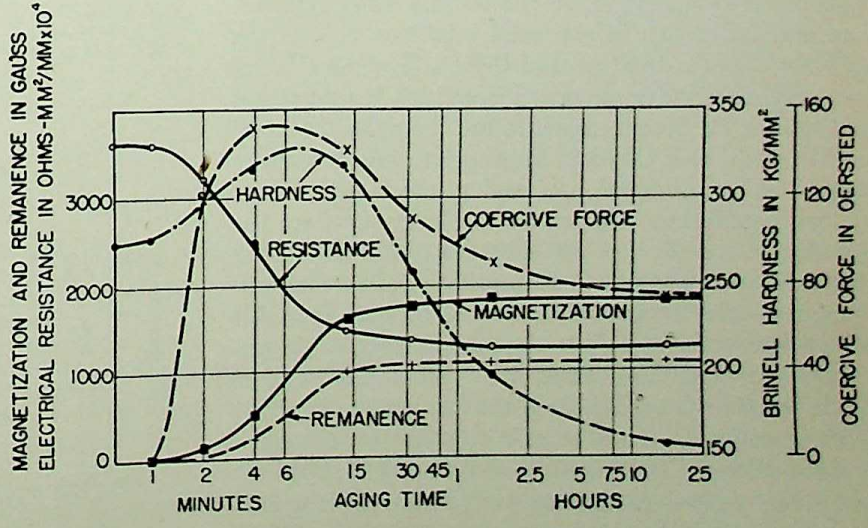


Fig. 3. Changes in properties of an Au–30 percent Ni alloy quenched from 900°C and aged designated intervals at 500°C. From Köster and Dannöhl (see reference 3).

* The broken part of the curve at the left is probably imaginary, limited because the alloys are no longer ferromagnetic.

[2] C. Kittel, Revs. Modern Phys. 21, 541 (1949).

CC-0. In Public Domain. Gurukul Kangri Collection, Haridwar

Digitized by Arya Samaj Foundation Chennai and eGangotri

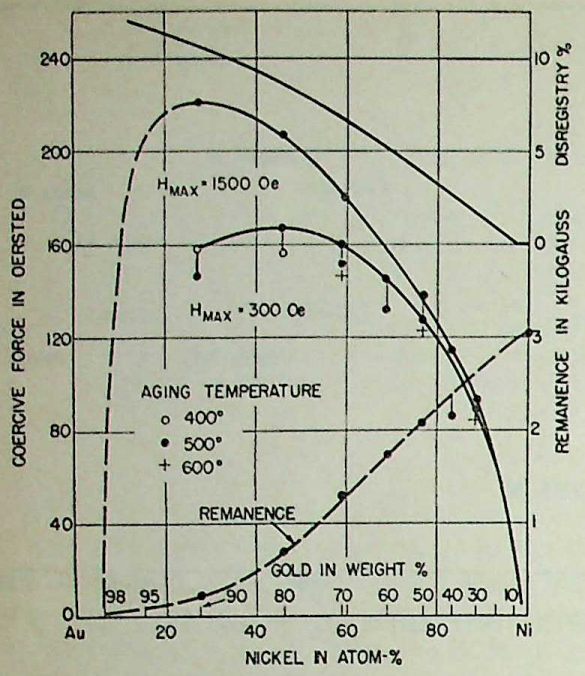


FIG. 4. Compositions dependence of maximum coercive force, remanence, and disregistry for Ni–Au alloys. From Köster and Dannöhl (see reference 3).

ing, was not provided for in theory. With no insight of the constitution of Ni-Au alloys, one might glibly conclude from Fig. 4 that these are alloys in which increasing coercive force with higher gold is associated with decreasing saturation intensity, increasing magnetostriction, or increasing magnetocrystalline anisotropy. In order to illustrate the types of information portrayed by the phase diagram and pertinent to an explanation of the composition dependence of magnetic properties, a brief description of the significance of the phase diagram follows.

Some features essential for an understanding of these alloys can be illustrated by Fig. 5, which represents schematically the phase diagram and lattice parameter variation for Ni-Au and also applies qualitatively to appropriate compositions in the ternary alloy systems. The miscibility gap in the solid solutions field is the basis for the heat treatment of these alloys. An alloy of composition X, when quenched from high temperatures and aged at T_1, decomposes into the two phases, of compositions $C\alpha_1$ and $C\alpha_2$ and appropriate lattice parameters. The weight fraction of each phase in the mixture at final equilibrium is given by the lever law from the sections of the tie line AC. For the nickel-rich phase α_2 the fraction is AB/AC. Regardless of alloy composition, in a series between $C\alpha_1$ and $C\alpha_2$ all heat-treatable alloys decompose at T_1 into the same phases, of compositions $C\alpha_1$ and $C\alpha_2$. Thus, bulk properties such as Curie temperature are those of the ferromagnetic phase, of composition $C\alpha_2$, and remain constant for the series of aged alloys. Consequently, direct variation of bulk properties such as saturation magnetization, magnetostriction, and magnetic anisotropy constants of the cubic ferromagnetic phase cannot be used to explain the composition variation of coercive force (Fig. 4). On the other hand, the effect of changing composition from $C\alpha_1$ to $C\alpha_2$ is to change the relative amounts of the two phases at equilibrium according to the lever law as pointed out above. This mixing obviously accounts for the changing residual nagnetization of the two-phase alloys, although the bulk properties of the ferromagnetic phase remain constant.

The phase diagram shows that at equilibrium, two features concerning the ferromagnetic phase α_2 change as the composition of the alloy is changed towards higher gold: first, the weight fraction of α_2 in the alloy decreases, and second, the composition and lattice parameter of the parent phase α_x becomes more different from that of α_2. The first feature expresses the ultimate packing factor for complete precipitation which should be considered in regard to the coercive force of fine particles as controlled by shape anisotropy. The second feature, when expressed as disregistry between the parent phase and the ferromagnetic precipitate (at top of Fig. 4), is related to the tetragonality which the lattice of the first particles to form must assume when they precipitate in the matrix. Both of these features change in the expected direction to explain the increasing coercive force with increasing gold content in the alloy.

The relationships between coercive force and the two features which possibly could be related to the variation with composition should now be examined. In Fig. 6 the ultimate packing factor by volume, which was obtained

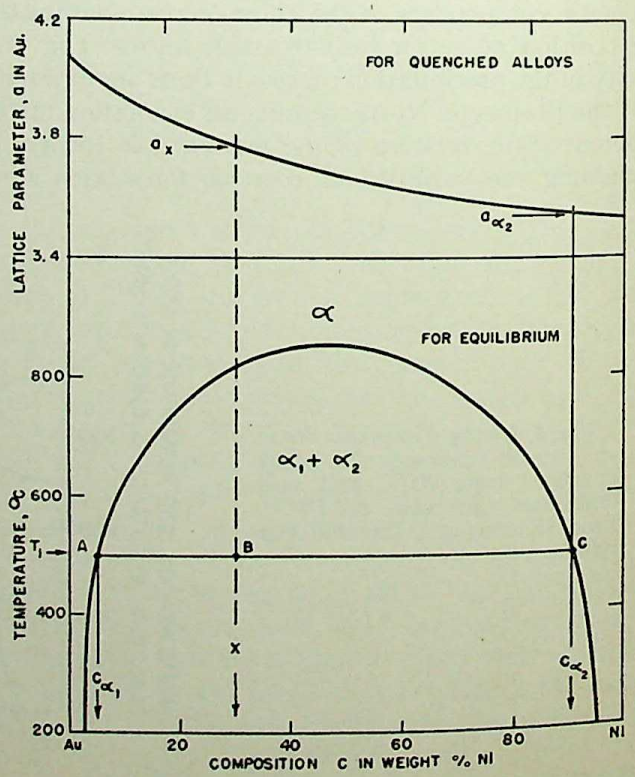


FIG. 5. Lattice parameter and miscibility gap in solid state of Ni–Au alloys.

CC-0. In Public Domain. Gurukul Kangri Collection, Haridwar

Digitized by Arya Samaj Foundation Chennai and eGangotri

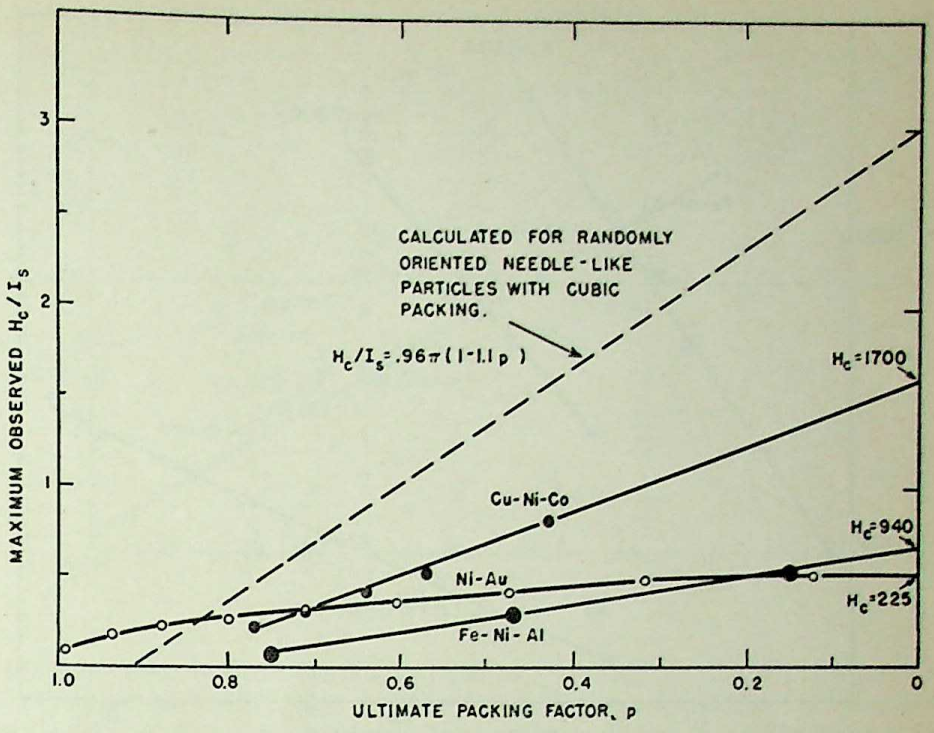


FIG. 6. Composition dependence for shape anisotropy.

from the corresponding phase diagrams[3–5] and corrected for density, is plotted against the observed ratio H_c/I_s for three series of alloys.†[6,7] The maximum observed coercive force H_c was obtained from published data for the variation of H_c with time for different aging temperatures. The intensity of magnetization at saturation was obtained from published data corresponding to the composition of the precipitate as determined from the phase diagrams. The plotted data show little tendency to group into a single curve. Thus, another variable must be considered to give a general relationship for coercive force. Comparison of the observed data with calculated data will be discussed later.

The relationship between coercive force and disregistry is shown in Fig. 7. The disregistry values δ were calculated from lattice parameter measurements for the supersaturated solid solutions[1,3,8,9] and equilibrium precipitates of compositions determined from the phase diagrams. When the quantities are plotted on logarithmic scales a straight line relationship results. This relation is particularly evident for the Ni-Au series, where most data were available. The data for the Cu-Ni-Co series were for maximum energy product, which apparently does not occur under the same aging conditions as maximum coercive force in the two alloys of greatest disregistry. This condition explains the departure of the line from the two points at the upper end of the series. A second point is given for a disregistry of 0.7 which is the maximum H_c of the alloy Cunico. The lines can be described by the relationship

$$\ln H_c = A \ln\delta + B, \qquad (1)$$

where the slope and intercept constants A and B have the following values for natural logarithms:

Alloy series	A	B	I_s
Fe–Ni–Al	1.48	9.48	1480
Cu–Ni–Co	1.15	7.13	1060
Ni–Au	0.45	4.37	432

It should be noted that the coefficients A and B decrease with saturation magnetization of the precipitate The relationship is given graphically in Fig. 8, from which empirical evaluations of the coefficients are possible. From these, a general relationship expressing the data for the three series of alloys would be

$$\ln H_c = 0.00103 I_s \ln\delta + 0.005 I_s + 2. \qquad (2)$$

It is interesting to compare the extrapolated values for zero packing, shown at the upper end of the curves in Fig. 6, with those for maximum disregistry (also zero packing) in the alloy series in Fig. 7. The latter give higher extrapolated values closer to those calculated for shape anisotropy. If it were possible to precipitate pure Fe with $I_s = 1714$ coherent with NiAl($\delta = 0.42$), then according to the empirical expression (2) the coercive force would reach 8300 oersteds, compared with 5200 oersteds calculated for randomly oriented needle-like particles. Thus, there tends to be some reasonable agree-

[3] W. Köster and W. Dannöhl, Z. Metallk. 28, 248 (1936).
[4] W. Dannöhl and H. Neumann, Z. Metallk. 30, 218 (1938).
[5] S. Kuiti, Rept. Aero. Res. Inst. Tokyo Imperial University 15, 601 (1940).
† Saturation values for the equilibrium precipitates of compositions shown by the phase diagrams were obtained from the work of Marian (reference 6), Sucksmith (reference 7), and Dannöhl (reference 4). Maximum coercive force values are from the work of Köster (reference 3), Dannöhl (reference 4), and Geisler (references 1 and 9).
[6] V. Marian, Ann. phys. 7(11), 459 (1937).
[7] W. Sucksmith, Proc. Roy. Soc. (London) A171, 525 (1939).
[8] Bradley, Cox, and Goldschmidt, J. Inst. Metals 67, 189 (1941).
[9] A. H. Geisler and J. B. Newkirk, Trans. Am. Inst. Mining Met. Engrs. 180, 101 (1949).

CC-0. In Public Domain. Gurukul Kangri Collection, Haridwar

Digitized by Arya Samaj Foundation Chennai and eGangotri

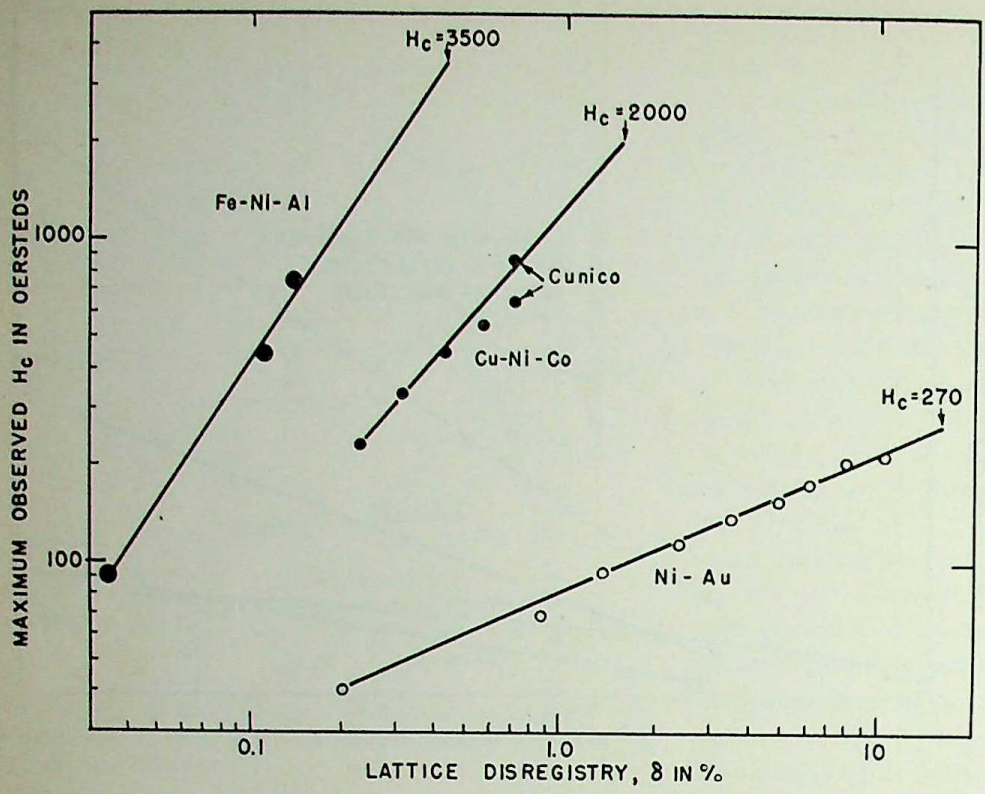


FIG. 7. Relation between maximum coercive force and precipitate disregistry or tetragonality.

ment of empirical and formal theory, regardless of the full magnitude difference when the comparison is made with the actually observed coercive forces of commercial alloys.

Attempts to fit the data for other alloys of the same type to the empirical expression are reasonably successful. The data given in Table I are based upon estimates of the composition and saturation magnetization of the precipitate phase in alloys with more than three components. The values of disregistry are based on lattice parameter measurements for the various alloys. The data are plotted in Fig. 9, where the line represents the relationship derived from the data for the three series of alloys. Cunife and the more complex Alnicos agree as well with the line as do Alnico 3, Cunico, and Au-30 percent Ni, alloys in the three series from which the expression was derived. Thus, it seems possible for the first time to justify the variation in coercive force among the commercial permanent magnet alloys of the simple precipitation type on the basis of fundamental properties of the precipitate: its saturation magnetization and its crystal lattice disregistry relative to the matrix. The relationship reconciles observations involving all three cubic ferromagnetic metals, Fe, Ni, and Co.

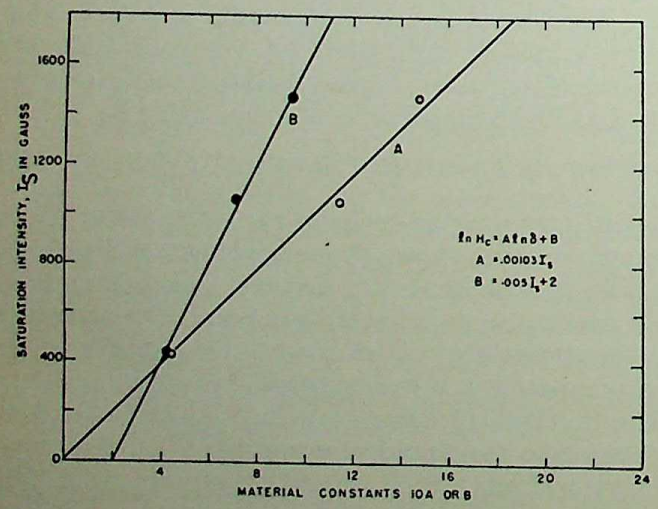


FIG. 8. Relation between intensity of magnetization at saturation and coefficients for the equations of curves in Fig. 7.

The role of disregistry in affecting the coercive force of fine precipitates could conceivably be threefold, involving all criteria which have been considered in the theory of the coercive force of fine particles.[2] In all three cases the effect is caused by low disregistry (under 10 percent), which promotes extensive coherent growth of the precipitate. First, disregistry will affect particle-shape anistropy; for when disregistry is low, the particles can grow as coherent plates or needles, to keep surface energy low with minimum strain energy. Increasing disregistry would lead to decreasing shape anistropy (inverse of desired relationship); for as the strain energy increases, coherency diminishes, and minimum surface energy requires a spherical shape. Second, higher disregistry leads to higher tetragonality at the coherent state, with an increased magnetic anisotropy of the precipitate. Third, the elastic strains for coherency entail high stresses, which increase to a limiting value with increasing disregistry. Since magnetostriction is not included, at least in the rough form of the empirical expression, it would seem that the third factor need not be considered. The first factor probably accounts for the direct dependence of coercive force on

CC-0. In Public Domain. Gurukul Kangri Collection, Haridwar

Digitized by Arya Samaj Foundation Chennai and eGangotri

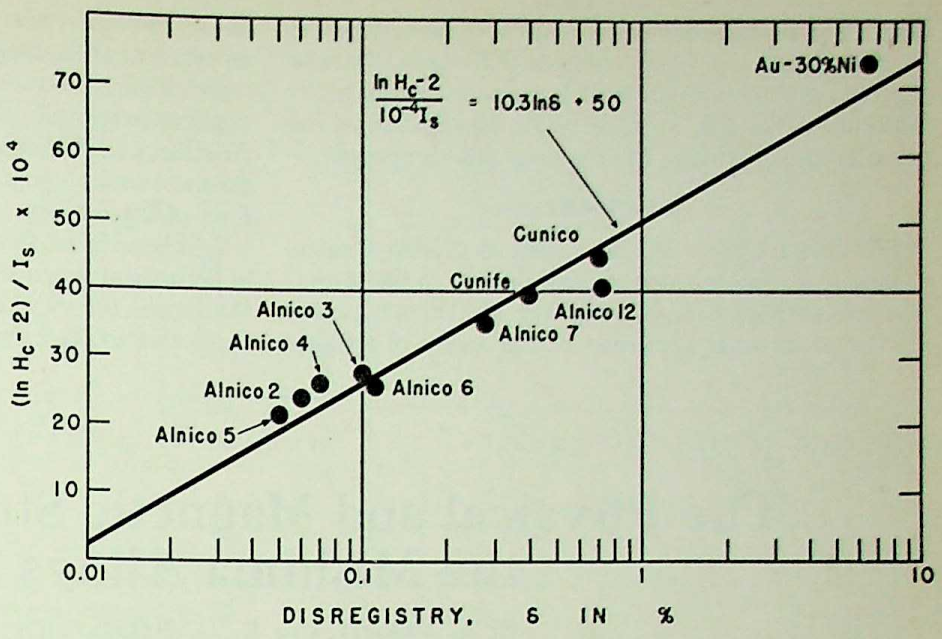


Fig. 9. Empirical relation for composition dependence of maximum coercive force, showing conformance of the commercial alloys and a Ni–Au alloy.

saturation magnetization as in theory; however, in the range of disregistry considered here the inverse relation to disregistry is not dominant. All of the alloys considered here have precipitate particles with appreciable shape anisotropy, 5 to 10 or more when the particles are large enough to resolve in the microscope. Thus, it would seem that the dominant role of disregistry is by means of its effect on crystal anisotropy. While absolute values were not considered, perhaps the expression is concerned only with the increasing magnetic anisotropy of a cubic lattice (a feature the alloys have in common) as tetragonality at the coherent state is increased. Evidence that this condition may be the case is found in the fact that the coefficients of Eq. (2) are not the same as those needed to explain the disregistry dependence of the coercive force of the CoPt type of ordering alloys, where the new phase at equilibrium may be tetragonal.

The departure of the calculated coercive forces listed in Table I from the observed could be attributed to deviation of the particle shape from the needle-like assumed for the theory. All the alloys have plate-like particles when of microscopically resolvable sizes, but it is known that a needle-like shape precedes the plate-like in some precipitation alloys. Correlation of coercive force with packing factor in Fig. 6 is based on the ultimate packing factor which obtains at complete equilibrium. This assumed value is probably greater than the value at maximum coercive force, where precipitation is only partly completed, and any correction would merely exaggerate the departure from calculated coercive force values. The saturation magnetization of the coherent precipitate was assumed to be that of the strained second phase at equilibrium. Although only slight departure would be expected, it is appreciable in other cases such as the precipitation of iron from copper solid soultions.

While disregistry and ultimate packing appear to be two factors which can be readily evaluated, it is possible that there are other less tangible factors which might explain the composition variation of coercive force in an alloy series. Other factors which cannot be readily evaluated quantitatively would include particle size and size distribuition, which may be implicit in the condition for maximum observed coercive force. The time of the maximum in the aging curve is probably controlled by the attainment of an optimum size distribution and packing of the more ferromagnetic precipitate.‡ These features depend upon nucleation and growth rates of the precipitate, which in turn are related to the free energy change on precipitation. Since free energy change goes through a maximum near the middle of the miscibility gap in the phase diagram, the nucleation rate would be a maximum here, leading to the narrowest size distribu-

TABLE I. Properties of the precipitation type of permanent magnet alloys

Alloy	Approximate composition of precipitate	Precipitate I_s	Precipitate δ	Maximum coercive force observed	Maximum coercive force calculated[b]
Alnico 2	[a]Fe–15%Co–4%Ni–4%Al–3%Cu	1800[a]	0.06	550	2450
Alnico 3	Fe–5%Ni–5%Al	1480	0.10	450	2010
Alnico 4	[a]Fe–10%Co–4%Ni–4%Al	1750[a]	0.07	700	2380
Alnico 5	[a]Fe–30%Co–3%Ni–3%Al random[c]	1900[a]	0.05	450	2620
Alnico 5DG	[a]Fe–30%Co–3%Ni–3%Al aligned	1900[a]	0.05	640	5500
Alnico 6	[a]Fe–30%Co–3%Ni–3%Al–2%Ti	1780[a]	0.11	750	2420
Alnico 7	[a]Fe–25%Co–4%Ni–4%Al–4%Ti	1500[a]	0.28	1200	2040
Alnico 12	[a]Fe–20%Co–5%Ni–5%Al–6%Ti	1200[a]	0.73	950	1630
Cunico	Co–29%Ni–7%Cu	1060	0.70	870	1440
Cunife	Fe–40%Ni–10%Cu	1100[a]	0.39	550	1500
Au–30%Ni	Ni–10%Au	432	6.51	180	590

[a] Estimated.
[b] Calculated for randomly oriented, needle-like particles with packing factor of 0.5, $H_c = 1.36 I_s$.
[c] Without field treatment during cooling.

‡ In alloys rich in the ferromagnetic component, which would be the continuous phase upon completion of precipitation, the pertinent "precipitate" would be the small impoverished shells surrounding the particles of the nonmagnetic phase at the state of partial precipitation.

CC-0. In Public Domain. Gurukul Kangri Collection, Haridwar

Digitized by Arya Samaj Foundation Chennai and eGangotri

tion. Thus, if size distribution alone were the controlling factor, the coercive force—composition curve would be expected to exhibit an inverted U shape analogous to the solubility limit (Fig. 5) rather than the continuous rise towards the side rich in the less magnetic component.

SUMMARY

The coercive force of alloys such as Ni-Au, Cunico, Cunife, and the Alnicos is related directly to the saturation magnetization and disregistry of the precipitate. The latter factor is a measure of the degree of tetragonality and strain which the precipitate must sustain to be coherent with the parent matrix at the state of high coercive force. Consideration of other factors such as the absolute magnitude of magnetic anisotropy, magnetostriction, and packing, which are incorporated in formal theories, seems unnecessary to rationalize the coercive force of these alloys.

It is hoped that this description of the various aspects of permanent magnet alloys will lead to an extension of the formal theory of fine particle magnets that will be applicable to the known alloys.

REVIEWS OF MODERN PHYSICS VOLUME 25, NUMBER 1 JANUARY, 1953

The Physical and Magnetic Structure of the Mishima Alloys

E. A. NESBITT AND R. D. HEIDENREICH

Bell Telephone Laboratories, Murray Hill, New Jersey

THE Mishima alloys[1] of the iron-nickel-aluminum system, discovered in 1932, have been the subject of many structural and magnetic investigations because of their interesting permanent magnet properties. Although a completely satisfactory equilibrium diagram has not yet evolved, many controversial points have been settled, and there has been substantial agreement by recent investigators[2–4] for the main reaction of the system. Because of these investigations, the permanent magnet properties have been attributed until now to a body-centered cubic precipitate which has approximately the same lattice spacing as its body-centered cubic matrix (2.86A). According to Bradley and Taylor,[5] this precipitate lattice under permanent magnet conditions conforms to the dimensions of the parent lattice. The idea of two body-centered cubic lattices of approximately the same spacing was also extended to the case of Alnico 5 in order to explain the high coercive force in this alloy. However, as a result of the recent discovery of a new face-centered cubic precipitate[6] in Alnico 5, which was found to be the agent responsible for the alloy's permanent magnet properties, it was decided to re-investigate the cause of the permanent magnet properties in the Mishima alloys.

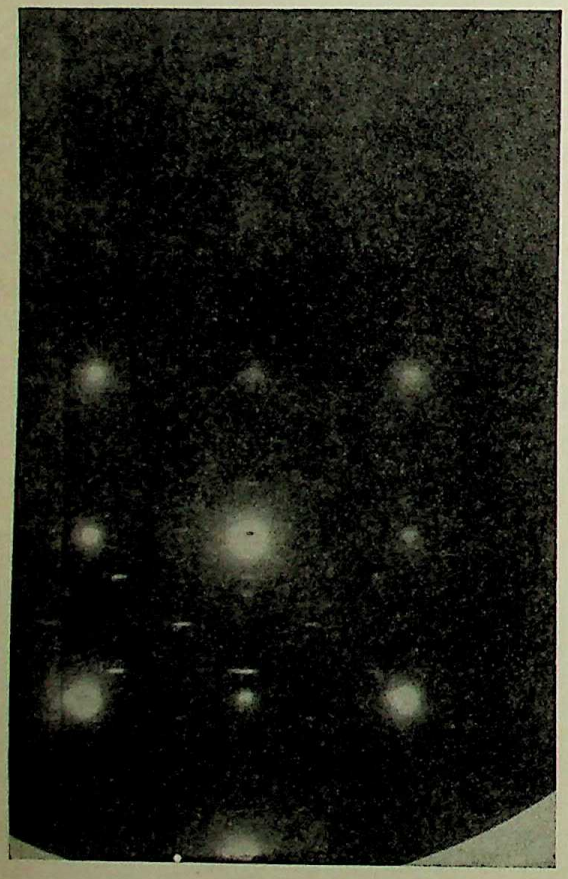


FIG. 1. Electron diffraction reflection pattern from Mishima single crystal (approx. Fe_2NiAl). (100) surface and electron beam along (100) direction. Array of needle-like spots indicates permanent magnet precipitate. Crystal cooled from 1300°C at 3°C per second, then aged at 600°C for 1 hour.

Figure 1 shows an electron diffraction pattern obtained on a (100) single crystal (approximately Fe_2NiAl) cooled from 1300°C at 3°C per second and aged at 600°C for 1 hour. The intense spots are those due to the body-centered cubic structure, and the less intense spots are superlattice reflections indicating that the alloy is ordered. The array of needle-like spots in this photograph

[1] Mishima, Stahl und Eisen 53, 79 (1933).

[2] A. J. Bradley and A. Taylor, Proc. Royal Soc. (London) 166, 353 (1938).

[3] S. Kiuti, Japan Nickel Rev. 9, 78 (1941).

[4] W. Dannohl, Arch. Eisenhüttenw. 15, 321 (1942).

[5] A. J. Bradley and A. Taylor, *Physics in Industry*, "Magnetism" (Institute of Physics, London, 1938), p. 91.

[6] R. D. Heidenreich and E. A. Nesbitt, J. Appl. Phys. 23, 35 (1952); E. A. Nesbitt and R. D. Heidenreich, J. Appl. Phys. 23, 366 (1952).

CC-0. In Public Domain. Gurukul Kangri Collection, Haridwar

Digitized by Arya Samaj Foundation Chennai and eGangotri

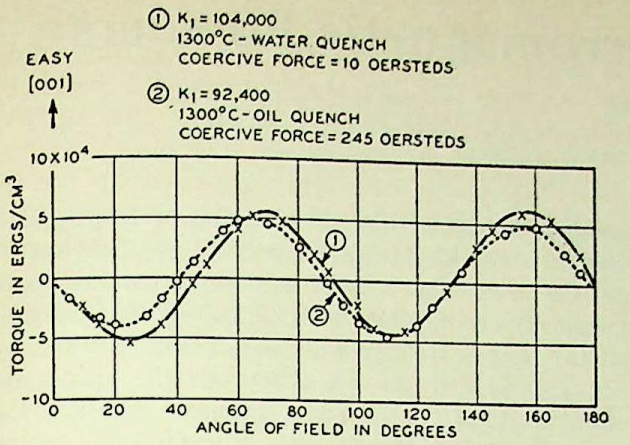


FIG. 2. Magnetic anisotropy of quenched Mishima single crystal (100) disks.

shows a new face-centered cubic phase of 10.0 angstroms cell size which is similar to the recently discovered Alnico 5 precipitate. The appearance of a second phase after this treatment is not surprising since the crystal has a coercive force of 435 oersteds.

Figure 2 shows torque curves obtained on water and oil quenched single crystals. Both curves show a simple fourfold symmetry and a [001] direction of easy magnetization. The water quenched sample has a value of 104 000 ergs per cm³ for K_1 which is slightly higher than the value of 92 400 ergs per cm³ obtained on the oil quenched sample. As we decrease the cooling rate of the crystals to obtain optimum permanent magnet properties, the measured anisotropy changes from positive to negative. This change in the sign of the anisotropy indicates that the anisotropy of the precipitate is opposite in sign to the anisotropy of the matrix. Figure 3 shows torque curves obtained on (100) crystals one of which was cooled at 10°C per second and the other at 10°C per second plus a bake at 820°C. Both curves

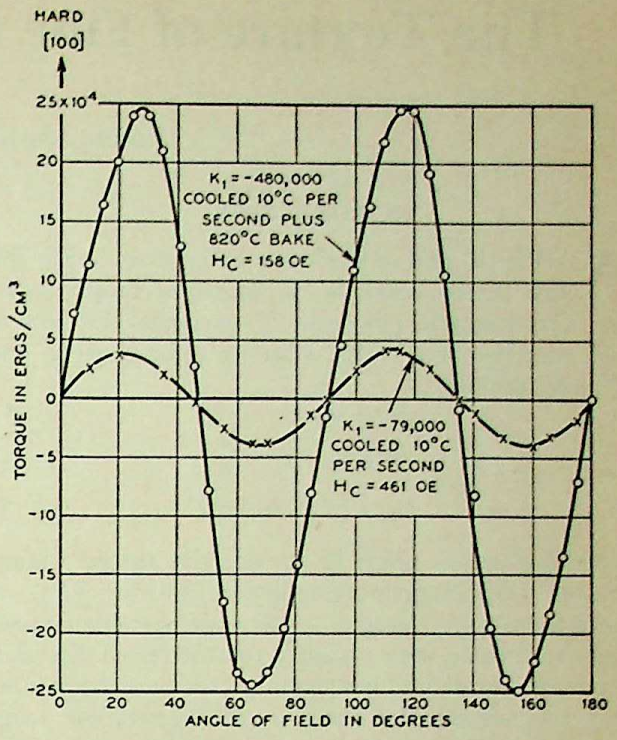


FIG. 3. Magnetic anisotropy of Mishima single crystal (100) disks.

show a simple fourfold symmetry and a [011] direction of easy magnetization. The sample cooled at 10°C per second has a K_1 value of −78 500 which is insufficient to account for the measured coercive force of 461 oersteds if we assume that the alloy is divided into single magnetic domains. However, the sample that was baked at 820°C yields a K_1 value of −480 000 ergs per cm³, which indicates that values of anisotropy exist in this alloy sufficient to account for all measured values of coercive force on the basis of the crystalline anisotropy of the precipitate and matrix.

CC-0. In Public Domain. Gurukul Kangri Collection, Haridwar

Digitized by Arya Samaj Foundation Chennai and eGangotri

The Texture of Fine Ferromagnetic Powders

L. WEIL

Institut Fourier, Grenoble, France

INTRODUCTION

A GREAT deal of work has been done during the last fifteen years on the magnetic properties of fine ferromagnetic powders. Of particular interest is their coercive force, which is known to be given by one of three formulas:

$$H_c=3\lambda\sigma/2J; \quad (1)$$

$$H_c=2K/J; \quad (2)$$

$$H_c=(N_2-N_1)J, \quad (3)$$

depending on the origin of the coercive force;[1–3] inner stresses (σ), magnetocrystalline anisotropy (K), or shape anisotropy (N_2 and N_1 being demagnetizing field coefficients) may give stability to a preferred direction of magnetization within the grain (λ is here the saturation magnetostriction and J the saturation magnetization). The materials are prepared by the general methods of making catalysts, from amalgams, by decomposition of carbonyls or even by mechanical crushing; the particle size should be small enough so that each grain comprises *only one domain*.[4] Theorists (Néel,[3] Kittel[5]) agree in stating that this condition is satisfied when the diameter of the grains becomes of the same order as the thickness of the Bloch walls in the same substance in the undivided state. For iron the critical diameter should therefore be about 300A; for nickel, it should be somewhat larger. These critical dimensions are confirmed by several noteworthy experiments; in particular, by means of x-rays (Bertaut[6]), by measurements of the heat of wetting in the case of iron (Weil[7]), and by means of electron microscopy for nickel (Kittel and Galt[8]). However, electron microscope photographs always show a very tight packing of the particles. In fact, in iron-amalgam, Mayer and Vogt[9] recently found by means of x-rays a diameter of 300A in agreement with a coercive force of 900 oersteds, but measured by ultrafiltration a much larger diameter of 10^4A.

THE SPONGES

We will show that these aspects are reconcilable. When speaking of very fine grains, the concept of separated grains is merely schematic: Particles stick together, somewhat like the elements of a sponge. A substance may be considered as made up of separated particles when the bridges between them are small enough. The sponge may well be as large as 1 micron; but the heat of wetting will nevertheless indicate the correct surface if the holes between the grains are communicating, and the x-rays will in any case give the correct diameter of the elements. Ultrafiltration, on the other hand, will indicate the size of the whole sponge.

From a magnetic point of view, the magnetic elements are single domains, while the sponges are not. In each element the direction of magnetization is different, and on every bridge there is a small Bloch wall. One of the two following alternatives may happen:

(1) The critical field for displacement of the wall is given by[10]

$$H=0.99\frac{\rho^3}{s^2}\left(\frac{K}{E}\right)^{\frac{1}{2}}\frac{2K+4\pi J^2K\rho^2/Ea^2}{Ja}, \quad (4)$$

where 2ρ = hole diameter; s = bridge diameter; K = anisotropy constant; a = lattice constant; J = saturation magnetization and E = Young's modulus. Thus, if H is small enough, the wall will move in fields smaller than those required for rotation, and the coercive force of the sponge will be given by formula (4) rather than by formulas (1), (2), or (3).

(2) The wall does not move before rotations take place.

As may be seen easily, alternative (1) happens when the bridges are large and the holes are small and ineffective. In the particular case of shape anisotropy (formula 3), for instance, the coercive force of compacts varies as $(1-d/d_0)$, where d/d_0 is the ratio of the density of the compact to that of the massive substance. This presupposes that all the holes are effective. If some holes are ineffective, the representative line will not go through the origin (see Fig. 1), but it will be shifted to the right by an amount corresponding to their relative volume. We found this true on a series of ferronickels (Fig. 1): Before sintering, for the four compositions, the line goes through the point $H_c=0$ when $(1-d/d_0)\cong 0$. However, after a low temperature sintering (300°C), a shift occurs and about 25 percent of the holes became ineffective.

It should be mentioned that, even when the field does not reach the critical value given by formula (4), but rather a lower value h, the wall may move, because of thermal fluctuations. The time of relaxation of this

[1] R. Becker, Z. Physik 62, 253 (1930).
[2] N. Akulov, Z. Physik 81, 790 (1933).
[3] L. Néel, Compt. rend. 224, 1550 (1947).
[4] L. Weil, Colloque de ferromagnetisme et antiferromagnetisme, Grenoble, 1951.
[5] C. Kittel, Revs. Modern Phys. 21, 541 (1949).
[6] E. F. Bertaut, Compt. rend. 229, 417 (1949).
[7] L. Weil, Compt. rend. 227, 42 (1948).
[8] Kittel, Galt, and Campbell, Phys. Rev. 77, 725 (1950).
[9] H. Mayer and E. Vogt, Z. Naturforsch. 7a, 334 (1952).
[10] L. Néel, Cahiers phys. 25, 21 (1944).

CC-0. In Public Domain. Gurukul Kangri Collection, Haridwar

Digitized by Arya Samaj Foundation Chennai and eGangotri

movement is[11,12]

$$\tau = c \exp\left[\frac{vJ(H-h)^{\frac{1}{2}}}{3kTH^{\frac{1}{2}}}\right],$$

where v is approximately the volume of the bridges. In this way, one may understand how some holes are effective at low temperatures and not at room temperature, in spite of only a small variation of H. For instance, Fig. 2 shows that at liquid nitrogen temperatures the effect of sintering on the coercive field of the above-mentioned ferronickels is much less pronounced than at room temperature.

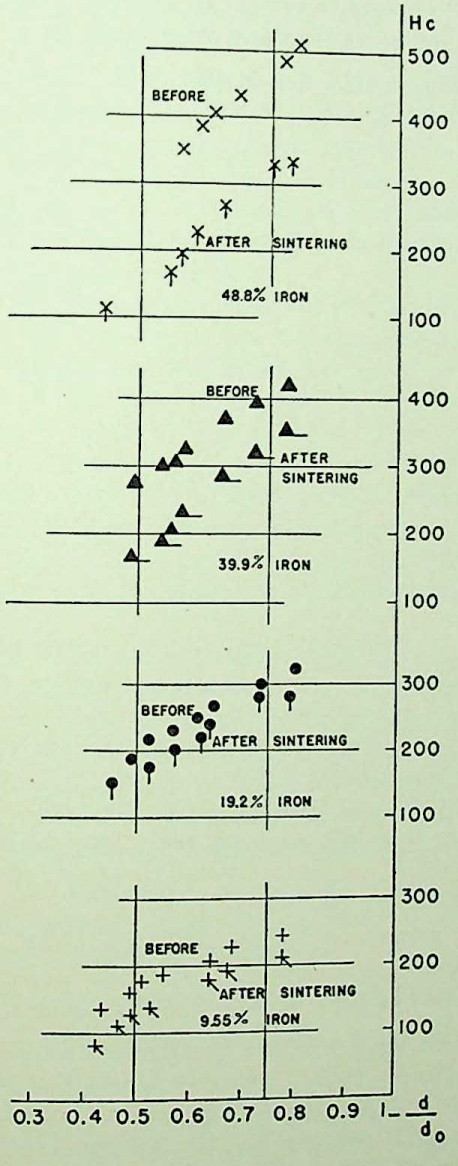


FIG. 1. Coercive force *vs* $1-(d/d_0)$, when (d/d_0) is the ratio of the density of the compact to that of the massive substance. Room temperature. Upper points, before sintering; lower points, after sintering.

[11] L. Weil, J. phys. et radium 12, 520 (1951).
[12] L. Néel, J. phys. et radium 11, 60 (1950).

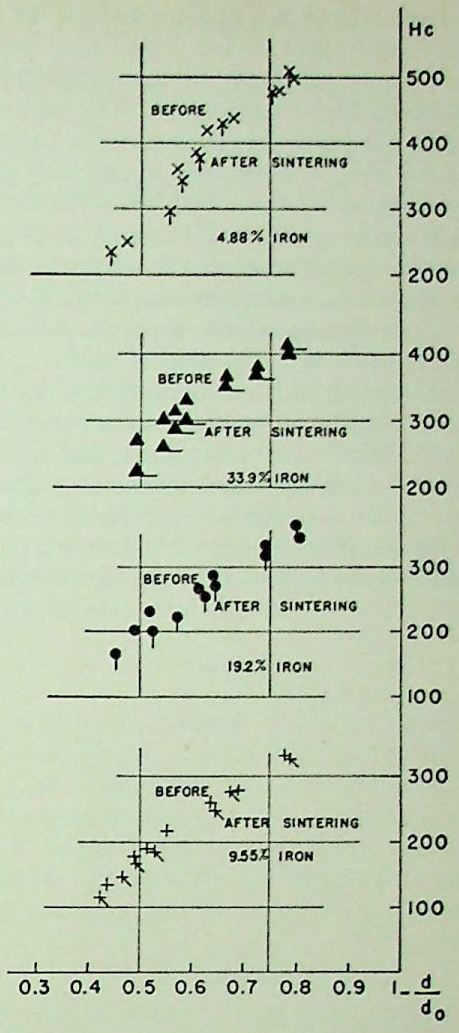


FIG. 2. Coercive force *vs* $1-(d/d_0)$, when (d/d_0) is the ratio of the density of the compact to that of the massive substance. Liquid nitrogen temperature. In each case the upper points indicate the values before sintering; the lower, after sintering.

SPONGES WITH VERY FINE ELEMENTS

When individual grains are very small, their magnetization may also turn spontaneously.[13] The relaxation time for such rotation is

$$\tau' \sim \exp[vJH'/kT],$$

where H' is approximately the coercive field [formulas (1), (2), or (3)]. When τ' is of the same order of magnitude as the time of measurement, the apparent critical field for such grains is of the order zero. In other words, if a fraction of the grains has a very small volume v, the mean coercive force of the powder will be smaller. Of course, the remanent magnetization will be reduced in proportion to the total volume of these small particles.

There is no experimental difference between a ferromagnetic body whose magnetization turns spontaneously during a measurement, and a paramagnetic body

[13] L. Néel, Compt. rend. 228, 664 (1949).

CC-0. In Public Domain. Gurukul Kangri Collection, Haridwar

Digitized by Arya Samaj Foundation Chennai and eGangotri

whose magnetization turns instantaneously. An explanation along these lines of the low coercive force of nickel and of iron Raney catalysts at room temperature, in spite of relatively high coercive force at liquid hydrogen temperatures, has previously been given by the author.[4]

As we have seen, at least from a magnetic point of view, there is little difference between separated grains and sponges made up of small elements connected by very narrow bridges. Therefore, the change in magnetic properties with temperature reported by Mayer and Vogt for their iron-amalgam sponges, which these authors attributed to a "rotational effect," is more probably associated with the temperature dependence of the probability for a spontaneous reversal of magnetization discussed above. Similarly, the increase in the coercive force of the same amalgam on aging from 20 oersteds to 900 oersteds is explainable by assuming that on aging—as is the case in every sintering process—the bridges become larger and consequently the holes become smaller and less effective, so that ultimately the sponges become effectively single grains and single domains of some hundred angstroms in diameter and, therefore, of high coercive force.

In spite of the beautiful results obtained by Elmore[14] on colloids, it would be incorrect to use a Langevin law to calculate the mean diameter of the sponge elements in the "paramagnetic" state. In colloids the particles are separated, while in a sponge, as we just pointed out, the particles are not independent. Moreover, the stopping of the Bloch walls on the bridges is temperature dependent, and, therefore, the "magnetic" diameter of the elements of the sponge is smaller, the lower the temperature. From this point of view, the magnetic granulometry used by Mayer and Vogt as well as by ourselves[15] appears to remain an approximate one, but probably not worse than any other method.

[14] W. C. Elmore, Phys. Rev. **54**, 1092 (1938).
[15] L. Weil, J. phys. et radium **12**, 23 (1951).

CC-0. In Public Domain. Gurukul Kangri Collection, Haridwar

Digitized by Arya Samaj Foundation Chennai and eGangotri

REVIEWS OF MODERN PHYSICS VOLUME 25, NUMBER 1 JANUARY, 1953

The Molecular Field Treatment of Antiferromagnetism

J. SAMUEL SMART

U. S. Naval Ordnance Laboratory, White Oak, Maryland

INTRODUCTION

THE first use of a molecular field concept was in Weiss' phenomenological theory of ferromagnetism.[1] The Weiss procedure was to take account of the interactions within a magnetic material by considering the total field acting on a given atom to consist of the applied magnetic field H_0 and an internal field which was assumed to be proportional to the average magnetization. In Néel's first papers[2] on antiferromagnetism he generalized this idea by dividing the magnetic lattice into two sublattices, each of which was acted on by a molecular field proportional and opposite to the magnetization of the other sublattice. Since that time Néel and other workers[3] have enlarged and refined Néel's methods. In this paper, we wish to discuss some of the results of such calculations.

We shall not concern ourselves here with the quantum-mechanical approaches to ferromagnetism and antiferromagnetism or with the relation of these results to the validity of the molecular field theory, although the usual Heisenberg interpretation of the molecular field coefficients will be used. It is worth noting, however, that the molecular field method seems to have considerably less theoretical justification for antiferromagnetism than for ferromagnetism, although the agreement with experiment is about the same for the two cases.

In the discussion to follow, only first and second nearest neighbor interactions will be considered, although the method can easily be extended to include the effects of more distant neighbors. We shall assume that both interactions may be either ferromagnetic or antiferromagnetic. For convenience in discussion, the various combinations are classified as indicated below.

Case	I	II	III	IV
Nearest neighbor interaction	*f*	*a*	*a*	*f*
Second nearest neighbor interaction	*f*	*a*	*f*	*a*

THE HIGH TEMPERATURE SUSCEPTIBILITY

We assume the material contains N magnetic atoms each with a magnetic moment $\mu=g\beta S_0$ where S_0 is the spin quantum number, g the gyromagnetic ratio, and β the Bohr magneton. In problems involving antiferromagnetic interactions it is necessary to divide the lattice of magnetic atoms into sublattices to take account of various possible types of magnetic ordering. The method of subdivision depends on the symmetry of the specific lattice, but there should be at least division into enough sublattices so that a given atom has neither first nor second nearest neighors on its own sublattice and only one kind of neighbors on any other sublattice. Let n be the number of sublattices required for the material considered. We limit ourselves to cases where the sublattices all have the same number of atoms, N/n.

We begin with a form of Langevin's equation for the high temperature susceptibility of a paramagnetic material

$$S=C'H/T, \tag{1}$$

where $g\beta S$ is the component of μ in the direction of the field H and $C'=g\beta S_0(S_0+1)/3k$. Let the internal field acting on an atom on the jth sublattice due to its neighbors on the kth sublattice be $\gamma_{jk}S_k$, where S_k is the value of S for sublattice k and γ_{jk} is the Weiss field coefficient. The γ_{jk} are simply related to the Weiss field coefficients, γ_1 and γ_2, for first and second nearest neighbor interactions.

$$\gamma_i=2Z_i|J_i|/g\beta, \quad i=1,2, \tag{2}$$

where Z_i is the number of ith nearest neighbors and J_i is the exchange interaction between electrons on ith neighbors. We have in general

$$\gamma_{jk}=f_{jk}{}^i\gamma_i, \tag{3}$$

where $f_{jk}{}^i$ is the fraction of the ith nearest neighbors of atom j on sublattice k.

We have chosen to define the γ_i as positive quantities and write in the sign of the interactions explicitly. Accordingly, we introduce the quantities $\epsilon_{jk}=\pm 1$, depending on whether the interaction between the jth and kth sublattices is ferromagnetic or antiferromagnetic.

The equations of state corresponding to (1) are then

$$S_j=(C'/T)\left[H_0+\sum_{k\neq j}^{n}\epsilon_{jk}\gamma_{jk}S_k\right], \quad j,k=1,2,\cdots,n. \tag{4}$$

From Eq. (4) we can easily calculate the susceptibility

$$\chi=(Ng\beta/nH_0)\textstyle\sum_j S_j=Ng\beta C'/(T-\theta), \tag{5}$$

where

$$\theta=C'\sum_{k\neq j}^{n}\epsilon_{jk}\gamma_{jk}. \tag{6}$$

It is found that the high temperature susceptibility of

[1] P. Weiss, J. phys. et radium 4, 661 (1907).
[2] L. Néel, Ann. phys. 18, 64 (1932); 5, 256 (1936).
[3] F. Bitter, Phys. Rev. 54, 79 (1938); J. H. Van Vleck, J. Chem. Phys. 9, 85 (1941); L. Néel, Ann. phys. 3, 137 (1948); P. W. Anderson, Phys. Rev. 79, 705 (1950); T. Nagamiya, Prog. Theoret. Phys. 6, 342 (1951); J. S. Smart, Phys. Rev. 86, 968 (1952).

CC-0. In Public Domain. Gurukul Kangri Collection, Haridwar

Digitized by Arya Samaj Foundation Chennai and eGangotri

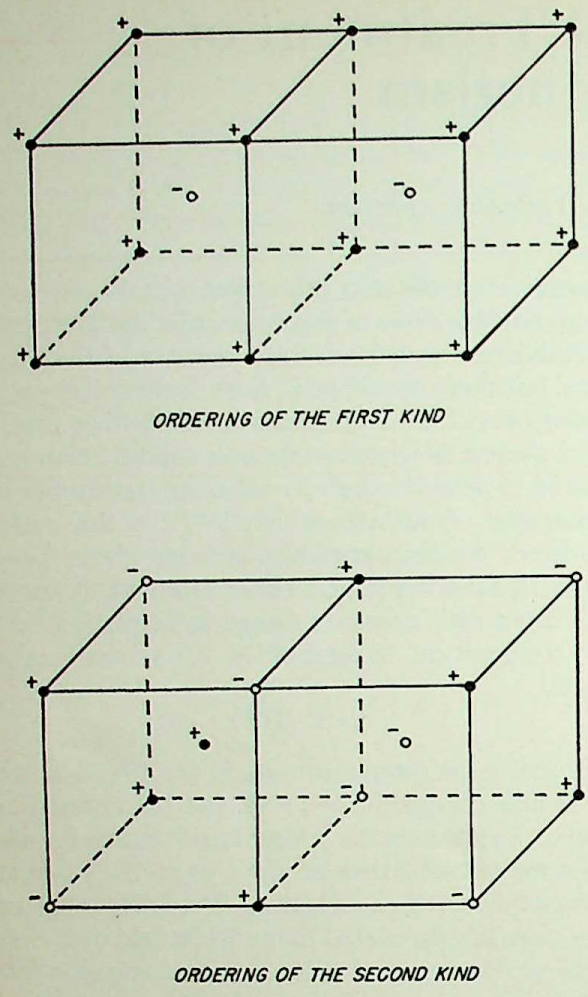


FIG. 1. Possible kinds of magnetic ordering for a body-centered cubic lattice.

an antiferromagnet can be fitted quite well to an equation of this form. The quantity θ so determined is usually (but not always) negative and is of the order of magnitude of the Curie temperature.

The possible Curie temperatures for the material can be found by setting $H_0=0$ in Eqs. (4) and finding what temperature allows nonzero solutions for the S_j. This procedure leads to solving a determinantal equation whose roots give the various Curie temperatures. We find, in general,

$$T_c=C'\sum_{k\neq j}^{n}\eta_{jk}\epsilon_{jk}\gamma_{jk} \tag{7}$$

and

$$S_j=\eta_{jk}S_k \quad \text{with} \quad \eta_{jk}=\eta_{kj}=\pm 1. \tag{8}$$

The η_{jk} are parameters which describe the type of ordering corresponding to a given Curie temperature; that is, there is a set of η_{jk} for each T_c.* If neither γ_1 nor γ_2 are zero, then three types of ordering are possible: (1) an antiferromagnetic arrangement with respect to nearest neighbors, (2) an antiferromagnetic arrangement with respect to second nearest neighbors, and (3) a ferromagnetic arrangement. The first two types have been designated by Van Vleck as antiferromagnetic ordering of the first and second kinds, respectively. As an example, Fig. 1 shows the two kinds of ordering for a b.c.c. lattice.

In practice, one is usually able to determine the magnetic configurations for the two types of ordering, and consequently the η_{jk} for each type, by inspection. Then θ and the T_c may be obtained from Eqs. (6) and (7) without the need of solving the determinantal equation. The kind of magnetic ordering which actually occurs will be that corresponding to the highest Curie temperature. This can be demonstrated, for example, by computing the Gibbs free energy for the various configurations, as is done in a later section of this paper.

These calculations help clarify the difference in the physical interpretations of θ and T_c. The quantity θ appearing in the susceptibility formula indicates the net effect of the internal fields in aiding or hindering the applied magnetic field in producing alignment. The θ for a particular material is obtained by adding algebraically the contributions from first and second nearest neighbor interactions as indicated by Eq. (6). T_c, on the other hand, depends on the actual magnetic structure below the Curie temperature and is essentially a measure of the energy required to bring the system from a state of perfect order to one where the long-range order is destroyed. To find T_c, we combine the same terms as were used in finding θ but with plus or minus signs according to whether or not the magnetic structure is favorable or unfavorable to a given interaction, as indicated by Eq. (7).

If θ and T_c are known, γ_1 and γ_2 may be calculated from Eqs. (6) and (7) for the antiferromagnetic case. (In the ferromagnetic case, where $\theta=T_c$, we have only one equation and can determine only the sum $(\gamma_1+\gamma_2)$.) However, a convenient way of demonstrating the relation between the experimental results and the Weiss field coefficients is to plot θ/T_c as a function of γ_2/γ_1. These curves are shown in Fig. 2 for a b.c.c. lattice. The Roman numerals labeling the curves refer to the type of interactions and the Arabic numerals to the kind of ordering. Thus, for Case II, the ordering is of the first or second kind depending on whether γ_2/γ_1 is less or greater than $\frac{1}{2}$. For Case III, the ordering is of the first kind for all values of γ_2/γ_1. For Case IV, the material is ferromagnetic for $\gamma_2/\gamma_1<\frac{1}{2}$ and antiferromagnetic with ordering of the second kind for $\gamma_2/\gamma_1>\frac{1}{2}$. Analogous results obtain for other types of lattice with cubic symmetry.

From Fig. 2 the theoretically possible values of θ/T_c for a b.c.c. antiferromagnet range from $+1$ to -3. For the f.c.c. lattice, which is of considerable experimental interest, the corresponding range is from $+1$ to -5. All known antiferromagnets have θ/T_c values which fall within the range appropriate to their magnetic lattice. We note that there are in general two possible

* In some cases, certain of the S_j are not related by equations of the form (8). This means that the magnetizations of some of the sublattices are completely uncorrelated as far as this simple theory goes.

CC-0. In Public Domain. Gurukul Kangri Collection, Haridwar

Digitized by Arya Samaj Foundation Chennai and eGangotri

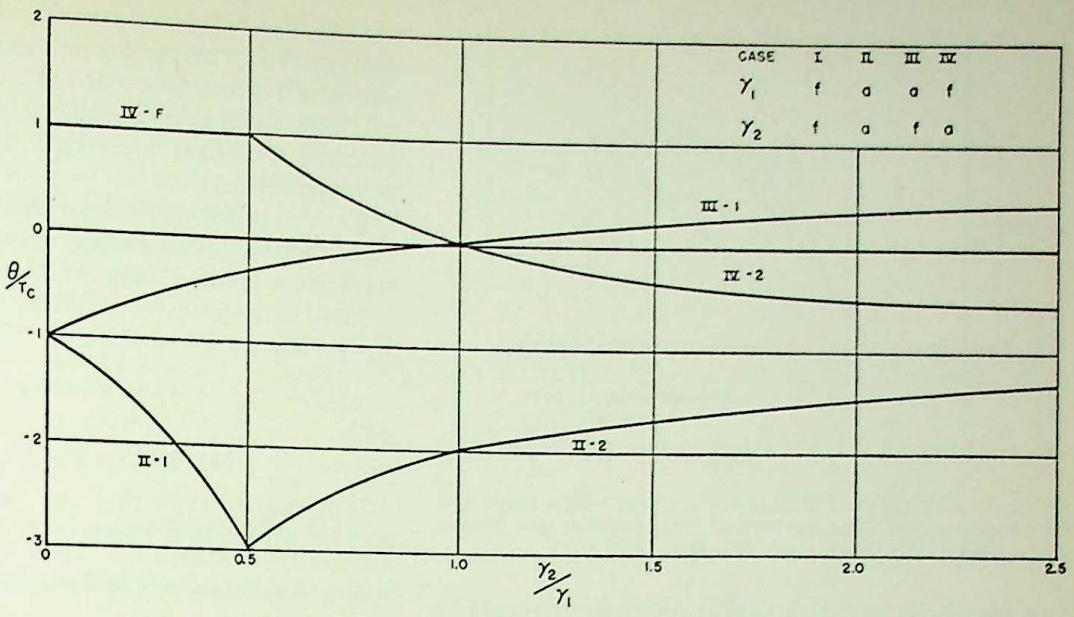


FIG. 2. θ/T_c values for body-centered cubic lattice. The Roman numerals on each curve refer to the signs of the interactions; the Arabic numerals refer to the kind of magnetic ordering.

values of γ_2/γ_1 for a given θ/T_c ratio. In order to determine the correct value of γ_2/γ_1, the magnetic structure must be established by neutron diffraction or susceptibility measurements on single crystals.

The determination of γ_1 and γ_2 by susceptibility measurements should be of considerable interest since there is at present no way of calculating these quantities theoretically. However, the existing experimental data is scant and sometimes not too accurate; also there is some question as to the degree of validity of the results of this simple theory. Brief reviews of the existing experimental data are given by Anderson and Smart.[3]

THE SUSCEPTIBILITY BELOW THE CURIE TEMPERATURE

For low temperatures, we can no longer use the approximation $\mu H/kT \ll 1$ which leads to Eq. (2), but we must instead write the exact equations of state

$$S_j = S_0 B(y_j), \tag{9}$$

where B is the Brillouin function for spin S_0 and $y_j = g\beta S_0 |\mathbf{H}_j|/kT$. In this case, S_j is the average spin per atom on the jth sublattice in the direction of $\mathbf{H}_j$. It is found, in a manner exactly analogous to the simple Weiss treatment of ferromagnetism, that the sublattices become spontaneously magnetized below T_c with their relative orientations specified by the η_{jk}. The temperature variation of the spontaneous magnetization of the individual sublattices is identical with that for a simple ferromagnet. The appearence of the spontaneous magnetization makes it necessary for us to consider cases in which the applied field H_0 and the molecular field are not collinear; we shall, however, consider only the possibility of a single antiferromagnetic axis. The calculation given below follows closely a method developed by Van Vleck.[3]

Let the total average spin per atom on the jth sublattice be given by

$$\mathbf{S}_j = \mathbf{S}_j^0 + \delta\mathbf{S}_j, \tag{10}$$

where $\mathbf{S}_j^0$ is the spontaneous value and $\delta\mathbf{S}_j$ the change produced by the external magnetic field. Using the above results and assuming all $\delta\mathbf{S}_j$ to be equal, we find that $\mathbf{H}_j$ may be written in the interesting and useful form

$$\mathbf{H}_j = \mathbf{H}_0 + (T_c/C')\mathbf{S}_j^0 + (\theta/C')\delta\mathbf{S}. \tag{11}$$

The total average spin S in the direction of the magnetic field $\mathbf{H}_0$ is given by

$$S = S_0\left[\sum_{j=1}^{n} B(y_j)\cos(\mathbf{H}_j, \mathbf{H}_0)\right]. \tag{12}$$

Combining Eqs. (11) and (12) and making approximations suggested by the fact that $|\mathbf{H}_0| \ll |\mathbf{H}_j|$, we find

$$\chi_{\parallel} = Ng\beta C' \frac{3S_0(S_0+1)^{-1}B'(y^0)}{T - 3S_0(S_0+1)^{-1}B'(y^0)\theta}, \tag{13a}$$

$$\chi_{\perp} = Ng\beta C'/(T_c - \theta) = \chi_{\parallel}(T_c) = \chi(T_c), \tag{13b}$$

where the parallel and perpendicular subscripts refer to the direction of the magnetic field with respect to the antiferromagnetic axis, and y^0 is the value of y_j with $\mathbf{H}_0 = 0$.

The powder susceptibility, which is what is usually obtained experimentally, is found for cubic crystals by combining $\chi_{\parallel}$ and $\chi_{\perp}$ in the ratio 1:2. Figure 3 shows the theoretical temperature variation of the powder susceptibility of MnO below the Curie temperature. The calculation was made by using the value $\theta/T_c = -5$ which was obtained from experimental susceptibility measurements on MnO above the Curie temperature. The theoretical prediction that $\chi(0)/\chi(T_c) = \frac{2}{3}$ is fairly well satisfied, but otherwise the agreement between theory and experiment is rather poor, the shapes of the curves being

CC-0. In Public Domain. Gurukul Kangri Collection, Haridwar

Digitized by Arya Samaj Foundation Chennai and eGangotri

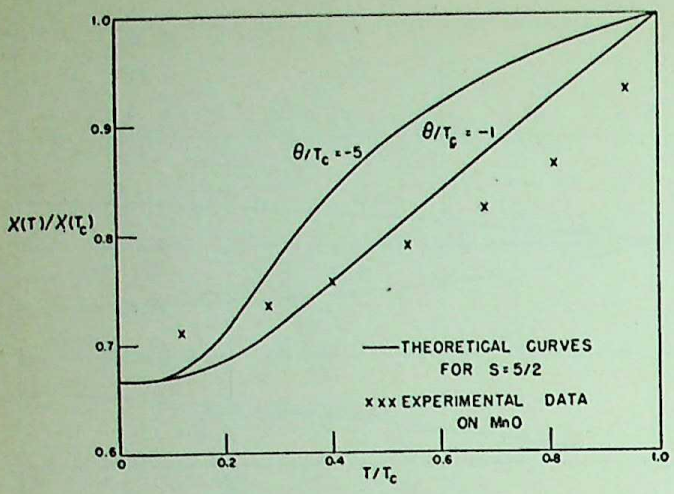


FIG. 3. $\chi(T)/\chi(T_c)$ *vs* T/T_c for a material with a single antiferromagnetic axis. The experimental data are taken from Bizette, Squire, and Tsai, Compt. rend. 207, 449 (1938).

considerably different. A similar discrepancy occurs for other antiferromagnetic compounds such as MnS, FeO, CoO, etc. It is difficult to say just why this discrepancy occurs. It is of interest to note that if more than one antiferromagnetic axis is assumed, then the theoretical $\chi-T$ curve becomes much more like the experimental one. Also, as Anderson has shown,[3] $\chi(0)/\chi(T_c)$ ratios different from $\frac{2}{3}$ are then allowed, and since the experimental values range from 0.30 to 0.90, a better over-all agreement between theory and experiment might be obtained. However, both the neutron and x-ray diffraction data on antiferromagnets are usually interpreted as being consistent with the idea of a single antiferromagnetic axis (MnO_2 is an exception). It is also possible that the reason for the discrepancy lies in a basic defect of the molecular field model. Ziman[4] has shown that a spin wave treatment considering only nearest neighbors gives results which are in good agreement with experiment (and also with the molecular field theory for nearest neighbors only), but no quantum-mechanical approach has been attempted which considers the effect of more distant neighbors.

MAGNETIC STRUCTURE TRANSITIONS

One of the interesting features of the results of the first section are that there are critical values of the ratio γ_2/γ_1 such that the orderings on either side of this critical value are of different kinds. This result suggests that, in addition to the usual Curie temperature transitions, there might sometimes occur transitions in which the magnetic ordering changes from one kind to another. Moreover, there is excellent experimental evidence[5] that transitions from a ferromagnetic to an antiferromagnetic arrangement occur in MnAs and MnBi. Garrett[6] and Ziman[7] have recently discussed the problem of phase transitions from an antiferromagnetic to a "ferromagnetic" state produced by application of a strong magnetic field. Using a model similar to Garrett's, the author[8] has recently examined the problem of changes in the type of magnetic ordering in zero applied field.

For this problem it is convenient to consider only the case of atoms having a single unpaired spin ($S_0=\frac{1}{2}$) and to define a reduced magnetization $\sigma=S/S_0=2S$ and a reduced temperature $\tau=T/T_c$. Then the Weiss-Langevin equation of state (9) takes the simple form

$$\sigma_j=\sigma=\tanh(\sigma/\tau), \tag{14}$$

with

$$\sigma_j=\eta_{jk}\sigma_k, \quad \eta_{jk}=\eta_{kj}=\pm 1. \tag{15}$$

It is easy to show that the entropy of this system may be written in the form

$$\mathcal{S}=Nk[\ln 2-(\tfrac{1}{2}\ln(1-\sigma)^2+\sigma\tanh^{-1}\sigma)]. \tag{16}$$

This result enables us to classify the types of transitions which may occur. If some of the sublattices merely reverse their direction of magnetization without changing σ, then the transition occurs without a change in entropy and is a second-order phase transition. On the other hand, if the specific magnetizations of the sublattices are changed as well as their directions the transition will in general be of the first order.

The free energy in zero field may be obtained by integrating $dG=-\mathcal{S}dT$. We find

$$G(T)=Nk\left[-T\ln 2+\frac{T_c}{2}\left(\sigma^2+\frac{\sigma\ln(1-\sigma^2)}{\tanh^{-1}\sigma}\right)\right], \tag{17}$$

with $G(T_c)=-NkT_c\ln 2$. Since the function of σ in Eq. (17) is zero for $\sigma=0$ and decreases monotonically for increasing σ (or decreasing T), the type of ordering with the highest Curie temperature will have the lowest free energy at all temperatures. Thus, as long as the equation of state has the form of Eq. (14), there will be no transition from one kind of ordering to another.

However, it seems likely that the molecular field coefficients γ_1 and γ_2 may actually depend in some way on the temperature, say because of thermal expansion of the lattice. This point has been particularly emphasized by Néel.[9] We assume that there is a simple linear variation of the form

$$\gamma_i=\gamma_{i0}(1+\alpha_i T), \quad i=1, 2. \tag{18}$$

This makes the effective field vary with temperature, giving an equation of state of the form

$$\sigma_j=\sigma=\tanh\left(\frac{1+\lambda\tau}{\tau}\sigma\right), \tag{19}$$

with $\sigma_j=\eta_{jk}\sigma_k$ as before. Here $\tau=T/T_c^0$, where T_c^0 is

[4] J. M. Ziman, Proc. Phys. Soc. (London) 65A, 540 (1952).
[5] C. Guillaud, J. phys. et radium 12, 223 (1951); A. Serres, J. phys. et radium 5, 146 (1947).
[6] C. G. B. Garrett, J. Chem. Phys. 19, 1154 (1951).
[7] J. M. Ziman, Proc. Phys. Soc. (London) 64A, 1108 (1951).
[8] J. S. Smart (unpublished work).
[9] L. Néel, Ann. phys. 8, 237 (1937).

CC-0. In Public Domain. Gurukul Kangri Collection, Haridwar

Digitized by Arya Samaj Foundation Chennai and eGangotri

the Curie temperature for $\alpha_1=\alpha_2=0$. The temperature coefficient λ is a function of the γ_{i0} and α_i, whose exact form depends on both the type of lattice and the type of ordering occurring. The principal effect of the temperature variation of the γ_i is to distort the normal $\sigma-\tau$ curve obtained for $\alpha_1=\alpha_2=0$. An example of this distortion is shown in Fig. 4 for the special case $\lambda=-0.23$.

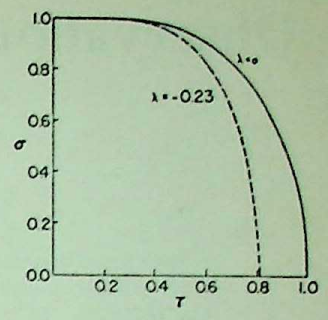


FIG. 4. Distortion of the normal $\sigma-\tau$ curve owing to temperature variation of the molecular field coefficients.

At any temperature T we have an "apparent Curie temperature" T_{ca}, given by

$$T_{ca}=T_c^0(1+\lambda\tau). \tag{20}$$

The actual Curie temperature is given by

$$T_c=T_c^0/(1-\lambda). \tag{21}$$

The entropy is, of course, the same function of σ as it was for the previous case. However, because of the different relation between σ and τ the free energy is now

$$G(T)=Nk\left[-T\ln 2+\frac{T_c^0}{2}\left(\frac{\sigma^2\tanh^{-1}\sigma+\sigma\ln(1-\sigma^2)}{\tanh^{-1}\sigma-\lambda\sigma}+\lambda\int_{\tau_c}^{\tau}\sigma^2 d\tau\right)\right], \tag{22}$$

with $\tau_c=T_c/T_c^0$.

Now let us consider two possible types of magnetic ordering, A and B, for a particular system. First, it is important to note that although γ_{10}, γ_{20}, α_1, and α_2 are the same for the A and B states, the temperature coefficients λ_A and λ_B are unequal since they are different functions of these four quantities. It is this difference which makes the structure transitions possible.

If, for example, the A state has the highest actual Curie temperature, then for temperatures just below T_{cA}, $G_A<G_B$. The condition that a transition occurs is then evidently $G_B(0)<G_A(0)$, or with the use of (22)

$$\lambda_A T_{CA}^0\int_0^{\tau_{CA}}\sigma_A^2 d\tau_A-\lambda_B T_{CB}^0\int_0^{\tau_{CB}}\sigma_B^2 d\tau_B<T_{CB}^0-T_{CA}^0, \tag{23}$$

where $\tau_A=T/T_{CA}^0$ and $\tau_B=T/T_{CB}^0$.

The theory described here is too simple to expect more than qualitative agreement with experiment. However, some of the predictions of the theory are supported by the observations of Guillaud and Serres.[5] It can be shown that if the temperature at which $\sigma_A=\sigma_B$ is T_σ, then in general $G_A(T_\sigma)\neq G_B(T_\sigma)$, so that the transitions should be expected to be first-order transitions, as is observed. Second, using the curves of Fig. 2 as an example, we see that a material which is ferromagnetic at low temperatures and antiferromagnetic at higher temperatures should have a θ/T_c value slightly less than unity. The observed value for MnAs is 0.72 and is the only known case where an antiferromagnet has a positive θ/T_c. Finally, the values of α_1 and α_2 required to give the observed transitions is of the order of magnitude of 10^{-4}/°K, in very good agreement with estimates (made by Néel[9]) based on other considerations.

CC-0. In Public Domain. Gurukul Kangri Collection, Haridwar

Digitized by Arya Samaj Foundation Chennai and eGangotri

Observations on Antiferromagnetic $CuCl_2 \cdot 2H_2O$ Crystals

C. J. GORTER

Kamerlingh Onnes Laboratorium, Leiden, The Netherlands

Four series of observations carried out in the Kamerlingh Onnes Laboratory on $CuCl_2 \cdot 2H_2O$ crystals are reviewed. The magnetization curves confirm the general picture given by the theoretical analysis of Gorter and Haantjes. At the lower temperature a sharp threshold field is found in the crystallographic *ac* plane with a minimum value of 6500 ϕ; at higher temperature its value increases somewhat.

Specific heat measurements reveal the existence of a short-range order tail above the sharp Néel temperature at which antiferromagnetism vanishes.

In the investigations on proton magnetic resonance a sharp transition is found between a nonsymmetrical paramagnetic resonance diagram and a symmetrical resonance diagram characteristic for antiferromagnetism. In this way it is found that the Néel temperature depends on the direction of the magnetizations.

It is possible to follow the turn-over of the magnetizations near the threshold field. The position of the protons and the nature of the sublattices have been determined. The sublattices do not exchange position within 10^{-4} sec. Microwave resonances have been observed at 9400 and at 4000 megacycles/sec. The absorption bands are confined to the neighborhood of the turn-over fields. General agreement with Ubbink's theoretical treatment is found.

INTRODUCTORY REMARKS

IN this review paper the chief results are given of four different kinds of investigations carried out by four teams of workers in the Kamerlingh Onnes Laboratory. On the whole the results are in agreement with the phenomenological theory described in another review paper.[1]

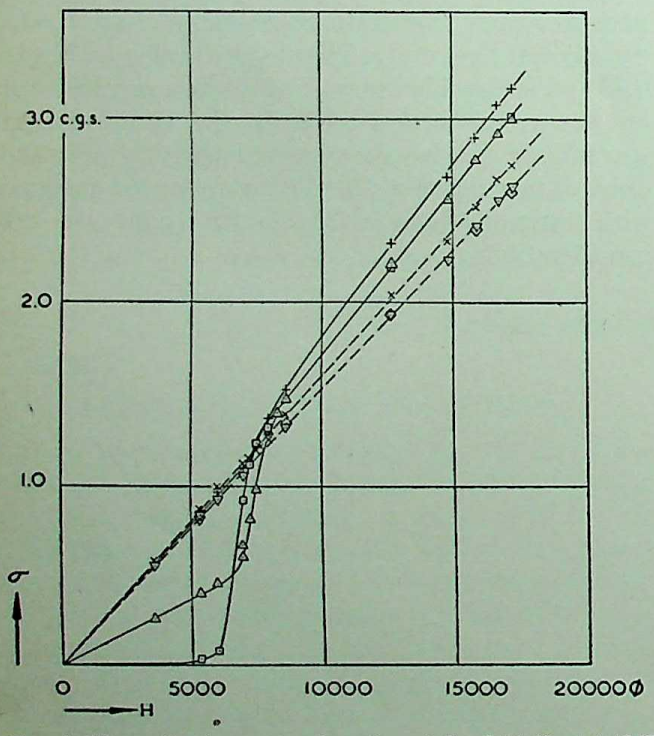


FIG. 1. Magnetization σ as a function of the field H. +4.1°K; field in the direction of the *a* axis. × 4.1°K; field in the direction of the *b* axis. △ 3.02°K; field in the direction of the *a* axis. ▽3.02°K; field in the direction of the *b* axis. ⊡ 1.57°K; field in the direction of the *a* axis. ◊ .57°K; field in the direction of the *b* axis.

[1] C. J. Gorter, Revs. Modern Phys. 25, 277 (1953).

They are presented as tests and confirmations of that theory which is presumed to be known. The historical order, however, was different: Many of the essential results had been collected before the theory in its present form had been set up, although at a later phase it was helpful in the classification of the data. For full details I refer to the original papers, which appeared in the Communications from the Kamerlingh Onnes Laboratory and in *Physica*.

MAGNETIZATION

By the usual Faraday method for the measurements of the magnetization parallel to a magnetic field,

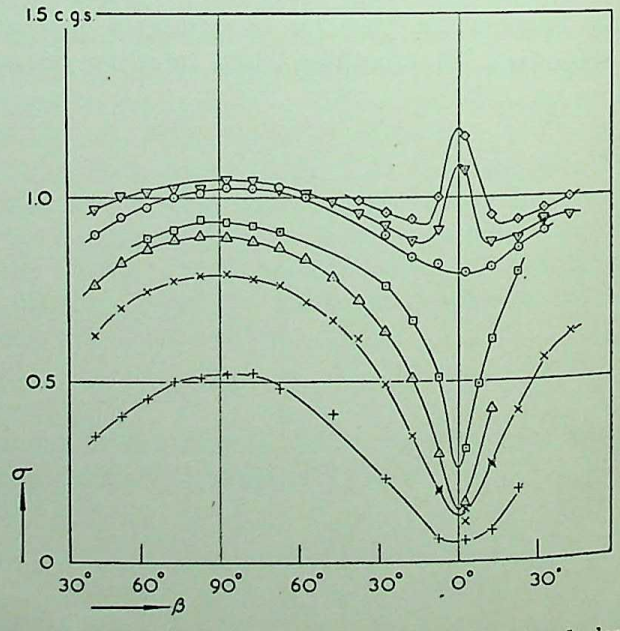


FIG. 2. Magnetization σ when the field H lies in the *ab* plane as a function of the angle between H and the *a* axis. Temperature 2.1°K. + $H=3600\ \phi$. × $H=5300\ \phi$. △ $H=6000\ \phi$. ⊡ $H=6300\ \phi$. ⊙ $H=7000\ \phi$. ▽ $H=7250\ \phi$. ◊ $H=7450\ \phi$.

CC-0. In Public Domain. Gurukul Kangri Collection, Haridwar

Digitized by Arya Samaj Foundation Chennai and eGangotri

Handel, Gijsman, and Poulis[2] investigated the hydrated copper chloride in the crystallographic *ab*, *ac*, and *bc* planes.[1] Between room temperature and the lowest liquid hydrogen temperatures the susceptibility χ follows the Curie-Weiss law,

$$\chi = \sigma/H = Ng^2\mu_B^2/k(T-\theta),$$

where μ_B is the Bohr magneton and k is Boltzmann's constant. g is found to be 2.19, 2.05, and 2.25 in the crystallographic *a*, *b*, and *c* directions, respectively, while $\theta = 5°K$.

At the lowest liquid helium temperatures (1.57°K), however, the magnetization remains very small when a field in the *a* direction up to 6500 ϕ is applied (Fig. 1). Then, in an interval of a few hundred oersted, the magnetization increases steeply. At still stronger fields the magnetization is simply proportional to the field strength. In the *b* and *c* directions the magnetization is proportional to the field at all field strengths used.

The three field independent susceptibilities are found to be approximately proportional to the squares of the three *g* factors just mentioned. This indicates that the antiferromagnetic exchange energy ($-\frac{1}{2}\alpha\mu^2$) is about 5×10^{-16} erg/ion and that its anisotropy is not higher than 1 percent.

It is clear that the threshold field at 6500 ϕ can be identified with the turn-over field discussed in reference 1. This leads to the result that the exchange energy, when the magnetizations in the sublattices are in the $\pm a$ directions, is 0.2 percent lower than in the $\pm b$ directions. When a constant field is rotated in the *ab* plane (Fig. 2), the susceptibility has a sharp minimum in the *a* direction, which, in agreement with the theoretical formulas, goes over into a narrow and small maximum at the threshold field strength. In the *ac* plane (Fig. 3), however, the corresponding curves at fields above 6500 ϕ consist of two clearly distinct parts. Near the *a* axis a platform develops which is separated

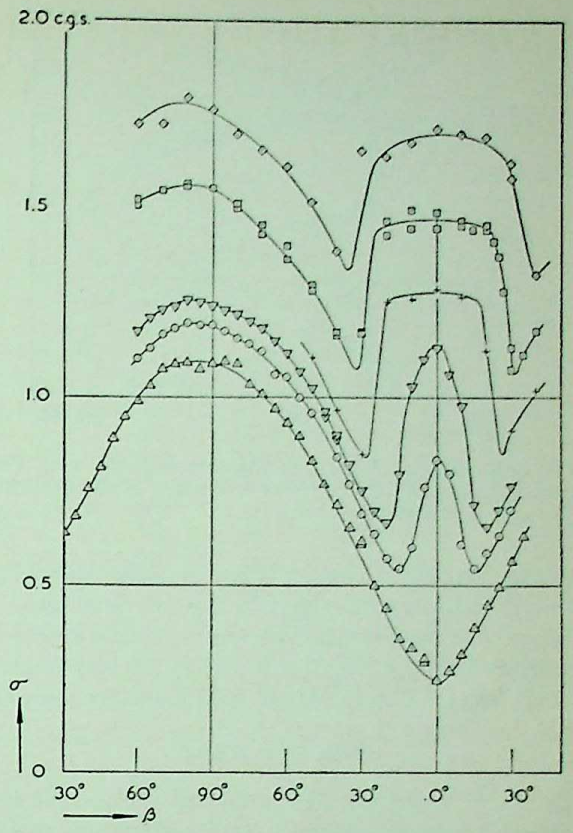


FIG. 3. Magnetization σ when the field H lies in the *ac* plane as a function of the angle between H and the *a* axis. Temperature 2.1°K. △ $H = 5660\ \phi$. ⊙ $H = 6640\ \phi$. ▽ $H = 6880\ \phi$. + $H = 7560\ \phi$. ⊡ $H = 8175\ \phi$. ◇ $H = 9225\ \phi$.

by a steep fall from a region where the magnetization behaves as if the threshold field had not yet been reached. Obviously the steep fall indicates the position of the hyperbola in the field space which separates the regions where the magnetizations in the sublattices remain in the *ac* plane from those where they have been turned over into the $\pm b$ directions. The shape of the hyperbola

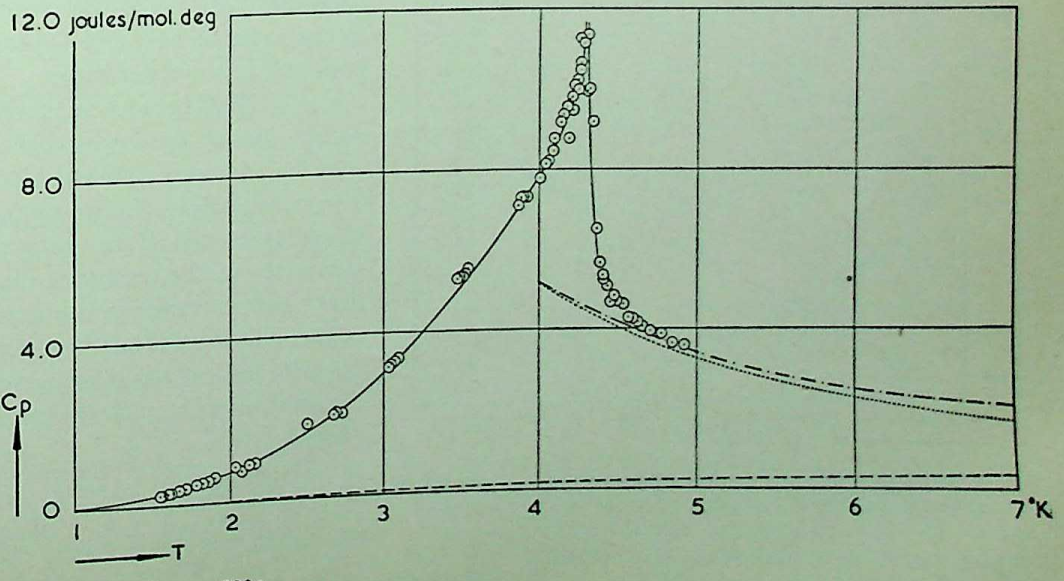


FIG. 4. Specific heat C_p as a function of temperature T. — — — specific heat caused by lattice waves. · · · · · tail caused by disappearing short-range order. —·—·—·sum of tail and lattice specific heat.

[2] Handel, Gijsman, and Poulis, Leiden Comm. 290c.

CC-0. In Public Domain. Gurukul Kangri Collection, Haridwar

Digitized by Arya Samaj Foundation Chennai and eGangotri

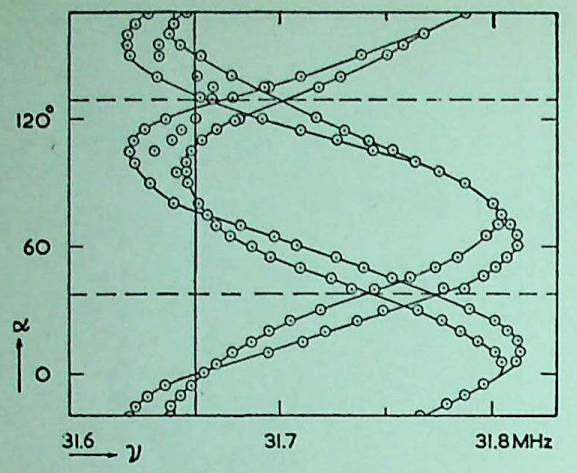


FIG. 5. Resonance diagram in the paramagnetic state. Proton magnetic resonance frequencies as a function of the angle in the *ab* plane. $T=14.3°K$; $H=7460$ ϕ.

indicates that the exchange in the $\pm c$ directions is again 0.8 percent higher than that in the $\pm b$ directions.

When the temperature increases, the low-field susceptibility in the *a* direction varies in the way predicted by Van Vleck.[3] The threshold field increases somewhat.

SPECIFIC HEAT

Dr. S. A. Friedberg has measured the specific heat.[4] It shows a lambda-anomaly with a steep fall at 4.3°K (Fig. 4) marking the Néel temperature θ_n. It is noteworthy that $-\frac{1}{2}k\theta_n$ is only about $\frac{2}{3}$ of the exchange energy as determined from the susceptibilities. At the high temperature side the specific heat has a tail which is approximately proportional to T^{-2}. In this tail apparently the short-range order disappears gradually. Below θ_n an entropy of about $0.40R$ is contained, while it is evaluated that the tail contains $0.25R$. Thus, the sum is not much smaller than the theoretical entropy value $R\ln 2=0.69R$.

According to Van Vleck's theoretical treatment, the exchange specific heat at high temperatures should be $3\alpha^2\mu^1/2zRT^2$, where z indicates the number of interacting antiferromagnetic neighbors.[5] This would lead to $z=3$ or $z=7$ depending on whether $\alpha\mu^2$ is deduced from θ_n and θ or from the susceptibilities in the antiferromagnetic region.

PROTON MAGNETIC RESONANCE

Poulis, Hardeman, and Bölger[6] have carried out elaborate investigations on the proton magnetic resonance. The observation of the frequency at which the nuclear magnetic resonance occurs gives a very accurate determination of the average local magnetic field at the spot where the nucleus happens to be located. Bloembergen discovered in the paramagneiic $CuSO_4\cdot 5H_2O$ that, when at low temperatures the average magnetization of the copper ions in the external field becomes large, the average local field may differ considerably from the external field. The observed splittings of the proton line are proportional to the external field and approximately inversely proportional to the temperature.

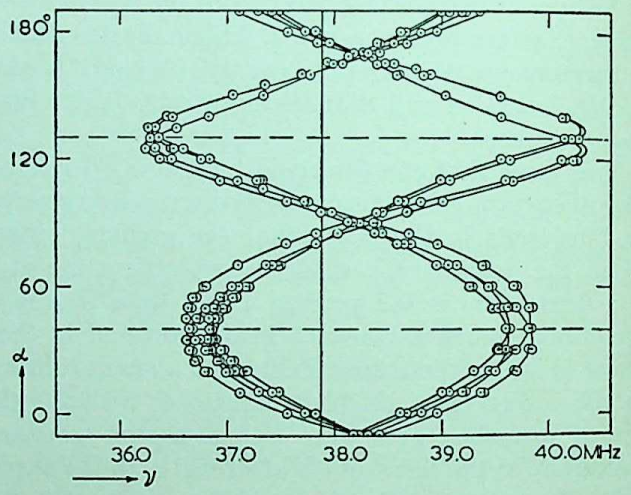


FIG. 7. Resonance diagram in the antiferromagnetic state above the threshold field H_c. *ab* plane; $T=3.02°K$; $H=8920$ ϕ.

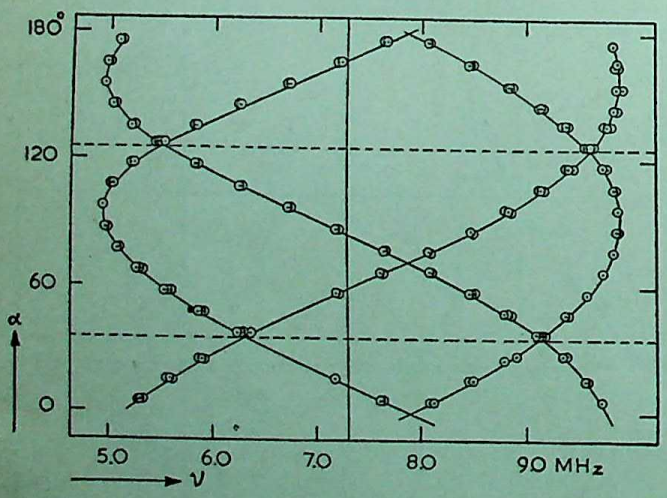


FIG. 6. Resonance diagram in the antiferromagnetic state below the threshold field H_c. *ab* plane; $T=3.03°K$; $H=1705$ ϕ.

$CuCl_2\cdot 2H_2O$ behaves similarly in the liquid hydrogen region, but at the lowest helium temperatures Poulis *et al.* found a very different kind of resonance diagram. The general width of the structure is independent of the temperature and of the external field, and a marked symmetry in the resonance diagram indicates that to every proton experiencing a certain field due to the copper ions there is another proton that feels an exactly opposite field. It was this observation which constituted the starting point of all the other observations on $CuCl_2\cdot 2H_2O$.

[3] J. H. Van Vleck, J. Chem. Phys. **9**, 85 (1941).
[4] S. A. Friedberg, Leiden Comm. 289[d].
[5] J. H. Van Vleck, J. Chem. Phys. **5**, 320 (1937).
[6] N. J. Poulis and G. E. G. Hardeman. Leiden Comm. 287[a], Physica **18**, 201 (1952); Leiden Comm. 288[b], Physica **18**, 315 (1952). Poulis, Hardeman, and Bölger, Leiden Comm. 289[a], Physica **18**, 429 (1952).

CC-0. In Public Domain. Gurukul Kangri Collection, Haridwar

Digitized by Arya Samaj Foundation Chennai and eGangotri

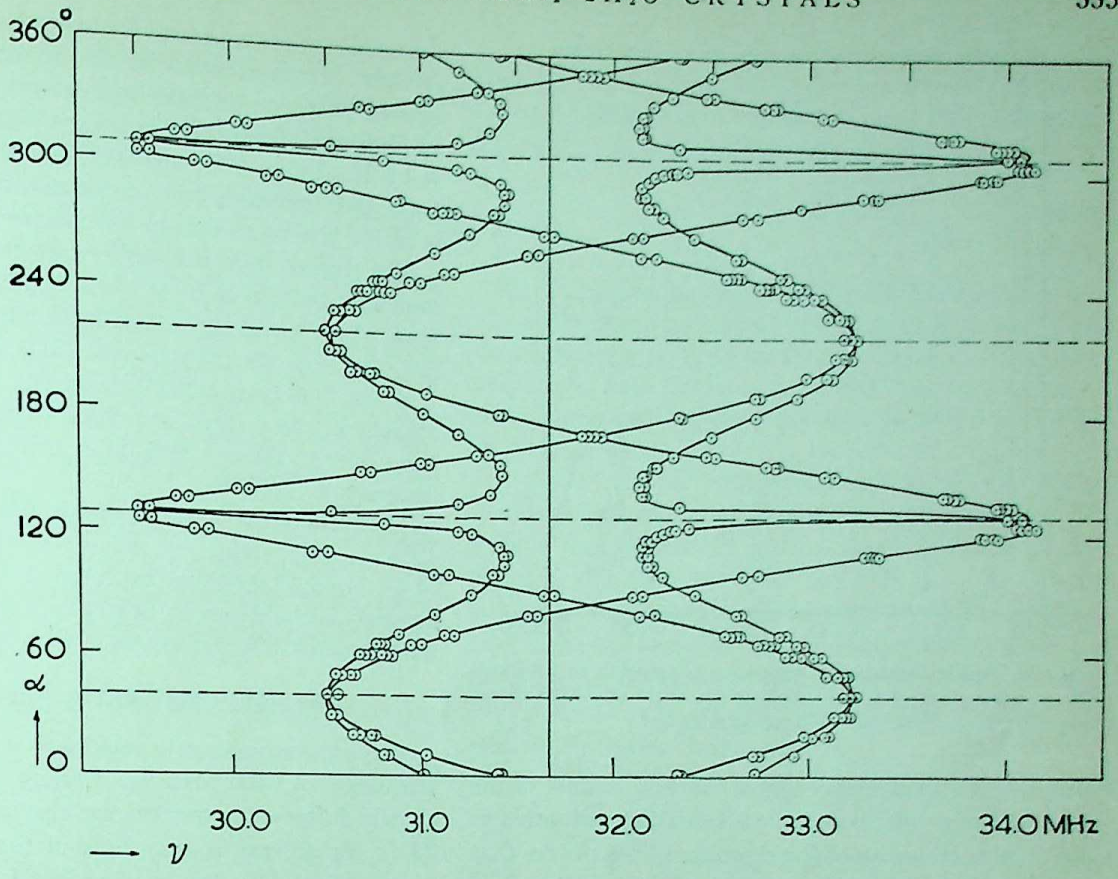


FIG. 8. Resonance diagram in antiferromagnetic state just blow the threshold field H_c. ab plane, $T = 3.47°K$; $H = 7460$ ϕ.

Below the threshold field the resonance diagram has a period of 360°, since the magnetizations in the two sublattices then remain in the neighborhood of the $\pm a$ directions. Above the threshold field, however, the magnetizations remain approximately perpendicular to the field.

After a rotation of 180° the magnetizations have also rotated over 180°, thus the relative orientation is the same; hence, the period of 180° in the diagram (Fig. 5).

Near the threshold field the resonance diagrams are complicated, and it is possible to follow the turning over of the magnetizations in detail.

It was not easy to find satisfactory locations for the protons and to divide the crystalline lattice in sublattices in a way that accounts for the many data in the paramagnetic as well as in the antiferromagnetic state. By trial and error a satisfactory arrangement was finally

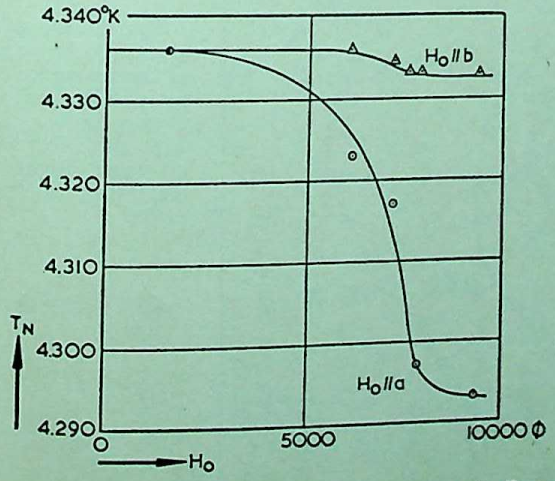


FIG. 9. Temperature at which the antiferromagnetic diagram is transformed into a paramagnetic resonance diagram as a function of a field in the a direction (⊙) and in the b direction (△).

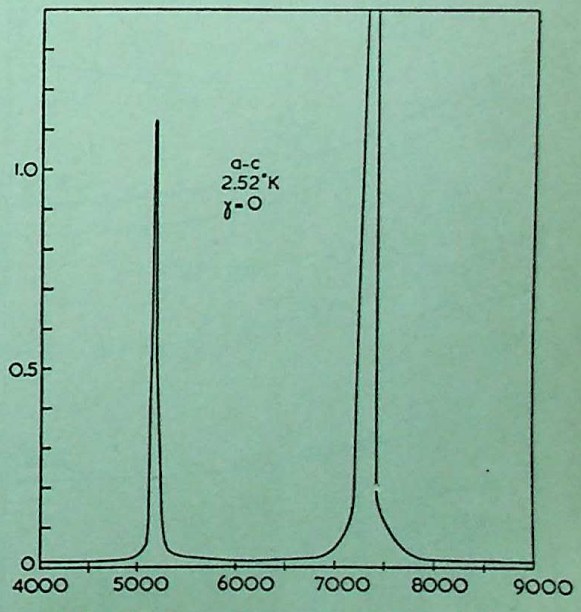


FIG. 10. Antiferromagnetic resonance absorption in arbitrary units as a function of a field in the a direction. $T = 2.52°K$; 9400 megacycles/sec.

CC-0. In Public Domain. Gurukul Kangri Collection, Haridwar

Digitized by Arya Samaj Foundation Chennai and eGangotri

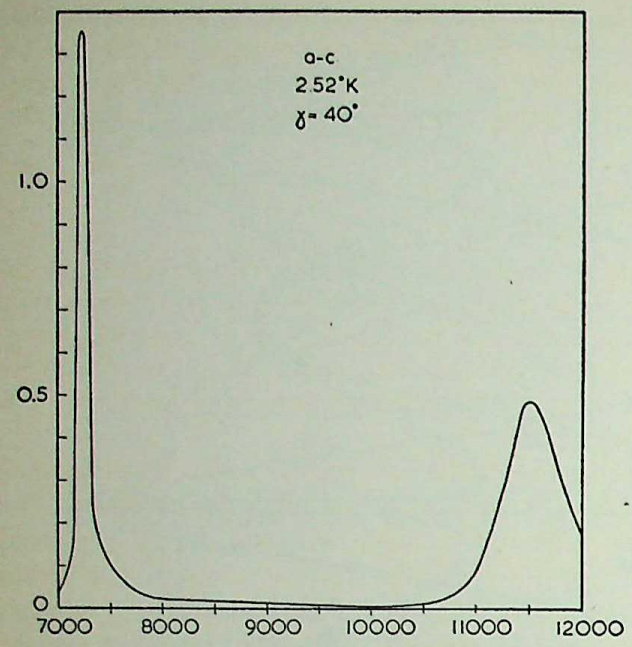


FIG. 11. Antiferromagnetic resonance absorption in arbitrary units as a function of a field making an angle of 40° in the *ac* plane with the *a* direction. 9400 megacycles/sec.

found in which successive copper layers parallel to the crystallographic *ab* plane have alternating spin-orientations. The narrowness of the resonance lines proves that the sublattices cannot exchange positions within 10^{-4} sec.

When the temperature increases, the width of the pattern of splittings decreases. This is obviously due to a decrease of the spontaneous magnetization on the sublattices. The dependence of this spontaneous magnetization, thus found, agrees up to about 4°K with that to be expected from Néel's theory with $S=\frac{1}{2}$ and $\theta_n=4.5$°K. Above 4°K, however, the spontaneous magnetization decreases much more rapidly. This behavior is rather similar to that of ferromagnetics.

The change from the antiferromagnetic to the paramagnetic pattern is quite abrupt. In a small external field, which leaves the magnetization near the favorable $\pm a$ direction, the change occurs at 4.33[7]°C.

When, however, a field above the threshold field is applied in the *a* direction which turns the magnetizations over to the $\pm b$ directions, this Néel temperature decreases to 4.29[2]°K.

The ratio of the width of the pattern at 4.4°K and at 15°K is only about 1.4, while theoretically $(15+5)/(4.4+5)=2.13$ should be expected. This, and the similar anomaly encountered in the susecptibilities, is connected with the two different values of the exchange energy.

ANTIFERROMAGNETIC RESONANCE

The antiferromagnetic resonance was studied at the frequency of 9400 MHz by Ubbink, Poulis, and Gerritsen.[7] A few experiments were also carried out at 4000 MHz. In general, it may be said that absorption has been observed in the neighborhood of the threshold hyperbola in the *ac* plane and that all results are in good agreement with Ubbink's theory (Figs. 6–12). When the constant field is situated in the *ac* plane, one absorption

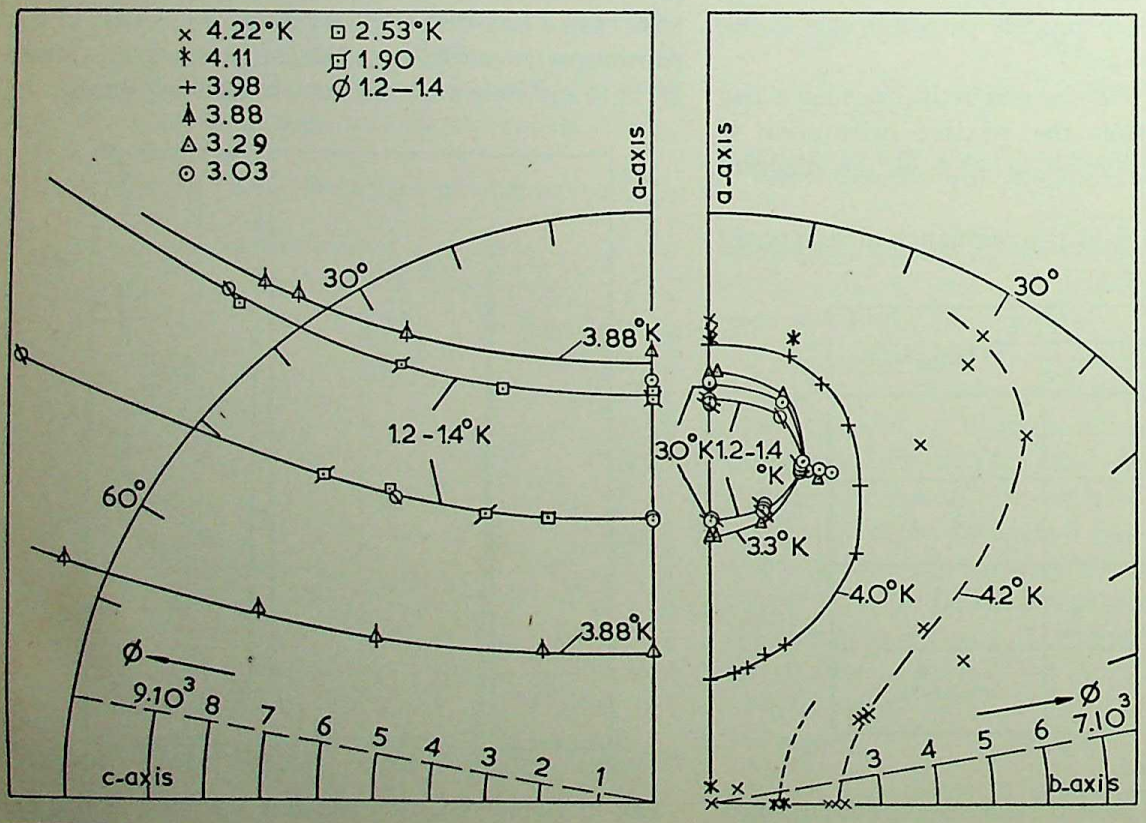


FIG. 12. Polar diagrams of the position of the resonance magnetic fields at 9400 megacycles/sec. Left-hand side: field in the *ac* plane. Right-hand side: field in the *ab* plane.

[7] Ubbink, Poulis, Gerritsen, and Gorter, Leiden Comm. 288[d], Physica 18, 361 (1952).

CC-0. In Public Domain. Gurukul Kangri Collection, Haridwar

Digitized by Arya Samaj Foundation Chennai and eGangotri

band is observed slightly below the threshold field and one slightly above it. When the constant field is situated in the *ab* plane, the two bands approach each other, merge, and vanish if the angle with the *a* axis increases.

The high frequency susceptibility increases anomalously at the low-field side of the lower band and not at the high-field side as it otherwise does. This is in agreement with the theoretical expectations.

DISCUSSION

M. LAX, *Syracuse University, Syracuse, New York:* It is not surprising, as Professor Gorter points out, that a deviation occurs from the Curie-Weiss law just above the Curie temperature, and that this deviation is not adequately explained by the classical molecular field theory. The deviation from the Curie-Weiss law originates in fluctuations of spin orientation that are neglected in the usual molecular field treatment. The spherical model which includes these fluctuations yields a molecular field coefficient that varies with temperature above the Curie temperature and thus can account qualitatively for the observed deviations.

F. KEFFER, *University of Pittsburgh, Pittsburgh, Pennsylvania.*

Mr. J. Kaplan has made an Ewald-Kornfeld calculation of the magnetic dipole field factors. By using these and anisotropy of the *g* factors, he finds a 1300-oersted anisotropic field between preferred and next-preferred axis, 12 oersted between preferred and third axis. This is clearly wrong.

Professor Kittel suggested using pseudo-dipole coupling between the exchange-coupled spins. This gives a dipole-like factor of order $J(g\text{-}2)^2$. By using this and the anisotropy of the *g* factors and adding to Kaplan's calculation, we find 500-oersted anisotropic field between preferred and next-preferred axis and 1000 oersted between preferred and third axis. This is in agreement as to order of size and direction as measured by Professor Gorter's group.

CC-0. In Public Domain. Gurukul Kangri Collection, Haridwar

Digitized by Arya Samaj Foundation Chennai and eGangotri

Magnetic Anisotropy of the Iron-Group Fluorides

J. W. STOUT AND L. M. MATARRESE *

Institute for the Study of Metals and Department of Chemistry, The University of Chicago, Chicago, Illinois

The magnetic anisotropy of single crystals of FeF_2 and CoF_2 has been measured over the temperature range 11 to 340°K. Like MnF_2, the anhydrous difluorides of iron and cobalt have the tetragonal rutile crystal structure, and the anisotropy results are compared with those found by Stout and Griffel for MnF_2. In all three compounds the magnetic susceptibility parallel to the crystallographic c axis is at room temperatures greater than that in a direction perpendicular to this axis. Because of the orbital magnetic moment the high temperature anisotropy is much greater for FeF_2 and CoF_2 than for MnF_2. As the temperature is lowered, the anisotropy changes sign and at 11°K has large negative values, indicating that the susceptibility parallel to the c axis becomes small. This indicates that at low temperatures there is an ordered antiferromagnetic arrangement with the elementary magnetic moments aligned parallel and antiparallel to the c axis. Such a magnetic structure has been found from neutron diffraction measurements by Shull and Erickson. The anomalous behavior of the magnetic anisotropy, associated with the antiferromagnetic ordering, is in the case of CoF_2 spread out over a much wider temperature range than in the case of MnF_2 and FeF_2. At the lowest temperatures the anisotropy of MnF_2 varies as T^2, whereas those of FeF_2 and CoF_2 vary as the fourth power of the temperature.

THE anhydrous difluorides of the elements manganese, iron, cobalt, and nickel all have the rutile-type crystal structure.[1] The tetragonal unit cell, containing two molecules, has values of c_0/a_0 in the neighborhood of two-thirds. The structure of the positive ion lattice may be thought of as made up of chains running parallel to the c axis. A given magnetic ion and its two nearest magnetic neighbors all lie in the same chain. The eight next nearest neighbors, in the directions of the body diagonal of the tetragonal unit cell, are more distant than the nearest neighbors by factors ranging from 1.12 in FeF_2 to 1.18 in NiF_2. The structure of MnF_2, which is typical, is shown in Fig. 1. Because of the tetragonal symmetry there is a possibility of anisotropy in the magnetic susceptibility. The symmetry requires that one of the principal axes of magnetic susceptibility lie along the c axis of the crystal, while the susceptibility must be the same in all directions normal to the c axis.

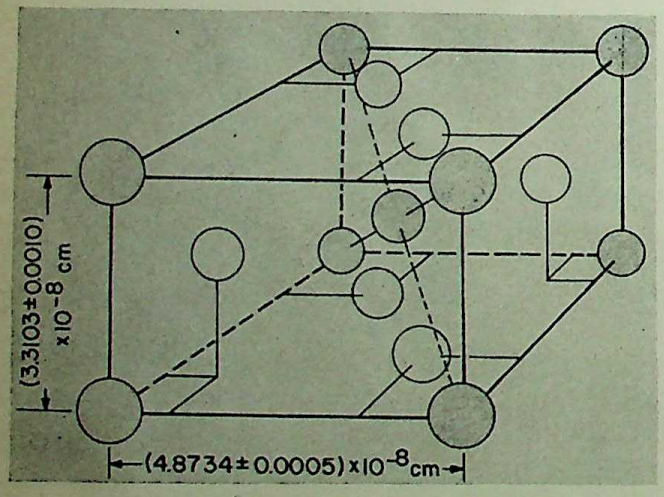


FIG. 1. Crystal structure of MnF_2. Solid circles are Mn^{++}, open circles are F^-.

From measurements of the magnetic susceptibiltiy by Bizette and Tsai,[2] and by de Haas, Schultz, and Koolhaas,[3] and from the heat capacity measurements of Stout and Adams,[4] manganese fluoride is known to be a typical antiferromagnetic material. It exhibits a maximum in the powder magnetic susceptibility and at about the same temperature a region of anomalously high heat capacity which is indicative of a cooperative phenomenon. The susceptibility data of Bizette and Tsai[5] indicate that FeF_2 is also antiferromagnetic, but, according to Bizette,[6] CoF_2 and NiF_2 are not.

The theory of antiferromagnetism proposed by Van Vleck[7] predicted that below the Curie temperature the magnetic susceptibility of an antiferromagnetic material should decrease with decreasing temperature in that direction along which the spins of two sublattices are aligned parallel and antiparallel, and should approach zero at the absolute zero of temperature. The susceptibility perpendicular to this direction would, according to the theory, remain constant below the Curie temperature. However, Van Vleck did not discuss why the direction of spin alignment should correspond to any particular direction with respect to the crystallographic axes. The exchange forces, which presumably cause the antiferromagnetic ordering, are themselves isotropic, so in a substance like MnF_2, where the magnetic ions are in an S state and consequently the anisotropy energy due to crystalline electrostatic fields would be

* Lindsay Light and Chemical Company Fellow, 1951.

[1] See (a) MnF_2, M. Griffel and J. W. Stout, J. Am. Chem. Soc. 72, 4351 (1950); (b) FeF_2 and CoF_2, A. Ferrari, Atti Acad. Lincei, [6] 3, 324 (1926); (c) NiF_2, Haendler, Patterson, and Bernard, J. Am. Chem. Soc. 74, 3167 (1952).

[2] H. Bizette and B. Tsai, Compt. rend. 209, 205 (1939).

[3] de Haas, Schultz, and Koolhaas, Physica 7, 57 (1940).

[4] J. W. Stout and H. E. Adams, J. Am. Chem. Soc. 64, 1535 (1942).

[5] H. Bizette and B. Tsai, Compt. rend. 212, 119 (1941).

[6] H. Bizette, Ann. phys. [12] 1, 295 (1946).

[7] J. H. Van Vleck, J. Chem. Phys. 9, 85 (1941).

CC-0. In Public Domain. Gurukul Kangri Collection, Haridwar

Digitized by Arya Samaj Foundation Chennai and eGangotri

very small, it was doubtful if any preferential direction of spin alignment would exist in a crystal.

In an investigation of this point Stout and Griffel[8] discovered by measurements on a single crystal of MnF_2 that at high temperatures the magnetic anisotropy is, as was expected, very small, but as the temperature is lowered below 70°K a rapid increase in anisotropy begins, reaching extraordinarily large values in the hydrogen temperature range. Figures 2 and 3 show the data on MnF_2. At high temperatures (Fig. 2) the magnetic susceptibility is greater parallel to the c axis; at 300°K the anisotropy is about 0.1 percent of the susceptibility. As the temperature is lowered the anisotropy rises at first as one would expect from the effect of an anisotropic crystalline field. At 120°K the curve reaches a maximum and then rapidly drops. The anisotropy passes through zero at about 77°K and at lower temperatures the greater susceptibility is perpendicular to the c axis. In Fig. 3, which shows the

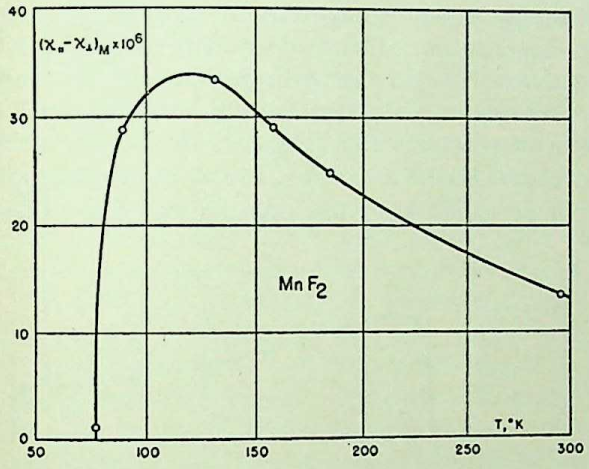


FIG. 2. Molal magnetic anisotropy of MnF_2. χ_{II} and $\chi_\perp$ are molal susceptibilities parallel and perpendicular to the c axis. Note that the ordinate scale is 1000 times that of Fig. 3.

anisotropy, $\chi_{II}-\chi_\perp$, below 100°K, the scale is one thousand times smaller than that of Fig. 2. By combining the results of the anisotropy measurements with the powder susceptibility data of de Haas, Schultz, and Koolhaas[3] one can calculate the susceptibilities parallel and perpendicular to the c axis. The curves for MnF_2 are shown in Fig. 4. Within the limits of error of the powder susceptibility data the susceptibility parallel to the c axis approaches zero at the absolute zero of temperature.

The observed magnetic behavior of MnF_2 at low temperatures is in qualitative agreement with the theory of Van Vleck,[7] provided one assumes that the alignment of the spins is parallel and antiparallel to the c axis of the crystal. This alignment of the spins has been confirmed by neutron diffraction measure-

[8] J. W. Stout and M. Griffel, (a) Phys. Rev. 76, 144 (1949); (b) J. Chem. Phys. 18, 1455 (1950).

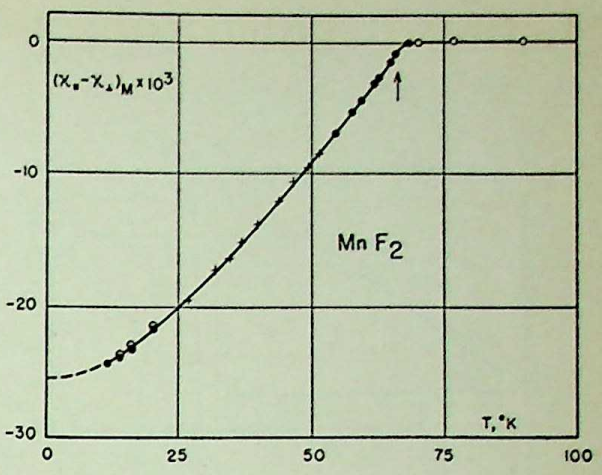


FIG. 3. Molal magnetic anisotropy of MnF_2. χ_{II} and $\chi_\perp$ are molal susceptibilities parallel and perpendicular to the c axis. The arrow indicates the temperature of the heat capacity maximum.

ments of Erickson and Shull[9] which, besides showing that the c axis is the direction along which alignment occurs, also demonstrate that the spins in a nearest-neighbor chain in the direction of the c axis are all aligned parallel to one another. Each chain is surrounded by four others with spin alignment antiparallel to it. The ordered magnetic structure consistent with the magnetic susceptibility and neutron diffraction data is shown in Fig. 5.

The small anisotropy observed in MnF_2 at high temperatures indicates that for each magnetic ion there is an anisotropy energy of a few tenths of a wave number favoring alignment of the spins along the c axis as compared to a perpendicular alignment. In the neighborhood of 100°K the long-range order, caused by the energetically much larger exchange forces, begins to appear in the crystal. As the temperature is lowered the extent of order continues to grow. One may think of the magnetic ions as clustered together in ordered

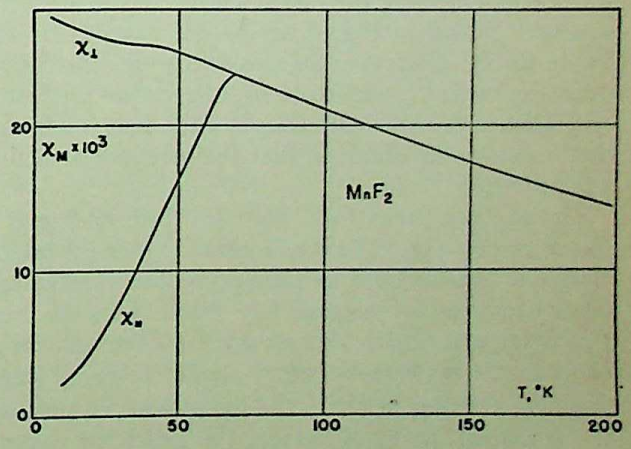


FIG. 4. Molal magnetic susceptibility of MnF_2 parallel and perpendicular to c axis of crystal.

[9] (a) R. A. Erickson and C. G. Shull, Phys. Rev. 83, 208 (1951); (b) R. A. Erickson, thesis, Agric. and Mech. College of Texas, June, 1952.

CC-0. In Public Domain. Gurukul Kangri Collection, Haridwar

Digitized by Arya Samaj Foundation Chennai and eGangotri

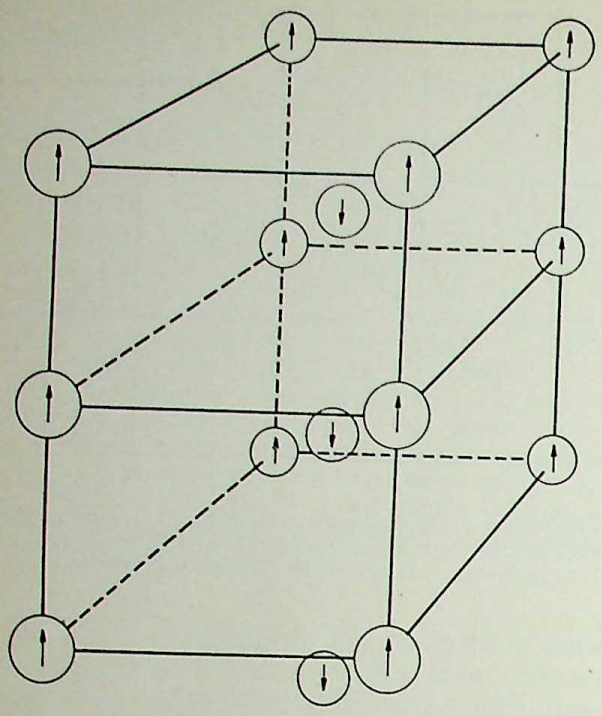


FIG. 5. Ordered magnetic structure of MnF_2, FeF_2, CoF_2. The arrows indicate the spin alignment parallel and antiparallel to the c axis. Only the positive ions are shown.

groups which grow in size as the temperature is lowered. The energy required to turn a group in the crystalline field is the small anisotropy energy per ion times the number of ions in a group, and if the number in a group increases rapidly this energy soon becomes large compared to kT. This explanation, suggested in qualitative form by Stout and Griffel,[8] has been quantitatively treated by Yosida[10] and by Keffer.[11] The latter author emphasizes the importance of the dipole forces which cause an anisotropy energy in addition to that of the crystalline field. Griffel and Stout[8b] had pointed out that the dipole forces would contribute to an anisotropy energy and, from their result that the spin alignment was along the c axis, suggested the magnetic structure shown in Fig. 5 as the one favored by the dipole forces. However, the possibility of other directional dependent forces made any theoretical prediction uncertain, and it was not until after the neutron diffraction results[9] were obtained that the magnetic structure was proved.

The magnetic ions Fe^{++} and Co^{++} are in D and F states, respectively. The interaction between the orbital motion of the electrons and the crystalline electrostatic fields produces in magnetically dilute salts of these ions a large magnetic anisotropy.[12] In the anhydrous fluorides the anisotropy energy should be much larger than was the case in MnF_2. As the number of electrons in the d shell increases beyond the half-filled position of manganous ion, one might also expect a decrease in the magnitude of the exchange energy. To investigate these effects we have measured the magnetic anisotropy of single crystals of FeF_2 and CoF_2. The detailed results of these measurements will be published elsewhere.

The observed magnetic anisotropy of FeF_2 is shown in Fig. 6. The points shown as filled circles were taken under isothermal conditions. Those indicated by crosses were obtained during a warming curve and because of possible temperature gradients are considerably less accurate. They serve, however, to show the general shape of the curve in the region between 20 and 60°K. Like MnF_2, the susceptibility at high temperatures is greater in the direction of the c axis, but the magnitude of the anisotropy at high temperatures is much greater, amounting at 300°K to 20 percent of the powder susceptibility. This is comparable to the anisotropy observed in dilute ferrous salts.[12] At high temperatures the anisotropy rises with decreasing temperature, but the curve bends over, reaching a maximum at about 95°K, and then drops rapidly. The anisotropy passes through zero at about 72°K and, as the temperature is lowered, rapidly drops to large negative values. In the hydrogen range the variation of anisotropy with temperature decreases at the lower temperatures and it appears that the curve will approach 0°K with zero slope. The magnetic susceptibility of powdered FeF_2 has been measured by Bizette

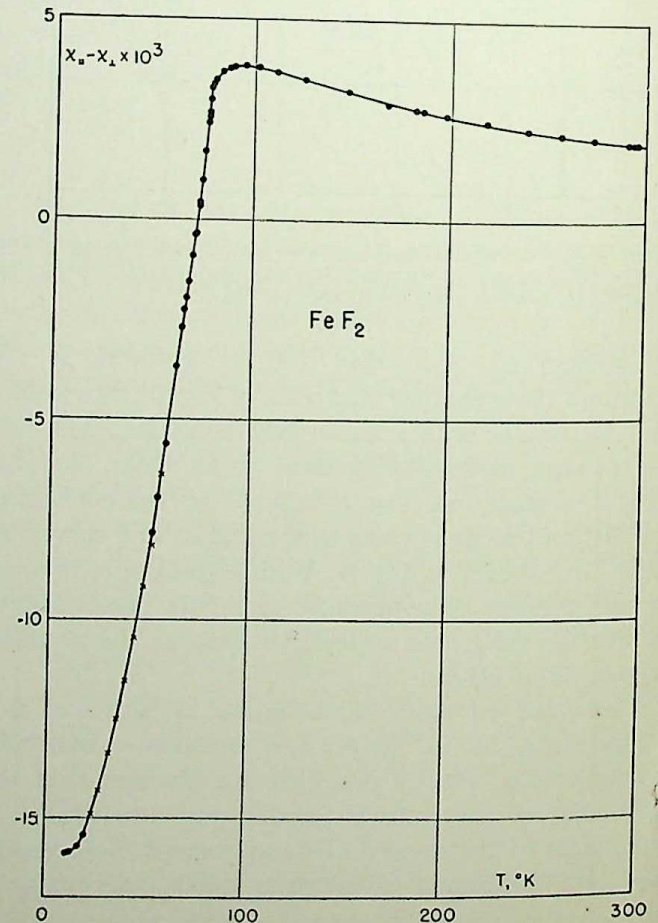


FIG. 6. Molal magnetic anisotropy of FeF_2. $\chi_\parallel$ and $\chi_\perp$ are molal susceptibilities parallel and perpendicular to the c axis.

[10] K. Yosida, Prog. Theoret. Phys. 6, 691 (1951).
[11] F. Keffer, Phys. Rev. 88, 608 (1952).
[12] Krishnan, Chakravorty, and Banerjee, Trans. Roy. Soc. 232, 99 (1932).

CC-0. In Public Domain. Gurukul Kangri Collection, Haridwar

Digitized by Arya Samaj Foundation Chennai and eGangotri

and Tsai.[5] By combining these data with out anisotropy values, the susceptibilities parallel and perpendicular to the c axis have been calculated. The curves are shown in Fig. 7. The powder susceptibility data do not extend below 63°K and the dotted portion of the curves is an extrapolation upon the assumption that the parallel susceptibiltiy, $\chi_{\parallel}$, approaches zero at 0°K. The powder susceptibility data do extend to a low enough temperature to show definitely the maximum in $\chi_{\parallel}$. Aside from the expected much larger anisotropy at high temperatures the curves for FeF_2 resemble those of MnF_2 and are in qualitative agreement with the behavior predicted by the theory of Van Vleck. The anisotropy data show that the alignment of the elementary magnets is in the direction of the c axis, in agreement with the neutron diffraction measurements of Erickson and Shull.[9] Figures 4 and 7 show the perpendicular susceptibility rising below the Curie temperature for MnF_2 and falling in the case of FeF_2. On the theory of Van Vleck[7] $\chi_{\perp}$ should be independent of temperature in this region. The variation in $\chi_{\perp}$ is much larger than the error in out anisotropy measurements, but because of possible errors in the powder susceptibilities, and the lack of data at hydrogen temperatures for FeF_2, the knowledge of the details of the variation of $\chi_{\perp}$ with temperature below the Curie points must await precise determination of the powder susceptibility, or preferably, measurements of the susceptibility of a single crystal along a known crystallographic direction.

The data for the magnetic anisotropy of CoF_2 are shown in Fig. 8. As was the case with MnF_2 and FeF_2, at the lowest temperatures the greater susceptibility of CoF_2 is that perpendicular to the c axis. The magnitude of the low temperature anisotropy in CoF_2 is unusually large, being twice that observed for MnF_2. On the Van Vleck theory[7] the Curie temperature, T_C, is related to the constant perpendicular susceptibility below the Curie temperature, $\chi_{\perp}$ (which is equal to the anisotropy at 0°K), by $T_C=\frac{1}{2}C/\chi_{\perp}$, C is the constant in the Curie-Weiss law, $\chi=C/(T+T_C)$, that describes the high temperature susceptibility. The observed Curie constants for colbalt salts[13] range from 2.4 to 3.4, so one might expect a Curie temperature for CoF_2 between 24 and 33°K. A similar calculation for MnF_2 and FeF_2 yields Curie temperatures of 88 and 120°K, respectively. These temperatures are roughly in agreement with those at which the rapid fall in anisotropy begins. However, in CoF_2 the anomalous behavior of the anisotropy extends to temperatures much higher than the Curie temperature calculated from the low temperature anisotropy data. By fitting Brillouin functions to his observed magnetic scattering intensity data, Erickson[9b] estimates the Curie temperatures as 75°K for MnF_2, 90°K for FeF_2, and 50°K for CoF_2.

The curve drawn in Fig. 8 between 20.4 and 53° is a smooth interpolation between these points. We have made measurements during warming between 20 and 60°K, and a preliminary calculation of the data indicates that at temperatures slightly above 20°K the anisotropy rises more steeply than the curve drawn and then decreases in slope until at a temperature of around 40°K it again rises steeply. Although these results may

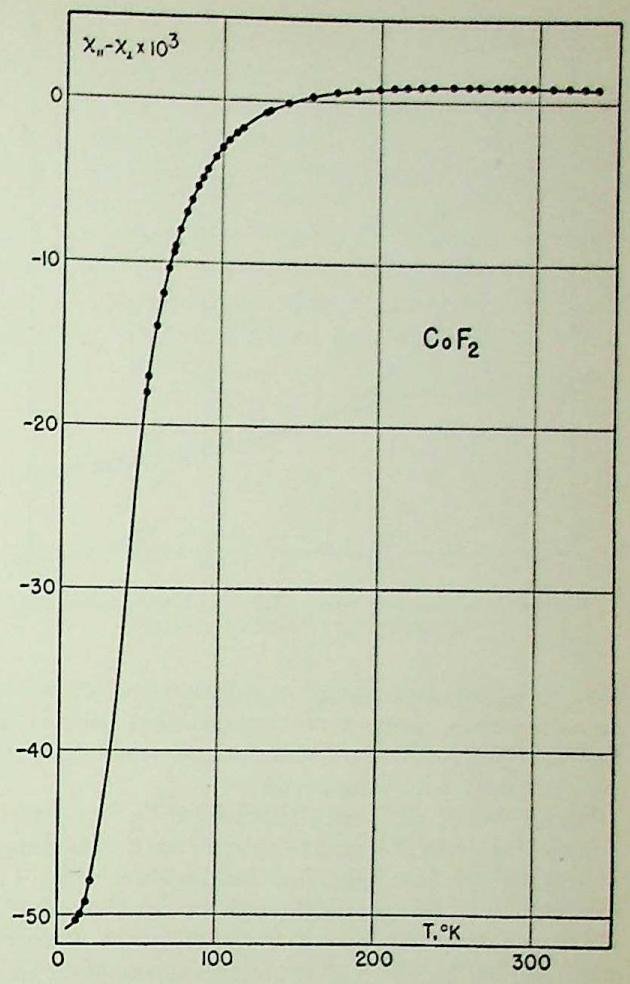


FIG. 8. Molal magnetic anisotropy of CoF_2. $\chi_{\parallel}$ and $\chi_{\perp}$ are molal susceptibilities parallel and perpendicular to the c axis.

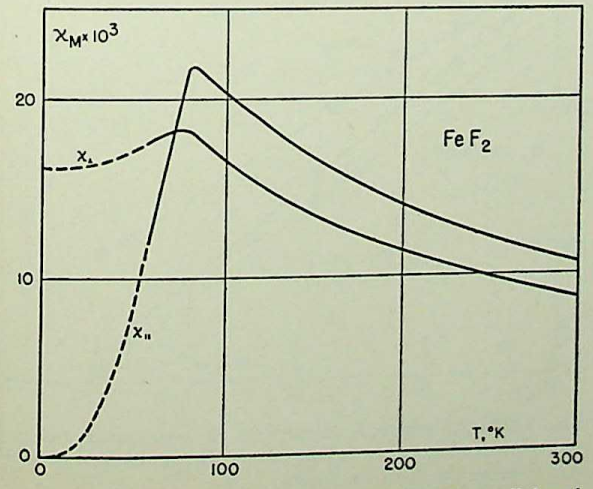


Fig. 7. Molal magnetic susceptibility of FeF_2 parallel and perpendicular to c axis of crystal.

[13] E. C. Stoner, *Magnetism and Matter* (Methuen and Company, London, 1934), p. 312.

CC-0. In Public Domain. Gurukul Kangri Collection, Haridwar

Digitized by Arya Samaj Foundation Chennai and eGangotri

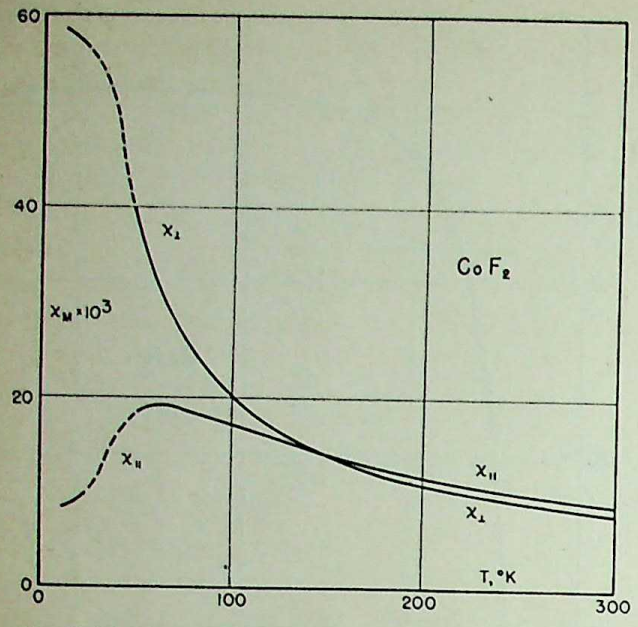


FIG. 9. Molal magnetic susceptibility of CoF_2 parallel and perpendicular to c axis of crystal.

be revised upon more complete calculation of the warming curve data, there is no question that between 20 and 60°K the absolute value of the anisotropy decreases monotonically with temperature.

Unlike MnF_2 and FeF_2 there is in CoF_2 no rapid change of slope in the anisotropy curve as the maximum is approached from the low temperature side. The anisotropy of CoF_2 passes through zero at about 146°K and rises slowly to a broad maximum in the neighborhood of 260°K. At higher temperatures there is a gradual fall in $\chi_\parallel - \chi_\perp$.

In CoF_2 we observed a small field dependence of anisotropy energy at the temperature of liquid hydrogen. The anisotropy increased by about 2 percent in going from 2000 to 10 000 gauss. No field dependence of anisotropy was observed for CoF_2 at higher temperatures, nor for MnF_2 and FeF_2 at any temperature.

Measurements of the powder susceptibility of CoF_2 have been made by de Haas and Schultz.[14] From these data and the anisotropy measurements we have calculated the susceptibilities parallel and perpendicular to the c axis. The curves are shown in Fig. 9. The data of de Haas and Schultz show a considerable decrease of the powder susceptibility with field at 14°K, whereas we found a slight increase in the anisotropy with field. In drawing the curves we have used the powder susceptibilities at high fields. The curve in Fig. 9 for $\chi_\parallel$ does not extrapolate to zero at 0°K; the value of the powder susceptibility would have to be decreased by 20 percent in order to obtain a curve extrapolating to zero. This rather surprising result should be verified by measurements of one of the principal susceptibilities using a single crystal specimen.

In the range from 11.5 to 20.4°K the temperature coefficient of the measured anisotropies decreases rapidly at the lower temperatures. This fact, together with the large value of the observed anisotropy, is evidence that the magnetic moments are aligned along the c axis of the crystal. Such an alignment has been found by Shull and Erickson[9] on the basis of neutron diffraction measurements. It appears clear from the neutron diffraction and magnetic anisotropy measurements that CoF_2 at low temperatures is antiferromagnetic, if by this term we mean an arrangement of magnetic moments ordered with respect to one another so that the net magnetic moment in the absence of a field is zero, and aligned along a certain direction in the crystal.

The spectacular drop in $\chi_\perp$ between 10 and 100°K and the gradual variation of the anisotropy curve before its maximum at 260°K is not consistent with a simple picture of antiferromagnetism based on exchange interactions between spins, together with an anisotropy energy. It is well known that over the range 1 to 300°K dilute cobalt salts do not obey Curie's law, and Schlapp and Penney[15] have pointed out that for Co^{++} ion the lowest orbital level in the presence of a cubic field will be triply degenerate. In addition, there is a spin degeneracy of four. These twelve lowest-lying states will be split by the spin-orbit coupling and by electrostatic fields of sufficiently low symmetry into six double degenerate levels. The separation in energy will be small enough so that, although at very low temperatures practically all of the magnetic ions are in the lowest level, at room temperature there will be an appreciable population in higher levels. If the exchange interactions, which can remove all spin degeneracy, are comparable in energy to the separation of the levels by spin-orbit interaction and anisotropic crystalline fields, then one would not expect any simple theory of antiferromagnetism to be applicable and it appears reasonable that the magnetic anomalies would be spread out over a larger temperature range than in a

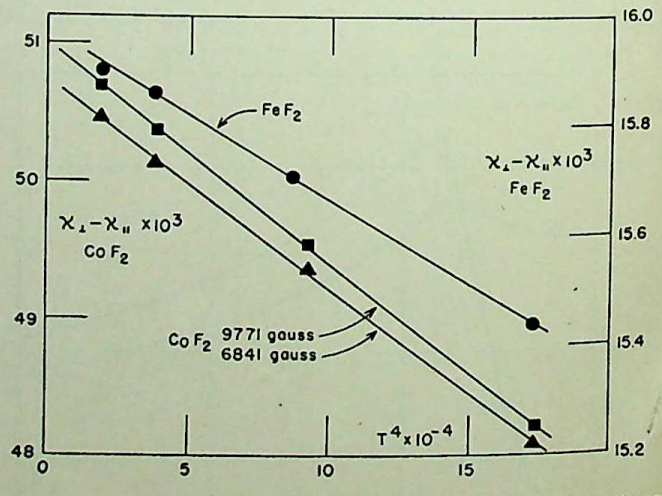


FIG. 10. Molal magnetic anisotropy at hydrogen temperatures *versus* fourth power of the temperature. The scale on the left is for CoF_2; that on the right for FeF_2.

[14] W. J. de Haas and B. H. Schultz, Physica 6, 481 (1939).

[15] R. Schlapp and W. G. Penney, Phys. Rev. 42, 666 (1932).

CC-0. In Public Domain. Gurukul Kangri Collection, Haridwar

Digitized by Arya Samaj Foundation Chennai and eGangotri

salt like MnF_2 where only the exchange interactions plus a small anisotropy energy need be considered.

By a treatment based on the spin-wave theory, Kubo[16] has shown theoretically that the magnetic anisotropy of a set of spins antiferromagnetically coupled together by exchange forces should at the low temperatures vary as T^2. The observed data[8] on MnF_2, at temperatures obtained with liquid and solid hydrogen, agree well with this relation. From these data Kubo calculates an approximate Curie temperature of 62°K which may be compared with the observed temperature, 66.5°K, of the heat capacity maximum. The observed anisotropies at the lowest temperatures of FeF_2 and CoF_2 do not, however, vary quadratically with temperature, but rather fit closely a function linear in the fourth power of the temperature. In Fig. 10 are shown the anisotropy data for FeF_2 and CoF_2 in the hydrogen range plotted against T^4. Within the accuracy of the measurements the points fall on straight lines. Because of the field dependence found for CoF_2, curves are given for two different magnetic field strengths.

[16] R. Kubo, Phys. Rev. 88, 568 (1952).

CC-0. In Public Domain. Gurukul Kangri Collection, Haridwar

Digitized by Arya Samaj Foundation Chennai and eGangotri

REVIEWS OF MODERN PHYSICS VOLUME 25, NUMBER 1 JANUARY, 1953

The Spin-Wave Theory as a Variational Method and Its Application to Antiferromagnetism

RYOGO KUBO*

Institute for the Study of Metals, The University of Chicago, Chicago, Illinois

The spin-wave theory in a modified form is applied to antiferromagnetism. The interaction between different modes of spin-waves, which is due to the higher order terms omitted in the customary spin-wave treatment, is taken into account in a self-consistent manner. It is shown that the interaction terms cause a change of the frequency spectrum of spin-waves which is equivalent to the existence of an anisotropic field. The upper limits of the ground levels are calculated. The variational method can also be applied to the discussions of the stable configurations of magnetization vectors in anisotropic and external fields, and it is consistent with the molecular field theory.

INTRODUCTION

THE spin-wave theory first invented by Bloch[1] as an approximate method of treating ferromagnets at low temperatures has recently been applied by several authors to antiferromagnets.[2–8] The main difference between the two cases lies in the fact that the theory remains approximate for antiferromagnets even at absolute zero, where it becomes rigorous for ferromagnets. The reason is simple; it is because the spin-wave theory applied to antiferromagnets necessarily starts from the assumption that there exists an ordered pattern of the sublattices at low temperatures, whereas the ground state of an antiferromagnet should be a singlet which is described by a very complicated combination of the patterns of the spin ordering.

The inverse pattern of an ordered pattern, that is, the spin configuration in which the directions of spins are just reversed, is also to be included in the linear combination. The interaction between the opposite orderings, however, will be so indirect that it can be neglected, and a fairly good approximation is obtained by taking the configurations near one of the ordered states.[2] The transition from such a state to its opposite pattern should be so slow that neutron diffraction experiments[9] can actually prove the ordering. Such a spin-wave treatment of antiferromagnets is a reasonable approximation to the ground states as has been discussed in detail by P. W. Anderson,[2] and it can be used to derive the thermodynamic properties[3] as well as the microwave absorption of antiferromagnets at low temperatures.[5–7]

It should be remembered here that the spin-wave theory customarily omits the higher order terms in the original Hamiltonian, which in the spin-wave language give the interactions between the different modes of the spin-waves and cause the broadening of resonance absorptions. Very little is known, however, concerning how these interactions effect the energy levels and the thermodynamic behavior of ferromagnets or antiferromagnets.[3] Obviously the contribution from the interaction terms is zero for ferromagnets at absolute zero, but it will be considerable at higher temperatures. It will be even greater for antiferromagnets, for which it is not zero at absolute zero. This is one of the reasons that one might feel somewhat skeptical about the spin-wave theory of antiferromagnets.

It should be also noticed that the neglect of interaction terms gives rise to a certain difficulty in the spin-wave theory. This is revealed, for example, in the fact that the fluctuation of the magnetization (of the sublattice in the case of antiferromagnets) diverges abnormally for both ferromagnets and antiferromagnets, or, more exactly, it is of the order of $N^{4/D}$, N being the total number of magnetic atoms or ions, and D the dimensionality of the lattice, if there exists no anisotropic field acting on the spins.[3] This abnormal fluctuation might, at first sight, be correlated with the free rotation of the resultant spin-moment in the absence of the anisotropic field. However, such an interpretation is inconsistent with the current picture that describes the spins primarily aligned by strong exchange forces, the resultant moment moving around in a relatively weak anisotropic field and also in an external field, if any. This picture requires the resultant moment to be a well-defined quantity with a normal fluctuation of the order of N. The fact that the spin-wave theory does not give such a picture may be regarded as a difficulty of the theory. Corresponding to this we have to suffer from many divergences if we apply simple perturbation methods to the interaction terms starting from the usual spin-wave approximation.

The purpose of the present paper is, in the first place, to examine the importance of these interactions terms, and secondly, to remove the difficulty mentioned above,

* On leave from the Department of Physics, University of Tokyo, Tokyo, Japan.

[1] F. Bloch, Z. Physik **61**, 206 (1930).
[2] P. W. Anderson, Phys. Rev. **86**, 694 (1952).
[3] R. Kubo, Phys. Rev. **86**, 929 (1952).
[4] I. Shoji, Busseiron-Kenkyu (in Japanese) **39**, 55 (1951).
[5] T. Nakamura, Prog. Theoret. Phys. **7**, 539 (1952).
[6] Keffer, Kaplan, and Yafet, Am. J. Phys. (to be published).
[7] J. M. Ziman, Proc. Phys. Soc. (London) **A65**, 540, 548 (1952).
[8] J. R. Tessman, Phys. Rev. **88**, 1132 (1952).
[9] C. G. Shull and J. S. Smart, Phys. Rev. **76**, 1256 (1949); Shull, Wollan, and Strausser, Phys. Rev. **83**, 333 (1951).

CC-0. In Public Domain. Gurukul Kangri Collection, Haridwar

Digitized by Arya Samaj Foundation Chennai and eGangotri

applying the spin-wave theory in a different form from the usual one, namely as a variational method. To do this, we choose a system of spin-waves with a certain spectrum of proper frequencies representing the best approximation of the spin-system. These spin-waves are different from those obtained in the usual spin-wave theory. They are determined in a self-consistent way, taking the interaction terms into account. Thus, for instance, the ground levels obtained are the best upper limit of the true values as far as we confine ourselves in the picture of spin-waves. This variational method will give a finite frequency for the spin-wave of infinite wavelength in the absence of an anisotropic field. This follows because, in antiferromagnets, where the spin-waves collide with each other even at absolute zero, the wave trains must be of finite length and accordingly the frequency of long waves cannot be exactly zero. The method proposed here can be applied to ferromagnets as well, but here we shall confine ourselves to antiferromagnets.

1. VARIATIONAL METHOD IN QUANTUM STATISTICS

First we describe in a general way the variational method employed. Let the Hamiltonian of the system under consideration be H. We define the variational functions for this Hamiltonian by the eigenfunctions of a suitable operator H_{tr}, called the trial Hamiltonian, which is assumed to be of the form

$$H_{tr}=\sum_r c_r X_r, \tag{1.1}$$

where X_r's are some known operators, and the sum should include the adjoint operators such as $c_r^* X_r^*$ if X_r is not Hermitian. The trial Hamiltonian should be selected of solvable form, and in most cases must be separable into components having only a few degrees of freedom, so that the eigenvalue problem of H_{tr} will be solved explicitly in the form

$$H_{tr}\Psi_n=\epsilon_n\Psi_n, \tag{1.2}$$

where Ψ_n and ϵ_n are naturally functions of the constants $\{c_r\}$. If such a trial Hamiltonian is properly chosen, the smallest diagonal element of H in the representation Γ diagonalizing H_{tr}, will be an approximation of the lowest level of H, the best approximation of which will be given by minimizing it with respect to the variational parameters $\{c_r\}$: As to the excited levels, there is a theorem proved by Peierls[10] which states that the approximate partition function

$$Z=\sum_n \exp(-H_{nn}/kT),$$

constructed by the diagonal elements of H in any representation, can never be larger than the true partition function of the system $Z_0=\text{trace}\exp(-H/kT)$. Therefore, at finite temperatures, the approximate free energy

$$F=-kT\log Z \tag{1.3}$$

should be minimized with respect to $\{c_r\}$. The calculated minimum of the free energy is the best approximation as far as we confine ourselves in the frame of the trial system set up by Eq. (1.1). The trial Hamiltonian itself might then be considered as a certain representation of the system at the temperature T.

The variational procedure of this program is simplified if the diagonal elements H_{nn} can be given in the form

$$H_{nn}=\bar{H}(\cdots, \bar{X}_r, \bar{X}_r^*, \cdots), \tag{1.4}$$

where $\bar{X}_r$ means the diagonal element of the operator X_r in the representation Γ. $\bar{X}_r$ is dependent on the quantum number n and on the parameters $\{c_r\}$. The diagonal elements of H_{tr}, or the eigenvalues, are expressed as

$$\epsilon_n=H_{tr}(n)=\sum_r c_r\bar{X}_r(n). \tag{1.5}$$

Then it can easily be proved that the extremum condition of F, Eq. (1.3), is reduced to a set of equations

$$\begin{aligned}&\frac{\partial\bar{H}}{\partial\bar{X}_r}=c_r \qquad r=1, 2, \cdots,\\ &\bar{X}_r=\frac{\partial F_{tr}}{\partial c_r} \qquad r=1, 2,\end{aligned} \tag{1.6}$$

where $\bar{H}$ is considered as a function of $\{\bar{X}_r\}$ in the form of Eq. (1.4) and F_{tr} is the "trial free energy" of the system represented by H_{tr}, that is,

$$F_{tr}=-kT\log\sum_n \exp(-\epsilon_n/kT). \tag{1.7}$$

The solution of Eq. (1.6) gives the most favorable values of the variational parameters and the averages of the operators X_r's at the temperature T. Inserting these values, the function $\bar{H}$ of Eq. (1.4) gives the average of the energy, and the equation

$$F=F_{tr}-\bar{H}_{tr}+\bar{H} \tag{1.8}$$

gives the free energy, which is an upper limit of the rigorous one. At absolute zero, the equations are reduced to

$$\begin{aligned}&\frac{\partial\bar{H}}{\partial\bar{X}_r}=c_r \qquad r=1, 2, \cdots,\\ &\bar{X}_r=\frac{\partial\bar{H}_{tr}{}^0}{\partial c_r} \qquad r=1, 2, \cdots,\end{aligned} \tag{1.9}$$

where $\bar{H}_{tr}{}^0$ means the lowest eigenvalue of H_{tr}. Of course, Eq. (1.9) is easily proved directly.

Applied to a many-electron system, Eq. (1.9) is nothing but the Hartree-Fock equation, provided that the set of our trial Hamiltonians covers the whole set of Hamiltonians corresponding to the one-body approxi-

[10] R. Peierls, Phys. Rev. 54, 918 (1938).

CC-0. In Public Domain. Gurukul Kangri Collection, Haridwar

Digitized by Arya Samaj Foundation Chennai and eGangotri

mation. Then Eq. (1.6) is the extension of the Hartree-Fock equation at finite temperatures. We shall not go further in this, but we see that the variational method used in the following just corresponds to the Hartree-Fock method in the sense that the coupled oscillators are represented in a self-consistent manner by a set of independent oscillators.

2. SPIN OPERATORS

The spin-wave theory is most conveniently formulated by using the "*spin deviation*" operators introduced by Holstein and Primakoff.[11] The spin deviation is defined by

$$n=S-S_z, \tag{2.1}$$

S being the magnitude of the spin and S_z its component along a given axis of quantization. In terms of the annihilation and creation operators a and a^*, which will be called the *spin-deviation operators* in the following, the other components are written as

$$\begin{aligned} S_x+iS_y&=(2S)^{\frac{1}{2}}\left(1-\frac{a^*a}{2S}\right)^{\frac{1}{2}}a, \\ S_x-iS_y&=(2S)^{\frac{1}{2}}a^*\left(1-\frac{a^*a}{2S}\right)^{\frac{1}{2}}, \end{aligned} \tag{2.2}$$

where a and a^* satisfy the commutation rule

$$aa^*-a^*a=1 \tag{2.3}$$

and

$$a^*a=n. \tag{2.4}$$

The merit of this formulation lies primarily in this commutation rule, which is much simpler than those for the spin operators. The spin-wave method consists, essentially, of writing the Hamiltonian in terms of the Fourier components of the spin-deviation operators defined over the whole crystal, and diagonalizing the expression by retaining only quadratic terms in the Fourier components. Naturally the equivalent approximation is obtained in a semiclassical way,[12] which has been adopted for antiferromagnets by Anderson.[2] But we prefer the Holstein-Primakoff expression, since we want to give rigorous expressions for the higher terms.

However, there is an inherent difficulty in this expression. Due to the commutation rule of Eq. (2.3), the spin-deviation operators have to be matrices of infinite dimensions in the representation diagonalizing n, Eq. (2.4). By definitions, (2.1) and (2.2), the parts where $n\geqq 2S+1$ (or $|S_z|>S$) is separated from the part $|S_z|\leqq S$. This separability no longer holds in the spin-wave formulation, so that the unwanted contributions will necessarily come in from the part $n\geqq 2S+1$.

[11] T. Holstein and H. Primakoff, Phys. Rev. 58, 1908 (1940).
[12] G. Heller and H. A. Kramers, Proc. Roy. Acad. Sci. Amsterdam, 37, 378 (1934); L. Hulthén, *ibid.* 39, 190 (1936); M. J. Klein and R. S. Smith, Phys. Rev. 80, 1111 (1951).

Therefore, if we wish to go a step further than the simple spin-wave theory, we have to supplement the definitions (2.1) and (2.2), which are primarily valid for $0\leqq n\leqq 2S$, by some definitions for $n\geqq 2S+1$.

Mathematically, the most convenient definition will be that which is periodic. Let us introduce a new operator $[n]$ refined by

$$\begin{aligned} &(n'|[n]|n'')=n'\delta_{n'n''}, \quad \text{for } 0\leqq n'\leqq 2S, \\ &(n'|[n]|n')=(n''|[n]|n''), \\ &\qquad\qquad \text{if } n'=n'', \text{ mod } (2S+1). \end{aligned} \tag{2.5}$$

$[n]$ is commutable with n, and so is a periodic function of n. With this we define the spin operators by

$$\begin{aligned} S_z&=S-[n], \\ S_x+iS_y&=(2S)^{\frac{1}{2}}fa, \\ S_x-iS_y&=(2S)^{\frac{1}{2}}a^*f, \end{aligned} \tag{2.6}$$

where f is a function of n defined by

$$f=\left(1-\frac{[n]}{2S}\right)^{\frac{1}{2}}([n]+1)^{\frac{1}{2}}(n+1)^{-\frac{1}{2}}. \tag{2.7}$$

In the representation where all the n's are diagonal, the Hamiltonian of a spin-system will correspond to a direct product of matrices, each of which is defined for each of the spins and, because of the definition (2.6), each composed of an infinite repetition of a $(2S+1)$-dimensional matrix. This Hamiltonian, which has an infinite dimension with respect to the spin-deviations, is to be distinguished from the usual Hamiltonian of the spin-system with $(2S+1)$-dimensions for each of the spins. Yet the new Hamiltonian has the same spectrum of the eigenvalues as the usual one. In particular, the upper limit of the lowest eigenvalue is the same for both. Thus the new Hamiltonian treated by the variational method gives the answer for the spin-system. The variational method will also be applied at finite temperatures using Eq. (2.6), although in this case it is less rigorous than at absolute zero because the virtual multiplicity introduced by the periodic definition of (2.6) might result in some errors.

An alternative of the definition (2.6) would be to introduce projection operators such as

$$\begin{aligned} (n'|\epsilon|n')&=1, \quad 0\leqq n'\leqq 2S \\ &=0, \quad 2S<n' \end{aligned}$$

and to multiply the density matrix of the spin-system by the product of such operators defined for all the spins. But this introduces mathematical difficulties, because then one has either to treat the problem approximately as for the spherical model of ferromagnets, or to abandon the simple commutation rule of Eq. (2.5) introducing the operators $\epsilon a\epsilon$ and $\epsilon a^*\epsilon$ instead of a and a^*. The latter method may be practical only for the case of $S=\frac{1}{2}$.[5]

CC-0. In Public Domain. Gurukul Kangri Collection, Haridwar

Digitized by Arya Samaj Foundation Chennai and eGangotri

3. DIAGONAL ELEMENTS OF THE HAMILTONIAN OF ANTIFERROMAGNETS IN SOME TRIAL REPRESENTATIONS

For simplicity we assume the Hamiltonian of an antiferromagnet to be

$$H_{ex}=J\sum_{\langle jk\rangle}\mathbf{S}_j\cdot\mathbf{S}_k \tag{3.1}$$

in the absence of anisotropy and of external fields. Assuming two opposite directions as the quantization axes of the spins on each of the sublattices, into which the lattice is assumed to be divided in the ordered state, we introduce the expressions for the spin operators by

$$\begin{aligned} S_{jz}&=S-[n]_j,\\ S_{jx}+iS_{jy}&=(2S)^{\frac{1}{2}}f_j a_j,\\ S_{jx}-iS_{jy}&=(2S)^{\frac{1}{2}}a_j^* f_j, \end{aligned} \tag{3.2}$$

and

$$\begin{aligned} S_{kz}&=-S+[n]_k,\\ S_{kx}+iS_{ky}&=(2S)^{\frac{1}{2}}b_k^* f_k,\\ S_{kx}-iS_{ky}&=(2S)^{\frac{1}{2}}f_k b_k, \end{aligned} \tag{3.3}$$

with $[n]$ and f defined by (2.5) and (2.7). Inserting Eqs. (3.2) and (3.3) in (3.1) one obtains

$$\begin{aligned} H_{ex}=&-\tfrac{1}{2}NJzS^2\\ &+zJS\Big(\sum_j[n]_j+\sum_k[n]_k\Big)-J\sum_{jk}[n]_j[n]_k\\ &+JS\sum_{jk}\{f_j a_j f_k b_k+a_j^* f_j b_k^* f_k\} \end{aligned} \tag{3.4}$$

which is, strictly speaking, different from (3.1) in that the dimensions of (3.4) is ∞^N, whereas that of (3.1) is $(2S+1)^N$.

Now let us introduce the Fourier components of the spin-deviation operators

$$\begin{aligned} a_\lambda&=(2/N)^{\frac{1}{2}}\textstyle\sum e^{ij\lambda}a_j\\ a_\lambda^*&=(2/N)^{\frac{1}{2}}\textstyle\sum e^{-ij\lambda}a_j^*\\ b_\lambda&=(2/N)^{\frac{1}{2}}\textstyle\sum e^{-ik\lambda}b_k\\ b_\lambda^*&=(2/N)^{\frac{1}{2}}\textstyle\sum e^{ik\lambda}b_k^*. \end{aligned} \tag{3.5}$$

Substituting these expressions into Eq. (3.4) we have a very complicated operator, which in itself may be beyond mathematical means. But we can give exact expressions for its diagonal elements in a certain family of representations.

The spin-wave approximation is obtained from Eq. (3.4) if we retain there only the quadratic terms of spin-deviation operators. This is given by

$$\begin{aligned} H_{\text{spin wave}}=&-\tfrac{1}{2}NJzS^2\\ &+zJS\sum_\lambda[a_\lambda^*a_\lambda+b_\lambda^*b_\lambda+\gamma_\lambda(a_\lambda b_\lambda+a_\lambda^*b_\lambda^*)], \end{aligned} \tag{3.6}$$

where

$$\gamma_\lambda=\sum_\rho e^{i\rho\lambda}/z$$

with ρ denoting the vectors to the nearest neighbors from a lattice point. The higher order terms of the spin-deviation operators omitted in Eq. (3.6) represent the interactions of the spin-wave modes. Now we define the trial Hamiltonians of the spin-waves by

$$H_{tr}=\sum_\lambda[c_{1\lambda}a_\lambda^*a_\lambda+c_{2\lambda}b_\lambda^*b_\lambda+c_{3\lambda}(a_\lambda b_\lambda+a_\lambda^*b_\lambda^*)], \tag{3.7}$$

which is a generalized form of Eq. (3.6). The operator (3.7) can easily be diagonalized to

$$\begin{aligned} H_{tr}=\sum_\lambda[&(n_{1\lambda}+\tfrac{1}{2})(\omega_\lambda^0+\Delta\omega_\lambda)\\ &+(n_{2\lambda}+\tfrac{1}{2})(\omega_\lambda^0-\Delta\omega_\lambda)-\tfrac{1}{2}(c_{1\lambda}+c_{2\lambda})], \end{aligned} \tag{3.8}$$

where

$$\omega_\lambda^0=[\{\tfrac{1}{2}(c_{1\lambda}+c_{2\lambda})\}^2-c_{3\lambda}^2]^{\frac{1}{2}},\quad \Delta\omega_\lambda=\tfrac{1}{2}(c_{1\lambda}-c_{2\lambda}).$$

The two modes with the same wave number λ correspond to the precessional motions of spins in opposite sense. These classical pictures have been discussed by Keffer *et al.*[6] More general forms of the trial Hamiltonian will be any quadratic form of spin-deviation operators, but for simplicity we shall not go into such generalizations. Equation (3.7) means that we confine ourselves to the representations where

$$\begin{aligned} &\text{diag } a_\lambda=\text{diag } a_\lambda^*=\text{diag } b_\lambda=\text{diag } b_\lambda^*=0,\\ &\text{diag } a_\lambda a_{\lambda'}=\text{diag } a_\lambda^*a_{\lambda'}=\text{diag } a_\lambda^*a_{\lambda'}^*\\ &\quad=\text{diag } a_\lambda b_{\lambda'}=\cdots=\text{diag } b_\lambda^*b_{\lambda'}^*=0 \text{ for } \lambda\neq\lambda'. \end{aligned} \tag{3.9}$$

These conditions allow us to derive exact expressions for the diagonal elements of H_{ex}, Eq. (3.4), provided that we make an additive condition that

$$\begin{aligned} &\text{diag } a_\lambda^*a_\lambda=0(1),\quad \text{diag } b_\lambda^*b_\lambda=0(1),\\ &\text{diag } a_\lambda b_\lambda=0(1),\quad \text{diag } a_\lambda^*b_\lambda^*=0(1). \end{aligned} \tag{3.10}$$

This means that we exclude those states where some modes of spin-waves are highly excited. One might suppose that such excitation may happen for the infinitely long waves, but we have to exclude such configurations because they correspond to the rotation of all the spins in phase.[3]

With the above conditions we can show the exact expression of the diagonal element of H_{ex} is given by

$$\begin{aligned} \text{diag } H_{ex}=&H_{ex}(A,B,C_\rho,C_\rho^*)\\ =&-\frac{N}{2}zJS^2\Big[1-\frac{1}{S}AG(A)-\frac{1}{S}BG(B)\\ &+\frac{1}{z}\sum_\rho F_{0\rho}(A,B,C_\rho,C_\rho^*)\\ &+\frac{1}{z}\sum_\rho F_{1\rho}(A,B,C_\rho,C_\rho^*)\Big], \end{aligned} \tag{3.11}$$

CC-0. In Public Domain. Gurukul Kangri Collection, Haridwar

Digitized by Arya Samaj Foundation Chennai and eGangotri

where

$$A=\frac{2}{N}\sum_{\lambda}\operatorname{diag} a_\lambda^* a_\lambda,$$

$$B=\frac{2}{N}\sum_{\lambda}\operatorname{diag} b_\lambda^* b_\lambda,$$

$$C_\rho=\frac{2}{N}\sum_{\lambda} e^{i\rho\lambda}\operatorname{diag} a_\lambda b_\lambda, \tag{3.12}$$

$$C_\rho^*=\frac{2}{N}\sum_{\lambda} e^{-i\rho\lambda}\operatorname{diag} a_\lambda^* b_\lambda^*,$$

and

$$G(A)=1-(2S+1)A^{2s}\{(1+A)^{2s+1}-A^{2s+1}\}^{-1}, \tag{3.13}$$

$$F_{0\rho}=\sum_{l=0}^{\infty}\sum_{m=0}^{\infty}\sum_{n=0}^{\infty}\binom{l+m}{l}\binom{l+n}{l}[l+m][l+n]$$
$$\times(A+AB-C_\rho C_\rho^*)^m(B+BA-C_\rho C_\rho^*)^n(C_\rho C_\rho^*)^l$$
$$\times[(1+A)(1+B)-C_\rho C_\rho^*]^{-1-2l-m-n}, \tag{3.14}$$

$$F_{1\rho}=C_\rho\sum_{l=0}^{\infty}\sum_{m=0}^{\infty}\sum_{n=0}^{\infty}(l+1)\binom{l+m+1}{l+1}\binom{l+n+1}{l+1}$$
$$\times f(l+m)f(l+n)(A+AB-C_\rho C_\rho^*)^m$$
$$\times(B+AB-C_\rho C_\rho^*)^n(C_\rho C_\rho^*)^l$$
$$\times[(1+A)(1+B)-C_\rho C_\rho^*]^{-2-2l-m-n}. \tag{3.15}$$

(See Appendix.) Since the diagonal elements of H_{ex} are expressed by Eq. (3.11) as was assumed in Eq. (1.4), we can apply the variational formulas given in Sec. 1.

4. GROUND LEVELS OF ANTIFERROMAGNETS

Now we shall go to the discussion of ground levels. In the absence of any anisotropy and magnetic field, we can assume in Eq. (3.8) that $c_{1\lambda}=c_{2\lambda}$ by symmetry. Then we have $A=B$ in Eq. (1.2) and Eqs. (1.9) are reduced to

$$\alpha=\frac{\partial\bar{H}_{ex}}{\partial C}\Big/\frac{\partial\bar{H}_{ex}}{\partial A},$$

$$A=B=-\tfrac{1}{2}+\frac{1}{N}\sum_{\lambda}(1-\alpha^2\gamma_\lambda^2)^{-\frac{1}{2}}, \tag{4.1}$$

$$C=C^*=-\frac{1}{N}\sum_{\lambda}\alpha\gamma_\lambda^2(1-\alpha^2\gamma_\lambda^2)^{-\frac{1}{2}},$$

where we assume that C_ρ is independent of ρ, which is true for cubic and also tetragonal systems. A and C are functions of α, which is the only parameter now remaining in our variational problem, although we started from a general assumption, Eq. (3.8) involving $(3/2)N$ parameters. Thus Eq. (4.1) gives the most favorable value of α. The functions A and C can be calculated from the expressions[2,3,13]

$$A_1(\sin\psi)=\frac{1}{\pi}K(\sin\psi)-\tfrac{1}{2},$$

$$C_1(\sin\psi)=-\frac{1}{\pi}\sin\psi D(\sin\psi),$$

$$A_2(\sin\psi)=\frac{2}{\pi^2}K^2\left(\sin\frac{\psi}{2}\right)-\tfrac{1}{2},$$

$$C_2(\sin\psi)=-\operatorname{cosec}\psi A_2(\sin\psi)$$
$$-\int_0^{\psi}A_2(\sin\theta)\sec\theta\cot^2\theta d\theta, \tag{4.2}$$

$$A_3(\sin\psi)=\frac{2}{\pi}\int_0^{\pi/2}A_2(\sin\psi\sin\theta)d\theta,$$

$$C_3(\sin\psi)=-\operatorname{cosec}\psi A_3(\sin\psi)$$
$$-\frac{2}{\pi}\int_0^{\pi/2}A_2(\sin\psi\sin\theta)\cot^2\theta d\theta,$$

where K and D are the complete elliptic integrals, or from the power series like

$$A_3(\sin\psi)=\tfrac{1}{2}\sum_{n=1}^{\infty}\left[2^{-2n}\binom{2n}{n}\right]^4\sin^{2n}\psi,$$

$$C_3(\sin\psi)=-\tfrac{1}{2}\sum_{n=1}^{\infty}(2n-1)^{-1}\left[2^{-2n}\binom{2n}{n}\right]^4\sin^{2n}\psi.$$

In these equations the suffices refer to the dimensionality of the lattice and the three-dimensional lattice is assumed here to be the body-centered type (CsCl type arrangement). Some examples of the numerical values of A and C are given in Table I.

If A and C are small enough, an approximate solution of Eq. (4.1) is given by

$$\alpha\simeq 1+[S^{-1}+4(1-1/2S)^{\frac{1}{2}}-4](A(1)-C(1))<1,$$

which can be used for three-dimensional cases. For example, if $S=1$, the most favorable value of α is around 0.975. In this case, the interaction between the spin-waves raises the frequency of long waves to a few percent of the frequency of the shortest waves. In effect, this is equivalent to a certain anisotropic field, which, if present, helps the ordering and produces a finite frequency for long waves. Therefore, if we start from the wave functions obtained by our variational method, all the divergent difficulties are removed and the fluctuations will always be normal.

Some numerical results of the preliminary calculations are shown in Table II. For convenience, we list

[13] G. N. Watson, Quart. J. Math. 9–10, 269 (1938); Quart. J. Pure and Appl. Math. 39, 27 (1908).

CC-0. In Public Domain. Gurukul Kangri Collection, Haridwar

Digitized by Arya Samaj Foundation Chennai and eGangotri

the values of c defined by the equation

$$E_{\text{ground}}=-\frac{N}{2}zJS^2(1+cS^{-1}). \tag{4.3}$$

Anderson[14] has proved by a variational argument that c lies in the limits

$$0<c<z^{-1}. \tag{4.4}$$

Our calculation replaces the lower limits of c in (4.4) by more accurate values. The spin-wave theory,[2,3] neglecting the higher terms, gives the approximate values of c:

$$c_\infty=-2[A(1)+C(1)], \tag{4.5}$$

which should be the limit of our values for $S=\infty$.

For one-dimensional cases, Eq. (4.5) gives surprizingly good agreement with the rigorous value $c=0.375$ calculated for $S=\frac{1}{2}$.[15] This agreement is more or less accidental, because the complete Hamiltonian evaluated by the wave function in the simple spin-wave approximation diverges in one dimensions. The most favorable values of α are actually smaller than 1. It is, however, remarkable that our c's are rather close to c_∞ for $S\geqq 1$.

In three dimensions, A and C are small even for $\alpha=1$, and our results are very close to the spin-wave approximation. This is because of a tendency for the higher terms to cancel. For example, the third term on the right-hand side of Eq. (3.4) contributes to c by 0.011 for $S=1$, but at the same time the higher expansion terms in the fourth term nearly compensate this increase.

One point which seems unfavorable for the variational method is that the theory fails to show the ground states of one-dimensional chains to be disordered. For example, the minimum of the energy plotted against $\alpha=\sin\psi$ occurs around $\psi\sim 65°$ for $S=1$, which gives $A\sim 0.23$. Thus the ground state of our variational method has a finite magnetization of the sublattice, which is generally given by the formula

$$M=\tfrac{1}{2}Ng\mu_0[S-AG(A)].$$

Most probably the one-dimensional antiferromagnets are disordered even at absolute zero.[2] The off-diagonal elements, neglected in the variational method, should then be very important in this case.

TABLE I. The functions A and C.

ψ	$A_1(\sin\psi)$	$C_1(\sin\psi)$	$A_2(\sin\psi)$	$C_2(\sin\psi)$	$A_3(\sin\psi)$	$C_3(\sin\psi)$
90°	∞	$-\infty$	0.1966	−0.2756	0.0593	−0.0958
80°	0.5038	−0.6831	0.1469	−0.2258	0.0534	−0.0898
70°	0.2973	−0.4696	0.1074	−0.1847	0.0433	−0.0795
60°	0.1865	−0.3475	0.0759	−0.1499	0.0329	−0.0679
50°	0.1161	−0.2618	0.0510	−0.1196		

[14] P. W. Anderson, Phys. Rev. 83, 1260 (1951).
[15] H. A. Bethe, Z. Physik 71, 205 (1931).

TABLE II. Numerical examples of c calculated by the variational method.

S	1/2	1	3/2	2	∞	1/z
Linear chain	0.198	0.323	0.345	0.330	0.363	0.5
Quadratic layer	0.147	0.197	0.212		0.1580	0.25
CsCl type	0.069	0.073	0.074	0.073	0.0730	0.125

5. ANTIFERROMAGNETS IN ANISOTROPIC AND EXTERNAL FIELDS

In the molecular field theory of antiferromagnets, which has been adopted by Nagamiya[16] and by Keffer and Kittel[17] for the calculation of resonance frequencies, each of the resultant moments of the sublattices, is pictured precessing in the resultant field due to the exchange forces, the anisotropic field, and the external field. The counterpart of this picture in the present analysis is as follows:

In Fig. 1, the crystallographic axes are given by (x_0, y_0, z_0). Let us assume the axes of the precessional motions of the spins of sublattices to be z' and z'', and take the bisector of these two axes as the y axis, the z axis being chosen orthogonal to y in the plane (z', z'', y), and the x axis orthogonal to y and z. Then the components of the spins on one of the sublattices can be represented by Eq. (2.6), choosing the axes (x, y', z') where y' is orthogonal to z' and x. Similarly, the spin-components of the other sublattices can be expressed with respect to the axes (x, y'', z''). Then the Hamiltonian of the spin-system is a function of the spin-deviation operators referred to the prescribed axes of precession, of the relative orientation of (x, y, z) with respect to the crystallographic axes and the applied magnetic field, and of the assumed distortion angle δ, the angle between z' and $-z''$, which can be assumed to be small. In this form, the odd power terms of the spin-deviation operators do not vanish, which means that torques remain making the precession axes deviate from the assumed directions. The variational method can be applied here in various ways. For instance, we can put δ equal to zero, and instead assume some finite shifts of equilibrium point, say ϵ, for the spin-wave oscillator of infinite wavelength, which should be determined in a variational way (in this case the spin-waves of finite wave numbers have the precessional axes in $z(-z)$ direction). Or, assuming ϵ to be zero, the most favorable value of δ can be determined. More generally we can seek the most favorable values of ϵ and δ, which means the spin-waves are precessing around z' and z'', except the longest spin-wave which has a little different axis of its precession.

In this way, we can first obtain the free energy of the system which depends on the other parameters left, that is, the orientation of (x, y, z) axes, the anisotropy constants, and the field strength. The most stable state of the antiferromagnet is that in which the free energy

[16] T. Nagamiya, Prog. Theoret. Phys. 6, 342, 350 (1951).
[17] F. Keffer and C. Kittel, Phys. Rev. 85, 329 (1952).

CC-0. In Public Domain. Gurukul Kangri Collection, Haridwar

Digitized by Arya Samaj Foundation Chennai and eGangotri

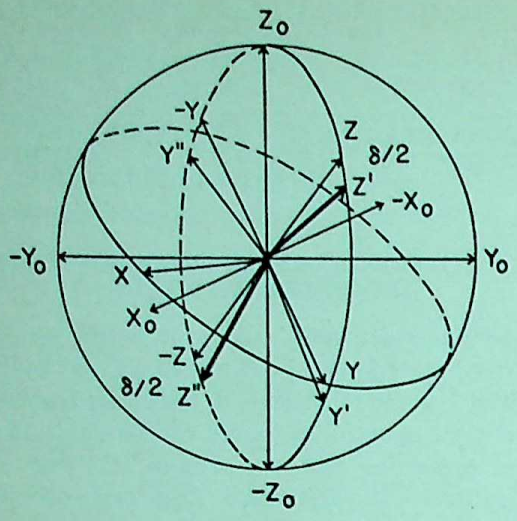


FIG. 1. Axes of quantization in anisotropic and external fields.

(or the energy at 0°K) is minimized with respect to the orientation. The calculation will not be carried out here, but we can show that the free energy is given in the form

$$F=F_{ex}+F_{anis}-\tfrac{1}{2}\chi_{\perp}(H_x^2+H_y^2)-\tfrac{1}{2}\chi_{\parallel}H_z^2. \quad (5.1)$$

Here F_{ex} means the free energy of the system in the absence of the anisotropic and the external fields, and F_{anis} is the additional free energy due to the anisotropic field. The last two terms are the magnetic energy due to the external field, and $\chi_{\parallel}$ and $\chi_{\perp}$ are the parallel and perpendicular susceptibilities. This expression is proved on the assumption that both the anisotropic field and the external field are far weaker than the exchange force, which allows us to use a perturbation method. If, for instance, the anisotropy is strong enough, F cannot be separated into such terms as in Eq. (5.1).

In Eq. (5.1) the first term F_{ex} is isotropic with respect to the orientation of the precessional axes, while the others are anisotropic. The stable orientation is dependent on the relative magnitudes of the anisotropic field and the applied field, so that the effective susceptibility is generally dependent on both the direction and the magnitude of the applied field.

These are the same conclusions one gets from the molecular field theory[16,18] except that the quantities in Eq. (5.1) have different functional forms as regards tempersture dependence, and that the anisotropic part of the free energy is calculated in a dynamical way. Some of such thermodynamic quantities have been studied by the author[3] in the frame of the spin-wave theory. The variational method does not change the results significantly for three-dimensional lattices, where the corrections due to the higher terms are small except in the case of fluctuations. For instance,

$$\chi_{\perp}\sim\frac{N}{2}\frac{g^2\mu_0^2}{zJ}$$

$$\chi_{\parallel}\sim\frac{4}{3}\frac{Ng^2\mu_0^2}{zJS}\left(\frac{kT}{zJS}\right)^2$$

at low temperatures. More detailed discussion is out of place here and will be given elsewhere.

APPENDIX

Any function of the operator $n=a^*a$ can be represented by

$$f(n)=\frac{1}{2\pi i}\oint \mathfrak{f}(x)x^n\frac{dx}{x}, \quad (A.1)$$

with the generating function $\mathfrak{f}$ defined by

$$\mathfrak{f}(x)=\sum_{n=0}^{\infty} f(n)x^{-n}. \quad (A.2)$$

The operator x^n is conveniently expanded as

$$x^n=\sum_{p=0}^{\infty}\frac{(x-1)^p}{p!}a^{*p}a^p. \quad (A.3)$$

Thus we have

$$\sum_j f(n_j)a_j{}^r f_2(n_{j+\rho})b_{j+\rho}{}^r$$
$$=(2\pi i)^{-2}\oint\oint \mathfrak{f}_1(x)x^{-1}dx\mathfrak{f}_2(y)y^{-1}dy$$
$$\times\sum_p\sum_q\frac{(x-1)^p}{p!}\frac{(y-1)^q}{q!}$$
$$\times\sum_j a_j{}^{*p}a_j{}^{p+r}b_{j+\rho}{}^{*q}b_{j+\rho}{}^{q+r}. \quad (A.4)$$

Now we define the notation

$$\operatorname{diag}\sum_j a_j{}^{*p}a_j{}^{p+r}b_{j+\rho}{}^{*q}b_{j+\rho}{}^{q+r}$$
$$=\frac{N}{2}(p,\ p+r,\ q,\ q+r)_\rho, \quad (A.5)$$

where "diag" means the diagonal elements of the operator in the representations satisfying the conditions (3.9) and (3.10). Then we can show that

$$(p,\ p+r,\ q,\ q+r)_\rho=(p+r)!\,q!$$
$$\times\frac{1}{2\pi i}\oint(A+C_\rho{}^*\zeta^{-1})^p(B+C_\rho\zeta)^{q+r}\zeta^{-r-1}d\zeta. \quad (A.6)$$

For instance,

$$\frac{N}{2}(p,\ p,\ q,\ q)_\rho$$
$$=(2/N)^{p+q}\sum_j\sum_\lambda\cdots\sum_\mu\cdots\sum_\nu\cdots\sum_\kappa\cdots$$
$$\operatorname{diag}\ a_{\lambda_1}{}^*\cdots a_{\lambda_p}{}^*a_{\mu_1}\cdots a_{\mu_p}b_{\nu_1}{}^*\cdots b_{\nu_q}{}^*b_{\kappa_1}\cdots b_{\kappa_q}$$
$$\times\exp[-i(\textstyle\sum\lambda-\sum\mu-\sum\nu+\sum\kappa)j+i(\sum\kappa-\sum\nu)\rho]$$
$$=\frac{N}{2}\sum_t p!q!\binom{p}{t}\binom{q}{q-t}A^tC_\rho{}^{*p-t}C_\rho{}^{p-t}B^{q-p-t}$$
$$=\frac{N}{2}p!q!\frac{1}{2\pi i}\oint(A+C_\rho{}^*\zeta^{-1})^p(B+C_\rho\zeta)^q\zeta^{-1}d\zeta,$$

[18] L. Néel, Ann. phys. 113 Serie 5, 232 (1936).

CC-0. In Public Domain. Gurukul Kangri Collection, Haridwar

Digitized by Arya Samaj Foundation Chennai and eGangotri

where the second formula obtained in a combinatory way is rigorous provided (3.10) holds. The general formula (A.6) can be established in like manner. Then the diagonal elements of (A.4) are expressed

$$\operatorname{diag}\sum_j f_1(n_j)a_j{}^r f_2(n_{j+\rho})b_{j+\rho}{}^r$$

$$=\tfrac{1}{2}N(2\pi i)^{-2}\oint\oint \mathfrak{f}_1(x)x^{-1}dx\mathfrak{f}_2(y)y^{-1}dy\Phi_{r\rho}(x,y), \quad \text{(A.7)}$$

with

$$\Phi_{r\rho}(x,y)=\sum_{p=0}^{\infty}\sum_{q=0}^{\infty}\frac{(x-1)^p}{p!}\frac{(y-1)^q}{q!}(p,p+r,q,q+r)_\rho$$

$$=\frac{1}{2\pi i}\oint\sum_p\sum_q\frac{(p+r)!}{p!}(x-1)^p(y-1)^q$$

$$\times(A+C_\rho{}^*\zeta^{-1})^p(B+C_\rho\zeta)^{q+r}\zeta^{-r-1}d\zeta,$$

which satisfy the recurrence formula

$$\partial\Phi_{r\rho}/\partial C_\rho{}^*=(x-1)(y-1)\Phi_{r+1,\rho}. \quad \text{(A.8)}$$

In particular,

$$\Phi_{0\rho}=[\{1-(x-1)A\}\{1-(y-1)B\}$$
$$-(x-1)(y-1)C_\rho C_\rho{}^*]^{-1},$$
$$\Phi_{1\rho}=C_\rho\Phi_{0\rho}{}^2. \quad \text{(A.9)}$$

The integral on the right-hand side of Eq. (A.7) can be carried out if the poles of the generating functions are known, or it can be done by expanding $\Phi_{r\rho}$ in x and y or $(x-1)$ and $(y-1)$. A simple example is

$$\operatorname{diag}\sum_j[n]_j$$

$$=\frac{N}{2}\frac{1}{2\pi i}\oint\sum_{n'=0}^{\infty}[n']x^{-n'}\{1-(x-1)A\}^{-1}x^{-1}dx$$

$$=\frac{N}{2}A\left[1-\frac{(2S+1)A^{2S}}{(1+A)^{2S+1}-A^{2S+1}}\right]\equiv\frac{N}{2}AG(A).$$

Equations (3.14) and (3.15) are obtained by the expansion

$$\Phi_{r\rho}=\sum_{l=0}^{\infty}\sum_{m=0}^{\infty}\sum_{n=0}^{\infty}\binom{l+m}{l}\binom{l+n}{l}x^{l+m}y^{l+n}$$

$$\times(A+AB-C_\rho C_\rho{}^*)^m(B+AB-C_\rho C_\rho{}^*)^n$$

$$\times(C_\rho C_\rho{}^*)^l[(1+A)(1+B)-C_\rho C_\rho{}^*]^{-1-2l-m-n}$$

and the similar expansion of $\Phi_{1\rho}$. Another useful expansion is

$$\Phi_{0\rho}=\sum_{l=0}^{\infty}\sum_{m=0}^{\infty}\sum_{m'=0}^{\infty}\binom{l+m}{l}\binom{l+m'}{l}$$

$$\times(x-1)^{l+m}(y-1)^{l+m'}A^mB^{m'}(C_\rho C_\rho{}^*)^l,$$

which give the formulas

$$F_{0\rho}=\sum_{l=0}^{\infty}\sum_{m=0}^{\infty}\sum_{m'=0}^{\infty}\binom{l+m}{l}\binom{l+n}{l}$$

$$\times\Delta^{l+m}[n]\Delta^{l+m'}[n]A^mB^{m'}(C_\rho C_\rho{}^*)^l,$$

$$F_{1\rho}=C_\rho\sum_{l=0}^{\infty}\sum_{m=0}^{\infty}\sum_{m'=0}^{\infty}(l+1)\binom{l+m+1}{l+1}\binom{l+m'+1}{l+1}$$

$$\times\Delta^{l+m}f\Delta^{l+m'}fA^mB^{m'}(C_\rho C_\rho{}^*)^l,$$

where the difference operator Δ^p means the pth difference of $[n]$ or $f(n)$ evaluated at $n=0$. Thus if the spins are of the magnitude S, $F_{0\rho}$ will be

$$F_{0\rho}=AB+C_\rho C_\rho{}^*-(2S+1)\{A^{2S+1}+B^{2S+1}\}+\cdots,$$
$$F_{i\rho}=C_\rho[1+2\{(1-\tfrac{1}{2}S)^{\frac{1}{2}}-1\}(A+B)+\cdots].$$

The function $F_{0\rho}$ can also be given in a closed form

$$F_{0\rho}=AG(A)BG(B)+C_\rho C_\rho{}^*\{1-G(A)-G(B)$$
$$\sum_\omega\sum_{\omega'}\omega\omega'[(1+A-\omega A)(1+B-\omega' B)$$
$$-(\omega-1)(\omega'-1)C_\rho C_\rho{}^*]^{-1}\},$$

where ω and ω' are the roots of the equations, $\omega^{2S+1}=1$ and $\omega'^{2S+1}=1$.

Some generalizations of these formulas are also possible. In particular, a useful generalization of Eq. (A.3) is

$$x^{(a^*+\epsilon^*)(a+\epsilon)}=\{1+\epsilon\epsilon^*(x-1)+O(\epsilon^3)\}$$
$$\times\{1+(x-1)\epsilon a^*+\tfrac{1}{2}(x-1)^2\epsilon^2a^{*2}+O(\epsilon^3)\}$$
$$\times\sum_{p=0}^{\infty}\frac{(x-1)^p}{p!}a^{*p}a^p\{1+(x-1)\epsilon^*a$$
$$+\tfrac{1}{2}(x-1)^2\epsilon^{*2}a^2+O(\epsilon^3)\},$$

which is employed for the treatments described in Sec. 5.

CC-0. In Public Domain. Gurukul Kangri Collection, Haridwar

Digitized by Arya Samaj Foundation Chennai and eGangotri

CC-0. In Public Domain. Gurukul Kangri Collection, Haridwar

Digitized by Arya Samaj Foundation Chennai and eGangotri

REVIEWS OF
MODERN PHYSICS

VOLUME 25, NUMBER 2 APRIL, 1953

On the Theory of the Ising Model of Ferromagnetism*

GORDON F. NEWELL AND ELLIOTT W. MONTROLL

Institute for Fluid Dynamics and Applied Mathematics, University of Maryland, College Park, Maryland

1. INTRODUCTION

IN his doctors dissertation of 1925, Ising[1]† proposed a simple model of ferromagnetism which has been the subject of considerable investigation during the past fifteen years. The model is based upon the view that ferromagnetism is caused by an interaction between the spins of certain electrons in the atoms making up a crystal.

We must therefore associate with each particle of the crystal, a spin coordinate σ. We imagine the particles to be rigidly fixed in the lattice, either neglecting the vibrations of the crystal or assuming that they act independently of the spin configuration and can therefore be considered separately. Instead of adopting the accepted model and considering σ as a vector spin, we consider σ as a scalar quantity which can achieve either of two values $\sigma=\pm 1$. The value $\sigma=1$ corresponds to a spin state with the spin in some preassigned direction, and $\sigma=-1$ corresponds to a spin in the opposite direction. The spin is considered to be either "up or down."

The interaction energy between two particles located at the jth and kth lattice points and having spins σ_j and σ_k, respectively, is postulated to be

$$E_{jk}=\begin{cases}-J\sigma_j\sigma_k & \text{if } j \text{ and } k \text{ are nearest neighbors}\\ 0 & \text{otherwise.}\end{cases} \tag{1.1}$$

Thus, we postulate that only particles on nearest neighbor lattice points interact; that the energy is $-J$ if the nearest neighbors have the same spin and $+J$ if they have unlike spins. The zero of energy has been conveniently chosen as the average of these two. The constant J, which appears as a parameter, is a measure of the strength of this coupling and must be determined from the physical properties of the system. J will be positive for a ferromagnetic system and negative for an antiferromagnetic system.

In addition to this energy, we postulate that the particles can interact with an external magnetic field. A magnetic moment μ is assigned to each lattice point, and the energy of interaction of the jth particle with the field is chosen to be

$$E_H=-\mu H\sigma_j. \tag{1.2}$$

The thermodynamic and magnetic properties of a crystal which contains N lattice points can be determined from the partition function

$$Z=\sum_{\sigma_1=\pm 1}\cdots\sum_{\sigma_N=\pm 1}\exp\{\tfrac{1}{2}K\sum_{j,k=1}^{N}a_{jk}\sigma_j\sigma_k+\mu\mathfrak{H}\sum_{j=1}^{N}\sigma_j\}, \tag{1.3}$$

where

$$a_{jk}=\begin{cases}1 & \text{if } j \text{ and } k \text{ are nearest neighbors}\\ 0 & \text{otherwise,}\end{cases} \tag{1.4}$$

$$K=J/kT, \quad \mathfrak{H}=H/kT. \tag{1.5}$$

For example, the internal energy per particle is given by

$$\bar{E}=N^{-1}kT^2\partial\log Z/\partial T \tag{1.6}$$

and the magnetization per particle by

$$M=N^{-1}\partial\log Z/\partial\mathfrak{H}. \tag{1.7}$$

If the only reason for studying the Ising partition function (1.3) is to advance the theory of ferromagnetism, then undue attention has been paid to this problem considering that the spin interaction used is a scalar one and that the lattice distances are fixed and do not depend on spin orientation. Actually the widespread interest in the model is primarily derived from

* This work was partially supported by the Office of Naval Research. Part of this paper was presented at the Washington Conference on Magnetism, September, 1952.

† References will be found under Bibliography at end of article.

CC-0. In Public Domain. Gurukul Kangri Collection, Haridwar

Digitized by Arya Samaj Foundation Chennai and eGangotri

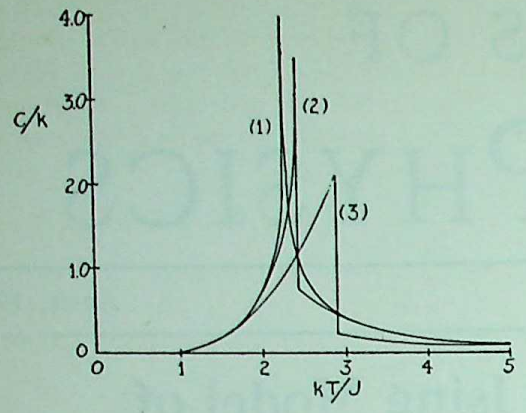


FIG. 1. The exact specific heat curve of the two-dimensional Ising lattice (curve 1) is compared with approximate curves of Kramer-Wannier (curve 2), and Bethe (curve 3) (see reference 3).

the fact that it is one of the simplest examples of a system of interacting particles which still has some features of physical reality in it. The model forms an excellent test case for any new approximate method of investigating systems of interacting particles. If a proposed method cannot deal with the Ising model, it can hardly be expected to be powerful enough to give reliable results in more complicated cases.

Underlying the interest in this problem as a study of some physical model, there rests the more fundamental question. Does the formalism of statistical mechanics predict phase transitions and, if so, how? We can hardly give satisfactory answers to these questions without examples. Even an artificial example is better than none. So far only a few examples have been successfully studied. One of these is the famous Einstein-Bose gas condensation and another is Onsager's brilliant analysis of the two-dimensional Ising model. A third is the spherical model of cooperative phenomena. The model and not some mathematical approximation is in each case the sole cause of the phase transition represented mathematically by a singularity in some of the thermodynamic quantities.

Even though the Ising model is not considered to be a very realistic model of ferromagnetism, it is equivalent to a very good model of a binary substitutional alloy and an interesting model of a gas or liquid.

It can easily be shown (see Appendix 1) that the grand partition function used to describe the order-disorder phenomenon in binary alloys has exactly the same mathematical form as that of an Ising ferromagnet in a magnetic field. An alloy with equal numbers of two atomic species is equivalent to the Ising model in the absence of an external field. The coordinate σ_j no longer represents a spin, but rather represents the two possible states of the jth lattice point. $\sigma_j=+1$ or -1 accordingly as the jth point is occupied by an atom of type 1 or type 2.

The "lattice" model of a gas or liquid is formed by dividing a given volume into a large number of cells of equal size, with each cell being occupied by either one or no molecules. An empty cell is represented by $\sigma=-1$ and a filled one by $\sigma=+1$. It is shown in Appendix 1 that the specific volume of a lattice gas is related to the magnetization of the Ising model.

The Ising model can also be related to a theory of adsorption of gases on surfaces.

This paper is a review of the work done on the Ising problem (and its equivalents) since the appearance of the comprehensive review of order-disorder phenomenon by Nix and Shockley.[2] Much of the emphasis in this period (and hence in this review) has been on the development of exact analytical expressions for thermodynamic quantities. It has been shown that critical phenomenon are not always accurately described by approximate theories.[3] For example, the critical temperature of the two-dimensional Ising problem is incorrectly given by approximate theories, as is the nature of the specific heat singularity. The exact specific heat curve derived by Onsager[4] is compared with the corresponding curves of various other theories in Fig. 1. It is to be noted that the form of the approximate curves at temperatures above the critical temperature are especially poor.

The thermodynamic properties of two-dimensional lattices of various sorts (with nearest neighbors interaction only) can now be derived by either of two methods. In the first, that used by Onsager, the partition function is expressed as the largest characteristic value of a certain matrix. This characteristic value was determined by Onsager using a complicated algebraic development. Through the use of spinors and the theory of Lie algebras, Kaufman[5,6] and van der Waerden (in an unpublished letter to Onsager, 1946) have simplified the Onsager analysis considerably and have given more motivation to the individual steps in his work. The second method, which has been developed recently by Kac and Ward[7] is based on the van der Waerden[8] combinational formulation of the partition function. The partition function is expressed in terms of the number of ways closed graphs with a given number of bonds can be constructed on a lattice. Finally a determinant is constructed such that each term in its expansion (by the definition of a determinant) corresponds to a closed graph. We shall discuss both of these methods in parts 2 and 4 of this paper.

To date no one has found exact expressions for (a) the partition function of a three-dimensional Ising lattice; (b) that of a two-dimensional lattice in a magnetic field; or (c) a two-dimensional lattice with interactions between next nearest neighbors as well as nearest neighbors. The first few terms in high and low temperature series for the partition functions of (a) and (b) will be reviewed in Sec. 7.

2. MATHEMATICAL FORMULATION OF PROBLEM

In this section we express the partition function (1.3) in several alternative forms so that we can proceed with both the matrix and combinational analysis of the two-dimensional lattices.

CC-0. In Public Domain. Gurukul Kangri Collection, Haridwar

Digitized by Arya Samaj Foundation Chennai and eGangotri

2.1 Matrix Formulation

Here we relate the partition function of the Ising model to the largest characteristic value of a certain matrix whose elements are functions of T and the coupling constants.[9–12] We first derive the required relations for a more general class of system than the Ising model and finally specialize to it.

We consider a lattice consisting of m "layers" of particles. We represent the possible states of the jth layer by ν_j. For a one-dimensional nearest neighbor system such as the Ising problem, the "layers" will be individual particles and ν_j will be described by the internal coordinates σ_j of these particles. For a two-dimensional lattice the "layers" will be rows of particle and ν_j will be given by the set of internal coordinates σ_k of all lattice points in the jth row. For a three-dimensional lattice, the "layer" will be a layer in the usual sense and ν_j will be given by the set of all internal coordinates of that layer.

In general the word "layer" will be used to describe any subdivision of the lattice into small (usually identical) parts but in such a way that the jth layer interacts only with the $j-1$th and $j+1$th layers. If there are interactions between nearest and next nearest lattice points, we choose a layer, in the one-dimensional case for example, to be a pair of particles which interacts only with a neighboring pair of particles. If the lattice has forces of finite range, we can still consider it a type of nearest neighbor system but with interacting units containing more than one lattice points.

The energy of such a system we assume to be of the form

$$V=\sum_{j=1}^{m-1} V(\nu_j, \nu_{j+1})+\sum_{j=1}^{m} V(\nu_j), \tag{2.1}$$

where $V(\nu_j, \nu_{j+1})$ is the interaction energy between the jth and $j+1$th layers, and $V(\nu_j)$ is the internal energy of the jth layer.

It is mathematically convenient to assign periodic boundary conditions by inserting an additional interaction $V(\nu_m, \nu_1)$ between the mth and first layers. Physically this is equivalent to bending the lattice into a ring, but, as one takes a larger and larger system, such surface effects become negligible.

The partition function of a system in which the mth layer is connected to the first is

$$Z=\sum_{\nu_1}\cdots\sum_{\nu_m}\prod_{j=1}^{m} P(\nu_j, \nu_{j+1}), \tag{2.2}$$

where

$$P(\nu_j, \nu_{j+1})=\exp\{-[V(\nu_j, \nu_{j+1})+\tfrac{1}{2}V(\nu_j)+\tfrac{1}{2}V(\nu_{j+1})]/kT\}. \tag{2.2a}$$

Notice that P is a function of a two-parameter set of numbers ν_j and ν_{j+1}, which we shall assume to be discrete. We may consider $\mathbf{P}$ as a matrix with matrix elements $P(\nu_j, \nu_{j+1})$ between the states ν_j and ν_{j+1}. Because of the particular choice of $\mathbf{P}$ with $\frac{1}{2}V(\nu_j)$ and $\frac{1}{2}V(\nu_{j+1})$, $\mathbf{P}$ is a symmetric matrix. It is sometimes convenient but not necessary to make $\mathbf{P}$ symmetric. We could have defined a matrix

$$P'(\nu_j, \nu_{j+1})=\exp\{-[V(\nu_j, \nu_{j+1})+V(\nu_j)]/kT\} \tag{2.2b}$$

which would substitute for $\mathbf{P}$ in (2.2).

One recognizes that the sum over ν_j in (2.2) yields simply the conventional matrix product. Indeed considering $\mathbf{P}$ as a matrix

$$Z=\text{trace}\,(\mathbf{P}^m)=\sum_j \lambda_j{}^m, \tag{2.3}$$

where $\{\lambda_j\}$ is the set of characteristic values of the matrix $\mathbf{P}$.

We are not usually interested in knowing Z exactly for arbitrary m but only

$$\lim_{m\to\infty} m^{-1}\log Z=\log\lambda_{\max}+\lim_{m\to\infty} m^{-1}\log[1+\sum_{j\geq 2}(\lambda_j/\lambda_{\max})^m].$$

Here we have factored out the largest eigenvalue $\lambda_{\max}$ and numbered the λ_j so that $\lambda_{\max}$ is λ_1. If $\lambda_{\max}$ is non-degenerate then $\lambda_j/\lambda_{\max}<1$ and $(\lambda_j/\lambda_{\max})^m\to 0$. Thus, the second term above does not contribute. Even if $\lambda_{\max}$ is degenerate or asymptotically degenerate as $m\to\infty$, the second term will not contribute unless the number of degenerate states or asymptotically degenerate states increase exponentially with m. To our knowledge such a situation has, however, not arisen in any applications; thus

$$\lim_{m\to\infty} m^{-1}\log Z=\log\lambda_{\max}. \tag{2.4}$$

Let us now find explicitly the matrix $\mathbf{P}$ for the one- and two-dimensional Ising lattice (without a magnetic field).

In the one-dimensional case ν_j is simply σ_j and

$$V(\sigma, \sigma')=-J\sigma\sigma', \quad V(\sigma)=0.$$

Hence (since $\sigma^2=1$),

$$P(\sigma, \sigma')=\exp(K\sigma\sigma')=(1+u\sigma\sigma')\cosh K,$$
$$u=\tanh K,$$

so that

$$\mathbf{P}=\begin{pmatrix} e^K & e^{-K} \\ e^{-K} & e^K \end{pmatrix}=e^K\mathbf{I}+e^{-K}\mathbf{C}, \tag{2.5}$$

where $\mathbf{I}$ is the identity matrix and

$$\mathbf{C}=\begin{pmatrix} 0 & 1 \\ 1 & 0 \end{pmatrix}, \quad \mathbf{C}^2=\mathbf{I}.$$

Another form for $\mathbf{P}$ is

$$\mathbf{P}=(2\sinh 2K)^{\frac{1}{2}}\exp(K^*\mathbf{C}), \tag{2.6a}$$

Digitized by Arya Samaj Foundation Chennai and eGangotri

where K^* is defined by

$$\tanh K^* = e^{-2K}, \quad \sinh 2K^* \sinh 2K = 1. \tag{2.6b}$$

Since the characteristic vectors of $\mathbf{C}$ are

$$\psi_1 = 2^{-\frac{1}{2}}\begin{pmatrix}1\\1\end{pmatrix} \quad \text{and} \quad \psi_2 = 2^{-\frac{1}{2}}\begin{pmatrix}1\\-1\end{pmatrix},$$

and every vector is a characteristic vector of the identity matrix

$$\lambda_1 = 2\cosh K, \quad \lambda_2 = 2\sinh K,$$
$$Z = (2\cosh K)^m + (2\sinh K)^m \sim (2\cosh K)^m. \tag{2.7}$$

The thermodynamic and magnetic properties of a one-dimensional Ising lattice are discussed in Appendix 2.

The matrix associated with the two-dimensional Ising lattice is much more complex. In the absence of a magnetic field, the potential energy $V(\nu)$ is the potential energy of interaction between neighboring particles in the same row. If n is the number of particles per row,

$$V(\nu) = -J' \sum_{j=1}^{n} \sigma_j \sigma_{j+1}.$$

This includes an interaction $\sigma_n \sigma_{n+1}$. For the purposes of obtaining greater symmetry, we impose periodic boundary conditions also in the rows by defining $\sigma_{n+1} \equiv \sigma_1$. Physically this means that the lattice is wrapped on a torus; it is periodic along both the rows and columns. We again anticipate that this device should have a negligible effect upon the physical properties of the system.

The potential energy between two neighboring rows is

$$V(\nu, \nu') = -J \sum_{j=1}^{n} \sigma_j \sigma_j'.$$

We have introduced here two different coupling constants J and J'. We thus consider the possibility that the lattice will have stronger couplings in one direction than the other. Wherever no additional complications arise from such a generalization we shall continue to consider $J \neq J'$ even though this generalization leads to no very interesting physical effects that $J = J'$ does not show.

Using (2.2b), we obtain

$$P'(\nu, \nu') = \exp(K \sum_{j=1}^{n} \sigma_j \sigma_{j+1} + K' \sum_{j=1}^{n} \sigma_j \sigma_j'); \tag{2.8}$$

$\mathbf{P}'$ is a matrix of dimension 2^n. A state ν is described by the values of $\sigma_1, \sigma_2, \cdots, \sigma_n$ with $\sigma_j = \pm 1$.

$\mathbf{P}'$ can be put into a more convenient form by factoring it into the product of simpler matrices.[3] We first make use of the following simple fact. If $(V_2)_{\nu\nu''}$ is a diagonal matrix with diagonal elements $(V_2)_\nu$,

$$(V_2)_{\nu\nu''} = (V_2)_\nu \delta_{\nu\nu''}$$

and $(V_1')_{\nu\nu'}$ any arbitrary matrix, then

$$(V_2 V_1')_{\nu\nu'} = \sum_{\nu''} (V_2)_\nu \delta_{\nu\nu''} (V_1')_{\nu''\nu'} = (V_2)_\nu (V_1')_{\nu\nu'}.$$

Notice that $\mathbf{P}'$ is of this form if we write

$$\mathbf{P}' = \mathbf{V}_2 \mathbf{V}_1',$$

$$(V_2)_{\nu\nu'} = \delta_{\sigma_1\sigma_1'} \delta_{\sigma_2\sigma_2'} \cdots \delta_{\sigma_n\sigma_n'} \exp(K' \sum_{j=1}^{n} \sigma_j \sigma_{j+1}), \tag{2.9}$$

$$(V_1')_{\nu\nu'} = \exp(K \sum_{j=1}^{n} \sigma_j \sigma_j') = \prod_{j=1}^{n} \exp(K \sigma_j \sigma_j').$$

Each of these two matrices can also be simplified. We notice that $\mathbf{V}_1$ is simply the nth direct product of the 2×2 matrices for the one-dimensional problem [Eq. (2.5)]. For some remarks about direct products see Appendix 3.

$$\mathbf{V}_1' = (e^K \mathbf{I} + e^{-K}\mathbf{C}) \times (e^K \mathbf{I} + e^{-K}\mathbf{C}) \times \cdots \times (e^K \mathbf{I} + e^{-K}\mathbf{C})$$
$$= (2\sinh 2K)^{n/2} \exp(K^*\mathbf{C}) \times \exp(K^*\mathbf{C}) \times \cdots \times \exp(K^*\mathbf{C}).$$

If we define

$$\mathbf{C}_j = \mathbf{I} \times \mathbf{I} \times \cdots \times \mathbf{I} \times \mathbf{C} \times \mathbf{I} \times \cdots \times \mathbf{I} \tag{2.10}$$

with $\mathbf{C}$ in the jth factor, then

$$\mathbf{V}_1' = (2\sinh 2K)^{n/2} \prod_{j=1}^{n} \exp(K^* \mathbf{C}_j).$$

To simplify $\mathbf{V}_2$ we define a matrix

$$\mathbf{s} = \begin{pmatrix}1 & 0\\0 & -1\end{pmatrix} \tag{2.11}$$

and

$$\mathbf{s}_j = \mathbf{I} \times \mathbf{I} \times \cdots \times \mathbf{I} \times \mathbf{s} \times \mathbf{I} \times \cdots.$$

$\mathbf{s}_j$ is also a diagonal matrix with diagonal elements $+1$ if the state ν has $\sigma_j = +1$ and -1 if $\sigma_j = -1$. In terms of these matrices $\mathbf{s}_j$, we may write

$$\mathbf{V}_2 = \exp(K' \sum_{j=1}^{n} \mathbf{s}_j \mathbf{s}_{j+1}). \tag{2.12}$$

If we define

$$\mathbf{V}_1 = \exp(K^* \sum_{j=1}^{n} \mathbf{C}_j), \tag{2.13}$$

then

$$\mathbf{P}' = (2\sinh 2K)^{n/2} \mathbf{V}_2 \mathbf{V}_1.$$

The symmetric matrix $\mathbf{P}$ of (2.2a) can be deduced in the same manner to be

$$\mathbf{P} = (2\sinh 2K)^{n/2} \mathbf{V}_2^{\frac{1}{2}} \mathbf{V}_1 \mathbf{V}_2^{\frac{1}{2}}.$$

This differs from $\mathbf{P}'$ only by a similarity transformation by $\mathbf{V}_2^{\frac{1}{2}}$. Since neither the eigenvalues nor $Z = \text{trace } \mathbf{P}^m$ are altered by a similarity transformation to $\mathbf{P}$, we again confirm that we can use either $\mathbf{P}$ or $\mathbf{P}'$.

CC-0. In Public Domain. Gurukul Kangri Collection, Haridwar

Digitized by Arya Samaj Foundation Chennai and eGangotri

It is easy to generalize the form of $\mathbf{P}'$ to include an interaction with a magnetic field. In this case

$$\mathbf{P}'=(2\sinh 2K)^{n/2}\mathbf{V}_3\mathbf{V}_2\mathbf{V}_1, \tag{2.14}$$

$$\mathbf{V}_3=\exp(\mu\mathfrak{H}\sum_{j=1}^{n}\mathbf{s}_j).$$

We shall return to this matrix method again in Secs. 3.2 and 4.

By imposing slightly different boundary conditions, Kramers and Wannier[9] showed that one could also formulate this problem with a different matrix. Whereas the matrix $\mathbf{P}$ represents the contribution to Z of an entire row of the lattice, we can define a matrix $\mathbf{M}$ which represents the contribution of only a single particle.

To do this we must choose "screw" boundary conditions. Instead of imposing an interaction between the nth and first particles of the same row (periodic boundary conditions), we let the nth particle of one row interact with the first particle of the next row. Thus the rows are connected to each other as on a screw. To eliminate any loose ends on the lattice, we connect the nth particle of the last (mth) row to the first particle of the first row. The rows of the lattice thus have the geometry of a helix with its ends connected to form a torus.

With this geometry, it is natural to number the particles consecutively from 1 to $n\times m$. The interaction between particles in the same column appears then as

$$-J\sigma_j\sigma_{j+n}$$

and that in the rows as

$$-J'\sigma_j\sigma_{j+1}.$$

The partition function for this system is

$$Z=\sum_{\sigma_1=\pm1}\cdots\sum_{\sigma_{nm}=\pm1}\exp[K'\sum_{j=1}^{nm}\sigma_j\sigma_{j+1}+K\sum_{j=1}^{nm}\sigma_j\sigma_{j+n}] \tag{2.15}$$

with

$$\sigma_{nm+j}\equiv\sigma_j.$$

We wish to represent this as a matrix product in such a way that the jth factor contributes the terms depending upon σ_j. Since the contribution of σ_j depends upon the state of the $j-n$th particle, it is still necessary to have a matrix of dimension 2^n. The physical significance of this matrix will be more apparent after the discussions of Sec. 3.2.

The appropriate matrix is defined by

$$M_{\sigma_n'\cdots\sigma_1',\sigma_n\cdots\sigma_1}\equiv\exp(K'\sigma_n'\sigma_n)\exp(K\sigma_n'\sigma_1)\prod_{j=1}^{n-1}\delta(\sigma_j'-\sigma_{j+1}). \tag{2.16}$$

The matrix connects the state $\sigma_1,\cdots,\sigma_n$ to the state $\sigma_n',\cdots,\sigma_1'$. Most of the matrix elements, however, are zero. They are nonzero only if $\sigma_1'=\sigma_2$, $\sigma_2'=\sigma_3$, $\cdots$, $\sigma_{n-1}'=\sigma_n$. σ_n' is the only "free" index and may be interpreted to be σ_{n+1}. The matrix thus may be considered to connect the states $\sigma_1,\cdots,\sigma_n$ to the state $\sigma_2,\cdots,\sigma_{n+1}$ and to produce a factor appropriate to describe the energy of interaction between σ_{n+1} and $\sigma_1,\cdots,\sigma_n$. Since the indices are dummy indices, we can also interpret it as connecting the state $\sigma_{j+1},\cdots,\sigma_{j+n}$ to the states $\sigma_{j+2},\cdots,\sigma_{j+n+1}$.

Regardless of how one interprets the matrix $\mathbf{M}$ one observes from (2.15) and (2.16) that

$$Z=\mathrm{trace}\mathbf{M}^{nm}=\sum_{j=1}^{2^n}\lambda_j{}^{nm}. \tag{2.17}$$

One can also express the matrix $\mathbf{M}$ in terms of simpler matrices. In addition to the matrices already defined by Eqs. (2.5), (2.10), and (2.11), we define a matrix

$$R_{\sigma_1'\cdots\sigma_n',\sigma_1\cdots\sigma_n}\equiv\delta(\sigma_1'-\sigma_2)\delta(\sigma_2'-\sigma_3)\cdots\times\delta(\sigma_{n-1}'-\sigma_n)\delta(\sigma_n'-\sigma_1). \tag{2.18}$$

This matrix merely cyclically permutes the n particles of one row. Thus, $\mathbf{R}^n=\mathbf{I}$. One easily deduces that[13]

$$\mathbf{M}=(2\sinh 2K)^{\frac{1}{2}}\exp(K'\mathbf{s}_n\mathbf{s}_{n-1})\exp(K^*\mathbf{C}_n)\mathbf{R}. \tag{2.19}$$

Loosely speaking one can say that the operator $\mathbf{R}$ turns the lattice from one point to the next, and the other factors introduce the appropriate Boltzmann factor for the new point.

Following the procedure above, one can also easily construct matrices appropriate for the three-dimensional lattice. One can in fact do this in at least three ways. By appropriate choice of boundary conditions, one can form matrices which represent the contribution to Z of an entire layer, a single row or a single particle in a manner analogous to that used in deducing $\mathbf{P}$ and $\mathbf{M}$ for the two-dimensional lattice. The matrices will in each case be of dimension 2^{lm} if the layers are l particles wide and m particles deep.

The reader may wish to try this as an exercise. Since there has been little progress toward solution of these matrices, we shall not discuss them in any detail.

2.2 Combinational Formulation

At high temperatures and zero magnetic field, an expansion of the partition function in powers of $\tanh^2 K$ can be constructed by counting the number of ways of forming closed paths of given length along the bonds of the lattice. This formulation of the problem was suggested by van der Waerden.[3] (Kirkwood[14] gave the first systematic approach to the order-disorder problem.)

We modify (1.3) slightly to read

$$Z=\sum_{\sigma_1=\pm1}\cdots\sum_{\sigma_N=\pm1}\prod_{n.n.}\exp(K\sigma_j\sigma_k).$$

The product over "$n.n.$" denotes the product over values of j and k corresponding to nearest neighbor

Digitized by Arya Samaj Foundation Chennai and eGangotri

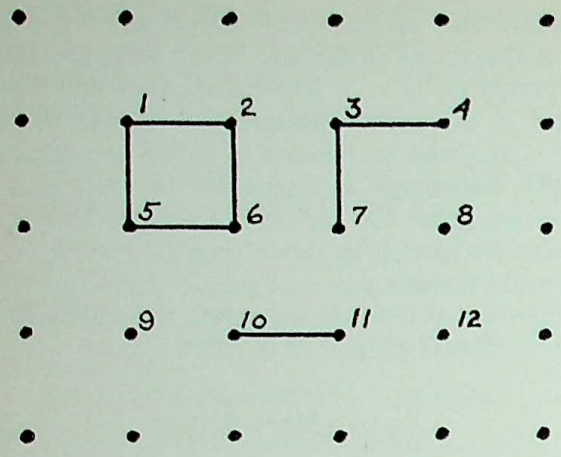


FIG. 2. An example of a graph connecting points of the lattice with no bond repeated.

points of the lattice. We next write[15]

$$\exp K\sigma_j\sigma_k=(1+u\sigma_j\sigma_k)\cosh K \qquad u=\tanh K \tag{2.20}$$

to give

$$Z=(\cosh K)^{cN/2}\sum_{\sigma_1=\pm1}\cdots\sum_{\sigma_N=\pm1}\prod_{n.n.}(1+u\sigma_j\sigma_k),$$

where c is the number of nearest neighbors of a given particle and $Nc/2$ is the total number of interactions. For the square lattice $c=4$. The formalism to this point, however, is also applicable to other lattices. For three-dimensional simple cubic lattices $c=6$.

We next expand the product

$$Z=(\cosh K)^{cN/2}\sum_{\sigma_1=\pm1}\cdots\sum_{\sigma_N=\pm1}\{1+u\sum_{n.n.}\sigma_i\sigma_j + u^2\sum_{n.n.}(\sigma_i\sigma_j)\sum_{n.n.}(\sigma_k\sigma_l)+\cdots\}. \tag{2.21}$$

The coefficient of u^l is the sum of products of $2l$ σ's. The σ's occur in pairs corresponding to nearest neighbors, and no such pair is to occur twice in the same product (by the simple rules of the expansion).

To obtain a convenient geometrical picture, we can associate with a pair $\sigma_i\sigma_j$, a bond connecting the neighbors i and j, and with the pair $\sigma_k\sigma_l$ another bond connecting k and l, etc. With each product of $2l$ σ's, we associate a "graph" or set of l bonds. Since pairs occur at most once in a given product, no bond is to appear more than once in the same graph. In Fig. 2 we have drawn the graph associated with the term

$$(\sigma_1\sigma_2)(\sigma_3\sigma_4)(\sigma_1\sigma_5)(\sigma_2\sigma_6)(\sigma_3\sigma_7)(\sigma_5\sigma_6)(\sigma_{10}\sigma_{11}).$$

Since

$$\sum_{\sigma=\pm1}\sigma=0, \qquad \sum_{\sigma=\pm1}\sigma^2=2, \tag{2.22}$$

the only terms of (2.21) which contribute to Z are those in which each σ_i occurs to an even power. Since a bond can appear only once in a term, σ_i can occur at most c times or 4 times for the square lattice. This also means that the only graphs of interest are those in which each lattice point is connected by an even number of bonds (0, 2, or 4 for the square net). We conclude from this that all contributing graphs must be the superposition of simple closed polygons (polygons with no loops) having no common sides. Also the converse is true; there is a nonzero term in Z for each such superposition of simple closed polygons. (Such polygons may have common points however.) For simplicity we shall call such graphs, "closed graphs" (Fig. 3).

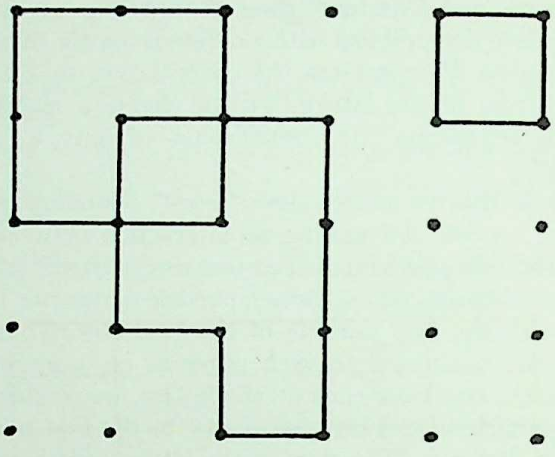


FIG. 3. An example of a closed graph in which each point is connected by 0, 2, or 4 bonds.

Each closed graph of m bonds contributes to Z a term $2^N u^m$ after summing over σ_1 to σ_N. Hence, the partition can be written as

$$Z=2^N(\cosh K)^{Nc/2}\sum_r n(r)\tanh^r K, \tag{2.23}$$

where $n(r)$ is the number of closed graphs of r bonds which can be constructed on the lattice. $n(0)=1$ and in a square or cubic lattice $n(r)=0$ unless r is even.

Equation (2.23) can be generalized to include more complex interactions. If, for example, K represents the interaction between lattice points of a square lattice which lie in the same row and K' that between pairs in the same column, then

$$Z=(\cosh K\cosh K')^N 2^N\sum_{r,s}n(r,s)\tanh^r K\tanh^s K', \tag{2.24}$$

where $n(r,s)$ is the number of closed graphs with $r+s$ bonds, r in the horizontal and s in the vertical direction.

Equation (2.24) is the starting point of the combinational derivation of the two-dimensional Onsager formulas by Kac and Ward.[7]

It is also possible to obtain a low temperature expansion of Z which involves a somewhat different combinational problem (except in the two-dimensional square lattice in which, as we shall see in the next section, both high and low temperature counting procedures are equivalent).

For any given state of the system, let

N_1 = number of σ's that are $+1$,

N_{12} = number of unlike pairs of nearest neighbors.

CC-0. In Public Domain. Gurukul Kangri Collection, Haridwar

Digitized by Arya Samaj Foundation Chennai and eGangotri

Since $Nc/2$ is the total number of nearest neighbor pairs (as before, c is the number of nearest neighbors for one lattice point),

$$\sum_{n.n.} \sigma_i\sigma_j = (Nc/2 - N_{12})(+1) + N_{12}(-1) = Nc/2 - 2N_{12},$$

$$\sum_{i=1}^{N} \sigma_i = N_1(+1) + (N - N_1)(-1) = N - 2N_1.$$

If $g(N, N_1, N_{12})$ is the number of ways a given N_1 and N_{12} can be chosen on a lattice of N points, then

$$Z = \exp(N\mathfrak{H}\mu) \exp(NcK/2) \sum_{N_1, N_{12}} g(N, N_1, N_{12}) \times \exp(-2KN_{12} - 2\mathfrak{H}\mu N_1). \quad (2.25)$$

In the absence of a magnetic field

$$Z = e^{NcK/2} \sum_r m(r) e^{-2Kr}, \quad (2.26)$$

where $m(r)$ is the number of ways r pairs of unlike neighbors can be arranged on a lattice.

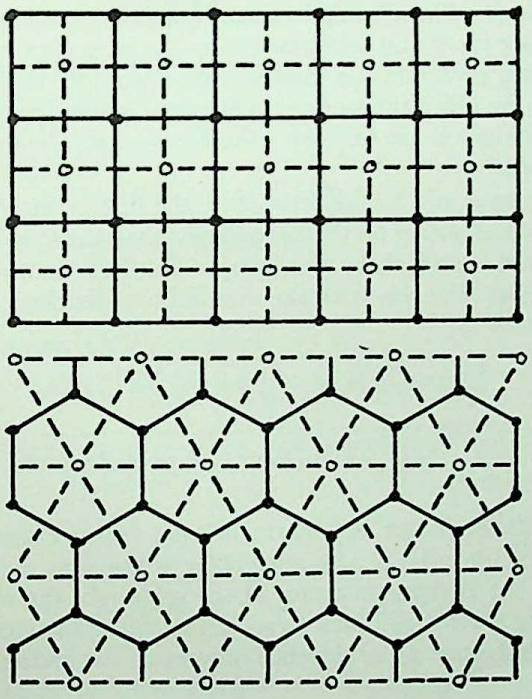


FIG. 4. A square lattice (above) hexagonal lattice (below) are illustrated by solid lines along the bonds joining nearest neighbors. The dual lattice, formed by bisecting the bonds of the original lattice, is similarly illustrated by the broken lines.

High and low temperature expansions based upon (2.24) and (2.25) will be discussed further in Sec. 7.

3. PHASE TRANSITIONS

3.1 Duality Theorems

Through certain symmetries in the matrix approach to the Ising problem, Kramers and Wannier[9] derived an interesting relation between the high and low temperature expansions for the partition function of a square lattice. Although this relation was not powerful enough to yield an analytic expression for the partition function, it was sufficient to locate the Curie point if we assume one existed. Onsager (see Wannier[3]) generalized this relation by a topological argument to a wider class of two-dimensional lattices.

Onsager constructed a "dual lattice" to a given lattice by drawing a bond through each bond of the original lattice and connecting these new bonds at points in the center of each unit cell of the original lattice. In Fig. 4 is shown the square lattice (solid line) and its dual (dotted lines) also a hexagonal lattice and its dual which is a triangular lattice. Since the dual of the square is also a square lattice, we describe it as self-dual.

To derive Wannier's duality theorem between the high and low temperature behavior by geometrical arguments, we consider the square lattice of Fig. 5. We represent lattice points with $\sigma = +1$ by dots and those with $\sigma = -1$ by $\times$. Each bond joining unlike spins is bisected by a bond of the dual lattice. It is clear that (except perhaps for points near the boundary of the lattice) this set of bonds on the dual lattice forms a closed graph of the type described in the preceeding section and that the number of bonds of the dual lattice is exactly the number of unlike pairs of the original lattice. Indeed there is a one-to-one correspondence between arrangements of bonds connecting unlike σ's on the original lattice and closed graphs of the same number of bonds on the dual lattice.

By comparing the definitions of $n(r)$ (2.23) and $m(r)$ (2.26), we notice that

$$\begin{aligned} m(r) &= n_D(r), \\ m_D(r) &= n(r), \end{aligned} \quad (3.1)$$

where the subscript D refers to functions on the dual lattice. These relations hold for other two-dimensional lattices as well as the square lattice used in the illustration. In the case of the square lattice, we can discard the subscript D because the dual lattice is the same as the original lattice.

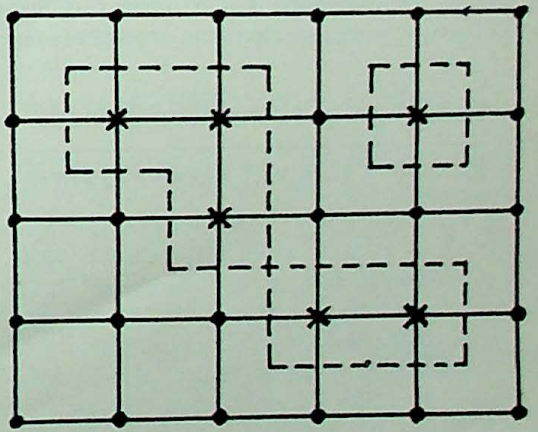


FIG. 5. An example to show that each configuration of "up spins" denoted by dots and "down spins" denoted by x can be described by a closed graph on the dual lattice. The bonds of the closed graph bisect bonds of the original lattice joining unlike pairs of spins.

Digitized by Arya Samaj Foundation Chennai and eGangotri

Using the definition of K^* given in (2.6b) and the relations (3.1), we see that the expressions (2.26) and (2.23) for Z are related as follows:

$$\begin{aligned} Z(K)e^{-NcK/2} &= \sum_r m(r)e^{-2Kr} \\ &= \sum_r n_D(r)\tanh^r K^* \\ &= Z_D(K^*)[2^{N_D}(\cosh K^*)^{N_D cD/2}]^{-1}. \end{aligned}$$

Since there is a bond of the dual lattice to each bond of the original lattice, $N_D c_D/2 = Nc/2$. The above can be simplified somewhat to read

$$Z(K) = Z_D(K^*)2^{-N_D}(2\sinh 2K)^{Nc/4}. \tag{3.2}$$

A large value of K^* is associated with a small value of K by (2.6b). Hence the partition function of one lattice at a high temperature is related to the partition function of its dual at a low temperature and vice versa.

In a self-dual lattice such as the square lattice, (3.2) implies that if a singularity exists at a temperature $T = J/kK$, then another singularity exists at a temperature $T^* = J/kK^*(K)$. If, however, as is intuitively expected, only one singularity exists, it must occur at $T = T^*$. From (2.6b) we see that this critical point is given by

$$|\sinh 2K_c| = 1, \quad K_c = \pm 0.4407$$

(K_c will be positive if J is positive, negative if J is negative). Substituting $T = T_c$ into (3.2), we see that (3.2) is identically satisfied so that we know the singularity is not a discontinuity of Z.

The above arguments cannot be directly applied to either the triangular or hexagonal lattices since these lattices are not self-dual. It is possible, however, to locate the Curie point. Onsager (see Wannier[3]) found another quite different relation between the triangular and hexagonal lattices, the so-called star-triangle transformation derived in Appendix 4. This relates the low temperature behavior of the triangular lattice to the low temperature behavior of the hexagonal lattice. Using both the star triangle and the dual transformations, one obtains a relation between the low and high temperature behaviors of the triangular lattice (also the hexagonal lattice). Thus, we can use the same arguments as above to deduce the Curie points of each of these lattices, assuming that one such exists.

3.2 Long-Range Order

The Ising lattice has many very interesting properties that would not generally be classified as thermodynamics. If, in the lattice, we should fix the spin configuration of part of the system, we might ask what effect this has upon the system as a whole. If when we fix the spin of one particle, particles far away from the fixed spin show a preference for some definite spin direction, we say that the system has a long-range order. We describe a system as ordered if the spins show a strong tendency toward some organized pattern. In a ferromagnet, for example, the spins of an ordered state are predominantly in the same direction.

Ashkin and Lamb[16] showed that long-range order in a nearest neighbor system is associated with a degeneracy or asymptotic degeneracy of the largest eigenvalue of the matrix $\mathbf{P}$ defined in Sec. 2.1.

Imagine that we build a large crystal by starting with a single layer and add new layers one at a time to the existing configuration. Suppose we should fix the state ν_0 of the original layer or, to be more general, suppose we assign a probability distribution $p_0(\nu_0)$ to the states ν_0.

We next add to the zero layer, the first layer of particles. Let $p_1(\nu_1)$ be the probability that the first layer is in the state ν_1 if the zero layer is distributed according to $p_0(\nu_0)$. We see that the equilibrium distribution is given by

$$p_1(\nu_1) = \frac{\sum_{\nu_0} \exp\{-[V(\nu_1,\nu_0)+V(\nu_1)]/kT\}p_0(\nu_0)}{\sum_{\nu_0,\nu_1} \exp\{-[V(\nu_1,\nu_0)+V(\nu_1)]/kT\}p_0(\nu_0)}. \tag{3.3a}$$

The denominator is a normalization factor chosen so that $\sum_{\nu_1} p_1(\nu_1) = 1$. The numerator is the sum over all ν_0 of the Boltzmann factor of the state ν_1 if the neighboring state is ν_0 times $p_0(\nu_0)$. In a similar manner, we see that since $p_2(\nu_2)$ depends only upon the state ν_1,

$$\begin{aligned} p_2(\nu_2) &= \frac{\sum_{\nu_1} \exp\{-[V(\nu_2,\nu_1)+V(\nu_2)]/kT\}p_1(\nu_1)}{\sum_{\nu_2,\nu_1} \exp\{-[V(\nu_2,\nu_1)+V(\nu_2)]/kT\}p_1(\nu_1)} \\ &= \frac{\sum_{\nu_1,\nu_0} \exp\{-[V(\nu_2,\nu_1)+V(\nu_1,\nu_0)+V(\nu_2)+V(\nu_1)]/kT\}p_0(\nu_0)}{\sum_{\nu_2,\nu_1,\nu_0} \exp\{-[V(\nu_2,\nu_1)+V(\nu_1,\nu_0)+V(\nu_2)+V(\nu_1)]/kT\}p_0(\nu_0)}. \end{aligned} \tag{3.4a}$$

In general, we find

$$p_m(\nu_m) = \frac{\sum_{\nu_{m-1}}\cdots\sum_{\nu_0} \exp\{-\sum_{j=1}^{m}[V(\nu_j)+V(\nu_j,\nu_{j-1})]/kT\}p_0(\nu_0)}{\sum_{\nu_m}\cdots\sum_{\nu_0} \exp\{-\sum_{j=1}^{m}[V(\nu_j)+V(\nu_j,\nu_{j-1})]/kT\}p_0(\nu_0)}. \tag{3.5a}$$

CC-0. In Public Domain. Gurukul Kangri Collection, Haridwar

Digitized by Arya Samaj Foundation Chennai and eGangotri

This procedure of adding one layer of particles at a time describes a Markov process. The probability distribution of the mth layer depends only upon the state of the $m-1$th layer. The usual theory of Markov processes is ideally suited to the analysis of this type of system.

We can simplify considerably the notation of Eqs. (3.3a) to (3.5a) by considering $\mathbf{p}_j$ to be a vector with components $p_j(\nu_j)$, $\mathbf{I}$ a vector with unit component for each state ν, and $\mathbf{P}'$ the matrix defined in Eq. (2.2b). The above equations can then be written in the usual matrix notation

$$\mathbf{p}_1=\frac{\mathbf{P}'\cdot\mathbf{p}_0}{\mathbf{I}\cdot\mathbf{P}'\cdot\mathbf{p}_0}, \tag{3.3b}$$

$$\mathbf{p}_2=\frac{\mathbf{P}'\cdot\mathbf{p}_1}{\mathbf{I}\cdot\mathbf{P}'\cdot\mathbf{p}_1}=\frac{(\mathbf{P}')^2\cdot\mathbf{p}_0}{\mathbf{I}\cdot(\mathbf{P}')^2\cdot\mathbf{p}_0}, \tag{3.4b}$$

$$\mathbf{p}_m=\frac{\mathbf{P}'\cdot\mathbf{p}_{m-1}}{\mathbf{I}\cdot\mathbf{P}'\cdot\mathbf{p}_{m-1}}=\frac{(\mathbf{P}')^m\cdot\mathbf{p}_0}{\mathbf{I}\cdot(\mathbf{P}')^m\cdot\mathbf{p}_0}. \tag{3.5b}$$

The matrix $\mathbf{P}'$ is similar to the symmetric matrix $\mathbf{P}$ and thus has a set of eigenvalues λ_j and complete set of eigenfunctions ψ_j. We can expand $\mathbf{p}_0$ in a series of these ψ_j,

$$\mathbf{p}_0=\sum_j c_j\psi_j. \tag{3.6}$$

By definition of the λ_j and ψ_j,

$$\mathbf{P}'\psi_j=\lambda_j\psi_j.$$

Therefore, (3.5b) becomes

$$\mathbf{p}_m=\Big[\sum_j c_j\lambda_j{}^m\psi_j\Big]\Big/\Big[\sum_j c_j\lambda_j{}^m(\mathbf{I}\cdot\psi_j)\Big]. \tag{3.7}$$

We again order the eigenvalues so that $\lambda_1\geq\lambda_2\geq\lambda_3\cdots$, so that if $c_1\neq 0$,

$$\mathbf{p}_m=\frac{\psi_1+\sum_{j\geq 2}(\lambda_j/\lambda_1)^m c_j\psi_j/c_1}{(\mathbf{I}\cdot\psi_1)+\sum_{j\geq 2}(\lambda_j/\lambda_1)^m c_j(\mathbf{I}\cdot\psi_j)/c_1}. \tag{3.8}$$

If λ_1 is neither degenerate nor asymptotically degenerate as $m\to\infty$, $(\lambda_j/\lambda_1)^m\to 0$ and

$$\mathbf{p}_m\to\psi_1/(\mathbf{I}\cdot\psi_1) \quad \text{as} \quad m\to\infty.$$

This means that the distribution of layers far from the original layer are independent of the coefficients c_j which describe the distribution of the zero layer. $\mathbf{p}_m$ is independent of $\mathbf{p}_0$. If there is no degeneracy, there is no long-range order.

If, on the other hand, the largest eigenvalue were degenerate, for example if $\lambda_1=\lambda_2>\lambda_3\cdots$, then

$$\mathbf{p}_m\to[c_1\psi_1+c_2\psi_2]/[c_1(\mathbf{I}\cdot\psi_1)+c_2(\mathbf{I}\cdot\psi_2)].$$

The distribution of a layer arbitrarily far from the original layer still depends upon c_2 and c_1 which in turn depend upon $\mathbf{p}_0$. A degeneracy of the largest eigenvalue therefore implies the existance of long-range order.

The question of what matrices have degenerate largest eigenvalues becomes a significant one. There is in some cases a definite answer to this question. Frobenius proved that if all the matrix elements of a finite matrix are positive and nonzero, then the largest eigenvalue is nondegenerate.

The matrix elements of $\mathbf{P}'$ are indeed positive and nonzero. It follows then that if we are to have long-range order, it is necessary that the number of states ν be infinite or become infinite as $m\to\infty$. In a two-dimensional lattice such as the Ising lattice, we are interested in the properties of lattices in which the number of particles per row is of the same order of magnitude as the number of rows. If we let $m\to\infty$, we must also let the number of particles per row $n\to\infty$, and the λ_j will depend upon m in the sense that as we add new layers (rows) we also wish to add new particles to the layers. As $m\to\infty$, the number of states per row also becomes infinite. Frobenius' theorem thus does not apply to a lattice infinite in two or more directions but it does forbid long-range order in most (if not all) systems of interest which are infinite in only one direction.[11,17]

Just as the matrix $\mathbf{P}$ describes a Markov process that gives the distribution of the mth layer in terms of the distribution of the $m-1$th layer, the matrix $\mathbf{M}$ discussed near the end of Sec. 2.1 described a Markov process giving the distribution of the particles $j+1$ to $j+n$ in terms of the distribution of the particles j to $j+n-1$. Notice that the "screw" boundary conditions make it possible to generate a lattice by iterating the procedure of adding a single particle at a time. This is not true of the periodic boundary conditions because one must change this procedure of adding single particles when one has filled a row and starts a new row. One can also build a three-dimensional lattice by an iterative procedure of adding single particles.

Frobenius' theorem does not directly apply to the matrix $\mathbf{M}$ because not all matrix elements of $\mathbf{M}$ are nonzero. There are equivalent theorems which do apply, however.

4. THE TWO-DIMENSIONAL SQUARE LATTICE

The solution of the two-dimensional square Ising lattice in zero magnetic field has been obtained in several ways. No one has found a short cut to success. All these methods are quite lengthy and very tricky. It would hardly be appropriate to describe in detail here all the various procedures. We shall discuss only one combinational method and one algebraic method.

Although the original solution by Onsager[4] could be easily followed from step to step, the motivations and over-all plan were obscure. In Sec. 4.2, we shall attempt to give some of the key steps in this original formulation and to describe, as we see it, the motivations that lead from one step to the next. We have

CC-0. In Public Domain. Gurukul Kangri Collection, Haridwar

Digitized by Arya Samaj Foundation Chennai and eGangotri

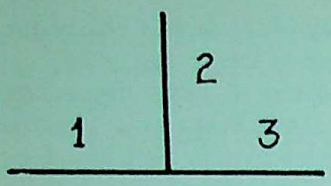


FIG. 6. Polygons containing the above type of connecting bonds are not to be counted.

chosen to discuss this method as the one example of an algebraic procedure not because we consider it the best, but because it affords an opportunity to present some ideas about it that have circulated privately but have never been published.

Interest in this problem reached a climax several years after Onsager's publication when Kaufman[5] described a simplified procedure based upon the theory of spinor representations of the rotation group. Her analysis was not only elegant but very clearly presented even to those not disciplined in the mathematical techniques employed. We shall have little to say about this procedure here for we see no way to add to or improve upon her analysis of the problem. For the details of this method, which in many ways still seems the most elegant despite more recent developments, we refer the reader to her original presentation.

Nambu[18] also independently discovered a method which was in principle very similar to Kaufman's.

Following these papers came a rapid sequence of minor refinements and applications. The method was also applied[13] to the matrix **M** discussed in Sec. 2 instead of the matrix **P** originally considered by Kaufman. It was also applied to other lattice types than the square lattice. Some of these supplementary calculations are discussed in Secs. 5 and 6.

In Sec. 4.1 we discuss one of the most recent techniques based upon the combinational procedure described in Sec. 2.2. This technique was discovered by Kac and Ward.[7] Domb has also solved the problem by obtaining recursion formulas for the $n(r)$ of Eq. (2.23). The method has not been published but has been described as being very lengthy.

The thermodynamic properties of the square lattice, based upon the results of Secs. 4.1 and 4.2, are summarized in Sec. 4.3.

4.1 Combinatorial Method

In this section we shall obtain an expression for the partition function of a two-dimensional square lattice by employing a combinatorial method, recently developed by Kac and Ward. This method is "elementary" in the sense that no spinors, Lie algebras, or other specialized algebraic techniques of the type used in the matrix method solution are required; however, it introduces some problems in topology that have not been rigorously solved. The starting point is the formula (2.24)

$$Z_{n,m}=(2\cosh K\cosh K')^{mn}\sum_{r,s} n(r,s)\tanh^r K\tanh^s K' \tag{4.1}$$

for the partition function of a square lattice of nm lattice points. Here $n(r, s)$ is the number of closed graphs with $r+s$ bonds, r in the horizontal and s in the vertical directions, which can be constructed on the lattice. The aim is to construct a matrix **A** whose determinant generates terms which are in a one-to-one correspondence with closed graphs on the lattice. We seek an **A** such that

$$Z_{n,m}=(2\cosh K\cosh K')^{mn}\det\mathbf{A}. \tag{4.2}$$

To see that there is a relation between determinants and closed graphs formed by connecting points on a lattice, let us examine the defining equation of the determinant of an Nth order matrix whose elements are A_{ij}

$$\det\mathbf{A}=\sum\pm A_{1k_1}A_{2k_2}\cdots A_{Nk_N}. \tag{4.3}$$

The set of indices $k_1, k_2, \cdots, k_N$ is some permutation of the indices $1, 2, \cdots, N$: the sum extends over all permutations, and the sign is $+$ or $-$ accordingly as the permutation is odd or even (it is even if an even number of interchanges of the indices $k_1, k_2, \cdots, k_N$ are required to put them in the order $1, 2, \cdots, N$).

It is well known in the theory of permutations that a given permutation can be expressed as a product of cyclic (see Carmichael, *Theory of Finite Groups*, Ginn and Company, 1937, p. 6) permutations, no two of which have a letter in common. Hence, the product of the A_{ik}'s in any term of (4.3) can be rearranged in the form

$$\pm(A_{i_1i_2}A_{i_2i_3}\cdots A_{i_{s(1)}i_1})(A_{j_1j_2}A_{j_2j_3}\cdots A_{j_{s(2)}j_1})\cdots \times(A_{l_1l_2}A_{l_2l_3}\cdots A_{l_{s(r)}l_1}). \tag{4.4}$$

The permutation $1, 2, 3\cdots N\rightarrow k_1, k_2, \cdots, k_N$ is thus described as a cyclic permutation of $i_1, i_2, i_3, \cdots, i_{s(1)}$ times a cyclic permutation of $j_1, j_2, j_3, \cdots, j_{s(2)}$, etc. The sign is $+$ or $-$ accordingly as the second indices

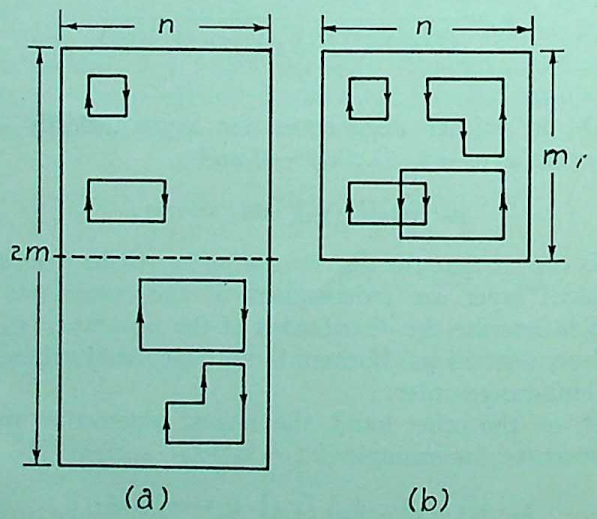


FIG. 7. Diagram (a) illustrates a closed graph on an $n\times 2m$ lattice, whereas (b) illustrates the corresponding oriented closed graph on an $n\times m$ lattice as described in the text.

CC-0. In Public Domain. Gurukul Kangri Collection, Haridwar

Digitized by Arya Samaj Foundation Chennai and eGangotri

$i_2, i_3, \cdots, i_{s(1)}, i_1; j_2 \cdots j_{s(2)}, j_1; \cdots$ represent an even or odd permutation of the first indices $i_1, i_2, \cdots i_{s(1)}; j_1, j_2 \cdots$. The number of interchanges necessary to bring $i_2, i_3, \cdots, i_{s(1)}, i_1$ into the order $i_1, i_2, i_3, \cdots, i_{s(1)}$ is $s(1)-1$ as one can easily see by interchanging successively the last and next to last numbers, the next to last and second from the last, etc. Thus, the sign is

$$(-1)^{s(1)-1}(-1)^{s(2)-1}(-1)^{s(3)-1}\cdots(-1)^{s(r)-1}. \quad (4.5)$$

We now ask in what way are the terms (4.4) similar to terms of the expansion of Z? First, we note that the cycles of (4.4) can be pictured as simple closed polygons. If the indices $i_1, i_2, \cdots$ represent points of a lattice and the matrix element $A_{i_1 i_2}$ represents a connection (bond) joining i_1 and i_2, then (4.4) is associated with the superposition of r simple closed polygons, one connecting the points $i_1, i_2, \cdots, i_{s(1)}$ another connecting $j_1, j_2, \cdots, j_{s(2)}$, etc.

This association is not quite what is required, for these polygons are somewhat different from the closed graphs of Z. The polygon $i_1, i_2, \cdots, i_{s(1)}$ has no point in common with $j_1, \cdots, j_{s(2)}$; they are *disjoint* polygons. As we saw in Sec. 2.2, the closed graphs of Z were not restricted to be the superposition of disjoint simple closed polygons but rather the superposition of simple closed polygons with no common sides.

This restriction on the polygons which generate Z suggests that perhaps we can establish a correspondence between the *sides* of these polygons and the indices of (4.4). Indeed, we can in this way come one step closer to success because the bonds of the simple closed polygons which generate the closed graphs are such that each bond joins another bond in a sequence which forms a cycle, but the same bond can appear in only one cycle. These are just the properties of the indices of (4.4).

In (4.4) we see that each bond is so represented as both a first and a last index of some A_{jk}, i.e., each bond is part of some polygon. In Z, however, not all points are parts of a graph. This can be remedied in a rather trivial manner. We interpret a cycle of order 1, an element A_{jj}, as indicating the absence of the jth bond in any polygon; the jth bond does not connect with anything except itself.

We have now established at least a one way correspondence between closed graphs of Z and terms of det **A**. There is for every closed graph a corresponding term in det **A**. There are many terms of det **A** which must be eliminated. The only nonzero matrix elements of $A_{jj'}$ would be those between two bonds j and j' having an end point in common; thus, most of the matrix elements would be zero.

There remain some very troublesome barriers to establishing a one-to-one correspondence between terms of Z and the terms of det **A**. The cycles $A_{i_1 i_2} A_{i_2 i_3} \cdots A_{i_{s(1)} i_1}$ and $A_{i_1 i_{s(1)}} \cdots A_{i_3 i_2} A_{i_2 i_1}$, which are inverses of each other, correspond to the same polygon. Also terms in the expansion of the determinant which correspond to cycles such as $A_{12}A_{21}$ or $A_{12}A_{23}A_{31}$ (see Fig. 6) are not related to any closed graphs on our lattice. The difficulty here seems to be rather fundamental. The terms of the determinant expansion seems to be more closely associated with oriented polygons, those traversed in a given direction. We must be able to distinguish between the two ends of a bond so that we can connect a new bond only to the "loose end" of its predecessor.

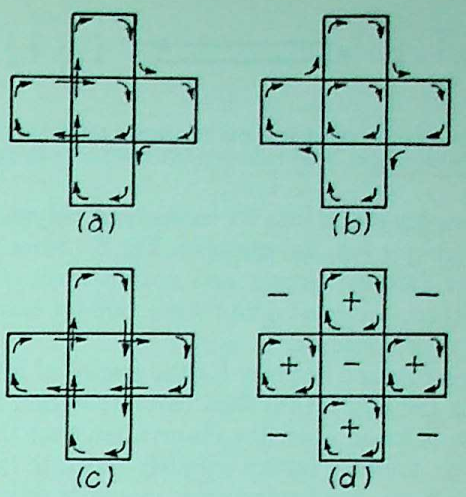


FIG. 8. The closed graph illustrated above can be oriented in many ways of which four examples are shown. Each is associated with a superposition of simple clockwise oriented polygons. If we first separate the space into two regions designated in (d) by + and −, then one can assign the unique orientation (d) to the closed graph by always choosing the bond orientation so that the + region is to the right of this direction.

Kac and Ward[7] overcame this hurdle by showing that the expansion of the partition function of an $n \times 2m$ lattice could be discussed in terms of oriented polygons on an $n \times m$ lattice. This correspondence is illustrated in Fig. 7. In the $n \times 2m$ lattice (a) upon which we draw the closed graphs that generate Z, we disregard those polygons which cross the center line. We are therefore really considering an $n \times 2m$ lattice consisting of two independent $n \times m$ lattices so that

$$Z_{n,2m} = Z_{nm}^2.$$

For any closed graph on the $n \times 2m$ lattice (7a), we construct oriented graphs on the $n \times m$ lattice (7b) in the following manner. We first adapt a rule for uniquely orienting the bonds of all graphs in Fig. 7a, a rule which is the same for both the upper and lower parts of Fig. 7a. Those graphs or parts of graphs in the upper half of (a) are transcribed on to (b). Those in the lower half of (a) are reflected across the center line and then transcribed on to (b). Kac and Ward suggested that the graphs in 7a be oriented "clockwise." This is a rule which is unambiguous if the graphs are simple closed polygons. It is also easily applied to the superposition of disjoint simple closed polygons each of which would be oriented clockwise.

Even though any closed graph is a superposition of simply closed polygons with no common sides, each of which would be oriented clockwise, the decomposition

CC-0. In Public Domain. Gurukul Kangri Collection, Haridwar

Digitized by Arya Samaj Foundation Chennai and eGangotri

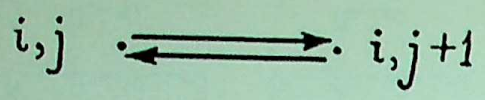


FIG. 9. An oriented polygon is not to contain this bond connection in which a right bond follows a left bond (or vice versa).

of a complex graph into its component polygons is not always unique (see, for example, Fig. 8). Since we want to count different graphs and not all ways of decomposing them, we must adapt some rule for extracting a unique decomposition.

Such a rule can be given for the graphs of interest by recalling the basis of the dual theorem in Sec. 3.1. This theorem is based upon the observation that the closed graphs on the dual lattice uniquely separate the lattice into two parts, one having spins in one direction (up or down) and the other part having the opposite spin (down or up). For any closed graph, it is possible to separate the space into two such parts which we desig- by + and − (see Fig. 8). One can then uniquely assign a direction of the bonds to be such that a + region is always to the right of the bond direction. The unique decomposition into simple closed polygons is achieved by choosing those polygons surrounding + regions and orienting them clockwise.

The problem of calculating Z has been described now as a problem of counting oriented closed graphs of the above type. The plan to write

$$Z_{n,2m}=Z_{n,m}^{2}=(2\cosh K\cosh K')^{2mn}\det \mathbf{A} \quad (4.6)$$

has been aided by the fact that det A does count oriented polygons, but we have achieved this goal at the expense of complicating the type of oriented graphs to be counted.

A bond in Fig. 7b can now appear at most twice, which means that it can no longer be associated in a one-to-one manner with the indices of (4.4). It will now be necessary to establish a two-to-one correspondence. Although the correspondence is not as elegant as one might have hoped, the scheme that finally leads to success is to associate directed bonds with the indices of (4.4).

A directed bond can be characterized by its direction and the lattice point toward which it is directed. Instead of numbering the bonds consecutively with a single index as in (4.4), it is convenient to replace these indices by a set of three parameters. The pair of variables (i, j) will be used to represent the row and column which locate the lattice point toward which the bond of interest is directed. The letter Γ will be used to represent the direction of the bond. Γ will have one of four values R, L, D, or U, depending on whether the bond is directed to the right, left, up or down. The symbol

$$A(i, j, \Gamma; i', j', \Gamma') \quad (4.7)$$

will replace the matrix element $A_{j,k}$ of (4.4). This symbol will be associated with an ordered pair of bonds, the first of which is in the direction Γ, directed toward the lattice point (i, j) and the second, which will be interpreted to start at (i, j), proceeds in the direction Γ' toward the lattice point (i', j'). The matrix (4.7) will be of dimension $4nm$ with 4 values of Γ for each of the nm lattice points.

Even though we have not yet completely established the desired one-to-one correspondence between unoriented graphs of Fig. 7a and the terms of det A, let us consider some properties that should be required of the matrix A.

As was indicated earlier in this section, in order to make the terms in the expansion of det A correspond only to oriented polygons on our lattice, we must set all matrix elements $A(i, j, \Gamma; i', j', \Gamma')$ equal to zero unless the point (i, j) can be connected by a bond in the direction Γ' to the point (i', j'). (The only exceptions to this are the diagonal elements which represent the bonds that are absent.) Of these possibilities we also wish to rule out those situations illustrated by Fig. 9 in which one step on a directed polygon is followed by a retracing of itself in the opposite direction. These rules can be summarized by the condition $A(i, j, \Gamma; i', j', \Gamma')=0$ unless

$$i=i', \quad j=j' \quad \text{and} \quad \Gamma=\Gamma', \quad (4.8a)$$
$$i=i', \quad j=j'+1, \quad \Gamma'=L, \quad \text{and} \quad \Gamma\neq R, \quad (4.8b)$$
$$i=i', \quad j=j'-1, \quad \Gamma'=R, \quad \text{and} \quad \Gamma\neq L, \quad (4.8c)$$
$$i=i'+1, \quad j=j', \quad \Gamma'=D, \quad \text{and} \quad \Gamma\neq U, \quad (4.8d)$$

or

$$i=i'-1, \quad j=j', \quad \Gamma'=U, \quad \text{and} \quad \Gamma\neq D. \quad (4.8e)$$

To make these conditions also valid at the boundary, we introduce periodic boundary conditions as in Sec. 2.1 by wrapping the lattice on a torus. We see then that the above conditions are invariant to rotations of the torus about either of its axes, i.e., to cyclic permutations of the indices $i\rightarrow i+1 (m\rightarrow m+1=1)$ or $j\rightarrow j+1 (n\rightarrow n+1=1)$. Indeed, we expect that the matrix elements themselves must be invariant to such transformations since these transformations leave the geometry of the lattice invariant.

In order to take advantage of the periodicity of the lattice, it is convenient to imagine the $4m\times n$th order matrix as consisting 4×4 blocks or as an $m\times n$th order matrix, the matrix elements of which are themselves 4×4 matrices. We use the convention that $\mathbf{A}(i, j; i', j')$ is for each i, j, i' and j' a 4×4 matrix with matrix elements $A(i, j, \Gamma; i', j', \Gamma')$. We realize that the matrices $\mathbf{A}(i, j; i', j')$ should be invariant to the cyclic transformations of the lattice, therefore

$$\mathbf{A}(i, j; i', j')=\mathbf{A}(0, 0; i'-i, j'-j). \quad (4.9)$$

In view of the conditions (4.8), the only independent matrices (4.9) that are not null matrices are $\mathbf{A}(0, 0; 0, 0)$, $\mathbf{A}(0, 0; 0, +1)$, $\mathbf{A}(0, 0; 0, -1)$, $\mathbf{A}(0, 0; +1, 0)$, and $\mathbf{A}(0, 0; -1, 0)$.

CC-0. In Public Domain. Gurukul Kangri Collection, Haridwar

Digitized by Arya Samaj Foundation Chennai and eGangotri

According to (4.8), A(0, 0, 0, 0) is a diagonal matrix, the diagonal elements of which correspond to the absence of a bond in a closed graph. All graphs are not weighted equally as seen by (4.1). The weight is assigned according to the number of vertical and horizontal bonds in the graph. Since the total number of possible bonds of a graph is fixed at $4nm$, this unequal weighting can be introduced either into the off diagonal matrices A(0, 0, 0; −1), etc., which in a certain sense count the number of such bonds or into A(0, 0, 0, 0) which counts the number of such bonds that are missing.

Another way of describing this freedom is to recall that multiplication of any row or column of a matrix by some constant changes the determinant into this constant times the original determinant. Thus, we can always replace a determinant, by a known multiple of another determinant all of whose diagonal elements are one.

We may, without any loss of flexibility, set

$$\mathrm{A}(0, 0, 0, 0) = \mathrm{I}_4, \tag{4.10a}$$

I_4 being the 4×4 identity matrix, and then choose the other matrices so as to give the desired weights.

We know that for every horizontal bond that appears in a graph, (4.4) must contain a factor $x = \tanh K$. The number of such bonds will be equal to the number of times a matrix element from A(0, 0, 0, ±1) appears in (4.4). To simplify notation we write

$$\mathrm{A}(0, 0, 0, \pm 1) \equiv x\mathrm{A}(0, \pm 1), \quad x = \tanh K, \tag{4.10b}$$

similarly

$$\mathrm{A}(0, 0, \pm 1, 0) \equiv y\mathrm{A}(\pm 1, 0), \quad y = \tanh K'. \tag{4.10c}$$

A(0, ±1) and A(±1, 0) will now be matrices independent of x and y. They will depend only upon the geometry of the lattice.

Most of the matrix elements of these matrices will also vanish as a result of (4.8). A(0, 1) must in fact be of the form

$$\mathrm{A}(0, +1) = \begin{pmatrix} \gamma & 0 & 0 & 0 \\ 0 & 0 & 0 & 0 \\ \beta & 0 & 0 & 0 \\ \alpha & 0 & 0 & 0 \end{pmatrix}, \tag{4.11a}$$

in which the matrix indices are taken in the order R, L, U, and D and γ, β, and α are as yet unspecified. Thus, γ corresponds to an element with $\Gamma = R$, $\Gamma' = R$; β corresponds to the element $\Gamma = U$, $\Gamma' = R$ and α to the element $\Gamma = D$, $\Gamma' = R$.

From A(0, −1), one uniquely determines also A(0, +1) and A(±1, 0). We ask that the matrix (4.7) be invariant to the interchange of x and y along with the transformation which rotates the positive horizontal direction into the positive vertical direction (a 90° rotation if the lattice were on a flat surface). Such a transformation preserves the topology of the graphs. Thus $A(i, j, \Gamma; i', j', \Gamma')$ must remain invariant if we simultaneously send $i \to j$, $j \to -i$, $i' \to j'$, $j' \to -i'$, $R \to U$, $U \to L$, $L \to D$, $D \to R$ and $x \leftrightarrow y$. It follows from this that

$$\mathrm{A}(+1, 0) = \begin{pmatrix} 0 & 0 & \alpha & 0 \\ 0 & 0 & \beta & 0 \\ 0 & 0 & \gamma & 0 \\ 0 & 0 & 0 & 0 \end{pmatrix}, \tag{4.11b}$$

$$\mathrm{A}(0, -1) = \begin{pmatrix} 0 & 0 & 0 & 0 \\ 0 & \gamma & 0 & 0 \\ 0 & \alpha & 0 & 0 \\ 0 & \beta & 0 & 0 \end{pmatrix}, \tag{4.11c}$$

$$\mathrm{A}(-1, 0) = \begin{pmatrix} 0 & 0 & 0 & \beta \\ 0 & 0 & 0 & \alpha \\ 0 & 0 & 0 & 0 \\ 0 & 0 & 0 & \gamma \end{pmatrix}. \tag{4.11d}$$

One might be tempted to also make A invariant to reflections. Although it is true that Z is invariant to reflections, the topology of the oriented polygons is not invariant; a reflection takes a clockwise polygon into a counterclockwise polygon. A will in fact not be invariant to reflections. α corresponds to a counterclockwise turn of $\pi/2$, β to a clockwise turn, and γ to no turn of connecting bonds (see Fig. 10).

The values of α, β, and γ are now to be chosen so that any term of the expansion of det A corresponding to a superposition of simple closed polygons of the prescribed type contributes $1 \times \tanh^r K \tanh^s K' = x^r y^s$ in accordance with (4.1). The substitution (4.10) assures that a term of the expansion will have the correct power of x and y but (4.5) indicates that we must choose α, β, and γ to give a positive sign.

Each simple closed polygon on a square lattice has an even number of bonds, therefore $s(j) - 1$ in Eq. (4.5) will be an odd number and the sign (4.5) will be $(-1)^r$. To make the terms positive, α, β, and γ must be chosen so that an additional factor of (-1) appears with each cycle in the expansion. A simple closed polygon directed in a clockwise direction has four more clockwise turns then counterclockwise turns. Thus, in (4.4) there will be 4 more powers of β than α for each clockwise cycle and 4 more powers of α than β for each counterclockwise cycle. There is for each cycle a factor of the form $(\alpha\beta)^n\beta^4$ or $(\alpha\beta)^n\alpha^4$ for some n. We can obtain the desired factor $(-1)^r$ if we choose $\alpha = \beta^{-1}$, $\alpha^4 = \beta^4 = -1$, and $\gamma = 1$. Thus,

$$\alpha = \exp(i\pi/4), \quad \beta = \exp(-i\pi/4), \quad \gamma = 1. \tag{4.12}$$

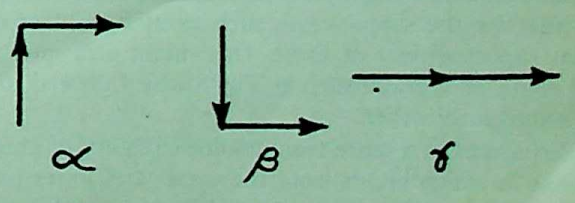


FIG. 10. The three types of bonds connections illustrated above correspond to the elements α, β, and γ in Eq. (4.11).

CC-0. In Public Domain. Gurukul Kangri Collection, Haridwar

Digitized by Arya Samaj Foundation Chennai and eGangotri

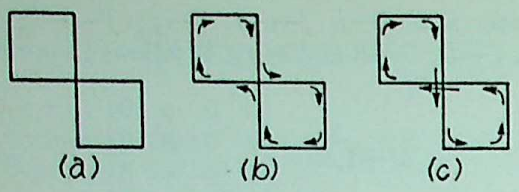


FIG. 11. The unoriented closed graph (a) corresponds to many oriented graphs. Among these are the unicursal paths (b) and (c) in which both polygons of (a) are traversed in a single cycle.

The matrix **A** has been completely specified on the basis of a few simple requirements which do, however, guarantee that det **A** will count correctly at least the simple closed polygons and superpositions of disjoint polygons on the lattice of Fig. 7b. The terms in det **A** which are associated with the bonds appearing in such graphs, consist of one term for each possible combination of clockwise and counterclockwise orientation of the disjoint polygons and each such combination does appear once in a figure such as 7b.

Det **A** also correctly counts many other types of graphs but there is as yet no proof that it correctly counts *all* possible graphs. Actually we know that there are some which are not counted correctly, namely those which "loop" the torus. Such failures would not be considered serious however since one would attribute them to the selection of periodic boundary conditions.

Kac and Ward considered a few simple cases of overlapping polygons and showed that they also are counted correctly.

One class of configurations which they considered was the graphs consisting of simple closed polygons on the lattice 7b which touch each other at single points only (no overlapping bonds). A simple example is given in Fig. 11a. A troublesome feature of such graphs is that det **A** includes terms corresponding to unicursal paths, i.e., those which traverse more than one polygon in a single cycle as illustrated in Figs. 11b and 11c. One readily sees that Fig. 11b has an excess of 4 clockwise turns and therefore is counted as a positive term, whereas 11c has an equal number of clockwise and counterclockwise turns and therefore contributes a negative term to det **A**. One can easily check that the net contribution of all unicursal paths of Fig. 11a is zero. Kac and Ward claim that this is true of the entire class of graphs which are composed of more than one polygon and in which each polygon has a point in common with at least one other polygon.

It is apparent that after the elimination of the unicursal paths, det **A** properly counts all possible graphs at least for the simple cases such as in Fig. 11 or disjoint superpositions of these. One might still question the count on a graph such as Fig. 8 which proved to be an annoyance earlier.

Perhaps even a more troublesome category of graphs is that in which bonds from the upper and lower parts of Fig. 7a overlap when transcribed onto Fig. 7b. Because of the choice of clockwise orientations in Fig. 7a, these double bonds may consist of either two bonds directed the same or two bonds directed oppositely. Since indices in (4.4) are never repeated in the same term, det **A** will not contain terms corresponding to graphs having an identical pair of bonds such as in Fig. 12a or Fig. 13a.

On the other hand, det **A** will count some superpositions of clockwise oriented polygons which have common sides forming a pair of oppositely directed bonds such as Figs. 12b and 13b, and even single polygons which loop back on themselves to form an oppositely directed pair as also illustrated within Fig. 13b and in Fig. 14. None of these graphs appear on the lattice of Fig. 7b because the graphs of Fig. 7a do not contain double bonds.

Kac and Ward did resolve the difficulties presented by the cases illustrated by Figs. 12 and 14. The contributions of Figs. 14a and 14b cancel as do all terms corresponding to similar type graphs. Regarding the situation in Figs. 12a and 12b, they pointed out that there is a one-to-one correspondence between graphs of type 12a and those of type 12b. Instead of counting the "allowed" polygons 12a, the determinant counts the "forbidden" polygons 12b.

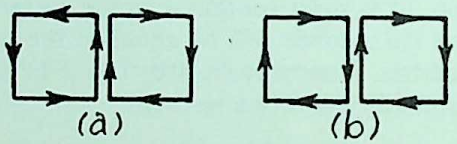


FIG. 12. (a) illustrates a superposition of simple closed polygons forming an identical pair of bonds. (b) illustrates a superposition of polygons forming an oppositely directed pair of bonds. Det **A** counts only type (b), whereas Fig. 7b contains only graphs of type (a).

A graph such as in Fig. 13 which contains both an identical pair and an oppositely directed pair of bonds was not considered. One cannot establish a one-to-one correspondence between allowed and forbidden paths by merely reversing the direction of one of the polygons as in Fig. 12.

It is certain that det **A** does correctly count all closed graphs since the partition function derived below checks (at least for large lattices) with that obtained by other methods. The manner in which some complicated graphs are counted is still uncertain, however. Although the analysis is as yet logically incomplete, the ideas presented are very praiseworthy.

It is worth pointing out here that this method of counting cannot be generalized in any obvious way to the three-dimensional problem nor to the two-dimensional problems with a magnetic field or longer-range interactions. The magnetic field problem involves a much more complicated counting procedure. One must keep account not only of the number of bonds in the polygon but also the area. The crossing of diagonal bonds in the next nearest neighbor problem causes

CC-0. In Public Domain. Gurukul Kangri Collection, Haridwar

Digitized by Arya Samaj Foundation Chennai and eGangotri

trouble, whereas in three dimensions, one encounters polygons with knots. Perhaps even more serious is the fact that a polygon in three dimensions does not divide the space into an "inside and outside." The solution above, thus, rests heavily upon the peculiar topological properties of this particular problem.

In view of the evidence presented above, we shall accept as correct the postulate that det **A** correctly counts closed graphs and proceed to obtain an explicit expression for Z based upon (4.6).

There would be little advantage in expressing Z in terms of det **A** if it were not for the fact that det **A** is invariant to any similarity transformation of **A**. In particular det **A** is equal to the product of the eigenvalues of **A**.

The matrix **A** is defined by Eqs. (4.7), (4.9), (4.10), (4.11), and (4.12), of which Eq. (4.10) represents the key to the simplification of det **A**. This equation expresses the cyclic character of **A** and immediately suggests that one transform the matrix **A** by a double Fourier expansion, thus transforming to a set of base vectors that are eigenfunctions of the two cyclic permutation operators (one for the vertical symmetry and one for the horizontal symmetry) that leave the lattice invariant.

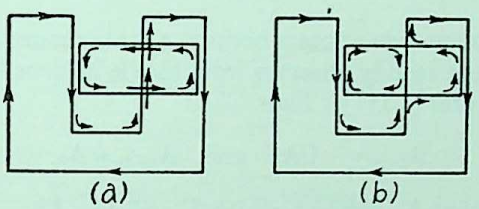


FIG. 13. A graphs such as (a) can appear as a graph in Fig. 7b but will not by counted by det **A** because it contains an identical pair of bonds. It also contains an oppositely directed pair. (b) illustrates another orientation of the same graph with no identical bond pairs.

We define a unitary matrix **R** of dimension $4nm$ with matrix elements

$$\mathbf{R}(k,l;k',l')=(nm)^{-\frac{1}{2}}\mathbf{I}_4\exp(2\pi ikk'/m+2\pi ill'/n). \quad (4.13)$$

The convention here is consistent with that used in Eq. (4.10). $\mathbf{I}_4$ is the 4×4 identity and $\mathbf{R}(k,l;k',l')$ is a 4×4 matrix. If we define **B**

$$\mathbf{B}\equiv\mathbf{RAR}^{-1}, \quad (4.14)$$

then $\det\mathbf{A}=\det\mathbf{B}$. One easily finds by using the orthogonality properties of the Fourier exponentials that

$$\mathbf{B}(k,l;k',l')=\delta_{kk'}\delta_{ll'}\sum_{s=1}^{n}\sum_{t=1}^{m}\mathbf{A}(0,0;t,s)\times\exp(-2\pi ikt/m-2\pi ils/n). \quad (4.15)$$

All elements of **B** vanish except those for which $k=k'$ and $l=l'$. Substituting Eq. (4.10) into (4.15), we find

$$\mathbf{B}(k,l;k,l)\equiv\mathbf{B}(k,l)=\mathbf{I}_4+y\mathbf{A}(1,0)\times\exp(-2\pi ik/m)+y\mathbf{A}(-1,0)\exp(2\pi ik/m)+x\mathbf{A}(0,1)\exp(-2\pi il/n)+x\mathbf{A}(0,-1)\exp(2\pi il/n)$$

$$=\begin{pmatrix}1+x\epsilon_l^{-1} & 0 & y\delta_k^{-1}\alpha & y\delta_k\alpha^{-1}\\ 0 & 1+x\epsilon_l & y\delta_k^{-1}\alpha^{-1} & y\delta_k\alpha\\ x\epsilon_l^{-1}\alpha^{-1} & x\epsilon_l\alpha & 1+y\delta_k^{-1} & 0\\ x\epsilon_l^{-1}\alpha & x\epsilon_l\alpha^{-1} & 0 & 1+y\delta_k\end{pmatrix}, \quad (4.16)$$

where

$$\epsilon=\exp(2\pi il/n),\quad \delta=\exp(2\pi ik/m),\quad \alpha=\exp(i\pi/4).$$

Since the eigenvalues of **A** are the eigenvalues of the $\mathbf{B}(k,l)$

$$\det\mathbf{A}=\prod_{k=1}^{m}\prod_{l=1}^{n}\det\mathbf{B}(k,l)$$

$$=\prod_{k=1}^{m}\prod_{l=1}^{n}\{(1+x^2)(1+y^2)-y(1-x^2)(\epsilon_l+\epsilon_l^{-1})-x(1-y^2)(\delta_k+\delta_k^{-1})\},$$

$$Z_{n,m}{}^2=2^{2nm}\prod_{k=1}^{m}\prod_{l=1}^{n}\{\cosh2K\cosh2K'-\sinh2K'\cos(2\pi l/n)-\sinh2K\cos(2\pi k/m). \quad (4.17)$$

The quantity of particular interest is

$$\lim_{n,m\to\infty}(nm)^{-1}\log Z$$

$$=\log2+\tfrac{1}{2}(mn)^{-1}\sum_{k=1}^{m}\sum_{l=1}^{n}\log[\cosh2K\cosh2K-\sinh2K'\cos(2\pi l/n)-\sinh2K\cos(2\pi k/m)]$$

$$=\log2+\tfrac{1}{2}\pi^{-2}\int_0^{\pi}\int_0^{\pi}\log(\cosh2K\cosh2K'-\sinh2K\cos w-\sinh2K'\cos w')dwdw'. \quad (4.18)$$

An attempt has been made by F. J. Murray[19] to apply a combinatorial approach to a three-dimensional lattice. The calculations have not yet been developed far enough to yield analytical results.

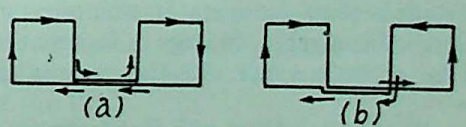


FIG. 14. Det **A** has terms corresponding to oriented polygons that "loop back on themselves" as illustrated by the two examples above. The terms corresponding to (a) and (b) cancel.

CC-0. In Public Domain. Gurukul Kangri Collection, Haridwar

Digitized by Arya Samaj Foundation Chennai and eGangotri

4.2 Algebraic Method

We now consider an algebraic procedure for finding the eigenvalue associated with the partition function for the two-dimensional square Ising lattice in zero magnetic field. We shall briefly outline Onsager's original solution with special emphasis on the method and motivations rather than the detailed algebra. For a more extensive discussion of the latter the reader is referred to Onsager's original presentation.[4]

As was shown in Sec. 2, the operator to be investigated is $\mathbf{V}_2\mathbf{V}_1$ [see Eqs. (2.12) and (2.13) for definitions]. It is convenient to express this in terms of two operators $\mathbf{A}_0$ and $\mathbf{A}_1$ defined by

$$\mathbf{A}_0=-\sum_{j=1}^{n}\mathbf{C}_j, \quad \mathbf{A}_1=\sum_{j=1}^{n}\mathbf{s}_j\mathbf{s}_{j+1} \tag{4.19}$$

with $\mathbf{s}_{n+j}\equiv\mathbf{s}_j$. (In the following we shall also have occasion to use the convention $\mathbf{C}_{n+j}\equiv\mathbf{C}_j$.) The matrices of interest are

$$\mathbf{V}_1=e^{-H^*\mathbf{A}_0} \quad \text{and} \quad \mathbf{V}_2=e^{H'\mathbf{A}_1}. \tag{4.20}$$

The general plan for solving this problem is to first perform some algebraic transformations. Starting from $\mathbf{A}_0$ and $\mathbf{A}_1$, we generate a Lie algebra (see Appendix 5) by forming the commutator $[\mathbf{A}_0, \mathbf{A}_1]$, then forming the commutators of this with $\mathbf{A}_0$ and $\mathbf{A}_1$. We continue to generate commutators of commutators until we obtain a set of operators such that the commutator of any two is a linear combination of operators already in the set.‡

One can, of course, generate a Lie algebra starting with any set of operators. Matrices of dimension 2^n will in many cases lead to a Lie algebra of 4^n elements, i.e., an algebra which contains as many independent elements as there are matrix elements in the matrix of dimension 2^n. The first fortunate feature of the operators $\mathbf{A}_0$ and $\mathbf{A}_1$ is that they generate a Lie algebra of only $3n-1$ linearly independent elements.

We next notice certain very convenient symmetries in the structure constants of the Lie algebra. Because of these symmetries we can, by applying linear transformations in the Lie algebra, decompose the Lie algebra into subalgebras of very simple structure. By expressing $\mathbf{A}_0$ and $\mathbf{A}_1$ in terms of these subalgebras we obtain a form of $\mathbf{V}_2\mathbf{V}_1$ which is readily factored into commuting matrices which can be diagonalized separately.

Attempts to apply this procedure to the three-dimensional problem or even the two-dimensional problem with a magnetic field are seriously hindered at an early stage because the operators of interest generate a much larger Lie algebra, so large in fact that it would seem to be of little value. All the various algebraic methods take advantage of very special properties of the operators, and it has not been possible to generalize them in any very interesting way.

The first step of the procedure is to generate a Lie algebra from $\mathbf{A}_0$ and $\mathbf{A}_1$. Rather than generate this element by element, we shall anticipate the results and write them in the most convenient form.

We define a set of operators

$$\begin{aligned}&\mathbf{P}_{a,a}=-\mathbf{C}_a,\\ &\mathbf{P}_{a,b}=\mathbf{s}_a\mathbf{C}_{a+1}\mathbf{C}_{a+2}\cdots\mathbf{C}_{b-1}\mathbf{s}_b \quad a\neq b,\end{aligned} \tag{4.21}$$

using the convention that $\mathbf{s}_{n+j}\equiv\mathbf{s}_j$ and $\mathbf{C}_{n+j}\equiv\mathbf{C}_j$. Thus,

$$\mathbf{A}_0=\sum_{a=1}^{n}\mathbf{P}_{a,a}, \quad \mathbf{A}_1=\sum_{a=1}^{n}\mathbf{P}_{a,a+1}. \tag{4.22}$$

These are but two operators of a set $\mathbf{A}_k$ which we define by

$$\mathbf{A}_k\equiv\sum_{a=1}^{n}\mathbf{P}_{a,a+k}. \tag{4.23}$$

There are $2n$ linearly independent $\mathbf{A}_k$. From (4.21) we see that

$$\begin{aligned}&\mathbf{P}_{a,a+k+n}=-\mathbf{U}\mathbf{P}_{a,a+k},\\ &\mathbf{U}\equiv\mathbf{C}_1\mathbf{C}_2\cdots\mathbf{C}_n.\end{aligned} \tag{4.24}$$

(The minus sign appears because $\mathbf{s}_j$ anticommutes with $\mathbf{C}_j$, as one readily observes from the definitions [(2.6a), (2.10), and (2.11)].) Thus

$$\mathbf{A}_{k+n}=-\mathbf{U}\mathbf{A}_k \quad \text{and} \quad \mathbf{A}_{k+2n}=\mathbf{A}_k. \tag{4.25}$$

(Note that $\mathbf{A}_k$ commutes with $\mathbf{U}$ and $\mathbf{U}^2=\mathbf{I}$.)

With the addition of a set of elements

$$\mathbf{G}_k=\tfrac{1}{4}[\mathbf{A}_k, \mathbf{A}_0], \tag{4.26}$$

we can define a complete Lie algebra containing the elements $\mathbf{A}_k$ and $\mathbf{G}_k$. The commutation rules for this algebra are (see reference 4, p. 127)

$$\begin{aligned}&[\mathbf{A}_j, \mathbf{A}_k]=4\mathbf{G}_{j-k},\\ &[\mathbf{A}_l, \mathbf{G}_{j-k}]=2(\mathbf{A}_{l+j-k}-\mathbf{A}_{l-j+k}),\\ &[\mathbf{G}_j, \mathbf{G}_k]=0.\end{aligned} \tag{4.27}$$

We have defined $2n$ operators $\mathbf{G}_k$ but actually only $n-1$ are linearly independent. Since $[\mathbf{A}_k, \mathbf{A}_j]=-[\mathbf{A}_j, \mathbf{A}_k]$, we see from (4.27) that $\mathbf{G}_m=-\mathbf{G}_{-m}=-\mathbf{G}_{2n-m}$. $\mathbf{G}_0=[\mathbf{A}_j, \mathbf{A}_j]=0$ because an operator always commutes with itself. $\mathbf{G}_n=[\mathbf{A}_{j+n}, \mathbf{A}_j]=[-\mathbf{U}\mathbf{A}_j, \mathbf{A}_j]=0$ because $\mathbf{U}$ also commutes with $\mathbf{A}_j$. We, therefore, have only $\mathbf{G}_1, \mathbf{G}_2, \cdots, \mathbf{G}_{n-1}$ as linearly independent operators.

We have seen so far that $\mathbf{A}_0$ and $\mathbf{A}_1$ generate a Lie algebra of only $3n-1$ elements ($2n$ $\mathbf{A}_k$'s and $n-1$ $\mathbf{G}_k$'s). We also observe that the structure of this Lie algebra is rather unique. Notice that if in (4.27) we replace $\mathbf{A}_j$ by $\mathbf{A}_{j+z}$, the commutation relations remain un-

‡ van der Waerden is credited with the observation that the algebra so generated and the transformations that follow belong to the theory of Lie algebras. The authors are indebted to Dr. Bruria Kaufman for describing this connection.

CC-0. In Public Domain. Gurukul Kangri Collection, Haridwar

Digitized by Arya Samaj Foundation Chennai and eGangotri

changed. From (4.27) alone there is no "preferred" $\mathbf{A}_j$; there is no way to single out one $\mathbf{A}_k$ as being different from all the others. The symmetry here is formally very similar to the symmetry of the cyclic matrix in Sec. 4.1, the cause of which could be traced to the fact that the crystal has cyclic symmetry, i.e., all particles in a row of the lattice are equivalent (with the periodic boundary conditions). The cyclic symmetry in (4.27) arises, however, from a different source. The periodicity in the lattice has already been incorporated into the $\mathbf{A}_j$ and $\mathbf{G}_k$ which are themselves invariant to a cyclic transformation of the lattice points. The cause of the cyclic symmetry in (4.27) is not obvious physically.

The existence of this symmetry, however, suggests the next step. From general properties of the group of cyclic permutations, one is assured that a Fourier transformation of the operators $\mathbf{A}_k$ and $\mathbf{G}_k$ will give an even simpler description of the Lie algebra. Just as a Fourier transformation of a cyclic matrix makes most of the matrix elements vanish, so also does a Fourier transformation to this cyclic Lie algebra make most of the structure constants vanish.

The Fourier transformation is achieved by introducing the operators

$$\begin{aligned}
\mathbf{X}_r &= (2n)^{-1} \sum_{m=1}^{2n} \mathbf{A}_m \cos(\pi r m/n), \\
\mathbf{Y}_r &= -(2n)^{-1} \sum_{m=1}^{2n} \mathbf{A}_m \sin(\pi m r/n), \qquad (4.28) \\
\mathbf{Z}_r &= i(2n)^{-1} \sum_{m=1}^{2n} \mathbf{G}_m \sin(m\pi r/n).
\end{aligned}$$

We notice that

$$\begin{aligned}
\mathbf{X}_r &= \mathbf{X}_{-r} = \mathbf{X}_{2n-r}, \\
\mathbf{Y}_r &= -\mathbf{Y}_{-r} = -\mathbf{Y}_{2n-r}, \qquad (4.29) \\
\mathbf{Z}_r &= -\mathbf{Z}_{-r} = -\mathbf{Z}_{2n-r}.
\end{aligned}$$

A check on the number of independent operators shows that there are $n-1$ independent $\mathbf{Y}_r$, $n-1$ independent $\mathbf{Z}_r$, but $n+1$ independent $\mathbf{X}_r$.

The commutation rules for these operators are easily calculated from (4.27) to be

$$\begin{aligned}
[\mathbf{X}_r, \mathbf{Y}_r] &= -2i\mathbf{Z}_r, \\
[\mathbf{Y}_r, \mathbf{Z}_r] &= -2i\mathbf{X}_r \quad 1 \leqslant r \leqslant n-1, \qquad (4.30) \\
[\mathbf{Z}_r, \mathbf{X}_r] &= -2i\mathbf{Y}_r.
\end{aligned}$$

All operators (including $\mathbf{X}_0$ and $\mathbf{X}_n$) commute with any other operator with a different subscript; thus, for $r \neq s$, $[\mathbf{X}_r, \mathbf{X}_s]=0$, $[\mathbf{X}_r, \mathbf{Y}_s]=0$, etc. The three operators $\mathbf{X}_r$, $\mathbf{Y}_r$, and $\mathbf{Z}_r$ (for each r) themselves form a Lie algebra which is a subalgebra of the complete set. We have, as predicted, decomposed the original Lie algebra into small subalgebras of very simple structure. The subalgebras are in fact very similar to those associated with the three-dimensional infinitesimal rotation group (see Appendix 5).

Our aim now is to express $\mathbf{V}_2\mathbf{V}_1$ in terms of this new set of operators and to take advantage of the simple structure (4.30). The relation (4.28) can be easily inverted by the usual rules of Fourier transforms to give $\mathbf{A}_m$ and $\mathbf{G}_m$ in terms of $\mathbf{X}_r$, $\mathbf{Y}_r$, and $\mathbf{Z}_r$. The result of this is

$$\begin{aligned}
\mathbf{A}_m &= \sum_{r=1}^{2n} [\mathbf{X}_r \cos(m\pi r/n) - \mathbf{Y}_r \sin(m\pi r/n)], \\
\mathbf{G}_m &= -i \sum_{r=1}^{2n} \mathbf{Z}_r \sin(mr\pi/n).
\end{aligned} \qquad (4.31)$$

In particular,

$$\mathbf{A}_0 = \sum_{r=1}^{2n} \mathbf{X}_r = \mathbf{X}_0 + 2\mathbf{X}_1 + 2\mathbf{X}_2 + \cdots + 2\mathbf{X}_{n-1} + \mathbf{X}_n,$$

$$\begin{aligned}
\mathbf{A}_1 &= \sum_{r=1}^{2n} [\mathbf{X}_r \cos(r\pi/n) - \mathbf{Y}_r \sin(\pi r/n)] \\
&= \mathbf{X}_0 + 2[\mathbf{X}_1 \cos(\pi/n) - \mathbf{Y}_1 \sin(\pi/n)] + \cdots \\
&\quad + 2[\mathbf{X}_{n-1} \cos((n-1)\pi/n) \\
&\quad - \mathbf{Y}_{n-1} \sin((n-1)\pi/n)] - \mathbf{X}_n. \qquad (4.32)
\end{aligned}$$

Substitution of (4.32) into (4.20) gives

$$\begin{aligned}
\mathbf{V}_2\mathbf{V}_1 = \exp\{K' \sum_{r=1}^{2n} [\mathbf{X}_r \cos(\pi r/n) \\
- \mathbf{Y}_r \sin(\pi r/n)]\} \exp\{-K^* \sum_{r=1}^{2n} \mathbf{X}_r\}. \qquad (4.33)
\end{aligned}$$

We can make valuable use of the commutation rules (4.30) by noting that if two operators $\mathbf{A}$ and $\mathbf{B}$ commute, then $e^{\mathbf{A}+\mathbf{B}} = e^{\mathbf{A}}e^{\mathbf{B}} = e^{\mathbf{B}}e^{\mathbf{A}}$. It is therefore possible to factor (4.33) into the product of commuting matrices:

$$\begin{aligned}
\mathbf{V}_2\mathbf{V}_1 &= \prod_{r=0}^{n} \mathbf{U}_r, \\
\mathbf{U}_r &= \exp\{2K'[\mathbf{X}_r \cos(\pi r/n) \\
&\quad - \mathbf{Y}_r \sin(\pi r/n)]\} \exp\{-2K^*\mathbf{X}_r\} \quad r \neq 0, n, \qquad (4.34) \\
\mathbf{U}_0 &= \exp\{(K'-K^*)\mathbf{X}_0\}, \\
\mathbf{U}_n &= \exp\{-(K'+K^*)\mathbf{X}_n\}.
\end{aligned}$$

The fact that the $\mathbf{U}_r$ commute with each other also implies that they can all be simultaneously diagonalized and that the eigenvalues of $\mathbf{V}_2\mathbf{V}_1$ are products of eigenvalues of the $\mathbf{U}_r$.

We can find the eigenvalues of the $\mathbf{U}_r$ by a somewhat indirect procedure. It is not wise to try to determine explicitly the matrices $\mathbf{X}_r$, $\mathbf{Y}_r$, and $\mathbf{Z}_r$ in the original

CC-0. In Public Domain. Gurukul Kangri Collection, Haridwar

Digitized by Arya Samaj Foundation Chennai and eGangotri

representation. The multiplication table of the $\mathbf{X}_r$, $\mathbf{Y}_r$, and $\mathbf{Z}_r$ is independent of representation as are also the eigenvalues. The latter are, with the help of a few rather simple bits of knowledge such as the dimension of the matrices, etc., determined by the former.

We have so far given only the commutation rules of the $\mathbf{X}_r$, $\mathbf{Y}_r$, and $\mathbf{Z}_r$. To proceed further we must also know $\mathbf{X}_r^2$, $\mathbf{Y}_r^2$, $\mathbf{Z}_r^2$, $\mathbf{X}_r\mathbf{Y}_r$, etc., which can be found by direct evaluation using the abstract properties of the $\mathbf{P}_{ab}$ (see reference 4, p. 129). The complete multiplication table is given below (the operators $\mathbf{R}_r$ are defined by the expressions below):

$$\left.\begin{aligned}
&\mathbf{X}_r^2=\mathbf{Y}_r^2=\mathbf{Z}_r^2=\mathbf{R}_r=\mathbf{R}_r^2,\\
&\mathbf{X}_r=\mathbf{R}_r\mathbf{X}_r=\mathbf{X}_r\mathbf{R}_r=i\mathbf{Y}_r\mathbf{Z}_r=-i\mathbf{Z}_r\mathbf{Y}_r\\
&\mathbf{Y}_r=\mathbf{R}_r\mathbf{Y}_r=\mathbf{Y}_r\mathbf{R}_r=i\mathbf{Z}_r\mathbf{X}_r=-i\mathbf{X}_r\mathbf{Z}_r\\
&\mathbf{Z}_r=\mathbf{R}_r\mathbf{Z}_r=\mathbf{Z}_r\mathbf{R}_r=i\mathbf{X}_r\mathbf{Y}_r=-i\mathbf{Y}_r\mathbf{X}_r
\end{aligned}\right\}\ 1\leqslant r\leqslant n-1,$$

$$\left.\begin{aligned}
&\mathbf{X}_r^2=\mathbf{R}_r=\mathbf{R}_r^2\\
&\mathbf{X}_r=\mathbf{R}_r\mathbf{X}_r=\mathbf{X}_r\mathbf{R}_r
\end{aligned}\right\} r=0,\ n. \tag{4.35}$$

From this table one can calculate any combination of products of $\mathbf{X}_r$, $\mathbf{Y}_r$, and $\mathbf{Z}_r$. The important features of the table are the following. The operators $\mathbf{X}_r$, $\mathbf{Y}_r$, and $\mathbf{Z}_r$ anticommute with each other and $\mathbf{X}_r^2$, $\mathbf{Y}_r^2$, and $\mathbf{Z}_r^2$ are all projection operators ($\mathbf{R}_r^2=\mathbf{R}_r$), i.e., they have eigenvalues either zero or one.

We can very easily establish that $\mathbf{R}_r$ is not the unit matrix and is truly a projection operator with some zero eigenvalues. From (4.28) we notice that since $\mathbf{A}_{m+n}=-\mathbf{U}\mathbf{A}_m$,

$$\mathbf{X}_r=(2n)^{-1}[\mathbf{I}-(-1)^r\mathbf{U}]\sum_{m=1}^{n}\mathbf{A}_m\cos(m\pi r/n).$$

Similarly $\mathbf{Y}_r$ and $\mathbf{Z}_r$ contain a factor $[\mathbf{I}-(-)^r\mathbf{U}]$.

The operator $\mathbf{U}$ defined in (4.24) plays a rather important role in this problem. $\mathbf{U}$ is the operator which changes all spins σ_j to $-\sigma_j$.

The eigenvalues and eigenfunctions of $\mathbf{U}$ are very simple. Since $\mathbf{U}^2=\mathbf{I}$, the eigenvalues are ±1. $\mathbf{U}$ operating on any state given by ν: $(\sigma_1, \sigma_2, \cdots, \sigma_n)$ changes it to a new state $\mathbf{U}\nu$: $(-\sigma_1, -\sigma_2, \cdots, -\sigma_n)$. For each pair of states ν and $\mathbf{U}\nu$ as described above, there is an "even" and an "odd" state given, respectively, by $\nu+\mathbf{U}\nu$ and $\nu-\mathbf{U}\nu$. In the "even space" $\mathbf{U}=\mathbf{I}'$ and in the "odd space" $\mathbf{U}=-\mathbf{I}'$. Each subspace is of dimension 2^{n-1}. In this representation $\mathbf{U}$ has the form

$$\begin{pmatrix}\mathbf{I}' & \mathbf{0}\\ \mathbf{0} & -\mathbf{I}'\end{pmatrix},$$

where $\mathbf{I}'$ is the 2^{n-1} identity matrix and $\mathbf{0}$ is the 2^{n-1} dimensional null matrix. In this same representation $\frac{1}{2}(\mathbf{I}+\mathbf{U})$ and $\frac{1}{2}(\mathbf{I}-\mathbf{U})$ are, respectively, the projection operators

$$\begin{pmatrix}\mathbf{I}' & \mathbf{0}\\ \mathbf{0} & \mathbf{0}\end{pmatrix}\quad\text{and}\quad\begin{pmatrix}\mathbf{0} & \mathbf{0}\\ \mathbf{0} & \mathbf{I}'\end{pmatrix}.$$

$\mathbf{V}_2$, $\mathbf{V}_1$, and all the operators used in describing them, including the $\{\mathbf{X}_r\}$, $\{\mathbf{Y}_r\}$, and $\{\mathbf{Z}_r\}$, commute with $\mathbf{U}$. This means that in the representation above, all these matrices must be of the general type

$$\begin{pmatrix}\mathbf{X} & \mathbf{0}\\ \mathbf{0} & \mathbf{X}'\end{pmatrix},$$

where $\mathbf{X}$ denotes some 2^{n-1} dimensional matrix. In particular, since $\mathbf{X}_r$, $\mathbf{Y}_r$, and $\mathbf{Z}_r$ contain $[\mathbf{I}-(-1)^r\mathbf{U}]$ as a factor, these operators must be of the type

$$\begin{pmatrix}\mathbf{X} & \mathbf{0}\\ \mathbf{0} & \mathbf{0}\end{pmatrix}\quad\text{for } r \text{ odd}$$

and

$$\begin{pmatrix}\mathbf{0} & \mathbf{0}\\ \mathbf{0} & \mathbf{X}'\end{pmatrix}\quad\text{for } r \text{ even}.$$

The nonsingular part of the projection operator $\mathbf{R}_r$ is at most of dimension 2^{n-1}.

Equipped with the multiplication table (4.35) and some simple properties of the $\mathbf{X}_r$, $\mathbf{Y}_r$, and $\mathbf{Z}_r$, we return again to the eigenvalue problem (4.34). Matrices such as (4.35) have been studied extensively, particularly in connection with representations of the rotation group and the Lie algebra discussed in Appendix 5. One need not be an expert on such things, however, to solve this problem.

We first observe that a transformation with $\exp(iz_r\mathbf{Z}_r)$, with z_r a constant, produces the following transformation of the $\mathbf{X}_r$, $\mathbf{Y}_r$, and $\mathbf{Z}_r$ ($r\neq0, n$):

$$\begin{aligned}
&\exp(iz_r\mathbf{Z}_r)\mathbf{X}_r\exp(-iz_r\mathbf{Z}_r)=\mathbf{X}_r\cos2z_r+\mathbf{Y}_r\sin2z_r,\\
&\exp(iz_r\mathbf{Z}_r)\mathbf{Y}_r\exp(-iz_r\mathbf{Z}_r)\\
&\qquad=-\mathbf{X}_r\sin2z_r+\mathbf{Y}_r\cos2z_r,\\
&\exp(iz_r\mathbf{Z}_r)\mathbf{Z}_r\exp(-iz_r\mathbf{Z}_r)=\mathbf{Z}_r.
\end{aligned}\tag{4.36}$$

If we imagine the $\mathbf{X}_r$, $\mathbf{Y}_r$, and $\mathbf{Z}_r$ to be orthogonal vectors, then the above similarity transformation also produces an orthogonal transformation of the vectors $\mathbf{X}_r$, $\mathbf{Y}_r$, and $\mathbf{Z}_r$. In general any orthogonal transformation of the $\mathbf{X}_r$, $\mathbf{Y}_r$, and $\mathbf{Z}_r$ can be produced by a similarity transformation of the type

$$\exp(z_r\mathbf{Z}_r+y_r\mathbf{Y}_r+x_r\mathbf{X}_r). \tag{4.37}$$

This correspondence between orthogonal transformations and similarity transformations is the basis for the theory of representations of the rotation group and also underlies the Dirac theory of the electron. A generalization of this is also the basis of Kaufman's scheme for solving the Ising problem.

If now we should expand the exponentials in (4.34) using the rules (4.35), we can express $\mathbf{U}_r$ as a constant plus a linear combination in $\mathbf{R}_r$, $\mathbf{X}_r$, $\mathbf{Y}_r$, and $\mathbf{Z}_r$. Note that any power of $\mathbf{X}_r$, for example, is either $\mathbf{X}_r$ or $\mathbf{R}_r$.

CC-0. In Public Domain. Gurukul Kangri Collection, Haridwar

Digitized by Arya Samaj Foundation Chennai and eGangotri

By using a transformation of the type (4.37), which leaves $\mathbf{R}_r$ invariant, we can eliminate $\mathbf{Z}_r$ and $\mathbf{Y}_r$. If we considered the linear expression in $\mathbf{X}_r$, $\mathbf{Y}_r$, and $\mathbf{Z}_r$ as a vector, then this procedure is identical to the rotation of coordinates so that the vector is along the "X axis."

It will not be necessary to find this transformation explicitly. We can easily show that $\mathbf{U}_r$ is transformed into the form

$$\mathbf{U}_r \sim (\mathbf{I}-\mathbf{R}_r)+\mathbf{R}_r\cosh\gamma_r+\mathbf{X}_r\sinh\gamma_r=\exp(\gamma_r\mathbf{X}_r) \quad (4.38)$$

($\sim$ indicates similarity). We already have argued that this expression will be linear in $\mathbf{R}_r$ and $\mathbf{X}_r$. In addition, we know from (4.34) that the projection $\frac{1}{2}(\mathbf{I}-\mathbf{R}_r)\mathbf{U}_r$ is a unit matrix (since $\mathbf{X}_r$, $\mathbf{Y}_r$, $\mathbf{Z}_r$, and $\mathbf{R}_r$ all vanish in this space) and is unaffected by the transformation (4.37). Furthermore, we see that transformation of (4.34) by $\exp(\frac{1}{2}\pi i\mathbf{Z}_r)$ changes both factors of $\mathbf{U}_r$ into their reciprocals, $\mathbf{X}_r\rightarrow-\mathbf{X}_r$ and $\mathbf{Y}_r\rightarrow-\mathbf{Y}_r$. $\mathbf{U}_r$ and $\mathbf{U}_r^{-1}$ are therefore similar and $|\det \mathbf{U}_r|=1$. Since this property also must be preserved by a similarity transformation, the coefficients of $\mathbf{R}_r$ and $\mathbf{X}_r$ are restricted in the manner indicated.

The problem of finding γ_r is very easy because the similarity transformation affects only the coefficients of $\mathbf{X}_r$, $\mathbf{Y}_r$, and $\mathbf{Z}_r$ leaving the coefficient of $\mathbf{R}_r$ unaltered. $\cosh\gamma_r$ is therefore the coefficient of $\mathbf{R}_r$ in the original expansion of $\mathbf{U}_r$:

$$\cosh\gamma_r=\cosh 2K'\cosh 2K^* - \sinh 2K'\sinh 2K^*\cos(r\pi/n). \quad (4.39)$$

Since $\mathbf{X}_r$, $\mathbf{Y}_r$, and $\mathbf{Z}_r$ commute with operators of a different index, we can apply the appropriate transformations for each r to $\mathbf{V}_2\mathbf{V}_1$ and bring all $\mathbf{U}_r$ simultaneous into the form (4.38).

We have thus established

$$\mathbf{V}_2\mathbf{V}_1\sim\exp[-\tfrac{1}{2}(\gamma_0\mathbf{X}_0+2\gamma_1\mathbf{X}_1+\cdots+2\gamma_{n-1}\mathbf{X}_{n-1}+\gamma_n\mathbf{X}_n)], \quad (4.40)$$

where

$$\gamma_0=K^*-K' \quad \text{and} \quad \gamma_n=K'+K^* \quad (4.41)$$

are also consistent with (4.39).

We have not as yet commented on the sign of the γ_j. The signs of γ_0 and γ_n are defined by (4.41) but except for $j=0$ and n, only $|\gamma_j|$ are defined by (4.39). This is all that is necessary, however, because the transformation $\exp(\frac{1}{2}i\pi\mathbf{Z}_r)$ sends $\mathbf{X}_r$ into $-\mathbf{X}_r$ [Eq. (4.36)]. Equation (4.40) is thus valid if we replace $\mathbf{X}_j$ by $-\mathbf{X}_j$ or γ_r by $-\gamma_r$, $(j\neq 0, n)$. For convenience we shall hereafter choose all γ_r, $(j\neq 0, n)$ as the positive solution of (4.39).

Since the $\mathbf{X}_r$ commute, they can all be simultaneously diagonalized. The $\mathbf{X}_r$ satisfy the equation

$$\mathbf{X}_r(\mathbf{X}_r^2-\mathbf{I})=0; \quad (4.42)$$

therefore they have eigenvalues $X_r=0$ or ± 1.

All eigenvalues of $\mathbf{V}_2\mathbf{V}_1$ must be of the type

$$\lambda=\prod_{r=0}^{n}\lambda_r,$$

$$\lambda_r=e^{\frac{1}{2}\gamma_r},\quad e^{-\frac{1}{2}\gamma_r}\quad\text{or}\quad 1\quad\text{for}\quad r=0,n, \quad (4.43)$$

$$\lambda_r=e^{\gamma_r},\quad e^{-\gamma_r}\quad\text{or}\quad 1\quad\text{for}\quad r\neq 0,n.$$

Unfortunately, the converse of this is not true; not all λ of the type (4.43) are eigenvalues of $\mathbf{V}_2\mathbf{V}_1$ (there are 3^{n+1} possible combinations of (4.43) but only 2^n eigenvalues). Even though the $\mathbf{X}_r$ can be simultaneously diagonalized, the subspace in which X_0 is $+1$ might be a space in which, for example, X_1 could be only $+1$. We are still confronted with the task of determining which combinations in (4.43) are allowed.

We can very easily eliminate a large number of the solutions of (4.43) by recalling that in the even space $(\mathbf{U}=+\mathbf{I}')$, $\mathbf{X}_r=0$ for all odd r, whereas in the odd space $(\mathbf{U}=-\mathbf{I}')$, $\mathbf{X}_r=0$ for all even r. We therefore know that either the λ_r with r odd are 1 (in the even space) or λ_r with r even are 1 (in the odd space),

$$\lambda=\lambda_1\lambda_3\lambda_5\cdots \quad\text{or}\quad \lambda=\lambda_0\lambda_2\lambda_4\cdots. \quad (4.44)$$

Whereas the spinor analysis method automatically gives all the eigenvalues and their degeneracies, the problem of completely disentangling the proper combinations of the above is at this state a rather tedious operation (although not a difficult one). Fortunately, we are interested only in the largest eigenvalue of $\mathbf{V}_2\mathbf{V}_1$ and perhaps also in any that are asymptotically degenerate with the largest.

The problem is to determine the simultaneous eigenvalues of the $\mathbf{X}_r$. To find at least some of these we consider

$$\mathbf{A}_0=-\sum_{j=1}^{n}\mathbf{C}_j=\sum_{r=0}^{2n-1}\mathbf{X}_r. \quad (4.45)$$

The $\mathbf{C}_j$ all commute and are very easily diagonalized simultaneously. Since $\mathbf{C}_j^2=\mathbf{I}$, the eigenvalues of $\mathbf{C}_j$ are ± 1 and since the $\mathbf{C}_j$ are direct product matrices, the eigenvalues of $\mathbf{C}_j$ do not depend in any way on the eigenvalues of other $\mathbf{C}_k$. The 2^n eigenvalues of $\mathbf{A}_0$ are given by

$$-A_0=\pm 1\pm 1\pm 1\pm\cdots\pm 1. \quad (4.46)$$

There are n terms in (4.46) and the 2^n solutions are obtained by selecting all possible combinations of the $\pm$ signs. If the $\mathbf{C}_j$ are all diagonalized, then $\mathbf{U}=\mathbf{C}_1\mathbf{C}_2\cdots\mathbf{C}_n$ is also diagonal and has the value ± 1 accordingly as the right side of (4.46) has an even or odd number of minus signs. In particular we note that the lowest eigenvalue of $\mathbf{A}_0$ is nondegenerate, belongs in the even space, and has the value

$$A_0=-n. \quad (4.47)$$

The next lowest eigenvalue of $\mathbf{A}_0$ is degenerate, belongs

CC-0. In Public Domain. Gurukul Kangri Collection, Haridwar

Digitized by Arya Samaj Foundation Chennai and eGangotri

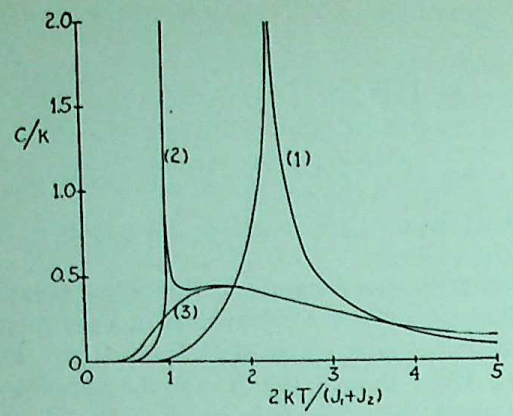


FIG. 15. The specific heat of the two-dimensional Ising lattice with (1) $J=J'$ (isotropic), (2) $J=100J'$, and (3) $J'=0$ (linear chain) (see reference 4).

in the odd space, and has the value

$$A_0=-n+2. \tag{4.48}$$

Returning to (4.45), we also recall that for $\mathbf{U}=+I'$, all $\mathbf{X}_r$ for r even vanish. There is one eigenfunction of the $\mathbf{X}_r$ which gives

$$A_0=-n=X_1+X_3+\cdots+X_{2n-1}$$
$$=\begin{cases}2X_1+2X_3+\cdots+2X_{n-2}+X_n & \text{for } n \text{ odd}\\ 2X_1+2X_3+\cdots+2X_{n-1} & \text{for } n \text{ even.}\end{cases}$$

Since the $\mathbf{X}_r$ can be only ±1 or 0, there is only one way that this equation can be satisfied, namely for all $\mathbf{X}_r$ (r odd) to have the value $\mathbf{X}_r=-1$.

This simple argument tells us that $\mathbf{V}_2\mathbf{V}_1$ has an eigenvalue

$$\lambda_+=\begin{cases}\exp[\tfrac{1}{2}(2\gamma_1+2\gamma_3+\cdots+2\gamma_{n-2}+\gamma_n)] & \text{for } n \text{ odd}\\ \exp[\tfrac{1}{2}(2\gamma_1+2\gamma_3+\cdots+2\gamma_{n-1})] & \text{for } n \text{ even}\end{cases} \tag{4.49}$$

or by extending the definition (4.39) of γ_j for $j>n$

$$\lambda_+=\exp[\tfrac{1}{2}(\gamma_1+\gamma_3+\cdots+\gamma_{2n-1})]. \tag{4.50}$$

By comparing this with other expressions in (4.44), we see that this is certainly the largest eigenvalue in the even space. The next largest in this space is smaller by at least a factor $e^{-\gamma_1}$. Comparison with the possible eigenvalues of the odd space shows that this is also larger than any of these but one of the possible eigenvalues of the odd space is asymptotically equal to the above, namely the solution with all positive exponentials.

There is one final question to be answered. Is the solution of (4.44)

$$\lambda=\exp[\tfrac{1}{2}(|\gamma_0|+\gamma_2+\gamma_4+\cdots+\gamma_{2n-2})]$$

really an eigenvalue of $\mathbf{V}_2\mathbf{V}_1$? To obtain a partial answer to this question we notice again (4.48) and observe that in the odd space, the smallest eigenvalue of $\mathbf{A}_0$ is

$$A_0=-n+2=X_0+X_2+\cdots+X_{2n-2}$$
$$=\begin{cases}X_0+2X_2+2X_4+\cdots+2X_{n-2}+X_n & \text{for } n \text{ even}\\ X_0+2X_2+2X_4+\cdots+2X_{n-1} & \text{for } n \text{ odd.}\end{cases}$$

The X_r cannot all simultaneously be -1 for this would contradict the above being the lowest eigenvalue of $\mathbf{A}_0$. The only possible solutions of the above are $X_0=+1$ and all other $X_j=-1$, $X_n=+1$ (for n even) and all other $X_j=-1$ or some $X_j=0$ ($j\neq0, n$) and all other $X_j=-1$. We shall not pursue further the question of which of these possibilities are really solutions (it turns out that they all are). The solution of particular interest is the case $X_0=+1$ all other $X_j=-1$, for this leads to the largest eigenvalue of $\mathbf{V}_2\mathbf{V}_1$ in the odd space:

$$\lambda_-=\exp[\tfrac{1}{2}(-\gamma_0+\gamma_2+\gamma_4+\cdots+\gamma_{2n-2})]. \tag{4.51}$$

If $K^*<K'$, $\gamma_0=K^*-K'$ is negative and for large n approaches the value of $-\gamma_1$. If $K^*<K'$, λ_- and λ_+ are asymptotically degenerate. At $K^*=K'$, γ_0 changes sign and for $K^*>K'$ the degeneracy no longer exists.

The situation here illustrates very nicely the predictions made in Sec. 3. There we predicted that if a phase transition exists, at least in the case $K'=K$, it occurs at $K'=K^*$, the point where this degeneracy disappears. We also saw that a degeneracy of the largest eigenvalue is associated with long-range order, thus the critical temperature truly represents a transition from an ordered to a disordered state.

To complete the analysis of this section, we find an asymptotic expression for Z. As shown by Eq. (2.4) a degeneracy of the above nature has no effect upon the thermodynamic properties derived from Z

$$\lim_{n,m\to\infty}(nm)^{-1}\log Z-\tfrac{1}{2}\log(2\sinh2K)$$
$$=\lim_{n\to\infty}(2n)^{-1}(\gamma_1+\gamma_3+\cdots+\gamma_{2n-1})$$
$$=\lim_{n\to\infty}(2n)^{-1}\sum_{r=1}^{n}\cosh^{-1}[\cosh2K'\cosh2K^*$$
$$-\sinh2K'\sinh2K^*\cos((2r-1)\pi/n)]$$
$$=(4\pi)^{-1}\int_0^{2\pi}d\omega\gamma(\omega), \tag{4.52}$$

$$\gamma(\omega)=\cosh^{-1}(\cosh2K'\cosh2K^*$$
$$-\sinh2K'\sinh2K^*\cos\omega).$$

This expression does not show the symmetry in K and K'. We can obtain a more symmetric form by converting (4.52) into a double integral using the relation

$$\int_0^{2\pi}\log(2\cosh x-2\cos\omega)d\omega=2\pi x.$$

CC-0. In Public Domain. Gurukul Kangri Collection, Haridwar

Digitized by Arya Samaj Foundation Chennai and eGangotri

This yields

$$\lim_{n,m\to\infty}(nm)^{-1}\log Z=\log 2$$
$$+\tfrac{1}{2}\pi^{-2}\int_0^{\pi}d\omega\int_0^{\pi}d\omega'\log(\cosh 2K\cosh 2K'$$
$$-\sinh 2K\cos\omega-\sinh 2K'\cos\omega'). \quad (4.53)$$

4.3 Thermodynamic Properties

In Secs. 4.1 and 4.2, we have derived by two quite different procedures the partition function of the two-dimensional square Ising lattice. The result of this calculation was

$$\lim_{n,m\to\infty}(nm)^{-1}\log Z=\log 2$$
$$+\tfrac{1}{2}\pi^{-2}\int_0^{\pi}\int_0^{\pi}\log(\cosh 2K\cosh 2K$$
$$-\sinh 2K\cos\omega-\sinh 2K'\cos\omega')d\omega d\omega'. \quad (4.18)$$

This expression shows the symmetry with respect to interchange of K and K'. One of the integrals is easily performed using the identity

$$\int_0^{\pi}\log(2\cosh x-2\cos\omega)d\omega=\pi x$$

to give the less symmetric form

$$\lim_{n,m\to\infty}(nm)^{-1}\log Z$$
$$=\tfrac{1}{2}\log(2\sinh 2K)+(2\pi)^{-1}\int_0^{\pi}\gamma(\omega)d\omega, \quad (4.52)$$

where

$$\cosh\gamma(\omega)=\cosh 2K'\cosh 2K^*$$
$$-\sinh 2K'\sinh 2K^*\cos\omega.$$

Although the above integrals are not of a common type, the thermodynamic functions involving derivatives of these integrals can be expressed in terms of elliptic functions. The analysis of these integrals for arbitrary K and K' is given in Onsager's paper. This analysis is considerably simplified if we let $K=K'$ as we shall do in the following. $\gamma(\omega)$ is then given by

$$\cosh\gamma(\omega)=\cosh 2K\,\mathrm{ctnh}2K-\cos\omega.$$

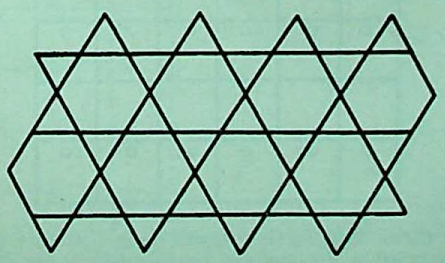


FIG. 16. The Kagomé lattice.

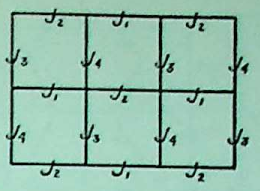


FIG. 17. A square lattice with four independent coupling constants denoted by J_1, J_2, J_3, and J_4.

The internal energy per particle is found from

$$\bar{E}=kT^2\partial[(nm)^{-1}\log Z]/\partial T \quad (1.6)$$
$$=-J\partial[(nm)^{-1}\log Z]/\partial K$$
$$=-J\coth 2K[1+2\pi^{-1}(2\tanh^2 2K-1)K_1(k_1)], \quad (4.54)$$

where

$$k_1=2\sinh 2K\cosh^{-2}2K$$

and $K_1(k_1)$ is the complete elliptic integral of the first kind,

$$K_1(k_1)=\int_0^{\pi/2}(1-k_1^2\sin^2\varphi)^{-\frac{1}{2}}d\varphi.$$

The critical point for this system has already been predicted in Sec. 3.1 as the point where $|\sinh 2K_c|=1$. For $K=K_c$, $k_1=1$ and $2\tanh^2 2K=1$. Even though $K_1(k_1)$ has a logarithmic singularity at $k_1=1$, the coefficient of $K_1(k_1)$ vanishes linearly with the result that $\bar{E}$ is continuous at T_c. There is no latent heat.

The specific heat is, however, given by

$$C=\partial\bar{E}/\partial T.$$

Since one of the terms of $\bar{E}$ is proportional to $|T-T_c|\times\log|T-T_c|$ near $T=T_c$, there is a term in C which is proportional to $\log|T-T_c|$. The specific heat has a logarithmic singularity at $T=T_c$.

The more complicated analysis of the general case $K\neq K'$ shows that the specific heat still has a logarithmic singularity at a temperature given by

$$\sinh 2K\sinh 2K'=1. \quad (4.55)$$

If we fix $J+J'$, the spin-spin internal energy at 0° Kelvin, and let J' become small. The critical temperature becomes smaller. If $J'=0$, the two-dimensional lattice degenerates into a system of independent one-dimensional chains which, as already seen, has no critical temperature. As $J'\to 0$, the critical point tends toward $T=0$ and finally disappears for $J'=0$. (See Fig. 15.)

5. OTHER LATTICES

The detailed analysis in the previous sections has been primarily restricted to properties of the square lattice. Other lattice types have been considered by several authors.[20–25] However, when these types have been successfully treated, the results have not differed in any very interesting way from the properties of the square net. We shall therefore only briefly summarize the calculations that have been done.

CC-0. In Public Domain. Gurukul Kangri Collection, Haridwar

Digitized by Arya Samaj Foundation Chennai and eGangotri

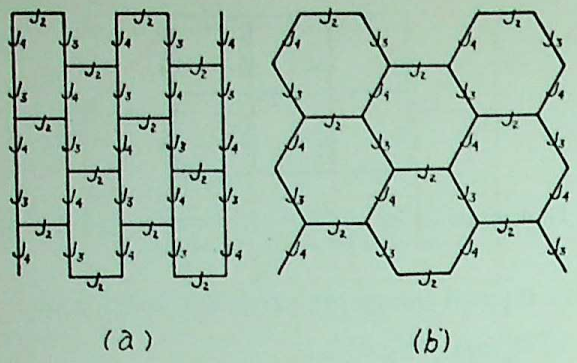


FIG. 18. (a) is obtained from Fig. 17 by setting $J_1=0$, thus eliminating the bond so designated. (a) can then be deformed into the hexagonal lattice (b). The partition function depends only upon the J's and the topology of the lattice.

The triangular and hexagonal lattices which have already been described in Sec. 3.1 can be solved exactly by essentially the same technique used for the square lattice. Another lattice that has been treated in the same way is the Kagomé lattice,[26] a woven bamboo pattern as shown in Fig. 16.

All these lattice types can be considered as special cases of a generalized square lattice.[27] In this generalized square lattice we introduce several interaction constants. For example, we may use four different constants, one for each of the four nearest neighbors as shown in Fig. 17. Each bond is labeled with its coupling constant.

The techniques used for solving the usual square net, particularly the method of spinor analysis, can with minor modifications solve this more complex lattice. It is in fact possible to solve exactly a square net with even more complex arrangements of coupling constants. The details of such will however not be given here.

We shall notice that from the solution of this lattice we obtain as special cases, the solution for both the triangular and hexagonal lattices. If we set $J_1=0$ we eliminate the bonds so designated. The resulting lattice shown in Fig. 18 is then deformable into the hexagonal lattice.

If, on the other hand, we take the limit $J\to\infty$, the spin pairs so coupled must take the same values. They therefore act as a single particle. The lattice resulting from bringing the particles joined by J_1 into a single particle gives the triangular lattice.

The Kagomé lattice is a special case of a more complex square lattice. The specialization is illustrated in Fig. 19 where we have designated by ∞ and 0 those bonds of the square lattice whose coupling constants are ∞ and 0, respectively.

With but a few special exceptions mentioned below, the properties of these lattices are of the same general type as the regular square lattice discussed in Sec. 4.3. They all exhibit a logarithmic singularity in the specific heat corresponding to a transition from an ordered to a disordered state. The critical temperature depends upon the values of the various coupling constants, for example, the critical temperature of the triangular lattice is given by the solution of

$$(\cosh 2K_2 \cosh 2K_3 \cosh 2K_4 + \sinh 2K_2 \sinh 2K_3 \sinh 2K_4)^2 = 2+\sinh^2 2K_2+\sinh^2 2K_3+\sinh^2 2K_4 \qquad K_j=J_j/kT. \quad (5.1)$$

The exceptions to this type of behavior are furnished by special antiferromagnetic lattices which have no "perfectly ordered" state. An example of such is the triangular lattice for which the three coupling constants are all exactly equal and negative $J_1=J_2=J_3<0$. Each particle tries to have its spin opposite to that of all its neighbors. One readily sees that it is not possible to arrange positive and negative spins so that each spin in the lattice is different than all its neighbors. There is no ordered state as for example in the rectangular and hexagonal lattices illustrated by Fig. 20.

This triangular lattice fails to have a transition if and only if one or three J_i's are negative and the two weakest $|J_i|$ are exactly equal. All these cases lack an ordered state. It is interesting that, if one or three J_i are negative and we let the two weakest $|J_i|$ approach equal values, the value of T_c becomes smaller and smaller until it finally disappears at $T_c=0$ much as the singularity in the two-dimensional square lattice vanished as we let one of the couplings go to zero.

Even in the general case $J_1\neq J_2\neq J_3$, it is possible to obtain both a dual transformation and a star-triangle transformation as in Sec. 2. These are obtained in the same manner as before but the algebra becomes more cumbersome. The fact that certain triangular lattices have no transition does not imply, however, that the hexagonal lattice has any such solutions of physical interest. By applying the star-triangle transformation to these special triangular lattices one finds that they correspond to hexagonal lattices with imaginary couplings. All hexagonal lattices with nonzero real coupling constants have phase transitions.

The triangular lattice may be considered as a first step toward the solution of a nearest and next nearest neighbor square net problem. We can deform the triangular lattice as shown in Fig. 21. It is then apparent

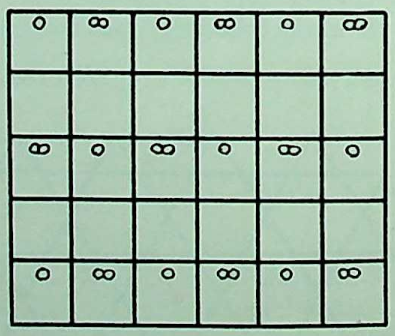


FIG. 19. By eliminating those bonds designated by 0 and joining points connected by the bonds ∞, one can deform the above lattice into the Kagomé lattice of Fig. 16.

CC-0. In Public Domain. Gurukul Kangri Collection, Haridwar

Digitized by Arya Samaj Foundation Chennai and eGangotri

that the triangular net is a square net with an additional interaction along one of the diagonals. Unfortunately, it has not been possible to solve the case of interactions along both diagonals. Indeed none of the cases considered involve interactions that "cross." The difficulties here are remindful of those in the three-dimensional lattice where the topology of closed paths involve knots. It would appear that this also may be a very difficult problem.

The partition function per particle Z_H, of a hexagonal lattice is given by[20]

$$\log(\tfrac{1}{2}Z_H)=\frac{1}{16\pi^2}\int_0^{2\pi}\int_0^{2\pi}\log\tfrac{1}{2}\{\cosh 2K_1\cosh 2K_2\times\cosh 2K_3+1-\sinh 2K_2\sinh 2K_3\cos\omega_1-\sinh 2K_3\sinh 2K_1\cos\omega_2-\sinh 2K_1\sinh 2K_2\cos(\omega_1+\omega_2)\}d\omega_1 d\omega_2.$$

That of a triangular lattice Z_T is given by

$$\log(\tfrac{1}{2}Z_T)=\frac{1}{8\pi^2}\int_0^{2\pi}\int_0^{2\pi}\log\{\cosh 2K_1\cosh 2K_2\times\cosh 2K_3+\sinh 2K_1\sinh 2K_2\sinh 2K_3-\sinh 2K_1\cos\omega_1-\sinh 2K_2\cos\omega_2-\sinh 2K_3\cos(\omega_1+\omega_2)\}d\omega_1 d\omega_2.$$

6. SPECIAL PROPERTIES OF THE TWO-DIMENSIONAL ISING LATTICE

6.1 Ferromagnetism

Perhaps the most interesting feature of the Ising lattice is its spontaneous magnetization, a necessary feature of any ferromagnet. Peierls[28] was the first to show that the Ising model was ferromagnetic and series expansions for the spontaneous magnetization were long ago given for low temperatures by van der Waerden[8] and Ashkin and Lamb.[16]

The magnetization per particle has already been defined as

$$M=N^{-1}\mu\sum_{j=1}^{N}\bar{\sigma}_j=N^{-1}\partial\log Z/\partial\mathfrak{H}. \tag{6.1}$$

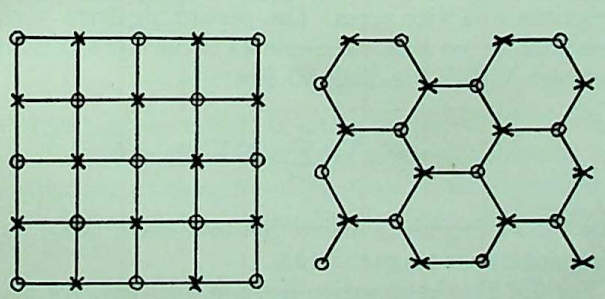


FIG. 20. For an antiferromagnetic square or hexagonal lattice, a state of "perfect order" exists. This state is illustrated with circle describing up (or down) spins and x describing down (or up) spins. Such a state does not exist for the triangular lattice.

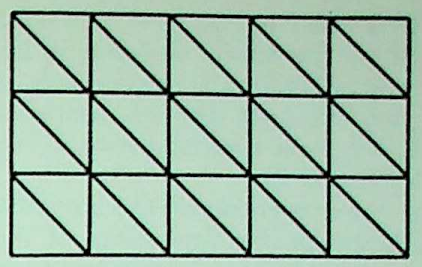


FIG. 21. A triangular lattice can be deformed into the above form which can be interpreted as a square lattice with interactions along one of the diagonal directions.

To be ferromagnetic, a system must have a discontinuity in $M(H, T)$ as a function of H at $H=0$ and T less than some critical temperature T_c. If we take the limit $M(H, T)$ as $H\to 0$ from positive values of H, then $M(0_+, T)>0$. The ferromagnet retains its magnetization in the direction of H even after the magnetic field is turned off. If, on the other hand, we let $H\to 0$ from the negative side, then $M(0_-, T)<0$.

The energy levels of the Ising lattice are given by

$$-J\sum_{n.n.}\sigma_i\sigma_j-\mu H\sum_{j=1}^{N}\sigma_j.$$

If we change the direction of the magnetic field ($H\to -H$) and all the spins ($\sigma_j\to-\sigma_j$), the energy remains unchanged. Since Z involves the sum over all $\sigma_j=\pm 1$ or $-\sigma_j=\pm 1$,

$$\begin{aligned}Z(H)&=Z(-H),\\ M(H)&=-M(-H).\end{aligned} \tag{6.2}$$

For any finite lattice $M(0)=0$. This is apparent since, for a finite lattice Z is a sum of a finite number of functions each analytic in H. Z and M must therefore be analytic in H, and $M(H)=-M(-H)$ implies $M(0)=0$. If, however, we allow the system to be infinite, Z becomes the limit of a sequence of analytic functions which is not necessary analytic. To calculate a spontaneous magnetization, it is necessary to first let $N\to\infty$, then let $H\to 0$. If we put $H=0$ first, we shall always obtain $M(0)=0$.

Although we do not have a solution of the Ising problem for arbitrary H, the spontaneous magnetization depends only upon the behavior of $Z(H, T)$ for small H to terms linear in H.

The existence of a spontaneous magnetization was first proved on the basis of the low temperature expansion of Z. Regarding Eq. (2.25), we note that because of the symmetry with respect to changing σ to $-\sigma$,

$$g(N, N_1, N_{12})=g(N, N-N_1, N_{12}),$$

where N_1 is the number of σ's that are $+1$ and $N-N_1$ the number that are -1. We combine the terms of (2.25) with $N>N/2$ and those with $N\equiv N/2$ to obtain

$$Z=2e^{NcK/2}\sum_{N_{12}}\sum_{N_1\le N/2}g(N, N_1, N_{12})\times\exp(-2KN_{12})\cosh[(N-2N_1)\mu\mathfrak{H}]. \tag{6.3}$$

CC-0. In Public Domain. Gurukul Kangri Collection, Haridwar

Digitized by Arya Samaj Foundation Chennai and eGangotri

(The one term with $N_1=N/2$ for N even is incorrect by a factor of 2 but this error is negligible for large N.)

For N is finite, (6.3) is a function only of $\mathfrak{H}^2$ and therefore gives $M(0)=0$. For low temperatures and positive K, the main contribution to Z comes from terms with $N_{12}\ll Nc/2$.

The existence or nonexistence of a spontaneous magnetization hinges on the dependence of N_1 on N_{12}. These two are certainly not independent quantities for example $N_{12}=0$ implies $N_1=0$ or N. In a one-dimensional lattice, there is, however, very little correlation between N_1 and N_{12} for $N_{12}>0$ because each unfavorable bond (joining unlike spins) gives a boundary between regions of $\sigma=+1$ and $\sigma=-1$. One can shift these boundaries almost at will. Such a shift leaves N_{12} unchanged but N_1 depends upon the length of the regions with $\sigma=+1$. One can make all regions with $\sigma=+1$ small to give a small N_1 or make them all large to give a large N_1.

In two or three dimensions, the situation is quite different. The correlation between N_1 and N_{12} is much stronger. The feature we will want to exploit is that small N_{12} implies small N_1 (or small $N-N_1$); if there are few unlike pairs, then most particles must have the same spin. This difference between the one-dimensional lattice and those of higher dimension is the cause of most of the marked dissimilarity of the thermodynamic and magnetic properties of the one-dimensional lattice.

The dependence of Z on H is contained in the factor $\cosh[(N-2N_1)\mu\mathfrak{H}]$ and the spontaneous magnetization comes from first allowing N to become infinite and then letting $\mu\mathfrak{H}\to 0$. The behavior of Z for small $\mathfrak{H}$ depends strongly on whether or not for most states $N-2N_1\to\infty$ as $N\to\infty$. Such is the case in two or three dimensions at sufficiently low temperatures because a low temperature implies that N_{12} is small for most states and therefore N_1/N is also small. (In one dimension such is not true.)

If $N_1/N\ll 1$ for most states as $N\to\infty$, then for any nonzero $\mu\mathfrak{H}$,

$$\cosh[(N-2N_1)\mu\mathfrak{H}]\to\tfrac{1}{2}\exp[(N-2N_1)|\mu\mathfrak{H}|]$$

for most states. Here lies the source of the spontaneous magnetization, for if we now let $|\mu\mathfrak{H}|\to 0$. Z contains terms linear in $|\mu\mathfrak{H}|$ leading to a nonzero magnetization for $\mathfrak{H}\to 0$ and a discontinuity. For very low temperature and small $\mathfrak{H}$,

$$Z(H)\sim Z(0)\cosh(N\mu\mathfrak{H})$$
$$M(H)\sim\mu\lim_{N\to\infty}\tanh(N\mu\mathfrak{H})=\begin{cases}\mu & \text{for } H>0\\ -\mu & \text{for } H<0\end{cases}\qquad(6.4)$$

(except in one dimension).

A closed expression for $M(0)$ as a function of T has not been derived by combinatorial methods although rather lengthy series expansions have been calculated (see Sec. 7). The spontaneous magnetization of the two-dimensional Ising lattice has been derived, however, using algebraic methods. This was done by Yang[29] (it was reported but never published by Onsager at the Cornell Phase Transition Conference, 1948) using a first-order perturbation of the solution of the Ising problem in zero field. We shall only indicate here the preliminary steps to this calculation. Although the basis for the method is quite obvious, the detailed calculations are both tricky and tedious.

In Eq. (2.14), the partition function is written as

$$Z=(2\sinh 2K)^{nm/2}\,\mathrm{trace}\,(\mathbf{V}_3\mathbf{V}_2\mathbf{V}_1)^m\sim(2\sinh 2K)^{mn/2}\lambda^m{}_{\max},$$

where $\lambda_{\max}$ is the largest eigenvalue of

$$\mathbf{V}_3\mathbf{V}_2\mathbf{V}_1=\mathbf{V}_2\mathbf{V}_1+\mu\mathfrak{H}(\sum_{j=1}^{n}\mathbf{s}_j)\mathbf{V}_2\mathbf{V}_1+\cdots.$$

We write $\lambda_{\max}=\lambda^0{}_{\max}+\mu\mathfrak{H}\lambda'_{\max}$ with $\lambda^0{}_{\max}$ the largest eigenvalue of $\mathbf{V}_2\mathbf{V}_1$ and we determine $\lambda'_{\max}$ by the usual first-order perturbation theory.

Perturbation theory is somewhat more elegant if the matrices are symmetric because then the eigenfunction are orthogonal. Instead of treating the matrix $\mathbf{V}_3\mathbf{V}_2\mathbf{V}_1$, Yang considers matrix $\mathbf{V}_1^{\frac{1}{2}}\mathbf{V}_3\mathbf{V}_2\mathbf{V}_1^{\frac{1}{2}}$ which is similar to the above but also symmetric. This is not a generalization of the symmetric matrix $\mathbf{P}$ of Sec. 2. Such a matrix would be $\mathbf{V}_2^{\frac{1}{2}}\mathbf{V}_3^{\frac{1}{2}}\mathbf{V}_1\mathbf{V}_3^{\frac{1}{2}}\mathbf{V}_2^{\frac{1}{2}}$. All three of these matrices are similar and therefore have the same eigenvalues. One should be able to carry through all the analysis irrespective of representation but to avoid confusion we use here the same matrix as Yang. We therefore write

$$\mathbf{V}_1^{\frac{1}{2}}\mathbf{V}_3\mathbf{V}_2\mathbf{V}_1^{\frac{1}{2}}=\mathbf{V}_1^{\frac{1}{2}}\mathbf{V}_2\mathbf{V}_1^{\frac{1}{2}}+\mu\mathfrak{H}\mathbf{V}_1^{\frac{1}{2}}\sum_{j=1}^{n}\mathbf{s}_j\mathbf{V}_2\mathbf{V}_1^{\frac{1}{2}}.$$

Perturbation theory warns us that we must distinguish between cases where $\lambda^0{}_{\max}$ is degenerate and cases where it is nondegenerate. We therefore consider separately the cases $T>T_c$ and $T<T_c$.

We have seen (Sec. 3.2) that for $T>T_c$, the largest eigenvalue of $\mathbf{V}_1^{\frac{1}{2}}\mathbf{V}_2\mathbf{V}_1^{\frac{1}{2}}$ is nondegenerate and its eigenfunction ψ_+ belongs to the space of even functions. Each of the matrices $\mathbf{V}_2$ and $\mathbf{V}_1$ commutes with $\mathbf{U}$, thus they send even functions into even functions and odd functions into odd functions. $\mathbf{s}_j$, however, anticommutes with $\mathbf{U}$, it sends even functions into odd functions and vice versa. The perturbing term above therefore has no diagonal elements in the representation in which $\mathbf{V}_1^{\frac{1}{2}}\mathbf{V}_2\mathbf{V}_1^{\frac{1}{2}}$ is diagonal and

$$\lambda'_{\max}=(\psi_+,\,\mathbf{V}_1^{\frac{1}{2}}\sum_{j=1}^{n}\mathbf{s}_j\mathbf{V}_2\mathbf{V}_1^{\frac{1}{2}}\psi_+)=0.$$

For $T>T_c$ there is no correction to λ linear in $\mathfrak{H}$, thus no spontaneous magnetization.

For $T<T_c$, the situation is quite different. We have seen that $\lambda^0{}_{\max}$ is then twofold degenerate in the limit $n\to\infty$. There is an eigenfunction ψ_+ in the even space and an eigenfunction ψ_- in the odd space. The perturba-

CC-0. In Public Domain. Gurukul Kangri Collection, Haridwar

Digitized by Arya Samaj Foundation Chennai and eGangotri

tion "splits" the degeneracy, and we have a situation quite analogous to the anomalous Zeeman effect in the quantum theory of the hydrogen atom.

The first step in a perturbation procedure is to consider separately those parts of the matrices corresponding to the space in which λ^0_{max} is degenerate. In this case we consider the 2×2 section of the matrices corresponding to the space ψ_+ and ψ_-. We wish to choose a representation in which the 2×2 part of both the zero-order and first-order matrices $\mathbf{V}_1^{\frac{1}{2}}\mathbf{V}_2\mathbf{V}_1^{\frac{1}{2}}$ and

$$\mathbf{V}_1^{\frac{1}{2}}\sum_{j=1}^{n}\mathbf{s}_j\mathbf{V}_2\mathbf{V}_1^{\frac{1}{2}},$$

respectively, are diagonal. This portion of the matrix $\mathbf{V}_1^{\frac{1}{2}}\mathbf{V}_2\mathbf{V}_1^{\frac{1}{2}}$ is simply λ^0_{max} times the 2×2 identity matrix and is invariant to any transformation of ψ_+ and ψ_-. It will be diagonal in any representation including that in which this part of the first-order matrix is diagonal. The 2×2 portion of the first-order matrix is symmetric and has zero diagonal elements in the representation ψ_+ and ψ_-. The first-order eigenfunctions are therefore $2^{\frac{1}{2}}(\psi_+\pm\psi_-)$ and

$$\lambda'_{max}=[2^{-\frac{1}{2}}(\psi_+ + \psi_-),\ \mathbf{V}_1^{\frac{1}{2}}\sum_{j=1}^{n}\mathbf{s}_j\mathbf{V}_2\mathbf{V}_1^{\frac{1}{2}}2^{-\frac{1}{2}}(\psi_+ + \psi_-)].$$

Since $\mathbf{V}_1^{\frac{1}{2}}\mathbf{V}_2\mathbf{V}_1^{\frac{1}{2}}(\psi_+ + \psi_-)=\lambda^0_{max}(\psi_+ + \psi_-)$,

$$\lambda'_{max}=\tfrac{1}{2}\lambda^0_{max}[(\psi_+ + \psi_-),\ \mathbf{V}_1^{\frac{1}{2}}\sum_{j=1}^{n}\mathbf{s}_j\mathbf{V}_1^{-\frac{1}{2}}(\psi_+ + \psi_-)]$$

$$=\lambda^0_{max}(\psi_-,\ \mathbf{V}_1^{\frac{1}{2}}\sum_{j=1}^{n}\mathbf{s}_j\mathbf{V}_1^{-\frac{1}{2}}\psi_+)$$

because $\mathbf{s}_j$ has no matrix elements connecting ψ_+ to ψ_+ or ψ_- to ψ_- but $\mathbf{s}_j$ is symmetric.

Using (6.1), we see that to order $\mathfrak{H}$,

$$M=n^{-1}\partial\log\lambda_{max}/\partial\mathfrak{H}=n^{-1}\mu\lambda'_{max}/\lambda^0_{max}$$

$$=n^{-1}\mu(\psi_-,\ \mathbf{V}_1^{\frac{1}{2}}\sum_{j=1}^{n}\mathbf{s}_j\mathbf{V}_1^{-\frac{1}{2}}\psi_+).$$

Since each point in the row is equivalent to any other point, each of the n values of j give the same contribution; therefore,

$$M=\mu(\psi_-,\ \mathbf{V}_1^{\frac{1}{2}}\mathbf{s}_1\mathbf{V}_1^{-\frac{1}{2}}\psi_+).$$

The magnetization is thus described by a single matrix element which formally looks quite simple. The evaluation of it is, however, rather complicated even though the answer is relatively simple. Yang[29] found for $K=K'$

$$|M(0)|=\mu(1+z^2)^{\frac{1}{4}}(1-z^2)^{-\frac{1}{4}}(1-6z^2+z^4)^{1/8} \qquad (6.5)$$
$$z=e^{-2K}.$$

Near the critical point $z=z_c=\sqrt{2}-1$, $M(0)$ has a branch point

$$M(0)\simeq\mu[4(\sqrt{2}+2)(z_c-z)]^{1/8}.$$

The magnetization $M(0, T)$ is shown in Fig. 22.§

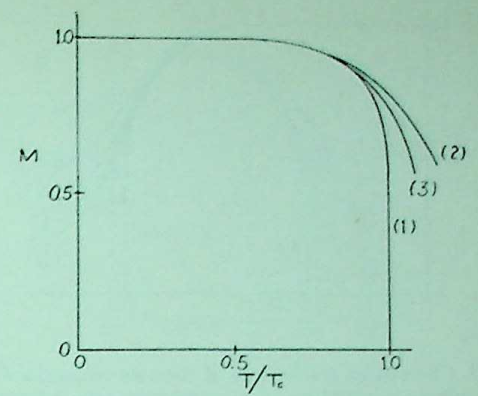


FIG. 22. The spontaneous magnetization of the two-dimensional Ising lattice is plotted *vs* the temperature (curve 1) (see reference 29). Curve (2) is an extrapolation of the low temperature series expansion in powers of $z=e^{-2K}$, including terms of order z^{12} [deduced by van der Waerden (see reference 8) and Ashkin and Lamb (see reference 16)]. Curve (3) is the expansion to terms of order z^{18} as given by Domb (see reference 34), the longest series known prior to Yang's exact treatment.

6.2 Correlations

Aside from the usual thermodynamic quantities, one is also interested in the correlations between spins at different lattice sites. Such correlations are observed experimentally in x-ray diffraction effects.

A great deal of literature exists on approximate theories of ferromagnetism and binary alloys based upon short-range and long-range correlations. A review of such work would carry us far away from our purpose here. This voluminous literature has been reviewed elsewhere.

Exact expressions for correlations have been calculated only for the two-dimensional square Ising lattice.[30] The correlation of the ith spin to the jth spin is defined as the average of σ_i if $\sigma_j=+1$. We may re-express this in many ways. It is also the average of σ_j if $\sigma_i=+1$, or the negative of the average of σ_i if $\sigma_j=-1$. The most convenient expression is the average of $\sigma_i\sigma_j$ written below as $\langle\sigma_i\sigma_j\rangle$. The equivalence of these definitions is apparent since $\sigma_i=+1$ with equal *a priori* probabilities.

$\langle\sigma_i\sigma_j\rangle$ is calculated from

$$\langle\sigma_i\sigma_j\rangle=Z^{-1}\sum_{\sigma_1=\pm1}\cdots\sum_{\sigma_N=\pm1}\sigma_i\sigma_j\exp(-E/kT). \qquad (6.6)$$

These averages are evaluated by again using matrix expressions. For a two-dimensional lattice, let σ_{jk} be the spin of the particle in the jth row and kth column.

§ *Note added in proof:* Formulas for the magnetization of the asymmetric square and triangular lattices have been presented by R. B. Potts [Phys. Rev. 88, 352 (1952)]. The formulas of the former were also given by C. H. Chang [Phys. Rev. 88, 1422 (1952)].

CC-0. In Public Domain. Gurukul Kangri Collection, Haridwar

Digitized by Arya Samaj Foundation Chennai and eGangotri

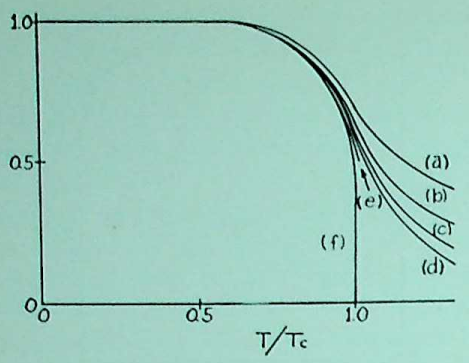


FIG. 23. Correlation coefficients of the two-dimensional square Ising lattice as a function of temperature (see reference 30); (a) $\langle\sigma_{11}\sigma_{12}\rangle$, (b) $\langle\sigma_{11}\sigma_{22}\rangle$, (c) $\langle\sigma_{11}\sigma_{13}\rangle$, (d) $\langle\sigma_{11}\sigma_{23}\rangle$, (e) $\langle\sigma_{11}\sigma_{14}\rangle$, and (f) M^2. Since, as one observes from the figure, these averages are monotone functions of the distance between the points, the long-range correlations approach a limit M^2 independent of direction on the lattice.

If ν_k represents the state of the kth row as in Sec. 2.1, then (6.6) can be written in the form

$$\langle\sigma_{jk}\sigma_{ab}\rangle = Z^{-1}\sum_{\nu_1=1}^{2^n}\cdots\sum_{\nu_m=1}^{2^n} P_{\nu_1\nu_2}\times\cdots \times P_{\nu_{j-1}\nu_j}(s_k)_{\nu_j\nu_j}P_{\nu_j\nu_{j+1}}\times\cdots \times P_{\nu_{a-1}\nu_a}(s_b)_{\nu_a\nu_a}P_{\nu_a\nu_{a+1}}\times\cdots\times P_{\nu_m\nu_1},$$

where $P_{\nu\nu'}$ is the matrix defined in Sec. 2.1. The above is again expressible as the trace of a matrix product,

$$\langle\sigma_{jk}\sigma_{ab}\rangle = Z^{-1}\,\text{trace}\,(\mathbf{P}^{j-1}\mathbf{s}_k\mathbf{P}^{a-j}\mathbf{s}_b\mathbf{P}^{m-a+1}) = Z^{-1}\,\text{trace}\,(\mathbf{s}_k\mathbf{P}^{a-j}\mathbf{s}_b\mathbf{P}^{m-a+j}). \quad (6.7)$$

The right side depends upon a and j only through the combination of $j-a$ as is to be expected physically as a result of the periodic boundary conditions. Also it depends upon k and a only through $k-a$ because the matrix $\mathbf{P}$ is invariant to a cyclic permutation of the particles in a row. One needs only consider $\langle\sigma_{11}\sigma_{ab}\rangle$. Also the correlations are independent of reflections about vertical or horizontal lines, they depend only upon $|a-1|$ and $|b-1|$, thus we need only consider $1<a\leq\frac{1}{2}m+1$ and $1<b\leq\frac{1}{2}n+1$.

Since the trace is invariant to a similarity transformation, we apply the transformation which diagonalizes $\mathbf{P}$. Let $\mathbf{\Psi}^r$ be this transformation matrix,

$$\langle\sigma_{11}\sigma_{ab}\rangle = (\sum_{l=1}^{2^n}\lambda_l{}^m)^{-1}\sum_{l=1}^{2^n}\lambda_l{}^{m-a+1}(\mathbf{\Psi}^{r-1}\mathbf{s}_1\mathbf{P}^{a-1}\mathbf{s}_b\mathbf{\Psi}^r)_{ll}. \quad (6.8)$$

Since $a-1\leq m/2$, $m-a+1$ will be large for m large and we need only consider the values of l corresponding to the largest eigenvalue. For $T>T_c$, the largest eigenvalue is nondegenerate and we neglect all l but one:

$$\langle\sigma_{11}\sigma_{ab}\rangle\simeq\lambda_{\max}{}^{-a+1}(\psi_+,\,\mathbf{s}_1\mathbf{P}^{a-1}\mathbf{s}_b\psi_+). \quad (6.8a)$$

For $T<T_c$ the largest eigenvalue is doubly degenerate, in which case

$$\langle\sigma_{11}\sigma_{ab}\rangle\simeq\tfrac{1}{2}\lambda_{\max}{}^{-a+1}[(\psi_+,\,\mathbf{s}_1\mathbf{P}^{a-1}\mathbf{s}_b\psi_+) + (\psi_-,\,\mathbf{s}_1\mathbf{P}^{a-1}\mathbf{s}_b\psi_-)]. \quad (6.8b)$$

The correlations between nearby point (a and b small) in an infinite lattice (m and $n\to\infty$) are used to describe "short-range order." Long-range order already discussed in Sec. 3.2 is described by the limit of $\langle\sigma_{11}\sigma_{ab}\rangle$ as a and $b\to\infty$ (after m and $n\to\infty$).

The correlations have been calculated by Kaufman and Onsager for several of the nearby pairs of points. The detailed evaluation of the matrix elements (6.8a,b) is again a rather tedious operation. The results of these calculations are plotted in Fig. 23.

Long-range order and spontaneous magnetization describe essentially the same thing as we shall see below. One can very easily see from (6.8) and (6.8a) that no long-range order exists for $T>T_c$. If we let $l=1$ correspond to the largest eigenvalue (it is nondegenerate), then

$$\langle\sigma_{11}\sigma_{ab}\rangle\to\lambda_1{}^{-a+1}(\mathbf{\Psi}^{r-1}\mathbf{s}_1\mathbf{\Psi}^r\mathbf{\Psi}^{r-1}\mathbf{P}^{a-1}\mathbf{\Psi}^r\mathbf{\Psi}^{r-1}\mathbf{s}_b\mathbf{\Psi}^r)_{11}$$

as $m\to\infty$

$$=\lambda_1{}^{-a+1}\sum_{j=1}^{2^n}(\mathbf{\Psi}^{r-1}\mathbf{s}_1\mathbf{\Psi}^r)_{1j}\lambda_j{}^{a-1}(\mathbf{\Psi}^{r-1}\mathbf{s}_b\mathbf{\Psi}^r)_{j1}$$

$$\to(\mathbf{\Psi}^{r-1}\mathbf{s}_1\mathbf{\Psi}^r)_{11}(\mathbf{\Psi}^{r-1}\mathbf{s}_b\mathbf{\Psi}^r)_{11}$$

as $a\to\infty$

$$=\langle\sigma_{11}\rangle\langle\sigma_{1b}\rangle=0$$

because both σ_{11} and σ_{1b} are zero. Thus, we again prove that long-range order cannot exist unless the largest eigenvalue is degenerate.

We might look at this from a slightly different point of view. Suppose $|M|=M(0_+,T)=-M(0_-,T)$ is the spontaneous magnetization per particle, N_1 the number of "up" spins and N_2 the number of "down" spins, then

$$|M|=|N_1-N_2|/N=\pm(N_1-N_2)/N,\quad N=N_1+N_2.$$

The $\pm$ is chosen accordingly as the magnetization is in the positive or negative direction (up or down). This gives

$$N_1/N=\tfrac{1}{2}(1\pm|M|),\quad N_2/N_1=\tfrac{1}{2}(1\mp|M|).$$

We now ask what is the average magnetization if one spin (call it σ_{11}) is positive? We use the symbol $Pr\{a\}$ to denote the probability of the event a. We have just deduced that

$$Pr\{\sigma_{11}>0\quad\text{if}\quad M=\pm|M|\}=\tfrac{1}{2}(1\pm|M|).$$

However,

$$Pr\{\sigma_{11}>0\quad\text{and}\quad M=\pm|M|\} = Pr\{\sigma_{11}>0\quad\text{if}\quad M=\pm|M|\}Pr\{M=\pm|M|\} = Pr\{M=\pm|M|\quad\text{if}\quad\sigma_{11}>0\}Pr\{\sigma_{11}>0\}.$$

CC-0. In Public Domain. Gurukul Kangri Collection, Haridwar

Digitized by Arya Samaj Foundation Chennai and eGangotri

In the absence of a magnetic field $Pr\{M=\pm|M|\}$ and $Pr\{\sigma_{11}=\pm 1\}$ are all $\frac{1}{2}$. Thus,

$$Pr\{M=\pm|M| \quad \text{if} \quad \sigma_{11}>0\}$$
$$=Pr\{\sigma_{11}>0 \quad \text{if} \quad M=\pm|M|\}=\tfrac{1}{2}(1\pm|M|).$$

We find that the average magnetization if $\sigma_{11}>0$ to be

$$|M|Pr\{M=|M| \quad \text{if} \quad \sigma_{11}>0\}$$
$$-|M|Pr\{M=-|M| \quad \text{if} \quad \sigma_{11}>0\}$$
$$=\tfrac{1}{2}|M|(1+|M|)-\tfrac{1}{2}|M|(1-|M|)=M^2.$$

M^2 is the conditional average of all spins if $\sigma_{11}>0$. It can also be expressed in terms of the correlations above

$$M^2=\lim_{m,n\to\infty}(nm)^{-1}\sum_{a=1}^{m}\sum_{b=1}^{n}\langle\sigma_{11}\sigma_{ab}\rangle.$$

As n and $m\to\infty$, no finite set of a, b contribute to this sum. We obtain a nonzero M^2 if and only if $\langle\sigma_{11}\sigma_{ab}\rangle$ is nonzero for arbitrarily large a and b. Thus, we see that the existence of long-range order is equivalent to the existence of a spontaneous magnetization.

7. THREE-DIMENSIONAL LATTICES

It has already been mentioned that the methods used in finding exact expressions for properties of two-dimensional lattices break down when they are applied to the investigation of three-dimensional lattices. However, the first few terms have been calculated in certain power series expansions for the partition function of three-dimensional Ising lattices. Expansions exist which are valid in the high and low temperature ranges. These have been obtained by both the matrix and combinatorial methods. Although it is impossible to base a rigorous discussion of critical phenomenon on these series, they give accurate results at temperatures not too close to the critical point and are useful for the estimation of the range of validity of approximate expressions for thermodynamic properties.

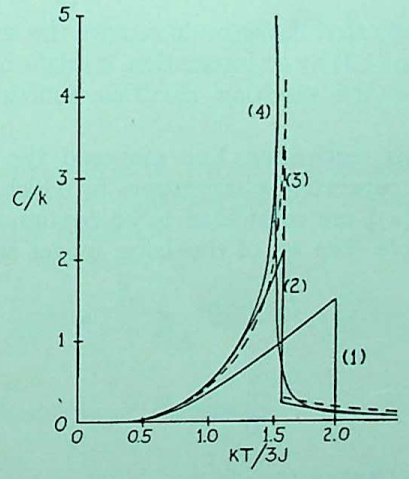


FIG. 24. Approximate specific heat curves for the three-dimensional cubic Ising lattice (see references 2, 31). In order of their apparent accuracy they are (1) Bragg-Williams approximation, (2) Bethe second approximation, (3) Kirkwood approximation, and (4) and extrapolation of high and low temperature expansions by Wakefield known to be accurate everywhere except near the critical point.

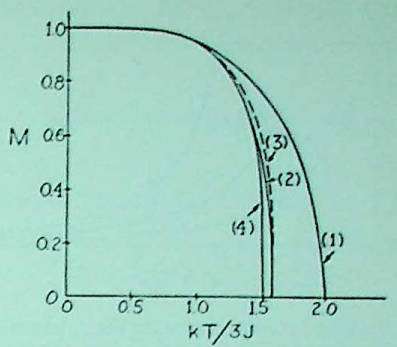


FIG. 25. Approximate spontaneous magnetization curves for the cubic lattice corresponding to the curves of Fig. 24.

Since Rushbrook[31] recently published a detailed review of the status of these series, we shall merely state the best available results for the simple, body-centered and face-centered cubic lattices and present specific heat and spontaneous magnetization curves (see Figs. 24 and 25) for the simple cubic lattice. These curves are compared with those computed on the basis of the Bragg-Williams and Bethe formulas.

A large number of articles have been written about series expansions. Some of the more recent ones are those of Rushbrook[32] and Wakefield;[33] Domb;[34] Trefftz;[35] Somers;[36] Ter Haar;[37] Oguchi;[38] Tanaka, Katsumori, and Toshima;[39] and Kikuchi.[40]

We shall consider only the case in which the interaction parameters in all directions are equal. We let

$$x=\tanh K. \tag{7.1}$$

Then the high temperature expansions for the Nth root of the partition function (in a lattice of N particles) are

a. simple cubic lattice

$$Z^{1/N}=2\cosh^3K(1+3x^4+22x^6+192x^8$$
$$+2070x^{10}+24\,943x^{12}+\cdots); \tag{7.2}$$

b. body-centered cubic

$$Z^{1/N}=2\cosh^4K(1+12x^4+148x^6+1860x^8+\cdots); \tag{7.3}$$

c. face-centered cubic

$$Z^{1/N}=2\cosh^6K(1+8x^3+33x^4+168x^5$$
$$+962x^6+5928x^7+\cdots). \tag{7.4}$$

The low temperature series for $N^{-1}\log Z$ are expressed in powers of $z=\exp(-2J/kT)$,

CC-0. In Public Domain. Gurukul Kangri Collection, Haridwar

Digitized by Arya Samaj Foundation Chennai and eGangotri

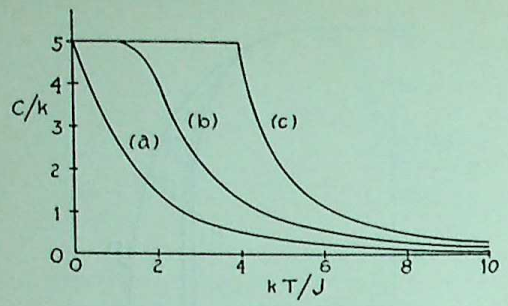


FIG. 26. Specific heat *vs* temperature for the spherical model in (a) one dimension, (b) two dimensions, and (c) three dimensions.

a. simple cubic lattice

$$z^{-1}\Big(z^6+3z^{10}-\frac{7}{2}z^{12}+15z^{14}-33z^{16}+\frac{313}{3}z^{18}-\frac{561}{2}z^{20}+849z^{22}-\frac{9847}{4}z^{24}+7485z^{26}-\frac{45\,069}{2}z^{28}+\cdots\Big); \quad (7.5)$$

b. body-centered cubic

$$z^{-2}\Big(z^8+4z^{14}-\frac{9}{2}z^{16}+28z^{20}-64z^{22}+\frac{145}{3}z^{24}+204z^{26}-786z^{28}+1164z^{30}+\frac{3691}{4}z^{32}-8760z^{34}+\cdots\Big); \quad (7.6)$$

c. face-centered cubic

$$z^{-3}\Big(z^{12}+6z^{22}-\frac{13}{2}z^{24}+8z^{30}+42z^{32}-120z^{34}+\frac{217}{3}z^{36}+24z^{28}+123z^{40}+126z^{42}-1623z^{44}+2418z^{46}+\cdots\Big). \quad (7.7)$$

The formulas for spontaneous magnetization are

a. simple cubic[11]

$$M/\mu=1-2z^6-12z^{10}+14z^{12}-90z^{14}+192z^{16}-792z^{18}+2148z^{20}-7716z^{22}+23\,262z^{24}-79\,512z^{26}+252\,054z^{28}+\cdots;$$

b. body-centered

$$M/\mu=1-2z^8-16z^{14}+18z^{16}-168z^{20}+384z^{22}-314z^{24}-1184z^{26}+6248z^{28}-9744z^{30}-10\,174z^{32}+\cdots;$$

c. face-centered

$$M/\mu=1-2z^{12}-24z^{22}+26z^{24}-48z^{30}-252z^{32}+720z^{34}-438z^{36}-192z^{36}-984z^{40}-1008z^{42}-\cdots.$$

It has frequently been conjectured that the partition function Z for a three-dimensional lattice is the simple generalization of the Onsager formula

$$\log\tfrac{1}{2}Z^{1/N}=\frac{1}{2(2\pi)^3}\int_0^{2\pi}\!\!\int\!\!\int \times\log(\cosh 2K_1\cosh 2K_2\cosh 2K_3-\sinh 2K_1\cos\omega_1-\sinh 2K_2\cos\omega_2-\sinh 2K_3\cos\omega_3)\,d\omega_1 d\omega_2 d\omega_3.$$

When the interaction constant in the z direction, K_3, vanishes this expression reduces to the correct two-dimensional formula (4.53). Unfortunately, if one sets $K_1=K_2=K_3=K$ the high temperature power series in $x=\tanh K$ is not the same as the exact series (7.2).

8. SPHERICAL MODEL

The partition function (1.3) of the Ising model (in the absence of a magnetic field, $\mathfrak{H}=0$) is a multiple sum whose summand is the exponential of a quadratic form in the σ's. The infinite integral over an exponential of a quadratic form whose real part is negative definite can be evaluated much easier than the sum by employing the formula

$$\int_{-\infty}^{\infty}\cdots\int \exp\Big(-\sum_{i,j=1}^{N}a_{ij}\sigma_i\sigma_j\Big)\,d\sigma_1\cdots d\sigma_N = \pi^{N/2}\,(\det|a_{jk}|)^{-\frac{1}{2}}. \quad (8.1)$$

This suggests that if one could replace the summation operation in (1.3) by an integration, it might be possible to evaluate the resulting partition function rather easily.

With this motivation Kac proposed the spherical model of cooperative phenomenon in which the spin variables $\{\sigma_j\}$ are considered to be continuous rather than discrete. The σ's of the Ising model satisfy the relations

$$\sigma_j^2=1, \quad j=1, 2, \cdots, N \quad (8.2)$$

$$\sum_{j=1}^{N}\sigma_j^2=N. \quad (8.3)$$

The spherical model is characterized by the relaxation of the strong conditions (8.2) and the postulation that the σ's can simultaneously have any real values which lie on the hypersphere (8.3).

There are certain properties of the spherical model which are physically unrealistic. For example, the fact

[11] *Note added in proof:* The coefficient of z^{26} is that given in reference 39, Wakefield (reference 33), however, gives 79530.

CC-0. In Public Domain. Gurukul Kangri Collection, Haridwar

Digitized by Arya Samaj Foundation Chennai and eGangotri

that the σ's are continuous suggests that the thermodynamic behavior should be classical at low temperatures (for example, the specific heat does not approach zero as $T\to 0$). On the other hand, the magnetic properties of the spherical model may resemble those of a real ferromagnetic more closely than does the Ising model. The two-dimensional spherical model has no transition while the corresponding Ising does. There is considerable evidence[41] that a real two-dimensional ferromagnet does not have a transition either; it has been suggested that the magnetic anisotropy of the Ising model induces the transition in two dimensions.

The attractive feature of the spherical model is that all its thermodynamic and magnetic properties can be calculated exactly in one, two, and three dimensions for any common type of lattice. Also the interaction of a particle with other than nearest neighbors can be introduced into the spherical model without causing any significant mathematical difficulties. In three dimensions a phase transition exists with long-range order below the critical temperature. The thermodynamic properties have been calculated by Berlin and Kac[42] and one of the authors.[43] Since the recent paper of Berlin and Kac is quite complete in all the details, we shall merely outline the methods used and summarize the results.

The partition function (normalized to unity as $T\to\infty$) of the spherical model in the absence of a magnetic field is

$$Z=A_N^{-1}\int\cdots\int_{\sum_{j=1}^{N}\sigma_j^2=N} d\sigma_1\cdots d\sigma_N \exp(\tfrac{1}{2}K\textstyle\sum a_{ij}\sigma_i\sigma_j), \quad (8.4)$$

where

$$A_N=\int\cdots\int_{\sum_{j=1}^{N}\sigma_j^2=N} d\sigma_1\cdots d\sigma_N=2\pi^{\frac{1}{2}N}N^{\frac{1}{2}(N-1)}/\Gamma(\tfrac{1}{2}N). \quad (8.5)$$

All other symbols have the meaning given to them in Sec. 1. One way of evaluating the partition function is to introduce the δ-function,

$$\delta(N-\sum_{j=1}^{N}\sigma_j^2)=\frac{1}{2\pi}\int_{-\infty}^{\infty}\exp\{iy(N-\sum_{j=1}^{N}\sigma_j^2)\}dy \quad (8.6)$$

into the integrands of (8.4) and (8.5). Since $\delta(N-\sum_{j=1}^{N}\sigma_j^2)$ vanishes, unless the sphericalization condition (8.3) is satisfied, the integration over the σ's can be allowed to extend over all real values, $-\infty<\sigma_j<\infty$ for all j. The integration over the σ's is then easily carried out by applying (8.1). The integration over the new variable y is performed by the method of steepest descents.

The final expression for the partition function of an s dimensional-simple cubic lattice is

$$\lim_{N\to\infty}\frac{1}{N}\log Z=-\tfrac{1}{2}-\tfrac{1}{2}\log 2K-\tfrac{1}{2}f(z_s)+Kz_s, \quad (8.7)$$

and the specific heat per particle is

$$C=\frac{k}{2}[1+2K^2dz_s/dK] \quad (8.8)$$

when a real position solution z_s exists for the equation

$$2K=\frac{1}{(2\pi)}\int_0^{2\pi}\cdots\int\frac{d\omega_1\cdots d\omega_s}{z_s-\cos\omega_1-\cdots-\cos\omega_s}. \quad (8.9)$$

The function $f(z_s)$ is defined by

$$f(z_s)=\frac{1}{(2\pi)^s}\int_0^{2\pi}\cdots\int\ln[z_s-\sum_{j=1}^{s}\cos\omega_j]d\omega_1\cdots d\omega_s. \quad (8.10)$$

When $s=1$ or 2, Eq. (8.9) has a solution z_s for all $0\le K\le\infty$; that is for all temperatures. Indeed, in these two cases z_s is an analytic function of K, as is the specific heat (8.8). No phase transitions occur.

In the three-dimensional case Eq. (8.9) has a real positive root z_s (which is ≥ 3) only when

$$T\ge T_c=3.9568J/k. \quad (8.11)$$

For $T<T_c$, it can be shown that the specific heat per particle is given by

$$C=\tfrac{1}{2}k, \quad T<T_c. \quad (8.12)$$

The function C/k is not analytic in this case. It has a singularity at $T=T_c$. The specific heat is plotted in Fig. 26. Notice that as $T\to 0$ it has a finite limit rather than zero, the corresponding limit in the Ising model. Berlin and Kac showed that the long-range correlation coefficient vanished at temperatures above T_c, while

$$\langle\sigma_j/\sigma_k\rangle_N/\langle\sigma_j^2\rangle_N^{\frac{1}{2}}\langle\sigma_k^2\rangle_N^{\frac{1}{2}}\to 1-(T/T_c), \quad T<T_c \quad (8.13)$$

as $|r_j-r_k|\to\infty$. The spontaneous magnetization is proportional to $(1-T/T_c)^{\frac{1}{2}}$ for $T<T_c$.

One might argue that the critical phenomenon discussed above are caused by a small number of excessively large spins [such are possible according to (8.3)]. However, the statistical weight of such spins is very small. It can be shown that

$$\langle\sigma_j^4\rangle_N=\begin{cases}3 & T>T_c\\ 3-2(1-T/T_c)^2 & \text{for } T\le T_c.\end{cases} \quad (8.14)$$

(Of course, $\sigma_j^4=1$ in the Ising model.) If on the average only one spin was abnormally large, say $\simeq\frac{1}{2}N^{\frac{1}{2}}$, and the rest small and equal, we would have $\langle\sigma_j^4\rangle$

CC-0. In Public Domain. Gurukul Kangri Collection, Haridwar

Digitized by Arya Samaj Foundation Chennai and eGangotri

$\sim N(1+9N^{-1})/16$ which is in contradiction to (8.14). Hence, we can say that the existance of even one very large spin is such an improbable event that it could hardly be responsible for the critical properties of the model.

The magnetic susceptibility of the spherical model in the presence of a homogeneous magnetic field $\mathfrak{H}$ is very similar to that given by the Curie-Weiss phenomenological theory of ferromagnetism. In the Curie-Weiss theory the susceptibility per particle is

$$\chi = T_c^*/\alpha^*[T - T_c^*],$$

where T_c^* is the transition temperature and α^* an empirical parameter. The spherical model with a simple cubic lattice yields

$$\chi = T_c/\alpha[Th(T) - T_c],$$

where $T_c \simeq 4J/k$ rather than the Curie-Weiss value $T_c^* = 6J/k$. The parameter $\alpha = 6J/\mu^2$ is to be identified with α^*. The quantity $h(T)$ is defined by

$$h(T) = T_c z_3(\mathfrak{H})/3T,$$

where $z_3(\mathfrak{H})$ is a positive real root of

$$2K = \frac{1}{(2\pi)^3}\int_0^{2\pi}\int\int \frac{d\omega_1 d\omega_2 d\omega_3}{z_3(\mathfrak{H}) - \cos\omega_1 - \cos\omega_2 - \cos\omega_3} + \frac{\mu^2\mathfrak{H}^2}{2k^2T^2K[z_3(\mathfrak{H}) - 3]}.$$

Berlin and Kac have shown that if one sets $T_c^* = \gamma T_c$,

$$\chi = (T_c^*/\alpha)/[T\gamma h(T) - T_c^*]. \qquad (8.15)$$

The combination $\gamma h(T)$ is, in the entire temperature range $T_c \leq T < \infty$, restricted by the inequality

$$3/2 \geq \gamma h(T) \geq 1.$$

Hence, Eq. (8.15) differs very slightly from the phenomenological Curie-Weiss law.

Interesting results have been obtained by Berlin and Thomsen[44] and Lax[45] by applying the sphericalization technique to the theory of electric dipole-dipole interaction in crystals. It can also be applied to a classical vector spin model of a ferromagnet.

APPENDIX 1

We stated in Sec. 1 that a very satisfactory model of a binary substitution alloy or a binary mixture is mathematically equivalent to the Ising model of a ferromagnet.[28] Also the Ising model is equivalent to a simplified model of a gas and liquid.[46] We shall here describe these models in more detail and show their relation to the Ising problem.

Let us first consider a binary system of N molecules of which on the average N_1 are of type 1 and N_2 are of type 2. These particles are distributed on lattice sights and the state of the system is described by giving the type of particle on each lattice sight. The energy of the system is chosen to be the sum of the energies of interacting pairs of nearest neighbors. The energy between pairs is written as $E_{ij} = E_{ji}$, if one member of the pairs is of the ith species and the other is of the jth species. Furthermore, we let the chemical potential of the jth species be μ_j.

The grand partition function of our system is

$$Z_A = \sum_{n_1+n_2=N}\sum_m \exp[(\mu_1 n_1 + \mu_2 n_2 - E_m)/kT]. \qquad (A1.1)$$

n_i has the significance of being the number of i type particles; m numbers the states of the system for fixed n_i; and E_m is the total energy of the system in the state m. The chemical potentials must be chosen in such a way that the system gives the preassigned composition.

$$N_i = \langle n_i\rangle = Z^{-1}\sum_{n_1+n_2=N}\sum_m n_i \times \exp[(\mu_1 n_1 + \mu_2 n_2 - E_m)/kT] = kT\partial \log Z/\partial\mu_i. \qquad (A1.2)$$

We again represent the "state" of the jth lattice point by $\sigma_j = \pm 1$. $\sigma_j = +1$ if the jth lattice point is occupied by a particle of type 1, and $\sigma = -1$ if it is occupied by a particle of type 2. $(1+\sigma_j)/2$ is 1 if the jth point has an atom of type 1 and zero if it has no atom of type 1. Thus,

$$n_1 = \tfrac{1}{2}\sum_{j=1}^{N}(1+\sigma_j), \qquad n_2 = \tfrac{1}{2}\sum_{j=1}^{N}(1-\sigma_j). \qquad (A1.3)$$

If i and j are a pair of nearest neighbors on the lattice, the expression

$$v(\sigma_i, \sigma_j) = \tfrac{1}{4}E_{11}(1+\sigma_i)(1+\sigma_j) + \tfrac{1}{4}E_{22}(1-\sigma_i)(1-\sigma_j) + \tfrac{1}{2}E_{12}(1-\sigma_i\sigma_j) \qquad (A1.4)$$

is E_{11}, E_{22}, or E_{12} accordingly as the i and j lattice points are occupied by two particles of type 1, two particles of type 2, or a mixed pair. $v(\sigma_i, \sigma_j)$ thus represents the energy between the pairs i and j. The total energy is given by

$$E_m = \sum_{i,j=1}^{N}\tfrac{1}{2}a_{ij}v(\sigma_i, \sigma_j), \qquad (A1.5)$$

where a_{ij} is as defined in 1.4. If we rewrite (A1.1) in the new notation of the σ_j, the sums over $n_1+n_2=N$ and m is equivalent to the multiple sum over all $\sigma_j = \pm 1$,

$$Z_A = \sum_{\sigma_1=\pm1}\cdots\sum_{\sigma_N=\pm1}\exp[(\mu_1 n_1 + \mu_2 n_2 - E_m)/kT],$$

CC-0. In Public Domain. Gurukul Kangri Collection, Haridwar

Digitized by Arya Samaj Foundation Chennai and eGangotri

where in view of (A1.3) to (A1.5)

$$\begin{aligned}
&\mu_1 n_1+\mu_2 n_2-E_m \\
&\quad=\tfrac{1}{2}\sum_{j=1}^{N}[\mu_1(1+\sigma_j)+\mu_2(1-\sigma_j)] \\
&\qquad-\tfrac{1}{2}\sum_{i,j=1}^{N} a_{ij}[\tfrac{1}{4}E_{11}(1+\sigma_i)(1+\sigma_j) \\
&\qquad+\tfrac{1}{4}E_{22}(1-\sigma_i)(1-\sigma_j)+\tfrac{1}{2}E_{12}(1-\sigma_i\sigma_j)] \\
&\quad=(N/8)[4\mu_1+4\mu_2-c(E_{11}+E_{22}+2E_{12})] \\
&\qquad+\tfrac{1}{4}[2\mu_1-2\mu_2-c(E_{11}-E_{22})]\sum_{j=1}^{N}\sigma_j \\
&\qquad-(1/8)(E_{11}+E_{22}-2E_{12})\sum_{i,j=1}^{N} a_{ij}\sigma_i\sigma_j. \qquad \text{(A1.6)}
\end{aligned}$$

c designates the number of nearest neighbors for a given particle

$$(\sum_{j=1}^{N} a_{ij}=c).$$

To finally transcribe this into the notation of the Ising problem, we define

$$\begin{aligned}
&\mu H=\tfrac{1}{4}[2\mu_1-2\mu_2-c(E_{11}-E_{22})]=\mu\mathfrak{H}kT \\
&J=-\tfrac{1}{4}(E_{11}+E_{22}-2E_{12})=KkT \qquad \text{(A1.7)} \\
&\alpha=(1/8)[4\mu_1+4\mu_2-c(E_{11}+E_{22}+2E_{12})],
\end{aligned}$$

so that

$$\begin{aligned}
Z_A&=\exp(N\alpha/kT)\sum_{\sigma_1=\pm1}\cdots\sum_{\sigma_N=\pm1} \\
&\qquad\times\exp\{K\sum_{i,j=1}^{N}\tfrac{1}{2}a_{ij}\sigma_i\sigma_j+\mu\mathfrak{H}\sum_{j=1}^{N}\sigma_j\} \qquad \text{(A1.8)} \\
&=\exp(N\alpha/kT)Z_I.
\end{aligned}$$

Z_I denotes the partition function for the Ising problem. We have thus established a simple relation between the Ising problem and the binary alloy.

The important thermodynamic functions of each are also related. For example, in the alloy

$$N_1=\langle n_1\rangle_{Av}=\tfrac{1}{2}\sum_{j=1}^{N}\langle(1+\sigma_j)\rangle_{Av}=(N/2)(1+\langle\sigma\rangle_{Av}).$$

The constant α has no effect upon any average so that $\langle\sigma\rangle_{Av}$ is the same as in the Ising problem, where the magnetization per particle is given by

$$M=\mu\langle\sigma\rangle_{Av},$$

thus,

$$N_1=(N/2)(1+M/\mu),\quad N_2=(N/2)(1-M/\mu). \qquad \text{(A1.9)}$$

If $H=0$, the Boltzmann factor is invariant to the transformation $\sigma_j=-\sigma_j$. Therefore, $M=-M=0$. The Ising lattice with $H=0$ thus corresponds to a binary alloy with $N_1=N_2=N/2$.

If J is positive, the Ising model is a model of a ferromagnet, if J is negative an antiferromagnet. In the binary alloy, J positive corresponds to a binary mixture which at low temperatures separates into two phases. J negative corresponds to a substitutional alloy, and a phase transition would be described as an order-disorder transition with the ordered state having type 1 and 2 particles on alternating lattice sites.

It will be shown in Sec. 6 that the Ising ferromagnet in two dimensions has a spontaneous magnetization (also in three dimensions), i.e., M as a function of H has a discontinuity at $H=0$ from $M=|M(0)|$ for $H=0_+$ to $M=-|M(0)|$ at $H=0_-$. Knowing the value of $M(0)$ for $H=0$, one deduces the critical composition from (A1.9).

The mathematical formulation of the "lattice gas" model is very similar to the above. As a starting point we choose the familiar expression for the grand partition function of a gas enclosed in a volume V,

$$Z_G(V,\mu,T)=\sum_{N=1}^{\infty} y^N Q_N/N!,$$

$$\begin{aligned}
&y=(2\pi mkT/h^2)^{\frac{3}{2}}\exp(\mu/kT), \qquad \text{(A1.10)} \\
&Q_N=\int_V\cdots\int d\tau_1 d\tau_2\cdots d\tau_N\exp(-U_N/kT).
\end{aligned}$$

y is known as the fugacity, μ is the chemical potential and U_N is the potential energy of a system with N particles. The other symbols have their customary meaning.

From the evaluation of Z, one deduces the pressure from

$$p=kT\lim_{V\to\infty} V^{-1}\log Z_G(V), \qquad \text{(A1.11)}$$

and the density is given by

$$\rho=\lim_{V\to\infty}\partial(V^{-1}\log Z_G)/\partial\log y. \qquad \text{(A1.12)}$$

Since either ρ or p in addition to V and T is usually known, one uses one of the above equations to select the value of μ which appears as a parameter in Z.

The lattice gas[47] is described by dividing V into cells of uniform size. For convenience we shall choose the units of V such that these cells are of unit size. U_N is expressed as a sum of the potential energies u between pairs of particles. u in turn is described in this model by

$$\begin{aligned}
&u=+\infty && \text{if the two atoms occupy the same lattice sight,} \\
&u=-4J && \text{if the two atoms are nearest neighbors,} \qquad \text{(A1.13)} \\
&u=0 && \text{otherwise.}
\end{aligned}$$

CC-0. In Public Domain. Gurukul Kangri Collection, Haridwar

Digitized by Arya Samaj Foundation Chennai and eGangotri

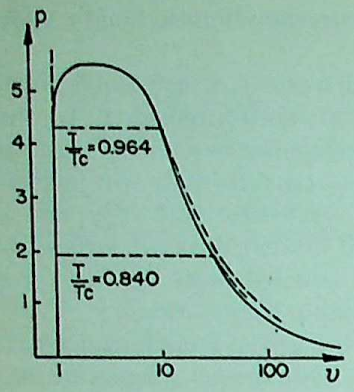


FIG. 27. $p-v$ diagram for the two-dimensional lattice gas (see reference 47). The solid curve is the exact boundary of the two-phase region. The dotted curves are the isotherms.

This interaction has the desirable feature of being very repulsive (infinitely so) at very short distances, attractive at intermediate distances, and zero at larger distances. It qualitatively represents the true interaction between gas molecules.

The infinite repulsion between particles in the same cell prohibits the occupation of a cell by more than one particle. The energy of the system can be described by giving for each cell the value of a set of coordinates σ_j, $1\leq j\leq V$. $\sigma_j=+1$ if the jth cell is occupied and -1 if unoccupied. In terms of the σ_j, U_N becomes

$$U_N=-J\sum_{i,j=1}^{V}\tfrac{1}{2}a_{ij}(\sigma_i+1)(\sigma_j+1). \qquad \text{(A1.14)}$$

Since the integrand of Q_N is a constant over-all cell, we can replace it by a multiple sum. There will be a term corresponding to each possible allocation of the N particles among the cells. For any choice of the σ_j there will be just $N!$ equal terms of the sum corresponding to the $N!$ permutation of the particles among each other which leave U_N invariant.

Since $\frac{1}{2}\sum(\sigma_j+1)$ is the number of particles in the lattice, we write

$$Q_N=N!\sum\cdots\sum\exp[(J/2kT)\sum_{i,j=1}^{V}a_{ij}(\sigma_i+1)(\sigma_j+1)],$$

where the multiple sum is over all $\sigma_j=\pm1$ with the restriction $\frac{1}{2}\sum(\sigma_j+1)=N$. When we substitute this into Z, the summation over N eliminates the restriction on the above sum, and we write

$$Z_G=\sum_{\sigma_1=\pm1}\cdots\sum_{\sigma_V=\pm1}y^{\frac{1}{2}\Sigma_j(\sigma_j+1)}\times\exp[\tfrac{1}{2}K\sum_{i,j=1}^{V}a_{ij}(\sigma_i+1)(\sigma_j+1)]$$

$$=\sum_{\sigma_1=\pm1}\cdots\sum_{\sigma_V=\pm1}\exp[\tfrac{1}{2}K\sum_{i,j=1}^{V}a_{ij}\sigma_i\sigma_j]\times\exp[(cK+\tfrac{1}{2}\log y)\sum_{j=1}^{V}\sigma_j]\exp[\tfrac{1}{2}(cK+\log y)V],$$

$$K\equiv J/kT,$$

where c is again the number of nearest neighbors of a particle and V is not only the volume but also the number of cells.

The formal similarity between Z_G and the partition function for the Ising problem is quite apparent. If we write

$$\log y=2(\mu H-Jc)/kT=2(\mu\mathfrak{H}-cK),$$

then

$$Z_G=\exp[(\mu\mathfrak{H}-\tfrac{1}{2}cK)V]\sum_{\sigma_1=\pm1}\cdots\sum_{\sigma_V=\pm1}\times\exp[\tfrac{1}{2}K\sum_{i,j=1}^{V}a_{ij}\sigma_i\sigma_j+\mu\mathfrak{H}\sum_{j=1}^{V}\sigma_j]$$

$$=\exp[(\mu\mathfrak{H}-\tfrac{1}{2}cK)V]Z_I. \qquad \text{(A1.15)}$$

From this, we can establish relationships between the thermodynamic properties of the Ising lattice and of the lattice gas. Since V is the number of lattice cells, the free energy per particle F of the Ising problem is

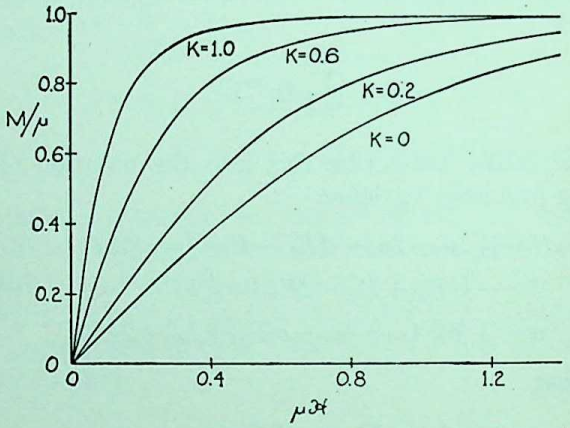


FIG. 28. Magnetization of the one-dimensional Ising chain as a function of the magnetic field $\mu\mathfrak{H}=\mu H/kT$ for several values of $K=J/kT$.

given by

$$Z_I=\exp(FV/kT),$$

and we find

$$p=kTV^{-1}\log Z_G=\mu H-\tfrac{1}{2}Jc+F. \qquad \text{(A1.16)}$$

The density is given by

$$\rho=\partial V^{-1}\log Z/\partial\log y=\tfrac{1}{2}V^{-1}\sum_{j=1}^{V}(\langle\sigma_j\rangle_{Av}+1)=\tfrac{1}{2}(1+M/\mu).$$

The specific volume v is given by

$$v=\rho^{-1}=2(1+M/\mu)^{-1}. \qquad \text{(A1.17)}$$

As was pointed out by Lee and Yang,[47] the $p-v$ isotherms of the lattice gas are closely related to the M, H isotherms of the Ising lattice. In particular a discontinuity in M gives a discontinuity in v. As has already been noted, the Ising lattice has a spontaneous magnetization or a discontinuity in M at $H=0$ for temperatures below the ferromagnetic Curie temperature T_c.

Although the two-dimensional Ising problem for arbitrary fields has not been evaluated, it is indeed

CC-0. In Public Domain. Gurukul Kangri Collection, Haridwar

Digitized by Arya Samaj Foundation Chennai and eGangotri

fortunate that the interesting part of the diagram for the two-dimensional lattice gas, namely the condensation curve, corresponds to $H=0$ for which we know all the necessary data. We know the magnetization has a jump from $|M|$ to $-|M|$ at $H=0$. We know both M and F as a function of T. The Curie temperature corresponds to the critical temperature above which no condensation occurs. The two-phase boundary is obtained by evaluating p and v for $H=0$ and is shown in Fig. 27.

In conjunction with their study of the lattice gas Yang and Lee have also proved many interesting theorems regarding the general properties of gases. They also announce the solution of the Ising problem in a magnetic field $\mathfrak{H}=i\pi/2$ or $H=i\pi kT/2$.

APPENDIX 2

Some of the properties of the one-dimensional Ising lattice were derived in Sec. 2. One must be an optimist to expect a one-dimensional system to behave like its two- or three-dimensional analog. If one is hopeful that techniques used to solve a one-dimensional problem will help solve a two- or three-dimensional problem, his optimism quickly subsides when he tries to apply them to the Ising lattice.

Despite this, we shall summarize here a few other properties of the one-dimensional Ising lattice. Although they may be rather useless, they are at least simple.

There is no difficulty in extending the analysis of Sec. 2 to include a magnetic field interaction. For such a system

$$P=\begin{pmatrix} e^{K+\mu\mathfrak{H}} & e^{-K} \\ e^{-K} & e^{K-\mu\mathfrak{H}} \end{pmatrix}, \qquad \text{(A2.1)}$$

and

$$\lambda_1=e^K\cosh\mu\mathfrak{H}+[e^{2K}\sinh^2\mu\mathfrak{H}+e^{-2K}]^{\frac{1}{2}}. \quad \text{(A2.2)}$$

λ_1 is analytic in T for $0<T<\infty$, thus there is no transition (see Sec. 3.2). It has no spontaneous magnetization since

$$M=kT\partial\log\lambda_1/\partial\mathfrak{H}$$
$$=(\mu\sinh\mu\mathfrak{H})[\sinh^2\mu\mathfrak{H}+e^{-2K}]^{-\frac{1}{2}} \quad \text{(A2.3)}$$

goes to zero as H goes to zero. M as a function of $\mathfrak{H}$ is shown in Fig. 28.

We note that for $\mathfrak{H}=0$

$$\lambda_1=2\cosh K,$$

and for $K=0$

$$\lambda_1=2\cosh\mu\mathfrak{H};$$

thus, the usual thermodynamic properties (excluding of course the magnetization) for a system of noninteracting particles ($J=0$) in a magnetic field are similar to those of a system of interacting particles with $H=0$. (This is not true in higher dimensions.)

Even though the system is well behaved, the properties of the system are quite sensitive to small magnetiz fields. If H is small compared with K, the term $e^{2K}\sinh^2\mu\mathfrak{H}$ in (A2.2) may not be small compared with e^{-2K}. We certainly anticipate even a small H to have a considerable effect at sufficiently low temperatures since it forces the spins to be all the same as $T\to 0$, but it turns out that H has an appreciable effect up to temperatures of the order

$$T\sim 2J[k\log(J/\mu\mathfrak{H})]^{-1},$$

a temperature which is rather insensitive to H. Figure 29 shows the specific heat *vs* temperature for some small values of H/J. In view of the spontaneous magnetization for two- or three-dimensional systems, they are also sensitive to small fields though in a quite different manner.

As a final remark on this problem, we note that for $H=0$, the partition function can be evaluated quite simply without appeal to the matrix method of Sec. 2.1 or without imposing the periodic boundary conditions.

$$Z(N)=\sum_{\sigma_1=\pm1}\cdots\sum_{\sigma_N=\pm1}\prod_{j=1}^{N-1}\exp(K\sigma_j\sigma_{j+1}).$$

Only one of the above factors involves σ_N, so we can first sum $\sigma_N=\pm1$.

$$Z(N)=\sum_{\sigma_1=\pm1}\cdots\sum_{\sigma_{N-1}=\pm1}[\prod_{j=1}^{N-2}\exp(K\sigma_j\sigma_{j+1})]2\cosh K\sigma_{N-1}.$$

σ_{N-1}, however, has only values ±1, and $\cosh K\sigma_{N-1}=\cosh K$.

$$Z(N)=2\cosh K\sum_{\sigma_1=\pm1}\cdots\sum_{\sigma_{N-1}=\pm1}[\prod_{j=1}^{N-2}\exp(K\sigma_j\sigma_{j+1})]$$
$$=2(\cosh K)Z(N-1).$$

By iterating this and noting that $Z(1)=2$, we obtain

$$Z(N)=2^N\cosh^{N-1}K.$$

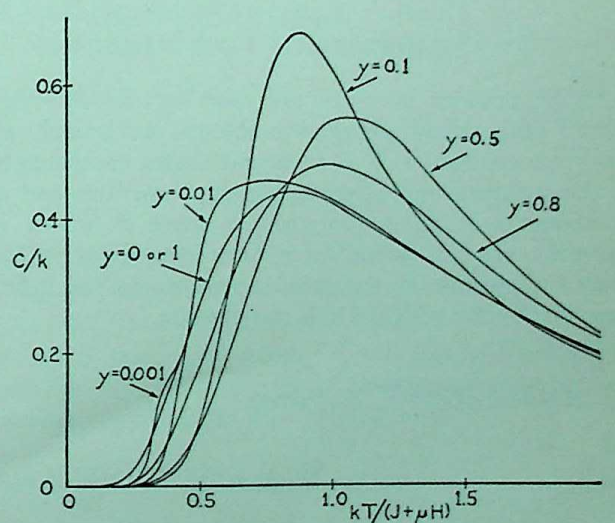


FIG. 29. Specific heat *vs* temperature for the one-dimensional Ising chain for several values of $y=\mu H/(J+\mu H)$. Temperature is measured in units $(J+\mu H)/k$ so that all curves have the same normalization.

CC-0. In Public Domain. Gurukul Kangri Collection, Haridwar

Digitized by Arya Samaj Foundation Chennai and eGangotri

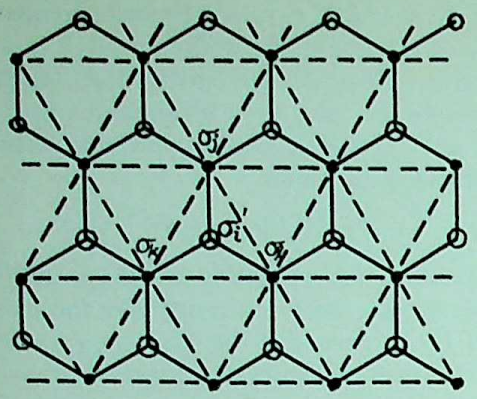


FIG. 30. Star-triangle transformation. The hexagonal lattice is shown by the solid line and its corresponding triangular lattice by the broken lines.

APPENDIX 3

We present here a brief review of the properties of direct product matrices used in Secs. 2.1 and 4.1.

Consider two matrices A and B of dimension n and m, respectively, with matrix elements A_{ij} and B_{kl}. The direct product $A\times B$ of A and B is defined as a matrix of dimension $m\times n$ with matrix elements,

$$(A\times B)_{ik,\,jl}=A_{ij}B_{kl}. \tag{A3.1}$$

The first index of $A\times B$ is the pair of first indices i and k of A and B usually considered to be ordered in dictionary order. For example, let n and m both be two

$$A=\begin{pmatrix}A_{11} & A_{12}\\ A_{21} & A_{22}\end{pmatrix},\quad B=\begin{pmatrix}B_{11} & B_{12}\\ B_{21} & B_{22}\end{pmatrix},$$

then

$$A\times B=\left(\begin{array}{cc:cc} A_{11}B_{11} & A_{11}B_{12} & A_{12}B_{11} & A_{12}B_{12}\\ A_{11}B_{21} & A_{11}B_{22} & A_{12}B_{21} & A_{12}B_{22}\\ \hdashline A_{21}B_{11} & A_{21}B_{12} & A_{22}B_{11} & A_{22}B_{12}\\ A_{21}B_{21} & A_{21}B_{22} & A_{22}B_{21} & A_{22}B_{22}\end{array}\right).$$

Direct product matrices are used extensively (disguised perhaps) in physical problems particularly in quantum mechanics. If x_j represent vector components in the n dimensional space in which A operates and y_l components in an m dimensional space in which B operates, we can define an $n\times m$ dimensional vector with components x_jy_l ordered according to the index pair (j, l) upon which $A\times B$ can operate.

Since

$$\sum_{j,\,l}(A\times B)_{ik,\,jl}x_jy_l=\sum_{j,\,l}A_{ij}B_{kl}x_jy_l$$

$$=(\sum_j A_{ij}x_j)(\sum_l B_{kl}y_l),$$

the direct product operating on a vector xy carries xy into the vector $(Ax)\,(By)$. $A\times B$ is thus the matrix representation of the product of an operation A which affects only the x_j components and an operation B which effects only the y_l components. In quantum mechanics the direct matrix product could be used, for example, to represent the product of an operation that affects only particle one-wave functions and an operator that affects only particle two-wave functions.

The most important property of direct product matrices is the manner in which they multiply. Let $A_1\times B_1$ and $A_2\times B_2$ be two direct product matrices. Then according to the usual rules of matrix multiplication,

$$[(A_1\times B_1)(A_2\times B_2)]_{ik,\,jl}$$

$$=\sum_{m,\,n}(A_1\times B_1)_{ik,\,mn}(A_2\times B_2)_{mn,\,jl}$$

$$=\sum_{m,\,n}(A_1)_{im}(B_1)_{kn}(A_2)_{mj}(B_2)_{nl}$$

$$=(A_1A_2)_{ij}(B_1B_2)_{kl}=(A_1A_2\times B_1B_2)_{ik,\,jl},$$

or

$$(A_1\times B_1)(A_2\times B_2)=A_1A_2\times B_1B_2. \tag{A3.2}$$

This relation is the key to almost all the theorems regarding direct products. We can immediately conclude that if T and T^* are transformations which diagonalize A and B, respectively, then $T\times T^*$ diagonalizes $A\times B$.

$$(T^{-1}\times T^{*-1})(A\times B)(T\times T^*)=(T^{-1}AT)\times(T^{*-1}BT)$$

is the direct product of two diagonal matrices which is also diagonal. If the eigenvalues of A are λ_j and those of B, $\lambda_k{}^*$, then $A\times B$ has eigenvalues $\lambda_j\lambda_k{}^*$.

APPENDIX 4

In Sec. 3.1, it was shown that one could locate the Curie point of a self-dual lattice by using the dual transformation (3.2). We stated that although the hexagonal lattice is not self-dual, one could find the Curie point by using the dual transformation in conjunction with the star-triangle transformation to be derived here.[3]

To derive the star-triangle transformation, we first divide the lattice into two sublattices with equal numbers of particles in the manner shown in Fig. 30. One sublattice is represented by dots, the other by circles. We shall represent the coordinates of the former by σ_k, $1\leq k\leq N/2$ and the latter by σ_k'. It is important to notice that a point of one lattice interacts only with points of the other lattice.

We write Z in the form

$$Z_H=\sum_{\sigma_1=\pm1}\cdots\sum_{\sigma_{N/2}=\pm1}\{\sum_{\sigma_1'=\pm1}\cdots\sum_{\sigma'_{N/2}=\pm1}$$

$$\times\exp(\sum_{n.n.}K_H\sigma_i\sigma_j')\}, \tag{A4.1}$$

where $K_H=J_H/kT$; J_H is the coupling constant for the hexagonal lattice.

CC-0. In Public Domain. Gurukul Kangri Collection, Haridwar

Digitized by Arya Samaj Foundation Chennai and eGangotri

Consider now only the quantity in braces, which we shall denote by $Z'(\sigma_1, \cdots, \sigma_{N/2})$. A σ_j' does not interact with other σ_k' and for any set of values of $\sigma_1, \sigma_2, \cdots, \sigma_{N/2}$, the σ_j' behave as independent particles. The summation over σ_j' are easily performed. If we let σ_j, σ_k, and σ_l be the three nearest neighbors of a point σ_i', then

$$Z'(\sigma_1, \cdots, \sigma_{N/2}) = \sum_{\sigma_1'=\pm 1} \cdots \sum_{\sigma'_{N/2}=\pm 1} \times \exp\Big[\sum_{i=1}^{N/2} K_H(\sigma_i'\sigma_j + \sigma_i'\sigma_k + \sigma_i'\sigma_l)\Big]$$

$$= \prod_{i=1}^{N/2} \Big\{ \sum_{\sigma_i'=\pm 1} \exp[K_H(\sigma_i'\sigma_j + \sigma_i'\sigma_k + \sigma_i'\sigma_l)] \Big\}$$

$$= \prod_{i=1}^{N/2} \Big\{ \sum_{\sigma_i'=\pm 1} (c_H + \sigma_i'\sigma_j s_H)(c_H + \sigma_i'\sigma_j s_H)(c_H + \sigma_i'\sigma_j s_H) \Big\}$$

$$= \prod_{i=1}^{N/2} \{2c_H{}^3 + 2s_H{}^2 c_H(\sigma_j\sigma_k + \sigma_j\sigma_l + \sigma_k\sigma_l)\},$$

where

$$c_H \equiv \cosh K_H, \quad s_H \equiv \sinh K_H.$$

Thus,

$$Z_H = 2^{N/2} \cosh^{3N/2} K_H \sum_{\sigma_1=\pm 1} \cdots \sum_{\sigma_{N/2}=\pm 1} \prod_{i=1}^{N/2} \times [1 + \tanh^2 K_H(\sigma_j\sigma_k + \sigma_j\sigma_l + \sigma_k\sigma_l)]. \quad \text{(A4.2)}$$

The manner in which the σ_k appear in (A4.2) suggests that we compare Z_H with the partition function for the triangular lattice represented in Fig. 30 by the dashed lines. We again use the index i to number the circles in Fig. 30 or the centers of alternating triangles. The partition function for this lattice can be written in the form

$$Z_T = \sum_{\sigma_1=\pm 1} \cdots \sum_{\sigma_{N/1}=\pm 1} \prod_{i=1}^{N/2} \exp[K_T(\sigma_j\sigma_k + \sigma_j\sigma_l + \sigma_k\sigma_l)].$$

However,

$$\exp[K_T(\sigma_j\sigma_k + \sigma_j\sigma_l + \sigma_k\sigma_l)] = (c_T + \sigma_j\sigma_k s_T)(c_T + \sigma_j\sigma_l s_T)(c_T + \sigma_k\sigma_l s_T) = c_T{}^3 + s_T{}^3 + c_T s_T(c_T + s_T)(\sigma_j\sigma_k + \sigma_j\sigma_l + \sigma_k\sigma_l)$$

with

$$c_T \equiv \cosh K_T, \quad s_T \equiv \sinh K_T.$$

Thus,

$$Z_T = (c_T{}^3 + s_T{}^3)^{N/2} \sum_{\sigma_1=\pm 1} \cdots \sum_{\sigma_{N/2}=\pm 1} \prod_{i=1}^{N/2} \times [1 + (\sigma_j\sigma_k + \sigma_j\sigma_l + \sigma_k\sigma_l) \times c_T s_T(c_T + s_T)/(c_T{}^3 + s_T{}^3)] \quad \text{(A4.3)}$$

comparing (A4.2) and (A4.3), we see that Z_T and Z_H will differ only by a known factor if we choose

$$c_T s_T(c_T + s_T)/(c_T{}^3 + s_T{}^3) = \tanh^2 K_H.$$

A somewhat neater version of this relation is

$$\exp 4K_T = 2\cosh 2K_H - 1. \quad \text{(A4.4)}$$

Under condition (A4.4), the partition function (A4.2) and (A4.3) are related by

$$Z_H(K_H)[2\sinh 2K_H]^{-N_H/2} = Z_T(K_T)[2\sinh 2K_T]^{-N_T/2}, \quad \text{(A4.5)}$$

where $N_H = N$ is the number of particles on the hexagonal lattice and $N_T = N/2$ is the number of particles on the triangular lattice.

Equations (A4.4) and (A4.5) give the results of the star-triangle transformation. We see from (A4.4) that a small K_T gives a small K_H and a large K_T a large K_H.

To also apply the dual-transformation we write (3.2) in the more symmetric form

$$Z_H(K_H)[2\sinh 2K_H]^{-N_H/2} = Z_T(K_H{}^*)[2\sinh 2K_H{}^*]^{-N_T/2}. \quad \text{(A4.6)}$$

Equations (A4.6) and (A4.5) together give

$$Z_T(K_T)[2\sinh 2K_T]^{-N_T/2} = Z_T(K_H{}^*)[2\sinh 2K_H{}^*]^{-N_T/2}. \quad \text{(A4.7)}$$

If we use (2.6b) to eliminate K_H from (A4.4), we obtain

$$[\exp(4K_T - 1][\exp(4K_H{}^*) - 1] = 4. \quad \text{(A4.8)}$$

Equations (A4.7) and (A4.8) describe a relation between the high and low temperature behavior of the triangular lattice. If a Curie point exists, it must occur $K_T = K_H{}^*$ or for $4K_T = \log 3$.

Similar relations for the hexagonal lattice give

$$Z_H(K_H)[2\sinh 2K_H]^{-N_H/2} = Z_H(K_T{}^*)[2\sinh 2K_T{}^*]^{-N_H/2}$$

with

$$\sinh K_H \sinh K_T{}^* = \tfrac{1}{2}.$$

The Curie point is at $\sinh^2 K_H = \frac{1}{2}$.

It is interesting to notice that in the triangular lattice $4K_T = \log 3$ has a solution only for $K > 0$. The antiferromagnetic triangular lattice ($K < 0$) has no Curie point (see Sec. 5). The properties of the hexagonal lattice are however invariant to $K_H \rightarrow -K_H$.

APPENDIX 5

A Lie algebra is a set of elements $x_1, x_2, x_3, \cdots$ (nondenumerable, however) upon which the usual rules of addition and multiplication by any complex number apply. The algebra includes $ax + by$ if x and y are ele-

CC-0. In Public Domain. Gurukul Kangri Collection, Haridwar

Digitized by Arya Samaj Foundation Chennai and eGangotri

ments, and a and b are any complex numbers. There is also defined another operation $[x, y]$ which satisfies the conditions

(a) $[x, y]+[y, x]=0$; (A5.1)

(b) $[[x, y], z]+[[y, z], x]+[[z, x], y]=0$; (Lie–Jacobi equation) (A5.2)

(c) if x and y are elements, then $[x, y]$ is also an element. The Lie algebra is in every respect the same as the usual abstract algebra except that the multiplication operation is replaced by the operation $[x, y]$ having the above properties. If x, y, and z are square matrices, a Lie algebra can be defined with the usual rules of addition of matrices and an operation $[x, y]=xy-yx$ the commutator of x and y. One readily checks that the commutator satisfies conditions (a) and (b).

A set of elements $x_1, x_2, \cdots, x_r$ are said to form a basis for a finite Lie algebra if there exists a set of numbers $\{c_{jk}{}^t\}$ which have the property

$$[x_j, x_k]=\sum_{t=1}^{r} c_{jk}{}^t x_t. \tag{A5.3}$$

These constants are called the structure constants of the algebra. The abstract properties of the algebra are completely described by the structure constants.

An important example of a Lie algebra is that associated with the three-dimensional rotations. According to Euler's theorem, any rotation in three dimensions can be decomposed into three successive rotations, one about the z axis, followed by one about the rotated x axis, and then one about the new z axis. A general rotation can also be considered as a vector (really a pseudovector) with components in the x, y, and z directions.

Let us consider an infinitesimal rotation through an angle γ about the z axis. The matrix for such a rotation is

$$\begin{pmatrix} \cos\gamma & -\sin\gamma & 0 \\ \sin\gamma & \cos\gamma & 0 \\ 0 & 0 & 1 \end{pmatrix} \sim \mathbf{I}_3+\gamma\mathbf{Z}+0(\gamma^2),$$

where

$$\mathbf{Z}=\begin{pmatrix} 0 & -1 & 0 \\ 1 & 0 & 0 \\ 0 & 0 & 0 \end{pmatrix}.$$

$\mathbf{I}_3$ is the identity matrix, and $0(\gamma^2)$ indicates order γ^2. Note that

$$\mathbf{Z}^{2n}=\begin{pmatrix} 1 & 0 & 0 \\ 0 & 1 & 0 \\ 0 & 0 & 0 \end{pmatrix}, \quad \mathbf{Z}^{2n+1}=\mathbf{Z};$$

hence, the direct expansion of $\exp\gamma\mathbf{Z}$ yields

$$\exp\gamma\mathbf{Z}=\begin{pmatrix} 0 & 0 & 0 \\ 0 & 0 & 0 \\ 0 & 0 & 1 \end{pmatrix}+\begin{pmatrix} 1 & 0 & 0 \\ 0 & 1 & 0 \\ 0 & 0 & 0 \end{pmatrix}\cos\gamma+\mathbf{Z}\sin\gamma$$

$$=\begin{pmatrix} \cos\gamma & -\sin\gamma & 0 \\ \sin\gamma & \cos\gamma & 0 \\ 0 & 0 & 1 \end{pmatrix}$$

which is a rotation through a finite angle γ about the z axis.

In a similar way, we can show that an infinitesimal rotation by an angle β about the y axis is given by

$$\mathbf{I}_3+\beta\mathbf{Y} \quad \text{with} \quad \mathbf{Y}=\begin{pmatrix} 0 & 0 & -1 \\ 0 & 0 & 0 \\ 1 & 0 & 0 \end{pmatrix},$$

and a rotation through a finite angle β by $\exp(\beta\mathbf{Y})$. An infinitesimal rotation α about the x axis is given by

$$\mathbf{I}_3+\alpha\mathbf{X} \quad \text{with} \quad \mathbf{X}=\begin{pmatrix} 0 & 0 & 0 \\ 0 & 0 & -1 \\ 0 & 1 & 0 \end{pmatrix},$$

and a finite rotation by $\exp(\alpha\mathbf{X})$.

Euler's theorem implies that any general rotation can be written as

$$\exp(\alpha\mathbf{Z})\exp(\beta\mathbf{Y})\exp(\gamma\mathbf{Z}).$$

It can also be written in the form

$$\exp[(\alpha\mathbf{X}+\beta\mathbf{Y}+\gamma\mathbf{Z})]$$

which is a rotation through an angle $(\alpha^2+\beta^2+\gamma^2)^{\frac{1}{2}}$.

The operators $\mathbf{X}$, $\mathbf{Y}$, $\mathbf{Z}$ take vectors into new vectors which are normal to the original one. For example,

$$\mathbf{Z}\cdot\begin{pmatrix} x \\ y \\ z \end{pmatrix}=\begin{pmatrix} -y \\ x \\ 0 \end{pmatrix}.$$

If we let $x_1=\mathbf{Z}$, $x_2=\mathbf{Y}$, and $x_3=\mathbf{X}$, the commutators of these operators generate a Lie algebra with the three base elements x_1, x_2, and x_3. We obtain

$$\begin{aligned} [x_1, x_2]&=x_3 \\ [x_3, x_1]&=x_2 \\ [x_2, x_3]&=x_1. \end{aligned} \tag{A5.4}$$

This structure constants of the algebra are

$$c_{ik}{}^t=0 \quad \text{except} \quad c_{12}{}^3=c_{31}{}^2=c_{23}{}^1=1.$$

There is also another representation of the Lie algebra defined by (A5.4). Consider the Pauli spin matrices

$$\mathbf{C}=\begin{pmatrix} 0 & 1 \\ 1 & 0 \end{pmatrix}, \quad \mathbf{s}=\begin{pmatrix} 1 & 0 \\ 0 & -1 \end{pmatrix}, \quad \text{and} \quad \mathbf{sC}=\begin{pmatrix} 0 & 1 \\ -1 & 0 \end{pmatrix}.$$

It is easy to see that the three operators $x_1=i\mathbf{s}/2$, $x_2=-i\mathbf{C}/2$, and $x_3=\mathbf{sC}/2$ have the same commutation rules as $\mathbf{X}$, $\mathbf{Y}$, and $\mathbf{Z}$.

CC-0. In Public Domain. Gurukul Kangri Collection, Haridwar

Digitized by Arya Samaj Foundation Chennai and eGangotri

BIBLIOGRAPHY

[1] E. Ising, Z. Physik **31**, 253 (1925).
[2] F. C. Nix and W. Shockley, Revs. Modern Phys. **10**, 1 (1938).
[3] G. H. Wannier, Revs. Modern Phys. **17**, 50 (1945).
[4] L. Onsager, Phys. Rev. **65**, 117 (1944).
[5] L. Onsager and B. Kaufman, Phys. Soc. Cambridge, Conference Report (1947) p. 137.
[6] B. Kaufman, Phys. Rev. **76**, 1232 (1949).
[7] M. Kac and J. C. Ward, Phys. Rev. **88**, 1332 (1952).
[8] B. L. van der Waerden, Z. Physik **118**, 473 (1941).
[9] H. A. Kramers and G. H. Wannier, Phys. Rev. **60**, 252 (1941).
[10] E. N. Lassettre and J. P. Howe, J. Chem. Phys. **9**, 747 (1941).
[11] E. Montroll, J. Chem. Phys. **9**, 706 (1941).
[12] R. Kubo, Busseiron Kenkyu **1** (1943).
[13] G. F. Newell, Phys. Rev. **78**, 444 (1950).
[14] J. Kirkwood, J. Chem. Phys. **6**, 70 (1938).
[15] W. Opechowski, Physica **4**, 181 (1937).
[16] J. Ashkin and W. E. Lamb, Jr., Phys. Rev. **64**, 159 (1943).
[17] L. van Hove, Physica **16**, 137 (1950).
[18] Y. Nambu, Prog. Theoret. Phys. **5**, 1 (1950).
[19] F. J. Murray, Ann. Math. **55**, 250 (1952).
[20] R. M. F. Houtappel, Physica **16**, 425 (1950).
[21] K. Husimi and I. Syozi, Prog. Theoret. Phys. **5**, 177 (1950).
[22] I. Syozi, Prog. Theoret. Phys. **5**, 341 (1950).
[23] H. N. V. Temperley, Proc. Roy. Soc. (London) **203A**, 202 (1950).
[24] G. H. Wannier, Phys. Rev. **79**, 357 (1950).
[25] G. F. Newell, Phys. Rev. **79**, 876 (1950).
[26] I. Syozi, Prog. Theoret. Phys. **6**, 306 (1951).
[27] T. Yamamoto, Prog. Theoret. Phys. **6**, 533 (1951).
[28] R. Peierls, Proc. Cambridge Phil. Soc. **32**, 477 (1936).
[29] C. N. Yang, Phys. Rev. **85**, 809 (1952).
[30] B. Kaufman and L. Onsager, Phys. Rev. **76**, 1244 (1949).
[31] G. S. Rushbrooke, J. chim. phys. (to be published).
[32] G. S. Rushbrooke, Nuovo cimento **6** (suppl. 2), 251 (1949).
[33] A. J. Wakefield, Proc. Cambridge Phil. Soc. **47**, 419, 799 (1951).
[34] C. Domb, Proc. Roy. Soc. (London) **196A**, 36 (1949); **199A**, 199 (1949); J. E. Brooks and C. Domb, Proc. Roy. Soc. (London) **207A**, 343 (1951).
[35] Eleanor Trefftz, Z. Physik **127**, 371 (1950).
[36] E. Somers, Ph.D. thesis, University of Pittsburgh (1949).
[37] D. ter Haar, Phys. Rev. **76**, 176 (1949).
[38] T. Oguchi, J. Phys. Soc. Japan **5**, 75 (1950); **6**, 27, 31 (1951).
[39] Tanaka, Katsumori, and Toshima, Prog. Theoret. Phys. **6**, 17 (1951).
[40] R. Kikuchi, Phys. Rev. **81**, 988 (1951).
[41] C. Herring and C. Kittel, Phys. Rev. **81**, 869 (1951).
[42] T. H. Berlin and M. Kac, Phys. Rev. **86**, 821 (1952).
[43] E. Montroll, Nuovo cimento **6** (suppl. 2), 1298 (1949).
[44] T. H. Berlin and J. S. Thomsen, J. Chem. Phys. **20**, 1368 (1952).
[45] M. Lax, J. Chem. Phys. **20**, 1351 (1952).
[46] C. N. Yang and T. D. Lee, Phys. Rev. **87**, 404 (1952).
[47] T. D. Lee and C. N. Yang, Phys. Rev. **87**, 410 (1952).

CC-0. In Public Domain. Gurukul Kangri Collection, Haridwar

Digitized by Arya Samaj Foundation Chennai and eGangotri

REVIEWS OF MODERN PHYSICS VOLUME 25, NUMBER 2 APRIL, 1953

The Energy Levels and the Structure of Light Nuclei

D. R. INGLIS

Argonne National Laboratory, Lemont, Illinois

A theoretical interpretation of the energy level sequences of the light nuclei of the p shell is developed, in the spirit of an exploratory survey. Phenomenological assumptions concerning the nuclear forces are used and the secular problem of intermediate coupling (between the Russell-Saunders and (jj) extremes) is in most cases treated by means of rough interpolations, so no exact energy agreement can be expected, but the order of states of various quantum numbers in the p-shell configuration can be approximately established. This order and the general density of levels agree with the observations, so far as they have been made, in enough cases to give some evidence for the validity of the general method of approach, though further refinements are needed.

The presentation is made with a number of introductory sections, intended to orient an uninitiated reader in various relevant aspects of the theory of nuclear structure, preceding the discussion of the interpretation of the levels of the individual nuclei. Section 1, an introduction, discusses the meaning of nuclear models. Section 2 deals with the phenomenological approximations to the specific nuclear forces and suggests various possible sources of the spin-orbit coupling. Sections 3 and 4 are primarily pedagogical, in that they explain and formulate well-established wave-mechanical fundamentals of two-body (as an example of many-body) systems. Section 3 treats the relation between symmetry and energy for two electrons or two neutrons, and Sec. 4 presents in some detail the relation of the total isobaric spin quantum number T to the more directly physical dynamical variables of a system of nucleons. Section 5 surveys the experimental data for the various polyads, or groups of isobars, arranged in such a way as to make apparent the matching in energy of the states of the same T but different neutron excess, after a correction has been applied for Coulomb energy differences. Section 6 is again pedagogical, reviewing the theory of intermediate coupling in atoms, and introducing the application to nuclei. Section 7 discusses explicitly and in some detail the interpretation of the energy level sequences observed in the various polyads, from $A=5$ to $A=17$, as well as some of the methods that have been used for making the crucial experimental assignments of angular momentum and parity of the various states. The degree of partial success of the interpretation leaves the impression that the (jj)-coupling scheme of heavy nuclei gives way to intermediate coupling in the light nuclei, and that some of the higher order deviations from this scheme may usefully be described as a partial transition to the nucleon clustering of the alpha-model in a few nuclei whose atomic number A is especially favorable for this clustering. Section 8 presents some details of the Coulomb energy calculations. Section 9 explains the remarkable appearance of double levels (which look like atomic doublets but are explained differently) in some of the nuclei near $A=30$, beyond the formal scope of this paper, and shows that the explanation does not apply to the similar occurrence of apparently fortuitous double levels in some of the nuclei of the p shell. Section 10 discusses the possible role of the alpha-model in influencing the states of some of the light nuclei. Section 11 discusses beta-decay, particularly in the case of C^{14} where there is an order-of-magnitude effect in need of explanation. One of the appendices treats the molecular problem of quadrupole coupling particularly in relation to the measurement of the quadrupole moment of Li^7 in polar molecules.

1. INTRODUCTION—NUCLEAR MODELS

THE increasing wealth of new material on the identification of angular momenta and parities of the excited states of light nuclei brings ever nearer the prospect of a more complete understanding of nuclear structure in this region. The gratifying success of the (jj)-coupling shell model (M49, H49, K50)* in explaining many features of heavier nuclei encourages the hope of finding some understanding also of the light nuclei in terms of simple models, but one encounters numerous difficulties in trying to apply the (jj) model alone to all the states of the light nuclei, especially to those of the p-shell nuclei He^4 to O^{16} and immediately beyond.

One had no *a priori* right to expect any model to apply well to a nucleus consisting of many nucleons attracted by short-range interactions, even after the success of the Hartree model in the quite different case of an atom with many electrons. The motion of most of the electrons is largely dictated by the overwhelmingly strong field of a body fixed at the center. Lacking this, and with attractive rather than repulsive interactions, it is not clear, for example, that the nucleons would not have at least an appreciable tendency to cluster into small groups, such as alphas (W37). Even if this were only a weak trend it could greatly complicate their behavior. If it were a very strong trend, it might again simplify matters and make the alpha-model valid (W37, I41). It has long been empirically apparent from regularities among such phenomena as nuclear moments that nuclei behave more simply than we had any *a priori* right to expect (S37, I41).

The somewhat surprisingly successful (jj) coupling shell model is of course a special case of the central (or Hartree) model of the nucleus. Its success indicates that the interaction of a single nucleon with all the others may be fairly well represented by an average central field, at least in heavy nuclei. But the success of this particular (jj) version of the central model indicates also that the spin-orbit coupling energy (I36, B37) is surprisingly large in nuclei. The spin-orbit coupling energy attempts to orient the spin $\boldsymbol{s}$ of a nucleon relative to the orbital angular momentum $\boldsymbol{l}$ of the same nucleon to form a total angular momentum quantum number j of the individual nucleon, to give the (jj)-coupling scheme, while the "exchange integral" of the

* References are given at the end of this article.

CC-0. In Public Domain. Gurukul Kangri Collection, Haridwar

Digitized by Arya Samaj Foundation Chennai and eGangotri

specific nuclear interactions competes with it in trying to bring about the (LS)-coupling scheme (H37, Wi37, F37), or "Russell-Saunders Coupling" as it is known in the analogous atomic problem, in which the total spin angular momentum S, summed over all the particles, is a constant of the motion and also the total orbital angular momentum L. Thus the observed approximation of heavy nuclei to (jj) coupling means in general terms that the spin-orbit coupling energy is large compared to the "exchange integral" in those nuclei.

The failure, in the p shell, of the (jj)-coupling version of the central model may be due either to a failure of the "(jj)-coupling" aspect or of the "central model" aspect, or both, and we shall see some evidence of both. The central model includes as special cases not only the (jj)-coupling version and the (LS)-coupling version, each of which is an extreme case having specially simple features, but also the whole range between them known as intermediate coupling, as was once well known in the theory of complex atomic spectra. It applies to a wide range of possible ratios of the two parameters, giving a variation of the possible energy level scheme analogous to the Paschen-Back transitions which are still widely known because of their applicability to atomic-beam and microwave spectroscopy. Intermediate coupling seems to be responsible for many features of the energy level schemes encountered in the latter half of the p shell, from B^{10} to O^{16}, while the failure of the complexities of intermediate coupling to account for some of the features of the still lighter nuclei in the first half of the p shell seems to be associated with the tendency for alpha-clustering to become important in these rather loosely-bound nuclei (or to some other manifestation of higher order perturbation theory as will be discussed further below).

An extreme case of the tendency for the formation of clusters of nucleons such as alphas within nuclear matter is of course represented by the alpha-model, and good reasons have been given for expecting the applicability of this model to light nuclei (W37, H38), especially to those within which the energy that may be ascribed to the mutual binding energy between alpha-clusters is small compared to the internal binding of these clusters. One can conceive of a transition between the central model and the alpha-model analogous to the intermediate-coupling transition within the central model, though it is more difficult to formulate explicitly. Thus one might think of setting up a sort of two-dimensional variation principle in which the wave functions of the various states are formed as a compromise between the three extremes, the (jj)-coupling model, the (LS)-coupling model, and the alpha-model. Fortunately, some approximation to the behavior of most nuclei seems to be possible without making use of all this complexity.

2. NUCLEON INTERACTIONS

Nuclear spectroscopy aims on the one hand to help to develop, on the other hand to get along without, a detailed knowledge of the nature of nuclear "forces." This seeming contradiction arises from the great difficulty of uncovering the profound laws of nature, and the hope of doing so in a stepwise fashion. It is too much to hope in the near future to calculate the energy levels of B^{11}, say, on the basis of a completely satisfactory meson theory of nuclear structure. Instead, one hopes to divide the problem up into a phenomenological one in which the interactions between nucleons are assumed to have one of several possible simple forms, it being determined by trial which form seems to have the greatest empirical validity, and a second step in which the phenomenological interaction thus selected is to be understood on the basis of a theory of the structure of the nucleons themselves, akin to the present meson theories which as yet are not entirely free from divergences. This review of the energy spectra of the light nuclei is concerned entirely with the first or phenomenological step, though we shall discuss briefly the relation of our assumed spin-orbit coupling energy to the second or "meson theory" step.

Phenomenological Specific Nuclear Interactions

Most practical attempts to formulate the sequence of nuclear states have been based on the assumption of central interactions between two nucleons written as a function of their distance apart, $V(r_{ij})$, multiplied by an exchange operator O_{ij}, which is variously written as a linear combination of operators such as P_{ij} or simply P, the space-exchange or Majorana operator which exchanges the space coordinates of the two nucleons in a wave function following it, the unit or "Wigner" operator 1 which does nothing, the space-spin exchange or Heisenberg operator PQ, and the spin-exchange or Bartlett operator Q. This usage and the saturation requirements of the coefficients with which the operators are combined is adequately reviewed in Rosenfeld's book (R48), where it is suggested (p. 234) that the most nearly satisfactory version of O_{ij} is perhaps

$$\begin{aligned} O_{ij} &= \boldsymbol{\tau}_i \cdot \boldsymbol{\tau}_j (0.1 + 0.23 \boldsymbol{\sigma}_i \cdot \boldsymbol{\sigma}_j) \\ &= (0.93P - 0.13 - 0.26PQ + 0.46Q). \end{aligned} \tag{1}$$

A simplified version that is almost equivalent to this in many rough calculations, because it keeps the large terms and contains the same proportion of terms involving spin exchange to those which do not, is

$$O_{ij} = 0.8P + 0.2Q. \tag{2}$$

As a similar part of the phenomenological step one usually assumes also a simple form of spin-orbit coupling operator, which we may write as a perturbation term to the Hamiltonian thus:

$$H' = \sum_i a_i \boldsymbol{l}_i \cdot \boldsymbol{s}_i = \sum a \boldsymbol{l} \cdot \boldsymbol{s}. \tag{3}$$

In most cases the parameter a will be the same for all nucleons under explicit consideration, they being all in

CC-0. In Public Domain. Gurukul Kangri Collection, Haridwar

Digitized by Arya Samaj Foundation Chennai and eGangotri

the same shell. This quantity a is the parameter which, by being large, can make the magnitude of the single-nucleon angular momentum vector $j=l+s$ a constant of the motion and thus account for the approximate physical existence of the (jj)-coupling scheme in heavy nuclei. This approach is not sufficiently refined to account for the quadrupole moment of the deuteron.

Still within the framework of the first or phenomenological step, there is another approach involving the assumption of a tensor interaction, in which $V(r_{ij})$ is multiplied by an operator

$$D_{ij}=3(\boldsymbol{\sigma}_i\cdot\mathbf{r})(\boldsymbol{\sigma}_j\cdot\mathbf{r})-\boldsymbol{\sigma}_i\cdot\boldsymbol{\sigma}_j, \qquad (4)$$

a term comparable in magnitude with the central interaction. In the treatment of the deuteron by Rarita and Schwinger (R41), which gives the quadrupole moment so nicely, neither term is given an exchange character and the lack of the saturation property has no dire consequences for this light nucleus or its immediate neighbors. The excitation energy, about 2.2 Mev, of the ^1S state of the deuteron is accounted for by the fact that (4) mixes some ^3D into the ^3S to make the ground state, but of course not into the ^1S. This separation, which is one of the two primary functions of the tensor interaction in this theory, is accomplished with the cruder interaction assumption, Eq. (2), as a result of the term in Q. If the tensor interaction were calculated for many cases in heavy nuclei in which Q provides energy splittings between certain states, the tensor interaction would presumably give somewhat similar splittings. In this sense we may think of the term in Q as an oversimplified sketch which preserves the main feature, a sort of caricature, of one aspect of the tensor force (which in turn is a caricature of the dim machinations of the mesons reserved for the second step). It is currently suspected that there may be a very short-range repulsive core to the nucleon interactions (J50), which could perhaps rescue the tensor-type interaction from its nonsaturating difficulties. If so, the saturation mechanism of the term of Eq. (2) in P could be looked on as a caricature, and it is to be hoped a useful caricature, of this aspect of the tensor interaction.

Spin-Orbit Interaction

There is still another aspect in which the phenomenological procedures implied by Eqs. (2) and (3) may be considered to have a significant parallelism to those implied by the use of the tensor interaction, Eq. (4), and this concerns the spin-orbit interaction. The tensor interaction (4) does contain the possibility of coupling spins $\boldsymbol{\sigma}_i$ to orbits which involve $\mathbf{r}_{ij}$, but in simple cases it does so only through the second-order and higher-order effects which involve excitation to other configurations. Feingold and Wigner (F50) have carried out extremely interesting calculations of this effect for He^5, and for Li^7, and for the effect which is not exactly spin-orbit coupling but closely analogous to the excitation of the deuteron plus effects arising from excitation of the core in Li^6. For the spin-orbit coupling with one and with three nucleons outside of an alpha-core, they obtain preliminary results which are somewhat small but of the right order of magnitude to account for the observed data. Very many extremely highly excited states of the alpha-core contribute to these results. The authors of this work have a feeling that in heavy nuclei analogous calculations will have the simplifying feature, as a result of statistical cancellations, that each nucleon outside a closed shell will because of its interaction with the nucleons of the closed shell have a spin-orbit coupling similar to that in He^5 and be very little affected by the coupling of other extra-shellular nucleons to the closed shell. These second-order contributions are thought to arise independently for the several nucleons in a manner somewhat analogous to the way in which the van der Waals forces, also of second order, are shown by London to add linearly for various pairs of molecules. Thus Feingold and Wigner feel that for heavy nuclei, Eq. (3) need not be an independent *ad hoc* hypothesis, but may be a higher-order consequence of Eq. (4).

It is desirable in exploratory work to use the simple assumptions implied by Eqs. (2) and (3) because of their easy tractability. We see that this may tentatively be justified by thinking of the term in Q in Eq. (2) as a caricature mainly of the first-order effects of the tensor interaction (4) (which has a greater claim to credibility because it accounts also for the quadruple moment of the deuteron), and by thinking of Eq. (3) as a manifestation of the second and higher order effects of the tensor interaction. The suspicion of the possible equivalence of Eq. (3) and the second-order aspects of Eq. (4) in heavy nuclei is analytically at such an extremely preliminary stage that it is not really clear that it exists, and least of all is it clear whether or how far it can be extended down from the heavier nuclei toward or into the p shell. For this reason we would be on extremely hazardous grounds in using Eq. (3) in the p shell if we felt dependent on this possible explanation for the adequacy of Eq. (3).

The most compelling reason for using Eq. (3) in the p shell is, of course, the empirical one: it is simple and has been successfully applied in heavy nuclei and also seems to correspond to the nuclear angular momentum values J for the ground states of the light nuclei. One wants to know how far down into the light nuclei it may be of use in accounting for all the available data. But there is also another possible source of spin-orbit coupling which may help to justify the exploratory use of Eq. (3), a direct manifestation of meson coupling to nucleon spin-orbit coupling without going through the intermediary of phenomenological nuclear forces. Both the Thomas-precession as a source of nuclear spin-orbit coupling (I36, B37), and the Feingold-Wigner higher order tensor-interaction effect (F50), have in common

CC-0. In Public Domain. Gurukul Kangri Collection, Haridwar

Digitized by Arya Samaj Foundation Chennai and eGangotri

the assumption that the coupling of the nucleons to the meson field contributes certain specific and intrinsic properties to the nucleons (their phenomenological interaction energies, their intrinsic magnetic moments) which may subsequently be introduced into the Hamiltonian for the quantum-mechanical calculation of spin-orbit coupling energies. In the case of the Thomas-precession, it is the acceleration of the nucleon as it circulates in its nebulous "orbit," a classical acceleration $(d^2\mathbf{r}/dt^2)=-\nabla V/M$ ascribed to the specific nucleon interactions such as Eq. (2) and so only indirectly to meson theory, that provides the spin-orbit coupling:

$$H'(r)=\hbar\mathbf{s}\cdot\boldsymbol{\omega}_T=\hbar\mathbf{s}\cdot(d\mathbf{r}/dt)\times(d^2\mathbf{r}/dt^2)/2c^2$$
$$=(\hbar^2/2M^2c^2)(r^{-1}dV/dr)\mathbf{l}\cdot\mathbf{s}. \quad (5)$$

Thus we have a coupling of the form, Eq. (3), with $(H'(r))_{Av}=H'$ and with the parameter

$$a=(\hbar^2/2M^2c^2)(r^{-1}dV/dr)_{Av} \quad (6)$$

proportional to $1/M^2$, M being of course the nucleon mass. One factor M arises from $(d^2\mathbf{r}/dt^2)$, that is, from an assumption concerning the interaction, and one from the expression for orbital angular momentum $M|\mathbf{r}\times(d\mathbf{r}/dt)|=l\hbar$. Here V is an effective (approximately central) potential energy $V(r_i)$ of one nucleon (i) in the field of all the others, an effective average of $V(r_{ij})$ summed over j, with exchange effects, Eq. (2), included in the averaging. The energy of the Thomas precession, Eq. (5), is now known to be inadequate in magnitude to account for more than a small fraction of the "observed" nuclear spin-orbit coupling: in atoms it is half as big as the magnetic spin-orbit coupling, but in light nuclei almost an order of magnitude larger than the magnetic coupling, the magnetic single-nucleon doublet splitting being of the order of 30 kev (I51), the Thomas-precession doublet splitting of the order of 100 kev, whereas the splittings needed to account for the empirical trends appear to be 1 Mev or considerably more, as we shall see in detail.

While Eq. (5) is thus inadequate in *magnitude*, its *form* still has considerable interest because this arises from requirements of relativistic and rotational invariance (F26, T26, D36, F36, B37) which are common to a larger class of assumptions than the particular phenomenological ones used in deriving Eq. (5), and in particular apply to the results of some meson theories. Thus a meson theory may give in the energy of the system a term of the form, Eq. (5), but with a different meaning for the symbols M and V. Unfortunately, meson theories are not yet far enough advanced in their application to all the appropriate phenomena that one can yet expect to find any agreement on the probable form of the final result. However, the hope that they will contribute mainly two-body interactions, and then only contribute to the spin-orbit coupling indirectly through the two-step arrangement we have discussed, seems to be an optimistic hope. The success of shell models as far as it goes does suggest that many-body interactions may, for a given three nucleons, say, be smaller than two-body forces for a given pair, to such an extent that the two-body forces predominate in determining the energy effects of orienting the vectors associated with the comparatively few nucleons in an unfilled shell. But when one counts among a large number of nucleons, there are enormously more many-body interactions than pair interactions. Thus it may be that the many-body interactions make a more important contribution to the total energy of the nucleus than to the energy separation of states within a configuration, which are determined by interactions within the unfilled shell.

These many-body interactions may perhaps be more properly described in terms of the coupling of the various nucleons to a common pool of mesons. In either description, they may be expected to be very important in determining the binding energy of one nucleon in an unfilled shell to the rest of the nucleus, the energy that determines the existence of the "shell." In the course of this complicated process, there would seem to be ample opportunity for the coupling between the single nucleon and the common meson field to give rise to a term of the properly invariant form, Eq. (5), directly, and not just through a two-step process involving specific nucleon properties such as M. The fact that M came in once through the nucleon angular momentum justifies its remaining as one factor in Eq. (5). The second factor M entered through the two-step treatment of the energy, and in a direct treatment is probably to be replaced by the π-meson mass, $\mu=278m\approx M/7$. Such a replacement of one factor M by μ has been suggested in early remarks of Teller and elsewhere (I49), then in connection with the particular assumption that the mesons concerned are pseudovector mesons (now out of favor on the basis of other phenomena) by Gaus (G49), and in a number of lectures by Heisenberg, who favored more specifically replacing M by $\mu/2$. With this replacement of M by μ, the question arises what should be done with V, and it has been argued in connection with the brief treatment by Gaus that V, although primarily the potential of the mesons in the field of the nucleon, or vice versa, as essentially the same thing as the potential of the nucleon in the nuclear potential well. While this point remains rather vague because it depends so sensitively on assumptions concerning the unformulated saturation properties of the meson field, it suggests that the main effect of a thorough meson theory may be to replace one factor M in Eq. (5) by μ or $\mu/2$, thus bringing the spin-orbit coupling parameter a in Eq. (3) up from the order of magnitude 100 kev to the order of 1 Mev or more. Such an effect could very well be additive both to the Thomas-precession coupling and to the second-order effect of tensor interactions, for which the Feingold-Wigner estimates have so far been somewhat smaller than needed, and might overwhelm them both. This possibility justifies proceeding in an

CC-0. In Public Domain. Gurukul Kangri Collection, Haridwar

Digitized by Arya Samaj Foundation Chennai and eGangotri

exploratory way on the basis of the attractively simple assumption, Eq. (3), with the parameter a quite large if need be.

To estimate a plausible dependence of the parameter a on atomic weight A one may assume that $\partial V/\partial r$ exists only on the surface of the nucleus, so that it may be replaced by $\Delta V/\Delta r$ in a surface layer Δr thick, or in a fraction $2\pi r^2\Delta r/(4\pi r^3/3)=(3/2)\Delta r/r$ of the nuclear volume. If this fraction be taken as the probability that the nucleon is in this layer, we have $(r^{-1}\partial V/\partial r)_{Av}=3(\Delta V/2r_0^2)A^{-2/3}$, where the nuclear radius is taken to be $r_0A^{1/3}$. For purposes of orientation concerning the magnitude of the spin-orbit coupling constant a in Eq. (3), we may replace one factor M by $\mu/2$, put $r_0=e^2/2mc^2$, and evaluate (6) thus:

$$a\approx(\hbar^2/M\mu c^2)(6m^2c^4\Delta V/e^4)A^{-2/3}$$
$$=(6\times137^2/1840\times278)\Delta VA^{-2/3}=0.22\Delta VA^{-2/3}. \quad (7)$$

For a nucleon entering a nucleus, ΔV is larger than the nucleon binding energy by a factor of about two or more because the kinetic energy is involved in the comparison. If we rather arbitrarily take $\Delta V=20$ Mev, we have $a=1.2$ Mev for Li^7, 0.125 Mev for Pb^{208}. The single-nucleon doublet splitting is $(l+\frac{1}{2})a$, which is 1.8 Mev for a ^2p splitting in Li^7, 0.75 Mev for a ^2i splitting in Pb^{208}. The latter is about a factor 3 smaller than needed to account for the energy jumps at the magic numbers in terms of the (jj)-coupling shell model.

There is another simple manner of taking the average (I36), which involves first the classical procedure of equating centripetal force to the mass times centripetal acceleration in a circular motion, and this yields an additional factor $l(l+1)r^{-2}$, leaving the doublet splitting approximately proportional to $l^3A^{-4/3}$ rather than to $lA^{-2/3}$, as would correspond roughly to the refinement that the probability distributions of orbits of higher l crowd toward the outer edge of the nucleus. This is mentioned only to emphasize the roughness of the above estimate, with its assumed uniform probability distribution among many other simplifications.

3. ENERGY CONTRIBUTIONS OF THE SPECIFIC NUCLEAR REACTIONS

Presuming, then, that some basis may eventually be found in meson theory for the validity of this procedure, we shall try to analyze the spacings of the energy states of light nuclei on the basis of the specific nuclear interactions with their exchange nature given by Eq. (2) and on the basis of an *ad hoc* spin-orbit coupling given by Eq. (3). The contribution of the spin-orbit coupling to the energies of nuclear states is in simple cases quite direct because the nucleons are involved singly: when the spin of a nucleon is "parallel" to its orbital angular momentum, the energy is thereby low (this being the sign empirically assumed, opposite to that for electrons in an atom). The specific nuclear interactions, Eq. (2), involve pairs of nucleons and for this reason we must invoke the distinction between direct integrals and exchange integrals, just as in the case of evaluating the effects of the Coulomb interaction between the electrons in an atom. Both types of integrals are altered by the exchange operators contained in them, but an important part of the separation between states is provided as in atoms by the fact that the sign with which the exchange integral enters depends on the symmetry of the wave function on interchange of the space coordinates of the particles. This effect puts triplets below singlets in an atom, an effect which may alternatively be described in the following well-known graphic way. The wave function of a two-electron system in a triplet state, being symmetric in spin, changes sign on interchange of the space coordinates of the two electrons, so is zero when they coincide and small if the two positions described by the space coordinates are near one another. Thus the probability of the electrons being close together is relatively small in the triplet state, which makes the average of the positive (repulsive) Coulomb interaction e^2/r_{12} relatively small, and the triplet lower than the singlet. In nuclei the origin of multiplet splittings is closely related to this: it would be the same with ordinary (Wigner) interactions except for a reversal in sign because we are dealing with attractive interactions (negative energy) between the nucleons, making singlets lie below triplets. This agrees with the observed tendency for the nuclear angular momenta J to be zero for the ground states of even-even nuclei, or for an even number of like nucleons in a shell. Because of the saturation property, nuclear forces are usually treated as exchange interactions, perhaps primarily space-exchange (Majorana) interactions as in Eq. (2). With a space-exchange interaction, the above explanation of a singlet-triplet separation is complicated by the fact that the quantity we are averaging is no longer just a function V but an operator VP which works on one pair of single-nucleon wave functions. The probability density is made up of the product of a wave function multiplied by itself, once before and once after the operator P. If the wave function is symmetric in interchange of the two particles, in the singlet, the operator P does not change anything and the attractive potential still gives a low energy (of large absolute magnitude). In the triplet, the wave function is antisymmetric and P has the effect of changing the sign of the average energy making the triplet energy small and positive rather than small and negative. Thus singlets continue to lie below triplets, but the separation is larger with a space-exchange interaction VP than with an ordinary interaction V. The same effect may be described more analytically in terms of the direct integral

$$L=\int\psi(r_1)\phi(r_2)V(r_{12})\psi(r_1)\phi(r_2)dv_1dv_2, \quad (8a)$$

CC-0. In Public Domain. Gurukul Kangri Collection, Haridwar

Digitized by Arya Samaj Foundation Chennai and eGangotri

and the exchange integral

$$K=\int \psi(r_1)\phi(r_2)V(r_{12})\phi(r_1)\psi(r_2)dv_1dv_2. \quad (8b)$$

Here ψ may in the simplest example be taken as a $1s$ wave function and ϕ a $2s$. With ordinary interactions the singlet and triplet energies are given by $L\pm K$, respectively, with L larger in magnitude than K, as is discussed further in Sec. 4. With anex change interaction the roles of L and K are interchanged, as may be seen from their definitions (8), making the energies $K\pm L$. The singlet-triplet separation is thus larger with the exchange operator than without it.

With several nucleons in the p shell, similar effects occur but, of course, with much more freedom of orientation of vectors, orbital as well as spin. In this case, only the p wave functions of the same shell are involved. We denote them by u_{m_l}, corresponding to the three projections $m_l=1, 0, -1$. In the definition, Eq. (8a), of L, both ψ and ϕ are replaced by u_0, with $m_l=0$. In K, one is u_0 and the other u_1 so as to give some meaning to the exchange operation. In terms of L and K thus defined, the energy separations of the various multiplets in the Russell-Saunders or (LS)-coupling scheme are given by Feenberg and Phillips (F37a) and the separations within the lowest (jj) configurations in the (jj)-coupling scheme by Kurath (K52). The physical basis for the separations in these cases is very much the same as in the simple case discussed above, though the computations are, of course, more involved.

In the approximation in which the range of $V(r_{12})$ is large compared to the nuclear radius, so that V may be considered constant throughout the region where the wave functions exist, K is zero because it reduces to this constant times the square of the integral expressing the orthogonality of ψ and ϕ. In the opposite extreme in which the range of $V(r_{12})$ is short compared to the size of the nucleus, known as the δ-function approximation, one obtains $K=L/3$. How much smaller K may be than L, within this range, depends on the details of the radial dependence of the wave functions and of the interaction. An evaluation based on oscillator wave functions and Gaussian radial dependence of V, with a reasonable estimate of their range parameters, yields a result (H51) near

$$L=6K, \quad (8c)$$

and we shall take this as the basis for numerical evaluations of the ratios of level spacings in the empirical comparisons made below.

Since the depth of the potential $V(r_{12})$ is known to be of the order of magnitude 20 Mev from general stability and scattering considerations, and L is reduced below this only by the failure of the two distributions to come within the range of V of one another, thus by perhaps a factor $\frac{1}{2}$ or $\frac{1}{3}$, it may be estimated that L is of the order of 6 to 10 Mev, and thus K of 1 Mev.

4. ISOBARIC SPIN

In the tabulations of multiplet spacings of Feenberg and Wigner and elsewhere (F37, F37a, K52) one finds the states listed according to the usual quantum numbers L and S of the (LS)-coupling scheme and also according to the isobaric spin quantum number T (or isotopic spin as it has been less aptly called since it was named long ago by Wigner, who agrees to this renaming of his child). This dynamical variable T, which was introduced by Wigner (Wi37) as a quantity which should be a constant of the motion or "good quantum number" with a charge-independent Hamiltonian, is attaining an increasing importance in experimental as well as theoretical physics with the discovery that it appears to help control reaction rates and provide valid selection rules in certain meson reactions as well as nuclear reactions. The usefulness of isobaric spin may be explained elegantly by saying that the Hamiltonian is invariant under rotations in isobaric-spin space (just as it is in ordinary space when there is no external field) if the nucleon isobaric spin vectors τ_i appear only in the form of scalar products as in the first line of Eq. (1), and this invariance makes the total isobaric spin T a good quantum number (just as is S when σ_i appears no more than through $\sigma_i\cdot\sigma_j$). A statement in this language is, however, apt to be too formal for those readers who want a more explicit and graphic description of how isobaric spin affects the energy of a nuclear state. A brief and completely nonmathematical statement of the usage of isobaric spin in these light nuclei is found in the introductory part of reference (Aj52).

Discussion of Ordinary Spin Preparatory to an Explanation of Isobaric Spin in a Simple Case

In preparation for a more complete explanation of the useful concept of isobaric spin in explicit analogy with the usual intrinsic spin of a system, we shall first formulate the dependence of the interaction energy on spin quantum number in an appropriate manner, more explicitly than was done in the more general remarks of Section 3. For the sake of clarifying the physical basis of the analogy, there are three aspects of the problem which we shall emphasize: (a) the formalism of single-particle "spin factors" of the wave function and the choice of the quantum numbers $\pm\frac{1}{2}$, (b) the Pauli principle in the case of "parallel spins," and (c) the Pauli principle in the more general case in which it selects four of the eight solutions of the two-body wave equation.

(a) A very essential feature of the discovery of electron "spin" by Goudsmit and Uhlenbeck was the recognition that there are in nature twice as many states as there are solutions of a one-electron equation of motion in three dimensions (wave equation in present terminology), and one ascribes to the electron another "degree of freedom" or coordinate or dynamical variable

CC-0. In Public Domain. Gurukul Kangri Collection, Haridwar

Digitized by Arya Samaj Foundation Chennai and eGangotri

(variously called $s_z=\frac{1}{2}\sigma_z$ or ω or σ) which can take on only two values rather than the continuous range of the three components of r. Just as the wave function $\psi(r)$ is in spherically symmetrical cases factorable into $R_{n,l}(r)Y_{l,m_l}(\theta,\phi)$ with factors specified by the three quantum numbers n, l, m_l, there is now a new factor of the wave function associated with the quantum number m_s, which can take on only two values, one for each of the Pauli spin wave functions α and β. In place of one wave function $\psi(r_i)$ we have two, $\psi(r_i)\alpha(s_{zi})$ and $\psi(r_i)\beta(s_{zi})$. The fact that there are two functions is important, and is the part which is most obviously convenient to carry over to the later discussion of the two charge states of a nucleon. Rosenfeld (R48) emphasizes the two-valuedness by calling the new coordinate a "dichotomic variable." Perhaps the simplest manifestation of electron spin is the observation that the energy given to an electron by a magnetic field H has two values, $\pm\mu_B H$, where μ_B is the Bohr magneton which in orbital motion is associated with the orbital angular momentum l of an electron in an atom, and now with the new coordinate is by analogy associated with "spin" angular momentum s. Because of this symmetry of the $\pm$ sign and because the proper values of a projection of an angular momentum jump by unit steps (in the unit h), we come to say the two values of m_s and of s_z are $\pm\frac{1}{2}$. The "spin" factor of the wave function associated with $m_s=\frac{1}{2}$ we call $\alpha(s_z)$ and the one with $m_s=-\frac{1}{2}$ we call $\beta(s_z)$. Their dependence on the two-valued coordinate s_z is as follows: $\alpha(\frac{1}{2})=1$, $\alpha(-\frac{1}{2})=0$, $\beta(\frac{1}{2})=0$, $\beta(-\frac{1}{2})=1$, so that the wave function $\psi\alpha=\psi(r)\alpha(s_z)$ has a value with "spin up" ($s_z=\frac{1}{2}$), none with "spin down," etc., as is familiar in one notation or another in most books on quantum mechanics [for example, reference (C35), pages 55–56, and reference (P35)].

(b) Consider now the problem of two particles in a potential well, one with a $1s$ wave function ψ and the other with a $2s$ wave function ϕ. Before introducing the interaction $V(r_{12})$ between them, one has solutions of the wave equation composed of simple products of the one-particle wave functions, such as

$$\psi(\mathbf{r}_1)\alpha(s_{z1})\phi(\mathbf{r}_2)\beta(s_{z2})=\psi(1)\phi(2)\alpha(1)\beta(2)\equiv\psi\phi\alpha\beta. \quad (9a)$$

Here we define the convention that, in the product of a pair of similar functions such as ψ and ϕ, the first shall refer to particle 1 and the second to particle 2. The association of particle 1, rather than particle 2, with the function $\psi\alpha$ in that product is artificial and has no physical meaning. A wave function that avoids stating more than one knows about this is formed by taking a sum of such products which is symmetric or antisymmetric in the exchange of the indices 1 and 2. The simplest wave-mechanical form of the Pauli principle is that, for two identical particles, such as two neutrons with α (i.e., "spin up"), the wave function must be antisymmetric (not symmetric) in interchange of $\mathbf{r}_1$ and $\mathbf{r}_2$, so that it vanishes when $\psi=\phi$, and there is thus no wave function in which two identical particles have the same set of quantum numbers. With "both spins up," the function similar to Eq. (9a) is $\psi\phi\alpha\alpha$, but in a system in which electrons 1 and 2 interact it is not a satisfactory approximate solution of the wave equation, corresponding to the fact that it erroneously associates electron 1 with the state ψ and 2 with ϕ whereas they may exchange. The function $\phi\psi\alpha\alpha$, with the electrons exchanged, is another possibility with the same energy before $V(r_{12})$ is introduced, but only the sum and the difference of the two are (approximate) solutions of the wave equation with $V(r_{12})$, as we shall see in a more general case below. Of these two solutions, the difference

$$(\psi\phi-\phi\psi)\alpha\alpha$$

vanishes in the special case $\psi=\phi$, and this is the one selected by the Pauli principle in keeping with the simple statement that "no two identical particles shall have the same set of quantum numbers." This two-electron wave function changes sign when we change the order of the factors ψ and ϕ, which is equivalent to exchanging $\mathbf{r}_1$ with $\mathbf{r}_2$, so may be said to be antisymmetric in the exchange of the coordinates of the two electrons.

(c) With "one spin up and one down" there are four primitive products, corresponding to either the association of α or β, and either electron 1 or 2, with the function ψ (the other with ϕ). With "both spins up" we had two and with "both spins down" there are two more, or eight in all. Eight independent linear combinations may be made of them, and the combinations that are solutions of the wave equation with $V(r_{12})$ may be expected to separate into space and spin factors, since V does not contain the spin coordinates. The salient experimental fact demanding the Pauli principle, the example in this simple case of the general workings of the vector model, is that there are only four physical states corresponding to these eight solutions, three (the ^3S separable by a magnetic field) with one value of the energy and one with another (the ^1S). Correspondingly, four of the eight [including the one selected in (b) above] are selected by the more general form of the Pauli principle, which states that the functions shall be antisymmetric in exchange of the particle-labeling indices, 1 and 2, or antisymmetric in "all the coordinates, including spin coordinates s_{zi}." This leaves us with the following familiar functions:

	M_S	S	Spectroscopic notation	Interaction energy
$\Psi_1=(\psi\phi-\phi\psi)\alpha\alpha$	1	1	^3S	$L-K$
$\Psi_2=(\psi\phi-\phi\psi)(\alpha\beta+\beta\alpha)$	0			
$\Psi_3=(\psi\phi-\phi\psi)\beta\beta$	-1			
$\Psi_4=(\psi\phi+\phi\psi)(\alpha\beta-\beta\alpha)$	0	0	^1S	$L+K$.

(9b)

We see that they change sign when we interchange the space functions ψ with ϕ and the spin functions, such

CC-0. In Public Domain. Gurukul Kangri Collection, Haridwar

Digitized by Arya Samaj Foundation Chennai and eGangotri

as α with β, which is equivalent to interchanging 1 with 2. These combinations (as well as the four symmetric ones that have been rejected) avoid stating more than we want to claim to know about the interacting particles; they do not specify which electron is in which state and they do not specify (in the second and fourth lines) whether α is associated with ψ and β with ϕ, or vice versa. That these functions are the proper solutions of the wave equation with interaction and leave the energy matrix diagonal, we shall see in the following paragraph.

The labels $M_S=m_{s1}+m_{s2}$ are convenient, and the further label S, which may be associated with the length of a "total spin" vector having projections M_S, denotes whether the "spin factor" is symmetric ($S=1$) or antisymmetric ($S=0$), in which cases the more important space factors are antisymmetric or symmetric, respectively. Now we introduce an interaction energy $V(r_{12})$, which is negative for two neutrons or positive, e^2/r_{12}, for two electrons, and calculate the interaction energy

$$\frac{1}{2}\int(\psi\phi\pm\phi\psi)V(\psi\phi\pm\phi\psi)dv_1dv_2=L\pm K, \quad (10)$$

where the "direct integral" L and the "exchange integral" K are

$$L=\int\psi\phi V\psi\phi dv_1dv_2$$

$$=\int\rho_\psi(1)\rho_\phi(2)V(r_{12})dv_1dv_2, \quad \rho_\psi=\psi^2,$$

$$K=\int\psi\phi V\phi\psi dv_1dv_2$$

$$=\int\rho_0(1)\rho_0(2)V(r_{12})dv_1dv_2, \quad \rho_0(1)=\psi(1)\phi(1),$$

as in Eq. (8). The exchange integral, being a self-energy of an "overlap density" ρ_0, which may have positive and negative regions, is smaller than the direct integral. For a reasonable function $|V|$ having a maximum when the particles are close together, K has the sign of V, which is negative between nucleons, so the singlet state, ^1S, with $S=0$, lies below the triplet states, ^3S, with $S=1$. The singlet-triplet separation is $2K$. (With a space-exchange or "Majorana" interaction VP in place of V, the role of L and K would be interchanged, as has been already mentioned, and the singlet-triplet separation would be larger, $2L$.)

If $H_0\Psi_a=E_0\Psi_a$, as is true for any of the functions $\Psi_a(1, 2)$ given by (9b), then with the interaction V included in the Hamiltonian, $H=H_0(r_1, r_2)+V(r_{12})$, we still have $H\psi_a=(E_0+\epsilon_a)\psi_a$ if $V\psi_a=\epsilon_a\psi_a$ [with ϵ given by Eq. (10)], without any added term in ψ_b, that is, if $V_{ab}=\int\Psi_bV\Psi_ad\tau_1d\tau_2=0$ for $a\neq b$. Thus the vanishing of the nondiagonal matrix elements V_{ab} is essential for the Ψ's to be proper solutions of the wave equation (in the approximation in which we neglect other states remote in energy). That the V_{ab} vanish can be seen from the orthogonality of the spin factors alone in Eq. (9b), since V does not operate on the spins s_i. Between different values of M_S, this is a simple result of conservation of S_z. Between the two states with $M_S=0$, the vanishing of V_{24} expresses the conservation of S. In this case the spin orthogonality may be formulated

$$\sum_{s_{z1}=\frac{1}{2}}^{-\frac{1}{2}}\sum_{s_{z2}=\frac{1}{2}}^{-\frac{1}{2}}[\alpha(s_{z1})\beta(s_{z2})+\beta(s_{z1})\alpha(s_{z2})]$$

$$\times[\alpha(s_{z1})\beta(s_{z2})-\beta(s_{z1})\alpha(s_{z2})]=1-1=0.$$

Here we use the familiar generalization that with the spin factors in the wave function the integral over $d\tau_i$ means an integral over the space coordinates, dv_i, and a sum over the two values of the spin coordinate s_{zi}. The same vanishing of V_{24} may be demonstrated also by the space factor, since the first member of Eq. (10) vanishes if modified to have one + and one − sign. These are some of the elements of familiar atomic spectroscopy which apply also to a pair of neutrons.

Explanation of Isobaric Spin for Simplified Nucleons

Let us now imagine that we might have spinless nucleons, both protons and neutrons (or nucleons with "spin up" will do as well, with less violence to nature, and let us, in this case, simply omit the common spin factor $\alpha\alpha$). Protons and neutrons differ so little in all properties but charge that we make the very important assumption (H32) that we can treat them as two states of a single type of particle, the nucleon, as is done in the theory of beta-decay. We can put either a proton into ψ in the potential well, or a neutron, two single-nucleon states which we can distinguish from one another by application of an electric potential, which adds an energy e or 0 multiplied by the potential.

(a) This factor e or 0 does not have the symmetry of the factor $\pm\mu_B$ in the magnetic energy of an electron, but it does have the same two-valuedness. The two-valuedness leaves the naming of the two values arbitrary, and it is this symmetry in the case of the electron spin that makes it convenient to take the two values $\pm\frac{1}{2}$. This choice led incidentally to a formulation of the "$V(r_{12})$ problem" in which the magnetic energy with its special symmetry played no direct role, and the formulation had a convenient elegance involving simpler quantum numbers than might have been encountered if we had not been guided by the magnetic symmetry in our choice, namely that the quantum numbers $S=1$ and 0 are associated with the "triplet" and "singlet"

CC-0. In Public Domain. Gurukul Kangri Collection, Haridwar

Digitized by Arya Samaj Foundation Chennai and eGangotri

energies of the two-electron system (the numbers of degenerate states being easy to remember in terms of a "vector model" concept). Because this formulation is both elegant and familiar, it is convenient in the discussion of nucleon charge to exploit the arbitrariness by proceeding arbitrarily in close analogy to the discussion of spin. With any other choice of numbers such as 1 and 0 to denote the two arbitrary values of the charge, it would be more difficult to remember what we had done, and would lead to the same physical results. Thus the closeness of the analogy of isobaric spin, as we shall formulate it, to intrinsic spin is somewhat artificial; it is a result of an easy, but arbitrary, choice. Isobaric spin has a very insistent physical meaning, nevertheless, in terms of states differing in energy and characterized by some sort of proper values T of a new dynamical variable that is conserved under appropriate circumstances. It is the codification of the quantum numbers that is arbitrary.

Thus with two charge states of a nucleon distinguishable in an electric potential the situation is almost exactly similar to the previous one wherein we had states $\psi\alpha$ and $\psi\beta$ distinguishable in a magnetic field (H32). With a neutron in the space-state ψ we shall call the wave function $\psi\nu$, or with a proton, $\psi\pi$, and similarly for the next lowest state $\phi\nu$ or $\phi\pi$. Here $\nu=\nu(t_z)$ is a function of the two-valued charge coordinate which we (arbitrarily) give the values $\pm\frac{1}{2}$, ν being associated with the quantum number $m_t=\frac{1}{2}$, etc., as for spin above.

(b) For two neutrons without spin, the situation is the same as for two electrons or two neutrons with "spin up," as discussed in (b) above. The solution allowed by the simple form of the Pauli principle is $(\psi\phi-\phi\psi)\nu\nu$.

(c) If we have a proton and a neutron and try to find simple product solutions before introduction of $V(r_{12})$, and if we treat the proton and neutron as quite different particles, not states of the nucleon, or if we claim to know that nucleon 1 is a proton, etc., there are only two states, a proton in ψ and a neutron in ϕ, or vice versa. Not only from old ideas about beta-decay and about the saturation of nuclear forces, but also even more convincingly from newer observations of exchange scattering at high energies, there are insistent suggestions of the nucleon concept, and of the exchange of identity of protons and neutrons when they interact. The possible existence of nucleon number 1 as either a proton or neutron, and of number 2 then as neutron or proton, makes the number of states of the neutron-proton system twice as great, or four. Of these we can make four independent linear combinations, two symmetric and two antisymmetric in the exchange of 1 and 2, and each a solution of the wave equation including an interaction $V(r_{12})$ that does not depend on the charge of the nucleons (in the same way that we made linear combinations of the spin functions that we showed to be solutions when V did not depend on spin). Because the simple statement of the Pauli principle applies to two neutrons in (b) just above, and because the simple generalization of the Pauli principle from (b) to (c), in the case of electrons, leads to the observed number of states, we here *assume* that the similar generalization from (b) to (c) may be made in the case of nucleons. The Pauli principle then states that the wave function shall be antisymmetric in interchange again of the particle-labeling indices 1 and 2, that is, of "all coordinates, including the charge coordinate or isobaric spin coordinate." All of this is independent of the choice of indices discussed in (a) above. Here the charge coordinate need only represent the two-valuedness, with π and ν vanishing or not depending on which of its two arbitrary values it takes, but from now on we shall let them be the convenient values $t_z=\pm\frac{1}{2}$.

On the basis of this new assumption concerning the scope of the Pauli principle, we discard the two symmetric states of the neutron-proton system. The physical necessity for the corresponding step for two electrons with spin in atoms could be verified by counting the number of states in multiplets. Unfortunately, the groupings of states in light nuclei are more complex and their identifications less complete, as we shall see, so this type of verification that states like the two discarded symmetric states (c) are really missing can come only with the success of a rather extensive interpretation of the various energy levels, but some fairly clear examples of it can be found in the cases discussed below. Another type of verification for the assumption that isobaric spin is a coordinate entering in the statement of the Pauli principle is found in the experimental evidence for conservation of isobaric spin T in reactions.

On this basis we select the four antisymmetric states of the system of two spinless s nucleons:

	M_T	T	Interaction energy
$(\psi\phi-\phi\psi)\nu\nu$	1	1	$L-K$
$(\psi\phi-\phi\psi)(\nu\pi+\pi\nu)$	0		
$(\psi\phi-\phi\psi)\pi\pi$	-1		
$(\psi\phi+\phi\psi)(\nu\pi-\pi\nu)$	0	0	$L+K$.

(11)

Again for convenience we use the labels M_T and T, analogous to M_S and S, and may use a vector concept in remembering how many states M_T are associated with each value of the isobaric spin T, as we shall call it, of the system. M_T may then be called isobaric spin projection. $M_T=1$ means two ν's, or the dineutron in this simplified potential-well model, $M_T=0$, the deuteron, and $M_T=-1$ means He^2, so M_T denotes which isobar we have. The state $T=1$ has substates in the three isobars, all with the same energy $L-K$ if we have just one $V(r_{12})$, or more generally if we have a "charge-independent Hamiltonian," independent of the distinction π and ν. With these peculiar spinless nucleons in this model, the ground state of the "deuteron" would have both nucleons in the lowest state ψ, and then in

CC-0. In Public Domain. Gurukul Kangri Collection, Haridwar

Digitized by Arya Samaj Foundation Chennai and eGangotri

our first excited configuration with ψ and ϕ populated, there would in this isobar be two excited states, one with $T=0$ and one with $T=1$. The physically significant fact would be that this $T=1$ ($M_T=0$) state would coincide in energy with the ground state of the dineutron ($T=1, M_T=1$) and of He^2 ($T=1, M_T=-1$), in this model. The reason for this fact is that the three $T=1$ states each have a minus sign in the space part of the wave function $(\psi\phi-\phi\psi)$. In the isobar $M_T=0$, the state with $T=1$ has a wave function of such symmetry that the Pauli principle would permit the two nucleons to be the same (both neutrons, e.g.). This is, in the simplest terms, how the $T=1$ state differs from the $T=0$ state in this isobar, and this symmetry difference affects the energy.

So far, in this simple example, the only difference between spin and isobaric spin is that states differing in spin projection may be distinguished by a magnetic field and those differing in isobaric spin projection by an electric field. When we go to a case in which the single-particle wave functions depend on angle and introduce orbital angular momentum operators, the projection quantum numbers of these may also be distinguished by a magnetic field in a way with which the behavior of spin operators may be put in close analogy, and in a way to preserve the classical property of conservation of angular momentum if the spin operators are associated with an intrinsic angular momentum of the particle. Thus the spin operators become associated with the Euclidian space of the laboratory, whereas the isobaric spin operators do not. One sometimes makes this distinction by referring to an isobaric spin projection operator as T_ζ rather than T_z. For a single nucleon one would have t_ζ or τ_ζ, analogous to s_z or σ_z, and m_t analogous to m_s.

Spin and Isobaric Spin Combined in a Simple Example

Now to get back to real, healthy nucleons, let us see how spin and isobaric spin are handled at the same time in this same simple example, at the same time introducing a more nearly realistic nuclear interaction, Eq. (2). It is convenient to list the states of the two-nucleon system by use of that form of the Pauli principle which states that no two nucleons may have the same set of quantum numbers, as is done in Table I. (States with negative M_S or M_T are omitted since they introduce nothing new.) The first line has the wave function

$$(\psi\phi-\phi\psi)\alpha\alpha,\ \nu\nu \qquad (9')$$

which combines the properties† $S=1$, $T=1$, of the first lines of Eqs. (9b) and (11), an antisymmetric space function of two neutrons with "spin up." The second and third lines are combined in the familiar way into the two antisymmetric combinations (one antisymmetric in space and the other in spin)

$$(\psi\phi\pm\phi\psi)(\alpha\beta\mp\beta\alpha)\nu\nu \qquad (9'')$$

which correspond to the second and fourth lines of Eq. (9b) for two neutrons, with $T=M_T=1$, $M_S=0$, and $S=0$ or 1, respectively. The fifth and sixth lines similarly have

$$(\psi\phi\pm\phi\psi)\alpha\alpha(\nu\pi\mp\pi\nu) \qquad (11')$$

corresponding to the second and fourth lines of Eq. (11) for a neutron and a proton with "spin up," with $S=M_S=1$, $M_T=0$ (deuteron), and $T=0$ or 1, respectively. From Eq. (10) we see that for an ordinary interaction V we have various states with $S=1$, $T=1$, all with energy $L-K$, whereas with $(S, T)=(1, 0)$ or $(0, 1)$ the energy is $L+K$, the difference again arising from the symmetry of the space factor.

TABLE I. States allowed for two nonequivalent s nucleons.

$\uparrow$ m_s	m_t	ϕ m_s	m_t	M_S	M_T	S	T	Energy calculated with (2) and (8c)
+	+	+	+	1	1	1	1	$-3K$
+	+	−	+	0	1	1	1	$-3K$
−	+	+	+	0	1	0	1	$4.2K$
+	+	+	−	1	0	1	1	$-3K$
+	−	+	+	1	0	1	0	$7K$
+	+	−	−	0	0	1	1	$-3K$
−	+	+	−	0	0	0	1	$4.2K$
+	−	−	+	0	0	1	0	$7K$
−	−	+	+	0	0	0	0	$-5K$

The degeneracy arising from the fact that $(S, T)=(1, 0)$ or $(0, 1)$ have the same energy with this simple interaction V is slightly confusing, so we list in Table I the energies derived from the assumed specific nuclear interaction, Eq. (2), specialized according to Eq. (8c). Through the spin-exchange operator, this differentiates between spin and isobaric spin, and thus lifts the degeneracy. These energies are calculated from the usual prescription $\int\Psi^*H\Psi dv$, taking care of the normalization, and with Ψ given by Eq. (11') the interaction energy is

$$0.8\int(\psi\phi\pm\phi\psi)^*V(\phi\psi\pm\psi\phi)dv/2$$

$$+0.2\int(\psi\phi\pm\psi\phi)^2Vdv/2$$

$$=0.8(\pm L+K)+0.2(L\pm K); \qquad (12)$$

the + sign applying to $T=0$ and the − to $T=1$. In such a calculation one sees that the space-exchange

† The demonstration that $S=1$ in this case, or that $(\mathbf{s}_1+\mathbf{s}_2)^2=S(S+1)=2$, is known from almost any textbook in quantum mechanics. It is simply that $(\mathbf{s}_1+\mathbf{s}_2)^2=\mathbf{s}_1^2+\mathbf{s}_2^2+2\mathbf{s}_1\cdot\mathbf{s}_2=\mathbf{s}_1^2+\mathbf{s}_2^2+2m_{s1}m_{s2}=\frac{3}{4}+\frac{3}{4}+\frac{1}{2}=2$. In the case $M_S=0$ of Eq. (10) the evaluation of $\mathbf{s}_1\cdot\mathbf{s}_2$ involves nondiagonal matrix elements, but the result is the same if the spin function is symmetric, or $S=0$ if antisymmetric. Exactly the same analysis applies to T in terms of the m_t's.

CC-0. In Public Domain. Gurukul Kangri Collection, Haridwar

Digitized by Arya Samaj Foundation Chennai and eGangotri

operator P operates to exchange ψ and φ in the second space factor only, and the summation (implied in the integral) over the other functions, being unaffected by any operators, comes in just as in the normalization and gives a factor unity. In the second term the spin-exchange operator Q in this case has no effect because of the symmetry of $\alpha\alpha$. Thus, we see that the two states differing in T have quite different energies. Let us see that one and only one of these energies corresponds to that of a state of another isobar, because of a similarity in space and spin symmetry.

The states of the other isobar, the dineutron, say, are obtained similarly by use of Eq. (9″):

$$0.8\int(\psi\varphi\pm\varphi\psi)V(\varphi\psi\pm\psi\varphi)dv/2$$

$$+0.2\int(\psi\varphi\pm\varphi\psi)^2Vdv(\alpha\beta\mp\beta\alpha)(\beta\alpha\mp\alpha\beta)/4$$

$$=0.8(\pm L+K)\mp0.2(L\pm K), \quad (13)$$

the upper sign applying to $S=0$, the lower to $S=1$, both with $T=M_T=1$. With the lower choice of signs the energies expressed by Eqs. (12) and (13) agree, but with the upper they do not, which means that the energy of the state $S=1$, $T=1$ calculated with the charge-independent interaction, Eq. (2) is the same for the isobaric spin projection $M_T=1$ or 0. That is, there is a state in the deuteron which should have the same energy as a state in the dineutron because the two states have the same dependence on space and spin coordinates.‡

Thus we may answer the question, "What is the physical property of a state with $T=1$ to distinguish it from a state with $T=0$ in the same nucleus?" by saying that it has a type of symmetry that would still be allowed by the Pauli principle even if one of the protons of the nucleus were a neutron. We have seen an example in which the calculation of the energy depends just on this type of symmetry. More generally, if the Hamiltonian is charge independent, that is, if it does not depend on the proportion of neutrons and protons among the nucleons involved, then the states of the same value of T in different isobars (that is, different values of M_T) have the same energy for much the same reason that makes the states of an atom with the same S but different M_S have the same energy when there is no external magnetic field and the Hamiltonian is thus orientation-independent. (In these cases, the operators S_z and T_z, of which M_S and M_T are quantum numbers, commute with the Hamiltonian.)

The main point of this explanation is that it shows in detail how the quantum number $T=1$ or 0 determines the symmetry that the Pauli principle will allow for the space and spin factors and through them has an influence on the energy of the system. That is why it is possible to write the physical operator in the first line of Eq. (1) in terms of the scalar product of the single-nucleon isobaric spin vectors $\boldsymbol{\tau}_i=2\mathbf{t}_i$, which have their physical effect only indirectly through the effects of symmetry on the evaluation of the space function (as indeed do also the spin vectors $\boldsymbol{\sigma}_i=2\mathbf{s}_i$ in this formulation or in the atomic singlet-triplet problem). A more elegant evaluation of an exchange interaction is possible in this form, since $\boldsymbol{\tau}\cdot\boldsymbol{\tau}$ or $\boldsymbol{\sigma}\cdot\boldsymbol{\sigma}$ is 1 for T or S equal to 1, -3 for T or S equal to 0, but this form is no more useful because the convenient tabulations of references (F37) and (K52) are presented in terms of the exchange operators.

With many particles, the symmetry is not as clear-cut as in the two-particle case. A function is in general neither completely symmetric in the exchange of the space coordinates of all pairs of particles, nor completely antisymmetric, but perhaps symmetric in interchange of some pairs, antisymmetric in others. The energy is still dependent on the degree of symmetry and the isobaric spin formalism provides more help to distinguish between the various symmetries than in the two-particle case where it is easier to explain.

Conservation of Spin and Isobaric Spin in Reactions

One aspect of the conservation of isobaric spin is then seen in the existence of states of a symmetry denoted by $T=1$ in isobars $M_T=1, 0$, and perhaps -1 as demonstrated by the fact that their energy differences may be estimated by treating the charge dependence of the Hamiltonian as a first-order perturbation, as is discussed further, from an empirical point of view, in the following section. Another way in which a quantity such as an angular momentum may appear as conserved is by remaining with its initial value, or within a group of initial values through a scattering process, or through a reaction involving the intermediate formation of a compound nucleus. For example, when only one orbital angular momentum is involved in the incident beam and one in the emergent beam, conservation of parity is assumed, and of course conservation of total angular momentum. When spin-orbit coupling is so small as to be small compared to the natural width of a compound state, it would be expected that spin angular momentum S would be conserved, and this process could be analyzed by expressing the various contributions s_i in

‡ To make a similar comparison for the $S=0$, $T=1$ and 0 states it is necessary to complete the discussion of Table I by considering the four $M_S=0$, $M_T=0$ states, in the last four lines. Note that lines six and seven match lines two and three in the m_s's and match line four in the m_t's, and similarly for the last two lines (matching line 5 in m_t). Thus the last four lines are antisymmetrized by taking the space-spin factor of Eq. (9″) multiplied by the isobaric spin factor of Eq. (11′), with three independent $\pm$ signs. Successive choice of one of the $\pm$ signs as $-$ gives the first three states (S, T) listed, and the last, (0, 0) is given by the remaining antisymmetric possibility with all three negative. The energies for the four choices of signs, with interaction, Eq. (2) specialized as in (8c), are listed in the last column of Table I, three of them agreeing, of course, with those obtained earlier because they agree with choices of signs made earlier in the space and spin factors.

CC-0. In Public Domain. Gurukul Kangri Collection, Haridwar

Digitized by Arya Samaj Foundation Chennai and eGangotri

terms of the spin operators, and analyzing the rate of change $\dot{S}$ in terms of these operators and the spin factors of the wave function. This $\dot{S}$ would be found to be small and S to be conserved to the extent that the dependence of the Hamiltonian on the s_i is small. Our choice of the isobaric spin operators and factors in the wave function in close analogy with those for ordinary spin provides us with a convenient dictionary with which to translate this expectation to isobaric spin, and leads us to expect T to be conserved in certain reactions. We shall see examples where the corresponding isobaric spin selection rule (A52a) forbids a transition that is indeed observed to be very weak. The conservation of the formal vector T is thus explained by comparing the formal operations with those associated with the physically familiar vector S of which we have physical reason to expect conservation, but here, just as with the energies, the physical meaning of the combination of formal vectors to make up T is to be understood in terms of the combination of space-spin symmetries of the parts of the system which is implied by the formal vectors and is difficult to calculate more directly.

Charge Independence As a Special Case of Charge Symmetry

We have seen that the conservation of isobaric spin follows from the assumption that the Hamiltonian is charge-independent, that is, that the specific nuclear interaction (neglecting the Coulomb interaction) between two nucleons is independent of their nature as neutrons or protons, the same for the three cases $n-n$, $n-p$, and $p-p$. Some of the consequences of charge independence also follow from the less restrictive assumption of charge symmetry, that is that the $n-n$ and $p-p$ interactions are identical, but not necessarily the same as the $n-p$ interaction, so that the Hamiltonian may be said to be symmetric in the interchange of all protons with all neutrons. Charge independence is a special case of charge symmetry. The great similarity of the energy separation in Li^7 and Be^7, each of which has four nucleons of one charge and three of the other, follows from the more general assumption of charge symmetry. There are other less obvious cases, particularly among the nuclei with $A=6$, 10, and 14, where some of the consequences of charge independence may not be considered to verify this special assumption because they are also consequences of the more general hypothesis of charge symmetry (Kr52). Because evidence for charge independence as quite a good approximation is found, as we shall see, particularly in the comparison of energies of states of the same T but different $|M_T|$, we shall not attempt to pursue the distinction further in the present survey. The Coulomb interaction between protons, which is considered to be the principal deviation from charge independence, constitutes just as large a deviation from charge symmetry, so the distinction does not appear to be very fruitful.

5. SURVEY OF THE EXPERIMENTAL DATA FOR THE POLYADS OF THE p SHELL, WITH COULOMB ENERGY ELIMINATED

Polyads

To bring into evidence the way in which the isobaric spin appears to be a fairly good quantum number, and to prepare for an interpretation in terms of isobaric spin, it is useful to present the data, not as associated with individual nuclei, but with the nuclei grouped into isobaric polyads after applying the "Coulomb correction," as has been done in Fig. 1. Isobaric spin T is, as we have seen, a dynamical variable not of a single nucleus, but of an isobaric set of nuclei, all with the same mass number A, and such a set of isobars we call a polyad, denoted by the symbol Py^A. Thus, Py^6 means $\cdots He^6+Li^6+Be^6+\cdots$. (The name "triad" or "isobaric triad" has been used for such a set of three isobaric nuclei in a recent review article by Lauritsen (L52), but in principle there are not only the states with $T=1$ spread over the three isobars, but also still higher groups of states with $T=2$ and so on up to $T=A/2$ spread over all $A+1$ isobars, so the name "polyad" seems more appropriate.) A polyad may alternatively be defined as a mechanical system of A nucleons, of which isobaric spin is a dynamical variable.

An extremely valuable compilation and digest of the far-flung experimental data on energy levels of light nuclei has been made by Lauritsen and his collaborators (H50, Aj52), and the level diagrams which they have tabulated form the starting point for any analysis such as this. Figure 1 is intended to give a survey of these data in a form to facilitate comparison and convey general impressions at a glance, and for this reason the proton-rich isobars are omitted except where their data contribute significantly to the identification of excited states. In Py^{10}, for example, only Be^{10} and B^{10} are shown, and the relative heights of their ground states are determined by making a "Coulomb correction," including a correction for the neutron-hydrogen mass difference.

Elimination of the Coulomb Energy and the Charge Independence of the Remaining Interaction

The correction is made in a simple manner on the basis of the assumption that the change in Coulomb energy on changing from four to five protons is the same in the difference $B^{10}-Be^{10}$ as in the difference of the other isobaric pair of the same elements, B^9-Be^9. (This assumption neglects the small effects of symmetry differences, and approximates a more careful theoretical correction about as well as the two steep theoretical curves in Fig. 18 are approximated by straight lines.) If we write the total nuclide ground-state mass energy, Mc^2, as $E(Z,A)=E_o(Z,A)+E_c(Z,A)+(ZM_H+NM_N)c^2$, the energy of binding (kinetic included) provided by the specific nuclear interactions being E_o, and the Coulomb

CC-0. In Public Domain. Gurukul Kangri Collection, Haridwar

Digitized by Arya Samaj Foundation Chennai and eGangotri

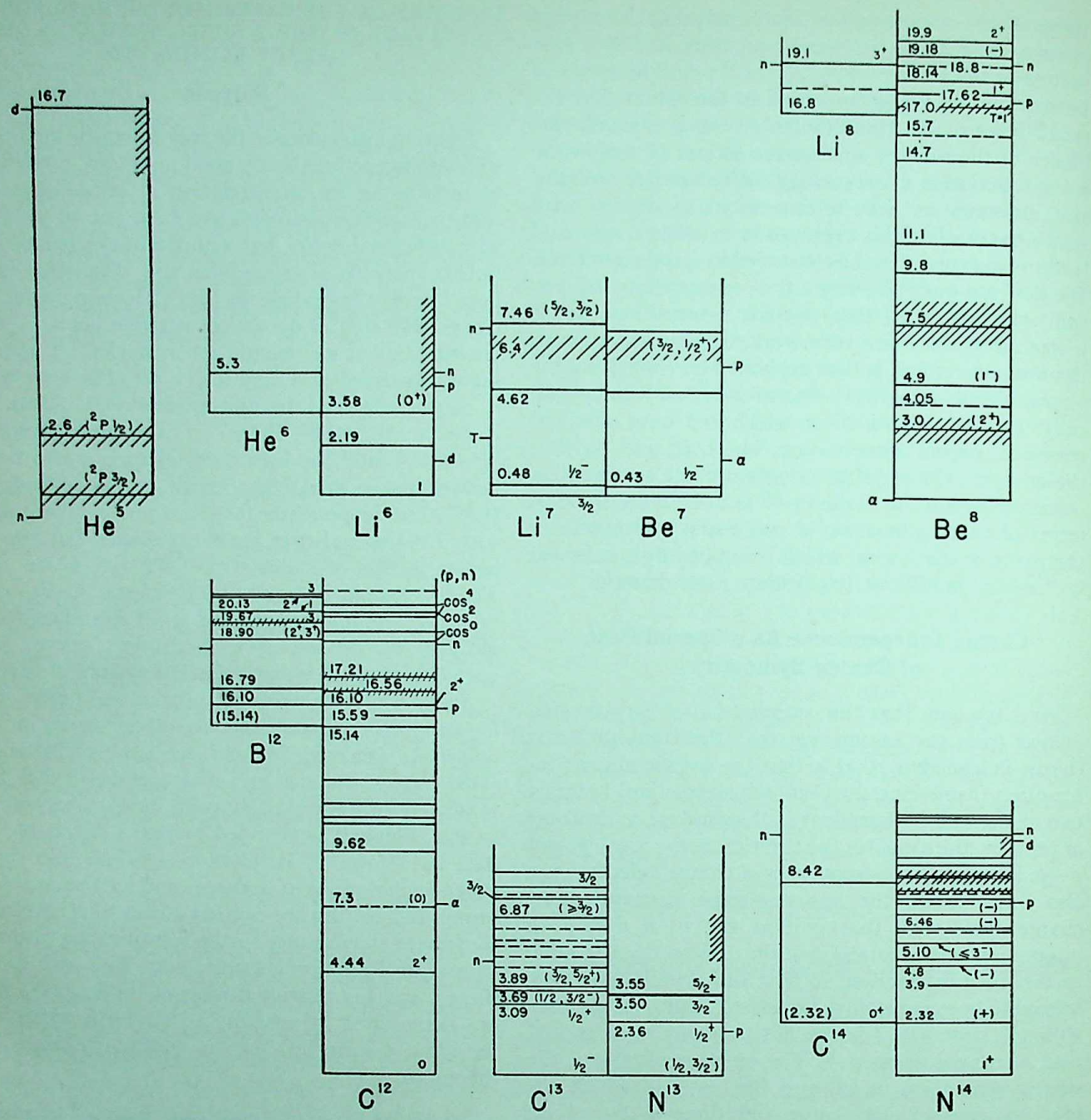


FIG. 1. Energy levels

energy E_c, then the ground-state energy difference $Be^{10}-B^{10}$ is

$$\Delta_{10}=E(4,10)-E(5,10)=E_o(4,10)-E_o(5,10)+E_c(4,10)-E_c(5,10)+(M_n-M_H)c^2=\Delta_{o,10}+\Delta_{c,10}+\Delta_{n,H}. \quad (14)$$

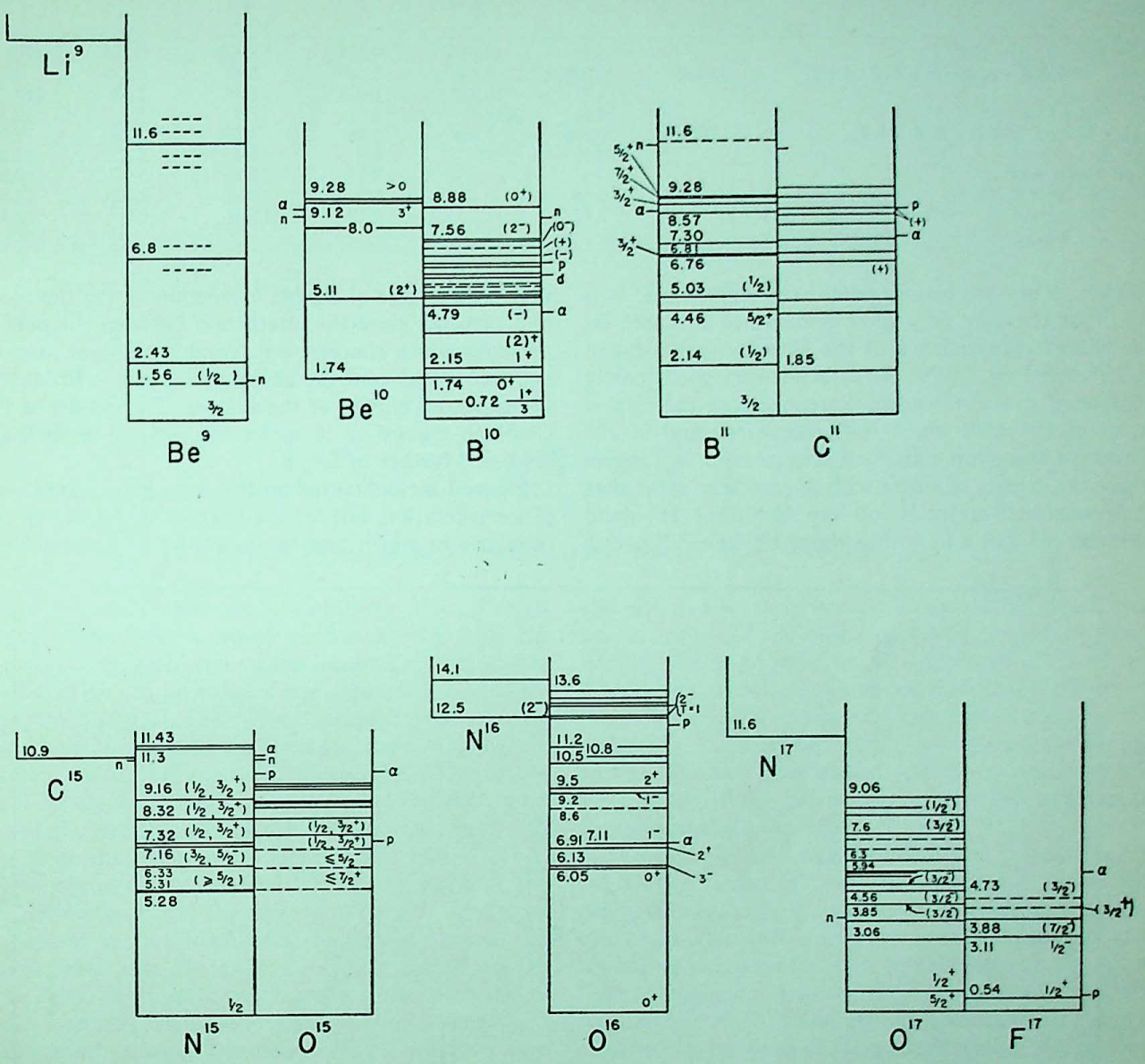
A similar equation holds with the 10 replaced by 9, with the differences Δ similarly defined. We assume that the specific nuclear interactions are symmetric (that is, the same between two protons as between two neutrons), which may be stated as $\Delta_{o,9}=0$, since taking this difference implies interchanging neutron number $N=5$ or 4 with proton number $Z=4$ or 5, and we further assume as just mentioned that $\Delta_{c,10}=\Delta_{c,9}$. We then have the $Be^{10}-B^{10}$ difference in binding energies provided by the specific nuclear Hamiltonian:

$$\Delta_{o,10}=\Delta_{10}-\Delta_9=E_o(4,10)-E_o(5,10). \quad (15)$$

If now we further assume that the specific nuclear interactions are charge-independent (that is, the same between a neutron and proton as between two neutrons or two protons) so as to expect isobaric spin T to be a good quantum number, we have this as an estimate of the excitation energy of the first state with $T=1$ above the ground state of the polyad, with the Coulomb energy differences of the charge projections $M_T=1,0$ eliminated. Thus from the observed differences in the mass-energy of the ground states of the two isobars the

CC-0. In Public Domain. Gurukul Kangri Collection, Haridwar

Digitized by Arya Samaj Foundation Chennai and eGangotri



of the p-shell polyads.

excitation energy of the state $T=1$, $M_T=1$ is estimated to be 1.625 Mev in a hypothetical idealized polyad having no Coulomb term in its Hamiltonian. There is an observed level in B^{10} at 1.74 Mev, and this is assumed to be the $T=1$, $M_T=0$ state. A measure of the exactness of the assumption of a charge-independent Hamiltonian is provided by the near equality of these two numbers, together with the plausibility of this identification, as dependent on the fact that the nearest other level is at 2.1 Mev and also in this case on the very spectacular failure of inelastic deuteron scattering (the deuteron has $T=0$) to excite the 1.74-Mev level (B53, A52a).

The data for the positron-emitting isobar C^{10} are in this case not so reliable (the positron energy end point being given to ± 100 kev) but indicate that the $M_T=-1$ component of the $T=1$ state lies at about 1.9 Mev, as indicated by the lines with δ in place of Δ in Table II. The regular progression from 1.625 to 1.74 to 1.9 Mev with added Coulomb energy may be a secondary effect of the Coulomb repulsion which, by expanding the nucleus, may slightly reduce the average of the specific nuclear interactions. A still more favorable indication of the charge independence of the interactions may then be obtained by comparing the average of 1.625 and 1.9 (or better 1.9_4) Mev, that is about 1.78 Mev, with 1.74 Mev, the average for $M_T=\pm 1$ with $M_T=0$.

A similar treatment of other polyads of the p shell is given in Table II. The data there used are taken from reference (L51) where possible, and otherwise from (L52) and (De52) and may in some cases involve an experimental uncertainty of the order of magnitude of

CC-0. In Public Domain. Gurukul Kangri Collection, Haridwar

Digitized by Arya Samaj Foundation Chennai and eGangotri

TABLE II. Differences in energies of binding, in Mev. Coulomb correction (including neutron-H, mass difference), and matching of states of isobaric spin $T=1$ in the even polyads.

A	4	6	8	10	12	14	16
Z	2	3	4	5	6	7	8
$\Delta_A=E(Z-1,A)-E(Z,A)$		3.55	15.985	0.556	13.370	0.155	(10)
$-\Delta_{A-1}=-E(Z-1,A-1)+E(Z,A-1)$	0.0185	(1.32)	0.863	1.069	1.98	2.221	2.705
$\Delta_A-\Delta_{A-1}$		(4.9)	16.848	1.625	15.35	2.38	(12.7)
$\delta_A=E(Z+1,A)-E(Z,A)$		(4.9)	(18.0)	(3.9)	17.6	5.1	15.5
$\delta_{A+1}=E(Z+1,A+1)-E(Z,A+1)$	(1.32)	0.863	1.069	1.98	2.221	2.705	2.749
$\delta_A-\delta_{A+1}$		(4.0)	(17)	1.9	15.4	2.4	12.8
Next higher level		—		2.15	15.59	3.7	12.95
Matched level in Z^A		3.58		1.74	15.14	2.32	12.51
Next lower level		2.17		0.72	(11.9)	0.0	12.44

100 kev. They are mainly beta-decay differences. It is seen that the only very good evidence of this sort for the charge independence of the Hamiltonian is found in Py^{10} and Py^{14}. In Py^{6} the fit is not very good (partly because of special uncertainties concerning the virtual states of Py^{5} with which it is compared) and in the others the first state with $T=1$ is quite high, in a region where the density of states with $M_T=0$ is so great that an approximate match is not very significant. It should be remarked that a fit within about 100 kev indicates a very high degree of charge independence (to the order of 1 percent) since the interaction between the pair of nucleons which changes, e.g., from neutron-neutron to neutron-proton contributes something like -10 Mev to the potential energy of the system. The details of the Coulomb energy as it varies through the p shell are discussed further in Sec. 8.

Figure 1 is constructed for the purpose of convenience of interpretation, not for the purpose of displaying the comparisons which test the exactness of the conserva-

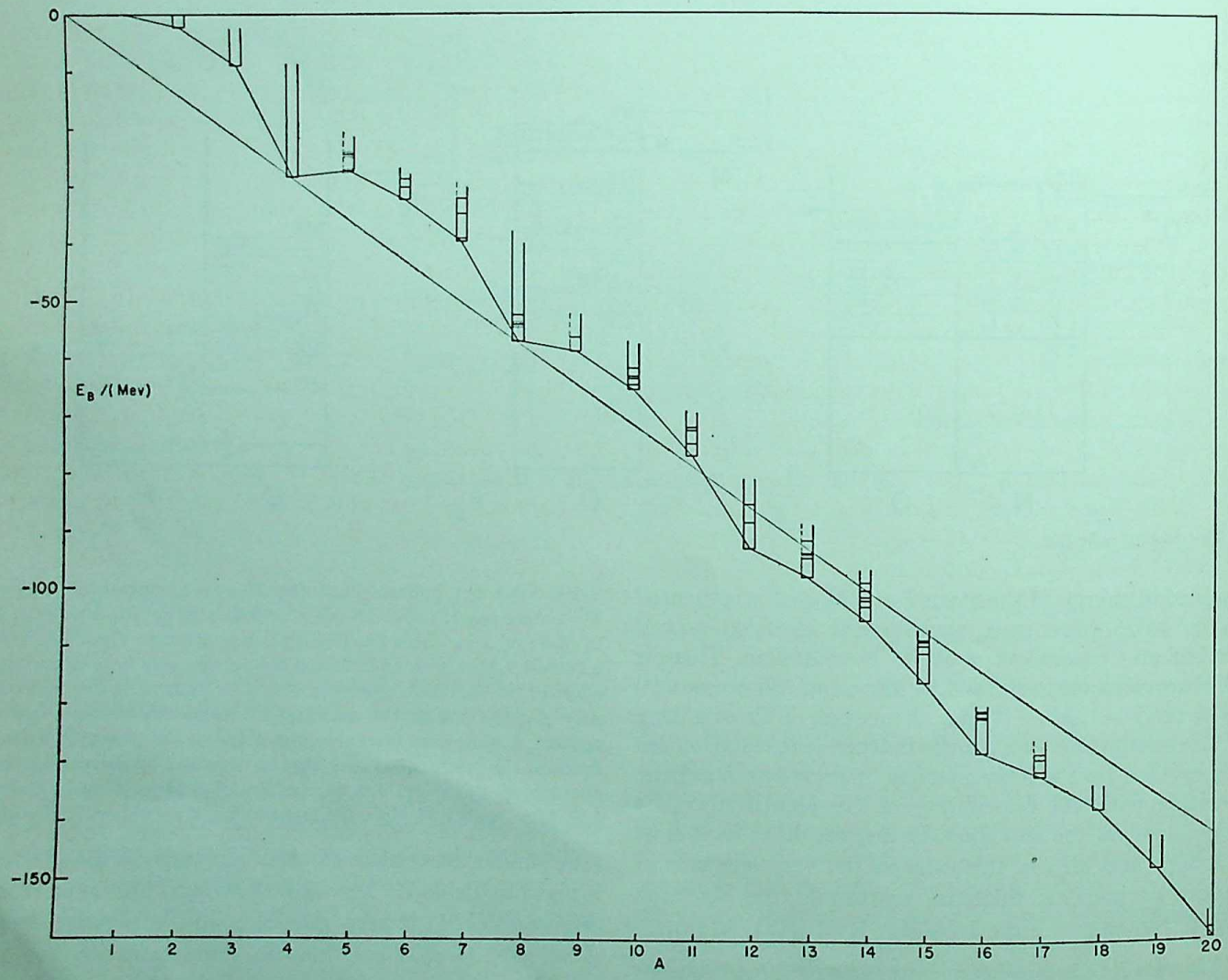


FIG. 2. Energies of binding of the states of the polyads.

CC-0. In Public Domain. Gurukul Kangri Collection, Haridwar

Digitized by Arya Samaj Foundation Chennai and eGangotri

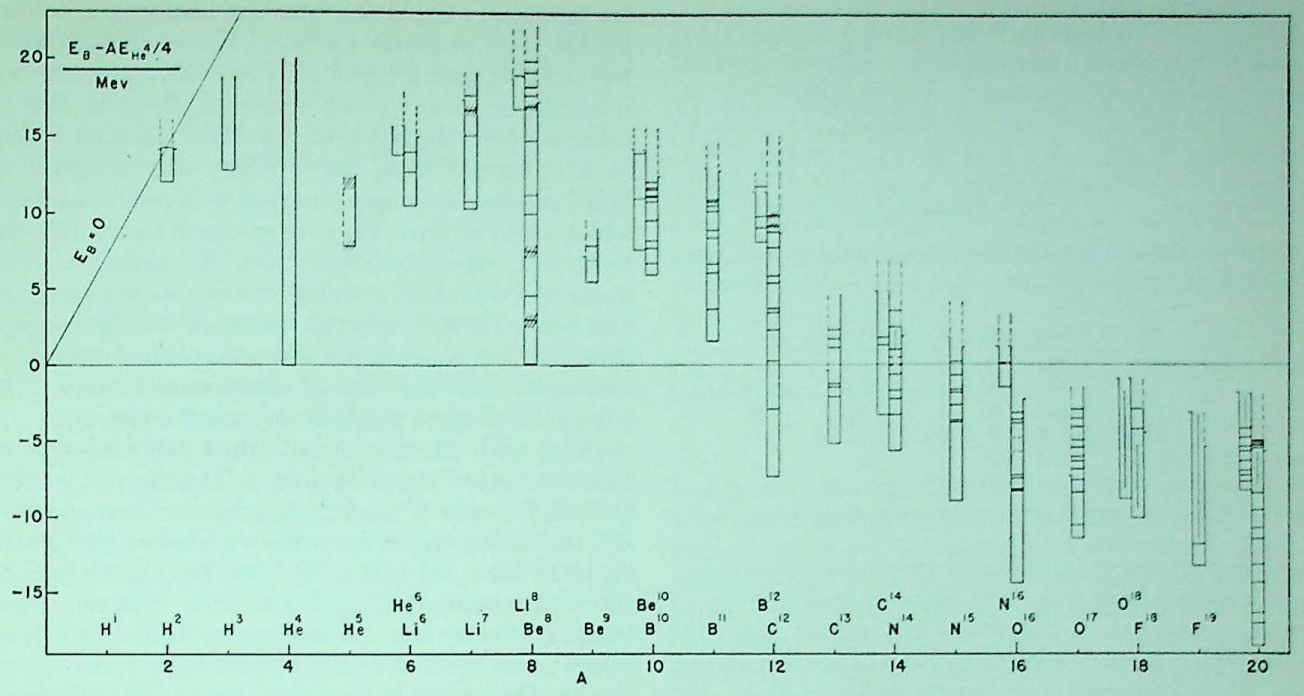


FIG. 3. Energies of binding relative to the binding per nucleon in an alpha.

tion of isobaric spin. In constructing Fig. 1 exact equality has been assumed of the $M_T=1$ with the $M_T=0$ charge projection of the lowest $T=1$ state after identification on the basis of the approximate equality found in Table II. (The identifications were actually made first in reference (L52) on the basis of a slightly different estimate of the Coulomb energies.) This makes Fig. 1 convenient for use in discussions of the interpretation of the energy spacings and sequence of levels, and facilitates the attempt to identify the higher $T=1$, $M_T=0$ states on the basis of the assumption that the Coulomb difference is the same for all $T=1$ states. In a similar way in the odd polyads, the ground states of the two isobars, with $M_T=\frac{1}{2}$ and $-\frac{1}{2}$, are placed on the same level in those cases in which the proton-rich isobar is shown. Thus we may say that an attempt has been made to display the data in Fig. 1 in such a way as to make it apply as well as possible to hypothetical polyads having no Coulomb terms in their Hamiltonians, although the spacings of levels within each isobar are obtained experimentally from a real nucleus in which it is assumed that the Coulomb terms contribute approximately equally to all states.

Trends in the Data

In Fig. 1 we see for each nucleus a number of horizontal lines representing observed energy levels, the excitation energy in the polyad being indicated, in Mev, by a number near the left side for many of the levels. In some cases a symbol appears near the right side indicating an experimental angular momentum and/or parity assignment. In cases in which this assignment is considered uncertain, it appears in parentheses ( ). Uncertain energy levels are indicated with broken lines. Levels observed to be broad are cross-hatched. Most of the spectral regions which have not been experimentally explored for the existence of levels are indicated by a vertical strip of cross-hatching at the right side. Outside the "boxes" containing the energy spectra are short lines labeled p, n, or α, indicating the level above which the nucleus is unstable relative to emission of these particles.

The ground-state angular momenta $\frac{3}{2}$, $\frac{3}{2}$, 3, $\frac{3}{2}$, for Li^7, Be^9, B^{10}, and B^{11} are what one expects from the compounding of $j=\frac{3}{2}$ vectors, as expected in the (jj)-coupling shell model in this first part of the p shell, and the values $\frac{1}{2}$, 1, $\frac{1}{2}$ for C^{13}, N^{14}, and N^{15} likewise may arise from the compounding of the $j=\frac{1}{2}$ vectors in the last part of the p shell. These are also the angular momenta expected on the basis of (LS) coupling (F37, R37) with the exception of B^{11} for which the low ^2P should be inverted because it is past the middle of the p shell.

Among the even polyads, there is a striking alternation in the excitation of the first state with $T=1$: in the $A=4n$ polyads Py^8, Py^{12}, and Py^{16} these excitation energies have large values in the range 12.5 to 16.7 Mev, while in the $A=4n+2$ polyads Py^6, Py^{10}, and Py^{14} they are much smaller, in the range 1.7 to 3.6 Mev. This appears to be an aspect of the "four structure" which seems to be associated with the symmetries available in (LS) coupling as clarified long ago by Wigner, Feenberg, and Phillips (W37, F37, F37a) and most apparent in the familiar "four structure" of the stability curve shown in Fig. 2. In exciting the ground state of Be^8 to the ground state of Li^8, for example, one has to break up a "four-group" of two neutrons and two protons

CC-0. In Public Domain. Gurukul Kangri Collection, Haridwar

Digitized by Arya Samaj Foundation Chennai and eGangotri

TABLE III. Number of states in the atomic configuration p^2, (LS) coupling.

m_1	m_s	m_1	m_s	M_L	M_S		M_L	$M_S=1$	0
1	+	1	−	2	0		2		1
1	+	0	+	1	1		1	1	2
:	:	:	:	:	:		0	1	3

TABLE IV. Number of states of two p electrons, (jj) coupling.

j_1	j_2	m_{j1}	m_{j2}	M	J	(jj) configuration	E	J
3/2	3/2	3/2	1/2	2	2	$p_{\frac{3}{2}}^2$	a	2, 0
		3/2	−1/2	1	2	$p_{\frac{3}{2}}p_{\frac{1}{2}}$	$-a/2$	2, 1
		3/2	−3/2	0	2	$p_{\frac{1}{2}}^2$	$-2a$	0
		1/2	−1/2	0	0			
3/2	1/2	3/2	1/2	2	2			
:	:	:	:	:	:			

whose spins cancel and whose interactions saturate in a particularly stable way, and make instead a group of three neutrons and one proton which cannot attain the same high symmetry relative to interchange of nucleons. (In the alpha-model, one has to excite an alpha, but much the same sort of effect prevails strongly in the central model in (LS) coupling, only weakly in (jj) coupling.) The odd polyads have relatively high excitation energies of the first $T=\frac{3}{2}$ states, presumably for this same reason in some cases and for reasons of shell structure in others.

Figure 2 is plotted in such a way as to display not only the "four structure" in the curve showing the stability of the ground states, but also to show in the same perspective the relative heights and thus the energies of binding of the excited states of the various polyads. Thus the energy spectra in Fig. 2 are small-scale versions of the energy spectra displayed in Fig. 1, standing on the stability curve for the ground states. One sees that the same four-structure is not in evidence for the energies of binding of the low states of higher isobaric spin. The stability curve of Fig. 2 is inverted relative to that shown by Feenberg and Phillips (F37a, Fig. 1), because they plotted binding energy, which is a positive quantity, the absolute magnitude of the negative "energy of binding" plotted in Fig. 2.

The straight line in Fig. 2 is drawn through the origin and the ground state of He^4. It thus represents the number of nucleons multiplied by the energy per nucleon in an alpha. In Fig. 3 the differences between the energy levels and this line are shown on a magnified scale, so as to exaggerate the four-structure and display the energy spectra on a larger scale. To see on this figure that Be^9 is stable, for example, one draws through the ground state of Be^8 a line parallel to the line $E_B=0$.

The most abundantly known energy levels are, of course, those of the more stable isobars of the various polyads, those with $M_T=0$ or $\pm\frac{1}{2}$. Among these, there is a striking variation in the density of the low states. In Py^7 one finds a low "doublet" and then a gap about ten times as wide as the "doublet" before the second excited state at about 4.6 Mev. The excited states of Be^8 start off with a broad state at 3 Mev and bear no resemblance to any other spectrum. Be^9 has two or perhaps three states below 2.5 Mev, then no others until at least 5 Mev, above which only a couple of broad maxima have been observed with poor resolution, which might be broad states or groups of states. B^{10} contrasts with the other light nuclei in having a more dense spectrum of low states, starting with a group of four below 2.2 Mev, of which one has $T=1$. Such a high density of low states in this odd-odd nucleus is somehow associated with the lack of exceptional symmetry in any one of them, to pull it down from the rest, or in (jj) coupling with the freedom to orient two $j=\frac{3}{2}$ vectors (nucleon "holes") in several ways. The contrast is most striking between B^{10} and the nearby even-even nucleus C^{12}, which has only a few widely spaced excited states up to 15 Mev, the first at $4\frac{1}{2}$ Mev. In this $A=4n$ case the wide spacing does appear to arise from an exceptional symmetry of a few low states, which pulls them down below the rest and is associated with the dip in the stability curve of Fig. 2 at $A=12$. The spectrum looks much more like (LS) coupling than (jj) coupling. In (jj) coupling, one would expect the first excited states to occur in a group of four, two of them with $T=1$, corresponding to the excitation of one $p_{\frac{3}{2}}$ nucleon to a $p_{\frac{1}{2}}$ state. (There are four states because there are two relative orientations of these two vectors; and either a proton or a neutron may be excited, which freedom of choice we may count in another way by saying that T may be 0 or 1.) The low states of Py^{13}, which are fairly dense after about 3 Mev, appear on the other hand to agree very nicely with the expectations of the (jj) model (K51). N^{14} has its first excited state at 2.3 Mev, and this has $T=1$ as expected for the $J=0$ orientation of two $p_{\frac{1}{2}}$ nucleons in the (jj) model, the other orientation $J=1$ being the ground state. Beginning at about 4 Mev there are numerous other states. The next nuclei N^{15} and O^{16} are very remarkable for having no excited states at all below 5.3 Mev and 6 Mev, respectively, and for then starting off in each case with a remarkably closely spaced pair of states. The large gap before the first excited state is doubtless associated with the end of the p shell, but in the case of N^{15} also seems to indicate that spin-orbit coupling is large. Beyond the closing of the shell at $A=16$, there are again many low states in O^{17}.

6. INTERMEDIATE COUPLING

From this survey we see that there is no consistent conformity of the energy spectra to the expectation of either (LS) or (jj) coupling. In (LS) coupling the various multiplets are characterized by values of the quantum numbers L and S, and the spacing between them is measured by the exchange integral K, as we have seen. In a graphic but still legitimate sense, K may be said to be a measure of the stiffness with which the

CC-0. In Public Domain. Gurukul Kangri Collection, Haridwar

Digitized by Arya Samaj Foundation Chennai and eGangotri

vectors $\mathbf{s}_i$ are coupled together to make a definite vector sum $\mathbf{S}$, and similarly the $\mathbf{l}_i$ to make $\mathbf{L}$. The separation of the states of various values of $\mathbf{J}=\mathbf{L}+\mathbf{S}$ within the multiplet is provided by a spin-orbit coupling perturbation which may be expressed in the form

$$H'=\Sigma a\mathbf{l}\cdot\mathbf{s}=A\mathbf{L}\cdot\mathbf{S} \tag{16}$$

just as in Eqs. (3) and (5) so far as the individual nucleons are concerned, but now with a collective or average spin-orbit parameter A characteristic of the multiplet. For a given multiplet, A is a multiple of a, with a positive constant near the beginning of a shell, a negative constant (for "holes") near the end of a shell, as is well known in atomic spectra. The approximation, Eq. (16) is a result of first-order perturbation theory, valid as long as the splittings within the multiplet, caused by a, are small compared to the separation of multiplets, caused by K. Thus we expect (LS) coupling to prevail if $a\ll K$, and similarly (jj) coupling if $a\gg K$, since a then measures the stiffness with which each $\mathbf{s}_i$ is coupled to $\mathbf{l}_i$ to make $\mathbf{j}_i$. In the central model, in which individual-nucleon wave functions are assumed to have an approximate meaning as a starting point, there is a broad region between the (LS) and (jj) extremes known as *intermediate coupling*, in which it may, in general, be said that a is of the same order of magnitude as K.

Derivation of the Intermediate-Coupling Transition for a Simple Case

Since the concept of intermediate coupling is taken over directly from the theory of complex atomic spectra (C35), it may be well to introduce our discussion of it by giving a simple example in an atomic case. It is, of course, just one of a number of effects in which a set of secular equations contains a parameter expressing a competition between two types of perturbing energy, such as the Paschen-Back effect in which external and internal fields compete in trying to orient the angular momentum vectors.

Let us consider the intermediate-coupling transition of an atom having two electrons in the same p shell, outside of closed shells, the configuration p^2. In (LS) coupling one counts the states allowed by the Pauli exclusion principle by constructing a little table starting as in Table III, which when completed gives the numbers of states for each M_L, M_S shown at the right side of Table III, enough to account for the multiplets ^1D, ^3P, ^1S. In atoms, triplets lie below singlets as we have seen, and the separations are given (S29) by $^1S=5K$, $^1D=2K$, $^3P=0$. By calculating $\Sigma am_l m_s$ in line 2 one sees that the spin-orbit energy, Eq. (3), of the $^3P_2$ is $a/2$ [or $A=a/2$ in Eq. (16)] from which one has by the Landé interval rule or by the usual vector-coupling formulas (or by further lines of Table III) that for $^3P_1$ it is $-a/2$ and for $^3P_0$ it is $-a$. At the risk of being redundant, one may count the states also in (jj) coupling, as in Table IV. The spin-orbit energies E listed for the configurations are calculated from Eq. (3), being $a/2$ for $p_{\frac{3}{2}}$ and $-a$ for $p_{\frac{1}{2}}$. In both extremes one finds two states with $J=2$, two with $J=0$, and one with $J=1$, so the energies in intermediate coupling are solutions of two quadratic secular equations, and one straight line $E=-a/2$ for $J=1$. For $J=2$ the quadratic equation which has as asymptotic values the (LS) and (jj) coupling energies we have listed is

$$E^2-(2K+a/2)E+aK-a^2/2=0, \tag{17}$$

and for $J=0$ we likewise have

$$E^2-(5K-a)E-5aK-2a^2=0. \tag{18}$$

In Fig. 4 we have plotted E/K as a function of a/K to show the solutions of these equations (after dividing through by K^2). The asymptotes showing the linear variation near (LS) coupling are shown at the left side, where $a\ll K$, and (jj) coupling is approached at the right side, where $a\ll K$. There are four energy differences between the five levels, and only two parameters, so the system is overdetermined and a verification of the adequacy of the theory by comparison with experiment is possible. Three of the levels may be used to determine a and K, after which the expected position of the two remaining levels may be calculated. Such comparisons in atomic spectra work out fairly well, but there are often discrepancies of the order of 10 percent or more to be ascribed to second and higher-order perturbations involving states of excited configurations (known as "configuration interaction").

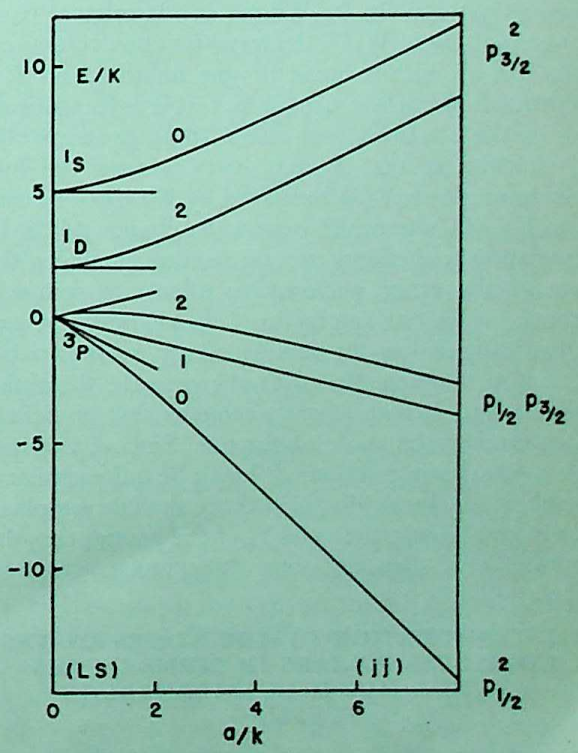


FIG. 4. The intermediate-coupling transition for the atomic configuration p^2.

CC-0. In Public Domain. Gurukul Kangri Collection, Haridwar

Digitized by Arya Samaj Foundation Chennai and eGangotri

Variation of the Parameters in Nuclei

It has recently been suggested that at least one important reason why the p-shell nuclei show no simple regularity of level spacing is the prevalence of intermediate coupling among such light nuclei (I52, H51). The fact that (jj) coupling seems to apply to the heavy nuclei does not necessarily imply that it should to the light nuclei, as the parameters a and K (or its more complicated equivalent) may vary, perhaps in a fairly regular manner, through the periodic table as suggested for a in Eq. (7). For K a similar variation may be estimated in the large-nucleus approximation by noting that K consists of summing the probability that an element of one "overlapping-density" function $\psi(r_1)\varphi(r_1)$ fall within the range of V of an element of another such function, which would make

$$K \sim R^{-3} \sim A^{-1}, \tag{19}$$

A here being atomic number again. Here we have again assumed that nuclear density is approximately constant from one nucleus to another, and this is shown to be valid even within the p shell, not only in the comparison of light with heavy nuclei, by the variation of Coulomb energies within the p shell, as discussed in Section 8. In the short-range approximation, Eq. (19), K thus varies more rapidly with atomic number than does the spin-orbit coupling parameter a in (7), which means that K might grow relative to a as one goes down from heavy nuclei, where $K \ll a$ as indicated by the success of (jj) coupling, to the lighter nuclei, and this would justify the existence of intermediate coupling in the latter. In the small-nucleus approximation (discussed so extensively by Wigner in his original paper on supermultiplets, Wi37) the wave-function volume elements are all within range of one another and K is independent of nuclear size (in fact, it is asymptotically zero), so that, in the actual case with range comparable with nuclear radius, K may vary among the light nuclei more slowly than indicated by Eq. (19). According to Eq. (7), one might expect the change ΔV in the average potential energy of a nucleon on coming within range of the other nucleons to affect its spin-orbit coupling, as well as the factor $A^{-\frac{1}{3}}$. ΔV does not vary as drastically as does the binding energy, so its variation may not have much effect, but of course the theoretical basis for Eq. (7) is sufficiently tenuous that no definite statement may be made about this. Since a variation of K a little less rapid than A^{-1} may be quite similar to that given to a by the factor $A^{-\frac{1}{3}}$, we shall for simplicity explore and discuss the validity of the assumption that the ratio a/K does not vary very much across the p shell.

7. INTERPRETATION OF THE STATES OF THE INDIVIDUAL POLYADS IN TERMS OF THE CENTRAL MODEL IN INTERMEDIATE COUPLING

In reference (I52) it was shown that the general spacing and sequence of the low levels of Py^{12}, which resembles (LS) coupling to the extent we have discussed above, and Py^{14}, which shows a closer resemblance to (jj) coupling, may both be understood in a rough sort of way as examples of intermediate coupling with approximately the same value of a/K, namely $a/K \approx 5$. The resemblance of one to one extreme and the other to the other extreme may be accounted for by refining the criterion for the validity of either extreme coupling. While (LS) coupling is valid when $K \gg a$, a less stringent criterion is this: the spacings of the first few states show some resemblance to (LS) coupling when the multiplet separations calculated in terms of K in (LS) coupling are large compared to a, for then A of Eq. (16) (or a in second order) does not have a chance to make states from the different multiplets come close to one another and thus disturb the general grouping. There could be some semblance to the general grouping into multiplets even if the spacing and order within a multiplet were disturbed, but in Py^{12} even this does not occur among the low states because the first three multiplets are singlets. The large spacing of these singlets is, as we have suggested, the result of the exceptional symmetry attainable in singlets in $A=4n$ nucleus, and this is what makes it look like (LS) coupling. In the polyad P^{14}, the order of states, with only slightly larger a/K, is the order given by (jj) coupling because in (LS) coupling K does not supply such large multiplet separations to compete so effectively with a.

Levels Arising from Excitation to a Higher Shell

One aspect of the energy spectra which was made clear by the examples just cited is the large extent of overlapping of the (jj) configurations (such as $p_{\frac{3}{2}}^{7}p_{\frac{1}{2}}$ with $p_{\frac{3}{2}}^{6}p_{\frac{1}{2}}^{2}$) on the one hand and of the (LS) multiplets on the other. Another aspect of the complexity is the overlapping of configurations, such as p^{10} with $p^{9}d$, for evidence of such inter-shell excitation was found in Py^{14} as low as about 4 Mev. This compares in order of magnitude with the evidence from the last two polyads of the p-shell, Py^{15} and Py^{16}, the high first excitation energy of which indicates, as we have seen above, that the inter-shell excitation there enters at about 5 or 6 Mev. It is apparent that the ground configuration spreads out over many Mev, and the configuration arising from inter-shell excitation is expected to do likewise, so we can expect no simple regularity in the excitation energy of the lowest state of the excited configuration, such as one might naively expect by postulating that the excitation energy of the lowest state obtained by exciting a p nucleon to the d shell is simply a definite amount of energy required to excite a p nucleon to the d shell, a single-nucleon or shell property that might carry over from one polyad to another in an oversimplified single-nucleon model.

A general survey of the data is enough to dissuade one from seeking any very simple regularities among the energy spectra of the light nuclei. What has been said of Py^{12} and Py^{14} suggests that at least the com-

CC-0. In Public Domain. Gurukul Kangri Collection, Haridwar

Digitized by Arya Samaj Foundation Chennai and eGangotri

plexity of intermediate coupling will have to be taken into account. Most polyads contain in their ground configurations so many p nucleons that it is not practicable to solve secular equations and draw exact curves giving the manner in which the energies of the various states should vary with the ratio a/K in intermediate coupling, in the basis of any definite interaction assumption. Our knowledge of the interactions is so meager that this is just as well. As was done (I52) for Py[12], it is perhaps sufficient to use a rather rough characterization of the specific nuclear interaction, Eq. (2), and spin-orbit coupling, Eq. (3), and then to treat the intermediate-coupling variation in a suitably rough manner by drawing smooth curves between the asymptotes which represent what is known in the relatively simple (LS) and (jj) extremes. We cannot of course hope to reproduce experimental data thus in any fine detail, but merely to understand general features, such as roughly the spacing of levels in different energy regions and perhaps their order, where identifications to distinguish the states from one another have been made. Future identifications will provide verifications or discrepancies, on the basis of which refinements in the interaction assumptions or general procedure may become justified.

We proceed now to discuss the individual polyads in that exploratory spirit. We discuss them in order of increasing mass as is customary for a review article, in spite of the fact that the first cases thus encountered are the most flagrant exceptions to the success of the intermediate coupling procedure, and will require a separate discussion later on.

He^5+Li^5

In this case both of the known low states, are not only virtual, being unstable with respect to single-nucleon emission, but are presumably very well described as single-particle states with all the excitation energy contained in a single nucleon, because of the exceptionally great stability of the alpha-particle which constitutes the s-shell core. We may say that one nucleon always has enough energy to escape, and under these circumstances we have no good approximation to a stationary state of the system, so that differences between different descriptions of what we mean by a "state" become especially severe. There seems to be general agreement that the low state is a $^2p_{\frac{3}{2}}$ and that the state several Mev above it may be interpreted, so far as it seems to exist, as a $^2p_{\frac{1}{2}}$, thus providing the fundamental instance of nuclear spin-orbit coupling, with the sign as anticipated (I36, B37) from the comparison with Li^7, a in Eq. (3) being negative. But the reaction and scattering methods of observation do not seem to agree very well at present on the doublet splitting: the broad peaks observed (Le51a, Ti51) in the reactions $T(T, n)He^5$ and $Li^6(\gamma, n)Li^5(p)He^4$ seem to indicate a doublet splitting of 2.5 or 2.6 Mev. Analysis (Hu52) of the $n+He^4$ scattering data shows the $P_{\frac{3}{2}}$ phase shift passing steeply up through 90° at 1.04 Mev (c.m.) and continuing to rise at higher energies, while the $P_{\frac{1}{2}}$ phase shift rises gently through 90° at 2.8 Mev, the ^2P splitting being thus only 1.76 Mev by this criterion. (See also A51, A52.) It may be that this $P_{\frac{3}{2}}$ shift in He^5 comes down again through 90° at a somewhat higher energy and that the broad reaction peak represents an average over this region of phase shift near 90°, or the discrepancy between the apparent 1.76 and 2.6 Mev doublet splittings may be an indication of the indefiniteness of the concept of a short-lived state in He^5 which would be even worse in Li^5. In Li^5 a $P_{\frac{3}{2}}$ phase shift is observed (Kre52, C49) of only about 35° at about 4.65 Mev contrasting with 115° at 3.4 Mev, which is about the equivalent energy, in He^5. It is enigmatic that the resonance peaks can be so similar (Le51, Ti51) in He^5 and Li^5 and the $P_{\frac{3}{2}}$ phase shifts apparently so different.

The methods of estimating a spin-orbit coupling parameter in terms of an assumption about ΔV, as in Eqs. (5) and (7), are not the same as in stable nuclei, and a special treatment is needed. There is, thus, no expectation of any semblance of continuity of a as it varies from He^5 to Li^6, even on the basis of this simple assumption.

With only one nucleon beyond the tightly closed s shell, intermediate coupling is, of course, meaningless. There seems to be no evidence of p-to-d shell excitation, even the states of the ground configuration being so broad as to be difficult to recognize. The single known state near 17 Mev probably arises from s-to-p excitation of the alpha-core, and should be one of several. Here the excitation energy is divided between nucleons, so the nucleus does not seem ready to come apart quite so quickly and the state is not so broad.

He^6+Li^6

Here the ground configuration, p^2, is simple enough and its states few enough that the secular equations can be written out explicitly and solved, with nothing more complicated than a cubic. The secular problem is only a slight extension of the atomic p^2 problem presented above in Eqs. (17) and (18). With two p nucleons rather than two p electrons we have the added coordinate of isobaric spin, which is handled very much as for the configuration $1s2s$ in Table I and Eqs. (9) above. Instead of the two-dimensional table at the right side of Table III, with M_L and M_S as its two dimensions, one has a three-dimensional assemblage of blocks, with M_T as the new dimension, consisting of the figure at the right side of Table III as one layer, for $M_T=1$, since the problem for two neutrons is the same as for two electrons, and another layer for $M_T=0$. With $M_T=0$ one obtains all integral vector sums that are possible with the vectors l_1, l_2, s_1 and s_2, not only the ^1S, ^3P, and ^1D which were obtained for $M_T=1$, and

CC-0. In Public Domain. Gurukul Kangri Collection, Haridwar

Digitized by Arya Samaj Foundation Chennai and eGangotri

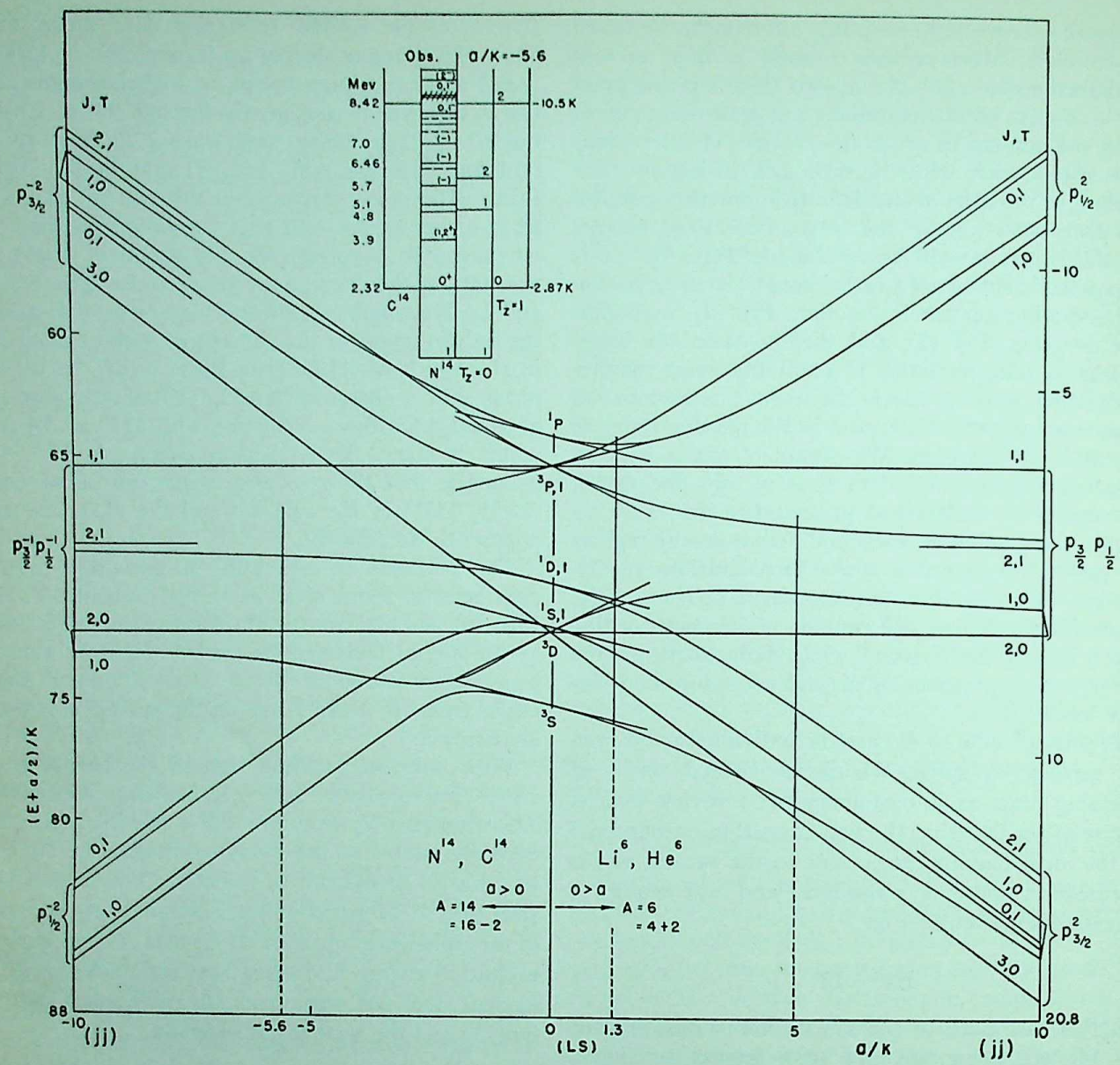


FIG. 5. Intermediate-coupling transition for the nuclear configuration p^2 and p^{-2} applying to the polyads Py^6 and Py^{14}.

thus have $T=1$, but also ^3S, ^1P, and ^3D which exist only for $M_T=0$, and thus have $T=0$. Among these latter multiplets we find three states with $J=1$, and thus have a cubic secular equation for their energies, besides two more linear equations. With the specialization of the specific nuclear interaction expressed by Eqs. (2) and (8c), the equations are to be found written explicitly in reference (I52), and the solutions of interest in Py^6 are portrayed in the right half of Fig. 5. The left half of Fig. 5 is intended for the discussion found below of Py^{14}, and is entered on the same graph because of the simple relationship between the states of two nucleons and the states of two "holes" in the p shell: the inversion of the spin-orbit coupling for holes means that the states in the configuration p^{-2} arise from the same secular equations as those of p^2, but with the opposite sign of the parameter a, so the energies for the two cases join continuously at $a=0$.

We see that all the states with $T=1$ on the right half of Fig. 5 correspond closely with those that are obtained by inverting Fig. 4, top for bottom. Figure 4 applies to two electrons, for which K is positive because of the repulsive interaction and a is positive because of the predominance of the magnetic term over the Thomas term (I36), and for a nuclear system with $T=1$, such as two neutrons or two protons, it applies with the ordinate inverted because of the change of sign of K for attractive forces, but with the abscissa unchanged because a too is here negative so a/K is the same as for electrons. The slope of the lines has been altered in Fig. 5, relative to Fig. 4, for the sake of symmetry and compactness of the figure, by plotting $(E+a/2)/K$ in place of E/K. The multiplet separations are taken from the paper of Feenberg and Phillips (F37a); the ratio between them for the $T=1$ multiplets is of course different from the ratio in the electron

CC-0. In Public Domain. Gurukul Kangri Collection, Haridwar

Digitized by Arya Samaj Foundation Chennai and eGangotri

case because of the different shape of the interaction function $V(r_{12})$, but after inversion the order of the multiplets is the same.

With the $T=0$ levels also on the figure, one sees that the ground (jj) configuration contains the four states that may be made by compounding two $j=\frac{3}{2}$ vectors, and that in the extreme (jj) coupling represented by the asymptotes they come in the order $(J, T)=(3, 0)$, $(0, 1)$, $(1, 0)$, and $(2, 1)$, a result derived also by a very different method, along with similar results for the other p-shell polyads, by Kurath (K52). Even with the approximation to (jj) coupling represented by the right side of the figure, where there is still a distinct division of the levels into groups according to their (jj) configurations, there has been a cross-over within the ground (jj) configuration making the lowest $T=1$ state the third excited state. This is indeed true experimentally (in contrast to the situation in Py^{14}), but still another cross-over is required, for the ground state is known to have $J=1$, whereas according to this theory $J=3$ is lowest near (jj) coupling and well into the region of intermediate coupling, down to $a/K\approx 4$. To match the observed spectrum with this scheme one has, therefore, to go down to rather low values of a/K, much lower than for the heavier polyads discussed below. Determining the parameters a and K requires using the two intervals between three levels, and the three lowest levels are used to determine the values $a/K=1.3$, $K=-1.23$ Mev, $a=-1.6$ Mev. The comparison between theory and experiment implied by these values is shown in Fig. 6(a). Unfortunately, the spectrum of Li^6 has not been explored much beyond the third level at 3.58 Mev, so there is only one further datum with which comparison may be made, the second $T=1$ level which experimentally is at about 5.3 Mev, theoretically at -4.9 $K=6$ Mev. The search for a couple of other low states in Li^6 arising from the ^3D will provide a crucial test of this straightforward but perhaps oversimplified interpretation.

Because smaller values of K and larger values of a seem to prevail in the somewhat heavier polyads, an attempt is made in Fig. 5 to see what can be done in the way of interpretation of the Py^6 spectrum in the neighborhood of $a/K\approx 5$, but here, of course, some other mechanism must be called upon in a rather *ad hoc* manner to explain the depression of the $J=1$ state below the $J=3$ state. This $J=1$ state is the only state that has a plausible stable counterpart in the alpha-model (alpha plus deuteron), so one might be tempted to ascribe the formation of this as the ground state to a variation theory in which some alpha-model wave function is mixed with a central-model wave function. The possible influence of the alpha-model in several polyads is discussed separately below. It may not be necessary to go to such arbitrary complexity because this rather special behavior of Py^6 (and perhaps a similar one in Py^7) may arise from their special place in the tensor-interaction theory of spin-orbit coupling of Feingold and Wigner (F52).

Li^7+Be^7

In this polyad, Py^7, the ground configuration is p^3, and the low states in (LS) coupling are provided by the multiplets ^2P, ^2F, ^4P, etc., as shown on the left side of Fig. 7(a), the separations again being taken from reference (F37), specialized for the interaction, Eq. (2), with (6). The multiplet splittings arising from spin-orbit coupling may, in this case, be calculated by the relatively simple method of trace invariance, without calculation of specific wave functions for the multiplet states, with the one exception that only the sum of the energies for the two doublets ^2P with $T=\frac{1}{2}$ are thereby given. The doublet splitting energy for one of these doublets, the one which includes the ground state, has been worked out in detail by Breit and Stehn (B38), so no further (LS) wave functions need be constructed. The calculation by trace invariance is outlined in Appendix 1. The result is that $A=a/3$ for each multiplet having $T=\frac{1}{2}$, and $A=0$ for the two doublets having $T=3/2$. This result is used to give the slopes of the (LS) asymptotes on the left side of Fig. 7(a).

In (jj) coupling the ground "(jj) configuration" is $p_{\frac{3}{2}}^3$, and the separation between the states of this (jj) configuration have been calculated by Kurath (K52). The next (jj) configuration is $p_{\frac{3}{2}}^2 p_{\frac{1}{2}}$, and because it lies above the region of present experimental interest, no great care has been used in plotting its (jj) asymptotes. [They are most of them drawn in broken lines because the energies expressible in K have not been used in plotting them, though these too have very recently been calculated (K52a).] The single-nucleon spin-orbit energies $a/2$ for $p_{\frac{3}{2}}$ and $-a$ for $p_{\frac{1}{2}}$ in this case give the total spin-orbit energy $3a/2$ for the ground (jj) configuration $p_{\frac{3}{2}}^2$ and zero for the next, $p_{\frac{3}{2}}^2 p_{\frac{1}{2}}$. Correspondingly, one set of (jj) asymptotes for E/K slopes sharply downward to the right (a being negative, as is K) in

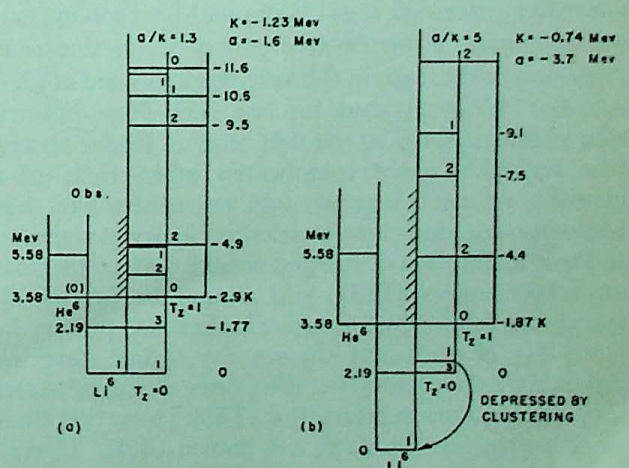


FIG. 6. Alternative interpretations of the energy levels of Py^6. (The energy 5.58 Mev is reduced to 5.3 Mev in the newer data as shown in Fig. 1.)

CC-0. In Public Domain. Gurukul Kangri Collection, Haridwar

Digitized by Arya Samaj Foundation Chennai and eGangotri

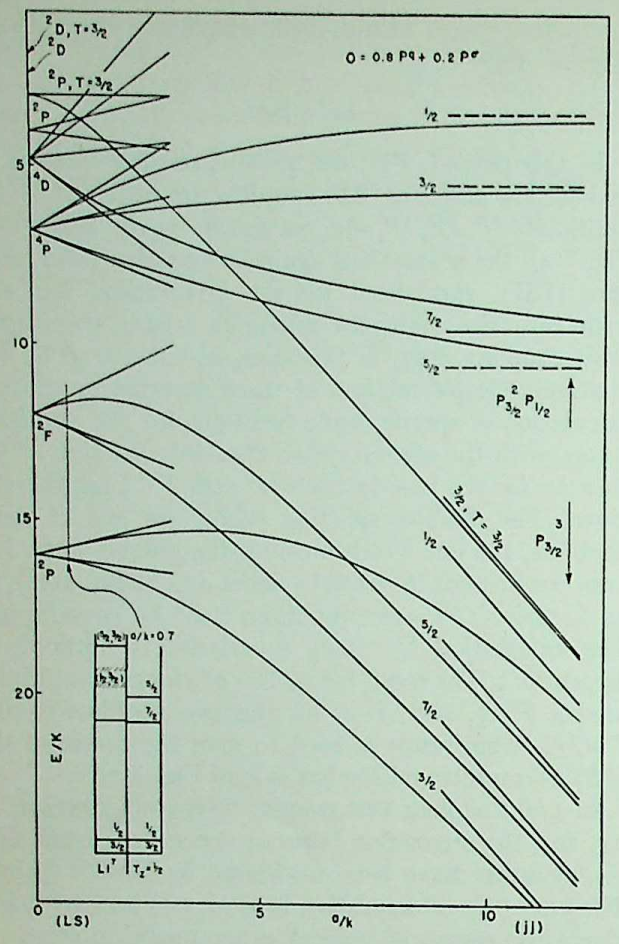


FIG. 7(a). Intermediate-coupling transition for the configuration p^3 applying to Py^7, with the interaction assumption (2). The insert shows that, even if one goes near (LS) coupling, it is not possible to obtain agreement between the ^2P and ^2F splittings.

Fig. 7(a), and the higher set is horizontal. Of the excited (jj) configuration, only a few of the lower states are shown in the figure.

An early discussion of intermediate coupling in nuclei (H51) was concerned with this configuration p^3. It was shown there that neither with a non-exchange (Wigner) nor with a space-exchange (Majorana) interaction alone can one obtain a low isolated pair of states similar to those observed except in the near neighborhood of (LS) coupling. With this true for two such very different simple interactions, it was felt that it would remain true for other more complicated interactions of a plausible nature. [Because only two states had then been observed, and there was contradictory evidence as to the identification of the first excited state, which has since been shown (Ph51, C52, Bu52) to have $J=\frac{1}{2}$, special emphasis which is now obsolete was put on the possibility of explaining the scarcity of low states by exploiting a degeneracy between three of the $p_{\frac{1}{2}}^3$ states with a non-exchange interaction (T52).] Now that three much higher excited states are known (Aj52, Tho52), it is of interest to explore this point in a little more detail. The interpolated intermediate-coupling pattern shown in Fig. 7(a) is that for the simple interaction, Eq. (2), which forms a basis for our discussion of other polyads. For the sake of indicating the sort of change that may be expected from a change in the interaction assumption, a similar intermediate-coupling scheme is shown in Fig. 7(b) for the somewhat different and perhaps more elegant interaction, Eq. (1), which also obeys the saturation requirements. It is seen that the main difference is that with Eq. (1) in place of Eq. (2) the first $T=\frac{3}{2}$ state is brought below the $J=\frac{1}{2}$ state in the ground (jj) configuration. The general pattern for the first four states in the intermediate-coupling region is altered very little. For this reason it seems satisfactory to proceed with the following rather preliminary discussion of other polyads on the basis of the interaction, Eq. (2), alone, for the sake of simplicity, realizing that it may ultimately be possible to improve the fit with experiment by introducing another interaction, and perhaps even to provide a selection of the most nearly adequate interaction law in this manner.

The attempt at an (LS) coupling interpretation is shown in the insert in Fig. 7(a). For the first three states one finds a match between theory and experiment with $a/K\approx 0.7$ but finds the ^2F much too narrow to account for the separation between the two sharp states at 4.6 and 7.5 Mev. The ratio of this separation to the low doublet splitting is 2.9 Mev/0.48 Mev$=6.0$. The ^2F splitting in the (LS) limit is only 7/3 times as great as the ^2P splitting, since $A=a/3$ for each in the doublet splitting formula $\Delta E=(L+\frac{1}{2})A$, and the curvatures away from the (LS) limit increase this discrepancy. Since the wave functions are relatively simple so near (LS) coupling, this discrepancy is based mainly on the assumption of the form of spin-orbit coupling, Eq. (3). It would be interesting to know whether the Feingold-Wigner treatment (F50) of the tensor interaction, even though a bit vague on the magnitude of the ^2P splitting itself, could give the ratio of the ^2F to ^2P splitting with sufficient accuracy for a significant comparison with these data.

Quite aside from the discrepancy based on Eq. (3), so small a value of a/K (which incidentally implies $a=-0.85$ Mev, $K=-1.2$ Mev) when compared with the much larger values found in the heavier polyads of the p-shell, seems incompatible with any simple assumption leading to Eq. (3). One might naively think that it is also incompatible when compared with the larger value of the doublet splitting in Py^5, which seems to be 2.6 Mev or more, since this might lead one to expect in Py^7 a ^2P splitting of 2.6 Mev/3$=$0.9 Mev or more, rather than about 0.48 Mev. The naiveté here lies in forgetting that the states of Py^5 are virtual so that their separation must be treated in a rather special way, as is being investigated by H. Hummel.

While the possible role of the alpha-model is to be discussed separately at greater length below, it may be pointed out here that the discrepancy does not necessarily throw one into a dependence upon the particular type of complexity of the second-order effects of the

CC-0. In Public Domain. Gurukul Kangri Collection, Haridwar

Digitized by Arya Samaj Foundation Chennai and eGangotri

tensor interaction. The type of alpha-model complexity discussed for Py^6 in connection with Fig. 6(b) may be operative here also. In this case one might identify the 4.6 and 7.5 Mev levels with 7/2 and 5/2 levels in intermediate coupling, perhaps in the neighborhood of $a/K \approx 4$ or 5, which would leave the 3/2 and 1/2 levels far apart and not much below these in the central model, but we might assume that they are physically much modified and depressed by a transition most of the way to the alpha-model, that is, by a strong admixture of alpha-model wave functions. The small separation of the two levels arising from the ^2P would then be a characteristic of the alpha-model, in which they are called in molecular terminology $^2\Sigma_u$ states ("doublet sigma ungerade"). The smallness of their splitting in first order presumably has something to do with the slow rotation of the "molecular framework" because the orbital angular momentum is divided between seven nucleons (I39, R48). In second order it is described in molecular discussions as "rho-type doubling" which is concerned with an interplay between conventional spin-orbit coupling as in Eq. (3) and the coriolis effects of the rotation in second-order perturbation theory. It has some reason to be small, although the separation of the rotational and other parts of the problem is not nearly as well justified in nuclei as in molecules where the electron mass is really very small compared to the mass factor in the moment of inertia.

The other attractive aspect of the possible participation of the alpha-model in Py^7 is the existence of a broad state at 6.4 Mev, identified as either $\frac{1}{2}^+$ or $\frac{3}{2}^+$, for the alpha-model has just one further low state besides the $^2\Sigma_u$ doublet, before going to higher rotational states which are apt to be too short-lived to be recognized, and that is one known as a $^2\Sigma_g$ in which the missing nucleon from two alphas is represented by a "hole" wave function which is even in the interchange of direction along the figure axis, rather than odd as in the $^2\Sigma_u$, and this lone excited state would indeed be a broad $\frac{1}{2}^+$ state. A state from the central model with this angular momentum and symmetry is found only among higher configurations such as p^2d, so would probably be intermixed only very weakly with this alpha-model state.

The difference between the doublet splitting 0.48 Mev in Li^7 and 0.43 Mev in Be^7 has been discussed about equally successfully in the central model with (LS) coupling (I51), in which case the classical magnetic term appears to play a somewhat larger role than the difference in size of the two nuclei, and in the alpha-model (F51). This discussion of the alpha-model is so general that it avoids any detailed specification of the source of the coupling and the difference in size of the nuclei arising from the Coulomb repulsion provides the entire spin-orbit coupling difference.

Li^7 is a nucleus that has attracted an extraordinary amount of interest, partly because it is, with its mirror Be^7, the lightest and thus, in one sense perhaps, the simplest stable nucleus in which the ground state in (LS) coupling is complicated enough to involve the problem of coupling an orbital moment L to a spin S. Its properties have therefore been scrutinized relatively carefully, and there have been among others some rather unfruitful excursions into speculation. One of these (I50a) arose from the fact that the $B^{10}(n, \alpha)Li^7$ reaction with thermal neutrons goes to the 480 kev state about 17 times as strongly as to the ground state. Since B^{10} has a large J-value, $J=3$, this anomalous ratio could be explained by the false assumption that the 480 kev state also has a large J, but it appears instead to arise from a not very unlikely, fortuitous cancellation in a matrix element, since this state has more recently been shown to have $J=\frac{1}{2}$. Another excursion arose from an "experimental determination" of the quadrupole moment Q of Li^7 which recently turns out to have been false even as to sign. All the simple models give a negative theoretical Q for Li^7, essentially because an orbit flattened in a plane normal to its angular momentum implies negative Q, and this sign persists in the various coupling schemes of nucleons here encountered. Attempts to find a theory (Av50, P50) that would be compatible with a positive Q serve now only to illustrate the "stability" and hence the reliability

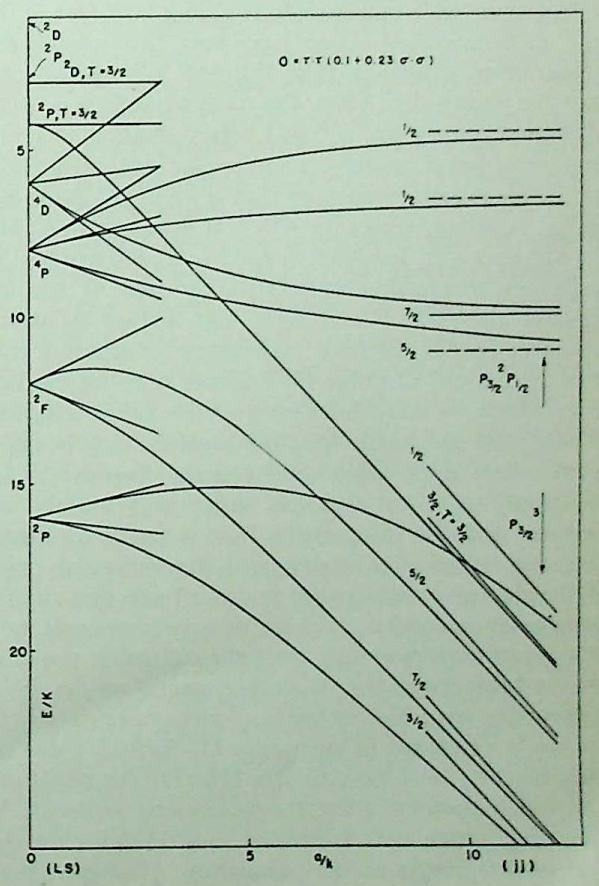


FIG. 7(b). Intermediate-coupling transition for the configuration p^3, with interaction assumption (1).

CC-0. In Public Domain. Gurukul Kangri Collection, Haridwar

Digitized by Arya Samaj Foundation Chennai and eGangotri

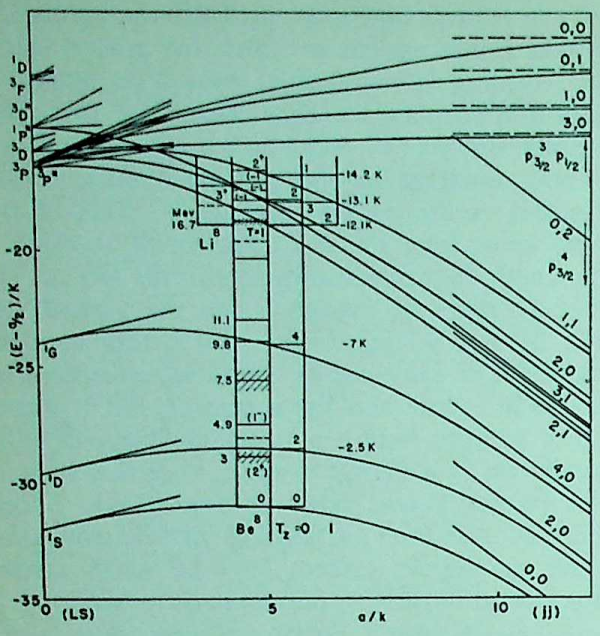


FIG. 8. Intermediate-coupling transition for the configuration p^4 applying to Py^8. In the notation for the multiplets of (LS) coupling, the asterisk (*) is used to denote $T=1$.

of some theoretical results based on models, for one had to go to great lengths of artifice to obtain a positive Q.

The weak link in the first "experimental determination" of Q of Li^7 was the molecular-theory calculation of the molecular quadrupole coupling constant q, for only qQ is measured. There have been two independent recent demonstrations that the first calculation of q gave the wrong sign. First, the measurement in Kusch's laboratory of qQ for Li^7 and other alkali nuclei in a number of polar as well as homopolar molecules (Lo52 and Table X below) showed that qQ had the same sign for Li^7 in all molecules for which it was measured, and the opposite sign for Na^{23} in each of a series of similar molecules, suggesting very strongly that Q has the opposite sign for Li^7 and Na^{23}, and further an atomic measurement in Bitter's laboratory (communication from P. Kusch) of Q for Na^{23} shows it to be positive, from which we may infer that Q for Li^7 is negative. (The sign of the atomic coupling constant may be calculated much more easily and reliably because it has contributions from electrons only, and mainly one electron, with no competition from a positive charge.) It is also possible to understand the molecular origin of the sign of q more easily in polar molecules than in homopolar molecules, because of a predominant term at a given nucleus arising from the charge on the other ion, and this shows that the experimental results are all compatible with each other and with a negative Q for Li^7, as is explained in Appendix II. Second, there has very recently become available (Har52) the result of a new calculation of q for the homopolar molecule Li_2 involving better wave functions, and this time the sign is altered from the earlier calculation, q being negative as a result of a more accurate representation of the lumping of the electron charge in the region between the nuclei because of the antisymmetry, as is discussed further in Appendix II. Thus Q_{Li^7} is now found to be negative, in agreement with the oblate charge distribution expected from the models.

Be^8+Li^8

A similar treatment of Py^8 is displayed in Fig. 8. The interaction, Eq. (2), is assumed, and the multiplet splittings are taken arbitrarily to be given by $A=a/5$. This represents interpolation between $A=a/3$ for Py^7 and $A=0$ for Py^{10}, at the middle of the p-shell where a "hole" is the same as a nucleon and the spin-orbit coupling constant A must according to the results of "hole theory" be the negative of itself, that is, zero. *Note added in proof.*—Recent calculation (C53) shows that the values of A/a should be 3/8, 3/8, and 1/12 for the $^3P^*$, ^3P, and ^3D in Fig. 8, respectively, rather than 1/5. The order of the first four levels is the same in (LS) coupling as in (jj) coupling, and remains the same in intermediate coupling. There is thus a great deal of latitude in the choice of the parameter a/K to obtain a rough comparison with the experimental spectrum, and the value $a/K=5$ has been chosen for this purpose, largely because about this value will be found to apply elsewhere, in the region Py^{10} to Py^{16}. In Py^8, a small value $a/K\approx 2$ could not be used because the density of states just beyond the first state with $T=1$ would be much greater than observed. Since Py^8 is thus not very near (LS) coupling, it is not very plausible to attribute the isolation of the low doublet in Li^7 to (LS) coupling in that adjacent nucleus.

At $a/K=5$ the energy scale has been chosen to fit the first $T=1$ state, $(J, T)=(2, 1)$, as indicated by the position of the ground state of Li^8, and we see in the overlaid insert in Fig. 8 that the broad states at 3 and 7.5 Mev lie considerably below the (2, 0) and (4, 0) theoretical levels. The 3-Mev state has been tentatively identified experimentally (T50, T51; see, however, W41) as (2, 0), and the fact that it is broad makes this assignment very likely because this is also the first excited state of the alpha-model, analogous to a molecular rotation state with Bose statistics of the constituent alphas. Such a state of the alpha-model is above the Coulomb-plus-centrifugal barrier (see Section 10), so it would be expected to be extremely short-lived and probably too broad to be recognized as a level at all. It is reasonable to assume that the 3-Mev level is a mixture of central-model wave functions, as given by the (2, 0) curve of Fig. 8, and alpha-model wave functions, the latter component accounting for the level width. The next rotational state of the alpha-model is a (4, 0) state, and it is reasonable to assume that the state corresponding to the (4, 0) curve in Fig. 8 is depressed and broadened by a similar admixture, giving rise to the 7.5-Mev state.

The prediction (of (LS), (jj), or intermediate coupling) is that the ground state of Li^8 is (2, 1), which is in

CC-0. In Public Domain. Gurukul Kangri Collection, Haridwar

Digitized by Arya Samaj Foundation Chennai and eGangotri

keeping with the fact that the beta-transition goes to the 3-Mev state of Be^8, but not to the ground state (or 7.5-Mev state). A further prediction of (jj) or intermediate coupling is that the first excited state of Li^8 is (3, 1), which corresponds to the identification 3^+ of a state at about 19 Mev in Py^8. There is a possibility that this is the second excited state of Li^8. The possible intervening state is shown by a broken line, and, if it exists, is high enough that it might have odd parity, arising from an excited configuration not shown on this graph. The experimental (3, 1) state lies above the theoretical, and this discrepancy would be more pronounced for larger values of a/K, nearer (jj) coupling. This is not to be considered a serious discrepancy, however, because this is the sort of separation which, in (jj) coupling for instance, is very sensitive to the choice of exchange operators, as we have seen in the comparison of Figs. 7(a) and 7(b). Thus it cannot be excluded that a/K is considerably larger than 5 in Py^8.

The existence of a state at 4.9 Mev (and perhaps one at 4.05 Mev) is rather surprising in this interpretation, because it does not correspond to any central-model state of the configuration p^4, and if it were purely a state of the alpha-model, in addition to those already mentioned, such as the vibration state discussed in Section 10 below (see Table V), it would be expected to be extremely broad (and probably for this reason unobservable). It lies at about the excitation energy at which the first state arising from the (jj) model excitation $p_{\frac{3}{2}} \rightarrow d_{5/2}$ appears in the nuclei C^{13} to O^{16}, but in Be^8 the corresponding excitation $p_{\frac{3}{2}} \rightarrow d_{5/2}$ would be expected to involve an excitation energy higher by something like the single-nucleon p-doublet splitting $-3a/2$. By tentatively taking $a/K=5$ we imply that $K=-1.38$ Mev, $a=-6.9$ Mev, $-3a/2=10.4$ Mev, so on an oversimplified single-nucleon picture we might expect the first level from the excited configuration $p_{\frac{3}{2}}{}^3 d_{5/2}$ to appear about 10 Mev higher than it seems to. However, there are also involved very great energies of interaction of the nucleons, of the sort indicated by the fact that the spread within the (jj) configuration $p_{\frac{3}{2}}{}^4$, after passing into intermediate coupling, is about 20 Mev, or even more if we include the (0, 2) state of higher isobaric spin, so that such predictions neglecting the variations in these interactions from one configuration to another cannot perhaps be expected to be accurate to much better than 10 Mev. It thus seems not entirely unreasonable to attribute the level at 4.9 Mev, and others such as those at 9.8 and 11.1 Mev, to the odd-parity configuration $p_{\frac{3}{2}}{}^3 d_{5/2}$. The 4.9-Mev state does indeed appear§ (Th51) to be odd, (1^-), and an experimental determination of the parities of the others will also be of interest.

§ The (n, γ) angular correlation following a (d, n) reaction (in the plane normal to the deuteron beam) is about of the form $(1-\frac{1}{2}\cos^2\theta)$, with rather poor statistics.

A similar situation is found in B^{10}, where the first odd state occurs at about 5 Mev.

The states of two alphas have J even, even parity, and $T=0$, and such states in Py^8 may be expected in general to be broad because of the rapidity of a possible break-up into alphas, others sharp even above the high thresholds for neutron and proton emission because the excitation energy is in this interpretation divided between many particles, and no admixture of alpha-model states is possible. The fact that there are, as far as known, just two broad excited states in the region below 15 Mev to correspond to the two theoretical excited states of the ground configuration, (2, 0) and (4, 0), is thus very satisfactory. The most recent compilation (Aj52) shows a third at 10 Mev, but it is not apparent that it is reliably established as a broad level.

The ground state of Li^8 is estimated to lie at 16.7 Mev in Py^8, and very recent evidence (T53, see also Ra52) of the preferential formation of the broad 16.9-Mev state of Be^8 resulting from conservation of T in the high-energy photodisintegration of C^{12} indicates that this lone nearby $T_z=0$ state is indeed the lowest one with $T=1$. This match in energy is an example of the importance of isobaric spin T as a fairly good quantum number as discussed in Section 4, above. The selection of the high state in competition with the lower states shows that it (or, at least, the more general charge symmetry) provides a significant selection rule, but the breadth of the state (presumably 2^+) caused by break-up into two alphas (competing only with gammas) indicates that the conservation is not perfect.

Note added in proof.—Very recent observations of the reaction $B^{10}(\gamma, d)Be^{8*}(2\alpha)$ and $B^{11}(\gamma, t)Be^{8*}(2\alpha)$ in photographic emulsions in Zuerich (S53) have shown that the Be^8 level previously observed only as a broad level at about 3 Mev may be resolved into three levels at 2.2 Mev, 2.9 Mev, and 3.4 Mev, and that these and the 4.0-Mev, 4.9-Mev, 6.9-(our 7.5) Mev, 9-(our 10) Mev, and 14.7-Mev levels have even J and even parity. (The statistics leave the resolution of the 3.4-Mev level quite doubtful.) The 2.2-Mev level has also been observed with doubtful statistics in the $Li^7(d, n)$ reaction (Tru52). A recent magnetic analysis (G53) of the reaction $Be^9(d, t)Be^8$ shows the 2.9-Mev level as broad [definitely broader than the central peak in (S53)], with a sharp peak attributed to an impurity that might hide the 3.4-Mev level, but the complete lack of a peak corresponding to the 2.2-Mev level may suggest that this state, if it exists, has too high J to be observed at the low energies involved, $E_d=1$ Mev, $E_t=2.2$ Mev. Some apparent confirmation of the suggestion that the alpha-model plays an important role in the Li and Be nuclei is found in the rather surprising fit (S53) of all but two of these levels to the alpha-model vibration-rotation scheme

$$E_{j,k}=(0.36J(J+1)+2.8K) \text{ Mev},$$

CC-0. In Public Domain. Gurukul Kangri Collection, Haridwar

Digitized by Arya Samaj Foundation Chennai and eGangotri

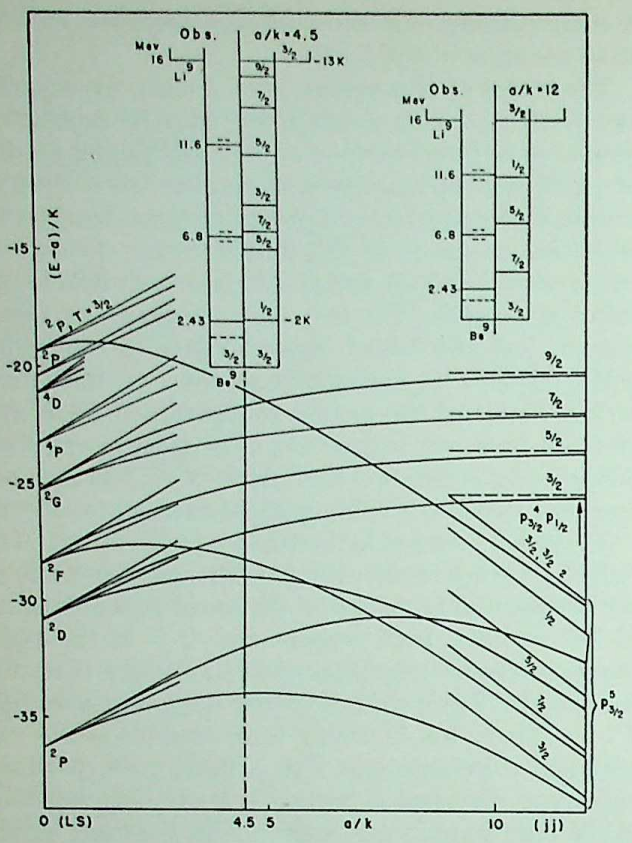


FIG. 9. Intermediate-coupling transition for the configuration p^5 applying to Py^9. The isobaric spin is $T=\frac{1}{2}$ except where indicated as $T=\frac{3}{2}$.

as in "Alpha-Model I":

Experimental energy	Alpha-Model I			Alpha-Model II		
Mev	Mev	J	K	Mev	J	K
14.7	14.7	6	0			
11.1 (odd?)						
9.7 (10)	9.8	4	1			
6.9 (7.5)	7.0	4	0	7.0	4	0
4.9	4.9	2	1	4.8	2	4
4.0				4.1	2	3
3.4				3.4	2	2
2.9	2.8	0	1	2.7	2	1
2.1	2.1	2	0	2.1	2	0
0	0	0	0	0	0	0

This scheme leaves the interpretation of the first excited state and the 7.5-Mev level about as above but with more complete participation of the alpha-model, and adds 14.7 Mev to the sequence. There are two unexplained states in the scheme "Alpha-Model I" and three in the central model with these new data. In the central model their even parity means that they would have to belong to doubly-excited configurations, analogous to the first excited state of O^{16} but involving greater spin-orbit energy. In the alpha-model, the presence of the lowest $T=1$ state at 17 Mev requires some explaining, for which the existence of the suspected excited state of the alpha at about 22 Mev would be helpful. The evidence for the latter is, however, conflicting and its existence is on the whole very doubtful (Ar50, Al51, Be51). In Section 10, there is a discussion of "The Low Barrier in the Alpha-Model of Be^8," in which it is estimated that the barrier for $J=0$ is less than about 0.9 Mev, on the assumption that the interaction between alphas provided by the specific nuclear forces is a simple well, attractive at large distances with a repulsive core. "Alpha-Model I" requires that these forces themselves provide a barrier at least about 2 Mev high, a nuclear repulsion between alphas beyond the attractive region. The large number and fairly regular spacing of the states from 2.1 to 4.9 Mev suggests the interpretation "Alpha-Model II," with a very small curvature at the bottom of the potential well and no need for a high barrier, but the lack of states $(J, K)=(0, 1)$, $(0, 2)$, $(4, 1)$, etc., is unexplained. There is still another possibility, involving $K=2$ and requiring a very high barrier, which accounts roughly for all but the doubtful 3.4-Mev level. Experimental assignments for the new states are needed to clarify the puzzle.

Li^9+Be^9

On the (jj)-coupling side of Py^9 we have first the configuration $p_{\frac{3}{2}}^5$, which is the same as $p_{\frac{3}{2}}^{-3}$ or three $p_{\frac{3}{2}}$ holes, and the order and separation of the states of this configuration are the same as in the low (jj) configuration $p_{\frac{3}{2}}^3$ of Py^7, as given by Kurath (K52). On the (LS) side there is no such similarity, since we are not yet quite halfway across the entire p shell, and the low ^2p is here followed by a ^2D before the ^2F. Because this is just one nucleon short of the middle of the shell (where multiplet splittings vanish), the multiplet splittings are expected to be very small, and we arbitrarily assume $A=a/10$ for all multiplets, and thus plot the (LS) asymptotes as very narrow doublets and quartets. The intermediate coupling transition is again drawn entirely by interpolation, Fig. 9, with smooth curves that approach the asymptotes in a reasonable fashion.

The observations on Be^9 are more incomplete than on most of the other light nuclei (it is much used as a target because of its availability in thin foils but infrequently attained as a final nucleus!). It is usually considered to have three low states, below 2.5 Mev, and no further states have been found (V51) in careful exploration up to 5 Mev with $B^{11}(d, \alpha)Be^9$. Beyond this, inelastic scattering of protons observed by NaI pulse-height analysis (Br51) shows broad maxima in a curve that does not dip down near zero between them, and indicates prominent excited states in Be^9 at 6.8 and 11.6 Mev, or groups of states clustering about these energies.

Of the states below 5 Mev, only two have been observed directly in the $B^{11}(d, \alpha)$ and $Be^9(p, p')$ data. The third, though absent in these investigations, is inferred from an analysis (Gu49) of the photo-excitation of Be^9 on the basis of a very crude model. The same analysis also infers that the 2.42-Mev level is a superposition of two states, an unresolved ^2D, though it appears experimentally to be very sharp. The model

CC-0. In Public Domain. Gurukul Kangri Collection, Haridwar

Digitized by Arya Samaj Foundation Chennai and eGangotri

used for Be^9 is a core of two alphas with a single neutron circulating in their field, and is subsequently treated for mathematical convenience as though the two alphas were coincident. Now that we seem to be forced in other light nuclei to the complexity of an intermediate-coupling interpretation, this model seems so crude that we may consider the photodisintegration not to have been adequately investigated, and we may, thus, be reasonably skeptical of the inference of a state at 1.56 Mev and of an associated preliminary assignment of a J to the state at 2.43 Mev.

One sees in Fig. 9 that there seems to be no possibility of obtaining in the intermediate-coupling scheme for the configuration p^5 just three low states, followed by a wide gap. For this reason, we must assume either that the inferred, unobserved state at 1.56 Mev does not exist or, as seems improbable but might be possible with such a large spread within each configuration, that one of the first two excited states belongs to an excited configuration such as p^4d. With this in mind, we have drawn the 1.56-Mev state with broken lines and ignore it in the comparison with experiment.

Because the slightly heavier nuclei suggest a ratio $a/K \approx 5$, we may attempt to match the 2.43-Mev state and the lowest states with $T=0$ and $T=1$ in this region. We thus find $a/K \approx 4.5$ (a value which is rough, *inter alia*, because it depends on the interpolation curves). In one of the inserts of Fig. 9 we see that this very satisfactorily implies first a wide gap extending from 2.43 Mev up beyond 5 Mev, and then several states which might cluster about the observed broad maxima (or some of them be lost in the background) in the higher region which has been explored only with poor resolution. If it should subsequently be found that there are only single states corresponding to these broad maxima, one might have to go to (jj) coupling to find so few widely spaced levels, as indicated in the second insert of Fig. 9, drawn for $a/K=12$, but this seems unlikely.

$Be^{10}+B^{10}$

Here we come to a polyad in which there are a considerable number of identifications of J's and parities, especially among the rather numerous low states (Aj52a, R52). The separations of the states, with the interaction given by Eqs. (2) and (6), are in (LS) coupling again taken from (F37), and in the ground (jj) configuration, $p_{\frac{3}{2}}^6$, they are the same as plotted in Fig. 5 for Py^6 and for the high states of Py^{14} in (jj) coupling. The separations of the (jj) asymptotes of many of the fairly low states in the excited configuration $p_{\frac{3}{2}}^5 p_{\frac{1}{2}}$ have very recently been calculated and kindly made available by Kurath (K52a), and make it possible to interpolate a fairly complete set of intermediate coupling curves between known asymptotes. This is done in Fig. 10, which is plotted with (jj) coupling on the left side (as for N^{14} in Fig. 5), and with the ordinate $[E-(3/2)a]/K$, in such a way that the (jj) asymptotes of the numerous states in the first excited (jj) configuration are horizontal.

The first excited configuration $p_{\frac{3}{2}}^5 p_{\frac{1}{2}}$ may be considered to be compounded by coupling the $p_{\frac{1}{2}}$ nucleon to the various levels of the $p_{\frac{3}{2}}^5$ partial configuration. This is, of course, artificial from a strict point of view, for the coupling between all nucleons is apt to be about equally strong, but the energy of the partial configuration does constitute a large contribution to the energy of the complete state, and there is a strong correlation between the lowest states of the excited configuration and those of the partial configuration. The calculated energies of the partial configurations (not including spin-orbit energy) are the same as already used in Py^7 and Py^9 above and are indicated by the horizontal lines in the upper left part of Fig. 10. Each of the states with $J=1$, 2, or 3 is associated with two partial configurations, as is indicated by broken lines in the figure, and the quantum numbers of the partial configuration, of course, do not remain constants of the motion after coupling on the $p_{\frac{1}{2}}$ nucleon. They do help in counting the number of states expected, and one sees that not all the states of the excited configuration have been plotted (the indication from the "Majorana" term alone being that the states omitted are too high to be of much interest).

This polyad is at the very middle of the p shell; its ground configuration may as well be called p^6 as p^{-6}. From the theory of holes, one knows that the spin-orbit

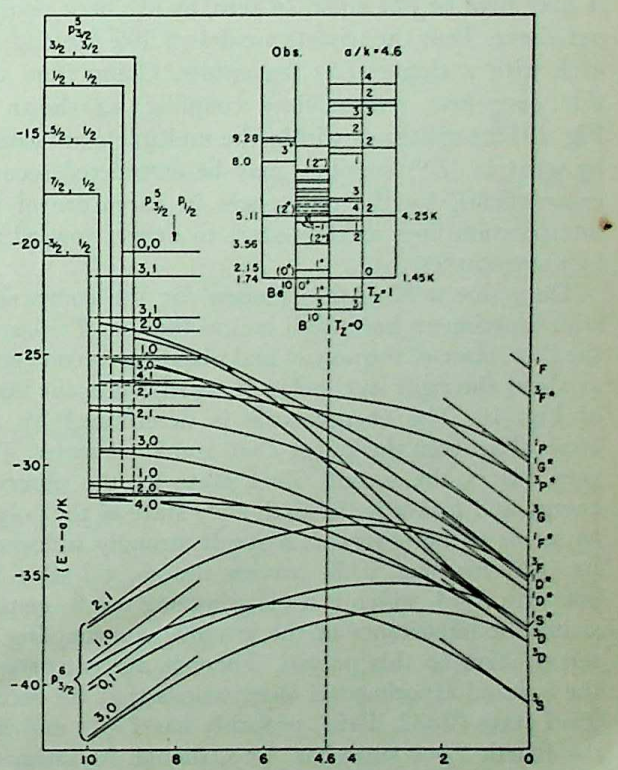


FIG. 10. Intermediate-coupling transition for the configuration p^6 applying to Py^{10}. The asterisk again denotes $T=1$. The ordinate is $(E-\frac{3}{2}a)/K$.

CC-0. In Public Domain. Gurukul Kangri Collection, Haridwar

Digitized by Arya Samaj Foundation Chennai and eGangotri

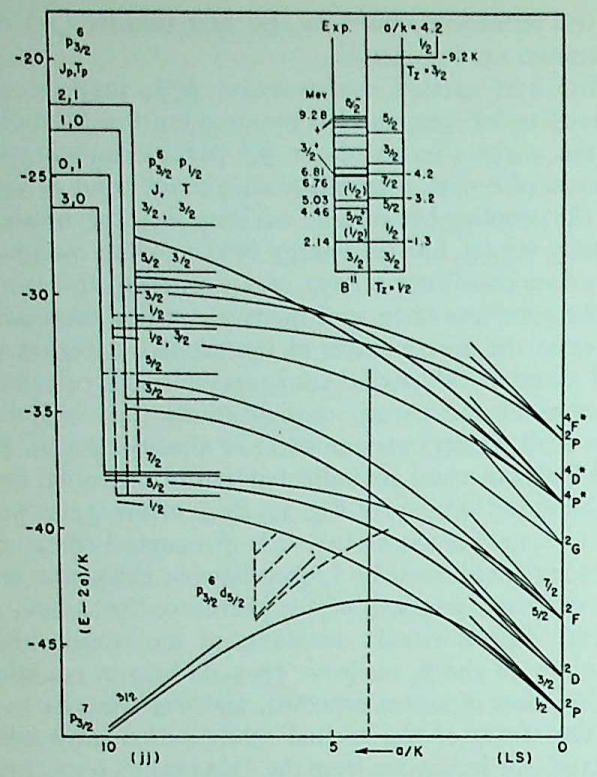


FIG. 11. Intermediate-coupling transition for the configuration p^5 applying to Py^{11}. The asterisk here denotes $T=\frac{3}{2}$, T being $\frac{1}{2}$ for the states not so marked.

coupling in any multiplet must be the negative of itself, and, therefore, the spin-orbit coupling parameter A may here be put equal to zero, as has been pointed out above. Thus the triplets are drawn, like the singlets, each with a single (LS) asymptote. Going from this side over into intermediate coupling, as shown in Fig. 10, the splittings within the multiplets are caused by what in (LS) coupling may be considered second-order effects, by the differences in curvature of the interpolation lines as they start to deflect toward the (jj) asymptotes.

The value $a/K=4.6$ is chosen for the comparison with experiment, because it makes the first $T=1$ state the third state of the polyad and places the second state at about the right level below it, as shown in the insert of Fig. 10. The energy scale is determined by the interval between the lowest $T=0$ and $T=1$ states. This then places the second $T=1$ state at the observed energy and makes it the sixth even state of the polyad as seems to be observed, a result strongly influenced by (LS) coupling, while leaving the ground state the one with $J=3$, which is a (jj)-coupling result, emphasizing the importance of the intermediate-coupling interpretation to this polyad. There is agreement with the isolated experimental observations that the second $T=1$ state (Co52, Th52) probably has $J=2^+$ and that the fourth $T=1$ state has $J=3$, though its estimated energy is too high. The first five states are observed to have even parity so should belong to this configuration, and of these the fourth and fifth together have the theoretical J's 1 and 2 as observed but in the wrong order, the experimental $J=1$ state being much lower than the theoretical level and the only sharp discrepancy encountered in this interpretaion. It does not seem possible to remove this discrepancy by reasonable use of the arbitrariness in drawing the interpolated energy curves. It is still a valuable accomplishment of the greater complexity of the intermediate-coupling interpretation that it may be made to fit the general features of level density and more special features of most of the assignments, including especially the existence of just one $T=1$ state among the first five, but the discrepancy shows its limitations and detracts from its persuasiveness. Whether it indicates inadequacy of the interaction assumption (2) or capricious intervention of configuration interaction, the discrepancy shows that we can claim no more than an incomplete understanding of general features in terms of a rather complicated scheme.

It is consistent with our treatment of the lighter polyads if we introduce here the further complexity of partial participation of alpha-model states to try to account for the discrepancy, for the state that appears to have been depressed by this or some other sort of configuration interaction does indeed have the J and parity of the ground state of the alpha-model, 1^+, corresponding to a nonrotating structure of two alphas and a deuteron or of three alphas and a deuteron hole. The use of this explanation is complicated by the fact that only the second 1^+ state appears to be strongly depressed by such an admixture of an alpha-model state. It is possible that further investigation would show that the second 1^+ state consists mostly of ^3S and thus resonates most strongly with the deuteron state (the pure deuteron having only about 4 percent of ^3D, though in the alpha-model of B^{10} this proportion might be altered). It is pointed out in the discussion of Py^{14} below that the ground state energy of N^{14} over most of the range of a/K plotted in Fig. 5 is near the extension of the (LS)-coupling asymptote of the $^3D_1$ state, and correspondingly that the wave function of this state consists mostly of $^3D_1$, as shown in Fig. 20. One may note that the second 1^+ state at $a/K=4.6$ in Fig. 10 is fairly near the extension of the (LS)-coupling asymptote of the ^3S, and there might correspondingly be the required preponderance of ^3S in the wave function, though it would require a more difficult calculation than in Py^{14} to show it.

There is a rather high density of B^{10} states at energies near 5 Mev and higher. This high density presumably corresponds to the contribution of excited configurations at these energies, and most of the lowest of the states so contributed would be expected to have odd parity, from the configurations p^5d and p^5s. The first three of this group of states, those at 4.79, 5.11, and 5.17 Mev, have indeed been tentatively identified as odd. If these identifications are all correct, we have the difficulty that the $T_z=1$ state observed at 5.11 Mev

CC-0. In Public Domain. Gurukul Kangri Collection, Haridwar

Digitized by Arya Samaj Foundation Chennai and eGangotri

would be expected to correspond to one of these, which would mean that the $T=1$ state in this region would be odd and would not correspond to the theoretical even (2, 1) state at $4.25K$. It would be surprising to have the first $T=1$ state of the odd configuration lie so low in the configuration. It is possible that the 5.11-Mev state in the Be^{10} column and the next higher state of B^{10} which is at 5.58 Mev (or possibly the uncertain state at 5.37 Mev) together form the components of the $T=1$ state, but the difference between 5.58 and 5.11 Mev would constitute a slightly larger deviation of apparent conservation of isobaric spin than is usual. It seems more likely either that one of the states at 5.11 or 5.17 Mev has even parity and $T=1$ or that there is another such state unobserved because of being practically coincident with one of them, or that the uncertain state indicated by the broken line at 5.37 Mev is the one in question. The possibility that the closely spaced pair at 5.11 and 5.17 Mev should arise from the coupling of an s nucleon to the p shell is discussed in Sec. 9.

In a shell with many nucleons in intermediate coupling, no single pair of states gives any indication of the magnitude of the spin-orbit parameter a, as may be obtained from a doublet splitting in a single-nucleon case such as O^{17}. By finding a rough fit in intermediate coupling with $a/K=4.6$, $K=-1.2$ Mev, we thus have a less direct estimate that $a=-5\frac{1}{2}$ Mev. The corresponding single-nucleon ^2p splitting in this part of the periodic table, or at least in this polyad, would be about 8 Mev.

$B^{11}+C^{11}$

In this case and in Py^{12} and Py^{13} the ground (jj) configuration contains only one state so the published calculations (K52) on the energies of the states of the ground (jj) configuration in (jj) coupling give no information concerning the separations of the (jj) asymptotes and left quite a lot of latitude in the drawing of the intermediate-coupling curves from known (LS) asymptotes to (jj) asymptotes of which only the slope was known. For the sake of filling in the information in the (jj) extreme, Dr. Kurath has very recently calculated the energies of the states in the first excited (jj) configuration for these polyads (K52a). This enables us to interpolate the intermediate-coupling curves between definite asymptotes, determined here again for the interaction assumptions, Eqs. (2) and (6), as in Fig. 11. This is an example of the sort of improvement in the theoretical basis of the intermediate-coupling interpretation that was anticipated in the introduction, and it enables us to present in Fig. 11 a second stage in the development of the interpretation. [It differs from the earlier, more imaginative, stage mainly in having the $J=7/2$ level considerably depressed, and in a similar evolution of Fig. 10 for Py^{10}, the state with the high value $J=4$, and $T=0$, also lies lower than was at first imagined, this depression of the high J's apparently being a characteristic of (jj) coupling.] At the same time a further step in the experimental clarification of the situation has become available in the J and parity determinations of Jones and Wilkinson (J52) for B^{11}, which are shown in Fig. 1 and in the insert of Fig. 11. Their assignment of even parity to the 4.46-Mev state means that there is, at most, one state of the odd ground configuration p^7 in the neighborhood of 5 Mev and forces us to go to a rather small value of a/K (and large value of K) in comparing theory with experiment. The comparison shown in the insert of Fig. 11 is for $a/K=4.2$ ($K=-1.65$ Mev, $a=-6.9$ Mev). The energy scale is determined to match the 2.14-Mev state in addition to the ground state. The experimental assignments at 4.46, 6.81, 8.93, 9.19, and 9.28 Mev are reported (J52) to have been made "with fair certainty," but those at 2.14 and 5.03 Mev involve further "reasonable assumptions," so we have indicated them in parentheses. In particular, the assignment $J=\frac{1}{2}$ at 5.03 Mev rather than, say, $J=5/2$ apparently leans very heavily on the failure to observe a gamma-transition from 9.19 to the 5.03 level with NaI pulse-height analysis. If the 5.03-Mev level should on further investigation be found to have $J=5/2$, there would be close agreement in the insert of Fig. 11. It seems more likely, however, that the state at 5.03 Mev is $\frac{1}{2}^+$ belonging to an excited configuration along with the 4.46-Mev state, and that the third and higher p^7 states are to be found at 6.76 Mev and above, in which case one might go to somewhat smaller a/K to obtain a closer fit.

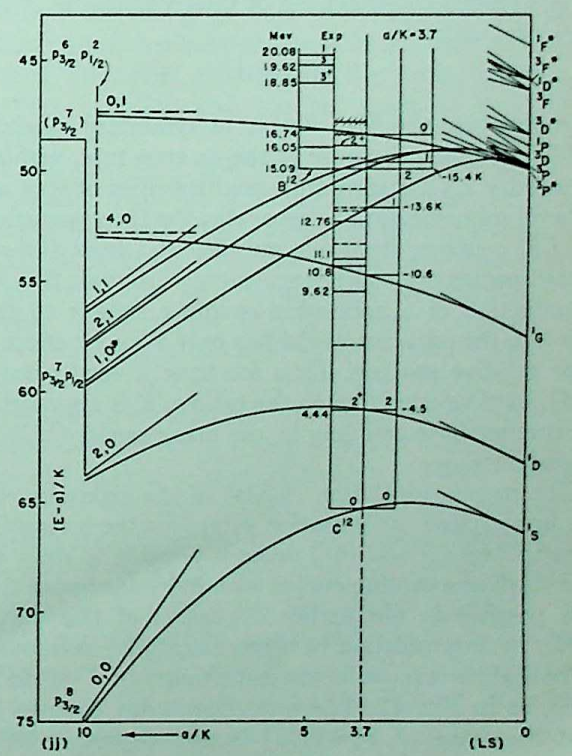


FIG. 12. Intermediate-coupling transition for the configuration p^6 applying to Py^{12}.

CC-0. In Public Domain. Gurukul Kangri Collection, Haridwar

Digitized by Arya Samaj Foundation Chennai and eGangotri

The "parentage" of the $p_{\frac{1}{2}}^6 p_{\frac{1}{2}}$ states in terms of the partial quantum numbers J_p, T_p of the $p_{\frac{1}{2}}^6$ "core" is shown in the upper left corner of Fig. 11. The spacings between the "core" states are the same as in Py^{10}. Cases of dual parentage are indicated by dotted lines (in these cases Kurath's results were obtained by solving secular equations, the low J, $T=\frac{1}{2}, \frac{1}{2}$ state having been "repelled" downward by the higher one, e.g.). In reference (J52) a frankly exploratory attempt was made to interpret the excited even levels in terms of a single-particle model, as though the $(J_p, T_p)=(0, 1)$ state were the only state of the "core," but because B^{10} has so many low states, the lowest with $J=3$, such a simplified explanation is not tenable. The more complex situation in the configuration $p_{\frac{1}{2}}^6 d_{5/2}$, for example, is suggested by the broken lines in Fig. 11, where an intermediate-coupling deviation from one of several (jj) asymptotes is schematically indicated at a position to account for the 4.46-Mev state.

The appearance (V51a) of two pairs of closely-spaced levels in B^{11}, one with a separation of 50 kev at 6.8 Mev and one with a separation of 90 kev at 9.2 Mev, does not very pressingly call for causal explanation, both because they are in fairly dense parts of the spectrum and because the lower one is not reproduced as a narrow double-level in the energy-level spectrum of the mirror nucleus C^{11}. (An explanation in terms of the configuration $p_{\frac{1}{2}}^6 s_{\frac{1}{2}}$, such as is discussed in Sec. 10 below, does not apply to the upper pair if the determination is correct that these two closely spaced levels have opposite parity, and if applied to the lower one would require special consideration of the complexities of this configuration.)

$B^{12}+C^{12}$

In this case the high degree of symmetry available in (LS) coupling (because of the $4n$ structure, with the periodicity 2×2 arising from multiplicities of spin and isobaric spin orientation) separates the three low states in (LS) coupling from one another and from the rest of the spectrum by such large energy intervals that the introduction of a spin-orbit coupling similar to that found in the adjacent nuclei has only a minor effect on their relative spacing. Thus we have a semblance of (LS) coupling even though the ratio a/K is appropriate for intermediate coupling in the other nuclei (I52), as remarked above.

The recent calculation (K52a) of the separations in the first excited configuration $p_{\frac{1}{2}}^7 p_{\frac{1}{2}}$ [for the interaction assumptions (2) and (6)] make it possible to draw the intermediate-coupling curves with more assurance than was possible in our earlier discussion of this polyad (I52), by interpolation between calculated asymptotes on both sides (except for the uncertainty in A on the LS side), as in Fig. 12. The most significant changes are that the state $(J, T)=(2, 1)$ is now depressed below $(1, 1)$, and that it is necessary to go to a lower value of (a/K) to fit the first two $T=0$ states and the first $T=1$ state. This is done in Fig. 12 at $(a/K)=3.7$, although this value is of course dependent on the indefinite drawing of the curves as well as on the interaction assumption.

An unsatisfactory feature of this set of curves as thus fitted is that this would make the ground state of B^{12} have $J=2$, whereas $J=1$ seems to be required by the existence of an allowed beta-transition to the ground state (and apparently also to the $J=2$ first excited state) of C^{12}. There is also very recent evidence, including some from photo-excitation and the $\Delta T=\pm1$ selection rule for dipole radiation (Ra52, T53), that the 15.09-Mev level of C^{12} has $(J, T)=(1^+, 1)$. (This energy level was called 15.14 Mev on an earlier energy scale which survives in Fig. 1.) With the ground state of B^{12} assumed to have $J=1^+$ and matched with this level, there is also a good match between the first excited state of B^{12} at 16.05 Mev and a 2^+ state of C^{12} at 16.10 Mev. Thus the first two $T=1$ states have $J=1$ and 2 both experimentally and theoretically, but they are close together theoretically in Fig. 12, and experimentally they are about 1 Mev apart in the reverse order. It would be possible to obtain the reverse order (and thus $J=1$ for the ground state of B^{12}) but not the observed separation by reasonable modifications in the drawing of the curves between the asymptotes shown in Fig. 12. This is high enough in the energy spectrum of the polyad that reasonable changes in the interaction assumption, Eq. (2) may make enough difference to invert the order of the (2, 1) and (1, 1) states also in the (jj) limit [compare Figs. 7 and 7(a)], and this would perhaps be an appropriate place for an investigation of such changes to start.

The experimental data now include several states at about 10 Mev and immediately above, and it is not yet clear which are the (4, 0) and (1, 0) states of the ground configuration p^8. The negative-parity states of the excited configurations p^7d and p^7s apparently start in this region of quite high energy (unless the doubtful state at 7.3 Mev exists), in contrast with the finding of the first even state of B^{11} as low as 4.46 Mev. Here again the exceptional symmetry attainable in the ground configuration of C^{12} seems to have pulled the low states down.

On the (LS) side, it has been assumed that the multiplets are regular (with the lowest J lowest) corresponding to having a more than half-filled shell, although it is not necessarily the case for multiplets of such complex parentage as these. The great density of multiplets above the first triplet indicate that there should be many states just above the first $T=1$ state, but no attempt has been made to draw in the curves beyond the first triplet [except one for which the (jj) asymptote is known]. Further experimental identifications of these high states will be required before their order can begin to make sense. It is apparent at least that the five available j identifications of high states of B^{12} are present among the $T=1$ multiplets.

CC-0. In Public Domain. Gurukul Kangri Collection, Haridwar

Digitized by Arya Samaj Foundation Chennai and eGangotri

The striking lack of resemblance to any simple result of (jj) coupling is epitomized by the fact that the first three states arise from three different (jj) configurations, the $J=0$ state of course from $p_{\frac{1}{2}}^8$, the $J=2$ state from $p_{\frac{1}{2}}^7 p_{\frac{3}{2}}$, and the $J=4$ state from $p_{\frac{1}{2}}^6 p_{\frac{3}{2}}^2$. They accordingly approach asymptotes of three different slopes.

The experimental assignment 2^+ for the 4.44-Mev state (Ha51, Th52, H52, Le52) is based on recent observations of the angular correlation in the reaction $B^{11}(p;\gamma_1,\gamma_2)C^{12}$. Any other assignment would have seemed anomalous, for this agrees with all the models.

$C^{13}+N^{13}$

This is another case in which the ground (jj) configuration contains only one state and the recent unpublished energies (K52a) for the five states of the first excited (jj) configuration have been used to provide definite (jj) asymptotes for the drawing of the curves in Fig. 13. These go over into states in as high as the sixth multiplet in (LS) coupling. All the states for which curves are not drawn in these multiplets would curve up to states of higher (jj) configurations, and so would contribute only very high states to the energy spectrum.

Experimentally, this polyad has been explored only for fairly low states in the two low mirror nuclei. The fact that it is not very stable relative to single-nucleon emission seems to induce an unusually large displacement (Th50, Th52a) between the mirror levels which lie between the proton threshold for N^{13} and the neutron threshold for C^{13} (see Fig. 1), so the comparison is made with the actual energies of C^{13} for which these levels are stable in this respect. There are some fine new possibilities for making unique or almost unique assignments of angular momentum from angular distribution of (d,p) or (d,n) stripping reactions near the forward direction (B51, Bh52, R51) and from elastic scattering resonances when the target nucleus, in this case C^{12}, has $J=0$, as is explained further a few paragraphs below, and quite a lot of information is available concerning the identification of the states.

By comparing the unique assignments of the resonant-scattering method in N^{13} with the not quite unique assignments of the stripping-reaction method in C^{13}, one may on the basis of the expected correspondence of mirror levels reasonably select the assignments in C^{13} as follows: $\frac{3}{2}^-$ at 3.69 Mev (3.50 Mev in N^{13}) and $5/2^+$ at 3.89 Mev (3.55 in N^{13}), in addition to the unique assignment $\frac{1}{2}^+$ at 3.09 Mev (2.36 in N^{13}), as has already been assumed above. The close juxtaposition of the $\frac{3}{2}^-$ and $5/2^+$ levels in N^{13} is here seen to be accidental.

Only one of the first three excited states of C^{13}, the one at 3.69 Mev, has the parity characteristic of the ground configuration. The energy scale in the insert of Fig. 13 is determined by matching the interval between this and the ground state, after arbitrarily selecting $a/K=5$ on the basis of experience with other, more

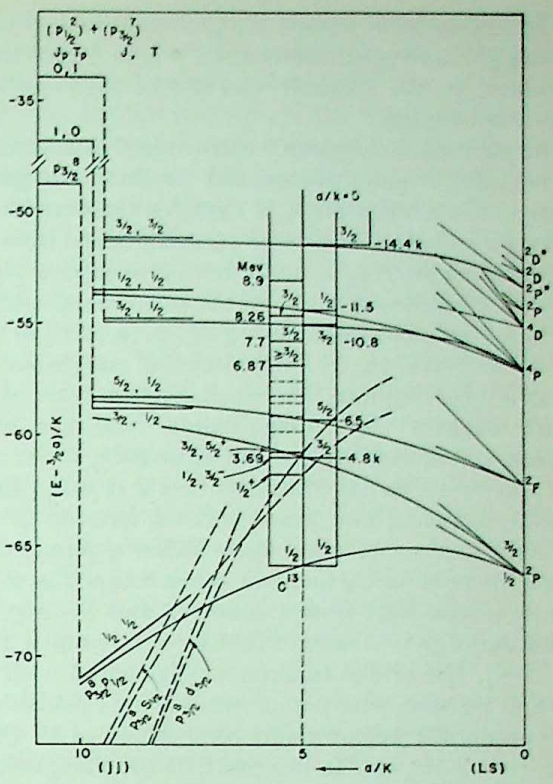


FIG. 13. Intermediate-coupling transition for the configuration p^7 applying to Py^{13}. The asterisk denotes $T=\frac{3}{2}$.

revealing, polyads. The theoretical values $J=\frac{1}{2}$ and $\frac{3}{2}$ for the first two states of this configuration then agree with the experimental assignments, the two states arising from the ^2P of (LS) coupling, inverted in the nuclear sense because of being in the last half of the p shell, but much distorted by the transition to intermediate coupling and too far apart to look like a doublet.

From the (jj)-coupling point of view, the mistake is sometimes made of thinking that, since the ground state consists of a single nucleon outside of a closed (jj) shell, the interval from the ground $J=\frac{1}{2}$ state to the first $J=\frac{3}{2}$ state is a measure of the single-nucleon doublet splitting, $\frac{3}{2}a$. This excitation is actually from the (jj) configuration $p_{\frac{1}{2}}^8 p_{\frac{3}{2}}$ to $p_{\frac{1}{2}}^7 p_{\frac{3}{2}}^2$, and thinking in a very simple (and still unjustifiably simple) way, one must at least consider that he is breaking up a pair of $p_{\frac{1}{2}}$ nucleons and forming a pair of $p_{\frac{3}{2}}$ nucleons (in keeping with the Mayer δ-function treatment (M50) which is valid only for large nuclei), and that the two pairing energies are different so that the observed interval is no measure of the single-nucleon $p_{\frac{1}{2}} \rightarrow p_{\frac{3}{2}}$ excitation energy. More properly, one notes that either a neutron or a proton may be excited, and in either case one can make a state with $(J,T)=(\frac{3}{2},\frac{1}{2})$, as may be described also by coupling the $p_{\frac{1}{2}}$ hole to the $(J_p,T_p)=(1,0)$ or $(0,1)$ states of the partial configuration $p_{\frac{1}{2}}^2$. Thus even in extreme (jj) coupling the mixing of these two states as solutions of the same secular equation tends to push

CC-0. In Public Domain. Gurukul Kangri Collection, Haridwar

Digitized by Arya Samaj Foundation Chennai and eGangotri

the lower one down toward the ground state and complicates the interpretation of the $J=\frac{1}{2}$ to $\frac{3}{2}$ excitation, so that it is not a simple measure of single-nucleon spin-orbit coupling.

The additional complexity encountered in intermediate coupling is more pronounced for these odd-parity states of the configuration p^9 than for the even-parity states p^8d and p^8s. The ground state is derived from the (jj)-coupling state $p_{\frac{3}{2}}{}^6p_{\frac{1}{2}}$ and other (jj)-coupling states formed by simple excitation of the least bound nucleon are $p_{\frac{3}{2}}{}^6d_{5/2}$ and $p_{\frac{3}{2}}{}^6s_{\frac{1}{2}}$, each with a full $p_{\frac{3}{2}}$ subshell so that the states have the characteristics of single-nucleon states in (jj) coupling. The single-nucleon state of the "extra nucleon" is distinguishable from the other nucleon states, only by its spin-orbit energy if it is $p_{\frac{1}{2}}$ but also by its radial wave function if it is $d_{5/2}$ or $s_{\frac{1}{2}}$. In (LS) coupling one may think of forming C^{13} by adding a nucleon to a C^{12} core. When a p nucleon is added, there is no energetic or other distinction of the added-nucleon state from the others, and we have the formation of a ^2P characterized by a communal $L=1$ and $S=\frac{1}{2}$, the added nucleon amalgamated with the rest and the spin-orbit parameter A being calculable by the appropriate vector-model composition of all the $\mathbf{l}_i$ with each other, etc. In intermediate coupling, most of this thorough mixing of the roles of the p nucleons persists, and these states of the system do not begin to resemble single-nucleon states until one gets to (jj) coupling, where the integrals L and K are too small compared to a to mix the (jj) configurations.

When instead a d nucleon (or an s nucleon) is added to the "C^{12} core," there remains a distinction between the added-nucleon state and the others in terms of the number of nodes of the radial wave function, for example, and in the problem of coupling the added nucleon to the "core," there appear integrals which we might call L_d and K_d, analogous to L and K except that they contain p and d wave functions where L and K contain only p functions, and which are expected to be considerably smaller than L and K because of the more complete cancellation of the positive and negative contributions to the integrals arising from the rapidly oscillating products of the different wave functions. It is this fact that in intermediate coupling tends to preserve the single-nucleon nature of the wave functions of the system. In (jj) coupling we have the single-nucleon semblance, as before, because in this case L_d and K_d are much too small to mix in the excited-core (jj) configurations, but as we pass to intermediate coupling, the $J_p=0$ to $J_p=2$ excitation of the core remains large, as we see in Fig. 12, of a magnitude determined both by K and by the spin-orbit parameter a (which make contributions of comparable magnitude in intermediate coupling) and the contributions of the K_d (and L_d) are presumably small in comparison, so the low $5/2^+$ state is composed almost entirely of the core state $J_p=0$ plus the $d_{5/2}$, with fairly little admixture of the core state $J_p=2$ plus the $d_{5/2}$, for example. Thus in this approximation the state of the system is expected to resemble a single-nucleon state, and the complexities of intermediate coupling are hidden within the core where they have no outside influence because $J_p=0$. In (LS) coupling the core again makes no contribution to the external properties of the low D and S states, because the core is in a ^1S state, and the parameter a is too small to mix in anything else.

In the course of making assignments to the states of N^{13} by examination of scattering resonances, the $\frac{3}{2}^-$ state, doubtless the mirror of the C^{13} state at 3.69 Mev, is found to have a "reduced width" only about a tenth as great as that of the $\frac{1}{2}^+$ and $5/2^+$ states which are presumably the mirror states of the 3.09- and 3.89-Mev states, respectively (J51). This small reduced width in single-nucleon scattering indicates that this $\frac{3}{2}^-$ state cannot be so well approximated as the others by a single-nucleon wave function, and this seems to be in accord with our intermediate-coupling interpretation. The same thing is indicated by the observation (R51) that the $C^{12}(d,p)C^{13}$ stripping reaction, in which a single neutron is added to the "core," gives the $\frac{3}{2}^-$ state with only a few percent of the yield of the $5/2^+$ state.

The order of the states associated with the $d_{5/2}$ and $s_{\frac{1}{2}}$ orbits in Py^{13} and in F^{19}, with $\frac{1}{2}^+$ below $5/2^+$, is opposite to that in Py^{17} in which the ground state $5/2^+$ is more than $\frac{1}{2}$ Mev below the $\frac{1}{2}^+$, and this seems like an anomaly if one tries to push the single-nucleon interpretation too far. The states of the system are probably most nearly like single-particle states in Py^{17}, in which the O^{16} "core" is in its ground state a filled p shell, not just a filled $p_{\frac{3}{2}}$ shell of (jj) coupling. As is discussed further below, the excited states of O^{16} not only begin at the high level 6 Mev, but the first of them is a O^+ state which would not change some properties if it were admixed and probably involves two-nucleon excitation which would greatly inhibit its being admixed, and the second excited state of the core has opposite parity which would probably inhibit its being admixed. Thus we may judge that the single-electron state $d_{5/2}$ lies below the $s_{\frac{1}{2}}$, at least in the potential well encountered in Py^{17}. It is possible that the potential well of the others would differ enough from this to change the order of the single-nucleon states, but it does not seem necessary to conclude that this is so, for the deviations from resemblance to single-particle states encountered in intermediate coupling, even if not very pronounced, could cause such an inversion of order. In Py^{13}, the resemblance of the $5/2^+$ and $\frac{1}{2}^+$ states to single-nucleon states in intermediate coupling depends on the integrals L_d and K_d being small. While no calculations have yet been made on the subject, it seems plausible that they could be of such a magnitude as to make enough admixture of excited states of the core to invert the order, and yet leave enough appearance of single-particle states to contrast strongly in the scattering and stripping results with the $\frac{3}{2}^-$ state in which

CC-0. In Public Domain. Gurukul Kangri Collection, Haridwar

Digitized by Arya Samaj Foundation Chennai and eGangotri

there is no distinction between core and added particle in the very thoroughly amalgamated situation of intermediate coupling.

If the single-nucleon state $d_{5/2}$ lies a little below $s_{\frac{1}{2}}$ (by an amount considerably less than the spin-orbit contribution to $d_{5/2}$) at the actual strength of spin-orbit coupling parameter a, as we may judge it does from O^{17} (neglecting any difference between shapes of potential wells), then it lies much lower than $s_{\frac{1}{2}}$ in extreme (jj) coupling attained by making a large and higher than $s_{\frac{1}{2}}$ in (LS) coupling with a small. Since also in C^{13} in both extremes the even nuclear states resemble single-nucleon states, the nuclear $5/2^+$ state would thus likewise lie above the $\frac{1}{2}^+$ state of C^{13} in (LS) coupling and below it in (jj) coupling. There is thus a cross-over of the intermediate-coupling curves somewhere between the two extremes, and it appears from the observed order of the levels in C^{13} that the cross-over occurs at a value of a/K higher than the actual one, as suggested by the broken lines in the lower part of Fig. 13 (where only the slopes of the (jj) asymptotes have been calculated). These sketched intermediate-coupling transitions for the $5/2^+$ and $\frac{1}{2}^+$ states are purely schematic. They are not properly functions of a/K but of a with K fixed, since otherwise the relation between K and the single-nucleon s, p, d energy differences would come into play.

The $\frac{3}{2}^-$ state of N^{13} has been interpreted elsewhere in papers which place too much emphasis on the closed-shell nature of the "$p_{\frac{1}{2}}^8$ core" (K51, J51), as arising from an anomalous depression of the next higher single-nucleon $p_{\frac{1}{2}}$ state, the $2p_{\frac{1}{2}}$ which in the oscillator model belongs to the same degenerate group as the first ^2f. The intermediate-coupling interpretation seems far preferable to pushing the single-nucleon model so far as to tolerate such a glaring exception to the usual order, especially in view of the small natural width of the $\frac{3}{2}^-$ level.

In this polyad there are only two known states in the ground configuration, so there are no verifiable relations between energy intervals to confirm the intermediate coupling scheme and one can make few predictions beyond the value $J=\frac{3}{2}$ for the first $T=\frac{3}{2}$ state, but the assignment data available do fit nicely into the intermediate-coupling scheme.

Two Methods of Assigning J's and Parities in C^{13}, N^{13}, and Other Nuclei

There are two new methods, one of which is conceptually new and the other of which has been only recently applied, to obtain angular momentum and parity assignments especially effectively in nuclei formed by adding one nucleon to a nucleus having $J=0$. The first is the analysis of the forward portion of the angular distribution of a (d, p) or (d, n) reaction, first made by Butler (B51). Attempts made earlier to obtain information concerning nuclear states from the angular distribution of (d, p) reactions failed to achieve unique assignments because the solidly backed targets used (H48) did not permit observation near the forward direction, and the analysis of the data (Di50) was too greatly complicated by the necessity of simultaneously making assignments to the rather numerous states of the compound nucleus contributing to the reaction.

It was found in this connection by Rotblat and his coworkers (R51) that at fairly high bombarding energies the (d, p) and (d, n) reactions have a strong forward or near forward peak in their angular distribution which may plausibly be attributed to a stripping process similar to that discussed earlier by Oppenheimer and Phillips in the case of heavy nuclei where barrier penetrability is more important. The process is pictured as the entry of one of the nucleons of the deuteron into the target nucleus while the other nucleon of the deuteron flies on its way, influenced in its direction and energy of flight both by the center-of-mass motion and the internal motion of the deuteron which it formerly shared. The way in which the internal motion is shared is determined by the fact that the final nucleus has very strong preferences for the energy and angular momentum of the nucleon with which it may be formed, and these preferences reflect the properties of the states which one wishes to ascertain. The beauty of this process is that it does not involve formation of a compound nucleus and the attendant complexity of trying to determine its properties at the same time.

The peak observed for a given reaction near the forward direction is so sharp that its analysis in spherical harmonics involves partial waves of several units of angular momentum, so high as to represent passage of the incident deuteron with quite a large collision parameter (or extrapolated distance of closest approach). This is possible only because of the large size of the deuteron and permits entry of only one of the nucleons into the target nucleus. Close enough collision for formation of a compound nucleus involves only about two or less units of angular momentum and consequently displays rather broad angular maxima spread out over all angles with rather low intensity.

The powerful analysis of Butler treats the various angular partial waves of the incoming beam, and determines the fate of each by joining incoming and outgoing wave functions in an annular region just outside the nucleus, before superposing the effects of the various outgoing waves. The results are fairly insensitive to the choice of the radius at which the joining is carried out, corresponding to the expectation that there is a region where the nucleon about to enter the nucleus is outside the influence of the deuteron potential, in the wings of the deuteron wave function, and not yet strongly attracted by the nuclear potential. The result of the analysis is to relate the shape and position of the near forward or forward peak to the angular momentum l_n with which the incoming nucleon is captured by the target nucleus. If the target nucleus is in a 0^+ state, as

CC-0. In Public Domain. Gurukul Kangri Collection, Haridwar

Digitized by Arya Samaj Foundation Chennai and eGangotri

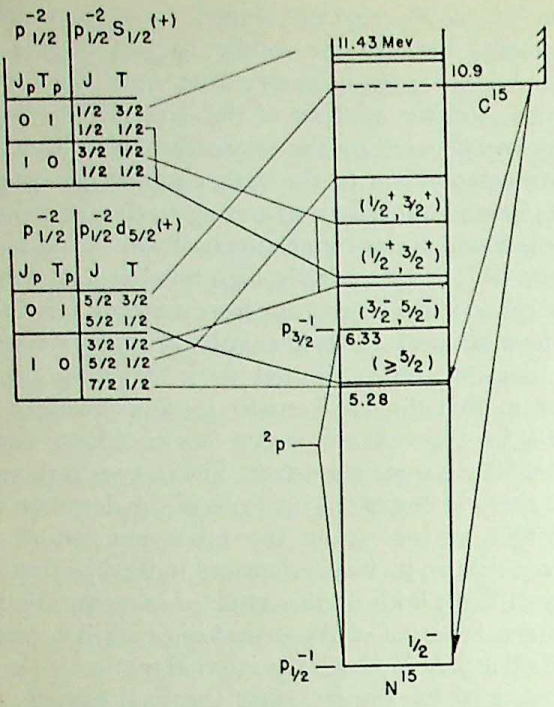


FIG. 14. (jj) configuration assignments to the states of Py^{15}. The "partial configurations" from which they arise are indicated in the left-hand columns, J_p and T_p being "partial quantum numbers" (of the two $p_{\frac{1}{2}}$ nucleons) which do not remain good quantum numbers in the complete system.

in the case of $C^{12}(d, p)C^{13}$, then the parity of the final nucleus, in the state being observed by selection of proton energy, is odd or even as l_n is odd or even, and the angular momentum of the final state is $l_n \pm \frac{1}{2}$. Thus in this most favorable case, J is not assigned uniquely but merely limited to a choice of two values, as one sees them listed in Fig. 1 and elsewhere.

A similar analysis based on the Born approximation, and thus differing radically from Butler's in the nature of its simplifying assumptions, has recently become available (Bh52, D52). It agrees completely with Butler's in providing assignments based on the position of the near forward peak, and seems to agree better with experimental results concerning the amplitude of the secondary maximum further from the forward direction.

There is a very similar phenomenon of pick-up of a nucleon from a nucleus by an incident particle in such reactions as $Be^9(d, t)Be^8$, characterized by a similar near forward peak, to which a similar analysis applies (B51, B52).

The second method which has only recently been extensively used to make assignments to the states of such nuclei as N^{13} is the detailed observation and analysis of the shape of elastic scattering resonances, as is possible now with the very nearly monoenergetic proton beams of a modern, well-controlled statitron. Most of the low states of light nuclei are far enough apart that the scattering may be analyzed in terms of the single-level scattering formula. The phase shift of the effective angular partial wave depends, in its Coulomb part on the orbital angular momentum l of the partial wave, in its resonant part on the "width" of the resonance, and the amplitude associated with this phase shift depends also on j. These properties of the scattered proton determine the parity and angular momentum of the state of the compound nucleus causing the resonance, in the simple case in which the target nucleus is 0^+. Probably because in a real "close-shell-plus-one-nucleon" nucleus such as O^{17} this also determines the value of the total orbital angular momentum vector L for the nucleus, these resonances have customarily been designated with symbols for nuclear multiplet levels, such as $P_{\frac{3}{2}}$, with a capital "P" which in atomic spectra implies that $L=1$, but these symbols are meant strictly merely to indicate parity and angular momentum. Thus we use, for example, $\frac{3}{2}^-$ in place of the $^2P_{\frac{3}{2}}$ of the experimental papers.

$C^{14}+N^{14}$

For this polyad we return to the left side of Fig. 5, since the configuration p^{-2}, or two nucleon "holes" in the p shell, has some similarity to the configuration p^2 discussed for Py^6. The order of the two low states of Py^{14} is that given by (jj) coupling, and the ratio of this interval to the interval up to the second state with $T=1$ is given by the transition curves at $a/K=-5.6$. Here a is the spin-orbit coupling parameter for a "hole," everywhere else in this paper it is for a single nucleon, since only here have we plotted the results for nucleons and holes on the same graph and used the "hole" nomenclature in labeling the (jj) configurations.

The prediction concerning energy levels is that there should be two even levels from this configuration in N^{14} somewhere in the region near 5 or 6 Mev, having $J=1$ and 2 in that order. Since odd parity has tentatively been assigned to most of the newly observed levels in that region and above (Be52), it appears that these two even levels may be the ones at 3.96 and 5.1 Mev, each about 1 Mev lower than given by the theoretical treatment. It would not be at all surprising if there should be another even level in the neighborhood of 6 Mev corresponding to the 6.05-Mev state in O^{16} as discussed below, arising from the doubly-excited configuration p^8d^2, and this might be the one at 5.7 Mev. Otherwise the levels in this region and immediately above are expected to arise from the singly-excited configurations p^9d and p^9s. The fact that they start at 4.8 Mev, so far as is well established, is consistent with the energies at which they begin to appear in the neighboring nuclei, with which no close agreement can be expected because of the complexities of intermediate coupling. There is no obvious reason that there should not be an odd $T=1$ level as low as or lower than the one we have assumed to be even at 8.42 Mev, and indeed recent observations (privately communicated by T. Lauritsen) suggest that there may be a $T=1$ level, which may be 0^- or 0^+ and is not shown in Fig. 1, at about 7 Mev.

CC-0. In Public Domain. Gurukul Kangri Collection, Haridwar

Digitized by Arya Samaj Foundation Chennai and eGangotri

One of the most puzzling facts known in light nuclei is the archeologically useful but apparently anomalous long life of C^{14}. Until recently the hope was entertained by those most interested in the theory of beta-decay that the puzzle could be relegated to those interested in nuclear structure by assuming (G51) that the C^{14} and N^{14} ground states have opposite parity, or else (F49) that the C^{14} state is a pure ^1S and the N^{14} ground state a pure ^3D. Both assumptions have been disproved by recent observations. The former possibility has vanished with the experimental proof, by means of the stripping-reaction technique, that the $T=0$ and 1 states have the same parity (Br52), and the latter possibility would require an isolated case of extreme (LS) coupling, with the order of the two low multiplets reversed from that in Fig. 5, and would lead one to expect two very low excited ^3D states of N^{14} that have escaped careful observation (Va52). The lifetime is about 10^6 times longer than expected. Either one must expect to find here some new principle of nuclear structure or of beta-theory to explain this, or one must accept it as chance cancellation in a matrix element to an accuracy of perhaps one part in 10^3. A calculation of the nuclear matrix element in intermediate coupling is discussed in detail in Sec. 11. It is there shown that a factor of about $10^{-\frac{1}{2}}$ in the matrix element, or 10 in the lifetime, appears naturally from the magnitude of the intermediate-coupling coefficients in the N^{14} wave function, but that the fortuitous cancellation required to give the remaining factor $10^{-5/2}$ in the matrix element does not occur in the ground configuration and must in this interpretation arise from a moderate amount of configuration mixing.

$C^{15}+N^{15}$

Here the ground (jj) configuration $p_{\frac{1}{2}}^{-1}$ has only one state $(J, T)=(\frac{1}{2}, \frac{1}{2})$ and the only excited (jj) configuration within the general configuration p^{-1}, namely, $p_{\frac{3}{2}}^{-1}$, has only one state, these two states being identical with the (LS) description of the two states $^2P_{\frac{1}{2}}$ and $^2P_{\frac{3}{2}}$ of a nucleus with a single p-nucleon "hole." Thus for this polyad the intermediate-coupling transition of the ground configuration consists merely of two straight lines. Experimental assignments of parity and not quite unique assignments of J have been made (B51) but they should be considered to some extent tentative because the observation of the near forward peaks did not cover the angles 0–15°. The (unresolved) pair of states at 5.3 Mev is exceptional in showing an approximately isotropic distribution with no forward peak, presumably indicating large angular momentum making possible a very large cross section for compound-nucleus formation.

A set of assignments of excited (jj) configurations consistent with these tentative experimental assignments, is shown in Fig. 14, and a very schematic representation of the intermediate-coupling transition of these states is shown in Fig. 15. The curvature of the lines suggests the direction of energy repulsion as the pairs of states with the same (J, T) are intermixed. The excited configurations are divided up into partial configurations mainly for the sake of convenience in counting the states by vector addition. For example, $p_{\frac{1}{2}}^{-2}(0)s_{\frac{1}{2}}$ in Fig. 14 indicates the $J=0$ state of the partial configuration $p_{\frac{1}{2}}^{-2}$, compounded with an $s_{\frac{1}{2}}$ nucleon. Since for $p_{\frac{1}{2}}^{-2}$, $J=0$ is associated with $T=1$ (as in the first excited state of Py^{14}), the addition of an $s_{\frac{1}{2}}$ nucleon with its $t=\frac{1}{2}$ gives states of the system with $T=\frac{3}{2}$ and $T=\frac{1}{2}$, each of course with $J=\frac{1}{2}$, as indicated in the upper left part of Fig. 15. The right column of Fig. 15 lists these assignments of angular momentum and parity, which have been arranged to agree with the experimental possibilities indicated in parentheses above the levels in Fig. 1. The only excited state observed to have negative parity, at 6.33 Mev, is, of course, assigned to the $p_{\frac{1}{2}}^{-1}$. This state does not mix in higher order with the states of opposite parity listed in the figure, but only with higher states obtained by double excitation. This 6.33-Mev excitation is thus the most direct measure we have of the doublet splitting of a p nucleon in a stable nucleus. Of the $T=\frac{3}{2}$ states, it is not clear from the available configuration assignments whether $J=5/2$ or $J=\frac{1}{2}$ should lie lower. The C^{15} beta-transition to the ground state is probably to be considered first forbidden ($\log ft=5.3$) (Fe51) and there is evidence (Hu50) for a transition to the 5.3-Mev or 6.33-Mev level, which to compete with the ground-state transition must be allowed. This would favor $J=5/2$ for the lowest $T=\frac{3}{2}$ state, as drawn in Fig. 14.

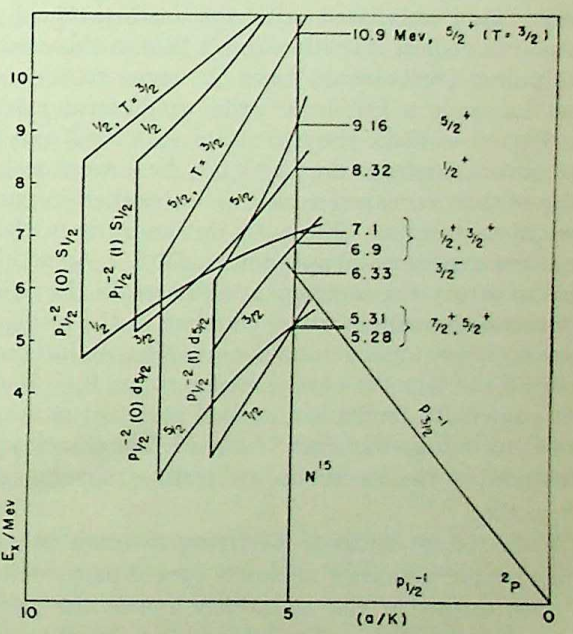


FIG. 15. Schematic intermediate-coupling transition for Py^{15}; including the first excited configurations. The numbers in parenthesis, (0) or (1), denote J_p.

CC-0. In Public Domain. Gurukul Kangri Collection, Haridwar

Digitized by Arya Samaj Foundation Chennai and eGangotri

The Closely Spaced Pairs in N^{15} and Other Nuclei

The grouping of the first two excited states into a very closely-spaced pair, with a separation of only 30 kev after a gap of 5.3 Mev and followed by a gap of 1 Mev, is very striking. It is particularly striking in combination with a similar close pairing of the first two excited states in the neighboring nucleus, O^{16}. Similar close pairing, though not of first excited states, has been noted in B^{10} and in B^{11}, where it was considered to be fortuitous and not very unlikely because of the density of nearby levels, and in N^{13}, where the accidental nature of the pairing is attested by the wider spacing of the levels in the mirror nucleus C^{13}. In the interpretation of Fig. 15 the close pairing in N^{15} is fortuitous. The chance that the first two levels should be only 30 kev apart in a spectrum starting off with averaging spacings of $\frac{1}{2}$ Mev is about 1/15. The chance in O^{16}, where the spacing is 80 kev, is about $\frac{1}{6}$. The chance that this should happen in two specified successive nuclei of which we have high resolution data is about 10^{-3}. The chance that it should happen in any two successive light nuclei out of about eight for which we have high resolution data is about 10^{-2}. But it is strange that it happens in the two with the highest first excitation energy—the probability of this happening fortuitously is about 10^{-3}. The unpleasantness of this is not mitigated by evidence to be cited below, concerning observed parities, that the close pairing in O^{16} is indeed fortuitous. Under these circumstances, one grasps at straws.

The most obvious assumption (I50) would be that the close pairs are caused by the coupling of an excited s-nucleon to the angular momentum vector of an almost filled p-shell, and that this coupling is very weak for some reason associated with the inadequacy of the phenomenological Hamiltonian (2). But in this case the two paired levels would have the same parity, so it does not apply to O^{16}. In N^{15}, this would mean modifying Fig. 15 to make the two states with $J=\frac{3}{2}$ and $\frac{1}{2}$ of the partial configuration $p_{\frac{1}{2}}^{-2}(1)s_{\frac{1}{2}}$ lie lowest and, in spite of their curvature which indicates their impurity, very close together. These J's do not agree with the tentative experimental assignment, $J \gtrsim 5/2$. An artificial way to satisfy this assignment and explain the pairing is to assume weak intershell coupling in the configuration $d_{5/2}{}^2(5)p_{\frac{1}{2}}$ arising from two-nucleon excitation, in spite of the fact the partial configuration $d_{5/2}{}^2(5)$ does not contribute to the low excited states of either O^{16} or O^{17}, as indicated in Figs. 16 and 17. The experimental situation is too uncertain to justify pursuing such conjecture.

While nature seems to be trying to teach us something by the frequency of closely spaced pairs, we have not yet learned it and tentatively ascribe the pairs in N^{15} and O^{16} to chance. The relation between these close pairs for which we have no causal explanation within the framework of the present analysis, and the close pairs observed in the odd-odd nuclei Na^{24}, Al^{28}, and P^{32}, for which an explanation is available involving an expected weak coupling of an s-nucleon spin to another j is discussed further in Sec. 9.

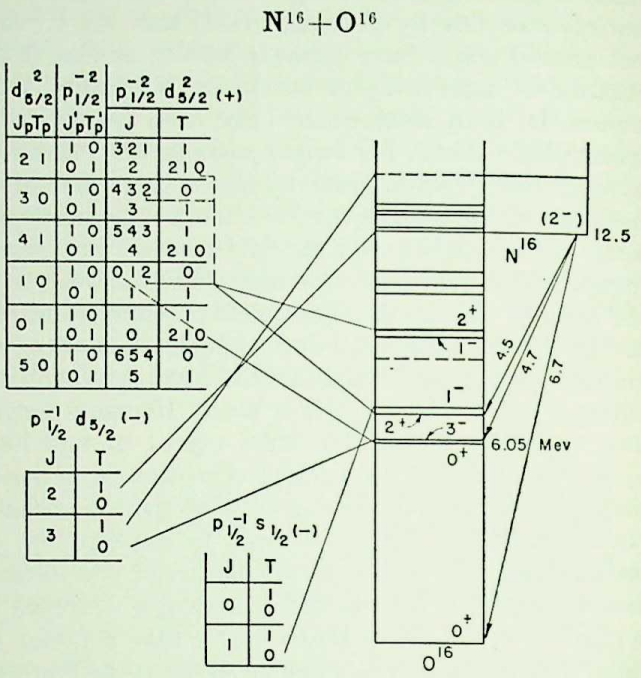


FIG. 16. (jj) configuration assignments to the states of Py^{16}.

Both here and in Py^{15}, the exceptionally high first excitation energy attests the influence of shell structure at the closing of the p shell. Another remarkable feature of the spectrum is the clustering of the first four excited states into two closely spaced pairs, the first pair separated by 80 kev (only a little more than 1 percent of the excitation energy) and the second pair by 200 kev (the same as between two states at the same excitation in N^{15}!) after a gap of about 800 kev.

As a result of recent careful studies of angular correlations we are fortunate in having experimental assignments of these first four excited states. The first has long been known to be 0^+ because of the fact that it does not emit gammas ($0^+ \rightarrow 0^+$ forbidden, the ground state of course being 0^+), and thus has time to emit electron-positron pairs. The second excited state has been shown by independent work in two laboratories (A50, B50) to be 3^-. Recent work at Cambridge (S52), mainly on alpha-gamma correlations, has identified the third and fourth excited levels as 2^+ and 1^-, respectively [although an earlier report (Fr51) on this work had given the preliminary result 2^+ and 2^- for these states]. It is possible that experimental clarification of further details will show that there is here very strong evidence for the validity of the alpha-model in this particular nucleus, which is particularly suited to this because it can be built as a compact cluster of four alphas (D40). This possibility is discussed further in Sec. 10. Pending further evidence, we wish, however, to view this nucleus here as a consistent part of a

CC-0. In Public Domain. Gurukul Kangri Collection, Haridwar

Digitized by Arya Samaj Foundation Chennai and eGangotri

sequence of nuclei to which the central model seems to apply.

Despairing of the hope of finding in the central model any simple cause for the close juxtaposition of states of opposite parity, as mentioned above, we regard the pairing as accidental and make the configuration assignments indicated in Fig. 16. The great complexity of the situation is typified by the fact that the first four excited states are ascribed to three different (jj) configurations, either with a $p_{\frac{1}{2}}$ nucleon excited to a $d_{5/2}$ state or to an $s_{\frac{1}{2}}$ state or with two $p_{\frac{1}{2}}$ nucleons excited to $d_{5/2}$ states. The perhaps rather surprising suggestion that the first excited state should result from two-nucleon excitation was first made by M. G. Mayer, who based it on the result of the short-range or δ-function approximation (M50) which states that two equivalent nucleons with large j have a large "pairing energy" when their j's add up to $J=0$. While the δ-function is not a good approximation (K50) in so small a nucleus as O^{16}, this result reflects the fact that this state has a high symmetry (upon nucleon exchange), and a high symmetry is doubtless one of the reasons why the $J=0$ and $J=2$ states of the two-nucleon excitation configuration have such low energy as to appear among the first four excited states. Another reason is that there is for each of these J's more than one state with the same (J, T), as indicated in Fig. 16, and the intermixing of these states pushes the lowest one down. It is a characteristic of our intermediate-coupling interpretation of the spectra of other light nuclei that a configuration is spread out over a wide energy region, and this doubly-excited configuration is so complicated, including very many states, that it is spread out over a very wide region and some of its states are low, one of them even lower than any of the states of the simpler singly excited configurations.

Note added in proof.—One would hope for some simplicity in the excited configuration $p_{\frac{1}{2}}^2 d_{\frac{5}{2}}^2$, arising from the expectation that the p–d exchange integrals are smaller than the p–p or d–d integrals. In this approximation one would expect to be able to estimate which states have the lowest energy from the energies of the two-nucleon partial configurations $p_{\frac{1}{2}}^2$ and $d_{\frac{5}{2}}^2$ separately, as is indeed implied in the above remarks of pairing energy in the δ-function approximation. Recent calculations of the energies of these partial configurations separately, by Flowers and Edmonds (Fl52), show that for reasonable ranges instead of the δ-function approximation, the next-to-lowest line of the two-nucleon excited configuration in Fig. 16 should lie lowest, that is, the first states of this configuration should be a group of three with $J=4, 5, 6$, $T=0$. We are left with no central-model explanation of the O^+ first excited state of O^{16}, which enhances the attractiveness of the alpha-model as an alternative. The possibility needs further investigation that the p–d exchange integrals might be responsible. The calculated result just quoted is dependent on the phenomenological representation (2) of the nuclear interactions. It is closely related to the explanation of the low state $J=3$ of $p_{\frac{3}{2}}^{-2}$ in B^{10}, and it is not apparent how to alter the interaction assumption to keep that experimentally satisfactory result and still obtain $J=0$ (rather than $J=5$) lowest in $d_{\frac{5}{2}}^2$. The intervention of the $(J, T) = (5, 0)$ state as the lowest state is due to the interplay of an excited proton and neutron along with a pair of either. If we were concerned with excitation only of a pair of neutrons or a pair of protons, it would have been $(0, 1)$, as was assumed above. There are other phenomena which would be clearer if neutron and proton excitation should be understood to act more nearly separately than we here expect them to. These phenomena are mentioned at the end of the discussion of the (jj) double levels of Na^{24}, about four pages below [see also (SG53)]. Some of these difficulties suggest that consideration of the deformability of the potential well which shapes the single-nucleon orbits (Ga53, W53) may provide a fruitful extension of this discussion of light nuclei.

The beta-decay to each of the (unresolved) pairs of excited levels is allowed, while that to the ground state is forbidden. (The log ft values appear on the transition lines in Fig. 16.) This suggests 2^- for the ground state of N^{16}, and such a state is available from one of the singly excited configurations, as indicated in the figure. It is satisfactory that the configuration $p_{\frac{1}{2}}^{-1} d_{5/2}$ should appear below $p_{\frac{1}{2}}^{-1} s_{\frac{1}{2}}$ among the $T=1$ states (as well as the $T=0$ states), both because one expects it to cover a wider energy spread and because the single-nucleon state $d_{5/2}$ appears according to the evidence of O^{17} to lie below $s_{\frac{1}{2}}$. It is further satisfactory that the $(J, T) = (2, 1)$ state should lie below the $(3, 1)$ state of $p_{\frac{1}{2}}^{-1} d_{5/2}$, because it agrees with a general rule (K52b) that, when a neutron hole, for instance, is coupled to a proton, the lowest state formed has $J=j_1+j_2-1$, that is, a total angular momentum quantum number one less than the maximum possible. Most examples are found with neutrons and protons in the same shell (for which the result follows for both the long-range and short-range extreme theoretical calculations, and presumably between), but the case of ${}_{19}K^{40}$ is very similar to the present case, configuration $d_{5/2}^{-1} f_{7/2}$, with two different shells involved. That the lowest state should be $J=j_1+j_2-1=4$, in agreement with observation, in this case with reasonable assumptions has been shown by Kurath (K52b), and similarly $J=2$ for N^{16}. There are only two states of this configuration in N^{16}, so the (jj)-coupling statement of which should be the lower should probably have significance also in intermediate coupling.

As we have suggested in connection with Be^8 above, the existence of states of the same symmetry in the alpha-model may influence the spacings and properties of the states encountered in the intermediate-coupling scheme, and O^{16} is a favorable place for this to happen because the first four excited states just discussed have

CC-0. In Public Domain. Gurukul Kangri Collection, Haridwar

Digitized by Arya Samaj Foundation Chennai and eGangotri

their counterparts among the low excited states of the alpha-model (Sec. 10).

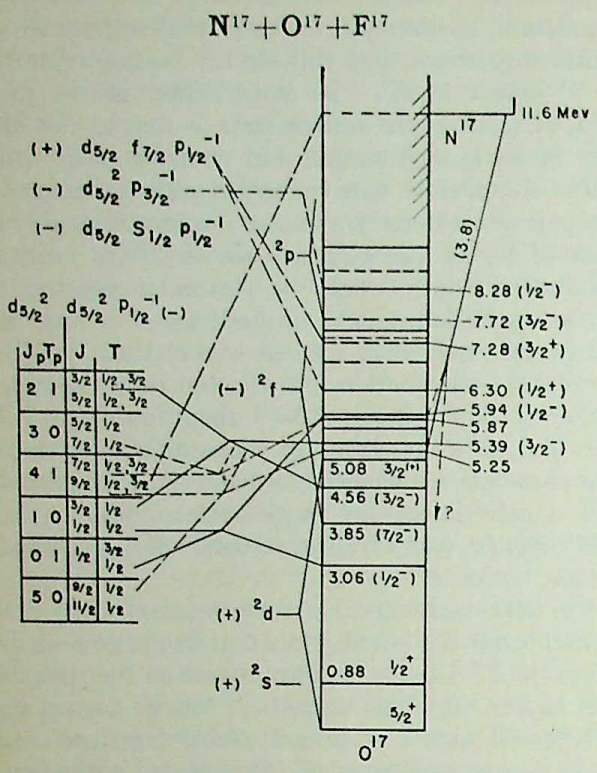


FIG. 17. (jj) configuration assignments to the states of Py^{17}.

In most of the low states of this polyad we have essentially a single nucleon outside of a closed p shell, and the existence of several states for this relatively loosely bound nucleon contributes several levels of moderate excitation energy, as shown in Fig. 17, in strong contrast to the closed-shell appearance of the O^{16} spectrum. The second excited state at about 3 Mev, however, does not fit into this single-nucleon scheme, and must be ascribed to an extra excitation from one shell to another, $p_{\frac{1}{2}}$ to $d_{5/2}$, similar to that responsible for the first excited state of O^{16}, the resultant low energy again resulting from "pairing" in the partial configuration $d_{5/2}^2$ (as was also suggested by Mrs. Mayer). In this case the excitation energy is lower because excitation of only one nucleon is necessary, to pair with a $d_{5/2}$ nucleon that is already there in the ground state. It is not so remarkable here as in O^{16} that this state lies low because here it arises from single-nucleon excitation, as do the other low excited states. It is more complicated than the others because the possibilities of vector addition give two $\frac{1}{2}^-$ states in this configuration and they are mixed to give the 3.09-Mev state as indicated in Fig. 17.

Note added in proof.—This interpretation, too, is cast in doubt by the calculated result (F152) that $(J_p, T_p) = (5, 0)$ lies lowest. Sufficient repulsion of the two $(J, T) = (\frac{1}{2}, \frac{1}{2})$ states again requires large p–d exchange integrals.

Partly by comparison with a state in F^{17} identified by a proton scattering resonance, the O^{17} state at 3.85 Mev is identified as the $7/2^-$ state corresponding to the single-nucleon state $f_{7/2}$, which it is very satisfactory to find here because it is expected to be the next single-nucleon state after the $d_{5/2}$ ground state and the $s_{\frac{1}{2}}$ just above it. Above this, the identifications are made by observation of the scattering resonances of neutrons on O^{16}. In the case of the 5.08-Mev state, there is some question whether it should be interpreted as an exceptionally strong $\frac{3}{2}^+$ resonance [with γ^2 about $\frac{1}{4}$ of the theoretical limit, according to Table I(17) of reference (Aj52)] or a $\frac{3}{2}^-$ resonance about as strong as the next few states above it (about 0.03 of the limit). The former possibility, $\frac{3}{2}^+$, is favored, partly because there is another level identified as $\frac{3}{2}^-$ only 50 kev below it and it does not seem likely that two such levels from the first excited configuration would occur so close together, but mainly because an exceptionally strong level $\frac{3}{2}^+$ is expected somewhere, namely, the single-nucleon-like $d_{\frac{3}{2}}$ state which is needed to join the ground state, essentially a $d_{5/2}$, to complete a ^2D. The single-nucleon-like level is expected to correspond to a much stronger resonance than the levels involving excitation of the "core," and this is the only level with the appropriate characteristics in the region up to above 8 Mev that has been properly explored.

Several levels next above this one have moderately weak resonances, apparently because they arise from excited configurations, and possible configuration assignments for them are suggested in Fig. 17. Above the $^2f_{7/2}$ single-nucleon state one expects to find the ^2p levels (with radial quantum number 2 corresponding to one radial node), first the $^2p_{\frac{3}{2}}$ and above it the $^2p_{\frac{1}{2}}$, and if one were to ignore the weakness of the resonances one might think to find the corresponding O^{17} states at 5.39 and 8.38 Mev, which would make a ^2p splitting of about 3 Mev related to the 5 Mev ^2d splitting roughly in the ratio of their $(2l+1)$. Because the single-nucleon-like levels corresponding to the ^2p are expected to be exceptionally strong, it seems preferable to recognize that these single-nucleon levels may be spread quite far apart in this nucleus, and to identify the strong level at 7.72 Mev with the $^2p_{\frac{3}{2}}$, as is done in the figure.

The beta-decay of N^{17} is observed under conditions of high energy bombardment and consequent strong contamination of other beta-decays, through the unusual circumstance that it gives rise to simultaneous neutron emission ("delayed" because it follows the beta) from excited states of O^{17}, the betas and neutrons being observed in coincidence (A49). The neutron energy measurements (H49) seem to indicate an intense transition to an O^{17} level at about 5.26 Mev ($E_n \approx 1.05$ Mev) and a weaker transition to a level at about 5.89 Mev ($E_n \approx 1.65$ Mev), which we take to be the levels at 5.25 and 5.87 Mev for which no identifications have been given because they have not been resolved in the neutron scattering experiments. It is not clear

CC-0. In Public Domain. Gurukul Kangri Collection, Haridwar

Digitized by Arya Samaj Foundation Chennai and eGangotri

to what extent they may have contributed to the neutron scattering and whether they may have falsified the identifications of the adjacent states from which they were not resolved, but it is possible that these states may have high J's and their contributions to the scattering may have been suppressed thereby. There are many other states of both parities and low J's in this region through which the $(\beta+n)$ process does not seem to go (though the neutron energy resolution is not good enough to make this certain). Therefore, it seems likely that these two states differ from the others in having high J's, and that the ground state of N^{17} also has high J. Either the $(J, T)=(7/2, \frac{3}{2})$ or $(9/2, \frac{3}{2})$ state of the configuration $d_{5/2}{}^2 p_{\frac{1}{2}}{}^{-1}$, assigned as the ground state of N^{17}, could accomplish this selection, and one could distinguish between these possibilities if it could be observed whether or not the beta-transition also goes to the $5/2^+$ ground state of O^{17}. The latter has been indicated among the tentative configuration assignments suggested in Fig. 17, along with similar suggested assignments from the same configuration for the presumed delayed-neutron states at 5.25 and 5.87 Mev. The favored beta-transition indicated by the value $\log ft=3.8$ is valid only if there is no transition to lower states, and is consistent with this assignment of initial and final states of the beta-decay to the same configuration.

8. COULOMB ENERGY IN THE CENTRAL MODEL

The central model, of which the (jj) model is a special case, is a model in which states of the system are formed of individual-nucleon wave functions which are solutions of a wave equation with a spherically symmetrical potential. The state of the system does not necessarily possess central symmetry. (With a statistical distribution of the direction of J, the over-all state has central symmetry, but not the magnetic substate.) This lack of central symmetry, which implies a correlation between the angular coordinates of two nucleons, is in part responsible for the multiplet separations in (LS) coupling and the separations within a (jj) multiplet in (jj) coupling. The Pauli asymmetry, which also implies a correlation of a different sort between the positions of the nucleons, is also and usually even more heavily responsible for these separations.

The lack of central symmetry may be described in terms of a flattening of the orbits of two nucleons almost into one plane when their orbital angular momenta l are nearly parallel or antiparallel (such as when $L=l_1+l_2$ is as large or small as possible), as compared to a closer approximation to spherical symmetry in states with intermediate values of L [or of J in (jj) coupling]. For example, the ^1S lies below the ^1D in the middle of Fig. 5, although they both have the Pauli antisymmetry in the spin factor, and this energy difference may be associated with the picture that the antiparallelism in the ^1S is exact, the vector sum $[L(L+1)]^{\frac{1}{2}}$ is exactly zero,

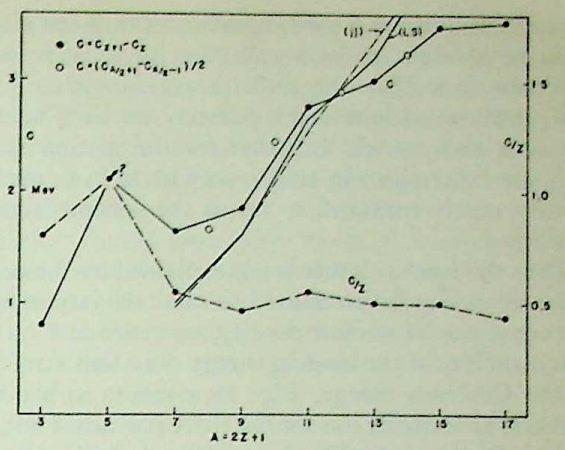


FIG. 18. The Coulomb energy differences of the mirror isobars. The curves are drawn between the points for the odd isobars only. The Coulomb energies differences per unit charge difference for the even isobars are indicated by open circles. The theoretical curves for (LS) and (jj) coupling assume a constant Coulomb exchange integral K_c.

whereas the corresponding parallelism in the ^1D is not exact, the two vectors of "length" $[l(l+1)]^{\frac{1}{2}}$ adding up vectorially to less than their arithmetic sum.

The Coulomb energy differences between the mirror nuclei are also affected by these considerations of nuclear "shape" and other correlations between the positions of the nucleons, and for this reason it is only an approximation to consider simply the electrostatic energy of a spherically symmetric charge cloud. The effect of the correlation considerations is, however, quite small. The Coulomb energy differences of the neighboring mirror pairs of isobars have been calculated both in (LS) coupling (F37) and in (jj) coupling (K52), and they are plotted in Fig. 18. (There the scale is quite arbitrary, the differences taken from Kurath's Table III (K52) being plotted with $17K_c=1$ Mev, K_c being the Coulomb exchange integral.) The experimental curve for the Coulomb difference C has a meaning for the p-shell only for $A=7$ and up, since $A=5$ is an anomalous case in which the ground states of both isobars are virtual. This portion of the experimental curve shows a rather pronounced four-structure, an alternation in slope with the points for $A=4n+1$ lying relatively low. The calculated (LS)-coupling curve is plotted in the same figure and shows a much weaker four-structure of the same sort. The (jj)-coupling curve is even more nearly a straight line. The fact that the theoretical curves are much too steep to follow the trend of the experimental curve indicates that K_c should not be taken constant across the p shell, as is done in Fig. 18. Instead it should decrease with increasing A, and a very good fit to the general trend (but with inadequate four-structure) may be obtained by assuming $K_c \sim A^{-1}$. This is exactly the variation one expects on the usual simple assumption of constant nuclear density, and range of interactions small compared to nuclear size; but it is perhaps somewhat surprising that it should

CC-0. In Public Domain. Gurukul Kangri Collection, Haridwar

Digitized by Arya Samaj Foundation Chennai and eGangotri

apply so well in the p shell. It indicates that the p shell is to be thought of as a collection of angular wave functions, but that the radial wave functions going with them are determined separately for each nucleus (or even each state), and that for the ground states they are determined in such a way as to keep nuclear density nearly constant, so far as the general trend is concerned.

Thus the four-structure is not explained by the correlations, but may be attributed to small deviations from the constancy of nuclear density, as dependent on the four-structure of the binding energy. The four structure of the Coulomb energy, Fig. 18, consists in the fact that C is abnormally low for the three polyads $A=9$, 13, and 17. Of these, $A=17$ is beyond the p shell, and may be low because a d orbit is larger than a p orbit. That and much more questionably the ground state of $A=13$ are cases where it is perhaps a better approximation than elsewhere to think of a "core" plus one nucleon, and this corresponds to the simple spherically symmetric model used by Bethe in discussing this effect (Be38, E41). The Coulomb difference C is a property of the last nucleon in its interaction with the "core," and its unusually small binding energy in Py^{13} leads one to expect it to have an abnormally diffuse probability distribution and thus an abnormally small value of C. In $A=9$ the experimental "binding energy of the last nucleon" is particularly low, being positive for the neutron in Be^9 but negative (-0.2 Mev) for the proton in B^9. Here it is probably not a good approximation to think of this low binding energy as belonging to any one nucleon, but even when shared among several it may have quite an effect on the nuclear size (contributing to a cooperative phenomenon). The virtual nature of B^9 makes this polyad an atypical case something like Py^5, though the influence of the virtual nature is probably much reduced by the sharing of energy between nucleons in B^9 (and indeed it seems in Fig. 18 that the sign of the influence is the opposite of that in Py^5).

9. THE NEUTRON-PROTON (jj)-COUPLING DOUBLE LEVELS

(jj) Double Levels in Atoms

In atomic spectra the only examples of real (jj) coupling are found in the configurations p^5s and d^9s involving the coupling of an s-electron spin to the j of an almost closed shell. Examples of (LS) coupling and quite frequently of intermediate coupling are found among the cases of coupling of two equivalent electrons. For example, the configuration p^2 shows a nice intermediate-coupling transition in Fig. 4[11] of reference (C35), going from GeI $4p^2$ with a moderately low principle quantum number and displaying a clear separation into the triplet and two singlets of (LS) coupling, and SnI $5p^2$ in which the multiplets may still be recognized, over to PbI $6p^2$ with a high principle quantum number, which is well out into intermediate coupling and even begins to show a grouping into the double-levels characteristic of (jj) coupling. But extreme (jj) coupling occurs only when one of the j's is an s-electron spin, and when the s electron has a high radial quantum number so that its charge distribution overlaps little with the almost closed shell. In the spectrum of un-ionized neon, for example, the four levels of the configuration $2p^53s$ are arranged in a singlet and triplet, with some deviation from the "interval rule" of (LS) coupling, and the $2p^54s$ and successively higher excitations progress across the region of intermediate coupling to (jj) coupling, until finally $2p^511s$ has two narrow (jj) double levels whose splitting is less than one percent of their separation.

(jj) Double Levels in Na, Al, and P

The reason that a high principle quantum number is required in atoms is that the exchange integral, arising from the Pauli antisymmetry of the two electrons, tends to separate the two levels $J=j\pm\frac{1}{2}$. For a neutron and a proton in a similar situation this is not so if the interaction between them does not involve the spin. Beautiful examples of (jj) double levels are for this reason found in the odd-odd nuclei in the region of filling of the second s orbit, in Na^{24}, Al^{28}, and P^{32} (as was recently pointed out by Maria G. Mayer at a conference in Pittsburgh). In the two latter nuclei (E51, E52, V52a), the ground states belong to double levels, the ground configuration of ${}_{13}Al^{28}$ being $d_{5/2}{}^{-1}s_{\frac{1}{2}}$ while in ${}_{15}P^{32}$ we have $s_{\frac{1}{2}}{}^3d_{\frac{3}{2}}$, since the $d_{5/2}$ orbit is filled at 14 nucleons and the s orbit at 16. The point is that the nuclear interactions as we treat them phenomenologically are only about one-fifth spin-exchange forces, and the rest does not involve the spin. This factor 0.2 from (2), say, is enough when combined with the fact that the two nucleons do not have the same radial wave function, to explain the small splitting of the double levels. Let us show that the large term not involving the spin gives no splitting. This is most easily done (as was suggested by Mrs. Mayer) by considering the problem of constructing the wave functions for the two values of J in the magnetic sublevel $M=0$, since the two simple product functions with which we start then have the same diagonal matrix element and the splitting is made only by the nondiagonal element between them. For the configuration $s^3d_{\frac{3}{2}}$, for example, let us define $d_{\frac{3}{2},\frac{1}{2}}=a$, $d_{\frac{3}{2},-\frac{1}{2}}=b$ (where the subscripts mean j, m_j) and write the two $M=0$ product wave functions for three neutrons and one proton of P^{32}:

$$\langle a^+\alpha^+\beta^+\beta^-\rangle, \qquad \langle b^+\alpha^+\beta^+\alpha^-\rangle. \tag{20}$$

The superscripts indicate isobaric spin projection, $+$ for a neutron and $-$ for a proton, α and β imply s-wave functions including these spin functions for spin up and down, the four factors are functions of the coordinates

CC-0. In Public Domain. Gurukul Kangri Collection, Haridwar

Digitized by Arya Samaj Foundation Chennai and eGangotri

of the four nucleons, respectively, and the pointed brackets mean "antisymmetrized sum." The matrix element between them is

$$H_{12}=(a^+\beta^-|\,V\,|b^+\alpha^-)-(a^+\beta^-|\,V\,|\alpha^-b^+). \quad (21)$$

The first term is zero because of spin orthogonality for the last nucleon if V does not operate on σ, and the second term is zero because of isobaric spin orthogonality (or another way of saying it is that "we don't have to antisymmetrize between a neutron and a proton"). Thus the levels $J=1$ and $J=2$ are degenerate so far as the main term $0.8P$ of (2) is concerned, and are split only by the small term in the spin-exchange operator Q which spoils the spin orthogonality. (Presumably it hereby represents what a tensor force would do, but this should be calculated.)

The same argument applies with the $d_{\frac{3}{2}}$ excess neutron replaced in excited states by $f_{7/2}$, $f_{5/2}$, $p_{\frac{3}{2}}$ and $p_{\frac{1}{2}}$, each giving an excited double level in P^{32}. In Al^{28} an excited double level may arise similarly from $d_{5/2}\rightarrow d_{\frac{3}{2}}$ excitation of the odd proton, leaving the spin of the s neutron the only neutron vector free to be oriented. In $_{11}Na^{24}$ the ground configuration does not contain an s nucleon [and the observations (Sp52) show the ground state to be single], and in the excited states of this nucleus the formation of the double levels is not quite so simple because there is the possibility of exciting either a proton or a neutron. Here the neutron excess comes into play in a somewhat different way from the way it does in P^{32} to avoid interaction between the states formed by these different types of excitation and leave intact any pairing into double levels that might be caused in some way similar to the same simple mechanism explained above. If we excite a $d_{5/2}$ neutron to the s orbit, we have a partially filled d shell $(d_{5/2})_{\text{prot}}{}^3(d_{5/2})_{\text{neut}}{}^4$ which possesses a low state of partial isobaric spin $T_P=\frac{1}{2}$, whereas proton excitation leaves the d shell $(d_{5/2})_{\text{prot}}{}^2(d_{5/2})_{\text{neut}}{}^5$, with its lowest $T_P=\frac{3}{2}$ and hence considerably higher energy that cannot be brought down by the weak coupling with an s nucleon. Hence the two excitations may be expected to act fairly independently, and each might give rise to a double level. In such a case we have, however, the coupling of an s-nucleon to a complex partial wave function of a d shell formed by the orientation of the vectors of both protons and neutrons, and it is not at all clear from simple considerations that an exchange integral of the Majorana term should be absent from the splitting $J=J_P\pm\frac{1}{2}$. If the excited nucleon is a neutron, to take the example just discussed, the d shell has an odd number of protons and an even number of neutrons. The fact that double levels appear in Na^{24} suggests that the s neutron is coupled only to the protons, as though the even number of neutrons were somehow suppressed from sharing in the complexity of the wave function of the d shell. This would be analogous in a simpler case to having the two $p_{\frac{3}{2}}$ neutrons of the configuration $p_{\frac{3}{2}}{}^3$ in the ground state of Li^7 form a partial resultant $J_P=0$ and ascribe all of the angular momentum to the $p_{\frac{3}{2}}$ proton, which is not in keeping with the way the energy of the ground state on the (jj) side of Fig. 6 was calculated. (It would give a Schmidt-line magnetic moment, whereas the magnetic moment calculated with proper neutron participation is close to that observed.)

Thus it is not clear why the even numbers of like nucleons should pair up to make their total angular momentum zero in such cases of only partly filled shells, but the double levels of Na^{24} suggests that they do. There are other indications that this happens in the intermediate and heavy nuclei, a set of probably related but enigmatic "queer facts." There are several cases in which the addition of two neutrons to go from one odd-even isotope to another changes the magnetic moment of a nucleus by only a small fraction of a percent. There are also several cases where the addition of two protons to an even-even nucleus changes the first excitation energy of a nucleus almost none at all.

A (jj) double level in a heavy nucleus. The ground state of the nucleus $_{81}Tl^{208}{}_{127}$ is a member of a double-level with a splitting of only 40 kev. This nucleus, though very heavy, is simple enough to discuss because of differing from a double closed shell by only one nucleon and one hole, and Pryce (Pr52) attributes the double-level to the configuration $(s_{\frac{1}{2}})_\pi{}^{-1}(g_{9/2})_\nu$. Its reason for being only 40 kev wide, as compared with about 300 kev for the quadruple-level attributed to $(d_{\frac{3}{2}})_\pi{}^{-1}(g_{9/2})_\nu$ is the same as for the double-levels in the much lighter nuclei here discussed.

(jj) Triple Levels in Si^{29} and Al^{28}

In $_{14}Si^{29}$ there is a triple level consisting of states at 4.840, 4.897, and 4.934 Mev, separated from the nearest neighbor by $\frac{3}{4}$ Mev (V52a). This may be ascribed to the excited configuration $d_{5/2}{}^{-1}s^2$, which is obtained from the ground configuration $d_{5/2}{}^{12}s$ by excitation of one $d_{5/2}$ nucleon into an s orbit. It is consistent with other examples that this excitation should "cost" about 5 Mev. The partial configuration s^2 can have a spin $S_p=1$ which couples to the $d_{5/2}{}^{-1}$ "hole" to give three states with $J=\frac{3}{2}$, 5/2, and 7/2 (a prediction of which verification would be of interest). Since the partial configuration $d_{5/2}{}^{-1}$ has only one state, it is consistent with this interpretation that there should be only one such triple level in Si^{29}. In $_{13}Al^{28}$ two triple levels (or more—the density of states is too high to be sure) have been observed at about this elevation, corresponding apparently to the excited configuration $d_{5/2}{}^{-2}s^2$, which also requires single-nucleon $d_{5/2}\rightarrow s$ excitation, and which could give rise to as many as four triple levels. Above the three fairly low double levels in $_{11}Na^{24}$ there is a region of high level density near 4 Mev which may be considered to contain as many as three triple levels, the narrowest with a total splitting of only 35 kev. In this case two-nucleon excitation to the configuration

CC-0. In Public Domain. Gurukul Kangri Collection, Haridwar

Digitized by Arya Samaj Foundation Chennai and eGangotri

$d_{5/2}s^2$ is required to obtain a partial spin $S_p=1$ which might give a triple level.

The reason for the small splitting of these triple levels is not as clear as in the case of the double levels, because the excited configurations required may be attained by either proton or neutron excitation, and the $S_p=1$ state of the partial configuration s^2 has $T=0$. Thus it necessarily involves both protons and neutrons, to be coupled to either protons or neutrons or both in the d shell. Lacking a more elegant suggestion, it is perhaps to be inferred that the different arrangement of nodes of the s and d orbits makes the coupling between them (an integral like K) quite small, suppressing the contribution of the leading term of Eq. (2) to the splitting.

The Possibility of (jj) Double Levels in Li^6, B^{10}, and N^{14}

The situation for the excited configuration $p_{\frac{1}{2}}^5 s_{\frac{1}{2}}$ in B^{10} has a slight similarity to that in Na^{24}, but differs from it drastically in the fact that this is a "self-mirrored" nucleus with no neutron excess. There is, thus, no energetic tendency to separate the states formed by neutron excitation from those formed by proton excitation. Even if we should invoke a not understood tendency for even numbers of nucleons to pair their j's to a zero resultant, as is suggested by the Na^{24} double levels, we should, because of the interference between neutron and proton excitation, still not expect double levels in B^{10} any more than in Li^6.

The lack of double levels caused by s excitation in Li^6+He^6 is a matter of easy calculation. We now use the notation a and b for the $m_j=\pm\frac{1}{2}$ projections of $p_{\frac{1}{2}}$:

$$\begin{aligned} a&=(2/3)^{\frac{1}{2}}z\alpha+(1/3)^{\frac{1}{2}}[(x+iy)/2^{\frac{1}{2}}]\beta,\\ b&=(2/3)^{\frac{1}{2}}z\beta+(1/3)^{\frac{1}{2}}[(x-iy)/2^{\frac{1}{2}}]\alpha, \end{aligned} \tag{22}$$

where $x\pm iy$ and z indicate the angular part of the p orbital. Then the four $M=0$ states are

$$a^+\beta^-,\quad b^+\alpha^-,\quad \beta^+a^-,\quad \alpha^+b^- \tag{23}$$

the superscripts again indicating the sign of the isobaric spin projection m_t. The secular determinant made from the matrix between these states, for an interaction not involving spin, is

$$\begin{vmatrix} -E & 0 & A & B \\ 0 & -E & B & A \\ A & B & -E & 0 \\ B & A & 0 & -E \end{vmatrix} = \begin{vmatrix} 0 & 0 & A & (B-E) \\ 0 & 0 & (B-E) & A \\ A & (B+E) & -E & 0 \\ (B+E) & A & 0 & -E \end{vmatrix} = 0, \tag{24}$$

where

$$\begin{aligned} B&=(a\beta|V|\alpha b)=(2/3)(zs|V|sz)\\ &=2(a\beta|V|\beta a)=2A \end{aligned} \tag{25}$$

since, because of the vanishing of integrals of odd powers and the equivalence of the three Cartesian coordinates,

$$\begin{aligned} &[(x+iy)^*s|V|s(x+iy)]/2\\ &\quad=[(xs|V|sx)+(ys|V|sy)]/2=(zs|V|sz). \end{aligned} \tag{26}$$

The diagonal elements have been omitted because they differ only in orientation or in the proton-neutron difference and are all equal. The factorization of the determinant into the product of two quadratics, as in the second member of Eq. (24), is accomplished by adding rows and subtracting columns, the third with the second and the fourth with the first. Thus we have the four distinct roots $\epsilon=\pm A, \pm 3A$, a ladder with three equal steps. (One might speculate as to whether the equal spacing between the first, second, and third $T=0$ excited states of B^{10} may indicate that they come from $p\rightarrow s$ excitation, were it not that they are observed to have even parity, and that the four odd theoretical levels have alternately $T=0$ and 1.) Thus the four levels do not fall into double levels. The same analysis applies to the configuration $p_{\frac{1}{2}}s$ of Py^{14} except for an interchange of the factors (2/3) with (1/3), and a sign of the coefficients which does not affect the result.

In B^{10} the two levels at 5.11 and 5.17 Mev appear to form a double level, the splitting between them being only 60 kev and the separation from the nearest other level being 220 kev. The ratio between these is not in itself very convincing. In such a densely populated part of the energy spectrum it is not very unlikely that levels will fall close together by chance. These two levels are both observed, and with comparable intensity, in the forward yield of low energy neutrons from the $Be^9(d, n)$ reaction as the deuteron energy is raised past their respective thresholds (Bo51). Since these are so strong that the first of them constitutes practically the threshold for the reaction, somewhat below 1 Mev, they are thought to involve capture of an s-proton, $l_p=0$, which would give them odd parity and require that their wave functions contain at least a major portion from the configuration p^5s. Thus it is very tempting to suppose that they correspond to the two orientations of an s-proton spin relative to another j or J_P. The fact that the states are prepared in such a way that the odd nucleon is a proton is not reason enough to expect that it remains so, without interference from the state formed by neutron excitation. As long as the interaction with the excited neutron state is represented by an exchange integral capable of making a splitting of the order of $\frac{1}{2}$ Mev or more, as would seem to be the most likely result of a complicated calculation on the basis of what we have said, the

CC-0. In Public Domain. Gurukul Kangri Collection, Haridwar

Digitized by Arya Samaj Foundation Chennai and eGangotri

prepared "excited proton state" could not remain undisturbed long enough to define an energy as sharply as 60 kev. Their juxtaposition may be accidental, or it may be related to the smaller than expected coupling suggested by the triple levels.

The Enigmatic Closely Spaced Pair in N^{15}

The double levels here discussed have been in odd-odd nuclei. Their occurrence and explanation does not seem to throw any light on the occurrence of closely spaced pairs in the odd-even nucleus N^{15} (even if we ignore the uncertain identification $J \gtrsim 5/2$ for the lower pair). Here one may excite a neutron to the s state and leave the rest of the nucleus in the $J_P=1$, $T_P=0$ state corresponding to the ground state of N^{14}, and this is not matched by proton excitation, but then J_P is made of a neutron as well as a proton and one would expect exchange splittings from the Pauli antisymmetry between the neutrons. Alternatively, one may form the $J_P=0$, $T_P=1$ state by either proton or neutron excitation to the s state, but then there is only one resultant angular momentum $J=\frac{1}{2}$, and the two isobaric spin states $T=\frac{1}{2}$ and $\frac{3}{2}$ resulting from the interference of the two excitations cannot form a $T=\frac{1}{2}$ double level such as observed at 5.3 Mev in N^{15} (far below the ground state of C^{15} at 10.9 Mev).

10. THE ALPHA-MODEL AS AN ALTERNATE POSSIBILITY AND AS AN OCCASIONAL ADMIXTURE

The intermediate-coupling interpretation presented above is a complex answer to a complicated experimental situation, in which there is no simple grouping of energy levels into consistent patterns of suggestive multiplets, but rather a variety of types of spacings as one compares the various polyads. This does not satisfy a physicist's natural desire for simplicity and elegance. It is probably true but disappointing. In accepting it with hesitance, one wishes to examine any alternative which might present the possibility of a simpler interpretation of the same data. Partly for this reason we discuss here the alpha-model, for which some rather persuasive arguments have been given in the past, before so many excited energy levels of the light nuclei were known, and before the success of the (jj)-coupling version of the central model became apparent in heavy nuclei. We discuss it also because it may actually contribute to the physical properties of some of the states of a few favorable nuclei and modify the properties that they would have in a pure central model, in the sense that the wave functions of the two models may in nature be, as we have already mentioned, intermixed. As an introduction to discussing the alpha-model as an admixture, we discuss it as an alternative, and show that it does not provide a simple and adequate source of the observed energy-level patterns.

TABLE V. Vibrational constants and excitation energies in the alpha-model, on the assumption of a standard harmonic "bond."

	Be^8	C^{12}	O^{16}
c	2	$(3)^{\frac{1}{2}}$	$2(2/3)^{\frac{1}{2}}$
b	1	3	6
n	2	3	4
$(c^2/nb)^{\frac{1}{2}}$	$2^{\frac{1}{2}}$	1/3	1/9
$\omega_1 \sim (bc^2/n)$	$2^{\frac{1}{2}}$	$3^{\frac{1}{2}}$	2
$\omega_2 \sim$		$(3/2)^{\frac{1}{2}}$	1
$\omega_3 \sim$			$2^{\frac{1}{2}}$
$(\omega_1+2\omega_2+3\omega_3)/2^{\frac{1}{2}}$	1	2.96	5.83
0^+	4.38	5.24	6.05 Mev
3^-		7.66	6.13
2^+	6.13	6.13	6.09
2^-			6.09
1^-		5.24	6.45

The Alpha-Model of O^{16}

The simplest and most hopeful application of the alpha-model is to nuclei which could consist solely of alphas, the even-even $A=4n$ nuclei, with no extra nucleons or "holes." Among the light nuclei these are the "dumbbell" or "diatomic molecule" Be^8, the equilateral triangle C^{12}, and the regular tetrahedron O^{16}, and we consider them in reverse order.

Dennison (D40) has shown that the first two excited states of O^{16} in the alpha-model should be the 0^+ state of uniform dilational vibration (which he identified with the well-known 6.05 Mev pair-emitting state) and the 3^- state corresponding to the rotation of an equilateral triangle, which is the base of the tetrahedron, about its threefold axis. This agrees with the experimental identification of the first two excited states. The difference in parity of the first two excited states is a natural consequence of the alpha-model, arising from the difference between dilational vibration and rotation of a body with threefold symmetry. In the central model we were forced instead to the interpretation, which might at first seem somewhat artificial but is probably correct, that the first excited state arises from two-nucleon excitation. Dennison estimated that the 3^- state of the alpha-model should come at about 4 or 5 Mev, dependent of course on an estimated moment of inertia to which the energy is inversely proportional. The mean distance of the alphas from the center was taken to be the same as that of the extra nucleon in O^{17} and F^{17}, as indicated by their Coulomb energy difference. It seems very reasonable to assume instead that this loosely bound extra nucleon has a considerably larger mean radial displacement than do the alphas, which revises the estimate of the rotational energy upward, in a direction to agree with the energy 6.13 Mev of the observed 3^- state.

The next two states in O^{16} also fall close together, though the 200-kev separation is great enough that theirs might more easily be a chance juxtaposition. It is a curious fact that the alpha-model predicts that the third and fourth excited states should indeed fall close

CC-0. In Public Domain. Gurukul Kangri Collection, Haridwar

Digitized by Arya Samaj Foundation Chennai and eGangotri

together. They arise from a mode of vibration in which the pairs of corners, like two dumbbells, both stretch and move so their centers of mass approach one another, or vice versa. There are two such modes corresponding to the possibility of reflecting one corner through the opposite face of the tetrahedron, and the levels are split by only the energy corresponding to the frequency of this inversion, which should be small. They have angular momentum and parity 2^+ and 2^-. The recent experimental result of French *et al.* (Fr52) is that they are actually 2^+ at 6.91 Mev and 1^- at 7.11 Mev. This experimental assignment, if final as it seems to be, precludes the possibility that the 200 kev splitting of the levels near 7 Mev is to be explained as the energy of the 2^+-2^- inversion frequency. It is to be noted, however, that this energy is expected by Dennison to be very much smaller than the other separations among the first five excited states, and might easily be too small to have been resolved. There is a third mode of vibration, in which one of the "dumbbells" shortens while the other lengthens, whose first excitation energy is expected to fall rather close to the 2^+ and 2^-, and indeed, is expected according to Dennison's analysis to fall quite near 7.1 Mev if the 2^+ and 2^- both fall very close to 6.9 Mev, as we shall show in more detail. It is, therefore, important for the question of the validity of the alpha-model to determine experimentally whether it might not be possible that the 2^+ and 2^- are very nearly degenerate at 6.91 Mev. Although the angular correlation experiments indicate that this level is 2^+, it must be considered whether it may not merely be predominantly 2^+ in a set of reactions, in which there may be some selection.

Dennison (D40) analyzed the frequencies of vibration in terms of the elastic constants a, for stretching, and b and c for types of bending. In making a comparison with the preliminary data available a dozen years ago, he pointed out that b and c must be much smaller than a and set $c=0$. In fitting the modern data, we determine the moment-of-inertia parameter A by putting $6\hbar^2/A=6.13$ Mev and the first vibration frequency from $\omega_1\hbar=6.05$ Mev. From the estimate $\epsilon_0\approx\epsilon_1/25$, we put $\epsilon_0=0$, which means assuming the 2^+ and 2^- degenerate, and have $\omega_2\hbar=6.91$ Mev$-3\hbar^2/A=3.85$ Mev. If we here too put $c=0$, we find from Dennison's relations $M\omega_1^2=4a+16b$ and $M\omega_2^2=a-2b$ that b is indeed small, $b=-a/13.8$, and from $M\omega_3^2=2a$ that $\omega_3\hbar=4.24$ Mev. After using the estimate $\epsilon_1\approx0.04\omega_3\hbar$ we evaluate the energy of the 1^- state as $2.125\hbar^2/A+0.96\omega_3\hbar=7.07$ Mev. Thus the assumption $c=0$ leads one to expect the separation between the 1^- and 2^+ (degenerate with 2^-) to be 160 kev, which compares very favorably with the observed 200 kev. (The value of c required to give an exact fit is about $-b/3$, the other numbers being not much changed.) From the estimate $\epsilon_0\approx0.003\omega_3\hbar$ one expects the nearly degenerate pair to be separated by about 13 kev, which should be capable of being resolved by a high resolution magnetic analyzer (and we intend to have a try at it).

Beyond 7.11 Mev, there appears to be a gap without levels for at least 1.5 Mev, with the next dependably observed level at 10.5 Mev. The next level listed by Dennison is a 4^+ at (10/6) 6.13 Mev$\approx$10.2 Mev. Thus again, if one can find a fifth level hiding in the observed group of four near 6 or 7 Mev, the grouping of these followed by a gap seems strongly indicative of some validity of the alpha-model, since no counterpart is found in merely taking note of the wide spread within excited configurations in the central model. Further experimental investigation of the possibility of states at 8.6 and 9.5 Mev will help clear up this point.

Comparison of C^{12} and Be^8 with O^{16}

One of the strongest empirical arguments for the applicability of the alpha-model to the even-even $4n$ nuclei is the one given by Hafstad and Teller when they showed that the mutual binding energy of the alphas per "inter-alpha bond" is quite nearly constant for a series of these nuclei. Their Fig. 2 shows that the linear relation holds for $n=3$, 4, 6, 7, and 8 while Ne^{20} ($n=5$) lies about ten percent low and Be^8 is the more serious exception, with about 2 Mev less binding energy than required. Among the light nuclei of special interest to this review, the significant part of this is that the energy of binding "relative to alphas" shown in Fig. 3 above lies twice as low for O^{16} (at -14.42 ± 0.06 Mev) as it is for C^{12} (at -7.28 ± 0.05 Mev), corresponding to the fact that a tetrahedron has twice as many edges as does a triangle, or that there are six bonds in the alpha-model of O^{16}, three in C^{12}.

This and the considerable degree of success of the alpha-model in accounting for assignments among the first few excited states of O^{16} make it tempting to apply the alpha-model at least to C^{12} on the assumption that the bonds between alphas have an individual reality such that they are simply additive and that their strength is not affected by whether or not the alphas are subject to the forces of other bonds at the same time. For simplicity we, of course, also represent the bonds in terms of the parabolic potential of a harmonic oscillator. In treating only the simple dilational mode of vibration, we may consider a system of n alphas equidistant, at a distance r, from the center of mass in a geometry such that there are b bonds between alphas at a distance $a=cr$ from each other. Then the potential energy of the system in dilational vibration is

$$V=(b/2)K(\delta a)^2=(bc^2/2)k(\delta r)^2, \tag{27}$$

and the kinetic energy

$$T=(n/2)M\dot{r}^2\rightarrow(n\hbar^2/2M)\partial^2/\partial r^2, \tag{28}$$

so that the normal frequency is $(bc^2/n)^{\frac{1}{2}}(K/M)^{\frac{1}{2}}$, the vibrational energy $(n+\frac{1}{2})$ times that, and the mean square amplitude of the zero-point vibration

$$(\delta a^2)_{Av}=(c^2/nb)^{\frac{1}{2}}(\hbar/2)(Mk)^{-\frac{1}{2}}. \tag{29}$$

CC-0. In Public Domain. Gurukul Kangri Collection, Haridwar

Digitized by Arya Samaj Foundation Chennai and eGangotri

These quantities are listed in Table V. There are other modes of vibration (W37, D40), the two we have discussed above for O^{16} and a similar one for C^{12}, and in the simple approximation, Eq. (27), which amounts to putting Dennisons constants $b=c=0$, ω_2 and ω_3 are related to the dilational frequency ω_1 as shown in Table V.

The fact that the mutual binding energy of the alphas is closely proportional to the number of bonds in C^{12} and O^{16} becomes an impressive argument for the use of the alpha-model with the same potential for each bond only after one notes that the vibrational zero-point energy in these structures is also closely proportional to the number of bonds, as was pointed out by Hafstad and Teller (H38) and is shown in the eighth line of Table V. In that line is given a number proportional to the sum of the vibrational frequencies multiplied by the number of modes of each frequency, and these numbers are almost equal to b in line 2. This indicates that Be^8 should also have this same binding energy per bond if the bonds were so simple. Actually, the bond potential is expected to be anharmonic, and the simplest deviation from our assumptions which could account for the low binding energy of Be^8 might be that the anharmonicity is more important in determining the ground state energy of Be^8 than in the other nuclei because the mean-square amplitude of the zero-point bond vibrations in the dilational mode is considerably greater in Be^8, as indicated in the fourth line of Table V. In C^{12} and O^{16}, the zero-point energy is divided between several bonds.

The rotations that go with these vibrations were discussed for O^{16}, and for C^{12} there is the similar symmetry requirement that the vibration ω_2 is accompanied by one unit of angular momentum about an axis normal to the figure axis (W37). If the alpha-model of C^{12} is considered to be a plane figure, the moment of inertia about this axis is half of that about the figure axis, which is the same as that in O^{16}, if a is the same as we here assume. Thus the rotation energy (H38) is proportional to $[J(J+1)-K^2/2]$. The consequent excitation energies are also listed in Table V, in units Mev, with the elastic constant of the bond determined by matching the 6.05-Mev state and the moment of inertia by matching the 6.13-Mev state of O^{16}. Some of the refinement of our earlier discussion of the states of O^{16} is here lost by having put Dennison's constant $b=0$, but this suffices to give a rough indication of where the levels in the other nuclei would be expected to lie if the bonds were similar in all of these nuclei. We run into the same difficulty that is encountered in trying to apply the central model in (jj) coupling to C^{12}: there are simply too many theoretical states accompanying the first excited state. There is one experimental level at 4.44 Mev and the possibility of another (that does not show up in all reactions (M51)) at 7.3 Mev, at most two in this general region. This is a qualitative discrepancy of a sort that is not apt to be removed by a more refined assumption concerning the nature of the bonds. It therefore does not seem possible to apply the alpha-model in any simple way to C^{12}.

The alpha-model might, however, be used to get us out of a possible difficulty with the intermediate-coupling interpretation of C^{12}. The possible level at 7.3 Mev has recently been shown to be probably a pair-emitting 0^+ level if it exists (Ha52, G52). The evidence is confusing and is based on very meagre observations because in the (α, n) reaction in which it is questionably observed polonium alphas on Be^9 seem to excite the level very weakly if at all. If the 0^+ level exists, it does not seem to arise in any simple way from the central model (double excitation from the $p_{\frac{3}{2}}$ shell in C^{12} being much more expensive than that from the $p_{\frac{1}{2}}$ shell giving rise to the 6.05-Mev state in O^{16}). It might possibly be that the other states are mostly central model (in intermediate coupling) with rather little tendency to cluster into alphas, but that the 7.3-Mev state is mostly the dilational-vibration 0^+ state of the alpha-model. The excitation energy 5.24 Mev listed for this state in Table V is what would be expected above a pure-alpha-model ground state and might instead be 7.3 Mev above the actual (more complicated) ground state. This happens to be just below the energy required for break-up into alphas. The other excited alpha-model states listed in Table V might be absent because of falling above this energy.

In Be^8 it is not clear, as it is in C^{12}, that there are too many fairly low excited states to be ascribed to the alpha-model if one simply assumes a harmonic bond. The number of states in the region 4 to 5 Mev is not experimentally certain—different experiments each give one state at a different energy, so there may be one, two, or perhaps three states in this region (where one solid and one broken line are shown in Fig. 1). If there were only one, this would be qualitatively compatible with the number of states in the alpha-model, the two states in Table V being at about 4.9 and 3 Mev, respectively, and the 4^+ state being at 7.5 Mev. One trouble with this supposition is that the harmonic assumption is expected to fail on the outside in the form of too low a potential barrier.

The Low Barrier in the Alpha-Model of Be^8

In making a simple estimate of the barrier height we consider the "rotational potential," or the term which enters the radial wave equation of the 2^+ state in the way a potential does in a one-dimensional equation,

$$V_{\text{rot}}=L(L+1)\hbar^2/4Ma^2=(15.3/x^2)mc^2, \qquad (30)$$

the Coulomb potential

$$V_c=4e^2/a=(4/x)mc^2, \qquad (31)$$

and the vibrational potential (harmonic term of the bond)

$$V_{\text{vib}}=(k/2)(\Delta a)^2=6.8(\Delta x)^2mc^2. \qquad (32)$$

Here we have put the distance between the alphas $=a=x(e^2/mc^2)$, $L=2$, and, by assuming the stiffness of the bonds the same as indicated by the 6.05-Mev state of O^{16}, $(k/M)=(11.8mc^2/\hbar)^2$, M being the nucleon mass. If we equate the kinetic energy of rotation at a fixed separation to the excitation energy of the 2.9-Mev state, we have $V_{\text{rot}}(x_0)=5.7mc^2$, or $x_0=1.64$, some sort of

CC-0. In Public Domain. Gurukul Kangri Collection, Haridwar

Digitized by Arya Samaj Foundation Chennai and eGangotri

average separation which we may take as an approximate equilibrium distance. From this the effective potential is assumed to rise according to Eq. (32) until it joins on to $V_{rot}+V_c$, which gives the potential outside the cut-off point. As the width of the potential hole V_{vib} we take the value where it is equal to the zero-point energy, which is at $\Delta x=0.66$, and take the cutoff roughly at $x_B=1.64+0.66=2.3$. This gives $V_c(x_B)=0.89$ Mev, $V_{rot}=1.48$ Mev, or a total barrier height of 2.37 Mev.

A slightly more refined estimate is made by taking into account the centrifugal stretching of the bond, which is one aspect of vibration-rotation interaction. Inside the top of the barrier, the bond energy is given V_0+V_{vib}, which includes V_c and applies to both nonrotating and rotating states. By equating the energy of the ground state, $0.17mc^2$, to V_0 plus the zero-point energy, $(11.8/2^4)mc^2$, we have $V_0=-4mc^2$. In the 2^+ state the effective potential is $V_0+V_{vib}+V_{rot}$, and it has a minimum at a separation x_2 greater than has the minimum without rotation by an amount $\Delta x_2=2.25/x_2^3$. Thus at the equilibrium separation in the rotating state the contribution of the bond energy to the total energy is greater than in the ground state by $V_{vib}(\Delta x_2)=34.4/x_2^6$. The two states also differ by the rotational energy $(V_{rot})_{Av}$ of the 2^+ state, and by the difference of the zero-point energies of the radial motion, both of which depend on wave functions in a detailed way. To avoid the use of wave functions, we assume that $(V_{rot})_{Av}\approx V_{rot}(x_2)$, since it is not clear whether this gives too large or too small an estimate, and that the radial zero-point contributions of V_{vib} plus kinetic energy are about the same in the two states. We then equate the energy difference to the excitation energy $5.7mc^2$:

$$15.3/x_2^2+34.4/x_2^6=5.7, \qquad (33)$$

which determines $x_2=1.81$. This includes only the simplest terms whose sign is clear without recourse to wave functions, and is obviously only a rough estimate. From this we have $\Delta x_2=0.38$ and thus the minimum of the potential energy curve representing the bond at $x_0=1.81-0.38=1.43$. If now we equate the expression for the effective potential inside, $V_0+V_{vib}+V_{rot}$, to that outside, $V_{rot}+V_c$, we find that they are equal at $\Delta x_B=0.92$, or $x_B=2.35$, the position of the top of the barrier. The barrier height is 2.29 Mev, composed of $V_c(x_B)=0.87$ Mev and $V_{rot}(x_B)=1.42$ Mev.

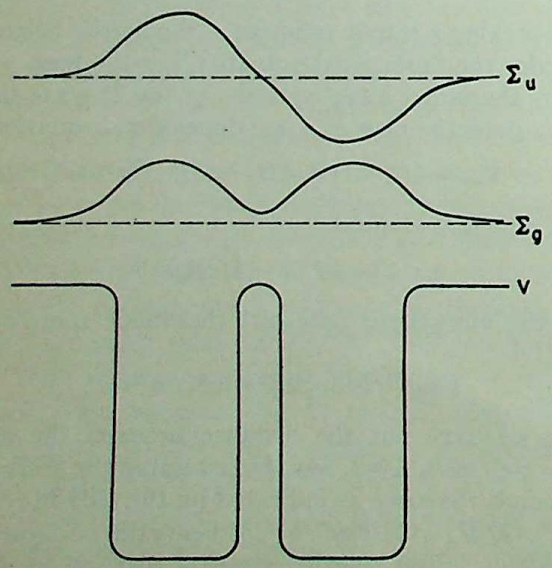


FIG. 19. Schematic potential and nucleon wave functions of an alpha-model of Be^8.

Though this estimate is rough, it makes it unlikely that the effective barrier in the 2^+ state is as high as 3 Mev. There are two phenomena that might make it possible to have a broad virtual state approximated by an alpha-model but slightly above the barrier: (1) the partial reflection of a particle just above a barrier (C29); (2) a possible division of the energy associated with vibration into effective energy of vibration in the one-dimensional problem and some other form such as "internal" energy of the "fluid" that makes up and binds the clusters. The partial reflection (1) is very weak at energies more than a very few percent above the barrier. It thus appears quite unlikely that a reasonable alpha-model would, without quite drastic and complicated modification, contain a 2^+ state near 3 Mev, and even less likely that it would have an excited vibration state 0^+ at this energy or above.

In the most recent previous treatment of these problems in this journal, Haefner (Ha51) has discussed the alpha-model both for Be^8 and C^{12}, as well as some other light nuclei. He does not make the questionable assumption of a standard harmonic bond, for which the principal support is the constancy of binding energy per bond, and thus does not try to compare different nuclei. In C^{12} he considers only rotational states and thus, by neglecting vibration, fails to find too many fairly low excited states. He also does not try to relate the spacing of states to the excitation of the first state of higher isobaric spin. When so few demands are made on the alpha-model, it looks more hopeful, even in C^{12}. In Be^8, he gives a new treatment of the radial motion, based on a bond potential which has no similarity to an harmonic approximation, but instead includes a short-range repulsion and a sudden cutoff to a Coulomb potential, which emphasizes the artificiality of the harmonic form in a problem with so much uncertainty of position. The reader is also referred to his discussion of the experimental situation. More recent experimental results (T51) on the photodisintegration of C^{12} show evidence for a long-range and a short-range peak in the alphas from the secondary break-up of Be^{8*} from the 3-Mev state, corresponding to forward and backward motion relative to the recoil direction, and this implies an angular correlation such that the 3-Mev state cannot be 0^+ (as it seems to be on the basis of alpha-alpha-scattering), thus providing further evidence that it must be 2^+. This is, however, not evidence for the alpha-model, since this assignment is expected in the (LS) model and in the (jj) model, so also in intermediate coupling as in the interpretation of Fig. 8. As was remarked above, a partial admixture of the alpha-model may account for the width of the state.

The Nucleon Coordinates in the Alpha-Model of Be^8

In those simple applications of the alpha-model to the vibration and rotation energies of the $4n$ nuclei,

CC-0. In Public Domain. Gurukul Kangri Collection, Haridwar

Digitized by Arya Samaj Foundation Chennai and eGangotri

we treat the alpha-model in terms of the coordinates of the alphas only. The coordinates of the individual nucleons are there ignored except in so far as they cause the alphas to obey Bose statistics. When we now turn to the discussion of the possible intermixture of alpha-model wave functions and central-model wave functions, it is necessary to look in more detail into the alpha-model, and to formulate it in terms of the same nucleon coordinates which appear also in the central model. Be^8 provides an appropriate example.

In the alpha-model we make assumptions similar to those made in the quantum treatment of molecular mechanics, in spite of the lack in the nucleus of a physical analog of the nuclei in a molecule. It is assumed that the angular correlations of the positions of the nucleons assemble them in clusters to a sufficient extent that there is a preferred "body-fixed" coordinate system whose motion may be treated as "adiabatic" in the sense that it is much slower than the motions of the nucleons within this coordinate system. The "self-consistent" field of the other nucleons is assumed to provide an effective ("Hartree") potential defined in this coordinate system, and such a potential V for Be^8 with two minima is indicated in Fig. 19. The distance between the two minima is assumed to vary so slowly as to be "adiabatic," corresponding to the vibration of the simple alpha-model discussed above, as is familiar in discussions of molecules.

The alpha-model wave functions in Be^8 are similar to "molecular orbitals." They may be assumed to have local maxima or minima near the potential minima, and may be either symmetric or antisymmetric in the change of direction of the figure axis, or z axis. The symmetric one, Σ_g, may be assumed to have lower energy because its smaller slope near the center of mass contributes less kinetic energy than does the greater slope in this part of the antisymmetric function Σ_u. These two functions, each with two spin and two isobaric spin projections, may accommodate eight nucleons, and are thus filled in Be^8.

Instead of starting a calculation with "molecular orbitals," one may start with "atomic orbitals" such as

$$\psi_1 \sim \exp[-(\beta/2)(x^2+y^2)] \exp[-(\alpha/2)(z+a)^2],$$
$$\psi_2 \sim \exp[-(\beta/2)(x^2+y^2)] \exp[-(\alpha/2)(z-a)^2]. \quad (34)$$

Gaussian functions each having a maximum at the center of an alpha on the z axis at a distance a from the center of mass. Then the "molecular orbitals" may be made as the sum and difference of these in the familiar Heitler-London fashion:

$$\Sigma_g \sim \psi_1+\psi_2,$$
$$\Sigma_u \sim \psi_1-\psi_2. \quad (35)$$

An Elliptical Model of Be^8

In discussing the possibility that the central-model wave functions may be mixed with alpha-model wave functions to form a good approximation to the actual wave function of a system, it is desirable at least to point out some of the difficulties of formulating the calculation of such an admixture. In doing so we shall first describe a very interesting calculation which has been carried out by Wergeland (We41) and has some slight similarity to the sort of calculation that would be necessary.

TABLE VI. Schematic wave functions for Be^8, indicated by occupation numbers of single-nucleon states.

	Eliptical model					(jj) model: s shell					
									m_j of p shell		
	ψ_3^+	ψ_3^-	ψ_4^+	ψ_4^-		s^+	s^-	3/2	1/2	−1/2	−3/2
proton	1	1	1	1	a	1	1		1	1	
neutron	1	1	1	1		1	1		1	1	
					b	1	1	1			1
						1	1	1			1
					c	1	1	1			1
						1	1		1	1	
					d	1	1	1	1		
						1	1			1	1
					e	1	1	1		1	
						1	1		1		1

The alpha-model wave functions in Be^8 are similar to "molecular orbitals." They may be assumed to have local maxima or minima near the potential minima, and may be either symmetric or antisymmetric in the change of direction of the figure axis, or z axis. The symmetric one, Σ_g, may be assumed to have lower energy because its smaller slope near the center of mass contributes less kinetic energy than does the greater slope in this part of the antisymmetric function Σ_u. These two functions, each with two spin and two isobaric spin projections, may accommodate eight nucleons, and are thus filled in Be^8.

Wergeland discusses the problem of the interaction of two alphas by means of an application of the variation principle in which the alpha-model wave function is modified by an admixture of another wave function which we may call an elliptical-model wave function. Thus he takes

$$\Psi = \Psi_H + \lambda \Psi_\alpha, \quad (36)$$

where Ψ_α is an antisymmetric sum of products of eight "molecular orbitals," Eq. (35), that is, an alpha-model wave function which may be written as a "Slater determinant," and Ψ_H is a similar wave function for the elliptical model, an antisymmetric sum of products of the anisotropic Gaussian functions

$$\psi_3 \approx \exp[-(\beta/2)(x^2+y^2)] \exp[-(\alpha/2)z^2],$$
$$\psi_4 \approx z\psi_3. \quad (37)$$

These functions have an ellipsoidal anisotropy, having two extension parameters α and β where one would suffice in a central model. Aside from this they are identical in form with the wave functions for the s shell and the particular $m_1=0$ one of the three wave functions for the p shell. The actual identity does not go so far, however, because they are written in terms of the coordinates of the body-fixed coordinate system of the alpha-model. The elliptical model thus is a special type of "Hartree model," but bears very little resemblance to the central model as discussed in the rest of this paper, since in the latter all three of the p-shell wave functions are populated, and in such a way as to provide special correlations between spin and orbital orientations. The elliptical model is sufficiently similar to the alpha-model [compare Eqs. (34) with (37)] to make the calculation of the mixing straightforward, and yet

CC-0. In Public Domain. Gurukul Kangri Collection, Haridwar

Digitized by Arya Samaj Foundation Chennai and eGangotri

contains enough of the concentration about the center of mass characteristic of the central model to exploit the feeling that an improvement of the energy may be obtained by mixing because an actual Be^8 nucleus may be intermediate between an alpha-model and something more concentrated at the center. It may be noted that ψ_3 and ψ_4 have the same symmetries as Σ_g and Σ_u, respectively, of the alpha-model. The main difference is that ψ_3 has a maximum at the center of mass where Σ_g has been assumed to have a minimum (Fig. 19).

The variation calculation is carried out (We41) by varying simultaneously λ, α, and β, with a fixed space-exchange (Majorana) interaction capable of providing enough binding for two separated alphas, and with various fixed values of the inter-alpha spacing $2a$. The resultant minimum energy as a function $2a$ then gives an interaction potential of the two alphas, which indeed has a nice dip inside of the Coulomb barrier, but a dip with a minimum a little above zero energy (the energy of two separated alphas), and thus not deep enough to give, after addition of the zero-point energy, a barely unstable ground state of Be^8. This still constitutes a very interesting treatment of the alpha-interaction problem. Its failure to provide a strong enough interaction with a simple one-term nucleon interaction is hardly surprising in the light of the failure of more elaborate second-order calculations (with more general nucleon interactions adjusted to the scattering and saturation demands) to provide enough binding in the central model of nuclei like Li^6, e.g., (I37). The value of λ found by Wergeland is $\lambda \approx 1.3$, suggesting that the nucleus prefers to remain somewhat closer to the alpha-model than to the elliptical model. The admixture is substantial, but the elliptical model resembles the alpha-model so much more than the central model that this result in itself may not be considered to show that the alpha-model approach is invalid.

The Ground-State Wave Function of Be^8 in the (jj) Version of the Central Model

In order to emphasize how small a part of the problem of the mixture of the central model and the alpha-model was carried out by Wergeland, we wish to compare his elliptical-model wave function with the central-model wave function of the ground state of Be^8 in the relatively simple case of pure (jj) coupling (not intermediate coupling). On the left side of Table VI, the complete occupancy of the single-nucleon functions ψ_3 and ψ_4 in the elliptical model wave function Ψ_H, for instance, is indicated by the occupation numbers "1" for both proton and neutron, for both ψ_3 and ψ_4 orbitals, and for both + and − spin orientations. The alpha-model is similar with Σ_g and Σ_u. Partial wave functions for the (jj) model are similarly indicated in Table VI. In terms of them, with a prime ($'$) indicating interchange of proton and neutron occupation numbers, the complete wave function of the ground state of Be^8 in the (jj) model (in the configuration $S^4p_{\frac{3}{2}}^4$) is

$$\Psi_{(jj)} = (3a+3b-2c-2c'+d+d'-e-e')/(30)^{\frac{1}{2}}. \quad (38)$$

With this more complicated wave function in place of Ψ_H, one could conceivably pursue a calculation similar to Wergeland's in order to calculate the expected degree of mixing of the central model and the alpha-model of the ground state of Be^8, as a simple example of a typical nuclear state. One might again allow an ellipsoidal distortion of the single-nucleon orbitals, but there might be more energetic tendency to resist this distortion, at least when one is near the central-model side, both because the $m_l = \pm 1$ states are occupied as much as the $m_l = 0$ state [within the $\psi_{mj}^{\frac{3}{2}}$ states given by Eq. (22), etc.] and because the spin-orbit term (3) in the Hamiltonian is an important contributor to the energy. This is the general sort of procedure that we imagine when we think of a partial admixture of alpha-model wave functions to modify the properties of specific nuclear states. It may be expected to be energetically advantageous only when a fairly low state of the alpha-model is available with the same symmetry (that is, J, T, and parity) as has the state of the central model under consideration.

In so complicated a calculation, it is not entirely clear that there would be only one local minimum as one varies λ. It might, for example, be possible to find a local minimum near the central model with little ellipsoidal distortion, and one near the alpha-model with much more, though this would seem a strange result of a variation procedure. The rise between them would then perhaps act as a potential barrier to isolate these as two essentially separate almost stationary states of the system, one resembling the central model and another at a different energy resembling more closely a state of the same symmetry of the alpha-model. The possibility of such a two-model interpretation of a nuclear energy spectrum has been discussed (I51) for Li^7 as a result of the preliminary identification (P52) of the 7.4 Mev state as having $J = \frac{3}{2}$, the same as that of the ground state. (It seemed that the only place one can find another $J = \frac{3}{2}$ state is from the other model.) While the relevant experimental measurements have not been completed, it appears on the basis of the available data that this excited state may instead have $J = 5/2$, so that such an unorthodox interpretation may not be required.

If, as seems more likely, there is effectively only one minimum for each such problem, then it may turn out that some states of a given nucleus resemble the central model rather closely, and others of other symmetries resemble the alpha-model, depending largely on which model provides the lower state of a given symmetry. In this case, each variation problem provides either a central model state (approximately) or an alpha-model state, but not both; or it might provide a state about midway between the models, as we presume to be the case among the low even-J states of Be^8.

CC-0. In Public Domain. Gurukul Kangri Collection, Haridwar

Digitized by Arya Samaj Foundation Chennai and eGangotri

The Alpha-Model States of Li^7

The alpha-model of a nucleus not containing $4n$ nucleons is described (H38) in terms of incomplete occupancy of molecular orbitals such as those shown in Fig. 19. The lowest state is described by saying that Σ_g is occupied by four nucleons and Σ_u by three, or alternatively that there is a Σ_u "hole." The wave function changes sign by interchanging the positive and negative z axis, which is physically the same as rotating the body-fixed coordinate system by 180° in space, so single valuedness requires that the rotational function be odd, with rotational quantum number 1, having a projection 0 along the body-fixed z axis, a $^2\Sigma_u$ as it is called in molecular spectroscopy. Such a doublet has two components depending on the relative orientation of spin and orbital moments, analogous to a ^2P in atomic spectra. In the interpretation given above these are supposed to account for the ground state and 0.48-Mev state, the "isolated low doublet," whose splitting is then largely an alpha-model characteristic. The other fairly low state in this model is the one described similarly as a Σ_g "hole," called a $^2\Sigma_g$, but like a ^2S it is a "doublet" having only one state. If this is at about 6.5 Mev as is supposed above, it has enough energy (and appropriate symmetry) to break up quickly into an alpha and a triton, so is expected to have short life and be broad, as is the state observed at that energy.

An alternative alpha-model of Li^7 would consist simply of an alpha and a triton, if they would attract each other. Its ground state would be a ^2S, and higher states similar to ^2P, etc., would arise from rotation. In view of the instability of He^5 and Be^8 and the large size of the triton, it seems unlikely that the alpha and triton would attract each other enough for this model to stick together. The model discussed above, consisting of Be^8 with a "hole," is favored by the importance of the exchange process, with resonance between the two positions of the "hole."

11. BETA-DECAY AND THE SURPRISING LONGEVITY OF C^{14}

General Situation of Beta-Decay in the p Shell

The squared matrix elements encountered in beta-decays of the various elements, or their reciprocals the ft values, vary so widely in order of magnitude that one might at first sight expect to find little meaning to a refined factor, such as $3^{\frac{1}{2}}$, by which a calculated matrix element might differ between two models, or between (LS) and (jj) coupling. Yet there is a similar variation of gamma-lifetimes, and once these transitions are sorted out according to their magnetic or electric multipole order, there is, at least among the very numerous magnetic 2^4-pole transitions, a very surprising exactitude with which they may be plotted on a straight line on the usual logarithmic plot (Go51). This phenomenon among the moderately heavy nuclei encourages the hope that matrix elements may have a fairly exact meaning in beta-decay, if ever we can calculate them. Attempts to compare the experimental matrix elements in the p-shell nuclei with those calculated with (LS) coupling on the one hand and with (jj) coupling on the other, always using the wave functions appropriate to a symmetric Hamiltonian, have indicated no uniform preference for either coupling scheme, which fact, in itself, is suggestive of the prevalence of intermediate coupling or other such complexity among these light nuclei (Fe50). Yet certain facts do appear particularly clearly in these light nuclei. The occurrence of several pairs of self-mirrored nuclei in this region gives rise to the highly favored or "super-allowed" transitions in which the nuclear matrix elements are expected to be unity because of the great similarity of the ground-state matrix elements of two mirror nuclei. Among the polyads centered about odd-odd nuclei, the allowed transition $He^6 \rightarrow Li^6$, with J changing from 0 to 1, shows that there must be a strong component of the Gamow-Teller operator,

$$V = g \sum_{\text{nucleons}} \tau_x \sigma, \tag{39}$$

effective in the transition, and the two examples of $0 \rightarrow 0$ transitions, $C^{10} \rightarrow B^{10}$ (0^+ state at 1.74 Mev) and $O^{14} \rightarrow N^{14}$ (0^+ state at 2.32 Mev), show that the Fermi operator, which is similar to Eq. (39) but lacks the factor σ, must also appear. Comparison of these cases and others shows that the two operators must be present with at least very roughly equal coefficients (Mo51, Bl52). [Those discussions are based on the assumption that in Li the contribution of the spin-orbit term, Eq. (3), is not large enough to cause a strong deviation from (LS) coupling, which does not seem to be quite assured in the light of the above review of the energy levels, so the equality of the coefficients may be only very rough.] The existence of a strong Gamow-Teller term demonstrated by the He^6 decay brings about what has probably been the most persistent puzzle in the study of beta-decay, the long life of C^{14}, which also involves a $0 \rightarrow 1$ transition. While this long life has made C^{14} a very useful radiological tool for archeology because of its cosmic-ray origin in the atmosphere (L49), it has been considered so anomalous that some rather farfetched *ad hoc* assumptions have at times been reluctantly introduced in an attempt to account for it, but have been disproved by subsequent experimental results, as has been mentioned in Sec. 7.

The Lifetime of C^{14} as Calculated in Intermediate Coupling

It has been recognized that the alternative to those unsuccessful *ad hoc* assumptions would be to admit a chance cancellation within a complicated matrix element, but the factor 10^6 by which the transition rate appears to be suppressed is so large as to make this explanation seem very unlikely, *a priori*. It happens

CC-0. In Public Domain. Gurukul Kangri Collection, Haridwar

Digitized by Arya Samaj Foundation Chennai and eGangotri

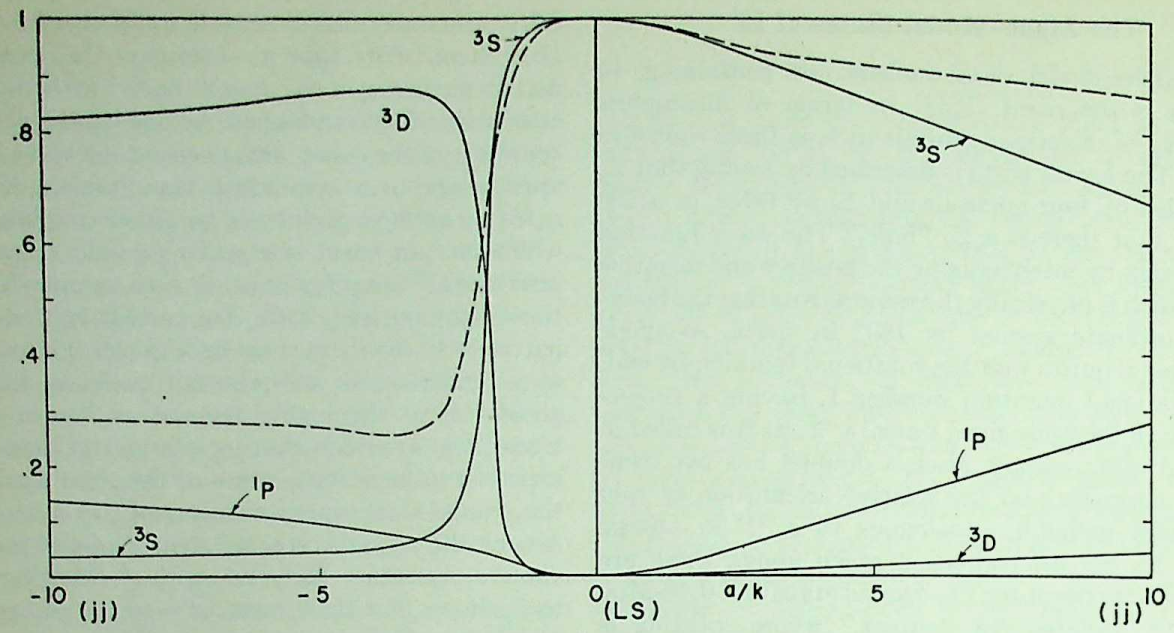


FIG. 20. The broken curve gives the nuclear matrix element for the beta-decay of C^{14} on the left and of He^6 on the right. The solid curves give the fractional constitution of the ground state of N^{14} (and Li^6), that is, the squares of the coefficients in the wave function, in terms of ^3S, ^1P, and ^3D.

that C^{14} is a part of the one polyad, Py^{14}, for which we have been able to present an analytic solution to the intermediate-coupling problem in the ground configuration. This makes it possible at least to calculate whether or not complete cancellation is possible with a reasonable value of the parameter a/K. We shall show that it is not possible within the ground configuration, but that the amount of configuration mixing required to supply the cancellation is not exorbitant.

The energies of the three $(J, T)=(1, 0)$ states plotted in Fig. 5 are derived from a cubic equation (4) of reference (I52), and from the energy matrix there given we may write the corresponding secular equations

$$\begin{aligned}(H_{11}-\epsilon_1)C_1+H_{12}C_2&=0,\\ H_{21}C_1+(H_{22}-\epsilon_1)C_2+H_{23}&=0,\\ H_{32}C_2+(H_{33}-\epsilon_1)&=0,\end{aligned}\tag{40}$$

with $H_{23}=H_{32}=(2/3)^{\frac{1}{2}}a$ [note misprint in (I52) on this point], $H_{33}=g+a/2$, etc. Similarly for the two (0, 1) states we have the secular equations

$$\begin{aligned}(H_{44}-\epsilon_2)C_4+H_{45}&=0,\\ H_{54}C_4+H_{55}-\epsilon_2&=0,\end{aligned}\tag{41}$$

with $H_{45}=-2^{\frac{1}{2}}a$, $H_{44}=-a/2$, $H_{55}=e+a/2$. Here e and g are energies arising from the specific nuclear interaction, Eq. (2), and when we specialized for $L=6K$, they became $e=6.6K$, $f=-8K$, $g=3K$. The C's are coefficients in the expansions of the wave functions

$$\begin{aligned}\psi(1, 0)&=N_1[C_1\psi(^3D_1)+C_2\psi(^1P_1)+\psi(^3S_1)],\\ \psi(0, 1)&=N_2[C_4\psi(^3P_0)+\psi(^1S_0)].\end{aligned}\tag{42}$$

With the Gamow-Teller interaction, Eq. (39), we have the matrix element for the beta-transition

$$\begin{aligned}\int\psi^*(1, 0)V\psi(0, 1)dv&=(1, 0|V|0, 1)\\ &=N_1N_2[C_2C_4(^1P_1|V|^3P_0)+(^3S_1|V|^1S_0)]\\ &=N_1N_2V_{35}\{(H_{45}/H_{32})[(H_{33}-\epsilon_1)/(H_{44}-\epsilon_2)]\\ &\qquad\times(V_{24}/V_{35})+1\}.\end{aligned}\tag{43}$$

This sum has only two terms because of L orthogonality, since the interaction operates on the spin and isobaric spin only, not on the space coordinates of the nucleons. There is a similar reduction of the number of terms, because of orthogonality in M_L, when we evaluate the two terms of the matrix of V in Eq. (43) using the expansions:

$$\begin{aligned}\psi_2&=\psi(^1P_1)=P^1(\alpha\beta-\beta\alpha)(\nu\pi-\pi\nu)/2,\\ \psi_3&=\psi(^3S_1)=S^0(\alpha\alpha)(\nu\pi-\pi\nu)/2^{\frac{1}{2}},\\ \psi_4&=\psi(^3P_0)=[P^1\beta\beta-P^0(\alpha\beta+\beta\alpha)/2^{\frac{1}{2}}\\ &\qquad+P^{-1}\alpha\alpha]\nu\nu/3^{\frac{1}{2}},\\ \psi_5&=\psi(^1S_0)=S^0(\alpha\beta-\beta\alpha)\nu\nu/2^{\frac{1}{2}}.\end{aligned}\tag{44}$$

Here we write two-nucleon wave functions to represent two holes in the p shell, on the assumption, to be justified in Appendix III, that holes behave as do nucleons in beta-decay as well as in energy matrices. We use a spectroscopic notation such as P^1 for L^{M_L} or $\psi_L{}^{M_L}$, the α and β are the usual Pauli spin functions, ν and π are analogous functions for isobaric spin, and within each product of two of these the first factor is associated with the first nucleon and the second with the second. There are three equal matrix elements of the form, Eq. (43) corresponding to the three states

CC-0. In Public Domain. Gurukul Kangri Collection, Haridwar

Digitized by Arya Samaj Foundation Chennai and eGangotri

$M_J=1$, 0, or -1 associated with $J=1$. It suffices to calculate with any one of them, and we select $M_J=1$ in writing and working with Eq. (44).

The wave functions, Eq. (44), are used to calculate both the matrix elements H_{ij} and V_{ij}, and the arbitrary choice of phase thus does not, of course, affect the final result. The same is true of the sign convention in the well-known operator

$$h^{-1}(J_x \pm iJ_y)\psi^m = [(j \mp m)(j+1 \pm m)]^{\frac{1}{2}}\psi^{m\pm 1},$$

which is used with $h^{-1}J_z\psi^m = m\psi^m$. Examples of this operator as we use it are $l^+c = 2^{\frac{1}{2}}b$, $l^+b = 2^{\frac{1}{2}}a$, $\frac{1}{2}\sigma^+\beta = s^+\beta = \alpha$, $t^+\pi = \nu$, etc., with positive square roots. We abbreviate $J_x \pm iJ_y = J^\pm$, $i \pm ij = i^\pm$, and the combinations of them with which we operate on the wave functions are

$$(\boldsymbol{l}\cdot\boldsymbol{s}) = \tfrac{1}{2}(l^+s^- + l^-s^+) + l_z s_z \qquad (45)$$

from Eq. (3), and from Eq. (39)

$$\tau_z\boldsymbol{\sigma} = (t^+ + t^-)(s^+\boldsymbol{i}^- + s^-\boldsymbol{i}^+ + 2s_z\boldsymbol{k}). \qquad (46)$$

The relevant beta-decay matrix elements are then

$$\begin{aligned} V_{24} &= ({}^1P_1 | V | {}^3P_0) = 3^{-\frac{1}{2}}(g/8) \\ &\quad \times [(\alpha\beta - \beta\alpha)(\nu\pi - \pi\nu) | \textstyle\sum \sigma^+\tau^- i^- | \beta\beta\nu\nu] \\ &= 3^{-\frac{1}{2}}(g/8)[(\alpha\beta - \beta\alpha)(\nu\pi - \pi\nu) | \alpha\beta\pi\nu - \beta\alpha\nu\pi] i^- \\ &= -3^{-\frac{1}{2}} g i^-, \end{aligned} \qquad (47)$$

and similarly

$$V_{35} = ({}^3S_1 | V | {}^1S_0) = g i^-. \qquad (48)$$

In verifying the spin-orbit elements H_{32} and H_{45} as given above, one further specifies $S^0 = 3^{-\frac{1}{2}}(ac + ca - bb)$, $P^1 = 2^{-\frac{1}{2}}(ab - ba)$, etc., in Eq. (44). Thus in the first term of the last number of Eq. (43) we find

$$(H_{45}/H_{32})(V_{24}/V_{35}) = 1, \qquad (49)$$

the sign being definitely positive. This is multiplied in the first term by the ratio of two expressions, each of the form $(\epsilon_i - H_{jj})$, and they both have the same sign because in solving secular equations of this sort one always obtains a lowest root lower than the lowest diagonal matrix element used, and we are here dealing with two lowest roots (ground states), ϵ_i. Thus there is no opportunity for the two terms in Eq. (43) to cancel one another, so it appears from this calculation that the long life of C^{14} may not be attributed to accidental cancellation within the matrix element here considered. Since there appears to be no other possibility within the framework of our present interpretation of nuclear structure and beta-decay (in the approximation in which we neglect configuration interaction), it is important to examine carefully all the assumptions involved in the determination of the relative sign of the two terms in Eq. (43). This is done in Appendix III. One must be careful because questions of phase sometimes arise when transferring from wave functions of particles to those of holes, and it is shown there explicitly that there is no change of relative sign in transferring the beta-decay matrix elements from particles to holes if the wave functions are those which give the usual change of sign in the more familiar transfer of the matrix of $\boldsymbol{l}\cdot\boldsymbol{s}$ from particles to holes.

Although there is no cancellation between the two terms in ground-configuration matrix element, the detailed nature of the coefficients in the wave functions do provide a little tendency to make the lifetime of C^{14} at least slightly longer than would without calculation be expected, by a factor of about 10 which is only a very small part of the factor 10^6 needed. This comes about because the ground state of N^{14}, well out in intermediate coupling to the left of the value $a/K \approx -3$, contains almost 90 percent of ^3D, only a little more than 10 percent of ^3S and ^1P combined. The behavior of the squares of the coefficients in the wave function is shown by the three full lines in Fig. 20. The interesting sudden cross-over in the vicinity of $a/K = -2$ is to be compared with the close approach of the two low (1, 0) energy curves in Fig. 5.

The cross-over of the ^3S and ^3D contributions is to be understood this way: without the influence of non-diagonal matrix elements, the ^3S and ^3D energy curves in Fig. 5 would follow their sloping (LS)-coupling asymptotes as straight lines which cross each other near $a/K = -2$, and further to the left the lowest (1, 0) state would be a pure ^3D following this straight line a little above the actual line drawn in Fig. 5 and a little above the (jj) asymptote, while to the right of $a/K = -2$ the lowest (1, 0) state would be a pure ^3S. The influence of the nondiagonal terms is to mix the two (LS)-coupling states quite completely where they came quite close together, in the region of the cross-over, and to mix the states only to a limited extent elsewhere, almost none at all in the vicinity of $a/K = 0$ where the non-diagonal elements vanish.

The effect that this suppression of the beta-decaying ^3S and ^1P components has on the matrix element is indicated by the broken line in Fig. 20, which gives $(1, 0 | V | 0, 1)/V_{35}$ from Eq. (43) with Eq. (49), that is, the nuclear matrix element relative to the $^1S \rightarrow {}^3S$ transition. For most of the region of a/K that is expected to apply to Py^{14} it has about one-third of the value that it has in the region appropriate to Py^6, and the square of this nuclear matrix element gives a factor 10 in the lifetime of C^{14} relative to He^6.

Other Possible Sources of the Cancellation

Since the required cancellation does not occur in the ground-configuration matrix element with charge-independent central interactions, and there remains a factor 10^5 in the lifetime of C^{14} to be explained, the question arises what modification of our assumptions could permit sufficient cancellation to occur, and whether the modification would invalidate our intermediate-coupling interpretation of the ground-configuration states as a plausible or useful approximation for other nuclear properties.

CC-0. In Public Domain. Gurukul Kangri Collection, Haridwar

Digitized by Arya Samaj Foundation Chennai and eGangotri

TABLE VIII. Spin-orbit energies of the electron configuration p^3 in the M_L, M_S representation.

m_l	m_s	m_l	m_s	m_l	m_s	M_L	M_S	$\Sigma m_l m_s = \Sigma(l \cdot s)$	AM_LM_S	A/a	M_S / M_L	1/2	3/2
1	+	1	−	0	+	2	$\frac{1}{2}$	0	$^2D, 0$	0	2	1	0
1	+	1	−	−1	+	1	$\frac{1}{2}$	0	$^2D, 0$	0	1	2	0
1	+	0	−	0	+	1	$\frac{1}{2}$		$\therefore {}^2P, 0$	0	0	3	1
1	+	0	+	−1	+	0	$\frac{3}{2}$	0	$^4S, 0$				

If we depart from the charge-independent Hamiltonian by introducing the Coulomb interaction we do not introduce any new contribution to this matrix element, for this still leaves J, L, and S conserved. The only state with the same J that could be admixed is the $(J, T)=(1, 1)$ state from the ^3P, but this is not admixed because it has a different (L, S) from any of the (LS)-coupling states contained in the ground state. The introduction of a tensor interaction also fails to admix any effective states of the ground configuration. Because a two-nucleon or two-hole wave function is purely symmetric or antisymmetric in space and the tensor interaction is symmetric, there is no mixture of the P multiplets with S or D, so the only nondiagonal matrix element of a tensor interaction is between the $^3S_1$ and the $^3D_1$. This would appear in the first equation of (40) but we used only the third in showing there is no cancellation, that is, it is only the ratio of the terms in the wave function ^3S to ^1P and not of these to ^3D that matters, so this tensor matrix element does not affect this result. (The influence of that nondiagonal tensor matrix element on ϵ_1 affects the detailed curves of Fig. 20, but not the lack of cancellation in the ground configuration p^{-2}.)

Thus we are forced to look to configuration mixing as a source of the apparently fortuitous cancellation that makes the lifetime of C^{14} so long. We may conveniently formulate the configuration mixing thus:

$$\psi(1, 0)=\sum_\alpha [c_{S\alpha}\psi_\alpha(^3S)+c_{P\alpha}\psi_\alpha(^1P)+c_{D\alpha}\psi_\alpha(^3D)],$$
$$\psi(0, 1)=\sum_\alpha [d_{S\alpha}\psi_\alpha(^1S)+d_{P\alpha}\psi_\alpha(^3P)], \quad (49)$$

where the summation index α indicates successively each of the configurations p^{-2}, $p^{-3}f$, $p^{-4}d^2$, $p^{-4}s^2$, etc., including many higher configurations. The beta-decay matrix element that must so nearly vanish is then

$$(1, 0|V|0, 1)=\sum[c_{S\alpha}d_{S\alpha}(^3S|V|^1S)_\alpha + c_{P\alpha}d_{P\alpha}(^1P|V|^3P)_\alpha]. \quad (50)$$

We have seen from Fig. 20 that c_{S1} and c_{P1} are each roughly equal to $c_{D1}/4$, and that their signs do not permit the two leading terms of Eq. (50) to cancel one another. If, for example, only one other configuration, $\alpha=2$, should contribute, it would be possible for Eq. (50) to vanish with $|c_{S2}|\approx c_{S1}/2\approx c_{D1}/8|d_{S2}|\approx d_{S1}/2$, and similarly for the subscripts P, or, as a second possibility, with $|c_{S2}|\approx c_{S1}\approx c_{D1}/4$, $d_{S2}\approx d_{S1}/4$, if the matrix elements like $(^3S|V|^1S)_\alpha$ do not depend strongly on the subscript. In the second possibility the mixture from the excited configuration appears with an amplitude $\frac{1}{4}$ or a probability $\frac{1}{16}$ relative to the leading term of each wave function. It is the probability rather than the amplitude that measures the modification of some properties of the state, such as magnetic moments.

Thus we see that it is possible for configuration mixing to provide the fortuitous cancellation without destroying the validity of the ground-configuration representation of the state as a valid approximation. Whether the fortuitous cancellation is not *a priori* so unlikely as to make it seem to be an unacceptable way to account for the long lifetime is another question. A factor 1/300 is needed in the matrix element. If the configuration mixing is just of the order of magnitude required, the probability that the cancellation should be so exact is somewhat more than 1/300. There are of the order of perhaps several dozen beta-transitions with J-values well enough known that an accident of this sort would have been recognized as troublesome. The probability that such an exact cancellation should have happened in any one of them is of course much greater than 1/300, and, indeed, not so improbable as to make implausible an otherwise acceptable interpretation of nuclei which requires this to have happened.

CONCLUSION

From the foregoing review we see that the situation in the p shell is more complicated than we might have hoped. An attempt has been made to outline the nature of the complexities as far as this can, at present, be done, with the expectation that this beginning may serve as a useful guide to further investigation, both experimental and theoretical. The type of agreement found between theory and experiment is such as to provide some indication but not very convincing proof that the intermediate-coupling interpretation is correct. The fact that the intermediate-coupling parameter a/K has been freely varied to fit the empirical needs of the various polyads, and that the range of variation about the rough mean value $|a/K|=5$ has become rather wide (from 3.7 in Py^{12} to 5.6 in Py^{14}) as slight refinements have become possible, leaves the uncomfortable feeling that such an array of rough fits might have been arranged even if the theory were not essentially correct. The variation of the energy parameters a and K individually is also disturbing. Surely the theory must be

CC-0. In Public Domain. Gurukul Kangri Collection, Haridwar

Digitized by Arya Samaj Foundation Chennai and eGangotri

TABLE IX. Further spin-orbit energies in the nucleon configuration p^3.

m_l	m_s	m_t	m_l	m_s	m_t	m_l	m_s	m_t	M_L	M_S	M_T	$\Sigma m_l m_s = \Sigma(\mathbf{l}\cdot\mathbf{s})$	$(A/a)M_L M_S$	A/a
1	+	+	0	+	+	1	+	−	2	1	$\frac{1}{2}$	1	$^4D, 1$	$^4D, \frac{1}{3}$
1	+	+	−1	+	+	1	+	−	1	1	$\frac{1}{2}$		$^4D, \frac{1}{2}$	
1	+	+	0	+	+	0	+	−				1	$^4P, \frac{1}{2}$	$^4P, \frac{1}{3}$
1	+	+	1	−	+	1	+	−	3	$\frac{1}{2}$	$\frac{1}{2}$	$\frac{1}{2}$	$^2F, \frac{1}{2}$	$^2F, \frac{1}{3}$
1	+	+	1	−	+	0	+	−	2	$\frac{1}{2}$	$\frac{1}{2}$		$^2D,^* 0$	
1	+	+	0	+	+	1	−	−					$^4D, \frac{1}{3}$	
1	+	+	0	−	+	1	+	−					$^2F, \frac{1}{3}$	
1	−	+	0	+	+	1	+	−				1	$^2D, \frac{1}{3}$	$^2D, \frac{1}{3}$

looked upon as exploratory and subject to verification or disproof by the accumulating evidence of further experimental assignments of quantum numbers as they increase in number and certainty. A propitious beginning of such verification has been made. The best that can be hoped is that the theory will merely have to be modified, and that the necessary modifications will be indicative of the more detailed nature of nuclear interactions, both specific and spin-orbit.

The reason for the peculiar behavior of the lightest p-shell nuclei, and the nature of the transition from these to the heavy nuclei, is here left in urgent need of further study and more detailed understanding. The intermediate-coupling interpretation is the most natural extension down toward light nuclei from the successful (jj)-coupling interpretation of the heavier nuclei, but its lack of spectacular and detailed success, even if that could hardly be expected, leaves one with some feeling of reservation concerning the general approach. Just as is sometimes said of other unfinished endeavors (such as the "majority plan" in the United Nations for the international control of atomic energy), we should perhaps stick by the approach we have already developed until something better is presented; but may its existence and its shortcomings stimulate the search both for improvements and for something better and more clearly acceptable.

In conclusion, there comes the opportunity to thank many colleagues for the help provided by their remarks on these varied subjects. They include Maria G. Mayer, Dieter Kurath, and Eugene P. Wigner for discussions and for communication of theoretical results before publication, Louis A. Turner for suggestions concerning parts of the presentation, Thomas Lauritsen and Fay Ajzenberg for sending preliminary sheets of the latest edition of their very valuable review of the experimental data, and William W. Buechner, Anthony P. French, Harry W. Fulbright, and Denys H. Wilkinson for communication and discussion of recent experimental findings.

APPENDIX I

Multiplet Splittings in Py[7]

Without the slight complication of isobaric spin, the calculation of multiplet splitting energies by trace invariance is familiar. In the three-electron configuration p^3, by way of example, the permitted multiplets are first found to be ^2D, ^2P, and ^4S by counting the numbers of sets of electron quantum numbers for each M_L, M_S, as listed in Table VIII, and the spin-orbit coupling parameter A for each multiplet is then calculated by trace invariance as in the right-hand columns of this table. It is remarkable that in this particular configuration all multiplet splittings vanish in first order. For three nucleons, when they each have the same charge with, say, $m_t=\frac{1}{2}$, the same calculation applies. Thus for the nucleon configuration p^3 there are, among others, three $T=\frac{3}{2}$ multiplets (which we denote by an asterisk), $^2D^*$, $^2P^*$, and $^4S^*$, each with zero multiplet splitting.

In Table IX a start is made of listing the allowed states having $M_T=\frac{1}{2}$. Aside from the $T=\frac{3}{2}$ multiplets already mentioned, these also require the $T=\frac{1}{2}$ multiplets ^2F, ^4D, ^2D, ^4P, ^2P, ^2P, and ^2S. In Table IX it is calculated by trace invariance that each of the first four of these have $A=a/3$, which suffices to show the method, and the table carried one step further shows that the sum of the A's for the two ^2P's is $(2/3)a$, which is all that this method of trace invariance can show. A detailed calculation of the ground-state wave functions (B38) shows that for the ground ^2P we have $A=a/3$, so this must be true for the remaining ^2P as well. Of course, A has no meaning for the ^4S and ^2S for which $L\cdot S=0$.

APPENDIX II

Nuclear Quadrupole Coupling in Polar Molecules

The sign and magnitude of a nuclear quadrupole moment Q are in most instances measured only indirectly through the effect on molecular energy levels which depend on the product of Qq, where q is the quadrupole coupling constant determined by the distribution of electric charge in the molecule. The calculation of q is difficult and in many cases unreliable because it depends on taking a difference, and sometimes a relatively small difference, between positive and negative contributions representing the competing effects of electronic charge and the charge of the other nucleus.

Although molecular binding forces are expressed in terms of "exchange forces," it must be remembered

CC-0. In Public Domain. Gurukul Kangri Collection, Haridwar

Digitized by Arya Samaj Foundation Chennai and eGangotri

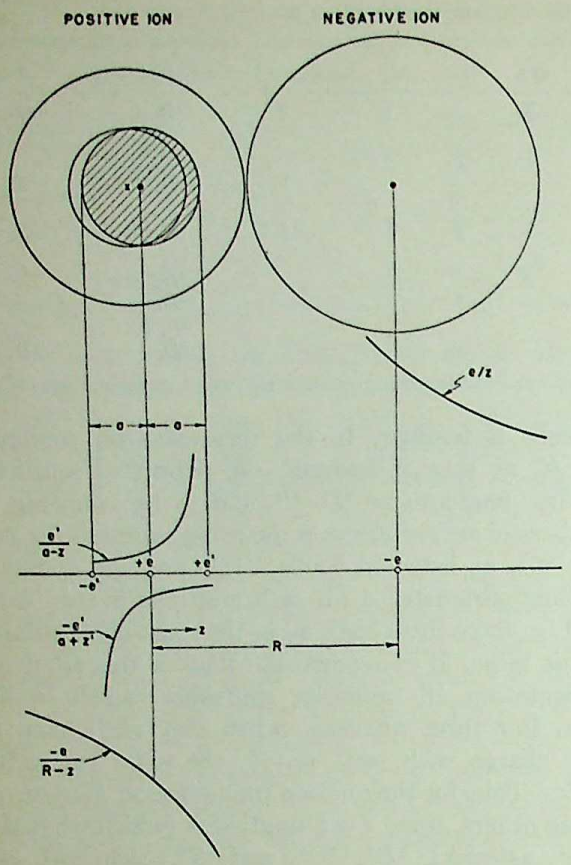


FIG. 21. Schematic charge redistribution in one of the ions of a polar molecule, and the terms of the potential which contribute to the calculation of the quadrupole coupling constant q at its nucleus.

that these are nothing but the result of making a quantum-mechanical average of the Coulomb interactions of the electrons and nuclei which constitute a molecule, and that the forces acting on a nucleus within the molecule are entirely electrical forces (aside from very small magnetic forces). It is important not to confuse the question of stability of a molecule at a given internuclear distance R with the question of the force acting on a nucleus, or the potential effective on the parts of the nucleus as it alters its orientation. In making this distinction, let us neglect zero-point vibration and consider a nonrotational state, so the molecule may be assumed to be at rest and in equilibrium at a constant internuclear distance. The equilibrium depends on the fact that, if R should be altered, the energy of the molecule would be higher after the electrons had readjusted their rapid motions to fit this adiabatic change. The total energy of the calculated ground state of the molecule, plotted against R, has a minimum at the equilibrium value of R. This statement says nothing about the electric potential in the vicinity of the nucleus. It may perfectly well be true that the nucleus is sitting at the top of a potential hill, but never slides off because the hill changes its height every time the nucleus moves a little. The electrons which determine the height of the hill are governed in their motions by the position of the nucleus. In a first-order treatment of hyperfine structure, which is a relatively small effect, we assume that the electrons are not appreciably affected in their motions by the orientation of the nonspherical nucleus, and thus use a potential function in this calculation. The "hill" is level on top, or the valley is level at the bottom, as the case may be (that is, there is no electric field acting on the nucleus, so that it may remain unaccelerated in its equilibrium position) but the sign of the quadrupole coupling constant q is negative or positive depending on whether the potential function is a hill or a valley, in the profile made by cutting along the internuclear axis z.

The charge distribution of a diatomic molecule has rotational symmetry about the z axis, and the potential in the neighborhood of a given nucleus resulting from all charges outside of (an arbitrarily small sphere surrounding) that nucleus may be described, in the light of the Laplace equation, by the derivatives

$$\partial^2V/\partial x^2=\partial^2V/\partial y^2=-\tfrac{1}{2}\partial^2V/\partial z^2,$$

that is, essentially by $\partial^2V/\partial z^2$, the first derivatives being zero because of the equilibrium. The nonspherical nature of the nucleus is defined by its quadrupole moment

$$Q=\sum_{\text{protons}}(3z_p^2-r_p^2)_{\text{Av}},$$

where z_p and r_p are proton coordinates in the nucleus, with the z_p axis the preferred one along the nuclear angular momentum, which in this section we traditionally call I (elsewhere J). With I oriented along the z axis of the molecule, the two coordinate systems coincide and the orientation energy is

$$\begin{aligned}\epsilon&=\tfrac{1}{2}e\sum_{\text{protons}}(x^2\partial^2V/\partial x^2+y^2\partial^2V/\partial y^2+z^2\partial^2V/\partial z^2)_{\text{Av}}\\&=\tfrac{1}{4}e\sum(2z^2-x^2-y^2)_{\text{Av}}\partial^2V/\partial z^2\\&=\tfrac{1}{4}eQ\partial^2V/\partial z^2\equiv\tfrac{1}{4}eQq,\end{aligned}$$

e being proton charge. In the orientation normal to this, with z_p along x, one obtains $\epsilon=-eQq/8$ (after using the symmetry of the nucleus about z_p). The quadrupole coupling constant q as here defined, $q=\partial^2V/\partial z^2$, agrees with the definition usually used in the experimental analysis (F45),

$$eq=\int de_j(3z_j^2-r_j^2)/r_j^5,$$

which is equal to

$$\int de_j\partial^2r_j^{-1}/\partial z_j^2.$$

In the case of a diatomic polar molecule, such as LiCl and the other alkali halides, the molecule may be assumed to consist essentially of two ions, and an important contribution to the electric potential at the

CC-0. In Public Domain. Gurukul Kangri Collection, Haridwar

Digitized by Arya Samaj Foundation Chennai and eGangotri

Li nucleus, say, is the Coulomb term $V_1=-e/r$ arising from the charge of the negative Cl ion. We shall show that one may plausibly conclude that this is the preponderant term in determining the sign of q.

If the ions remained unpolarized (spherically symmetrical), V_1 would be the only potential acting on the nucleus and the nucleus would be accelerated by an electric field E_1. The field to annul this must be supplied by polarization, and, since polarization forces are comparatively short-ranged, this must come primarily from the ion in which the nucleus is located. The simplest model for polarization would be to consider that the nucleus moves away from the center of a uniformly filled sphere of electron charge, but this is too simple. In the Thomas-Fermi approximation to atomic theory, for example, it is known that the electron density increases toward the center, and correspondingly, there is a tendency for the nucleus, if displaced, to carry the electron density in its immediate vicinity along with it. As a simple model intended to describe this effect, with a discontinuity replacing a gradual change, let us consider that the polarization of the positive ion (for example) is accomplished by moving the nucleus and all the electron charge within a sphere of radius a about it bodily to the right, as sketched in Fig. 21, by application of an imaginary constraint. In this step we have introduced no new electric force acting on the nucleus: the total force of all the electrons in the positive ion on its nucleus remains zero, because the nucleus is at the center of a spherical distribution of charge and, at the same time, inside of a spherical shell, each of which makes zero field. In this step, we have, however, piled up the charge in the region of overlap and thus made it necessary to occupy high energy parts of momentum space in one crescent-shaped segment, and have left another empty. If we relax the constraint, the most marked readjustment to this inequitable situation is expected to be that some of the charge from the overlapped segment will settle in the empty segment. Electrically, this readjustment is roughly equivalent to placing a positive charge, let us say e', at about a distance a to the right of the nucleus, and a negative charge $-e'$ at about the same distance to the left. The corresponding equivalent charges and potentials are shown in the lower part of Fig. 21.

The electric potential caused by all other charges (the electron cloud and the other nucleus) at and near the nucleus of the positive ion is the sum of three terms, which along the z axis are

$$V_1(z)=-e/(R-z),$$
$$V_2(z)=e'/(a-z),$$
$$V_3(z)=-e'/(a+z).$$

The z components of the corresponding electric fields are $E_i=-dV_i/dz$, and from the vanishing of the total electric field at the nucleus we have $E_2=E_3=-E_1/2$,

TABLE X. Observed sign of qQ for various nuclei in various molecules (Lo52), and the sign of Q deduced.

Nucleus	Homopolar	Other ion F	Cl	I	Br	K	Tl	Q	Config.
Li^7	+	+	+	+	+			−	$p_{3/2}^3$
Na^{23}	−	−	−	−	−			+	$(\pi d_{5/2})^3(\nu d_{5/2})^4$
$_{19}K_{20}^{39}$	−	−						+	$(\pi d_{3/2})^{-1}$
$_{37}Rb_{48}^{85}$	−	−						+	$(\pi f_{5/2})^{-1}$
$_{55}Cs_{78}^{133}$	+	+						−	$(\pi g_{7/2})^{-3}$
$_{17}Cl^{35,37}$						−	−	−	$(\pi d_{3/2})$

in the approximation in which the similar polarization of the other ion is here neglected. Thus the two polarization terms in the electric field have the same sign and combine to annul the ionic term.

Among the corresponding contributions $q_i=\partial^2 V_i/\partial z^2$ to the quadrupole coupling constant q, the two polarization terms annul one another in this approximation, for $q_2=-q_3$, corresponding to the fact that the curve resulting from e' is concave upward and the curve resulting from $-e'$ is concave downward in Fig. 21. This leaves the quadrupole coupling $q=q_1$ with the sign determined simply by the sign of the charge on the other ion, corresponding to the downward curvature of the curve due to $-e$ in Fig. 21. Thus q is in this approximation expected to be negative at the Li nucleus and a similar treatment of the polarization of the other ion makes it positive at the Cl nucleus in the molecule LiCl, for example.

This oversimplified approximation is of course only a beginning of a calculation, intended to give some initial insight into the quadrupole coupling process, and it is gratifying that it does seem to have a simple correspondence with the observed results. The next higher terms in such a calculation may be of two types. First, there are those involving a difference in the curvatures q_2 and q_3, which might be troublesome, being individually larger in magnitude than the presumably dominant term q_1 by a factor $R/2a$, because of the shorter range a in the equations $q_2=E_2/a$, etc. These are essentially higher approximations in the treatment of the polarization of the ion caused by the application of the constant field E_1. Second, there are the effects of the ionic distortion caused by the derivatives of E_1, that is, by q_1 applied to the electrons, and their subsequent effect on the nuclear orientation. Since E_1 curves downward in Fig. 21, the corresponding potential energy for electrons curves upward and the electrons tend to shun the z axis, concentrating slightly near the xy plane. This makes the electric potential acting on the bulges of the nucleus lower in the xy plane, opposing the direct effect of the downward curvature of E_1 to make it lower along the z axis. The electrons thus tend to shield the nucleus from q_1.

Note added in proof.—The extent of this shielding is being investigated by Foley and Sessler (according to a private communication). By a spherical-harmonic

CC-0. In Public Domain. Gurukul Kangri Collection, Haridwar

Digitized by Arya Samaj Foundation Chennai and eGangotri

expansion of the potential applied to an atom and a perturbation-theory expansion of the statistical atom, they estimate that the shielding can be as high as 90 percent.

The consistency of the experimental results seems to indicate that these higher order effects still leave q_1 dominant in determining the sign of q. The measured signs (Lo52) of the products qQ are shown in Table X. The sign of Q, deduced from the rule that the sign of q is the sign of the charge on the other ion in the case of the alkali halides, is also listed. The (jj) configurations are listed. In the case of Li^7, where the (jj) model apparently does not apply, Q is expected to be negative on any reasonably simple model (essentially because the configuration p^3 is near the beginning of the p shell), and it is very gratifying to have the experimental evidence in favor of this expectation, since this was not clear earlier when the evidence depended on an uncertain calculation of q in Li_2.

Recent results (F52) show that q at the Cl nucleus in KCl is very sensitive to vibrational quantum numbers, so presumably to internuclear distance. This suggests (Du52) that the molecule is not quite completely ionic, and that a small admixture of a nonspherical $2p^{-1}$ shell in Cl contributes very significantly to q, so that the variation of the admixture with internuclear distance may account for the variation of q. The p electrons in Cl tend to overlap with the other atom to contribute some valence binding, and the corresponding sign of the quadrupole polarization of the atom makes a negative contribution to q, opposite to the contribution of the charge of the positive K ion. The small atomic admixture to the K ion (or the Li ion in LiCl, etc.) involves an s electron so does not appreciably affect q at its nucleus, so our conclusions concerning Q_{Li} are unaffected.

The signs of Q listed for K, Rb, and Cl are also in keeping with expectations based on the theory of nuclear structure, negative at the beginning of a subshell corresponding to an orbit spread out in a flat distribution near a plane normal to J, and positive for proton "holes" near the end of a subshell. In the cases of Na^{23} and Cs^{133} we do not have such a simple possibility with just one proton or "hole" in addition to closed subshells, so the shell-model expectation is not so clear. The Na^{23} configuration is complex enough that anything could happen, but in this case Q has been measured (by F. Bitter *et al.*, private communication from P. Kusch) to be positive by an atomic method not involving the uncertainty of a molecular q. This gives us our only direct verification of the signs here deduced. The Cs^{133} configuration listed should have positive Q, being nearer the end of a subshell, but the higher pairing energy (M50) of the competing nucleon level $h_{11/2}$ would favor the configuration $h_{11/2}{}^4g_{7/2}$, which woulp have a negative Q as observed, if the h protons pair to give zero.

For the polar molecules, a more physical argument may be given leading to the same picture of polarization of the ions, and not involving the temporary application of imaginary constraints. When an ion containing only closed electron shells begins to overlap with another ion, one may expect the angular factor of the electron distribution, originally isotropic, to begin to be affected by admixture of higher configurations (electrons being partially excited to higher shells) in such a way as to move electrons away from the region of overlap and over to the far side of the ion. This suggests that in case of modest overlap, the angular redistribution is most important near the outside of the ion and the parameter a in Fig. 21 should be approximately equal to $R/2$. In this case the curvature of the individual curves involving e' is about equal to that of the ionic term and higher approximations (such as the existence of radial as well as angular redistribution) are not apt to be more important than the terms already discussed.

Purely classically, one may describe the same effect by thinking of the balance of electric forces. The two ions must attract one another electrically, either in the unpolarized or polarized approximation. Thus some of the matter in each ion is accelerated toward the other ion, while the average charge distribution remains fixed. There is a reciprocal flux of electrons between the ions, which in their effective z motion come to rest on the far side of the ion and start back. It is their relatively low probability density in the region between the nuclei, where their z motion is rapid, and high density in the region where they come to rest that provides the polarization of the ion which we have described.

The signs of qQ for the homopolar molecules Li_2, etc., are also listed in Table X. Here the calculation of the sign of q appears to be more difficult because q is zero in the approximation corresponding to the one we have discussed, there being no simple Coulomb term from the charge on the "other ion." The deviation from spherical symmetry of the separate atoms is influenced by the symmetry of the electron wave function in the space coordinates and the consequent tendency for the electrons to concentrate in the region of atomic overlapping between the two nuclei. This effect appears to predominate, for it gives the negative sign observed for q in the alkali molecules, but it has to compete with the effect of the penetration of one nucleus into the initially spherical screening charge distribution of the other atom. It is perhaps gratifying that the effect predominates which sets in first as the atoms begin to overlap, but in an actual molecule the result might be expected to be a fairly delicate balance between the positive and negative contributions of electron and nuclear charge. That the balance is not extremely delicate is suggested by the consistency with which the homopolar value of q agrees with the value at the nucleus of the positive ion in Table X.

CC-0. In Public Domain. Gurukul Kangri Collection, Haridwar

Digitized by Arya Samaj Foundation Chennai and eGangotri

APPENDIX III

Transfer from Particles to Holes in the Theory of Beta-Decay

A convenient notation for calculations of beta-decay and other matrix elements is to list terms in a wave function according to entries of nucleons as 1, rather than 0, in a little table with rows and columns labeled with the quantum numbers of the substates of the p shell as follows:

$m_l=$	1		0		−1			a		b		c	
$m_s=$	$\frac{1}{2}$	$-\frac{1}{2}$	$\frac{1}{2}$	$-\frac{1}{2}$	$\frac{1}{2}$	$-\frac{1}{2}$		α	β	α	β	α	β
m_t $\frac{1}{2}$	1	0	0	0	0	0	or ν	1	0	0	0	0	0
$-\frac{1}{2}$	0	0	0	1	0	0	π	0	0	0	1	0	0.

Of course one need not bother to write the labels of the rows and columns in calculating. A "term" indicated thus is understood to be antisymmetric in exchange of the nucleons, and normalized. In our previous notation, the "term" given in this example is

$$(ab\alpha\beta\nu\pi - ba\beta\alpha\pi\nu)/2^{\frac{1}{2}} = \left|\begin{matrix} 1 & 0 & 0 & 0 & 0 & 0 \\ 0 & 0 & 0 & 1 & 0 & 0 \end{matrix}\right|.$$

This is a two-nucleon "term" applying to Li^6, and the ten-nucleon "term" of N^{14} associated with this one according to a generalization for nucleons of the systematization used by Condon and Shortley (C35, p. 284) in their treatment of the matrix of $l\cdot s$, is

$$\left|\begin{matrix} 1 & 1 & 1 & 1 & 1 & 0 \\ 1 & 1 & 0 & 1 & 1 & 1 \end{matrix}\right|,$$

which has the same value of M_L, M_S, and M_T. The nucleons are numbered in standard order consecutively from left to right across the upper row and then across the lower row, in the first term of the antisymmetric sum of products implied by this symbol.

The first line of Eq. (44) can be written

$$\psi_2 = \psi(^1P_1{}^1) = 8^{-\frac{1}{2}}(ab-ba)(\alpha\beta-\beta\alpha)(\nu\pi-\pi\nu)$$

$$= \tfrac{1}{2}\left\{ \left|\begin{matrix} 1 & 0 & 0 & 0 & 0 & 0 \\ 0 & 0 & 0 & 1 & 0 & 0 \end{matrix}\right| + \left|\begin{matrix} 0 & 0 & 0 & 1 & 0 & 0 \\ 1 & 0 & 0 & 0 & 0 & 0 \end{matrix}\right| - \left|\begin{matrix} 0 & 1 & 0 & 0 & 0 & 0 \\ 0 & 0 & 1 & 0 & 0 & 0 \end{matrix}\right| - \left|\begin{matrix} 0 & 0 & 1 & 0 & 0 & 0 \\ 0 & 1 & 0 & 0 & 0 & 0 \end{matrix}\right| \right\},$$

and for ten nucleons we have for this $^1P_1$ state and correspondingly for the $^3S_1$, the $^3P_0$ and the $^1S_0$ states, respectively, the wave functions

$$\psi_2 = \tfrac{1}{2}\left\{ - \left|\begin{matrix} 1 & 1 & 1 & 1 & 1 & 0 \\ 1 & 1 & 0 & 1 & 1 & 1 \end{matrix}\right| + \left|\begin{matrix} 1 & 1 & 0 & 1 & 1 & 1 \\ 1 & 1 & 1 & 1 & 1 & 0 \end{matrix}\right| + \left|\begin{matrix} 1 & 1 & 1 & 1 & 0 & 1 \\ 1 & 1 & 1 & 0 & 1 & 1 \end{matrix}\right| - \left|\begin{matrix} 1 & 1 & 1 & 0 & 1 & 1 \\ 1 & 1 & 1 & 1 & 0 & 1 \end{matrix}\right| \right\},$$

$$\psi_3 = 3^{-\frac{1}{2}}\left\{ \left|\begin{matrix} 1 & 1 & 1 & 1 & 1 & 0 \\ 1 & 0 & 1 & 1 & 1 & 1 \end{matrix}\right| - \left|\begin{matrix} 1 & 0 & 1 & 1 & 1 & 1 \\ 1 & 1 & 1 & 1 & 1 & 0 \end{matrix}\right| + \left|\begin{matrix} 1 & 1 & 1 & 0 & 1 & 1 \\ 1 & 1 & 1 & 0 & 1 & 1 \end{matrix}\right| \right\},$$

$$\psi_4 = -6^{-\frac{1}{2}}\left\{ 2^{\frac{1}{2}} \left|\begin{matrix} 1 & 1 & 1 & 1 & 1 & 1 \\ 1 & 0 & 1 & 0 & 1 & 1 \end{matrix}\right| + \left|\begin{matrix} 1 & 1 & 1 & 1 & 1 & 1 \\ 0 & 1 & 1 & 1 & 1 & 0 \end{matrix}\right| + \left|\begin{matrix} 1 & 1 & 1 & 1 & 1 & 1 \\ 1 & 0 & 1 & 1 & 0 & 1 \end{matrix}\right| + 2^{\frac{1}{2}} \left|\begin{matrix} 1 & 1 & 1 & 1 & 1 & 1 \\ 1 & 1 & 0 & 1 & 0 & 1 \end{matrix}\right| \right\},$$

$$\psi_5 = 3^{-\frac{1}{2}}\left\{ \left|\begin{matrix} 1 & 1 & 1 & 1 & 1 & 1 \\ 0 & 1 & 1 & 1 & 1 & 0 \end{matrix}\right| - \left|\begin{matrix} 1 & 1 & 1 & 1 & 1 & 1 \\ 1 & 0 & 1 & 1 & 0 & 1 \end{matrix}\right| + \left|\begin{matrix} 1 & 1 & 1 & 1 & 1 & 1 \\ 1 & 1 & 0 & 0 & 1 & 1 \end{matrix}\right| \right\}.$$

CC-0. In Public Domain. Gurukul Kangri Collection, Haridwar

Digitized by Arya Samaj Foundation Chennai and eGangotri

Here the sign has been changed (C35, p. 285) of each ten-nucleon "term" having odd M_L, from the sign of its two-nucleon counterpart, for reasons which we shall see presently.

Thus we have, for example,

$$\tfrac{1}{2}\sum l^+s^- \left|\begin{matrix}1&0&0&0&0&0\\0&0&0&1&0&0\end{matrix}\right| = 0, \quad \tfrac{1}{2}\sum l^-s^+ \left|\begin{matrix}1&0&0&0&0&0\\0&0&0&1&0&0\end{matrix}\right| = 2^{-\frac{1}{2}} \left|\begin{matrix}1&0&0&0&0&0\\0&0&0&0&1&0\end{matrix}\right|,$$

with only one term because the operator s^+ on the spin function α of the first nucleon gives zero. The corresponding examples for ten nucleons are

$$\tfrac{1}{2}\sum l^+s^- \left|\begin{matrix}1&1&1&1&1&0\\1&1&0&1&1&1\end{matrix}\right| = 0, \quad \tfrac{1}{2}\sum l^-s^+ \left|\begin{matrix}1&1&1&1&1&0\\1&1&0&1&1&1\end{matrix}\right| = 2^{-\frac{1}{2}} \left|\begin{matrix}1&1&1&1&1&0\\1&0&1&1&1&1\end{matrix}\right|.$$

Here the number of effective operations in the sum is limited because the antisymmetry gives zero if more than one nucleon is recorded in the same space, and the only effective operation is one that changes the seventh nucleon from $a\beta$ to $b\alpha$, with no change from the standard order of nucleon numbers. Thus the relation between the corresponding terms is the same in the two-nucleon and ten-nucleon cases in these examples and continues similarly (C35) for all the operations involving l^+s^- and l^-s^+, which change M_L by one unit. The change of sign introduced into the wave functions for "terms" of odd M_L, as mentioned above, makes the contribution to the matrix element have opposite sign in the two cases, in keeping with the familiar fact that the spin-orbit coupling energy for two holes is the opposite of that for two particles. In the operations involving $\sum l_z s_z$ the summation gives the opposite sign in the ten-nucleon case from the two-nucleon case, a familiar fact which constitutes the most elementary part of the theory of holes. Thus the matrix of $\sum \mathbf{l}\cdot\mathbf{s}$ has opposite sign for particles and holes.

The beta-decay operator works somewhat differently. We have, for example,

$$t^+s^- \left|\begin{matrix}1&0&0&0&0&0\\0&0&0&1&0&0\end{matrix}\right| = 0; \quad t^+s^- \left|\begin{matrix}0&0&0&1&0&0\\1&0&0&0&0&0\end{matrix}\right| = -\left|\begin{matrix}0&1&0&1&0&0\\0&0&0&0&0&0\end{matrix}\right|,$$

$$t^+s^- \left|\begin{matrix}1&1&1&1&1&0\\1&1&0&1&1&1\end{matrix}\right| = -\left|\begin{matrix}1&1&1&1&1&1\\1&1&0&1&0&1\end{matrix}\right|; \quad t^+s^- \left|\begin{matrix}1&1&0&1&1&1\\1&1&1&1&1&0\end{matrix}\right| = 0.$$

In the two-nucleon case which has a nonvanishing result, a negative sign appears because the second nucleon has been moved by the operation into a position where the first nucleon should appear in the standard order, and a permutation introducing a negative sign must be affected before the symbol implying standard order may be used. Similarly in the ten-nucleon case, the effective operation moves a nucleon, in this case the ninth, upward toward the right to put it ahead of an odd number of other nucleons, in this case three, placing it where nucleon number six should be, and an odd permutation is required to get it back where it belongs in the standard order (so as to match a term in the other wave function appearing in the calculation of the matrix element). The two two-nucleon terms operated upon in this example differ from one another only in an interchange of neutrons and protons, and always appear together in the wave functions we consider, the same being true of the two ten-nucleon terms, so the operator acting on the sum of the two terms has just the corresponding effect, including the same negative sign, in the two cases. The generalization of the theorem here illustrated involves showing that the permutation to compensate the operator always has the same "parity" in the two cases, essentially because one fills in places in the table in adjacent pairs when filling up the shell from the particle case to the hole case.

While this theorem is sufficient, we may complete the explicit demonstration of a lack of cancellation by listing the results of the operations involved in calculating the four crucial matrix elements:

$$\sum l\cdot s\psi_2 = (\tfrac{1}{4})\left\{ \left|\begin{matrix}1&1&1&1&1&0\\1&1&0&1&1&1\end{matrix}\right| + \left|\begin{matrix}1&1&0&1&1&1\\1&1&1&1&1&0\end{matrix}\right| + \left|\begin{matrix}1&1&1&1&0&1\\1&1&1&0&1&1\end{matrix}\right| + \left|\begin{matrix}1&1&1&0&1&1\\1&1&1&1&0&1\end{matrix}\right| \right.$$

$$\left. -2^{\frac{1}{2}} \left|\begin{matrix}1&1&1&1&1&0\\1&0&1&1&1&1\end{matrix}\right| - 2^{\frac{1}{2}} \left|\begin{matrix}1&0&1&1&1&1\\1&1&1&1&1&0\end{matrix}\right| + 2^{\frac{1}{2}} \left|\begin{matrix}1&1&1&0&1&1\\1&1&1&0&1&1\end{matrix}\right| \right\},$$

CC-0. In Public Domain. Gurukul Kangri Collection, Haridwar

Digitized by Arya Samaj Foundation Chennai and eGangotri

$$\sum l\cdot s\psi_5=-3^{-\frac{1}{2}}\left\{\begin{vmatrix}1&1&1&1&1&1\\&&&&&\\0&1&1&1&1&0\end{vmatrix}+\begin{vmatrix}1&1&1&1&1&1\\&&&&&\\1&0&1&1&0&1\end{vmatrix}+2^{\frac{1}{2}}\begin{vmatrix}1&1&1&1&1&1\\&&&&&\\1&1&0&1&0&1\end{vmatrix}+2^{\frac{1}{2}}\begin{vmatrix}1&1&1&1&1&1\\&&&&&\\1&0&1&0&1&1\end{vmatrix}\right\},$$

$$\sum\tau_x\sigma\psi_2=i^+\begin{vmatrix}1&1&1&1&1&1\\&&&&&\\1&1&0&1&0&1\end{vmatrix}+\cdots,$$

$$\sum\tau_x\sigma\psi_3=3^{-\frac{1}{2}}i^+\left\{\begin{vmatrix}1&1&1&1&1&1\\&&&&&\\0&1&1&1&1&0\end{vmatrix}-\begin{vmatrix}1&1&1&1&1&1\\&&&&&\\1&0&1&1&0&1\end{vmatrix}-\begin{vmatrix}1&1&1&1&1&1\\&&&&&\\1&1&0&0&1&1\end{vmatrix}+\cdots\right\}.$$

Here the dots indicate that terms have been omitted having the wrong M_T. The matrix elements are

$$({}^3S_1|H'|{}^1P_1)/a=(\psi_3,\sum l\cdot s\psi_2)=-(2/3)^{\frac{1}{2}},$$
$$({}^3P_0|H'|{}^1S_0)/a=(\psi_4,\sum l\cdot s\psi_5)=2^{\frac{1}{2}},$$
$$({}^3P_0|\mathbf{V}|{}^1P_1)/g=(\psi_4,\sum\tau_x\boldsymbol{\sigma}\psi_2)=-3^{-\frac{1}{2}}\mathbf{i}^+,$$
$$({}^1S_0|\mathbf{V}|{}^3S_1)/g=(\psi_5,\sum\tau_x\boldsymbol{\sigma}\psi_3)=\mathbf{i}^+.$$

The ratio of the first two divided by the ratio of the last two is $+1$, just as it appeared in Eq. (47) as calculated for the two-nucleon case, and this is the sign which gives no cancellation in the ground-configuration beta-decay matrix element to the ground state of Py[14]. With the arbitrary phases of the ψ's chosen so that the nondiagonal as well as the diagonal matrix elements of H' have the opposite sign, those of $\mathbf{V}$ have the same sign, for holes as for particles.

BIBLIOGRAPHY

A49 L. W. Alvarez, Phys. Rev. **75**, 1127 (1949).
A50 Wayne Arnold, Phys. Rev. **79**, 170 (1950); **80**, 34 (1950).
Ar50 Argo, Gittings, Hemmendinger, Jarvis, and Taschek, Phys. Rev. **78**, 691 (1950).
Al51 J. C. Allred, Phys. Rev. **84**, 695 (1951).
Av50 R. Avery and C. H. Blanchard, Phys. Rev. **78**, 704 (1950).
A51 R. K. Adair, Phys. Rev. **82**, 750 (1951); Bashkin, Petree, and Mooring, Phys. Rev. **82**, 378 (1951); H. Staub and H. Tatel, Phys. Rev. **58**, 820 (1940).
Aj51 F. Ajzenberg, Phys. Rev. **82**, 43 (1951).
Aj51a F. Ajzenberg, Phys. Rev. **83**, 693 (1951).
Ar51 Arfken, Biedenharn, and Rose, Phys. Rev. **84**, 89 (1951).
A52 R. K. Adair, Phys. Rev. **86**, 155 (1952).
A52a R. K. Adair, Phys. Rev. **87**, 1041 (1952).
Aj52 F. Ajzenberg and T. Lauritsen, Revs. Modern Phys. **24**, 321 (1952); see (H50). It is a matter for apology to the observers that most of the extensive data on which this interpretation is based are referred to only indirectly through these very convenient reviews.
Aj52a F. Ajzenberg, Phys. Rev. **88**, 298 (1952).
B37 G. Breit, Phys. Rev. **51**, 248 (1937).
B38 G. Breit and G. R. Stehn, Phys. Rev. **53**, 459 (1938).
Be38 H. A. Bethe, Phys. Rev. **54**, 436 (1938).
B50 Barnes, French, and Devons, Nature **166**, 145 (1950).
B51 S. T. Butler, Proc. Roy. Soc. (London) **208A**, 559 (1951); N. Austern and S. T. Butler, Phys. Rev. **90**, 365(A) (1953).
Be51 J. Benveniste and B. Cork, Phys. Rev. **83**, 894 (1951).
Bo51 T. W. Bonner and J. W. Butler, Phys. Rev. **83**, 1091 (1951).
Br51 R. Britten, Phys. Rev. **82**, 295 (1951); U. S. Atomic Energy Commission Report NYO 970.
B52 S. T. Butler and E. E. Salpeter, Phys. Rev. **88**, 133 (1952).
Be52 R. E. Benenson, Phys. Rev. **87**, 207(A) (1952).
Bh52 Bhatia, Huang, Huby, and Newns, Phil. Mag. **7**, 485 (1952).
B152 J. M. Blatt, Phys. Rev. **89**, 83 (1953). It was in a preliminary communication that (LS) coupling in Py[6] was used as implied in the text.
Br52 D. A. Bromley and L. M. Goldman, Phys. Rev. **86**, 790 (1952).
Bu52 W. H. Burke and J. R. Risser, Phys. Rev. **87**, 294 (1952).
B53 Bockelman, Browne, Buechner, and Sperduto, Phys. Rev. **90**, 340(A) (1953).
C29 Condon and Morse, *Quantum Mechanics* (McGraw-Hill Book Company, Inc., New York, 1929).
C35 Condon and Shortley, *Atomic Energy States* (Cambridge University Press, Cambridge, 1935).
C49 C. L. Critchfield and D. C. Dodder, Phys. Rev. **76**, 602 (1949); Frier, Lampi, Sleator, and Williams, Phys. Rev. **75**, 1345 (1949).
C50 C. D. Curling and J. O. Newton, Nature **166**, 339 (1950).
C52 C. M. Class and S. S. Hanna, Phys. Rev. **87**, 247 (1952).
Co52 Cohen, Shefroth, Class, and Hanna, Phys. Rev. **87**, 205 (1952).
C53 E. A. Crosbie, private communication. Some of the ground-configuration results of reference (K52), and further second-order deviations from extreme-coupling asymptotes, are implied in a recent summary, Phys. Rev. **90**, 138 (1953).
D36 S. Dancoff and D. R. Inglis, Phys. Rev. **51**, 784 (1936); see errata Phys. Rev. **82**, 182 (1951).
D40 D. M. Dennison, Phys. Rev. **57**, 454 (1940).
D50 S. M. Dancoff, Phys. Rev. **77**, 775A; **78**, 382 (1950).
Di50 L. Diesendruck, dissertation, The Johns Hopkins University, 1950.
D52 P. B. Daitch and J. B. French, Phys. Rev. **87**, 900 (1952).
De52 Dewan, Pepper, Allen, and Almquist, Phys. Rev. **86**, 416 (1952).
Du52 J. Duchesne, J. Chem. Phys. **20**, 1804 (1952).
E41 D. Elliott and L. D. P. King, Phys. Rev. **60**, 489 (1941).
E51 Enge, Buechner, Sperduto, and Van Patter, Phys. Rev. **83**, 31 (1951).
E52 Enge, Buechner, and Sperduto, Phys. Rev. **88**, 963 (1952).
F26 J. Frenkel, Z. Physik **37**, 243 (1926).
F36 W. H. Furry, Phys. Rev. **51**, 784 (1936).
F37 E. Feenberg and E. Wigner, Phys. Rev. **51**, 95 (1937); E. Feenberg and M. Phillips, Phys. Rev. **51**, 597 (1937).
F45 B. T. Feld and W. E. Lamb, Jr., Phys. Rev. **67**, 15 (1945); Eq. II(5).
F49 E. Feenberg and K. C. Hammack, Phys. Rev. **75**, 1877 (1949).
F50 A. M. Feingold and E. P. Wigner, Phys. Rev. **79**, 221A (1950), and valued expository remarks thereon by Professor Wigner.
Fe50 E. Fermi and M. G. Mayer, private communication.
Fee50 E. Feenberg and G. Trigg, Revs. Modern Phys. **22**, 399 (1950).
F51 E. Feenberg, Phys. Rev. **81**, 644 (1951).

CC-0. In Public Domain. Gurukul Kangri Collection, Haridwar

Digitized by Arya Samaj Foundation Chennai and eGangotri

Fe51 A. M. Feingold, Revs. Modern Phys. **23**, 10 (1951).
Fr51 O. R. Frisch, International Conference, Chicago, September 1951, Proc., p. 54.
F52 Fabricand, Carlson, Lee, and Rabi, Phys. Rev. **86**, 607 (1952).
Fl52 B. H. Flowers and A. R. Edmonds, Proc. Roy. Soc. (London) **A215**, 120 (1952).
G49 H. Gauss, Z. Naturforsch. **4A**, 721 (1949).
Gu49 E. Guth and C. J. Mullin, Phys. Rev. **76**, 234, 682 (1949).
G51 E. Gerjuoy, Phys. Rev. **81**, 62 (1951).
Go51 M. Goldhaber and A. W. Sunyar, Phys. Rev. **83**, 906 (1951).
G52 Guier, Bertini, and Roberts, Phys. Rev. **85**, 426 (1952).
G53 R. W. Gelinas and S. S. Hanna, Phys. Rev. **89**, 483 (1953).
Ga53 S. Gallone and C. Salvetti, Nuovo cimento **10**, 145 (1953).
H32 W. Heisenberg, Z. Physik **77**, 1 (1932).
H37 F. Hund, Z. Physik **105**, 202 (1937).
H38 L. R. Hafstad and E. Teller, Phys. Rev. **54**, 681 (1938).
H48 N. P. Heydenburg and D. R. Inglis, Phys. Rev. **73**, 230 (1948).
H49 Haxel, Jensen, and Suess, Phys. Rev. **75**, 1766 (1949); Naturwiss. **36**, 155 (1949).
H50 Hornyak, Lauritsen, Morrison, and Fowler, Revs. Modern Phys. **22**, 291 (1950). The next revision, "Energy Levels IV" (Aj52), appeared just as the present paper was about to go to press, and complete references to the experimental data are to be found there. Professor Lauritsen and Dr. Ajzenberg have very kindly communicated prepublication copies of many of the valuable charts and tables. In spite of this, there remain some trivial differences in the numbers given for the energies in Fig. 1 and in (Aj52).
Hu50 Hudspeth, Swann, and Heydenburg, Phys. Rev. **77**, 736 (1950).
H51 H. H. Hummel and D. R. Inglis, Phys. Rev. **81**, 910; **83**, 1078 (1951).
Ha51 R. R. Haefner, Revs. Modern Phys. **23**, 228 (1951).
H52 Hubbard, Nelson, and Jacobs, Phys. Rev. **87**, 378 (1952).
Ha52 G. Harries and G. W. Davies, Proc. Phys. Soc. (London) **65A**, 564 (1952).
Har52 E. G. Harris and M. A. Melanoff, Bull. Am. Phys. Soc. **27**, 5 (1952).
Hu52 P. Huber and E. Baldinger, Helv. Phys. Acta **25**, 435 (1952).
I36 D. R. Inglis, Phys. Rev. **50**, 783 (1936).
I37 D. R. Inglis, Phys. Rev. **51**, 531 (1937); H. Margenau and K. G. Carrol, Phys. Rev. **54**, 705 (1938); W. J. Kroeger, Phys. Rev. **54**, 1048 (1938).
I39 D. R. Inglis, Phys. Rev. **56**, 1175 (1939).
I41 D. R. Inglis, Phys. Rev. **60**, 837 (1941).
I49 D. R. Inglis, Phys. Rev. **75**, 1767 (1949).
I50 D. R. Inglis, Phys. Rev. **78**, 616 (1950).
I50a D. R. Inglis, Phys. Rev. **81**, 914 (1950).
I51 D. R. Inglis, Phys. Rev. **82**, 181 (1951).
I51a D. R. Inglis, Phys. Rev. **81**, 914 (1951).
I52 D. R. Inglis, Phys. Rev. **87**, 915 (1952).
I52a D. R. Inglis, Phys. Rev. **85**, 492 (1952).
J50 R. Jastrow, Phys. Rev. **81**, 165 (1950).
J51 H. L. Jackson and A. I. Galonsky, Phys. Rev. **84**, 401 (1951).
J52 G. A. Jones and D. H. Wilkinson, Phys. Rev. **88**, 423 (1952).
K50 D. Kurath, Phys. Rev. **80**, 98 (1950).
K51 Koester, Jackson, and Adair, Phys. Rev. **83**, 1250 (1951).
K52 D. Kurath, Phys. Rev. **88**, 804 (1952).
K52a D. Kurath, recent unpublished calculation.
K52b D. Kurath, Phys. Rev. **87**, 218 (1952).
Kr52 N. M. Kroll and L. L. Foldy, Phys. Rev. **88**, 1177 (1952).
Kre52 Kreger, Kerman, and Jentschke, Phys. Rev. **86**, 593 (1952).
Ki53 King, Dismuke, and Way, Table of log *ft* values: October, 1952 (Oak Ridge National Laboratory Report ORNL 1450.)
L49 Libby, Anderson, and Arnold, Science **109**, 227; **110**, 679 (1949).
L51 Li, Whaling, Fowler, and Lauritsen, Phys. Rev. **83**, 512 (1951).
La51 H. H. Landon, Phys. Rev. **83**, 1081 (1951).
Le51 L. T. Leland and H. M. Agnew, Phys. Rev. **82**, 559 (1951).
L52 T. Lauritsen, Annual Reviews of Nuclear Science **1**, 67 (1952).
Le52 G. M. Lewis, Phil. Mag. **43**, 690 (1952).
Lo52 Logan, Cote, and Kusch, Phys. Rev. **86**, 280 (1952).
M49 M. G. Mayer, Phys. Rev. **75**, 1969 (1949); **78**, 16 (1950).
M50 M. G. Mayer, Phys. Rev. **78**, 22 (1950).
M51 R. Malm and W. W. Buechner, Phys. Rev. **81**, 519 (1951).
Mo51 S. A. Moszkowski, Phys. Rev. **82**, 118 (1951).
P35 L. Pauling and E. B. Wilson, *Introduction to Quantum Mechanics* (McGraw-Hill Book Company, Inc., New York, 1935), pp. 209–218.
P50 R. D. Present, Phys. Rev. **80**, 43 (1950).
Ph51 Phillips, Heydenburg, and Cowie, Phys. Rev. **85**, 742(A) (1951).
P52 Murray Peshkin and A. J. F. Siegert, Phys. Rev. **87**, 735 (1952).
Pr52 M. H. L. Pryce, Proc. Phys. Soc. (London) **A65**, 773 (1952).
R41 W. Rarita and J. Schwinger, Phys. Rev. **59**, 209, 436, 556 (1941).
R48 L. Rosenfeld, *Nuclear Forces* (North-Holland, Amsterdam 1948).
R49 Rasmussen, Hornyak, and Lauritsen, Phys. Rev. **76**, 581 (1949); Chao, Lauritsen, and Rasmussen, Phys. Rev. **76**, 582 (1949).
R51 J. Rotblat, Nature **167**, 1027 (1951); Phys. Rev. **83**, 1271 (1951).
R52 Hugh T. Richards, Remarks at the Pittsburgh Conference on Nuclear Physics, p. 33, June, 1952 (to be published).
Ra52 L. A. Radicati, Phys. Rev. **87**, 521 (1952).
S29 J. C. Slater, Phys. Rev. **34**, 1293 (1929).
S37 T. Schmidt, Z. Physik **106**, 358 (1937).
S52 J. Seed and A. P. French, Phys. Rev. **88**, 1007 (1952).
Sp52 A. Sperduto and W. W. Buechner, Phys. Rev. **88**, 574 (1952).
S53 P. Stoll, private communication; Erdös, Stoll, and Scherrer, to appear in Helv. Phys. Acta. See also W. E. Burcham and J. M. Freeman, Phil. Mag. **41**, 921 (1950); O. Rochat and P. Stoll, Helv. Phys. Acta **25**, 451 (1952); H. Glättli and P. Stoll, Helv. Phys. Acta **25**, 455 (1952); R. Müller and P. Stoll, Nuovo cimento **9**, 1232 (1952), J. D. Jackson and D. I. Wanklyn, Phys. Rev. **90**, 381(A) (1953).
SG53 G. Scharff-Goldhaber, Phys. Rev. **90**, 587 (1953).
T26 L. H. Thomas, Phil. Mag. **3**, 1 (1926).
Th50 R. G. Thomas, Phys. Rev. **80**, 136 (1950).
T51 V. L. Telegdi, Phys. Rev. **84**, 600 (1951); V. L. Telegdi and W. Zunti, Helv. Phys. Acta **23**, 744 (1950).
Th51 J. Thirion and T. Muller, Compt. rend. **232**, 1093 (1951).
Ti51 E. W. Titterton and T. A. Brinkley, Proc. Phys. Soc. (London) **64A**, 212 (1951).
T52 I. Talmi, Helv. Phys. Acta **25**, 185 (1952).
Th52 R. G. Thomas and T. Lauritsen, Phys. Rev. **88**, 966 (1952).
Th52a R. G. Thomas, Phys. Rev. **88**, 1109 (1952).
Tho52 D. M. Thompson, Phys. Rev. **88**, 954 (1952).
Tr52 L. Trainor, Phys. Rev. **85**, 962 (1952).
Tru52 Trumpy, Grotdal, and Graue, Nature **170**, 1118 (1952).
T53 V. Telegdi and M. Gell-Mann, private communication.
V51 Van Patter, Serduto, Huang, Strait, and Buechner, Phys. Rev. **81**, 233 (1951).
V51a Van Patter, Buechner, and Sperduto, Phys. Rev. **82**, 248 (1951).
V52 Van Patter, Endt, Sperduto, and Buechner, Phys. Rev. **86**, 502 (1952).
V52a D. M. Van Patter and W. W. Buechner, Phys. Rev. **87**, 51 (1952).
Va52 Van de Graaff, Sperduto, Buechner, and Enge, Phys. Rev. **86**, 966 (1952).
W37 J. A. Wheeler, Phys. Rev. **52**, 1088, 1107 (1937); J. A. Wheeler and E. Teller, Phys. Rev. **53**, 778 (1938).
We37 W. Wefelmeier, Z. Physik **107**, 332 (1937).
Wi37 E. Wigner, Phys. Rev. **51**, 106 (1937). Anticipated in the concept T by B. Cassen and E. U. Condon, Phys. Rev. **50**, 846 (1936).
W41 J. A. Wheeler, Phys. Rev. **59**, 16 (1941).
We41 Harald Wergeland, Norske Videnskabers Selskabs Skrifter, 1 (1941).
W50 S. D. Warshaw, Phys. Rev. **80**, 111 (1950).
W53 J. A. Wheeler and D. L. Hill, Phys. Rev. **90**, 366(A) (1953); K. W. Ford, Phys. Rev. **90**, 366(A) (1953).

CC-0. In Public Domain. Gurukul Kangri Collection, Haridwar

Digitized by Arya Samaj Foundation Chennai and eGangotri

REVIEWS OF MODERN PHYSICS VOLUME 25, NUMBER 2 APRIL, 1953

Gravitational Motion

A. E. SCHEIDEGGER

Imperial Oil Limited, Calgary, Alberta, Canada

1. INTRODUCTION

AMONG classical field theories, the theory of gravitation, also called general relativity theory, occupies a somewhat peculiar place. Unlike most other field theories, the field equations of relativity theory are nonlinear. This implies that many facts, well known in linear theories, have no analogs in general relativity theory, and conversely. The equations of motion of the gravitational field are contained in the field equations, a fact which does not apply for the motion of an electron in the electromagnetic field. Conversely, it is difficult to define the notion of a "wave" in relativity theory, for the linear principle of superposition is crucial for the existence of waves, at least in the sense that the notion of a "wave" is normally used.

Since the gravitational field manifests itself in the motion of its sources, the problem of finding the equations of motion is of fundamental importance. This problem has been puzzling theoretical physicists for a long time, and more or less convincing solutions have been given on several occasions. Today, the problem can be considered as solved, but the attempts and partial solutions are scattered over a variety of journals and over a long period of time. Thus, it is the object of this review article to summarize the methods that lead from the gravitational field equations to the equations of motion and to outline the physical implications of those methods. In addition, we shall discuss here some amplified aspects of the general methods which have grown mainly out of the personal association of the author with Dr. Infeld and the correspondence of the latter with Dr. Einstein. Although this article does not aim to consist entirely of original research, it will be found that many parts are presented in a way not published heretofore. In addition, the contents of Sec. 5 and of parts of Sec. 6 are believed to be original.

The plan for this review is as follows. After a brief introductory section on the notation and the principal contents of general relativity theory, the reader will find an exposition of the Einstein-Infeld-Hoffmann method. The aim was to give enough material of the calculations so that a reference to the unpublished notes deposited at the Institute of Advanced Studies[1] is no longer necessary. This is especially the case for the discussion of the two-body problem in the following section. Then the methods of integration of the differential equations of motion are studied and a new way is presented by which this aim can be achieved. The influence of the coordinate conditions and of general coordinate transformations upon the equations of motion are also investigated. Subsequently, the possibility of gravitational radiation of moving bodies in their own field and the possible reaction of such radiation upon their motion is discussed. Finally, a review of the attempts is given of generalizing the Einstein-Infeld-Hoffmann method to other field theories than that of gravitation.

It is hoped that this review will be found to be a useful summary of the work done on the question of gravitational motion during the last twenty years, and a suitable basis for carrying research into the yet unknown.

2. NOTATION

This paper will use extensively well-known facts of tensor calculus and general relativity. Unfortunately, no over-all accepted notation has been established so that it is necessary to list the notations and abbreviations which will be used.

We shall represent the four-dimensional time-space continuum by the coordinates

$$x^0, x^1, x^2, x^3,$$

where x^0 denotes time, the others the three space-coordinates. Since time often plays a different role in physics than the other three coordinates, we shall use a specific notation as follows. Wherever x^μ is written with a *Greek* index, it is understood to represent either time or one of the space coordinates. On the other hand, if we write x^m with a *Latin* index, we mean by this that x^m is one of the space coordinates only. This convention is extended to all indices such that a Greek index assumes the values 0–3, a Latin index 1–3.

We denote differentiation with respect to a world coordinate by a stroke. Thus, for any entity T we have

$$T_{|\alpha} \equiv \partial T/\partial x^\alpha. \tag{2.1}$$

We shall further denote the metric in the continuum of the x^α's by the ten functions

$$g_{\alpha\beta}(x^\mu) = g_{\beta\alpha}(x^\mu). \tag{2.2}$$

Then the length of the world-line $x^\mu = \xi^\mu(t)$ is given by

$$s_{12} = \int_1^2 \left\{ \sum_{\alpha\beta} g_{\alpha\beta}[x^\mu = \xi^\mu(t)] \frac{d\xi^\alpha}{dt} \frac{d\xi^\beta}{dt} \right\}^{\frac{1}{2}} dt. \tag{2.3}$$

Furthermore, we shall use the summation convention. In an expression containing entities with indices (any kind) or power exponents, it is understood that one has to sum over the whole range of any such symbol

[1] Einstein, Infeld, and Hoffmann, appendix to Ann. Math. 39, 66 (1938), unpublished notes deposited at the Institute for Advanced Studies, Princeton, New Jersey.

CC-0. In Public Domain. Gurukul Kangri Collection, Haridwar

Digitized by Arya Samaj Foundation Chennai and eGangotri

that appears twice. In cases where we want to consider one single term only, although a symbol of the above kind appears twice, we shall use brackets in order to indicate that the summation convention does not apply.

There is no unique way for assigning to a particular world point a set of coordinates x^β. We could equally well take another set of numbers $x^{\beta*}$ (with the same properties as described above) for describing our world. The passing from one set of coordinates to another one is called a coordinate transformation and may be expressed mathematically in the following way:

$$x^{\beta*}=f^\beta(x^\alpha). \tag{2.4}$$

The starred and the unstarred "systems" of coordinates represent the same four-dimensional universe and in both the length of a line must be expressible according to (2.3).

Tensors are entities satisfying the following transformation law under a coordinate transformation (2.4):

$$t_\mu{}^{\sigma*}=\frac{\partial x^\alpha}{\partial x^{\mu*}}\frac{\partial x^{\sigma*}}{\partial x^\beta}t_\alpha{}^\beta. \tag{2.5}$$

The quantities $g_{\alpha\beta}$ form a tensor, the metric tensor of the world. We may define the contravariant metric tensor $g^{\alpha\beta}$ by the equation

$$g_{\alpha\beta}g^{\beta\gamma}=\delta_\alpha{}^\gamma=\begin{cases}1 & \text{for} \quad \alpha=\gamma\\ 0 & \text{for} \quad \alpha\neq\gamma\end{cases}. \tag{2.6}$$

With the help of the metric tensor we can rise or lower indices of any tensor:

$$g_{\alpha\beta}T^\beta=T_\alpha; \quad g^{\alpha\beta}T_\beta=T^\alpha. \tag{2.7}$$

A set of functions $y_A(x^\beta)$ defined in all points of the world is called a "field." A is an index running from 1 to N, N being the total number of algebraically independent "components" of the field at one world point. The components of the field (also called field variables) are subject to a set of functional relationships

$$L^B(y_A)=0; \quad B=1\cdots N \tag{2.8}$$

which are termed field equations. They can be expressed as the Euler Lagrangian equations of a variational principle

$$\delta\int_V Ld^4x=0 \tag{2.9}$$

taken in the domain V, where the field equations are to be satisfied.

The field variables of general relativity theory are the components $g_{\alpha\beta}$ of the metric tensor of the world. Instead of $g_{\alpha\beta}$ one could equally well use any linear combinations of them or also the components of the metric tensor density

$$\mathfrak{g}_{\alpha\beta}=(-g)^{\frac{1}{2}}g_{\alpha\beta}. \tag{2.10}$$

One also could use the contravariant entities instead of the covariant ones.

The field variables in relativity theory are subject to the following nonlinear field equations (see references 2, 3, 4)

$$G^{\alpha\beta}=0. \tag{2.11}$$

The notation is chosen as follows:

(a) Christoffel symbols

$$\left\{\begin{matrix}\lambda\\ \iota\kappa\end{matrix}\right\}=\tfrac{1}{2}g^{\lambda\sigma}(g_{\iota\sigma|\kappa}+g_{\kappa\sigma|\iota}-g_{\iota\kappa|\sigma})\equiv g^{\lambda\sigma}[\iota\kappa,\ \sigma]. \tag{2.12}$$

(b) Covariant derivatives

$$t\ldots{}^{\iota}{}_{\ldots,\sigma}=t\ldots{}^{\iota}{}_{\ldots|\sigma}+\cdots+\left\{\begin{matrix}\iota\\ \rho\sigma\end{matrix}\right\}t\ldots{}^{\rho}{}_{\ldots}+\cdots \tag{2.13}$$

$$t\ldots{}_{\kappa\ldots;\sigma}=t\ldots{}_{\kappa\ldots|\sigma}-\cdots-\left\{\begin{matrix}\rho\\ \eta\sigma\end{matrix}\right\}t\ldots{}_{\rho\ldots}-\cdots \tag{2.14}$$

(c) Curvature tensor

$$R_{\iota\kappa\lambda\cdot}{}^{\nu}=\left\{\begin{matrix}\nu\\ \lambda\iota\end{matrix}\right\}_{|\kappa}-\left\{\begin{matrix}\nu\\ \lambda\kappa\end{matrix}\right\}_{|\iota}-\left\{\begin{matrix}\nu\\ \sigma\iota\end{matrix}\right\}\left\{\begin{matrix}\sigma\\ \lambda\kappa\end{matrix}\right\}+\left\{\begin{matrix}\nu\\ \sigma\kappa\end{matrix}\right\}\left\{\begin{matrix}\sigma\\ \lambda\iota\end{matrix}\right\}, \tag{2.15}$$

$$R_{\alpha\beta\gamma\cdot}{}^{\beta}=R_{\alpha\gamma}; \quad R=g^{\alpha\beta}R_{\alpha\beta}; \tag{2.16}$$

$$G_{\alpha\beta}=R_{\gamma\delta}g^{\gamma\alpha}g^{\delta\beta}-\tfrac{1}{2}Rg^{\alpha\beta}. \tag{2.17}$$

The field equations (2.11) are equivalent to

$$R_{\alpha\beta}=0. \tag{2.18}$$

The field variables satisfy the Bianchi identities

$$R_{\alpha\beta\gamma\cdot}{}^{\delta}{}_{;\theta}+R_{\beta\theta\gamma\cdot}{}^{\delta}{}_{;\alpha}+R_{\theta\alpha\gamma\cdot}{}^{\delta}{}_{;\beta}=0. \tag{2.19}$$

The latter are a geometrical property of the metric tensor and thus are closely connected with the postulate of the general covariance of our theory.

A trivial rigorous solution of the field equations (2.18) is the flat Minkowski metric $\eta_{\alpha\beta}$. If we choose the units of space and time so that the velocity of light is equal to 1, the Minkowski metric may be represented by the following matrix:

$$\eta^{\alpha\beta}=\eta_{\alpha\beta}=\begin{bmatrix}+1 & 0 & 0 & 0\\ 0 & -1 & 0 & 0\\ 0 & 0 & -1 & 0\\ 0 & 0 & 0 & -1\end{bmatrix}. \tag{2.20}$$

The Minkowski metric represents the empty space.

---

[2] P. G. Bergmann, *Introduction to the Theory of Relativity* (Prentice-Hall Inc., New York, 1942).

[3] A. S. Eddington, *The Mathematical Theory of Relativity* (Cambridge University Press, Cambridge, 1923).

[4] R. C. Tolman, *Relativity, Thermodynamics and Cosmology* (Oxford University Press, London, 1934).

CC-0. In Public Domain. Gurukul Kangri Collection, Haridwar

Digitized by Arya Samaj Foundation Chennai and eGangotri

3. THE DIFFERENTIAL EQUATIONS OF MOTION

It has been recognized some twenty years ago by Einstein and Grommer[5] that in general relativity theory the equations of motion follow from the field equations. Earlier, it was assumed that a "geodesic principle" governs the relativistic motion of bodies. By this one understood some generalization of the fact that a small body in the gravitational field of a big one moves along a geodesic line of the "external" field. This is a similar concept as in Newtonian mechanics where the field equations are completed by the equations of motion, that is by putting the acceleration of each particle equal to the negative gradient of the field due to the other particles present. Thus, the geodesic principle would play in general theory the role of the equations of motion.

When it became known that the relativistic equations of motion are contained in the field equations, it had to be questioned how the geodesic principle, whose validity for sufficiently small particles in a large field was all but established, could be fitted into the new scheme. This problem has been investigated by Infeld and Schild.[6] These authors were able to show that the geodesic principle (for sufficiently small particles) can be deduced from the field equations, and that it is not necessary to postulate it separately.

In order to obtain the relativistic equations of motion from the field equations, one has to recur to an approximation procedure. This is due to the fact that the motion of the sources cannot completely be determined unless such effects as spontaneous emission of radiation are specifically excluded. This exclusion is accomplished by assuming that all the motions are "slow" in the sense that differentiation with respect to x^0 reduces the order of magnitude of the term concerned at every stage of the approximation procedure.

An outline of this procedure was given for the first time by Einstein, Infeld, and Hoffmann in 1938.[1,7] Shortly thereafter there appeared an improved treatment by Einstein and Infeld.[8] In these first attempts there remained some ambiguities and logical difficulties unsolved. Later, however, the theory was developed further and a completely new treatment was given by Einstein and Infeld in 1949.[9] The method of Einstein and co-workers has been modified by Hu[10] and Papapetrou[11] so as to treat the masses present in the field as extended sources instead of as poles. Whereas this treatment saves some labor when it comes to the actual calculations of the equation of motion, it seems that the Einstein-Infeld-Hoffmann method is simpler from a logical standpoint, especially if the later amendments to that method are used.

In order to perform the approximation procedure, the field variables are split into a part representing the vacuum and another representing the deviation from it. Accordingly, they are written as follows:

$$g_{\alpha\beta}=\eta_{\alpha\beta}+h_{\alpha\beta}, \tag{3.1}$$

$$g^{\alpha\beta}=\eta^{\alpha\beta}+h^{\alpha\beta}, \tag{3.2}$$

where $h_{\alpha\beta}$ is not assumed to be small. It turns out to be convenient to replace the h's by the following linear combinations:

$$\gamma_{\alpha\beta}=h_{\alpha\beta}-\tfrac{1}{2}\eta_{\alpha\beta}\eta^{\gamma\delta}h_{\gamma\delta}. \tag{3.3}$$

The original field equations are as given in (2.11), but one may take any linear combination thereof. According to the choice (3.3) of field variables, it will be convenient to choose the following field equations:

$$-2(R_{\gamma\vartheta}-\tfrac{1}{2}\eta_{\gamma\vartheta}\eta^{\alpha\beta}R_{\alpha\beta})=0. \tag{3.4}$$

Introducing everywhere the γ's instead of the h's, one can write Eq. (3.4) in the following way:

$$\left.\begin{aligned}\phi_{00}+2\Lambda_{00}&=0\\ \phi_{0n}+2\Lambda_{0n}&=0\\ \phi_{mn}+2\Lambda_{mn}&=0\end{aligned}\right\}, \tag{3.5}$$

where

$$\left.\begin{aligned}\phi_{00}&=-\gamma_{00|ss}\\ \phi_{0m}&=-\gamma_{0m|ss}+\gamma_{0s|0s}\\ \phi_{mn}&=-\gamma_{mn|ss}+\gamma_{ms|ns}+\gamma_{ns|ms}-\delta_{mn}\gamma_{rs|rs}\end{aligned}\right\} \tag{3.6}$$

and

$$\left.\begin{aligned}2\Lambda_{00}&=\gamma_{sr|sr}+2\Lambda'_{00}\\ 2\Lambda_{0m}&=\gamma_{ms|s0}-\gamma_{00|m0}+2\Lambda'_{0m}\\ 2\Lambda_{mn}&=-\gamma_{0m|0n}-\gamma_{0n|0m}+2\delta_{mn}\gamma_{0s|0s}+\gamma_{mn|00}\\ &\qquad-\delta_{mn}\gamma_{00|00}+2\Lambda'_{mn}\end{aligned}\right\}. \tag{3.7}$$

In these formulas, all the linear terms are written out explicitly, while $\Lambda'_{\mu\nu}$ stands for all the nonlinear terms in the γ's.

With any function F_{st} one can form the integral

$$\oint_S F_{st}n_t dS \tag{3.8}$$

over an arbitrary closed surface S that does not pass through any singularities of F. In Eq. (3.8)

$$n_t=\cos(x_t, \mathbf{n}) \tag{3.9}$$

are the components of the normal unit vector to the surface. The words "normal" and "unit" are used in the conventional sense to designate the corresponding

[5] A. Einstein and J. Grommer, Sitz. Berl. Akad. Wiss. 1927, 1
[6] L. Infeld and A. E. Schild, Revs. Modern Phys. **21**, 408 (1949).
[7] Einstein, Infeld, and Hoffman, Ann. Math. **39**, 66 (1938).
[8] A. Einstein and L. Infeld, Ann. Math. **41**, 455 (1940).
[9] A. Einstein and L. Infeld, Can. J. Math. **1**, 209 (1949).
[10] N. Hu, Proc. Roy. Irish Acad. **51A**, 87 (1947).
[11] A. Papapetrou, Proc. Phys. Soc. (London) **A64** 57 (1951).

CC-0. In Public Domain. Gurukul Kangri Collection, Haridwar

Digitized by Arya Samaj Foundation Chennai and eGangotri

functions of the coordinates which are implied by these terms in Euclidian geometry.

If one takes as F the left-hand sides of the field equations (3.5), one ends up with (since the surface integrals of ϕ vanish)

$$\oint_S \Lambda_{\beta k} n_k dS = 0, \tag{3.10}$$

which imples

$$\phi_{\alpha n|n} = 0; \quad \Lambda_{\alpha n|n} = 0. \tag{3.11}$$

The aim is to develop every function $f(x^\beta)$ into a power series in $1/c \equiv \lambda$:

$$f(x^\mu) = \lambda^0 {}_0f + \lambda^1 {}_1f + \lambda^2 {}_2f + \cdots = \sum_{k=0}^{\infty} \lambda^k {}_kf. \tag{3.12}$$

The left-lower indices indicate the order of the term. If the function f varies quickly in space, but slowly in x^0, then one is justified in not treating all its derivatives in the same fashion. The derivatives with respect to x^0 will be of a higher order than space derivatives. One can formalize this procedure by introducing an auxiliary time

$$\tau = x^0 \lambda, \tag{3.13}$$

so that derivatives with respect to t can be treated on the same footing as the space derivatives

$$f_{10} = \partial f/\partial x^0 = \partial f/\partial \tau \quad \lambda = \lambda f_{,0} \equiv \lambda \dot{f}. \tag{3.14}$$

In other words, the "stroke" differentiation of a quantity with respect to x^0 can be replaced by the "comma" differentiation with respect to τ if the power of $\lambda = 1/c$ with which this quantity is associated is simultaneously raised by one.

With this notation, the γ's may be developed into a power series as follows:

$$\left.\begin{aligned} \gamma_{00} &= \lambda^2 {}_2\gamma_{00} + \lambda^4 {}_4\gamma_{00} + \lambda^6 {}_6\gamma_{00} + \cdots && \text{(a)} \\ \gamma_{0m} &= \lambda^3 {}_3\gamma_{0m} + \lambda^5 {}_5\gamma_{0m} + \cdots && \text{(b)} \\ \gamma_{mn} &= \lambda^4 {}_4\gamma_{mn} + \lambda^6 {}_6\gamma_{mn} + \cdots && \text{(c)} \end{aligned}\right\}. \tag{3.15}$$

The start with different powers of λ is an assumption which can be justified heuristically. It will be seen that Eq. (3.15) leads to a possible solution of the field equations. It is, however, possible to retain all the terms in Eq. (3.15), instead of only alternating powers of λ. This would lead to solutions analogous to those in electromagnetic theory representing radiation. It is for this reason that one calls the omitted terms in Eq. (3.15) "*radiation*" terms.

Going back to the field equations (3.5)–(3.7), one can introduce the γ's into the latter in their power series development. Spontaneous radiation is excluded by the assumption that all the γ's vary slowly in time and quickly in space; in other words, by assuming that all the γ's are of such a type that Eq. (3.14) applies. Thus, according to Eq. (3.5)–(3.7), the field equations are split into the following equations for each approximation step

$$\left.\begin{aligned} {}_{2k-2}\phi_{00} + 2\,{}_{2k-2}\Lambda_{00} &= 0 && \text{(a)} \\ {}_{2k-1}\phi_{0m} + 2\,{}_{2k-1}\Lambda_{0m} &= 0 && \text{(b)} \\ {}_{2k}\phi_{mn} + 2\,{}_{2k}\Lambda_{mn} &= 0 && \text{(c)} \end{aligned}\right\}. \tag{3.16}$$

Let us now assume that ${}_2\gamma_{00} \cdots {}_{2k-4}\gamma_{00}$; ${}_3\gamma_{0m} \cdots {}_{2k-3}\gamma_{0m}$; and ${}_4\gamma_{mn} \cdots {}_{2k-4}\gamma_{mn}$ are all known. Then Eq. (3.16), if solved will yield ${}_{2k-2}\gamma_{00}$, ${}_{2k-1}\gamma_{0m}$, ${}_{2k}\gamma_{mn}$; and if such a procedure converges, one can determine the field to any approximation desired. The structure of the equations indicate that one really can set all the odd terms in γ_{00}, γ_{mn} and the even ones in γ_{0m} equal to zero. This amounts to taking "zero" as solutions of Eq. (3.16) for half-interger k's.

There are, however, at every stage of the approximation procedure the conditions (3.10) and (3.11) to be satisfied. It can be shown that the divergence condition for ϕ (3.11) is automatically satisfied in each approximation step. On the other hand, the surface conditions (3.10) are not generally satisfied; they are the conditions which lead to the equations of motion.

To start the approximation procedure one has to solve the following equations:

$$\left.\begin{aligned} {}_2\gamma_{00,\,ss} &= 0, && \text{(a)} \\ -{}_3\gamma_{0m,\,ss} + {}_3\gamma_{0s,\,ms} &= 2\gamma_{00,\,0m}. && \text{(b)} \end{aligned}\right\} \tag{3.17}$$

The character of the entire solution will depend on the choice of the harmonic function one takes as a solution of (3.17a). The term ${}_2\gamma_{00}$ is the gravitational potential as one would find it if one were to use Newtonian theory instead of general relativity theory. Since one is interested in a solution representing p particles in the Newtonian approximation, one has to write

$${}_2\gamma_{00} = 2\varphi; \quad \varphi = \sum_{A=1}^{p} (-2\,{}^A m\,{}^A\psi); \tag{3.18a}$$

$${}^A\psi = \{(x^k - {}^AX^k)(x^k - {}^AX^k)\}^{-\frac{1}{2}} = ({}^Ar)^{-1}. \tag{3.18b}$$

Here, ${}^Ar$ is the "distance" in space of a point from the Ath singularity. Now, introducing ${}_2\gamma_{00}$ into (3.17b) and again obtaining three equations for the three functions ${}_3\gamma_{0m}$, one observes that the latter is only soluble if the ${}^Am$'s are constant in time. Only then the conditions (3.10) are satisfied for that stage of the approximation procedure.

Going on, one observes that at every step of the approximation one has to solve equations of the type of Eqs. (3.16). Since one has the surface condition (3.10), Eqs. (3.16) are consistent only if one has

$$\oint_{SA} 2\,{}_{2k-1}\Lambda_{0r} n_r dS \equiv {}_{2k-1}{}^AC_0 = 0, \tag{3.19}$$

$$\oint_{SA} 2\,{}_{2k}\Lambda_{mr} n_r dS \equiv {}_{2k}{}^AC_m = 0. \tag{3.20}$$

CC-0. In Public Domain. Gurukul Kangri Collection, Haridwar

Digitized by Arya Samaj Foundation Chennai and eGangotri

Herein, S^A is representing a surface around the Ath singularity. If S^A would not enclose a singularity, then the surface integrals in (3.19/20) would be trivially zero. The Λ's in Eqs. (3.19/20) are already known. Thus it is likely to happen that the C's in (3.19) and (3.20) are not zero, so that Eqs. (3.16) cannot be integrated. However, by adding single poles to the *previous* γ's one can insure the integrability of Eq. (3.16b), and by adding dipoles the integrability of Eq. (3.16c). It is easily seen that adding poles to the original solution ${}_{2k-2}\gamma_{00}$

$$ {}_{2k-2}\gamma_{00} \rightarrow {}_{2k-2}\gamma_{00} - 4\,{}_{2k-2}{}^{A}m\,{}^{A}\psi \tag{3.21} $$

changes ${}_{2k-1}{}^{A}C_0$ into

$$ {}_{2k-1}{}^{A}C_0 \rightarrow {}_{2k-1}{}^{A}C_0 - 4_{2k-2}{}^{A}\dot{m}. \tag{3.22} $$

Similarly, if one replaces ${}_{2k-2}\gamma_{00}$ (containing the additional poles) by

$$ {}_{2k-2}\gamma_{00} \rightarrow {}_{2k-2}\gamma_{00} - {}_{2k-2}{}^{A}S_r\,{}^{A}\psi_{,r} \tag{3.23} $$

(i.e. adding dipoles), ${}_{2k}{}^{A}C_m$ is changed into

$$ {}_{2k}{}^{A}C_m \rightarrow {}_{2k}{}^{A}C_m - {}_{2k-2}{}^{A}\ddot{S}_m. \tag{3.24} $$

Therefore, it can be made zero by choosing

$$ {}_{2k-2}{}^{A}\ddot{S}_m = {}_{2k}{}^{A}C_m. \tag{3.25} $$

By proceeding in this way, one accumulates single poles and dipoles; the additional expressions in γ_{00} are

$$ \sum \lambda^{2k-2}(4_{2k-2}{}^{A}m\,{}^{A}\psi + {}_{2k-2}{}^{A}S_r\,{}^{A}\psi_{,r}). \tag{3.26} $$

However, since negative masses are not known, gravitational dipoles have no physical meaning. Thus, one has, at the end of the approximation procedure, to annihilate all these additional dipoles by taking

$$ \sum \lambda^{2k-2}\,{}_{2k-2}{}^{A}S_r = 0. \tag{3.27} $$

Differentiating this twice yields

$$ \sum \lambda^{2k}\,{}_{2k-2}{}^{A}\ddot{S}_m = \sum \lambda^{2k}\,{}_{2k}{}^{A}C_m = 0. \tag{3.28} $$

These are the $3p$ differential equations of motion of the kth approximation.

One may impose at every step of the approximation procedure four coordinate conditions in the form of four nontensorial equations involving the field variables. The fact that this is possible is due to the existence of four (Bianchi) identities between the field variables. The coordinate conditions if properly chosen, may be of considerable help if one is going to actually carry out the calculations of the approximation procedure.

One may notice that the field equations (3.16) would permit that arbitrary multipoles be added to the γ_{00}'s at every step of the approximation. The integrability conditions for the *subsequent* step, however, fix what multiples have to be chosen and make, for given coordinate conditions, the solution unique at every step of the procedure.

4. THE TWO-BODY PROBLEM

Let us now apply the procedure outlined in Sec. 3 to the task of finding the differential equations of motion of the two-body problem. For the actual calculations it will turn out to be convenient to assume the following coordinate conditions

$$ \left.\begin{aligned} {}_{2k-1}\gamma_{0s,\,s} - {}_{2k-2}\gamma_{00,\,0} &= 0, \quad (a)\\ {}_{2k}\gamma_{mn,\,n} &= 0. \quad (b) \end{aligned}\right\} \tag{4.1} $$

The solution of the first approximation corresponding to Eq. (3.18) becomes for the two-body problem

$$ \left.\begin{aligned} {}_{2}\gamma_{00} &= 2\varphi; \quad \varphi = -2\{{}^{1}m\,{}^{1}\psi - {}^{2}m\,{}^{2}\psi\}, \quad (a)\\ {}^{1}\psi &= [(x^k - Y^k)(x^k - Y^k)]^{\frac{1}{2}} = \frac{1}{{}^{1}r}, \quad (b)\\ {}^{2}\psi &= [(x^k - Z^k)(x^k - Z^k)]^{\frac{1}{2}} = \frac{1}{{}^{2}r}, \quad (c) \end{aligned}\right\} \tag{4.2} $$

Y^k, Z^k being the coordinates of the two bodies. This solution determines the character of the entire solution for the field equations.

For going on, one needs the explicit forms of all the occurring Λ's, g's, etc. It follows from Eqs. (3.1) and (3.2) that

$$ \left.\begin{aligned} g_{00} &= 1 + \lambda^2\,{}_{2}h_{00} + \lambda^4\,{}_{4}h_{00} + \cdots, \quad (a)\\ g_{0m} &= \lambda^3\,{}_{3}h_{0m} + \lambda^5\,{}_{5}h_{0m} + \cdots, \quad (b)\\ g_{mn} &= -\delta_{mn} + \lambda^2\,{}_{2}h_{mn} + \lambda^4\,{}_{4}h_{mn} + \cdots, \quad (c) \end{aligned}\right\} \tag{4.3} $$

and similarly

$$ \left.\begin{aligned} g_{00} &= 1 + \lambda^2\,{}_{2}h^{00} + \lambda^4\,{}_{4}h^{00} + \cdots, \quad (a)\\ g^{0m} &= \lambda^3\,{}_{3}h^{0m} + \lambda^5\,{}_{5}h^{0m} + \cdots, \quad (b)\\ g^{mn} &= -\delta_{mn} + \lambda^2\,{}_{2}h^{mn} + \lambda^4\,{}_{4}h^{mn} + \cdots. \quad (c) \end{aligned}\right\} \tag{4.4} $$

Therefore, from Eq. (4.2)

$$ {}_{2}h_{00} = \varphi, \tag{4.5} $$

$$ {}_{2}h_{mn} = \varphi\delta_{mn}. \tag{4.6} $$

The general property (2.6) of the metric tensor allows one to express all the contravariant h's by the covariant ones.

Thus, one obtains

$$ {}_{2}h^{00} = -\varphi; \quad {}_{4}h^{00} = -{}_{4}h_{00} + \varphi\varphi, \tag{4.7} $$

$$ {}_{3}h^{m0} = {}_{3}h_{m0}; \quad {}_{5}h^{m0} = {}_{5}h_{m0}, \tag{4.8} $$

$$ {}_{2}h^{mn} = -\delta_{mn}\varphi; \quad {}_{4}h^{mn} = -{}_{4}h_{mn} - \varphi\varphi\delta_{mn}. \tag{4.9} $$

Moreover, one observes that generally ${}_{k}h^{0m}$ contains ${}_{k}h_{0m}$ only linearly, so that one may write

$$ {}_{k}h^{0m} = {}_{k}h_{0m} + \text{terms not containing } {}_{k}h_{0m}. \tag{4.10} $$

The next step is to write down the field equations explicitly in terms of the h's. They are already split into terms denoted by Λ and ϕ. The ϕ's are already found explicitly, and the Λ's may be represented in the

CC-0. In Public Domain. Gurukul Kangri Collection, Haridwar

Digitized by Arya Samaj Foundation Chennai and eGangotri

following way

$$\left.\begin{aligned} \Lambda_{00} &= \tfrac{1}{2}L_{00}+\tfrac{1}{2}L_{ss}, && \text{(a)}\\ \Lambda_{0m} &= L_{0m}, && \text{(b)}\\ \Lambda_{mn} &= L_{mn}-\tfrac{1}{2}\delta_{mn}L_{ss}+\tfrac{1}{2}\delta_{mn}L_{00}, && \text{(c)} \end{aligned}\right\} \quad (4.11)$$

with

$$2L_{00} = 2h_{0s|0s}-h_{ss|00} -2(h^{\alpha\beta}[00,\beta])_{|\alpha}+2(h^{\alpha\beta}[0\alpha,\beta])_{|0} +2\left\{\begin{matrix}\alpha\\0\beta\end{matrix}\right\}\left\{\begin{matrix}\beta\\\alpha 0\end{matrix}\right\}-2\left\{\begin{matrix}\alpha\\00\end{matrix}\right\}\left\{\begin{matrix}\beta\\\alpha\beta\end{matrix}\right\}, \quad (4.12)$$

$$2L_{0n} = -2(h^{\alpha\beta}[0n,\beta)_{|\alpha}+2(h^{\alpha\beta}[m\alpha,\beta])_{|0} +2\left\{\begin{matrix}\alpha\\m\beta\end{matrix}\right\}\left\{\begin{matrix}\beta\\\alpha 0\end{matrix}\right\}-2\left\{\begin{matrix}\beta\\m0\end{matrix}\right\}\left\{\begin{matrix}\alpha\\\beta\alpha\end{matrix}\right\}, \quad (4.13)$$

$$2L_{mn} = -h_{0n|0m}-h_{0m|0n}+h_{mn|00} -2(h^{\alpha\beta}[mn,\beta])_{|\alpha}+2(h^{\alpha\beta}[m\alpha,\beta])_{|n} +2\left\{\begin{matrix}\alpha\\m\beta\end{matrix}\right\}\left\{\begin{matrix}\beta\\\alpha n\end{matrix}\right\}-2\left\{\begin{matrix}\alpha\\mn\end{matrix}\right\}\left\{\begin{matrix}\beta\\\alpha\beta\end{matrix}\right\}. \quad (4.14)$$

The next step is to insert the power series for all the h's into the above equations. Then one can split the latter into corresponding equations for every power of λ.

The result is, if one uses the coordinate conditions,

$$2_3\Lambda_{0m}=0, \quad (4.15)$$

$$2_4\Lambda_{mn} = -{}_3\gamma_{0m,0n}-{}_3\gamma_{0n,0m}+2\delta_{mn}\varphi_{,00} -2\varphi\varphi_{,mn}-\varphi_{,m}\varphi_{,n}+\tfrac{3}{2}\delta_{mn}\varphi_{,s}\varphi_{,s}, \quad (4.16)$$

$$2_4\Lambda_{00} = -\tfrac{3}{2}\varphi_{,s}\varphi_{,s}, \quad (4.17)$$

$$2_5\Lambda_{0m} = \varphi_{,s}\,{}_3\gamma_{0s,m}-\varphi_{,sm}\,{}_3\gamma_{0s}-3\varphi_{,0}\varphi_{,m}, \quad (4.18a)$$

$$\begin{aligned} 2_6\Lambda_{mn} = &-{}_5\gamma_{0m,0n}-{}_5\gamma_{0n,0m}+\delta_{mn}\,{}_4\gamma_{00,00}\\ &+{}_4\gamma_{mn,00}-\varphi\,{}_4\gamma_{00,mn}-\varphi\,{}_4\gamma_{ss,mn}\\ &-\varphi_{,mn}\,{}_4\gamma_{00}-\varphi_{,mn}\,{}_4\gamma_{ss}+\varphi_{,ms}\,{}_4\gamma_{ns}\\ &+\varphi_{,ns}\,{}_4\gamma_{ms}-\delta_{mn}\varphi_{,sr}\,{}_4\gamma_{sr}-2\varphi_{,s}\,{}_4\gamma_{mn,s}\\ &+\varphi_{,s}\,{}_4\gamma_{ms,n}+\varphi_{,s}\,{}_4\gamma_{ns,m}-\tfrac{1}{2}\varphi_{,m}\,{}_4\gamma_{ss,n}\\ &-\tfrac{1}{2}\varphi_{,n}\,{}_4\gamma_{ss,m}-\tfrac{1}{2}\varphi_{,n}\,{}_4\gamma_{00,m}-\tfrac{1}{2}\varphi_{,m}\,{}_4\gamma_{00,n}\\ &+\tfrac{3}{2}\delta_{mn}\varphi_{,s}\,{}_4\gamma_{rr,s}+\tfrac{3}{2}\delta_{mn}\varphi_{,s}\,{}_4\gamma_{00,s}\\ &-{}_3\gamma_{0s}\,{}_3\gamma_{0n,ms}-{}_3\gamma_{0s}\,{}_3\gamma_{0m,ns}\\ &+2\,{}_3\gamma_{0s}\,{}_3\gamma_{0s,mn}+\tfrac{1}{2}\delta_{mn}\,{}_3\gamma_{0s,r}\,{}_3\gamma_{0r,s}\\ &-\tfrac{3}{2}\delta_{mn}\,{}_3\gamma_{0s,r}\,{}_3\gamma_{0s,r}+{}_3\gamma_{0s,m}\,{}_3\gamma_{0s,n}\\ &+{}_3\gamma_{0m,s}\,{}_3\gamma_{0n,s}-\varphi_{,0n}\,{}_3\gamma_{0m}-\varphi_{,0m}\,{}_3\gamma_{0n}\\ &+2\delta_{mn}\,{}_3\gamma_{0s}\varphi_{,0s}-\varphi_{,0}\,{}_3\gamma_{0m,n}\\ &-\varphi_{,0}\,{}_3\gamma_{0n,m}-\varphi_{,n}\,{}_3\gamma_{0m,0}-\varphi_{,m}\,{}_3\gamma_{0n,0}\\ &+2\varphi\,{}_3\gamma_{0m,0n}+2\varphi\,{}_3\gamma_{0n,0m}-2\delta_{mn}\varphi\varphi_{,00}\\ &+2\varphi\varphi\varphi_{,mn}-\varphi\varphi_{,m}\varphi_{,n}+\tfrac{3}{2}\delta_{mn}\varphi\varphi_{,s}\varphi_{,s}\\ &+\tfrac{1}{2}\delta_{mn}\varphi_{,0}\varphi_{,0}. \end{aligned} \quad (4.18b)$$

Starting now the calculations of the field variables, one has to solve the following equations:

$$\left.\begin{aligned} {}_2\gamma_{00,ss} &= 0, && \text{(a)}\\ {}_3\gamma_{mn,ss} &= 0, && \text{(b)}\\ {}_4\gamma_{mn,ss} &= 2_4\Lambda_{mn}. && \text{(c)} \end{aligned}\right\} \quad (4.19)$$

It is convenient to introduce here a slightly new notation by putting

$$\varphi = f+g; \quad f=-2\,{}^1m\,{}^1\psi; \quad g=-2\,{}^2m\,{}^2\psi. \quad (4.20)$$

Equation (4.19a) has been solved already to yield (4.2). Using the coordinate condition (4.1) one obtains therefore

$${}_3\gamma_{0n} = 4({}^1m\,{}^1\psi\dot{Y}^n+{}^2m\,{}^2\psi\dot{Z}^n). \quad (4.21)$$

The surface integral (3.19) vanishes; thus the next step is to determine

$$\left.\begin{aligned} {}_4{}^1C_m &= \frac{1}{4\pi}\oint_1 2_4\Lambda_{ms}n_s dS,\\ {}_4{}^2C_m &= \frac{1}{4\pi}\oint_2 2_4\Lambda_{ms}n_s dS. \end{aligned}\right\} \quad (4.22)$$

If one wishes to finish the approximation procedure here, the differential equations of motion of the 4th approximation are

$${}_4{}^1C_m=0; \quad {}_4{}^2C_m=0. \quad (4.23)$$

Therefore, all one has to do is to calculate those surface integrals. The result of this calculation is

$$\left.\begin{aligned} {}_4{}^1C_m(\tau) &= 4\,{}^1m(\ddot{Y}^m+\tfrac{1}{2}\tilde{g}_{,m}) = 0,\\ {}_4{}^2C_m(\tau) &= 4\,{}^2m(\ddot{Z}^m+\tfrac{1}{2}\tilde{f}_{,m}) = 0, \end{aligned}\right\} \quad (4.24)$$

where

$$\tilde{g}_{,m}\equiv g_{,m} \quad \text{for} \quad x^s=Y^s; \quad \tilde{f}_{,m}\equiv f_{,m} \quad \text{for} \quad x^s=Z^s.$$

These are the equations of the Newtonian approximation of general relativity theory.

In order to go beyond the Newtonian approximation, one has to calculate ${}_4\gamma_{mn}$. It is to be found from the equation

$${}_4\gamma_{mn,ss}=2_4\Lambda_{mn}. \quad (4.25)$$

These equations are integrable only if one assumes Newtonian motion in the lower approximation. Otherwise one would have to add dipoles. Yet if one wishes to proceed only to the sixth approximation, one may ignore these additional dipoles since they do not influence the surface integrals. Thus, the solution for ${}_4\gamma_{mn}$ is in the neighborhood of the *first* singularity,

$$\begin{aligned} {}_4\gamma_{mn} = &\{f[(x^n-Y^n)\dot{Y}^m+(x^m-Y^m)\dot{Y}^n\\ &-\delta_{mn}(x^s-Y^s)\dot{Y}^s]\}_{,0}+\{g[(x^n-Z^n)\dot{Z}^m\\ &+(x^m-Z^m)\dot{Z}^n-\delta_{mn}(x^s-Z^s)\dot{Z}^s]\}_{,0}\\ &+(7/4)\,{}^1r^2f_{,m}f_{,n}+(7/4)^2r^2g_{,m}g_{,n}\\ &+\alpha_{mn}f+\beta_{mn}g. \end{aligned} \quad (4.26)$$

CC-0. In Public Domain. Gurukul Kangri Collection, Haridwar

Digitized by Arya Samaj Foundation Chennai and eGangotri

The last two expressions are determined by the coordinate conditions and are found to be

$$\alpha_{mn}=2\dot{Y}^m\dot{Y}^n+\delta_{mn}\tilde{g};\quad \beta_{mn}=2\dot{Z}^m\dot{Z}^n+\delta_{mn}\tilde{f};$$
$$\tilde{f}=f(r);\quad \tilde{g}=g(r);\quad r^2=(Y^s-Z^s)(Y^s-Z^s). \tag{4.27}$$

Moreover, ${}_4\gamma_{ss}$ can be calculated rigorously. The result is

$${}_4\gamma_{ss}=-2\,{}^1m\,{}^1r_{,00}-2\,{}^2m\,{}^2r_{,00}+(7/4)\varphi^2+\alpha f+\beta g \tag{4.28}$$

with

$$\alpha=2\dot{Y}^s\dot{Y}^s+\tfrac{1}{2}\tilde{g};\quad \beta=2\dot{Z}^s\dot{Z}^s+\tfrac{1}{2}f. \tag{4.29}$$

Now, the next field equations are

$$\left.\begin{aligned} &{}_4\gamma_{00,\,rr}=2_4\Lambda_{00}=-\tfrac{3}{2}\varphi_{,s}\varphi_{,s}, && \text{(a)}\\ &{}_5\gamma_{0m,\,ss}=2_5\Lambda_{0m}=\varphi_{,s}\,{}_3\gamma_{0s,\,m} && \\ &\qquad -\varphi_{,sm}\,{}_3\gamma_{0s}-3\varphi_{,0}\varphi_{,m}, && \text{(b)}\\ &{}_6\gamma_{mn,\,ss}=2_6\Lambda_{mn}. && \text{(c)} \end{aligned}\right\} \tag{4.30}$$

The solution of (4.30a) is simply

$${}_4\gamma_{00}=-\tfrac{3}{2}\varphi^2-4_4{}^1m\,{}^1\psi-4_4\,{}^2m^2\psi. \tag{4.31}$$

One knows from the general theory that the arbitrary harmonic functions have to be determined in such a way as to make (4.30b) self-consistent, that is, the corresponding surface integral must vanish:

$$\frac{1}{4\pi}\oint(2_5\Lambda'_{-0m}-{}_4\gamma_{00,\,0m})n_m dS=0. \tag{4.32}$$

The next step is to calculate the ${}_5\gamma_{0s}$. Including only relevant terms that can enter into the equations of motion of the sixth approximation, one obtains near the first singularity

$$\begin{aligned} {}_5\gamma_{0m}=&-(7/4)\,{}^1r_{,m}f_{,s}\dot{Y}^s+\tfrac{3}{4}f^2\dot{Y}^m\\ &+\tfrac{3}{2}(x^s-Y^s)(\dot{Y}^s-\dot{Z}^s)f\tilde{g}_{,m}\\ &-(x^m-Y^m)(\dot{Y}^s-\dot{Z}^s)f\tilde{g}_{,s}\\ &+\tfrac{1}{2}(x^s-Y^s)f_{,m}\dot{Z}^s[g+\tilde{g}_{,r}(x^r-Y^r)]\\ &+(x^s-Y^s)(f\tilde{g}_{,s}\dot{Z}^m+f_{,m}\tilde{g}\dot{Z}^s)+\alpha_{0m}f. \end{aligned} \tag{4.33}$$

Again α_{0m} is determined from the coordinate condition. The result is

$$\alpha_{0m}=-\dot{Y}^s\dot{Y}^s\dot{Y}^m+\tilde{g}\dot{Y}^m-\tilde{g}\dot{Z}^m. \tag{4.34}$$

One has to insert all these values for the field variables into the expressions for ${}_6\Lambda_{mn}$ and to calculate the surface integrals

$${}_6{}^1C_m=\frac{1}{4\pi}\oint 2_6\Lambda_{mn}n_n dS. \tag{4.35}$$

The result of this calculation is

$$\left.\begin{aligned} {}_6{}^1C_m=&-4\,{}^1m\,{}^2m\left\{\left(\dot{Y}^s\dot{Y}^s+\tfrac{3}{2}\dot{Z}^s\dot{Z}^s\right.\right.\\ &\left.-4\dot{Y}^s\dot{Z}^s-4\frac{{}^2m}{r}-5\frac{{}^1m}{r}\right)\frac{\partial(1/r)}{\partial Y^m}\\ &+[4\dot{Y}^s(\dot{Z}^m-\dot{Y}^m)+3\dot{Y}^m\dot{Z}^s-4\dot{Z}^s\dot{Z}^m]\\ &\left.\times\frac{\partial(1/r)}{\partial Y^s}+\frac{1}{2}\frac{\partial^3 r}{\partial Y^s\partial Y^n\partial Y^m}\dot{Z}^s\dot{Z}^n.\right\} \end{aligned}\right. \tag{4.36}$$

Thus, the differential equations of motion of this stage of the approximation procedure are

$$\lambda^4\,{}_4{}^1C_m+\lambda^6\,{}_6{}^1C_m=0. \tag{4.37}$$

It is possible to absorb the parameter λ by changing the units of mass and time. The final result of the 6th approximation is, then,

$$\begin{aligned} &\ddot{Y}^m-{}^2m\frac{\partial(1/r)}{\partial Y^m}\\ &={}^2m\left\{\left(\dot{Y}^s\dot{Y}^s+\tfrac{3}{2}\dot{Z}^s\dot{Z}^s-4\dot{Y}^s\dot{Z}^s-4\frac{{}^2m}{r}-5\frac{{}^1m}{r}\right)\frac{\partial(1/r)}{\partial Y^m}\right.\\ &\quad+[4\dot{Y}^s(\dot{Z}^m-\dot{Y}^m)+3\dot{Y}^m\dot{Z}^s+3\dot{Z}^s\dot{Z}^m]\frac{\partial(1/r)}{\partial Y^s}\\ &\quad\left.+\frac{1}{2}\frac{\partial^3 r}{\partial Y^s\partial Y^n\partial Y^m}\dot{Z}^s\dot{Z}^n.\right\} \end{aligned} \tag{4.38}$$

The equations of motion for the other body are obtained from that one above by an obvious substitution. These differential equations can be integrated as will be shown in the next section of this paper.

5. INTEGRATION OF THE DIFFERENTIAL EQUATIONS OF MOTION

If one is to integrate the differential equations of motion as found in Sec. 4, one has to keep in mind that the latter were found by an approximation procedure. Thus an *exact* integration of the differential Eq. (4.38) does *not* yield exact equations of motion. It is, therefore, reasonable to assume a similar power series development with respect to the parameter λ for the Y, Z as this was done for the γ's. Then, in order to solve the differential equations of the sixth approximation, one needs to take into account in Y, Z only terms up to the power λ^6, for the higher order terms are not contained in the differential equations anyway.

Robertson[12] has integrated the differential equations of motion for the two-body problem (4.38). He ac-

[12] H. P. Robertson, Ann. Math. 39, 101 (1938).

CC-0. In Public Domain. Gurukul Kangri Collection, Haridwar

Digitized by Arya Samaj Foundation Chennai and eGangotri

counted for the fact that the solution can be accurate only up to the 6th order by simply omitting in the left-hand side of (4.38) all terms of any order higher than Newtonian. The result is that up to the sixth order in λ the orbit of a double star in general relativity theory differs in its secular behavior from the classical orbit only in an advance of perihelion equal to that which an infinitesimal planet, describing the same relative orbit, would undergo in the field of a star whose mass is the sum of those of the two components of the double star.

The fact that the differential equations of motion are solved by an expansion of the coordinates of the particles into a power series of the parameter λ (i.e., the same parameter with respect to which Einstein, Infeld, and Hoffmann's approximation procedure is performed) suggests that it might be possible to tie together the two approximation procedures. The notion of accuracy "up to" a certain order, intuitively conceived above, can be formulated mathematically by a specific notation. Let us take any field expression

$$ {}_{2k}S\cdots \tag{5.1}$$

(e.g., $S=\phi, C$) where the dots stand for indices. The left subscript indicates that one considers the $2k$th approximation of S. S may depend on terms containing Y, Z (both together denoted by X), i.e., the coordinates of the two sources in the two-body problem. If one introduces into such a field quantity motion up to some approximation, ${}_{2k}S$ will not be of the $2k$th order; for one observes

$$ {}_{2k}S({}_0X+{}_2X)={}_{2k}S({}_0X)+\frac{\partial}{\partial {}_0X}({}_{2k}S){}_2X+\cdots, \tag{5.2}$$

which shows that ${}_{2k}S({}_0X+{}_2X)$ is really an expression containing terms of the $2k$th and *higher* orders.

However, if one wants to keep all the terms of the $2k$th order in a certain equation involving S's, then these do not only originate from ${}_{2k}S$, since the lower orders of S combine with the higher order of X to yield terms of the order $2k$. Therefore, it is impossible to split an equation containing such S's depending on the X's into λ-terms *before* the development for the X's is inserted. Thus, if one desires to have an accuracy up to all terms of order $2k$, one has to write the expression for S as follows:

$$ {}_{[2k]}S({}_{[2k]}X), \tag{5.3}$$

the square brakets having the meaning that one has to take the sum of all the terms up to the denoted order.

It is possible to reformulate the approximation procedure by use of this notation. The field equations are up to the $2k$th order

$$\begin{aligned}
&{}_{[2k-2]}\phi_{00}({}_{[2k-4]}X)+2\,{}_{[2k-2]}\Lambda_{00}({}_{[2k-4]}X)=0, && \text{(a)}\\
&{}_{[2k-1]}\phi_{0m}({}_{[2k-4]}X)+2\,{}_{[2k-1]}\Lambda_{0m}({}_{[2k-4]}X)=0, && \text{(b)}\\
&{}_{[2k]}\phi_{mn}({}_{[2k-4]}X)+2\,{}_{[2k]}\Lambda_{mn}({}_{[2k-4]}X)=0. && \text{(c)}
\end{aligned} \tag{5.4}$$

For $k=2$ those equations are identical with those for $k=2$ in Sec. 3, since there is no difference between the equations "up to" and "of" the second order. Thus, the beginning of the procedure is identical with that in Sec. 3.

Let us now assume that one has solved the Eqs. (5.4) up to the order $2k-1$. The next equations to be solved are then Eqs. (5.4) as they stand. These equations are solvable only if one assumes that the surface conditions (3.19) and (3.20) are satisfied. Thus, the integrability condition for (5.4b) leads to the adding of poles in the previous γ, whereas the integrability condition for Eq. (5.4c) determines the new corrective terms in the series expansion for the motion; for, these integrability conditions are

$$ \oint_S 2\,{}_{[2k]}\Lambda_{mn}({}_{[2k-4]}X)dS={}_{[2k]}{}^SC_m({}_{[2k-4]}X)=0. \tag{5.5}$$

Written out more explicitly this is

$$\begin{aligned}
&{}_4{}^SC_m({}_0X+\cdots+{}_{2k-4}X)\\
&\quad+{}_6{}^SC_m({}_0X+\cdots+{}_{2k-6}X)+\cdots+{}_{2k}{}^SC_m({}_0X)=0.
\end{aligned} \tag{5.6}$$

Since the corrective functions ${}_{2k-4}X$ appear only in ${}_4C$, Eqs. (5.6) are of the second order. One has thus a procedure whereby the motion is determined step by step to a higher accuracy.

The version of Einstein, Infeld, and Hoffmann's approximation procedure presented here has been suggested by Dr. Infeld. It is from a technical standpoint considerably simpler than that of Sec. 3 involving the dipoles. However, it should be noted that theoretically this new version tells one less than that of Sec. 3. The method of Sec. 3 uses physical notions such as dipoles whose annihilation, again a physical procedure, yields the equations of motion. The present method exemplified by Eq. (5.6), however, adjusts the corrective terms in the motion so as to make the *equations* consistent. Thus, it is seen that one is completely tied up with the representation of the motion in a particular coordinate system, which is not so satisfactory.

6. COORDINATE CONDITIONS

We have mentioned on several previous occasions that one can change the gravitational equations of motion in form by changing the coordinate conditions. It must be expected that the different solutions of the field equations thus obtained can be transformed into each other by simple coordinate transformations. This question has been studied by Infeld and Scheidegger.[13] Earlier it had been shown by Einstein and Infeld[9] that the most general solutions of the field equations that can be obtained by rejecting the coordinate condi-

[13] L. Infeld and A. E. Scheidegger, Can. J. Math. 3, 195 (1951).

CC-0. In Public Domain. Gurukul Kangri Collection, Haridwar

Digitized by Arya Samaj Foundation Chennai and eGangotri

tions are

$$ {}_{k-2}\gamma_{00}{}^{*} = {}_{k-2}\gamma_{00} \qquad \text{(a)} $$

$$ {}_{k-1}\gamma_{0m}{}^{*} = {}_{k-1}\gamma_{0m} + {}_{k-1}a_{0,m} \qquad \text{(b)} \quad (6.1) $$

$$ {}_{k}\gamma_{mn}{}^{*} = {}_{k}\gamma_{mn} + {}_{k}a_{m,n} + {}_{k}a_{n,m} - \delta_{mn}\, {}_{k-1}a_{0,0} \qquad \text{(c)} $$

and

$$ {}_{k}\gamma_{mn}{}^{*} = {}_{k}\gamma_{mn} + {}_{k}b_{m,n} + {}_{k}b_{n,m} - \delta_{mn}\, {}_{k}b_{r,r} \qquad \text{(a)} $$

$$ {}_{k}\gamma_{00}{}^{*} = {}_{k}\gamma_{00} + {}_{k}b_{r,r} \qquad \text{(b)} \quad (6.2) $$

$$ {}_{k+1}\gamma_{0m}{}^{*} = {}_{k+1}\gamma_{0m} + {}_{k+1}b_{0,m} + {}_{k}b_{m,0}, \qquad \text{(c)} $$

where the functions a_0, a_m and b_0, b_m are arbitrary. We shall prove here that it is possible to obtain the solutions γ^* from the γ's by a suitable coordinate transformation.

A general coordinate transformation is given as follows:

$$ x^{\beta} = x^{\beta}(x^{\alpha^*}) = T^{\beta}(x^{\alpha^*}). \tag{6.3} $$

Thus, the task is to calculate the transformed γ's which can be done straightforwardly starting from the transformation law of the metric tensor

$$ g_{\mu\nu}{}^{*} = T^{\rho}{}_{|\mu} T^{\sigma}{}_{|\nu}\, g_{\rho\sigma}. \tag{6.4} $$

When applying Eqs. (6.4) one has to be careful that one takes the same world point as argument in all the functions which occur. Thus, in addition to the tensorial transformation (6.4) one has to perform inside the g's a substitution of the variables x^{β} by x^{β^*} according to Eq. (6.3).

In conformity with the general methods of the approximation procedure one has to expand the metric tensor $g_{\alpha\beta}$ into a power series with respect to the parameter λ. However, now *all* the terms instead of only alternating ones have to be kept.

Furthermore, it was assumed in the original solution that the motion of the particles is "slow" which made it necessary to introduce the "comma-differentiation" for $g_{\mu\nu}$. It is natural to require that the motion remains "slow" in the starred coordinate system. Thus one has to assume that the derivatives of T^{μ}, too, are subject to the "comma-differentiation." Therefore, the transformation of the metric tensor represents itself as follows:

$$ \begin{aligned} g_{mn}{}^{*} &= T^{r}{}_{,m} T^{s}{}_{,n} g_{rs} + T^{0}{}_{,n} T^{s}{}_{,n} g_{0s} \\ &\quad + T^{r}{}_{,m} T^{0}{}_{,n} g_{r0} + T^{0}{}_{,m} T^{0}{}_{,n} g_{00}, \\ \frac{1}{\lambda} g_{m0}{}^{*} &= T^{r}{}_{,m} T^{s}{}_{,0} g_{rs} + T^{0}{}_{,m} T^{s}{}_{,0} g_{0s} \\ &\quad + T^{r}{}_{,m} T^{0}{}_{,0} g_{r0} + T^{0}{}_{,m} T^{0}{}_{,0} g_{00}, \\ \frac{1}{\lambda^2} g_{00}{}^{*} &= T^{r}{}_{,0} T^{s}{}_{,0} g_{rs} + 2 T^{0}{}_{,0} T^{s}{}_{,0} g_{0s} + T^{0}{}_{,0} T^{0}{}_{,0} g_{00}. \end{aligned} \tag{6.5} $$

Equations (6.5) apply quite independently from whether for T an expansion in λ is used or not.

Furthermore, one observes that in the usual solution the lowest terms different from zero are of the order λ^2, apart from constant ones ${}_0 g_{\alpha\beta} = \eta_{\alpha\beta}$. It will be convenient to confine oneself to coordinate systems where this same property holds. This means that in every coordinate system which is admitted for consideration, one has the flat Miskowskian metric as a first approximation of the gravitational field. This restriction of the coordinate transformations is justified by a remark of Papapetrou[14] who has proved that a change of the coordinate conditions will never affect the Newtonian approximation of general relativity. Thus, one is justified to assume that the coordinate transformation T^{μ} differs from the identity transformation only by terms proportional to λ^2:

$$ T^{\mu} = x^{\mu} + \lambda^{k}\, {}_{k}f^{\mu}; \quad k \geqslant 2. \tag{6.6} $$

As the indices 0 and k have to be treated differently, one has to distinguish between two cases.

(a) Only the space coordinates are transformed by a single transormation of the order λ^k,

$$ x^{r} = T^{r} = x^{r^*} + \lambda^{k}{}_{(k)} T^{r}(x^{\beta^*}), \qquad \text{(a)} $$

$$ x^{0} = T^{0} = x^{0^*}. \qquad \text{(b)} \tag{6.7} $$

If this is inserted into Eqs. (6.5) and everything expressed in γ's, one obtains

$$ {}_{k}\gamma_{mn}{}^{*} = {}_{k}\gamma_{mn} + \delta_{m\,|}\, {}_{k}T^{s}{}_{,s} - {}_{k}T^{m}{}_{,n} - {}_{k}T^{n}{}_{,m}, \qquad \text{(a)} $$

$$ {}_{k}\gamma_{00}{}^{*} = {}_{k}\gamma_{00} - {}_{k}T^{s}{}_{,s}, \qquad \text{(b)} \quad (6.8) $$

$$ {}_{k+1}\gamma_{0m}{}^{*} = {}_{k+1}\gamma_{0m} - {}_{k}T^{s}{}_{,0}. \qquad \text{(c)} $$

One observes that only the kth and higher approximations are influenced.

(b) Only the time coordinates are changed by a single transformation of the order λ^k,

$$ x^{0} = T^{0} = x^{0^*} + \lambda^{k}{}_{(k)} T^{0}(x^{\beta^*}), \qquad \text{(a)} $$

$$ x^{m} = x^{m^*}. \qquad \text{(b)} \tag{6.9} $$

In a similar way the following occurs:

$$ {}_{k+1}\gamma_{mn}{}^{*} = {}_{k+1}\gamma_{mn} + \delta_{mn}\, {}_{k}T^{0}{}_{,0}, \qquad \text{(a)} $$

$$ {}_{k}\gamma_{0n}{}^{*} = {}_{k}\gamma_{0n} + {}_{k}T^{0}{}_{,n}, \qquad \text{(b)} \quad (6.10) $$

$$ {}_{k+1}\gamma_{00}{}^{*} = {}_{k+1}\gamma_{00} + {}_{k}T^{0}{}_{,0}. \qquad \text{(c)} $$

By combining the cases (a) and (b) arbitrarily one obtains the most general coordinate transformation within the restrictions imposed here. Thus one may, for instance, consider the following combination:

$$ x^{m} = x^{m^*} + \lambda^{k}{}_{(k)} T^{m}, \qquad \text{(a)} $$

$$ x^{0} = x^{0^*} + \lambda^{k-1}{}_{(k-1)} T^{0}. \qquad \text{(b)} \tag{6.11} $$

[14] A. Papapetrou, Proc. Phys. Soc. (London) A64, 302 (1951).

CC-0. In Public Domain. Gurukul Kangri Collection, Haridwar

Digitized by Arya Samaj Foundation Chennai and eGangotri

This yields the following transformation of the Y's:

$$
\begin{aligned}
&{}_{k-1}\gamma_{0m}{}^{*} = {}_{k-1}\gamma_{0m} + T^{0}{}_{,m}, && \text{(a)}\\
&{}_{k}\gamma_{mn}{}^{*} = {}_{k}\gamma_{mn} + \delta_{mn}\,{}_{k}T^{s}{}_{,s} - {}_{k}T^{m}{}_{,n} \\
&\qquad\qquad - {}_{k}T^{n}{}_{,m} + \delta_{mn}\,{}_{k-1}T^{0}{}_{,0}, && \text{(b)}\quad (6.12)\\
&{}_{k}\gamma_{00}{}^{*} = {}_{k}\gamma_{00} - {}_{k}T^{s}{}_{,s} + {}_{k-1}T^{0}{}_{,0}, && \text{(c)}
\end{aligned}
$$

which produces the formulas of Einstein and Infeld quoted in Eqs. (6.1) if one sets

$$
\begin{aligned}
&{}_{k}T^{m} = -\,{}_{k}a_{m}, && \text{(a)}\\
&{}_{k-1}T^{0} = {}_{k-1}a_{0}. && \text{(b)}
\end{aligned}
\qquad (6.13)
$$

Similarly, one can obtain the other set of Einstein and Infeld's formulas, quoted as Eqs. (6.2), by choosing a somewhat different combination of the coordinate transformations, (6.7) and (6.9), namely

$$
\begin{aligned}
&x^{s} = x^{s*} + \lambda^{k}{}_{(k)}T^{s}, && \text{(a)}\\
&x^{0} = x^{0*} + \lambda^{k+1}{}_{(k+1)}T^{0}. && \text{(b)}
\end{aligned}
\qquad (6.14)
$$

This yields the following transformation of the γ's

$$
\begin{aligned}
&{}_{k}\gamma_{mn}{}^{*} = {}_{k}\gamma_{mn} + \delta_{mn}\,{}_{k}T^{s}{}_{,s} - {}_{k}T^{m}{}_{,n} - {}_{k}T^{n}{}_{,m}, && \text{(a)}\\
&{}_{k+1}\gamma_{0m}{}^{*} = {}_{k+1}\gamma_{0m} - {}_{k}T^{s}{}_{,0} + {}_{k+1}T^{0}{}_{,m}, && \text{(b)}\quad (6.15)\\
&{}_{k}\gamma_{00}{}^{*} = {}_{k}\gamma_{00} - {}_{k}T^{s}{}_{,s}, && \text{(c)}
\end{aligned}
$$

which is identical with (6.2) if one puts

$$
\begin{aligned}
&{}_{k}T^{s} = -\,{}_{k}b_{s}, && \text{(a)}\\
&{}_{k+1}T^{0} = {}_{k+1}b_{0}. && \text{(b)}
\end{aligned}
\qquad (6.16)
$$

The results contained in Eqs. (6.13) and (6.16) show that coordinate transformations produce all the changes in the γ's which Einstein and Infeld[9] found possible by rejecting the coordinate conditions in the kth step of the approximation procedure. Thus, having the usual solution, all the different solutions which result from the arbitrariness in the approximation procedure can be obtained simply by an appropriate coordinate transformation, and conversely.

7. COORDINATE TRANSFORMATIONS

The next question to be investigated is the possible influence of the coordinate transformations which were under consideration in Sec. 6, upon the equations of motion. This question has been studied previously up to the Newtonian approximation by Papapetrou,[14] and generally by Infeld and Scheidegger.[13] However, a new approach will be used here, which appears somewhat simpler.

Assume that the field equation be solved up to the order λ^{2k+1}. Thus, one knows the following quantities:

$$
\begin{aligned}
&{}_{2}\gamma_{00} \cdots {}_{2k}\gamma_{00}, && \text{(a)}\\
&{}_{3}\gamma_{0m} \cdots {}_{2k+1}\gamma_{0m}, && \text{(b)}\quad (7.1)\\
&{}_{4}\gamma_{mn} \cdots {}_{2k}\gamma_{mn}. && \text{(c)}
\end{aligned}
$$

Furthermore, the equations of motion of the corresponding order are

$$
\begin{aligned}
&\lambda^{4}{}_{4}{}^{1}C(Y,Z) + \cdots + \lambda^{2k}{}_{2k}{}^{1}C(Y,Z) = 0, && \text{(a)}\\
&\lambda^{4}{}_{4}{}^{2}C(Y,Z) + \cdots + \lambda^{2k}{}_{2k}{}^{2}C(Y,Z) = 0. && \text{(b)}
\end{aligned}
\qquad (7.2)
$$

One has to consider now two cases where in the first, one leaves all the Eqs. (7.1–2) unaltered, but in the second, one performs a coordinate transformation. The aim is to compare the equations of motion of higher approximation in those two cases.

To simplify the calculations involved, it turns out to be convenient to make some special assumptions. Firstly, the transformation T be of the form

$$T^{\beta} = x^{\beta*} + \lambda^{2k}{}_{(2k)}T^{\beta} \qquad (7.3)$$

as before. Secondly, noting that one needs the behavior of the expressions for ${}_{2k}T^{\beta}$ only in the neighborhood of the world lines of the particles, and thus, that they can be developed near the world lines into a Taylor series, one assumes that the occurring space derivatives near those lines shall vanish up to a 4th order. One may call such a coordinate transformation an infinitesimal one; because of all the group property all others can be obtained by repetitions of such infinitesimal transformations. Thirdly, one assumes that only ${}_{2k}T^{m}$ is different from zero, whereas ${}_{2k}T^{0}$ vanishes. These assumptions restrict, of course, the transformations considered to a large extent; it will be seen, however, that the admitted ones are still general enough for all purposes.

Thus, one has near the first world line the following coordinate transformation:

$$x^{m} = x^{m*} + \lambda^{2k}{}_{(2k)}{}^{1}T^{m}(x^{\beta*}). \qquad (7.4)$$

An example for a choice of ${}_{2k}{}^{1}T^{m}$ satisfying all the above requirements would be near the world line Y

$${}_{2k}{}^{1}T^{m} = F^{m}(\tau) + [(x^{s} - Y^{s})(x^{s} - Y^{s})]^{5/2} f^{m}(\tau). \qquad (7.5)$$

Then, the only γ which is influenced in form up to the order $2k+1$ is ${}_{2k+1}\gamma_{0k}$. It becomes near the first world line, according to Eqs. (6.8),

$${}_{2k+1}\gamma_{0k}{}^{*} = {}_{2k+1}\gamma_{0m} - {}_{2k}{}^{1}T^{m}{}_{,0}. \qquad (7.6)$$

When calculating the higher approximations, one is interested only in terms which contain T^{m}; the other ones are the terms which one would have got without the coordinate transformation. Thus, keeping only terms containing T's, one obtains the formal difference betweeen the equations of motion in the old and in the new coordinate systems. We may note that one can use the standard coordinate conditions (4.1) throughout; for, (7.6) satisfies these conditions and for the later steps one is free to choose any coordinate conditions one likes.

To proceed with the approximation, one has to calculate the quantities denoted by ${}_{2k+2}L_{mn}$ and ${}_{2k+2}L_{00}$

CC-0. In Public Domain. Gurukul Kangri Collection, Haridwar

Digitized by Arya Samaj Foundation Chennai and eGangotri

in Eqs. (4.12)–(4.14). An inspection of the terms shows that a contribution containing T's could only come from the linear terms. Those, however, vanish because they all contain space-derivatives of ${}_{2k}T$. From these statements we conclude that the additional terms in ${}_{2k}\Lambda_{mn}$ are just zero, so that we find

$$ {}_{2k+2}\Lambda_{mn}{}^{*} = {}_{2k+2}\Lambda_{mn}(x^{*}). \tag{7.7} $$

The corresponding surface integrals, therefore, remain unchanged; a fact which shows that an alteration of terms at the $2k$th step within the prescriptions of the approximation procedure never affects the differential equations of motion of the $2k+2$nd step. This is in conformity with the cited statement of Papapetrou[14] who observed that an infinitesimal coordinate transformation will not change the Newtonian approximation.

Thus, an infinitesimal coordinate transformation of the order λ^{2k} will affect only terms from ${}_{2k+4}C$ onward in the equations of motion. The object is to calculate the first term which is affected. In the old coordinate system the equations of motion are

$$ \begin{aligned} &\lambda^{4}\,{}_{4}{}^{1}C_{m}(Y,Z)+\lambda^{6}\,{}_{6}{}^{1}C_{m}(Y,Z) \\ &\qquad +\cdots+\lambda^{2k+4}\,{}_{2k+4}{}^{1}C_{m}=0, \quad \text{(a)} \\ &\lambda^{4}\,{}_{4}{}^{2}C_{m}(Y,Z)+\lambda^{6}\,{}_{6}{}^{2}C_{m}(Y,Z) \\ &\qquad +\cdots+\lambda^{2k+4}\,{}_{2k+4}{}^{2}C_{m}=0. \quad \text{(b)} \end{aligned} \tag{7.8} $$

Transforming the coordinate system at the $2k$th step by an infinitesimal transformation (7.4) will change somehow Eqs. (7.8). If one performs the *substitution* (7.4) in Eqs. (7.8) one obtains that same *old* condition for the motion of the particles concerned, but now expressed in the *new* coordinate system. The substitution (7.4) is equivalent to saying that one has to replace in (7.8)

$$ \begin{aligned} Y^{n} \quad &\text{by} \quad Y^{n*}+\lambda^{2k}{}_{(2k)}T^{n}(Y^{*}), \quad \text{(a)} \\ Z^{n} \quad &\text{by} \quad Z^{n*}+\lambda^{2k}{}_{(2k)}T^{n}(Z^{*}). \quad \text{(b)} \end{aligned} \tag{7.9} $$

It will be seen that the substitution (7.4) does not only yield the old equations of motion in the new coordinate system, but the new equations of motion altogether. For, one observes that generally the new equations of motion will contain terms with λ^{j} where $j>2k+4$. However, one has made the assumption that ${}_{2k}T$ is of the order λ^{0} in the total domain where it is defined so that one can be sure that all the terms involving T in the transformed equations of motion are actually of the order indicated by the power of λ by which they are multiplied. If one keeps in mind that the method for solving the differential equations is by making a similar development for the solution, namely

$$ Y^{*}={}_{0}Y^{*}+\lambda^{2}\,{}_{2}Y^{*}+\cdots $$

and that in the latter in any case only terms up to the order λ^{2k+4} are reliable, then one can discard all the terms of higher order than $2k+4$th arising from the coordinate substitution,—which proves the sufficiency of the substitution. The argument may not seem quite legitimate, but it would certainly be legitimate if the old C's are of such a type that in performing the substitution terms of higher order than $2k+4$ just do not occur. This is actually the case in one significant application which will be given below as follows:

Consider the equations of motion of the 6th order; i.e., in the old coordinate system

$$ \begin{aligned} &\lambda^{4}\,{}_{4}{}^{1}C_{m}(Y,Z)+\lambda^{6}\,{}_{6}{}^{1}C_{m}(Y,Z)=0, \quad \text{(a)} \\ &\lambda^{4}\,{}_{4}{}^{2}C_{m}(Y,Z)+\lambda^{6}\,{}_{6}{}^{2}C_{m}(Y,Z)=0. \quad \text{(b)} \end{aligned} \tag{7.10} $$

All the occurring C's have been calculated by Einstein, Infeld, and Hoffmann[5] and are listed in the earlier sections of this paper as Eqs. (4.24) and (4.36). Perform now the coordinate transformation (7.4) which alters (7.10) by the corresponding substitution

$$ \begin{aligned} &\lambda^{4}\,{}_{4}{}^{1}C_{m}(Y^{*}+\lambda^{2}\,{}_{2}T(Y^{*}),Z^{*}+\lambda^{2}\,{}_{2}T(Z^{*})) \\ &\qquad +\lambda^{6}\,{}_{6}{}^{1}C_{m}(Y^{*},Z^{*})=0, \quad \text{(a)} \\ &\lambda^{4}\,{}_{4}{}^{2}C_{m}(Y^{*}+\lambda^{2}\,{}_{2}T(Y^{*}),Z^{*}+\lambda^{2}\,{}_{2}T(Z^{*})) \\ &\qquad +\lambda^{6}\,{}_{6}{}^{2}C_{m}(Y^{*},Z^{*})=0. \quad \text{(b)} \end{aligned} \tag{7.11} $$

For the calculations it is very convenient to have assumed that

$$ \begin{aligned} {}_{2}T(Y^{*})={}_{2}T(Z^{*})={}_{2}T_{,k}(Y^{*})={}_{2}T_{,k}(Z^{*}) \\ ={}_{2}T_{,0}(Y^{*})={}_{2}T_{,0}(Z^{*})=0, \end{aligned} \tag{7.12} $$

as this effects that one has T^{m} equal to zero on the first world line. Thus, one finds near the first world line

$$ \begin{aligned} {}_{2}T^{m}&=(x^{s}-Y^{s})(x^{s}-Y^{s})f^{m}(\tau), \quad \text{(a)} \\ {}_{2}T^{m}{}_{,k}&=2(x^{k}-Y^{k})f^{m}(\tau), \quad \text{(b)} \end{aligned} \tag{7.13} $$

and

$$ {}_{2}T^{m}{}_{,0}=-2(x^{k}-Y^{k})\dot{Y}^{k}+(x^{s}-Y^{s})(x^{s}-Y^{s})\dot{f}^{m}(\tau), \tag{7.14} $$

which are all zero on the line; but

$$ {}_{2}T^{m}{}_{,00}=2\dot{Y}^{k}\dot{Y}^{k}f(\tau)+\textit{terms zero on the line.} \tag{7.15} $$

Thus, the last term can be put equal to any arbitrary function of time.

Under these assumptions ${}_{4}C^{m}$ changes into

$$ \begin{aligned} {}_{4}{}^{1}C_{m} \quad &\text{into} \quad {}_{4}{}^{1}C_{m}+4\,{}^{1}mT^{m}{}_{,00}(Y^{*})\lambda^{2}, \quad \text{(a)} \\ {}_{4}{}^{2}C_{m} \quad &\text{into} \quad {}_{4}{}^{2}C_{m}+4\,{}^{2}mT^{m}{}_{,00}(Z^{*})\lambda^{2}. \quad \text{(b)} \end{aligned} \tag{7.16} $$

Hence, one obtains the following equations of motion of the 6th order:

$$ \begin{aligned} &\lambda^{4}\,{}_{4}{}^{1}C(Y^{*},Z^{*})+\lambda^{6}\{4\,{}^{1}m\,{}_{4}T^{m}{}_{,00}(Y^{*})+{}_{6}{}^{1}C_{m}\}=0, \quad \text{(a)} \\ &\lambda^{4}\,{}_{4}{}^{2}C(Y^{*},Z^{*})+\lambda^{6}\{4\,{}^{2}m\,{}_{4}T^{m}{}_{,00}(Z^{*})+{}_{6}{}^{2}C_{m}\}=0. \quad \text{(b)} \end{aligned} \tag{7.17} $$

CC-0. In Public Domain. Gurukul Kangri Collection, Haridwar

Digitized by Arya Samaj Foundation Chennai and eGangotri

It is readily seen that it is possible to choose the transformation T in such a way that the coefficient of λ^6 in the equations of motion of the 6th order vanishes. Considering the expression (7.13) for T near the first world line, one observes that one can annihilate the 6th order terms in Eq. (7.17a) simply by putting

$$f(\tau) = -{}_6{}^1C_m\{1/(4\dot{Y}^k\dot{Y}^{k\,1}m)\}, \tag{7.18}$$

which, at the same time, insures one that ${}_2T$ is actually of the order λ^0 as required (except for $\dot{Y}^k=0$, a singular case which can easily be avoided by a translation of the origin). A similar procedure leads to the annihilation of the 6th order term in (7.17b).

Thus, we obtain equations of motion of the 6th order which do not contain any 6th order terms at all. This argument can be generalized for transformations of the $2j$th order

$$x^m = x^{m*} + \lambda^{2j}{}_{(2j)}T^m(x^*). \tag{7.19}$$

All the calculations are identical to those above; one has simply to apply them everywhere to the corresponding order of the equations. Thus, it is again possible to construct a coordinate transformation such that the equations of the order i are transformed so as to contain no terms of the order $2j \leq i$. One can do that a sufficient number of times and thus finally end up with Newtonian equations of motion.

Thus we may shortly summarize the results of this section as follows.

It is always possible to construct such a coordinate transformation that the differential equations of motion have Newtonian form. In other words, the Newtonian form is a standard form to which the differential equations of motion can be reduced. As to the physical significance of this formalism, one has to observe, first of all, that it does *not* mean that the motion is just the same as it would be nonrelativistically in such a specially chosen coordinate system. Only the *form* of the differential equations is Newtonian; one must keep in mind, however, that the *metric* is by no means Galilean. Thus, the relativistic corrections of the motion are only transferred into the metric of the universe. Infeld[15] has demonstrated this recently explicitly for the case of the two-body problem.

So far, this does not yield any new conceptions. One may note, however, that the above statement about the possible Newtonian form of the equations of motion can be formulated in a slightly different way. For, one observes that it is the same as saying that, at every step of the approximation procedure, one can reach the vanishing of the surface integrals concerned by choosing the coordinate system in an appropriate way. This shows that one really has a new version of Einstein, Infeld, and Hoffmann's method for solving Einstein's field equations, which is equivalent to that introducing and annihilating dipoles.

[15] L. Infeld, Can. J. Math. 5, 17 (1953).

8. THE PROBLEM OF GRAVITATIONAL RADIATION

In every field theory the problem of radiation is very closely connected with the problem of motion of a particle in that field. This is best seen in the electromagnetic case where the motion of a particle may be slowed down on account of a radiation damping effect by the field.

The gravitational field in space and time is in many respects very analogous to the electromagnetic field. From this analogy one might expect that moving bodies radiate gravitational waves and undergo a damping of their motion in a manner similar to moving charged particles. However, one will have to be very careful in defining what one means by "radiation of gravitational waves." In the usual way of speaking about "waves" the linear superposition principle is crucial for their existence. Since this superposition principle does not hold in nonlinear relativity theory one will have to study the analogy between electrodynamics and relativity in great detail so as to see whether the notion of a "wave" makes sense in the latter. To do this, one needs a formulation of electrodynamics which resembles the approximation procedure leading to the relativistic equations of motion of masses. This formulation was given by Infeld[16] as follows.

One can write down the field equations of electrodynamics in the following form

$$\begin{aligned} &\gamma_{0|ss} - \gamma_{0|00} = -\rho, && \text{(a)} \\ &\gamma_{m|ss} - \gamma_{m|ss} = \rho\dot{X}^m, && \text{(b)} \\ &\gamma_{m|ss} = \gamma_{0|0}. && \text{(c)} \end{aligned} \tag{8.1}$$

Here γ_0 is the electric, γ_m the magnetic potential, ρ the charge density and $\dot{X}^m$ the velocity vector of the charges. If the velocity of all the charged particles is small compared with the velocity of light, one may assume γ_0 as of the order λ^2 and γ_m as of the order λ^3. Under these circumstances, the field variables γ vary slowly in time but quickly in space. This compels one to introduce the "comma-differentiation" as before. If one assumes that all the charges are concentrated in particles and the latter described by singularities of the field, then Eq. (8.1) takes the following form outside of the singularities:

$$\begin{aligned} &\gamma_{0,\,ss} = \lambda^2\,\gamma_{0,\,00}, && \text{(a)} \\ &\gamma_{m,\,ss} = \lambda^2\,\gamma_{m,\,00}, && \text{(b)} \\ &\gamma_{m,\,n} = \lambda\gamma_{0,\,0}. && \text{(c)} \end{aligned} \tag{8.2}$$

If one expands the γ's in power series of λ, taking the lowest powers of expansion to be of the order indicated by the assumptions about the γ's, the Eqs. (8.2) split into

$$\begin{aligned} &{}_k\gamma_{0,\,ss} = {}_{k-2}\gamma_{0,\,00}, && \text{(a)} \\ &{}_{k+1}\gamma_{m,\,ss} = {}_{k-1}\gamma_{m,\,00}, && \text{(b)} \\ &{}_{k+1}\gamma_{m,\,m} = {}_k\gamma_{0,\,0}. && \text{(c)} \end{aligned} \tag{8.3}$$

[16] L. Infeld, Phys. Rev. 53, 836 (1938).

CC-0. In Public Domain. Gurukul Kangri Collection, Haridwar

Digitized by Arya Samaj Foundation Chennai and eGangotri

The fact that (8.3) connects only ${}_k\gamma_0$ with ${}_{k+2}\gamma_0$ and ${}_{k+1}\gamma_m$ with ${}_{k-1}\gamma_m$ permits one to set all the odd ${}_k\gamma_0$ and all the even ${}_k\gamma_m$ equal to zero.

Consider now the case of one point-singularity with its motion represented by X^s. (It is obvious how to generalize the ensuing statements for many particles.) The Eqs. (8.3) in the lowest order lead to the solution (choosing the particle at the origin and at rest for $t=0$)

$$\begin{aligned} {}_2\gamma_0 &= e/r, && \text{(a)} \\ {}_3\gamma_m &= -e\dot{X}/r, && \text{(b)} \\ r^2 &= (x^s-X^s)(x^s-X^s). && \text{(c)} \end{aligned} \tag{8.4}$$

The nature of the whole solution is determined by this initial choice of the harmonic functions for ${}_2\gamma_0$ and ${}_3\gamma_m$, if one agrees not to introduce any arbitrary harmonic functions in the further approximation steps. One obtains then

$$\begin{aligned} {}_{2k}\gamma_0 &= \frac{e}{(2k-2)!}\frac{d^{2k-2}}{d\tau^{2k-2}}(r^{2k-3}), && \text{(a)} \\ {}_{2k+1}\gamma_m &= \frac{-e}{(2k-2)!}\frac{d^{2k-2}}{d\tau^{2k-2}}(r^{2k-3}\dot{X}^m). && \text{(b)} \end{aligned} \tag{8.5}$$

This corresponds to a standing wave, that is to $\frac{1}{2}$ advanced $+\frac{1}{2}$ retarded potential, as discussed long ago by Nordstrøm[17] and Page.[18]

If one wants to retain in the expressions for γ all the powers of λ, then one has to make an arbitrary choice for ${}_3\gamma_0$, ${}_4\gamma_m$. The odd and even powers of λ do not mix since the electrodynamic field Eqs. (8.1) are linear and of the second order. Take for ${}_3\gamma_0$ and ${}_4\gamma_m$ the following simple harmonic functions satisfying (8.3) for $k=3$:

$$\begin{aligned} {}_3\gamma_0 &= 0, && \text{(a)} \\ {}_4\gamma_m &= ed^2X/d\tau^2. && \text{(b)} \end{aligned} \tag{8.6}$$

This leads to

$$\begin{aligned} {}_{2k+1}\gamma_0 &= -\frac{e}{(2k-1)!}\frac{d^{2k-1}}{d\tau^{2k-1}}(r^{2k-2}), && \text{(a)} \\ {}_{2k+2}\gamma_m &= \frac{e}{(2k-1)!}\frac{d^{2k-1}}{d\tau^{2k-1}}(r^{2k-2}\dot{X}^m). && \text{(b)} \end{aligned} \tag{8.7}$$

The general power series for the γ's, if (8.5) and (8.7) are inserted, represent a retarded potential. Therefore one is justified to call the terms of Eqs. (8.7) "radiation terms." They change the standing potential, if added, into a solution with radiation.

Now, one observes that the electromagnetic equations (8.3) as discussed here are analogous to a corresponding set in general relativity theory, namely (3.16) and (4.1). The two sets of equations differ only by the additional index "0" in the gravitational case. In both cases the right-hand sides are known and determined by the previous approximation steps, for the Λ's in the gravitational case are known functions of the γ's.

This analogy with electrodynamics induces one to seek in the gravitational case a solution which corresponds to the retarded potential in electrodynamics. Such a solution might properly be expected to represent gravitational radiation. The analogy suggests to choose for ${}_3\gamma_{00}$ and ${}_4\gamma_{0m}$ the following expressions in the case of two particles:

$$\begin{aligned} {}_3\gamma_{00} &= 0, && \text{(a)} \\ {}_4\gamma_{0m} &= -4^1m^m\dot{Y}-4^2m\ddot{Z}^m. && \text{(b)} \end{aligned} \tag{8.8}$$

One should note, however, that in electrodynamics the "radiation terms" initiated by the choice (8.7) can be calculated by themselves and simply inserted into the power series for the γ's. In relativity theory the assumption of (8.8) will not only initiate "radiation terms," but will also alter all the γ's as calculated without the radiation.

The introduction of radiation in relativity theory by analogy with electrodynamics as given above, may seem somewhat artificial. However, it is also possible to arrive at gravitational radiation terms by a more physical argument. True enough, one cannot speak of radiation or waves in relativity theory in the usual way, due to its nonlinear field equations, but one can set up a linear approximation of the theory as shown for instance by Eddington[3] where the notion of waves is sensible. Setting as usual

$$g_{\alpha\beta} = \eta_{\alpha\beta} + h_{\alpha\beta} \tag{8.9}$$

and assuming $h_{\alpha\beta}$ to be *small*, one can neglect all terms involving the h's more than linearly. Then one has correct to the first order, outside of the singularities of the field (reference 3, p. 128 ff),

$$\eta^{\alpha\beta}(h_{\beta\mu}-\tfrac{1}{2}\eta_{\beta\mu}\eta^{\sigma\rho}h_{\sigma\rho})_{|\alpha}=0, \tag{8.10}$$

$$\Box\eta^{\alpha\beta}(h_{\beta\mu}-\tfrac{1}{2}\eta_{\beta\mu}\eta^{\rho\sigma}h_{\rho\sigma})=0, \tag{8.11}$$

where $\Box$ denotes the d'Alembertian operator. Introducing the γ's instead of the h's yields

$$\begin{aligned} \gamma_{\alpha 0|0}-\gamma_{\alpha s|s} &= 0, && \text{(a)} \\ \Box\gamma_{\alpha\beta} &= 0. && \text{(b)} \end{aligned} \tag{8.12}$$

Setting $\alpha=0$ yields

$$\begin{aligned} \gamma_{00|0} &= \gamma_{0s|s}, && \text{(a)} \\ \Box\gamma_{0\beta} &= 0. && \text{(b)} \end{aligned} \tag{8.13}$$

These equations are precisely identical with (8.1), if one omits in (8.13) the additional index 0 and sets $\rho=0$ which means that the particles are represented as singularities of the field. Hence, it follows that one may deduce from (8.13) exactly the same solutions as one did from (8.1) (see for instance Infeld and Wallace[19]).

[17] C. Nordstrøm, Proc. Acad. Amsterdam 22, 145 (1920).
[18] L. Page, Phys. Rev. 24, 296 (1924).
[19] L. Infeld and P. R. Wallace, Phys. Rev. 57, 797 (1940).

CC-0. In Public Domain. Gurukul Kangri Collection, Haridwar

Digitized by Arya Samaj Foundation Chennai and eGangotri

One can take over all the formulas from (8.4) to (8.7). Thus one obtains the result that the standing as well as the retarded potential is an exact solution of the linearized field equations. Gravitational radiation exists in the linearized theory in the conventional sense.

It is customary to regard the linearized theory as a first approximation to exact general relativity theory. Therefore, if one wants to retain radiation terms in the development for the field variables, then it is reasonable to request that the first term starting the radiation terms is equal to that which one had found starting radiation terms in the linear approximation. Thus, one is again led to the assumption that this term must be of the form given in Eqs. (8.8). Taking this term and inserting it into Einstein, Infeld and Hoffmann's approximation procedure should yield a physical effect which represents ordinary radiation in the limiting case of a weak field represented by linearized equations.

Generalizing the argument above, one is not forced to start the "radiation terms" with the choice of ${}_4\gamma_{0m}$ as this was done in (8.8). One can ask whether it would be possible to start the omitted terms in the original development for the γ's at any stage of the approximation procedure, say in the $2k$th.

The prescriptions of Einstein, Infeld, and Hoffmann imply that one never must add arbitrarily to a field variable any additional poles or higher harmonic functions. On the other hand, the first equation starting the radiation terms is (keeping the usual coordinate conditions) one of the following:

$$\begin{aligned} &{}_{2k+1}\gamma_{00,\,ss}=0 && \text{(a)}\\ \text{or}\quad &\\ &{}_{2k}\gamma_{0m,\,ss}=0 && \text{(b)}\\ \text{or}\quad &\\ &{}_{2k+1}\gamma_{mn,\,ss}=0. && \text{(c)} \end{aligned} \tag{8.14}$$

If one wishes to take for one of these γ's a solution $\neq 0$ which is nowhere singular in space (including infinity), one observes that the only possibility is γ equal to a function of τ. Thus, one can start "radiation terms" only with one of the following possibilities:

$$\begin{aligned} &{}_{2k+1}\gamma_{00}=f_{00}(\tau) && \text{(a)}\\ \text{or}\quad &\\ &{}_{2k}\gamma_{0m}=f_{0m}(\tau) && \text{(b)}\\ \text{or}\quad &\\ &{}_{2k+1}\gamma_{mn}=f_{mn}(\tau). && \text{(c)} \end{aligned} \tag{8.15}$$

It is readily seen that the particular choice (8.8) suggested by the electromagnetic analogy is indeed of the form (8.15) since Y, Z are functions of τ only.

Concluding, we may summarize the contents of this section by stating that gravitational radiation in connection with gravitational motion can formally be introduced by analogy with electrodynamics. Whether this formal definition of radiation will represent any physical effects (as which one would expect radiation damping of the moving bodies) remains to be seen.

9. RADIATION DAMPING OF GRAVITATIONAL MOTION

All early attempts to obtain radiation damping effects in general relativity theory started from the electromagnetic analogy as expressed by Eq. (8.8). In particular, starting with the assumption (8.8), Infeld[16] has calculated the equation of motion up to the order λ^7.

It is readily seen that with this assumption one obtains

$${}_5\Lambda_{mn}=0. \tag{9.1}$$

Therefore, the equations of motion are not changed up to the fifth order by assuming a radiation term.

If one desires to go on in the approximation schedule, the next equations that one is faced with are

$$\begin{aligned} &{}_5\gamma_{00,\,ss}=0, && \text{(a)}\\ &{}_6\gamma_{0m,\,ss}=0, && \text{(b)}\\ &{}_7\gamma_{mn,\,ss}={}_5\gamma_{00,\,0}. && \text{(c)} \end{aligned} \tag{9.2}$$

As solutions of these equations, one can conveniently take

$${}_5\gamma_{00}=\frac{2}{3}\frac{d^3}{d\tau^3}\{{}^1m\,{}^2r^2+{}^2m\,{}^2r^2\}, \tag{9.3}$$

$${}_6\gamma_{0m}=-4\frac{d}{d\tau}\{{}^1m\dot{Y}^m+{}^2m\dot{Z}^m\} -\frac{2}{3}\frac{d^3}{d\tau^3}\{{}^1m\,{}^1r^2\,\dot{Y}^m+{}^2m\,{}^2r^2\,\dot{Z}^m\}, \tag{9.4}$$

which is in analogy with the corresponding electrodynamic equations. Then, one can calculate ${}_7\Lambda_{mn}$ in a similar way as this has been done before. The result is

$$\begin{aligned} 2\,{}_7\Lambda_{mn}=&-{}_6\gamma_{0m,\,0n}-{}_6\gamma_{0n,\,0m}+\delta_{mn}\,{}_5\gamma_{00,\,00}\\ &-\varphi\,{}_5\gamma_{00,\,mn}-{}_5\gamma_{00}\varphi_{,\,mn}-\tfrac{1}{2}{}_5\gamma_{00,\,m}\,\varphi_{,\,n}\\ &-\tfrac{1}{2}{}_5\gamma_{00,\,n}\,\varphi_{,\,m}+\tfrac{3}{2}\delta_{mn}\,{}_5\gamma_{00,\,s}\,\varphi_{,\,s}, \end{aligned} \tag{9.5}$$

which leads to

$${}_7{}^1C_m=\oint {}_7\Lambda_{mn}n_n dS=-(4/3)\,{}^1m\{{}^1m\ddot{Y}^m+{}^2m\ddot{Z}^m\}. \tag{9.6}$$

But again, because of the Newtonian equations of motion, the right-hand side is not of the 7th, but at least of the 9th order; i.e., if one considers the equations of motion up to the 7th or 8th order, one obtains *no* contribution from inserting the radiation terms (8.8) into the usual approximation schedule.

Taking this result, Hu[10] went on in the approximation procedure and calculated the equations of motion up to the 9th order. This involves a tremendous amount of calculations which will not be reproduced here. The

CC-0. In Public Domain. Gurukul Kangri Collection, Haridwar

Digitized by Arya Samaj Foundation Chennai and eGangotri

result is (${}^1m={}^2m=m$)

$$ {}_9{}^1C_n=-\frac{17}{60}Y^s\frac{d^5}{d\tau^5}\{m^2Y^sY^n\}+\frac{8}{3}Y^s\frac{d^4}{d\tau^4}\{m^2Y^s\dot{Y}^n\}. \quad (9.7) $$

Carrying out the differentiation with respect to time, and eliminating after each stage of differentiation the second derivatives by the Newtonian equations of motion, one obtains finally

$$ {}_9{}^1C_n=\frac{84}{5}m^4\dot{Y}^n/r^4 \quad (9.8) $$

and a similar equation for the second particle. From this position Hu calculated the "loss" of energy per unit time as given by

$$ -\dot{E}=-\frac{84}{5}m^4v^2/r^4=-(42/5)m^5/r^5 \quad (9.9) $$

with

$$ v^2=\dot{Y}^s\dot{Y}^s=m/2r \quad (9.10) $$

for a circular orbit. The sign in Eq. (9.9) means that the total energy defined in Newtonian mechanics as

$$ E=mv^2-2m^2/r \quad (9.11) $$

is *increased* by the radiation "damping" force. This result is rather strange from the point of view of Newtonian mechanics, according to which the energy can only be radiated out at the loss of the total energy. Physically, this result, if correct, has the meaning that the radiation damping force makes the particles move spirally away from each other, which is rather unbelievable.

Such are the results obtained by direct calculations. The most natural thing of taking the term ${}_4\gamma_{0m}=(8.8)$ for starting the radiation expansion, as suggested by electrodynamic analogy, leads obviously to an unbelievable result when physically interpreted in the conventional way, as shown above.

Thus, one is strongly induced to look for another approach to the problem of gravitational radiation damping. In this instance, it has been observed by Scheidegger[20] that a clue for the proper interpretation of the "radiation terms" might be provided by the remarks of Sec. 6 on coordinate conditions. There it was shown that one can create additional terms in the usual solutions of Einstein, Infeld, and Hoffmann's approximation procedure according to Eqs. (6.1) and (6.2) by a mere infinitesimal coordinate transformation. This statement gives us the clue for the proper interpretation of the radiation terms. It is easily seen that the terms which were chosen to start the radiation expansion can be obtained from the usual solution by putting in (6.7),

$$ {}_3T^m=4\,{}^1m\dot{Y}^m+4\,{}^2m\dot{Z}^m. \quad (9.12) $$

[20] A. E. Scheidegger, Proc. Second Can. Math. Congr. 218 (1949).

Thus, the starting term (8.8) is just of such a form that it can be created by an infinitesimal coordinate transformation. Therefore, it can also be wiped out by the concerning inverse transformation. But after this inverse transformation, one has no radiation terms, the metric tensor is that which one had before radiation terms were inserted, the equations of motion are the original ones (without the radiation), and thus the old solutions of the relativistic field equations without the radiation terms are regained.

It may be noted that the coordinate system containing the radiation terms with the particular assumption (9.12) does not even require a departure from the usual coordinate conditions, since ${}_4\gamma_{0m,0}={}_3\gamma_{00,0}=0$.

One may ask now whether there are other possibilities for inserting radiation terms. It was seen generally that a term starting the radiation expansion is of the form (8.15). Let us take first the following possibility:

$$ {}_{2k}\gamma_{0m}=f_m(\tau). \quad (9.13) $$

This yields formally an even γ_{0m} which is different from zero. However, we note again that (9.13) can be created by a coordinate transformation of the usual solution by putting in Eq. (6.7),

$$ {}_{2k-1}T^m=-\int f_m d\tau. \quad (9.14) $$

Hence, it also may be destroyed by the corresponding inverse coordinate transformation.

The second possibility to start a radiation expansion is with ${}_{2k+1}\gamma_{mn}$. Thus, one assumes

$$ {}_{2k+1}\gamma_{mn}=f_{mn}(\tau), \quad (9.15) $$

where again f_{mn} is an arbitrary function of time. However, this term, too, can be obtained from the usual solution by a coordinate transformation. It is of the form (6.1) if one sets

$$ \begin{aligned} {}_{2k}a_m&=\tfrac{1}{2}f_{ms}x^s, && \text{(a)}\\ {}_{2k-1}a_0&=\tfrac{1}{2}\int f_{ss}d\tau. && \text{(b)} \end{aligned} \quad (9.16) $$

It has been shown in Sec. 6 that all such terms can be obtained or annihilated by an infinitesimal coordinate transformation.

Finally, it remains to investigate what happens if a radiation term is inserted for γ_{00} at a certain stage of the approximation procedure

$$ {}_{2k+1}\gamma_{00}=f(\tau). \quad (9.17) $$

In order to annihilate it, one may construct the following coordinate transformation:

$$ \begin{aligned} {}_{2k}T_0&=\tfrac{1}{4}\int f(\tau)d\tau, && \text{(a)}\\ {}_{2k+1}T^s&=-\tfrac{1}{4}f(\tau)x^s. && \text{(b)} \end{aligned} \quad (9.18) $$

CC-0. In Public Domain. Gurukul Kangri Collection, Haridwar

Digitized by Arya Samaj Foundation Chennai and eGangotri

According to Eq. (6.12) one finds indeed that the old $_{2k+1}\gamma_{00}$ is changed into (9.17), whereas all the other field variables are unaffected up to the considered approximation. Therefore, the corresponding inverse coordinate transformation again effects the annihilation of (9.17).

These results provide now an easy explanation of the radiation terms obtained by direct calculations.

First, one observes that all the additional terms of the form (6.1) or (6.2) added to the usual solutions do not affect the equations of motion in the next stage of the approximation. All the radiation terms can be brought into a linear combination of (6.1)and (6.2). Hence, one obtains the result that adding a radiation term at a certain stage of the approximation procedure leaves unaltered the equations of motion in the next one.

Second, having explicitly shown that all the radiation terms whatsoever can be destroyed by coordinate transformations, one observes that the terms that had been found by straightforward calculations must be entirely due to the particular choice of the coordinate system. Thus, there is no radiation damping of gravitational motion.

Actually, part of the results of this section could have been deduced directly from the structure of the gravitational field equations as observed by Scheidegger,[21] for it is well known (see Bergmann, reference 2, p. 188) that in the linearized theory only the waves where $\gamma_{st}\neq 0$ (so-called transverse-transverse waves) have a physical meaning, as the others can be annihilated by coordinate transformations. Now, it should be noted that the linearized theory should be identical to the first approximation of the exact theory, thus implying that radiation terms of the type $\gamma_{00}\neq 0$ or $\gamma_{0m}\neq 0$ can be wiped out by a suitable coordinate transformation in the lowest approximation of Einstein, Infeld, and Hoffmann's method. Hence, it follows that such terms cannot represent any physical effects. Thus, the only gravitational waves for which the possibility of annihilation by coordinate transformation is not obvious beforehand are the transverse-transverse waves. They have to be treated in the manner demonstrated earlier in this section.

In conclusion, it should be remarked that some theoretical physicists do not entirely agree with all the conclusions given in this and the last sections. Whereas it is undisputed that there is no physical reality to gravitational radiation *as defined in Section 8*, it has been questioned whether this is the *only* possible way to define gravitational radiation. The difficulty is that so far no satisfactory definition of "real" (as against apparent) radiation is to be found in literature. Until such a definition can be given, one will have to contend with giving (by analogies) reasonable definitions of gravitational radiation and to test whether those definitions will lead to physically real effects. This is the approach used by Infeld and Scheidegger.[13] It is the opinion of these authors that this is also the *only* way to obtain the radiation of a two-body system if there is any. The argument for this is largely one of principle, namely, if the gravitational motion of a system of two bodies in otherwise empty space is to be determined by the initial conditions implying position and velocities of the bodies only, then there is no room for additional boundary conditions that would determine in which of several choices of "stages" ("with" or "without" radiation) the system would be at a later instant. It seems to the writer logically impossible that a system whose behavior is thought to be completely determined by the initial conditions (according to the causalistic relativity theory) should have the freedom of several "behaviors." Since a solution fitting the initial conditions has been found, this is not only a solution, but the *only* solution of the problem. Nothing, of course, is being said of the possibility of gravitational radiation if the system is subjected to additional forces and not only to the gravitational ones originating from itself.

Nevertheless, the argument given in the last paragraph has been and still is being questioned by noted experts in relativity[22] who maintain that a different approach from that of Einstein, Infeld, and Hoffmann to the two-body problem and a different definition of "radiation" might lead to a different behavior of the system from that presented in the previous sections of this paper. To this date, however, nothing of such a different approach is to be found in the literature.

10. THE EINSTEIN-INFELD-HOFFMANN FORMALISM; IN GENERAL COVARIANT NONLINEAR FIELD THEORIES

In the last section the deduction of the equations of motion in general relativity theory was studied. It would be interesting to know whether the procedure outlined there is restricted to relativity theory or whether it might be possible to generalize it in such a way that it provides one with a scheme allowing to find equations of motion in any given nonlinear field theory.

Recently Bergmann[23] has made an attempt to set up a general covariant scheme for many types of field theories. Then, relativity theory would appear as a special case in this formalism. The principal aim in Bergmann's[23] investigations was to bring all these field theories into a Hamiltonian form so that their quantization would be possible (see Bergmann and Brunings[24]). In the classical part of his work, however, he points out some features which are connected with the equations of motion. One of his statements is that it should be possible to deduce in a covariant nonlinear theory the equations of motion of the sources from the field equations. If this is true, then it must be possible

[21] A. E. Scheidegger, Phys. Rev. 82, 883 (1951).

[22] Private communications, notably from Dr. P. G. Bergmann, Syracuse University, Syracuse, New York.

[23] P. G. Bergmann, Phys. Rev. 75, 680 (1949).

[24] P. G. Bergmann and J. Brunings, Revs. Modern Phys. 21, 480 (1949).

CC-0. In Public Domain. Gurukul Kangri Collection, Haridwar

Digitized by Arya Samaj Foundation Chennai and eGangotri

to find Lorentz's equations of motion of an electron in a generalized nonlinear theory of the electromagnetic field, (see the attempts of Born,[25] Born and Infeld,[26] Infeld,[27,28] Infeld and Wallace[19]) in the same way as the equations of motion of stars are found in general relativity theory. Up to now it has not yet been possible to deduce the equations of motion of an electron from an electrodynamic field theory.

We denote the field variables by y_A, $(A=1\cdots N)$, where N is the number of algebraically independent components. It will be assumed that the field equations can be deduced from a variational principle of the form

$$\delta I=\delta\int_V L(y_A, y_{A|\beta})d^4x=0, \tag{10.1}$$

satisfied in the four-dimensional domain V. L is an algebraic function of y_A and $y_{A|\beta}$ only. The field equations which result from the (infinitesimal) variation of the field variables in the interior of V are

$$L^A\equiv\frac{\partial L}{\partial y_A}-\left(\frac{\partial L}{\partial y_{A|\beta}}\right)_{|\beta}=0. \tag{10.2}$$

With respect to an infinitesimal coordinate transformation,

$$x^\mu=x^\mu-\epsilon\xi^\mu, \tag{10.3}$$

the field variables are assumed to transform according to a law having the form

$$\bar\delta y_A\equiv y_A{}^*-y_A=\epsilon(F_{A\mu}{}^{B\nu}\xi^\mu{}_{|\nu}-y_{A|\mu}\xi^\mu)+0(\epsilon^2). \tag{10.4}$$

The $F_{A\alpha}{}^{B\beta}$ are numbers characteristic for the type of field variables used. It should be noted that $\bar\delta y_A$ are the changes of the y_A as functions of their *arguments* (and not as functions of the world point only); hence, the second term in (10.4).

The field Eqs. (10.2) must be covariant. If the Lagrangian, in the face of an infinitesimal coordinate transformation, adds a divergence, then that condition is sufficient (though possibly not necessary) to assure covariant field equations. For, in this case, the infinitesimal change in the integral I can be expressed by means of a surface integral, and it must be assumed that the coordinate transformation is the identity on the boundary of our volume of integration. Thus, one has

$$\bar\delta L=\epsilon Q^\mu{}_{|\mu}+0(\epsilon^2), \tag{10.5}$$

where the Q^β are functions of the ξ^β and their derivatives. Then, the transformation laws of the field equations can be computed straightforwardly to be

$$\bar\delta L^B=\epsilon\{-F_{A\mu}{}^{B\nu}\xi^\mu{}_{|\nu}L^A-(L^B\xi^\mu)_{|\mu}\}+0(\epsilon^2). \tag{10.6}$$

A further remarkable property of this scheme is that the field variables must fulfill 4 identities, namely,

$$(F_{A\mu}{}^{B\nu}y_BL^A)_{|\nu}+y_{A|\mu}L^A=0 \tag{10.7}$$

(generalized Bianchi identities).

The expressions L^A contain the field variables and their first and second derivatives. The second derivatives occur only linearly, and their coefficients can be represented in the form

$$L^A=L^{AB\alpha\gamma}y_{B|\alpha\gamma}+\cdots. \tag{10.8}$$

Thus, the third derivatives occur only linearly in the identities (10.7) and those must cancel each other. It follows that the coefficients $L^{AB\alpha\gamma}$ must satisfy the identities

$$\{F_{A\beta}{}^{B\gamma}L^{AC\alpha\delta}+F_{A\beta}{}^{B\alpha}L^{AC\delta\gamma}+F_{A\beta}{}^{B\delta}L^{AC\gamma\alpha}\}y_B=0. \tag{10.9}$$

To deduce the equations of motion from the above scheme, one has to apply an approximation procedure. The solutions of the field equations are to be obtained as a power series in a certain parameter λ

$$y_A={}_0y_A+\lambda\,{}_1y_A+\lambda^2\,{}_2y_A+\cdots=0. \tag{10.10}$$

The time differentiation is thought to raise the order of the differentiated term; thus, the "comma" differentiation is used in the same sense as before.

The zeroth approximation of the approximation procedure shall be a "trivial" solution, a rigorous solution of the field equations in which all field variables are constants. The first approximation will yield

$${}_0L^{ABrs}{}_1y_{B,rs}=0. \tag{10.11}$$

The solutions ${}_1y_B$ will generally not be defined throughout space. At each instant of time there will be certain three-dimensional domains in which the field equations have no bounded solutions. However, only such solutions will be considered in which each one of these singular regions can be surrounded by a closed surface S on which the field equations are satisfied. Proceeding to the next approximation, the equations have the form

$${}_0L^{ABrs}{}_2y_{B,rs}=-{}_2L^A({}_0y+\lambda\,{}_1y). \tag{10.12}$$

The right-hand sides will be the L^A of the second order formed from the first-order solutions. The left-hand sides satisfy identically the four relationships

$$F_{A\alpha}{}^{Ct}{}_0y_C({}_0L^{ABrs}{}_2y_{B,rs})_{,t}=0 \tag{10.13}$$

irrespective of the choice of the second-order field variables. On a surface S surrounding a singularity, on which (10.12) are to be satisfied, one has then

$$0\equiv\oint F_{\alpha\mu}{}^{Ct}{}_0y_C\,{}_0L^{ABrs}{}_2y_{B,rs}n_tdS$$

$$=-\oint_S F_{A\mu}{}^{Ct}{}_0y_C\,{}_2L^A({}_0y+\lambda\,{}_1y)n_tdS, \tag{10.14}$$

[25] M. Born, Proc. Roy. Soc. (London) A143, 410 (1934).
[26] M. Born and L. Infeld, Proc. Roy. Soc. (London) A144, 485 (1934).
[27] L. Infeld, Proc. Cambridge Phil. Soc. 32, 127 (1936).
[28] L. Infeld, Proc. Cambridge Phil. Soc. 33, 70 (1937).

CC-0. In Public Domain. Gurukul Kangri Collection, Haridwar

Digitized by Arya Samaj Foundation Chennai and eGangotri

which represent for that singularity inside S the three equations of motion and the law of conservation of "mass."

To investigate the possibility of the existence of equations of motion in different nonlinear field theories, one has to apply Eq. (10.14) systematically to certain types of possible field variables. The results quoted here have been deduced by Scheidegger.[29]

Starting with field theories using one scalar field variable only, one sets

$$y_A = \phi. \tag{10.15}$$

Then, the transformation of the field variables is given by just the last term in Eq. (10.14) so that the coefficients $F_{A\alpha}{}^{B\beta}$ all vanish

$$F_{A\alpha}{}^{B\beta} = 0. \tag{10.16}$$

The surface conditions, therefore, become trivial identities, and one gets the result that no equations of motion can be deduced in any scalar field theory whatsoever.

The next more complicated type of field variables are vectors. Thus,

$$y_A = A_\beta. \tag{10.17}$$

Using the infinitesimal transformation

$$x^{\beta *} = x^\beta - \epsilon\xi^\beta, \tag{10.18}$$

one obtains the following change of the field variables (except for the term originating in the coordinate substitution):

$$A_\mu{}^* = (\delta_{\rho\mu} - \epsilon\xi^\rho{}_{|\mu})A_\rho = \delta_{\rho\mu}A_\rho - \epsilon\xi^\eta{}_{|\lambda}\delta_{\rho\eta}\delta_{\mu\lambda}A_\rho. \tag{10.19}$$

Hence,

$$F_{\mu\eta}{}^{\rho\lambda} = -\delta_{\rho\eta}\delta_{\mu\lambda}. \tag{10.20}$$

The calculation of the surface condition with these coefficients (denoting the "trivial" solution, constant in space and time, by a_α) yields

$$0 = -\oint F_{\alpha\mu}{}^{\gamma t}a_\gamma L^\alpha n_t dS = a_\mu \oint L^t n_t dS. \tag{10.21}$$

This shows that the four conditions of Eq. (10.14) reduce to only one in every vector theory whatsoever. This one condition, however, cannot be sufficient for determining the motion of the singularity to which it refers; it is just the conservation law for the pole strength of that singularity.

Thus, one concludes that the analogous procedure to that of Einstein, Infeld, and Hoffmann cannot be set up for a covariant vector theory. Electromagnetic theory is a covariant vector theory; the field variables are the components of the potential vector ϕ_α. Even in a nonlinear generalization such as that of Born and Infeld[25–28] there are, therefore, no equations of motion.

Thus one may state that a covariant field theory has to be at least a tensor field theory so that it is possible to obtain equations of motion from the field equations.

[29] A. E. Scheidegger, Helv. Phys. Acta 23, 740 (1950).

CC-0. In Public Domain. Gurukul Kangri Collection, Haridwar

Digitized by Arya Samaj Foundation Chennai and eGangotri

REVIEWS OF MODERN PHYSICS VOLUME 25, NUMBER 2 APRIL, 1953

Table of Isotopes

J. M. Hollander, I. Perlman, and G. T. Seaborg

Department of Chemistry and Radiation Laboratory, University of California, Berkeley, California

THE table on pages 476–612 represents a complete list of all the radioactive and stable isotopes of the elements, together with a number of their salient features, as recorded in the literature or by private communication by approximately December, 1952.

A primary objective has been to retain as much of the compactness of the previous editions as is consistent with an adequate coverage of the multitudes of nuclear data presently available.

A new system of references has been employed. Each paper is represented by the code symbol of the first author, followed by the year in which the paper was published. If two or more papers by one author have appeared during a single year, these are distinguished by the small letters *a*, *b*, *c*, etc., following the main reference. For example, 16H is the code symbol given to O. Hahn; thus, the references 16H41, 16H41a, and 16H41b represent three papers published in 1941 of which O. Hahn is the first author. The code symbols given to the authors are arranged alphabetically only with respect to the first letter of their names.

A description of the entries in the various columns is given below, followed by a table listing some frequently used abbreviations.

ISOTOPE

The first column lists the atomic numbers, chemical symbols, and mass numbers of the nuclear species. Separate entries have been made for each nuclear state whose half-life has been experimentally determined. Metastable excited states are denoted by the superscript "m" following the mass number, and for those cases in which two or more isomeric states are known, they are distinguished by the use of the superscripts "m_1," "m_2," etc.

CLASS AND IDENTIFICATION

The degree of certainty of each isotopic assignment is indicated by a letter, according to the following code:

A Element and mass number certain
B Element certain and mass number probable
C Element probable and mass number certain or probable
D Element certain and mass number not well established
E Element probable and mass number not well established or unknown (mass number not listed means that it is unknown)
F Insufficient evidence
G Assignment probably in error

Data which have been shown to be in error have in general been eliminated from the table. A few isotopes have been quoted so widely in the literature, however, that it was felt some reference should be made to them. For these cases the G rating has been adopted, and reference made both to the original work and to that which has supplanted it.

The means by which the mass assignments were made are next tabulated. In general, several references are given here, the first of which denotes the probable discoverer of the isotope (except in the cases of the old natural radioactivities). Following this, references are given to the paper or papers which contributed most significantly toward giving the isotope its best or present rating. Some indication of the experimental methods used in making the various assignments may be had from the following symbolism:

chem	Chemical separations, establishing uniquely the chemical identity (atomic number) of the isotope
genet	Proven genetic relationships (by chemical or other means) with other isotopes whose mass assignments are presumably known
genet energy levels	Proof of isobaric relationship with an identified nuclide by observation of identical energy levels following decay of both, implying decay to the same product
excit	Loosely refers to energetic considerations which have aided in making the mass assignment. Some of these might be (1) excitation or yield experiments to establish the nuclear reaction which produces the isotope (2) bombardments with low energy particles, in which possible products are few (3) mass calculations, or other estimates or measurements of Q values (4) in a few cases, use of fission yield data in making assignments
cross bomb	Studies of yields of the isotope in several different types of bombardments, in which the target elements as well as the projectiles have been varied
n-capt	Cases where bombardments with slow neutrons ($n-\gamma$ reactions) have provided key evidence in the mass assignments

CC-0. In Public Domain. Gurukul Kangri Collection, Haridwar

Digitized by Arya Samaj Foundation Chennai and eGangotri

sep isotopes — The use of target elements enriched or depleted in a certain isotope

mass spect — Identification of the mass number by means of a mass spectrograph

resonance neutron activation — Identification of a nuclear isomer by observing both isomers upon irradiation with filtered neutrons

decay charac — Identification of expected or predicted decay characteristics

PERCENT ABUNDANCE

The relative isotopic abundances for the elements are given in accordance with the "best values" listed in the report (1B50) by K. T. Bainbridge and A. O. Nier. In some of the light elements, reference is made also to papers which discuss source variations in isotope abundances.

TYPE OF DECAY

The observed modes of decay have been listed for all radioactive nuclei. In cases of branched decay between two or more modes, the branching ratios are listed wherever they are known. Symbols used are

β^- Negative beta-particle (negatron) emission

β^+ Positive beta-particle (positron) emission

α Alpha-particle emission

EC Orbital electron capture. It may be assumed that x-rays have been observed or actually identified in virtually all cases of orbital electron capture listed. If the ratio of L electron capture to K electron capture has been determined, it is given here as L/K

IT Isomeric transition (transition from upper to lower isomeric state of same nucleus)

n Neutron emission

When experimenters have searched for and failed to find a particular mode of decay, this is indicated, for example, as "no β^+." Experimental upper limits are frequently given, but no theoretically predicted limits have been quoted.

Among the heavy alpha-emitting isotopes, calculations by means of closed radioactive decay cycles have shown that many of these isotopes are thermodynamically stable against β^-, β^+, or EC decay. This has been indicated by the term "β-stable," followed by an abbreviation for the principle of conservation of energy, which is used in the calculations.

HALF-LIFE

Half-life values are listed without qualification where the determination has been a direct measurement of decay rate. In other cases, the experimental methods have been described with the aid of the following symbols:

sp act — Determination by weighing a long-lived isotope of known purity

delay coinc — Measurement of the time interval between two successive nuclear events (such as β^- and γ-emission) thus establishing the lifetime of the state responsible for the second event. By this method, half-lives between 10^{-3} sec and 10^{-10} sec have been determined.

yield — Estimation of half-life from the amount of activity resulting from a nuclear reaction whose cross section (or yield) is known or estimated

genet — Measurement of the half-life of a parent activity by determining the yield of a daughter activity as a function of time, where periodic chemical separations of daughter from parent have been performed

An attempt has been made to list the best value or values first. However, in a few cases where many values of comparable precision have been reported, and no choice seemed obvious, an average value for the half-life has been listed; this is explicitly stated, and references are given to all the papers whose values contributed to that average. Also, among the natural radioactivities an average value is often used which was taken from an international committee summary report (1C31).

PARTICLE ENERGIES

The particle energies are followed by other relevant information pertaining to the decay scheme, and by a description of the experimental methods used in obtaining the data. In cases of complex alpha-structure or several partial beta-spectra, the relative abundances of the various groups within that mode of decay are given in parentheses.

Beta-particle energies correspond to the upper limits of the spectra.

Alpha-particle energies have been quoted only where the investigator has actually measured them. Where he has determined only the relative abundances of alpha-groups or the energy differences between groups, this has been indicated as in the following example:

$$\alpha_0(10 \text{ percent}),\ \alpha_{50}(75 \text{ percent}),\ \alpha_{80}(15 \text{ percent}),$$

meaning that 75 percent of the alpha-particles lead to a state 50 kev above the ground state, and that 15 percent of the alpha-particles lead to a state 80 kev above the ground state.

The term "long-range α" is the classical designation for alpha-particle groups emitted from excited states of the listed nuclide, and the energies therefore are not included in the Q_α value, which applies to the ground state to ground-state transition. These alpha-groups

CC-0. In Public Domain. Gurukul Kangri Collection, Haridwar

Digitized by Arya Samaj Foundation Chennai and eGangotri

occur in competition with gamma-ray emission, following the beta-decay of the parent nuclide.

Conversion electron energies are listed only when it is not known in which shell internal conversion takes place or when no attempt was made by the experimenter to relate the electrons with observed or unobservable gamma-rays; in all other cases, entries are made in the column for gamma-transitions.

Experimental methods are described as follows:

abs	Absorption
spect	Magnetic deflection (magnetic spectrograph or spectrometer or counter with magnetic field)
scint spect	Measurement of pulses produced by a scintillating crystal or solution
ion ch	Measurement of pulse sizes in ionization chamber or proportional counter
cl ch	Cloud chamber (with magnetic field in case of beta-particles)
coinc abs	Beta- and gamma-coincidence counters with absorbers
coinc spect	Coincidence counters arranged with a spectrometer or spectrometers

GAMMA-TRANSITIONS

Gamma-transitions are described by the following information, in so far as reliable data permit:

Energy of the gamma-quantum. When internal conversion electrons form the basis for the energy determination, the energy listed in this column is always that of the corresponding gamma-ray transition.

Abundances of gamma-rays. This may be given as the number of unconverted gamma-rays emitted per 100 disintegrations. Where an absolute abundance has not been determined, often the relative unconverted gamma-ray abundances have been measured. These are tabulated as $\gamma_1/\gamma_2/\gamma_3 \approx 2/1/5$, for example.

Internal conversion coefficients. These are given for each gamma-transition as the ratio of the number of conversion electrons emitted to the number of unconverted gamma-quanta emitted, and are expressed as e/γ. Where conversion coefficients for individual electron shells have been determined, they are denoted as e_K/γ, e_L/γ, etc.

Conversion coefficient ratios. Where the ratios of internal conversion coefficients in several electron shells have been measured, they are listed as K/L, L/M, $K/L+M$, $K/L/M$, $L_I/L_{II}/L_{III}$, etc.

Gamma-rays associated with short-lived isomers have been listed as entries both of the isomer and of its parent.

When an author states that gamma-radiation is present, but reports no energy determination, this is indicated by the symbol "γ." Conversely, when attempts to find gamma-radiation have failed, this has been indicated by "no γ."

X-rays have been mentioned only when they are the prominent radiation observed in measuring an activity, or when the observation and identification of x-rays has been crucial in the characterization of an isotope.

The symbols used to describe the methods employed for the determination of gamma-ray energies or for the elucidation of decay schemes are as follows:

spect	Secondary electrons observed with magnetic spectrograph or spectrometer
spect conv	Internal conversion electrons observed with magnetic spectrograph or spectrometer
scint spect	Measurement of pulses produced by a scintillating crystal or solution
cryst spect	Direct measurement by diffraction of gamma-rays with a bent crystal spectrometer
abs	Absorption of the gamma-rays
abs conv	Absorption of internal conversion electrons
abs sec	Absorption of secondary electrons
coinc	Studies of coincidences or lack of coincidences ($\gamma-\gamma$, γ-conv, conv-conv, $\beta-\gamma$, etc.) with coincidence counters, and, in some cases, spectrometers
coinc abs	Coincidence studies using absorber techniques
cl ch recoil	Secondary electrons observed in cloud chamber with magnetic field
pair spect	Magnetic analysis of positron-electron pairs produced by gamma-rays in a thin radiator
Be$-\gamma-n$, $D-\gamma-n$, or $D-\gamma-p$ reactions	Measurements of neutron or proton energies from these reactions

DISINTEGRATION ENERGY AND SCHEME

The disintegration energy, or Q value, of a nuclear transformation is defined as the mass difference (expressed in Mev) between the initial and final systems under consideration. For radioactive decay processes, Q is equal to the sum of the particle kinetic energy, nuclear recoil energy, and the energy of any gamma-rays necessary to de-excite the final nucleus to its ground state. For positron decay, the energy equivalent to $2m_0c^2$ has been included in the Q value. Where Q values have been estimated or calculated by the authors of this compilation, the special reference "HPS" is used; otherwise, reference is made to the paper from which the quoted value is taken. In most instances Q values have been obtained from decay data; where this is not the case, the method is indicated.

Energy level diagrams have been drawn in many cases; these are not necessarily complete representations of the data, but sometimes include only those features which are reasonably well established and unambiguous. Heights of the various energy levels above the ground state are indicated at the side of the drawing. Similarly,

CC-0. In Public Domain. Gurukul Kangri Collection, Haridwar

Digitized by Arya Samaj Foundation Chennai and eGangotri

the total angular momentum (spin) and parity of the states have been included in some cases, where these quantum numbers could be inferred with some confidence from determinations of conversion coefficients, K/L ratios, ft values, etc. We have relied heavily on the interpretation of decay data by Goldhaber and Hill (18G52).

For β^-, β^+, α or EC decay, the percentage figures given in the decay drawings total 100 percent for *each* mode of decay, thus expressing only the relative abundances of various groups within that mode of decay. (Branching ratios between the several modes of decay are found in the "Type of Decay" column.) In the case of gamma-radiation, however, the percentages given refer to the fraction of the total disintegrations of that isotope which give rise to the gamma-ray and its conversion electron. This has been done because of the difficulty of assigning a gamma-ray to a particular mode of decay.

Measured values for the mechanical or spin moment I of stable or long-lived isotopes have also been given in this column. Except as supplemented by more recent data, the values given here are taken from the compilation by Mack (87M50).

METHOD OF PRODUCTION AND GENETIC RELATIONSHIPS

The observed nuclear reactions (giving the target element, projectile, and outgoing particle, in order) by which the radioactive isotopes are formed, and the corresponding references are listed (p-proton, n-neutron, α-alpha-particle, d-deuteron, t-triton, γ-gamma-ray or x-ray, e-electron, π-pi-meson, C-carbon ion). In cases in which the target material is not the naturally occurring element, but one enriched or depleted in a particular isotope, the isotope responsible for the reaction is indicated. No means for identifying the source or energy of the projectile is given.

In nuclear reactions with high energy projectiles, multiple particle ejection is common. Rather than attempt to state definitely the path by which the product nucleus was reached, these spallation reactions are briefly represented by the abbreviation "spall" followed by the symbol of the target element. High energy fission reactions are similarly represented by the words "spall-fission," and thermal or low energy neutron fission simply by "fission."

The criterion for listing genetic relationships has been with few exceptions that these relationships be demonstrated experimentally; for example, by chemical "milking" of daughter activities, analysis of growth-decay curves, or in the case of short-lived isomers, by delayed coincidence experiments. The listing of these parent-daughter relationships gives some warning to the reader as to what he may expect in the way of radiation from a given isotope, since a sufficiently short-lived daughter's radiation will usually be observed with that of the parent.

A few further abbreviations are listed below:

NNES–PPR	Volumes of the National Nuclear Energy Series, Plutonium Project Record, McGraw-Hill Book Company, Inc., New York
[ ]	Properties listed in brackets have not been observed directly, but have been inferred from other experimental data
est, calc	Estimated or calculated from theoretical or empirical considerations
HPS	Refers to the authors of this compilation
lim	Experimental upper limit
emuls	Photographic emulsion

A considerable fraction of the effort necessary to produce this table consisted of abstracting the literature and organizing the data over the past few years. We are greatly indebted to Marjorie Hollander for her efficacious handling of this work, and in addition for her preparation of the drawings.

It is a pleasure to acknowledge the generous help and constructive criticism which we have received from our friends and colleagues, and to thank many of the authors whose measurements are cited for their aid in evaluating data familiar to them. We are especially grateful to Dr. Gerhart Friedlander for his invaluable assistance in checking the entire draft.

We would also like to express our appreciation to Mildred Davis for the speed and accuracy with which she prepared the manuscript.

The compilation of this table was supported by the U. S. Atomic Energy Commission.

CC-0. In Public Domain. Gurukul Kangri Collection, Haridwar

Digitized by Arya Samaj Foundation Chennai and eGangotri

Rapid Method for Calculating Log(ft) Values

[From S. A. Moszkowski, Phys. Rev. 82, 35 (1951).]

Figures 1–5 permit the rapid calculation of log(ft) for a given type of decay, given energy, half-life, etc. The notation is: E_0 for $\beta^{\pm}$ emission is the maximum kinetic energy of the particles in Mev; E_0 for K-electron capture is the disintegration energy in Mev. When a β^+ emission and K-electron capture go from and to the same level, E_0 for K capture = E_0 for β^+ emission + 1.02 Mev. Z is the atomic number of the initial nucleus, t is the total half-life, and p is the percentage of decay occurring in the mode under consideration. When no branching occurs, $p = 100$.

PROCEDURE FOR OBTAINING LOG(FT)

(1) First obtain log(f_0t), using Fig. 1. E_0 is read off the left-hand side of the E_0 column for K-electron capture, and off the right-hand side for $\beta^{\pm}$ emission. Put a straight edge over the given values of E_0 and t and note where it crosses the column of log(f_0t) values.

(2) Then read off log(C) from Figs. 2, 3, and 4 for β^-, β^+, and K-electron capture, respectively.

(3) Get Δ log(ft) from Fig. 5 if $p < 100$. When $p = 100$, Δ log(ft) = 0.

(4) Log(ft) = log(f_0t) + log(C) + Δ log(ft).

These graphs have been reproduced with the kind permission of Dr. Moszkowski. For details concerning their construction, significance, and range of usefulness, reference should be made to the original paper.

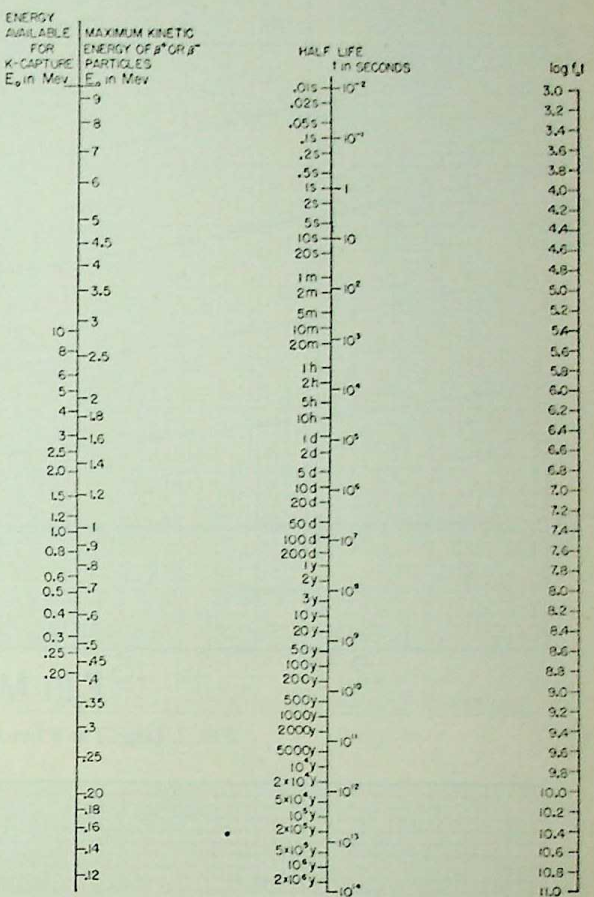


FIG. 1. Log(f_0t) as a function of E_0 and t.

(Figures 2–5 are on pages 474 and 475.)

CC-0. In Public Domain. Gurukul Kangri Collection, Haridwar

Digitized by Arya Samaj Foundation Chennai and eGangotri

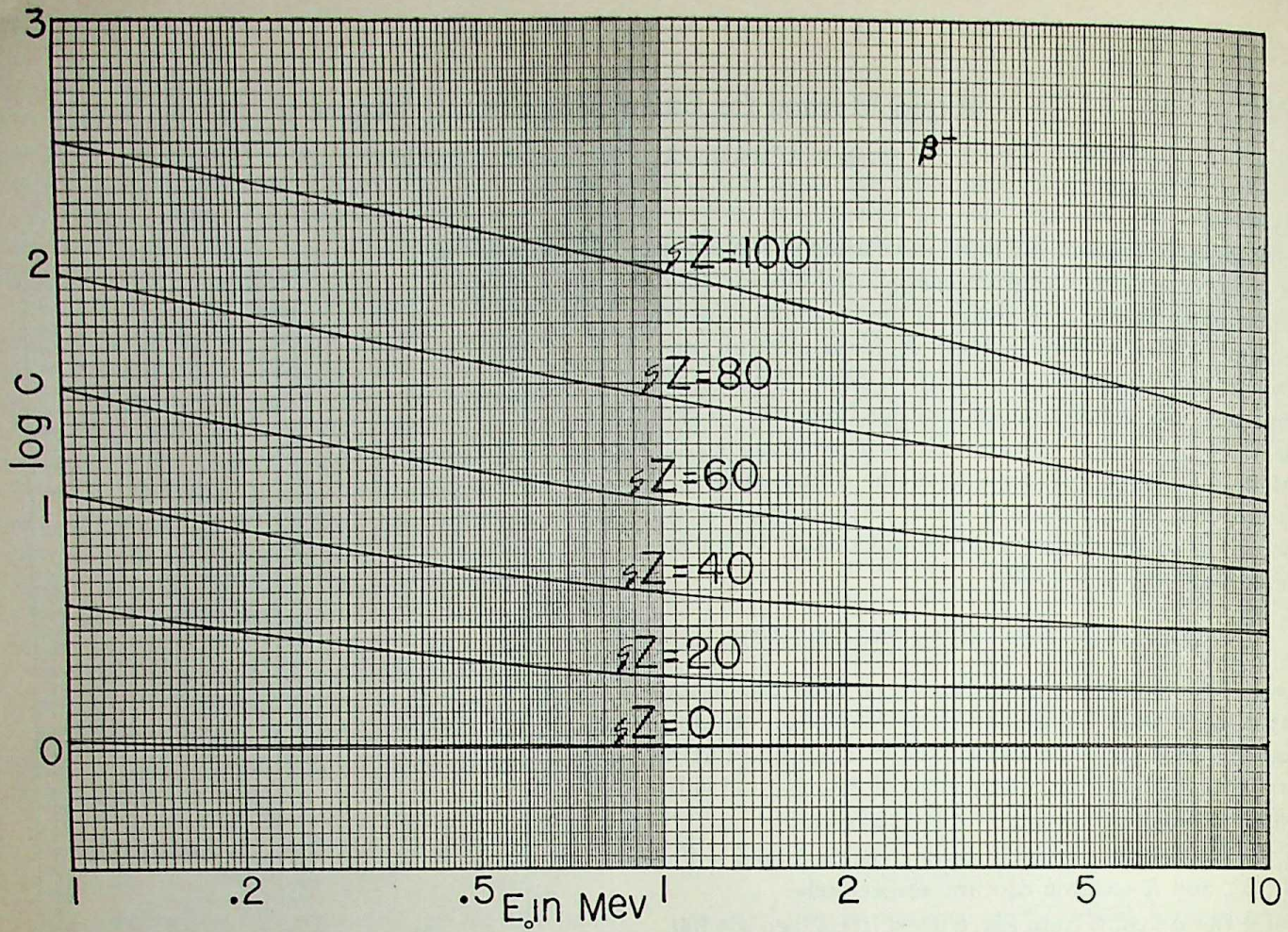
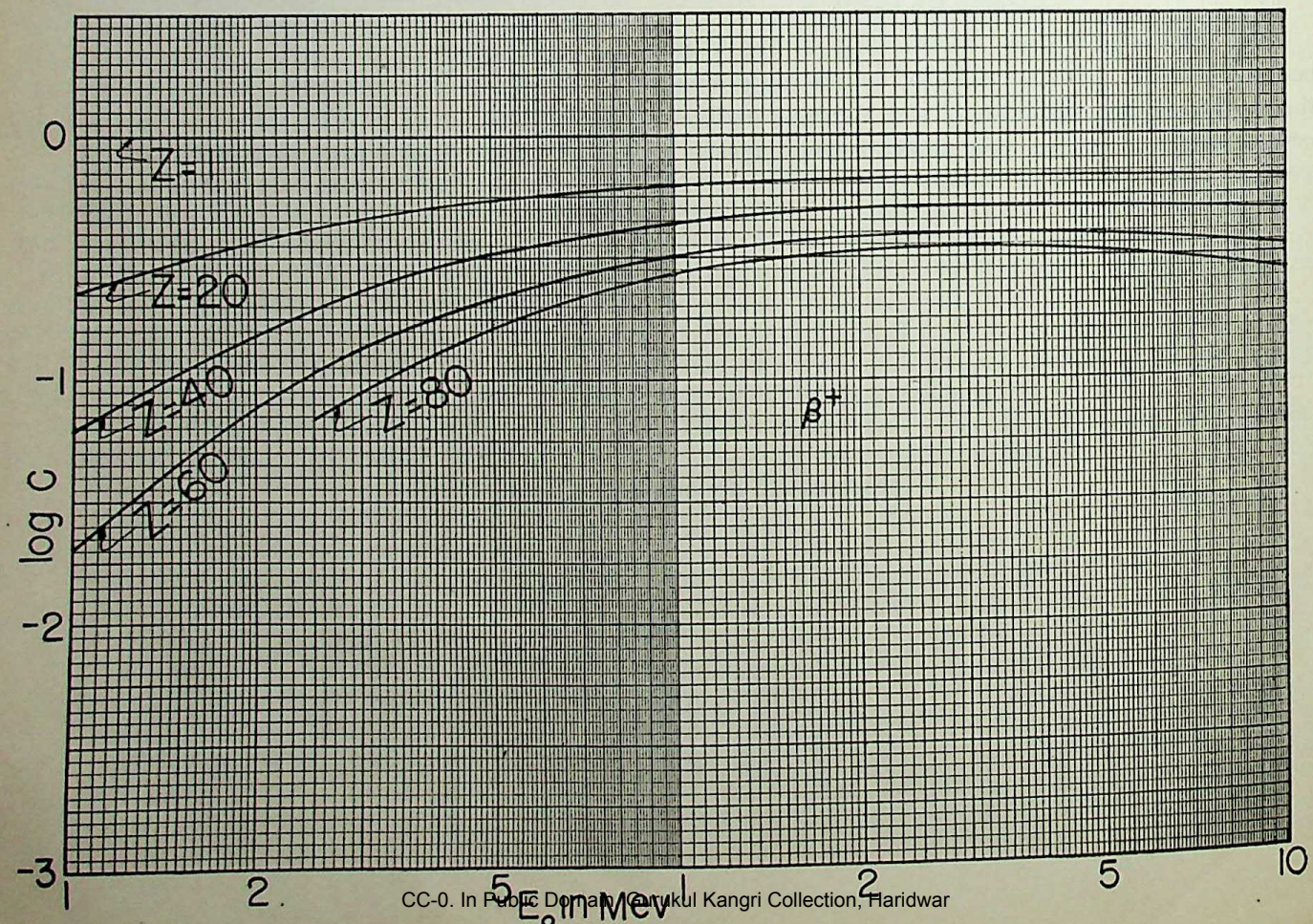


FIG. 2. Log(C) as a function of E_0 and Z for β^- emission.



CC-0. In Public Domain. Panmukul Kangri Collection, Haridwar

Digitized by Arya Samaj Foundation Chennai and eGangotri

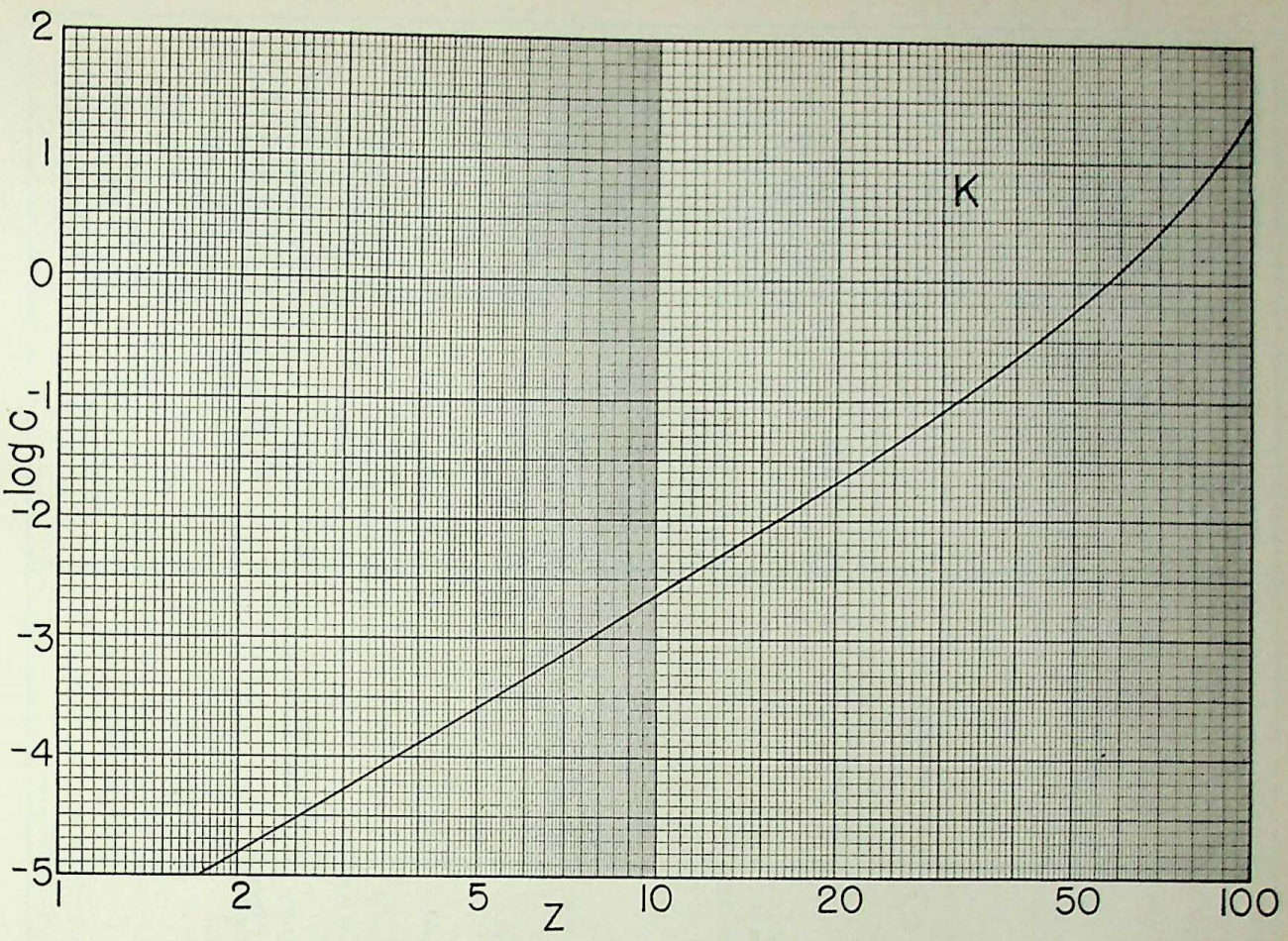


FIG. 4. Log(C) as a function of Z for K-electron capture.

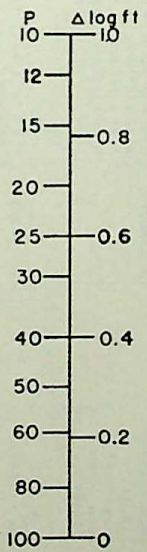
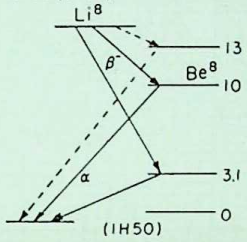


FIG. 5. $\Delta \log(ft)$ as a function of p.

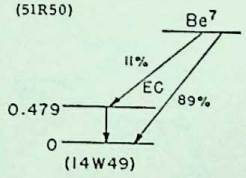
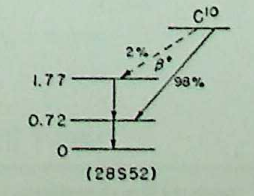
(Table of Isotopes begins on next page.)

CC-0. In Public Domain. Gurukul Kangri Collection, Haridwar

Isotope Z A	Class and identification	Percent abundance	Type of decay	Half-life	Energy of radiation in Mev: Particles	Energy of radiation in Mev: Gamma-transitions	Disintegration energy and scheme	Method of production and genetic relationships
$0n^1$	A recoil nuclei, conservation of momentum (18C32); observation of n-α reaction (4F32, 87H33)		β^- (18C35, 26S50)	12.8 m (2R51); 10-30 m (26S50)	0.78 p-β^- spect coinc (2R51)		Q_β^- 0.7823 (16L51) n^1, I = 1/2 (87M50)	Be-α-n (18C32); spall reactions in general; fission (92H39, 27A39, 118S39); parent H^1 (26S50, 2R50)
$1H^1$		99.9849 - 99.9861 (diff sources) (52K51); 99.9851 (1V38)					H^1, I = 1/2 (87M50)	
H^2		0.0139-0.0151 (diff sources) (52K51); 0.0149 (1V38)					H^2, I = 1 (87M50)	
H^3	A chem, sep isotopes, excit (6A39, 6A40a)		β^- (6A39, 6A40a)	12.46 y genet (12J50); 12.4 y sp act (11J51); 12.1 y genet (8N47)	0.01795 spect (10L52b); 0.0183 ion ch (21C49); 0.0194 spect (26H51); 0.0189 ion ch (24H49); 0.0186 (72S49a, calc from 12J49); 0.0180 abs bremsstrahlung Zr, Ta (17G49); others (22B49, 21C48, 35K51b, 5I51)	no γ (18G46)	Q_β^- 0.019 (HPS) H^3, I = 1/2 (87M50)	D-d-p (6A39, 6A40a); D-n-γ (3Z43); He^3-n-p (19C48, 28H48); Li-n-t (4O40); Be-d-t (4O40a, 6A40a); B-n-t, N-n-t (20C41); spall reactions (33B52)
$2He^3$		1.3×10^{-4} (atmos), 1.7×10^{-5} (wells) (7A46, 19C49)					He^3, I = 1/2 (87M50)	
He^4		~100					He^4, I = 0 (87M50)	
He^6	A chem (23B36, 23B36a), cross bomb, excit, chem (27S46)		β^- (23B36b)	0.823 s (9A50); 0.82 s (27H49); 0.84 s (12R49); 0.85 s (27S46)	3.50 spect (16W52); 3.2 abs (12R49); 3.5 abs (27S46); others (23B36b, 16K48, 2P50, 35A50)	no γ (16K48, 27S46)	Q_β^- 3.50 (16W52); Q_β^- 3.55 (36D52)	Be-n-α (23B36, 9P37, 27S46, 16K48, 2P50); Li-γ-p (25B47, 44S52a)
$3Li^6$		7.52 (17L38)					Li^6, I = 1 (87M50)	
Li^{7m}	A excit (4E49)		IT (4E49)	5.2×10^{-14} s Doppler broadening (4E49)		~0.48 spect (4E49)		B-n-α (4E49)
Li^7		92.48 (17L38)					Li^7, I = 3/2 (87M50)	
Li^8	A excit (22C35, 11L37); n-capt, sep isotopes, genet (28H47)		β^-, 2α (11L37)	0.825 s (11R51); 0.88 s (26B37, 3O47, 10B49); 0.85 s (44S52a); 0.89 s (28H47)	β^-: 13 (~90%), ~6 (~5%), ~3 (~5%) spect (1H50); <13 (~2%) β-γ coinc abs (5V51a); 12.0 cl ch (26B37); abs (3O47); two α's: total energy 3.2, 7-9 cl ch (27B48)	no γ (13R37, 26B37); γ (very weak) β-γ coinc (5V51a)	Q_β^- 15.99 (9V52) 	Li-n-γ (15K36, 10P46, 28H47); Li^7-n-γ (28H47); Li-d-p (22C35, 5D35, 1F37, 26B37, 11L37, 1H50, 1Y50); spall C, N, Ne, A, Kr, Xe (13W50); Be-γ-p (3O47, 44S52a, 40T52); B-n-α (18L39); B-γ-2p, B-γ-2pn (44S52a)
Li^9	B excit, cross bomb (20G51)		β^-, n (20G51, 78H52)	0.168 s (20G51); 0.170 s (78H52); 0.19 s (44S52a)				Be-d-2p (20G51); B-p-3p, B-d-3pn (20G51); B-γ-2p (44S52a); C-d-4pn, C-p-4p (20G51); C-p-4p (78H52)

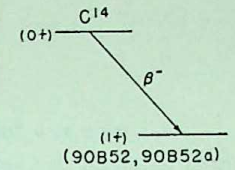
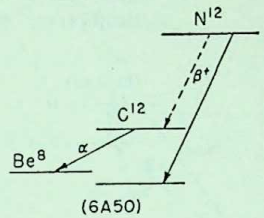
Digitized by Arya Samaj Foundation Chennai and eGangotri

CC-0. In Public Domain. Gurukul Kangri Collection, Haridwar

Isotope Z A	Class and identification	Percent abundance	Type of decay	Half-life	Energy of radiation in Mev: Particles	Energy of radiation in Mev: Gamma-transitions	Disintegration energy and scheme	Method of production and genetic relationships
$_4Be^7$	A chem, cross bomb, excit (13R38)		EC (13R38)	52.93 d (24S49); 53.61 d (58K52); 54.3 d (55B47); 54.5 d (29B49)		0.479 spect (4E48, 11T49); 0.478 spect (1H49); 0.485 spect (17K48); coinc abs (4Z42); 0.474 spect (5Z48a); γ (11%) (14W49), (10-13%) (10T49) (Be^7 formation yield - γ ratio); others (15R46, 7S47b)	Q_{EC} 0.864 p-n-threshold (51R50) 	Li-d-n (13R38, 14R38, 14R38a, 4Z42); Li-p-n (39H39, 39H40); B-p-α (14R38a, 17M39); B-d-αn (12M46); spall C (4D50, 74M51), Al, Cu, Ag, Au (74M51)
Be^8	A observation of Be-γ-n reaction (18C35)		2α	<2 x 10^{-14} s photo-dis O^{16} emuls (26W51); <5 x 10^{-14} s photo-dis O^{16} emuls (18M52); 10^{-15} - 10^{-17} s calc (15W41)	energy of each α in center of mass system: 0.039 spect (41C51); 0.045 spect (12T49); 0.051 ion ch (40H49); 0.043 range emuls (23C50)		$Q_α$ 0.078 (41C51); $Q_α$ 0.089 (12T49); $Q_α$ 0.103 (40H49); $Q_α$ 0.085 (23C50)	Be-p-d (12T49); Be-γ-n (18C35, 40H49); O-γ-2α (18M51, 53L52)
Be^9		100 (6N37)					Be^9, I = 3/2 (100S51, 77H51)	
Be^{10}	A chem (12M46a); chem, mass spect (11P46)		$β^-$ (12M46a)	2.5 x 10^6 y sp act + mass spect (12M47); 2.9 x 10^6 y yield (28H47a)	0.555 spect (15F52); 0.560 spect (13A50); abs (12M46a, 12M47); 0.553 ion ch (11F49a); others (28H49, 16W49, 41H49, 11B50a)	no γ (12M47, 19L47, 28H49)	$Q_β^-$ 0.56 (HPS)	Be-d-p (12M46a, 19L47); Be-n-γ (28H47a, 13A50, 11B50a); B-n-p (9E48); C-n-α (28H46)
$_5B^8$	A excit, cross bomb (6A50)		$β^+$, 2α (6A50)	0.46 s (102B52a); 0.61 s (44S52a)	$β^+$: 13.7 abs (6A50); spect (44S52a)		$Q_β^+$ 18 (calc from 6A50)	B-γ-2n, B-γ-3n (44S52a); B-p-t (6A50); Be-p-2n (6A50); C-p-nα (6A50); C-γ-p3n (44S52a); spall reactions (33B52)
B^{10}		18.45 - 18.98 (13T48)					B^{10}, I = 3 (87M50)	
B^{11}		81.02 - 81.55 (13T48)					B^{11}, I = 3/2 (87M50)	
B^{12}	A excit (22C35a, 1F36)		$β^-$ (22C35a)	0.027 s delay coinc (3J48a, 30B51); 0.022 s delay coinc (25B39)	13.43 spect (1H50); 13.3 abs (30H48); 12 cl ch (26B37); ~9 (~4%) coinc abs (5V51a)	~4.5 β-γ coinc abs (5V51)		B-d-p (22C35a, 1F36, 30B51); C^{14}-d-α (32H50b); N^{15}-n-α (3J48a)
$_6C^{10}$	A chem, sep isotopes (28S48, 28S49)		$β^+$ (28S49)	19.1 s (28S49)	2.2 abs (28S49)	0.72 (~100%), 1.05 (~2%) scint spect (28S52)		B-p-n, B^{10}-p-n (28S48, 28S49, 28S52); C-γ-2n (44S52a)

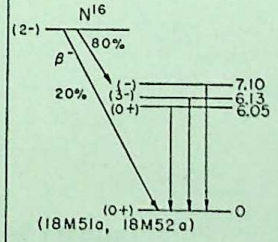
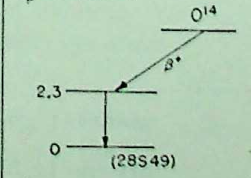
CC-0. In Public Domain. Gurukul Kangri Collection, Haridwar

Digitized by Arya Samaj Foundation Chennai and eGangotri

Isotope Z A	Class and identification	Percent abundance	Type of decay	Half-life	Energy of radiation in Mev: Particles	Energy of radiation in Mev: Gamma-transitions	Disintegration energy and scheme	Method of production and genetic relationships
$_6C^{11}$	A excit (22C34, 35H34); chem, excit (33B39)		β^+ (22C34)	20.4 m (30S41); 20.5 m (29S41, 12P48, 25C50); 20.0 m (7S44a, 4D51)	0.99 spect (7S44a); 0.981 spect (14T41); 0.95 cl ch (5D40)	no γ, β-γ coinc (7S46a)	Q^+_β 2.0 (HPS)	Be-α-2n (12M46b); Be-He^3-n (1P52); B-d-n (26C35, 2Y35, 1F36); B-p-γ (22C34a, 33B39); B-p-n (33B39); C-γ-n (10B46, 12P48, 25C50, 55S51, 22E52, 44S52a); C-n-2n (1P37, 110S51, 30B52); C-d-dn (6T47); C-p-pn (27C47, 82H52); C-He^3-α (1P52); C-α-an (12M46b, 6T47); N-p-α (33B39); N-n-p3n (16K47); N-γ-p2n (10B46); N-π^--3n (21T51a); O-γ-an (10B46, 85H52); O-n-α2n (12M47a); O-π^--p4n (21T51a); spall Cu (57G51)
C^{12}		98.892 (limestone CO_2)(6N50)					C^{12}, I = 0 (87M50)	
C^{13}		1.108 (limestone CO_2)(6N50)					C^{13}, I = 1/2 (87M50)	
C^{14}	A chem, cross bomb, excit (16R41)		β^- (1K40)	5568 y weighted average of 3E50, 11J49, 21M50, and 20M51, all by sp act + mass spect (3L51); others (31H49, 17R46, 31H48, 10N48, 1Y48, 17W48)	0.155 spect (15F49, 18W50); 0.156 spect (28C48); 0.154 spect (2L47a), abs (29S47); 0.155 ion ch (10A49); no conv, spect (2L47a); E (average) 0.045 calorimetric (12J52)	no γ (16R41)	Q^-_β 0.155 (HPS); C^{14}, I = 0 (87M50)  (90B52, 90B52a)	C-d-p (16R40, 16R41); C-n-γ (20L45); N-n-p (16R41, 20L45); O-n-α (19M47)
C^{15}	C excit, sep isotopes (32H50)		β^- (32H50)	2.4 s (32H50a)	8.8 abs (32H50a)	5.5 β-γ coinc abs (32H52)		C^{14}-d-p (32H50, 32H50a, 32H52); not found by: C^{14}-n-γ (1Y50)
$_7N^{12}$	A excit, sep isotopes (6A49)		β^+, $\beta^+3\alpha$ (6A50)	0.0125 s delay coinc (6A49)	β^+: 16.6 abs (6A49); α: ~4 total energy of three α's (6A50)		 (6A50)	C-p-n, C^{12}-p-n (6A49, 6A50); N-γ-2n (33P52)

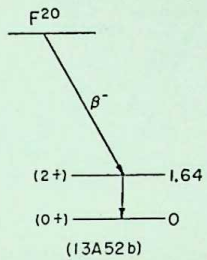
CC-0. In Public Domain. Gurukul Kangri Collection, Haridwar

Digitized by Arya Samaj Foundation Chennai and eGangotri

Isotope Z A	Class and identification	Percent abundance	Type of decay	Half-life	Energy of radiation in Mev: Particles	Energy of radiation in Mev: Gamma-transitions	Disintegration energy and scheme	Method of production and genetic relationships
$_7N^{13}$	A excit (4C34, 22C34)		β^+ (22C34)	9.93 m (5W39a); 10.1 m (7S45); 10.2 m (28C48a)	1.24 spect (7S45); 1.25 spect (28C48a); 1.20 spect (1H48); 1.22 spect (14T41); others (21L39, 53K43)	no γ >0.135, <0.700 (10L47, 7S46a)	Q^+_β 2.26 (HPS)	B-a-n (4C34, 8E35, 18R37); C-d-n (22C34, 33H35, 2Y35, 26C35, 1F36); C-p-γ (33H35, 26C35); C^{13}-p-n (11A50); N-n-2n (1P37, 34H43); N-d-t (34B42); N-γ-n (10B46, 12P48, 22E52, 44S52a); O-n-p3n (16K47); O-γ-p2n (85H52); spall Al (74M52)
N^{14}		99.635 (6N50)					N^{14}, I = 1 (87M50)	
N^{15}		0.365 (6N50)					N^{15}, I = 1/2 (87M50)	
N^{16}	A excit (22L34, 16F34)		β^- (22L34, 16F34)	7.35 s (35B47); 7.5 s (28H46a); 7.3 s (27S46)	~10.3 (~20%), ~4.3 (~40%), ~3.8 (~40%) cl ch (35B47); 10, 3.5 abs (27S46); 10 cl ch (28H46a)	γ_1 6.13, γ_2 7.10 (γ_2/γ_1 0.08) pair spect (18M51a); 6.2, 6.7 abs sec, cl ch pair (35B46)	Q^-_β 10.3 (35B47)  (18M51a, 18M52a)	N-n-γ (28H46a, 41F52); N-d-p (1F36); O-n-p (7C37, 26S43, 35B47, 18M51a); F-n-a (22L34, 16F34, 3N36, 2N36, 9P37)
N^{17}	A chem, cross bomb (6A49a, 18K48, 27C48)		β^-, n (18K48)	4.14 s (18K48); 4.15 s (32S51)	β^-: 3.7 β-recoil coinc abs (6A49a); n: 0.9 (mean) O^{16} recoil in ion ch (6A49a); 1.0 (mean) p recoil in cl ch (36H49)		Q^-_β 8.7 (6A49a)	spall O, F, Na, Mg, Al, Si, P, S, Cl, K (27C48, 18K48); C^{14}-a-p (31S51); O-n-p (83C49); O^{18}-γ-p (32S51); F-γ-2p (44S52a)
$_8O^{14}$	B chem, excit (28S49)		β^+ (28S49)	76.5 s (28S49)	1.8 abs (28S49)	2.3 coinc abs sec (28S49)	Q^-_β 5.1 (28S49) 	N-p-n (28S49); O-γ-2n (44S52a)
O^{15}	A chem, excit (22L34a, 12M35); excit (1F36, 19K39)		β^+ (22L34a)	118.0 s (2P49); 126 s (12M35, 37B39); 127 s (35D51)	1.683 spect (36B50); 1.68 abs (28S49)	no γ (2P50b)	Q^+_β 2.70 (HPS)	C-a-n (19K39); N-d-n (22L34a, 12M35, 1F36, 36B50); N-p-γ (2D38, 35D51); O-γ-n (37B39, 34H43, 10B46, 12P48, 22E52, 44S52a); O-n-2n (1P37); O-He^3-a (1P52)

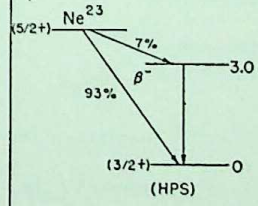
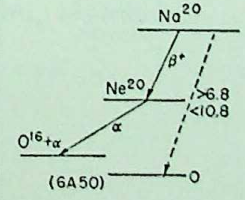
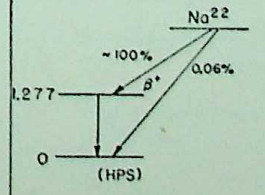
CC-0. In Public Domain. Gurukul Kangri Collection, Haridwar

Digitized by Arya Samaj Foundation Chennai and eGangotri

Isotope Z A	Class and identification	Percent abundance	Type of decay	Half-life	Energy of radiation in Mev: Particles	Energy of radiation in Mev: Gamma-transitions	Disintegration energy and scheme	Method of production and genetic relationships
$_8O^{16}$		99.759 (air O_2) (6N50); O^{16}/O^{18} variation $\lesssim$ ~4% (13T49, 1K46)					O^{16}, I = 0 (87M50)	
O^{17}		0.037 (air O_2) (6N50)					O^{17}, I = 5/2 (3A51)	
O^{18}		0.204 (air O_2) (6N50)					O^{18}, I = 0 (91M51)	
O^{19}	A excit (3N36); n-capt (22M43)		β^- (22M43)	29.4 s (11F44a); 29.5 s (28H46a); 27.0 s (35B47a)	4.5 (30%), 2.9 (70%) abs (35B47a); 4.1 abs (11F44a); ~3.2 abs (34H45)	1.6 abs (11F44a)		O-n-γ (22M43, 2S46, 2S47); F-n-p (12A35, 3N36)
$_9F^{17}$	A cross bomb (19W34, 8E34a); chem, excit (12N35, 37H35, 2D38)		β^+ (12N35)	70 s (12N35, 2P50c); 60 s (86H52); 66 s (46L51); 72 s (12P48); 74 s (2D38)	1.72 spect (2P50c); 1.7 abs (46L51); 2.1 cl ch (17K36)	no γ (2P51, 51R51)	Q^+_β 2.74 (HPS)	N-α-n (19W34, 8E34a, 18R37); O-d-n (12N35, 1F36, 2P50c); O-p-γ (2D38); F-γ-2n (10B46, 12P48, 86H52)
F^{18}	A chem (26S37); chem, sep isotopes, excit (2D38)		β^+ (26S37)	112 m (26S37, 12P48, 47B49); 115 m (34H43); 107 m (2D38)	0.649 spect (19R51); 0.635 spect (47B49); others (3Y38, 9K41, 20K45, 38H48)	no γ (16K48, 47B49)	Q^+_β 1.67 (19R51)	O-α-pn (2T47a); O^{18}-p-n (2D38); O-d-n (3Y38, 3D40, 20W41); O-He^3-p (1P52); O-t-n (20K45); F-n-2n (1P37); F-d-t (9K41, 34B42); F-γ-n (34H43, 10B46, 12P48, 22E52, 86H52); F-p-pn (19R51); Ne-d-α (26S37); Na-γ-αn (10B46, 85H52); spall Al (74M52, 74M52a), Cu (57G51, 74M52a), Cl, Ag, Au (74M52a)
F^{19}		100 (1A20)					F^{19}, I = 1/2 (87M50)	
F^{20}	A excit (22C35, 1F36, 3N36)		β^- (22C35)	10.7 s (33S50); 12 s (22C35)	5.41, no ~7 β^- (lim 1%) spect (13A52b); 5.33 (97%), 6.7 (3%) spect (47L50); 5.0 spect, abs (3J50); others (38B40)	1.631, no 2.5 γ (lim 0.2%) spect, Be-γ-n reaction (13A52b); 1.64, no 2.5 γ spect, γ-γ coinc (47L50); 1.64, 2.5 (weak) spect, abs sec (3J50); 2.2 cl ch recoil (38B40); γ (coinc with 5.0 β^-) β-γ coinc (21C40, 3J50).	Q^-_β 7.04 (13A52b)  (13A52b)	F-d-p (22C35, 1F36, 33S50, 3J50, 13N50, 13A52c); F-n-γ (3N36, 2S47, 21K50); Na-n-α (3N36)

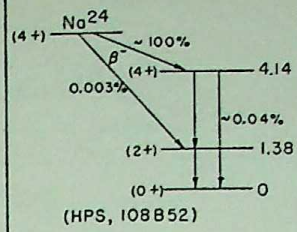
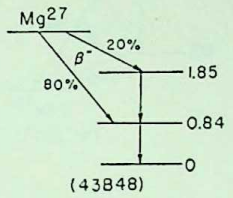
CC-0. In Public Domain. Gurukul Kangri Collection, Haridwar

Digitized by Arya Samaj Foundation Chennai and eGangotri

Isotope Z A	Class and identification	Percent abundance	Type of decay	Half-life	Energy of radiation in Mev: Particles	Energy of radiation in Mev: Gamma-transitions	Disintegration energy and scheme	Method of production and genetic relationships
$_{10}Ne^{19}$	A cross bomb, excit (21W39)		β^+ (21W39)	18.2 s (28S49); 18.5 s (34S52); 20.3 s (21W39)	2.18 spect (34S52); 2.2 cl ch (21W39); 2.3 abs (28S49)	no γ (21W39, 34S52)	Q^+_β 3.20 (HPS)	F-p-n (21W39, 47B51a, 34S52)
Ne^{20}		90.92 (6N50a)					Ne^{20}, I = 0 (87M50)	
Ne^{21}		0.257 (6N50a)					Ne^{21}, I = 3/2 (87M50)	
Ne^{22}		8.82 (6N50a)					Ne^{22}, I = 0 (87M50)	
Ne^{23}	A excit (12A35); chem (23B37, 9P37)		β^- (14P40)	40.2 s (36B50a); 40.7 s (34H44a); 40 s (12A35, 23B37)	4.21 (~93%), 1.18 (~7%) spect (36B50a); 4.3 abs (35B46a, calc from 14P40); 4.1 abs (14P40)	~3 abs (2P50a)	Q^-_β 4.21 (2P50a) 	Ne-n-γ (41F52); Ne-d-p (22W40); Ne^{22}-d-p (14P40, 36B50a, 2P50a); Na-n-p (12A35, 3N36, 9P37, 23B37); Mg-n-α (12A35)
$_{11}Na^{20}$	A excit (6A50)		β^+, α (6A50, 44S51a)	0.385 s (102B52a); 0.23 s (44S51a)	$3.5 < \beta^+ < 7.3$ est (44S51a)			Ne-p-n (6A50); Na-γ-3n (44S51a, 44S52a)
Na^{21}	A excit (29C40a)		β^+ (14P40)	22.8 s (34S52); 23 s (29C40a)	2.50 spect (34S52); 2.53 spect (52B51b)	no γ (34S52)		Ne^{20}-p-γ (40B47); Ne-p-n (29C40a); Ne-d-n (14P40); Mg-p-a (34S52); Mg^{24}-p-a (39B48)
Na^{22}	A chem, excit (17F35)		β^+ ~100%, no EC (21G46)	2.60 y (23L49); 2.8 y (36S39)	0.542 spect (23M50); 0.575 spect (21G46); ~1.8 (0.06%) spect (56W52); ~1.8 (0.004%) cl ch (25M49); others (23L37, 2O39)	1.277 spect (13A49); 1.30 (coinc with β^+) spect, β-γ coinc (21G46); 1.3 spect (2O39) others (85S51)	Q^+_β 2.84 (HPS) Na^{22}, I = 3 (87M50) 	F-a-n (17F35, 23L37, 24M37); Ne-d-n (23L37); Ne^{21}-p-γ (40B47); Na-n-2n (41B46, 35S47); Mg-d-a (23L37, 13A49); spall Mg, Mg^{25}, Mg^{26} (92M51), Fe (45R52), Cu (42B51a)
Na^{23}		100 (37S36a)					Na^{23}, I = 3/2 (87M50)	

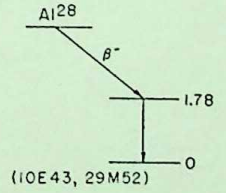
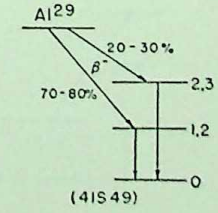
CC-0. In Public Domain. Gurukul Kangri Collection, Haridwar

Digitized by Arya Samaj Foundation Chennai and eGangotri

Isotope Z A	Class and identification *	Percent abundance	Type of decay	Half-life	Energy of radiation in Mev: Particles	Energy of radiation in Mev: Gamma-transitions	Disintegration energy and scheme	Method of production and genetic relationships
$_{11}Na^{24}$	A chem, excit (16F34, 1L35)		β^- (1L35)	15.06 h (39S51); 15.04 h (29S50); 15.10 h (31C50); 15.0 h (38S51, 23W49)	1.390 spect, coinc (7S46b, 7S47); 1.4 spect (24L39); 4.17 (0.003%), no 5.5 β^-, spect (15T51); lim 4.15 β^-, 0.01% spect (22G50); others (42H48)	γ_1 1.3679, γ_2 2.7535 spect (12H52); γ_1 1.380, γ_2 2.758 spect (7S46b); 1.380, 2.765 spect (20R49); γ_2 (e/γ 3 x 10^{-6}) (7S50b); 2.748 spect (21K50a); 2.755 spect (6W50); γ_1 (coinc with γ_2) spect, β-γ, γ-γ coinc (4E43); γ-γ coinc abs (28C46); 3.7 (0.04%) D-γ-p ion ch (101B51); ~4 (0.05%) spect (15T51); others (9B50, 4I41, 26M43, 41M50, 85B50a, 85S51, 55C50, 108B52)	Q^-_β 5.53 (HPS) Na^{24}, I = 4 (101S51)  (HPS, 108B52)	Na-d-p (1L35, 2V36a); Na-n-γ (12A35, 2S47); Mg-d-α (35H35); Mg-n-p (12A35); Mg-γ-p (10B46, 42H47, 22E52); Al-n-α (12A35, 74M52); Al-d-pα (30C46, 30C47); Al-γ-n2p (10B46, 22E52, 42S52); Al-p-3pn (82H52); Si-γ-n3p (?) (10B46); spall Al (39F52), Fe (45R52), Cu (42B51a, 57G51), Sn (42B51); spall-fission Cu (42B51), U (6F51)
Na^{25}	B excit (34H43a)		β^- (34H43a)	58 s (35B47a); 62 s (12P48, 10B46, 34H43a); 60 s (21R44)	3.7 (~55%), 2.7 (~45%) abs (35B47a); 3.4 abs (34H44a); 3.3 abs (21R44)	>0.5 (weak) abs (35B47a)	Q^-_β 3.7 (35B47a)	Mg-γ-p (34H44a, 10B46, 22E52); Mg-n-p (34H44a, 35B47a); Al-γ-2p (10B46, 12P48, 22E52, 42S52)
$_{12}Mg^{23}$	A excit, cross bomb (21W39)		β^+ (21W39)	11.9 s (34H43); 12.3 s (52B51a); 11.6 s (21W39)	2.99 scint spect (52B51a); 2.8 cl ch (21W39)	no γ (21W39)		Na-p-n (21W39, 2D40); Mg-γ-n (34H42, 34H43, 10B46, 25B47, 27M49, 22E52)
Mg^{24}		78.60 (24W48)					Mg^{24}, I = 0 (87M50)	
Mg^{25}		10.11 (24W48)					Mg^{25}, I = 5/2 (87M50, 3A51a)	
Mg^{26}		11.29 (24W48)					Mg^{26}, I = 0 (87M50)	
Mg^{27}	A chem, excit (12A35, 35H35)		β^- (35H35)	9.45 m (3S52); 9.6 m (10E43); 10.0 m (32C39); 10.2 m (35H35)	1.80 (80%), 0.9 (20%) spect (43B48); 1.8 cl ch (10E43, 32C39); 1.7 abs (28M40); ~1.8 (coinc with γ) β-γ coinc (35B47a)	γ_1 1.01, γ_2 0.84 (γ_1 coinc with γ_2) spect, γ-γ coinc (43B48); 1.02, 0.84, 0.64 spect (4I41); 1.05 cl ch recoil (10E43)	Q^-_β 2.64 (43B48)  (43B48)	Mg-d-p (35H35); Mg-n-γ (12A35, 2S47); Al-n-p (12A35, 16F34, 74M52)
Mg^{28}	A chem, genet (37L53, 44S53)		β^- (37L53, 44S53)	21.2 h (37L53); 21.3 h (44S53)	0.3-0.4 abs (37L53)	<0.1 abs (37L53)		Si-γ-2p, Mg-α-2p (44S53); spall Cl (37L53); parent Al^{28} (37L53, 44S53)
$_{13}Al^{24}$	A excit, decay charac (102B52)		β^+ or EC, α (p?) (102B52a)	2.3 s (102B52)				Mg-p-n (102B52)
Al^{25}	B excit, sep isotopes (39B48)		β^+ (39B48)	7.3 s (39B48)				Mg^{25}-p-n (39B48)

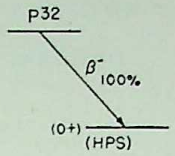
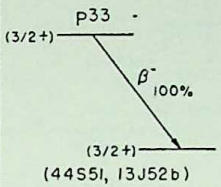
CC-0. In Public Domain. Gurukul Kangri Collection, Haridwar

Digitized by Arya Samaj Foundation Chennai and eGangotri

Isotope Z A	Class and identification	Percent abundance	Type of decay	Half-life	Energy of radiation in Mev: Particles	Energy of radiation in Mev: Gamma-transitions	Disintegration energy and scheme	Method of production and genetic relationships
$_{13}Al^{26}$	A excit (17F34); cross bomb (34H43, 39B48)		β^+ (17F34)	6.5 s (30K51); 6.3 s (39B48); 7.0 s (21W39, 14A48, 12P48); 7.2 s (25W48)	2.8 abs (14A48); 3.0 cl ch (21W39); 3.4 abs (35B46a, calc from 17F34)			Na-α-n (17F34, 24M37); Mg-p-n (21W39); Mg^{26}-p-n (39B48); Mg-p-γ (21C39, 16T46); Al-γ-n (34H41, 34H42, 34H43, 10B46, 25B47, 12P48, 22E52)
Al^{27}		100 (1B50)					Al^{27}, I = 5/2 (87M50)	
Al^{28}	A chem, excit (4C34a, 4C34b, 16F34); chem, cross bomb (12A35)		β^- (12M35a)	2.27 m (106B52b); 2.07 m (40S48); 2.30 m (10E43)	2.865 spect (29M52); 2.75 (coinc with γ) coinc abs (35B47a); 3.01 spect (43B48); no 4.6 β^- (29M52)	1.782 spect (29M52); 1.80 spect (43B48); 1.80 abs sec (35B47a); 1.82 spect (4I41)	Q^-_β 4.65 (29M52)  (10E43, 29M52)	Mg-α-p (8E36, 18R37); Al-d-p (12M35a, 29M52); Al-n-γ (12A35, 2S47, 9O49, 50H51, 29M52); Si-n-p (12A35, 35B47a); Si-γ-p (10B46, 42H47); P-n-α (12A35); daughter Mg^{28} (37L53)
Al^{29}	A excit, cross bomb (32B39)		β^- (32B39)	6.56 m (41S49); 6.7 m (32B39)	2.5 (~70%), 1.4 (~30%) (both coinc with γ) β-γ coinc abs (41S49); ~2.5 cl ch, abs (32B39)	1.2 (~80%) (coinc with 2.5 β^-), 2.3 (~20%) coinc abs sec (41S49)	Q^-_β 3.8 (41S49)  (41S49)	Mg-α-p (8E36, 32B39, 14H39, 41S49); Al-α-2p (I12S51); Si-n-p (21F43); Si-γ-p (10B46, 42H47, 12P48); P-γ-2p (10B46, 12P48)
$_{14}Si^{27}$	A excit (22K39)		β^+ (30M40)	4.9 s (12E41, 29C40a); 4.5 s (25W48); 5.4 s (52B51a)	3.48 scint spect (52B51a); 3.5 cl ch (33B40); 3.7 cl ch (30M40)			Mg-α-n (12E41); Al-p-n (22K39, 30M40, 29C40a, 33B40, 76C51); Si-γ-n (34H44, 25B47, 25W48)
Si^{28}		92.27 (1B50)					Si^{28}, I = 0 (87M50)	
Si^{29}		4.68 (1B50)					Si^{29}, I = 1/2 (87M50)	
Si^{30}		3.05 (1B50)					Si^{30}, I = 0 (87M50)	
Si^{31}	A n-capt (12A35); chem, excit (12N35a)		β^- (12N35a)	2.62 h (33C38, 55W51); 2.65 h (29M52a); 2.6 h (48L50); 2.8 h (12N37, 15A40) 2.7 h (15P49)	1.471 spect (29M52a); 1.486 spect (47W52); 1.48 abs (55W51)	0.17, 0.52, ~1 (weak) (?) abs (80C52); no γ (12N37)	Q^-_β 1.47 (29M52a)	Si-d-p (12N35a, 12N37, 17K36); Si-n-γ (12A35, 2S47); Si-He^3-2p (1P52); P-n-p (12A35, 1P37); S-n-α (42S36, 33C38); spall Fe (45R52)
Si^{32}	B chem, genet (37L53)		β^- (37L53)	~100 y yield (37L53)	Soft β^- (37L53)			spall Cl, parent P^{32} (37L53)

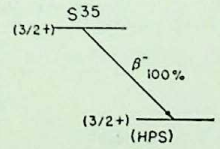
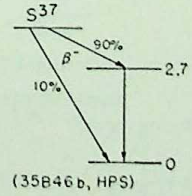
CC-0. In Public Domain. Gurukul Kangri Collection, Haridwar

Digitized by Arya Samaj Foundation Chennai and eGangotri

Isotope Z A	Class and identification	Percent abundance	Type of decay	Half-life	Energy of radiation in Mev: Particles	Energy of radiation in Mev: Gamma-transitions	Disintegration energy and scheme	Method of production and genetic relationships
$_{15}P^{29}$	B excit (21W41)		β^+ (21W41)	4.57 s (30R52); 4.6 s (21W41)	3.6 cl ch (21W41)	1.28 (2.5%), 2.42 (0.5%), scint spect, γ-γ coinc (30R52)		Si-p-n (21W41); Si-d-n (14D48); P-γ-2n (?) (10B46)
P^{30}	A excit (4C34, 17F34)		β^+ (4C34)	2.55 m (18R37); 2.18 m(33C38)	3.5 spect (24M41); 3.4 abs (35B46a, calc from 17F34); 3.0 cl ch (33B40)			Al-α-n (17F34, 4C34, 18R37); Si-p-n (33B39, 33B40); Si-He^3-p (6A39, 1P52); P-n-2n (1P37); P-γ-n (37B39, 10B46, 12P48); S-d-α (42S36); Cl-γ-an (85H52)
P^{31}		100 (1A20)					P^{31}, I = 1/2 (87M50)	
P^{32}	A chem, n-capt (12A35)		β^- (21L37)	14.30 d (12C38, 45B50); 14.35 d (23K48); 14.07 d (31M40); 14.60 d (38S51)	1.701 spect (average of 44S51, 29M52a, 13J52b, 8H51b, 16A50, 18W50a, 10L49, 7S46b); E (average) 0.70 ion ch (77C52)	no γ (17K36, 7S46b)	Q^-_β 1.702 (HPS) 	Si-d-γ (11?S51); Si-α-p (18F35); Si-He^3-p (1P52); P-d-p (12N37); P-n-γ (2S47); S-n-p (12A35); S-d-α (42S36); Cl-n-α (12A35); Cl-γ-an, Cl-γ-t (85H52); Cl-d-pa (17T47); spall Fe (45R52), Cu (32M48, 42B51a)
P^{33}	A chem, cross bomb (44S51)		β^- (13J52b, 44S51)	25.4 d (58W52); 24.8 d (13J52b); 25 d (44S51)	0.27 spect (44S51); 0.26 spect (13J52b); 0.25 abs (58W52)	no γ (44S51, 58W52)	Q^-_β 0.27 (44S51) 	S-n-p (44S51, 13J52b, 58W52); S-γ-p (44S51, 13J52b); Cl-γ-α, Cl-γ-2p (44S51, 13J52b)
P^{34}	B excit (10C40a); chem, excit, cross bomb (35B46b)		β^- (6Z45)	12.4 s (35B46b); 12.7 s (10C40a)	5.1 (75%), 3.2 (25%) abs (35B46b)			S-n-p (10C40a, 6Z45, 35B46b); Cl-n-α (6Z45, 34H45, 35B46b)
$_{16}S^{31}$	A excit, cross bomb (21W41, 12E41)		β^+ (21W41)	3.18 s (12E41); 3.2 s (21W41, 52B51a); 2.6 s (27M49)	3.85 cl ch (21W41); 3.87 cl ch (12E41a); 4.1 scint spect (52B51a)			Si-α-n (19K40, 12E41, 12E41a); P-p-n (21W41); S-γ-n (34H41, 34H42, 34H43, 25B47, 27M49)
S^{32}		95.018 (meteoritic sulfur) (76M50a); terrestrial S^{32}/S^{34} variation $\leq$5% (41T50)					S^{32}, I = 0 (87M50)	

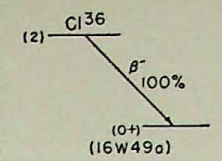
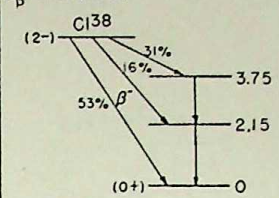
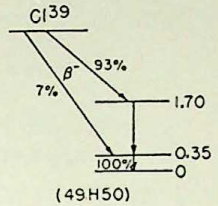
Digitized by Arya Samaj Foundation Chennai and eGangotri

CC-0. In Public Domain. Gurukul Kangri Collection, Haridwar

Isotope Z A	Class and identification	Percent abundance	Type of decay	Half-life	Energy of radiation in Mev: Particles	Energy of radiation in Mev: Gamma-transitions	Disintegration energy and scheme	Method of production and genetic relationships
$_{16}S^{33}$		0.750 (meteoritic sulfur) (76M50a)					S^{33}, I = 3/2 (87M50)	
S^{34}		4.215 (meteoritic sulfur) (76M50a)					S^{34} I = 0 (87M50)	
S^{35}	A chem, excit (17A36); chem, cross bomb, excit (1K41); sep isotopes (1K42)		β^- (3L39)	87.1 d (44H43) 88 d (26L40, 1K41)	0.1670 spect (10L50c); 0.167 spect (45H51), abs (29S47); 0.169 spect (46B48), abs (1Y48a); 0.168 spect (23G50); 0.166 spect (18A48); 0.168 ion ch (56C49)		Q^-_β 0.167 (HPS) S^{35}, I = 3/2 (87M50) 	S-n-γ (2S47); S-d-p (34C39, 1K41); Cl-n-p (17A36, 26L40, 1K41, 3M49); Cl^{35}-n-p (1K42); Cl-d-a (1K41); spall Fe (45R52)
S^{36}		0.017 (meteoritic sulfur) (76M50a)					S^{36}, I = 0 (87M50)	
S^{37}	B chem, excit cross bomb (6Z45, 35B46b)		β^- (6Z45)	5.04 m (35B46b); 5.0 m (28H46b)	4.3 (10%), 1.6 (90%) abs (6Z45, 35B46b); 1.4, ~4 abs (28H46b)	2.7 abs sec (35B46b); 2.75 abs sec (28H46b)	Q^-_β 4.3 (HPS)  (35B46b, HPS)	S-n-γ (28H46b); Cl-n-p (6Z45, 35B46b)
$_{17}Cl^{33}$	A excit (46H40); excit (21W41)		β^+ (21W41)	2.8 s (46H40, 45S48); 2.4 s (21W41); 1.8 s (52B51a)	4.13 cl ch (21W41); 4.4 scint spect (52B51a)			S-d-n (46H40, 45S48); S-p-n (21W41); Cl-γ-2n (52B51a)
Cl^{34}	A chem excit (17F34); chem, excit (42S36)		β^+ (17F34; 44B38)	33.2 m (25W48); 33.0 m (12P48); 33 m (42S36, 44B38)	4.5 (46%), 2.6 (28%), 1.3 (26%) spect (19R51); 5.1 (~80%), 2.4 (~20%) cl ch (38H46)	3.22, 2.10, 1.16 scint spect (18T51); 3.3, 2.1, 0.145 spect, spect conv (19R51); 3.4 cl ch recoil (38H46)	Q^+_β 5.6 (19R51)	Al-C^{12}-an (4M50); P-a-n (17F34, 18R37, 44B38); S-d-n (42S36, 38H46); S-a, pn (28S40); S-p-n (19R51); S-t-n (20K45); Cl-n-2n (1P37); Cl-p-pn (19R51); Cl-γ-n (37B39, 34H43, 12P48, 25W48, 22E52); spall Fe (45R52), Cu (42B51a)
Cl^{35}		75.4 (6N36)					Cl^{35}, I = 3/2 (87M50)	

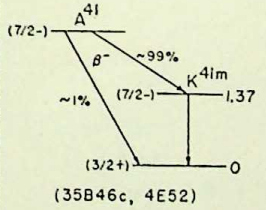
CC-0. In Public Domain. Gurukul Kangri Collection, Haridwar

Digitized by Arya Samaj Foundation Chennai and eGangotri

Isotope Z A	Class and identification	Percent abundance	Type of decay	Half-life	Energy of radiation in Mev: Particles	Energy of radiation in Mev: Gamma-transitions	Disintegration energy and scheme	Method of production and genetic relationships
$_{17}Cl^{36}$	A chem, n-capt (31G41)		β^- (31G41); no β^+ (lim 0.01%) (16W49a); (lim 0.03%) (14J49)	4.4×10^5 y sp act (16W49a); 3.6×10^5 y sp act (22R49); 2.0×10^5 y yield (22R49); 2×10^6 y yield (28H47b); $\sim 10^6$ y yield (10O47)	0.714 spect (15F52); 0.66 abs (10O47); 0.64 abs (31G41); others (16W49b, 16W51)	no γ (16W49a)	Q^-_β 0.714 (16W49b, 15F52) Cl^{36}, I = 2 (87M50, 27J51)  (16W49a)	Cl-n-γ (31G41, 10O47, 2S47); Cl-d-p (31G41)
Cl^{37}		24.6 (6N36)					Cl^{37}, I = 3/2 (87M50)	
Cl^{38}	A chem, n-capt (12A35); chem, sep isotopes (14K40)		β^- (17K36)	37.29 m (31C50); 37.5 m (47H37, 21C40a); 37.0 m (2V36a, 5S45); 38.5 m (15H46)	4.81 (53%), 2.77 (16%), 1.11 (31%) spect (10L50); 5.0, 2.8, 1.1 spect (27W39); spect, coinc abs (27W41); 5.2 (53%), 2.70 (11%), 1.19 (36%) spect (15H46)	γ_1 2.15, γ_2 1.60 (γ_1/γ_2 = 1.3) spect (15H46); γ_1 2.19, γ_2 1.64 (γ_1 coinc with γ_2) spect, coinc (4I41); 2.15, 1.65 spect (21C40a); no 3.75 γ (lim 0.03%) Be-γ-n reaction (33M49)	Q^-_β 4.81 (HPS)  (10L50, 15H46)	Cl-d-p (17K36, 2V36a); Cl-n-γ (12A35, 14K40, 19A41, 2S47); Cl^{37}-n-γ (14K40); K-n-α (47H37); spall Fe (45R52), Co (29W52), Cu (32M48, 42B51a); spall-fission Cu (42B51)
Cl^{39}	A chem (32M48a); chem, excit (49H49)		β^- (49H49)	55.5 m (49H49); ~1 h (32M48a, 48H49)	1.65 (93%), 2.96 (7%) abs (49H50)	1.35, 0.35 (coinc with 1.65 β^-) coinc abs sec (49H50)	Q^-_β 3.3 (49H50)  (49H50)	A-γ-p (49H49, 49H50); spall Fe (45R52), Co (29W52), Cu (32M48a, 42B51a), As (48H49)
$_{18}A^{35}$	A excit (21W41, 19K40)		β^+ (12E41a, 21W41)	1.88 s (12E41a); 1.84 s (45S48)	4.38 cl ch (21W41); 4.41 cl ch (12E41a)		Q^+_β 5.4 (HPS)	S-α-n (19K40, 45S48); Cl-p-n (21W41)
A^{36}		0.337 (6N50)					A^{36}, I = 0 (87M50)	
A^{37}	A chem, cross bomb (28W41)		EC (28W44, 46R52); EC (L/K 0.087) (17P49)	35.0 d (56M52); 34.1 d (28W44)		no γ, Cl K_α-x (28W44)	Q_{EC} ~0.8 continuous γ spectrum (38A52); Q_{EC} 0.816 p-n threshold (51R50)	S-α-n (28W41, 28W44); Cl-d-2n (28W41, 28W44); Cl-p-n (28W41, 28W44, 47B51a); K-d-α (28W41, 28W44); Ca-n-α (28W41, 28W44)
A^{38}		0.063 (6N50)						
A^{39}	B chem, excit (8Z52)		β^- (48B50)	~265 y sp act (8Z52)	0.565 spect (48B50)	no $\gamma > 0.3$ (lim 0.1%) (48B50)	Q^-_β 0.57 (HPS)	A-n-γ (32K52); K-n-p (48B50, 8Z52)

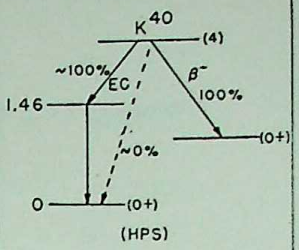
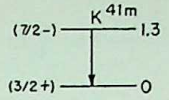
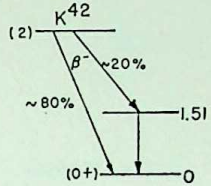
Digitized by Arya Samaj Foundation Chennai and eGangotri

CC-0. In Public Domain. Gurukul Kangri Collection, Haridwar

Isotope Z A	Class and identification	Percent abundance	Type of decay	Half-life	Energy of radiation in Mev: Particles	Energy of radiation in Mev: Gamma-transitions	Disintegration energy and scheme	Method of production and genetic relationships
$_{18}A^{40}$		99.600 (6N50)					A^{40}, I = 0 (87M50)	
A^{41}	A chem, excit (26S36)		β^- (26S36)	109 m (35B46c); 110 m (26S36)	1.245 (~100%) spect (36B50); 1.18 (99.3%), 2.5 (0.7%) abs, coinc abs (35B46c); others (26S36, 17K36)	1.37 cl ch recoil (23R36); 1.3 (coinc with 1.2 β^-) β-γ coinc, abs sec (35B46c); γ (e/γ ~0) spect conv (36B49)	Q^-_β 2.5 (35B46c)  (35B46c, 4E52)	A-d-p (26S36, 36B49, 36B50); A-n-γ (26S36); K-n-p (47H37, 35B46c); parent K^{41m} (4E52)
A^{42}	A chem, genet (32K52)		β^- (32K52)	$\geq$3.5 y (32K52)				A-n-γ (sec order reaction) (32K52); parent K^{42} (32K52)
$_{19}K^{37}$	C excit (27L48)		β^+ (52B51a)	1.3 s (27L48); 1.2 s (52B51a)	4.6 scint spect (52B51a)			K-γ-2n (27L48, 52B51a)
K^{38}	A chem, cross bomb (47H37, 14H37)		β^+ (47H37)	7.7 m (47H37, 18R37, 58G51); 7.5 m (24R47); 7.6 m (12P48)	2.8 spect (58G51); 2.5 abs (24R47); others (18R37)	2.16 scint spect (18T51); ~2.1 abs sec (24R47)	see Cl^{38}	Cl-a-n (47H37, 18R37, 14H37, 24R47); K-n-2n (1P37); K-p-pn (18T51, 58G51); K-γ-n (34H42, 34H43, 12P48, 22E52); Ca-d-a (47H37)
K^{39}		93.08 (6N50); K^{39}/K^{41} variations (81C43)					K^{39}, I = 3/2 (87M50)	

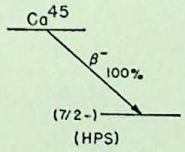
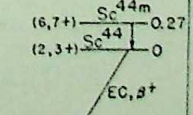
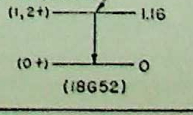
CC-0. In Public Domain. Gurukul Kangri Collection, Haridwar

Digitized by Arya Samaj Foundation Chennai and eGangotri

Isotope Z A	Class and identification	Percent abundance	Type of decay	Half-life	Energy of radiation in Mev: Particles	Energy of radiation in Mev: Gamma-transitions	Disintegration energy and scheme	Method of production and genetic relationships
$_{19}K^{40}$	A chem (1T05, 54C06); chem, mass spect (15S37)	0.0119 (6N50)	β^- 89%, EC 11% (3I50); β^- ~88%, EC (K) ~12% (46S50); β^- ~93%, EC (K) ~7% (36C50); assuming EC/γ = 1, β^- 90%, EC 10% (19F50, 76H50); β^- 91%, EC 9% (48S50); β^- 89%, EC 11% (27G51); β^- 94%, EC 6% (65M52); no β^+ (lim 0.06%) (37C51); no β^+ (lim 0.002%) (11B50b); $\beta^+ \leq 0.1\%$ (25G51b)	t_{β^-} sp act (uncorr. for EC): 1.32×10^9 y (47S49, 48S50); 1.26×10^9 y (17D51, 17D51a); 1.29×10^9 y (19F50); 1.49×10^9 y (27G50, 76H50, 25G51); 1.42×10^9 y (46S50); others (20A48, 20F49, 111S50); $t_{1/2}$ 1.2×10^9 y calc from average t_{β^-} and EC/β^- (HPS)	1.33 spect (15F52); 1.36 spect (13A50a); 1.36 scint spect (11B50c); 1.35 spect coinc (16D46); 1.41 abs (42H46, 42H48); 1.28 scint spect (25G51)	1.46 scint spect (11B50b, 25G51a); 1.48 scint spect (55H50); 1.47 scint spect (18P50); 1.54 (with EC) abs, coinc (42H46); 1.55 abs (26G47); γ (with EC) (34M47, 16P52); γ/β^- 0.12 sp act (average of 19F50, 47S49, 48S50, 25G51, 20F49, 27G48, 46S49, 76H50); EC/γ ~1 (35M51, 46S50, 16P52)	Q_{β^-} 1.33 (HPS) Q_{EC} 1.63 (26R50, HPS) K^{40}, I = 4 (87M50)  (HPS)	natural source (1T05, 54C06)
K^{41m}	A genet (4E52)		IT (4E52)	6.7×10^{-9} s delay coinc (4E52)		~1.3 scint spect (4E52)	 (4E52, 18G52)	daughter A^{41} (4E52)
K^{41}		6.91 (6N50)					K^{41}, I = 3/2 (87M50)	
K^{42}	A chem, n-capt (12A35); chem, cross bomb (71H35, 71H36)		β^- (17K36)	12.44 h (7S47c); 12.5 h (38S51, 35L52a); 12.4 h (47H37)	3.58 (75%), 2.04 (25%) spect (7S47c); 3.60, 1.9 spect (6P47); 3.5 (~70%) (not coinc with γ), ~1.8 (~30%) abs, coinc (35B47a)	1.51 spect (7S47c); 1.50 spect (6P47); 1.5 (17%) scint spect (35L52a)	Q_{β^-} 3.6 (HPS)  (HPS)	A-α-pn (11O49); K-d-p (47H37); K-n-γ (12A35, 47H37, 2S47); Ca-n-p (71H35, 47H37); Sc-n-α (71H36, 47H37, 35B47a); spall Co (29W52), Cu (57G51); daughter A^{42} (32K52)
K^{43}	B chem, excit (11O49)		β^- (11O49)	22.4 h (11O49)	0.81, 0.24 spect, abs (11O49)	~0.4 abs (11O49)		A-α-p (11O49)
K^{44}	E chem, excit (30W37)		β^- (30W37)	18 m (30W37)				Ca-n-p (30W37, 30W40)
$_{20}Ca^{39}$	B excit (34H43, 27M49)		β^+ (34H43)	1.06 s (34H43) 1.1 s (52B51a)	5.1 scint spect (52B51a)			Ca-γ-n (34H43, 25W48, 27M49)
Ca^{40}		96.97 (6N38a)					Ca^{40}, I = 0 (87M50)	

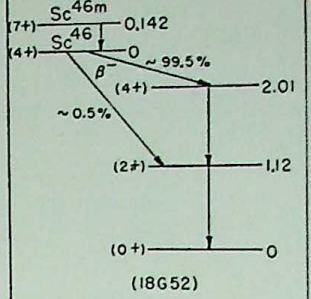
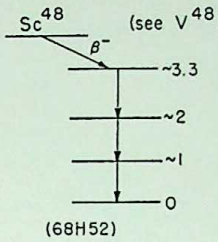
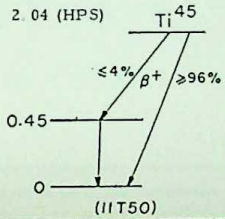
CC-0. In Public Domain. Gurukul Kangri Collection, Haridwar

Digitized by Arya Samaj Foundation Chennai and eGangotri

Isotope Z A	Class and identification	Percent abundance	Type of decay	Half-life	Energy of radiation in Mev: Particles	Energy of radiation in Mev: Gamma-transitions	Disintegration energy and scheme	Method of production and genetic relationships
$_{20}Ca^{41}$	B chem, n-capt sep isotopes (60B51)		EC (60B51)	1.1×10^5 y yield (60B52a)		K K_α-x (60B51)		Ca-n-γ (49S51, 60B51)
Ca^{42}		0.64 (6N38a)						
Ca^{43}		0.145 (6N38a)						
Ca^{44}		2.06 (6N38a)						
Ca^{45}	A chem, excit, cross bomb (30W40)		β^- (30W40)	152 d (36M47); 180 d (30W40)	0.254 spect (23M50a); 0.255 scint spect (24K50); 0.260 abs (29S48); 0.26 abs (50S50); E (average) 0.075 ion ch (77C52)	no γ (29S48, 37M49, 25K46); others (52M51)	Q^-_β 0.254 (HPS) 	Ca-d-p (30W40); Ca-n-γ (30W40, 2S47); Sc-n-p (30W40, 25K46); Sc-d-2p (51H48); Ti-n-α (38C48, 63H48); spall Fe (45R52), Cu (42B51a); spall-fission Bi (11G49)
Ca^{46}		0.0033 (6N38a)						
Ca^{47}	A (36M47); chem, genet (42B51a)		β^- (36M47)	4.8 d (42B51a); 5.8 d (36M47)	1.2 abs (42B51a); 1.1 abs (36M47)	1.3 abs (36M47)		Ca-d-p (36M47); spall Fe (45R52), Cu (42B51a); parent Sc^{47} (42B51a)
Ca^{48}		0.185 (6N38a)		$t_{\beta^-} > 2 \times 10^{16}$ y sp act (28J52)				
Ca^{49}	A chem, n-capt, sep isotopes (38M50)		β^- (38M50)	8.5 m (38M50)	~2.7 abs (38M50)	hard (38M50)		Ca^{48}-n-γ, Ca-n-γ (38M50)
$_{21}Sc^{41}$	A excit (12E41)		β^+ (12E41a)	0.873 s (98M52); 0.87 s (12E41)	4.94 cl ch (12E41)			Ca-d-n (12E41, 12E41a); Ca-p-γ (39T52)
Sc^{43}	A chem, excit (17F35)		β^+ (17F35)	3.92 h (53H45); 4 h (30W40a)	1.18 (72%), 0.77 (28%) spect (93H52); 1.12 abs, spect (53H45); 1.4 cl ch (30W37a); abs (30W40a)	0.375, no higher γ (lim 15%) spect (93H52); 1.65 abs (53H45); 1.0 abs (30W40a)		Ca-α-p (17F35, 30W40a); Ca-d-n (30W37a, 53H45); Ca-p-n (2D38, 53H45); spall Fe (45R52), Co (29W52), Cu (42B51a)
Sc^{44m}	A chem, excit cross bomb (30W37a)		IT (30W40a)	2.44 d (53H45); 2.4 d (49B50); 2.2 d (30W40a)		0.271 spect, spect conv (49B50); 0.269 spect conv (51S42); 0.26 spect conv (2H41); 0.28 abs conv (53H45)		K^{41}-α-n (49B50); K-α-n (30W40a, 53H43); Ca-d-n (30W37a, 51S42, 53H43); Ca-p-n (2D38); Sc-n-2n (31B38, 53H45); Ti-d-α (30W37b); spall Fe (45R52), Co (29W52), Cu (42B51a)
Sc^{44}	A chem, excit (10C38)		β^+, EC (53H45)	3.92 h (53H45); 4.0 h (49B50); 4.1 h (30W40a, 51S42)	1.463 spect (49B50); 1.45 spect (51S42); 1.5 abs (39C50, 30W40a)	1.16 spect spect conv (49B50); 1.18 coinc abs sec (39C50)	Q^+_β 3.64 (18G52) 	K^{41}-α-n (49B50); K-α-n (30W40a, 53H43); Ca-d-n (30W37a, 51S42, 53H43); Ca-p-n (2D38); Sc-n-2n (31B38, 53H43); Sc-γ-n (37B39); Ti-d-α (53H44); spall Co (29W52), Cu (42B51a); spall-fission Br (42B51)

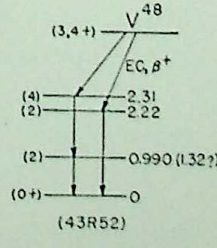
CC-0. In Public Domain. Gurukul Kangri Collection, Haridwar

Digitized by Arya Samaj Foundation Chennai and eGangotri

Isotope Z A	Class and identification	Percent abundance	Type of decay	Half-life	Energy of radiation in Mev: Particles	Energy of radiation in Mev: Gamma-transitions	Disintegration energy and scheme	Method of production and genetic relationships
$_{21}Sc^{45}$		100 (28L50)					Sc^{45}, I = 7/2 (87M50)	
Sc^{46m}	A n-capt, resonance neutron activation (18G48)		IT (18G48)	19.5 s (38M51)		0.142 (K/L ~10) spect conv (82B52); 0.135 scint spect (38M51)	 (18G52)	Sc-n-γ (18G48, 38M51)
Sc^{46}	A n-capt, chem (71H36); chem, excit, cross bomb (30W37c)		β^-, no EC (40M47); β^-, EC (weak) (30W39); no β^+ (lim 0.0016%) (41M51)	85 d (30W39); 84 d (19P51)	0.36 spect (22F47, 40M47, 20P48); 0.36 abs (52S50); 0.34 abs (14N50); 1.2 (~0.5%) spect (19P51); no 1.5 β^- (lim 0.05%) cl ch (52S50); no 1.5 β^- (lim 0.06%) spect (39M50); 1.5 (~2%) spect (20P48); abs (14N50)	γ_1 0.89, γ_2 1.12 spect, spect conv (20P48); 0.88, 1.12 spect (22F47); 0.90, 1.12 spect (40M47); γ_1 (e/γ 1.7 x 10^{-4}), γ_2 (e/γ 0.98 x 10^{-4}) spect conv (39M50); γ_1 (e/γ 1.4 x 10^{-4}), γ_2 (e/γ 0.61 x 10^{-4}) spect conv (19P51a); γ_1 (coinc with 0.36 β^- and γ_2) β-γ, γ-γ coinc (15J48, 52S50, 26M48); γ_1 (coinc with 1.5 β^- and γ_2) delay coinc (14N50)	Q^-_β 2.37 (18G52)	Ca-α-p (30W40a); Sc-d-p (30W37c, 30W39) Sc-n-γ (71H36, 30W37c, 2S47); Ti-d-α (30W37b); Ti-n-p (30W37b, 63H48); spall Fe (45R52), Cu (42B51a)
Sc^{47}	A chem, cross bomb (53H45a); sep isotopes (26K49)		β^- (53H45a)	3.43 d (26K49)	0.61 abs (26K49)	γ (26K49)		Ca-α-p (53H45a); Ca-d-n (53H45a); Ca-p-γ (53H45a); Ti-γ-p (22E52); Ti-n-p (63H48); Ti^{49}-d-α (26K49); spall Fe (45R52), Cu (42B51a); daughter Ca^{47} (42B51a)
Sc^{48}	A chem, excit (30W37b); sep isotopes (26K49)		β^- (30W37b)	44 h (30W40a, 26M42, 53H45a, 26K49)	0.64 spect (51S42); 0.57 abs (53H45a, 26K49)	γ_1 1.33, γ_2 0.98, γ_3 ~1.0 scint spect, γ-γ coinc (68H52); 1.32, 0.99, no 2.3 γ (lim 0.1%) scint spect (69M52); 1.33, 0.98 spect (6P46); 1.35 spect (26M42, 26M43a); 1.33 abs (53H45a)	Q^-_β 3.87 (74S51a)  (68H52)	Ca-p-n (53H43); Ca-d-2n (51S42, 26M42, 53H43, 26M43a); Ti-n-p (30W37b, 1P37, 30W40a, 26M43a); Ti^{50}-d-α (26K49); Ti-d-α (53H44); V-n-α (30W37b, 1P37, 30W40a); spall Fe (45R52)
Sc^{49}	B chem, excit, cross bomb (30W40a)		β^- (30W40a)	57 m (30W40a)	1.8 abs (30W40a)	no γ (30W40a)		Ca-d-n (30W40a); Ti-n-p (30W40a); Ti-γ-p (42H47, 22E52)
$_{22}Ti^{43}$	E excit (45S48)			0.6 s (45S48)				Ca-α-n (45S48)
Ti^{45}	A chem, cross bomb, excit (21A41)		β^+, EC (27K50)	3.09 h (27K50); 3.05 h (11T50); 3.08 h (21A41)	1.02 (≥96%), 0.57 (≤4%) spect (11T50); 1.00 spect (27K50); 1.2 cl ch (21A41)	0.45 (weak), (no 0.8 γ) spect (11T50); 0.80 spect, abs (27K50)	Q^+_β 2.04 (HPS)  (11T50)	Ca-α-n (21A41); Sc-p-n (21A41, 11T50, 27K50), Sc-d-2n (21A41, 11T50); Ti-n-2n (21A41); Ti-γ-n (34H43b, 34H44, 25W48, 22E52); spall Fe (45R52), Cu (42B51a, 74M52)

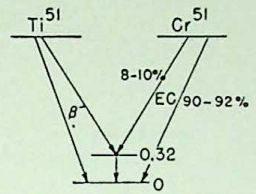
Digitized by Arya Samaj Foundation Chennai and eGangotri

CC-0. In Public Domain. Gurukul Kangri Collection, Haridwar

Isotope Z A	Class and identification	Percent abundance	Type of decay	Half-life	Energy of radiation in Mev: Particles	Energy of radiation in Mev: Gamma-transitions	Disintegration energy and scheme	Method of production and genetic relationships
$_{22}Ti^{46}$		7.95 (6N38a)						
Ti^{47}		7.75 (6N38a)						
Ti^{48}		73.45 (6N38a)						
Ti^{49}		5.51 (6N38a)					Ti^{49}, I = 7/2 (?) (29J52)	
Ti^{50}		5.34 (6N38a)						
Ti^{51}	B n-capt (2S47)		β^- (2S47)	5.82 m (3S52); 5.75 m (2B52); 6 m (24S49a, 38M50, 2S47)	1.7, 1.35 (coinc with 0.32 γ) scint spect (38M52); 2.2 (~30%), 1.9 (~70%) abs, spect (60K52); 1.6 abs (24S49a)	0.320, 0.910 (weak) scint spect (2B52); 0.32 scint spect (38M51a, 60K52)	see Cr^{51}	Ti-n-γ (2S47, 38M50)
$_{23}V^{46}$	E excit (98M52)		β^+ (98M52)	0.40 s (98M52)	>6.0 scint spect (98M52)			Ti-p-n (98M52)
V^{47}	A chem, excit, cross bomb (12O42); chem, sep isotopes (26K49)		β^+ (30W37b)	33 m (26K49, 12O42, 30W37b)	1.7 abs (26K49); 2.0 abs (35B46a, calc from 30W37b); ~1.9 abs (12O42, 30W37b)	γ (26K49)		Ti-d-n (30W37b, 12O42); Ti-p-n (12O42) Ti^{47}-p-n (26K49) spall Fe (45R52)
V^{48}	A chem, excit, cross bomb (30W37c, 30W37b)		β^+ 58%, EC 42% (21G46); β^+, EC (30W39, 53H44)	16.0 d (30W37b)	0.69 (~95%), ~0.8 (~5%) spect (43R52); 0.72 spect (6P46); 0.6 abs (53H44) 1.0 cl ch (30W37b)	γ_1 0.99, γ_2 1.32 (γ_2 coinc with γ_1), γ_3 2.29 (γ_3/γ_2 = 0.017) scint spect (69M52); γ_1 0.99, γ_2 1.32, γ_3 2.22 scint spect, β^+-γ, γ-γ coinc (43R52); γ_1 0.98, γ_2 1.33 (γ_2 coinc with γ_1, both coinc with β^+) spect, β-γ coinc (6P46); γ_1 (e/γ 2 x 10^{-4}), γ_2 (e/γ 8 x 10^{-5}) spect conv (7Z52); γ_3 2.22 (~2%), no 2.3 γ (lim 0.5%) scint spect (18T52); γ_1 0.99, γ_2 1.32 spect conv (20R49); γ_1 (coinc with γ_2) γ-γ coinc (34J52)	Q^+_β 4.02 (43R52)  (43R52)	Sc-α-n (30W37c); Ti-d-n (30W37b); Ti-p-n (2D40, 18T52); Cr-d-α (30W37b, 6P46); spall Fe (45R52), Cu (32M48, 42B51a); daughter Cr^{48} (45R52)
V^{49}	D chem (30W39, 29T40); excit (43H49, est from 10C49)		EC (30W39)	635 d (10C49) ~600 d (30W39)		0.119, 0.081 spect conv (10C49)		Ti-d-n (30W39); V-n-2n (?) (10C49)
V^{50}		0.24 (43H49, 28L49)					Q^-_β 1.18, Q^+_β 2.39 (23J52); V^{50}, I = 6 (56K52)	

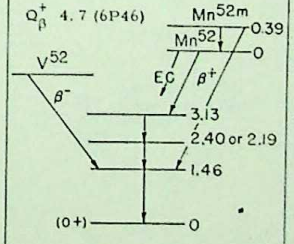
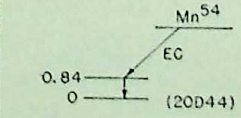
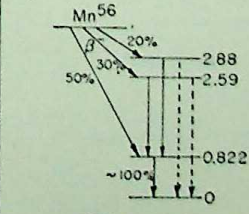
CC-0. In Public Domain. Gurukul Kangri Collection, Haridwar

Digitized by Arya Samaj Foundation Chennai and eGangotri

Isotope Z A	Class and identification	Percent abundance	Type of decay	Half-life	Energy of radiation in Mev: Particles	Energy of radiation in Mev: Gamma-transitions	Disintegration energy and scheme	Method of production and genetic relationships
$_{23}V^{51}$		99.76 (43H49, 28L49)					V^{51}, I = 7/2 (87M50, 97B51c)	
$V^{52(m?)}$	A chem, n-capt (12A35); cross bomb, excit (30W37b)		β^- (12A35); IT (25R50)	3.76 m (3S52); 3.74 m (42M47); 3.75 m (12A35)	2.1 abs (3D40a); 2.6 cl ch (4Y42); conv: 0.25, β^- with V^{52}, abs, β-γ, β-conv coinc (25R50)	1.5 abs (42M47); 1.3 abs (28G48); ~1.5 γ with V^{52} (25R50)		V-n-γ (12A35, 30W37b, 1P37, 2S47, 9O49, 25R50, 50H51); V-d-p (30W37b); Cr-n-p (30W37b, 1P37); Cr-γ-p (42H47); Cr^{54}-d-α (15N50); Mn-n-α (12A35, 30W37b, 1P37)
V^{52}	F n-capt (25R50)		β^- (25R50)	2.6 m (25R50)	2.7 cl ch (4Y42)	1.5 abs (42M47)		V-n-γ (25R50)
$V^{52,50m}$	F V^{52}: (10C49); V^{50m}: (43H49)			16 h (10C49)				V-n (10C49)
V^{53}	B chem, sep isotopes, excit (88H52)		β^- (88H52)	23 h (88H52)	~0.6 abs (88H52)			Cr^{54}-γ-p (88H52)
$_{24}Cr^{48}$	B chem, genet (45R52)		EC (45R52)	~23 h (45R52)				spall Fe, parent V^{48} (45R52)
Cr^{49}	A chem, excit, cross bomb (12O42)		β^+ (12O42)	41.9 m (12O42); 45 m (34H44)	1.45 abs, cl ch (12O42)	0.18, 1.55 abs (12O42)		Ti-α-n (12O42); Cr-n-2n (12O42); Cr-γ-n (34H44, 12P49); spall Fe (45R52), Co (29W52), Cu (32M48, 42B51a, 74M52), As (48H50)
Cr^{50}		4.31 (24W48)						
Cr^{51}	A chem, excit, cross bomb (30W40b); chem, genet (50B50)		EC (16B45a, 30W40b); no β^+ (16B45a, 28K49, 35L52)	27.8 d (35L52); 26.5 d (30W40b)		0.330 (~3%, e_K/γ ~0.02), spect spect conv (16B45a); 0.32 (8%, e/γ very small) scint spect, x-γ coinc (35L52); 0.323 spect, spect conv (28K49); 0.320 (single γ) spect (17K48); 0.32 spect conv (43M46); others (52M51, 28K49, 13A50b)	 (38M51a, 14S52a, 35L52)	Ti-α-n (30W40b); V-p-n (16B45a); Cr-d-p (30W40b, 22A40); Cr-n-γ (30W40b, 2S47); Cr-n-2n (22A40); spall Fe (45R52), Cu (32M48, 42B51a), As (48H50); daughter Mn^{51} (50B50)
Cr^{52}		83.76 (24W48)						
Cr^{53}		9.55 (24W48)					Cr^{53}, I = 3/2 (97B51)	
Cr^{54}		2.38 (24W48)						
Cr^{55}	G not found: sep isotopes, excit, cross bomb (15N50); chem, excit (32M50)			~2 h (18D40)				Cr-n (18D40, 22A40, 2S47); Cr-d (22A40)

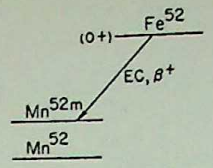
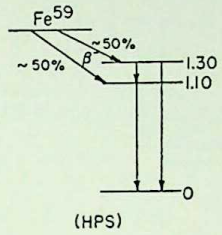
Digitized by Arya Samaj Foundation Chennai and eGangotri

CC-0. In Public Domain. Gurukul Kangri Collection, Haridwar

Isotope Z A	Class and identification	Percent abundance	Type of decay	Half-life	Energy of radiation in Mev: Particles	Energy of radiation in Mev: Gamma-transitions	Disintegration energy and scheme	Method of production and genetic relationships
$_{25}Mn^{49}$, Mn^{50}	E excit (39T52, 98M52)		β^+ (98M52)	0.28 s (98M52); ~0.5 s (39T52)	>6.3 scint spect (98M52)			Cr-p-2n (39T52); Cr-p-n (98M52)
Mn^{51}	A chem, cross bomb (12L37, 12L38); chem, genet (50B50)		β^+ (12L37)	44.3 m (50B50); 46 m (12L38)	2.4 abs (35B46a, calc from 12L38); 2.0 abs (12L38)			Cr-d-n (12L38, 50B50); Cr-p-γ (2D38, 5D39); Fe-γ-p2n (42S52); spall Fe (45R52), Cu (32M48, 42B51a, 74M52); parent Cr^{51} (50B50)
Mn^{52m}	A chem (19D37); chem, excit, cross bomb (12L37, 12L38)		β^+ 99+%, IT (?) ~0.05% (1O47)	21.3 m (40H40); 21 m (12L38, 19D37)	2.66 spect (1O47); 2.2 cl ch (40H40)	1.46 (coinc with β^+) spect, β-γ coinc (1O47); 0.392 (0.05%) (with IT?) spect conv (1O47)	Q^+_β 5.1 (1O47)	Cr-p-n (40H40); Fe-d-α (19D37, 12L38); Fe-γ-pn (22E52, 42S52); daughter Fe^{52} (32M48)
Mn^{52}	A chem, excit, cross bomb (12L37, 12L38)		EC 65%, β^+ 35% (21G46)	6.0 d (29H50); 6.2 d (84H51); 6.5 d (12L38); 6 d (32M48)	0.58 spect (6P46); 0.75 abs (19T48); 0.77 cl ch (40H40)	γ_1 0.73, γ_2 0.94, γ_3 1.46 (γ_1 coinc with γ_2 and γ_3, all coinc with β^+) spect, β-γ coinc (6P46)	Q^+_β 4.7 (6P46)  (18G52, HPS)	Cr-p-n (40H40); Cr-d-2n (6P46); Fe-d-α (12L38); spall Fe (45R52), Co (29W52), Cu (32M48, 42B51a, 74M52), As (48H50); spall-fission U (6F51)
Mn^{54m}	F sep isotopes (40C51)		β^- (40C51)	2.1 m (40C51)				Fe^{54}-n-p, Fe^{54}-d-2p (40C51)
Mn^{54}	A chem, excit, cross bomb (12L37, 12L38)		EC (6A38); no β^+, no β^- (12L38, 20D44)	310 d (12L38)		0.84 spect, x-γ coinc (20D44); 0.85 abs (12L38)	 (20D44)	V-α-n (12L38); Cr-d-n (12L38); Cr-p-n (2D40); Fe-d-α (12L38, 20D44); spall Fe (45R52) Cu (42B51a)
Mn^{55}		100 (37S36a)					Mn^{55}, I = 5/2 (97B51a)	
Mn^{56}	A chem, n-capt (12A35)		β^- (12A35)	2.576 h (106B52a); 2.59 h (12L38, 9B50)	2.81 (50%), 1.04 (30%), 0.65 (20%) spect (7S46c); 2.86 (60%), 1.05 (25%), 0.75 (15%) spect (4E43a); 2.88, 1.04 spect (14T41)	γ_1 0.822, γ_2 1.77, γ_3 2.06 ($\gamma_1/\gamma_2/\gamma_3$ = 10/3/2) spect (7S46c); (γ_2/γ_3 = 1.0) spect (5S51); γ_1 0.85, γ_2 1.81, γ_3 2.13 ($\gamma_1/\gamma_2/\gamma_3$ = 10/3/2) spect, β-γ coinc (4E43a); ~2.7 (~0.1%), ~3.0 (~0.2%) D-γ-p ion ch (9B50)	Q^-_β 3.63 (7S46c)  (7S46c, 4E43a)	Cr-α-p (18R37); Mn-n-γ (12A35, 2S47, 9C49, 50H51); Mn-d-p (12L38); Fe-d-α (12L38); Fe-n-p (12A35); Fe-γ-p (12P48, 22E52); Co-γ-2pn (22E52); Co-n-α (12A35); spall Fe (45R52), Co (29W52), Cu (32M48, 42B51a, 74M52), As (48H50)
Mn^{57}	B chem, cross bomb (112S51)		β^- (112S51)	7 d (112S51)	1.0 spect (112S51)			Mn-α-2p, Cr-α-p (112S51)

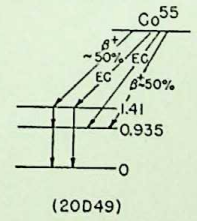
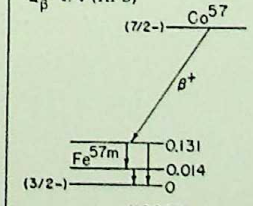
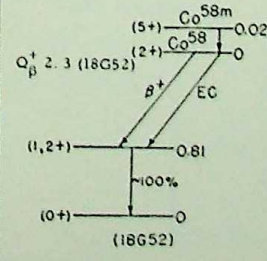
CC-0. In Public Domain. Gurukul Kangri Collection, Haridwar

Digitized by Arya Samaj Foundation Chennai and eGangotri

Isotope Z A	Class and identification	Percent abundance	Type of decay	Half-life	Energy of radiation in Mev: Particles	Energy of radiation in Mev: Gamma-transitions	Disintegration energy and scheme	Method of production and genetic relationships
$_{26}Fe^{52}$	A chem, genet (32M48)		EC 60%, β^+ 40% (23F51)	8.3 h (23F52b); 7.8 h (32M48)	~0.55 abs (32M48); ~0.6 abs (23F51)	no γ >0.5 scint spect (23F51)	 (23F51, HPS)	Cr-α-2n (23F51); Fe-γ-2n (42S52); spall Fe (45R52), Co (29W52), Cu (32M48, 51B50, 23F51, 42B51a, 74M52); parent Mn^{52m} (32M48); not parent Mn^{52} (lim 5%) (23F51)
Fe^{53}	A chem (18R37); chem, excit, cross bomb (12L38a)		β^+ (18R37)	8.9 m (18R37, 12L38a)	2.5 scint spect (52B51); 2.6 abs (15N50)	no γ (15N50)		Cr^{50}-α-n (15N50); Cr-α-n (18R37, 12L38a); Fe-n-2n (12L38a); Fe-γ-n (34H42, 34H44, 52B51, 22E52, 42S52); Fe^{54}-γ-n (12P49); spall Cu (32M48, 42B51a, 74M52)
Fe^{54}		5.84 (6V41)						
Fe^{55}	A chem, excit (12L39a)		EC, no β^+ (16B46b, 94M51)	2.94 y (53B50); 3.0 y (53S51)		no γ (6P46a); ~0.07 (0.002%), Mn K-x (16B46b)	Q_{EC} 0.21 continuous γ spectrum (94M51, 94M51a)	Mn-d-2n (51H48); Mn-p-n (2V40, 16B46b); Fe-d-p (12L39a); spall Co (93M51), Cu (42B51a, 93M51); daughter Co^{55} (12L41)
Fe^{56}		91.68 (6V41)						
Fe^{57m}	A genet (20D50)		IT (20D50)	1.1×10^{-7} s delay coinc (20D50)		0.014 spect (20D50)	see Co^{57}	daughter Co^{57} (20D50)
Fe^{57}		2.17 (6V41)						
Fe^{58}		0.31 (6V41)						
Fe^{59}	A chem, excit, cross bomb (12L38a)		β^- (12L38a)	45.1 d (53S51); 47.1 d (22T51); 45.5 d (29G43); 46 d (54S47)	0.460 (~50%), 0.257 (~50%) spect, β-γ coinc abs (20D42); 0.45, no 0.26 β^- spect (48M51)	γ_1 1.295, γ_2 1.097 spect (12H50); γ_1 1.29, γ_2 1.10 (not coinc with γ_1) spect, γ-γ coinc (48M51); 1.30, 1.10 spect (20D42); γ_1 (e_K/γ 0.84×10^{-4}), γ_2 (e_K/γ 1.45×10^{-4}) spect conv (93B52); 0.195 (2.5%, coinc with 1.1 γ) scint spect, γ-γ coinc (44M52); others (52M51)	 (HPS)	Fe-d-p (12L38a, 20D42); Fe-n-γ (26S42, 4W43, 2S47); Co-n-p (12L38a, 2I46); Co-d-2p (17T48); spall Cu (32M48, 51B50, 42B51a, 74M52), As (48H50); spall-fission Ta (22N52), Bi (11G49), U (6F51)
Fe^{60}	E chem (6F51)		β^- (6F51)	8.4 h (6F51)	~1.5 abs (6F51)			spall-fission U (6F51)

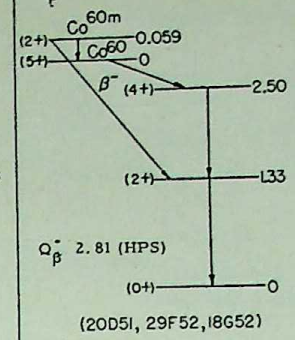
CC-0. In Public Domain. Gurukul Kangri Collection, Haridwar

Digitized by Arya Samaj Foundation Chennai and eGangotri

Isotope Z A	Class and identification	Percent abundance	Type of decay	Half-life	Energy of radiation in Mev: Particles	Energy of radiation in Mev: Gamma-transitions	Disintegration energy and scheme	Method of production and genetic relationships
$_{27}Co^{54}$	E excit (98M52)		β^+ (98M52)	0.18 s (98M52)	>7.4 scint spect (98M52)			Fe-p-n (98M52)
Co^{55}	A chem (19D37); chem, cross bomb, genet (12L41)		β^+ ~60%, EC ~40% (calc from 20D49)	18.2 h (19D37)	1.50 (~50%), 1.01 (~50%) spect (20D49); 1.50 spect (24L39)	γ_1 0.477 (γ/β^+ 0.3, e/γ 0.0007), γ_2 0.935 (γ/β^+ 1.4, e/γ 0.0005), γ_3 1.41 (γ/β^+ 0.3, e/γ 0.00004) spect, spect conv, β-γ coinc (20D49); others (85S51)	Q^+_β 3.45 (20D49)  (20D49)	Fe-d-n (19D37, 12L41, 20D49); Fe-p-γ (12L38b, 12L41); Ni-γ-p2n (42S52); spall Fe (45R52), Co (29W52), Cu (32M48, 42B51a, 74M52), As (48H50); parent Fe^{55} (12L41)
Co^{56}	A chem, excit, cross bomb (12L41)		EC, β^+ (4E43a, 28C42)	72 d (12L41); 80 d (28C42)	1.50 (coinc with γ_1 and γ_2) spect (4E43a); 1.2 abs (12L41, 28C42)	γ_1 0.845, γ_2 1.26 (coinc with γ_1), γ_3 1.74, γ_4 2.01, γ_5 2.55, γ_6 3.25 ($\gamma_1/\gamma_2/\gamma_3/\gamma_4/\gamma_5/\gamma_6$ = 1.0/0.5/0.2/0.1/0.2/0.2) spect, β-γ coinc (4E43a); others (85S51)	Q^+_β 4.6 (4E43a)	Fe-d-2n (12L41, 16J41, 21P42, 4E43a); Fe-a-np (12L41); Co-p-p3n (29W52); Ni-d-a (12L41, 28C42, 4E43a); Ni-γ-pn (42S52); spall Fe (45R52), Cu (42B51a); daughter Ni^{56} (44S52, 32W52)
Co^{57}	A chem, excit, cross bomb (12L41)		β^+ (12L41)	270 d (12L41)	0.26 abs (12L41)	0.119, 0.131 spect (4E43a); 0.117 (e/γ large, K/L 7), 0.130 (e/γ large, K/L 7) spect, spect conv (21P42); with Fe^{57m}: 0.014 spect (20D50)	Q^+_β 1.4 (HPS)  (18G52)	Fe-d-n (12L38b, 22P38, 54B39, 12L41); Fe-p-γ (12L41); parent Fe^{57m} (20D50); daughter Ni^{57} (23F52)
Co^{58m}	A chem, excit (55S50)		IT, no β^+ (55S50)	9.2 h (25C50); 9.0 h (37A52); 8.8 h (55S50)		0.025 (e/γ large, K/L 1.9) spect conv (55S50)		Mn-a-n, Co-d-p2n, Co-n-2n, Ni-n-p, Ni-d-2p (55S50); Fe^{58}-p-n (37A52); Co-γ-n (25C50); spall Cu (55S50, 74M52)
Co^{58}	A chem, excit, cross bomb (12L41)		EC 85%, β^+ 15% (21G46)	72 d (12L41)	0.47 spect (20D44); 0.4 abs (12L41)	0.81 spect, β-γ coinc (20D44); ~0.81 (e/γ 0.0003) spect conv (55S50); 0.6 abs (12L41)	Q^+_β 2.3 (18G52)  (18G52)	Mn-a-n (12L38b, 12L41); Fe-d-n (12L38b, 22P38, 54B39, 12L41); Fe^{58}-p-n (37A52); Fe-p-n (12L38b); Fe-a-np (12L41); Fe-p-γ (12L41); Co-p-pn (29W52); Ni-n-p (7V38, 12L41, 20D44); spall Cu (51B50, 42B51a, 74M52), As (48H50)
Co^{59}		100 (45M41)					Co^{59}, I = 7/2 (87M50, 97B51d)	

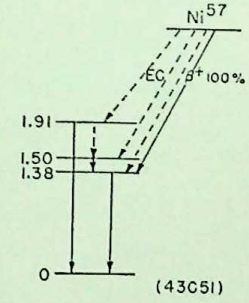
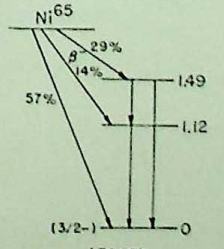
CC-0. In Public Domain. Gurukul Kangri Collection, Haridwar

Digitized by Arya Samaj Foundation Chennai and eGangotri

Isotope Z A	Class and identification	Percent abundance	Type of decay	Half-life	Energy of radiation in Mev: Particles	Energy of radiation in Mev: Gamma-transitions	Disintegration energy and scheme	Method of production and genetic relationships
$_{27}Co^{60m}$	A n-capt (6H37a); chem, excit, cross bomb (12L41)		IT 99+%, β^- 0.28% (20D51)	10.1 m (106B52b); 10.7 m (12L41)	1.56 spect (6P47); 1.35 spect (15N42); 1.28 spect (20D45)	0.0589 (K/L 4.6) spect conv (42C50); 0.059 scint spect (31K51); 0.056 spect conv (20D45)	Q^-_β 2.89 (HPS)  Q^-_β 2.81 (HPS) (20D51, 29F52, 18G52)	Co-n-γ (6H37a, 12L37, 12L41, 20D42a, 2S47); Co-d-p (15N42); Ni-n-p (6H37b, 12L41)
Co^{60}	A n-capt (37S36); chem, excit, cross bomb (12L41)		β^- (27R37)	5.27 y (22T51); 5.3 y (12L41, 53B50, 38S51)	0.306 spect (29F52); 0.318 spect (31W50a); 0.310 spect (43M47)	γ_1 1.3316, γ_2 1.1715 cryst spect (29L49); 1.3316, 1.1715 spect γ-γ coinc (16D51); γ_1 (e/γ 1.24×10^{-4}), γ_2 (e/γ 1.72×10^{-4}) spect conv (29F52); γ_1 (e/γ 1.29×10^{-4}), γ_2 (e/γ 1.73×10^{-4}) spect conv (31W50, 31W50a); γ_1 (e/γ 1.8×10^{-4}), γ_2 (e/γ 2.3×10^{-4}) spect conv (7S50); others (17B50, 44M50a, 13A49, 36A52, 37D51, 85B50a, 85S51)		Co-d-p (12L38b, 54B39, 12L41, 20D42a, 15N42); Co-n-γ (27R37, 12L38b, 12L41, 2S47, 1Y51); Ni-d-α (12L41); Cu-n-α (12M46c); spall-fission Bi (66B51)
Co^{61}	A chem, excit, cross bomb, sep isotopes, mass spect (23P47)		β^- (23P47)	99.0 m (56S51); 105 m (23P49); 110 m (48H50)	1.42 (~55%), 1.00 (~45%) abs (56S51); 1.3 abs (23P49)	~0.5 abs (56S51); no γ (23P49, 29K48)	Q^-_β 1.4 (HPS)	Co-α-2p (112S51); Co-t-p (29K48); Ni-γ-p (12P48, 56S51, 22E52); Ni^{64}-p-α (23P47, 23P49); Ni^{61}-n-p (23P47, 23P49); Ni-d-αn, Cu-n-αn (23P47, 23P49); Cu-γ-2p (12P48); Cu-γ-α (49H51); spall Cu (32M48, 42B51a, 74M52), As (48H50); spall-fission Ag (42B51), U (6F51)
Co^{62}	A chem, sep isotopes (23P49)		β^- (23P49)	13.9 m (23P49)	2.3 abs (23P49)	1.3 (coinc with β^-) abs, β-γ coinc (23P49)		Ni^{62}-n-p (23P49)
Co^{62}	E cross bomb, sep isotopes (23P49)		β^- (23P49)	1.6 m (23P49)		γ (23P49)		Ni^{62}-n-p, Ni^{64}-d-α (23P49)
Co^{64}	F cross bomb, sep isotopes (23P49)			~5 m (23P49)				Ni^{64}-n-p (23P49)
$_{28}Ni^{56}$	A chem (32W52); chem, sep isotopes, genet (44S52)		EC ~100%, no β^+ (lim 1%) (44S52)	6.4 d (44S52); 6.0 d (32W52)		γ_1 0.17, γ_2 0.28, γ_3 0.48, γ_4 0.81, γ_5 0.96, γ_6 1.33, γ_7 1.58, γ_8 1.75 ($\gamma_1/\gamma_2/\gamma_3/\gamma_4/\gamma_5/\gamma_6/\gamma_7/\gamma_8$ = 1.0/0.3/0.4/0.8/0.1/0.05/0.15/0.02) scint spect (44S52); 0.14, 0.77, >1.4 scint spect (32W52)		Fe-α-2n (32W52); Fe^{54}-α-2n (44S52); spall Zn (32W52); parent Co^{56} (44S52, 32W52)

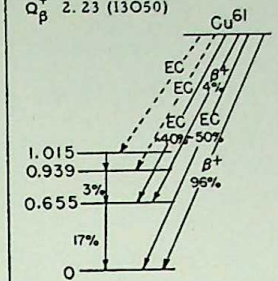
CC-0. In Public Domain. Gurukul Kangri Collection, Haridwar

Digitized by Arya Samaj Foundation Chennai and eGangotri

Isotope Z A	Class and identification	Percent abundance	Type of decay	Half-life	Energy of radiation in Mev: Particles	Energy of radiation in Mev: Gamma-transitions	Disintegration energy and scheme	Method of production and genetic relationships
$_{28}Ni^{57}$	A chem, excit, cross bomb (12L38c)		β^+ 50%, EC 50% (23F50)	36 h (46M49, 12L38c)	0.835 spect (43C51); 0.845 spect (23F50)	γ_1 1.91, γ_2 1.38 (γ_2/γ_1 = 6) spect (43C51); γ_1 1.90, γ_2 1.39 (γ_2/γ_1 = 5) scint spect (44S52); 0.128 spect, spect conv (43C51); 0.120, 1.9 scint spect, spect conv, β-γ coinc (23F50)	Q^+_β 3.24 (43C51)  (43C51)	Fe-α-n (12L38c, 14D41, 15N42a, 46M49, 23F50, 43C51); Co-p-3n (29W52); Ni-n-2n (12L38c, 14D41, 15N42a, 80M52); Ni-He^3-α (1P52); Ni-γ-n (34H44, 12P48, 12P49, 22E52, 42S52); spall Cu (32M48, 42B51a, 74M52), As (48H50); parent Co^{57} (23F52)
Ni^{58}		67.76 (24W48)						
Ni^{59}	A chem, cross bomb, n-capt (44C45); chem, sep isotopes, n-capt (48B51)		EC (23F49)	8×10^4 y yield (48B51); 8×10^5 y yield (33W51); ~3×10^5 y yield (23F49)		Co-K-x, no γ (33W50, 33W51); Co-K-x (48B51, 23F49)		Fe-α-n (44C45); Co-d-2n (48B51); Ni-n-γ (44C45, 33W50); Ni^{58}-n-γ (48B51); Ni-d-p (44C45)
Ni^{60}		26.16 (24W48)						
Ni^{61}		1.25 (24W48)						
Ni^{62}		3.66 (24W48)						
Ni^{63}	A chem, n-capt, sep isotopes (48B51)		β^- (23F49, 48B51)	85 y yield (48B51); 61 y yield (33W51)	0.067 ion ch (48B51); 0.063 ion ch (33W49)			Ni-n-γ (23F49, 33W49, 33W50, 48B51); Ni^{62}-n-γ (48B51)
Ni^{64}		1.16 (24W48)						
Ni^{65}	A n-capt (6R35); chem, sep isotopes, excit (54S46, 45C46)		β^- (6H37b)	2.564 h (57S49); 2.6 h (12L38c, 46M49)	2.10 (57%), 1.01 (14%), 0.60 (29%) spect (7S49)	1.49, 1.12, 0.37 spect, β-γ, γ-γ coinc (7S49); others (54W51)	Q^-_β 2.10 (7S49)  (7S49)	Ni-d-p (12L38c, 15N42a); Ni-n-γ (6H37b, 14D41, 15N42a, 2S47, 46M49); Ni^{64}-n-γ (45C46); Cu-n-p (6H37b); Cu^{65}-n-p (54S46); Cu^{65}-t-He^3 (29K51); Cu-d-2p (32M48, 51B50); Zn-n-α (6H37b); spall Cu (74M52), As (48H50); spall-fission Ta (22N52), Bi (11G49), U (6O48, 6F51)
Ni^{66}	A chem, genet (11G49)		β^- (11G49)	56 h (11G49, 48H50)				spall As (48H50); spall-fission Ta (22N52), Bi (11G49), U (6F51); parent Cu^{66} (11G49)

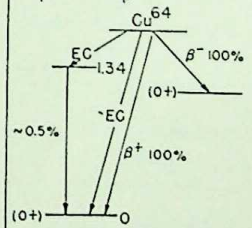
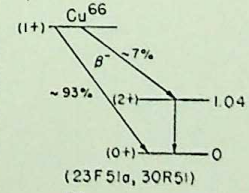
CC-0. In Public Domain. Gurukul Kangri Collection, Haridwar

Digitized by Arya Samaj Foundation Chennai and eGangotri

Isotope Z A	Class and identification	Percent abundance	Type of decay	Half-life	Energy of radiation in Mev: Particles	Energy of radiation in Mev: Gamma-transitions	Disintegration energy and scheme	Method of production and genetic relationships
$_{29}Cu^{58}$	B chem (5D39); chem, excit, sep isotopes (30L47)		β^+ (5D39)	7.9 m (5D39); 10 m (30L47)				Ni-p-n (5D39); Ni^{58}-p-n (30L47)
Cu^{58}	C excit (39T52, 98M51)		β^+ (98M51)	3.04 s (98M51); 2.6 s (39T52)	>7.5 scint spect (98M51)			Ni-p-n (39T52, 98M51)
Cu^{59}	E chem (5D39); excit, sep isotopes (30L47)		β^+ (5D39)	81 s (5D39, 30L47)				Ni-p-γ (5D39); Ni^{58}-p-γ (30L47)
Cu^{60}	A chem, excit, sep isotopes, mass spect (30L47)		β^+ (30L47)	24.6 m (30L47)	1.8, 3.3 (<5%) abs (30L47)	1.5 abs (30L47)		Ni-p-n (30L47); Ni^{60}-p-n, Ni^{60}-d-2n, Ni^{58}-α-pn (30L47); spall Cu (42B51a), As (48H48a)
Cu^{61}	A chem, excit (18R37a); chem, excit, sep isotopes (30L47, 29K50)		β^+ 68%, EC 32% (28C51); β^+ 72%, EC 28% (55B50); β^+ 75%, EC 25% (34H49)	3.33 h (28C48b); 3.4 h (6T37a, 18R37, 29K50); 3.3 h (48H50)	1.205 (96%), 0.55 (4%) spect (13O50); 1.23 spect (16B45b)	γ_1 0.655 (γ/β^+ 0.25, e/γ ~0), γ_2 0.284 (γ/β^+ 0.05, e/γ 0.015), γ_3 0.076 (γ/β^+ 0.01, e/γ large) spect, spect conv (13O50); γ_1 (17%), γ_2 (3%), γ_3 (~0.6%) (calc from 28C51, 13O50); 0.652, 0.279, 0.070 (K/L ~10) spect, spect conv (56B50)	Q^+_β 2.23 (13O50)  (13050, 28C51, HPS)	Ni-d-n (6T37a); Ni-p-n, Ni-p-γ (58S38, 5D39); Ni^{61}-p-n (30L47); Ni-He^3-d (1P52); Ni-α-p (18R37, 29K50); Cu-γ-2n (12P48, 22E52); Zn-γ-p2n (55S51, 42S52); spall Cu (32M48, 42B51a, 74M52), As (48H50); spall-fission Bi (66B51), U (6F51)
Cu^{62}	A excit (6H37a); excit, cross bomb (18R37, 58S38, 37B39); chem, sep isotopes (30L47)		β^+ (6H37a)	10.1 m (30L47); 10.0 m (18R37); 9.9 m (12P48); 10.5 m (6H37a)	2.92 spect (61H50); abs (30K50); 2.83 spect (25B49)	0.56 abs (19T47)		Co-α-n (18R37); Ni-p-n, Ni-p-γ (58S38); Ni^{60}-α-pn (48G50); Cu-n-2n (6H37b, 80M52, 30B52); Cu-p-pn (48G50); Cu-γ-n (37B39, 34H43, 34H43b, 55K52, 25B49, 12P48, 22J50, 55S51, 22E52); Cu-e^--e^-n (59S48); Cu-d-t (9K40a, 9K41a); Zn-γ-pn (55S51, 22E52, 42S52); spall Cu (32M48, 42B51a, 74M52), As (48H50); daughter Zn^{62} (32M48)
Cu^{63}		69.1 (57B47)					Cu^{63}, I = 3/2 (87M50)	

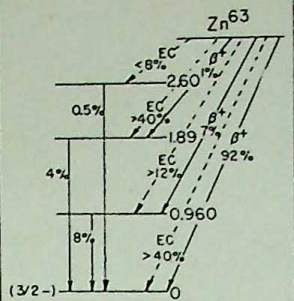
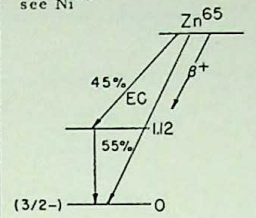
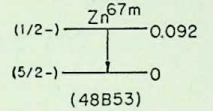
CC-0. In Public Domain. Gurukul Kangri Collection, Haridwar

Digitized by Arya Samaj Foundation Chennai and eGangotri

Isotope Z A	Class and identification	Percent abundance	Type of decay	Half-life	Energy of radiation in Mev: Particles	Energy of radiation in Mev: Gamma-transitions	Disintegration energy and scheme	Method of production and genetic relationships
$_{29}Cu^{64}$	A chem, n-capt (12A35); excit (2V36); chem, excit (5D39)		EC 42%, β^- 39%, β^+ 19% (HPS, calc from average of K/β^+ and β^-/β^+); K/β^+ 2.2 (24P51); K/β^+ 2.3 (28R50); K/β^+ 1.8 (34H49); K/β^+ 2.7 (55B50); β^-/β^+ 2.0 (55B49, 28C48c); β^-/β^+ 2.1 (16B46a); $\frac{\beta^+ + EC}{\beta^-}$ 1.62 (28R50)	12.80 h (29R50); 12.74 h (53S51); 12.88 h (57S49); 12.8 h (2V36, 48H50)	β^-: 0.571 spect (28C48c, 13O49); 0.570 spect (6P47); 0.58 spect (20T39, 14T41) β^+: 0.657 spect (28C48c, 13O49); 0.644 spect (6P47); 0.65 spect (14T41); 0.66 spect (20T39)	γ (with EC) coinc (16B46a); γ (1% of EC) (HPS, calc from 20D47, 27K50, 28R50); 1.34 (weak) spect (17K48); 1.35 (γ/β^+ 0.025) spect (20D47); 1.33 scint spect (11B50d); (γ/β^+ 0.023) abs (10V52); 1.38 (γ/β^+ 0.032) abs (27K50); ~1.34 (e_K/γ ~1.3 x 10^{-4}) spect conv (93B52); γ (e/γ <0.005) spect conv (47M48)	Q^-_β 0.57, Q^+_β 1.68 (HPS)  (HPS)	Ni-p-n (58S38, 5D39); Ni-He^3-p (1P52); Cu-d-p (2V36); Cu-n-γ (6H37b, 2S47); Cu-n-2n (6H37b, 74M52); Cu-p-pn (23R46, 42B51a); Cu-t-d (29K51); Cu-γ-n (34H43b, 34H44, 22J50, 12P49, 55S51, 22E52); Zn-n-p (12A35, 6H37b); Zn-γ-pn (55S51, 22E52); spall Cu (32M48, 42B51a), As (48H50); spall-fission Bi (66B51), U (6F51)
Cu^{65}		30.9 (57B47)					Cu^{65}, I = 3/2 (87M50)	
Cu^{66}	A n-capt (12A35); excit (7C37)		β^- (12A35)	5.10 m (3S52); 5.12 m (53S51); 5.17 m (30R51); 5.18 m (46C50); 5.2 m (23F51a)	2.63 (91%), 1.5 (9%) spect (23F51a); 2.7 (~94%), 1.65 (~6%) scint spect, β-γ coinc (30R51)	1.044 (γ/β^- 0.10, e/γ <3 x 10^{-3}) spect, spect conv (23F51a); 1.05 scint spect (30R51, 94M51a)	Q^-_β 2.63 (23F51a)  (23F51a, 30R51)	Cu-n-γ (12A35, 2S47, 9O49, 50H51); Cu-d-p (31L40); Zn-n-p (6H37b); Ga-n-a (7C37); daughter Ni^{66} (11G49)
Cu^{67}	A chem (11G49); chem, cross bomb, sep isotopes (29K50)		β^- (11G49)	58.5 h (29K50); 61.0 h (80S52); 56 h (11G49); 61 h (48H50)	0.38 (67%), 0.57 (33%) spect (80S52); 0.54 abs (29K50)	0.191 (e/γ 0.01, K/L ~8), 0.096 (e/γ 0.09, K/L 7.4) scint spect, spect conv, β-γ coinc (80S52)	see Ga^{67}	Ni^{64}-a-p (29K50); Cu-a-2p (11S51); Cu-t-p (29K51); Zn^{67}-n-p (29K50); Zn-γ-p (23D48, 55S51, 22E52) spall As (48H50); spall-fission Bi (11G49, 66B51), U (6F51)
$_{30}Zn^{62}$	A chem, genet (32M48); excit (48G50)		EC ~90%, β^+ ~10% (61H50)	9.33 h (61H50); 9.5 h (32M48)	0.66 spect (61H50)	0.0418 (K/L >6) spect conv (61H50)		Ni-He^3-n (1P52); Ni^{60}-a-2n (48G50); Cu-p-2n (48G50); Zn-γ-2n (55S51, 22E52, 42S52); spall Cu (32M48, 61H50, 51B50, 42B51a), As (48H50); parent Cu^{62} (32M48)

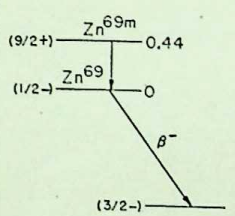
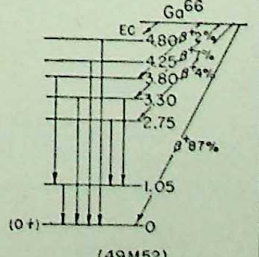
CC-0. In Public Domain. Gurukul Kangri Collection, Haridwar

Digitized by Arya Samaj Foundation Chennai and eGangotri

Isotope Z A	Class and identification	Percent abundance	Type of decay	Half-life	Energy of radiation in Mev: Particles	Energy of radiation in Mev: Gamma-transitions	Disintegration energy and scheme	Method of production and genetic relationships
$_{30}Zn^{63}$	A chem, excit (37B37, 6H37b, 18R37)		β^+ 93%, EC 7% (34H47)	38.3 m (34H47, 58S38); 38.5 m (5D39)	2.36 (92%), 1.40 (7%), 0.5 (~1%) spect (34H47); 2.32 spect (14T41)	0.960 (~8%, e/γ 2 x 10^{-4}), 1.89 (~4%, e/γ ~0), 2.60 (~0.5%, e/γ ~0) spect, spect conv, abs, γ-γ coinc (34H47)	Q^+_β 3.38 (34H47)  (34H47)	Ni-α-n (18R37); Ni^{60}-α-n (48G50); Cu-p-n (58S38, 5D39, 47B51b, 48G50); Cu-d-2n (31L40, 14T41); Zn-n-2n (6H37b, 1P37); Zn-γ-n (37B39, 12P49, 55S51, 22E52, 42S52); Zn-γ-3n (55S51); spall Cu (32M48, 51B50, 42B51a), As (48H50)
Zn^{64}		48.89 (1B50)					Zn^{64}, I = 0 (87M50)	
Zn^{65}	A chem (22P38); chem, excit, cross bomb (12L39)		EC (K) 97.5%, β^+ 2.5% (95M52, 4Y52) EC 99+%, β^+ 0.7% (calc from 30G51, 24F51, 21G46a)	250 d (12L39); 245 d (22P38)	0.325 spect (48M49); 0.32 spect (6P47)	1.120 spect conv (48M49); 1.125 spect, spect conv (12H50); 1.114 spect (48M49); 1.112 (e/γ 2.3 x 10^{-4}) spect conv (31W50); 1.127 scint spect (25G51a); 1.12 spect (13J49); γ (46% of EC) x-e coinc (21G46a); γ (44% of EC) x-γ coinc (24F51); γ/β^+ ≃ 65 γ-γ coinc (30G51); 0.21 (coinc with β^+, e/γ ~0.1) β-γ, β-conv coinc (47C50)	see Ni^{65}  (21G46a, 24F51, 95M52)	Cu-d-2n (22P38); Cu-p-n (58B38, 47B51b); Cu-t-n (29K51); Zn-d-p (12L39); Zn-n-γ (42S39, 2S47); spall Cu (42B51a), As (48H50); daughter Ga^{65} (12L39b)
Zn^{66}		27.81 (1B50)					Zn^{66}, I = 0 (87M50)	
Zn^{67m}	A genet (48B53, 47M52)		IT (47M52, 48B53)	8.5×10^{-6} s delay coinc (48B53); 9×10^{-6} s delay coinc (47M52)		0.092 (e_K/γ 0.63, K/L 7) scint spect (48B53); 0.092 (e/γ 0.6) scint spect (47M52)	see Ga^{67}  (48B53)	daughter Ga^{67} (48B53, 47M52)
Zn^{67}		4.11 (1B50)					Zn^{67}, I = 5/2 (87M50, 38D52)	
Zn^{68}		18.56 (1B50)					Zn^{68}, I = 0 (87M50)	

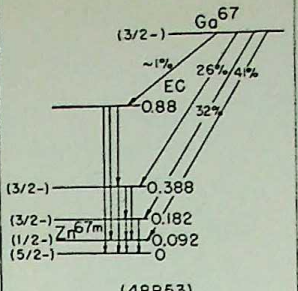
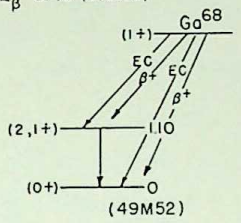
CC-0. In Public Domain. Gurukul Kangri Collection, Haridwar

Digitized by Arya Samaj Foundation Chennai and eGangotri

Isotope Z A	Class and identification	Percent abundance	Type of decay	Half-life	Energy of radiation in Mev: Particles	Energy of radiation in Mev: Gamma-transitions	Disintegration energy and scheme	Method of production and genetic relationships
$_{30}Zn^{69m}$	A chem, excit (6T38); chem, excit, cross bomb (12L39, 14K39)		IT (14K39)	13.8 h (12L39)		0.437 (e/γ 0.049) spect, conv (91S52b); 0.436 (e/γ ~0.065) spect conv, scint spect (23D52); 0.439 (e/γ ~0.04) spect, spect conv (2H41); 0.440 spect (28G41); 0.450 (e/γ ~0.06) (16N44)	 (18G52) Q^-_β 0.90 (HPS, 12L39)	Zn-d-p (12L39, 14K39, 6V39); Zn-n-γ (6T38, 12L39, 2S47); Ga-d-α (12L39); Ga-n-p (12L39); spall As (48H50); parent Zn^{69} (14K39)
Zn^{69}	A chem, n-capt (6H37b); chem, excit, cross bomb (12L39, 14K39)		β^- (6H37b)	57 m (12L39); 51 m (48H48b); 52 m (7H49)	0.897 spect (23D52); 0.914 spect (91S52b); others (14K39, 12L39, 35B46a)	no γ (12L39)		Zn^{70}-γ-n (7H49); Zn-d-p (12L39, 14K39, 6V39); Zn-n-γ (6H36, 6T38, 2S47, 50H51, 42S39); Ga-d-α (12L39); Ga-n-p (12L39); spall As (48H48a); daughter Zn^{69m} (14K39)
Zn^{70}		0.62 (1B50)						
Zn^{71}	E n-capt, cross bomb (28H46b)		β^- (28H46b)	2.2 m (28H46b)	2.1 abs (28H46b)			Zn-n-γ, Ge-n-α (28H46b)
Zn^{72}	A chem, genet (60S46, 60S51)		β^- (60S51)	49.0 h (60S51)	~0.3 (95%), ~1.6 (5%) abs (60S51)	γ (60S51)		As-p-4p (112S51); spall As (48H50); spall-fission Bi (11G49), U (6F51); fission Th (21T51), U (60S51), Pu (61S51a); parent Ga^{72} (60S51)
$_{31}Ga^{65}$	A chem, genet (12L39b)		EC (6A38); β^+ >50% (25A52)	15 m (6A38, 12L39b)	2.2 (25A52)	0.054, 0.117 spect conv (6V39)		Cu-He^3-n (1P52); Zn-d-n (6A38, 12L39b); Zn-p-γ (2D40); parent Zn^{65} (12L39b)
Ga^{66}	A chem, excit (50M37, 18R37a)		β^+ 64%, EC 36% (49M52); β^+ 66%, EC 34% (10L50a)	9.45 h (10L50a); 9.4 h (18R37, 59B38); 9.2 h (49M50, 50M37)	4.144 (87%), 1.4 (4%), 0.88 (7%), 0.40 (2%) spect (10L50a); 4.15 (87%), 1.38 (4%), 0.90 (7%), 0.40 (2%) spect (49M52)	γ_1 1.05, γ_2 1.7, γ_3 2.2, γ_4 2.75 coinc with γ_1), γ_5 3.3, γ_6 4.25, γ_7 4.8 ($\gamma_1/\gamma_2/\gamma_3/\gamma_4/\gamma_5/\gamma_6/\gamma_7$ = 3.7/0.3/0.5/2.9/0.5/0.2/0.2) spect, γ-γ coinc abs (49M52); γ_1 1.04, γ_2 1.38, γ_3 1.90, γ_4 2.17, γ_5 2.40, γ_6 2.75, γ_7 3.24, γ_8 3.41, γ_9 3.78, γ_{10} 4.12, γ_{11} 4.33, γ_{12} 4.83 ($\gamma_1/\gamma_2/\gamma_3/\gamma_4/\gamma_5/\gamma_6/\gamma_7/\gamma_8/\gamma_9/\gamma_{10}/\gamma_{11}/\gamma_{12}$ = ~1.5/~0.2/0.14/0.24/0.10/1.00/0.09/0.14/0.08/0.07/0.21/0.09) scint spect, pair scint spect (58M52); 1.06, 2.75, 3.25, 4.27, 4.8 scint spect (55H50); 1.03, 2.75, 4.8 spect, spect conv (10L50a)	Q^+_β 5.16 (23F51a)  (49M52)	Cu-α-n (50M37, 18R37, 10L50a); Zn-p-n (59B38, 49M50); spall Cu (second order reaction) (42B51a, 29W52), spall As (48H50); spall-fission Sn, Ba (42B51); daughter Ge^{66} (48H49)

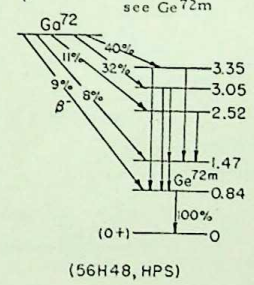
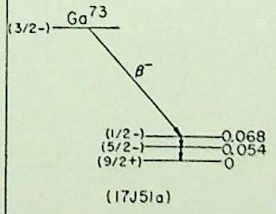
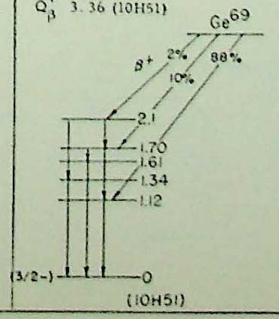
CC-0. In Public Domain. Gurukul Kangri Collection, Haridwar

Digitized by Arya Samaj Foundation Chennai and eGangotri

Isotope Z A	Class and identification	Percent abundance	Type of decay	Half-life	Energy of radiation in Mev: Particles	Energy of radiation in Mev: Gamma-transitions	Disintegration energy and scheme	Method of production and genetic relationships
$_{31}Ga^{67}$	A chem, excit (50M38a, 50M38); chem, excit, cross bomb (6A38)		EC (6A38); no β^+ (lim 0.01%) (47M52); no β^+ (49M52, 48B53)	77.9 h (22T51); 78.2 h (51M48)		γ_1 0.090 (e_K/γ 0.074), γ_2 0.092 (with Zn^{67m}, e_K/γ 0.63, K/L 7), γ_3 0.182 (e_K/γ 0.011, K/L ~12.5), γ_4 0.206 (e_K/γ 0.029, K/L ~14), γ_5 0.296 (e_K/γ 0.0029), γ_6 0.388 (e_K/γ 0.0019), γ_7 0.496, γ_8 0.790, γ_9 0.880 ($\gamma_1/\gamma_2/\gamma_3/\gamma_4/\gamma_5/\gamma_6/\gamma_7/\gamma_8/\gamma_9$ = 0.073/1.00/0.81/0.021/0.54/0.13/0.004/0.002/0.004) spect conv, scint spect, conv-γ, γ-γ coinc (48B53); γ_2 0.092 (e/γ 0.28, K/L 6.5), γ_3 0.182 (e/γ 0.0091, K/L 9), γ_4 0.205 (e/γ 0.0055), γ_5 0.298 (e/γ 0.0025), γ_6 0.388 (e/γ 0.0017) ($\gamma_2/\gamma_3/\gamma_4/\gamma_5/\gamma_6$ = 62/21/2/12/3) spect, spect conv, conv-γ coinc (49M52); γ_1 0.090 (4%), γ_2 0.092 (with Zn^{67m}, 46%, e/γ 0.6), γ_3 0.182 (21.5%), γ_4 0.20 (2%), γ_5 0.30 (12.5%), γ_6 0.39 (4.5%), γ_7 ~0.50 (<1%), γ_9 ~0.85 (≤1%), γ_{10} ~1.05 (<1%) scint spect, γ-γ coinc (47M52); others (2H41, 10C42, 28G41, 7S52)	 (48B53)	Cu-α-γ (112S51); Cu-He^3-n (1P52); Zn-d-n (6A38, 31G38, 6V39); Zn-α-p (50M38); Zn-p-n (59B38, 6V39); Ge-γ-p2n (42S52); spall Cu (second order reaction) (42B51a), As (48H50); daughter Ge^{67} (48H49); parent Zn^{67m} (48B53, 47M52)
Ga^{68}	A chem, excit (37B37); chem, excit (18R37)		β^+ ~85%, EC ~15% (49M52)	68 m (18R37, 12P48)	1.88 (~96%), 0.77 (~4%) spect (49M52); 2.0 abs (35B46a, calc from 50M37); 1.9 abs (18R37, 50M37); cl ch (50M37)	1.10 spect (49M52)	Q^+_β 2.90 (49M52)  (49M52)	Cu-α-n (18R37, 50M37); Zn-p-n (2D38, 59B38, 49M50); Zn-p-γ (?) (2D38); Zn-d-n (31G38, 6V39); Ga-n-2n (1P37); Ga-γ-n (37B37, 37B39, 12P48); Ge-γ-pn (12P49, 42S52); Ge-d-α (42S41); spall Cu (second order reaction) (42B51a, 29W52), spall As (48H50); daughter Ge^{68} (48H48a)
Ga^{69}		60.2 (3I48)					Ga^{69}, I = 3/2 (87M50)	
Ga^{70}	A chem, n-capt (12A35); chem, excit (2D38)		β^- (2D38)	20.3 m (61B47); 20 m (12A35)	1.65 spect (56H48); 1.62 abs (61B47); ~1.6 cl ch (42S39a)			Zn-p-n (2D38); Zn-α-p (50M38); Ga-n-γ (12A35, 2S47); Ga-n-2n (1P37); Ga-γ-n (37B39, 12P48); Ge-d-α (42S41); Ge-n-p (42S41); As-γ-αn (85H52); spall As (48H50)
Ga^{71}		39.8 (3I48)					Ga^{71}, I = 3/2 (87M50)	

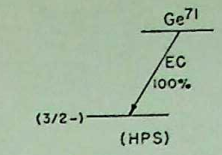
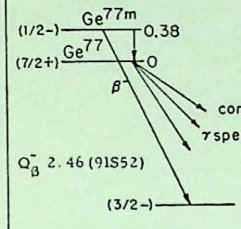
Digitized by Arya Samaj Foundation Chennai and eGangotri

CC-0. In Public Domain. Gurukul Kangri Collection, Haridwar

Isotope Z A	Class and identification	Percent abundance	Type of decay	Half-life	Energy of radiation in Mev: Particles	Energy of radiation in Mev: Gamma-transitions	Disintegration energy and scheme	Method of production and genetic relationships
$_{31}Ga^{72}$	A chem, n-capt, excit (12L38a, 42S39)		β^- (42S39)	14.3 h (26M43a, 60S51); 14.1 h (42S39, 9B50)	3.15 (9%), 2.52 (8%), 1.5 (11%), 0.9 (32%), 0.6 (40%) spect (56H48); 3.17 (8%), 2.57 (8%), 1.7 (?) (3%), 1.5 (?) (7%), 1.00 (26%), 0.74 (23%), 0.6 (?) (25%) spect (14M48)	γ_1 2.491, γ_2 2.508 (γ_1/γ_2 0.63) spect (12H52); 2.51 (26%), 2.21 (33%), 1.87 (8%), 1.59 (5%), 1.20 (?) (<2%), 1.05 (5%), 0.84 (100%), 0.68 (<2%), 0.63 (24%) spect, spect conv (56H48); $\gamma_1\gamma_2$ 2.50 (15%), γ_3 2.18 (33%), γ_4 1.81 (10%), γ_5 1.57, γ_6 1.47, γ_7 1.30 ($\gamma_5+\gamma_6+\gamma_7$ 28%), γ_8 1.05 (15%), γ_9 0.835 (100%), γ_{10} 0.691 (5%), γ_{11} 0.631 (54%) spect, spect conv (14M48); 3.4 (~0.03%), 3.1 (~0.1%) D-γ-p ion ch (9B50)	Q^-_β 4.0 (56H48, 14M48) see Ge^{72m}  (56H48, HPS)	Ga-d-p (12L38a); Ga-n-γ (42S39, 2S47, 60S51); Ge-n-p (42S41, 60S51); As-d-ap (16C47); As-γ-He^3, As-γ-2pn (85H52); spall-fission Sn, Ba (42B51), Tl (2T47b), Bi (11G49, 13P47), U (6O47, 6F51); fission Th (21T51), U (60S51); daughter Zn^{72} (60S51); parent Ge^{72m} (28B48)
Ga^{73}	B chem, excit (60S46, 60S51)		β^- (60S51)	5.0 h (60S51)	1.4 abs (60S51)	0.0135, 0.054 spect conv (17J51a)	 (17J51a)	Ge-n-p (60S51); Ge-γ-p (12P49); As-γ-2p (85H52); As-α-α2p (11S51); spall-fission Bi (11G49); fission U (60S51)
$_{32}Ge^{66}$	A chem, genet (48H49)		β^+ (?) (48H50)	~150 m (48H50)				spall Cu (second order reaction) (42B51a), spall Ge (48H49), As (48H50); parent Ga^{66} (48H49)
Ge^{67}	A chem, genet (48H49)		β^+ (48H50)	21 m (48H50)				spall Cu (second order reaction) (42B51a), spall Ge (48H49), As (48H50); parent Ga^{67} (48H49)
Ge^{68}	A chem (50M38); chem, genet (48H48b)		EC (48H48b)	250 d (48H50)				spall Cu (second order reaction) (42B51a), spall As (48H48a, 48H50); Zn-α-2n (50M38); parent Ga^{68} (48H48a, 48H50)
Ge^{69}	A chem (50M38); chem, excit, cross bomb (51M48)		EC ~67%, β^+ ~33% (51M48); β^+ (50M38)	39.6 h (51M48); 39.7 h (12D42); 40 h (48H50); 37 h (50M38)	1.215 (88%), 0.610 (10%), 0.22 (2%) spect (10H51)	1.610, 1.340, 1.12, 0.870, 0.576, 0.388, 0.090 spect, β-γ coinc (10H51)	Q^+_β 3.36 (10H51)  (10H51)	Zn-a-n (50M38, 51M48); Ga-d-2n (13S41a, 51M48, 10H51); Ga-p-n (12D42); Ge-n-2n (42S41, 51M48); Ge-γ-n (34H44, 42S52); spall As (48H50)

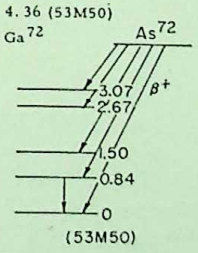
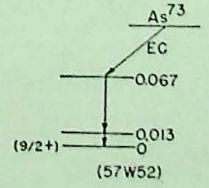
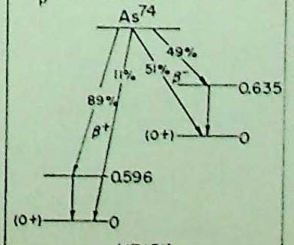
CC-0. In Public Domain. Gurukul Kangri Collection, Haridwar

Digitized by Arya Samaj Foundation Chennai and eGangotri

Isotope Z A	Class and identification	Percent abundance	Type of decay	Half-life	Energy of radiation in Mev: Particles	Energy of radiation in Mev: Gamma-transitions	Disintegration energy and scheme	Method of production and genetic relationships
$_{32}Ge^{70}$		20.55 (3I48a)					Ge^{70}, I = 0 (35T49)	
Ge^{71}	A chem, excit, cross bomb (13S41a); sep isotopes, n-capt (22R50)		EC, no β^+ (51M48, 26M49)	11.4 d (51M48); 11.3 d (12D42); 11 d (26M49, 13S41a)		no γ (13S41a, 26M49, 51M48); Ga K-x (2S47, 51M48, 26M49)		Ga-d-2n (13S41a, 51M48); Ga-p-n (12D42); Ge-d-p (13S41a, 51M48); Ge-n-γ (2S47, 51M48, 26M49); Ge^{70}-n-γ (22R50); spall As (48H50); daughter As^{71} (48H49)
Ge^{72m}	A genet (28B48)		IT (28B48)	2.9×10^{-7} s delay coinc (52M51); 5×10^{-7} s delay coinc (28B48)		0.7 (e/γ very high) coinc abs conv (28B48, 52M51)	see Ga^{72}	daughter Ga^{72} (28B48); daughter As^{72} (14S50b)
Ge^{72}		27.37 (3I48a)					Ge^{72}, I = 0 (35T49)	
Ge^{73}		7.67 (3I48a)					Ge^{73}, I = 9/2 (35T49)	
Ge^{74}		36.74 (3I48a)					Ge^{74}, I = 0 (35T49)	
Ge^{75m}	A excit (9F52); cross bomb, n-capt, sep isotopes (91S52c)		IT (9F52)	42 s (9F52); 48 s (91S52c)	conv: 0.14 abs (9F52)	0.175 scint spect (91S52c); ~0.150 scint spect (24C52)		Ge^{74}-n-γ (91S52c); Ge-n-γ (9F52, 24C52); As-n-p (9F52, 91S52c)
Ge^{75}	A chem, excit, cross bomb (13S41a); n-capt, sep isotopes (22R50)		β^- (13S41a)	82 m (51M48); 89 m (13S41a); 79 m (22R50)	1.137 (85%, not coinc with γ), 0.614 (15%) spect (91S52c); 1.2 abs (13S41a); 1.3 abs (22R50)	0.265 (e/γ very small), 0.418, 0.572, other γ's spect, spect conv, scint spect (91S52c); 0.25 (~10%) (22R50); no γ (51M48)	Q^-_β 1.14 (91S52c)	Ge^{74}-n-γ (22R50, 91S52c); Ge-n-γ (42S39, 42S41, 2S47); Ge-d-p (42S39, 42S41, 13S41a); Ge-n-2n (42S41, 13S41a); Ge-γ-n (34H44, 12P49); As-n-p (42S41, 13S41a, 51M48); Se-n-α (42S41, 13S41a)
Ge^{76}		7.67 (3I48a)					Ge^{76}, I = 0 (35T49)	
Ge^{m}	E n-capt (24C52)		IT (24C52)	~0.35 s (24C52)		~0.06 scint spect (24C52)		Ge-n-γ (24C52)
Ge^{77m}	A cross bomb, genet, n-capt (23A47); sep isotopes (22R50)		β ~50%, IT ~50% calc (42F52); β^-, IT (14M52)	59 s (23A47); 57 s (22R50)	2.8 abs (23A47)	0.38 scint spect (14M52)		Ge-n-γ, parent As^{77} (23A47, 22R50); Ge^{76}-n-γ (22R50)
Ge^{77}	A chem, excit, cross bomb (13S41a)		β^- (42S41)	12 h (13S41a, 61S51, 22R50)	2.196 (42%, coinc with γ), 1.379 (35%), 0.71 (23%) spect (91S52); others (14M52, 61S51, 22R50, 26M49)	0.042, 0.073 (coinc with 0.213 and 0.264 γ), 0.213, 0.264, 0.368, 0.418, 0.564, 1.105, 1.75 spect, β-γ, γ-γ coinc (91S52); 0.209, 0.268, 0.300, 0.327, 0.366, 0.408, 0.425, 0.466 spect conv (91S52); 0.6, 0.3 (coinc with β^-) abs, β-γ coinc (22R50)		Ge^{76}-n-γ (22R50); Ge-n-γ (42S39, 42S41, 2S47); Ge-d-p (42S41, 13S41a, 88S52); Se-n-α (13S41a); fission Th (21T51), U (61S46, 61S51), U^{233} (61S48); parent As^{77} (61S46, 61S51)

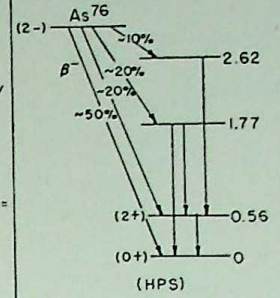
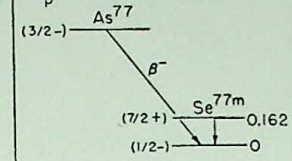
CC-0. In Public Domain. Gurukul Kangri Collection, Haridwar

Digitized by Arya Samaj Foundation Chennai and eGangotri

Isotope Z A	Class and identification.	Percent abundance	Type of decay	Half-life	Energy of radiation in Mev: Particles	Energy of radiation in Mev: Gamma-transitions	Disintegration energy and scheme	Method of production and genetic relationships
$_{32}Ge^{78}$	B chem, genet (61S46, 61S51)		β^- (61S51)	2.1 h (61S51)	~0.9 abs (61S51)	γ (61S51)		fission U, parent As^{78} (61S51)
$_{33}As^{70}$	D chem (48H49, 48H50)		β^+ (48H50)	52 m (48H50)				As-d-p6n, daughter Se^{70} (48H50); not found: Ge^{70}-p (37A52)
As^{71}	A chem (42S41); chem, genet (48H49); mass spect (104B52)		EC (48H50); EC, β^+ (51M48a)	60 h (48H50); 50 h (51M48a)		0.162 spect conv (53M50)		Ga-α-2n (53M50); Ge-d-n (51M48a); As-d-p5n (48H50); parent Ge^{71} (48H49)
As^{72}	A chem, excit (14M47); chem, excit, sep isotopes (51M48a)		EC, β^+ (51M48a)	26 h (51M48a, 2V40); 27 h (48H50)	3.34 (19%), 2.50 (62%), 1.84 (12%), 0.67 (5%), 0.27 (2%) spect (53M50); 2.8 abs (14M47, 51M48a)	0.835, others up to 3.0 (weak) spect (53M50)	Q^+_β 4.36 (53M50) see Ga^{72}  (53M50)	Ga-α-n (14M47, 51M48a, 53M50); Ge-p-n (2V40); As-d-p4n (48H50); Se^{74}-d-α (51M48a); daughter Se^{72} (48H48a)
As^{73}	A chem (42S39b); chem, excit, cross bomb, sep isotopes (51M48a); mass spect (17J51a)		EC (4E43b); no β^+ (4E43b, 51M48a)	76 d (51M48a); 90 d (42S39b, 53M50)		0.0135 (L/M 5.4), 0.0539 (K/L+M 5.6) spect conv, conv-conv coinc (17J51a, 17J52); 0.052 spect conv (4E43b, 53M50)	 (57W52)	Ge-d-n (42S39b, 4E43b); Ge^{70}-α-p (51M48a); Ge-α-p (51M48a, 53M50); As-d-p3n (48H50); Se^{76}-p-α (25F51)
As^{74}	A excit (48C38); chem, excit (42S39b)		β^- 53%, β^+ 47% (17J51); β^- ~67%, β^+ ~33% (53M50)	17.5 d (51M48a); 19.0 d (48H50); 16 d (42S39b)	β^-: 1.36 (51%), 0.69 (49%) spect (17J51); 1.45 (47%), 0.82 (53%) spect (53M50) β^+: 1.53 (11%), 0.92 (89%) spect (17J51); 0.96 spect (53M50)	Y_1 0.596, Y_2 0.635 (Y_1/Y_2 = 4) spect, β-γ coinc (17J51); 0.593 spect (53M50); 0.582 spect (20D41)	Q^-_β 1.36 (17J51) Q^+_β 2.55 (17J51)  (17J51)	Ga-α-n (51M48a); Ge-d-n (42S39b, 42S41, 2I42); Ge-p-n (2D40); As-n-2n (48C38, 42S39b); As-d-p2n (48H50); Se-d-α (23F40); Br-γ-an (85H52); spall-fission Bi (11G49)

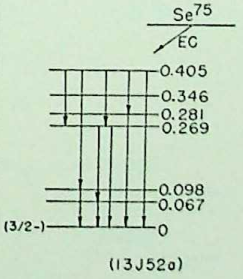
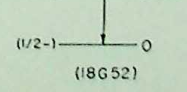
CC-0. In Public Domain. Gurukul Kangri Collection, Haridwar

Digitized by Arya Samaj Foundation Chennai and eGangotri

Isotope Z A	Class and identification	Percent abundance	Type of decay	Half-life	Energy of radiation in Mev: Particles	Energy of radiation in Mev: Gamma-transitions	Disintegration energy and scheme	Method of production and genetic relationships
$_{33}As^{75}$		100 (6N37)					As^{75}, I = 3/2 (87M50, 29J52)	
As^{76}	A chem, n-capt (12A35)		β^-, no β^+: β^+ lim 0.03% (63B47); β^+ lim 0.07% (41M51); β^+ lim 0.1% (16W48)	26.8 h (34W42); 26.3 h (14M40); 26.1 h (3P48)	3.04 (60%), 2.49 (25%), 1.29 (15%) spect (7S47d); 3.15 (54%), 2.57 (21%), 1.4 (19%), 0.4 (7%) spect (54M51); 3.15 (~40%), 2.7 (~30%), 1.1 (~30%) spect, β-γ coinc (3P48)	0.55, 1.20, 1.70 spect (7S47d); 0.557, 1.22, 1.78 (weak) spect (16W48); 0.558 (e_K/γ 0.002) spect conv (7T52); γ_1 0.57, γ_2 1.25, γ_3 1.84, γ_4 2.15 ($\gamma_1/\gamma_2/\gamma_3/\gamma_4$ = 1/0.4/weak/weak) spect (43M46); 0.58, 1.20, 1.76, 2.02, no 2.3-2.7 γ (lim 0.01%) scint spect, γ-γ coinc (62B51); γ_1 0.555, γ_2 0.648, γ_3 1.210, γ_4 1.410, γ_5 2.06 ($\gamma_1/\gamma_2/\gamma_3/\gamma_4/\gamma_5$ = 1/0.1/0.25/0.02/0.06) spect (57H51); 0.568 (e/γ ~0), 1.25 (e/γ ~0) spect, spect conv (54M49, 54M51); others (52M51)	Q^-_β 3.1 (HPS)  (HPS)	Ge-p-n (2V40); As-d-p (6T36, 48C38); As-n-γ (12A35, 48C38, 9O49, 50H51); Se-n-p (42S39b); Se-γ-p (42H47); Se-d-α (23F40); Br-n-α (48C38); Br-γ-an, Br-γ-He^3 (85H52)
As^{77}	A chem, genet (61S46, 61S51)		β^- (61S51)	38 h (18H50, 21T51); 40 h (61S51)	0.700 spect (43C51a); 0.679 spect (13J51); no conv (43C51a, 13J51)	no γ (43C51a, 13J51)	Q^-_β 0.70 (43C51a)  (43C51a, 18G52)	Br-γ-α (85H52); spall-fission Bi (11G49), Th (7N49a), U (6F51); fission Th (21T51), U (61S51), U^{233} (61S48); daughter Ge^{77} (61S51); daughter Ge^{77m} (23A47, 22R50); not parent Se^{77m} (lim 2%) (56M50a)
As^{78}	B chem (26S37a); excit (48C38)		β^- (26S37a)	90 m (61S51, 64B51); 80 m (48C38); 65 m (26S37a, 42S39b)	4.1 (~70%), 1.4 (~30%) abs (61S51); 1.4 cl ch (42S39b)	0.27 abs (42S39b); no γ coinc with 4.1 β^- (74S51a)	Q^-_β 4.1 (74S51a)	Br-n-α (26S37a, 48C38, 42S39b, 64B51); Br-γ-He^3 (85H52); Se-n-p (42S39b); fission U, daughter Ge^{78} (61S46, 61S51)
As^{78}	F chem (64B51)			~40 m (64B51)				fission U, daughter (?) Ge^{78} (64B51)
As^{79}	D chem (65B50)		β^- (11V52)	9 m (65B50); 10 m (11V52)	~2.1 abs (11V52)			Se-γ-p (65B50); Se-n-pn (11V52)
$_{34}Se^{70}$	D chem (48H49, 48H50)		β^+ (48H50)	~44 m (48H50)				As-d-7n, parent As^{70} (48H50)
Se^{72}	A chem, genet (48H48a)		EC (48H50)	9.7 d (48H50)				As-d-5n, parent As^{72} (48H48a, 48H50)

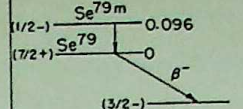
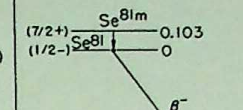
CC-0. In Public Domain. Gurukul Kangri Collection, Haridwar

Digitized by Arya Samaj Foundation Chennai and eGangotri

Isotope Z A	Class and identification	Percent abundance	Type of decay	Half-life	Energy of radiation in Mev: Particles	Energy of radiation in Mev: Gamma-transitions	Disintegration energy and scheme	Method of production and genetic relationships
$Se^{73(m?)}$	A chem (48H48a); chem, excit, sep isotopes (49C48)		β^+, EC, IT 20% (?) (62S51)	7.1 h (49C48, 62S51); 6.7 h (48H50)	1.68 (1%), 1.318 (88%), 0.750 (10%), 0.25 (1%) spect (62S51)	γ_1 0.0671 (conv in Se, K/L 7.6), γ_2 0.361 (K/L 8.6), γ_3 0.860, γ_4 1.310 ($\gamma_1/\gamma_2/\gamma_3/\gamma_4$ = 10/163/11/8) spect, spect conv (62S51)	Q^+_β 2.70 (62S51)	Ge-α-n (49C48, 62S51); Ge^{70}-α-n (49C48); As-d-4n (48H50); spall-fission Bi (66B51)
Se^{74}		0.87 (24W48)					Se^{74}, I = 0 (55G50)	
Se^{75}	A chem, excit (2D40, 4K42); sep isotopes, n-capt (10C50)		EC, no β^+ (26F47, 49C48, 10C50)	127 d (49C48); 128 d (10C50); 115 d (26F47); 120 d (48H50)		γ_1 0.067, γ_2 0.077, γ_3 0.098 (K/L ~11, e/γ ~8), γ_4 0.124 (e/γ ~0.3), γ_5 0.138 (e/γ ~0.1), γ_6 0.203, γ_7 0.269 (e/γ ~0.09), γ_8 0.281, γ_9 0.308, γ_{10} 0.405 (e/γ ~0.001) ($\gamma_2/\gamma_3/\gamma_4/\gamma_5/\gamma_7/\gamma_8/\gamma_{10}$ = 0.14/~0.007/~0.02/0.21/0.70/~0.05/0.14) spect, spect conv, γ-γ coinc (13J52a); 0.025, 0.066, 0.081, 0.097, 0.121, 0.136, 0.199, 0.265, 0.280, 0.305, 0.402 spect conv (10C50); 0.076, 0.099 (?), 0.123, 0.137, 0.267, 0.283, 0.405 spect (11T48); 0.098 (e/γ large), all other γ (e/γ very small) spect, spect conv (75M51); others (52M51)	 (13J52a)	As-p-n (2D40); As-d-2n (4K42, 26F47, 49C48, 48H50); Se-n-γ (2S47, 26F47, 11T48, 13J52a); Se^{74}-n-γ (10C50)
Se^{76}		9.02 (24W48)					Se^{76}, I = 0 (55G50)	
Se^{77m}	A n-capt (23A47); sep isotopes, n-capt (18G48a); genet (43C51b)		IT (23A47)	17.5 s (23A47, 32G49, 43C51b)		0.162 (K/L 4.6) spect conv (31R52); 0.160 (e/γ large) spect, spect conv (43C51b); 0.165 spect conv (19O52); abs (9F50); others (38M51, 31K51, 32G49, 23A47)	see Br^{77}  (18G52)	Se-n-γ (23A47); Se^{76}-n-γ (18G48a); Se-x rays (32G49); daughter Br^{77} (43C51b, 43C51); not daughter As^{77} (lim 2%) (56M50a)
Se^{77}		7.58 (24W48)					Se^{77}, I = 1/2 (55G50, 32D51)	
Se^{78}		23.52 (24W48)					Se^{78}, I = 0 (55G50, 32D51)	

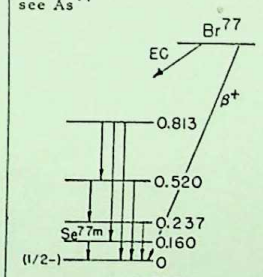
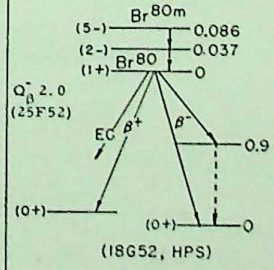
CC-0. In Public Domain. Gurukul Kangri Collection, Haridwar

Digitized by Arya Samaj Foundation Chennai and eGangotri

Isotope Z A	Class and identification	Percent abundance	Type of decay	Half-life	Energy of radiation in Mev: Particles	Energy of radiation in Mev: Gamma-transitions	Disintegration energy and scheme	Method of production and genetic relationships
$_{34}Se^{79m}$	A excit, n-capt (9F50, 9F50b); n-capt, sep isotopes (31R52)		IT (9F50b)	3.5 m (31R52); 3.9 m (9F50)		0.096 (K/L 2.9) spect conv (31R52)	 (18G52, HPS)	Se^{78}-n-γ (31R52); Se-n-γ, Se-n-2n (9F50, 9F50b); Br-n-p (9F50b)
Se^{79}	B chem, spect (?) (26P49)		β^- (26P49)	$\lesssim 6.5 \times 10^4$ y sp act (est fission yield) (26P49)	0.160 abs (26P49); ~0.150 abs (32K50)	no γ (26P49)	Se^{79}, I = 7/2 (83H52)	fission U (26P49)
Se^{80}		49.82 (24W48)					Se^{80}, I = 0 (87M50)	
Se^{81m}	A chem, excit, cross bomb (26S37a); sep isotopes, n-capt (32L47); mass spect (67B49)		IT (20L40)	56.5 m (25W48); 57 m (26S37a, 20L40); 59 m (33G51)		0.103 (K/L 3.0) spect conv (31R52); 0.104 (e/γ very large, K/L ~3.9) spect conv (67B49); 0.099 (K/L ~4) spect conv (2H41)		Se-d-p (26S37a, 20L40); Se-n-γ (26S37a, 6H37, 2S47); Se^{80}-n-γ (32L47); Br-n-p (26S37a, 20L40); fission U (33G51); parent Se^{81} (20L40)
Se^{81}	A chem, genet (20L40)		β^- (20L40)	17 m (33G51); 18 m (9F50); 19 m (20L40); 13.6 m (25W48)	1.38 spect (67B49); 1.5 abs (20L40, 33G51); no conv (31R52)	no γ (33G51)	Q^-_β 1.38 (67B49, 33G51) (3/2-) (18G52)	Se-d-p (26S37a, 20L40); Se-n-γ (26S37a, 6H37, 2S47); Se-γ-n (37B39); Br-n-p (20L40); spall-fission Bi (66B51); fission U (33G51); daughter Se^{81m} (20L40)
Se^{82}		9.19 (24W48)					Se^{82}, I = 0 (55G50)	
Se^{83}	A chem, genet (23A47)		β^- (23A47)	67 s (23A47)	3.4 abs (23A47); no conv (31R52)			Se-n-γ (23A47); fission U (63S47); parent Br^{83} (23A47)
Se^{83}	A chem, excit, cross bomb (26S37a); chem, genet (20L40)		β^- (26S37a)	25 m (33G51a); 26 m (31R52); 30 m (20L40)	1.5 abs (33G51a, 31R52)	0.950, 0.176, 0.061 (?), 0.04 (?) spect conv, scint spect (31R52); 1.1, 0.37, 0.17 abs (33G51a)		Se-d-p (26S37a, 20L40); Se-n-γ (26S37a, 20L40, 2S47); fission Th (72B51), U (33G51a); parent Br^{83} (20L40, 33G51a)
Se^{84}	A chem, genet (33G46)		β^- (33G46)	~2 m (33G51b, 20E51)				fission U, parent Br^{84} (33G51b, 20E51)
$_{35}Br^{74}$	D chem (13H51)		β^+, EC (13H51)	~35 m (13H51)				Cu-C-3n (13H51)
Br^{75}	B chem, cross bomb, sep isotopes (35W48)		β^+, EC (35W48)	1.6 h (13H51); 1.7 h (35W48)	1.70 (46%), 0.8 (20%), 0.6 (15%), 0.3 (19%) spect (25F52); ~1.8 abs (13H51)	~0.6 abs (25F52)		Cu-C-2n (13H51); Se^{74}-d-n (35W48); Se^{74}-p-γ (35W48, 25F52)
Br^{76}	A chem (48H48); chem, excit (13H51); chem, sep isotopes (25F52)		β^+ (48H48)	17.2 h (25F52); 16.5 h (13H51); 15.7 h (48H48)	3.57 (46%), 1.7 (10%), 1.1 (11%), 0.8 (14%), 0.6 (19%) spect (25F52); 3.5 spect (13H51)	1.2, 0.96, 0.75, 0.68, 0.42, 0.37, 0.33, 0.25 spect, spect conv (25F52); ~2 abs (48H48)	Q^+_β 4.6 (25F52)	As-α-3n (48H48, 13H51); Se^{76}-p-n (25F52)

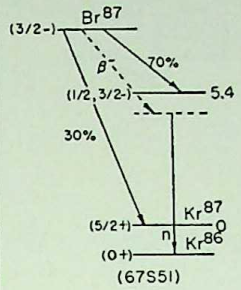
CC-0. In Public Domain. Gurukul Kangri Collection, Haridwar

Digitized by Arya Samaj Foundation Chennai and eGangotri

Isotope Z A	Class and identification	Percent abundance	Type of decay	Half-life	Energy of radiation in Mev: Particles	Energy of radiation in Mev: Gamma-transitions	Disintegration energy and scheme	Method of production and genetic relationships
$_{35}Br^{77}$	A chem, sep isotopes (35W48)		EC 95%, β^+ 5% (35W48)	57 h (48H48, 13H51); 58 h (35W48)	0.336 spect (43C51); 0.36 spect (48H48); abs, spect (35W48)	γ_1 0.160, γ_2 0.237, γ_3 0.284, γ_4 0.298, γ_5 0.520, γ_6 0.641, γ_7 0.813 ($\gamma_1/\gamma_2/\gamma_3/\gamma_4/\gamma_5/\gamma_6/\gamma_7$ = 0.6/20/0.2/0.2/100/8.6/25) spect, spect conv (43C51); 0.160, 0.234, 0.299, 0.521 spect conv, x-γ coinc (25F52)	see As^{77}  (43C51)	As-α-2n (48H48, 13H51, 43C51); Se^{74}-α-p (35W48); Se^{76}-d-n (35W48, 25F52); parent Se^{77m} (43C51, 43C51b)
Br^{78}	A chem, excit (26S37a)		β^+ (26S37a)	6.4 m (26S37a); 6.5 m (13H51).	2.4 abs (35B46a, calc from 26S37a); 2.3 abs (26S37a)	0.108, 0.046 spect conv (6V39)		As-α-n (26S37a, 13H51); Se-d-n (26S37a); Se-p-n (59B38, 6V39); Br-γ-n (7C37, 37B39); Br-n-2n (6H37)
Br^{79}		50.52 (9W46)					Br^{79}, I = 3/2 (87M50)	
Br^{80m}	A chem, n-capt (12A35); chem, excit, cross bomb (26S37a)		IT (24S39)	4.58 h (41M51); 4.5 h (26S37a); 4.4 h (59B38)		0.049, 0.037 (e/γ ~1.3) ion ch (32R50); 0.048, 0.036 spect conv (33L50); 0.049, 0.037 spect conv (6V39); 0.049 (L_I/L_{III} 1.0) spect conv (63M52a); 0.048 (e/γ very large), 0.037 (e/γ ~1) abs (35G40); others (52W51)		Se-d-2n (35W48, 25F52); Se-α-p (35W48); Se-p-n (59B38, 6V39, 25F52); Br-n-γ (24A36, 26S37a, 24S39, 34G46, 2S47); Br-d-p (26S37a); Br-γ-n (37B39); Br-n-2n (1P37); spall-fission Ta (22N52), Bi (66B51), U (6F51); fission Th (?) (9P40, 9P41)
Br^{80}	A chem, n-capt (12A35); chem, excit, cross bomb (26S37a); chem, genet (24S39)		β^- ~92%, β^+ ~3%, EC ~5% (calc from 41M51, 28R50); β^+/β^- 0.037 (41M51); $\frac{\beta^+ + EC}{\beta^-}$ 0.09 (28R50); β^+/β^- 0.028 (34L51); β^+/β^- 0.03 (63B47)	18 m (26S37a, 24S39)	β^-: 1.99 (85%), 1.1 (15%) spect (34L52); 1.97 (80%), 1.1 (11%), 0.7 (9%) spect (25F52); 1.99 spect (33L50); others (34L51, 50C48, 24A36) β^+: 0.87 spect (34L51); 1.0 spect (16D49); 0.73 abs (63B47)	>0.6 abs (21D40); <0.5 abs (26S37a, 59B38); no γ (34L52)	 (18G52, HPS)	Se-p-n (59B38); Br-n-γ (26S37a, 34G46, 2S47, 9O49); Br-d-p (26S37a); Br-γ-n (37B39); Br-n-2n (1P37); daughter Br^{80m} (24S39, 21D40, 64S41)
Br^{81}		49.48 (9W46)					Br^{81}, I = 3/2 (87M50)	
Br^{82}	A chem, n-capt (33K35); chem, excit, cross bomb (26S37a)		β^- (33K35); no EC or β^+ (lim 0.03%) (28R50); no β^+ (lim 0.02%) (41M51)	35.87 h (31C50); 36.0 h (68B50); 35.1 h (36W51); 35.7 h (38S51)	0.465 spect, β-γ coinc (33R41, 20D42b)	γ_1 0.547, γ_2 0.608, γ_3 0.692, γ_4 0.766, γ_5 0.823, γ_6 1.031, γ_7 1.312 spect conv, spect (7S49a); γ_1 0.535, γ_2 0.602, γ_4 0.750, γ_6 1.020, γ_7 1.292, γ_8 1.445 ($\gamma_1/\gamma_4/\gamma_6/\gamma_7/\gamma_8$ = 3.7/3.5/1.0/0.85/0.40) spect (16D52); 0.547, 0.615, 0.682, 0.752, 0.822, 1.026, 1.306, 1.453 spect (57H51a); 1.7-2.0 (0.14%) Be-γ-n reaction (33M49); 0.07, 0.05 abs conv (69B44); others (52M51)		Se-p-n (59B38, 6R41a); Se-d-2n (26S37a, 56M51); Br-n-γ (33K35, 26S37a, 2S47); Br-d-p (26S37a, 56M51); Rb-n-α (26S37a); spall-fission Ta (22N52), Hg (63S52), Tl (2T47b), Pb (13P47a), Bi (66B51, 13P47, 11G49), U (6O48, 6F51); fission U (2F51)

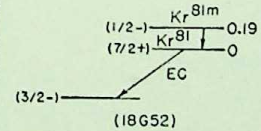
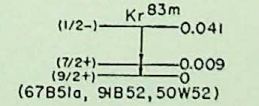
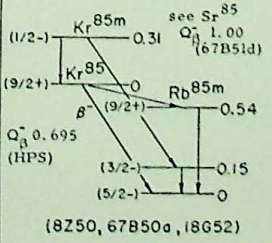
CC-0. In Public Domain. Gurukul Kangri Collection, Haridwar

Digitized by Arya Samaj Foundation Chennai and eGangotri

Isotope Z A	Class and identification	Percent abundance	Type of decay	Half-life	Energy of radiation in Mev: Particles	Energy of radiation in Mev: Gamma-transitions	Disintegration energy and scheme	Method of production and genetic relationships
$_{35}Br^{83}$	A chem, excit (26S37a)		β^- (26S37a)	2.33 h (20L40, 49H51a); 2.4 h (33G51a, 26S37a)	0.940 spect (23D51); 0.94 spect (25F52)	no γ (26S37a, 33G51a); ~0.046 (?) cl ch (50W52)		Se-d-n (26S37a, 25F52); Rb-γ-α (49H51a); spall-fission Ta (22N52), Hg (63S52), Pb (13P47a), Bi (13P47, 11G49, 66B51), Th (7N49a), U (6O48); fission Th (6B39, 20L40, 21T51, 72B51), U (20L40, 65S40, 57M41, 33G51a), U^{233} (61S48), Pu (32K48, 61S51a); daughter Se^{83}, parent Kr^{83m} (20L40, 65S40, 57M41, 33G51a)
Br^{84}	A chem (22D39); chem, excit (70B43)		β^- (22D39)	30 m (65S40); 32 m (23D51); 33 m (32K51)	4.68 (40%), 3.56 (9%), 2.53 (16%), 1.72 (35%) spect (23D51)	0.89, 1.89 scint spect (10L52d)		Rb-n-α (70B43); spall-fission Bi (13P47a), U (6F51); fission Th (72B51), U (22D39, 16H39a, 16H39b, 65S40, 57M41, 70B43, 32K51); daughter Se^{84} (33G51b)
Br^{85}	A chem (65S40); chem, genet (66S43)		β^- (65S40)	3.00 m (63S49); 3.0 m (65S40, 70B43)	2.5 abs (63S49)	no γ (63S49)		fission U (65S40, 70B43, 66S43, 63S49); parent Kr^{85} (66S43, 63S49)
Br^{87}	A chem (65S40, 26S47); chem, genet (70B43, 63S49)		β^-, β^-n (~2% of disintegrations) (19L51a)	55.6 s (n) (28H48a); 55.0 s (n) (34R47); 56.1 s (β^-) (63S49)	β^-: 2.6 (70%), 8.0 (30%) abs (67S51); n (mean): 0.25 abs paraffin (28H48a); 0.30 p recoil in cl ch (71B46)	5.4, others ~3 abs, abs sec, γ-γ coinc (67S51)	Q^-_β ~8 (?) (67S51)  (67S51)	fission U (65S40, 26S47, 63S47a, 63S49), U^{235} (34R47, 28H48a), Pu (34R47); parent Kr^{87} (70B43, 66S43, 63S49); parent Kr^{86} (2% of dis) (26S47, 63S49)
Br^{88}	A chem, genet (63S49)		β^- (63S49)	15.5 s (63S49)				fission U, parent Kr^{88} (63S49)
Br^{89}	D chem (63S47a)		β^-, β^-n (26S47a, 28H48a)	4.51 s (n) (28H48a); 4.45 s (n) (34R47)	n (mean): 0.43 abs paraffin (28H48a); 0.65 p recoil in cl ch (71B46)			fission U (63S47a, 26S47a, 63S49), U^{235} (34R47, 28H48a); parent Kr^{89} (?), parent Kr^{88} (?) (51C51)
$_{36}Kr^{77}$	B chem, sep isotopes (35W48a)		EC 70%, β^+ 30% (35W48a)	1.1 h (35W48a)	1.7 abs (35W48a)	γ (35W48a)		Se-α-n, Se^{74}-α-n (35W48a)
Kr^{78}		0.354 (6N50a)						

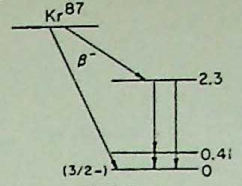
CC-0. In Public Domain. Gurukul Kangri Collection, Haridwar

Digitized by Arya Samaj Foundation Chennai and eGangotri

Isotope Z A	Class and identification	Percent abundance	Type of decay	Half-life	Energy of radiation in Mev: Particles	Energy of radiation in Mev: Gamma-transitions	Disintegration energy and scheme	Method of production and genetic relationships
$_{36}Kr^{79m}$	D chem (29C40b)		IT (?), no β^+ (29C40b)	55 s (29C40b)		0.127 spect conv (29C40b)		Br-p-n (33B40a, 29C40b)
Kr^{79}	A chem (29C40b); chem, sep isotopes (35W48a); mass spect (104B52)		EC 95% (L/K 0.27), β^+ 5% (12R52a, 12R52b); EC (K) ~90%, β^+ ~10% (67B51); EC ~98%, β^+ ~2% (35W48a)	34.5 h (12R52); 34 h (33B40a, 35W48a, 29C40b)	0.595 spect (67B51); 0.6 abs (58H51)	0.263 (e/γ ~0.02), 0.044 spect conv (67B51); 0.2 abs (58H51)		Se-a-n (52C41); Se^{76}-a-n (35W48a); Br-d-2n (30C44); Br-p-n (33B40a, 29C40b); Kr-d-p (26S37a, 52C41); Kr-n-γ (58H51, 67B51)
Kr^{80}		2.27 (6N50a)						
Kr^{81m}	A chem (29C40b); genet (7K50)		IT, no β^+ (29C40b)	13 s (29C40b); ~10 s (7K50)		0.193 spect conv (7K50); 0.187 spect conv (29C40b)	 (18G52)	Br-p-n (33B40a, 29C40b); daughter Rb^{81} (7K50)
Kr^{81}	A chem, mass spect (28R50a)		EC (28R50a)	2.1×10^5 y sp act (28R50a)		0.012 abs, Br K-x (28R50a)		Kr-n-γ (28R50a)
Kr^{82}		11.56 (6N50a)					Kr^{82}, I = 0 (87M50)	
Kr^{83m}	A chem, genet (20L40); mass spect (67B50)		IT (20L40)	114 m (67B51a, 21R46); 113 m (20L40)		0.0322 (e/γ very large, K/L+M 0.35), 0.0093 (e/γ very large, L/M ~3) spect conv (67B51a); 0.032 (K/L 0.32), 0.009 (e/γ ~10) ion ch (91B52); 0.046, 0.029 spect conv (2H41)	 (67B51a, 91B52, 50W52)	Se-a-n (52C41); Kr-d-p (52C41); Kr-n-γ, Kr-x rays (37W45); fission U, daughter Br^{83} (20L40); daughter Rb^{83} (53C50)
Kr^{83}		11.55 (6N50a)					Kr^{83}, I = 9/2 (87M50)	fission U (mass spect) (13T47, 13T48a)
Kr^{84}		56.90 (6N50a)					Kr^{84}, I = 0 (87M50)	fission U (mass spect) (13T47, 13T48a)
Kr^{85m}	A chem (26S37a); chem, mass spect (34K49)		β^- 77%, IT 23% (67B51d)	4.36 h (34K49); 4.4 h (35W48a); 4.5 h (58H51, 26S37a); 4.6 h (21R46, 66S43)	0.855 spect (67B51d); 0.85 abs (70B43a); 0.95 abs (58H51); 0.75 abs (34K49)	0.150 (e/γ 0.057, coinc with β^-), 0.305 spect conv, β-γ coinc (67B50a, 67B51d); 0.17, 0.37 abs (58H51)	 (8Z50, 67B50a, 18G52)	Se-a-n (35W48a); Kr-d-p (26S37a, 52C41); Kr-n-γ (21R45, 58H51); Rb-n-p, Sr-n-a (70B43); fission U, daughter Br^{85} (66S43, 63S49)
Kr^{85}	A chem (58H51a); chem, mass spect (13T47)		β^- (58H51a)	9.4 y (13T48a); ~10 y (58H51a)	0.695 (99+%), 0.15 (0.65%) spect, β-γ coinc abs (8Z50); 0.74 abs (58H51a)	0.54 (coinc with 0.15 β^-) scint spect, abs, β-γ coinc (8Z50)		Kr-n-γ (58H51); fission U (13T47, 58H51a)
Kr^{86}		17.37 (6N50a)					Kr^{86}, I = 0 (87M50)	fission U (mass spect) (13T47, 13T48a); daughter Br^{87} (2% of dis) (26S47, 63S49)

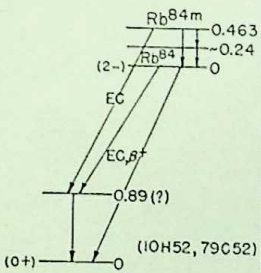
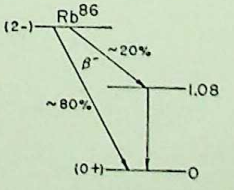
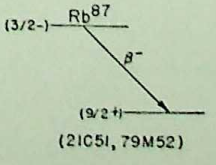
CC-0. In Public Domain. Gurukul Kangri Collection, Haridwar

Digitized by Arya Samaj Foundation Chennai and eGangotri

Isotope Z A	Class and identification	Percent abundance	Type of decay	Half-life	Energy of radiation in Mev: Particles	Energy of radiation in Mev: Gamma-transitions	Disintegration energy and scheme	Method of production and genetic relationships
$_{36}Kr^{87}$	A chem, (26S37a); chem, mass spect (34K49)		β^- (26S37a)	78 m (34K49); 75 m (66S43, 63S49); 74 m (26S37a)	3.63 (75%), 1.27 (25%) spect (30T52a); others (34K49, 70B43a)	0.41, 1.89, ~2.3 scint spect (30T52a)	Q^-_β 3.6 (30T52a)  (30T52a)	Kr-n-γ (21R46, 58H51); Kr-d-p (26S37a); Rb-n-p (70B43); fission U (70B43, 66S43); daughter Br^{87} (66S43, 70B43, 63S49)
Kr^{88}	A chem (6H39); chem, genet (20L39); chem, mass spect (34K49)		β^- (20L39)	2.77 h (34K49); 2.8 h (36G40, 63S49)	2.8 (20%), 0.9 (12%), 0.52 (68%) spect (30T52b); 2.4 (weak), ~0.5 abs (4J48, 34K49)	0.028 (coinc with 0.5 β^-, e/γ ~0.1, K/L+M 8) spect conv, β-γ coinc (30T52b)		fission Th (20L39, 25A39), U (6H39, 16H40a, 36G40, 16H40b); parent Rb^{88} (20L39, 25A39, 6H39, 16H40a, 36G40, 16H40b); daughter Br^{88} (63S49)
Kr^{89}	A chem, genet (36G40, 66S40); mass spect (35K51a)		β^- (36G40)	3.18 m (35K51a); 2.6 m (24D51); 2.5 m (16H43a)	4.0 abs (35K51a); 3.9 calc from average recoil energy (35K51)			fission U, parent Rb^{89} (36G40, 66S40, 16H40b, 16H43, 17B51, 35K51a); spall-fission U (11O51); fission Pu (26A51)
Kr^{90}	A chem, genet (24D51a); mass spect (35K51a)		β^- (24D51a)	33 s (35K51a, 32K46)	3.2 abs (35K51a)			fission U, ancestor Sr^{90} (24D51a, 24D51); fission Pu (26A51); parent Rb^{90} (35K51a)
Kr^{91}	A chem, genet (16H40c); mass spect (35K51a)		β^- (16H40c)	9.8 s (24D51); 10 s (35K51a); ~6 s (11O51)	~3.6 abs (35K51a)			fission U, ancestor Y^{91} (16H40c, 17B51, 24D51a, 24D51); spall-fission U (11O51); fission Pu (26A51) parent Rb^{91}, parent Rb^{91m} (35K51a)
Kr^{92}	B chem, genet (16H40a, 24D51)		β^- (16H40a)	3.0 s (24D51)				fission Th (16H40), U (16H40a, 16H40b, 16H43), Pu (26A51); ancestor Y^{92} (24D51)
Kr^{93}	B chem, genet (16H42, 70S51)		β^- (16H42)	2.0 s (24D51)				fission U, ancestor Y^{93} (70S51); spall-fission U (11O51); fission Pu (26A51)
Kr^{94}	B chem, genet (16H43a, 24D51)		β^- (16H43a)	1.4 s (24D51)				fission U, ancestor Y^{94} (16H43a, 24D51)
Kr^{95}	A chem, genet (24D51a)		β^- (24D51a)	short (24D51a)				fission U, ancestor Zr^{95} (24D51a)
Kr^{97}	B chem, genet (26A51)		β^- (26A51)	~1 s (24D51)				fission U, ancestor Zr^{97} (26A51, 24D51); fission Pu (26A51)
$_{37}Rb^{81}$	A chem, mass spect (10R49)		EC 87%, β^+ 13% (7K50)	4.7 h (7K50)	0.990 spect (7K50)	0.95 abs (7K50)		Br-α-2n (10R49, 7K50); parent Kr^{81} (7K50)
Rb^{82m}	B chem, genet (54L52)		β^+ (54L52)	1.25 m (54L52)	~3 abs (54L52); see Sr^{82}			daughter Sr^{82} (54L52)
Rb^{82}	A chem (59H40); chem, mass spect (10R49)		EC 94%, β^+ 6% (7K50)	6.3 h (7K50)	0.775 (76%), 0.175 (24%) spect (10H52); 0.670 spect (7K50)	0.188, 0.248, 0.322, 0.390, 0.423, 0.465, 0.558, 0.610, 0.690, 0.768, 0.818, 1.020, 1.314, 1.464 spect conv, spect (10H52)		Br-α-n (59H40, 10R49, 7K50); Kr-d-2n (59H40); not daughter Sr^{82} (lim 0.01%) (54L52)

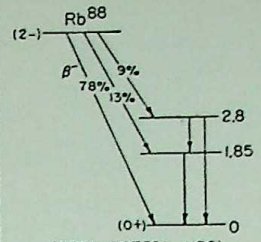
CC-0. In Public Domain. Gurukul Kangri Collection, Haridwar

Digitized by Arya Samaj Foundation Chennai and eGangotri

Isotope Z A	Class and identification	Percent abundance	Type of decay	Half-life	Energy of radiation in Mev: Particles	Energy of radiation in Mev: Gamma-transitions	Disintegration energy and scheme	Method of production and genetic relationships
$_{37}Rb^{83}$	A chem, mass spect (7K50)		EC (7K50)	83 d (53C50); 107 d (7K50)		-0.45, -0.15 spect conv (53C50)		Br-α-2n (7K50); daughter Sr^{83} (53C50); parent Kr^{83m} (53C50)
Rb^{84m}	B chem (59H40); chem, excit (9F50a)		IT, EC (weak) (79C52); EC (9F50a)	23 m (9F50a); 20 m (59H40)		γ_1 0.463 (not coinc with γ_2 or γ_3), γ_2 0.239, γ_3 -0.239 (coinc with γ_2), γ_4 0.890 (γ_1/γ_4 = 7) scint spect, γ-γ coinc (79C52)		Br-α-n (59H40); Rb-n-2n (9F50a, 79C52)
Rb^{84}	A chem, cross bomb (63B47); chem, mass spect (7K50)		EC, β^+, β^- (?) (7K50, 73B50); EC/β^+ ~13 (7K50); β^+/β^- ~6.2 (73B50)	34 d (7K50); 38 d (73B50)	β^+: 1.629 (39%), 0.822 (58%), 0.373 (?) (3%) spect (10H52); 1.5 spect (7K50); 1.3 abs (73B50)	0.890 scint spect, spect conv (10H52); 0.85 abs (7K50); 0.8 abs (73B50)		Br-α-n (7K50, 73B50); Kr-α-pn, Kr-d-2n (73B50); Rb-n-2n (63B47); Sr-d-α (63B47)
Rb^{85m}	A genet (14S52)		IT (14S52)	0.9×10^{-6} s delay coinc (14S52)		0.513 spect, spect conv (11T51, 14S52)	see Sr^{85} and Kr^{85}	daughter Sr^{85} (14S52)
Rb^{85}		72.15 (6N50a)					Rb^{85}, I = 5/2 (87M50)	fission U (mass spect) (38W52)
Rb^{86m}	B chem, excit, n-capt (9F51)		IT, no EC (12P52); EC (9F51)	0.99 m (12P52); 1.06 m (9F51)		0.57 scint spect (12P52); 0.78 abs (9F51)		Rb-n-γ, Rb-n-2n (9F51)
Rb^{86}	A chem, n-capt (26S37a); chem, excit (2H41a)		β^- (2H41a); no β^+ (lim 0.002%) (41M51); no EC (lim 0.04%) (12P52)	19.5 d (2H41a)	β_1 1.82 (80%), β_2 0.72 (20%) spect (5Z48); β_1 1.79 spect (96M52); β_1 1.76, β_2 0.670 (coinc with γ) β-γ coinc spect (23M51); β_1 1.82 (~67%), β_2 0.56 (~33%) abs (15J48); β_2 0.72 (coinc with γ) β-γ coinc spect (55M50); β_2 0.67 scint spect (27P51); β_2 (12%) β-γ coinc (26M50)	1.076 spect (55M50); 1.081 spect (5Z48); 1.12 (coinc with β_2) coinc abs sec, β-γ coinc (15J48); others (85S51)	Rb^{86}, I = 2 (98B51) Q^-_β 1.8 (5Z48)  (5Z48, HPS)	Rb-n-γ (26S37a, 69S38, 2S47); Rb-γ-n (34H44); Sr-d-α (2H41a); spall-fission Bi (11G49, 66B51), U (6F51); fission U (2F51a)
Rb^{87}	A chem (1T05, 54C06); chem, genet (16H37a, 8M37); chem, mass spect (40H37)	27.85 (6N50a)	β^- (1T05, 54C06)	6.0×10^{10} y sp act (37H48, 37H48a, 37K49, 50L52); 6.4×10^{10} y sp act (79M52); 6.2×10^{10} y sp act (21C51); 7.6×10^{10} y (55C51, calc from 21C51); 6.3×10^{10} y yield (65S38); 5.8×10^{10} y sp act (10E46)	0.275 spect (21C51); scint spect (50L52); 0.270 scint spect (11B50e); others (36K35, 34T52, 3L39, 14O41, 12S46)	no γ (21C51, 79M52, 50L52)	Rb^{87}, I = 3/2 (87M50) Q^-_β 0.27 (21C51)  (21C51, 79M52)	natural source (1T05, 54C06); fission U (mass spect) (38W52); parent Sr^{87} (mass spect) (16H37a, 8M37)

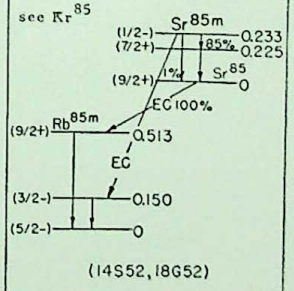
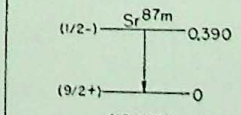
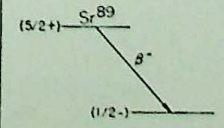
CC-0. In Public Domain. Gurukul Kangri Collection, Haridwar

Digitized by Arya Samaj Foundation Chennai and eGangotri

Isotope Z A	Class and identification	Percent abundance	Type of decay	Half-life	Energy of radiation in Mev: Particles	Energy of radiation in Mev: Gamma-transitions	Disintegration energy and scheme	Method of production and genetic relationships
$_{37}Rb^{88}$	A chem (26S37a); chem, genet (20L39, 36G40, 16H39a)		β^- (16H39a)	17.8 m (36G40, 2B51); 17.7 m (30T52b); 17.5 m (34W42); 18 m (16H40b, 26S37a)	5.30 (78%), 3.6 (13%), 2.5 (9%) spect (30T52b); 5.13 (66%), 3.29 (19%), 2.0 (15%) spect (2B51); 5.20 (~66%), 3.6 (~17%), 1.8 (~17%) abs (37G51)	2.8, 1.86, 0.90 spect (2B51); γ_1 3.0, γ_2 1.7 (γ_1/γ_2 ~ 1/10) abs sec, β-γ coinc (37G51)	see Y^{88} Q^-_β 5.30 (30T52b)  (2B51, 30T52b, HPS)	Rb-n-γ (26S37a, 1P37, 69S38, 2S47); fission Th (25A39), Pa (2G39); fission U, daughter Kr^{88} (6H39, 20L39, 36G40, 16H40a, 16H40b)
Rb^{89}	A chem, genet (36G40, 66S40)		β^- (36G40)	15.4 m (36G40); 15.5 m (16H40b)	4.5 abs (35B46a, calc from 36G40); 3.8 abs (36G40)	γ (35B46a)		fission U, daughter Kr^{89} (36G40, 66S40, 16H40b, 16H43, 17B51); parent Sr^{89} (36G40, 16H40a, 16H40b, 16H43)
Rb^{90}	A chem, genet (35K51a)		β^- (35K51a)	2.74 m (35K51a)	5.7 abs (35K51a)	γ (35K51a)		fission U, daughter Kr^{90}, parent Sr^{90} (24D51a, 24D51, 35K51a)
Rb^{91}	A chem, genet (35K51a)		β^- (35K51a)	1.67 m (35K51a); [short] (24D51a, 17B51, 11O51, 24D51, 16H40c)	4.6 abs (35K51a)	γ (35K51a)		fission U, daughter Kr^{91}, parent Sr^{91} (35K51a); ancestor Y^{91} (24D51a, 16H40c)
Rb^{91}	A chem, genet (35K51a)		β^- (35K51a)	14 m (35K51a)	3.0 abs (35K51a)	γ (35K51a)		fission U, daughter Kr^{91}, parent Sr^{91} (35K51a)
Rb^{92}	D chem, genet (16H40a)		β^- (16H40a)	80 s (16H40a); [short] (17B51, 24D51)				fission U, daughter Kr^{92} (24D51); ancestor Y^{92} (16H40a, 16H40c, 16H40, 16H43, 24D51)
Rb^{93}	[B] genet (16H42, 17B51)		[β^-] (16H42)	[short] (17B51, 24D51, 24D51a, 16H42, 16H43)				fission U, daughter Kr^{93} (17B51, 24D51, 24D51a); ancestor Y^{93} (16H42, 16H43, 17B51)
Rb^{94}	[B] genet (16H43, 16H43a)		[β^-] (16H43, 16H43a)	[short] (24D51, 16H43, 16H43a)				fission U, daughter Kr^{94}, ancestor Y^{94} (16H43, 16H43a, 24D51)
Rb^{95}	[A] genet (24D51a)		[β^-] (24D51a)	[short] (24D51a)				fission U, daughter Kr^{95}, ancestor Zr^{95} (24D51a)
Rb^{97}	[A] genet (24D51)		[β^-] (24D51)	[short] (24D51)				fission U, daughter Kr^{97}, ancestor Zr^{97} (24D51); fission U^{235}, Pu (26A51)

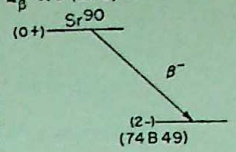
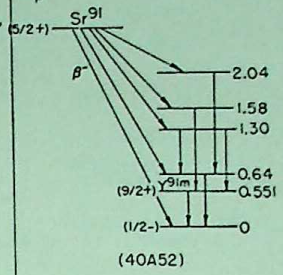
CC-0. In Public Domain. Gurukul Kangri Collection, Haridwar

Digitized by Arya Samaj Foundation Chennai and eGangotri

Isotope Z A	Class and identification	Percent abundance	Type of decay	Half-life	Energy of radiation in Mev: Particles	Energy of radiation in Mev: Gamma-transitions	Disintegration energy and scheme	Method of production and genetic relationships
$_{38}Sr^{81}$	B chem, genet (53C50)		EC, β^+ (53C50)	29 m (53C50)	conv (53C50)			spall Rb, parent Rb^{81} (53C50)
Sr^{82}	A chem, excit (53C50); mass spect (97M52)		EC, β^+ (?) (53C50)	27 d (97M52); 25 d (53C50)	β^+ with Rb^{82m} (54L52); 3.15 spect (53C50)	0.95, -0.40, -0.15 spect conv, abs (53C50)		spall Rb (53C50); daughter Y^{82} (78C52); parent Rb^{82m}, not parent Rb^{82} (lim 0.01%) (54L52)
Sr^{83}	A chem, genet (53C50); mass spect (97M52)		EC, β (53C50)	33 h (97M52); 38 h (53C50)	1.15 spect (53C50); 1.35 abs (97M52)	0.040, 0.074, 0.101, 0.151, 0.165 spect conv (53C50)		spall Rb, parent Rb^{83} (53C50); daughter Y^{83} (78C52)
Sr^{84}		0.56 (6N38b)						
Sr^{85m}	A chem, excit (2D40a)		IT 86%, EC 14% (14S52)	70 m (2D40a)		0.0075 (e/γ very large), 0.150 (with EC), 0.225 (e/γ 0.031, K/L ~5.5), 0.233 (e/γ ~0.04) scint spect, spect conv, x-γ coinc (14S52); 0.233, 0.152 spect conv (11T51)	see Kr^{85}  (14S52, 18G52)	Rb-p-n (2D40a); Rb-d-2n (11T51); Sr^{84}-n-γ (14S52)
Sr^{85}	A chem, excit (2D40a)		EC (35L51, 11T51); no β^+ (11T51)	65 d (11T51); 66 d (2D40a)		with Rb^{85m}: 0.513 spect, spect conv (11T51); 0.513 (~100%, e/γ 0.008) spect conv, x-γ coinc, scint spect (14S52); 0.514 (~100%, e/γ 0.007, K/L ~12) spect, spect conv, coinc abs (2E52)		Rb-p-n (2D40a); Rb-d-2n (11T51, 35L51, 2E52); parent Rb^{85m} (14S52); daughter Y^{85} (78C52)
Sr^{86}		9.86 (6N38b)					Sr^{86}, I = 0 (87M50)	
Sr^{87m}	A chem, excit (71S37); chem, excit, cross bomb, genet (2D40a)		IT (2D40a)	2.80 h (58M51, 8H51b); 2.75 h (2D40a)		0.388 (K/L+M 5.79) spect conv (59G52); 0.390 (e/γ 0.28, K/L+M 6.9) spect conv, x-conv coinc (58M51); 0.388 (K/L+M 5.5) spect conv (79B52); 0.388 spect conv (11T51); 0.394 (K/L 7.2) spect conv (8H51b); 0.386 spect conv (2H41)	 (18G52)	Rb-p-n (2D39); Sr-n-n (2D40a, 35R40, 35R40a); Sr-x rays, Sr-e-e (37W45a); Sr-d-p (71S37); Sr-n-γ (71S37, 2D39, 35R40, 2S47, 2S47a); Sr-p-p (?) (2D40a); daughter Y^{87} (2D39, 2D40a, 58M50, 18H51b, 58M51); Zr-n-α (42S40)
Sr^{87}		7.02 (6N38b)					Sr^{87}, I = 9/2 (87M50)	
Sr^{88}		82.56 (6N38b)					Sr^{88}, I = 0 (87M50)	
Sr^{89}	A chem, excit (71S37); chem, mass spect (60H48)		β^- (71S37)	53 d (1N51); 54 d (36L39); 55 d (71S39, 11G49)	1.463 spect (10L49); 1.48 spect (17N44); 1.5 spect (72S49, 4W44, 11R47); cl ch (71S39)	no γ (1N51, 71S39, 71S37); others (52M51)	see Zr^{89} Q^-_β 1.46 (10L49)  (18G52)	Sr-d-p (71S37, 71S39); Sr-n-γ (71S37, 71S39, 2S47); Y-n-p (42S38); Zr-n-α (?) (42S40); spall-fission Pt (2T47b), Pb (13P47a), Bi (2T47b, 11G49, 66B51), Th (7N49a), U (6O48, 11O51, 6F51); fission Th (72B51, 21T51), U^{233} (38G48, 61S48), U^{235} (38G46), Pu (28F51); fission U, daughter Rb^{89} (36G40, 16H40a, 16H40b, 16H43, 38G46)

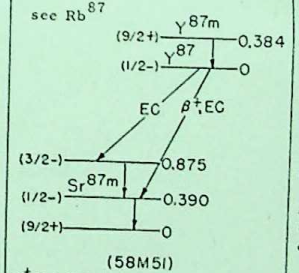
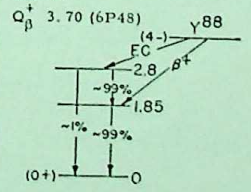
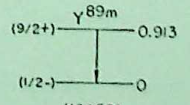
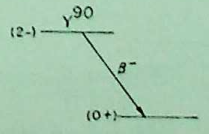
CC-0. In Public Domain. Gurukul Kangri Collection, Haridwar

Digitized by Arya Samaj Foundation Chennai and eGangotri

Isotope Z A	Class and identification	Percent abundance	Type of decay	Half-life	Energy of radiation in Mev: Particles	Energy of radiation in Mev: Gamma-transitions	Disintegration energy and scheme	Method of production and genetic relationships
Sr^{90}	A chem, genet (16H42); chem, mass spect (60H48, 38W52)		β^- (18N51)	19.9 y (28P50)	0.61 spect (47M48a); 0.54 spect (23L50); 0.53 spect (74B49); 0.6 abs (38G46, 33G51c)	no γ (33G51c, 39G43)	Q^-_β 0.6 (HPS) 	spall-fission Bi (11G49), Th (7N49a); fission Th (21T51), U^{233} (38G48), U^{235} (38G46); fission U, daughter Rb^{90} (24D51a, 24D51, 35K51a, 38W52); parent Y^{90} (16H42, 16H43, 38G46, 18N51)
Sr^{91}	A chem, genet (40G41); chem, excit (66S43a)		β^- (40G41)	9.7 h (28F51a); 10 h (16H43)	2.665 (26%), 2.03 (4%), 1.36 (29%), 1.09 (33%), 0.62 (7%) spect (40A52); 3.2 (~60%), 1.3 (~40%) abs (28F51a)	0.551 (with Y^{91m}, K/L+M 6.0), 0.64, 0.66, 0.747, 1.025, 1.413 (coinc with 0.630 γ) spect, scint spect, γ-γ coinc (40A52)	Q^-_β 2.66 (40A52) 	Zr-n-α (66S43a); spall-fission Pt (2T47b), Hg (π^-) (63S52), Pb (13P47a), Bi (13P47a, 13P47, 66B51), Th (7N49a), U (6F51), U (C) (13H51); fission Th (72B51, 21T51), Pu (32K48, 28F51); fission U, parent Y^{91m}, parent Y^{91} (40G41, 16H43, 28F51a); daughter 1.7 m Rb^{91}, 14 m Rb^{91} (35K51a)
Sr^{92}	B chem, genet (40G41)		β^- (40G41)	2.7 h (40G41)				spall-fission Th (7N49a); fission Th (72B51), U (16H40a, 16H43, 16H43a, 32K51a, 17B51), Pu (32K48); parent Y^{92} (40G41, 58H51b)
Sr^{93}	B chem (36L39); chem, genet (16H43)		β^- (36L39)	7 m (36L39)				fission U (36L39, 16H42, 16H43); parent Y^{93} (16H43, 16H43a)
Sr^{94}	B chem, genet (16H43, 16H43a)		β^- (16H43, 16H43a)	~2 m (16H43, 16H43a)				fission U (16H43, 16H43a, 24D51); parent Y^{94} (16H43, 16H43a)
Sr^{95}	[A] genet (24D51a)		β^- (24D51a)	short (24D51a)				fission U, ancestor Zr^{95}, descendent Kr^{95} (24D51a)
Sr^{97}	[A] genet (24D51)		β^- (24D51)	short (24D51)				fission U, ancestor Zr^{97}, descendent Kr^{97} (24D51, 26A51)
$_{39}Y^{82}$	B chem, genet (78C52)			70 m (78C52)				spall Y, parent Sr^{82} (78C52)
Y^{83}	B chem, genet (78C52)			3.5 h (78C52)				spall Y, parent Sr^{83} (78C52)
Y^{84}	B chem, excit, sep isotopes (36R49)		β^+, EC (36R49)	3.7 h (36R49)	2.0 abs (36R49)	γ (36R49)		Sr^{84}-d-2n, Sr^{84}-p-n (36R49)
Y^{85}	B chem, genet (78C52)			5 h (78C52)				spall Y, parent Sr^{85} (78C52)

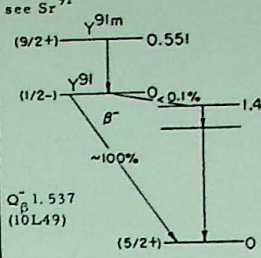
CC-0. In Public Domain. Gurukul Kangri Collection, Haridwar

Digitized by Arya Samaj Foundation Chennai and eGangotri

Isotope Z A	Class and identification	Percent abundance	Type of decay	Half-life	Energy of radiation in Mev: Particles	Energy of radiation in Mev: Gamma-transitions	Disintegration energy and scheme	Method of production and genetic relationships
$39Y^{86}$	B chem, excit, sep isotopes (53C51)		β^+ (53C51)	14.6 h (53C51, 8H51b)	1.80 (~50%), 1.19 (~50%) spect (8H51b)	1.4 abs (8H51b); ~1.3 abs (53C5i)		Sr-p-3n, Sr^{88}-p-3n (53C51); spall Nb, daughter Zr^{86} (8H51b)
Y^{87m}	A chem (71S39); chem, excit, cross bomb (2D40a)		IT (2D40a); no β^+ (8H51b)	14 h (2D40a, 8H51b, 58M51)		0.381 (K/L+M 5.41) spect conv (59G52); 0.384 (e/γ 0.28) spect conv, ion ch, conv-x coinc (58M51); 0.389 spect conv (8H51b); no γ >1 (58M51); conv >1 (8H51b)	see Rb^{87}  (58M51) Q^+_β 2.1 (58M51)	Sr-d-n (71S39, 2D40a, 58M50, 58M51); Sr-p-n (2D40a, 58M51); spall Nb, daughter Zr^{87} (8H51b); parent Y^{87} (58M50, 8H51b, 58M51)
Y^{87}	A chem (71S39); chem, excit, cross bomb (2D40a)		EC 99+%, β^+ ~0.3% (58M51); EC, β^+ (weak) (36R50)	80.0 h (58M51); 80 h (2D40a, 8H51b)	0.7 spect (58M51, 36R50)	0.485 (e/γ 0.0035) spect conv, scint spect, γ-x coinc (58M51); 0.390 (with Sr^{87m})		Sr-p-n (2D40a, 58M51); Sr-d-n (71S39, 2D40a, 58M51, 58M50); Sr^{84}-α-p (36R50); spall Nb (8H51b), Sb (37L50); daughter Y^{87m} (58M50, 8H51b, 58M51); parent Sr^{87m} (2D40a, 37L50, 58M50, 8H51b, 58M51)
Y^{88}	A chem (2D40a); chem, excit (2H42); mass spect (60H48)		EC (2D40a); EC 99+%, β^+ 0.19% (6P48)	104 d (10O46); 105 d (2D40a)	0.83 spect (6P48)	0.908 (e/γ 0.0003), 1.853 (e/γ 0.0001), 2.76 spect conv, spect (6P48); ~0.9 (e_K/γ 0.00034), ~1.85 (e_K/γ 0.00017) spect conv (44M52b); 0.908, 1.89 spect, γ-γ coinc (25D41); 1.87 Be-γ-n reaction (17S41); 2.8 (~1%) D-γ-n reaction (41G44)	see Rb^{88} Q^+_β 3.70 (6P48)  (6P48, HPS)	Sr-d-2n (29P40, 2H42, 41G44, 17B50); Sr-p-n (2D40a); Y-n-2n (2H42, 10O46); daughter Zr^{88} (8H51b)
Y^{88}	G not found: chem, cross bomb, sep isotopes (36R49)		β^+ (71S37)	2.0 h (71S39)				Sr-d (71S37, 71S39); Sr-p (2D40b, 2D40a); Y-n (71S37)
Y^{89m}	A chem, genet (18G51)		IT (18G51)	~14 s (18G51)		0.913 spect conv (73S51); 0.917 spect conv (8H51b); ~0.9 (K/L+M 7.0) spect conv (79B52); 0.92 (e/γ 0.01) spect conv, scint spect (74S51, 18G51)	 (18G52)	Y-n-n, daughter Zr^{89} (18G51)
Y^{89}		100 (1D39)					Y^{89}, I = 1/2 (87M50)	
Y^{90}	A chem, excit, cross bomb (71S37); chem, mass spect (60H48)		β^- (71S37)	61 h (37B46, 71S37); 62 h (11G49); 65 h (18N51)	2.18 spect (10L49); 2.24 spect (23L50); 2.25 spect (74B49); 2.27 spect (96M52); 2.2 spect, abs (33G51c); E (average) 0.90 ion ch (77C52)	no γ (33G51c, 74B49, 39G43); 1.4 (0.4%) abs (11S52); others (52M51)	Q^-_β 2.18 (10L49)  (74B49)	Y-d-p (71S37); Y-n-γ (71S37, 42S38, 2S47); Zr-n-p, Zr-d-α (42S40); Nb-n-α (42S38a, 42S40a); spall-fission Pt, Tl (2T47b), Bi (13P47, 11G49); fission Th (21T51); fission U, daughter Sr^{90} (16H42, 16H43, 38G46, 18N51)

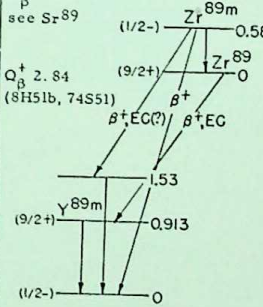
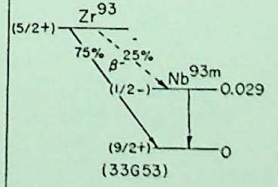
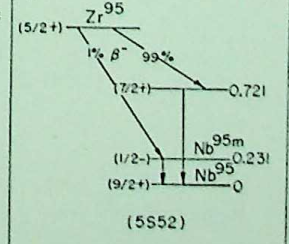
CC-0. In Public Domain. Gurukul Kangri Collection, Haridwar

Digitized by Arya Samaj Foundation Chennai and eGangotri

Isotope Z A	Class and identification	Percent abundance	Type of decay	Half-life	Energy of radiation in Mev: Particles	Energy of radiation in Mev: Gamma-transitions	Disintegration energy and scheme	Method of production and genetic relationships
$_{39}Y^{91m}$	A chem, genet (40G41)		IT (40G41)	51.0 m (28F51a); 50 m (40G41)		0.551 (K/L+M 6.00) scint spect (59G52); 0.61 (e/γ ~0.1) abs, abs conv (28F51a)	see Sr^{91}  (10L49, 28F51a, 40A52)	Zr-n-p (66S43a); fission U, daughter Sr^{91} (40G41, 16H43, 28F51a)
Y^{91}	A chem, genet (16H40c, 16H43); chem, mass spect (72B51a, 60H48)		β^- (16H40c)	61 d (38G46, 10L49); 57 d (40G41, 16H40c, 19J44)	1.537 spect (10L49); 1.54 spect (15O49); 1.55 spect (16W49c, 24K49); 1.56 spect (16A50, 96M52)	1.2, 0.2 (both <0.1%) abs, coinc abs sec, γ-γ coinc (10L49)		Zr-n-p (66S43a); spall Sb (37L50); spall-fission Bi (11G49), U (11O51); fission Th (72B51), U^{233} (38G48), Pu (28F51, 13E51); fission U, daughter (~60%) Sr^{91} (40G41, 16H43, 28F51a)
Y^{92}	B chem (36L39); fission fragment range (32K48)		β^- (36L39)	3.60 h (40A52a); 3.5 h (28A43, 16H43a, 36L39)	3.60, 2.7, 1.3 spect (40A52a); 3.5 abs (58H51b); 3.4 abs (40G41); 3.6 abs (70B43a)	0.6 abs (40G41); 0.7 - 1.1 abs (58H51b)		Zr-n-p (42S40, 66S43a, 28A43); fission Hg (π) (63S52); fission Th (72B51), Pu (32K48); fission U, daughter Sr^{92} (40G41, 58H51b)
Y^{93}	B chem (16H43, 72B46, 72B51b, 70S51); fission fragment range (32K48)		β^- (72B51b)	10.0 h (72B51b); 11.5 h (16H43)	3.1 abs (72B51b)	0.7 abs (72B51b)		spall-fission U (6O48); fission Th (72B51), Pu (32K48); fission U, daughter Sr^{93} (16H43, 16H43a, 72B51b)
Y^{94}	B chem (16H43, 16H43a); fission fragment range (32K48)		β^- (16H43, 16H43a)	16.5 m (75B49); 20 m (24D51b, 16H43)	5.4 abs (75B49)	1.4 abs (75B49)		Zr-n-p (66S43a); fission U (16H43, 16H43a, 24D51b), Pu (32K48); daughter Sr^{94} (16H43, 16H43a)
Y^{95}	B chem, sep isotopes, excit (20K49)		β^- (20K49)	10.5 m (20K49); <1.5 h (70S51)				Zr^{96}-γ-p (20K49)
Y^{97}	[A] genet (24D51)		β^- (24D51)	short (24D51)				fission U, descendent Kr^{97}, parent Zr^{97} (24D51, 26A51)
$_{40}Zr^{86}$	[B] chem, genet (8H51b)		EC (8H51b)	~17 h genet (8H51b)				spall Nb, parent Y^{86} (8H51b)
Zr^{87}	A chem, excit, sep isotopes (36R49); chem, genet (8H51b)		β^+, EC (36R49)	94 m (8H51b); 120 m (36R49)	2.10 spect (8H51b); 2.0 abs (36R49)	0.65, 0.35 abs (36R49)		Sr-α-n, Sr^{84}-α-n (36R49); spall Nb, parent Y^{87m} (8H51b); Mo-γ-αn (85H52)
Zr^{88}	B chem, genet (8H51b)		EC (8H51b)	85 d (8H52)		0.406 spect conv (8H51b)		spall Nb, parent Y^{88} (8H51b)

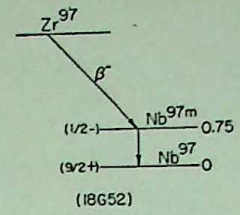
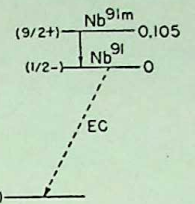
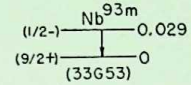
CC-0. In Public Domain. Gurukul Kangri Collection, Haridwar

Digitized by Arya Samaj Foundation Chennai and eGangotri

Isotope Z A	Class and identification	Percent abundance	Type of decay	Half-life	Energy of radiation in Mev: Particles	Energy of radiation in Mev: Gamma-transitions	Disintegration energy and scheme	Method of production and genetic relationships
$_{40}Zr^{89m}$	A chem, excit (2D40a)		IT, β^+ (weak) (73S51)	4.4 m (73S51); 4.5 m (2D40a)	2.5, ~0.85 (both weak) (β^+/0.59 γ = 0.004) spect, scint spect, β-γ coinc abs (73S51, 73S52)	0.586 (e/γ 0.07, K/L+M 5.4) scint spect, spect conv (79B52, 73S51); 1.53 (~7%) scint spect (73S52)	Q^+_β ~3.4 see Sr^{89}  (73S51, 73S52, HPS)	Y-p-n (2D40a); Zr-n-2n (?) (28A43); Zr-γ-n (73S51)
Zr^{89}	A chem, excit (42S38, 2D40a)		EC ~75%, β^+ ~25% (18G51)	79.3 h (74S51); 77 h (8H51b); 78 h (2D40a); 80 h (11O43)	0.910 spect (8H51b); 0.905 spect (74S51); 0.890 spect (73S51)	γ (with Y^{89m}): 0.92 (e/γ 0.01) spect conv, scint spect (74S51, 18G51); 0.913 spect conv (73S51); 0.917 spect conv (8H51b); ~0.9 (K/L+M 7.0) spect conv (79B52)	Q^+_β 2.84 (8H51b, 74S51)	Y-d-2n (11O43, 18G51); Y-p-n (2D40a); Zr-n-2n (42S38, 42S40); Zr-γ-n (73S51); spall Nb (8H51b); Mo-n-α (42S40); parent Y^{89m} (18G51)
Zr^{90}		51.46 (24W48)						
Zr^{91}		11.23 (24W48)					Zr^{91}, I = 5/2 (87M50)	
Zr^{92}		17.11 (24W48)						
Zr^{93}	B chem (61S50)		β^- (61S50)	9.5×10^5 y sp act (33G53)	0.063 scint spect (33G53)	no γ (33G53)	Q^-_β 0.063 (33G53)  (33G53)	fission U (61S50, 76B50); parent Nb^{93m} (33G53)
Zr^{94}		17.40 (24W48)						
Zr^{95}	A chem (2G40, 42S40); chem, genet (39G51)		β^- (42S40)	65 d (17B51a, 38G46); 66 d (2G48); 63 d (42S40)	0.371 (99%), 0.84 (1%) spect (5S52); 0.39 (98%), ~1.0 (2%) spect (17N51); 0.365 (95%), ~0.60 (weak), ~1.1 (weak) spect (88S51b); ~0.4 (98%), ~1.0 (2%) abs (17B51a); 0.40 abs (26M48a); 0.40, 0.88 β-γ coinc abs, abs (14M51)	0.721 (e/γ 0.0024), no 0.92 γ spect, spect conv (5S52); 0.73, 0.92 (?) spect conv (17N51); 0.88 abs (17B51a); 0.91 coinc abs sec (26M48a); others (52M51)	Q^-_β 1.09 (5S52)  (5S52)	Zr-n-γ (42S40, 2S47); Zr-d-p (42S40, 20J51); Mo-n-α (42S40); spall-fission Bi (11G49, 66B51), Th (7N49a); fission U^{233} (38G48, 61S48), Pu (28F51); fission U, parent (~1%) Nb^{95m}, parent (~99%) Nb^{95} (62H49, 17B51a, 20J51, 61S51b)
Zr^{96}		2.80 (24W48)						

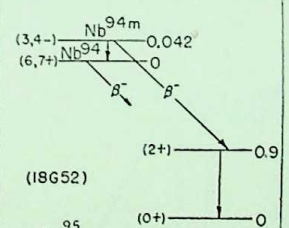
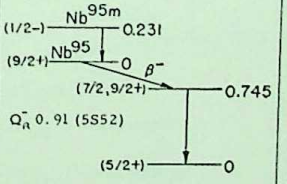
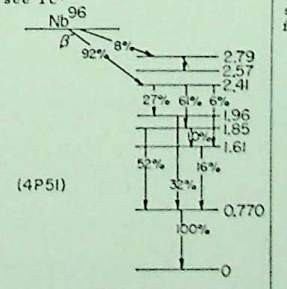
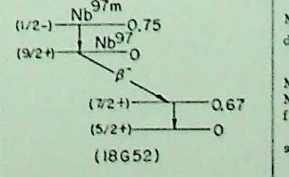
CC-0. In Public Domain. Gurukul Kangri Collection, Haridwar

Digitized by Arya Samaj Foundation Chennai and eGangotri

Isotope Z A	Class and identification	Percent abundance	Type of decay	Half-life	Energy of radiation in Mev: Particles	Energy of radiation in Mev: Gamma-transitions	Disintegration energy and scheme	Method of production and genetic relationships
$_{40}Zr^{97}$	A chem (2G40); chem, n-capt, sep isotopes (50B50a, 26M52)		β^- (2G40)	17.0 h (50B50a, 26M52, 32K51b, 2G40)	1.91 spect (50B50a); 1.9 abs (75S49); 2.2 abs (32K51b); 2.5 abs (26M52)	with Nb^{97m}: 0.747 (e/γ 0.015) spect, spect conv, β-γ coinc, γ-γ coinc, β-conv coinc (50B50a)	Q^-_β 2.66 (50B50a)  (18G52)	Zr^{96}-n-γ (50B50a, 26M52); Zr-n-γ (42S40, 2S47); Mo-n-α (42S40); spall-fission Bi (66B51), Th (7N49a), U (6O47); fission Th (21T51), U (2G40, 16H41a), Pu (32K48) parent Nb^{97m} (50B50a); descendent Kr^{97} (24D51)
Zr^m	E (24C52)		IT (24C52)	0.83 s (24C52)		~0.50 scint spect (24C52)		Zr-n (24C52)
$_{41}Nb^{90}$	A chem, excit, cross bomb (20J51); chem, sep isotopes, cross bomb (76B49b, 29K49)		β^+ (20J51)	15.0 h (29K49); 15 h (76B49b); 18 h (20J51)	1.2 abs (29K49); ~1.7 abs (76B49b)	0.14, 1.14, 2.23 scint spect (76B51d); 2.0 abs (29K49)		Zr-d-2n (20J51); Zr^{90}-d-2n (29K49); Mo-d-α (20J51); Mo^{92}-d-α (29K49, 76B49b); Mo-γ-pn (22E52); daughter Mo^{90} (43D52)
Nb^{91m}	A chem, excit (20J51); chem, sep isotopes (16O51)		IT (76B49b)	64 d (76B49b); 60 d (20J51)		0.1045 (e/γ ~50, K/L 2.1) spect conv, scint spect (16O51); 0.105 (K/L+M 2.1) spect conv (4P51); Nb x (76B49b, 16O51)	 (18G52)	Zr^{90}-d-n (16O51); Zr-d-n (20J51); Mo^{94}-d-αn (76B49b)
Nb^{91}	B genet (16O51)		[EC] (16O51)	long (16O51)		Zr x (16O51)		[Zr^{90}-d-n, daughter Nb^{91m}] (16O51)
Nb^{92}	B chem, excit (8J52a)		EC (8J52a)	~13 h (8J52a)		2.35 scint spect (8J52a)		Nb-p-pn (8J52a)
Nb^{92}	A chem, excit (42S38a)		EC, no β^- (lim 0.05%) (4P51); EC, no β^- (8J52a)	10.1 d (29K47); 9.8 d (60M48); 11 d (42S40a, 42S38a)	β^- (?): 1.3 cl ch (42S40a), abs (29K47); 0.6 abs (59M44)	0.930 (with EC) spect (4P51); 0.933, 1.84 (weak) scint spect (18T52); 1.0 abs (59M44, 29K47); 1.1 abs (1P45); Zr-x (1P45)		Y-α-n (1P45); Zr-p-n (59M44); Nb-γ-n (60M48, 22E52); Nb-n-2n (42S38a, 42S40a); Nb-d-t (37W46, 29K47); Mo-n-p (42S40); Mo^{94}-d-α (76B49b)
Nb^{92}	G not found: chem, excit (76B49b)		β^- (37W46)	21.6 h (37W46)				Nb-d (37W46)
Nb^{93m}	B genet (33G53)		IT (33G53)	3.65 y (33G53)		0.0292 (e/γ very large, K/L 0.14) spect conv (33G53)	 (33G53)	daughter Zr^{93} (33G53)
Nb^{93}		100 (37S36a)					Nb^{93}, I = 9/2 (87M50)	

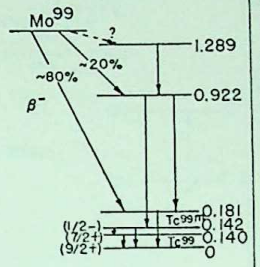
CC-0. In Public Domain. Gurukul Kangri Collection, Haridwar

Digitized by Arya Samaj Foundation Chennai and eGangotri

Isotope Z A	Class and identification	Percent abundance	Type of decay	Half-life	Energy of radiation in Mev: Particles	Energy of radiation in Mev: Gamma-transitions	Disintegration energy and scheme	Method of production and genetic relationships
41 Nb^{94m}	A n-capt, excit (1P37, 42S38a, 18G46b, 29K46)		IT 99+%, β^- -0.1% (18G46b)	6.6 m (42S40a)	1.3 abs (18G46b)	0.0415 (e/γ large, K/L/M = 0.31/1.00/0.36) spect conv (42C50); 0.056 (e/γ large) abs conv (18G46b); 0.9 (weak) scint spect (38M51a); Nb K-x (18G46a, 18G46b)	 (18G52)	Nb-n-γ (1P37, 42S38a, 42S40a, 18G46a, 18G46b, 2S47); Nb-d-p (29K46, 37W46)
Nb^{94}	[A] n-capt (18G46b); chem, n-capt (63H52)		[β^-] (18G46b)	>5 x 10^4 y yield (63H52); >>100 y yield (18G46b, 18G48a)				Nb-n-γ (18G46b)
Nb^{95m}	A chem (13E46, 13E51a); chem, genet (61S51b)		IT (61S51b)	90 h (61S51b, 62H49); 84 h (5S52)		0.231 (e/γ very large) spect conv (5S52); 0.232 (K/L+M ~3.5) spect conv (4P51); 0.216 (e/γ very large) spect conv (62H49); Nb K-x (61S51b)	see Zr^{95} 	Mo^{97}-d-α (76B49b); fission U, daughter (~1%) Zr^{95} (62H49, 17B51a, 20J51, 61S51b); spall-fission U (6F51); parent Nb^{95} (61S51b, 19L51)
Nb^{95}	A chem (39G46, 39G51); chem, excit, cross bomb (20J51)		β^- (39G51)	35 d (13E51b); 37 d (20J51)	0.160 spect (29F52); 0.159 spect (5S52); 0.148 spect (88S51b); 0.146 spect (62H49); 0.15 spect (17N51a); others (26M48b)	0.745 (e/γ 0.0024) spect, spect conv (5S52); 0.758 (e/γ 0.002) spect, spect conv (62H49); 0.77 (e/γ 0.0016, K/L = 4) spect conv (29F52); 0.77 spect, spect conv (17N51a); 0.75 spect conv (11R47)	Q^-_α 0.91 (5S52) (5S52)	Mo^{97}-d-α (76B49b); Mo-d-α (20J51); spall-fission Bi (66B51), U (6F51); fission U, daughter (~99%) Zr^{95} (62H49, 17B51a, 61S51b)
Nb^{96}	A chem, excit, sep isotopes (29K49a)		β^- (29K49a)	23.35 h (29K49a); 22.9 h (76B51)	0.750 (92%), 0.37 (8%) spect (4P51); 0.686 (92%), 0.37 (8%) spect (31J52); 0.75 spect (76B51)	0.216 (7%, e/γ <23 x 10^{-3}), 0.238 (10%, e/γ <16 x 10^{-3}), 0.451 (27%, e/γ 4 x 10^{-3}), 0.560 (61%, e/γ 1.7 x 10^{-3}), 0.770 (100%, e/γ 1.2 x 10^{-3}), 0.804 (6%, e/γ 1.3 x 10^{-3}), 0.840 (16%, e/γ 1.2 x 10^{-3}), 1.078 (52%, e/γ 0.5 x 10^{-3}), 1.187 (32%, e/γ 0.3 x 10^{-3}) spect conv, spect (4P51); 0.455, 0.545, 0.745, 0.9, 1.05, 1.1 spect, spect conv (31J52)	Q^-_β 3.16 (4P51, 74S51a) see Tc^{96}  (4P51)	Zr^{96}-p-n (29K49a); Mo^{98}-d-α (76B51); spall-fission Bi (66B51); fission U (68C51a)
Nb^{97m}	A chem, excit, sep isotopes, genet (50B50a)		IT (50B50a)	60 s (50B50a)		0.747 (e/γ 0.015, K/L ≥4) spect, spect conv, β-γ coinc, γ-γ coinc, β-conv coinc (50B50a)	 (18G52)	Mo^{98}-γ-p (50B50a); daughter Zr^{97} (50B50a)
Nb^{97}	A chem, genet (2G40)		β^- (2G40)	72.1 m (26M52); 74 m (50B50a); 75 m (2G40)	1.267 spect (50B50a); 1.35 abs (75S49); 1.4 abs (32K51b, 26M52)	0.665 (e/γ ~0.0015) spect, spect conv (50B50a); 0.7 abs, β-γ coinc (26M52)		Mo-n-p (42S40); Mo-γ-p (42H47, 12P48, 22E52); fission U (2G40, 32K51b), Pu (32K51b); spall-fission U (6F51)
Nb^{98}	E chem, sep isotopes (76B49b)		β^- (76B49b)	30 m (76B49b)				Mo^{100}-d-α (76B49b)
Nb^{99}	B chem, excit sep isotopes (23D50)		β^- (23D50)	2.5 m (23D50)	3.2 abs (23D50)			Mo^{100}-γ-p (23D50)

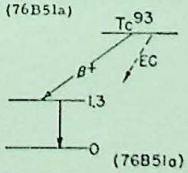
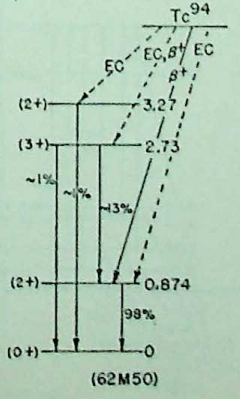
CC-0. In Public Domain. Gurukul Kangri Collection, Haridwar

Digitized by Arya Samaj Foundation Chennai and eGangotri

Isotope Z A	Class and identification	Percent abundance	Type of decay	Half-life	Energy of radiation in Mev: Particles	Energy of radiation in Mev: Gamma-transitions	Disintegration energy and scheme	Method of production and genetic relationships
$_{42}Mo^{90}$	B chem, genet (43D52)		β^+, EC (43D52)	5.7 h genet (43D52)		~0.1, other γ's abs (43D52)		spall Nb (43D52); parent Nb^{90} (43D52)
Mo^{91}	A excit (37B37a); chem, excit (42S38); chem, sep isotopes, excit (29K49, 23D49)		β^+ (42S38)	15.5 m (23D49, 25W48); 17 m (29K49, 37B39, 42S38)	3.7 abs (23D49); 2.7 cl ch (42S40)	no γ (23D49)		Mo-γ-n (37B39, 25W48, 22E52); Mo-n-2n (6H37, 42S38, 42S40, 30B52); Mo^{92}-n-2n (29K49); Mo^{92}-γ-n (23D49)
Mo^{91}	B chem, sep isotopes (23D49)		β^+ (23D49)	75 s (23D49); 73 s (25W48)	2.6 abs (23D49)	0.3 abs (23D49)		Mo^{92}-γ-n (23D49); Mo-γ-n (25W48)
Mo^{92}		15.86 (9W46)					Mo^{92}, I = 0 (87M50)	
Mo^{93m}	D chem, excit (29K46); chem, excit, cross bomb, sep isotopes (29K50a); chem, excit (76B52b); possibly Mo^{92m} or Mo^{94m} (HPS)		IT (29K50a)	6.95 h (76B52b); 6.75 h (29K50a)		0.262 (K/L 2.9), 0.69, 1.51 spect, spect conv (19R51); 0.256 (K/L 2.8), 0.7, 1.5 spect conv, scint spect (13A50b); 0.30 (e/γ 9), 0.70 (e/γ 0.005), 1.7 (e/γ ~0) abs, abs conv, spect conv, conv-γ coinc (29K50a); γ_1 0.29, γ_2 0.69, γ_3 1.46 ($\gamma_1/\gamma_2/\gamma_3$ = 0.6/1/1) scint spect (76B52b) others (85S51)		Zr^{90}-α-n (29K50a); Zr-α-n (29K46); Nb-p-n (29K46, 19R51, 76B52b); Nb-d-2n (29K46, 37W46, 29K50a); Mo^{94}-n-2n (29K50a); not found by: Mo^{92}-n-γ (76B50a); Mo^{94}-γ-n (23D49); Mo^{92}-d-p (29K50a); not daughter Tc^{93} (76B50a)
Mo^{93}	B chem, n-capt (76B49)		EC (76B49)	>2 y (76B49)		Nb K-x (76B49)		Mo-n-γ (76B49)
Mo^{94}		9.12 (9W46)					Mo^{94}, I = 0 (87M50)	
Mo^{95}		15.70 (9W46)					Mo^{95}, I = 5/2 (87M50)	
Mo^{96}		16.50 (9W46)					Mo^{96}, I = 0 (87M50)	
Mo^{97}		9.45 (9W46)					Mo^{97}, I = 5/2 (87M50)	
Mo^{98}		23.75 (9W46)					Mo^{98}, I = 0 (87M50)	
Mo^{99}	A chem, n-capt, excit (42S38, 42S40)		β^- (42S38)	67 h (13S39); 68.3 h (10C49); 63.5 h (25W48); 64 h (42S40)	1.23 (~80%), 0.45 (~20%), ~0.08 (weak) (?) spect (2B50a); 1.23 (87%), 0.54 (13%) spect (62M51); 1.25, others, spect (54M51); 1.2 abs (32K51c)	γ_1 0.040, γ_2 0.181 (K/L 5), γ_3 0.367, γ_4 0.741, γ_5 0.780 ($\gamma_3/\gamma_4/\gamma_5$ = 10/100/14) spect, spect conv (2B50a); 0.728, 0.360 (weak), 0.182 (weak) spect, β-γ, γ-γ coinc (62M51); 0.179, 0.168 spect conv (10C49); γ_4 0.745, γ_5 0.780, γ_6 0.850 ($\gamma_4/\gamma_5/\gamma_6$ = 100/50/30) spect (54M51); with Tc^{99m}: 0.0018, 0.140 (62M49, 62M51); 0.142 (63M51)	Q^-_β 1.37 (2B50a)  (18G52)	Zr-α-n (14E46); Mo-d-p (13S39); Mo-n-γ (42S38, 13S39, 61M47, 2S47, 26M48c, 62M49); Mo^{98}-n-γ (61M47a); Mo-n-2n (42S40); Mo-γ-n (25W48, 22E52); spall Sb (37L50); spall-fission Pt, Tl (2T47b), Bi (13P47, 11G49, 66B51), Th (7N49a); fission Th (16H39d, 72B51, 21T51), U^{233} (61S48), U (16H39e, 24S40, 32K51c), Pu (32K48, 28F51); parent Tc^{99m} (13S39, 24S40, 62M49, 33G51e)

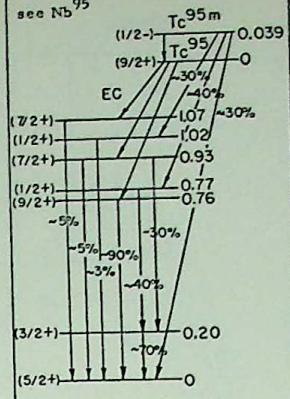
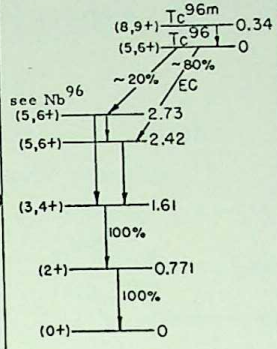
Digitized by Arya Samaj Foundation Chennai and eGangotri

CC-0. In Public Domain. Gurukul Kangri Collection, Haridwar

Isotope Z A	Class and identification	Percent abundance	Type of decay	Half-life	Energy of radiation in Mev: Particles	Energy of radiation in Mev: Gamma-transitions	Disintegration energy and scheme	Method of production and genetic relationships
$_{42}Mo^{100}$		9.62 (9W46)					Mo^{100}, I = 0 (87M50)	
Mo^{101}	A chem, n-capt (42S40); chem, n-capt, sep isotopes (61M47a)		β^- (42S40)	14.6 m (3M41); 14 m (16H41b)	1.2, 2.1 abs (31R52); ~1.0, 2.2 abs (3M41); 1.9 abs (42S40)	0.191 (K/L ~6), 0.960 (coinc with 1.2 β^-) spect conv, scint spect, β-γ, γ-γ coinc (31R52); 0.15 scint spect (38M51a)		Mo-n-γ (42S40b, 42S40, 24S40a, 3M41, 2S47, 50H51); Mo^{100}-n-γ (61M47a); parent Tc^{101} (42S40b); fission U, parent Tc^{101} (24S40a, 37B41, 16H41, 16H41b, 3M41)
Mo^{102}	D chem (16H41)		β^- (16H41)	12 m (16H41); 11 m (76B49a)				fission U, parent Tc^{102} (16H41, 16H41b, 76B49a)
Mo^{105}	B chem, genet (70B43b)		β^- (70B43b)	~5 m (66S47)				fission U, ancestor Ru^{105} (70B43b)
$_{43}Tc^{92}$	D chem, sep isotopes (61M48)		β^+, EC (76B52c)	4.3 m (76B52c)	4.1 abs (76B52c)	1.3 abs (61M48)		Mo^{92}-d-2n (61M48)
Tc^{92}	D chem, excit, sep isotopes (29K48a)		EC (29K48a)	43.5 m (62M50); 47 m (29K48a)		0.389 spect, spect conv (62M50); 1.50 abs conv (29K48a)		Mo^{92}-d-2n, p-n (29K48a); Mo-p-n (62M50)
Tc^{93}	A chem (13S39); chem, excit, sep isotopes (29K48a)		EC 93%, β^+ 7% (29K48a, 76B51d)	2.75 h (29K48a) 2.7 h (61M48, 5D39)	0.800 spect (76B51a); 0.83 abs (29K48a)	1.34 (coinc with β^+) scint spect, β-γ coinc abs (76B51d); 2.00 abs (29K48a); 2.4 abs (61M48)	Q^+_β 3.1 (76B51a)  (76B51a)	Mo^{92}-d-n (29K48a, 61M48); Mo-d-n (13S39); Mo-p-γ (5D39, 29K48a); not parent (7h) Mo^{93m} (76B50a)
Tc^{94}	B chem, excit (42G47); chem, excit, sep isotopes (61M48a)		β^+ ~75%, EC ~25% (62M50)	53 m (62M50); 50 m (61M48a)	2.41 (coinc with γ) spect, β-γ coinc (62M50); 2.5 abs (61M48a)	0.874 (e/γ ~10^{-3}), 1.85, 2.73, 3.27 spect, spect conv (62M50); 0.9 abs (61M48a)	Q^+_β 4.30 (62M50)  (62M50)	Mo-p-n (42G47, 34H48, 62M50); Mo^{94}-d-2n (61M48a); daughter Ru^{94} (12V52)

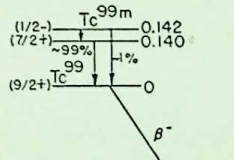
Digitized by Arya Samaj Foundation Chennai and eGangotri

CC-0. In Public Domain. Gurukul Kangri Collection, Haridwar

Isotope Z A	Class and identification	Percent abundance	Type of decay	Half-life	Energy of radiation in Mev: Particles	Energy of radiation in Mev: Gamma-transitions	Disintegration energy and scheme	Method of production and genetic relationships
$_{43}Tc^{95m}$	A chem (12C37, 12C39); chem, sep isotopes (61M48b)		EC 96+%, IT ~3%, β^+ 0.2-0.6% (62M50, 62M50a)	60 d (62M50); 52 d (14E47); 62 d (12C39)	0.4 cl ch (62M50)	γ_1 0.810 (e/γ 0.001), γ_2 0.201 (e/γ 0.036), γ_3 0.570 (e/γ 0.002), γ_4 1.02 ($\gamma_1/\gamma_2/\gamma_3/\gamma_4$ = 0.3/0.7/0.4/0.03) spect, spect conv, γ-γ coinc (62M50); 0.0390 spect conv (62M50a); 0.80, 0.20, 0.58, 1.03 scint spect (76B51a); 0.8, 0.2 abs (14E47, 61M48b)	see Nb^{95}  (62M50, 62M50a, 18G52)	Mo-d-n (12C37, 12C39, 14E46); Mo-p-n (14E47); Mo^{95}-d-2n (61M48b)
Tc^{95}	A chem, sep isotopes (1E48, 61M48a)		EC (1E48); no β^+ (62M50)	20.0 h (1E48); 20 h (61M48a)		0.762 (~90%), 0.932 (~5%), 1.071 (~5%) spect conv, γ-γ coinc (62M50); 0.76, 1.07, no 0.93 γ scint spect (76B51d); 0.78 abs (1E48)		Mo-a-p, Mo-p-n, Mo^{92}-a-p (1E48); Mo^{95}-d-2n (61M48a); Mo-p-n (62M50)
Tc^{96m}	B chem, excit (62M50); chem, excit, sep isotopes (62M52)		IT (62M50)	51.5 m (62M50)		0.0344 (K/L 1.2) spect conv (62M50); Tc K-x (62M50)	 (62M50, 76B51a, 62M52, 18G52)	Mo^{96}-p-n (62M52); Mo-p-n (62M50)
Tc^{96}	A chem (15E39); chem, excit, cross bomb (14E47); chem, excit, sep isotopes (61M48b)		EC (61M48b); no β^+ (62M50)	4.20 d (31C50); 4.35 d (62M50); 4.2 d (61M48b); 4.3 d (14E47)		γ_1 1.119 (e/γ 3 x 10^{-4}), γ_2 0.842 (e/γ 6 x 10^{-4}), γ_3 0.806 (e/γ 6 x 10^{-4}), γ_4 0.771 (e/γ 6 x 10^{-4}), γ_5 0.312 (K/L 6.4) ($\gamma_1/\gamma_2/\gamma_3/\gamma_4/\gamma_5$ = 0.17/1.00/0.82/1.00/0.0052) spect, spect conv, γ-γ coinc (62M50); 1.65, 1.89, 2.39 (?) (all weak) scint spect (76B51a)		Nb-a-n (14E47); Mo-p-n (15E39, 14E47, 62M50); Mo-d-n (14E47, 13S39); Mo^{96}-d-2n (61M48b)
Tc^{97m}	A chem (22P37, 12C37); chem, genet (61M47b); excit, sep isotopes (61M48b)		IT (2H41, 14E47)	90 d (61M48b); 91 d (2H41); 95 d (14E47)		0.0958 (K/L+M 1.6) spect conv (62M50); 0.097 (K/L ~2) spect conv (2H41); 0.097 (e/γ very large) abs conv (61M48b); 0.108 (e/γ large) abs conv (14E47)		Mo^{97}-d-2n (61M48b); Mo-d-n (12C37, 22P37, 12C39); Mo-p-n (14E47); daughter Ru^{97} (61M47b)
Tc^{97}	[A] genet (76B51b)		[EC] (76B51b)	$>10^4$ y yield (76B51b)				[daughter Tc^{97m}] (76B51b)

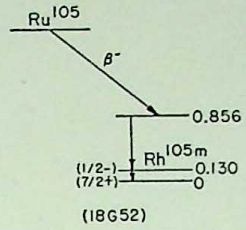
CC-0. In Public Domain. Gurukul Kangri Collection, Haridwar

Digitized by Arya Samaj Foundation Chennai and eGangotri

Isotope Z A	Class and identification	Percent abundance	Type of decay	Half-life	Energy of radiation in Mev: Particles	Energy of radiation in Mev: Gamma-transitions	Disintegration energy and scheme	Method of production and genetic relationships
$_{43}Tc^{99m}$	A chem, genet (13S39)		IT (13S39)	6.04 h (1B52); 5.9 h (33G51e); 6.6 h (13S39)		0.1403 (K/L 7.7), 0.1423 (~1%, K/L ~2.5) spect conv (63M51); 0.1412 (e/γ 0.11, K/L/M+N = 7.9/1/0.3), 0.0018 (e/γ very large) spect conv (62M49, 62M51); 0.140 (K/L ~9) spect, spect conv (2B50a); 0.139 (K/L ~10) spect conv (54M51)		Ru-n-p (76B47); fission Th (72B51), U (24S40, 16H41, 33G51e); daughter Mo^{99} (13S39, 24S40, 62M49, 33G51e, 63M51); parent Tc^{99} (13S39, 16H41)
Tc^{99}	A chem (25L46, 53S46); chem, mass spect (3I47)		β^- (25L51, 53S51a)	2.12×10^5 y sp act (30F51); 2.2×10^5 y sp act (26P51)	0.290 spect (15F52); 0.292 spect (23T51); 0.296 spect (39W52); 0.30 spect (24K50a)	no γ (61M47, 53S51a, 30F51)	Q^-_β 0.29 (15F52, 23T51) (5/2+) (62M51, 63M51, 18G52) Tc^{99}, I = 9/2 (48K51)	fission U (3I47, 25L51, 53S51a); daughter Tc^{99m} (13S39, 16H41); descendent Mo^{99} (61M47)
Tc^{100}	A sep isotopes (64H52); sep isotopes, n-capt (76B52)		β^- (64H52)	15.8 s (76B52); 17.5 s (64H52)	2.8 abs (76B52); 2.4 abs (64H52)	0.55 scint spect (76B52c)		Mo^{100}-p-n (64H52); Mo-p-n (2D40); Tc^{99}-n-γ (76B52)
Tc^{101}	A chem, genet (42S40b)		β^- (42S40b)	14.0 m (3M41, 16H41b); 14.5 m (12P48); 16.5 m (60M48)	1.20 (>95%) abs; β-γ coinc (76B51d); 1.2 abs (42S40); 1.3 abs (3M41)	0.307 (coinc with β^-, K/L ~6) spect conv, β-γ coinc, scint spect (31R52); 0.30 (coinc with β^-), 0.56 (weak) scint spect, β-γ coinc (76B51a); 0.26 scint spect (38M51a); no 0.56 γ (31R52)		Mo^{100}-d-n (61M48); Ru-γ-p (12P48, 60M48); Rh-γ-2p (22E52); fission U, daughter Mo^{101} (24S40a, 37B41, 16H41, 16H41b, 3M41); daughter Mo^{101} (42S40b)
Tc^{102}	E genet (16H41)		β^- (16H41)	<25 s (76B49a); <1 m (16H41)				daughter Mo^{102} (16H41, 16H41b, 76B49a)
Tc^{105}	B chem, genet (70B43b)		β^- (70B43b)	short (70B43b)				fission U, daughter Mo^{105} parent Ru^{105} (70B43b)
Tc^{107}	[E] genet (70B43b)		[β^-] (70B43b)	<1.5 m (70B43b)				[fission U, parent Ru^{107}] (70B43b)
$_{44}Ru^{94}$	D chem, genet (12V52)		EC (12V52)	~57 m genet (12V52)				Mo-a-2n, parent Tc^{94} (12V52)
Ru^{95}	A chem, cross bomb, sep isotopes (1E48)		EC, β^+ (1E48)	1.65 h (1E48)	1.1 abs (1E48)	1.0, 0.5 abs (1E48)		Mo-a-n, Mo^{92}-a-n (1E48); Ru-n-2n (1E48); Ru-γ-n (60M48)
Ru^{96}		5.7 (16E43)						
Ru^{97}	A chem, excit (23S46); chem, cross bomb, sep isotopes (1E48)		EC (23S46)	2.8 d (23S46, 60M48)		0.217 spect (53M50a); 0.23 abs (23S46)		Mo^{94}-a-n (1E48); Ru-d-p (23S46); Ru-n-γ (23S46); Ru-n-2n (1E48); Ru-γ-n (60M48); spall Sb (37L50); parent Tc^{97m} (61M47b)
Ru^{98}		2.2 (16E43)						
Ru^{99}		12.8 (16E43)					Ru^{99}, I = 5/2 (19O52)	

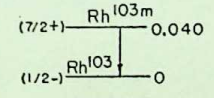
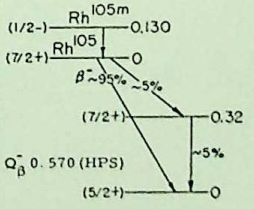
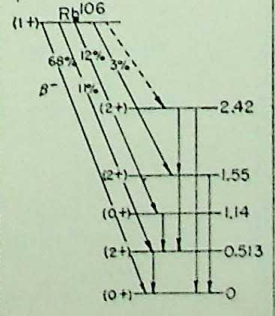
CC-0. In Public Domain. Gurukul Kangri Collection, Haridwar

Digitized by Arya Samaj Foundation Chennai and eGangotri

Isotope Z A	Class and identification	Percent abundance	Type of decay	Half-life	Energy of radiation in Mev: Particles	Energy of radiation in Mev: Gamma-transitions	Disintegration energy and scheme	Method of production and genetic relationships
$_{44}Ru^{100}$		12.7 (16E43)						
Ru^{101}		17.0 (16E43)					Ru^{101}, I = 5/2 (19O52)	
Ru^{102}		31.3 (16E43)						
Ru^{103}	A excit (12L36); chem (5N42, 39G46); chem, excit (23S51, 23S51b)		β^- (5N42)	39.8 d (38K50); 42 d (23S51); 41 d (77B45, 15H48); 45 d (5N42, 60M48)	0.217 (~99%), 0.698 (~1%) spect (38K50, 38K51c); 0.222 (94%), 0.684 (6%) spect (53M50a); 0.205 (strong), 0.670 (weak) spect (79S50); 0.350 (50%), 0.665 (50%) spect (15H48); 0.2 (92%), 0.7 (8%) abs, β-γ coinc (26M50)	0.498 (coinc with 0.22 β^-, e/γ ~0.01) spect, spect conv, β-γ coinc (38K50, 38K51c); 0.498 spect (46K52); 0.494 (e_K/γ 0.006, K/L 6.5) spect, spect conv (53M50a); 0.499 (K/L 8.5), 0.611 (K/L 4), 0.295 (?), 0.053 (K/L 1.0) spect conv (10C52); others (26M50, 23E52, 52M51); with Rh^{103m}: 0.040 (38K50, 53M50a, 79S50, 37W45, 10C52)	Q^-_β 0.75 (38K51c)	Ru-d-p (12L36, 23S51); Ru-n-γ (23S51, 7D38); Ru-γ-n (60M48); spall Sb (37L50); spall-fission Pb (13P47a), Bi (11G49); fission Th (72B51, 21T51), U^{233} (38G48, 61S48), U (5N41, 5N42, 39G51a, 23S51f), Pu (28F51); parent Rh^{103m} (23S51b)
Ru^{104}		18.3 (16E43)						
Ru^{105}	A chem (24S41); chem, excit (23S51c)		β^- (5N41)	4.5 h (76S51, 23S51d, 23S51a); 4.4 h (77B45)	1.150 spect (23D51); 1.15 spect (90S52); 1.3 abs (23S51d, 23S51a, 77B45)	0.726 (coinc with β^-) spect, β-γ coinc (23D51); 0.75 abs (23S51d); 0.7 abs (77B45); with Rh^{105m}: 0.130 (29A51, 23D51a, 90S52)	Q^-_β 2.01 (23D51)  (18G52)	Ru-n-γ (7D38, 23S51c); Ru-d-p (12L36, 23S51c); spall Sb (37L50); spall-fission Pt (2T47b), Hg (π) (63S52), Tl (2T47b), Pb (13P47a), Bi (13P47, 11G49), U (6O48, 6F51); fission Th (24S41, 72B51), U (7D38, 5N41, 24S41, 70B43b, 77B45, 76S51, 23S51d); descendent Mo^{105} (70B43b), parent Rh^{105m} (23D51), ancestor Rh^{105} (5N41, 77B45, 76S51, 23S51c)
Ru^{106}	A chem (39G46, 33G46a); chem, mass spect (60H48)		β^- (39G51a, 33G51f)	1.0 y (33G51f, 66S46)	0.0392 spect (16A50); 0.038 spect (3F50b)	no γ (76S51a, 16A50)		spall Sb (37L50); spall-fission Bi (11G49), Th (7N49a), U (6F51); fission Th (72B51, 21T51), U^{233} (38G48, 61S48), U (33G51f), Pu (28F51); parent Rh^{106} (33G51f)
Ru^{107}	D chem (70B43b, 33G51g)		β^- (70B43b)	4 m (33G51g, 70B43b)	~4 abs (70B43b)			fission U, parent Rh^{107} (33G51g, 70B43b)
$_{45}Rh^{99}$	D chem (1E49)		β^+ (90S52)	4.5 h (90S52)	0.74 spect (90S52)			Ru-p-n (1E49, 90S52); Ru-d-n (1E49, 90S52)
Rh^{100}	B chem (23S51e); chem, genet (37L48)		EC ~95%, β^+ ~5% (37L48)	19.4 h (37L48); 21 h (23S51e)	3.0 spect (37L48)	1.2 abs (37L48); 1.8 abs (23S51e)		Ru-d-n (23S51e); daughter Pd^{100} (37L48)
Rh^{101}	B chem, excit (23S51g)		EC (23S51g)	4.3 d (37L48); 5.9 d (23S51g)		0.300, 0.148 spect conv (90S52); 0.35 spect conv, abs (37L48)		Ru-p-n (90S52); Ru-d-n (23S51g, 90S52); daughter Pd^{101} (37L48)

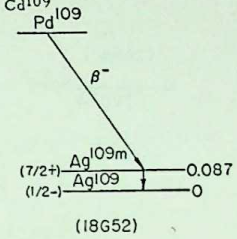
CC-0. In Public Domain. Gurukul Kangri Collection, Haridwar

Digitized by Arya Samaj Foundation Chennai and eGangotri

Isotope Z A	Class and identification	Percent abundance	Type of decay	Half-life	Energy of radiation in Mev: Particles	Energy of radiation in Mev: Gamma-transitions	Disintegration energy and scheme	Method of production and genetic relationships
$_{45}Rh^{102}$	A chem, excit (64M41)		β^-, β^+ (64M41); EC (?) (23S51h)	210 d (64M41); 215 d (15H47)	β^-: 1.0 cl ch (15H45); 1.1 abs (64M41) β^+; 1.1 cl ch (15H45)			Ru-d-n (23S51h); Rh-n-2n (64M41, 15H45); Rh-γ-n (60M48, 22E52)
Rh^{103m}	A chem, excit (9F44); chem (33G46a, 33G51f); chem, genet (23S51b)		IT (9F44, 37W45)	57 m (33G51f); 56 m (53M50a); 52 m (9F47); 45 m (37W45)		0.0400 (K/L+M 0.2) spect conv, β-γ coinc (38K50, 38K51c); 0.0404 (e/γ very large) spect conv (53M50a); 0.0396 (K/L 0.1) spect conv (10C52); 0.040 spect conv (79S50); abs conv (37W45); 0.042 abs conv (9F47)	 (18G52)	Rh-d-pn, Rh-p-p (15H48); Rh-n-n (9F44); Rh-e⁻-e⁻, Rh-x rays (37W45); fission U, daughter Ru^{103} (23S51b); daughter Pd^{103} (48B46, 53M50a)
Rh^{103}		100 (57C43)					Rh^{103}, I = 1/2 (49K50)	
Rh^{104m}	A n-capt (12A35)		IT (17P38, 28A43a)	4.4 m (32C39); 4.7 m (38M51, 58C47); 4.3 m (9F47)		0.052 scint spect (38M51); scint spect, ion ch (31K51); others (28A43a, 14O40, 15H47)		Ru-p-n (2D40); Rh-n-γ (12A35, 1P37, 17P38, 34G46, 2S47, 50H51); Pd-γ-p (42H47); parent Rh^{104} (17P38, 9F47)
Rh^{104}	A n-capt (12A35); genet (17P38)		β^- (17P38)	44 s (12A35, 17P38)	2.6 spect (15H47); 2.3 abs (18S43); cl ch (32C39); 2.5 abs (28M40)	0.04, 0.18, 0.95 abs, abs conv (58C47)		Rh-n-γ (12A35, 17P38, 34G46); daughter Rh^{104m} (17P38, 9F47)
Rh^{105m}	A chem, genet (23D51)		IT (23D51)	45 s (23D51)		0.130 (e/γ ~3, K/L 1.5) scint spect, spect conv (29A52); 0.127 spect conv (90S52)	 (18G52)	daughter Ru^{105}, parent Rh^{105} (23D51)
Rh^{105}	A chem, genet (5N41); chem, genet (23S51c)		β^- (5N41)	36.5 h (23S51c); 37 h (77B45); 34 h (5N41)	0.570 (~96%), 0.25 (~4%) spect (23D51, 23D51a); 0.57 spect (90S52); 0.26 (~10%) β-γ coinc abs (76B52a)	0.322 (~10%, coinc with 0.26 β^-), 0.157 (very weak), 0.080 (?) scint spect, β-γ coinc abs (76B52a); 0.320 (~3%) scint spect (23D51a); ~0.3 (~8%, not coinc with 0.6 β^-) abs, β-γ coinc (26M51); 0.33 (weak) abs (23S51i)		Ru-d-n (23S51i, 90S52); Rh-t-p (29K48); Pd-γ-p (12P48); spall-fission U (6F51); fission Th (72B51, 21T51), U (5N41, 76S51), Pu (32K48); descendent Ru^{105} (5N41, 77B45, 76S51, 23S51c), daughter Rh^{105m} (23D51)
Rh^{106}	A chem, genet (33G46a, 33G51f)		β^- (33G51f)	30 s (33G51f); 40 s (66S46)	3.53 (68%), 3.1 (11%), 2.44 (12%), 2.0 (3%), others (6%) spect (13A52); 3.55 (82%), 2.30 (18%) spect (6P47a); 3.5, ~2.3 abs, β-γ coinc (15J49)	γ_1 0.513 (e_K/γ 0.004, K/L 8), γ_2 0.624 (e_K/γ 0.002), γ_3 0.87, γ_4 1.045, γ_5 1.55, γ_6 2.41 ($\gamma_1/\gamma_2/\gamma_3/\gamma_4/\gamma_5/\gamma_6$ = 100/53/3/8/2.5/1) spect, scint spect, spect conv (13A52); 0.510, 0.622 spect conv (10C52); 0.51 (17%), 0.73 (17%), 1.25 (~1%) spect, β-γ, γ-γ coinc (6P47a); ~0.5 (e_K/γ 0.005), ~0.7 (e_K/γ <0.003) spect conv (44M50); others (39A52)	Q_β^- 3.53 (13A52)  (13A52)	fission U, daughter Ru^{106} (38G46, 33G51f); fission Pu (28F51)

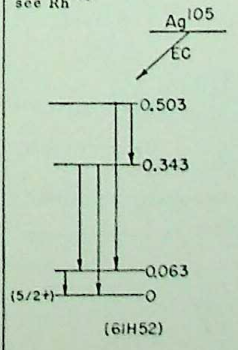
CC-0. In Public Domain. Gurukul Kangri Collection, Haridwar

Digitized by Arya Samaj Foundation Chennai and eGangotri

Isotope Z A	Class and identification	Percent abundance	Type of decay	Half-life	Energy of radiation in Mev: Particles	Energy of radiation in Mev: Gamma-transitions	Disintegration energy and scheme	Method of production and genetic relationships
$_{45}Rh^{107}$	D chem, genet (70B43b)		β^- (70B43b)	26 m (33G51g); 24 m (70B43b)	1.2 abs (70B43b)			Pd-γ-p (22E52); fission U, daughter Ru^{107} (70B43b, 33G51g)
Rh^{109}	[A] genet (77S51)		[β^-] (77S51)	<1 h (77S51)				[fission U, parent Pd^{109}] (77S51)
$_{46}Pd^{100}$	B chem, excit (37L48)		EC (37L48)	4.0 d (37L48)		0.09, 1.8 abs (37L48)		Rh-d-5n (37L48); spall Sb (37L48, 37L50); parent Rh^{100} (37L48)
Pd^{101}	B chem, genet (37L48)		EC 90%, β^+ 10% (37L48, 1E49)	8 h (37L50); 9 h (1E49)	2.3 spect (37L48); 0.5 abs (1E49)	no γ (37L48)		Ru-α-n (1E49); Rh-d-4n (37L48); spall Sb (37L48, 37L50); parent Rh^{101} (37L48)
Pd^{102}		0.8 (37S36a)						
Pd^{103}	A chem, genet (48B46a); chem, excit (36M47)		EC (48B46a)	17.0 d (36M47, 48B46a)		Rh K-x (36M47, 53M50a); no γ (36M47, 53M50a); with Rh^{103m}: 0.040 (38K50, 53M50a, 79S50, 10C52)		Rh-α-p3n (53M50a); Rh-d-2n (36M47, 37L48); Rh-p-n (36M47); Pd-n-γ (48B46a, 78S50); spall Sb (37L50); parent Rh^{103m} (48B46a, 53M50a)
Pd^{104}		9.3 (37S36a)						
Pd^{105m}	E excit (9F52a)		IT (9F52a)	~23 s (9F52a)		0.20 (e/γ ~0.4) (9F52a)		Pd-n-2n, Pd-n-n (9F52a)
Pd^{105}		22.6 (37S36a)					Pd^{105}, I = 5/2 (99B51)	
Pd^{106}		27.2 (37S36a)						
Pd^{107}	B chem (26P49a)		β^- (26P49a)	$\sim 7 \times 10^6$ y sp act (26P49a)	~0.04 abs (26P49a)			fission U (26P49a)
Pd^{108}		26.8 (37S36a)						
Pd^{109m}	D n-capt (31K51); excit, cross bomb, n-capt (9F52a)		IT (31K51, 9F52a)	4.8 m (9F52a)		0.173 scint spect (31K51); 0.160 (e/γ ~0.6) (9F52a)		Pd-n-2n, Pd-n-γ (9F52a); Ag-n-p (9F52a)
Pd^{109}	A n-capt (12A35); chem, excit (39K37); chem, mass spect (37R46, 67B49a)		β^- (39K37)	13.6 h (11M53); 13.1 h (25W48); 13 h (39K37, 77S51); 14.1 h (60M48)	0.961 spect (20K52); 0.95 spect (7S49b, 38K51c); others (2H46, 39K37, 77S51)	with Ag^{109m}: 0.087 (e/γ ≥11, K/L+M 1.3) spect conv (7S49b); no γ (77S51); others (52M51)	Q^-_β 1.05 (HPS) see Cd^{109}  (18G52)	Pd-γ-n (12P48, 60M48, 25W48, 22E52); Pd-d-p (39K37); Pd-n-γ (12A35, 39K37, 2S47, 9O49, 50H51); Ag-d-2p (2H46, 112S51); Ag-n-p (4F38b); Ag-t-He^3 (29K47a); spall Sb (37L50), Ta (22N52); spall-fission Bi (11G49, 66B51), U (6F51); fission Th (21T51), U (77S51), U^{233} (61S48), Pu (32K48); parent Ag^{109m} (24S41, 7S49b, 77S51)
Pd^{110}		13.5 (37S36a)						

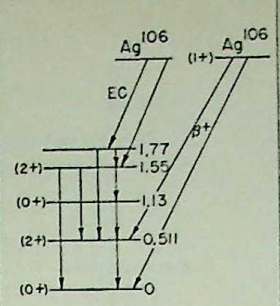
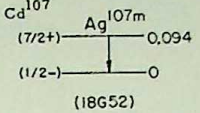
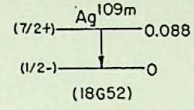
CC-0. In Public Domain. Gurukul Kangri Collection, Haridwar

Digitized by Arya Samaj Foundation Chennai and eGangotri

Isotope Z A	Class and identification	Percent abundance	Type of decay	Half-life	Energy of radiation in Mev: Particles	Energy of radiation in Mev: Gamma-transitions	Disintegration energy and scheme	Method of production and genetic relationships
$_{46}Pd^{111m}$	B chem, genet (66M52)		IT 75%, β^- 25% (66M52)	5.5 h (66M52)		0.16, 1.77 scint spect (66M52)		Pd-d-p, parent Ag^{111} (66M52)
Pd^{111}	A n-capt (12A35); chem, genet (24S41)		β^- (39K37)	22 m (66M52); 26 m (24S41)	2.13 spect (20K52); 2.15 spect (66M52); 3.5 abs (70B43b)	0.38, 0.56, 0.65, 0.73 scint spect (66M52)		Pd-d-p (12A35, 39K37); Pd-n-γ (12A35, 39K37, 2S47); spall Sb (37L50); spall-fission Bi (66B51); fission Th (24S41), U (24S41, 5N40a); parent Ag^{111} (39K37, 24S41)
Pd^{112}	A chem, genet (5N40a, 24S41)		β^- (5N40a)	21 h (77S51)	0.2 abs (77S51)	no γ (77S51)		In-p-4p, Pd-α-2p (112S51); spall Sb (37L50); spall-fission Bi (11G49, 66B51), Th (7N49a), U (6F51); fission Th (24S41, 21T51), U^{233} (61S48), Pu (32K48); fission U, parent Ag^{112} (5N40a, 5N40b, 24S41, 77S51)
$_{47}Ag^{102}$	E excit (17E39)			16 m (17E39)				Pd-p-n (17E39)
Ag^{104}	B excit (17E39); chem, excit, sep isotopes (11M52a)		β^+, EC (37L50)	1.2 h (17E39, 11M52a)				Pd-p-n (17E39); Cd^{106}-d-α (11M52a); spall Sb (37L50)
Ag^{104}	B chem, genet (32J52); chem, excit, sep isotopes (11M52a)		β^+ (32J52)	27 m (32J52)	2.70 spect (32J52)	0.118, 0.556, 0.148 (?), 0.179 (?) spect conv (32J52)		Cd^{106}-d-α (11M52a); daughter Cd^{104} (32J52)
Ag^{105}	A excit (17E39); chem, excit (16B47a)		EC (44G50)	40 d (44G50); 45 d (17E39)		0.0625 (e/γ very large, K/L >5), 0.280 (coinc with 0.063 γ, K/L 8), 0.343 (K/L 5.8), 0.440 (K/L 7), weak γ's: 0.154, 0.181, 0.391 spect conv, spect, γ-γ coinc (61H52); 0.064, 0.220 (weak), 0.278, 0.340, 0.437 (weak) spect (53M50b); 0.281, 0.319, 0.331, 0.345, 0.393, 0.443 spect conv (32J52); others (17E39, 20D42c)	see Rh^{105}  (61H52)	Rh-α-2n (16B47a, 44G50, 53M50b, 61H52); Pd-p-n (17E39, 44G50); Pd-d-2n (44G50, 53M50b, 61H52); Pd-α-p (44G50); spall Sb (37L50)

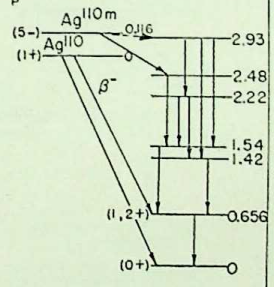
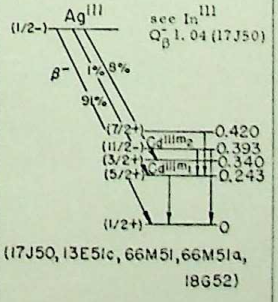
CC-0. In Public Domain. Gurukul Kangri Collection, Haridwar

Digitized by Arya Samaj Foundation Chennai and eGangotri

Isotope Z A	Class and identification	Percent abundance	Type of decay	Half-life	Energy of radiation in Mev: Particles	Energy of radiation in Mev: Gamma-transitions	Disintegration energy and scheme	Method of production and genetic relationships
$_{47}Ag^{106}$	A excit (37B37a, 6H37); chem, excit, cross bomb (39K37, 1P38)		β^+ (39K37); β^- (?) ~2% (79B51)	24.0 m (79B51); 24.5 m (1P38); 24.4 m (2D38); 24.3 m (60M48)	β^+: 1.95, 1.5 spect (79B51); 2.0 abs (4F38b); 1.9 cl ch (1P38) β^- (?): 0.45 spect (79B51); conv: ~0.5 (weak) spect conv (79B51)	~0.5, >0.6 (weak) spect conv, scint spect, abs (79B51) no γ (4F38b, 1P38)	 see Rh^{106} (18G52)	Rh-α-n (1P38, 19K39, 16B47a); Pd-d-n (39K37, 1P38); Pd-p-γ (2D38); Pd-p-n (2D38, 17E39); Ag-n-2n (6H37, 1P38); Ag-d-t (29K47); Ag-γ-n (37B37a, 37B39, 60M48, 55S51, 22E52, 79B51); Ag-e⁻-e⁻n (59S48); Ag-d-p2n (9K40b); Cd-n-p (1P38)
Ag^{106}	A chem, excit, cross bomb (39K37, 1P38)		EC (65H44)	8.2 d (1P38); 8.3 d (44G49); 7.5 d (39K37)		0.220, 0.409, 0.511 (K/L 8), 0.620, 0.717, 0.815, 1.04, 1.24, 1.55 spect conv (61H52); 0.515, 0.722, 1.04, 1.54 spect (53M50b); 0.72, 1.06, 1.63 spect (20D42c)		Rh-α-n (1P38, 16B47a, 53M50b, 61H52); Pd-d-n (39K37, 1P38, 61H52); Pd-p-n (2D38, 17E39); Ag-n-2n (1P38, 39K37, 36S51); Cd-n-p (1P38); spall Sb (37L50)
Ag^{107m}	A chem, genet (6A40, 2H41b)		IT (6A40)	44.3 s (16B45d, 16B47); 44 s (40W51)		0.094 (e/γ ~16, K/L 0.92) spect conv (16B47); 0.093 spect conv (6V39, 2H41)	see Cd^{107}  (18G52)	Ag-e⁻-e⁻ (37W45b); Ag-n-n (9F44); Ag-γ-γ (31F41, 37W45b, 24T45); Ag^{107}-γ-γ (40W51); daughter Cd^{107} (6A40, 2H41b, 16B45c, 2H46, 16B47)
Ag^{107}		51.35 (24W48)					Ag^{107}, I = 1/2 (87M50)	
Ag^{108}	A chem, n-capt (12A35); excit, cross bomb (1P38)		β^- 98.5%, EC 1.5% (12P52)	2.3 m (12A35, 12P48, 60M48, 37B39); 2.4 m (9F44)	1.5 scint spect (45G52)	0.45, 0.66 scint spect (12P52); 0.43, 0.60 scint spect (45G52)		Pd-p-n (2D38, 17E39); Ag-n-γ (12A35, 9F44, 2S47, 9O49, 50H51, 36S51); Ag-e⁻-e⁻n (59S48); Ag^{107}-n-γ (9F44a); Ag-γ-n (37B39, 12P48, 60M48, 22E52); Ag-d-p (9K39, 9K40b); Cd-n-p (1P38)
Ag^{109m}	A chem, genet (2H41b)		IT (2H41b)	39.2 s (16B46c, 16B47); 40 s (40W51, 2H41b, 37W45b)		0.0875 spect conv (10C50b); 0.087 (e_K/γ ~6, K/L+M 0.75) spect conv (34H52); 0.087 (e/γ ≥11, K/L+M 1.3) spect conv (7S49b); 0.087 spect conv (2H46, 16B47)	 (18G52)	daughter Pd^{109} (24S41, 7S49b); Ag-n-n (9F44); Ag-γ-γ (31F41, 37W45b, 24T45); Ag^{109}-γ-γ (40W51); Ag-e⁻-e⁻ (37W45b); daughter Cd^{109} (2H41b, 16B45c, 2H46)
Ag^{109}		48.65 (24W48)					Ag^{109}, I = 1/2 (87M50)	

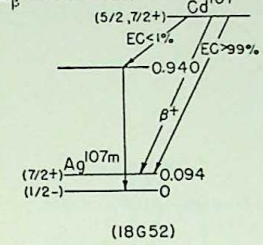
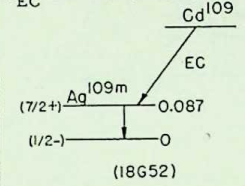
CC-0. In Public Domain. Gurukul Kangri Collection, Haridwar

Digitized by Arya Samaj Foundation Chennai and eGangotri

Isotope Z A	Class and identification	Percent abundance	Type of decay	Half-life	Energy of radiation in Mev: Particles	Energy of radiation in Mev: Gamma-transitions	Disintegration energy and scheme	Method of production and genetic relationships
$_{47}Ag^{110m}$	A chem, n-capt (35R38); resonance neutron activation (18G46c); chem, sep isotopes, n-capt (18G46d); chem, mass spect (67B49a)		β^-, IT (7S49c, 56M50, 10C50a); IT $\geq$3% (7S49c); no EC (lim 3%) (20D47a); no β^+: lim β^+/β^- 0.002% (2E49); lim β^+/β^- 0.05% (41M51)	270 d (44G50, 10C50a); 225 d (12L38d)	with Ag^{110m} and Ag^{110}: 0.087 (~58%), 0.530 (~35%), 2.12 (~3%), 2.86 (~3%), others (?) spect (7S49c); 0.088 (65%), 0.520 (33%), 2.89 (~2%) spect (31A51); 0.590, 2.24, 2.91 spect (88S51a), 0.09 (coinc with γ), 0.57 (coinc with γ), 0.19 (?) abs, β-γ coinc (46M49); 0.09, 0.59 cl ch (2E49); 0.59 spect (11R47)	0.116 (e/γ very large, K/L 1.3), 0.656 (e/γ 0.0025), 0.676, 0.706, 0.759, 0.814, 0.885, 0.935, 1.389, 1.516 spect conv, spect, β-γ coinc, γ-γ coinc (7S49c); 0.116 (conv in Ag), 0.438, 0.446, 0.471, 0.499, 0.542, 0.575, 0.619, 0.657, 0.677, 0.705, 0.723, 0.764, 0.817, 0.884, 0.937, 1.384, 1.504 spect, spect conv (10C50a); 0.116 (K/L+M 1.8), 0.447, 0.618, 0.655 (K/L+M 4.3), 0.687, 0.706 (K/L+M 6.6), 0.740, 0.759 (K/L+M 6.5), 0.815 (K/L+M 4.1), 0.883 (K/L+M 4.2), 0.932 (K/L+M 6.5), 1.386 (K/L+M 6.5), 1.480, 1.506 (K/L+M 4.5) spect conv (31A51); 0.656 (K/L+M 14) spect conv (40K52); 0.66, 0.90, 1.40 spect conv, spect (11R47); ~0.7, ~0.9 (coinc with 0.7 γ) γ-γ coinc abs (5Y49); $1.7 < \gamma < 2.2$ Be-γ-n reaction (38M50a); others (52M51)	see In^{110} Q^-_β 3.02 (7S49c)  (7S49c, 18G52)	Pd-d-2n (44G50); Ag-n-γ (35R38, 12L38d, 30A38, 14M38, 2S47); Ag^{109}-n-γ (18G46d); Ag^{109}-d-p (44G50); Ag-d-p (9K39, 9K40b, 65H44a); spall Sb (37L50); parent Ag^{110} (56M50)
Ag^{110}	A n-capt (12A35); sep isotopes, n-capt (9F44a); chem, genet (56M50)		β^- (1P38)	24.2 s (42H46a); 22 s (12A35, 1P38)	2.24 (~60%), 2.82 (~40%) scint spect (45G51a)	0.66, ~0.9 (weak) scint spect (45G51a)	Q^-_β 2.90 (HPS)	Ag-n-γ (12A35,46G36,9F44,2S47); Ag^{109}-n-γ (9F44a); Cd-n-p (1P38); Cd-γ-p (42H46a, 42H47); daughter Ag^{110m} (56M50)
Ag^{111m}	F genet (80S52)			[<5 m] (80S52)				Pd-d-n, parent Cd^{111m_2} (80S52)
Ag^{111}	A chem, excit (39K37); chem, excit, cross bomb (1P38)		β^- (39K37)	7.6 d (61S51c); 7.5 d (17J50, 39K37, 1P38)	1.04 (91%), 0.80 (1%), 0.70 (8%) spect (17J50); 1.06 spect (66M51, 53M50b); 1.1 (93.5%), 0.7 (6.5%) abs (78S50)	γ_1 0.243 (e/γ <0.08), γ_2 0.340 (e/γ ~0.015) (γ_2/γ_1 ~ 8) spect, spect conv, β-γ coinc, γ-γ coinc (17J50); 0.33 (~6.5%) abs (78S50)	 (17J50, 13E51c, 66M51, 66M51a, 18G52)	Pd-d-n (39K37, 1P38, 9Z49); Pd-a-p (1P38); Ag-a-2p (66M51); Ag-t-p (29K47a); Cd-n-p (1P38); Cd-γ-p (42H47, 23D49a); spall Sb (37L50), Ta (22N52); spall-fission Bi (11G49, 66B51), Th (7N49a), U (6O48, 6F51), U (C) (13H51); fission Th (21T51), U (5N40a, 24S41, 61S51c), Pu (28F51); parent Cd^{111m_1} (13E51c), daughter Pd^{111} (39K37, 24S41, 17J50), daughter Pd^{111m} (66M52)
Ag^{112}	A chem, excit, cross bomb (1P38)		β^- (1P38)	3.20 h (74S51a); 3.2 h (1P38)	4.2 scint spect (27P51a); 3.6 abs (77S51); 3.5 abs (74S51a)	0.625, 1.40 (40A52b); 0.86 abs (77S51); no γ coinc with 3.5 β^- (74S51a)		Cd-n-p (1P38); Cd-γ-p (42H47); In-n-a (1P38); spall Sb (37L50); spall-fission Bi (66B51), U (6O47, 6F51); fission Th (21T51), U^{233} (61S48); fission U, daughter Pd^{112} (5N40a, 5N40b, 24S41, 77S51)

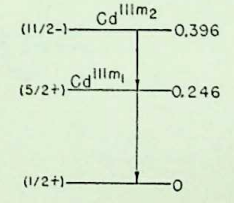
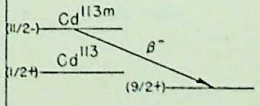
CC-0. In Public Domain. Gurukul Kangri Collection, Haridwar

Digitized by Arya Samaj Foundation Chennai and eGangotri

Isotope Z A	Class and identification	Percent abundance	Type of decay	Half-life	Energy of radiation in Mev: Particles	Energy of radiation in Mev: Gamma-transitions	Disintegration energy and scheme	Method of production and genetic relationships
$_{47}Ag^{113}$	A chem (21T47); chem, sep isotopes, excit (23D49a)		β^- (21T47)	5.3 h (21T47, 23D49a)	2.0 scint spect (27P51a); 2.1 abs (23D49a); 2.2 abs (21T47)	no γ (21T47, 23D49a)	Q^-_β 2.0 (HPS)	Cd^{114}-γ-p (23D49a); Cd-γ-p (23D49a); spall-fission Bi (66B51), U (6F51); fission U (21T47)
Ag^{114}	B chem (21T47, 66S47); chem, excit, sep isotopes (23D49a)		β^- (23D49a)	2 m (23D49a); 3 m (66S47)	hard β^- (23D49a)			Cd^{114}-n-p (23D49a); fission U (21T47, 66S47)
Ag^{115}	A chem (21T47, 66S47); chem, excit, sep isotopes (23D49a)		β^- (21T47)	20 m (23D49a, 66S47); 21 m genet (1W52); 22 m (21T47)	~3 abs (21T47, 23D49a)	no γ (23D49a)		Cd-γ-p (23D49a); Cd^{116}-γ-p (23D49a); fission U (21T47, 66S47); parent (91%) Cd^{115}, parent (9%) Cd^{115m} (1W52)
$_{48}Cd^{104}$	B chem, excit (32J52)		β^+ (32J52)	59 m (32J52)	0.93 spect (32J52)	0.0666 (K/L+M ~10), 0.0835 (K/L+M ~15), 0.124, 0.134, other γ's spect conv (32J52)		Ag-p-4n (32J52); parent (24 m) Ag^{104} (32J52)
Cd^{105}	B cross bomb (44G50); chem, excit (32J52)		EC, β^+ (44G50)	57 m (44G50); 55 m (32J52); 65 m (54K52)	1.68 spect (32J52); 1.5 abs (44G50)	0.0255, 0.0494, 0.0525, 0.262, 0.293, 0.308, 0.312, 0.317, 0.321, 0.341, 0.347, 0.433, 2.1 spect conv, scint spect (32J52)		Pd-α-n (44G50); Ag-p-3n (32J52, 54K52); Cd-n-2n (44G50)
Cd^{106}		1.215 (28L48)						
Cd^{107}	A chem (5D39); chem, n-capt, sep isotopes (2H46)		EC 99+%, β^+ 0.31% (16B45d, 55B50)	6.7 h (5D39)	0.32 spect (16B45d, 16B45e)	0.846 (0.4%, e/γ ~10^{-3}) spect, spect conv (16B45d, 16B45e); 0.7 abs (2H41); with Ag^{107m}: 0.094 (16B45c, 16B47, 6V39, 2H41)	Q^+_β 1.43 (16B45d)  (18G52)	Ag-p-n (5D39, 6V39); Ag-d-2n (9K39, 6A40, 9K40b, 2H41b); Ag-α-p3n (2H46); Cd^{106}-n-γ (2H46, 18G46d); spall Sb (37L50); spall-fission U (6F51); parent Ag^{107m} (6A40, 2H41b, 16B45c, 2H46, 16B47)
Cd^{108}		0.875 (28L48)						
Cd^{109}	A chem (9K40b); chem, n-capt, sep isotopes (2H46)		EC (L/K 0.28) (38M52); EC (16B46c); no β^+ (26D51)	470 d (44G50); 330 d (16B46c)		with Ag^{109m}: 0.0875 spect conv (10C50b); 0.087 (e_K/γ ~6, K/L+M 0.75) spect conv (34H52); 0.087 (e/$\gamma \geq$11, K/L+M 1.3) spect conv (7S49b)	see Pd^{109} Q_{EC} 0.16 calc (38M52)  (18G52)	Pd-α-n (44G50); Ag-d-2n (9K40b, 2H41b, 44G50); Ag-α-pn (2H46); Cd^{108}-n-γ (2H46, 10C50b, 59C51); spall Sb (37L50); parent Ag^{109m} (2H41b, 16B45c, 2H46, 16B46c)

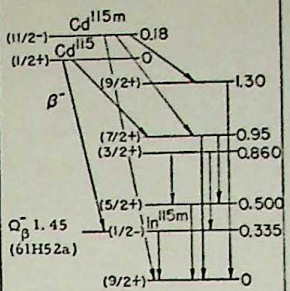
CC-0. In Public Domain. Gurukul Kangri Collection, Haridwar

Digitized by Arya Samaj Foundation Chennai and eGangotri

Isotope Z A	Class and identification	Percent abundance	Type of decay	Half-life	Energy of radiation in Mev: Particles	Energy of radiation in Mev: Gamma-transitions	Disintegration energy and scheme	Method of production and genetic relationships
$_{48}Cd^{110}$		12.39 (28L48)					Cd^{110}, I = 0 (87M50)	
Cd^{111m_2}	A chem (27D38); chem, sep isotopes, n-capt (18G48a)		IT (31F41, 37W45b)	48.6 m (66M51); 48.7 m (37W45b)		γ_1 0.150 (e/γ ~3, K/L 2.0), γ_2 0.246 (e/γ 0.064, K/L 5.1) spect conv (66M51, 66M51a); γ_1 (e/γ 2.3) (calc from 14S51, 66M51); γ_1 0.149, γ_2 0.247 scint spect (14S51); γ_1 0.146, γ_2 0.235 spect conv (15H48a)	see Ag^{111} and In^{111}  (17J50, 13E51c, 66M51, 18G52)	Pd^{108}-α-n (2H48); Pd-α-n (66M51); Ag-α-pn (2H48, 66M51); Cd-n-n or Cd-n-γ (27D38, 15H48a); Cd-γ-γ (31F41, 37W45b, 24T45); Cd^{112}-n-2n (66M51); Cd-e^--e^- (37W45b); Cd^{110}-n-γ (18G48a, 52M51); fission U (5N40a, 5N40b); spall-fission U (6F51); parent Cd^{111m_1} (20D50, 52M51); daughter (0.01%) In^{111} (66M51a)
Cd^{111m_1}	A genet (20D49a)		IT (20D49a)	8×10^{-8} s delay coinc (20D50, 63B50, 52M51); 10×10^{-8} s delay coinc (13E51c)		0.247 scint spect (52M51)		daughter Cd^{111m_2} (20D50, 52M51); daughter In^{111} (20D49a, 63B50); daughter Ag^{111} (13E51c)
Cd^{111}		12.75 (28L48)					Cd^{111}, I = 1/2 (87M50)	
Cd^{112}		24.07 (28L48)					Cd^{112}, I = 0 (87M50)	
Cd^{113m}	A chem, excit (44G49); chem, excit, sep isotopes (60C50,59C51)		β^- (60C50)	5.1 y (60C50)	0.59 scint spect (59C51); 0.5 abs (60C50)		 (18G52)	Cd-d-p (60C50); Cd-n-γ or Cd-n-n (60C50); Cd^{112}-d-p (60C50); Cd^{112}-n-γ (59C51); fission U^{235} (1W52)
Cd^{113}		12.26 (28L48)					Cd^{113}, I = 1/2 (87M50)	
Cd^{114}		28.86 (28L48)					Cd^{114}, I = 0 (87M50)	

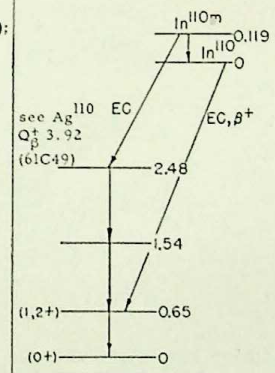
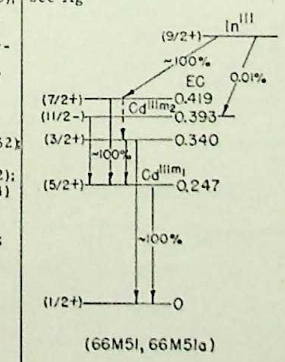
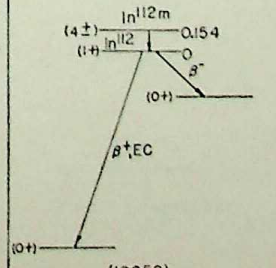
CC-0. In Public Domain. Gurukul Kangri Collection, Haridwar

Digitized by Arya Samaj Foundation Chennai and eGangotri

Isotope Z A	Class and identification	Percent abundance	Type of decay	Half-life	Energy of radiation in Mev: Particles	Energy of radiation in Mev: Gamma-transitions	Disintegration energy and scheme	Method of production and genetic relationships
$_{48}Cd^{115m}$	A chem (10C39); chem, excit (2S47b); chem, sep isotopes, n-capt (10C50b)		β^- (10C39)	43 d (2S47b, 10C50b); 44 d (33G51h)	1.61 (~98%), 0.7 (~2%), ~0.3 (weak) spect (61H52a); 1.5 abs (2S47b, 10C50b, 1W52); 1.4 abs; 0.4 (coinc with γ, ~1%) β-γ coinc abs (47G50); 1.7 abs (33G51h); ~0.8 (~1.4%) abs (13E51d)	0.46, 0.50, 0.96, 1.28 scint spect, γ-γ coinc (61H52a); γ_1 0.48, γ_2 0.94 (coinc with γ_1), γ_3 1.30 (not coinc with γ_1 or γ_2) ($\gamma_1/\gamma_2/\gamma_3$ = 13/100/40) scint spect, γ-γ coinc (13E52); others (56G49, 52M51)	Q^-_β 1.63 (61H52a)  (18G52)	Cd-d-p (10C39); Cd-n-γ (2S47, 2S47b); Cd^{114}-n-γ (10C50b); Cd^{116}-γ-n (1W52); In-n-p (2S47b); spall Sb (37L50); spall-fission Bi (11G49), Th (7N49a), U (6O48, 6F51); fission Th (21T51), U (67M51), U^{233} (61S48), U^{235} (1W52), Pu (33G51h, 28F51); daughter (9%) Ag^{115} (1W52)
Cd^{115}	A chem (10C37); chem, genet (18G38); chem, sep isotopes, n-capt (10C50b)		β^- (10C37)	53 h (1W52); 54 h (10C50b); 56 h (24L40, 67M51a)	1.11 (58%), 0.58 (42%) spect (10L52); 1.11 (~60%), 0.59 (~40%) spect (61H52a); ~1 (~85%), ~0.5 (~15%) β-γ coinc abs (1W52); others (26M49a, 10C50b, 67M51a)	0.335 (with In^{115m}), 0.360, 0.500, 0.525 scint spect, γ-γ coinc (61H52a); 0.522 spect (28D50); 0.336, 0.344, 0.349, 0.363 (?), 0.369, 0.424, 0.452, 0.525, 0.559, 0.713 spect conv (10C50b); with In^{115m}: 0.334 (10L52, 24L40, 61H49, 61H52a, 28D50, 20K51)	Q^-_β 1.45 (61H52a)	Cd-d-p (10C37, 10C39); Cd-n-γ (18G38, 14M37, 2S47); Cd^{114}-n-γ (10C50b); Cd-n-2n (18G38); Cd-γ-n (60M48); In-n-p (2S47b); spall Sb (37L50); spall-fission Th (7N49a), U (6O48, 6F51); fission Th (21T51), U^{233} (61S48), U^{235} (1W52), U (5N40a, 5N40b, 67M51a); parent In^{115m} (18G38, 10C39, 5N40b, 67M51a, 1W52, 10L52); daughter (91%) Ag^{115} (1W52)
Cd^{116}		7.58 (28L48)					Cd^{116}, I = 0 (87M50)	
Cd^{117m}	A chem, excit (10C39)		IT (51C52a)	3.0 h (51C52a); 2.9 h (25A52); 2.8 h (24L40); 2.7 h (67M51b)		with Cd^{117} (51C52a): ~1.2 abs (25A52)		Cd-d-p (10C39, 51C52a, 25A52); Cd-n-γ (14M37, 18G38, 2S47, 51C52a); spall-fission U (6F51); fission U (5N40a, 5N40b, 67M51b); parent In^{117} (18G38, 24L40, 67M51b), via Cd^{117} (51C52a)
Cd^{117}	A chem, genet (51C52a)		β^- (51C52a)	~50 m (51C52a)	~1.6, ~3.0 abs (51C52a)			Cd-n-γ, Cd-d-p, parent In^{117}, parent In^{117m} (51C52a)
$_{49}In^{107}$	A chem, sep isotopes (68M49); mass spect (97M52)		β^+ (68M49)	30 m (97M52); 33 m (68M49)	~2 spect (68M49)			Cd^{106}-p-γ, Cd^{106}-d-n (68M49)
In^{108}	A chem, sep isotopes (68M49); mass spect (97M52)		β^+ (68M49)	50 m (97M52, 66M51); ~55 m (68M49)	2.31 spect (66M51); 2.2 abs (37L50); ~2 spect (68M49)	0.285 (<5%, K/L ≥3) spect conv (66M51)	Q^+_β 3.3 (66M51)	Cd^{108}-d-2n (68M49); daughter Sn^{108} (68M49, 37L50, 66M51)
In^{109}	A chem, excit (25T47); chem, mass spect (48G48); chem, excit, sep isotopes (68M49)		β^+, EC (25T47, 68M49)	4.3 h (68M49); 4.2 h (66M51); 6.5 h (25T47); 5.2 h (48G48)	0.75 abs (68M49); ~2 (weak) (25T47)	0.427, 0.347, 0.205 (K/L 3), 0.058 (K/L 0.9) spect conv (66M51)		Ag-α-2n (25T47, 48G48, 66M51); Cd^{106}-α-p, Cd^{108}-d-n, Cd^{108}-p-γ (68M49)

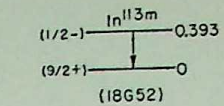
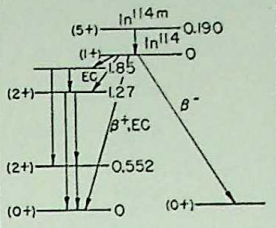
CC-0. In Public Domain. Gurukul Kangri Collection, Haridwar

Digitized by Arya Samaj Foundation Chennai and eGangotri

Isotope Z A	Class and identification	Percent abundance	Type of decay	Half-life	Energy of radiation in Mev: Particles	Energy of radiation in Mev: Gamma-transitions	Disintegration energy and scheme	Method of production and genetic relationships
$_{49}In^{110m}$	A chem (48G48); chem, genet energy levels Ag^{110} (66M51a, 35B51)		EC 99+%, IT ~0.3% (66M51)	5.0 h (66M51); 4.9 h (35B51); ~5 h (48G48)		0.119 (with IT, K/L 4.5), 0.935, 0.885, 0.661 spect conv (66M51); 0.119 (weak), 0.937, 0.887, 0.654 spect conv (35B51)	 (35B51, 61C49, 18G52)	Ag-a-3n (48G48, 66M51)
In^{110}	A chem (58B39); chem, excit, mass spect (48G48)		β^+, EC (61C49)	66 m (58B39, 35B51); 65 m (48G48)	2.25 spect (61C49)	0.654 spect conv (35B51); 0.677 (e/γ 0.005) spect, spect conv (61C49)		Ag-a-n (19K39a, 25T47a, 48G48); Cd-p-n (58B39); Cd-d-2n (24L40)
In^{111}	A chem (10C39); chem, excit (25T47a, 48G48); mass spect (48G48)		EC (24L40); no β^+ (lim 0.06%) (66M51); no β^+ (48G48)	2.84 d (66M51); 2.7 d (58B39, 10C39)		0.172 (~100%, e/γ 0.12, K/L 6.6), 0.247 (~100%, e/γ 0.064, K/L 5.19), 0.330 (weak), 0.093 (weak) spect, spect conv, conv-conv coinc abs (66M51); 0.173 (e/γ 0.09, K/L ~8), 0.247 (e/γ 0.04, K/L ~5) γ-conv, conv-conv, γ-γ coinc (56B49); 0.171 (K/L+M 7.03), 0.246 (K/L+M 4.79) spect conv (59G52); 0.173 (K/L+M 6.6), 0.247 (K/L+M 5.3) spect conv (34H52); 0.173 (K/L 6.6), 0.247 (K/L 5.4) spect conv (24L40); 0.25 (coinc with 0.17 γ) scint spect, γ-γ delay coinc (69M51); others (36A51, 36A51a)	see Ag^{111}  (66M51, 66M51a)	Ag-a-γ (112S51); Ag-a-2n (24L40, 25T47a, 48G48, 66M51); Cd-p-n (58B39); Cd-a-p (66M51); Cd-d-n (24L40); In-n-3n (10C39); spall Sb (37L50); parent (0.01%) Cd^{111m_2} (66M51a); parent Cd^{111m_1} (20D49a, 63B50)
In^{112m}	A chem (58B39); chem, cross bomb, excit (81S42); chem, excit (25T47a)		IT (81S42, 25T47a)	20.9 m (35B52); 20 m (58B39); 23 m (25T47a)		0.154 (e/γ >4) spect conv (61C49); 0.16 spect conv (58B39); 0.16 (e/γ large) abs (25T47a)	 (18G52)	Ag-a-n (81S42, 25T47a); Cd-d-n (24L40); Cd-p-n (58B39); In-n-2n (81S42, 25T47a); parent In^{112} (81S42, 25T47a, 49G50)
In^{112}	A chem, cross bomb, excit (81S42); chem, excit (25T47a)		β^-, β^+, EC (25T47a, 61C49); β^-/β^+ 2.7 (61C49)	14.5 m (35B52)	β^+: 1.74 spect (61C49); 1.7 spect (24L40) β^-: 0.67 spect (61C49)			Ag-a-n (81S42, 25T47a); In-n-2n (81S42, 25T47a); daughter In^{112m} (81S42, 25T47a, 49G50)

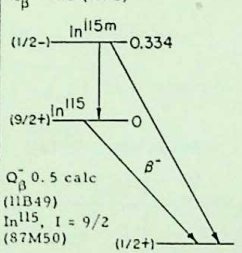
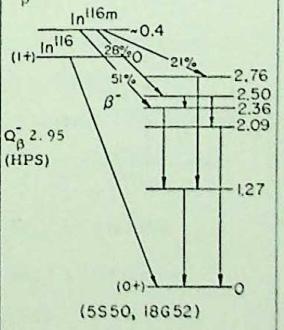
CC-0. In Public Domain. Gurukul Kangri Collection, Haridwar

Digitized by Arya Samaj Foundation Chennai and eGangotri

Isotope Z A	Class and identification	Percent abundance	Type of decay	Half-life	Energy of radiation in Mev: Particles	Energy of radiation in Mev: Gamma-transitions	Disintegration energy and scheme	Method of production and genetic relationships
$_{49}In^{m}$	E (31K52)		IT (31K52)	2.5 s (31K52)		0.153 scint spect (31K52)		In^{113}-n (31K52)
In^{113m}	A chem, excit, genet (58B39)		IT (58B39)	104 m (24L40) 105 m (58B39)		0.392 (K/L+M 4.21) spect conv (59G52); 0.393 spect conv (10C51a); 0.39 spect conv (58B39); 0.39 (K/L 5.4) spect conv (24L40); 0.39 (e/γ 0.55) scint spect (62C52); ~0.39 (e/γ 0.35, K/L 5.4) spect conv, ion ch (26T51)	 (18G52)	Cd-p-n (58B39); Cd-d-n (24L40); In-n-n (63C48); In-γ-γ (11D47); daughter Sn^{113} (58B39, 24S40a)
In^{113}		4.23 (24W48)					In^{113}, I = 9/2 (87M50)	
In^{114m}	A chem, n-capt, excit (24L37, 14M38)		IT, no EC (82S52)	49 d (58B39)		γ_1 with In^{114m}, γ_2, γ_3, γ_4, γ_5, γ_6 with In^{114}: γ_1 0.190, γ_2 0.552, γ_3 0.722, γ_4 1.27 ($\gamma_1/\gamma_2/\gamma_3/\gamma_4$ = 100/18.6/18.6/1.2) spect (53M49); γ_1 0.192 (e/γ 4.2, K/L 1.10) spect conv, scint spect (82S51); γ_1 0.190 (K/L/M = 1.18/1.00/0.18) spect conv. (59G52); γ_1 0.191 spect conv (10C48); γ_1 (K/L 1.30) spect conv (40K52); γ_1 0.192 (e/γ 4, K/L 1.1), γ_2 0.55, γ_3 0.72 spect conv (56B49a); γ_1 (e/γ 4) spect conv (10L49a); γ_1 (K/L 1.16) spect conv (88S51a); γ_4/γ_2 ~0.06 scint spect, γ-γ coinc (23K52); γ_5 0.576, γ_6 1.30 (coinc with γ_2) spect, γ-γ coinc (25J52)	 (HPS, 18G52, 25J52)	Cd-p-n (58B39); Cd-d-n (24L40, 46M49); In-n-γ (24L37, 14M38, 46M49); In-d-p (24L40); In-γ-n (25W48, 22E52); In-n-2n (24L40); spall Sb (37L50); parent In^{114} (49G50)
In^{114}	A excit (7C37, 37B37a, 24L37); n-capt, sep isotopes (18G48a)		β^- ≤97%, EC ≥3%, β^+ ~0.01% (82S52); β^- 99+%, β^+ 0.015% (25J52); β^- 99+%, β^+ ~0.01% (56B49a)	72 s (24L37, 58B39)	β^-: 1.984 spect (25J52); 1.98 spect (24L40); 2.01 spect (88S51a); 2.05 abs (46M49) β^+: ~1 abs (25J52); 0.65 spect (56B49a)		Q^-_β 1.98 (25J52) Q^+_β 2.07 p-n threshold (66M51)	Cd-p-n (58B39); In-n-2n (24L37, 1P37); In-γ-n (37B37a, 7C37, 25W48, 22E52); In^{113}-n-γ (18G48a); daughter In^{114m} (49G50)

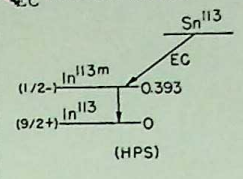
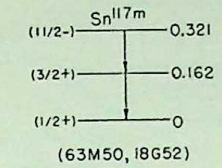
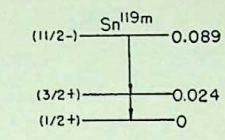
CC-0. In Public Domain. Gurukul Kangri Collection, Haridwar

Digitized by Arya Samaj Foundation Chennai and eGangotri

Isotope Z A	Class and identification	Percent abundance	Type of decay	Half-life	Energy of radiation in Mev: Particles	Energy of radiation in Mev: Gamma-transitions	Disintegration energy and scheme	Method of production and genetic relationships
$_{49}In^{115m}$	A chem, excit (18G38)		IT (24L39), β^- (11B49); IT 95%, β^- 5% (10L52)	4.50 h (11D47); 4.53 h (24L40)	0.83 spect (11B49)	0.335 (e/γ 0.98, K/L+M 3.76) spect conv (10L52, 59G52); 0.338 (e/γ ~1, K/L 5.0, K/L+M 4.0) spect conv (24L40); 0.335 (K/L 5.3) spect conv (20K51); 0.337 spect, spect conv (61H49); 0.336 spect (28D50)	Q^-_β 0.83 (HPS)  (18G52)	Cd-d-n (24L40); In-n-n (18G38, 63C48); In-p-p (58B39, 58B39a); In-α-α (38L39); In-e-e (64C40, 41W43, 41W49); In-γ-γ (17P38a, 64C39, 70M49, 83S51); fission Th (21T51), U (5N40a); daughter Cd^{115} (18G38, 10C39, 5N40b, 67M51a, 1W52, 10L52)
In^{115}	A chem, sep isotopes (71M50)	95.77 (24W48)	β^- (71M50, 63C51)	6×10^{14} y sp act (71M50); $\sim 10^{14}$ y sp act (63C51)	0.63 abs (71M50)		Q^-_β 0.5 calc (11B49) In^{115}, I = 9/2 (87M50)	natural source (71M50)
In^{116m}	A chem, n-capt (12A35); chem, excit, n-capt (24L37)		β^- (24L37)	53.93 m (57S49); 54.31 m (38R50); 54.05 m (50G47)	1.00 (51%), 0.87 (28%), 0.60 (21%) spect, β-γ coinc (5S50); 0.85 spect (10C39); cl ch (48C40); 0.7 β-γ coinc abs (26M48d)	2.090 (25%), 1.487 (21%), 1.274 (75%, e/γ 5.7×10^{-4}), 1.085 (54%, e/γ 8.4×10^{-4}), 0.406 (25%), 0.137 (3%) spect conv (5S50); 0.137, 0.171 spect conv (11K50a); others (20D42c, 48C40, 24L40, 18J45, 42W47)	Q^-_β 3.36 (5S50)  (5S50, 18G52)	Cd-p-n (58B39); In-n-γ (12A35, 14M38a, 34G46, 2S47, 50H51); In-d-p (24L37)
In^{116}	A n-capt (12A35); excit, n-capt (24L37)		β^- (24L37)	13 s (12A35, 10C39)	2.95 abs (35B46a, calc from 24L40); 2.8 cl ch (10C39)	no γ (14M38a)	Q^-_β 2.95 (HPS)	Cd-p-n (2D40), In-n-γ (12A35, 24L37, 34G46, 2S47), In-d-p (24L37), Sn-γ-p (42H47)
In^{117m}	A chem, genet (51C52a)		IT, β^- (51C52a)	~70 m (51C52a)	see In^{117}			daughter Cd^{117} (51C52a)
In^{117}	A chem, excit (10C39)		β^- (10C39)	~2.5 h (51C52a); 1.95 h (24L40); 1.90 h (67M51b)	with In^{117m} (?) (51C52a); 1.726 spect (20K51); 1.73 spect (10C39); 1.95 abs (67M51b) with In^{117}; 0.7 abs (51C52a)	0.161, 0.558 scint spect (20K51)		Cd-d-n (10C39, 24L40); Sn-γ-p (42H47); fission U (5N40a, 5N40b, 67M51b), Pu (32K48); daughter Cd^{117m} (18G38, 24L40, 67M51b); daughter Cd^{117} (51C52a)
In^{118}	B excit, sep isotopes (23D49b)		β^- (23D49b)	4.5 m (23D49b)	1.5 abs (23D49b)	γ (23D49b)		Sn^{119}-γ-p (23D49b)
In^{119}	B chem, excit, sep isotopes (23D49b)		β^- (23D49b)	17.5 m (23D49b)	2.7 abs (23D49b)	no γ (23D49b)		Sn^{120}-γ-p (23D49b)

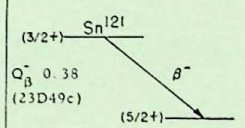
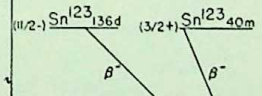
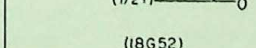
CC-0. In Public Domain. Gurukul Kangri Collection, Haridwar

Digitized by Arya Samaj Foundation Chennai and eGangotri

Isotope Z A	Class and identification	Percent abundance	Type of decay	Half-life	Energy of radiation in Mev: Particles	Energy of radiation in Mev: Gamma-transitions	Disintegration energy and scheme	Method of production and genetic relationships
$_{50}Sn^{108}$	B chem, sep isotopes (68M49)		EC (68M49)	4.0 h (66M51); 4.5 h (68M49)				Cd^{106}-α-2n (68M49); Cd-α-2n (66M51); parent In^{108} (68M49, 37L50, 66M51); spall Sb (37L50)
Sn^{111}	B chem, sep isotopes (66H49)		EC ~71%, β^+ ~29% (66M51)	35.0 m (66H49); 35 m (66M51)	1.51 spect (66M51); 1.5 abs (66H49)			Cd-α-3n (66M51); Cd^{108}-α-n (66H49)
Sn^{112}		0.95 (1B50)						
Sn^{113}	A chem, excit (58B39, 12L39c)		EC, no β^+ (58B39); EC (L/K ~0.8) (26T51)	112 d (19N50); 118 d (10C51a); 105 d (58B39)		with In^{113m}: 0.393 (10C51a, 58B39, 24L40, 62C52, 26T51); 0.401 (weak), 0.255 (weak) spect conv (10C51a); no 0.09 γ (65C47, 26T51, 10C51a, 63M51a, 28B51)	EC 0.43 calc (26T51)  (HPS)	Cd-α-n (12L39c); In-p-n (58B39); In-d-2n (65C47); Sn-d-p (12L39c); Sn-γ-n (60M48); Sn-n-γ (2S47, 28B51); Sn^{112}-n-γ (19N50, 63M51a, 10C51a); spall Sb (37L50); parent In^{113m} (58B39, 24S40a)
Sn^{114}		0.65 (1B50)						
Sn^{115}		0.34 (1B50)					Sn^{115}, I = 1/2 (87M50)	
Sn^{116}		14.24 (1B50)					Sn^{116}, I = 0 (87M50)	
Sn^{117m}	A chem (12L39c); chem, sep isotopes, cross bomb (68M50)		IT (68M50)	14.0 d (10C51a); 15 d (19N50)		0.159 (e/γ very large, K/L 2.2), 0.162 (e_K/γ 0.10) spect conv, e-γ coinc, x-γ coinc (63M50); 0.156 (e/γ large, K/L ~7), 0.159 spect conv (10C51a); 0.157 (K/L 2.2) spect conv (61H50a); 0.152 (K/L 2.4) spect conv (19N50)	 (63M50, 18G52)	Cd^{114}-α-n (68M50); Cd-α-n (12L39c); Sn^{116}-n-γ (63M50, 19N50); Sn^{116}-d-p, Sn^{118}-n-2n (68M50); Sn^{117}-n-n (68M50, 19N50); spall Sb (37L50)
Sn^{117}		7.57 (1B50)					Sn^{117}, I = 1/2 (87M50)	
Sn^{118}		24.01 (1B50)					Sn^{118}, I = 0 (87M50)	
Sn^{119m}	A chem, n-capt, sep isotopes (63M50)		IT (63M50)	~250 d (63M50); ~245 d (19N50)		γ_1 0.0653 (K/L 0.51, L/M ~4), γ_2 0.0242 (L/M ~4) spect conv (67H51); γ_2 0.0238 (e/γ ~7) scint spect, ion ch, γ-γ coinc (28B51); γ_1 0.065, γ_2 0.024 scint spect, ion ch conv (17S51b); γ_1 0.064 (K/L 0.82) spect conv (19N50)	 (17S51b, 28B51, 18G52)	Sn^{118}-n-γ (63M50, 19N50, 17S51b, 28B51)
Sn^{119}		8.58 (1B50)					Sn^{119}, I = 1/2 (87M50)	
Sn^{120}		32.97 (1B50)					Sn^{120}, I = 0 (87M50)	

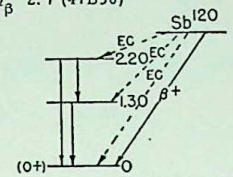
CC-0. In Public Domain. Gurukul Kangri Collection, Haridwar

Digitized by Arya Samaj Foundation Chennai and eGangotri

Isotope Z A	Class and identification	Percent abundance	Type of decay	Half-life	Energy of radiation in Mev: Particles	Energy of radiation in Mev: Gamma-transitions	Disintegration energy and scheme	Method of production and genetic relationships
$_{50}Sn^{121m}$	E sep isotopes, n-capt (19N50)		β^- (19N50)	>400 d (19N50)	0.42 spect (19N50)			Sn^{120}-n-γ (19N50)
Sn^{121}	A chem, excit (12L39c); chem, sep isotopes (37L48a)		β^- (12L39c)	27.5 h (19N50); 28 h (23D49c); ~27 h (6F51)	0.383 spect (23D49c); 0.4 abs (37L48a); 0.35 abs (39L49)	no γ (23D49c, 37L48a, 7N49b); others (52M51)	 (18G52)	Sn-d-p (12L39c); Sn-n-γ (12L39c, 2S47); Sn^{120}-d-p (37L48a, 39L49, 7N49b); Sn^{120}-n-γ (39L49, 23D49c, 19N50); Sn^{122}-n-2n (39L49); Sb-d-α (37L50); spall-fission Th (7N49a), U (6O48, 6F51)
Sn^{122}		4.71 (1B50)						
Sn^{123}	A chem (12L39c); chem, sep isotopes, excit (7N49b, 39L49, 19N50)		β^- (12L39c)	39.5 m (23D49c); 40 m (12L39c, 39L49, 19N50); 41.5 m (60M48); 39 m (7N49b)	1.26 spect (23D49c); 1.3 abs (39L49); 1.1 abs (19N50)	0.153 spect conv, β-e coinc (23D49c); 0.153 scint spect (76B51c); others (52M51)	Q^-_β -1.4 (HPS) 	Sn-d-p (12L39c); Sn-n-γ (2S47); Sn-n-2n (1P37); Sn-γ-n (60M48, 7H49); Sn^{124}-d-t (7N49b); Sn^{122}-n-γ (23D49c, 39L49, 19N50); Sn^{124}-n-2n (39L49)
Sn^{123}	A chem (40L46, 40L51); chem, sep isotopes, cross bomb (39L49)		β^- (40L51)	136 d (38G51); 125 d (10C51a); 130 d (39L49, 7N49b, 40L51); 126 d (19N50)	1.42 spect (24K50b); 1.3 abs (39L49)	no γ (39L49, 7N49b, 19N50, 10C51a, 38G51)	Q^-_β -1.4 (HPS)  (18G52)	Sn^{122}-n-γ (39L49, 19N50); Sn^{122}-d-p, Sn^{124}-n-2n (39L49); Sn^{124}-d-t (7N49b); Sb-n-p (7N49b); spall-fission Th (7N49a), U (6F51); fission U (38G46, 40L51), U^{233} (38G48, 38G51), U^{235} (38G51)
Sn^{124}		5.98 (1B50)		double β^- decay: (lower limit, by sp act) $>2 \times 10^{17}$ y (41K52, 32F52, 70H52); $>10^{17}$ y (72M52); $>10^{16}$ y (41L51, 25P52)				
Sn^{125}	A chem, excit, n-capt (12L39c); chem, sep isotopes (23D50a, 39L49, 19N50)		β^- (12L39c)	9.5 m (19N50); 9.8 m (39L49)	2.04, 1.17, 0.51 (?) spect (23D50a); 2.06, ~0.5 abs (19N50)	0.326, others >1 (weak) spect, spect conv (23D50a); 0.38 (coinc with 2.06 β) abs, β-γ coinc (19N50); 1.37 (weak) scint spect (76B51c)	Q^-_β ~2.4 (HPS)	Sn-d-p (12L39c); Sn-n-γ (12L39c, 23S47, 2S47); Sn^{124}-n-γ (39L49, 23D50a, 19N50)
Sn^{125}	A chem (12L39c); chem, excit, sep isotopes (39L49); chem, sep isotopes, n-capt, genet (19N50)		β^- (12L39c)	9.4 d (19N50); 10.0 d (39L49); 9.5 d (7N49b)	2.37 (~95%), 0.40 (~5%) spect (61H50b); 2.33 spect (24K50b); ~0.5 (10%) β-γ coinc abs (26M52a); others (65C47, 7N49b, 39L49, 77S51a)	1.90 scint spect, abs (76B51d); 1.67 coinc abs sec (26M52a)	Q^-_β ~2.4 (HPS)	Sn-n-γ (12L39c, 2S47); Sn-d-p (12L39c, 65C47); Sn^{124}-n-γ (39L49, 19N50); Sn^{124}-d-p (39L49); spall-fission Th (7N49a), U (6F51); fission U^{233} (61S48, 38G51), U (16H43b, 77S51a), U^{235} (38G51); parent Sb^{125} (19N50); not parent Sb^{125} (7N49b)

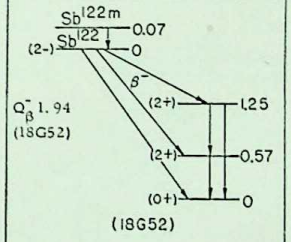
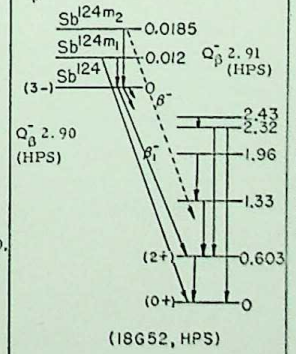
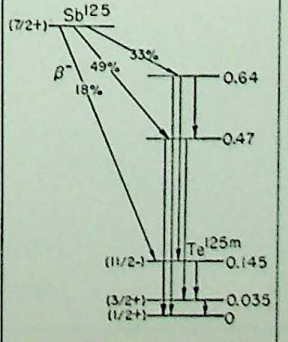
CC-0. In Public Domain. Gurukul Kangri Collection, Haridwar

Digitized by Arya Samaj Foundation Chennai and eGangotri

Isotope Z A	Class and identification	Percent abundance	Type of decay	Half-life	Energy of radiation in Mev: Particles	Energy of radiation in Mev: Gamma-transitions	Disintegration energy and scheme	Method of production and genetic relationships
$_{50}Sn^{126}$	B chem, genet (80B51)		β^- (80B51)	~50 m yield (80B51)				fission U^{235}, parent Sb^{126} (80B51)
Sn^{127}	A chem, genet (80B51)		β^- (80B51)	1.5 h yield (80B51)				fission U^{235}, parent Sb^{127} (80B51)
$_{51}Sb^{116}$	A chem, excit, mass spect (27T49)		β^+ (27T49)	60 m (27T49)	~1.45 spect (27T49)			In-α-3n (27T49)
Sb^{117}	A chem (12L39d); chem, excit, mass spect (27T49)		EC (65C47)	2.8 h (65C47, 27T49)		0.156 spect conv (27T49)		In-α-2n (27T49); Sn-d-n (12L39d, 65C47); Sn-p-n (65C47); spall I (π) (51W52)
Sb^{118}	B excit (27R40)		β^+ (37L48a)	3.5 m (37L48a); 3.6 m (27R40)	3.1 abs, spect (37L48a)			In-α-n (38L39, 27R40); Sn-p-n (2D40); daughter Te^{118} (37L48a)
Sb^{118}	A chem, cross bomb (65C47); chem, excit, mass spect (27T49)		EC (65C47)	5.1 h (65C47, 27T49)	e ~0.2 abs (65C47)	0.260 spect conv (27T49); 1.5 abs (65C47)		In-α-n (65C47, 27T49); Sn-d-n (65C47)
Sb^{119}	B chem, cross bomb (65C47)		EC (65C47)	39 h (65C47, 37L48a)		no γ (65C47); Sn K-x (65C47, 37L48a)		Sn-d-n, Sn-p-n (65C47); spall Sb (37L48a); daughter Te^{119} (37L48a)
Sb^{120}	D chem, sep isotopes (37L48a)		EC (37L48a)	6.0 d (37L48a)		~1.1 abs (37L48a)		Sb-d-p2n (37L48a); Sn^{120}-d-2n (37L48a); spall-fission Bi (11G49); not found: Sn-p, Sb-γ (47B51); Sb-x rays (30K51a)
Sb^{120}	A chem, excit (37B39, 6H37, 7C37); chem, excit, cross bomb (12L37a)		β^+, EC (47B50)	16.4 m (22J50); 16.6 m (12P48); 17 m (6H37, 12L39d)	1.70 spect (47B50)	γ_1 0.90, γ_2 1.30, γ_3 2.20 ($\gamma_1/\gamma_2/\gamma_3$ ~ 0.08/0.35/0.04) (e/γ very small) spect (47B50)	Q^+_β 2.7 (47B50)  (47B50)	Sn-d-n (12L39d); Sn-p-n (47B50); Sn^{120}-d-2n (37L48a); Sb-n-2n (1P37, 6H37, 21J44, 7C37); Sb-γ-n (37B39, 12P48, 27M49, 25W48, 22J50); Sb-d-t (9K41a); Sb-p-pn (23R46)
Sb^{121}		57.25 (24W48)					Sb^{121}, I = 5/2 (87M50)	

CC-0. In Public Domain. Gurukul Kangri Collection, Haridwar

Digitized by Arya Samaj Foundation Chennai and eGangotri

Isotope Z A	Class and identification	Percent abundance	Type of decay	Half-life	Energy of radiation in Mev: Particles	Energy of radiation in Mev: Gamma-transitions	Disintegration energy and scheme	Method of production and genetic relationships
$_{51}Sb^{122m}$	A chem, n-capt, sep isotopes (38M47)		IT (38M47)	3.5 m (38M47)		0.068 scint spect (38M51); 0.059, 0.074 ion ch (31K51)	 Q^-_β 1.94 (18G52) (18G52)	Sb-n-γ (38M47); Sb^{121}-n-γ (38M51, 31K51)
Sb^{122}	A chem (12A35); chem, cross bomb (12L39d)		β^- (12L39d)	2.80 d (47B51); 2.8 d (12L39b)	β_2 1.46 (coinc with γ) β-γ coinc spect (23M51); β_1 1.94, β_2 1.36 spect (43M46); β_1 1.8, β_2 1.2 abs, coinc abs (26M48d); β_1 1.8 abs (14M40)	0.568 spect (28C48d, 28K48); 0.57 spect conv (11R47); 0.56 (e_K/γ 0.0049), 0.68 (51G52)		Sn-d-2n (12L39d); Sn-p-n (47B51); Sb-d-p (12L39d); Sb-γ-n (22J50, 47B51); Sb-n-γ (12A35, 12L39d, 2S47, 50H51); spall Sb (37L50), I (π) (51W52); spall-fission Bi (11G49)
Sb^{123}		42.75 (24W48)					Sb^{123}, I = 7/2 (87M50)	
Sb^{124m_2}	A chem, n-capt, sep isotopes (38M47)		IT, β^- (38M47)	21 m (38M47)		0.0185 (e/γ very large) (18G50)	Q^-_β 2.92 (HPS)	Sb-n-γ, Sb^{123}-n-γ (38M47)
Sb^{124m_1}	A chem, n-capt, sep isotopes (38M47)		IT, β^- (38M47)	1.3 m (38M47)	3.2 abs (38M47)	0.012 (e/γ very large) (18G50)		Sb-n-γ, Sb^{123}-n-γ (38M47)
Sb^{124}	A chem (12L37a); chem, excit, cross bomb (12L39d)		β^- (12L39d); nσ β^+, no EC (10L50b)	60 d (12L39d)	β_1 2.291 (21%), β_2 1.69 (7%), β_3 0.95 (7%), β_4 0.68 (26%), β_5 0.50 (39%) spect (28C48d, 10L50b); β_1 2.37 (21%), β_2 1.62 (8%), β_3 1.00 (9%), β_4 0.65 (44%), β_5 0.48 (18%) spect (28K48); β_4 0.654 spect (7J47); others (54H43, 47M47, 43M46, 14M40, 37W47)	0.121, 0.607, 0.653, 0.730, 1.708, 2.04 spect, spect conv (28C48d, 10L50b); 0.61 γ (40-50%, e_K/γ 0.0043) spect, spect conv (44M52a); 0.61 γ (e_K/γ 0.0036) spect conv (94H52); 0.603 (~100%, e/γ ~0.002), 0.650, 0.714, 1.708, 2.06 spect, spect conv (28K48); 0.598, 0.645, 0.817, 1.67, 2.07 spect (13J49b); others (11R47, 14M40, 42W47, 52M51, 85S51, 89S52, 39D51, 39D51a, 42K45, 47M47)	 Q^-_β 2.90 (HPS) (18G52, HPS)	Sn-p-n (47B51); Sn-d-2n (12L39d); Sb-d-p (12L39d, 54H43, 42K45); Sb-n-γ (12L39d, 2S47); spall Sb (37L50); Te-d-α (28T38); I-n-α (12L39d); spall-fission Bi (11G49)
Sb^{125}	A chem (12L39d); chem, n-capt (84S51)		β^- (67C51)	~2.7 y (40L51a)	0.616 (18%), 0.299 (49%), 0.128 (33%) spect (7S49d); 0.621, 0.288, others (?) spect (28K49); others (38G46, 15J49, 26M49b, 84S51)	0.637, 0.601, 0.465, 0.425, 0.175, 0.035 spect, spect conv, coinc (7S49d); 0.646 (weak, e/γ very small), 0.609 (strong), 0.466 (weak, e/γ very small), 0.431 (strong), 0.174 (strong), 0.125 (weak) spect, spect conv, coinc (28K49); with Te^{125m}: 0.110, 0.035 (28B52, 10C51a, 7S49d, 28K49, 67H49a)	Q^-_β 0.76 (7S49d)  (7S49d, 18G52)	Sn-d-n (12L39d); Sn-n-γ, β⁻ decay (7S49d, 23F48, 84S51); spall-fission Th (7N49a); fission U^{233} (38G48), U (67C51, 40L51a, 84S51); parent Te^{125m} (23F48, 28K49); daughter (9.4 d) Sn^{125} (19N50); not daughter (9.4 d) Sn^{125} (7N49b)

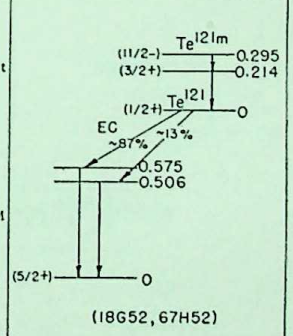
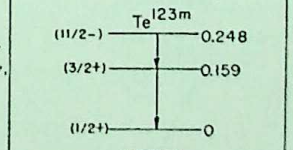
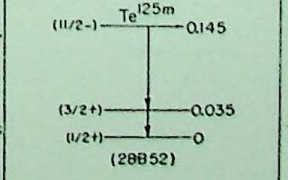
CC-0. In Public Domain. Gurukul Kangri Collection, Haridwar

Digitized by Arya Samaj Foundation Chennai and eGangotri

Isotope Z A	Class and identification	Percent abundance	Type of decay	Half-life	Energy of radiation in Mev: Particles	Energy of radiation in Mev: Gamma-transitions	Disintegration energy and scheme	Method of production and genetic relationships
$_{51}Sb^{126}$	B chem, excit (80B51)		β^- (80B51)	9 h (80B51)	~1 abs (80B51)	0.90, ~0.4 (both coinc with β^-) scint spect, β-γ-coinc (80B51)		fission U^{235} daughter Sn^{126} (80B51)
Sb	E chem (80B51)		β^- (80B51)	10 m (80B51)				fission U^{235} (80B51)
Sb^{-126}	D chem (38G46)		β^- (38G46)	28 d (38G46); ~30 d (80B51)	1.9 (38G46)			fission U (38G46), U^{235} (80B51)
Sb^{127}	A chem, genet (32A39)		β^- (32A39)	93 h (76S51b); 95 h (38G46)	1.2 abs (76S51b); 0.8 abs (38G46)	0.72 abs (76S51b)		fission U^{233} (61S48), U^{235} (38G51, 80B51), U (32A39, 38G46, 76S51b), Pu (32K48); parent Te^{127} (32A39, 33G51i); parent (84%) Te^{127}, parent (16%) Te^{127m} (78B48); daughter Sn^{127} (80B51)
Sb^{129}	A chem, genet (32A39)		β^- (32A39)	4.2 h (32A39)				fission U (32A39), Pu (32K48); parent Te^{129} (32A39)
Sb^{130}	D chem, excit (fission yield) (80B52)		β^- (80B52)	40 m (80B52)				fission U^{235} (80B52)
Sb^{130}	D chem, excit (fission yield) (30P52a)		β^- (80B52)	12 m (30P52a); 10 m (80B52)				fission U (80B52, 30P52a)
Sb^{131}	A chem, genet (30P51, 68C51)		β^- (30P51)	23.1 m (30P51); ~20 m (68C51)				fission U, parent Te^{131}, parent Te^{131m} (30P51, 68C51)
Sb^{132}	B chem, genet (32A39)		β^- (32A39)	2 m (30P51); ~5 m (32A39); ~2 m (68C51)				fission U (32A39, 30P51, 68C51); parent Te^{132} (32A39, 30P52a)
Sb^{133}	B chem, genet (30P51)		β^- (30P51)	4.4 m (30P51); 4.2 m (68C51)				fission U (30P51, 68C51); parent Te^{133m} (30P51)
$Sb^{134,135}$	D chem (30P51)		β^- (30P51)	~50 s (30P51); 45 s (68C51)				fission U (30P51, 68C51)
$_{52}Te^{<118}$	D chem (37L48a)		β^+ (37L48b)	2.5 h (37L48a)				spall Sb (37L48a), I (π) (51W52)
Te^{118}	B chem, genet (37L48a)		EC (37L48a)	6.0 d (37L48a)		no γ (?) (37L48a)		Sb-d-5n, parent (4 m) Sb^{118} (37L48a, 37L50); spall I (π) (51W52); spall-fission Bi (11G49)
Te^{119}	B chem, genet (37L48a)		EC (37L48a)	4.5 d (37L48a)	conv: 0.2, 0.5 spect conv (37L48a)	1.6 abs (37L50)		Sb-d-4n, parent Sb^{119} (37L48a, 37L50); spall-fission Bi (11G49)
Te^{120}		0.089 (1B50)						

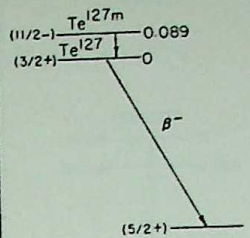
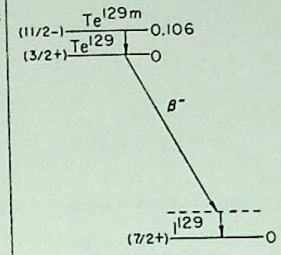
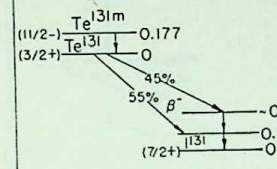
CC-0. In Public Domain. Gurukul Kangri Collection, Haridwar

Digitized by Arya Samaj Foundation Chennai and eGangotri

Isotope Z A	Class and identification	Percent abundance	Type of decay	Half-life	Energy of radiation in Mev: Particles	Energy of radiation in Mev: Gamma-transitions	Disintegration energy and scheme	Method of production and genetic relationships
$_{52}Te^{121m}$	A chem, excit, cross bomb (13S40); chem, n-capt, sep isotopes (10C51a)		IT (14E46a)	154 d (67H51d); 143 d (14E46a); 125 d (13S40); 140 d (10C51a)		γ_1 0.082 (e/γ very large, K/L 0.75), γ_2 0.213 (e_K/γ 0.09, K/L 7.3) (γ_2 coinc with γ_1) spect conv, conv-γ coinc, conv-conv coinc (43K50); γ_1 0.0818, γ_2 0.214 spect conv (10C51a); others (67H49, 81B46, 82B46, 6Y45, 20D50, 4K42a)	 (18G52, 67H52)	Sn-α-n (13S40); Sb-d-2n (13S40, 14E46a, 43K50); Sb-p-n (13S40, 14E46a); spall Sb (37L50); Te^{120}-n-γ (10C51a); parent Te^{121} (82B46)
Te^{121}	A chem, genet (14E46a, 82B46)		EC (14E46a)	17 d (14E46a); ~16 d (82B46)		γ_1 0.506 (13%, e/γ ~0.018, K/L+M 6), γ_2 0.573 (87%, not coinc with γ_1, e/γ 0.009, K/L+M 6) spect conv, scint spect (67H52); 0.575 spect conv (10C51a); ~0.61 (e_K/γ 0.004) spect conv (43K50); 0.6 abs (14E46a)		Sb-d-2n (14E46a); Sb-p-n (14E46a); daughter Te^{121m} (82B46); daughter I^{121} (74M50)
Te^{122}		2.46 (1B50)						
Te^{123m}	A chem, n-capt, sep isotopes (67H49)		IT (67H49)	104 d (67H51d); 121 d (10C51a)		γ_1 0.0885 (e/γ very large, K/L 0.68), γ_2 0.159 (e_K/γ 0.18, K/L 8.9) (γ_1 coinc with γ_2) spect conv, γ-conv coinc, conv-conv coinc, abs (43K50); γ_1 0.0887, γ_2 0.159 spect conv (10C51a); γ_1 (L_I/L_{III} 0.5) spect conv (63M52a); γ_2 (e_K/γ 0.19) scint spect (52M52e); no 0.25 γ (lim 0.5%) scint spect (68H51); others (4K42a, 67H49, 20D50, 52M52)	 (18G52)	Sb-d-2n (43K50); Te^{122}-n-γ (67H49, 43K50, 68H51, 10C51a)
Te^{123}		0.87 (1B50)					Te^{123}, I = 1/2 (87M50)	
Te^{124}		4.61 (1B50)						
Te^{125m}	A chem, genet (23F48)		IT (23F48)	58 d (67H49a, 67H51d)		0.110 (e_K/γ ~160, K/L+M 1.15), 0.0355 (e_K/γ ~11.7, K/L/M = 7.3/1.0/0.18) spect conv, ion ch, scint spect, x-γ coinc, x-x coinc (28B52); 0.110, 0.0353 spect conv (10C51a); 0.110 (K/L+M 1.1), 0.035 spect conv (7S49d); 0.110 (K/L 1.2) spect conv (28K49); 0.109 (e/γ >100, K/L ~1.5, L/M ~3.5) spect conv (67H49a); others (67H49, 23F50a, 52M51, 28B49)	see Sb^{125}  (28B52)	Te^{124}-n-γ (67H49); daughter Sb^{125} (23F48, 28K49); not daughter I^{125} (lim 0.05%) (23F51b)
Te^{125}		6.99 (1B50)					Te^{125}, I = 1/2 (87M50)	
Te^{126}		18.71 (1B50)					Te^{126}, I = 0 (87M50)	

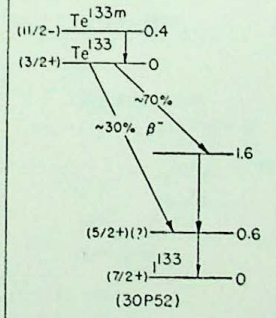
CC-0. In Public Domain. Gurukul Kangri Collection, Haridwar

Digitized by Arya Samaj Foundation Chennai and eGangotri

Isotope Z A	Class and identification	Percent abundance	Type of decay	Half-life	Energy of radiation in Mev: Particles	Energy of radiation in Mev: Gamma-transitions	Disintegration energy and scheme	Method of production and genetic relationships
$_{52}Te^{127m}$	A chem, excit, genet (13S40)		IT (13S40)	115 d (10C51a); 90 d (13S40)		0.0885 (K/L 0.75) spect conv (67H49, 67H49a); 0.0887 spect conv (10C51a); 0.086 (e/γ very large, K/L 0.75) spect conv (2H41)	 (18G52)	Te-n-γ (13S40, 2S47); Te-d-p (13S40); Te^{126}-n-γ (67H49); I-n-p (13S40); fission U (38G46, 33G51i, 43W48), U^{233} (61S48, 38G48, 38G51), U^{235} (38G51); parent Te^{127} (13S40, 33G51i, 43W51); daughter (16%) Sb^{127} (78B48)
Te^{127}	A chem (28T38, 32A39); chem, excit, cross bomb (13S40)		β⁻ (32A39)	9.3 h (13S40)	0.7 abs (33G51i)	no γ (33G51i)		Te-n-γ (13S40, 2S47); Te-d-p (28T38, 13S40); Te-n-2n (28T38); I-n-p (13S40); fission U (32A39, 13S40, 43W48, 33G51i), U^{233}, U^{235} (38G51); daughter Te^{127m} (13S40, 33G51i, 43W51); daughter Sb^{127} (32A39, 33G51i), (84%) (78B48)
Te^{128}		31.79 (1B50)					Te^{128}, I = 0 (87M50)	
Te^{129m}	A chem, genet (13S40)		IT (13S40)	33.5 d (10C51a); 32 d (13S40, 1N51a)		0.1060 spect conv (10C51a); 0.106 (K/L ~4) spect conv (67H49); 0.102 (e/γ very large, K/L ~1) spect conv (2H41)	 (18G52, HPS)	Te^{128}-n-γ (67H49); Te-n-γ (13S40, 2S47); Te-d-p (13S40); Te-n-2n (28T38); Te-γ-n (25W48); fission U (16H43b, 38G46, 43W48, 1N51a, 30P51a), U^{233} (38G48, 38G51), U^{235} (38G51); parent Te^{129} (13S40, 38G46, 43W51)
Te^{129}	A chem, excit (37B39, 13S40)		β⁻ (13S40)	72 m (13S40); 70 m (32A39, 33G51i); 67 m (25W48)	1.8 spect (11R47); 1.7 abs (33G51i)	0.3, 0.8 abs (33G51i)		Te-n-γ (13S40, 2S47); Te-d-p (13S40, 28T38); Te-γ-n (37B39, 25W48); Te-n-2n (6H37, 28T38); fission Th (72B51), U (32A39, 16H43b, 38G46, 43W48, 1N51a); daughter Te^{129m} (13S40, 38G46, 43W51); daughter Sb^{129} (32A39)
Te^{130}		34.49 (1B50)		double beta decay; $\sim 10^{21}$ y Xe ratios, mass spect (3I50b)			Te^{130}, I = 0 (87M50)	
Te^{131m}	A chem, genet (13S40)		IT (13S40)	30 h (32A39, 13S40)		0.177 (K/L 2) spect conv (2H41)	 (18G52, 37G52)	Te-n-γ (13S40, 2S47); Te-d-p (13S40); spall-fission U (6F51); fission U (32A39, 16H39a, 32K51d, 43W51, 30P51a); parent Te^{131} (32A39, 13S40, 43W51); daughter Sb^{131} (68C51)
Te^{131}	A chem, excit (13S40)		β⁻ (13S40)	24.8 m (37G52); 25 m (13S40)	2.0 (~55%), 1.4 (~45%) abs, β-γ coinc (37G52)	0.16, 0.7 abs (37G52)		Te-d-p (13S40); Te-n-γ (13S40, 2S47, 37G52); fission U (32A39); daughter Te^{131m} (32A39, 13S40, 43W51); parent I^{131} (32A39, 13S40, 30P51, 68C51); daughter Sb^{131} (30P51, 68C51)

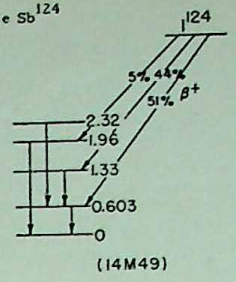
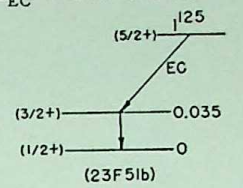
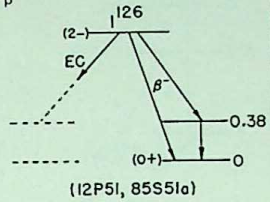
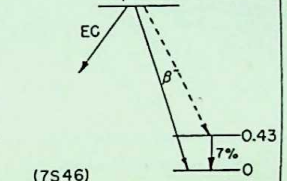
CC-0. In Public Domain. Gurukul Kangri Collection, Haridwar

Digitized by Arya Samaj Foundation Chennai and eGangotri

Isotope Z A	Class and identification	Percent abundance	Type of decay	Half-life	Energy of radiation in Mev: Particles	Energy of radiation in Mev: Gamma-transitions	Disintegration energy and scheme	Method of production and genetic relationships
$_{52}Te^{132}$	B chem (32A39); fission fragment range (32K48)		β^- (32A39)	77.7 h (30P51a); 77 h (32A39)	0.22 spect (10L51a); 0.3, ~0.1 (?) abs (1N51b); ~0.3 abs (70B43a)	0.231 scint spect (10L51a); 0.22 abs (1N51b)		Te-a-2p (11S51); spall-fission Th (7N49a); fission Th (16H39d, 72B51, 21T51), U (32A39, 16H39e, 16H39a, 1N51b, 30P51a), Pu (32K48); daughter Sb^{132} (32A39, 30P52a); parent I^{132} (32A39, 16H39e, 16H39a, 1N51b, 44W51)
Te^{133m}	A chem, genet (32A39)		IT (30P52)	63 m (30P52); 60 m (32A39, 16W40)		~0.4 scint spect (30P52); with Te^{133}: 0.6, 1.0 abs (30P52)		fission U (32A39, 16H39a, 24S40, 16W40, 30P51), Pu (32K48); parent Te^{133} (30P52); ancestor I^{133} (32A39, 16H39a, 24S40, 16W40, 16W45, 30P51); daughter Sb^{133} (30P51)
Te^{133}	A chem, genet (30P52)		β^- (30P52)	2 m (30P52)	2.4 (~30%), 1.3 (~70%) abs (30F52)	0.6, 1.0 abs (30P52)		daughter Te^{133m} (30P52); parent I^{133} (30P52a)
Te^{134}	B chem, genet (32A39)		β^- (32A39)	44 m (30P51a); 43 m (32A39)				fission Th (9P40), U (32A39, 16H39a, 30P51a), Pu (32K48); parent I^{134} (32A39, 16H39a, 30P51a)
Te^{135}	[A] genet (22D40)		β^- (22D40)	<2 m (33G51j, 32K51e, 22D40)				fission U, parent I^{135} (33G51j, 32K51e)
Te	E chem (16H43b)		β^- (16H43b)	~1 m (16H43b)				fission U (16H43b)
$_{53}I^{120}$	D chem (74M50)		β^+ (74M50)	30 m (74M50)	4.0 abs, spect (74M50)			spall Sn (second order reaction) (74M51); Sb-a-5n (74M50)
I^{121}	B chem, genet (74M50)		β^+ (74M50)	1.5 h (40D52); 1.8 h (74M50)	1.2 abs, spect (74M50); 1.2, 4.0 (weak) (40D52); conv: 0.185 spect (74M50)			spall Sn (second order reaction) (74M51); Sb-a-4n, parent Te^{121} (74M50); daughter Xe^{121} (37T52, 8H52b, 40D52)
I^{122}	A chem, excit (74M50); sep isotopes (7Y51)		β^+ (74M50)	3.6 m (7Y51); 3.4 m (40D52), 4 m (74M50)	2.9 abs (74M50); 3.1 abs (7Y51)			Sb-a-3n (74M50); Te^{122}-p-n (7Y51); daughter Xe^{122} (37T52, 8H52b, 40D52)
I^{123}	A chem, excit (74M50); chem, sep isotopes (14M49)		EC (74M50)	13.0 h (14M49); 13 h (74M50)		0.159 spect, spect conv (14M49)		spall Sn (second order reaction) (74M51); Sb-a-2n (74M50); Sb^{121}-a-2n (14M49); daughter Xe^{123} (37T52, 8H52b, 40D52)

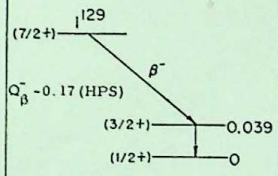
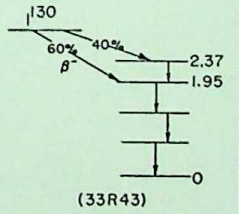
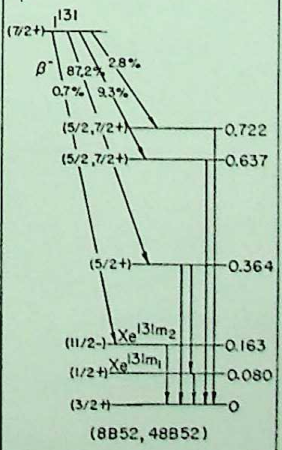
CC-0. In Public Domain. Gurukul Kangri Collection, Haridwar

Digitized by Arya Samaj Foundation Chennai and eGangotri

Isotope Z A	Class and identification	Percent abundance	Type of decay	Half-life	Energy of radiation in Mev: Particles	Energy of radiation in Mev: Gamma-transitions	Disintegration energy and scheme	Method of production and genetic relationships
$_{53}I^{124}$	A chem, excit, cross bomb (12L38e)		EC ~70%, β^+ ~30% (74M50)	4.5 d (74M50); 4.0 d (12L38e, 2D40)	2.20 (51%), 1.50 (44%), 0.7 (5%) spect (14M49); 2.1 spect, abs (74M50)	0.603, 0.73, 1.72, 1.95 spect, spect conv (14M49); no γ coinc with 2.2 β^+, β-γ coinc (85S51); γ-γ, β-γ coinc (37M49)	see Sb^{124}  (14M49)	spall Sn (second order reaction) (74M51); Sb-a-n (12L38e, 74M50); Sb-a-3n (74M50); Sb^{121}-a-n (74M50); Te-p-n (2D40); spall-fission Bi (11G49, 66B51)
I^{125}	A chem (17R46a); chem, excit (33G47); genet (67B51b)		EC (L/K 0.23) (38M52); EC (L/K 0.3) (23F51b); no β^+ (33G47)	60.0 d (23F51b); 56 d (17R46a)		0.035 ion ch (23F51b); 0.0355, no 0.109 γ spect conv (67B51b)	see Te^{125m} Q_{EC} ~0.13 calc (38M52)  (23F51b)	Sb-a-2n (74M50); Te-d-n (17R46a, 33G47); spall-fission Bi (11G49, 66B51); daughter Xe^{125} (67B51b); not parent Te^{125m} (lim 0.05%) (23F51b)
I^{126}	A excit (28T38); chem, excit, cross bomb (12L38e)		EC ~58%, β^- ~40%, β^+(?) ~2% (12P51)	13.0 d (12L38e); 13 d (28T38)	β^-: 1.268 (27%), 0.85 (73%) spect (14M49); 1.24 (~25%), 0.85 (~75%) spect (12P51); 0.865 spect (23M51a)	with β^-: 0.382 spect conv, β-γ coinc (12P51); 0.395 spect, spect conv (14M49); with EC: 0.64 (weak) scint spect, x-γ coinc, γ-γ coinc (12P51); others (85S51)	Q^-_β 1.27 (12P51)  (12P51, 85S51a)	spall Sn (second order reaction) (74M51); Sb-a-n (12L38e, 74M50); Te-d-n (12L38e); Te-p-n (2D40); I-n-2n (12L38e, 28T38, 12P51); I-γ-n (12P49, 27M49, 3O50); spall-fission Bi (11G49, 66B51)
I^{127}		100 (6N37)					I^{127}, I = 5/2 (87M50)	
I^{128}	A chem, n-capt (12A35)		β^- 95.0%, EC + β^+ 5.0% (28R50); EC/β^- 0.063 (41M51a)	24.99 m (69H41)	2.02 spect (7S46)	0.428 (7%) spect (7S46)	Q^-_β 2.0 (7S46)  (7S46)	I-n-γ (12A35, 28T38, 2S47, 7S46, 9O49, 50H51); Te-d-2n (12L38e); Te-p-n (2D40)

CC-0. In Public Domain. Gurukul Kangri Collection, Haridwar

Digitized by Arya Samaj Foundation Chennai and eGangotri

Isotope Z A	Class and identification	Percent abundance	Type of decay	Half-life	Energy of radiation in Mev: Particles	Energy of radiation in Mev: Gamma-transitions	Disintegration energy and scheme	Method of production and genetic relationships
$_{53}I^{129}$	A chem, n-capt (32K47)		β^- (32K47)	1.72×10^7 y sp act (32K51f); 3×10^7 y sp act (26P49b)	0.12 scint spect (38M52); 0.12 abs (26P49b); 0.12 ion ch (83B50); 0.13 abs (32K51f)	0.039 (coinc with β^-, e_K/γ ~6, K/L ~40) ion ch, β-γ coinc (83B50)	I^{129}, I = 7/2 (87M50)  (83B50, 30T52, 18G52)	fission U (32K47, 26P49b, 83B50)
I^{130}	A chem, cross bomb (12L38e)		β^- (12L38e)	12.6 h (12L38e)	1.03 (~60%), 0.61 (~40%) spect (33R43)	0.744 (e_K/γ 0.003), 0.667 (e_K/γ 0.004), 0.537 (e_K/γ 0.007), 0.417 (coinc with 0.6 β^-, e_K/γ 0.012) ($e_K >> e_L$ for all γ's) spect, spect conv, β-γ, γ-γ coinc (33R43)	 (33R43)	Te-d-2n (12L38e); Te-p-n (2D40); I^{129}-n-γ (32K47); Cs-n-α (16W40)
I^{131}	A chem (12L38e); chem, genet (13S40)		β^- (12L38e)	8.141 d (39S51a); 8.05 d (106B52); 8.16 d (17K51); 8.04 d (38S51)	0.815 (0.7%), 0.608 (87.2%), 0.335 (9.3%), 0.250 (2.8%) spect, β-γ coinc (8B52); 0.810, 0.606, 0.335, 0.250 spect, β-γ coinc (24K51); 0.807, 0.606, 0.339 spect (40R52); E (average) 0.189 ion ch (77C52); see also: (69C52, 11B52, 8V51, 20N51, 10C51b, 30T51, 11B51, 22F50, 28K49, 44M48, 25D42)	0.080 (2.2%, coinc with 0.284 γ, e_K/γ 1.73, K/L 7), 0.163 (coinc with Xe^{131m2}), 0.284 (5.3%, coinc with 0.608 β^-, e_K/γ 0.047, K/L 5), 0.364 (80%, coinc with 0.608 β^-, e_K/γ 0.018, K/L 8), 0.637 (9%, coinc with 0.335 β^-, e_K/γ 0.0037, K/L 9), 0.722 (3%, coinc with 0.250 β^-, e_K/γ 0.0028, K/L 8) spect, spect conv, β-γ delay coinc, scint spect (8B52, 8B52a); γ_1 0.080133, γ_2 0.28413, γ_3 0.36418 ($\gamma_1/\gamma_2/\gamma_3$ = 5/9/100) cryst spect (29L49a); γ_2 0.284 (e_K/γ 0.052, K/L 3.3), γ_3 0.364 (e_K/γ 0.021, K/L 5.6), γ_4 0.638 (e_K/γ 0.0040), γ_5 0.723 (e_K/γ 0.0034) ($\gamma_2/\gamma_3/\gamma_4/\gamma_5$ = 6/100/10/3) spect, spect conv (93H52a); 0.080 (4.3%, with 0.283 γ, e/γ 1.83) γ-γ, x-γ coinc, scint spect (69C52a); see also: (11B52, 48B52, 69C52, 86S52, 8V51, 30T51, 24K51, 10C51b, 22F50, 28K49, 48B49, 44M48, 13O48, 25D42, 40R52, 52W51, 24E51)	Q^-_β 0.972 (8B52)  (8B52, 48B52)	Te-d-n (12L38e, 33R41a); spall-fission Th (7N49a), U (16F41, 6O47, 6F51); fission Th (21T51), U (32A39, 16H39a, 38G46, 23S51), 32K51g), U^{233} (1Y47, 38G48, 61S48, 38G51), U^{235} (1Y47, 38G51), Pu (28F51); daughter Te^{131} (12L38e, 32A39, 16H39a, 13S40, 30P51, 68C51); parent (~1%) Xe^{131m2} (48B49, 67B50b); parent Xe^{131m1} (14G51a)
I^{132}	B chem, genet (32A39)		β^- (32A39)	2.4 h (32A39); 2.3 h (16H39a)	2.2, 0.9 abs (1N51b); 1.5 abs (75S49); ~1.4 abs (70B43a)	γ_1 0.69, γ_2 1.41, γ_3 2.0 ($\gamma_1/\gamma_2/\gamma_3$ = 37/4/1), γ_4 ~0.8 (very weak) scint spect, γ-γ coinc (46M51); 0.6, 1.4 abs (1N51b)		spall-fission U (16F41, 6O47); fission Th (72B51, 21T51), U (32A39, 16H39a, 9P40, 38G46, 1N51b), U^{233} (38G48); daughter Te^{132} (32A39, 16H39a, 16H39e, 1N51b, 44W51)

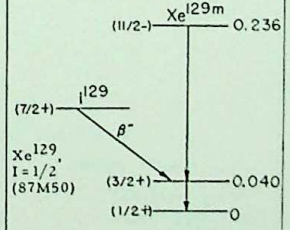
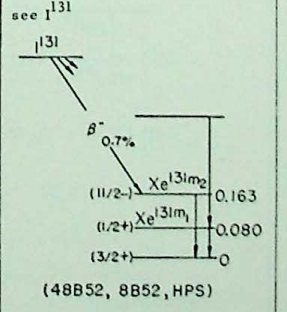
CC-0. In Public Domain. Gurukul Kangri Collection, Haridwar

Digitized by Arya Samaj Foundation Chennai and eGangotri

Isotope Z A	Class and identification	Percent abundance	Type of decay	Half-life	Energy of radiation in Mev: Particles	Energy of radiation in Mev: Gamma-transitions	Disintegration energy and scheme	Method of production and genetic relationships
$_{53}I^{133}$	A chem (32A39); chem, genet (16W40)		β^- (32A39, 16H39a)	20.5 h (106B52); 22.4 h (30P51a)	1.3 (~91%), 0.4 (~9%) abs (30P52a); 1.4 (~94%), 0.5 (~6%) abs, β-γ coinc (48B49a); 1.4 abs (23S51j)	0.53 (94%), 0.85 (5%), 1.4 (1%) scint spect, γ-γ coinc (48B49a); 0.53 spect (6P47b); 0.55 abs (23S51j)		spall-fission Pb (2T47b), U (16F41, 6O47); fission U (32A39, 16H39a, 24S40, 16W40, 30P51, 23S51k), Pu (28F51); daughter Te^{133} (32A39, 16H39a, 24S40, 16W40, 16W45, 30P51); parent Xe^{133} (24S40, 16W40, 16W45); parent (2.4%) Xe^{133m} (8Z51, 24K51a)
I^{134}	B chem (32A39); fission fragment range (32K48)		β^- (32A39)	52.5 m (30P51a); 51 m (32L49); 54 m (32A39)	1.6 (~70%), 2.8 (~30%), hard β (weak) abs (30P52a); 1.5-1.75, 3.5-4.2 abs (32L49)	>2.2 (weak) D-γ-n reaction (32L49); >1 abs (32K51h)		spall-fission U (16F41); fission Th (22D39), U^{235} (1Y47, 38G51), U (16H39a, 32A39, 9P40, 9P40a, 32L49, 32K51h, 30P51a), Pu (32K48, 28F51); daughter Te^{134} (16H39a, 32A39, 30P51a)
I^{135}	A chem, genet (22D40, 24S40)		β^- (22D40, 24S40)	6.68 h (6P47b); 6.7 h (33G51j, 32K51e)	0.5 (35%), 1.0 (40%), 1.4 (25%) spect (6P47b); 1.4 abs (32K51e); 1.5 abs (23S51j)	1.8, 1.27 spect (6P47b); 1.3 abs (23S51j); 1.6 abs (32K51e); 2.4 (1.1%) abs (32L49)		spall-fission U (6O47); fission Th (72B51), U (24S40, 16W40, 22D40, 16W45, 6P47b, 33G51j, 32K51e), Pu (28F51); daughter Te^{135} (33G51j, 32K51e); parent (~30%) Xe^{135m}, parent (~70%) Xe^{135} (6P47b); parent Xe^{135m} (40G40, 16W45); parent Xe^{135} (24S40, 22D40, 40G40, 16W45)
I^{136}	D chem (65S40)		β^- (65S40)	86 s (84S49)	6.5 abs (84S49)	1.4, 2.9 scint spect, abs (84S49, 99M52)		fission U (65S40, 66S43, 84S49), U^{233}, Pu (84S49)
I^{137}	A chem (65S40, 26S47); chem, genet (66S43, 63S49)		β^-, β^-n (~6% of disintegrations) (19L51a)	22.0 s (n) (28H48a); 22.5 s (n) (34R47); 19.3 s genet (63S49)	n (mean): 0.56 abs paraffin (28H48a); 0.67 p recoil in cl ch (71B46)			fission U (65S40, 66S43, 26S47, 34R47, 63S47a, 63S49), Pu (34R47); parent Xe^{137} (66S43, 63S49)
I^{138}	A chem, genet (63S49)		β^- (63S49)	5.9 s (63S49)				fission U, ancestor Cs^{138} (63S49)
I^{139}	A chem, genet (63S49)		β^- (63S49)	2.7 s (63S49)				fission U, parent Xe^{139}, ancestor Ba^{139} (63S49)
$_{54}Xe^{121}$	B chem, genet (37T52, 8H52b, 40D52)			40 m (40D52); 70 m (37T52); ~60 m (8H52b)				I-p-7n (37T52, 8H52b, 40D52); parent I^{121} (37T52, 8H52b, 40D52)
Xe^{122}	A chem, genet (37T52, 8H52b, 40D52)			19.5 h (37T52); 20.0 h (40D52); 19 h (8H52b)				I-p-6n (37T52, 8H52b, 40D52); parent I^{122} (37T52, 8H52b, 40D52)
Xe^{123}	A chem, genet (37T52, 8H52b, 40D52)		β^+ (40D52)	2.1 h (37T52); 1.7 h (40D52); ~2 h (8H52b)				I-p-5n (37T52, 8H52b, 40D52); parent I^{123} (37T52, 8H52b, 40D52)
Xe^{124}		0.096 (6N50a)						

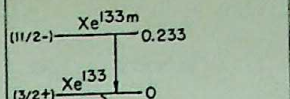
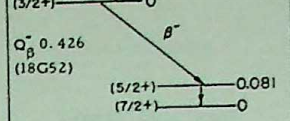
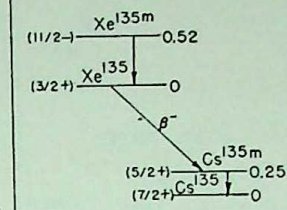
CC-0. In Public Domain. Gurukul Kangri Collection, Haridwar

Digitized by Arya Samaj Foundation Chennai and eGangotri

Isotope Z A	Class and identification	Percent abundance	Type of decay	Half-life	Energy of radiation in Mev: Particles	Energy of radiation in Mev: Gamma-transitions	Disintegration energy and scheme	Method of production and genetic relationships
$_{54}Xe^{125}$	A chem, sep isotopes (33A50); chem, mass spect (67B51b)		EC, no β^+ (67B51b, 33A50)	18 h (67B51b); 20 h (33A50)		0.054 (K/L ~4.3), 0.096, 0.106, 0.187 (K/L ~4.6), 0.243 spect conv; 0.460 scint spect (67B51b)		Te^{122}-α-n (33A50); Xe-n-γ (67B51b); parent I^{125} (67B51b)
Xe^{126}		0.090 (6N50a)						
Xe^{127}	D chem (29C40b)		IT (?) (29C40b)	75 s (29C40b)		0.125, 0.175 spect conv (29C40b)		I-p-n (29C40b)
Xe^{127}	A chem (29C40b); chem, sep isotopes (33A50); mass spect (67B51c)		EC (67B51c)	34 d (29C40b); 32 d (33A50); 25 d (67B51d)		0.057, 0.145, 0.170, 0.200, 0.365 spect conv, scint spect (67B51c)		Te^{124}-α-n (33A50); I-p-n (29C40b); I-d-2n (11O42); Xe-n-γ (44C44, 67B51c); daughter Cs^{127} (33F50)
Xe^{128}		1.919 (6N50a)						
Xe^{129m}	A chem, mass spect (67B51c)		IT (67B51c)	8.0 d (67B51c)		0.196 (K/L+M 2.1) spect conv (67B51c); 0.040 (K/L+M 4.3) spect conv (30T52, 30T52c)	 (30T52, 18652)	Xe-n-γ (67B51c)
Xe^{129}		26.44 (6N50a)						
Xe^{130}		4.08 (6N50a)						
Xe^{131m_2}	A chem (44C44); chem, genet (48B49); mass spect (67B50b)		IT (48B49, 44C44)	12.0 d (67B50b)		0.163 (K/L+M 1.9, L/M 3.4) spect conv (67B50b, 67B51c); 0.163 (K/L+M 1.7) spect conv (8V51); 0.165 (e/γ ~20) abs conv, abs (48B49)	see I^{131}  (48B52, 8B52, HPS)	Xe-n-n (44C44); daughter (~1%) I^{131} (48B49, 67B50b); not daughter Cs^{131} (43C51c); daughter Cs^{131} (70C50)
Xe^{131m_1}	A genet (14G51a)		IT (14G51a)	4.8×10^{-10} s delay coinc (14G51a, 8B52a)		0.080 scint spect (14G51a, 8B52a)		daughter I^{131} (14G51a, 8B52a)
Xe^{131}		21.18 (6N50a)					Xe^{131}, I = 3/2 (87M50)	fission U (mass spect) (13T47)
Xe^{132}		26.89 (6N50a)					Xe^{132}, I = 0 (87M50)	fission U (mass spect) (13T47)

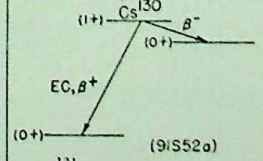
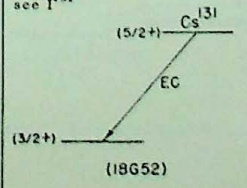
CC-0. In Public Domain. Gurukul Kangri Collection, Haridwar

Digitized by Arya Samaj Foundation Chennai and eGangotri

Isotope Z A	Class and identification	Percent abundance	Type of decay	Half-life	Energy of radiation in Mev: Particles	Energy of radiation in Mev: Gamma-transitions	Disintegration energy and scheme	Method of production and genetic relationships
$_{54}Xe^{133m}$	A chem (24K50c); mass spect (67B51a)		IT (24K50c)	2.3 d (67B51a); 2.1 d (24K51a)		0.233 (K/L 2.9) spect conv (67B51a); 0.235 (e_K/γ 4.2) spect conv, scint spect (24K51a)		Xe-n-γ (67B51a); fission U (24K50c, 67B50c); daughter (2.4%) I^{133} (8Z51, 24K51a)
Xe^{133}	A chem (20L39, 22D40, 24S40); chem, excit (16W40); mass spect (13T47, 30T49)		β^- (22D40)	5.270 d (76M50); 5.3 d (18E51)	0.345 spect (67B50c); 0.34 abs (18E51); 0.35 abs (13E51e)	with Cs^{133m}: 0.081 (K/L 5.9) spect conv (67B50c); 0.08 γ (e_K/γ 1.8, K/L+M 6.0) scint spect, β-γ delay coinc (14G53); -0.085 abs (13E51e); 0.08 cl ch (84B51)	 (18G52)	Te-α-n (52C41); Xe-d-p (52C41); Xe-n-γ (21R43, 44C44); Xe-n-2n (21R43); Cs-n-p (16W40, 44C44, 16W45); Ba-n-α (16W40, 66S43b, 44C44, 16W45); fission U (24S40, 22D40, 16W40, 70B43a, 16W45, 13T47, 18E51, 84B51, 13E51e); daughter I^{133} (24S40, 16W40, 16W45); parent Cs^{133} (8Z51); parent Cs^{133m} (14G53)
Xe^{134}		10.44 (6N50a)					Xe^{134}, I = 0 (87M50)	fission U (mass spect) (13T47)
Xe^{135m}	A chem, genet (40G40, 16W45)		IT (16W45)	15.6 m (21R43); 15.3 m (6P47b); 13 m (1N51c)		0.52 spect (6P47b); 0.5 (e/γ ~0.2) abs, abs conv (16W45, 1N51c)	 (18G52, 14G53)	Xe-n-2n (21R43); Xe-n-γ (21R43, 21R46); Ba-n-α (66S43b); fission U (40G40, 16W45, 13T47); daughter I^{135} (40G40, 16W45); daughter (~30%) I^{135} (6P47b); parent Xe^{135} (16W45)
Xe^{135}	A chem (24S40, 22D40); chem, excit (16W40); mass spect (30T49)		β^- (24S40)	9.13 h (60B52); 9.2 h (7N51, 58H51c); 9.1 h (30T49)	0.905 spect (67B51); 0.93 spect (6P47b); 0.95 abs (70B43a); 0.9 abs (16W45); 1.0 abs (7N51, 58H51c)	with Cs^{135m}: 0.250 (e_K/γ 0.05) spect conv, β^--conv coinc (67B51, 67B51d); 0.248 (K/L 7.0) spect conv, scint spect, β-γ delay coinc (14G53); 0.25 spect (6P47b)	Q_β^- 1.15 (67B51)	Xe-n-γ, Xe-n-2n (21R43); Xe-d-p (52C41); Ba-n-α (16W40, 66S43b, 16W45); fission U (24S40, 22D40, 84B51); daughter I^{135} (24S40, 22D40, 40G40, 16W45); daughter (~70%) I^{135} (6P47b); daughter Xe^{135m} (16W45); parent Cs^{135} (63S49a); parent Cs^{135m} (14G53)
Xe^{136}		8.87 (6N50a)					Xe^{136}, I = 0 (87M50)	fission U (mass spect) (13T47); daughter I^{137} (~6% of dis) (19L51a)
Xe^{137}	A chem (66S43); mass spect (30T49)		β^- (66S43)	3.9 m (63S49); 3.8 m (66S43); 3.4 m (21R43)	~4 abs (66S43, 70B43a)			Xe-n-γ (21R43, 66S43b, 63S49); fission U (66S43, 63S49, 33G51k); daughter I^{137} (66S43, 63S49); parent Cs^{137} (21T51b, 33G51k)
Xe^{138}	A chem (16H39a); mass spect (30T49)		β^- (16H39a)	17 m (36G40)				fission U (16H39a, 16H40a, 36G40, 66S43b); parent Cs^{138} (16H39a, 36G40, 66S43b)

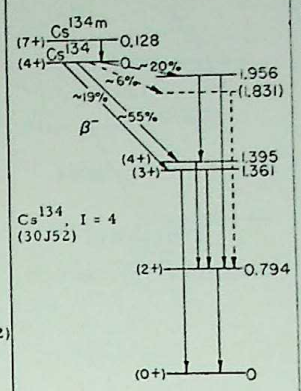
CC-0. In Public Domain. Gurukul Kangri Collection, Haridwar

Digitized by Arya Samaj Foundation Chennai and eGangotri

Isotope Z A	Class and identification	Percent abundance	Type of decay	Half-life	Energy of radiation in Mev: Particles	Energy of radiation in Mev: Gamma-transitions	Disintegration energy and scheme	Method of production and genetic relationships
$_{54}Xe^{139}$	A chem, genet (16H39a, 6H39)		β^- (16H39a, 6H39)	41 s (24D51)				fission Th (25A39, 16H40); fission U, parent Cs^{139} (16H39a, 6H39, 16H40a); ancestor Ba^{139} (16H39a, 6H39, 24D51); daughter I^{139} (63S49)
Xe^{140}	A chem, genet (16H40a)		β^- (16H40a)	16.0 s (24D51); 9.8 s (11O51)				fission Th (16H40); fission U, ancestor Ba^{140} (16H40a, 24D51a, 24D51, 11O51)
Xe^{141}	A chem, genet (17B51)		β^- (17B51)	1.7 s (32K46, 11O51); 3 s (24D51)				fission U, ancestor La^{141} (17B51); fission U, ancestor Ce^{141} (24D51a, 24D51, 11O51)
Xe^{143}	A chem, genet (17B51)		β^- (17B51)	1.0 s (24D51)				fission U, ancestor Ce^{143} (17B51, 24D51);
Xe^{144}	A chem, genet (24D51a)		β^- (24D51a)	~1 s (24D51)				fission U, ancestor Ce^{144} (24D51a, 24D51)
$_{55}Cs^{125}$	A chem, mass spect (73M52)		β^+ (73M52)	45 m (73M52)	2.03 spect (73M52)			I-a-6n (73M52)
Cs^{127}	A chem, mass spect (33F50)		β^+ (33F50)	5.5 h (33F50)	1.2 spect, abs (33F50)			I-a-4n (33F50); parent Xe^{127} (33F50); daughter Ba^{127} (37L52)
Cs^{128}	B chem, genet (33F51)		β^+, EC (37L52)	3.8 m (37L52); 3.1 m (33F51)	3.0 abs (33F50a, 32T50, 37L52)			daughter Ba^{128} (33F51, 37L52)
Cs^{129}	A chem, mass spect (33F50)		EC, no β^+ (33F50)	31 h (33F50)	conv: ~0.3 abs (33F50)	~0.5 abs (33F50)		I-a-2n (33F50); daughter Ba^{129} (33F50a, 32T50)
Cs^{130}	A chem (27R48); chem, excit (91S52a); chem, mass spect (73M52)		β^+, EC, β^- (β^+/β^- 27.5) (91S52a)	30 m (91S52a); ~30 m (27R48, 33F50)	β^+: 1.97 spect (91S52a); β^-: 0.442 spect (91S52a)	no γ (91S52a); Xe K-x (91S52a)	Q^-_β 0.442, Q^+_β 2.99 (91S52a)  (91S52a)	I-a-n (27R48, 33F50, 91S52a)
Cs^{131}	A chem, genet (32K47a); chem, mass spect (7K49)		EC, no β^+ (28F47, 43C51c, 38K51d)	9.6 d (1Y49); 10.2 d (32K47a); 10.0 d (5Y47)		no γ (43C51c, 32K47a, 38K51d, 113S52); Xe K-x (43C51c, 5Y47, 1Y49, 32K47a, 28F47); ~0.1 abs conv, abs (5Y47, 1Y49)	see I^{131}  (18G52)	I-a-γ (112S51); daughter Ba^{131} (32K47a, 5Y47, 1Y49, 43C51c); not parent Xe^{131m_2} (43C51c); parent (?) Xe^{131m_2} (70C50)
Cs^{132}	B chem, excit (44C44)		EC (44C44)	7.1 d (44C44)		0.668 scint spect (10L51a); 0.62 abs, abs conv (44C44)		Cs-n-2n (44C44, 10L51a)

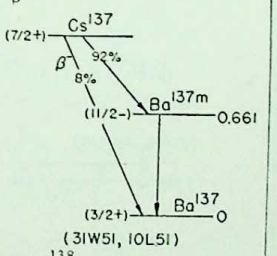
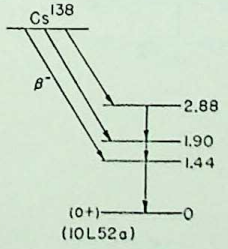
CC-0. In Public Domain. Gurukul Kangri Collection, Haridwar

Digitized by Arya Samaj Foundation Chennai and eGangotri

Isotope Z A	Class and identification	Percent abundance	Type of decay	Half-life	Energy of radiation in Mev: Particles	Energy of radiation in Mev: Gamma-transitions	Disintegration energy and scheme	Method of production and genetic relationships
$_{55}Cs^{133m}$	A genet (14G53)		IT (14G53)	6.0×10^{-9} s delay coinc (14G53)		see Xe^{133}; -0.081 (e_K/γ 1.8, K/L+M 6.0) scint spect, β-γ delay coinc (14G53)		daughter Xe^{133} (14G53)
Cs^{133}		100 (6N37)					Cs^{133}, I = 7/2 (87M50)	
Cs^{134m}	A chem, n-capt (12A35, 77M35); chem, excit, n-capt (45K40)		IT (6P47, 18G48a, 42C50)	3.2 h (5S45); 3 h (45K40)		0.128 (K/L/M = 64.3/100/18.6) spect conv (42C50); 0.128 (e_K/γ 2.2) scint spect (14S51); 0.128 (L_{II}/L_{III} -1) spect conv (63M52a); others (6P47, 18G48a, 5S45)	 Cs^{134}, I = 4 (30J52) (87S52)	Cs-n-γ (12A35, 77M35, 45K40, 2S47); Cs-d-p (45K40)
Cs^{134}	A n-capt (30A38); chem, n-capt, excit (45K40)		β⁻ (45K40); no EC (lim 4%) (31W50); no EC (lim 5%) (7S48); no β⁺ (lim 0.009%) (41M51)	2.3 y (33G51ℓ) 1.7 y (45K40)	0.648 (75%), 0.09 (25%) spect (20P51); 0.65 spect (31W50); 0.66 (~72%), 0.09 (~28%) spect (4E47); 0.676, 0.640, ~0.08 (~24%) spect (87S52); 0.60, 0.09 abs, β-γ coinc abs (37M49); others (7S47e, 45K40, 6P47, 37W47)	0.561 (e_K/γ 0.005), 0.567 (e_K/γ 0.007), 0.601 (e/γ 0.005, K/L 6.0), 0.794 (e/γ 0.002, K/L 6.0), 1.037 (weak, K/L 4.5), 1.164 (weak, K/L 6.2), 1.365 (weak, K/L 6.1) spect conv (87S52); 0.560 (e/γ 0.008), 0.602 (e/γ 0.0053), 0.799 (e/γ 0.0025), 1.037 (weak), 1.170 (weak), 1.363 (with 0.09 β⁻, e/γ 0.00062) spect conv, β-γ coinc (31W50); 0.040 crit abs (47R52); γ_1 0.570, γ_2 0.601, γ_3 0.793, γ_4 1.024, γ_5 1.11, γ_6 1.35 ($\gamma_1/\gamma_2/\gamma_3/\gamma_6$ = 0.35/0.94/1.0/0.017) spect (88S51); γ_1 0.57, γ_2 0.60, γ_3 0.79 ($\gamma_1/\gamma_2/\gamma_3$ = 0.26/1.0/1.0) spect (4E47); no 1.96 γ (lim 10^{-4}%) Be-γ-n reaction (23W50); others (7S48, 20P51, 6P47, 20D50, 8B49, 45W50, 17B50, 44M50a, 85S51, 85B50, 39R51, 61K52)		Cs-n-γ (30A38, 69S38, 45K40, 2S47); Cs-d-p (45K40); Ba-d-α (51H43)
Cs^{135m}	A genet (14G53)		IT (14G53)	2.8×10^{-10} s delay coinc (14G53)		0.248 (K/L 7.0) spect conv, scint spect, β-γ delay coinc (14G53)	see Xe^{135}	daughter Xe^{135} (14G53)
Cs^{135}	A chem, genet (63S49a); chem, mass spect (3I49a)		β⁻ (63S49a)	3.0×10^6 y sp act (8Z49); 2.1×10^6 y yield (63S49a)	0.21 abs (63S49a); ~0.19 abs (8Z49)	no γ (63S49a, 8Z49)	Cs^{135}, I = 7/2 (87M50)	daughter Xe^{135} (63S49a); fission U (8Z49, 38W52)
Cs^{136}	A chem (33G46, 33G51m); chem, excit (33G49)		β⁻ (33G51m)	13.7 d (33G49)	0.35 abs (33G49); 0.28 β-γ coinc abs (28F51b)	~0.9 abs (33G49); 1.2 β-γ coinc abs (28F51b); two γ's (33G49)		La-n-α (44C44, 33G49); spall-fission Th (7N49a), U (6F51); fission Th (21T51), U^{233} (38G48, 38G51), U^{235} (38G51, 33G51m), Pu (28F51b, 33G51m)

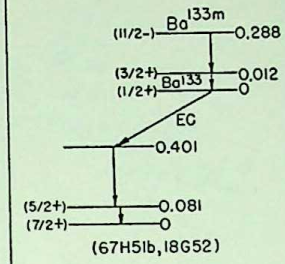
CC-0. In Public Domain. Gurukul Kangri Collection, Haridwar

Digitized by Arya Samaj Foundation Chennai and eGangotri

Isotope Z A	Class and identification	Percent abundance	Type of decay	Half-life	Energy of radiation in Mev: Particles	Energy of radiation in Mev: Gamma-transitions	Disintegration energy and scheme	Method of production and genetic relationships
$_{55}Cs^{137}$	A chem, genet (78M41); chem, mass spect (60H46a, 3I49a)		β^- (78M41)	33 y (33G51n, 38W52)	β_1 0.523 spect (16A50); β_1 0.51 (92%), β_2 1.17 (8%) spect (10L51); β_1 0.521, β_2 ~1.2 spect (20P49); β_1 0.518, β_2 ~1.18 spect (15O49); others (31W51, 10L49, 31T48)	with Ba^{137m}: 0.6616 cryst spect (100M52); see Ba^{137m}: others (10L50d, 79B52, 31W51, 80H52, 40K52, 14M49a, 31T48, 20P49, 15O49)	Cs^{137}, I = 7/2 (87M50) Q^-_β 1.2 (HPS)  (31W51, 10L51)	spall-fission Th (7N49a); fission Th (21T51), U (60H48, 3I49a, 33G51n, 38W52), U^{233} (38G48, 38G51), U^{235} (38G51), Pu (28F51); parent Ba^{137m} (13E48, 31T48); daughter Xe^{137} (21T51b, 33G51k)
Cs^{138}	A chem (16H39a, 6H39); chem, mass spect (30T49)		β^- (16H39a)	32.9 m (19E51); 33 m (25A39, 16H39a); 32 m (33G51k, 36G40)	3.40 (coinc with 1.4 γ), ~2.9, ~2.0 spect, β-γ coinc abs (10L52a); 2.68 spect (30T49); 2.65 abs (35B46a, calc from 36G40)	γ_1 0.463, γ_2 0.98, γ_3 1.44 (coinc with γ_1 and γ_2) spect conv, scint spect, β-γ, γ-γ coinc (10L52a); 1.2 abs (33G51k, 19E51)	see La^{138} Q^-_β 4.84 (10L52a)  (10L52a)	Ba-n-p (66S43b); fission Th (25A39, 16H40), Pa (2G39), U (6H39, 16H40a); daughter Xe^{138} (16H40a, 36G40, 66S43b); descendent I^{138} (63S49)
Cs^{139}	A chem, genet (16H39a, 6H39)		β^- (16H39a)	9.5 m (63S50); 10 m (25A39, 6H39); 7 m (16H40a)				fission Th (25A39), U (16H39a, 6H39, 16H40a); daughter Xe^{139} (16H39a, 6H39, 16H40, 16H40a); descendent I^{139} (63S49); parent Ba^{139} (16H39a, 6H39, 16H40, 16H40a, 63S50)
Cs^{140}	A chem (16H40a); chem, genet (63S50)		β^- (16H40a)	66 s (63S50)				fission U (16H40a, 63S50); parent Ba^{140} (63S50)
Cs^{141}	[A] genet (17B51)		[β^-] (17B51)	short (17B51, 24D51, 11O51)				[daughter Xe^{141}] (17B51, 24D51, 11O51); [ancestor La^{141}] (17B51)
Cs^{142}	D chem, genet (16H42a)		β^- (16H42a)	~1 m (16H42a)				fission U, parent Ba^{142} (16H42a)
Cs^{143}	[A] genet (17B51)		[β^-] (17B51)	short (17B51, 24D51, 11O51)				[daughter Xe^{143}] (17B51, 24D51) [ancestor Ce^{143}] (17B51, 24D51)
Cs^{144}	[A] genet (24D51a)		[β^-] (24D51a)	short (24D51a, 24D51)				[daughter Xe^{144}] (24D51); [ancestor Ce^{144}] (24D51a, 24D51)

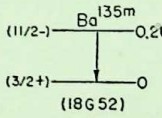
CC-0. In Public Domain. Gurukul Kangri Collection, Haridwar

Digitized by Arya Samaj Foundation Chennai and eGangotri

Isotope Z A	Class and identification	Percent abundance	Type of decay	Half-life	Energy of radiation in Mev: Particles	Energy of radiation in Mev: Gamma-transitions	Disintegration energy and scheme	Method of production and genetic relationships
$_{56}Ba^{127}$	A chem, genet (37L52)			~12 m (37L52)				Cs-d-8n, Cs-p-7n (37L52); parent Cs^{127} (37L52)
Ba^{128}	B chem (33F50a, 32T50)		EC (37L52)	2.4 d (33F50a, 32T50)				Cs-d-7n (37L52); Cs-p-6n (33F50a, 32T50, 37L52); parent Cs^{128} (33F51, 37L52)
Ba^{129}	A chem, genet (32T50, 33F50a)		β^+ (33F50a, 32T50)	2.0 h (33F50a); 1.8 h (32T50)	hard β^+ (32T50)			Cs-p-5n (33F50a, 32T50); parent Cs^{129} (33F50a, 32T50)
Ba^{130}		0.101 (6N38b)						
Ba^{131}	A chem, n-capt, excit (32K47a)		EC (32K47a); no β^+ (5Y47, 28F47)	12.0 d (32K47a); 11.7 d (5Y47)		γ_1 0.122 (K/L 6.0), γ_3 0.214 (K/L 2.8, e_K/γ ~0.18), γ_4 0.241, γ_5 0.370 (e_K/γ ~0.01), γ_6 0.494 (K/L 2.5, e_K/γ ~0.005), ~0.043 (?), ~0.065 (?), ~0.108 (?) ($\gamma_3/\gamma_4/\gamma_5/\gamma_6$ = 10/4/7/100) spect, spect conv (25E52); γ_1 0.122, γ_2 0.196, γ_3 0.213, γ_4 0.241, γ_5 0.371, γ_6 0.497 ($\gamma_1/\gamma_2/\gamma_3/\gamma_4/\gamma_5/\gamma_6$ = 1.3/4.4/5.3/1.4/12/100) spect (43C51c); 0.122 (e/γ 0.8, K/L ~3.5), 0.206 (e/γ 0.15), 0.372 (e/γ 0.03), 0.494 (e/γ 0.01) spect, spect conv, γ-γ, conv-conv coinc (38K50a); ~0.5 (coinc with ~0.2 γ) γ-γ coinc abs (39C51); γ_7 1.2 abs (32K47a, 39C51); (γ_6/γ_7 ~4) (39C51); others (28D50a, 10Z50)		Ba-n-γ (32K47a, 5Y47, 1Y49, 28D50a, 10Z50, 43C51c); parent Cs^{131} (32K47a, 5Y47, 1Y49, 43C51c); spall-fission Bi (11G49)
Ba^{132}		0.097 (6N38b)						
Ba^{133m}	A chem, excit (10C41, 2D40)		IT (10C41)	38.8 h (46W43a); 38.9 h (5Y48)		0.276 (e_K/γ ~3) spect conv, scint spect (67H51a); 0.0117 (e/γ ~130) γ-γ coinc, ion ch (67H51b); 0.276 (K/L 3.2) spect conv (10C41)		Cs-p-n (2D40); Cs-d-2n (10C41, 67H51a, 67H51b); Ba-γ-n (60M48); Ba-n-γ (5Y48); spall-fission Pb (13P47a), Bi (13P47, 11G49); parent Ba^{133} (5Y48)
Ba^{133}	A chem, n-capt, excit (32K47a); chem, genet (5Y48)		EC (32K47a)	~9.5 y (32K52a)		0.320 (e/γ 0.02), 0.085 (e/γ 0.3, K/L ~10) abs, abs conv, cl ch (5Y48); 0.36 abs, abs conv (32K47a)		Ba-n-γ (32K47a); daughter Ba^{133m} (5Y48)
Ba^{134}		2.42 (6N38b)					Ba^{134}, I = 0 (87M50)	

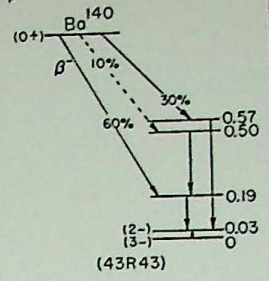
CC-0. In Public Domain. Gurukul Kangri Collection, Haridwar

Digitized by Arya Samaj Foundation Chennai and eGangotri

Isotope Z A	Class and identification	Percent abundance	Type of decay	Half-life	Energy of radiation in Mev: Particles	Energy of radiation in Mev: Gamma-transitions	Disintegration energy and scheme	Method of production and genetic relationships
$_{56}Ba^{135m}$	A chem (45K40); chem, n-capt, sep isotopes (67H51a)		IT (46W43, 5Y48)	28.7 h (5Y48)		0.269 (e_K/γ ~3.5, K/L ~2) spect conv, scint spect (67H51a); 0.267 spect conv, spect, scint spect (39C51a)		Ba-n-γ, Ba-n-2n (45K40); Ba-d-p (46W43, 39C51a); Ba^{134}-n-γ (67H51a); spall-fission U (6O47)
Ba^{135}		6.59 (6N38b)					Ba^{135}, I = 3/2 (87M50)	
Ba^{136}		7.81 (6N38b)					Ba^{136}, I = 0 (87M50)	
Ba^{137m}	A n-capt (12A35); chem, genet (31T48, 13E48)		IT (31T48)	2.60 m (14M49a); 2.63 m (31T48); 2.5 m (13E48)		0.6616 cryst spect (100M52); γ_1 0.661 (K/L+M 4.64) spect conv (10L50d, 59G52); 0.661 (K/L/M+N = 5.5/1.0/0.27) spect conv (79B52); γ_1 (e_K/γ 0.097) spect, spect conv (31W51); γ_1 (e_K/γ 0.095) scint spect (80H52); 0.662 (K/L+M 4.57) spect conv (40K52); 0.663 (e_K/γ 0.13, K/L 4.8) spect conv (14M49a); γ_1 (e_K/γ 0.08, K/L 5.0) spect conv (15O49); 0.663 (e/γ 0.14) spect conv, x-conv coinc (31T48); 0.669 spect conv (20P49)	see Cs^{137}	Ba-n-2n (1P37, 45K40); Ba-n-γ (12A35); daughter Cs^{137} (13E48, 31T48)
Ba^{137}		11.32 (6N38b)					Ba^{137}, I = 3/2 (87M50)	
Ba^{138}		71.66 (6N38b)					Ba^{138}, I = 0 (87M50)	
Ba^{139}	A chem, n-capt (12A35); chem, excit (1P38a)		β^- (1P37a)	85.0 m (24D51c); 84 m (92S48); 86 m (1P37a, 16H40a)	2.27 spect (92S48); 2.3 abs (32K51i, 70B43a)	0.163 (26%, e/γ 0.20, K/L = 6), 1.05 (0.6%) spect conv, abs, coinc (92S48); ~0.163 (e_K/γ 0.28) scint spect (52M52e)		Ba-d-p (1P37a, 45K40, 92S48); Ba-n-γ (12A35, 1P37, 2S47, 1Y49a); La-n-p (1P38a); Ce-n-α (46W43); spall-fission U (γ) (42L40), U (6F51); fission Th (25A39, 16H40, 72B51), U (6H39, 16H39a, 24D51), U^{235} (38G51), Pu (32K48, 28F51); daughter Cs^{139} (16H39a, 6H39, 16H40, 16H40a, 63S50); descendent Xe^{139} (16H39a, 6H39, 24D51)

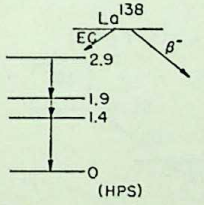
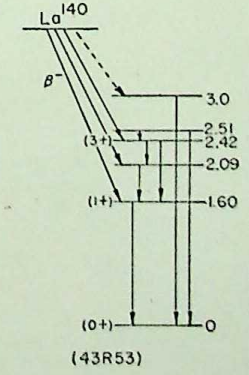
CC-0. In Public Domain. Gurukul Kangri Collection, Haridwar

Digitized by Arya Samaj Foundation Chennai and eGangotri

Isotope Z A	Class and identification	Percent abundance	Type of decay	Half-life	Energy of radiation in Mev: Particles	Energy of radiation in Mev: Gamma-transitions	Disintegration energy and scheme	Method of production and genetic relationships
$_{56}Ba^{140}$	A chem, genet (16H39, 16H39a)		β^- (16H39a)	12.80 d (13E51f, 77S47)	1.022 (60%), 0.480 spect (86B49, 43R53); 1.05 spect (4W51); 0.99, 0.47 spect (35L49); 1.0 (~75%), ~0.4 (~25%) abs (13E51g)	0.0296, 0.132, 0.162, 0.304, 0.537 spect conv (10C51c); 0.160, 0.310, 0.535 spect (35L49); 0.03, 0.16, 0.31, 0.54 spect, spect conv, scint spect, γ-γ coinc (86B49, 43R53), others (4W51, 26M49c)	Q^-_β 1.05 (43R53) 	Ba-n-γ (second order reaction) (32K51k); spall-fission Th (6O47, 7N49a), U (6O48, 6F51); fission Th (72B51, 21T51), U (16H39, 6H39, 16H40a, 36G40, 38G46, 63S50, 24D51, 24D51a, 17B51, 11O51, 4W51, 13E51f, 13E51g), U^{233} (61S48, 38G51), U^{235} (38G51), Pu (32K48, 28F51) descendent Xe^{140} (16H40a, 17B51, 24D51, 24D51a, 11O51); parent La^{140} (16H39, 16H39a, 16H40a, 36G40, 16H42a, 38G46, 28F51c)
Ba^{141}	A chem, genet (16H42a)		β^- (16H42a)	18 m (16H42a, 52G51)	2.8 abs (32L48)	γ (52G51)		fission Th (16H39c, 16H39), U (16H42a, 52G51, 52G51a); photo-fission U (42L40); daughter Cs^{141} (16H42a); parent La^{141} (16H42a); descendent Xe^{141} (17B51, 11O51, 24D51)
Ba^{142}	D chem, genet (16H42a)		β^- (16H42a)	6 m (16H42a)				fission Th (16H39c, 16H39), U (16H42a); photo-fission U (42L40); daughter Cs^{142} (16H42a); parent La^{142} (16H42a)
Ba^{143}	B chem (16H39)		β^- (16H42a)	<0.5 m (16H42a)				fission Th (16H39c), U (16H39c, 16H39, 16H42a, 24D51, 17B51, 11O51); [descendent Xe^{143}] (17B51, 24D51)
Ba^{144}	[A] genet (24D51)		β^- (24D51)	short (24D51, 24D51a)				[fission U, descendent Xe^{144}, ancestor Ce^{144}] (24D51, 24D51a)
$_{57}La^{131}$	A chem, mass spect (53G51)		β^+ (53G51)	58 m (53G51)	1.6 abs (53G51)			spall Ba (53G51)
La^{132}	A chem, mass spect (53G51)		β^+ (53G51)	4.5 h (53G51)	3.5 abs (53G51)	1.0 abs (53G51)		spall Ba (53G51)
La^{133}	A chem, mass spect (21N50)		EC, β^+ (weak) (21N50)	4.0 h (21N50)	~1.2 abs, spect (21N50); conv: 0.26 spect conv (21N50)	0.8 abs (21N50)		Cs-α-4n (21N50); daughter Ce^{133} (93S51)
La^{134}	B chem, genet (93S51)		β^+ ~44%, EC ~56% (93S51)	6.5 m (93S51)	2.7 abs, spect (93S51)	no γ (93S51)		daughter Ce^{134} (93S51)
La^{135}	A chem (81M42); chem, excit (73C48); chem, mass spect (21N50)		EC (81M42, 73C48)	19 h (21N50); 19.5 h (73C48);		0.76 (weak) abs (73C48); 0.88 abs (46W43b)		Cs-α-2n (73C48, 21N50); Ba-d-n (81M42, 46W43b); Ba-p-n (46W43b); daughter Ce^{135} (73C48)

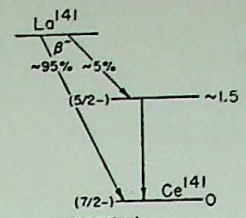
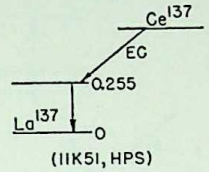
Digitized by Arya Samaj Foundation Chennai and eGangotri

CC-0. In Public Domain. Gurukul Kangri Collection, Haridwar

Isotope Z A	Class and identification	Percent abundance	Type of decay	Half-life	Energy of radiation in Mev: Particles	Energy of radiation in Mev: Gamma-transitions	Disintegration energy and scheme	Method of production and genetic relationships
$_{57}La^{136}$	A chem (3M47); chem, excit, sep isotopes (36R50a)		EC ~67%, β^+ ~33% (21N50)	9.5 m (21N50); 9.0 m (36R50a); 10 m (3M47)	2.1 spect (21N50); abs (3M47); 1.8 abs (36R50a)			Cs-α-n (21N50, 36R50a); Ba-d-n (3M47); Ba^{135}-d-n, Ba^{136}-d-2n (36R50a)
La^{137}	C mass spect (3I48b)			>400 y yield (73C48); >30 y yield (3I48b)				[daughter Ce^{137}] (3I48b, 73C48)
La^{138}	A chem, mass spect (3I47a)	0.089 (3I47a)	EC (18P51); β^- ~6% (85M52a)	~2.0×10^{11} y sp act (18P51); ~7×10^{10} y sp act (85M52a)	1.0 abs (85M52a)	γ_1 1.39, γ_2 0.81, γ_3 0.54 ($\gamma_1/\gamma_2/\gamma_3$ = 1/0.65/0.3) scint spect (18P51); 1.0, 0.54 scint spect (11B50f)	see Cs^{138} 	natural source (11B50f, 18P51)
La^{139}		99.911 (3I47a)					La^{139}, I = 7/2 (87M50)	
La^{140}	A n-capt (82M35); chem, excit, n-capt (1P38a); chem, mass spect (60H48)		β^- (1P38a)	40.0 h (72B51d, 9B50, 46W43b); 40.4 h (77S47); 39.5 h (37B46)	1.32 (~70%), 1.67 (~20%), 2.26 (~10%), others <1.3 (very weak) spect (86B49, 43R53); 0.90, 1.40, 2.12 spect (1O46); 1.45, 2.2 spect (4W51a); others (46W43b, 37B46)	γ_2 0.3286, γ_3 0.4867, γ_4 0.8151, γ_5 1.596 spect (12H52); γ_1 0.093, γ_2 0.335, γ_3 0.490, γ_4 0.820, γ_5 1.600, γ_6 2.50, γ_7 3.0 (weak) spect, spect conv, γ-γ coinc (86B49, 43R53); γ_1 0.093, γ_2 0.335, γ_3 0.49, γ_4 0.82, γ_5 1.62, γ_6 2.55 ($\gamma_1/\gamma_2/\gamma_3/\gamma_4/\gamma_5/\gamma_6$ = <1/3/22/16/56/3) scint spect (87B51); 0.069, 0.110, 0.131, 0.173, 0.241, 0.265, 0.329, 0.431, 0.486, 0.752, 0.816, 0.926, 1.597, 1.904 spect conv (10C51d); γ_2 0.335, γ_3 0.49, γ_4 0.87, γ_5 1.65, γ_6 2.3 ($\gamma_2/\gamma_3/\gamma_4/\gamma_5/\gamma_6$ = 2/5/10/77/6) spect (11R47); γ_2 0.335, γ_3 0.49, γ_4 0.83, γ_5 1.63, γ_6 ~2.3 ($\gamma_2/\gamma_3/\gamma_4/\gamma_5/\gamma_6$ = 1/10/20/100/5) spect (43M46); γ_5 (coinc with 2.3 β^- and γ_4) scint spect, β-γ, γ-γ coinc (39R51a); 2.55 (~4%), 2.9 (~0.1%) D-γ-p ion ch (9B50); 2.49 (~3%) D-γ-n, Be-γ-n reactions (42W47); others (26M48a)	Q^-_β 3.86 (39R51a, 43R53)  (43R53)	Ba-d-γ (?) (46W43b); La-d-p (1P37a, 1P38a, 81M42, 46W43b); La-n-γ (82M35, 1P38a, 40G42, 81M42, 46W43b, 2S47); Ce-n-p (46W43b); fission Th (72B51, 21T51), U (16H39, 16H39a, 16H40a, 36G40, 16H42a, 38G46, 28F51c), U^{233} (38G48, 38G51), U^{235} (38G47), Pu (28F51); spall-fission U (6F51) daughter Ba^{140} (16H39, 16H39a, 16H40a, 36G40, 38G46, 28F51c)

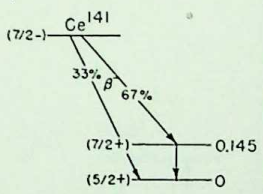
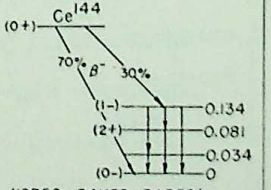
CC-0. In Public Domain. Gurukul Kangri Collection, Haridwar

Digitized by Arya Samaj Foundation Chennai and eGangotri

Isotope Z A	Class and identification	Percent abundance	Type of decay	Half-life	Energy of radiation in Mev: Particles	Energy of radiation in Mev: Gamma-transitions	Disintegration energy and scheme	Method of production and genetic relationships
$_{57}La^{141}$	A chem (16H42a); chem, genet (50B51, 23D51b)		β^- (16H42a)	3.7 h (32K51j); 3.5 h (16H42a)	2.43 (~95%), 0.9 (~5%) spect (23D51b)	1.3-1.6 (?, weak) scint spect, β-γ coinc (23D51b)	 (23D51b)	La-n-γ (second order reaction) (32K49); fission Th (4C39, 72B51), U (16H42a, 32K51j); daughter Ba^{141} (16H42a); descendent Xe^{141} (17B51); parent Ce^{141} (50B51, 23D51b)
La^{142}	D chem (16H42a)		β^- (32K51j)	74 m (16H42a); 77 m (32K51j)		γ (32K51j)		fission Th (16H39c), U (16H42a, 32K51j); daughter Ba^{142} (16H42a)
La^{143}	A chem, genet (54G51)		β^- (54G51)	~19 m genet (54G51); ~15 m (16H43b)				fission U (16H42a, 16H43b, 54G51); parent Ce^{143} (54G51)
La^{144}	[A] genet (24D51a)		[β^-] (24D51a)	short (24D51a)				[descendent Xe^{144}, parent Ce^{144}] (24D51a)
$_{58}Ce^{133}$	A chem, genet (93S51)		EC, β^+ (93S51)	6.30 h (93S51)	1.3 spect, abs (93S51)	1.8 abs (93S51)		La-p-7n (93S51); parent La^{133} (93S51)
Ce^{134}	B chem, excit (93S51)		EC (93S51)	72.0 h (93S51)		K-x, no γ (93S51)		La-p-6n (93S51); spall Ta (22N52); parent La^{134} (93S51)
Ce^{135}	A chem, genet (73C48)		EC, $\beta^+ \leq 1\%$ (93S51)	22 h (93S51)	0.81 spect (93S51)			La-d-6n (73C48); La-p-5n (93S51); spall Ta (22N52); parent La^{135} (73C48)
Ce^{136}		0.193 (3I47a)						
Ce^{137}	A chem, excit (73C48); n-capt, sep isotopes (67H51c)		EC, no β^+ (73C48)	36 h (73C48)		0.257 (K/L ~4) spect conv (67H51c); 0.253 (K/L ~10) spect conv (11K51)	 (11K51, HPS)	La-d-4n (73C48); La-p-3n (93S51); Ce^{136}-n-γ (67H51c, 11K51); [parent La^{137}] (3I48b, 73C48)
Ce^{138}		0.250 (3I47a)						
Ce^{139}	A chem (1P43); chem, excit, cross bomb (1P48, 36M47); n-capt, sep isotopes (67H51c)		EC (36M47)	140 d (1P43, 1P48)		0.166 (K/L ~10), 0.275 spect conv (11K51); 0.166 (K/L $\geq$4) spect conv (67H51c); ~0.8 abs (1P48)		Ba-α-n (1P43, 1P48); La-d-2n (1P43, 36M47, 1P48); Ce^{138}-n-γ (67H51c, 11K51); Ce-n-γ (83M50); spall-fission Bi (11G49); daughter Pr^{139} (93S51)
Ce^{140}		88.48 (3I47a)						

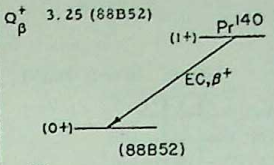
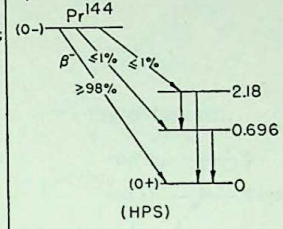
CC-0. In Public Domain. Gurukul Kangri Collection, Haridwar

Digitized by Arya Samaj Foundation Chennai and eGangotri

Isotope Z, A	Class and identification	Percent abundance	Type of decay	Half-life	Energy of radiation in Mev: Particles	Energy of radiation in Mev: Gamma-transitions	Disintegration energy and scheme	Method of production and genetic relationships
$_{58}Ce^{141}$	A chem (16H40c); chem, excit, n-capt, cross bomb (1P43, 72B51e); chem, mass spect (60H48)		β^- (16H40c)	33.1 d (49W49); 32.5 d (3F50c); 30.6 d (1P48) [J]	0.581 (33%), 0.442 (67%) spect (3F50c); 0.58 (29%), 0.44 (71%) spect (38K51c); 0.56 (30%), 0.41 (70%) spect (92S48a), 0.56 spect, β-γ coinc abs (11T49a); others (26M49e, 94S50, 1P48, 37B46)	0.145 (e_K/γ 0.25, K/L 5.5) spect conv, spect (3F50c); ~0.14 (e_K/γ 0.46) scint spect (80H52a); 0.142 (e_K/γ 0.48) scint spect (17J52a); 0.145 (K/L ~7) spect conv (67H51c); 0.144 (e/γ ~0.33, K/L 6.5) spect conv (38K51, 38K51c); 0.146 spect conv (11K51, 11T49a); 0.141 (coinc with β^-) spect conv, β-conv coinc (92S48a); 0.14 (coinc with β^-) scint spect, β-γ coinc (23D51b); others (94S50, 26M49e, 4B49, 42H47a, 52M51)	Q^-_β 0.58 (3F50c)  (3F50c, 38K51c)	Ba-α-n (1P43, 1P48); Ce-d-p (1P43, 1P48, 72B51e, 50B51); Ce-n-γ (1P43, 10C48a, 72B51e); Ce-n-2n (1P43, 1P48, 72B51e); Pr-n-p (1P43); spall Ta (22N52); spall-fission Bi (11G49), U (6F51); fission Th (72B51, 21T51), U (16H40c, 50B51), U^{235} (38G51), Pu (28F51) daughter La^{141} (50B51, 23D51b); descendent Xe^{141} (11O51, 24D51)
Ce^{142}		11.07 (3I47a)						
Ce^{143}	A chem (63S46, 1P43); chem, cross bomb (1P48); chem, genet (72B51e); mass spect (3I48b)		β^- (63S46)	33 h (72B51e, 95S50, 37B46); 34 h (38K51c); 36 h (4B49, 1P43)	β_1 1.39, β_2 1.09, β_3 0.71 ($\beta_1/\beta_2/\beta_3$ = 1.0/1.3/1.0) spect (50B52); β_1 1.37, β_2 1.09, β_3 0.37 (?) (β_2/β_1 1.4) spect (38K51c)	0.035, 0.126, ~0.160, 0.289, 0.356, 0.660, 0.720 spect, spect conv, scint spect (50B52); γ_1 0.057 (K/L ~1), γ_2 0.283 (K/L ~6), γ_3 0.649, γ_4 0.705 ($\gamma_2/\gamma_3/\gamma_4$ = 4.5/1/1) spect, spect conv, β-γ coinc (38K51, 38K51c); 0.0575 (K/L <1), 0.291 (K/L ~10), 0.348 spect conv (11K51); others (95S50)		Ce-d-p (1P43, 1P48, 72B51e); Ce-n-γ (1P43, 37B46, 1P48, 72B51e); Ce^{142}-n-γ (11K51); spall-fission Th (7N49a), U (6O48, 6F51); fission Th (72B51), U (17B51, 24D51, 63S51), Pu (32K48); daughter La^{143} (54G51); parent Pr^{143} (1P43, 37B46, 72B51e); descendent Xe^{143} (17B51, 24D51)
Ce^{144}	A chem (16H40c); chem, mass spect (60H48)		β^- (16H40c)	282 d (53S51); 275 d (50B51a); 290 d (19J44)	0.300 (70%), 0.170 (30%, coinc with 0.134 γ, with 0.080 γ) spect, β-γ coinc (34P52); 0.304 (70%) spect (19P52); 0.17 (coinc with 0.134 γ) β-γ coinc (24K52); others (70C52, 17N51b, 6P47, 26M50a)	0.0337, 0.054, 0.0807 (e/γ large, K/L ~4), 0.100, 0.134 (K/L ~9) spect conv, spect (19P52); 0.034, 0.041, 0.047, 0.054 (K/L <1), 0.081 (K/L ~5), 0.095, 0.101, 0.135 (K/L ~10) spect conv (11K51); 0.0547, 0.079 (K/L 6.3), 0.134 (K/L 8.3), 0.231 (K/L 1.7) spect conv (70C52); ~0.132 (K/L 5.3) spect conv (40K52); 0.695, 1.50, 2.18 spect (15T50); others (13A52a, 2E51)	Q^-_β 0.304 (19P52)  (19P52, 24K52, 34P52)	spall-fission Th (7N49a), U (6O48); fission Th (21T51), U (16H40c, 70B43a, 24D51, 7N51a, 50B51a), U^{233} (38G48, 61S48, 38G51), U^{235} (38G51), Pu (28F51); parent Pr^{144} (16H43b, 39G43, 7N51a); descendent Xe^{144} (24D51, 24D51a)
Ce^{145}	G not found: (78C52a)			~1.8 h (72B51f)				not found: fission U (78C52a); fission U (24D51, 72B51f); parent Pr^{145} (72B51f)
Ce^{146}	D chem, genet (40G43)		β^- (40G43)	14.6 m (53S45); 11 m (40G46)	~0.9 abs (78C52a)	soft γ (78C52a)		fission U, parent Pr^{146} (40G43, 16H43b, 53S45, 40G46)

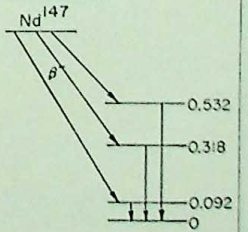
CC-0. In Public Domain. Gurukul Kangri Collection, Haridwar

Digitized by Arya Samaj Foundation Chennai and eGangotri

Isotope Z A	Class and identification	Percent abundance	Type of decay	Half-life	Energy of radiation in Mev: Particles	Energy of radiation in Mev: Gamma-transitions	Disintegration energy and scheme	Method of production and genetic relationships
$_{59}Pr^{137}$	B chem, mass spect (44D52)		β^+ (44D52)	1.4 h (44D52)	1.8 (44D52)			Ce-p-4n (44D52)
Pr^{138}	A chem, excit (93S51); chem, mass spect (44D52)		EC ~90%, β^+ ~10% (93S51)	2.0 h (93S51, 44D52)	1.4 abs, spect (93S51)	0.2, ~0.5, 1.3 abs (93S51)		Ce-p-3n (93S51, 44D52)
Pr^{139}	A chem, genet (93S51); chem, mass spect (44D52)		EC ~94%, β^+ ~6% (93S51)	4.2 h (44D52); 4.5 h (93S51)	1.0 abs spect (93S51)	1.0 abs (93S51)		Ce-p-2n (93S51, 44D52); parent Ce^{139} (93S51)
Pr^{140}	A excit (12A35); excit (1P38a)		β^+ 58%, EC 42% (88B52)	3.4 m (29D42); 3.5 m (1P38a)	2.23 spect (88B52)	no γ (88B52)	Q^+_β 3.25 (88B52)  (88B52)	Ce-p-n (93S51); Pr-n-2n (12A35, 1P38a, 29D42); Pr-γ-n (34H45, 12P49); daughter Nd^{140} (2W49, 88B52)
Pr^{141}		100 (3I48c)					Pr^{141}, I = 5/2 (87M50)	
Pr^{142}	A n-capt (12A35, 82M35)		β^- (29D42); no β^+ or EC (lim 0.5%) (28R50b)	19.2 h (37B46); 19.1 h (13J50); 19.3 h (29D42)	2.15 (~96%), 0.64 (~4%) spect (13J50); 2.23, 0.66 spect (41R50); 2.14 spect (96M52, 29D42); 2.23 spect (6P47); 2.22, 0.22 abs, β-γ coinc abs (26M49d); 2.5, ~0.4 abs, β-γ coinc abs (15J49)	γ_1 0.135, γ_2 1.59 (γ_1/γ_2 <0.2) spect, spect conv (41R50); 1.58 spect (13J50, 13J52); 0.134, 0.329, 0.490, 0.624 spect conv; 2.1 abs (10C48); 1.5 coinc abs sec (15J49)	Q^-_β 2.23 (13J50, 26M49d)	La-a-n (29D42); Ce-p-n (29D42); Pr-d-p (29D42); Pr-n-γ (12A35, 82M35, 1P37, 1P38a, 29D42, 2S47); Nd-n-p (1P37, 1P38a); spall-fission U (6F51)
Pr^{143}	A chem (72B51g, 19J44); mass spect (60H46a)		β^- (72B51g, 19J44)	13.7 d (15F49a); 13.8 d (72B51h); 13.5 d (1P48)	0.932 spect (15F49a); 0.922 spect (49B50a); 0.920 spect (11T49a); 0.92 spect (38K51); 0.84 abs (26M49e)	no γ (72B51g, 72B51h, 1P48)	Q^-_β 0.93 (HPS)	Ce-d-n (1P48); spall-fission U (6F51); fission U (16H43b, 19J44, 72B51g), Pu (28F51) daughter Ce^{143} (1P43, 37B46, 72B51e)
Pr^{144}	A chem, genet (7N51a, 16H43b, 39G43)		β^- (7N51a)	17.5 m (7N51a, 77S51b); 17 m (16H43b)	2.97 (>99%), other β's (<1%) spect (19P52); 2.32 (<1%, coinc with 0.69 γ), 0.81 (<1%) spect, β-γ coinc (24K52); 2.95 (~95%), 0.87 (~5%) spect (10L52c); 2.97 (~90%), 2.3 (~5%), 0.86 (~5%) spect (13A52a); 2.99 spect (6P47); others (17N51b, 19J44, 50B51a, 70B43a, 16H43b, 26M50a, 70C52)	γ_1 0.0603, γ_2 0.696, γ_3 1.5, γ_4 2.19 (γ_2, γ_3, γ_4 weak) scint spect, spect, spect conv (19P52); γ_2 0.695, γ_3 1.48, γ_4 2.19 ($\gamma_2/\gamma_3/\gamma_4$ = 1/0.4/1.1) spect, β-γ, γ-γ coinc (13A52a); γ_1 0.061 (K/L <1) spect conv (11K51); others (17N51b, 77S51b)	Q^-_β 3.0 (13A52a, 19P52) 	fission Th (21T51), Pu (28F51); spall-fission U (6F51); daughter Ce^{144} (16H43b, 39G43, 7N51a)
Pr^{145}	G not found: (78C52a)			4.5 h (72B51f)				not found: fission U (78C52a); fission U (72B51f); daughter Ce^{145} (72B51f)
Pr^{146}	D chem (40G43)		β^- (40G43)	24.0 m (20K51a); 24.6 m (53S45a); 25 m (40G46)	3.8 abs (78C52a); ~3 abs (53S45a)	0.490, 0.78 scint spect (20K51a); 1.4 abs (53S45a)		fission U, daughter Ce^{146} (40G43, 16H43b, 53S45, 40G46)

CC-0. In Public Domain. Gurukul Kangri Collection, Haridwar

Digitized by Arya Samaj Foundation Chennai and eGangotri

Isotope Z A	Class and identification	Percent abundance	Type of decay	Half-life	Energy of radiation in Mev: Particles	Energy of radiation in Mev: Gamma-transitions	Disintegration energy and scheme	Method of production and genetic relationships
$_{60}Nd^{138}$	D chem, excit (93S51)		β^+ (93S51)	22 m (93S51)	~2.4 abs (93S51)			Pr-p-4n (93S51)
Nd^{139}	A chem, genet (93S51)		EC ~90%, β^+ ~10% (93S51)	5.50 h (93S51)	3.1 abs, spect (93S51)	1.3 abs (93S51)		Pr-p-3n (93S51); ancestor Ce^{139} (93S51)
Nd^{140}	A chem, excit, genet (2W49)		EC (88B52)	3.3 d (2W49)		Pr K-x (88B52)		Pr-p-2n (93S51); Pr-d-3n (2W49); parent Pr^{140} (2W49, 88B52); spall-fission U (6F51)
Nd^{141}	A excit (47K42); chem, excit (2W49)		EC ~98%, β^+ ~2% (2W49)	2.42 h (2W49); 2.5 h (47K42)	0.7 abs (2W49); 0.8 abs (47K42)	1.2 (weak) abs (2W49)		Pr-p-n (47K42, 2W49); Pr-d-2n (2W49); Nd-n-2n (1P38a, 47K42); Nd-γ-n (47K42)
Nd^{142}		27.13 (3I48c)						
Nd^{143}		12.20 (3I48c)					Nd^{143}, I = 7/2 (97B50, 88M51)	fission U^{235} (mass spect) (3I50a)
Nd^{144}		23.87 (3I48c)						fission U^{235} (mass spect) (3I50a)
Nd^{145}		8.30 (3I48c)					Nd^{145}, I = 7/2 (97B50, 88M51)	fission U^{235} (mass spect) (3I50a)
Nd^{146}		17.18 (3I48c)						fission U^{235} (mass spect) (3I50a)
Nd^{147}	A chem, genet (84M47, 84M51a)		β^- (84M47, 84M51)	11.3 d (average of 3IR52, 2E51a, 38K51a, 84M51, 37B46)	0.83 (~60%), 0.60 (~15%), 0.38 (~25%) spect (2E51a); 0.78 (~65%), 0.35 (~32%) spect (38K51a); 0.83, 0.60, 0.38 spect (3IR52)	0.0918 (K/L_I = 6.4) spect conv (63M52); γ_1 0.0918 (e/γ ~0.9, K/L+M 6.5), γ_2 0.309, γ_3 0.391, γ_4 0.520 ($\gamma_1/\gamma_2/\gamma_3/\gamma_4$ = 66/1/2/32) spect (38K51a); γ_1 (K/L/M = 7.55/1/0.096) spect conv (91S52d); 0.0912 (K/L 4.9), 0.121, 0.197, 0.231, 0.260, 0.273, 0.301, 0.318, 0.398, 0.441, 0.532 (K/L ~6) (all weak except 0.091 γ) spect conv, γ-γ, β-γ coinc (3IR52); 0.0915 (coinc with 0.83 β^-), 0.320, 0.534 spect conv, β-conv coinc (2E51a); others (26M50b, 52M51)	Q^-_β 0.92 (3IR52)  (3IR52, 2E51a, HPS)	Nd-d-p (47K42); Nd-n-γ (37B46, 84M47, 10C48b, 84M51b); fission U (84M51); spall-fission U (6F51); parent Pm^{147} (84M47, 84M51a)
Nd^{148}		5.72 (3I48c)						U^{235}-n-fission (mass spect) (3I50a)
Nd^{149}	A excit (1P38a); chem, genet (84M51b)		β^- (1P38a)	2.0 h (37B46, 1P38a); 1.8 h (3IR52); 1.7 h (84M51b)	1.5, 1.1, 0.95 spect (3IR52); 1.5 abs (84M51b); 1.6 abs (37B46)	0.030, 0.097 (K/L 0.9), 0.112, 0.114 (K/L ~5), 0.124, 0.188, 0.198, 0.211 (K/L ~7), 0.226, 0.240, 0.266 (K/L ~10), 0.424, 0.538, 0.650 spect, spect conv, scint spect, coinc (3IR52); others (52M51)	Q^-_β 1.5 (3IR52)	Nd-n-2n (1P38a); Nd-d-p (1P38a); Nd-n-γ (1P38a, 37B46, 84M51b); parent Pm^{149} (42K52)
Nd^{150}		5.60 (3I48c)	β^- (?) (85M52, 3L34)	>2 x 10^{15} y sp act (85M52); >10^{13} y sp act (21C52)				fission U^{235} (mass spect) (3I50a)

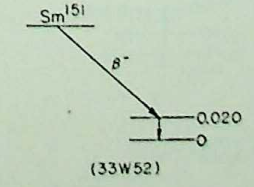
CC-0. In Public Domain. Gurukul Kangri Collection, Haridwar

Digitized by Arya Samaj Foundation Chennai and eGangotri

Isotope Z A	Class and identification	Percent abundance	Type of decay	Half-life	Energy of radiation in Mev: Particles	Energy of radiation in Mev: Gamma-transitions	Disintegration energy and scheme	Method of production and genetic relationships
$_{60}Nd^{151}$	B n-capt (84M51b); sep isotopes, n-capt, Pm K-L-M difference (31R52)		β^- (31R52)	15 m (51C52); 12 m (31R52, 84M51b)	1.93 spect (31R52)	0.085, 0.110, 0.117 (K/L 4), 0.421, 0.73, 1.14 spect conv, scint spect, β-γ, γ-γ coinc (31R52); Pm K-x (31R52)		Nd-n-γ (84M51b); Nd^{150}-n-γ, parent Pm^{151} (31R52)
$_{61}Pm^{141}$	B chem, excit (34F52)		β^+ (34F52)	20 m (34F52)	2.4-2.8 spect (34F52)			Nd^{142}-p-2n (34F52)
$Pm^{142,143}$	D chem, excit (2W50a)		EC (2W50a)	250-280 d (43L52a); 285 d (2W50a)		0.95 abs (2W50a)		Pr-α-2n (2W50a, 34F52); Nd-p-n (43L52a)
$Pm^{143,144}$	D chem (34F52)		EC (34F52)	200-400 d (34F52); 300-350 d (43L52a)		0.65, 0.44, 0.17 scint spect (34F52)		Pr-α-n, Pr-α-2n (34F52); $Nd^{143,144}$-p-n (34F52); Nd-p-n (43L52a)
Pm^{145}	F sep isotopes (43L52a)		β^+ (43L52a)	14-18 d (43L52a)	0.45 (43L52a)			Nd-p-n (43L52a)
Pm^{145}	A chem, genet (65B51, 26P52)		EC (65B51)	~30 y yield (65B51)		Nd K, L-x (65B51, 26P52)		daughter Sm^{145} (65B51, 26P52)
Pm^{146}	B chem, excit (34F52)		β^- (?) (34F52)	~1 y (34F52); 1-2 y (43L52a)	0.7 abs (34F52); 0.75 (43L52a)			Nd^{146}-p-n (34F52); Nd-p-n (43L52a)
Pm^{147}	A chem (84M47, 84M51a); mass spect (60H48)		β^- (39G43, 72B51i)	2.6 y (53S51); 2.3 y yield (31I50a)	0.223 spect (10L50c); 0.227 spect (39W52a, 33L49); 0.229 spect (16A50)	no γ (84M47, 84M51a, 77S51c)	Q^-_β 0.223 (HPS)	fission U (39G43, 72B51i, 77S51c, 84M51a), U^{233} (38G48, 38G51), U^{235} (31I50a, 38G51); daughter Nd^{147} (84M47, 84M51a); parent Sm^{147} (42R50)
Pm^{148}	A chem, n-capt, mass spect (26P47)		β^- (47K43)	5.3 d (47K43, 26P47)	~2.5 abs (26P47); 2 abs (47K43)	~0.8 abs (26P47)		Nd-p-n (47K43); Nd^{148}-p-n (43L52, 34F52); Nd-d-2n (47K42, 47K43); Nd-α-p (47K42); Pm^{147}-n-γ (26P47); spall-fission U (6F51)
Pm^{148}	B excit, sep isotopes (43L52); chem (6F51)		β^- (43L52)	42 d (34F52); 43 d (6F51); 48 d (43L52)	2.4 (weak), 0.6 spect (6F51); 2.7 (weak), 0.7 abs (34F52); 1.7, 0.6 abs (43L52)	0.9 abs (6F51); 1.0 abs (34F52); 0.5 abs (43L52)		Nd^{148}-p-n (43L52, 34F52); spall-fission U (6F51)
Pm^{149}	A chem (84M47, 84M51c); chem, mass spect (31I47b)		β^- (84M47, 84M51c)	54 h (34F52); 55 h (31I47b); 50 h (31R52, 38K51c); 47.5 h (37B46); 47 h (84M51c, 16W42, 44L41)	1.05 spect (38K51a, 31R52, 34F52); others (26M49f, 37B46, 84M51c)	0.285 (coinc with β^-, K/L 8), ~1.3 (weak) spect conv, abs, β-γ coinc (31R52); no γ (38K51a); ~0.2 (coinc with β^-) β-γ coinc abs (26M49f); others (52M51)		Nd^{150}-p-2n (34F52); Nd-d-n, Sm-n-p, Sm-γ-p (44L41); fission U (84M47, 84M51c), Pu (32K48); spall-fission U (6F51); daughter Nd^{149} (42K52)
Pm^{150}	A excit, sep isotopes (43L52); chem, excit, sep isotopes (34F52)		β^- (43L52)	2.7 h (43L52, 34F52, 47K43)	2.01 (~70%), 3.00 (~30%) spect (34F52); 2.4 abs (43L52)	1.4, 0.3 abs (34F52)		Nd-p-n, Nd-d-2n (47K43); Nd^{150}-p-n (34F52, 43L52)

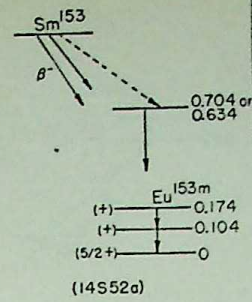
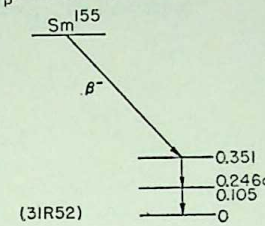
CC-0. In Public Domain. Gurukul Kangri Collection, Haridwar

Digitized by Arya Samaj Foundation Chennai and eGangotri

Isotope Z A	Class and identification	Percent abundance	Type of decay	Half-life	Energy of radiation in Mev: Particles	Energy of radiation in Mev: Gamma-transitions	Disintegration energy and scheme	Method of production and genetic relationships
$_{61}Pm^{151}$	B genet, Sm K-L-M differences (31R52)		β^- (31R52)	27.5 h (31R52)	1.1 abs (31R52)	0.065 (K/L 0.3), 0.066 (K/L 0.3), 0.070 (K/L 0.3), 0.100 (K/L ~5), 0.116, 0.144 (K/L ~9), 0.163 (K/L ~7), 0.168 (K/L ~3), 0.177 (K/L ~9), 0.208 (K/L ~4), 0.232, 0.240, 0.275 (K/L >10), 0.340 (K/L ~9), 0.715 spect conv, scint spect (31R52)		daughter Nd^{151} (31R52); fission U (51C52)
Pm	E (1P38a); chem (6F51)		β^- (1P38a)	12.5 h (6F51, 1P38a)				Nd-d- (1P38a); spall-fission U (6F51)
$_{62}Sm^{143}$	E chem (65B50)			8 m (65B50)				Sm-γ-n (65B50)
Sm^{144}		3.16 (3I48d)						
Sm^{145}	A mass spect (3I47c); chem (65B51); chem, sep isotopes, n-capt (26P52)		EC (65B51, 31R52)	~410 d (65B51); >150 d (10C48b); >72 d (3I47c)		0.061 (K/L 1.0) spect conv (31R52)		Sm^{144}-n-γ (26P52); Sm-n-γ (3I47c, 10C48b, 65B51); parent Pm^{145} (65B51, 26P52)
Sm^{147}	A chem (71H32); sep isotopes, mass spect (48W50); chem, genet, mass spect (42R50)	15.07 (3I48d)	α (71H32, 3L33)	$t_{1/2}$ corrected for abundance of Sm^{147} (HPS): 1.4×10^{11} y sp act (45L47); 1.5×10^{11} y sp act (72H35); 1×10^{11} y sp act (31P49)	2.18 ion ch (10J50); 2.14 range emuls (74C46); 2.1 range emuls (73H49); 2.0 cl ch (72H35); others (92B49)		Sm^{147}, I = 7/2 (105B52); Sm^{147}, I = 5/2 (88M51)	natural source (71H32, 3L33, 72B48, 1D48); daughter Pm^{147} (42R50); fission U^{235} (mass spect) (3I50a)
Sm^{148}		11.27 (3I48d)						
Sm^{149}		13.84 (3I48d)					Sm^{149}, I = 7/2 (105B52); Sm^{149}, I = 5/2 (88M51)	fission U^{235} (mass spect) (3I50a)
Sm^{150}		7.47 (3I48d)						
Sm^{151}	A mass spect (3I47c, 3I50a); chem (84M49)		β^- (3I47c)	73 y (7K52); ~120 y yield (3I50a)	0.076 spect (16A50, 39W52b); 0.079 spect (24K49e); 0.074 spect (84M49); no conv (31R52)	0.019 (coinc with β^-) ion ch, β-γ coinc (33W52); 0.021 ion ch (17S50); 0.021 scint spect (39W52b); no γ (84M49, 31R52); others (52M51)	 (33W52)	Sm-n-γ (3I47c); fission U (84M49); fission U^{235} (mass spect) (3I50a)
Sm^{152}		26.63 (3I48d)						fission U^{235} (mass spect) (3I50a)

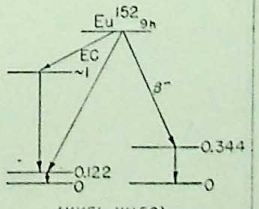
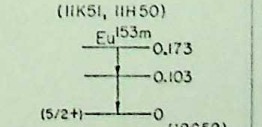
CC-0. In Public Domain. Gurukul Kangri Collection, Haridwar

Digitized by Arya Samaj Foundation Chennai and eGangotri

Isotope Z A	Class and identification	Percent abundance	Type of decay	Half-life	Energy of radiation in Mev: Particles	Energy of radiation in Mev: Gamma-transitions	Disintegration energy and scheme	Method of production and genetic relationships
$_{62}Sm^{153}$	A n-capt, excit (1P38a); mass spect (60H46, 3I47b); chem (51W51)		β^- (47K42)	47 h (51W51, 37B46, 47K42, 31R52)	0.80, 0.70 (coinc with 0.101 γ) scint spect, β-γ coinc (87B52); 0.68 (~67%), 0.80 (~33%) spect (11H50); 0.70 spect (7S51); 0.82 spect (31R52); 0.78 abs (82B48); 0.73 abs (51W51)	γ_1 0.070 (e_K/γ 3.1), γ_2 0.104 (e_K/γ 1.2, coinc with γ_3 or γ_4), γ_3 0.530, γ_4 ~0.60 ($\gamma_1/\gamma_2/\gamma_3/\gamma_4$ = 100/425/1.0/0.3) scint spect, γ-γ coinc (14S52a); 0.069 (e_K/γ 3.8), 0.103 (e_K/γ 1.2, K/L+M 3.5) scint spect (52M52e); 0.070, 0.103 (coinc with 0.07 γ, e_K/γ 0.65, K/L ~6), 0.530 (weak) scint spect, spect conv, conv-conv coinc (7S51); 0.070 (weak, e/γ >10), 0.101 (e/γ ~3), no higher γ, scint spect, γ-γ coinc (87B52); 0.070 (K/L 3.5, $L_I/L_{II}/L_{III}$ = 26/1.3/1.3), 0.104 (K/L 6.5, $L_I/L_{II}+L_{III}$ = 43/2.3) spect conv (63M52a, 63M52b); 0.070 (coinc with 0.103 γ, K/L 0.29), 0.103 (K/L 3.5), 0.582 (weak) spect conv, γ-γ coinc (31R52); 0.069, 0.103 spect conv (67H48a); 0.102 (e/γ >2.5) spect conv, β-γ, β-conv coinc (11H50); others (43M46, 82B48)	 (14S52a)	Nd-α-n (47K42); Sm-n-γ (71H36, 1P38a, 44L41, 16W42, 60H46, 2S47, 51W51); Sm-n-Zn (1P38a, 47K42); Sm-d-p (44L41, 47K42); Sm-γ-n (44L41); spall-fission Th (7N49a), U (6F51); fission U^{233} (61S48), U^{235}, Pu (51W51); parent Eu^{153m} (52M50)
Sm^{154}		22.53 (3I48d)						fission U^{235} (mass spect) (3I50a)
Sm^{155}	B n-capt (12A35, 82M35); chem (51W51a)		β^- (47K42)	23.5 m (31R52); 25 m (51W51a); 21 m (1P38a)	1.8 (coinc with both γ's) abs, β-γ coinc (31R52); 1.9 abs (51W51a); 1.8 abs (47K42)	γ_1 1.05 (K/L 3.6), γ_2 0.246 (coinc with γ_1, K/L ~8) (γ_1/γ_2 ~1) spect, spect conv, γ-γ coinc (31R52)	Q^-_β 2.2 (31R52)  (31R52)	Sm-n-γ (12A35, 82M35, 71H36, 1P38a, 44L41, 2S47, 3I47c, 51W51a); Sm-d-p (44L41, 47K42); fission U^{235} (51W51a), Pu (51W51a); parent Eu^{155} (3I47c)
Sm^{156}	A chem, genet (51W51b)		β^- (51W51b)	~10 h (51W51b)	0.9 abs (51W51b)			fission U (51W51b); spall-fission U (6F51); parent Eu^{156} (51W51b)
$_{63}Eu^{144}$	C excit, sep isotopes (74H52)		β^+ (74H52)	18 m (74H52)	2.4 spect (74H52)			Sm^{144}-p-n (74H52)
Eu^{145}	A chem, genet, sep isotopes, excit (74H51)		EC (74H51)	5 d (74H51)	conv: 0.2 abs (74H51)			Sm^{147}-p-3n (74H51); daughter Tb^{149} (74H51)
Eu^{146}	C excit, sep isotopes (74H51)		EC (74H51)	38 h (74H51)	conv: 0.4 abs (74H51)			Sm^{144}-α-pn, Sm^{147}-d-3n (74H51)
Eu^{147}	B chem, excit, sep isotopes (74H51)		EC 99+%, α ~10^{-3}%, no β^+ (74H51)	24 d (74H51)	α: 2.88 ion ch (74H51) conv: 0.2 abs (74H51)			Sm^{147}-p-n (74H51); Sm-d-2n, 3n (42R52)

CC-0. In Public Domain. Gurukul Kangri Collection, Haridwar

Digitized by Arya Samaj Foundation Chennai and eGangotri

Isotope Z A	Class and identification	Percent abundance	Type of decay	Half-life	Energy of radiation in Mev: Particles	Energy of radiation in Mev: Gamma-transitions	Disintegration energy and scheme	Method of production and genetic relationships
$_{63}Eu^{148}$	A chem (84M51d); excit, sep isotopes (74H51, 86M52)		EC, no β^+ (74H51)	59 d (86M52); 54 d (2W50b); 50 d (74H51); 53 d (84M51d)	conv: 0.4 abs (74H51, 2W50b)	0.57 scint spect (74H52); 1.0, 0.4 abs (84M51d, 2W50b); 0.7 abs (86M52)		Sm^{148}-p-n (74H51, 86M52); Sm-p-n (2W50b); Sm-d-n (47K43, 84M51d)
Eu^{149}	E sep isotopes, excit (74H52)			~120 d (74H52)		~0.4 scint spect (74H52)		Sm^{149}-p-n (74H52)
Eu^{150}	A chem, excit (65B50); chem, excit, sep isotopes (74H52); excit, sep isotopes (86M52)		β^- (86M52)	15.0 h (2W50b); 15 h (65B50); 13.1 h (86M52)	1.8 spect (2W50b); 0.8, other β's (86M52)			Sm^{150}-p-n (74H52, 86M52); Sm-p-n (2W50b); Eu-γ-n (65B50)
Eu^{151}		47.77 (43H48)					Eu^{151}, I = 5/2 (87M50)	fission U (mass spect) (3I50a)
Eu^{152}	A n-capt, mass spect (3I47d); chem (84M49a)		EC, β^- (60H49)	13 y (7K52); 5.3 y yield (60H49)	1.58, others spect (11H50); 1.58, 0.75 spect (68S48); 1.7 (~20%), 0.9 (~80%) abs (84M49a)	0.122 (conv in Sm), 0.123 (conv in Gd), 0.244, 0.344, 0.720, 0.964, 1.086 spect conv (11K51, 10C50c); 0.121, 0.244, 0.344 spect conv (43K52); 0.121 (coinc with 0.244 γ), 0.123 (coinc with 0.344 γ), 0.244, 0.344 (not coinc with 0.244 γ) conv-conv coinc spect (35F50); others (11H50, 68S48)		Eu-n-γ (3I47d, 2S47)
Eu^{152}	A n-capt (82M35); n-capt, excit (1P38a); mass spect (60H46, 60H49)		β^-, EC (60H49)	9.2 h (1P38a, 60H49); 9.3 h (37B46)	1.880, 0.55 (?) (weak) spect (11H50); 1.88 spect (20T39)	γ_1 0.122 (conv in Sm, K/L ~4), γ_2 0.344 (conv in Gd, K/L ~10) spect conv (11K51); 0.122, 0.336 (coinc with β) pair spect, β-γ coinc (107S51); 0.120 (coinc with 0.9 or 0.8 γ), 0.94, 0.82 (not coinc with 0.9 γ) spect, spect conv, β-conv, γ-γ coinc (11H50); others (52W51, 20T39, 10C50c, 35F50, 23R39)	 (11K51, 11H50)	Eu-n-γ (82M35, 1P38a, 71H36, 5F41b, 2S47, 60H49); Eu-n-2n (1P38a); Eu-d-p (5F39, 5F41b)
Eu^{153m}	A genet (52M50)		IT (52M50)	3.0×10^{-9} s delay coinc (52M50)		0.069 (e_K/γ 3.8), 0.103 (e_K/γ 1.2, K/L+M 3.5) scint spect (52M52e)	 (18G52)	daughter Sm^{153} (52M50)
Eu^{153}		52.23 (43H48)					Eu^{153}, I = 5/2 (87M50)	fission U (mass spect) (3I50a)
Eu^{154}	A n-capt (69S38); mass spect (3I47d, 60H49); chem (84M49a)		β^- (60H49)	16 y (7K52); 5.4 y yield (60H49)	1.9 (~10%), 0.7 (~40%), 0.3 (~50%) abs (84M49a, calc from 60H49); ~0.7 (coinc with hard γ), 0.3 abs, β-γ coinc abs (84M49a); with Eu^{154} and Eu^{155}: 1.88, 0.90, 0.59, 0.25, 0.14 spect, β-γ coinc abs (24K50d); others (37B46, 26K48, 11H50, 37W47)	0.336, 0.778, 1.116 spect conv (11K51); with Eu^{154} and Eu^{155}: 0.085, 0.101, 0.725, 1.005, 1.288 spect (24K50d); 0.122 spect conv (43K52); others (26K48, 10C48b)		Eu-n-γ (69S38, 5F39, 5F41b, 2S47); Eu-d-p (5F41b, 26K48); Eu^{153} (fission product)-n-γ (84M49a); fission U (24K50d)

CC-0. In Public Domain. Gurukul Kangri Collection, Haridwar

Digitized by Arya Samaj Foundation Chennai and eGangotri

Isotope Z A	Class and identification	Percent abundance	Type of decay	Half-life	Energy of radiation in Mev: Particles	Energy of radiation in Mev: Gamma-transitions	Disintegration energy and scheme	Method of production and genetic relationships
$_{63}Eu^{155}$	A chem (51W51c); mass spect (60H49)		β^- (51W51c)	1.7 y (31R52); yield (60H49); 2.0 y (51W51c)	0.154 (80%), 0.243 (20%) spect, β-γ, γ-γ coinc (84M49a); see Eu^{154} β's (24K50d)	0.060 (weak), 0.087 (K/L ~8), 0.106 (K/L ~8), 0.132 (weak) spect conv (31R52); 0.085, 0.099 crit abs Pb, Pt (84M49a); 0.084 crit abs Tl, Hg (51W51c); 0.015 ion ch, β-γ coinc (33W52); see Eu^{154} γ's (24K50d)		Sm-d-n (47K43); Eu-n-γ (second order reaction) (60H49); spall-fission Th (7N49a); fission U (51W51c, 84M49a); daughter Sm^{155} (31I47c)
Eu^{156}	A chem (51W51b); mass spect (31I47b, 31I47c)		β^- (51W51b)	15.4 d (51W51b, 31I47c)	~0.5 (60%), 2.4 (40%) abs (51W51b)	2.0 abs (51W51b)		Eu-n-γ (second order reaction) (31I47c); spall-fission Th (7N49a), U (6O48, 6F51); fission U (51W51b), Pu (28F51); daughter Sm^{156} (51W51b)
Eu^{157}	D chem (51W51d)		β^- (51W51d)	15.4 h (51W51d)	~1.0 (~75%), ~1.7 (~25%) abs (51W51d)	0.6, 0.2 abs (51W51d)		spall-fission Th (7N49a); fission U (51W51d), Pu (32K48)
Eu^{158}	D chem (51W51d)		β^- (51W51d)	60 m (51W51d)	2.6 abs (51W51d)	γ (51W51d)		fission U (51W51d)
Eu^{159}	F excit (65B50)			20 m (65B50)				Gd-γ-p (?) (65B50)
$_{64}Gd^{148}$	B chem, excit, sep isotopes (42R52)		α, EC (?) (42R52)	>35 y (42R52)	α: 3.16 ion ch (42R52)			Sm-α-3n, Sm^{147}-α-3n (42R52); Eu-p-4n (42R52); spall Dy (42R52)
Gd^{149}	B chem, excit, sep isotopes, cross bomb (74H51)		EC 99+%, α ~10^{-3}% (42R52)	9 d (74H51)	α: 3.0 ion ch (74H51); conv: 0.35 abs (74H51)			Sm-α-2n, Sm^{147}-α-2n (74H51, 42R52); Eu-p-3n (74H51)
Gd^{150}	D chem (42R52)		α (42R52)	long (42R52)	α: 2.7 ion ch, range emuls (42R52)			Eu-d-3n (42R52)
Gd^{151}	B chem, excit (63H50)		EC, no β^+ (63H50)	150 d (63H50)		0.265 (e/γ large) abs (63H50)		Eu-d-2n (5F41b, 26K48, 63H50)
Gd^{152}		0.20 (1B50)						
Gd^{153}	A mass spect (3I47c); chem, n-capt (63H50)		EC, no β^+ (63H50)	236 d (63H50); 225 d (24K49a)		0.104 (K/L 5.2) spect conv (10C52c); 0.100 spect conv, abs (24K49a); 0.106 (e/γ >0.9) abs (63H50); others (10C48b)		Eu-d-2n (63H50); Gd-n-γ (3I47c, 10C48b, 24K49a, 63H50)
Gd^{154}		2.15 (1B50)						
Gd^{155}		14.73 (1B50)						
Gd^{156}		20.47 (1B50)						
Gd^{157}		15.68 (1B50)						
Gd^{158}		24.87 (1B50)						
Gd^{159}	B n-capt (2S47); chem (65B49, 63H50)		β^- (26K48)	18.0 h (65B49, 65B50, 26K48); 17.9 h (24K49b); ~24 h (63H50)	0.9 abs (26K48, 65B49)	0.055, 0.38 abs (65B49); ~0.3 abs (26K48); others (52M51)		Gd-n-γ (2S47, 24K49b, 65B49, 63H50); Gd-d-p (26K48); Gd-γ-n (65B50)
Gd^{160}		21.90 (1B50)						
Gd^{161}	C n-capt (3I46); n-capt, excit (65B49)		β^- (38M49)	3.6 m (65B49, 24K49b); 3.5 m (26K48); 3.3 m (38M49); 4.5 m (3I46)	1.5 abs (24K49c); ~2 (38M49)	0.37 abs (24K49c); ~0.07 (38M49)		Gd-n-γ (3I46, 26K48, 65B49, 38M49, 24K49b); parent Tb^{161} (24K49b, 24K49c)

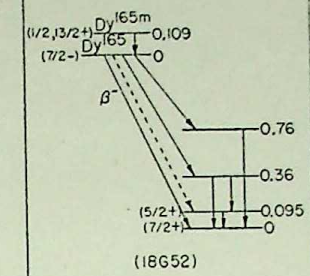
CC-0. In Public Domain. Gurukul Kangri Collection, Haridwar

Digitized by Arya Samaj Foundation Chennai and eGangotri

Isotope Z A	Class and identification	Percent abundance	Type of decay	Half-life	Energy of radiation in Mev: Particles	Energy of radiation in Mev: Gamma-transitions	Disintegration energy and scheme	Method of production and genetic relationships
$_{65}Tb^{149}$	A chem, mass spect (42R50)		α, EC (?) (42R52)	4.1 h (42R52)	α: 3.955 spect (42R52); 3.95 ion ch (42R52)			spall Gd, Dy (3T49, 42R52), Tb, Yb (42R52); parent Eu^{145} (74H51)
Tb^{151}	D chem, excit (42R52)		α, EC (?) (42R52)	19 h (42R52)	3.44 ion ch (42R52)			spall Eu (42R52), Gd, Tb, Dy (42R52)
Tb^{153}	B chem, excit (2W50c)		EC (2W50c)	5.1 d (2W50c)		1.2, 0.2 abs (2W50c)		Eu-α-2n (2W50c)
Tb^{154}	B chem, excit (2W50c)		EC 99+%, β^+ ~0.5% (2W50c)	17.2 h (2W50c)	2.6 spect (2W50c)	1.3 abs (2W50c)		Eu-α-n, Eu-α-3n (2W50c); Gd-p-n (2W50c)
Tb^{155}	D chem, excit (2W50c)		EC (2W50c)	190 d (2W50c)		1.4 abs (2W50c)		Eu-α-2n (2W50c)
Tb^{156}	B chem, excit (2W50c)		EC >75%, β^+ <25% (2W50c)	5.0 h (2W50c)	~1.3 abs (2W50c)			Eu-α-n (2W50c); Gd-p-n (2W50c)
Tb^{157}	B chem, excit, cross bomb (2W50c)		EC (2W50c)	4.7 d (2W50c)		1.4 abs (2W50c)		Gd-p-n (2W50c)
Tb^{159}		100 (43H48)					Tb^{159}, I = 3/2 (87M50)	
Tb^{160}	A n-capt (37B43); mass spect (3147c); chem (6F51)		β^- (37B43); no β^+ (82B50)	73.5 d (37B46); 71 d (82B50); 76 d (10C50d)	0.860 (43%), 0.521 (41%), 0.396 (16%) spect (82B50); ~0.90 β^- (coinc with 0.085 γ) scint spect, β-γ coinc (52M52)	0.962, 0.876, 0.410, 0.391, 0.375, 0.298, 0.282, 0.215, 0.196, 0.176, 0.093, 0.087 spect, spect conv (10C50d); 0.970, 0.886, 0.300, 0.200, 0.085 spect conv (82B50); with Dy^{160m}: 0.085 (e_K/γ 1.7) scint spect (52M52a); others (10C48b)		Gd-d-2n (26K48); Tb-n-γ (37B43, 37B46, 2S47); spall-fission U (6F51); parent Dy^{160m} (52M52, 52M52a)
Tb^{161}	B excit (26K48); chem, excit (24K49c)		β^- (26K48)	6.75 d (65B49); 6.8 d (10C52c); 7.2 d (63H50); 7 d (24K49a)	0.5 abs (63H50, 65B49, 24K49a)	0.049 (L/M 3.7) spect conv (10C52c); 0.026 ion ch (17S50); 0.05 abs (65B49, 24K49a)		Gd-d-n (26K48, 65B49); spall-fission U (6F51); daughter Gd^{161} (24K49b, 24K49c)
$Tb^{162,163}$	E excit (65B50)			14 m (65B50)				Dy-γ-p (?) (65B50)
$_{66}Dy^{<153}$	E cross bomb (42R52)		α (42R52)	7 m (42R52)	4.21 ion ch (42R52)			Nd-C-spall, Tb-p (42R52)
$Dy^{<153}$	E cross bomb (42R52)		α (42R52)	19 m (42R52)	4.06 ion ch (42R52)			spall Tb, Dy (42R52)
$Dy^{<153}$	D chem (42R52)		α (42R52)	2.3 h (42R52)	3.61 ion ch (42R52)			Nd-C-spall, Tb-p (42R52)
Dy^{156}		0.0524 (3149b)						
Dy^{158}		0.0902 (3149b)						
Dy^{159}	B chem, n-capt (24K49d); chem, cross bomb (65B51a)		EC (24K49d)	134 d (65B51a); 140 d (24K49d)		Tb K, L-x (65B51a)		Tb-d-2n (65B51a); Dy-n-γ (24K49d, 65B51a)

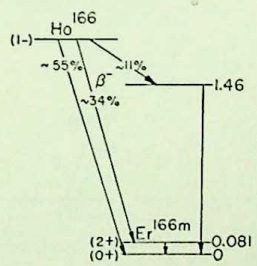
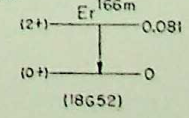
CC-0. In Public Domain. Gurukul Kangri Collection, Haridwar

Digitized by Arya Samaj Foundation Chennai and eGangotri

Isotope Z A	Class and identification	Percent abundance	Type of decay	Half-life	Energy of radiation in Mev: Particles	Energy of radiation in Mev: Gamma-transitions	Disintegration energy and scheme	Method of production and genetic relationships
$_{66}Dy^{160m}$	A genet (52M52)		IT (52M52a)	1.8 x 10^{-9} s delay coinc (52M52a)		0.085 (e_K/γ 1.7) scint spect (52M52a)		daughter Tb^{160} (52M52, 52M52a)
Dy^{160}		2.294 (3I49b)						
Dy^{161}		18.88 (3I49b)						
Dy^{162}		25.53 (3I49b)						
Dy^{163}		24.97 (3I49b)						
Dy^{164}		28.18 (3I49b)						
Dy^{165m}	A n-capt (9F44b); n-capt, sep isotopes (3I47e)		IT (9F44b)	1.25 m (9F46)		0.109 (K/L 0.08) spect conv (42C50); 0.102 scint spect (31K51); 0.102 spect conv (15H48)		Dy-n-γ (9F44b, 9F46, 2S47, 18G47, 42C50); Dy^{164}-n-γ (3I47e)
Dy^{165}	A n-capt (71H36, 82M35); n-capt, sep isotopes (3I47e); mass spect (3I47f)		β^- (1P38a)	139.2 m (109S52); 140 m (37B46); 145 m (5S46)	1.25, 0.88, 0.42 spect (5S46); others (72C42, 16D41, 10E41)	0.0951 (K/L_I 6.4) spect conv (63M52); 0.0878 spect conv (42C50); 0.091, 0.36, 0.76 spect, spect conv (5S46); others (43M46, 52M51, 52M52, 52W51)	 (18G52)	Dy-n-γ (82M35, 71H36, 1P38a, 1M40, 2S47, 24K49d); Dy^{164}-n-γ (3I47e)
Dy^{166}	A chem, genet (24K49d)		β^- (24K49d)	82 h (65B50a); 81 h (24K49d)	0.2 abs (65B50a); 0.4 abs (24K49d)			Dy-n-γ (second order reaction) (24K49d, 65B50a); spall-fission U (6F51); parent Ho^{166} (24K49d, 65B50a)
$_{67}Ho$	E excit (42R52)		α (42R52)	4 m (42R52)	α: 4.2 ion ch (42R52)			Dy-p (42R52)
Ho^{160}	C excit (2W50c)		EC 99+%, β^+ ~0.5% (2W50c)	22.5 m (2W50c)	~1.3 abs (2W50c); conv: 0.2 abs (2W50c)	~1.2 abs (2W50c)		Tb-α-3n (2W50c)
Ho^{161}	B chem, excit (2W50c)		EC (2W50c)	4.6 h (2W50c)	conv: 0.1 abs (2W50c)	1.1 abs (2W50c)		Tb-α-2n, Dy-p-n, Dy-d-n (2W50c)
Ho^{162}	B chem, excit (2W50c)		EC ~85%, β^- ~15% (2W50c)	65.0 d (2W50c)	β^-: 0.8 spect, abs (2W50c); conv: 0.1 abs (2W50c)	~1 abs (2W50c)		Tb-α-n, Dy-p-n, Dy-d-2n (2W50c)
Ho^{163}	B chem, excit, cross bomb (2W50c)		EC (2W50c)	5.20 d (2W50c)	conv: 0.4 abs (2W50c)	~0.5, 1.4 abs (2W50c)		Dy-p-n, Dy-d-n, Dy-d-2n (2W50c)
Ho^{164}	A excit (1P38a)		β^- (2W50c)	34.0 m (2W50c); 41.5 m (25W50)	0.95 spect (2W50c)	no γ (2W50c)		Dy-p-n (2W50c); Ho-n-2n (1P38a, 25W50); Ho-γ-n (25W48)

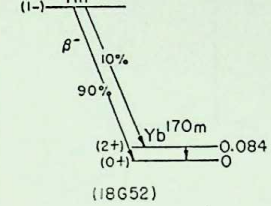
CC-0. In Public Domain. Gurukul Kangri Collection, Haridwar

Digitized by Arya Samaj Foundation Chennai and eGangotri

Isotope Z A	Class and identification	Percent abundance	Type of decay	Half-life	Energy of radiation in Mev: Particles	Energy of radiation in Mev: Gamma-transitions	Disintegration energy and scheme	Method of production and genetic relationships
$_{67}Ho^{165}$		100 (28L50)					Ho^{165}, I = 7/2 (87M50)	
Ho^{166}	A n-capt (71H36); mass spect (3I47d); chem (24K49b)		β^- (71H36)	27.3 h average of (24K49b, 3I47d, 37B46, 22G49, 10C49a, 31A50)	1.84 (~89%), 0.55 (~11%) spect (7S50a); 1.88 spect (22G49); 1.84 (86%), 0.66 (14%) spect (31A50); 1.85 spect (24K49); 1.90 cl ch, abs (97S50)	0.080 (e_K/γ 1.9, K/L+M 0.25), 1.38 (coinc with 0.08 γ) scint spect, γ-γ coinc (14S52a); 0.081 (K/L 0.07, $L_I/L_{II}/L_{III}$ = <0.1/0.72/1.00) spect conv (63M52); 0.080 (e_L/γ ~0.4, K/L <1), 1.36 (weak) spect, spect conv, β-conv coinc (7S50a); 0.081 (e_K/γ 1.9) scint spect (52M52a); 0.081, 0.9 spect conv, abs (10C49a); 0.081, ~1.5 (weak) spect conv, β-γ coinc (31A50); 0.080, 1.2 (weak) spect conv, abs (22G49)	 (14S52a)	Ho-n-γ (71H36, 1P38a, 1M40, 2S47); spall-fission U (6F51); daughter Dy^{166} (24K49d, 65B50a); parent Er^{166m} (52M50a, 52M52a, 63M52)
Ho^{166}	B chem, excit (65B52)		β^- (65B52)	>30 y (65B52)	1.1 (~8%), 0.28 (~46%), 0.18 (~46%) abs (65B52)	0.212 (coinc with 1.1 β), 0.280 (coinc with 0.73 and 0.83 γ), 0.725, 0.830, 0.095 (very weak) scint spect, γ-γ, β-γ coinc (65B52)		Ho-n-γ (65B52)
$Ho^{167,169}$	E excit (65B50)			96 m (65B50)				Er-γ-p (65B50)
$_{68}Er^{160,161}$	D chem (6F51)		β^+ (?) (6F51)	~17 h (6F51)				spall-fission U (6F51)
Er^{162}		0.136 (60H50)						
Er^{163}	D chem (6F51)		β^+ (?) (6F51)	~65 h (6F51)				spall-fission U (6F51)
Er^{164}		1.56 (60H50)						
Er^{165}	A chem, excit (65B50b); excit (29K52)		EC (65B50b)	10.0 h (65B50b); 9.9 h (29K52); 11.2 h (2W50d)	conv: ~0.2, 1.1 (weak) abs (29K52)	1.1 abs (2W50d); no γ (65B50b)		Dy-α-3n (2W50d); Ho-p-n (65B50b, 29K52); Ho-d-2n (29K52)
Er^{166m}	A genet (52M50a)		IT (52M50a)	1.7×10^{-9} s delay coinc (52M50a)		0.081 (e_K/γ 1.9) scint spect (52M52a); 0.081 (K/L 0.07) spect conv (63M52)	see Ho^{166}  (18G52)	daughter Ho^{166} (52M50a, 63M52, 52M52a)
Er^{166}		33.41 (60H50)						
Er^{167}		22.94 (60H50)					Er^{167}, I = 7/2 (97B51b)	
Er^{168}		27.07 (60H50)						
Er^{169}	B chem, n-capt (24K48)		β^- (24K48)	9.4 d (24K48); 9 d (65B50)	0.33 spect (24K48); 0.33 scint spect (11B49a)	no γ (24K48, 11K51)		Er-γ-n (65B50); Er-n-γ (24K48); spall-fission U (6F51)

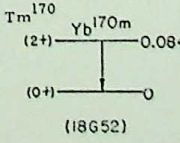
CC-0. In Public Domain. Gurukul Kangri Collection, Haridwar

Digitized by Arya Samaj Foundation Chennai and eGangotri

Isotope Z A	Class and identification	Percent abundance	Type of decay	Half-life	Energy of radiation in Mev: Particles	Energy of radiation in Mev: Gamma-transitions	Disintegration energy and scheme	Method of production and genetic relationships
$_{68}Er^{170}$		14.88 (60H50)						
Er^{171}	B n-capt (71H36, 23N35); chem (24K48)		β^- (24K48)	7.5 h (24K48, 11K51)	1.49 (~6%), 1.05 (~72%), 0.67 (~22%) spect, β-γ coinc (24K48)	0.113 (K/L ~10), 0.118 (K/L ~0.5), 0.126 (K/L ~2), 0.176, 0.295 (K/L ~10), 0.308 (K/L ~10), 0.420, no 0.8 γ spect conv (11K51); 0.113 (e/γ large, coinc with 1.05 β and 0.31 γ), 0.31 (coinc with 1.05 β), 0.81 spect, spect conv, β-γ coinc (24K48); ~0.1 (e/γ 1.3) β-γ delay coinc (10D48)		Er-n-γ (71H36, 1P38a, 24K48, 37B46, 23N35); parent Tm^{171} (24K48); parent Tm^{171m} (10D48)
Er^m	E n-capt (38M49a)		IT (38M49a)	2.5 s (38M49a, 45G51)		0.210 (e_K/γ 0.55) scint spect (45G51, 24C51a)		Er-n-γ (38M49a, 45G51)
$_{69}Tm^{166}$	B chem, excit (2W49a)		EC 99+%, β^+ ~0.5% (2W49a)	7.7 h (2W49a)	β^+: 2.1 spect (2W49a); conv: 0.24, ~1 spect, abs (2W49a)	1.7 abs (2W49a)		Ho-α-3n (2W49a); Er-p-n (2W49a); daughter Yb^{166} (6F51)
Tm^{167}	B chem, excit (2W49a)		EC, no β^+ (2W49a)	9.6 d (2W49a)	conv: 0.21 abs (2W49a)	0.22, 0.95 abs (2W49a)		Ho-α-2n (2W49a); Er-p-n (2W49a); spall Ta (2W49a)
Tm^{168}	A chem, excit (2W49a)		EC, β^- (?) ~2% (2W49a)	85 d (2W49a)	conv: 0.16, 0.5 abs (2W49a)	0.21, 0.85 abs (2W49a)		Ho-α-n (2W49a); Er-p-n (2W49a); Tm-n-2n (2W49a)
Tm^{169m}	A genet (10D48)		IT (10D48)	all delay coinc: 0.658×10^{-6} s (27F50); 0.67×10^{-6} s (75M51a); 0.7×10^{-6} s (52M51); 0.60×10^{-6} s (14S51a)		see γ's of Yb^{169}		daughter Yb^{169} (10D48, 27F50, 52M51, 14S51a, 75M51a)
Tm^{169}		100 (7L50)					Tm^{169}, I = 1/2 (87M50)	
Tm^{170}	A n-capt (23N36, 71H36); chem (24K48a)		β^- (37B46a); no EC (lim 0.3%), no β^+ (lim 0.01%) (14G52)	129 d (24K49b); 120 d (42C50); 127 d (37B46a)	0.968 (76%), 0.884 (24%) spect (14G52); 0.970 (~90%), 0.886 (~10%) spect (36F49); 0.970, 0.88 spect, β-γ coinc (44R52); 0.990 spect (16A50); others (14G49, 22G49a, 97S50, 9S49a)	0.0841 (3%, e_K/γ 1.6, K/L/M = 1/2.6/0.75) spect conv, β-γ coinc (14G52); γ (~3%, e/γ 9.4, K/L+M 0.22) x-γ coinc, scint spect (1N50); 0.085 (K/L 0.16, $L_I/L_{II}/L_{III}$ = <0.1/0.83/1.00) spect conv (63M52); 0.085 (e_K/γ 1.5) scint spect (52M52a); 0.084 (e/γ 4, K/L/M ~1/6.9/2.1) spect, spect conv, β-γ coinc (36F49); γ (e/γ >10, K/L+M 0.1) spect conv, scint spect (7S51); 0.085 spect conv (16A50, 42C50, 9S49a); others (22G50a, 4E50a, 1N50a, 10C49a, 52R52)	Q^-_β 0.970 (36F49)  (18G52)	Tm-n-γ (71H36, 23N36, 2S47); Tm-d-p (24K48a); parent Yb^{170m} (8B50, 52M52a, 14G52)

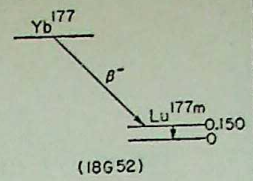
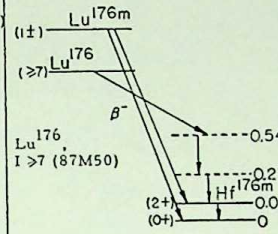
CC-0. In Public Domain. Gurukul Kangri Collection, Haridwar

Digitized by Arya Samaj Foundation Chennai and eGangotri

Isotope Z A	Class and identification	Percent abundance	Type of decay	Half-life	Energy of radiation in Mev: Particles	Energy of radiation in Mev: Gamma-transitions	Disintegration energy and scheme	Method of production and genetic relationships
$_{69}Tm^{171m}$	B genet (10D48)		IT (10D48)	2.5×10^{-6} s delay coinc (10D48)		0.113 (e/γ 1.3) spect conv, β-γ coinc (10D48); 0.113 (e/γ large) spect conv, β-γ coinc (24K48)		daughter Er^{171} (10D48)
Tm^{171}	B chem, genet (24K48)		β^- (24K48)	680 d (24K49b)	0.10 spect (24K48a)			daughter Er^{171} (24K48)
$Tm^{172(?)}$	E chem (6F51)		β^- (6F51)	2-3 d (6F51)				spall-fission U (6F51)
$Tm^{>171}$	E excit (65B50)			19 m (65B50)				Yb-γ-p (?) (65B50)
$_{70}Yb^{166}$	D chem, genet (6F51)		EC (6F51)	62 h (6F51)				spall-fission U, parent Tm^{166} (6F51)
Yb^{168}		0.140 (1B50)						
Yb^{169}	A n-capt (37B46a); chem, excit (24K48a)		EC (37B46a)	31.8 d (49W49); 32.4 d (10C50e); 33 d (37B46a, 75M51a)		γ_1 0.023, γ_2 0.064, γ_3 0.095, γ_4 0.110 (e/γ 1.6), γ_5 0.120, γ_6 0.133 (e/γ 0.2), γ_7 0.143, γ_8 0.160, γ_9 0.178 (e/γ 0.8), γ_{10} 0.198 (e/γ 0.4), γ_{11} 0.308 (e/γ 0.04); ($\gamma_2/\gamma_4/\gamma_6/\gamma_9/\gamma_{10}/\gamma_{11}$ = 1.3/2.1/2.0/1.0/1.7/0.6) spect, spect conv, delay coinc (75M51a); 0.063, 0.094, 0.110, 0.131, 0.177, 0.198, 0.308 spect conv (10C50e); 0.109, 0.130, 0.177, 0.198, 0.307 scint spect, delay coinc (14S51a)		Tm-d-2n (24K48a); Yb-n-γ (34A45, 37B46a, 3I48a); spall-fission U (6F51); parent Tm^{169m} (10D48, 27F50, 52M51, 14S51a, 75M51a)
Yb^{170m}	A genet (8B50)		IT (8B50)	1.57×10^{-9} s delay coinc (14G52); 1.6×10^{-9} s delay coinc (52M52a)		0.0841 (e_K/γ 1.6, K/L/M = 1/2.6/0.75) spect conv, β-γ coinc (14G52); 0.085 (e_K/γ 1.5) scint spect (52M52a)	see Tm^{170}  (18G52)	daughter Tm^{170} (8B50, 14G52, 52M52a)
Yb^{170}		3.03 (1B50)						
Yb^{171}		14.31 (1B50)					Yb^{171}, I = 1/2 (87M50)	
Yb^{172}		21.82 (1B50)						
Yb^{173}		16.13 (1B50)					Yb^{173}, I = 5/2 (87M50)	
Yb^{174}		31.84 (1B50)						
Yb^{175}	A n-capt (37B46a, 34A45); mass spect (3I47f); chem (24K49b)		β^- (34A45)	102 h (3I47f); 99 h (37B46a); 101 h (34A45)	0.50, 0.13 abs (37B46a); 0.45 cl ch (34A45)	0.138, 0.259, 0.283, 0.396 spect conv (10C50e); others (52M51)		Yb-n-γ (34A45, 37B46a, 3I47f, 24K49b); Yb-γ-n (65B50)
Yb^{176}		12.73 (1B50)						

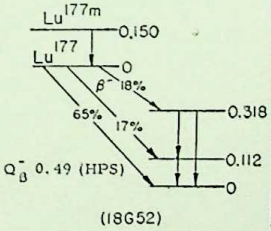
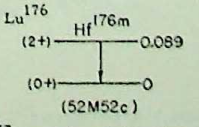
CC-0. In Public Domain. Gurukul Kangri Collection, Haridwar

Digitized by Arya Samaj Foundation Chennai and eGangotri

Isotope Z A	Class and identification	Percent abundance	Type of decay	Half-life	Energy of radiation in Mev: Particles	Energy of radiation in Mev: Gamma-transitions	Disintegration energy and scheme	Method of production and genetic relationships
$_{70}Yb^{177}$	B n-capt (82M35, 71H36); chem (24K49b)		β^- (37B46a)	1.8 h (52M51); 1.9 h (34A45); 2.4 h (37B46a)	1.3 abs (37B46a); 1.2 cl ch (34A45)	0.150 (K/L 3) spect conv, β-γ coinc (52M51)	 (18G52)	Yb-n-γ (82M35, 71H36, 1P38a, 37B46a, 3I47f); parent Lu^{177m} (52M49, 52M51)
Yb^m	E n-capt (38M49a)		IT (38M49a)	6 s (38M49a, 31K51)		0.212, 0.104 (?) scint spect (31K51); 0.200 abs (38M49a); Yb K-x (38M49)		Yb-n-γ (38M49a, 38M49, 31K51)
Yb^m	E n-capt (38M49a)		IT (38M49a)	50 s (38M49a)		~0.025, Yb L-x abs (38M49a)		Yb-n-γ (38M49a, 38M49)
Yb^m	E n-capt (31K51)			0.15 s (31K52)		0.455 scint spect (31K52)		Yb-n-γ (31K51)
$_{71}Lu^{170}$	B chem, excit (2W51)		EC (2W51)	1.7 d (2W51)		~2.5 abs (2W51)		Tm-α-3n, spall Ta (2W51)
Lu^{171}	B chem, excit (2W51)		EC (2W51)	8.5 d (2W51)		~1.2 abs (2W51)		Tm-α-2n, Yb-p-n, spall Ta (2W51); daughter Hf^{171} (2W51)
Lu^{171}	D chem, excit (2W51)		EC (2W51)	~600 d (2W51)		~1 abs (2W51)		Tm-α-2n (2W51)
Lu^{172}	B chem, excit (2W51)		EC (2W51)	6.70 d (2W51)		1.2 abs (2W51)		Tm-α-n, Yb-p-n (2W51); daughter Hf^{172} (2W51)
Lu^{172}	B chem, excit (2W51)		β^+, EC (?) (2W51)	4.0 h (2W51)	1.2 abs (2W51)			Tm-α-n, Yb-p-n, Lu-p-p3n (2W51)
Lu^{173}	B chem, excit (2W51)		EC (2W51)	~500 d (2W51)		~0.2, 0.8 abs (2W51)		Yb-p-n, Lu-p-p2n (2W51); daughter Hf^{173} (2W51)
Lu^{174}	A chem, excit (2W51)		EC ~80%, β^- ~20% (2W51)	165 d (2W51)	β^-: 0.6 abs (2W51)	~1 abs (2W51)		Lu-n-2n, Lu-d-p2n, Lu-p-pn, Hf-d-α (2W51)
Lu^{175}		97.40 (60H50)					Lu^{175}, I = 7/2 (87M50)	
Lu^{176m}	A n-capt (77M35a, 82M35); chem, excit (2W48)		β^-, no IT (17S52)	3.67 h (34A45); 3.7 h (37B46a)	1.1, 1.2 (17S52); 1.3 cl ch (34A45); 1.2 abs (9F43)	0.0889 ($K/L_{II}/L_{III}$ = 0.24/0.71/1.00) spect conv (63M52); 0.089 (e_K/γ 1.3) scint spect, β-γ delay coinc (52M52c); 0.089 (e/γ large, K/L 0.1) scint spect (17S52)	 Lu^{176}, I >7 (87M50) (18G52)	Lu-d-p (2W51, 2W48); Lu-n-γ (77M35a, 82M35, 71H36, 9F43, 37B46a, 34A45, 2S47, 24K49b, 31A50a); Lu-γ-γ (11D47a, 65B50); parent Hf^{176m} (52M52c)
Lu^{176}	A chem (52H38); mass spect (8M39)	2.60 (60H50)	β^-, no EC (17S52a)	7.5×10^{10} y sp act (3L39a)	0.40 abs (9F47a, 9F43)	0.089, 0.180, 0.270 scint spect (17S52a)		natural source (52H38, 8M39)

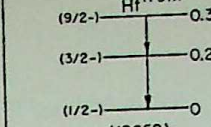
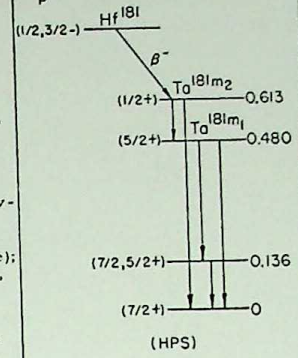
Digitized by Arya Samaj Foundation Chennai and eGangotri

CC-0. In Public Domain. Gurukul Kangri Collection, Haridwar

Isotope Z A	Class and identification	Percent abundance	Type of decay	Half-life	Energy of radiation in Mev: Particles	Energy of radiation in Mev: Gamma-transitions	Disintegration energy and scheme	Method of production and genetic relationships
$_{71}Lu^{177m}$	B genet (52M49)		IT (52M49)	1.3×10^{-7} s delay coinc (52M49, 52M51)		0.150 (K/L 3) scint spect, β-γ coinc (52M51, 52M49)	 (18G52)	daughter Yb^{177} (52M49, 52M51)
Lu^{177}	A n-capt (71H36); mass spect (3147f); chem, excit (2W48)		β^- (37B46a)	6.8 d (37B46a, 2W48); 7.0 d (30D49); 6.6 d (9F43, 34A45)	0.495 (65%), 0.37 (17%), 0.17 (18%) spect (30D49); 0.475 spect (31A50a)	0.112 (e_K/γ 0.81), 0.206 (e_K/γ 0.04), 0.318 (~5%) scint spect, γ-γ coinc (52M52d); 0.112, 0.206, 0.317 (very weak) spect, spect conv (30D49); 0.112 (K/L/M = 1/2/0.5), 0.205 spect conv (31A50a); 0.113, 0.209 spect conv (10C49a); others (52M51)		Lu-n-γ (71H36, 9F43, 34A45, 37B46a, 2S47, 24K49b, 31A50a); Lu-d-p (2W48)
$Lu^{178,179}$	D chem (65B50)			22 m (65B50)				Hf-γ-p (65B50)
$_{72}Hf^{170}$	D chem (2W51)		β^+ (2W51)	112 m (2W51)	2.4 spect (2W51)	no γ (2W51)		Lu-p-6n (2W51)
Hf^{171}	B chem, genet, excit (2W51)		EC (2W51)	16.0 h (2W51)		1.4 abs (2W51)		Yb-α-3n, Lu-p-5n (2W51); parent (8.5 d) Lu^{171} (2W51)
Hf^{172}	B chem, genet (2W51)		EC (2W51)	~5 y (2W51)		~0.28, 0.8 abs, spect conv (2W51)		Yb-α-2n, Yb-α-3n, Lu-p-4n, spall Ta (2W51); parent (6.7 d) Lu^{172} (2W51)
Hf^{173}	B chem, excit, genet (2W51)		EC (2W51)	23.6 h (2W51)		~1 abs (2W51)		Yb-α-n, Yb-α-2n, Yb-α-3n, Lu-p-3n (2W51); parent Lu^{173} (2W51)
Hf^{174}		0.18 (75H49)						
Hf^{175}	A chem, excit (2W49b); n-capt, sep isotopes (82B51); mass spect (12H51a)		EC (2W49b)	70 d (2W49b)		0.089, 0.113, 0.228, 0.318, 0.342 (K/L 4.9), 0.431 spect conv (82B52); 1.5 abs (2W49b)		Lu-d-2n, Lu-p-n (2W49b); Hf-n-γ (12H51a); Hf^{174}-n-γ (82B51)
Hf^{176m}	A genet (52M52c)		IT (52M52c)	1.35×10^{-9} s delay coinc (52M52c)		0.089 (e_K/γ 1.3) scint spect, β-γ coinc (52M52c)	see Lu^{176}  (52M52c)	daughter Lu^{176m} (52M52c)
Hf^{176}		5.15 (75H49)						
Hf^{177}		18.39 (75H49)					Hf^{177}, I = 1/2 or 3/2 (87M50)	
Hf^{178}		27.08 (75H49)					Hf^{178}, I = 0 (87M50)	

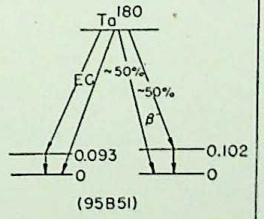
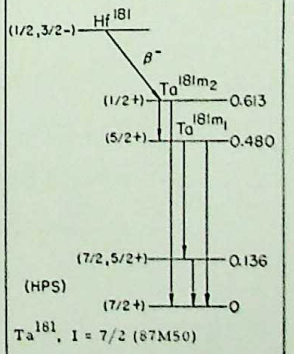
CC-0. In Public Domain. Gurukul Kangri Collection, Haridwar

Digitized by Arya Samaj Foundation Chennai and eGangotri

Isotope Z A	Class and identification	Percent abundance	Type of decay	Half-life	Energy of radiation in Mev: Particles	Energy of radiation in Mev: Gamma-transitions	Disintegration energy and scheme	Method of production and genetic relationships
$_{72}Hf^{179m}$	A n-capt (9F44b); n-capt, sep isotopes (82B51, 38M51b)		IT (9F46)	19 s (9F44b, 38M51b)		0.160, 0.217 scint spect, spect conv (82B51); ~0.150, 0.215 scint spect, conv-γ coinc (38M51b); 0.150 (e/γ very large, K/L 0.9) spect conv (15H48a); 0.220 scint spect (31K51)		Hf -n-γ (9F44b, 9F46, 38M51); Hf^{178}-n-γ (38M51b, 82B51)
Hf^{179}		13.78 (75H49)					Hf^{179}, I = 1/2 or 3/2 (87M50)	Hf^{179}-n-γ (82B51)
Hf^{180m}	B chem, n-capt, sep isotopes (82B51)		IT (82B51)	5.5 h (82B51)		0.057, 0.093, 0.214, 0.330, 0.442 spect conv, γ-conv coinc (82B51)		
Hf^{180}		35.44 (75H49)					Hf^{180}, I = 0 (87M50)	
Hf^{181}	A chem, n-capt (71H38); mass spect (12H51a); sep isotopes, n-capt (82B51)		β^- (71H38)	45 d (10C50f, 22R50); 47 d (43B48a)	0.408 spect (29F52); 0.420 spect (82B51); 0.410 spect (4E50); 0.404 spect (71C49); 0.460 spect (43B48a)	γ_1 0.133, γ_2 0.136, γ_3 0.344, γ_4 0.481, γ_5 0.611 spect conv, β-conv, conv-conv, β-γ coinc (82B51); γ_1 0.133, γ_2 0.136, γ_3 0.345, γ_4 0.481, γ_5 0.615 spect conv (4E50); γ_1 0.133 (K/L ~1), γ_2 0.136 (K/L ~0.2), γ_3 0.345, γ_4 0.481, γ_5 0.612 (γ_1 and γ_2 coinc with γ_3, γ_1 coinc with γ_4, γ_4 not coinc with γ_3) spect conv, conv-conv coinc (10C50f); γ_1 (e_K/γ 0.51), γ_4 (e_K/γ 0.034) scint spect, γ-γ coinc (52M52e); γ_1 0.130 (e/γ 0.90, K/L+M 0.6), γ_2 0.134 (e/γ ~3, K/L+M ~8), γ_3 0.340 (e/γ ~0.1), γ_4 0.474 (e/γ 0.030, K/L+M 4.0) spect conv (29F52); γ_1 0.132, γ_2 0.135 (K/L ~8), γ_3 0.345, γ_4 0.481 (γ_1/γ_2 ~5, γ_4/γ_3 ~8) spect, spect conv (12H51a); γ_1 0.130 (e_K/γ ~1.3), γ_2 0.134, γ_3 0.337 (K/L ~3.6), γ_4 0.471 (K/L ~3) (γ_3/γ_4 ~2.5) spect conv, β-γ, conv-conv coinc (71C49); γ_3 0.347 (K/L ~5.0), γ_4 0.485 (K/L ~5.2) spect, spect conv (13J49a); others (43B48a, 10C47, 24N47, 3V48, 26M49a, 49W49a, 63B50, 20D50a, 32P50, 27F50a, 35F50, 52M51, 4B48, 4B49, 14L49)	Q^-_β 1.02 (HPS) 	Hf-n-γ (71H38, 2S47); Hf^{180}-n-γ (82B51); Ta-n-p (24N47); spall-fission U (6F51); parent Ta^{181m_1} (4E50, 63B50, 52M51); parent Ta^{181m_2} (10D48, 4B48, 4E50, 63B50, 52M51)
Hf^m	E (24C52)		IT (24C52)	~3.5 s (24C52)				Hf-n (24C52)

CC-0. In Public Domain. Gurukul Kangri Collection, Haridwar

Digitized by Arya Samaj Foundation Chennai and eGangotri

Isotope Z A	Class and identification	Percent abundance	Type of decay	Half-life	Energy of radiation in Mev: Particles	Energy of radiation in Mev: Gamma-transitions	Disintegration energy and scheme	Method of production and genetic relationships
$_{73}Ta^{176}$	B chem, excit (2W48, 2W50e)		EC (2W50e)	8.0 h (2W50e)	conv: 0.1, 0.2, ~1 abs (2W50e)	~2 abs (2W50e)		Lu-α-3n (2W50e); spall Ta (2W48); daughter W^{176} (2W50e)
Ta^{177}	B chem, excit (2W48, 2W50e)		EC (2W50e)	53 h (2W50e)	conv: 0.1 abs (2W50e)	~1.4 (weak) abs (2W50e)		Lu-α-2n, Lu-α-3n, Hf-p-n (2W50e); spall Ta (2W48); daughter W^{177} (2W50e)
Ta^{178}	B chem, excit (2W50e)		EC ~97%, β^+ ~3% (2W50e)	2.1 h (2W50e)	β^+: ~1 abs (2W50e); conv: ~0.1 abs (2W50e)	1.3-1.5 abs (2W50e)		Lu-α-n, Hf-p-n, Ta-p-p3n (2W50e)
Ta^{178}	B chem, genet (2W50e)		EC ~94%, β^+ ~6% (2W50e)	9.35 m (2W50e)	β^+: 1.06 spect (2W50e); conv: 0.08 spect conv (2W50e)	~1.5 abs (2W50e)		Hf-p-n (2W50e); daughter W^{178} (2W50e)
Ta^{179}	D chem, excit (2W50e)		EC (2W50e)	~600 d (2W50e)	conv: ~0.1 abs (2W50e)	~0.7 (weak) abs (2W50e)		Lu-α-n, Hf-p-n, Ta-p-p2n (2W50e)
Ta^{180}	A chem, excit (17O38)		EC ~79%, β^- ~21%, no β^+ (lim 0.005%) (95B51)	8.15 h (95B51); 8.00 h (2W50e); 8.2 h (17O38)	0.71 (~50%), ~0.61 (~50%) spect (95B51); 0.7 spect (2W50e); abs (83M51)	γ_1 0.093 (K/L ~0.15), γ_2 0.102 ($\gamma_1 + \gamma_2$: e/γ ~5), γ_3 0.2, γ_4 0.4 (γ_3 and γ_4 very weak) spect conv, scint spect, β-γ, x-γ coinc (95B51); 1.3 abs (2W50e)	 (95B51)	Ta-n-2n (1P37, 17O38, 2W50e); Ta-γ-n (27M49, 55S51, 95B51); Ta-p-pn (96B49, 2W50e); W^{182}-γ-pn (83M51)
Ta^{181m_2}	A genet (10D48)		IT (10D48)	2.2×10^{-5} s delay coinc (10D48, 4E50, 63B50); 2.0×10^{-5} s delay coinc (4B48)		see γ's of Hf^{181}		daughter Hf^{181} (10D48, 4B48, 4E50, 63B50, 52M51)
Ta^{181m_1}	A genet (63B50)		IT (63B50)	1.2×10^{-8} s delay coinc (4E50); 1.1×10^{-8} s delay coinc (63B50); 1×10^{-8} s delay coinc (52M51)		see γ's of Hf^{181}	 Ta^{181}, I = 7/2 (87M50)	daughter Hf^{181} (4E50, 63B50, 52M51)
Ta^{181}		100 (24W48)						
Ta^m	E n-excit (24C49, 24C52)		IT (45G50)	0.33 s (24C49, 45G50, 31K51)		Ta L-x (45G50, 31K51)		Ta-n (24C49, 45G50, 31K51)

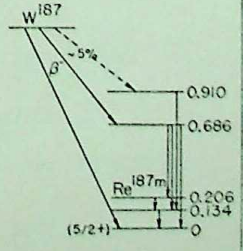
CC-0. In Public Domain. Gurukul Kangri Collection, Haridwar

Digitized by Arya Samaj Foundation Chennai and eGangotri

Isotope Z A	Class and identification	Percent abundance	Type of decay	Half-life	Energy of radiation in Mev: Particles	Energy of radiation in Mev: Gamma-transitions	Disintegration energy and scheme	Method of production and genetic relationships
$_{73}Ta^{182m}$	A chem, n-capt (2S47, 15H48a)		IT (15H48a); IT ~95%, β^- ~5% (2W50e)	16.5 m (15H48a); 16.2 m (2S47)	β^-: 0.6 abs (2W50e)	0.180 (K/L 0.25) spect conv (15H48a); 0.180 (e_K/γ 0.8) scint spect (14S51)		Ta-n-γ (2S47, 15H48a, 2W50e)
Ta^{182}	A chem, n-capt (37F36, 17O38)		β^- (76H40)	111 d (21E52, 38S51); 113 d (9S49c); 117 d (2S47, 11Z43)	0.525, other β's, spect (7J49); 0.53 spect (86B49a); others (11R47, 7J47, 24N47)	γ_1 0.065714, γ_2 0.067736, γ_3 0.084667, γ_4 0.10009, γ_5 0.11366, γ_6 0.11640, γ_7 0.15241, γ_8 0.15637, γ_9 0.17936, γ_{10} 0.19831, γ_{11} 0.22205, γ_{12} 0.22927, γ_{13} 0.26409, γ_{14} 1.121, γ_{15} 1.188, γ_{16} 1.223 (rel intens: γ_1 9, γ_2 100, γ_3 6, γ_4 46, γ_5 9, γ_6 2, γ_7 43, γ_8 14, γ_9 19, γ_{10} 9, γ_{11} 45, γ_{12} 24, γ_{13} 27, γ_{14} 352, γ_{15} 157, γ_{16} 334) cryst spect (100M52); 0.046, 0.058, 0.065, 0.067, 0.075, 0.077, 0.084, 0.100, 0.113, 0.134, 0.143, 0.152, 0.178, 0.198, 0.221, 0.228, 0.245, 0.262 spect conv (10C50e); 1.121, 1.189, 1.219 spect, spect conv (10C51e); 0.082, 0.098, 0.112, 0.122, 0.132, 0.141, 0.157, 0.165, 0.172, 0.198, 0.222, 0.243, 0.255, 0.264, 0.290 (?), 0.299 (?), 0.324, 1.133, 1.219, 1.237 spect, spect conv (86B49a); 0.224, 0.232, 0.260, 0.268, 0.280, 0.320, 0.342, 0.362, 0.392, 0.412, 0.421, 0.526, 0.565, 0.607, 0.624, 0.728, 0.763, 0.780, 0.892, 0.935, 0.993, 1.133, 1.215, 1.231 spect (18O50); others (4G49, 11R47, 10C49b, 13E50, 94S50, 98S48, 4B49, 52M51, 52W51)		Ta-n-γ (37F36, 17O38, 76H40, 2S47, 1M48); Ta-d-p (17O38, 11Z43, 31S50); W-d-α, W-n-p (33T51)
Ta^{183}	B chem, excit (65B50)		β^- (2W50f)	5.2 d (65B52c); 6.0 d (83M51); 6.1 d (2W50f)	0.65 scint spect (65B52c); 0.6 abs (2W50f, 83M51)	0.24 scint spect (65B52c); γ (2W50f)		W-n-p (2W50f, 65B52c); W-γ-p (65B50, 83M51)
Ta^{184}	B chem, excit (65B52c)		β^- (65B52c)	9.3 h (65B52c)	1.4 abs (65B52c)	0.410, 0.86, 1.10 scint spect (65B52c)		W-n-p, W^{184}-n-p (65B52c)
Ta^{185}	A chem, excit (65B50); excit, sep isotopes (23D50)		β^- (23D50)	48 m (83M51, 65B50)	1.6, 0.15 (conv?) abs (83M51); 1.7 abs (23D50)			W-γ-p (65B50, 83M51); W^{186}-γ-p (23D50)
$_{74}W^{176}$	B chem, genet (2W50e)		EC 99+%, β^+ ~0.5% (2W50e)	80 m (2W50e)	β^+: ~2 abs (2W50e); conv: ~0.1, ~0.2 abs (2W50e)	~1.3 abs (2W50e)		Ta-p-6n (2W50e, 22N52); parent Ta^{176} (2W50e)
W^{177}	B chem, genet (2W50e)		EC (2W50e)	130 m (2W50e)	conv: 0.13, ~0.4 abs (2W50e)	~0.5, 1.2 abs (2W50e)		Ta-p-5n (2W50e, 22N52); parent Ta^{177} (2W50e)

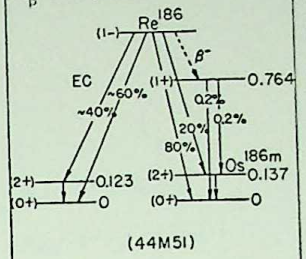
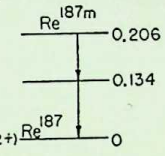
CC-0. In Public Domain. Gurukul Kangri Collection, Haridwar

Digitized by Arya Samaj Foundation Chennai and eGangotri

Isotope Z A	Class and identification	Percent abundance	Type of decay	Half-life	Energy of radiation in Mev: Particles	Energy of radiation in Mev: Gamma-transitions	Disintegration energy and scheme	Method of production and genetic relationships
$_{74}W^{178}$	B chem, genet (2W50e)		EC (2W50e)	21.5 d (2W50e)		~0.3 (weak) abs (2W50e)		Ta-p-4n (2W50e, 22N52); parent 9.4 m Ta^{178} (2W50e)
W^{179}	D chem, excit (2W50e)		EC (2W50e)	30 m (2W50e)				Ta-p-3n (2W50e)
W^{179}	D chem, excit (2W50e)		EC or IT (2W50e)	5.2 m (2W50e)				Ta-p-3n (2W50e)
W^{180}		0.135 (9W46)						
W^{181}	A chem, excit (2W47); chem, n-capt (37L51)		EC (2W47)	140 d (2W47)		0.030, 0.600, 0.800 scint spect (13A50b); 1.8 (weak) abs (2W47)		Ta-d-2n (2W47); Ta-p-n (96B49); W-n-γ (13A50b, 37L51); not parent Ta^{181m3} (38M51c)
W^{182}		26.4 (9W46)					W^{182}, I = 0 (87M50)	
W^{183m}	B sep isotopes, n-capt (38M49)		IT (38M49)	5.5 s (38M49, 24C52a)	conv: 0.08 abs (38M49a)	0.12, 0.17 scint spect (24C52a)		W^{182}-n-γ (38M49); W-n-γ (38M49, 31K51)
W^{183}		14.4 (9W46)					W^{183}, I = 1/2 (87M50)	
W^{184}		30.6 (9W46)					W^{184}, I = 0 (87M50)	
W^{185m}	C excit, sep isotopes (23D50)		IT (23D50)	1.85 m (23D50)	conv: 0.075 scint spect (23D50)			W^{186}-γ-n (23D50)
W^{185}	A chem, excit, n-capt (64M40)		β^- (64M40)	73.2 d (9S48a); 75 d (5F40a)	0.428 spect (68S48); 0.43 spect (20P48, 9S48a); others (23S45a)	0.134 spect conv (10C49); others (23S45a, 65C47a, 4B49, 52M51)		W-n-γ (64M40, 5F40a, 2S47, 10C49); W-n-2n (64M40, 5F40a); W-d-p (5F40a); Re-d-a (5F40a)
W^{186}		28.4 (9W46)					W^{186}, I = 0 (87M50)	
W^{187}	A chem, n-capt (12A35); chem, n-capt, excit (64M40)		β^- (64M40)	24.1 h (5F40a); 24.0 h (64M40)	1.33 (30%), 0.63 (70%) spect (20P48); 1.32 (≥12%), 0.63 (≥65%), ~0.38 (≤23%) spect (2L49); 1.34, ~0.65 spect (15H48b); others (23S45a, 43M46)	0.07200, 0.13425, 0.4795, 0.6189, 0.6861 cryst spect (100M52); γ_1 0.072 (coinc with γ_2, delay coinc with γ_3), γ_2 0.134 (coinc with γ_1, γ_4, and γ_7, delay coinc with γ_3), γ_3 0.480 (ϵ_K/γ 0.022, delay coinc with γ_1 and γ_2, not coinc with γ_4 or γ_6), γ_4 0.552 (coinc with γ_2), γ_5 0.618 (not coinc with other γ's), γ_6 0.69, γ_7 0.775 (coinc with γ_2) ($\gamma_2/\gamma_3/\gamma_4/\gamma_5/\gamma_6/\gamma_7$ = 0.45/1.00/0.31/0.42/1.48/0.23) scint spect (14S52a); 0.133, 0.204, 0.478, 0.615, 0.680, 0.767 spect conv (2L49); 0.129, 0.462, 0.652 spect conv, β-γ, γ-γ coinc (15H48b); 0.078, 0.138 spect conv (86B49b); others (6V41a, 72C42, 20P48, 9J51)	Q_β^- 1.33 (HPS)  (14S52a)	W-n-γ (12A35, 77M35b, 64M40, 5F40a, 2S47, 10C49); W-d-p (5F40a, 20P48); spall U (6O48); parent Re^{187m} (10D48, 4F49, 52M51)
W^{188}	A chem, genet (37L51)		β^- (37L51)	65 d genet (37L51)				W-n-γ (second order reaction) (13A50c, 37L51, 37L51a); parent Re^{188} (37L51, 37L51a)

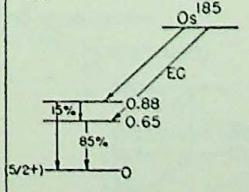
CC-0. In Public Domain. Gurukul Kangri Collection, Haridwar

Digitized by Arya Samaj Foundation Chennai and eGangotri

Isotope Z A	Class and identification	Percent abundance	Type of decay	Half-life	Energy of radiation in Mev: Particles	Energy of radiation in Mev: Gamma-transitions	Disintegration energy and scheme	Method of production and genetic relationships
$_{75}Re^{182}$	B chem, excit (2W50g); chem, sep isotopes (31D50)		EC (2W50g)	12.7 h (2W50g); 14 h (31D50)		0.110, 0.127, 0.222, 0.250, 0.346 spect conv, spect (2W50g)		Ta-α-3n (2W50g); W-p-n (2W50g); W^{182}-d-2n (31D50); daughter Os^{182} (93S50)
Re^{182}	D (182) chem, excit (2W50g); (183) chem, sep isotopes (31D50)		EC (2W50g)	64.0 h (2W50g); 67 h (31D50)		0.110, 0.127, 0.222, 0.250, 0.346 spect conv, spect (2W50g)		Ta-α-3n, W-p-n (2W50g); W^{182}-d (31D50)
Re^{183}	B chem, excit (2W50g)		EC (2W50g)	155 d (33T51); 120 d (93S50)		0.081, 0.252 spect conv (2W50g)		Ta-α-2n, W-p-n (2W50g); W-d-n, W-α-p (33T51); daughter Os^{183} (93S50)
Re^{184}	A chem, excit (5F40a); chem, excit (2W50g)		EC (2W50g)	50 d (2W50g, 33T51)		0.159, 0.206, 0.244, 0.784, 0.89 spect conv (4W52); 0.043, 0.159, 0.205, 0.285 spect, spect conv (2W50g); 1.0 abs (33T51, 29C40)		Ta-α-n (2W50g); W-α-pn (33T51); W-p-n (2W50g); W-d-n (29C40, 5F40a, 33T51); Re-n-2n (2W50g, 5F40a)
Re^{184}	B chem, excit (2W50g)		EC or IT (2W50g)	2.2 d (2W50g)		0.043, 0.159 spect, spect conv (2W50g)		Ta-α-n (2W50g); W-p-n (2W50g)
Re^{185}		37.07 (24W48)					Re^{185}, I = 5/2 (87M50)	
Re^{186}	A n-capt (8K35); n-capt, excit (99S39); chem, n-capt, excit (5F40a); mass spect (43H47)		β^- ~95%, EC ~5%, no β^+ (lim 10^{-5}%) (44M51); β^- ~91%, EC ~9% (82S51a)	92.8 h (24G47); 91 h (10C48); 90 h (99S39)	1.07 (80%), 0.93 (20%) spect (44M51); 1.070 (73%), 0.942 (27%) spect (82S51a); 1.090 (67%), 0.95 (30%), 0.64 (3%) spect (22G49a); 1.063 spect (10L49); 1.07 spect (86B49a)	with β^-: γ_1 0.137 (e_K/γ ~0.35, K/L/M = 0.6/1/0.2), 0.627, 0.764 spect, spect conv, β-γ, γ-γ coinc (44M51); γ_1 0.136 (e_K/γ 0.37, K/L/M = 0.6/1/0.2) spect, spect conv, β-conv, γ-γ coinc (82S51a); with EC: γ_2 0.123 (~2%), γ_1/γ_2 = 9 (44M51); γ_2 0.122 (3%, e_K/γ 0.45, K/L 0.6) (82S51a); others (22G49a, 10C48, 86B49a)	Q_{β^-} 1.07 (44M51)  (44M51)	W-d-2n (5F40a); W-p-n (29C40); Re-γ-n (12P48); Re-n-γ (8K35, 99S39, 5F40a, 8Y40, 2S47); Re-n-2n (99S39, 8Y40, 5F40a); Re-d-p (5F40a, 66C50); spall Re (66C50); parent Os^{186m} (52M51a)
Re^{187m}	A genet (10D48)		IT (10D48)	5.3×10^{-7} s delay coinc (4B49); 5.5×10^{-7} s delay coinc (52M51)		0.133 ($e_K/\gamma \leq 3.2$, K/L ~5) scint spect (52M52b); see γ's of W^{187}	see W^{187}  (14S52a) Re^{187}, I = 5/2 (87M50)	daughter W^{187} (10D48, 4B49, 52M51)
Re^{187}	A chem (25N48)	62.93 (24W48)	β^- (25N48)	4×10^{12} y sp act (25N48, 63S48)	0.400 ion ch (42D52); 0.043 abs (25N48)	no γ, no x (42D52)		natural source (25N48, 63S48)

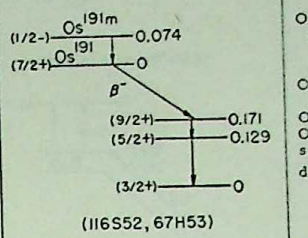
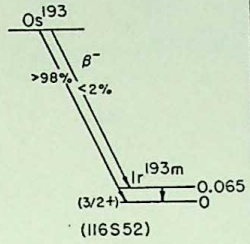
CC-0. In Public Domain. Gurukul Kangri Collection, Haridwar

Digitized by Arya Samaj Foundation Chennai and eGangotri

Isotope Z A	Class and identification	Percent abundance	Type of decay	Half-life	Energy of radiation in Mev: Particles	Energy of radiation in Mev: Gamma-transitions	Disintegration energy and scheme	Method of production and genetic relationships
$_{75}Re^{188m}$	C n-capt, sep isotopes (63M52d, 63M52b)		IT (63M52d)	22 m (63M52d); 17 m (65B50)		0.0635, 0.092, 0.106 spect conv, scint spect (63M52b)		Re^{187}-n-γ (63M52b); Os-γ-p (?) (65B50)
Re^{188}	A chem, n-capt (12A35); n-capt, excit (99S39); chem, n-capt, excit (5F40a); mass spect (43H47)		β^- (99S39)	16.9 h (37L51); 18.9 h (24G47); 18 h (1P37)	2.07 (coinc with 0.152 γ) spect, β-γ coinc (44R52a); 2.10 spect (86B49a); 2.05 abs (24G47); others (26M48b, 99S39)	0.152 (70%, e_K/γ 0.05, K/L 0.42), 0.476 (3%), 0.638 (6%), 0.933 (5%), 1.3 (5%) spect, abs, spect conv (44R52a); 0.15, 0.48, 0.64, 0.95, 1.40 spect (86B49a); 0.16, 0.48, 0.64, 0.94, 1.43 spect (43M46); 1.39 coinc abs (26M48b); 0.154 spect conv (10C48)		Re-n-γ (8K35, 12A35, 1P37, 99S39, 5F40a, 8Y40, 2S47); Re-d-p (5F40a, 24G47, 66C50); spall U (6O48); spall Re (66C50); daughter W^{188} (37L51, 37L51a)
Re^{189}	D chem (37L51, 33T51)		β^- (37L51, 33T51)	150 d (37L51); 250-300 d (33T51)	0.2 abs (37L51, 33T51)	1.0 abs (33T51)		W-α-p (33T51); Re-n-γ (second order reaction) (37L51)
Re	E chem (37L51)		β^- (37L51)	≥5 y (37L51)	0.75 abs (37L51)			Re-n-γ (second order reaction) (?) (37L51)
$_{76}Os^{182}$	B chem, genet (93S50)		EC, no β^+ (93S50)	24.0 h (93S50)				Re-p-4n (93S50); parent Re^{182} (93S50)
Os^{183}	B chem, genet (93S50)		EC (93S50)	12.0 h (93S50)	conv: 0.15, 0.42 spect conv (93S50)	0.3, 1.6 abs (93S50)		Re-p-3n (93S50); parent Re^{183} (93S50)
Os^{184}		0.018 (6N37a)						
Os^{185}	B chem, cross bomb (24G47, 50K48)		EC (L/K ~0.35) (69M51a); no β^+ (2B50b)	97 d (50K48, 33T51); 95 d (24G47)		γ_1 0.648, γ_2 0.878 (γ_1/γ_2 ~6) spect, γ-γ coinc (2B50b); γ_1 0.65, γ_2 0.88 (γ_1/γ_2 6.1) scint spect (69M51b); 0.235, 0.653 spect conv (11GS52)	Q_{EC} ~1.0 calc (69M51a)  (2B50b, 69M51b, HPS)	Re-d-2n (24G47, 66C50); Re-p-n (93S50); Os-n-γ (50K48)
Os^{186m}	A genet (52M51a)		IT (52M51a)	8×10^{-10} s delay coinc (52M51a)		0.137 scint spect (52M51a)	see Re^{186}	daughter Re^{186} (52M51a)
Os^{186}		1.59 (6N37a)						
$Os^{187m(?)}$	E chem (66C50)			35 h (66C50)				daughter Ir^{187} (?) (66C50)
Os^{187}		1.64 (6N37a)						
Os^{188}		13.3 (6N37a)						

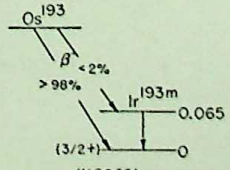
CC-0. In Public Domain. Gurukul Kangri Collection, Haridwar

Digitized by Arya Samaj Foundation Chennai and eGangotri

Isotope Z A	Class and identification	Percent abundance	Type of decay	Half-life	Energy of radiation in Mev: Particles	Energy of radiation in Mev: Gamma-transitions	Disintegration energy and scheme	Method of production and genetic relationships
$_{76}Os^{189}$		16.1 (6N37a)					Os^{189}, I = 1/2 (87M50)	
$Os^{190m(?)}$	E chem (66C50)			6 h (66C50)				daughter 12 d Ir^{190} (?) (66C50)
Os^{190m}	D chem, genet (66C50)			9.5 m (66C50)				daughter 3 h Ir^{190} (66C50)
Os^{190}		26.4 (6N37a)						
Os^{191m}	A chem, genet (116S52)		IT, no β^- (lim 5%) (116S52)	14 h (116S52)		0.0742 ($L_I/L_{II}/L_{III}$ = 42/24/100) spect conv (116S52)	 (116S52, 67H53)	Os-n-γ, Os-γ-n, parent Os^{191} (116S52)
Os^{191}	A n-capt (12Z40); chem, n-capt (13S41b); chem, excit (23F48a, 116S52)		β^- (13S41b)	16.0 d (66C50); 16.1 d (9S48a); 15.0 d (50K48)	0.143 spect (38K51b); 0.142 spect (9S48a); others (50K48, 13S41b, 37W47, 26M48b, 2B50b)	γ_1 0.0417 (L_{II}/L_{III} = 32/40, e/γ large), γ_2 0.129 (coinc with γ_1, $K/L_I/L_{II}/L_{III}$ = 100/30/11/6) spect conv, conv-conv coinc (116S52); γ_1 (e_K/γ 1.36) (116S52, calc from 38K51b); 0.042 (L/M 1.8), 0.128 (e_K/γ ~0.5, K/L 2.1) spect conv (38K51b, 38K51c); 0.041, 0.128 spect conv, spect (2B50b); 0.039, 0.127 spect conv (9S48a); 0.129 spect conv (10C47)	Q^-_β 0.313 (38K51b)	Os-n-γ (13S41b, 12Z40, 2S47, 116S52); Os-d-p (66C50); Os-γ-n (23F48a, 116S52); spall U (6O48); daughter Os^{191m} (116S52)
Os^{192}		41.0 (6N37a)						
Os^{193}	A n-capt (8K35, 12Z40); chem, n-capt (13S41b); chem, excit (23F48a, 116S52)		β^- (13S41b)	30.6 h (66C50); 31.9 h (24G47); 32 h (13S41b); 30 h (12Z40)	1.10 spect (2B50b); 1.05 scint spect (52M50b); 1.15 abs (66C50, 26M48b)	with Ir^{193m}: 0.066 spect conv (116S52); 0.065 scint spect, β-γ delay coinc (52M50b); no γ (2B50b); others (24G47, 26M48b)	Q^-_β 1.17 (HPS)  (116S52)	Os-n-γ (8K35, 12Z40, 13S41b, 2S47); Os-d-p (24G47, 66C50); Ir-d-2p (24G47); spall U (6F51); parent Ir^{193m} (52M50b, 52M51); not found: Os-γ-n (23F48a, 116S52)
Os^{194}	A chem, genet (37L50a)		[β^-] (37L50a)	~700 d (37L51)				Os-n-γ (second order reaction) (37L50a, 37L51); parent Ir^{194} (37L50a, 37L51)
$_{77}Ir^{187}$	B chem, excit, sep isotopes (66C50)		EC 99+%, β^+ ~0.2% (66C50)	11.8 h (66C50)	β^+: 2.2 spect (66C50); conv: 0.3, 1.2 spect conv (66C50)	~1.3 abs (66C50)		Re-α-2n, Re^{185}-α-2n (66C50); Os-d-3n (66C50); parent Os^{187m} (?) (66C50)
Ir^{188}	B chem, excit, sep isotopes (66C50)		EC 99+%, β^+ ~0.3% (66C50)	41.5 h (66C50)	β^+: 2.0 spect (66C50); conv: 0.2, 0.9 spect conv (66C50)	~1.8 abs (66C50)		Re-α-n, Re-α-3n, Re^{187}-α-3n (66C50); Os-d-2n, Os-d-3n (66C50)

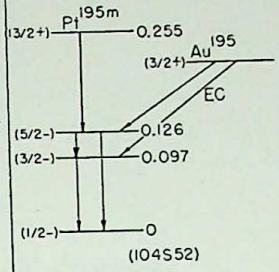
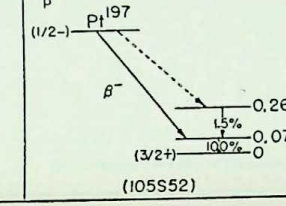
CC-0. In Public Domain. Gurukul Kangri Collection, Haridwar

Digitized by Arya Samaj Foundation Chennai and eGangotri

Isotope Z A	Class and identification	Percent abundance	Type of decay	Half-life	Energy of radiation in Mev: Particles	Energy of radiation in Mev: Gamma-transitions	Disintegration energy and scheme	Method of production and genetic relationships
$_{77}Ir^{190}$	D chem, excit, sep isotopes (66C50)		β^+, EC (?) (66C50)	3.2 h (66C50)	β^+: 1.7 spect (66C50); conv: 0.2, 0.8 spect conv (66C50)			Re-a-n, Re^{187}-a-n (66C50); Os-d-n, Os-d-2n (66C50); parent 9.5 m Os^{190m} (66C50)
Ir^{190}	B chem, excit (24G47); chem, excit, sep isotopes (66C50)		EC (24G47)	12.6 d (66C50); 10.7 d (24G47)		0.2, 0.6 abs (66C50); 0.3 abs (24G47)		Re-a-n, Re^{187}-a-n (66C50); Os-d-n (24G47, 66C50); Ir-n-2n (24G47); parent 6 h Os^{190m} (?) (66C50)
Ir^{191}		38.5 (37S36a)					Ir^{191}, I = 3/2 (99B50); Ir^{191}, I = 1/2 (94B49)	
Ir^{192m}	A n-capt (12M37); resonance neutron activation (18G47a)		IT (18G47a)	1.42 m (15H48a); 1.5 m (12M37)		0.057 spect conv (42C50); 0.056 spect conv (15H48a); γ (continuum) scint spect (38M51); γ (e_L/γ >400) ion ch (31K51)		Ir-n-γ (12M37, 18G47a, 2S47)
Ir^{192}	A n-capt (12A36); mass spect (37R46); chem (2W48a)		EC, β^- (10C51f); no β^+ (lim 0.008%) (41M51)	74.37 d (51K51); 74.5 d (38S51); 74.7 d (66C50)	0.66 spect (88S51a); 0.67 spect (2L47); 0.68 coinc abs (37W47); 0.6 abs (26M48a, 24G47)	γ_1 0.13633, γ_2 0.20131, γ_3 0.20574, γ_4 0.29594, γ_5 0.30845, γ_6 0.31646, γ_7 0.46798, γ_8 0.4848, γ_9 0.5884, γ_{10} 0.6045, γ_{11} 0.6129 (rel abund γ_1 4, γ_2 10, γ_3 75, γ_4 380, γ_5 370, γ_6 990, γ_7 300, γ_8 11, γ_9 11, γ_{10} 14, γ_{11} 5) cryst spect (100M52); 0.136, 0.151 (or 0.156), 0.169 (or 0.173), 0.201, 0.206, 0.283, 0.295, 0.308, 0.316, 0.396 (or 0.400), 0.415, 0.434 (or 0.438), 0.467, 0.484, 0.589, 0.604, 0.611 spect conv (10C51f); 0.775, 0.870 scint spect (50R52); others (103S51, 2L47, 20D50, 4B49, 67H48b, 52W51, 98S48, 56G49, 88S51a, 52M51)	Q^-_β 1.58 (50R52)	Os-d-2n (24G47, 66C50); Ir-n-γ (12A36, 12M37, 24J38, 2S47); Ir-n-2n (24G47); Ir-d-p (24G47, 2W48a); Pt-d-a (2W48a); Pt-γ-pn (25C52)
Ir^{193m}	B genet (52M50b)		IT (52M50b)	5.7×10^{-9} s delay coinc (52M50b)		0.065 scint spect, β-γ delay coinc (52M50b)	 (116S52)	daughter Os^{193} (52M50b, 52M51)
Ir^{193}		61.5 (37S36a)					Ir^{193}, I = 3/2 (99B50, 94B49)	
Ir^{194}	A n-capt (12A35); mass spect (37R46); chem (2W48a)		β^- (12M37)	19.0 h (24G47); 19.5 h (53W41); 19 h (12A35, 12M37)	2.18 spect (53W41); 2.2 spect (24A36); 2.1 abs (53W41, 24G47); 0.5 β-γ coinc abs (26M48a)	γ_1 0.290, γ_2 0.326, γ_3 1.51 ($\gamma_1/\gamma_2/\gamma_3$ = 1/5/1) spect (89B52); 0.328 spect conv (10C51f); 1.7-2.2 (0.14%) Be, D-γ-n reaction (23W50); others (4B49, 26M48a, 42C50, 37L51)		Ir-n-γ (12A35, 1P37, 2S47, 12M37, 24J38); Ir-d-p (24G47, 2W48a); Pt-γ-p, Pt-γ-pn (25C52)
Ir^{195}	D chem, excit (25C52)		β^- (25C52)	140 m (25C52, 65B52b)	1.8 abs (65B52b); ~1 abs (25C52)	0.49, 0.84 scint spect (65B52b)		Pt-γ-p (25C52); Pt-n-p (65B52b)
Ir^{196}	D chem, excit (65B52b)		β^- (65B52b)	9 d (65B52b)	~0.08 abs (65B52b)	γ (65B52b)		Pt-n-p (65B52b)

CC-0. In Public Domain. Gurukul Kangri Collection, Haridwar

Digitized by Arya Samaj Foundation Chennai and eGangotri

Isotope Z A	Class and identification	Percent abundance	Type of decay	Half-life	Energy of radiation in Mev: Particles	Energy of radiation in Mev: Gamma-transitions	Disintegration energy and scheme	Method of production and genetic relationships
$_{77}Ir^{197}$	D chem, excit (25C52, 65B52b)		β^- (65B52b)	7 m (25C52, 65B52b)	1.65, 0.6 abs (65B52b)	γ (65B52b)		Pt-γ-p (25C52); Pt-n-pn (65B52b)
Ir^{198}	E excit (65B52b)		β^- (65B52b)	45 s (65B52b)	3.6 abs (65B52b)	0.78 scint spect (65B52b)		Pt-n-p (65B52b)
$_{78}Pt^{190}$		0.012 (28L49a)						
Pt^{191}	B chem, excit (2W48a, 90M52)		EC (2W48a)	3.00 d (2W49c, 90M52)		0.083, 0.096, 0.173 spect (116S52a); 0.6, 1.5 abs, abs conv (2W49c)		Ir-d-2n (2W48a, 2W49c); Pt-n-2n (2W48a, 2W49c); daughter Au^{191} (2W48a, 2W49c, 90M52)
Pt^{192}		0.78 (3I47g)						
Pt^{193m}	B chem, excit (2W48a, 90M52)		IT (116S52a); EC (2W48a)	4.33 d (2W49c); 4.6 d (90M52)		0.135 (K/L 0.28, $L_I/L_{II}/L_{III}$ 1/0/2) spect conv (116S52a); 0.2, 1.5 abs (2W49c)		Ir-d-2n (2W49c); Pt-n-γ, Pt-n-2n, Pt-d-p (2W49c); Pt-γ-n (116S52a); daughter Au^{193} (2W49c, 90M52)
Pt^{194}		32.8 (3I47g)					Pt^{194}, I = 0 (87M50)	
Pt^{195m}	B chem (12M37); chem, genet (104S52)		IT (104S52)	3.5 d (15H48a); 3.8 d (104S52); 4.4 d (79H52); 3.3 d (12M37)		0.029 (e/γ >7.5), 0.097 (e/γ 9.0, K/L 5.7), 0.126, 0.129 (e/γ very large, K/L 0.26) spect, spect conv, γ-conv coinc (104S52); 0.099, 0.130 (K/L 0.1) spect conv (10C52a); 0.126 (K/L 0.23) spect conv (15H48a)	 (104S52)	Pt-n-γ (26M48e, 79H52, 104S52, 12M37, 1P37, 2S47, 34H51); Pt-d-p (9K41b); Pt-γ-n (25C52); daughter Au^{195} (180 d) (104S52)
Pt^{195}		33.7 (3I47g)					Pt^{195}, I = 1/2 (87M50)	
Pt^{196}		25.4 (3I47g)					Pt^{196}, I = 0 (87M50)	
Pt^{197m}	B chem (28S41); chem, excit, cross bomb (25C52)		IT (15H48a)	78 m (15H48a); 80 m (28S41); 88 m (25C52)		0.337 (e/γ very large, K/L 1.3) spect conv (15H48a)		Pt-d-p (28S41); Pt-n-2n (28S41); Pt-γ-n (60M48, 25C52); Hg-n-α (28S41); Au-n-p (?) (2W50f)
Pt^{197}	A chem (10C36); chem, excit (12M37)		β^- (12M37)	18 h (12M37); 17.4 h (10C52a)	0.670 spect (105S52, 34H51); 0.7 abs (9K41b, 28S41)	0.077, 0.191 (K/L 6.0) spect conv (10C52a); 0.077, 0.191 spect, spect conv (105S52); others (4B49)	see Au^{197m}, Hg^{197} Q^-_β 0.75 (105S52)  (105S52)	Pt-n-γ (12M37, 28S41, 2S47, 79H52); Pt-d-p (10C36, 9K41b, 28S41, 9K42, 2W48a); Pt-γ-n (25C52, 25W48); Pt-n-2n (28S41); Hg-n-α (28S41)

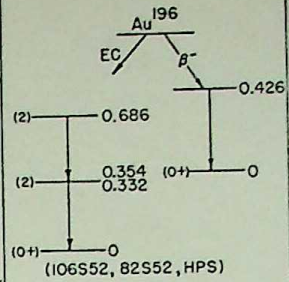
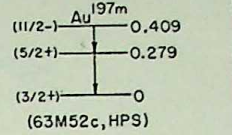
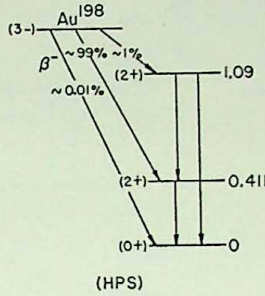
CC-0. In Public Domain. Gurukul Kangri Collection, Haridwar

Digitized by Arya Samaj Foundation Chennai and eGangotri

Isotope Z A	Class and identification	Percent abundance	Type of decay	Half-life	Energy of radiation in Mev: Particles	Energy of radiation in Mev: Gamma-transitions	Disintegration energy and scheme	Method of production and genetic relationships
$_{78}Pt^{198}$		7.23 (3I47g)						
Pt^{199}	A n-capt (77M35b, 12A35); chem, n-capt, excit (28S41)		β^- (12M37)	31 m (12M37)	1.8 abs (9K41b, 28S41)			Pt-n-γ (12A35, 77M35b, 12M37, 28S41, 2S47, 50H51); Pt-d-p (28S41, 9K41b, 10C36); Hg-n-α (28S41)
Pt	F n-capt (10C50g)		β^- (10C50g)	82 d (10C50g)	0.5 abs (10C50g)	0.6 abs (10C50g)		Pt-n-γ (10C50g)
$_{79}Au^{183-187}$	D chem, excit (3T49)		EC, β^+, α ~0.01% (3T49)	4.3 m (42R52)	α: 5.07 ion ch (42R52)			spall Pt (42R52), Au (3T49, 42R52)
Au^{191}	B chem, genet (2W49c, 90M52)		EC (2W49c)	18 h (90M52); ~1 d (2W49c)		0.053, 0.064, 0.111, 0.123, 0.166, 0.250, 0.405 spect conv (90M52)		Ir-α-4n (2W49c); Pt-d-3n (2W49c); parent Pt^{191} (2W48a, 2W49c, 90M52); daughter Hg^{191} (90M52)
Au^{192}	B chem, excit (2W49c); chem, genet (42T52, 33F52)		EC, β^+ (2W49c)	5.0 h (42T52); 4.7 h (2W49c); 4.1 h (33F52)	β^+: ~1.9 abs (2W49c); conv: ~0.4 abs (2W49c)	2-3 abs (2W49c)		Ir-α-3n (2W49c); Pt-d-2n (2W49c); daughter Hg^{192} (33F52, 42T52)
Au^{193}	B chem, genet (2W49c, 90M52)		EC (2W49c)	15.8 h (2W49c, 90M52); 15.3 h (33F52)		0.051, 0.060, 0.084, 0.093, 0.109, 0.165, 0.177, 0.235 spect conv (90M52)		Ir-α-2n (2W49c); Pt-d-n, Pt-d-3n (2W49c); parent Pt^{193} (2W49c, 90M52); daughter Hg^{193} (33F52, 90M52)
Au^{194}	B chem, excit (2W49c)		EC ~97%, β^+ ~3% (2W49c)	39.5 h (2W49c); 39 h (82S49)	1.8 abs (2W49c)	0.291 (e/γ 0.054, K/L 2), 0.328 (e/γ 0.19, K/L 2), 0.466 (weak), 1.48 (e/γ 0.0026), 2.1 spect, spect conv (82S49)		Ir-α-3n (2W49c); Pt-d-2n, Pt-d-3n (2W49c); Pt-p-n (82S49)
Au^{195m}	B chem, genet (34H52a)		IT (34H52a)	0.5 m (34H52a)		0.056, 0.259 spect conv (34H52a)		daughter Hg^{195m} (34H52a)
Au^{195}	B chem, excit (2W49c); chem, genet (30D52)		EC (2W49c)	180 d (82S49, 30D52); 185 d (2W49c)		0.0308, 0.0990, 0.130 spect conv (30D52); 0.029 (L/M 4.6), 0.097 (K/L 5.8), 0.126 spect, spect conv, γ-conv coinc (104S52); others (34H51, 82S49)	see Pt^{195m}	Ir-α-2n (2W49c); Pt-d-n, Pt-d-2n, Pt-d-3n (2W49c); Pt-p-n (82S49); daughter Hg^{195m} (30D52)

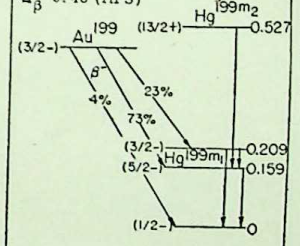
CC-0. In Public Domain. Gurukul Kangri Collection, Haridwar

Digitized by Arya Samaj Foundation Chennai and eGangotri

Isotope Z A	Class and identification	Percent abundance	Type of decay	Half-life	Energy of radiation in Mev: Particles	Energy of radiation in Mev: Gamma-transitions	Disintegration energy and scheme	Method of production and genetic relationships
$_{79}Au^{196}$	B chem, excit (12M37)		EC or IT (2W49c)	14.0 h (2W49c); 13 h (12M37)				Au-n-2n (12M37, 2W49c); spall U (?) (6F51)
Au^{196}	A chem, excit (12M37)		EC ~95%, β^- ~5% (82S49); EC ~80%, β^- ~20% (2W49c)	5.55 d (2W49c); 5.60 d (82S49)	β^-: 0.27 spect (106S52); 0.30 spect (82S49); 0.34 abs (2W49c)	with EC: 0.332, 0.354 spect conv (106S52); 0.330 (K/L 1.7), 0.358 (K/L 1.7) spect conv (82S49); with β^-: 0.426 (e_L/γ 0.007, L/M+N 3.5), no 0.175 γ spect conv, β-conv coinc (106S52); 0.175 spect conv (82S49)	 (106S52, 82S52, HPS)	Pt-d-n (9K41b, 2W49c, 106S52); Pt-p-n (82S49); Au-n-2n (12M37, 2W49c); Au-γ-n (25W48); spall U (?) (6F51)
Au^{197m}	A excit (37W45a)		IT (37W45a)	7.4 s (40F47); 7.5 s (37W45a)		0.130 ($e_K/\gamma \leq 2.0$, K/L/M = 1/7.5/3.6), 0.279 (e_K/γ ~0.3) spect conv (63M52c); 0.273 spect conv, conv-conv coinc (34H48a); 0.275 scint spect (24C52); 0.25 abs conv (37W45a)	 (63M52c, HPS)	Au-γ-γ (37W45a); Au-n-n (37W45a, 40F47); daughter 25 h Hg^{197} (40F47)
Au^{197}		100 (1D35a)					Au^{197}, I = 3/2 (87M50)	
Au^{198}	A chem, n-capt (12A35, 12M37)		β^- (12M37); no EC (lim 0.2%) (38M52); no EC (lim 0.4%) (25R49); no β^+ (lim 0.003%) (41M51)	2.69 d (57S49, 9S49b); 2.73 d (38S51, 33D46); 2.66 d (69C51)	β_1 0.963 spect (average of 9S48, 2L49a, 10L49, 82S49, 107S49, 4E51); β_2 0.290 (coinc with 0.680 γ) β-γ coinc spect (48B51a); β_3 1.37 (0.01%) spect (4E51)	γ_1 0.41177 cryst spect (100M52, 34D48); γ_1 0.4116 spect (29L51); γ_1 (e_K/γ 0.031, K/L 3.1, L/M 3.3) spect conv (50S52); γ_1 (e_K/γ 0.03, K/L 3, L/M 3.3) spect, spect conv (7S49e); γ_1 (e_K/γ 0.029, K/L 2.1, L/M 4.3) spect conv (82S49); γ_1 (e_K/γ 0.026, K/L 2.2, L/M 4) spect conv (107S49); γ_1 (e_K/γ 0.03, K/L+M 2.3) spect conv (29F52); γ_1 (L_{II}/L_{III} 2.5) spect conv (63M52a); γ_2 0.676 (0.5%, e_K/γ 0.034, K/L 5.7), γ_3 1.088 (0.1%, e_K/γ 0.005, K/L 6.3) spect, spect conv (4E51, 4E51a, 6W52); γ_2 0.680 (1%, coinc with 0.411 γ and 0.29 β^-), γ_3 1.09 (~0.2%) scint spect, β-γ coinc (48B51a); γ_2 0.673 (1.4%), γ_3 1.08 (0.3%) spect (57H51b); γ_2 0.67 (1.4%, coinc with 0.411 γ), γ_3 1.09 (0.3%) scint spect, γ-γ coinc (69C51a, 69C51); others (18P50a, 2L48, 2L49a, 9S49b, 31A50a, 12H50, 38T49, 4F44, 72C42, 7S47g, 15J48, 25R48, 52M51)	Q_β^- 1.374 (HPS)  (HPS)	Au-n-γ (12A35, 12M37, 1P37, 16D41, 2S47, 50H51); Au-d-p (9K41c); Hg-n-p (28S41); Pt-p-n (82S49, 82S48); spall U (6O48)

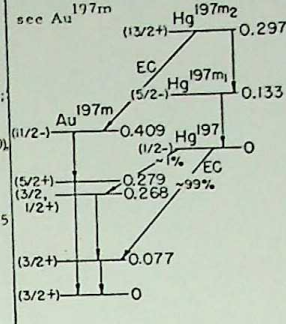
CC-0. In Public Domain. Gurukul Kangri Collection, Haridwar

Digitized by Arya Samaj Foundation Chennai and eGangotri

Isotope Z A	Class and identification	Percent abundance	Type of decay	Half-life	Energy of radiation in Mev: Particles	Energy of radiation in Mev: Gamma-transitions	Disintegration energy and scheme	Method of production and genetic relationships
$_{79}Au^{199}$	A chem, genet (12M37)		β^- (9K41b)	3.15 d (8B52b); 3.2 d (104S52); 3.3 d (12M37)	0.460, 0.297 (coinc with 0.158 γ), 0.250 (coinc with 0.207 γ) β-γ spect coinc (8B52a); ~0.47 β^- (not coinc with γ) β-γ coinc (1I53); 0.47 (~4%), 0.30, 0.25 spect (108S51); 0.443 (~7%), 0.291 spect (104S52); 0.32 spect (86B49a); abs (37M49); others (26M48e, 9K41b)	γ_1 0.050 (e_L/γ 6), γ_2 0.159 (e_K/γ 0.19, K/L 0.6), γ_3 0.209 (e_K/γ 0.54, K/L 5.4) ($\gamma_1/\gamma_2/\gamma_3$ = 0.84/100/23.8) spect, spect conv, γ-γ coinc (108S51); γ_1 (coinc with γ_2), γ_3 (not coinc with γ_1 or γ_2) scint spect, γ-γ coinc (1I53); 0.050, 0.158 (e_K/γ 0.24, K/L 0.73, L/M 3.3), 0.208 (e_K/γ 0.62, K/L ~5.6, L/M ~4) spect, spect conv, scint spect, γ-γ, β-γ coinc (7S51); 0.0498, 0.159 (K/L 0.56, L/M 3.6), 0.208 (K/L 4.5) spect conv (10C52a); others (104S52, 86B49a, 37M49, 26M48e, 67H50, 67H50a, 63M52a, 4B49, 34H51, 10C50g)	see Tl^{199}, Hg^{199} Q^-_β 0.46 (HPS)  (108S51, 104S52, 18G52)	Pt-d-n (9K41b); Au-n-γ (second order reaction) (67H50a); Hg-n-p (28S41); daughter Pt^{199} (12M37, 86B49a, 37M49, 67H50); parent Hg^{199m1} (14G51a, 8B52a)
Au^{200}	B chem (28S41); chem, sep isotopes, excit (65B52a)		β^- (28S41)	48 m (65B52a, 28S41)	2.2 abs (65B52a); ~2.5 abs (28S41)	1.13, 0.39 scint spect (65B52a)		Hg-n-p (28S41, 3M42); Hg^{201}-γ-p (65B52a); Tl-n-α (3M42)
Au^{201}	B chem, excit, sep isotopes (65B50, 65B52a)		β^- (65B52a)	26 m (65B52a)	1.5 abs (65B52a)	0.55 scint spect (65B52a)		Hg-γ-p (65B50); Hg^{202}-γ-p (65B52a)
$Au^{202,204}$	E excit (65B52a)		β^- or IT (65B52a)	25 s (65B52a)				Hg-n-p (65B52a)
Au^{203}	B chem, excit, sep isotopes (65B52a)		β^- (65B52a)	55 s (65B52a)	1.9 abs (65B52a)	0.69 scint spect (65B52a)		Hg-n-pn (65B52a); Hg^{204}-γ-p (65B52a)
$_{80}Hg^{<195}$	E chem (3T49)		α (3T49)	0.7 m (42R52)	α: 5.60 ion ch (42R52)			spall Au (3T49)
Hg^{189}	D chem, excit (42T52)			30 m (42T52)				spall Au (42T52)
Hg^{190}	D chem, excit (42T52)			90 m (42T52)				spall Au (42T52)
Hg^{191}	D chem, excit (90M52)		EC (90M52)	12.4 h (90M52)				spall Au, parent Au^{191} (90M52)
Hg^{192}	D chem, excit (33F52, 90M52)		EC (90M52); β^+ (33F52)	5.7 h (33F52); 8.4 h (90M52)	1.18 spect (33F52)	1.4 abs (33F52)		spall Au (90M52, 33F52); parent Au^{192} (33F52, 42T52)
Hg^{193}	B chem, excit (33F52, 90M52)		EC (33F52)	10.0 h (33F52); 14.5 h (?), 29.0 h (?) (90M52)				Au-p-5n (33F52, 90M52); parent Au^{193} (33F52, 90M52)

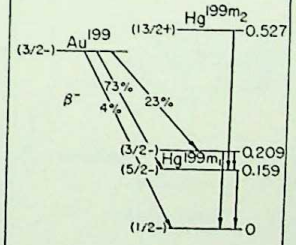
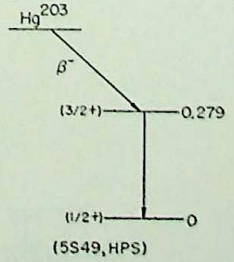
CC-0. In Public Domain. Gurukul Kangri Collection, Haridwar

Digitized by Arya Samaj Foundation Chennai and eGangotri

Isotope Z A	Class and identification	Percent abundance	Type of decay	Half-life	Energy of radiation in Mev: Particles	Energy of radiation in Mev: Gamma-transitions	Disintegration energy and scheme	Method of production and genetic relationships
$_{80}Hg^{195m}$	B chem, excit (30D52, 33F52)		EC, IT (30D52)	38 h (30D52); ~31 h (33F52); 40 h (34H52a)		0.036, 0.056 (coinc with Au^{195m}), 0.122, 0.259 (coinc with Au^{195m}) spect conv (34H52a); 0.037, 0.056, 0.122 (conv in Hg), 0.206, 0.261, 0.318, 0.558 spect conv (30D52)		Au-d-4n (34H52a); Au-p-3n (30D52, 33F52); parent Au^{195} (30D52); parent Au^{195m} (34H52a)
Hg^{195}	B chem, excit (30D52)		EC (30D52)	9.5 h (30D52, 34H52a)		0.061, 0.179, 0.600, 0.780 spect conv (90M52); 0.061, 0.179 spect conv (34H52a)		Au-p-3n (30D52)
Hg^{196}		0.146 (6N50a)						
Hg^{197m_2}	A n-capt (17A36a); chem (12M37); chem, excit, cross bomb (16W41, 23F43)		IT 97%, EC 3% (104S52)	23 h (23F43, 34H51); 25 h (12M37)		with IT: 0.133 (e_K/γ 0.5, K/L/M+N = 1.0/2.4/0.8), 0.164 (e_K/γ 4.6, K/L/M+N = 1.0/2.3/1.2) spect conv, γ-γ coinc (40F50, 34H51); 0.134 (K/L <0.1), 0.165 (K/L ~0.25) spect conv (10C52b); 0.134 ($L_I/L_{II}/L_{III}$ = 0.05/1.1/1.0), 0.165 ($L_I/L_{II}/L_{III}$ = 1.0/<0.1/1.5) spect conv (63M52c); with EC: 0.191 (e_K/γ ~1.7, K/L ~6), 0.275 (weak, e_K/γ ~0.5, K/L ~5) spect conv, γ-γ coinc (40F50, 34H51); others (2H42a, 6V41b, 34H48a, 40F47, 40F50a)	see Au^{197m}  (63M52c, 104S52, HPS)	Pt-α-n (28S41); Au-d-2n (16W41, 9K41c, 23F43); Hg-n-2n (12M37, 23F43, 16W41); Hg-n-γ (17A36a, 16W41, 23F43); Hg-d-p (9K40); parent (3%) Au^{197m} (40F50, 104S52); parent Hg^{197m_1} (20D50, 52M50c)
Hg^{197m_1}	A genet (52M50c, 20D50)		IT (52M50c, 20D50)	7.0×10^{-9} s delay coinc (52M50c); 8×10^{-9} s delay coinc (20D50)		0.13 scint spect (20D50)		daughter Hg^{197m_2} (20D50, 52M50c)
Hg^{197}	A chem, excit, cross bomb (16W41, 23F43)		EC (23F43)	65 h (34H51); 66 h (10C52b); 64 h (23F43)		0.077 (e_L/γ 2.5, L/M 3.6), 0.191 (e_K/γ ~1.7, K/L ~6) spect conv, γ-γ coinc (34H51, 40F50); 0.077 ($L_I/L_{II}/L_{III}$ = 1.0/0.45/0.34) spect conv (63M52c); 0.078 (L_I/M 4), 0.191 (K/L ~9) spect conv (10C52b); 0.077, 0.278 spect conv (30D52); others (2H42a, 40F47, 34H48a)		Au-d-2n (23F43, 16W41); Hg-n-2n (23F43, 16W41); Hg-n-γ (23F43, 16W41)
Hg^{198}		10.02 (6N50a)					Hg^{198}, I = 0 (87M50)	

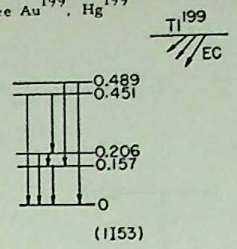
CC-0. In Public Domain. Gurukul Kangri Collection, Haridwar

Digitized by Arya Samaj Foundation Chennai and eGangotri

Isotope Z A	Class and identification	Percent abundance	Type of decay	Half-life	Energy of radiation in Mev: Particles	Energy of radiation in Mev: Gamma-transitions	Disintegration energy and scheme	Method of production and genetic relationships
$_{80}Hg^{199m_2}$	A chem, excit (6H37, 12M37); mass spect (67B49b)		IT (23F43)	44 m (15H47a, 60M48); 43 m (12M37, 6H37)		0.155 (e/γ 0.25, K/L <0.4), 0.368 (e/γ >11, K/L 1.6) spect conv (15H48a); 0.159 (L_{II}/L_{III} 1.6) spect conv (63M52a); 0.16 γ (coinc with 0.37 γ) scint spect, γ-γ coinc (11I53); others (15H47a, 37M49)	see Au^{199}, Tl^{199}  (108S51, 104S52, 18G52)	Pt-α-n (28S41); Hg-n-2n (12M37, 1P37, 6H37, 67B49b); Hg-n-n (23F43, 16W41, 67B49b); Hg-d-p (9K40); Hg-γ-n (60M48, 37W45a); Hg-γ-γ (16W41)
Hg^{199m_1}	A genet (14G51a)		IT (14G51a)	2.4×10^{-9} s delay coinc (8B52a)		0.158 spect conv, β-γ coinc (14G51a, 8B52a)		daughter Au^{199} (14G51a, 8B52a)
Hg^{199}		16.84 (6N50a)					Hg^{199}, I = 1/2 (87M50)	
Hg^{200}		23.13 (6N50a)					Hg^{200}, I = 0 (87M50)	
Hg^{201}		13.22 (6N50a)					Hg^{201}, I = 3/2 (87M50)	
Hg^{202}		29.80 (6N50a)					Hg^{202}, I = 0 (87M50)	
Hg^{203}	A excit (9K40); chem, excit, n-capt (16W41, 23F43); mass spect (5S49a, 67B49a)		β⁻ (23F43)	47.9 d (10C52b); 45.9 d (33W51a); 46.5 d (35L51a); 43.5 d (9S48b)	0.208 β-γ coinc spect (5S49, 5S49a); 0.210 spect (33W51a); 0.205 spect (9S48b); others (37W47)	0.279 (e/γ 0.27, K/L 3) spect, spect conv, β-γ coinc (5S49, 5S49a, 12H50); 0.278 (e_K/γ 0.19, K/L+M 3.7) spect, spect conv (33W51a); ~0.28 (e_K/γ 0.23) scint spect (80H52); 0.279 (K/L ~10) spect conv (10C52b); 0.286 (e/γ 0.3, K/L 3) spect conv (9S48b); others (43M46, 11B50, 4B49, 100B50, 20D50, 52M51)	Q^-_β 0.487 (5S49, 5S49a) see Pb^{203}  (5S49, HPS)	Hg-n-γ (23F43, 16W41, 31I7b, 2S47); Hg-n-2n (16W41, 28S41, 23F43); Hg-d-p (9K40); Hg^{202}-n-γ (35L51a); Tl-n-p (3M42)
Hg^{204}		6.85 (6N50a)					Hg^{204}, I = 0 (87M50)	
Hg^{205}	A n-capt, excit (9K40, 9K42); sep isotopes, n-capt (35L51a)		β⁻ (9K40)	5.5 m (3M42, 9K40); 5.6 m (35L51a)	1.8 abs (35L51a); 1.6 abs (9K40)			Hg-d-p (9K40, 9K42); Hg-n-γ (23F43, 16W41, 2S47); Hg^{204}-n-γ (35L51a); Tl-n-p (3M42); Pb-n-α (3M42)

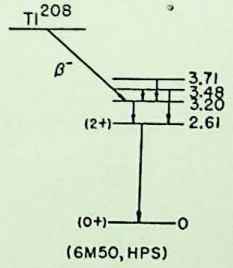
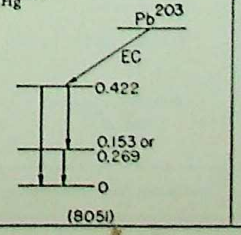
CC-0. In Public Domain. Gurukul Kangri Collection, Haridwar

Digitized by Arya Samaj Foundation Chennai and eGangotri

Isotope Z A	Class and identification	Percent abundance	Type of decay	Half-life	Energy of radiation in Mev: Particles	Energy of radiation in Mev: Gamma-transitions	Disintegration energy and scheme	Method of production and genetic relationships
81 Tl^{198}	B chem, excit (7O49)		EC (7O49)	1.8 h (7O49)	conv: ~0.4 abs (7O49)	several γ's, abs (7O49)		Au-α-3n (7O49); daughter Pb^{198} (4N50)
Tl^{199}	A chem (9K40); chem, excit (7O49); genet (energy levels Hg^{199}) (1I53)		EC (7O49); no β^+ (1I51)	7 h (7O49)		0.049, 0.078, 0.103, 0.157, 0.206, 0.245, 0.332, 0.454, 0.490 spect conv, γ-γ coinc (1I51, 1I53)	see Au^{199}, Hg^{199}  (1I53)	Au-α-2n (7O49, 1I51); Hg-d-2n (9K40); daughter Pb^{199} (4N50)
Tl^{200}	A chem, excit (7O49)		EC (7O49); no β^+ (1I51)	27 h (7O49)		0.365, 0.577, 0.622, 0.829, 1.210, 1.360 spect conv (1I51); ~0.4, 1.6 abs (4N50)		Au-α-n (7O49, 1I51); Hg-d-2n (9K40); daughter Pb^{200} (4N50)
Tl^{201}	B chem, excit, cross bomb (4N50)		EC (4N50)	72 h (4N50)		0.210 spect conv, abs (4N50)		Au-α-γ (1I2S51); Hg-d-2n (9K40); daughter Pb^{201} (4N50)
Tl^{202}	A chem, excit (9K40, 5F41)		EC (9K40, 3M42); EC (L/K ~1), no β^+ or β^- (2W50)	12.5 d (80M52); 11.5 d (2W50); 11.8 d (5F41)		0.435 spect conv, abs (2W50); 0.431 scint spect (80M52)		Hg-d-2n (9K40, 2W50); Tl-n-2n (9K40, 5F41, 3M42, 80M52)
Tl^{203}		29.50 (1B50)					Tl^{203}, I = 1/2 (87M50)	
Tl^{204}	B chem, n-capt (5F40)		β^- ~98%, EC ~2% (33L52); β^- ~98.5%, EC ~1.5% (38M52)	3.5 y (5F41); 2.7 y (3V45)	0.765 spect (33L52); 0.760 scint spect (38M52); 0.783 spect (9S49); 0.77 spect (6P47); others (4H47a, 5F41, 6E50)	no γ (lim 0.01%) (38M52a); no γ (lim 0.5%) (6E50); no γ (5F41); Hg K-x (33L52, 14M52a)	Q^-_β 0.77 (13S53)	Tl-n-γ (5F40, 2S47); Tl-γ-n (7H49); Tl-d-p (9K40, 5F41)
Tl^{205}		70.50 (1B50)					Tl^{205}, I = 1/2 (87M50)	
Tl^{206}	A n-capt (4P35); chem, genet (7B47); excit, sep isotopes (4N50a)		β^- (5F40, 9K42)	4.19 m (3S52); 4.23 m (5F40); 4.3 m (13A51)	1.51 spect (13A51); 1.65 abs (5F41); 1.8 abs (9K40); no conv (13A51)	no γ (5F40, 7B47, 13A51)	Q^-_β 1.51 (13A51)	Tl-n-γ (4P35, 1P37, 6H37); Tl^{205}-n-γ (4N50a); Tl-d-p (5F40, 9K40); daughter Bi^{210} (RaE) (7B47); daughter (long-lived) Bi^{210} (4N50a)
Tl^{207} (AcC")	A chem, genet (1C31)		β^-	4.79 m (3S52); 4.77 m (5F40); 4.76 m (1C31, 3S39)	1.44 abs (6E50); 1.47 abs (3S39a); 1.6 abs (6L38)	0.870 (~0.5%) (11S41)	Q^-_β 1.44 (13S53)	Pb-n-p (6B40); Pb-γ-p (10B46); natural source, daughter Bi^{211} (AcC)

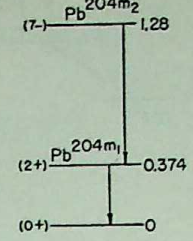
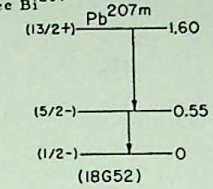
CC-0. In Public Domain. Gurukul Kangri Collection, Haridwar

Digitized by Arya Samaj Foundation Chennai and eGangotri

Isotope Z A	Class and identification	Percent abundance	Type of decay	Half-life	Energy of radiation in Mev: Particles	Energy of radiation in Mev: Gamma-transitions	Disintegration energy and scheme	Method of production and genetic relationships
$_{81}Tl^{208}$ (ThC'')	A chem, genet (1C31)		β^-	3.1 m (1C31)	1.792 spect (6M48); 1.795 spect (14H34); 1.805 spect, β-γ coinc (4F48); 1.72 spect (7S47); 1.82 abs (3S33); β^- >1.792 (?) (<1%) spect (6M48)	2.62 (~100%, e/γ ~0.002), 0.859 (~15%, e/γ ~0.02), 0.582 (~80%, e/γ ~0.02), 0.510 (~25%, e/γ ~0.08), 0.277 (~10%, e/γ ~0.3) spect, spect conv (6M50); 2.6143 spect (49L52); 0.51085 spect (49L51); 2.6147 spect conv (110B51); 2.616, 0.510 spect (12H51); 2.615 spect (6W50); 2.58 (100%), 0.575 (100%), 0.51 (50%) spect (2J47); 2.62, 0.582, 0.510, 0.277 spect conv (8E32); 2.62, 0.868, 0.581, 0.502 spect (8B48); 2.62 scint spect (11B50); no 3.2 γ (8B48, 9B50)	Q^-_β 4.99 (13S53)  (6M50, HPS)	natural source, daughter Bi^{212} (ThC)
Tl^{209}	A chem, genet (4H50)		β^- (4H50)	2.2 m (4H50)	1.99 spect (39W53); 1.8 abs (4H50)	0.12 scint spect (39W53)	Q^-_β 3.92 calc (13S53)	daughter Bi^{213}, parent Pb^{209} (4H47, 11E47)
Tl^{210} (RaC'')	A chem, genet (1C31)		β^-	1.32 m (1C31); 1.5 m (9B50); ~1.3 m (8D37)	1.8 cl ch (6L38); 2.0 abs (8D37)	no γ >2.8, D-γ-p reaction (9B50)	Q^-_β 5.39 calc (13S53)	natural source, daughter Bi^{214} (RaC), parent Pb^{210} (RaD)
$_{82}Pb^{198}$	B chem, genet (7K51)		EC (7K51)	25 m (7K51)				Tl-p-6n (7K51); parent Tl^{198} (7K51, 4N50); daughter Bi^{198} (4N50)
Pb^{199}	B chem, genet (4N50)		EC (4N50)	~80 m (4N50)				daughter Bi^{199}, parent Tl^{199} (4N50)
Pb^{200}	A chem, genet (4N50)		EC (4N50)	18 h (4N50)		0.139, 0.320 spect conv (8O51)		daughter Bi^{200}, parent Tl^{200} (4N50)
Pb^{201m}	D chem, excit (89H52)		IT (89H52)	50 s (89H52)		0.25, 0.42, 0.67 scint spect (89H52)		Tl-p-3n (89H52)
Pb^{201}	B chem (5H46); chem, genet (4N50)		EC (4N50)	8 h (4N50)				Tl-d-4n (5H46); daughter Bi^{201}, parent Tl^{201} (4N50)
Pb^{202m}	E excit (89H52)		IT (89H52)	5.6 s (89H52)		0.89 scint spect (89H52)		Tl-p-2n (89H52)
Pb^{202}		$<4 \times 10^{-4}$ (9D49)		>500 y genet, yield (2T47, 4N50)				Tl-d (2T47)
Pb^{203}	B chem, excit (3M42); chem, excit, cross bomb (2T47)		EC (3M42, 8O51)	52 h (5F40, 2T47); 54 h (9K40, 12D42)		0.153, 0.269, 0.422 spect conv (8O51); 0.270, 0.420 abs conv (3M42); 0.270, ~0.470 spect, spect conv (9L44)	see Hg^{203}  (8O51)	Tl-d-2n (5F40, 9K40, 5F41, 2T47); Tl-p-n (12D42); Pb-n-2n (3M42); Pb^{204}-n-2n (2T47); Pb-γ-n (10B46)

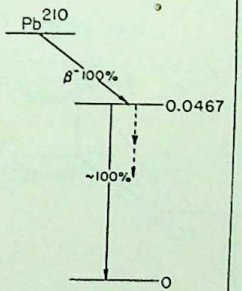
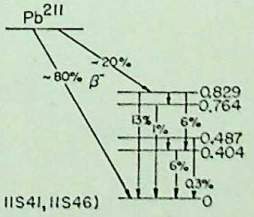
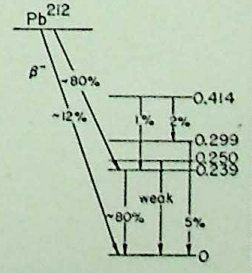
CC-0. In Public Domain. Gurukul Kangri Collection, Haridwar

Digitized by Arya Samaj Foundation Chennai and eGangotri

Isotope Z A	Class and identification	Percent abundance	Type of decay	Half-life	Energy of radiation in Mev: Particles	Energy of radiation in Mev: Gamma-transitions	Disintegration energy and scheme	Method of production and genetic relationships
Pb^{204m_2} 82	B chem (5F41); chem, excit, genet (2T47, 7K51)		IT (3M42)	68 m (3M42); 65 m (5F41)		0.905 (e/γ ~0.1, K/L 1.5), 0.374 (with Pb^{204m_1}, e/γ ~0.05, K/L 2.1) spect conv, abs conv, abs (14S50); 0.90 abs conv (3M42); 1.1 abs conv, abs (5F41)	see Bi^{204} 	Tl-d-n (5F41); Tl-d-3n (2T47); Pb-n-n (7D39, 3M42); Pb-γ-2n (10B46); daughter Bi^{204} (2T47, 14S50, 7K51), ~4% (2T47); parent Pb^{204m_1} (14S50)
Pb^{204m_1}	B genet (14S50)		IT (14S50)	3×10^{-7} s delay coinc (14S50)		0.374 (see γ's of Pb^{204m_2})		daughter Pb^{204m_2} (14S50); daughter Bi^{204} (14S52b)
Pb^{204}		1.48 (6N38)					Pb^{204}, I = 0 (87M50)	
Pb^{206}		23.6 (6N38)					Pb^{206}, I = 0 (87M50)	
Pb^{207m}	A excit, sep isotopes (24C51); chem, genet (23F52c)		IT (24C50)	0.84 s (24C52); 0.82 s (51L51); 0.80 s (89H52)		0.55, 1.05 scint spect (24C51); 0.5, 1.1 scint spect (23F52c)	see Bi^{207} 	Pb^{207}-n-n (24C51); Pb-n-n (51L51); daughter Bi^{207} (23F52c); not daughter Po^{211} (lim 0.005%) (23F52a)
Pb^{207}		22.6 (6N38)					Pb^{207}, I = 1/2 (87M50)	
Pb^{208}		52.3 (6N38)					Pb^{208}, I = 0 (87M50)	
Pb^{209}	A chem (6T37, 9K40); chem, sep isotopes (5F41a)		β^- (9K40, 5F41)	3.22 h (5F41); 2.75 h (9K40)	0.635 spect (47W52a); 0.620 spect (39W53); 0.68 spect (11R47); others (9K40, 5F41, 19L44)	no γ, no conv (4W44, 47W52a); no γ (19L44, 39W53)	Q^-_β 0.64 (13S53)	Pb-d-p (6T37, 9K40, 5F41, 5F41a, 9K42, 3H50); Pb-n-γ (3M42); Bi-d-2p (11 2S51); Bi-n-p (3M42); daughter Po^{213} (4H47, 11E47, 11M49); daughter Tl^{209} (11E47, 4H47)

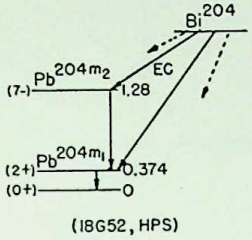
CC-0. In Public Domain. Gurukul Kangri Collection, Haridwar

Digitized by Arya Samaj Foundation Chennai and eGangotri

Isotope Z A	Class and identification	Percent abundance	Type of decay	Half-life	Energy of radiation in Mev: Particles	Energy of radiation in Mev: Gamma-transitions	Disintegration energy and scheme	Method of production and genetic relationships
$_{82}Pb^{210}$ (RaD)	A chem, genet (1C31)		β^-	22 y (1C31)	0.018 ion ch (5I52); 0.018 scint spect, β-γ coinc (87B52a); 0.017 ($\leq$90%), 0.056 ($\geq$10%) ion ch (33J52); others (8L39, 12S46)	γ_1 0.0465, no other γ between 0.016 and 0.060 (lim ~2% of γ_1) cryst spect (26E52); γ_1 0.0467, no other γ (lim 5% of γ_1) cryst spect (88B52a); 0.0467 (3.5%) spect conv, abs (24B30, 8S31, 19G32, 6D33); γ_1 (e_L/γ ~16, $L_I/L_{II}/L_{III}/M$ = 1.0/0.09/0.019/0.29) spect conv (6C50); γ_1 (e/γ ~23) spect conv (33L51); γ_1 (e/γ ~17, using γ = 3.5%) spect conv (14B51); 0.032, 0.037, 0.0467 cryst spect (8F52); 0.065 (<0.2%), 0.0467 (2.8%), 0.043 (0.2%), 0.037 (0.2%), 0.032 (0.4%), 0.023 (~1%), 0.007 (~10%) cryst spect, cl ch, abs (9T46); others (9T43, 10C51, 4T52a, 63C52, 35C52)	Q^-_β 0.065 (5I52)  (26E52, HPS)	natural source, daughter Tl^{210} (RaC''), daughter Po^{214} (RaC'), parent Bi^{210} (RaE)
Pb^{211} (AcB)	A chem, genet (1C31)		β^-	36.1 m (3S39); 36.0 m (1C31)	1.39 (~80%), ~0.5 (~20%) abs (3S39a)	0.065, 0.083, 0.404, 0.425, 0.487, 0.764, 0.829 spect, spect conv, abs (11S42); 0.829 (5%) (54M44); 0.8 abs (3S39a)	Q^-_β 1.4 (13S53)  (11S41, 11S46)	natural source, daughter Po^{215} (AcA), parent Bi^{211} (AcC)
Pb^{212} (ThB)	A chem, genet (1C31)		β^-	10.6 h (1C31)	0.355, 0.589 spect, β-γ coinc (4F48); 0.331, 0.569 (~12%) spect (6M48a); 0.340 spect (6G49); 0.36 spect (3S33)	γ_3 0.2386 spect conv (49L51); γ_1 0.115, γ_2 0.176, γ_3 0.238, γ_4 0.249, γ_5 0.299 spect conv (8E32); γ_3 0.238 (~40%), γ_5 0.300 (~4%) spect (6M50); γ_3 (L_I/L_{II} ~18, M_I/M_{II} ~4.3) spect conv (117S52); γ_3 (e/γ ~1), γ_5 (e/γ ~0.3) (calc from 9F39, 6M48a, 6M50); γ_3 0.238 spect (7S44)	Q^-_β 0.58 (13S53)  (11S46, 4F48, 6M48a)	natural source, daughter Po^{216} (ThA), parent Bi^{212} (ThC)

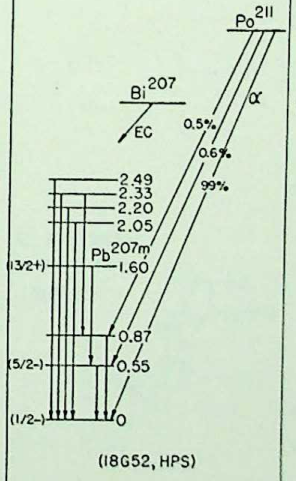
CC-0. In Public Domain. Gurukul Kangri Collection, Haridwar

Digitized by Arya Samaj Foundation Chennai and eGangotri

Isotope Z A	Class and identification	Percent abundance	Type of decay	Half-life	Energy of radiation in Mev: Particles	Energy of radiation in Mev: Gamma-transitions	Disintegration energy and scheme	Method of production and genetic relationships
$_{82}Pb^{214}$ (RaB)	A chem, genet (1C31)		β^- (3S33, 7R36)	26.8 m (1C31)	0.65 spect (3S33); 0.72 spect (8C41)	γ_1 0.05323, γ_2 0.24192, γ_4 0.29522, γ_5 0.35199 ($\gamma_2/\gamma_4/\gamma_5$ = 0.2/0.55/1.0) cryst spect (100M52); γ_1 0.0528, γ_2 0.2410, γ_3 0.2578, γ_4 0.2942, γ_5 0.3509 spect (7S44); γ_1 (1.6%) crit abs (9T43a); γ_2 (K/L_I ~6.7), γ_4 (K/L_I ~6.7), γ_5 (K/L_I ~5.9) spect conv (59K51); 0.053, 0.241, 0.257, 0.294, 0.350 spect (8E34); 0.053, 0.242, 0.295, 0.351 spect conv (10C51)		natural source, daughter Po^{218} (RaA), parent Bi^{214} (RaC)
$_{83}Bi^{<198}$	E (2T48); chem (4N50)		α (2T48)	1.7 m (4N50)	6.2 ion ch (4N50)			spall Pb (2T48, 4N50)
Bi^{198}	B chem (2T48); chem, genet (4N50)		EC 99+%, α 5×10^{-2}% (4N50)	7 m genet (4N50)	5.83 ion ch (4N50)			spall Pb (2T48, 4N50); parent Pb^{198} (4N50)
Bi^{199}	B chem (2T48); chem, genet (4N50)		EC 99+%, α 10^{-2}% (4N50)	~25 m genet (4N50)	5.47 ion ch, abs mica (4N50)			spall Pb (4N50, 2T48); parent Pb^{199} (4N50)
Bi^{200}	B chem, genet (4N50)		EC (4N50)	35 m genet (4N50)				spall Pb, parent Pb^{200} (4N50)
Bi^{201}	B chem (2T48); chem, genet (4N50)		EC 99+%, α 3×10^{-3}% (4N50)	62 m (4N50)	5.15 ion ch (4N50)			spall Pb (2T48, 4N50); parent Pb^{201} (4N50)
Bi^{201}	B chem, genet (4N50)		EC (4N50)	~2 h genet (4N50)				spall Pb, parent Pb^{201} (4N50)
Bi^{202}	B chem, genet (7K51)		EC (7K51)	95 m (7K51)				daughter Po^{202} (7K51)
Bi^{203}	B chem, genet (4N50)		EC (4N50); α ~10^{-5}% (15D52a)	12 h genet (4N50)	α: 4.85 range emuls (15D52a)			spall Pb, parent Pb^{203} (4N50); daughter Po^{203} (7K51)
Bi^{204}	B chem, sep isotopes, cross bomb (2T47)		EC, no β^+ (2T47)	12 h (2T47)	conv: ~0.2, ~0.8 (weak), abs, spect (2T47)	0.217 spect conv (14S50a)	 (18G52, HPS)	Pb^{204}-d-2n (2T47); Pb-d-2n (14S50); daughter Po^{204} (7K51); Tl-α-3n, parent (~4%) Pb^{204m_2} (2T47); parent Pb^{204m_1} (14S52b)
Bi^{205}	B chem, genet, sep isotopes (7K51)		EC (7K51)	14.5 d (7K51)		0.431, 0.527, 0.550, 0.746, 1.84 spect conv (7K51)		daughter Po^{205} (7K51); daughter At^{209} (12B51)

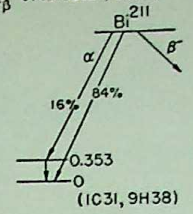
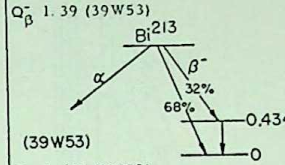
Digitized by Arya Samaj Foundation Chennai and eGangotri

CC-0. In Public Domain. Gurukul Kangri Collection, Haridwar

Isotope Z A	Class and identification	Percent abundance	Type of decay	Half-life	Energy of radiation in Mev: Particles	Energy of radiation in Mev: Gamma-transitions	Disintegration energy and scheme	Method of production and genetic relationships
$_{83}Bi^{206}$	B chem, sep isotopes (5F41a, 2T47)		EC (9L44); EC, no β^+ (13A51a)	6.4 d (9K40)		0.182, 0.234, 0.260, 0.341, 0.396, 0.470, 0.505, 0.536, 0.590, 0.803, 0.880, 0.889, 1.020, 1.097, 1.720 spect, spect conv, γ-γ coinc (13A51a); others (9K40, 5F41, 2T47a)		Tl-α-3n (2T47); Pb-d-2n (5F41, 5F41a, 9K40, 13A51a); Pb^{207}-d-3n (2T47); Pb^{206}-d-2n (5F41a); daughter Po^{206} (2T47a); daughter At^{210} (4N50b)
Bi^{207}	B chem, genet (4N51)		EC (5G50, 4N51)	~50 y genet (4N51)		0.56, 1.1 (coinc with 0.56 γ) scint spect, γ-γ coinc (7G51a); 0.064 or 0.137, 0.565, 1.063, 1.46, 2.05, 2.20, 2.33, 2.49 spect conv (4N51); with Pb^{207m}: 0.5, 1.1 scint spect (23F52c)	 (18G52, HPS)	Pb-d-3n (4N51); daughter At^{211} (4N51); parent Pb^{207m} (23F52c)
Bi^{208}	F chem (4N51)		EC (4N51)	long (4N51)		no γ (?) (4N51)	Q_a 3.2 calc (13S53)	Pb-d-2n (4N51)
Bi^{209}		100 (6N38b)					Bi^{209}, I = 9/2 (87M50) Q_a 3.2 calc (13S53)	
Bi^{209}	G α's not seen (9IH52)		α (7F51)	$>>10^{17}$ y sp act (9IH52); 3×10^{17} y sp act (7F51)	~3.15 range emulsion (7F51)			
Bi^{210} (RaE)	A chem, genet (1C31)		β^- 99+%, α 5×10^{-5}% (7B47)	5.02 d (111B52); 4.85 d (7S47f); 5.0 d (1C31); 5.1 d (15H45a)	β^-: 1.17 spect (10L37, 9F39a, 9N40, 2Z49, 10L49)	no γ (19G36, 6L47, 10C51)	Q_{β}^- 1.17, Q_a 5.06 calc (13S53)	natural source, daughter Pb^{210} (RaD), parent Po^{210} (RaF); parent Tl^{206} (7B47); Pb-d-γ (112S51); Pb-α-pn (2T47); Bi-d-p (12L36, 10C40, 47H40); Bi-n-γ (7M48, 2S47)
Bi^{210}	A chem, genet (4N50a); chem, mass spect (52L52)		α, β^- or IT (~0.3%) (52L52)	$\sim 10^6$ y yield (52L52)	4.93 ion ch (52L52)		Q_a 5.03 (52L52)	Bi-n-γ, parent Tl^{206} (4N50a); parent Po^{210} (52L52)

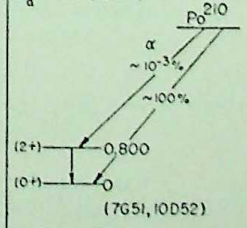
CC-0. In Public Domain. Gurukul Kangri Collection, Haridwar

Digitized by Arya Samaj Foundation Chennai and eGangotri

Isotope Z A	Class and identification	Percent abundance	Type of decay	Half-life	Energy of radiation in Mev: Particles	Energy of radiation in Mev: Gamma-transitions	Disintegration energy and scheme	Method of production and genetic relationships
$_{83}Bi^{211}$ (AcC)	A chem, genet (1C31)		α 99.68%, β^- 0.32% (1C31)	2.16 m (1C31)	α: 6.618 (84%), 6.272 (16%) spect (9H38, 1R31); 6.621 (82.6%), 6.274 (17.4%) spect (13V52)	0.350 abs (3S39a); -0.35 (e_K/γ = 0.18, K/L 5.5) (4T52b, 10F52); 0.354 abs (16H25)	Q_α 6.746 (13S53); Q^-_β 0.61 calc (13S53)  (1C31, 9H38)	natural source, daughter Pb^{211} (AcB), parent Po^{211} (AcC'), parent Tl^{207} (AcC'')
Bi^{212} (ThC)	A chem, genet (1C31)		β^- 66.3%, α 33.7% (6K38)	60.5 m (1C31)	α: 6.086 (27.2%), 6.047 (69.9%), 5.765 (1.7%), 5.622 (0.15%), 5.603 (1.1%), 5.481 (0.016%) spect (48R51); 6.082 (27%), 6.042 (70%), 5.760 (1.8%), 5.618 (0.2%), 5.599 (1.1%) spect (11L34); β^-: 2.250 spect (6M48a); 2.256 spect, β-γ coinc (4F48); others (7C48, 3S33)	with α: 0.040 (strong), 0.144, 0.164, 0.288, 0.328, 0.432, 0.452, 0.472, other γ's, spect, spect conv (11S37, 11S46); 0.040 (~4%) coinc abs (21K47); ($e/\gamma \geq 14$ calc from 21K47, 9F39, 14B49); 0.295 spect conv (117S52); with β^-: 2.20, 1.81 (~7%), 1.61 (~7%), 1.34 (~5%), 1.03 (~6%), 0.83 (~19%), 0.72 (~19%) spect (2J47) (intensities calc from 2J47); 0.726 (~6%, e/γ 0.015) spect (6M50); others (5L47)	Q_α 6.203, Q^-_β 2.25 (13S53)	natural source, daughter Pb^{212} (ThB), parent Po^{212} (ThC') and Tl^{208} (ThC'')
Bi^{213}	A chem, genet (11E47, 4H47)		β^- 98%, α 2% (11E47, 4H50a, 39W53)	47 m (4H47); 46 m (11E47)	β^-: 1.39 (68%), 0.959 (32%) spect (39W53); ~1.3 abs (4H47, 11E47); α: 5.86 ion ch (11E47); 6.0 ion ch (4H47)	0.434 spect conv, scint spect (39W53)	Q_α 5.97 (13S53); Q^-_β 1.39 (39W53)  (39W53)	daughter At^{217}, parent Po^{213} (4H47, 11E47, 4H50a); parent Tl^{209} (4H50)
Bi^{214} (RaC)	A chem, genet (1C31)		β^- 99+%, α 0.04% (1C31)	19.7 m (1C31)	α: 5.505 (45%), 5.444 (55%) spect (11L34); 5.52 (37%), 5.47 (46%), 5.33 (17%) spect (7C48a); β^-: 3.17 (~23%), 1.65 (~77%) spect (8C41, 5L47); 3.15 spect, abs (3S33)	with β^-: γ_1 0.6094 cryst spect (100M52); γ_1 0.606 (K/L 5.6), γ_2 0.766, γ_3 0.933, γ_4 1.120 (K/L 6.7), γ_5 1.238 (K/L 5.9), γ_6 1.379, γ_7 1.520, γ_8 1.761 (K/L 6.7), γ_9 1.820, γ_{10} 2.200, γ_{11} 2.420 ($\gamma_1/\gamma_2/\gamma_3/\gamma_4/\gamma_5/\gamma_6/\gamma_7/\gamma_8/\gamma_9/\gamma_{10}/\gamma_{11}$ ~ 9/1.3/1.1/2.6/1.0/0.9/0.7/3.2/0.2/1.00/0.5) spect, spect conv (59K52, 5M50); 0.426, 0.498, 0.607, 0.766, 0.933, 1.120, 1.238, 1.379, 1.414, 1.761, 2.193 spect conv (8E34); 0.609, 0.769, 0.935, 1.122, 1.241, 1.419, 1.766 spect conv (10C51); with α: 0.0625, 0.191 spect conv (10C51); others (8E30, 8C41)	Q_α 5.610 (13S53); Q^-_β 3.17 (8C41)	natural source, daughter Pb^{214} (RaB), daughter At^{218}, parent Po^{214} (RaC'), parent Tl^{210} (RaC''); descendent Fr^{222} (8H51a)
Bi^{215}	A chem, genet (8H53)		β^- (8H53)	8 m (8H53)			Q^-_β 2.01 est (60G53)	natural source, daughter At^{219}, parent Po^{215} (8H53)

CC-0. In Public Domain. Gurukul Kangri Collection, Haridwar

Digitized by Arya Samaj Foundation Chennai and eGangotri

Isotope Z A	Class and identification	Percent abundance	Type of decay	Half-life	Energy of radiation in Mev: Particles	Energy of radiation in Mev: Gamma-transitions	Disintegration energy and scheme	Method of production and genetic relationships
$_{84}Po^{200}$	B chem, genet (7K51a)		EC, α (7K51a)	11 m (7K51a)	5.84 ion ch (7K51a)			Bi-p-10n, parent Bi^{200} (7K51a)
Po^{201}	B chem, genet (7K51a)		EC, α (7K51a)	18 m (7K51a)	5.70 ion ch (7K51a)			Bi-p-9n, parent Bi^{201} (7K51a)
Po^{202}	B chem, genet, excit (7K51)		EC, α (7K51)	52 m genet (7K51)	5.59 ion ch (7K51)			Bi-p-8n, Pb-α-spall, parent Bi^{202} (7K51)
Po^{203}	B chem, genet (7K51)		EC (7K51) -	47 m genet (7K51)				Bi-p-7n, Pb-α-spall, parent Bi^{203} (7K51)
Po^{204}	B chem, genet (7K51)		EC ~99%, α ~1% (7K51)	3.8 h (7K51)	5.37 ion ch (7K51)			Bi-p-6n, Pb-α-spall, parent Bi^{204}, parent Pb^{200} (7K51)
Po^{205}	B chem, genet, sep isotopes, excit (7K51)		EC 99+%, α 0.074% (17H51a)	1.5 h genet (7K51)	5.2 ion ch (7K51a)			Pb^{204}-α-3n, parent Bi^{205} parent Pb^{201} (7K51)
Po^{206}	B chem, genet, sep isotopes (2T47a)		EC ~90%, α ~10% (2T47a)	9 d (2T47a)	5.218, 5.064 spect (4R52b); 5.21 ion ch (7K51a)	0.8 abs (2T47a)	$Q_α$ 5.321 (HPS)	Pb^{204}-α-2n, parent Bi^{206} (2T47a)
Po^{207}	B chem, excit, sep isotopes (2T47a)		EC 99+%, α ~10^{-2}% (2T47a)	5.7 h (2T47a)	5.10 ion ch (7K51a)	1.3 abs (2T47a)		Pb^{206}-α-3n (2T47a)
Po^{208}	A chem, excit, sep isotopes (2T47a)		α (2T47a)	2.93 y (2T50)	5.108 spect (4A52b); 5.109 spect (4R52b); 5.10 ion ch (7K51a)	no γ (2T47a, 18H51)	$Q_α$ 5.208, Q_{EC} 1.3 calc (13S53)	Pb^{206}-α-2n (2T47a); Pb^{207}-α-3n (2T47a); Bi-d-3n (2T47a, 10K49); Bi-p-2n (4L47); daughter Em^{212}, daughter 1.7 h At^{208} (8H50); daughter 7.0 h At^{208} (12B51)
Po^{209}	A chem, excit (10K49)		α >90%, EC ≤10% est (13P50)	~100 y yield (10K50)	4.877 spect (4A52b); 4.86 ion ch (7K51a)	0.87 (1%), 0.55 (0.5%), 0.2 (0.2%), 0.1 (0.07%) scint spect (18H51)	$Q_α$ 4.972 (13S53)	Bi-d-2n (10K49)
Po^{210}	A chem, genet (1C31)		α; β stable (cons energy) (HPS)	138.3 d (5B49); 140 d (1C31)	5.298 spect (9H38, 16S51); 5.303 spect (7C46); ~4.5 (weak) α-γ coinc, scint spect (10D52)	$γ_1$ 0.800 (e/γ ~0.03, K/L 3.7) spect, spect conv (13A51a); $γ_1$ 0.804 scint spect (18P52); $γ_1$ 0.784 spect conv (10C51); $γ_1$ 0.773 spect (7S47a); $γ_1$ (1.8 x 10^{-3}%, e/γ ~0.07), no 0.08 γ ion ch, crit abs, γ-γ coinc (7G51); $γ_1$ (1.6 x 10^{-3}%) abs (3R52); 0.77 (~10^{-3}%), 0.084 (~10^{-3}%) abs (1Z48); others (10D47, 49R52, 63B52)	$Q_α$ 5.401 (13S53) 	natural source, daughter Bi^{210} (RaE); Pb^{208}-α-2n (2T47a); Bi-d-n (47H40, 10C40); Bi-p-γ (10K50); daughter At^{210} (10K49); daughter (long-lived) Bi^{210} (52L52)
Po^{211} (AcC')	A genet (1C31)		α; β stable (cons energy) (HPS)	0.52 s (13L51)	7.434 spect (11L34); 6.88 (0.50%), 6.56 (0.53%), no 6.34 α (lim 0.02%) spect (74H52a); 6.90 (0.6%), 6.57 (0.5%), 6.34 (0.1%) ion ch (4N51)		$Q_α$ 7.58 (13S53) see Bi^{207}	natural source, daughter Bi^{211} (AcC); daughter At^{211} (11C40, 11C40a); daughter Em^{215} (11M52); not parent Pb^{207m} (23F52a)
Po^{211}	D chem, excit, sep isotopes (114S51)		α (114S51)	25 s (114S51)	7.14 ion ch (114S51)			Pb^{208}-α-n (114S51)

CC-0. In Public Domain. Gurukul Kangri Collection, Haridwar

Digitized by Arya Samaj Foundation Chennai and eGangotri

Isotope Z A	Class and identification	Percent abundance	Type of decay	Half-life	Energy of radiation in Mev: Particles	Energy of radiation in Mev: Gamma-transitions	Disintegration energy and scheme	Method of production and genetic relationships
$_{84}Po^{212}$ (ThC')	A genet (1C31)		α	3.04×10^{-7} s delay coinc (4B49); 3.0×10^{-7} s delay coinc (11H48); others (3J48, 4V49, 11D39, 16B43)	8.776 spect (15B36, 9H38); long range α's: 10.536 (0.017%), 10.417 (0.002%), 9.489 (0.004%) spect (48R51)		Q_α 8.946 (13S53)	natural source, daughter Bi^{212} (ThC); daughter Em^{216} (11M49)
Po^{213}	A genet (4H47, 11E47)		α (4H47, 11E47)	4.2×10^{-6} s delay coinc (3J48)	8.336 ion ch (11E47, 5C48); 8.34 ion ch (4H50a)		Q_α 8.496 (13S53)	daughter Bi^{213}, parent Pb^{209} (4H47, 11E47); daughter Em^{217} (11M49)
Po^{214} (RaC')	A genet (1C31)		α; β stable (cons energy) (HPS)	1.637×10^{-4} s delay coinc (13D50); -1.5×10^{-4} s delay coinc (11D39, 6R41, 5W42, 4J43, 14L47, 4B48); 1.4×10^{-4} s delay coinc (5R47)	7.680 spect (15B36, 9H38); 7.683 spect (16S51); long range α's: 9.069 (0.002%), others 8.280-10.509 spect (11L34)		Q_α 7.826 (13S53)	natural source, daughter Bi^{214} (RaC), parent Pb^{210} (RaD); daughter Em^{218} (4S48)
Po^{215} (AcA)	A genet (1C31)		α 99+%, β^- 5×10^{-4}% (5K44, 8A50)	1.83×10^{-3} s delay coinc (5W42)	7.365 spect (11L34)		Q_α 7.505, Q_β^- 0.8 calc (13S53)	natural source, daughter Em^{219} (An), parent Pb^{211} (AcB); parent At^{215} (5K44)
Po^{216} (ThA)	A genet (1C31)		α; β stable (cons energy) (HPS); α 99+%, β^- 0.014% (5K43)	0.158 s (5W42)	α: 6.774 spect (15B36, 9H38)		Q_α 6.902 (13S53)	natural source, daughter Em^{220} (Tn), parent Pb^{212} (ThB); parent At^{216} (5K43) (?)
Po^{217}	C genet (9M52b)		α (9M52b)		6.5 ion ch (9M52b)		Q_α 6.7, Q_β^- 1.3 est (13S53)	daughter Em^{221} (9M52b)
Po^{218} (RaA)	A chem, genet (1C31)		α 99+%, β^- 0.03% (5K43a)	3.05 m (1C31)	α: 5.998 spect (15B36, 9H38)		Q_α 6.110, Q_β^- 0.33 calc (13S53)	natural source, daughter Em^{222} (Rn), parent Pb^{214} (RaB); parent At^{218} (5K43a)
$_{85}At^{<202}$	D chem, excit (12B51)		α, EC (12B51)	43 s (12B51)	6.50 ion ch (12B51)			Bi-α-spall (12B51)
$At^{<203}$	D chem, excit (12B51)		α, EC (12B51)	1.7 m (12B51)	6.35 ion ch (12B51)			Bi-α-spall (12B51)
At^{203}	D chem, excit (12B51)		α, EC (12B51)	7 m (12B51, 13H51)	6.10 ion ch (12B51)			Bi-α-10n (12B51); Au-C-6n (13H51, 4M50)
At^{204}	B chem, excit, genet (12B51)		EC (12B51)	~25 m genet (12B51)				Bi-α-9n, parent Po^{204} (12B51)
At^{205}	B chem, excit, genet (12B51)		α, EC (12B51)	25 m (12B51, 13H51)	5.90 ion ch (12B51)			Bi-α-8n, parent Po^{205} (12B51); Au-C-4n (4M50, 13H51)
At^{206}	B chem, excit, genet (12B51)		EC (12B51)	2.6 h genet (12B51)				Bi-α-7n, parent Po^{206} (12B51)

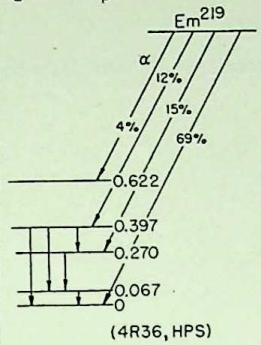
CC-0. In Public Domain. Gurukul Kangri Collection, Haridwar

Digitized by Arya Samaj Foundation Chennai and eGangotri

Isotope Z A	Class and identification	Percent abundance	Type of decay	Half-life	Energy of radiation in Mev: Particles	Energy of radiation in Mev: Gamma-transitions	Disintegration energy and scheme	Method of production and genetic relationships
$_{85}At^{207}$	B chem, excit, genet (2T48a, 12B51)		EC ~90%, α ~10% (2T48a, 12B51)	2.0 h (12B51)	5.75 ion ch (12B51)			Bi-α-6n (2T48a, 12B51); parent Po^{207}, parent Bi^{203} (12B51)
At^{208}	B chem, excit, genet (12B51)		EC (12B51)	6.3 h genet (12B51)				Bi-α-5n, parent Po^{208} (12B51)
At^{208}	A chem, genet (8H50)		EC 99+%, α 0.5% (8H50)	1.7 h (8H50)	5.65 ion ch (8H50)			daughter Fr^{212}, parent Po^{208} (8H50, 9M52a)
At^{209}	B chem, genet, excit (12B51)		EC ~95%, α ~5% (12B51)	5.5 h (12B51)	5.65 ion ch (12B51)	0.2, 0.8 scint spect (89M52)		Bi-α-4n, parent Po^{209}, parent Bi^{205} (12B51)
At^{210}	A chem, excit, genet (10K49)		EC 99+%, α 0.17% (74H52a); EC 99+%, α 0.1% (4N50b)	8.3 h (10K49)	5.519 (32%), 5.437 (31%), 5.355 (37%) spect (74H52a)	0.25, 1.15, 1.40 scint spect (74H52a); 1.0 abs, abs conv (10K49)		Bi-α-3n, parent Po^{210} (10K49, 12B51); parent Bi^{206} (4N50b)
At^{211}	A chem, excit, genet (11C40, 10K49)		α 40.9%, EC 59.1% (4N51)	7.5 h (11C40, 10K49); 7.3 h (17H51)	5.862 spect (74H52a); 5.89 ion ch (2T48a, 12B51)		Q_α 5.975, Q_{EC} 0.9 est (13S53)	Bi-α-2n (11C40, 11C40a, 10K49, 12B51); spall Th, U (20B52, 13S47)
At^{212}	E excit (7W48)		α (7W48)	0.25 s (7W48)				Bi-α-n (7W48)
At^{213}	E genet, decay charac (57K51)		α (57K51)		9.2 range emuls (57K51)			descendent Pa^{225} (57K51)
At^{214}	B genet (11M49)		α (11M49)	~2×10^{-6} s est (11M51)	8.78 ion ch (11M49, 11M51)		Q_α 8.95, Q_{EC} 1.05 calc (13S53)	daughter Fr^{218} (11M49, 11M51)
At^{215}	A genet (5K44, 13G48)		α (5K44, 13G48)	~10^{-4} s delay coinc (13G48, 11M51); short (5K44)	8.00 ion ch (13G48, 11M51); 8.4 ion ch (5K44)		Q_α 8.15, Q_{β^-} 0.0 calc (13S53)	daughter Fr^{219}, parent Bi^{211} (AcC) (13G48, 11M51); natural source, daughter Po^{215} (AcA), parent Bi^{211} (AcC) (5K44)
At^{216}	A genet (13G48)		α (5K43, 13G48)	~3×10^{-4} s delay coinc (11M49, 11M51); short (<54 s) (5K43)	7.79 ion ch (13G48, 11M51); 7.64 ion ch (5K43)		Q_α 7.94, Q_{β^-} 2.03 calc, Q_{EC} 0.46 calc (13S53)	daughter Fr^{220}, parent Bi^{212} (ThC) (13G48, 11M51); natural source, parent Bi^{212} (ThC) (5K43); daughter Po^{216} (ThA) (5K43); note Po^{216} β-stable (HPS)
At^{217}	A genet (11E47, 4H47)		α (11E47, 4H47)	0.018 s delay coinc (4H47, 4H50a); 0.021 s delay coinc (11E47)	7.02 ion ch (5C48); 7.00 ion ch (4H47)		Q_α 7.15, Q_{β^-} 0.65 calc (13S53)	daughter Fr^{221}, parent Bi^{213} (11E47, 4H47, 4H50a)
At^{218}	E genet (5K43a)		α (5K43a); α 99+%, β^- 0.1% (3W48)	1.5-2.0 s (3W48); several sec (?) (5K43a)	α: 6.63 range (5K43a); 6.7 ion ch (3W48)		Q_α 6.75, Q_{β^-} 2.67 calc (13S53)	natural source, daughter Po^{218} (RaA), parent Bi^{214} (RaC) (5K43a, 3W48)
At^{219}	A chem, genet (8H53)		α ~97%, β^- ~3% (8H53)	0.9 m (8H53)	α: 6.27 ion ch (8H53)		Q_α 6.39, Q_{β^-} 1.45 est (13S53)	natural source, daughter Fr^{223} (AcK), parent Em^{219} (An), parent Bi^{215} (8H53)

CC-0. In Public Domain. Gurukul Kangri Collection, Haridwar

Digitized by Arya Samaj Foundation Chennai and eGangotri

Isotope Z A	Class and identification	Percent abundance	Type of decay	Half-life	Energy of radiation in Mev: Particles	Energy of radiation in Mev: Gamma-transitions	Disintegration energy and scheme	Method of production and genetic relationships
86 Em^{208}	D chem (9M52b)		EC ~80%, α ~20% (9M52b)	23 m (9M52b)	6.138 spect (9M52)			spall Th (9M52b)
Em^{209}	B chem, genet (9M52a)		EC ~80%, α ~20% (9M52a)	30 m (9M52b)	6.02 ion ch (9M52a)			Pb-C-spall, spall Th (9M52a); daughter Ra^{213}, parent At^{209} (9M52a)
Em^{210}	B chem, genet (9M52a)		α >95%, EC <5% (9M52b)	2.7 h (9M52a); 2.1 h (13G49)	6.036 spect (9M52); 6.02 ion ch (9M52a)		$Q_α$ 6.153 (13S53)	spall Th (13G49, 9M52a); Pb-C-spall (9M52a); parent Po^{206} (9M52a)
Em^{211}	A chem, genet (9M52a)		EC 75%, α 25% (9M52a)	16 h (9M52a)	5.847 (33%), 5.778 (67%) spect (9M52); 5.82 ion ch (9M52a)			Pb-C-spall, parent At^{211} (9M52a)
Em^{212}	A chem, genet (8H50, 13G49)		α (8H50)	23 m (13G49, 8H50, 9M52a)	6.262 spect (9M52); 6.23 ion ch (9M52a)		$Q_α$ 6.382 (13S53)	spall Th (13G49); daughter Fr^{212}, parent Po^{208} (8H50, 9M52a)
Em^{215}	B genet (11M52)		α (11M52)	~10^{-6} s est (11M52)	8.6 ion ch (11M52)			daughter Ra^{219}, parent Po^{211} (AcC') (11M52)
Em^{216}	A genet (11M49, 11M51)		α (11M49, 11M51); β stable (cons energy) (HPS)	~10^{-4} s est (11M51)	8.01 ion ch (7O50)		$Q_α$ 8.16 (13S53)	daughter Ra^{220}, parent Po^{212} (ThC') (11M49, 11M51)
Em^{217}	A genet (11M49, 11M51)		α (11M51); β stable (cons energy) (HPS)	~10^{-3} s delay coinc (11M51)	7.74 ion ch (11M51)		$Q_α$ 7.89 (13S53)	daughter Ra^{221}, parent Po^{213} (11M49, 11M51)
Em^{218}	A genet (4S48)		α (4S48); β stable (cons energy) (HPS)	0.019 s delay coinc (4S48)	7.12 ion ch (1J48)		$Q_α$ 7.25 (13S53)	daughter Ra^{222}, parent Po^{214} (RaC') (4S48)
Em^{219} (An)	A chem, genet (1C31)		α	3.92 s (1C31)	6.824, 6.559, 6.434 spect (11L34); $α_0$ (69%), $α_{270}$ (15%), $α_{397}$ (12%), $α_{622}$ (4%) spect (4R36)	0.067, 0.124, 0.198 (strong), 0.267, 0.321, 0.392, 0.589 (weak) spect conv (11S37); 0.123, 0.270, 0.590 cryst spect (8F40)	$Q_α$ 6.951, $Q_β^-$ 0.26 calc (13S53)  (4R36, HPS)	natural source, daughter Ra^{223} (AcX), parent Po^{215} (AcA); daughter At^{219} (8H53)
Em^{220} (Tn)	A chem, genet (1C31)		α; β stable (cons energy) (HPS)	54.5 s (1C31)	6.282 spect (15B36, 9H38)		$Q_α$ 6.398 (13S53)	natural source, daughter Ra^{224} (ThX), parent Po^{216} (ThA)
Em^{221}	A chem, genet (9M52a)		$β^-$ ~80%, α ~20% (9M52b)	25 m (9M52b)			$Q_α$ 6.0 est, $Q_β^-$ 0.9 est (13S53)	Th-p-spall, parent Fr^{221} (9M52a); parent Po^{217} (9M52b)

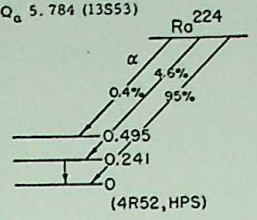
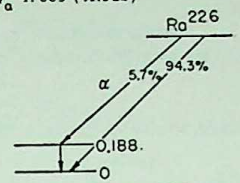
CC-0. In Public Domain. Gurukul Kangri Collection, Haridwar

Digitized by Arya Samaj Foundation Chennai and eGangotri

Isotope Z A	Class and identification	Percent abundance	Type of decay	Half-life	Energy of radiation in Mev: Particles	Energy of radiation in Mev: Gamma-transitions	Disintegration energy and scheme	Method of production and genetic relationships
$_{86}Em^{222}$ (Rn)	A chem, genet (1C31)		α; no β^- (lim 10^{-4}%) (5K46)	3.825 d (22T51, 1C31)	5.486 spect (15B36, 9H38)		Q_α 5.587 (13S53)	natural source, daughter Ra^{226}, parent Po^{218} (RaA)
$_{87}Fr^{212}$	A chem, genet (8H50); chem, mass spect (9M52a)		EC 56%, α 44% (8H50)	19.3 m (8H50)	6.409 (37%), 6.387 (39%), 6.339 (24%) spect (8H52c); 6.36 ion ch (8H51)			spall Th (8H50), parent Em^{212} (8H50, 9M52a)
Fr^{217}	E genet, decay charac (57K51)		α (57K51)		8.3 range emuls (57K51)			descendent Pa^{225} (57K51)
Fr^{218}	B genet (11M49, 11M51)		α (11M51)	5×10^{-3} s est (11M51)	7.85 ion ch (11M51)		Q_α 8.00, Q_{EC} 1.8 calc (13S53)	daughter Ac^{222}, parent At^{214} (11M49, 11M51)
Fr^{219}	A genet (13G48)		α (13G48); β stable (cons energy) (HPS)	0.02 s delay coinc (11M51)	7.30 ion ch (11M51)		Q_α 7.44 (13S53)	daughter Ac^{223}, parent At^{215} (13G48, 11M49, 11M51)
Fr^{220}	A genet (13G48)		α (13G48)	27.5 s (11M51)	6.69 ion ch (11M51)		Q_α 6.81, Q_β^- 1.27 calc, Q_{EC} 0.87 calc (13S53)	daughter Ac^{224}, parent At^{216} (13G48, 11M49, 11M51)
Fr^{221}	A chem, genet (4H47, 11E47)		α (11E47, 4H47)	4.8 m (4H50a); 5 m (11E47)	6.30 ion ch (4H47, 5C48); 6.30 (~75%), 6.05 (~25%) ion ch (4H50a)	0.220 spect conv, scint spect (39W53)	Q_α 6.42, Q_β^- 0.24 calc (13S53)	daughter Ac^{225}, parent At^{217} (11E47, 4H47, 5C48, 4H50a); daughter Em^{221} (9M52a)
Fr^{222}	A chem, genet (8H50a)		β^- 99+%, α 0.01-0.1% (8H51a)	14.8 m (8H50a)			Q_α 6.00 est, Q_β^- 2.04 est, Q_{EC} 0.02 est (13S53)	spall Th, parent Ra^{222}, ancestor Bi^{214} (8H50a, 8H51a)
Fr^{223} (AcK)	A chem, genet (7P39, 7P39b)		β^- (7P39a, 8G47); α 4×10^{-3}% (8H53)	21 m (7P39)	β^-: 1.2 cl ch (7P39a, 7P39b, 6L50)	0.09 abs (6L44, 7P46); ~0.330 (6%) abs, 0.0486 (27%) crit abs (6L50)	Q_α 5.60 est, Q_β^- 1.19 calc (13S53)	natural source, daughter Ac^{227}, parent Ra^{223} (AcX) (7P39, 7P39a, 7P39b, 7P41, 7P46, 8G47, 6L50); parent At^{219} (8H53)
$_{88}Ra^{213}$	B chem, genet (9M52a)		α (9M52a)	2.7 m (9M52c)	6.90 ion ch (9M52c)			Pb-C-spall, spall Th, parent Em^{209} (9M52a)
Ra^{219}	B genet (11M52)		α (11M52)	~10^{-3} s est (11M52)	8.0 ion ch (11M52)		Q_α 8.1 (13S53)	daughter Th^{223}, parent Em^{215} (11M52)
Ra^{220}	A genet (11M49, 11M51)		α (11M51)	3×10^{-2} s est (11M51)	7.43 ion ch (7O50)		Q_α 7.57 (13S53)	daughter Th^{224}, parent Em^{216} (11M49, 11M51)
Ra^{221}	A chem, genet (11M49, 11M51)		α (11M51)	30 s (11M51)	6.71 ion ch (11M51)		Q_α 6.83 (13S53)	daughter Th^{225}, parent Em^{217} (11M49, 11M51)
Ra^{222}	A chem, genet (4S48)		α (4S48); β stable (cons energy) (HPS)	38 s (4S48)	6.51 ion ch (1J48)		Q_α 6.63 (13S53)	daughter Th^{226}, parent Em^{218} (4S48); daughter Fr^{222} (8H51a)

CC-0. In Public Domain. Gurukul Kangri Collection, Haridwar

Digitized by Arya Samaj Foundation Chennai and eGangotri

Isotope Z A	Class and identification	Percent abundance	Type of decay	Half-life	Energy of radiation in Mev: Particles	Energy of radiation in Mev: Gamma-transitions	Disintegration energy and scheme	Method of production and genetic relationships
$_{88}Ra^{223}$ (AcX)	A chem, genet (1C31)		α; β stable (cons energy) (HPS)	11.2 d (1C31)	5.860 (weak), 5.730 (9%), 5.704 (53%), 5.596 (24%), 5.528 (9%), 5.487 (2%), 5.419 (3%) spect (4R52b); 5.750 (11%), 5.719 (53%), 5.607 (25%), 5.540 (9%), 5.433 (2%) spect (4A52a); no 6.0-6.1 α (lim 0.5%) (13H50); others (11L34, 4R36, 4R37)	0.144, 0.155, 0.180, 0.270, 0.340 cryst spect (8F40); 0.026, 0.064, 0.081, 0.099, 0.116, 0.154, 0.164, 0.180, 0.232, 0.268, 0.280, 0.322, 0.348, 0.444 spect conv (11S37)	Q_α 5.855 (13S53)	natural source, daughter Th^{227} (RdAc), daughter Fr^{223} (AcK), parent Em^{219} (An); daughter Ac^{223} (11M51); spall U (13S47, 6O47, 6F51)
Ra^{224} (ThX)	A chem, genet (1C31)		α; β stable (cons energy) (HPS)	3.64 d (1C31)	5.681 (95%), 5.448 (4.6%), 5.194 (0.4%) spect (4R49); 5.681 spect (15B36); 5.66 ion ch (2C45)	0.241 (e_K/γ 0.1) spect conv (4R52); no γ (1M28, 4F49)	Q_α 5.784 (13S53)  (4R52, HPS)	natural source, daughter Th^{228} (RdTh), parent Em^{220} (Tn); spall U (13S47, 6O47, 6F51)
Ra^{225}	A chem, genet (11E47, 4H47)		β^- (11E47, 4H47); no α (lim 0.1%) (9M52c)	14.8 d (4H50a); 14 d (11E47)	~0.31 spect (3F52a); ~0.2 abs (4H50a); <0.05 abs (11E47)			daughter Th^{229} parent Ac^{225} (11E47, 4H47, 4H50a); spall U (6F51)
Ra^{226}	A chem, genet (1C31)		α; β stable (cons energy) (HPS)	1622 y sp act (2K49a); 1631 y sp act (3C46); 1590 y sp act (1C31)	α_0 4.777 spect (4R52b); α_0 (94.3%), α_{188} (5.7%) spect (4A52c); α_0 (95.2%), α_{186} (4.8%) ion ch (7K51a); α_0 (93.5%), α_{187} (6.5%) spect (4R49a); others (109B51)	0.186 spect conv (10C51); ~0.19 (e/γ 0.88, K/L ~0.5) α-conv coinc abs (14V52); 0.188 (16H24, 7R36); (e/γ ~0.5) (8S43)	Q_α 4.863 (4R52b)  (4A52a, HPS)	natural source, daughter Th^{230} (Io), parent Em^{222} (Rn)
Ra^{227}	A n-capt, genet (8P49)		β^- (8P49, 6F50)	41.2 m (107B52)	1.30 spect (107B52)	0.291, 0.498 scint spect (107B52)		Ra-n-γ, parent Ac^{227} (8P49); spall U (6F50)
Ra^{228} ($MsTh_1$)	A chem, genet (1C31)		β^-	6.7 y (1C31)	~0.012 (?) cl ch (6L48, 6L49a); 0.053 spect, abs (8L39)	~0.03 cl ch (6L48, 6L49)	Q^-_β ~0.04 (13S53)	natural source, daughter Th^{232}, parent Ac^{228} ($MsTh_2$)
Ra^{229}	[B] n-capt, genet (41D52)		[β^-] (41D52)	[short] (41D52)				[Ra^{228}-n-γ, parent Ac^{229}] (41D52)
Ra^{230}	D chem (5J52)		β^- (5J52)	1 h (5J52)	1.2 abs, spect (5J52)			spall Th, parent Ac^{230} (5J52)
$_{89}Ac^{221}$	E genet, decay charac (57K51)		α (57K51)		7.6 range emuls (57K51)			descendent Pa^{225} (57K51)
Ac^{222}	B genet (11M49, 11M51)		α (11M51)	5.5 s (11M52)	6.96 ion ch (11M51)		Q_α 7.09, Q_{EC} 2.26 calc (13S53)	daughter Pa^{226}, parent Fr^{218} (11M49, 11M51)
Ac^{223}	A genet (13G48)		α 99%, EC 1% (11M51)	2.2 m (11M51)	6.64 ion ch (11M51)		Q_α 6.76, Q_{EC} 0.64 calc (13S53)	daughter Pa^{227}, parent Fr^{219}, parent Ra^{223} (AcX) (13G48, 11M49, 11M51)
Ac^{224}	A chem, genet (13G48)		EC ~90%, α ~10% (11M51)	2.9 h (11M51)	6.17 ion ch (11M51)		Q_α 6.28, Q_{EC} 1.37 calc, Q^-_β 0.29 calc (13S53)	daughter Pa^{228}, parent Fr^{220}, parent Ra^{224} (ThX), (13G48, 11M49, 11M51)

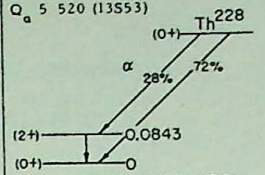
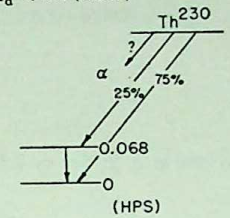
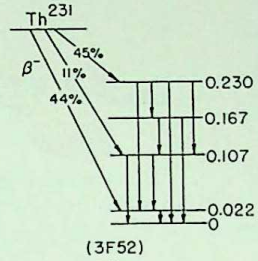
CC-0. In Public Domain. Gurukul Kangri Collection, Haridwar

Digitized by Arya Samaj Foundation Chennai and eGangotri

Isotope Z A	Class and identification	Percent abundance	Type of decay	Half-life	Energy of radiation in Mev: Particles	Energy of radiation in Mev: Gamma-transitions	Disintegration energy and scheme	Method of production and genetic relationships
$_{89}Ac^{225}$	A chem, genet (4H47, 11E47)		α (11E47, 4H47); β stable (cons energy) (HPS)	10.0 d (4H50a, 11E47)	5.80 ion ch (4H50a, 5C48)		$Q_α$ 5.90 (13S53)	daughter Ra^{225}, parent Fr^{221} (4H47, 11E47, 4H50a); daughter Pa^{229} (8H49a); daughter Th^{225} (11M49, 11M51); spall Th (17H50), U (6O47)
Ac^{226}	A chem, genet (6S48)		$β^-$ (6S48)	29 h (6S50)	1.17 abs (17H50)		$Q_α$ 5 44 est, Q_{EC} 0.6 est, $Q_{β^-}$ 1.07 est (13S53)	spall U, daughter Pa^{230}, parent Th^{226} (6S48, 6S50); spall Th (17H50, 11M50); daughter Pa^{230}, parent Th^{226} (11M50)
Ac^{227}	A chem, genet (1C31)		$β^-$ ~99% (7P39, 8P49a); α 1.2% (2M14, 7P39, 7P46, 8P49a)	22.0 y (13H50a); 21.7 y (4C44); 13.5 y (1C31)	α: 4.942 spect (4R52b); 4.94 (100%) ion ch (13G48a); others (3G47) $β^-$: 0.04 spect (3F50); ~0.02 cl ch (7P46); <0.03 abs (6L44)	0.037 (weak) abs (6L43, 6L44, 7P46); (0.2%) (6L50)	Ac^{227}, I = 3/2 (36T51) $Q_α$ 5.03, $Q_{β^-}$ ~0.08 calc (13S53)	natural source, daughter Pa^{231}, parent Th^{227} (RdAc); parent Fr^{223} (AcK) (7P39, 7P46); daughter Ra^{227} (8P49)
Ac^{228} ($MsTh_2$)	A chem, genet (1C31)		$β^-$	6.13 h (1C31)	2.18 (10%), 1.85 (9%), 1.72 (7%), 1.15 (53%), 0.66 (8%), 0.46 (13%) spect (82C52); 2.03, 1.74, 1.10 spect (5J51); others (4F38, 6L38, 3L39)	0.058, 0.129, 0.184, 0.338, 0.462, 0.914, 0.969 spect conv (13B24); 0.333, 0.462, 0.913, 0.968 spect (5T26); 0.063, 0.146, 0.186, 0.338, 0.533, 0.590, 0.905 spect conv (5J51)	$Q_α$ 4.66 est, $Q_{β^-}$ 2.18 (13S53)	natural source, daughter Ra^{228} ($MsTh_1$), parent Th^{228} (RdTh)
Ac^{229}	B chem, n-capt (41D52)		$β^-$ (41D52)	66 m (41D52)			$Q_{β^-}$ 1.0 est (13S53)	daughter Ra^{229} (41D52)
Ac^{230}	F genet (5J52)		$β^-$ (5J52)	<1 m genet (5J52)	~2.2 abs, spect (5J52)			daughter Ra^{230} (5J52)
$_{90}Th^{223}$	B genet (11M52)		α (11M52)	~0.1 s est (11M52)	7.55 ion ch (11M52)		$Q_α$ 7.69 (13S53)	daughter U^{227}, parent Ra^{219} (11M52)
Th^{224}	A genet (11M49, 11M51)		α (11M51); β stable (cons energy) (HPS)	~1 s est (11M51)	7.13 ion ch (7O50)		$Q_α$ 7.26 (13S53)	daughter U^{228}, parent Ra^{220} (11M49, 11M51)
Th^{225}	A chem, genet (11M49, 11M51)		α ~90%, EC ~10% (11M51)	8.0 m (11M51)	6.57 ion ch (11M51)		$Q_α$ 6.69, Q_{EC} 0.55 calc (13S53)	daughter U^{229}, parent Ra^{221}, parent Ac^{225} (11M49, 11M51)
Th^{226}	A chem, genet (4S48)		α (4S48); β stable (cons energy) (HPS)	30.9 m (4S48)	$α_0$ (78%), $α_{117}$ (22%) spect (21S52); 6.30 ion ch (1J48)		$Q_α$ 6.41 (13S53)	daughter U^{230}, parent Ra^{222} (4S48); daughter Ac^{226} (6S48, 6S50)

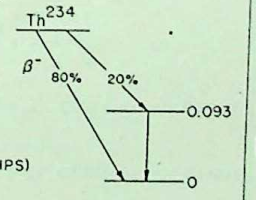
CC-0. In Public Domain. Gurukul Kangri Collection, Haridwar

Digitized by Arya Samaj Foundation Chennai and eGangotri

Isotope Z A	Class and identification	Percent abundance	Type of decay	Half-life	Energy of radiation in Mev: Particles	Energy of radiation in Mev: Gamma-transitions	Disintegration energy and scheme	Method of production and genetic relationships
$_{90}Th^{227}$ (RdAc)	A chem, genet (1C31)		α; β stable (cons energy (HPS)	18.6 d (8P49b); 18.9 d (1C31)	6.030 (19%), 6.001 (5%), 5.972 (21%), 5.952 (13%), 5.922 (~2%), 5.860 (4%), 5.796 (2%), 5.749 (17%), 5.728 (~1%), 5.704 (15%), 5.651 (~2%) spect (4R52b); 6.049 (20%), 6.017 (4%), 5.988 (25%), 5.966 (4%), 5.922 (~1%), 5.868 (2.5%), 5.815 (~1%), 5.764 (20%), 5.742 (4%), 5.717 (15%), 5.672 (2.5%) spect (11L34)	0.050, 0.057, 0.080, 0.101, 0.113, 0.129, 0.208, 0.240, 0.258 cryst spect (8F40); 0.050 (3%), 0.120 (13%), 0.280 (50%) abs (3R50); 0.050 (5%), 0.125 (10%), 0.270 (26%) abs (3B44); 0.050 (~3%), 0.125 (23%) abs (9T42)	$Q_α$ 6.138 (13S53)	natural source, daughter Ac^{227}, parent Ra^{223} (AcX); daughter Pa^{227} (13G48, 11M51); spall U (6O47)
Th^{228} (RdTh)	A chem, genet (1C31)		α; β stable (cons energy) (HPS)	1.90 y (1C31)	5.423 (72%), 5.338 (28%) spect (4R49b)	0.0843 spect conv (4R52a); 0.083 (e/γ 12) α-conv coinc abs (14V52); 0.083 (2.1%, e/γ = 10) crit abs (3R53); others (1M28, 11S41a, 3R50, 103B51)	$Q_α$ 5.520 (13S53)  (4R49b, 4R52α, HPS)	natural source, daughter Ac^{228} ($MsTh_2$), parent Ra^{224} (ThX); daughter U^{232} (9G49); daughter Pa^{228} (13G48b, 11M51)
Th^{229}	A chem, genet (11E47, 4H47)		α; β stable (cons energy) (HPS)	7340 y genet (4H50a); ~10^4 y genet (11E47)	5.02 (~10%), 4.94 (~20%), 4.85 (~70%) ion ch (4H50a)		$Q_α$ 5.11 (13S53)	daughter U^{233}, parent Ra^{225} (11E47, 4H47, 4H50a)
Th^{230} (Io)	A chem, genet (1C31)		α; β stable (cons energy) (HPS)	8.0×10^4 y sp act (8H49b); 8.2×10^4 y genet (1C30)	4.682 (~75%), 4.613 (~25%), 4.51 (?) (weak) spect (4R48); 4.66 range air (1G22), ion ch (2C44, 2C45)	0.068, 0.228 (very weak) spect conv (4R51); 0.068 (0.85%), 0.140 (0.33%), 0.240 (0.05%) abs (4C48); ~0.07 (coinc with α, e/γ ~46) ~ α-conv coinc abs (14V52, 10F51); ~0.068 (0.5%), 0.190 (0.3%) abs (3R50); ~0.07 (coinc with α), ~0.2 (coinc with α) α-γ, α-conv coinc abs (5P51); others (6J51, 5W39)	$Q_α$ 4.765 (13S53)  (HPS)	natural source, daughter U^{234} (U_{II}), parent Ra^{226}; daughter Pa^{230} (4S48a)
Th^{231} (UY)	A chem, genet (1C31)			25.64 h (1J51); 25.5 h (3K49); 24.6 h (1C31); 24.0 h (12G32)	0.302 (44%), 0.216 (11%), 0.094 (45%) spect (3F52); 0.39 (~20%), 0.19 (~40%), 0.10 (~40%) spect (10S51); 0.2 abs (5E37, 1J51)	γ_1 0.022, γ_2 0.059, γ_3 0.063, γ_4 0.085, γ_5 0.107, γ_6 0.122, γ_7 0.167, γ_8 0.208, γ_9 0.230 ($\gamma_2+\gamma_3/\gamma_4/\gamma_5/\gamma_6/\gamma_7/\gamma_8/\gamma_9$ = 0.40/1.00/0.065/0.02/0.018/0.003/0.001) spect conv, scint spect (3F52); 0.059, 0.063, 0.082, 0.120 spect conv (10S51); 0.035 (>80%), 0.210 abs (3K49)	$Q_α$ 4.19 calc (13S53) $Q^-_β$ 0.324 (3F52)  (3F52)	natural source, daughter U^{235} (AcU), parent Pa^{231}; Th-n-2n (5N38, 13S52)
Th^{232}	A chem, genet (1C31)	100 (1A35, 1D36)	α; β stable (cons energy) (HPS)	1.39×10^{10} y sp act (6K38); spont fission: 1.4×10^{18} y (24S52)	3.98 ion ch (2C45); 3.98 range emuls (7F51a); 4.20 ion ch (1S37)	~0.055 (coinc with 24% of α) α-conv coinc emuls (15D52); ~0.075 (coinc with ~20% of α) α-conv coinc emuls (5A52)	$Q_α$ 4.05 (13S53)	natural source, parent Ra^{228} ($MsTh_1$)

CC-0. In Public Domain. Gurukul Kangri Collection, Haridwar

Digitized by Arya Samaj Foundation Chennai and eGangotri

Isotope Z A	Class and identification	Percent abundance	Type of decay	Half-life	Energy of radiation in Mev: Particles	Energy of radiation in Mev: Gamma-transitions	Disintegration energy and scheme	Method of production and genetic relationships
$_{90}Th^{233}$	A chem, n-capt (1M38)		β^- (13S47a)	23.3 m (2B50); 23.5 m (13S47a); 23.6 m (31R52); 23 m (2G41)	1.23 spect (2B50, 31R52); 1.24 spect (3F53); 1.2 abs (13S52)	0.098 (0.25%), 0.172 (0.03%), 0.350 (0.004%), 0.448 (0.1%), 0.662 (0.05%) scint spect (3F53); no γ (2B50, 31R52)	Q_a 3.79 est, Q_β^- 1.23 (13S53)	Th-n-γ (1M38, 13S47a, 13S41, 2G41); Th-d-p (9G49); parent Pa^{233} (1M38)
Th^{234} (UX_1)	A chem, genet (1C31)		β^-	24.10 d (3K48); 24.1 d (3S39); 24.5 d (1C31)	0.205 (~80%), 0.111 (~20%) spect (16B46); 0.192 (56%), 0.104 (44%) spect (19H50); 0.190 spect (7J46); 0.20, 0.1 abs (4F38a)	0.090 (e/γ ~0.2) spect conv (19H50); 0.093 (~20%, e_L/γ ~0.34), 0.180 (4.5%) spect conv, abs (16B46); 0.092 (1M23)	Q_β^- 0.20 (13S53) 	natural source, daughter U^{238}, parent Pa^{234} (UX_2)
Th^{235}	[B] n-capt, genet (20H50)		[β^-] (20H50)	<<10 m genet (20H50)				[Th^{234}-n-γ, parent Pa^{235}] (20H50)
$_{91}Pa^{225}$	E excit, decay charac (57K51)		α (57K51)	2.0 s (57K51)				spall Th, ancestor Ac^{221} Fr^{217}, At^{213} (57K51)
Pa^{226}	B chem, genet (11M49, 11M51)		α (11M51)	1.8 m (11M51)	6.81 ion ch (11M51)		Q_a 6.93, Q_{EC} 2.8 calc (13S53)	spall Th, parent Ac^{222} (11M49, 11M51, 11M52)
Pa^{227}	A chem, genet (13G48)		α ~85%, EC ~15% (11M51)	38.3 m (11M51)	6.46 ion ch (11M51)		Q_a 6.58, Q_{EC} 1.08 calc (13S53)	spall Th, parent Ac^{223}, parent Th^{227} (RdAc) (13G48, 11M51); daughter Np^{231} (13G48b); spall U (6O48)
Pa^{228}	A chem, genet (13G48)		EC ~98%, α ~2% (11M51)	22 h (11M51)	6.09 (75%), 5.85 (25%) ion ch (11M51)		Q_a 6.20, Q_{EC} 2.05 calc (13S53)	spall Th, daughter U^{228}, parent Ac^{224}, parent Th^{228} (RdTh) (13G48, 11M49, 11M51)
Pa^{229}	A chem, genet (8H49a)		EC 99+%, α 0.25% (21S51); EC ~99%, α ~1% (11M51)	1.5 d (8H48)	5.69 ion ch (11M48); 5.66 ion ch (8H48)		Q_a 5.79, Q_{EC} 0.37 calc (13S53)	Th^{230}-d-3n, parent Ac^{225} (8H49a); daughter U^{229} (11M51)
Pa^{230}	A chem, genet, excit (4S48)		EC ~92%, β^- ~8% (4S49); α ~0.003% (11M50)	17.7 d (5O49), 17.0 d (4S48)	β^-: ~0.43 abs (5O49)	0.94 abs (5O49)	Q_a 5.45 est, Q_β^- 0.57 est, Q_{EC} 1.28 est (13S53)	Th-d-4n, Th-α-p5n, parent U^{230} (4S48); Th^{230}-d-2n (8H49a); Pa-d-p2n, Pa-α-an (5O49); U^{233}-d-an (8H49); parent Th^{230} (Io), parent Ac^{226} (11M50)
Pa^{231}	A chem, genet (1C31)		α; β stable (cons energy) (HPS)	3.43×10^4 y sp act (8W49); 3.2×10^4 y sp act (2G30)	5.042 (11%), 5.002 (47%), 4.938 (25%), 4.838 (3%), 4.720 (11%), 4.660 (1-3%) spect (4R49c, 13C51); ~5.0 (85%), ~4.7 (15%) ion ch (2C44, 9T46a, 13G48a)	0.034, 0.038, 0.057, 0.064, 0.082, 0.102, 0.198, 0.259, 0.301, 0.331, 0.357, 0.383 spect conv (10F52a); 0.095, 0.294, 0.323 spect conv (1M28a); 0.027 (9%), 0.087, 0.100, 0.30 (4%) aba, crit abs (3R52a); 0.044, 0.066 cl ch (4T52); 0.027 crit abs, ion ch (17S51); others (4S46, 4T49)	Pa^{231}, I = 3/2 (87M50) Q_a 5.131 (13S53)	natural source, daughter Th^{231} (UY), parent Ac^{227}; Th-d-3n (4S48); daughter U^{231} (14C50)

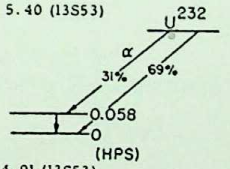
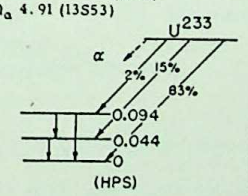
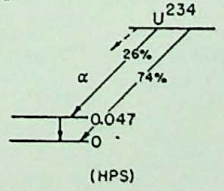
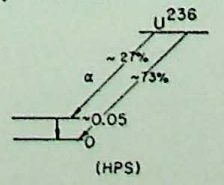
CC-0. In Public Domain. Gurukul Kangri Collection, Haridwar

Digitized by Arya Samaj Foundation Chennai and eGangotri

Isotope Z A	Class and identification	Percent abundance	Type of decay	Half-life	Energy of radiation in Mev: Particles	Energy of radiation in Mev: Gamma-transitions	Disintegration energy and scheme	Method of production and genetic relationships
$_{91}Pa^{232}$	A chem, genet (9G49)		β^- (9G49); no EC (lim 2%) (88B52a)	1.32 d (1J50); 1.4 d (5O49); 1.6 d (9G49)	0.99 (~30%), 0.64 (~10%), 0.28 (~60%) spect (35P52); ~0.28 abs (1J48b)	~0.23 (~30%), 1.05 (~100%) abs (1J48b); 0.21, 1.0 abs (5O49)	Q_α 4.70 est, Q^-_β 1.48, Q_{EC} 0.61 est (13S53)	Th-d-2n (9G49, 4S48, 1J50); Th-α-p3n (4S48); Pa-d-p (5O49); Pa-n-γ (1J50); parent U^{232} (9G49, 5O49)
Pa^{233}	A chem, genet (1M38, 2G41, 13S41)		β^- (1M38, 2G41, 13S41)	27.4 d (2G41)	0.530, 0.430 spect (3F51); 0.5 abs (13S52); ~0.2 spect, abs (21H41, 2L47, 11K50); ~0.7 spect (11F44)	0.029, 0.041, 0.058, 0.076, 0.087, 0.105, 0.273, 0.302, 0.313, 0.342, 0.377, 0.400, 0.416 spect conv (11K50); 0.028, 0.040, 0.058, 0.076, 0.087, 0.105, 0.302, 0.343, 0.417 spect conv (7K51b); 0.0287, 0.0405, 0.0754, 0.0870 (rel abund 100/75/3/3) cryst spect (88B52a); 0.084, 0.298, 0.309, 0.337 spect conv (2L47); no γ >~0.4 abs (11K50)	Q_α 4.46 est, Q^-_β 0.53 (13S53)	daughter Th^{233} (1M38, 2G41, 13S41, 16H41a, 13S47a); parent U^{233} (13S47a); daughter Np^{237} (4H47); Th-d-n (4S48, 9G49); Th-α-p2n (4S48); daughter Np^{237} (15M47)
Pa^{234} (UX_2)	A chem, genet (1C31)		β^- 99+%, IT 0.15% (4F38a, 16B45)	1.175 m (11ZB51); 1.14 m (1C31)	2.32 (80%), 1.50 (13%), 0.60 (?) (~7%) spect (19H50); 2.32 (98%) spect (16B45)	0.817 (e_K/γ 0.04) spect conv (19H50); 0.394 (with IT, 0.15%, e/γ ~1), ~0.9 (~2%), ~1.5 (~0.2%) spect, spect conv (16B45); 0.822, 0.806, 0.782 (weak, e/γ large) spect conv (16B43a)	Q^-_β 2.32 (16B45)	natural source, daughter Th^{234} (UX_1), parent U^{234} (U_{II})
Pa^{234} (UZ)	A chem, genet (1C31)		β^-	6.7 h (1C31)	~1.2 (10%), 0.45 (90%) spect (16B45); 1.6, 0.6 abs (4F38a)	0.85 (two γ's) abs, β-γ coinc (16B45); ~0.7 (two γ's) abs, γ-γ coinc (4F38a, 4F38b)	Q^-_β 2.2 (?) est (13S53); Q^-_β 1.95 (4F49)	natural source, parent U^{234} (U_{II}); Pa^{233}-n-γ (50K52)
Pa^{235}	B chem, excit, sep.isotopes (11M50); genet (20H50)		β^- (11M50, 20H50)	23.7 m (11M50); 23 m (20H50)	1.4 abs (11M50)	no γ, abs (11M50)		U^{238}-p-α, U^{238}-d-αn (11M50); daughter Th^{235} (20H50)
$_{92}U^{227}$	B chem, genet (11M52)		α (11M52)	1.3 m (11M52)	6.8 ion ch (11M52)		Q_α 7.14 est (13S53)	Th-α-9n, parent Th^{223} (11M52)
U^{228}	A chem, genet (11M49, 11M51)		α ~80%, EC ~20% (11M51)	9.3 m (11M51)	6.67 ion ch (7O50)		Q_α 6.79, Q_{EC} 0.30 calc (13S53)	Th-α-8n, parent Th^{224}, parent Pa^{228} (11M49, 11M51); daughter Pu^{232} (8J48)
U^{229}	A chem, genet (11M49, 11M51)		EC ~80%, α ~20% (11M51)	58 m (11M51)	6.42 ion ch (11M51)		Q_α 6.53, Q_{EC} 1.29 calc (13S53)	Th-α-7n, parent Th^{225}, parent Pa^{229} (11M49, 11M51)
U^{230}	A chem, genet (4S48)		α (4S48); β stable (cons energy) (HPS)	20.8 d (4S48)	5.85 ion ch (1J48); α_0 (77%), α_{70} (23%) spect (21S52)		Q_α 5.95 (13S53)	daughter Pa^{230}, parent Th^{226}, Th-α-6n (4S48); daughter Pa^{230}, Pa-d-3n, Pa-α-p4n (5O49); daughter Pu^{234} (13P49); spall U (6O47)
U^{231}	A chem, sep isotopes, excit (5O49); genet (14C50)		EC 99+%, α 5.5×10^{-3} % (14C50)	4.3 d (14C50); 4.2 d (5O49)	5.45 ion ch (14C50)	0.051, 0.064, 0.076 spect conv (8O50)	Q_α 5.55, Q_{EC} 0.34 calc (13S53)	Pa^{231}-d-2n, Pa^{231}-α-p3n (5O49); Th-α-5n (14C50, 8O50); parent Th^{227}, parent Pa^{231} (14C50)

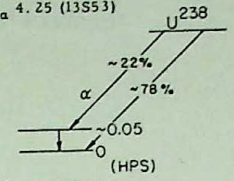
Digitized by Arya Samaj Foundation Chennai and eGangotri

CC-0. In Public Domain. Gurukul Kangri Collection, Haridwar

Isotope Z A	Class and identification	Percent abundance	Type of decay	Half-life	Energy of radiation in Mev: Particles	Energy of radiation in Mev: Gamma-transitions	Disintegration energy and scheme	Method of production and genetic relationships
$_{92}U^{232}$	A chem, genet (9G49)		α (9G49); β stable (cons energy) (HPS)	70 y yield (8J49); ~30 y yield (9G49)	5.31 range Al (1J48a); 5.27 range air (12K44); α_0 (69%), α_{58} (31%) spect (21S52)	~0.060 (coinc with 30% of α) α-conv coinc emuls (15D52)	Q_α 5.40 (13S53) 	daughter Pa^{232}, parent Th^{228} (RdTh) (9G49); daughter Pu^{236} (8J49); daughter Pa^{232}, Pa^{231}-d-n, Pa^{231}-α-p2n (5O49); Th-α-4n (7N49)
U^{233}	A chem, genet (13S47a, 13S52)		α (13S52); β stable (cons energy) (HPS)	1.62×10^5 y sp act + mass spect (8H52a); 1.63×10^5 y sp act + mass spect (15L45); 1.2×10^5 y yield (13S52)	4.823 ion ch (5C48); α_0 (83%), α_{44} (15%), α_{94} (2%) spect (4A52a); 4.80 abs air (15C47); others (11E47)	0.0428 (0.05%), 0.0561 (0.01%) ion ch (12W52); ~0.043, ~0.056, 0.099 α-conv coinc emuls (113B52); 0.04, 0.08 (0.8%, e/γ ~8), 0.31 (0.1%, e/γ ~3) abs (4S52); 0.04, 0.09, 0.36 (all coinc with α) α-γ, α-conv coinc abs (5P51)	Q_α 4.91 (13S53) 	daughter Pa^{233} (13S47a); parent Th^{229} (11E47, 4H47)
U^{234} (U_{II})	A chem, genet, mass spect (1C31)	0.0058 (1B50)	α; β stable (cons energy) (HPS)	2.48×10^5 y sp act (12F52); 2.52×10^5 y sp act, sp act + mass spect (13K52, 13K49); 2.67×10^5 y yield (10G49); 2.35×10^5 y sp act + mass spect (15C46); spont fission: 2×10^{16} y (13G52)	4.763 ion ch (2C44); α_0 (74%), α_{47} (26%) spect (4A52a); 4.76 ion ch (1S39, 13G51); 4.78 range air (18S37), ion ch (3A47)	0.050, 0.117 scint spect (17S51a); γ_1 0.053, γ_2 0.093, γ_3 0.118 ($\gamma_1/\gamma_2/\gamma_3$ = 1/~0.2/0.4) scint spect (11B52a); 0.055 (coinc with α, e/γ large) α-conv coinc emuls (4T52); 0.065 (coinc with α, e/γ large) α-γ coinc abs, α-conv coinc abs (5P51); others (10M47, 17S51)	Q_α 4.85 (13S53) 	natural source, daughter Pa^{234} (UX_2 and UZ), parent Th^{230} (Io)
U^{235} (AcU)	A chem, mass spect (1C31)	0.715 (1B50)	α; β stable (cons energy) (HPS)	7.13×10^8 y sp act (12F52); 7.07×10^8 y radiogenic Pb ratios (6N39); spont fission: 1.9×10^{17} y (24S52)	4.58 (10%), 4.47 (?) (~3%), 4.40 (83%), 4.20 (4%) ion ch (13G51); 4.39 ion ch (15V52)	γ_1 0.094, γ_2 0.143, γ_3 0.184, γ_4 0.289, γ_5 0.386 ($\gamma_1/\gamma_2/\gamma_3/\gamma_4/\gamma_5$ = 0.9/0.2/1.0/0.1/0.05) scint spect (11B52a); 0.187 abs (20S52); 0.167 abs (10M49)	Q_α 4.66 (13S53) U^{235}, I = 5/2 (102S50)	natural source, parent Th^{231} (UY)
U^{236}	A chem, n-capt, mass spect (9W45, 13G51a)		α (13G51a); β stable (cons energy) (HPS)	2.39×10^7 y sp act (12F52); 2.46×10^7 y sp act (1J51a)	4.499 ion ch (1J51a); 4.5 ion ch (13G51a)	~0.050 (coinc with 27% of α) α-conv coinc emuls (15D52)	Q_α 4.58 (13S53) 	U^{235}-n-γ (9W45, 13G51a, 1J51a)

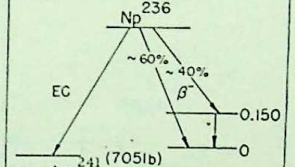
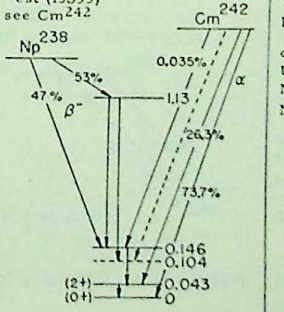
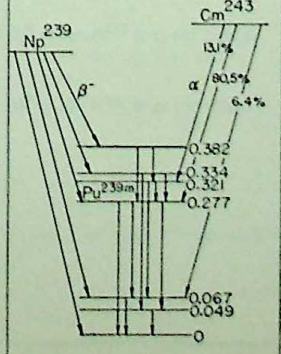
CC-0. In Public Domain. Gurukul Kangri Collection, Haridwar

Digitized by Arya Samaj Foundation Chennai and eGangotri

Isotope Z A	Class and identification	Percent abundance	Type of decay	Half-life	Energy of radiation in Mev: Particles	Energy of radiation in Mev: Gamma-transitions	Disintegration energy and scheme	Method of production and genetic relationships
$_{92}U^{237}$	A chem, excit (5N40, 12M40)		β^- (5N40, 12M40)	6.75 d (81H52); 6.63 d (13M48); 6.8 d (1W48)	0.245, other β^- (weak) spect (3F53); ~0.23 spect (13M48)	γ_1 0.027, γ_2 0.043, γ_3 0.059, γ_4 0.165, γ_5 0.207 (e_K/γ 1.6, K/L 5.0), γ_6 0.269, γ_7 0.334, γ_8 0.370, γ_9 0.430 ($\gamma_3/\gamma_5/\gamma_7$ = 37/21/2.5) scint spect, spect conv (3F53); 0.0598 cryst spect (88B52a); 0.032, 0.057, 0.204, 0.260 abs, spect conv (13M48); 0.14, 0.23, 0.53 abs (17B43)	Q_β^- 0.514 (3F53)	U-n-2n (12M40, 5N40, 1W48, 2A44); parent Np^{237} (1W48); daughter Pu^{241} (2K45, 13S49); U-d-t (17B43, 2A44, 8J49); U-α-an (8J49)
U^{238} (U_I)	A chem, genet, mass spect (1C31)	99.28 (1B50)	α; β stable (cons energy) (HPS)	4.49×10^9 y sp act (13K49); 4.51×10^9 y sp act (6N39); spont fission: 8.0×10^{15} y (24S52, 17S46)	4.18 ion ch (3A47, 2C44); 4.21 range (1S39)	~0.045 (coinc with 22% of α) α-conv coinc emuls (15D52); 0.048 (coinc with 23% of α) α-conv coinc emuls (1Z52); ~0.050 (coinc with 24% of α) α-conv coinc emuls (5A52a)	Q_α 4.25 (13S53) 	natural source (18B96), parent Th^{234} (UX_1)
U^{239}	A n-capt (1M37)		β^- (12M39)	23.54 m (14M43); 23.5 m (4F47, 13M47)	1.21 spect (3F53); 1.20 abs (4F47, 4F47a); 1.2 abs (1W42, 14M42); 1.12 spect (5S47)	0.0736 spect conv, scint spect (3F53); 0.073 spect conv, abs (5S47); 0.076, >0.3 (<10%) abs (4F47, 4F47a)	Q_β^- 1.28 (3F53); Q_α 4.12 est (13S53)	U-n-γ (1M37, 2I39, 12M39, 22S42); parent Np^{239} (12M40a, 22S42); U-d-p (13S49a)
U^{240}	A chem, n-capt (4S49a)		β^- (4S49a)	~18 h genet (4S49a)				U-n-γ (second order reaction) (4S49a); parent Np^{240} (8H48b)
$_{93}Np^{231}$	A chem, genet, excit, sep isotopes (15M50)		α (15M50)	~50 m (15M50)	6.28 ion ch (15M50)		Q_α 6.39, Q_{EC} 1.92 calc (13S53)	U^{238}-d-9n, U^{233}-d-4n, U^{235}-d-6n, parent Pa^{227} (15M50)
Np^{232}	D chem (15M50)		EC (15M50)	~13 m (15M50)		hard γ (15M50)	Q_α 6.04 est, Q_{EC} 2.7 est (13S53)	U^{233}-d-3n (15M50)
Np^{233}	A chem, excit, sep isotopes (15M50, 7O51)		EC 99+%, α ~10^{-3}% (15M50)	35 m (15M50)	5.53 ion ch (15M50); conv: ~0.3 (15M50)		Q_α 5.63, Q_{EC} 1.09 calc (13S53)	U^{233}-d-2n, U^{235}-d-4n (15M50); U^{233}-p-n (7O51)
Np^{234}	A chem, excit, genet, sep isotopes (8J49)		EC (L/K ~1) (7O51a); no α (lim 0.01%) (8H49); no β^+ (8H49)	4.40 d (8H49); 4.4 d (5O49)		0.177, 0.442, 0.803, 1.42 spect conv (7O51a); 1.9 abs (8H49, 5O49)	Q_α 5.39 est, Q_{EC} 1.8 est (13S53)	U^{235}-d-3n, U^{235}-α-p4n (8J49); U^{235}-p-2n (11G46); U^{233}-d-n (8H49); U^{233}-α-p2n (8H49, 13P49); Pa^{231}-α-n (5O49); daughter Pu^{234} (13P49)
Np^{235}	A chem, excit, sep isotopes (8J49)		EC (L/K >9) (8J52); α ~5×10^{-3}% (8J52)	410 d (8J52)	5.06 ion ch (8J52)		Q_α 5.15, Q_{EC} 0.17 calc (13S53)	U^{235}-d-2n (8J49, 8J52); U^{233}-α-pn (8H49)

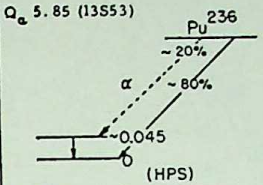
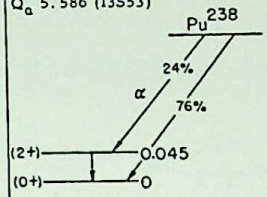
CC-0. In Public Domain. Gurukul Kangri Collection, Haridwar

Digitized by Arya Samaj Foundation Chennai and eGangotri

Isotope Z A	Class and identification	Percent abundance	Type of decay	Half-life	Energy of radiation in Mev: Particles	Energy of radiation in Mev: Gamma-transitions	Disintegration energy and scheme	Method of production and genetic relationships
$_{93}Np^{236}$	A chem, genet, sep isotopes, excit (8J49)		β^- ~33%, EC ~67% (L/K ~2) (7O51b)	22 h (8J49)	0.51 (~60%), 0.36 (~40%) spect (7O51b)	0.150 (e/γ large) spect conv (7O51b)	Q_a 5.00 est, Q_β^- 0.63 est, Q_{EC} 1.03 est (13S53)  see Am^{241} (7O51b)	U^{235}-d-n, U^{235}-a-p2n, U-d-4n (8J49); Np^{237}-d-p2n (8J49a); U^{233}-a-p (8H49); Np^{237}-n-2n (13G45, 13F50); parent Pu^{236} (8J49, 8J49a, 8H49, 13G52)
Np^{237m}	A genet (103B52)		IT (103B52)	6.3×10^{-8} s delay coinc (103B52)		0.060 scint spect (103B52)	see Am^{241} (7O51b)	daughter Am^{241} (103B52)
Np^{237}	A chem, genet, excit (1W48)		α (1W48); β stable (cons energy) (HPS)	2.20×10^6 y sp act (15M48)	4.77 ion ch (13G48c)	soft γ's (coinc with 80% of α) α-conv coinc emuls (15D52); soft γ, spect conv (15M45)	Np^{237}, I = 5/2 (87M50) Q_a 4.97 est (13S53)	daughter U^{237} (1W48); parent Pa^{233} (15M47)
Np^{238}	A chem, genet, n-capt, sep isotopes (13S46)		β^- (13S46, 13S49a)	2.10 d (3F50a); 2.0 d (13S49a)	1.272 (47%), 0.258 (53%) spect, spect coinc (3F50a); 1.39, 0.22 abs (1J49)	0.043, 0.047, 0.103 (L/M 1.6), 0.983, 1.03 (1.03 γ/0.98 γ = 1) spect, spect conv, β-γ, β-x coinc (3F50a); no 0.047 γ (63M52a, 4A52a); 1.1 abs (13S49a); 0.075, 1.2 abs, abs conv (1J49)	Q_a 4.83 est, Q_β^- 1.42, Q_{EC} 0.38 est (13S53) see Cm^{242}  (4A52a)	U-d-2n (13S46, 13S49a, 14K49); U^{238}-d-2n (14K49); parent Pu^{238} (13S46, 14K49, 1J49, 8J49); daughter Am^{242} (13S49, 6S50a); U^{238}-a-p3n, U^{235}-a-p (8J49); Np^{237}-n-γ (1J49); Np^{237}-d-p (8J49a)
Np^{239}	A chem, n-capt, genet, excit (12M39, 12M40a)		β^- (12M40a)	2.33 d (1W42); 2.35 d (4F42); 2.3 d (3P46)	0.715, 0.654, 0.44, 0.33 spect (7T51); 0.718 (4.8%), 0.655 (1.7%), 0.441 (31%), 0.380 (10%), 0.329 (52%) spect (3F53); 0.705 (7%, not coinc with γ), 0.435 (46%), 0.310 (47%) spect (14G51); 1.179, 0.676, 0.403, 0.288 spect (5S47); others (22H45, 11F49)	0.049, 0.057, 0.061, 0.067 (coinc with 0.210 γ), 0.210, 0.227, 0.276 (last 3 γ's coinc with 0.435 β^-, 0.276 γ not coinc with 0.227 γ) spect conv, β-γ, γ-γ coinc (14G51); 0.013, 0.019, 0.044, 0.049, 0.057, 0.061, 0.067, 0.077, 0.105, 0.209, 0.228, 0.254, 0.277, 0.285, 0.316, 0.334 spect conv (3F53); 0.044, 0.049, 0.057, 0.061, 0.068, 0.105, 0.209, 0.228, 0.254, 0.277, 0.286 spect conv (7T51); 0.023, 0.049, 0.057, 0.061, 0.068, 0.106, 0.209, 0.228, 0.277 spect conv (11F49); 0.0576, 0.0618 cryst spect (26J52); 0.057, 0.061, 0.067, 0.206, 0.227, 0.275 spect conv (5S47); others (4F42, 22H45, 3P46)	Q_β^- 0.715 (3F53, 14G51)  (4A52a)	daughter U^{239} (12M40a, 22S42); parent Pu^{239} (14K46, 13S49a); U-d-n (13S46, 13S49a, 8J49); U-a-p2n (8J49); daughter Am^{243} (6S50a)

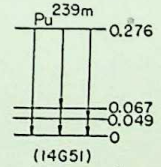
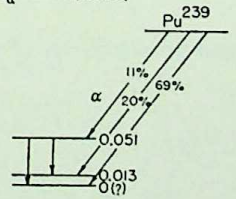
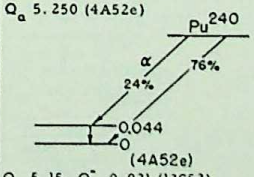
CC-0. In Public Domain. Gurukul Kangri Collection, Haridwar

Digitized by Arya Samaj Foundation Chennai and eGangotri

Isotope Z A	Class and identification	Percent abundance	Type of decay	Half-life	Energy of radiation in Mev: Particles	Energy of radiation in Mev: Gamma-transitions	Disintegration energy and scheme	Method of production and genetic relationships
$_{93}Np^{240}$	A chem, genet (8H48b)		β^- (8H48b)	7.3 m (8H48b)	~1.3 abs (8H48a)			daughter U^{240} (8H48b)
Np^{241}	B chem, cross bomb (7O51a)		β^- (7O51a)	60 m (7O51a)	0.89 spect (7O51a)	0.15, 0.20, 0.26, 0.58 spect conv (7O51a); ~0.7 abs (7O51a)		U^{238}-α-p (7O51a)
$_{94}Pu^{232}$	B chem, sep isotopes, excit, genet (7O51a)		α >2%, EC ≤98% (7O51a)	36 m (7O51a)	6.58 ion ch (7O51a)		Q_α 6.70, Q_{EC} 0.96 est (13S53)	U^{235}-α-7n, U^{233}-α-5n, parent U^{228} (7O51a)
Pu^{234}	A chem, genet, sep isotopes, excit (8H49, 13P49)		α ~4%, EC ~96% (7O51a, 23H52a)	9.0 h (7O51a); 8.5 h (13P49)	6.19 ion ch (7O51a); 6.2 ion ch (13P49)		Q_α 6.30, Q_{EC} 0.21 est (13S53)	U^{233}-α-3n (8H49, 13P49, 7O51a); U^{235}-α-5n (7O51a); parent U^{230}, parent Np^{234} (13P49, 7O51a); daughter Cm^{238} (23H52a)
Pu^{235}	B chem, excit, sep isotopes (7O51a)		EC 99+%, α ~0.002% (7O51a)	26 m (7O51a)	5.85 ion ch (7O51a)		Q_α 5.95, Q_{EC} 1.14 calc (13S53)	U^{233}-α-2n, U^{235}-α-4n (7O51a)
Pu^{236}	A chem, excit, sep isotopes, cross bomb, genet (8J49)		α (8J49); β stable (cons energy) (HPS)	2.7 y (8J49); spont fission: 3.5×10^9 y (13G52)	5.75 range air (8J49); 5.75 ion ch (13G53)	~0.045 (coinc with 20% of α) α-conv coinc emuls (15D52)	Q_α 5.85 (13S53)  (HPS)	U^{235}-α-3n, U^{238}-α-6n (8J49); Np^{237}-d-3n (8J49a); U^{233}-α-n (8H49, 13P49); daughter Cm^{240} (13S49b); daughter Np^{236} (8J49, 8J49a, 8H49, 13G52)
Pu^{237}	B chem, sep isotopes, cross bomb (8J49)		EC (8J49)	~40 d (8J49)		K, L-x, no γ (8J49)	Q_α 5.72 est, Q_{EC} 0.21 est (13S53)	U^{235}-α-2n, U-α-5n (8J49); Np^{237}-d-2n (8J49a)
Pu^{238}	A chem, sep isotopes, excit (13S46, 13S46a, 13S49a)		α (13S46); β stable (cons energy) (HPS)	89.6 y (1J50a); 92 y genet (13S49b); 77 y genet (1J49); spont fission: 3.8×10^{10} y (24S52)	5.492 (76%), 5.450 (24%) spect (4A52a); 5.47 range air (8T49); 5.51 range air (15C47)	0.045 spect conv (8O51); ~0.040 (coinc with 23% of α) α-conv coinc emuls (15D52); ~0.04 (e/γ ~700) α-γ coinc, scint spect (4A52d)	Q_α 5.586 (13S53)  (HPS)	U^{238}-d-2n (13S46, 13S49a, 14K49, 7E42, 8J49); U^{238}-α-4n, U^{235}-α-n (8J49); daughter Np^{238} (8J49, 1J49, 13S46a, 14K49); daughter Cm^{242} (13S49b)

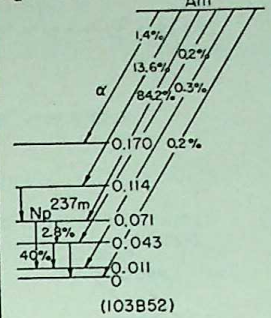
CC-0. In Public Domain. Gurukul Kangri Collection, Haridwar

Digitized by Arya Samaj Foundation Chennai and eGangotri

Isotope Z A	Class and identification	Percent abundance	Type of decay	Half-life	Energy of radiation in Mev: Particles	Energy of radiation in Mev: Gamma-transitions	Disintegration energy and scheme	Method of production and genetic relationships
$_{94}Pu^{239m}$	A genet (14G51)		IT (14G51)	1.1 x 10^{-9} s delay coinc (14G51)		0.049, 0.067, 0.210, 0.227, 0.276 spect conv, coinc (14G51)	see Np^{239}, Cm^{243}  (14G51)	daughter Np^{239}, parent Pu^{239} (14G51)
Pu^{239}	A chem, genet, mass spect (14K46)		α (14K46); β stable (cons energy) (HPS)	24,360 y sp act (10W51); 24,400 y sp act (11W46, 14F45); 24,300 y sp act (16C49); 24,100 y calorimetric (96S47); spont fission: 5.5 x 10^{15} y (24S52)	5.150 (69%), 5.137 (20%), 5.099 (11%) spect (4A52e); 5.147 (~70%), 5.097 (~30%) spect (4R50); 5.14 ion ch (10J48); 5.15 range air (15C47); 5.13 ion ch (17C51); 5.13 range air (8T49); conv: ~0.10 (weak) α-conv coinc emuls (15D52, 5A51)	γ_1 0.039, γ_2 0.0531, γ_3 0.100, γ_4 0.124, γ_5 0.384 ($\gamma_1/\gamma_2/\gamma_3/\gamma_4/\gamma_5$ = 0.4/1.4/1.1/0.5/0.3) spect conv, scint spect (3F52b); 0.0385 (2 x 10^{-3}%), 0.0520 (7 x 10^{-3}%) ion ch (12W51, 12W52); ~0.035, 0.05 α-conv coinc emuls (15D52); 0.05 α-conv coinc emuls (5A51); others (11I52)	Q_α 5.238 (13S53)  (4A52a, HPS)	daughter Np^{239} (14K46, 13S49a); U^{238}-α-3n (8J49); Pu^{238}-n-γ (9R48, 19B48)
Pu^{240}	A chem, n-capt, mass spect (15C44, 14F46, 21B44)		α (8J49); β stable (cons energy) (HPS)	6580 y genet (31S1); 6240 y sp act (11W51); 6760 y sp act (10W51)	5.162 (76%), 5.118 (24%) spect (4A52e)	0.0496 spect conv, scint spect (3F52b)	Q_α 5.250 (4A52e)  (4A52e)	Pu^{239}-n-γ (15C44, 14F46, 21B44); U^{238}-α-2n (8J49)
Pu^{241}	A chem, n-capt, mass spect, excit, genet (13S49, 13S49b, 13G50)		β^- 99+%, α ~10^{-3}% (13S49, 3T50e)	14 y genet (3T50e)	α: 4.91 ion ch (3T50e); β^-: 0.021 spect (3F52b); ~0.02 abs (13S49)	γ_1 0.100, γ_2 0.145 (γ_1/γ_2 = 5) scint spect (3F52b)	Q_α 5.15, Q_{β^-} 0.021 (13S53)	Pu^{240}-n-γ (13G50, 3T50e); U^{238}-α-n (13S49); parent Am^{241} (13S49, 16C49a); parent U^{237} (2K45, 13S49)
Pu^{242}	A chem, mass spect, n-capt, genet (3T50e)		α (3T50e); β stable (cons energy) (HPS)	~5 x 10^5 y genet (3T50e)	4.88 ion ch (3T50e)		Q_α 4.96 (13S53)	Pu^{241}-n-γ (3T50e, 3I49); daughter Am^{242m} (8O50a)
Pu^{243}	B chem, n-capt, cross bomb (25S51)		β^- (25S51)	4.98 h (81H52a); 5.0 h (25S51, 3T51)	0.39 spect (3T51); ~0.45 abs (25S51)	0.095, 0.12 spect conv (3T51)	Q_α 4.82 est, Q_{β^-} 0.67 est (13S53)	Pu^{242}-n-γ (25S51, 3T51); parent Am^{243} (3T51)
$_{95}Am^{237}$	B chem, excit (23H52a)		EC 99+%, α 0.005% (23H52a)	~1.3 h (23H52a)	6.01 ion ch (23H52a)		Q_α 6.20 est, Q_{EC} 1.6 est (13S53)	Pu^{239}-d-4n, Pu^{239}-p-3n (23H52a)
Am^{238}	B chem, excit (6S50a)		EC (6S50a); no α (lim 3 x 10^{-4}%) (23H52a)	2.1 h (23H52a)	conv (6S50a)		Q_α 5.99 est, Q_{EC} 2.22 est (13S53)	Pu^{239}-d-3n (6S50a, 23H52a)

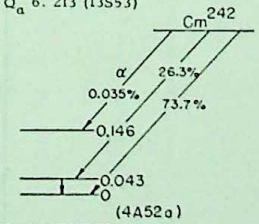
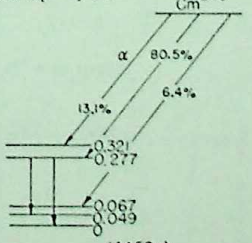
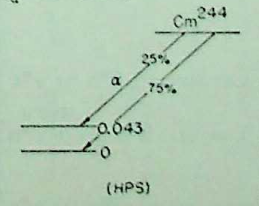
CC-0. In Public Domain. Gurukul Kangri Collection, Haridwar

Digitized by Arya Samaj Foundation Chennai and eGangotri

Isotope Z A	Class and identification	Percent abundance	Type of decay	Half-life	Energy of radiation in Mev: Particles	Energy of radiation in Mev: Gamma-transitions	Disintegration energy and scheme	Method of production and genetic relationships
$_{95}Am^{239}$	B chem, excit (13S49)		EC 99+%, α 0.003% (23H52a)	12 h (13S49)	5.75 ion ch (23H52a)	0.3 (10%) scint spect (23H52a); 0.3 abs conv (13S49)	$Q_α$ 5.85, Q_{EC} 0.78 calc (13S53)	Np^{237}-α-2n (13S49); Pu^{239}-p-n (6S50a); Pu^{239}-d-2n (13S49, 23H52a); Pu^{239}-α-p3n (23H52a)
Am^{240}	B chem, excit (13S49); chem, excit, cross bomb (6S50a)		EC (13S49); no α (lim 0.2%) (23H52a)	50 h (13S49); 53 h (23H52a)		no γ >0.7 (23H52a)	$Q_α$ 5.76 est, $Q^-_β$ 0.02 est, Q_{EC} 1.54 est (13S53)	Np^{237}-α-n (13S49); Pu^{239}-d-n (13S49, 6S50a, 23H52a); Pu^{239}-α-p2n (23H52a)
Am^{241}	A chem, n-capt, excit, mass spect (13S49)		α (13S49); β stable (cons energy) (HPS)	470 y sp act (20H52a); 475 y sp act (16C50)	5.546 (0.23%), 5.535 (0.34%), 5.503 (0.21%), 5.476 (84.2%), 5.433 (13.6%), 5.379 (1.4%) spect (4A52); 5.48 ion ch (13G48c); 5.47 range air (8T49)	$γ_1$ 0.0597 (40%, e/γ <1.5, with Np^{237m}), $γ_2$ 0.0263 (2.8%, e/γ ≤20), $γ_3$ 0.0209, $γ_4$ 0.0173, $γ_5$ 0.0135 ($γ_1/γ_2/γ_3/γ_4/γ_5$ = 1/0.069/0.155/0.56/0.32) ion ch, α-γ delay coinc (103B52); $γ_1$ 0.0598, $γ_2$ 0.0264 ($γ_1/γ_2$ = 1/0.30) cryst spect (88B52a), 0.0590, 0.0414, 0.0264 spect conv, scint spect (3F52b); others (13S49, 8O51, 5P51, 15D52)	Am^{241}, I = 5/2 (38F52) $Q_α$ 5.639 (13S53)  (103B52)	daughter Pu^{241} (13S49, 16C49a); parent Np^{237m} (103B52)
Am^{242m}	A chem, n-capt, genet (16M49, 13S49b)		$β^-$ 60%, EC (L) 20%, IT 20% (8O51)	16.01 h (44K52); 15.7 h (20H49a); 16 h (16M49)	0.628 spect (8O50a); 0.63 abs (15G50)	0.035, 0.038, 0.053 spect conv (8O51)	$Q^-_β$ 0.68 (HPS)	Am^{241}-n-γ (16M49, 13S49); parent Cm^{242} (16M49, 13S49b); parent Pu^{242} (8O50a)
Am^{242}	A chem, genet, mass spect, n-capt (13S49, 6S50a)		$β^-$, EC, α (8O51); (α/$β^-$ 0.01) (6S50a)	~100 y genet (6S50a)	$β^-$: 0.593 spect (8O51); ~0.5 abs (13S49)	0.038, 0.053 spect conv (8O51)	$Q_α$ 5.44 calc, $Q^-_β$ 0.65, Q_{EC} 0.86 est (13S53)	Am^{241}-n-γ, parent Cm^{242}, parent Np^{238} (13S49, 6S50a, 13S49b)
Am^{243}	A chem, mass spect (6S50a)		α (6S50a)	~10^4 y genet (6S50a)	5.267 (~90%), 5.226 (~10%) spect (4A52a); 5.27 ion ch (13G51b)	0.075 (coinc with 90% of α) α-γ coinc, scint spect (4A52a); 0.076 scint spect (89M52a)	$Q_α$ 5.430, $Q^-_β$ 0.00 calc (13S53)	Am^{242}-n-γ, parent Np^{239} (6S50a); daughter Pu^{243} (3T51)
Am^{244}	B chem, n-capt (6S50a)		$β^-$ (6S50a)	~25 m (6S50a)				Am^{243}-n-γ (6S50a)

CC-0. In Public Domain. Gurukul Kangri Collection, Haridwar

Digitized by Arya Samaj Foundation Chennai and eGangotri

Isotope Z A	Class and identification	Percent abundance	Type of decay	Half-life	Energy of radiation in Mev: Particles	Energy of radiation in Mev: Gamma-transitions	Disintegration energy and scheme	Method of production and genetic relationships
$_{96}Cm^{238}$	B chem.(6S48a); chem, genet (23H52a)		EC <90%, α >10% (75C52)	2.5 h (6S48a)	6.50 ion ch (6S48a)		Q_a 6.61, Q_{EC} 0.8 est (13S53)	Pu^{239}-α-5n (6S48a); parent Pu^{234} (23H52a)
Cm^{239}	D chem, excit (75C52)		EC ~100%, no α (lim 0.1%) (75C52)	~3 h (75C52)			Q_a 6.50 est, Q_{EC} 1.8 est (13S53)	Pu^{239}-α-4n (75C52)
Cm^{240}	A chem, genet (13S49b)		α (13S49b); no EC (lim 0.5%) (23H52)	26.8 d (13S49b); spont fission: 7.9×10^5 y (13G52)	6.25 ion ch (23H52); 6.3 range air (13S49b)		Q_a 6.37 (13S53)	Th-C-4n (23H52a); Pu^{239}-α-3n (13S49b, 23H52)
Cm^{241}	B chem, excit (13S49b, 23H52)		EC 99+%, α 0.2% (23H52a)	35 d (23H52)	5.90 ion ch (23H52a)		Q_a 6.3 est, Q_{EC} 0.9 est (13S53)	Pu^{239}-α-2n, Am^{241}-p-n (23H52, 23H52a)
Cm^{242}	A chem, genet (13S49b); mass spect (10R50)		α (13S49b); β stable (cons energy) (HPS)	162.5 d (24H50); 162 d (8J48a); spont fission: 7.2×10^6 y (24H51)	6.110 (73.7%), 6.066 (26.3%), 5.965 (0.035%) spect (4A52, 4A52d); 6.118 ion ch (20H52); 6.08 ion ch (13G48c)	0.043 spect conv (8O51); ~0.04 (e/γ ~600) α-γ coinc, scint spect (4A52d); ~0.045 (coinc with 23% of α) α-conv coinc emuls (15D52); ~0.04 (coinc with α) α-conv coinc (5P51)	see Np^{238} Q_a 6.213 (13S53)  (4A52a)	Pu^{239}-α-n (13S49b); daughter Am^{242} (13S49b, 13G50); Am^{241}-d-n (3T50a); daughter Cf^{246} (25H51)
Cm^{243}	A chem, mass spect, genet (10R50)		α (10R50)	~100 y genet (3T50b)	5.985 (6.4%), 5.777 (80.5%), 5.732 (13.1%) spect (4A52d); 5.89 (15%), 5.79 (85%) ion ch (3T50b)	0.226, 0.277 (both γ's coinc with 5.777 α) scint spect (4A52d)	Q_a 6.15 (4A52a) Q_{EC} 0.00 calc (13S53) see Np^{239}, Pu^{239m}  (4A52a)	Cm^{242}-n-γ (10R50); daughter Bk^{243} (3T50b)
Cm^{244}	A chem, mass spect (10R50)		α (10R50); β stable (cons energy) (HPS)	19 y (3T52); spont fission: 1.4×10^7 y (13G52)	5.798 (75%), 5.755 (25%) spect (4A52d)		Q_a 5.895 (13S53)  (HPS)	daughter Am^{244}, Cm^{243}-n-γ (10R50)
Cm^{245}	B chem, decay charac, genet (25H51)		α (25H51)	>500 y (25H51)	~5.6 ion ch (25H51)			daughter Bk^{245} (25H51)

CC-0. In Public Domain. Gurukul Kangri Collection, Haridwar

Digitized by Arya Samaj Foundation Chennai and eGangotri

Isotope, Z A	Class and identification	Percent abundance	Type of decay	Half-life	Energy of radiation in Mev		Disintegration energy and scheme	Method of production and genetic relationships
					Particles	Gamma-transitions		
$_{97}Bk^{243}$	A chem, n-capt, genet (3T50, 3T50b)		EC 99+%, α ~0.1% (3T50b)	4.6 h (3T50b)	6.72 (30%), 6.55 (53%), 6.20 (17%) ion ch (3T50b)		Q_a 6.83, Q_{EC} 1.46 calc (13S53)	Am^{241}-α-2n (3T50, 3T50b); Cm^{242}-d-n (25H51); parent Cm^{243} (3T50b)
Bk^{244}	D chem, decay charac (3T52)		EC (3T52)	~5 h (3T52)			Q_a 6.63 est, Q_{EC} 2.27 est (13S53)	Am^{241}-α-n (3T52)
Bk^{245}	B chem, excit, decay charac (25H51)		EC 99+%, α ~0.1% (25H51)	4.95 d (25H51)	6.33 (18%), 6.15 (48%), 5.90 (34%) ion ch (25H51)		Q_a 6.44, Q_{EC} 0.67 est (13S53)	Am^{243}-α-2n (3T52); Cm^{244}-d-n, Cm^{242}-α-p (25H51); parent Cm^{245} (25H51)
$_{98}Cf^{244}$	B chem, excit, decay charac (3T50c)		α, EC (?) (3T50d)	45 m (3T50d)	7.15 ion ch (3T50d)		Q_a 7.27, Q_{EC} 0.7 est (13S53)	U-C-6n (13G51c); Cm^{242}-α-2n (3T50c, 3T50d)
Cf^{246}	A chem, genet (13G51c)		α (13G51c); β stable (cons energy) (HPS)	35.7 h (25H51); spont fission: ~2000 y (3T52)	6.75 ion ch (13G51c)		Q_a 6.86 (13S53)	U-C-4n (13G51c); Cm^{243}-α-n, Cm^{244}-α-2n (25H51); parent Cm^{242} (25H51)

Digitized by Arya Samaj Foundation Chennai and eGangotri

CC-0. In Public Domain. Gurukul Kangri Collection, Haridwar

Digitized by Arya Samaj Foundation Chennai and eGangotri

1A20 F. W. Aston, Phil. Mag. 40, 628 (1920)

1A35 F. W. Aston, Proc. Roy. Soc. (London) 149A, 396 (1935)

2A44 M. B. Allen, University of California Radiation Laboratory Classified Report RL-4.6.270 (July 1944)

3A47 F. Alder, P. Huber, and F. Metzger, Helv. Phys. Acta 20, 234 (1947)

3A51 F. Alder and F. C. Yu, Phys. Rev. 81, 1067 (1951)

3A51a F. Alder and F. C. Yu, Phys. Rev. 82, 105 (1951)

4A52 F. Asaro, F. L. Reynolds, and I. Perlman, Phys. Rev. 87, 277 (1952)

4A52a F. Asaro and I. Perlman, private communication (Nov. 1952)

4A52b F. Asaro and W. J. Heiman, private communication (Aug. 1952)

4A52c F. Asaro and I. Perlman, Phys. Rev. 88, 129 (1952)

4A52d F. Asaro, S. G. Thompson, and I. Perlman, private communication (Nov. 1952)

4A52e F. Asaro and I. Perlman, Phys. Rev. 88, 828 (1952)

5A51 G. Albouy and J. Teillac, Compt. rend. 232, 326 (1951)

5A52 G. Albouy, J. phys. et radium 13, 309 (1952)

5A52a G. Albouy and J. Teillac, Compt. rend. 234, 829 (1952)

6A38 L. W. Alvarez, Phys. Rev. 54, 486 (1938)

6A39 L. W. Alvarez and R. Cornog, Phys. Rev. 56, 613 (1939)

6A40 L. W. Alvarez, A. C. Helmholz, and E. Nelson, Phys. Rev. 57, 660 (1940)

6A40a L. W. Alvarez and R. Cornog, Phys. Rev. 57, 248 (1940)(A)

6A49 L. W. Alvarez, Phys. Rev. 75, 1815 (1949)

6A49a L. W. Alvarez, Phys. Rev. 75, 1127 (1949)

6A50 L. W. Alvarez, Phys. Rev. 80, 519 (1950)

7A46 L. T. Aldrich and A. O. Nier, Phys. Rev. 70, 983 (1946)

8A50 P. Avignon, J. phys. et radium 11, 521 (1950)

9A50 R. Ashapa and G. Grimm, reported in Columbia University Document CUD-53 (June 1950)

10A49 J. Angus, A. L. Cockroft, and S. C. Curran, Phil. Mag. 40, 522 (1949)

11A50 R. E. Adamson, Jr., W. W. Buechner, W. M. Preston, C. Goodman, and D. M. Van Patter, Phys. Rev. 80, 985 (1950)

12A35 E. Amaldi, O. D'Agostino, E. Fermi, B. Pontecorvo, R. Rasetti, and E. Segrè, Proc. Roy. Soc. (London) 149A, 522 (1935)

12A36 E. Amaldi and E. Fermi, Ricerca sci. 7, Part I, 56 (1936)

13A49 D. E. Alburger, Phys. Rev. 76, 435 (1949)

13A50 D. E. Alburger, C. Eggler, and D. J. Hughes, Phys. Rev. 77, 726 (1950)

13A50a D. E. Alburger, Phys. Rev. 78, 629 (1950)

13A50b D. E. Alburger, E. der Mateosian, G. Friedlander, M. Goldhaber, J. W. Mihelich, G. Scharff-Goldhaber, and A. W. Sunyar, reported in Brookhaven National Laboratory Unclassified Report BNL-82 (Nov. 1950)

13A50c D. E. Alburger, E. der Mateosian, and M. Goldhaber, reported in Brookhaven National Laboratory Unclassified Report BNL-64 (July 1950)

13A51 D. E. Alburger and G. Friedlander, Phys. Rev. 82, 977 (1951)

13A51a D. E. Alburger and G. Friedlander, Phys. Rev. 81, 523 (1951)

13A52 D. E. Alburger, Phys. Rev. 88, 339 (1952)

13A52a D. E. Alburger and J. Kraushaar, Phys. Rev. 87, 448 (1952)

13A52b D. E. Alburger, Phys. Rev. (to be published) (1952)

14A48 H. R. Allan and C. A. Wilkinson, Proc. Roy. Soc. (London) 194A, 131 (1948)

15A40 W. D. Allen and C. Hurst, Proc. Phys. Soc. (London) 52, 501 (1940)

16A50 H. M. Agnew, Phys. Rev. 77, 655 (1950)

17A36 E. B. Andersen, Z. physik. Chem. 32B, 237 (1936)

17A36a E. B. Andersen, Nature 137, 457 (1936)

18A48 R. D. Albert and C. S. Wu, Phys. Rev. 74, 847 (1948)

19A41 H. Akabori, et al., Proc. Phys.-Math. Soc. Japan 23, 599 (1941)

20A48 L. H. Ahrens and R. D. Evans, Phys. Rev. 74, 279 (1948)

21A41 J. S. V. Allen, M. L. Pool, J. D. Kurbatov, and L. L. Quill, Phys. Rev. 60, 425 (1941)

22A40 T. Amaki, T. Iimori, and A. Sugimoto, Phys. Rev. 57, 751 (1940)

23A47 J. R. Arnold and N. Sugarman, J. Chem. Phys. 15, 703 (1947)

24A36 A. I. Alichanian, A. I. Alichanov, and B. S. Dzhelepov, Physik. Z. Sowjetunion 10, 78 (1936)

25A39 A. H. W. Aten, Jr., C. J. Bakker, and F. A. Heyn, Nature 143, 679 (1939)

25A52 A. H. W. Aten, Jr. and M. Boelhouwer, Physica 18, 651 (1952)

26A51 R. M. Adams and H. Finston, NNES-PPR 9, 1791 (1951)

27A39 H. L. Anderson, E. Fermi, and H. B. Hanstein, Phys. Rev. 55, 797 (1939)

28A43 M. Ageno, Nuovo cimento 1, 33 (1943)

28A43a M. Ageno, Nuovo cimento 1, 415 (1943)

29A52 P. Axel and R. B. Duffield, private communication (Oct. 1952)

30A38 K. Alexeeva, Compt. rend. U.R.S.S. 18, 553 (1938)

31A50 N. M. Anton'eva, A. A. Bashilov, B. S. Dzhelepov, and A. V. Zolotavin, Doklady Akad. Nauk, S.S.S.R. 70, 397 (1950)

31A50a N. M. Anton'eva, A. A. Bashilov, B. S. Dzhelepov, and A. V. Zolotavin, Doklady Akad. Nauk, S.S.S.R. 70, 597 (1950); Izv. Akad. Nauk, S.S.S.R. 14, 299 (1950)

31A51 N. M. Anton'eva, A. A. Bashilov, and B. S. Dzhelepov, Doklady Akad. Nauk, S.S.S.R. 77, 41 (1951)

32A39 P. Abelson, Phys. Rev. 56, 1 (1939)

33A50 D. L. Anderson and M. L. Pool, Phys. Rev. 77, 142 (1950)

34A45 H. Atterling, E. Bohr, and T. Sigurgeirsson, Arkiv Mat., Astron. Fysik 32A, No. 2 (1945)

35A50 K. Artemov and B. Dzhelepov, Uspekhi Fiz. Nauk 41, 189 (1950)

36A51 H. Aeppli, A. S. Bishop, H. Frauenfelder, M. Walter, and W. Zünti, Phys. Rev. 82, 550 (1951); Helv. Phys. Acta 24, 355 (1951)

36A51a H. Aeppli, H. Albers-Schönberg, A. S. Bishop, H. Frauenfelder, and E. Heer, Phys. Rev. 84, 370 (1951)

36A52 H. Aeppli, H. Frauenfelder, E. Heer, and R. Rüetschi, Phys. Rev. 87, 379 (1952)

36A52a H. Aeppli, H. Albers-Schoenberg, H. Frauenfelder, and P. Scherrer, Helv. Phys. Acta 25, 339 (1952)

37A52 C. J. Avery, K. C. Kaericher, and M. L. Pool, Phys. Rev. 87, 216 (1952)(A)

38A52 C. E. Anderson, G. W. Wheeler, and W. W. Watson, Phys. Rev. 87, 668 (1952)

39A52 G. B. Arfken, E. D. Klema, and F. K. McGowan, Phys. Rev. 86, 413 (1952)

40A52 D. P. Ames, M. E. Bunker, and L. M. Langer, Phys. Rev. (in press) (1952)

CC-0. In Public Domain. Gurukul Kangri Collection, Haridwar

Digitized by Arya Samaj Foundation Chennai and eGangotri

40A52a D. P. Ames, M. E. Bunker, and J. W. Starner, reported in Los Alamos Scientific Laboratory Classified Report WASH-75 (Jan. 1952)

40A52b D. P. Ames, M. E. Bunker, and B. M. Sorensen, reported in Los Alamos Scientific Laboratory Classified Report WASH-66 (March 1952)

1B50 K. T. Bainbridge and A. O. Nier, National Research Council Nuclear Energy Series, Preliminary Report No. 9 (Dec. 1950)

1B52 K. T. Bainbridge, M. Goldhaber, and E. Wilson, private communication (Oct. 1952)

2B50 M. E. Bunker, L. M. Langer, and R. J. D. Moffat, Phys. Rev. 80, 468 (1950)

2B50a M. E. Bunker and R. Canada, Phys. Rev. 80, 961 (1950)

2B50b M. E. Bunker, R. Canada, and A. C. G. Mitchell, Phys. Rev. 79, 610 (1950)

2B51 M. E. Bunker, L. M. Langer, and R. J. D. Moffat, Phys. Rev. 81, 30 (1951)

2B52 M. E. Bunker and J. W. Starner, reported in Los Alamos Scientific Laboratory Classified Report WASH-76 (May 1952)

3B44 M. Bachelet and P. Savel, Cahiers phys. No. 19, 51 (1944)

4B48 D. E. Bunyan, A. Lundby, A. H. Ward, and D. Walker, Proc. Phys. Soc. (London) 61, 300 (1948)

4B49 D. E. Bunyan, A. Lundby, and D. Walker, Proc. Phys. Soc. (London) 62A, 253 (1949)

5B49 W. H. Beamer and W. E. Easton, J. Chem. Phys. 17, 1298 (1949)

6B39 E. Bretscher and L. G. Cook, Nature 143, 559 (1939)

6B40 E. Bretscher and L. G. Cook, Nature 146, 430 (1940)

7B47 E. Broda and N. Feather, Proc. Roy. Soc. (London) 190A, 20 (1947)

8B48 R. E. Bell and L. G. Elliott, Can. J. Research 26A, 379 (1948)

8B49 R. E. Bell and H. E. Petch, Phys. Rev. 76, 1409 (1949)

8B50 R. E. Bell and R. L. Graham, Phys. Rev. 78, 490 (1950)

8B52 R. E. Bell and R. L. Graham, Phys. Rev. 86, 212 (1952)

8B52a R. E. Bell, R. L. Graham, and H. E. Petch, Can. J. Phys. 30, 35 (1952)

8B52b R. E. Bell, R. L. Graham, and L. Yaffe, Can. J. Phys. (in press) (1952)

9B50 G. R. Bishop, R. Wilson, and H. Halban, Phys. Rev. 77, 416 (1950)

10B46 G. C. Baldwin and G. S. Klaiber, Phys. Rev. 70, 259 (1946)

10B49 G. C. Baldwin, Phys. Rev. 76, 182 (1949)(A)

11B49 P. R. Bell, B. H. Ketelle, and J. M. Cassidy, Phys. Rev. 76, 574 (1949)

11B49a P. R. Bell and J. M. Cassidy, reported in Oak Ridge National Laboratory Unclassified Report ORNL-481 (Dec. 1949)

11B50 P. R. Bell, Science 112, 7 (1950)

11B50a P. R. Bell and J. M. Cassidy, Phys. Rev. 77, 301 (1950)

11B50b P. R. Bell and J. M. Cassidy, Phys. Rev. 79, 173 (1950)

11B50c P. R. Bell, B. Weaver, and J. M. Cassidy, Phys. Rev. 77, 399 (1950)

11B50d P. R. Bell, J. M. Cassidy, W. H. Jordan, and R. C. Davis, Oak Ridge National Laboratory Classified Report ORNL-782 (Oct. 1950)

11B50e P. R. Bell, J. M. Cassidy, and R. C. Davis reported in Oak Ridge National Laboratory Unclassified Report ORNL-694 (June 1950)

11B50f P. R. Bell, J. M. Cassidy, W. H. Jordan, and R. C. Davis, reported in Oak Ridge National Laboratory Unclassified Report ORNL-782 (Oct. 1950)

11B51 P. R. Bell, J. M. Cassidy, and G. G. Kelley, Phys. Rev. 82, 103 (1951)

11B52 P. R. Bell, R. C. Davis, J. E. Francis, and J. Cassidy, reported in Oak Ridge National Laboratory Unclassified Report ORNL-1092 (Jan. 1952)

11B52a P. R. Bell, R. C. Davis, J. E. Francis, and J. M. Cassidy, reported in Oak Ridge National Laboratory Unclassified Report ORNL-1164 (April 1952)

12B51 G. W. Barton, Jr., A. Ghiorso, and I. Perlman, Phys. Rev. 82, 13 (1951)

13B24 D. H. Black, Proc. Roy. Soc. (London) 106A, 632 (1924)

14B49 D. K. Butt, unpublished data quoted in (4F49)

14B51 D. K. Butt and W. D. Brodie, Proc. Phys. Soc. (London) 64A, 791 (1951)

15B36 G. H. Briggs, Proc. Roy. Soc. (London) 157A, 183 (1936)

16B43 H. Bradt and P. Scherrer, Helv. Phys. Acta 16, 259 (1943)

16B43a H. Bradt, H.-G. Heine, and P. Scherrer, Helv. Phys. Acta 16, 455 (1943)

16B45 H. Bradt and P. Scherrer, Helv. Phys. Acta 18, 405 (1945); and private communication to R. W. Stoughton (Feb. 1947)

16B45a H. Bradt, P. C. Gugelot, O. Huber, H. Medicus, P. Preiswerk, and P. Scherrer, Helv. Phys. Acta 18, 259 (1945)

16B45b H. Bradt, P. C. Gugelot, O. Huber, H. Medicus, P. Preiswerk, and P. Scherrer, Helv. Phys. Acta 18, 252 (1945)

16B45c H. Bradt, P. C. Gugelot, O. Huber, H. Medicus, P. Preiswerk, and P. Scherrer, Helv. Phys. Acta 18, 256 (1945)

16B45d H. Bradt, P. C. Gugelot, O. Huber, H. Medicus, P. Preiswerk, and P. Scherrer, Phys. Rev. 68, 57 (1945)

16B45e H. Bradt, P. C. Gugelot, O. Huber, H. Medicus, P. Preiswerk, and P. Scherrer, Helv. Phys. Acta 18, 351 (1945)

16B46 H. Bradt and P. Scherrer, Helv. Phys. Acta 19, 307 (1946); Phys. Rev. 71, 141 (1947) (A)

16B46a H. Bradt, P. C. Gugelot, O. Huber, H. Medicus, P. Preiswerk, P. Scherrer, and R. Steffen, Helv. Phys. Acta 19, 219 (1946)

16B46b H. Bradt, P. C. Gugelot, O. Huber, H. Medicus, P. Preiswerk, P. Scherrer, and R. Steffen, Helv. Phys. Acta 19, 222 (1946)

16B46c H. Bradt, P. C. Gugelot, O. Huber, H. Medicus, P. Preiswerk, P. Scherrer, and R. Steffen, Helv. Phys. Acta 19, 218 (1946)

16B47 H. Bradt, P. C. Gugelot, O. Huber, H. Medicus, P. Preiswerk, P. Scherrer, and R. Steffen, Helv. Phys. Acta 20, 153 (1947)

16B47a H. L. Bradt and D. J. Tendam, Phys. Rev. 72, 1117 (1947)

17B43 E. L. Brady and W. Rubinson, reported in Metallurgical Laboratory Classified Report CC-724 (June 1943)

17B50 E. L. Brady and M. Deutsch, Phys. Rev. 78, 558 (1950)

17B51 E. L. Brady and N. Sugarman, NNES-PPR 9, 613 (1950)

17B51a E. L. Brady, D. W. Engelkemeir, and E. P. Steinberg, NNES-PPR 9, 711 (1951)

18B96 H. Becquerel, Compt. rend. 122, 420, 501, 559, 609, 762, 1086 (1896)

19B48 R. J. Bruehlman, W. C. Bentley, and E. K. Hyde, reported in Argonne National Laboratory Classified Report ANL-4215 (Oct. 1948)

CC-0. In Public Domain. Gurukul Kangri Collection, Haridwar

Digitized by Arya Samaj Foundation Chennai and eGangotri

20B52 Berkeley Chemistry Group, unpublished results (1947-1952)

21B44 A. A. Bartlett, D. F. Swinehart, and R. W. Thompson, Los Alamos Scientific Laboratory Classified Reports LA-168 (Nov. 1944); LA-327 (July 1945); LA-561 (May 1946)

22B49 W. J. Byatt, F. T. Roger, Jr., and A. Waltner, Phys. Rev. 75, 909 (1949)

23B36 T. Bjerge, Nature 137, 865 (1936)

23B36a T. Bjerge, Nature 138, 400 (1936)

23B36b T. Bjerge and K. J. Broström, Nature 138, 400 (1936)

23B37 T. Bjerge, Nature 139, 757 (1937)

24B30 S. Bramson, Z. Physik 66, 721 (1930)

25B39 R. A. Becker and E. R. Gaerttner, Phys. Rev. 56, 854 (1939) (A)

25B47 R. A. Becker, A. O. Hanson, and B. C. Diven, Phys. Rev. 71, 466 (1947) (A)

25B49 R. A. Becker, F. S. Kirn, and W. L. Buck, Phys. Rev. 76, 1406 (1949)

26B37 D. S. Bayley and H. R. Crane, Phys. Rev. 52, 604 (1937)

27B48 T. W. Bonner, J. E. Evans, C. W. Malich, and J. R. Risser, Phys. Rev. 73, 885 (1948)

28B48 J. C. Bowe, M. Goldhaber, R. D. Hill, W. E. Meyerhof, and O. Sala, Phys. Rev. 73, 1219 (1948) (A)

28B49 J. C. Bowe and G. Scharff-Goldhaber, Phys. Rev. 76, 437 (1949)

28B51 J. C. Bowe and P. Axel, Phys. Rev. 84, 939 (1951)

28B52 J. C. Bowe and P. Axel, Phys. Rev. 85, 858 (1952)

29B49 J. F. Bonner, Jr., U. S. Atomic Energy Commission Unclassified Document AECU-107 (Feb. 1949)

30B51 J. E. Brolley, Jr., D. H. Cooper, W. S. Hall, M. S. Livingston, and L. K. Schlacks, Phys. Rev. 83, 990 (1951)

30B52 J. E. Brolley, Jr., J. L. Fowler, and L. K. Schlacks, Phys. Rev. 88, 618 (1952)

31B38 W. E. Burcham, M. Goldhaber, and R. D. Hill, Nature 141, 510 (1938)

32B39 H. A. Bethe and W. J. Henderson, Phys. Rev. 56, 1060 (1939)

33B39 W. H. Barkas, Phys. Rev. 56, 287 (1939)

33B40 W. H. Barkas, E. C. Creutz, L. A. Delsasso, R. A. Sutton, and M. G. White, Phys. Rev. 58, 383 (1940)

33B40a W. H. Barkas, E. C. Creutz, L. A. Delsasso, and R. A. Sutton, Phys. Rev. 57, 1087 (1940) (A)

33B52 W. H. Barkas, R. W. Deutsch, and H. Tyren, private communication (Sept. 1952)

34B42 L. B. Borst, Phys. Rev. 61, 106 (1942) (A)

35B46 E. Bleuler, P. Scherrer, M. Walter, and W. Zünti, Helv. Phys. Acta 19, 421 (1946)

35B46a E. Bleuler and W. Zünti, Helv. Phys. Acta 19, 375 (1946)

35B46b E. Bleuler and W. Zünti, Helv. Phys. Acta 19, 137 (1946)

35B46c E. Bleuler, W. Bollman, and W. Zünti, Helv. Phys. Acta 19, 419 (1946)

35B47 E. Bleuler, P. Scherrer, M. Walter, and W. Zünti, Helv. Phys. Acta 20, 96 (1947)

35B47a E. Bleuler and W. Zünti, Helv. Phys. Acta 20, 195 (1947)

35B51 E. Bleuler, J. W. Blue, and A. C. Johnson, Phys. Rev. 82, 333 (1951) (A)

35B52 E. Bleuler, A. K. Stebbins, and D. J. Tendam, reported in Purdue University Progress Report II (June 1952)

36B49 H. Brown and V. Perez-Mendez, Phys. Rev. 75, 1276 (1949)

36B50 H. Brown and V. Perez-Mendez, Phys. Rev. 78, 649 (1950)

36B50a H. Brown and V. Perez-Mendez, Phys. Rev. 78, 812 (1950)

37B37 W. Bothe and W. Gentner, Z. Physik 106, 236 (1937)

37B37a W. Bothe and W. Gentner, Naturwiss. 25, 90, 126, 191 (1937)

37B39 W. Bothe and W. Gentner, Z. Physik 112, 45 (1939)

37B41 W. Bothe and A. Flammersfeld, Naturwiss. 29, 194 (1941)

37B43 W. Bothe, Naturwiss. 31, 551 (1943)

37B46 W. Bothe, Z. Naturforsch. 1, 179 (1946)

37B46a W. Bothe, Z. Naturforsch. 1, 173 (1946)

38B40 J. C. Bower and W. E. Burcham, Proc. Roy. Soc. (London) 173A, 379 (1940)

39B48 H. Bradner and J. D. Gow, Phys. Rev. 74, 1559 (1948) (A)

40B39 K. J. Broström, J. Koch, and T. Lauritsen, Nature 144, 830 (1939)

40B47 K. J. Broström, T. Huus, and J. Koch, Nature 160, 498 (1947)

41B46 D. S. Ballantine, reported in Oak Ridge National Laboratory Classified Report Mon N-150 (Aug. 1946)

42B51 R. E. Batzel and G. T. Seaborg, Phys. Rev. 82, 607 (1951)

42B51a R. E. Batzel, D. R. Miller, and G. T. Seaborg, Phys. Rev. 84, 671 (1951)

43B48 J. Beneš, A. Hedgran, and N. Hole, Arkiv Mat., Astron. Fysik 35A, No. 12 (1948)

43B48a J. Beneš, A. Ghosh, A. Hedgran, and N. Hole, Nature 162, 261 (1948); Arkiv Mat., Astron. Fysik 35A, No. 33 (1948)

44B38 H. Brandt, Z. Physik 108, 726 (1938)

45B50 J. G. Bayly, Can. J. Research 28A, 520 (1950)

46B48 J. L. Berggren and R. K. Osborne, Phys. Rev. 74, 1240 (1948) (A)

47B49 J. P. Blaser, F. Boehm, and P. Marmier, Phys. Rev. 75, 1953 (1949)

47B50 J. P. Blaser, F. Boehm, and P. Marmier, Helv. Phys. Acta 23, 623 (1950)

47B51 J. P. Blaser, F. Boehm, P. Marmier, and H. Wäffler, Helv. Phys. Acta 24, 245 (1951)

47B51a J. P. Blaser, F. Boehm, P. Marmier, and P. Scherrer, Helv. Phys. Acta 24, 465 (1951)

47B51b J. P. Blaser, F. Boehm, P. Marmier, and D. C. Peaslee, Helv. Phys. Acta 24, 3 (1951)

48B46 A. R. Brosi, private communication (June 1946)

48B46a A. R. Brosi, reported in Oak Ridge National Laboratory Classified Reports Mon N-150 (Aug. 1946); Mon N-229 (Jan. 1947)

48B49 A. R. Brosi, T. W. DeWitt, and H. Zeldes, Phys. Rev. 75, 1615 (1949)

48B49a A. R. Brosi and P. M. Gross, Jr., reported in Oak Ridge National Laboratory Classified Report ORNL-499 (Dec. 1949)

48B50 A. R. Brosi, H. Zeldes, and B. H. Ketelle, Phys. Rev 79, 902 (1950)

48B51 A. R. Brosi, C. J. Borkowski, E. E. Conn, and J. C. Griess, Jr., Phys. Rev. 81, 391 (1951)

48B51a A. R. Brosi, B. H. Ketelle, H. Zeldes, and E. Fairstein, Phys. Rev. 84, 586 (1951)

48B52 A. R. Brosi, B. H. Ketelle, and H. Zeldes, reported in Oak Ridge National Laboratory Classified Report ORNL-1116 (Feb. 1952)

48B53 A. R. Brosi, B. H. Ketelle, H. Zeldes, and F. M. Porter, Phys. Rev. (to be published) (1953)

49B50 J. A. Bruner and L. M. Langer, Phys. Rev. 79, 606 (1950)

49B50a J. Bruner, L. M. Langer, and R. D. Moffat, Phys. Rev. 77, 747 (1950) (A)

CC-0. In Public Domain. Gurukul Kangri Collection, Haridwar

Digitized by Arya Samaj Foundation Chennai and eGangotri

50B50 W. H. Burgus and J. W. Kennedy, J. Chem. Phys. 18, 97 (1950)

50B50a W. H. Burgus, J. D. Knight, and R. J. Prestwood, Phys. Rev. 79, 104 (1950)

50B51 W. H. Burgus and N. E. Ballou, NNES-PPR 9, 1184 (1951)

50B51a W. H. Burgus, L. Winsberg, J. A. Seiler, and W. Rubinson, NNES-PPR 9, 1195 (1951)

50B52 W. H. Burgus, Phys. Rev. 88, 1129 (1952)

51B50 F. O. Bartell, A. C. Helmholz, S. D. Softky, and D. B. Stewart, Phys. Rev. 80, 1006 (1950)

52B51 F. I. Boley and L. J. Laslett, Phys. Rev. 83, 215 (1951) (A)

52B51a F. I. Boley and D. J. Zaffarano, Phys. Rev. 84, 1059 (1951)

52B51b F. I. Boley and D. J. Zaffarano, Iowa State College Unclassified Report ISC-154 (July 1951)

53B50 G. L. Brownell and C. J. Maletskos, Phys. Rev. 80, 1102 (1950)

54B39 G. Barresi and B. N. Cacciapuoti, Ricerca sci. 10, 464 (1939)

55B47 R. Bouchez, R. Daudel, P. Daudel, and R. Muxart, J. phys. et radium 8, 336 (1947)

55B49 R. Bouchez and G. Kayas, J. phys. et radium 10, 110 (1949)

55B50 R. Bouchez, S. R. de Groot, R. Nataf, and H. A. Tolhoek, J. phys. et radium 11, 105 (1950)

56B49 F. Boehm, O. Huber, P. Marmier, P. Preiswerk, and R. Steffen, Helv. Phys. Acta 22, 69 (1949)

56B49a F. Boehm and P. Preiswerk, Helv. Phys. Acta 22, 331 (1949)

56B50 F. Boehm, J. P. Blaser, P. Marmier, and P. Preiswerk, Phys. Rev. 77, 295 (1950)

57B47 H. S. Brown and M. G. Inghram, Phys. Rev. 72, 347 (1947)

58B38 S. W. Barnes and G. Valley, Phys. Rev. 53, 946 (1938) (A)

58B39 S. W. Barnes, Phys. Rev. 56, 414 (1939)

58B39a S. W. Barnes and P. W. Aradine, Phys. Rev. 55, 50 (1939)

59B38 J. H. Buck, Phys. Rev. 54, 1025 (1938)

60B51 F. Brown, G. C. Hanna, and L. Yaffe, Phys. Rev. 84, 1243 (1951)

60B52 F. Brown and L. Yaffe, Can. J. Chem. (in press) (1952)

60B52a F. Brown, G. C. Hanna, and L. Yaffe, private communication (Sept. 1952)

61B47 E. C. Barker, reported in Oak Ridge National Laboratory Classified Report Mon P-269 (March 1947)

62B51 J. K. Bair and F. Maienschein, Phys. Rev. 81, 463 (1951)

63B47 W. C. Barber, Phys. Rev. 72, 1156 (1947)

63B50 W. C. Barber, Phys. Rev. 80, 332 (1950)

63B52 W. C. Barber and R. H. Helm, Phys. Rev. 86, 275 (1952)

64B51 R. A. Brightsen, K. Shure, C. Fisher, and C. D. Coryell, Phys. Rev. 81, 298 (1951) (A)

65B49 F. D. S. Butement, Phys. Rev. 75, 1276 (1949)

65B50 F. D. S. Butement, Nature 165, 149 (1950); Proc. Phys. Soc. (London) 64A, 395 (1951)

65B50a F. D. S. Butement, Proc. Phys. Soc (London) 63A, 532 (1950)

65B50b F. D. S. Butement, Proc. Phys. Soc (London) 63A, 775 (1950)

65B51 F. D. S. Butement, Nature 167, 400 (1951)

65B51a F. D. S. Butement, Proc. Phys. Soc (London) 64A, 428 (1951)

65B52 F. D. S. Butement, Proc. Phys. Soc. (London) 65A, 254 (1952)

65B52a F. D. S. Butement and R. Shillito, Proc. Phys. Soc. (London) (in press)(1952)

65B52b F. D. S. Butement and A. J. Poë, unpublished data (Oct. 1952)

65B52c F. D. S. Butement, private communication (Oct. 1952)

66B51 W. Biller, reported in University of California Radiation Laboratory Classified Report UCRL-1507 (Oct. 1951)

67B49 I. Bergström and S. Thulin, Phys. Rev. 76, 1718 (1949)

67B49a I. Bergström, S. Thulin, N. Svartholm, and K. Siegbahn, Arkiv Fysik 1, 281 (1949)

67B49b I. Bergström and S. Thulin, Phys. Rev. 76, 313 (1949)

67B50 I. Bergström, S. Thulin, and G. Andersson, Phys. Rev. 77, 851 (1950)

67B50a I. Bergström and S. Thulin, Phys. Rev. 79, 537 (1950)

67B50b I. Bergström, Phys. Rev. 80, 114 (1950)

67B50c I. Bergström and S. Thulin, Phys. Rev. 79, 538 (1950)

67B51 I. Bergström, Phys. Rev. 82, 112 (1951)

67B51a I Bergström, Phys. Rev. 81, 638 (1951)

67B51b I. Bergström, Phys. Rev. 82, 111 (1951)

67B51c I. Bergström, Nature 167, 634 (1951)

67B51d I. Bergström, reported in M. Siegbahn Commemorative Volume, p 307 (Uppsala 1951); Arkiv Fysik 5, 191 (1952)

68B50 E. Berne, Phys. Rev. 77, 568 (1950)

69B44 A. Berthelot, Ann. phys. 19, 219 (1944)

70B43 H. J. Born and W. Seelmann-Eggebert, Naturwiss. 31, 86 (1943)

70B43a H. J. Born and W. Seelmann-Eggebert, Naturwiss. 31, 201 (1943)

70B43b H. J. Born and W. Seelmann-Eggebert, Naturwiss. 31, 420 (1943)

71B46 M. Burgy, L. A. Pardue, H. B. Willard, and E. O. Wollan, U. S. Atomic Energy Commission Declassified Document MDDC-16 (June 1946)

72B46 N. E. Ballou, reported in J. Am. Chem. Soc. 68, 2411 (1946)

72B48 N. E. Ballou, Phys. Rev. 73, 630 (1948)

72B51 N. E. Ballou, W. H. Burgus, J. B. Dial, L. E. Glendenin, H. Finston, M. F. Ravely, B Schloss, and N. Sugarman, NNES-PPR 9, 1410 (1951)

72B51a N. E. Ballou, T. B. Novey, D. E. Engelkemeir, E. L. Brady, and J. A. Seiler, NNES-PPR 9, 675 (1951)

72B51b N. E. Ballou, NNES-PPR 9, 695 (1951)

72B51d N. E. Ballou, W. Rubinson, and L. E. Glendenin, NNES-PPR 9, 1115 (1951)

72B51e N. E. Ballou and W. H. Burgus, NNES-PPR 9, 1168 (1951)

72B51f N. E. Ballou, NNES-PPR 9, 1151 (1951)

72B51g N. E. Ballou, NNES-PPR 9, 1176 (1951)

72B51h N. E. Ballou, W. H. Burgus, and J. A. Marinsky, NNES-PPR 9, 1181 (1951)

72B51i N. E. Ballou, NNES-PPR 9, 1220 (1951)

73B50 C. Beckham and M. L. Pool, Phys. Rev. 80, 125 (1950) (A)

74B49 C. H. Braden, L. Slack, and F. B. Shull, Phys. Rev. 75, 1964 (1949)

75B49 L. J. Brown and S. Katcoff, J. Chem. Phys. 17, 497 (1949)

CC-0. In Public Domain. Gurukul Kangri Collection, Haridwar

Digitized by Arya Samaj Foundation Chennai and eGangotri

76B47 G. E. Boyd and Q. V. Larson, reported in Oak Ridge National Laboratory Classified Report Mon N-229 (Jan. 1947)

76B49 G. E. Boyd and Q. V. Larson, reported in Oak Ridge National Laboratory Classified Report ORNL-499 (Dec. 1949)

76B49a G. E. Boyd and Q. V. Larson, reported in Oak Ridge National Laboratory Classified Report ORNL-286 (Sept. 1949)

76B49b G. E. Boyd, reported in Oak Ridge National Laboratory Classified Report ORNL-229 (Feb. 1949)

76B50 G. E. Boyd and Q. V. Larson, reported in Oak Ridge National Laboratory Classified Report ORNL-685 (June 1950)

76B50a G. E. Boyd and Q. V. Larson, reported in Oak Ridge National Laboratory Classified Report ORNL-607 (March 1950)

76B51 G. E. Boyd and B. H. Ketelle, reported in Oak Ridge National Laboratory Classified Report ORNL-870 (March 1951)

76B51a G. E. Boyd and B. H. Ketelle, Phys. Rev. 83, 216 (1951) (A)

76B51b G. E. Boyd, Record Chem. Progress (Kresge-Hooker Sci. Lib.) 12, 67 (1951)

76B51c G. E. Boyd, reported in Oak Ridge National Laboratory Classified Report ORNL-870 (March 1951)

76B51d G. E. Boyd and B. H. Ketelle, reported in Oak Ridge National Laboratory Classified Report ORNL-1053 (Oct. 1951)

76B52 G. E. Boyd, Q. V. Larson, and G. W. Parker, Phys. Rev. 86, 1051 (1952)

76B52a G. E. Boyd, Phys. Rev. 86, 578 (1952)

76B52b G. E. Boyd and R. A. Charpie, Phys. Rev. 88, 681 (1952)

76B52c G. E. Boyd, private communication (Nov. 1952)

77B45 E. Bohr and N. Hole, Arkiv Mat., Astron. Fysik 32A, No. 15 (1945)

78B48 J. Beydon, Compt. rend. 227, 1159 (1948)

79B51 W. L. Bendel, F. J. Shore, and R. A. Becker, Phys. Rev. 83, 677 (1951)

79B52 W. L. Bendel, F. J. Shore, H. N. Brown, and R. A. Becker, Phys. Rev. 87, 195 (1952) (A)

80B51 J. W. Barnes and A. J. Freedman, Phys. Rev. 84, 365 (1951)

80B52 J. W. Barnes, private communication (May 1952)

81B46 P. T. Bittencourt and M. Goldhaber, Phys. Rev. 70, 780 (1946)

82B46 S. B. Burson, P. T. Bittencourt, R. B. Duffield, and M. Goldhaber, Phys. Rev. 70, 566 (1946)

82B48 S. B. Burson and C. O. Muehlhause, Phys. Rev. 74, 1264 (1948) (A)

82B50 S. B. Burson, K. W. Blair, and D. Saxon, Phys. Rev. 77, 403 (1950)

82B51 S. B. Burson, K. W. Blair, H. B. Keller, and S. Wexler, Phys. Rev. 83, 62 (1951)

82B52 S. B. Burson and W. C. Rutledge, Phys. Rev. 86, 633 (1952) (A)

83B50 C. J. Borkowski and A. R. Brosi, reported in Oak Ridge National Laboratory Classified Report ORNL-607 (March 1950)

84B51 H. Behrens, Z. Naturforsch. 6a, 249 (1951)

85B50 J. R. Beyster and M. L. Wiedenbeck, Phys. Rev. 79, 411 (1950)

85B50a J. R. Beyster and M. L. Wiedenbeck, Phys. Rev. 79, 728 (1950)

86B49 L. A. Beach, C. L. Peacock, and R. G. Wilkinson, Phys. Rev. 76, 1624 (1949)

86B49a L. A. Beach, C. L. Peacock, and R. G. Wilkinson, Phys. Rev. 76, 1585 (1949)

86B49b L. A. Beach, C. L. Peacock, and R. G. Wilkinson, Phys. Rev. 75, 211 (1949)

87B51 R. C. Bannerman, G. M. Lewis, and S. C. Curran, Phil. Mag. 42, 1097 (1951)

87B52 R. C. Bannerman, Proc. Phys. Soc. (London) 65A, 565 (1952)

87B52a R. C. Bannerman and S. C. Curran, Phys. Rev. 85, 134 (1952)

88B52 C. I. Browne, J. O. Rasmussen, J. P. Surls, and D. F. Martin, Phys. Rev. 85, 146 (1952)

88B52a C. I. Browne and I. Perlman, unpublished data (1952)

89B52 D. T. Baker, E. Bleuler, and R. M. Steffen, reported in Purdue University Progress Report II (June 1952)

90B52 D. A. Bromley and L. M. Goldman, Phys. Rev. 86, 790 (1952)

90B52a D. A. Bromley, Phys. Rev. 88, 565 (1952)

91B52 P. T. Barrett, Proc. Phys. Soc. (London) 65A, 450 (1952)

92B49 E. Bestenreiner and E. Broda, Nature 164, 658 (1949)

93B52 D. Brower, G. Hinman, G. Lang, R. Leamer, and D. Rose, Phys. Rev. 86, 1054 (1952)

94B49 G. J. Bene, P. M. Denis, and R. C. Extermann, Helv. Phys. Acta 22, 606 (1949)

95B51 H. N. Brown, W. L. Bendel, F. J. Shore, and R. A. Becker, Phys. Rev. 84, 292 (1951)

96B49 J. W. Burkig and J. R. Richardson, Phys. Rev. 76, 586 (1949) (A)

97B50 B. Bleaney and H. E. D. Scovil, Proc. Phys. Soc. (London) 63A, 1369 (1950)

97B51 B. Bleaney and K. D. Bowers, Proc. Phys. Soc. (London) 64A, 1135 (1951)

97B51a B. Bleaney and D. J. E. Ingram, Proc. Roy. Soc. (London) 205A, 336 (1951)

97B51b B. Bleaney and H. E. D. Scovil, Proc. Phys. Soc. (London) 64A, 204 (1951)

97B51c B. Bleaney, D. J. E. Ingram, and H. E. D. Scovil, Proc. Phys. Soc. (London) 64A, 601 (1951)

97B51d B. Bleaney and D. J. E. Ingram, Proc. Roy. Soc. (London) 208A, 143 (1951)

98B51 E. H. Bellamy, Nature 168, 556 (1951)

99B50 P. Brix, H. Kopfermann, and W. v. Siemans, Naturwiss. 37, 397 (1950)

99B51 P. Brix and A. Stendel, Naturwiss. 38, 431 (1951)

100B50 D. Binder, Phys. Rev. 77, 291 (1950)

101B51 L. E. Beghian, G. R. Bishop, and H. Halban, Phys. Rev. 83, 186 (1951)

102B52 A. C. Birge, Phys. Rev. 85, 753 (1952) (A)

102B52a A. C. Birge, private communication (Oct. 1952)

103B51 J. K. Beling, B. T. Feld, and I. Halpern, Phys. Rev. 84, 155 (1951)

103B52 J. K. Beling, J. O. Newton, and B. Rose, Phys. Rev. 87, 670 (1952); 86, 797 (1952)

104B52 D. F. Bracher and A. R. Crathorn, Nature 169, 364 (1952)

105B52 G. S. Bogle and H. E. D. Scovil, Proc. Phys. Soc. (London) 65A, 360 (1952)

106B52 R. M. Bartholomew, F. Brown, R. C. Hawkings, W. F. Merritt, and L. Yaffe, Can. J. Chem. (in press) (1952)

106B52a R. M. Bartholomew, R. C. Hawkings, W. F. Merritt, and L. Yaffe, Can. J. Chem. (in press) (1952)

106B52b R. M. Bartholomew, F. Brown, W. D. Howell, W. Shorey, and L. Yaffe, Can. J. Phys. (in press) (1952)

107B52 J. P. Butler and B. G. Harvey, private communication (Oct. 1952)

108B52 S. D. Bloom, Phys. Rev. 88, 312 (1952)

109B51 G. Bastin-Scoffier, Compt. rend. 233, 945 (1951)

CC-0. In Public Domain. Gurukul Kangri Collection, Haridwar

Digitized by Arya Samaj Foundation Chennai and eGangotri

110B51 W. L. Brown, Phys. Rev. 83, 271 (1951)

111B52 F. Begemann and F. G. Houtermans, Z. Naturforsch. 7a, 143 (1952)

112B51 F. Barendregt and Sj. Tom, Physica 17, 817 (1951)

113B52 K. Maack Bisgård, Proc. Phys. Soc. (London) 65A, 677 (1952)

1C30 M. Curie and S. Cotelle, Compt. rend. 190, 1289 (1930)

1C31 M. Curie, A. Debierne, A. S. Eve, H. Geiger, O. Hahn, S. C. Lind, St. Meyer, E. Rutherford, and E. Schweidler, Revs. Modern Phys. 3, 427 (1931). Summarizes results of various investigators.

2C44 F. L. Clark, H. J. Spencer-Palmer, and R. N. Woodward, British Declassified Report BR-522 (Oct. 1944)

2C45 F. L. Clark, H. J. Spencer-Palmer, and R. N. Woodward, British Unclassified Report BR-584 (March 1945)

3C46 L. F. Curtiss, private communication (July 1946); value derived from average of values given in following references: Ward, Wynn-Williams, and Cave, Proc. Roy. Soc. (London) 125, 713 (1929); Jedrzejowski, Ann. phys. 9, 128 (1928); Braddick and Cave, Proc. Roy. Soc. (London) 121, 367 (1928); Gregoire, Ann. phys. 2, 161 (1934); Gleditsch and Foyn, Am. J. Sci. 29, 253 (1935)

4C34 I. Curie and F. Joliot, Compt. rend. 198, 254 (1934)

4C34a I. Curie and F. Joliot, J. phys. et radium 5, 153 (1934)

4C34b I. Curie, F. Joliot, and P. Preiswerk, Compt. rend. 198, 2089 (1934)

4C39 I. Curie and P. Savitch, Compt. rend. 208, 343 (1939)

4C44 I. Curie and G. Bouissières, Cahiers phys. No. 26, 1 (1944)

4C48 I. Curie, Compt. rend. 227, 1225 (1948); J. phys. et radium 10, 381 (1949)

5C48 T. E. Cranshaw and J. A. Harvey, Can. J. Research 26A, 243 (1948)

6C50 L. Cranberg, Phys. Rev. 77, 155 (1950)

7C37 W. Y. Chang, M. Goldhaber, and R. Sagane, Nature 139, 962 (1937)

7C46 W. Y. Chang, Phys. Rev. 69, 60 (1946)

7C48 W. Y. Chang and T. Coor, Phys. Rev. 74, 1196 (1948)

7C48a W. Y. Chang, Phys. Rev. 74, 1195 (1948)

8C41 A. A. Constantinov and G. D. Latyshev, J. Phys. (U.S.S.R.) 5, 239 (1941)

9C38 S. P. Choong and J. Surugue, J. phys. et radium 9, 437 (1938)

10C36 J. M. Cork and E. O. Lawrence, Phys. Rev. 49, 788 (1936)

10C37 J. M. Cork and R. L. Thornton, Phys. Rev. 51, 608 (1937)

10C38 J. M. Cork and R. L. Thornton, Phys. Rev. 53, 866 (1938)

10C39 J. M. Cork and J. L. Lawson, Phys. Rev. 56, 291 (1939)

10C40 J. M. Cork, J. Halpern, and H. Tatel, Phys. Rev. 57, 371 (1940)

10C40a J. M. Cork and W. Middleton, Phys. Rev. 58, 474 (1940)

10C41 J. M. Cork and G. P. Smith, Phys. Rev. 60, 480 (1941)

10C42 J. M. Cork, L. N. Hadley, Jr., and C. V. Kent, Phys. Rev. 61, 388 (1942) (A)

10C47 J. M. Cork, R. G. Shreffler, and C. M. Fowler, Phys. Rev. 72, 1209 (1947)

10C48 J. M. Cork, R. G. Shreffler, and C. M. Fowler, Phys. Rev. 74, 1657 (1948)

10C48a J. M. Cork, R. G. Shreffler, and C. M. Fowler, Phys. Rev. 73, 1220 (1948) (A)

10C48b J. M. Cork, R. G. Shreffler, and C. M. Fowler, Phys. Rev. 74, 240 (1948)

10C49 J. M. Cork, H. B. Keller, and A. E. Stoddard, Phys. Rev. 76, 575 (1949)

10C49a J. M. Cork, H. B. Keller, and A. E. Stoddard, Phys. Rev. 76, 986 (1949)

10C49b J. M. Cork, H. B. Keller, J. Sazynski, W. C. Rutledge, and A. E. Stoddard, Phys. Rev. 75, 1778 (1949)

10C50 J. M. Cork, W. C. Rutledge, C. E. Branyan, A. E. Stoddard, and J. M. LeBlanc, Phys. Rev. 79, 889 (1950)

10C50a J. M. Cork, W. C. Rutledge, C. E. Branyan, A. E. Stoddard, W. J. Childs, and J. M. LeBlanc, Phys. Rev. 80, 286 (1950)

10C50b J. M. Cork, W. C. Rutledge, A. E. Stoddard, C. E. Branyan, and J. M. LeBlanc, Phys. Rev. 79, 938 (1950)

10C50c J. M. Cork, H. B. Keller, W. C. Rutledge, and A. E. Stoddard, Phys. Rev. 77, 848 (1950)

10C50d J. M. Cork, C. E. Branyan, W. C. Rutledge, A. E. Stoddard, and J. M. LeBlanc, Phys. Rev. 78, 304 (1950)

10C50e J. M. Cork, H. B. Keller, W. C. Rutledge, and A. E. Stoddard, Phys. Rev. 78, 95 (1950)

10C50f J. M. Cork, A. E. Stoddard, W. C. Rutledge, C. E. Branyan, and J. LeBlanc, Phys. Rev. 78, 299 (1950)

10C50g J. M. Cork, A. E. Stoddard, W. C. Rutledge, C. E. Branyan, and J. M. LeBlanc, Phys. Rev. 77, 843 (1950)

10C51 J. M. Cork, C. E. Branyan, A. E. Stoddard, H. B. Keller, J. M. LeBlanc, and W. J. Childs, Phys. Rev. 83, 681 (1951)

10C51a J. M. Cork, A. E. Stoddard, C. E. Branyan, W. J. Childs, D. W. Martin, and J. M. LeBlanc, Phys. Rev. 84, 596 (1951)

10C51b J. M. Cork, W. C. Rutledge, A. E. Stoddard, C. E. Branyan, and W. J. Childs, Phys. Rev. 81, 482 (1951)

10C51c J. M. Cork, J. M. LeBlanc, A. E. Stoddard, D. W. Martin, C. E. Branyan, and W. J. Childs, Phys. Rev. 83, 856 (1951)

10C51d J. M. Cork, A. E. Stoddard, J. M. LeBlanc, C. E. Branyan, D. W. Martin, and W. J. Childs, Phys. Rev. 83, 856 (1951)

10C51e J. M. Cork, W. J. Childs, C. E. Branyan, W. C. Rutledge, and A. E. Stoddard, Phys. Rev. 81, 642 (1951)

10C51f J. M. Cork, J. M. LeBlanc, A. E. Stoddard, W. J. Childs, C. E. Branyan, and D. W. Martin, Phys. Rev. 82, 258 (1951)

10C52 J. M. Cork, J. M. LeBlanc, F. B. Stumpf, and W. H. Nester, Phys. Rev. 86, 575 (1952)

10C52a J. M. Cork, J. M. LeBlanc, F. B. Stumpf, and W. H. Nester, Phys. Rev. 86, 415 (1952)

10C52b J. M. Cork, D. W. Martin, J. M. LeBlanc, and C. E. Branyan, Phys. Rev. 85, 386 (1952)

10C52c J. M. Cork, J. M. LeBlanc, W. H. Nester, and F. B. Stumpf, Phys. Rev. 88, 685 (1952)

11C40 D. R. Corson, K. R. MacKenzie, and E. Segrè, Phys. Rev. 57, 459, 1087 (1940)

11C40a D. R. Corson, K. R. MacKenzie, and E. Segrè, Phys. Rev. 58, 672 (1940)

12C37 B. N. Cacciapuoti and E. Segrè, Phys. Rev. 52, 1252 (1937)

12C38 B. N. Cacciapuoti, Nuovo Cimento 15, 213 (1938)

12C39 B. N. Cacciapuoti, Phys. Rev. 55, 110 (1939)

13C51 E. Cotton, Ann. phys. 6, 481 (1951)

CC-0. In Public Domain. Gurukul Kangri Collection, Haridwar

Digitized by Arya Samaj Foundation Chennai and eGangotri

14C50 W. W. T. Crane and I. Perlman, unpublished data (1950)

15C44. O. Chamberlain, G. W. Farwell, and E. Segrè, Los Alamos Scientific Laboratory Classified Report LAMS-131 (Sept. 1944)

15C46 O. Chamberlain, D. Williams, and P. Yuster, Phys. Rev. 70, 580 (1946)

15C47 O. Chamberlain, J. W. Gofman, E. Segrè, and A. C. Wahl, Phys. Rev. 71, 529 (1947)

16C47 B. B. Cunningham and H. H. Hopkins, Jr., unpublished work (Feb. 1947)

16C49 B. B. Cunningham and L. B. Werner, J. Am. Chem Soc. 71, 1521 (1949); NNES-PPR 14B, 51 (1949)

16C49a B. B. Cunningham, NNES-PPR 14B, 1363 (1949)

16C50 B. B. Cunningham, S. G. Thompson, and H. R Lohr, unpublished data (1950)

17C51 M. Conjeaud and V. Naggiar, Compt. rend. 232, 499 (1951)

18C32 J. Chadwick, Proc. Roy. Soc. (London) 136A, 692 (1932)

18C35 J. Chadwick and M. Goldhaber, Proc. Roy. Soc. (London) 151A, 479 (1935)

19C48 J. H. Coon, M. Goldblatt, R. Nobles, and C. F. Robinson, U. S. Atomic Energy Commission Declassified Document AECD-2190 (July 1948)

19C49 J. H. Coon, Phys. Rev. 75, 1355 (1949)

20C41 R. Cornog and W. F. Libby, Phys. Rev. 59, 1046 (1941)

21C39 S. C. Curran and J. E. Strothers, Proc. Roy. Soc. (London) 172A, 72 (1939)

21C40 S. C. Curran and J. E. Strothers, Proc. Cambridge Phil. Soc. 36, 252 (1940)

21C40a S. C. Curran, P. I. Dee, J. E. Strothers, Proc. Roy. Soc. (London) 174A, 546 (1940)

21C48 S. C. Curran, J. Angus, and A. L. Cockroft, Nature 162, 302 (1948)

21C49 S. C. Curran, J. Angus, and A. L. Cockroft, Phys. Rev. 76, 853 (1949)

21C51 S. C. Curran, D. Dixon, and H. W. Wilson, Phys. Rev. 84, 151 (1951); Phil. Mag. 43, 82 (1952)

21C52 S. C. Curran, D. Dixon, and H. W. Wilson, private communication (Sept. 1952)

22C34 H. R. Crane and C. C. Lauritsen, Phys. Rev. 45, 430 (1934)

22C34a H. R. Crane and C. C. Lauritsen, Phys. Rev. 45, 497 (1934)

22C35 H. R. Crane, L. A. Delsasso, W. A. Fowler, and C. C. Lauritsen, Phys. Rev. 47, 971 (1935)

22C35a H. R. Crane, L. A. Delsasso, W. A. Fowler, and C. C. Lauritsen, Phys. Rev. 47, 887 (1935)

23C50 J. Crussard, Compt. rend. 231, 141 (1950)

24C49 E. C. Campbell and W. M. Good, Phys. Rev. 76, 195 (1949) (A)

24C50 E. C. Campbell and M. Goodrich, Phys. Rev. 78, 640 (1950) (A)

24C51 E. C. Campbell and M. Goodrich, private communication (Oct. 1951)

24C51a E. C. Campbell, J. H. Kahn, and M. Goodrich, reported in Oak Ridge National Laboratory Unclassified Report ORNL-1164 (April 1951)

24C52 E. C Campbell, private communication (Oct. 1952)

24C52a E. C. Campbell and M. Goodrich, private communication (Oct. 1952)

25C50 D. Christian and D. S. Martin, Jr., Phys. Rev. 80, 1110 (1950)

25C52 D. Christian, R. F. Mitchell, and D S Martin, Jr., Phys Rev. 86, 946 (1952)

26C35 J. D. Cockcroft, C. W. Gilbert, and E. T. S. Walton, Proc. Roy. Soc. (London) 148A, 225 (1935)

27C47 W. W. Chupp and E. M. McMillan, Phys. Rev. 72, 873 (1947)

27C48 W. W. Chupp and E. M. McMillan, Phys. Rev. 74, 1217 (1948) (A)

28C42 C. S. Cook and P. W. McDaniel, Phys. Rev. 62, 412 (1942)

28C46 C. S. Cook, E. T. Jurney, and L. M. Langer, Phys. Rev. 70, 985 (1946)

28C48 C. S. Cook, L. M. Langer, and H. C. Price, Jr., Phys. Rev. 74, 548 (1948)

28C48a C. S. Cook, L. M. Langer, H. C. Price, Jr., and M. B. Sampson, Phys. Rev. 74,502 (1948)

28C48b C. S. Cook and L. M. Langer, Phys. Rev. 74, 227 (1948)

28C48c C. S. Cook and L. M. Langer, Phys. Rev. 73, 601 (1948)

28C48d C. S. Cook and L. M. Langer, Phys Rev. 73, 1149 (1948)

28C51 C. S. Cook, Phys. Rev. 83, 462 (1951)

29C40 E. C. Creutz, W. H. Barkas, and N. H. Furman, Phys. Rev. 58, 1008 (1940)

29C40a E. C. Creutz, J. G. Fox, and R. Sutton, Phys. Rev. 57, 567 (1940) (A)

29C40b E. C. Creutz, L. A. Delsasso, R. B. Sutton, M. G. White, and W. H. Barkas, Phys. Rev. 58, 481 (1940)

30C44 E. T. Clarke and J. W. Irvine, Jr., Phys. Rev. 66, 231 (1944)

30C46 E. T. Clarke and J. W. Irvine, Jr., Phys. Rev. 69, 680 (1946) (A)

30C47 E. T. Clarke, Phys. Rev. 71, 187 (1947)

31C50 J. W. Cobble and R. W. Atterbury, Phys. Rev. 80, 917 (1950)

32C39 E. C. Crittenden, Jr., Phys. Rev. 56, 709 (1939)

33C38 J. Cichocki and A. Soltan, Compt. rend. 207, 423 (1938)

34C39 R. A. Cooley, D. M. Yost, and E. M. McMillan, J. Am. Chem. Soc. 61, 2970 (1939)

35C52 H. Craig, Phys. Rev. 85, 688 (1952)

36C50 M. Ceccarelli, G. Quareni, and A. Rostagni, Phys. Rev. 80, 909 (1950)

37C51 S. A. Colgate, Phys Rev. 81, 1063 (1951)

38C48 W. O. Caster and T. P. Kohman, private communication (1948)

39C50 W. H. Cuffey, Phys. Rev. 79, 180 (1950)

39C51 W. H. Cuffey, Phys. Rev. 82, 461 (1951)

39C51a W. H. Cuffey and R. Canada, Phys. Rev. 83, 654 (1951)

40C51 D. O. Caldwell and H. F. Stoddart, Phys. Rev. 81, 660 (1951) (A)

41C51 R. R. Carlson, Phys. Rev. 84, 749 (1951)

42C50 R. L. Caldwell, Phys. Rev. 78, 407 (1950)

43C51 R. Canada and A. C. G. Mitchell, Phys. Rev. 83, 955 (1951)

43C51a R. Canada and A. C. G. Mitchell, Phys. Rev. 81, 485 (1951)

43C51b R. Canada, W. H. Cuffey, A. E. Lessor, and A. C. G. Mitchell, Phys. Rev. 82, 750 (1951)

43C51c R. Canada and A. C. G. Mitchell, Phys. Rev. 83, 76 (1951)

44C44 M. Camac, Metallurgical Laboratory Declassified Report CC-2409 (Dec. 1944)

44C45 M. Camac and L. Brown, Metallurgical Laboratory Classified Report CP-2407 (Feb. 1945)

45C46 E. E. Conn, A. R. Brosi, J. A. Swartout, A. E. Cameron, R. L. Carter, and D. G. Hill, Phys. Rev. 70, 768 (1946)

CC-0. In Public Domain. Gurukul Kangri Collection, Haridwar

Digitized by Arya Samaj Foundation Chennai and eGangotri

46C50 A. G. W. Cameron and L. Katz, Phys. Rev. 80, 904 (1950)

47C50 R. A. Cohn and J. D. Kurbatov, Phys. Rev. 78, 318 (1950) (A)

48C38 B. R. Curtis and J. M. Cork, Phys. Rev. 53, 681 (1938) (A)

48C40 B. R. Curtis and J. R. Richardson, Phys. Rev. 57, 1121 (1940)

49C48 W. S. Cowart, M. L. Pool, D. A. McCown, and L. L. Woodward, Phys. Rev. 73, 1454 (1948)

50C48 S. D. Chatterjee and N. K. Saha, Indian J. Phys. 22, 515 (1948)

51C51 C. D. Coryell, unpublished data quoted in NNES-PPR 9, 2013 (Appendix 3) (1951)

51C52 C. D. Coryell, private communication (Oct., 1952)

51C52a C. D. Coryell, P. Levêque, and H. G. Richter, unpublished data (Oct. 1952)

52C41 E. P. Clancy, Phys. Rev. 60, 87 (1941)

53C50 S. V. Castner, M.S. Thesis, University of California Radiation Laboratory Unclassified Report UCRL-942 (Oct. 1950); Phys. Rev. 88, 1126 (1952)

53C51 S. V. Castner, University of California Radiation Laboratory Unclassified Report UCRL-1099 (Jan. 1951)

54C06 N. R. Campbell and A. Wood, Proc. Cambridge Phil. Soc. 14, 15 (1906); N. R. Campbell, Proc. Cambridge Phil. Soc 14, 211 (1907); 557 (1908)

55C50 G. Charpak and F. Suzor, J. phys. et radium 11, 633 (1950)

55C51 G. Charpak and F. Suzor, Compt. rend. 233, 1356 (1951)

56C49 A. L. Cockroft and G. M. Insch, Phil. Mag. 40, 1014 (1949)

57C43 A. A. Cohen, Phys. Rev. 63, 219 (1943) (A)

58C47 P. Chudom and C. O. Muehlhause, reported in Argonne National Laboratory Classified Report CP-3801 (May 1947)

59C51 J. M. Cassidy, Phys. Rev. 83, 483 (1951) (A)

60C50 W. L. Carss, J. R. Gum, and M. L. Pool, Phys. Rev. 80, 1028 (1950)

61C49 S. A. Chowdary, reported in Purdue University Unclassified Report NP-943 (June 1949)

62C52 T. B. Cook, Jr. and S. K. Haynes, Phys. Rev. 86, 190 (1952)

63C48 S. G. Cohen, Nature 161, 475 (1948)

63C51 S. G. Cohen, Nature 167, 779 (1951)

63C52 S. G. Cohen and A. A. Jaffe, Phys. Rev. 86, 800 (1952)

64C39 G. B. Collins, B. Waldman, E. M. Stubblefield, and M. Goldhaber, Phys. Rev. 55, 507 (1939)

64C40 G. B. Collins and B. Waldman, Phys. Rev. 57, 1088 (1940) (A)

65C47 K. D. Coleman and M. L. Pool, Phys. Rev. 72, 1070 (1947)

65C47a K. D. Coleman, R. Nudenberg, and M. L. Pool, Phys. Rev. 72, 164 (1947) (A)

66C50 T. C. Chu, Phys. Rev. 79, 582 (1950)

67C51 G. W. Campbell, N. R. Sleight, and W. H Sullivan, NNES-PPR 9, 931 (1951)

68C51 G. B. Cook, British Atomic Energy Report AERE C/R-729 (June 1951)

68C51a G. B. Cook, reported in British Classified Report AERE-PR-20 (April 1951)

69C51 P. E. Cavanagh, J. F. Turner, D. V. Booker, and H. J. Dunster, Proc. Phys. Soc. (London) 64A, 13 (1951)

69C51a P. E. Cavanagh, Phys. Rev. 82, 791 (1951)

69C52 P. E. Cavanagh, Phil. Mag. 43, 221 (1952)

69C52a P. E. Cavanagh, Phil. Mag. 43, 648 (1952)

70C50 L. S. Cheng and J. D. Kurbatov, Phys. Rev. 78, 319 (1950) (A)

70C52 L. S. Cheng, G. John, and J. D. Kurbatov, Phys. Rev. 86, 632 (1952) (A); 85, 487 (1952)

71C49 K. Y. Chu and M. L. Wiedenbeck, Phys. Rev. 75, 226 (1949)

72C42 A. F. Clark, Phys. Rev. 61, 242 (1942)

73C48 J. B. Chubbuck and I. Perlman, Phys. Rev. 74, 982 (1951)

74C46 P. Cuer and C. M. G. Lattes, Nature 158, 197 (1946)

75C52 R. J. Carr and G. H. Higgins, private communication (Aug. 1952)

76C51 J. M. Cassels, T. C. Randle, T. G. Pickavance, and A. E. Taylor, Phil. Mag. 42, 215 (1951)

77C52 R. S. Caswell, Phys. Rev. 86, 82 (1952)

78C52 A. A. Caretto and E. O. Wiig, J. Am. Chem. Soc. 74, 5235 (1952)

78C52a A. A. Caretto and S. Katcoff, private communication (Sept. 1952)

79C52 R. S. Caird and A. C. G. Mitchell, Phys. Rev. (in press) (1952)

80C52 P. G. Cobb, reported in Purdue University Progress Report II (June 1952)

81C43 K. L. Cook, Phys. Rev. 64, 278 (1943)

82C52 C. G. Campbell, W. J. Henderson, and J. Kyles, Phil. Mag. 43, 126 (1952); private communication (Oct. 1952)

83C49 R. A. Charpie, K. H. Sun, B. Jennings, and J. F. Nechaj, Phys. Rev. 76, 1255 (1949)

1D35 A. J. Dempster, Nature 135, 993 (1935)

1D35a A. J. Dempster, Nature 136, 65 (1935)

1D36 A. J. Dempster, Nature 138, 120 (1936)

1D39 A. J. Dempster, Phys. Rev. 55, 794 (1939)

1D48 A. J. Dempster, Phys. Rev. 73, 1125 (1948)

2D38 L. A. Dubridge, S. W. Barnes, J. H. Buck, and C. V. Strain, Phys. Rev. 53, 447 (1938)

2D39 L. A. Dubridge and J. Marshall, Phys. Rev. 56, 706 (1939)

2D40 L. A. Dubridge, private communication to G. T. Seaborg (1940); includes work of entire Rochester group

2D40a L. A. Dubridge and J. Marshall, Phys. Rev. 58, 7 (1940)

2D40b L. A. Dubridge and J. Marshall, Phys. Rev. 57, 348 (1940) (A)

3D40 W. L. Davidson, Jr., Phys. Rev. 57, 1086 (1940) (A)

3D40a W. L. Davidson, private communication (1940)

4D50 J. M. Dickson and T. C. Randle, Nature 166, 235 (1950)

4D51 J. M. Dickson and T. C. Randle, Proc. Phys. Soc. (London) 64A, 902 (1951)

5D35 L. A. Delsasso, W. A. Fowler, and C. C Lauritsen, Phys. Rev. 48, 848 (1935)

5D39 L. A. Delsasso, L. N. Ridenour, R. Sherr, and M. G. White, Phys. Rev. 55, 113 (1939)

5D40 L. A. Delsasso, M. G. White, W. Barkas, and E. C. Creutz, Phys Rev 58, 586 (1940)

6D33 G. von Droste, Z. Physik 34, 17 (1933)

7D38 H. DeVries and J Veldkamp, Physica 5, 249 (1938)

7D39 H. DeVries and G. Diemer, Physica 6, 599 (1939)

CC-0. In Public Domain. Gurukul Kangri Collection, Haridwar

Digitized by Arya Samaj Foundation Chennai and eGangotri

8D37 S. Devons and G. J. Neary, Proc. Cambridge Phil Soc. 33, 154 (1937)

9D49 H. E. Duckworth, R. F. Black, and R. F. Woodcock, Phys. Rev. 75, 1616 (1949)

10D47 S. DeBenedetti and E. H. Kerner, Phys. Rev. 71, 122 (1947)

10D48 S. DeBenedetti and F. K. McGowan, Phys. Rev. 74, 728 (1948)

10D52 S. DeBenedetti and G. H. Minton, Phys. Rev. 85, 944 (1952)

11D39 J. V. Dunworth, Nature 144, 152 (1939)

11D47 J. V. Dunworth and B. Pontecorvo, Proc. Cambridge Phil. Soc. 43, 123 (1947)

11D47a J. V. Dunworth and B. Pontecorvo, Proc. Cambridge Phil. Soc. 43, 429 (1947)

12D42 G. Dessauer, private communication (May 1942)

13D50 G. von Dardel, Phys. Rev 79, 734 (1950)

14D41 R. L. Doran and W. J Henderson, Phys Rev. 60, 411 (1941)

14D48 R. L. Doran and W. J. Henderson, private communication from K. Lark-Horowitz (1948)

15D52 D. C. Dunlavey and G. T. Seaborg, Phys Rev 87, 165 (1952)

15D52a D. C. Dunlavey and G. T. Seaborg, Phys Rev 85, 757 (1952) (A)

16D41 B. S. Dzhelepov and A. A. Konstantinov, Compt. rend U.S.S.R. 30, 701 (1941)

16D46 B. Dzhelepov, M. Kopjova, and E. Vorbjov, Phys. Rev. 69, 538 (1946)

16D49 B. S. Dzhelepov, N. M. Anton'eva, and S. A. Shestopalova, Doklady Akad Nauk, S.S.S.R. 64, 309 (1949)

16D51 B. Dzhelepov, N. Zhukovskii, and Yu. Kholnov, Doklady Akad. Nauk, S.S.S.R. 77, 233 (1951)

16D52 B. Dzhelepov and A. Silantov, Doklady Akad. Nauk, S.S.S.R. 85, 533 (1952)

17D51 C. F. G. Delaney, Phys. Rev 81, 158 (1951)

17D51a C. F. G. Delaney, Sci. Proc Roy. Dublin Soc 25, 251 (1951)

18D40 G. Dickson, P. W. McDaniel, and E. J. Konopinski, Phys. Rev. 57, 351 (1940) (A)

19D37 B. T. Darling, B. R. Curtis, and J. M. Cork, Phys. Rev. 51, 1010 (1937) (A)

20D41 M. Deutsch and A. Roberts, Phys Rev. 60, 362 (1941)

20D42 M. Deutsch, J. R. Downing, L. G. Elliott, J. W. Irvine, Jr., and A. Roberts, Phys. Rev. 62, 3 (1942)

20D42a M. Deutsch and L. G. Elliott, Phys. Rev 62, 558 (1942) (A)

20D42b M. Deutsch, Phys. Rev. 61, 672 (1942)

20D42c M. Deutsch, A. Roberts, and L. G. Elliott, Phys Rev. 61, 389 (1942) (A)

20D44 M. Deutsch and L. G. Elliott, Phys. Rev. 65, 211 (1944)

20D45 M. Deutsch, L. G. Elliott, and A. Roberts, Phys. Rev. 68, 193 (1945)

20D47 M. Deutsch, Phys. Rev. 72, 729 (1947)

20D47a M. Deutsch, Phys. Rev. 72, 527 (1947) (A)

20D49 M. Deutsch and A. Hedgran, Phys. Rev. 75, 1443 (1949)

20D49a M. Deutsch and D. T. Stevenson, Phys. Rev. 76, 184 (1949) (A)

20D50 M. Deutsch and W. E. Wright, Phys. Rev. 77, 139 (1950)

20D50a M. Deutsch and A. Hedgran, Phys. Rev. 79, 400 (1950)

20D51 M. Deutsch and G. Scharff-Goldhaber, Phys. Rev. 83, 1059 (1951)

21D40 D. DeVault and W. F. Libby, Phys. Rev. 58, 688 (1940)

22D39 R. W. Dodson and R. D. Fowler, Phys Rev. 55, 880 (1939)

22D40 R. W. Dodson and R. D. Fowler, Phys. Rev. 57, 966 (1940)

23D48 R. B. Duffield and J. D. Knight, private communication (Oct. 1948)

23D49 R. B. Duffield and J. D. Knight, Phys. Rev. 76, 573 (1949)

23D49a R. B. Duffield and J. D. Knight, Phys. Rev. 75, 1613 (1949)

23D49b R. B. Duffield and J. D. Knight, Phys. Rev. 75, 1967 (1949)

23D49c R. B. Duffield and L. M. Langer, Phys. Rev. 76, 1272 (1949)

23D50 R. B. Duffield, L. Hsiao, and E. N. Sloth, Phys. Rev. 79, 1011 (1950)

23D50a R. B. Duffield and L. M. Langer, Phys. Rev. 77, 743 (1950) (A)

23D51 R. B. Duffield and L. M. Langer, Phys. Rev. 81, 203 (1951)

23D51a R. B. Duffield, reported in U. S. Atomic Energy Commission Classified Report WASH-62 (Dec. 1951)

23D51b R. B. Duffield and L. M. Langer, Phys. Rev. 84, 1065 (1951)

23D52 R. B. Duffield and L. M. Langer, Phys. Rev. (to be published) (1952)

24D51 C. R. Dillard, R. M. Adams, H. Finston, and A. Turkevich, NNES-PPR 9, 624 (1951)

24D51a C. R. Dillard, R. M. Adams, H. Finston, and A. Turkevich, NNES-PPR 9, 616 (1951)

24D51b C. R. Dillard, R. M. Adams, H. Finston, and A. Turkevich, NNES-PPR 9, 692 (1951)

24D51c C. R. Dillard, H. Finston, and R. M. Adams, NNES-PPR 9, 1101 (1951)

25D41 J. R. Downing, M. Deutsch, and A. Roberts, Phys. Rev. 60, 470 (1941)

25D42 J. R. Downing, M. Deutsch, and A. Roberts, Phys. Rev. 61, 686 (1942)

26D51 B. Dreyfus, J. K. Major, and P. Radvanyi, Compt. rend. 232, 617 (1951)

27D38 M. Dodé and B. Pontecorvo, Compt. rend. 207, 287 (1938)

28D50 E. B. Dale and J. D. Kurbatov, Phys. Rev. 80, 126 (1950) (A)

28D50a E. B. Dale, E. D. Richert, T. A. Redfield, and J. D. Kurbatov, Phys. Rev. 80, 763 (1950)

29D42 J. W. DeWire, M. L. Pool, and J. D. Kurbatov, Phys. Rev. 61, 564 (1942)

30D49 D. G. Douglas, Phys. Rev. 75, 1960 (1949)

30D52 D. G. Douglas, J. S. Foster, and A. L. Thompson, private communication (Oct. 1952)

31D50 T. Dybvig and M. L. Pool, Phys. Rev 80, 126 (1950) (A)

32D51 S. P. Davis and F. A. Jenkins, Phys. Rev. 83, 1269 (1951)

33D46 G. Diemer and H. Groendijk, Physica 11, 396 (1946)

34D48 J. W. M. DuMond, D. A. Lind, and B. B. Watson, Phys. Rev. 73, 1392 (1948)

35D51 D. B. Duncan and J. E. Perry, Phys Rev. 82, 809 (1951)

36D52 J. T. Dewan, T. P. Pepper, K. W. Allen, and E. Almqvist, Phys. Rev. 86, 416 (1952)

37D51 S. Das and S. K. Sen, Indian J. Phys. 25, 451 (1951)

38D52 S. S. Dharmatti and H. E. Weaver, Jr., Phys. Rev. 85, 927 (1952)

39D51 E. K. Darby and W. Opechowski, Phys. Rev. 83, 676 (1951)

CC-0. In Public Domain. Gurukul Kangri Collection, Haridwar

Digitized by Arya Samaj Foundation Chennai and eGangotri

39D51a E. K. Darby, Can. J. Phys. 29, 569 (1951)

40D52 B. Dropesky and E. O. Wiig, Phys. Rev. 88, 683 (1952)

41D52 F. Depocas and B. G. Harvey, Phys. Rev. 85, 499 (1952)

42D52 D. Dixon, McNair, and S. C. Curran, Physica (in press) (1952)

43D52 R. M. Diamond, private communication (Nov. 1952)

44D52 C. Dahlstrom, J. S. Foster, and A. L. Thompson, private communication (Oct. 1952)

1E48 D. T. Eggen and M. L. Pool, Phys. Rev. 74, 57 (1948)

1E49 D. T. Eggen and M. L. Pool, Phys. Rev. 75, 1464 (1949) (A)

2E49 W. S. Emmerich and J. D. Kurbatov, Phys. Rev. 75, 1446 (1949)

2E51 W. S. Emmerich, G. John, and J. D. Kurbatov, Phys. Rev. 82, 968 (1951)

2E51a W. S. Emmerich and J. D. Kurbatov, Phys. Rev. 83, 40 (1951)

2E52 W. S. Emmerich and J. D. Kurbatov, Phys. Rev. 85, 149 (1952)

3E50 A. G. Engelkemeir and W. F. Libby, Rev. Sci. Instr. 21, 550 (1950)

4E43 L. G. Elliott, M. Deutsch, and A. Roberts, Phys. Rev. 63, 386 (1943)

4E43a L. G. Elliott and M. Deutsch, Phys. Rev. 64, 321 (1943)

4E43b L. G. Elliott and M. Deutsch, Phys. Rev. 63, 457 (1943) (A)

4E47 L. G. Elliott and R. E. Bell, Phys. Rev. 72, 979 (1947)

4E48 L. G. Elliott and R. E. Bell, Phys. Rev. 74, 1869 (1948)

4E49 L. G. Elliott and R. E. Bell, Phys. Rev. 76, 168 (1949) (A) and private communication from R. L. Graham (Sept. 1952)

4E50 L. G. Elliott, R. E. Bell, et al., reported in Chalk River Laboratory Classified Report PR-P-7 (Aug. 1950)

4E50a L. G. Elliott et al., reported in Chalk River Laboratory Classified Report PR-P-8 (Nov. 1950)

4E51 L. G. Elliott and J. L. Wolfson, Phys. Rev. 82, 333 (1951) (A)

4E51a L. G. Elliott et al., reported in Chalk River Laboratory Classified Reports PR-P-12 (Nov. 1951) and PR-P-13 (Feb. 1952)

4E52 L. G. Elliott, Phys. Rev. 85, 942 (1952)

5E37 Z. V. Erchova, J. phys. et radium 8, 501 (1937)

6E50 H. D. Evans, Proc. Phys. Soc. (London) 63A, 575 (1950)

7E42 S. G. English and R. A. James, reported in Metallurgical Laboratory Classified Report CN-261 (Sept. 1942)

8E30 C. D. Ellis and G. H. Aston, Proc. Roy. Soc. (London) 129A, 180 (1930)

8E32 C. D. Ellis, Proc. Roy. Soc. (London) 138A, 318 (1932)

8E33 C. D. Ellis and N. F. Mott, Proc. Roy. Soc. (London) 141A, 502 (1933)

8E34 C. D. Ellis, Proc. Roy. Soc. (London) 143A, 350 (1934)

8E34a C. D. Ellis and W. J. Henderson, Proc. Roy. Soc. (London) 146A, 206 (1934)

8E35 C. D. Ellis and W. J. Henderson, Nature 135, 429 (1935)

8E36 C. D. Ellis and W. J. Henderson, Proc. Roy. Soc. (London) 156A, 358 (1936)

9E48 C. Eggler, D. J. Hughes, and C. Huddleston, Phys. Rev. 74, 1239 (1948) (A)

10E41 S. Eklund, Arkiv Mat., Astron. Fysik 28A, No. 3 (1941)

10E43 S. Eklund and N. Hole, Arkiv Mat., Astron. Fysik 29A, No. 26 (1943)

10E46 S. Eklund, Arkiv Mat., Astron. Fysik 33A, No. 14 (1946)

11E47 A. C. English, T. E. Cranshaw, P. Demers, J. A. Harvey, E. P. Hincks, J. V. Jelley, and A. N. May, Phys. Rev. 72, 253 (1947)

12E41 D. R. Elliott and L. D. P. King, Phys. Rev. 60, 489 (1941)

12E41a D. R. Elliott and L. D. P. King, Phys. Rev. 59, 403 (1941)

13E46 D. W. Engelkemeir and E. L. Brady, reported in J. Am. Chem. Soc. 68, 2411 (1946)

13E48 D. W. Engelkemeir, U. S. Atomic Energy Commission Declassified Document AECD-2125 (July 1948)

13E50 D. W. Engelkemeir, M. S. Freedman, and J. May, Argonne National Laboratory Unclassified Report ANL-4473 (June 1950)

13E51 D. W. Engelkemeir, J. A. Seiler, E. P. Steinberg, and L. Winsberg, NNES-PPR 9, 1354 (1951)

13E51a D. W. Engelkemeir and E. L. Brady, NNES-PPR 9, 746 (1951)

13E51b D. W. Engelkemeir, E. L. Brady, and E. P. Steinberg, NNES-PPR 9, 722 (1951)

13E51c D. W. Engelkemeir, Phys. Rev. 82, 552 (1951)

13E51d D. W. Engelkemeir, reported in Argonne National Laboratory Classified Report ANL-4526 (Jan. 1951)

13E51e D. W. Engelkemeir and N. Sugarman, NNES-PPR 9, 1052 (1951)

13E51f D. W. Engelkemeir, M. S. Freedman, L. E. Glendenin, and R. P. Metcalf, NNES-PPR 9, 1104 (1951)

13E51g D. W. Engelkemeir, NNES-PPR 9, 1108 (1951)

13E52 D. W. Engelkemeir, reported in Argonne National Laboratory Classified Report ANL-4717 (April 1952)

14E46 J. E. Edwards and M. L. Pool, Phys. Rev. 69, 253 (1946) (A)

14E46a J. E. Edwards and M. L. Pool, Phys. Rev. 69, 140 (1946)

14E47 J. E. Edwards and M. L. Pool, Phys. Rev. 72, 384 (1947)

15E39 D. Ewing, T. Perry, and R. McCreary, Phys. Rev. 55, 1136 (1939) (A)

16E43 H. Ewald, private communication to S. Flügge and J. Mattauch, Ber. deut. chem. Ges. 76A, 1 (1943); Z. physik 122, 487 (1944)

17E39 T. Enns, Phys. Rev. 56, 872 (1939)

18E51 N. Elliott, NNES-PPR 9, 1047 (1951)

19E51 H. B. Evans, L. E. Glendenin, and R. P. Metcalf, NNES-PPR 9, 1081 (1951)

20E51 R. R. Edwards, H. Gest, and T. H. Davies, NNES-PPR 9, 237 (1951)

21E52 G. G. Eichholz and L. A. Ficko, Phys. Rev. 86, 794 (1952)

22E52 L. S. Edwards and F. A. MacMillan, Phys. Rev. 87, 377 (1952)

23E52 V. O. Erikson, G. Jenssen, and A. Sunde, Physica 18, 91 (1952)

24E51 E. W. Emery, Phys. Rev. 83, 679 (1951)

25E52 M. W. Elliott, L. S. Cheng, J. R. Haskins, and J. D. Kurbatov, Phys. Rev. 88, 263 (1952)

26E52 G. T. Ewan and M. A. S. Ross, Nature 170, 760 (1952)

CC-0. In Public Domain. Gurukul Kangri Collection, Haridwar

Digitized by Arya Samaj Foundation Chennai and eGangotri

1F36 W. A. Fowler, L. A. Delsasso, and C. C. Lauritsen, Phys. Rev. 49, 561 (1936)

1F37 W. A. Fowler and C. C. Lauritsen, Phys. Rev. 51, 1103 (1937)

2F51 M. H. Feldman, L. E. Glendenin, and R. R. Edwards, NNES-PPR 9, 598 (1951)

2F51a M. H. Feldman and L. E. Glendenin, NNES-PPR 9, 654 (1951)

3F50 M. Freedman, J. May, R. Pairs, W. Ramler, and M. Rusnak, reported in Argonne National Laboratory Classified Report ANL-4380 (March 1950)

3F50a M. S. Freedman, A. H. Jaffey, and F. Wagner, Jr., Phys. Rev. 79, 410 (1950)

3F50b M. S. Freedman and E. P. Steinberg, reported in Argonne National Laboratory Classified Report ANL-4427 (July 1950)

3F50c M. S. Freedman and D. W. Engelkemeir, Phys. Rev. 79, 897 (1950)

3F51 M. Freedman and F. Wagner, Jr., reported in Argonne National Laboratory Classified Report ANL-4526 (Jan. 1951)

3F52 M. S. Freedman, F. Wagner, Jr., A. H. Jaffey, and J. May, Phys. Rev. (in press) (1952)

3F52a M. Freedman, J. May, M. Rusnak, and F. Wagner, Jr., reported in Argonne National Laboratory Classified Report ANL-4717 (April 1952)

3F52b M. S. Freedman, F. Wagner, Jr., and D. W. Engelkemeir, Phys. Rev. 88, 1155 (1952)

3F53 M. S. Freedman, F. Wagner, Jr., D. W. Engelkemeir, J. R. Huizenga, and L. B. Magnusson, Phys. Rev. (to be published) (1953)

4F32 N. Feather, Proc. Roy. Soc. (London) 136, 709 (1932); 142, 689 (1933)

4F38 N. Feather, Proc. Cambridge Phil. Soc. 34, 115 (1938)

4F38a N. Feather and E. Bretscher, Proc. Roy. Soc. (London) 165A, 530 (1938)

4F38b N. Feather and J. V. Dunworth, Proc. Roy. Soc (London) 168A, 566 (1938)

4F42 N. Feather, British Classified Report CPB-83 (1942)

4F44 N. Feather and J. Dainty, Proc. Cambridge Phil. Soc. 40, 57 (1944)

4F47 N. Feather and R. S. Krishnan, Proc. Cambridge Phil. Soc. 43, 267 (1947)

4F47a N. Feather, Nature 160, 749 (1947)

4F48 N. Feather, J. Kyles, and R. W. Pringle, Proc. Phys. Soc. (London) 61, 466 (1948)

4F49 N. Feather, Nucleonics 5, No. 1, 22 (1949)

5F39 K. Fajans and D. W. Stewart, Phys. Rev. 56, 625 (1939)

5F40 K. Fajans and A. F. Voigt, Phys. Rev. 58, 177 (1940)

5F40a K. Fajans and W. H Sullivan, Phys. Rev. 58, 276 (1940)

5F41 K. Fajans and A. F. Voigt, Phys. Rev. 60, 619 (1941)

5F41a K. Fajans and A. F. Voigt, Phys. Rev. 60, 626 (1941)

5F41b K. Fajans and A. F. Voigt, Phys. Rev. 60, 533 (1941)

6F50 R. L. Folger, University of California Radiation Laboratory Declassified Report UCRL-937 (Oct. 1950)

6F51 R. L. Folger, P. C. Stevenson, and G. T. Seaborg, University of California Radiation Laboratory Classified Report UCRL-1195 Revised (May 1951)

7F51 H. Faraggi and A. Berthelot, Compt. rend. 232, 2093 (1951)

7F51a H. Faraggi, Ann. phys. 6, 325 (1951)

8F40 M. Frilley, J. phys. et radium 1, 34 (1940)

8F52 M. Frilley, B. G. Gokhale, and M. Valadares, Compt. rend. 232, 50 (1952)

9F39 A. Flammersfeld, Z. Physik 114, 227 (1939)

9F39a A. Flammersfeld, Z. Physik 112, 727 (1939)

9F43 A. Flammersfeld and J. Mattauch, Naturwiss. 31, 66 (1943)

9F44 A. Flammersfeld, Naturwiss. 32, 36 (1944)

9F44a A. Flammersfeld and O. Bruna, Naturwiss. 32, 70 (1944)

9F44b A. Flammersfeld, Naturwiss 32, 68 (1944)

9F46 A. Flammersfeld, Z. Naturforsch. 1, 190 (1946)

9F47 A. Flammersfeld and O. Bruna, Z. Naturforsch. 2a, 241 (1947)

9F47a A. Flammersfeld, Z. Naturforsch. 2a, 86 (1947)

9F50 A. Flammersfeld and C. Ythier, Z. Naturforsch. 5a, 401 (1950)

9F50a A. Flammersfeld, Z. Naturforsch. 5a, 687 (1950)

9F50b A. Flammersfeld and W. Herr, Z. Naturforsch. 5a, 569 (1950)

9F51 A. Flammersfeld, Z. Naturforsch. 6a, 559 (1951)

9F52 A. Flammersfeld, Z. Naturforsch. 7a, 295 (1952)

9F52a A. Flammersfeld, Z. Naturforsch. 7a, 296 (1952)

10F51 P. Falk-Vairant and J. Teillac, J. phys. et radium 12, 659 (1951)

10F52 P. Falk-Vairant, J. Teillac, and C. Victor, J. phys et radium 13, 313 (1952)

10F52a P. Falk-Vairant, Compt. rend. 235, 796 (1952)

11F44 H. W. Fulbright, reported in Metallurgical Laboratory Classified Report CP-1954 (Aug. 1944)

11F44a H. W. Fulbright, W. Bentz, K. Booth, R. G. Gilbert, H. Huth, A. Knudson, H. Meier, H. Plew, C. A. Potter, W. Rall, A. A. Schulke, and M. Waldner, Metallurgical Laboratory Classified Report CP-1357 (Feb. 1944)

11F49 H. W. Fulbright, NNES-PPR 14B, 1011 (1949)

11F49a H. W. Fulbright and J. C. D. Milton, Phys. Rev. 76, 1271 (1949)

12F52 E. H. Fleming, Jr., A. Ghiorso, and B. B. Cunningham, Phys. Rev. 88, 642 (1952)

13F50 P. R. Fields, G. L. Pyle, and J. F. Mech, reported in Argonne National Laboratory Classified Report ANL-4469 (June 1950)

14F45 G. W. Farwell, J. E. Roberts, A. Spane, and A. C. Wahl, Los Alamos Scientific Laboratory Classified Report LAMS-293 (Oct. 1945)

14F46 G. W. Farwell, E. Segrè, A. Spane, and C. E. Wiegand, Los Alamos Scientific Laboratory Classified Report LA-490 (April 1946)

15F49 L. Feldman and C. S. Wu, Phys. Rev. 75, 1286 (1949) (A)

15F49a L. Feldman, L. Lidofsky, P. Macklin, and C. S. Wu, Phys. Rev. 76, 1888 (1949)

15F52 L. Feldman and C. S. Wu, Phys. Rev. 87, 1091 (1952)

16F34 E. Fermi, E. Amaldi, O. d'Agnostino, F. Rasetti, and E. Segrè, Proc. Roy. Soc. (London) 146A, 483 (1934)

16F41 E. Fermi and E. Segrè, Phys. Rev. 59, 680 (1941)

17F34 O. R. Frisch, Nature 133, 721 (1934)

17F35 O. R. Frisch, Nature 136, 220 (1935)

18F35 H. Fahlenbrach, Z. Physik 96, 503 (1935)

19F50 W. R. Faust, Phys. Rev. 78, 624 (1950)

20F49 J. J. Floyd and L. B. Borst, Phys. Rev. 75, 1106 (1949)

21F43 B. T. Feld, reported in Metallurgical Laboratory Classified Report CP-1016 (Oct. 1943)

22F47 I. Feister and L. F. Curtiss, J. Research Natl. Bur. Standards 38, 411 (1947)

22F50 I. Feister and L. F. Curtiss, Phys. Rev. 78, 179 (1950)

CC-0. In Public Domain. Gurukul Kangri Collection, Haridwar

Digitized by Arya Samaj Foundation Chennai and eGangotri

23F40 G. Friedlander, private communication (1940)

23F43 G. Friedlander and C. S. Wu, Phys. Rev. 63, 227 (1943)

23F48 G. Friedlander, M. Goldhaber, and G. Scharff-Goldhaber, Phys Rev 74, 981 (1948)

23E48a G Friedlander and M. L. Perlman, private communication (Sept. 1948)

23F49 G. Friedlander, reported in Brookhaven National Laboratory Unclassified Report BNL-AS-2 (June 1949)

23F50 G. Friedlander, M. L. Perlman, D. Alburger, and A. W. Sunyar, Phys Rev. 80, 30 (1950)

23F50a G. Friedlander, M. L. Perlman, and G. Scharff-Goldhaber, Phys Rev 80, 1103 (1950)

23F51 G Friedlander and J. M. Miller, Phys. Rev 84, 588 (1951)

23F51a G Friedlander and D. E Alburger, Phys Rev 84, 231 (1951)

23F51b G. Friedlander and W. C. Orr, Phys. Rev. 84, 484 (1951)

23F52 G. Friedlander and M. L. Perlman, private communication (Aug. 1952)

23F52a G. Friedlander, A. Ghiorso, and I. Perlman, unpublished data (Sept. 1952)

23F52b G. Friedlander and J. M. Miller, private communication (Oct. 1952)

23F52c G. Friedlander, private communication (Dec. 1952)

24F51 S. E. Furberg, Nature 168, 1005 (1951)

25F51 S. C. Fultz and M L. Pool, Phys. Rev 83, 875 (1951) (A)

25F52 S. C. Fultz and M. L. Pool, Phys. Rev. 86, 347 (1952)

26F47 H. N. Friedlander, L. Seren, and S. H. Turkel, Phys. Rev. 72, 23 (1947)

27F50 E. W. Fuller, Proc Phys. Soc. (London) 63A, 1044 (1950)

27F50a E. W. Fuller, Proc. Phys. Soc. (London) 63A, 1348 (1950)

28F47 B. J. Finkle, Phys. Rev. 72, 1260 (1947)

28F51 B. Finkle, E. J. Hoagland, S. Katcoff, and N. Sugarman, NNES-PPR 9, 1368 (1951)

28F51a B. Finkle, S. Katcoff, and N. Sugarman, NNES-PPR 9, 663 (1951)

28F51b B. Finkle, D. W. Engelkemeir, and N. Sugarman, NNES-PPR 9, 1083 (1951)

28F51c B. Finkle and N. Sugarman, NNES-PPR 9, 1121 (1951)

29F52 C. Y. Fan, Phys. Rev. 87, 252 (1952)

30F51 S. Fried, A. H. Jaffey, N. F. Hall, and L. E. Glendenin, Phys. Rev. 81, 741 (1951)

31F41 J. R. Feldmeier and G. B. Collins, Phys. Rev. 59, 937 (1941)

32F52 E. L. Fireman and D. Schwarzer, Phys. Rev. 86, 451 (1952)

33F50 R. W. Fink, F. L. Reynolds, and D. H. Templeton, Phys. Rev. 77, 614 (1950)

33F50a R. W. Fink and D. H. Templeton, J. Am. Chem. Soc. 72, 2818 (1950)

33F51 R. W. Fink and E. O. Wiig, J. Am. Chem. Soc. 73, 2365 (1951)

33F52 R. W. Fink and E. O. Wiig, J. Am. Chem. Soc. 74, 2457 (1952)

34F52 V. Kistiakowsky Fischer, Ph. D. Thesis, University of California Radiation Laboratory Unclassified Report UCRL-1629 (Jan. 1952); Phys. Rev. 87, 859 (1952)

35F50 C. M. Fowler and R. G. Shreffler, Rev. Sci. Instr. 21, 740 (1950)

36F49 J. S. Fraser, Phys. Rev. 76, 1540 (1949)

37F36 V. Fomin and F. G. Houtermans, Physik Z. Sowjetunion 9, 273 (1936)

38F52 M. S. Fred and F. S. Tompkins, Phys. Rev. (in press) (1952)

39F52 S. C. Fung and I. Perlman, Phys. Rev. 87, 623 (1952)

40F47 H. Frauenfelder, P. C. Gugelot, O. Huber, H. Medicus, P. Preiswerk, P. Scherrer, and R Steffen, Helv Phys. Acta 20, 238 (1947)

40F50 H. Frauenfelder, O. Huber, A. de-Shalit, and W Zünti, Phys. Rev 79, 1029 (1950)

40F50a H. Frauenfelder, M. Walter, and W Zünti, Phys. Rev. 77, 557 (1950)

41F52 A. J. Ferguson and J. H. Montague, Phys. Rev 87, 215 (1952) (A)

42F52 A W Fairhall, private communication (Dec 1952)

1G22 H Geiger, Z. Physik 8, 45 (1922)

2G30 A. V. Grosse, J. Am. Chem. Soc. 52, 1742 (1930); Naturwiss. 20, 505 (1932)

2G39 A. V. Grosse, E. T. Booth, and J. R. Dunning, Phys Rev. 56, 382 (1939)

2G40 A. V. Grosse and E. T. Booth, Phys. Rev. 57, 664 (1940)

2G41 A. V. Grosse, E T. Booth, and J. R. Dunning, Phys. Rev 59, 322 (1941)

2G48 A. V. Grosse and E. T. Booth, J. Am. Chem. Soc. 70, 465 (1948)

3G47 R. G. Grégoire and M. Perey, Compt rend. 225, 733 (1947)

4G49 C. H. Goddard and C. S. Cook, Phys. Rev. 76, 1419 (1949)

5G50 L. S. Germain, Phys Rev. 80, 937 (1950)

6G49 L. V. Groshev and L. Y. Shavtvalov, Doklady Akad Nauk S.S S.R. 68, 257 (1949)

7G51 M. A. Grace, R. A. Allen, D. West, and H. Halban, Proc. Phys. Soc. (London) 64A, 493 (1951)

7G51a M. A. Grace and J. R. Prescott, Phys. Rev. 84, 1059 (1951)

8G47 M. Guillot and M. Perey, Compt. rend 225, 330 (1947)

9G49 J. W. Gofman and G. T. Seaborg, NNES-PPR 14B, 1427 (1949)

10G49 A. S. Goldin, G. B. Knight, P. A. Macklin, and R. L. Macklin, Phys. Rev. 76, 336 (1949)

11G46 R. H. Goeckermann, P. R. O'Connor, and W. J. Knox, private communication (1946)

11G49 R. H. Goeckermann and I. Perlman, Phys. Rev. 76, 628 (1949)

12G32 O. Gratias and C. H. Collie, Proc. Roy. Soc. (London) 135A, 299 (1932)

13G44 A. Ghiorso, reported in Metallurgical Laboratory Classified Reports CK-1511 (April 1944); CS-1657 (May 1944)

13G45 A. Ghiorso, unpublished data (1945)

13G48 A. Ghiorso, W. W. Meinke, and G. T. Seaborg, Phys. Rev. 74, 695 (1948)

13G48a A. Ghiorso, J. M. Hollander, and I. Perlman, U. S. Atomic Energy Commission Declassified Document AECD-2232 (July 1948)

13G48b A. Ghiorso, L. B. Magnusson, and G. T. Seaborg, unpublished data (July 1948)

13G48c A. Ghiorso, unpublished data (1948)

13G49 A. Ghiorso, W. W. Meinke, and G. T. Seaborg, Phys. Rev. 76, 1414 (1949)

CC-0. In Public Domain. Gurukul Kangri Collection, Haridwar

Digitized by Arya Samaj Foundation Chennai and eGangotri

13G50 A. Ghiorso, R. A. James, L. O. Morgan, and G. T. Seaborg, Phys. Rev. 78, 472 (1950)

13G51 A. Ghiorso, Phys. Rev. 82, 979 (1951)

13G51a A. Ghiorso, J. W. Brittain, W. M. Manning, and G. T. Seaborg, Phys. Rev. 82, 558 (1951)

13G51b A. Ghiorso, unpublished data (1951)

13G51c A. Ghiorso, S. G. Thompson, K. Street, Jr., and G. T. Seaborg, Phys. Rev. 81, 154 (1951)

13G52 A. Ghiorso, G. H. Higgins, A. E. Larsh, G. T. Seaborg, and S. G. Thompson, Phys. Rev. 87, 163 (1952) and private communication (Nov. 1952)

13G53 A. Ghiorso, unpublished rumor (1953)

14G49 R. L. Graham and D. H. Tomlin, Nature 164, 278 (1949)

14G51 R. L. Graham and R. E. Bell, Phys. Rev. 83, 222 (1951) (A)

14G51a R. L. Graham and R. E. Bell, Phys. Rev. 84, 380 (1951)

14G52 R. L. Graham, J. L. Wolfson, and R. E. Bell, Can. J. Phys. 30, 459 (1952)

14G53 R. L. Graham and R. E. Bell, Can. J. Phys. (to be published) (1953)

15G50 J. M. Grunlund, B. G. Harvey, N. Moss, and L. Yaffe, Phys. Rev. 78, 69 (1950)

16G47 M. Goldblatt, E. S. Robinson, and R. W. Spence, Phys. Rev. 72, 973 (1947)

17G49 E. R. Graves and D. I. Meyer, Phys. Rev. 76, 183 (1949) (A)

18G38 M. Goldhaber, R. D. Hill, and L. Szilard, Phys. Rev. 55, 47 (1939); Nature 142, 521 (1938)

18G46 M. Goldhaber and R. D. O'Neal, private communication (Dec. 1946)

18G46a M. Goldhaber and W. J. Sturm, Phys. Rev. 70, 111 (1946) (A)

18G46b M. Goldhaber, C. O. Muehlhause, and W. J. Sturm, reported in Metallurgical Laboratory Classified Report CF-3574 (Oct. 1946)

18G46c M. Goldhaber, Phys. Rev. 70, 89 (1946)

18G46d M. Goldhaber, L. Jacobs, and D. J. Williams, reported in Argonne National Laboratory Classified Report CP-3647 (Nov. 1946)

18G47 M. Goldhaber and C. O. Muehlhause, reported in Argonne National Laboratory Classified Report ANL-4010 (Sept. 1947)

18G47a M. Goldhaber, C. O. Muehlhause, and S. H. Turkel, Phys. Rev. 71, 372 (1947)

18G48 M. Goldhaber and C. O. Muehlhause, Phys. Rev. 74, 1877 (1948)

18G48a M. Goldhaber and C. O. Muehlhause, Phys. Rev. 74, 1248 (1948) (A)

18G50 M. Goldhaber, private communication listed in Natl. Bur. Standards Circular No. 499 (Sept. 1950)

18G51 M. Goldhaber, E. der Mateosian, G. Scharff-Goldhaber, A. W. Sunyar, M. Deutsch, and N. S. Wall, Phys. Rev. 83, 661 (1951)

18G52 M. Goldhaber and R. D. Hill, Revs. Modern Phys. 24, 179 (1952)

19G38 J. A. Gray, Nature 130, 738 (1932)

19G36 J. A. Gray and J. F. Hinds, Phys. Rev. 49, 477 (1936)

20G51 W. L. Gardner, N. Knable, and B. J. Moyer, Phys. Rev. 83, 1054 (1951)

21G46 W. M. Good, D. Peaslee, and M. Deutsch, Phys. Rev. 69, 313 (1946)

21G46a W. M. Good and W. C. Peacock, Phys. Rev. 69, 680 (1946) (A)

22G49 P. J. Grant and J. M. Hill, Nature 163, 524 (1949)

22G49a P. J. Grant and R. Richmond, Nature 163, 840 (1949); Proc. Phys. Soc. (London) 62A, 573 (1949)

22G50 P. J. Grant, Proc. Phys. Soc. (London) 63A, 1298 (1950)

22G50a P. J. Grant, Nature 165, 1018 (1950)

23G50 L. Gross and D. R. Hamilton, Phys. Rev. 80, 484 (1950)

24G47 L. J. Goodman and M. L. Pool, Phys. Rev. 71, 288 (1947)

25G51 M. L. Good, Phys. Rev. 83, 1054 (1951)

25G51a M. L. Good, Phys. Rev. 81, 891 (1951)

25G51b M. L. Good, Phys. Rev. 81, 1058 (1951)

26G47 E. Gleditsch and T. Gráf, Phys. Rev. 72, 640 (1947)

27G48 T. Gráf, Phys. Rev. 74, 831 (1948)

27G50 T. Gráf, Phys. Rev. 79, 1014 (1950)

27G51 T. Gráf, Arkiv Fysik 3, 171 (1951)

28G41 A. Guthrie, Phys. Rev. 60, 746 (1941)

28G48 A. Guthrie, private communication from K. Lark-Horowitz (1948)

29G43 J. Govaerts, Bull. Soc. Roy. Sci. Liege 12, 555 (1943); Chem. Zentr. I, 634 (1944)

30G51 G. M. Griffiths, Phys. Rev. 83, 852 (1951)

31G38 D. C. Grahame and G. T. Seaborg, Phys. Rev. 54, 240 (1938) (A)

31G41 D. C. Grahame and H. J. Walke, Phys. Rev. 60, 909 (1941)

32G49 D. N. Gideon, W. C. Miller, and B. Waldman, Phys. Rev. 75, 329 (1949) (A)

33G46 L. E. Glendenin, reported in J. Am. Chem. Soc. 68, 2411 (1946)

33G46a L. E. Glendenin and E. P. Steinberg, reported in J. Am. Chem. Soc. 68, 2411 (1946)

33G47 L. E. Glendenin and R. R. Edwards, Phys. Rev. 71, 742 (1947)

33G49 L. E. Glendenin, Ph.D. Thesis, Massachusetts Institute of Technology Unclassified Report NP-1242 (Dec. 1949)

33G51 L. E. Glendenin, NNES-PPR 9, 596 (1951)

33G51a L. E. Glendenin, NNES-PPR 9, 592 (Editor's note) (1951)

33G51b L. E. Glendenin, NNES-PPR 9, 590 (Editor's note) (1951)

33G51c L. E. Glendenin and C. D. Coryell, NNES-PPR 9, 687 (1951)

33G51e L. E. Glendenin, NNES-PPR 9, 773 (1951)

33G51f L. E. Glendenin and E. P. Steinberg, NNES-PPR 9, 793 (1951)

33G51g L. E. Glendenin, NNES-PPR 9, 849 (1951)

33G51h L. E. Glendenin, NNES-PPR 9, 895 (1951)

33G51i L. E. Glendenin, NNES-PPR 9, 979 (Editor's note) (1951)

33G51j L. E. Glendenin and R. P. Metcalf, NNES-PPR 9, 992 (1951)

33G51k L. E. Glendenin and J. D. Knight, NNES-PPR 9, 1074 (1951)

33G51l L. E. Glendenin, NNES-PPR 9, 1931 (1951)

33G51m L. E. Glendenin, NNES-PPR 9, 1092 (1951)

33G51n L. E. Glendenin and R. P. Metcalf, NNES-PPR 9, 1067 (1951)

33G53 L. E. Glendenin and E. P. Steinberg, Phys. Rev. (to be published) (1953)

34G46 N. Goldstein and W. Spatz, reported in Metallurgical Laboratory Classified Report CF-3574 (Oct. 1946)

35G40 A. P. Grinberg and L. I. Roussinow, Phys. Rev. 58, 181 (1940)

36G40 G. N. Glasoe and J. Steigman, Phys. Rev. 58, 1 (1940)

37G51 K. Geiger, Ann. Physik 9, 293 (1951); Z. Naturforsch. 6a, 54 (1951)

CC-0. In Public Domain. Gurukul Kangri Collection, Haridwar

Digitized by Arya Samaj Foundation Chennai and eGangotri

37G52 K. Geiger, Z. Naturforsch. 7a, 579 (1952)

38G46 W. E. Grummitt and G. Wilkinson, Nature 158, 163 (1946)

38G47 W. E. Grummitt, J. Gueron, G. Wilkinson, and L. Yaffe, Can. J. Research 25B, 357, 364 (1947)

38G48 W. E. Grummitt and G. Wilkinson, Nature 161, 520 (1948)

38G51 W. E. Grummitt and G. Wilkinson, Chalk River Laboratory Declassified Report CRC-470 (March 1951)

39G43 B. L. Goldschmidt and F. Morgan, National Research Council of Canada, Atomic Energy Project Report MC-11 (Aug. 1943)

39G46 B. L. Goldschmidt and I. Perlman, reported in J. Am. Chem. Soc. 68, 2411 (1946)

39G51 B. L. Goldschmidt and I. Perlman, NNES-PPR 9, 709 (1951)

39G51a B. L. Goldschmidt and I. Perlman, NNES-PPR 9, 790 (1951)

40G40 H. Götte, Naturwiss. 28, 449 (1940)

40G41 H. Götte, Naturwiss. 29, 496 (1941)

40G42 H. Götte, Naturwiss. 30, 108 (1942)

40G43 H. Götte, reported in (16H43b)

40G46 H. Götte, Z. Naturforsch. 1, 377 (1946)

41G44 G. R. Gamertsfelder, Phys. Rev. 66, 288 (1944)

42G47 P. C. Gugelot, O. Huber, H. Medicus, P. Preiswerk, P. Scherrer, and R. Steffen, Helv. Phys. Acta 19, 418 (1947); 20, 240 (1947)

43G48 H. F. Gunlock and M. L. Pool, Phys. Rev. 74, 1264 (1948)

44G49 J. R. Gum, L. E. Thompson, and M. L. Pool, Phys. Rev. 76, 184 (1949) (A)

44G50 J. R. Gum and M. L. Pool, Phys. Rev. 80, 315 (1950)

45G50 M. Goodrich and E. C. Campbell, Phys. Rev. 79, 418 (1950) (A)

45G51 M. Goodrich, reported in Oak Ridge National Laboratory Unclassified Report ORNL-940 (March 1951)

45G51a M. Goodrich, Phys. Rev. 82, 759 (1951)

45G52 M. Goodrich and E. C. Campbell, Phys. Rev. 85, 742 (1952) (A) and private communication (Nov. 1952)

46G36 E. R. Gaerttner, J. J. Turin, and H. R. Crane, Phys. Rev. 49, 793 (1936)

47G50 P. S. Gill, C. E. Mandeville, and E. Shapiro, Phys. Rev. 80, 284 (1950); Indian J. Phys. 33, 566 (1950)

48G48 S. N. Ghoshal, Phys. Rev. 73, 417 (1948)

48G50 S. N. Ghoshal, Phys. Rev. 80, 939 (1950)

49G50 G. J. Goldsmith and E. Bleuler, J. Phys. Colloid Chem. 54, 717 (1950)

50G47 A. C. Graves and R. L. Walker, Phys. Rev. 71, 1 (1947)

51G52 M. J. Glaubman and F. R. Metzger, Phys. Rev. 87, 203 (1952) (A)

52G51 A. Goldstein, NNES-PPR 9, 1096 (1951)

52G51a A. Goldstein, R. P. Schuman, and W. Rubinson, NNES-PPR 9, 1188 (1951)

53G51 M. M. Gransden and W. S. Boyle, Phys. Rev. 82, 447 (1951)

54G51 H. Gest and R. R. Edwards, NNES-PPR 9, 1144 (1951)

55G50 S. Geschwind, H. Minden, and C. H. Townes, Phys. Rev. 78, 174 (1950)

56G49 R. L. Garwin, Phys. Rev. 76, 1876 (1949)

57G51 D. H. Greenberg and J. M. Miller, Phys. Rev. 84, 845 (1951)

58G51 D. Green and J. R. Richardson, Phys. Rev. 83, 891 (1951) (A)

59G52 G. A. Graves, L. M. Langer, and R. D. Moffat, Phys. Rev. 88, 344 (1952)

1H48 W. F. Hornyak, C. B. Dougherty, and T. Lauritsen, Phys. Rev. 74, 1727 (1948)

1H49 W. F. Hornyak, T. Lauritsen, and V. K. Rasmussen, Phys. Rev. 76, 731 (1949)

1H50 W. F. Hornyak and T. Lauritsen, Phys. Rev. 77, 160 (1950)

2H41 A. C. Helmholz, Phys. Rev. 60, 415 (1941)

2H41a A. C. Helmholz, C. Pecher, and P. R. Stout, Phys. Rev. 59, 902 (1941)

2H41b A. C. Helmholz, Phys. Rev. 60, 160 (1941) (A)

2H42 A. C. Helmholz, Phys. Rev. 62, 301 (1942) (A)

2H42a A. C. Helmholz, Phys. Rev. 61, 204 (1942) (A)

2H46 A. C. Helmholz, Phys. Rev. 70, 982 (1946)

2H48 A. C. Helmholz and C. L. McGinnis, Phys. Rev. 74, 1559 (1948) (A)

3H50 J. A. Harvey, reported in Massachusetts Institute of Technology Progress Report NP-1586 (April 1950)

4H47 F. Hagemann, L. I. Katzin, M. H. Studier, A. Ghiorso, and G. T. Seaborg, Phys. Rev. 72, 252 (1947)

4H47a F. Hagemann, reported in Argonne National Laboratory Classified Report CC-3780 (March 1947)

4H50 F. Hagemann, Phys. Rev. 79, 534 (1950)

4H50a F. Hagemann, L. I. Katzin, M. H. Studier, G. T. Seaborg, and A. Ghiorso, Phys. Rev. 79, 435 (1950)

5H46 J. J. Howland, D. H. Templeton, and I. Perlman, University of California Radiation Laboratory Declassified Report BC-31 (Nov. 1946)

6H36 F. A. Heyn, Nature 138, 723 (1936)

6H37 F. A. Heyn, Nature 139, 842 (1937)

6H37a F. A. Heyn, Physica 4, 160 (1937)

6H37b F. A. Heyn, Physica 4, 1224 (1937)

6H39 F. A. Heyn, A. H. W. Aten, Jr., and C. J. Bakker, Nature 143, 516 (1939)

7H49 A. O. Hanson, R. B. Duffield, J. D. Knight, B. C. Diven, and H. Palevsky, Phys. Rev. 76, 578 (1949)

8H48 E. K. Hyde, M. H. Studier, and R. J. Bruehlman, reported in Argonne National Laboratory Classified Report ANL-4112 (March 1948)

8H48a E. K. Hyde and M. H. Studier, reported in Argonne National Laboratory Memorandum ANL-WMM-445 (Dec. 1948)

8H48b E. K. Hyde and M. H. Studier, Argonne National Laboratory Classified Report ANL-4182 (Aug. 1948)

8H49 E. K. Hyde, M. H. Studier, and A. Ghiorso, NNES-PPR 14B, 1622 (1949)

8H49a E. K. Hyde, M. H. Studier, H. H. Hopkins, Jr., and A. Ghiorso, NNES-PPR 14B, 1439 (1949)

8H49b E. K. Hyde, NNES-PPR 14B, 1435 (1949)

8H50 E. K. Hyde, A. Ghiorso, and G. T. Seaborg, Phys. Rev. 77, 765 (1950)

8H50a E. K. Hyde and A. Ghiorso, University of California Radiation Laboratory Unclassified Report UCRL-593 (Feb. 1950)

8H51 E. K. Hyde, A. Ghiorso, and G. T. Seaborg, unpublished results (Aug. 1951)

8H51a E. K. Hyde and A. Ghiorso, unpublished data (May 1951)

8H51b E. K. Hyde and G. D. O'Kelley, Phys. Rev. 82, 944 (1951)

8H52 E. K. Hyde, private communication (May 1952)

CC-0: In Public Domain. Gurukul Kangri Collection, Haridwar

Digitized by Arya Samaj Foundation Chennai and eGangotri

8H52a E. K. Hyde, NNES-PPR 17B, 46 (1952) (classified)

8H52b E. K. Hyde and H. B. Mathur, private communication (June 1952)

8H52c E. K. Hyde and F. Asaro, private communication (Dec. 1952)

8H53 E. K. Hyde and A. Ghiorso, Phys. Rev. (to be published) (1953); University of California Radiation Laboratory Unclassified Report UCRL-2019 (Nov. 1952)

9H38 M. G. Holloway and M. S. Livingston, Phys. Rev. 54, 18 (1938). Summarizes results of various investigators.

10H51 C. M. Huddleston and A. B. Smith, Phys. Rev. 84, 289 (1951)

10H52 C. M. Huddleston and A. C. G. Mitchell, Phys. Rev (in press) (1952)

11H48 J. M. Hill, Proc. Cambridge Phil. Soc 44, 440 (1948)

11H50 J. M. Hill and L. R. Shepherd, Proc. Phys Soc. (London) 63A, 126 (1950)

12H50 A. Hedgran, K. Siegbahn, and N. Svartholm, Proc. Phys. Soc. (London) 63A, 960 (1950)

12H51 A. Hedgran, Phys. Rev. 82, 128 (1951)

12H51a A. Hedgran and S. Thulin, Phys. Rev. 81, 1072 (1951)

12H52 A. Hedgran and D. Lind, Arkiv Fysik 5, 177 (1952)

13H50 J. M. Hollander, A. Ghiorso, and I. Perlman, reported in University of California Radiation Laboratory Classified Report UCRL-923 (Sept. 1950)

13H50a J. M. Hollander and R. F. Leininger, Phys Rev. 80, 915 (1950)

13H51 J. M. Hollander, Ph.D. Thesis, University of California Radiation Laboratory Unclassified Report UCRL-1396 (July 1951)

14H34 W. J. Henderson, Proc. Roy. Soc. (London) 147A, 572 (1934)

14H37 W. J. Henderson, L. N. Ridenour, M. G. White, and M. C. Henderson, Phys. Rev. 51, 1107 (1937)

14H37a W. J. Henderson and L. N. Ridenour, Phys. Rev. 52, 40 (1937)

14H39 W. J. Henderson and R. L. Doran, Phys. Rev. 56, 123 (1939)

15H45 N. Hole, Arkiv Mat., Astron. Fysik 32A, No. 3 (1945)

15H45a N. Hole, Arkiv Mat., Astron. Fysik 31B, No. 9 (1945)

15H46 N. Hole and K. Siegbahn, Arkiv Mat., Astron. Fysik 33A, No. 9 (1946)

15H47 N. Hole, Arkiv Mat., Astron. Fysik 34B, No. 5 (1947)

15H47a N. Hole, Arkiv Mat., Astron. Fysik 34B, No. 19 (1947)

15H48 N. Hole, Arkiv Mat., Astron. Fysik 36A, No. 2 (1948)

15H48a N. Hole, Arkiv Mat., Astron. Fysik 36A, No. 9 (1948)

15H48b N. Hole, J. Benes, and A. Hedgran, Arkiv Mat., Astron. Fysik 35A, No. 35 (1948)

16H24 O. Hahn and L. Meitner, Z. Physik 26, 161 (1924)

16H25 O. Hahn and L. Meitner, Z. Physik 34, 795 (1925)

16H37a O. Hahn, F. Strassmann, and E. Walling, Naturwiss. 25, 189 (1937)

16H39 O. Hahn and F. Strassmann, Naturwiss. 27, 11 (1939)

16H39a O. Hahn and F. Strassmann, Naturwiss. 27, 529 (1939)

16H39b O. Hahn and F. Strassmann, Physik Z. 40, 673 (1939)

16H39c O. Hahn and F. Strassmann, Naturwiss. 27, 89 (1939)

16H39d O. Hahn, F. Strassmann, and S. Flügge, Naturwiss. 27, 544 (1939)

16H39e O. Hahn and F. Strassmann, Naturwiss. 27, 451 (1939)

16H40 O. Hahn and F. Strassmann, Naturwiss. 28, 61 (1940)

16H40a O. Hahn and F. Strassmann, Naturwiss. 28, 54 (1940)

16H40b O. Hahn and F. Strassmann, Naturwiss. 28, 455 (1940)

16H40c O. Hahn and F. Strassmann, Naturwiss. 28, 543 (1940)

16H41 O. Hahn and F. Strassmann, Naturwiss. 29, 369 (1941)

16H41a O. Hahn and F. Strassmann, Naturwiss. 29, 285 (1941)

16H41b O. Hahn and F. Strassmann, Z. Physik 117, 789 (1941)

16H42 O. Hahn, F. Strassmann, and H. Götte, Abhandl. preuss. Akad. Wiss. Math.-naturw. Klasse, No. 3 (1942)

16H42a O. Hahn and F. Strassmann, Naturwiss. 30, 324 (1942)

16H43 O. Hahn and F. Strassmann, Naturwiss 31, 249 (1943)

16H43a O. Hahn and F. Strassmann, Z. Physik 121, 729 (1943)

16H43b O. Hahn and F. Strassmann, Naturwiss. 31, 499 (1943)

17H50 K. L. Hall and D. H. Templeton, University of California Radiation Laboratory Unclassified Report UCRL-957 (Oct. 1950)

17H51 K. L. Hall and D. H. Templeton, unpublished data (Aug. 1951)

17H51a K. L. Hall, University of California Radiation Laboratory Unclassified Report UCRL-1460 (Aug. 1951)

18H50 W. J. Heiman and A. Voigt, Iowa State College Unclassified Report ISC-89 (June 1950)

18H51 W. J. Heiman and D. F. Martin, unpublished data (Aug. 1951)

19H50 M. Heerschap, O. P. Hok, and G. J. Sizoo, Physica 16, 767 (1950)

20H49a B. G. Harvey and N. Moss, reported in Chalk River Laboratory Report CRR-427 (Dec. 1949)

20H50 B. G. Harvey and B. I. Parsons, Phys. Rev. 80, 1098 (1950)

20H52 B. G. Harvey, private communication to S. G. Thompson (Feb. 1952)

20H52a B. G. Harvey, Phys. Rev. 85, 482 (1952)

21H41 E. Haggstrom, Phys. Rev. 59, 322 (1941)

22H45 J. Halperin and D. E. Koshland, Jr., Clinton Laboratory Classified Report CN-3422x (June 1945)

23H52 G. H. Higgins and K. Street, Jr., Phys. Rev. 86, 252 (1952)

23H52a G. H. Higgins, Ph.D. Thesis, University of California Radiation Laboratory Unclassified Report UCRL-1796 (June 1952)

24H49 G. C. Hanna and B. Pontecorvo, Phys. Rev 75, 983 (1949)

24H50 G. C. Hanna, B. G. Harvey, and N. Moss, Phys. Rev. 78, 617 (1950)

24H51 G. C. Hanna, B. G. Harvey, N. Moss, and P. R. Tunnicliffe, Phys Rev. 81, 466 (1951)

25H51 E. K. Hulet, S. G. Thompson, A. Ghiorso, and K. Street, Jr., Phys. Rev 84, 366 (1951)

26H51 D. R. Hamilton, W. P. Alford, and L. Gross, Phys. Rev. 83, 215 (1951) (A)

27H49 J. E. R. Holmes, Proc. Phys. Soc. (London) 62A, 293 (1949)

28H46 D. J. Hughes and C. Eggler, private communication (Oct. 1946)

28H46a D. J. Hughes and W. D. B. Spatz, private communication (Oct. 1946)

28H46b D. J. Hughes, J. Wallace, E. Goldfarb, C. Eggler, H. Murdock, and N. Goldstein, reported in Argonne National Laboratory Classified Reports CP-3647 (Nov. 1946); CF-3574 (Oct. 1946)

28H47 D. J. Hughes, D. Hall, C. Eggler, and E. Goldfarb, Phys. Rev. 72, 646 (1947)

28H47a D. J. Hughes, C. Eggler, and C. M. Huddleston, Phys. Rev. 71, 269 (1947)

28H47b D. J. Hughes, C. Eggler, and N. Goldstein, reported in Argonne National Laboratory Classified Report CP-3801 (May 1947)

28H48 D. J. Hughes and C. Eggler, Phys. Rev. 73, 809 (1948)

CC-0. In Public Domain. Gurukul Kangri Collection, Haridwar

Digitized by Arya Samaj Foundation Chennai and eGangotri

28H48a D. J. Hughes, J. Dabbs, A. Cahn, and D. Hall, Phys. Rev. 73, 111 (1948)

28H49 D. J. Hughes, C. Eggler, and C. M. Huddleston, Phys. Rev. 75, 515 (1949)

29H50 T. H. Handley, reported in Oak Ridge National Laboratory Classified Report ORNL-867 (Dec. 1950)

30H48 F. L. Hereford, Phys. Rev. 74, 574 (1948)

31H48 R. C. Hawkings, R. F. Hunter, W. B. Mann, and W. H. Stevens, Phys. Rev. 74, 696 (1948)

31H49 R. C. Hawkings, R. F. Hunter, W. B. Mann, and W. H. Stevens, Can. J. Research 27B, 545 (1949)

32H50 E. L. Hudspeth, C. P. Swann, and N. P. Heydenburg, Phys. Rev. 77, 736 (1950)

32H50a E. L. Hudspeth, C. P. Swann, and N. P. Heydenburg, Phys. Rev. 80, 643 (1950)

32H50b E. L. Hudspeth and C. P. Swann, Phys. Rev. 78, 337 (1950) (A)

32H52 E. L. Hudspeth, W. B. Rose, and N. P. Heydenburg, Phys. Rev. 85, 742 (1952) (A)

33H35 L. R. Hafstad and M. A. Tuve, Phys. Rev. 48, 306 (1935)

34H41 O. Huber, O. Lienhard, P. Scherrer, and H. Wäffler, Phys. Rev. 60, 910 (1941)

34H42 O. Huber, O. Lienhard, P. Scherrer, and H. Wäffler, Helv. Phys. Acta 15, 312 (1942)

34H43 O. Huber, O. Lienhard, P. Scherrer, and H. Wäffler, Helv. Phys. Acta 16, 33 (1943)

34H43a O. Huber, O. Lienhard, P. Scherrer, and H. Wäffler, Helv. Phys. Acta 16, 431 (1943)

34H43b O. Huber, O. Lienhard, and H. Wäffler, Helv. Phys. Acta 16, 226 (1943)

34H44 O. Huber, O. Lienhard, and H. Wäffler, Helv. Phys. Acta 17, 195 (1944)

34H44a O. Huber, O. Lienhard, P. Scherrer, and H. Wäffler, Helv. Phys. Acta 17, 139 (1944)

34H45 O. Huber, O. Lienhard, P. Scherrer, and H. Wäffler, Helv. Phys. Acta 18, 221 (1945)

34H47 O. Huber, H. Medicus, P. Preiswerk, and R. Steffen, Helv. Phys. Acta 20, 495 (1947)

34H48 O. Huber, P. Marmier, H. Medicus, P. Preiswerk, and R. Steffen, Phys. Rev. 73, 1208 (1948)

34H48a O. Huber, R. Steffen, and F. Humbel, Helv. Phys. Acta 21, 192 (1948)

34H49 O. Huber, R. Rüetschi, and P. Scherrer, Helv. Phys. Acta 22, 375 (1949)

34H51 O. Huber, F. Humbel, H. Schneider, and A. de Shalit, Helv. Phys. Acta 24, 127, 629 (1951)

34H52 O. Huber, F. Humbel, H. Schneider, and A. de Shalit, Helv. Phys. Acta 25, 3 (1952)

34H52a O. Huber, R. Joly, P. Scherrer, and N. F. Verster, Helv. Phys. Acta 25, 621 (1952) and private communication (Sept. 1952)

35H34 M. C. Henderson, M. S. Livingston, and E. O. Lawrence, Phys. Rev. 45, 428 (1934)

35H35 M. C. Henderson, Phys. Rev. 48, 855 (1935)

36H49 E. Hayward, Phys. Rev. 75, 917 (1949)

37H35 O. Haxel, Z. Physik 93, 400 (1935)

37H48 O. Haxel, F. G. Houtermans, and M. Kemmerich, Phys. Rev. 74, 1886 (1948)

37H48a O. Haxel and F. G. Houtermans, Z. Physik 124, 705 (1948)

38H46 Zah-Wei Ho, Phys. Rev. 70, 782 (1946)

38H48 Zah-Wei Ho, Compt. rend. 226, 1187 (1948)

39H39 J. E. Hill and G. E. Valley, Phys. Rev. 55, 678 (1939) (A)

39H40 J. E. Hill, Phys. Rev. 57, 567 (1940) (A)

40H37 A. Hemmendinger and W. R. Smythe, Phys. Rev. 51, 1052 (1937)

40H40 A. Hemmendinger, Phys. Rev. 58, 929 (1940)

40H49 A. Hemmendinger, Phys. Rev. 75, 1267 (1949)

41H49 S. G. Hughes and W. E. Stephens, Phys. Rev. 75, 1286 (1949) (A)

42H46 O. Hirzel and H. Wäffler, Helv. Phys. Acta 19, 216 (1946)

42H46a O. Hirzel and H. Wäffler, Helv. Phys. Acta 19, 214 (1946)

42H47 O. Hirzel and H. Wäffler, Helv. Phys. Acta 20, 373 (1947)

42H47a O. Hirzel, P. Stoll, and H. Wäffler, Helv. Phys. Acta 20, 241 (1947)

42H48 O. Hirzel and H. Wäffler, Phys. Rev. 74, 1553 (1948)

43H47 D. C. Hess, Jr., R. J. Hayden, and M. G. Inghram, Phys. Rev. 72, 730 (1947)

43H48 D. C. Hess, Jr., Phys. Rev. 74, 773 (1948)

43H49 D. C. Hess, Jr. and M. G. Inghram, Phys. Rev. 76, 1717 (1949)

44H43 R. H. Hendricks, L. C. Bryner, M. D. Thomas, and J. O. Ivie, J. Phys. Chem. 47, 469 (1943)

45H51 R. B. Heller, E. F. Sturcken, and A. H. Weber, Phys. Rev. 83, 848 (1951)

46H40 J. B. Hoag, Phys. Rev. 57, 937 (1940)

47H37 D. G. Hurst and H. Walke, Phys. Rev. 51, 1033 (1937)

47H40 D. G. Hurst, R. Latham, and W. B. Lewis, Proc. Roy. Soc. (London) 174A, 126 (1940)

48H48 H. H. Hopkins, Jr. and B. B. Cunningham, private communication (Aug. 1948)

48H48a H. H. Hopkins, Jr. and B. B. Cunningham, Phys. Rev. 73, 1406 (1948)

48H49 H. H. Hopkins, Jr., Ph.D. Thesis, University of California Radiation Laboratory Report UCRL-312 (March 1949)

48H50 H. H. Hopkins, Jr., Phys. Rev. 77, 717 (1950)

49H49 R. N. H. Haslam, L. Katz, H. E. Johns, and H. J. Moody, Phys. Rev. 76, 704 (1949)

49H50 R. N. H. Haslam, L. Katz, H. J. Moody, and H. M. Skarsgard, Phys. Rev. 80, 318 (1950)

49H51 R. N. H. Haslam, L. A. Smith, and J. G. V. Taylor, Phys. Rev. 84, 840 (1951)

49H51a R. N. H. Haslam and H. M. Skarsgard, Phys. Rev. 81, 479 (1951)

50H51 V. Hummel and B. Hammermesh, Phys. Rev. 82, 67 (1951)

51H43 J. G. Hamilton, reported in Metallurgical Project Classified Report (work performed at Berkeley) CH-843 (Aug. 1943)

51H48 J. G. Hamilton, private communication (Sept. 1948)

52H38 M. Heyden and W. Wefelmeier, Naturwiss. 26, 612 (1938)

53H43 C. T. Hibdon, M. L. Pool, and J. D. Kurbatov, Phys. Rev. 63, 462 (1943) (A)

53H44 C. T. Hibdon, M. L. Pool, and J. D. Kurbatov, Phys. Rev. 65, 351 (1944) (A)

53H45 C. T. Hibdon, M. L. Pool, and J. D. Kurbatov, Phys. Rev. 67, 289 (1945)

53H45a C. T. Hibdon and M. L. Pool, Phys. Rev. 67, 313 (1945)

54H43 E. B. Hales and E. B. Jordan, Phys. Rev. 64, 202 (1943)

55H50 R. Hofstadter and J. A. McIntyre, Phys. Rev. 80, 631 (1950)

56H48 S. K. Haynes, Phys. Rev. 74, 423 (1948)

57H51 P. Hubert, J. phys. et radium 12, 823 (1951)

57H51a P. Hubert and J. Laberrigue-Frolow, Compt. rend. 232, 2420 (1951)

57H51b P. Hubert, Compt. rend. 232, 2201 (1951)

58H51 E. J. Hoagland and N. Sugarman, NNES-PPR 9, 642 (1951)

CC-0. In Public Domain. Gurukul Kangri Collection, Haridwar

Digitized by Arya Samaj Foundation Chennai and eGangotri

58H51a E. J. Hoagland and N. Sugarman, NNES-PPR 9, 635 (1951)

58H51b E. J. Hoagland and S. Katcoff, NNES-PPR 9, 660 (1951)

58H51c E. J. Hoagland and N. Sugarman, NNES-PPR 9, 1031 (1951)

59H40 J. O. Hancock and J. C. Butler, Phys. Rev. 57, 1088 (1940) (A)

60H46 R. J. Hayden and M. G. Inghram, Phys. Rev. 70, 89 (1946)

60H46a R. J. Hayden and L. G. Lewis, Phys. Rev. 70, 111 (1946) (A)

60H48 R. J. Hayden, Phys. Rev. 74, 650 (1948)

60H49 R. J. Hayden, J. H. Reynolds, and M. G. Inghram, Phys. Rev. 75, 1500 (1949)

60H50 R. J. Hayden, D. C. Hess, Jr., and M. G. Inghram, Phys. Rev. 77, 299 (1950)

61H49 R. W. Hayward and A. C. Helmholz, Phys. Rev. 75, 1469 (1949) (A)

61H50 R. W. Hayward, Phys. Rev. 79, 541 (1950)

61H50a R. W. Hayward, Phys. Rev. 79, 542 (1950)

61H50b R. W. Hayward, Phys. Rev. 79, 409 (1950)

61H52 R. W. Hayward, Phys. Rev. 85, 760 (1952) (A) and private communication (Oct. 1952)

61H52a R. W. Hayward, Phys. Rev. 87, 202 (1952) (A) and private communication (Oct. 1952)

62H49 J. E. Hudgens, Jr. and W. S. Lyon, Phys. Rev. 75, 206 (1949)

63H48 R. E. Hein and A. F. Voigt, Phys. Rev. 74, 1265 (1948) (A)

63H50 R. E. Hein and A. F. Voigt, Phys. Rev. 79, 783 (1950)

63H52 R. E. Hein, C. M. Fowler, and R. H. McFarland, Phys. Rev. 85, 138 (1952)

64H52 R. A. House, R. L. Colligan, D. N. Kundu, and M. L. Pool, Phys. Rev. 86, 654 (1952) (A)

65H44 L. K. Hurst and M. L. Pool, Phys. Rev. 65, 60 (1944) (A)

65H44a L. K. Hurst and M. L. Pool, Phys. Rev. 65, 351 (1944) (A)

66H49 R. A. Hinshaw and M. L. Pool, Phys. Rev. 76, 358 (1949)

67H48 R. D. Hill and J. W. Mihelich, Phys. Rev. 74, 1874 (1948)

67H48a R. D. Hill, Phys. Rev. 74, 78 (1948)

67H48b R. D. Hill and W. E. Meyerhof, Phys. Rev. 73, 812 (1948)

67H49 R. D. Hill, Phys. Rev. 76, 333 (1949)

67H49a R. D. Hill, G. Scharff-Goldhaber, and G. Friedlander, Phys. Rev. 75, 324 (1949)

67H50 R. D. Hill, Phys. Rev. 79, 413 (1950)

67H50a R. D. Hill and J. W. Mihelich, Phys. Rev. 79, 275 (1950)

67H51 R. D. Hill, Phys. Rev. 83, 865 (1951)

67H51a R. D. Hill and F. R. Metzger, Phys. Rev. 83, 455 (1951)

67H51b R. D. Hill, G. Scharff-Goldhaber, and M. McKeown, Phys. Rev. 84, 382 (1951)

67H51c R. D. Hill, Phys. Rev. 82, 449 (1951)

67H51d R. D. Hill, Phys. Rev. 81, 470 (1951)

67H52 R. D. Hill, P. Axel, and A. W. Sunyar, private communication (Sept. 1952)

67H53 R. D. Hill and J. W. Mihelich, Phys. Rev. (to be published) (1953)

68H51 B. Hammermesh and V. Hummel, Phys. Rev. 84, 381 (1951)

68H52 B. Hammermesh, V. Hummel, L. Goodman, and D. Engelkemeir, Phys. Rev. 87, 528 (1952)

69H41 D. E. Hull and H. Seelig, Phys. Rev. 60, 553 (1941)

70H52 B. G. Hogg and H. E. Duckworth, Phys. Rev. 86, 567 (1952)

71H32 G. Hevesy and M. Pahl, Nature 130, 846 (1932)

71H35 G. Hevesy and H. Levi, Nature 135, 580 (1935)

71H36 G. Hevesy and H. Levi, Kgl. Danske Videnskab. Selskab, Mat.-fys. Medd. 14, No. 5 (1936); Nature 137, 185 (1936)

71H38 G. Hevesy and H. Levi, Kgl. Danske Videnskab Selskab, Mat.-fys. Medd. 15, No. 11 (1938)

72H35 R. Hosemann, Z. Physik 99, 405 (1935)

73H49 C. Haenny, M. Najar, and M. Gailloud, Helv. Phys. Acta 22, 611 (1949)

74H51 R. W. Hoff, J. O. Rasmussen, and S. G. Thompson, Phys. Rev. 83, 1068 (1951)

74H52 R. W. Hoff, unpublished data (July 1952)

74H52a R. W. Hoff and F. Asaro, private communication (Aug. 1952)

75H49 R. F. Hibbs, U. S. Atomic Energy Commission Unclassified Report AECU-556 (Aug. 1949)

76H40 F. G. Houtermans, Naturwiss. 28, 578 (1940)

76H50 F. G. Houtermans, O. Haxel, and J. Heintze, Z. Physik 128, 657 (1950)

77H51 J. Hatton, B. V. Rollin, and E. F. W. Seymour, Phys. Rev. 83, 672 (1951)

78H52 R. B. Holt, R. N. Thorn, and R. W. Wanick, Phys. Rev. 87, 378 (1952)

79H52 B. C. Haldar, Phys. Rev. 87, 158 (1952)

80H52 R. L. Heath and P. R. Bell, Phys. Rev. 87, 176 (1952) (A)

80H52a R. L. Heath, Phys. Rev. 87, 1132 (1952)

81H52 J. R. Huizenga and K. F. Flynn, private communication (June 1952)

81H52a J. R. Huizenga, D. W. Engelkemeir, and P. R. Fields, private communication (June 1952)

82H52 N. M. Hintz, Phys. Rev. 86, 1042 (1952)

83H52 W. A. Hardy, G. Silvey, and C. H. Townes, Phys. Rev. 85, 494 (1952)

84H51 H. R. Haymond, W. R. Garrison, and J. G. Hamilton, J. Chem. Phys. 19, 382 (1951)

85H52 R. B. Holtzman and N. Sugarman, Phys. Rev. 87, 633 (1952)

86H52 R. J. Horsley, R. N. H. Haslam, and H. E. Johns, Phys. Rev. 87, 756 (1952)

87H33 W. D. Harkins, D. M. Gans, and H. W. Newson, Phys. Rev. 44, 529 (1933)

88H52 L. Hsiao and R. B. Duffield, private communication (Oct. 1952)

89H52 N. J. Hopkins, Phys. Rev. 88, 680 (1952)

91H52 E. P. Hincks and C. H. Millar, Abstract 106, June Meeting, Roy. Soc. Canada (1952)

92H39 H. v. Halban, Jr., F. Joliot, and L. Kowarski, Nature 143, 470, 680 (1939)

93H52 J. R. Haskins, J. E. Duval, L. S. Cheng, and J. D. Kurbatov, Phys. Rev. 88, 876 (1952)

93H52a J. R. Haskins and J. D. Kurbatov, Phys. Rev. 88, 884 (1952)

94H52 D. R. Hutchinson and M. L. Wiedenbeck, Phys. Rev. 88, 699 (1952)

CC-0. In Public Domain. Gurukul Kangri Collection, Haridwar

Digitized by Arya Samaj Foundation Chennai and eGangotri

1I51 H. I. Israel and R. G. Wilkinson, Phys. Rev. 83, 1051 (1951)

1I52 H. I. Israel, Phys. Rev. 88, 682 (1952)

1I53 H. I. Israel, C. H. Pruett, and R. G. Wilkinson, Phys. Rev. (to be published) (1953)

2I39 J. W. Irvine, Jr., Phys. Rev. 55, 1105 (1939)

2I42 J. W. Irvine, Jr., J. Phys. Chem. 46, 910 (1942)

2I46 J. W. Irvine, Jr., Oak Ridge National Laboratory Classified Report Mon C-142 (Sept. 1946)

3I46 M. G. Inghram and R. J. Hayden, U. S. Atomic Energy Commission Declassified Document MDDC-525 (Dec. 1946)

3I47 M. G. Inghram, D. C. Hess, Jr., and R. J. Hayden, Phys. Rev. 72, 1269 (1947)

3I47a M. G. Inghram, R. J. Hayden, and D. C. Hess, Jr., Phys. Rev. 72, 349, 967 (1947)

3I47b M. G. Inghram, D. C. Hess, Jr., R. J. Hayden, and G. W. Parker, Phys. Rev. 71, 743 (1947)

3I47c M. G. Inghram, R. J. Hayden, and D. C. Hess, Jr., Phys. Rev. 71, 643 (1947)

3I47d M. G. Inghram and R. J. Hayden, Phys. Rev. 71, 130 (1947)

3I47e M. G. Inghram, A. E. Shaw, D. C. Hess, Jr., and R. J. Hayden, Phys. Rev. 72, 515 (1947)

3I47f M. G. Inghram, R. J. Hayden, and D. C. Hess, Jr., Phys. Rev. 71, 270 (1947)

3I47g M. G. Inghram, D. C. Hess, Jr., and R. J. Hayden, reported in Argonne National Laboratory Classified Report ANL-4012 (Aug. 1947)

3I47h M. G. Inghram, D. C. Hess, Jr., and R. J. Hayden, Phys. Rev. 71, 561 (1947)

3I48 M. G. Inghram, D. C. Hess, Jr., H. S. Brown, and E. Goldberg, Phys. Rev. 74, 343 (1948)

3I48a M. G. Inghram, D. C. Hess, Jr., and R. J. Hayden, reported in Argonne National Laboratory Classified Report ANL-4082 (Jan. 1948)

3I48b M. G. Inghram and D. C. Hess, Jr., Phys. Rev. 74, 627 (1948)

3I48c M. G. Inghram, D. C. Hess, Jr., and R. J. Hayden, Phys. Rev. 74, 98 (1948)

3I48d M. G. Inghram, D. C. Hess, Jr., and R. J. Hayden, Phys. Rev. 73, 180 (1948)

3I49 M. G. Inghram and D. C. Hess, Jr., reported in Argonne National Laboratory Classified Report ANL-4355 (Oct. 1949)

3I49a M. G. Inghram, D. C. Hess, Jr., and J. H. Reynolds, Phys. Rev. 76, 1717 (1949)

3I49b M. G. Inghram, R. J. Hayden, and D. C. Hess, Jr., Phys. Rev. 75, 693 (1949); 74, 1724 (1948)

3I50 M. G. Inghram, H. S. Brown, C. Patterson, and D. C. Hess, Phys. Rev. 80, 916 (1950)

3I50a M. G. Inghram, R. J. Hayden, and D. C. Hess, Jr., Phys. Rev. 79, 271 (1950)

3I50b M. G. Inghram and J. H. Reynolds, Phys. Rev. 78, 822 (1950)

3I51 M. G. Inghram, D. C. Hess, P. R. Fields, and G. L. Pyle, Phys. Rev. 83, 1250 (1951)

4I41 J. Itoh, Proc. Phys.-Math. Soc. Japan 23, 605 (1941)

5I51 G. M. Insch and S. C. Curran, Phil. Mag. 42, 892 (1951)

5I52 G. M. Insch, J. G. Balfour, and S. C. Curran, Phys. Rev. 85, 805 (1952)

1J48 A. H. Jaffey, quoted by M. H. Studier and E. K. Hyde, Phys. Rev. 74, 591 (1948)

1J48a A. H. Jaffey, unpublished data (1948)

1J48b A. H. Jaffey and Q. Van Winkle, Argonne National Laboratory Classified Report ANL-4193 (Oct. 1948), NNES-PPR 17B, 729 (1952) (classified)

1J49 A. H. Jaffey and L. B. Magnusson, NNES-PPR 14B, 978 (1949)

1J50 A. H. Jaffey and E. K. Hyde, Phys. Rev. 79, 280 (1950)

1J50a A. H. Jaffey and J. Lerner, reported in Argonne National Laboratory Classified Report ANL-4411 (Feb. 1950)

1J51 A. H. Jaffey, J. Lerner, and S. Warshaw, Phys. Rev. 82, 498 (1951)

1J51a A. H. Jaffey, H. Diamond, A. Hirsch, and J. Mech, Phys. Rev. 84, 785 (1951)

2J47 A. Johansson, Arkiv Mat., Astron. Fysik 34A, No. 9 (1947)

3J48 J. V. Jelley, Can. J. Research 26A, 255 (1948)

3J48a J. V. Jelley and E. B. Paul, Proc. Cambridge Phil. Soc. 44, 133 (1948)

3J50 J. V. Jelley, Proc. Phys. Soc. (London) 63A, 538 (1950); Phil. Mag. 41, 1199 (1950)

4J43 J. C. Jacobsen and T. Sigurgeirsson, Det. Kgl. Danske Vid. Sels. 20, No. 11 (1943)

4J48 J. C. Jacobsen and O. Kofoed-Hansen, Phys. Rev. 73, 675 (1948)

5J51 W. A. Jenkins and G. D. O'Kelley, unpublished data (April 1951)

5J52 W. A. Jenkins and G. T. Seaborg, Phys. Rev. 85, 758 (1952) (A)

6J51 C. J. D. Jarvis and M. A. S. Ross, Proc. Phys. Soc. (London) 64A, 535 (1951)

7J46 S. Jnanananda, Phys. Rev. 69, 570 (1946)

7J47 S. Jnanananda, Phys. Rev. 72, 1124 (1947)

7J49 S. Jnanananda, J. Sci. Ind. Research (India) 8B, No. 9, 147 (1949)

8J48 R. A. James, D. A. Orth, and G. T. Seaborg, unpublished data (July 1948)

8J48a R. A. James, reported in University of California Radiation Laboratory Memorandum MB-IP-247 (Jan. 1948)

8J49 R. A. James, A. E. Florin, H. H. Hopkins, Jr., and A. Ghiorso, NNES-PPR 14B, 1604 (1949)

8J49a R. A. James, S. G. Thompson, and H. H. Hopkins, Jr., NNES-PPR 14B, 1634 (1949)

8J52 R. A. James, A. Ghiorso, and D. A. Orth, Phys. Rev. 85, 369 (1952)

8J52a R. A. James, private communication (Oct. 1952)

9J51 J. Jacquesson and A. Lataste, Compt. rend. 232, 1822 (1951)

10J48 W. P. Jesse and H. Forstat, Phys. Rev. 73, 926 (1948)

10L50 W. P. Jesse and J. Sadanskis, Phys. Rev. 78, 1 (1950)

11J49 W. M. Jones, Phys. Rev. 76, 885 (1949)

11J51 W. M. Jones, Phys. Rev. 83, 537 (1951)

12J49 G. H. Jenks, J. A. Ghormley, and F. H. Sweeton, Phys. Rev. 75, 701 (1949)

12J50 G. H. Jenks, F. H. Sweeton, and J. A. Ghormley, Phys. Rev. 80, 990 (1950)

12J52 G. H. Jenks and F. H. Sweeton, Phys. Rev. 86, 803 (1952)

13J49 E. N. Jensen, L. J. Laslett, and W. W. Pratt, Phys. Rev. 76, 430 (1949)

13J49a E. N. Jensen, Phys. Rev. 76, 958 (1949)

CC-0. In Public Domain. Gurukul Kangri Collection, Haridwar

Digitized by Arya Samaj Foundation Chennai and eGangotri

13J49b E. N. Jensen, reported in Iowa State College Unclassified Report ISC-46 (July 1949)

13J50 E. N. Jensen, L. J. Laslett, and D. J. Zaffarano, Phys. Rev. 80, 862 (1950)

13J51 E. N. Jensen, R. T. Nichols, and J. Clement, Phys. Rev. 81, 143 (1951)

13J52 E. N. Jensen, L. J. Laslett, and D. J. Zaffarano, Phys. Rev. 86, 1047 (1952)

13J52a E. N. Jensen, L. J. Laslett, D. S. Martin, Jr., F. J. Hughes, and W. W. Pratt, Phys. Rev. (to be published)(1952)

13J52b E. N. Jensen, R. T. Nichols, J. Clement, and A. Pohm, Phys. Rev. 85, 112 (1952)

14J49 F. Johnston and J. E. Willard, Phys. Rev. 75, 528 (1949)

15J48 E. T. Jurney, Phys. Rev. 74, 1049 (1948)

15J49 E. T. Jurney, Phys. Rev. 76, 290 (1949)

16J41 A. S. Jensen, Phys. Rev. 60, 430 (1941)

17J50 S. Johansson, Phys. Rev. 79, 896 (1950)

17J51 S. Johansson, Y. Cauchois, and K. Siegbahn, Phys. Rev. 82, 275 (1951)

17J51a S. Johansson, reported in M. Siegbahn Commemorative Volume, p 183 (Uppsala, 1951)

17J52 S. Johansson, Arkiv Fysik 4, 273 (1952)

17J52a S. Johansson, Arkiv Fysik 3, 533 (1952)

18J45 S. Jashemski and N. Goldstein, reported in Metallurgical Laboratory Classified Report CP-2984 (May 1945)

19J44 F. Joliot, Compt. rend. 218, 733 (1944)

20J51 L. Jacobson and R. Overstreet, NNES-PPR 9, 735 (1951)

21J44 P. Jensen, Z. Physik 122, 387 (1944)

22J50 H. E. Johns, L. Katz, R. A. Douglas, and R. N. H. Haslam, Phys. Rev. 80, 1062 (1950)

23J52 W. H. Johnson, Jr., Phys. Rev. 87, 166 (1952)

24J38 R. Jaeckel, Z. Physik 110, 330 (1938)

25J52 M. W. Johns, C. D. Cox, R. J. Donnelly, and C. C. McMullen, Phys. Rev. 87, 1134 (1952)

26J52 H. Jaffe and I. Perlman, unpublished data (Aug. 1952)

27J51 C. M. Johnson and W. Gordy, Phys. Rev. 83, 1249 (1951)

28J52 J. W. Jones and T. P. Kohman, Phys. Rev. 85, 941 (1952)

29J52 C. D. Jeffries, H. Loeliger, and H. H. Staub, Phys. Rev. 85, 478 (1952)

30J52 V. Jaccarino, B. Bederson, and H. H. Stroke, Phys. Rev. 87, 676 (1952)

31J52 D. R. Jones, S. C. Fultz, and M. L. Pool, Phys. Rev. 86, 654 (1952) (A)

32J52 F. A. Johnson, Abstract 76, June Meeting, Roy. Soc. Canada (1952) and private communication (Oct. 1952)

33J52 A. A. Jaffe and S. G. Cohen, Phys. Rev. 86, 1041 (1952)

34J52 P. S. Jastram and C. E. Whittle, Phys. Rev. 87, 1133 (1952)

1K40 M. D. Kamen and S. Ruben, Phys. Rev. 58, 194 (1940) (A)

1K41 M. D. Kamen, Phys. Rev. 60, 537 (1941)

1K42 M. D. Kamen, Phys. Rev. 62, 303 (1942) (A)

1K46 M. D. Kamen, Bull. Am. Museum Nat. Hist. 87, 103 (1946)

2K45 T. P. Kohman, J. A. Swartout, and W. H. Sullivan, Hanford Engineer Works Report (H)CN-3212 (Oct. 1945)

2K49 T. P. Kohman, private communication (1949)

2K49a T. P. Kohman, D. P. Ames, and J. Sedlet, NNES-PPR 14B, 1675 (1949)

3K48 G. B. Knight and R. L. Macklin, Phys. Rev. 74, 1540 (1948)

3K49 G. B. Knight and R. L. Macklin, Phys. Rev. 75, 34 (1949)

4K42 C. V. Kent, J. M. Cork, and W. G. Wadey, Phys. Rev. 61, 389 (1942) (A)

4K42a C. V. Kent and J. M. Cork, Phys. Rev. 62, 297 (1942) (A)

5K43 B. Karlik and T. Bernert, Naturwiss. 31, 492 (1943)

5K43a B. Karlik and T. Bernert, Naturwiss. 31, 298 (1943); Z. Physik 123, 51 (1944)

5K44 B. Karlik and T. Bernert, Naturwiss. 32, 44 (1944)

5K46 B. Karlik and T. Bernert, Naturwiss. 33, 23 (1946)

6K38 A. F. Kovarik and N. I. Adams, Jr., Phys. Rev. 54, 413 (1938)

6K41 A. F. Kovarik and N. I. Adams, Jr., J. Appl. Phys. 12, 296 (1941) (A)

7K49 D. G. Karraker, F. L. Reynolds, and D. H. Templeton, University of California Radiation Laboratory Unclassified Report UCRL-285 (Feb. 1949)

7K50 D. G. Karraker and D. H. Templeton, Phys. Rev. 80, 646 (1950)

7K51 D. G. Karraker and D. H. Templeton, Phys. Rev. 81, 510 (1951)

7K51a D. G. Karraker, A. Ghiorso, and D. H. Templeton, Phys. Rev. 83, 390 (1951)

7K51b D. G. Karraker, unpublished data (May 1951)

7K52 D. G. Karraker, R. J. Hayden, and M. G. Inghram, Phys. Rev. 87, 901 (1952)

8K35 I. V. Kurtchatov, G. D. Latyshev, L. M. Nemenov, and I. P. Selinov, Physik. Z. Sowjetunion 8, 589 (1935)

9K39 R. S. Krishnan and D. H. T. Gant, Nature 144, 547 (1939)

9K40 R. S. Krishnan and E. A. Nahum, Proc. Cambridge Phil. Soc. 36, 490 (1940)

9K40a R. S. Krishnan and T. E. Banks, Nature 145, 777 (1940)

9K40b R. S. Krishnan, Proc. Cambridge Phil. Soc. 36, 500 (1940)

9K41 R. S. Krishnan, Nature 148, 407 (1941)

9K41a R. S. Krishnan and T. E. Banks, Proc. Cambridge Phil. Soc. 37, 317 (1941)

9K41b R. S. Krishnan and E. A. Nahum, Proc. Cambridge Phil. Soc. 37, 422 (1941)

9K41c R. S. Krishnan, Proc. Cambridge Phil. Soc. 37, 186 (1941)

9K42 R. S. Krishnan and E. A. Nahum, Proc. Roy. Soc. (London) 180A, 321, 333 (1942)

10K49 E. L. Kelly and E. Segrè, Phys. Rev. 75, 999 (1949)

10K50 E. L. Kelly, Ph.D. Thesis, University of California Classified Report UCRL-1044 (Dec. 1950)

11K50 H. B. Keller and J. M. Cork, Phys. Rev. 79, 1030 (1950)

11K50a H. B. Keller, reported in Argonne National Laboratory Classified Report ANL-4437 (April 1950)

11K51 H. B. Keller and J. M. Cork, Phys. Rev. 84, 1079 (1951)

12K44 M. Kahn and G. A. Linenberger, reported in Los Alamos Scientific Laboratory Classified Report LAMS-151 (Oct. 1944)

CC-0. In Public Domain. Gurukul Kangri Collection, Haridwar

Digitized by Arya Samaj Foundation Chennai and eGangotri

13K49 C. A. Kienberger, Phys. Rev. 76, 1561 (1949)

13K52 C. A. Kienberger, Phys. Rev. 87, 520 (1952)

14K39 J. W. Kennedy, G. T. Seaborg, and E. Segrè, Phys. Rev. 56, 1095 (1939)

14K40 J. W. Kennedy and G. T. Seaborg, Phys. Rev. 57, 843 (1940)

14K46 J. W. Kennedy, G. T. Seaborg, E. Segrè, and A. C. Wahl, Phys. Rev. 70, 555 (1946); NNES-PPR 14B, 5 (1949)

14K49 J. W. Kennedy, M. L. Perlman, E. Segrè, and A. C. Wahl, NNES-PPR 14B, 79 (1949)

15K36 K. S. Knol and J. Veldkamf, Physica 3, 145 (1936)

16K47 W. J. Knox, Phys. Rev. 72, 1254 (1947)

16K48 W. J. Knox, Phys. Rev. 74, 1192 (1948)

17K36 F. N. D. Kurie, J. R. Richardson, and H. C. Paxton, Phys. Rev. 49, 368 (1936)

17K48 F. N. D. Kurie and M. Ter-Pogossian, Phys. Rev. 74, 677 (1948)

17K51 F. N. D. Kurie, unpublished data quoted in (39S51a)

18K48 K. Knable, E. O. Lawrence, C. E. Leith, B. J. Moyer, and R. L. Thornton, Phys. Rev. 74, 1217 (1948) (A)

19K39 L. D. P. King, W. J. Henderson, and J. R. Risser, Phys. Rev. 55, 1118 (1939) (A)

19K39a L. D. P. King and W. J. Henderson, Phys. Rev. 56, 1169 (1939)

19K40 L. D. P. King and D. R. Elliott, Phys. Rev. 58, 846 (1940)

20K45 J. D. Knight, T. B. Novey, C. V. Cannon, and A. Turkevich, Metallurgical Laboratory Classified Report CC-2605 (April 1945)

20K49 J. D. Knight, W. H. Burgus, and R. J. Prestwood, private communication listed in NNES-PPR 9, 2063 (1951) (ref. K14)

20K51 J. D. Knight and G. A. Cowan, reported in Los Alamos Scientific Laboratory Classified Report WASH-58 (March 1951) and private communication (Oct. 1952)

20K51a J. D. Knight and D. P. Ames, reported in Los Alamos Scientific Laboratory Classified Report WASH-62 (Dec. 1951)

20K52 J. D. Knight and L. Baggett, private communication (April 1952)

21K47 B. B. Kinsey, Phys. Rev. 72, 526 (1947) (A)

21K50 B. B. Kinsey, G. A. Bartholomew, and W. H. Walker, Phys. Rev. 78, 481 (1950)

21K50a B. B. Kinsey, et al., reported in Chalk River Laboratory Classified Report PR-P-6 (March 1950)

22K39 G. Kuerti and S. N. Van Voorhis, Phys. Rev. 56, 614 (1939)

23K48 E. D. Klema and A. O. Hanson, Phys. Rev. 73, 106 (1948)

23K52 E. D. Klema and F. K. McGowan, Phys. Rev. 87, 524 (1952)

24K48 B. H. Ketelle and W. C. Peacock, Phys. Rev. 73, 1269 (1948) (A)

24K48a B. H. Ketelle and G. E. Boyd, reported in Oak Ridge National Laboratory Classified Report ORNL-65 (July 1948)

24K49 B. H. Ketelle, reported in Oak Ridge National Laboratory Classified Report ORNL-286 (Sept. 1949)

24K49a B. H. Ketelle, reported in Oak Ridge National Laboratory Classified Report ORNL-336 (May 1949)

24K49b B. H. Ketelle, reported in Oak Ridge National Laboratory Classified Report ORNL-229 (Feb. 1949)

24K49c B. H. Ketelle, reported in Brookhaven National Laboratory Unclassified Report BNL-C-9 (Aug. 1949)

24K49d B. H. Ketelle, Phys. Rev. 76, 1256 (1949)

24K49e B. H. Ketelle and G. W. Parker, Phys. Rev. 76, 1416 (1949)

24K50 B. H. Ketelle, Phys. Rev. 80, 758 (1950)

24K50a B. H. Ketelle and J. W. Ruch, Phys. Rev. 77, 565 (1950)

24K50b B. H. Ketelle, C. M. Nelson, and G. E. Boyd, Phys. Rev. 79, 242 (1950) (A)

24K50c B. H. Ketelle, A. R. Brosi, and H. Zeldes, Phys. Rev. 80, 485 (1950)

24K50d B. H. Ketelle, reported in Oak Ridge National Laboratory Classified Report ORNL-607 (March 1950)

24K51 B. H. Ketelle, H. Zeldes, A. R. Brosi, and R. A. Dandl, Phys. Rev. 84, 585 (1951); H. Zeldes, A. R. Brosi, and B. H. Ketelle, Phys. Rev. 81, 642 (1951)

24K51a B. H. Ketelle, A. R. Brosi, and H. Zeldes, reported in Oak Ridge National Laboratory Classified Report ORNL-870 (March 1951)

24K52 B. H. Ketelle and A. R. Brosi, private communication (Oct. 1952)

25K46 J. X. Khym, Oak Ridge National Laboratory Classified Report Mon C-61 (Feb. 1946)

26K48 N. L. Krisberg, M. L. Pool, and C. T. Hibdon, Phys. Rev. 74, 44 (1948)

26K49 N. L. Krisberg and M. L. Pool, Phys. Rev. 75, 1693 (1949)

27K50 H. E. Kubitschek, Phys. Rev. 79, 23 (1950)

28K48 B. D. Kern, D. J. Zaffarano, and A. C. G. Mitchell, Phys. Rev. 73, 1142 (1948)

28K49 B. D. Kern, A. C. G. Mitchell, and D. J. Zaffarano, Phys. Rev. 76, 94 (1949)

29K46 D. N. Kundu and M. L. Pool, Phys. Rev. 70, 111 (1946) (A)

29K47 D. N. Kundu and M. L. Pool, Phys. Rev. 71, 140 (1947) (A)

29K47a D. N. Kundu and M. L. Pool, Phys. Rev. 72, 101 (1947)

29K48 D. N. Kundu and M. L. Pool, Phys. Rev 73, 22 (1948)

29K48a D. N. Kundu and M. L. Pool, Phys. Rev. 74, 1775 (1948)

29K49 D. N. Kundu and M. L. Pool, Phys. Rev. 76, 183 (1949) (A)

29K49a D. N. Kundu and M. L. Pool, Phys. Rev. 75, 1690 (1949)

29K50 D. N. Kundu and M. L. Pool, Phys. Rev. 78, 488 (1950)

29K50a D. N. Kundu, J. L. Hult, and M. L. Pool, Phys. Rev. 77, 71 (1950)

29K51 D. N. Kundu and M. L. Pool, Phys. Rev. 84, 481 (1951)

29K52 D. N. Kundu, J. D. Service, and M. L. Pool, Phys. Rev. 87, 203 (1952) (A)

30K50 L. Katz, A. S. Penfold, H. J. Moody, R. N. H. Haslam, and H. E. Johns, Phys. Rev. 77, 289 (1950)

30K51 L. Katz and A. G. W. Cameron, Phys. Rev. 84, 1115 (1951)

30K51a L. Katz and A. G. W. Cameron, Can. J. Phys. 29, 518 (1951)

31K51 J. H. Kahn, Oak Ridge National Laboratory Unclassified Report ORNL-1089 (Nov. 1951)

31K52 J. H. Kahn and E. C. Campbell, private communication (Oct. 1952)

32K46 S. Katcoff and A. Goldstein, U. S. Atomic Energy Commission Declassified Document MDDC-293 (April 1946)

32K47 S. Katcoff, Phys. Rev. 71, 826 (1947)

32K47a S. Katcoff, Phys. Rev. 72, 1160 (1947)

32K48 S. Katcoff, J. A. Miskel, and C. W. Stanley, Phys. Rev. 74, 631 (1948)

CC-0. In Public Domain. Gurukul Kangri Collection, Haridwar

Digitized by Arya Samaj Foundation Chennai and eGangotri

32K49 S. Katcoff, J. A. Leary, K. A. Walsh, R. A. Elmer, S. S. Goldsmith, L. D. Hall, E. G. Newbury, J. J. Povelites, and J. S. Waddell, J. Chem. Phys. 17, 421 (1949)

32K50 S. Katcoff, reported in Brookhaven National Laboratory Unclassified Report BNL-39 (Jan. 1950)

32K51 S. Katcoff, B. Finkle, and N. Sugarman, NNES-PPR 9, 587 (1951)

32K51a S. Katcoff and E. J. Hoagland, NNES-PPR 9, 659 (1951)

32K51b S. Katcoff and B. Finkle, NNES-PPR 9, 705 (1951)

32K51c S. Katcoff, NNES-PPR 9, 765 (1951)

32K51d S. Katcoff, NNES-PPR 9, 980 (1951)

32K51e S. Katcoff, C. R. Dillard, H. Finston, B. Finkle, J. A. Seiler, and N. Sugarman, NNES-PPR 9, 1005 (1951)

32K51f S. Katcoff, O. A. Schaeffer, and J. M. Hastings, Phys. Rev. 82, 688 (1951)

32K51g S. Katcoff, B. Finkle, N. Sugarman, L. E. Glendenin, and L. Winsberg, NNES-PPR 9, 1017 (1951)

32K51h S. Katcoff, B. Finkle, E. J. Hoagland, N. Sugarman, L. E. Glendenin, and R. P. Metcalf, NNES-PPR 9, 982 (1951)

32K51i S. Katcoff, B. Finkle, and N. Sugarman, NNES-PPR 9, 1097 (1951)

32K51j S. Katcoff, NNES-PPR 9, 1147 (1951)

32K51k S. Katcoff, NNES-PPR 9, 1400 (1951)

32K52 S. Katcoff, Phys. Rev. 87, 886 (1952)

32K52a S. Katcoff, reported in Brookhaven National Laboratory Unclassified Report BNL-149 (March 1952)

33K35 B. Kurtchatov, I. Kurtchatov, L. Myssowsky, and L. Roussinov, Compt. rend. 200, 1201 (1935)

34K49 J. Koch, O. Kofoed-Hansen, P. Kristensen, and W. Drost-Hansen, Phys. Rev. 76, 279 (1949)

35K51 O. Kofoed-Hansen and P. Kristensen, Phys. Rev. 82, 96 (1951)

35K51a O. Kofoed-Hansen and K. O. Nielsen, Phys. Rev. 82, 96 (1951); Kgl. Danske Videnskab. Selskab, Mat. fys. Medd. 26, No. 7 (1951)

35K51b O. Kofoed-Hansen, Phil. Mag. 42, 1448 (1951)

36K35 O. Klemperer, Proc. Roy. Soc. (London) 148A, 638 (1935)

37K49 M. Kemmerich, Z. Physik 126, 399 (1949)

38K50 E. Kondaiah, Phys. Rev. 79, 891 (1950)

38K50a E. Kondaiah, Arkiv Fysik 2, 295 (1950)

38K51 E. Kondaiah, Phys. Rev. 83, 471 (1951)

38K51a E. Kondaiah, Phys. Rev. 81, 1056 (1951)

38K51b E. Kondaiah, Arkiv Fysik 3, 47 (1951)

38K51c E. Kondaiah, reported in M. Siegbahn Commemorative Volume, p 411 (Uppsala, 1951)

38K51d E. Kondaiah, Arkiv Fysik 2, 295 (1951)

39K37 J. D. Kraus and J. M. Cork, Phys. Rev 52, 763 (1937)

40K52 W. C. Kelly, Phys Rev. 85, 101 (1952)

41K52 M. I. Kalkstein and W. F. Libby, Phys. Rev. 85, 368 (1952)

42K45 P. G. Kruger and W. E. Ogle, Phys. Rev. 67, 273 (1945)

42K52 P. Kruger and C. D. Coryell, private communication (Oct. 1952)

43K50 R. Katz, R. D. Hill, and M. Goldhaber, Phys. Rev 78, 9 (1950)

43K52 R. Katz and M. R. Lee, Phys. Rev. 85, 1038 (1952)

44K52 T. K. Keenan, R. A. Penneman, and B. B. McInteer, Phys. Rev. 87, 204 (1952) (A)

45K40 D. C. Kalbfell and R. A. Cooley, Phys. Rev 58, 91 (1940)

46K52 A. W. Knudsen, Phys. Rev. 86, 571 (1952)

47K42 J. D. Kurbatov, D. C. MacDonald, M. L. Pool, and L. L. Quill, Phys. Rev. 61, 106 (1942) (A)

47K43 J. D. Kurbatov and M. L. Pool, Phys. Rev. 63, 463 (1943) (A)

48K51 K. G. Kessler and W. F. Meggers, Phys. Rev. 80, 905 (1951)

49K50 H. Kuhn and K. G. Woodgate, Nature 166, 906 (1950); Proc. Phys. Soc. (London) 64A, 1090 (1951)

50K48 L. I. Katzin and M. Pobereskin, Phys. Rev 74, 264 (1948)

50K52 L. I. Katzin and F. Hagemann, NNES-PPR 17B, 582 (1952) (classified)

51K51 J. Kastner, Can. J. Phys. 29, 480 (1951)

52K51 I. Kirshenbaum, J. Graff, and H. Forstat, NNES Div. III, 4A, 393 (1951)

53K43 S. Kikuchi, et al., Proc. Phys.-Math. Soc. Japan 25, 502 (1943)

54K52 P. Kofstad and G. T. Seaborg, reported in University of California Radiation Laboratory Classified Report UCRL-1770 (April 1952)

55K52 V. E. Krohn, Jr. and E. F. Shrader, Phys. Rev 87, 685 (1952)

56K52 C. Kikuchi, M. H. Sirvetz, and V. W. Cohen, Phys. Rev. 88, 142 (1952)

57K51 J. D. Keys, Ph. D. Thesis, McGill University (1951)

58K52 J. Kraushaar, E. Wilson, and K. T. Bainbridge, private communication (Oct. 1952)

59K51 S. Kageyama, J. Phys. Soc. Japan 6, 285 (1951)

59K52 S. Kageyama, J. Phys. Soc. Japan 7, 93 (1952)

60K52 L. Koester, H. Maier-Leibnitz, T. Mayer-Kuckuk, K. Schmeiser, and G. Schulze-Pillot, Z. Physik 133, 319 (1952)

61K52 R. M. Kloepper, E. S. Lennox, and M. L. Wiedenbeck, Phys. Rev. 88, 695 (1952)

1L35 E. O. Lawrence, Phys. Rev. 47, 17 (1935)

2L47 P. W. Levy, Phys. Rev. 72, 352 (1947)

2L47a P. W. Levy, Phys. Rev. 72, 248 (1947)

2L48 P. W. Levy and E. Greuling, Phys. Rev. 73, 83 (1948)

2L49 P. W. Levy, reported in Oak Ridge National Laboratory Unclassified Report ORNL-312 (March 1949); U. S. Atomic Energy Commission Unclassified Document AECU-173 (March 1949)

2L49a P. W. Levy and E. Greuling, Phys Rev. 75, 819 (1949)

3L33 W. F. Libby and W. M. Latimer, J. Am. Chem. Soc. 55, 433 (1933)

3L34 W. F. Libby, Phys. Rev. 45, 845 (1934)

3L39 W. F. Libby and D. D. Lee, Phys. Rev. 55, 245 (1939)

3L39a W. F. Libby, Phys. Rev 56, 21 (1939)

3L51 W. F. Libby, private communication (Oct. 1951)

4L47 E. J. Lofgren, reported by (2T47a)

5L47 G. D. Latyshev, Revs. Modern Phys. 19, 132 (1947)

6L38 M. Lecoin, J. phys et radium 9, 81 (1938)

6L43 M. Lecoin, M. Perey, and San-Tsiang Tsien, Compt. rend. 217, 146 (1943)

6L44 M. Lecoin, M. Perey, and San-Tsiang Tsien, Cahiers phys. No. 26, 10 (1944)

CC-0. In Public Domain. Gurukul Kangri Collection, Haridwar

Digitized by Arya Samaj Foundation Chennai and eGangotri

6L47 M. Lecoin, Compt. rend. 224, 912 (1947)

6L48 M. Lecoin, M. Perey, and J. Teillac, Compt. rend. 227, 121 (1948)

6L49 M. Lecoin, M. Perey, and M. Riou, J. phys. et radium 10, 390 (1949)

6L49a M. Lecoin, M. Perey, and J. Teillac, J. phys. et radium 10, 33 (1949)

6L50 M. Lecoin, M. Perey, M. Riou, and J. Teillac, J. phys. et radium 11, 227 (1950)

7L50 C. R. Lagergren and M. E. Kettner, Phys. Rev. 80, 102 (1950)

8L39 D. D. Lee and W. F. Libby, Phys. Rev. 55, 252 (1939)

9L44 A. L. Lutz, M. L. Pool, and J. D. Kurbatov, Phys. Rev. 65, 61 (1944) (A)

10L37 L. M. Langer and M. D. Whitaker, Phys. Rev. 51, 713 (1937)

10L47 L. M. Langer, C. S. Cook, and M. B. Sampson, Phys. Rev. 71, 906 (1947)

10L49 L. M. Langer and H. C. Price, Jr., Phys. Rev. 76, 641 (1949)

10L49a L. M. Langer and H. C. Price, Jr., reported by (53M49)

10L50 L. M. Langer, Phys. Rev. 77, 50 (1950)

10L50a L. M. Langer and R. D. Moffat, Phys. Rev. 80, 651 (1950)

10L50b L. M. Langer, R. D. Moffat, and H. C. Price, Jr., Phys. Rev. 79, 808 (1950)

10L50c L. M. Langer, J. W. Motz, and H. C. Price, Jr., Phys. Rev. 77, 798 (1950)

10L50d L. M. Langer and R. D. Moffat, Phys. Rev. 78, 74 (1950)

10L51 L. M. Langer and R. D. Moffat, Phys. Rev. 82, 635 (1951)

10L51a L. M. Langer and G. Ford, reported in U. S. Atomic Energy Commission Classified Report WASH-62 (Dec. 1951)

10L52 L. M. Langer, R. D. Moffat, and G. A. Graves, Phys. Rev. 86, 632 (1952) (A)

10L52a L. M. Langer, R. B. Duffield, and C. W. Stanley, private communication (Sept. 1952)

10L52b L. M. Langer and R. J. D. Moffat, Phys. Rev. 88, 689 (1952)

10L52c L. M. Langer, private communication (Oct. 1952)

10L52d L. M. Langer and R. B. Duffield, private communication (Oct. 1952)

11L34 W. B. Lewis and B. V. Bowden, Proc. Roy. Soc. (London) 145A, 235 (1934). Summarizes the results of various investigators. Values recalculated according to (9H38)

11L37 W. B. Lewis, W. E. Burcham, and W. Y. Chang, Nature 139, 24 (1937)

12L36 J. J. Livingood, Phys. Rev. 50, 425 (1936)

12L37 J. J. Livingood, F. Fairbrother, and G. T. Seaborg, Phys. Rev. 52, 135 (1937)

12L37a J. J. Livingood and G. T. Seaborg, Phys. Rev. 52, 135 (1937)

12L38 J. J. Livingood and G. T. Seaborg, Phys. Rev. 54, 391 (1938)

12L38a J. J. Livingood and G. T. Seaborg, Phys. Rev. 54, 51 (1938)

12L38b J. J. Livingood and G. T. Seaborg, Phys. Rev. 53, 847 (1938)

12L38c J. J. Livingood and G. T. Seaborg, Phys. Rev. 53, 765 (1938)

12L38d J. J. Livingood and G. T. Seaborg, Phys. Rev. 54, 88 (1938)

12L38e J. J. Livingood and G. T. Seaborg, Phys. Rev. 54, 775 (1938)

12L39 J. J. Livingood and G. T. Seaborg, Phys. Rev. 55, 457 (1939)

12L39a J. J. Livingood and G. T. Seaborg, Phys. Rev. 55, 1268 (1939)

12L39b J. J. Livingood and G. T. Seaborg, unpublished data (1939)

12L39c J. J. Livingood and G. T. Seaborg, Phys. Rev. 55, 667 (1939)

12L39d J. J. Livingood and G. T. Seaborg, Phys. Rev. 55, 414 (1939)

12L41 J. J. Livingood and G. T. Seaborg, Phys. Rev. 60, 913 (1941)

13L51 R. F. Leininger, E. Segrè, and F. N. Spiess, Phys. Rev. 82, 334 (1951) (A)

14L47 A. Lundby, Forsvarets Forskning Institutt, Arbok (1947), 13

14L49 A. Lundby, Phys. Rev. 76, 1809 (1949)

15L45 G. A. Linenberger, reported in Los Alamos Scientific Laboratory Classified Report LAMS-256 (May 1945)

16L51 C. W. Li, W. Whaling, W. A. Fowler, and C. C. Lauritsen, Phys. Rev. 83, 512 (1951)

17L38 H. Lu, Phys. Rev. 53, 845 (1938)

18L39 A. M. Lawrance, Proc. Cambridge Phil. Soc. 35, 304 (1939)

19L44 J. S. Levinger, Metallurgical Laboratory Declassified Report CP-2267 (Oct. 1944)

19L47 J. Levinger and E. Meiners, Phys. Rev. 71, 586 (1947)

19L51 J. S. Levinger, NNES-PPR 9, 757 (1951)

19L51a J. S. Levinger, E. P. Meiners, M. B. Sampson, A. H. Snell, and R. G. Wilkinson, NNES-PPR 9, 603 (1951)

20L39 A. Langsdorf, Jr., Phys. Rev. 56, 205 (1939)

20L40 A. Langsdorf, Jr. and E. Segrè, Phys. Rev. 57, 105 (1940)

20L45 A. S. Langsdorf, Jr. and R. L. Purbrick, Metallurgical Laboratory Classified Report CP-3272 (Oct. 1945)

21L37 E. M. Lyman, Phys. Rev. 51, 1 (1937)

21L39 E. M. Lyman, Phys. Rev. 55, 1123 (1939) (A)

22L34 M. S. Livingston, M. C. Henderson, and E. O. Lawrence, Phys. Rev. 46, 325 (1934) (A)

22L34a M. S. Livingston and E. M. McMillan, Phys. Rev. 46, 437 (1934)

23L37 L. J. Laslett, Phys. Rev. 52, 529 (1937)

23L49 L. J. Laslett, Phys. Rev. 76, 858 (1949)

23L50 L. J. Laslett, E. N. Jensen, and A. Paskin, Phys. Rev. 79, 412 (1950)

24L37 J. L. Lawson and J. M. Cork, Phys. Rev. 52, 531 (1937)

24L39 J. L. Lawson, Phys. Rev. 56, 131 (1939)

24L40 J. L. Lawson and J. M. Cork, Phys. Rev. 57, 982 (1940)

25L46 D. C. Lincoln and W. H Sullivan, reported in J. Am. Chem. Soc. 68, 2411 (1946)

25L51 D. C. Lincoln and W. H Sullivan, NNES-PPR 9, 778 (1951)

26L40 H. Levi, Nature 145, 588 (1940)

27L48 R. V. Langmuir, Phys. Rev. 74, 1559 (1948) (A)

28L48 W. T. Leland and A. O. Nier, Phys. Rev. 73, 1206 (1948)

28L49 W. T. Leland, Phys. Rev. 76, 1722 (1949)

CC-0. In Public Domain. Gurukul Kangri Collection, Haridwar

Digitized by Arya Samaj Foundation Chennai and eGangotri

28L49a W. T. Leland, Phys. Rev. 76, 992 (1949)

28L50 W. T. Leland, Phys. Rev. 77, 634 (1950)

29L49 D. A. Lind, J. R. Brown, and J. W. M. DuMond, Phys. Rev. 76, 591 (1949) (A)

29L49a D. A. Lind, J. Brown, D. Klein, D. Muller, and J. DuMond, Phys. Rev. 75, 1544 (1949)

29L51 D. Lind and A. Hedgran, reported in M. Siegbahn Commemorative Volume, p 283 (Uppsala, 1951)

30L47 C. E. Leith, A. Bratenahl, and B. J. Moyer, Phys. Rev. 72, 732 (1947)

31L40 R. S. Livingston and B. T. Wright, Phys. Rev. 58, 656 (1940)

32L47 H. A. Levy and M. H. Feldman, reported in Oak Ridge National Laboratory Classified Report Mon N-432 (Dec. 1947)

32L48 H. A. Levy and B. Zemel, reported in Oak Ridge National Laboratory Classified Report ORNL-176 (Nov. 1948)

32L49 H. A. Levy and M. H. Feldman, reported in Oak Ridge National Laboratory Classified Report ORNL-286 (Sept. 1949)

33L49 L. Lidofsky, P. Macklin, and C. S. Wu, Phys. Rev. 76, 1888 (1949)

33L50 L. J. Lidofsky, P. A. Macklin, and C. S. Wu, Phys. Rev. 78, 318 (1950) (A)

33L51 L. Lidofsky, P. Macklin, and C. S. Wu, reported in Columbia University Report CU-97 (Nov. 1951)

33L52 L. Lidofsky, P. Macklin, and C. S. Wu, Phys. Rev. 87, 391 (1952)

34L51 J. Laberrigue-Frolow, Compt. rend. 232, 1201 (1951)

34L52 J. Laberrigue-Frolow, Compt. rend. 234, 2599 (1952)

35L49 W. S. Lyon, reported in Oak Ridge National Laboratory Classified Report ORNL-286 (Sept. 1949)

35L51 W. S. Lyon and D. J. Coombe, reported in Oak Ridge National Laboratory Classified Report ORNL-1088 (Oct. 1951)

35L51a W. S. Lyon, Phys. Rev. 82, 276 (1951)

35L52 W. S. Lyon, Phys. Rev. 87, 1126 (1952)

35L52a W. S. Lyon and B. Kahn, reported in Oak Ridge National Laboratory Classified Report ORNL-1276 (Oct. 1952)

36L39 C. Lieber, Naturwiss. 27, 421 (1939)

37L48 M. Lindner and I. Perlman, Phys. Rev. 73, 1202 (1948)

37L48a M. Lindner and I. Perlman, Phys. Rev. 73, 1124 (1948)

37L48b M. Lindner and I. Perlman, unpublished data (May 1948)

37L50 M. Lindner and I. Perlman, Phys. Rev. 78, 499 (1950)

37L50a M. Lindner and J. S. Coleman, Phys. Rev. 78, 67 (1950)

37L51 M. Lindner, Phys. Rev. 84, 240 (1951)

37L51a M. Lindner and J. S. Coleman, J. Am. Chem. Soc 73, 1610 (1951)

37L52 M. Lindner and R. Osborne, private communication (July 1952)

37L53 M. Lindner, Phys. Rev. (to be published) (1953)

38L39 K. Lark-Horowitz, J. R. Risser, and R. N. Smith, Phys. Rev. 55, 878 (1939)

39L49 J. C. Lee and M. L. Pool, Phys. Rev. 76, 606 (1949)

40L46 G. R. Leader, reported in J. Am. Chem. Soc. 68, 2411 (1946)

40L51 G. R. Leader, NNES-PPR 9, 919 (1951)

40L51a G. R. Leader and W. H Sullivan, NNES-PPR 9, 934 (1951)

41L51 J. S. Lawson, Phys. Rev. 81, 299 (1951) (A)

42L40 A. Langer and W. E. Stephens, Phys. Rev. 58, 759 (1940)

43L52 J. K. Long and M. L. Pool, Phys. Rev. 85, 137 (1952)

43L52a J. K. Long, M. L. Pool, and D. N. Kundu, Phys. Rev. 88, 171 (1952) (A)

44L41 H. B. Law, M. L. Pool, J. D. Kurbatov, and L. L. Quill, Phys. Rev. 59, 936 (1941) (A)

45L47 C. M. G. Lattes, E. G. Samuel, and P. Cuer, Anais acad. brasil. cienc. 19, 1 (1947)

46L51 M. J. W. Laubenstein, R. A. Laubenstein, L. J. Koester, and R. C. Mobley, Phys. Rev. 81, 654 (1951) (A)

47L50 R. M. Littauer, Phil. Mag. 41, 1214 (1950)

48L50 E. Lüscher, R. Ricamo, P. Scherrer, and W. Zünti, Helv. Phys. Acta 23, 561 (1950)

49L51 G. Lindström, Arkiv Fysik 4, 1 (1951); Phys. Rev. 83, 465 (1951)

49L52 G. Lindström, Phys. Rev. 87, 678 (1952)

50L52 G. M. Lewis, Phil. Mag. 43, 1070 (1952)

51L51 J. Lascoux and G. Vendryes, Compt. rend. 233, 858 (1951)

52L52 H. B. Levy and I. Perlman, Phys. Rev. 85, 758 (1952) (A); unpublished data (Nov. 1952)

53L52 D. L. Livesey and C. L. Smith, Proc. Phys. Soc (London) 65A, 758 (1952)

54L52 L. M. Litz, S. A. Ring, and W. P. Balkwell, private communication (Nov. 1952)

1M23 L. Meitner, Z. Physik 17, 54 (1923)

1M28 L. Meitner, Z. Physik 52, 637, 645 (1928)

1M28a L. Meitner, Z. Physik 50, 15 (1928)

1M37 L. Meitner, O. Hahn, and F. Strassmann, Z. Strassmann, Z. Physik 106, 249 (1937)

1M38 L. Meitner, F. Strassmann, and O. Hahn, Z. Physik 109, 538 (1938)

1M40 L. Meitner, Arkiv Mat., Astron. Fysik 27A, No. 17 (1940)

1M48 L. Meitner, Ann. Physik 3, 115 (1948)

2M14 S. Meyer, V. F. Hess, and F. Paneth, Wien. Ber. 123, 1459 (1914)

3M41 W. Maurer and W. Ramm, Naturwiss. 29, 368 (1941); Z. Physik 119, 334 (1942)

3M42 W. Maurer and W. Ramm, Z. Physik 119, 602 (1942)

3M47 W. Maurer, Z. Naturforsch. 2a, 586 (1947)

3M49 W. Maurer, Z. Naturforsch. 4a, 150 (1949)

4M50 J. F. Miller, J. G. Hamilton, T. M. Putnam, H. R. Haymond, and G. B. Rossi, Phys. Rev. 80, 486 (1950)

5M50 M. Miwa and S. Kageyama, J. Phys. Soc. Japan 5, 416 (1950)

6M48 D. G. E. Martin, H. O. W. Richardson, and Yun-Kuei Hsü, Proc. Phys. Soc. (London) 60, 466 (1948)

6M48a D. G. E. Martin and H. O. W. Richardson, Proc. Roy. Soc. (London) 195A, 287 (1948)

6M50 D. G. E. Martin and H. O. W. Richardson, Proc. Phys. Soc. (London) 63A, 223 (1950)

7M48 K. R. MacKenzie, private communication (1948)

8M37 J. Mattauch, Naturwiss. 25, 189 (1937)

8M39 J. Mattauch and H. Lichtblau, Z. Physik 111, 514 (1939)

CC-0. In Public Domain. Gurukul Kangri Collection, Haridwar

Digitized by Arya Samaj Foundation Chennai and eGangotri

9M52 F. F. Momyer, F. Asaro, and E. K. Hyde, private communication (Aug. 1952)

9M52a F. F. Momyer, E. K. Hyde, A. Ghiorso, and W. E. Glenn, Phys. Rev. 86, 805 (1952)

9M52b F. F. Momyer, A. Ghiorso, and E. K. Hyde, private communication (Aug. 1952)

9M52c F. F. Momyer and E. K. Hyde, unpublished data (Dec. 1952)

10M47 R. L. Macklin and G. B. Knight, Phys. Rev. 72, 435 (1947)

10M49 R. L. Macklin, Phys. Rev. 76, 595 (1949)

11M48 W. W. Meinke, A. Ghiorso, and G. T. Seaborg, unpublished data (July 1948)

11M49 W. W Meinke, A. Ghiorso, and G. T. Seaborg, Phys. Rev. 75, 314 (1949)

11M50 W. W. Meinke and G. T. Seaborg, Phys. Rev. 78, 475 (1950)

11M51 W. W. Meinke, A. Ghiorso, and G. T. Seaborg, Phys. Rev. 81, 782 (1951)

11M52 W. W. Meinke, A. Ghiorso, and G. T. Seaborg, Phys. Rev. 85, 429 (1952)

11M52a W. W. Meinke and K. L. Hall, private communication (Oct. 1952)

11M53 W. W. Meinke, Phys. Rev. (to be published) (1953)

12M35 E. M. McMillan and M. S. Livingston, Phys. Rev. 47, 452 (1935)

12M35a E. M. McMillan and E. O. Lawrence, Phys Rev. 47, 343 (1935)

12M37 E. M. McMillan, M. Kamen, and S. Ruben, Phys. Rev. 52, 375 (1937)

12M39 E. M. McMillan, Phys. Rev. 55, 510 (1939)

12M40 E. M. McMillan, Phys. Rev. 58, 178 (1940)

12M40a E. M. McMillan and P. H. Abelson, Phys. Rev. 57, 1185 (1940)

12M46 E. M. McMillan, private communication (June 1946)

12M46a E. M. McMillan and S. Ruben, Phys. Rev. 70, 123 (1946)

12M46b E. M. McMillan and T. M. Putnam, private communication (July 1946)

12M46c E. M. McMillan, W. J. Knox, and R. H. Goeckermann, private communication (June 1946)

12M47 E. M. McMillan, Phys. Rev. 72, 591 (1947)

12M47a E. M. McMillan, private communication (Jan. 1947)

13M47 L. Melander, Acta Chem. Scan. 1, 169 (1947)

13M48 L. Melander and H. Slätis, Phys. Rev. 74, 709 (1948); Arkiv Mat., Astron. Fysik 36A, No. 15 (1949)

14M37 A. C. G. Mitchell, Phys. Rev. 51, 995 (1937)

14M38 A. C. G. Mitchell, Phys. Rev. 53, 269 (1938)

14M38a A. C. G. Mitchell and L. M. Langer, Phys. Rev. 53, 505 (1938)

14M40 A. C. G. Mitchell, L. M. Langer, and P. W. McDaniel, Phys. Rev. 57, 1107 (1940)

14M42 A. C. G. Mitchell, L. M. Langer, and L. J. Brown, Metallurgical Project Classified Report (work performed at Indiana University) CN-409 (Dec. 1942)

14M43 A. C. G. Mitchell, L. Slotin, J. Marshall, V. A. Nedzel, L. J. Brown, and J. R. Pruett, Metallurgical Laboratory Classified Report CP-597 (April 1943)

14M47 A. C. G. Mitchell, E. T. Jurney, and M. Ramsey, Phys. Rev. 71, 825 (1947)

14M48 A. C. G. Mitchell, D. J. Zaffarano, and B. D. Kern, Phys. Rev. 73, 1424 (1948)

14M49 A. C. G. Mitchell, J. Y. Mei, F. C. Maienschein, and C. L. Peacock, Phys. Rev. 76, 1450 (1949)

14M49a A. C. G. Mitchell and C. L. Peacock, Phys. Rev. 75, 197 (1949)

14M51 A. C. G. Mitchell and L. J. Brown, NNES-PPR 9, 717 (1951)

14M52 A. C. G. Mitchell and A. B. Smith, Phys. Rev. 85, 153 (1952)

14M52a A. C. G. Mitchell and R. S. Caird, Phys. Rev. 87, 388 (1952)

15M45 L. B. Magnusson and A. Ghiorso, unpublished data (1945)

15M47 L. B. Magnusson and T. J. LaChapelle, unpublished data (1947)

15M48 L. B. Magnusson and T. J. LaChapelle, J. Am. Chem. Soc. 70, 3534 (1948); NNES-PPR 14B, 39 (1949)

15M50 L. B. Magnusson, S. G. Thompson, and G. T. Seaborg, Phys. Rev. 78, 363 (1950)

16M49 W. M. Manning and L. B. Asprey, NNES-PPR 14B, 1595 (1949)

17M39 H. Maier-Leibnitz, Naturwiss. 26, 614 (1939)

18M51 C. H. Millar and A. G. W. Cameron, Phys. Rev. 81, 316 (1951) (A)

18M51a C. H. Millar, G. A. Bartholomew, and B. B. Kinsey, Phys. Rev. 81, 150 (1951)

18M52 C. H. Millar and A. G. W. Cameron, private communication (Oct. 1952)

18M52a C. H. Millar, G. A. Bartholomew, and B. B. Kinsey, private communication (Oct. 1952)

19M47 A. N. May and E. P. Hincks, Can. J. Research 25A, 77 (1947)

20M51 G. G. Manov and L. F. Curtiss, J. Research Natl. Bur. Standards 46, 328 (1951)

21M50 W. W. Miller, R. Ballentine, W. Bernstein, L. Friedman, A. O. Nier, and R. D. Evans, Phys. Rev. 77, 714 (1950)

22M43 J. Marshall, reported in Metallurgical Laboratory Classified Report CP-718 (June 1943)

23M50 P. A. Macklin, L. J. Lidofsky, and C. S. Wu, Phys. Rev. 78, 318 (1950) (A)

23M50a P. A. Macklin, L. Feldman, L. Lidofsky, and C. S. Wu, Phys. Rev. 77, 137 (1950)

23M51 P. A. Macklin, L. I. Lidofsky, and C. S. Wu, Phys. Rev. 82, 334 (1951) (A)

23M51a P. Macklin, L. Lidofsky, and C. S. Wu, reported in Columbia University Unclassified Report CU-96 (June 1951)

24M37 C. Magnan, Compt. rend. 205, 1147 (1937)

24M41 C. Magnan, Ann. phys. 15, 5 (1941)

25M49 K. H. Morganstern and K. P. W. Wolf, Phys. Rev. 76, 1261 (1949)

26M42 C. E. Mandeville, Phys. Rev. 62, 555 (1942)

26M43 C. E. Mandeville, Phys. Rev. 63, 387 (1943)

26M43a C. E. Mandeville, Phys. Rev. 64, 147 (1943)

26M48 C. E. Mandeville and M. V. Scherb, Phys. Rev. 73, 141 (1948)

26M48a C. E. Mandeville and M. V. Scherb, Phys. Rev. 73, 1434 (1948)

26M48b C. E. Mandeville, M. V. Scherb, and W. B. Keighton, Phys. Rev. 74, 888 (1948)

26M48c C. E. Mandeville and M. V. Scherb, Phys. Rev. 73, 848 (1948)

26M48d C. E. Mandeville and M. V. Scherb, Phys. Rev 73, 340 (1948)

26M48e C. E. Mandeville, M. V. Scherb, and W. B Keighton, Phys. Rev. 74, 601 (1948)

26M49 C. E. Mandeville, Y. H. Woo, M. V. Scherb, W. B. Keighton, and E. Shapiro, Phys. Rev. 75, 1528 (1949)

CC-0. In Public Domain. Gurukul Kangri Collection, Haridwar

Digitized by Arya Samaj Foundation Chennai and eGangotri

26M49a C. E. Mandeville, M. V. Scherb, and W. B Keighton, Phys. Rev. 75, 221, 329 (1949)

26M49b C. E. Mandeville and E. Shapiro, Phys. Rev. 75, 897 (1949)

26M49c C. E. Mandeville and E. Shapiro, Phys. Rev. 76, 718 (1949)

26M49d C. E. Mandeville, Phys. Rev. 75, 1017 (1949)

26M49e C. E. Mandeville and E. Shapiro, Phys. Rev. 75, 1834 (1949)

26M49f C. E. Mandeville and M. V. Scherb, Phys. Rev. 76, 186 (1949) (A)

26M50 C. E. Mandeville and E. Shapiro, Phys. Rev. 77, 439 (1950)

26M50a C. E. Mandeville and E. Shapiro, Phys. Rev. 79, 243 (1950) (A)

26M50b C. E. Mandeville and E. Shapiro, Phys. Rev. 79, 391 (1950)

26M51 C. E. Mandeville and E. Shapiro, Phys. Rev. 82, 953 (1951); J. Franklin Inst. 253, 145 (1952)

26M52 C. E. Mandeville, E. Shapiro, R. I. Mendenhall, E. R. Zucker, and G. L. Conklin, Phys. Rev. 86, 813 (1952)

26M52a C. E. Mandeville, E. Shapiro, R. I. Mendenhall, E. R. Zucker, and G. L. Conklin, Phys. Rev. 88, 554 (1952)

27M49 J. McElhinney, A. O. Hanson, R. A. Becker, R. B. Duffield, and B. C. Diven, Phys. Rev. 75, 542 (1949)

28M40 B. L. Moore, Phys. Rev. 57, 355 (1940) (A)

29M52 H. T. Motz and D. E. Alburger, Phys. Rev. 86, 165 (1952)

29M52a H. T. Motz, Phys. Rev. 85, 501 (1952)

30M40 R. L. McCreary, G. Kuerti, and S. N. Van Voorhis, Phys. Rev. 57, 351 (1940) (A)

31M40 D. Mulder, G. W. Hoeksema, and G. J. Sizoo, Physica 7, 849 (1940)

32M48 D. R. Miller, R. C. Thompson, and B. B. Cunningham, Phys. Rev. 74, 347 (1948)

32M48a D. R. Miller, Ph.D. Thesis, University of California Radiation Laboratory Declassified Report UCRL-142 (July 1948)

32M50 D. R. Miller, Phys. Rev. 78, 808 (1950)

33M49 V. Myers and A. Wattenberg, Phys. Rev. 75, 992 (1949)

34M47 H. A. Meyer, G. Schwachheim, and M. D. de Souza Santos, Phys. Rev. 71, 908 (1947)

35M51 P. Morrison, Phys. Rev. 82, 209 (1951)

36M47 D. E. Matthews and M. L. Pool, Phys. Rev. 72, 163 (1947) (A)

37M49 J. L. Meem, Jr. and F. Maienschein, Phys. Rev. 76, 328 (1949)

38M47 E. der Mateosian, M. Goldhaber, C. O. Muehlhause, and M. McKeown, Phys. Rev. 72, 1271 (1947)

38M49 E. der Mateosian, M. Goldhaber, and A. Smith, reported in Argonne National Laboratory Classified Report ANL-4237 (Jan. 1949)

38M49a E. der Mateosian and M. Goldhaber, Phys. Rev. 76, 187 (1949) (A)

38M50 E. der Mateosian and M. Goldhaber, Phys. Rev. 79, 192 (1950)

38M50a E. der Mateosian, M. Goldhaber, and D. E. Alburger, reported in Brookhaven National Laboratory Unclassified Report BNL-39 (Jan. 1950)

38M51 E. der Mateosian and M. Goldhaber, Phys. Rev. 82, 115 (1951)

38M51a E. der Mateosian, Phys. Rev. 83, 223 (1951) (A)

38M51b E. der Mateosian and M. Goldhaber, Phys. Rev. 83, 843 (1951)

38M51c E. der Mateosian and M. Goldhaber, unpublished data quoted in (18G52)

38M52 E. der Mateosian, private communication (Oct. 1952)

38M52a E. der Mateosian, G. Friedlander, M. Goldhaber, and A. W. Sunyar, quoted in (18G52)

39M50 M. L. Moon, M. A. Waggoner, and A. Roberts, Phys. Rev. 79, 905 (1950)

40M47 A. E. Miller and M. Deutsch, Phys. Rev. 72, 527 (1947) (A)

41M50 W. Mims, H. Halban, and R. Wilson, Nature 166, 1027 (1950)

41M51 W. Mims and H. Halban, Proc. Phys. Soc. (London) 64A, 311 (1951)

41M51a W. B. Mims and H. Halban, Proc. Phys. Soc. (London) 64A, 753 (1951)

42M47 J. Martelly, Ann. phys. 2, 555 (1947)

43M46 L. C. Miller and L. F. Curtiss, Phys. Rev. 70, 983 (1946)

43M47 L. C. Miller and L. F. Curtiss, J. Research Natl. Bur. Standards 38, 359 (1947)

44M48 F. Metzger and M. Deutsch, Phys. Rev. 74, 1640 (1948)

44M50 F. Metzger, Phys. Rev. 79, 398 (1950)

44M50a F. Metzger and M. Deutsch, Phys. Rev. 78, 551 (1950)

44M51 F. R. Metzger and R. D. Hill, Phys. Rev. 82, 646 (1951)

44M52 F. R. Metzger, Phys. Rev. 85, 727 (1952) (A)

44M52a F. R. Metzger, Phys. Rev. 86, 435 (1952)

44M52b F. R. Metzger and H. C. Amacher, Phys. Rev. 88, 147 (1952)

45M41 J. J. Mitchell, H. S. Brown, and R. D. Fowler, Phys. Rev. 60, 359 (1941)

46M49 F. Maienschein and J. L. Meem, Jr., Phys. Rev. 76, 899 (1949)

46M51 F. C. Maienschein, J. K. Bair, and W. B. Baker, Phys. Rev. 83, 477 (1951)

47M47 W. E. Meyerhof and G. Scharff-Goldhaber, Phys. Rev. 72, 273 (1947)

47M48 W. E. Meyerhof and M. Goldhaber, Phys. Rev. 74, 348 (1948)

47M48a W. E. Meyerhof, Phys. Rev. 74, 621 (1948)

47M52 W. E. Meyerhof, L. G. Mann, and H. I. West, Jr., private communication (Oct. 1952)

48M49 K. C. Mann, D. Rankin, and P. N. Daykin, Phys. Rev. 76, 1719 (1949)

48M51 K. C. Mann and G. H. Hanson, Phys. Rev. 83, 893 (1951) (A)

49M50 A. Mukerji and P. Preiswerk, Helv. Phys. Acta 23, 516 (1950)

49M52 A. Mukerji and P. Preiswerk, Helv. Phys. Acta 25, 387 (1952)

50M37 W. B. Mann, Phys. Rev. 52, 405 (1937)

50M38 W. B. Mann, Phys. Rev. 54, 649 (1938)

50M38a W. B. Mann, Phys. Rev. 53, 212 (1938) (A)

51M48 D. A. McCown, L. L. Woodward, and M. L. Pool, Phys. Rev. 74, 1311 (1948)

51M48a D. A. McCown, L. L. Woodward, and M. L. Pool, Phys. Rev. 74, 1315 (1948)

52M49 F. K. McGowan, Phys. Rev. 76, 1730 (1949)

52M50 F. K. McGowan, Phys. Rev. 80, 482 (1950)

52M50a F. K. McGowan, Phys. Rev. 80, 923 (1950)

52M50b F. K. McGowan, Phys. Rev. 79, 404 (1950)

CC-0. In Public Domain. Gurukul Kangri Collection, Haridwar

Digitized by Arya Samaj Foundation Chennai and eGangotri

52M50c F. K. McGowan, Phys. Rev. 77, 138 (1950)

52M51 F. K. McGowan, Oak Ridge National Laboratory Unclassified Report ORNL-952 (March 1951)

52M51a F. K. McGowan, Phys. Rev. 81, 1066 (1951)

52M52 F. K. McGowan, Phys. Rev. 85, 142 (1952)

52M52a F. K. McGowan, Phys. Rev. 85, 151 (1952)

52M52b F. K. McGowan and E. D. Klema, reported in Oak Ridge National Laboratory Unclassified Report ORNL-1164 (April 1952)

52M52c F. K. McGowan, Phys. Rev. 87, 542 (1952)

52M52d F. K. McGowan, E. D. Klema, and P. R. Bell, Phys. Rev. 85, 152 (1952)

52M52e F. K. McGowan, private communication (Oct. 1952)

53M49 J. Y. Mei, A. C. G. Mitchell, and D. J. Zaffarano, Phys. Rev. 76, 1883 (1949)

53M50 J. Y. Mei, A. C. G. Mitchell, and C. M. Huddleston, Phys. Rev. 79, 19 (1950)

53M50a J. Y. Mei, C. M. Huddleston, and A. C. G. Mitchell, Phys. Rev. 79, 429 (1950)

53M50b J. Y. Mei, C. M. Huddleston, and A. C. G. Mitchell, Phys. Rev. 79, 1010 (1950)

54M44 N. Marty, J. phys. et radium 5, 276 (1944)

54M49 N. Marty, J. Labeyrigue, and H. Langevin, Compt. rend. 228, 1722 (1949)

54M51 N. Marty-Wollman, Ann. phys. 6, 662 (1951)

55M50 H. R. Muether and S. L. Ridgway, Phys. Rev. 80, 750 (1950)

56M50 J. Miskel, Phys. Rev. 79, 403 (1950)

56M50a J. Miskel and G. Friedlander, reported in Brookhaven National Laboratory Unclassified Report BNL-39 (Jan. 1950)

56M51 J. A. Miskel and A. C. Wahl, Phys. Rev. 84, 700 (1951)

56M52 J. A. Miskel and M. L. Perlman, Phys. Rev. 87, 543 (1952)

57M41 A. Moussa and L. Goldstein, Phys. Rev. 60, 534 (1941); Compt. rend. 212, 986 (1941)

58M50 L. G. Mann and P. Axel, Phys. Rev. 80, 759 (1950)

58M51 L. G. Mann and P. Axel, Phys. Rev. 84, 221 (1951)

58M52 L. G. Mann and W. E. Meyerhof, Phys. Rev. 87, 202 (1952) (A) and private communication with H. I. West, Jr. (Oct. 1952)

59M44 W. N. Moquin and M. L. Pool, Phys. Rev. 65, 60 (1944) (A)

60M48 D. L. Mock, R. C. Waddel, L. W. Fagg, and R. A. Tobin, Phys. Rev. 74, 1536 (1948)

61M47 E. E. Motta, Q. V. Larson, and G. E. Boyd, Phys. Rev. 72, 1270 (1947)

61M47a E. E. Motta, Q. V. Larson, and G. E. Boyd, reported in Oak Ridge National Laboratory Classified Report Mon N-432 (Dec. 1947)

61M47b E. E. Motta, G. E. Boyd, and A. R. Brosi, Phys. Rev. 71, 210 (1947)

61M48 E. E. Motta and G. E. Boyd, Phys. Rev. 73, 1470 (1948)

61M48a E. E. Motta and G. E. Boyd, Phys. Rev. 74, 220 (1948)

61M48b E. E. Motta and G. E. Boyd, Phys. Rev. 74, 344 (1948)

62M49 H. Medicus, D. Maeder, and H. Schneider, Helv. Phys. Acta 22, 603 (1949)

62M50 H. Medicus, P. Preiswerk, and P. Scherrer, Helv. Phys. Acta 23, 299 (1950)

62M50a H. Medicus and P. Preiswerk, Phys. Rev. 80, 1101 (1950)

62M51 H. Medicus, D. Maeder, and H. Schneider, Helv. Phys. Acta 24, 72 (1951); Phys. Rev. 81, 652 (1951) (A)

62M52 H. Medicus and H. T. Easterday, Phys. Rev. 85, 735 (1952) (A)

63M50 J. W. Mihelich and R. D. Hill, Phys. Rev. 79, 781 (1950)

63M51 J. W. Mihelich, M. Goldhaber, and E. Wilson, Phys. Rev. 82, 972 (1951)

63M51a J. W. Mihelich, reported in Brookhaven National Laboratory Unclassified Report BNL-93 (March 1951)

63M52 J. W. Mihelich and E. L. Church, Phys. Rev. 85, 690 (1952)

63M52a J. W. Mihelich, Phys. Rev. 87, 646 (1952)

63M52b J. W. Mihelich, private communication (Oct. 1952)

63M52c J. W. Mihelich and A. de Shalit, private communication (Nov. 1952)

63M52d J. W. Mihelich, Bull. A. P. S. 27, No. 5, Abstract V3 (1952)

64M40 O. Minakawa, Phys. Rev. 57, 1189 (1940)

64M41 O. Minakawa, Phys. Rev. 60, 689 (1941)

65M52 A. K. Mousuf, Phys. Rev. 88, 150 (1952)

66M51 C. L. McGinnis, Phys. Rev. 81, 734 (1951)

66M51a C. L. McGinnis, Phys. Rev. 83, 686 (1951)

66M52 C. L. McGinnis, Phys. Rev. 87, 202 (1952) (A) and private communication (Oct. 1952)

67M51 R. P. Metcalf, NNES-PPR 9, 891 (1951)

67M51a R. P. Metcalf, NNES-PPR 9, 898 (1951)

67M51b R. P. Metcalf, NNES-PPR 9, 905 (1951)

68M49 E. C. Mallary and M. L. Pool, Phys. Rev. 76, 1454 (1949)

68M50 E. C. Mallary and M. L. Pool, Phys. Rev. 77, 75 (1950)

69M51 M. M. Miller, C. H. Pruett, and R. G. Wilkinson, Phys. Rev. 84, 849 (1951)

69M51a M. M. Miller and R. G. Wilkinson, Phys. Rev. 83, 1050 (1951)

69M51b M. M. Miller and R. G. Wilkinson, Phys. Rev. 82, 981 (1951)

69M52 M. M. Miller, Phys. Rev. 88, 516 (1952)

70M49 W. C. Miller and B. Waldman, Phys. Rev. 75, 425 (1949)

71M50 E. A. Martell and W. F. Libby, Phys. Rev. 80, 977 (1950)

72M52 J. A. McCarthy, Phys. Rev. 87, 194 (1952) (A)

73M52 H. B. Mathur, M. Michel, T. O. Passell, and E. K. Hyde, private communication (Dec. 1952)

74M50 L. Marquez and I. Perlman, Phys. Rev. 78, 189 (1950)

74M51 L. Marquez and I. Perlman, Phys. Rev. 81, 953 (1951)

74M52 L. Marquez, Phys. Rev. 88, 225 (1952)

74M52a L. Marquez, Phys. Rev. 86, 406 (1952)

75M51 D. S. Martin, Jr. and F. J. Hughes, reported in Iowa State College Classified Report ISC-137 (May 1951)

75M51a D. S. Martin, Jr., E. N. Jensen, F. J. Hughes, and R. T. Nichols, Phys. Rev. 82, 579 (1951)

76M50 J. Macnamara, C. B. Collins, and H. G. Thode, Phys. Rev. 78, 129 (1950)

76M50a J. Macnamara and H. G. Thode, Phys. Rev. 78, 307 (1950)

77M35 J. C. McLennan, L. G. Grimmett, and J. Read, Nature 135, 505 (1935)

77M35a J. C. McLennan and W. H. Rann, Nature 136, 831 (1935)

CC-0. In Public Domain. Gurukul Kangri Collection, Haridwar

Digitized by Arya Samaj Foundation Chennai and eGangotri

77M35b J. C. McLennan, L. G. Grimmett, and J. Read, Nature 135, 147 (1935)

78M41 M. Melhase, unpublished data, University of California, Berkeley (Sept. 1941)

79M52 M. H. MacGregor and M. L. Wiedenbeck, Phys. Rev. 86, 420 (1952)

80M52 H. C. Martin and B. C. Diven, Phys. Rev. 86, 565 (1952)

81M42 K. E. Mounce, M. L. Pool, and J. D. Kurbatov, Phys. Rev. 61, 389 (1942) (A)

82M35 J. K. Marsh and S. Sugden, Nature 136, 102 (1935)

83M50 A. J. Moses and D. S. Martin, Jr., Phys. Rev. 79, 467 (1950)

83M51 A. J. Moses and D. S. Martin, Jr., Phys. Rev. 84, 366 (1951)

84M47 J. A. Marinsky, L. E. Glendenin, and C. D. Coryell, J. Am. Chem. Soc. 69, 2781 (1947)

84M49 J. A. Marinsky, reported in Massachusetts Institute of Technology Unclassified Report NP-1272 (July 1949)

84M49a J. A. Marinsky, L. E. Glendenin, and F. Metzger, reported in Massachusetts Institute of Technology Unclassified Report NP-1727 (July 1949)

84M51 J. A. Marinsky and L. E. Glendenin, NNES-PPR 9, 1229 (1951)

84M51a J. A. Marinsky and L. E. Glendenin, NNES-PPR 9, 1243 (1951)

84M51b J. A. Marinsky and L. E. Glendenin, NNES-PPR 9, 1264 (1951)

84M51c J. A. Marinsky and L. E. Glendenin, NNES-PPR 9, 1254 (1951)

84M51d J. A. Marinsky and L. E. Glendenin, NNES-PPR 9, 1969 (1951)

85M52 G. I. Mulholland and T. P. Kohman, Phys. Rev. 85, 144 (1952)

85M52a G. I. Mulholland and T. P. Kohman, Phys. Rev. 87, 681 (1952)

86M52 R. C. Mack, D. I. Prickett, and M. L. Pool, Phys. Rev. 86, 633 (1952) (A)

87M50 J. E. Mack, Revs. Modern Phys. 22, 64 (1950)

88M51 K. Murakawa and J. S. Ross, Phys. Rev. 82, 967 (1951)

89M52 D. F. Martin, unpublished data (Aug. 1952)

89M52a D. F. Martin, R. W. Hoff, G. H. Higgins, and S. G. Thompson, reported in University of California Radiation Laboratory Classified Report UCRL-1770 (April 1952)

90M52 J. H. Moon and A. L. Thompson, Phys. Rev. 83, 892 (1951) (A) and private communication (Oct. 1952)

91M51 S. L. Miller, A. Javan, and C. H. Townes, Phys. Rev. 82, 454 (1951)

92M51 J. W. Meadows and R. B. Holt, Phys. Rev. 83, 1257 (1951)

93M51 J. M. Miller and G. Friedlander, Phys. Rev. 84, 589 (1951)

94M51 D. Maeder and P. Preiswerk, Phys. Rev. 84, 595 (1951)

94M51a D. Maeder and P. Preiswerk, Helv. Phys. Acta 24, 625 (1951)

95M52 J. K. Major, Compt. rend. 234, 2276 (1952); Phys. Rev. 86, 631 (1952) (A)

96M52 J. Moreau and J. Perez y Jorba, Compt. rend. 235, 38 (1952)

97M52 K. C. Maclure, Ph.D. Thesis, McGill University (Sept. 1952)

98M51 W. M. Martin, Ph.D. Thesis, McGill University (1951)

98M52 W. M. Martin and S. W. Breckon, Can. J. Phys. (to be published) (1952)

99M52 M. McKeown and S. Katcoff, private communication (Oct. 1952)

100M52 D. E. Muller, H. C. Hoyt, D. J. Klein, and J. W. M. DuMond, Phys. Rev. 88, 775 (1952)

1N50 T. B. Novey, reported in Argonne National Laboratory Classified Report ANL-4427 (July 1950)

1N50a T. B. Novey, Phys. Rev. 78, 66 (1950)

1N51 T. B. Novey, D. W. Engelkeimeir, E. L. Brady, and L. E. Glendenin, NNES-PPR 9, 678 (1951)

1N51a T. B. Novey, NNES-PPR 9, 976 (1951)

1N51b T. B. Novey, W. H Sullivan, C. D. Coryell, A. S. Newton, N. R. Sleight, and O. Johnson, NNES-PPR 9, 958 (1951)

1N51c T. B. Novey and J. D. Knight, NNES-PPR 9, 1043 (1951)

2N36 R. Naidu and R. E. Siday, Proc. Phys. Soc. (London) 48, 332 (1936)

3N36 M. E. Nahmias and R. J. Walen, Compt. rend. 203, 71 (1936)

4N50 H. M. Neumann and I. Perlman, Phys. Rev. 78, 191 (1950)

4N50a H. M. Neumann, J. J. Howland, Jr., and I. Perlman, Phys. Rev. 77, 720 (1950)

4N50b H. M. Neumann, A. Ghiorso, and I. Perlman, unpublished data (1950)

4N51 H. M. Neumann and I. Perlman, Phys. Rev. 81, 958 (1951)

5N38 Y. Nishina, T. Yasaki, K. Kimura, and M. Ikawa, Nature 142, 874 (1938)

5N40 Y. Nishina, T. Yasaki, H. Ezoe, K. Kimura, and M. Ikawa, Phys. Rev. 57, 1182 (1940)

5N40a Y. Nishina, T. Yasaki, K. Kimura, and M. Ikawa, Phys. Rev. 58, 660 (1940)

5N40b Y. Nishina, T. Yasaki, H. Ezoe, K. Kimura, and M. Ikawa, Nature 146, 24 (1940)

5N41 Y. Nishina, T. Yasaki, K. Kimura, and M. Ikawa, Phys. Rev. 59, 677 (1941)

5N42 Y. Nishina, K. Kimura, T. Yasaki, and M. Ikawa, Z. Physik 119, 195 (1942)

6N36 A. O. Nier and E. E. Hanson, Phys. Rev. 50, 722 (1936)

6N37 A. O. Nier, Phys. Rev. 52, 933 (1937)

6N37a A. O. Nier, Phys. Rev. 52, 885 (1937)

6N38 A. O. Nier, J. Am. Chem. Soc. 60, 1571 (1938)

6N38a A. O. Nier, Phys. Rev. 53, 282 (1938)

6N38b A. O. Nier, Phys. Rev. 54, 275 (1938)

6N39 A. O. Nier, Phys. Rev. 55, 150 (1939). Values recalculated according to (6K41)

6N50 A. O. Nier, Phys. Rev. 77, 789 (1950)

6N50a A. O. Nier, Phys. Rev. 79, 450 (1950)

7N49 A. S. Newton, Phys. Rev. 75, 209 (1949)

7N49a A. S. Newton, Phys. Rev. 75, 17 (1949)

7N49b A. S. Newton and W. R. McDonell, University of California Radiation Laboratory Unclassified Report UCRL-395 (July 1949)

7N51 A. S. Newton, W. H Sullivan, O. Johnson, and R. Nottorf, NNES-PPR 9, 1028 (1951)

7N51a A. S. Newton, A. Kant, and R. E. Hein, NNES-PPR 9, 1200 (1951)

8N47 A. Novick, Phys. Rev. 72, 972 (1947)

CC-0. In Public Domain. Gurukul Kangri Collection, Haridwar

Digitized by Arya Samaj Foundation Chennai and eGangotri

9N40 G. J. Neary, Proc. Roy. Soc. (London) 175A, 71 (1940)

10N48 L. D. Norris and M. G. Inghram, Phys. Rev. 73, 350 (1948)

11N37 S. Nishida, Proc. Phys.-Math. Soc. Japan 19, 809 (1937)

12N35 H. W. Newson, Phys. Rev. 48, 790 (1935)

12N35a H. W. Newson, Phys. Rev. 48, 482 (1935) (A)

12N37 H. W. Newson, Phys. Rev. 51, 624 (1937)

13N50 Y. A. Nemilov and L. I. Gedeonov, Doklady Akad. Nauk S.S.S.R. 70, 219 (1950)

14N50 B. D. Nag, S. Sen, and S. Chatterjee, Indian J. Phys. 24, 479 (1950)

15N42 M. E. Nelson, M. L. Pool, and J. D. Kurbatov, Phys. Rev. 62, 1 (1942)

15N42a M. E. Nelson, M. L. Pool, and J. D. Kurbatov, Phys. Rev. 61, 428 (1942)

15N50 M. E. Nelson and M. L. Pool, Phys. Rev. 77, 682 (1950)

16N44 B. D. Nag-Chowdhury, Proc. Nat. Inst. Sci. India 10, 317 (1944), Chem. Abs. 42, 4452b (1948)

17N44 V. A. Nedzel and E. C. Barker, reported in Metallurgical Laboratory Classified Report CP-1728 (June 1944)

17N51 V. A. Nedzel, NNES-PPR 9, 719 (1951)

17N51a V. A. Nedzel, NNES-PPR 9, 732 (1951)

17N51b V. A. Nedzel, NNES-PPR 9, 1213 (1951)

18N51 R. W. Nottorf, NNES-PPR 9, 682 (1951)

19N50 C. M. Nelson, B. H. Ketelle, and G. E. Boyd, Oak Ridge National Laboratory Unclassified Report ORNL-828 (Nov. 1950)

20N51 G. J. Nijgh, N. F. Verster, R. H. Nussbaum, R. Van Lieshout, and C. J. Bakker, Physica 17, 658 (1951)

21N50 R. A. Naumann, F. L. Reynolds, and I. Perlman, Phys. Rev. 77, 398 (1950)

22N52 W. E. Nervik, reported in University of California Radiation Laboratory Classified Report UCRL-1632 (Jan. 1952)

23N35 E. Neuninger and E. Rona, Anz. Akad. Wiss. Wien, Math.-naturw. Klasse 72, 275 (1935)

23N36 E. Neuninger and E. Rona, Anz. Akad. Wiss. Wien, Math.-naturw. Klasse 73, 159 (1936)

24N47 H. Neuert, Z. Naturforsch. 2a, 432 (1947)

25N48 S. N. Naldrett and W. F. Libby, Phys. Rev 73, 487 (1948)

1O46 R. K. Osborne and W. C. Peacock, Phys. Rev. 69, 679 (1946) (A)

1O47 R. K. Osborne and M. Deutsch, Phys. Rev. 71, 467 (1947) (A)

2O39 F. Oppenheimer and E. P. Tomlinson, Phys. Rev 56, 858 (1939) (A)

3O47 W. Ogle, L. Brown, and R. Conklin, Phys. Rev 71, 378 (1947)

3O50 W. E. Ogle, L. J. Brown, and A. N. Carson, Phys. Rev. 78, 63 (1950)

4O40 R. D. O'Neal and M. Goldhaber, Phys. Rev 58 574 (1940)

4O40a R. D. O'Neal and M. Goldhaber, Phys. Rev. 57, 1086 (1940) (A)

4O41 R. D. O'Neal, Phys. Rev. 60, 359 (1941)

5O49 D. W. Osborne, R. C. Thompson, and Q. Van Winkle, NNES-PPR 14B, 1397 (1949)

6O47 P. R. O'Connor and G. T. Seaborg, unpublished data (1947)

6O48 P. R. O'Connor and G. T. Seaborg, Phys. Rev. 74, 1189 (1948)

7O49 D. A. Orth, L. Marquez, W. J. Heiman, and D. H. Templeton, Phys. Rev. 75, 1100 (1949)

7O50 D. A. Orth, A. Ghiorso, and G. T. Seaborg, unpublished data (April 1950)

7O51 D. A. Orth and R. A. Glass, unpublished data (March 1951)

7O51a D. A. Orth and K. Street, Jr., unpublished data (1951)

7O51b D. A. Orth and G. D. O'Kelley, Phys. Rev. 82, 758 (1951)

8O50 G. D. O'Kelley and F. L. Reynolds, reported in University of California Radiation Laboratory Classified Report UCRL-550 (Jan. 1950)

8O50a G. D. O'Kelley, G. W. Barton, Jr., W. W. T. Crane, and I. Perlman, Phys. Rev. 80, 293 (1950)

8O51 G. D. O'Kelley, Ph.D. Thesis, University of California Radiation Laboratory Unclassified Report UCRL-1243 (May 1951)

9O49 A. Orsini, Anais faculdade farm. odontol., Univ. São Paulo 7, 9 (1949)

10O46 R. T. Overman, U. S. Atomic Energy Commission Declassified Document MDDC-354 (Sept. 1946)

10O47 R. T. Overman, U. S. Atomic Energy Commission Declassified Document AECD-857 (April 1947)

11O42 R. Overstreet, L. Jacobson, K. Scott, and J. G. Hamilton, Metallurgical Project Declassified Report (work performed at Berkeley) CH-379 (Dec. 1942)

11O43 R. Overstreet and L. Jacobson, reported in Metallurgical Project Classified Report (work performed at Berkeley) CH-498 (Feb. 1943)

11O49 R. Overstreet, L. Jacobson, and P. R. Stout, Phys. Rev. 75, 231 (1949)

11O51 R. Overstreet and L. Jacobson, NNES-PPR 9, 621 (1951)

12O42 J. J. O'Connor, M. L. Pool, and J. D. Kurbatov, Phys. Rev. 62, 413 (1942)

13O48 G. E. Owen, D. Moe, and C. S. Cook, Phys. Rev. 74, 1879 (1948); 75, 1270 (1949)

13O49 G. E. Owen and C. S. Cook, Phys. Rev. 76, 1726 (1949)

13O50 G. E. Owen, C. S. Cook, and P. H. Owen, Phys. Rev. 78, 686 (1950)

14O40 Z. Ollano, Ricerca sci. 11, 568 (1940)

14O41 Z. Ollano, Nuovo cimento 18, 11 (1941)

15O49 J. S. Osoba, Phys. Rev. 76, 345 (1949)

16O51 J. Ovadia and P. Axel, Phys. Rev. 82, 332 (1951) (A)

17O38 O. Oldenberg, Phys. Rev. 53, 35 (1938)

18O50 F. E. O'Meara, Phys. Rev. 79, 1032 (1950)

19O52 J. Orring, Arkiv Fysik 4, 469 (1952), reported in M. Siegbahn Commemorative Volume, p 197 (Uppsala, 1951)

20O52 J. Owen and J. H. E. Griffiths, (to be published) (1952)

1P37 M. L. Pool, J. M. Cork, and R. L. Thornton, Phys. Rev. 52, 239 (1937)

1P37a M. L. Pool and J. M. Cork, Phys. Rev. 51, 1010 (1937) (A)

1P38 M. L. Pool, Phys. Rev. 53, 116 (1938)

1P38a M. L. Pool and L. L. Quill, Phys. Rev. 53, 437 (1938)

1P43 M. L. Pool and J. D. Kurbatov, Phys. Rev. 63, 463 (1943) (A)

1P45 M. L. Pool and J. E. Edwards, Phys. Rev. 67, 60 (1945) (A)

CC-0. In Public Domain. Gurukul Kangri Collection, Haridwar

Digitized by Arya Samaj Foundation Chennai and eGangotri

1P48 M. L. Pool and N. L. Krisberg, Phys. Rev. 73, 1035 (1948)

1P52 M. L. Pool and D. N. Kundu, private communication (Nov. 1952)

2P49 V. Perez-Mendez and H. Brown, Phys. Rev. 76, 689 (1949)

2P50 V. Perez-Mendez and H. Brown, Phys. Rev. 77, 404 (1950)

2P50a V. Perez-Mendez and H. Brown, Phys. Rev. 78, 812 (1950)

2P50b V. Perez-Mendez and P. Lindenfeld, reported in Columbia University Unclassified Document CUD-56 (Aug. 1950)

2P50c V. Perez-Mendez and P. Lindenfeld, Phys. Rev. 80, 1097 (1950)

2P51 V. Perez-Mendez and P. Lindenfeld, Phys. Rev. 83, 864 (1951)

3P46 K. Philipp and J. Riedhammer, Z. Naturforsch. 1, 372 (1946)

3P48 K. Philipp and F. Rehbein, Z. Physik 124, 225 (1948)

4P35 P. Preiswerk and H. von Halban, Compt. rend. 201, 722 (1935)

4P51 P. Preiswerk and P. Stähelin, Helv. Phys. Acta 24, 300 (1951)

5P51 C. A. Prohaska, Ph.D. Thesis, University of California Radiation Laboratory Unclassified Report UCRL-1395 (Aug. 1951)

6P46 W. C. Peacock and M. Deutsch, Phys. Rev. 69, 306 (1946)

6P46a W. C. Peacock, R. D. Evans, J. W. Irvine, W. M. Good, A. F. Kip, S. Weiss, and J. G. Gibson, J. Clin. Invest. 25, 605 (1946)

6P47 W. C. Peacock, J. W. Jones, and R. T. Overman, reported in Oak Ridge National Laboratory Classified Report Mon N-432 (Dec. 1947)

6P47a W. C. Peacock, Phys. Rev. 72, 1049 (1947)

6P47b W. C. Peacock, A. R. Brosi, and A. D. Bogard, reported in Oak Ridge National Laboratory Classified Reports Mon N-432 (Dec. 1947); ORNL-65 (July 1948); ORNL-176 (Nov. 1948)

6P48 W. C. Peacock and J. W. Jones, U. S. Atomic Energy Commission Declassified Document AECD-1812 (March 1948)

7P39 M. Perey, Compt. rend. 208, 97 (1939); J. phys. et radium 10, 435 (1939)

7P39a M. Perey and M. Lecoin, J. phys. et radium 10, 439 (1939)

7P39b M. Perey and M. Lecoin, Nature 144, 326 (1939)

7P41 M. Perey and M. Lecoin, Compt. rend. 212, 893 (1941)

7P46 M. Perey, J. chim. phys. 43, 155, 269 (1946)

8P49 S. Peterson, NNES-PPR 14B, 1393 (1949)

8P49a S. Peterson and A. Ghiorso, NNES-PPR 14B, 1395 (1949)

8P49b S. Peterson and A. Ghiorso, NNES-PPR 14B, 1424 (1949)

9P37 A. Polessitsky, Physik Z. Sowjetunion 12, 339 (1937)

9P40 A. Polessitsky and N. Nemerovsky, Compt. rend. U.R.S.S. 28, 217 (1940)

9P40a A. Polessitsky and M. Orbeli, Compt. rend. U.R.S.S. 28, 215 (1940)

9P41 A. Polessitsky, N. Nemerovsky, M. Orbeli, and N. Baronckik, J. Phys. (U.S.S.R.) IV, 284 (1941)

10P46 M. J. Poole and E. B. Paul, Nature 158, 482 (1946)

11P46 A. K. Pierce and F. W. Brown, III, Phys. Rev. 70, 779 (1946)

12P48 M. L. Perlman and G. Friedlander, Phys. Rev. 74, 442 (1948)

12P49 M. L. Perlman, Phys. Rev. 75, 988 (1949)

12P51 M. L. Perlman and G. Friedlander, Phys. Rev. 82, 449 (1951)

12P52 M. L. Perlman and R. Schwartz, private communication (Oct. 1952)

13P47 I. Perlman, R. H. Goeckermann, D. H. Templeton, and J. J. Howland, Jr., Phys. Rev. 72, 352 (1947)

13P47a I. Perlman, J. J. Howland, Jr., and D. H. Templeton, unpublished data (1947)

13P49 I. Perlman, P. R. O'Connor, and L. O. Morgan, NNES-PPR 14B, 1651 (1949)

13P50 I. Perlman, A. Ghiorso, and G. T. Seaborg, Phys. Rev. 77, 26 (1950)

14P40 E. Pollard and W. W. Watson, Phys. Rev. 58, 12 (1940)

15P49 D. D. Phillips, U. S. Atomic Energy Commission Unclassified Report AECU-404 (June 1949)

16P52 M. Paganelli and G. Quareni, Phys. Rev. 86, 423 (1952); Nuovo cimento 9, 324 (1952)

17P38 B. Pontecorvo, Phys. Rev. 54, 542 (1938)

17P38a B. Pontecorvo and A. Lazard, Compt. rend. 208, 99 (1938)

17P49 B. Pontecorvo, D. H. W. Kirkwood, and G. C. Hanna, Phys. Rev. 75, 982 (1949)

18P50 R. W. Pringle, S. Standil, and K. I. Roulston, Phys. Rev. 77, 841 (1950)

18P50a R. W. Pringle and S. Standil, Phys. Rev. 80, 762 (1950)

18P51 R. W. Pringle, S. Standil, H. W. Taylor, and G. Fryer, Phys. Rev. 84, 1066 (1951)

18P52 R. W. Pringle, H. W. Taylor, and S. Standil, Phys. Rev. 87, 384 (1952)

19P51 F. T. Porter and C. S. Cook, Phys. Rev. 81, 640 (1951)

19P51a F. T. Porter and C. S. Cook, Phys. Rev. 81, 298 (1951) (A)

19P52 F. T. Porter and C. S. Cook, Phys. Rev. 87, 464 (1952)

20P48 C. L. Peacock and R. G. Wilkinson, Phys. Rev. 74, 297 (1948)

20P49 C. L. Peacock and A. C. G. Mitchell, Phys. Rev. 75, 1272 (1949)

20P51 C. L. Peacock and J. L. Braud, Phys. Rev. 83, 484 (1951) (A)

21P42 E. H. Plesset, Phys. Rev. 62, 181 (1942)

22P37 C. Perrier and E. Segrè, J. Chem. Phys. 5, 713 (1937); 7, 155 (1939)

22P38 C. Perrier, M. Santangelo, and E. Segrè, Phys. Rev. 53, 104 (1938)

23P47 T. J. Parmley and B. J. Moyer Phys. Rev. 72, 82 (1947)

23P49 T. J. Parmley, B. J. Moyer, and R. C. Lilly, Phys. Rev. 75, 619 (1949)

24P51 E. Plassmann and F. R. Scott, Phys. Rev. 84, 156 (1951)

25P52 R. M. Pearce and E. K. Darby, Phys. Rev. 86, 1049 (1952)

26P47 G. W. Parker, P. M. Lantz, M. G. Inghram, D. C. Hess, Jr., and R. J. Hayden, Phys. Rev. 72, 85 (1947)

26P49 G. W. Parker, G. E. Creek, G. M. Hebert, P. M. Lantz, and W. J. Martin, reported in Oak Ridge National Laboratory Classified Report ORNL-499 (Dec. 1949)

26P49a G. W. Parker, G. E. Creek, G. M. Hebert, and P. M. Lantz, reported in Oak Ridge National Laboratory Classified Report ORNL-336 (May 1949)

CC-0. In Public Domain. Gurukul Kangri Collection, Haridwar

Digitized by Arya Samaj Foundation Chennai and eGangotri

26P49b G. W. Parker, G. E. Creek, G. M. Hebert, P. M. Lantz, and W. J. Martin, reported in Oak Ridge National Laboratory Classified Report ORNL-286 (Sept. 1949)

26P51 G. W. Parker, reported in Oak Ridge National Laboratory Classified Report ORNL-870 (March 1951)

26P52 G. W. Parker and W. J. Martin, private communication (Oct. 1952)

27P51 J. P. Palmer and L. J. Laslett, U. S. Atomic Energy Commission Unclassified Report AECU-1220 (March 1951)

27P51a J. P. Palmer, Phys. Rev. 82, 772 (1951) (A)

28P50 R. I. Powers and A. F. Voigt, Phys. Rev. 79, 175 (1950)

29P40 C. Pecher, Phys. Rev. 58, 843 (1940)

30P51 A. C. Pappas, Phys. Rev. 81, 299 (1951) (A)

30P51a A. C. Pappas and C. D. Coryell, Phys. Rev. 81, 329 (1951) (A)

30P52 A. C. Pappas, Phys. Rev. 87, 162 (1952)

30P52a A. C. Pappas, private communication (Oct. 1952)

31P49 E. Picciotti, Compt. rend. 229, 117 (1949)

32P50 W. W. Pratt, Phys. Rev. 80, 289 (1950)

33P52 W. K. H. Panofsky and D. Reagan, Phys. Rev. 87, 543 (1952)

34P52 I. Pullman and P. Axel, private communication (Oct. 1952)

35P52 T. Passel, W. A. Jenkins, and W. W. T. Crane, reported in University of California Radiation Laboratory Classified Report UCRL-1770 (April 1952)

1R31 E. Rutherford, C. E. Wynn-Williams, and W. B. Lewis, Proc. Roy. Soc (London) 133A, 351 (1931)

2R50 J. M. Robson, Phys. Rev. 78, 311 (1950)

2R51 J. M. Robson, Phys. Rev. 83, 349 (1951)

3R50 M. Riou, J. phys. et radium 11, 185 (1950); Compt. rend. 228, 678 (1949)

3R52 M. Riou, J. phys. et radium 13, 244 (1952)

3R52a M. Riou, Compt. rend. 234, 1157 (1952)

3R53 M. Riou, Ann. phys. (to be published) (1953)

4R36 S. Rosenblum, M. Guillot, and M. Perey, Compt. rend. 202, 1274 (1936)

4R37 S. Rosenblum, M. Guillot, and M. Perey, Compt. rend. 204, 175 (1937)

4R48 S. Rosenblum, M. Valadares, and J. Vial, Compt. rend. 227, 1088 (1948)

4R49 S. Rosenblum, M. Valadares, M. Perey, and J. Vial, Compt. rend. 229, 1009 (1949)

4R49a S. Rosenblum, M. Guillot, and G. Bastin-Scoffier, Compt. rend. 229, 191 (1949)

4R49b S. Rosenblum, M. Valadares, and M. Perey, Compt. rend. 228, 385 (1949)

4R49c S. Rosenblum, E. Cotton, and G. Bouissières, Compt. rend. 229, 825 (1949)

4R50 S. Rosenblum, M. Valadares, and B. Goldschmidt, Compt. rend. 230, 638 (1950)

4R51 S. Rosenblum and M. Valadares, Compt. rend. 232, 501 (1951)

4R52 S. Rosenblum, M. Valadares, and M. Guillot, Compt. rend. 234, 1767 (1952)

4R52a S. Rosenblum, M. Valadares, and M. Guillot, Compt. rend. 235, 238 (1952)

4R52b S. Rosenblum, M. Perey, M. Valadares, and M. Guillot, private communication (Oct. 1952)

5R47 S. Rowlands, Nature 160, 191 (1947)

6R35 J. Rotblat, Nature 136, 515 (1936)

6R41 J. Rotblat, Proc. Roy. Soc. (London) 177A, 260 (1941)

6R41a J. Rotblat, Nature 148, 371 (1941)

7R36 F. Rasetti, "Elements of Nuclear Physics," Prentice-Hall, Inc., New York (1936)

8R40 R. Ringo, Phys. Rev. 58, 942 (1940); 59, 107 (1941). Values recalculated according to (9H38)

9R48 G. Reed, Jr., W. M. Manning, and W. Bentley, reported in Argonne National Laboratory Classified Report ANL-4112 (March 1948)

10R49 F. L. Reynolds, D. G. Karraker, and D. H. Templeton, Phys. Rev 75, 313 (1949)

10R50 F. L. Reynolds, E. K. Hulet, and K. Street, Jr., Phys. Rev. 80, 467 (1950)

11R47 W. Rall and R. G. Wilkinson, Phys. Rev. 71, 321 (1947)

11R51 W. Rall and K. G. McNeill, Phys. Rev. 83, 1244 (1951)

12R52 P. Radvanyi, Compt. rend. 234, 1275 (1952)

12R52a P. Radvanyi, Compt. rend. 235, 289 (1952)

12R52b P. Radvanyi, Compt. rend. 235, 428 (1952)

13R37 L. H. Rumbaugh, R. B. Roberts, and L. R. Hafstad, Phys. Rev. 51, 1106 (1937)

13R38 L. H. Rumbaugh, R. B. Roberts, and L. R. Hafstad, Phys. Rev. 54, 657 (1938)

14R38 R. B. Roberts and N. P. Heydenburg, Phys. Rev. 53, 929 (1938) (A)

14R38a R. B. Roberts, N. P. Heydenburg, and G. L. Locher, Phys. Rev. 53, 1016 (1938)

15R46 S. Rubin, Phys. Rev. 69, 134 (1946) (A)

16R40 S. Ruben and M. D. Kamen, Phys. Rev. 57, 549 (1940)

16R41 S. Ruben and M. D. Kamen, Phys. Rev. 59, 349 (1941)

17R46 A. F. Reid, J. R. Dunning, S. Weinhouse, and A. V. Grosse, Phys. Rev. 70, 431 (1946)

17R46a A. F. Reid and A. S. Keston, Phys. Rev. 70, 987 (1946)

18R37 L. N. Ridenour and W. J. Henderson, Phys. Rev. 52, 889 (1937)

18R37a L. N. Ridenour and W. J. Henderson, Phys. Rev. 51, 1102 (1937)

19R51 L. Ruby and J. R. Richardson, Phys. Rev. 83, 698 (1951)

20R49 J. E. Robinson, M. Ter-Pogossian, and C. S. Cook, Phys. Rev. 75, 1099 (1949)

21R43 W. Riezler, Naturwiss. 31, 326 (1943)

21R44 W. Riezler, Physik Z. 45, 191 (1944)

21R46 W. Riezler, Naturwiss. 33, 53 (1946)

22R49 S. A. Reynolds, reported in Oak Ridge National Laboratory Classified Report ORNL-286 (Sept. 1949)

22R50 S. A. Reynolds, reported in Oak Ridge National Laboratory Classified Report ORNL-867 (Dec. 1950)

23R36 J. R. Richardson and F. N. D. Kurie, Phys. Rev. 50, 999 (1936)

23R39 J. R. Richardson, Phys. Rev. 55, 609 (1939)

23R46 J. R. Richardson and B. T. Wright, Phys. Rev. 70, 445 (1946) (A)

24R47 M. M. Ramsey, J. L. Meem, Jr., and A. C. G. Mitchell, Phys. Rev. 72, 639 (1947)

25R48 G. A. Renard, Compt. rend. 226, 1269 (1948)

25R49 G. A. Renard, Compt. rend. 228, 387 (1949)

25R50 G. A. Renard, Ann. phys. 5, 385 (1950)

CC-0. In Public Domain. Gurukul Kangri Collection, Haridwar

Digitized by Arya Samaj Foundation Chennai and eGangotri

26R50 T. R. Roberts and A. O. Nier, Phys. Rev. 79, 198 (1950) (A)

27R37 J. R. Risser, Phys. Rev. 52, 768 (1937)

27R40 J. R. Risser, K. Lark-Horowitz, and R. N. Smith, Phys. Rev. 57, 355 (1940) (A)

27R48 J. R. Risser and R. N. Smith, private communication from K. Lark-Horowitz (1948)

28R50 J. H. Reynolds, Phys. Rev. 79, 789 (1950)

28R50a J. H. Reynolds, Phys. Rev. 79, 886 (1950)

28R50b J. H. Reynolds, reported in Argonne National Laboratory Classified Report ANL-4515 (Oct. 1950)

29R50 E. Rabinowicz, Proc. Phys. Soc. (London) 63A, 1040 (1950)

30R51 H. Roderick, W. E. Meyerhof, and L. G. Mann, Phys. Rev. 84, 887 (1951)

30R52 H. Roderick, O. Lonsjo, and W. E. Meyerhof, private communication (Oct. 1952)

31R52 W. C. Rutledge, J. M. Cork, and S. B. Burson, Phys. Rev. 86, 775 (1952)

32R50 P. Rothwell and D. West, Proc. Phys. Soc. (London) 63A, 539 (1950)

33R41 A. Roberts, J. R. Downing, and M. Deutsch, Phys. Rev. 60, 544 (1941)

33R41a A. Roberts and J. W. Irvine, Jr., Phys. Rev. 59, 936 (1941)

33R43 A. Roberts, L. G. Elliott, J. R. Downing, W. C. Peacock, and M. Deutsch, Phys. Rev. 64, 268 (1943)

34R47 W. C. Redman and D. Saxon, Phys. Rev. 72, 570 (1947)

35R38 H. Reddemann and F. Strassmann, Naturwiss. 26, 187 (1938)

35R40 H. Reddemann, Naturwiss. 28, 110 (1940)

35R40a H. Reddemann, Z. Physik 116, 137 (1940)

36R49 B. E. Robertson, W. E. Scott, and M. L. Pool, Phys. Rev. 76, 1649 (1949)

36R50 B. E. Robertson, W. E. Scott, and M. L. Pool, Phys. Rev. 78, 318 (1950) (A)

36R50a B. E. Robertson, W. L. Carss, and M. L. Pool, Phys. Rev. 77, 747 (1950) (A)

37R46 Wilfrid Rall, Phys. Rev. 70, 112 (1946) (A)

38R50 B. Russell and A. Wattenberg, U. S. Atomic Energy Commission Declassified Document AECD-2926 (Dec. 1950)

39R51 B. L. Robinson and L. Madansky, Phys. Rev. 84, 604 (1951)

39R51a B. L. Robinson and L. Madansky, Phys. Rev. 84, 1067 (1951)

40R52 D. Rose, G. Hinman, and L. G. Lang, Phys. Rev. 86, 863 (1952)

41R50 E. R. Rae, Proc. Phys. Soc. (London) 63A, 292 (1950)

42R50 J. O. Rasmussen, F. L. Reynolds, S. G. Thompson, and A. Ghiorso, Phys. Rev. 80, 475 (1950)

42R52 J. O. Rasmussen, Jr., S. G. Thompson, and A. Ghiorso, Phys. Rev. (to be published) (1952)

43R52 P. L. Roggenkamp, C. H. Pruett, and R. G. Wilkinson, Phys. Rev. (in press) (1952)

43R53 P. L. Roggenkamp, C. H. Pruett, and R. G. Wilkinson, Phys. Rev. (to be published) (1953)

44R52 R. Richmond and H. Rose, Phil. Mag. 43, 367 (1952)

44R52a R. Richmond, P. J. Grant, and H. Rose, Proc. Phys. Soc. (London) 65A, 484 (1952)

45R52 G. Rudstam, P. C. Stevenson, and R. L. Folger, Phys. Rev. 87, 358 (1952)

46R52 G. W. Rodeback and J. S. Allen, Phys. Rev. 86, 446 (1952)

47R52 H. N. Ritland and F. H. Schmidt, private communication (Oct. 1952)

48R51 A. Rytz, Compt. rend. 233, 790 (1951)

49R52 W. Robinson and W. Bernstein, Phys. Rev. 86, 545 (1952)

50R52 K. I. Roulston and R. W. Pringle, Phys. Rev. 87, 930 (1952)

51R50 H. T. Richards, R. V. Smith, and C. P. Browne, Phys. Rev. 80, 524 (1950)

51R51 H. T. Richards, Phys. Rev. 83, 694 (1951)

52R52 H. Rose, Phil. Mag. 43, 1146 (1952)

1S37 J. Schintlmeister, Sitzber. Akad. Wiss. Wien. Abt. IIa, 146, 371 (1937)

1S39 J. Schintlmeister and K. Lintner, Sitzber. Akad. Wiss. Wien, Abt. IIa, 148, 279 (1939)

2S46 L. Seren, W. E. Moyer, and W. Sturm, Phys. Rev. 70, 561 (1946)

2S47 L. Seren, H. N. Friedlander, and S. H. Turkel, Phys. Rev. 72, 888 (1947)

2S47a L. Seren, H. N. Friedlander, and S. H. Turkel, Phys. Rev. 71, 454 (1947)

2S47b L. Seren, D. Engelkemeir, W. Sturm, H. N. Friedlander, and S. Turkel, Phys. Rev. 71, 409 (1947)

3S33 B. W. Sargent, Proc. Roy. Soc. (London) 139A, 659 (1933). Summarizes the results of various investigators.

3S39 B. W. Sargent, Can. J. Research 17A, 103 (1939)

3S39a B. W. Sargent, Can. J. Research 17A, 82 (1939). Phys. Rev. 54, 232 (1938)

3S52 B. W. Sargent, L. Yaffe, and A. P. Gray, Can. J. Phys. (in press) (1952)

4S46 M. H. Studier, Argonne National Laboratory Classified Report CP-3642 (Dec. 1946), NNES-PPR 17B, 634 (1952) (classified)

4S48 M. H. Studier and E. K. Hyde, Phys. Rev. 74, 591 (1948)

4S48a M. H. Studier and R. J. Bruehlman, private communication (Oct. 1948)

4S49 M. H. Studier and R. J. Bruehlman, reported in Argonne National Laboratory Classified Report ANL-4252 (Feb. 1949)

4S49a M. H. Studier and E. K. Hyde, unpublished data (Feb. 1949)

4S52 M. H. Studier, NNES-PPR 17B, 50 (1952) (classified)

5S45 H. Slätis, Arkiv Mat., Astron. Fysik 32A, No. 16 (1945)

5S46 H. Slätis, Arkiv Mat., Astron. Fysik 33A, No. 17 (1946)

5S47 H. Slätis, Nature 160, 579 (1947); Arkiv Mat., Astron. Fysik 35A, No. 3 (1948)

5S49 H. Slätis and K. Siegbahn, Arkiv Mat., Astron. Fysik 36A, No. 21 (1949)

5S49a H. Slätis and K. Siegbahn, Phys. Rev. 75, 318 (1949)

5S50 H. Slätis, S. J. du Toit, and K. Siegbahn, Phys. Rev. 78, 498 (1950); Arkiv Fysik 2, 321 (1950)

5S51 H. Slätis and K. Siegbahn, reported in M. Siegbahn Commemorative Volume, p 153 (Uppsala, 1951)

5S52 H. Slätis and L. Zappa, Arkiv Fysik 5, 26 (1952)

6S48 K. Street, Jr., R. A. James, and G. T. Seaborg, unpublished data (July 1948)

6S48a K. Street, Jr., A. Ghiorso, D. A. Orth, and G. T. Seaborg, unpublished data (Oct. 1948)

CC-0. In Public Domain. Gurukul Kangri Collection, Haridwar

Digitized by Arya Samaj Foundation Chennai and eGangotri

6S50 K. Street, Jr., unpublished data quoted in Phys. Rev. 78, 475 (1950)

6S50a K. Street, Jr., A. Ghiorso, and G. T. Seaborg, Phys. Rev. 79, 530 (1950)

7S44 K. Siegbahn, Arkiv Mat., Astron. Fysik 30A, No. 20 (1944)

7S44a K. Siegbahn and E. Bohr, Arkiv Mat., Astron. Fysik 30B, No. 3 (1944)

7S45 K. Siegbahn and H. Slätis, Arkiv Mat., Astron. Fysik 32A, No. 9 (1945)

7S46 K. Siegbahn and N. Hole, Phys. Rev. 70, 133 (1946)

7S46a K. Siegbahn and S. E. Petersson, Arkiv Mat. Astron. Fysik 32B, No. 5 (1946)

7S46b K. Siegbahn, Phys. Rev. 70, 127 (1946)

7S46c K. Siegbahn, Arkiv Mat., Astron. Fysik 33A, No. 10 (1946)

7S47 K. Siegbahn and A. Johansson, Arkiv Mat., Astron. Fysik 34A, No. 10 (1947)

7S47a K. Siegbahn and H. Slätis, Nature 159, 471 (1947); Arkiv Mat., Astron. Fysik 34A, No. 15 (1947)

7S47b K. Siegbahn, Arkiv Mat., Astron. Fysik 34B, No. 6 (1947)

7S47c K. Siegbahn, Arkiv Mat., Astron. Fysik 34B, No. 4 (1947)

7S47d K. Siegbahn, Arkiv Mat., Astron. Fysik 34A, No. 7 (1947)

7S47e K. Siegbahn and M. Deutsch, Phys. Rev. 71, 483 (1947) (A)

7S47f K. Siegbahn and H. Slätis, Arkiv Mat., Astron. Fysik 34A, No. 6 (1947)

7S47g K. Siegbahn, Proc. Roy. Soc. (London) 189A, 527 (1947)

7S48 K. Siegbahn and M. Deutsch, Phys. Rev. 73, 410 (1948); A. Hedgran, K. Siegbahn, and N. Svartholm, Proc. Phys. Soc. (London) 63A, 960 (1950)

7S49 K. Siegbahn and A. Ghosh, Phys. Rev. 76, 307 (1949); Arkiv Mat., Astron. Fysik 36A, No. 19 (1949)

7S49a K. Siegbahn, A. Hedgran, and M. Deutsch, Phys. Rev. 76, 1263 (1949)

7S49b K. Siegbahn, E. Kondaiah, and S. Johansson, Nature 164, 405 (1949)

7S49c K. Siegbahn, Phys. Rev. 75, 1277 (1949); 77, 233 (1950)

7S49d K. Siegbahn and W. Forsling, Arkiv Fysik 1, 505 (1949)

7S49e K. Siegbahn and A. Hedgran, Phys. Rev. 75, 523 (1949)

7S50 K. Siegbahn and M. Deutsch, Arkiv Fysik 2, 9 (1950), Phys. Rev. 77, 680 (1950)

7S50a K. Siegbahn and H. Slätis, Arkiv Fysik 1, 559 (1950)

7S50b K. Siegbahn and S. der Toit, Arkiv Fysik 2, 211 (1950)

7S51 K. Siegbahn, reported in M. Siegbahn Commemorative Volume, p 199 (Uppsala, 1951)

7S52 K. Siegbahn, Arkiv Fysik 4, 223 (1952)

8S31 E. Stahel, Z. Physik 68, 1 (1931); Helv. Phys. Acta 8, 651 (1935)

8S43 E. Stahel and W. Johner, J. phys. et radium 5, 97 (1943)

9S48 D. Saxon, Phys. Rev. 73, 811 (1948)

9S48a D. Saxon, Phys. Rev. 74, 1264 (1948) (A)

9S48b D. Saxon, Phys. Rev. 74, 849 (1948)

9S49 D. Saxon and J. Richards, Phys. Rev. 76, 982 (1949)

9S49a D. Saxon and J. Richards, Phys. Rev. 76, 186 (1949) (A)

9S49b D. Saxon and R. Heller, Phys. Rev. 75, 909 (1949)

9S49c D. Saxon, reported in Argonne National Laboratory Classified Report ANL-4237 (Jan. 1949)

10S51 P. H. Stoker, O. P. Hok, and G. J. Sizoo, Physica 17, 164 (1951)

11S37 J. Surugue, Ann. phys. 8, 484 (1937)

11S38 J. Surugue, J. phys. et radium 9, 438 (1938)

11S41 J. Surugue, Compt. rend. 212, 337 (1941)

11S41a J. Surugue and San-Tsiang Tsien, Compt. rend. 213, 172 (1941)

11S42 J. Surugue, J. phys. et radium 4, 71 (1942)

11S46 J. Surugue, J. phys. et radium 7, 145 (1946)

12S46 A. K. Saha, Proc. Nat. Inst. Sci. India 12, No. 3, 159 (1946)

13S39 G. T. Seaborg and E. Segrè, Phys. Rev. 55, 808 (1939)

13S40 G. T. Seaborg, J. J. Livingood, and J. W. Kennedy, Phys. Rev. 57, 363 (1940)

13S41 G. T. Seaborg, J. W. Gofman, and J. W. Kennedy, Phys. Rev. 59, 321 (1941)

13S41a G. T. Seaborg, J. J. Livingood, and G. Friedlander, Phys. Rev. 59, 320 (1941)

13S41b G. T. Seaborg and G. Friedlander, Phys. Rev. 59, 400 (1941)

13S46 G. T. Seaborg, E. M. McMillan, J. W. Kennedy, and A. C. Wahl, Phys. Rev. 69, 366 (1946); NNES-PPR 14B, 1 (1949)

13S46a G. T. Seaborg, A. C. Wahl, and J. W. Kennedy, Phys. Rev. 69, 367 (1946); NNES-PPR 14B, 3 (1949)

13S47 G. T. Seaborg, B. B. Cunningham, H. H. Hopkins, Jr., M. Lindner, D. R. Miller, P. R. O'Connor, I. Perlman, and R. C. Thompson, Phys. Rev. 72, 740 (1947) (A)

13S47a G. T. Seaborg, J. W. Gofman, and R. W. Stoughton, Phys. Rev. 71, 378 (1947)

13S49 G. T. Seaborg, R. A. James, and L. O. Morgan, NNES-PPR 14B, 1525 (1949)

13S49a G. T. Seaborg, A. C. Wahl, and J. W. Kennedy, NNES-PPR 14B, 13 (1949)

13S49b G. T. Seaborg, R. A. James and A. Ghiorso, NNES-PPR 14B, 1554 (1949)

13S52 G. T. Seaborg, J. W. Gofman, and R. W. Stoughton, NNES-PPR 17B, 31 (1952) (classified)

13S52a G. T. Seaborg, Phys. Rev. 85, 157 (1952)

13S53 G. T. Seaborg, R. A. Glass, and S. G. Thompson, J. Am. Chem. Soc. (to be published) (1953)

14S50 A. W. Sunyar, D. Alburger, G. Friedlander, M. Goldhaber, and G. Scharff-Goldhaber, Phys. Rev. 79, 181 (1950)

14S50a A. W. Sunyar, D. Alburger, G. Friedlander, M. Goldhaber, and G. Scharff-Goldhaber, Phys. Rev. 78, 326 (1950) (A)

14S50b A. W. Sunyar, G. Friedlander, and M. Goldhaber, reported in Brookhaven National Laboratory Unclassified Report BNL-39 (Jan. 1950)

14S51 A. W. Sunyar, Phys. Rev. 83, 864 (1951)

14S51a A. W. Sunyar and J. W. Mihelich, Phys. Rev. 81, 300 (1951) (A)

14S52 A. W. Sunyar, J. W. Mihelich, G. Scharff-Goldhaber, M. Goldhaber, N. S. Wall, and M. Deutsch, Phys. Rev. 86, 1023 (1952)

14S52a A. W. Sunyar, private communication (Oct. 1952)

14S52b A. W. Sunyar, D. E. Alburger, G. Friedlander, M. Goldhaber, and G. Scharff-Goldhaber, unpublished data quoted in (18G52)

15S37 W. R. Smythe and A. Hemmendinger, Phys. Rev. 51, 178 (1937)

16S51 W. J. Sturm and V. Johnson, Phys. Rev. 83, 542 (1951)

CC-0. In Public Domain. Gurukul Kangri Collection, Haridwar

Digitized by Arya Samaj Foundation Chennai and eGangotri

17S41 G. Scharff-Goldhaber, Phys. Rev. 59, 937 (1941) (A)

17S46 G. Scharff-Goldhaber and G. S. Klaiber, Phys. Rev. 70, 229 (1946)

17S50 G. Scharff-Goldhaber, E. der Mateosian, M. McKeown, and A. W. Sunyar, Phys. Rev. 78, 325 (1950) (A)

17S51 G. Scharff-Goldhaber and M. McKeown, Phys. Rev. 82, 123 (1951)

17S51a G. Scharff-Goldhaber, reported in Brookhaven National Laboratory Unclassified Report BNL-103 (June 1951)

17S51b G. Scharff-Goldhaber, E. der Mateosian, M. Goldhaber, G. W. Johnson, and M. McKeown, Phys. Rev. 83, 480 (1951)

17S52 G. Scharff-Goldhaber, E. der Mateosian, and J. W. Mihelich, Phys. Rev. 85, 734 (1952) (A)

17S52a G. Scharff-Goldhaber, private communication (Oct. 1952)

18S37 G. J. Sizoo and S. A. Wytzes, Physica 4, 791 (1937)

18S43 G. J. Sizoo and L. F. C. Friele, Physica 10, 57 (1943)

19S51 G. J. Sayag, Compt. rend. 232, 2091 (1951)

20S52 B. F. Scott, NNES-PPR 17B, 638 (1952) (classified)

21S51 L. M. Slater and G. T. Seaborg, unpublished data (Aug. 1951)

21S52 L. M. Slater and F. Asaro, private communication (Aug. 1952)

22S42 K. Starke, Naturwiss. 30, 107, 577 (1942)

23S45a W. H Sullivan, Phys. Rev. 68, 277 (1945)

23S46 W. H Sullivan, N. R. Sleight, and E. M. Gladrow, Phys. Rev. 70, 778 (1946)

23S47 W. H Sullivan, J. A. Swartout, and H. E. Wyatt, reported in Oak Ridge National Laboratory Classified Report Mon N-243 (Feb. 1947)

23S51 W. H Sullivan, N. R. Sleight, and E. M. Gladrow, NNES-PPR 9, 832 (1951)

23S51a W. H Sullivan, N. R. Sleight, and E. M. Gladrow, NNES-PPR 9, 820 (1951)

23S51b W. H Sullivan, N. R. Sleight, and E. M. Gladrow, NNES-PPR 9, 842 (1951)

23S51c W. H Sullivan, N. R. Sleight, and E. M. Gladrow, NNES-PPR 9, 817 (1951)

23S51d W. H Sullivan, N. R. Sleight, and E. M. Gladrow, NNES-PPR 9, 808 (1951)

23S51e W. H Sullivan, N. R. Sleight, and E. M. Gladrow, NNES-PPR 9, 1953 (1951)

23S51f W. H Sullivan, N. R. Sleight, and E. M. Gladrow, NNES-PPR 9, 838 (1951)

23S51g W. H Sullivan, N. R. Sleight, and E. M. Gladrow, NNES-PPR 9, 1949 (1951)

23S51h W. H Sullivan, N. R. Sleight, and E. M. Gladrow, NNES-PPR 9, 1945 (1951)

23S51i W. H Sullivan, N. R. Sleight, and E. M. Gladrow, NNES-PPR 9, 824 (1951)

23S51j W. H Sullivan, O. Johnson, and R. Nottorf, NNES-PPR 9, 984 (1951)

23S51k W. H Sullivan and S. Katcoff, NNES-PPR 9, 1015 (1951)

24S39 E. Segrè, R. S. Halford, and G. T. Seaborg, Phys. Rev. 55, 321 (1939)

24S40 E. Segrè and C. S. Wu, Phys. Rev. 57, 552 (1940)

24S40a E. Segrè, J. W. Kennedy, and G. T. Seaborg, unpublished work (1940)

24S41 E. Segrè and G. T. Seaborg, Phys. Rev. 59, 212 (1941)

24S49 E. Segrè and C. Wiegand, Phys. Rev. 75, 39 (1949)

24S49a E. Segrè, unpublished data quoted in E. Segrè and A. C. Helmholz, Revs. Modern Phys. 21, 271 (1949)

24S52 E. Segrè, Phys. Rev. 86, 21 (1952), some values recalculated according to more recent half-life determinations (HPS)

25S51 J. C. Sullivan, G. L. Pyle, M. H. Studier, P. R. Fields, and W. M. Manning, Phys. Rev. 83, 1267 (1951)

26S36 A. H. Snell, Phys. Rev. 49, 565 (1936)

26S37 A. H. Snell, Phys. Rev. 51, 143 (1937) (A)

26S37a A. H. Snell, Phys. Rev. 52, 1007 (1937)

26S42 A. H. Snell et al., reported in Metallurgical Laboratory Classified Report CP-257 (Sept. 1942)

26S43 A. H. Snell, M. B. Sampson, and J. S. Levinger, Metallurgical Laboratory Classified Report CP-1176 (Dec. 1943)

26S47 A. H. Snell, J. S. Levinger, E. P. Meiners, Jr., M. B. Sampson, and R. G. Wilkinson, Phys. Rev. 72, 545 (1947); NNES-PPR 9, 603 (1951)

26S47a A. H. Snell, V. A. Nedzel, H. W. Ibser, J. S. Levinger, R. G. Wilkinson, and M. B. Sampson, Phys. Rev. 72, 541 (1947)

26S50 A. H. Snell, F. Pleasonton, and R. V. McCord, Phys. Rev. 78, 310 (1950)

27S46 H. S. Sommers, Jr. and R. Sherr, Phys. Rev. 69, 21 (1946)

28S40 R. Sherr, Phys. Rev. 57, 937 (1940)

28S41 R. Sherr, K. T. Bainbridge, and H. H. Anderson, Phys. Rev. 60, 473 (1941)

28S48 R. Sherr, H. R. Muether, and M. G. White, Phys. Rev. 74, 1239 (1948) (A)

28S49 R. Sherr, H. R. Muether, and M. G. White, Phys. Rev. 75, 282 (1949)

28S52 R. Sherr and J. Gerhart, Phys. Rev. 86, 619 (1952) (A)

29S41 A. K. Solomon, Phys. Rev. 60, 279 (1941)

29S47 A. K. Solomon, R. G. Gould, and C. B. Anfinsen, Phys. Rev. 72, 1097 (1947)

29S48 A. K. Solomon and L. E. Glendenin, Phys. Rev. 73, 415 (1948)

29S50 A. K. Solomon, Phys. Rev. 79, 403 (1950)

30S41 J. H. C. Smith and D. B. Cowie, J. Appl. Phys. 12, 78 (1941)

31S50 K. H. Sun, F. A. Pecjak, R. A. Charpie, and J. F. Nichaj, Phys. Rev. 78, 338 (1950) (A)

31S51 K. H. Sun, B. Jennings, W. E. Shoupp, and A. J. Allen, Phys. Rev. 82, 267 (1951)

32S51 W. E. Stephens, J. Halpern, and R. Sher, Phys. Rev. 82, 511 (1951)

33S50 S. C. Snowdon, Phys. Rev. 78, 299 (1950)

34S52 G. Schrank and J. R. Richardson, Phys. Rev. 86, 248 (1952)

35S47 W. Spatz, N. Goldstein, C. Huddleston, and E. Goldfarb, reported in Argonne National Laboratory Classified Report CP-3750 (Feb. 1947)

36S39 N. K. Saha, Trans. Bose Res. Inst. (Calcutta) 14, 57 (1939-1941); Chem. Abstracts 42, 4501 (1948)

36S51 N. K. Saha and K. Gopalakrishnan, Proc. Nat. Inst. Sci. India 17, 301 (1951)

37S36 M. B. Sampson, L. N. Ridenour, and W. Bleakney, Phys. Rev. 50, 382 (1936)

37S36a M. B. Sampson and W. Bleakney, Phys. Rev. 50, 732 (1936)

38S51 W. K. Sinclair and A. F. Holloway, Nature 167, 365 (1951)

39S51 J. H. Sreb, Phys. Rev. 81, 469 (1951)

39S51a J. H. Sreb, Phys. Rev. 81, 643 (1951)

40S48 A. Szalay and E. Csangor, Phys. Rev. 74, 1063 (1948)

41S49 L. Seidlitz, E. Bleuler, and D. J. Tendam, Phys. Rev. 76, 861 (1949)

CC-0. In Public Domain. Gurukul Kangri Collection, Haridwar

Digitized by Arya Samaj Foundation Chennai and eGangotri

42S36 R. Sagane, Phys. Rev. 50, 1141 (1936)

42S38 R. Sagane, S. Kojima, G. Miyamoto, and M. Ikawa, Phys. Rev. 54, 542 (1938)

42S38a R. Sagane, S. Kojima, G. Miyamoto, and M. Ikawa, Phys. Rev. 54, 970 (1938)

42S39 R. Sagane, Phys. Rev. 55, 31 (1939)

42S39a R. Sagane, S. Kojima, and G. Miyamoto, Proc. Phys.-Math. Soc. Japan 21, 728 (1939)

42S39b R. Sagane, S. Kojima, G. Miyamoto, and M. Ikawa, Proc. Phys.-Math. Soc. Japan 21, 660 (1939)

42S40 R. Sagane, S. Kojima, G. Miyamoto, and M. Ikawa, Phys. Rev. 57, 1179 (1940)

42S40a R. Sagane, S. Kojima, G. Miyamoto, and M. Ikawa, Proc. Phys.-Math. Soc. Japan 22, 174 (1940)

42S40b R. Sagane, S. Kojima, G. Miyamoto, and M. Ikawa, Phys. Rev. 57, 750 (1940)

42S41 R. Sagane, G. Miyamoto, and M. Ikawa, Phys. Rev. 59, 904 (1941)

42S52 R. Sagane, Phys. Rev. 85, 926 (1952)

44S51 R. K. Sheline, R. B. Holtzman, and C. Y. Fan, Phys. Rev. 83, 919 (1951)

44S51a R. K. Sheline, Phys. Rev. 82, 954 (1951)

44S52 R. K. Sheline and R. W. Stoughton, Phys. Rev. 87, 1 (1952)

44S52a R. K. Sheline, Phys. Rev. 87, 557 (1952)

44S53 R. K. Sheline and N. R. Johnson, Phys. Rev. 89, 520 (1953)

45S48 A. D. Schelberg, M. B. Sampson, and A. C. G. Mitchell, Rev. Sci. Instr. 19, 458 (1948)

46S49 G. A. Sawyer and M. L. Wiedenbeck, Phys. Rev. 76, 1535 (1949)

46S50 G. A. Sawyer and M. L. Wiedenbeck, Phys. Rev. 79, 490 (1950)

47S49 R. W. Stout, Phys. Rev. 75, 1107 (1949)

48S50 F. W. Spiers, Nature 165, 356 (1950)

49S51 V. L. Sailor and J. J. Floyd, Phys. Rev. 82, 960 (1951)

50S50 L. Simons, Soc. Scien. Fennica Comm. Phys.-Math. 15, No. 9 (1950)

50S52 L. Simons, Phys. Rev. 86, 570 (1952)

51S42 G. P. Smith, Phys. Rev. 61, 578 (1942)

52S50 B. N. Sorensen, B. M. Dale, and J. D. Kurbatov, Phys. Rev. 79, 1007 (1950)

53S45 R. P. Schuman, reported in Metallurgical Laboratory Classified Report CN-2929 (May 1945)

53S45a R. P. Schuman, reported in Metallurgical Laboratory Classified Report CN-2799 (April 1945)

53S46 R. P. Schuman, reported in J. Am. Chem. Soc. 68, 2411 (1946)

53S51 R. P. Schuman and A. Camilli, Phys. Rev. 84, 158 (1951)

53S51a R. P. Schuman, NNES-PPR 9, 783 (1951)

54S46 J. A. Swartout, G. E. Boyd, A. E. Cameron, C. P. Keim, and C. E. Larson, Phys. Rev. 70, 232 (1946)

54S47 J. A. Swartout, reported in Oak Ridge National Laboratory Classified Report Mon N-243 (Feb. 1947)

55S50 K. Strauch, Phys. Rev. 79, 487 (1950)

55S51 K. Strauch, Phys. Rev. 81, 973 (1951)

56S51 L. A. Smith, R. N. H. Haslam, and J. G. V. Taylor, Phys. Rev. 84, 842 (1951)

57S49 L. M. Silver, Phys. Rev. 76, 589 (1949) (A); Can. J. Physics 29, 59 (1951)

58S38 C. V. Strain, Phys. Rev. 54, 1021 (1938)

59S48 L. S. Skaggs, J. S. Laughlin, A. O. Hanson, and J. J. Orlin, Phys. Rev. 73, 420 (1948)

60S46 J. M. Siegel and L. E. Glendenin, reported in J. Am. Chem. Soc. 68, 2411 (1946)

60S51 J. M. Siegel and L. E. Glendenin, NNES-PPR 9, 549 (1951)

61S46 E. P. Steinberg and D. W. Engelkemeir, reported in J. Am. Chem. Soc. 68, 2411 (1946)

61S48 E. P. Steinberg, J. A. Seiler, A. Goldstein, and A. Dudley, U. S. Atomic Energy Commission Declassified Document MDDC-1632 (Jan. 1948)

61S50 E. P. Steinberg and L. E. Glendenin, Phys. Rev. 78, 624 (1950)

61S51 E. P. Steinberg and D. W. Engelkemeir, NNES-PPR 9, 566 (1951)

61S51a E. P. Steinberg and M. S. Freedman, NNES-PPR 9, 1378 (1951)

61S51b E. P. Steinberg, NNES-PPR 9, 750 (1951)

61S51c E. P. Steinberg and L. E. Glendenin, NNES-PPR 9, 877 (1951)

62S51 F. R. Scott, Phys. Rev. 84, 659 (1951)

63S46 N. Sugarman and N. E. Ballou, reported in J. Am. Chem. Soc. 68, 2411 (1946)

63S47 N. Sugarman, private communication (April 1947)

63S47a N. Sugarman, J. Chem. Phys. 15, 544 (1947)

63S48 N. Sugarman and H. Richter, Phys. Rev. 73, 1411 (1948)

63S49 N. Sugarman, J. Chem. Phys. 17, 11 (1949)

63S49a N. Sugarman, Phys. Rev. 75, 1473 (1949)

63S50 N. Sugarman and H. Richter, J. Chem. Phys. 18, 174 (1950)

63S51 N. Sugarman, N. E. Ballou, D. W. Engelkemeir, and W. H. Burgus, NNES-PPR 9, 1163 (1951)

63S52 N. Sugarman, Phys. Rev. 86, 604 (1952) (A)

64S41 R. E. Siday, Proc. Roy. Soc. (London) 178A, 189 (1941)

65S38 F. Strassmann and E. Walling, Ber. deut. chem. Ges. 71B, 1 (1938)

65S40 F. Strassmann and O. Hahn, Naturwiss. 28, 817 (1940)

66S40 W. Seelmann-Eggebert, Naturwiss. 28, 491 (1940)

66S43 W. Seelmann-Eggebert and H. J. Born, Naturwiss. 31, 59 (1943)

66S43a W. Seelmann-Eggebert, Naturwiss. 31, 510 (1943)

66S43b W. Seelmann-Eggebert, Naturwiss. 31, 491 (1943)

66S46 W. Seelmann-Eggebert, Naturwiss. 33, 279 (1946)

66S47 W. Seelmann-Eggebert and F. Strassmann, Z. Naturforsch. 2a, 80 (1947)

67S51 A. F. Stehney and N. Sugarman, U. S. Atomic Energy Commission Declassified Document AECD-3047 (Jan. 1951); Phys. Rev. (in press) (1952)

68S48 F. B. Shull, Phys. Rev. 74, 917 (1948)

69S38 H. Scheichenberger, Anz. Akad. Wiss. Wien, Math.-naturw. Klasse 75, 108 (1938)

70S51 B. Selikson and J. M. Siegel, NNES-PPR 9, 699 (1951)

71S37 D. W. Stewart, J. L. Lawson, and J. M. Cork, Phys. Rev. 52, 901 (1937)

71S39 D. W. Stewart, Phys. Rev. 56, 629 (1939)

72S49 L. Slack, C. H. Braden, and F. B. Shull, Phys. Rev. 75, 1965 (1949)

72S49a L. Slack, G. E. Owen, and H. Primakoff, Phys. Rev. 75, 1448 (1949)

73S51 F. J. Shore, W. L. Bendel, and R. A. Becker, Phys. Rev. 83, 688 (1951)

73S52 F. J. Shore, H. N. Brown, W. L. Bendel, and R. A. Becker, Phys. Rev. 87, 202 (1952) (A)

74S51 K. Shure and M. Deutsch, Phys. Rev. 82, 122 (1951)

74S51a K. Shure, Ph.D. Thesis, Massachusetts Institute of Technology (May 1951)

CC-0. In Public Domain. Gurukul Kangri Collection, Haridwar

Digitized by Arya Samaj Foundation Chennai and eGangotri

75S49 F. Suzor, Ann. phys. 4, 269 (1949)

76S51 N. R. Sleight, NNES-PPR 9, 805 (1951)

76S51a N. R. Sleight, T. B. Novey, and L. E. Glendenin, NNES-PPR 9, 846 (1951)

76S51b N. R. Sleight and W. H Sullivan, NNES-PPR 9, 928 (1951)

77S47 J. A. Seiler, reported in Argonne National Laboratory Classified Report ANL-4000 (Aug. 1947)

77S51 J. A. Seiler, NNES-PPR 9, 860 (1951)

77S51a J. A. Seiler, NNES-PPR 9, 910 (1951)

77S51b J. A. Seiler and L. Winsberg, NNES-PPR 9, 1206 (1951)

77S51c J. A. Seiler and L. Winsberg, NNES-PPR 9, 1225 (1951)

78S50 A. Storruste, Phys. Rev. 79, 193 (1950)

79S50 A. J. Saur, P. Axel, L. G. Mann, and J. Ovadia, Phys. Rev. 79, 237 (1950) (A)

80S52 P. C. Stevenson and H. G. Hicks, private communication (April 1952)

81S42 R. N. Smith, Phys. Rev. 61, 389 (1942)

82S48 R. Steffen, O. Huber, F. Humbel, and W. Zünti, Helv. Phys. Acta 21, 194 (1948)

82S49 R. M. Steffen, O. Huber, and F. Humbel, Helv. Phys. Acta 22, 167 (1949)

82S51 R. M. Steffen, Phys. Rev. 83, 166 (1951)

82S51a R. M. Steffen, Phys. Rev. 82, 827 (1951)

82S52 R. M. Steffen, private communication (Oct. 1952)

83S51 E. J. Schillinger, Jr., B. Waldman, and W. C. Miller, Phys. Rev. 83, 320 (1951)

84S49 C. W. Stanley and S. Katcoff, J. Chem. Phys. 17, 653 (1949)

84S51 C. W. Stanley and L. E. Glendenin, NNES-PPR 9, 947 (1951)

85S51 D. T. Stevenson and M. Deutsch, Phys. Rev. 83, 1202 (1951)

85S51a D. T. Stevenson and M. Deutsch, Phys. Rev. 84, 1071 (1951)

86S52 D. Schiff, Phys. Rev. 85, 727 (1952) (A)

87S52 F. H. Schmidt and G. L. Keister, Phys. Rev. 86, 632 (1952) (A) and private communication (Oct. 1952)

88S51 V. S. Shpinel, Zhur. Eksptl.' i Teoret. Fiz. 21, 853 (1951)

88S51a V. S. Shpinel and N. V. Forafontov, Zhur. Eksptl. i Teoret. Fiz. 21, 1376 (1951)

88S51b V. S. Shpinel, Zhur. Eksptl.' i Teoret. Fiz 21, 1370 (1951)

89S52 R. Stump, Phys. Rev. 86, 249 (1952)

90S52 C. L. Scoville, S. C. Fultz, and M. L. Pool, Phys. Rev. 85, 1046 (1952)

91S52 A. B. Smith, Phys. Rev. 86, 98 (1952)

91S52a A. B. Smith, A. C. G. Mitchell, and R. S. Caird, Phys. Rev. 87, 454 (1952)

91S52b A. B. Smith and A. C. G. Mitchell, private communication (Oct. 1952)

91S52c A. B. Smith, R. S. Caird, and A. C. G. Mitchell, Phys. Rev. 88, 150 (1952)

91S52d A. B. Smith and A. C. G. Mitchell, Phys. Rev. 87, 1128 (1952)

92S48 L. R. Shepherd and J. M. Hill, Nature 162, 566 (1948)

92S48a L. R. Shepherd, Research (London) 1, 671 (1948)

93S50 B. J. Stover, Phys. Rev. 80, 99 (1950)

93S51 B. J. Stover, Phys. Rev. 81, 8 (1951)

94S50 W. Steuber, Ph. D. Thesis, University of Illinois (1950)

95S50 E. Shapiro and C. E. Mandeville, Phys. Rev. 78, 319 (1950) (A)

96S47 J. W. Stout and W. M. Jones, Phys. Rev. 71, 582 (1947)

97S50 G. F. Snelling and E. W. Titterton, British Atomic Energy Commission Unclassified Report AERE-G/M-55 (Sept. 1950)

98S48 M. V. Scherb and C. E. Mandeville, Phys. Rev. 73, 1401 (1948)

99S39 K. Sinma and F. Yamasaki, Phys. Rev. 55, 320 (1939)

100S51 N. A. Schuster and G. E. Pake, Phys. Rev. 81, 886 (1951)

101S51 K. F. Smith, Nature 167, 942 (1951)

102S50 G. L. Stukenbroeker and J. R. McNally, Jr., J. Opt. Soc. Am. 40, 336 (1950)

103S51 W. W. Schoof and R. D. Hill, Phys. Rev. 83, 892 (1951) (A)

104S52 A. de Shalit, O. Huber, and H. Schneider, Helv Phys. Acta 25, 279 (1952)

105S52 H. Schneider, O. Huber, F. Humbel, and A. de Shalit, Helv. Phys. Acta 25, 259 (1952)

106S52 P. Stähelin, Phys. Rev. 87, 374 (1952)

107S49 L. Ya. Shavtvalov, Zhur. Eksptl.' i Teoret. Fiz. 19, 633 (1949)

107S51 L. Ya. Shavtvalov, Zhur. Eksptl.' i Teoret. Fiz. 21, 1123 (1951)

108S51 P. M. Sherk and R. D. Hill, Phys Rev. 83, 1097 (1951)

109S52 R. Sher, H. J. Kouts, and K. W. Downes, Phys. Rev. 87, 523 (1952)

110S51 J. Sharpe and G. H. Stafford, Proc. Phys. Soc (London) 64A, 211 (1951)

111S50 B. Smaller, J. May, and M. Freedman, Phys. Rev. 79, 940 (1950)

112S51 H. D. Sharma, Ph. D. Thesis, University of California Radiation Laboratory Unclassified Report UCRL-1265 (May 1951)

113S52 W. L. Stirling and M. Goodrich, Phys. Rev. 87, 176 (1952) (A)

114S51 F. N. Spiess, Ph. D. Thesis, University of California Unclassified Report UCRL-1494 (Oct. 1951)

115S52 A. Sorruste, Ph. D. Thesis, University of Oslo (1952)

116S52 J. B. Swan and R. D. Hill, Phys. Rev. 88, 831 (1952)

116S52a J. B. Swan, W. M. Portnoy, and R. D. Hill, Bull. Am. Phys. Soc. 27, No. 5, Abstract V4 (1952)

117S52 D. A. Silverston, Proc. Phys. Soc. (London) 65A, 344 (1952)

118S39 L. Szilard and W. H. Zinn, Phys. Rev. 55, 799 (1939)

1T05 J. J. Thomson, Phil. Mag. 10, 584 (1905)

2T47 D. H. Templeton, J. J. Howland, Jr., and I. Perlman, Phys. Rev. 72, 766 (1947)

2T47a D. H. Templeton, J. J. Howland, Jr., and I. Perlman, Phys. Rev. 72, 758 (1947)

2T47b D. H. Templeton, R. H. Goeckermann, J. J. Howland, Jr., and I. Perlman, unpublished data (Jan. 1947)

2T48 D. H. Templeton and I. Perlman, Phys. Rev. 73, 1211 (1948)

2T48a D. H. Templeton, A. Ghiorso, and I. Perlman, unpublished data (June 1948)

2T50 D. H. Templeton, Phys. Rev. 78, 312 (1950)

CC-0. In Public Domain. Gurukul Kangri Collection, Haridwar

Digitized by Arya Samaj Foundation Chennai and eGangotri

3T49 S. G. Thompson, A. Ghiorso, J. O. Rasmussen, and G. T. Seaborg, Phys. Rev. 76, 1406 (1949)

3T50 S. G. Thompson, A. Ghiorso, and G. T. Seaborg, Phys. Rev. 77, 838 (1950)

3T50a S. G. Thompson, A. Ghiorso, and K. Street, Jr., private communication (1950)

3T50b S. G. Thompson, A. Ghiorso, and G. T. Seaborg, Phys. Rev. 80, 781 (1950)

3T50c S. G. Thompson, K. Street, Jr., A. Ghiorso, and G. T. Seaborg, Phys. Rev. 78, 298 (1950)

3T50d S. G. Thompson, K. Street, Jr., A. Ghiorso, and G. T. Seaborg, Phys. Rev. 80, 790 (1950)

3T50e S. G. Thompson, K. Street, Jr., A. Ghiorso, and F. L. Reynolds, Phys. Rev. 80, 1108 (1950)

3T51 S. G. Thompson, K. Street, Jr., A. Ghiorso, and F. L. Reynolds, Phys. Rev. 84, 165 (1951)

3T52 S. G. Thompson, E. K. Hulet, and A. Ghiorso, private communication (Aug. 1952)

4T49 J. Teillac, Compt. rend. 229, 650 (1949)

4T50 J. Teillac, Compt. rend. 230, 1056 (1950)

4T52 J. Teillac, Ann. phys. 7, 396 (1952)

4T52a J. Teillac, P. Falk-Vairant, and C. Victor, J. phys. et radium 13, 143 (1952); Compt. rend. 233, 1025 (1951)

4T52b J. Teillac, P. Falk-Vairant, and C. Victor, Compt. rend. 234, 1051 (1952)

5T26 J. Thibaud, Ann. phys. 5, 73 (1926)

6T36 R. L. Thornton, Phys. Rev. 49, 207 (1936) (A)

6T37 R. L. Thornton and J. M. Cork, Phys. Rev. 51, 383 (1937) (A)

6T37a R. L. Thornton, Phys. Rev. 51, 893 (1937)

6T38 R. L. Thornton, Phys. Rev. 53, 326 (1938) (A)

6T47 R. L. Thornton and R. W. Senseman, Phys. Rev. 72, 872 (1947)

7T51 E. P. Tomlinson, H. W. Fulbright, and J. J. Howland, Jr., Phys. Rev. 83, 223 (1951) (A)

7T52 E. P. Tomlinson and S. L. Ridgway, Phys. Rev. 88, 170 (1952) (A)

8T49 W. Thiel and A. H. Jaffey, reported in Argonne National Laboratory Classified Report ANL-4370 (Nov. 1949)

9T42 San-Tsiang Tsien, J. phys. et radium 3, 1 (1942); Compt. rend. 217, 685 (1943)

9T43 San-Tsiang Tsien, Compt. rend. 216, 765 (1943)

9T43a San-Tsiang Tsien, Compt. rend. 217, 599 (1943)

9T46 San-Tsiang Tsien, Phys. Rev. 69, 38 (1946)

9T46a San-Tsiang Tsien, M. Bachelet, and G. Bouissières, Phys. Rev. 69, 39 (1946)

10T49 C. M. Turner, Phys. Rev. 76, 148 (1949); U. S. Atomic Energy Commission Unclassified Document AECU-432 (July 1949)

11T48 M. Ter-Pogossian, J. E. Robinson, and C. S. Cook, Phys. Rev. 75, 995 (1948)

11T49 M. Ter-Pogossian, J. E. Robinson, and H. Goddard, Phys. Rev. 76, 453 (1949) (A)

11T49a M. Ter-Pogossian, C. S. Cook, C. H. Goddard, and J. E. Robinson, Phys. Rev. 76, 909 (1949)

11T50 M. Ter-Pogossian, C. S. Cook, F. T. Porter, K. H. Morganstern, and J. Hudis, Phys. Rev. 80, 360 (1950); 81, 285 (1951)

11T51 M. Ter-Pogossian and F. T. Porter, Phys. Rev. 81, 1057 (1951)

12T49 A. V. Tollestrup, W. A. Fowler, and C. C. Lauritsen, Phys. Rev. 76, 428 (1949)

13T47 H. G. Thode and R. L. Graham, Can. J. Research 25A, 1 (1947)

13T48 H. G. Thode, J. Macnamara, F. P. Lossing, and C. B. Collins, J. Am. Chem. Soc. 70, 3008 (1948)

13T48a H. G. Thode, Nucleonics 3, No. 3, 14 (1948)

13T49 H. G. Thode, Research 2, 154 (1949)

14T41 A. A. Townsend, Proc. Roy. Soc. (London) 177A, 357 (1941)

15T50 J. F. Turner, reported in British Atomic Energy Commission Report AERE-PR-18 (Oct. 1950)

15T51 J. F. Turner and P. E. Cavanagh, Phil. Mag. 42, 636 (1951)

16T46 R. Tangen, Kgl. Norske Videnskab. Selskab. Skr. No. 1 (1946)

17T47 C. A. Tobias and C. Levinthal, private communication (Jan. 1947)

17T48 C. A. Tobias, private communication (Sept. 1948)

18T51 H. K. Ticho, Phys. Rev. 84, 847 (1951)

18T52 H. K. Ticho, D. Green, and J. R. Richardson, Phys. Rev. 86, 422 (1952) and private communication (Oct. 1952)

19T47 R. C. Thompson and D. R. Miller, private communication (Jan. 1947)

19T48 R. C. Thompson and D. R. Miller, private communication (Jan. 1948)

20T39 A. W. Tyler, Phys. Rev. 56, 125 (1939)

21T47 A. Turkevich, reported in Argonne National Laboratory Classified Report ANL-4010 (Sept. 1947)

21T51 A. Turkevich and J. B. Niday, Phys. Rev. 84, 52 (1951)

21T51a A. Turkevich and J. B. Niday, Phys. Rev. 84, 1253 (1951)

21T51b A. Turkevich, E. P. Steinberg, B. Finkle, and N. Sugarman, NNES-PPR 9, 1070 (1951)

22T51 J. Tobailem, Compt. rend. 233, 1360 (1951)

23T51 S. I. Taimuty, Phys. Rev. 81, 461 (1951)

24T45 B. Trumpy and J. J. Orlin, Bergens Museums Årbok, Naturv. Rekke Nr. 7 (1945)

25T47 D. J. Tendam and H. L. Bradt, Phys. Rev. 72, 527 (1947) (A)

25T47a D. J. Tendam and H. L. Bradt, Phys. Rev. 72, 1118 (1947)

26T51 D. A. Thomas, S. K. Haynes, C. D. Broyles, and H. C. Thomas, Phys. Rev. 82, 961 (1951)

27T49 G. M. Temmer, Phys. Rev. 76, 424 (1949)

28T38 G. F. Tape and J. M. Cork, Phys. Rev. 53, 676 (1938) (A)

29T40 L. A. Turner, Phys. Rev. 58, 679 (1940)

30T49 S. Thulin, I. Bergström, and A. Hedgran, Phys. Rev. 76, 871 (1949)

30T51 S. Thulin, Phys. Rev. 83, 860 (1951)

30T52 S. Thulin and I. Bergström, Phys. Rev. 85, 1055 (1952)

30T52a S. Thulin, Phys. Rev. 87, 684 (1952)

30T52b S. Thulin, Arkiv Fysik 4, 363 (1952); reported in M. Siegbahn Commemorative Volume, p 163 (Uppsala, 1951)

30T52c S. Thulin, Arkiv Fysik (in press) (1952)

31T48 J. Townsend, M. Cleland, and A. L. Hughes, Phys. Rev. 74, 499 (1948)

32T50 C. C. Thomas, Jr. and E. O. Wiig, J. Am. Chem. Soc. 72, 2818 (1950)

33T51 S. E. Turner and L. O. Morgan, Phys. Rev. 81, 881 (1951)

34T52 Y. Tomozawa, M. Umezawa, and S. Nakamura, Phys. Rev. 86, 791 (1952)

35T49 C. H. Townes, J. M. Mays, and B. P. Dailey, Phys. Rev. 76, 700 (1949)

CC-0. In Public Domain. Gurukul Kangri Collection, Haridwar

Digitized by Arya Samaj Foundation Chennai and eGangotri

36T51 F. S. Tompkins, M. Fred, and W. F. Meggers, Phys. Rev. 84, 168 (1951)

37T52 D. E. Tilley, Abstract 77, June Meeting, Roy. Soc. Canada (1952)

38T49 B. V. Thosar, Proc. Phys. Soc. (London) 62A, 739 (1949)

39T52 H. Tyren, unpublished data (March 1952)

40T52 B. L. Tucker and E. C. Gregg, Phys. Rev. 87, 907 (1952)

41T50 A. P. Tudge and H. G. Thode, Can. J. Research 28B, 567 (1950)

42T52 A. L. Thompson, private communication (Oct. 1952)

1V38 R. J. Voskuyl, Ph.D. Thesis, Harvard University (1938)

2V36 S. N. Van Voorhis, Phys. Rev. 50, 895 (1936)

2V36a S. N. Van Voorhis, Phys. Rev. 49, 889 (1936) (A)

2V40 S. N. Van Voorhis, private communication (1940)

3V45 A. F. Voigt, private communication (Jan. 1945)

3V48 A. F. Voigt and B. J. Thamer, Phys. Rev. 74, 1264 (1948) (A)

4V49 F. W. Van Name, Jr., Phys. Rev. 75, 100 (1949)

5V51 G. Vendryes, Compt. rend. 232, 1549 (1951)

5V51a G. Vendryes, Compt. rend. 233, 391 (1951)

6V39 G. E. Valley and R. L. McCreary, Phys. Rev. 56, 863 (1939)

6V41 G. E. Valley and H. H. Anderson, Phys. Rev. 59, 113 (1941) (A)

6V41a G. E. Valley, Phys. Rev. 59, 686 (1941)

6V41b G. E. Valley, Phys. Rev. 60, 167 (1941) (A)

7V38 O. Viktorin, Proc. Cambridge Phil. Soc. 34, 612 (1938)

8V51 N. F. Verster, G. J. Nijgh, R. Van Lieshout, and C. J. Bakker, Physica 17, 637 (1951)

9V52 D. M. Van Patter, Massachusetts Institute of Technology Unclassified Report MIT-NSE-Tech. Rep. 57 (Jan. 1952)

10V52 H. T. Vlaar and A. H. W. Aten, Jr., Physica 18, 275 (1952)

11V52 P. J. Van der Haack, A. E. de Vries, and A. H. W. Aten, Jr., Physica 18, 20 (1952)

12V52 A. Van der Weil and A. H. W. Aten, Jr., Physica 18, 356 (1952)

13V52 G. Vieira and L. Salgueiro, Compt. rend. 234, 1765 (1952)

14V52 C. Victor, J. Teillac, P. Falk-Vairant, and G. Bouissières, J. phys. et radium (to be published) (1952)

15V52 R. Vestergaard and E. Haeffner, Arkiv Fysik 3, 557 (1952)

1W42 A. C. Wahl and G. T. Seaborg, Metallurgical Project Classified Report (work performed at Berkeley) CN-266 (Sept. 1942)

1W48 A. C. Wahl and G. T. Seaborg, Phys. Rev. 73, 940 (1948); NNES-PPR 14B, 21 (1949)

1W52 A. C. Wahl and N. A. Bonner, Phys. Rev. 85, 570 (1952)

2W47 G. Wilkinson, Nature 160, 864 (1947)

2W48 G. Wilkinson and H. G. Hicks, Phys. Rev. 74, 1733 (1948)

2W48a G. Wilkinson, Phys. Rev. 73, 252 (1948)

2W49 G. Wilkinson and H. G. Hicks, Phys. Rev. 75, 1687 (1949)

2W49a G. Wilkinson and H. G. Hicks, Phys. Rev. 75, 1370 (1949)

2W49b G. Wilkinson and H. G. Hicks, Phys. Rev. 75, 696 (1949)

2W49c G. Wilkinson, Phys. Rev. 75, 1019 (1949)

2W50 G. Wilkinson, Phys. Rev. 79, 1014 (1950)

2W50a G. Wilkinson and H. G. Hicks, University of California Radiation Laboratory Unclassified Report UCRL-751 (June 1950)

2W50b G. Wilkinson and H. G. Hicks, Phys. Rev. 80, 491 (1950)

2W50c G. Wilkinson and H. G. Hicks, Phys. Rev. 79, 815 (1950)

2W50d G. Wilkinson and H. G. Hicks, University of California Radiation Laboratory Unclassified Report UCRL-744 (June 1950)

2W50e G. Wilkinson, Phys. Rev. 80, 495 (1950)

2W50f G. Wilkinson, reported in Massachusetts Institute of Technology Unclassified Report NP-1879 (Oct. 1950)

2W50g G. Wilkinson and H. G. Hicks, Phys. Rev. 77, 314 (1950)

2W51 G. Wilkinson and H. G. Hicks, Phys. Rev. 81, 540 (1951)

3W48 R. J. Walen, Compt. rend. 227, 1090 (1948); J. phys. et radium 10, 95 (1949)

4W43 R. Wilkinson and J. S. Levinger, reported in Metallurgical Laboratory Classified Report CP-641 (May 1943)

4W44 R. Wilkinson, W. Rall, and E. Meiners, reported in Metallurgical Laboratory Classified Report CP-2090 (Sept. 1944)

4W51 R. G. Wilkinson and W. Rall, NNES-PPR 9, 1124 (1951)

4W51a R. G. Wilkinson, W. Rall, L. C. Miller, and L. F. Curtiss, NNES-PPR 9, 1128 (1951)

4W52 R. G. Wilkinson, private communication (Oct. 1952)

5W39 A. G. Ward, Proc. Cambridge Phil. Soc. 35, 322 (1939)

5W39a A. G. Ward, Proc. Cambridge Phil. Soc. 35, 523 (1939)

5W42 A. G. Ward, Proc. Roy. Soc. (London) 181A, 183 (1942)

6W50 J. L. Wolfson, Phys. Rev. 78, 176 (1950)

6W52 J. L. Wolfson, private communication (Oct. 1952)

7W48 M. Weissbluth, T. M. Putnam, and E. Segrè, private communication (July 1948)

8W49 Q. Van Winkle, R. G. Larson, and L. I. Katzin, J. Am. Chem. Soc. 71, 2585 (1949)

9W45 D. Williams and P. Yuster, Los Alamos Scientific Laboratory Classified Report LAMS-195 (Jan. 1945)

9W46 D. Williams and P. Yuster, Phys. Rev. 69, 556 (1946)

10W51 J. C. Wallmann, Ph.D. Thesis, University of California Radiation Laboratory Classified Report UCRL-1255 (April 1951)

11W46 E. F. Westrum, Jr., R. W. Greenlee, and J. C. Hindman, Metallurgical Laboratory Classified Report CC-3894 (Nov. 1946)

11W51 E. F. Westrum, Jr., Phys. Rev. 83, 1249 (1951)

12W51 D. West and J. K. Dawson, Proc. Phys. Soc. (London) 64A, 586 (1951)

12W52 D. West, J. K. Dawson, and C. J. Mandleberg, Phil. Mag. 43, 875 (1952)

CC-0. In Public Domain. Gurukul Kangri Collection, Haridwar

Digitized by Arya Samaj Foundation Chennai and eGangotri

13W50 S. C. Wright, Phys. Rev. 77, 742 (1950) (A)

14W49 R. M. Williamson and H. T. Richards, Phys. Rev. 76, 614 (1949)

15W41 J. A. Wheeler, Phys. Rev. 59, 27 (1941)

16W40 C. S. Wu, Phys. Rev. 58, 926 (1940)

16W41 C. S. Wu and G. Friedlander, Phys. Rev. 60, 747 (1941)

16W42 C. S. Wu and E. Segrè, Phys. Rev. 61, 203 (1942) (A)

16W45 C. S. Wu and E. Segrè, Phys. Rev. 67, 142 (1945)

16W48 C. S. Wu, W. W. Havens, Jr., and L. J. Rainwater, Phys. Rev. 74, 1248 (1948) (A)

16W49 C. S. Wu and L. Feldman, Phys. Rev. 76, 698 (1949)

16W49a C. S. Wu, C. H. Townes, and L. Feldman, Phys. Rev. 76, 692 (1949)

16W49b C. S. Wu and L. Feldman, Phys. Rev. 76, 693 (1949)

16W49c C. S. Wu and L. Feldman, Phys. Rev. 76, 696 (1949)

16W51 C. S. Wu and L. Feldman, Phys. Rev. 82, 457 (1951)

16W52 C. S. Wu, B. M. Rustad, V. Perez-Mendez, and L. Lidofsky, Phys. Rev. 87, 1140 (1952)

17W48 A. S. Weil and J. R. Dunning, Columbia University Document CUD-9 (Feb. 1948)

18W50 S. D. Warshaw, Phys. Rev. 80, 111 (1950)

18W50a S. D. Warshaw, J. J. L. Chen, and G. L. Appleton, Phys. Rev. 80, 288 (1950)

19W34 L. Wertenstein, Nature 133, 564 (1934)

20W41 S. B. Welles, Phys. Rev. 59, 679 (1941)

21W39 M. G. White, L. A. Delsasso, J. G. Fox, and E. C. Creutz, Phys. Rev. 56, 512 (1939)

21W41 M. G. White, E. C. Creutz, L. A. Delsasso, and R. R. Wilson, Phys. Rev. 59, 63 (1941)

22W40 W. W. Watson and E. Pollard, Phys. Rev. 57, 1082 (1940) (A)

23W49 R. Wilson and G. R. Bishop, Proc. Phys. Soc. (London) 62, 457 (1949). Value recalculated in (38S51)

23W50 R. Wilson, Phys. Rev. 79, 1004 (1950)

24W48 J. R. White and A. E. Cameron, Phys. Rev. 74, 991 (1948)

25W48 H. Wäffler and O. Hirzel, Helv. Phys. Acta 21, 200 (1948)

25W50 H. Wäffler, Helv. Phys. Acta 23, 239 (1950)

26W51 J. J. Wilkins and F. K. Goward, Proc. Phys. Soc. (London) 64A, 849 (1951)

27W39 Y. Watase and J. Itoh, Proc. Phys.-Math. Soc. Japan 21, 626 (1939)

27W41 Y. Watase, Proc. Phys.-Math. Soc. Japan 23, 618 (1941)

28W41 P. K. Weimer, J. D. Kurbatov, and M. L. Pool, Phys. Rev. 60, 469 (1941)

28W44 P. K. Weimer, J. D. Kurbatov, and M. L. Pool, Phys. Rev. 66, 209 (1944)

29W52 G. Wagner and E. O. Wiig, J. Am. Chem. Soc. 74, 1101 (1952)

30W37 H. Walke, Phys. Rev. 52, 663 (1937)

30W37a H. Walke, Phys. Rev. 52, 400 (1937)

30W37b H. Walke, Phys. Rev. 52, 777 (1937)

30W37c H. Walke, Phys. Rev. 52, 669 (1937)

30W39 H. Walke, E. J. Williams, and G. R. Evans, Proc. Roy. Soc. (London) 171A, 360 (1939)

30W40 H. Walke, F. C. Thompson, and J. Holt, Phys. Rev. 57, 177 (1940)

30W40a H. Walke, Phys. Rev. 57, 163 (1940)

30W40b H. Walke, F. C. Thompson, and J. Holt, Phys. Rev. 57, 171 (1940)

31W50 M. A. Waggoner, M. L. Moon, and A. Roberts, Phys. Rev. 80, 420 (1950)

31W50a M. A. Waggoner, M. L. Moon, and A. Roberts, Phys. Rev. 78, 295 (1950)

31W51 M. A. Waggoner, Phys. Rev. 82, 906 (1951); 80, 489 (1950)

32W52 W. J. Worthington, Jr., Phys. Rev. 87, 158 (1952)

33W49 H. W. Wilson and S. C. Curran, Phil. Mag. 40, 631 (1949)

33W50 H. W. Wilson, Phys. Rev. 79, 1032 (1950)

33W51 H. W. Wilson, Phys. Rev. 82, 548 (1951)

33W51a H. W. Wilson and S. C. Curran, Phil. Mag. 42, 762 (1951)

33W52 H. W. Wilson and G. M. Lewis, Proc. Phys. Soc. (London) 65A, 656 (1952)

34W42 G. L. Weil, Phys. Rev. 62, 229 (1942)

35W48 L. L. Woodward, D. A. McCown, and M. L. Pool, Phys. Rev. 74, 870 (1948)

35W48a L. L. Woodward, D. A. McCown, and M. L. Pool, Phys. Rev. 74, 761 (1948)

36W51 F. P. W. Winteringham, Nature 167, 155 (1951)

37W45 M. L. Wiedenbeck, Phys. Rev. 68, 237 (1945)

37W45a M. L. Wiedenbeck, Phys. Rev. 68, 1 (1945)

37W45b M. L. Wiedenbeck, Phys. Rev. 67, 92 (1945)

37W46 M. L. Wiedenbeck, Phys. Rev. 70, 435 (1946)

37W47 M. L. Wiedenbeck and K. Y. Chu, Phys. Rev. 72, 1164 (1947)

38W52 D. R. Wiles, B. W. Smith, R. Horsley, and H. G. Thode, Chalk River Laboratory Classified Report CRC-493 (Jan. 1952)

39W52 F. Wagner, Jr. and M. S. Freedman, Phys. Rev. 86, 631 (1952) (A)

39W52a F. Wagner, Jr. and M. S. Freedman, Phys. Rev. (to be published) (1952)

39W52b F. Wagner, Jr., M. S. Freedman, and D. Engelkemeir, U. S. Atomic Energy Commission Declassified Document AECD-3304 (Feb. 1952)

39W53 F. Wagner, Jr., M. S. Freedman, D. W. Engelkemeir, and L. B. Magnusson, Phys. Rev. (to be published) (1953)

40W51 E. J. Wolicki, B. Waldman, and W. C. Miller, Phys. Rev. 82, 486 (1951)

41W43 B. Waldman and M. L. Wiedenbeck, Phys. Rev. 63, 60 (1943) (A)

41W49 B. Waldman, W. C. Miller, and D. Gideon, Phys. Rev. 76, 181 (1949) (A)

42W47 A. Wattenberg, Phys. Rev. 71, 497 (1947)

43W48 R. R. Williams, Jr., J. Chem. Phys. 16, 513 (1948)

43W51 R. R. Williams, Jr., NNES-PPR 9, 220 (1951)

44W51 W. E. Winsche, L. G. Stang, Jr., and W. D. Tucker, Nucleonics 8, No. 3, 14 (1951)

45W50 A. H. Williams and M. L. Wiedenbeck, Phys. Rev. 78, 822 (1950)

46W43 K. E. Weimer, M. L. Pool, and J. D. Kurbatov, Phys. Rev. 63, 59 (1943) (A)

46W43a K. E. Weimer, M. L. Pool, and J. D. Kurbatov, Phys. Rev. 64, 43 (1943) (A)

46W43b K. E. Weimer, M. L. Pool, and J. D. Kurbatov, Phys. Rev. 63, 67 (1943)

47W52 A. H. Wapstra, Phys. Rev. 86, 561 (1952)

47W52a A. H. Wapstra, Phys. Rev. 86, 562 (1952)

CC-0. In Public Domain. Gurukul Kangri Collection, Haridwar

Digitized by Arya Samaj Foundation Chennai and eGangotri

48W50 B. Weaver, Phys. Rev. 80, 301 (1950)

49W49 D. Walker, Proc. Phys. Soc. (London) 62A, 799 (1949)

49W49a D. Walker and E. W. Fuller, Nature 164, 226 (1949)

50W52 J. Walker, Proc. Phys. Soc. (London) 65A, 449 (1952)

51W51 L. Winsberg, NNES-PPR 9, 1273 (1951)

51W51a L. Winsberg, NNES-PPR 9, 1284 (1951)

51W51b L. Winsberg, NNES-PPR 9, 1302 (1951)

51W51c L. Winsberg, NNES-PPR 9, 1311 (1951)

51W51d L. Winsberg, NNES-PPR 9, 1292 (1951)

51W52 L. Winsberg, private communication (Oct. 1952)

52W51 W. E. Wright and M. Deutsch, Phys. Rev. 82, 277 (1951)

53W41 C. M. Witcher, Phys. Rev. 60, 32 (1941)

54W51 T. Wiedling and A. Carlsson, Phys. Rev. 83, 181 (1951)

55W51 A. Wennerblom, K. E. Zimen, and E. Ehn, Svensk Kem. Tid. 63, 207 (1951)

56W52 B. T. Wright, Phys. Rev. (to be published) (1952); Bull. Am. Phys. Soc. 27, No. 5, Abstract Q2 (1952)

57W52 J. Welker, A. Schardt, J. J. Howland, Jr., and G. Friedlander, private communication (Nov. 1952)

58W52 T. Westermark, Phys. Rev. 88, 573 (1952); private communication (Oct. 1952)

1Y47 L. Yaffe and C. E. MacKintosh, Can. J. Research 25B, 371 (1947)

1Y48 L. Yaffe and J. M. Grunlund, Phys. Rev. 74, 696 (1948)

1Y48a L. Yaffe and K. M. Justus, Can. J. Research 26B, 734 (1948)

1Y49 L. Yaffe, M. Kirsch, S. Standil, and J. M. Grunlund, Phys. Rev. 75, 699 (1949)

1Y49a L. Yaffe, B. W. Sargent, M. Kirsch, S. Standil, and J. M. Grunlund, Phys. Rev. 76, 617 (1949)

1Y50 L. Yaffe and W. H. Stevens, Phys. Rev. 79, 893 (1950)

1Y51 L. Yaffe, R. C. Hawkings, W. F. Merritt, and J. H. Craven, Phys. Rev. 82, 553 (1951)

2Y35 D. M. Yost, L. N. Ridenour, and K. Shinohara, J. Chem. Phys. 3, 133 (1935)

3Y38 T. Yasaki and S. Watanabe, Nature 141, 787 (1938)

4Y42 T. Yuasa, Compt. rend. 215, 414 (1942)

4Y52 T. Yuasa, Compt. rend. 235, 366 (1952)

5Y47 F. Yu, D. Gideon, and J. D. Kurbatov, Phys. Rev. 71, 382 (1947)

5Y48 F. Yu and J. D. Kurbatov, Phys. Rev. 74, 34 (1948)

5Y49 F. Yu, L. Cheng, and J. D. Kurbatov, Phys. Rev. 75, 1287 (1949) (A)

6Y45 R. S. Yalow and M. Goldhaber, Phys. Rev. 67, 59 (1945)

7Y51 J. N. Young, M. L. Pool, and D. N. Kundu, Phys. Rev. 83, 1060 (1951)

8Y40 H. Yamasaki and K. Sinma, Sci. Papers Inst. Phys. Chem. Research (Tokyo) 37, 10 (1940)

1Z48 B. Zajac, E. Broda, and N. Feather, Proc. Phys. Soc. (London) 60, 501 (1948)

1Z52 B. Zajac, Phil. Mag. 43, 264 (1952)

2Z49 A. S. Zavel'skii, G. Ya. Umarov, and S. K. Matushevskii, Zhur. Eksptl' i Teoret. Fiz. 19, 1136 (1949)

3Z43 W. H. Zinn, A. Wattenberg, and J. West, reported in Metallurgical Laboratory Classified Report CP-781 (July 1943)

4Z42 I. Zlotowski and J. H. Williams, Phys. Rev. 62, 29 (1942)

5Z48 D. J. Zaffarano, B. D. Kern, and A. C. G. Mitchell, Phys. Rev. 74, 682 (1948)

5Z48a D. J. Zaffarano, B. D. Kern, and A. C. G. Mitchell, Phys. Rev. 74, 105 (1948)

5Z51 D. J. Zaffarano and F. I. Boley, Phys. Rev. 83, 223 (1951) (A)

6Z45 W. Zünti and E. Bleuler, Helv. Phys. Acta 18, 263 (1945)

7Z52 W. Zobel, reported in Purdue University Progress Report II (June 1952)

8Z49 H. Zeldes, A. R. Brosi, G. W. Parker, G. M. Hebert, and G. E. Creek, reported in Oak Ridge National Laboratory Classified Report ORNL-286 (June 1949)

8Z50 H. Zeldes, B. H. Ketelle, and A. R. Brosi, Phys. Rev. 79, 901 (1950)

8Z51 H. Zeldes, B. H. Ketelle, and A. R. Brosi, reported in Oak Ridge National Laboratory Classified Report ORNL-1036 (Sept. 1951)

9Z52 H. Zeldes, B. H. Ketelle, A. R. Brosi, C. R. Fultz, and R. F. Hibbs, Phys. Rev. 86, 811 (1952)

9Z49 K. E. Zimen, Z. Naturforsch. 4a, 95 (1949)

10Z50 E. L. Zimmerman, E. B. Dale, D. G. Thomas, and J. D. Kurbatov, Phys. Rev. 80, 908 (1950)

11Z43 R. V. Zumstein, J. D. Kurbatov, and M. L. Pool, Phys. Rev. 63, 59 (1943) (A)

12Z40 E. Zingg, Helv. Phys. Acta 13, 219 (1940)

CC-0. In Public Domain. Gurukul Kangri Collection, Haridwar

Digitized by Arya Samaj Foundation Chennai and eGangotri

CC-0. In Public Domain. Gurukul Kangri Collection, Haridwar

Digitized by Arya Samaj Foundation Chennai and eGangotri

REVIEWS OF
MODERN PHYSICS

VOLUME 25, NUMBER 3 JULY, 1953

Acoustic Radiation Pressure of Plane Compressional Waves*

F. E. BORGNIS
California Institute of Technology, Pasadena, California

Both electromagnetic and acoustic waves exert forces of radiation upon an obstacle placed in the path of the wave, the forces being proportional to the mean energy density of the wave motion. In electromagnetics the action of these forces is relatively easily understood through the concept of Maxwell's electromagnetic stress tensor.

The physical processes leading to these forces in a sound wave have been found to be considerably more complex; the difficulties belong to the fact that the acoustic wave equation is not linear and that a beam of finite cross section is subject to effects caused by the surrounding medium.

Though many papers have been devoted to the subject and though various theoretical approaches have been made, some difficulties still seem to stand in the way of a clear understanding of the physics of the problem.

The purpose of the present study is especially to throw light on the physical aspects. The approach adopted, which uses the momentum theorem, is believed to serve this purpose especially well. The expression for the radiation pressure is given in both Eulerian and Lagrangian coordinate systems.

Special consideration is given to liquids of constant compressibility, since in such media the processes involved can be dealt with mathematically in a simple manner. The general case of a plane reflector with arbitrary reflection coefficient is treated; the *modus operandi* of the forces at the interface between liquid and obstacle is explained for some special cases, including the radiation forces on the interface between two nonmiscible liquids.

Finally, a general relation is established between the energy density and the pressure caused by radiation falling normally upon a plane reflector, which, under certain assumptions, is valid in any fluid and at any amplitude.

1. INTRODUCTION

THE concept of radiation pressure originated in electrodynamics. According to Maxwell's equations and his concept of the electrodynamic stress tensor, a plane surface of perfect conductivity emitting normally a plane electromagnetic wave undergoes a reacting force per unit area equal to the total energy density E of the emitted wave. Also, such a plane wave, striking perpendicularly a plane and totally absorbing surface, exerts a radiation pressure equal to E.

Lord Rayleigh was the first to formulate a theory of radiation pressure resulting from compressional acoustic waves in fluids. He established a relation which gives the time-average value of the pressure produced upon a piston by a plane wave of infinite cross section in a fluid, and he showed that this mean pressure is proportional to the mean mechanical energy density $\bar{E}$ of the periodic wave motion. He found that the factor of proportionality was not in general unity, but dependent on the special law relating the pressure p to the density in the fluid under consideration.

The actual radiation pressure, however, as encountered in an acoustic beam under ordinary experimental conditions, is different from Rayleigh's "pressure of vibrations." Rayleigh's result,[1] which is often quoted, applies to a theoretical case rather than to what is usually measured.

The equations describing the motion of acoustic waves are nonlinear (with the one exception of the Lagrangian wave equation in a fluid of constant com-

* Work performed under U. S. Office of Naval Research Contract Nonr-220(02).

[1] Lord Rayleigh, Phil. Mag. 3, 338 (1902) and 10, 364 (1905). For example, in a gas under adiabatic conditions, Rayleigh's pressure amounts to $(1+\gamma_c)\bar{E}_i$ at a perfect reflector and at small amplitudes. γ_c = ratio of the specific heats and $\bar{E}_i$ = mean energy density of the incident wave = one-half of the total mean energy density in a standing wave.

CC-0. In Public Domain. Gurukul Kangri Collection, Haridwar

Digitized by Arya Samaj Foundation Chennai and eGangotri

pressibility). For many purposes, it is sufficient to "linearize" these equations and to retain only first-order terms of the velocities or particle displacements, regarding them as small quantities. Radiation pressure, however, is connected with energy densities, which are quadratic terms containing the squares of velocities or displacements. Any theory dealing with acoustic radiation pressure, therefore, must retain at least all second-order terms, to be valid even at small amplitudes.

The fact that radiation pressure is a second-order quantity and that the vibrational amplitudes are usually very small in comparison with the acoustic wavelength λ, explains its relatively small numerical value in comparison with the values of the periodically alternating first-order pressures encountered in acoustical waves. Whereas the first-order pressure amounts to maximal values up to kilograms per cm^2, acoustic radiation pressure only reaches values of the order of grams or dynes of force per cm^2. Nevertheless, radiation pressure is an important quantity in the experimental determination of acoustic intensity.

Since Rayleigh's investigations, a considerable number of papers have been devoted to the subject, many of which, however, do not deal adequately with certain peculiar difficulties inherent in the problem.

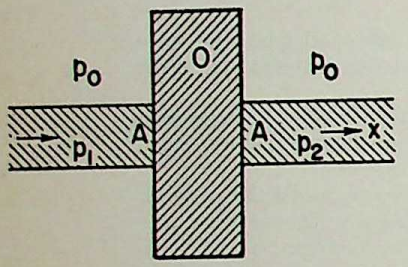


FIG. 1. Acoustic beam of finite cross section A incident upon a plane obstacle 0, and passing through undisturbed regions in which the hydrostatic pressure is p_0.

L. Brillouin[2] seems to have been the first to give a comprehensive approach to the subject, especially in pointing out the tensorial character of what is usually called radiation "pressure." Indeed, this quantity is not a "pressure" in the sense ordinarily understood in hydrodynamics. Brillouin published his first paper on the subject as early as 1925; various authors, however, in later papers on the same subject, seem not to have paid proper attention to Brillouin's approach.

In what follows, a study is presented of the forces exerted upon a plane obstacle by plane compressional waves in a fluid, meeting the obstacle at normal incidence.[3]

Special attention is devoted to throwing light upon the actual physical processes involved. For this reason, a different approach from that used by Brillouin has been chosen; the study also goes further in the consideration of certain details than has been done hitherto.

[2] L. Brillouin, Ann. phys. (X) 4, 528 (1925).

[3] The case of oblique incidence can easily be solved, if the forces resulting from radiation pressure at normal incidence are known. See, for example, F. E. Borgnis, J. Acoust. Soc. Am. 24, 468 (1952).

2. STATEMENT OF THE PROBLEM

In dealing with plane waves, some idealizing assumptions must be made. Plane waves cannot strictly be realized experimentally. Still, if the width of the acoustic beam is large in comparison with the wavelength, the concept of plane waves gives a good approximation, especially in the case of the high frequencies used in ultrasonics. Under most experimental conditions, the acoustic beam in any fluid is surrounded by regions of the same fluid. Reasoning as in geometrical optics, we assume that only the region inside the beam is subject to the acoustical wave motion, whereas the region surrounding the beam is assumed to be undisturbed; that is, we disregard diffraction effects at the edge of the beam and assume uniformity of wave motion over the cross section of the beam. The beam is supposed to fall normally upon a plane obstacle, entirely immersed and at rest in the fluid (Fig. 1). This obstacle causes reflection at its front surface; it may absorb partially or totally the penetrating wave energy. The transmitted part leaves the rear of the obstacle as a purely progressive wave.

The interaction of the obstacle with the plane wave motion can be described completely by an amplitude reflection coefficient γ, an amplitude transmission coefficient δ, and the phase angles θ and θ' of the reflected and transmitted waves with respect to the phase of the incident wave; a plane wave motion in the acoustic beam is thus uniquely determined.

Considerable complications in the measurement of radiation pressure are caused by the fact that the acoustic field sets up a steady streaming in the medium. Two effects have been made responsible for this mass flow: first, the so-called "pumping effect," which may occur at the source of radiation and by which fluid is sucked into the beam and set in motion in the direction of the wave propagation. Second, owing to viscous forces, the wave motion generates what is called the "hydrodynamic flow;" a steady vortical motion is set up in the fluid, causing a steady streaming along the beam in the direction of the incident wave and returning outside the beam. The phenomenon of hydrodynamic flow is inseparably associated with acoustic radiation in a fluid. Like the latter, it is an effect of second order; it cannot be treated without taking into account at least second-order terms in the hydrodynamic equations.[4]

In order to measure the forces due to radiation only, these forces must be separated from those caused by the steady mass flow of the fluid. Usually, some sort of screening is resorted to, consisting of thin films, transparent to radiation but preventing the flow from exerting forces upon the obstacle. Such screens are located close and parallel to the surface of the obstacle,

[4] C. Eckart, Phys. Rev. 73, 68 (1948); J. J. Markham, Phys. Rev. 86, 497 (1952); P. J. Westervelt, J. Acoust. Soc. Am. 25, 60 (1953).

CC-0. In Public Domain. Gurukul Kangri Collection, Haridwar

Digitized by Arya Samaj Foundation Chennai and eGangotri

and it is commonly assumed that in this way the forces caused by acoustic radiation can be measured with sufficient accuracy.

A separation of the forces in question may also be achieved by a low-frequency intensity modulation of the beam and measuring the radiation pressure by a device which responds to the modulation but not to the steady forces of the mass flow nor to the unmodulated wave.[5]

Since we are only concerned with forces caused by radiation, viscous forces are not taken into account in this paper.

3. GENERAL FORMULA FOR THE ACOUSTIC RADIATION PRESSURE

In order to obtain the force exerted upon 0 in Fig. 1, we apply Newton's theorem of equivalence of the time rate of change in momentum to the forces acting upon 0. To keep 0 in time average at rest, we have to apply a force F, equal and opposite to that caused by the quantity which we call radiation pressure. Denoting by P this radiation pressure, that is, the force *per unit area* of the beam of total area A, F amounts to PA, since we are assuming uniformity over the cross section A.

The other force acting on 0 is due to the "dynamic" pressure p_d and is given by $\oint p_d \mathbf{da}$ over the entire surface of 0. In absence of acoustic waves, the pressure p_d is the undisturbed hydrostatic pressure p_0; when variation with depth is ignored, p_0 is constant over the whole surface and $\oint p_d \mathbf{da} = p_0 \oint \mathbf{da} = 0$.

If an acoustic wave motion is present, the hydrostatic pressure p_0 becomes "modulated" over the affected parts of 0 by the "excess pressure" p of the acoustic waves; the resultant pressure may be called the "dynamic pressure" $p_d = p_0 + p$. Forces are counted positive in the positive x direction (Fig. 1), which is the direction of propagation of the incident wave; the force upon 0 due to the action of p_d is $\oint p_d \mathbf{da} = \oint p \mathbf{da} = (p_1 - p_2)A$.

Next we establish the expression for the time rate of change of momentum of 0. As we have to assume continuity of particle displacement at the interface between the fluid and the surface of 0, mechanical motion is transferred to 0. Let ρ be the density and $\mathbf{u}$ the velocity vector of mass elements in 0; the "momentum-density" then is given by $\rho\mathbf{u}$. The quantities p, ρ, and $\mathbf{u}$ are considered as functions of x, y, z, and t, the coordinates belonging to a system fixed in space. 0 may be regarded as having a large inertia, so that its center of gravity may be assumed to be practically at rest, although parts of 0 undergo small and rapid mechanical movements.

In order to compute the change of momentum and to express it by values of the density and the velocity of the *fluid*, we visualize an imaginary surface S stationary in space and in close neighborhood of the surface of 0, but at any time entirely within the fluid. Owing to the law of action and reaction, it is permissible to extend the integrations involved over the surface S instead of over the actual surface of 0.

The momentum of 0 can change in two ways: (a) by a "local" change *in time* of $\rho\mathbf{u}$ within volume elements of 0; the rate of change of this momentum is given by $(d/dt)\int_V \rho\mathbf{u}dV$; (b) by a "convectional" change of $\rho\mathbf{u}$ in the course of the displacement *in space* of mass elements of 0.†

The volume integral of the convectional change in momentum of 0 can be transformed into the surface integral over the entire surface of S in Fig. 2 of the "flux of momentum" crossing S per unit time; the integral amounts to $\oint_S (\rho\mathbf{u})(\mathbf{u}\cdot\mathbf{n})da$,[6] Indeed, during a time element dt the "flux of momentum" crossing a surface element da of S is given by $(\rho\mathbf{u})(\mathbf{u}\cdot\mathbf{n})dadt$, $\rho\mathbf{u}$ being the density of momentum and $(\mathbf{u}\cdot\mathbf{n})$ the normal velocity across S. The surface integral results from a gain or loss in momentum of mass elements in the course of their displacements within 0.

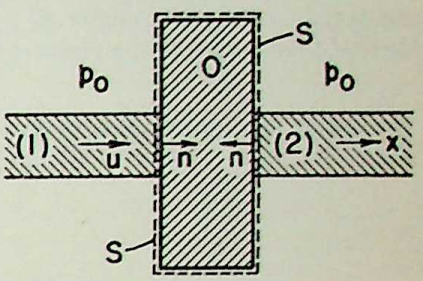


FIG. 2. Imaginary surface S enclosing 0 and stationary in space. n is the inner normal, u the (positive) particle velocity.

In our one-dimensional problem, the total flux of momentum *entering* S per unit time is given by $(\rho_1 u_1^2 - \rho_2 u_2^2)A$; the minus sign of $\rho_2 u_2^2$ expresses the fact that this quantity is the flux *leaving* S, when u is positive in the positive x direction. The parts of S outside the beam give no contribution, as the fluid there is assumed to be at rest.

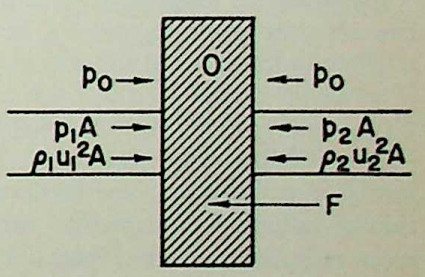


FIG. 3. Directions of the forces acting upon 0.

It may be noted that ρu^2 is always a positive quantity, independent of the sign of u. Owing to the equivalence between force and rate of change of momentum, the

[5] A. Barone and M. Nuovo, Ricerca sci. 21, 516 (1951).

† The *total* change of a quantity q is $Dq/Dt = \partial q/\partial t + (\mathbf{u}\cdot\nabla)q$; the first term is called the local change, the latter term the convectional change of q.

[6] See, for example, L. M. Milne-Thomson, *Theoretical Hydrodynamics* (The Macmillan Company, New York, 1950), p. 72, or *Handbuch der Physik* (Julius Springer, Berlin, 1925), Vol. VII, p. 22.

CC-0. In Public Domain. Gurukul Kangri Collection, Haridwar

Digitized by Arya Samaj Foundation Chennai and eGangotri

terms $(\rho_1 u_1^2)$ and $-(\rho_2 u_2^2)$, representing the flux of momentum entering and leaving S per unit time, may be treated as if they represented forces acting upon S and directed always in the sense of the *inner* normal of S (Fig. 2), whatever the direction of motion of the particles crossing S may be. Nothing, however, indicates that such forces *really* act on the front and rear surfaces of S; only their *sum* has a physical meaning, as it integrates the convectional changes of momentum per unit time of all mass elements within S.

Summing up all the forces acting upon 0 (Fig. 3) and assuming that they are balanced by the external force F necessary to keep the center of gravity of 0 in equilibrium,‡ we arrive at the equation

$$\oint_S p_0 \mathbf{da} + (p_1 + \rho_1 u_1^2 - p_2 - \rho_2 u_2^2)A - F - (d/dt) \times \int_V \rho u dV = 0, \quad (1)$$

where the last integral is taken over the volume bounded by S.

Since we are interested only in the time average of the radiation pressure, we average Eq. (1) over a full period. Assuming a periodic character of the wave motion and periodicity in time of $\int_V \rho u dV$, the time average of $(d/dt)\int_V \rho u dV$ vanishes; also $\oint_S p_0 \mathbf{da} = 0$, disregarding variation of p_0 with depth. From Eq. (1) we obtain, after replacing F by $P_t A$,

$$\bar{P}_t = \bar{p}_1 + \langle \rho_1 u_1^2 \rangle - \bar{p}_2 - \langle \rho_2 u_2^2 \rangle, \quad (2)$$

where the angular parenthesis denotes the average value.

This is the general expression for the *total* mean radiation pressure $\bar{P}_t$ exerted upon 0 in the present case.

Equation (2) suggests regarding $\bar{P}_t$ as consisting of two separate parts $\bar{P}_1$ and $\bar{P}_2$, belonging to the wave motions in front and at the rear of 0. $\bar{P}_1$ can be thought of as being caused by the wave motion in front of 0, $\bar{P}_2$ by an "emitted" wave leaving 0 at its rear. It may be recalled that F was defined as the force necessary to keep 0 in equilibrium; the direction of F is opposite to that of radiation pressure. We can, therefore, define a mean radiation pressure $\bar{P}$ per unit area of a plane compressional wave by

$$\bar{P} = \bar{p} + \langle \rho u^2 \rangle. \quad (3)$$

As so defined, $\bar{P}$ is always directed in the sense of the *inner* normal of the surface interacting with the acoustic wave, whether the surface is thought of as receiving or as emitting radiation.

As a generalization of the expression (3), the mean radiation pressure upon an obstacle of arbitrary shape in an acoustic field can obviously be written

$$\langle \mathbf{P} \rangle = \bar{p}\mathbf{n} + \langle \rho \mathbf{u}(\mathbf{u} \cdot \mathbf{n}) \rangle, \quad (4)$$

where $\mathbf{u}$ now stands for the vector of the velocity $\mathbf{u}(x, y, z)$, and $\mathbf{n}$, as before, is the vector of the inner normal on the surface element da.[7] In the general case, the acoustic radiation may also exert shearing forces upon the obstacle, resulting in a torque upon 0.

The procedure of attributing to each surface element of S a radiation force of amount $\bar{P}$, as defined by Eqs. (3) or (4), has its analogy in electrodynamics, where Poynting's radiation vector $\mathbf{S} = \mathbf{E} \times \mathbf{H}$ is assigned to each surface element of an irradiated surface. What is, in fact, derived in both cases is the total force or the total electromagnetic radiation belonging to a closed surface; from the surface integral, however, no rigorous conclusion can be drawn with regard to the distribution over the elements of the surface of derived quantities such as $\langle \mathbf{P} \rangle$ or $\mathbf{S}$. Still the concept of a radiation pressure $\bar{P}$ as defined in Eqs. (3) and (4) is very useful and leads, if properly applied, to correct results.

Incidentally, an expression analogous to Eq. (4) is well known in hydrodynamics in connection with what has been called "Euler's momentum theorem."§

4. BRILLOUIN'S STRESS TENSOR IN FLUIDS

From the foregoing considerations, Brillouin's concept of a tensor describing the dynamical stresses acting upon a fluid under acoustic motion can easily be obtained. The general result of Eq. (4) may equally well be applied to a volume V belonging to the *fluid*. We consider a unit volume in the fluid and describe the force exerted upon it in the x direction by the component T_{xx} of a general stress tensor; the tensor components T_{xx}, T_{yy}, T_{zz} are here positive in the sense of the inner normal, that is, in the sense of the positive pressure. Equation (4), then, gives in the one-dimensional case

$$\oint_S \bar{P} da = (\bar{T}_{xx})_1 - (\bar{T}_{xx})_2 = -\int_1^2 (\partial \bar{T}_{xx}/\partial x) dx = \oint_S (\langle p + \rho u^2 \rangle) \cos a,$$

whence by use of a well-known integral transformation

$$-\int_1^2 \frac{\partial \bar{T}_{xx}}{\partial x} dx = -\int_V \frac{\partial}{\partial x}(\langle p + \rho u^2 \rangle) dx dy dz = -\int_1^2 \frac{\partial}{\partial x}(\langle p + \rho u^2 \rangle) dx,$$

since $(\langle p + \rho u^2 \rangle)$ is a function of x only and $dydz = 1$. The fluid, therefore, can be thought of as subjected in the

‡ Viscous forces at the interface between 0 and the fluid are excluded. Any viscous forces inside 0 cancel out.

[7] See P. J. Westervelt, J. Acoust. Soc. Am. 23, 312 (1951), Eq. (8).

§ See L. M. Milne-Thomson, reference 6, p. 74.

CC-0. In Public Domain. Gurukul Kangri Collection, Haridwar

Digitized by Arya Samaj Foundation Chennai and eGangotri

x direction to a dynamical stress component

$$\bar{T}_{xx}=p_0+(\langle p+\rho u^2\rangle)=\bar{p}_d+\langle\rho u^2\rangle. \tag{5}$$

Since the particle velocities in the y and z directions are zero, the pressure $\bar{p}_d=p_0+\bar{p}$ is the only force acting in those directions. Thus,

$$\bar{T}_{yy}=\bar{T}_{zz}=\bar{p}_d. \tag{6}$$

These forces acting in the fluid can be described by use of the dynamical stress tensor introduced by Brillouin:[8]

$$\begin{vmatrix} \bar{p}_d+\langle\rho u^2\rangle & 0 & 0 \\ 0 & \bar{p}_d & 0 \\ 0 & 0 & \bar{p}_d \end{vmatrix}. \tag{7}$$

In the absence of acoustic wave motion $\langle\rho u^2\rangle=0$ and $\bar{p}_d=p_0$; the liquid is under the hydrostatic pressure p_0 only, which is the same in every direction. If the acoustic wave is present, the fluid undergoes a non-isotropic state of stress: the stress component $\bar{T}_{xx}$ differs from $\bar{T}_{yy}$ and $\bar{T}_{zz}$ by $\langle\rho u^2\rangle$, that is by the mean flux of momentum density through a stationary area normal to the x direction. Moreover, as is shown later, the pressure p_0 is changed in time average to the mean dynamic pressure $\bar{p}_d=p_0+\bar{p}$, where $\bar{p}$ is found to be proportional to the energy density of the wave motion.

If the fluid is bounded by a plane material surface normal to x, the mean normal stress $\bar{T}_{xx}=\bar{p}_d+\langle\rho u^2\rangle$ is transferred to unit area of this surface; thus, we are led back to the expression for $\bar{P}$, as defined in Eq. (3). At oblique incidence the radiation tensor transforms like the tensor in Eq. (7). In order to attain the final value of $\bar{P}$, the expressions for the tensor components must be completed; since $\bar{p}_d$ will turn out to be different from the pressure p_0 in the undisturbed medium, the interaction between the two regions inside and outside the beam must be considered.

5. A GENERAL RELATION FOR THE MEAN EXCESS PRESSURE, AND FOR THE "RAYLEIGH-PRESSURE"

The mean excess pressure $\bar{p}$ depends upon the properties of the fluid under consideration, that is, upon the relation $p(\rho)$ between pressure and density. $\bar{p}$ finally follows from the solution for the wave motion. Since $\bar{p}$ is related to an area fixed in space, the solution of the so-called *Eulerian* equation of motion is indicated. In this equation the quantities p, ρ, and $\mathbf{u}$ are regarded as functions of x, y, z, and t, the coordinates belonging to a system at rest. A velocity $\mathbf{u}(x, y, z, t)$, for example, means the velocity that would be observed at the point (x, y, z) at the time t; since the fluid is in motion, different particles of the fluid are found at the same point (x, y, z) at a different time t'. In other words, p, ρ, and $\mathbf{u}$ are *not* associated with *particles*, but with a fixed point in space.

Often, however, a solution for the wave motion can more easily be established by using the *Lagrangian* equation of motion. Here the quantities p, ρ, and $\mathbf{u}$ are related to special particles and the solution describes the change in time of p, ρ, and $\mathbf{u}$, which would be noted by an observer at the instantaneous positions of the particles. In order to mark the difference between Eulerian and Lagrangian quantities, we shall denote the latter by p^*, ρ^*, and $\mathbf{u}^*$. The particles themselves are characterized by their original positions at rest, the coordinates of which may be a, b, c; their instantaneous positions are denoted by the displacements ξ, η, ζ (which are functions of a, b, c, t) from their original positions. The *actual* position of a particle with respect to a fixed system is therefore given by $x=a+\xi$; $y=b+\eta$, $z=c+\zeta$. For example, a solution for $\mathbf{u}(a, b, c, t)$ in Lagrangian coordinates indicates the velocity found at the actual position $a+\xi$, $b+\eta$, $c+\zeta$ of the particle, the rest position of which was a, b, c.

The relation between a Lagrangian quantity q^* and the corresponding Eulerian quantity q is expressed by

$$\begin{aligned} q^*(a, b, c, t)&=q\{a+\xi(t), b+\eta(t), c+\zeta(t), t\} \\ &=q\{x(t), y(t), z(t), t\} \end{aligned} \tag{8}$$

since the positions and velocities of particles are given by

$$\begin{aligned} x(t)&=a+\xi(a, b, c, t); \quad dx/dt=u_x=\partial\xi/\partial t \\ y(t)&=b+\eta(a, b, c, t); \quad dy/dt=u_y=\partial\eta/\partial t \\ z(t)&=c+\zeta(a, b, c, t); \quad dz/dt=u_z=\partial\zeta/\partial t. \end{aligned} \tag{9}$$

If ξ, η, ζ are known functions of (a, b, c, t), the inversion of the system (9) allows one to express a, b, c as functions of (x, y, z, t). By insertion of a, b, c, so found, into q^* of Eq. (8), one obtains the corresponding quantity q in Eulerian coordinates. The inversion of the system (9) cannot ordinarily be accomplished by functions of closed form; one has rather to resort to power developments.‖

Our further considerations will be limited to *small amplitudes* of the acoustic wave motion; that is, terms of third and higher order of amplitudes will be neglected. In compressible liquids, the amplitudes that are so far experimentally obtainable in plane waves are always small; in gases, owing to the nonlinearity of the wave equation, the mathematical difficulties in dealing with finite amplitudes are beyond the scope of the present paper.

Returning to the one-dimensional case under consideration, we will now establish a relation between p and p^*, that is, between the mean pressure p at a fixed position, as needed in Eq. (3) for P, and the mean pressure p^* related to an oscillating particle. Such a relation is very useful, because in acoustics solutions

[8] L. Brillouin, reference 2. Also, "*Les Tenseurs en Mécanique et en Élasticité*" (Dover Publications, New York, 1946), pp. 290, 302. It is proved by Brillouin that the forces can actually be represented by a tensor, that is, that they transform like a tensor.

‖ See F. E. Borgnis, Technical Report No. 1A, March 10, 1953, under U. S. Office of Naval Research Contract Nonr-220(02).

CC-0. In Public Domain. Gurukul Kangri Collection, Haridwar

Digitized by Arya Samaj Foundation Chennai and eGangotri

for p^* are often easier to find than solutions for p. According to Eq. (8), $p\{a+\xi(a,t)\}=p^*(a,t)$: by substituting a for $a+\xi$, we have $p(a,t)=p^*\{a-\xi(a-\xi,t)\}$. Regarding ξ, p, and p^* as small first-order quantities and neglecting terms of order higher than second, we may write

$$p(a)=p^*(a-\xi)=p^*(a)-\xi(\partial p^*/\partial a). \tag{10}$$

The Lagrangian equation of motion in one dimension is known to be

$$\rho_0\frac{\partial^2\xi(a,t)}{\partial t^2}=-\frac{\partial p^*(a,t)}{\partial a}, \tag{11}$$

where ρ_0 is the *undisturbed* density. This equation is rigorous, with nothing neglected.[9]

From Eqs. (10) and (11), we find, using customary abbreviations denoting partial derivatives,

$$\bar{p}=\bar{p}^*-(\langle\xi p_a{}^*\rangle)=\bar{p}^*+\rho_0(\langle\xi\xi_{tt}\rangle).$$

Now we can write $\xi\xi_{tt}\equiv(\xi\xi_t)_t-(\xi_t)^2$; taking the time average and assuming ξ and its derivative as periodic in time, we find $\langle(\xi\xi_{tt})\rangle=-\langle(\xi_t)^2\rangle=-\langle u^{*2}\rangle$, since $u^*=\xi_t$. Thus, we obtain

$$\bar{p}(a)=\bar{p}^*(a)-\rho_0\langle u^{*2}\rangle(a). \tag{12}$$

Denoting first- and second-order terms by the subscripts 1 and 2, we have, excluding a continuous particle velocity u_0,

$$\begin{aligned} &u=u_1+u_2, \quad && p=p_1+p_2, && \rho=\rho_0+\rho_1+\rho_2\\ &u^*=u_1{}^*+u_2{}^*, && p^*=p_1{}^*+p_2{}^*, && \rho^*=\rho_0+\rho_1{}^*+\rho_2{}^*. \end{aligned} \tag{13}$$

To the second order twice the kinetic energy is $2E_{\text{kin}}=\rho u^2=\rho_0 u_1{}^2=E_{\text{kin}}{}^*=\rho^* u^{*2}=\rho_0 u^{*2}$ as seen from Eq. (13), because u^2 differs from u^{*2} in terms higher than the second. Also, in this approximation $\bar{E}_{\text{kin}}{}^*=\bar{E}_{\text{pot}}{}^*$, and the total energy density $\bar{E}^*=\bar{E}_{\text{kin}}{}^*+\bar{E}_{\text{pot}}{}^*=2\bar{E}_{\text{kin}}{}^*=\langle\rho u^{*2}\rangle=\langle\rho_0 u^{*2}\rangle$. Consequently, we have at small amplitudes

$$\bar{E}=\bar{E}^*=\langle\rho u^2\rangle=\langle\rho u^{*2}\rangle=\rho_0\langle u^2\rangle=\rho_0\langle u^{*2}\rangle, \tag{14}$$

and hence, from Eq. (12)

$$\bar{p}(a)=\bar{p}^*(a)-\bar{E}^*(a)=\bar{p}^*(a)-\bar{E}(a). \tag{15}$$

This general relation between the mean pressure $\bar{p}$ at a fixed coordinate a, and the mean pressure $\bar{p}^*$ which would be observed by moving with the particle around a, is independent of the special function $p(\rho)$.[10] Equation (15) enables us to find the mean Eulerian excess pressure $\bar{p}$, when p^* and u^* in Lagrangian coordinates are known.

Inserting Eq. (15) in Eq. (3), with consideration of Eq. (14), we obtain

$$\bar{P}=\bar{p}+\langle\rho u^2\rangle=\bar{p}^*. \tag{16}$$

Thus, the radiation pressure can equally well be expressed by the mean pressure averaged in time over a unit area *moving with the particles* at the interface between fluid and obstacle.

Some authors dealing with the present subject identify radiation pressure with the mean Eulerian excess pressure $\bar{p}$ only. Most problems in acoustics are usually treated only to the first order of approximation; within this approximation the second-order term $\langle\rho u^2\rangle$ is neglected and $\bar{p}$ becomes identical with $\langle p^*\rangle$. Radiation pressure, however, is a second-order quantity. If Eulerian quantities are used, the term $\langle\rho u^2\rangle$ (as well as at least second-order terms in $\bar{p}$) are essential; only in the case of a perfectly rigid reflector ($u=0$) does the identification of the radiation pressure with $\bar{p}$ lead to accurate results.[11] If Lagrangian quantities are used, at least second-order terms in $\langle p^*\rangle$ have to be taken into account.

From the physical point of view, it appears natural to reason that the radiation force exerted upon a material surface which (unless it belongs to a perfectly stiff reflector) is in periodic motion, should be obtained by averaging in time the excess pressure on the moving surface, as indicated by Eq. (16). Indeed, as Eq. (16) shows, this is perfectly correct in dealing with a beam of infinite width, or of finite width but not in communication with undisturbed regions of static pressure p_0; in these cases both the Lagrangian quantity $\bar{p}^*$ and the Eulerian quantity $\langle(p+\rho u^2)\rangle$ constitute a correct expression for the radiation force. Nevertheless, the case of infinite width is, of course, purely theoretical; the case of finite width could be conceived as represented by a beam filling completely a closed cylindrical tube with perfectly rigid walls. Experimentally, however, it seems hardly feasible to measure radiation pressure by such a device.

G. Hertz and H. Mende[10] introduced the notation "*Rayleigh pressure*" for the Lagrangian quantity $\bar{p}^*$, that is, the excess pressure averaged in time over a moving surface. Therefore, according to the statements above, the Rayleigh pressure can be identified with the radiation pressure in an *infinitely extended* beam, not in communication with undisturbed regions.

Practically, however, the acoustic beam is of finite width and interacts under almost all conditions with undisturbed regions. This interaction plays a fundamental part in producing the actual radiation forces, because it changes the dynamic pressure in the beam in a way which will be treated below. It is this change in pressure that leads to the actual expression for the radiation pressure. The expressions for $\bar{P}$ in Eq. (16),

[9] See, for example, H. Lamb, *Theory of Sound* (Edwin Arnold, London, 1910), p. 176; also *Hydrodynamics* (University Press, Cambridge, 1936), p. 479.

[10] See G. Hertz and H. Mende, Z. Physik 114, 354 (1939); also F. Borgnis, Z. Physik 134, 363 (1953), where it is shown that Eq. (15) holds also for finite amplitudes. In the present paper, it is sufficient to know its validity at small amplitudes.

[11] F. Bopp, Ann. Physik 38, 495 (1940).

CC-0. In Public Domain. Gurukul Kangri Collection, Haridwar

Digitized by Arya Samaj Foundation Chennai and eGangotri

therefore, have to be modified, because they fail to take into account this phenomenon of interaction.

6. MEAN EXCESS PRESSURE AND ENERGY DENSITY IN LIQUIDS OF CONSTANT COMPRESSIBILITY

The case of liquids offers the least complicated analytical access to the quantities involved and, therefore, affords the most perspicuous physical insight into the problem. This advantage is due to the fact that in liquids we can assume *constant compressibility*. This concept introduces a simple analytical relation between the hydrodynamic pressure p_d and the relative change in volume $\Delta V/V$ of a volume element having the original volume V, on which a pressure Δp_d is exerted. The compressibility is by definition

$$\beta = -\frac{\Delta V}{V}\frac{1}{\Delta p_d}. \tag{17}$$

For acoustic waves one uses normally the adiabatic value of β, though the processes are certainly not strictly adiabatic. Still, the exact value of β will not be very much affected, even if the process is not strictly adiabatic; this conclusion follows from the fact that the difference between the adiabatic and isothermal compressibility amounts to only a few percent for liquids forming drops and under normal conditions of temperature and pressure. Over *large* ranges of pressure the compressibility is not constant. Still, within the range of excess pressures encountered in acoustic waves, which in plane waves rarely exceed about 30 atmos, the compressibility for both positive and negative pressures can be regarded as practically constant.[12]

In the one-dimensional case, the relative change of a unit volume element is $\Delta V/V = \partial\xi/\partial a$, where ξ denotes the particle displacement in the Lagrangian sense. Hence, we have from Eq. (17) with $\Delta p_d = p^*$,

$$p^* = -(1/\beta)\cdot(\partial\xi/\partial a). \tag{18}$$

In a plane wave, the volume element is stretched and compressed only in the x direction; this causes, however, a dynamic pressure which is a scalar and, therefore, the same in every direction. The relation (18) is exact by definition for media with constant compressibility; no higher terms in ξ are involved.

The exact one-dimensional Lagrangian equation (11) gives, with Eq. (18),

$$\rho_0\frac{\partial^2\xi(a,t)}{\partial t^2} = \frac{1}{\beta}\frac{\partial^2\xi(a,t)}{\partial a^2}. \tag{19}$$

The well-known solution for plane acoustic waves generated by a simple harmonic piston motion of angular frequency ω and located, for example, at any $a = \pm 2\pi n/k$, is

$$\xi(a,t) = \xi_0\{\sin(\omega t - ka) + \gamma\sin(\omega t + ka + \theta)\}, \tag{20}$$

where $\omega/k = c = (1/\beta\rho_0)^{\frac{1}{2}}$ (c = phase velocity). This solution is rigorous, including finite amplitudes, subject only to the limitation that the solution (20) remains unique. This limitation excludes amplitudes so large that one particle can overtake the one in front of it. The amplitude ξ_0 is thus limited to values smaller than $\lambda/4\pi$.

From Eq. (20) we obtain immediately the velocity $u^*(a,t) = \partial\xi/\partial t$ as

$$u^*(a,t) = \omega\xi_0\{\cos(\omega t - ka) + \gamma\cos(\omega t + ka + \theta)\}. \tag{21}$$

The excess pressure, according to Eq. (18), is

$$p^*(a,t) = (k\xi_0/\beta)\{\cos(\omega t - ka) - \gamma\cos(\omega t + ka + \theta)\}. \tag{22}$$

The constants γ and θ are the amplitude reflection coefficient and the phase angle of the reflected wave with respect to the incident wave.

The mean energy density follows from Eqs. (14) and (21):

$$\bar{E}^*(a) = (\rho_0/\tau)\int_0^\tau u^{*2}(a,t)\,dt, \quad (\tau = 2\pi/\omega),$$

whence

$$\bar{E}^*(a) = \bar{E}_i\{1 + 2\gamma\cos(2ka + \theta) + \gamma^2\}, \tag{23}$$

where the mean energy density of the *incident wave* is denoted by

$$\bar{E}_i = \tfrac{1}{2}\rho_0\omega^2\xi_0^2. \tag{24}$$

Since $\bar{p}^*(a) = 0$ according to Eq. (22) in liquids of constant compressibility, Eq. (15) becomes, by use of Eq. (23),

$$\bar{p}(x) = -\bar{E}_i[1 + 2\gamma\cos(2kx + \theta) + \gamma^2], \tag{25}$$

where x is now written for the Eulerian coordinate; it is a matter of notation only whether we call this variable x or a.

With the same change in notation we have, according to Eq. (23), $\langle\rho u^2\rangle = \bar{E} = \bar{E}_i\{1 + 2\gamma\cos(2kx + \theta) + \gamma^2\}$ and with Eq. (25) we obtain $\bar{P} = \bar{p} + \langle\rho u^2\rangle = 0$. This relation, which holds for an infinitely extended beam or a beam not communicating with undisturbed regions, shows that the mean decrease of pressure due to the acoustic field is just compensated by the flux of momentum density at any x; the tensor component $\bar{T}_{xx}$ in Eq. (7) becomes p_0 in this case. Thus, no radiation pressure would be found in liquids of constant compressibility, when the beam does not interact with outside regions. This is obviously in contradiction to experimental results, because, as already pointed out, the radiation pressure actually encountered is essentially due to the interaction of the beam with the surrounding medium; this effect will be treated in the following section.

[12] See, for example, the tables in N. E. Dorsey, *Properties of Ordinary Water-Substance* (Reinhold Publishing Corporation, New York, 1940).

CC-0. In Public Domain. Gurukul Kangri Collection, Haridwar

Digitized by Arya Samaj Foundation Chennai and eGangotri

7. INTERACTION BETWEEN ACOUSTIC BEAM AND SURROUNDING UNDISTURBED MEDIUM, AND THE RESULTANT RADIATION PRESSURE

Equation (25) indicates that the mean dynamic excess pressure produced by the periodic wave motion varies periodically along x, except when the incident wave falls upon a perfect absorber ($\gamma=0$). Along its circumference the beam is bordered by the parts of the fluid unaffected by the wave motion. The boundary conditions require continuity of stress, that is of $\bar{T}_{yy}$ and $\bar{T}_{zz}$; both amount to $\bar{p}_d=p_0+\bar{p}$ as seen from the stress tensor (7). The instantaneous stresses T_{yy} and T_{zz} have been replaced by their time averages $\bar{T}_{yy}$ and $\bar{T}_{zz}$, since it is sufficient to postulate that the balance of stresses has to be maintained in time average. Since the pressure outside is assumed to be p_0, the continuity of stress requires that $p_0=\bar{T}_{yy}=\bar{T}_{zz}=\bar{p}_d=p_0+\bar{p}$, or: $\bar{p}=0$.

Thus, if no reflected wave is present, $\bar{p}(x)=-\bar{E}_i$ according to Eq. (25), the total dynamic pressure being $\bar{p}_d=p_0-\bar{E}_i$ inside the beam and p_0 outside. In order to establish the same amount of pressure at the boundary of the beam, the beam will be compressed and its mean density raised by the outside pressure p_0 until the dynamic pressure inside the beam equals p_0.

If a reflected wave is present, the case is more complicated, owing to the second-order periodic change of $\bar{p}$ along x, as expressed by Eq. (25). It is not possible to fulfill exactly the boundary conditions at the interface between beam and undisturbed medium, since the pressure is independent of x in the medium, while periodic in x within the beam; this dilemma results from our idealized assumption of a sharp boundary between the two regions. Actually, the periodic variation of p inside the beam will change gradually into the constant pressure p_0 in the undisturbed medium. However, it is reasonable to assume that this change is essentially performed within a region of transition which is small in comparison with the width of the beam, if the latter is large compared with the acoustic wavelength. Theoretically, this region of transition might extend to infinity. Within this "edge region" of the beam a more complicated (vortical) motion of particles will occur; a closer theoretical investigation of this effect is beyond our scope.

A reasonable way to satisfy the boundary condition at the edge of the beam is the assumption that by reaction of the surrounding medium *the average value in space* of the dynamic pressure $\bar{p}_d=p_0+\bar{p}$ is brought to p_0; inside the beam $\bar{p}_d$ then varies periodically along the x axis around the value p_0.¶

If the average value of p in *time and space* is denoted by $\langle\langle p\rangle\rangle$, the boundary condition at the edge of the beam thus leads us to the condition $\langle\langle p\rangle\rangle=0$ inside the beam. However, if there is no interaction with the surrounding undisturbed medium, it is found from Eq. (25) that $\langle\langle p\rangle\rangle=1/\lambda\int_0^\lambda\bar{p}(x)dx=-\bar{E}_i(1+\gamma^2)$, where λ denotes the acoustic wavelength. The beam, therefore, will undergo a mean compression, which raises the pressure by the opposite amount $\langle\langle p_0'\rangle\rangle=+\bar{E}_i(1+\gamma^2)$ in order to bring the total *space and time average* of p in the beam to p_0. The mean "effective dynamic pressure" in the beam can then be expressed as

$$(\bar{p}_d)_{\text{eff}}=p_0+\bar{p}+p_0'=p_0-2\gamma\bar{E}_i\cos(2kx+\theta), \quad (26)$$

from which expression we indeed obtain $\langle\langle p_d\rangle\rangle_{\text{eff}}=p_0$. The resultant mean stress tensor in the fluid according to Eq. (7), upon introducing $\langle p_d\rangle_{\text{eff}}$ and $\langle\rho u^2\rangle=\bar{E}(x)$ from Eq. (23), becomes

$$\begin{vmatrix} p_0+\bar{E}_i(1+\gamma^2) & 0 & 0 \\ 0 & p_0-2\gamma\bar{E}_i\cos(2kx+\theta) & 0 \\ 0 & 0 & p_0-2\gamma\bar{E}_i\cos(2kx+\theta) \end{vmatrix}. \quad (27)$$

The stress tensor averaged in time *and space* becomes

$$\begin{vmatrix} p_0+\bar{E}_i(1+\gamma^2) & 0 & 0 \\ 0 & p_0 & 0 \\ 0 & 0 & p_0 \end{vmatrix}, \quad (27a)$$

thus satisfying the boundary conditions for $\langle\langle T_{yy}\rangle\rangle$ and $\langle\langle T_{zz}\rangle\rangle$, both of which now equal p_0.

Finally, we calculate the value of the radiation pressure, taking into account the additional pressure $\bar{p}_0'=\bar{E}_i(1+\gamma^2)$ resulting from the interaction between beam and undisturbed medium.

From Eqs. (3) and (23) we have

$$\bar{P}=\bar{p}+\langle\rho u^2\rangle=\bar{p}+\bar{E}_i\{1+2\gamma\cos(2kx+\theta)+\gamma^2\}. \quad (28)$$

Replacing $\bar{p}$ by the "effective excess pressure,"

$$\bar{p}_{\text{eff}}=\bar{p}+\bar{p}_0'=\bar{p}+\bar{E}_i(1+\gamma^2)=-2\gamma\bar{E}_i\cos(2kx+\theta), \quad (29)$$

we find for the radiation pressure from Eq. (28):

$$\bar{P}=\bar{E}_i(1+\gamma^2). \quad (30)$$

This result agrees, as it should, with the tensor component $\bar{T}_{xx}$ in Eq. (27).

For a perfect absorber ($\gamma=0$), $\bar{P}=\bar{E}_i$; for a perfect reflector ($\gamma^2=1$), $\bar{P}=2\bar{E}_i$. The radiation pressure is independent of the phase angle between incident and reflected wave.

One might construe $\bar{P}$ in Eq. (30) as consisting of two parts, $\bar{P}_i=\bar{E}_i$ and $\bar{P}_r=\gamma^2\bar{E}_i$, $\bar{P}_i$ caused by the incident wave only and $\bar{P}_r$ by the reflected wave, whose mean energy density is $\gamma^2\bar{E}_i$. In adopting this view,[8] one might say that the incident wave of energy density

¶ F. Bopp (reference 11) uses the same assumption, basing it on the premise that a nonvanishing average value in space of $\bar{p}$ would be neutralized by a lateral flow of fluid into or out from the beam.

CC-0. In Public Domain. Gurukul Kangri Collection, Haridwar

Digitized by Arya Samaj Foundation Chennai and eGangotri

$\bar{E}_i$ is completely absorbed by the obstacle, leading to a radiation pressure $\bar{P}_i=\bar{E}_i$, while at the same time, the obstacle re-emits a reflected wave of energy density $\gamma^2\bar{E}_i$, the obstacle undergoing a *reactional* radiation pressure $\bar{P}_r=\gamma^2\bar{E}_i$. This concept yields the right numerical value for the radiation pressure; it does not, however, afford an insight into the physical background of the forces really acting at the surface of the obstacle. That mechanism will become apparent from the following section.

8. JOINT ACTION OF THE DYNAMIC PRESSURE AND THE FLUX OF MOMENTUM IN PRODUCING RADIATION PRESSURE IN LIQUIDS

Considering the interface between liquid and obstacle at $x=0$, we find the following Eulerian components acting at the interface by applying Eqs. (23) and (25) to the plane x (or a) $=0$:

$$\bar{p}=-\bar{E}_i(1+\gamma^2+2\gamma\cos\theta), \tag{31}$$

$$\bar{p}_0'=\bar{E}_i(1+\gamma^2), \tag{32}$$

$$\langle\rho u^2\rangle=\bar{E}_i(1+\gamma^2+2\gamma\cos\theta), \tag{33}$$

the sum of which amounts to the radiation pressure $\bar{P}=\bar{E}_i(1+\gamma^2)$ actually measured. The joint *modus operandi* of these forces may be demonstrated by a discussion of certain examples.

(a) Perfect Absorber ($\gamma=0$)

An incident wave is absorbed completely by an obstacle, the surface particles of which follow exactly the movement of the fluid particles in the pure progressive wave at the interface. No reflected wave is set up in this case and $\gamma=0$.**

The mean excess pressure $\bar{p}(x)$ caused by the periodic particle movement is $-\bar{E}_i$ and is constant throughout the beam [Eq. (25)]; by interaction with the surrounding medium $\bar{p}$ is exactly compensated throughout the beam by $\bar{p}_0'=\bar{E}_i$ [Eq. (32)], so that the total mean pressure equals p_0 in the beam. The radiation pressure $\bar{P}_i$ is solely a consequence of the flux of momentum ρu^2 and therefore equals $\bar{P}=\langle\rho u^2\rangle=\bar{E}_i$.

(b) Perfect Reflector ($\gamma=1$)

If the obstacle does not absorb any energy, the entire energy of the incident wave is returned as a reflected wave of the same amplitude. By interference, the two waves cause a standing wave (in a nonviscous liquid), with periodic variation in excess pressure $\bar{p}(x)$, as well as in $\langle\rho u^2\rangle(x)$ along the axis of the beam.

Perfect reflection can be achieved by both a perfectly *stiff* and a perfectly *soft* reflector. The particles at the surface of the perfectly stiff reflector are considered as absolutely immovable; the boundary condition at the interface between fluid and reflector is, therefore, expressed as $u(0,t)=u^*(0,t)=0$ at any t, u being the velocity component normal to the boundary. From Eq. (21) we find that the boundary condition $u^*(0,t)=0$ requires $\gamma=1$ and $\theta=\pi$ in the one-dimensional case. On the other hand, a perfectly soft reflecting surface is characterized by $p^*(0,t)=0$ at any t; a reflection of this kind occurs at the plane free surface of a liquid, where the condition must be satisfied that the pressure shall be continuous as we pass from liquid to air. Since the pressure in air can be assumed to be constant and equal to p_0 (disregarding the negligible wave motion transmitted into the air), the Lagrangian excess pressure p^* must vanish at the free surface of the liquid. The boundary condition $p^*(0,t)=0$ is satisfied by $\gamma=1$ and $\theta=0$, as seen from Eq. (22).

First we consider the *perfectly stiff* reflector: The mean flux of momentum $\langle\rho u^2\rangle$ vanishes at the interface because here $u=0$; the radiation pressure is now due entirely to the dynamic pressure in the liquid. According to Eq. (31), $\bar{p}=0$, since $\gamma=1$ and $\theta=\pi$. However, by interaction between beam and surrounding medium, all values of $\bar{p}$ distributed along the x axis are raised by an amount $\bar{p}_0'=2\bar{E}_i$ [Eq. (32)], which leads to the actual radiation pressure $\bar{P}=2\bar{E}_i$.

At the *perfectly soft* reflector we find from Eq. (31), with $\gamma=1$ and $\theta=0$, that $\bar{p}=-4\bar{E}_i$; from Eq. (32), $\bar{p}_0'=2\bar{E}_i$; and from Eq. (33), $\langle\rho u^2\rangle=4\bar{E}_i$. Three effects act jointly in this case: First, the mean pressure $\bar{p}$ amounts to $-4\bar{E}_i$ per unit area of the free surface; second, by interaction between beam and surrounding medium $\bar{p}$ is raised by an amount $\bar{p}_0'=2\bar{E}_i$, that is, to $-2\bar{E}_i$; third, the mean flux of momentum equals $4\bar{E}_i$, because, owing to the reflection, the resultant velocity amplitude $u(0,t)$ is twice as large as that belonging to the incident wave alone [Eq. (21)]. Thus, in the sum the radiation pressure amounts to $\bar{P}=4\bar{E}_i-2\bar{E}_i=2\bar{E}_i$, just as was found for the perfectly stiff reflector.

Figure 4 illustrates the distribution of pressure and flux of momentum for the two cases of perfect reflection.

(c) General Case ($0\leq\gamma\leq1$; $-\pi\leq\theta\leq\pi$)

In general, where the incident energy is partially absorbed and partially reflected, the force upon the obstacle is due to both effects: the effective excess pressure $\bar{p}_{\text{eff}}=\bar{p}+\bar{p}_0'$, and the quantity $\langle\rho u^2\rangle$. Each of the quantities $\bar{p}$ and $\langle\rho u^2\rangle$ depends on γ and θ, as indicated by Eqs. (31) and (33), but their *sum* does not; it cancels out in liquids of constant compressibility,

** One practicable approach to a perfect absorber is the acoustic "hohlraum," that is, a cavity with acoustically insulating walls, filled with an absorbing medium, and provided with a small window through which the acoustic beam is admitted. Such a device has been applied for measuring acoustic intensities in water in the form of a cylindrical tube; for frequencies in the megacycle range, the absorption of energy is practically complete in a tube that is not excessively long. The plane of the window, therefore, serves as a totally absorbing surface. Another practicable solution is the use of a 90° wedge (F. Borgnis, J. Acoust. Soc. Am. 24, 468 (1952).

CC-0. In Public Domain. Gurukul Kangri Collection, Haridwar

Digitized by Arya Samaj Foundation Chennai and eGangotri

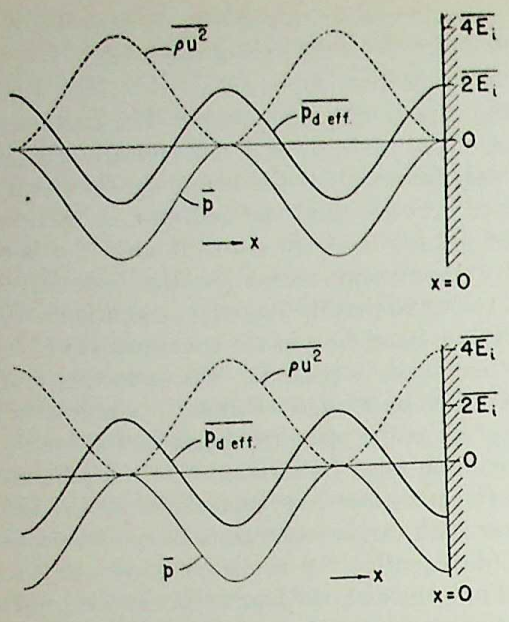


FIG. 4. Distribution of the mean excess pressure $\bar{p}$ resulting from the acoustic wave motion alone; the mean effective dynamic pressure $(\bar{p}_d)_{eff}=\bar{p}+\bar{p}_0'$ resulting from both the wave motion and the interaction of the beam with the surrounding medium; and the mean flux of momentum $\langle\rho u^2\rangle$, in the neighborhood of the boundary of a perfectly stiff reflector (above), and a perfectly soft reflector (below), in a liquid of constant compressibility.

reducing the Rayleigh pressure to zero. The radiation pressure encountered in a beam of finite width is a mere consequence of the mean compression of the beam by the outside medium, that is, of the term $\bar{p}_0'=\bar{E}_i(1+\gamma^2)$.

The Rayleigh pressure $\bar{p}+\langle\rho u^2\rangle$ does not vanish, however, if the compressibility is not constant, as in gases. For example, in a purely progressive wave in a gas under adiabatic conditions and in the neighborhood of the source $\bar{p}^*=\bar{p}+\langle\rho u^2\rangle=(1+\gamma_c)\bar{E}_i/4$ at small amplitudes (γ_c=ratio of the specific heats).

As an example of a general case, we treat in the following section the radiation pressure produced at the interface between two nonmiscible liquids.

9. RADIATION PRESSURE UPON A PLANE INTERFACE BETWEEN TWO NONMISCIBLE LIQUIDS

Let an acoustic beam of plane waves fall normally upon the plane interface between two nonmiscible liquids 1 and 2. The static pressure p_0 outside the beam may be regarded as constant and the same in both liquids. The "obstacle" is reduced in this case to the interface between the two liquids. In liquid 1 we assume a progressive wave of energy density $\bar{E}_{i1}$; this incident wave causes, in general, a reflected wave in liquid 1 and a transmitted wave in liquid 2. The waves in 1 produce a radiation pressure $\bar{P}_1=\bar{E}_{i1}(1+\gamma^2)$, while the transmitted wave causes a reactional radiation pressure $\bar{P}_2=-\bar{E}_{t2}$, where $\bar{E}_{t2}$ is the mean energy density of the progressive wave transmitted into liquid 2. The total radiation pressure, according to the result of Eq. (2), is then given by

$$\bar{P}=\bar{P}_1+\bar{P}_2=\bar{E}_{i1}(1+\gamma^2)-\bar{E}_{t2}. \tag{34}$$

Since the interface does not absorb energy, the balance of the power transmitted requires $c_2\bar{E}_{t2}=c_1(1-\gamma^2)\bar{E}_{i1}$. Hence, we obtain from Eq. (34):

$$\bar{P}=E_{i1}\{1-c_1/c_2+\gamma^2(1+c_1/c_2)\}. \tag{35}$$

At normal incidence the coefficient of reflection is known to be $\gamma=(1-m)/(1+m)$, where $m=\rho_2c_2/\rho_1c_1$, ρ and c being the undisturbed densities and velocities of sound in the respective media.[13]

Equation (35) shows that for special values of c_2/c_1 and ρ_2/ρ_1, the pressure $\bar{P}$ at the interface becomes zero. Inserting the above value of γ in Eq. (35), we obtain the following condition for vanishing radiation pressure:

$$c_2/c_1=(\rho_1/\rho_2)\{2(\rho_2/\rho_1)-1\}^{\frac{1}{2}}. \tag{36}$$

According to this, $\bar{P}$ becomes zero only if the two liquids are arranged so that $\rho_1<2\rho_2$; moreover, c_2/c_1 has to obey Eq. (36). If c_2/c_1 is *smaller* than indicated by Eq. (36), $\bar{P}$ is found from Eq. (35) to become *negative*. In this case, the direction of $\bar{P}$ is *opposite* to the direction of propagation of the incident wave. This effect is caused by the fact that c_2/c_1 is now small enough to make the energy density $\bar{E}_{t2}$ exceed $\bar{E}_{i1}(1+\gamma^2)$ in Eq. (35).[14]

These two quantities represent the additional pressures $\bar{p}_0'$ on the two sides of the interface because of the compression of the beam by the surrounding medium. The mean Lagrangian pressure $\bar{p}^*$ on both sides of the interface is zero when the liquids have constant compressibility, and therefore does not contribute to the radiation pressure. The actual physical forces to which the interface is subjected result from the difference in compression of the acoustic beam on both sides of the partition.

10. GENERAL REMARKS ON THE RADIATION PRESSURE IN GASES

The relation between pressure and density in gases leads to a nonlinear Lagrangian wave equation, the rigorous solution of which can be obtained only by series development. As is well known, the wave form in gases becomes distorted in the course of the propagation. This fact is expressed by a variation in space of the amplitudes of higher terms in the series developments; more and more wave energy is transferred from the fundamental mode, which holds in the immediate neighborhood of the source, to higher harmonics in the course of the wave propagation.[15]

It is difficult to obtain a strict solution of the wave

[13] H. Lamb, *Theory of Sound* (Edwin Arnold, London, 1910), p. 169.

[14] G. Hertz and H. Mende (reference 10) have demonstrated this effect. If $\rho_1\geqslant 2\rho_2$, $\bar{P}$ in Eq. (35) is always positive, that is, in the direction of the incident wave.

[15] Reference 13, p. 174.

CC-0. In Public Domain. Gurukul Kangri Collection, Haridwar

Digitized by Arya Samaj Foundation Chennai and eGangotri

equation even for small amplitudes, if a reflected wave is present. A rigorous treatment would require consideration of absorption, because the amplitude of each higher harmonic is determined by its particular rate of absorption.[16]

A procedure for computing the radiation pressure for the general case of reflection, such as was applied in the previous sections for compressible liquids, is hardly feasible for gases, owing to the mathematical difficulties involved. Still, the insight into the physical processes that has been gained from the treatment of liquids can be used to establish a very general expression for the radiation pressure in all fluids. It will be shown that the formula $\bar{P}=\bar{E}_i(1+\gamma^2)$ holds in any fluid, that is, also in gases, at small amplitudes, at least under the idealized assumptions introduced in the present treatment.

11. A GENERAL EXPRESSION FOR THE RADIATION PRESSURE IN FLUIDS

By multiplying the one-dimensional Eulerian equation of continuity $\rho_t+(\rho u)_x=0$ by u and adding the equation so obtained to the Eulerian equation of motion $\rho(u_t+uu_x)+p_x=0$, a well-known form of the equation of motion in one dimension is obtained:

$$(\rho u)_t+(\rho u^2)_x+p_x=0. \tag{37}$$

In Eqs. (37) to (39), p may be regarded as representing either the excess pressure or the total dynamic pressure p_d. Considering a purely harmonic motion of the acoustic source and assuming that Eq. (37) has solutions periodic in time, we find by averaging Eq. (37) in time and integrating with respect to x,

$$\langle\rho u^2\rangle+\bar{p}=C, \tag{38}$$

where C is a constant independent of x and t, but not, in general, of the wave amplitude. Next, averaging Eq. (38) also in *space*, we obtain

$$\langle\langle\rho u^2\rangle\rangle+\langle\langle p\rangle\rangle=C. \tag{39}$$

Regarding for the moment p as the *total* dynamic pressure, we apply the same conclusions concerning p that were used in Sec. 7, namely, that owing to the interaction between beam and surrounding medium, the total mean Eulerian pressure averaged in *time and space* along the beam may reasonably be assumed equal to the undisturbed outside pressure p_0, or in other words, that $\langle\langle p\rangle\rangle=p_0$. Inserting this condition in Eq. (39) and substituting C so obtained from Eq. (39) in Eq. (38), we find

$$\langle\rho u^2\rangle+(\bar{p}-p_0)=\langle\langle\rho u^2\rangle\rangle. \tag{40}$$

Now $(\bar{p}-p_0)$ is what we previously called the mean excess pressure $\bar{p}$, and $\langle\langle\rho u^2\rangle\rangle=2\langle\langle E\rangle\rangle_{\text{kin}}=\langle\langle E\rangle\rangle_{\text{total}}+(\langle\langle E\rangle\rangle_{\text{kin}}-\langle\langle E\rangle\rangle_{\text{pot}})$. Therefore, from Eq. (40) and according to the definition of radiation pressure in Eq. (3), we have††

$$\bar{P}=2\langle\langle E\rangle\rangle_{\text{kin}}=\langle\langle E\rangle\rangle_{\text{total}}+(\langle\langle E\rangle\rangle_{\text{kin}}-\langle\langle E\rangle\rangle_{\text{pot}}). \tag{41}$$

Equation (41), which includes the interaction between beam and surrounding medium, gives the radiation pressure for a beam of finite width in any fluid and on any plane reflecting surface. With the assumption $\langle\langle p\rangle\rangle=p_0$, which led to Eq. (40), Eq. (41) is valid for finite amplitudes, since no restriction was introduced in this respect in the derivation. Whether this assumption is valid or not at *finite* amplitudes is an open question.

At small amplitudes, where we limit ourselves to terms up to the second order, it is sufficient to know the *first*-order solution in u, as already mentioned in Sec. 5. This is correct, at least, within a distance not too far from the origin of the wave motion; or, if absorption is assumed to be exactly zero, within a not too large time interval after the wave motion started. Owing to the transfer of wave energy from the fundamental to higher harmonics, as mentioned in Sec. 10, the amplitudes of these harmonics increase with distance from the origin (Earnshaw's solution), and also with time in absence of absorption. At larger distances, therefore, the terms of higher order may no longer be negligible. On the other hand, absorption is always present, limiting the amplitudes of the harmonics. It is only in a medium with constant compressibility that the fundamental wave is propagated without producing higher harmonics, preserving its original shape everywhere.

To the first order the solution for u of the Lagrangian wave equation is given in any fluid by Eq. (21). Moreover, $\langle\langle E\rangle\rangle_{\text{pot}}=\langle\langle E\rangle\rangle_{\text{kin}}$ at small amplitudes, and therefore $2\langle\langle E\rangle\rangle_{\text{kin}}=\langle\langle E\rangle\rangle_{\text{total}}=\bar{E}_i(1+\gamma^2)$, as seen from Eq. (23). Consequently, we find from Eq. (41) that the expression

$$\bar{P}=2\bar{E}_{\text{kin}}=\bar{E}_i(1+\gamma^2)=\tfrac{1}{2}\rho_0\omega^2\xi_0^2(1+\gamma^2) \tag{42}$$

is valid both in liquids and gases, when terms of third and higher order in $k\xi_0=2\pi\xi_0/\lambda$ are excluded. Eq. (42) agrees with Eq. (30), which was found to hold for liquids of constant compressibility.

Since $\bar{E}_i(1+\gamma^2)$ is the mean total energy density encountered at the surface of the plane reflector, Eq. (42) states that *at small amplitudes the radiation pressure of a finite beam of plane compressional waves equals the mean total energy density at the reflecting surface.* This result is independent of the special law connecting pressure and density in the fluid under consideration. At larger amplitudes, according to Eq. (41), the total energy density must be replaced by $2\langle\langle E\rangle\rangle_{\text{kin}}$, that is twice the average in time and space of the kinetic energy density.

[16] See P. J. Westervelt, J. Acoust. Soc. Am. 22, 319 (1950), Sec. VI, and F. E. Borgnis, Technical Report No. 1A, March 10, 1953, under U. S. Office of Naval Research Contract Nonr-220(02).

†† An analogous derivation was applied to the special case of a perfectly stiff reflector by F. Bopp (reference 11).

CC-0. In Public Domain. Gurukul Kangri Collection, Haridwar

Digitized by Arya Samaj Foundation Chennai and eGangotri

It may be recalled that the expressions for the radiation pressure given in Eqs. (41) and (42) represent only the force that may be attributed to one side of the reflector. A force of the same kind, equal to the energy density behind the reflector, but opposite in sign, has to be attributed to the opposite side.‡‡ Only the *sum* of these two forces has a physical significance; it represents both the change in momentum per unit time to which the wave motion is subjected in passing through a partition, and the effects of interaction between beam and surrounding medium on both sides of the partition.

The *total* radiation pressure $\bar{P}_t$ exerted upon a partition by a finite beam is, therefore, under the assumption leading to Eq. (41), given by

$$\bar{P}_t = (\langle\langle\rho u^2\rangle\rangle)_1 - (\langle\langle\rho u^2\rangle\rangle)_2 = 2(\langle\langle E\rangle\rangle_{\text{kin}})_1 - 2(\langle\langle E\rangle\rangle_{\text{kin}})_2, \quad (43)$$

where, as before, the indices 1 and 2 denote the two sides of the partition (Fig. 2). At small amplitudes, $2\langle\langle E\rangle\rangle_{\text{kin}}$ can be replaced on both sides by the total energy density $\langle\langle E\rangle\rangle$; the total radiation pressure then equals the difference in energy densities on both sides of the partition. A similar result, namely, that the radiation pressure is equal to the difference between two energy densities, is also well known in electrodynamics.

BIBLIOGRAPHY

A good survey of the literature on the subject, covering the period before 1927, is found in *Handbuch der Physik*, Vol. VIII (Berlin, 1927), pp. 148, 149, 579, and 580. Below is given a selected list of papers of special interest in relation to the present treatment; the list also includes some papers quoted in the text.

‡‡ In the special cases of a perfect absorber or of a perfect reflector this force at the rear is zero.

R. T. Beyer, "Radiation pressure in a sound wave," Am. J. Phys. **18**, 25 (1950).

P. Biquard, "Ultrasonic waves," Rev. acoust. **1**, 93 and 315 (1932).

F. E. Borgnis, (a) "Theory of Acoustic Radiation Pressure," Technical Report No. 1A (March 10, 1953), under U. S. Office of Naval Research Contract Nonr-220(02); (b) "Acoustic radiation pressure of plane compressional waves at oblique incidence," J. Acoust. Soc. Am. **24**, 468 (1952); (c) "On the physics of acoustic radiation pressure," Z. Physik **134**, 363 (1953).

F. Bopp, "Energetic considerations on acoustic radiation pressure," Ann. Physik **38**, 495 (1940).

L. Brillouin, (a) "The tensions of radiation and their interpretation in terms of classical mechanics and relativity," J. phys. et radium **6**, 337 (1925); (b) "On the tensions of radiation," Ann. phys. **4**, 528 (1925); (c) "The tensions of radiation and their interpretation," Physica **5**, 396 (1925); (d) "Radiation pressure and 'tension,'" Rev. acoust. **5**, 99 (1936).

G. Hertz, "Acoustic radiation pressure in liquids and gases in connection with the equation of state," Physik. Z. **41**, 546 (1940).

G. Hertz and H. Mende, "Acoustic radiation pressure in liquids," Z. Physik **114**, 354 (1939).

J. S. Mendousse, "On the theory of acoustic radiation pressure," Proc. Am. Acad. Arts Sci. **78**, 148 (1950).

J. H. Poynting, "Radiation pressure," Phil. Mag. **9**, 393 (1905).

Lord Rayleigh, (a) "On the pressure of vibrations," Phil. Mag. **3**, 338 (1902) or "Collected Papers," Vol. 5, 41; (b) "On the momentum and pressure of gaseous vibrations and on the connection with the virial theorem," Phil. Mag. **10**, 364 (1905) or "Collected Papers," Vol. 5, 262.

G. Richter, "On the problem of acoustic radiation pressure," Z. Physik **115**, 97 (1940).

C. Schaefer, (a) "On the theory of acoustic radiation pressure," Ann. Physik **35**, 473 (1939); (b) "On the discussion concerning acoustic radiation pressure," Z. Physik **115**, 109 (1940).

A. Schoch, "On the question of the momentum of a sound wave," Z. Naturforsch. **7a**, 273 (1952).

W. Weaver, "The pressure of sound," Phys. Rev. **15**, 399 (1920).

P. J. Westervelt, "The theory of steady forces caused by sound waves," J. Acoust. Soc. Am. **23**, 312 (1951).

CC-0. In Public Domain. Gurukul Kangri Collection, Haridwar

Digitized by Arya Samaj Foundation Chennai and eGangotri

The Thermal Expansion of Anisotropic Metals

B. G. CHILDS
Atomic Energy Research Establishment, Harwell, Berkshire, England

A review of the present state of knowledge of the variation with temperature of the thermal expansion of anisotropic metals. The theoretical significance of the experimental data is discussed.

INTRODUCTION

THE thermal expansion of a noncubic crystal can be specified completely in terms of the linear expansion coefficients, α_x α_y α_z, measured along three mutually perpendicular axes. These axes, in the case of the rhombic and tetragonal systems, correspond with the crystallographic axes. In the hexagonal and rhombohedral systems the axis of highest rotational symmetry coincides with one of the expansion axes; the direction of the second expansion axis is chosen arbitrarily. In the monoclinic system one of the expansion axes coincides with the b axis of the crystal and the direction of one of the other two expansion axes depends upon the particular crystal under consideration, while in the triclinic system there is, in general, no relation between the crystal and expansion axes.

The thermal expansion coefficient α_{lmn}, in the direction having direction cosines l, m, n with the coordinate axes, is given by

$$\alpha_{lmn}=\alpha_x l^2+\alpha_y m^2+\alpha_z n^2,$$

which, for the three uniaxial systems that comprise the majority of anisotropic metals, reduces to

$$\alpha_\theta=\alpha_{\parallel}\cos^2\theta+\alpha_\perp\sin^2\theta,$$

where θ is the angle between the given direction and the principal axis, and $\alpha_{\parallel}$ and $\alpha_\perp$ are the expansion coefficients in the directions parallel and perpendicular to the principal axis.

A complete specification of the expansion of such a crystal requires a knowledge of the two, or three, expansion coefficients as functions of temperature over the whole range from the absolute zero to the melting point. In the past, relatively little attention has been paid to the study of the expansion of anisotropic metals, and for only 10 out of the 34 metals that have anisotropic structures have values for the expansion coefficients been obtained at more than one temperature. Some of these values must, in addition, be regarded as uncertain. Even less information is available for anisotropic alloys.

In view of the practical and fundamental importance of the subject the lack of interest in the expansion of anisotropic substances is remarkable. For example, much information with regard to the directional dependence of the binding forces and lattice vibrations in anisotropic metals can be obtained from a study of the expansion of such bodies. In order to stimulate interest, therefore, experimental data for the expansion of anisotropic metals are summarized in this paper, and a brief account of the theoretical relations that have been derived for the observed behavior is given.

I. HUME-ROTHERY'S CLASSIFICATION

In dealing with the experimental results it is convenient to adopt Hume-Rothery's classification (1)* in which the elements in the periodic table are separated (by continuous lines) into four classes (see Fig. 1). Class I, at the extreme left of the table, comprises those metals that crystallize in the three typically metallic structures, the face- and body-centered cubic systems and the hexagonal close-packed system with an axial ratio of 1.63. In these structures each atom has 8 or 12 equidistant neighbors so that, to a first approximation, the force field acting on the atom may be considered as spherically symmetrical. Consequently, these metals show relatively slight anisotropy in their elastic and thermal properties.

Elements in Class III include metals and semimetals with a valency of four or more. These tend to form structures in which the atoms are bound by covalent forces into clusters of $(8-N)$ atoms, where N is the valency. The binding forces between clusters are weaker than those within the clusters, and consequently, considerable anisotropy results. Thus, the atoms in selenium and tellurium with 6 electrons in their outer shells form into spiral chains, each atom having two nearest neighbors. The expansion in the direction of the chains is markedly different from that in the direction perpendicular to the chains.

Class II includes metals with structures intermediate between those of Class I and III. Thus zinc and cadmium possess structures which, though hexagonal close-packed, have axial ratios of 1.86 and 1.89, respectively, instead of 1.63.

Class IV consists of nonmetals and is therefore not of interest here.

II. CLASS I METALS

For thermal expansion, as also for many other properties, magnesium (Fig. 2) is virtually isotropic—more so, in fact, than iron. At room temperature, where the coefficients differ to the greatest extent, $\alpha_\perp$ is 95 per-

* Numbers in parentheses refer to Bibliography at end of paper.

CC-0. In Public Domain. Gurukul Kangri Collection, Haridwar

Digitized by Arya Samaj Foundation Chennai and eGangotri

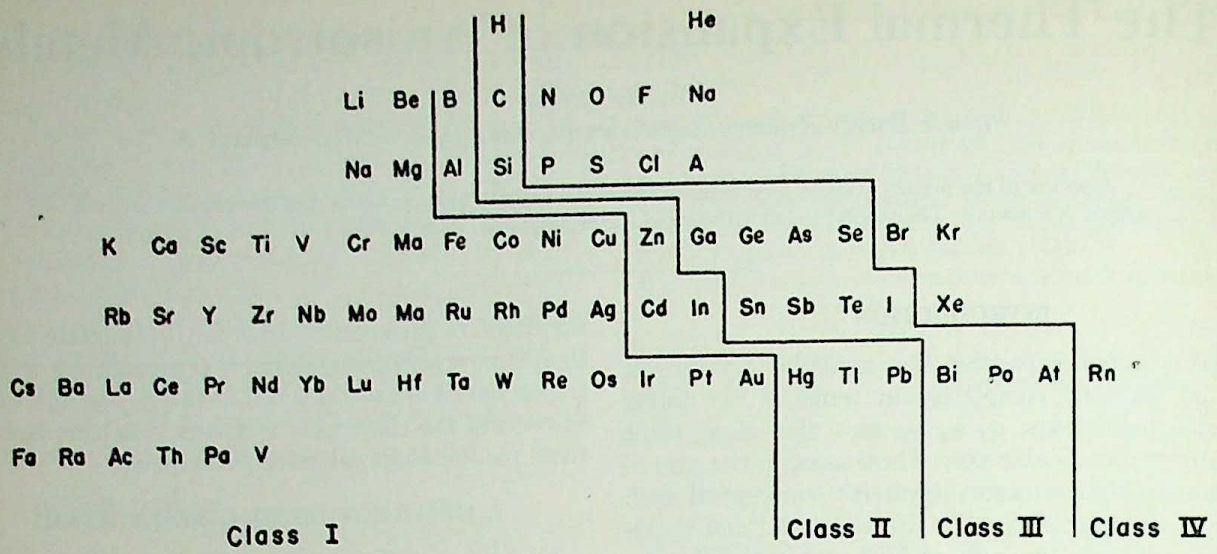


FIG. 1. Hume-Rothery's classification of the elements.

cent of α_{II}. Both $\alpha_{\perp}$ and α_{II} increase monotonically with temperature, the increase being particularly marked between 0 and 300°K and above 600°K. This kind of variation is found also for several other metals. The chief feature of interest in magnesium, however, is the excellent agreement between the values obtained by Hume-Rothery and Raynor (5) who measured the expansion of the magnesium lattice by an x-ray diffraction method, and those obtained by Goens and Schmid (3) who used a Henning comparator to measure the expansion of bulk single crystals of various orientations. This agreement between values obtained by these two essentially different methods, though of general occurrence, is not necessarily to be expected. It depends, on the one hand, upon the degree of perfection of the bulk crystals and the extent to which they deform plastically when loaded, and, on the other hand, upon the amount of strain which is present, because of the anisotropy, in the polycrystalline specimens used in the x-ray measurements. The other results for magnesium appear to be somewhat less accurate, but even so, there is no systematic disagreement between the crystal measurements of Bridgman (2) and the lattice measurements of the other investigators.

Beryllium (Fig. 3) is also relatively isotropic, though less so than magnesium. There is some discrepancy between the results of Gordon (7) and those of Owen and Richards (9), though both used x-ray methods. This discrepancy is particularly marked at the lower temperatures, where Gordon finds a steep fall, below about 420°K, in the values of the coefficients. Because of the high Debye temperature (1000°K) of beryllium such a fall may be expected so that it is likely that Gordon's results are the more reliable. The bulk crystal values for the expansion coefficients of beryllium obtained by Bridgman (2) and by Treco (10) do not deviate systematically from the lattice expansion values obtained by the other investigators.

In Table I expansion data for osmium, ruthenium, α-cobalt, zirconium, rhenium, and α uranium are given. Osmium and ruthenium, as expected from their strong binding forces and consequently high melting points and low compressibilities, have small expansion coefficients. These depend only slightly on temperature and do not differ greatly. Zirconium, rhenium, and α uranium are exceptions to the Hume-Rothery classification. They are all strongly anisotropic in their thermal expansion. Uranium has a complex orthorhombic structure below 650°C, and one of its expansion coefficients is negative.

III. CLASS II METALS

The expansion coefficients of all the five anisotropic metals in Class II have been measured. In Fig. 4 $\alpha_{\perp}$ for zinc is shown. Except for the inaccurate results of Austin (13), there is good agreement, particularly between the lattice expansion measurements of Owen and Yates (16) and the bulk crystal data of Grüneisen and Goens (15). The general dependence of $\alpha_{\perp}$ on temperature is similar to that for magnesium, except that it becomes negative at about 70°K.

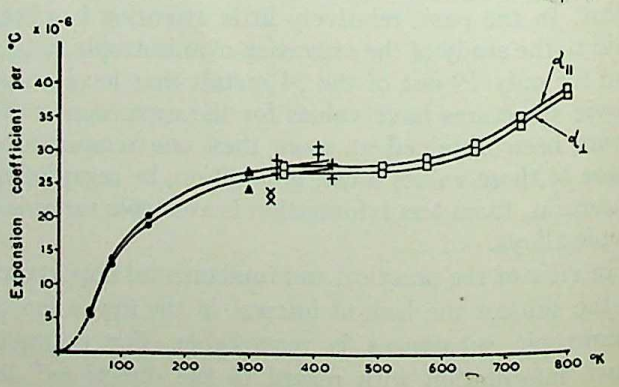


FIG. 2. α_{II} and $\alpha_{\perp}$ for magnesium. ▲ Bridgman (2). ● Goens and Schmid (3). + Hannawalt and Frevel (4). □ Hume-Rothery and Raynor (5). × Shinoda (6).

CC-0. In Public Domain. Gurukul Kangri Collection, Haridwar

Digitized by Arya Samaj Foundation Chennai and eGangotri

For α_{II}, however, there is not such good agreement (Fig. 5). In the overlapping region the results of Owen and Yates (16) are lower than those of Grüneisen and Goens (15) and are probably less accurate. The remarkable feature is the rapid rise of α_{II} to a large maximum value at 120°K followed by a progressive fall to the melting point.

Cadmium (Fig. 6), as expected from its similar crystal structure and axial ratio, behaves similarly to zinc; α_{II} has a high maximum value, and $\alpha_{\perp}$ a negative value at low temperatures. An additional feature of interest

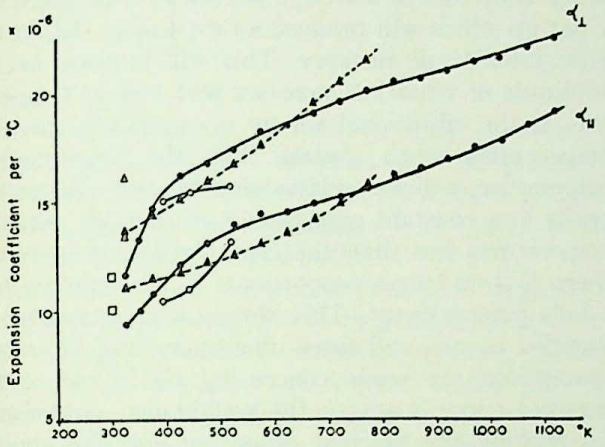


FIG. 3. α_{II} and $\alpha_{\perp}$ for beryllium. △ Bridgman (2). ● Gordon (7). ○ Kossolapow and Trapesnikow (8). ▲ Owen and Richards (9). □ Treco (10).

is that at 523°K cadmium becomes isotropic in expansion.

Mercury (Fig. 7), unlike zinc and cadmium, is only feebly anisotropic in expansion. This is remarkable since its linear compressibilities are in the ratio 1:5 and,

TABLE I. Expansion coefficients of some metals in Class I.

Metal	Structure	$10^6\alpha_{II}$ per °C	$10^6\alpha_{\perp}$ per °C	Temp. °C	Reference
Os (c.p.)	hexagonal	5.9– 8.35	4.0–5.85	50–550	9
Ru (c.p.)	hexagonal	8.8–11.7	5.9–7.65	50–550	9
α-Co (c.p.)	hexagonal	16.1	12.6	60	6
Zr (c.p.)	hexagonal	2.5	14.3	80	6
Re (c.p.)	hexagonal	12.5	4.7	20	11
		$10^6\alpha_a$	$10^6\alpha_b$ $10^6\alpha_c$		
α-U	orthorhombic	23	−3.5 17	150	12

more especially, since the direction of greatest expansion corresponds to the direction of smallest compressibility or strongest binding.

For thallium and indium, which have hexagonal close-packed and tetragonal structures, respectively, only single mean values of the expansion coefficients are available. These are for thallium at 60°C, $\alpha_{II}=72\times10^{-6}$, $\alpha_{\perp}=9\times10^{-6}$, and for indium at 50°C, $\alpha_{II}=11.7\times10^{-6}$, $\alpha_{\perp}=45.0\times10^{-6}$ in deg^{-1}C. Both metals are thus highly anisotropic.

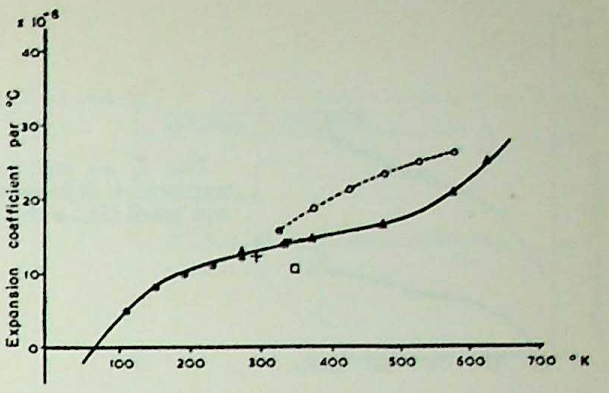


FIG. 4. $\alpha_{\perp}$ for zinc. ○ Austin (13). + Bridgman (14). ● Grüneisen and Goens (15). ▲ Owen and Yates (16). □ Shinoda (17). ▼ Staker (18).

IV. CLASS III METALS

In Class III only tin and bismuth have been investigated thoroughly. Using an interferometric method and bulk crystals, Childs and Weintroub (23) found

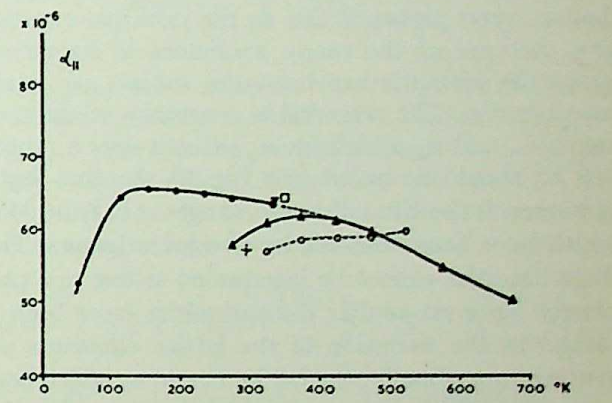


FIG. 5. α_{II} for zinc. ○ Austin (13). + Bridgman (14). ● Grüneisen and Goens (15). ▲ Owen and Yates (16). □ Shinoda (17). ▼ Staker (18).

that for tin α_{II} was approximately twice $\alpha_{\perp}$ and that both coefficients increased almost linearly with temperature from room temperature to the melting point (see Fig. 8). The single values obtained by the other in-

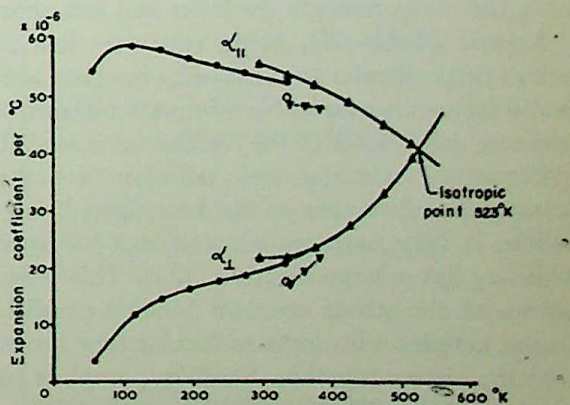


FIG. 6. α_{II} and $\alpha_{\perp}$ for cadmium. ● Grüneisen and Goens (15). ▼ Kossolapow and Trapesnikow (19). ▲ Owen and Roberts (20). ○ Shinoda (6).

CC-0. In Public Domain. Gurukul Kangri Collection, Haridwar

Digitized by Arya Samaj Foundation Chennai and eGangotri

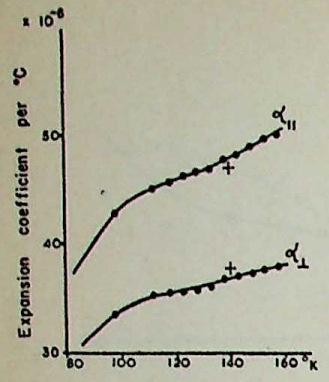


FIG. 7. $\alpha_{\parallel}$ and $\alpha_{\perp}$ for mercury. + Grüneisen and and Sckell (21). ● Hill (22).

vestigators differ considerably from those of Childs and Weintroub; two lattice expansion values lie above the curves, and one bulk crystal result lies below. This separation between the lattice and crystal results may not be significant, however, in view of the disagreement between the individual values in the two groups.

Bismuth, antimony, and arsenic have a rhombohedral structure in which the atoms are arranged in double layers perpendicular to the principal expansion axis. Because of the many anomalies in its physical properties bismuth has been the subject of detailed investigation. The remarkable constancy of the coefficients $\alpha_{\parallel}$ and $\alpha_{\perp}$, which for $\alpha_{\parallel}$ extends over a range of 360°K, should be noted (see Fig. 9). Another feature of interest is the discontinuous changes at 258 and 345°K which have been observed by two investigators. These discontinuities cannot be interpreted as due to a phase change since no similar discontinuities have been observed in the variation of the lattice constants with temperature. Finally, the fall in $\alpha_{\parallel}$ and $\alpha_{\perp}$ which begins near the melting point and which has been found by Buchta and Goetz (29) to be due to the presence of small amounts of impurity should be noted.

The relatively looser structure of antimony perpendicular to the layers makes antimony more anisotropic than bismuth. The coefficients (Fig. 10), similar to those for bismuth, do not appear to vary appreciably with temperature, but this is not established definitely since the measurements are fewer and less accurate.

Arsenic (Table II), being relatively less strongly bound perpendicular to the layers even than antimony, is still more anisotropic. No information about the temperature dependence of the coefficients is available.

Hexagonal selenium and tellurium are the most anisotropic substances so far investigated. $\alpha_{\parallel}$ for selenium is very negative even at room temperatures, while $\alpha_{\perp}$ has a large positive value. This is in consequence of the strong covalent binding parallel to the chains, coupled with weak molecular type forces which hold the chains together. Similarly, graphite, with an hexagonal layer structure, has a relatively large $\alpha_{\parallel}$ in the direction of weak molecular binding and a negative $\alpha_{\perp}$ in the direction of the strong covalent forces.

V. THEORY AND DISCUSSION

A physical explanation of the thermal expansion of substances may be given by considering Fig. 11 in which the potential energy E of a pair of atoms is plotted as a function of their distance d apart. The important feature of this curve is the lack of symmetry about the minimum at the equilibrium distance d_0. Thus the displacement from the equilibrium position required to produce a given change in potential energy is greater for an increase than for a decrease in d. Hence, if the atoms vibrate longitudinally, corresponding to the lattice vibrations of a solid, a net outward pressure will be set up which will produce an expansion, Δd, in the mean interatomic distance. This will increase as the amplitude of vibration increases with rise in temperature. If the vibrational energy is quantized, then for temperatures much greater than the characteristic temperature, a linear relationship between Δd and E results in a constant expansion coefficient α, while at temperatures less than the characteristic temperature where E is no longer proportional to the temperature, α falls progressively. This simple argument can be extended to two and three dimensions and, if certain assumptions are made concerning the shape of the potential curve, leads to the well-known Grüneisen's law relating the thermal expansion and the specific heat of isotropic substances.

For anisotropic substances the general situation is very similar, but for these the dependence of the potential energy curve, and consequently of the linear compressibilities on direction, has two important consequences. The first is that at low temperatures lattice vibrations will be excited preferentially in the direction of greatest compressibility on account of the lower vibrational frequencies. Thus, initially, the expansion parallel to this direction will be greater than in the perpendicular direction. The second is that an expansion in one direction is accompanied by an elastic contraction in the perpendicular directions, the magnitude of which is determined by the magnitude of the expansion and, for the principal directions, by the elastic coefficients s_{12}, s_{13}, s_{23}. This contraction may be sufficiently

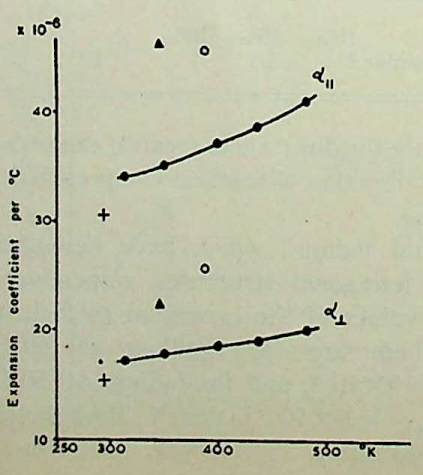


FIG. 8. $\alpha_{\parallel}$ and $\alpha_{\perp}$ for tin. + Bridgman (14). ● Childs and Weintroub (23). ▲ Kossolapow and Trapesnikow (8). ○ Shinoda (17).

CC-0. In Public Domain. Gurukul Kangri Collection, Haridwar

Digitized by Arya Samaj Foundation Chennai and eGangotri

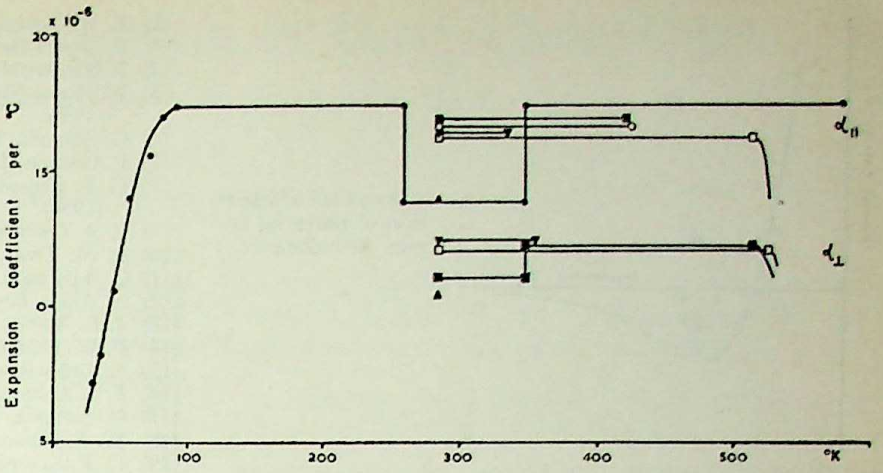


FIG. 9. $\alpha_{\parallel}$ and $\alpha_{\perp}$ for bismuth. ▲ Bridgman (14). ▼ Fizeau (24). ● Jacobs and Goetz (25). ■ Jay (26). ○ Ho and Goetz (27). □ Roberts (28).

great to overcome the intrinsically small expansion in these directions at low temperatures and produce a net contraction. This occurs for zinc, cadmium, graphite, selenium, tellurium, and uranium, and probably also for thallium, indium, and arsenic.

This qualitative treatment has been applied by Grüneisen and Goens (15) to anisotropic (hexagonal) crystals and by making several simplifying assumptions they have derived theoretical relationships for $\alpha_{\parallel}$ and $\alpha_{\perp}$. They have used these to interpret their experimental results for zinc and cadmium at low temperatures. Commencing with the thermodynamical relations, if X_x and Z_z are the "thermal pressures,"

$$\alpha_{\perp}=\alpha_x=\alpha_y=\frac{1}{l_x}\left(\frac{\partial l_x}{\partial T}\right)_p=\frac{1}{V}\int_0^T\left(\frac{\partial C_p}{\partial X_x}\right)\frac{dT}{T},$$

$$\alpha_{\parallel}=\alpha_z=\frac{1}{l_z}\left(\frac{\partial l_z}{\partial T}\right)_p=\frac{1}{V}\int_0^T\left(\frac{\partial C_p}{\partial Z_z}\right)\frac{dT}{T},$$

where V is the volume and C_p the specific heat at constant pressure; C_p is replaced by C_v, the specific heat at constant volume, and the Born (35) expression for C_v is substituted. This expression takes account of the variation of the limiting frequencies, i.e., the characteristic temperatures Θ^j, with the nature and direction of the lattice vibrations. Grüneisen and Goens (15) obtained

$$\alpha_x=(s_{11}+s_{12})q_x+s_{13}q_z,$$

$$\alpha_z=2s_{13}q_x+s_{33}q_z,$$

TABLE II. Expansion coefficients of some metals in Class III.

Metal	Structure	$10^6\alpha_{\parallel}$ per °C	$10^6\alpha_{\perp}$ per °C	Temp. °C	Reference
As	rhombohedral	43	3	6	31
C	hexagonal	27.6–29.0	−1.5–0.9	85–750	32
Te	hexagonal	−1.7	27.5	45	33
		−1.6	27.2	25	14
Se	hexagonal	−17.9	74.1	45	33
		$10^6\alpha_a$ $10^6\alpha_b$	$10^6\alpha_c$ $10^6\alpha_\beta$		
Se	monoclinic	−1.5 84.7	63.3 5.5	20	34

where

$$q_x=\frac{R}{V}\sum_{j=1}^{3}\int\gamma_x{}^jD\left(\frac{\Theta_x{}^j}{T}\right)\frac{d\Omega}{4\pi}$$

and

$$q_z=\frac{R}{V}\sum_{j=1}^{3}\int\gamma_z{}^jD\left(\frac{\Theta^j}{T}\right)\frac{d\Omega}{4\pi}$$

are the so-called "thermal pressure coefficients," D is the Debye function, $\gamma_x{}^j=(\partial\log\Theta_x{}^j/\partial\log l_x)$, etc., and $j=1, 2, 3$ refers to the acoustical modes of vibration. Finally as in the Debye theory of specific heats the distinction between the Θ^j's and the γ^j's is removed and mean values (indicated by $\langle\ \rangle$) substituted so that

$$\alpha_x=\frac{3R}{V}\left[(s_{11}+s_{12})\langle\gamma_x\rangle D\left(\frac{\langle\Theta_x\rangle}{T}\right)+s_{13}\langle\gamma_z\rangle D\left(\frac{\langle\Theta_z\rangle}{T}\right)\right],$$

$$\alpha_z=\frac{3R}{V}\left[2s_{13}\langle\gamma_x\rangle D\left(\frac{\langle\Theta_x\rangle}{T}\right)+s_{33}\langle\gamma_z\rangle D\left(\frac{\langle\Theta_z\rangle}{T}\right)\right].$$

The values of $\langle\gamma\rangle$ and $\langle\Theta\rangle$ have to be chosen empirically to give agreement between the theoretical and experimental values of α.

In Fig. 12 the agreement which can be obtained with

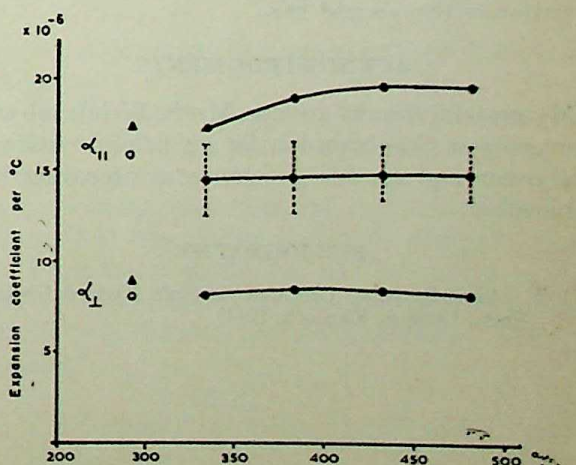


FIG. 10. $\alpha_{\parallel}$ and $\alpha_{\perp}$ for antimony. ○ Bridgman (14). ▲ Fizeau (24). ● Hidnert (30).

CC-0. In Public Domain. Gurukul Kangri Collection, Haridwar

Digitized by Arya Samaj Foundation Chennai and eGangotri

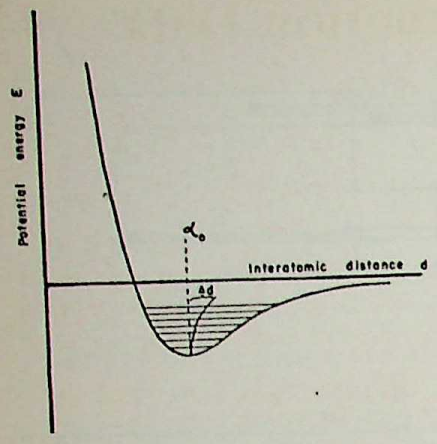


FIG. 11. The variation of potential energy with distance.

experiment is illustrated for the case of zinc. The values used by Grüneisen and Goens were $\langle\gamma_x\rangle = 2.04$, $\langle\gamma_z\rangle = 1.68$ which are of the same order as those for isotropic substances, and $\langle\Theta_x\rangle = 320°K$, $\langle\Theta_z\rangle = 200°K$, compared with $\Theta = 250°K$ from specific heat measurements. The agreement, however, is not a true measure of the correctness of the formulas, because the various approximations and simplifications are obscured by the choice of the values for the $\langle\gamma\rangle$'s and $\langle\Theta\rangle$'s. For example, the elastic coefficients are assumed to be independent of temperature. It must be remembered also that the assumptions involved in the Debye theory regarding the frequency spectrum of the lattice vibrations, introduced errors at low temperatures, and the assumption of the equality of C_p and C_v introduces error at high temperatures. (For a modification of the Grüneisen-Goens theory applicable at high temperatures see Riley (36).)

CONCLUSION

It should be clear from the above summary both of the experimental data and of the theoretical formulas for the expansion of anisotropic metals that it is desirable that much additional information be obtained, by accurate measurement, of the linear expansion coefficients over wide ranges of temperature and, by calculation from the elastic coefficients, of the spatial variation of the γ's and Θ's.

ACKNOWLEDGMENTS

My grateful thanks are due Mr. S. Weintroub of the University of Southampton for his helpful criticism of this paper and for his assistance in preparing it for publication.

BIBLIOGRAPHY

(1) W. Hume-Rothery, *The Metallic State* (Oxford University Press, London, England, 1931).
(2) P. W. Bridgman, Proc. Am. Acad. Arts Sci. **67**, 345 (1932).
(3) E. Goens and E. Schmid, Physik. Z. **37**, 385 (1936).
(4) J. Hannawalt and L. Frevel, Z. Krist. **98**, 84 (1937).
(5) W. Hume-Rothery and G. V. Raynor, J. Inst. Metals **65**, 379 (1939).
(6) G. Shinoda, Kyoto Coll. Sci. Mem. **A17**, 27 (1934).
(7) P. Gordon, J. Appl. Phys. **20**, 908 (1949).
(8) G. F. Kossolapow and A. K. Trapesnikow, Z. Krist. **94**, 53 (1936).
(9) E. A. Owen and T. L. Richards, Phil. Mag. **22**, 304 (1936).
(10) R. M. Treco, J. Metals **188**, 1274 (1950).
(11) C. Agte et al., Naturwiss. **19**, 109 (1931).
(12) N. Allen, Report BR-718 (1946).
(13) J. B. Austin, Physics **3**, 240 (1932).
(14) P. W. Bridgman, Proc. Am. Acad. Arts Sci. **60**, 305 (1925).
(15) E. Grüneisen and E. Goens, Z. Physik **29**, 141 (1924).
(16) E. A. Owen and E. L. Yates, Phil. Mag. **17**, 113 (1934).
(17) G. Shinoda, Kyoto Coll. Sci. Mem. **A16**, 193 (1933).
(18) W. P. Staker, Phys. Rev. **61**, 653 (1942).
(19) G. F. Kossolapow and A. K. Trapesnikow, Z. Krist. **91**, 410 (1935).
(20) E. A. Owen and E. W. Roberts, Phil. Mag. **22**, 290 (1936).
(21) E. Grüneisen and O. Sckell, Ann. Physik **19**, 387 (1934).
(22) D. M. Hill, Phys. Rev. **48**, 620 (1935).

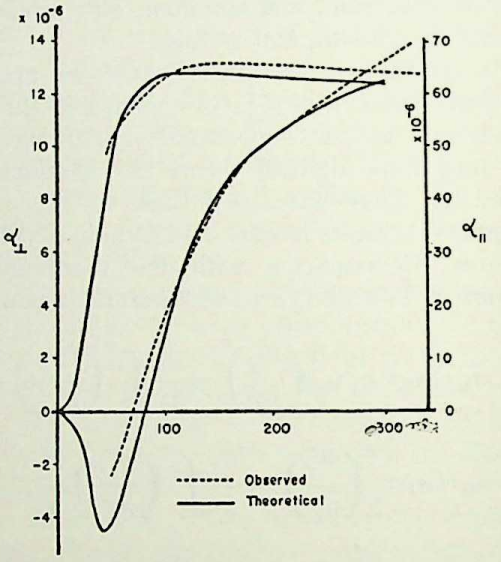


FIG. 12. Theoretical and observed values of $\alpha_\parallel$ and $\alpha_\perp$ for zinc, after Grüneisen and Goens (reference 15).

(23) B. G. Childs and S. Weintroub, Proc. Phys. Soc. (London) **63B**, 267 (1950).
(24) A. H. Fizeau, Compt. rend. **68**, 1125 (1869).
(25) R. B. Jacobs and A. Goetz, Phys. Rev. **51**, 159 (1937).
(26) A. H. Jay, Proc. Roy. Soc. (London) **A143**, 465 (1934).
(27) T. L. Ho and A. Goetz, Phys. Rev. **43**, 213 (1933).
(28) J. K. Roberts, Proc. Roy. Soc. (London) **A106**, 385 (1924).
(29) J. W. Buchta and A. Goetz, Phys. Rev. **46**, 1092 (1934).
(30) P. Hidnert, J. Research Natl Bur. Standards **14**, 523 (1935).
(31) P. W. Bridgman, Proc. Am. Acad. Arts Sci. **67**, 29 (1932).
(32) J. B. Nelson and D. P. Riley, Proc. Phys. Soc. (London) **57**, 477 (1945).
(33) M. Straumanis, Z. Krist. **102**, 432 (1940).
(34) C. J. Newton and M. Y. Colby, Acta Cryst. **4**, 477 (1951).
(35) M. Born, *Atomtheorie des festen Zustandes* (Leipzig, 1923).
(36) D. P. Riley, Proc. Phys. Soc. (London) **57**, 486 (1945).

CC-0. In Public Domain. Gurukul Kangri Collection, Haridwar

Digitized by Arya Samaj Foundation Chennai and eGangotri

The Fourier Inversion of Diffraction Data

JÜRG WASER, *The Rice Institute, Houston, Texas*

AND

VERNER SCHOMAKER, *California Institute of Technology, Pasadena, California*

THERE are two methods, generally speaking, which are used to analyze experimental diffraction data in terms of structure. The one consists in the theoretical calculation of the scattering pattern for various models and comparison with the observed pattern. The other, taking advantage of the trigonometric form of the equations, consists in Fourier inversion, to obtain structural information directly. We may remark that the two methods are equivalent in principle, but that actually they do not entirely replace each other. For example, in the study of gas-molecule structure by electron diffraction, where the two methods are called the correlation method and the radial distribution method, certain aspects of the experimentally determined intensity function are usually better known than others: The correlation method is much better suited to this situation than the less laborious radial distribution method, which requires essentially indiscriminate use of the intensity data. In practice, the radial distribution method is often used to narrow the choice of possible models and parameter values, while the visual method serves to analyze the remaining possibilities.

In this paper many of the problems connected with the use of the Fourier methods will be discussed. Some of these problems have been handled satisfactorily in one way or another before, but we intend to deal with them from a unified point of view, at the core of which are two simple facts of Fourier theory. They are that the Fourier transform of a sum of products is again a sum, the sum of the transforms of these products. The nature of these transforms is discussed most simply with the aid of the convolution or folding theorem, which states that multiplication of two functions corresponds to the folding of their transforms, as discussed in Sec. 3.

A main problem in the inversion of diffraction data arises from the absence of experimental data for scattering angles greater than a limiting angle; it and related problems are treated by considering the effect of modifying the observed intensity function, by multiplication with suitable factors before inversion. A number of such factors—we call them *modification functions*—are discussed and a general treatment of a special class of them is attempted. Next, the difficulties are considered which arise from the presence in the intensity function of the atomic scattering factors and temperature factors, leading to a generalization to include such effects in a *complete* modification function. These matters are all first illustrated by the special one-dimensional case of the electron-diffraction pattern, and later applied to x-ray diffraction of liquids and amorphous solids. Final sections deal with the application of modification functions to the analysis of crystal structures.

1. THE RADIAL DISTRIBUTION FUNCTION IN ELECTRON DIFFRACTION

The structure sensitive part of the expression which describes the scattering of fast electrons by gas molecules not involving internal rotations is of the form[1]

$$sI'(s)=\text{const}\sum_{ij}{}'\frac{[Z_i-f_i(s)][Z_j-f_j(s)]}{s^4r_{ij}}\times\exp(-a_{ij}s^2)\sin sr_{ij}, \quad (1\text{-}1)$$

where the sum extends over all pairs of atoms of a molecule, atom i having atomic number Z_i and x-ray form factor $f_i(s)$. The effect on the scattering of zero-point and temperature variation of the interatomic distance r_{ij} is described by the so-called temperature factor $\exp(-a_{ij}s^2)$, in which a_{ij} is given by one-half the mean-square variation $\langle\delta r_{ij}^2\rangle_{Av}$ of r_{ij}. The variable s is $(4\pi/\lambda)\sin(\varphi/2)$, where φ is the angle between incident and scattered beam and λ the electron wavelength.

The factor $(Z_i-f_i(s))$ is often nearly proportional to the average $\langle(Z-f(s))/Z\rangle_{Av}$ taken over all atoms, so that (1-1) may be approximated by

$$sI'(s)\approx\text{const}\left\langle\frac{Z-f(s)}{Z}\right\rangle_{Av}^2\times\frac{\exp(-as^2)}{s^4}\sum_{ij}{}'\frac{Z_iZ_j}{r_{ij}}\sin sr_{ij}\exp(-\delta a_{ij}s^2), \quad (1\text{-}2)$$

where a is a convenient reference value of the a_{ij} and $\delta a_{ij}=a_{ij}-a$.

The film exposure due to the electrons scattered according to (1-1) or (1-2) is superposed on a smooth, structure-insensitive background caused by the "atomic" elastic scattering (described by the terms with $i=j$, which in (1-1) were omitted from the complete expression), by inelastic scattering, and by processes occasioned by imperfections of the experimental arrangement. It will become evident, however, that the expression

$$sI''(s)=\sum_{ij}{}'\frac{Z_iZ_j}{r_{ij}}\exp(-\delta a_{ij}s^2)\sin sr_{ij} \quad (1\text{-}3)$$

[1] L. O. Brockway, Revs. Modern Phys. 8, 231 (1936).

CC-0. In Public Domain. Gurukul Kangri Collection, Haridwar

Digitized by Arya Samaj Foundation Chennai and eGangotri

obtained by suppressing the monotonic factor in front of the summation symbol in (1-2) or an expression of the form of

$$sI'''(s)=\frac{1}{\sum_i(Z_i-f_i(s))^2}\times\sum_{ij}{}'\frac{[Z_i-f_i(s)][Z_j-f_j(s)]}{r_{ij}}\times\exp(-\delta a_{ij}s^2)\,\sin sr_{ij} \quad (1\text{-}4)$$

obtained by dividing (1-1) by $\sum_i[Z_i-f_i(s)]^2$, or some similar factor, are more convenient for the radial distribution method. Furthermore, (1-3) and (1-4) are the more natural functions to use if diffraction photographs are to be interpreted visually, because what is apparent to the eye is approximately the ratio of the fluctuating part of the intensity distribution to some smooth background.[1] In the correlation method, functions of one of these forms calculated for molecular models of interest are directly compared with the observed intensity distribution.

For the discussion of the radial distribution method the further simplified function

$$sI(s)=\left(\frac{2}{\pi}\right)^{\frac{1}{2}}\sum_{ij}{}'\frac{Z_iZ_j}{r_{ij}}\sin sr_{ij}, \quad (1\text{-}5)$$

which describes the structure sensitive part of the scattering by a rigid molecule made up of point atoms, is a convenient starting point. The factor $(2/\pi)^{\frac{1}{2}}$ provides a suitable normalization. Such a molecule is characterized by a distance spectrum which may formally be expressed by the radial distribution function

$$r^2D_o(r)=\sum'_{ij}Z_iZ_j\delta(r-r_{ij}), \quad (1\text{-}6)$$

where $\delta(r)$ is the Dirac delta function, defined by the two conditions[2]

$$\delta(r)=0 \quad \text{unless } r=0 \quad (1\text{-}7)$$

and

$$\int_{-\infty}^{\infty}\delta(r)dr=1.$$

The function $r^2D_o(r)$ has infinitely high and infinitely narrow peaks for values of r which represent interatomic distances. With it Eq. (1-5) may be expressed by

$$sI(s)=(2/\pi)^{\frac{1}{2}}\int_0^{\infty}rD_o(r)\sin srdr. \quad (1\text{-}8)$$

Sine inversion[3] of (1-8) yields

$$rD(r)=(2/\pi)^{\frac{1}{2}}\int_0^{\infty}sI(s)\sin srds, \quad (1\text{-}9)$$

where $rD(r)$ is essentially $rD_o(r)$ except that it is antisymmetrical because $\sin sr$ is odd, whereas $rD_o(r)$ was defined as vanishing for negative r; $rD(r)$ may also be expressed as

$$rD(r)=\sum_{ij}{}'\frac{Z_iZ_j}{r_{ij}}[\delta(r-r_{ij})-\delta(r+r_{ij})]. \quad (1\text{-}10)$$

The problem now is to obtain from the actually observed intensity curve, which is known for a finite range of s only, a radial distribution function which is a faithful representation of the distance spectrum of the molecules.

2. THE LIMITATION OF OBSERVED DATA

If the integration in (1-9) is not extended over the whole range in which the integrand is different from zero, the resulting function shows certain spurious maxima and minima which may make its interpretation very laborious if not impossible. Bragg and West[4] discussed such effects in the case of the two-dimensional Fourier series of crystal structure analysis and pointed out a close analogy to diffraction effects which occur in an optical image in consequence of the finite aperture of the optical system.

These spurious features may be greatly diminished or entirely eliminated by multiplying the integrand of (1-9) by a suitable factor. The function $\exp(-as^2)$ is often used for this purpose, with a chosen so that the resulting integrand has a negligible value beyond the upper limit of s for which experimental data are available. This function has been called the artificial temperature factor, a name suggested by its identity in form to the temperature factors in the intensity formula (1-1). Sommerfeld used this convergence factor in his doctorate thesis,[5] where he succeeded in obtaining with its aid the first precise result concerning the validity of the Fourier integral theorem. Bragg and West,[4] who referred to it as an "arbitrary temperature factor," introduced its use in crystal structure analysis, and Dégard[6] introduced it in electron diffraction investigations, at the suggestion of Professor L. Pauling. A convergence factor of this type was perhaps first introduced by Weierstrass[7] who used the factor $r^{-n^2}(r<1)$ in his discussion of Fourier series.

Quite a different mode of procedure was early used by

[2] P. A. M. Dirac, *Quantum Mechanics* (Oxford University Press, London, 1947), third edition, p. 58. An example of a δ-function pertinent to Fourier theory is $\delta(x)=\int_{-\infty}^{\infty}\exp(-2\pi ihx)dh$.

[3] The background of Fourier theory needed for our discussion is expounded in various textbooks. See, for example, H. S. Carslaw, *Fourier Series and Integrals* (Macmillan and Company, Ltd., London, 1930) and W. Rogosinski, *Fourier Series* (Chelsea Publishing Company, New York, 1950). Special points will be referred to standard treatises.

[4] W. L. Bragg and J. West, Phil. Mag. 10, 823 (1930).

[5] H. S. Carslaw, reference 3, p. 321.

[6] C. Dégard, Ph.D. thesis, University of Liège, 1937.

[7] M. Bôcher, Annals of Math. 7, 81 (1906), footnote, p. 103.

CC-0. In Public Domain. Gurukul Kangri Collection, Haridwar

Digitized by Arya Samaj Foundation Chennai and eGangotri

Havighurst, Compton, and James and Firth[8] and has been applied recently by van Reijen[9] in an x-ray analysis of the electron distribution in diamond. It consists in using extrapolated values at large values of s, where $sI(s)$ (or the structure factor in the crystal case) is not experimentally accessible. Although an exact knowledge of $sI(s)$ for even an arbitrarily small range of s would define $sI(s)$ for all values of s, such knowledge (as would define $sI(s)$ and all its derivatives at a given point) can never be obtained experimentally, however small the experimental error, and the extrapolation must be carried out judiciously. Even so, it is difficult to judge the uniqueness of the results, and deceptively false distributions can be produced.[10] For the case of atomic scattering, Hauptman and Karle[11] have recently discussed the use of the criterion that the distribution function should be everywhere positive as an aid towards a unique extrapolation of $sI(s)$. Nevertheless, it would seem that more than the criterion of nonnegativeness is required—perhaps also the more complex condition of smoothness of the distribution function and conditions about its asymptotic behavior, e.g., that for finite molecules $rD(r)$ must vanish when r exceeds a certain value.

In electron diffraction the absence of data for s less than some minimum value presents a similar problem which also has often been handled by extrapolation, usually either by use of the theoretical intensities for an approximate model of the molecule or even by some gross appeal to experience.[12] Since the desire is here to locate interatomic distances with precision rather than to study the distribution of the outer electrons, and since the low frequency components contributed by the inner part of the intensity pattern have very little effect on the locations of the peaks of the radial distribution function, this is a valid procedure of convenience, just as the extrapolation beyond the upper limit of s in the crystal case is above reproach if it is only the broad, diffuse aspects of the distribution function about which information is desired. If the extrapolation to $s=0$ is not used,[13] the problem of convergence is similar to the ones discussed earlier in this paragraph; heretofore, however, it does not seem to have been handled by the explicit use of a convergence factor.

[8] R. J. Havighurst, Phys. Rev. **29**, 1 (1927); A. H. Compton and S. K. Allison, *X-Rays in Theory and Experiment* (D. Van Nostrand Company, Inc., New York, 1935), second edition; R. W. James and E. M. Firth, Proc. Roy. Soc. (London) **A117**, 62 (1927).

[9] L. L. van Reijen, Physica **9**, 461 (1942); J. O. Bouman, *X-Ray Crystallography* (North Holland Publishing Company, Amsterdam, 1951), Chap. 3.

[10] D. W. J. Cruickshank, Acta Cryst. **2**, 65 (1949), see (10.1), (10.2), and appendix; H. Viervoll, Skrifter Norske Videnskaps Akad., Oslo, Mat- Naturv. Kl. No. 2, 1950.

[11] H. Hauptman and J. Karle, Phys. Rev. **77**, 491 (1950).

[12] See, for example, Shaffer, Schomaker, and Pauling, J. Chem. Phys. **14**, 659 (1946).

[13] H. Viervoll, Acta Chem. Scand. **1**, 120 (1947).

3. THE FOLDING THEOREM AND MODIFICATION FUNCTIONS

We shall now consider[14] the problem of the convergence factor and, more generally, of the change in $rD(r)$ to

$$rD'(r)=(2/\pi)^{\frac{1}{2}}\int_0^\infty sI(s)M(s)\sin srds, \qquad (3\text{-}1)$$

which occurs if $sI(s)$ is multiplied by a modification function $M(s)$. In this discussion the folding theorem of Fourier integrals[3,15,16] is very useful. If $f(x)$, $F(t)$ and $g(x)$, $G(t)$ are two sets of Fourier transforms such that

$$\begin{aligned} f(x)&=(2\pi)^{-\frac{1}{2}}\int_{-\infty}^{\infty}F(t)\exp(itx)dt,\\ F(t)&=(2\pi)^{-\frac{1}{2}}\int_{-\infty}^{\infty}f(x)\exp(-itx)dx,\\ g(x)&=(2\pi)^{-\frac{1}{2}}\int_{-\infty}^{\infty}G(t)\exp(itx)dt,\\ G(t)&=(2\pi)^{-\frac{1}{2}}\int_{-\infty}^{\infty}g(x)\exp(-itx)dx, \end{aligned} \qquad (3\text{-}2)$$

then the Fourier transform of the product $f(x)\cdot g(x)$ is given by

$$\begin{aligned} R(t)&=(2\pi)^{-\frac{1}{2}}\int_{-\infty}^{\infty}f(x)\cdot g(x)\exp(-itx)dx\\ &=(1/2\pi)\int_{-\infty}^{\infty}f(x)\int_{-\infty}^{\infty}G(u)\exp(iux)du\exp(-itx)dx\\ &=(1/2\pi)\int_{-\infty}^{\infty}G(u)\int_{-\infty}^{\infty}f(x)\exp[-ix(t-u)]dxdu\\ &=(2\pi)^{-\frac{1}{2}}\int_{-\infty}^{\infty}G(u)F(t-u)du. \end{aligned} \qquad (3\text{-}3)$$

The function $R(t)$ is known as the folding ("Faltung"), resultant, or convolution of G and F. Inversely, the Fourier transform of $R(t)$ is

$$(2\pi)^{-\frac{1}{2}}\int_{-\infty}^{\infty}R(t)\exp(itx)dt=f(x)\cdot g(x), \qquad (3\text{-}4)$$

so that the multiplication of two functions corresponds to the folding of their transforms in Fourier transform space and inversely. The indicated derivation is only a

[14] J. Waser, Ph.D. thesis, California Institute of Technology, 1944.

[15] E. L. Titchmarsh, *Introduction to the Theory of Fourier Integrals* (Oxford University Press, London, 1937).

[16] S. Bochner, *Vorlesungen über Fouriersche Integrale* (Akademische Verlagsgesellschaft, Leipzig, 1932).

CC-0. In Public Domain. Gurukul Kangri Collection, Haridwar

Digitized by Arya Samaj Foundation Chennai and eGangotri

formal one, but the result can be shown to be valid for the functions considered here.[15,16]

An important example is provided by the Gaussian distribution function:

$$\begin{aligned} f(x)&=\exp(-ax^2),\\ F(t)&=(2a)^{-\frac{1}{2}}\exp(-t^2/4a),\\ g(x)&=\exp(-bx^2),\\ G(t)&=(2b)^{-\frac{1}{2}}\exp(-t^2/4b),\\ f(x)g(x)&=\exp[-(a+b)x^2],\\ R(t)&=[2(a+b)]^{-\frac{1}{2}}\exp[-t^2/4(a+b)]. \end{aligned} \tag{3-5}$$

The transform of a Gaussian is again a Gaussian, and the half-widths at half-height, $0.83(a)^{-\frac{1}{2}}$ and $0.83(4a)^{\frac{1}{2}}$ (one finds $\exp(-0.83)^2=0.5$), are in a reciprocal relation. Since the resultant $R(t)$ is the transform of the product $f(x)g(x)$, it must be Gaussian, as shown, with half-width equal to the square root of the sum of the squares of the half-widths of $F(t)$ and $G(t)$.

For the special case that $f(x)$ is odd and $g(x)$ even [the latter so that $f(x)g(x)$ is odd], the above formulas become after absorbing factors $\pm i$

$$\begin{aligned} f(x)&=(2/\pi)^{\frac{1}{2}}\int_0^\infty F(t)\,\sin txdt=-f(-x),\\ F(t)&=(2/\pi)^{\frac{1}{2}}\int_0^\infty f(x)\,\sin txdx=-F(-t);\\ g(x)&=(2/\pi)^{\frac{1}{2}}\int_0^\infty G(t)\,\cos txdt=g(-x),\\ G(t)&=(2/\pi)^{\frac{1}{2}}\int_0^\infty g(x)\,\cos txdx=G(-t);\\ R(t)&=(2/\pi)^{\frac{1}{2}}\int_0^\infty f(x)\cdot g(x)\,\sin txdx\\ &=(2\pi)^{-\frac{1}{2}}\int_{-\infty}^\infty F(u)G(t-u)du=-R(-t). \end{aligned} \tag{3-6}$$

For our problem we identify the odd function $sI(s)$ with $f(x)$, the even function $M(s)$ with $g(x)$, the distribution function $rD(r)$ with $F(t)$, and the cosine transform of $M(s)$,

$$T(r)=(2/\pi)^{\frac{1}{2}}\int_0^\infty M(s)\,\cos srds=T(-r), \tag{3-7}$$

with $G(t)$. The result is

$$rD'(r)=(2\pi)^{-\frac{1}{2}}\int_{-\infty}^\infty uD(u)T(r-u)du, \tag{3-8}$$

which of course pertains to any $uD(u)$ of mathematically allowable form, and is in particular not tied to the very special $rD(r)$ defined by (1-9) and (1-10), which merely serves to provide a simple example. The integrand of (3-8) may be written in several equivalent ways by changing the variable of integration or taking advantage of the symmetries of $T(u)$ and $uD(u)$. Correspondingly, the folding process may be viewed in several ways. The one indicated in (3-8) may be described by the following three steps: (1) Superposition of $uD(u)$ with a (reflected) $T(u)$ whose origin has been shifted by r. (2) Multiplication of corresponding values. (3) Integration over u. This has to be repeated for all (positive) values of r, and is in general a complicated procedure. For the idealized $rD(r)$ (1-10) the result is, however, simply

$$rD'(r)=(2\pi)^{-\frac{1}{2}}\sum_{ij}{}'\frac{Z_iZ_j}{r_{ij}}[T(r-r_{ij})-T(r+r_{ij})], \tag{3-9}$$

which entails the replacement of the infinitely sharp peaks of $rD(r)$ (1-10) by the features of the function $T(r)$. This suggests that the folding for a continuous distribution may also be viewed in terms of a decomposition of $rD(r)$ into a suitably weighted array of δ-functions, which are then to be replaced by T's and summed. It should be noted that the features of $T(r+r_{ij})$, though centered at $r=-r_{ij}$, may extend across the origin to positive values of r, so that the second term in (3-10) may in some cases be of practical importance.

There are of course other combinations of odd and even functions $f(x)$ and $g(x)$ besides the one discussed here in detail. They lead to equations analogous to (3-6), which are at times very useful.

4. EXAMPLES OF MODIFICATION FUNCTIONS

A useful modification function must substantially equal zero outside the s range for which $sI(s)$ is known (or assumed); moreover, the transform $T(r)$ should be such as to make analysis of the resulting $rD'(r)$ in terms of the desired distribution function $rD(r)$ straightforward and economical. In general, the useful transforms will have a main peak flanked by subsidiary features; it will be desired to have the main peak sharp, for resolving closely spaced peaks, and the subsidiary features weak, to minimize the influence of a given peak on all the others. Unfortunately, these requirements are not entirely compatible, and compromise has to be made in the interest of convenience.

Convenience, it must be realized, is all that is ever achieved in practical Fourier analysis: An integral equation

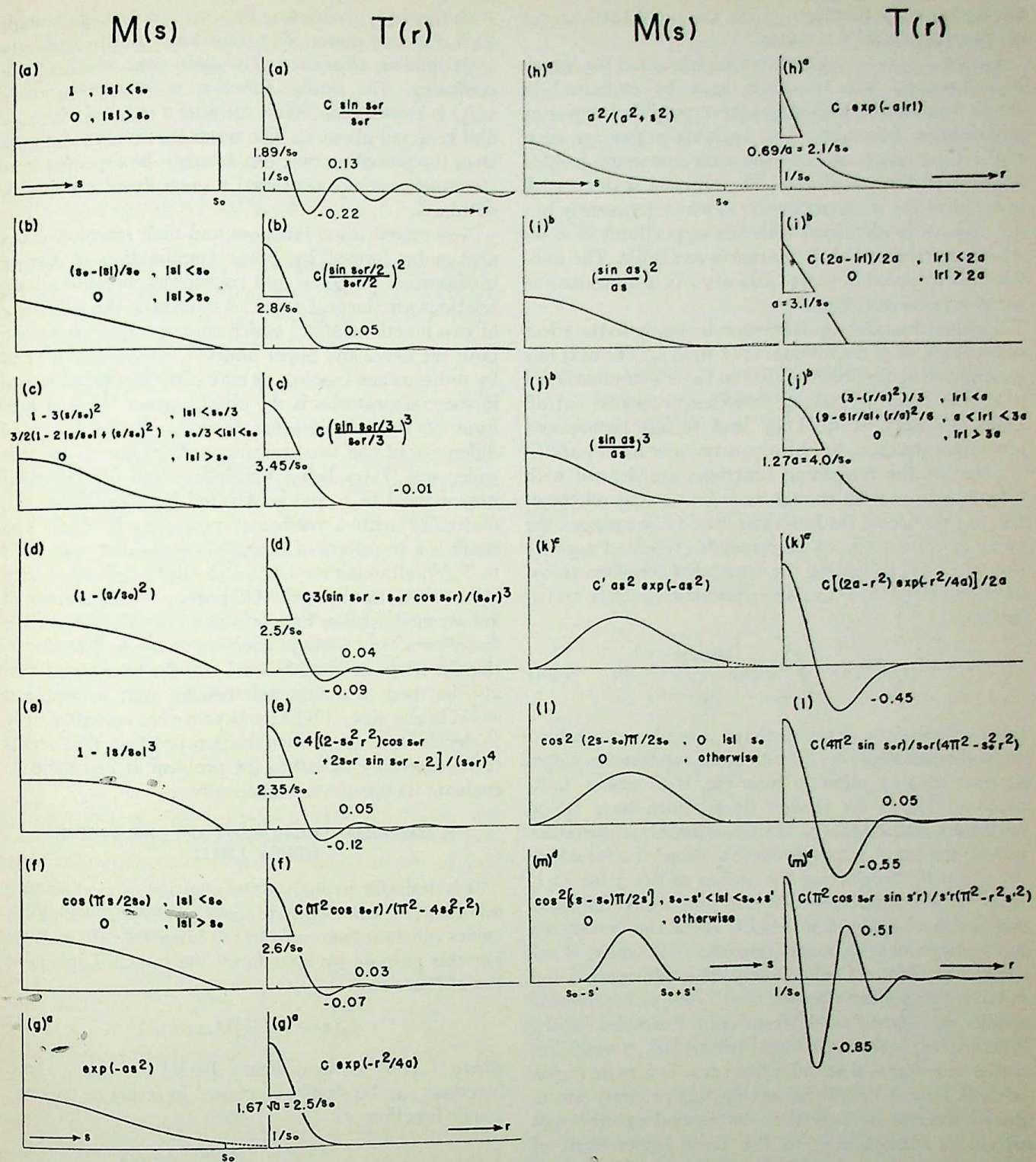
$$sI(s)=(2/\pi)^{\frac{1}{2}}\int_0^\infty rD(r)\,\sin rsdr \tag{4-1}$$

is merely transformed into another integral equation

$$rD'(r)=(2\pi)^{-\frac{1}{2}}\int_{-\infty}^\infty uD(u)T(r-u)du, \tag{4-2}$$

CC-0. In Public Domain. Gurukul Kangri Collection, Haridwar

Digitized by Arya Samaj Foundation Chennai and eGangotri



[a] For a chosen such as to make $M(s_0) = 0.1$.
[b] For a chosen such that the first zero of $M(s_0)$ falls on s_0.
[c] The graphs correspond to C' and a chosen such as to make $M_{max} = 1.0$ and $M(s_0) = 0.10$.
[d] The graphs correspond to $s' = s_0/2$.

FIG. 1. Examples of modification functions $M(s)$ and their transforms $T(r)$.

which still has to be solved in one way or another. For the applications considered here the convenience achieved is indeed often very great. Even more important is the circumstance that in practice no unique solution is possible without the use of assumptions based on external knowledge—and these assumptions can usually be introduced by far the more easily and naturally into the consideration of the transformed Eq. (4-2). Prime examples are the many successful interpretations which have been made of incomplete

CC-0. In Public Domain. Gurukul Kangri Collection, Haridwar

Digitized by Arya Samaj Foundation Chennai and eGangotri

electron density functions in the course of the analysis of complex crystal structures.

Figure 1 presents a number of functions for which both function and transform may be expressed in simple form and which might have possible interest as modification functions. The ordinate scales are such that all the functions have the same maximum height; likewise all the transforms. The abscissa scales are all in terms of the same parameter s_o which frequently but not always is identified with the upper limit of s for which experimental information is available. The half-width is included in most cases also. It is a measure of the sharpness of the peak.

The first function (a) corresponds simply to the effect of breaking off of the integral in (1-9) at s_o. The next five examples (the first corresponds to Fejér's summation of a Fourier series by taking first Cesàro means) cut off more gradually at s_o. They lead to less pronounced secondary maxima, but also to a broader main peak.

Some of the remaining functions are defined with reference to s_o even though they do not cut off there. But in practice all the functions have to be assigned the value zero for $s>s_o$, as corresponds [repeated application of (3-3)] to folding the illustrated complete transforms with $(\sin s_o r)/s_o r$. The resulting effective transforms

$$T'(r)=(2\pi)^{-\frac{1}{2}}\int_{-\infty}^{\infty}T(u)\frac{\sin s_o(r-u)}{s_o(r-u)}du \qquad (4\text{-}3)$$

are of somewhat changed shape, usually with added secondary maxima, in a way that one can learn to judge, at least roughly, directly from the $M(s)$ values, indicated in Fig. 1 by broken lines, which have to be neglected. Function (g) is the artificial temperature factor; the graph corresponds to a value of a for which $M(s_o)=0.10$. Neglecting the values of $M(s)$ for $s>s_o$ leads to a transform which has practically the same half-width at half-height ($\sim 2.7/s_o$) as the one shown but shows weak secondary maxima;[17] actually, it resembles transform b quite closely. The transforms h and k will suffer similar changes, and i and j considerably smaller and somewhat different ones. Examples i and j (and b and c) involve the form $[(\sin as)/as)]^n$, which has cosine transforms that differ from zero in a finite region $|r|\leqq na$ only.[16] Functions having this property are of special interest because they correspond exactly—not merely approximately—to the finite upper limit of integration; a general treatment of them is given below.

Functions k and l are of interest if it is desired to give the inner part of $sI(s)$ especially small weight, perhaps either because the small angle data were unreliable or in order to discriminate between terms of $rD(r)$ which had different real temperature factors (i.e., values of $\langle \delta r_{ij}^2 \rangle_{Av}$). Modification functions such as these of course also tend to emphasize large values of s, and so lead to transforms with relatively sharp main maxima and correspondingly high resolving power. The transforms shown both have large minima adjacent to the main peak which can be confusing. The similar function m is appropriate if $sI(s)$ is known in a certain range of s only, of width $2s'$ and centered about s_o. The transform is more complex than the preceding two, just as might be expected from the more severely restricted s range from which it is obtained.

New modification functions and their transforms can always be formed by linear combination of known modification functions and transforms, because all the relations are linear. Of special interest is the difference of two functions $M_a(s)$ which corresponds to replacing both the lower and upper limits of integration in (1-9) by finite values ($s_1<s_2$), as may often be desirable and in some laboratories is the usual practice.[13] The transform of this modification function is the weighted difference of the two transforms $T_1(r)$ and $T_2(r)$, the wider one $T_1(r)$ being multiplied with a coefficient proportional to s_1 and subtracted from the other one multiplied with a coefficient proportional to s_2. The result is a transform of increased complexity, compared to $T_a(r)$, although for $s_1 \ll s_2$ this additional complexity is not very troublesome. Of course, multiplication of known modification functions and convolution of their transforms (and perhaps even convolution of modification functions and multiplication of the transforms) can also be used to obtain new results. And in practical work, in any case, it is likely to prove convenient simply to decide upon some modification function that seems to be especially suited to the problem at hand and to evaluate its transform numerically.

5. GENERAL TREATMENT OF THE FINITE UPPER LIMIT

It is desirable to analyze the question of modification functions, we now designate them by $M_F(s)$, which have values different from zero in the range $0\leqq|s|\leqq s_o$ only. For this purpose we introduce[18] the so-called spherical Bessel functions[19]

$$j_n(x)=(\pi/2x)^{\frac{1}{2}}J_{n+\frac{1}{2}}(x), \qquad (5\text{-}1)$$

where $J_{n+\frac{1}{2}}(x)$ is an ordinary Bessel function. These functions can be simply expressed in terms of trigonometric functions as

$$j_n(x)=(-1)^n(2x)^n\frac{d^n}{d(x^2)^n}\left(\frac{\sin x}{x}\right), \qquad (5\text{-}2)$$

the first few members of the set being

$$j_0(x)=(\sin x)/x, j_1(x)=(\sin x)/x^2-(\cos x)/x$$

and

$$j_2(x)=(3/x^3-1/x)\sin x-(3\cos x)/x^2.$$

[17] V. Schomaker, Ph.D. thesis, California Institute of Technology, 1938.

[18] J. Waser, Phys. Rev. 85, 745 (1952).

[19] For example, L. I. Schiff, *Quantum Mechanics* (McGraw-Hill Book Company, Inc., New York, 1949).

CC-0. In Public Domain. Gurukul Kangri Collection, Haridwar

Digitized by Arya Samaj Foundation Chennai and eGangotri

The $j_{2k}(x)$ (of even order) have the desired property[16,20] of possessing a cosine transform which is different from zero in a finite range only, since

$$\int_0^\infty j_{2k}(x)\cos xt\,dx=\begin{cases}(\pi/2)(-1)^k P_{2k}(t), & |t|<1\\ 0, & |t|>1\end{cases}, \quad (5\text{-}3)$$

$$\int_0^1 P_{2k}(t)\cos xt\,dt=(-1)^k j_{2k}(x). \quad (5\text{-}4)$$

Here $P_{2k}(t)$ is the Legendre polynomial of (even) order $2k$. Since the Legendre polynomials form a complete set of orthogonal functions it is an easy matter to expand any reasonably well behaved $M_F(s)$ as

$$M_F(s)=\begin{cases}\sum_k(\pi/2)^{\frac{1}{2}}a_k(-1)^k P_{2k}(s/s_o), & |s|<s_o\\ 0, & |s|>s_o\end{cases}, \quad (5\text{-}5)$$

where $M_F(s)$ is regarded as even so that only even polynomials occur in the expansion. The cosine transform of $M_F(s)$ is then

$$T_F(r)=\sum_k a_k j_{2k}(rs_o). \quad (5\text{-}6)$$

The question as to what transforms $T_F(r)$ exist is accordingly the question of what class of functions can be represented as expansions of the type (5-6), which, if they exist, can be found with the help of the orthogonality and normalization relations

$$\int_0^\infty j_n(x)j_m(x)dx=\begin{cases}0, & m\neq n\\ \frac{1}{2}\pi/(2n+1), & m=n\end{cases}. \quad (5\text{-}7)$$

It is obvious, of course, that this class is limited (the $j_n(x)$ do not form a complete set), but there seems to be no simple criterion for characterizing functions of this type.[21]

Figure 2 shows the first few $T_F(r)$ and $M_F(s)$ components. The first,

$$j_0(s_o r)=\frac{\sin s_o r}{s_o r} \quad \text{and} \quad M_F(s)=\begin{cases}1, & |s|\leqslant s_o\\ 0, & |s|>s_o\end{cases},$$

are of course already familiar.[22]

[20] G. H. Watson, *Theory of Bessel Functions* (Cambridge University Press, Cambridge, 1944).

[21] See the analysis of the similar case of the Neumann expansion in Bessel functions in references 15 and 20.

[22] The integral (see references 16 and 20)

$$\text{const}\int_{-\infty}^{\infty}\frac{\sin s_o'(r-u)}{s_o'(r-u)}j_{2k}(s_o u)du=j_{2k}(s_o r), \quad s_o'\geqslant s_o,$$

expresses in perhaps surprising form a property obvious from the Fourier transform, possessed by any $M_F(s)$, namely, that the transform is unchanged if the integration is broken off at a point $s_o'\geqslant s_o$. The analogous expression for the special case that $M_F(s)$ itself represents a cutoff (at s_o) is

$$\text{const}\int_{-\infty}^{\infty}\frac{\sin s_o u}{s_o u}\frac{\sin s_o'(r-u)}{s_o'(r-u)}du=\begin{cases}\frac{\sin s_o r}{s_o r}, & s_o\leqslant s_o'\\ \frac{\sin s_o' r}{s_o' r}, & s_o\geqslant s_o'.\end{cases}$$

The examples shown in Figs. 1 and 2 show interesting generalities about which the following remarks appear pertinent. Perhaps the most notable are the indications, confirmed by all our experience, that suppression of subsidiary features of $T(r)$ gives rise to a broadening of the main peak. The properties of $T(r)$ at small values of r are exhibited by the expansion in ascending powers of r:

$$(\pi/2)^{\frac{1}{2}}T(r)=\int_0^{s_o}M(s)ds-\tfrac{1}{2}r^2\int_0^{s_o}s^2M(s)ds+r^4/4!\int_0^{s_o}s^4M(s)ds+\cdots, \quad (5\text{-}8)$$

having as coefficients the even moments of $M(s)$. For large values of r an expansion in inverse powers of r, obtained by repeated partial integration is more appropriate:

$$(\pi/2)^{\frac{1}{2}}T(r)=M(s_o)\frac{\sin s_o r}{r}+\frac{M'(s_o)}{r^2}\cos s_o r-\frac{M''(s_o)}{r^3}\sin s_o r+\cdots. \quad (5\text{-}9)$$

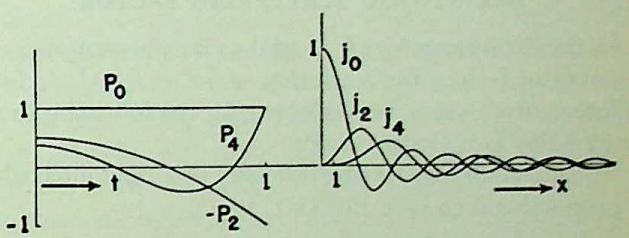


FIG. 2. The first three Legendre and circular Bessel functions of even order.

The first of these expansions confirms the further observation from Fig. 1 that sharp peaks—in the sense of initial curvature—correspond to modification functions which give greatest weight to large s values, whereas the second expansion gives substance to the impression that the dying out of subsidiary features depends on the smoothness with which $M(s)$ reaches zero at s_o.

These expansions show in a broad way the connection between the sharpness of the main peak and the extent of the subsidiary features, but the details are not clear. The sharpest transform shown in Figs. 1 and 2 is $T_a(r)=j_0(r)$, but (5-8) shows that still sharper peaks can be obtained simply by increasing the second moment of $M(s)$ while holding the area of $M(s)$ constant: The limiting case is the useless one of $M(s)=\delta(s-s_o)$.

A rather attractive criterion, on the other hand, might be that for a given peak height

$$T(0)=(2/\pi)^{\frac{1}{2}}\int_0^{s_o}M(s)ds, \quad (5\text{-}10)$$

CC-0. In Public Domain. Gurukul Kangri Collection, Haridwar

Digitized by Arya Samaj Foundation Chennai and eGangotri

the square fluctuation of $T(r)$

$$\int_0^\infty T^2(r)dr=(1/2\pi)\int_0^\infty M^2(s)ds \qquad (5\text{-}11)$$

(Parseval's relation)[15,16] should be minimized. This leads by a simple variation treatment to just the step function

$$M(s)=\begin{cases}1 & |s|\leq s_o\\ 0 & |s|>s_o\end{cases}, \qquad (5\text{-}12)$$

a result that is unchanged in higher dimensions. Since this result does not seem to be especially well suited to practice, it is evident that more subtle criteria play a decisive role in determining the usefulness of a modification function and its transform. These criteria will depend very much on the information desired and indeed a given problem may warrant making several inversions with different modification functions in order to facilitate different stages and aspects of the interpretation, such as separation of overlapping peaks, location and verification of the presence of small peaks, determination of peak areas, etc.

6. THE ATOMIC SCATTERING FACTOR

In the expression for $sI(s)$ used so far the assumption is contained that the variation of $[Z_i-f_i(s)]/Z_i$ for different atoms may be neglected. In the following this assumption is no longer made.

The molecular scattering intensity of a rigid molecule is proportional to [see Eq. (1-1)]

$$sI_m(s)=\left(\frac{2}{\pi}\right)^{\frac{1}{2}}\sum_{ij}'\frac{(Z_i-f_i(s))(Z_j-f_j(s))}{r_{ij}s^4}\sin sr_{ij}$$

$$=\left(\frac{2}{\pi}\right)^{\frac{1}{2}}\sum_{ij}'\frac{\psi_i(s)\psi_j(s)}{r_{ij}}\sin sr_{ij}, \qquad (6\text{-}1)$$

where

$$\frac{Z_i-f_i(s)}{s^2}=\psi_i(s) \qquad (6\text{-}2)$$

is the atomic form factor for electrons. When the function $s^5I_m(s)$ is inverted[14] the contributions of each $\sin sr_{ij}/sr_{ij}$ term to the resulting radial distribution function is centered at r_{ij} and has a (symmetrical) shape characteristic of atoms i and j:

$$T_{ij}(r)=\left(\frac{2}{\pi}\right)^{\frac{1}{2}}\int_0^\infty s^4\psi_i(s)\psi_j(s)\cos sr\,ds, \qquad (6\text{-}3)$$

so that

$$rD(r)=\left(\frac{2}{\pi}\right)^{\frac{1}{2}}\int_0^\infty s^5I_m(s)\sin sr\,ds \qquad (6\text{-}4)$$

is given by

$$(2\pi)^{-\frac{1}{2}}\sum_{ij}'r_{ij}^{-1}\int_{-\infty}^\infty[\delta(u-r_{ij})-\delta(u+r_{ij})]T_{ij}(r-u)du$$

$$=(2\pi)^{-\frac{1}{2}}\sum_{ij}'r_{ij}^{-1}[T_{ij}(r-r_{ij})-T_{ij}(r+r_{ij})]. \qquad (6\text{-}5)$$

The second term in the bracket makes $rD(r)$ antisymmetrical, as it did in (1-10) and (3-9).

The (ideal) peak shape may also be expressed as the result of a folding process

$$T_{ij}(r)=(2\pi)^{-\frac{1}{2}}\int_{-\infty}^\infty t_i(u)t_j(r-u)du, \qquad (6\text{-}6)$$

where we made use of the cosine transform $t_i(r)$ of $s^2\psi_i(s)$:

$$t_i(r)=(2/\pi)^{\frac{1}{2}}\int_0^\infty s^2\psi_i(s)\cos sr\,dr. \qquad (6\text{-}7)$$

The atomic form factor $\psi_i(s)$ is related to the density of scattering matter $\rho_i(r)$ of atom i by the equation[1]

$$s^2\psi_i(s)=\text{const}\int_0^\infty\rho_i(r)\frac{\sin sr}{sr}r^2dr \qquad (6\text{-}8)$$

and inversely

$$r\rho_i(r)=\text{const}\int_0^\infty s^2\psi_i(s)(s\sin sr)ds, \qquad (6\text{-}9)$$

which upon comparison with (6-7) yields

$$r\rho_i(r)=-\text{const}\frac{dt_i(r)}{dr} \qquad (6\text{-}10)$$

so that

$$t_i(r)=\text{const}\int_r^\infty u\rho_i(u)du. \qquad (6\text{-}11)$$

Similar relationships are valid for radial distribution functions obtained from the scattering of x-rays and neutrons as well. The ideal peak shapes for such distribution curves may be obtained by inversion of a product as in (6-3) or by operations (6-6) and (6-11). For figures showing the peak shape expected for light atoms like oxygen reference should be made to a paper by Viervoll[23] who chose the latter method for his calculations. If instead of inverting $s^5I_m(s)$, other functions such as (1-4) are inverted, other peak shapes $T_{ij}(r)$ result, but each peak shape is again dependent on the partners i and j and can be calculated by a formula analogous to (6-3).

For a nonrigid molecule with no internal rotation each term in $sI_m(s)$ would be multiplied by a different temperature factor $\exp(-a_{ij}s^2)$ [see Eq. (1-1)], the trans-

[23] H. Viervoll, Skrifter Norske Videnskaps Akad., Oslo, Mat. Naturv. Kl. No. 2 (1950).

CC-0. In Public Domain. Gurukul Kangri Collection, Haridwar

Digitized by Arya Samaj Foundation Chennai and eGangotri

form of which is the Gaussian $(4a_{ij}\pi)^{-\frac{1}{2}}\exp(-r^2/4a_{ij})$. The contribution $rD_{ij}(r)$ by a pair of atoms will then be the resultant of this Gaussian and the transform $T_{ij}(r)$ (6-3):

$$rD_{ij}(r)=(8a_{ij}\pi^2)^{-\frac{1}{2}} \times\int_{-\infty}^{\infty}\exp(-u^2/4a_{ij})T_{ij}(r-u)du. \quad (6\text{-}12)$$

Each peak in $rD(r)$ may thus contain the transform of a different temperature factor as well as of different form factors.

The fundamental meaning of the temperature factor is of course just this—that the real radial distribution peak is not infinitely sharp but has a finite width due to molecular vibrations. It is interesting that for molecules of the class under discussion the function $(4a_{ij}\pi)^{-\frac{1}{2}}\exp(-r^2/4a_{ij})$ is an appropriate approximation for $r^2D(r)/r_{ij}$ [rather than for $rD(r)$, as given by (6-4)] and that accordingly the conventional temperature factor corresponds to an $r^2D(r)$ equal to the assumed distribution multiplied by the factor r/r_{ij}. This remark[17] suggests simple corrections to the usual temperature factor; the first, for the example of intensity formula (1-1) alters the terms $\exp(-a_{ij}r^2)\sin r_{ij}s$ to the form

$$\left(1+\frac{2a_{ij}}{r_{ij}^2}\right)\exp\left[-\left(1+\frac{2a_{ij}}{r_{ij}^2}\right)a_{ij}s^2\right]\sin\left(1-\frac{2a_{ij}}{r_{ij}^2}\right)r_{ij}s,$$

in which the correction to r_{ij}, at least, will sometimes be important. In the derivation of the temperature factor by James,[24] based on the assumption of normal vibrations, a series expansion is used, the range of validity of which was not established. Karle and Karle,[25] on the other hand, modified the distribution characteristic for normal vibrations [it is not strictly Gaussian in $r^2D(r)$] by multiplication with r/r_{ij} and solved the remaining problem in closed form. Corrections of the sort mentioned above are evidently required, however, for all but the lowest order term, which is nothing more than the usual temperature factor.

The radial distribution functions of molecules involving large temperature librations[26] or internal rotations[27] contain peaks characteristically distorted by being folded with wide probability distributions, analogous to (6-12).

The application of the analysis of modification functions given in the previous section to the functions $rD(r)$ of this section is straightforward. For a given applied modification function, with transform $T(r)$, each contribution to the resulting distribution function will correspond to the folding operation

$$\int_{-\infty}^{\infty}uD_{ij}(u)T(r-u)du, \quad (6\text{-}13)$$

where $rD_{ij}(r)$, of course, describes the peak which would have been obtained by inverting the unmodified scattering function $s^5I_m(s)$ in the range $0\leq s<\infty$.

All these results [like (6-5), (6-12), (6-13)] involve symmetrical transforms T. This makes it clear why it is preferable to construct $rD'(r)$ rather than $D'(r)$ or $r^2D'(r)$ which might at first glance appear to be the more natural functions to evaluate, because of their more obvious physical interpretation, as evidenced in one instance by the above discussion of the real temperature factor [folding the scattering density $\rho(r)$ with itself and integrating over all orientations leads to $4\pi r^2D(r)$]. The great advantage of $rD'(r)$, as has also been stressed by Viervoll,[23] is that of being composed additively of *symmetrical* peaks whose position, as our discussion shows, is not influenced by any of the multiplicative factors affecting the molecular scattering intensity—either term by term or as a whole. Neither $r^2D'(r)$ nor $D'(r)$ has this important property.

Interpretation of a radial distribution curve should obviously be made in terms of the various expected peak shapes. This may be a simple problem, provided suitable modification functions have been applied. In special cases, however, as instanced by serious overlap of peaks, it becomes necessary to take the expected peak shape into explicit account. This is, of course, the main problem and has to be handled by trial and error—by subtracting peaks from $rD'(r)$, by constructing a synthetic distribution curve, or by other methods. Brief expositions are given by Viervoll.[23] The use of several distribution functions made with different modification functions may be helpful. The expected peak shapes are best calculated by allowing for all the effects on the intensity side [$M(s)$, $\psi_i(s)$, $\psi_j(s)$, temperature factor], and then inverting the complete modification function as in (6-3) rather than by using the several folding processes (6-6), (6-12), and (6-13) in turn, at least if numerical facilities for cosine as well as sine inversion are available.

With regard to the widths of the various peaks the rule may be used that the square of the half-width of a peak is approximately equal to the sum of the squares of the half-widths expected from the various items discussed above, a rule which is rigidly true only if all the modifying effects are Gaussian (3-5). In particular, the half-widths due to the step function $M_a(s)$ and the usual artificial temperature factor $M_g(s)$ (Fig. 1) are $1.9/s_o$ and $2.7/s_o$, respectively, and approximate corrections to obtain the natural peak widths can be made accordingly. For more exact information detailed analysis (or synthesis) of the peak shape is necessary.

[24] R. W. James, Physik. Z. 33, 737 (1932).
[25] J. Karle and I. M. Karle, J. Chem. Phys. 18, 957 (1950).
[26] P. Debye, J. Chem. Phys. 9, 55 (1941); J. Karle, J. Chem. Phys. 15, 202 (1947).
[27] J. Karle and H. Hauptman, J. Chem. Phys. 18, 875 (1950).

CC-0. In Public Domain. Gurukul Kangri Collection, Haridwar

Digitized by Arya Samaj Foundation Chennai and eGangotri

7. LIQUIDS AND AMORPHOUS SOLIDS

The foregoing discussion illuminates the following confusing notions to be found in the literature on distribution functions for amorphous substances and liquids:[28]

(1) When several kinds of atoms are involved, "simple Fourier inversion [of the part of the scattering intensity due to interatomic interactions] is no longer possible . . . and . . . approximations have to be used."

(2) The number of interatomic interactions at a given distance is found by inversion of the suitably modified interatomic part of the intensity function and multiplication by r, to obtain an *atomic* distribution function whose peaks have areas proportional to the *numbers* of atom pairs involved in the interactions (as well as to the products of effective atomic numbers).

The Fourier *transform* of the interatomic part of the scattering function can of course always be calculated and (in the ideal case of perfect data for an infinite range) may be regarded as a radial distribution function of scattering density—of electron density in the x-ray case. However, if it is realized that the intensity function can be written as a sum of terms characteristic of different kinds of *pairs* of atoms (rather than of different kinds of atoms), it is clear that all these terms can be *inverted*. And the sum of these terms is identical with the above transform, in consequence of the linearity of the inversion process.

A concrete formulation for the case of x-rays will perhaps be helpful. As stated, the interatomic part $sI(s)$ of the scattering function is the sum

$$sI(s)=\sum_{n\leqslant m} si_{nm}(s) \tag{7-1}$$

of terms $si_{nm}(s)$

$$si_{nm}(s)=(2/\pi)^{\frac{1}{2}}\int_0^\infty rd_{nm}(r)\,\sin srdr, \tag{7-2}$$

each of which concerns atoms of kinds n and m only. Here $rd_{nm}(r)=rd_{mn}(r)$ is a radial distribution function of electron density for atom pairs of kind (n, m): $4\pi r^2 d_{nm}(r)$ is the result of folding the electron density due to atoms of kind n with that due to atoms of kind m and integrating over all orientations. Inversion of (7-2) and (7-1) yields (7-3) and (7-4):

$$rd_{nm}(r)=(2/\pi)^{\frac{1}{2}}\int_0^\infty si_{nm}(s)\,\sin srds; \tag{7-3}$$

$$rD(r)=(2/\pi)^{\frac{1}{2}}\int_0^\infty sI(s)\,\sin srds=\sum_{n\leqslant m} rd_{nm}(r). \tag{7-4}$$

Each of the electronic distribution functions $rd_{nm}(r)$ may be analyzed in terms of an "atomic" distribution function $r\Delta_{nm}(r)$ defined by

$$si_{nm}(s)=f_n(s)f_m(s)(2/\pi)^{\frac{1}{2}}\int_0^\infty r\Delta_{nm}(r)\,\sin srdr, \tag{7-5}$$

with $f_n(s)$ the atom form factor for atoms of kind n, so that $r\Delta_{nm}(r)$ is given by

$$r\Delta_{nm}(r)=(2/\pi)^{\frac{1}{2}}\int_0^\infty \frac{si_{nm}(s)}{f_n(s)f_m(s)}\sin srds. \tag{7-6}$$

The relation between $r\Delta_{nm}(r)$ and $rd_{nm}(r)$ is again one of folding:

$$rd_{nm}(r)=(2\pi)^{-\frac{1}{2}}\int_{-\infty}^\infty u\Delta_{nm}(u)t_{nm}(u-r)du; \tag{7-7}$$

$$t_{nm}(r)=(2/\pi)^{\frac{1}{2}}\int_0^\infty f_n(s)f_m(s)\,\cos srds. \tag{7-8}$$

Relations analogous to (6-6)–(6-11) connect $t_{nm}(r)$ with the electron densities of atoms n and m.

While this clarifies the meaning of $rD(r)$ in terms of the atomic distribution functions $r\Delta_{nm}(r)$, it is also evident that the problem of separating $rD(r)$ into its components will be difficult if not hopeless, since each $r\Delta_{nm}(r)$ may itself be a complicated function with many features. Frequently, especially for light atoms, the functions $f_n(s)$ are approximately proportional to each other:

$$f_n(s)\approx K_n\frac{\sum_m f_m(s)}{\sum_m Z_m}=K_n f_e(s), \tag{7-9}$$

where K_n is a constant approximately equal to the atomic number Z_n and $f_e(s)$ is the average scattering power per electron. The functions $t_{nm}(r)$ reduce in this case to

$$t_{nm}(r)\approx K_nK_m(2/\pi)^{\frac{1}{2}}\times\int_0^\infty f_e^2(s)\,\cos srds=K_nK_m t_e(r), \tag{7-10}$$

so that all distribution functions $rd_{nm}(r)$ assume similar character. It then becomes possible either to analyze $rD(r)$ in terms of the general peak shape $t_e(r)$, or to form by inversion of $si(s)/f_e^2(s)$ a distribution function

$$r\Delta(r)=\left(\frac{2}{\pi}\right)^{\frac{1}{2}}\int_0^\infty \frac{sI(s)}{f_e^2(s)}\sin srds \approx\sum_{n\leqslant m} K_nK_m r\Delta_{nm}(r) \tag{7-11}$$

which is the weighted sum of the various atomic distribution functions. (The actual peak shapes may, of course, be further modified as discussed previously.)

This result, although essentially similar to the usual

[28] For example, R. W. James, *The Optical Principles of the Diffraction of X-Rays* (Macmillan and Company, Ltd., London, 1950), p. 504.

CC-0. In Public Domain. Gurukul Kangri Collection, Haridwar

Digitized by Arya Samaj Foundation Chennai and eGangotri

one,[28] differs from it in being stated explicitly in terms of the different kinds of atom pairs and in being closely related to the precise formulas (7-4) to (7-8) so as to suggest the correct interpretation of $rD(r)$ in terms of atomic distribution functions even when the approximation (7-9) is no longer valid. It is now evident that the difficulties in the conventional exposition are caused by the introduction of functions $\rho_m(r)$ which are characteristic of atoms rather than of atom pairs.

For homoatomic liquids the situation as discussed so far becomes trivial, in agreement with the usual discussion, since all terms in (7-1) and (7-11) reduce to one. However, the analysis of $rD(r)$ into characteristic subdistributions (e.g., temperature-factor Gaussians), as will often be desirable, is in principle just as complex for homoatomic as for heteroatomic liquids, since each subdistribution will have its own characteristic shape (e.g., width). For molecular liquids, indeed, this added bit of complexity can be turned to advantage, since it will usually permit a separation of the intramolecular components of $rD(r)$, which are generally the sharper ones by a large margin from the intermolecular components. The total effect is especially favorable if the desired intramolecular terms are not only the sharper ones but also have the greater weight, pair for pair, as when strongly scattering complex, rigid molecules are dispersed in a weakly scattering, molecularly simple solvent.[29]

Although the general discussion of modification functions given previously applies to this section also, some special remarks seem to be called for.

The modification of $sI(s)$ by multiplication with $f_e^{-2}(s)$ in the construction of $r\Delta(r)$ (7-11) has besides the desirable effect of sharpening peaks the undesirable one of introducing subsidiary features of a nature which may significantly encumber the analysis of the distribution function. This is all the more troublesome, if the distribution function is no longer interpretable in terms of characteristic distances but rather has to be regarded just as a distribution function or a sum of distribution functions in their own rights. This point has been stressed by Finbak.[30]

The conventional multiplication of $rD'(r)$ (the direct result of the inversion) by r is unfortunate because it is in $rD'(r)$ rather than $r^2D'(r)$ that the various multiplicative factors, like form factors and modification factors, leave symmetrical peaks symmetrical and unshifted. It seems appropriate, therefore, even in the case of the atomic distribution function $r\Delta'(r)$ (7-11) not to multiply it with r, but rather to compare it directly with the theoretical function $r^2\Delta_{th}(r)$ of interest divided by r. (The usual additive parabolic term[28] $r^2\Delta_0(\Delta_0=\text{const})$ is of course to be replaced by a linear term $r\Delta_0$. This term arises from the fact that in practice the integral in the inversion (7-4) is assumed to have a negligible value as s approaches zero. However, if the intensity due to a particle of constant scattering density is calculated, it is found to be concentrated at very small values of s, of the order D^{-1} where D is the linear dimension of the particle. This small angle scattering is essentially the same for particles of nonuniform scattering density. Its omission from an inversion like (7-4) has the consequence that the resulting function represents the difference between the actual distribution function and that corresponding to a uniform, average scattering density.)

[29] Vaughan, Sturdivant, and Pauling, J. Am. Chem. Soc. 72, 5477 (1950); O. Kratky and W. Worthmann, Monatsh. Chem. 76, 263 (1947); E. Rumpf, Ann. Physik 9, 704 (1931).

[30] C. Finbak, Acta Chem. Scand. 3, 1279, 1293 (1949).

8. EXTENSION TO SEVERAL DIMENSIONS

In order to extend the previous results to Fourier series such as are used in crystal structure analysis, it seems essential to introduce alternative representations by means of Fourier integrals. In order to illustrate this procedure and to give incidentally yet another example of the power of the folding theorem, the connection between the Fourier transform of the electron density and the structure factors for a crystal will first be established along the lines of Ewald's classic paper.[31]

The electron density of an ideal crystal of infinite size is a triply periodic function,

$$\rho(\mathbf{r})=\rho(\mathbf{r}+n_1\mathbf{a}_1+n_2\mathbf{a}_2+n_3\mathbf{a}_3),$$
$$n_i=\cdots-2,-1,0,1,2\cdots,\quad i=1,2,3, \tag{8-1}$$

of the position vector with the vector periods $\mathbf{a}_1$, $\mathbf{a}_2$, and $\mathbf{a}_3$, which define the unit cell of the translation lattice of the crystal. In terms of the reciprocal lattice vectors, $\mathbf{h}=h_1\mathbf{b}_1+h_2\mathbf{b}_2+h_3\mathbf{b}_3$,

$$h_i=\cdots,-2,-1,0,1,2\cdots, \tag{8-2}$$

$$\mathbf{a}_i\cdot\mathbf{b}_j=\delta_{ij}, \tag{8-3}$$

the Fourier expansion of $\rho(\mathbf{r})$ takes the form[32]

$$\rho(\mathbf{r})=v_r^{-1}\sum_{\mathbf{h}}F_{\mathbf{h}}\exp(-2\pi i\mathbf{h}\cdot\mathbf{r}), \tag{8-4}$$

where v_r is the volume of the unit cell and the sum includes all reciprocal lattice points.

The coefficients $F_{\mathbf{h}}$ in this expansion are the structure factors

$$F_{\mathbf{h}}=\int_{\text{unit cell}}\rho(\mathbf{r})\exp(2\pi i\mathbf{h}\cdot\mathbf{r})dv_r. \tag{8-5}$$

If the crystal is not of infinite extent or if $\rho(\mathbf{r})$ is not otherwise really periodic, the above formulation is no longer strictly valid; in any case it is convenient to consider the Fourier transform of $\rho(\mathbf{r})$—we shall call it $F(\mathbf{q})$—for the entire crystal. The two functions are

[31] P. P. Ewald, Proc. Phys. Soc. (London) 52, 167 (1940).

[32] M. von Laue, *Röntgenstrahlinterferenzen* (2nd ed., Akademische Verlagsgesellschaft, Leipzig, 1948); W. H. Zachariasen, *Theory of X-Ray Diffraction in Crystals* (John Wiley and Sons, Inc., New York, 1945); R. W. James, *The Optical Principles of the Diffraction of X-Rays* (Macmillan and Company, Ltd., London, 1950).

CC-0. In Public Domain. Gurukul Kangri Collection, Haridwar

Digitized by Arya Samaj Foundation Chennai and eGangotri

symmetrically related,[31] with $F(\mathbf{q})$ a function of the continuously variable vector $\mathbf{q}=q_1\mathbf{b}_1+q_2\mathbf{b}_2+q_3\mathbf{b}_3$ in reciprocal space:

$$F(\mathbf{q})=\int_{\text{crystal}}\rho(\mathbf{r})\exp(2\pi i\mathbf{q}\cdot\mathbf{r})dv_{\mathbf{r}}; \tag{8-6}$$

$$\rho(\mathbf{r})=\int F(\mathbf{q})\exp(-2\pi i\mathbf{q}\cdot\mathbf{r})dv_{\mathbf{q}}. \tag{8-7}$$

(The normalization factor corresponding to $(2/\pi)^{\frac{1}{2}}$ of earlier sections becomes unity here due to the inclusion of the factor 2π in the exponent; the variable $\mathbf{q}$ is related to s by $s=2\pi|\mathbf{q}|$.) The integral in (8-7) extends over the whole of reciprocal space.

To establish the connection of the pair (8-4) and (8-5) with the pair (8-6) and (8-7), we note that an infinite periodic crystal may be represented by the folding of the contents of one unit cell into the *lattice function*, which is a sum of δ functions, each situated at a lattice point. The Fourier transform of this lattice function is the so-called *Laue function for infinite crystals*,[32] $L(\mathbf{q})$, which again consists of a collection of δ functions, each multiplied with $1/v_{\mathbf{r}}$ and situated at a reciprocal lattice point.

The Fourier transform

$$F_c(\mathbf{q})=\int_{\text{unit cell}}\rho(\mathbf{r})\exp(2\pi i\mathbf{q}\cdot\mathbf{r})dv_{\mathbf{r}} \tag{8-8}$$

of the electron density of one specified unit cell is related to $F(\mathbf{q})$ by

$$F(\mathbf{q})=F_c(\mathbf{q})L(\mathbf{q})=v_{\mathbf{r}}^{-1}\textstyle\sum_{\mathbf{h}}F_{\mathbf{h}}\delta(\mathbf{q}-\mathbf{h}), \tag{8-9}$$

since the folding of the contents of the specified unit cell with the lattice function to obtain $\rho(\mathbf{r})$ corresponds to multiplication of the transform $F_c(\mathbf{q})$ by the transform $L(\mathbf{q})$. Accordingly, $F(\mathbf{q})$, which refers to a strictly periodic, infinite crystal, is an essentially discontinuous function, proportional to the appropriate structure factor at each reciprocal lattice point and zero elsewhere, as is also evident from the representation of $\rho(\mathbf{r})$ by the Fourier series (8-4). The $F_{\mathbf{h}}$ are a sampling, at reciprocal lattice points, of the continuous transform $F_c(\mathbf{q})$ for a unit cell. It will be noted that although $F_c(\mathbf{q})$ in general depends upon which unit cell is specified, the samples $F_{\mathbf{h}}$ do not.

As Ewald[31] has discussed, the folding theorem is very useful in understanding the effect of crystal size on the shape of reflections. If a shape function be introduced which has the value unity inside the crystal and zero outside, then the electron density of an actual crystal is simply the product of the electron density of the infinite crystal with this shape function. This corresponds to the folding in Fourier space of the discrete transform (8-9) with the transform of the shape function. The resulting transform of the finite crystal consists therefore in a set of broadened features of finite extension in reciprocal space, identical in shape, but scaled proportionally to the structure factors. The crystal reflections are correspondingly broadened, as is the range of small angle-scattering which would be expected in the absence of interdomain and interparticle interference. (For small-angle scattering, of course, these latter effects usually dominate. Their consideration, like the consideration of crystal imperfections, rests fundamentally on the entire density function and its transform, but the manipulation of an ideal density function by multiplication and/or folding will often be profitable,[32a] as it is in our example of the finite crystal.)

The special shape function which covers exactly a specified unit cell leads to an interesting result. For definiteness, let this unit cell be situated with its center at $\mathbf{r}_o$ from the origin and have edges parallel to the crystal axes. The shape transform is then

$$v_{\mathbf{r}}\exp(2\pi i\mathbf{q}\cdot\mathbf{r}_o)\prod_{j=1}^{3}\frac{\sin\pi q_j}{\pi q_j}, \tag{8-10}$$

and the corresponding expression for the transform of the contents of one unit cell is

$$F_c(\mathbf{q})=\exp(2\pi i\mathbf{q}\cdot\mathbf{r}_o)\sum_{\mathbf{h}}F_{\mathbf{h}}\prod_{j=1}^{3}\frac{\sin\pi(q_j-h_j)}{\pi(q_j-h_j)}. \tag{8-11}$$

This is the inverse of the sampling picture exposed above: From the samples $F_{\mathbf{h}}$ the transform of a unit cell can be reconstructed by what is known as (three-dimensional) trigonometric interpolation.[33]

Expression (8-11) may suggest a direct determination at least of $|F_c(\mathbf{q})|$, the zeros of which (at any rate in the centrosymmetrical case) might provide important clues to changes in sign between adjacent structure factors. But this is not possible, for the phases of the $F_{\mathbf{h}}$ are as pertinent in (8-11) as are the amplitudes, and knowledge of the phase is essential in the construction of $|F_c(\mathbf{q})|$ also. Even more important, $F_c(\mathbf{q})$ has meaning only in regard to a unit cell of arbitrary shape and position; the phase of $F_c(\mathbf{q})$, in (8-11), would change if the origin were shifted and even more drastic changes would occur if a unit cell of different shape were to be singled out. The only invariant property of all possible interpolations (8-11) is that they have identical values for reciprocal lattice vectors $\mathbf{q}=\mathbf{h}$. All this is to be expected since unit cells, although useful in describing crystals, have no physical reality. Even more generally, it is arbitrary to generate the whole crystal by folding the complete contents of one unit cell with the lattice function, inasmuch as other functions extending over possibly many unit cells may be folded with the lattice function

[32a] For example, R. Hosemann, Z. Physik **128**, 1, 465 (1950); R. Hosemann and S. N. Bagchi, Acta Cryst. **5**, 612 (1952).

[33] E. T. Whittaker, Proc. Roy. Soc. (Edinburgh) **35**, 181 (1915); *Interpolatory Function Theory* (Cambridge University Press, Cambridge, 1935).

CC-0. In Public Domain. Gurukul Kangri Collection, Haridwar

Digitized by Arya Samaj Foundation Chennai and eGangotri

to obtain the same $\rho(\mathbf{r})$. This is especially pertinent in the case of the Patterson function: interpolation of $|F_\mathbf{h}|^2$ according to (8-11) yields the transform of one specified unit cell of the Patterson function, but except for $\mathbf{q}=\mathbf{h}$ this transform is not equal to $|F_c(\mathbf{q})|^2$ even when corresponding unit cells have been chosen. Nevertheless, a case for which (8-11) has practical significance is considered at the end of Sec. 10.

It is quite another matter when the unit cell of a molecular crystal is chosen to contain one or a small number of relatively rigid molecules. It may then be possible by external influences continuously to change the size and shape of the unit cell without changing the configurations of the molecules. In this way various samplings of $F_c(\mathbf{q})$, now characteristic of the molecules, may be made from which information about the signs of the structure factors may be deduced in centrosymmetrical cases. This idea was used by Perutz[34] and coworkers in determining the signs of some x-ray reflections of methemoglobin, for which the unit cell size and shape depend on the extent of hydration of the protein.

Projections of three-dimensional density are often useful. Consider first the projection ρ_2 along a crystallographic axis, upon a plane. If the projection axis is inclined it is convenient to project onto a perpendicular plane rather than the plane of the other two crystallographic axes in order that the projections of spherically symmetrical functions shall show circular symmetry. In practice the distinction involves merely the choice of scales and axes for plotting the projected function. We call the axis of projection $\mathbf{a}_3$, the projections of the other two axes $\mathbf{a}_1'$ and $\mathbf{a}_2'$, and the coordinates of $\mathbf{r}$ in this "monoclinic" system of axes x_1', x_2', and x_3'. Further, $\mathbf{R}_2$ is the projection of $\mathbf{r}$, A the area of the projection of the unit cell, $\mathbf{Q}$ the projection of $\mathbf{q}$ on the plane of $\mathbf{b}_1$ and $\mathbf{b}_2$ (which is parallel to the projection plane), and $dA_\mathbf{Q}$ the surface element of that plane; finally, $\mathbf{b}_3$ may be replaced by $\mathbf{b}_3'$ so as to obtain a triple $\mathbf{b}_1$, $\mathbf{b}_2$, $\mathbf{b}_3'$, reciprocal to $\mathbf{a}_1'$, $\mathbf{a}_2'$, $\mathbf{a}_3$.

The projection of $\rho(\mathbf{r})$ is given by

$$\begin{aligned}\rho_2(\mathbf{R}_2) &= \int_{-\infty}^{\infty} \rho(\mathbf{r}) a_3 dx_3' \\ &= \int_{-\infty}^{\infty} a_3 dx_3' \int_{-\infty}^{\infty} b_3' dq_3' \exp(-2\pi i q_3' x_3') \\ &\quad \times \int_{-\infty}^{\infty} dA_\mathbf{Q} F(q_1, q_2, q_3) \exp(-2\pi i \mathbf{Q}\cdot\mathbf{R}_2) \\ &= \int_{-\infty}^{\infty} F(\mathbf{Q}) \exp(-2\pi i \mathbf{Q}\cdot\mathbf{R}_2) dA_\mathbf{Q}, \qquad (8\text{-}12)\end{aligned}$$

where use of the δ-function of footnote 3 has been made. It should be noted that the projection $\rho_2(\mathbf{R}_2)$ is determined by the values of $F(\mathbf{Q})$ in the plane $(\mathbf{b}_1, \mathbf{b}_2)$ parallel to our plane of projection rather than by a projection of $F(\mathbf{q})$ onto it. The expression (8-12) is furthermore not dependent on periodicity of $\rho(\mathbf{r})$ and differs from the more conventional one

$$\int_0^1 \rho(\mathbf{r}) a_3 dx_3' = A^{-1} \sum_{h_1, h_2} F_{h_1 h_2 0} \times \exp(-2\pi i (h_1 x_1' + h_2 x_2')) \qquad (8\text{-}13)$$

by a factor N_3, the number of layers of (the now periodic) $\rho(\mathbf{r})$ projected in (8-12). (The factor N_3, while obvious in the relationship between the sides of (8-12) and (8-13) pertaining to real space, enters on the transform side of (8-12) through the fact that the Laue function for a one-dimensional crystal of N_3 unit cells has the value N_3 at $q_3=0$).

For the line projection of the electron density, the line on which the projected values are recorded is preferably chosen perpendicular to the directions of projection, which are parallel to a crystallographic plane, for definiteness called (100). We introduce the symbols $\mathbf{a}_1'$ and $\mathbf{R}_1$ for the projections of $\mathbf{a}_1$ and $\mathbf{r}$ and $\mathbf{B}$ for the projection of $\mathbf{q}$ on $\mathbf{b}_1$. The line projection is given by

$$\rho_1(\mathbf{R}_1) = \int_{-\infty}^{\infty} F(\mathbf{B}) \exp(-2\pi i \mathbf{R}_1\cdot\mathbf{B}) dB, \qquad (8\text{-}14)$$

the derivation being analogous to that of ρ_2 and $\rho_1(\mathbf{R}_1)$ being related to

$$\int_0^1 \int_0^1 \rho(\mathbf{r}) (\mathbf{a}_2 \times \mathbf{a}_3) dx_2 dx_3 = (a_1')^{-1} \sum_{h_1=-\infty}^{\infty} F_{h_1 00} \exp(-2\pi i h_1 x_1') \qquad (8\text{-}15)$$

in a similar way. The expression (8-14) again does not depend on any periodicity of $\rho(\mathbf{r})$, and the line projection is determined by the values of $F(\mathbf{q})$ along a parallel line in reciprocal space.

These relationships are symmetrical in the sense that the line or plane *section* of a function and the line or plane *projection* of its transform are also mutual transforms.

We are of course here mainly interested in the consequences of breaking off the Fourier series after a finite number of terms and, more generally, in the effects of any modification of the coefficients by multiplication with a function of $\mathbf{q}$. As has become evident in earlier sections the complete modification function may be regarded as the product of all factors in the expression to be transformed which are functions just of the variable of integration. Such factors are the imposed convergence and sharpening factors as well as the natural form and temperature factors. We shall some-

[34] Boyes-Watson, Davidson, and Perutz, Proc. Roy. Soc. (London) A191, 83 (1947); for the latest report, see W. L. Bragg and M. F. Perutz, Proc. Roy. Soc. (London) A213, 425 (1952).

CC-0. In Public Domain. Gurukul Kangri Collection, Haridwar

Digitized by Arya Samaj Foundation Chennai and eGangotri

times single out one or the other of them or, again, treat the complete product, but the nature of the modification function under discussion will always be obvious from the context. A general treatment of these effects appears unfeasible for multidimensional Fourier series without the use of the integral representation.

If

$$\rho'(\mathbf{r}) = \int_{-\infty}^{\infty} M(\mathbf{q}) F(\mathbf{q}) \exp(-2\pi i \mathbf{q}\cdot\mathbf{r}) dv_{\mathbf{q}}$$

$$= (v_r)^{-1} \sum_{\mathbf{h}} M_{\mathbf{h}} F_{\mathbf{h}} \exp(-2\pi i \mathbf{h}\cdot\mathbf{r}) \qquad (8\text{-}16)$$

is the electron density function resulting from the series with modified coefficients and if the transform of $M(\mathbf{q})$ is

$$T(\mathbf{r}) = \int_{-\infty}^{\infty} M(\mathbf{q}) \exp(-2\pi i \mathbf{q}\cdot\mathbf{r}) dv_{\mathbf{q}}, \qquad (8\text{-}17)$$

then the (three-dimensional) folding theorem implies

$$\rho'(\mathbf{r}) = \int_{-\infty}^{\infty} T(\mathbf{u}) \rho(\mathbf{r}-\mathbf{u}) dv_{\mathbf{u}} \qquad (8\text{-}18)$$

in complete analogy to (3-3). The corresponding two- and one-dimensional formulas are

$$\rho_2'(\mathbf{R}_2) = \int_{-\infty}^{\infty} T_2(\mathbf{U}) \rho_2(\mathbf{R}_2-\mathbf{U}) dA_{\mathbf{U}} \qquad (8\text{-}19)$$

and

$$\rho_1'(\mathbf{R}_1) = \int_{-\infty}^{\infty} T_1(\mathbf{U}) \rho_1(\mathbf{R}_1-\mathbf{U}) dU, \qquad (8\text{-}20)$$

where T_2 and T_1 are the respective projections of T.

9. RADIAL FUNCTIONS

In this section modification functions $M(\mathbf{q})$ will be discussed which depend on the length only of $\mathbf{q}$. Such functions have been called *radial functions*[16] and their transforms can be reduced to one dimension by introducing appropriate polar coordinates into (8-17):

$$T(r) = \int_0^{\infty}\int_0^{\pi}\int_0^{2\pi} M(q) \times \exp(-2\pi i q r \cos\vartheta) d\varphi \sin\vartheta d\vartheta q^2 dq, \qquad (9\text{-}1)$$

$$T(r) = 2/r \int_0^{\infty} M(q) \sin(2\pi q r) q dq.$$

The projection $T_2(R_2)$ of $T(r)$ onto a plane is given by the two-dimensional transform

$$T_2(R_2) = \int_{-\infty}^{\infty} M(Q) \exp(-2\pi i \mathbf{Q}\cdot\mathbf{R}_2) dA_{\mathbf{Q}}$$

$$= \int_0^{\infty}\int_0^{2\pi} M(Q) \exp(2\pi i Q R_2 \cos\varphi) d\varphi Q dQ$$

$$= 2\pi \int_0^{\infty} Q M(Q) J_o(2\pi Q R_2) dQ. \qquad (9\text{-}2)$$

The line projection $T_1(R_1)$, finally, is given by the one-dimensional transform

$$T_1(R_1) = \int_{-\infty}^{\infty} M(B) \exp(-2\pi i R_1 B) dB$$

$$= 2\int_0^{\infty} M(B) \cos(2\pi R_1 B) dB. \qquad (9\text{-}3)$$

which is of the form already encountered in previous sections. Writing $T_3(r)$ for $T(r)$ and abandoning the formal distinction between r, R_2 and R_1 makes possible a combination of the three formulas (9-1) to (9-3) into one[16]

$$T_i(r) = 2\pi r^{1-(i/2)} \int_0^{\infty} M(q) q^{i/2} J_{(i/2)-1}(2\pi q r) dq, \qquad (9\text{-}4)$$

where $J_{(i/2)-1}$ is the Bessel function of order $(i/2)-1$. Between T_1 and T_3 there exist the direct relations

$$T_3(r) = -\frac{1}{2\pi r}\frac{d}{dr} T_1(r)$$

and (9-5)

$$T_1(r) = 2\pi r \int_r^{\infty} T_3(u) du,$$

so that functions T_3 can be obtained from all functions $T_1(r)$ listed in Fig. 1 simply by differentiation and division by $-2\pi r$; T_2 is connected directly with T_3 and T_1 by the equations

$$T_i(r) = 2\int_r^{\infty} u T_{i+1}(u) (u^2-r^2)^{-\frac{1}{2}} du$$

and (9-6)

$$T_{i+1}(r) = -\frac{1}{\pi}\int_r^{\infty} \frac{dT_i(u)}{du} (u^2-r^2)^{-\frac{1}{2}} du; \quad i = 1, 2.$$

The effect of breaking off a three-, two-, or one-dimensional series by not using terms with $|\mathbf{q}| > q_o$ can be judged by considering the respective transforms of

$$M(q) = \begin{cases} 1, & |q| \leqslant q_o \\ 0, & |q| > q_o \end{cases}; \qquad (9\text{-}7)$$

namely,

$$T_i(r) = 2\pi r^{1-(i/2)} \int_0^{q_o} q^{i/2} J_{(i/2)-1}(2\pi q r) dq$$

$$= (q_o/r)^{i/2} J_{i/2}(2\pi q_o r), \qquad (9\text{-}8)$$

CC-0. In Public Domain. Gurukul Kangri Collection, Haridwar

Digitized by Arya Samaj Foundation Chennai and eGangotri

where the relation[35]

$$\int x^n J_{n-1}(x)dx = x^n J_n(x) \tag{9-9}$$

has been used. Written out in terms of $s_o = 2\pi q_o$, the three transforms are

$$T_1(r) = \frac{s_o}{\pi} j_0(s_o r) = \frac{1}{\pi r} \sin s_o r,$$

$$T_2(r) = \frac{s_o}{2\pi r} J_1(s_o r),$$

and (9-10)

$$T_3(r) = T(r) = \frac{s_o^2}{2\pi^2 r} j_1(s_o r)$$

$$= \frac{1}{2\pi^2 r^3}[\sin s_o r - s_o r \cos s_o r].$$

The first is familiar from the earlier discussion, and all have been derived by van Reijen,[10] and from a different point of view, by James,[36] who also discusses their shape. The effects of breaking off are evidently less serious the higher the dimensionality, which is not surprising if it is remembered that the section $T_i(r)$ is determined by the projection of $M(q)$ so that the *effective* break-off is more gradual the higher the dimensionality.

An example of a convergence factor which is zero outside the limiting sphere and whose transform can be expressed analytically is example d of Fig. 1,

$$M(q) = \begin{cases} 1-(q/q_o)^2, & |q| \le q_o \\ 0, & |q| > q_o \end{cases}; \tag{9-11}$$

the corresponding transforms, obtained by partial integration and the aid of (9-9), are

$$T_i(r) = \frac{q_o^{(i/2)-1}}{\pi r^{(i/2)+1}} J_{(i/2)+1}(2\pi q_o r), \tag{9-12}$$

$$T_1(r) = \frac{2}{\pi r} j_1(s_o r) = \frac{2}{\pi s_o^2 r^3}[\sin s_o r - s_o r \cos s_o r],$$

$$T_2(r) = \frac{1}{\pi r^2} J_2(s_o r),$$

and (9-13)

$$T_3(r) = T(r) = \frac{s_o}{\pi^2 r^2} j_2(s_o r)$$

$$= \frac{1}{\pi^2 s_o^2 r^5}[(3-(s_o r)^2)\sin s_o r - 3 s_o r \cos s_o r].$$

Again $s_o = 2\pi q_o$ has been introduced for easier comparison with Fig. 1. In keeping with the foregoing remark the present $T_1(r)$ (9-13) is essentially identical with the previous $T_3(r)$ (9-10). The transforms (9-10) and (9-13) are shown in Fig. 3.

The foregoing emphasis on the reduction which is afforded by the use of polar coordinates must not be taken to mean that this is always the best procedure. There are no doubt many counter examples. One is the familiar transform $T_3(r) = (2a)^{-\frac{1}{2}} \exp(-\pi r^2/2a)$ of the modification function $\exp(-2\pi a q^2)$, for which the projections are easily found by direct integration, either projection or transformation, in Cartesian coordinates (not the coordinates relative to the lattice vectors except for orthogonal crystals), whereas the use of polar coordinates proves unfruitful. The projections are

$$T_i(r) = (2a)^{(-i/2)} \exp(-\pi r^2/2a); \quad i = 1, 2.$$

The anisotropic Gaussian modification function, an important nonradial function, can be handled just as

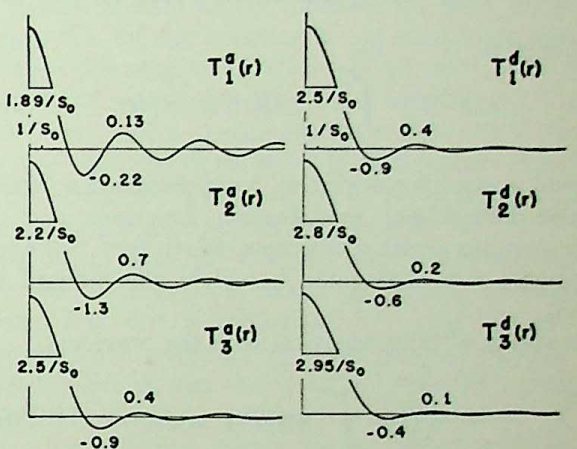


FIG. 3. One-, two-, and three-dimensional transforms corresponding to modification functions (a) and (d) of Fig. 1.

readily in this way. From our example, again, a whole series of mutual transforms and their sections and projections may be derived very simply by differentiation with respect to a. Two, (g) and (k), are shown in Fig. 1; another is the pair

$$M(q) = 4\pi^2 q^4 \exp(-2\pi a q^2),$$

$$T_3(r) = (2a)^{-7/2}[15 - 10\pi r^2/a + \pi^2 r^4/a^2] \exp(-\pi r^2/2a),$$

which has proved most useful in affording a Patterson function with near maximal resolving power. (The alterations corresponding to the necessary finite cutoff are in this case almost entirely negligible.)

10. SERIES TRANSFORMS

It may be useful sometimes, especially in numerical work, to calculate the series transform of a modification function, rather than the integral transform. This transform must again be folded with the original func-

[35] H. B. Dwight, *Tables of Integrals* (Macmillan and Company, Ltd., New York, 1934), 835.1.
[36] R. W. James, Acta Cryst. 1, 132 (1948).

CC-0. In Public Domain. Gurukul Kangri Collection, Haridwar

Digitized by Arya Samaj Foundation Chennai and eGangotri

tion, but the folding integral, in keeping with the periodic property of the series transform, now extends over one unit cell only. The simple development follows.

Consider the series representation (8-4) of $\rho(\mathbf{r})$:

$$\rho(\mathbf{r}) = v_r^{-1} \sum_{\mathbf{h}} F_{\mathbf{h}} \exp(-2\pi i \mathbf{h}\cdot\mathbf{r}); \tag{10-1}$$

$$F_{\mathbf{h}} = \int_{\text{unit cell}} \rho(\mathbf{r}) \exp(2\pi i \mathbf{h}\cdot\mathbf{r}) dv_r.$$

When the coefficients are modified by multiplication with $M_{\mathbf{h}}$, the series becomes

$$\rho''(\mathbf{r}) = v_r^{-1} \sum_{\mathbf{h}} M_{\mathbf{h}} F_{\mathbf{h}} \exp(-2\pi i \mathbf{h}\cdot\mathbf{r})$$

$$= v_r^{-1} \int_{\text{unit cell}} \rho(\mathbf{t}) \sum_{\mathbf{h}} M_{\mathbf{h}} \exp[2\pi i \mathbf{h}\cdot(\mathbf{t}-\mathbf{r})] dv_t,$$

which on writing $K(\mathbf{r})$ for the series transforms of $M_{\mathbf{h}}$,

$$K(\mathbf{r}) = v_r^{-1} \textstyle\sum_{\mathbf{h}} M_{\mathbf{h}} \exp(-2\pi i \mathbf{h}\cdot\mathbf{r}), \tag{10-2}$$

simplifies to

$$\rho''(\mathbf{r}) = \int_{\text{unit cell}} \rho(\mathbf{t}) K(\mathbf{r}-\mathbf{t}) dv_t. \tag{10-3}$$

Pepinsky and his associates[37] have discussed a number of one-dimensional modification functions and the corresponding series transforms, which they call kernel functions, $K(\mathbf{r})$ being the kernel in the integral Eq. (10-3).

Of course $\rho''(\mathbf{r})$ is identical with the previous

$$\rho'(\mathbf{r}) = \int_{-\infty}^{\infty} \rho(\mathbf{t}) T(\mathbf{r}-\mathbf{t}) dv_t, \tag{10-4}$$

where $T(\mathbf{r})$ is the integral transform of any $M(\mathbf{q})$ interpolated from the values $M(\mathbf{h})$, if only it $[M(\mathbf{q})]$ satisfies the general requirements for the Fourier theorems. Correspondingly, any one of the $T(\mathbf{r})$ on folding with the lattice function results in the same transform $K(\mathbf{r})$, which contains the contributions to a given unit cell of $T(\mathbf{r})$ as displaced successively by all the lattice vectors $\mathbf{l}$:

$$\textstyle\sum_{\mathbf{l}} T(\mathbf{r}+\mathbf{l}) = K(\mathbf{r}) = v_r^{-1} \sum_{\mathbf{h}} M_{\mathbf{h}} \exp(-2\pi i \mathbf{h}\cdot\mathbf{r}). \tag{10-5}$$

This equation is essentially Poisson's summation formula.[15,16]

The development so far tends to emphasize $M_{\mathbf{h}}$ and $K(\mathbf{r})$ and to make $M(\mathbf{q})$ and $T(\mathbf{r})$ appear arbitrary and comparatively unimportant. Nevertheless, it is profitable to adopt the point of view that $M(\mathbf{q})$ and $T(\mathbf{r})$ are the important fundamental functions, with $M(\mathbf{q})$ chosen as smooth as possible relative to the reciprocal lattice spacing and $T(\mathbf{r})$ accordingly restricted to relatively small values of $|\mathbf{r}|$, and that $M_{\mathbf{h}}$ and $K(\mathbf{r})$ depend upon them *and* the particular lattice under consideration. For although direct use of $K(\mathbf{r})$, the series transform, has the apparent advantage of at once taking into account the influence on a given peak of $\rho(\mathbf{r})$ by all the peaks of a set equivalent by the lattice translations, so that only the peaks within a unit cell have to be considered explicitly, the extra complexity of $K(\mathbf{r})$, as compared to a suitable $T(\mathbf{r})$, is likely to prove troublesome in practical work as well as general analysis. In effect, the use of the integral transform decomposes a complex total process into two simpler steps.

Some evident features of the situation are the following. In the first place $K(\mathbf{r})$ will lack radial symmetry. In practical work with actual density functions, it will therefore be much more difficult to handle, interaction for interaction, than radially symmetrical functions, which are readily obtained as integral transforms; and the advantage that follows from the smaller number of interactions that have to be considered may be lost. Even numerical evaluation of $K(\mathbf{r})$ is comparatively difficult, since a multidimensional sum has to be evaluated for a very large number of values of $\mathbf{r}$, whereas for $T(\mathbf{r})$ the radially symmetrical cases need to be evaluated in only one direction and by use of polar coordinates may always be reduced (see Sec. 9) to one-dimensional integrals. (Depending on the case and the computational facilities, however, it may be more convenient to deal with the original integral, with other coordinates.) A particular $M(\mathbf{q})$ and $T(\mathbf{r})$, once found satisfactory for a particular investigation, are apt to be suitable for other crystals of roughly similar elastic properties studied with the same equipment, regardless of the unit cell, whereas $K(\mathbf{r})$ evidently has to be calculated anew except in cases of precise isomorphism. On the analytical side, $T(\mathbf{r})$ can often be found in closed form, whereas the analytical evaluation of $K(\mathbf{r})$ would appear to be limited to a few one-dimensional cases and to products of these one-dimensional sums. It is important that even when $T(\mathbf{r})$ is not evaluated exactly, the general point of view affords an insight into the overlap problem which may in fact be adequate; if $K(\mathbf{r})$ has not been evaluated and the integral point of view is rejected, this insight is lacking. Finally, we remark that a radially symmetrical modification function can always be chosen which will restrict the significant overlap to closely neighboring peaks and that in this approximation (except for the smallest unit cells) the practical distinction between the series and integral transforms disappears. In this case it may be the more convenient to evaluate the series, for one especially simple direction of $\mathbf{r}$.

These relations between series and integral transforms afford an elegant and precise understanding of the approximation of the general (one or multidimensional) Fourier integral by a sum spaced at the points of an

[37] R. Pepinsky, Abstracts of Washington Meeting of the American Crystallographic Association, February, 1951.

CC-0. In Public Domain. Gurukul Kangri Collection, Haridwar

Digitized by Arya Samaj Foundation Chennai and eGangotri

arbitrary (one or multidimensional) lattice.[38] This sum will be the folding of the desired transform with the Laue function of the lattice, or stated differently, the sum multiplied by the "volume" of the unit cell of the lattice is the result of superposing the desired transform with its repetitions at all points of a lattice reciprocal to the original one. The approximation will be good only if the unit cell of the original lattice is small enough so there is no important overlap between the repeated transforms. With decreasing lattice spacing, accordingly, the approximation (sum) for compact transforms will converge very rapidly once the lattice spacing is small enough; most remarkably, the sum for any transform which is restricted to a finite range of $\mathbf{r}$ becomes exact in that finite range, for a certain spacing of terms and for smaller spacings is quite independent of the spacing.

The interplay of the series and integral points of view also suggests the discussion of a number of minor questions not always correctly stated, which concern the convergence of the ordinary electron density series and the amount of information it contains regarding the shape $\rho_i(\mathbf{r})$ of the contribution of a particular atom i.

Thus, it is sometimes said[39] that the resolving power of the series will be low unless the number of terms is large. That there should be an effect which is characteristic just of the number of terms seems obvious. However, the fundamental peak shape given by the integral transform is determined solely by the complete modification function, of which the cutoff incidentally limits the number (but not the spacing) of terms, and if the number of terms is varied by varying the spacing, the resolving power is affected only in so far as the overlap of lattice-equivalent peaks is involved.

Again, it is obvious that the series will be affected much or little by a certain increase of the radius of cutoff according to the magnitude of terms so admitted, and concern is consequently sometimes expressed over the question of whether, even when the typical $F_\mathbf{h}$ has fallen to a low value, a number of especially strong reflections may happen to be just outside the sphere of reflection, so as to invalidate the conclusion that the only effects of increasing the cut-off radius slightly would correspond to the resulting slight changes in peak shape. The resolution of this situation depends upon the observation that only if the Fourier series is well converged, in the sense that $T(\mathbf{r})$ does not have relatively large oscillations extending to relatively large values of $\mathbf{r}$, will it be true that small changes in $T(\mathbf{r})$, caused perhaps by small changes in the cutoff, will have only small effects on $\rho'(\mathbf{r})$. For otherwise the background, on the average small, resulting from the essentially random superposition of large numbers of these oscillating contributions will typically show large relative variations when these oscillations are but little changed. Accordingly, a well-resolved Fourier series, perhaps by virtue of an imposed convergence factor, will not exhibit large changes when the complete modification function is changed slightly; correspondingly, a density series, for example, which is naturally well resolved will not change sharply as the cutoff is changed. In other words the type of sudden resurgence of strong F's presumed at the beginning of this paragraph cannot actually occur.

Lastly, it has been remarked[40] that if a good experimental determination of the atom form factor is to be desired from crystal reflections, a crystal of large unit cell, affording by its many reflections many samples of $f(\sin\vartheta/\lambda)$, must be used. But the essential problem is again peak overlap, a problem which would indeed be ameliorated if the unit cell could be expanded without adding more atoms, which of course it cannot in actual crystals. The obvious solution lies rather in reducing the temperature far enough to minimize the effects of thermal vibrations and in suitably decreasing the wavelength. Further still, the present considerations lead to an understanding of the problem of how to choose among the infinite number of possible interpolations between the samples of $f(\sin\vartheta/\lambda)$ afforded by a given crystal and wavelength. One must compute $\rho(\mathbf{r})$, partition it into atoms—perhaps quite arbitrarily if there is overlap—and transform one of them to obtain $f(\sin\vartheta/\lambda)$. If the atoms are well resolved in $\rho(\mathbf{r})$, the reasonable partitioning is accomplished—assuming for the present one atom at $\mathbf{r}_o$ per unit cell—by taking the contents of a unit cell centered at $\mathbf{r}_o$ whose boundaries do not slice atoms. But this is equivalent to modifying $\rho(\mathbf{r})$ by multiplication with the unit cell shape function discussed in Sec. 8, and the result for $f(\sin\vartheta/\lambda)$, given by Eq. (8-11), is obtained by folding the transform of this shape function with the reciprocal lattice, as weighted with the observed $F_\mathbf{h}$. With more than one atom in the unit cell, or with a lattice so skewed that all possible choices of the unit would slice atoms, the $f_i(\sin\vartheta/\lambda)$ may still be obtained, in an approximation of validity corresponding to the magnitude of any overlap, by the same procedure, now to be carried out with appropriate shape functions—not necessarily parallelepipeds—centered at the respective atoms. Although it is really $\rho'(\mathbf{r})$ and complete atomic modification functions $M_i(\mathbf{h})$ which have to be manipulated, it will be noted that approximations to the true $M_i(\mathbf{q})$ are nevertheless obtained by this procedure and that the $f_i(\sin\vartheta/\lambda)$ inside the cutoff then follow by dividing out the real temperature factors—if they are known—and the imposed modification function. Overlap will be affected by the imposed modification function in a way so complicated, however, as to preclude the use of any formula like (8-11), so that if overlap is important, it becomes necessary somehow to analyze $\rho'(\mathbf{r})$ in terms of the transform of the products of the respective temperature factors by the imposed

[38] An example is provided by the calculation of structure factors by Fourier summation described by D. Sayre, Acta Cryst. 4, 362 (1951), who also discusses the nature of the approximation involved.

[39] For example, reference 28, bottom of p. 370.

[40] Reference 4, p. 825.

CC-0. In Public Domain. Gurukul Kangri Collection, Haridwar

Digitized by Arya Samaj Foundation Chennai and eGangotri

modification function, to suitably decompose the peaks of the resulting $\rho(\mathbf{r})$, if they still overlap, and to calculate their transforms.

11. CONCLUDING REMARKS

It is obvious that the general discussions given in earlier sections pertain to several dimensions as well. A number of specific additional remarks follow.

Modification functions may again be useful to improve convergence of Fourier series, but it is evident that the resulting peak shape will in general depend on the number of dimensions (see Fig. 3; comparison is of course possible only for radial functions), the Gaussian being an exception and the effects of cutoff being less severe the greater the number of dimensions. [The last point may also be seen from general arguments, as in the remark following (9-10) or from a development analogous to (5-9).] Nevertheless, the feasibility of introducing convergence factors does not seem to be generally recognized. For example, the atom form factors describing the scattering of thermal neutrons are constants, so that the only cause for a general decrease of intensities at high scattering angles is the motion of the atoms, and Lonsdale[41] has commented that "only trial and error methods of structure analysis are possible." However, a suitable convergence factor will always lead to sound Fourier maps, as has also been remarked by Thewlis,[42] and the only serious question is the universal one of how to make the compromise between desirable simplicity of interpretation and the concomitant undesirable loss of essential resolving power. But for some crystals the natural temperature effect will already provide adequate convergence with the current experimental conditions, and there is always the possibility, for harder crystals, of shortening the wavelength and so increasing the power of resolution.

Booth[43] has raised objections to the use of a convergence factor on the grounds that they "introduce errors greater than for the elimination of which [they are] applied." In support of this contention he shows a table containing the maximum errors of peak positions which may be caused by terminating a one-, two-, or three-dimensional series, as well as a table of the maximum errors caused by using different artificial temperature factors in a three-dimensional sum. However, these tables would appear to pertain only to the very specific example underlying them, that of two neighbors at a distance of 1.4A (or larger) having radial, Gaussian density distributions of a width characteristic for organic crystals. Unfortunately, no lower distance limit of 1.4A exists for Patterson functions or for projections of the electron density; different results would further be expected for heavier atoms, harder crystals, low temperature data, or neutron diffraction data; finally a number of distant peaks may cause significant shifts in a terminated series, whereas the peak broadening due to a convergence factor will affect close neighbors only. Again, the advantage of using a convergence factor lies in the simplicity of its transform, which facilitates detailed analysis of peak shapes should any be required.

A recently proposed way[44] of handling the breaking-off error is the now often used back-shift method which involves comparison of the Fourier map based on observational data with a similar map obtained from calculated structure factors, all terms which were lacking in the first sum being omitted in the second one also. Alternately,[45] an $F_o - F_c$ synthesis may be carried out using as coefficients the difference between calculated and observed structure factors. Accurate knowledge of the form and temperature factors is a very important requirement, to which, it seems, too little attention is ordinarily given. Weighting with a suitable modification function will be helpful in this connection if the accuracy of the assumed form and temperature factors can be estimated as a function of $\mathbf{h}$.

These methods are equivalent to the peak by peak analysis discussed above. They have the advantage of dealing with the crystal as a whole and thus, if the peaks have not been made reasonably compact, may actually entail less calculation. In a peak by peak analysis, on the other hand, in which important interactions only need to be dealt with in detail, the assumed peak shapes (which is to say the form, temperature, and imposed modification factors) are necessarily checked, or else the correct peak shapes can be taken directly from the map under analysis, at least if it is not hopelessly complicated. If the thermal motions are anisotropic with principal axes oriented unsymmetrically to the principal symmetry elements of the crystal, as often happens, it is inconvenient to make appropriate precise structure factor calculations and the present direct analysis should be especially advantageous.

Van Reijen[9] seems inclined to favor inclusion of extrapolated coefficients in order to avoid termination errors while still making full use of far-out reflections. If not really correct, however, such an extrapolation will lead to error. Indeed, van Reijen's (110) projection of diamond, which he gives as an example, shows questionable high frequency details near the centers of the carbon six-rings which presumably must be attributed either to extrapolation errors or possibly to experimental errors in high order terms.

Imposed modification functions need not be limited to convergence factors and a number of other functions have been found useful so far. Sharpening of peaks by multiplying structure factors with $f_e^{-1}(s)$ or similar

[41] K. Lonsdale, Nature **164**, 205 (1949).

[42] J. Thewlis, Ann. Repts. Progress Chem. (Chem. Soc., London) **47**, 420 (1950).

[43] A. D. Booth, Proc. Roy. Soc. (London) **A188**, 77 (1946) **190**, 482 (1947); Nature **157**, 517 (1946).

[44] A. D. Booth, Proc. Roy. Soc. (London) **A188**, 77 (1946); *Fourier Technique in X-Ray Organic Structure Analysis* (Cambridge University Press, Cambridge, 1948).

[45] W. Cochran, Acta Cryst. **4**, 408 (1951).

CC-0. In Public Domain. Gurukul Kangri Collection, Haridwar

Digitized by Arya Samaj Foundation Chennai and eGangotri

functions is an example. Sharpening is especially important for Patterson functions, where resolution is the crucial consideration, and the limited experience so far seems to show that even in addition to sharpening with $f_e^{-2}\exp(as^2)$ a further emphasis of the far-out data (to be sure with suitable smoothing at the cutoff), as in the examples derived from the Gaussian, mentioned in Sec. 9, is most helpful. Such functions are likely to vanish at the origin, so that the integral of their transform is zero. This requires that the desirable sharp, high peak at the center of the transform at least be balanced by negative values elsewhere, but this is less serious in the three-dimensional case, to which one is forced for even moderately large unit cells, than it is for lower dimensionality, inasmuch as the negative region is of greater extent relative to the central peak. Even so, although it apparently has not yet so turned out in practice,[46] a transform with integral zero could well be most confusing in failing to reveal unresolved concentrations of peaks such as would seem to be possible over regions of atomic or possibly even molecular size. It seems that here is a prime example where the concurrent use of more than one suitably chosen modification function should prove profitable.

As in the one-dimensional cases, the peak shapes for $\rho'(\mathbf{r})$ and $P'(\mathbf{r})$ may be evaluated either by inverting the complete modification function or by folding the transforms of its several factors, the single inversion, usually, being the easier to perform while the successive foldings provide the clearer picture of the situation. Viervoll[23] discusses peak shapes for $\rho(\mathbf{r})$ and $P(\mathbf{r})$ and gives some actual examples. For the shape of ideal Patterson peaks,

$$P_{ij}(r)=\int_{-\infty}^{\infty}\rho_i(t)\rho_j(|\mathbf{t}+\mathbf{r}|)dv_t,$$

involving spherically symmetrical atoms, Viervoll[23] uses the expression

$$\frac{2\pi}{r}\int_0^{\infty}t\rho_i(t)\int_{|t-r|}^{t+r}u\rho_j(u)dudt,$$

which follows immediately (Viervoll gives a lengthy derivation) from the substitution

$$|\mathbf{t}+\mathbf{r}|=(r^2+t^2+2rt\cos\vartheta)^{\frac{1}{2}}.$$

In a procedure for subtracting the peaks corresponding to certain atoms in a Fourier map, Finbak and Norman[47] use what amounts to an arbitrary, unsymmetrical modification function. The peak shape is obtained by setting up a Fourier series corresponding to one specific atom at its most probable position. This series—our series transform $K(\mathbf{r})$ except for a shifted origin—is terminated in the same way as the original series. In addition Finbak and Norman propose that coefficients be omitted where no terms are available in the original series due to unobservably low intensity of the corresponding x-ray reflection. This corresponds to the omission of terms in back-shift and F_o-F_c syntheses mentioned above. Nevertheless, Finbak and Norman's proposal may lead to grave complications, because the corresponding $M_{\mathbf{h}}$ has scattered zeros and an excessively complicated transform; and we believe it should be adopted only in those cases of duress, important to be sure, where relatively high background or low sensitivity of the instruments of detection lead to a significantly high value for the maximum unobservable $F_{\mathbf{h}}$. Analysis of Fourier maps in terms of such transforms, although possible and more accurate, would in general be very difficult, and the general advisability of the procedure is not demonstrated by Finbak and Norman's example, for which the number of missing large terms is very small. It will be appreciated that if certain reflections were unobservably weak, compared to the strongest reflections, the contribution of the corresponding terms, left out of the original Fourier map, is small and can be neglected in good approximation. In this approximation the original Fourier map still corresponds to a superposition of simple peaks and may be so interpreted, the negligible size of the unobservable terms being a consequence of structure rather than of complexity of atom shapes. Correspondingly, the subtraction of a complex peak shape would only change into complex features the basically simple peaks (possibly complicated by overlap) present in the original map and could not be stopped after dealing with a few peaks, as otherwise would usually be the case. Furthermore a new Fourier would usually have to be evaluated should a change of parameters be desirable, since a simple translation of the transform can only be executed if it is a cover operation of the grid for which the values have been calculated. Again simple peak shapes prove much less cumbersome.

Two related examples can be found in a recent paper by Magnéli.[48] He first considers a one-dimensional structure whose period contains a sequence of eight equidistant lines, the last line of one period and the first line of the next one being at half that distance. The Fourier coefficients of this structure are either large or comparatively small[49] due to the existence of a pseudo-sublattice. Magnéli shows diagrams of the following sums evaluated using a convergence factor such that only terms with $n\leq 40$ are of any significance: (1) corresponding to the above structure, (a) the complete sum and (b) an incomplete sum, including only the four largest terms with $n=0, 7, 8, 15$, which function shows false detail; (2) the series transform $K(\mathbf{r})$ corresponding

[46] Shoemaker, Donohue, Schomaker, and Corey, J. Am. Chem. Soc. 72, 2328 (1950); J. Donohue and K. N. Trueblood, Acta Cryst. 5, 414 (1952).

[47] C. Finbak and N. Norman, Acta Chem. Scand. 2, 813 (1948).

[48] A. Magnéli, Acta Cryst. 4, 447 (1951).

[49] The effect of such pseudo-sublattices on the distribution of Fourier coefficients has been discussed by V. Vand, Acta Cryst. 4, 104 (1951), and by J. W. Jeffery, Proc. Phys. Soc. (London) A64, 1003 (1951), in terms of concepts expounded in the foregoing.

CC-0. In Public Domain. Gurukul Kangri Collection, Haridwar

Digitized by Arya Samaj Foundation Chennai and eGangotri

to a line at the origin, with (a) all terms and (b) only the four terms corresponding to (1b), the last result being of considerable complexity. Magnéli points out how the incomplete sum for the structure (1b) can be understood as resulting from a superposition of the incomplete series transforms (2b). However, while this is undoubtedly true, the omitted coefficients are by no means small and if the coefficients with $n=6$, 9, 22, 23, 30, whose magnitudes average about 20 percent of that of the largest term, are included a graph results whose main peaks stand out clearly and correspond in position to the original structure. The subsidiary features of this graph are clearly recognizable as such, the largest one being about one-third of the size of the smallest main peak and comparable in size to the subsidiary features of a sum which includes *all* terms with $n\leq 30$. The original structure can thus clearly be reconstructed from this graph despite the fact that the magnitude of many of the terms omitted is still above 5 percent of the size of the largest term. These terms are not really negligible and a detailed complete analysis of the graph would of course require the corresponding incomplete $K(\mathbf{r})$.

An alternative to using this complex transform in cases where the magnitude of the terms which cannot be determined experimentally is relatively large, is to substitute theoretical values for the missing coefficients. This will result in simple peaks provided the parameters used in the calculation of the substituted terms are close to their correct values. This procedure is a special case of one proposed by Cochran[50] which permits giving different weights to different observed values. The use of theoretical values in this way of course increases the provisional character of the electron density function, which usually is considerable anyhow because of the necessity of using theoretical values for the phase angle values of the coefficients.

Magnéli's second example is two-dimensional and concerns his (010) projection of β tungsten oxide. The structure is analogous to the one-dimensional example just discussed, being characteristic of the transform of the tungsten form factor, modified by the omission of a large number of terms and thus comprising a complex system of peaks. Again the original Fourier map may be interpreted in terms of simple transforms, and it is interesting that Magnéli's solution of the structure actually does rest on this point of view.

[50] W. Cochran, Nature **161**, 765 (1948); Acta Cryst. **1**, 138 (1948).

CC-0. In Public Domain. Gurukul Kangri Collection, Haridwar

Digitized by Arya Samaj Foundation Chennai and eGangotri

Least-Squares Adjustment of the Atomic Constants, 1952

JESSE W. M. DUMOND,
California Institute of Technology, Pasadena, California

AND

E. RICHARD COHEN,
North American Aviation, Incorporated, Downey, California

1. THE GROUP KNOWN AS THE ATOMIC CONSTANTS

THIS review is concerned with the determination of the numerical values of an interesting subgroup of the general constants and conversion factors of physics and chemistry known as the atomic constants. No clear-cut definition of this subgroup exists, and, indeed, with the passage of time it has been found convenient to include in it more and more members of the parent group because of the improvements (partly theoretical and partly in the form of increased experimental precision) in our knowledge of the interrelations between the members. As of the present date we may, perhaps somewhat arbitrarily, enumerate the following six interrelated constants as the primary atomic constants: N, Avogadro's number; e, the electronic charge; m, the electronic rest-mass;[1] h, Planck's constant; c, the velocity of light; and λ_g/λ_s, the important conversion factor which converts x-ray wavelengths from the arbitrary Siegbahn x units (in which at 18° C the grating constant of the cleavage planes of calcite is $d_{18}=3029.45\ x$ units) to milliangstrom units. (We shall call this latter conversion factor for brevity simply λ.) Certain important constants such as $R_\infty=2\pi me^4h^{-3}c^{-1}$, the Rydberg fundamental wave number of spectroscopy; $F=Ne$, the Faraday constant of electrochemistry; $\alpha=2\pi e^2/(hc)$, Sommerfeld's fine-structure constant; $a_0=h^2/(4\pi^2me^2)$, Bohr's fundamental radius, and many others are closely related to the six named above by well-established formulas. In a few cases, certain rather accurately known "auxiliary constants" such as R_0, the gas constant, must be combined with these, as, for example, to compute the Stefan-Boltzman radiation constant $\sigma=(2/15)\pi^5R_0^4c^{-2}h^{-3}N^{-4}$ in the Stefan-Boltzman σT^4 law.

Thus there is a large group of very important fundamental numerical values, which are so interlaced and interconnected by known, well-established relationships that a precise knowledge of only about five of them, together with five or six very accurately known auxiliary constants, is all that is needed to establish the values of the entire group with considerable certainty. The choice of which particular set of five atomic constants we shall call our primary ones is to some extent arbitrary or dictated by mathematical convenience. Once they are selected, these primary constants are the "unknowns" whose values it shall be our object to determine by the method of least-squares, so as to form a consistent set which does the least violence to all our known sources of information with as much accuracy as the present state of our knowledge permits as regards both the values themselves and their standard errors. From the "best" (least-squares adjusted) values of these unknowns, combined with whatever auxiliary constants may be needed, all the other atomic constants and conversion factors will be computed. In the present instance, we have selected α, c, e, N, and λ as the five primary unknowns.

The reader accustomed to the textbook accounts of how such atomic constants as e, h, and m were measured for the first time in famous and historically important experiments such as R. A. Millikan's oil-drop experiment or his studies of the photoelectric effect, Planck's interpretation of the experimental curves of blackbody radiation, or J. J. Thomson's deflection experiments on cathode rays, may be surprised to see how little remains of these traditional methods in the present high precision evaluation. These earlier methods, which were of great value for the progress of knowledge at the time and which still possess immense historical importance, are now so greatly surpassed in accuracy by more modern, though sometimes less direct, methods that, although the earlier results are not inconsistent with the later ones, they would carry no significant weight if included in a least-squares solution.

2. RECENT HIGH PRECISION EXPERIMENTAL DATA

Undoubtedly the greatest single contribution to the progress of our knowledge of the atomic constants is to be found in the monumental pioneer work of R. T. Birge,[2] who by his painstaking and persistent life-long effort has certainly done more than any other person to separate truth from error and bring order out of chaos

[1] We omit the usual subscript zero since we shall need to use this later with a different meaning.

[2] R. T. Birge, Revs. Modern Phys. 1, 1 (1929); Phys. Rev. 40, 207 (1932); Phys. Rev. 40, 228 (1932); Phys. Rev. 42, 736 (1932); Nature 133, 648 (1934); Nature 134, 771 (1934); Phys. Rev. 48, 918 (1935); Nature 137, 187 (1936); Phys. Rev. 54, 972 (1938); Am. Phys. Teacher 7, 351 (1939); Phys. Rev. 55, 1119 (1939); Phys. Rev. 57, 250 (1940); Phys. Rev. 58, 658 (1940); Phys. Rev. 60, 766 (1941); Repts. Progr. Phys. VIII, 90 (1942); Am. J. Phys. 13, 63 (1945).

CC-0. In Public Domain. Gurukul Kangri Collection, Haridwar

Digitized by Arya Samaj Foundation Chennai and eGangotri

in this field. His 1929 and 1942 general reviews are all-time models of meticulous care in studying a huge mass of primary data, searching out errors, sifting and evaluating to separate the chaff from the wheat, and they are required reading for a proper understanding of this subject.

Rapid evolution in the direction of much higher accuracy of the data bearing on the atomic constants has occurred since 1947; undoubtedly partly the result of the stimulus given the subject by the many analyses of Birge and others during the preceding two decades, but chiefly made possible by the intense development since World War II of microwave and atomic beam techniques for the study of proton resonance in magnetic fields, the fine structure of energy levels in hydrogen and deuterium, the magnetic moments, spin gyromagnetic ratios, nuclear magnetic resonance frequencies, and cyclotron frequencies of fundamental particles such as protons and electrons, etc. Great improvements have also been made thanks to microwave cavity resonance and high frequency Kerr cell techniques in the measurement of the velocity of light. Unfinished work is also under way at the National Bureau of Standards to improve the accuracy of the electrochemical evaluations of the Faraday: (1) by the electrolysis of silver in which both the *anodic silver lost* and the *cathodic silver deposited* are weighed and compared and re-solution of the silver in the electrolyte is minimized by using for that medium a solution of silver perchlorate in perchloric acid, and (2) by anodically oxidizing sodium oxalate. Finally, a great advance in the accuracy of our knowledge of the atomic weights of light atoms has been gained through the determination of these by the measurement of nuclear reaction energies.

Of these modern experiments those used in the least-squares adjustment of this review are (1) the precision determination at the U. S. National Bureau of Standards of γ, the gyromagnetic ratio of the proton by Thomas, Driscoll, and Hipple; (2) the magnetic moment of the proton expressed in nuclear magnetons (ratio ω_c/ω_p of the cyclotron frequency to the magnetic resonance frequency of the proton in a given magnetic field) as obtained, (a) with the U. S. National Bureau of Standards "Omegatron" of Sommer, Thomas, and Hipple and also (b) at Stanford University with the inverse cyclotron of Bloch and Jeffries; (3) the fine structure separation ΔE_D of the $2^2P_{\frac{3}{2}}-2^2P_{\frac{1}{2}}$ levels in deuterium using the atomic beam magnetic resonance method performed by Dayhoff at Columbia; and (4) the ratio of the electron magnetic moment to the proton magnetic moment measured by Koenig, Kusch, and Prodell, also at Columbia University. References and numerical results for all the above work are given in Secs. 6 and 7. No attempt will be made here to describe experimental details of the techniques.

Since the discovery by Willis Lamb of the slight shift in the hydrogen levels, as a result of a remarkable program[3] of studies at Columbia University of the fine and hyperfine structure of the hydrogen spectrum, a complete reexamination and recalculation of the experimental data on which the determinations of R_∞, R_H, and R_D are based becomes necessary. A very thorough and complete study of the masses of the light atoms based on measurements of nuclear reaction energies has been made by Li, Whaling, Fowler, and Lauritsen at California Institute of Technology. For references and results of these studies see Sec. 7.

The all important velocity of light has received much attention in the period during and following World War II, with greatly improved accuracy resulting. Several excellent and concise reviews[4–7] of the situation concerning this constant at different epochs have been given of which that of Mulligan is to be recommended. The recent important high precision measurements of this constant are those of Hansen and Bol[8] at Stanford, using microwave cavity resonance with a cavity of fixed length; Bergstrand[9–10] in Norway, using Kerr cell-modulated visible light (the "Geodimeter"); cavity resonance work with a cavity of variable length by Essen;[11] at National Physical Laboratory, Teddington, England, using cavity resonance in a cavity of variable length; Froome,[12] also at NPL, using a free-space microwave interferometer; and Aslakson[13] using Shoran.

All the measurements just cited indicate quite unequivocally that the earlier weighted average value arrived at by Birge,[4] based chiefly on earlier measurements by Michelson, Pease, and Pearson[14] with the rotating mirror method in an evacuated tube and by Anderson,[15] using Kerr cell modulation, namely, 299 776 km/sec, was low by about 15 or 16 km/sec. As a matter of fact, if the Michelson, Pease, and Pearson and the Anderson values had been excluded from Birge's weighted average, the remainder of the data he considered, which included the remarkably accurate determination of the ratio of the electrical units by Rosa and

[3] Willis E. Lamb, Jr., and Robert C. Retherford, "Fine-structure of the hydrogen atom," Part I, Phys. Rev. **79**, 549 (1950); Part II, Phys. Rev. **81**, 222 (1951); Part III, Phys. Rev. **85**, 259 (1952); Part IV, Phys. Rev. **86**, 1014 (1952); Part V and Part VI (unpublished Columbia reports at the date of writing).

[4] R. T. Birge, Reps. Progr. Phys. **VIII**, 92–101 (1941).

[5] L. Essen, Nature **165**, 582 (1950).

[6] J. F. Mulligan, Am. J. Phys. **20**, 165 (1952).

[7] E. S. Dayhoff, Survey of Microwave Interferometers and Measurements of the Velocity of Light for the National Bureau of Standards Office of Basic Instrumentation, September 2, 1952, OBI Project 7507, 14.9 Project 1459.

[8] Kees Bol, thesis, Stanford University, 1950; Phys. Rev. **80**, 298 (1950). Unfortunately W. W. Hansen's untimely death came before this experiment was finished.

[9] Erik Bergstrand, Nature **163**, 338 (1949); **165**, 405 (1950).

[10] Erik Bergstrand, Arkiv Fysik **2**, 119 (1950); **3**, 479 (1951).

[11] L. Essen, Proc. Roy. Soc. (London) **A204**, 260 (1950); Nature **167**, 258 (1951).

[12] K. D. Froome, Proc. Roy. Soc. (London) **A213**, 123 (1952).

[13] C. I. Aslakson, Nature **164**, 711 (1949); Trans. Am. Geophys. Union **30**, 475 (1949).

[14] Michelson, Pease, and Pearson, Astrophys. J. **82**, 26 (1935).

[15] W. C. Anderson, J. Opt. Soc. Am. **31**, 187 (1941).

CC-0. In Public Domain. Gurukul Kangri Collection, Haridwar

Digitized by Arya Samaj Foundation Chennai and eGangotri

Dorsey,[16] would have yielded a weighted average not inconsistent with the present newer values.[17] These newer values are not all of equal reliability or accuracy, however, and in particular the Hansen and Bol result disagrees with the others by being some 3 kilometers per sec too low, a disagreement which, though small judged by earlier standards, is uncomfortably large relative to the claimed probable errors.

E. S. Dayhoff, in a privately circulated report,[7] criticizes the Hansen and Bol measurements because the resonant frequencies of not enough different modes of vibration were measured to obtain the requisite amount of information (especially as regards the skin depth) for an experiment otherwise so carefully and ingeniously designed to give such high precision. In Essen's (1950) results his cavity appeared to be about 2×10^{-4} cm larger in electrical diameter than it actually was mechanically because of the effective skin depth, and this was 2.8 times the calculated skin depth. Dayhoff concludes that this was probably because of polishing the silvered surface whose conductivity close to the surface, it appears, can be thus greatly decreased by the effect of cold working associated with polishing. Such an effect would increase Hansen and Bol's estimated skin depth correction of 3 km/sec to 8 km/sec and would bring their value of c into substantial agreement with the others. Table I lists these recent results with their estimated standard errors.

Note added in proof.—Dr. E. L. Ginzton of Stanford has recently pointed out to us that the above-mentioned interpretation of Essen's results as transmitted to us by Dr. Dayhoff is open to some question. Dr. Ginzton is of the opinion that the effect of possible variations in the diameter of Essen's cavity as a function of axial position are not properly taken into account in the Teddington measurements and that this might account for part of the discrepancy between the NPL and the Stanford results. This work on c is being continued at Stanford by Ginzton.

TABLE I. Experimental values of the velocity of light in vacuum.

Author	Date of publication	Reference	Method[a]	Velocity km/sec
Aslakson	1949	13	Shoran	299 792 ±3.5
Hansen and Bol	1950	8	FLCR	299 789.3±1.2
Essen	1950	11	VLCR	299 792.5±4.5
Bergstrand	1951	10	Geodimeter	299 793.1±0.32
Froome	1952	12	FSMWI	299 792.6±0.7

[a] FLCR = Fixed length cavity resonance. VLCR = Variable length cavity resonance. FSMWI = Free space microwave interferometer.

3. THE METHOD OF LEAST SQUARES

The first man to apply the method of least squares in a thoroughgoing way to obtain a consistent set of "best" adjusted values for the atomic constants was a former student of Birge, Frank G. Dunnington.[18] There are two uses which can be made of a least-squares solution of this sort: (1) It may be used on a fairly consistent overdetermined set of equations to determine the adjusted best values of the constants. (2) It may be used on an inconsistent set of equations as a tool to ascertain, if possible, which of the equations contains the concealed systematic error. At the time of Dunnington's work, because progress in refining the experiment of Duane and Hunt on the short-wavelength limit of the continuous x-ray spectrum was still not very advanced and for other reasons, there was a disturbing lack of consistency among the equations for determining the atomic constants. Dunnington's chief preoccupation in his paper was with this question of locating the cause of inconsistency. His attack consisted in performing a series of least-squares adjustments in each of which one item was omitted in an effort to see which item was the cause of inconsistency. Other least-squares solutions,[19–22] on the other hand, made subsequent to Dunnington's have been performed chiefly to determine "best" compromise values of the constants from a reasonably consistent set of data.

It is clear that in the quest for the "best" consistent set of values of the constants the entire situation of their complicated interrelatedness requires the application of some unbiased analytic technique. That is to say, one must (1) decide which if any of the quantities which we have chosen to call the primary atomic constants are known with sufficient accuracy relative to the rest, so that they can be practically eliminated from the category of "unknowns" and treated as known numbers (merely to save labor); (2) set up as many independent equations as there are reliable determinations of functions of the unknowns; and finally, (3) solve for the "best" compromise values of the unknowns. Considerably more such equations can be set up than the number of unknowns. Because of both random and systematic errors in the experimental determinations represented by the different equations, these latter may, in general, be expected to be more or less incompatible. The method of least squares then supplies a well-known mathematical technique for obtaining the "best compromise" values of the unknowns to satisfy all the equations approximately.

[16] E. B. Rosa and N. E. Dorsey, Bull. Bur. Standards 3, 433 (1907).

[17] *A posteriori* reasons to account for systematic errors in the Michelson, Pease, and Pearson and the Anderson determinations are not hard to find. The base line of the first mentioned determination was on very unstable alluvial soil, while the different transit times of the electrons in the detecting tube in Anderson's work constituted a possible source of systematic error which he recognized clearly himself. This latter objection is avoided in Bergstrand's "Geodimeter."

[18] F. G. Dunnington, Revs. Modern Phys. 11, 68 (1939).

[19] J. W. M. DuMond and E. R. Cohen, Revs. Modern Phys. 20, 82 (1948).

[20] J. W. M. DuMond and E. R. Cohen, Reports to National Research Council, Committee on Constants and Conversion Factors of Physics, December, 1950.

[21] J. A. Bearden and H. M. Watts, Phys. Rev. 81, 73 (1951); 81, 160 (1951).

[22] J. W. M. DuMond and E. R. Cohen, Ann. Sci. 40, 447 (1952).

CC-0. In Public Domain. Gurukul Kangri Collection, Haridwar

Digitized by Arya Samaj Foundation Chennai and eGangotri

If we examine all the different experiments described in the previous section, we find that in the majority of cases the individual measurements do not measure one of the primary unknown quantities, but rather some function of several of them. Furthermore, the function whose numerical value is determined by such an experiment can be expressed in most cases (except for quantities which can be considered as accurately calculable correction factors) as a simple product of powers, positive or negative, of the primary variables of the form

$$N^{i_\mu}e^{j_\mu}m^{k_\mu}\cdots=A_\mu(1-r_\mu),\quad \mu=1,2,3,\cdots,N_{Eq}, \tag{3.1}$$

wherein A_μ is the numeric which results from the measurement and N, e, m, etc., are the primary variables. If we were to put true values of these variables (which we do not know) into the left-hand side of Eq. (3.1) we would, in general, not obtain the number A_μ, since it is the result of measurement and therefore subject to error. We must include the factor $1-r_\mu$ in order that Eq. (3.1) shall be a valid equation. We do not know the true values of the primary variables so that we cannot compute r_μ from this. The quantity r_μ is the actual relative error in the measured quantity A_μ, and this is, of course, beyond our ken. We know only an estimate of some of the parameters of its probability distribution. The most probable value of the error is zero, since the numeric quoted as the result of an experiment is, to the best of knowledge, the number which is most likely to be the correct value of the quantity being measured. Furthermore, we have an estimate of the root-mean-square deviation of the relative error σ_μ, and we shall restrict ourselves momentarily to a Gaussian[23] distribution for the errors such that the probability of the error r_μ lying between the values r and $r+dr$ is

$$P_\mu\{r<r_\mu<r+dr\}=\frac{1}{(2\pi)^{\frac{1}{2}}\sigma_\mu}\exp(-r^2/2\sigma_\mu{}^2)dr. \tag{3.2}$$

When we omit the factors $1-r_\mu$ from Eqs. (3.1) the system is, in general, overdetermined; we have N_{Eq} equations and only q variables ($q<N_{Eq}$), so that a solution is impossible (except for the very improbable situation in which all of the experimental data are exactly compatible). When we introduce the quantities r_μ, we increase the number of unknowns to $q+N_{Eq}$, there being one residual for each observational equation, and we are able to satisfy the equations in infinitely many ways. It is now necessary to find some additional conditions which will allow us to choose that one solution, from the infinitely many which are available to us, which represents the "best" choice. This "best" choice can be based on the Axiom of Maximum Likelihood:

"Of all the possible choices for the set of residuals (r_μ), the best choice is that whose probability of occurrence is maximum."

The probability of obtaining simultaneously the set of values, $r_1, r_2, r_3, \cdots, r_{NEq}$ is the product of the probabilities of obtaining each value separately, provided these errors are all independent. (The importance of this proviso will soon become evident.) Therefore,

$$P(r_1, r_2, r_3, \cdots)=(2\pi)^{-\frac{1}{2}N_{Eq}}[\sigma_1\sigma_2\sigma_3\cdots\sigma_{N_{Eq}}]^{-1}\times\exp\left\{-\tfrac{1}{2}\left(\frac{r_1{}^2}{\sigma_1{}^2}+\frac{r_2{}^2}{\sigma_2{}^2}+\frac{r_3{}^2}{\sigma_3{}^2}+\cdots\right)\right\}. \tag{3.3}$$

This probability will be a maximum when the sum in the exponent is a minimum. This then is the "least-squares" condition: The N_{Eq} equations (3.1) are solved for the residuals r_μ written as functions of the unknown variables N, e, m, $\cdots$ and we seek that set of values for the variables which minimizes the sum of the squares of the quotient of each residual divided by its standard deviation.

If the distribution of the errors is other than Gaussian, it is difficult to formulate an analytic procedure based on the condition of Maximum Likelihood but it has been shown[24] that, independent of any assumptions about the exact distribution of the errors of the A_μ save that the σ_μ exist (i.e., are finite) in each case, this least-squares condition is equivalent to the condition that the resultant solution shall be that set which has minimum root-mean-square deviations. [See following article by E. R. Cohen; Revs. Modern Phys. **25**, 709 (1953).]

For convenience in effecting the least-squares adjustment, the system of Eqs. (3.1) is "linearized." We adopt origin values N_0, e_0, m_0, etc., which have been chosen sufficiently close to our expected solution that any set of values N, e, m, in which we are likely to be interested will differ from these individual origin values by only small relative amounts; that is, $N_0, e_0, m_0, \cdots$ are so chosen that $x_N=(N-N_0)/N_0$, $x_e=(e-e_0)/e_0$, $x_m=(m-m_0)/m_0$, $\cdots$ are always small, and we then express the experimental measurements in terms of these dimensionless variables $x_N, x_e, x_m, \cdots$. To each type of experimental determination of a function of the type (3.1) there corresponds a hyperplane

$$i_\mu x_N+j_\mu x_e+k_\mu x_m+\cdots=a_\mu-r_\mu, \tag{3.4}$$

which is tangent to the curved surface (3.1). The constant a_μ is given by $a_\mu=(A_\mu-A_{\mu 0})/A_{\mu 0}$, in which $A_{\mu 0}$ is the value of the function f when the origin values $N_0, e_0, m_0, \cdots$ are inserted. The orientation of this plane in the hyperspace depends on the exponents $i_\mu, j_\mu, k_\mu, \cdots$ of (3.1) [i.e., the coefficients $i_\mu, j_\mu, k_\mu, \cdots$

[23] The Gaussian distribution is not uniquely implied by these two parameters, A_μ and σ_μ, and the least-squares procedure can, in fact, be justified *without recourse to any presumed probability distribution of errors*. The introduction of such a distribution is convenient and makes possible a more direct development.

[24] E. Whittaker and G. Robinson, *Calculus of Observations* (Blackie & Sons, London, 1944), fourth edition, p. 224.

CC-0. In Public Domain. Gurukul Kangri Collection, Haridwar

Digitized by Arya Samaj Foundation Chennai and eGangotri

of (3.4)], while the origin distance of the plane depends on a_μ. The entire status of our knowledge regarding the "best" values of e, m, and h to fit the data is contained in the way these various planes intersect each other to define some compromise point, taking into consideration the relative reliability of the positioning of each plane, i.e., the magnitude of the standard error, σ_μ. The function $Q=\sum(r_\mu^2/\sigma_\mu^2)$, which is to be minimized, is therefore an expression of the second degree in the variables x_N, x_e, x_m, etc., and the minimum condition is obtained by equating to zero each of the partial derivatives of Q taken with respect to each variable in turn. It is easy to show that this process is equivalent to the following simple recipe for forming the so-called "normal equations": Write down the system of eqs. (3.4) omitting the residue r_μ in each case. Assign to each equation a weight

$$p_\mu=C/\sigma_\mu^2, \tag{3.5}$$

where the constant C may have any convenient numerical value. To obtain the normal equation associated with a given variable (i.e., the one which expresses the condition that the partial derivative of Q with respect to that variable shall vanish), multiply each of the linearized observational equations (with r_μ omitted!) by the coefficient of the variable in question in that equation and by the weight assigned to that equation. These individual expressions are then added together to give a single "normal" equation. Repeat for each variable, and in this way construct a set of q simultaneous equations for the q unknown quantities x_N, x_e, x_m, etc.

The solution is completed by inserting the values obtained for the x's into the original set of observational equations (3.4) and finding the associated residuals; the values of the residuals computed using the solution of the normal equations we shall denote as R_μ (a number) to be distinguished from r_μ which is a function of the variables x_N, x_e, $\cdots$. The minimum value of the quadratic expression Q is usually denoted by the symbol χ^2

$$\chi^2=\sum(R_\mu^2/\sigma_\mu^2). \tag{3.6}$$

An important measure of the consistency of the entire set of equations is given by χ^2 divided by the difference between the number of equations N_{Eq} and the number of unknowns q. The expectation value of $[\chi^2/(N_{Eq}-q)]^{\frac{1}{2}}$ is unity; this quantity is the generalization to multidimensional space of R. T. Birge's[25] ratio of the measures of external and internal consistency. The difference $N_{Eq}-q$ is known as the "number of degrees of freedom" of the system.

A word of caution about the actual method of formulating the equations of least-squares from the data as applied to the atomic constants is in place at this point. The general form of the primitive equations of observation is given in Eq. (3.1) above. In each such equation A_μ is a number with an estimated relative standard error σ_μ, the result of reduction of some particular experimental observations, which, if care to avoid it has not been exercised, *may be correlated observationally* with some of the other A_μ by reason of the fact that one and the same error-contributing component (such as, for example, c) may have been used in reducing the data to arrive at both A_μ's.

Now, it is an important point, which has never been emphasized in even the most advanced texts on least squares, that the observational equations must be observationally independent, if the above classical procedure of effecting least-squares adjustment is to be followed. This is because one cannot otherwise assign simple independent weights to the different equations. If, on the contrary, the equations are observationally correlated, the standard errors of the a's can only be measured by an error matrix involving correlation coefficients corresponding to all possible pairs of a's as well as individual standard errors for each a, and the weights must be replaced by a "weight matrix," the inverse of the error matrix, to express the situation fully. The process of least-squares adjustment can then be formulated[26] in matrix algebra in a manner quite analogous to the simpler case of independent a's but with considerable increase in labor.

The easy and obvious way out of this difficulty is to recast the entire system of equations in such a way as to remove the observational correlations between the a's. This amounts to finding a transformation which diagonalizes the error and weight matrices. It may be impossible to do this, however, without transferring some of the quantities with larger standard errors from the category of the known a's to the category of the unknown x's and also to write for each of these an extra observational equation in which the new unknown x is equated to its appropriate input datum a, the numerical result of direct measurements. This, of course, complicates the problem by increasing the number of unknowns to be adjusted, but it in no way affects the original overdetermination $(N_{Eq}-q)$ of the set, since an additional observational equation is added for each new unknown introduced.

4. CALCULATION OF STANDARD ERRORS AND CORRELATION COEFFICIENTS

The reliability of the output values of any least-squares adjustment must, in general, be described not only by stating the standard deviation for each numerical result but also by specifying certain quantities known as *correlation coefficients, r_{ij} for each pair of results*. The numerical output values, of e, m, h, c, etc., are of little use unless functions of these can be combined to compute other derived values. Now the standard devia-

[25] R. T. Birge, Phys. Rev. **40**, 213–224 (1932).

[26] This formulation was, we believe, given for the first time by J. W. M. DuMond and E. R. Cohen, Report to the National Research Council on the Atomic Constants, December, 1950. See also E. R. Cohen, Phys. Rev. **81**, 162 (1951).

CC-0. In Public Domain. Gurukul Kangri Collection, Haridwar

Digitized by Arya Samaj Foundation Chennai and eGangotri

tions of such derived values must be computed, as we shall show in this section, by formulas which involve not only the standard deviations of the values entering into the function but also the correlation coefficients r_{ij} connecting all possible pairs of those values.

The calculation of error estimates in such a situation may be unfamiliar to many physicists. There is no escape from this added complication in the computation of precision measures, however, since it reflects the complexity inherent in the sources of our knowledge of the adjusted values. A comprehension of the content of this section is, therefore, essential to the correct use of the adjusted output values given here.

Each quantity subject to random or accidental error (frequently known as a "random variable") may conveniently be thought of as a sample taken at random from a group or "universe" of values which group themselves around a mean value according to some frequency law. This frequency law we shall usually assume to be the normal or Gaussian law. For each such random variable x_i, one is to think then of the implied universe of values in the background which it is presumed would be obtained by repeated measurements on it. This universe may be described by giving some of its parameters. Thus, if the universe is known to be Gaussian, for example, then prescription of its first and second moments, i.e., its mean value x_i and its variance σ_i^2 are sufficient. (The standard deviation σ_i is the root-mean-square deviation from the mean of this universe of values.)

Two such random quantities are observationally independent, if the random selection of a sample value from one universe in no wise affects or biases the free selection of a sample from the other universe. If, however, two variables are connected by a strict functional relationship so that the value of *either one is uniquely determined by the other*, the variables are completely correlated and the correlation coefficient connecting them has the absolute value unity. Random samples can no longer be selected freely and independently from the two universes because of the functional condition which ties the selections rigidly together. Having selected a sample value from one universe at random, the second selection is now completely dictated in value. On the other hand, if one of the two random variables is a function of the other *and also of still other completely independent random variables*, then the first two will be partially but not completely correlated, and the correlation coefficient connecting them will have an absolute value somewhere between zero and unity. The problem of correlated errors has been pointed up in a previous article in this journal[27] (q.v.), and it was shown there that, in general, the distribution in probability of the possible solutions of the set of eqs. (3.4) is represented by a hyperellipsoid of probability in the constants space whose major axes are skew to the coordinate axes. Because of this the probability distribution of a particular variable is dependent upon the specification of the values of all the other variables. The extent of this dependence is expressed by correlation coefficients. There exists then in the hyperspace of our primary variables a hyperellipsoid of error whose principal axes will lie, in general, oblique to the axes of any of the primary variables in a way which depends on the precision (and consequent weights) to be attached to the various input data. The various standard deviations σ_i of the different linearized unknowns x_i together with the correlation coefficients r_{ij} connecting all possible pairs of unknowns can be systematized in the form of a square matrix whose derivation from the normal equations we shall now describe.

For definiteness, let us now consider a system with four unknowns. We shall write the (linearized) observationally independent equations in the form

$$i_\mu x_1+j_\mu x_2+k_\mu x_3+l_\mu x_4=a_\mu-r_\mu, \qquad \mu=1, 2, 3 \cdots N_{Eq}, \quad (4.1)$$

and to each of the N_{Eq} equations we assign a weight $p_\mu=C/\sigma_\mu^2$ (see Eq. 3.5), in which σ_μ is the standard error of the constant term a_μ. We construct the normal equations in accord with the instructions of the previous section and these can be written in the form

$$\begin{aligned} b_{11}x_1+b_{12}x_2+b_{13}x_3+b_{14}x_4&=c_1,\\ b_{21}x_1+b_{22}x_2+b_{23}x_3+b_{24}x_4&=c_2,\\ b_{31}x_1+b_{32}x_2+b_{33}x_3+b_{34}x_4&=c_3,\\ b_{41}x_1+b_{42}x_2+b_{43}x_3+b_{44}x_4&=c_4. \end{aligned} \quad (4.2)$$

The quantities b_{ij} are symmetric, $(b_{ij}=b_{ji})$;

$$b_{11}=\sum_\mu p_\mu i_\mu^2, \quad b_{12}=b_{21}=\sum_\mu p_\mu i_\mu j_\mu,$$

$$b_{22}=\sum_\mu p_\mu j_\mu^2, \quad (4.3)$$

and it should be apparent from the form of these four quantities exactly how the other twelve b_{ij} may be constructed. The constant terms of the normal equation c_j are calculated in a similar way:

$$c_1=\sum_\mu p_\mu i_\mu a_\mu, \quad c_2=\sum_\mu p_\mu j_\mu a_\mu, \text{ etc., } \cdots \quad (4.4)$$

It is well known that the solution of the set of eqs. (4.2) can be written in the form

$$\begin{aligned} x_1&=d_{11}c_1+d_{12}c_2+d_{13}c_3+d_{14}c_4,\\ x_2&=d_{21}c_1+d_{22}c_2+d_{23}c_3+d_{24}c_4,\\ x_3&=d_{31}c_1+d_{32}c_2+d_{33}c_3+d_{34}c_4,\\ x_4&=d_{41}c_1+d_{42}c_2+d_{43}c_3+d_{44}c_4, \end{aligned} \quad (4.5)$$

in which the sixteen numbers d_{ij} bear an inverse relationship to the set of numbers b_{ij}; the element d_{ij} is equal to the minor of b_{ji} in the determinant of the b's divided by the determinant itself. All the information

[27] J. W. M. DuMond and E. R. Cohen, Revs. Modern Phys. 20, 91–94 (1948).

CC-0. In Public Domain. Gurukul Kangri Collection, Haridwar

Digitized by Arya Samaj Foundation Chennai and eGangotri

required for the complete solution of the problem of least squares is contained in the sixteen b's (or equivalently in the sixteen d's) and the four c's. In addition to the "best" values of the x's, we are equally interested in determining the precision measures which must be assigned to them. The x's are not accurately determined quantities, since they are computed from numbers which are the results of experiments and therefore are subject to error. Using the definition of the c's from Eq. (4.4) in Eq. (4.5) allows us to express our solution in terms of the directly observed quantities a_μ. There is some error associated with each quantity a_μ. This error, which we shall call E_μ, is unknown (if it were known we should remove the error by correcting the quantity a_μ); we know an estimate of the mean square value of this error, however, and we can, therefore, make an estimate of the mean square error in a function of the a_μ. The error ϵ_i in x_i, which is produced by errors E_1 in a_1, E_2 in a_2, E_3 in a_3, etc., can be calculated from the partial derivative of x_i taken with respect to a_μ:

$$\epsilon_i=\frac{\partial x_i}{\partial a_1}E_1+\frac{\partial x_i}{\partial a_2}E_2+\frac{\partial x_i}{\partial a_3}E_3+\cdots. \tag{4.6}$$

The errors E_μ are to be considered as random variables; they may be positive or negative. Since the numeric a_μ is presumably the best estimate available for this quantity, we expect E_μ to be zero. On the other hand, the mean value of E_μ^2 is estimated to be σ_μ^2, so that σ_μ is an estimate of root mean square error in a_μ.

If we calculate the mean value of ϵ_i^2 we find

$$\sigma_{x_i}^2=\langle\epsilon_i^2\rangle=\left(\frac{\partial x_i}{\partial a_1}\right)^2\sigma_1^2+\left(\frac{\partial x_i}{\partial a_2}\right)^2\sigma_2^2+\left(\frac{\partial x_i}{\partial a_3}\right)^2\sigma_3^2+\cdots+2\left(\frac{\partial x_i}{\partial a_1}\frac{\partial x_i}{\partial a_2}\right)\langle E_1E_2\rangle+2\left(\frac{\partial x_i}{\partial a_1}\frac{\partial x_i}{\partial a_3}\right)\langle E_1E_3\rangle+\cdots, \tag{4.7}$$

in which the $\langle\ \rangle$ about a quantity denotes the operation of taking the average value of that quantity. Since the a's have been assumed to be observationally independent, the errors in two different a's are in no way related to each other, and the average value of the product of two different errors vanishes, since for any value of one error the other may be averaged out to zero. Thus, in such a case, the cross product terms in Eq. (4.7) disappear, and we have the law of the propagation of independent errors

$$\sigma_{x_i}^2=\langle\epsilon_i^2\rangle=\sum_\mu\left(\frac{\partial x_i}{\partial a_\mu}\right)^2\sigma_\mu^2. \tag{4.8}$$

When the differentiations are actually carried out we find, after some straightforward but somewhat lengthy algebraic manipulation, that the mean square error in x_i is given simply by Cd_{ii}. Thus, the diagonal elements of the matrix (d) are directly related to the standard errors of the solution. It may also be shown that the off-diagonal elements of matrix (d) are similarly related to the mean value of the product of the errors in two different variables:

$$\langle\epsilon_i\epsilon_j\rangle=Cd_{ij}. \tag{4.9}$$

For this reason we refer to the matrix (d_{ij}) as the "error matrix" of the solution. It is important to realize that the mean value of the product of the errors of two different x's does not vanish, because these quantities are not independent in terms of the observational quantities a_μ, each x_i being expressed ultimately in the least-squares procedure by some linear combination of the a_μ.

The extent of this correlation can be best expressed by defining the "correlation coefficient" r_{ij} connecting the two variables x_i and x_j by the relationship

$$r_{ij}=d_{ij}/(d_{ii}d_{jj})^{\frac{1}{2}}. \tag{4.10}$$

It can be shown that r_{ij} must lie between the limits -1 and $+1$. If the two variables are uncorrelated, in the sense that an error in one is completely independent of an error in the other, $r_{ij}=0$; at the other extreme, if the two variables are functionally related to the extent that an error in one completely determines the error in the other $r_{ij}=\pm1$, the sign depending on whether a positive error in one variable is associated with a positive or a negative error in the other. Once we have calculated the error matrix, it is no longer necessary to express a function of the x's in terms of the independent quantities a_μ in order to calculate its standard error, as long as we realize that the errors in the x's are correlated. If we have any function $f(x_1, x_2, x_3, x_4)$, the error in the function arising from specified errors ϵ_1, ϵ_2, ϵ_3, ϵ_4 in the x's is

$$\epsilon_f=\alpha_1\epsilon_1+\alpha_2\epsilon_2+\alpha_3\epsilon_3+\alpha_4\epsilon_4, \tag{4.11}$$

where $\alpha_i=\partial f/\partial x_i$, and the mean square error (variance) of f is given by

$$\sigma_f^2=\langle\epsilon_f^2\rangle=\sum_{ij}\alpha_i\alpha_j\langle\epsilon_i\epsilon_j\rangle=C\sum_{ij}\alpha_i\alpha_jd_{ij}. \tag{4.12}$$

The quantity C is the constant relating the "weight" of an observation to its variance; our *a priori* choice for this constant (its value by "internal consistency") is

$$C_I=p_\mu\sigma_\mu^2 \text{ (internal)}. \tag{4.13}$$

It is possible also to make an *a posteriori* estimate of C (its value by "external consistency") based on the statistical agreement of the least-squares solution. We expect the quantity $\chi^2/(N_{Eq}-q)$ to be equal to unity; if this is not so, we make an *a posteriori* readjustment in the scale of our standard deviation and define

$$C_E=C_I\chi^2/(N_{Eq}-q)=\sum_\mu p_\mu R_\mu^2/(N_{Eq}-q) \text{ (external)}. \tag{4.14}$$

CC-0. In Public Domain. Gurukul Kangri Collection, Haridwar

Digitized by Arya Samaj Foundation Chennai and eGangotri

Equation (4.12) gives us the generalized law of the propagation of errors; written out in terms of the standard deviation and the correlation coefficients of the variables it becomes

$$\sigma_f^2=\sum_{i=1}^{4}\alpha_i^2\sigma_{x_i}^2+2\sum_{i<j}r_{ij}\alpha_i\sigma_{x_i}\alpha_j\sigma_{x_j}, \qquad (4.15)$$

and this form must be used rather than an expression of the form (4.8), if we are dealing with correlated variables (i.e., if the correlation coefficients r_{ij} do not vanish).

As an example of the importance of the correlation coefficient, let us consider now an extreme case. We can write the function $f(x)=x^{s+t}$ as $f(x)=x^s x^t$ and in this latter form, if we consider the two factors to be independent, we would calculate the relative standard error of f to be $(s^2+t^2)^{\frac{1}{2}}$ times the relative standard error of x, whereas in the original form the relative error in f is $(s+t)$ times the relative error in x. However, we have neglected the effect of the correlation coefficient which is this case is $r=+1$ so that the correct expression for the relative error in f, when written in the second form, is $(s^2+t^2+2st)^{\frac{1}{2}}$, and *not* $(s^2+t^2)^{\frac{1}{2}}$, times the relative error in x, and we have thereby resolved the paradox. This method of computing errors (Eq. 4.15) will be called the method of the ellipsoid of error, because it is the analytical equivalent of constructing two parallel planes tangent to either side of the ellipsoid of error and normal to a given axis in the hyperspace of the unknowns (the axis for the linear function, f) to find the domain of standard deviation $\pm\sigma_f$ cut off by those planes on that axis.

The generalized formula of errors is the one used in calculating the error measures of all the derived quantities in obtaining our least-squares adjusted general table of output values in this paper. Now, it is true that a certain valid objection could be raised to the practice of giving only the standard deviations of the derived output values, for these values are definitely *not* observationally independent, in general. To give, however, a complete matrix of standard deviations *and correlation coefficients* connecting all possible pairs of all the derived values would obviously be too cumbersome. We must emphasize, however, that when any of these output values are used in formulas to compute other quantities, it is strictly *incorrect* to compute the probable error of the resultant quantities by the ordinary formula of propagation of errors for observationally independent quantities. The correct probable error may be either greater or less than this because of the cross-product terms. When two correlated quantities are to be combined, the standard error of the resultant can be calculated only if the correlation coefficient is also known or if the quantities are re-expressed in terms of variables whose correlation coefficients are known. A numerical example of such a computation is given in Sec. 10.

5. REJECTION OF CERTAIN INPUT DATA FOR THE PRESENT LEAST-SQUARES ADJUSTMENT

Two criteria have been followed in selecting data for use in the present adjustment. (1) Reject data of such low numerical accuracy that the corresponding weight of the observational equation would imply negligible influence on the entire solution. (2) Reject data which, even though accurately measured, suffer from uncertainties in theoretical interpretation.

The hyperfine structure shift of hydrogen in the $^2S_{\frac{1}{2}}$ state, $\Delta\nu_H$ would furnish an important datum connecting the quantities α, c, R_∞, and μ_p/μ_e, the ratio of the magnetic moments of proton and electron, were it not for the uncertainty regarding a certain correction term. The shift $\Delta\nu_H$ has been measured by the atomic beam magnetic resonance method with a precision of 6 ppm in 1947 at Columbia University by Nafe and Nelson,[28,29] but more recently, and much more accurately, with a probable error of only 0.2 ppm by the same method by Prodell and Kusch[30] at the same laboratory. This remarkable measurement is absolute in the sense that a microwave frequency which can be directly compared to a fundamental time standard is resonated with an atomic energy level difference. The relationship which is originally due to Fermi[31] is

$$\Delta\nu_H=\frac{16\alpha^2}{3}cR_\infty\left(\frac{\mu_p}{\mu_e}\right)\left(\frac{\mu_e}{\mu_0}\right)^2 \times(1+\tfrac{3}{2}\alpha^2)\left(1+\frac{m}{m_p}\right)^{-3}\mathcal{E}\mathcal{P}. \qquad (5.1)$$

In this formula μ_p is the magnetic moment of the proton and μ_e that of the electron; μ_e/μ_0 is the ratio[32] of the electron moment to the Bohr magneton. The factor $(1+\frac{3}{2}\alpha^2)$ is Breit's relativistic correction term, and the next parenthesis is the reduced mass correction term. The last two factors $\mathcal{E}$ and $\mathcal{P}$, whose importance was first pointed out by Bethe and Longmire,[33] correct for the finite extension of the electron and proton dipoles; the magnitude of the former effect has been calculated by Karplus and Klein,[34] but there has only been an order of magnitude estimate for the latter which could be in error by a few parts in 10^5. The present state of meson theory holds little promise that a better estimate will be soon forthcoming. Thus, although the accuracy of the measurement is better than 1 part in 10^6, the theoretical uncertainty is sufficiently large that we have no recourse for the present but to reject this datum.

Under the direct measurements of the Faraday by electrochemical methods we have felt obliged to omit the provisional values obtained from the measurements

[28] J. E. Nafe and E. B. Nelson, Phys. Rev. **73**, 718 (1948).
[29] E. B. Nelson and J. E. Nafe, Phys. Rev. **75**, 1194 (1949).
[30] A. G. Prodell and P. Kusch, Phys. Rev. **79**, 1009 (1950).
[31] E. Fermi, Z. Physik **60**, 320 (1930).
[32] R. Karplus and N. M. Kroll, Phys. Rev. **77**, 536 (1950).
[33] H. A. Bethe and C. Longmire, Phys. Rev. **75**, 306 (1949).
[34] R. Karplus and A. Klein, Phys. Rev. **85**, 972 (1952).

CC-0. In Public Domain. Gurukul Kangri Collection, Haridwar

Digitized by Arya Samaj Foundation Chennai and eGangotri

by Craig and Hoffman with sodium oxalate and with silver. In a preliminary least-squares adjustment we have found that the recently revised values of the sodium oxalate measurements (revised chiefly because of revisions in the chemists international atomic weights) fall considerably out of line with the other observational equations. This by itself would constitute insufficient reason for omitting this datum but a letter from D. N. Craig, dated August 29, 1952, clearly states that work is still in progress to establish (1) the exactness of the assumed chemical reaction, (2) the isotopic composition of the sodium oxalate, and (3) the purity of the sodium oxalate. Dr. Craig concludes, "Consequently, we are not in a position to change the preliminary value which appeared in the Physical Review." We reject the silver value of Craig and Hoffman, because it is presumed also to be only preliminary.

The Faraday values for silver and for iodine which have been kindly furnished by Dr. Vinal based on earlier work are definitive, and hence we have retained them, although they disagree by more than 3 times the internally estimated probable error of the difference between them.

The items listed as Eqs. (6.9) to (6.11) are obtained from measurements of the short wavelength limit of the continuous x-ray spectrum. These measurements have traditionally been called measurements of h/e, whereas what is measured is the dc voltage applied to an x-ray tube and the wavelength in Siegbahn x units of the emitted continuous x-ray spectrum quantum limit. Factors like c and λ_g/λ_s, which were once treated as auxiliary fixed constants, have in the present adjustment acquired the status of unknown variables, and we must, therefore, be careful to recognize exactly what the observed quantity in this experiment really is. Clearly this experiment measures, after appropriate corrections, the conversion constant between the energy in electron volts and the wavelength (in Siegbahn x units) of electromagnetic quanta.

6. CHOICE OF THE UNKNOWNS AND THE PRIMITIVE OBSERVATIONAL EQUATIONS

Wherever more than one important determination of a given datum exists and is deemed worthy of inclusion in our adjustment, *we write a separate observational equation for each of the determinations* instead of following the almost universal past practice of taking a weighted average of all similar determinations and treating this as a single datum for which only one observational equation need be written. This method is the more logical one, since it permits the determination of separate normalized residues for each separate datum and gives a more correct measure of χ^2. Clearly with this method $N_{Eq}-q$, the number of "degrees of freedom" (or of overdetermination) in the least-squares solution will be larger and should give a truer picture of the real consistency situation. Also (and of more direct utility) the separate normalized residues for each determination can be independently computed and assessed.

In order to avoid hidden observational correlations, care has been taken in formulating the primitive equations of observation (6.1) to (6.13) to see that the numeric, the right-hand member of each equation, is the result of a single determination and not the combined result of two or more determinations. For example, Dayhoff quotes in his recent report on the fine structure of hydrogen and deuterium a value of the fine structure constant α. What he actually measured, however, was the frequency separation ΔE_D between the levels $2^2P_{\frac{3}{2}}$ and $2^2P_{\frac{1}{2}}$ in deuterium and his value of α was computed from ΔE_D by the use of a formula involving R_∞, c, and correction factors depending on α and on the ratio M_d/D of the mass of the deuteron to the mass of the deuterium atom. Consequently, in Eq. (6.13) we have equated his measured numeric ΔE_D to the appropriate function of all the quantities involved along with α.

The precision measures given are standard errors σ (as distinguished from "probable error," equal to $0.6745\,\sigma$ for a Gaussian distribution). The absolute standard error is given immediately following each numerical value and the relative standard error in parts per million (ppm) is given in parentheses after this. When experimenters report "limits of error," we have followed the rule of dividing these by two to obtain the standard error.

The physical scale of atomic weights is used throughout in quoting numerical values.

The primitive equations of observation are the following, Eqs. (6.1) to (6.13):

The *velocity of light* as obtained by K. D. Froome[12] at the British National Physical Laboratory with a microwave interferometer:

$$c=(299792.6\pm0.7)\times10^5 \text{ cm sec}^{-1} \quad (2.3 \text{ ppm}). \quad (6.1)$$

The same constant as obtained by Bergstrand[9,10] with visible light over long base lines using his "geodimeter" (Kerr cell modulation)

$$c=(299793.1\pm0.32)\times10^5 \text{ cm sec}^{-1} \quad (1.1 \text{ ppm}). \quad (6.2)$$

The results of determinations of the *Faraday* by the electrolysis of iodine and of silver, respectively, as recently recomputed from old data[35] by G. W. Vinal,[36] utilizing the latest international atomic weights (chemical scale) and conversion factors for the absolute electrical units.

(Iodine) $Ne/c=9652.15\pm0.13$ emu (g mole)$^{-1}$ (phys. scale) (13 ppm). (6.3)

(Silver) $Ne/c=9651.29\pm0.19$ emu (g mole)$^{-1}$ (phys. scale) (20 ppm). (6.4)

[35] G. W. Vinal and S. J. Bates, Bull. Bur. Standards **10**, 425 (1914); G. W. Vinal and W. M. Bouvard, Bull. Bur. Standards **13**, 147 (1916).

[36] G. W. Vinal, November 22, 1949 and corrected for new atomic mass of iodine (1951) (private communication by J. A. Hipple, December 14, 1951).

CC-0. In Public Domain. Gurukul Kangri Collection, Haridwar

Digitized by Arya Samaj Foundation Chennai and eGangotri

The *magnetic moment of the proton* μ' (uncorrected for diamagnetism), expressed in nuclear magnetons $\mu_n = eh/4\pi m_p c$, as obtained by Bloch and Jeffries,[37] using the method of the inverse cyclotron,

$$\mu' = 2.792365 \pm 0.00010 \text{ (36 ppm)} \quad (6.5)$$

and the same constant as obtained by Sommer, Thomas, and Hipple,[38] using the "omegatron,"

$$\mu' = 2.792685 \pm 0.00003 \text{ (11 ppm)}. \quad (6.6)$$

The *gyromagnetic ratio for the proton* γ, as obtained at the U. S. National Bureau of Standards by Thomas, Driscoll, and Hipple[39] before making the diamagnetic correction,

$$\gamma = \mu' Ne/(M_p c) = (2.67523 \pm 0.00006) \times 10^4 \text{ sec}^{-1} \text{ gauss}^{-1} \text{ (23 ppm)}. \quad (6.7)$$

The *conversion factor* $\lambda = \lambda_0/\lambda_s$ from the Siegbahn nominal scale of x-ray wavelengths (expressed in x units) to milliangstroms as recommended for general adoption by Sir Lawrence Bragg[40] after consultation with Professor Manne Siegbahn, Professor B. E. Warren (of the Massachusetts Institute of Technology), and Dr. H. Lipson (of the College of Technology, Manchester, England), and with due consideration given to the analysis of the various sources of primary data by R. T. Birge (see last article of reference 2).

$$\lambda = \lambda_0/\lambda_s = 1.002020 \pm 0.000030 \text{ (30 ppm)}. \quad (6.8)$$

Three recent precision determinations[41–43] of the *short wavelength limit* of the continuous x-ray spectrum (a) by G. Felt at 24 500 volts, (b) by Bearden, Johnson, and Watts at 10 000 volts and at 6000 volts, and (c) by Bearden and Schwarz at 8000, 9800, and 19600 volts, to obtain the conversion constant from wavelengths in x units on the Siegbahn nominal scale to quantum energy in electron volts, emu:

(G. Felt)

$$hc^2/(\lambda e) = (12370.02 \pm 0.63) \text{ emu cm (51 ppm)}, \quad (6.9)$$

(B. J. and W.)

$$hc^2/(\lambda e) = (12371.03 \pm 0.48) \text{ emu cm (40 ppm)}, \quad (6.10)$$

(B. and S.)

$$hc^2/(\lambda e) = (12370.77 \pm 1.03) \text{ emu cm (83 ppm)}. \quad (6.11)$$

The value of *Avogadro's number multiplied by* λ^3 as obtained by R. T. Birge[2] from his analysis of a considerable number of measurements of the densities of crystals, the geometry of their unit cells and their grating constants expressed on the Siegbhan nominal scale of x units:

$$N\lambda^3 = (6.06179 \pm 0.00023) \times 10^{23} \text{ (g mole)}^{-1} \text{ (physical) (38 ppm)}. \quad (6.12)$$

The *fine-structure separation in deuterium*, $2^2P_{\frac{3}{2}} - 2^2P_{\frac{1}{2}}$, ΔE_D, measured in frequency units by Dayhoff,[44] using the atomic beam magnetic resonance method,

$$\Delta E_D = (1/16)\alpha^2 R_\infty c\left[1 + (5/8)\alpha^2 + (\alpha/\pi)\left(1 - 5.946\frac{\alpha}{\pi}\right)\right] M_d/D = (10971.59 \pm 0.10)10^6 \text{ sec}^{-1} \text{ (9 ppm)}. \quad (6.13)$$

7. AUXILIARY CONSTANTS AND EQUATIONS

It will be noted that the quantities[45] involved in expressing the above thirteen primitive observational equations are N, e, m, h, c, α, μ', λ, R_∞, and the masses M_p, D, and M_d on the physical scale of atomic masses. Certain of these quantities are so accurately known from measurements that they can be safely regarded as fixed auxiliary constants, since their relative standard errors are so small as to contribute negligibly when combined in formulas along with the other quantities. These are (a) the masses on the physical scale of atomic masses M_p, D, and M_d along with which we list also H, since it will be needed in computing derived quantities, (b) the Rydberg fundamental wave number R_∞, (c) the ratio of the electron magnetic moment to the proton magnetic moment very recently measured to 0.6 ppm at Columbia by Koenig, Kusch, and Prodell.

The four atomic masses are obtained, with great accuracy by the method of measuring nuclear reaction energies:[46]

$$H = 1.008142 \pm 0.000003 \text{ (Physical Scale) (3 ppm)}, \quad (7.1)$$

$$H/M_p = 1.00054461 \text{ (Computed using } Nm = 0.00054875) \text{ (Physical Scale)}, \quad (7.2)$$

$$D = 2.014735 \pm 0.000006 \text{ (Physical Scale) (3 ppm)}, \quad (7.3)$$

$$D/M_d = 1.00027244 \text{ (Computed using } Nm = 0.00054875) \text{ (Physical Scale)}. \quad (7.4)$$

[37] F. Bloch and C. D. Jeffries, Phys. Rev. **80**, 305 (1950); C. D. Jeffries, Phys. Rev. **81**, 1040 (1951).
[38] Sommer, Thomas, and Hipple, Phys. Rev. **82**, 697 (1951).
[39] Thomas, Driscoll, and Hipple, J. Research Natl. Bur. Standards **44**, 569 (1950); Phys. Rev. **78**, 787 (1950).
[40] Sir Lawrence Bragg, Acta Cryst. **1**, 46 (1948); J. Sci. Instr. **24**, 27 (1947).
[41] G. Felt, thesis, California Institute of Technology (1951).
[42] Bearden, Johnson, and Watts, Phys. Rev. **81**, 70 (1951).
[43] J. A. Bearden and G. Schwarz, Phys. Rev. **79**, 674 (1950).
[44] Edward S. Dayhoff, Preprinted Report No. VI on Fine Structure of the Hydrogen Atom, Columbia University (1952).
[45] All the quantities enumerated here appear explicitly in Eqs. (6.1) to (6.13) except m. Because of the Rydberg relationship (R_∞ being so accurately known that we treat it as an exact auxiliary constant) the value of m is implied by the other quantities through the equation $m = 4\pi e^2 R_\infty \alpha^{-3} c^{-2}$, and we therefore list m along with the rest.
[46] Li, Whaling, Fowler, and Lauritsen, Phys. Rev. **83**, 512 (1951).

CC-0. In Public Domain. Gurukul Kangri Collection, Haridwar

Digitized by Arya Samaj Foundation Chennai and eGangotri

The numerical value of R_∞ has recently been recomputed[47] taking into consideration the modifications required by the Lamb shift:

$$R_\infty = 109737.311 \pm 0.012 \text{ cm}^{-1} \quad (0.11 \text{ ppm}). \quad (7.5)$$

The measurement at Columbia by Koenig, Prodell, and Kusch[48] of the ratio of the electron magnetic moment to the proton magnetic moment μ' (without diamagnetic correction) is so accurate as to warrant its inclusion in the category of auxiliary fixed constants

$$[M_p/(Nm\mu')](1+\alpha/2\pi-2.973\ \alpha^2/\pi^2) = 658.2288 \pm 0.0004 \quad (0.6 \text{ ppm}). \quad (7.6)$$

In addition to the above, there are available two exact auxiliary equations connecting the quantities involved which can be used to reduce the number of variables of the least-squares adjustment. These are the equation expressing α in terms of e, h, and c and the equation for the Rydberg expressed in terms of e, α, c, and m. Solving these for h and m, respectively, we have

$$h = 2\pi e^2/(\alpha c) \quad (7.7)$$

$$m = 4\pi e^2 R_\infty/(\alpha^3 c^2). \quad (7.8)$$

Using the value $1/\alpha = 137.04$, the correction factor μ_e/μ_0 for the anomalous magnetic moment of the electron can be computed with amply sufficient accuracy (less than 0.1 ppm) and it is, therefore, also treated as an auxiliary constant

$$\mu_e/\mu_0 = (1+\alpha/2\pi-2.973\ \alpha^2/\pi^2) = 1.0011453. \quad (7.9)$$

8. FORMATION OF THE LINEARIZED EQUATIONS OF OBSERVATION IN FIVE VARIABLES

We now use Eqs. (7.3)–(7.9) to reduce the number of variables in our solution. None of the original error measures of Eqs. (6.1) to (6.13) are appreciably influenced by the introduction of these very much more accurate auxiliary constants. Hence, the numerics of the new transformed set can be considered to be essentially just as uncorrelated with each other as were the original ones. The new set (with the physical units suppressed) is given below. With these we show on the left the numbers of the earlier equations involved in obtaining each equation. The equations in square brackets are those which contribute negligibly to the error:

(6.1)		$c = 2.997926\times10^{10}$	(2.3 ppm)	(8.1)
(6.2)		$c = 2.997931\times10^{10}$	(1.1 ppm)	(8.2)
(6.3)		$Ne/c = 9652.15$	(13 ppm)	(8.3)
(6.4)		$Ne/c = 9651.29$	(20 ppm)	(8.4)
(6.5)	[7.5] [7.6] [7.8] [7.9]	$Ne^2/(\alpha^3c^2) = 3.979879\times10^{-10}$	(36 ppm)	(8.5)
(6.6)	[7.5] [7.6] [7.8] [7.9]	$Ne^2/(\alpha^3c^2) = 3.979423\times10^{-10}$	(11 ppm)	(8.6)
(6.7)	[7.5] [7.6] [7.8] [7.9]	$\alpha^3c/e = 2.425517\times10^{13}$	(23 ppm)	(8.7)
(6.8)		$\lambda = 1.002020$	(30 ppm)	(8.8)
(6.9)	[7.7]	$ec/(\lambda\alpha) = 1968.750$	(51 ppm)	(8.9)
(6.10)	[7.7]	$ec/(\lambda\alpha) = 1968.911$	(40 ppm)	(8.10)
(6.11)	[7.7]	$ec/(\lambda\alpha) = 1968.869$	(83 ppm)	(8.11)
(6.12)		$N\lambda^3 = 0.606179\times10^{24}$	(38 ppm)	(8.12)
(6.13)	[7.3] [7.4] [7.5]	$\alpha^2c = 1.596412\times10^{6}$	(9 ppm)	(8.13)

We adopt the following origin values:

$$\alpha_0 = 0.007297000$$
$$c_0 = 2.997900\times10^{10}$$
$$e_0 = 4.802200\times10^{-10}$$
$$N_0 = 0.6025000\times10^{24}$$
$$\lambda_0 = 1.0020200$$
$$(\alpha^2c)_0 = 1.596268\times10^{6}$$
$$(Ne/c)_0 = 9651.174$$
$$(\alpha^3c/e)_0 = 2.425548\times10^{13}$$
$$(Ne^2/\alpha^3c^2)_0 = 3.978966\times10^{-10}$$
$$(ec/\lambda\alpha)_0 = 1968.959$$
$$(N\lambda^3)_0 = 0.6061585\times10^{24}:$$

and define the linearized unknowns $x_1 \cdots x_5$ as follows

$$\alpha = \alpha_0(1+10^{-6}\ x_1)$$
$$c = c_0(1+10^{-6}\ x_2)$$
$$e = e_0(1+10^{-6}\ x_3)$$
$$N = N_0(1+10^{-6}\ x_4)$$
$$\lambda = \lambda_0(1+10^{-6}\ x_5),$$

so that the x's are the relative deviations of the primitive variables from the origin values expressed in ppm.

[47] E. R. Cohen, Phys. Rev. 88, 353 (1952).
[48] Koenig, Prodell, and Kusch, Phys. Rev. 88, 191 (1952).

CC-0. In Public Domain. Gurukul Kangri Collection, Haridwar

Digitized by Arya Samaj Foundation Chennai and eGangotri

We can now write our linearized equations of observation as follows:

Linearized Equations of Observation

						Weight $=1/\sigma^2$	
		x_2			$=$ 8.7± 2.3	0.198	(8.14)
		x_2			$=$ 10.3± 1.1	0.830	(8.15)
		$-x_2$	$+x_3$	$+x_4$	$=$ 101 ±13	0.0058	(8.16)
		$-x_2$	$+x_3$	$+x_4$	$=$ 12 ±20	0.0025	(8.17)
$-3x_1$	$-2x_2$	$+2x_3$	$+x_4$		$=$ 229 ±36	0.0008	(8.18)
$-3x_1$	$-2x_2$	$+2x_3$	$+x_4$		$=$ 115 ±11	0.0083	(8.19)
$3x_1$	$+x_2$	$-x_3$			$=-$ 13 ±23	0.0019	(8.20)
				x_5	$=$ 0 ±30	0.0011	(8.21)
$-x_1$	$+x_2$	$+x_3$			$-x_5=-106$ ±51	0.0004	(8.22)
$-x_1$	$+x_2$	$+x_3$			$-x_5=-$ 24 ±40	0.0006	(8.23)
$-x_1$	$+x_2$	$+x_3$			$-x_5=-$ 46 ±83	0.00015	(8.24)
				x_4	$+3x_5=$ 35 ±38	0.0007	(8.25)
$2x_1$	$+x_2$				$=$ 90 ± 9	0.0123	(8.26)

9. THE LEAST-SQUARES SOLUTION

The normal equations are now formed from the equations of observation (8.14) to (8.26), according to the classical rule. They are:

Normal Equations

	α	c	e	N	λ	Const	
α	$0.14935x_1$	$+0.08375x_2$	$-0.06145x_3$	$-0.02730x_4$	$+0.00115x_5=$	-1.2095	(9.1)
c	$0.08375x_1$	$+1.08605x_2$	$-0.04545x_3$	$-0.02650x_4$	$-0.00115x_5=$	8.3784	(9.2)
e	$-0.06145x_1$	$-0.04545x_2$	$+0.04775x_3$	$+0.02650x_4$	$-0.00115x_5=$	2.8522	(9.3)
N	$-0.02730x_1$	$-0.02650x_2$	$+0.02650x_3$	$+0.01810x_4$	$+0.00210x_5=$	1.7780	(9.4)
λ	$0.00115x_1$	$-0.00115x_2$	$-0.00115x_3$	$+0.00210x_4$	$+0.00855x_5=$	0.13720	(9.5)

The solution of this system of linear equations gives the least-squares adjusted values of the unknowns. The solution together with the corresponding values of the primitive variables are given in Table II.

Substituting these values of the x's into the linearized equations of observation (8.14) to (8.26), one obtains the residues R_i by which each of these thirteen equations fails to balance. Dividing each of these residues by the standard deviation assigned to the observed constant in the equation, we obtain the column of "normalized residues" labeled Case I in Table III, together with the value of $\chi^2=(\Sigma R_i^2/\sigma_i^2)$ and of $r_e/r_i=[\chi^2/(N-q)]^{\frac{1}{2}}$, the ratio of external to internal consistency.

The expectation value of χ^2 for Case I is $N-q=13-5=8$. The actual value 52.1 is seen to be much larger. This corresponds to a ratio of error by external consistency to error by internal consistency of $r_e/r_i=(52.1/8)^{\frac{1}{2}}=2.55$. This large value of χ^2 we interpret as probably meaning that the estimated uncertainties (standard deviations) attached to the various input measurements were throughout somewhat too small. We have used the values given by the experimenters themselves, reduced whenever necessary to the scale of standard deviation. We tend to this view rather than to the alternative possibility that systematic errors are present (though, of course, such a possibility cannot be completely refuted) for the following reason. We have plotted the normalized residues on probability integral graph paper to see if they conform satisfactorily to a normal probability integral distribution curve, which

TABLE II. Least-squares adjusted values.

Linearized unknowns	Primitive variables
$x_1=$ 36.1	$\alpha=0.007297264$
$x_2=$ 9.80	$c=2.9979294\times10^{10}$ cm sec^{-1}
$x_3=$ 142.1	$e=4.802882\times10-10$ esu
$x_4=-45.9$	$N=0.6024723\times10^{24}$ (g mole)$^{-1}$ (Phys.)
$x_5=$ 42.9	$\lambda=1.002063$

TABLE III. Normalized residues of observational equations.

	R_i/σ_i Case I	R_i/σ_i Case II	R_i/σ_i Case III	R_i/σ_i Case IV
(8.14) c, Froome	0.49	0.49	0.58	0.58
(8.15) c, Bergstrand	−0.46	−0.45	−0.27	−0.28
(8.16) F, Vinal (I)	−1.11		−1.42	
(8.17) F, Vinal (Ag)	3.72		3.51	
(8.18) μ', B J	−3.36	−3.06	−3.12	−2.92
(8.19) μ', STH	−0.44	0.52	0.35	0.96
(8.20) γ, TDH	−0.47	1.29	−1.03	0.21
(8.21) λ, Bragg	1.42	0.53	1.01	0.42
(8.22) h/e, Felt	3.58	3.34		
(8.23) h/e, BJW	2.37	2.09		
(8.24) h/e, BS	1.45	1.31		
(8.25) $N\lambda^3$, Birge	1.26	1.47	−0.42	−0.18
(8.26) ΔE_D, Dayhoff	−0.88	−0.68	−0.15	−0.06
	$\chi^2=52.1$	31.9	26.9	10.15
	$r_e/r_i=2.55\pm0.90$	2.31±0.95	2.32±1.04	1.84±1.06

CC-0. In Public Domain. Gurukul Kangri Collection, Haridwar

Digitized by Arya Samaj Foundation Chennai and eGangotri

on such paper would appear as a straight line.[49] If one or two of the observational equations were subject to a large systematic error, one would expect these to exhibit residues inconsistent with the rest, i.e., departing markedly from the curve for the normal distribution. Fig. 1 shows this plot, and the fluctuations from the normal do not appear to be larger than one would expect for a sample with eight degrees of freedom. We have also performed three additional least-squares adjustments designated as Case II, Case III, and Case IV. In Case II Eqs. (8.16) and (8.17), the two Faraday determinations by electrochemistry, were omitted. In Case III Eqs. (8.22), (8.23), and (8.24), the three x-ray determinations of the quantum limit of the continuous spectrum, were omitted. In Case IV both complete sets of determinations were omitted. Table III gives the normalized residues for these four cases together with the resulting

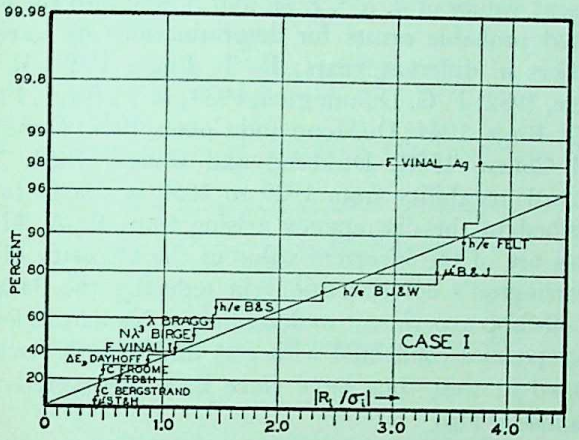


FIG. 1. The normalized residues $|R_i/\sigma_i|$ for a least squares adjustment of the entire thirteen input observational data are here shown as abscissas plotted without regard to algebraic sign in order of increasing absolute magnitude on probability graph paper whose ordinates are so distorted from a linear scale of percent as to rectify probability integral graphs for Gaussian distributions into straight lines of different slopes for different values of χ^2. The straight line shown corresponds to $\chi^2=52.1$, the result for this case in which there are thirteen input equations and eight degrees of freedom. The ratio of the error by external to that by internal consistency is $R_E/R_I=2.55\pm0.90$.

values of χ^2. The normalized residues for each of the four cases are shown in Figs. 1 to 4, and all are approximately equally satisfactory. The values of χ^2 and of r_e/r_i also are not significantly more plausible or satisfactory for Cases II, III, and IV than for Case I. For these reasons, then, we think that the large value of r_e/r_i in Case I probably does not reflect any single large isolated case of systematic error among the thirteen input data. We are basing our adjusted output values

[49] We are indebted to Professor John Tukey of Princeton for pointing out to us that for the case of a small number of degrees of freedom it is very unlikely that the residuals should be exactly normally distributed. In the present instance let it be understood therefore that we are merely *comparing* the actual distribution of residuals with a normal distribution as a type-form but without any implication as to what precisely their expected distribution *should* be.

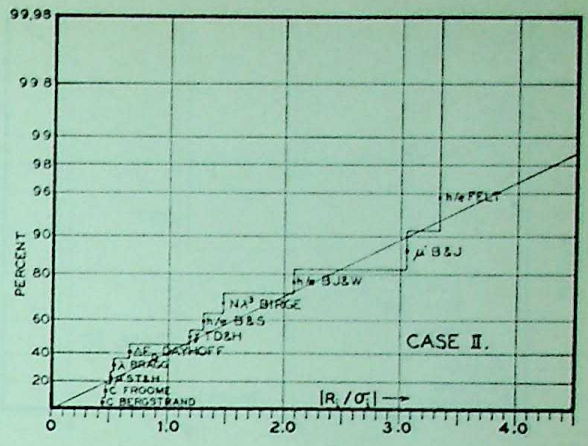


FIG. 2. The normalized residues $|R_i/\sigma_i|$ for a least squares adjustment of all input data save the two electrochemical measurements of the Faraday plotted in similar manner to those of Fig. 1. The straight line shown corresponds to $\chi^2=31.9$, the result for this case in which there are eleven input equations and six degrees of freedom. The ratio of the error by external to that by internal consistency is $R_E/R_i=2.31\pm0.95$.

on Case I, because it reflects the results of more input data than the other cases.

Adopting the error by external consistency as the measure of error we obtain the error elements shown in Table IV.

In computing the standard deviation of any function of α, c, e, N, and λ, the appropriate elements of the error matrix must be used in Eq. (4.15) as explained in Sec. 4. The tables of atomic constants and conversion factors have been computed using the least squares adjusted values of α, c, e, N, and λ given above together with the auxiliary constants given in the tables, and the standard deviation of derived values following each ($\pm$) sign has been computed from Eq. (4.15), using values from the error matrix of Table IV. The reader must realize that if he uses any of these values (either the unknowns α, c, e, N, λ, or tabular values derived

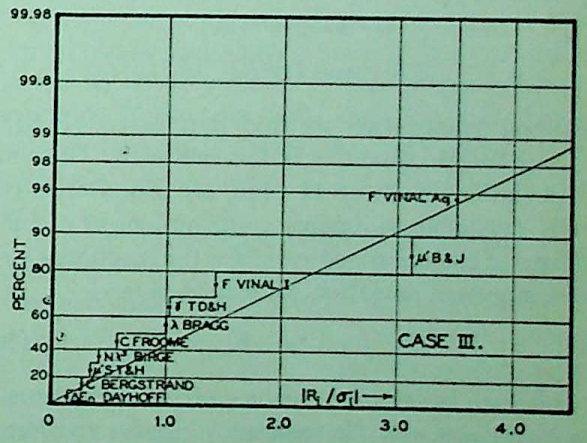


FIG. 3. The normalized residues $|R_i/\sigma_i|$ for a least squares adjustment of all input data save the three x-ray measurements of the short wavelength limit of the continuous spectrum plotted in similar manner to those of Fig. 1. The straight line shown corresponds to $\chi^2=26.9$, the result for this case in which there are ten input equations and five degrees of freedom. The ratio of the error by external to that by internal consistency is $R_E/R_i=2.3\pm1.0$.

CC-0. In Public Domain. Gurukul Kangri Collection, Haridwar

Digitized by Arya Samaj Foundation Chennai and eGangotri

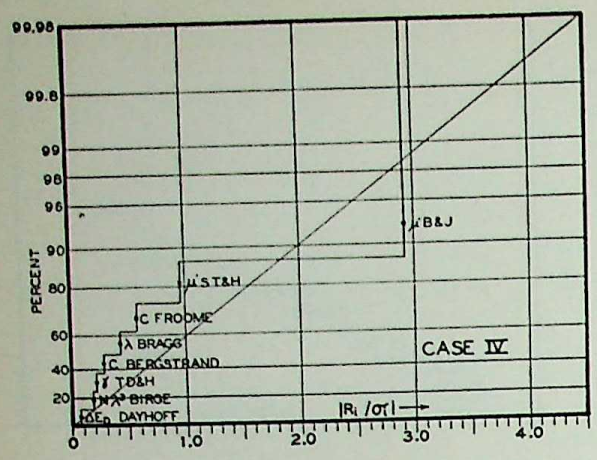


FIG. 4. The normalized residues $|R_i/\sigma_i|$ for a least squares adjustment of all input data save the three x-ray measurements of the short wavelength limit of the continuous spectrum and the two electrochemical measurements of the Faraday plotted in similar manner to those of Fig. 1. The straight line shown corresponds to $\chi^2=10.2$, the result for this case in which there are eight input equations and three degrees of freedom. The ratio of the error by external to that by internal consistency is $R_E/R_i=1.8\pm1.1$.

from these) in further computations, he *must* compute the standard deviation of his results by this more generalized method. We give the following example as an illustration.

10. ILLUSTRATIVE EXAMPLE OF COMPUTATION OF THE STANDARD DEVIATION OF A FUNCTION OF TABULAR VALUES OBTAINED IN THE PRESENT LEAST-SQUARES ANALYSIS

Compute the standard deviation for the ionization energy $I_0=e^2/(2a_0)$ of a hydrogen atom. The Bohr radius is $a_0=h^2/(4\pi^2me^2)$. This is expressed as a function of two variables h and m which are not explicit members of our set of unknowns α, c, e, N, and λ. We have, however, relations (7.7) and (7.8) which relate h and m to those unknowns,

$$(7.7)\quad h=2\pi e^2/(\alpha c)$$

$$(7.8)\quad m=4\pi e^2R_\infty/(\alpha^3c^2),$$

and upon substitution we find that $a_0=\alpha/(4\pi R_\infty)$ so that our desired quantity is $I_0=2\pi R_\infty e^2/\alpha$. The standard deviation in R_∞ (0.11 ppm, see Eq. 7.5) is completely negligible as against contributions of e^2 and α. In terms of the linearized variables the function $\varphi=e^2/\alpha$ whose standard deviation we seek then is

$$f=2x_3-x_1, \qquad (10.1)$$

in which we see that the values of the coefficients are $\alpha_3=2$ and $\alpha_1=-1$. (In general, whatever the form of the primitive function φ the α_j's are determined from it by the formula $\alpha_j=(\partial\varphi/\partial u_j)(u_j/\varphi)$, wherein u_j is one of the primitive unknowns, i.e., in the present solution α, c, e, N, or λ). It remains then simply to apply formula (4.15) to obtain σ_f^2 which, written out for this case, is

$$\sigma_f^2=\alpha_1^2\sigma_1^2+\alpha_3^2\sigma_3^2+2\alpha_1\alpha_3\sigma_1\sigma_3r_{13} \qquad (10.2)$$

$$=\sigma_1^2+4\sigma_3^2-4\sigma_1\sigma_3r_{13}. \qquad (10.3)$$

From the error matrix given in Table IV, we find

$$\sigma_1^2=128;\quad \sigma_3^2=1981;\quad \sigma_1\sigma_3r_{13}=365$$

$$\sigma_f^2=128+7924-1460=6592$$

$$\sigma_f=(6592)^{\frac{1}{2}}=81.1 \text{ ppm}.$$

11. DISCUSSION OF THE RESULTS

It is of interest to examine the results of the various analyses for "best" values of the atomic constants made over the last quarter century to obtain an impression as to what progress toward precision and stabilization of the values has been accomplished. Accordingly, we have plotted in Fig. 5 the relative deviations from the present values of h, α^{-1}, e, m, and N and also the estimated probable errors for determinations by various authors in different years: R. T. Birge, 1929; R. T. Birge, 1932; F. G. Dunnington, 1939; R. T. Birge, 1941; R. T. Birge, 1944; DuMond and Cohen, 1947; DuMond and Cohen, 1950; DuMond and Cohen, 1952. The marked instability from 1929 to 1939 is chiefly to be ascribed to the discrepancy arising from R. A. Millikan's use of the incorrect value of the viscosity of air (Harrington's determination) in reducing the data of his oil-drop experiment to determine e. Numerous lesser discrepancies connected with e/m and with h/e which existed at that time have since been discovered and eliminated also.

The improvement as regards both stability and precision has been so great after 1939 that we have felt it worthwhile also to represent the last thirteen years in Fig. 6 to a scale of deviation fivefold that in Fig. 5.

Examination of these charts, especially Fig. 6, shows that the adjusted "best" values have changed in the last two years by from five to nine times the estimated probable errors of the December 1950 evaluation.

TABLE IV. Error elements (external consistency), Case I.

	Error matrix, $v_{ij}=\sigma_i\sigma_jr_{ij}$ (in ppm²)				
	α	c	e	N	λ
α	128	− 3.30	365	− 355	118
c	− 3.30	6.34	− 4.13	10.47	− 1.82
e	365	− 4.13	1981	−2454	820
N	−355	10.47	−2454	3568	−1158
λ	118	− 1.82	820	−1158	1140

	Standard errors σ_i (in ppm)				
	α	c	e	N	λ
	11.33	2.52	444	59.7	33.8

	Correlation coefficients r_{ij}				
	α	c	e	N	λ
α	1.000	−0.116	0.714	−0.521	0.308
c	−0.116	1.000	−0.036	0.070	−0.021
e	0.714	−0.036	1.000	−0.923	0.546
N	−0.521	0.070	−0.923	1.000	−0.574
λ	0.308	0.021	0.546	−0.574	1.000

CC-0. In Public Domain. Gurukul Kangri Collection, Haridwar

Digitized by Arya Samaj Foundation Chennai and eGangotri

Although the changes are small in the absolute sense (the largest being 224 ppm, for h) they are, at first sight, disturbingly large relative to the estimated probable errors of December, 1950. However, we believe the explanation for this is not hard to find, if we recall that the December, 1950 values, unlike the present ones, were afflicted with a systematic uncertainty because of the two uncertain Bethe-Longmire correction terms for the finite spatial extension of the nuclear and electronic dipoles, in the formula connecting $\Delta\nu_H$, the hydrogen hyperfine structure shift, with the Sommerfeld constant α. We supplied each numerical output value in the solution with a so-called Γ-coefficient to facilitate revising the numerical values when more accurate information became available regarding the exact magnitude of the Bethe-Longmire correction terms. We find that if we assign the value $\Gamma = 86.2 \pm 9$ ppm, that is to say if we increase G^2 in the formula

$$\Delta\nu_H = \frac{\alpha^2}{4\pi^2}(\mu_p/\mu_0)R_\infty c G^{-2}, \qquad (11.1)$$

by 86.2 ppm[50] (see p. 180 ff of the December, 1950 report), then the application of the resulting corrections to the five variables depicted in Fig. 6 simultaneously brings all of them fairly satisfactorily into agreement with the values obtained in the present adjustment. This is shown with the dotted lines in Fig. 6.

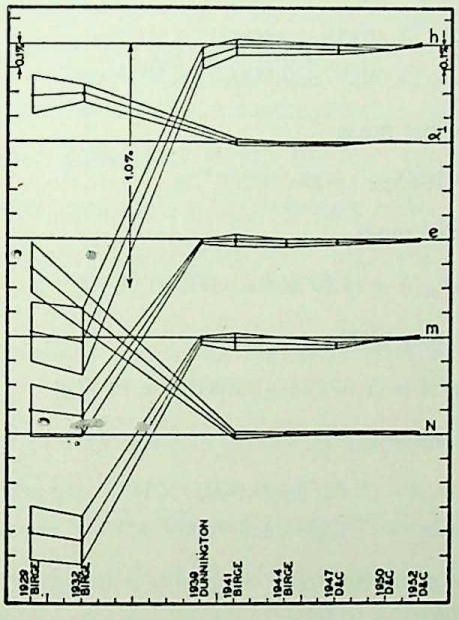


FIG. 5. History of relative fluctuations in the best adjusted values and probable errors of five atomic constants h, α^{-1}, e, m, and N over a 23-year interval. Fluctuations plotted as percent deviations from the present 1952 values. Probable errors rather than standard deviations are plotted to conform with the older usage prevailing through most of the interval. The large fluctuations in the first decade are chiefly due to the effects of Millikan's use of Harrington's erroneous value of the viscosity of air in reducing his oil-drop data to calculate e.

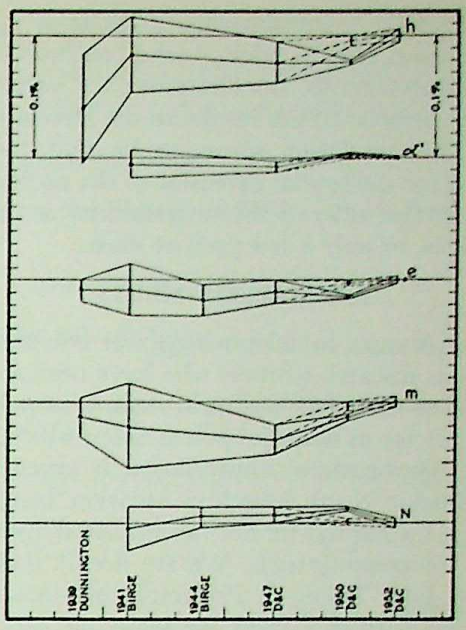


FIG. 6. History of relative fluctuations in the best adjusted values and probable errors of five atomic constants h, α^{-1}, e, m, and N over a 13 year interval plotted to five times larger scale of fluctuation than in Fig. 5. The fluctuations plotted are the percent deviations from the present 1952 values. As in Fig. 5, probable errors rather than standard deviations are plotted as the indices of precision. The full lines are plotted through the December, 1950 values and their probable errors as they were stated in the tables without applying any Γ-coefficient correction for the then uncertain Bethe-Longmire dipole correction terms. The dotted lines are plotted through the revisions required in the December, 1950 values, if these are modified by applying a Γ-coefficient correction to each output value with $\Gamma = 86.2$ ppm, as explained in the text.

In addition to the shift in the values of the constants, a change of 86.2 ppm in G^2 increases the probable errors of the 1950 output data by a factor of 1.48, if one uses external consistency (which has now become the larger measure of error) in place of the internal consistency used in the 1950 report. The evaluation of the variation of χ^2 and, hence, of the measure of the errors by external consistency is contained in Table XXXVII of that report.

The general conclusion seems to be a reassuring one, namely, that the constants are settling down to stable values and that successive determinations, even though many quite new and different types of data may enter, not only exhibit smaller and smaller precision measures by external consistency but also yield values which remain reasonably close to the limits set by preceding precision measures.

The Bethe-Longmire correction factor for the spatial

[50] This increase of 86.2 ppm was computed by solving for a new value of G^2 to compare with the 1950 value, $G^2 = 0.004751364$. The new value G^2 was obtained from Eq. (11.1), using our present new adjusted best values of α and c and a value of μ_p/μ_0 consistent with the results of Koenig, Kusch, and Prodell (reference 60) Eq. 7.6, corrected for diamagnetism using Ramsey's correction (1.000027). The new value of G^2 thus is not afflicted with any uncertainty regarding the Bethe-Longmire nuclear correction term as was the 1950 value. We regret to point out a misprint in the cited formula for $\Delta\nu_H$ near the bottom of p. 180 of the December, 1950 report (reference 33), in which a factor $c/4\pi^2$ was omitted. It should read as does Eq. 11.1.

CC-0. In Public Domain. Gurukul Kangri Collection, Haridwar

Digitized by Arya Samaj Foundation Chennai and eGangotri

extension of the electronic dipole has been computed by R. Karplus and A. Klein,[34] who conclude that this part of the correction alone requires a Γ value of 96.2 ppm to be applied to the results of the December, 1950 report. The conclusion seems to be that the factor correcting for the spatial extension of the nuclear dipole must be of the order of the uncertainties in the above calculations, or only a few ppm at most.

ACKNOWLEDGMENTS

It is a pleasure to acknowledge our indebtedness to the various research workers who have been so kind as to furnish us with their results in advance of publication or to clarify for us doubtful points about which we have inquired. Our grateful appreciation is given to Mrs. Melba Nead of North American Aviation, Incorporated (Downey, California) for her careful and diligent assistance in the computations. We are deeply indebted to Professor John Tukey of Princeton, who has read our manuscript with care from the viewpoint of a mathematical statistician and has made a number of helpful suggestions for its correction and improvement. The work has been carried out as part of the activity of a contract financially supported by the U. S. Office of Naval Research and the U. S. Atomic Energy Commission.

TABLE OF LEAST SQUARES—ADJUSTED OUTPUT VALUES (NOVEMBER, 1952)

I. Auxiliary Constants Used

These auxiliary constants are quantities which are uncorrelated (observationally) with the variables of the least-squares adjustment.

Rydberg wave number for infinite mass[51]

$R_\infty = 109737.309 \pm 0.012$ cm^{-1}

Rydberg wave numbers for the light nuclei

$R_H = 109677.576 \pm 0.012$ cm^{-1}
$R_D = 109707.419 \pm 0.012$ cm^{-1}
$R_{He^3} = 109717.345 \pm 0.012$ cm^{-1}
$R_{He^4} = 109722.267 \pm 0.012$ cm^{-1}

Atomic mass of neutron

$n = 1.008982 \pm 0.000003$

Atomic mass of hydrogen

$H = 1.008142 \pm 0.000003$

Atomic mass of deuterium

$D = 2.014735 \pm 0.000006$

Gas constant per mole (physical scale)

$R_0 = (8.31662 \pm 0.00038) \times 10^7$ erg mole^{-1} deg^{-1} C.

Standard volume of a perfect gas (physical scale)

$V_0 = 22420.7 \pm 0.6$ cm^3 atmos mole^{-1}

II. Least-Squares Adjusted Output Values

(The quantity following each ± sign is the standard error by external consistency)

Velocity of light

$c = 299792.9 \pm 0.8$ km sec^{-1}

Avogadro's constant (physical scale)

$N = (6.02472 \pm 0.00036) \times 10^{23}$ (g mole)$^{-1}$

Loschmidt's constant (physical scale)

$L_0 = N/V_0 = (2.68713 \pm 0.00016) \times 10^{19}$ cm^{-3}

Electronic charge

$e = (4.80288 \pm 0.00021) \times 10^{-10}$ esu
$e' = e/c = (1.60207 \pm 0.00007) \times 10^{-20}$ emu

Electron rest mass

$m = (9.1085 \pm 0.0006) \times 10^{-28}$ g

Proton rest mass

$m_p = M_p/N = (1.67243 \pm 0.00010) \times 10^{-24}$ g

Neutron rest mass

$m_n = n/N = (1.67474 \pm 0.00010) \times 10^{-24}$ g

Planck's constant

$h = (6.6252 \pm 0.0005) \times 10^{-27}$ erg sec
$h = h/(2\pi) = (1.05444 \pm 0.00009) \times 10^{-27}$ erg sec

Conversion factor from Siegbahn x units to millian-stroms

$\lambda_g/\lambda_s = 1.002063 \pm 0.000034$

Faraday constant (physical scale)

$F = Ne = (2.89360 \pm 0.00007) \times 10^{14}$ esu (g mole)$^{-1}$
$F' = Ne/c = (9652.01 \pm 0.25)$ emu (g mole)$^{-1}$

Charge-to-mass ratio of the electron

$e/m = (5.27299 \pm 0.00016) \times 10^{17}$ esu g^{-1}
$e'/m = e/(mc) = (1.75888 \pm 0.00005) \times 10^7$ emu g^{-1}

Ratio h/e

$h/e = (1.37943 \pm 0.00005) \times 10^{-17}$ erg sec (esu)$^{-1}$

[51] This differs from the value $R_\infty = 109737.311 \pm 0.012$ cm^{-1} given by E. R. Cohen (reference 47) and which was used in the least squares adjustment. In reference 47 a tentative value $Nm = 5.48785 \times 10^{-4}$ for the atomic mass of the electron was used with the proviso (page 359) that "an increase of 1 part per million in the electron mass will produce an increase of 0.00005 cm^{-1} in the Rydberg." (The coefficient 0.0005 cm^{-1} in the text is a typographical error.) The present value has, therefore, been revised using this coefficient to accord with our present output value of Nm and similar modifications have been made in the Rydberg values of the light nuclei.

CC-0. In Public Domain. Gurukul Kangri Collection, Haridwar

Digitized by Arya Samaj Foundation Chennai and eGangotri

Fine structure constant

$$\alpha = e^2/(hc) = (7.29726 \pm 0.00008) \times 10^{-3}$$
$$1/\alpha = 137.0377 \pm 0.0016$$
$$\alpha/2\pi = (1.161396 \pm 0.000013) \times 10^{-3}$$
$$\alpha^2 = (5.32501 \pm 0.00012) \times 10^{-5}$$
$$1-(1-\alpha^2)^{\frac{1}{2}} = (0.266254 \pm 0.000006) \times 10^{-4}$$

Atomic mass of the electron (physical scale)

$$Nm = (5.48760 \pm 0.00013) \times 10^{-4}$$

Ratio of mass of hydrogen to mass of proton[52]

$$H/H^+ = \left[1 - \frac{Nm}{H}(1-\tfrac{1}{2}\alpha^2)\right]^{-1}$$
$$= 1.000544610 \pm 0.000000013$$

Atomic mass of proton

$$H^+ = 1.007593 \pm 0.000003$$

Ratio of proton mass to electron mass

$$H^+/Nm = 1836.13 \pm 0.04$$

Reduced mass of electron in hydrogen atom

$$\mu = mH^+/H = (9.1035 \pm 0.0006) \times 10^{-28} \text{ g}$$

Schrödinger constant for a fixed nucleus

$$2m/\hbar^2 = (1.63844 \pm 0.00016) \times 10^{27} \text{ erg}^{-1} \text{ cm}^{-2}$$

Schrödinger constant for the hydrogen atom

$$2\mu/\hbar^2 = (1.63755 \pm 0.00016) \times 10^{27} \text{ erg}^{-1} \text{ cm}^{-2}$$

First Bohr radius

$$a_0 = \hbar^2/(me^2) = (5.29171 \pm 0.00006) \times 10^{-9} \text{ cm}$$
$$= \alpha/(4\pi R_\infty)$$

Radius of electron orbit in normal H^1, referred to center of mass

$$a_0' = a_0(1-\alpha^2)^{\frac{1}{2}} = (5.29157 \pm 0.00006) \times 10^{-9} \text{ cm}$$

Separation of proton and electron in normal H^1

$$a_0'' = a_0' R_\infty / R_H = (5.29445 \pm 0.00006) \times 10^{-9} \text{ cm}$$

Compton wavelength of the electron

$$\lambda_{ce} = h/(mc) = (24.2625 \pm 0.0006) \times 10^{-11} \text{ cm}$$
$$= \alpha^2/(2R_\infty)$$
$$\lambda\!\!\!^{-}_{ce} = \lambda_{ce}/(2\pi) = (3.86150 \pm 0.00009) \times 10^{-11} \text{ cm}$$
$$= \alpha^2/(4\pi R_\infty)$$

Compton wavelength of the proton

$$\lambda_{cp} = h/m_p c = (13.2139 \pm 0.0004) \times 10^{-14} \text{ cm}$$
$$\lambda\!\!\!^{-}_{cp} = \lambda_{cp}/(2\pi) = (2.10307 \pm 0.00007) \times 10^{-14} \text{ cm}$$

[52] The binding energy of the electron in the hydrogem atom has been included in the quantity. The mass of the electron when found in the hydrogen atom is not m, but more correctly $m(1-\frac{1}{2}\alpha^2+\cdots)$.

Compton wavelength of the neutron

$$\lambda_{cn} = h/m_n c = (13.1958 \pm 0.0004) \times 10^{-14} \text{ cm}$$
$$\lambda\!\!\!^{-}_{cn} = \lambda_{cn}/(2\pi) = (2.10017 \pm 0.00007) \times 10^{-14} \text{ cm}$$

Classical electron radius

$$r_0 = e^2/(mc^2) = (2.81784 \pm 0.00010) \times 10^{-13} \text{ cm}$$
$$= \alpha^3/(4\pi R_\infty)$$
$$r_0^2 = (7.9402 \pm 0.0005) \times 10^{-26} \text{ cm}^2$$

Thompson cross section

$$\frac{8}{3}\pi r_0^2 = (6.65196 \pm 0.0005) \times 10^{-25} \text{ cm}^2$$

Fine structure doublet separation in hydrogen

$$\Delta E_H = \frac{1}{16} R_H \alpha^2 \left[1 + \frac{\alpha}{\pi} + \left(\frac{5}{8} - \frac{5.946}{\pi^2}\right)\alpha^2\right]$$
$$= 0.365869 \pm 0.000008 \text{ cm}^{-1}$$
$$= 10968.49 \pm 0.25 \text{ Mc sec}^{-1}$$

Fine structure separation in deuterium

$$\Delta E_D = \Delta E_H R_D / R_H = 0.365969 \pm 0.000008 \text{ cm}^{-1}$$
$$= 10971.48 \pm 0.25 \text{ Mc/sec}^{-1}$$

Zeeman displacement per gauss

$$(e/mc)/(4\pi c) = (4.66879 \pm 0.00015) \times 10^{-5} \text{ cm}^{-1} \text{ gauss}^{-1}$$

Boltzmann's constant

$$k = R_0/N = (1.38042 \pm 0.00010) \times 10^{-16} \text{ ergs deg}^{-1}$$
$$k = (8.6164 \pm 0.0004) \times 10^{-5} \text{ ev deg}^{-1}$$
$$1/k = 11605.7 \pm 0.5 \text{ deg ev}^{-1}$$

First radiation constant

$$c_1 = 8\pi hc = (4.9919 \pm 0.0004) \times 10^{-15} \text{ erg cm}$$

Second radiation constant

$$c_2 = hc/k = (1.43884 \pm 0.00008) \text{ cm deg}$$

Atomic specific heat constant

$$c_2/c = (4.79946 \pm 0.00027) \times 10^{-11} \text{ sec deg}$$

Wein displacement law constant[53]

$$\lambda_{\max} T = c_2/(4.96511423) = 0.28979 \pm 0.00005 \text{ cm deg.}$$

Stefan-Boltzmann constant

$$\sigma = (\pi^2/60)(k^4/\hbar^3 c^2) = (0.56686 \pm 0.00005) \times 10^{-4} \text{ erg cm}^{-2} \text{ deg}^{-4} \text{ sec}^{-1}$$

Sackur-Tetrode constant

$$S_0/R_0 = \tfrac{5}{2} + \ln\{(2\pi R_0)^{\frac{3}{2}} h^{-3} N^{-4}\}$$
$$= -5.57324 \pm 0.00011$$
$$S_0 = -(46.3505 \pm 0.0017) \times 10^7 \text{ erg mole}^{-1} \text{ deg}^{-1}$$

[53] The numerical constant 4.96511423 is the root of the transcendental equation $x = 5(1-e^{-x})$.

CC-0. In Public Domain. Gurukul Kangri Collection, Haridwar

Digitized by Arya Samaj Foundation Chennai and eGangotri

Bohr magneton

$$\mu_0 = he/(4\pi mc) = \tfrac{1}{2}e\lambda_{ce} = (0.92732 \pm 0.00006) \times 10^{-20} \text{ erg gauss}^{-1}$$

Anomalous electron moment correction

$$\left[1 + \frac{\alpha}{2\pi} - 2.973\frac{\alpha^2}{\pi^2}\right] = \mu_e/\mu_0 = 1.001145356 \pm 0.000000013$$

Magnetic moment of the electron

$$\mu_e = (0.92838 \pm 0.00006) \times 10^{-20} \text{ erg gauss}^{-1}$$

Nuclear magneton

$$\mu_n = he/(4\pi m_p c) = \mu_0 Nm/\mathrm{H}^+ = (0.505038 \pm 0.000036) \times 10^{-23} \text{ erg gauss}^{-1}$$

Proton moment

$$\mu = 2.79277 \pm 0.00006 \text{ nuclear magnetons}$$
$$= (1.41045 \pm 0.00009) \times 10^{-23} \text{ erg gauss}^{-1}$$

Gyromagnetic ratio of the proton in hydrogen, uncorrected for diamagnetism

$$\gamma' = (2.67520 \pm 0.00008) \times 10^4 \text{ radians sec}^{-1} \text{ gauss}^{-1}$$

Gyromagnetic ratio of the proton (corrected)

$$\gamma = (2.67527 \pm 0.00008) \times 10^4 \text{ radians sec}^{-1} \text{ gauss}^{-1}$$

Multiplier of (Curie constant)$^{\frac{1}{2}}$ to give magnetic moment per molecule

$$(3k/N)^{\frac{1}{2}} = (2.62178 \pm 0.00017) \times 10^{-20} (\text{erg mole deg}^{-1})^{\frac{1}{2}}$$

Mass-Energy conversion factors

$$1 \text{ g} = (5.60999 \pm 0.00025) \times 10^{26} \text{ Mev}$$
$$1 \text{ electron mass} = 0.510984 \pm 0.000016 \text{ Mev}$$
$$1 \text{ atomic mass unit} = 931.162 \pm 0.024 \text{ Mev}$$
$$1 \text{ proton mass} = 938.232 \pm 0.024 \text{ Mev}$$
$$1 \text{ neutron mass} = 939.526 \pm 0.024 \text{ Mev}$$

Quantum energy conversion factors

$$1 \text{ ev} = (1.60207 \pm 0.00007) \times 10^{-12} \text{ erg}$$
$$E/\tilde{\nu} = (1.98620 \pm 0.00016) \times 10^{-16} \text{ erg cm}$$
$$E\lambda_g = (12397.8 \pm 0.5) \times 10^{-8} \text{ ev-cm}$$
$$E\lambda_x = 12372.2 \pm 0.4 \text{ kilovolt } x \text{ units}$$
$$E/\nu = (6.6252 \pm 0.0005) \times 10^{-27} \text{ erg sec}$$
$$E/\nu = (4.13544 \pm 0.00015) \times 10^{-15} \text{ ev-sec}$$
$$\tilde{\nu}/E = (5.0347 \pm 0.0004) \times 10^{15} \text{ cm}^{-1} \text{ erg}^{-1}$$
$$\tilde{\nu}/E = (8065.98 \pm 0.30) \text{ cm}^{-1} \text{ ev}^{-1}$$
$$\nu/E = (1.50938 \pm 0.00012) \times 10^{26} \text{ sec}^{-1} \text{ erg}^{-1}$$
$$\nu/E = (2.41812 \pm 0.00009) \times 10^{14} \text{ sec}^{-1} \text{ ev}^{-1}$$

de Broglie wavelengths, λ_D of elementary particles[54]

Electrons

$$\lambda_{De} = (7.27373 \pm 0.00016) \text{ cm}^2 \text{ sec}^{-1}/v$$
$$= (1.55226 \pm 0.00008) \times 10^{-13} \text{ cm (erg)}^{\frac{1}{2}}/(E)^{\frac{1}{2}}$$
$$= (1.226377 \pm 0.000032) \times 10^{-7} \text{ cm (ev)}^{\frac{1}{2}}/(E)^{\frac{1}{2}}$$

Protons

$$\lambda_{Dp} = (3.96145 \pm 0.00013) \times 10^{-3} \text{ cm}^2 \text{ sec}^{-1}/v$$
$$= (3.62261 \pm 0.00020) \times 10^{-15} \text{ cm (erg)}^{\frac{1}{2}}/(E)^{\frac{1}{2}}$$
$$= (2.86208 \pm 0.00012) \times 10^{-9} \text{ cm (ev)}^{\frac{1}{2}}/(E)^{\frac{1}{2}}$$

Neutrons

$$\lambda_{Dn} = (3.95599 \pm 0.00013) \times 10^{-3} \text{ cm}^2 \text{ sec}^{-1}/v$$
$$= (3.62005 \pm 0.00020) \times 10^{-15} \text{ cm (erg)}^{\frac{1}{2}}/(E)^{\frac{1}{2}}$$
$$= (2.86005 \pm 0.00012) \times 10^{-9} \text{ cm (ev)}^{\frac{1}{2}}/(E)^{\frac{1}{2}}$$

Energy of 2200 m/sec neutron

$$E_{2200} = 0.0252977 \pm 0.0000006 \text{ ev}$$

Velocity of 1/40 ev neutron

$$v_{0.025} = 2187.017 \pm 0.028 \text{ m/sec}$$

The Rydberg and related derived constants

$$R_\infty = 109737.309 \pm 0.012 \text{ cm}^{-1}$$
$$R_\infty c = (3.289847 \pm 0.000008) \times 10^{15} \text{ sec}^{-1}$$
$$R_\infty hc = (2.17961 \pm 0.00018) \times 10^{-11} \text{ erg}$$
$$\frac{R_\infty hc^2 \times 10^{-8}}{e} = 13.6050 \pm 0.0005 \text{ ev}$$

Hydrogen ionization potential

$$I_0 = 13.5978 \pm 0.0005 \text{ ev}$$
$$= R_H \frac{hc^2}{e}\left[1 + \frac{\alpha^2}{4} + \cdots\right] \times 10^{-8}$$

[54] These formulas apply only to nonrelativistic velocities. If the velocity of the particle is not negligible compared to the velocity of light c or the energy not negligible compared to the rest mass energy, we must use $\lambda_D = \lambda_c[\epsilon(\epsilon+2)]^{-\frac{1}{2}}$, where λ_c is the appropriate Compton wavelength and ϵ is the kinetic energy measured in units of the particle rest mass.

CC-0. In Public Domain. Gurukul Kangri Collection, Haridwar

Digitized by Arya Samaj Foundation Chennai and eGangotri

REVIEWS OF MODERN PHYSICS VOLUME 25, NUMBER 3 JULY, 1953

The Basis for the Criterion of Least Squares

E. RICHARD COHEN

Atomic Energy Research Department, North American Aviation, Inc., Downey, California

THERE have been many who have objected to the use of the method of least squares on the grounds that it assumes the Gaussian curve for the probability distribution of the error in any particular measurement. This is the formulation which is indicated in Sec. 3 of the preceding article.[1] The objection is indeed valid that the assumption of the Gaussian distribution is often unwarranted in many experimental configurations. However, the problem of determining a "best" set of values which can be computed from an overdetermined system of equations is essentially the problem of determining an analytic basis on which one can define the adjective "best." The condition of least squares serves as one such analytic criterion. This says nothing in itself of what could be called the *physical* interpretation of the criterion. It is recognized, in general, that the method of least squares corresponds to the "Axiom of Maximum Likelihood," if the distribution functions of all the errors are Gaussian. Gauss himself was able to justify the method on a much wider base, and in 1821 he published a theory which replaces this axiom with an "Axiom of Minimum Error" or "Axiom of Maximum Weight."[2] The definition of "best" is not to be made on the basis of that solution which is most likely to be correct, but on that solution which is most accurate and to which can, therefore, be attached the greatest statistical weight. (The statistical weight of a statistical variable is defined in the present sense as the reciprocal of the variance, i.e., the reciprocal of the mean square error of the quantity.)

Consider then an overdetermined set of N_{Eq} equations expressing relationships between q variables. We can find an infinite number of solutions for the q variables depending on how we choose to combine the equations. We can think of this process as one in which some set of $q-1$ of the equations are used to express $q-1$ of the variables in terms of one particular variable, say x_1. These values are then to be substituted into the remaining $N_{Eq}-q+1$ equations to give a set of $N_{Eq}-q+1$ values for the variable x_1. Any of these numerical values is a possible choice for the variable x_1 and, in general, we would want to take some weighted average of these numerical values. The numerical value of such an average depends both on the weights attached to the elements which go to make up the average and on the numerical values of these elements. Ultimately, therefore, the value ascribed to x_1 depends on $N_{Eq}-q$ independent parameters which specify the *mathematical form* of the average (there is one condition to restrict the choice of the $N_{Eq}-q+1$ weights; this is the condition that their sum is unity) and N_{Eq} quantities which are either the observational numerics or quantities directly deduced from them (such as relative deviations from a set of origin values) which determine the *numerical value* of the average.

The numerical value of x_1 is thus expressed as a linear combination of N_{Eq} numerical quantities, each of which has associated with it a mean square error. If the numerical quantities are observationally independent, we can assert that the mean square error of x_1 is the sum of certain coefficients, depending on the $N_{Eq}-q$ free parameters, times the mean square errors of the N_{Eq} observational numerics. The Axiom or Condition of Minimum Error states that the "best" choice for x_1 is that one whose error is a minimum with respect to the possible variation of the free parameters. We shall show below that this condition is equivalent to the condition of least squares, although the results cannot, in general, be identified as corresponding to that set which has maximum likelihood, except in the case when the distribution function for the errors is specified to be Gaussian. This is, however, an advantage for one can easily construct distributions (for example, rectangular distributions) for which the condition of maximum likelihood has no unique solution. Furthermore, the development of the condition of minimum error is quite general in regard to the forms of the error distribution functions; all that is specified is the mean square error, so that the range of applicability of the theory of least squares is extended from Gaussian distributions to the much larger class of distributions with finite second moments.

AN EXAMPLE

As an elementary example of the method and in order to clarify the concepts involved, let us consider a problem which is perhaps the simplest possible example. We have two measurements of the quantity x; these two measurements are a_1 and a_2, in general, $a_1 \neq a_2$. We also assume that each measurement represents a single selection from a universe of values. We let the probability distribution of the first measurement be $P_1(\xi)$ such that the probability is $P_1(\xi)d\xi$, that the result of a measurement of the quantity x by the specified pro-

[1] J. W. M. DuMond and E. R. Cohen, Revs. Modern Phys. 25, 691 (1953).

[2] E. Whittaker and G. Robinson, *Calculus of Observations* (Blackie & Sons, London, 1944), fourth ed., p. 224.

CC-0. In Public Domain. Gurukul Kangri Collection, Haridwar

Digitized by Arya Samaj Foundation Chennai and eGangotri

cedure shall lie between the values ξ and $\xi+d\xi$. Similarly, the second measurement of x is to be characterized by the probability distribution $P_2(\eta)$. We need not make any detailed specification of the form of the distribution functions P_1 and P_2; it is not even necessary that the two functions have similar form. We impose upon them only the restriction that the distributions have finite second moments.

If we have two measurements of x then we can take some average value to use as the "best" choice. There are, however, several different choices for this average and we can write

$$x_0(\alpha)=\alpha a_1+(1-\alpha)a_2, \tag{1}$$

where α is any real number, although intuitively we would prefer that $0\leq\alpha\leq 1$ because this is the condition that x_0 lies between the values a_1 and a_2. Defined in this way, the mean of the universe of values of x_0 is

$$\begin{aligned}\bar{x}_0&=\int\int[\alpha\xi+(1-\alpha)\eta]P_1(\xi)P_2(\eta)d\xi d\eta\\&=\alpha\int\xi P_1(\xi)d\xi\cdot\int P_2(\eta)d\eta\\&\quad+(1-\alpha)\int P_1(\xi)d\xi\cdot\int\eta P_2(\eta)d\eta.\end{aligned}\tag{2}$$

Now each probability distribution is assumed to be normalized so that

$$\int P_1(\xi)d\xi=1;\quad\int P_2(\eta)d\eta=1, \tag{3}$$

and furthermore, if there are no systematic errors in either measurement, the expectation value of each measurement is x

$$\int\xi P_1(\xi)d\xi=x;\quad\int\eta P_2(\eta)d\eta=x. \tag{4}$$

Therefore, Eq. (2) reduces to

$$\bar{x}_0=\alpha x+(1-\alpha)x=x, \tag{5}$$

so that the expectation value of the average is indeed the quantity we are trying to measure independent of the value of the parameter α which determines the particular average. But we now ask the question, "How accurate is this average; what is its standard deviation?" If we let ϵ^2 be the mean square deviation of the universe from which x_0 is extracted, we have, by the usual definition,

$$\begin{aligned}\epsilon^2&=\int\int[\alpha\xi+(1-\alpha)\eta-x]^2P_1(\xi)P_2(\eta)d\xi d\eta\\&=\int\int[\alpha(\xi-x)+(1-\alpha)(\eta-x)]^2P_1(\xi)P_2(\eta)d\xi d\eta\\&=\alpha^2\int(\xi-x)^2P_1(\xi)d\xi\int P_2(\eta)d\eta\\&\quad+(1-\alpha)^2\int P_1(\xi)d\xi\int(\eta-x)^2P_2(\eta)d\eta\\&\quad+2\alpha(1-\alpha)\int(\xi-x)P_1(\xi)d\xi\int(\eta-x)P_2(\eta)d\eta,\\\epsilon^2&=\alpha^2\int(\xi-x)^2P_1(\xi)d\xi+(1-\alpha)^2\int(\eta-x)^2P_2(\eta)d\eta.\end{aligned}\tag{6}$$

The two integrals in the last form of Eq. (6) are the variances (the mean square errors), respectively, of the first and of the second measurements. These quantities are defined to be σ_1^2 and σ_2^2. The expression for the error in the average in terms of the errors of the numbers entering into the average is, therefore,

$$\epsilon^2=\alpha^2\sigma_1^2+(1-\alpha)^2\sigma_2^2. \tag{7}$$

We find that, although the expectation value of the average is independent of α, the error in the average *is* a function of α: for $\alpha=0$ we have $\epsilon^2=\sigma_2^2$ and for $\alpha=1$ we have $\epsilon^2=\sigma_1^2$; we may reasonably ask whether a proper choice of α might not result in a value of ϵ^2 which is smaller than either of these, and indeed, what choice of α yields the minimum value of ϵ^2? By completing the square we can write Eq. (7) as,

$$\begin{aligned}\epsilon^2&=\alpha^2(\sigma_1^2+\sigma_2^2)-2\alpha\sigma_2^2+\sigma_2^2\\&=\frac{\alpha^2(\sigma_1^2+\sigma_2^2)^2-2\alpha\sigma_2^2(\sigma_1^2+\sigma_2^2)+\sigma_2^4+\sigma_1^2\sigma_2^2}{\sigma_1^2+\sigma_2^2}\\&=\frac{\sigma_1^2\sigma_2^2+[\alpha(\sigma_1^2+\sigma_2^2)-\sigma_2^2]^2}{\sigma_1^2+\sigma_2^2}.\end{aligned}\tag{8}$$

Since α appears now only in a term which can never be negative, we see immediately that the minimum value of ϵ^2 occurs when the square bracket vanishes. This is achieved when $\alpha=\sigma_2^2/(\sigma_1^2+\sigma_2^2)$; the minimum value of ϵ^2 corresponding to this choice is

$$\epsilon_0^2=\sigma_1^2\sigma_2^2/(\sigma_1^2+\sigma_2^2),$$

and the corresponding value of x_0 which we indicate by x_0 is

$$\mathrm{x}_0=\epsilon_0^2\left(\frac{a_1}{\sigma_1^2}+\frac{a_2}{\sigma_2^2}\right). \tag{9}$$

CC-0. In Public Domain. Gurukul Kangri Collection, Haridwar

Digitized by Arya Samaj Foundation Chennai and eGangotri

The "weights" to be attached to measured quantities in order to compute the "best" average are therefore proportional to the reciprocal of the mean square error of each measurement. If we define the statistical weights

$$w_1=1/\sigma_1^2 \quad w_2=1/\sigma_2^2, \tag{10}$$

we have two important formulas

$$x_0=(w_1a_1+w_2a_2)/(w_1+w_2), \tag{9.1}$$

$$w_0=1/\epsilon_0^2=w_1+w_2. \tag{8.1}$$

The first of these essentially justifies the nomenclature of "statistical weight" for the reciprocal variance, since it is this quantity which determines the importance of the measurement in the computation of the average. The second formula shows that when this "best" average is obtained the weight of the result (computed as the reciprocal of the variance of the average) is just the sum of the weights of the components and, furthermore, that this is the maximum weight ascribable to any average. Any other linear combination of the two observations would have a weight which is less than the sum of the individual weights and is, therefore, an inefficient average which "wastes weight." The weight of the average w as a function of the weights assigned to the individual measurements and the choice of the average value is indicated in Fig. 1. The measurement x_1 has variance $\sigma_1^2=1/w_1$, and the measurement x_2 has variance $\sigma_2^2=1/w_2$. Each value of α corresponds to a particular value of x_0, and the statistical weight of this average value is a function not only of the parameter α but also of the statistical weights of x_1 and x_2. The statistical weight of the average is a maximum (equal to the sum of the weights of the individual components), when the weighting employed in computing the average is determined by the statistical weights of the components.

THE GENERALIZED THEORY*

We can now establish a generalized theory of least squares in which the individual equations are not observationally independent.[3] Let there be q variables which are connected by N equations. The numerical constants in these equations are interrelated and are determined by a set of n observationally independent quantities s_α. We shall assume that the equations can all be linearized so that the system is

$$\begin{aligned}
&a_{11}x_1+a_{12}x_2+a_{13}x_3+\cdots+a_{1q}x_q=c_1\\
&a_{21}x_1+a_{22}x_2+a_{23}x_3+\cdots+a_{2q}x_q=c_2\\
&\cdots\cdots\cdots\cdots\cdots\cdots\cdots\cdots\\
&a_{N1}x_1+a_{N2}x_2+a_{N3}x_3+\cdots+a_{Nq}x_q=c_N,
\end{aligned} \tag{11}$$

where the constants c_μ are numerical quantities which are explicit functions of the quantities s_α.

In the discussion to follow it will be useful to introduce two conventions: One is the Einstein summation convention; in any product a repeated index is to be summed over all values permissible to it unless specifically indicated to the contrary. The other is the use of different characters to indicate the range of the index. Roman letters $(i, j, k, \cdots)$ shall be used for indices relating to the unknowns and, therefore, have the range

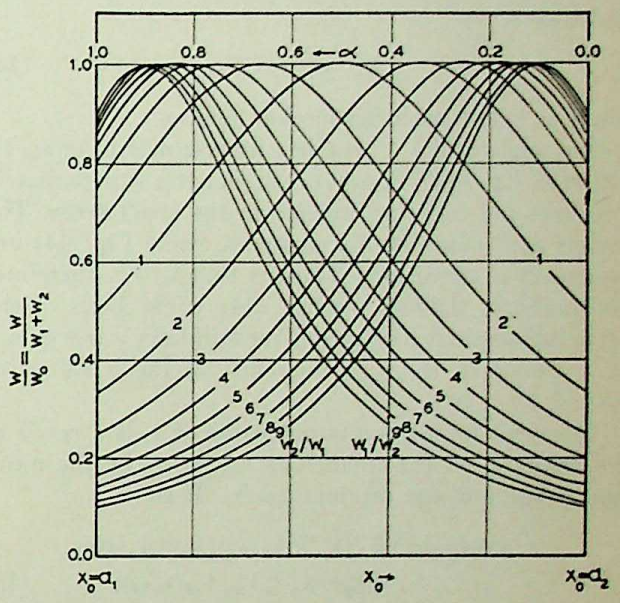


FIG. 1. The weight assignable to the average of two observed quantities as a function of the statistical weights of those quantities and the weighting parameter α of the average. The weight of the average is a maximum if α is determined by the statistical weights.

1 to q; Greek letters from the middle of the alphabet $(\mu, \nu, \sigma, \cdots)$ shall be used for indexes relating to the observational equations and have the range 1 to N; Greek letters from the start of the alphabet $(\alpha, \beta, \cdots)$ shall be used for indexes relating to the observationally independent variables and have the range 1 to n. It is thus possible to identify a quantity with two indexes as a square or a nonsquare matrix by noting whether the indices are of the same type or not.

Since the c_μ are functions of s_α the *statistically independent* variations ϵ_α in s_α will produce *statistically correlated* variations η_μ in c_μ:

$$\begin{aligned}
&\epsilon_\alpha=ds_\alpha,\\
&\eta_\mu=dc_\mu=A_{\mu\alpha}\epsilon_\alpha,
\end{aligned} \tag{12}$$

where $A_{\mu\alpha}=\partial c_\mu/\partial s_\alpha$ are the derivatives of the computed

* Note added in proof: Professor J. W. Tukey of Princeton University has kindly pointed out to the author that this generalized system of least squares is not new. R. L. Plackett, Biometrika **36**, 458 (1949) has traced the origins to Laplace and Markoff as well as to Gauss. A. C. Aitken, Proc. Roy. Soc. Edinburgh **55**, 42 (1933), has also presented a generalization equivalent to the present development.

[3] J. W. M. DuMond and E. R. Cohen, Report to the National Research Council on the Atomic Constants, December, 1950. See also E. R. Cohen, Phys. Rev. **81**, 162 (1951).

CC-0. In Public Domain. Gurukul Kangri Collection, Haridwar

Digitized by Arya Samaj Foundation Chennai and eGangotri

observational quantities with respect to the fundamental independently measured quantities s_α.

We wish to find the most accurate values of x_i which can be computed from Eq. (11). To find each x_i we need a set of multipliers $\lambda_\mu^{(i)}$ by which to multiply the N observational equations so that we obtain

$$x_i=\lambda_\mu^{(i)}c_\mu=\lambda_\mu^{(i)}a_{\mu j}x_j. \tag{13}$$

Equation (13) is to be understood as follows: Each of the N individual equations of observation (identified by a particular value of the index μ) is to be multiplied by a number λ_μ, there being a set of N numbers for each variable x_i. These numbers are to be so chosen that when the equations are then summed the coefficient of each x other than the specific x_i is zero, while the coefficient of x_i is unity. This, therefore, implies that there are q conditions on each of the q sets of N multipliers,

$$\lambda_\mu^{(i)}a_{\mu j}=\delta_{ij}, \tag{14}$$

where δ_{ij} is the usual Kronecker symbol.

One might call $\lambda_\mu^{(i)}$ the left inverse matrix to $a_{\mu i}$ by virtue of Eq. (14). However, $a_{\mu i}$ is not a square matrix and does not have an inverse in the strict sense. The matrix $\lambda_\mu^{(i)}$ contains Nq elements, while Eq. (14) imposes only q^2 conditions. The fact that $\lambda_\mu^{(i)}$ is, therefore, not uniquely defined by Eq. (14) is the basis of the entire subsequent discussion. We still have a free choice of $f=N-q$ of the $\lambda_\mu^{(i)}$ for each of the q values of $i=1, 2, 3 \cdots q$.

The error in the computed value of x_i is a result of the errors ϵ_α in the quantities s_α; let v_{ij} be the mean square value of the product $dx_i dx_j$. Then

$$\begin{aligned} v_{ij}=\langle dx_i dx_j\rangle&=\langle(\lambda_\mu^{(i)}A_{\mu\alpha}\epsilon_\alpha)(\lambda_\nu^{(j)}A_{\nu\beta}\epsilon_\beta)\rangle \\ &=\lambda_\mu^{(i)}\lambda_\nu^{(j)}A_{\mu\alpha}A_{\nu\beta}\langle\epsilon_\alpha\epsilon_\beta\rangle. \end{aligned} \tag{15}$$

The ϵ_α are, however, independently observed quantities and are completely unrelated, one to the other, so that

$$E_{\alpha\beta}\equiv\langle\epsilon_\alpha\epsilon_\beta\rangle=\overline{\epsilon_\alpha^2}\delta_{\alpha\beta}. \tag{16}$$

We must now choose the $\lambda_\mu^{(i)}$ in such a way as to minimize the value of the variance of x_i; hence we must minimize the expression

$$v_{ii}=\lambda_\mu^{(i)}\lambda_\nu^{(i)}A_{\mu\alpha}A_{\nu\beta}E_{\alpha\beta} \text{ (not summed on } i) \tag{17}$$

consistent with the restrictions imposed on $\lambda_\mu^{(i)}$ by Eq. (14). We therefore introduce q^2 Lagrangian multipliers $L_j^{(i)}$, so that we may then take independent variations of $\lambda_\mu^{(i)}$ in the expression

$$\lambda_\mu^{(i)}\lambda_\nu^{(j)}A_{\mu\alpha}A_{\nu\beta}E_{\alpha\beta}-2L_j^{(i)}\{\lambda_\mu^{(i)}a_{\mu j}-\delta_{ij}\} \text{ (not summed on } i). \tag{18}$$

Differentiating this expression and making use of the symmetry of $E_{\alpha\beta}$, we obtain

$$L_j^{(i)}a_{\mu j}=\lambda_\nu^{(i)}S_{\nu\mu}, \tag{19}$$

where

$$S_{\nu\mu}=S_{\mu\nu}=\sum_\alpha A_{\mu\alpha}A_{\nu\alpha}\overline{\epsilon_\alpha^2}.$$

$S_{\nu\mu}$ is the error matrix of the observational equations. The diagonal elements of $S_{\nu\mu}$ are simply the variances of the numerical constants c_μ. If these numbers are uncorrelated, by which we imply that any given s_α occurs in only one of the c_μ's, the product $A_{\mu\alpha}A_{\nu\alpha}$ (not summed on α) will be different from zero only for $\mu=\nu$ and $S_{\nu\mu}$ will be a diagonal matrix. This is the only case usually considered in most discussions of the theory of least squares; the recognition that $S_{\nu\mu}$ need not be diagonal constitutes what is here referred to as the "generalized theory of least squares." The weight matrix of the observational equations, $\pi_{\mu\nu}$, is defined as the inverse of the error matrix so that

$$\pi_{\mu\nu}S_{\nu\tau}=\delta_{\mu\tau}=S_{\mu\nu}\pi_{\nu\tau}. \tag{20}$$

If we therefore multiply Eq. (19) by the weight matrix $\pi_{\mu\tau}$, we obtain the result

$$\begin{aligned} L_j^{(i)}a_{\mu j}\pi_{\mu\tau}&=\lambda_\nu^{(i)}S_{\nu\mu}\pi_{\mu\tau} \\ &=\lambda_\nu^{(i)}\delta_{\nu\tau}, \\ L_j^{(i)}a_{\mu j}\pi_{\mu\nu}&=\lambda_\nu^{(i)}. \end{aligned} \tag{21}$$

This defines $\lambda_\nu^{(i)}$ in terms of the Lagrangian multipliers. Insertion of Eq. (21) into Eq. (14) gives us

$$L_j^{(i)}a_{\mu j}\pi_{\mu\nu}a_{\nu k}=\delta_{ik}, \tag{22}$$

so that $L_j^{(i)}$ must be the inverse of the symmetric matrix $P_{ij}=a_{\mu i}\pi_{\mu\nu}a_{\nu j}$ (P_{ij} is symmetric since $\pi_{\mu\nu}$ is symmetric; the symmetry of this latter matrix follows directly from the symmetry of $S_{\mu\nu}$). We have therefore established also the symmetry of $L_j^{(i)}$ ($L_j^{(i)}=L_i^{(j)}$).

We now return to Eq. (13) and write [using Eq. (21)]

$$x_i=\lambda_\mu^{(i)}c_\mu=L_j^{(i)}a_{\nu j}\pi_{\nu\mu}c_\mu. \tag{23}$$

This is the solution for the "best" choice for the x_i; Eq. (23) is, however, just the solution of the system of equations

$$P_{ji}x_i=a_{\nu j}\pi_{\nu\mu}c_\mu, \tag{24}$$

and these are exactly the same equations as one obtains from the condition of least squares. The basic quadratic form associated with Eq. (24) and from which Eq. (24) can be deduced as the condition that the quadratic form have its minimum value (i.e., the "least-squares" condition) is

$$Q=\sum_{\mu\nu}\Big(\sum_i a_{\mu i}x_i-c_\mu\Big)\pi_{\mu\nu}\Big(\sum_j a_{\nu j}x_j-c_\nu\Big). \tag{25}$$

In particular, in the case where the variables c_μ are themselves observationally independent (which is equivalent to $S_{\mu\nu}$ being diagonal), we find that $\pi_{\nu\mu}$ is a diagonal matrix and its diagonal elements, which we may write simply as p_μ, are just the usual statistical weights to be ascribed to each observational equation.

CC-0. In Public Domain. Gurukul Kangri Collection, Haridwar

Digitized by Arya Samaj Foundation Chennai and eGangotri

Under these conditions the quadratic form, Eq. (25), reduces to the more familiar expression

$$Q=\sum_{\mu}(\sum_{i}a_{\mu i}x_i-c_\mu)^2p_\mu, \tag{25.1}$$

and Eq. (24) reduces to the usual normal equations

$$\sum_{i}(\sum_{\mu}p_\mu a_{\mu j}a_{\mu i})x_i=\sum_{\mu}p_\mu a_{\mu j}c_\mu. \tag{24.1}$$

Since Eqs. (23) and (24) are actually the same equations as one would obtain from the condition of least squares, we have shown not only that the axiom of maximum statistical weight is equivalent to the axiom of maximum likelihood for a Gaussian distribution but, furthermore, that the usual normal equations of least squares correspond to the condition of maximum statistical weight, even in those cases where the condition of maximum likelihood is impossible of simple analytic formulation or is ambiguous. One of these ambiguous cases occurs even when the error distributions are Gaussian if the c_μ are observationally correlated in such a way that the matrix $S_{\nu\mu}$ cannot be diagonalized, which is in general the case if $n>N$. In the earlier discussion[2] of the generalized theory the present writer was not fully appreciative of this ambiguity which was left unresolved. Although the quadratic form Eq. (25) was presented as the proper generalization of the simpler expression (25.1), the proof was semi-intuitive and was based on plausibility arguments rather than a firm logical foundation. The present formulation achieves this and has the further advantage of admitting to consideration by the condition of least squares a much wider class of error distribution functions than merely the Gaussian.

CC-0. In Public Domain. Gurukul Kangri Collection, Haridwar

Digitized by Arya Samaj Foundation Chennai and eGangotri

An Introduction to Spinors*

W. L. Bade and Herbert Jehle

Brace Laboratory of Physics, University of Nebraska, Lincoln, Nebraska

CONTENTS

I. Introduction.
II. Transformations of Tensors.
III. Transformations of Spinors.
IV. The Fundamental Spinor.
V. Algebraic Properties of Spinors.
VI. Special Spin Transformations.
VII. The Connection Between World Tensors and Spinors.
VIII. Lorentz Transformations and Spin Transformations.
IX. The Maxwell-Lorentz and Dirac Equations.
X. Spinor Analysis.

IN order to give a satisfactory account of the Lorentz-covariance of Dirac's equation for the electron, it is necessary to attribute certain transformation properties to the four-component wave function appearing there. In 1929, van der Waerden (20)[1] devised an *algebra of spinors* which plays a role in the transformation theory of such wave functions analogous to that played in special relativity theory by tensor algebra. Four years later, in 1933, van der Waerden and Infeld (14) presented a *spinor analysis* which liberated the formalism from the restrictions of special relativity theory and permitted the employment of spinors against the background of a general Riemannian metric. In addition, many other contributions to the subject appeared.

The purpose of the present article is to offer an exposition of spinor calculus which will be more elementary and more accessible than those which constitute the original literature.

I. INTRODUCTION

As a preliminary to description of the spinor formalism, the following brief discussion is intended to show how the concept of spinors arises. This discussion will also serve to define the notations to be used in this article.[2]

Schrödinger's representation in nonrelativistic quantum mechanics is characterized by the equations

$$H\psi=ih\partial\psi/\partial t, \quad P_x\psi=-ih\partial\psi/\partial x, \cdots. \tag{I 1}$$

Our choice for the metric of special relativity theory is

$$g_{00}=1, \quad g_{11}=g_{22}=g_{33}=-1, \quad g_{kl}=0 \quad (k\neq l). \tag{I 2}$$

With the four-velocity $u^k=dx^k/ds$ we can form the free-particle world momentum

$$mcu_k=(E/c, -P_x, -P_y, -P_z).$$

We choose the sign of the four potential in such a way as to retain the conventional form of the field equations (IX 2) and (IX 4):

$$\phi_k=(-V, A_x, A_y, A_z). \tag{I 3}$$

When a charged particle is in an electromagnetic field, its total energy is $H=E+qV$. The world momentum of a particle in a field should have the property that its time-like component is H/c. This consideration[3] leads to

$$P_k=mcu_k-(q/c)\phi_k. \tag{I 4}$$

With the relativistic generalization of (I 1), $P_k\psi=ih\partial_k\psi$ (where $\partial_k\equiv\partial/\partial x^k$), one can construct a single second-order wave equation:

$$g^{kl}[ih\partial_k+(q/c)\phi_k][ih\partial_l+(q/c)\phi_l]\psi=m^2c^2\psi, \tag{I 5}$$

by virtue of $g^{kl}u_ku_l=1$. Equation (I 5) is linearized, following Dirac, to[4]

$$\Gamma^k(\partial_k+i\epsilon\phi_k)\psi=\kappa\psi, \tag{I 6}$$

with the conditions

$$\Gamma^k\Gamma^l+\Gamma^l\Gamma^k=-2g^{kl}1. \tag{I 7}$$

For abbreviation, we have set

$$\epsilon=-q/(hc), \quad \mu=mc/h.$$

It is well known that (I 7) can be satisfied with matrices having four rows and columns, but not with matrices having fewer rows and columns.

* The authors wish to express their indebtedness to the University of Nebraska Research Council, which generously supported this work.

[1] Arabic numerals enclosed by parentheses and inserted into the text refer to items in the List of References at the end of this paper.

The fundamental mathematical discoveries underlying the theory of spinors were made by Cartan (13) and Weyl (12), Chap. III, Sec. 8c.

[2] The spinor notation used is taken from the paper of Infeld and van der Waerden (14). Gaussian units are used for electromagnetic quantities; the charge of a particle is denoted by q.

Spinor analysis necessitates the choice (I 2) for the signature of the special relativistic metric, unless one would load some of the formulas of Sec. VII with minus signs in a very ugly way. This would be most disturbing in Eqs. (VII 6) and (VII 11). The signature (I 2), however, implies the inconvenience that spatial contravariant and covariant vector components differ in sign, whereas in nonrelativistic quantum theory we work with a spatial metric +++ which makes it possible to equate a covariant to a contravariant vector: $mdx/dt=P_x=-ih\partial/\partial x$. We make the transition to a relativistic metric (I 2) by identifying these P_x, P_y, P_z with the contravariant components.

[3] For a more precise way of arriving at (I 4), consult Corben and Stehle (3), p. 349.

[4] See Hill and Landshoff (43), and the numerous references given there.

CC-0. In Public Domain. Gurukul Kangri Collection, Haridwar

Digitized by Arya Samaj Foundation Chennai and eGangotri

However, the conditions

$$\sigma^{k*}\sigma^{l}+\sigma^{l*}\sigma^{k}=-g^{kl}1 \tag{I 8}$$

(asterisk denotes complex conjugate), which bear a certain resemblance to (I 7), can be satisfied with the two-row matrices

$$\sigma^0=\frac{1}{\sqrt{2}}\begin{pmatrix}0&1\\-1&0\end{pmatrix},\quad \sigma^1=\frac{1}{\sqrt{2}}\begin{pmatrix}-1&0\\0&1\end{pmatrix},$$
$$\sigma^2=\frac{1}{\sqrt{2}}\begin{pmatrix}i&0\\0&i\end{pmatrix},\quad \sigma^3=\frac{1}{\sqrt{2}}\begin{pmatrix}0&1\\1&0\end{pmatrix}. \tag{I 9}$$

Since (I 7) can be satisfied with

$$\Gamma^k=\sqrt{2}\begin{pmatrix}0&\sigma^k\\\sigma^{k*}&0\end{pmatrix},$$

because of (I 8), Dirac's equation (I 6) can be written as a set of two two-component equations:

$$\sqrt{2}\sigma^k(\partial_k+i\epsilon\phi_k)\chi=\mu\xi$$
$$\sqrt{2}\sigma^{k*}(\partial_k+i\epsilon\phi_k)\xi=\mu\chi, \tag{I 10}$$

where the ψ of (I 6) is written as[5]

$$\psi=\begin{pmatrix}\xi\\\chi\end{pmatrix}.$$

Now, the covariance of Eqs. (I 8) and (I 10) can be viewed in either of two ways:

View (A). The quantities $\partial_k+i\epsilon\phi_k$ certainly transform as components of a covariant world vector. One can assume that the σ^k transform simply as components of a contravariant world vector. Then (I 8) and (I 10) are covariant with respect to Lorentz transformations. However, taking the σ^k as world vector components violates the spirit if not the letter of the relativity idea, for the following reason: As components of a world vector, the σ^k will have the especially simple values (I 9) only in certain frames of reference. In consequence, the four equations which appear when (I 10) is written out in full will not be the same in all Lorentz frames.

View (B). The alternative is to consider the σ^k as *fixed* matrices; then, to maintain the covariance of the Eqs. (I 10), it will be necessary to attribute some new transformation properties to the wave functions ξ, χ. When this procedure is carried out, with development of an appropriate mathematical formalism, the wave functions ξ and χ are renamed *spinors*.

The matrices appearing in (I 10) can be written out in the following way:

$$\chi=(\chi^\dot{\rho}),\quad \xi=(\xi^\dot{\rho}),\quad \sigma^k=(\sigma^{k\dot{\rho}}{}_\rho),$$
$$\chi^*=(\chi^{\dot{\rho}}),\quad \xi^*=(\xi^{\rho}),\quad \sigma^{k*}=(\sigma^{k\rho}{}_{\dot{\rho}}).$$

Note should be taken of the following conventions:

1. Latin indexes run from 0 to 3.
2. Greek indexes take the values 1, 2 (or $\dot{1}$, $\dot{2}$).
3. The meaning of the "dotted indexes," as in $\xi^{\dot{\rho}}$, will be discussed later in more detail; for the moment, it suffices to establish that adding a dot above every Greek index in a spin quantity means taking the complex conjugate of the quantity. (Two dots on the same index mean the same as none at all.)

Now (I 10) can be written

$$\sqrt{2}\sigma^{k\dot{\nu}}{}_\rho(\partial_k+i\epsilon\phi_k)\chi^\rho=\mu\xi^{\dot{\nu}},$$
$$\sqrt{2}\sigma^{k\nu}{}_{\dot{\rho}}(\partial_k+i\epsilon\phi_k)\xi^{\dot{\rho}}=\mu\chi^{\nu}. \tag{I 11}$$

When we undertake to elaborate on the view (B) as to the covariance of (I 10) or (I 11) (namely, that the σ^k are constant matrices), the new transformation properties which must be attributed to ξ, χ will involve transformations in the "space" of the Greek indexes. These transformations are called "spin transformations." All quantities in this space which transform according to a linear homogeneous law of any sort are called "spin tensors" or "spinors."

In Sec. II to Sec. VI there is developed a formalism for the transformation theory of spinors. Sections VII and VIII deal with the connections between spin quantities and world quantities. In Sec. IX, the Maxwell-Lorentz equations and the Dirac equation for the electron are written out in spinor notation. Finally, in Sec. X we sketch Infeld and van der Waerden's spinor analysis and its application as a gauge-covariant formalism.

II. TRANSFORMATIONS OF TENSORS

The pattern after which the formalism of spin transformations is modeled is that of the transformations of tensors. To make the development of the spinor formalism more intelligible, we shall review this pattern briefly in the present section.

A contravariant world vector A^k transforms according to the rule

$$A'^l=a^l{}_kA^k,\quad A^l=a^{-1l}{}_kA'^k, \tag{II 1}$$

where the quantities $a^{-1l}{}_k$ are solutions of the set of equations $a^m{}_la^{-1l}{}_k=\delta^m{}_k$. To obtain the rule for transforming covariant world vectors, it is sufficient to require the invariance of the scalar product A^lB_l of such a vector B_l with an arbitrary contravariant vector. This requirement leads to the rule

$$B_l=B_k'a^k{}_l,\quad B_l'=B_ka^{-1k}{}_l. \tag{II 2}$$

Tensors of higher rank transform as outer products of world vectors.

[5] In the special case $\xi=\chi^*$, the first member of (I 10) reduces to the two-component equation $\sqrt{2}\sigma^k(\partial_k+i\epsilon\phi_k)\chi=\mu\chi^*$ discussed by H. Jehle, Phys. Rev. 75, 1609 (1949) and J. Serpe, 76, 1538 (1949). For comparison of our notation with that of Infeld and van der Waerden, see footnote 15.

CC-0. In Public Domain. Gurukul Kangri Collection, Haridwar

Digitized by Arya Samaj Foundation Chennai and eGangotri

Using the fundamental metric tensor g_{kl} one can generally construct invariants of the form $g_{kl}A^kA^l=\text{inv}$, and can lower contravariant indexes, $A_l=A^kg_{kl}$. The tensor g_{kl} is symmetric, $g_{kl}=g_{lk}$; hence also $A_l=g_{lk}A^k$.

It is desirable further to have a tensor which raises covariant indexes, i.e., $A^k=A_lg^{lk}=A^mg_{ml}g^{lk}$. Hence we define g^{lk} by $g_{ml}g^{lk}=\delta_m{}^k$, so that g^{lk} is just the inverse of g_{lk}. As a further consequence, $g_{kl}A^kA^l=g^{kl}A_kA_l$.

III. TRANSFORMATIONS OF SPINORS

We establish for spinors the same form of transformation law as (II 1):

$$\psi'^\lambda=\Lambda^\lambda{}_\kappa\psi^\kappa,\quad \psi^\lambda=\Lambda^{-1\lambda}{}_\kappa\psi'^\kappa \tag{III 1}$$

(Greek indexes = 1, 2). Here ψ^λ is a spinor of first rank and $\Lambda^\lambda{}_\kappa$ is the matrix of transformation coefficients. For the present, we restrict the transformations $\Lambda^\lambda{}_\kappa$ only by requiring them to be nonsingular: $|\Lambda^\lambda{}_\kappa|\neq 0$. In general, any quantity with Greek indexes is liable to have complex components.

To obtain invariance of the form $\chi_\lambda\psi^\lambda$ with respect to spin transformations, it is necessary to establish the rule for transforming covariant spinors,

$$\chi_\lambda=\chi'_\kappa\Lambda^\kappa{}_\lambda,\quad \chi'_\lambda=\chi_\kappa\Lambda^{-1\kappa}{}_\lambda, \tag{III 2}$$

the same form as (II 2) for covariant world vectors.

We shall denote by $\psi^{\dot\lambda}$ the contravariant spinor whose components are conjugate complex to those of ψ^λ, and which transforms according to the law

$$\psi'^{\dot\lambda}=\Lambda^{\dot\lambda}{}_{\dot\kappa}\psi^{\dot\kappa},\quad \psi^{\dot\lambda}=\Lambda^{-1\dot\lambda}{}_{\dot\kappa}\psi'^{\dot\kappa}. \tag{III 3}$$

Here the transformation coefficients $\Lambda^{\dot\lambda}{}_{\dot\kappa}$ are conjugate complex to the $\Lambda^\lambda{}_\kappa$. Similarly, we shall denote by $\chi_{\dot\lambda}$ the spinor whose components are conjugate complex to those of χ_λ, and which transforms according to the law

$$\chi_{\dot\lambda}=\chi'_{\dot\kappa}\Lambda^{\dot\kappa}{}_{\dot\lambda},\quad \chi'_{\dot\lambda}=\chi_{\dot\kappa}\Lambda^{-1\dot\kappa}{}_{\dot\lambda}. \tag{III 4}$$

A contravariant spin vector may transform either like ψ^λ [by (III 1)] or like $\psi^{\dot\lambda}$ [by (III 3)]; the transformation matrix may be either $\Lambda^\kappa{}_\lambda$ or $\Lambda^{\dot\kappa}{}_{\dot\lambda}$. Similarly, a covariant spin vector may transform either by (III 2) or by (III 4). The transformation rules for spinors of higher rank are defined by the requirement that such spinors transform like outer products of spin vectors. Quite generally, an undotted contravariant index transforms like ψ^λ, a dotted one like $\psi^{\dot\lambda}$. Thus, for example, $\eta^{\mu\alpha}{}_{\dot\nu}$ transforms like $\psi^\mu\xi^\alpha\chi_{\dot\nu}$, i.e.,

$$\eta'^{\dot\rho\beta}{}_{\dot\sigma}=\Lambda^\rho{}_\mu\Lambda^\beta{}_\alpha\eta^{\mu\alpha}{}_{\dot\nu}\Lambda^{-1\dot\nu}{}_{\dot\sigma}.$$

The essential purpose of the "dotted index" notation is to distinguish these two transformation laws in spin space. Summation is to be permitted only over a dotted subscript and a dotted superscript, or over an undotted subscript and an undotted superscript. As a consequence of this restriction, the invariance of such expressions as $\psi^{\dot\lambda}\chi_{\dot\lambda}$ and $\alpha^{\mu\nu}\chi_\mu\xi_\nu$ becomes apparent on inspection, while non-invariant forms such as $\sum_\mu\psi^\mu\chi_{\dot\mu}$ are prevented from appearing.

It has sometimes been customary to let ψ^λ, $\psi^{\dot\lambda}$ represent arbitrary unrelated spinors transforming according to (III 1) and (III 3), respectively. In this case ψ^λ and $\psi^{\dot\lambda}$ are not necessarily conjugate complex to one another. However, the convention that $\psi^{\dot1}=(\psi^1)^*$, $\psi^{\dot2}=(\psi^2)^*$ (and analogously for all other spinors) is a convenient one, and we shall adhere to it.

In any second-rank spinor, as $\eta^{\dot\lambda}{}_\rho$, and in any spin transformation $\Lambda^\lambda{}_\kappa$, we make the further convention that the first index numbers the rows and the second index numbers the columns when such quantities are written out as matrices.

IV. THE FUNDAMENTAL SPINOR

In the preceding section, we have defined contravariant and covariant spinors in terms of their transformation properties. As yet, however, we have no means of finding the covariant components of a spinor when only its contravariant components are known, or conversely. In world space, the raising and lowering of indexes is accomplished by means of the metric tensor g_{kl} or g^{kl}. In the present section, we shall introduce an analogous "metric spinor"[6] for raising and lowering spin indexes.

We shall denote this fundamental spinor by $\gamma_{\mu\nu}$. With it, we can construct the invariant bilinear form

$$\chi^\mu\psi^\nu\gamma_{\mu\nu}=\chi'^\mu\psi'^\nu\gamma'_{\mu\nu}. \tag{IV 1}$$

This form is naturally invariant with any covariant spin tensor $\gamma_{\mu\nu}$. However, we select $\gamma_{\mu\nu}$ to be an *antisymmetric* spinor

$$\gamma_{\mu\nu}=\begin{pmatrix}0 & \gamma_{12}\\ -\gamma_{12} & 0\end{pmatrix}. \tag{IV 2}$$

The reason for this choice is the following one: In Sec. VII and VIII we shall establish a connection between spinors and spin transformations, on the one hand, and tensors and world transformations, on the other. Now, in world space, the case of special relativity is distinguished by unusual simplicity in that the metric tensor g_{kl} is invariant under Lorentz transformations. We should like the corresponding case in spin space to be similarly distinguished. This implies choosing $\gamma_{\mu\nu}$ to be invariant under unimodular spin transformations $|\Lambda^\rho{}_\kappa|=1$, since the entire connection between spin space and world space is based on the known isomorphism between the binary unimodular group and the restricted Lorentz group (see Sec. VIII). The antisymmetric tensor (IV 2) indeed satisfies this requirement:

$$\gamma'_{\mu\nu}=\gamma_{\lambda\kappa}\Lambda^{-1\lambda}{}_\mu\Lambda^{-1\kappa}{}_\nu=\gamma_{12}[(\Lambda^{-1})^1{}_\mu(\Lambda^{-1})^2{}_\nu-(\Lambda^{-1})^2{}_\mu(\Lambda^{-1})^1{}_\nu];$$

[6] This "metric" has the singular property that it assigns to all vectors in spin space the "length" zero; see Sec. V. Such an "Hermitizing matrix" was first introduced by Bargmann (30). See also van der Waerden (20), Pauli (27), and Kofink (47).

CC-0. In Public Domain. Gurukul Kangri Collection, Haridwar

Digitized by Arya Samaj Foundation Chennai and eGangotri

and since the second factor is zero for $\mu=\nu$, we obtain

$$\gamma'_{\mu\nu}=\gamma_{\mu\nu}|\Lambda^{-1\lambda}{}_{\kappa}|, \tag{IV 3}$$

so that with unimodular transformations, $\gamma'_{\mu\nu}=\gamma_{\mu\nu}$. A similar investigation shows that symmetric spinors are not invariant under such transformations.

We can now make use of the invariance of the expression (IV 1) to introduce a rule for lowering spin superscripts: Since covariant spin vectors are defined by the requirement that their scalar products with contravariant spin vectors be invariant,

$$\chi'_{\dot\nu}\psi'^{\dot\nu}=\chi_\mu\psi^\mu, \tag{IV 4}$$

it follows that we can define a covariant χ_ν by

$$\chi_\nu=\chi^\mu\gamma_{\mu\nu}=-\gamma_{\nu\mu}\chi^\mu. \tag{IV 5}$$

The second equation follows from the antisymmetry of $\gamma_{\mu\nu}$. It should be remarked that to lower a superscript without change of sign, the spin metric $\gamma_{\mu\nu}$ has to be written *after* the spinor whose index is to be lowered. (It is assumed that summation indices are placed adjacent, as in matrix multiplication.)

We establish the same rule for dotted indexes,

$$\chi_{\dot\nu}=\chi^{\dot\mu}\gamma_{\dot\mu\dot\nu},$$

with

$$\gamma_{\dot\mu\dot\nu}=(\gamma_{\mu\nu})^*.$$

It is now desired to define a $\gamma^{\mu\nu}$ which will raise subscripts. Because of (IV 5),

$$\chi_\nu\psi_\lambda=\chi^\mu\psi^\kappa\gamma_{\mu\nu}\gamma_{\kappa\lambda},$$

and a second-rank spinor $\gamma^{\nu\lambda}$ should have its indexes lowered by just this same rule. Thus

$$\gamma_{\nu\lambda}=\gamma^{\mu\kappa}\gamma_{\mu\nu}\gamma_{\kappa\lambda}=-\gamma_{\nu\mu}\gamma^{\mu\kappa}\gamma_{\kappa\lambda}.$$

From this equation it follows that

$$\begin{aligned}\gamma_{\nu\mu}\gamma^{\mu\kappa}&=-\delta_\nu{}^\kappa=-\begin{pmatrix}1&0\\0&1\end{pmatrix},\\ \gamma^{\mu\kappa}\gamma_{\kappa\lambda}&=-\delta^\mu{}_\lambda=-\begin{pmatrix}1&0\\0&1\end{pmatrix};\end{aligned} \tag{IV 6}$$

and so we define

$$\gamma^{\mu\nu}=\begin{pmatrix}0&1/\gamma_{12}\\-1/\gamma_{12}&0\end{pmatrix}. \tag{IV 7}$$

The formula for raising covariant spin indexes is now, because of (IV 5) and (IV 6),

$$\chi^\mu=\gamma^{\mu\lambda}\chi_\lambda=-\chi_\lambda\gamma^{\lambda\mu}. \tag{IV 8}$$

In the case without change of sign, the $\gamma^{\mu\lambda}$ is written *before* the spinor whose index is being raised.

The spinors $\gamma_{\lambda\mu}$, $\gamma^{\lambda\mu}$ are determined by a single complex number, say γ_{12}. The quantity

$$\gamma=\gamma_{12}\gamma_{\dot1\dot2} \tag{IV 9}$$

is real and positive. The forms

$$\gamma_{\lambda\mu}=\begin{pmatrix}0&1\\-1&0\end{pmatrix}\gamma^{\frac12}e^{i\vartheta},\quad \gamma^{\lambda\mu}=\begin{pmatrix}0&1\\-1&0\end{pmatrix}\gamma^{-\frac12}e^{-i\vartheta} \tag{IV 10}$$

are often useful.

The spinors $\delta_\nu{}^\mu$ and $\delta^\mu{}_\nu$ appearing in (IV 6) could be written $\delta_\nu{}^\mu=\delta^\mu{}_\nu=\gamma_\nu{}^\mu=-\gamma^\mu{}_\nu$, since it is evident from (IV 6) that they are just the forms of the fundamental spinor which have one covariant and one contravariant index.[7] These spinors $\gamma_\nu{}^\kappa$ and $\gamma^\mu{}_\lambda$ are invariant, since for example

$$\begin{aligned}\gamma'^\kappa{}_\nu&=-\delta'^\kappa{}_\nu=-\Lambda^\kappa{}_\lambda\delta^\lambda{}_\mu\Lambda^{-1\mu}{}_\nu\\&=-\Lambda^\kappa{}_\lambda\Lambda^{-1\lambda}{}_\nu=-\delta^\kappa{}_\nu=\gamma^\kappa{}_\nu.\end{aligned}$$

V. ALGEBRAIC PROPERTIES OF SPINORS

When performing calculations with spinors, it is essential to have at hand a number of relations which state the important algebraic properties of spinors. Some of these relations, which are frequently of use in manipulating expressions containing spinors, are written down in this section.

We first note some relations involving the fundamental spinor $\gamma^{\alpha\beta}$ (and arbitrary spinors $\eta_{\alpha\beta\gamma}$):

$$\gamma^{\alpha\beta}=-\gamma^{\beta\alpha}, \tag{V 1}$$

$$\gamma^{\alpha\beta}\gamma^{\gamma\delta}+\gamma^{\beta\gamma}\gamma^{\alpha\delta}+\gamma^{\gamma\alpha}\gamma^{\beta\delta}=0, \tag{V 2}$$

$$\gamma^{\alpha\beta}\eta_{\alpha\beta\gamma}+\gamma^{\alpha\beta}\eta_{\gamma\alpha\beta}+\gamma^{\alpha\beta}\eta_{\beta\gamma\alpha}=0. \tag{V 3}$$

They are easily verified by going through the possible numerical values of the indexes. Similar relations hold for $\gamma^{\dot\alpha\dot\beta}$, $\gamma_{\alpha\beta}$, $\gamma_{\dot\alpha\dot\beta}$.

Making use of these basic relations, we find the following formal properties of spinors:

A. Contraction proceeds just as with tensors, e.g.,

$$\varphi^{\dot\lambda\mu}\zeta_{\dot\rho\mu\sigma}{}^\kappa=\eta^{\dot\lambda}{}_{\dot\rho\sigma}{}^\kappa.$$

Summation can occur only over a dotted subscript and a dotted superscript, or over an undotted subscript and an undotted superscript.

B. Scalar multiplication of two spinors is "anticommutative" in the following sense:

$$\chi_\nu\psi^\nu=\chi_\nu\gamma^{\kappa\nu}\psi_\kappa=-\gamma^{\kappa\nu}\chi_\nu\psi_\kappa=-\chi^\kappa\psi_\kappa=-\psi_\kappa\chi^\kappa. \tag{V 4}$$

C. The absolute value of any spinor of *odd* rank is zero. For example,

$$\chi_\nu\chi^\nu=-\chi_\nu\chi^\nu=0,$$

from (V 4). But $\eta_{\lambda\nu}\eta^{\lambda\nu}=\eta^{\lambda\nu}\eta_{\lambda\nu}$ (by a similar raising and lowering of indexes) need not be zero.

D. The contraction of a symmetrical spinor is zero. Let $\eta_{\lambda\nu}=\eta_{\mu\lambda}$. The contraction is[8]

$$\eta_\lambda{}^\lambda=\gamma^{\lambda\mu}\eta_{\lambda\mu}=-\gamma^{\mu\lambda}\eta_{\lambda\mu}=-\gamma^{\mu\lambda}\eta_{\mu\lambda}=-\eta_\mu{}^\mu=0. \tag{V 5}$$

[7] Analogously, in world space $g_k{}^l=\delta_k{}^l$; but $g^l{}_k=\delta^l{}_k$.

[8] It should perhaps be remarked that $\eta_\lambda{}^\lambda$ is not the sum of the diagonal elements of either $\eta_{\lambda\mu}$ or $\eta^{\lambda\mu}$.

CC-0. In Public Domain. Gurukul Kangri Collection, Haridwar

Digitized by Arya Samaj Foundation Chennai and eGangotri

E. Let $\eta_{\lambda\mu}=-\eta_{\mu\lambda}$ be an antisymmetric spinor. Its contraction is, with reference to (IV 7),

$$\eta_\lambda{}^\lambda=\gamma^{\lambda\mu}\eta_{\lambda\mu}=(\eta_{12}-\eta_{21})/\gamma_{12}=2\eta_{12}/\gamma_{12}=-2\eta_{21}/\gamma_{12}.$$

Hence

$$\eta_{\lambda\mu}=\tfrac{1}{2}\eta_\alpha{}^\alpha\gamma_{\lambda\mu}$$

or

$$\eta_{\lambda\mu}-\eta_{\mu\lambda}=\eta_\alpha{}^\alpha\gamma_{\lambda\mu}. \tag{V 6}$$

Equation (V 6) holds for a *general* spinor of second rank, since the symmetrical part vanishes on both sides.

F. Equation (V 3) can be put into the special forms

$$\begin{gathered}\xi_\alpha\eta^\alpha\zeta_\gamma+\xi_\gamma\eta_\alpha\zeta^\alpha+\xi^\alpha\eta_\gamma\zeta_\alpha=0,\\ \eta_\alpha{}^\alpha{}_\gamma+\eta_{\gamma\alpha}{}^\alpha+\eta^\alpha{}_{\gamma\alpha}=0.\end{gathered} \tag{V 7}$$

Similarly, (V 2) gives

$$\eta_\alpha{}^\alpha{}_\gamma{}^\gamma+\eta_{\alpha\beta}{}^{\beta\alpha}+\eta^\gamma{}_{\beta\gamma}{}^\beta=0. \tag{V 8}$$

VI. SPECIAL SPIN TRANSFORMATIONS

So far no restrictions have been placed on the spin transformations $\Lambda^\lambda{}_\kappa$, except that they be nonsingular. Two kinds of specialization of $\Lambda^\lambda{}_\kappa$ will be of interest:

(A) $$\Lambda^\lambda{}_\kappa=\delta^\lambda{}_\kappa e^{i\varphi/2}, \tag{VI 1}$$

where φ is an arbitrary real function of $(xyzt)$. It will be shown in Sec. 10 that (VI 1) represents a gauge transformation.

B. *Unimodular* spin transformations

$$|\Lambda^\lambda{}_\kappa|=|\Lambda^{\dot\lambda}{}_{\dot\kappa}|=|\Lambda^{-1\lambda}{}_\kappa|=|\Lambda^{-1\dot\lambda}{}_{\dot\kappa}|=1. \tag{VI 2}$$

Such transformations will be shown in Sec. VIII to represent Lorentz transformations (not including inversions). In problems where special relativity theory is applicable one can restrict himself to unimodular spin transformations (VI 2) and because of (IV 3) can choose for the $\gamma_{\mu\nu}$ the simple invariant values

$$\gamma_{\mu\nu}=\begin{pmatrix}0 & 1\\ -1 & 0\end{pmatrix}=\gamma^{\mu\nu}. \tag{VI 3}$$

In this way one recovers, from the general theory which we have partially described, the special spinor algebra presented in van der Waerden's original 1929 paper.

In the case of this specialization, one can introduce the spin metric $\gamma_{\mu\nu}$ (VI 3) in a very simple way. Under unimodular spin transformations, both

$$\chi^1\psi^2-\chi^2\psi^1 \quad\text{and}\quad \chi_1\psi^1+\chi_2\psi^2 \tag{VI 4}$$

are invariant. Hence one can define covariant components χ_ν of a spinor χ^ν by identifying the two expressions (VI 4)

$$\chi_1=-\chi^2, \quad \chi_2=\chi^1.$$

This procedure immediately gives (VI 3) when one sets $\chi_\nu=\chi^\mu\gamma_{\mu\nu}$.

The possibility of establishing such a simple scheme rests upon the fact that $\gamma_{\mu\nu}$ and $\gamma^{\mu\nu}$ are invariant in respect to unimodular spin transformations, as is evident from (IV 3) and (IV 7). Section VIII of the present article will discuss this special spinor algebra in some detail.

VII. THE CONNECTION BETWEEN WORLD TENSORS AND SPINORS

An Hermitean[9] second-rank spinor

$$A_{\dot\lambda\mu}=A_{\mu\dot\lambda} \tag{VII 1}$$

is determined by four real numbers. One can therefore make correspond to every real world vector A_k, in a unique way, such an Hermitean spinor (VII 1), whose components are linear functions of the components of the vector

$$A_{\dot\lambda\mu}=\sigma^k{}_{\dot\lambda\mu}A_k. \tag{VII 2}$$

Here the "mixed quantities" $\sigma^k{}_{\dot\lambda\mu}$ must be Hermitean,

$$\sigma^k{}_{\dot\lambda\mu}=\sigma^k{}_{\mu\dot\lambda}, \tag{VII 3}$$

since the A_k are real and $A_{\dot\lambda\mu}$ in (VII 2) is assumed to be Hermitean. If (VII 2) is to have significance independently of particular coordinate systems, then $\sigma^k{}_{\dot\lambda\mu}$ must transform as a contravariant four-vector in respect to general world transformations and, independently, as a second-rank spinor in respect to spin transformations.

Let us assume that the metrics g_{kl} and $\gamma_{\mu\nu}$, in world space and in spin space, respectively, are given. The invariant quadratic form $g^{kl}A_kA_l$ in the world vector components A_k has the signature $+---$. The Hermitean spinor $A_{\dot\lambda\mu}$ has an invariant of just this same signature, namely,

$$A^{\dot\lambda\mu}A_{\dot\lambda\mu}=\gamma^{\dot\lambda\dot\rho}\gamma^{\mu\nu}A_{\dot\rho\nu}A_{\dot\lambda\mu}=(2/\gamma)|A_{\dot\lambda\mu}|, \tag{VII 4}$$

where we have used the form (IV 10) for $\gamma^{\mu\nu}$. To show that this expression has the desired signature, we can set $A_{\dot1\dot1}=a+b$, $A_{\dot2\dot2}=a-b$, $A_{\dot1\dot2}=c+id$, $A_{\dot2\dot1}=c-id$, from which

$$A_{\dot1\dot1}A_{\dot2\dot2}-A_{\dot1\dot2}A_{\dot2\dot1}=a^2-b^2-c^2-d^2.$$

The correspondence $A_k\rightarrow A_{\dot\lambda\mu}$ transforms the invariant expression (VII 4) into a quadratic form in the A_k. We arbitrarily identify this quadratic form with the fundamental metrical form $g^{kl}A_kA_l$:

$$g^{kl}A_kA_l=\gamma^{\dot\lambda\dot\rho}\gamma^{\mu\nu}A_{\dot\rho\nu}A_{\dot\lambda\mu}=\gamma^{\dot\lambda\dot\rho}\gamma^{\mu\nu}\sigma^k{}_{\dot\rho\nu}\sigma^l{}_{\dot\lambda\mu}A_kA_l$$

identically in A_k. Thus

$$\sigma^{k\dot\lambda\mu}\sigma^l{}_{\dot\lambda\mu}=\gamma^{\dot\lambda\dot\rho}\gamma^{\mu\nu}\sigma^k{}_{\dot\rho\nu}\sigma^l{}_{\dot\lambda\mu}=g^{kl}. \tag{VII 5}$$

Equation (VII 5) gives 10 conditions which must be satisfied by the 16 real parameters determining the Hermitean quantities $\sigma^k{}_{\dot\rho\nu}$. On the basis of (VII 5) we

[9] The transpose of $A_{\dot\lambda\mu}$ is $A_{\dot\mu\dot\lambda}$, while the complex conjugate of the last spinor is $A_{\mu\dot\lambda}$. The dot in a dotted index belongs to the position of the index. Taking the transpose of a second-rank spinor interchanges rows and columns, but does not alter the fact that the first index in each component is dotted, the second not.

CC-0. In Public Domain. Gurukul Kangri Collection, Haridwar

Digitized by Arya Samaj Foundation Chennai and eGangotri

can solve (VII 2) for the A_k:

$$\sigma^{l\dot{\lambda}\mu}A_{\dot{\lambda}\mu}=\sigma^{l\dot{\lambda}\mu}\sigma^{k}{}_{\dot{\lambda}\mu}A_k=g^{lk}A_k;$$
$$A^l=\sigma^{l\dot{\lambda}\mu}A_{\dot{\lambda}\mu}. \qquad \text{(VII 6)}$$

World tensors of higher rank can also be made to correspond to certain spinors by means of an obvious extension of the rules (VII 2), (VII 6). For example, if T_{kl} is a world tensor of second rank, we define

$$T^{\dot{\mu}\nu\dot{\rho}\sigma}=\sigma^{k\dot{\mu}\nu}\sigma^{l\dot{\rho}\sigma}T_{kl}. \qquad \text{(VII 7)}$$

The inverse equation is

$$T^{kl}=\sigma^{k\dot{\mu}\nu}\sigma^{l\dot{\rho}\sigma}T_{\dot{\mu}\nu\dot{\rho}\sigma}. \qquad \text{(VII 8)}$$

If one substitutes (VII 6) back into (VII 2), he obtains

$$A_{\dot{\lambda}\mu}=\sigma^{k}{}_{\dot{\lambda}\mu}g_{kl}\sigma^{l\dot{\rho}\sigma}A_{\dot{\rho}\sigma},$$

which can be satisfied identically only if

$$g_{kl}\sigma^{k}{}_{\dot{\lambda}\mu}\sigma^{l\dot{\rho}\sigma}=\delta_{\dot{\lambda}}{}^{\dot{\rho}}\delta_{\mu}{}^{\sigma}=\gamma_{\dot{\lambda}}{}^{\dot{\rho}}\gamma_{\mu}{}^{\sigma}. \qquad \text{(VII 9)}$$

By raising indexes one obtains the equivalent relation

$$g_{kl}\sigma^{k\dot{\lambda}\mu}\sigma^{l\dot{\rho}\sigma}=\gamma^{\dot{\lambda}\dot{\rho}}\gamma^{\mu\sigma}. \qquad \text{(VII 10)}$$

On the basis of (VII 5), it is clear that we can also equate the invariant *bilinear* forms in world space and in spin space:

$$A_{\dot{\lambda}\mu}B^{\dot{\lambda}\mu}=A_kB^k. \qquad \text{(VII 11)}$$

The expression $\gamma_{\dot{\lambda}\dot{\rho}}(\sigma^{k\dot{\lambda}\mu}\sigma^{l\dot{\rho}\nu}+\sigma^{l\dot{\lambda}\mu}\sigma^{k\dot{\rho}\nu})$ is antisymmetric in the indexes μ and ν, and hence is equal to a multiple of $\gamma^{\mu\nu}$, say $h^{kl}\gamma^{\mu\nu}$. If one multiples by $\gamma_{\nu\sigma}$ and considers the rule for lowering indexes, it follows that

$$\sigma^{k\dot{\lambda}\mu}\sigma^{l}{}_{\dot{\lambda}\sigma}+\sigma^{l\dot{\lambda}\mu}\sigma^{k}{}_{\dot{\lambda}\sigma}=h^{kl}\delta^{\mu}{}_{\sigma}.$$

In order to determine h^{kl}, we set $\mu=\sigma$, sum over μ and compare with (VII 5). The result is $h^{kl}=g^{kl}$. Thus

$$\sigma^{l\dot{\mu}\dot{\lambda}}\sigma^{k}{}_{\dot{\lambda}\sigma}+\sigma^{k\dot{\mu}\dot{\lambda}}\sigma^{l}{}_{\dot{\lambda}\sigma}=g^{kl}\delta^{\mu}{}_{\sigma}. \qquad \text{(VII 12)}$$

VIII. LORENTZ TRANSFORMATIONS AND SPIN TRANSFORMATIONS

In this section, and in the next, we restrict ourselves to the special metric (I 2) and to Lorentz transformations. As already mentioned in Sec. VI, these restrictions characterize the special spinor calculus presented by van der Waerden in his original 1929 paper.

The theme of Sec. VII was the possibility of establishing, quite generally, correspondences between world tensors of any rank and spinors with certain special symmetry properties. The present section deals with the further possibility, which arises in the case of the specialization to Lorentz frames and transformations, of establishing a coordination between world transformations and unimodular spin transformations.[10]

[10] This possibility is founded essentially on the existence, in world space and in spin space, of quadratic forms having the same signature. See Sec. VII.

We choose for the spin metric $\gamma_{\mu\nu}$ the simple form

$$\gamma_{\mu\nu}=\begin{pmatrix}0&1\\-1&0\end{pmatrix}. \qquad \text{(VI 3)}$$

Then (VII 10) is satisfied with

$$\sigma^{0\dot{\rho}\sigma}=\frac{1}{\sqrt{2}}\begin{pmatrix}1&0\\0&1\end{pmatrix},\quad \sigma^{1\dot{\rho}\sigma}=\frac{1}{\sqrt{2}}\begin{pmatrix}0&1\\1&0\end{pmatrix},$$
$$\sigma^{2\dot{\rho}\sigma}=\frac{1}{\sqrt{2}}\begin{pmatrix}0&-i\\i&0\end{pmatrix},\quad \sigma^{3\dot{\rho}\sigma}=\frac{1}{\sqrt{2}}\begin{pmatrix}1&0\\0&-1\end{pmatrix}, \qquad \text{(VIII 1)}$$

as can be verified by direct calculation. By lowering indexes, using (VI 3), one finds[11]

$$\sigma^{0\dot{\rho}}{}_{\sigma}=\frac{1}{\sqrt{2}}\begin{pmatrix}0&1\\-1&0\end{pmatrix},\quad \sigma^{1\dot{\rho}}{}_{\sigma}=\frac{1}{\sqrt{2}}\begin{pmatrix}-1&0\\0&1\end{pmatrix},$$
$$\sigma^{2\dot{\rho}}{}_{\sigma}=\frac{1}{\sqrt{2}}\begin{pmatrix}i&0\\0&i\end{pmatrix},\quad \sigma^{3\dot{\rho}}{}_{\sigma}=\frac{1}{\sqrt{2}}\begin{pmatrix}0&1\\1&0\end{pmatrix}, \qquad \text{(VIII 2)}$$

and

$$\sigma^{0}{}_{\dot{\rho}\sigma}=\frac{1}{\sqrt{2}}\begin{pmatrix}1&0\\0&1\end{pmatrix},\quad \sigma^{1}{}_{\dot{\rho}\sigma}=\frac{1}{\sqrt{2}}\begin{pmatrix}0&-1\\-1&0\end{pmatrix},$$
$$\sigma^{2}{}_{\dot{\rho}\sigma}=\frac{1}{\sqrt{2}}\begin{pmatrix}0&-i\\i&0\end{pmatrix},\quad \sigma^{3}{}_{\dot{\rho}\sigma}=\frac{1}{\sqrt{2}}\begin{pmatrix}-1&0\\0&1\end{pmatrix}. \qquad \text{(VIII 3)}$$

Here our exposition has, so to speak, returned to its starting point. The set of matrices $\sigma^{k\dot{\rho}}{}_{\sigma}$ (VIII 2) is identical with the set σ^k (I 9), the study of whose transformation properties initiated the entire development. Moreover, the relations (I 8) are completely equivalent to (VII 12), from which they can be obtained by raising and lowering indexes. As a matter of fact we are now prepared to carry to completion the program sketched at the end of Sec. I.

This program consisted essentially in considering the matrices σ^k and the wave functions ξ, χ in (I 10) as spinors, and in seeking to discover how the wave functions must transform with a Lorentz transformation if the σ^k are to remain constant while the equations remain covariant. Since it was assumed in Sec. VII that the mixed quantities $\sigma^{k\dot{\rho}}{}_{\sigma}$ transform like world vector components in respect to world transformations and like spin tensor components in respect to spin transformations, these quantities can remain constant when a Lorentz transformation is made only if an appropriate spin transformation is made at the same time. That is to say, the $\sigma^{k\dot{\rho}}{}_{\sigma}$ can be held constant only by coordinating a suitably chosen spin transformation with the Lorentz transformation. Moreover, we desire to

[11] Note that the matrices (VIII 1) and (VIII 3) are all Hermitean, while some of those of the set (VIII 2) are not.

CC-0. In Public Domain. Gurukul Kangri Collection, Haridwar

Digitized by Arya Samaj Foundation Chennai and eGangotri

maintain the choice (VI 3) of $\gamma_{\mu\nu}$ when such spin transformations are made.

We therefore determine conditions that the $\sigma^{k\dot{\rho}}{}_{\sigma}$ and $\gamma_{\mu\nu}$ have fixed values, for example (VIII 2) and (VI 3), independent of particular frames in spin space and world space. It is clear from (IV 3) that $\gamma_{\mu\nu}$ is left invariant only by unimodular spin transformations

$$|\Lambda^{\sigma}{}_{\nu}| = 1. \tag{VI 2}$$

Equation (VI 2) determines two of the eight real parameters specifying $\Lambda^{\sigma}{}_{\nu}$. The remaining six parameters permit us to coordinate $\Lambda^{\sigma}{}_{\nu}$ to a six-parameter Lorentz transformation. Let $a^{k}{}_{l}$ be a Lorentz transformation. Then $a^{k}{}_{l}$ and the spin transformation $\Lambda^{\sigma}{}_{\nu}$, applied in concert, leave the $\sigma^{k\dot{\rho}}{}_{\sigma}$ invariant if

$$\sigma^{k\dot{\rho}}{}_{\sigma} = \sigma'^{k\dot{\rho}}{}_{\sigma} = a^{k}{}_{l}\Lambda^{\dot{\rho}}{}_{\dot{\mu}}\sigma^{l\dot{\mu}}{}_{\nu}\Lambda^{-1\nu}{}_{\sigma},$$

i.e., if

$$a^{k}{}_{l}\sigma^{l\dot{\mu}}{}_{\nu} = \Lambda^{-1\dot{\mu}}{}_{\dot{\rho}}\sigma^{k\dot{\rho}}{}_{\sigma}\Lambda^{\sigma}{}_{\nu}. \tag{VIII 4}$$

When a Lorentz transformation $a^{k}{}_{l}$ is given, these equations can be solved in a straightforward way, if they can be solved at all; together with (VI 2), they suffice to determine $\Lambda^{\sigma}{}_{\nu}$ up to algebraic sign. Thus there are exactly two spin transformations corresponding to every Lorentz transformation which is represented at all in spin space, namely $\pm\Lambda^{\sigma}{}_{\nu}$, where $\Lambda^{\sigma}{}_{\nu}$ is a unimodular solution of (VIII 4).

On account of the invariance of $\gamma_{\mu\nu}$ and $\gamma^{\mu\nu}$ in respect to unimodular transformations, the $\Lambda^{\sigma}{}_{\nu}$ determined by (VIII 4) and (VI 2) will, when coordinated with the given Lorentz transformation, hold constant not only $\sigma^{k\dot{\rho}}{}_{\sigma}$ but also $\sigma^{k\dot{\rho}\sigma}$ and $\sigma^{k}{}_{\dot{\rho}\sigma}$.

All the Lorentz transformations constitute a group. From (I 2) and the defining equation

$$g_{kl} = g'_{mn}a^{m}{}_{k}a^{n}{}_{l} = g'_{kl},$$

it is clear that the determinant of every Lorentz transformation is either $+1$ or -1. The transformations with determinant $+1$ constitute a subgroup of the full group, the so-called *restricted* Lorentz group. The transformations with determinant -1 are called inversions.

If one undertakes to solve (VIII 4), for the spin transformation corresponding to an inversion in world space, in place of a solution he gets a self-contradictory set of equations. The following argument shows that, in general, there is no unimodular spin transformation which will hold the σ's constant when a Lorentz transformation of determinant -1 is made in world space: The identity transformation in spin space corresponds to the identity Lorentz transformation. All the spin transformations of determinant $+1$ can be produced in a continuous way from the identity transformation, i.e., can be arrived at by application of infinitesimal transformations of determinant $+1$. An infinitesimal transformation in spin space corresponds to an infinitesimal Lorentz transformation. Hence the Lorentz transformations corresponding to unimodular spin transformations can be reached continuously from the identity transformation, which has determinant $+1$. But every Lorentz transformation has determinant $+1$ or -1, and the ones with determinant -1 are not infinitesimal (they are inversions). Thus only the positive Lorentz transformations correspond to unimodular spin transformations.

It is important for the purpose of discussing the reflection covariance of equations that we be able to represent inversions, somehow, in spin space. We should therefore like to coordinate with each negative Lorentz transformation some sort of spin transformation, such that when the two are performed together the matrices $\sigma^{m\dot{\rho}}{}_{\sigma}$ are left invariant. This can be accomplished as follows:

An arbitrary inversion may be regarded as being composed of the reflection

$$c^{l}{}_{m} = \begin{bmatrix} 1 & 0 & 0 & 0 \\ 0 & 1 & 0 & 0 \\ 0 & 0 & -1 & 0 \\ 0 & 0 & 0 & 1 \end{bmatrix} \tag{VIII 5}$$

and a positive Lorentz transformation $a^{k}{}_{l}$. We coordinate with the latter, as usual, a spin transformation $\Lambda^{\sigma}{}_{\nu}$ which is a unimodular solution of (VIII 4).

With the special reflection (VIII 5) we shall coordinate a new kind of transformation which is defined in the following way: To each spinor $\eta^{\mu}{}_{\nu\dot{\sigma}}$ (for example) we make correspond a new spinor $\eta^{C\mu}{}_{\nu\dot{\sigma}}$, whose components are conjugate complex to the corresponding components of $\eta^{\mu}{}_{\nu\dot{\sigma}}$, and which obeys the same transformation law as does $\eta^{\mu}{}_{\nu\dot{\sigma}}$. Thus $\eta^{C\mu}{}_{\nu\dot{\sigma}}$ has the same components as $\eta^{\dot{\mu}}{}_{\dot{\nu}\sigma}$, but transforms quite differently. The new transformation, which we shall coordinate with (VIII 5), is then defined by

$$\eta^{\mu}{}_{\nu\dot{\sigma}} \longrightarrow \eta^{C\mu}{}_{\nu\dot{\sigma}}$$

for all spinors η. It is clear from this definition that

$$(\eta^{C\mu}{}_{\nu\dot{\sigma}})^{C} = \eta^{\mu}{}_{\nu\dot{\sigma}}.$$

When this C transformation and the reflection (VIII 5) are performed together, the $\sigma^{m\dot{\rho}}{}_{\sigma}$ are left invariant:

$$(c^{l}{}_{m}\sigma^{m\dot{\rho}}{}_{\sigma})^{C} \equiv c^{l}{}_{m}\sigma^{Cm\dot{\rho}}{}_{\sigma} = \sigma^{l\dot{\rho}}{}_{\sigma}. \tag{VIII 6}$$

This result is easy to verify by reference to (VIII 2); for $l=2$,

$$(c^{2}{}_{m}\sigma^{m\dot{\rho}}{}_{\sigma})^{C} = (-\sigma^{2\dot{\rho}}{}_{\sigma})^{C} = \sigma^{2\dot{\rho}}{}_{\sigma},$$

since the components of $\sigma^{2\dot{\rho}}{}_{\sigma}$ are pure imaginary and the C transformation does not affect the Λ-transformation properties. It is similarly clear that

$$(c^{l}{}_{m}\sigma^{m\dot{\rho}\sigma})^{C} = \sigma^{l\dot{\rho}\sigma}, \quad (c^{l}{}_{m}\sigma^{m}{}_{\dot{\rho}\sigma})^{C} = \sigma^{l}{}_{\dot{\rho}\sigma}.$$

An arbitrary inversion can be expressed in the form $a^{k}{}_{l}c^{l}{}_{m}$, where $|a^{k}{}_{l}| = 1$ and $c^{l}{}_{m}$ is (VIII 5). With this inversion we coordinate the spin transformation which consists in first performing the C transformation, then performing the unimodular Λ-transformation corre-

CC-0. In Public Domain. Gurukul Kangri Collection, Haridwar

Digitized by Arya Samaj Foundation Chennai and eGangotri

sponding to $a^k{}_l$ by (VIII 4). With this coordination, the σ's are evidently kept invariant.

Using (VIII 6), we can now formulate the covariance of equations with respect to the reflection (VIII 5), and hence with respect to all negative Lorentz transformations. For example, (VII 6) becomes

$$A'^l = c^l{}_m A^m = c^l{}_m \sigma^{m\dot\rho\sigma} A_{\dot\rho\sigma} = \sigma^{Cl\dot\rho\sigma} A_{\dot\rho\sigma}$$

or

$$A'^l = \sigma^{l\dot\rho\sigma} A^C{}_{\dot\rho\sigma},$$

by virtue of the reality of the components of A'^l. Just as with the positive Lorentz transformations, we are able to express the transformed world vector components in terms of the transformed spinor components by means of the *original* σ's and an equation of the same form as (VII 6). This means that (VII 6) is covariant with respect to the reflection $c^l{}_m$ (VIII 5). But evidently (VII 6) is also covariant with respect to positive Lorentz transformations $a^k{}_l$. Hence it is covariant with respect to any inversion $a^k{}_l c^l{}_m$.

The covariance of the Dirac set (I 11) with respect to inversions is proved in a similar way. We substitute into (I 11) the expression

$$\partial_k + i\epsilon\phi_k = c^l{}_k(\partial'_l + i\epsilon\phi'_l),$$

where $c^l{}_m$ is given by (VIII 5). The result is, by (VIII 6),

$$\sqrt{2}\sigma^{Cl\dot\nu}{}_\rho(\partial'_l + i\epsilon\phi'_l)\chi^\rho = \mu\xi^{\dot\nu},$$
$$\sqrt{2}\sigma^{Cl\nu}{}_{\dot\rho}(\partial'_l + i\epsilon\phi'_l)\xi^{\dot\rho} = \mu\chi^\nu.$$

In order to recover the original σ's, we perform the C transformation on these equations:

$$\sqrt{2}\sigma^{l\dot\nu}{}_\rho(\partial'_l - i\epsilon\phi'_l)\chi^{C\rho} = \mu\xi^{C\dot\nu},$$
$$\sqrt{2}\sigma^{l\nu}{}_{\dot\rho}(\partial'_l - i\epsilon\phi'_l)\xi^{C\dot\rho} = \mu\chi^{C\nu}.$$

Taking complex conjugates so as to return to a form similar to that of (I 11), we obtain finally

$$\sqrt{2}\sigma^{l\nu}{}_{\dot\rho}(\partial'_l + i\epsilon\phi'_l)\chi^{C\dot\rho} = \mu\xi^{C\nu},$$
$$\sqrt{2}\sigma^{l\dot\nu}{}_\rho(\partial'_l + i\epsilon\phi'_l)\xi^{C\rho} = \mu\chi^{C\dot\nu}.$$

Upon comparison with (I 11), this is seen to be the same set of equations. The correspondence between the transformed and the untransformed spinors χ, ξ is

$$\chi^\rho \longrightarrow \xi^{C\rho}, \quad \xi^{\dot\rho} \longrightarrow \chi^{C\dot\rho}.$$

As these various spinors are only determined as solutions of (I 11) and the transformed set of equations, this interchange of names is not significant. Thus the Dirac set (I 11) is covariant with respect to (VIII 5), and hence with respect to all inversions.[12]

To every positive Lorentz transformation there correspond two unimodular spin transformations, which are negatives of one another and are solutions of (VI 2) and (VIII 4). This correspondence maintains product relations: i.e., if

$$a^k{}_l \longrightarrow \Lambda^\rho{}_\mu, \quad b^m{}_k \longrightarrow \Omega^\kappa{}_\rho$$

then

$$\sigma^{\kappa\dot\rho}{}_\sigma = a^k{}_l \Lambda^{\dot\rho}{}_{\dot\mu} \sigma^{l\dot\mu}{}_\nu \Lambda^{-1\nu}{}_\sigma$$

and

$$\sigma^{m\dot\kappa}{}_\lambda = (b^m{}_k a^k{}_l)(\Omega^\kappa{}_{\dot\rho}\Lambda^{\dot\rho}{}_{\dot\mu})\sigma^{l\dot\mu}{}_\nu(\Lambda^{-1\nu}{}_\sigma \Omega^{-1\sigma}{}_\lambda),$$

so that

$$b^m{}_k a^k{}_l \longrightarrow \Omega^\kappa{}_\rho \Lambda^\rho{}_\mu.$$

When to every element of a group there is made correspond some linear transformation of an n-dimensional vector space (over a specified field) onto itself, such that to the product of two group elements there always corresponds the product of the transformations representing those elements, this correspondence is called a representation of the group, of degree n. Spin space, as already presented, is a two-dimensional vector space over the field of complex numbers. It is now apparent that the correspondence of unimodular spin transformations to positive Lorentz transformations gives a representation (of degree 2) of the restricted Lorentz group. This is a two-valued representation, since to each positive Lorentz transformation there correspond two spin transformations.

As an example of the coordination of spin transformations to Lorentz transformations, consider the special Lorentz transformation,

$$x' = x\cosh\phi - ct\sinh\phi,$$
$$ct' = ct\cosh\phi - x\sinh\phi,$$

from an original frame K to a new frame K' moving along the x axis of K with velocity

$$V = c\tanh\phi$$

relative to K. By solving Eqs. (VIII 4) in this case, one finds the corresponding spin transformation to be either of the pair

$$\Lambda^\mu{}_\sigma = \pm\begin{pmatrix}\cosh(\phi/2) & \sinh(\phi/2)\\ \sinh(\phi/2) & \cosh(\phi/2)\end{pmatrix}.$$

Another kind of special Lorentz transformation is a rotation in space. In this case the Lorentz transformation coefficients satisfy the conditions

$$a^0{}_0 = 1, \quad a^0{}_k = a^m{}_0 = 0 \quad (k, m \neq 0).$$

Then the first equation of the set

$$\sigma^{m\dot\mu\nu} = a^m{}_k \Lambda^{\dot\mu}{}_{\dot\rho} \Lambda^\nu{}_\sigma \sigma^{k\dot\rho\sigma}$$

[see (VIII 4), (III 1), (III 3)] reads

$$\begin{pmatrix}\Lambda^{\dot1}{}_{\dot1} & \Lambda^{\dot1}{}_{\dot2}\\ \Lambda^{\dot2}{}_{\dot1} & \Lambda^{\dot2}{}_{\dot2}\end{pmatrix}\begin{pmatrix}1 & 0\\ 0 & 1\end{pmatrix}\begin{pmatrix}\Lambda^1{}_1 & \Lambda^2{}_1\\ \Lambda^1{}_2 & \Lambda^2{}_2\end{pmatrix} = \begin{pmatrix}1 & 0\\ 0 & 1\end{pmatrix}, \quad \text{(VIII 7)}$$

[12] The two-component equation mentioned in footnote 5 is not reflection covariant: (VIII 5) carries it into

$$\sqrt{2}\sigma^{k\dot\nu}{}_\rho c^l{}_k(\partial'_l + i\epsilon\phi_{l'})\chi^\rho = \mu\chi^{\dot\nu},$$

i.e.,

$$\sqrt{2}\sigma^{k\dot\nu}{}_\rho(\partial'_l - i\epsilon\phi'_l)\chi^{C\rho} = \mu\chi^{C\dot\nu},$$

which is the charge-conjugate of the original equation.

For the theory of charge-conjugation, see Kramers (48) and (7), Sec. 63 and 64. Charge conjugation in the Dirac theory is best discussed on the basis of (IX 31).

CC-0. In Public Domain. Gurukul Kangri Collection, Haridwar

Digitized by Arya Samaj Foundation Chennai and eGangotri

because of the form of $\sigma^{0\dot{\mu}\nu}$ in (VIII 1). Equation (VIII 7) is just the *unitary* condition, often written $\Lambda^*\tilde{\Lambda}=1$ or $\Lambda^\dagger\Lambda=1$.

Thus spatial rotations can be represented by spin transformations which are not only unimodular but also unitary. The matrix elements of such spin transformations are called the Cayley-Klein parameters representing the rotation.

It may be of some utility to have the spin transformations representing a general spatial rotation written down in terms of the Euler angles.[13] The spin transformations corresponding to a rotation φ about the z axis are

$$\Phi^{\dot{\rho}}{}_{\dot{\nu}}=\pm\begin{pmatrix} e^{-i\varphi/2} & 0 \\ 0 & e^{i\varphi/2}\end{pmatrix};$$

those corresponding to a rotation θ about the new x axis are

$$\Theta^{\dot{\sigma}}{}_{\dot{\rho}}=\pm\begin{pmatrix} \cos(\theta/2) & -i\sin(\theta/2) \\ -i\sin(\theta/2) & \cos(\theta/2)\end{pmatrix};$$

and those representing a rotation ψ about the new z axis have the same form as $\Phi^{\dot{\rho}}{}_{\dot{\nu}}$, but with ψ substituted for φ. The spin transformation $\Lambda^{\dot{\mu}}{}_{\dot{\nu}}$ representing the entire rotation in space which is specified by the Euler angles φ, θ, ψ is obtained by multiplying the matrices representing the separate rotations

$$\Lambda^{\dot{\mu}}{}_{\dot{\nu}}=\Psi^{\dot{\mu}}{}_{\dot{\sigma}}\Theta^{\dot{\sigma}}{}_{\dot{\rho}}\Phi^{\dot{\rho}}{}_{\dot{\nu}}$$

$$=\pm\begin{pmatrix} e^{-i(\varphi+\psi)/2}\cos(\theta/2) & -ie^{i(\varphi-\psi)/2}\sin(\theta/2) \\ -ie^{-i(\varphi-\psi)/2}\sin(\theta/2) & e^{i(\varphi+\psi)/2}\cos(\theta/2)\end{pmatrix}. \qquad \text{(VIII 8)}$$

The following rule is a convenient mnemonic device: The spin transformation corresponding to a rotation through angle θ about the kth Cartesian coordinate axis ($k=1, 2, 3$) is

$$\Lambda_k=1\cos(\theta/2)-i\sigma^k\sin(\theta/2),$$

where σ^k are the last three of the set of matrices $\sigma^{k\dot{\rho}\sigma}$ (VIII 1). One can verify this result by direct calculation. Its significance is discussed by Corben and Stehle (3) in relation to the representation of rotations by quaternions.

IX. THE MAXWELL-LORENTZ AND DIRAC EQUATIONS

In Sec. I it was seen that the concept of spinors arises in a study of the transformation properties of the wave functions in Dirac's equation for the electron. Now that a complete spinor algebra is at hand, it is of interest to see how the Dirac equation can be written entirely in spinor notation. At the same time, it will also be useful to have the fundamental equations of the theory of electromagnetism written out in terms of spinors.[14] In this section we shall assume that we have to deal only with Lorentz frames and transformations, so that the special spinor calculus presented in Sec. VIII will be applicable.

Because of the continuity equation

$$\partial_k j^k=0, \qquad \text{(IX 1)}$$

the Maxwell-Lorentz equations for the antisymmetric field tensor F^{kl},

$$\partial_l F^{kl}=(4\pi/c)j^k, \qquad \text{(IX 2)}$$

$$\partial_m F_{kl}+\partial_k F_{lm}+\partial_l F_{mk}=0, \qquad \text{(IX 3)}$$

give only $3+3=6$ independent relations. Equation (IX 3) is satisfied identically if the electromagnetic field tensor is written in terms of the four-potential ϕ_k (I 3):

$$F_{kl}=\partial_k\phi_l-\partial_l\phi_k. \qquad \text{(IX 4)}$$

The remaining three Eqs. (IX 2) do not suffice to determine the four components of ϕ_k; this ambiguity signifies that we can subject ϕ_k to a gauge transformation without altering F_{kl}. If we fix the gauge by means of the Maxwell-Lorentz condition

$$\partial_k\phi^k=0, \qquad \text{(IX 5)}$$

Eqs. (IX 2) become

$$g^{kl}\partial_k\partial_l\phi^m=-(4\pi/c)j^m. \qquad \text{(IX 6)}$$

It is immediately clear that (IX 1) and (IX 5) can be written in terms of Hermitean spinors of second rank by means of (VII 11). We define

$$\begin{aligned}\partial_{\dot{\mu}\nu}&=\sigma^k{}_{\dot{\mu}\nu}\partial_k,\\ j^{\dot{\mu}\nu}&=\sigma^{k\dot{\mu}\nu}j_k,\\ \phi^{\dot{\mu}\nu}&=\sigma^{k\dot{\mu}\nu}\phi_k,\end{aligned} \qquad \text{(IX 7)}$$

in accordance with (VII 2). Then (IX 1) becomes

$$\partial_{\dot{\mu}\nu}j^{\dot{\mu}\nu}=0, \qquad \text{(IX 8)}$$

because of (VII 11). Similarly, (IX 5) becomes

$$\partial_{\dot{\mu}\nu}\phi^{\dot{\mu}\nu}=0. \qquad \text{(IX 9)}$$

Equation (IX 6) can also be written over into spinor form without difficulty. Because of (VII 11), the d'Alembertian becomes

$$g^{kl}\partial_k\partial_l=\partial_{\dot{\mu}\nu}\partial^{\dot{\mu}\nu}, \qquad \text{(IX 10)}$$

and since the $\sigma^{k\dot{\rho}\sigma}$ are constants so long as we deal only with special relativity theory, it follows that (IX 6) can be written

$$\partial_{\dot{\mu}\nu}\partial^{\dot{\mu}\nu}\phi_{\dot{\rho}\sigma}=-(4\pi/c)j_{\dot{\rho}\sigma}. \qquad \text{(IX 11)}$$

[13] To avoid ambiguity, let us state here that we have chosen the Euler angles as given in Goldstein (6), p. 107. The same book contains an instructive discussion of the Cayley-Klein parameters.

[14] The spinor form of the Maxwell equations was presented by Laporte and Uhlenbeck (15). In this same paper the Dirac equations were derived from a spinor variational principle, and some new relations following from the Dirac equations were given.

In part of our derivation of the spinor form of Maxwell's equations, we follow unpublished lectures of Dirac.

CC-0. In Public Domain. Gurukul Kangri Collection, Haridwar

Digitized by Arya Samaj Foundation Chennai and eGangotri

The field tensor F^{kl} can, of course, be expressed in terms of a fourth-rank spinor by means of (VII 8):

$$F^{kl}=\sigma^{k\dot\mu\nu}\sigma^{l\dot\rho\sigma}F_{\dot\mu\nu\dot\rho\sigma}. \qquad \text{(IX 12)}$$

However, F^{kl} is antisymmetric, and this fact permits us to express it in terms of a spinor of only second rank, which is not Hermitean but symmetric. The proof of this theorem will be given for the field tensor F^{kl}, but it will naturally remain valid if F^{kl} is replaced by an arbitrary antisymmetric contravariant world tensor of second rank.

From $F^{kl}=-F^{lk}$ and (IX 12),

$$F_{\dot\rho\sigma\dot\mu\nu}=-F_{\dot\mu\nu\dot\rho\sigma}. \qquad \text{(IX 13)}$$

Because the $\sigma^{k\dot\mu\nu}$ are Hermitean, it also follows that

$$F_{\dot\mu\nu\dot\rho\sigma}=F_{\nu\dot\mu\sigma\dot\rho}. \qquad \text{(IX 14)}$$

The reduction to second rank is to be carried out by using

$$\eta_{\lambda\mu}-\eta_{\mu\lambda}=\eta_\alpha{}^\alpha\gamma_{\lambda\mu}. \qquad \text{(V 6)}$$

Using (IX 13), we write

$$F_{\dot\mu\nu\dot\rho\sigma}=\tfrac{1}{2}(F_{\dot\mu\nu\dot\rho\sigma}-F_{\dot\rho\sigma\dot\mu\nu})$$
$$=\tfrac{1}{2}(F_{\dot\mu\nu\dot\rho\sigma}-F_{\dot\mu\sigma\dot\rho\nu})+\tfrac{1}{2}(F_{\sigma\dot\mu\nu\dot\rho}-F_{\sigma\dot\rho\nu\dot\mu}),$$

by adding and subtracting a term and using (IX 14). Finally, applying (V 6) to this result,

$$F_{\dot\mu\nu\dot\rho\sigma}=\tfrac{1}{2}(F_{\dot\mu\dot\rho}\gamma_{\nu\sigma}+F_{\sigma\nu}\gamma_{\dot\mu\dot\rho}), \qquad \text{(IX 15)}$$

where

$$F_{\sigma\nu}\equiv F_{\sigma\dot\alpha\nu}{}^{\dot\alpha}. \qquad \text{(IX 16)}$$

A proof that $F_{\sigma\nu}$ is symmetric goes

$$F_{\sigma\dot\alpha\nu}{}^{\dot\alpha}=-F_{\sigma\dot\alpha\nu\dot\beta}\gamma^{\dot\beta\dot\alpha}=+F_{\nu\dot\beta\sigma\dot\alpha}\gamma^{\dot\beta\dot\alpha}=-F_{\nu\dot\beta\sigma\dot\alpha}\gamma^{\dot\alpha\dot\beta}=+F_{\nu\dot\beta\sigma}{}^{\dot\beta}$$

by using (IV 8), (IX 13), (IV 7), and (IV 8) (in that order). Note that

$$2F_{kl}F^{kl}=F_{\sigma\nu}F^{\sigma\nu}+F_{\dot\rho\dot\mu}F^{\dot\rho\dot\mu}. \qquad \text{(IX 16a)}$$

When ϕ_k and ∂_k are expressed in terms of the spinors $\phi_{\dot\mu\nu}$ and $\partial_{\dot\mu\nu}$ introduced in (IX 7), Eq. (IX 4) becomes

$$F^{kl}=\sigma^{k\dot\mu\nu}\sigma^{l\dot\rho\sigma}(\partial_{\dot\mu\nu}\phi_{\dot\rho\sigma}-\partial_{\dot\rho\sigma}\phi_{\dot\mu\nu}).$$

By comparison with (IX 12),

$$F_{\dot\mu\nu\dot\rho\sigma}=\partial_{\dot\mu\nu}\phi_{\dot\rho\sigma}-\partial_{\dot\rho\sigma}\phi_{\dot\mu\nu}.$$

Then, from (IX 16), with use of (IX 14),

$$F_{\nu\sigma}=\partial_{\nu\dot\alpha}\phi_\sigma{}^{\dot\alpha}-\partial_\sigma{}^{\dot\alpha}\phi_{\nu\dot\alpha}=\partial_{\nu\dot\alpha}\phi_\sigma{}^{\dot\alpha}+\partial_{\sigma\dot\alpha}\phi_\nu{}^{\dot\alpha}. \qquad \text{(IX 17a)}$$

This result can be simplified still further by remarking that

$$\partial_{\nu\dot\alpha}\phi_\sigma{}^{\dot\alpha}-\partial_{\sigma\dot\alpha}\phi_\nu{}^{\dot\alpha}=\partial_{\beta\dot\alpha}\phi^{\beta\dot\alpha}\gamma_{\nu\sigma}=0$$

because of (V 6) and the Maxwell-Lorentz condition (IX 9). Thus

$$F_{\sigma\nu}=2\partial_{\sigma\dot\alpha}\phi_\nu{}^{\dot\alpha}. \qquad \text{(IX 17)}$$

Now we can write the field Eqs. (IX 2) over into spinor form. Consider the expression

$$\partial^\sigma{}_{\dot\mu}F_{\sigma\nu}=2\partial^\sigma{}_{\dot\mu}\partial_{\sigma\dot\alpha}\phi_\nu{}^{\dot\alpha},$$

where (IX 17) has been used. The differential operators on the right can be combined to form the d'Alembertian (IX 10) as follows: Since

$$\partial^\sigma{}_{\dot\mu}\partial_{\sigma\dot\alpha}\phi_\nu{}^{\dot\alpha}=-\partial_{\sigma\dot\mu}\partial^\sigma{}_{\dot\alpha}\phi_\nu{}^{\dot\alpha},$$

we have

$$2\partial^\sigma{}_{\dot\mu}\partial_{\sigma\dot\alpha}\phi_\nu{}^{\dot\alpha}=(\partial_{\sigma\dot\alpha}\partial^\sigma{}_{\dot\mu}-\partial_{\sigma\dot\mu}\partial^\sigma{}_{\dot\alpha})\phi_\nu{}^{\dot\alpha}=\partial_{\sigma\dot\rho}\partial^{\sigma\dot\rho}\phi_{\nu\dot\mu}=\partial_{\sigma\dot\rho}\partial^{\sigma\dot\rho}\phi_{\dot\mu\nu}$$

by (V 6). Thus

$$\partial^\sigma{}_{\dot\mu}F_{\sigma\nu}=-(4\pi/c)j_{\dot\mu\nu}, \qquad \text{(IX 18)}$$

by comparison with (IX 11).

Now let us write the Dirac equation (I 6) entirely over into spinor form. By raising and lowering indexes in (I 11), which may conveniently be taken as a starting point, we obtain

$$\begin{aligned}\sqrt{2}\sigma^k{}_{\dot\mu\rho}(\partial_k+i\epsilon\phi_k)\chi^\rho&=\mu\xi_{\dot\mu}\\ \sqrt{2}\sigma^{k\nu\dot\sigma}(\partial_k+i\epsilon\phi_k)\xi_{\dot\sigma}&=-\mu\chi^\nu.\end{aligned} \qquad \text{(IX 19)}$$

When (IX 7) is taken into account, these equations become

$$\begin{aligned}\sqrt{2}(\partial_{\dot\mu\rho}+i\epsilon\phi_{\dot\mu\rho})\chi^\rho&=\mu\xi_{\dot\mu},\\ \sqrt{2}(\partial^{\nu\dot\sigma}+i\epsilon\phi^{\nu\dot\sigma})\xi_{\dot\sigma}&=-\mu\chi^\nu.\end{aligned} \qquad \text{(IX 20)}$$

which is a spinor form of Dirac's equation.[15]

The current is

$$j^k=q\sigma^{k\dot\mu\nu}(\chi_{\dot\mu}\chi_\nu+\xi_{\dot\mu}\xi_\nu). \qquad \text{(IX 21)}$$

This quantity transforms as a world vector. Its components are real, since the combinations $\chi_{\dot\mu}\chi_\nu$ and $\xi_{\dot\mu}\xi_\nu$ are Hermitean. Let

$$j_{\dot\mu\nu}=q(\chi_{\dot\mu}\chi_\nu+\xi_{\dot\mu}\xi_\nu). \qquad \text{(IX 22)}$$

Then, by (VII 11),

$$\partial_k j^k=\partial^{\dot\mu\nu}j_{\dot\mu\nu}=q(\partial_{\dot\mu\nu}\chi^{\dot\mu}\chi^\nu+\partial^{\dot\mu\nu}\xi_{\dot\mu}\xi_\nu)$$
$$=q\{(\partial_{\dot\mu\nu}\chi^{\dot\mu})\chi^\nu+\chi^{\dot\mu}(\partial_{\dot\mu\nu}\chi^\nu)$$
$$+(\partial^{\dot\mu\nu}\xi_{\dot\mu})\xi_\nu+\xi_{\dot\mu}(\partial^{\dot\mu\nu}\xi_\nu)\}.$$

Taking Dirac's set (IX 20) into account, one sees that this quantity is identically zero:

$$\partial_k j^k=\partial^{\dot\mu\nu}j_{\dot\mu\nu}=0. \qquad \text{(IX 23)}$$

The Schwarzschild-Darwin variational principle takes the form derived by Laporte and Uhlenbeck, with a Lagrangian density

$$\begin{aligned}L=&i\{\chi^\lambda\partial_{\lambda\dot\mu}\chi^{\dot\mu}-\xi^\lambda\partial_{\lambda\dot\mu}\xi^{\dot\mu}-\chi_{\dot\mu}\partial^{\dot\mu\lambda}\chi_\lambda+\xi_{\dot\mu}\partial^{\dot\mu\lambda}\xi_\lambda\}\\ &+\sqrt{2}\mu i(-\chi^\lambda\xi_\lambda+\chi^{\dot\lambda}\xi_{\dot\lambda})+2\epsilon\phi^{\dot\mu\lambda}(\chi_{\dot\mu}\chi_\lambda+\xi_{\dot\mu}\xi_\lambda)\\ &-(1/16\pi\hbar)[(\partial^{\nu}{}_{\dot\lambda}\phi^{\nu\dot\lambda}+\partial^{\nu}{}_{\dot\lambda}\phi^{\mu\dot\lambda})(\partial_\mu{}^{\dot\sigma}\phi_{\nu\dot\sigma}+\partial_\nu{}^{\dot\sigma}\phi_{\mu\dot\sigma})\\ &+(\partial^{\dot\mu}{}_\lambda\phi^{\dot\nu\lambda}+\partial^{\dot\nu}{}_\lambda\phi^{\dot\mu\lambda})(\partial_{\dot\mu}{}^\sigma\phi_{\dot\nu\sigma}+\partial_{\dot\nu}{}^\sigma\phi_{\dot\mu\sigma})].\end{aligned} \qquad \text{(IX 24)}$$

When forming the Euler-Lagrange equations, it is necessary to recognize that this Lagrangian can be considered as a function

$$L(\phi^{\dot\mu\lambda},\Sigma\partial^{\dot\mu}{}_\lambda\phi^{\dot\nu\lambda},\ldots;\chi^\lambda,\textstyle\sum\partial^{\dot\mu\lambda}\chi_\lambda;\ldots) \qquad \text{(IX 25)}$$

[15] Our choice of the σ's coincides with that of Infeld and van der Waerden; our χ^ρ and $\xi_{\dot\sigma}$ are their ψ and $-i\chi$.

CC-0. In Public Domain. Gurukul Kangri Collection, Haridwar

Digitized by Arya Samaj Foundation Chennai and eGangotri

of the indicated spinors of first and second rank, as a function

$$\mathfrak{L}(\phi^{\dot\mu\lambda}, \partial^{\dot\mu}{}_{\rho}\phi^{\dot\rho\lambda}; \chi^{\lambda}, \partial^{\dot\mu\rho}\chi_{\lambda}; \ldots) \qquad \text{(IX 26)}$$

of the much more numerous spinors of higher rank, or as a function

$$\mathrm{L}(\phi^{\dot\mu\lambda}, \partial_k\phi^{\dot\mu\lambda}; \chi^{\lambda}, \partial_k\chi^{\lambda}; \ldots).$$

By a simple transformation using (VIII 3), (IX 7), the Euler-Lagrange equations can be put into the spinor form

$$0=\partial_k\frac{\partial \mathrm{L}}{\partial(\partial_k\chi^{\dot\lambda})}-\frac{\partial \mathrm{L}}{\partial\chi^{\dot\lambda}}=\partial_{\rho\dot\sigma}\frac{\partial\mathfrak{L}}{\partial(\partial_{\rho\dot\sigma}\chi^{\dot\lambda})}-\frac{\partial\mathfrak{L}}{\partial\chi^{\dot\lambda}}.$$

Because of the particular form of L, these equations become

$$\begin{aligned}0&=-\frac{\partial\mathfrak{L}}{\partial\chi^{\dot\lambda}}+\partial_{\rho\dot\sigma}\delta^{\dot\sigma}{}_{\dot\lambda}\frac{\partial\mathfrak{L}}{\partial(\partial_{\rho}i\chi^{\dot i})}\\&=-\frac{\partial\mathfrak{L}}{\partial\chi^{\dot\lambda}}+\partial_{\rho\dot\lambda}\frac{\partial\mathfrak{L}}{\partial(\partial_{\rho\dot\imath}\chi^{\dot\imath})}\\&=-\frac{\partial L}{\partial\chi^{\dot\lambda}}+\partial_{\rho\dot\lambda}\frac{\partial L}{\partial(\Sigma\partial_{\rho\dot\alpha}\chi^{\dot\alpha})}.\end{aligned} \qquad \text{(IX 27)}$$

In this last equation, the summation over $\dot\alpha$ is to be taken before the differentiation is performed, contrary to the usual rule that a doubly occurring index indicates summation of the entire expression.

By simple algebraic transformations, observing the somewhat strange-looking identity

$$\partial_k\frac{\partial \mathrm{L}}{\partial(\partial_k\eta)}=\partial^{\dot\sigma\lambda}\frac{\partial\mathfrak{L}}{\partial(\partial^{\dot\sigma\lambda}\eta)}\equiv+\partial_{\dot\sigma}{}^{\lambda}\frac{\partial\mathfrak{L}}{\partial(\partial_{\dot\sigma}{}^{\lambda}\eta)}, \qquad \text{(IX 28)}$$

we obtain

$$\begin{aligned}&-\frac{\partial L}{\partial\chi^{\dot\lambda}}+\partial_{\rho\dot\lambda}\frac{\partial L}{\partial(\Sigma\partial_{\rho\dot\alpha}\chi^{\dot\alpha})}=0,\\&-\frac{\partial L}{\partial\xi_{\lambda}}+\partial^{\dot\sigma\lambda}\frac{\partial L}{\partial(\Sigma\partial^{\dot\sigma\alpha}\xi_{\alpha})}=0,\\&-\frac{\partial L}{\partial\phi_{\nu\dot\sigma}}+\partial_{\mu}{}^{\dot\sigma}\frac{\partial L}{\partial(\Sigma\partial_{\mu}{}^{\dot\alpha}\phi_{\nu\dot\alpha})}\\&\qquad+\partial_{\dot\mu}{}^{\nu}\frac{\partial L}{\partial(\Sigma\partial_{\dot\mu}{}^{\alpha}\phi_{\dot\sigma\alpha})}=0.\end{aligned} \qquad \text{(IX 29)}$$

These equations are the Dirac equations (IX 20) and the Maxwell-Lorentz equations (IX 18) with current (IX 22).

The conservation laws for the current and the energy-momentum tensor can be derived directly from the Lagrangian. We refer the reader to the original literature and former review articles for discussions of these topics.[16]

We wish to close this section with a brief discussion of the relation between the form (I 6) of the Dirac equation (in which the indexes 0, 1, 2, 3 appear in a symmetrical way) and the more commonly quoted form. When

$$i\Gamma^k(-i\partial_k+\epsilon\phi_k)\psi-\mu\psi=0 \qquad \text{(I 6)}$$

is multiplied by $-i\Gamma^0$, it becomes

$$\begin{aligned}\{&-\Gamma^0\Gamma^0(i\partial_0-\epsilon\phi_0)+\Gamma^0\Gamma^1(-i\partial_1+\epsilon\phi_1)\\&+\Gamma^0\Gamma^2(-i\partial_2+\epsilon\phi_2)+\Gamma^0\Gamma^3(-i\partial_3+\epsilon\phi_3)+i\mu\Gamma^0\}\psi=0.\end{aligned}$$

If each Γ or the whole operator $\{\ \}$ is subjected to a similarity transformation $\Lambda^{-1}\Gamma\Lambda$ with

$$\Lambda=\begin{bmatrix}1&0&1&0\\0&1&0&1\\0&i&0&-i\\-i&0&i&0\end{bmatrix}, \qquad \text{(IX 30)}$$

this equation is brought into the form[17]

$$\{(i\partial_0-\epsilon\phi_0)+\rho_1\sum_{k=1}^{3}\sigma_k(-i\partial_k+\epsilon\phi_k)+\rho_3\mu\}\Psi=0. \qquad \text{(IX 31)}$$

In this nonrelativistic notation, the Dirac equation is more convenient for the description of spin; and the four components of Ψ fall into a pair of big Ψ functions and a pair of small ones.

X. SPINOR ANALYSIS

In tensor analysis, one considers covariant derivatives of tensors in affinely connected manifolds. We shall pursue a similar procedure in spinor analysis, following in detail the excellent exposition of Infeld and van der Waerden (14).

Covariant differentiation is introduced in world space by means of an affine connection $\Gamma^k{}_{rs}$:

$$A_{r;s}=\partial_s A_r-A_k\Gamma^k{}_{rs},\quad A^r{}_{;s}=\partial_s A^r+A^k\Gamma^r{}_{ks}. \qquad \text{(X 1)}$$

In a similar way, we now define covariant derivatives of spinors

$$\psi_{\alpha;s}=\partial_s\psi_\alpha-\Gamma^{\rho}{}_{\alpha s}\psi_\rho,\quad \psi^{\alpha}{}_{;s}=\partial_s\psi^\alpha+\Gamma^{\alpha}{}_{\rho s}\psi^\rho, \qquad \text{(X 2)}$$

in which we consider the spinors ψ_α, ψ^α as functions of the space-time point specified by the world coordinates x^s. Note that the "product rule" holds for covariant differentiation:

$$(\psi_\alpha\chi^\alpha)_{;s}=\partial_s(\psi_\alpha\chi^\alpha)=\psi_{\alpha;s}\chi^\alpha+\psi_\alpha\chi^\alpha{}_{;s}. \qquad \text{(X 3)}$$

The requirement that $\psi_{\alpha;s}$ and $\psi^{\alpha}{}_{;s}$ transform as spin vectors in respect to spin transformations leads to the

[16] See Pauli (62), Møller and Rosenfeld (61), Rosenfeld (65), and Belinfante (51).

[17] See Dirac (4) and Hill and Landshoff (43). Here ρ_1, ρ_3, σ_k denote the four-row matrices used by Dirac. These σ_k are, of course, not the σ's of the present paper.

CC-0. In Public Domain. Gurukul Kangri Collection, Haridwar

Digitized by Arya Samaj Foundation Chennai and eGangotri

following rule for transforming $\Gamma^{\alpha}{}_{\rho s}$:

$$\Lambda^{\rho}{}_{\sigma}\Gamma'^{\alpha}{}_{\rho s}=\Lambda^{\alpha}{}_{\rho}\Gamma^{\rho}{}_{\sigma s}-\partial_s\Lambda^{\alpha}{}_{\sigma}. \tag{X 4}$$

In order to have a consistent formalism, we desire that the complex conjugates of $\psi_{\alpha;s}$ and $\psi^{\alpha}{}_{;s}$ be, respectively, $\psi_{\dot\alpha;s}$ and $\psi^{\dot\alpha}{}_{;s}$. Then the covariant derivatives of the complex conjugate spinors $\psi_{\dot\alpha}$, $\psi^{\dot\alpha}$ are given by placing a dot above every Greek index in (X 2), where $\Gamma^{\dot\rho}{}_{\dot\alpha s}=(\Gamma^{\rho}{}_{\alpha s})^*$. Moreover, an arbitrary spin tensor is differentiated covariantly like an outer product of spin vectors, for example

$$\eta^{\dot\lambda}{}_{\mu;s}=\partial_s\eta^{\dot\lambda}{}_{\mu}+\Gamma^{\dot\lambda}{}_{\dot\rho s}\eta^{\dot\rho}{}_{\mu}-\Gamma^{\sigma}{}_{\mu s}\eta^{\dot\lambda}{}_{\sigma}. \tag{X 5}$$

In Sec. VII there was established a correspondence between arbitrary world vectors A_k and Hermitean spinors $A_{\dot\lambda\mu}$ by means of the mixed quantities $\sigma^{k}{}_{\dot\lambda\mu}$:

$$A^k=\sigma^{k\dot\lambda\mu}A_{\dot\lambda\mu}.$$

The quantities $A^{k}{}_{;s}$ and $A_{\dot\lambda\mu;s}$ transform as covariant world tensors on the index s. It is natural to require that the connection between these quantities should be as between any other quantities $A^{k}{}_{s}$ and $A_{\dot\lambda\mu s}$, *viz.*,

$$A^{k}{}_{;s}=\sigma^{k\dot\lambda\mu}A_{\dot\lambda\mu;s}. \tag{X 6}$$

Covariant differentiation of any tensor or spinor equation obeys the "product rule," as in (X 3). Thus (X 6) has as a consequence

$$\begin{aligned}\sigma^{k\dot\lambda\mu}{}_{;s}&=0\\ &=\partial_s\sigma^{k\dot\lambda\mu}+\Gamma^{k}{}_{rs}\sigma^{r\dot\lambda\mu}+\Gamma^{\dot\lambda}{}_{\dot\rho s}\sigma^{k\dot\rho\mu}+\Gamma^{\mu}{}_{\sigma s}\sigma^{k\dot\lambda\sigma}.\end{aligned} \tag{X 7}$$

We assume that the $\Gamma^{k}{}_{rs}$ are the Christoffel symbols $\left\{\begin{matrix}rs\\k\end{matrix}\right\}$, i.e., that the notion of parallel transfer is introduced[18] in connection with the metric g_{kl}. The metric establishes geodesics defined by parallel transfer of dx^k/ds. At the same time, $g_{kl}(dx^k/ds)(dx^l/ds)=1$ is invariant, so that g_{kl} also goes into itself when subjected to parallel transfer along a geodesic. Hence

$$g^{kl}{}_{;s}=0. \tag{X 8}$$

Christoffel's choice

$$\Gamma^{k}{}_{rs}=\Gamma^{k}{}_{sr}, \tag{X 9}$$

together with (X 8), determines the $\Gamma^{k}{}_{rs}$ uniquely in terms of the metric. Formula (X 9) represents 4.6 real equations.

We now proceed to study the spinor affinities $\Gamma^{\alpha}{}_{\rho s}$, considering the $\gamma_{\mu\nu}$ and the $\sigma^{k\dot\lambda\mu}$ to be given as functions of space and time. Because of

$$g^{kl}=\sigma^{k\dot\lambda\mu}\sigma^{l}{}_{\dot\lambda\mu}=\sigma^{k\dot\lambda\mu}\sigma^{l\dot\rho\sigma}\gamma_{\dot\rho\dot\lambda}\gamma_{\sigma\mu} \tag{VII 5}$$

and (X 7), (X 8) we take

$$0=(\gamma_{\dot\rho\dot\lambda}\gamma_{\sigma\mu})_{;s}=\gamma_{\dot\rho\dot\lambda;s}\gamma_{\sigma\mu}+\gamma_{\dot\rho\dot\lambda}\gamma_{\sigma\mu;s}. \tag{X 10}$$

This equation has only one distinct nonvanishing component,

$$\begin{aligned}0=\partial_s(\gamma_{1\dot2}\gamma_{12})&-\Gamma^{1}{}_{1s}\gamma_{1\dot2}\gamma_{12}-\Gamma^{\dot2}{}_{2s}\gamma_{1\dot2}\gamma_{12}\\ &-\Gamma^{1}{}_{1s}\gamma_{1\dot2}\gamma_{12}-\Gamma^{2}{}_{2s}\gamma_{1\dot2}\gamma_{12}.\end{aligned} \tag{X 11}$$

With the abbreviation (IV 9), $\gamma_{1\dot2}\gamma_{12}=\gamma$, this becomes

$$\begin{aligned}\partial_s\gamma-(\Gamma^{\alpha}{}_{\alpha s}+\Gamma^{\dot\alpha}{}_{\dot\alpha s})\gamma&=0,\\ \Gamma^{\alpha}{}_{\alpha s}+\Gamma^{\dot\alpha}{}_{\dot\alpha s}&=\partial_s\ln\gamma.\end{aligned} \tag{X 12}$$

Equations (X 10) and (X 11) can be interpreted to signify that covariant differentiation preserves volumes in spin space. (Compare with the Infeld-van der Waerden paper cited above.)

The Eqs. (X 12) are 4 real equations for the $\Gamma^{\alpha}{}_{\rho s}$. The symmetry conditions (X 9), when we insert $\Gamma^{k}{}_{rs}$, $\Gamma^{k}{}_{sr}$ from (X 7), are 24 more real conditions on the $\Gamma^{\alpha}{}_{\beta s}$. These 28 conditions are not sufficient to determine the 8.4 real and imaginary parts of the 2.2.4 complex quantities $\Gamma^{\alpha}{}_{\beta s}$. Four real parameters remain arbitrary. As a matter of fact, if Eqs. (X 7) and (X 12) are satisfied, they remain satisfied when one leaves the $\Gamma^{k}{}_{rs}$ unchanged but replaces the $\Gamma^{\mu}{}_{\rho s}$ and $\Gamma^{\dot\mu}{}_{\dot\rho s}$ by

$$\Gamma^{\mu}{}_{\rho s}+i\epsilon\Phi_s\delta^{\mu}{}_{\rho} \quad\text{and}\quad \Gamma^{\dot\mu}{}_{\dot\rho s}-i\epsilon\Phi_s\delta^{\dot\mu}{}_{\dot\rho}.$$

There thus appears here an arbitrary real quantity ϕ_s which is defined by

$$\Gamma^{\alpha}{}_{\alpha s}-\Gamma^{\dot\alpha}{}_{\dot\alpha s}=4i\epsilon\phi_s. \tag{X 13}$$

We investigate the transformation property of this quantity. In respect to world transformations, ϕ_s behaves like a covariant world vector. With transformations in spin space, one can set $|\Lambda^{\rho}{}_{\sigma}|=\Delta e^{i\varphi}$ (Δ positive real) and obtain

$$\phi'_s=\phi_s-\partial_s\varphi/2\epsilon. \tag{X 14}$$

This follows from the transformation Eq. (X 4):

$$\Gamma'^{\alpha}{}_{\alpha s}=\Gamma^{\alpha}{}_{\alpha s}-\partial_s\ln|\Lambda^{\rho}{}_{\sigma}|$$

and its complex conjugate. ϕ_s thus transforms with a transformation of the form

$$\Lambda^{\rho}{}_{\sigma}=\delta^{\rho}{}_{\sigma}e^{i\varphi/2} \tag{X 15}$$

exactly as the four-potential is supposed to do according to Weyl's principle of gauge invariance. We therefore identify ϕ_s with the electromagnetic potential vector.

From (IV 10), namely $\gamma_{12}=\gamma^{\frac12}e^{i\theta}$, it follows that $\partial_s\theta$ transforms just as $2\epsilon\phi_s$ does,

$$\partial_s\theta'=\partial_s\theta-\partial_s\varphi.$$

[Apply (IV 3) with the general expression $|\Lambda^{-1}{}^{\rho}{}_{\sigma}|=\Delta^{-1}e^{-i\varphi}$ to $\theta=-\frac12 i(\ln\gamma_{12}-\ln\gamma_{1\dot2})$.] Therefore $2\epsilon\phi_s-\partial_s\theta$ is a vector which is invariant with respect to gauge transformations.

From (X 12), (X 13) one can calculate that

$$\begin{aligned}\Gamma^{\alpha}{}_{\alpha s}&=2i\epsilon\phi_s+\partial_s\ln\gamma^{\frac12},\\ \Gamma^{\dot\alpha}{}_{\dot\alpha s}&=-2i\epsilon\phi_s+\partial_s\ln\gamma^{\frac12}.\end{aligned} \tag{X 16}$$

[18] See Schrödinger (9), Chap. IX.

CC-0. In Public Domain. Gurukul Kangri Collection, Haridwar

Digitized by Arya Samaj Foundation Chennai and eGangotri

Hence, also taking (X 5) and (IV 10) into account, the differential equations for the fundamental spinors are

$$\gamma^{\lambda\mu}{}_{;s}=i\gamma^{\lambda\mu}(2\epsilon\phi_s-\partial_s\theta),$$
$$\gamma_{\lambda\mu;s}=-i\gamma_{\lambda\mu}(2\epsilon\phi_s-\partial_s\theta). \quad \text{(X 17)}$$

The Riemann-Christoffel tensor is

$$R^r{}_{kps}=-\partial_s\Gamma^r{}_{kp}+\partial_p\Gamma^r{}_{ks}-\Gamma^h{}_{kp}\Gamma^r{}_{hs}+\Gamma^h{}_{ks}\Gamma^r{}_{hp}. \quad \text{(X 18)}$$

Similarly, we can form, in spin space, the mixed tensor

$$P^{\mu}{}_{\lambda ps}=-\partial_s\Gamma^{\mu}{}_{\lambda p}+\partial_p\Gamma^{\mu}{}_{\lambda s}-\Gamma^{\rho}{}_{\lambda p}\Gamma^{\mu}{}_{\rho s}+\Gamma^{\rho}{}_{\lambda s}\Gamma^{\mu}{}_{\rho p}, \quad \text{(X 19)}$$

and the corresponding one with dotted Greek indices. The contraction of the former gives, by (X 16), the electromagnetic field intensity

$$-P^{\dot\rho}{}_{\dot\rho ps}=P^{\rho}{}_{\rho ps}=2i\epsilon(\partial_p\phi_s-\partial_s\phi_p)=2i\epsilon F_{ps}. \quad \text{(X 20)}$$

By definition of the curvature tensors, we have

$$\chi^{\rho}{}_{;ps}-\chi^{\rho}{}_{;sp}=\chi^{\sigma}P^{\rho}{}_{\sigma sp} \quad \text{(X 21)}$$

and hence also

$$\sigma^{k\dot\lambda\mu}{}_{;ps}-\sigma^{k\dot\lambda\mu}{}_{;sp}=\sigma^{k\dot\rho\mu}P^{\dot\lambda}{}_{\dot\rho sp}+\sigma^{k\dot\lambda\rho}P^{\mu}{}_{\rho sp}+\sigma^{r\dot\lambda\mu}R^k{}_{rsp}. \quad \text{(X 22)}$$

Because of (X 7), the left-hand side vanishes. Hence we arrive at a relation between R and P. This relation can be solved for R or for P, e.g.,

$$P^{\lambda}{}_{\rho sp}=\tfrac{1}{2}R_{krsp}\sigma^{k\lambda\dot r}\sigma^{r}{}_{\dot r\rho}+i\epsilon F_{sp}\delta^{\lambda}{}_{\rho}. \quad \text{(X 23)}$$

If the world space under consideration is flat, the theory can be reduced to a gauge-covariant modification of the 1929 spinor calculus presented in Sec. VIII. In this case, the conditions (VII 5), (X 7), (X 9), (X 12), and (X 13) can be satisfied by taking (I 2) and (VIII 1) for g_{kl} and $\sigma^{k\dot\rho\sigma}$, respectively, and taking

$$\gamma_{\mu\nu}=\begin{pmatrix}0 & 1\\ -1 & 0\end{pmatrix}e^{i\theta}, \quad \text{(X 24)}$$

$$\Gamma^k{}_{rs}=\left\{\begin{matrix} rs \\ k \end{matrix}\right\}=0, \quad \text{(X 25)}$$

$$\Gamma^{\beta}{}_{\alpha s}=i\epsilon\phi_s\delta^{\beta}{}_{\alpha}. \quad \text{(X 26)}$$

These forms are all maintained when one carries out in world space an arbitrary positive Lorentz transformation and at the same time applies in spin space the unimodular spin transformation corresponding thereto by (VIII 4). They are also maintained under gauge transformations (X 15).

With the special metrics (I 2) and (X 24) given, the $\sigma^{k\dot\rho\sigma}$ appearing in (VIII 1) are not the only ones which satisfy (VII 5). One still has the freedom to apply an arbitrary (positive or negative) Lorentz transformation on the index k, or to apply an arbitrary unimodular spin transformation on the indices $\dot\rho$, σ. That is, however, the *only* freedom which one has. For the condition (VII 5) means, according to its derivation, that with the correspondence $A_{\dot\rho\sigma}\rightarrow A_k$ the quadratic form $\gamma^{\dot\lambda\dot\rho}\gamma^{\mu\sigma}A_{\dot\lambda\mu}A_{\dot\rho\sigma}$ is brought over into $g^{kl}A_kA_l$, and such a linear correspondence is completely determined up to a linear transformation which leaves the latter quadratic form invariant, i.e., up to a Lorentz transformation.

In Infeld and van der Waerden's spinor analysis, gauge transformations are represented as spin transformations of form (X 15). As a consequence, any generally covariant equation between tensors, spinors, and their covariant derivatives is *ipso facto* gauge-covariant. We have adopted a specialization to the case of flat space-time which has the advantage of retaining this property. It may be instructive to contrast this specialization with other possible specializations and modifications of Infeld and van der Waerden's spinor analysis.

One such modification would be achieved by replacing (X 10) by the stronger assumption $\gamma_{\mu\nu;s}=0$. This procedure would have the advantage that it would permit the raising and lowering of Greek indexes in covariant derivatives by the natural-looking rule $\xi_{\nu;s}=\xi^{\mu}{}_{;s}\gamma_{\mu\nu}$, which is *not* valid in Infeld and van der Waerden's formalism. This stronger assumption would, however, eliminate from the theory the four arbitrary real quantities ϕ_s, which were interpreted as components of the electromagnetic potential. In Eqs. (X 13), (X 16), and (X 17), $2\epsilon\phi_s$ would be replaced by $\partial_s\theta$. Thus the possibility of using spinor analysis as a gauge-covariant formalism would be lost. In the case of flat space-time, the selection of (I 2), (VI 3), (VIII 1), and (X 25) for g_{kl}, $\gamma_{\mu\nu}$, $\sigma^{k\dot\rho\sigma}$, and $\Gamma^k{}_{rs}$ would reduce this modification exactly to the 1929 spinor calculus of Sec. VIII, since the choice $\gamma=1$, $\theta=0$ (VI 3) would entail $\Gamma^{\beta}{}_{\alpha s}=0$.

Reverting to Infeld and van der Waerden's form of spinor analysis (that is, rejecting the assumption $\gamma_{\mu\nu;s}=0$), we note that in specializing to the case of flat space-time we could have achieved a closer approach to the 1929 theory by selecting (VI 3) in place of (X 24). Had we made this choice, the resulting specialization would differ from the 1929 spinor calculus only by having (X 26) in place of $\Gamma^{\beta}{}_{\alpha s}=0$. This is another enticing simplification which, if adopted, would entail the loss of gauge covariance. The choice (VI 3) could not be maintained under gauge transformations, since these are not unimodular [see (IV 3)].

Let us now write the equations of the Dirac theory over into the gauge-covariant formalism provided by the specialization [(I 2), (VIII 1), (X 24), (X 25), (X 26)] which we actually chose to adopt. In our previous discussions of the Dirac theory (Sec. I and Sec. IX), we have worked within the framework of the 1929 spinor calculus, which provides for Lorentz covariance but not gauge covariance. In making the transition to a gauge-covariant theory, we subject Eqs. (I 11) to manipulations admissible under the Lorentz group and the unimodular spin group, in order

CC-0. In Public Domain. Gurukul Kangri Collection, Haridwar

Digitized by Arya Samaj Foundation Chennai and eGangotri

to bring them into a form in which the differential operators ∂_k and potentials ϕ_k appear only in the gauge-covariant combinations produced by covariant differentiation. Equations (IX 19) have such a form and were obtained by subjecting (I 11) to just such manipulations; they can at once be written

$$\begin{aligned}\sqrt{2}\sigma^k{}_{\dot\mu\rho}\chi^\rho{}_{;k}&=\sqrt{2}(\sigma^k{}_{\dot\mu\rho}\chi^\rho)_{;k}=\mu\xi_{\dot\mu}\\ \sqrt{2}\sigma^{k\nu\dot\sigma}\xi_{\dot\sigma;k}&=\sqrt{2}(\sigma^{k\nu\dot\sigma}\xi_{\dot\sigma})_{;k}=-\mu\chi^\nu,\end{aligned}\qquad\text{(X 27)}$$

by using (X 2), (X 7), and (X 26). Equations (X 27) are the Dirac equations in the spin frame with $\gamma=1$ and $\theta=0$, and have gauge-covariant form; hence they are the Dirac equations in any spin frame with $\gamma=1$, θ arbitrary.

The conservation theorem for the current $j_{\dot\mu\nu}$ (IX 22) takes the form $j^k{}_{;k}=(\sigma^{k\dot\mu\nu}j_{\dot\mu\nu})_{;k}=\sigma^{k\dot\mu\nu}j_{\dot\mu\nu;k}=0$, and can easily be derived in gauge-covariant fashion using the Dirac equations (X 27) and their complex conjugates.

The second-order equation can be derived in the following way: From (X 27),

$$[\sigma^{k\nu\dot\sigma}(\sigma^l{}_{\dot\sigma\rho}\chi^\rho)_{;l}]_{;k}=\sigma^{k\nu\dot\sigma}\sigma^l{}_{\dot\sigma\rho}\chi^\rho{}_{;lk}=-\tfrac{1}{2}\mu^2\chi^\nu.$$

Using (VII 12), one obtains

$$g^{lk}\chi^\nu{}_{;lk}-\sigma^{l\nu\dot\sigma}\sigma^k{}_{\dot\sigma\rho}\chi^\rho{}_{;lk}=-\tfrac{1}{2}\mu^2\chi^\nu.$$

Taking account of the fact that l and k are summation indexes, and using (X 21),

$$g^{lk}\chi^\nu{}_{;lk}+\sigma^{l\nu\dot\sigma}\sigma^k{}_{\dot\sigma\rho}P^\rho{}_{\alpha lk}\chi^\alpha=-\mu^2\chi^\nu.$$

This is the second-order equation for χ^ν. If we use (X 2), (X 26), and (X 23), setting $R_{krsp}=0$ since we are working in a flat world space, we obtain

$$g^{lk}(\partial_k+i\epsilon\phi_k)(\partial_l+i\epsilon\phi_l)\chi^\nu+i\epsilon F_{lk}\sigma^{l\nu\dot\sigma}\sigma^k{}_{\dot\sigma\rho}\chi^\rho=-\mu^2\chi^\nu,$$

which is the Schrödinger-Klein-Gordon equation including the spin interaction term. A similar equation holds for $\xi_{\dot\sigma}$.

The Lagrangian density (IX 24) can be written in the form

$$\begin{aligned}L=i[&\chi^\lambda(\sigma^k{}_{\lambda\dot\mu}\chi^{\dot\mu})_{;k}-\chi^{\dot\mu}(\sigma^k{}_{\dot\mu\lambda}\chi^\lambda)_{;k}-\xi_\lambda(\sigma^{k\lambda\dot\mu}\xi_{\dot\mu})_{;k}\\ &+\xi_{\dot\mu}(\sigma^{k\dot\mu\lambda}\xi_\lambda)_{;k}]+\sqrt{2}\mu i(-\chi^\lambda\xi_\lambda+\chi^{\dot\lambda}\xi_{\dot\lambda})\\ &+(1/16\pi\hbar)(F^{\mu\nu}F_{\mu\nu}+F^{\dot\mu\dot\nu}F_{\dot\mu\dot\nu}),\end{aligned}$$

by use of (IX 17), (X 2), (X 7), and (X 26). The last term is equal to $(1/8\pi\hbar)F^{kl}F_{kl}$, by (IX 16a). The invariance of this Lagrangian density with respect to general spin transformations implies the covariance of the whole theory, in particular with respect to gauge transformations.

LIST OF REFERENCES

We cannot attempt to give a comprehensive literature list for spinor calculus and its related fields. Instead we shall mention, beneath each of the following subheadings, a few of the important publications which might be of interest or of aid to the reader.

A. Books

1. L. de Broglie, *Théorie Générale des Particules à Spin* (Gauthier-Villars, Paris, 1943).
2. E. Cartan, *Leçons sur la Théorie des Spineurs* (*Actualités Scientifiques et Industrielles*, No. 643 and 701, Hermann, Paris, 1938).
3. H. C. Corben and P. Stehle, *Classical Mechanics* (John Wiley and Sons, Inc., New York, 1950).
4. P. A. M. Dirac, *The Principles of Quantum Mechanics* (Oxford University Press, London, 1947), third edition.
5. A. S. Eddington, *Fundamental Theory* (Cambridge University Press, Cambridge, 1946).
6. H. Goldstein, *Classical Mechanics* (Addison-Wesley Press, Cambridge, 1950).
7. H. A. Kramers, *Quantentheorie des Elektrons und der Strahlung* (Akademische Verlagsgesellschaft, Leipzig, 1938).
8. W. Pauli, *Handbuch der Physik*, H. Geiger and K. Scheel, editors (Springer, Berlin, 1933), second edition, Vol. 24, Part 1, pp. 83–272.
9. E. Schrödinger, *Space-Time Structure* (Cambridge University Press, Cambridge, 1950).
10. O. Veblen, *Projective Relativitätstheorie* (Springer, Berlin, 1933).
11. B. L. van der Waerden, *Die gruppentheoretische Methode in der Quantenmechanik* (Springer, Berlin, 1932).
12. H. Weyl, *Gruppentheorie und Quantenmechanik* (Hirzel, Leipzig, 1928).

B. Spinors

13. E. Cartan, Bull. Soc. Math. France **41**, 53 (1913).
14. L. Infeld and B. L. van der Waerden, Sitzber. preuss. Akad. Wiss., Physik.-math. Kl. 380 (1933).
15. O. Laporte and G. E. Uhlenbeck, Phys. Rev. **37**, 1380, 1552 (1931).
16. W. T. Payne, Am. J. Phys. **20**, 253 (1952).
17. A. Proca, J. phys. et radium **8**, 363 (1937).
18. A. Sommerfeld, Ber. Akad. Wiss. Wien **145**, 639 (1936).
19. O. Veblen, Proc. Nat. Acad. Sci. **19**, 462, 503 (1933); Science **80**, 415 (1934).
20. B. L. van der Waerden, Nachr. Akad. Wiss. Göttingen, Math.-physik. Kl. 100 (1929).
21. E. T. Whittaker, Proc. Roy. Soc. (London) **158A**, 38 (1937).

C. Semivectors

The theory of semivectors, originated by Einstein and Mayer, was a parallel development to spinor calculus.

22. V. Bargmann, Helv. Phys. Acta **7**, 57 (1934).
23. J. Blaton, Z. Physik **95**, 337 (1935).
24. A. Einstein and W. Mayer, Sitzber. preuss. Akad. Wiss., Physik.-math. Kl. 522 (1932); Proc. K. Akad Amsterdam **36**, 497, 615 (1933).
25. J. A. Schouten, Z. Physik **84**, 92 (1933).

D. Projective Relativity Theory

The relation of spinors to projective geometry was elucidated chiefly by Veblen and by Schouten and van Dantzig, in connection with their efforts to formulate a unified projective field theory.

26. H. J. Bhabha, Proc. Cambridge Phil. Soc. **32**, 622 (1936).
27. W. Pauli, Ann. Physik **18**, 305, 337 (1933).
28. J. A. Schouten and D. van Dantzig, Ann. Math. **34**, 271 (1933).

CC-0. In Public Domain. Gurukul Kangri Collection, Haridwar

Digitized by Arya Samaj Foundation Chennai and eGangotri

29. O. Veblen, Comptes Rendus du Congrès International des Mathematiciens (Oslo, 1936), p. 111; Proc. Natl. Acad. Sci. **19**, 979 (1933) and **20**, 85 (1934).

E. The Vierbein Formalism

As a method for formulating the relativistic invariance of wave equations, spinor calculus was preceded by the "Vierbein" formalism.

30. V. Bargmann, Sitzber. preuss. Akad. Wiss., Physik.-math. Kl., 346 (1932).
31. V. Fock, Z. Physik **57**, 261 (1929).
32. V. Fock and D. Iwanenko, Compt. rend. **188**, 1470 (1929).
33. T. Levi-Civita, Sitzber. preuss. Akad. Wiss., Physik.-math. Kl. 240 (1933).
34. B. Podolsky, Phys. Rev. **37**, 1398 (1931).
35. E. Schrödinger, Sitzber. preuss. Akad. Wiss., Physik.-math. Kl. 105 (1932).
36. H. Tetrode, Z. Physik **50**, 336 (1928).
37. T. Y. Thomas, Proc. Natl. Acad. Sci. **16**, 761 (1930).
38. H. Weyl, Proc. Natl. Acad. Sci. **15**, 323 (1929).

F. Relativistic Quantum Theory

Here we list a few of the very many papers on relativistic quantum mechanics which are of some interest in connection with spinors.

39. H. J. Bhabha, Proc. Indian Acad. Sci. A **21**, 241 (1945); Revs. Modern Phys. **17**, 200 (1945).
40. P. A. M. Dirac, Proc. Roy. Soc. (London) **155A**, 447 (1936).
41. W. Elsasser, Z. Physik **69**, 1 (1931).
42. V. Fock, J. phys. et radium **10**, 392 (1929).
43. E. L. Hill and R. Landshoff, Revs. Modern Phys. **10**, 87 (1938).
44. L. Infeld, Physik. Z. **33**, 475 (1932).
45. C. W. Kilmister, Proc. Roy. Soc. (London) **199A**, 517 (1949).
46. O. Klein, Arkiv Mat. Astron. Fys., Stockholm **25A**, No. 15 (1937).
47. W. Kofink, Math. Z. **51**, 702 (1949).
48. H. A. Kramers, Proc. K. Akad. Amsterdam **40**, 814 (1937).
49. W. Pauli and J. Solomon, J. phys. et radium **3**, 452 (1932).
50. A. Proca, J. phys. et radium **7**, 347 (1936).

G. Possible Relativistic Wave Equations

The papers listed in this section are samples illustrating developments in which spinors have played an important role.

51. F. J. Belinfante, Physica **7**, 305, 449 (1940).
52. R. J. Duffin, Phys. Rev. **54**, 1114 (1938).
53. M. Fierz, Helv. Phys. Acta **12**, 3 (1939).
54. M. Fierz and W. Pauli, Proc. Roy. Soc. (London) **173A**, 211 (1939).
55. W. H. Furry, Phys. Rev. **54**, 56 (1938).
56. Harish-Chandra, Proc. Roy. Soc. (London) **192A**, 195 (1948).
57. N. Kemmer, Proc. Roy. Soc. (London) **173A**, 91 (1939).
58. H. A. Kramers, F. J. Belinfante and J. K. Lubanski, Physica **8**, 597 (1941).
59. J. K. Lubanski, Physica **9**, 310, 325 (1942).
60. E. Majorana, Nuovo cimento **14**, 171 (1937).
61. C. Møller and L. Rosenfeld, Kg. Danske Videnskab. Selskab, Mat.-fys. Medd. **20**, No. 12 (1943).
62. W. Pauli, Revs. Modern Phys. **13**, 203 (1941).
63. W. Pauli and F. J. Belinfante, Physica **7**, 177 (1940).
64. W. Pauli and M. Fierz, Helv. Phys. Acta **12**, 297 (1939).
65. L. Rosenfeld, Mémoires Sci. Acad. roy. Belg. **18**, Fasc. 6 (1940).
66. J. Serpe, Bull. Soc. Roy. Sci., Liège **18**, 266 (1949); Physica **18**, 295 (1952).
67. A. H. Taub, Phys. Rev. **56**, 799 (1939).
68. J. S. de Wet, Phys. Rev. **58**, 236 (1940).
69. C. N. Yang and J. Tiomno, Phys. Rev. **79**, 495 (1950).
70. H. Yukawa *et al.*, Proc. Phys.-Math. Soc. Japan **17**, 48 (1935); **19**, 1084 (1937); **20**, 319 (1938); **20**, 720 (1938).

H. Representations of the Lorentz Group

Some further mathematical developments.

71. V. Bargmann, Ann. of Math. **48**, 568 (1947).
72. V. Bargmann and E. P. Wigner, Proc. Natl. Acad. Sci. **34**, 211 (1948).
73. R. Brauer and H. Weyl, Am. J. Math. **57**, 425 (1935).
74. P. A. M. Dirac, Proc. Roy. Soc. (London) **183A**, 284 (1945).
75. Harish-Chandra, Proc. Roy. Soc. (London) **189A**, 372 (1947); Phys. Rev. **71**, 793 (1947).
76. E. P. Wigner, Ann. Math. **40**, 149 (1939); Z. Physik **124**, 665 (1947).

CC-0. In Public Domain. Gurukul Kangri Collection, Haridwar

Digitized by Arya Samaj Foundation Chennai and eGangotri

Theory of Angular Correlation of Nuclear Radiations*

L. C. BIEDENHARN† AND M. E. ROSE

Oak Ridge National Laboratory, Oak Ridge, Tennessee

CONTENTS

	Page
I. Definition of the Angular Correlation Process	729
II. General Formulation	731
A. Introduction	731
B. Statistical Interpretation of Fano	734
C. The Tensor Parameters of the Radiation	735
D. Relation to Nuclear Reactions	737
E. The Double Correlation	739
(1) The general double-correlation function	739
(2) Direction-direction correlation	740
F. Symmetry Properties of the Double Correlation	741
G. Relation to the Falkoff-Uhlenbeck Method	742
III. Special Cases of Angular Correlation	743
A. Gamma Radiation	743
(1) General properties	743
(2) Correlation function for unpolarized radiation	745
(3) Correlation function for linear polarization-direction correlation	748
B. Spinless Particles	751
C. Conversion Electrons	752
D. Beta Radiation	759
(1) Description of the problem	759
(2) Explicit calculation	760
IV. Magnetic Effects in Angular Correlation	766
A. The Correlation Function with Spin-Coupling	767
B. Magnetic Interaction	768
C. External Magnetic Fields	769
(1) The delayed correlation	769
(2) The average correlation	770
D. Paschen Back Effect	770
V. Triple Correlation	772
A. Correlation with Intermediate Radiation Unobserved	773
B. Parallel Radiations	775

I. DEFINITION OF THE ANGULAR CORRELATION PROCESS

IT is a well-known fact that the coincidence observation of two radiations emitted by a nucleus yields a correlation in their relative propagation directions. This fact, which was first pointed out by Dunworth (22),[1] has been utilized very extensively as a method for measuring various properties of nuclear energy levels, and rather elaborate development of the theory is now available thanks to the efforts of many investigators (30, 57, 65). In the following we shall attempt to synthesize these various theoretical developments with particular emphasis on the interpretation which must be given to the various possible formulations of the theory (Sec. II). At the same time it is our purpose to discuss in detail the various special cases of angular correlation with which the experimentalist is apt to be confronted (Sec. III, IV, and V), and to provide a reasonably complete set of numerical results so that the present article, it is hoped, can be used as a "handbook" of angular correlation, so far as the theory is concerned. We shall not attempt a discussion of specific experimental results inasmuch as such discussion as is pertinent at present will be given in a companion article by Frauenfelder (34, see also 21 and 35). However, as will be seen from the following, it is necessary to recognize the relation of the theory, as it appears here, to the circumstances under which the observations may be carried out.

The simplest type of angular correlation process consists of the measurement of the coincidence rate of two successive nuclear radiations as a function of the angle between the propagation directions of these radiations. We shall refer to such a process as a direction-direction (double) cascade. The principal information obtainable from such a measurement is the angular momenta of the nuclear levels involved and that of the emitted radiations. In addition, in all cases except emission of electromagnetic radiation a determination of relative parity can be made. The case of γ correlations in which at least one of the transitions is not a pure multipole also provides a more sensitive means of obtaining the mixing ratio (ratio of intensities of magnetic to electric multipoles) than total intensity (for example, conversion coefficient) measurements do.[2] Possible generalizations and alternative processes in which one is interested are: (1) the polarization-direction correlation in which, for one of the radiations, the polarization state is also measured (thereby fixing relative parity for pure multipole γ-radiation) and (2) the case of nonsuccessive radiations where more than two radiations are involved in the cascade. The latter case, in which one may also observe the propagation vectors of two radiations only, is properly classified as a triple correlation, Sec. V. This list of alternative correlations processes is not meant to be complete. In particular, in the above we have omitted reference to the correlation process in a magnetic field (internal or external) which merits

* This paper is based on work performed for the U. S. Atomic Energy Commission at the Oak Ridge National Laboratory.

† Now at Yale University.

[1] Numbers in parentheses refer to references which are arranged alphabetically in bibliography at end of paper. Equation numbers are prefixed by the customary abbreviation "Eq." wherever ambiguity may arise. The bibliography should represent a fairly complete guide to the literature as of September, 1952.

[2] An additional parameter depending on nuclear structure resulting from the correlation observation is the relative phase of electric and magnetic multipole matrix elements, see further Sec. II and references (3) and (55).

CC-0. In Public Domain. Gurukul Kangri Collection, Haridwar

Digitized by Arya Samaj Foundation Chennai and eGangotri

separate consideration, Sec. IV. In the following references to the angular correlation without qualifying phrases or adjectives will generally be concerned with the direction-direction double cascade in which the radiations are emitted consecutively.

From a descriptive point of view a simple physical explanation of the existence of the angular correlation can be given as follows: If we consider only one transition, either the first or second, then clearly the angular distribution of the emitted radiation is isotropic. Proofs of this result too numerous to mention have been given in the literature; it is moreover obvious (or expected, to say the least) from the fact that no direction in space has been singled out. Each substate (magnetic sublevel of an isolated nucleus) emits anisotropically but on summing over these substates with equal populations and random (relative) phases, so that the sum is incoherent, the total intensity is independent of angle. However, in the angular correlation process the angular distribution of one radiation is observed when it is known that the other has a *fixed* direction. The prescription of a fixed direction, of course, singles out a direction in space; stated otherwise, the observation of the aforementioned propagation vector acts as a kind of projection operation in giving different weights to the various substates. In other words it gives information about the substates of the nuclear level formed after the emission of this radiation. In particular it asserts that these sublevels are not uniformly populated.[3] Consequently, the radiation subsequently emitted will not be isotropic [except in very rare cases where isotropy results as an accident (9)].

This rather elementary point is belabored in order to emphasize the fact that the quantitative description of the angular correlation process depends critically on the fact that we are considering an *isolated* nucleus. It is also clear that isolated here means that there is no appreciable interaction depending on the orientation of the nuclear spin in the intermediate state of the cascade. Even more specifically, the assumption is that the mean life for emission of the second radiation is short compared to the precession period of the nuclear spin, in the intermediate state, under the influence of possible spin couplings.

We may now examine the circumstances under which this assumption may realistically be regarded as valid. In general, it is clear that the only interactions of importance are those for which the energy splittings in the intermediate state are of the order of or larger than the total width of this intermediate state.

We first consider direct interactions. Then there are two well-known types of spin couplings to be considered: (1) the coupling of the intermediate state magnetic moment to a magnetic field and (2) the coupling of the quadrupole moment in the intermediate state to an electric field gradient. Since the intermediate state angular momentum j must fulfill $j \geqslant 1$ in order to have an anisotropic correlation neither of these couplings can be ruled out *a priori*. It is evident that the presence of such spin-couplings will attenuate the correlation in the sense that it will be more isotropic than that of a bare nucleus. Experimentally it is observed that the correlation can be wiped out entirely, although a detailed description of the physical circumstances giving rise to this effect cannot be given at present.

We may now examine the importance of the spin-couplings listed below.

(1) Magnetic Coupling

Here we are primarily concerned with hyperfine fields. The multiplet splitting caused by hyperfine interaction ranges from 10^{-3} to about 1 cm^{-1} corresponding to precession periods τ_{hfs} in the range 10^{-7} to 10^{-10} or perhaps 10^{-11} sec.[4] Therefore, for some cases, high energy and small angular momentum of the second radiation, no coupling effect would be important. However, a majority of cases, for which angular correlation would be a useful tool, fall into the range of lifetime corresponding to important hfs coupling perturbative effects. An indication of how these affect the angular correlation is given in Sec. IV. Of course, no difficulty arises if for the ground state the electronic shell has zero angular momentum, $J_e=0$. However, even if such were the case the electron shell cannot be expected to remain in the ground state, or indeed, to remain in any stationary state. The nuclear recoil in a heavy particle reaction and/or excitation and ionization resulting from β-emission or K capture which will initiate the cascade in almost every case will also initiate a chain of electronic transitions. Thus, following K capture (or internal conversion, as well) the emission of Auger electrons and x-rays transfers a K hole to the outer orbits and, in the case of the former, results in the formation of a multiply-charged ion (20). While these electronic transitions generally proceed very rapidly [$10^{-15}-10^{-14}$ sec—see (62)], it is to be expected that in most cases a non-negligible magnetic interaction will occur in the equilibrium state. In those cases in which $J_e=0$ for the ground state, one may attempt to eliminate the magnetic coupling by providing the radioactive nucleus with an environment such that the transition to the electronic ground state is very rapid. Presumably this is what is accomplished by the surface film technique [embedding in thin metallic layers formed by evaporation, electrodeposition, etc. (1, 33, 73) and by the use of dilute ionic

[3] As an example, in the emission of spinless particles the magnetic quantum numbers (defined with respect to the propagation direction) of the two states connected by the transition must be the same. Thus, in the simple case of a $j=0\rightarrow j=1$ transition, only one of the substates ($m_j=0$) is populated.

[4] This, of course, is based on the very reasonable assumption that nuclear magnetic moments in excited states are of the same order of magnitude as ground state moments. It also involves the equally reasonable assumption that the electronic states involved in the correlation have roughly the same properties as those involved in optical transitions.

CC-0. In Public Domain. Gurukul Kangri Collection, Haridwar

Digitized by Arya Samaj Foundation Chennai and eGangotri

solutions (48, 73)]. However, the physical processes involved are not very well understood at present, and there is no *a priori* method whereby one may be sure that all spin-coupling has been eliminated.

(2) Quadrupole Coupling

The quadrupole interactions may be as large as 100 megacycles, or $\tau_Q \sim 10^{-8}$ sec. While not as large as the magnetic interaction, the quadrupole interaction cannot be ignored for a very appreciable number of cascades (1a). Little needs to be added to the above except to say that the formation of an environment which has the property of eliminating magnetic interactions must also eliminate field gradients at the nucleus.

It would seem that an alternative procedure, which avoids the complications of imperfectly understood solid-state properties of thin films and the properties of dilute solutions could be utilized wherein the correlation is observed in a strong external magnetic field. Then, under conditions of complete Paschen-Back effect the spins are decoupled even if quadrupole coupling is present. As discussed in Sec. IV, one of the radiations must then be parallel, or nearly parallel, to the field. However, the very preliminary and admittedly meager experimental evidence [correlation in Ni^{60}, (36)] indicates that little or no decoupling takes place even with fields of the order 10^4 gauss. There seems to be no reason to doubt the validity of the reasoning with regard to spin decoupling by such a field for an isolated atom. In the actual source the presence of indirect couplings between neighboring ions may explain the failure of the strong field method. The presence of such couplings would, of course, imply an effect of chemical environment on the angular correlation. Even if this is the case a combination of a strong field and suitably prepared (magnetically dilute) sources may produce the desired spin decoupling. Whether one uses these sources with or without a magnetic field, an additional complication arises in observing charged particles due to multiple scattering which is necessarily present with the requisite thicknesses. However, corrections can be made if the scattering is not excessive (32). Even with thin sources the presence of a strong field could be tolerated only for correlations not involving light charged particles.

In any case the difficulties discussed above are such that little or no help can be expected in the way of quantitative calculations. Certainly, the technique of preparing suitable sources which is closely associated with the question of understanding the concomitant physical problems, is largely an experimental one. Nevertheless, the starting point for the analysis of any experimental results must be the theory for the isolated, uncoupled nucleus. This must be so whether the angular correlation is regarded as a method of nuclear spectroscopy or as a method of investigating nonstationary state processes in the solid (or liquid) state.[5] For this reason, and because the purely nuclear aspect of the theory is so well developed, we restrict our attention chiefly to the angular correlation without spin-coupling. The only noteworthy exception is the case in which hfs and other internal couplings can be eliminated. Then the application of a magnetic field, for which the coupling is completely defined, permits a determination of the intermediate state gyromagnetic ratio and magnetic moment by comparison with the zero-field correlation, (2, 5). This will be discussed in Sec. IV. It goes almost without saying that, for purposes of nuclear spectroscopy, every effort to eliminate the essentially unknown spin-coupling should be made. To the extent that this can be done the results of this paper would apply to the observed correlation, and the correlation measurement becomes an extremely valuable tool for the investigation of nuclear properties. It should be emphasized, however, that in many cases the spin-coupling effects are either too small to be observed or are small enough so as not to render ambiguous spin (and parity) assignments. Recent experimental results on Co^{60} shows that when care is taken in the preparation of sources and in making appropriate corrections for geometry and statistics the agreement with theory is excellent.

II. GENERAL FORMULATION

A. Introduction

It is our purpose in this section to set up the problem of the angular correlation of successive nuclear radiations in the most general fashion possible in order to provide a common framework for the discussion of the various specialized problems of practical interest. The detailed applications appear in succeeding sections. The common features of all correlation problems is to be found in the fact that they involve an initial nuclear state of sharp angular momentum j_1 and parity that undergoes successive transformations either emitting or absorbing radiations through intermediate nuclear states of sharp angular momenta j_a, $j_b \cdots$ with sharp parity and terminating as a nucleus with sharp angular momentum j_2 and parity. The properties of the radiations, the observation or lack thereof of their directions of motion, polarization properties, the presence or absence of perturbation of the intermediate nuclear states by external fields (magnetic (hfs) and possibly quadrupole interactions) condition the specific correlation discussed. Our general assumption of sharp angular momenta and parity for the nuclear states is restrictive, however, and distinguishes the correlation problem from, say, the closely related problem of the angular distribution of nuclear reactions (15, 16). One addi-

[5] It is perhaps worthy of note that this interweaving of nuclear and atomic as well as solid-state physics arises from the fact that we are interested in the *angular* properties of the nuclear transitions and because the nuclear lifetimes are long enough to compare with the characteristic transition times for the atomic and solid state processes.

CC-0. In Public Domain. Gurukul Kangri Collection, Haridwar

Digitized by Arya Samaj Foundation Chennai and eGangotri

tional restriction will be made in the general formulation: namely, that the initial and final nuclear states are randomly oriented. This is a mild delimitation of the problem, excluding only such specialized processes as the radiations from oriented nuclei in certain crystalline lattices at very low temperatures (72). It turns out that in several instances such problems can nonetheless be treated as special cases of our formulation. In any case such processes are not our immediate concern.

The initial and final transitions thus occupy a preferred position in this formulation, and focusing our attention on the two transitions leading from and to these states we can write the general correlation function in the form

$$W(\mathrm{A}_1, \mathrm{A}_2; \mathrm{A}', \mathrm{A}'', \cdots) \sim \mathfrak{S}\sum \langle j_1 m_1 | H_1(\mathrm{A}_1) | j_a m_a\rangle^* \times \langle j_1 m_1 | H_1(\mathrm{A}_1) | j_a m_a'\rangle S(m_a m_a'; m_n m_n') \times \langle j_n m_n | H_2(\mathrm{A}_2) | j_2 m_2\rangle^* \langle j_n m_n' | H_2(\mathrm{A}_2) | j_2 m_2\rangle. \quad (1)$$

Here the summation $\sum$ is over m_1, m_a, m_a', m_n, m_n', m_2, and the symbol $\mathfrak{S}$ refers to the averaging over all of the unobserved properties of the radiations. As indicated irrelevant constant factors have been omitted since we are interested only in the dependence of the correlation function on observed parameters A_1 and A_2 such as propagation directions, polarization. We omit scale factors in the sequel usually without comment. Further, in Eq. (1) $H_1(\mathrm{A}_1)$ is the interaction Hamiltonian for the emission of the initial radiation described by the set of vectors A_1 and H_2 describes the emission of the second radiation in a similar way; $S(m_a m_a'; m_n m_n')$ is a matrix that describes all the other properties of the correlation (the intermediate radiations and extraneous perturbations, see Secs. IV and V). The vectors $\mathrm{A}', \mathrm{A}'' \cdots$ describe intermediate observed radiations and are contained in the S coefficient. For the emission of two successive radiations this matrix represents the spin coupling of the nucleus in the intermediate state with extranuclear fields. In the following sections the form of this matrix will be derived in detail as it is needed for the cases of interest. For the simple case of two successive radiations (double cascade), i.e., where only the initial and final radiations occur and the intermediate state of spin $j_a = j_n = j$ is unperturbed, $S(m_a m_a'; m_n m_n') = \delta(m_a m_n)\delta(m_a' m_n')$. In such cases the superfluous subscripts a and n will be omitted. For the same case but with the intermediate state perturbed by hfs, or for the case where but a single unobserved radiation connects intermediate states j_a and j_n and the states j_a and j_n are unperturbed [see reference (42)] $S = \delta(m_a - m_a', m_n - m_n') f(m_a, m_a', m_n)$. This particular form may be deduced in general for those cases that do not introduce any new angular information. The case of an external magnetic field with incomplete Paschen-Back effect constitutes an example to the contrary.

We may rearrange Eq. (1) so as to bring it to the more useful form:

$$W(\mathrm{A}_1\mathrm{A}_2\mathrm{A}'\mathrm{A}''\cdots) \sim \sum E^{(1)}(m_a m_a') S(m_a m_a'; m_n m_n') E^{(2)}(m_n' m_n). \quad (2)$$

The summation is to be carried out over m_a, m_a', m_n and m_n', and we have defined:‡

$$E^{(1)}(m_a m_a') \equiv \mathfrak{S}_1 \sum_{m_1} \langle j_1 m_1 | H_1 | j_a m_a\rangle^* \times \langle j_1 m_1 | H_1 | j_a m_a'\rangle \quad (3)$$

with $\mathfrak{S}_1$ designating an average over the unobserved properties of radiation 1; E^2 is defined in a similar manner. These E matrices are Hermitian so that $E(mm') = E^*(m'm)$. The interpretation of the E matrices is given below in Sec. II-B.

The rearrangement leading to Eq. (2) is of more than calculational interest, since it allows one to break the angular correlation problem into much simpler parts: the initial and final transitions (which may now be considered independently and, moreover, involve the same kind of treatment), and the link between these radiations which depends on spin-coupling in the intermediate state. The E matrices can be greatly simplified by the methods of Racah (63, 64, 65), as originally shown by Gardner (38). To do this we first expand the interaction Hamiltonian H_1 for the emission of a particle along the quantization (z) axis in terms of tensor operators with definite angular momentum, parity, and time-reversal properties:

$$H_1(\mathrm{A}_1) = \sum_{L,M,\pi} \alpha(LM, \pi; \mathrm{A}_1) T(\hat{LM}, \pi; \hat{\mathrm{X}}_1). \quad (4)$$

Here the $\alpha(LM, \pi; \mathrm{A})$ are variables that characterize the particle emitted, and the $T(LM, \pi)$ are irreducible nuclear operators of degree L (see Eq. (5) below) with parity $\pi = \pm 1$. The arguments X_1 refer to nuclear configuration and spin coordinates. Note that L can be a half-integer as well as an integer. For a transition with a definite angular momentum and parity change, i.e., a pure multipole transition, only a single one of the $T(LM, \pi)$ enters. In the following sections, the $\alpha(LM, \pi)$ or their equivalent are given explicitly for the cases of interest. For the present purpose it suffices to say that the $\alpha(LM, \pi)$ are characteristic parameters of the particles; for example, for alpha particles the $\alpha(LM, \pi)$ vanish unless $\pi = (-)^L$ and $M = 0$ since the projection

‡ *Note added in proof.*—We recognize that, strictly speaking, the H operators are not Hermitian but are the emission (or absorption) parts of Hermitian operators. Actually in Eq. (2) $E^{(2)}(m_n' m_n)$ should be replaced by a density matrix constructed in the same way except that H_2 is replaced by H_2^+. The distinction between these two density matrices is a phase $(-)^\nu$, [see Eq. (38), for example], which would appear in every correlation function. However, except in the impractical case in which the circular polarization of *two* γ-rays is measured, ν will be an even integer, and the distinction is academic.

CC-0. In Public Domain. Gurukul Kangri Collection, Haridwar

Digitized by Arya Samaj Foundation Chennai and eGangotri

of orbital angular momentum along the axis of motion (z axis in the present notation) must be zero and no spin angular momentum is involved. In this case the parity is related to the angular momentum L by $\pi=(-)^L$. For γ-rays $M=\pm 1$ only, because of the transverse character of the electromagnetic field, and now for given L (multipolarity) the π index essentially characterizes the transitions as electric or magnetic. Other cases in which we shall be interested, especially Dirac particles, are somewhat more complicated and will be examined in connection with the special cases treated in the sequel.

If we are interested in the radiation emitted in an arbitrary direction, we make use of the rotational properties of the T operators and transform them to a new set of axes. The operators $T(LM, \pi)$ transform as $(2L+1)$ dimensional irreducible representations of the 3-dimensional rotation group, that is

$$T(LM, \pi; \mathrm{X}_1)=\sum_\mu T(L\mu, \pi; \mathrm{X}_1')D(L, \mu M; \mathfrak{R}), \quad (5)$$

where the X_1 and X_1' refer to the original and rotated coordinate system, respectively. The argument $\mathfrak{R}$ of the rotation matrix D is a rotation, with Euler angles $\alpha\beta\gamma$, such that the coordinate system describing the radiation (propagation vector and polarization direction) is carried over into the quantization coordinate system. The three Euler angles are necessary, so far as problems considered below are concerned, only in the case of emission of linearly polarized light. If the observation of the radiation does not include a measurement of linear polarization, the angle γ is ignorable and can be set equal to zero. In this case the azimuth angle α is meaningful only in the E matrix but, as will be seen and as is to be expected, for the correlation only a single angle β will be pertinent. However, until the two links in the correlation function are formed the rotation $\mathfrak{R}$ will define a direction (α, β) which will coincide with the propagation direction. With $\mathfrak{k}$ denoting the *unit* vector in this direction we shall write $\mathfrak{k}$ as argument of the rotation matrix in this case. (We follow the practice of using boldface German letters for unit vectors.)

Introducing Eq. (4) and Eq. (5) into Eq. (3) and dropping the subscript a we find

$$E^{(1)}(mm')=\mathfrak{S}_1\sum\alpha^*(LM, \pi)\alpha(L'M', \pi') \times D^*(L, \mu M)D(L', \mu'M')\langle j_1m_1|T(L\mu, \pi)|jm\rangle^* \times\langle j_1m_1|T(L'\mu', \pi')|jm'\rangle, \quad (6)$$

and the summation is now over m_1, L, M, μ, π and L', M', μ', π'. Now the Wigner-Eckart theorem (77) gives

$$\langle j_1m_1|T(L\mu, \pi)|jm\rangle =C(j_1Lj; m_1m-m_1)(j_1\|T(L\pi)\|j)\delta(\pi, \pi_1\pi_a), \quad (7)$$

where π_1 and π_a are the parities of the nuclear states and $C(j_1Lj; m_1m-m_1)$ is the vector addition coefficient or Wigner coefficient[6] corresponding to the addition of j_1 and L with components m_1 and $m-m_1$ to give a resultant j with component m (19), while $(j_1\|T\|j)$ is a reduced matrix element. We use now the relation (77)

$$D^*(L, \mu M)=(-)^{M-\mu}D(L, -\mu, -M) \quad (8)$$

and the Clebsch-Gordan series (77)

$$D(L, -\mu, -M)D(L', \mu'M') =\sum_\nu C(LL'\nu; -\mu\mu')C(LL'\nu; -MM') \times D(\nu, \mu'-\mu, M'-M). \quad (9)$$

Using Eqs. (7), (8), and (9) in Eq. (6) yields

$$E^{(1)}(mm')=\mathfrak{S}_1\sum(-)^{M-m+m_1}(j_1\|T(L\pi)\|j)^* \times(j_1\|T(L'\pi)\|j)\alpha^*(LM, \pi) \times\alpha(L'M'\pi)C(j_1Lj; m_1m-m_1) \times C(j_1L'j; m_1\,m'-m_1)C(LL'\nu; -MM') \times C(LL'\nu; m_1-m, m'-m_1) \times D(\nu, m'-m, M'-M; \mathfrak{R}). \quad (10)$$

The summation here is over m_1, L, L', ν, M and M'. We can perform the m_1 sum using Racah's techniques

$$\sum_{m_1}(-1)^{-m+M+m_1}C(j_1Lj; m_1m-m_1) \times C(j_1L'j; m_1m'-m_1)C(LL'\nu; m_1-m, m'-m_1) =(2j+1)(-)^{j_1-m+M}C(jj\nu; m, -m') \times W(jjLL'; \nu j_1). \quad (11)$$

---

[6] Equation (7) is in the form given by Wigner (77). At first glance it appears that this result implies the convention

$$(a|H|b)\equiv\int\psi_b^*H\psi_a d\tau.$$

Although this is a perfectly legitimate convention, we prefer to use the more commonly used notation in which the indices a and b are interchanged in the left- (or right-) hand side of the above. It would then appear that the proper manner in which the Wigner-Eckart theorem should be written is

$$\langle j_1m_1|T(L\mu, \pi)|jm\rangle =B(jj_1)(j_1\|T(L\pi)\|j)C(jLj_1; mm_1-m)\delta(\pi, \pi_1\pi_a), \quad (7a)$$

where $B(jj_1)$ is a constant depending only on the indicated arguments and its specification merely fixes the normalization of the reduced matrix element $(j_1\|T(L\pi)\|j)$. For example, Racah [(63), his Eq. (28)] writes the Wigner-Eckart theorem in this form with $B(jj_1)=(2j_1+1)^{-\frac{1}{2}}$. Actually Eqs. (7) and (7a) give identical results with the understanding that different definitions of the reduced matrix elements are involved in each case. To see this in a simple way we consider that the tensor operator $T(LM, \pi)$ in Eq. (7) is actually the adjoint of $T(LM, \pi)$ in Eq. (7a) where the phase choice is $T+(LM, \pi)=(-)^{L-M}T(L-M, \pi)$, say, (see Sec. II-C below). That is, we replace emission by absorption which doesn't have any effect on the results. Then, if we equate the corresponding sides of Eqs. (7) and (7a), we find that the reduced matrix elements differ by a phase $(-)^L$, aside from j and j_1 dependent factors which are nonessential and which can moreover be removed by suitable normalization. Thus, our result given in Eq. (38) below can be transcribed to Racah's form by insertion of a phase factor $(-)^{L_1+L_1'+L_2+L_2'}$ which is equivalent to a redefinition of the reduced matrix elements. Here and throughout we suppress the third magnetic quantum number in the Clebsch-Gordan (vector addition) coefficients since it is always the sum of the first two.

CC-0. In Public Domain. Gurukul Kangri Collection, Haridwar

Digitized by Arya Samaj Foundation Chennai and eGangotri

Following Racah we also define the set of parameters

$$c_{\nu\tau}(LL')\equiv\mathfrak{S}_1\sum_M \alpha^*(LM,\pi)\alpha(L'\tau+M,\pi) \times(-)^{L-M}C(LL'\nu;-M,\tau+M). \quad (12)$$

Then Eq. (10) reduces to

$$E^{(1)}(mm')=\sum(-)^{j_1-m+L}(2j+1)(j_1\|T(L\pi)\|j)^* \times(j_1\|T(L'\pi)\|j)c_{\nu\tau}(LL')C(jj\nu;m,-m') \times W(jjLL';\nu j_1)D(\nu,m'-m,\tau;\mathfrak{R}), \quad (13)$$

and the sum is over L, L', ν and τ.

The various terms in Eq. (13) have a clear-cut meaning. The factors $(j_1\|T(L\pi)\|j)$ are physical parameters (that is, reduced matrix elements) characteristic of the nuclear transition involved and, in particular, of the state emitting or absorbing radiation, and are thus independent of orientation and of the directions of motion. These are physical parameters in the sense that they are dependent on a physical model. The factors $c_{\nu\tau}(LL')$ are characteristic of the particles emitted, and upon the multipolarity and parity of the transitions considered through the parameters $\alpha(LM,\pi)$, but are, in addition, dependent on the information specified as defined by the physical experiment under discussion. This is clear by virtue of the averaging process indicated in Eq. (12). The remaining factors are to be interpreted as intrinsically geometrical in nature in contrast to the foregoing factors which are determined by the physics of the process.

Some general properties of the $c_{\nu\tau}$ can be obtained rather readily. If only the direction of motion of the particle is observed, then $c_{\nu 0}$ alone differs from zero. This can be seen simply from the fact that the angle γ refers to a rotation about the direction of motion, and the physical experiment by assumption is independent of γ. Thus $\tau=0$. Similarly if the experiment measures circular polarization, the experimental results are again independent of γ and $\tau=0$. Thus, for this case only $c_{\nu 0}\neq 0$. These conclusions can be verified in detail for each specific case from the definitions given above.

B. Statistical Interpretation of Fano (30)

A number of fruitful interpretations of the formalism of angular correlation are possible and have been given in the literature. At this point we consider an interesting interpretation of the meaning of Eq. (13) in terms of the density matrix as given by Fano. The density or statistical matrix was introduced into quantum mechanics to provide for the discussion of states about which less than maximal information is available. This is exactly the situation we have used earlier where we assumed the initial nuclear state was randomly oriented (an impure state) and only limited information provided on the state of the radiation (only its direction of motion specified, as is the usual case). The treatment of the problem was first to describe it as if we had maximal information, that is, the procedure is to introduce pure states and then average our final result to accord with our limited knowledge. The use of the Racah functions appeared as an algebraic convenience to handle the sums. As pointed out by Blatt (16) and especially by Fano (30), a direct procedure should be possible that never introduces the extraneous details of this method. In carrying out this program by means of the density matrix the geometrical significances of the Racah functions will become more apparent.

Consider a pure state ψ defined by an expansion in terms of an complete orthonormal set of wave functions $u_j{}^m$, i.e.,

$$\psi=\sum_m a_m u_j{}^m.$$

One constructs the matrix

$$P_{mm'}=a_{m'}{}^*a_m.$$

Then all properties of the state ψ, that is to say, the mean value of any arbitrary operator F can be found from the trace rule

$$\langle F\rangle=\sum_{mm'} a_{m'}{}^*a_m F_{m'm}=tr(FP).$$

The state ψ is therefore completely described by the density matrix P. The density matrix, however, can also describe impure states, which can be looked upon as the weighted sum of the density matrices P_n of pure states; thus $P=\sum_n p_n P_n$ where p_n are the weight factors.

The matrix $E(mm')$ introduced above is seen to be the density matrix of the intermediate state j. The information on the intermediate state j, as represented by the matrix $E(mm')$, has its origin in the coupling of the density matrices for the initial state, about which we know only its spin j_1, and the radiation, about which we also have limited information. Equations (4) and (5) can be considered as the expansion of the radiation into pure states, $T(L\mu,\pi)$, with coefficients $\sum_M D(L,\mu M)\alpha(LM,\pi;\mathrm{A}_1)$, while the initial state is expanded on the set $\psi_{j_1}{}^{m_1}$. Equation (6) is then the expression of the density matrix for the state j in terms of the density matrices of the initial and radiation states.

In more detail one has for the initial state

$$\psi_{\mathrm{in}}=\sum_{m_1} A(m_1)\psi_{j_1}{}^{m_1},$$

for the radiation

$$\psi_{\mathrm{rad}}=\sum_{LM} B(LM)\psi_L{}^M, \quad (14)$$

and for the resultant state

$$\psi_{\mathrm{res}}=\sum_m C(jm)\psi_j{}^m,$$

where

$$C(jm)=\sum_{m_1LM} A(m_1)B(LM)\langle jm|LM|j_1m_1\rangle.$$

CC-0. In Public Domain. Gurukul Kangri Collection, Haridwar

Digitized by Arya Samaj Foundation Chennai and eGangotri

Forming the density matrices for the resultant state, in which the transition ends, one obtains

$$P_{mm'}(\text{res})=\sum P_{m_1m_1'}(\text{in})P_{LML'M'}(\text{rad}) \times\langle jm|LM|j_1m_1\rangle\langle jm'|L'M'|j_1m_1\rangle^*. \quad (15)$$

The summation is over the indices L, L', M, M', m_1 and m_1'. Equation (15) is the desired relation for the density matrices, but it is in a very unwieldy form. Fano introduced at this stage the concept of "statistical tensors" $R(kq)$, defined by the relation

$$R(kq, jj')=\sum_{mm'}{}^{j}(-)^{j-m}C(jj'k; m, -m') \times P(jj'mm')\delta(m', m-q), \quad (16)$$

where $P(jj'mm')$ is the density matrix for states not sharp in j.

This step is motivated by the observation that the density matrix is dependent upon the choice of the quantization axes, and under rotation of coordinates transforms as the Kronecker product of the two representations $\mathbf{j}'$ and $\mathbf{j}$. This product, $(\mathbf{j}')^*\times\mathbf{j}$ is, of course, completely reducible into a sum of terms with rank k, $(|j'-j|\leqslant k\leqslant j'+j)$, and, in the usual fashion, the coefficient of each representation is the vector addition coefficient, which allows us to separate each term by means of Eq. (16).

For a completely random state but with sharp j we know that the density matrix $P(jj'mm')=\delta(jj')\delta(mm')$ and using Eq. (16) we find that only the scalar $R(00, jj)$ can be defined; i.e., a random state looks spherically symmetric, as is to be expected. In general a state of spin j can define tensors of rank less than or equal to $2j$, as Eq. (16) shows. Using the unitary property of the vector addition coefficients, we can invert Eq. (16) to give the density matrix in terms of the tensor parameters. Introducing the tensor parameters in Eq. (15) gives the result

$$P_{mm'}(\text{res})=\sum_{kq}(-1)^{j-m}C(jjk; m, -m') \times R(kq)\delta(q, m-m') \quad (17a)$$

with

$$R(kq)=\sum(j_1\|L\|j)^*(j_1\|L'\|j)R(k_1q_1) \times R(k_rq_r)C(k_rk_1k; q_r, -q_1)\delta(q_1, q_r+q) \times\{\sum_{\alpha}(2\alpha+1)(2j+1)[(2k_1+1)(2k_r+1)]^{\frac{1}{2}} \times(-1)^{L'+q_r+k_1+\alpha}W(j_1\alpha j_1L; jk_1) \times W(j\alpha jL'; j_1k)W(k_1\alpha k_rL'; Lk)\}. \quad (17b)$$

The first summation is over L, L', k_1, q_1, k_r, q_r. The bracketed term in Eq. (17b) is essentially a recoupling coefficient that allows one to relate the tensor parameters of the initial and radiation states to the tensor parameters of the resultant state. The tensor parameters of the initial state represent the coupling $\mathbf{j}_1+\mathbf{j}_1=\mathbf{k}_1$, while the radiation tensor parameters represent the coupling $\mathbf{L}+\mathbf{L}'=\mathbf{k}_r$.[7] The tensor parameters of the resultant state, however, are expressed in the system $\mathbf{j}+\mathbf{j}=\mathbf{k}$ with $\mathbf{j}=\mathbf{L}+\mathbf{j}_1=\mathbf{L}'+\mathbf{j}_1$. The bracketed coefficient in Eq. (17b) is just the change of coupling coefficient to go from the coupling of resultant tensor parameters,

$$(\mathbf{j}_1+\mathbf{L})+(\mathbf{j}_1+\mathbf{L}')=\mathbf{k},$$

to the coupling

$$(\mathbf{j}_1+\mathbf{j}_1=\mathbf{k}_1)+(\mathbf{L}+\mathbf{L}'=\mathbf{k}_r)=\mathbf{k}. \quad (18)$$

For the present problem where the initial state is random, only the scalar tensor parameter is defined, i.e., $k_1=q_1=0$. Then

$$R(kq)=\sum_{LL'}(j_1\|L\|j)^*(j_1\|L'\|j)R(k, -q; LL'; \text{rad}) \times(2j+1)(-1)^{L'+q+j-j_1}W(jjLL'; kj_1). \quad (19)$$

Using Eq. (19) in Eq. (17a) we find

$$P_{mm'}(\text{res})=\sum_{kq}\sum_{LL'}(-)^{m+L'-j_1+q}(2j+1) \times C(jjk; m, -m')\delta(q, m'-m) \times R(kq; LL'; \text{rad})(j_1\|L\|j)^* \times(j_1\|L'\|j)W(jjLL'; kj_1). \quad (20)$$

Comparing Eqs. (20) and (13) gives the desired interpretation of Fano. Namely, (a) the $(-1)^{j-m}C(jj\nu; m, -m')$ is the coefficient that relates the tensor parameters to the density matrix, (b) $W(jjLL'; \nu j_1)$ is the coefficient that changes the coupling schemes, (c) the $(j_1\|L\|j)$ are physical coefficients that weight the various multipoles (d) finally, $(-)^{L+L'+q}\sum_\tau c_{\nu\tau}(LL') \times D(\nu, q\tau; \Re)$, which appear in Eq. (13), [see also Eqs. (42a) and (71) below] are the tensor parameters of the radiation [$R(kq)$ in Eq. (20)] which express directly the information available on the radiation by virtue of the physical measurements performed. For example, if the radiation were unobserved only a scalar parameter can be defined, and Eq. (20) shows that the intermediate nuclear state is also random.

C. The Tensor Parameters of the Radiation

This formulation shows that the key point of the correlation problem is the determination of the tensor parameters of the radiations. Let us limit ourselves for the moment to a single emergent nonrelativistic[8] particle. Then the tensor parameters of this radiation are obtained from the measurements:

(1) the type of particle (this includes its spin magnitude),

(2) the detection of its direction of motion,

(3) a spin polarization measurement (carried out, we shall assume, with respect to a set of coordinates defined by the direction of motion).

---

[7] The order in which the vectors $\mathbf{L}$ and $\mathbf{L}'$ are added is important for the phases, (19).

[8] By this we mean that the spin is treated in Pauli approximation.

CC-0. In Public Domain. Gurukul Kangri Collection, Haridwar

Digitized by Arya Samaj Foundation Chennai and eGangotri

The measurement of a direction of motion is, of course, the basic correlation measurement. Interpreted quantum-mechanically it means that the particle is in a plane wave state, $\exp(i\mathbf{K}_\sigma\cdot\mathbf{r}_\sigma)$ (leaving aside the irrelevant center of mass motion). The subscript σ here is a particle label. The spin measurements determine the spin wave function to be $\chi_s{}^m$, assuming for the moment that the observation corresponds to pure m states, rather than to a more general linear combination of m states. This information must now be used to deduce the density matrix for the radiation in terms of eigenstates of the total angular momentum.

We employ the Rayleigh plane wave expansion

$$e^{iKz}=2\pi^{\frac{1}{2}}\sum_l j_l(Kr)(2l+1)^{\frac{1}{2}}(i^lY_l{}^0).$$

The $j_l(Kr)$ are, of course, the spherical Bessel functions. We shall use the set of functions $(i^lY_l{}^0)$ as our angle functions since they have the time-reversal property we desire, namely,

$$K_0(i^lY_l{}^m)=(-)^{l-m}Y_l{}^{-m},$$

where K_0 is here the complex conjugation operation. Similarly we choose a representation such that

$$K_t\chi_s{}^m=(-)^{s-m}\chi_s{}^{-m}.$$

For example, the time reversal operator K_t for a spin $\frac{1}{2}$ particle is $K_t=i\sigma_yK_0$. In the coordinate system determined by the direction of motion we have therefore

$$e^{iKz}\chi_s{}^M=\sum_l j_l(Kr)[4\pi(2l+1)]^{\frac{1}{2}}(i^lY_l{}^0)\chi_s{}^M$$
$$=\sum_{J,l}[4\pi(2l+1)]^{\frac{1}{2}}j_l(Kr)\times C(lsJ;0M)\Phi_{J,l}{}^M, \quad (21)$$

where

$$\Phi_{J,l}{}^M\equiv\sum_\mu C(lsJ;\mu,M-\mu)(i^lY_l{}^\mu)\chi_s{}^{M-\mu} \quad (21a)$$

and

$$K_t\Phi_{J,l}{}^M=(-)^{J-M}\Phi_{J,l}{}^{-M}. \quad (21b)$$

The wave functions $\Phi_{J,l}{}^m$ combine with the initial state wave functions, $\psi_{j_1}{}^{m_1}$, to form the compound state $\psi_j{}^m$. Since the Hamiltonian that effects this combination is invariant under rotations and commutes with the time reversal operator K_t, we find that the reduced matrix elements, the "physical parameters," appearing in Eq. (20) for example, are purely real. To see this we note that

$$(j_1m_1;JlM|H|jm)=(j_1Jl\|H\|j)C(j_1Jj;m_1M)$$

and

$$(j_1Jl\|H\|j)^*C(j_1Jj;m_1M)$$
$$=(K_tj_1m_1;K_tJlM|H|K_tjm)$$
$$=(-)^{j_1-m_1+J-M-j+m}(j_1Jl\|H\|j)C(j_1Jj;-m_1,-M)$$

or

$$(j_1Jl\|H\|j)^*=(j_1Jl\|H\|j). \quad (22)$$

This result is the general form of a theorem enunciated for special cases by Lloyd (55), by Longmire and Messiah (59), and by Fuchs (37). These authors have stated the theorem, for electromagnetic radiation and β particles, in the form of the reality of the product of interfering matrix elements. This, of course, follows trivially from Eq. (22). The foregoing is not intended as a rigorous demonstration of the phase theorem. However, a rigorous proof of this theorem, which moreover demonstrates the fact that it is generally valid and does not depend on the use of perturbation theory, is given below in Sec. II-D (see Eq. (30) and following text).

For an arbitrary direction of motion, we use the property of the $\Phi_{J,l}{}^M$ that this set of wave functions transforms with a $2J+1$ dimensional representation of the rotation group. Hence

$$(e^{iKz}\chi_s{}^m)'=2\pi^{\frac{1}{2}}\sum_{J,M}D(J,Mm;\mathfrak{k})\sum_l(2l+1)^{\frac{1}{2}}j_l(Kr)\times C(lsJ;0m)\Phi_{J,l}{}^M,$$

where the prime refers to the rotated coordinate system.

The parity of the states $\Phi_{J,l}{}^M$ is $\pi_\sigma(-)^l$ where π_σ is the intrinsic parity of the particle σ. Hence we note that only states with l's differing by an *even* integer can mix. The density matrix for the radiation is

$$E(JMl;J'M'l')=4\pi[(2l+1)(2l'+1)]^{\frac{1}{2}}\times C(l'sJ';0m)C(lsJ;0m)\times D^*(J',M'm)D(J,Mm). \quad (23)$$

If, instead of $\chi_s{}^m$ being measured, the measurement fixes the spin function to be the linear combination $\chi_s=\sum_m a_m\chi_s{}^m$ then the density matrix is

$$E(J'M'l';JMl)=4\pi[(2l+1)(2l'+1)]^{\frac{1}{2}}\sum_{mm'}a_{m'}{}^*a_m\times C(l'sJ';0m')C(lsJ;0m)D^*(J',M'm')D(J,Mm).$$

Introducing the concept of tensor parameters leads to the results

$$R(k_\sigma q_\sigma;\text{spin})=\sum_{mm'}(-)^{s-m}a_{m'}{}^*a_m\times C(ssk_\sigma;m,-m')\delta(q_\sigma,m-m'), \quad (24a)$$

and

$$R(kq,JJ'll';\text{rad})=\sum_{k_\sigma q_\sigma\lambda}(-)^{J-J'+l+q-q_\sigma-\lambda+k}\times[(2k+1)(2k_\sigma+1)(2J+1)(2J'+1)\times(2l+1)(2l'+1)]^{\frac{1}{2}}R(k_\sigma q_\sigma)C(l'k_\sigma\lambda;0q_\sigma)\times C(lk\lambda;0q_\sigma)D(k,qq_\sigma)W(l'J'k_\sigma s;s\lambda)\times W(lskJ';J\lambda). \quad (24b)$$

If no measurement is made on the spin polarization then $k_\sigma=q_\sigma=0$. The result for the tensor parameters of the radiation is then

$$R(kq,JJ'll')=(-)^{J-s+q}\times[(2J+1)(2J'+1)(2l+1)(2l'+1)]^{\frac{1}{2}}\times C(ll'k;00)W(lJl'J';sk')D(k,q0;\mathfrak{k}). \quad (25)$$

CC-0. In Public Domain. Gurukul Kangri Collection, Haridwar

Digitized by Arya Samaj Foundation Chennai and eGangotri

This example shows the general feature of all correlation problems: that the tensor parameters of the radiation are basically no more and no less than the *information contained in the transformation from linear momentum to angular momentum representations*, suitably coupled with the information obtained from a spin polarization measurement, if such is present. The situation for relativistic particles, and photons, needs to be treated more carefully, but the essentials are completely analogous to the nonrelativistic case above. We give the results in detail in Sec. III.

D. Relation to Nuclear Reactions

It is instructive to consider now the relstion of the angular correlation problem to the very closely related problem of the angular distribution of nuclear reactions, and scattering (78). In so doing one can eliminate any reference to perturbation theory, or to the specific interactions responsible for the transitions, and concentrate solely on the properties of angular momenta which account for the correlation phenomena (23). As this implies, the angular correlation formalism is very general and is based on fundamental quantum-mechanical concepts.

Consider a (compound) state of an excited nucleus with angular momentum J and parity π that can decay into pairs of particles of spins j_1 and j_2, respectively. The specific pair will be denoted by α (channel label); the vector sum of $\mathbf{j}_1$ and $\mathbf{j}_2$ will be denoted by $\mathbf{s}$ (channel spin).

In the region where the particle pair α are well separated, that is, the "external region" where the only interparticle interaction is, at most, the Coulomb interaction, the two particles will be in relative motion with angular momentum l, and we can write the eigenstates with sharp energy in the form

$$\psi(JM\pi)=\hat{\psi}(JM;\alpha ls;\text{in}) + \sum_{\alpha' l' s'} S(J\pi;\alpha ls;\alpha' l' s')\psi(JM;\alpha' l' s';\text{out}), \quad (26)$$

where

$$\hat{\psi}(JM;\alpha ls)\equiv \pm(ir_s v_s^{\frac{1}{2}})^{-1}\exp\pm i\left(K_s r_s-\frac{l\pi}{2}\right)\sum_{m\nu} \times C(j_1 j_2 s;m_1,\nu-m_1)C(slJ;\nu,M-\nu) \times\chi_{j_1}^{m_1}\chi_{j_2}^{m_2}Y_l^{M-\nu}(\vartheta,\varphi). \quad (26a)$$

(The $\chi_{j_i}^{m_i}$ are the wave functions of the particles i, while v_s is their relative velocity. For an in-going spherical wave we use the minus signs in Eq. (26a); for an outgoing wave, the plus signs are used.) $S(J\pi;\alpha ls;\alpha' l' s')$ is the scattering matrix, which must be unitary and symmetric in order to satisfy the two requirements of (1) conservation of the total number of systems and (2) reciprocity. The wave functions given above are continuable into the internal region, and are therefore suitable eigenfunctions to use as a basis for describing the compound state. The compound state is assumed to be a pure state, decaying into pairs of particles which are detected by the apparatus envisaged. According to the preceding discussion, the detection of a direction of motion of a particle corresponds to information which determines the density matrix of the compound state. Such information, when combined with the information that leads to this state, yields an angular correlation.

The states given by Eq. (26) are, however, not pure states, since the in- and out-going parts correspond to different mixtures of the various channels. What we desire is an eigenstate of the scattering matrix, that is, a state (we label it by n) composed of all channels, pairs of particles and orbital angular momenta, with the weights $X(n,\alpha ls)$, such that the in- and out-going parts belong to the same mixture. Since this is an eigenstate of the scattering matrix, we have by definition

$$\sum_{\alpha' l' s'} S(J\pi;\alpha ls;\alpha' l' s')X(n,\alpha' l' s')=e^{2i\delta_n}X(n,\alpha ls) \quad (27)$$

with real δ_n. The desired state is therefore

$$\psi(JM\pi,n)=\sum_{\alpha ls} X(n,\alpha ls) \times\{\psi(JM;\alpha ls;\text{in})+e^{2i\delta_n}\psi(JM;\alpha ls;\text{out})\}. \quad (28)$$

Strictly speaking, since the compound state is decaying, the energy is unsharp and one should take a summation of the states above over an energy range. We shall not put this in evidence since it does not affect the arguments that follow.

The experiment envisaged measures now the type of particles (α) and their spin magnitudes (j_1 and j_2) as well as their (back-to-back) direction of motion. Hence we must expand the wave function above into eigenstates of the linear momentum, exactly the situation considered in Sec. II-C above. When this is done, one finds for the density matrix of the compound state

$$E(JJMM')=\tfrac{1}{2}\sum(-)^{s-M}i^{l'-l}(2J+1) \times[(2l+1)(2l'+1)]^{\frac{1}{2}}C(ll'\nu;00) \times C(JJ\nu;M,-M')X(n,\alpha ls) \times X^*(n,\alpha l's)W(JJll';\nu s) \times D(\nu,M-M',0;\mathfrak{k}), \quad (29)$$

and the summation is to be carried out over s, l, l' and ν.

This result has just the form given in Eq. (20); since (a) $[(2l+1)(2l'+1)]^{\frac{1}{2}}C(ll'\nu;00)D(\nu,M'-M,0;\mathfrak{k})$ are the tensor parameters of the radiation, inasmuch as no spin polarization is considered, (b) $C(JJ\nu;M,-M')\times(-)^{s-M}$ are the coefficients that connect the tensor parameters with the density matrix, and (c) the $W(JJll';\nu s)$ are the change of coupling or Racah coefficients. The $X(n,\alpha ls)$, $X^*(n,\alpha l's)$ are the "physical parameters" that give the weights with which various subsystems mix in the nth eigenstate.

It remains only to observe that the $X(n,\alpha ls)$ are (or can be chosen to be) *real*. Since the $X(n,\alpha ls)$ corre-

CC-0. In Public Domain. Gurukul Kangri Collection, Haridwar

Digitized by Arya Samaj Foundation Chennai and eGangotri

spond in a perturbation calculation to the reduced matrix elements, one sees in particular that the relative phase of any mixture of reduced matrix elements is always 0 or π.

The proof for the reality of the $X(n, \alpha ls)$ is immediate. Since $S^+=S^{-1}$ (unitary property) and $\tilde{S}=S$ (symmetric property), we see that S can be always written in the form $S=U^{-1}e^{i\Delta}U$ where U is real and orthogonal and Δ is real and diagonal.

Since

$$SX(n)=e^{2i\delta_n}X(n)$$
$$=U^{-1}e^{i\Delta}UX(n),$$

we have then

$$e^{i\Delta}UX(n)=e^{2i\delta_n}UX(n),$$

and we can choose $UX(n)$ to have the form of a column vector with unity in the nth place, zero elsewhere. Designating this column vector by w_n, that is,

$$\text{trans}w_n=(\cdots 0\,0\,0\,1\,0\cdots),$$

we have

$$X(n)=U^{-1}w_n. \tag{30}$$

Then $X(n, \alpha ls)$ is real since U is real. This is the proof of the reality of the matrix elements, and *a fortiori*, of the theorem on relative phases of interfering matrix elements, referred to in subsection C above.

Previous proofs of the reality of the reduced matrix elements have involved the commutability of the interactions with time reversal operators. The above proof also uses time reversal but in a concealed fashion since the properties of the S matrix were deduced from demanding reciprocity. The form of the proof above shows that this result on the relative phase of the reduced matrix elements is more general than the strict applicability of the equations would indicate. For photon emission or absorption, the use of wave functions as in the above equations is dubious at best. However (78), the form of the results should nonetheless hold, and, indeed, the result on the relative phase of the matrix elements has been verified for photon emission directly, (55). Since the generalization to relativistic wave functions can be readily carried out (42a), the result can be seen to be valid in this case also.

In the double cascade correlation experiment, the initial compound state is randomly oriented and the observation of the first radiation determines the density matrix of the residual compound state. This introduces only formal changes as compared to the case considered above where the observation of the radiation determined the density matrix of the *radiating* state. As a result, however, one sees that the cascade correlation involves the properties (i.e., the "physical parameters" $X(n, \alpha ls)$) of *two* compound states, unlike the nuclear reaction problem where the same compound state occurs in both transitions. An additional distinction, as mentioned earlier, is the fact that the nuclear reaction cannot in general be considered as occurring via a pure state; rather one must add with equal weights, the contributions of all spins (J), parities (π) and eigenstates (n) of the compound system.

The density matrix for a compound state where J, π, n are not sharp has the form

$$E(JJ'MM')=\tfrac{1}{2}\sum(-)^{s-M}i^{l'-l}$$
$$\times[(2J+1)(2J'+1)(2l+1)(2l'+1)]^{\frac{1}{2}}$$
$$\times C(ll'\nu;00)C(JJ'\nu;M,-M')$$
$$\times W(lJl'J';s\nu)D(\nu,M'-M,0;\mathfrak{k})$$
$$\times X(n,\alpha ls)X(n',\alpha'l's)$$
$$\times\begin{Bmatrix}\exp[2i(\delta_n-\delta_{n'})] & \text{out}\\ 1 & \text{in}\end{Bmatrix}, \tag{31}$$

and the sum is over s, l, l', ν; the "out" and "in" refer to the compound state decaying or being formed, respectively. For a nuclear reaction, we have the *same* compound state formed by an incident radiation (1) and decaying into an outgoing radiation (2). The angular distribution has the form (see Eqs. (35) and (38) below),

$$W(\mathfrak{k}_1,\mathfrak{k}_2)=\sum E(JJ'MM';1)E^*(JJ'MM';2), \tag{32}$$

with the summation over M, M', J, J', π, π', n and n'. In Eq. (32) $\mathfrak{k}_1$ and $\mathfrak{k}_2$ are the unit propagation vectors of the radiations (1) and (2). The sum over J, J', π, π', n, n' is necessary since the reaction proceeds via all compound states. The sum over M' and M is readily performed giving the result

$$W(\mathfrak{k}_1,\mathfrak{k}_2)=\tfrac{1}{4}\sum_L B_L P_L(\mathfrak{k}_1\cdot\mathfrak{k}_2),$$

where

$$B_L=\sum X(n,\alpha l_1 s)X(n',\alpha l_1' s)X(n,\alpha' l_2 s')$$
$$\times X(n',\alpha' l_2' s')(-)^{s-s'}\exp[2i(\delta_{n'}-\delta_n)]$$
$$\times[i^{l_1'-l_1+L}\{(2J+1)(2J'+1)(2l_1+1)(2l_1'+1)\}^{\frac{1}{2}}$$
$$\times C(l_1l_1'L;00)W(l_1Jl_1'J';sL)]$$
$$\times[i^{l_2'-l_2+L}\{(2J+1)(2J'+1)(2l_2+1)(2l_2'+1)\}^{\frac{1}{2}}$$
$$\times C(l_2l_2'L;00)W(l_2Jl_2'J';s'L)]. \tag{33}$$

The latter sum is over J, J', l_1, l_1', l_2, l_2', s, s', n, n'. The quantities in square brackets are just the $Z(l_1Jl_1'J';s\nu)$ coefficients arising in the angular distribution of nuclear reactions and defined in reference (15).

The sum over n, n' can be carried out since we note that this is just the "spectral form" of the scattering matrix. That is,

$$\sum_n X(n,\alpha l_1 s)X(n,\alpha' l_2 s')e^{-2i\delta_n}$$
$$=S^+(J\pi;\alpha l_1 s;\alpha' l_2 s') \tag{34a}$$

$$\sum_{n'} X(n',\alpha l_1' s)X(n',\alpha' l_2' s')e^{2i\delta_{n'}}$$
$$=S(J'\pi';\alpha l_1' s;\alpha' l_2' s'). \tag{34b}$$

CC-0. In Public Domain. Gurukul Kangri Collection, Haridwar

Digitized by Arya Samaj Foundation Chennai and eGangotri

Finally if we wish to find the scattering angular distribution as well as the reaction distribution, we must cancel the cross section given above for no reaction, i.e., $S=1$. In other words, we replace S by $S-1$ in the above formula for the reaction cross section, and it becomes valid for scattering as well. Putting these steps together we find for the differential cross section

$$W(\mathbf{f}_1, \mathbf{f}_2)\sim d\sigma_{\alpha\alpha'}=\frac{1}{4}\frac{\lambda\!\!\!^{-}_{\alpha}{}^2}{(2j+1)(2j_0+1)}\sum_L B_L P_L(\mathbf{f}_1\cdot\mathbf{f}_2),$$

where j and j_0 are the spins of incident particle and target nucleus and $\lambda\!\!\!^{-}_{\alpha}$ is the reduced wavelength in the incident channel α;

$$B_L=\sum(S(J\pi)-1)^{+}(S(J'\pi')-1)(-)^{s-s'}\times Z(l_1Jl_1'J';sL)Z(l_2Jl_2'J';s'L). \quad (34)$$

The sum in the expression for B_L is over J, J', π, π', l_1, l_1', l_2, l_2', s, s'. This is exactly the result for nuclear scattering and reactions given in reference (15).

We emphasize again that this simple reduction of the distribution to its dependence on the scattering matrix was possible only because (a) we summed over all possible compound states, and (b) the two radiations involved the *same* compound state. The angular correlation problem is distinguished from the above by just these features, and we therefore must give our results in the less compact spectral form.

E. The Double Correlation

We consider here the correlation of two successive radiations for the case of an unperturbed intermediate state. In (1) below the general form of the correlation function is obtained. In (2) the direction-direction correlation is considered. The polarization-direction correlation is of practical interest only in the case of an observation of the linear polarization of γ rays and for this reason we defer the discussion of this correlation to Sec. III.

1. The General Double Correlation Function

Here, and in the following, we make explicit use of our choice of phases for which the reduced matrix elements are *real*. They are not Hermitian (i.e., symmetric). Instead

$$(2j+1)^{\frac{1}{2}}(j_1\|L\|j)=(-)^{j_1+L-j}(2j_1+1)^{\frac{1}{2}}(j\|L\|j_1).$$

Having set up the density matrices $E(mm')$, the problem now is to relate this to the correlation function of a simple two radiation correlation. Let us suppose that the intermediate nucleus is unperturbed, i.e., that $S(m_am_a';m_nm_n')=\delta(m_am_n)\delta(m_a'm_n')$. Then using Eqs. (2) and (13) we have

$$\begin{aligned}W&=\sum_{mm'}E^{(1)}(mm')E^{(2)*}(mm')\\&=(2j+1)^2\sum C_{\nu_1\tau_1}(L_1L_1')C_{\nu_2\tau_2}{}^{*}(L_2L_2')\\&\quad\times(-1)^{j_1-j_2+L_1-L_2}(j_1\|L_1\|j)(j_1\|L_1'\|j)\\&\quad\times(j_2\|L_2\|j)(j_2\|L_2'\|j)C(jj\nu_1;m,-m')\\&\quad\times C(jj\nu_2;m,-m')W(jjL_1L_1';\nu_1j_1)\\&\quad\times W(jjL_2L_2';\nu_2j_2)D(\nu_1,m'-m,\tau_1;\mathfrak{R}_1)\\&\quad\times D^{*}(\nu_2,m'-m,\tau_2;\mathfrak{R}_2). \quad (35)\end{aligned}$$

The summation in Eq. (35) is over $\pi_1\pi_2L_1L_1'L_2L_2'\nu_1\nu_2\tau_1\tau_2mm'$. $\mathfrak{R}_1$ and $\mathfrak{R}_2$ are the rotations corresponding to radiations 1 and 2 as explained below Eq. (5). We can perform the sum over m holding $\mu\equiv m-m'$ fixed. This involves

$$\sum_m C(jj\nu_1;m\mu-m)C(jj\nu_2;m\mu-m)=\delta(\nu_1\nu_2). \quad (36)$$

That is, $\nu_1=\nu_2=\nu$. Finally we can perform the sum over μ

$$\begin{aligned}\sum_\mu D(\nu,\mu\tau_1;\mathfrak{R}_1)D^{*}(\nu,\mu\tau_2;\mathfrak{R}_2)&=\sum_\mu D(\nu,\mu\tau_1;\mathfrak{R}_1)D(\nu,\tau_2\mu;\mathfrak{R}_2^{-1})\\&=D(\nu,\tau_2\tau_1;\mathfrak{R}_2^{-1}\mathfrak{R}_1) \quad (37)\end{aligned}$$

and $\mathfrak{R}_2^{-1}$ is the inverse rotation to $\mathfrak{R}_2$. The rotation $\mathfrak{R}_2^{-1}\mathfrak{R}_1$ is that rotation which carries the coordinate system of the first radiation into the coordinate system of the second radiation. We designate the Euler angles of the $\mathfrak{R}_2^{-1}\mathfrak{R}_1$ rotation by $\alpha\beta\gamma$. The result is

$$\begin{aligned}W(\alpha\beta\gamma)\sim\sum(-1)^{L_1+L_2}&C_{\nu\tau_1}(L_1L_1')C_{\nu\tau_2}{}^{*}(L_2L_2')\\&\times(j_1\|L_1\|j)(j_1\|L_1'\|j)(j_2\|L_2\|j)(j_2\|L_2'\|j)\\&\times W(jjL_1L_1';\nu j_1)W(jjL_2L_2';\nu j_2)\\&\times D(\nu,\tau_2\tau_1;\alpha\beta\gamma). \quad (38)\end{aligned}$$

The sum is over L_1, L_1', L_2, L_2', τ_1, τ_2, and ν. This is the form of the general double correlation as given by Racah (65) and equivalently by Lloyd (57).

It is of interest to note that the sum performed in Eq. (37) furnishes a direct proof of the conjecture of Falkoff and Uhlenbeck (26) since it shows in particular thst only the angles of the reference axes attached to $\mathbf{f}_1$ measured with respect to $\mathbf{f}_2$ are significant in the correlation.[9] In other words, one may arbitrarily pick either of the radiations to define the coordinate axes without loss of generality—the principle of spectroscopic stability in another terminology. This fact has been extensively discussed in the literature from many points of view, see especially (44) and (26, 53, 51, 71, 75). It should be noted further that the density matrix may or may not be diagonal for this choice of axes, the diagonality being irrelevant (75).

[9] In fact, if only propagation vectors are measured, the only non-ignorable angle is β which is the angle between $\mathbf{f}_1$ and $\mathbf{f}_2$, the unit vectors in the propagation directions. See paragraph (2) below.

CC-0. In Public Domain. Gurukul Kangri Collection, Haridwar

Digitized by Arya Samaj Foundation Chennai and eGangotri

For the important cases where the intermediate state is not unperturbed (hfs, for example), the correlation calculation is more difficult but the methods are the same. We shall discuss these cases in Sec. IV.

2. Direction-Direction Correlation

Of greatest interest is the angular correlation in which one observes only the propagation vectors $\mathbf{f}_1$ and $\mathbf{f}_2$ of the two radiations and, as discussed in subsection II-A, for this case $\tau_1=\tau_2=0$ in Eq. (38) and α and γ are ignorable. Then, using

$$D(\nu, \lambda 0; \alpha\beta 0)=\left(\frac{4\pi}{2\nu+1}\right)^{\frac{1}{2}} Y_\nu^{\lambda *}(\beta, \alpha), \qquad (39a)$$

and thus

$$D(\nu, 00; \alpha\beta 0)=P_\nu(\cos\beta)=P_\nu(\mathbf{f}_1\cdot\mathbf{f}_2), \qquad (39b)$$

where P_ν is the Legendre polynomial, Eq. (38) becomes

$$W(\beta)=\sum(-)^{L_1+L_2}c_{\nu 0}(L_1L_1')c_{\nu 0}(L_2L_2') \times(j_1\|L_1\|j)(j_1\|L_1'\|j)(j_2\|L_2\|j) \times(j_2\|L_2'\|j)W(jjL_1L_1';\nu j_1) \times W(jjL_2L_2';\nu j_2)P_\nu(\cos\beta). \qquad (40)$$

The sum is over ν, L_1, L_1', L_2, and L_2'. As discussed in subsection G below, ν is an even integer in the range 0 to the smallest even integer of the set $2(L_1)_{\max}$, $2(L_2)_{\max}$ or $2j$. Here $(L_1)_{\max}$ is the largest value assumed by L_1 and/or L_1' and similarly for $(L_2)_{\max}$.

Equation (40) refers to the correlation in which the emitted radiation is a superposition of different angular momentum states. This case may occur not infrequently in the emission of α particles (Sec. III-B). Also, in the case of unfavorable parity change in γ-ray emission, a superposition of magnetic dipole and electric quadrupole has been observed to occur in several instances. Perhaps the more interesting case is the one in which only one of the transitions is not pure and consists in the superposition of only two angular momenta L_1 and L_1', say. Then the correlation function becomes

$$W(\beta)=W_I(\beta)+W_{II}(\beta)+W_{III}(\beta), \qquad (41)$$

where

$$W_I(\beta)=(-)^{L_1+L_2}(j_2\|L_2\|j)^2(j_1\|L_1\|j)^2 \times\sum_\nu c_{\nu 0}(L_1L_1)c_{\nu 0}(L_2L_2)W(jjL_1L_1;\nu j_1) \times W(jjL_2L_2;\nu j_2)P_\nu(\cos\beta), \qquad (41a)$$

$$W_{II}(\beta)=(-)^{L_1'+L_2}(j_2\|L_2\|j)^2(j_1\|L_1'\|j_1)^2 \times\sum_\nu c_{\nu 0}(L_1'L_1')c_{\nu 0}(L_2L_2)W(jjL_1'L_1';\nu j_1) \times W(jjL_2L_2;\nu j_2)P_\nu(\cos\beta), \qquad (41b)$$

$$W_{III}(\beta)=(-)^{L_2}(j_2\|L_2\|j)^2(j_1\|L_1\|j)(j_1\|L_1'\|j) \times\sum_\nu[(-)^{L_1}c_{\nu 0}(L_1L_1')+(-)^{L_1'}c_{\nu 0}(L_1'L_1)] \times c_{\nu 0}(L_2L_2)W(jjL_1L_1';\nu j_1) \times W(jjL_2L_2;\nu j_2)P_\nu(\cos\beta). \qquad (41c)$$

W_I is the correlation function which applies when the first transition is pure with radiation angular momentum L_1. Similarly, W_{II} applies when the first radiation angular momentum is L_1' only. W_{III} is an interference term which (see subsection II-F) does not contribute to the total intensity. In this term the minimum $\nu=2$. The maximum value of ν is the smallest even integer of the sets $2(L_1L_2j)$, $2(L_1'L_2j)$, $(L_1+L_1', 2L_2, 2j)$ in W_I, W_{II}, and W_{III}, respectively, (see subsection II-F). As written the correlation function W is not normalized so as to be necessarily positive definite. However, the insertion of a factor $(-)^{j_1-j_2}$ will insure this.

It will be observed that for both transitions pure the reduced matrix elements are merely scale factors so that in this case the correlation function can be written

$$W(\beta)=(-)^{L_1+L_2}\sum_\nu c_{\nu 0}(L_1L_1)c_{\nu 0}(L_2L_2) \times W(jjL_1L_1;\nu j_1)W(jjL_2L_2;\nu j_2)P_\nu(\cos\beta). \qquad (41d)$$

The result for the double correlation given in Eq. (40) shows that a useful representation of the correlation functions for different radiations is obtained as follows: (a) we adopt a standard cascade, *viz*, the $\gamma-\gamma$ cascade. For a transition in which a γ ray is emitted the $c_{\nu 0}(LL')$ will be denoted by $c_\nu(LL';\gamma)$. (b) For any other type of particle (x) emitted, the $c_{\nu 0}(LL')$ will be denoted by $c_\nu(LL';x)$. (c) We define the particle parameters $b_\nu(LL';x)$ by[10]

$$b_\nu(LL';x)=c_\nu(LL';x)/c_\nu(LL';\gamma). \qquad (42)$$

From the discussion following Eq. (20) we have in this case $(\tau=0)$ for the tensor parameters of radiation of type x

$$R(\nu q, LL';x)=(-)^{q+L'+L}D(\nu, q0;\mathbf{f})c_{\nu 0}(LL';x). \qquad (42a)$$

Therefore an alternative definition of the particle parameters is

$$b_\nu(LL';x)=R(\nu q, LL';x)/R(\nu q, LL';\gamma), \qquad (42b)$$

and it is to be noted that the ratio is independent of q. (d) The correlation function as written in Eq. (41 a, b, c) may be expressed in the form

$$W=\sum_i W_i, \qquad (43)$$

where $i=I, II, III$, and each of these may be written in the form

$$W_i=\sum_\nu A_\nu^{(i)}P_\nu(\cos\beta). \qquad (43a)$$

In Sec. III-A results are given whereby the coefficients $A_\nu^{(i)}$ for the standard $\gamma-\gamma$ correlation may be immediately obtained. We denote these coefficients by

[10] In subsequent applications involving pure radiations it is sometimes convenient to adopt a normalization in which $b_0(LL';x)=1$. This, of course, can always be accomplished by redefining b_ν as $c_\nu(LL';x)c_0(LL';\gamma)/c_\nu(LL';\gamma)c_0(LL';x)$.

CC-0. In Public Domain. Gurukul Kangri Collection, Haridwar

Digitized by Arya Samaj Foundation Chennai and eGangotri

$A_\nu^{(i)}(\gamma\gamma)$. Then, if a radiation (x) replaces the pure γ, the correlation function is

$$W(\beta)=\sum_i \sum_\nu b_\nu(L_2L_2;x)A_\nu^{(i)}(\gamma\gamma)P_\nu(\cos\beta). \quad (43b)$$

When the mixed γ-radiation is replaced by the radiation x, the coefficients $A_\nu^{(I)}$ and $A_\nu^{(II)}$ are merely multiplied by $b_\nu(L_1L_1;x)$ and $b_\nu(L_1'L_1';x)$, respectively. For the interference term we first note that

$$(-)^L c_\nu(LL';\gamma)=(-)^{L'}c_\nu(L'L;\gamma) \quad (44)$$

as is shown in Sec. III-A. Therefore the factor by which $A_\nu^{(III)}$ is to be multiplied is

$$\tfrac{1}{2}[b_\nu(LL';x)+b_\nu(L'L;x)].$$

(e) For the correlation of radiations x and y the correlation function is obtained by performing the steps given in (d) for each particle. Thus, for the $x-y$ correlation with both radiations pure the correlation function is[11]

$$W_{x-y}(\beta)=\sum_\nu b_\nu(L_1L_1;x)b_\nu(L_2L_2;y) \times A_\nu^{(I)}(\gamma\gamma)P_\nu(\cos\beta). \quad (45)$$

Of course, the choice of the $\gamma-\gamma$ correlation as the standard one is arbitrary. We could have chosen the $\alpha-\alpha$ correlation which, from the point of view of analytical simplicity and availability of numerical results, would have been almost equally suitable. However, the fact that the parity restriction precludes the mixing of even and odd L militates against this choice. For γ-rays the parity for given L depends on the character of the radiation (electric or magnetic) and mixtures of all L, L' pairs (consistent with angular momentum conservation) are permissible in principle. Of course, in the case of γ rays $L\geqslant 1$ and the omission of the $L=0$ value is a slight disadvantage when one wishes to consider the emission of radiations with a mixture of $L=0$ and a nonvanishing L (in the emission of α or β particles, for example). However, in this infrequently occurring case direct use of Eq. (40) can be made.

F. Symmetry Properties of the Double Correlation

The double-correlation problem shows a number of symmetries, which are the consequence of (a) the "Hermitian" character of the matrix elements, (b) the invariance of the interactions [Eq. (4)] under reversal of coordinates and/or time reversal and (c) the special symmetries characteristic of particular observations, (for example, observing only a direction of propagation). Consider first the Hermitian symmetry. From Eq. (1), particularized to simple double correlation, ($S(m_am_a';m_nm_n'$) a unit matrix), we find that the Hermitian property requires the correlation function for $j_1(L_1)j(L_2)j_2$ to be identical with that corresponding to $j_2(L_2)j(L_1)j_1$. That is, initial and final states as well as first and second radiations may be reversed without any change in the correlation. This "degeneracy" is present even when the intermediate state is perturbed (Secs. IV and V-B). In the tabulation of the coefficients for the double correlation, given in Sec. III, use is made of this symmetry.

This symmetry property was apparent from Eq. (2). This property, it can be seen, holds even for non-Hermitian H operators. For example, in the case of no spin-coupling considered here, the correlation function is given by the trace of the product of the two density matrices; i.e., $W=tr(E^1E^2)=tr(E^2E^1)$ and the density matrices E^1 and E^2 are defined in precisely corresponding ways. The symmetry is not entirely obvious in Eq. (38) but can be readily checked by using

$$c_{\nu\tau}^*(LL')=(-)^{L+L'-\tau}c_{\nu,-\tau}(L'L),$$

which is directly derivable from the definition given in Eq. (12), and the unitary character of the rotation group matrices D^ν. It must be emphasized, however, that this symmetry was built into the theory, so to speak by our definition of the reduced matrix elements. Thus, Lloyd [(56) and especially (52)] writes the reduced matrix elements so that they always appear in the form $(j_f\|L\|j_i)$ where j_f and j_i, respectively, refer to final and initial states in each transition of the cascade. This differs from our convention only for the second transition of the cascade. Using the fact that Hermitian conjugation of the reduced matrix elements introduces a factor $(-)^{j_f-j_i+L}$, one finds that for the second transition

$$(j\|L_2\|j_2)(j\|L_2'\|j_2)=(-)^{L_2-L_2'}(j_2\|L_2\|j)(j_2\|L_2'\|j).$$

Consequently, with Lloyd's definition of the reduced matrix elements one must introduce a sign change in the interference term w_{III} when the second transition is a mixture with $|L_2-L_2'|$ an odd integer—the practical case (and the first pure), but no sign change if the first transition is a similar mixture (the second pure). This point is emphasized because the sign of the reduced matrix element product $(j_i\|L_i\|j)(j_i\|L_i'\|j)$ (with $|L_i'-L_i|=1$) can be measured and any attempt to compare a calculation of this phase on the basis of some nuclear model with the measured result must take into account the definition of the matrix elements used in the analysis of the experimental data.

The invariance of the interaction to time inversion allows us to conclude that the relative phase of the reduced matrix elements appearing in Eq. (38) is 0 or π. This point has already been discussed in subsections II-C and -D above.

[11] For the K conversion-conversion correlation the validity of Eq. (45) is based on the fact that the lifetime of the K shell hole, formed after the first conversion, is much shorter than the lifetime of the intermediate nuclear state, (62). Therefore, when the second conversion transition occurs the atomic state is initially the same as for the first conversion transition. If this were not the case, there would be appreciable interference contributions between the two alternative ways of reaching the final state corresponding to the two possible orders of emission of the two K electrons (50).

CC-0. In Public Domain. Gurukul Kangri Collection, Haridwar

Digitized by Arya Samaj Foundation Chennai and eGangotri

In order to derive the properties of $W(\mathbf{f}_1\cdot\mathbf{f}_2)$ under coordinate reversal ($\beta\to\pi-\beta$), we shall assume (a) that the parity is a good quantum number and (b) that our measurements do not distinguish between right and left-handed coordinate systems. The only possible cases where the latter would not apply involve measurements of circular polarization of γ rays and/or polarization of spin $\frac{1}{2}$ particles and these cases are not particularly amenable to experiment. In the case where only a direction of motion is observed, the tensor parameters of the radiation involve $D(\nu, q0; \mathbf{f})$ which under reflection is multiplied by $(-)^\nu$. Since this must be identical with the tensor parameters before reflection we deduce that ν is *even*. The correlation is therefore symmetric around $\beta=\frac{1}{2}\pi$. If the second condition is violated (imagine for example measuring the circular polarization of gamma-rays), then the argument is invalid, and in fact odd values of ν enter. In contrast to some arguments hitherto advanced, the good quantum number property of the parity is insufficient to guarantee that only even ν enter the double correlation. For linear polarized gammas, the measurements are unchanged by coordinate reflection and thus ν is indeed even in this case.

The *complexity* of the double correlation, that is the number of Legendre polynomials with $\nu>0$ that enter Eq. (40), has been the subject of much discussion in the literature, (24, 79, 80). In the formulation above the allowed values for ν are determined by the properties of the Racah coefficients, so that this question is solved in detail. The Racah coefficient $W(abcd; ef)$ vanishes unless we satisfy the triangle conditions (abe), (cde), (acf), and (bdf). A triangle condition such as (abe) implies that a, b, and e can form a triangle (including the case of vanishing area). As a result, we see from Eq. (40) that ν is restricted by

$$(1)\quad 0\leqslant\nu\leqslant 2j,$$
$$(2)\quad 0\leqslant\nu\leqslant 2(L_1)_{\max},$$
$$(3)\quad 0\leqslant\nu\leqslant 2(L_2)_{\max}.$$

In the light of the density matrix formulation these rules are fairly obvious. For a radiation of multipolarity 2^L, we can define tensor parameters of rank at most $2L$. Since these tensor parameters determine the tensor parameters of the intermediate state, it is clear that the rank of the tensor parameters of the intermediate state is less than or equal to the minimum of $(2L, 2j)$. Finally, the tensor parameters of the intermediate state determine the tensor parameters of the second radiation, which must therefore be the minimum of $2(L_1, L_2, j)$. If j is a half-integer then j in the above is replaced by $j-\frac{1}{2}$. Of course, for $j=\frac{1}{2}$ one always has $\nu=0$ only and therefore an isotropic correlation function.

Of course, an experimental determination of the maximum ν is difficult if the coefficient of the Legendre polynomial with maximum ν is small. However, the coefficient of P_2 is almost always sufficiently large to give an observable anisotropy. Thus, if isotropy is observed one can conclude (a) in the case of γ emission (or conversion electrons) $j=0$ for even-mass nuclei and $j=\frac{1}{2}$ for odd-mass nuclei; (b) for particles which can have $L=0$ (α particles, β decay, nucleons) either one of the L's has a zero value or $j=0$ or $\frac{1}{2}$ depending on the mass number of the nucleus in the intermediate state.

G. Relation to the Falkoff-Uhlenbeck Method (26)

It is useful at this point to show the relation of the present methodology to the procedures of Falkoff-Uhlenbeck. Falkoff and Uhlenbeck consider the angular correlation problem in two steps, wherein each transition is represented in terms of the emission of a particle current multiplied by suitable weight factors (the relative probability of transitions between various sublevels of the nuclear states involved, see Eq. (47) below). In the case of gamma emission, this current is the familiar Poynting flux from an array of multipoles all with the same magnetic quantum number. Since the Falkoff-Uhlenbeck procedure considers the radiation with a well-defined magnetic quantum number, emerging from a completely defined initial state, it is clear that the intermediate state similarly has a fixed magnetic quantum number. Consequently, their procedure is more restrictive than the procedure given in the foregoing, in that it does not make provision for coherent processes in general. Lacking the flexibility to handle coherent processes, the Falkoff-Uhlenbeck procedure forces one to link the two successive emissions via an incoherent intermediate state, which is simply enough accomplished by letting one or the other of the two radiations define the quantization axis for the problem, subject only to the restriction (necessary in the Falkoff-Uhlenbeck method) that the choice must diagonalize the density matrix (see discussion at the end of II-E). It is for this reason that the "choice of axes" held such a central position in their work.

To show the relation of the two procedures in more detail let us consider the double correlation problem for the unperturbed intermediate state. The correlation is then

$$W(\mathbf{f}_1\cdot\mathbf{f}_2)=\mathfrak{S}\sum_{m_1m_2m}|\langle j_1m_1|H_1(\mathbf{f}_1)|jm\rangle|^2\times|\langle jm|H_2(\mathbf{f}_2)|j_2m_2\rangle|^2. \quad (46)$$

Here we have made the sums incoherent by taking $\mathbf{f}_1$ (for example) to define the quantization axis. Falkoff and Uhlenbeck now introduce the function

$$\mathfrak{S}|\langle j_1m_1|H(\mathbf{f})|jm\rangle|^2\equiv[C(j_1Lj; m_1, m-m_1)]^2F_L{}^{m-m_1}(\beta) \quad (47)$$

for a pure multipole transition. Hence

$$W(\mathbf{f}_1\cdot\mathbf{f}_2)\sim\sum_{m_1m_2m}[C(jL_1j; m_1, m-m_1)]^2\times F_{L_1}{}^{m-m_1}(0)[C(jL_2j_2; m, m_2-m)]^2F_{L_2}{}^{m_2-m}(\beta), \quad (48)$$

CC-0. In Public Domain. Gurukul Kangri Collection, Haridwar

Digitized by Arya Samaj Foundation Chennai and eGangotri

again for pure multipoles and unpolarized radiations. The result for polarized radiation can be obtained from Eq. (50) below. In this form the angular correlation problem has a very simple physical interpretation. Equation (48) states that the populations of the sublevels m of the intermediate state are determined by the current associated with the first radiation, $F_{L_1}{}^{m-m_1}(0)$, multiplied by the Zeeman intensity coefficients $[C(j_1L_1j; m_1, m-m_1)]^2$. The subsequent radiation is the product then of the flux of the second radiation, $F_{L_2}(\beta)$, the Zeeman intensity coefficients and the population of the intermediate sublevels obtained from the first transition. Of course, as pointed out earlier, it is equally valid to choose $\mathbf{f}_2$ as the axis of quantization.

The connection with the density matrix formulation is easily seen to be

$$E_{mm}{}^{(1)} \sim \sum_{m_1} [C(j_1L_1j, m_1, m-m_1)]^2 F_{L_1}{}^{m-m_1}(\beta). \quad (49)$$

It is more convenient to consider Eq. (47) (generalized for mixed multipoles), however, to define the mixed flux $F_{LL'}{}^M$ (49). Introducing Eqs. (4), (5), (7), (9), yields

$$\begin{aligned} F_{LL'}{}^M(\beta, \alpha) &= \sum_\nu (j_1\|L\|j)(j_1\|L'\|j) \\ &\quad \times C(LL'\nu; M, -M)(-)^M \\ &\quad \times \mathfrak{S} \sum_{\mu\mu'} \alpha^*(L\mu, \pi)\alpha(L'\mu', \pi)(-)^\mu \\ &\quad \times C(LL'\nu; -\mu, \mu')D(\nu, 0\mu'-\mu; \mathbf{f}_1) \\ &= \sum_{\nu\tau} c_{\nu\tau}(LL')(j_1\|L'\|j)(j_1\|L\|j) \\ &\quad \times \left(\frac{4\pi}{2\nu+1}\right)^{\frac{1}{2}} (-)^{L'-\nu} Y_\nu{}^\tau(\beta\alpha) \\ &\quad \times (-1)^M C(LL'\nu; M, -M). \quad (50) \end{aligned}$$

The $F_{LL'}{}^M$ of reference (49) is normalized differently and is, in fact, the above without the reduced matrix elements.

This form for the generalized $F_{LL'}{}^M$ shows a number of interesting features. (a) In order that the use of the Falkoff-Uhlenbeck procedure be correct, it is necessary that the choice of axes diagonalize the density matrix. This will not be the case unless $\tau=0$. (An example when $\tau\neq0$ is an experiment detecting linearly polarized γ-rays.) We must thus choose the other radiation to define the axis, if it has $\tau=0$, or if not, apply the more general techniques discussed earlier. (b) The integrated intensity from the $F_{LL'}{}^M(\beta\alpha)$ consists of only the term with $\nu=\tau=0$. Since $C(LL'0; M, -M)$ vanishes unless $L=L'$ we see that only the $F_{LL}{}^M(\beta)$, i.e., the "self terms," contribute to the integrated intensity. The interference terms affect the angular distribution but not the total intensity. This was shown first by Casimir (18). As shown earlier, this result follows from the general correlation function given in Eq. (38). (c) One of the central problems for angular correlations is the determination of the particle parameters of the radiation, depending on the $c_{\nu\tau}(LL')$. From Eq. (50) it is clear that the problem of determining $F_{LL'}{}^M(\beta\alpha)$ is completely equivalent to that of determining the $c_{\nu\tau}(LL')$. In practice, the formulation of a radiation problem in terms of the emitted flux is generally simpler conceptually than the equivalent formulation in terms of the tensor parameters for the radiation. Consequently, the relation given in Eq. (50) is very often useful.

It remains only to observe that introducing Eq. (50) into Eq. (49), and using Eq. (11) twice, reduces the correlation function $W(\mathbf{f}_1, \mathbf{f}_2)$ to the form of Eq. (38). As noted before the radiation that is chosen to define the axes must have $\tau=0$ so that the Falkoff-Uhlenbeck procedure is not completely general even for the double correlation. However, the use of the $F_{LL'}{}^M(\beta\alpha)$ to define the particle parameters is nonetheless completely general.

III. SPECIAL CASES OF ANGULAR CORRELATION

In this section we take up the correlation in the case of specific radiations. We consider in turn the tensor parameters for (a) gamma radiation (b) alpha particles, (c) conversion electrons, and (d) β particles. It follows from Sec. II-E that from these results one can immediately obtain the correlation function for the double cascade in which any pair of these radiations (e.g., $\gamma-\gamma$, $\beta-\gamma$, etc.) are emitted. The numerical results are presented in the form of tables given below.

A. Gamma Radiation

(1) General Properties

We shall describe the photon field by means of the vector potential, which we shall treat as the "wave function" for the light quantum, (42). The tensor parameters of the quantum, according to our general recipe, are then found from the transcription of the measured plane wave states, taking proper account of polarization, into the spherical eigenfunction states natural to the description of the nuclear process. The intrinsic (unit) spin of the photon will be described by the wave function $\chi_1{}^P$, the sharp momentum of the γ-ray by $e^{i\mathbf{K}\cdot\mathbf{r}}$. The transverse nature of light waves allows P to be ±1 only, measured in a coordinate system attached to the direction of motion. Thus P is a polarization index ($P=-1$ corresponding to right circular polarization). Because of this restriction, a polarization measurement determines the spin state to be a linear combination of these two basic states, with complex coefficients, that is,

$$\chi_* = a\chi_1{}^1 + b\chi_1{}^{-1}; \quad |a|^2 + |b|^2 = 1. \quad (51)$$

A convenient description of an arbitrary polarization is

CC-0. In Public Domain. Gurukul Kangri Collection, Haridwar

Digitized by Arya Samaj Foundation Chennai and eGangotri

obtained by introducing the rotation matrices for spin $\frac{1}{2}$,

$$\chi_s=\sum_\mu D(\tfrac{1}{2},\tfrac{1}{2}\mu;0ba)\chi_1{}^{2\mu}. \tag{52}$$

Of course, $\mu=\pm\frac{1}{2}$. The Euler angles b, a constitute a full description of a completely polarized quantum, and are, of course, closely related to the Stokes parameters, as shown in detail later. Setting the first Euler angle in Eq. (52) equal to zero merely fixes a nonessential constant phase. Consider now the wave function (vector potential) for a circularly polarized plane wave quantum travelling along the z direction[12]

$$\chi_1{}^P e^{iKz}=\sum_l (2l+1)^{\frac{1}{2}}(4\pi)^{\frac{1}{2}} j_l(Kr) i^l Y_l{}^0(\mathbf{r})\chi_1{}^P. \tag{52a}$$

Using the vector addition model we write

$$i^l Y_l{}^0\chi_1{}^P=\sum_{L=l\pm1,\,l} C(l1L;0P)\Phi_{L,l}{}^P, \tag{53}$$

where

$$\Phi_{Ll}{}^P=i^l\sum_\tau C(l1L;P-\tau,\tau)Y_l{}^{P-\tau}\chi_1{}^\tau. \tag{53a}$$

Thus

$$\begin{aligned}\chi_1{}^P e^{iKz}=(2\pi)^{\frac{1}{2}}\sum_L[&(L+1)^{\frac{1}{2}} j_{L-1}(Kr)\Phi^P{}_{L,L-1}\\ &+L^{\frac{1}{2}} j_{L+1}(Kr)\Phi^P{}_{L,L+1}\\ &-P(2L+1)^{\frac{1}{2}} j_L(Kr)\Phi^P{}_{L,L}].\end{aligned} \tag{54}$$

In Eq. (54) the first two terms correspond to an electric multipole vector potential and the last term to a magnetic multipole potential.

If we rotate the coordinate system, so that the wave propagates in an arbitrary direction $\mathfrak{k}$, we note that the spin direction rotates (rigidly) with the propagation direction so that we rotate the $\Phi_{L,l}{}^P$ as a single entity.

$$\begin{aligned}(\chi_1{}^P e^{iKz})'=\pi\sum_{L,M}&(2L+1)^{\frac{1}{2}}D(L,MP;\mathfrak{R})\\ &\times(A^e(LM)+(-P)A^m(LM)).\end{aligned} \tag{55}$$

The $A^e(LM)$ and $A^m(LM)$ are the usual (standing wave) vector potentials, (42), normalized to $(\pi^2\hbar K)^{-1}$ quanta-sec, redefined only to the extent of a phase. For magnetic multipoles (m) this phase is i^L, for electric multipoles (e) it is i^{L+1}, since we require that $K_t A^{e,m}(LM)=(-1)^{L-M}A^{e,m}(L-M)$ in order to make the reduced matrix elements explicitly real.

At present, it is experimentally feasible to measure only unpolarized and linearly polarized gamma-rays (17). Nonetheless we shall not specialize our treatment at the outset to these important cases alone but rather shall handle a general partially polarized gamma-quantum and specialize at the end to the relevant cases. Let us represent the result of the polarization measurement by the vector $\mathbf{P}$; that is to say, a vector with the Euler angles a, b as azimuth and polar angles, respectively, in a coordinate frame attached to the direction of motion. Note that this polarization vector is *not* along the direction of the electric field vector, $\mathbf{E}$. Then our measured state is represented by

$$\begin{aligned}(\chi_s e^{iKz})'=\pi\sum_{LM\mu}&(2L+1)^{\frac{1}{2}}D(\tfrac{1}{2},\tfrac{1}{2}\mu;\mathfrak{P})\\ &\times D(L,M2\mu;\mathfrak{R})[A^e(LM)-2\mu A^m(LM)].\end{aligned} \tag{56}$$

We write the phase (-2μ), that occurs for magnetic multipoles only, in the form $[\pi(-)^L]^{\frac{1}{2}+\mu}$ when π is the parity of the radiation. Here $\pi=(-)^{L+1}$ for magnetic multipoles and $\pi=(-)^L$ for electric multipoles. Then we can treat all the multipoles symmetrically

$$\begin{aligned}(\chi_s e^{iKz})'=\pi\sum&(2L+1)^{\frac{1}{2}}D(\tfrac{1}{2},\tfrac{1}{2}\mu;\mathfrak{P})\\ &\times D(L,M2\mu;\mathfrak{R})[\pi(-)^L]^{\frac{1}{2}+\mu}A^\pi(L,M),\end{aligned} \tag{57}$$

where $A^\pi(L,M)=A^e(L,M)$ and $A^m(L,M)$ for $\pi=(-)^L$ and $(-)^{L+1}$, respectively. The sum is over L, M, μ, and π.[13]

The tensor parameters of the radiation, with parity a good quantum number, are obtained as described in Sec. II-B and one finds[14]

$$\begin{aligned}R(\nu q,LL'\pi)=&[(2L+1)(2L'+1)]^{\frac{1}{2}}\\ &\times\sum(-)^{(\frac{1}{2}+\mu)L+(\frac{1}{2}+\mu')L'}(-)^{L-M}\pi^{\mu-\mu'}\\ &\times C(LL'\nu;M,-M')\delta(q,M-M')\\ &\times D^*(\tfrac{1}{2},\tfrac{1}{2}\mu';\mathfrak{P})D(\tfrac{1}{2},\tfrac{1}{2}\mu;\mathfrak{P})\\ &\times D^*(L',M'2\mu;\mathfrak{R})D(L,M2\mu;\mathfrak{R}).\end{aligned} \tag{58}$$

The sum is over M, M', μ, μ'. Now

$$\begin{aligned}D^*(\tfrac{1}{2},\tfrac{1}{2}\mu';\mathfrak{P})&D(\tfrac{1}{2},\tfrac{1}{2}\mu;\mathfrak{P})\\ &=\tfrac{1}{2}\delta(\mu\mu')+\tfrac{1}{2}|\mathbf{P}|(-)^{\frac{1}{2}-\mu}D(1,00;\mathfrak{P})\delta(\mu\mu')\\ &\quad+2^{-\frac{1}{2}}|\mathbf{P}|(-)^{\frac{1}{2}+\mu}D(1,02\mu;\mathfrak{P})\delta(\mu,-\mu').\end{aligned} \tag{59}$$

To account for partial polarization, we have assigned a magnitude to the polarization vector, $0\leqslant|\mathbf{P}|\leqslant1$, such that $|\mathbf{P}|=0$ corresponds to unpolarized γ rays and $|\mathbf{P}|=1$ corresponds to completely polarized γ-rays.

Using Eq. (9) we find that the tensor parameter consist of three terms

$$R(\nu q,LL'\pi)=R_I+R_{II}+R_{III}. \tag{60}$$

The first term is

$$\begin{aligned}R_I\equiv(-)^{q+L'+1}&[(2L+1)(2L'+1)]^{\frac{1}{2}}\\ &\times C(LL'\nu;1-1)D(\nu,q0;\mathfrak{k})\end{aligned} \tag{60a}$$

[12] To clarify the notation we observe that

$$\chi_1{}^1=\begin{pmatrix}1\\0\\0\end{pmatrix}\quad\chi_1{}^{-1}=\begin{pmatrix}0\\0\\1\end{pmatrix}$$

and denoting the vector potential by $\mathbf{A}$, Eq. (52a) gives $-2^{-\frac{1}{2}}(A_x+iA_y)$ for $P=1$ and $2^{-\frac{1}{2}}(A_x-iA_y)$ for $P=-1$.

[13] The distinction between the numeric π (occurring in Eq. (57) and elsewhere) and the parity symbol should be fairly obvious. Wherever π occurs in the tensor parameters $R(\nu q)$, it refers to parity.

[14] Since the tensor parameters refer here to γ rays, we have suppressed the radiation index γ and to emphasize the parity dependence the π symbol is put in evidence in the $R(\nu q)$.

CC-0. In Public Domain. Gurukul Kangri Collection, Haridwar

Digitized by Arya Samaj Foundation Chennai and eGangotri

for ν an even integer. This is the polarization independent term.

$$R_{II}\equiv(-)^{q+L'+1}|\mathbf{P}|[(2L+1)(2L'+1)]^{\frac{1}{2}} \times C(LL'\nu;1-1)D(1,00;\mathfrak{P})D(\nu,q0;\mathfrak{k}) \quad (60b)$$

for ν an *odd* integer. This is the "circular" polarization contribution.

$$R_{III}\equiv(-)^{q}\pi 2^{-\frac{1}{2}}|\mathbf{P}|[(2L+1)(2L'+1)]^{\frac{1}{2}} \times C(LL'\nu;11)[D(1,01;\mathfrak{P})D(\nu,q2;\mathfrak{R}) -(-)^{\nu}D(1,0-1;\mathfrak{P})D(\nu,q-2;\mathfrak{R})]. \quad (60c)$$

This is the linear polarization contribution. There is no restriction on ν at this stage of the calculation, but, since the reduced matrix elements are explicitly real, the $R(\nu q)$ are restricted to be "real" in the sense that $K_0R(\nu q)=(-)^{-q}R(\nu-q)$ (see II-C). This condition implies that ν is an *even* integer in R_{III}.

The tensor parameters for the most general partially polarized γ quanta have thus been obtained. Having introduced a magnitude for $\mathbf{P}$ to describe the degree of polarization, it is now clear that this description in terms of $\mathbf{P}$ corresponds to the Stokes parameter description of a quantum of unit intensity with polarization vector $\mathbf{P}$ in the Poincaré sphere (29).

For the cases of interest we have first unpolarized γ-rays; $|\mathbf{P}|=0$. Then

$$R(\nu q,LL'\pi)=(-)^{q+L'+1}[(2L+1)(2L'+1)]^{\frac{1}{2}} \times C(LL'\nu;1-1)D(\nu,q0;\mathfrak{k}), \quad (61)$$

where ν is an even integer, and

$$c_{\nu 0}(LL')=(-)^{L-\nu}C(LL'\nu;1-1) \times[(2L+1)(2L'+1)]^{\frac{1}{2}}. \quad (62)$$

If linear polarization is measured, the Euler angles of $\mathbf{P}$ are a, $b=\pi/2$, so that $D(1,00;\mathfrak{P})=0$ and $D(1,0\pm1;\mathfrak{P})=\mp2^{-\frac{1}{2}}e^{\pm ia}$. Then one finds

$$R(\nu q,LL'\pi) =[(2L+1)(2L'+1)]^{\frac{1}{2}}[(-)^{q+L'+1} \times C(LL'\nu;1-1)D(\nu,q0;\mathfrak{k}) +\tfrac{1}{2}(-)^{q+1}\pi C(LL'\nu;11)(e^{ia}D(\nu,q2;\mathfrak{R}) +e^{-ia}D(\nu,q-2;\mathfrak{R}))]. \quad (63)$$

The first term is simply R_I which is polarization independent. The second term is the contribution of the linear polarization, (R_{III}). It should be noted that the tensor parameters for linear polarization, in contrast to the unpolarized case, depend explicitly upon the parity of the radiation. It is this feature which motivates one to perform the more difficult polarization measurements, and shows, incidentally, that a polarization-polarization correlation (in which one measures the polarization of both quanta) has essentially nothing new to offer over the simpler direction-polarization correlations (60). The origin of this dependence on parity is not far to seek, since it is simply an expression of the duality theorem for multipole radiation. Changing the parity of the radiation but keeping L, L' fixed takes $e\leftrightarrow m$ multipoles, which by duality, takes $\mathbf{E}\rightarrow\mathbf{H}$, $\mathbf{H}\rightarrow-\mathbf{E}$, thus changing a by 180°; this reverses the sign of the linear polarization term, R_{III}. The usual linear polarization angle (defined by the $\mathbf{E}$ vector) is here $\frac{1}{2}a$. Since $D(L,q\pm2;\alpha\beta\gamma)=e^{iq\alpha}e^{\pm i2\gamma}\ d(L,q\pm2;\beta)$ (where $d(L,\mu\mu';\beta)$ is the Jacobi polynomial), one sees that the polarization angle a can be absorbed into γ, i.e., $\gamma\rightarrow\gamma+\frac{1}{2}a$. This introduces the usual polarization angle into the formalism above, see Eq. (73) below.

(2) *Correlation Function for Unpolarized Radiation*

Only the first term in Eq. (63) for the γ-tensor parameter enters and using Eqs. (40) and (42a) the $\gamma-\gamma$ correlation function is

$$W(\beta)=\sum(j_1\|L_1\|j)(j_1\|L_1'\|j)(j_2\|L_2\|j)(j_2\|L_2'\|j) \times C(L_1L_1'\nu;1-1)C(L_2L_2'\nu;1-1) \times W(jjL_1L_1';\nu j_1)W(jjL_2L_2';\nu j_2) \times[(2L_1+1)(2L_1'+1)(2L_2+1)(2L_2'+1)]^{\frac{1}{2}} \times P_\nu(\cos\beta). \quad (64)$$

The sum is over L_1L_1', L_2L_2' and ν.

For the cascade emission of a mixed 2^{L_1} plus $2^{L_1'}$ pole and a pure 2^{L_2} pole the correlation is, explicitly,

$$W(\beta)=(j_1\|L_1\|j)^2w_I+(j_1\|L_1'\|j)^2w_{II} +2(j_1\|L_1\|j)(j_1\|L_1'\|j)w_{III}, \quad (65)$$

where

$$w_I=(2L_1+1)(2L_2+1) \times\sum_{\nu\geq0}C(L_1L_1\nu;1-1)C(L_2L_2\nu;1-1) \times W(jjL_1L_1;\nu j_1)W(jjL_2L_2;\nu j_2)P_\nu(\cos\beta) \quad (65a)$$

is the correlation function for a pure $2^{L_1}-$pure 2^{L_2} pole cascade, w_{II} is the same as w_I but with L_1' replacing L_1 and

$$w_{III}=[(2L_1+1)(2L_1'+1)]^{\frac{1}{2}}(2L_2+1) \times\sum_{\nu\geq2}C(L_1L_1'\nu;1-1)C(L_2L_2\nu;1-1) \times W(jjL_1L_1';\nu j_1)W(jjL_2L_2;\nu j_2)P_\nu(\cos\beta) \quad (65b)$$

is the interference term. See also Eqs. (70, 70a, 70b, 70c). The correlation function for two mixed radiations can be readily obtained from Eq. (64). In practice the γ-ray mixture will be a 2^L and 2^{L+1} pole mixture. Then if $L_1=L$, the first term of Eq. (64) refers to the 2^L pole radiation and the second to the 2^{L+1} pole. From (Appendix A11)

$$C(LL0;1-1)W(jjLL;0j_1) =(-)^{j_1-j-1}(2L+1)^{-1}(2j+1)^{\frac{1}{2}} \quad (66)$$

it follows that the 2^{L_1+1} pole to 2^{L_1} pole intensity ratio is

CC-0. In Public Domain. Gurukul Kangri Collection, Haridwar

Digitized by Arya Samaj Foundation Chennai and eGangotri

TABLE I(a). $F_2(1j_1j)$ for integer spins.

j \ j_1	0	1	2	3	4
1	0.7071	−0.3536	0.0707	0	0
2	0	0.4183	−0.4183	0.1195	0
3	0	0	0.3464	−0.4330	0.1443
4	0	0	0	0.3134	−0.4387
5	0	0	0	0	0.2944

TABLE Ib. $F_2(2j_1j)$ for integer spins.

j \ j_1	0	1	2	3	4
1	0	−0.3535	0.3535	−0.1010	0
2	−0.5976	−0.2988	0.1281	0.3415	−0.1707
3	0	−0.4949	−0.1237	0.2268	0.3093
4	0	0	−0.4477	−0.0448	0.2645
5	0	0	0	−0.4206	0

TABLE I(c). $F_4(2j_1j)$ for integer spins.

j \ j_1	0	1	2	3	4
2	−1.069	0.7127	−0.3054	0.0764	−0.0085
3	0	−0.4467	0.6700	−0.4467	0.1489
4	0	0	−0.3044	0.6087	−0.4981
5	0	0	0	−0.2428	0.5665

TABLE I(d). $F_2(3j_1j)$ for integer spins.

j \ j_1	0	1	2	3	4
1	0	0	−0.4243	0.5303	−0.1768
2	0	−0.7171	−0.1793	0.3287	0.4482
3	−0.8660	−0.6495	−0.2742	0.1443	0.4330
4	0	−0.7835	−0.4701	−0.0855	0.2678
5	0	0	−0.7360	−0.3680	0.0170

TABLE I(e). $F_4(3j_1j)$ for integer spins.

j \ j_1	0	1	2	3	4
2	0	0.0891	−0.1336	0.0891	−0.0297
3	0.2132	0.0355	−0.1066	−0.0355	0.1044
4	0	0.1453	−0.0484	−0.1012	0.0132
5	0	0	0.1159	−0.0773	−0.0852

TABLE I(f). $F_6(3j_1j)$ for integer spins.

j \ j_1	0	1	2	3	4
3	1.3056	−0.9792	0.5440	−0.2176	0.0593
4	0	0.4214	−0.7585	0.6895	−0.3831
5	0	0	0.2420	−0.6049	0.6979

TABLE I(g). $F_2(4j_1j)$ for integer spins.

j \ j_1	0	1	2	3	4
1	0	0	0	−0.4293	0.6010
2	0	0	−0.7257	−0.0726	0.4288
3	0	−0.8763	−0.5258	−0.0956	0.2995
4	−0.9687	−0.8234	−0.5554	−0.2101	0.1447
5	0	−0.9099	−0.6825	−0.3787	−0.0437

TABLE I(h). $F_4(4j_1j)$ for integer spins.

j \ j_1	0	1	2	3	4
2	0	0	0.1718	−0.3436	0.2811
3	0	0.4112	−0.1371	−0.2866	0.0374
4	0.6034	0.3017	−0.0901	−0.2860	−0.1408
5	0	0.4814	0.0802	−0.2239	−0.2592

TABLE I(i). $F_6(4j_1j)$ for integer spins.

j \ j_1	0	1	2	3	4
3	0	0.0218	−0.0392	0.0356	−0.0198
4	0.0674	−0.0034	−0.0346	0.0104	0.0243
5	0	0.0387	−0.0290	−0.0190	0.0242

TABLE I(j). $F_8(4j_1j)$ for integer spins.

j \ j_1	0	1	2	3	4
4	−1.4809	1.1847	−0.7539	0.3770	−0.1450
5	0	−0.3893	0.7785	−0.8384	0.5989

related to the ratio of reduced matrix elements by

$$\delta^2 \equiv \frac{I_{L_1+1}}{I_{L_1}} = \frac{(j_1\|L_1+1\|j)^2}{(j_1\|L_1\|j)^2}. \tag{67}$$

Very often $I_{L_1+1}/I_{L_1} \ll 1$ and only linear terms in δ need be retained, (56). Of course, while the correlation function for pure multipoles is parity independent, the case of mixed multipoles gives a parity determination only if it is assumed that a M_L, E_{L+1} mixture is much more likely than an E_L, M_{L+1} mixture (76a).

It should also be emphasized that the presence of interference in the correlation may change the correlation markedly and the correlation measurement is a sensitive method for the determination of mixture ratios.

Equations (64) and (65) define the standard $\gamma-\gamma$ correlation. In particular Eq. (65a) is the standard $\gamma-\gamma$ correlation for pure multipoles. We write the latter in the form

$$w(\beta) = \sum_\nu A_\nu P_\nu(\cos\beta) \tag{68}$$

and renormalize so that $A_0 = 1$ corresponding to unit value for the average of the correlation function w. Then

$$A_\nu = F_\nu(L_1 j_1 j) F_\nu(L_2 j_2 j), \tag{69a}$$

where

$$F_\nu(Lj_1j) = (-)^{j-j_1-1}(2j+1)^{\frac{1}{2}}(2L+1) \times C(LL\nu; 1-1) W(jjLL; \nu j_1) \tag{69b}$$

so that also $F_0 = 1$.

CC-0. In Public Domain. Gurukul Kangri Collection, Haridwar

Digitized by Arya Samaj Foundation Chennai and eGangotri

TABLE I(k). $F_2(1j_1j)$ for half-integer spins.

j \ j_1	1/2	3/2	5/2	7/2	9/2	11/2	13/2
3/2	0.5000	−0.4000	0.1000	0	0	0	0
5/2	0	0.3742	−0.4276	0.1336	0	0	0
7/2	0	0	0.3273	−0.4364	0.1528	0	0
9/2	0	0	0	0.3028	−0.4404	0.1651	0
11/2	0	0	0	0	0.2876	−0.4425	0.1738
13/2	0	0	0	0	0	0.2774	−0.4437

TABLE I(l). $F_2(2j_1j)$ for half-integer spins.

j \ j_1	1/2	3/2	5/2	7/2	9/2	11/2	13/2
3/2	−0.5000	0	0.3571	−0.1429	0	0	0
5/2	−0.5345	−0.1909	0.1909	0.3245	−0.1909	0	0
7/2	0	−0.4676	−0.0779	0.2494	0.2962	−0.2182	0
9/2	0	0	−0.4325	−0.0197	0.2752	0.2752	−0.2359
11/2	0	0	0	−0.4109	0.0158	0.2890	0.2596
13/2	0	0	0	0	−0.3962	0.0396	0.2972

TABLE I(m). $F_4(2j_1j)$ for half-integer spins.

j \ j_1	1/2	3/2	5/2	7/2	9/2	11/2	13/2
5/2	−0.6172	0.7054	−0.3968	0.1176	−0.0147	0	0
7/2	0	−0.3581	0.6367	−0.4775	0.1736	−0.0253	0
9/2	0	0	−0.2684	0.5857	−0.5124	0.2102	−0.0338
11/2	0	0	0	−0.2237	0.5505	−0.5309	0.2359
13/2	0	0	0	0	−0.1970	0.5254	−0.5418

TABLE I(n). $F_2(3j_1j)$ for half-integer spins.

j \ j_1	1/2	3/2	5/2	7/2	9/2	11/2	13/2
3/2	0	−0.6000	0.1500	0.5000	−0.2500	0	0
5/2	−0.8018	−0.4410	0.0267	0.4009	0.4009	−0.3341	0
7/2	−0.8183	−0.5455	−0.1637	0.2182	0.4474	0.3273	−0.3819
9/2	0	−0.7569	−0.4129	−0.0275	0.3028	0.4541	0.2753
11/2	0	0	−0.7191	−0.3319	0.0522	0.3476	0.4504
13/2	0	0	0	−0.6934	−0.2774	0.1040	0.3744

TABLE I(o). $F_4(3j_1j)$ for half-integer spins.

j \ j_1	1/2	3/2	5/2	7/2	9/2	11/2	13/2
5/2	0.1543	−0.0772	−0.0772	0.1029	−0.0444	0.0070	0
7/2	0.1709	−0.0190	−0.1076	−0.0069	0.1019	−0.0627	0.0121
9/2	0	0.1281	−0.0660	−0.0932	0.0278	0.0935	−0.0735
11/2	0	0	0.1067	−0.0849	−0.0778	0.0469	0.0850
13/2	0	0	0	0.0940	−0.0940	−0.0653	0.0585

It is clear that for the numerical tabulation of the pure $\gamma-\gamma$ correlation it is most economical to tabulate only the F_ν and this gives a complete numerical description of the correlation. In Tables I(a) through I(j) we give numerical values for the F_ν for $L=1, 2, 3, 4$ and all the necessary ν values and for $j_1=0, 1, 2, 3, 4$ and $j\leqslant 5$ (integer values). In Tables I(k) through I(t) we give F_ν for the same range of L and ν and for all half-integer values of j_1 in the range $\frac{1}{2}$ to 13/2 inclusive and for all pertinent $j\leqslant 13/2$.

In using the tables one selects an F value (for each ν) corresponding to each transition and then the correlation function is completely defined by Eqs. (68) and (69a).

For the correlation in which one γ-ray is not pure we can use the normalization given above if the intensity ratio δ^2 is introduced in Eq. (65). The correlation function is simply

$$W=w_I+\delta^2 w_{II}+2\delta w_{III}, \qquad (70)$$

where δ^2 is the ratio of intensities of the $2^{L'}$ pole to that

CC-0. In Public Domain. Gurukul Kangri Collection, Haridwar

Digitized by Arya Samaj Foundation Chennai and eGangotri

TABLE I(p). $F_6(3j_1j)$ for half-integer spins.

j \ j_1	1/2	3/2	5/2	7/2	9/2	11/2	13/2
7/2	0.6528	−0.8704	0.6528	−0.3165	0.0989	−0.0183	0.0015
9/2	0	0.3077	−0.6714	0.6994	−0.4304	0.1614	−0.0344
11/2	0	0	0.1998	−0.5533	0.6916	−0.4918	0.2075
13/2	0	0	0	0.1498	−0.4793	0.6741	−0.5287

TABLE I(q). $F_2(4j_1j)$ for half-integer spins.

j \ j_1	1/2	3/2	5/2	7/2	9/2	11/2	13/2
3/2	0	0	−0.6071	0.2429	0.5409	−0.3091	0
5/2	0	−0.8113	−0.3245	0.1711	0.4898	0.3924	−0.4130
7/2	−0.9274	−0.6889	−0.3397	0.0482	0.3734	0.5059	0.2867
9/2	−0.9358	−0.7444	−0.4558	−0.1155	0.2127	0.4466	0.4861
11/2	0	−0.8890	−0.6326	−0.3175	0.0122	0.3001	0.4770
13/2	0	0	−0.8573	−0.5572	−0.2266	0.0934	0.3521

TABLE I(r). $F_4(4j_1j)$ for half-integer spins.

j \ j_1	1/2	3/2	5/2	7/2	9/2	11/2	13/2
5/2	0	0.2976	−0.2976	−0.1082	0.2976	−0.1602	0.0291
7/2	0.5128	0.0733	−0.2597	−0.2131	0.1235	0.2474	−0.2188
9/2	0.5322	0.1693	−0.1762	−0.2786	−0.0800	0.2065	0.1893
11/2	0	0.4434	0.0171	−0.2509	−0.2363	0.0087	0.2372
13/2	0	0	0.3906	−0.0651	−0.2744	−0.1916	0.0668

TABLE I(s). $F_6(4j_1j)$ for half-integer spins.

j \ j_1	1/2	3/2	5/2	7/2	9/2	11/2	13/2
7/2	0.0435	−0.0348	−0.0071	0.0317	−0.0259	0.0110	−0.0025
9/2	0.0492	−0.0213	−0.0269	0.0195	0.0172	−0.0292	0.0167
11/2	0	0.0320	−0.0326	−0.0123	0.0264	0.0061	−0.0284
13/2	0	0	0.0240	−0.0348	−0.0024	0.0275	−0.0014

TABLE I(t). $F_8(4j_1j)$ for half-integer spins.

j \ j_1	1/2	3/2	5/2	7/2	9/2	11/2	13/2
9/2	−0.6623	0.9633	−0.8429	0.5187	−0.2316	0.0741	−0.0162
11/2	0	−0.2624	0.6460	−0.8075	0.6460	−0.3533	0.1330
13/2	0	0	−0.1497	0.4791	−0.7336	0.6904	−0.4315

of the 2^{L_1} pole and

$$w_I=\sum_\nu A_\nu(L_1L_2)P_\nu(\cos\beta), \tag{70a}$$

$$w_{II}=\sum_\nu A_\nu(L_1'L_2)P_\nu(\cos\beta), \tag{70b}$$

where the A_ν are given in Eq. (69a) and

$$w_{III}=(-)^{j-j_1-1}[(2j+1)(2L_1+1)(2L_1'+1)]^{\frac{1}{2}} \times\sum_\nu G_\nu(L_1L_1'j_1j)F_\nu(L_2j_2j)P_\nu(\cos\beta), \tag{70c}$$

where F_ν is given in Eq. (69b) and

$$G_\nu(L_1L_1'j_1j)=C(L_1L_1'\nu;1-1)W(jjL_1L_1';\nu j_1) \tag{70d}$$

symmetric in L_1 and L_1'.

In Tables II(a) through II(l) numerical values of the coefficients $G_\nu(LL'j_1j)$ are presented for $\nu=2$, 4, 6, $L=1$, 2, 3 with $L'=L+1$ and the range of j_1 and j is the same as Table I. In the table headings the first argument in G_ν is the value of L. Special cases of the mixed correlation were considered by Ling and Falkoff (49).

(3) *Correlation Function for Linear Polarization-Direction Correlation (45)*

The correlation function which applies here was given in Eq. (38). In order to make direct use of the results of this section we evaluate the $e_{\nu\tau}$ from the tensor param-

CC-0. In Public Domain. Gurukul Kangri Collection, Haridwar

Digitized by Arya Samaj Foundation Chennai and eGangotri

TABLE II(a). $G_2(1j_1j)$ for integer spins.

j \ j_1	1	2	3	4
1	0.1581	0.0707	0	0
2	−0.1080	0.0707	0.0756	0
3	0	−0.0926	0.0423	0.0704
4	0	0	−0.0809	0.0289
5	0	0	0	−0.0725

TABLE II(b). $G_2(2j_1j)$ for integer spins.

j \ j_1	1	2	3	4
1	0	−0.0617	−0.0369	0
2	−0.0404	0.0432	−0.0132	−0.0382
3	0.0296	−0.0378	0.0279	0
4	0	0.0298	−0.0322	0.0195
5	0	0	0.0284	−0.0279

TABLE II(c). $G_4(2j_1j)$ for integer spins.

j \ j_1	1	2	3	4
2	0.0753	0.0604	0.0246	0.0047
3	−0.0667	0	0.0472	0.0332
4	0	−0.0507	−0.0171	0.0346
5	0	0	−0.0409	−0.0224

TABLE II(d). $G_2(3j_1j)$ for integer spins.

j \ j_1	1	2	3	4
1	0	0	0.0326	0.0223
2	0	0.0246	−0.0213	0.0027
3	0.0145	−0.0203	0.0193	−0.0105
4	−0.0114	0.0168	−0.0180	0.0141
5	0	−0.0125	0.0161	−0.0155

TABLE II(e). $G_4(3j_1j)$ for integer spins.

j \ j_1	1	2	3	4
2	0	−0.0331	−0.0382	−0.0199
3	−0.0386	0.0180	0.0194	−0.0190
4	0.0317	−0.0242	−0.0033	0.0221
5	0	0.0295	−0.0138	−0.0106

TABLE II(f). $G_6(3j_1j)$ for integer spins.

j \ j_1	1	2	3	4
3	0.0429	0.0429	0.0259	0.0101
4	−0.0429	−0.0153	0.0206	0.0286
5	0	−0.0288	−0.0236	0.0071

eters. By making use of (see Eq. (20) *et seq.*)

$$R(\nu q, LL'\pi)=(-)^{q+L'+L}\sum_{\tau} D(\nu, q\tau; \mathfrak{R})c_{\nu\tau}(LL'\pi), \quad (71)$$

and we have used the fact that we are concerned only with linear polarization (therefore $\mathfrak{R}$ appears instead of $\mathfrak{k}$). Comparing Eqs. (71) and (63) we see that

$$c_{\nu\tau}(LL'\pi)=(-)^{L+1}e^{\frac{1}{2}i\tau a}[(2L+1)(2L'+1)]^{\frac{1}{2}} \times\begin{Bmatrix} C(LL'\nu;1-1) \\ \frac{1}{2}(-)^{\sigma'} \quad C(LL'\nu;11)\end{Bmatrix}, \quad (72)$$

where the uppper line in the bracket refers to $\tau=0$, and the lower refers to $\tau=\pm 2$. Also $\sigma'=1$ for magnetic and 0 for electric radiation and the prime in σ' denotes the $2^{L'}$ multipole.

For pure multipoles in which the polarization of the first (2^{L_1} pole) quantum is observed and correlated with the direction of a 2^{L_2} pole quantum, we obtain the correlation function

$$W_1(\beta,\varphi)=\sum_{\nu} A_\nu\left\{P_\nu+(-)^{\sigma_1}\frac{C(L_1L_1\nu;11)}{C(L_1L_1\nu;1-1)} \times\left[\frac{(\nu-2)!}{(\nu+2)!}\right]^{\frac{1}{2}}\cos 2\varphi P_\nu^2(\cos\beta)\right\}, \quad (73)$$

where A_ν is defined in Eq. (69a and b) and σ_1 refers to radiation 1. In Eq. (73) φ is the angle between the polarization vector and the normal to the $\mathfrak{k}_1-\mathfrak{k}_2$ plane and P_ν^2 is the associated Legendre polynomial; in the second term of Eq. (73) $\nu\geqslant 2$. The explicit dependence on the character of the radiation will be noted. Equivalent results have been obtained by Zinnes (81) and Lloyd (58).

The ratio of vector addition coefficients can be expressed in the form

$$\frac{C(LL\nu;11)}{C(LL\nu;1-1)}=\frac{2\nu(\nu+1)L(L+1)}{\nu(\nu+1)-2L(L+1)}\left[\frac{(\nu-2)!}{(\nu+2)!}\right]^{\frac{1}{2}} \quad (74)$$

with ν even, so that with Table I numerical results for the correlation function for linear polarization can be readily obtained. Special cases have been considered by Falkoff (25).

If the linear polarization of the second quantum is measured, the correlation function is obtained by interchanging L_1 and L_2 which affects only the ratio of vector addition coefficients given in Eq. (74) and the phase $(-)^\sigma$ if the radiations are of different character. Designating this correlation function by W_2, what will be observed is the average correlation function

$$W=\eta_{12}W_1+\eta_{21}W_2,$$

where η_{12} is the over-all efficiency for detection of photon 1 in the polarization sensitive detector and photon 2 in the polarization insensitive detector, while η_{21} is the over-all efficiency for the photons interchanged.

The importance of the relative over-all detector efficiencies η_{12} and η_{21} can be seen as follows. If the efficiencies are the same (so that $W\sim W_1+W_2$) the polarization sensitive term in W will be absent if

$$\frac{\nu(\nu+1)-2L_2(L_2+1)}{\nu(\nu+1)-2L_1(L_1+1)}=\pm\frac{L_2(L_2+1)}{L_1(L_1+1)}$$

CC-0. In Public Domain. Gurukul Kangri Collection, Haridwar

Digitized by Arya Samaj Foundation Chennai and eGangotri

TABLE II(g). $G_2(1j_1j)$ for half-integer spins.

j \ j_1	1/2	3/2	5/2	7/2	9/2	11/2	13/2
3/2	−0.1118	0.1000	0.0764	0	0	0	0
5/2	0	−0.1000	0.0535	0.0732	0	0	0
7/2	0	0	−0.0863	0.0345	0.0677	0	0
9/2	0	0	0	−0.0764	0.0246	0.0628	0
11/2	0	0	0	0	−0.0691	0.0187	0.0586
13/2	0	0	0	0	0	−0.0635	0.0148

TABLE II(h). $G_2(2j_1j)$ for half-integer spins.

j \ j_1	1/2	3/2	5/2	7/2	9/2	11/2	13/2
3/2	0	0.0535	−0.0286	−0.0391	0	0	0
5/2	0.0261	−0.0405	0.0344	−0.0049	−0.0366	0	0
7/2	0	0.0302	−0.0349	0.0231	0.0031	−0.0332	0
9/2	0	0	0.0292	−0.0299	0.0168	0.0066	−0.0305
11/2	0	0	0	0.0275	−0.0262	0.0129	0.0082
13/2	0	0	0	0	0.0259	−0.0234	0.0102

TABLE II(i). $G_4(2j_1j)$ for half-integer spins.

j \ j_1	1/2	3/2	5/2	7/2	9/2	11/2	13/2
5/2	−0.0753	0.0225	0.0551	0.0308	0.0070	0	0
7/2	0	−0.0578	−0.0111	0.0402	0.0339	0.0096	0
9/2	0	0	−0.0452	−0.0205	0.0300	0.0334	0.0109
11/2	0	0	0	−0.0375	−0.0235	0.0233	0.0320
13/2	0	0	0	0	−0.0322	−0.0243	0.0187

TABLE II(j). $G_2(3j_1j)$ for half-integer spins.

j \ j_1	1/2	3/2	5/2	7/2	9/2	11/2	13/2
3/2	0	0	−0.0298	0.0119	0.0234	0	0
5/2	0	−0.0195	0.0225	−0.0149	−0.0020	0.0215	0
7/2	−0.0094	0.0165	−0.0193	0.0164	−0.0074	−0.0063	0.0193
9/2	0	−0.0122	0.0166	−0.0167	0.0123	−0.0035	−0.0079
11/2	0	0	−0.0126	0.0156	−0.0145	0.0095	−0.0013
13/2	0	0	0	−0.0124	0.0145	−0.0127	0.0076

TABLE II(k). $G_4(3j_1j)$ for half-integer spins.

j \ j_1	1/2	3/2	5/2	7/2	9/2	11/2	13/2
5/2	0	0.0405	0.0078	−0.0282	−0.0238	−0.0068	0
7/2	0.0295	−0.0317	0.0045	0.0222	−0.0122	−0.0241	−0.0092
9/2	0	0.0310	−0.0183	−0.0078	0.0208	−0.0037	−0.0223
11/2	0	0	0.0280	−0.0104	−0.0122	0.0178	0.0009
13/2	0	0	0	0.0251	−0.0057	−0.0137	0.0150

TABLE II(l). $G_6(3j_1j)$ for half-integer spins.

j \ j_1	1/2	3/2	5/2	7/2	9/2	11/2	13/2
7/2,	−0.0526	0	0.0312	0.0292	0.0142	0.0039	0.0005
9/2	0	−0.0347	−0.0213	0.0128	0.0268	0.0178	0.0060
11/2	0	0	−0.0244	−0.0242	0.0030	0.0227	0.0188
13/2	0	0	0	−0.0187	−0.0236	−0.0023	0.0190

CC-0. In Public Domain. Gurukul Kangri Collection, Haridwar

Digitized by Arya Samaj Foundation Chennai and eGangotri

for all possible ν; the $(+,-)$ sign refers to the case of radiations of (different, same) character. This actually occurs for

(a) radiations of opposite character and $L_1=L_2$,

(b) radiations of the same character, and L_1, $L_2=1$, 2 or 2, 1 and for no other cases.[15] In both cases there is an *over-all* parity change in the cascade. Therefore, if there is no polarization effect, with equal efficiencies, there must have been an over-all parity change (61), but the converse does not follow. That is, it is not true (as has been stated (61)) that the cascades in which a polarization effect is observed ($\eta_{12}=\eta_{21}$) correspond to no over-all parity charge. It should be recognized that when the detector efficiencies are unequal there will also be cases in which the polarization can cancel, or nearly cancel, accidentally. No conclusions should be drawn in such a case and the relative detector efficiencies should be varied.

As mentioned above, when one of the radiations is a mixture, the correlation function depends on the parity change in the transition in which the mixed radiation is emitted. To determine the parity change in the transition in which the pure radiation is emitted one may make a polarization-direction correlation, observing the polarization of the pure radiation. Of course, unless one can devise detectors for which the efficiency is zero for the mixed radiation going to the polarization sensitive detector, it is also necessary to consider the case in which the polarization of the mixed radiation is observed. We therefore consider these two cases. We consider a M_{L_1}, E_{L_1+1} (or alternatively, E_{L_1}, M_{L_1+1}) mixture. The pure radiation is again a 2^{L_2} pole.

(*a*) *Polarization-direction correlation with polarization of pure radiation measured.*—From Eqs. (38) and (72) we find for the correlation function

$$\bar{W}_1=\bar{w}_I+\delta^2\bar{w}_{II}+2\delta\bar{w}_{III}, \tag{73a}$$

where δ^2 is the intensity ratio $I(L_1+1)/I(L_1)$ and

$$\bar{w}_I=\sum_\nu A_\nu(L_1L_2)\mathcal{P}_\nu(L_2L_2;\beta\varphi). \tag{73b}$$

This is the polarization-direction correlation for the pure 2^{L_1}-pure 2^{L_2} pole. Here we define

$$\mathcal{P}_\nu(L\Sigma';\beta\varphi)=P_\nu(\cos\beta)+(-)^{\sigma(L')}\times\left[\frac{(\nu-2)!}{(\nu+2)!}\right]^{\frac{1}{2}}\frac{C(LL'\nu;11)}{C(LL'\nu;1-1)}\cos2\varphi P_\nu^2(\cos\beta). \tag{73c}$$

The notation is the same as in Eq. (73) and the parity index $\sigma(L')$ is determined by the character of the $2^{L'}$ pole. Thus, in Eq. (73b) the phase $(-)^{\sigma(L_2)}$ is -1 for M_{L_2} radiation, 1 for E_{L_2} radiation. In a similar way $\bar{w}_{II}$ is the correlation function for a pure 2^{L_1+1} pole-2^{L_2} pole and is obtained by replacing L_1 by L_1+1 in Eq. (73b)

$$\bar{w}_{II}=\sum_\nu A_\nu(L_1+1,L_2)\mathcal{P}_\nu(L_2L_2;\beta\varphi) \tag{73d}$$

and $\bar{w}_{III}$ is the interference term

$$\bar{w}_{III}=(-)^{j-j_1-1}[(2j+1)(2L_1+1)(2L_1+3)]^{\frac{1}{2}}\times\sum_\nu G_\nu(L_1L_1+1\,j_1j)F_\nu(L_2j_2j)\mathcal{P}_\nu(L_2L_2;\beta\varphi). \tag{73e}$$

In Eq. (73e) $\nu\geqslant 2$.

(*b*) *Polarization-direction correlation with polarization of mixed radiation measured.*—An entirely similar procedure gives for the correlation function

$$\bar{W}_2=\bar{w}_I'+\delta^2\bar{w}_{II}'+2\delta\bar{w}_{III}'. \tag{73f}$$

Here, δ is as in Eq. (73a) and

$$\bar{w}_I'=\sum_\nu A_\nu(L_1L_2)\mathcal{P}_\nu(L_1L_1;\beta\varphi) \tag{73g}$$

$$\bar{w}_{II}'=\sum_\nu A_\nu(L_1+1,L_2)\mathcal{P}_\nu(L_1+1,L_1+1;\beta\varphi), \tag{73h}$$

which are the polarization-direction correlations for pure multipoles and

$$\bar{w}_{III}'=(-)^{j-j_1-1}[(2j+1)(2L_1+1)(2L_1+3)]^{\frac{1}{2}}\times\sum_\nu G_\nu(L_1L_1+1\,j_1)F_\nu(L_2j_2j)\times\mathcal{P}_\nu(L_1L_1+1;\beta\varphi) \tag{73i}$$

which is the interference term. Again in Eq. (73i) $\nu\geqslant 2$. In Eq. (73i) one needs (52)

$$\frac{C(LL'\nu;11)}{C(LL'\nu;1-1)}=\left[\frac{(\nu-2)!}{(\nu+2)!}\right]^{\frac{1}{2}}(L'-L)(L'+L+1), \tag{73j}$$

where $L+L'+\nu$ is an odd integer. Equivalent results have been obtained by Zinnes (81).

In the actual observation the quantity measured is, of course, the weighted average of $\bar{W}_1$ and $\bar{W}_2$ with weight factors given by the over-all detector efficiencies for the pure radiation and the mixed radiation going to the polarization sensitive detector, respectively. The results given above have a common normalization and can be averaged directly.

B. Spinless Particles

The only spinless particle in which we are interested is the alpha particle and the specific results given here apply to this case. However, for other nuclear particles (neutrons, protons, deuterons) for which only directions of motions are observed, the results given here could apply equally well in the manner indicated below.

The determination of the tensor parameters for alpha particles is a very simple problem, as one might expect, since the only possible measurement is the determination of a direction of motion, uncomplicated by any spin polarization questions. Let us first omit consideration of the charge of the emitted particles. Then the physical measurement determines that the particle is in the plane wave state, $e^{i\mathbf{K}\cdot\mathbf{r}}$, and in accord with the discussion of Sec. II-C, the tensor parameters of the radiation are determined from the transformation to

[15] Aside from the trivial cases ($j=0$ or $\frac{1}{2}$) there is one other case which leads to *complete* isotropy; *viz.*, a cascade in which $j_1=\frac{3}{2}$, $j=\frac{3}{2}$ with pure quadrupole emission (9).

CC-0. In Public Domain. Gurukul Kangri Collection, Haridwar

Digitized by Arya Samaj Foundation Chennai and eGangotri

angular momentum eigenfunctions. Using the well-known Rayleigh formula we have

$$e^{i\mathbf{K}\cdot\mathbf{r}}=4\pi\sum_{lm} j_l i^l Y_l^m(\mathbf{r})Y_l^{m*}(\mathbf{f})$$
$$=\sum_{lm}[(2l+1)4\pi]^{\frac{1}{2}} j_l(Kr)D(l,m0;\mathbf{f})i^l Y_l^m(\mathbf{r}). \quad (75)$$

The tensor parameters, $R(\nu q)$, of this radiation are

$$R(\nu q, ll'\pi)=4\pi(2l+1)^{\frac{1}{2}}(2l'+1)^{\frac{1}{2}}\sum_m (-)^{l-m}$$
$$\times D^*(l', q-m, 0;\mathbf{f})D(l, m0;\mathbf{f})$$
$$\times C(ll'\nu; mq-m). \quad (76)$$

By use of Eq. (9), we find that

$$R(\nu q, ll'\pi)=4\pi[(2l+1)(2l'+1)]^{\frac{1}{2}}(-)^{l-q}$$
$$\times C(ll'\nu;00)D(\nu, q0;\mathbf{f}). \quad (77)$$

In order that parity be a good quantum number for the radiation (as indicated by the variable $\pi_l=(-)^l=(-)^{l'}$ in the notation for $R(\nu q)$), we must require that l and l' differ by an even integer. Since the vector addition coefficient, $C(ll'\nu;00)$, vanishes for $l+l'+\nu\neq$ even integer we see that ν is even.

In terms of the $c_{\nu\tau}$ of Eq. (12) we find

$$c_{\nu\tau}=\delta(\tau 0)(-)^l[(2l+1)(2l'+1)]^{\frac{1}{2}}C(ll'\nu;00). \quad (78)$$

If we now consider charged particles the changes that occur are of two kinds. Firstly the discrimination against the emission of high angular momentum particles will become less marked, because of the Coulomb barrier, so that the interference of different angular momenta will be more pronounced. This effect[16] is, of course, contained in the physical parameters (the relative size of the reduced matrix elements) and does not influence the tensor parameters above. The second effect is to introduce phase shifts, $e^{i\delta_l(Z)}$, multiplying the lth spherical wave of our basis.[17]

The result for charged, spinless particles (alpha particles) is found to be

$$c_{\nu\tau}(\alpha)=4\pi\delta(\tau 0)(-)^l e^{i(\delta_l-\delta_{l'})}[(2l+1)(2l'+1)]^{\frac{1}{2}}$$
$$\times C(ll'\nu;00). \quad (78a)$$

For a single angular momentum,[16] the phase shift difference drops out. However, for those cases in which more than one angular momentum is important the phase shifts will remain and may change the correlation functions appreciably. We consider explicitly only the former case. Since we have chosen the gamma-ray correlation to be the standard directional correlation, the most useful parameters are the b_ν, defined in Eq. (42). Using the results of the preceding section we find for pure multipoles (unique orbital angular momentum l) that (normalized to $b_0=1$)

$$b_\nu(ll;\alpha)=-C(ll\nu;00)/C(ll\nu;1-1)$$
$$=\frac{2l(l+1)}{2l(l+1)-\nu(\nu+1)}. \quad (79)$$

The $\alpha-\gamma$ correlation, for example, is then

$$W_{\alpha-\gamma}(\beta)=\sum_\nu A_\nu\frac{2l(l+1)}{2l(l+1)-\nu(\nu+1)}P_\nu(\cos\beta), \quad (80)$$

with A_ν from Eq. (69a, b) with l replacing L_1 or L_2 according as to whether the α particle is emitted in the $j_1\rightarrow j$ or $j\rightarrow j_2$ transition.

The results can be extended to the emission or absorption of a nuclear particle with a pure angular momentum in the following way. If l is the particle angular momentum, i its intrinsic spin and I the target nucleus then the channel spin s is any of the values consistent with

$$\mathbf{s}=\mathbf{i}+\mathbf{I}.$$

Assume for the moment that only a single value of s need be considered. The correlation is then the same as for α particles if j_1, the initial state angular momentum is replaced by s. For the more realistic case wherein more than one channel spin is relevant, the correlation is an incoherent sum over s of such contributions with weight factors corresponding to the relative probability for the occurrence of the channel spin s in the assumed pure compound state. An example of this procedure is given in reference (11).

C. Conversion Electrons

For heavy elements in which conversion electrons are more prevalent than γ rays, it may be advantageous to measure the correlation with such electrons. The problem of correlations involving conversion electrons, in either or both transitions, has been considered by a number of authors. A preliminary discussion was given by Fierz (31) and nonrelativistic approximations applicable to electric conversion of s electrons were considered by Berestetzky (10) and Gardner (38, 39). An approximate but incomplete consideration of magnetic conversion was also given by Gardner (40), see also Ling (50). The relativistic treatment of the conversion of an s electron was given by Rose, Biedenharn, and Arfken (68) and numerical results were given for the K shell when the conversion transition is pure. For mixed conversion transitions the results appeared in a later publication by the same authors (70). At present all numerical results in a relativistic calculation are limited to K conversion correlation (69, 68).

The internal conversion process is viewed as the ejection of an extranuclear electron, originally in a stationary state (say the K shell), via the electromag-

[16] This question is discussed at length by H. A. Bethe, Revs. Modern Phys. 9, 69 (1937), see Sec. 72.

[17] We may consider the Coulomb potential to be screened, so as to eliminate the logarithmic terms. In the final result the limit for zero screening can be taken. Also from Eq. (78a) below it is seen that the logarithmic term would drop out in any case since only phase differences enter.

CC-0. In Public Domain. Gurukul Kangri Collection, Haridwar

Digitized by Arya Samaj Foundation Chennai and eGangotri

magnetic field which is excited by a nuclear transition. The tensor parameters of the radiation are nonetheless the tensor parameters of the nuclear gamma radiation for we have but substituted, in place of a direct observation of the gamma radiation, an indirect observation of its effect on the surrounding electrons. The tensor parameters of the gamma radiation are thus determined by the coupling of (a) the tensor parameters of the ejected electron-fixed by our observation of a plane wave state with a definite direction of motion but unobserved spin orientation, and (b) the tensor parameters of the initial state of the electron, which are quite simple since this state is random.

The first problem is to determine the tensor parameters of the final state of the ejected electrons. For the moment, let us neglect the effect of the Coulomb field on the motion of the electrons.

The observations imply that the ejected electrons are detected in plane wave states, $e^{iKz}D_\tau$, where we have taken the direction of motion to define the z axis and the D_τ are Dirac plane wave spinors (with $\tau=+$ taken to be spin "up," i.e., along the z axis and $\tau=-$, spin "down"). In relativistic units and with $K=p$

$$D_+=\begin{bmatrix}-p/E+1\\0\\1\\0\end{bmatrix};\quad D_-=\begin{bmatrix}0\\p/E+1\\0\\1\end{bmatrix}. \tag{81}$$

Since the spin is not observed, we must average over τ. These plane wave states can be expanded into a sum of Dirac spherical eigenfunctions, $\phi_\kappa{}^\mu$, (references 68, 67 and Eq. (83) below) and the result is

$$e^{iKz}D_\tau=-\left(\frac{\pi}{p(E+1)}\right)^{\frac{1}{2}}\sum_\kappa(4\pi|\kappa|)^{\frac{1}{2}}i^{-l(\kappa)}\times[-S(\kappa)]^{\tau-\frac{1}{2}}\phi_\kappa{}^\tau. \tag{82}$$

$\kappa=\pm(j+\frac{1}{2})$ for $j=l\mp\frac{1}{2}$ and l determines the parity (67). The sum is over all positive and negative integers, except zero. The notation is

$$\begin{aligned}S(\kappa)&\equiv\text{sign of }\kappa=\pm1\\ l(\kappa)&=|\kappa|+\tfrac{1}{2}[S(\kappa)-1]\\ j&=|\kappa|-\tfrac{1}{2}\end{aligned} \tag{82a}$$

$$\phi_\kappa{}^\mu=\left(\frac{p}{\pi}\right)^{\frac{1}{2}}\begin{pmatrix}i(E-1)^{\frac{1}{2}}j_{l(-\kappa)}(pr)\chi_{-\kappa}{}^\mu\\-S(\kappa)(E+1)^{\frac{1}{2}}j_{l(\kappa)}(pr)\chi_\kappa{}^\mu\end{pmatrix} \tag{83}$$

$$\chi_\kappa{}^\mu=\sum_\tau C(l(\kappa)\tfrac{1}{2}j;\mu-\tau,\tau)\chi_{\frac{1}{2}}{}^\tau Y_{l(\kappa)}{}^{\mu-\tau}. \tag{83a}$$

$\chi_{\frac{1}{2}}{}^\tau$ in Eq. (83a) is a Pauli spinor and μ is the eigenvalue of the z component of the total angular momentum j. The total energy $E=(p^2+1)^{\frac{1}{2}}$.

For convenience we give the following properties of the central field spinors which are used below

$$(\boldsymbol{\sigma}\cdot\mathbf{L}+1)\chi_\kappa{}^\mu=-\kappa\chi_\kappa{}^\mu \tag{83b}$$

$$\sigma_\tau\chi_\kappa{}^\mu=-\chi_{-\kappa}{}^\mu, \tag{83c}$$

and $\boldsymbol{\sigma}$ is the usual Pauli spin operator, $\mathbf{L}$ the orbital angular momentum operator.

If now our measuring axes are taken to be arbitrarily oriented with respect to the direction of motion of the plane wave (but the spin still quantized along this direction of motion), we must consider the above equation in a rotated system of coordinates. Since the $\phi_\kappa{}^\mu$ transform like wave functions with total angular momentum $j=|\kappa|-\frac{1}{2}$, we find

$$(e^{iKz}D_\tau)'=\frac{2\pi}{[p(E+1)]^{\frac{1}{2}}}\sum_{\kappa\mu}|\kappa|^{\frac{1}{2}}i^{-l(\kappa)}\times[-S(\kappa)]^{\tau-\frac{1}{2}}D(j,\mu\tau)\phi_\kappa{}^\mu. \tag{84}$$

The prime again denotes rotated.

The tensor parameters for the electron in the continuum are now readily seen to be (discarding a factor $2\pi/[p(E+1)]^{\frac{1}{2}}$)

$$\begin{aligned}R(\nu q,\kappa\kappa')&=\sum_{\mu\mu'\tau}(-)^{j-\mu}i^{l(\kappa')-l(\kappa)}C(jj'\nu;\mu,-\mu',q)\\&\quad\times[S(\kappa)S(\kappa')]^{\tau-\frac{1}{2}}|\kappa\kappa'|^{\frac{1}{2}}D^*(j',\mu'\tau)D(j,\mu\tau)\\&=i^{l(\kappa')-l(\kappa)}(-)^{\kappa+q}|\kappa\kappa'|^{\frac{1}{2}}D(\nu,q0;\mathbf{f})\\&\quad\times\sum_\tau[-S(\kappa)S(\kappa')]^{\tau-\frac{1}{2}}C(jj'\nu;\tau,-\tau).\end{aligned} \tag{85}$$

$\mathbf{f}$ is the unit propagation vector for the electron and $j'=|\kappa'|-\frac{1}{2}$. Using now the identity $(2l+1)^{\frac{1}{2}}C(l\tfrac{1}{2}j;0\tau)=|\kappa|^{\frac{1}{2}}[-S(\kappa)]^{\tau+\frac{1}{2}}$, one readily works out the sum over τ from

$$\begin{aligned}\sum_\tau[-S(\kappa)S(\kappa')]^{\tau+\frac{1}{2}}C(jj'\nu;\tau,-\tau)&=[(2l+1)(2l'+1)]^{\frac{1}{2}}(-)^{j+j'-\nu}\\&\quad\times C(ll'\nu;00)W(ljl'j';\tfrac{1}{2}\nu).\end{aligned} \tag{86}$$

Hence the tensor parameters of the ejected electron can be written in the simpler form

$$\begin{aligned}R(\nu q,\kappa\kappa')&=i^{l(\kappa')-l(\kappa)}(-)^{\nu+q+j'-\frac{1}{2}}\\&\quad\times[(2l+1)(2l'+1)|\kappa\kappa'|]^{\frac{1}{2}}S(\kappa)S(\kappa')\\&\quad\times C(ll'\nu;00)W(ljl'j';\tfrac{1}{2}\nu)D(\nu,q0;\mathbf{f}).\end{aligned} \tag{87}$$

So far we have calculated the tensor parameters for the field-free case. If there is a central field, decreasing more rapidly at infinity than a Coulomb field, then the only effects are to modify the radial part of the base wave function $\phi_\kappa{}^\mu$ and to multiply these functions by a phase shift $e^{i\Delta_\kappa}$. The tensor parameters are then

$$\begin{aligned}R(\nu q,\kappa\kappa')&=[(2l+1)(2l'+1)|\kappa\kappa'|]^{\frac{1}{2}}\\&\quad\times(-)^{\nu+q+j'-\frac{1}{2}}i^{l(\kappa')-l(\kappa)}\exp[i(\Delta_\kappa-\Delta_{\kappa'})]\\&\quad\times S(\kappa)S(\kappa')C(ll'\nu;00)W(ljl'j';\tfrac{1}{2}\nu)\\&\quad\times D(\nu,q0;\mathbf{f}).\end{aligned} \tag{88}$$

For the Coulomb field the well-known logarithmic term in the phase shift enters, but this clearly drops out in the above expression since only differences of the phase shifts enter and the logarithmic terms are inde-

CC-0. In Public Domain. Gurukul Kangri Collection, Haridwar

Digitized by Arya Samaj Foundation Chennai and eGangotri

pendent of κ and the phase shift difference is therefore independent of r. Hence the above expression applies to the Coulomb case as well. The phase shift Δ_κ is equal to $\delta_\kappa(Z)-\delta_\kappa(0)$ in the notation of reference (67) and the arguments here refer to the atomic number; thus Δ_κ vanishes in the case of no field. The phase shift $\delta_\kappa(0)=\frac{1}{2}\pi[\frac{1}{2}(1+S(\kappa))-|\kappa|]$. The absolute *sign* of the phase shifts (the relative signs are unique) in Eq. (88) above is determined from the requirement that the Green's function for the emission of the electrons corresponds to outgoing waves at infinity. Strictly speaking, this method of deriving the tensor parameters from the field-free tensor parameters is ambiguous in regard to the absolute sign of the phase shifts. A more thorough derivation which treats this point in detail is given in (68).

Since the tensor parameters of the initial state ($\kappa=-1$) are $R(\nu q;\text{in})=\delta_{\nu 0}\delta_{q0}$ it is now a simple matter to determine the radiation parameters, using the procedure discussed in connection with Eq. (17b). The result is

$$R(\nu q, LL'\pi)=\sum_{\kappa\kappa'}|\kappa\kappa'|^{\frac{1}{2}}W(\tfrac{1}{2}jL'\nu;Lj')Q(\kappa L\sigma)\times Q^*(\kappa' L'\sigma')R(\nu q,\kappa\kappa'). \quad (89)$$

The $Q(\kappa L\sigma)$ are the reduced matrix elements for the electronic transition from $\kappa_i=-1$ to κ by an outgoing 2^L pole electromagnetic field and parity $(-)^{L+\sigma}$. These are defined explicitly in references (68) and (69). The same sign and normalization conventions are used here. The σ parameter (Sec. III-A) is used in the Q's in lieu of the parity symbol π. Since for pure multipoles we have two possible κ values for the final state ($\kappa=L$, $-L-1$ for electric multipoles and $\kappa=-L$, $L+1$ for magnetic multipoles), there will always be coherent mixing of the final states, and thus the Coulomb phase shifts, as well as the relative size of the electronic matrix elements, will become important. In general, exact calculation of these matrix elements using Dirac wave functions for the Coulomb field is consequently essential [see further, (68)].

The radiation tensor parameters for a pure 2^L multipole ($\sigma=\sigma'$) are then

$$R(\nu q, LL\sigma)=\sum_{\kappa\kappa'}[(2l+1)(2l'+1)]^{\frac{1}{2}}|\kappa\kappa'|Q(\kappa L\sigma)\times Q^*(\kappa' L\sigma)(-)^{L+q}i^{l(\kappa')-l(\kappa)}\times\exp[i(\Delta_\kappa-\Delta_{\kappa'})]C(ll'\nu;00)\times S(\kappa)S(\kappa')D(\nu,q0;\mathfrak{f})W(ljl'j';\tfrac{1}{2}\nu)\times W(LjLj';\tfrac{1}{2}\nu) \quad (90)$$

and $l\equiv l(\kappa)$, $l'\equiv l(\kappa')$.

Using the fact that for 2^L-poles the allowed κ values are L, $-L-1$ one finds in both cases, $l(\kappa)=L$. The above equation then takes the simpler form

$$\begin{aligned}R(\nu q, LL\epsilon)&=(2L+1)(-)^{L+q}C(LL\nu;00)D(\nu,q0;\mathfrak{f})\\&\times\{L^2|Q(LL\epsilon)|^2W^2(LLL-\tfrac{1}{2}L-\tfrac{1}{2};\nu\tfrac{1}{2})\\&+(L+1)^2|Q(-L-1L\epsilon)|^2W^2(LLL+\tfrac{1}{2}L+\tfrac{1}{2};\nu\tfrac{1}{2})\\&-2L(L+1)Re[(e^{i\Delta_L}Q(LL\epsilon))^*e^{i\Delta_{-L-1}}\\&\times Q(-L-1,L\epsilon)]W^2(LLL-\tfrac{1}{2}L+\tfrac{1}{2};\nu\tfrac{1}{2})\}. \quad (91)\end{aligned}$$

The occurrence of $C(LL\nu;00)$ shows that ν is an even integer. If we use the relation

$$C(LL\nu;1-1)=C(LL\nu;00)\frac{\nu(\nu+1)-2L(L+1)}{2L(L+1)}$$

for ν even and the explicit formulas for the Racah coefficients (see Appendix, A8, A9, A10) then $R(\nu q, LL\epsilon)$ takes the form

$$\begin{aligned}R(\nu q, LL\epsilon)&=\frac{2L(L+1)(2L+1)}{\nu(\nu+1)-2L(L+1)}\\&\times(-)^{L+q}C(LL\nu;1-1)D(\nu,q0;\mathfrak{f})\\&\times\Big\{|Q(LL\epsilon)|^2\frac{(2L-\nu)(2L+\nu+1)}{4(2L+1)^2}\\&+|Q(-L-1,L,\epsilon)|^2\frac{(2L+1-\nu)(2L+2+\nu)}{4(2L+1)^2}\\&-\frac{\nu(\nu+1)}{2(2L+1)^2}Re[(e^{i\Delta_L}Q(LL\epsilon))^*e^{i\Delta_{-L-1}}\\&\times Q(-L-1,L,\epsilon)]\Big\} \quad (92)\end{aligned}$$

or

$$\begin{aligned}R(\nu q, LL\epsilon)&=\{(-)^{L+q+1}(2L+1)\\&\times C(LL\nu;1-1)D(\nu,q0;\mathfrak{f})\}\\&\times\frac{L(L+1)}{2(2L+1)^2}[2L(L+1)-\nu(\nu+1)]^{-1}\\&\times\Big[\frac{|T_\epsilon|^2}{L}2(2L+1)+2(L+1)(2L+1)\\&-\nu(\nu+1)\Big(\frac{|T_\epsilon|^2}{L^2}-\frac{2}{L}\mathrm{Re}(T_\epsilon)+1\Big)\Big], \quad (93)\end{aligned}$$

where we have used the definition

$$T_\epsilon\equiv L\frac{e^{i\delta_L}Q(LL\epsilon)}{e^{i\delta_{-L-1}}Q(-L-1,L,\epsilon)};$$

$$\Delta_\kappa=\delta_\kappa-\frac{\pi}{2}\Big[\frac{1+S(\kappa)}{2}-|\kappa|\Big]. \quad (94)$$

CC-0. In Public Domain. Gurukul Kangri Collection, Haridwar

Digitized by Arya Samaj Foundation Chennai and eGangotri

The term in curly brackets in Eq. (93) will be recognized as just the tensor parameters for pure 2^L pole γ rays. We can therefore write, after a little algebraic manipulation, that the particle parameter b_ν' for conversion electrons [see Eq. (42b)] has the form

$$b_\nu'(LLe)=\frac{|Q(-L-1,L,e)|^2}{2L(2L+1)}(|T_e|^2+L(L+1))\times\left[1+\frac{\nu(\nu+1)}{2L(L+1)-\nu(\nu+1)}\frac{L}{2L+1}\times\frac{|L+1+T_e|^2}{L(L+1)+|T_e|^2}\right]$$
$$=c_e(L)\left[1+\frac{\nu(\nu+1)}{2L(L+1)-\nu(\nu+1)}\frac{L}{2L+1}\times\frac{|L+1+T_e|^2}{L(L+1)+|T_e|^2}\right]\equiv c_e(L)b_\nu(LLe). \quad (95)$$

In this last equation the conversion coefficient, $c_e(L)$ (aside from a factor-reference (69)), has been inserted, so that the $b_\nu(LLe)$ may be normalized to $b_0=1$. Thus

$$b_\nu(LLe)=1+\frac{\nu(\nu+1)}{2L(L+1)-\nu(\nu+1)}\frac{L}{2L+1}\times\frac{|L+1+T_e|^2}{L(L+1)+|T_e|^2}. \quad (95a)$$

The tensor parameters for pure magnetic multipoles may also be put in this explicit form by similar manipulation, involving explicit formulas for the Racah coefficients given in the Appendix (A6, A8, A9, A10). The result is

$$R(\nu q,LLm)=\{(-)^{L+1+q}(2L+1)\times C(LL\nu;1-1)D(\nu,q0;\mathfrak{k})\}\times\frac{|Q(-LLm)|^2L}{2(L+1)(2L+1)}(L+1+L|T_m|^2)\times\left[1+\frac{\nu(\nu+1)}{2L(L+1)-\nu(\nu+1)}\times\frac{L(L+1)}{2L+1}\frac{|1-T_m|^2}{L+1+L|T_m|^2}\right]$$
$$=R(\nu q,LL;\gamma)c_m(L)b_\nu(LLm). \quad (96)$$

The notation is $c_m(L)\equiv$ the 2^L multipole conversion coefficient (69), that is,

$$c_m(L)=\frac{L}{2(L+1)(2L+1)}|Q(-L,L,m)|^2\times(L+1+L|T_m|^2) \quad (96a)$$

and

$$T_m\equiv-\frac{L+1}{L}\frac{e^{i\delta_{L+1}}Q(L+1,L,m)}{e^{i\delta_{-L}}Q(-L,L,m)}. \quad (96b)$$

Therefore,

$$b_\nu(LLm)=1+\frac{\nu(\nu+1)}{2L(L+1)-\nu(\nu+1)}\times\frac{L(L+1)}{2L+1}\frac{|1-T_m|^2}{L+1+L|T_m|^2}. \quad (97)$$

From Eqs. (95a) and (97) it is clear that for both electric and magnetic transitions the normalized coefficients $b_\nu(LL;e/m)$ for $\nu>2$ are readily obtained from the corresponding coefficients $b_2(LL;e/m)$ by the recurrence formula

$$b_\nu(LL;e/m)=1+\frac{\nu(\nu+1)[L(L+1)-3]}{3[2L(L+1)-\nu(\nu+1)]}\times[b_2(LL;e/m)-1]. \quad (98)$$

As a result, one need tabulate only the coefficients b_2. Tables III(a)–III(l) give $b_2(LL;e)$ and $b_2(LL;m)$ for the K shell for 12 values of Z in the range 10–96, 5 or 6 values of the transition energy ($\equiv kmc^2$) and $L=1$ through 5.

The experimental problem of observing correlations with conversion electrons is somewhat complicated by the multiple scattering that is necessarily present with thick sources. If thick sources are necessary, the requisite corrections can be made as described by Frankel, (32).

For purposes of extrapolation the following limiting cases may be of interest. For small k values, in the case of $b_2(LLe)$, extrapolation toward threshold can be made with the aid of the nonrelativistic limit

$$b_2(LLe)=\frac{L(L+1)}{L(L+1)-3}\quad(\alpha Z\ll1;k\ll1).$$

For the magnetic transitions, the "nonrelativistic" limit for $b_2(LLm)$ is Z, k dependent.

The high-energy limit can be obtained by using the Casimir approximation [asymptotic forms of the radial Dirac functions are used (67)]. One finds immediately that

$$Q(\kappa,L,m)\to Ne^{-i\delta_\kappa}(\kappa-1)\frac{1}{[L(L+1)]^{\frac{1}{2}}}(\delta_{\kappa,-L}+\delta_{\kappa,L+1})$$
$$Q(\kappa,L,e)\to Ne^{-i\delta_\kappa}(\kappa+1)\frac{1}{[L(L+1)]^{\frac{1}{2}}}(\delta_{\kappa,L}+\delta_{\kappa,-L-1})$$

where N is an irrelevant normalization constant. Thus $T_e\to-(L+1)$ and $T_m\to1$. As a result one finds that both $b_\nu(LLe)$ and $b_\nu(LLm)$ approach the value unity (68). This implies that at high energies the conversion electrons for pure multipoles give the same correlation function as the corresponding cascade with a photon replacing the conversion electron.

For $Z=0$ arbitrary k one finds $b_\nu(LLm)=1$ (for all ν) and

$$b_2(LLe)=1+\frac{12L}{[L(L+1)-3][(L+1)k^2+4L^2]}.$$

CC-0. In Public Domain. Gurukul Kangri Collection, Haridwar

Digitized by Arya Samaj Foundation Chennai and eGangotri

TABLE III(a). b_2 Coefficients for $Z=10$.[a]

	$k=0.3$	0.5	1.0	1.8	3.0	5.0
E_1	−1.8624	−1.6544	−1.0000	−0.1757	0.4157	0.7506
E_2	1.9611	1.9015	1.7023	1.4281	1.2176	1.0942
E_3	1.3209	1.3020	1.2376	1.1458	1.0737	1.0316
E_4	1.1699	1.1600	1.1264	1.0777	1.0389	1.0163
E_5	1.1069	1.1007	1.0796	1.0489	1.0243	1.0100
M_1	0.9288	0.9551	0.9769	0.9875	0.9930	0.9963
M_2	1.0291	1.0186	1.0100	1.0058	1.0035	1.0020
M_3	1.0115	1.0073	1.0040	1.0024	1.0015	1.0010
M_4	1.0070	1.0045	1.0024	1.0015	1.0009	1.0006
M_5	1.0050	1.0032	1.0017	1.0010	1.0007	1.0004

[a] E_L, M_L designate electric, magnetic 2^L-pole transitions, respectively.

TABLE III(b). b_2 Coefficients for $Z=20$.

	$k=0.3$	0.5	1.0	1.8	3.0	5.0
E_1	−1.8539	−1.6419	−1.0000	−0.2077	0.3730	0.7188
E_2	1.9527	1.8850	1.6717	1.4004	1.2044	1.0913
E_3	1.3167	1.2940	1.2219	1.1290	1.0632	1.0270
E_4	1.1670	1.1546	1.1159	1.0661	1.0311	1.0126
E_5	1.1047	1.0966	1.0718	1.0403	1.0184	1.0071
M_1	0.7685	0.8430	0.9119	0.9488	0.9696	0.9830
M_2	1.0931	1.0637	1.0369	1.0226	1.0144	1.0087
M_3	1.0361	1.0248	1.0145	1.0091	1.0061	1.0038
M_4	1.0214	1.0149	1.0087	1.0055	1.0036	1.0024
M_5	1.0149	1.0104	1.0061	1.0038	1.0026	1.0017

TABLE III(c). b_2 Coefficients for $Z=30$.

	$k=0.3$	0.5	1.0	1.8	3.0	5.0
E_1	−1.8452	−1.6292	−1.0000	−0.2411	0.3260	0.6815
E_2	1.9411	1.8631	1.6338	1.3679	1.1877	1.0874
E_3	1.3105	1.2827	1.2018	1.1099	1.0518	1.0225
E_4	1.1625	1.1466	1.1022	1.0531	1.0232	1.0090
E_5	1.1009	1.0903	1.0615	1.0308	1.0126	1.0045
M_1	0.5810	0.6951	0.8130	0.8830	0.9261	0.9560
M_2	1.1646	1.1206	1.0755	1.0491	1.0328	1.0210
M_3	1.0623	1.0460	1.0292	1.0193	1.0132	1.0091
M_4	1.0362	1.0271	1.0172	1.0114	1.0079	1.0054
M_5	1.0246	1.0186	1.0119	1.0079	1.0055	1.0038

TABLE III(d). b_2 Coefficients for $Z=40$.

	$k=0.3$	0.5	1.0	1.8	3.0	5.0
E_1	−1.8361	−1.6160	−1.0000	−0.2759	0.2743	0.6375
E_2	1.9246	1.8333	1.5863	1.3298	1.1703	1.0824
E_3	1.3008	1.2662	1.1764	1.0885	1.0400	1.0174
E_4	1.1549	1.1346	1.0849	1.0392	1.0156	1.0058
E_5	1.0944	1.0804	1.0485	1.0209	1.0075	1.0024
M_1	0.4009	0.5359	0.6898	0.7908	0.8583	0.9095
M_2	1.2298	1.1787	1.1205	1.0831	1.0586	1.0398
M_3	1.0850	1.0668	1.0454	1.0317	1.0228	1.0160
M_4	1.0486	1.0387	1.0266	1.0186	1.0136	1.0096
M_5	1.0325	1.0262	1.0182	1.0128	1.0093	1.0067

TABLE II(c). b_2 Coefficients for $Z=54$.

	$k=0.3$	0.5	1.0	1.8	3.0	5.0
E_1	−1.8231	−1.5966	−1.0000	−0.3273	0.1936	0.5624
E_2	1.8868	1.7698	1.4983	1.2660	1.1402	1.0737
E_3	1.2764	1.2293	1.1303	1.0564	1.0241	1.0113
E_4	1.1347	1.1068	1.0546	1.0200	1.0067	1.0027
E_5	1.0765	1.0579	1.0269	1.0085	1.0022	1.0007
M_1	0.1917	0.3244	0.4961	0.6231	0.7174	0.7974
M_2	1.3024	1.2518	1.1863	1.1390	1.1054	1.0778
M_3	1.1094	1.0919	1.0686	1.0514	1.0393	1.0295
M_4	1.0613	1.0521	1.0393	1.0297	1.0228	1.0172
M_5	1.0403	1.0346	1.0264	1.0200	1.0154	1.0118

TABLE III(f). b_2 Coefficients for $Z=64$.

	$k=0.3$	0.5	1.0	1.8	3.0	5.0
E_1	−1.8129	−1.5819	−1.0000	−0.3661	0.1293	0.4972
E_2	1.8400	1.6984	1.4152	1.2131	1.1162	1.0668
E_3	1.2444	1.1876	1.0905	1.0344	1.0149	1.0085
E_4	1.1082	1.0768	1.0311	1.0088	1.0027	1.0019
E_5	1.0540	1.0354	1.0122	1.0025	1.0006	1.0010
M_1	0.0800	0.1954	0.3566	0.4842	0.5837	0.6736
M_2	1.3410	1.2952	1.2312	1.1817	1.1446	1.1131
M_3	1.1220	1.1064	1.0840	1.0660	1.0527	1.0415
M_4	1.0677	1.0596	1.0474	1.0375	1.0299	1.0236
M_5	1.0441	1.0392	1.0316	1.0251	1.0201	1.0159

For a *mixed* conversion transition the tensor parameters are found from Eq. (89). We specialize now to a magnetic 2^L and electric 2^{L+1} mixture. If we choose the unprimed variables to refer to the magnetic multipole, κ is restricted to $-L$, $L+1$ (and $\sigma=1$) while κ' is restricted to $L+1$, $-L-2$ (and $\sigma'=0$). $R(\nu q)$ then consists of four terms which, by using Eq. (A7) of the Appendix, can be reduced to

$$R(\nu q)[L, L+1, \pi=(-)^L] = (-)^{L+q}D(\nu, q0; 1)C(LL+1\nu; 1-1)\Omega \quad (99)$$

and

$$\Omega=\tfrac{1}{2}(L+1)\left[\frac{L(L+2)}{(2L+1)(2L+3)}\right]^{\frac{1}{2}}\{Q(-L, L, m) \times Q^*(L+1, L+1, e)e^{i(\Delta-L-\Delta_{L+1})}+Q(-L, L, m) \times Q^*(-L-2, L+1, e)e^{i(\Delta-L-\Delta-L-2)} -Q(L+1, L, m)Q^*(L+1, L+1, e) -Q(L+1, L, m)Q^*(-L-2, L+1, e) \times e^{i(\Delta_{L+1}-\Delta-L-2)}\}$$

$$=\tfrac{1}{2}(L+1)\left[\frac{L(L+2)}{(2L+1)(2L+3)}\right]^{\frac{1}{2}} \times\{Q(-L, L, m)e^{i\Delta-L}-Q(L+1, L, m)e^{i\Delta L+1}\} \times\{Q(L+1, L+1, e)e^{i\Delta L+1} +Q(-L-2, L+1, e)e^{i\Delta-L-2}\} \quad (99a)$$

Comparing these results with the tensor parameters for mixed multipole γ rays, [Eq. (60a)], and noting again that the γ-ray reduced matrix elements are real, we find

$$b_\nu'[L, L+1, \pi=(-)^L]=\tfrac{1}{2}(L+1)\frac{[L(L+2)]^{\frac{1}{2}}}{(2L+1)(2L+3)} \times\mathrm{Re}\{[Q(-L, L, m)e^{i\Delta-L} -Q(L+1, L, m)e^{i\Delta L+1}] \times[Q(L+1, L+1, e)e^{i\Delta L+1} +Q(-L-2, L+1, e)e^{i\Delta-L-2}]^*\}. \quad (100)$$

CC-0. In Public Domain. Gurukul Kangri Collection, Haridwar

Digitized by Arya Samaj Foundation Chennai and eGangotri

TABLE III(g). b_2 Coefficients for $Z=72$.

	$k=0.3$	0.5	1.0	1.8	3.0	5.0
E_1	−1.8041	−1.5693	−1.0000	−0.3986	0.0735	0.4368
E_2	1.7801	1.6155	1.3348	1.1678	1.0968	1.0615
E_3	1.2039	1.1423	1.0572	1.0194	1.0096	1.0074
E_4	1.0772	1.0480	1.0147	1.0031	1.0017	1.0027
E_5	1.0311	1.0171	1.0038	1.0004	1.0009	1.0021
M_1	0.0152	0.1104	0.2520	0.3687	0.4615	0.5460
M_2	1.3647	1.3242	1.2645	1.2158	1.1781	1.1455
M_3	1.1296	1.1160	1.0950	1.0773	1.0637	1.0517
M_4	1.0716	1.0645	1.0533	1.0436	1.0358	1.0292
M_5	1.0464	1.0422	1.0352	1.0289	1.0238	1.0195

TABLE III(h). b_2 Coefficients for $Z=78$.

	$k=0.3$	0.5	1.0	1.8	3.0	5.0
E_1	−1.7968	−1.5592	−1.0000	−0.4240	0.0288	0.3861
E_2	1.7133	1.5325	1.2672	1.1339	1.0832	1.0584
E_3	1.1621	1.1023	1.0344	1.0111	1.0075	1.0082
E_4	1.0499	1.0269	1.0059	1.0013	1.0024	1.0042
E_5	1.0149	1.0065	1.0007	1.0007	1.0022	1.0036
M_1	−0.0189	0.0589	0.1808	0.2838	0.3652	0.4365
M_2	1.3789	1.3427	1.2874	1.2408	1.2039	1.1717
M_3	1.1343	1.1220	1.1025	1.0855	1.0719	1.0601
M_4	1.0739	1.0676	1.0573	1.0479	1.0403	1.0336
M_5	1.0478	1.0440	1.0376	1.0316	1.0266	1.0222

TABLE III(i). b_2 Coefficients for $Z=83$.

	$k=0.5$	1.0	1.8	3.0	5.0
E_1	−1.5499	−1.0000	−0.4460	−0.0103	0.3399
E_2	1.4467	1.2083	1.1073	1.0734	1.0569
E_3	1.0680	1.0188	1.0071	1.0078	1.0100
E_4	1.0125	1.0016	1.0016	1.0041	1.0062
E_5	1.0014	1.0003	1.0020	1.0040	1.0053
M_1	0.0347	0.1279	0.2166	0.2853	0.3407
M_2	1.3562	1.3051	1.2609	1.2255	1.1944
M_3	1.1265	1.1083	1.0922	1.0789	1.0673
M_4	1.0698	1.0603	1.0514	1.0439	1.0373
M_5	1.0453	1.0394	1.0338	1.0289	1.0245

TABLE III(j). b_2 Coefficients for $Z=88$.

	$k=0.5$	1.0	1.8	3.0	5.0
E_1	−1.5404	−1.0000	−0.4687	−0.0514	0.2899
E_2	1.3461	1.1503	1.0841	1.0661	1.0573
E_3	1.0367	1.0081	1.0059	1.0097	1.0129
E_4	1.0033	1.0007	1.0036	1.0068	1.0088
E_5	1.0001	1.0018	1.0044	1.0064	1.0075
M_1	−0.0012	0.0820	0.1548	0.2086	0.2457
M_2	1.3678	1.3214	1.2803	1.2468	1.2176
M_3	1.1302	1.1137	1.0985	1.0858	1.0745
M_4	1.0718	1.0630	1.0547	1.0475	1.0410
M_5	1.0465	1.0411	1.0358	1.0312	1.0269

TABLE III(k). b_2 Coefficients for $Z=92$.

	$k=0.5$	1.0	1.8	3.0	5.0
E_1	−1.5321	−1.0000	−0.4875	−0.0856	0.2470
E_2	1.2581	1.1081	1.0696	1.0631	1.0596
E_3	1.0172	1.0044	1.0081	1.0128	1.0166
E_4	1.0004	1.0022	1.0064	1.0097	1.0114
E_5	1.0015	1.0043	1.0069	1.0086	1.0095
M_1	−0.0160	0.0511	0.1105	0.1522	0.1743
M_2	1.3758	1.3335	1.2951	1.2636	1.2362
M_3	1.1330	1.1179	1.1036	1.0912	1.0805
M_4	1.0731	1.0651	1.0572	1.0503	1.0440
M_5	1.0473	1.0424	1.0374	1.0329	1.0287

TABLE III(l). b_2 Coefficients for $Z=96$.

	$k=0.5$	1.0	1.8	3.0	5.0
E_1	−1.5231	−1.0000	−0.5069	−0.1213	0.2013
E_2	1.1701	1.0734	1.0603	1.0634	1.0643
E_3	1.0050	1.0042	1.0115	1.0173	1.0207
E_4	1.0013	1.0057	1.0103	1.0132	1.0146
E_5	1.0046	1.0075	1.0098	1.0112	1.0117
M_1	−0.0253	0.0258	0.0719	0.1019	0.1106
M_2	1.3828	1.3446	1.3093	1.2801	1.2548
M_3	1.1354	1.1214	1.1081	1.0965	1.0862
M_4	1.0744	1.0670	1.0596	1.0531	1.0471
M_5	1.0480	1.0435	1.0389	1.0346	1.0306

Here one uses the result that interchanging L and $L+1$ in Ω changes this factor into its negative complex conjugate.

This result can be greatly simplified by the introduction of the T_e and T_m given earlier for the pure multipole case, as well as the explicit introduction of the conversion coefficients $c_e(L+1)$ and $c_m(L)$:

$$b_\nu'[L, L+1, \pi=(-)^L]$$

$$=[c_e(L+1)c_m(L)]^{\frac{1}{2}}\left[\frac{L(L+2)}{(2L+1)(2L+3)}\right]^{\frac{1}{2}}$$

$$\times\frac{\mathrm{Re}\left\{e^{i(\theta_e-\theta_m)}\left(1+\frac{L+1}{LT_m}\right)^*\left(1-\frac{L+1}{T_e}\right)\right\}}{\left[\left(1+\frac{L+1}{L|T_m|^2}\right)\left(1+\frac{(L+2)(L+1)}{|T_e|^2}\right)\right]^{\frac{1}{2}}}, \quad (101)$$

where we have defined

$$\frac{Q(L+1, L, m)}{|Q(L+1, L, m)|}=e^{i\theta_m}, \quad (101a)$$

$$\frac{Q(L+1, L+1, e)}{|Q(L+1, L+1, e)|}=e^{i\theta_e}. \quad (101b)$$

This is just the result given in reference (70). The b_ν' here defined is that coefficient by which one multiplies the cross term in a mixed 2^L, 2^{L+1} multipole γ-ray correlation to convert this term into the corresponding term of a mixed conversion electron correlation. It should be noted that this coefficient is independent of ν.

Just as for the pure multipole cases, we normalize by dividing out the conversion coefficient terms, in this case removing $[c_e(L+1)c_m(L)]^{\frac{1}{2}}$. Let

$$b[L, L+1, \pi=(-)^L]=b_\nu'(L, L+1, \pi)[c_e(L+1)c_m(L)]^{\frac{1}{2}}.$$

Then the correlation function for a cascade involving a mixed conversion electron (E_{L+1}, M_L mixture) and a

CC-0. In Public Domain. Gurukul Kangri Collection, Haridwar

Digitized by Arya Samaj Foundation Chennai and eGangotri

TABLE IV(a). Mixed conversion particle parameter b for $k=0.3$.

Z	$L=1$	2	3	4
10	−0.1928	−0.1899	−0.1898	−0.1909
20	−0.1989	−0.2083	−0.2166	−0.2243
30	−0.1979	−0 2287	−0.2491	−0.2669
40	−0.1894	−0.2536	−0.2905	−0.3225
54	−0.1483	−0.2916	−0.3692	−0.4311
64	−0.08891	−0.3130	−0.4353	−0.5235
72	−0.006616	−0.3200	−0.4825	−0.5857
78	0.08917	−0.2972	−0.4953	−0.6059

TABLE IV(b). Mixed conversion particle parameter b for $k=0.5$.

Z	$L=1$	2	3	4
10	−0.3094	−0.3032	−0.3016	−0.3020
20	−0.3203	−0.3288	−0.3365	−0.3447
30	−0.3244	−0.3567	−0.3772	−0.3958
40	−0.3198	−0.3877	−0.4251	−0.4576
54	−0.2924	−0.4383	−0.5106	−0.5658
64	−0.2490	−0.4759	−0.5785	−0.6460
72	−0.1908	−0.5003	−0.6242	−0.6947
78	−0.1266	−0.5126	−0.6486	−0.7094
83	−0.05448	−0.5077	−0.6527	−0.7118
88	0.03913	−0.4913	−0.6447	−0.6951
92	0.1322	−0.4610	−0.6231	−0.6728
96	0.2419	−0.4144	−0.5895	−0.6410

TABLE IV(c). Mixed conversion particle parameter b for $k=1.0$.

Z	$L=1$	2	3	4
10	−0.5417	−0.5324	−0.5291	−0.5287
20	−0.5557	−0.5643	−0.5715	−0.5792
30	−0.5623	−0.5948	−0.6150	−0.6324
40	−0.5593	−0.6267	−0.6610	−0.6869
54	−0.5324	−0.6665	−0.7209	−0.7563
64	−0.4902	−0.6867	−0.7552	−0.7903
72	−0.4370	−0.6976	−0.7697	−0.7986
78	−0.3822	−0.6966	−0.7694	−0.7907
83	−0.3246	−0.6882	−0.7620	−0.7792
88	−0.2547	−0.6717	−0.7461	−0.7596
92	−0.1892	−0.6490	−0.7241	−0.7404
96	−0.1148	−0.6272	−0.7056	−0.7181

pure γ multipole is

$$W(\beta)=I_m c_m(L)W_m(\beta)+I_e c_e(L+1)W_e(\beta)$$
$$\pm 2(I_e I_m)^{\frac{1}{2}}[c_m(L)c_e(L+1)]^{\frac{1}{2}}bW_{em}(\beta). \quad (102)$$

Here the conversion coefficients can be taken from reference (69) since only a common factor has been dropped. In Eq. (102) I_m and I_e are proportional to the intensities of the magnetic and electric radiations in the mixed transition (Eq. 67) and the sign in the third (interference) term depends on the nuclear structure and must be regarded as an adjustable parameter. This sign is the same as in the mixed γ-pure γ-correlation. In Eq. (102) W_m is the correlation function for a pure magnetic 2^L pole (M_L) conversion electron replacing the mixed radiation

$$W_m(\beta)=\sum_\nu b_\nu(LLm)A_\nu P_\nu(\cos\beta), \quad (102a)$$

where A_ν is obtained from Eq. (69a) by setting $L_1=L$.

TABLE IV(d). Mixed conversion particle parameter b for $k=1.8$.

Z	$L=1$	2	3	4
10	−0.7533	−0.7473	−0.7451	−0.7449
20	−0.7608	−0.7709	−0.7785	−0.7850
30	−0.7609	−0.7906	−0.8075	−0.8200
40	−0.7504	−0.8063	−0.8314	−0.8472
54	−0.7104	−0.8159	−0.8506	−0.8675
64	−0.6574	−0.8100	−0.8505	−0.8651
72	−0.5958	−0.7979	−0.8400	−0.8501
78	−0.5363	−0.7819	−0.8248	−0.8317
83	−0.4768	−0.7634	−0.8075	−0.8129
88	−0.4078	−0.7411	−0.7868	−0.7901
92	−0.3453	−0.7170	−0.7640	−0.7703
96	−0.2763	−0.6955	−0.7455	−0.7489

TABLE IV(e). Mixed conversion particle parameter b for $k=3.0$.

Z	$L=1$	2	3	4
10	−0.8826	−0.8805	−0.8805	−0.8813
20	−0.8829	−0.8909	−0.8977	−0.9033
30	−0.8770	−0.8981	−0.9101	−0.9181
40	−0.8614	−0.8991	−0.9148	−0.9236
54	−0.8149	−0.8878	−0.9093	−0.9170
64	−0.7564	−0.8674	−0.8926	−0.8990
72	−0.6895	−0.8443	−0.8717	−0.8761
78	−0.6255	−0.8230	−0.8525	−0.8544
83	−0.5623	−0.8009	−0.8325	−0.8339
88	−0.4897	−0.7758	−0.8101	−0.8108
92	−0.4248	−0.7535	−0.7903	−0.7912
96	−0.3540	−0.7296	−0.7696	−0.7705

TABLE IV(f). Mixed conversion particle parameter b for $k=5.0$.

Z	$L=1$	2	3	4
10	−0.9507	−0.9501	−0.9509	−0.9521
20	−0.9481	−0.9531	−0.9572	−0.9604
30	−0.9410	−0.9511	−0.9579	−0.9632
40	−0.9263	−0.9463	−0.9549	−0.9590
54	−0.8835	−0.9266	−0.9382	−0.9410
64	−0.8271	−0.9014	−0.9162	−0.9184
72	−0.7591	−0.8759	−0.8940	−0.8941
78	−0.6915	−0.8508	−0.8721	−0.8722
83	−0.6229	−0.8266	−0.8514	−0.8523
88	−0.5430	−0.8004	−0.8292	−0.8296
92	−0.4712	−0.7763	−0.8085	−0.8110
96	−0.3931	−0.7527	−0.7888	−0.7909

Similarly W_e is the correlation function for a pure electric 2^{L+1} pole (E_{L+1}) conversion electron replacing the mixed radiation

$$W_e(\beta)=\sum_\nu b_\nu(L+1, L+1, e)A_\nu P_\nu(\cos\beta), \quad (102b)$$

and here A_ν is obtained from Eq. (69a) by replacing L_1 by $L+1$. The interference term W_{em} is given in Eq. (70c) if one sets $L_1=L$, $L_1'=L+1$.

Of course, as mentioned above, the interference term (which is absent in the total conversion coefficient) constitutes a sensitive indicator of mixtures. Numerical results for this mixed conversion correlation coefficient $b[L, L+1, \pi=(-)^L]$ are given in Table IV(a)–IV(f).

Corresponding to the discussion of limiting cases for the pure conversion transitions one may examine the coefficient b for the mixed conversion transition for these limits. It is of in-

CC-0. In Public Domain. Gurukul Kangri Collection, Haridwar

Digitized by Arya Samaj Foundation Chennai and eGangotri

terest to inquire whether in the high-energy limit the conversion electrons in a mixed transition behave like photons as was the case for the pure transitions. To examine this question in a general way we consider the high-energy limit of $R(\nu q)$. By use of Eq. (89) and the notation $\epsilon=(-)^{\sigma}$, one sees that

$$R(\nu q, LL'\pi)\rightarrow|N|^2(-)^{L+q}[L(L+1)L'(L'+1)]^{-\frac{1}{2}}D(\nu, q0; \mathbf{f})\times\sum_{\kappa\kappa'}[(2l+1)(2l'+1)]^{\frac{1}{2}}|\kappa\kappa'|(\kappa+\epsilon)(\kappa'+\epsilon')\times(\delta_{\kappa,\epsilon L}+\delta_{\kappa,-\epsilon(L+1)})(\delta_{\kappa',\epsilon'L'}+\delta_{\kappa',-\epsilon'(L'+1)})\times C(ll'\nu;00)W(ljl'j';\tfrac{1}{2}\nu)W(LjL'j';\tfrac{1}{2}\nu). \quad (89a)$$

There are three cases to consider: (a) electric 2^L-electric $2^{L'}$ poles, (b) magnetic 2^L-magnetic $2^{L'}$ poles (for both of these $L-L'$ is an even integer), and (c) electric 2^L-magnetic $2^{L'}$ poles (here $L-L'$ is an odd integer). We note that for all cases we have $|\kappa|(\kappa+\epsilon)=S(\kappa)L(L+1)$.

Consider the $E-E$ case first. Then $l=L$, $l'=L'$ and we have

$$R(\nu q, LL'; EE)\rightarrow|N|^2(-)^{L+q}\times[L(L+1)(2L+1)L'(L'+1)(2L'+1)]^{\frac{1}{2}}C(LL'\nu;00)\times D(\nu, q0; \mathbf{f})\sum_{\kappa\kappa'}S(\kappa)S(\kappa')W^2(LjL'j';\tfrac{1}{2}\nu)$$

$$=\tfrac{1}{2}|N|^2(-)^{L+q+1}[(2L+1)(2L'+1)]^{\frac{1}{2}}C(LL'\nu;1-1)D(\nu, q0; \mathbf{f}),$$

where we have used the results

$$\sum_{\kappa\kappa'}S(\kappa)S(\kappa')W^2(LjL'j';\tfrac{1}{2}\nu)=\frac{L(L+1)+L'(L'+1)-\nu(\nu+1)}{4L(L+1)L'(L'+1)}$$

and

$$C(LL'\nu;1-1)=C(LL'\nu;00)\frac{\nu(\nu+1)-L(L+1)-L'(L'+1)}{2[L(L+1)L'(L'+1)]^{\frac{1}{2}}}$$

for ν an even integer.

From Eq. (61) we find therefore

$$R(\nu q, LL'; EE)\rightarrow\tfrac{1}{2}|N|^2R(\nu q, LL'; \gamma)$$

using $L-L'=$ even integer.

Exactly the same results holds for the magnetic-magnetic case if we first employ the identity given in (A6) of the Appendix

The $E-M$ case presents no additional difficulties if we use the identity given in (A7) of the Appendix. Using this one gets

$$R(\nu q, LL'; E-M)\rightarrow\tfrac{1}{2}|N|^2(-)^{L+q+1}\times[(2L+1)(2L'+1)]^{\frac{1}{2}}C(LL'\nu;1-1)D(\nu, q0; \mathbf{f})=-\tfrac{1}{2}|N|^2R(\nu q, LL'; \gamma).$$

(The use of the identity (A7) shows, moreover, that the $b_\nu(LL'; E-M)$ are always independent of ν. We found this to be true earlier for the special case of $E_{L+1}-M_L$ mixtures.)

Collecting our results, we can now assert that the high-energy conversion electron correlation is exactly the same as the correlation with a photon replacing the conversion electron, except that all cross-terms involving electric and magnetic multipoles have the *opposite* sign.

The $Z=0$ limit for the $E_{L+1}-M_L$ mixture is found to be

$$b=\left[1+\frac{4}{k^2}\frac{L+1}{L+2}\right]^{-\frac{1}{2}}.$$

The nonrelativistic limit is Z, k dependent.

D. Beta Radiation

1. Description of the Problem

The problem of determining the particle parameters b_ν, for β radiation is analogous to the determination of the b_ν for internal conversion electron emission, as treated in III-C above. In the latter case, one considers a bound electron, a K shell electron to be explicit, making a transition to an outgoing wave state. In the β-decay case the initial state is considered to be a Dirac particle without charge or rest mass, a neutrino, which undergoes a transition from a plane wave state into an outgoing wave electron state.[18] The fact that the initial state is characterized by zero charge and rest mass does not change the formalism of III-C in any essential way. The physical measurement in both the β-decay and internal conversion cases is the same, namely, one observes the direction of motion $\mathbf{f}$ of the emitted electron.

The direction of motion of the neutrino and its spin polarization are, of course, unobserved. Consequently, the initial state is random, exactly as was the case for the conversion problem. In contrast, however, we can no longer confine our attention to an initial state with $\kappa=-1$.

The simplicity which arises in the conversion of an s electron ($\kappa=-1$) is twofold. First, the fact that κ is fixed removes a summation and second, this particular value of κ (for which $j=\frac{1}{2}$) allows considerable algebraic simplification. Equivalent remarks would apply for $p_{\frac{1}{2}}$ electrons ($\kappa=1$).

From the point of view of precedure, however, there is a one-to-one correspondence between the treatment of the two problems, although the greater complexity of detail for the β-decay problem tends to obscure this parallelism. The origin of this complexity is to be found in the difference in the interactions. Whereas in the conversion problem one has a field interaction (electromagnetic) with known coupling, in the β-decay problem one deals with a point interaction (between leptons and nucleons) with essentially unknown coupling. This coupling must be some combination of the five relativistic invariants that can be formed with the four Dirac spinors, corresponding to the four spin $\frac{1}{2}$ particles involved, i.e., contraction of the covariants scalar (S), vector (V), tensor (T), axial vector (A) and pseudoscalar (P), (47). We shall consider only pure invariants in the following, although the treatment of mixtures would add no difficulty in principle.

As a model for the β-radiation problem, let us consider the essential steps involved in the conversion problem. By making a multipole expansion of the electromagnetic field, and with the justifiable neglect of the finite size of the nucleus, one separates the interaction into a sum of terms, each of which is factorable into a product of nuclear and electronic matrix elements (76). The separate terms in the expansion are characterized by their transformation properties, indicated by L and π. The analogous step for the β-radiation problem

[18] We follow the customary formulation of the theory in which the emission of *two* particles is equivalent to the emission of a particle and the absorption of an antiparticle. Thus, for negative electron emission the initial state is actually an antineutrino (charge-conjugate neutrino) state. To discuss positron emission one applies the charge conjugation operator to the entire system and, as is well known, this is equivalent to reversing the sign of the external field, that is, Z is changed to $-Z$ in the result for the negative electron case.

For the present problem there is no distinction between Dirac and Majorana neutrinos.

CC-0. In Public Domain. Gurukul Kangri Collection, Haridwar

Digitized by Arya Samaj Foundation Chennai and eGangotri

is effected by an expansion of the point interaction (a δ function) into spherical harmonics, Eq. (104), with appropriate modifications for each of the five invariants, *SVTAP*, as required (see Eq. (103b) and the discussion following). However, L and π do not constitute a sufficient description of these "multipoles" and an additional index α is used to distinguish between them. Having separated the nuclear and electronic matrix elements by this procedure, the tensor parameters, and hence the particle parameters $b_\nu(\beta)$, follow exactly as in III-C.

The procedure whereby the β-decay process is described as an analog of the conversion process clearly necessitates the use of the angular momentum representation, in contrast to methods previously used (27, 37, 47). This is, understandably, the natural representation for angular correlation problems. Analogous to the ordering of the contributions of the various possible multipoles in the electromagnetic (or conversion) problems by the retardation expansion, is the corresponding ordering which here leads to the usual classification in terms of orders of forbiddenness of the β-transitions. The results obtained below appear most most directly in terms of a notation different than that already familiar in β-decay theory and therefore tables of transcriptions to the customary notation are given.

The $\beta-x$ correlation has been treated by Falkoff and Uhlenbeck (27) who considered free electrons. The formalism for the case of electrons in a Coulomb field was given by Fuchs (37) and that paper also gives explicit results for the Z dependence valid for light nuclei. For heavy emitters results of sufficient precision require numerical evaluation[19] of certain combinations of electronic radial functions, see Table VII and Table 10 of reference 37.

2. *Explicit Calculation*

The Hamiltonian density H for the β-decay interaction, corresponding to the emission of negative electrons, is taken to be a scalar formed by the contraction of covariants made up of the lepton and nucleon wave functions, evaluated at the same point in space. The most general form for H is

$$H=\sum_s C_s(\Psi_{N_f}{}^+|O_s|\Psi_{N_i}):(\psi_e{}^+|O_s|\psi_\nu). \qquad (103)$$

In Eq. (103) the sign : means contraction. The $^+$ symbol is the Pauli adjoint, $\psi^+=i\psi^*\gamma_4$. The interactions O_s are

S	V	T	A	P
1	γ_μ	$\gamma_\mu\gamma_\nu$	$\gamma_\mu\gamma_\nu\gamma_\tau$	$\gamma_\mu\gamma_\nu\gamma_\tau\gamma_\sigma$.

(103a)

Of course, in Eq. (103) above the O_s operators appearing are in the separate nucleon and lepton spaces, respectively.

The C_s can be taken to be real constants. Since we shall treat only pure interactions, we can take $C_s=g\delta_{ss'}$ where g is the coupling constant. The γ_μ are Dirac operators; the Greek indices in Eq. (103a) run from 1 to 4. A product such as $\gamma_\mu\gamma_\nu\gamma_\tau$ implies that all combinations of μ, ν, τ are to be used, subject to $\mu>\nu>\tau$.

It is our aim now to classify the operators in the nucleon space by their rotational properties (L) and parity (π). One can accomplish this most easily by the following two steps: (a) Formally separate the nucleon and lepton spaces by introducing the delta function, $\delta(\mathbf{r}_N-\mathbf{r}_L)$ (integrating over the lepton space), and (b) by classifying the interaction O_s by their 3-space rotational properties. This latter step is easily accomplished by introducing the Dirac direct product notation for the γ's, i.e., $\gamma_4=\rho_3$, $\gamma_k=\rho_2\sigma_k$. Under 3-space rotations the ρ transform as scalars, the σ as a vector. Under reflections ($\pi_{Op}=\rho_3P_s$ where P_s mean space inversion), ρ_3, σ are unchanged, while ρ_1 and ρ_2 change sign. The interactions O_s become in this representation

	S	V	T	A	P
Scalar	1	ρ_3		$i\rho_2$	ρ_1
Vector		$\rho_2\boldsymbol{\sigma}$	$i\rho_1\boldsymbol{\sigma}$ $i\boldsymbol{\sigma}$	$i\rho_3\boldsymbol{\sigma}$	.

(103b)

In order to avoid possible confusion we repeat that the "scalar" and "vector" here refer to the transformation properties of the constituents of the O_s operators under 3-space rotations and not under Lorentz transformations. The phase i is fixed by direct substitution of the ρ and σ operators in (103a). A real phase (±1) has been ignored since it disappears under contraction.[20] Next one introduces the expansion for the delta function

$$\delta(\mathbf{r}_N-\mathbf{r}_L)=\frac{1}{r^2}\delta(r_N-r_L)\sum_{L,M}Y_L{}^{M*}(\mathbf{r}_N)Y_L{}^M(\mathbf{r}_L). \qquad (104)$$

For the "scalar" part of the interactions, i.e., those with the operators 1, ρ_k, this provides the desired multipole expansion since we may write for the nucleon operators

$$\left\{\begin{matrix}1\\ \rho_k\end{matrix}\right\}Y_L{}^{M*}(\mathbf{r}_N)$$

$$\times\left[\int d\Omega\left(\psi_e{}^+\left|\left\{\begin{matrix}1\\ \rho_k\end{matrix}\right\}Y_L{}^M(\mathbf{r}_L)\right|\psi_\nu\right)\right]_{r_L=r_N}. \qquad (104a)$$

Here the integration is over the common lepton angular variables. This operator is a function of r_N, it will be observed, but it is customary to evaluate it at $r_N=R$, the nuclear radius. In the sequel we shall refer to the first part (the coefficient of the term in square brackets) as the nuclear operator and the term in square brackets will be referred to as the lepton matrix element.

For the "vector" part of the interactions, one uses instead of the delta function the unit dyadic delta

[19] This work has been undertaken at this laboratory. In addition, it is necessary to change the sign of the phase δ which appears in the formal results of reference (37).

[20] An alternative way to fix the phase i is to check the requirement of commutability with the time reversal operator $K_t=i\sigma_yK_0$.

CC-0. In Public Domain. Gurukul Kangri Collection, Haridwar

Digitized by Arya Samaj Foundation Chennai and eGangotri

function:

$$\mathbf{I}\delta(\mathbf{r}_N-\mathbf{r}_L)=\frac{1}{r^2}\delta(r_N-r_L)\sum_{J,M,L}\times\mathbf{\Phi}^{M+}{}_{J,L}(\mathbf{r}_N)\mathbf{\Phi}^{M}{}_{J,L}(\mathbf{r}_L). \quad (105)$$

The orthonormal vector functions $\mathbf{\Phi}^{M}{}_{J,L}$ have the operational definitions

$$\mathbf{\Phi}^{M}{}_{J=L,L-1}=[L(2L+1)]^{-\frac{1}{2}}(r\nabla+L\mathbf{r})Y_L{}^{M} \quad (105a)$$

$$\mathbf{\Phi}^{M}{}_{J=L,L}=[L(L+1)]^{-\frac{1}{2}}\mathbf{L}Y_L{}^{M} \quad (105b)$$

$$\mathbf{\Phi}^{M}{}_{J=L,L+1}=[(L+1)(2L+1)]^{-\frac{1}{2}}\times(r\nabla-(L+1)\mathbf{r})Y_L{}^{M}. \quad (105c)$$

An equivalent definition of these vector eigenfunctions was given in Eq. (53a) except that, for convenience, the phase i^l appearing in that definition has been omitted here. (The magnetic quantum number M which replaces P in that definition is not restricted to the values ±1.) Here $\mathbf{L}$ is again the rotation operator, $-i\mathbf{r}\times\nabla$.

Using this formalism the operators corresponding to (104a) for the "vector" parts become

$$\begin{Bmatrix}1\\ \rho_k\end{Bmatrix}\boldsymbol{\sigma}\cdot\mathbf{\Phi}^{M+}{}_{J,L}\times\left[\int d\Omega\left(\psi_e{}^{+}\middle|\begin{Bmatrix}1\\ \rho_k\end{Bmatrix}\boldsymbol{\sigma}\cdot\mathbf{\Phi}^{M}{}_{J,L}\middle|\psi_\nu\right)\right]_{r_L=r_N}. \quad (105d)$$

The terminology, nuclear operator and lepton matrix element, already introduced applies here also.

For low values of J, $L\leqslant3$ the operators $\boldsymbol{\sigma}\cdot\mathbf{\Phi}^{M}{}_{J,L}$ are the familiar tensor operators which appear explicitly in Konopinski-Uhlenbeck (47). The correspondences are given in Table V. The great advantage of using the functions $\boldsymbol{\sigma}\cdot\mathbf{\Phi}^{M}{}_{J,L}$ is that by means of the operational definitions, Eqs. (105a, b, c), one can readily evaluate the lepton matrix elements, $\int d\Omega(\psi_e{}^{+}|(1 \text{ or } \rho_k)\boldsymbol{\sigma}\cdot\mathbf{\Phi}|\psi_\nu)$.

For clarity, the various interaction operators are tabulated below in Table VI. These operators are characterized by their rotational properties (L) and their parity (π). Since this is insufficient to distinguish them completely, a third index α is introduced as shown explicitly.

The lepton wave functions are plane waves at infinity (using once more the technique of a screened Coulomb field so that the concept of a plane wave is meaningful) and we again go to the spherical eigenfunction representation. The coefficients of the expansion, in the now familiar way, lead to the tensor parameters of the electron and neutrino [Eq. (88)], the latter being trivial since the neutrino state is random. We denote the electron quantum numbers by κ, μ; the neutrino by κ_ν, μ_ν. We must now evaluate the lepton matrix elements

$$M(\kappa_\nu;L\pi\alpha)=\left[\int d\Omega(\phi_\kappa{}^{\mu}(e)^{+}|O_\alpha|\phi_{\kappa_\nu}{}^{\mu_\nu}(\nu))\right]_{r_L=R}. \quad (106)$$

The operators O_α are explicitly given in Table VI.

Making use of the operational form of the $\mathbf{\Phi}^{M}{}_{J,L}$ one readily evaluates the (lepton) matrix elements, $M(\kappa\kappa_\nu;L\pi\alpha)$. It is convenient to split off the magnetic quantum number dependence, i.e., to define reduced

TABLE V. Correspondence of operators.[a]

Interaction	Operator	$K-U$	L
S	$Y^{M}{}_{L}$	β	0
		$\beta\mathbf{r}$	1
V	$\rho_3Y^{M}{}_{L}$	$R^{\beta}{}_{\mu\nu}/r^2$	2
		1	0
		$\mathbf{r}$	1
	$\rho_3\boldsymbol{\sigma}\cdot\mathbf{\Phi}^{M}{}_{L,L}$	$R_{\mu\nu}/r^2$	2
		$\boldsymbol{\alpha}\times\mathbf{r}$	1
	$\rho_2\boldsymbol{\sigma}\cdot\mathbf{\Phi}^{M}{}_{L,L-1}$	$\boldsymbol{\alpha}$	1
		$A_{\mu\nu}/r$	2
T	$\boldsymbol{\sigma}\cdot\mathbf{\Phi}^{M}{}_{L,L}$	$\beta\boldsymbol{\sigma}\times\mathbf{r}$	1
		$T^{\beta}{}_{ij}/r^2$	2
	$\rho_1\boldsymbol{\sigma}\cdot\mathbf{\Phi}^{M}{}_{L,L+1}$	$\beta\boldsymbol{\alpha}\cdot\mathbf{r}$	0
	$\rho_1\boldsymbol{\sigma}\cdot\mathbf{\Phi}^{M}{}_{L,L-1}$	$\beta\boldsymbol{\alpha}$	1
		$A^{\beta}{}_{ij}/r$	2
	$\boldsymbol{\sigma}\cdot\mathbf{\Phi}^{M}{}_{L,L-1}$	$\beta\boldsymbol{\sigma}$	1
		$B^{\beta}{}_{\mu\nu}/r$	2
		$S^{\beta}{}_{ijk}/r^2$	3
	$\boldsymbol{\sigma}\cdot\mathbf{\Phi}^{M}{}_{L,L+1}$	$\beta\boldsymbol{\sigma}\cdot\mathbf{r}$	0
A	$\rho_3\boldsymbol{\sigma}\cdot\mathbf{\Phi}^{M}{}_{L,L}$	$\boldsymbol{\sigma}\times\mathbf{r}$	1
		T_{ij}/r^2	2
	$i\rho_2Y^{M}{}_{L}$	γ_5	0
	$\rho_3\boldsymbol{\sigma}\cdot\mathbf{\Phi}^{M}{}_{L,L+1}$	$\boldsymbol{\sigma}\cdot\mathbf{r}$	0
	$\rho_3\boldsymbol{\sigma}\cdot\mathbf{\Phi}^{M}{}_{L,L-1}$	$\boldsymbol{\sigma}$	1
		$B_{\mu\nu}/r$	2
		S_{ijk}/r^2	3
P	$\rho_1Y^{M}{}_{L}$	$\beta\gamma_5$	0
		$\beta\gamma_5\mathbf{r}$	1
		$R^{\beta\gamma_5}{}_{\mu\nu}/r^2$	2

[a] Whereas the operator given here is associated with the use of the Pauli adjoint (in forming matrix elements) the $K-U$ equivalent is associated with the ordinary Hermitian conjugate nuclear wave function.

TABLE VI. Lepton operators.[a]

$\pi=(-1)^L$		$\pi=(-1)^{L+1}$	
α	Operator	α	Operator
S	$Y^{M}{}_{L}$	P	$\rho_1Y^{M}{}_{L}$
T_0	$i\boldsymbol{\sigma}\cdot\mathbf{\Phi}^{M}{}_{L,L}$	T_0'	$i\rho_1\boldsymbol{\sigma}\cdot\mathbf{\Phi}^{M}{}_{L,L}$
V	$\rho_3Y^{M}{}_{L}$	A	$i\rho_2Y^{M}{}_{L}$
A_0	$i\rho_3\boldsymbol{\sigma}\cdot\mathbf{\Phi}^{M}{}_{L,L}$	V_0	$\rho_2\boldsymbol{\sigma}\cdot\mathbf{\Phi}^{M}{}_{L,L}$
T_1	$i\rho_1\boldsymbol{\sigma}\cdot\mathbf{\Phi}^{M}{}_{L,L+1}$	T_1'	$i\boldsymbol{\sigma}\cdot\mathbf{\Phi}^{M}{}_{L,L+1}$
T_{-1}	$i\rho_1\boldsymbol{\sigma}\cdot\mathbf{\Phi}^{M}{}_{L,L-1}$	T'_{-1}	$i\boldsymbol{\sigma}\cdot\mathbf{\Phi}^{M}{}_{L,L-1}$
V_1	$\rho_2\boldsymbol{\sigma}\cdot\mathbf{\Phi}^{M}{}_{L,L+1}$	A_1	$i\rho_3\boldsymbol{\sigma}\cdot\mathbf{\Phi}^{M}{}_{L,L+1}$
V_{-1}	$\rho_2\boldsymbol{\sigma}\cdot\mathbf{\Phi}^{M}{}_{L,L-1}$	A_{-1}	$i\rho_3\boldsymbol{\sigma}\cdot\mathbf{\Phi}^{M}{}_{L,L-1}$

[a] The indexes in the first and third columns, on the T, V, and A symbols refer to the three $\mathbf{\Phi}$ functions introduced in Eqs. (105a, b, c). The prime distinguishes the two operators of different parity for given L.

CC-0. In Public Domain. Gurukul Kangri Collection, Haridwar

Digitized by Arya Samaj Foundation Chennai and eGangotri

TABLE VII. Reduced matrix elements.[a]

α	$Q(\kappa\kappa_\nu; L\pi\alpha)$
(a) $\pi=(-1)^L$	
S	$(f_\kappa g_{\kappa_\nu}-g_\kappa f_{\kappa_\nu})(\kappa\|L\|-\kappa_\nu)$
V	$-(f_\kappa g_{\kappa_\nu}+g_\kappa f_{\kappa_\nu})(\kappa\|L\|-\kappa_\nu)$
T_0	$i(\kappa+\kappa_\nu)(f_\kappa g_{\kappa_\nu}+g_\kappa f_{\kappa_\nu})(\kappa\|L\|-\kappa_\nu).N_0$
A_0	$-i(\kappa+\kappa_\nu)(f_\kappa g_{\kappa_\nu}-g_\kappa f_{\kappa_\nu})(\kappa\|L\|-\kappa_\nu).N_0$
T_1	$-i[f_\kappa f_{\kappa_\nu}(L+1-\kappa-\kappa_\nu)+g_\kappa g_{\kappa_\nu}(L+1+\kappa+\kappa_\nu)](\kappa\|L\|-\kappa_\nu).N_1$
T_{-1}	$-i[f_\kappa f_{\kappa_\nu}(-L-\kappa-\kappa_\nu)+g_\kappa g_{\kappa_\nu}(-L+\kappa+\kappa_\nu)](\kappa\|L\|-\kappa_\nu).N_{-1}$
V_1	$[f_\kappa f_{\kappa_\nu}(L+1-\kappa-\kappa_\nu)-g_\kappa g_{\kappa_\nu}(L+1+\kappa+\kappa_\nu)](\kappa\|L\|-\kappa_\nu).N_1$
V_{-1}	$[f_\kappa f_{\kappa_\nu}(-L-\kappa-\kappa_\nu)-g_\kappa g_{\kappa_\nu}(-L+\kappa+\kappa_\nu)](\kappa\|L\|-\kappa_\nu).N_{-1}$
(b) $\pi=(-)^{L+1}$	
P	$i(f_\kappa f_{\kappa_\nu}+g_\kappa g_{\kappa_\nu})(\kappa\|L\|\kappa_\nu)$
A	$i(f_\kappa f_{\kappa_\nu}-g_\kappa g_{\kappa_\nu})(\kappa\|L\|\kappa_\nu)$
T_0'	$i(\kappa_\nu-\kappa)(f_\kappa f_{\kappa_\nu}-g_\kappa g_{\kappa_\nu})(\kappa\|L\|\kappa_\nu)N_0$
V_0	$-(\kappa_\nu-\kappa)(f_\kappa f_{\kappa_\nu}+g_\kappa g_{\kappa_\nu})(\kappa\|L\|\kappa_\nu).N_0$
T_1'	$-i[f_\kappa g_{\kappa_\nu}(\kappa-\kappa_\nu-L-1)+g_\kappa f_{\kappa_\nu}(\kappa-\kappa_\nu+L+1)](\kappa\|L\|\kappa_\nu).N_1$
T_{-1}'	$i[f_\kappa g_{\kappa_\nu}(-\kappa+\kappa_\nu-L)-f_{\kappa_\nu}g_\kappa(\kappa-\kappa_\nu-L)](\kappa\|L\|\kappa_\nu).N_{-1}$
A_1'	$-i[f_\kappa g_{\kappa_\nu}(-\kappa+\kappa_\nu+L+1)+g_\kappa f_{\kappa_\nu}(\kappa-\kappa_\nu+L+1)](\kappa\|L\|\kappa_\nu).N_1$
A_{-1}'	$i[f_\kappa g_{\kappa_\nu}(\kappa-\kappa_\nu+L)-f_{\kappa_\nu}g_\kappa(\kappa-\kappa_\nu-L)](\kappa\|L\|\kappa_\nu).N_{-1}$

[a] $N_\mu=[1-\delta(\mu,1)+(2-\mu^2)L]^{\frac{1}{2}}[L(L+1)(2L+1)]^{-\frac{1}{2}}$.

matrix elements $Q(\kappa\kappa_\nu; L\pi\alpha)$ (the analog of the $Q(\kappa L\pi)$ of III-C).

$$M(\kappa\kappa_\nu; L\pi\alpha)\equiv Q(\kappa\kappa_\nu; L\pi\alpha)C(Lj_\nu j; M\mu_\nu). \quad (107)$$

Table VII gives the explicit forms for these reduced matrix elements. In Table VII the f_κ and g_κ are radial wave functions for the electron which are given explicitly in reference (67). The notation differs from that used in (67) only in the use of κ as an index. Note also that the normalization is to one particle in a sphere of unit radius. Moreover, in Table VII, f and g are evaluated at R. The radial functions with κ_ν as index refer to the neutrino. The identification of the radial functions can be made by the definition

$$\phi_\kappa{}^\mu=\begin{pmatrix}-if_\kappa\chi_{-\kappa}{}^\mu\\ g_\kappa\chi_\kappa{}^\mu\end{pmatrix},$$

which may be compared with Eq. (83), noting that for the neutrino $E=p$, ($E-1$ and $E+1\rightarrow E$).

In Table VII the reduced angular matrix elements are given by

$$(\kappa|L|\kappa_\nu)=(-)^{j_\nu-\frac{1}{2}}\left[\frac{(2j_\nu+1)(2l+1)(2l_\nu+1)}{4\pi}\right]^{\frac{1}{2}}$$
$$\times C(ll_\nu L,00)W(jlj_\nu l_\nu;\tfrac{1}{2}L), \quad (108)$$

where again $l\equiv l(\kappa)$, $l_\nu\equiv l(\kappa_\nu)$ and similarly for j and j_ν. It is useful to note that $(-\kappa|L|-\kappa_\nu)=(\kappa|L|\kappa_\nu)$. The occurrence of the matrix element with $-\kappa_\nu$ replacing κ_ν in the case $\pi=(-)^L$ should be noted. The two cases, $\pi=(-)^L$ and $\pi=(-)^{L+1}$, can be considered together by introducing the notation $\delta=\pi(-)^{L+1}$. Then the reduced matrix elements in Eq. (108) have the common form $(\kappa|L|\delta\kappa_\nu)$.

The formal work of determining the tensor parameters of the nuclear transition is complete, upon using Eq. (89), which couples the electron and neutrino tensor parameters, noting that now an additional summation, over κ_ν, is required

$$R(\nu q, L\pi\alpha; L'\pi\alpha')=\sum_{\kappa\kappa'\kappa_\nu}Q(\kappa\kappa_\nu; L\pi\alpha)$$
$$\times Q^*(\kappa'\kappa_\nu; L'\pi\alpha')|\kappa\kappa'|^{\frac{1}{2}}W(jj_\nu\nu L'; Lj')$$
$$\times R(\nu q, \kappa\kappa'; el), \quad (109)$$

where the tensor parameter for the β-particle $R(\nu q, \kappa\kappa'; el)$ is given explicitly in Eq. (87). The summation is over all κ_ν, which thus sums all states of the neutrino with equal weight but incoherently. The electron states, on the other hand, are seen to interfere coherently, as is to be expected.

The reflection symmetry (that is, symmetry about 90° in the angle between the two radiations) follows from Eq. (109). From Eq. (108) one sees that

$$l(\kappa)+l(\delta\kappa_\nu)+L=\text{even integer}$$

with $\delta=\pi(-)^{L+1}$ and

$$l(\kappa')+l(\delta'\kappa_\nu)+L'=\text{even integer}$$

with $\delta'=\pi(-)^{L'+1}$. From the results of III-C, the tensor parameter for the electron vanishes unless

$$l(\kappa)+l(\kappa')+\nu=\text{even integer}.$$

CC-0. In Public Domain. Gurukul Kangri Collection, Haridwar

Digitized by Arya Samaj Foundation Chennai and eGangotri

Moreover, $L-L'$ and $\delta-\delta'$ have the same character (are both even or both odd). Therefore it follows that ν is always an even integer which guarantees the reflection symmetry (since ν is always the degree of the Legendre polynomial in the correlation function). This result is a direct consequence of the fact that the β-transition is characterized by a definite parity change π (so that no interference between π and $-\pi$ is possible) and that only a propagation direction $\mathbf{f}$ is observed.

At this point we may verify from Eq. (109) that isotropy is obtained in the following two cases: (a) the limit of zero electron momentum (since this implies that Q vanishes unless $\kappa=\pm 1$; but then $j(\kappa)=\frac{1}{2}$ and the Racah coefficient $W(jj_\nu\nu L'; Lj')$ with $j=j'=\frac{1}{2}$ vanishes unless $\nu=0$, which means isotropy). (b) If the energy spectrum has the allowed shape (this implies that the energy correction factor (47) is independent of the electron momentum, which in turn implies that $\kappa=\pm 1$. Hence $\nu=0$ as in (a).

One can reduce the large number of nuclear operators that are seen to occur in the β-decay problem to manageable proportions, by making the customary "order of forbiddenness" expansion. The physical basis of this is twofold: firstly, the lepton matrix elements, $Q(\kappa\kappa_\nu; L\pi\alpha)$, are functions of the small parameters (pR) and (qR), i.e., the ratio of the nuclear radius to the electron and neutrino de Broglie wavelengths, respectively.[20] At least in the small Z limit, one can classify the Q in terms of the lowest order of (pR) and (qR) occurring. Secondly, some of the nuclear operators involve the off-diagonal operators (in the Dirac space), ρ_1 and ρ_2; hence since small and large components of the nuclear wave function are thereby coupled, the nuclear matrix elements are of the order v/c (where v is the nucleon velocity). This is a small quantity of the same order as (pR) or (qR). We shall evaluate the "order of forbiddenness" in the $Z=0$ limit and assume that this same ordering holds for $Z\neq 0$. Table VIII lists the results.

TABLE VIII. Order of forbiddenness classification.[a]

$\pi=(-1)^L$		$\pi=(-1)^{L+1}$	
α	Order of forbiddenness	α	Order of forbiddenness
S	L	P	$L+1$
T_0	L	T_0'	$L+1$
V	L	A	$L+1$
A_0	L	V_0	$L+1$
T_1	$L+2$	T_1'	$L+1$
T_{-1}	L	T'_{-1}	$L-1$
V_1	$L+2$	A_1	$L+1$
V_{-1}	L	A_{-1}	$L-1$

[a] The operator in each case is as in Table VI.

It will be observed from Table VIII that the well-known correlation between order of forbiddenness and parity is obtained. That is, successive orders of forbiddenness are characterized by opposite parity change and the allowed transitions correspond to parity change "no" $(\pi=1)$.

TABLE IX. Interfering operators for the Lth forbidden transitions $(\pi=(-)^L)$.[a]

Interaction	Operators
S	$Y^M{}_L$
V	$i\rho_2\boldsymbol{\sigma}\cdot\boldsymbol{\Phi}^M{}_{L-1,L-1}$; $\rho_2 Y^M{}_L$; $\rho_2\boldsymbol{\sigma}\cdot\boldsymbol{\Phi}^M{}_{L,L-1}$; $\rho_2\boldsymbol{\sigma}\cdot\boldsymbol{\Phi}^{M(\mathrm{x})}{}_{L-2,L-1}$
T	$i\boldsymbol{\sigma}\cdot\boldsymbol{\Phi}^M{}_{L,L}$; $i\rho_1\boldsymbol{\sigma}\cdot\boldsymbol{\Phi}^{M(\mathrm{x})}{}_{L-2,L-1}$; $i\rho_1\boldsymbol{\sigma}\cdot\boldsymbol{\Phi}^M{}_{L,L-1}$; $i\rho_1\boldsymbol{\sigma}\cdot\boldsymbol{\Phi}^{M(\mathrm{x})}{}_{L-1,L-1}$; $i\boldsymbol{\sigma}\cdot\boldsymbol{\Phi}^{M(\mathrm{x})}{}_{L-1,L}$; $i\boldsymbol{\sigma}\cdot\boldsymbol{\Phi}^M{}_{L+1,L}$
A	$i\rho_5\boldsymbol{\sigma}\cdot\boldsymbol{\Phi}^M{}_{L,L}$; $i\rho_2 Y^{M(\mathrm{x})}{}_{L-1}$; $i\rho_5\boldsymbol{\sigma}\cdot\boldsymbol{\Phi}^{M(\mathrm{x})}{}_{L-1,L}$; $i\rho_5\boldsymbol{\sigma}\cdot\boldsymbol{\Phi}^M{}_{L+1,L}$
P	$\rho_1 Y^M{}_{L-1}$

[a] The operators marked with a cross (x) are generally omitted as small corrections to operators with the same parity and L but two orders of forbiddenness lower, provided the L value is large enough for this latter operator to exist.

Specification of the order of forbiddenness and the nature of the interaction $(SVTAP)$ does not uniquely select a nuclear operator, as is also well known. In general, interference between various operator matrix elements occur, and this is illustrated in Table IX. In this table interferences occur for a given pure interaction wherever there is more than one entry (V, T, A). These interferences are of two types. (a) Interference between operators of different rotational properties (indicated by the first subscript on $\boldsymbol{\Phi}^M{}_{JL}$). This type of interference is the analog of the E_L, $M_{L'}$ multipole mixtures in the case of electromagnetic radiation. (b) Interference between different operators of the same rotational properties. Interferences of type (b) occur in the total intensity of β-emission whereas those of type (a) are present only in angular distributions (37).

For the T and A interactions, for given L, there is a single operator $i\boldsymbol{\sigma}\cdot\boldsymbol{\Phi}^M{}_{L+1,L}$ which does not interfere with any others. This is the unique matrix element case in the Gamow-Teller interactions.

Having determined the $R(\nu q, L\pi\alpha; L'\pi\alpha')$ by Eq. (109), it is now a straightforward matter to define the particle parameters b_ν for β-radiation. The first step is to weight $R(\nu q, L\pi\alpha; L'\pi\alpha')$ by the reduced nuclear matrix elements

$$R(\nu q, LL'; \beta)=\sum_{\alpha\alpha'} M_N(L\pi\alpha)M_N{}^*(L'\pi\alpha') \times R(\nu q, L\pi\alpha; L'\pi\alpha'). \quad (110)$$

The nuclear reduced matrix elements, $M_N(L\pi\alpha)$, are defined as usual to be

$$(\Psi_{J'\mu'}|O_\alpha{}^{+(L\pi)}|\Psi_{J,\mu}) \equiv M_N(L\pi\alpha)C(J'LJ;\mu'M)\delta(\mu, M+\mu'). \quad (111)$$

Here the primed Ψ functions refer to initial state and the unprimed Ψ's to the final state. The relative phases of these reduced matrix elements are real, i.e., $M_N(L\pi\alpha) \times M_N{}^*(L'\pi\alpha')$ is a real number, see Sec. II. The b_ν parameters are then obtained from Eq. (42b).

[20] That is, p and q are the electron and neutrino momenta, respectively.

CC-0. In Public Domain. Gurukul Kangri Collection, Haridwar

Digitized by Arya Samaj Foundation Chennai and eGangotri

TABLE X. Partial particle parameters for β radiation.[a]

Matrix element product	b_ν
First forbidden	
$S:\ \left\|\int \beta\mathbf{r}\right\|^2_{(L=1)}$	$b_0=\frac{1}{4}\left[\frac{1}{3}(q^2+p^2)-\frac{2}{9}\frac{qp^2}{E}+\frac{2\xi}{3}\left(\frac{p^2}{E}-q\right)+\xi^2\right]$
	$b_2=\frac{p^2}{6}\left(\frac{2q}{3E}-1-\frac{2\xi}{E}\right)$
$V:\ \left\|\int \mathbf{r}\right\|^2_{(L=1)}$	$q\to -q$ in $\left\|\int \beta\mathbf{r}\right\|^2$
$\left\|\int \boldsymbol{\alpha}\right\|^2_{(L=1)}$	$b_0=\frac{1}{4}$
$\pm\left\|\int \boldsymbol{\alpha}\right\|\left\|\int \mathbf{r}\right\|_{(L=1)}$	$b_0=\frac{1}{2}\left(\frac{q}{3}+\frac{p^2}{3E}+\xi\right)$
	$b_2=-p^2/3E$
$T:\ \left\|\int \beta\boldsymbol{\alpha}\right\|^2_{(L=1)}$	Same as $\left\|\int \boldsymbol{\alpha}\right\|^2$
$\left\|\int \beta\boldsymbol{\sigma}\times\mathbf{r}\right\|^2_{(L=1)}$	$b_0=\frac{1}{4}\left[\frac{1}{6}(q^2+p^2)+\frac{2}{9}\frac{qp^2}{E}+\frac{2}{3}\left(\frac{p^2}{E}+q\right)\xi+\xi^2\right]$
	$b_2=\frac{p^2}{6}\left(\frac{q}{3E}+\frac{1}{4}+\frac{\xi}{E}\right)$
$\pm\left\|\int \beta\boldsymbol{\sigma}\times\mathbf{r}\right\|\left\|\int \beta\boldsymbol{\alpha}\right\|_{(L=1)}$	$b_0=\frac{1}{2}\left[\frac{1}{3}\left(q+\frac{p^2}{E}\right)+\xi\right]$
	$b_2=p^2/6E$
$\sum_{ij}\|B_{ij}{}^\beta\|^2_{(L=2)}$	$b_0=\frac{1}{48}(q^2+p^2)$
	$b_2=\frac{7}{240}p^2$
$A:\ \left\|\int \boldsymbol{\sigma}\times\mathbf{r}\right\|^2_{(L=1)}$	$q\to -q$ in $\left\|\int \beta\boldsymbol{\sigma}\times\mathbf{r}\right\|^2$
$\sum_{ij}\|B_{ij}\|^2_{(L=2)}$	Same as $\sum_{ij}\|B_{ij}{}^\beta\|^2$
$P:\ \left\|\int \beta\gamma_5\mathbf{r}\right\|^2_{(L=1)}$	Same as $\left\|\int \beta\mathbf{r}\right\|^2$
Second forbidden	
$S:\ \sum_{ij}\|R_{ij}{}^\beta\|^2_{(L=2)}$	$b_0=\frac{q^4+p^4}{120}+\frac{1}{36}q^2p^2-\frac{qp^2}{90E}(q^2+p^2)+\xi\left[\frac{1}{60}\left(\frac{p^4}{E}-2q^2\right)-\frac{1}{36}qp^2\left(1-\frac{2q}{E}\right)\right]+\frac{\xi^2}{12}\left(q^2+\frac{1}{4}p^2\right)$
	$b_2=\frac{p^2}{30}\left\{\frac{p^2}{2}+\frac{7}{6}q^2-\frac{1}{15}\frac{q}{E}(7q^2+10p^2)+\xi\left[\frac{3p^2+7q^2}{3E}-\frac{7q}{6}\right]+\frac{7}{8}\xi^2\right\}$
	$b_4=-\frac{p^4}{60}\left(\frac{3}{4}-\frac{q}{E}+\frac{3}{2}\frac{\xi}{E}\right)$

[a] The cross terms which occur in Table X are to be taken only once since a factor 2 has been inserted in the corresponding b_ν.

The determination of the $b_\nu(\beta)$ is complicated by the coherent mixing of different operators, for different α, having the same L and π, and the same order of forbiddenness. Table IX shows that this occurs for the V, T, A interactions (for example, T_0 and T_{-1} mix as do V and V_{-1}).

In order to give explicit results for the parameters b_ν it would be necessary to evaluate the nuclear matrix elements $M_N(L\pi\alpha)$ in the cases where interference occurs. Then the b_ν are obtained at once from Eqs. (42b), (109) and (110). In the absence of information concerning the nuclear matrix elements one is forced to resort to the usual artifice of treating these as adjustable parameters. In the cases where there is no interference between matrix elements with different L values, the matrix elements which occur in the angular correlation are the same as those which occur in the total intensity. Thus, the pertinent matrix element could be empirically determined from an analysis of the β spectrum. In any case it is important to define partial parameters $b_\nu(LL';\beta\alpha\alpha')$ as follows:

$$b_\nu(LL';\beta\alpha\alpha')=\frac{R(\nu q, L\pi\alpha, L'\pi\alpha')}{R(\nu q, LL';\gamma)}. \tag{112}$$

When there are no interferences (for example S, P interactions and the favorable parity change transitions for Gamow-Teller interactions) these parameters, defined by Eq. (112), constitute the factors by which the $\gamma-x$ correlation is modified. When interference is present, the required parameters are weighted sums of the partial parameters of Eq. (112) with weight factors given by the product of matrix elements appearing in Eq. (110).

CC-0. In Public Domain. Gurukul Kangri Collection, Haridwar

Digitized by Arya Samaj Foundation Chennai and eGangotri

TABLE X.—*Continued.*

Matrix element product	b_ν
Second forbidden—*continued*	
V: $\left\|\int \boldsymbol{\alpha}\times\mathbf{r}\right\|^2_{(L=1)}$	Same as $\left\|\int \boldsymbol{\sigma}\times\mathbf{r}\right\|^2$
$\sum_{ij}\|R_{ij}\|^2_{(L=2)}$	$q\rightarrow -q$ in $\sum_{ij}\|R_{ij}^{\beta}\|^2$
$\sum_{ij}\|A_{ij}\|^2_{(L=2)}$	Same as $\sum_{ij}\|B_{ij}\|^2$
$\pm\|\sum_{ij} R_{ij}A_{ij}^*\|_{(L=2)}$	$b_0=\frac{1}{12}\left[\frac{1}{5}\left(q^3+\frac{p^4}{E}\right)+\frac{1}{3}qp^2\left(1+\frac{q}{E}\right)+\xi\left(q^2+\frac{1}{2}p^2\right)\right]$
	$b_2=\frac{p^2}{30}\left[\frac{p^2}{E}+\frac{7}{6}q\left(1+\frac{q}{E}\right)+\frac{7}{4}\xi\right]$
	$b_4=-\frac{1}{40}\frac{p^4}{E}$
T: $\sum_{ij}\|A_{ij}^{\beta}\|^2_{(L=2)}$	Same as $\sum_{ij}\|B_{ij}\|^2$
$\sum_{ij}\|T_{ij}^{\beta}\|^2_{(L=2)}$	$b_0=\frac{1}{360}\left[\frac{1}{2}(q^2+p^2)+\frac{5}{3}q^2p^2+\frac{qp^2}{E}(p^2+q^2)\right]+\frac{\xi}{120}\left[q^3+\frac{5}{6}qp^2+\frac{1}{2}\frac{p^4}{E}+\frac{5}{3}\frac{q^2p^2}{E}\right]+\frac{5\xi^2}{240}\left(q^2+\frac{1}{4}p^2\right)$
	$b_2=\frac{p^2}{60}\left[\frac{1}{6}\left(\frac{p^2}{2}+\frac{7}{6}q^2+\frac{qp^2}{E}\right)+\frac{\xi}{4}\left(\frac{7}{3}q+\frac{p^2}{E}\right)+\frac{7}{16}\xi^2\right]$
	$b_4=\frac{p^4}{360}\left(\frac{q}{E}+\frac{3\xi}{2E}+\frac{1}{2}\right)$
$\pm\|\sum_{ij} T_{ij}^{\beta}A_{ij}^{\beta*}\|_{(L=2)}$	$b_0=\frac{1}{120}\left\{q^3+\frac{p^4}{E}+\frac{5}{3}qp^2\left(1+\frac{q}{E}\right)+5\xi\left(q^2+\frac{1}{2}p^2\right)\right\}$
	$b_2=\frac{p^2}{120}\left(\frac{7}{3}q+\frac{p^2}{E}+\frac{7}{2}\xi\right)$
	$b_4=\frac{1}{120}\frac{p^4}{E}$
$\sum_{ijk}\|S_{ijk}^{\beta}\|^2_{(L=3)}$	$b_0=\frac{1}{864}\left[\frac{1}{5}(p^2+q^2)+\frac{2}{3}q^2p^2\right]$
	$b_2=\frac{p^2}{3780}\left(p^2+\frac{7}{3}q^2\right)$
	$b_4=\frac{11p^4}{15120}$
A: $\sum_{ij}\|T_{ij}\|^2_{(L=2)}$	$q\rightarrow -q$ in $\sum_{ij}\|T_{ij}^{\beta}\|^2$
$\sum_{ijk}\|S_{ijk}\|^2_{(L=3)}$	Same as $\sum_{ijk}\|S_{ijk}^{\beta}\|^2$
P: $\sum_{ij}\|R_{ij}^{\beta\gamma_5}\|^2_{(L=2)}$	Same as $\sum_{ij}\|R_{ij}^{\beta}\|^2$

Pending numerical work in progress we give the analytical results of Fuchs (37), valid for light elements, for the $b_\nu(LL';\beta\alpha\alpha')$ in Table X below. In this table the notation in common use has been employed. E is the total energy of the electron ($E=(p^2+1)^{\frac{1}{2}}$ and $q=E_0-E$, where E_0 is the end point energy). The Coulomb field effect is contained in the terms with $\xi\equiv\alpha Z/2R$, where α is the fine structure constant. When no entry is given the corresponding parameter (b_ν) is zero. In the table the pseudoscalar interaction, $\beta\gamma_5\mathbf{r}$, has been grouped with the first forbidden case although in actuality the pseudoscalar interaction can only enter in mixtures and from this point of view it might more appropriately be classed with second forbidden (in harmony with the discussion above). A similar remark applies to $\sum_{ij}|R_{ij}^{\beta\gamma_5}|^2$.

The matrix elements

$$\int\boldsymbol{\alpha},\quad \int\beta\boldsymbol{\sigma}\cdot\mathbf{r},\quad \int\beta\boldsymbol{\alpha},\quad \int\beta\boldsymbol{\alpha}\cdot\mathbf{r},\quad \int\boldsymbol{\sigma}\cdot\mathbf{r},\quad \int\beta\gamma_5$$

by themselves give isotropy as expected. Since $\xi\gg 1$, especially for heavy elements, the matrix elements

$$\int\mathbf{r},\quad \int\beta\mathbf{r},\quad \int\boldsymbol{\sigma}\times\mathbf{r},\quad \int\beta\boldsymbol{\sigma}\times\mathbf{r},\quad \int\beta\gamma_5\mathbf{r},\quad \int\boldsymbol{\alpha}\times\mathbf{r}$$

by themselves give a very weak correlation ($b_0\gg b_2$). The matrix elements

$$B_{ij},\ B_{ij}^{\beta},\ A_{ij},\ A_{ij}^{\beta},\ S_{ijk},\ S_{ijk}^{\beta}$$

by themselves give a correlation which is virtually Z independent and large. The remaining matrix elements

CC-0. In Public Domain. Gurukul Kangri Collection, Haridwar

Digitized by Arya Samaj Foundation Chennai and eGangotri

are characterized by a correlation intermediate in magnitude.

In Table X above interference terms of type (b) are explicitly given. For interference terms of type (a) we distinguish two cases; namely, (1) those involving interference with a rotationally symmetric operator ($L=0$) like $\beta\boldsymbol{\sigma}\cdot\mathbf{r}$, or γ^5 and (2) those involving interferences between operators for both of which $L\neq 0$. This procedure is necessary because in the standard correlation ($\gamma-\gamma$) there is no counterpart for the first case.

Interferences involving one operator with $L=0$ are given by Fuchs (37) for the following cases: $B_{ij}{}^{\beta}$ with $\int\beta\boldsymbol{\sigma}\cdot\mathbf{r}$, B_{ij} and $\int\boldsymbol{\sigma}\cdot\mathbf{r}$, B_{ij} and $\int\gamma_5$. In these cases we give the results in the form of the $\beta-\gamma$ correlation function. Noting that for the B_{ij} operator $L=2$, we find

$$W=B^2\sum_{\nu}A_\nu b_\nu(B_{ij})P_\nu(\cos\beta)+5M_0{}^2C_0 +2BM_0DF_2(Ljj)P_2(\cos\beta),$$

where F_2 is given in Eq. (69b), (note that $j_1=j$) and and $B^2=\sum_{ij}|B_{ij}|^2$, M_0 is the matrix element of $L=0$ operator and $b_\nu(B_{ij})$ is obtained from Table X. The constants C_0 and D for each case are as follows:

T: $M_0=\int\beta\boldsymbol{\sigma}\cdot\mathbf{r}$

$$C_0=\frac{1}{9}(q^2+p^2)-\frac{2}{9}\frac{qp^2}{E}+\frac{2\xi}{3}\left(\frac{p^2}{E}-q\right)+\xi^2$$

$$D=(54)^{-\frac{1}{2}}p^2\left(1-\frac{q}{E}+\frac{3\xi}{E}\right).$$

For the axial vector interaction with $M_0=\int\boldsymbol{\sigma}\cdot\mathbf{r}$ the constants are obtained by changing q to $-q$ in the above. The remaining operator gives

A: $M_0=\int\gamma_5$

$$C_0=1$$

$$D=6^{-\frac{1}{2}}(p^2/E).$$

For the other interfering terms we can express the results most simply by giving the values of the partial particle parameters b_ν as before. The cases considered were interferences between B_{ij} (or $B_{ij}{}^{\beta}$) with $L=1$ operators for which we may write the matrix element as M_1. Then we give only the particle parameter b_2' for the cross term (since only $\nu=2$ enters in those cases). The correlation function for β-(pure) 2^L pole γ ray is then

$$W=\tfrac{1}{5}B^2\sum_{\nu}A_\nu(2,L)b_\nu(B_{ij})P_\nu +\tfrac{1}{3}M_1{}^2\sum_{\nu}A_\nu(1,L)b_\nu(M_1)P_\nu-2M_1Bb_2'A_2'P_2,$$

where

$$A_2'=(2j+1)^{\frac{1}{2}}G_2(12j_1j)F_2(Lj_2j)$$

is obtained from the mixed-pure $\gamma-\gamma$ correlation. The coefficients b_2' are

T: $B^2=\sum_{ij}|B_{ij}{}^{\beta}|^2$

$$M_1=\int\beta\boldsymbol{\sigma}\times\mathbf{r},\quad b_2'=\frac{p^2}{4(30)^{\frac{1}{2}}}\left(\frac{1}{2}+\frac{q}{3E}+\frac{\xi}{E}\right)$$

$$M_1=\int\beta\alpha,\qquad b_2'=\frac{1}{4(30)^{\frac{1}{2}}}\frac{p^2}{E},$$

A: $B^2=\sum_{ij}|B_{ij}|^2$

$$M_1=\int\boldsymbol{\sigma}\times\mathbf{r},\quad b_2'=\frac{p^2}{4(30)^{\frac{1}{2}}}\left(\frac{1}{2}-\frac{q}{3E}+\frac{\xi}{E}\right).$$

As was pointed out by Fuchs (37) the existence of these interference terms can give rise to a situation in which the energy spectrum has very nearly an allowed shape and a strongly anisotropic correlation. An example would be one in which $\int\beta\alpha$ dominates. Alternatively, it is possible to have an almost isotropic correlation together with a strongly energy dependent correction factor for the β spectrum.

In all cases the normalization is such that integration of the angular correlation function gives the energy spectrum for the β transition, that is, b_0 is, to within an energy independent constant, equal to the usual energy-correction factor. Therefore, the integrated angular correlation is obtained by integrating the product of the angular correlation function and the allowed energy spectrum over the appropriate energy range.

IV. MAGNETIC FIELD EFFECTS IN ANGULAR CORRELATION

In this section we wish to consider three questions: (a) the effect on the angular correlation of the magnetic interaction due to the electron shell, (b) the role of an applied magnetic field in the angular correlation when no hyperfine interaction is present, and (c) the spin decoupling effect of an external magnetic field. In connection with (a) the fundamental assumption is made that the nucleus is coupled to a system which remains in a stationary state throughout the nuclear cascade. Our concern here is to indicate at least qualitatively, that the hyperfine interaction does affect the correlation function in an important way. The primary point of interest in connection with (b) is the possibility of measuring the gyromagnetic ratio and the magnetic moment (sign and magnitude) in the short-lived intermediate state. As would be expected, the elimination of hyperfine interaction in this case must be accomplished by the use of suitable prepared sources since the Paschen-Back effect discussed in (c) imposes

CC-0. In Public Domain. Gurukul Kangri Collection, Haridwar

Digitized by Arya Samaj Foundation Chennai and eGangotri

geometrical requirements which make the measurement considered in (b) impossible.

A. The Correlation Function with Spin-Coupling

The starting point for all the effects here considered is the formalism developed by Goertzel (42). One considers the nucleus as part of a larger system (atom or ion) from which the radiations are emitted. The energy levels in the cascade are designated by the labels A, B, and C for initial, intermediate and final levels, respectively. Due to the spin-coupling these energy levels will now be nondegenerate; the substates of A, B, and C are designated by α, β, and γ, respectively.

While it is not essential to specify the nature of the radiation emitted, it is convenient, for concreteness, to discuss the emission of γ rays. Then in the first transition the radiation emitted is described by the index ρ, the second by σ—these indices giving the propagation vector and polarization of the emitted photons. With only slight changes we follow Goertzel's notation (but with units such that $h=1$, and with a different sign convention on the time dependence); then the equations of "motion" for the probability amplitudes are

$$i\dot{a}_\alpha=\epsilon_\alpha a_\alpha+\sum_{\beta\rho}(\alpha|H_\rho|\beta)b_{\beta\rho}, \tag{113a}$$

$$i\dot{b}_{\beta\rho}=\epsilon_{\beta\rho}b_{\beta\rho}+\sum_{\alpha}(\alpha|H_\rho|\beta)^*a_\alpha+\sum_{\gamma\sigma}(\beta|H_\sigma|\gamma)c_{\gamma\rho\sigma}, \tag{113b}$$

$$i\dot{c}_{\gamma\rho\sigma}=\epsilon_{\gamma\rho\sigma}c_{\gamma\rho\sigma}+\sum_{\beta}(\beta|H_\sigma|\gamma)^*b_{\beta\rho}, \tag{113c}$$

where a, b, and c refer to initial, intermediate, and final state, respectively. Also

$$\epsilon_{\beta\rho}=\epsilon_\beta+\omega_\rho, \quad \epsilon_{\gamma\rho\sigma}=\epsilon_\gamma+\omega_\rho+\omega_\sigma, \tag{113d}$$

where ω_ρ and ω_σ are the quantum energies radiated, while ϵ_α, ϵ_β and ϵ_γ are eigenvalues of the zero-order Hamiltonian where the latter contains everything but the radiation operators H_ρ, H_σ.

With the initial condition

$$a_\alpha=e^{i\phi_\alpha} \quad (t=0),$$

where ϕ_α is a random phase, the above equations can be solved to give $c(t=\infty)$. This is conveniently done, for example, by the Laplace transform method (76). Thus, introducing

$$A_\alpha(s)=\int_0^\infty e^{-st}a_\alpha(t)dt$$

and similar definitions for $B_{\rho\sigma}(s)$ and $C_{\gamma\rho\sigma}(s)$ in terms of $b_{\beta\rho}$ and $c_{\gamma\rho\sigma}$, respectively, Eqs. (113) become

$$w_1A_\alpha=ie^{i\phi_\alpha}+\sum_{\beta\rho}(\alpha|H_\rho|\beta)B_{\beta\rho}, \tag{114a}$$

$$w_2B_{\beta\rho}=\sum_{\alpha}(\alpha|H_\rho|\beta)^*A_\alpha+\sum_{\gamma\sigma}(\beta|H_\sigma|\gamma)C_{\gamma\rho\sigma}, \tag{114b}$$

$$w_3C_{\gamma\rho\sigma}=\sum_{\beta}(\beta|H_\sigma|\gamma)^*I_{\beta\rho}. \tag{114c}$$

Here

$$w_1=is-\epsilon_\alpha, \quad w_2=is-\epsilon_{\beta\rho}, \quad w_3=is-\epsilon_{\gamma\rho\sigma}. \tag{114d}$$

Neglecting all but the first terms on the right-hand side of Eqs. (114) gives A to zero order, B to first order, and C to second order in the radiation coupling. This result, which gives the correlation function of Eq. (114) with $S(m_am_a';m_nm_n')=\delta(m_am_n)\delta(m_a'm_n')$, contains no radiation damping and hence no spin-coupling effects. Using these results in Eq. (114) to obtain A to first order, thence B to third order and finally C to fourth order, one obtains the desired final result for $C_{\gamma\rho\sigma}$. Carrying out the inverse Laplace transform we find

$$\lim_{t\to\infty}c_{\gamma\rho\sigma}=\sum_{\alpha\beta}\frac{e^{-i\phi_\alpha}(\alpha|H_\rho|\beta)^*(\beta|H_\sigma|\gamma)^*e^{i(\omega_\rho+\omega_\sigma+\epsilon_\gamma)t}}{(\omega_\rho+\omega_\sigma-\epsilon_{\alpha,\gamma}-i\gamma_A)(\omega_\sigma-\epsilon_{\beta,\gamma}-i\gamma_B)}, \tag{115}$$

where $\epsilon_{\alpha,\gamma}=\epsilon_\alpha-\epsilon_\gamma$, etc., and[21]

$$\gamma_A=i\sum_{\beta\rho}\frac{|(\alpha|H_\rho|\beta)|^2}{w_2}, \tag{116a}$$

$$\gamma_B=i\sum_{\gamma\sigma}\frac{|(\beta|H_\sigma|\gamma)|^2}{w_3}. \tag{116b}$$

These quantities are real and independent of s and of the sublevel labels α, β, respectively (76). The total transition probabilities from levels A and B are in fact $2\gamma_A$ and $2\gamma_B$, respectively.

Averaging over the phases ϕ_α with

$$\langle e^{i(\phi_\alpha-\phi_{\alpha'})}\rangle_{Av}=\delta_{\alpha\alpha'}$$

and summing $|c_{\gamma\rho\sigma}(\infty)|^2$ from (115) over all polarization states of the emitted radiations gives finally the correlation function for propagation directions defined by the unit vectors $\mathbf{f}_\rho$, $\mathbf{f}_\sigma$:

$$\begin{aligned}W(\mathbf{f}_\rho,\mathbf{f}_\sigma)&=\mathfrak{S}_{\rho\sigma}\int_0^\infty d\omega_\rho\int_0^\infty d\omega_\sigma\sum_\gamma\langle|\lim_{t\to\infty}c_{\gamma\rho\sigma}|^2\rangle_{Av}\\&=\sum_{\alpha\beta\beta'\gamma}\mathfrak{S}_{\rho\sigma}\frac{(\alpha|H_\rho|\beta)^*(\beta|H_\sigma|\gamma)^*(\alpha|H_\rho|\beta')(\beta'|H_\sigma|\gamma)}{1+i\epsilon_{\beta\beta'}\tau}.\end{aligned} \tag{117}$$

Here, $\mathfrak{S}_{\rho\sigma}$ denotes the polarization average for the two radiations. Irrelevant constant factors have been discarded in obtaining Eq. (117). We have introduced the mean life of the intermediate state

$$\tau=1/2\gamma_B. \tag{118}$$

As expected on physical grounds only the intermediate state lifetime enters. The scale of the coupling

[21] Goertzel's Eqs. (4a) and (4b) and also his Eq. (5) contain misprints.

CC-0. In Public Domain. Gurukul Kangri Collection, Haridwar

Digitized by Arya Samaj Foundation Chennai and eGangotri

effects is clearly defined by the comparison of the "multiplet" splittings $\epsilon_{\beta\beta'}$ and $1/\tau$ in corresponding units. Comparing with the no spin-coupling case of Sec. II we see that the effect of this coupling is to introduce the energy denominator $(1+i\epsilon_{\beta\beta'}\tau)^{-1}$. It will be noted that even if the coupling is extremely large, $\epsilon_{\beta\beta'}\to\infty$ $(\beta\neq\beta')$, the result expressed by Eq. (117) would imply that the correlation is not completely eliminated. In this case the terms $\beta=\beta'$ would yield a "minimum" correlation which would, in general, be less anisotropic than the no spin-coupling case, but would not be isotropic. This is not surprising in view of the assumptions made. The spin-coupling is expected to attenuate the correlation due to the transitions taking place between substates of different nuclear spin orientation in the intermediate nuclear state. However, these transitions (or, speaking classically, precession) of the nuclear spin vector does not represent a complete loss of information. In some actual experimental cases it is observed that the anisotropy actually disappears

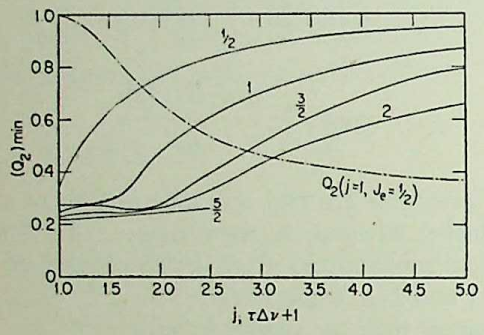


FIG. 1. The solid curves give the minimum attenuation factor $(Q_2)_{\min}$ *versus* the intermediate state spin j, see Eq. (124a). The numbers affixed to the curves give the value of J_e. $(Q_2)_{\min}$ gives a lower limit for the attenuation of the correlation for dipole transitions or for $j<2$. The dashed curve gives the full attenuation factor Q_2 as a function of $\tau\Delta\nu$ for $J_e=\frac{1}{2}$ and $j=1$ ($\tau\equiv$intermediate state lifetime, $\Delta\nu=$hfs doublet splitting). For $J_e=\frac{1}{2}$, $Q_\nu=1-[1-(Q_\nu)_{\min}](\tau\Delta\nu)^2[1+(\tau\Delta\nu)^2]^{-1}$ for any j.

(within the accuracy of the measurements), and it may be concluded that the above assumptions are invalid.

B. Magnetic Interaction

Here we consider an isolated atom (or ion) and represent the coupling by the usual hyperfine interaction $a\mathbf{j}\cdot\mathbf{J}_e$ where J_e is the angular momentum of the electron shell, assumed constant. The labels β, β' correspond to the zero-field quantum numbers F, m_F, where in the customary notation $\mathbf{F}=\mathbf{j}+\mathbf{J}_e$ and m_F is the eigenvalue of F_z.

We introduce the density matrix as in Sec. II

$$E^{(1)}(\beta\beta')=\mathfrak{S}_\rho\sum_\alpha(\alpha|H_\rho|\beta)^*(\alpha|H_\rho|\beta'),$$
$$E^{(2)}(\beta\beta')=\mathfrak{S}_\sigma\sum_\gamma(\gamma|H_\sigma|\beta)^*(\gamma|H_\sigma|\beta'), \tag{119}$$

and write Eq. (117) in the form

$$W=\sum_{\beta\beta'}\frac{E^{(1)}(\beta\beta')E^{(2)}(\beta'\beta)}{1+i\epsilon_{\beta\beta'}\tau}. \tag{120}$$

The reality of the result in Eq. (120) follows from the Hermitian property of $E^{(i)}$ (as does that of Eq. (117) from the Hermitian property of the matrix element occurring therein). Since the matrix elements of H_ρ and H_σ are diagonal in all non-nuclear quantum numbers, the density matrix is very easily written in terms of the decoupled (strong field) representation. In this case we introduce the projection quantum numbers m and μ for the nucleus and electrons, respectively. Then, for example,

$$E^{(1)}(mm')=(-)^{j_1-m}(2j+1)\sum_\nu C(jj\nu;m,-m')\times W(jjLL;\nu j_1)D(\nu,m'-m,0;\mathfrak{f}_1) \tag{121}$$

for a pure 2^L pole. In Eq. (121) ν is even and, as usual, the transition is represented by $j_1\to j$. We shall write $\mathfrak{f}_1$ and $\mathfrak{f}_2$ for $\mathfrak{f}_\rho$ and $\mathfrak{f}_\sigma$, respectively. The density matrix in the weak field representation is obtained by the usual unitary transformation defined by the vector addition coefficients $C(jJ_eF;m\mu)$ (and $m_F=m+\mu$). A straightforward calculation gives

$$\begin{aligned}E(Fm_F;F'm_F')&=(-)^{J_e+m_F-J_1}[(2F+1)(2F'+1)]^{\frac{1}{2}}(2j+1)\sum_\nu\\&\times C(LL\nu;1-1)C(FF'\nu;-m_Fm_F')\\&\times W(jjFF';\nu J_e)W(jjLL;\nu j_1)\\&\times D(\nu,-\Delta m_F0;\mathfrak{f}),\end{aligned} \tag{122}$$

where

$$\Delta m_F=m_F-m_F'.$$

Inserting Eq. (122) into Eq. (120), summing over m_F (keeping Δm_F fixed) and using

$$\sum_{m_F}C(FF'\nu;m_F,-m_F')C(FF'\bar\nu;m_F,-m_F')=\delta(\nu\bar\nu),$$

we find

$$\begin{aligned}W=\sum_{FF'}\sum_{\Delta m_F}(2F+1)(2F'+1)&\frac{W^2(jjFF';\nu J_e)}{1+i\epsilon_{FF'}\tau}\\&\times C(L_1L_1\nu;1-1)C(L_2L_2\nu;1-1)\\&\times W(jjL_1L_1;\nu j_1)W(jjL_2L_2;\nu j_2)\\&\times D^*(\nu,-\Delta m_F0;\mathfrak{f}_1)D(\nu,-\Delta m_F0;\mathfrak{f}_2).\end{aligned} \tag{122a}$$

Carrying out the sum over Δm_F as before and comparing with Eqs. (65a) and (68), we recognize that the correlation function can be written in the form

$$W=\sum_\nu A_\nu Q_\nu P_\nu(\cos\beta), \tag{123}$$

which differs from the ordinary $\gamma-\gamma$ correlation by

CC-0. In Public Domain. Gurukul Kangri Collection, Haridwar

Digitized by Arya Samaj Foundation Chennai and eGangotri

the additional attenuation factors Q_ν. These are

$$Q_\nu=\frac{1}{2J_e+1}\sum_{FF'}(2F+1)(2F'+1)\frac{W^2(jjFF';\nu J_e)}{1+(\epsilon_{FF'}\tau)^2}. \quad (124)$$

In Eq. (124) a normalization factor $(2J_e+1)^{-1}$ has been inserted so that $Q_0=1$ and $Q_\nu(\tau=0)=1$. The result given in Eq. (124) was originally given by Alder (4).[22] It is clear that this result also applies to correlations with mixed radiations.

In order to obtain an idea as to the order of magnitude of the hyperfine coupling effect one may insert

$$\epsilon_{FF'}=\frac{a}{2}[F(F+1)-F'(F'+1)].$$

Then, for particular values of j or J_e and of ν one can evaluate the sums in Eq. (124). For numerical results, however, it is easier to use the Racah Tables (13) and perform the sums arithmetically. A few cases are shown in Fig. 1 [see also (4)]. Here the "minimum" correlation factors $(Q_\nu)_{\min}$ are shown:

$$(Q_\nu)_{\min}=\frac{1}{2J_e+1}\sum_{F}(2F+1)^2W^2(jjFF;\nu J_e). \quad (124a)$$

From Fig. 1 we may draw the qualitative conclusion that, even if the assumption of a stationary state for the electronic shell is valid, the magnetic interaction produces a small alteration of the correlation only for $J_e=\frac{1}{2}$ and $j\gtrsim 5$ with the additional restriction that at least one of the radiations be a dipole. Hence we can conclude that, in general, the effect is not a minor one.

C. External Magnetic Fields

Here we shall assume that $J_e=0$. That this situation can be realized in practice is made highly plausible by the results of Aeppli *et al.* (1, 2). We are interested in the possibility of using an external field to measure the nuclear gyromagnetic ratio and for this purpose two methods have been suggested[23]:

(1) The delayed correlation (54).

(2) The average correlation in a field. Of these two methods (2) has been successfully applied experimentally (2).

(1) *The Delayed Correlation*

One measures the coincidence rate per dt (steradians^{-2} sec^{-1}) in the case that a time delay between t and $t+dt$ is introduced between the successive radiations. The spin precession in the presence of a magnetic field clearly alters the angular correlation only if a nonzero time delay exists. Conversely, without a field the time delay only affects the total intensity but not the angular correlation of the radiations.

The perturbation theory formalism leading to the correlation function in this case is very similar to that discussed in subsection A of this Section but with the following alterations. We observe the first radiation at time t_1, say. Then t_1 is taken as the time origin for the emission of the second radiation. If we designate the interval between t_1 and the time at which the second radiation is observed by t we have as initial conditions

$$b_{\beta\rho}=b_{\beta\rho}{}^{(0)}, \quad c_{\gamma\rho\sigma}=0: \quad t=0$$

to use with the equations of motion

$$w_2B_{\beta\rho}=ib_{\beta\rho}{}^{(0)}+\sum_{\gamma\sigma}(\beta|H_\sigma|\gamma)C_{\gamma\rho\sigma}$$

$$w_3C_{\gamma\rho\sigma}=\sum_{\beta}(\beta|H_\sigma|\gamma)^*B_{\beta\rho},$$

and $b_{\beta\rho}{}^{(0)}$ is obtained by a solution of the equations for A_α and $B_{\beta\rho}$ in which only the matrix elements of H_ρ are involved. The desired probability is then

$$\frac{d}{dt}\int|c_{\gamma\rho\sigma}(t)|^2d\omega\sigma.$$

The result for the probability that radiations 1 and 2 be emitted in the direction $\vartheta_1\varphi_1$ and $\vartheta_2\varphi_2$, respectively, with a time delay t to $t+dt$ is, per dt,

$$W_d(\vartheta_1\varphi_1;\vartheta_2\varphi_2;t)$$

$$=\frac{1}{\tau}e^{-t/\tau}\Re\sum_{\alpha\beta\beta'\gamma}(\alpha|H_1|\beta)^*(\alpha|H_1|\beta')(\beta|H_2|\gamma)^*\times(\beta'|H_2|\gamma)e^{i\epsilon_{\beta\beta'}t}. \quad (125)$$

In the external field H,

$$\epsilon_{\beta\beta'}=\mu_N g(H/h)(m-m')=\omega_0(m-m'), \quad (125a)$$

where ω_0 is the Larmor frequency, μ_N the nuclear magneton, g the nuclear gyromagnetic ratio in the intermediate state, and m is the projection of the nuclear spin on the quantization axis (≡direction of magnetic field). Here $\alpha, \beta, \beta', \gamma$ all have the significance of nuclear magnetic quantum numbers for the appropriate states. In particular, $\beta, \beta'=m, m'$.

---

[22] The same result can also be obtained in an essentially equivalent manner by transforming the radiation matrix elements with the unitary (vector addition coefficients) transformation to obtain [see (42) and Eq. (2)]

$$S(m_am_a';m_nm_n')=\delta(m_a-m_a',m_n-m_n')S(m_am_nm_a')$$
$$S(mm'm'')=(2J_e+1)^{-1}\Sigma(1+\epsilon_{FF'}\tau)^{-2}\delta(\mu+m,\mu'+m')$$
$$\times C(jJ_eF;m\mu)C(jJ_eF;m'\mu')C(jJ_eF';m''\mu)C(jJ_eF';m'+m''-m,\mu')$$

and the sum is over F, F', μ, μ'. Application of the algebraic relations of the Racah coefficients [Appendix Eq. (A5)] yields the result given in Eq. (124). It is also possible to generalize the foregoing to other radiations x, y. It is easily seen that the only change is the insertion of the parameters $b_\nu(x)$ in the density matrices Eq. (121) and Eq. (122) and $b_\nu(x)b_\nu(y)$ in Eq. (122a). Thus, Q_ν is independent of the nature of the radiation.

[23] A third method, which would utilize an rf field so that at resonance one would observe a maximum attenuation in anisotropy, is actually impractical. The intermediate state lifetime and the available rf power are such that only a very small and probably unobservable effect would take place.

CC-0. In Public Domain. Gurukul Kangri Collection, Haridwar

Digitized by Arya Samaj Foundation Chennai and eGangotri

Since a rotation around the quantization axis through an angle α multiplies the product of the elements of the two density matrices in (125) by $e^{i\alpha(m-m')}$ it follows that

$$W_d(\vartheta_1\varphi_1;\vartheta_2\varphi_2;t)=\frac{1}{\tau}e^{-t/\tau}W_0(\vartheta_1\varphi_1;\vartheta_2,\ \varphi_2+\omega_0 t) \quad (126)$$

which is Lloyd's result (54). The delayed coincidence correlation may be regarded as the result of imparting to the instantaneous (or zero field) correlation W_0 a precession around the external field with the Larmor frequency. In this form the result seems an almost self-evident application of Larmor's theorem.

Expressing the W_0 correlation function in the usual form we find[24]

$$W_d=\frac{4\pi}{\tau}e^{-t/\tau}\sum_\nu \frac{A_\nu}{2\nu+1}\sum_{M=-\nu}^{\nu} \times Y_\nu^M(\mathbf{f}_1)Y_\nu^{M*}(\mathbf{f}_2)e^{-iM\omega_0 t}. \quad (127)$$

As one may expect, the delayed correlation contrasts with the average correlation (see paragraph (2) below) in that it provides a possible means of measuring g without measuring the mean life τ. However, this is only a formal difference and does not correspond to any essential difference in experimental techniques involved. We note in passing that interchanging the propagation directions $\mathbf{f}_1$ and $\mathbf{f}_2$ is equivalent to changing the sign of ω_0 or to changing the direction of the field. Hence, the sign of the g factor is determinable only if the over-all detector efficiencies changes when $\mathbf{f}_1$ and $\mathbf{f}_2$ are interchanged. In addition, if the radiations and the field are coplanar, then reversing the directions of $\mathbf{f}_1$ and $\mathbf{f}_2$ is equivalent to changing the direction of $\mathbf{H}$. Since reversing the directions of $\mathbf{f}_1$ and/or $\mathbf{f}_2$ does not change W_d, it follows that a determination of the sign of g requires non-coplanarity of $\mathbf{f}_1$, $\mathbf{f}_2$ and $\mathbf{H}$. A particular case of coplanarity is coincidence between $\mathbf{H}$ and either $\mathbf{f}_1$ or $\mathbf{f}_2$. In this case the effect of the magnetic field disappears. This result is of interest in connection with the question discussed in IV-D below.

(2) *Average Correlation*

If an external field is applied and the correlation measured without regard to delay time (that is, all coincidences are accepted), the correlation function is

$$\bar{W}=\int_0^\infty W_d dt=4\pi\sum_\nu \frac{A_\nu}{2\nu+1}\sum_M \frac{Y_\nu^M(\mathbf{f}_1)Y_\nu^{M*}(\mathbf{f}_2)}{1+iM\omega_0\tau}. \quad (128)$$

Aside from the irrelevant factor 4π, Eq. (128) is equivalent to the result given by Alder (5).[25] A convenient way in which to carry out the measurement is the arrangement in which the magnetic field is perpendicular to the plane of the radiations. In this case

$$\bar{W}=\sum_{n=0}^{n_m}\frac{B_n}{1+(2n\omega_0\tau)^2}[\cos 2n\phi+2n\omega_0\tau\sin 2n\phi], \quad (129)$$

where $\phi=\varphi_1-\varphi_2$ is the angle between $\mathbf{f}_1$ and $\mathbf{f}_2$ and the coefficients B_n are given by

$$B_n=(2-\delta_{n0})\sum_{k=n}^{k_{\max}}\frac{A_{2k}}{2^{4k}}\frac{(2k+2n)!(2k-2n)!}{[(k+n)!(k-n)!]^2}. \quad (129a)$$

Here $2k=\nu$ and $2n_m=2k_{\max}=\nu_{\max}$. These are, of course, just the coefficients of the zero-field correlation when expanded in $\cos 2n\phi$. The same remarks relative to the sign of g made under (1) apply here. Thus, for equal over-all efficiencies

$$\bar{W}=\sum_{n=0}^{n_m}\frac{B_n}{1+(2n\omega_0\tau)^2}\cos 2n\phi, \quad (129b)$$

while with unequal efficiencies the sign of g is determined. Thus, if the efficiency for the arrangement $\mathbf{f}_1$ in the direction $\frac{1}{2}\pi$, φ_1 and $\mathbf{f}_2$ in the direction $\frac{1}{2}\pi$, φ_2 is η_{12} while η_{21} corresponds to $\mathbf{f}_1(\frac{1}{2}\pi,\ \varphi_2)$ and $\mathbf{f}_2(\frac{1}{2}\pi,\ \varphi_1)$, the observed correlation would be

$$\bar{W}=\sum_n\frac{B_n}{1+(2n\omega_0\tau)^2}\times\left[\cos 2n\phi+\frac{\eta_{12}-\eta_{21}}{\eta_{12}+\eta_{21}}2n\omega_0\tau\sin 2n\phi\right]. \quad (129c)$$

Since the zero-field correlation should serve to determine the intermediate spin j, the magnetic moment in this excited state can also be measured. Such a measurement, first suggested by Brady and Deutsch (17) and by Sunyar *et al.* (74), has been carried out by the Swiss group for the case of the Cd^{111} cascade (2). It is clear that this method requires a measurement of the intermediate state lifetime but where this is not feasible it is not to be expected that any other method will be workable.

D. Paschen-Back Effect

In Sec. I reference was made to the fact that it would be highly desirable to be able to eliminate the magnetic (and quadrupole) interaction by using a strong field. In this paragraph we wish to discuss the requirements which such a procedure would have to fulfill. In doing so we assume that we deal with an isolated atom (ion) recognizing that in an actual experiment a different situation may apply in some cases. It will be sufficient to consider that the spin part of the zero-order Hamiltonian contains the following three terms (a) magnetic

[24] The time-dependent factor $e^{-t/\tau}$ is, or course, of no consequence for the present application. It is, however, needed for the following, see paragraph (2) below.

[25] This result can also be obtained from Eq. (117) using Eq. (125a).

CC-0. In Public Domain. Gurukul Kangri Collection, Haridwar

Digitized by Arya Samaj Foundation Chennai and eGangotri

interactions between external field and electron moment, (b) magnetic interaction between external field and nuclear moment, and (c) hyperfine coupling between electrons and nucleus. If the spins can be decoupled under these circumstances then, as will be clear from the following, it will follow *a fortiori* that any weaker couplings like the quadrupole-electric field gradient terms will cause no trouble.

The discussion is conveniently divided into two parts: First, we show that if there is a strong Paschen-Back effect on the electrons (electron Zeeman energy$\gg$hyperfine splitting) then there is no first-order effect on the matrix elements in Eq. (117). Starting from the strong field representation in which m and μ are good quantum numbers, the matrix elements are transformed by an infinitesimal unitary matrix

$$S=1+\sigma, \quad \sigma\ll 1,$$

where σ is antihermitian and has zero diagonal matrix elements. Also σ is diagonal in $m_F=m+\mu$. Clearly σ is of order $a/\mu_e H$ where the hyperfine energy is $a\mathbf{j}\cdot\mathbf{J}_e$ and μ_e is the magnetic moment of the electron shell.

Now the argument consists in showing that only diagonal matrix elements of σ enter in modifying Eq. (117). Since we are concerned with first-order effects we consider one matrix element at a time. Labeling the perturbed states by $\bar{m}$ and $\bar{\mu}$ and designating the perturbed and unperturbed wave functions by Ψ and Φ, respectively, the unitary transformation in question may be written in the form

$$\Psi(\bar{m}\bar{\mu})=\sum_{m\mu}(m\mu|\bar{m}\bar{\mu})\Phi_{j^m}\Phi_{J_e{}^\mu}.$$

Then,

$$(\alpha|H_1|\beta)=\sum_{m\mu}(\bar{m}_1|H_1|m)\delta(\bar{\mu}_1\mu)(m\mu|\bar{m}\bar{\mu}), \tag{130a}$$

$$(\beta|H_2|\gamma)=\sum_{m'\mu'}(m'|H_2|\bar{m}_2)\delta(\mu'\bar{\mu}_2)(m'\mu'|\bar{m}\bar{\mu}), \tag{130b}$$

$$(\alpha|H_1|\beta')=\sum_{m''\mu''}(\bar{m}_1|H_1|m'')\delta(\bar{\mu}_1\mu'')\times(m''\mu''|\bar{m}'\bar{\mu}'), \tag{130c}$$

$$(\beta'|H_2|\gamma)=\sum_{m'''\mu'''}(m'''|H_2|\bar{m}_2)\delta(\mu'''\bar{\mu}_2)\times(m'''\mu'''|\bar{m}'\bar{\mu}'), \tag{130d}$$

where the subscripts 1 and 2 on the magnetic quantum numbers refer to the initial and final states, respectively. If we consider the first term perturbed, the transformation coefficients in the remaining three matrix elements must reduce to the elements of the identity transformation. Thus

$$m'=\bar{m}, \quad \mu'=\bar{\mu}; \quad m''=\bar{m}', \quad \mu''=\bar{\mu}'; \quad m'''=\bar{m}', \quad \mu'''=\bar{\mu}'.$$

From these results it follows that

$$\mu=\bar{\mu}_1=\mu''=\bar{\mu}'=\bar{\mu}.$$

Hence, since $m+\mu=\bar{m}+\bar{\mu}$,

$$m=\bar{m}, \tag{131a}$$

and only diagonal elements of $(m\mu|\bar{m}\bar{\mu})$ enter. In an entirely equivalent fashion one can show that

$$m'=\bar{m}, \quad \mu'=\bar{\mu}, \tag{131b}$$

by considering the second matrix element (130b) to be transformed and the remaining ones unchanged, and similarly with Eqs. (130c) and (130d). It follows then that to first order there is no change in the matrix elements.

We now consider the energy denominator in Eq. (117). If the matrix elements of the spin-dependent zero-order Hamiltonian are evaluated in the m, μ representation we need consider only diagonal matrix elements; off-diagonal matrix elements will all be of second order in $a/\mu_e H$ compared to the leading terms. Then the difference of two diagonal elements $\epsilon_\beta-\epsilon_{\beta'}$ will contain three terms corresponding to the three interaction energies listed above; electron and nuclear Zeeman energies and hyperfine energy. Among other terms there will be those for which $\mu=\mu'$, and the usually large electron Zeeman energy difference will vanish in this case. The spins will then be decoupled only if the nuclear Zeeman energy splitting is large compared to the hyperfine splitting. Clearly, this demands impractically large fields.

However, if one of the radiations is parallel to the field this requirement on the field is considerably relaxed. Then starting from state A (or C) with a fixed nuclear projection quantum number m_1 or m_2 and considering the fact that the radiation carries off ± 1 unit of angular momentum with respect to the field direction, the value of m in the intermediate state is fixed:

$$m=m_1\pm 1 \quad \text{or} \quad m=m_2\pm 1,$$

depending on which of the two radiations is parallel to the field. Since the two polarization states of the quantum do not interfere and are added incoherently only one of these possible values will occur. Consequently, we now have $m=m'$. Since the energy matrix is diagonal in $m+\mu$, it follows that $\mu=\mu'$ and $\epsilon_\beta=\epsilon_{\beta'}$ for all pairs of states. Consequently, the energy denominator reduces to unity and all first-order effects vanish. The magnitude of the second-order effects shows that the criterion for a strong field is that the electron Zeeman energy be large compared to the hyperfine splitting. That is, if the over-all hyperfine multiplet is $\Delta\nu$ in cm^{-1}, one must require that

$$(H/2\times 10^4\Delta\nu)^2\gg 1, \tag{132}$$

where H is in gauss (42). In many cases fields of order 5×10^3 to 10^4 gauss would presumably be adequate. Of course, if such a procedure were successful one would not have the opportunity to measure the intermediate state magnetic moment. The application of the Paschen-

CC-0. In Public Domain. Gurukul Kangri Collection, Haridwar

Digitized by Arya Samaj Foundation Chennai and eGangotri

Back effect would, of course, necessarily be confined to the $\gamma-\gamma$ correlation. The only attempt to carry out such an experiment was made by Frauenfelder *et al.* (36) for the Ni^{60} $\gamma-\gamma$ cascade. No effect of the magnetic field was observed, and it appears that condition (132) is not fulfilled in this case. *Note added in proof.*—A decoupling experiment with a metallic In^{111} source has also given a negative result. This problem has now been beautifully clarified by the experiments of Albers-Schönberg, Hänni, Heer, Novey, and Scherrer [Phys. Rev. **90**, 322 (1953)] and the work of A. Abragam and R. V. Pound (unpublished). The quadrupole coupling, which is in general quite significant, and in particular important in the In metal, will attenuate the correlation unless one of the radiations lies along the symmetry axis of the single crystal source. The importance of quadrupole coupling has since been discussed by A. Abragam and R. V. Pound [Eq. (1a) and Phys. Rev. **90**, 993 (1953)] and by Alder, Albers-Schönberg, Heer and Novey (to be published in Helv. Phys. Acta.).

Finally, we may inquire into the stringency of the parallelism requirement. How accurately must this be fulfilled? To investigate this point, we consider the relevant part of the correlation function; *viz.*,

$$\mathcal{S}\equiv\sum_{M\mu}\frac{Y_\nu^M(\mathbf{f}_1)Y_\nu^{M*}(\mathbf{f}_2)}{1+M(Z_1+Z_2)}, \tag{133}$$

where $Z_1=i\mu_N g_N(H/h)\tau$, $Z_2=2ia\mu\tau\equiv 2\mu\zeta$ are the $i\omega t$ products for the nuclear Zeeman and the hyperfine energies. If we neglect the hyperfine energy, $\mathcal{S}$ would become

$$\mathcal{S}_0=\sum_{M\mu}\frac{Y_\nu^M(\mathbf{f}_1)Y_\nu^{M*}(\mathbf{f}_2)}{1+Z_1M}.$$

We therefore consider the difference

$$\Delta\mathcal{S}=\mathcal{S}-\mathcal{S}_0=-\sum_{M\mu}\frac{MZ_2Y_\nu^M(\mathbf{f}_1)Y_\nu^{M*}(\mathbf{f}_2)}{(1+Z_1M)[1+(Z_1+Z_2)M]}$$

$$\equiv-\sum_{M\mu}\Delta_M\mathcal{S}.$$

Then for $J_e=\frac{1}{2}$, $\mu=\pm\frac{1}{2}$

$$\Delta_M\mathcal{S}=-\frac{Y_\nu^M(\mathbf{f}_1)Y_\nu^{M*}(\mathbf{f}_2)2M^2\zeta^2}{(1+Z_1M)[(1+MZ_1)^2-M^2\zeta^2]}. \tag{134a}$$

The case of interest is $|\zeta|\gg 1$, $|Z_1|\sim 1$ and then

$$\Delta_M\zeta\sim 2\frac{Y_\nu^M(\mathbf{f}_1)Y_\nu^{M*}(\mathbf{f}_2)}{1+Z_1M}. \tag{134b}$$

Since $\Delta_0\mathcal{S}=0$, it follows that $\Delta_M\mathcal{S}\sim\Theta^M$ where Θ is the angle between the field and the (nearly parallel) radiation. Thus, at worst, $\Delta\mathcal{S}\sim\Theta$. It is seen that this conclusion is equally valid for arbitrary J_e. It is also valid from Eq. (134a) without the assumptions leading to Eq. (134b). Consequently, the parallelism requirement is not very stringent.

V. TRIPLE CORRELATION

The principal results of this paper are contained in the description of double-cascade process (Secs. II and III) where, when unpolarized radiations are observed, we deal with a two-vector problem. In the foregoing the only exception was the process of correlation in an external magnetic field wherein a third direction is introduced.

There is another important exception and this concerns the case in which three radiations are involved. These need not all be emitted radiations (thus, an absorption can equally well replace the first emitted radiation), and one need not observe all three radiations. For example, in the case of non s proton, or neutron, capture the compound nucleus formed after capture of the nuclear particle may decay by a cascade of two (or more) γ-rays, say. Then the correlation of the second γ-ray with the incident beam constitutes a special case of a three-vector problem or a triple correlation even though the correlation does not depend on the *direction* of the unobserved intervening radiation. Alternatively, there are several cases reported in the literature, [for example, (66)] in which there are three γ radiations observed in cascade. The correlation between all three (11) or between the first and third (8) will often be of relevance. The latter observation which, in some cases, may present no greater difficulty than the more usual type of measurement involved in double correlation, is useful in that it provides confirmation of assignments of angular momenta and parity obtained from observing the correlation between successive radiations taken in pairs. In a few cases the correlation of first and third radiations may resolve ambiguities resulting from the analysis of double correlation measurements (8).

The correlation between three propagation directions represents a complicated problem both from the experimental and theoretical point of view, and it is probable that only the special cases discussed below will be of major interest. In the following we present the formalism for the general case of three γ rays in cascade and then proceed to the special cases. The case in which one of the γ ray emissions is replaced by the absorption of a nucleon of nonvanishing orbital angular momentum has also been treated (11). Here the main complication arises from channel-spin degeneracy, and this complication would be aggravated if one considered a correlation such as $d-p-\gamma$ [proceeding by compound nucleus formation rather than stripping (14a)].

We consider the triple γ-cascade in which three pure multipoles are emitted. *Note added in proof.*—The extension to triple correlations with mixed multipoles is straightforward. (See R. K. Osborn and M. E. Rose, Oak Ridge National Laboratory Report No. 1560 and M. E. Rose, Oak Ridge National Laboratory Report No. 1555.) The nuclear angular momenta will be

CC-0. In Public Domain. Gurukul Kangri Collection, Haridwar

Digitized by Arya Samaj Foundation Chennai and eGangotri

denoted by j_0, j_1, j_2, and j_3 in order of ascending energy (or the emission problem), and we consider emission of 2^{L_0}, 2^{L_1}, and 2^{L_2} poles in "temporal" order. The cascade is thus designated by $j_0(L_0)j_1(L_1)j_2(L_2)j_3$. In view of remarks made above consideration of the added complication with mixed radiations does not seem worth while at present. The envisaged process can then be interpreted in terms of the formalism already established in Sec. II by treating the intermediate transition $j_1(L_1)j_2$ as constituting a link between the first and third transitions. It thus provides a certain coupling coefficient of the form $S(m_a m_a'; m_n m_n')$. The two end links $j_0(L_0)j_1$ and $j_2(L_2)j_3$ are characterized by density matrices of the form

$$\begin{aligned}&\sum_{m_0 P} C(j_0 L j; m_0 m-m_0)C(j_0 L j; m_0 m'-m_0)\\&\qquad\times D(L, m-m_0, P)D^*(L, m'-m_0, P)\\&=\sum_{m_0 P \nu_0}(-)^{m'-m_0-P}C(j_0 L j; m_0, m-m_0)\\&\quad\times C(j_0 L j; m_0, m'-m_0)C(LL\nu_0; m-m_0, m_0-m')\\&\qquad\times C(LL\nu_0; P, -P)D(\nu_0, m-m', 0)\\&=2(2j+1)\sum_{\nu_0}(-)^{m'+j_0-P}C(LL\nu_0; 1-1)\\&\quad\times C(jj\nu_0; -m'm)W(LLjj; \nu_0 j_0)\\&\qquad\times D(\nu_0, m-m', 0)\end{aligned}\tag{135}$$

by use of the Clebsch-Gordan series Eq. (9) and the usual Racah relations (see Appendix). In Eq. (135) ν_0 is even and the notation is, in part, descriptive of the first transition. For the first transition $j=j_1$, $L=L_0$ while for the third $j=j_3$, $L=L_2$ and j_0 is replaced by j_2. Of course, the arguments of the D matrices are $\mathbf{f}_0$ and $\mathbf{f}_2$, respectively. In all cases $P=\pm 1$.

For the intermediate step, the second transition, one obtains the coupling coefficient

$$\begin{aligned}&S(m_1 m_1'; m_2 m_2')\\&=\sum_P C(j_1 L_1 j_2; m_1 m_2-m_1)C(j_1 L_1 j_2; m_1' m_2'-m_1')\\&\quad\times D(L_1, m_2-m_1, P; \mathbf{f}_1)D^*(L_1, m_2'-m_1'; P; \mathbf{f}_1)\\&=2(-)^{1+m_1'-m_2'}\sum_{\nu_1} C(L_1 L_1 \nu_1; 1-1)\\&\quad\times C(L_1 L_1 \nu_1; m_2-m_1, m_1'-m_2')\\&\quad\times C(j_1 L_1 j_2; m_1, m_2-m_1)C(j_1 L_1 j_2; m_1' m_2'-m_1')\\&\qquad\times D(\nu_1, m_2-m_2'-m_1+m_1', 0; \mathbf{f}_1)\end{aligned}\tag{136}$$

and ν_1 is even.

Discarding scale factors we obtain for the correlation function

$$\begin{aligned}&W(\mathbf{f}_0, \mathbf{f}_1, \mathbf{f}_2)\\&=\sum(-)^{m_2+m_2'}C(L_0 L_0 \nu_0; 1-1)C(L_1 L_1 \nu_1; 1-1)\\&\quad\times C(L_2 L_2 \nu_2; 1-1)W(L_0 L_0 j_1 j_1; \nu_0 j_0)\\&\quad\times W(L_2 L_2 j_2 j_2; \nu_2 j_3)C(j_1 j_1 \nu_0; -m_1' m_1)\\&\quad\times C(j_2 j_2 \nu_2; -m_2' m_2)C(L_1 L_1 \nu_1; m_2-m_1, m_1'-m_2')\\&\quad\times C(j_1 L_1 j_2; m_1 m_2-m_1)C(j_1 L_1 j_2; m_1' m_2'-m_1')\\&\quad\times D(\nu_0, m_1-m_1', 0; \mathbf{f}_0)\\&\quad\times D(\nu_1, m_2-m_2'-m_1+m_1', 0; \mathbf{f}_1)\\&\qquad\times D^*(\nu_2, m_2-m_2', 0; \mathbf{f}_2),\end{aligned}\tag{137}$$

and the sum is over ν_0, ν_1, ν_2, (all even) and m_1, m_1', m_2, m_2'.

We define

$$\mu_1=m_1-m_1'$$
$$\mu_2=m_2-m_2'$$

and perform the sums over m_1 and m_2 keeping μ_1 and μ_2 fixed. This summation is performed by repeating application of the Racah relations (Appendix Eq. (A5)) and after a somewhat lengthy but straightforward calculation we obtain for the triple correlation function the result

$$\begin{aligned}W(\mathbf{f}_0\mathbf{f}_1\mathbf{f}_2)&=\sum F_{\nu_0}(L_0 j_0 j_1)F_{\nu_2}(L_2 j_3 j_2)\\&\quad\times\Gamma(j_1 L_1 j_2; \nu_0\nu_1\nu_2)A_{\nu_0\nu_1\nu_2}(\mathbf{f}_0, \mathbf{f}_1, \mathbf{f}_2),\end{aligned}\tag{138}$$

where the sum is over ν_0, ν_1, ν_2 and the notation of Eq. (69b) has been introduced. Also

$$\begin{aligned}&\Gamma(j_1 L_1 j_2; \nu_0\nu_1\nu_2)\\&=(2\nu_2+1)^{-\frac{1}{2}}C(L_1 L_1 \nu_1; 1-1)\sum_\lambda(2\lambda+1)\\&\quad\times W(\nu_0\nu_1 j_2 j_2; \nu_2\lambda)W(\nu_1\lambda L_1 j_1; j_2 L_1)\\&\qquad\times W(j_1 j_1\lambda j_2; \nu_0 L_1),\end{aligned}\tag{138a}$$

and

$$\begin{aligned}A_{\nu_0\nu_1\nu_2}(\mathbf{f}_0\mathbf{f}_1\mathbf{f}_2)&=\sum_{\mu_1\mu_2}C(\nu_1\nu_0\nu_2; \mu_2-\mu_1, \mu_1)\\&\quad\times Y_{\nu_0}^{\mu_1*}(\mathbf{f}_0)Y_{\nu_1}^{\mu_2-\mu_1*}(\mathbf{f}_1)Y_{\nu_2}^{\mu_2}(\mathbf{f}_2).\end{aligned}\tag{138b}$$

The limits on the λ sum in Eq. (138a) are given by the triangular inequalities defined by the Racah coefficient (see Appendix). Equation (138) is the general form for the triple correlation of three pure multipole γ rays. Aside from the fact that one can choose the polar axis along any one of the unit vectors $\mathbf{f}_0$, $\mathbf{f}_1$, or $\mathbf{f}_2$ (which eliminates one of the summations in Eq. (138b) the result is clearly rather cumbersome and involves laborious calculations before numerical results can be obtained. For this purpose the tabulation of reference (13) is helpful. In the following we consider certain special cases which may be of interest.

A. Correlation with Intermediate Radiation Unobserved (8)

If the correlation between only the first and third radiation is observed, the appropriate correlation function is obtained from Eq. (138) by integration over $\mathbf{f}_1$. Then, from Eq. (138b), we find $\nu_1=0$, $\mu_2=\mu_1$ and, using the addition theorem for spherical harmonics, $A_{\nu_0\nu_1\nu_2}(\mathbf{f}_0\mathbf{f}_1\mathbf{f}_2)$ reduces to

$$A=\frac{2\nu+1}{(4\pi)^{\frac{1}{2}}}P_\nu(\mathbf{f}_0\cdot\mathbf{f}_2)\delta(\nu_0\nu_2)\delta(\nu_1 0)\qquad(\nu=\nu_0).\tag{139}$$

Using this result in (138a) one obtains

$$\begin{aligned}\Gamma&=(-)^{L-1}[(2\nu+1)(2j_2+1)(2L_1+1)]^{-1}\\&\quad\times W(j_1 j_1 j_2 j_2; \nu L_1),\end{aligned}\tag{140}$$

CC-0. In Public Domain. Gurukul Kangri Collection, Haridwar

Digitized by Arya Samaj Foundation Chennai and eGangotri

TABLE XI(a). Values of the coefficient a_2 [Eq. (142)] for the case in which either the first and/or third radiations are dipole. The triad $\Delta_3\Delta_2\Delta_1$ are defined in Eq. (142a). The double entry at the top of column 3, for example, means that a_2 is the same for the decay schemes j_3+1 (1) j_3+1 (1) j_3(1) j_3 and j_3 (1) j_3 (1) j_3+1 (1) j_3+1, as explained in the text. In general the number in parentheses following $\Delta_3\Delta_2\Delta_1$ is δ, the difference in spins of the lowest state—see Eq. (142b).

j_3	$\Delta_3\Delta_2\Delta_1$ 0 0 0	0 1 0	0 2 0	0 0 1	0 1 1
		0 −1 0(−1)	0 −2 0(−2)	−1 0 0(−1)	−1 −1 0(−2) 0 2 1(0) −1 −2 0(−3)
0	...	...	...	...	...
1/2	0	0	0	0	0
1	−0.0625	0.0875	0.0750	0.0125	−0.0250
3/2	0.0320	0.1280	0.1143	−0.0080	−0.0400
2	0.0875	0.1500	0.1375	−0.0250	−0.0500
5/2	0.1202	0.1633	0.1524	−0.0376	−0.0571
3	0.1406	0.1719	0.1625	−0.0469	−0.0625
7/2	0.1542	0.1777	0.1697	−0.0540	−0.0667
4	0.1636	0.1820	0.1750	−0.0595	−0.0700
9/2	0.1704	0.1851	0.1790	−0.0639	−0.0727
5	0.1755	0.1875	0.1821	−0.0675	−0.0750
11/2	0.1794	0.1893		−0.0705	−0.0769
6	0.1824	0.1908		−0.0730	−0.0786
13/2	0.1848			−0.0751	
7	0.1868			−0.0769	
∞	0.2000	0.2000	0.2000	−0.1000	−0.1000

j_3	0 1 −1	0 −1 1	1 0 0	1 1 0	0 2 −1
	1 −1 0(0)	−1 1 0(0)	0 0 −1(−1)	0 −1 −1(−2) 1 2 0(1) 0 −2 −1(−2)	1 −2 0(−1)
0	...	...	0.1250	−0.1750	...
1/2	0	—	−0.0400	−0.1600	0
1	−0.0875	0	−0.0875	−0.1500	−0.0600
3/2	−0.1120	0	−0.1051	−0.1429	−0.0857
2	−0.1200	−0.0175	−0.1125	−0.1375	−0.0982
5/2	−0.1224	−0.0320	−0.1156	−0.1333	−0.1047
3	−0.1228	−0.0429	−0.1169	−0.1300	−0.1083
7/2	−0.1222	−0.0510	−0.1172	−0.1273	−0.1104
4	−0.1213	−0.0573	−0.1170	−0.1250	−0.1114
9/2	−0.1203	−0.0622	−0.1166	−0.1231	−0.1118
5	−0.1193	−0.0662	−0.1161	−0.1214	−0.1121
11/2	−0.1183	−0.0694	−0.1155		
6	−0.1174	−0.0721	−0.1149		
13/2		−0.0744			
7		−0.0763			
∞	−0.1000	−0.1000	−0.1000	−0.1000	−0.1000

j_3	−1 2 0	1 0 1	1 0 −1	−1 0 1	1 1 −1
	0 −2 1(−1)	−1 0 −1(−2)			1 −1 −1(−1) 1 2 −1(1) 1 −2 −1(−1)
0	...	−0.0250	−0.2500	...	0.1750
1/2	...	0.0100	0.0500	...	0.1400
1	0	0.0250	0.0875	...	0.1200
3/2	0	0.0329	0.0920	0	0.1071
2	−0.0150	0.0375	0.0900	−0.0025	0.0982
5/2	−0.0286	0.0405	0.0867	0.0020	0.0917
3	−0.0393	0.0425	0.0835	0.0071	0.0867
7/2	−0.0476	0.0439	0.0806	0.0117	0.0827
4	−0.0542	0.0450	0.0780	0.0156	0.0795
9/2	−0.0594	0.0458	0.0758	0.0189	0.0769
5	−0.0636	0.0464	0.0739	0.0216	0.0747
11/2	−0.0671	0.0469	0.0722	0.0240	
6	−0.0700	0.0473	0.0707	0.0260	
13/2				0.0277	
7				0.0292	
∞	−0.1000	0.0500	0.0500	0.0500	0.0500

j_3	$\Delta_3\Delta_2\Delta_1$ 1 −1 1	−1 1 1	0 0 2	2 0 0	0 1 2
	−1 1 −1 (−1)	−1 −1 1(−1) −1 2 1(0) −1 −2 1(−2)	−2 0 0(−2)	0 0 −2(−2)	−2 −1 0(−3) 0 2 2(0) −2 −2 0(−4)
0	0	...	...	0.1250	...
1/2	0	...	0	0.1502	0
1	0.0175	0	−0.0179	0.1607	0.0357
3/2	0.0280	0	0.0114	0.1652	0.0571
2	0.0343	0.0050	0.0357	0.1670	0.0714
5/2	0.0383	0.0100	0.0536	0.1674	0.0816
3	0.0409	0.0143	0.0670	0.1671	0.0893
7/2	0.0428	0.0179	0.0771	0.1666	0.0952
4	0.0441	0.0208	0.0850	0.1658	0.1000
9/2	0.0451	0.0233	0.0913	0.1650	0.1039
5	0.0459	0.0255	0.0964	0.1642	0.1071
11/2	0.0465	0.0274	0.1007		0.1099
6	0.0470	0.0288	0.1042		0.1123
13/2		0.0302	0.1073		
7		0.0314	0.1099		
∞	0.0500	0.0500	0.1429	0.1429	0.1429

j_3	2 −1 0	0 −1 2	2 1 0	1 0 2	2 0 −1
	0 1 −2(−1)	−2 1 0(−1)	0 −1 −2(−3) 0 −2 −2(−3) 2 2 0(1)	−2 0 −1(−3) −1 0 −2(−2) 2 0 1(1)	1 0 −2(−1)
0	0.1250	...	0.2143	0.0357	−0.1250
1/2	0.1600	...	0.2041	−0.0143	−0.1314
1	0.1714	0	0.1964	−0.0357	−0.1286
3/2	0.1749	0	0.1905	−0.0470	−0.1238
2	0.1754	0.0250	0.1857	−0.0536	−0.1193
5/2	0.1746	0.0457	0.1819	−0.0579	−0.1151
3	0.1733	0.0613	0.1786	−0.0607	−0.1114
7/2	0.1719	0.0729	0.1759	−0.0627	−0.1083
4	0.1704	0.0819	0.1734	−0.0643	−0.1056
9/2	0.1690	0.0889		−0.0654	−0.1031
5	0.1677	0.0946		−0.0663	−0.1010
11/2		0.0991		−0.0670	
6		0.1030		−0.0676	
13/2		0.1063			
7		0.1090			
∞	0.1429	0.1429	0.1429	−0.0714	−0.0714

j_3	1 1 −2	1 −1 2	−1 0 2	−1 −1 2
	2 −1 −1(0) 1 −1 −2(−1) 2 1 −1(1) 1 −2 −2(−1) 2 2 −1(2)	−2 1 −1(−2) −1 1 −2(−1) 2 −1 1(1)	−2 0 1(−1)	−2 1 1(0) −1 −1 2(1) −2 −1 1(−1) −1 2 2(1) −2 −2 1(−2)
0	−0.2500	0	...	...
1/2	−0.2000	0	...	...
1	−0.1714	−0.0250	...	...
3/2	−0.1530	−0.0400	0	...
2	−0.1403	−0.0490	0.0036	0
5/2	−0.1310	−0.0547	−0.0029	0
3	−0.1239	−0.0584	−0.0101	−0.0071
7/2	−0.1181	−0.0611	−0.0167	−0.0143
4	−0.1136	−0.0630	−0.0223	−0.0204
9/2	−0.1099	−0.0644	−0.0270	−0.0256
5	−0.1067	−0.0656	−0.0309	−0.0297
11/2		−0.0664	−0.0343	−0.0333
6		−0.0671	−0.0371	−0.0364
13/2			−0.0396	−0.0391
7			−0.0417	−0.0411
∞	−0.0714	−0.0714	−0.0714	−0.0714

and the correlation functions assume the simple form

$$W(\beta)=N\sum_{\nu}F_\nu(L_0j_0j_1)F_\nu(L_2j_3j_2)\times W(j_1j_1j_2j_2;\nu L_1)P_\nu(\cos\beta), \quad (141)$$

where β is the angle between $\mathbf{f}_0$ and $\mathbf{f}_2$. In Eq. (141) N is a normalizing factor fixed so that $\langle W\rangle_{\text{Av}}=1$.

$$N=(-)^{L_1-j_1-j_2}[(2j_1+1)(2j_2+1)]^{-\frac{1}{2}}. \quad (141a)$$

From the Racah inequalities we find that upper limit

CC-0. In Public Domain. Gurukul Kangri Collection, Haridwar

Digitized by Arya Samaj Foundation Chennai and eGangotri

on ν is

$$\nu_{\max}=2\ \min(L_0, L_2, j_1, j_2), \qquad (141b)$$

the multipolarity of the unobserved radiation does not affect $\nu_{\max}$.

We write the correlation function (141) in the form

$$W(\beta)=\sum_{\nu} a_\nu P_\nu(\cos\beta);\quad a_0=1. \qquad (142)$$

Tables XI(a) and (b) contain numerical results for the coefficients a_ν in the case of cascades for which L_0, L_1, $L_2\leqslant 2$ (dipole, quadrupole only), and the only cases omitted are those in which a dipole crossover would be competing with a quadrupole transition. In such cases, it is assumed, the triple cascade would be improbable. In Tables XI we have adopted the notation

$$\Delta_i=j_{i-1}-j_i, \qquad (142a)$$

and $L_i=1$ when $\Delta_i=0, \pm1$ while $L_i=2$ when $\Delta_i=\pm2$. In Tables XI the coefficients a_2 and a_4 have been given for various possible j_3 (usually ground state angular momentum) and a particular set of Δ's, represented in the order $\Delta_3\Delta_2\Delta_1$. The tables have been made more compact by noting that different sets of Δ's correspond to the same a_2 (or a_4) if the spin of the lowest state is j_3' (instead of j_3). The triad of numbers $\Delta_3\Delta_2\Delta_1$ at the head of column are used when the lowest state has a spin given by the first column. For the additional entries $\Delta_3'\Delta_2'\Delta_1'(\delta)$ appearing immediately below $\Delta_3\Delta_2\Delta_1$ the results for $a_2(a_4)$ apply with the lowest state spin given by

$$j_3'=j_3-\delta. \qquad (142b)$$

Table XI(a) refers to transitions in which either L_0 or $L_2=1$ so that $\nu_{\max}=2$. The entries are the a_2 coefficients. In Table XI(b) both L_0 and $L_2=2$ and a_2 and a_4 are given. The extension of these numerical results is easily obtained by using Table I and the Racah coefficient tabulation of reference (13).

It is interesting to note that in at least two cases an observation of the first and third radiations removes an ambiguity which would be present if only successive radiations were observed. For example, consider the pair of decay schemes $j_0, j_1, j_2, j_3=0, 1, 1, 2$ and $0, 2, 1, 1$, respectively. For each of these $a_2=-0.250$ for the correlation of the first two γ-rays and -0.025 for the correlation of the last two. However, for the correlation of the first and third γ rays $a_2=-0.0250$ and 0.1250 for the two levels schemes, respectively. A similar resolution of ambiguity applies in the comparison of the levels with $j_0, j_1, j_2, j_3=\frac{1}{2}, 3/2, 3/2, 5/2$ and $\frac{1}{2}, 5/2, 3/2, 3/2$.

B. Parallel Radiations

An alternative procedure, whereby corroborative evidence may be obtained for the angular momentum assignment in the triple cascade, is to observe the radiations with one pair of them parallel, or antiparallel.

TABLE XI (b). Values of the coefficients a_2 and a_4 for both first and third radiations quadrupole. The notation is the same as in Table XI(a).

j_3	$\Delta_3\Delta_2\Delta_1$ 2 0 2 $-2\ 0\ -2\ (-4)$ a_2	a_4
0	0.0510	−0.0060
1/2	0.0671	−0.0013
1	0.0765	0.0015
3/2	0.0826	0.0033
2	0.0867	0.0045
∞	0.1020	0.0091

Let the two parallel (or antiparallel) radiations be designated by the indices p, q and the other radiation by the index r. Then taking the polar axis along $\mathbf{f}_p$ or $\mathbf{f}_q$ we find that $\mu_1=\mu_2=0$ in all cases and hence

$$\Lambda=\left[\frac{(2\nu_0+1)(2\nu_1+1)(2\nu_2+1)}{(4\pi)^3}\right]^{\frac{1}{2}} \times C(\nu_1\nu_0\nu_2;00)P_{\nu_r}(\cos\beta_r) \qquad (143)$$

for both parallel and antiparallel radiation (since all ν are even). Here β_r is the angle between $\mathbf{f}_r$ and $\mathbf{f}_p$ or $\mathbf{f}_q$ and ν_r is ν_0 if $\mathbf{f}_1$ and $\mathbf{f}_2$ are parallel, $\nu_r=\nu_1$ if $\mathbf{f}_0$ and $\mathbf{f}_2$ are parallel, $\nu_r=\nu_2$ if $\mathbf{f}_0$ and $\mathbf{f}_1$ are parallel. No further simplification is possible. Apart from scale factors the angular correlation function is now

$$W(\beta_r)=\sum_{\nu_0\nu_1\nu_2} F_{\nu_0}(L_0j_0j_1) \times F_{\nu_2}(L_2j_3j_2)\Gamma(j_1L_1j_2;\nu_0\nu_1\nu_2) \times[(2\nu_0+1)(2\nu_1+1)(2\nu_2+1)]^{\frac{1}{2}} \times C(\nu_1\nu_0\nu_2;00)P_{\nu_r}(\cos\beta_r). \qquad (144)$$

The *complexity* of the correlation function depends on which pair of radiations are made parallel (or antiparallel) since $\nu_{\max}$ may be different for ν_0, ν_1, ν_2. If the first two radiations are parallel ($\nu_r=\nu_2$)

$$(\nu_2)_{\max}=2\ \min[\min(L_0, j_1)+L_1, j_2, L_2].$$

If the first and third radiations are parallel ($\nu_r=\nu_1$)

$$(\nu_1)_{\max}=2\ \min[\min(L_0, j_1)+\min(L_2, j_2), L_1]$$

as is shown in reference (8). Also, if the second and third radiations are parallel ($\nu_r=\nu_0$)

$$(\nu_0)_{\max}=2\ \min[L_0, j_1, \min(L_2j_2)+L_1].$$

If one of the intermediate spins j_1, j_2 is 0 or $\frac{1}{2}$, then isotropy results whenever the 0 or $\frac{1}{2}$ spin "joins" the radiations $\mathbf{f}_r$ and $\mathbf{f}_p$ (or $\mathbf{f}_q$). Thus if $j_2=0$ or $\frac{1}{2}$ one obtains isotropy when the first and second radiations are parallel and if $j_1=0$ or $\frac{1}{2}$ the correlation is isotropic for the second and third radiations parallel. However, unless *both* j_1 and $j_2=0$ or $\frac{1}{2}$, the correlation with first and third radiations parallel will not, in general, be isotropic.

It is clear that the triple correlation process in which

CC-0. In Public Domain. Gurukul Kangri Collection, Haridwar

Digitized by Arya Samaj Foundation Chennai and eGangotri

any one of the γ rays is replaced by another particle is obtained from the above by the usual procedure of insertion of the particle parameters: $b_{\nu 0}(x)$ if the first γ ray is replaced by another particle, and similarly for the other transitions. If one of the particles is a proton or neutron, the procedure described in Sec. III(B) should be followed. Some special cases for the $p-\gamma-\gamma$ correlation have been worked out in reference (8).

APPENDIX: VECTOR ADDITION AND RACAH COEFFICIENT RELATIONS

Throughout the text repeated use is made of a number of symmetry relations and other properties of the vector addition coefficients $C(j_1j_2j_3;\ m_1m_2)$ and the Racah coefficients $W(abcd;ef)$. These are given below.

1. Vector Addition Coefficient

Interchange of the angular momentum quantum numbers is made by use of the symmetry properties

$$\begin{aligned}
&C(j_1j_2j_3;\ m_1m_2)\\
&\quad=(-)^{j_1+j_2-j_3}C(j_2j_1j_3;\ m_2m_1)\\
&\quad=(-)^{j_1+j_2-j_3}C(j_1j_2j_3;\ -m_1-m_2)\\
&\quad=(-)^{j_1-m_1}[(2j_3+1)/(2j_2+1)]^{\frac{1}{2}}\\
&\qquad\qquad\times C(j_1j_3j_2;\ m_1,\ -m_3)\\
&\quad=(-)^{j_2+m_2}[(2j_3+1)/(2j_1+1)]^{\frac{1}{2}}\\
&\qquad\qquad\times C(j_3j_2j_1;\ -m_3m_2)\\
&\quad=(-)^{j_1-j_3+m_2}[(2j_3+1)/(2j_1+1)]^{\frac{1}{2}}\\
&\qquad\qquad\times C(j_2j_3j_1;\ m_2-m_3). \qquad \text{(A1)}
\end{aligned}$$

The explicit form for $C(ll'\nu;00)$ (with $l+l'+\nu=2g$ = even integer) is

$$C(ll'\nu;00)=(-)^{g+\nu}(2\nu+1)^{\frac{1}{2}}\frac{\Delta(ll'\nu)g!}{(g-l)!(g-l')!(g-\nu)!}, \qquad \text{(A2)}$$

where

$$\Delta(ll'\nu)=\left[\frac{(l+l'-\nu)!(l-l'+\nu)!(l'+\nu-l)!}{(l+l'+\nu+1)!}\right]^{\frac{1}{2}}.$$

The vector addition coefficient which occurs in the γ-ray correlations is

$$C(ll'\nu;1-1)=\frac{1}{2}\frac{\nu(\nu+1)-l(l+1)-l'(l'+1)}{[l(l+1)l'(l'+1)]^{\frac{1}{2}}}\times C(ll'\nu;00). \qquad \text{(A3)}$$

In all cases

$$C(j_10j_3;\ m_10)=\delta_{j_1j_3}.$$

2. Racah Coefficients

The Racah coefficients vanish unless the triads abe, cde, bdf, and acf form a triangle. The symmetry properties are

$$\begin{aligned}
W(abcd;ef)&=W(badc;ef)=W(cdab;ef)\\
&=W(acbd;fe)=(-)^{e+f-a-d}W(ebcf;ad)\\
&=(-)^{e+f-b-c}W(aefd;bc), \qquad \text{(A4)}
\end{aligned}$$

and others obtained by combining the operations indicated.

The Racah recoupling is accomplished by means of

$$\begin{aligned}
&C(j_1j_2j;\ m_1m_2)C(jj_3j_4;\ m_1+m_2,\ m_3)\\
&\quad=\sum_s(2s+1)^{\frac{1}{2}}(2j+1)^{\frac{1}{2}}C(j_2j_3s;\ m_2m_3)\\
&\qquad\times C(j_1sj_4;\ m_1,\ m_2+m_3)W(j_1j_2j_4j_3;\ js) \qquad \text{(A5)}
\end{aligned}$$

and variants of (A5) obtained by using (A1) and/or (A4). In Section III(C) we make use of the relations

$$\begin{aligned}
&[(2l+1)(2l'+1)]^{\frac{1}{2}}C(ll'\nu;00)W(ljl'j';\tfrac{1}{2}\nu)\\
&\quad=[(2L+1)(2L'+1)]^{\frac{1}{2}}C(LL'\nu;00)\\
&\qquad\times W(LjL'j';\tfrac{1}{2}\nu), \qquad \text{(A6)}
\end{aligned}$$

where $l=l(\kappa)=|\kappa|+\frac{1}{2}[S(\kappa)-1]$, ($S(\kappa)$ = sign of κ) and $l'=l(\kappa')$ with

$$\kappa=-L \quad\text{and}\quad L+1$$

and

$$\kappa'=-L' \quad\text{and}\quad L'+1$$

In (A6) ν is an even integer and $j=|\kappa|-\frac{1}{2}$, $j'=|\kappa'|-\frac{1}{2}$

$$\begin{aligned}
&C(LL'\nu;1-1)\\
&\quad=-2\left(\frac{L'+1}{L'}\right)^{\frac{1}{2}S(\kappa')}\left(\frac{L}{L+1}\right)^{\frac{1}{2}S(\kappa)}\\
&\qquad\times[(2L+1)(2L'+1)(2l+1)(2l'+1)]^{\frac{1}{2}}\\
&\qquad\times S(\kappa)S(\kappa')C(ll'\nu;00)W(ljl'j';\tfrac{1}{2}\nu)\\
&\qquad\times W(LjL'j';\tfrac{1}{2}\nu), \qquad \text{(A7)}
\end{aligned}$$

where the notation is as above except that now

$$\kappa=L \quad\text{and}\quad -L-1$$
$$\kappa'=-L' \quad\text{and}\quad L'+1.$$

Also

$$W^2(LLL-\tfrac{1}{2}L-\tfrac{1}{2};\ \nu\tfrac{1}{2})=\frac{(2L-\nu)(2L+\nu+1)}{4L^2(2L+1)^2}, \qquad \text{(A8)}$$

$$W^2(LLL+\tfrac{1}{2}L+\tfrac{1}{2};\ \nu\tfrac{1}{2})=\frac{(2L+1-\nu)(2L+2+\nu)}{4(L+1)^2(2L+1)^2}, \qquad \text{(A9)}$$

$$W^2(LLL+\tfrac{1}{2}L-\tfrac{1}{2};\ \nu\tfrac{1}{2})=\frac{\nu(\nu+1)}{4L(L+1)(2L+1)^2}. \qquad \text{(A10)}$$

If any parameter in W vanishes the value of the Racah coefficient is

$$W(abcd,\ 0f)=(-)^{b+c-f}[(2b+1)(2c+1)]^{-\frac{1}{2}}\delta_{ab}\delta_{cd}. \qquad \text{(A11)}$$

BIBLIOGRAPHY

(1a) A. Abragam and R. V. Pound, Phys. Rev. **89**, 1306 (1953).
(1) Aeppli, Bishop, Frauenfelder, Walter, and Zunti, Phys. Rev. **82**, 550 (1951).
(2) Aeppli, Albers—Schonberg, Bishop, Frauenfelder, and Heer, Phys. Rev. **84**, 370 (1951).
(3) Aeppli, Frauenfelder, and Walter, Helv. Phys. Acta **24**, 335 (1951).

CC-0. In Public Domain. Gurukul Kangri Collection, Haridwar

Digitized by Arya Samaj Foundation Chennai and eGangotri

(4) K. Alder, Phys. Rev. **83**, 1266 (1951).
(5) K. Alder, Phys. Rev. **84**, 369 (1951).
(6) K. Alder, Helv. Phys. Acta, **25**, 235 (1952).
(7) Arfken, Biedenharn, and Rose, Oak Ridge National Laboratory Report No. 1103.
(8) Arfken, Biedenharn, and Rose, Phys. Rev. **86**, 761 (1952).
(9) Arfken, Biedenharn, and Rose, Phys. Rev. **84**, 89 (1951).
(10) V. B. Berestetzky, J. Exptl. Theoret. Phys. (U.S.S.R.) **18**, 1057 (1948).
(11) Biedenharn, Arfken, and Rose, Phys. Rev. **83**, 586 (1951).
(12) L. C. Biedenharn, J. Math. Phys. (M.I.T.) **XXXI**, 287 (1953).
(13) L. C. Biedenharn, Oak Ridge National Laboratory Report No. 1098.
(14) Biedenharn, Blatt, and Rose, Revs. Modern Phys. **25**, 249 (1953).
(14a) Biedenharn, Boyer, and Charpie, Phys. Rev. **88**, 517 (1952); G. R. Satchelor and J. A. Spiers, Proc. Phys. Soc. (London) **A65**, 980 (1952); L. J. Gallaher and W. H. Cheston, Phys. Rev. **88**, 684 (1952).
(15) J. M. Blatt and L. C. Biedenharn, Revs. Modern Phys. **25**, 258 (1953).
(16) J. M. Blatt and L. C. Biedenharn, Phys. Rev. **82**, 123 (1951).
(17) E. L. Brady and M. Deutsch, Phys. Rev. **78**, 558 (1947).
(18) H. B. Casimir, Archieves der Musée Teyler, Series III, VIII; (1936).
(18a) F. Coester and J. M. Jauch, Helv. Phys. Acta **XXVI**, 3 (1953).
(19) E. U. Condon and G. H. Shortley, *Theory of Atomic Spectra* (Cambridge University Press, Cambridge, 1935).
(20) E. P. Cooper, Phys. Rev. **61**, 1 (1942).
(21) M. Deutsch, Repts. Progr. Phys. **14**, 196 (1951).
(22) J. W. Dunworth, Rev. Sci. Instr. **11**, 167 (1940).
(23) L. Eisenbud, J. Franklin. Inst. **251**, 231 (1951).
(24) E. Eisner and R. Sachs, Phys. Rev. **72**, 680 (1947).
(25) D. L. Falkoff, Phys. Rev. **73**, 518 (1948).
(26) D. L. Falkoff and G. E. Uhlenbeck, Phys. Rev. **79**, 323 (1950).
(27) D. L. Falkoff and G. E. Uhlenbeck, Phys. Rev. **79**, 334 (1950).
(28) D. L. Falkoff, Phys. Rev. **82**, 98 (1951).
(29) U. Fano, J. Opt. Soc. Am. **39**, 859 (1949).
(30) U. Fano, Natl. Bur. Standards Report No. 1214 (1951). Phys. Rev. **90**, 577 (1953).
(31) M. Ferz, Helv. Phys. Acta **22**, 489 (1949).
(32) S. Frankel, Phys. Rev. **83**, 673 (1951).
(33) H. Frauenfelder, Phys. Rev. **82**, 549 (1951).
(34) H. Frauenfelder, (to be published).
(35) H. Frauenfelder, *Ann. Reviews of Nuclear Science*, (Annual Review, Inc., Stanford, 1953), Vol. 2.
(36) Frauenfelder, Aeppli, Heer, and Ruetschi, Phys. Rev. **87**, 379 (1952).
(37) M. Fuchs, Ph.D. dissertation (University of Michigan, (1951).
(38) J. W. Gardner, Proc. Phys. Soc. (London) **A62**, 763 (1949).
(39) J. W. Gardner, Proc. Phys. Soc. (London) **A64**, 238 (1951).
(40) J. W. Gardner, Proc. Phys. Soc. (London) **A64**, 1136 (1951).
(41) J. W. Gardner, Phys. Rev. **82**, 283 (1951).
(42) G. Goertzel, Phys. Rev. **70**, 897 (1946).
(42a) G. Goertzel, Phys. Rev. **73**, 1463 (1948).
(43) M. Goldhaber and A. W. Sunyar, Phys. Rev. **83**, 906 (1951).
(44) D. R. Hamilton, Phys. Rev. **58**, 122 (1940).
(45) D. R. Hamilton, Phys. Rev. **74**, 782 (1948).
(46) H. A. Jahn, Proc. Roy. Soc. (London) **A205**, 192 (1951).
(47) E. Konopinski and G. E. Uhlenbeck, Phys. Rev. **60**, 308 (1941).
(48) J. C.Kluyver and M. Deutsch, Phys. Rev. **87**, 203 (1952).
(49) D. S. Ling and D. L. Falkoff, Phys. Rev. **76**, 1639 (1949).
(50) D. S. Ling, Ph.D. dissertation (University of Michigan, (1948).
(51) B. A. Lippmann, Phys. Rev. **81**, 162 (1951).
(52) S. P. Lloyd, Ph.D. dissertation (University of Illinois, 1951).
(53) S. P. Lloyd, Phys. Rev. **80**, 118 (1950).
(54) S. P. Lloyd, Phys. Rev. **82**, 277 (1951).
(55) S. P. Lloyd, Phys. Rev. **81**, 161 (1951).
(56) S. P. Lloyd, Phys. Rev. **83**, 716 (1951).
(57) S. P. Lloyd, Phys. Rev. **85**, 904 (1952).
(58) S. P. Lloyd, Phys. Rev. **88**, 906 (1952).
(59) C. L. Longmire and A. M. L. Messiah, Phys. Rev. **83**, 464 (1951).
(60) J. E. MacDonald and D. L. Falkoff, Phys. Rev. **83**, 875 (1951).
(61) F. Metzger and M. Deutsch, Phys. Rev. **78**, 551 (1950).
(62) L. Pincherle, Nuovo cimento **12**, 81 (1935).
(63) G. Racah, Phys. Rev. **62**, 438 (1942).
(64) G. Racah, Phys. Rev. **63**, 367 (1943).
(65) G. Racah, Phys. Rev. **84**, 910 (1951).
(66) B. L. Robinson and L. Madansky, Phys. Rev. **84**, 604 (1951).
(67) M. E. Rose, Phys. Rev. **51**, 484 (1937).
(68) Rose, Biedenharn, and Arfken, Phys. Rev. **85**, 5 (1952).
(69) Rose, Goertzel, Spinrad, Harr, and Strong, Phys. Rev. **83**, 79 (1951).
(70) M. E. Rose and L. C. Biedenharn, Oak Ridge National Laboratory Report No. 1324.
(71) J. A. Spiers, Phys. Rev. **80**, 491 (1950).
(72) J. A. Spiers, Nature **161**, 807 (1948).
(73) R. M. Steffen, private communication.
(74) Sunyar, Alburger, Friedlander, Goldhaber, and Scharff-Goldhaber, Phys. Rev. **79**, 181 (1950).
(75) H. A. Tolhoek and S. R. deGroot, Phys. Rev. **83**, 189, 845 (1951).
(76) N. Tralli and G. Goertzel, Phys. Rev. **83**, 399 (1951).
(76a) V. F. Weisskopf, Phys. Rev. **83**, 1073 (1951).
(77) E. P. Wigner, *Gruppentheorie* (Friedrich Vieweg and Sohn, Braunschweig).
(78) E. P. Wigner and L. Eisenbud, Phys. Rev. **72**, 29 (1947).
(79) L. Wolfenstein and R. G. Sachs, Phys. Rev. **73**, 528 (1948).
(80) C. N. Yang, Phys. Rev. **74**, 764 (1948).
(81) I. Zinnes, Phys. Rev. **80**, 386 (1950).

CC-0. In Public Domain. Gurukul Kangri Collection, Haridwar

Digitized by Arya Samaj Foundation Chennai and eGangotri

CC-0. In Public Domain. Gurukul Kangri Collection, Haridwar

Digitized by Arya Samaj Foundation Chennai and eGangotri

CC-0. In Public Domain. Gurukul Kangri Collection, Haridwar

Digitized by Arya Samaj Foundation Chennai and eGangotri

CC-0. In Public Domain. Gurukul Kangri Collection, Haridwar

Digitized by Arya Samaj Foundation Chennai and eGangotri

REVIEWS OF
MODERN PHYSICS

VOLUME 25, NUMBER 4 OCTOBER, 1953

Passage of Heavy Particles through Matter*

S. K. ALLISON,† *Institute for Nuclear Studies, The University of Chicago, Chicago, Illinois*

AND

S. D. WARSHAW, *Argonne Cancer Research Hospital, The University of Chicago, Chicago, Illinois*

I. INTRODUCTION

IF the short summary article by Taylor (Ta52)[1] is excepted, for at least ten years there has been no review published in the periodical literature, either descriptive or discursive by nature, on the subject of experiments in atomic penetration. The present article is therefore intended to remedy this lack, without going into the detailed description of all such phenomena that can be found in the definitive chapter by Bethe and Ashkin in the book, *Experimental Nuclear Physics* (Be53). However, since the closing date on experimental data for that article was 1951, and since at least a few special topics deserve more detail than could be practically included in that chapter, the present article will attempt to supplement it and bring the experimental picture more up to date.

The scope of this article will be limited to the penetration of charged atomic particles through matter, thereby excluding experiments done with mesons or electrons. From the point of view of theory, this is not an important distinction, since except for a few special modifications the accepted basic theory is as good for one kind of charged particle as another. However, it is just these modifications which also make the experimental techniques—between the use of protons and electrons for example—different enough to warrant a separate writing. Those theoretical topics pertinent to the measurement of penetration parameters, the value of these parameters, and factors affecting the accuracy or interpretation of the experiments, will first be discussed; this will be done at the risk of repeating other reviews, but is included for the sake of coherency. There will first be a general discursive section on the phenomena involved; this will include discussion on stopping by ionization of a medium with presentation of the Bethe-Bloch equation and of its validity; discussion of range relation and definitions and calculation from stopping power; the general effects of fluctuation phenomena; a short presentation of some phenomena that are not related directly to ionization of single atoms, but affect the penetration to a more or less significant degree depending, e.g., on the energy of the incident particle: polarization of the medium, charge exchange phenomena, chemical binding, scattering, etc.

As remarked above, Taylor has reviewed the 1952 status of range-energy relations and has included an extensive bibliography; therefore, this article will not attempt to present a comprehensive coverage of the literature (except for work completed since Taylor's article and prior to June, 1953). The usefulness of the range-energy relations, as such, becomes small in the low-energy region, since the preparation and storage of suitable absorbing foils, while possible, becomes a major undertaking. Therefore, the discussion of experimental work in this article will be split into two parts: "low energy," or less than an arbitrarily set 2 Mev (protons), and "high energy," or greater than 2 Mev. The range-energy relations will be given only casual mention in the low-energy part, while measurements on absolute stopping powers will receive brief treatment in the high-energy part. The point of view for the high-energy sections will be that of the experimenter who wishes to determine beam energy and energy spread by means of absorption curves.

* Closed June, 1953.

† Member of National Research Council Committee on Penetration of Charged Particles in Matter.

[1] References in parentheses are given in the Bibliography.

CC-0. In Public Domain. Gurukul Kangri Collection, Haridwar

Digitized by Arya Samaj Foundation Chennai and eGangotri

II. DISCUSSION OF PHENOMENA

A. Physical Basis of Stopping

While the physical basis of the stopping phenomena has been well understood for some time (Bo48), discrepancies between theory and experiment can be ascribed to the mathematical difficulties involved in an accurate collision theory. Stated concisely, the problem is: a charged particle with a given kinetic energy passes through a region containing atoms of one kind or another. What is the energy of this particle when it leaves the region? An obvious simplifying assumption is first to consider the region as made up of many isolated atoms, calculate the contribution of a single incident particle-atom collision, and then sum over all atoms. This approximation will turn out to be justified for all but the highest velocity incident particles. In the second place, the numerical value of such a sum must be interpreted as some kind of average value, since each collision will lead, not to some definite, final state of the collision pair, but rather to a probability describing that state; hence, the kinetic energy of the particles in a beam that has passed through such a region will be distributed according to the laws of chance, and for a completely unambiguous interpretation, the essential parameters of this distribution (the "straggling") must be known. Having granted that collisions of the incident particle with single atoms can be summed in an interpretable way, it must still be assumed that the incident particle retains its identity and description: an incident proton can pick up an orbital electron and spend some of its time as a neutral atom at low energy or be lost through a nuclear reaction at high energy.

The collision occurring between one of the atomic electrons and the passing particle (the energy transferred to the nucleus being—usually—small) is considered in the actual calculation of the energy transferred to an atom by ionization. For this calculation the Born approximation may be used: obtain the matrix element for an electronic transition (induced by the field of the passing particle) to a given final state, average over all initial and final electronic states, and then sum over all electrons in the medium. Since the chance that the final electron state will be in the continuum is large, and since these states are easily observable as ionization current, the stopping process is said to produce ionization energy loss. However, part of the energy of the incident particle clearly goes to electronic transitions between discrete states, with the subsequent emission of photons; indeed, after the moving particle has lost so much energy that it has little chance of ionizing an atom, it still moves far enough to produce many atoms in excited states. For this reason the observed range (defined below) will differ according to the type of detector used: an experiment that measures ionization (e.g., with an ionization chamber) will give a slightly shorter range than one using, say, a scintillation counter, which responds to excited atoms. The assumptions made for the Born approximation are that the change of momentum during the collision be small, which can be shown (Mo49, Bo48) to reduce to the condition that Zv_0/v is much less than unity, where $v_0=e^2/h$ is the Bohr velocity, or, in energy units (for protons), that E in Mev is greater than $0.025Z^2$. Hence, for all but the lightest elements (Z less than 10) the low-energy (proton E less than 2 Mev) application of the theory, even ignoring such extraneous effects as charge exchange, is quite dubious. At very high energies, in the full relativistic form the formula would predict a continuous increase in the rate of energy loss, but for the breakdown of the approximation of isolated atoms in the stopping material. For collisions at distances larger than atomic dimensions, some account must be made of the effect of neighboring atoms of the stopping material; polarization of the entire medium by the incident particle produces a decrease in the field of this particle that is effective in the transfer of energy, with a consequent decrease in the energy loss. However, since the distant collisions play an important role only at high energies, in the nonrelativistic case there should be only a small effect, with the important exception of stopping in materials containing a large fraction of conduction electrons. The polarization phenomena should be expected to become significant (A.Bo49) when $mv^2 \gg h\omega_A$ (where $\omega_A^2=\omega_a^2+(1-\alpha)\nu^2$, ω_a corresponding to the binding energy of an isolated atom, $\alpha \lesssim 1$ a numerical constant, and $\nu^2=4\pi ne^2/m$, with n the electron density). Thus in the case of the light elements (beryllium, carbon), there can be a relatively large effect even at moderate energy. At extremely high energy the effect of polarization is to make the stopping power a constant function of energy rather than a continuously increasing one. (See Be53, Fe40, Ha48, Sc51, St52).

B. Simple Theory of Stopping

The theoretical factors most generally applicable to experimental use are the mean range, the average rate of energy loss, the specific ionization, and the straggling parameter; these are all related in a fairly straightforward way, this being made clear from the simplified classical theory, in which the differential cross section for the transfer of energy between T and $T+dT$ is

$$d\sigma=\frac{2\pi e^4z^2}{mv^2}\frac{dT}{T^2}, \tag{1}$$

where e is the electronic charge and z is the atomic number of the incident particle. Thus, the average rate of loss is obtained by integrating the product $Td\sigma$ (the maximum value being $T_m=2mv^2$, the minimum of the order of the mean excitation potential I) over all possible transfers, the specific ionization by integrating $d\sigma$ over all transfers that result in a free electron-ion pair, the mean square deviation in energy loss by integrating $T^2d\sigma$ over all possible transfers, etc. The mean range

CC-0. In Public Domain. Gurukul Kangri Collection, Haridwar

Digitized by Arya Samaj Foundation Chennai and eGangotri

is obtained in a simple way from the mean rate of loss as

$$R_m=\int_E^0 dE(dx/dE). \tag{1'}$$

The mean square deviation from the mean range (if we assume that the distribution is Gaussian) can be shown to be (Bo48)

$$\sigma_R^2=\int_0^E P(dE/dx)^{-3}dE, \tag{2}$$

where $P=4\pi ne^4z^2$.

Actually the distribution in energy loss is not strictly Gaussian, but is rather such that greater losses than the most probable are favored, when collisions between particles of the same order of magnitude of mass are considered as contributing to the net loss. Thus, the ionization loss of electrons or the nuclear collision loss for protons leads to a distinctly non-Gaussian distribution. However, in the high-energy range, nuclear collisions contribute little to the stopping and for the electronic collisions the most probable and the average energy loss are very nearly identical. If one uses the accurate quantum-mechanical theory, the result of the integration over all possible energy transfers gives the average rate of loss as (Li37)

$$-\frac{dE}{dx}=\frac{4\pi e^4z^2}{mv^2}N\left[Z\left(\log\frac{2mv^2}{I}-\log(1-\beta^2)-\beta^2\right)-C_K\right], \tag{3}$$

where the relativistic correction term has been included. In Eq. (3): N is the number of atoms of the stopping material per cubic centimeter; z is the atomic number of the incident particle; Z is the atomic number of the stopping material; β = particle velocity/velocity of light; $C_K(1/\eta)$ is a correction term for binding in the K shell (see below); and

$$\eta=\frac{mE}{M(Z-\sigma)^2Ry}=[v/(Z-\sigma)v_0]^2,$$

where $v_0=e^2/\hbar$, with σ a screening constant (approximately 0.3 for light elements) such that $(Z-\sigma)e$ gives the effective source strength of the field in which the K electrons move. Here I, the mean excitation potential, is a measure of the least (on the average) energy that can be transferred to a bound electron. A good part of the experimental work in the field has been concerned with measurements of I, which is assumed to be a velocity independent parameter and shown by Bloch (Bl33) to be proportional to the atomic number Z for high Z materials. In terms of more easily calculable constants the first factor in (3) can be written

$$8\pi a_0^2Ry\cdot z^2NZ\frac{Ry}{E}\cdot\frac{M}{m}\cdot\frac{\gamma^2}{1-\gamma},$$

TABLE II-1. $C_K(1/\eta)$: Correction for K-shell binding in light elements.[a]

Proton energy Mev	$\frac{1}{(Z-0.3)^2\eta}$	C_K Be	C	Al
0.6	0.0414	0.895	0.900	...
0.8	0.0311	0.780	0.972	...
1.0	0.0248	0.680	0.981	...
1.2	0.0207	0.596	0.951	...
1.4	0.0177	0.531	0.901	...
1.6	0.0155	0.475	0.852	0.380
1.8	0.0137	0.421	0.800	0.552
2.0	0.0124	0.390	0.758	0.613
2.2	0.0113	0.359	0.716	0.700
2.4	0.0104	0.330	0.678	0.767
2.6	0.0096	0.310	0.638	0.820
2.8	0.0087	0.288	0.597	0.861
3.0	0.0083	0.270	0.570	0.892
4.0	0.0062	0.208	0.451	0.975
5.0	0.0049	0.160	0.361	0.880[b]

[a] From the curve of Fig. 2 in M. C. Walske, Phys. Rev. 88, 1283 (1952), for the three elements θ_k was taken as 0.7. The last decimal is, of course, doubtful.

[b] Above this energy the correction in Al is less than 1 percent.

where M is the rest mass of the incident particle, a_0 the Bohr radius, γ the Lorentz factor $1/(1-\beta^2)^{\frac{1}{2}}$, and E the kinetic energy.

In the low-energy range, the Born approximation for heavy materials would fail, since the inner electrons move at very high velocities compared to the incident protons, and a correction for binding in the inner electron shells must be applied. This is done by subtracting the number C_K from the logarithmic term in the Bethe-Bloch formula. These corrections have been calculated most recently by Walske (Wa52) and earlier by Brown (Br50), and still earlier given by Livingston and Bethe (Li37) in their 1937 review; in all of these, the correction is given as a function of the particle velocity in units of K-shell electron velocity.‡ Some representative values from Walske's article are given in Table II-1.

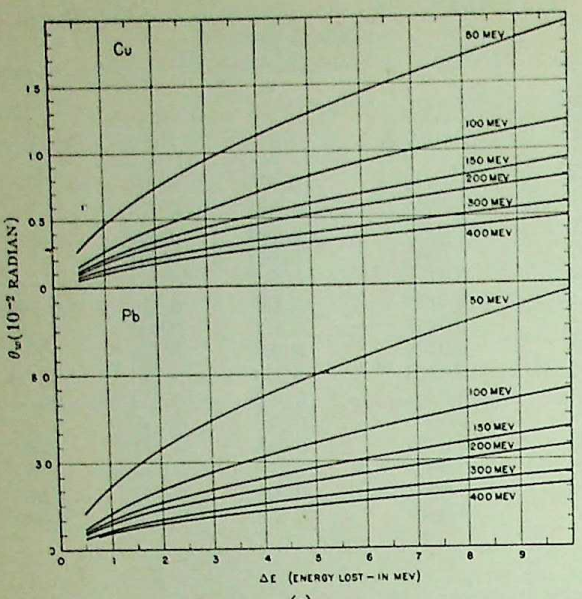
The Bethe-Bloch equation then stands as an approximation valid in a restricted energy range (which differs for different particles and materials) and requiring the measurement of a parameter, the mean excitation potential; further, this parameter is velocity dependent, at least at high energy, because of polarization phenomena (and incorporating this effect into the excitation potential), although at most energies it is relatively constant except for binding corrections.

For protons in the energy range 20 kev to about 2 Mev, there is no satisfactory theory, and recourse must be made to empirical data. Below 20 kev the statistical theory of Fermi and Teller (Fe49) has not been directly verified (however, see Sec. III). In heavy materials, a crude statistical argument (Bo48) gives a $Z^{\frac{1}{2}}/v$ dependence of the stopping power at lower energies. Experimental agreement with this is only qualitative (Wa49).

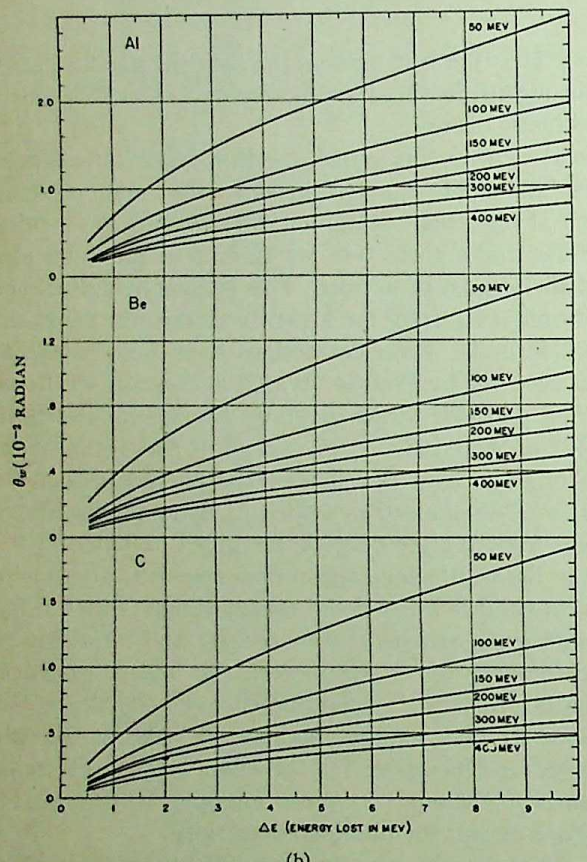
‡ It should be pointed out that in the widely used tables calculated by Aron (Ar51) the wrong C_K correction was evidently used: instead of calculating the ratio v/v_K, Aron apparently used four times this value.

CC-0. In Public Domain. Gurukul Kangri Collection, Haridwar

Digitized by Arya Samaj Foundation Chennai and eGangotri



(a)



(b)

FIG. 1(a+b). The effective rms (unprojected) scattering angle θ_w as a function of energy lost in the scattering material.

Experimentally, the measurement of range may be done by obtaining the curve for the number of particles remaining in a beam as a function of the thickness of the material the beam has to pass through and identifying a point on that curve with the mean range. By definition this point would be the thickness R_m of material for which one-half of the particles have been absorbed by the ionization process; the ideal absorption curve for monoergic protons would have such a form that the derivative dN/dx, where $N(x)$ is the number of particles counted for absorber thickness x, would be a Gaussian. However, in practice this is almost never the case. If the mean range is defined as above, such that one-half of the incident beam travels a distance greater than R_m and one-half less than R_m, then clearly because of small-angle multiple scattering of the beam (that is, angles small enough so that the detector still sees the entire beam) the observed mean range being the projection of many short segments of trajectory, each randomly oriented to the axis of the beam, will be smaller than the "true" mean range. The effect of scattering is most significant, of course, near the end of the range. Following Mather and Segrè (Ma51) the difference between observed and true ranges may be written as

$$R_{\text{obs}}=\sum_i l_i\cos\theta_i \doteq \sum l_i\left(1-\frac{\theta_i^2}{2}\right)=R_m-\tfrac{1}{2}\sum l_i\theta_i^2, \quad (4)$$

where l_i is the distance between the ith and $(i+1)$th small angle collision, and θ_i the direction with respect to the beam axis after the ith collision. An approximation of the value of θ_i was obtained from William's formula (Wi45),

$$\langle\theta_i^2\rangle=\frac{Zm}{M}\log(E_0/E_i). \quad (5)$$

By assuming that R is roughly proportional to $E^{1.75}$, writing the sum as an integral and integrating, we get $(R_m-R_{\text{obs}})/R_m=Z/6440$. It is, therefore, of the order of 1 percent for copper.

Other authors (Bl51) have used somewhat more accurate expressions for the mean square scattering angle with a resulting formula for the range correction that differs in form from the above expression but only by a

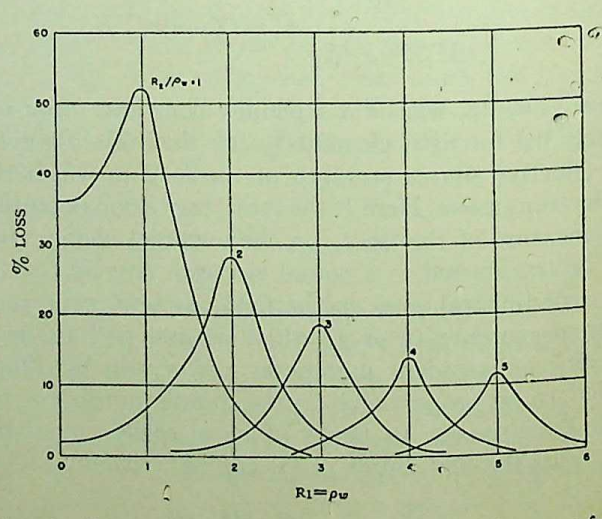


FIG. 1c. From reference Di53: Fractional beam loss as a function of detector and source geometry; R_1=source radius; R_2=detector radius; $\rho_w=S\theta_w$, with S=source-detector distance.

CC-0. In Public Domain. Gurukul Kangri Collection, Haridwar

Digitized by Arya Samaj Foundation Chennai and eGangotri

small amount numerically. This is

$$\langle\theta^2\rangle=\int_{-R_m}^{-x} ZPG(pv)^{-2}dx, \tag{6}$$

where P is defined above, $G=2\log 181Z^{-\frac{1}{3}}$, x is the residual range, and p, v are the momentum and velocity of the incident particle. The range correction is then $\delta R/R=ZPG/C$, where it has been assumed that $(pv)^{-2}=Cx$. For Al, $C=2.6\times10^{-8}$, for Cu, $C=8.9\times10^{-8}$. A full discussion of the multiple scattering theory (Ro41, Gr50, Sc50, Mo51, Be53) is beyond the scope of this paper. The correction is, in most cases, small, and relatively large errors in the correction are of little consequence. However, for aid in the interpretation of some experiments, it is useful to have an estimate of the beam spread as it is passed through relatively thin targets. To this end we have calculated curves for the mean square angle of scatter (at several high energies) as a function of the energy lost in the target, using an approximate form of Moliere's (Mo51) expression for the scattering angle, and Aron's table for the energy loss. Both of these are sufficiently accurate for this purpose. Moliere's expression gives an angle which is not properly identified as the spread of a Gaussian distribution in scattering angles. His distribution function has a leading term which is Gaussian, but there are also higher order terms (making the resulting curve slightly greater for small angles and smaller than Gaussian at larger angles) resulting from a smooth transition from multiple to single scattering. Following Hanson, *et al.* (Ha51) let θ_w be the $1/e$ width of an effective Gaussian distribution, fit to Moliere's theory. Then as given in (Ha51)

$$\theta_w^2=\theta_1^2(B-1.2), \tag{7}$$

where

$$\theta_1^2=\frac{4\pi NZ(Z+1)xe^4}{p^2v^2},$$

$$\theta_a^2=\left(\frac{hZ^{\frac{1}{3}}}{0.885pa_0}\right)^2\left[1.13+3.76\left(\frac{Z}{137\beta}\right)^2\right],$$

x is the thickness of the stopping material, and $B(\theta_1/\theta_a)$ is the auxilliary function tabulated by Moliere (see also reference Be53). The group of curves in Fig. 1 gives θ_w for several elements and energies. In this connection, the evaluation of particle loss resulting from the multiple scattering that has been made by Dickinson and Dodder (Di53) is of interest. Figure 1(c) gives the calculated fractional loss as a function of detector radius R_2, the foil radius R_1, and the average normal displacement $\rho_w=S\theta_w$, with S the foil-detector distance. (These curves were actually calculated with Moliere's $\langle\theta^2\rangle_{Av}$, but the difference, for this application, is negligibly small.)

At higher energies, nuclear collisions may occur which attenuate the beam intensity, thereby changing the shape of the absorption curve, and thus the point corresponding to the mean range. If N_0 is the initial beam flux, then R_m would be the thickness x of the absorber for which the flux N is $\frac{1}{2}N_0$; if the fraction f is attenuated, $1-f$ remaining, then this point should be at $(1-f)N_0/2$. The fraction f may be calculated from the data of Kirschbaum (Ki52) which is shown in Fig. 2, giving σ_{abs} as a function of the nuclear mass A. In Kirschbaum's work, the cross section was measured by observing the average slope of the integral absorption curve for a beam of protons passing through a variable thickness of absorbing material. The point just to the left of the knee of the curve was taken as the running point for attenuation measurements. The cross section is then given at the average energy of the beam in the attenuator. The significance of this type of measurement in the interpretation of nuclear reactions is beyond the scope of this work, but the use of this technique makes the results directly applicable to the correction for range. (Also on Fig. 2 the data of Perry (Pe51) and Bernardini, *et al.* (Be51) are shown, with some evidence of a different slope.) While an exponential fit to the energy variation probably has no theoretical significance, for present purposes it is convenient to represent Kirschbaum's data by the empirical relation $\sigma_{abs}=\sigma_0\exp(-E/\epsilon)$, where $\sigma_0=\pi r_0^2A^{\frac{2}{3}}$ is the geometric cross section ($r_0=1.37\times10^{-13}$ cm) $\epsilon=400A^{0.14}$ Mev, and E is the average energy of the protons in the attenuator. The absorption curve is very steep near the end of the range so that the range will be insensitive to rather large errors in the determination of $f\doteq0.9R_m\sigma_{abs}$, where R_m is expressed in atoms/cm^2 and the factor 0.9 gives an approximately correct "running point." Included in f, of course, should be the contribution from large angle Coulomb scattering, which will depend on the geometry of the experimental arrangements.

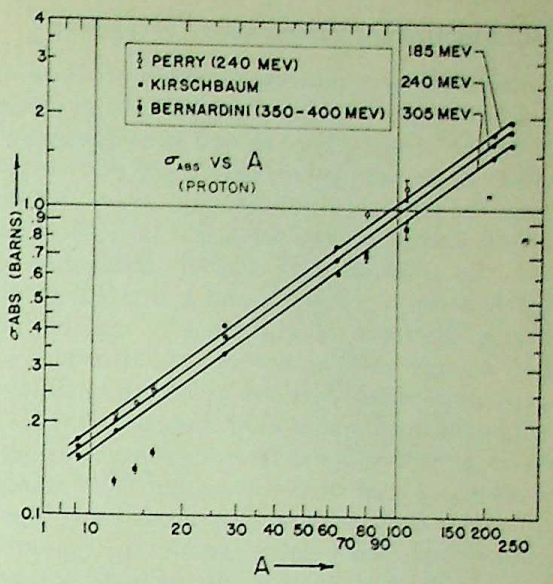


FIG. 2. Experimental high-energy nuclear absorption cross section (for protons) *versus* atomic weight.

CC-0. In Public Domain. Gurukul Kangri Collection, Haridwar

Digitized by Arya Samaj Foundation Chennai and eGangotri

C. Fluctuation Phenomena: Straggling

The statistical nature of the stopping produces also a fluctuation in the distance traveled by the incident particle before being stopped as well as a corresponding fluctuation of the total energy loss by the particle. This is because the number of collisions necessary to reduce the particle energy to zero will vary, since the energy that may be transferred in a single collision is distributed between a minimum and a maximum value. For incident electrons, *all* of the energy may be transferred in a single collision, so that the distribution in range may show many particles with very small range; for protons the maximum is only about 1/460 times the initial energy, so that the differential range distribution should be sharp and nearly Gaussian. The standard deviation, σ_R, from the rectified mean range due to straggling was obtained experimentally by Mather and Segrè (Ma51) by measuring the Bragg ionization curve for 340-Mev protons in various materials; the mean range was obtained by assuming a Gaussian distribution of range about the mean, with a spread measured by σ_R, and by fitting this curve to the measured curve near the end of the range. They found that the center of the Gaussian fit the data best where the ionization was 0.82 times its maximum value. For elements from Be to Pb, $\sigma_{R(\text{exp})}$ varied from 0.91 to 1.90 g/cm^2, while the theoretical value $\sigma_{R(\text{theoret})}$ (see above) varied from 0.65 to 1.35. The difference was attributed to a small but significant energy spread in the initial beam which was then calculated to be 0.5 percent. These authors also found that the distribution was not truly Gaussian, but rather slightly skewed toward shorter ranges.

The same group had earlier measured $\sigma_{R(\text{exp})}$ in copper and again determined that agreement with theory was good if the beam spread was only about 0.5 percent. In the same year Bloembergen and Van Heerden (Bl51) determined the straggling parameter s, for protons from above 35 Mev to 115 Mev in lead, aluminum, and copper from integral range curves. The parameter here is defined as the difference between the mean and extrapolated range, where the extrapolated range is determined by the intercept with the R axis of the tangent drawn on the absorption curve at the $N_0/2$ point. Comparison with theory was made by calculating $\sigma_{R(\text{theoret})}$, including the effect of multiple scattering as well as the range straggling effect; σ_s, the contribution from scattering, is a function of the mean square deviation of the normal angle from the beam direction near the end of the range. The quantity $(\sigma_s^2+\sigma^2_{R(\text{theoret})})$ agreed well with $\sigma^2_{R(\text{exp})}$ with σ_s calculated from the formulas given by Livingston and Bethe (Li37). (It should be noted that S is related to σ_R by $S=(\pi/2)^{\frac{1}{2}}\sigma_R$ if a Gaussian is assumed.)

The value of the range straggling is generally small. Using the value for σ_R given above (Eq. 2) and substituting from the Bethe-Bloch formula, while neglecting the variation of the logarithmic factor, one finds

$$\frac{\sigma_R^2}{R_m^2}=\frac{4m}{M}\cdot\frac{1}{\log(2mv^2/I)} \tag{8}$$

for light stopping materials, and

$$\sigma_R^2/R_m^2=3m/4M \tag{8'}$$

for heavy materials, where m/M is the ratio of electron to incident particle mass. These relations have been verified for practical purposes (the straggling is of the order of 1 percent) by Madsen and Venkateswarlu (Ma48) at low energy. At high energy, Tobias (To51) using 190-Mev deuterons in aluminum finds a straggling effect of 0.017 or about twice the theoretical value given by Wilson (Wi47) in the expression,

$$\sigma_R/R_m=0.24(E/Mc^2)^{-0.1}(Mc^2)^{-\frac{1}{2}}, \tag{9}$$

which was derived by approximating the logarithmic factor above with a power function (Mc^2 = rest energy of proton in Mev).

The extrapolated range may be expressed in terms of the mean range and the straggling parameter by expanding $R(N)$ in a Taylor series (where unit flux is incident);

$$R(N)=R_m+(N-\tfrac{1}{2})\left(\frac{dR}{dN}\right)_{N=\frac{1}{2}};$$

if a Gaussian of spread σ_R is assumed, then

$$R(N)=R_m+\left(\frac{\pi}{2}\right)^{\frac{1}{2}}\sigma_R. \tag{10}$$

The slight amount of skewness found by Mather and Segre can, perhaps, be quantitatively explained by the calculation of Caldwell (Ca52) who obtained (using the work of Lewis (Le52)) values for the theoretical integral range distribution of fast (2–500 Mev) protons in aluminum to show how the distribution differs from Gaussian. The difference is small: for 200-Mev protons in aluminum, the lengthening of the mean range because of this is only 0.021 percent. Since, however, this calculation is better than the range straggling curves published in previous reviews, Caldwell's curve is reproduced here (Fig. 3).

The energy loss straggling theory has been worked out by Landau (La44) and improved by Blunck and Leisegang (Bl49); these authors give the distribution in energy loss for not too thick slabs of stopping material. A first approximation to the loss straggling is given by Bohr (Bo48) as the spread of a Gaussian distribution, with the resulting spread independent of particle velocity; this neglects the effect of collisions which, though infrequent, result in relatively large energy transfers and produce a tail on the loss curve favoring larger loss. This corresponds to the tail on the

CC-0. In Public Domain. Gurukul Kangri Collection, Haridwar

Digitized by Arya Samaj Foundation Chennai and eGangotri

range distribution mentioned above, with shorter range favored. The distribution given by Landau contains this effect, which, however, is small enough so that most conventional energy measuring equipment is not able to resolve the components contributing to the smear. Using a calibrated proportional counter with pulse-height discrimination, and 32-Mev protons, Igo, Clark, and Eisberg (Ig53) were able to show the "Landau" effect in fair agreement with their measurement. Experiments with electrons verify this distribution and the effect is much more striking (see Be53). At lower proton energy, the simple Bohr formula is a fair approximation for "not too thin" (but not thick enough to make a large energy loss) absorbing foil. This has been shown by Madsen and Venkateswarlu (Ma48b) working at energies under 2 Mev with beryllium and mica as foils and using the resonance radiation from aluminum and fluorine targets as energy indicators (see Sec. III).

While in principle the measurements of absolute stopping power with finite resolving power equipment should be corrected by a fold of the resolution curve in the Landau distribution or some other appropriate distribution, the corrections at high energy are shown to be small, and therefore the fold has not been made. At lower energies somewhat simpler techniques have been used; these will be discussed in the section on results of measurement in the low-energy region.

D. Other Related Phenomena

At the extreme low-energy end of the picture, the increasing dominance of collisions of the incident particle with entire atoms of the stopping region, large-angle Coulomb scattering, and charge exchange phenomena make experimental determinations of the range in even gaseous materials rather uninterpretable. While the range in centimeters can be extended at will by using the gas at variable pressure, the first two effects produce large energy loss and hence a large range straggling, with no resulting ionization, and reduce the precision enormously. Furthermore, loss by ionization is becoming less important since the effective charge of the moving particle (see below) is approaching zero as electrons are picked up.

1. Charge Exchange Phenomena

Although charge exchange phenomena are properly a separate subject for discussion from stopping or range relations—with which this article is largely concerned—in order that low-energy experimental data on stopping be understood, it is necessary that some attention be paid to the charge state of the incident beam. Furthermore, while very early work in this field has been published (see, for example, reference Ru33), much of the early results failed to give quantitative or reproducible values for the parameters involved in the theory. More recently, interest in this field has been stimulated by

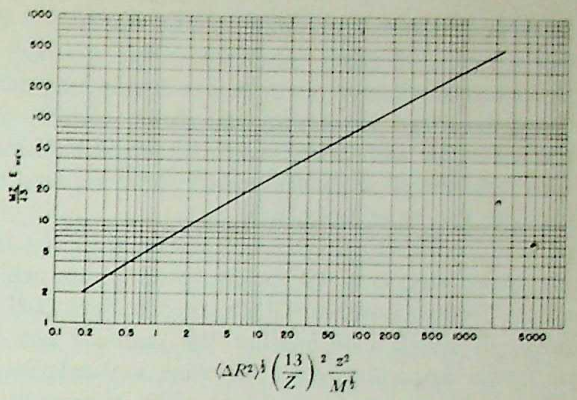


FIG. 3. Curve from reference Ca52 for the straggling about the mean range as a function of energy. Z is the atomic number of the stopping material, z of the incident particle; and M is the ratio of particle to proton mass.

studies of the ranges of fission fragments, in which case the charge exchange collisions and "hard" collisions play an important role. The practical desire of experimentalists to obtain multiply charged ion beams for accelerators has also stimulated recent work. Therefore a brief description of the existing theory of charge exchange will be given in this section and a fairly complete summary of recent measurements (performed largely by the Chicago group) will be given in Sec. III, on low-energy measurements.

A proton moving through material can capture an electron into a bound state; subsequent to this capture, the moving hydrogen atom can then lose its electron, the experimental picture then being one in which stopping power measurements are being made with a "particle" that is sometimes a singly charged proton and the remainder of the time a neutral system with a relatively widely separated proton-electron pair. If the cross sections for capture and loss were known, the relative fractions of time that the system is in either of these states could be calculated, and if the effective stopping power of the neutral system can be determined, then the measured energy loss of an incident low-energy proton can become interpretable. Thus, using a simple estimate for the stopping power for a neutral hydrogen atom§ and estimates of the cross sections for capture and loss given by Bohr (Bo48), Warshaw (Wa49b) argued that except where the capture cross section (σ_c) and the loss cross section (σ_l) become nearly equal—for proton velocity approaching v_0, about 25-kev energy—Eq. (3) could be used without introducing any essential modification from this source at least. Indeed, it has been argued by Isenberg (Is50) that bound states of hydrogen atoms in metals cannot exist, which would make the motivation

§ The effective charge for the neutral atom will be zero for distant collision, impact parameter≫Bohr radius. For the close collisions, the effective field of the electronic collision partner will be screened by the bound electron of the hydrogen atom. The choice (stopping for H^0) = 0.46 (stopping for H^+) corresponds to an effective electronic charge of about $0.7e$ (i.e., a "screening constant" of about 0.3). The estimate was made, however, by actually using, in the matrix element for the energy transfer, the potential of the (1*s*) hydrogen atom, rather than of a bare proton.

CC-0. In Public Domain. Gurukul Kangri Collection, Haridwar

Digitized by Arya Samaj Foundation Chennai and eGangotri

for such an analysis also nonexistent, except for the case of stopping in gases. The case of the stopping of highly charged, massive particles like fission fragments has been discussed by Knipp and Teller (Kn41) and most recently by Bell (Be53a) who obtained values for the effective charge of the fragments and compared the results with recent experiments.

Bohr has pointed out that for heavy stopping materials, those electrons will be captured whose orbital velocities are comparable with v, the incident particle velocity, in which case neither the classical nor the quantum-mechanical (Born approximation) calculation is accurate. However, to obtain an order of magnitude, Bohr applies Eq. (1) and using a statistical argument to select those electrons which, after a collision resulting in their removal, will be captured into any bound state, he estimates

$$\sigma_c = 4\pi a_0^2 z^5 Z^{\frac{1}{3}} (v_0/v)^6. \tag{11}$$

References to more accurate early calculations for capture cross sections have been listed by Hall (Ha50). Of these, that by Brinkman and Kramers (Br30) gives a variation like v^{-12} for capture from a $1S$ state into a $1S$ state for $v \gg v_0$. In an actual experiment, of course, capture need not be $1S \rightarrow 1S$, and the sum over the different possibilities (Mo49) modifies the exponent to a smaller value. However, as will be shown in Sec. III, the Brinkman-Kramers theory gives much too large values, a discrepancy which can be attributed to failure of the Born approximation in the experimental energy region (Ri52), but which, as has been pointed out by Bates and Dalgarno (Ba52) and Jackson and Schiff (Ja53), is more likely caused by an incorrect choice of interaction potential. The first authors do not include the contribution to the cross section for capture into excited states, and while their energy variation is nearly what is observed, their magnitude is about 1.5 times too small. Jackson and Schiff do, however, obtain quite good agreement with experiment.

The loss cross section can be estimated more directly, the problem being essentially that of the ionization energy loss, but now in a coordinate frame moving with the incident particle. Again using Eq. (1) and integrating over the range $I_b < T < \infty$, where $I_b = z^2 Ry$ is the binding energy of the electron, one gets

$$\sigma_l = 4\pi a_0^2 Z(Z+1) z^{-2} (v_0/v)^2, \tag{12}$$

where the term linear in Z can be shown (Bo48) to account for the nuclear interaction. This formula is to be viewed as good for light stopping materials. Bohr argues that for intermediate Z materials, where screening may play a dominant role, one gets, to an order of magnitude

$$\sigma_l = \pi a_0^2 Z^{\frac{1}{3}} z^{-1} (v_0/v). \tag{12'}$$

Thus it is expected that for protons the ratio $\sigma_l/\sigma_c \sim Z^{\frac{1}{3}} E^{5/2}$; i.e., nearly independent of Z and rapidly increasing for $E \gtrsim 25$ kev. This is actually rather close to what is observed.

2. Collisions with Nucleus

For the *nuclear* stopping contribution to energy loss, the classical theory (Bo48) may be applied. Since the transfer of energy to a single heavy nucleus can be a large fraction of the proton energy, a distribution in loss more nearly like the Landau type (La44) than Gaussian may result. No measurements seem to be available at present which could refer specifically to the nuclear stopping contribution; for particles as light as protons and alpha particles, nuclear stopping effects play a very subordinate role, becoming significant, however, for more massive particles like fission fragments (Bo48, Bø40).

3. Chemical Additivity; Effect of Phase of Stopping Substance

This discussion of related phenomena will conclude with a short discussion on the stopping properties of compounds. Much of the experimental work has been stimulated by studies of the effect of radiation on living systems, in which the energy absorption takes place in a medium containing several atomic species. It is then necessary to inquire whether the average absorption can be represented as a sum over the different atoms even when these are chemically bound to each other. If strict additivity were correct, the stopping power could be represented—adding energy increments along the path—by Eq. (3) with an effective ionization potential, defined by

$$\log I_{\text{eff}} = \frac{\sum a_k Z_k \log I_k}{\sum a_k Z_k},$$

where the compound has the formula $A_{a_1}{}^1 \cdots A_{a_k}{}^k \cdots A_{a_N}{}^N$. In at least one theoretical calculation for the stopping properties of compounds (Hi38) the use of the additivity property has been indicated. Several measurements at low energy and one measurement at high energy differ on the presence or absence of the additivity rule. The careful work by Thompson (Th52), using 340-Mev protons from the Berkeley cyclotron and a variety of organic compounds (containing C, H, O, N, and Cl) as targets to slow the protons to 200 Mev, shows that to at least 1 percent the relative stopping power is additive; however he found small (i.e., less than 1 percent with a stated experimental precision of better than 1 part per 1000) but measurable deviations from the additivity rule, these deviations depending, for example, on the molecular structure of the compound (see Table II-2). In Thompson's work relative stopping ratio $S = (R/A)_{\text{Cu}}/(R/A)$, where A is the atomic weight and R the range in grams per square centimeter. This is a molal stopping power relative to copper and he shows that, theoretically, for the compound $A_a B_b$, $S = aS_A + bS_B$, and is nearly independent of energy as long as the Bethe-Bloch equation is valid. The conventionally defined relative stopping power is the ratio of stopping cross sections (energy loss per atom per unit area) generally relative to air.

CC-0. In Public Domain. Gurukul Kangri Collection, Haridwar

Digitized by Arya Samaj Foundation Chennai and eGangotri

Another recent measurement of the stopping by compounds has been that of Wenzel and Whaling (We52, also Fr51) who obtained the stopping cross section in the low-energy range (20 to 500 kev) of D_2O ice to about 4 percent accuracy; this measurement disagreed with previous measurements (Cr42) taken on D_2O vapor but does agree with the Hirschfeld and Magee calculation for water. These authors conclude that additivity might be indicated except for the uncertainty in the knowledge of theoretical values; they point out that there is evidence that the stopping depends on the phase of the stopping material (that is the assumption of isolated noninteracting atoms is not valid). However, the theory shows that there should be little effect on the stopping due to molecular binding, hence (except for polarization phenomena which would cause denser media to be less effective, per unit mass, than the equivalent gases, but only slightly) there should be no difference between the phases. Several measurements with alpha particles in water, including the old experiments of Michl (Mi14) and Phillip (Ph23) and the more recent measurements of Appleyard (Ap51), show a difference between condensed and vapor phases of about 15 percent. These experiments have been criticized by de Carvalho and Yagoda (Ca53) who, using a photographic method, concluded that the difference between water and ice stopping properties is nonexistent, and that the measured relative stopping power for each agrees with an additivity theory. They give the measured integral molecular stopping power of H_2O as 1.56 ± 0.02 at 5.3-Mev alphas, and for RaC′ alpha particles, as compared with a computed 1.54. Other evidence favoring the additivity rule is given by Ellis, Rossi, and Failla, (El52) who measured and compared the stopping power of CH_2, in thin foil and gaseous form. They used Po alpha particles and, after passing these through acetylene gas to a windowless ionization chamber, interposed a foil of polystyrene and observed the changes of ionization. Within the experimental uncertainty of about 5 percent, the indication is that the stopping properties of solid and gaseous phases are equivalent. Furthermore, the measured stopping power agreed with theory.

TABLE II-2. Effective stopping power of bound elements.[a]

Element	Binding	Molal stopping rel. to Cu	S mass stopping rel. to Al[b]	I_{eff}[c] ev
H	Saturated	0.04797±0.0007	2.647	15.3
	Unsaturated	0.04879±0.0001	2.692	12.8
C	Saturated	0.24627±0.0002	1.141	67.6[d]
	Unsaturated	0.24674±0.001	1.143	66.5
	Highly chlorinated	0.2509 ±0.0008	1.162	57.5
N	NH_2, NO_3	0.2785 ±0.0025	1.106	88.5
	in ring	0.2870 ±0.002	1.140	68.1
O	$-O-$	0.3187 ±0.002	1.108	87.6
	$O=$	0.3226 ±0.001	1.122	78.6
Cl	All	0.6335 ±0.004	0.994	151.9

[a] From Thompson's thesis, UCRL-1910.
[b] Converted from molal stopping power, using Cu/Al value from Bakker and Segrè, Table IV-1
[c] Using $I_{Al}=151$ ev.
[d] Compare 58.5 ev given by (Pr52).

III. METHODS OF MEASUREMENT AND RESULTS IN THE ENERGY REGION 25–2000 KEV

This section is intended to be a summary of the results of experimental investigations on the stopping power of matter for particles of atomic mass and of kinetic energies in the range 25 to 2000 kev. Following some general remarks concerning range-energy relations in this energy region, part A will deal with the stopping powers of metals and solids, part B will summarize the stopping powers of gases, and part C will deal with experiments on charge exchange.

As already remarked, in the lower part of the energy interval with which this section is concerned, the range measurements begin to lose their usefulness as a method of measuring energy. The stopping powers of solids for the moving particles becomes so great that the preparation of foils through which they can pass, although possible, becomes a major effort in itself (see Sa52 and Gr52), and the use of a set of such delicate foils for range determinations is impracticable. Although the range in centimeters can be extended at will by using a gas at variable pressure as the stopping medium, the "range" in the lower-energy interval becomes noticeably dependent on the geometry. If no collimation of the rays is attempted, the straggling of the range is detrimental to precision. This straggling arises from the increasing dominance of collisions in which the momentum and energy are shared with an entire atom of the stopping medium, producing no ionization but resulting in large energy loss and large change in direction. The loss of energy by ionization of the stopping medium is fading out of the picture because the effective charge of the moving particle, due to electron capture, is approaching zero. Hence, if particles are accepted for range measurement which can have suffered significant deviations|| in direction, an appreciable fraction of their energy loss has occurred by a process in which the loss of energy in a single event is large related to the total energy. Thus, to a certain extent, we approach the behavior of high energy photons in passing through matter, where the entire energy of the photon may be lost in a single event, and one does not speak of a range, but merely of an exponential diminution with distance (St52).

Furthermore, in such uses, the "range" will depend on the method used for detecting the particles. They may retain their ability to eject secondary electrons from a sensitive surface after they have ceased to be able to ionize a gas, and hence their "secondary-electron-ejecting range" may be greater than their "gas-ionization range."

|| See Bo48, definition of θ_a, Pp. 20, 47.

CC-0. In Public Domain. Gurukul Kangri Collection, Haridwar

Digitized by Arya Samaj Foundation Chennai and eGangotri

A. The Stopping Power of Metals and Solids for Protons, Deuterons, and Helium Ions

Much of our present knowledge of the stopping power of metals and mica for protons and helium ions in the energy region 25 to 2000 kev arises from a series of experimental investigations carried out at the University of Chicago, in Copenhagen, and at The Ohio State University.¶ The stopping power of D_2O ice has been measured for protons and deuterons in a part of this energy range at the California Institute of Technology (We52).

1. Measurements by the Chicago Group

The investigations at Chicago published by Wilcox (Wi48), Hall and Warshaw (Ha49), Warshaw (Wa49a, b), and Kahn (Ka53), were all carried out in essentially the same manner, using, with small variations, the experimental equipment shown in Fig. 4.

Protons, deutrons, or He^+ ions were accelerated in a Cockcroft-Walton accelerator, for the lower-energy ranges, or, in the case of Kahn's work, in a 2-Mev van de Graaff generator. The desired ionic constituent of the accelerated beam was magnetically sorted and directed to a scattering target, or in some cases to a target giving disintegration particles for which stopping power measurements were to be made. The particles scattered at 90°, or those from the nuclear disintegration, were passed through a compartment in which a foil could be placed in their path at the will of the investigator. On leaving this compartment, the particles passed into a cylindrical electrostatic analyzer in which their energy was determined from the applied potential necessary to bend them 90° and focus them on a slit, behind which was some sort of particle detector.

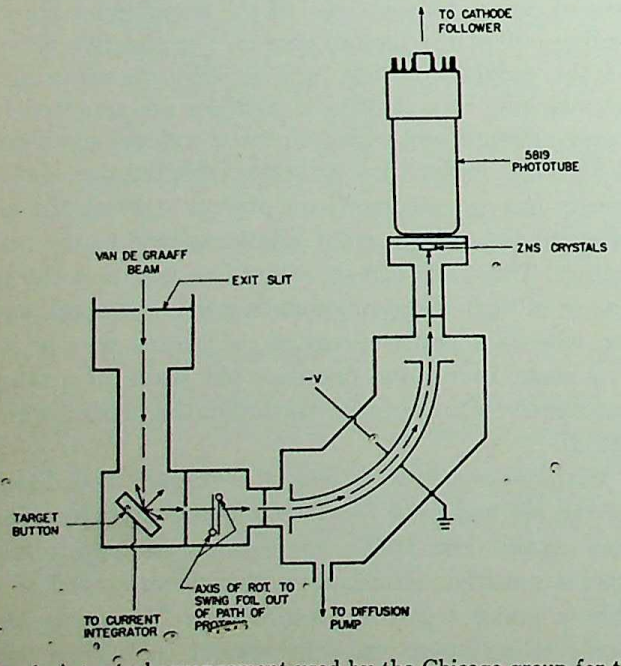


FIG. 4. A typical arrangement used by the Chicago group for the measurement of the stopping power of metal foils.

¶ Chilton, Cooper, and Harris (private communication).

The reason for the use of the scattered beam for passage through the foil rather than the direct beam from the accelerator is essentially a practical one. Although foils which can transmit the direct beam from the accelerator can be produced, they are very apt to be fractured, especially in the preparatory stages of an experiment, in which the beam is being focused, or the accelerator tube is in unsteady operation. There is no necessity to conserve intensity in such experiments, and the loss of it in scattering is unimportant. To avoid loss of homogeneity in energy in the beam on scattering, a very thin, 0.008 mg/cm², layer of gold evaporated on a solid beryllium backing was used. The intensity of scattering from the light beryllium is so low with respect to that from gold that it is negligible, and furthermore the Be-scattered protons only retain 80 percent of their energy (see Wi48, Fig. 2) and are not seen at all in the experiments in which beams are transmitted by foils which remove 10 percent or less of the incident energy.

The procedure for measuring the energy loss was quite simple. With the high-energy ion source in steady operation, the energy profile of the scattered beam was obtained by varying the potential on the electrostatic analyzer; see Fig. 5. The foil was then swung into the scattered beam, and the energy profile of the scattered particles which is transmitted was again obtained. In most cases, the foil was then swung out of the beam and the energy profile run again, to make sure that the kevatron or van de Graaff voltage had not drifted during the "foil in" measurement. The energy loss ΔE in the foil was measured between the ordinates of symmetry of the foil and no-foil curves. Strictly speaking, as Landau (La44) has calculated (see Sec. II), there should not be an ordinate of symmetry in the foil profile even if one exists in the no-foil profile. Kahn (unpublished) investigated his profiles using the results of Landau's work and estimated that the nonrandom error** introduced into his dE/dx values through lack of symmetry in the foil curves was negligibly small compared to errors from other sources, such as determination of foil thickness. By choice of appropriate foils, the energy losses were kept to approximately 10 percent of the original energy.

The major source of error in the Chicago stopping power measurements was the determination of foil thicknesses, which for metals were on the order of 0.1 mg/cm². The early work of Wilcox (Wi48) proved to be mainly valuable in showing, unfortunately in retrospect, that commercially rolled or beaten foils are not always reliable for measurements of the present type (see Ha49 and Wa49b). This point will be returned to later. A technique for the preparation of evaporated

** There is no error introduced at all if the results of measurement are taken to be the "most probable loss" rather than "average loss." The "most probable" will, of course, be slightly less than the "average."

CC-0. In Public Domain. Gurukul Kangri Collection, Haridwar

Digitized by Arya Samaj Foundation Chennai and eGangotri

metal foils has been described by Warshaw (Wa49a), as follows:

"Carefully cleaned glass slides were first coated with a weakly adherent plastic film by immersion in a 5 percent solution of pyroxylin in a 50 percent mixture of ether and alcohol; the slide was withdrawn in such a way that the excess liquid could drain off. The concentration of the pyroxylin was not found to be critical, but best results were obtained when the liquid flowed easily, and was still just concentrated enough to form a barely visible coat on the glass when dry. (Pyroxylin is sold as "Parlodion" by the Mallinckrodt Chemical Company.) The coated slide was then placed in a vacuum evaporator, on a wire rack at a convenient distance from the source, and, using standard evaporation techniques (St45), covered with metal. After evaporation, the edges of the film on the glass were roughed with a sharp knife, and the film cut across at about 2 cm intervals. The slide was then immersed at about a 45° angle to the surface of a dish of distilled water. The surface tension of the water was usually enough to peel the plastic film off the glass, carrying the foil with it, and leaving the foil and backing floating on the water surface. If the Parlodion solution was too dilute, the water generally failed to disengage even the edges of the foil; it was then necessary to soak the slide in an ether-alcohol mixture for a few minutes, and free the foil completely by working at the edges with a wire loop forceps. However, if the foil were freed under the surface of the liquid, it generally curled up, indicating that it was deposited in a highly strained state. This, of course, made mounting difficult. Small local strains also developed, very often, around dust particles and water bubbles in the plastic solution; therefore absolute alcohol was used and the solution prepared as dust free as possible and stored in a clean, glass-stoppered bottle.

For mounting the foils, it was convenient to use a small brass frame, about 1.5×2 cm, with a 2 mm wall. This was placed under the floating foil and raised carefully so that the surface tension would not cause any rupture. The last few wrinkles were removed with the aid of a soft brush dipped in alcohol and the foil then washed free of the plastic by dipping it, mounted on the frame, into the ether-alcohol, at right angles to the liquid surface."

Three methods have, at various times, been used by the Chicago group in measuring foil thicknesses.

(a) *Weighing.*—Kahn determined the mg/cm² of his foils by weighing a known area on a microbalance.†† Simultaneously with the deposition of the evaporated metal for the foil proper, a deposit was collected through an aperture of known area on a weighed platinum foil, a subsequent weighing of which indicated, by difference, the number of mg/cm² laid down. The glass microscope slide for the receipt of the foil itself, and the platinum foil were rotated over the source of evaporation many times during the deposition, to insure uniformity of deposit. The deposits were 2.856±0.006 cm² in area, and the error in determining the amount of evaporated metal by weighing ranged from ±1 percent for 200 micrograms of deposit to ±0.5 percent for deposits of the order of 1 milligram.

(b) *Interferometry.*—For this purpose,

"a mirror from a Michelson interferometer was placed in the evaporator bell jar at the same time as the coated slide, and in as nearly the same geometry as possible, but with half the mirror covered by a shield. The deposit of metal on half the mirror then corresponded to the amount deposited on the glass slide. Fringes were obtained with yellow (Na-D) light and the relative displacement of the two sets of fringes—one set from each half of the mirror—then gave the linear thickness of the foil in half wave-length units, after the displacement was first estimated using white light to determine the integral number of fringe displacements. It was found most convenient to make an enlarged photograph of the fringes, and determine the displacements from this with a traveling microscope. The probable error, obtained by measuring a large number of displacements separately, was about ±2 percent. The linear thickness was then converted to mg/cm² by using the usual bulk density of the metal."

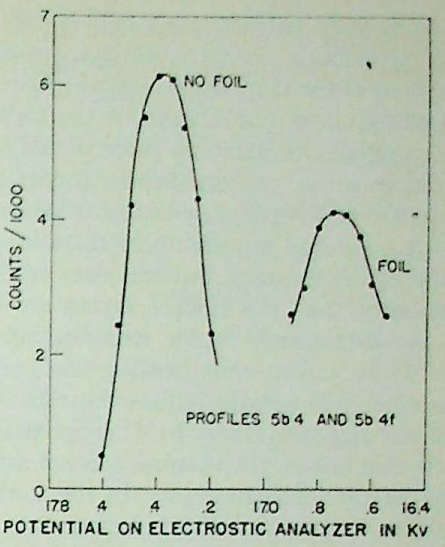


FIG. 5. Analysis of the incident (no foil) beam and the transmitted (foil) beam in the experiments of Kahn (Ka53). The energies of the protons focused on the detector (Fig. 4) are obtained by multiplying the abscissas by 45.23.

The use of the bulk density for the conversion of the interferometric thickness to mg/cm² may be questioned; there is some metallurgical evidence that for surface deposits considerably thinner than the present foils, a density 10 percent less than for bulk metal should be used.§§ For the foils used in this work which were several thousand atomic layers thick, there is less reason to expect a density uncertainty. To investigate this point, Warshaw estimated the amount of metal in his foils, whose thickness had been measured interferometrically, by quantitative chemical analysis, as follows.

(c) *Gravimetric chemical analysis.*—This could, of course, be used as a primary method of thickness determination, but Warshaw (Wa49a) used it to verify his use of bulk metal density in connection with the interferometric method for thickness. Foils which had been deposited on the glass slides for interferometric measurements were subdivided into accurately defined areas, which were then dissolved off in acid, and quantitatively analyzed by titrating the 8-hydroxy quiniline precipitate against standard bromate, according to well-known methods (Ko36). The accuracy of such a chemical determination was about ±1.5 percent; when used in connection with the interferometric thickness measurements, it indicated that the density of the evaporated foil was not more than 2 percent lower than the density of the bulk material.

The possibility that surface films may form over the

†† Type FDJ, manufactured by Wm. Ainsworth and Son, Inc., Denver, Colorado.

§§ L. Schultz, Institute for the Study of Metals, University of Chicago (private communication).

CC-0. In Public Domain. Gurukul Kangri Collection, Haridwar

Digitized by Arya Samaj Foundation Chennai and eGangotri

foils in the vacuum, increase the loss of energy, and thus introduce systematic errors, is always present. It will lead to values of the stopping power which are too high. Unfortunately, it is not always, or in fact, usually, possible to weigh the identical piece of foil which was introduced into the vacuum before and after the determination of ΔE. A run may be discarded as bad if the ΔE from a given foil appears to increase in magnitude with time in the vacuum, but this does not dispose of the possibility that the surface layers are laid down almost instantaneously upon introduction into the vacuum. It is known that heating the target before bombardment will greatly reduce the rate of accumulation of any deposit (Ha38, Br51, page 965), but heating of the thin foils in the vacuum was not attempted in the work of the Chicago group. In the work of Kahn (Ka53), the van de Graaff accelerator was evacuated with a mercury vapor diffusion pump, trapped with liquid nitrogen. The foil chamber and electrostatic analyzer were evacuated from a separated system with an organic oil (not a silicone) diffusion pump. A valve in the high-vacuum line between pump and foil was always closed except when the pump was trapped with liquid nitrogen. A series of measurements carried on for four days on the same foil showed no increase in ΔE, but the most that can really be said concerning the Chicago group experiments in this respect is that all precautions were taken to minimize the deposition outside of actually heating the foils.

2. *The Copenhagen Experiments*

The experiments in Copenhagen on the stopping power of solids for protons have been carried out by Madsen and Venkateswarlu (Ma48a, b), Huus and Madsen (Hu49), and Madsen (Ma53). The technique used by these investigators for the measurement of ΔE was quite different from that of the Chicago group. A van de Graaff generator was used as a proton source and a target material was selected which showed sharp resonances for gamma ray or neutron production. When a foil was interposed in the beam, it was necessary to increase the energy of the proton beam to excite the gamma rays or neutrons, and this energy increase gives the energy loss in the foil. Madsen found the following resonances to be useful for such measurements, one criterion being that the material show no other resonances in the immediate vicinity:

$F(p, \gamma)$	at 339 kev and at 660 kev;
$Al(p, \gamma)$	at 630, 986, and 1255 kev;
$Cl(p, \gamma)$	at 860 kev;
$Cl^{35}(p, n)$	at 1974 kev.

The neutrons or gamma rays were detected by standard counting techniques.

The foils were placed in a rotating holder which could either interpose them in the proton beam or leave it unhindered for the measurement of the initial energy.

Besides the foils, so-called "sandwich targets" were prepared and used. Madsen describes these in the following way:

> "On three or four discs of the supporting material (copper or or silver), a layer containing the energy indicator (fluorine, aluminum, or chlorine) was evaporated. One or two discs were removed from the evaporation chamber, while the stopping substance (Be, Al, Au, Ag, or Bi) was evaporated on the energy indicator layer. In this way, heating of the foil is avoided and a greater beam current can be applied. Moreover, a decrease in intensity of the radiation from the energy indicator, caused by scattering, is thus prevented."

Although the sandwich targets had certain advantages, a satisfactory absolute measurement of their thickness was not obtained, and the energy loss of such targets was always compared with that from a free foil of known thickness in order to obtain the target thickness. Having done this at a certain energy, the calibrated sandwich target could then be used for stopping power determinations at higher energy. For instance, with an aluminum indicating layer, the thickness of the sandwich foil could be found by comparison with a free foil at the 986-kev $Al(p, \gamma)$ resonance, and then the sandwich target used for measurements at the higher, 1255-kev resonance in aluminum.

In addition to measuring the stopping power of his foils, Madsen recorded the energy straggling of the beam caused by the randomness of the stopping process within the material. This resulted in an increase in the width of the resonance curve of the indicator when the foil was in the beam. Although the presence of energy straggling was obvious in the curves taken by the Chicago group, no record of it was kept.

3. *Experiments at Ohio State University*

Measurements of the stopping powers of metals and gases for protons in the low-energy range have been carried out at Ohio State University under the direction of J. N. Cooper (Ch53). The technique used was that of Madsen and Venkateswarlu (Ma48a, b) and the proton energies were in the region 450–1100 kev. Commercial foils of copper and nickel have been used, and the results indicate curves of dE/dx which run parallel to those of Kahn (Ka53), but are from 3 to 5 percent lower in dE/dx value for the same energy. Such a discrepancy is uncomfortably large, but not seriously outside the combination of internal consistency and systematic errors with which stopping power work is now being carried out. The use of commercial foils has been criticized by Warshaw (Wa49b), who found that the apparent stopping power for protons varied as much as 30 percent in foils of the same weight per unit area where a large area was taken for weighing purposes and the beam sent through a randomly selected small area in the larger one. Mention is made below of a technique used by the Ohio State group to investigate the consistency in thickness of their commercial foils. We may also note that the stopping power for protons measured by Wilcox from commercial gold leaf proved

CC-0. In Public Domain. Gurukul Kangri Collection, Haridwar

Digitized by Arya Samaj Foundation Chennai and eGangotri

to be approximately 15 percent low after evaporated gold foils had been prepared and used.

4. Correction for Foils of Finite Thickness

Since all foils used in dE/dx measurements are of finite thickness, there can, of course, be no sharp quantitative distinction between "thick" and "thin" foils. But it is of some use to make the rough distinction that a foil which, in a given experiment, absorbs more than 20 percent of the incident ion energy should be thought of as "thick," for that ion and energy. The prevailing practice is to measure the energy loss E_0-E_t, and to set the quotient $(E_0-E_t)/t=-(dE/dx)$, assigning the energy $\frac{1}{2}(E_0+E_t)\equiv E_{Av}$ as the energy to which the measurement of dE/dx pertains. If the variation of dE/dx with energy is rapid in the interval E_0-E_t, such a procedure is only approximate, and we will now inquire into the validity of the approximation. If an analytic expression is known or assumed for the variation of dE/dx with E, the correction can be calculated. The following rather general treatment of the problem is the suggestion of Harvey Casson.

Let it be known or assumed that

$$dE/dx=-1/f(E),$$

so that we have, on integrating from $x=0$ to $x=t$,

$$t=\int_{Et}^{E_0} f(E)dE.$$

The problem may now be stated: find an effective energy E_e (with $E_0>E_e>E_t$) such that

$$(E_0-E_t)/t\equiv\Delta E/t=-(dE/dx)_{Ee};$$

from this and the definition of $f(E)$,

$$f(E_e)=\frac{1}{\Delta E}\int_{E_t}^{E_0} f(E)dE.$$

Now let $E=E_0(1-\epsilon)$ and expand $f(E)$ near E_0, for small ϵ, in the form

$$f(E)=\sum_{n=1}^{\infty} A_n\epsilon^n.$$

If we substitute this expansion in both the right and left sides of the above integral, we get, on integrating,

$$\sum A_n\epsilon^n=\sum\frac{A_n}{n+1}\epsilon^n.$$

This can be put into the form of a series expansion of ϵ_e as a function of ΔE by successive differentiation with respect to ΔE and observing that $\epsilon_e=0$ for $\Delta E=0$. If one equates coefficients to a Taylor expansion of

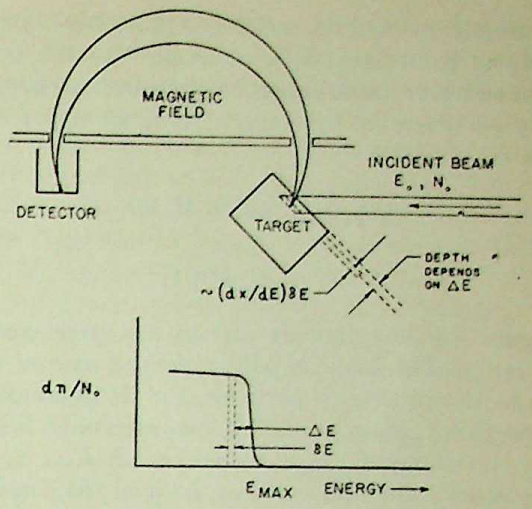


FIG. 6. Schematized spectrometer and spectrum for determination of dE/dx from scattering.

$\epsilon_e(\Delta E)$, one then gets

$$\epsilon_e=\tfrac{1}{2}\frac{\Delta E}{E_0}\left(1+\frac{A_2}{6A_1}\left(\frac{\Delta E}{E_0}\right)+\cdots\right)$$

or, to second-order terms,

$$E_e=E_{Av}\left(1-\frac{A_2}{12A_1}\frac{\Delta E^2}{E_0E_{Av}}\right).$$

If we take $dE/dx=-(A/E)\log bE$, expansion of f and substitution of coefficients gives

$$E_e=E_{Av}\left(1-\frac{1}{24}\frac{(B+2)}{B(1-B)}\frac{\Delta E^2}{E_0E_{Av}}\right)\cdots, \qquad (13)$$

where

$$B=\log bE.$$

If, however $dE/dx\sim E^{-\frac{1}{2}}$ (as in Bohr's estimate for low-energy stopping in heavy elements),

$$E_e=E_{Av}\left(1+\frac{1}{48}\frac{\Delta E^2}{E_{Av}E_0}\right). \qquad (13')$$

In any case, the correction is clearly small.

5. Stopping Power Determined by Intensity of Scattering and by Displacement of the Scattering Edge

Wenzel and Whaling (We52) have used a technique for measuring the stopping power of solids which does not involve the preparation of a foil. The particles whose stopping power is to be measured are scattered from a thick target, and some of the scattered particles are accepted into a momentum (magnetic) or energy (electrostatic) analyzer. The counting rate for the scattered particles passing through the analyzer depends directly on the stopping power of the target material for the beam particles. Figure 6 illustrates the

CC-0. In Public Domain. Gurukul Kangri Collection, Haridwar

Digitized by Arya Samaj Foundation Chennai and eGangotri

essential features of the method. The scattered particles emerging from the target at angle θ to the primary beam will have a continuous energy spectrum because of stopping losses in the target, with an upper energy limit E_{max}, where

$$E_{max}=E_0\phi(m, M, \theta), \quad \text{and} \quad \phi(m, M, \theta)\lesssim 1, \tag{14}$$

because of momentum transfer to the target nuclei on scattering. The analyzer will transmit a narrow energy spread δE of scattered particles, and let us assume that the analyzer field is set so that the interval δE is located near an energy $E_{max}-\Delta E$, where $\Delta E/E_{max}$ is small, that is, near the upper energy limit of the continuum. More precisely, δE is the spread in energy accepted, from a point in the target, by the analyzer at a single field setting. This δE, multiplied by $(dE/dx)^{-1}$ and by a suitable geometric factor depending on the inclinations of the incident and scattered ray to the normal to the target face, will determine the thickness of a layer (in general, buried beneath the target surface) in which the measured scattering originated.

In order to obtain reliable dE/dx values, cases must be chosen in which the scattering cross section is known, and this usually means that beam particle and target must be chosen such that one can be sure that pure Rutherford scattering, uncomplicated by nuclear force fields, is taking place. The differential scattering cross section is then (Da14)

$$\frac{d\sigma}{d\omega}=\left(\frac{zZe^2}{mv^2}\right)^2 \operatorname{cosec}^3\theta \frac{[\cot\theta\pm(\operatorname{cosec}^2\theta-(m/M)^2)^{\frac{1}{2}}]^2}{(\operatorname{cosec}^2\theta-(m/M)^2)^{\frac{1}{2}}}. \tag{15}$$

- $d\sigma$ is the differential cross section per target nucleus for scattering into differential solid angle $d\omega$ at scattering angle θ in the laboratory system.
- m; M are the masses of the projectile and target nuclei, respectively.
- z; Z are the atomic numbers of beam and target nuclei.
- v is the speed of the projectile nucleus in the laboratory system.
- θ is the scattering angle in the laboratory.

Both experiment and detailed calculation show that the continuous energy spectrum is quite flat near its upper energy limit at E_{max}, and if the analyzer is set so that $\Delta E/E_{max}\sim 1$ percent, the counting rate is independent of ΔE.

The solid angle of acceptance of the analyzer Ω, in steradians, can be calculated from the geometry of the instrument, or may be found experimentally by quantitative scattering experiments in which the pertinent dE/dx values are known from foil measurements.

It is not advisable to give a general formula for dE/dx from this method, where magnetic or electrostatic analysis, in different target geometries, may be used. A simple case is an electrostatic analysis with an instrument aperture of such a shape that all the scattered particles which are accepted leave essentially at the same angle to the target face normal. (Such is not the case, for instance, in the spherical analyzer of Allison and Casson (Al53).) Also, for simplicity, we consider a target geometry such that incident and scattered rays make the same angle with the normal to the target face. Then we have

$$\delta n/N_0=N_T(dE/dx)^{-1}\cdot(d\sigma/d\omega)\cdot\delta E\cdot\Omega, \tag{16}$$

where

- $\delta n/N_0$ is the fraction of the incident beam particles detected per second as focused, scattered particles;
- N_T is the number of target nuclei per cm^3;
- δE is the energy interval, in electron-kilovolts, accepted by the analyzer from a point in the target, at a given field setting. δE is calculable from the orbit characteristics and object aperture dimensions of the instrument;
- dE/dx is the stopping power in kilovolts per cm of the target material for beam particles of energy $(E_{max}-\Delta E)$;
- $d\sigma/d\omega$ is the differential scattering cross section, Eq. (15);
- Ω is the solid angle or acceptance of the analyzer in steradians.

Variants of this equation, suitable to their own instruments, have been given by various experimenters (We52, Sn50, Br51).

Wenzel and Whaling (We52) have also used a method for dE/dx in solids which depends on the displacement of the scattering edge at E_{max} (Fig. 6) in case a layer of material of Z different from that of the thick target forms on its surface. This effect is often seen in scattering experiments in which a layer of carbon is forming over the target surface because of imperfect vacuum conditions. In their experiments D_2O ice was formed on the face of a copper target cooled with liquid nitrogen. The Z's in the D_2O are so low that the Coulomb scattering is small compared to that of the copper substrate, but also, and of more importance, there is the fact that the relatively large momentum and energy transfers to the D and O nuclei throw the energies of the particles scattered from them well below E_{max} for the substrate. Thus, after energy or momentum analysis, the copper scattering edge is free of contamination from D or O scattering, as from the bare target. If one can be sure that layers of frozen material are formed which retain their same thickness during the time necessary for several experimental runs, the shifts of the copper scattering edge to lower energies are directly interpretable as relative values of dE/dx for the surface layer at different beam energies.

CC-0. In Public Domain. Gurukul Kangri Collection, Haridwar

Digitized by Arya Samaj Foundation Chennai and eGangotri

6. Discussion and Tables

With the exception of the results on beryllium and mica, all the Copenhagen data are based on dE/dx values obtained from commercial (rolled or beaten) metal foils. We will first discuss the data on beryllium and mica foils, which were specially prepared in the laboratory for the measurements.

Data Obtained from Foils Prepared in the Laboratory

Beryllium.—The data of Madsen, *et al.* shown in Table III-1 were taken on weighed, evaporated foils. Hence, the technique of foil preparation was similar to that of the Chicago group. Furthermore, there is in general good agreement between Kahn and Madsen where their data overlap. In the region 500 to 1150 kev the largest discrepancy is at 1133 kev where Madsen's value of 203 lies 5 percent above Kahn's curve of dE/dx in kev×cm²/mg *vs* energy. At 455 kev Madsen reports a dE/dx value of 377 kev×cm²/mg from a Be foil in which the loss of energy was 230 kev or 40.3 percent of the incident proton energy. At 436 kev, Kahn's value for dE/dx is 347 in these units. Madsen's results show that the energy straggling for this determination, compared to the energy, was very much larger than for his other determinations on beryllium, and we have not attached sufficient reliability to it to modify the Kahn-Warshaw curve in its vicinity.

Unfortunately, in the case of beryllium, the absolute error in Kahn's data may be the greatest of all his experiments because of his difficulties in obtaining a piece of foil large enough for a reliable weight determination. Kahn states that the error in absolute value may possibly be 15 percent. In the region above 1150 kev, near 1276 kev, the dE/dx value of Madsen is 11 percent greater than that of Kahn, and this has caused us to raise the stopping power values in this region close to the results reported by Madsen. The combined data of Madsen, Kahn, and Warshaw has been used to construct the beryllium curve of Fig. 7 and the beryllium data in Table III-7.

Mica.—Mica, of course, is a substance of possibly variable composition; the variety used by Kahn is properly known as muscovite. Foil thicknesses were measured gravimetrically in both researches, but Madsen investigated his foils for homogeneity using an interferometric method due to Tolansky (To45, To47). The stopping power values obtained by Madsen in the region 400–1100 kev lie slightly above a smooth curve through Kahn's points, the largest discrepancy being 6.7 percent for the values of 1072 kev. Madsen's point at 1279 kev lies exactly coincident with Kahn's value of 143 kev×cm²/mg at 1245 kev, and we interpolate to Madsen's point at 2000 kev with considerable confidence. Values from Kahn and Madsen appear in Fig. 8 and in Table III-7.

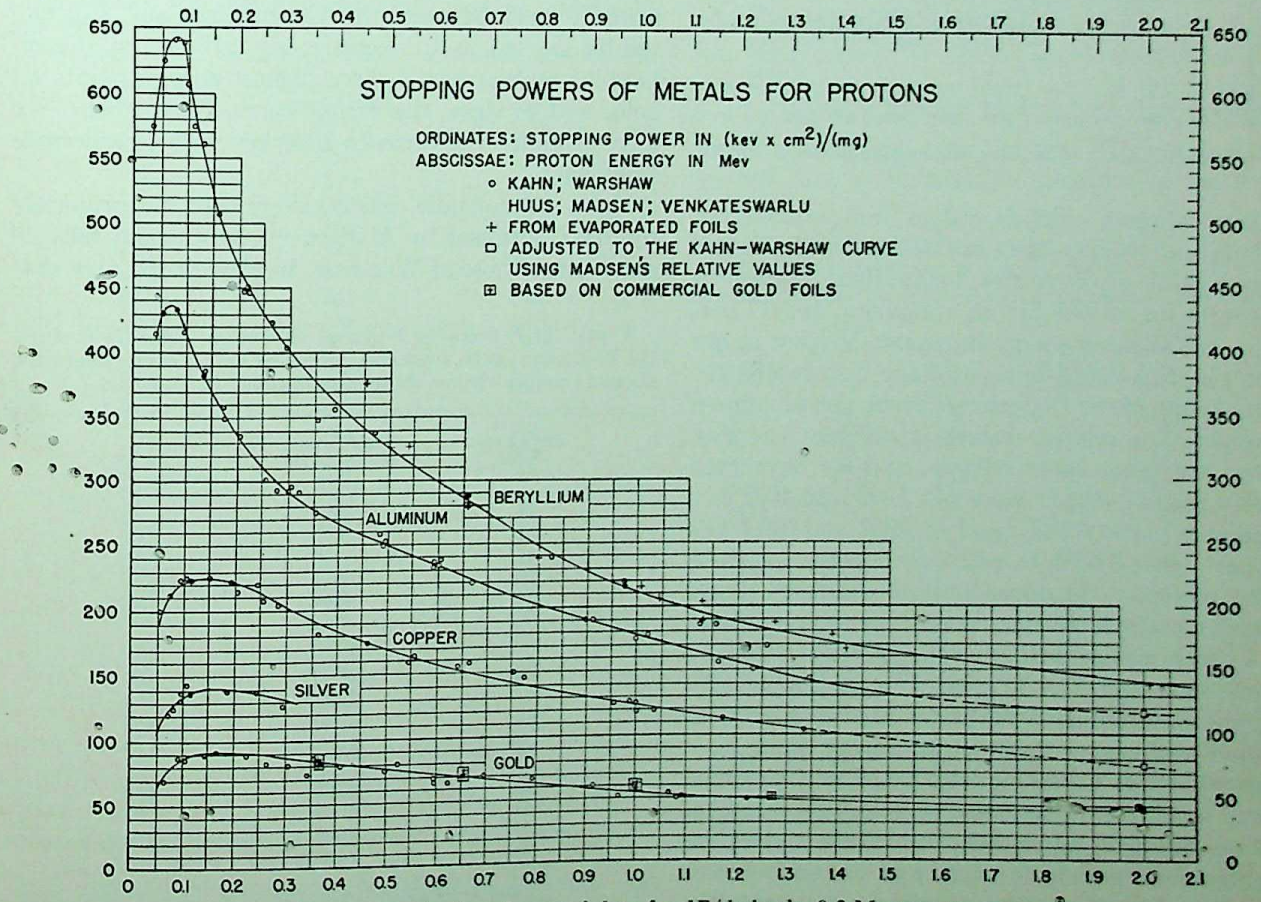


Fig. 7. Combined equipmental data for dE/dx in the 0-2-Mev proton range.

CC-0. In Public Domain. Gurukul Kangri Collection, Haridwar

Digitized by Arya Samaj Foundation Chennai and eGangotri

Data Obtained from Commercial Foils

The Copenhagen data on Al, Cu, Ag, and Au all depend, in their absolute value, on stopping powers measured in commercial foils. In some cases Madsen used "sandwich" foils in which a layer of the stopping substance was evaporated over a layer of detecting material on a solid mounting. However, the thickness of these "sandwich" foils was always determined by comparing the energy loss (or sometimes the straggling) with that produced by a weighed commercial foil.

The Chicago group has had trouble with commercial foils in the past. Warshaw (Wa49b), who investigated the reliability of commercial aluminum foils for dE/dx measurements, reports as follows:

". . . four rolled and two evaporated foils were used to determine the stopping power in aluminum. The surface densities of the commercial foils were determined by accurately weighing known areas (about 50 cm²). The resulting curves from the commercial foils deviated as much as 30 percent from the average curve. On the other hand, data from both of the evaporated foils fell on the same curve (within the standard deviation of all points), and furthermore, within 8 percent of the average of the curves obtained from the commercial foils."

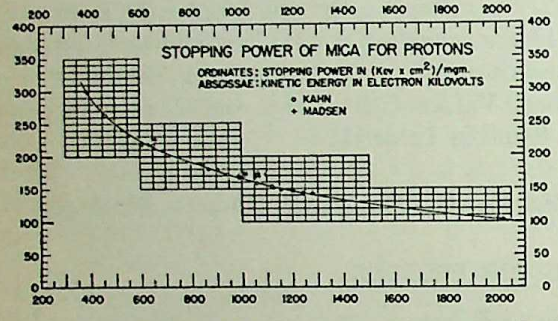


FIG. 8. Data of Kahn and Madsen on stopping power of mica.

In fact, Madsen's dE/dx values from commercial aluminum and copper foils fall seriously off Kahn's curves, typical discrepancies being that Madsen is 11.4 percent low at 689 kev in aluminum, and 17 percent low at the same energy in copper. In view of our experiences with rolled foils, we have disregarded the absolute values of the Copenhagen results on aluminum and copper. The relative values at different energies, however, are much more reliable, and we have used Madsen's relative dE/dx values at 1993 and 1022 kev in aluminum (ratio 0.643), and at 2002 and 1012 kev in copper (ratio 0.623) to establish a point for these stopping powers at the upper limit of our energy range. By taking the absolute values at the lower voltages from Kahn's curve, we find a dE/dx value of 112 at 1993 kev for aluminum, and 75.4 at 2002 kev for copper. We have used these adjusted results of Madsen's work to continue Kahn's curve to the upper energy limit.

Madsen's dE/dx values for gold, based on commercial foils, and in some cases adjusted to gold from measurements on bismuth, agree well with Kahn's data on evaporated foils, which, in turn, join on smoothly to Warshaw's gold values. The agreement may possibly be fortuitous, because in the Chicago laboratory the stopping power for protons obtained by Wilcox (Wi48) in a commercial gold foil was 14 percent lower than Warshaw and Kahn's evaporated foil values, and Wilcox was led to incorrect (Ha49) conclusions regarding deuteron *vs* proton stopping powers using different commercial foils of gold. The extended region of agreement in gold between the Copenhagen and Chicago results has led us to decrease our estimate of the reliability of Warshaw's three highest energy points on gold, and to draw the dE/dx curve above them. We have extended the curve to 2000 kev with considerable confidence.

Kahn did not take data on silver, and unfortunately the data obtained by Madsen on commercial foils do not overlap those of Warshaw. In view of the fact that

TABLE III-1. Stopping power of beryllium metal for protons. (C. B. Madsen, *et al.* from evaporated foil.)

Energy loss in foil (kev)	Mean proton energy in foil (kev)	dE/dx kev×cm²/mg
230	455	377
73	540	329
62	661	279
64	662	288
69	665	282
53	798	239
48	1010	216
48	1010	216
53	1013	216
126	1049	207
42	1133	189
45	1135	203
42	1276	188
108	1310	177
39.5	1392	178
101	1422	166
85	2016	139

TABLE III-2. Stopping power of aluminum metal for protons. (C. B. Madsen, *et al.*, from commercial Al foil.) (These values run about 11 percent below those recommended in Table III-7.)

Energy loss in foil (kev)	Mean proton energy in foil (kev)	dE/dx kev×cm²/mg
58	368	252
95	387	250
42	681	182
70	695	185
38.5	1005	167
59.5	1016	157
72	1020	150
82	1025	164
31	1270	135
53	1281	139
23	1986	100
37	1993	98
37	1993	100[a]
39	1994	105[a]

[a] "Sandwich" target calibrated from commercial foil.

CC-0. In Public Domain. Gurukul Kangri Collection, Haridwar

Digitized by Arya Samaj Foundation Chennai and eGangotri

TABLE III-3. Stopping power of copper metal for protons. (C. B. Madsen, *et al.*, from commercial copper foil.) (These data run 14–20 percent below those recommended in Table III-7.)

Energy loss in foil (kev)	Mean proton energy in foil (kev)	dE/dx kev ×cm²/mg
73	376	149
90	384	155
60	690	122
70	695	121
53.5	1012	109
53.0	1012	106
56.5	1014	98
46	1278	94
51	1281	88
35	1991	72
46	1997	79
41.4	1994	70
54	2001	64[a]
56	2002	67[a]

[a] "Sandwich" target, Cl indicator, calibrated at 860 kev.

Madsen's values of dE/dx from commercial foils of Al and Cu do not lie on the Kahn-Warshaw curves for those elements, we have not used his silver values to extend Warshaw's silver points to higher energies, but have tabulated them separately.

Tables III-1 to III-5 contain the experimental results

TABLE III-4. Stopping power of silver metal for protons. (C. B. Madsen, *et al.*, based on commercial silver foil.) (This is the only available experimental data on Ag above 350 kev.)

Energy loss in foil (kev)	Mean proton energy in foil (kev)	dE/dx kev ×cm²/mg
69	369	137[a]
60	370	143
60	370	143
51	365	142
84	381	142
209	445	138
22.8	641	101[b]
22.6	641	96[b]
32.5	646	114[b]
36	678	100
44	683	100
64	692	108
47.5	880	93[d]
33	1003	91
34.7	1004	82
38.5	1005	80
40	1006	82
53	1012	90
130	1051	86
15.9	1263	71[b]
15.9	1263	71[b]
29.6	1270	68[b]
29	1989	59
47.5	1998	59[c]
90	2019	60

[a] "Sandwich" target, fluorine indicator, calibrated at 660 kev.
[b] "Sandwich" target, aluminum indicator, calibrated at 986 kev.
[c] "Sandwich" target, chlorine indicator, calibrated at 860 kev.
[d] "Sandwich" target, chlorine indicator, calibrated at 1974 kev.

TABLE III-5. Stopping power of gold metal for protons. (C. B. Madsen, *et al.*, from commercial gold foils.)

Energy loss in foil (kev)	Mean proton energy in foil (kev)	dE/dx kev ×cm²/mg
38.5	359	85
42	360	81
44	366	82[a]
41.9	651	71[b]
42.9	652	72[b]
49.4	655	76[b]
27	999	60
30	1000	58
31	1001	61
49.5	1009	59
29.6	1270	50[b]
29	1988	43[c]
28.7	1988	43[c]
34	1991	41

[a] Bi "sandwich" target; fluorine indicator, calibrated at 660 kev.
[b] Bi "sandwich" target; aluminum indicator, calibrated at 986 kev.
[c] Bi "sandwich" target, chlorine indicator, calibrated at 860 kev.

on dE/dx at present available to us from the Copenhagen group.

At Ohio State University (Ch53) measurements of stopping powers of metal foils for protons have been carried out using the shift-in-resonance technique of Madsen. The foils used were those commercially available from the Chromium Corporation of America, and varied in surface density from 0.67 to 2 mg/cm². The thickness variation from point to point on the thin foils was tested by allowing alpha particles from polonium to traverse a small area of the foil and observing the variation in range as the point of transmission was varied over the foil. The conclusion was reached that if the average thickness of the foils, as

TABLE III-6. Data of Chilton, Cooper, and Harris (see reference Ch53) on the stopping power of nickel and of copper for protons.

Proton energy (kev)	Nickel kev ×cm² / mg	Prob. error %	Proton energy (kev)	Copper kev ×cm² / mg	Prob. error %
527	172.3	1.5	446	171.1	
704	148.7	2.0	532	160.0	
718	150.1	3.0	603	152.0	1.5
739	142.8	2.0	713	141.6	1.5
741	141.7	2.0	755	138.7	2.0
755	145.6	1.5	812	133.2	1.5
757	146.5	1.5	949	121.5	2.0
915	128.4	3.0	996	116.0	1.5
935	125.8	2.0	1006	113.3	2.0
941	133.7	2.0	1050	114.5	2.0
949	128.5	2.0			
951	128.5	2.0			
977	129.1	3.0			
1000	127.5	2.0			
1007	122.0	2.0			
1046	120.6	2.5			
1047	122.1	2.5			
1057	120.9	2.0			

CC-0. In Public Domain. Gurukul Kangri Collection, Haridwar

Digitized by Arya Samaj Foundation Chennai and eGangotri

determined by weighing known areas, was used, the variation in thickness would not account for more than a 1 percent error in dE/dx.

The results of the investigations on Ni and Cu are given in Table III-6. The measured dE/dx values lie from 4 to 5 percent below those on the Kahn-Warshaw curve (in the case of copper) as shown in Fig. 7 and Table III-7.

7. *Stopping Power of Solid D_2O for Protons and Deuterons*

Stimulated by the interest in the cross sections of the (d, d) and (t, d) reactions, Wenzel and Whaling (We52) have measured the stopping power of D_2O ice for protons and deuterons by the methods previously described. The results, stated in terms of the molecular stopping power in electronvolts per molecule per cm² are believed to contain a probable error of 4 percent, and are given in Table III-8.

It was found by experiment, as indicated by theory, that the stopping powers for protons and deuterons of the same speed are equal. Thus, the table may be used for the stopping power of D_2O ice for deuterons, by assuming that the value given for each proton energy applies to deuterons of twice that energy.

TABLE III-7. The proton energy loss as a function of energy.

Proton energy (kev)	dE/dx (kev×cm²/mg) Be	Mica (Muscovite)	Al	Cu	Au
25	546				
50	617		422	185	61
75	640		439	212	77
100	615		416	221	87
150	521		366	225	90
200	468		334	222	91
250	433		314	212	90
300	405		293	202	86
350	381	312	279	190	84
400	360	286	268	183	81
450	342	266	258	175	79
500	325	250	250	169	76
550	311	236	241	162	74
600	298	224	233	156	72
650	284	214	224	151	70
700	272	204	217	146	68
750	266	196	210	141	66
800	251	189	202	138	64
850	241	182	196	133	62
900	232	176	190	129	60
950	223	171	183	127	58
1000	215	165	177	124	56
1050	206	160	171	120	54
1100	198	154	165	117	52
1150	192	150	159	113	51
1200	188	146	154	110	49
1250	182	143	148	108	48
1300	178	139	143	105	47
1350	175	136	139	102	46
1400	171	133	135	100	45
1500	164	127	127	96	44
1600	158	122	123	91	42
1700	152	117	120	88	42
1800	148	112	117	83	42
1900	144	108	115	79	42
2000	139	102	112	75	42

TABLE III-7A. Conversion factors for expressing stopping powers of metals in various units.

Given units	Units desired: kev×cm²/mg	ev×cm²/atom	erg/cm	kev/cm
kev×cm²/mg	Au 1	327×10^{-18}	309×10^{-7}	193×10^{2}
	Ag 1	179	168	105
	Cu 1	106	143	89.3
	Al 1	44.8	43.2	27.0
	Be 1	15.0	29.6	18.5
ev×cm²/atom	3.06×10^{15}	Au 1	9.46×10^{10}	5.91×10^{19}
	5.59	Ag 1	9.39	5.86
	9.43	Cu 1	13.57	8.47
	22.2	Al 1	9.66	6.03
	66.7	Be 1	19.87	12.35
erg/cm	3.24×10^{1}	1.057×10^{-11}	Au 1	6.243×10^{3}
	5.95	1.065	Ag 1	6.243
	6.99	0.737	Cu 1	6.243
	23.2	1.035	Al 1	6.243
	33.8	0.503	Be 1	6.243
kev/cm	5.18×10^{-5}	1.692×10^{-18}	1.602×10^{-9}	Au 1
	9.524	1.706	1.602	Ag 1
	11.20	1.181	1.602	Cu 1
	37.0	1.658	1.602	Al 1
	54.0	0.809	1.602	Be 1

8. *Recommended Low-Energy Stopping Power Values for Protons in Metals and Mica; Formulas for Interpolation and Extrapolation*

Figures 7 and 8 and the numerical values in Table III-7 present a set of dE/dx values for protons in metals and mica, obtained by averaging weighted values from the experiments of Warshaw (Wa49b), Kahn (Ka53), and the values communicated to us from Copenhagen by Madsen. The data of Chilton, Cooper, and Harris (Ch53), given in Table III-6, were received at too late a date to be included in the averaging process. In copper, where there are serious discrepancies between the results of Kahn and Madsen, the data of Chilton, *et al.* lie slightly below, but close to, Kahn's results. It seems reasonable to suppose that the recommended values in the figure and the table are correct to within 5 percent.

Light elements.—For the light elements, the fastest moving electron may still have lower speed than that of the moving ion for relatively low energy (see Sec. II), and therefore it is expected that the Bethe-Bloch equation for stopping power, with values of I empirically fit, can be used at these low energies. Further, the constancy of these values of I can be used as a test of the validity, and therefore usefulness, of the theory.

Beryllium.—Table III-9 shows considerable variations in the value of I for Be in the region 1000–2000 kev, when I is calculated from experimental values. However, the fact that I is in the argument of the

CC-0. In Public Domain. Gurukul Kangri Collection, Haridwar

Digitized by Arya Samaj Foundation Chennai and eGangotri

TABLE III-8. Molecular stopping power of D_2O ice for protons.[a]

Proton energy (kev)	Stopping power in ev×cm²/molecule
18	15.6×10^{-15}
20	17.4
30	20.4
40	22.6
50	23.5
60	24.0
70	24.1
80	24.0
100	23.7
125	23.0
200	20.1
300	16.0
400	13.3
500	11.6
540	11.2

[a] See reference We52.

logarithm makes it quite sensitive to fluctuations in the experimental value of dE/dx. Madsen and Venkateswarlu (Ma48a) found that $I=64$ ev gave the best fit to their data between 500- and 1500-kev proton energy. A value of $I=57$ ev will fit the curve of Fig. 7 to within 3 percent in the range 1600–2000 kev and can be recommended for cautious interpolation and extrapolation in and beyond this region. Using this value for I, we obtain the following formula for protons in beryllium, with E in kev,

$$\frac{dE}{dx}(\text{kev}\times\text{cm}^2/\text{mg}) = -\frac{6.385\times10^4}{E}\log_e(3.818\times10^{-2}E) + \frac{1.597\times10^4}{E}C_K, \quad E>1600 \text{ kev}, \quad (17)$$

with C_K values from TableII–1. The K-correction term affects dE/dx by 4 percent at 2000 kev, and its effect decreases above this proton energy.

Aron (Ar51) has computed stopping powers for protons in beryllium from 1 Mev to 10^4 Mev using $I=59$ ev [and, of course, for the higher energies, the relativistic Eq. (3)]. The value of I used by Aron was consistent with that found in the experimental work of Mather and Segrè (Ma51) on the range-energy relation for protons in beryllium at 340 Mev, and we see that the value of I appears to be essentially the same at 1600 kev and 340 Mev. Aron's calculated numerical values of dE/dx for a given I are slightly different (2.3 percent higher at 2 Mev) than those calculated in this report (see note in Sec. II).

As previously mentioned in this report, the experimental errors in the stopping experiments on beryllium are unfortunately large, and better data might reveal a more constant value of I than is exhibited in Table III-9.

Aluminum.—If one uses a value of $I=162$ ev for aluminum, the nonrelativistic Bethe equation for dE/dx for protons in the metal becomes (E in kev)

$$\frac{dE}{dx}(\text{kev}\times\text{cm}^2/\text{mg}) = -\frac{6.944\times10^4}{E}\log_e(1.344\times10^{-2}E) + \frac{5.34\times10^3}{E}C_K. \quad (18)$$

This expression, with values of C_K from Table II-1 will fit the numerical values of the data at 1400 and 2000 kev within 5 percent. Bloembergen and van Heerden (Bl51) found $I=159$ for 70-Mev protons in aluminum, and Mather and Segrè (Ma51) found $I=148$ at 340 Mev. The value indicated above as fitting the data around 2000 kev is nearer to the value found for 70-Mev protons (see Sec. IV).

Heavier elements.—In the case of the heavier elements, nickel, copper, silver, and gold, the simple stopping power equation cannot be used in the energy region of this section, and thus a theoretical guide for interpolation and extrapolation is not available.

It may be noted that there is a large discrepancy between the dE/dx values of Pb for 1- and 2-Mev protons as calculated by Aron (Ar51) and as inferred from measurements on the nearby element, gold. Assuming that the stopping power in ev×cm²/atom varies as $Z^{\frac{1}{2}}$, and using the observed values 56 and 42 in kev ×cm²/mg for gold at 1000 and 2000 kev, one finds the stopping power in these units for Pb should be 54 and 40 in kev×cm²/mg at 1 and 2 Mev, respectively. Aron's calculated values are 71 and 51.

9. *Stopping Power of Gold for Helium Ions*

There is need for more work by experimental physicists on the stopping power of metals and solids for helium ions. At high energies, above 2 Mev, where the moving particle is always He^{++}, the atomic stopping powers should be calculable from Eq. (3), with the I appropriate to protons. There is, however, no theory at present capable of including the lower-energy region where the forms He^0, He^+ also appear in the moving beam.

TABLE III-9. I from experimental data: beryllium.

Proton energy (kev)	dE/dx (observed)	$I_{calc.}$ (ev)
1000	215	64
1200	185	70
1400	166	71
2000	140	50

CC-0. In Public Domain. Gurukul Kangri Collection, Haridwar

Digitized by Arya Samaj Foundation Chennai and eGangotri

The only direct measurements of stopping power for helium ions in solids in our energy region are those of Wilcox (Wi48), and these unfortunately are vitiated in that the commercial gold foils he used evidently led to errors in related experiments (Wa49b, Ha49). Fortunately, however, Wilcox published values of the loss of energy of protons in these same gold foils, and through the recent reliable data for the stopping of protons in gold we are able to deduce what the effective thickness of his gold foils was. In this way the data of Fig. 9 were computed; Wilcox's original dE/dx values have been increased about 14 percent. Because of the uncertainty of the correction and the evidence of some internal errors of measurement from the spread of his points at higher energies where the disintegration alpha particles from $Be^9(p, \alpha)Li^6$ were used, there may well be 15 percent error in the results summarized in the figure.

B. The Stopping Powers of Gases for Various Ions

The first direct measurement of the stopping powers of gases for ions of energies within the range (20–2000 kev) of this report seems to have been made by Crenshaw (Cr42). The beam of protons or deuterons, of kinetic energies in the range 60–340 kev, was passed through a differentially pumped gas absorption cell, and the effect of introduction of the gas in lowering the energy of the transmitted beam was determined by magnetic analysis of the emergent particles. This early work has been repeated and extended by several investigators with greater accuracy than in the original, and Crenshaw's data will not be included here.

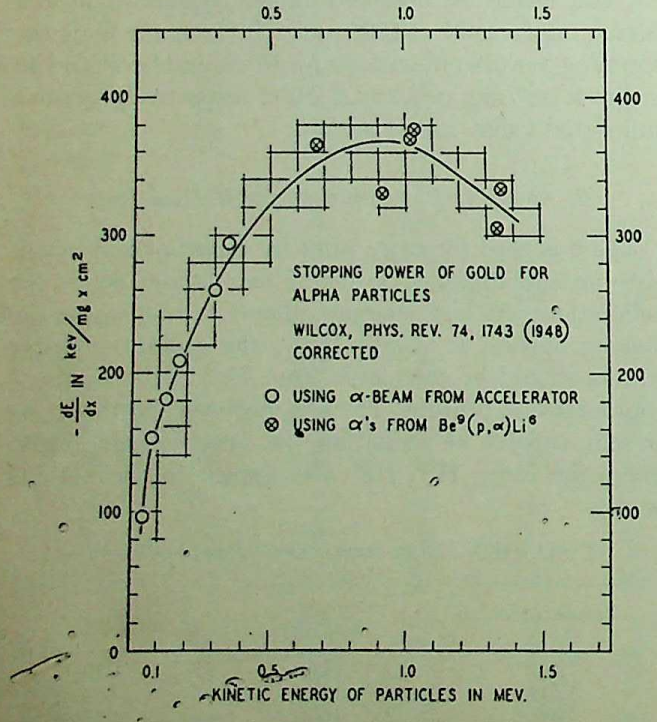


FIG. 9. The stopping power of gold for Alpha particles; corrected (see text, Sec. IIIA-1) from reference Wi48.

As discussed above, the range, as a quantitative measure of energy, loses much of its significance in the energy region under consideration. Evans, Stier, and Barnett (Ev53) have shown that if ions of He^+, N^+, Ne^+, and A^+ in the energy region 20 to 250 kev are admitted to various stopping gases, the range which is measured is a function of the geometry, and, if an ionization chamber of too small an aperture is used, the result in gm/cm² may appear to have a pressure dependence. We shall therefore emphasize in this report what can be learned about dE/dx itself, although, as we shall show, the present measurements give only the energy loss resulting from electronic impacts, whereas the losses due to atomic impacts in which large exchanges of energy and momentum occur, become increasingly important as the mass of the moving particles increases.

1. Methods

(a) *Methods used by the Chicago group.*—Figure 10 indicates schematically the technique used by Weyl (We53). The gases H_2, D_2, He, N_2, and Ne were at

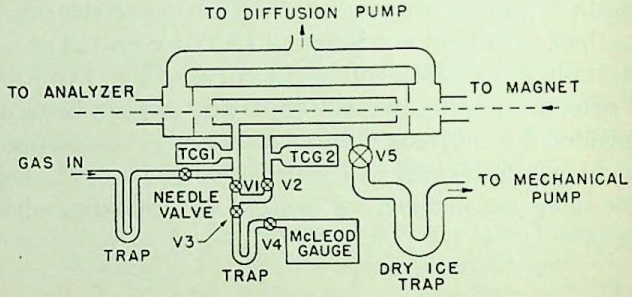


FIG. 10. Schematic of the gas absorption cell and associated equipment used by Weyl (see reference We53) for measurement of dE/dx in gases.

separate times fed into the low voltage arc of the Cockcroft-Walton accelerator, or "kevatron," for short. The accelerated ion beams were magnetically analyzed and the singly charged components H^+, H_2^+, D^+, He^+, N^+, or Ne^+ were directed toward a gas absorption cell which the beam then traversed. After passing through the gas cell, which could either be evacuated or filled with the gas whose stopping power was to be measured, the energy of the emergent beam was measured by electrostatic deflection in a 90° cylindrical analyzer (Al38).

The gas absorption cell consisted of a thin-walled cylinder 2.54 cm in internal diameter and 76.53 cm long, with holes in its ends 0.038 cm in diameter so that the ion beam could enter, traverse it longitudinally, and leave. The cell was enclosed in a larger tube 5.40 cm in outside diameter, and compartments at both ends of the cell were designed so that the pressure could be reduced in stages from approximately 0.5 mm in the cell to less than 10^{-5} mm Hg in the kevatron itself, and in the electrostatic analyzer. Thus, the only matter traversed by the ion beam from the low voltage arc

CC-0. In Public Domain. Gurukul Kangri Collection, Haridwar

Digitized by Arya Samaj Foundation Chennai and eGangotri

to the ZnS scintillator at the object focus of the cylindrical electrostatic analyzer was the gas whose stopping power was being determined. The pressure of the gas in the cell was measured by a sensitive McLeod gauge.

Weyl adopted a simple procedure which made the energy analysis of the beam after traversal of the gas cell independent of slight fluctuations in beam intensity. The 0.038-cm diameter entrance aperture to the absorption cell was so small that fluctuations of intensity within the focal spot of the beam affected the current through the cell. The outer plate of the cylindrical electrostatic analyzer, which would normally be grounded, was connected to a 60-cycle ac supply. The phase of this biasing ac could be shifted, and the impressed wave had an amplitude of 250-volts rms symmetrically above and below ground potential. Thus the ion beam leaving the analyzer was kept in 60-cycle oscillatory motion across the exit slit in front of the ZnS scintillator.

The output of the photomultiplier (see Fig. 4), which was activated by the light from the ZnS, was connected

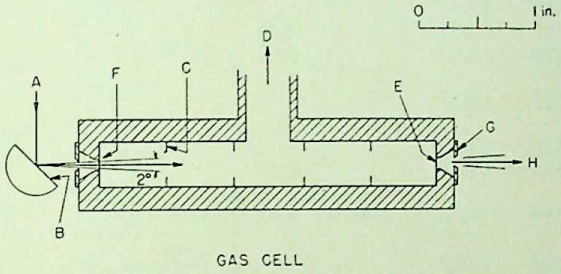


FIG. 11. Gas cell for dE/dx measurements as used by investigators at the California Institute of Technology (see reference Du52). *A*. Monoenergetic proton beam. *B*. Target (gold plated on copper). *C*. Baffles to prevent scattering from the walls. *D*. To manometer and gas handling equipment. *E*, *F*. Aluminum foil windows. *G*. Limiting aperture, 0.131-cm diameter.

to the vertical deflection plates of a cathode ray oscilloscope, and the horizontal sweep of the scope was driven by the biasing ac. By shifting the phase of the ac with respect to the phase of the 60-cycle ac on which the kevatron was operated, an oscilloscope trace with a single extremum could be produced. (More complicated curves resulted if the sweep was in arbitrary phase relationship with the ripple in the kevatron high voltage.) Fluctuations in beam intensity moved this extremum vertically, but only its horizontal location was needed to measure the beam energy by electrostatic deflection. The energy loss in the gas was determined by first adjusting the phase of the detector voltage so that a single peak appeared on the oscilloscope screen at a given (marked) abscissa, with no gas in the cell; the analyzer voltage for this condition then gave the initial energy. As gas was admitted to the cell, the peak moved horizontally and the shift in analyzer voltage required to bring the peak back to its original condition was taken as the energy loss. By using the analyzer constant (19.77 kev/kv) and correcting the

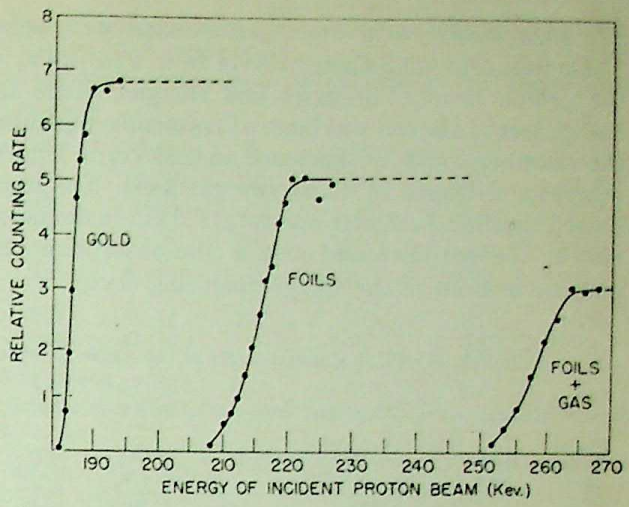


FIG. 12. Gas stopping power measurement by the California Institute of Technology group. "Gold": energy analysis of scattered protons from a gold target, see Fig. 11. "Foils": same spectrum degraded in energy by passage through foil windows. "Foils plus gas": additional energy loss when gas is introduced to the chamber.

McLeod gauge reading to 0°C, the stopping power was calculated.

(b) *Methods used at California Institute of Technology.*—Recently a group of investigators (Du52) at Pasadena have made measurements on the stopping power of a large number of gases for protons. The energy region covered was 30–600 kev. The gases were contained in an absorption tube 7.3 cm long, the entrance and exit ports being closed with aluminum foils each 4.5×10^{-2} mg/cm² in thickness (Fig. 11). The protons which were measured were scattered from a gold layer backed by copper, and the shift of the high-energy edge (Fig. 12) produced by admitting gas to the cell, through which the scattered beam passed, indicated the stopping power. A correction must be made because the gas has lowered the energy of the protons striking the second aluminum foil, and hence its stopping power has been changed (see Table III-7). The energy of the scattered beam which emerged from the absorption cell was determined in a magnetic momentum analyzer.

(c) *Method used at Los Alamos.*—Phillips (Ph53) has measured the stopping power of various gases for protons in the energy range 10–80 kev. The gases were contained in an absorption cell (see Fig. 13) by the use of

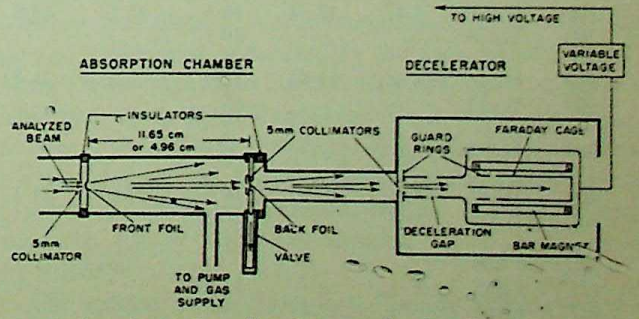


FIG. 13. Gas absorption cell and proton deceleration chamber used by J. A. Phillips (see reference Ph53).

CC-0. In Public Domain. Gurukul Kangri Collection, Haridwar

Digitized by Arya Samaj Foundation Chennai and eGangotri

SiO foils (Sa52) over the entrance and exit holes. These foils caused an energy loss of from 5 to 10 kev in the proton beam. For gases and energies where the energy loss in the cell was large at reasonable pressures, the chamber could be shortened to 4.86 cm in length; otherwise a length of 11.65 cm was used. The beam passed through 3 circular apertures 0.5 cm in diameter, two at the entrance and exit of the absorption cell, and one in front of the energy analyzing device.

The foil at the exit port of the absorption cell was mounted on a sliding valve so that it could be completely retracted from the line of motion of the beam, allowing a measurement of the loss in energy in the entrance foil alone. An investigation was made of the bowing out of the foils when gas was admitted to the cell, and it was found that the effect added 0.26 ± 0.03 cm to the length of the cell as defined by the planes of the window-supporting frames.

TABLE III-10. Stopping powers of the noble gases for protons in the energy range 20–1000 kev. Atomic stopping powers in $(\text{ev}\times\text{cm}^2/\text{atom})\times10^{15}$.

Proton energy (kev)	Reference	He	Ne	A	Kr	Xe
20	Ph53	4.83	···	23.3	26.0	···
30	Ph53	5.77	···	27.2	30.0	···
40	Ph53	6.51	···	30.0	33.4	···
40	Du52	6.67	10.6	31.4	35.6	50.0
40	We53	···	···	32	···	···
50	Ph53	7.07	···	31.4	35.5	···
50	Du52	6.97	11.9	33.4	38.3	52.6
50	We53	···	···	33	···	···
60	Ph53	7.26	···	31.6	36.6	···
60	Du52	7.22	12.8	34.3	39.8	53.5
60	We53	···	···	33	···	···
70	Ph53	7.33	···	30.7	36.9	···
70	Du52	7.33	13.45	34.4	40.5	53.5
70	We53	···	···	33	···	···
80	Ph53	7.41	···	29.2	37.2	···
80	Du52	7.37	13.95	34.1	40.5	53.2
80	We53	···	···	33	···	···
90	Du52	7.37	14.3	33.5	40.3	52.0
90	We53	···	···	32	···	···
100	Du52	7.30	14.6	32.6	39.8	50.6
100	We53	···	···	31.5	···	···
150	Du52	6.37	14.6	28.2	35.0	45.2
150	We53	···	···	29	···	···
190	We53	5.4	···	···	···	···
200	Du52	5.55	14.10	24.5	30.7	41.8
200	We53	···	···	25.5	···	···
250	Du52	4.91	13.20	21.6	27.4	38.6
250	We53	···	···	22	···	···
290	We53	4.4	···	···	···	···
300	Du52	4.41	12.34	19.5	25.1	35.8
300	We53	···	···	19.7	···	···
350	Du52	4.01	11.50	17.9	23.3	33.4
350	We53	···	···	18	···	···
360	We53	3.7	···	···	···	···
400	Du52	3.69	10.75	16.6	22.0	31.4
400	We53	···	···	16.5	···	···
420	Ch53	···	···	···	22.65	···
421	Ch53	···	···	14.87	···	···
422	Ch53	···	10.37	···	···	···
424	Ch53	···	9.70	···	···	···
437	Ch53	···	···	···	···	26.3
441	Ch53	···	···	···	···	26.4
450	Du52	3.42	10.15	15.55	20.9	29.8
476	Ch53	···	···	14.81	···	···
500	Du52	3.18	9.58	14.7	19.9	28.6
516	Ch53	···	···	···	20.75	···
517	Ch53	···	9.38	···	···	···
519	Ch53	···	8.91	14.28	···	···
527	Ch53	···	···	···	21.30	···
536	Ch53	···	···	···	···	24.1
538	Cu53	···	···	···	···	25.1
550	Du52	2.99	9.09	13.9	19.1	27.4
567	Ch53	···	···	13.71	···	···
600	Du52	2.81	8.65	13.3	18.4	26.4
662	Ch53	···	···	11.67	···	···
665	Ch53	···	···	···	18.07	···
668	Ch53	···	7.88	···	···	···
675	Ch53	···	···	···	17.95	···
679	Ch53	···	···	···	20.72	···
679	Ch53	···	···	···	19.85	···
713	Ch53	···	···	12.39	···	···
730	Ch53	···	7.27	···	···	···
733	Ch53	···	7.26	···	17.21	···
743	Ch53	···	···	···	16.98	···
748	Ch53	···	···	···	···	18.95
750	Ch53	···	···	···	···	20.22
778	Ch53	···	···	11.66	···	···
929	Ch53	···	6.22	10.19	14.81	···
930	Ch53	···	6.38	···	···	···
932	Ch53	···	···	10.24	···	···
941	Ch53	···	···	···	14.77	···
943	Ch53	···	···	···	···	16.99
969	Ch53	···	···	···	···	16.80
971	Ch53	···	···	10.20	···	···
988	Ch53	···	5.86	···	···	···
989	Ch53	···	···	9.82	14.22	···
992	Ch53	···	6.30	···	···	···

CC-0. In Public Domain. Gurukul Kangri Collection, Haridwar

Digitized by Arya Samaj Foundation Chennai and eGangotri

TABLE III-11. Stopping powers of the gases hydrogen, oxygen, nitrogen, and air for protons in the energy range 30–1000 kev. [Stopping powers in (ev×cm²/atom)×10¹⁵.]

Proton energy (kev)	Reference	H_2	N_2	Air	O_2
20	Ph53	5.11	13.0	...	11.17
30	Ph53	5.58	14.5	...	13.0
30	Du52	5.84	16.1	15.5	...
30	We53	...	...	15.5	...
40	Ph53	6.14	15.4	...	13.9
40	Du52	6.25	17.1	16.48	15.2
40	We53	...	...	16.5	...
50	Ph53	6.51	16.2	...	14.7
50	Du52	6.43	17.8	17.16	16.4
50	We53	...	...	17.5	
60	Ph53	6.51	16.7	...	15.1
60	Du52	6.45	18.2	17.7	16.9
60	We53	...	...	17.5	...
70	Ph53	6.32	...	...	15.3
70	Du52	6.36	18.5	17.9	17.15
70	We53	...	...	16.8	...
80	Ph53	5.58	...	...	15.2
80	Du52	6.23	18.5	17.9	17.15
80	We53	...	...	17.2	...
90	Du52	6.04	18.25	17.72	17.25
90	We53	...	...	17.6	...
100	Du52	5.83	17.9	17.5	17.17
100	We53	...	...	17.3	...
150	Du52	4.70	16.1	15.98	16.13
150	We53	...	...	15.5	...
200	Du52	3.90	14.2	14.2	14.70
200	We53	...	...	13.5	...
245	We53	3.05	...	...	...
250	Du53	3.33	12.5	12.74	13.26
250	We53	...	...	12.3	...
300	Du52	2.91	11.2	11.56	11.99
300	We53	...	...	11.2	...
350	Du52	2.60	10.13	10.60	11.01
350	We53	...	...	10.3	...
400	Du52	2.35	9.34	9.79	10.23
400	We53	...	...	9.6	...
406	Ch53	...	9.30	...	...
406	Ch53	...	9.32	...	...
450	Du52	2.14	8.62	9.05	9.45
450	We53	...	...	8.9	...
452	Ch53	...	8.62	...	...
500	Du52	1.97	8.08	8.39	8.84
501	Ch53	...	8.42	...	...
502	Ch53	...	8.16	...	...
541	Ch53	...	7.62	...	...
550	Du52	1.82	7.61	7.9	8.38
600	Du52	1.70	7.21	7.51	7.91
648	Ch53	...	6.47	...	...
648	Ch53	...	6.87	...	...
716	Ch53	...	6.40	...	...
717	Ch53	...	6.15	...	...
748	Ch53	...	5.98	...	...
914	Ch53	...	5.09	...	...
942	Ch53	...	5.05	...	...
973	Ch53	...	4.80	...	...
974	Ch53	...	5.30	...	...
1001	Ch53	...	4.85	...	...

The energy analyzing device was a beam decelerator which had been previously developed for other work. The device measured the deceleration voltage which was required just to bring the charged ions of the beam to rest, a procedure which was possible because of the low voltages used in the experiment.

(d) *Measurements at the Ohio State University.*—Measurements of the stopping power of gaseous nitrogen, Ne, A, Kr, and Xe have been made at Ohio State University (Ch53) with protons from their van de Graaff generator. The energies lie in the interval 400 to 1000 kev. Details have not yet been published concerning the gas absorption cell used. The energy loss measurement was by the displaced resonance technique which they used in their foil measurements, and which was also used by Madsen (Sec. III-A).

2. *Results and Discussion of the Measurements on the Stopping Powers of Gases for Protons*

The results of various recent investigations of the stopping powers of gases for protons of energies 20–1000 kev are given in Tables III-10 to III-13. The Chicago group (We53) and the group at Pasadena (Du52) have each measured the stopping powers of argon and air for 30–450 kev protons, and there is remarkably good agreement between their results, which were taken in quite different geometries and with different energy analysis technique.

In general the results from the Ohio State group (Ch53) agree well with the Pasadena group where they overlap, but there is some discrepancy in the stopping power of xenon as measured in the two investigations. Near 450 kev the Ohio State values are some 10 percent less than those from Pasadena. Since most impurities in xenon would lower the stopping power of the mixture, in the absence of other information it would seem prudent to give the greater weight to the results showing higher stopping power, i.e., those from Pasadena.

The measurements from Los Alamos (Ph53) show a more systematic divergence from those of other investigations. In the case of the stopping power of argon

CC-0. In Public Domain. Gurukul Kangri Collection, Haridwar

Digitized by Arya Samaj Foundation Chennai and eGangotri

TABLE III-12. Stopping powers of various inorganic gases for protons in the energy range 20–600 kev. Molecular stopping powers in (ev×cm²/molecule)×10¹⁵.

Proton energy (kev)	Reference	NH_3	H_2O	NO	CO_2	N_2O	CCl_4
20	Ph53	···	21.4	···	30.9	···	104.2
30	Du52	29.7	···	···	···	···	···
30	Ph53	···	23.6	···	37.2	···	114.6
40	Du52	32.0	25.0	32.6	44.2	47.0	···
40	Ph53	···	26.1	···	41.1	···	128.4
50	Du52	33.6	26.1	34.5	46.8	48.6	···
50	Ph53	···	27.2	···	43.9	···	132.1
60	Du52	34.6	26.9	35.7	48.4	49.9	···
60	Ph53	···	27.7	···	45.0	···	134.0
80	Du52	34.4	27.6	36.6	50.2	50.9	···
80	Ph53	···	···	···	45.4	···	134
90	Du52	33.9	27.5	36.6	50.5	51.0	···
100	Du52	33.5	27.3	36.4	50.5	50.7	···
150	Du52	30.1	24.7	33.2	47.1	47.0	···
200	Du52	25.6	22.0	29.7	42.5	42.0	···
250	Du52	22.3	19.7	26.7	38.1	37.6	···
300	Du52	19.9	17.9	24.1	34.6	34.0	···
350	Du52	17.9	16.2	22.0	31.6	31.0	···
400	Du52	16.4	15.0	20.3	29.2	28.6	···
450	Du52	15.1	13.9	18.9	27.0	26.6	···
500	Du52	14.0	13.0	17.6	25.2	25.0	···
550	Du52	13.1	12.2	16.6	23.7	23.5	···
600	Du52	12.3	···	15.7	22.4	22.2	···

TABLE III-13. Stopping powers of certain organic gases for protons in the energy range 30–600 kev. Molecular stopping powers in (ev×cm²/molecule)×10¹⁵ (see reference Du52).

Proton energy (kev)	CH_4	C_2H_2	C_2H_4	C_6H_6
30	37.4	43.4	···	116.0
40	39.7	47.4	54.4	126.0
50	40.9	49.5	57.4	133.0
60	41.3	49.8	58.7	135.7
70	41.2	49.2	58.8	135.5
80	40.8	48.0	58.0	134.4
90	40.0	46.7	56.7	133.5
100	38.9	45.0	55.5	131.7
150	33.6	38.5	48.8	116.5
200	28.6	32.9	41.4	102.0
250	24.8	29.0	36.1	89.2
300	22.0	25.9	32.0	79.8
350	19.8	23.5	28.8	72.2
400	18.1	21.4	26.2	66.3
450	16.65	19.7	24.1	61.4
500	15.5	18.4	22.4	57.3
550	14.5	17.2	20.9	53.9
600	13.6	16.2	19.6	51.0

for protons, the Los Alamos results are always lower than the Chicago-Pasadena average, by amounts varying from 5 to 15 percent. The Los Alamos values for nitrogen and oxygen are also lower than the California values, by approximately the same percentage. Correspondence and discussion between the investigators involved has up to the present given no clear reason for the discrepancy. The close agreement on argon and air between the Chicago and Pasadena groups would seem, at present, to give superior weight to their results. The Los Alamos results on protons in helium and hydrogen gases are much closer to those resulting from the work of other investigators.

The question may be raised as to whether the energy losses measured in these experiments include those arising from all possible events in the gas. In the next sub-section of this report an argument will be presented indicating that these experiments, because of their good geometry, measure only those losses which are incurred in interactions with practically free electrons, and exclude those events in which a large momentum is transferred to an atom of the gas.

3. Stopping Powers of Gases for Particles Heavier than Protons

A Cockcroft-Walton accelerator or a van de Graaff generator will accelerate any positive ion which can be produced at its high-voltage electrode, and, using a low-voltage capillary arc, beams of He^+, N^+, Ne^+ ions are readily obtained. If, as in Weyl's apparatus (Fig. 11), there are no foils in the path of the beam, these ions can be passed through a gas in a differentially pumped chamber and the resultant degradations in energy studied. Thus, Weyl (We53) has obtained results on the loss of energy of ions heavier than protons which have passed through a gas without having undergone any large angle deflections. These results are shown in Table III-14.

In the experiments with these heavier ions, a phenomenon becomes outstanding which is already observable to a considerable extent with hydrogen beams, namely, the great diminution in intensity of the transmitted beam when gas is admitted to the absorption cell. This of course means that with the ions of higher Z the occurrence of nuclear scattering, with its large angular deviations and higher energy losses, is becoming more and more prevalent. The recent work at Oak Ridge (Ev53) shows clearly the marked spreading of the beam when such heavy ions are stopped in a gas.

Weyl's gas absorption tube was 74 cm long, 2.22 cm in internal diameter, and the entrance and exit apertures were circular, and 0.038 cm in diameter. Under these circumstances an event in the gas which deviated the ion as much as 5×10^{-4} radians from its direction of motion would remove it from the beam. Bohr's formula (Bo41) for the contribution to dE/dx from the screened nuclear, or "hard," collisions is

$$\left.\frac{dE}{dx}\right|_{\text{"hard"}} = \frac{4\pi e^4 z^2 Z^2}{Mv^2} \log\left(\frac{1}{\mu v^2}\frac{a^{\text{scr}}}{zZe^2}\right) \frac{\text{erg}\times\text{cm}^2}{\text{atom}}, \quad (19)$$

CC-0. In Public Domain. Gurukul Kangri Collection, Haridwar

Digitized by Arya Samaj Foundation Chennai and eGangotri

where z, Z are the atomic numbers of the moving particle and the stopping nucleus, respectively; M is now the atomic mass of the nucleus, and μ is the reduced mass of nucleus and particle; v is the velocity of the particle in cm/sec; and a^{scr} is the distance between particle and nucleus when the electronic screening has set a limit to the action of the nuclear charges. a^{scr} may be calculated with sufficient accuracy from the formula

$$a^{scr}=a_0(z^{-1}+Z^{-1}),$$

in which a_0 is the Bohr radius. The formula for losses by ionization of the medium has been given as Eq. (3). Although the square of the nuclear charge of the moving ion apparently appears in the numerator in the expression for both types of interaction, it is actually the ionic charge that is effective in ionization of the medium, and the nuclear charge that is effective in nuclear scattering. The latter is not energy-dependent, but in the electronic collisions we are dealing with a function of the ion energy which tends to zero at the lower velocities where the moving ion has been neutralized by the capture and retention of electrons from the stopping medium. Thus, for heavy moving ions of relatively high kinetic energy but low velocity, the loss of energy by "hard" collisions assumes much importance, although we must remember that even a neutral moving atom has a possibility of ionizing the medium, as pointed out above (Sec. II-D-1).

At kinetic energies of a few hundred kilovolts the moving ions of He, N, and Ne are to a considerable extent singly ionized; their effective Z for ionization of the medium lies between 0 and 2. Thus, we cannot neglect the contribution of "hard" scattering to the total energy loss in an experiment in poor geometry.

This means that if monoenergetic neon ions were liberated isotropically from a point in an atmosphere of argon gas, and note made of the average energy of the neon ions which passed in any direction through a spherical surface in the gas centered on the source, the stopping power of the argon gas would appear considerably greater than that observed in Weyl's experiments. Many of the neon ions would have suffered large angle deviations with high energy transfers to argon atoms within the spherical volume.

Calculation of the stopping power for hard collisions of neon ions in argon at 400 kev from Eq. (19) gives 15×10^{-15} ev$\times$cm^2/atom. Weyl's observed dE/dx from electronic collisions was 86×10^{-15} and at most 85 percent of this energy loss would go into a type of collision producing electronic excitation in the gas. It has been pointed out (Al53) that this may be a factor in explaining the lowered efficiency of heavy ions in producing scintillations (presumably by electronic enounters) in sensitized crystals.

The energy loss in hard collisions falls off rapidly as the deviation in the collision decreases, or, in other words, as the impact parameter increases. Bohr has shown (Bo48) that the contribution to dE/dx from the "hard" scattering may be neglected in cases in which the deviation in path of the ions is less than an angle θ_a', where this angle is given by

$$\theta_a'=s_{min}/a^{scr}, \tag{20}$$

where s_{min} is the closest approach of the two nuclei in a head-on collision and is given by

$$s_{min}=2zZe^2/\mu v^2, \tag{21}$$

TABLE III-14. Electronic stopping powers of various gases for helium, nitrogen, and neon ions.[a] Atomic stopping powers in (ev$\times$cm^2/atom)$\times10^{15}$.

Moving ion	Kinetic energy (kev)	Gas H_2	He	Air	Argon
Helium	150	8.6	10.2	30.6	63.3
	175	9.4	11.0	43.3	57.0
	200	10.2	11.7	33.7	60.0
	250	11.0	13.2	36.3	66.0
	300	11.4	14.4	38.5	71.0
	350	11.9	15.5	40.5	75.0
	400	12.3	16.7	42.3	79.0
Nitrogen	150	12.7	16.7	...	...
	175	13.3	17.7	...	...
	200	13.8	18.7	52.6	90
	250	15.2	20.5	59.0	102
	300	17.0	22.2	64.5	114
	350	17.7	23.7	70.0	125
	400	18.5	25.0	74.5	135
Neon-20	150	...	10.5	...	...
	175	6.9	11.8	...	...
	200	7.3	12.8	...	63
	250	7.9	14.3	46	70
	300	8.8	16.0	50.5	77
	350	9.6	17.5	54.5	83
	400	10.3	18.0	58	86

[a] See reference We53.

TABLE III-15. Conversion factors for expressing the stopping power of gases in various units.

Given units	Units desired				
	(kev$\times$cm^2)/mg		(ev$\times$cm^2)/atom	ergs/cm at N.T.P.[a]	kev/cm at N.T.P.
(kev$\times$cm^2)/mg	H_2 1		1.673×10^{-18}	1.440×10^{-10}	0.0899
	He 1		6.645	2.881×10^{-10}	0.1786
	Air 1		24.05	2.070×10^{-9}	1.293
	Argon 1		66.29	2.855×10^{-9}	1.782
(ev$\times$cm^2)/atom	5.977×10^{17}	H_2 1		8.610×10^{7}	5.375×10^{14}
	1.505	He 1		4.305	2.688
	0.4158	Air 1		8.610	5.375
	0.1508	Argon 1		4.305	2.688
erg/cm at N.T.P.	69.42×10^{3}	1.162×10^{-3}	H_2 1	6.243×10^{5}	
	34.95	2.323	He 1	6.243	
	4.828	1.162	Air 1	6.243	
	3.498	2.323	Argon 1	6.243	
kev/cm at N.T.P.	11.12	1.861×10^{-17}	1.602×10^{-9}	H_2 1	
	5.599	3.722	1.602	He 1	
	0.7734	1.861	1.602	Air 1	
	0.5612	3.722	1.602	Argon 1	

[a] N.T.P. means 0°C, 760-mm Hg.

CC-0. In Public Domain. Gurukul Kangri Collection, Haridwar

Digitized by Arya Samaj Foundation Chennai and eGangotri

where μ is the reduced mass of the two colliding atoms. For neon ions of 400-kev kinetic energy in argon we compute that $\theta_a' = 6.3\times10^{-2}$ radian. Since, as we have seen, an angular deviation greater than 5×10^{-4} radian would throw the ion out of Weyl's detecting system, it is, *a fortiori*, certain that only electronic impacts were involved in the stopping power he measured. Table III-16 gives an idea of the influence of the mass of the moving ion on the fraction of the energy loss due to "hard" collisions.

Another interesting feature of the results for the heavy ions is shown in the fact that, for example, the stopping power of helium gas is the same for helium or neon ions at 150-kev kinetic energy, although the nuclear charges of the moving ions differ by a factor of five. According to present theories, the proper independent variable to use in discussing stopping power is not the energy but the velocity. We should thus compare the electronic stopping power of helium gas for helium ions at 150 kev with its stopping for neon ions at 750 kev. If the effective Z's of the two moving ions were the same, the same electronic stopping power would be found. A rather hazardous extrapolation of the data would indicate that the stopping power of helium for 750-kev neon ions would lie between 25 and 30 (in units $(\text{ev}\times\text{cm}^2/\text{atom})\times10^{15}$), compared to the value of 10.2 observed for helium ions. The square root of the ratio, 1.6, might give an indication of the relative effective charges of neon and helium ions moving through helium gas with the same velocity (about 2.6×10^8 cm/sec). This highly qualitative comment is made with the thought of foreshadowing the kind of conclusion that may be drawn in the future if more abundant and more precise data become available.

If we compare the stopping power of hydrogen gas for nitrogen and neon ions we are studying a case in which the two moving ions have quite dissimilar outer electronic structures, in contrast to the two noble gas ions mentioned in the preceding paragraph. Nitrogen ions of 280-kev kinetic energy have the same velocity as do 400-kev neon ions (about 2×10^8 cm/sec). The stopping power of hydrogen gas for such nitrogen ions is observed to be 16 (in the above units), to be compared with 10.3 for neon ions of the same velocity. The higher stopping power for the lower atomic number must be due to the relatively loose structure of the outermost nitrogen electrons, in contrast to the relatively tightly bound noble gas structure of neon.

TABLE III-16. Estimate of the ratio of energy loss in hard collisions to that in electronic collisions in argon gas. (Estimates at 400-kev kinetic energy.)

Moving particle	$a^{scr}\times10^9$ cm	Computed dE/dx for "hard" collisions. $(\text{ev}\times\text{cm}^2)/\text{atom}\times10^{15}$	Observed dE/dx from electronic encounters	Ratio of "hard" to electronic losses
H	5.6	0.02	16	0.12
D	5.6	0.04	25	0.2
He	2.9	0.25	79	0.3
Ne	0.82	15.0	87	17.2

The charge exchange cycle, in which a moving charged ion captures and then loses an electron produces as its result a pair of ions in the stopping medium, and thus is a mode of transfer of energy from the moving ion to the gas. The cross sections for capture and loss of electrons by hydrogen beams in air are known through the work of the Chicago group (Mo50, Ri51, Ka51). These data on protons allow us to put a lower limit on the energy loss due to charge exchange in such cases. We shall estimate this loss in hydrogen and in air at an energy where the electron capture and loss cross sections are equal. This is 52 kev in hydrogen and 25 kev in air. At this energy the two cross sections are each 6.3×10^{-17} cm^2 in hydrogen and 24×10^{-17} cm^2 in air. Since only one-half of the ions at this energy are singly charged and can pick up an electron, we have to divide the above cross section by two. Multiplying this by the ionization potential, since at least this amount of energy must have been given up, leads to 0.49×10^{-15} $\text{ev}\times\text{cm}^2/\text{atom}$ in hydrogen and 1.8×10^{-15} as a lower limit to the energy losses by charge exchange in air. The total measured energy loss cross sections for protons in hydrogen and air are 6.4 and 14×10^{-15} (ev cm^2), respectively. Hence, the charge exchange phenomenon accounts for at least 7.7 percent of the observed stopping power of hydrogen gas for 52-kev protons, and 14 percent of that of air for 25-kev protons. At higher ion velocities the electron capture cross section decreases rapidly, and therefore the effect of charge exchange in the stopping of protons becomes negligible.

For the heavier ions, which move much more slowly at kinetic energy values equivalent to those of protons, charge exchange is certainly an important mechanism for energy transfer, but in the complete absence of data, speculation must be considered futile.

C. Capture and Loss of Electrons by Moving Ions in the Energy Range 20–7000 Kev

1. Reduction of Experimental Data to Cross Sections

An introductory statement (Sec. II-D) has already mentioned enough of the theory to motivate the following summary of experimental work. It is, however, necessary to give some analysis for the interpretation of observations in terms of collision cross sections. These cross sections will be expressed per atom of material through which the ions are passing; in the general form σ_{if}, the initial index represents the number of electronic charges on the ion before the event, the final index the number after the event. Thus, σ_{01} applied to He ions concerns the loss of an electron by a moving neutral He atom, while $\sigma_{0\bar{1}}$ applied to H ions concerns the capture of an electron by a moving, neutral H atom.

CC-0. In Public Domain. Gurukul Kangri Collection, Haridwar

Digitized by Arya Samaj Foundation Chennai and eGangotri

Although the simplest independent variable to use in setting up equations concerning the effect would seem to be the distance along the path of the ion, experiments are almost always conducted by varying the pressure (p) in a vessel which encloses a constant length (l) along the path of the ion, as schematically represented in Fig. 14, and the equations given here will apply to the composition of a beam which is leaving such a variable pressure chamber.

The equations for capture and loss when only two charged states of the ion are concerned (0 and 1) were given at an early date by Wien (Rü33) and are reproduced here in terms of cross sections, rather than the mean free paths used more frequently in Wien's time.

In the first simple case we are concerned only with the two cross sections σ_{01} and σ_{10}. In the region above 20-kev kinetic energy charge exchange in a hydrogen beam should be describable in terms of these only since we may neglect the fraction of negative hydrogen ions

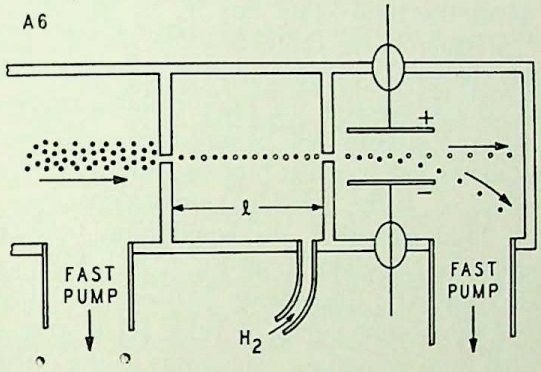


FIG. 14. Schematic representation of an experimental arrangement for the study of charge equilibrium in hydrogen ions passing through hydrogen gas. Neutral H atoms appear in the beam emerging from the charge exchange space of length l and the beam is then electrostatically analyzed. A similar setup was used by Snitzer (Sn53) with magnetic analysis and helium ions.

present (Ph53a, Ri51). Let n_1 be the flux of protons in the beam, n_0 the flux of neutral hydrogen atoms, $N=n_0+n_1$ the constant total flux of hydrogen, and $\pi=Ll\xi p/RT$ the measure of the number of gas atoms per square centimeter of the target. Here L is Avogadro's number, l the thickness of the gas target, ξ the number of atoms per molecule in the gas which is at pressure p, absolute temperature T; R is the gas constant 8.31×10^7 erg/mol C°. Then,

$$\begin{aligned} dn_0/d\pi &= n_1\sigma_{10}-n_0\sigma_{01}, \\ dn_1/d\pi &= -n_1\sigma_{10}+n_0\sigma_{01}, \end{aligned} \tag{22}$$

with solutions

$$\begin{aligned} n_1 &= \eta_1 \exp[-\pi(\sigma_{01}+\sigma_{10})]+\eta_2, \\ n_0 &= -\eta_1 \exp[-\pi(\sigma_{01}+\sigma_{10})]+\sigma_{10}\eta_2/\sigma_{01}, \end{aligned} \tag{22'}$$

where η_1, η_2 are constants of integration that will be deduced in the discussion of the various types of experiment.

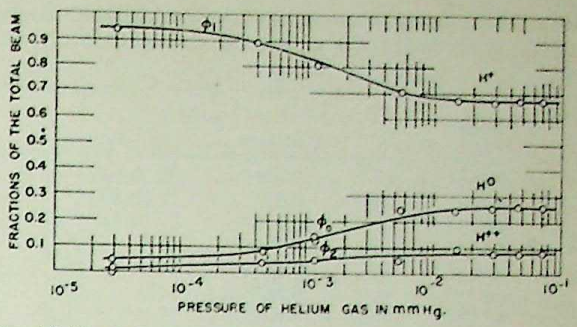


FIG. 15. Typical approach to equilibrium in the charge exchange process. This is 340-kev He^+ incident on He gas in the arrangement of Fig. 14 with $l=74$ cm.

In a system where there are three possible charge states, such as helium ions in motion, three simultaneous differential equations in n_0, n_1, n_2 can be written, of which two are independent because $n_0+n_1+n_2=N$. Here σ_{02} and σ_{20} correspond to events in which two electrons are transferred in a single encounter; while these are probably small compared to cross sections for single electron transfers, in the absence of experimental verification of this supposition they will be retained in the equations. Thus,

$$\begin{aligned} dn_1/d\pi &= n_0(\sigma_{01}-\sigma_{21})-n_1(\sigma_{21}+\sigma_{12}+\sigma_{10})+N\sigma_{21}; \\ dn_0/d\pi &= -n_0(\sigma_{01}+\sigma_{02}+\sigma_{20})+n_1(\sigma_{10}-\sigma_{20})+N\sigma_{20}; \\ n_2 &= N-n_0-n_1. \end{aligned} \tag{23}$$

The general solution of (23) can be obtained in a straightforward manner; in the special and interesting case where the boundary condition is such that for $\pi=0$, $n_1=N$, $n_0(0)=n_2(0)=0$, the solution may be written

$$\frac{n_1}{N}=\phi_1+(k_1e^{-q\pi}+k_2e^{q\pi})\exp\left(-\frac{\pi}{2}\sum\sigma_{if}\right).$$

$$\frac{n_0}{N}=\phi_0+\left(k_1\frac{q+S}{b}e^{-q\pi}-k_2\frac{q-S}{b}e^{q\pi}\right)\times\exp\left(-\frac{\pi}{2}\sum\sigma_{if}\right), \tag{23'}$$

where $2S=\sigma_{12}+\sigma_{21}+\sigma_{10}-\sigma_{01}-\sigma_{02}-\sigma_{20}$; $a=(\sigma_{01}-\sigma_{21})\times(\sigma_{10}-\sigma_{20})$; $b=\sigma_{01}-\sigma_{21}$; $q^2=S^2+a^2$; and $k_1=[(q-S)\times(N-\phi_1)-b\phi_0]/2q$; $k_2=[(q+S)(N-\phi_1)+b\phi_0]/2q$; and where ϕ_0, ϕ_1 are the limiting values of the beam fractions as π becomes large; these are the equilibrium values.

If a moving ion beam, homogeneous in velocity, impinges on a slab of matter and traverses it, a charge equilibrium is rapidly attained which is characterized by the set of fractions ϕ_i. Figure (15) shows the approach to equilibrium for a beam of helium ions, originally all He^+, as the pressure was increased in a charge exchange tube containing helium through which they were passed. In a tube length of 74 cm we see that equilibrium has been attained in the emergent beam when the pressure of the gas has reached 0.01-mm Hg.

CC-0. In Public Domain. Gurukul Kangri Collection, Haridwar

Digitized by Arya Samaj Foundation Chennai and eGangotri

TABLE III-17. Direct measurement of the equilibrium fraction of protons in hydrogen beams passing through hydrogen gas and air.[a]

Energy (kev)	ϕ_1 in Hydrogen	ϕ_1 in Air
20	0.231	0.405
30	0.315	0.500
40	0.419	0.545
50	0.500	...
59[a]	0.61	
60	0.56	
66.7[a]	0.67	
73.0[a]	0.73	

[a] *a* values are from reference Ri51, other values from reference Ba32. Values by Bartels are from a smooth curve through his data.

This approach to equilibrium is already shown in Eq. (23′) but for a simpler illustration, and for later use, we may continue the analysis of the hydrogen case whose general solution is Eq. (22′). In this set, put $n_0=0$ and $n_1=N$ for $\pi=0$ and obtain

$$\begin{aligned} n_1/N&=\phi_1+\phi_0\exp[-\pi(\sigma_{01}+\sigma_{10})],\\ n_0/N&=\phi_0(1-\exp[-\pi(\sigma_{01}+\sigma_{10})]), \end{aligned} \qquad (22'')$$

where the ϕ's may be expressed as

$$\phi_1=\sigma_{01}/(\sigma_{01}+\sigma_{10}),\quad \phi_0=\sigma_{10}/(\sigma_{01}+\sigma_{10}). \qquad (22''')$$

The appearance of the sum of the capture and loss cross sections in (22″) is important because it illustrates that the rate of approach to equilibrium is governed by a cross section sum which is larger than the individual cross sections involved in the phenomena. It is a characteristic and simplifying feature of this process that charge equilibrium is attained in a variable pressure tube at pressures so low that no appreciable diminution of energy of the beam occurs in traversing the length of the tube. Thus, a mathematical treatment need not, at the present stage of experimental accuracy, concern itself with variation of the cross sections with velocity.

The variation of the various beam fractions with pressure for the case of three possible charge stages has already been given as Eqs. (23′), with the characteristic appearance of the sum of all possible cross sections. The equilibrium values ϕ_i may be expressed as

$$\begin{aligned} \phi_0&=[\sigma_{10}(\sigma_{21}+\sigma_{20})+\sigma_{20}\sigma_{12}]/D,\\ \phi_1&=[\sigma_{21}(\sigma_{02}+\sigma_{01})+\sigma_{01}\sigma_{20}]/D,\\ \phi_2&=[\sigma_{02}(\sigma_{10}+\sigma_{12})+\sigma_{12}\sigma_{01}]/D, \end{aligned} \qquad (23'')$$

where

$$D=\sigma_{12}(\sigma_{01}+\sigma_{02}+\sigma_{20})+\sigma_{10}(\sigma_{21}+\sigma_{02}+\sigma_{20})+\sigma_{21}(\sigma_{01}+\sigma_{02})+\sigma_{01}\sigma_{20},$$

and if the cross sections involving double electron transfers may be neglected, these simplify to

$$\begin{aligned} \phi_0&=\sigma_{10}\sigma_{21}/D_0,\\ \phi_1&=\sigma_{01}\sigma_{21}/D_0,\\ \phi_2&=\sigma_{01}\sigma_{12}/D_0, \end{aligned} \qquad (23''')$$

where $D_0=\sigma_{01}(\sigma_{12}+\sigma_{21})+\sigma_{10}\sigma_{21}$.

2. *Experimental Values of the Equilibrium Fractions in Gases*

(*a*) *Hydrogen beams.*—The experimental work on this problem prior to 1933 has been summarized in (Rü33). The older work which seems most reliable in the energy range above 20 kev is that of Bartels (Ba30, Ba32). Other measurements by Meyer (Me37) do not agree as well with subsequent results.

Recently equilibrium fractions were measured by Ribe (Ri51) for hydrogen beams in hydrogen gas. In his work an initially nearly 100 percent pure proton beam was passed into a gas chamber in which the path length was 12.70 cm. The current collected from the proton constituent of the beam was measured in a Faraday cup and the decrease in this current noted as hydrogen gas was admitted into the chamber. Table III-17 gives the results of Bartels and of Ribe.

It is assumed, for the experiments leading to the values of Table III-17, that the current measured in the Faraday cup when there is no gas in the path of the beam gives the total beam flux N. If, however, this "zero" pressure beam contains some neutral atoms, caused by imperfect vacuum or neutralization of some protons on the walls of the beam-defining apertures, too small a total beam will be indicated, and the true fraction of the flux which is protons will be lower than that measured. If the individual cross sections σ_{10} and σ_{01} have been measured, the equilibrium fraction of protons can be calculated from Eq. (22‴). Ribe found a small systematic discrepancy between the directly measured equilibrium values of Table III-17 and those calculated from σ_{01} and σ_{10}, which was in the direction to be explained by the presence of a small neutral component of the "zero-pressure" beam.

Table III-18 gives computed values of ϕ_1 based on cross sections measured by the Chicago group (Mo50, Ri51 for hydrogen beams in hydrogen gas, and Ka51 for hydrogen beams in air). The equilibrium fractions for air have been calculated from formulas given by Kanner (Ka51) and quoted later in this section.

TABLE III-18. Equilibrium fractions of protons in a hydrogen ion beam in hydrogen and air, computed from measured capture and loss cross sections.

Energy in kev	ϕ_1 in H_2	ϕ_1 in Air
30	...	0.530
40	0.342	0.582
50	0.487	0.643
60	0.602	0.674
70	0.692	0.723
80	0.756	0.764
90	0.796	0.800
100	0.841	0.831
110	0.865	0.860
120	0.899	0.883
130	0.910	0.902
140	0.933	...
150	0.944	...

CC-0. In Public Domain. Gurukul Kangri Collection, Haridwar

Digitized by Arya Samaj Foundation Chennai and eGangotri

TABLE III-19. Equilibrium fractions of the various charged states in a helium ion beam traversing the gases H_2, He, Air, and Argon (Sn53).[a]

Ion energy (kv)	H_2 ϕ_0	H_2 ϕ_1	H_2 ϕ_2	He ϕ_0	He ϕ_1	He ϕ_2	Air ϕ_0	Air ϕ_1	Air ϕ_2	Argon ϕ_0	Argon ϕ_1	Argon ϕ_2
100	0.63	0.37	...	0.59	0.41	...	0.50	0.50	...	0.53	0.47	...
120	0.57	0.43	...	0.54	0.45	...	0.43	0.57	...	0.48	0.52	...
140	0.52	0.48	...	0.51	0.48	0.01	0.38	0.62	...	0.42	0.58	...
160	0.47	0.53	...	0.47	0.52	0.015	0.34	0.66	...	0.37	0.63	...
180	0.41	0.57	0.015	0.43	0.55	0.02	0.28	0.69	0.025	0.33	0.67	...
200	0.36	0.62	0.02	0.40	0.57	0.025	0.26	0.71	0.03	0.28	0.70	0.02
220	0.32	0.66	0.025	0.38	0.59	0.03	0.23	0.73	0.035	0.24	0.73	0.03
240	0.28	0.69	0.03	0.35	0.61	0.035	0.21	0.74	0.05	0.21	0.75	0.04
260	0.25	0.72	0.035	0.32	0.63	0.04	0.19	0.75	0.065	0.18	0.77	0.055
280	0.22	0.73	0.05	0.30	0.65	0.05	0.17	0.75	0.08	0.16	0.77	0.07
300	0.19	0.75	0.06	0.28	0.67	0.06	0.15	0.76	0.095	0.15	0.77	0.085
320	0.17	0.75	0.075	0.25	0.68	0.07	0.14	0.75	0.11	0.13	0.76	0.11
340	0.15	0.76	0.095	0.23	0.69	0.085	0.13	0.74	0.13	0.11	0.75	0.13
360	0.13	0.75	0.12	0.21	0.70	0.095	0.12	0.73	0.15	0.095	0.74	0.16
380	0.12	0.74	0.14	0.19	0.71	0.11	0.11	0.72	0.17	0.085	0.73	0.19
400	0.10	0.74	0.16	0.17	0.71	0.12	0.095	0.71	0.19	0.07	0.71	0.22
420	0.095	0.73	0.18	0.16	0.71	0.13	0.08	0.70	0.21	0.06	0.69	0.25
440	0.085	0.72	0.20	0.14	0.71	0.15	0.07	0.69	0.24	0.055	0.66	0.28
460	0.08	0.70	0.22	0.13	0.70	0.17	0.065	0.68	0.26	0.05	0.64	0.30
480	...	...	...	0.11	0.68	0.20	0.055	0.66	0.29	0.045	0.62	0.33

[a] ϕ_0 is the fraction of the total number of ions which is neutral at any time, and the subscripts 1 and 2 refer to He^+ and He^{++}, respectively.

(*b*) *Helium ions.*—A study of the charge equilibrium of a helium ion beam in the gases H_2, He, air, and argon has recently been published by Snitzer (Sn53). The original beam of He^+ ions obtained from a 500-kev Cockcroft-Walton accelerator or kevatron was passed through apparatus similar to that of Fig. 14, with magnetic deflection replacing electrostatic; the length of the tube was 74 cm. The equilibrated beam (with pressures of the order of 0.01 mm Hg) on leaving the tube passed into a circular chamber kept at high vacuum between the pole pieces of an electromagnet. This separated the three beam fractions by virtue of their different charge, and sent them through separate exit apertures; since the fractions all contained ions of the same average kinetic energy, a calorimetric measurement could be expected to indicate correctly the beam flux without requiring an investigation of the detector response to the charge of the particle incident on it. The use of such a detector is novel enough to warrant some descriptive detail.

Each beam fraction was detected on one of three identical targets. These consisted of a thin walled tube of nickel foil 0.0025 cm thick, 0.5 cm long and 0.3 cm in diameter. A No. 27A thermistor (a 0.05 cm diameter bead of a composition having a high temperature coefficient of electrical resistance) was placed on the axis of the foil tube and received heat by radiation from it. Ion beams of the order of 10^{-8} amperes produced temperature rises from 10–50°C at the various energies used. The lower values of the temperature rise ΔT were directly proportional to the power incident on the nickel foil; the higher values had a small radiation and conduction loss correction. This correction was determined as follows. The nickel tube targets were mounted on electrically insulating supports so that when one of the beams impinged on such a target a current flowed which was the sum of the rates of collection of positive charge from the beam and from the loss of secondary electrons, but which was directly proportional to the flux of ions in the beam. Thus, relative values of beam currents and temperature rises could be obtained by varying the kevatron beam at the same kinetic energy, and the losses thus were experimentally determined.

The results of Snitzer on the equilibrium fractions of He ions in various gases are given in Table III-19 and are shown graphically for air in Fig. 16.

As discussed briefly in Sec. II-D, one would expect than when the ratio $\gamma = v/v_0$ is of the order unity, the probabilities of capture and loss will be equal, and one-half of the moving ions will be neutral at a given moment. This expectation seems surprisingly well fulfilled for hydrogen and helium ions in air. The energy of a hydrogen ion beam at $\gamma = 1$ is 24.8 kev; for a helium ion beam it is 99.2 kev. At 25 kev the value of ϕ_1 for hydrogen ions in air is 0.50 from a slight extrapolation of Table III-18, and from Table III-19 we see that for helium ions in air ϕ_1 and ϕ_0 are 0.50 at 100 kev. For helium ions moving in hydrogen, helium, or argon gas the γ values for $\phi_1 = \phi_0 = 0.50$ range from 1.08 in argon

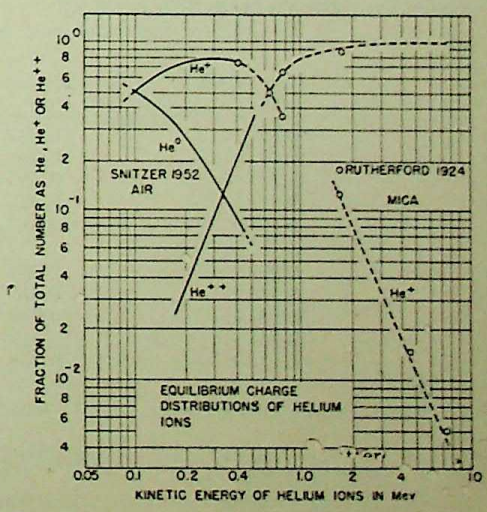


FIG. 16. Equilibrium charge fractions of He ions in air, including older results for He ions emerging from mica.

CC-0. In Public Domain. Gurukul Kangri Collection, Haridwar

Digitized by Arya Samaj Foundation Chennai and eGangotri

to 1.21 for helium or hydrogen gas. The largest discrepancy occurs in the case of hydrogen ions moving in hydrogen gas where the 50–50 point occurs at $\gamma=1.44$.

3. *Equilibrium Ratios on Emerging from Solids*

(*a*) *Hydrogen ions.*—The fraction of the hydrogen ions which are charged on emerging from metal foils in a vacuum has been investigated by Hall (Ha50). In his experiments protons in the energy region 20–400 kev were passed through a metal foil and, in the emergent, equilibrated beam the charged constituent could be deflected out of the beam by an electric field. The total equilibrated beam, or its neutral component, was measured by the scintillations caused in a KI(Tl) crystal, as detected by a photomultiplier tube. Since charge equilibrium is established after the penetration of a few atomic layers in the crystal, there can be no difference in its response to beams of originally neutral or charged hydrogen ions. The ratio of the photomultiplier currents with and without the electric deflection gives ϕ_0, the fraction of the total equilibrated beam which is neutral. Hall's results are given in Table III-20.

As we shall see below, in discussing charge equilibrium for emergent helium ions, most investigators have found that the composition of the equilibrium mixture is independent of the metal or solid in which it is produced. Hall found that he could not distinguish between the hydrogen in equilibria produced in beryllium, aluminum, and silver foils. The composition of the beam emergent from gold, however, contained more neutrals than beams from the lighter elements.

In discussing Hall's results, we may make the following remarks. His low-energy data did not take account of the possibility of H^- in the emergent beam. According to Phillips and Ribe (Ph53a and Ri51), about 4 percent of the equilibrated hydrogen beam may have been negatively charged at 20 kev. Also there is some doubt whether the entire equilibrating effect of a foil may not be due to a surface layer of foreign material. Such a layer, even if only between 5 and 10 atoms thick, would impress its own characteristic equilibrium on the emergent ions irrespective of the foil material. It is known that in the rather poor vacuum ($p \lesssim 10^{-6}$ mm Hg) used in this type of work, many metals take on a coating of absorbed oxygen, or even a layer of organic material from diffusion pump oil. Only very high vacuum techniques, such as the fresh evaporation of the foil material at pressures less than 10^{-8} mm, and its use as an equilibrating foil under baked-out high vacuum conditions would give one the right to assume that the effects of surface layers were being minimized. Such techniques have not, as yet, been applied in the work of the Chicago group.

TABLE III-20. Equilibrium fraction of protons (ϕ_1) in the total emergent hydrogen ion beam from metal foils.[a]

Hydrogen ion energy (kev)	Be, Al, or Ag foil ϕ_1	Au foil ϕ_1
25	0.56	0.56
50	0.68	0.68
74	0.75	0.75
99	0.82	0.80
124	0.87	0.85
149	0.909	0.886
174	0.939	0.910
198	0.954	0.935
223	0.968	0.952
248	0.976	0.968
298	(1−0.0159)	(1−0.0164)
347	(1−0.0113)	(1−0.0124)
397	(1−0.0050)	(1−0.0101)

[a] See reference Ha50.

(*b*) *Helium ions.*—Following the discovery by Henderson (He22) in 1922 that alpha particles emitted from a radioactive source and deviated in a magnetic field always show evidence of a singly as well as a doubly charged component, this phenomenon was the subject of several investigations at the Cavendish Laboratory and elsewhere (Ru24, Br27, He25, Ja27). Even from the bare source (RaC′) singly charged α particles were always found, and slowing down the particles by interposing a mica foil increased the fraction of singly charged ions. Detection was by counting scintillations on a ZnS screen after magnetic deflection of the particles. The work on natural alpha particles up to 1933 has been summarized by Geiger (Ge33).

Henderson (He25) extended the work of Rutherford on equilibrium produced in mica by using metal foils to slow down the particles. Except at the lowest energy used by Rutherford (405 kev), the equilibrium fraction of He^0 is so small that the ratio $n_1/(n_1+n_2)$, which may be computed from the experimental data, which give n_1/n_2, is not appreciably different from n_1/N, that is, from ϕ_1. Snitzer found $\phi_0=0.095$ for 400-kev helium ions in air and we have, in Table III-21, altered Rutherford's $n_1/n_2=0.75$ to $\phi_1=0.68$. We assume that the equilibrium mixture will contain approximately this same fraction of neutrals.

The results of Rutherford and of Henderson are summarized in Table III-21. The remarks made previously concerning the effect of foreign layers on the foil surfaces apply here but with less force, since at the relatively high energies of their work a thicker surface layer is needed to impress its characteristic equilibrium.

The charge composition of helium ions which have been scattered from a metal surface has been investigated by the Chicago group (Al53a) in some experiments as yet unpublished.

In these experiments a beam of monoenergetic He^+ ions was allowed to impinge upon thin and thick targets of gold, and a thick target of nickel. The helium ions scattered at 85°16′ from the beam, which struck the surfaces at a glancing angle of 45°, were examined in a spherical electrostatic analyzer for the ratio He^{++}/He^+.

CC-0. In Public Domain. Gurukul Kangri Collection, Haridwar

Digitized by Arya Samaj Foundation Chennai and eGangotri

TABLE III-21. The equilibrium fraction of He^+ in helium ions emerging from foils.[a]

Energy (kev)	Material	Reference	Fraction of total No. of helium ions which are singly charged
406	Mica	Ru24	0.68[b]
590	Mica	Ru24	0.60
640	Mica	Ru24	0.50
787	Mica	Ru24	0.346
1260	Mica	He25	0.156
1260	Gold	He25	0.137
1355	Mica	He25	0.138
1521	Silver	He25	0.116
1696	Mica	Ru24	0.12
1935	Mica	He25	0.0610
1935	Gold	He25	0.0654
2323	Aluminum	He25	0.0446
2408	Mica	He25	0.0389
2408	Mica	He25	0.0370
2408	Gold	He25	0.0415
2408	Gold	He25	0.0374
2719	Mica	He25	0.0325
2719	Gold	He25	0.0356
3406	Gold	He25	0.0235
4262	Copper	He25	0.0148
4440	Mica	Ru24	0.0150
4915	Mica	He25	0.0120
6028	Mica	He25	0.0079
6028	Gold	He25	0.0088
7680	As emitted from source on Pt wire	He25	0.0062
7680	As emitted from source	Ru24	0.0050

[a] See reference Ru24, He25.
[b] Rutherford's result was 0.75 for $He^+/(He^+ + He^{++})$; we assume that He^0 was present to about 10 percent.

The analyzer had such a large aperture that the electric currents arising from the transport of charge by the scattered ions were of the order 10^{-13} amperes and could be read on a recording electrometer. Charge equilibrium was established among the scattered helium ions *after* electrostatic deflection by interposing a foil in their path before their impact on the collecting probe. Thus, the same mixture of He^+ and He^{++} arrived at the probe irrespective of whether the charge on the analyzer was set for the transmission of the He^+ or He^{++} constituent. A NaI(Tl) scintillator was also used as a detector, the incident He^+ beam being depressed and reduced to the point where individual counting was possible. The data obtained from the NaI(Tl) detector and from the relative currents collected at the probe gave He^{++}/He^+ ratios which agreed to within 10 percent. Unfortunately, the method can give no information about neutrals, since it depends on electrostatic analysis, and in the energy range covered (150–450 kev) the fraction of neutrals cannot be ignored.

The ratio He^{++}/He^+ in scattered helium ions from metal surfaces is given in Fig. 17. It will be seen from Fig. 17 that the ratio He^{++}/He^+ in ions which have been charge equilibrated by scattering from a metal surface (nickel or gold) is considerably greater than when charge equilibrium has been produced by passage through air. There is considerable interest at present in the best method for producing multiply charged ions by stripping a moving ion beam; if these experiments are confirmed it would seem that, in this energy range, passage through a foil is considerably superior to equilibration in a gas for this purpose.

Snitzer's results for air, and Rutherford's for mica are shown in Fig. 16,|| || giving an idea of the behavior over the range 100–7000 kev. Rutherford measured his ratios He^+/He^{++} for helium ions emerging from mica and assumed that these would be the ratios at charge equilibrium in air. The present evidence would indicate that this is a questionable assumption, at least in the lower-energy region. It is seen that between its maximum value of about 0.75 in air at 300 kev, the fraction ϕ_1 has sunk by a factor of 150 to 5×10^{-3} at 7680 kev.

4. *Measurements of the Cross Sections for Capture and Loss of Electrons*

The equilibrium fractions discussed in the preceding section give ratios of the probabilities of capture and loss. In order to measure the probabilities separately, experiments involving the transient conditions, before equilibrium has been established, must be performed. Most of the measurements of individual cross sections have been made using one of the following methods.

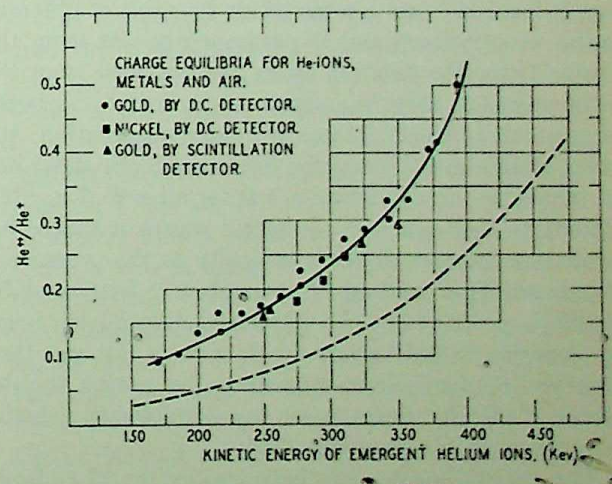


FIG. 17. Charge equilibria in He ions scattered by metals and transmitted by air.

|| || The Rutherford values were entered incorrectly in a similar figure (Fig. 7) in Snitzer's paper (see reference Sn53).

CC-0. In Public Domain. Gurukul Kangri Collection, Haridwar

Digitized by Arya Samaj Foundation Chennai and eGangotri

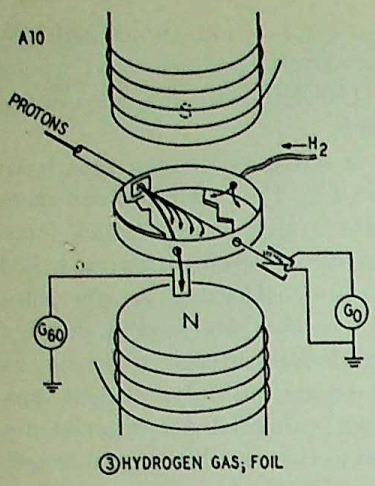


FIG. 18. Essentials of an experiment to measure σ_{01}, σ_{10} for hydrogen ions in hydrogen gas. Both beams decrease in intensity as gas is admitted. Any protons formed in the atomic beam are removed by the magnetic field and any atoms formed in the proton beam fly off tangentially (not shown).

(*a*) *Methods.*—(i) An arrangement similar to that of Fig. 14 is used. In a two component system, such as hydrogen ions above 20-kev kinetic energy, two measurements are carried out. The equilibrium fraction of protons ϕ_1, is measured by increasing the gas pressure until a pressure-independent mixture emerges from the tube. Then, at a lower pressure, before equilibrium has been established, a value of n_1/N is observed and the gas pressure noted. If one uses $\phi_0+\phi_1=1$ in Eqs. (22″), one finds these observations are sufficient for the calculation of the cross sections. This method was used by Bartels (Ba30).

(ii) The essentials of this second method are shown in Fig. 18, as applied to a situation in which one of the ionic states is neutral in charge. A mixed ion beam (produced, in the figure, by bringing the beam to charge equilibrium in its passage through a foil) is passed into a chamber which is in a strong magnetic field. The various charged states proceed through the chamber on orbits of different radii. A detector is placed on one of the beams, and gas is admitted to the chamber. There is a decrease in beam intensity because of the fact that when the charge of the moving ion changes due to capture or loss, the new ion moves on an orbit of different radius of curvature and is permanently lost from the beam. Thus, the new ion types are removed from the beam as fast as they are formed. If, for instance, a beam of neutral hydrogen atoms is under observation, the effect of method (ii) may be mathematically described as imposing the condition $n_1=0$ for all π in Eq. (22), leading to $dn_0/n_0 d\pi=-\sigma_{01}$, which means a simple exponential decrease in beam intensity as the pressure is increased. This method was apparently first used by Rutherford (Ru24), who produced the mixed beam by covering a RaC′ source with a mica foil and then observed σ_{12} for helium ions in air by noting the decrease of the He^+ beam as air was admitted to a deviation chamber in a magnetic field.

The method has recently been applied by the Chicago group (Mo50, Ri51, Ka51) to the study of σ_{10} and σ_{01} for hydrogen ions in hydrogen gas and in air.

Both methods (i) and (ii) impose rather arbitrary experimental definitions of the concepts "capture" and "loss." The only criterion established by the methods is that something has happened to the moving ion which changes the radius of curvature of its orbit in a magnetic field. Thus, "capture," as here observed, includes addition of an electron into an excited, and perhaps metastable, state of the resultant ion, but "loss" does not include events in which an electron in the moving ion

TABLE III-22. Experimental cross sections, in square centimeters, per atom of material traversed, for electron capture and loss.

Beam kinetic energy (kev)	Hydrogen beam in hydrogen gas		Hydrogen beam in air	
	Capture $\times 10^{17}$	Loss $\times 10^{17}$	Capture $\times 10^{17}$	Loss $\times 10^{17}$
31.4	...	...	20.8	...
34.0	15.2	...	...	...
38.2	17.6	...	...	...
40.6	...	...	16.0	...
40.8	...	...	...	24.4
41.4	...	...	...	23.1
43.0	...	...	15.6	...
44.5	9.1	6.7	...	...
48.3	7.6	...	...	...
48.7	7.0	...	...	...
49.4	...	...	13.4	...
50.8	...	6.4	...	...
53.9	5.7	...	...	...
55.7	...	...	11.6	...
56.6	...	...	11.5	...
58.1	...	...	10.1	...
62.5	3.8	...	...	...
63.0	...	...	9.7	...
65.6	...	...	9.3	...
67.0	...	...	...	22.2
70.5	...	5.7	...	...
73.0	2.8	...	6.8	...
77.0	...	...	7.1	...
81.1	1.8	...	...	...
88.8	1.4	...	...	...
103	0.84	...	...	...
105	...	...	...	20.8
107	...	...	...	21.0
109	0.74	...	...	...
112	...	4.7	...	...
114	...	...	3.4	...
117	...	...	2.7	20.6
120	0.48	...	...	...
122	...	...	2.7	...
123	...	4.3	...	...
128	0.41	...	...	...
142	...	...	...	19.8
149	0.23	...	...	...
153	...	3.8	...	...
156	...	...	...	18.8
193	...	...	...	17.4
204	...	3.2	...	...
252	...	...	...	14.4
263	...	2.8	...	...
280	...	...	...	14.5
305	...	2.4	...	...
321	...	2.3	...	...
325	...	...	...	13.6

CC-0. In Public Domain. Gurukul Kangri Collection, Haridwar

Digitized by Arya Samaj Foundation Chennai and eGangotri

is excited to a state which is bound. Thus, the role of the well-known highly metastable states in He I in these phenomena is still open for further experimentation, and this means that the light emitted by the moving ions must be investigated.

(*b*) *Capture and loss cross sections for hydrogen beams in hydrogen gas.*—The results of the Chicago group on hydrogen in charge exchange are shown in Table III-22 and Fig. 19. From these, it is clear that the capture and loss values are of the order of geometric atomic cross sections for $\gamma(=v/v_0)$ near unity since $\pi a_0^2=8.8\times10^{-17}$ cm^2, where a_0 is the Bohr radius.

For the case of hydrogen ions traversing air, Kanner found that his data on the cross sections per average air atom could be represented empirically as follows:

$$\sigma_{01}=(24.54-0.866E/E_0)\times10^{-17}\ \text{cm}^2;$$
$$\sigma_{10}=41.1\exp(-0.562E/E_0)\times10^{-17}\ \text{cm}^2; \qquad (24)$$

and the equilibrium data of Table III-18 were computed (for air) from these equations. Here, $E_0=24.8$ kev; E is the kinetic energy in electron kilovolts.

The two cross sections behave quite differently with energy; in hydrogen Montague estimated that σ_{01} varies as $1/E^n$ where $n=0.70\pm0.05$. σ_{10}, however, has $n=3.5$, a fivefold increase in the magnitude of the exponent. Thus, a fast moving hydrogen atom is quickly stripped of its electron and has little probability of capturing another. We also note that the two probabilities for hydrogen ions in air are considerably larger at the same ion velocity (factors varying from 2.5 to 5) than they are in hydrogen gas.

(*c*) *Capture and loss cross section for helium ions.*—The experimental information at present available concerning capture and loss cross sections for helium ions is due to the work of Rutherford (Ru24) and some incidental observations of Snitzer (Sn53) in connection with his work on equilibrium fractions in helium.

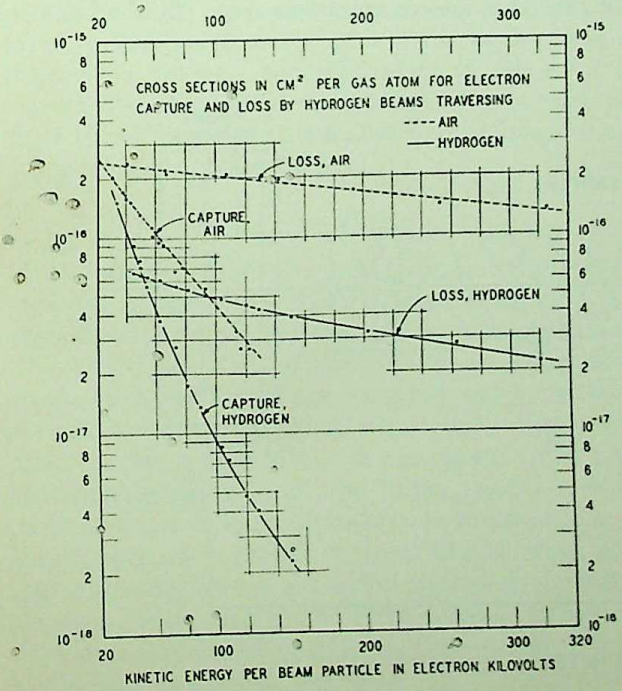


FIG. 19. Cross sections per atom of traversed gas for capture (σ_{10}) and loss (σ_{01}) of electrons by hydrogen ions in motion.

TABLE III-23. Some capture and loss cross sections for helium ions above 100 kev in kinetic energy.[a]

Energy kev	Gas		Cross section
131*	Helium	σ_{01}	1.72×10^{-16} cm^2 (±30%)
		σ_{10}	1.72×10^{-16} cm^2 (±30%)
340*	Helium	σ_{01}	8.3×10^{-17} cm^2 (±20%)
		σ_{10}	3.1×10^{-17} cm^2 (±20%)
		σ_{12}	1.4×10^{-17} cm^2 (±20%)
		σ_{21}	1.2×10^{-17} cm^2 (±20%)
646	Air	σ_{12}	6.2×10^{-17} cm^2
		σ_{21}	6.2×10^{-17} cm^2
1696	Air	σ_{12}	3.7×10^{-17} cm^2
		σ_{21}	5.01×10^{-18} cm^2
4440	Air	σ_{12}	2.38×10^{-17} cm^2
		σ_{21}	3.56×10^{-19} cm^2
6780	Air	σ_{12}	1.68×10^{-17} cm^2
		σ_{21}	8.43×10^{-20} cm^2

[a] Starred values from reference Sn53; other values from reference Ru24.

Rutherford obtained σ_{12}, the cross section per air atom for loss of an electron by He^+, using method (ii) as previously described. The mixed beam of various charge states was varied in energy from 650 to 6780 kev by using mica foils of different stopping powers over the RaC′ source. At these energies helium ions which have interacted with matter in their path are essentially only of the charge types He^+, He^{++}. Scintillations due to the He^+ beam were observed in a good vacuum; as air was admitted to the portion of the path in the magnetic field these diminished in number because of the process $He^+\rightarrow He^{++}+e^-$. This gave the mean free path or loss cross section σ_{12} directly for air. In order to obtain the capture cross section σ_{12}, Rutherford measured the equilibrium fractions in mica, and assumed that these same fractions would be applicable to air, which is somewhat questionable. On this assumption, he was able to compute σ_{21} for helium ions from the relation [see Eqs. (23‴)] $\sigma_{21}=\sigma_{12}\phi_1/\phi_2$. His results are given in Table III-23.

Snitzer, in his paper on the equilibrium fractions (Sn53), reports some tests of the attainment of equilibrium from which cross sections may be deduced. If the helium beam enters the gas chamber as He^+, the initial rates of growth of He^0 and He^{++}, and decay of He^+ may be found by imposing the conditions of (23′) for small, but not zero, values of π on Eq. (23). Then the initial part of the curves are given by

$$n_2/N=\pi\sigma_{12};$$
$$n_1/N=1-\pi(\sigma_{12}+\sigma_{10}); \qquad (25)$$
$$n_0/N=\pi\sigma_{10}.$$

CC-0. In Public Domain. Gurukul Kangri Collection, Haridwar

Digitized by Arya Samaj Foundation Chennai and eGangotri

These equations serve to give estimates of σ_{12} and σ_{10} from the initial rates of change. Then from the equilibrium values, σ_{01} and σ_{21} may be calculated. This is clearly a slight modification of method (i), previously described.

Estimates of the cross sections applicable to helium ions at a few scattered energy values above 100 kev are given in Table III-23.

IV. HIGH-ENERGY MEASUREMENTS

In the high-energy region, measurements are unfortunately meager, with the methods necessarily differing somewhat from those used at low energies and, at least in the region above about 15 Mev, restricted to those few laboratories blessed with synchrocyclotrons. For purposes of verifying the theory, experiments have been largely concerned with the extraction of the value of I, the mean excitation potential, from the range and stopping power data; for use in other experimental work, the points on a range energy curve are sufficient.

Three forms of data are available. The absolute stopping power, or direct measurement of direct energy loss, consists of passing a well-collimated beam of known initial energy through a slab of stopping material of thickness Δx, determining the energy decrement ΔE, and calculating $\Delta E/\Delta x$. This corresponds to a popular practice at low energy except that magnetic analysis is most conveniently used for energy measurement, rather than electrostatic. From the value $\Delta E/\Delta x$, the value of I may be determined by fitting Eq. (3) to observation, and from a curve of dE/dx *vs* E, the range energy relation can be obtained as described in Sec. II.

The relative stopping power is determined by finding the thickness Δx_s of some standard substance (air at low energies, aluminum, copper at high energies) that reduces the beam energy the same amount as the thickness Δx of the material investigated. This can be done without actually measuring the energy loss, by sending the beam through just enough standard material to stop the particles, removing a known thickness and replacing the amount removed with enough thickness of the sample to produce the same effect near the end of the ionization (Bragg) or integral range curve. Then if we apply Eq. (3),

$$S=\frac{(Z/A)}{(Z/A)_s}\frac{\log(2mv^2/I)-\log(1-\beta^2)-\beta^2}{\log(2mv^2/I_s)-\log(1-\beta^2)-\beta^2}$$

(mass stopping power),

in which the velocity v may be taken as the average velocity in Δx.

A. Methods

1. Berkeley

The data of the Berkeley group consist of the range measurements at 340 Mev (Ma51b) and the relative stopping power measurements by Bakker and Segrè (Ba51) and Thompson (Th52). With small modifications from one experiment to another the techniques were as follows.

(*a*) *Relative stopping power.*—The external beam of the synchrocyclotron—obtained either by electrostatic deflection or by scattering—was allowed to pass through a hole in the shielding material and collimated to diameters of the order of $\frac{1}{4}$ in.; a steering magnet then bent the beam (about 20°) into the cave area through, for example, a $\frac{1}{2}$-in. diameter×40-in. long collimating tube. In Thompson's work (see Fig. 20) the beam of

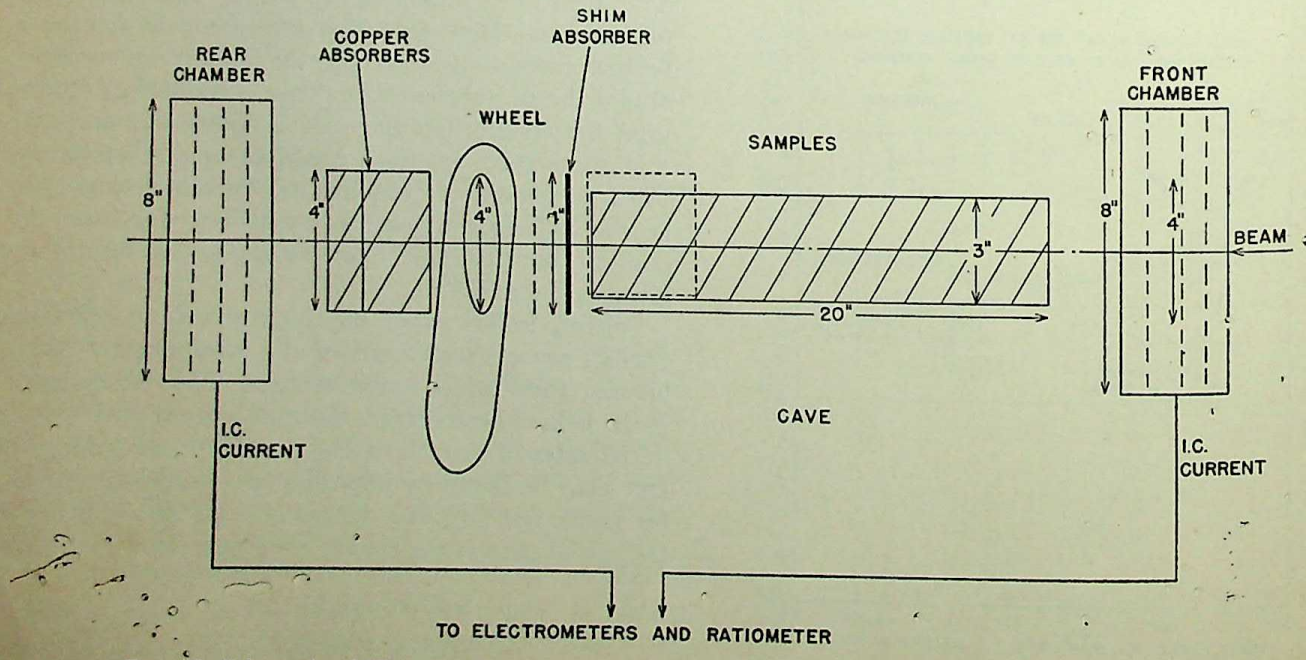


FIG. 20. Schematic of Thompson's (see reference Th52) apparatus for measurement of relative stopping power. The "shim absorbers" were used to make the energy loss in all the samples nearly equal.

CC-0. In Public Domain. Gurukul Kangri Collection, Haridwar

Digitized by Arya Samaj Foundation Chennai and eGangotri

protons first traversed a thin ionization chamber which served as a beam monitor; after this chamber the beam entered a sample of the material whose stopping properties were to be determined and following this an

". . . energy wheel with 12 slots containing step variations of copper of about 0.3 gm/cm² each. These were stamped with a circular die 4″ in diameter from 12.5 mil selected copper and carefully weighed. After the wheel was located a set of 4 absorbers working in a guillotine-like arrangement in such a way that any choice of these absorbers could be added or removed from the beam path by means of remote controls at a position outside the shielding. Next in the beam path were a predetermined number of copper blocks of 4″ square cross-sections and varying thickness. Each block was milled plane, flat and parallel to 0.2 mil and weighed to an accuracy of about 1 part in 50,000. Finally the rear ionization chamber was used to measure dE/dx near the end of the range."

The ratio of the currents from the two ionization chambers (read directly on an ingenious modification of a Leeds and Northrup Speedomax to a ratiometer) as a function of copper thickness respresented the raw data: the result is the end of the Bragg curve including the hump. The abscissa corresponding to 0.8 of the peak ionization value was then taken as the range in copper of the protons. With the thickness of the sample known precisely, and the measurement repeated with copper replacing the sample, the relative stopping power of the material could then be calculated.

(*b*) *Range.*—The range measurements (Ma51b) used roughly the same experimental arrangement (now with 1-in. collimation) with the addition that the beam first passed through Mather's (Ma51a) Čerenkov radiation apparatus, with which a precise measurement of the initial velocity of the beam could be made. After the beam energy was determined, the flux monitored, the beam passed through the copper absorber wheel, through a stack of plates of the metal being studied, and then into the second ionization chamber. The range is then given as the sum of the thickness of the main absorber and the equivalent thickness of the copper absorber wheel and chamber windows (less than 10 percent of the main absorber), this equivalence being calculated from (Ba51).

2. Los Angeles

(*c*) *Range.*—Hubbard and MacKenzie (Hu52) measured the range of 18-Mev protons in aluminum by using the internal beam of the 41-in. synchrocyclotron at UCLA. The beam was allowed to strike a heavy target on the median plane of the cyclotron and a fraction of the upward scattered component (the "axially scattered" beam) was used in the experiment. At a given azimuthal distance from the target, and above the median plane, a Faraday cage was interposed at an accurately known radius; in front of the cage, which was connected to an electronic electrometer, foils of aluminum were placed, one after another, in order to determine the absorber thickness that corresponded to a stoppage of one-half the beam. In this experiment, and in those of (Sa51 and Bl51), the beam energy could

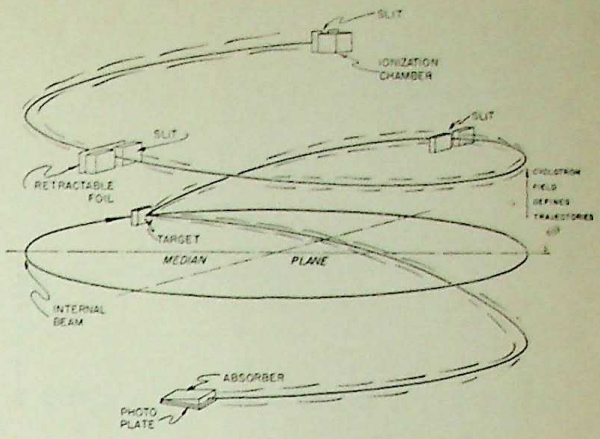


FIG. 21. Schematic illustrating internal beam cyclotron experiments. The "upper" experiment is similar to (Sa51), the "lower" to (Bl51).

be determined quite precisely since the magnetic field was referred in each case to the nuclear magnetic resonance frequency and the accuracy of the trajectory from target to detector is limited only by the patience of the plotter.¶¶

(*b*) *Absolute stopping power.*—The work of Sachs and Richardson (Sa51, Sa53) appears to be the first measurement of high-energy absolute stopping power. The cyclotron arrangement was similar to that of Hubbard and MacKenzie. They used the internal beam of the cyclotron, again with an axial deflection that allowed conveniently large intensities on the foil of stopping material and a precise value of the beam energy as measured by the cyclotron field itself. From the foil of high Z material (thorium) placed in the dee and on the median plane, those protons which multiply scattered upwards through angles small enough so that they were not captured by the dee, described a circular path inside the cyclotron, and 180° after scattering passed through a foil of the stopping material and then another 210° (20° past the scatterer, to take advantage of vertical focusing conditions in the cyclotron) to an ionization chamber detector whose radial position could be changed precisely from outside the vacuum tank. The shifts of radial position of the chamber with the foil "in" and "out" and a knowledge of the magnetic field along the trajectory (defined by a slit as in Fig. 21) then gave the energy loss in the foil.

3. Harvard

Again using the internal synchrocyclotron beam Bloembergen and van Heerden (Bl51) obtained the range-energy relation in aluminum, copper and lead, with an energy region stretching from 35–120 Mev. They used a tungsten scatterer (Fig. 21) and the down-

¶¶ In this connection it might be pointed out that a simple though somewhat less accurate method of determining the particle trajectory in an experiment of this type is the well-known floating wire method, described by J. Loeb, L'Onde Electrique 27, 27 (1947) and L. Cranberg, AECU 1670.

CC-0. In Public Domain. Gurukul Kangri Collection, Haridwar

Digitized by Arya Samaj Foundation Chennai and eGangotri

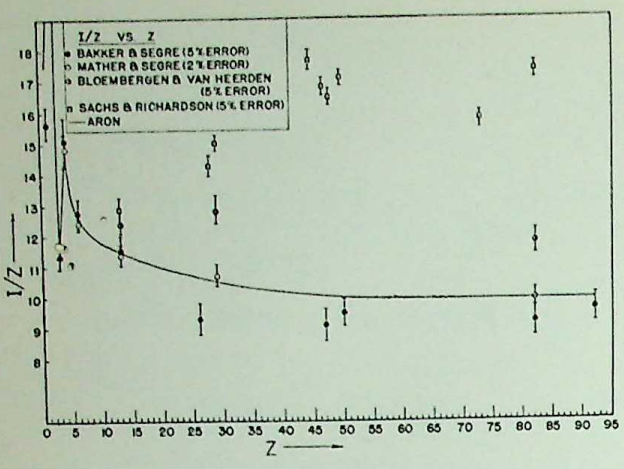


FIG. 22. Experimental determination of mean excitation potentials: I/Z *vs* Z. The errors given are orders of magnitude only.

ward scattered component was then detected by a photographic plate on a radius 180° after the scattering event; in front of the plate was a tapered absorber made of the stopping material. This absorber was made in the shape of a 30–60 triangular wedge, about 10-in. long, and the position of the absorber edge was located on the film with light marks. The photographic density along the direction parallel to the scattered beam, and at a given radius, then (after conversion by standard methods to particle flux) gave directly the integral absorption curve for an energy corresponding to the radius selected. Scanning the film in the direction perpendicular to the beam (along the cyclotron radius) yielded a measure of the energy spread in the beam, presumably resulting from the radial oscillation of the paths of the protons striking the target.

B. Experimental Results

From the total range (R) measurements (see Sec. II) the value of I can be calculated (Ar51) by using a trial value, I_1 from earlier experimental work, and computing the difference $R(I)-R(I_1)=R_{\text{exp}}-R(I_1)$. Aron, combining the results of a number of high-energy experiments and theoretical calculations, has calculated an extensive set of tables of dE/dx and range as a function of proton energy (Ar51). Since these tables represent the most definitive summary of experimental data taken up to the date of their calculation they can be used for comparison of subsequent data with theory. The smooth curve in Fig. 22 for the ratio I/Z *vs* Z gives the values used by Aron in his tables. Note that according to the Bloch theory I/Z should be constant for the heavy materials, and independent of incident particle energy. Hence, deviations from the theory should show up in a velocity-dependent excitation potential. It should be noted, of course, that the value of I is quite sensitive to error in the observations, since in both the absolute and relative stopping power methods what is really determined is $\log I$ rather than I itself. In the absolute method, the relative error $\delta I/I$ is the stopping number B (say of the order of 10) times the relative error in the stopping power. Since a one percent error or greater in stopping is common, this means a five to ten percent error in the excitation potential derived from this data. The relation between range error and error in I is (Si52)

$$\delta R/R=\left[2+\frac{E}{R(dE/dR)}\right]\frac{\delta I}{I}.$$

In terms of the use of calculated tables for absorption measurements, this is fortunate, since the range values are therefore not sensitive to the chosen value of this parameter. For purposes of verifying the theory, it means that much more precise experiments will have to be done.

Experimental data for protons have been recently obtained at 10 Mev at Birmingham, at 18 Mev on the Los Angeles synchrocyclotron, between 35 and 120 Mev at Harvard, and at 340 Mev at Berkeley. At 10 Mev Simmons (Si52) using the external beam of the Birmingham cyclotron, scanned nuclear track plates (C2 emulsion) for range distribution of the proton beam after passing the beam through Al absorbers. Using Rotblatt's (Ro51) range-energy curve for the emulsion to determine the beam energy and Smith's range tables to convert to aluminum range, he found that Smith's range was about 0.8 percent too low and that $I_{\text{Al}}=155\pm3$ ev.

The principal result given by Sachs and Richardson is a list of ionization potentials fitted by the Bethe-Bloch equation. Their original values for aluminum differed only slightly (156 ± 3 ev compared with 150 ± 20 ev) from the value obtained by Wilson (Wi41) with a relative stopping power technique, but they later (Sa53) recomputed their I using more recent numbers for the fundamental constants with the result $I_{\text{Al}}=168\pm3$ ev, considerably different from both lower-energy values from absolute measurements (Warshaw-Kahn) and higher-energy values from relative measurements. The results of (Hu52) and (Bl51) should be of comparable accuracy since the techniques—at least for the energy measurement—were so similar. Thus, the low initial energy measurement is given with a stated error of 0.11 percent (18.00 ± 0.02 Mev), and the higher initial energy error is stated to vary from 0.2 percent to 0.3 percent. At 18 Mev the measured mean range is 477.0 ± 0.5 mg/cm² of aluminum, compared with 468.7 mg/cm² given in Aron's table. In the higher-energy region, there were smaller, but still significant deviations of the experimental from theoretical range*** of the order of about 1 percent greater than theoretical in the lower end. This results for both aluminum and copper.

For lead the experimental range was about 1 percent lower than theory. Note that the direction of the

*** While Bloembergen and van Heerden compared their data with the earlier tables of Smith (see reference Sm47), these are essentially identical with Aron's for aluminum.

CC-0. In Public Domain. Gurukul Kangri Collection, Haridwar

Digitized by Arya Samaj Foundation Chennai and eGangotri

deviation is the same in both of these last measurements although the magnitudes of the deviations are different.

Bloembergen and van Heerden computed the value of the mean excitation potential from their range data with the result that I_{exp} is considerably larger than that used by Aron. They give a corrected value for I_{Al} (the corrected I corresponding to the experimental range, in turn corrected for small angle scattering as in Sec. II) as 161 ev in the region 50 to 75 Mev and 164 ev in the region 75 to 120 Mev. Since the error in I_{Al} is about 5 ev, the difference is possibly not significant. Hubbard and MacKenzie get substantially the same corrected value for I_{Al}: 170±19 ev. Both of these values are therefore in essential agreement with the recomputed I_{Al} from Sach's data.

No data for energies greater than 340 Mev are at present available, although much work at this energy has been reported by the group at Berkeley. In the series of measurements by Bakker and Segrè (Ba51) the stopping power relative to aluminum of elements from H to U were determined, with the initial energy obtained from the orbit radius at deflection from the cyclotron. By use of the general method (Bragg curve) outlined above, the relative mass stopping power was measured to about 1 percent error (5 percent for hydrogen, obtained by a difference method using graphite and CH_2), thus yielding the ionization potential to about 5–10 percent if there were no errors in the value used for the potential of the standard substance (Al). For I_{Al} they used 150 ev from Wilson's (Wi41) data, which they stated was accurate to about 3 percent. A careful analysis of the pertinent data on air and aluminum has been made by Bogaardt and Koudijs (Bo51) who find that the best value for I_{air} in the region between 2 Mev and 10 Mev is 77.5 ev, rather than the 80.5 ev used by Wilson. Since Wilson's 150 ev for I_{Al} was based on the older value of I_{air}, they changed this to $I_{Al}=151\pm3$ ev, an increase small enough to discount in interpreting Bakker and Segrè's work. Agreement with the low-energy data of Madsen and Venkateswarlu could be taken to confirm the high-energy values (but see below).

Later in the same year, Mather and Segrè reported a set of range values for elements from Be to Pb, again using an ionization chamber for detection, and with the initial velocity of the protons (340 Mev) determined precisely by Mather's (Ma51a) Čerenkov counter method. Mean rectified range on the Bragg curve was taken at the distance (see Sec. II) where the ionization fell to 0.82 of its peak value.

Also at Berkeley, the results of Thompson's work on chemical additivity yields the ionization potential of H_2, C, N_2, O_2, Cl; these however, are based on stopping powers relative to copper, for which Thompson took $I_{Cu}=279$ ev, as in the work of Bakker and Segrè. The values of the mean excitation potentials obtained by the aforementioned authors are summarized in Table IV-2, and a summary of existing data is in Table IV-1.

TABLE IV-1. Summary of recent high-energy data.[a]

A. All elements

Element	Bakker-Segrè (Ba50) S(rel to Al) 340 Mev	Mather-Segrè (Ma51) Range (gm/cm²) 340 Mev	Thompson (Th52) S(rel to Al)[c] 270 Mev	Tobias, *et al.* (To49) S(rel to Al) 180-Mev deuterons	Bloembergen-van Heerden (Bl51) S(rel to Al) 70 Mev
H_2	2.634	...	2.605	2.57	...
Li	1.062	...	...	...	...
Be	1.024	76.73	...	1.02	...
C	1.124	70.03	1.137	1.12	...
N_2	...	...	1.126	1.10	...
O_2	...	...	1.108	1.08	...
Al	1.000[d]	79.02[b]	1.000[d]	1.000[d]	1.000[e]
Cl	...	...	0.999	...	...
Fe	0.906	...	...	0.889	...
Cu	0.875	91.8[b]	...	0.867	0.819
Ag	0.789	...	...	...	...
Sn	0.751	107.41	...	0.719	...
W	0.680	...	...	...	...
Pb	0.660	123.6	...	0.613	0.612
U	0.630	...	...	...	...

B. Results for aluminum

Observer	Initial energy (Mev)	I_{Al}(ev)	Method	Value
Simmons (Si52)	10	155±3	Range	0.1410+0.0001 gm/cm²
Sachs-Richardson (Sa53)	18	168±3	Abs. dE/dx	22.07±0.6 Mev/gm/cm²
Hubbard-MacKenzie (Hu52)	18	162±2.5	Range	0.4769±0.0005 gm/cm²
Bloembergen-van Heerden (Bl51)	66.1[f]	162±5	Range	4.774±0.008 gm/cm²
Mather-Segrè (Ma51)	340	147.9±3	Range	79.02±0.5 gm/cm²

[a] The complete data of (Sa52) were not given in their article.
[b] Average range for two energies differing by < 1 percent.
[c] Converted from original as in Table II-2.
[d] Reference value.
[e] Actually Cu was the reference material; they also give experimental range as a function of energy from 35–120 Mev.
[f] Typical value of a set of energies.

CC-0. In Public Domain. Gurukul Kangri Collection, Haridwar

Digitized by Arya Samaj Foundation Chennai and eGangotri

TABLE IV-2. Summary of recent high-energy measurements of mean excitation potentials, I (ev).

Element	Z	Sachs-Richardson (Sa53) 18 Mev	Bloembergen-van Heerden (Bl51) 60 Mev[a]	Bakker-Segrè (Ba50) 340 Mev	Mather-Segrè (Ma51) 340 Mev[a]	Thompson (Th52) 270 Mev[e]
H	1	...	...	15.6[c]	...	18.0[d]
Li	3	...	...	34.0	...	...
Be	4	...	...	60.4	59.0	...
C	6	...	...	76.4	74.4	69.7
N	7	...	...	...	...	75.9[d]
O	8	...	...	...	...	87.6[d]
Al	13	168±3	162±5	150[b]	147.9±3	...
Cl	17	...	...	...	...	151.9
Fe	26	...	...	243	...	...
Ni	28	399	...	...	...	...
Co	29	435	370	279	309.9±3	...
Rh	45	799	...	...	...	...
Ag	47	796	...	428	...	...
Cd	48	792	...	...	...	...
Sn	50	853	...	479	...	...
Ta	73	1148	...	...	...	...
W	74	...	...	697	...	...
Au	79	1383	...	...	...	...
Pb	82	...	970	758	810.7±12	...
U	92	...	...	881	...	...

[a] Averaged over the several energies given in the original article.
[b] Taken as reference value, from Wilson.
[c] CH_2-carbon difference.
[d] Liquid target.
[e] These have been recalculated using Thompson's data and $I_{Al}=151$ ev.

The values of I/Z are also plotted in Fig. 22. Here it is seen that considerable deviations occur from the constancy of this quantity I/Z. These deviations, it has been noted by Sachs and Richardson (Sa53), cannot be explained by shell corrections and seem to give evidence of a velocity dependent I. Since each set of values reported was taken at a different energy, and with varying techniques, it would be more satisfactory to settle this question with data taken over a fairly large band of energies and with the same techniques. However, if it is granted that the variation in I is real, then some general tendencies are apparent.

It would then be advantageous to have some kind of semi-empirical method for obtaining the values of I for any Z and any energy. Lindhard and Scharf (Li52, 53) showed, using a dimensional argument and a Fermi-Thomas model, that the stopping number per electron, $B=(1/NZ)(dE/dx)(mv^2/4\pi e^4)$ (with the relativistic terms added to the right side when necessary), should be a function of Z/v^2 only. Following their suggestion, one may plot measured values of this quantity as a function of the logarithm of the dimensionless variable $x=v^2/v_0^2Z$, and the result should be a straight line if the Bloch formula is correct, with the log$x$ intercept giving the value of $I_0=I/Z$, or a smooth curve in any event. Figure 23 reproduces the curve from this paper, with the addition of points by Bloembergen and van Heerden and Thompson at high energy and Chilton, *et al.* at low energy. The curve is asymptotically straight (for $x\gtrsim 100$), and if the asymptote is projected back, the intercept gives $I_0=10.2$ ev. Then, if one writes $I=I_0Zf(x)$, $f(x)=\log(4Rx/I_0)-B(x)$ and f may be determined from the figure. This has been done (only by taking graphical differences from the smooth curves shown) with the result given in Fig. 24. Evidently, as particle energy changes by a factor of 100, I changes by a factor of nearly 2. The maximum in the curve means also that a low-energy measurement of I may agree with one at high energy and still leave the intermediate energy stopping power not exactly calculable from the common result.

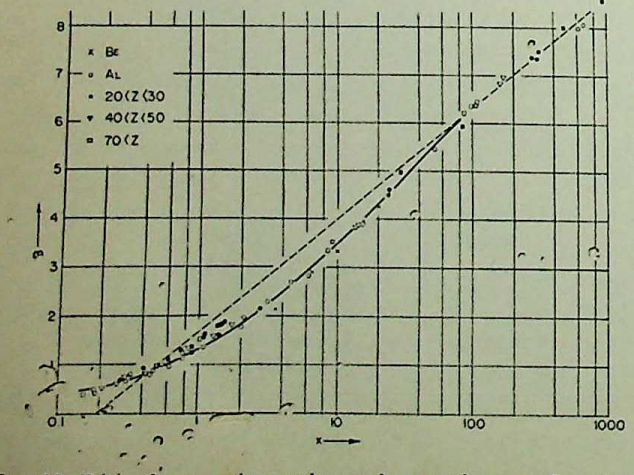


FIG. 23. $B(x)$, the experimental stopping number as a function of the variable $x=v^2/v_0^2Z$, reproduced from (Li53).

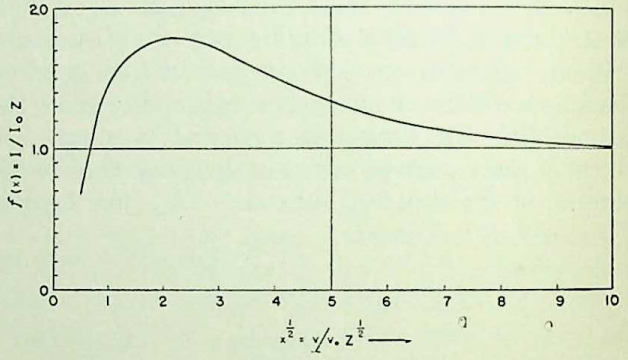


FIG. 24. The approximate energy variation of the mean excitation potential: $f(x)=I/I_0Z$ with $I_0=10.2$ ev.

BIBLIOGRAPHY

Al38 Allison, Skaggs, and Smith, Jr., Phys. Rev. **54**, 171 (1938).

Al53 S. K. Allison and Harvey Casson, Phys. Rev. **90**, 880 (1953).

Al53a Allison, Casson, and Weyl (to be published).

Ap51 R. K. Appleyard, Proc. Cambridge Phil. Soc. **47**, (2) 443 (1951).

Ar51 W. A. Aron, Thesis: "The Passage of Charged Particles Through Matter," University of California, (UCRL 1325).

Ba30 H. Bartels, Ann. Physik **6**, 957 (1930).

Ba32 H. Bartels, Ann. Physik **13**, 373 (1932).

Ba51 C. J. Bakker and E. Segre, Phys. Rev. **81**, 489 (1951).

Ba52 D. R. Bates and A. Dalgarno, Proc. Phys. Soc. (London) **A55**, 919 (1952).

Be51 Bernardini, Booth, and Lindenbaum, Phys. Rev. **82**, 307 (1951).

Be53 H. Bethe and J. Ashkin, *Experimental Nuclear Physics*, E. Segrè, editor. (John Wiley and Sons, Inc., New York, 1953), Chapter 2.

Be53a G. I. Bell, Phys. Rev. **90**, 548 (1953).

Bl33 F. Bloch, Ann. Physik. **16**, 285 (1933).

Bl51 Bloembergen and van Heerden, Phys. Rev. **83**, 561 (1951).

CC-0. In Public Domain. Gurukul Kangri Collection, Haridwar

Digitized by Arya Samaj Foundation Chennai and eGangotri

Bl49 O. Blunck and L. Leisegang, Z. Physik. **128**, 500 (1950).

Bø40 Bøgild, Brøstrøm, and Lauritsen, Math-fys. Medd. Acad. Copenhagen **18**, 4 (1940).

Bo41 N. Bohr, Phys. Rev. **59**, 270 (1941).

A.Bo49 A. Bohr, Kgl. Danske Videnskab. Selskab. Mat-fysk. Medd. **24**, 19 (1949).

Bo48 N. Bohr, Kgl. Danske Videnskab. Selskab. Mat-fysk. Medd. **18**, 8 (1948).

Bo51 M. Bogaardt and B. Koudijs, Physica **17**, 703 (1951).

Br27 G. H. Briggs, Proc. Roy. Soc. (London) **A114**, 241 (1927).

Br30 H. C. Brinkman and H. A. Kramer, Proc. Acad. Sci. Amsterdam **33**, 973 (1930).

Br41 Brunings, Knipp, and Teller, Phys. Rev. **60**, 657 (1941).

Br50 L. M. Brown, Phys. Rev. **79**, 297 (1950).

Br51 Browne, Craig, and Williamson, Rev. Sci. Instr. **22**, 952 (1951).

Ca52 D. O. Caldwell, Phys. Rev. **88**, 131 (1952).

Ca53 H. G. DeCarvalho and H. Yagoda, Phys. Rev. **88**, 273 (1953).

Ch53 Chilton, Cooper, and Harris, Bull. Am. Phys. Soc. **28**, 71 (1953).

Cr42 C. M. Crenshaw, Phys. Rev. **62**, 54 (1942).

Da14 C. G. Darwin, Phil. Mag. **27**, 499 (1914).

Di53 W. C. Dickinson and D. C. Dodder, Rev. Sci. Instr. **24**, 428 (1953).

Du52 Dunbar, Reynolds, Wenzel, and Whaling, Bull. Am. Phys. Soc. **27**, 6 (1952).

El52 Ellis, Rossi, and Failla, Phys. Rev. **86**, 562 (1952).

Ev53 Evans, Stier, and Barnett, Phys. Rev. **90**, 825 (1953).

Fe40 E. Fermi, Phys. Rev. **57**, 485 (1940).

Fe47 E. Fermi and E. Teller, Phys. Rev. **22**, 399 (1947).

Fr51 A. P. French and F. G. P. Seidl, Phil. Mag. **42**, 537 (1951).

Ge33 H. Geiger, Handbuch der Physik **22/2**, 221 (1933).

Gr50 Groetzinger, Berger, and Ribe, Phys. Rev. **77**, 584 (1950).

Gr52 A. C. Graves and D. K. Froman, *Miscellaneous Physical and Chemical Techniques of the Los Alamos Project* (McGraw-Hill Book Company, Inc., New York, 1952).

Ha38 G. T. Hatch, Phys. Rev. **54**, 165 (1938).

Ha48 O. Halpern and H. Hall, Phys. Rev. **73**, 477 (1948).

Ha49 T. A. Hall and S. D. Warshaw, Phys. Rev. **75**, 891 (1949).

Ha50 T. A. Hall, Phys. Rev. **79**, 509 (1950).

Ha51 Hanson, Lanzl, Lyman, and Scott, Phys. Rev. **84**, 634 (1951).

Ha52 E. L. Hubbard and K. R. MacKenzie, Phys. Rev. **85**, 107 (1952).

He22 G. H. Henderson, Proc. Roy. Soc. (London) **A102**, 496 (1922).

He25 G. H. Henderson, Proc. Roy. Soc. (London) **A109**, 157 (1925).

Hi48 J. O. Hirschfelder and J. L. Magee, Phys. Rev. **73**, 207 (1948).

Hu49 T. Huus and C. B. Madsen, Phys. Rev. **76**, 323 (1949).

Hu52 E. L. Hubbard and K. R. MacKenzie, Phys. Rev. **85**, 107 (1952).

Ig53 Igo, Clark, and Eisberg, Phys. Rev. **89**, 879 (1953).

Is50 I. Isenberg, Phys. Rev. **79**, 736 (1950).

Ja27 J. C. Jacobson, Nature **117**, 341 (1927).

Ja53 J. D. Jackson and H. Schiff, Phys. Rev. **89**, 359 (1953).

Ka51 H. Kanner, Phys. Rev. **84**, 1211 (1951).

Ka53 D. Kahn, Phys. Rev. **90**, 503 (1953).

Ki52 A. J. Kirschbaum, Thesis, University of California (Berkeley 1952) UCRL 1967.

Kn41 J. Knipp and E. Teller, Phys. Rev. **59**, 659 (1941).

Ko36 I. M. Kolthoff and E. B. Sandell, *Quantitative Inorganic Analysis* (Macmillan Company, New York, 1936), p. 306.

La44 W. Landau, J. Phys. (U.S.S.R.) **8**, 201 (1944).

Le52 L. Lewis, Phys. Rev. **85**, 20 (1952).

Li37 S. Livingston and H. A. Bethe, Revs. Modern Phys. **9**, 264 (1937).

Li52 J. Lindhard and M. Scharff, Phys. Rev. **85**, 1058 (1952).

Li53 J. Lindhard and M. Scharff, Kgl. Danske Videnskab. Selskab. Mat-fys Medd. **27**, 15 (1953).

Ma48a C. B. Madsen and P. Venkateswarlu, Phys. Rev. **74**, 648 (1948).

Ma48b C. B. Madsen and P. Venkateswarlu, Phys. Rev. **76**, 1782 (1948).

Ma51 R. Mather and E. Segrè, Phys. Rev. **84**, 191 (1951).

Ma53 M. Madsen, private communication.

Me37 H. Meyer, Ann. Physik **30**, 635 (1937).

Mi14 W. Michl, Sitzber. Akad. Wiss. Wein, Math-naturw. Kl. **123**, 1965 (1914).

Mo49 N. F. Mott and H. S. W. Massey, *The Theory of Atomic Collisions* (Oxford University Press, New York, 1949).

Mo50 J. Montague, Phys. Rev. **81**, 1026 (1950).

Mo51 G. Moliere, Z. Naturforsch. **3a**, 78 (1948).

Pe52 A. M. Perry, Phys. Rev. **85**, 497 (1952).

Ph23 K. Phillip, Z. Physik **17**, 23 (1923).

Ph53 J. A. Phillips, Phys. Rev. **90**, 532 (1953).

Ph53a J. A. Phillips, Bull. Am. Phys. Soc. **28**, 31 (1953).

Ri51 F. Ribe, Phys. Rev. **83**, 1217 (1951).

Ro41 B. B. Rossi and K. I. Greisen, Revs. Modern Phys. **13**, 240 (1941).

Ro51 J. Rotblatt, Nature, **167**, 550 (1951).

Rü33 E. Rüchardt, Handbuch der Physik **22/2**, 103 (1933).

Ru24 E. Rutherford, Phil. Mag. **4**, 277 (1924).

Sa51 D. C. Sachs and J. R. Richardson, Phys. Rev. **83**, 834 (1951).

Sa53 D. C. Sachs and J. R. Richardson, Phys. Rev. **89**, 1165 (1953).

Sa52 G. A. Sawyer, Rev. Sci. Instr. **23**, 604 (1952).

Sc50 W. T. Scott and H. S. Snyder, Phys. Rev. **78**, 223 (1950).

Sc51 M. Schoenberg, Nuovo Cimento **8**, 159 (1951).

Sc52 W. T. Scott, Phys. Rev. **85**, 245 (1952).

Si52 D. H. Simmons, Proc. Phys. Soc. (London) **A65**, 454 (1952).

Sm47 J. H. Smith, Phys. Rev. **71**, 32 (1947).

Sn50 Snyder, Rubin, Fowler, and Lauritsen, Rev. Sci. Instr. **21**, 852 (1950).

Sn53 E. Snitzer, Phys. Rev. **89**, 1237 (1953).

St45 J. Strong, *Procedures in Experimental Physics* (Prentice-Hall, Inc., New York, 1945), Chapter 4.

St52 R. Sternheimer, Phys. Rev. **88**, 851 (1952).

Ta52 A. E. Taylor, Repts. Prog. in Phys. **15** (1952).

Th52 T. Thompson, Thesis, University of California (Berkeley 1952) UCRL 1910.

To45 S. Tolansky, Proc. Roy. Soc. (London) **A186**, 261 (1945).

To47 S. Tolansky, Proc. Roy. Soc. (London) **A191**, 182 (1947).

To51 C. Tobias, AECD-2099-A.

Wa49a S. D. Warshaw, Rev. Sci. Instr. **20**, 623 (1949).

Wa49b S. D. Warshaw, Phys. Rev. **76**, 1759 (1949).

Wa52 W. C. Walske, Phys. Rev. **88**, 1283 (1952).

We52 W. A. Wenzel and Ward Whaling, Phys. Rev. **87**, 499 (1952).

We53 P. K. Weyl, Phys. Rev. **91**, 289 (1953).

Wi41 R. R. Wilson, Phys. Rev. **60**, 749 (1941).

Wi47 R. R. Wilson, Phys. Rev. **71**, 385 (1947).

Wi48 H. A. Wilcox, Phys. Rev. **74**, 1743 (1948).

Wi45 E. J. Williams, Revs. Modern Phys. **17**, 217 (1945).

CC-0. In Public Domain. Gurukul Kangri Collection, Haridwar

Digitized by Arya Samaj Foundation Chennai and eGangotri

REVIEWS OF MODERN PHYSICS VOLUME 25, NUMBER 4 OCTOBER, 1953

On Statistical Estimation in Physics

M. ANNIS,* W. CHESTON,† AND H. PRIMAKOFF

Washington University,‡ St. Louis, Missouri

The problem of the estimation of parameters determined statistically from physical measurements is discussed. Emphasis is placed on the fundamental role played by the prior probability distribution for the parameter. The validity of "maximum likelihood" estimation is examined with particular reference to the case of the estimation of a parameter which actually has an unique but (originally) unknown magnitude. Situations in which the prior probability distribution for the parameter is completely unknown are treated and a method is described for the calculation of this distribution from appropriate experimental data. Many examples are given throughout from the field of cosmic radiation.

I. INTRODUCTION

THE current paper is the outgrowth of an attempt by the authors to understand certain statistical considerations associated with the determination of elementary particle parameters on the basis of cosmic-ray measurements. We could not discover the answers to several questions which appeared relevant to the problem in any references easily available to physicists and were therefore forced to work out the conclusions below—many of our results are no doubt implicitly or perhaps even explicitly contained in the literature on probability and statistics. Nevertheless, we communicate these results in their present form in the hope that others may possibly find them useful, and with the intention of arousing further interest in the subject.

In physics, a situation frequently arises in which one desires to determine a physical quantity, which we shall call θ, characteristic of either a class of individual particles (e.g., the mean-life of a class of individual (unstable) particles of the same kind) or a class of systems of particles (e.g., the temperature of a class of stars); however, this physical quantity θ cannot in any sense be "measured" directly. Instead, one measures directly another set of n quantities, x_1, x_2, $x_3 \cdots x_n$, which we shall call x_i, which are not related to θ in a simple one-to-one fashion (i.e., θ is not uniquely determined by the set x_i). What we do know on the basis of some theoretical consideration is the probability that the set x_i lie in the interval dx_i (i.e., that, simultaneously, x_1 is between x_1 and x_1+dx_1, x_2 between x_2 and x_2+dx_2, etc.) for a given value of θ. We shall denote this probability function by $G(\theta;\ x_1,\ x_2 \cdots x_n) \times dx_1 dx_2 \cdots dx_n \equiv G(\theta; x_i)dx_i$. (In our notation, the quantity before the semi-colon is a parameter and the quantities after the semi-colon are variables.) However, having measured the set x_i directly, we should like to know the probability that θ lies in $d\theta$ for these given values of the set x_i. We shall denote this latter probability (the so-called posterior probability) by $H(x_1,\ x_2 \cdots x_n; \theta)d\theta \equiv H(x_i; \theta)d\theta$. The question now arises: "What relationship, if any, exists between the two probability functions $G(\theta; x_i)dx_i$ and $H(x_i; \theta)d\theta$?"

In order to answer the question posed above, we define another probability function (the so-called prior probability), $P(\theta)d\theta$. $P(\theta)d\theta$ is the probability that, in the type of experiment performed, θ lies in $d\theta$, independent of the values of the x_i. In the same manner, we may define the probability that, in a measurement of the set x_i, the x_i lie in dx_i, independent of the values of θ. We designate this latter probability by the expression $Q(x_1,\ x_2,\ \cdots x_n)dx_1 \cdots dx_n \equiv Q(x_i)dx_i$.

It is not superfluous to mention that all the four probability functions defined may be understood, in a physical context, in the sense of the corresponding, in principle observable, relative frequencies; the normalizability of these probability functions with respect to their variables may then be demanded. It should also be mentioned that our whole treatment can be generalized in a straightforward manner to the case of the existence of several parameters $\theta_1, \cdots, \theta_m$; the essential conclusions obtained below are also valid in the case of such a generalization.

II. CASE OF KNOWN PRIOR PROBABILITY DISTRIBUTION

An intimate relationship exists among the probability functions defined in Sec. I. To exhibit this relationship, we define a function $S(\theta, x_i)d\theta dx_i$ as the simultaneous probability that θ lies in $d\theta$ while the set x_i lie in dx_i. By the rules of combining probabilities, this simultaneous probability is the probability that the x_i lie in dx_i for given θ, multiplied by the probability that θ lies in $d\theta$, independent of the values of x_i; i.e.,

$$S(\theta, x_i)dx_i d\theta = P(\theta)d\theta \cdot G(\theta; x_i)dx_i. \tag{1a}$$

On the other hand, this simultaneous probability can also be expressed as the probability that θ lies in $d\theta$ for given values of the x_i multiplied by the probability that the x_i lie in dx_i, independent of θ; i.e.,

$$S(\theta, x_i)dx_i d\theta = Q(x_i)dx_i \cdot H(x_i; \theta)d\theta. \tag{1b}$$

* Present address: Institute of Physics, University of Padua, Padua, Italy.

† Present address: Department of Physics, University of Minnesota, Minneapolis, Minnesota.

‡ Assisted by the joint program of the U. S. Office of Naval Research and the U. S. Atomic Energy Commission.

CC-0. In Public Domain. Gurukul Kangri Collection, Haridwar

Digitized by Arya Samaj Foundation Chennai and eGangotri

Combining the results of Eqs. (1a) and (1b), we may write a relationship between $G(\theta; x_i)dx_i$ and $H(x_i; \theta)d\theta$ usually attributed to Bayes, namely,

$$Q(x_i)H(x_i; \theta)dx_i d\theta = P(\theta)G(\theta; x_i)d\theta dx_i \qquad (2a)$$

or

$$H(x_i; \theta) = P(\theta)G(\theta; x_i)/Q(x_i). \qquad (2b)$$

Equation (2b) may be written in a slightly altered form if we remember the normalization of $H(x_i; \theta)$. Integrating both sides of Eq. (2a) over the variable θ, we note that

$$Q(x_i)dx_i \cdot \int H(x_i; \theta)d\theta = Q(x_i)dx_i$$

$$= \left[\int P(\theta)G(\theta; x_i)d\theta\right] \cdot dx_i, \qquad (2c)$$

it being understood that all integrals contained in this paper extend over the complete range of the integration variable unless otherwise explicitly stated. Therefore, we see that

$$H(x_i; \theta) = \frac{P(\theta)G(\theta; x_i)}{\int P(\theta)G(\theta; x_i)d\theta}. \qquad (2d)$$

We can also write an expression analogous to Eq. (2c) for the probability function $P(\theta)$, via Eq. (2a). This is

$$P(\theta) = \int Q(x_i)H(x_i; \theta)dx_i. \qquad (2e)$$

One should now remember that $G(\theta; x_i)dx_i$ is usually known on the basis of theoretical considerations. It is to be noted, therefore, that any statements we make about $H(x_i; \theta)$ must depend upon our knowledge of the function $P(\theta)d\theta$. If this last function is known via some physical theory and/or a set of previously performed experiments, Eq. (2d) offers us an exact solution for the posterior probability function $H(x_i; \theta)d\theta$; i.e., we can state what the probability is that θ lies in $d\theta$ with our measured values of the set x_i. It is also obvious from Eq. (2d) that $H(x_i; \theta)d\theta$ cannot be determined if $P(\theta)d\theta$ is completely unknown. In many cases, it is, however, not necessary that $P(\theta)d\theta$ be completely known as a function of θ in order to make statements with significance in a probability sense. Such cases will be discussed in detail in subsequent sections of this paper.

We shall now examine more carefully the case where $P(\theta)d\theta$ is a known function of the parameter θ. The existence of the probability function $H(x_i; \theta)d\theta$ allows us here to answer the question, "What is the probability that the parameter θ lies in $d\theta$ for a given set of the x_i?" The answer to this question is given by exhibiting $H(x_i; \theta)$ as in Fig. 1(a) or 1(b).

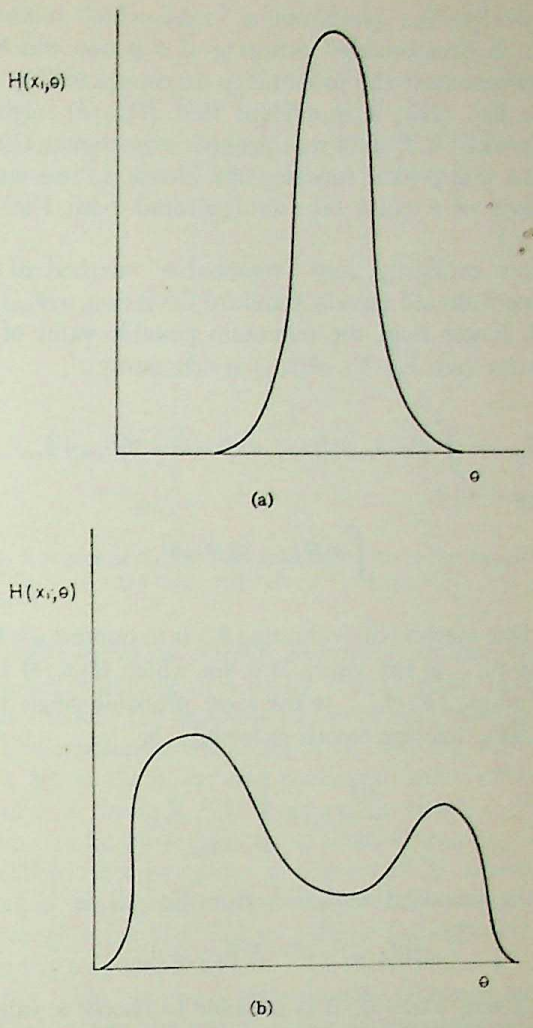


FIG. 1. The posterior probability function, $H(x_i; \theta)$, plotted as a function of θ, (a) in the case where a single estimate of θ might be given, and (b) in the case where no single estimate of θ can be quoted.

When $H(x_i; \theta)$ has the form shown in Fig. 1(a) (i.e., a single, well-defined peak), there is little doubt that one can quote a single value of θ which has "statistical significance." On the other hand, if $H(x_i; \theta)$ looks somewhat as in Fig. 1(b) with widely different θ's having comparable probabilities, it is perhaps unwise to quote a single value for θ. However, in a particular case, the information in Fig. 1(b) could conceivably still be valuable.

When $H(x_i; \theta)$ is well peaked as in Fig. 1(a), it is frequently useful to quote a single "statistically significant" value or estimate for θ, *viz.*, θ_{est}, with an appropriately defined standard deviation. (One should point out that this standard deviation is taken as the standard deviation of the posterior probability distribution about θ_{est} and hence is one measure of the statistical accuracy of the estimate.) Of course one can also easily answer any questions concerning the probability of θ lying within a certain range about θ_{est}. This procedure is only useful if the value of θ_{est} and the standard deviation is not sensitive to the method used

CC-0. In Public Domain. Gurukul Kangri Collection, Haridwar

Digitized by Arya Samaj Foundation Chennai and eGangotri

to calculate θ_{est} (assuming a "reasonable" method is used). A "reasonable" estimate of θ is one which lies somewhere near the probability maximum in Fig. 1(a). From Eq. (2b), it is evident that $H(x_i;\theta)$ might be well peaked if $P(\theta)$ is well peaked, even though $G(\theta;x_i)$ is not a well-peaked function of θ. Hence, a "reasonable" estimate of θ must take into account both $P(\theta)$ and $G(\theta;x_i)$.

More explicitly, any "reasonable" method of estimating θ should have a standard deviation, $\sigma(\theta_{est})$, not much larger than the minimum possible value of this quantity (see Eq. 7). $\sigma^2(\theta_{est})$ is defined by

$$\sigma^2(\theta_{est})=\int(\theta-\theta_{est})^2H(x_i;\theta)d\theta=\overline{\theta^2}-\overline{2\theta}\,\theta_{est}+\theta_{est}^2, \quad (3)$$

where

$$\int\theta^sH(x_i;\theta)d\theta\equiv\overline{\theta^s}.$$

1. One method of evaluating θ_{est} is to quote $\theta_{est}=\theta_{m.p.}$, where $\theta_{m.p.}$ is the value of θ, for which $H(x_i;\theta)$ has a maximum; i.e., $\theta_{m.p.}$ is the most probable single value of θ. The defining equation for $\theta_{m.p.}$ is

$$\frac{\partial H}{\partial\theta}(x_i;\theta)\Big]_{\theta=\theta_{m.p.}}=0 \quad (4)$$

and the standard deviation, from Eq. (3), is

$$\sigma^2(\theta_{m.p.})=\theta^2-2\bar{\theta}\,\theta_{m.p.}+\theta_{m.p.}^2. \quad (5)$$

2. Using Eq. (3), it is possible to choose a value of θ_{est} which minimizes the standard deviation of the estimate. To do this, we differentiate Eq. (3) with respect to θ_{est} and set the derivative equal to 0, yielding a defining equation for θ_{est}. One finds

$$\theta_{est}=\bar{\theta} \quad (6)$$

with standard deviation

$$\sigma^2(\bar{\theta})=\overline{\theta^2}-\bar{\theta}^2. \quad (7)$$

3. To minimize the *relative* standard deviation, we solve Eq. (3) for $\sigma^2(\theta_{est})/\theta_{est}^2$, and set the derivative of this quantity with respect to θ_{est} equal to zero. We obtain

$$\theta_1=\overline{\theta^2}/\bar{\theta} \quad (8)$$

with relative standard deviation

$$\sigma^2(\theta_1)/\theta_1^2=1-\bar{\theta}^2/\overline{\theta^2}. \quad (9)$$

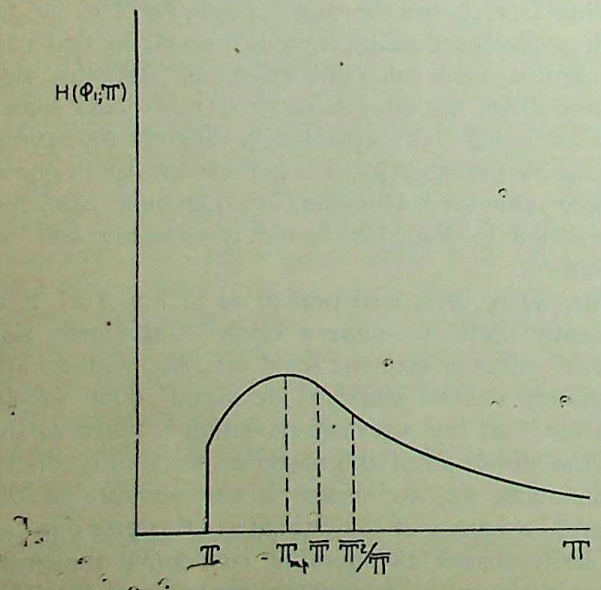


FIG. 2. The posterior probability, $H(\phi_i;\Pi)$, plotted as a function of $\Pi=pc\beta$. The relative position of the different estimates of Π is also shown.

Example from the Theory of Multiple Coulomb Scattering

One measures the n-projected angles of multiple scattering of a particle in the n plates of a multiplate cloud chamber and from this scattering data, one desires to find an estimate of $\Pi=pc\beta$ for the particle (p=momentum; $c\beta$=velocity), assuming that Π does not change while the particle is traversing the chamber. In this case the parameter θ becomes the physical quantity Π and the x_i become ϕ_i, the projected angle of multiple scattering in the ith plate.

From the theory of multiple Coulomb scattering, the probability that ϕ_i lies in $d\phi_i$, $f(\phi_i)d\phi_i$, is given as

$$f(\phi_i)d\phi_i=(2\pi GQ)^{-\frac{1}{2}}\exp\{-\phi_i^2/2GQ\}d\phi_i. \quad (10)$$

Equation (10) is an approximation, good only for $\phi_i^2<2GQ$, where G and Q are defined by Olbert.[1] However we shall assume that Eq. (10) holds for all ϕ_i, the resultant error in the final answer being less than 10 percent.

In the above approximation, G depends only on the material in the plates, while Q depends on the material in the plates, and in addition, is inversely proportional to Π^2. Hence we can define a quantity A independent of Π by the equation

$$A=\Pi(2GQ)^{\frac{1}{2}} \quad (11)$$

so that Eq. (10) becomes

$$f(\phi_i)d\phi_i=N_1\Pi\exp\{-\phi_i^2\Pi^2/A^2\}d\phi_i, \quad (12)$$

where N_1 is a normalization factor, independent of ϕ_i and Π.

Since the angles of multiple scattering in the n plates are statistically independent, it is evident that

$$G(\Pi;\phi_i)=f(\phi_1)f(\phi_2)\cdots f(\phi_n)$$
$$=N_1{}^n\Pi^n\exp\left\{-\frac{\Pi^2}{A^2}\sum_{i=1}^{n}\phi_i{}^2\right\}. \quad (13)$$

Let us now assume that the prior probability distribution for Π is a power law, i.e.,

$$P(\Pi)=\begin{matrix}0; & \Pi<\Pi_0\\ N_2\Pi^{-\gamma}; & \Pi\geqq\Pi_0,\end{matrix} \quad (14)$$

where N_2 is a normalization factor, and γ is an empirically determined constant ($\gamma\approx3$ in many cases). $H(\phi_i;\Pi)$ may then be evaluated from Eqs. (2d) and (13). (14) yielding

$$H(\phi_i;\Pi)=\begin{matrix}0; & \Pi<\Pi_0\\ N_3\Pi^{n-\gamma}\exp\left\{-\frac{\Pi^2}{A^2}\sum_{i=1}^{n}\phi_i{}^2\right\}; & \Pi\geqq\Pi_0.\end{matrix} \quad (15)$$

$H(\phi_i;\Pi)$ is plotted in Fig. 2 as a function of Π.

[1] S. Olbert, Phys. Rev. 87, 319 (1952).

CC-0. In Public Domain. Gurukul Kangri Collection, Haridwar

Digitized by Arya Samaj Foundation Chennai and eGangotri

The most probable value of Π is, from Eqs. (15) and (4),

$$\Pi_{\text{m.p.}} = \begin{cases} \Pi_0; & n \leqq \gamma \\ (m/2)^{\frac{1}{2}} A \left(\sum_{i=1}^{n} \phi_i^2\right)^{-\frac{1}{2}}; & n > \gamma, \end{cases} \tag{16}$$

where $m = n - \gamma$. Using Eq. (3), we find that the corresponding standard deviation is (for $\Pi_0 \ll \Pi_{\text{m.p.}}$)

$$\sigma(\Pi_{\text{m.p.}}) = \Pi_{\text{m.p.}} \{2 + 1/m - 2(2/m)^{\frac{1}{2}} \Gamma(1+m/2)/\Gamma(\tfrac{1}{2}+m/2)\}^{\frac{1}{2}}. \tag{17}$$

Under the same assumption, the mean value of Π, i.e., the estimate of Π which minimizes the standard deviation, is (Eqs. (15) and (6))

$$\langle \Pi \rangle_{\text{Av}} = \frac{\Gamma(1+m/2)}{\Gamma(\frac{1}{2}+m/2)} A \left(\sum_{i=1}^{n} \phi_i^2\right)^{-\frac{1}{2}}, \tag{18}$$

with standard deviation (Eq. 7)

$$\sigma(\langle \Pi \rangle_{\text{Av}}) = \langle \Pi \rangle_{\text{Av}} \left\{ \frac{m+1}{2} \frac{\Gamma^2(\frac{1}{2}+m/2)}{\Gamma^2(1+m/2)} - 1 \right\}^{\frac{1}{2}}, \tag{19}$$

and the estimate of Π which minimizes the *relative* standard deviation is (Eqs. (15) and (8))

$$\Pi_1 = \langle \Pi^2 \rangle_{\text{Av}} / \langle \Pi \rangle_{\text{Av}} = \frac{m+1}{2} \frac{\Gamma(\frac{1}{2}+m/2)}{\Gamma(1+m/2)} A \left(\sum_{i=1}^{n} \phi_i^2\right)^{-\frac{1}{2}}, \tag{20}$$

with standard deviation (Eq. (9))

$$\sigma(\Pi_1) = \Pi_1 \left\{ 1 - \frac{2}{m+1} \frac{\Gamma^2(1+m/2)}{\Gamma^2(\frac{1}{2}+m/2)} \right\}^{\frac{1}{2}}. \tag{21}$$

Each of these estimates is shown in Fig. 2. For all of these estimates

$$\lim_{m \to \infty} \sigma(\Pi_{\text{est}}) = \Pi_{\text{est}} (2m)^{-\frac{1}{2}}. \tag{22}$$

(For $m = 6$, Eq. (22) agrees to within a few percent with Eqs. (17), (19) and (21).)

From Eqs. (16) to (21) it is evident that for $m = (n - \gamma) > 6$, and for $\Pi_0 \ll \Pi_{\text{m.p.}}$; $\Pi_{\text{m.p.}}$, $\langle \Pi \rangle_{\text{Av}}$ and Π_1 are nearly the same. If $n \gg \gamma$, all of these estimates are effectively independent of $P(\Pi)$, the prior probability distribution in Π, so that uncertainties in detail about $P(\Pi)$ make little difference in the Π estimates.

We have mentioned previously that whenever it is desired to ascribe a numerical value to a statistically determined physical parameter such as θ, it is essential that at least some aspects of the nature of the prior probability function $P(\theta)d\theta$ be known. We have treated the case in which $P(\theta)d\theta$ is a known function of θ. It is, however, not necessary that $P(\theta)$ be completely known as a function of θ; on the other hand, one must at least know whether $P(\theta)$ is: (1) a continuous function of θ, (2) a linear combination of δ functions of θ, or (3) a single δ-function of θ. Put in another way, one should know: (1) whether all values of θ are possible, (2) whether only certain discrete values of θ are possible, or (3) whether θ has a certain unique but as yet unknown value. On the other hand, if $P(\theta)d\theta$ is completely unknown, steps must be taken, in general, to delimit at least some of its aspects. Such steps will now be described.

III. PROCEDURE FOR FINDING AN UNKNOWN PRIOR PROBABILITY DISTRIBUTION

In the previous section, we have assumed that the prior distribution in the physical parameter, $P(\theta)d\theta$, is known. This is often not the case. Indeed, in some situations this prior distribution may actually be the chief quantity which is sought. Before we outline the procedure for finding $P(\theta)$ under these circumstances, we shall describe the experimental work that must be done.

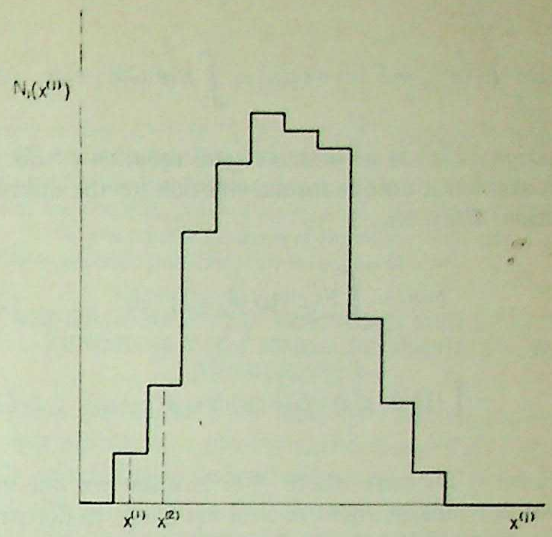


FIG. 3. A plot of $N_j(x^{(j)})$, the number of times the variable x had the measured value $x^{(j)}$, *versus* $x^{(j)}$.

The experiment described in II (i.e., the observation of a set of the x_i for one particular value of θ) is repeated M times. If $P(\theta)$ is a function which is different from zero for more than one value of θ, then one expects that θ will not be unique in this set of M experiments. Each of the experiments will, in general, correspond to a different value of θ. Let us assume for simplicity that there is only one value of x in each of the M experiments (i.e., in *each* experiment $G(\theta; x_i)$ becomes $G(\theta; x)$); then the result of the experiments will look, for example, somewhat as illustrated in Fig. 3, where $N_j(x^{(j)})\Delta x$ is the number of times that the measured value x falls between $x^{(j)} - (\Delta x/2)$ and $x^{(j)} + (\Delta x/2)$, Δx being the difference between adjacent $x^{(j)}$'s. Since θ is not fixed during the M experiments, we do not expect $N_j(x^{(j)})$ to be well peaked unless $P(\theta)$ is well peaked. To convert the $N_j(x^{(j)})$ to a relative frequency distribution, we remember that

$$\sum_{j=1}^{\infty} N_j(x^{(j)})\Delta x = M,$$

so the distribution sought is simply

$$F_j(x^{(j)}) = N_j(x^{(j)})/M,$$

where $F_j(x^{(j)})\Delta x$ is the relative frequency with which x lies between $x^{(j)} - \Delta x/2$ and $x^{(j)} + \Delta x/2$. In the limit of small Δx and large M, $F_j(x^{(j)})$ becomes $F(x)$, a continuous distribution in x. It is to be noted that the (prior) probability distribution for x, previously called $Q(x)$, must now be identified with the relative frequency distribution in x, $F(x)$.

The problem then is to find $P(\theta)$ having been given $F(x)$ from experiment and knowing the distribution function, $G(\theta; x)$, from theory. By use of Eq. (2c), we

CC-0. In Public Domain. Gurukul Kangri Collection, Haridwar

Digitized by Arya Samaj Foundation Chennai and eGangotri

find

$$\lim_{\substack{M\to\infty\\ \Delta x\to 0}} F_j(x^{(j)}) = F(x) = Q(x) = \int P(\theta)G(\theta; x)d\theta. \quad (23a)$$

Equation (23a) is a *linear integral equation of the first kind*, and has a unique formal solution for the unknown function, $P(\theta)$, *viz.*,

$$P(\theta) = \int F(x')\{G(\theta; x')\}^{-1}dx', \quad (23b)$$

where

$$\int \{G(\theta; x')\}^{-1}G(\theta; x)d\theta = \delta(x-x'). \quad (23c)$$

Thus, in the case where $P(\theta)$ is unknown one must repeat the measurement of x (θ *not* fixed) to determine $F(x)=Q(x)$ and then use Eq. (23b) to calculate $P(\theta)$. Of course, in the special case where $P(\theta)$ is a linear combination of δ functions of θ or a single δ function of θ, Eq. (23b) will simply indicate that fact.

Comparison of Eqs. (23b) and (2e) (or of Eqs. (2c) and (2e)) should not lead one to the conclusion that $H(x';\theta)=\{G(\theta;x')\}^{-1}$; this conclusion is obviously wrong, if only because $H(x';\theta)$ depends on $P(\theta)$ (see Eq. (2b)) and $\{G(\theta;x')\}^{-1}$ does not. More explicitly, if $H(x';\theta)$ were equal to $\{G(\theta;x')\}^{-1}$, Eq. (23c) would indicate that

$$\int H(x';\theta)G(\theta;x)d\theta = \delta(x-x'),$$

and this last is impossible since H and G, being both probability distributions, are everywhere positive as functions of θ for any x', x. Thus the reasons for the validity of (23b) and (2e) are quite different; the former follows from (23a) as a consequence of the δ function relation between $G(\theta;x)$ and $\{G(\theta;x)\}^{-1}$, the latter on the other hand follows from (2a) as a consequence of the interconnected definitions of $Q(x)$, $P(\theta)$, $G(\theta;x)$, $H(x;\theta)$ in Eqs. (2).

Example from the Theory of Multiple Coulomb Scattering

Many particles are observed to reach the end of their range in one of the plates of a multiplate cloud chamber. The problem is to estimate the masses and relative frequencies of occurrence of the different particles. We shall assume that each particle is observed to penetrate n plates before reaching the end of its range.

Following Annis *et al.*[2] we define a variable, η_i, by the relationship

$$\eta_i \equiv \phi_i R_i^{\alpha}, \quad (24)$$

where ϕ_i is the projected angle of scattering in the ith plate, and R_i is the residual range of the particle in the ith plate. The exponent $\alpha=0.553$ for all materials, and is defined by the equation

$$R/mc^2 = A_Z(\Pi/mc^2)^{1/\alpha}, \quad (25)$$

where $\Pi=pc\beta$ as before, m is the mass of the particle, R is the range of a particle with given Π, and A_Z is a constant for a given scattering material. Equation (25) allows us to write the distribution in η_i in a form analogous to Eq. (11);

$$f(\eta_i) \cong (2\pi)^{-\frac{1}{2}}\rho^{-1}\exp\{-\eta_i^2/2\rho^2\}, \quad (26)$$

where ρ is a constant for a given particle, independent of the residual range, and depending on the mass of the particle through the relation $\rho \sim m^{1-\alpha}$. From Eq. (26) it is evident that ρ has the dimensions of η_i.

Let us now define the mean square value of the η_i by the equation

$$s^2 = n^{-1}\sum_{i=1}^{n}\eta_i^2, \quad (27)$$

and let $G(\rho;s)ds$ be the probability for given ρ (i.e., given m), that s lies in ds. Then,

$$G(\rho;s)ds = \int\cdots\int f(\eta_1)\cdots f(\eta_n)d\eta_1\cdots d\eta_n, \quad (28)$$

the region of integration in Eq. (28) being over those values of the η_i for which Eq. (27) holds. The integral in Eq. (28) can be readily performed and the result is

$$G(\rho;s) = B\rho^{-n}s^{n-1}\exp\{-(1/2)ns^2/\rho^2\}, \quad (29)$$

where B is a constant independent of ρ and s.

Let us now suppose that we have observed M particles reach the end of their range in the chamber and we calculate s for each of these particles. If $F_i(s^{(i)})\,\Delta s$ is defined as the relative frequency with which s lies between $s^{(i)}-(\Delta s/2)$ and $s^{(i)}+(\Delta s/2)$, the (normalized) $F_i(s^{(i)})$ function might look somewhat as shown in Fig. 4. In this case, Eq. (23a) has approximately the form (if $M\to\infty$ and $\Delta\rho\to 0$)

$$F_i(s^{(i)}) = \sum_{j=1}^{\infty} P_j(\rho^{(j)})G(\rho^{(j)};s^{(i)})\Delta\rho, \quad (30)$$

where $P_j(\rho^{(j)})\Delta\rho$, is the (unknown) probability that ρ lie between $\rho^{(j)}-\Delta\rho/2$ and $\rho^{(j)}+\Delta\rho/2$. Here $\Delta\rho$ is at our disposal, and since ρ has the dimensions of s, let us take $\Delta\rho=\Delta s$. It is evident from Fig. 4, that the right-hand side of Eq. (30) is zero for $i>N$. This implies that $P_j(\rho^{(j)})<0$ for some values of j (since $G(\rho^{(j)};s^{(i)})$ is always positive), but since $P_j(\rho^{(j)})$ is a probability, $P_j(\rho^{(j)})\geqq 0$ for all j. The contradiction arises because of the experimental approximation that $F_i(s^{(i)})=0$ for $i>N$. In other words, we can say immediately that $P_j(\rho^{(j)})=0$ for $\rho^{(j)}<s^{(1)}$ and for $\rho^{(j)}>s^{(N)}$ to the approximation considered here, and the sum in Eq. (30) becomes a finite sum over those values of $\rho^{(j)}$ between $s^{(1)}$ and $s^{(N)}$.

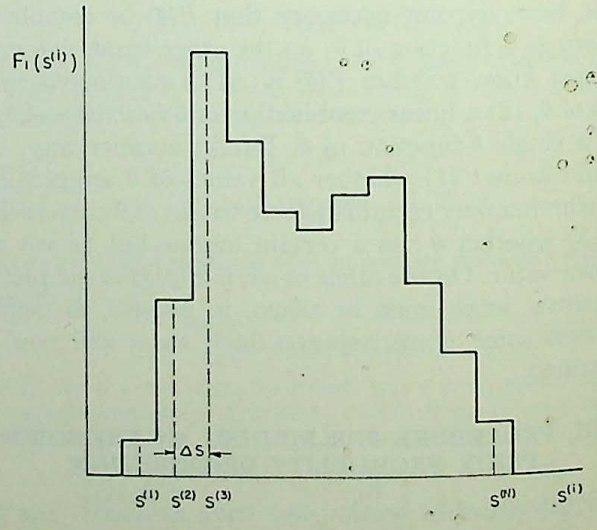


FIG. 4. The form that the data might take in a measurement of the multiple scattering of many particles. The relative frequency $F_i(s^{(i)})$ of different values of $s^{(i)}$ is plotted *versus* the measured $s^{(i)}$.

[2] Annis, Bridge, and Olbert, Phys. Rev. 89, 1216 (1953).

CC-0. In Public Domain. Gurukul Kangri Collection, Haridwar

Digitized by Arya Samaj Foundation Chennai and eGangotri

If one places

$$\Delta\rho = \Delta s, \qquad F_i(s^{(i)}) = f_i, \qquad P_j(\rho^{(j)}) = p_j, \tag{31}$$

and

$$(\Delta\rho)G(\rho^{(j)}; s^{(i)}) = g_{ji},$$

Eq. (30) becomes

$$f_i = \sum_{j=1}^{N} p_j g_{ji}; \quad i = 1, 2, \cdots, N, \tag{32}$$

where f_i and the g_{ji} are known and the p_j are unknown. There are N equations in Eq. (32) with N unknowns, so that we can solve immediately for the p_j. Explicitly,

$$p_j = |g_{ji}^{-1}| \sum_{i=1}^{N} f_i G_{ji}, \tag{33}$$

where $|g_{ji}|$ is the determinant of the g_{ji} and G_{ji} is the cofactor of g_{ji}. In addition, the "statistical errors" assigned to the p_j are related to the "statistical errors" in the f_i's by the equation

$$\epsilon^2(p_j) = |g_{ji}|^{-2} \sum_{i=1}^{N} G_{ji}^2 \epsilon^2(f_i), \tag{34}$$

the $\epsilon^2(f_i)$ being conventionally calculated from the experimentally determined f_i (i.e., $\epsilon^2(f_i) = f_i$).

Our final solution has then the form shown in Fig. 5. The horizontal "errors" are simply the channel widths $\Delta\rho$ and the vertical "errors" are the $\epsilon(p_j)$ calculated from the $\epsilon(f_i)$ by Eq. (34).

Example: The Measurement of Mean Lives of Unstable Particles

M individual unstable particles are observed to decay in the gas of a very large cloud chamber. It is desired to find the relative abundances and the mean lives of the different species of unstable particles present. In this case, $F_i(t^{(i)})\Delta t$ is the observed relative frequency with which the particle life span t lies between $t^{(i)} - \Delta t/2$ and $t^{(i)} + \Delta t/2$, $P_j(\tau^{(j)})\Delta\tau$ is the unknown relative abundance of particles with mean life τ between $\tau^{(j)} - \Delta\tau/2$ and $\tau^{(j)} + \Delta\tau/2$, and

$$G(\tau; t) = \tau^{-1} \exp\{-t/\tau\}. \tag{35}$$

Then, exactly as in the previous example, we have, approximately,

$$F_i(t^{(i)}) = \sum_{j=1}^{N} P_j(\tau^{(j)}) G(\tau^{(j)}; t^{(i)}) \Delta\tau, \tag{36}$$

whence, setting $f_i = F_i(t^{(i)})$, $P_j(\tau^{(j)}) = p_j$, $(\Delta\tau)G(\tau^{(j)}, t^{(i)}) = g_{ji}$, Eq. (33) follows as before (analogous to the previous case, one can take $\Delta\tau = \Delta t \equiv$ life-span channel width in the $F_j(t^{(j)})$ histogram). If now, for example, $p_j\Delta\tau = P_j(\tau^{(j)})\Delta\tau$ is "large" ($\gtrsim 1$) for only one $\tau^{(j)}$, one has reliable evidence of the existence of only a single species of unstable particles with mean-life near $\tau^{(j)}$.

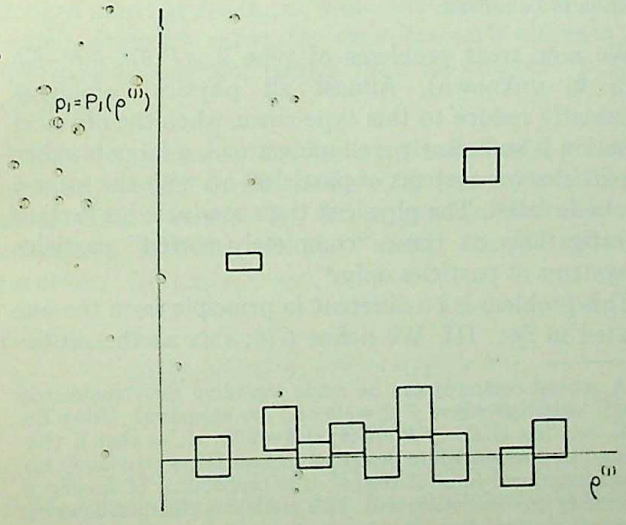


FIG. 5. A possible result of the calculation described in the text concerning the spectrum of masses incident on a cloud chamber. The relative frequency of occurrence of different values of $\rho^{(j)} \sim m_j^{-(1-\alpha)}$ is plotted as a function of $\rho^{(j)}$. Note that the result is consistent with two discrete mass values.

IV. CASE OF COMPLETELY UNKNOWN AND OF DELTA-FUNCTION TYPE PRIOR PROBABILITY DISTRIBUTION

In this section we shall treat two related problems. In both problems, a measurement of a set of the x_i is made on a single system which is one of a class of systems, the value of the parameter θ being fixed for the set of the x_i. It is desired to estimate the value of θ corresponding to the set x_i. The difference between the problems lies in our knowledge of the (prior) probability, $P(\theta)d\theta$, that θ lies in $d\theta$. Problems of type 1 are those in which we have no prior knowledge whatever about the value of θ for any of the systems. Problems of type 2 are those in which we know that in *each* system of the class of systems considered, the value of θ is fixed and the same, i.e., $P(\theta)d\theta = \delta(\theta - \theta_0)d\theta$; however the numerical value of θ_0 is unknown.

The occurrence of situations in which $P(\theta) = \delta(\theta - \theta_0)$ is generally accepted by physicists as a valid description of the properties of a certain class of systems (e.g., a certain type of elementary particles) about which it is known that several parameters other than θ (i.e., ψ, $\chi \cdots$) have the same value for all the systems in the class. The systems are then assumed to be identical in every way and are therefore characterized by the same value of the θ parameter ($= \theta_0$). Thus in the example of elementary particles, θ may be the mean life of the particular type of particles, ψ the mass of this type, χ the charge, etc.

Problem of Type 1

A μ meson enters a multiplate cloud chamber and scatters through angles ϕ_i upon traversing the n plates of the chamber. It is desired to find the product $\Pi = pc\beta$ for the meson. Here Π is the same for every member of the set ϕ_i; however, we do not know the (prior) probability that Π lies in $d\Pi$ independent of the data on the particular scattering angles ϕ_i.

Problem of Type 2

Measurements are made of the life spans (t_i) of a number, N, of "μ mesons" selected by the parent particles (π mesons) from which they are born, the daughter particles (electrons) into which they decay, etc., i.e., the identification of these particles as "μ mesons" is independent of the measurements of the t_i. It is desired to find the mean life, τ, of the μ mesons. Here we know that $P(\tau)d\tau = \delta(\tau - \tau_0)d\tau$ by our selection or sorting procedure but we do not know the numerical value of τ_0.

We first consider problems of type 1, i.e., problems where no independent information whatever is available about $P(\theta)$. The first thing that is evident is that *in*

CC-0. In Public Domain. Gurukul Kangri Collection, Haridwar

Digitized by Arya Samaj Foundation Chennai and eGangotri

this case there is no rigorous way to find $H(x_i;\theta)$, i.e., there is no way to estimate θ and to quote a standard deviation in this estimate which may not be grossly in error. To justify this statement, we need only examine Eq. (2b) for $H(x_i;\theta)$. Since we have no information about $P(\theta)$, we must make some assumption about the form of $P(\theta)$ in order to estimate θ (e.g., we might take $P(\theta)=$constant). Having made this assumption, it is then a simple matter to use one of the methods described in Sec. II to estimate θ, and then to evaluate the standard deviation in this estimate. However, $P(\theta)$ is here actually unknown, and may have a form which makes our estimate of θ differ from the true θ by an amount large compared to the quoted standard deviation (e.g., $P(\theta)$ may be sharply peaked for values of θ at which $G(\theta;x_i)$ is flat and small.) *Hence, we see immediately that there is a certain degree of arbitrariness in any procedure one adopts in the case where* $P(\theta)$ *is completely unknown; this arbitrariness can eventually be removed only if enough individual measurements of the set* x_i *are made so that, as in the previous section, an integral equation for* $P(\theta)$, *Eq. (23), can be set up and solved.*

Let us, however, consider a possible, yet ultimately arbitrary, procedure, in the case in which $P(\theta)$ is completely unknown and only one measurement of the set x_i is available. We suggest, essentially following Laplace, that in this case, the least unreasonable choice for $P(\theta)$ is $P(\theta)=$constant. We further suggest that one take θ_{est} as $\theta_{\text{m.p.}}$, defined by (see Eq. (4))

$$\frac{\partial H(x_i;\theta)}{\partial\theta}\Big]_{\theta=\theta_{\text{m.p.}}} = \text{const}\frac{\partial G(\theta;x_i)}{\partial\theta}\Big]_{\theta=\theta_{\text{m.p.}}} = 0, \quad (37)$$

and that one quote a "statistical error" or "figure of merit" for the estimate, $\epsilon(\theta_{\text{m.p.}})$, given by (see below—Eq. (47) *et seq.*)

$$\epsilon(\theta_{\text{m.p.}}) = \left\{-\frac{\partial^2}{\partial\theta^2}\log G(\theta;x_i)\Big]_{\theta=\theta_{\text{m.p.}}}\right\}^{-\frac{1}{2}}. \quad (38)$$

In view of the necessary arbitrariness of this or any other procedure for estimating θ when $P(\theta)$ is completely unknown, it is always well to indicate explicitly that $P(\theta)$ has been taken as constant in the derivation of such an estimate.

One reason for suggesting the estimate of Eq. (37) is that this estimate has an interesting property, observed by many authors and by R. A. Fisher,[3] in particular, which allows one to resolve a certain ambiguity in the problem. The ambiguity in question is the following.

In any physical problem, the choice of θ is usually not unique. There may be many different physical quantities, related one to another in a simple one-to-one fashion, which might be chosen as θ. For example, in the case of radioactive decay of a group of nuclei of the same species, θ can be taken as either the mean life τ, or the reciprocal mean life, $\lambda=1/\tau$. If one assumes $P_1(\tau)$ is a constant, this is not consistent with taking $P_2(\lambda)$ constant. Indeed,

$$P_1(\tau)=P_2(\lambda)\left|\frac{d\lambda}{d\tau}\right|=P_2(\lambda)\tau^{-2}.$$

Hence, $P_1(\tau)=$constant and $P_2(\lambda)=$constant are two very different physical assumptions.

If one now takes τ as θ, and the corresponding $P_1(\tau)$ as constant, one can find a $\tau_{\text{m.p.}}$. If one takes λ as θ, and the corresponding $P_2(\lambda)$ as constant, one can similarly find $\lambda_{\text{m.p.}}$. However, it turns out that $\lambda_{\text{m.p.}}=1/\tau_{\text{m.p.}}$, so that the arbitrariness in the choice of the parameter θ (with the corresponding $P(\theta)$ always taken as constant) does not lead to any ambiguity in the estimate $\theta_{\text{m.p.}}$. This property holds in general and is perhaps the strongest reason for adopting the $\theta_{\text{m.p.}}$ estimate.

To prove the last remark we let $\theta=\theta(\phi)$ be any function of ϕ, where ϕ is a new parameter. We must then prove that $\theta_{\text{m.p.}}$ is equal to $\theta(\phi_{\text{m.p.}})$, where $\theta_{\text{m.p.}}$ is calculated assuming $P_\theta(\theta)=$constant, and $\phi_{\text{m.p.}}$ is calculated assuming $P_\phi(\phi)=$constant.

$\theta_{\text{m.p.}}$ is defined by Eq. (37), i.e.,

$$\frac{\partial G(\theta;x_i)}{\partial\theta}\Big]_{\theta=\theta_{\text{m.p.}}}=0, \quad (39)$$

and $\phi_{\text{m.p.}}$ is defined, similarly, by

$$\frac{\partial G(\theta(\phi);x_i)}{\partial\phi}\Big]_{\phi=\phi_{\text{m.p.}}}=0. \quad (40)$$

But

$$\frac{\partial G}{\partial\phi}(\theta(\phi);x_i)=\frac{\partial G}{\partial\theta}(\theta(\phi);x_i)\cdot\frac{d\theta(\phi)}{d\phi}.$$

If $d\theta(\phi)/d\phi$ does not equal zero, we can write Eq. (40) as

$$\frac{\partial G}{\partial\theta}(\theta(\phi);x_i)\Big]_{\phi=\phi_{\text{m.p.}}}=0, \quad (41)$$

so that from Eqs. (39) and (41), it is evident that

$$\theta(\phi_{\text{m.p.}})=\theta_{\text{m.p.}}, \quad (42)$$

which is to be proved.

We now treat problems of type 2, ($P(\theta)=\delta(\theta-\theta_0)$ with θ_0 unknown). Almost all physical problems eventually reduce to this type since, when the physical situation is sufficiently well understood, a large number of particles (or systems of particles) all with the same θ can be isolated. The physicist then conducts his further investigations on these "completely sorted" particles or systems of particles only.[4]

This problem is no different in principle from the one treated in Sec. III. We define $G(\theta;x)dx$ as the proba-

[3] Fisher, R. A., *Contributions to Mathematical Statistics* (John Wiley and Sons, Inc., New York, 1950).

[4] A general comment can be made regarding this "completely sorted" situation where $P(\theta)=\delta(\theta-\theta_0)$ (θ_0 unknown). Using Eq. (23a), one has $Q(x)=\int P(\theta)G(\theta;x)d\theta=G(\theta_0;x)$, so that if $Q(x)$ is found by the procedure described in Sec. III, a previously unknown functional form of $G(\theta;x)$ (the probability of finding x, knowing θ) may be determined. This method is clearly followed in deducing physical laws from experimental data. On the other hand, it is quite evident from Eq. (23a) that if nothing is known concerning $P(\theta)$, a previously unknown $G(\theta;x)$ cannot be deduced from the experimental data summarized by $Q(x)$. Unfortunately, this latter situation is usually encountered when the "sorting" is incomplete.

CC-0. In Public Domain. Gurukul Kangri Collection, Haridwar

Digitized by Arya Samaj Foundation Chennai and eGangotri

bility, for fixed θ, that the measured quantity x lies in dx. (For simplicity, we again assume that the set x_i measured in any single experiment has only one member, x.) Exactly as before, we measure a large number of x's, $x^{(1)}, \cdots, x^{(M)}$, and so can define a distribution in x, $F(x)=Q(x)$. In this case, however, we know that θ is unique, and all we wish to find is this unique value of θ.

The solution for $P(\theta)$ is (from Eq. (23b))

$$P(\theta)=\int F(x)\{G(\theta;x)\}^{-1}dx, \tag{43}$$

and, of course, we would hope that this solution is consistent with the original assumption that $P(\theta)$ is a δ function about the unique value of $\theta(\theta=\theta_0)$. Moreover θ_0 can now be immediately found. If, on the other hand, our solution is not consistent with the δ function assumption, we immediately suspect a systematic error of some kind.

The rigorous solution to the problem, given by Eq. (43), suffers however from several disadvantages:

1. It is rather laborious for practical calculation. The steps that have to be carried out are summarized in the examples done in Sec. III.

2. It is difficult to assign a "statistical error" or "figure of merit" to the estimate of θ. There is strictly no meaningful probability statement that can be made about any estimate in the case where $P(\theta)$ is known to be a single δ function, e.g., the statement, "θ has a probability of 0.1 to be greater than, say, θ_1" is obviously meaningless since this probability, by hypothesis, is either 1 or 0. However, it is still useful to have some number which is a "figure of merit" for the estimate. This number cannot have a relation to any statements about probability (=relative frequency), but instead must indicate, in some well-defined but ultimately arbitrary sense, the experimenter's estimate of the over-all precision which may be assigned to the value of θ.

There is, however, another approach to the present problem, which, as we shall see, is free from both of these disadvantages. In this approach one defines, essentially following R. A. Fisher,[3] the "likelihood function," $G(\theta;x_1x_2\cdots x_M)$, as

$$G(\theta;x_1\cdots x_M)\equiv G(\theta;x^{(1)})G(\theta;x^{(2)})\cdots G(\theta;x^{(M)}),\quad (x_i\equiv x^{(i)}); \tag{44}$$

$G(\theta;x_1\cdots x_M)$ is formally identical with the previously defined function which gives the probability that for given θ, the set $x_i=x^{(i)}$ lies in dx_i. This likelihood function, considered as a function of θ with the x_i given, will, as we show later, have a very sharp maximum at some value of θ, $\theta=\theta_l$, if M is large enough. θ_l is then taken as the "maximum likelihood" estimate of the actual unique value of θ, θ_0. More precisely, θ_l is defined by the equation

$$\frac{\partial G}{\partial\theta}(\theta;x_1\ldots x_M)\Big]_{\theta=\theta_l}=0, \tag{45}$$

formally, the same equation which defines the estimate, $\theta_{m.p.}$, calculated from the corresponding $H(x_i;\theta)$ with $P(\theta)$ taken as constant (see Eq. (4)). A justification of this procedure of estimating θ_0 by θ_l, based on physical arguments, may now be attempted as follows:

Suppose that the likelihood function $G(\theta;x_1,\cdots,x_M)$ becomes an infinitely sharply peaked function in θ as M approaches infinity, i.e., suppose

$$\lim_{M\to\infty} G(\theta;x_1\ldots x_M)\sim\delta(\theta-\theta');$$

$$\theta'=\lim_{M\to\infty}\text{ function of } x_1\ldots x_M. \tag{46}$$

(In all of the examples treated in this paper, Eq. (46) is obviously satisfied.) Put in another way, Eq. (46) states that for sufficiently large M, the value of θ, $\theta=\theta'(x_1\cdots x_M)$, is determined uniquely by a set of values of the x_j. It is evident from Eq. (45) that θ_l as defined by Eq. (45) is then the same as θ' defined in Eq. (46), at least in the case where M is sufficiently large. Hence, if Eq. (46) holds, the likelihood function gives (for finite M):

(1) a relatively easy way to find the estimate $\theta_l(x_1,\cdots,x_M)$, and

(2) a well-defined but nevertheless ultimately arbitrary "figure of merit" or "statistical error" for this estimate. For with M large but finite, the "width" of the likelihood function tells us how close we are to the optimum situation where $G(\theta;x_1\cdots x_M)$ becomes an infinitely sharply peaked function of θ. We therefore suggest that this "figure of merit" be defined as the quantitative measure of the width of $G(\theta;x_1\cdots x_M)$, i.e., we define[5]

$$\epsilon(\theta_l)\equiv\left\{-\frac{\partial^2}{\partial\theta^2}\log G(\theta;x_1\ldots x_M)\Big]_{\theta=\theta_l}\right\}^{-\frac{1}{2}}$$

$$=\left\{-G^{-1}\frac{\partial^2 G}{\partial\theta^2}\Big]_{\theta=\theta_l}\right\}^{-\frac{1}{2}}. \tag{47}$$

This definition of $\epsilon(\theta_l)$ is motivated by the fact that for large but finite M, $G(\theta;x_1\cdots x_M)$ is well approximated

[5] In Eq. (47) we have implicitly assumed that the set x_i is given exactly by the measurements. However, if any x_i is itself uncertain as a consequence of the limited precision of the x_i measurement, then the $\epsilon(\theta_l)$ has an additional contribution. This contribution is discussed in Sec. V and shown to be small with proper design of the experiment, in cases of practical interest.

CC-0. In Public Domain. Gurukul Kangri Collection, Haridwar

Digitized by Arya Samaj Foundation Chennai and eGangotri

(as in all the examples of this paper) by

$$G(\theta; x_1 \ldots x_M) \cong G(\theta_l; x_1 \ldots x_M) \times \exp\left\{ \left[\frac{\partial^2}{\partial \theta^2} \log G(\theta; x_1 \ldots x_M) \right]_{\theta=\theta_l} \cdot \tfrac{1}{2}(\theta-\theta_l)^2 \right\}. \quad (48)$$

The expression for θ_l given by Eq. (45) (with the "statistical error" given by Eq. (47)) is (for M large but finite) a good approximation to θ' when Eq. (46) is true. *However, Eq. (46) must hold in every case where θ actually has a unique value $\theta=\theta_0$, with, in addition, $Lim_{M\to\infty}\theta'(x_1 \cdots x_M)$ being just equal to θ_0.* For, suppose Eq. (46) with $\theta'=\theta_0$ did not hold as $M\to\infty$. This would mean that, as $M\to\infty$, θ was not uniquely determined as θ_0 by the set of the x_i, and this is counter to our hypothesis that each member of the set of the x_i obeys the probability distribution $G(\theta; x)$ with $\theta=\theta_0$. Hence as $M\to\infty$, the likelihood function $G(\theta; x_1 \cdots x_M)$ must approach an infinitely sharply peaked function of θ centered at $\theta'(x_1, \cdots, x_M)=\theta_0$, so that $\theta_l(x_1 \cdots x_M)\to\theta_0$ as $M\to\infty$.

As we have mentioned previously, the physical quantity one chooses as θ is not unique; thus there are many quantities related in a one-to-one fashion any one of which can be chosen as the parameter θ. The previous discussion shows that the maximum likelihood estimate of θ, θ_l given by Eq. (45) is independent of this lack of uniqueness. However, $\epsilon(\theta_l)$, as given by Eq. (47), will in general depend in a sensitive way on the choice of the parameter θ; thus from Eqs. (47), (39), (40), we have

$$\epsilon(\theta_l) = \epsilon(\phi_l) \left| \left[\frac{d\theta(\phi)}{d\phi} \right]_{\phi=\phi_l} \right|. \quad (49)$$

Example: Measurement of Mean Life of a Moving Particle in a Cloud Chamber; the Mean Life Assumed Unique

In this example we assume that by means of an experimental sorting procedure we have isolated a set of identical particles each of which has the same mean life, $1/\lambda=1/\lambda_0$. If a particle has mean life $1/\lambda$, then

$$\exp\{-\lambda t\}\lambda dt \quad (50)$$

is the probability that it will decay in dt at t. However, if the observing chamber is of finite size, and if T is the maximum value of t that can be observed, then the probability of observing a decay in dt at $t \leqq T$ becomes

$$G(\lambda; t)dt = \exp\{-\lambda t\}(1-\exp\{-\lambda T\})^{-1}\lambda dt, \quad (51)$$

and the corresponding likelihood function is ($t^{(j)} \equiv t_j$ is the life span of the jth particle and T_j is the maximum value of $t^{(j)}$ that could be observed)

$$G(\lambda; t_1 \cdots t_M) = \prod_{j=1}^{M} \exp\{-\lambda t^{(j)}\}(1-\exp\{-\lambda T_j\})^{-1}\lambda. \quad (52)$$

The maximum likelihood estimate of λ is now given by (Eq. (45)),

$$1/\lambda_l = M^{-1} \sum_{j=1}^{M} t^{(j)} + M^{-1} \sum_{j=1}^{M} T_j(\exp\{\lambda_l T_j\}-1)^{-1}. \quad (53)$$

Equation (53) can be solved for λ_l by a process of iteration. In the case where $T_j \gg 1/\lambda_l$, the solution for λ_l becomes

$$1/\lambda_l \cong t_{\text{mean}} + M^{-1} \sum_{j=1}^{M} T_j(\exp\{T_j/t_{\text{mean}}\}-1)^{-1}, \quad (54)$$

where

$$t_{\text{mean}} \equiv M^{-1} \sum_{j=1}^{M} t^{(j)}.$$

For the "figure of merit," Eq. (47) gives

$$\epsilon(\lambda_l) = \lambda_l\left(M - \sum_{j=1}^{M} (\lambda_l T_j)^2 \exp\{-\lambda_l T_j\}/[1-\exp\{-\lambda_l T_j\}]^2\right)^{-\frac{1}{2}}, \quad (55)$$

where the effect, for given M, of the finite T_j in increasing $\epsilon(\lambda_l)$ is clearly shown.[6]

Example

If the decay of the individual particles is detected by a counter with background rate b, then $G(\lambda; t)dt$, the probability per particle of observation of a count in dt, is

$$G(\lambda; t)dt = (b+\lambda \exp\{-\lambda t\})(bT+1-\exp\{-\lambda T\})^{-1}dt; \quad \int_0^T G(\lambda; t)dt = 1, \quad (56)$$

whence

$$G(\lambda; t_1 \cdots t_M) = \prod_{j=1}^{M} (b+\lambda \exp\{-\lambda t^{(j)}\})(bT+1-\exp\{-\lambda T\})^{-1}. \quad (57)$$

($T_j = T =$ maximum possible observed value of $t^{(j)} \equiv t_j$; T is determined from the time at which the counting rate is reduced to a value near the background rate.) The maximum likelihood estimate of λ is, if $b \ll \lambda_l \exp(-\lambda_l T)$,

$$1/\lambda_l \cong t_{\text{mean}} + \frac{T\exp\{-\lambda_l T\}}{bT+1-\exp\{-\lambda_l T\}} + \frac{b}{\lambda_l^2} M^{-1} \sum_{j=1}^{M} (1-\lambda_l t_j)\exp\{\lambda_l t_j\}; \quad (58)$$

and since for large M,

$$M^{-1} \sum_{j=1}^{M} f(t_j) \approx \int_0^T f(t)G(\lambda_l; t)dt \quad \text{(where } f(t) \text{ is any function of } t\text{)}, \quad (59)$$

we obtain

$$1/\lambda_l \cong t_{\text{mean}} + \frac{T\exp\{-\lambda_l T\}}{bT+1-\exp\{-\lambda_l T\}} + \frac{bT}{1-\exp\{-\lambda_l T\}}\left(\frac{T}{2} - \lambda_l^{-1}\right). \quad (60)$$

For small b, $\epsilon(\lambda_l)$ is given in terms of λ_l again by Eq. (55).

Example

The very fact that physical situations exist in which a "sorting" procedure can be performed to separate particles with a unique value of θ implies that workers in different laboratories can carry out the same sorting procedure, and then estimate the unique value of θ. The question arises, "How must one proceed in order to combine these estimates of θ from the different laboratories to form a 'combined estimate' and what is the 'statistical error' or 'figure of merit' of this 'combined estimate'?"

We will show how one proceeds in a simple case and quote the results for one other simple case.

Consider that N different laboratories have carried out the same sorting procedure to isolate a group of particles and have then estimated the unique value of the reciprocal mean life λ_0. Calling the jth maximum-likelihood estimate of λ_0, $(\lambda_l)_j$, and

[6] See Fretter, May, and Nakada, Phys. Rev. 89, 168 (1953); W. L. Alford and R. B. Leighton, Phys. Rev. 90, 622 (1953); M. S. Bartlett, Phil. Mag. 44, 249 (1953).

CC-0. In Public Domain. Gurukul Kangri Collection, Haridwar

Digitized by Arya Samaj Foundation Chennai and eGangotri

assuming that the maximum measurable time T is infinite, we find the likelihood function for the jth laboratory is (see Eqs. (52) and (53))

$$G_j(\lambda; t_k)=\lambda^J \exp\{-\lambda \sum_{k=1}^{J} t_k\}, \tag{61}$$

where J is the number of particles seen to decay by the jth laboratory, i.e., $J=J(j)$.

From Eq. (61)

$$1/(\lambda_l)_j=J^{-1}(j) \sum_{k=1}^{J(j)} t_k \tag{62}$$

with "statistical error,"

$$\epsilon[(\lambda_l)_j]=J^{-\frac{1}{2}}(j)(\lambda_l)_j.$$

The over-all likelihood function is

$$G(\lambda; (\lambda_l)_j)=\prod_{j=1}^{N} \lambda^{J(j)} \exp\{-\lambda \sum_{k=1}^{J(j)} t_k\}$$

$$=\lambda^M \exp\{-\lambda \sum_{j=1}^{N} J(j)/(\lambda_l)_j\}, \tag{63}$$

where

$$M \equiv \sum_{j=1}^{N} J(j). \tag{64}$$

It is evident from Eq. (63) that λ_l, the combined maximum likelihood estimate of λ_0, is given by

$$1/\lambda_l=M^{-1} \sum_{j=1}^{N} J(j)/(\lambda_l)_j \tag{65}$$

and

$$\epsilon(\lambda_l)=M^{-\frac{1}{2}}\lambda_l.$$

In practice, however, one does not in general know the values of the $J(j)$, hence it is useful to express our result for λ_l and $\epsilon(\lambda_l)$ in terms of the $(\lambda_l)_j$ and $\epsilon[(\lambda_l)_j]$. From Eqs. (63–65) we obtain

$$1/\lambda_l=\frac{\sum_{j=1}^{N} (\lambda_l)_j/\{\epsilon[(\lambda_l)_j]\}^2}{\sum_{j=1}^{N} \{(\lambda_l)_j\}^2/\{\epsilon[(\lambda_l)_j]\}^2} \tag{66}$$

and

$$\{\epsilon(\lambda_l)\}^{-2}=\lambda_l^{-2} \sum_{j=1}^{N} \{(\lambda_l)_j\}^2/\{\epsilon[(\lambda_l)_j]\}^2.$$

Referring now to the problem of combining mass values from N different laboratories, we call $(\rho_l)_j$ the maximum likelihood estimate of the parameter ρ_0 by the jth laboratory (according to example of Sec. III, $\rho_0 \sim (m)^{-0.417}$), and the corresponding "statistical error." A calculation similar to the one carried out above gives

$$\rho_l^2=\frac{\sum_{j=1}^{N} \{(\rho_l)_j\}^4/\{\epsilon[(\rho_l)_j]\}^2}{\sum_{j=1}^{N} \{(\rho_l)_j\}^2/\{\epsilon[(\rho_l)_j]\}^2} \tag{67}$$

and

$$\{\epsilon(\rho_l)\}^{-2}=\rho_l^{-2} \sum_{j=1}^{N} \{(\rho_l)_j\}^2/\{\epsilon[(\rho_l)_j]\}^2,$$

where ρ_l is the combined maximum likelihood estimate of ρ_0 and $\epsilon(\rho_l)$ is the corresponding "statistical error."

We note from Eqs. (66) and (67) that the rule for combining estimated mass values is not the same as the rule for combining estimated reciprocal mean lives. In general, the rule for combining the $(\theta_{est})_j=(\theta_l)_j$ depends on the functional form of the corresponding $G(\theta; x_1, \cdots, x_{J(j)})$.

V. EFFECT ON THE ESTIMATES OF IMPERFECT EXPERIMENTAL PRECISION IN THE DIRECTLY MEASURED QUANTITIES

It sometimes arises in practice that one can easily derive from theory an expression for $G'(\theta; y_1, \cdots, y_N) \equiv G'(\theta; y_i)$, where $G'(\theta; y_i)dy_i$ is the probability that the quantities y_i lie in dy_i for given θ, but that the y_i cannot be "measured exactly." However, one can "measure exactly" a set of quantities x_i which are related to the y_i through another probability distribution. For instance one may have

$$g(y_i; x_i)dx_i=(2\pi)^{-N/2} \prod_{j=1}^{N} \sigma_j^{-1} \times \exp\{-(x_j-y_j)^2/2\sigma_j^2\}dx_j; \tag{68}$$

i.e., each of the x_j may be distributed statistically in Gaussian fashion about the y_j. In this case, the likelihood function becomes

$$G(\theta; x_1 \ldots x_N) \equiv G(\theta; x_i)$$

$$=\int \cdots \int G'(\theta; y_i)g(y_i; x_i)dy_i. \tag{69}$$

Let us now expand $G'(\theta; y_i)$ in a Taylor series about the values $y_1=x_1$, $y_2=x_2$, etc.:

$$G'(\theta; y_i)=G'(\theta; y_i=x_i)+\sum_{j=1}^{N} (y_j-x_j)\frac{\partial G'(\theta; x_i)}{\partial x_j}$$

$$+\tfrac{1}{2} \sum_{j,k=1}^{N} (y_j-x_j)(y_k-x_k)\frac{\partial^2 G'(\theta; x_i)}{\partial x_j \partial x_k}+\ldots; \tag{70}$$

and let us introduce the additional assumption that $g(y_i; x_i)$, considered as a function of the y_i, is sharply peaked for $y_i \approx x_i$, whereas $G'(\theta; y_i)$ is relatively slowly varying in the region of $y_i \approx x_i$. Then, substituting Eq. (70) into Eq. (69) and neglecting terms above 2nd order in (y_j-x_j) in Eq. (70), we get

$$G(\theta; x_i)=G'(\theta; x_i)+\tfrac{1}{2} \sum_{j=1}^{N} \sigma_j^2 \frac{\partial^2 G'(\theta; x_i)}{\partial x_j^2}+\ldots. \tag{71}$$

Equation (71) can be used in Eq. (2) to derive the posterior probability $H(\theta; x_i)$ or it can be used directly to estimate θ from the exactly measured x_i in the case when θ is independently known to be unique (see Sec. IV). If θ is unique the maximum likelihood estimate of θ, θ_l, is given by

$$\left[\frac{\partial G'(\theta; x_i)}{\partial \theta}+\tfrac{1}{2} \sum_{j=1}^{N} \sigma_j^2 \frac{\partial^3 G'(\theta; x_i)}{\partial \theta \partial x_j^2}+\ldots\right]_{\theta=\theta_l}=0, \tag{72}$$

CC-0. In Public Domain. Gurukul Kangri Collection, Haridwar

Digitized by Arya Samaj Foundation Chennai and eGangotri

while if θ obeys a known prior distribution law, $P(\theta)$, θ_l is given by

$$\left[\frac{\partial H'(\theta;x_i)}{\partial\theta}+\tfrac{1}{2}\sum_{j=1}^{N}\sigma_j{}^2\frac{\partial^3 H'(\theta;x_i)}{\partial\theta\partial x_j{}^2}+\cdots\right]_{\theta=\theta_l}=0, \quad (73)$$

where

$$H'(\theta;x_i)=P(\theta)G'(\theta;x_i)\Big/\int P(\theta)G'(\theta;x_i)d\theta.$$

The relative "error" in θ_l, $\epsilon(\theta_l)/\theta_l$ will not be changed appreciably if the correction terms in Eqs. (72) and (73) are not large, i.e., if $\sigma_j{}^2/x_j{}^2$ is not large. If the correction terms are large, the formulas in (72) and (73) are inadequate; therefore in either case it is of little use to derive from them a new formula for $\epsilon(\theta_l)$. In this situation, the problem must be re-examined and improved methods to measure the y_i devised.

Example from the Theory of Multiple Coulomb Scattering. "Noise Level Scattering"

Let us consider again the example treated at the end of Sec. II. We shall now assume that each of the n measured angles of "apparent" multiple scattering ϕ_i obeys a Gaussian distribution about the corresponding "real" angle of multiple scattering ψ_i, with standard deviation σ. The magnitude of σ is a measure of the "noise level scattering." In this case (see Eq. (73) and Eqs. (13) and (15)),

$$\begin{aligned}&\theta\rightarrow\Pi\\&y_i\rightarrow\psi_i\\&x_i\rightarrow\phi_i\\&\sigma_j\rightarrow\sigma=\text{constant}\end{aligned} \quad (74)$$

and

$$H'(\Pi;\phi_i)=\text{const}\Pi^m\exp\left\{-\frac{\Pi^2}{A^2}\sum_{i=1}^{n}\phi_i{}^2\right\},$$

where $m=n-\gamma$ as before, and we assume $\Pi_0\ll\Pi_{\text{m.p.}}$ Substituting in Eq. (73), and remembering that the second term in Eq. (73) is small, we find

$$\Pi_{\text{m.p.}}=(m/2)^{\frac{1}{2}}A\{\sum_{i=1}^{n}\phi_i{}^2-(n-2\gamma)\sigma^2\}^{-\frac{1}{2}}. \quad (75)$$

Comparison of Eq. (16) with Eq. (75) shows that the estimate of $\Pi=pc\beta$ is increased when one takes into account the noise-level scattering.

The formula given in Eq. (75) does not at first glance agree with the formula given by Olbert.[1] (We have σ^2, where Olbert has $2\sigma^2$.) The reason for this apparent discrepancy is a difference in the definition of σ from the one used by Olbert. A possible method of measuring the σ we have defined in Eq. (68) is given below.

Allow N tracks of very great momentum to penetrate the plates of the cloud chamber. (The momentum must be great enough so that the real scattering is negligible compared to the noise-level scattering.) In this case the distribution in scattering angles is given by Eq. (68) with $y_i\rightarrow\psi_i\cong 0$ and $x_i\rightarrow\phi_i$; i.e.,

$$g(\sigma;\phi_i)d\phi_i=(2\pi)^{-N/2}\sigma^{-N}\exp\{-(1/2\sigma^2)\sum_{j=1}^{N}\phi_j{}^2\}\prod_{j=1}^{N}d\phi_j \quad (76)$$

is the probability that for fixed (unique but unknown) σ each of the ϕ_i lie in $d\phi_i$. σ can now be estimated from $g(\sigma;\phi_i)$ by the method of maximum likelihood (Sec. IV), and is given by

$$\sigma_l=\{N^{-1}\sum_{j=1}^{N}\phi_j{}^2\}^{\frac{1}{2}}. \quad (77)$$

VI. THE "ESTIMATE DISTRIBUTION"

Suppose an experiment is performed in which the information is available that the parameter θ is unknown but fixed and unique ($\theta=\theta_0$) for the set $x_i\equiv x^{(i)}$. The likelihood function for the experiment may then be constructed, namely $G(\theta;x_i)dx_i$, and an estimate of the parameter $\theta_{\text{est}}=f_{\text{est}}(x_1,\cdots,x_N)$, e.g., the maximum likelihood estimate $\theta_l=\theta_{\text{est}}$, may be calculated. We now ask "What is the probability that θ_{est} lies in $d\theta_{\text{est}}$ if the value of the parameter is assumed to be θ_0?" This question may be answered by constructing the function $R(\theta_0;\theta_{\text{est}})d\theta_{\text{est}}$ which is the probability that θ_{est} lies in $d\theta_{\text{est}}$ for θ assumed to be θ_0; $R(\theta_0;\theta_{\text{est}})d\theta_{\text{est}}$ is given by Eq. (78):

$$R(\theta_0;\theta_{\text{est}})d\theta_{\text{est}}=\int\cdots\int dx_1\ldots dx_N G(\theta_0;x_1\ldots x_N), \quad (78)$$

where the integration over the set dx_i is carried out under the restriction imposed by the equation

$$\theta_{\text{est}}\leqq f_{\text{est}}(x_1\ldots x_N)\leqq\theta_{\text{est}}+d\theta_{\text{est}}. \quad (79)$$

Thus,

$$\begin{aligned}&R(\theta_0;\theta_{\text{est}})d\theta_{\text{est}}\\&=\Big[\int\cdots\int dx_1\ldots dx_N G(\theta_0;x_1\ldots x_N)\\&\qquad\times\delta(\theta_{\text{est}}-f_{\text{est}}(x_1\ldots x_N))\Big]d\theta_{\text{est}}. \quad (80a)\end{aligned}$$

The probability function $R(\theta_0;\theta_{\text{est}})$ will be called the "estimate distribution" and can be used to answer questions of the type: "What will be the probability that θ_{est} is, e.g., equal to or greater than some ϑ_a if the value of the parameter θ is assumed to be θ_0?" This probability, $J(\theta_0,\theta_a)$, is obtained directly from the estimate distribution $R(\theta_0;\theta_{\text{est}})$, and is

$$J(\theta_0,\theta_a)=\int_{\theta_a}^{\infty}R(\theta_0,\theta_{\text{est}})d\theta_{\text{est}}, \quad (80b)$$

with $J(\theta_0,-\infty)=1$.

Using Eq. (80a), we find averages over the estimate distribution can be expressed as follows:

$$\begin{aligned}\langle\theta_{\text{est}}\rangle&\equiv\int\theta_{\text{est}}R(\theta_0;\theta_{\text{est}})d\theta_{\text{est}}\\&=\int f_{\text{est}}(x_1\ldots x_N)G(\theta_0;x_1\ldots x_N)dx_1\ldots dx_N, \quad (81a)\\\langle(\theta_{\text{est}}-\theta_0)^2\rangle&\equiv\int(\theta_{\text{est}}-\theta_0)^2R(\theta_0;\theta_{\text{est}})d\theta_{\text{est}}\\&=\int(f_{\text{est}}(x_1\ldots x_N)-\theta_0)^2\\&\qquad\times G(\theta_0;x_1\ldots x_N)dx_1\ldots dx_N, \quad (81b)\end{aligned}$$

etc. It can then be proved[7] (under suitable restrictions)

[7] Cramer, H., *Mathematical Methods of Statistics* (Princeton University Press, Princeton, 1946), Chapters 32 and 33.

CC-0. In Public Domain. Gurukul Kangri Collection, Haridwar

Digitized by Arya Samaj Foundation Chennai and eGangotri

that for $\theta_{est}=f_{est}(x_1, \cdots, x_N)=\theta_l$, θ_{est} "converges in probability" to the true value of $\theta=\theta_0$, i.e.

$$\lim_{N\to\infty}\langle\theta_l\rangle\to\theta_0. \tag{81c}$$

One can also show[7] (under suitable restrictions) that

$$\langle(\theta_l-\theta_0)^2\rangle<\langle(\theta_{est}-\theta_0)^2\rangle \tag{81d}$$

for any fixed finite N and any $\theta_{est}\neq\theta_l$. Equations (81c) and (81d) constitute additional powerful arguments in favor of maximum likelihood estimation in the case of an unique but unknown parameter.

Suppose a single charged particle which stops in a multiplate cloud chamber has a certain angle of multiple scattering in each of the plates of the chamber. From these angles of multiple scattering (and the range) one can estimate the mass of the particle: θ_{est} = mass estimate = a definite function of the multiple-scattering angles. One can then calculate the probability that a particle of known mass, e.g., a proton, appears to exhibit a mass equal to or greater than the above θ_{est}, i.e., appears to scatter as little or less than the observed particle. This calculation involves constructing the estimate distribution for θ_{est} (Eqs. (80)) and hence the estimate distribution for the angles of multiple scattering. However, questions of the inverse type—"What is the probability that a particle which scatters the observed amount is, say, a proton?"—are meaningless since this probability is, by hypothesis, one or zero.

As a further illustration of the use of the estimate distribution, suppose a "sorting" has been made in two experiments with the result that for each experiment the information is available that the parameter θ has an unique value (which may be different, in general) in the two experiments. Then the simultaneous probability that the estimate of θ from the first experiment lies in $d\theta_{est}^{(1)}$ and that the estimate of θ from the second experiment lies in $d\theta_{est}^{(2)}$ for a unique value of θ, θ_0, assumed the same in both experiments, is

$$R(\theta_0;\theta_{est}^{(1)},\theta_{est}^{(2)})d\theta_{est}^{(1)}d\theta_{est}^{(2)} = R(\theta_0;\theta_{est}^{(1)})d\theta_{est}^{(1)}R(\theta_0;\theta_{est}^{(2)})d\theta_{est}^{(2)}.$$

Example

Suppose two experiments are performed on the life spans of two sets of unstable particles. In addition, it is assumed on the basis of the sorting procedure used that within each experiment the particles are identical. It is now desired to know if the results of the two experiments are consistent with the assumption that the mean life of *both sets* of particles is the *same*, in other words, if the *two sets* of particles are the *same*. The probability in experiment 1 that the estimate of τ lies in $d\tau_{est}^{(1)}$ for a unique mean life assumed equal to τ_0 is given by Eq. (80a). We shall take this estimate to be

$$\tau_{est}^{(1)}=\tau_l^{(1)}=t_{mean}^{(1)}\equiv N^{-1}\sum_{i=1}^{N}t_i^{(1)}$$

(See Eq. (54) with $T_j\to\infty$), where N is the number of life spans measured in experiment 1. Then

$$R(\tau_0;\tau_{est}^{(1)})d\tau_{est}^{(1)}=\left[\int dt_1^{(1)}\cdots dt_N^{(1)}\prod_{i=1}^{N}\tau_0^{-1} \times\exp\{-t_i^{(1)}/\tau_0\}\delta(\tau_{est}^{(1)}-N^{-1}\sum_{j=1}^{N}t_j^{(1)})\right]d\tau_{est}^{(1)}$$

and by use of the integral representation of the δ function

$$\delta(x-a)=(2\pi)^{-1}\int_{-\infty}^{\infty}\exp\{i\alpha(x-a)\}d\alpha,$$

the integral over $dt_1^{(1)}\cdots dt_N^{(1)}$ may be performed yielding

$$R(\tau_0;\tau_{est}^{(1)})d\tau_{est}^{(1)} =\frac{i^N}{2\pi}\left(\frac{N\tau_{est}^{(1)}}{\tau_0}\right)\int_{-\infty}^{\infty}\frac{\exp\{i\beta\}d\beta}{\{\beta-iN\tau_{est}^{(1)}/\tau_0\}^N}\left(\frac{d\tau_{est}^{(1)}}{\tau_{est}^{(1)}}\right).$$

Finally, via the calculus of residues,[8]

$$R(\tau_0;\tau_{est}^{(1)})d\tau_{est}^{(1)} =\frac{N^N}{(N-1)!}\left(\frac{\tau_{est}^{(1)}}{\tau_0}\right)^N\exp\left\{\frac{-N\tau_{est}^{(1)}}{\tau_0}\right\}\frac{d\tau_{est}^{(1)}}{\tau_{est}^{(1)}}. \tag{82}$$

In a similar manner, the estimate distribution for the second experiment, again for a unique mean life assumed equal to τ_0, is

$$R(\tau_0;\tau_{est}^{(2)})d\tau_{est}^{(2)} =\frac{M^M}{(M-1)!}\left(\frac{\tau_{est}^{(2)}}{\tau_0}\right)^M\exp\left\{\frac{-M\tau_{est}^{(2)}}{\tau_0}\right\}\frac{d\tau_{est}^{(2)}}{\tau_{est}^{(2)}},$$

where M is the number of life spans measured in experiment 2. Thus

$$R(\tau_0;\tau_{est}^{(1)},\tau_{est}^{(2)})d\tau_{est}^{(1)}d\tau_{est}^{(2)} =\frac{N^N}{(N-1)!}\frac{M^M}{(M-1)!}\frac{(\tau_{est}^{(1)})^N(\tau_{est}^{(2)})^M}{\tau_0^{N+M}} \cdot\exp\left\{\frac{-N\tau_{est}^{(1)}+M\tau_{est}^{(2)}}{\tau_0}\right\}\frac{d\tau_{est}^{(1)}}{\tau_{est}^{(1)}}\frac{d\tau_{est}^{(2)}}{\tau_{est}^{(2)}}, \tag{83}$$

so that the simultaneous probability for experiment 1 to yield a value of τ_{est} between $\tau_{est}^{(1)}-\epsilon(\tau_{est}^{(1)})$ and $\tau_{est}^{(1)}+\epsilon(\tau_{est}^{(1)})$, and experiment 2 a value of τ_{est} between $\tau_{est}^{(2)}-\epsilon(\tau_{est}^{(2)})$ and $\tau_{est}^{(2)}+\epsilon(\tau_{est}^{(2)})$ is

$$\int_{\tau_{est}^{(2)}-\epsilon(\tau_{est}^{(2)})}^{\tau_{est}^{(2)}+\epsilon(\tau_{est}^{(2)})}\int_{\tau_{est}^{(1)}-\epsilon(\tau_{est}^{(1)})}^{\tau_{est}^{(1)}+\epsilon(\tau_{est}^{(1)})}R(\tau_0;\tau_{est}^{(1)\prime},\tau_{est}^{(2)\prime}) \times d\tau_{est}^{(1)\prime}d\tau_{est}^{(2)\prime}. \tag{84}$$

If now this last expression calculated from the observed $t_i^{(1)}$, $t_i^{(2)}$ (see Eqs. (54) and (55)) is "very much less than one," whatever the choice of τ_0, it is not "likely" that the mean life of *both* sets of particles is actually the *same*. If, on the other hand, a value of τ_0 can be found for which this expression is not "very much less than one," it is "likely" that *both* sets of particles have the *same* mean life, τ_0. (From Eq. (83) we find that in the optimum situation in which $\tau_{est}^{(1)}=\tau_{est}^{(2)}$, $\epsilon(\tau_{est}^{(1)})=\epsilon(\tau_{est}^{(2)})$, and τ_0 is taken as $\tau_{est}^{(1)}$, Eq. (84) gives approximately one-half.) Obviously, both of the preceding qualitative statements can be made quantitative by a definite (though ultimately arbitrary) numerical specification of "very much less than one," and "likely."

Example

Another interesting case of the use of the estimate distribution involves the following problem previously considered and solved by Sard and Sard.[9] In a cosmic-ray counting experiment the observed number of coincidences in a certain time interval is x,

[8] In this problem, the integral on the right-hand side of Eq. (78) may be performed directly because of the simple relationship for τ_{est}, namely

$$\tau_{est}=(1/N)\sum_{i=1}^{N}t_i.$$

In this case

$$R(\tau_0;\tau_{est})d\tau_{est}=\tau_0^{-N}\exp\{-N\tau_{est}/\tau_0\}\int dt_1\cdots dt_N,$$

where the integral is the volume in N-dimensional t space contained between the two hypersurfaces defined by τ_{est} and $\tau_{est}+d\tau_{est}$. This volume is proportional to $(\tau_{est})^{N-1}d\tau_{est}$, so that

$$R(\tau_0;\tau_{est})=A\left(\frac{\tau_{est}}{\tau_0}\right)^N\tau_{est}^{-1}\exp\{-N\tau_{est}/\tau_0\},$$

in agreement with Eq. (82). The normalization constant A may be determined by requiring that $\int R(\tau_0;\tau_{est})d\tau_{est}=1$. This simple method of evaluating the right-hand side of Eq. (78) will work whenever $G(\theta_0;x_i)$ can be written as a function of θ_0 and θ_{est} only.

[9] A. Sard and R. Sard, Rev. Sci. Instr. 20, 526 (1949).

CC-0. In Public Domain. Gurukul Kangri Collection, Haridwar

Digitized by Arya Samaj Foundation Chennai and eGangotri

the calculated number of chance coincidences in the same time interval is β, and the parameter θ to be estimated is the mean number of true coincidences in the time interval. It then follows that the probability distribution for x, given θ, i.e., the likelihood function, is Poissonian:[9]

$$G(\theta; x)=\frac{(\theta+\beta)^x}{x!}\exp\{-(\theta+\beta)\}. \tag{85}$$

The maximum likelihood estimate of θ, θ_l, is then given by

$$\left.\frac{\partial G(\theta; x)}{\partial\theta}\right]_{\theta=\theta_l}=0; \quad \text{whence, } \theta_l=x-\beta. \tag{86}$$

By use of Eqs. (78), (79), the estimate distribution with $\theta_{\text{est}}=\theta_l=x-\beta$, is given as

$$R(\theta_0; \theta_{\text{est}})d\theta_{\text{est}}=\int G(\theta_0; x)dx$$

with

$$\theta_{\text{est}}+\beta\leqq x\leqq\theta_{\text{est}}+\beta+d\theta_{\text{est}},$$

so that

$$R(\theta_0; \theta_{\text{est}})d\theta_{\text{est}}=G(\theta_0; \theta_{\text{est}}+\beta)d\theta_{\text{est}}$$
$$=\frac{(\theta_0+\beta)^{\theta_{\text{est}}+\beta}}{(\theta_{\text{est}}+\beta)!}\exp\{-(\theta_0+\beta)\}d\theta_{\text{est}}. \tag{87}$$

Thus the Poissonian property of $G(\theta_0; x)$ implies that $R(\theta_0; \theta_{\text{est}})$ with $\theta_{\text{est}}=\theta_l$ is also Poissonian in the variable $\theta_{\text{est}}+\beta$. Further the "statistical error" or "figure of merit" assigned by Eq. (47) to θ_l is given by

$$\epsilon^2(\theta_l)=x, \tag{88}$$

so that we can write

$$\theta_0\approx(x-\beta)\pm x^{\frac{1}{2}}$$

in agreement with the results of Sard and Sard.[9] It is also possible to calculate (for $\theta_{\text{est}}=\theta_l=x-\beta$)

$$\langle\theta_{\text{est}}\rangle=\langle\theta_{\text{est}}+\beta\rangle-\beta$$
$$\equiv\int(\theta_{\text{est}}+\beta)R(\theta_0; \theta_{\text{est}})d\theta_{\text{est}}-\beta$$
$$=\int(\theta_{\text{est}}+\beta)\left\{\frac{(\theta_0+\beta)^{\theta_{\text{est}}+\beta}}{(\theta_{\text{est}}+\beta)!}\exp\{-(\theta_0+\beta)\}\right\}$$
$$\times d\theta_{\text{est}}-\beta=\theta_0,^{10} \tag{89}$$

and similarly

$$\langle\theta_{\text{est}}^2\rangle\equiv\int\theta_{\text{est}}^2R(\theta_0; \theta_{\text{est}})d\theta_{\text{est}}=\theta_0^2+(\theta_0+\beta), \tag{91}$$

so that

$$\langle\theta_{\text{est}}^2\rangle-\langle\theta_{\text{est}}\rangle^2=\theta_0+\beta=\langle\theta_{\text{est}}\rangle+\beta. \tag{92}$$

Equation (92) can be used as a check on the internal consistency of the coincidence counting data. Specifically, Eq. (92) gives (since $\theta_{\text{est}}=\theta_l=x-\beta$)

$$M^{-1}\sum_{\gamma=1}^{M}(x^{(\gamma)}-\beta)^2-\{M^{-1}\sum_{\gamma=1}^{M}(x^{(\gamma)}-\beta)\}^2=M^{-1}\sum_{\gamma=1}^{M}x^{(\gamma)}, \tag{93}$$

where $x^{(\gamma)}$ is the number of coincidences during a definite time interval γ (say, one day).

VII. CONCLUSION

In this paper we have attempted to find a relationship between the probability functions $H(x_i; \theta)$ and $G(\theta; x_i)dx_i$ defined in Sec. I. In other words, we have attempted to answer the question, "How does one proceed to estimate a physical parameter θ, given a set x_i of physical data related to θ through a theoretically derived and/or experimentally confirmed probability function $G(\theta; x_i)dx_i$; in addition, what statistical significance does this estimate and any quoted 'error' possess?"

The above problem has, of course, been treated in the literature in great detail. In fact, R. A. Fisher[3] has actually constructed a "maximum likelihood" theory of estimation essentially independent of the prior probability $P(\theta)$. On the other hand, in the present paper we attempt to formulate a treatment of estimation consistent with a partial knowledge of $P(\theta)$. Specifically:

1. If $P(\theta)d\theta$ is known initially, the procedure to follow is given in Sec. II. If a single measurement of the set x_i is made, the corresponding value of θ can be estimated and meaningful probability statements can be made concerning this estimate, θ_{est}; e.g., we can give the probability that θ lies between $\theta_{\text{est}}+\sigma(\theta_{\text{est}})$ and $\theta_{\text{est}}-\sigma(\theta_{\text{est}})$.

2. If $P(\theta)d\theta$ is initially completely unknown, one can always find it on the basis of sufficient experimental data using the procedure in Sec. III.

3. If $P(\theta)d\theta$ is initially completely unknown and *only one measurement of the set x_i is made*, there is an intrinsic degree of arbitrariness in any estimation procedure. Nevertheless we suggest in Sec. IV that in this case one take all values of θ as having the same prior probability and that one quote an estimate $\theta_{\text{m.p.}}$ formally equivalent to the "maximum likelihood" estimate. The corresponding "statistical error" in $\theta_{\text{m.p.}}$ as well as $\theta_{\text{m.p.}}$ itself, however, are now quantities about which one can make no statements which are meaningful in the sense of probability = relative frequency.

4. If $P(\theta)d\theta$ is initially known to be a single δ function about an unknown value of θ [$P(\theta)=\delta(\theta-\theta_0)$ where θ_0 is unknown], and if one measurement of the set x_i is made, the procedure is similar to that in (3) above, but we believe that its justification rests on firmer ground (Sec. IV). One can here quote an estimate of θ, the "maximum likelihood" estimate, and a "figure of merit" (or "statistical error") for this estimate (see also Sec. V). However, it is still intrinsic to the problem that no really meaningful probability statement (in the sense probability = relative frequency) can be made about the "statistical error" associated with the estimate. On the other hand, this "statistical error," and indeed the estimate itself, possesses a significance in the sense of a suitable statement of the relative degree of belief which can be objectively assigned to the possible θ values; we feel that such a significance is greater when $P(\theta)=\delta(\theta-\theta_0)$ with θ_0 unknown, than in the corresponding case just above where nothing is known about $P(\theta)$ (see also Sec. VI).

One of the authors (M.A.) wishes to thank Professor Bruno Rossi for very helpful discussions. We also wish to thank Professor Robert Sard for his helpful comments.

[10] The estimate distribution $R(\theta_0; \theta_{\text{est}})d\theta_{\text{est}}$ permits the definition of the so-called "unbiased" estimate through the relation

$$\theta_0=\langle\theta_{\text{est}}\rangle\equiv\int d\theta_{\text{est}}\theta_{\text{est}}R(\theta_0; \theta_{\text{est}})$$
$$=\int f_{\text{est}}(x_1\cdots x_N)G(\theta_0; x_1\cdots x_N)dx_1\cdots dx_N, \tag{90}$$

any θ_{est} satisfying the condition in Eq. (90) being called "unbiased." Thus any θ_{est} is unbiased provided that its average over the estimate distribution is equal to the true (or assumed) value θ_0 of the parameter θ. Eq. (89) shows that the $\theta_{\text{est}}=\theta_l$ of the present example ($N=1$!!) is unbiased. (It is to be noted that Eq. (81c) proves the "unbiasedness" in general of maximum likelihood estimates only in the limit $N\to\infty$.)

CC-0. In Public Domain. Gurukul Kangri Collection, Haridwar

Digitized by Arya Samaj Foundation Chennai and eGangotri

REVIEWS OF MODERN PHYSICS VOLUME 25, NUMBER 4 OCTOBER, 1953

Virial Coefficients and Models of Molecules in Gases*

TARO KIHARA

Department of Physics, University of Tokyo, Tokyo, Japan

CONTENTS

I. The Second and the Third Virial Coefficients for Spherical Molecules
1. Introduction
2. Square-Well Potential
3. Lennard-Jones Potential
4. Inverse-Power Repulsive Potential
II. Criticism of the Lennard-Jones Potential
5. Transport Properties of Gases
6. Stability of Crystal Structures
III. The Second Virial Coefficient for Nonspherical Molecules
7. Rigid Convex Body
8. Parallel Bodies of a Convex Core
9. Core Model

GENERAL INTRODUCTION

THE equation of state of gases may be expressed in the form

$$pv=kT(1+Bv^{-1}+Cv^{-2}+\cdots),$$

where p is the pressure, v is the volume per molecule, k is the Boltzmann constant, and T is the (absolute) temperature. In this expression B, C, $\cdots$, which are functions of the temperature, are called the second, third, $\cdots$virial coefficients. These coefficients indicate the deviation of a real equation of state from that of the ideal gas. It is a great success of statistical physics that these virial coefficients have been given in terms of the interaction between molecules, or the intermolecular potential. In fact, each virial coefficient is represented as an integral of a function of the intermolecular potential.

Besides the equation of state, the viscosity, isotopic thermal diffusion, and other transport properties of a gas are also intimately related to the intermolecular potential. In fact, each one of these properties is expressed in terms of effective cross sections for molecular collisions, which are also determined by the intermolecular potential.

The objective of the present article is to collect information about intermolecular potentials obtained from these properties of gases, particularly that by Japanese workers in recent years. In order to make the limits of our problem clear, we confine ourselves to pure, nonpolar, nonquantum gases.

For our purpose it is advisable to use suitable models of molecules. A suitable model must have both of the following two merits: (1) The model approximates real molecules (accuracy). (2) Necessary integrals can be evaluated for the model (integrability).

A molecular theory of matter is usually based upon the assumption that the total potential energy is equal to the sum of the potential energies between pairs of molecules. We also have to assume this additivity of the intermolecular potential.

I. THE SECOND AND THE THIRD VIRIAL COEFFICIENTS FOR SPHERICAL MOLECULES

1. Introduction

For spherically symmetric molecules, such as the rare gases, the potential energy between molecules, U, is a function only of the distance between the centers of molecules, r. In terms of r_{ij}, the distance between two molecules i and j, and by means of a function

$$f(r)=\exp[-U(r)/kT]-1, \tag{1.1}$$

the expressions for the second and the third virial coefficients, derived from statistical mechanics,[1] are

$$B=-\tfrac{1}{2}\int f(r_{12})d\tau_1=-2\pi\int_0^\infty f(r)r^2dr, \tag{1.2}$$

$$C=-\tfrac{1}{3}\int\int f(r_{12})f(r_{13})f(r_{23})d\tau_1 d\tau_2, \tag{1.3}$$

where

$$d\tau_i\equiv dx_i dy_i dz_i,$$

(x_i, y_i, z_i) being the position of the molecule i.

There is a temperature, T_B, such that

$$B(T)>0 \quad \text{for} \quad T>T_B,$$
$$B(T)<0 \quad \text{for} \quad T<T_B.$$

The T_B is called the Boyle temperature, because Boyle's law holds better for this temperature than for other temperatures. Relative to the Boyle temperature, let us define a volume v_B by

$$v_B=\left(T\frac{dB}{dT}\right)_{T=T_B}.$$

It may be suitable to call this v_B van der Waals' molecular volume, since it is equal to the term concerned with molecular volume in van der Waals'

* This work was carried out at the University of Wisconsin U. S. Naval Research Laboratory, Madison, Wisconsin.

[1] J. E. Mayer and M. G. Mayer, *Statistical Mechanics* (John Wiley and Sons, Inc., New York, 1940).

CC-0. In Public Domain. Gurukul Kangri Collection, Haridwar

Digitized by Arya Samaj Foundation Chennai and eGangotri

TABLE I. Boyle temperature T_B and van der Waals volume v_B for the rare gases.

	T_B°K	v_B A³
Ne	123	35.5
A	410	67.4
Kr	594	78.5
Xe	772	114

equation of state. The values of T_B and v_B for the rare gases are given in Table I.

Taking the characteristic values T_B and v_B as units, let us consider dimensionless "reduced virial coefficients"

$$B^*\left(\frac{T}{T_B}\right)=\frac{B(T)}{v_B},\quad C^*\left(\frac{T}{T_B}\right)=\frac{C(T)}{{v_B}^2},$$

in which B^* is normalized as

$$B^*(1)=0,\quad [dB^*(t)/dt]_{t=1}=1.$$

The B^* and C^* for the rare gases, which have been obtained from observed values given in Table II, are shown in Figs. 2 and 5 in the following two sections.

TABLE II. Second and third virial coefficients for the rare gases.

	T°K	B A³	$C\times10^{-2}$ A⁶	Reference
Ne	65.2	−34.8	15.5	a
	90.6	−13.6	12.2	
	123	0.2	6.1	
	173	10.7	5.5	
	223	15.1	6.3	
	273	17.7	7.0	
	373	19.7	...	
	473	21.7	...	
	573	22.8	...	
	673	22.8	...	
A	173	−106.8	...	a
	223	−62.7	48	
	273	−36.7	46	
	323	−18.3	33	
	373	−7.1	31	
	423	1.9	27	
	473	7.8	27	
	573	18.6	...	
Kr	273	−104.5	76	b
	323	−71.1	62	
	373	−47.9	54	
	423	−31.2	48	
	473	−18.5	44	
	523	−9.5	45	
	573	−1.9	44	
Xe	290	−229	175	c
	323	−184	146	
	373	−135	113	
	423	−100.9	96	
	473	−75.4	84	
	523	−55.2	74	
	573	−39.1	67	

[a] L. Holborn and J. Otto, Z. Physik. 33, 1 (1925).
[b] Beattie, Brierley, and Barriault, J. Chem. Phys. 20, 1615 (1952).
[c] Beattie, Barriault, and Brierley, J. Chem. Phys. 19, 1222 (1951).

2. Square-Well Potential[2]

The simplest model for which both the second and the third virial coefficients have been calculated is that of the square-well potential:

$$U(r)=\begin{cases}\infty & \text{for} \quad r<\sigma\\ -\epsilon & \text{for} \quad \sigma<r<g\sigma\\ 0 & \text{for} \quad g\sigma<r\end{cases}\qquad(2.1)$$

(Fig. 1). Here σ means the collision radius between molecules or, in our case of one-component gases, the diameter of a molecule.

Substituting (2.1) into (1.1), we have

$$f(r)=\begin{cases}-1 & \text{for} \quad r<\sigma\\ x & \text{for} \quad \sigma<r<g\sigma\\ 0 & \text{for} \quad g\sigma<r,\end{cases}$$

where

$$x=\exp(\epsilon/kT)-1.\qquad(2.2)$$

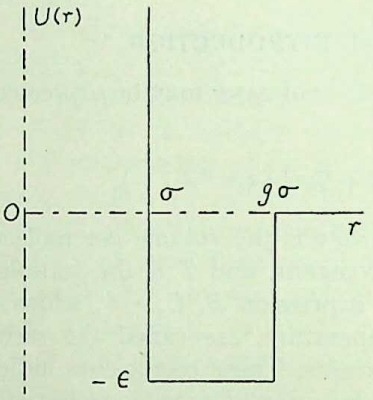


FIG. 1. Square-well potential.

The second virial coefficient (1.2) is expressed as a linear function of this x:

$$B=4v_0[1-(g^3-1)x],\qquad(2.3)$$

in which

$$v_0\equiv\frac{\pi}{6}\sigma^3$$

is the volume of the molecule.

Relations between T_B and ϵ and between v_B and v_0 are calculated to be

$$\frac{\epsilon}{kT_B}=\ln\frac{g^3}{g^3-1},\qquad(2.4)$$

$$\frac{v_B}{4v_0}=g^3\ln\frac{g^3}{g^3-1}.\qquad(2.5)$$

The third virial coefficient can be expressed as a cubic function of x;

$$3C=I^{(0)}-3xI^{(1)}+3x^2I^{(2)}-x^3I^{(3)}.\qquad(2.6)$$

[2] T. Kihara, Nippon Sugaku-Buturigakukaisi 17, 11 (1943).

CC-0. In Public Domain. Gurukul Kangri Collection, Haridwar

Digitized by Arya Samaj Foundation Chennai and eGangotri

Here $I^{(i)}$ are values of $\int\int d\tau_1 d\tau_2$ integrated over the following regions.

$$I^{(0)}: \quad r_{12}<\sigma, \quad r_{13}<\sigma, \quad r_{23}<\sigma;$$
$$I^{(1)}: \quad \sigma<r_{12}<g\sigma, \quad r_{13}<\sigma, \quad r_{23}<\sigma;$$
$$I^{(2)}: \quad \sigma<r_{12}<g\sigma, \quad \sigma<r_{13}<g\sigma, \quad r_{23}<\sigma;$$
$$I^{(3)}: \quad \sigma<r_{12}<g\sigma, \quad \sigma<r_{13}<g\sigma, \quad \sigma<r_{23}<g\sigma.$$

Let $W(a, b, c)$ generally be the value of $\int\int d\tau_1 d\tau_2$ integrated over the region

$$r_{12}<a, \quad r_{13}<b, \quad r_{23}<c.$$

Since W is symmetric with respect to a, b, c, it is sufficient to calculate it in the case $a\geqq b$, $a\geqq c$. It is clear that W is given by

$$W(a, b, c)=4\pi\int_0^c V(a, b, r)r^2dr,$$

in which $V(a, b, c)$ means the volume of the overlapping part of two spheres of radii a and b having a distance r between centers:

$$V(a, b, r)=(\pi/12)[r^3-6r(a^2+b^2)+8(a^3+b^3) -3(a^2-b^2)^2r^{-1}]$$
when $a-b\leqq r\leqq a+b$,
$$=(4\pi/3)b^3$$
when $r\leqq a-b$.

We obtain, therefore,

$$W(a, b, c)=(\pi^2/18)[a^6+b^6+c^6+18a^2b^2c^2 +16(b^3c^3+c^3a^3+a^3b^3) -9\{a^4(b^2+c^2)+b^4(c^2+a^2)+c^4(a^2+b^2)\}]$$
when $a\leqq b+c$,
$$=(16\pi^2/9)b^3c^3$$
when $a\geqq b+c$.

In terms of this function, $I^{(i)}$ in (2.6) are given by

$$I^{(0)}=W(\sigma, \sigma, \sigma),$$
$$I^{(1)}=W(g\sigma, \sigma, \sigma)-I^{(0)},$$
$$I^{(2)}=W(g\sigma, g\sigma, \sigma)-I^{(0)}-2I^{(1)},$$
$$I^{(3)}=W(g\sigma, g\sigma, g\sigma)-I^{(0)}-3I^{(1)}-3I^{(2)}.$$

Thus we obtain finally

$$C=2v_0^2[5-(g^6-18g^4+32g^3-15)x +(-2g^6+36g^4-32g^3-18g^2+16)x^2 -(6g^6-18g^4+18g^2-6)x^3] \quad \text{for} \quad g\leqq 2,$$
$$=2v_0^2[5-17x+(32g^3-18g^2-48)x^2 -(5g^6-32g^3+18g^2+26)x^3] \quad \text{for} \quad g\geqq 2.$$

For example

$$C=2v_0^2(5-17x+136x^2-162x^3) \quad \text{for} \quad g=2.$$

Figure 2 shows these virial coefficients in the reduced forms. From Fig. 2 and consulting Fig. 3, we see the following facts:

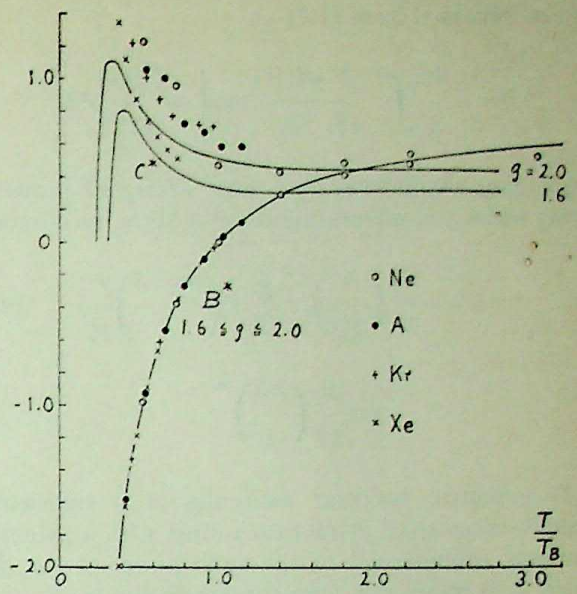


FIG. 2. Reduced virial coefficients compared with curves for the square-well potential.

1. The third virial coefficient C^* is sensitive to the shape of the potential, whereas the second virial coefficient B^* is insensitive to it.

2. If the bowl of the assumed potential is not sufficiently wide, the calculated C^* is too small.

3. The adequate value of g for the rare gases is about 2.0.

3. Lennard-Jones Potential

Assuming that

$$U(r)=\frac{\lambda}{r^n}-\frac{\mu}{r^m}=U_0\left[\frac{m}{n-m}\left(\frac{r_0}{r}\right)^n-\frac{n}{n-m}\left(\frac{r_0}{r}\right)^m\right], \quad (3.1)$$
$$\lambda, \mu>0, \quad n>m>3,$$

Lennard-Jones[3] evaluated the second virial coefficient (1.2) in the form of a power series. Integrating by parts,

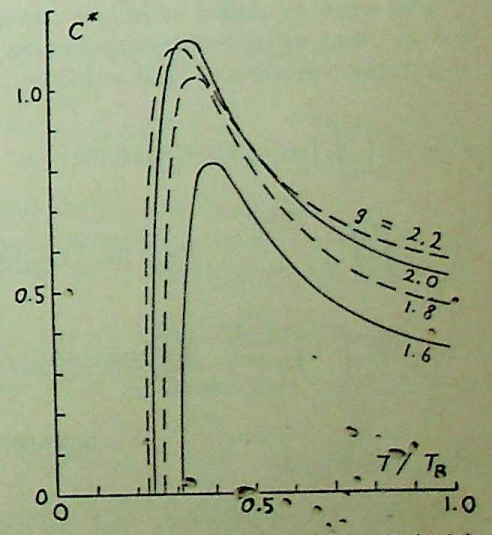


FIG. 3. Reduced third virial coefficient calculated for the square-well potential.

[3] Lennard-Jones, Proc. Roy. Soc. (London) **A106**, 463 (1924), Proc. Phys. Soc. (London) **A43**, 461 (1931).

CC-0. In Public Domain. Gurukul Kangri Collection, Haridwar

Digitized by Arya Samaj Foundation Chennai and eGangotri

he first obtained from (1.2)

$$B=-\frac{2\pi}{3}\int_0^\infty \frac{1}{kT}\frac{dU(r)}{dr}\exp\left[-\frac{U(r)}{kT}\right]r^3dr.$$

Expanding $\exp(\mu/r^mkT)$ of $\exp[-U(r)/kT]$ into a power series and integrating term by term, he obtained

$$B=-\frac{2\pi}{n}\left(\frac{\lambda}{kT}\right)^{3/n}\sum_{t=0}^{\infty}\Gamma\left(\frac{tm-3}{n}\right)\frac{y^t}{t!}, \qquad (3.2)$$

$$y\equiv\frac{\mu}{kT}\left(\frac{kT}{\lambda}\right)^{m/n}.$$

Two neutral nonpolar molecules at a sufficiently large distance apart attract each other with a potential inversely proportional to the sixth power of the distance. It is reasonable, therefore, to choose $m=6$.

The expression (3.2) can be transformed into

$$B=\frac{2\pi}{3}r_0^3F_3\left(\frac{U_0}{kT}\right), \qquad (3.3)$$

where

$$F_3(z)=-\frac{3}{n}\sum_{t=0}^{\infty}\frac{1}{t!}\Gamma\left(\frac{tm-3}{n}\right)\left(\frac{n}{m}\right)^t\left(\frac{m}{n-m}z\right)^{[(n-m)t+3]/n}.$$

(The suffix 3 indicates that this function is one of the F_s in section 9. In the case $m=6$, $n=12$, the F_s are given in Table X.) In the case $m=6$, the Boyle temperature, T_B, and the van der Waals volume, v_B, are related to the model constants as follows:

$$kT_B=4.57U_0,\quad v_B=1.00r_0^3 \quad \text{for} \quad n=9;$$
$$kT_B=3.44U_0,\quad v_B=1.20r_0^3 \quad \text{for} \quad n=12;$$
$$kT_B=1.17U_0,\quad v_B=2.46r_0^3 \quad \text{for} \quad n=\infty.$$

The series expansion technique can also be applied to the third virial coefficient.[4] Let us transform the integration variables of (1.3) as follows:

$$C=-\tfrac{1}{3}\int\int f(r_{12})f(r_{13})f(r_{23})d\tau_1d\tau_2$$

$$=-\int\int_{r_{12}>r_{13},\ r_{12}>r_{23}} f(r_{12})f(r_{13})f(r_{23})d\tau_1d\tau_2$$

$$=-4\pi^2\int_0^{\frac{1}{2}}\int_{1-(1-y^2)^{\frac{1}{2}}}^{(1-y^2)^{\frac{1}{2}}}\int_0^\infty f(r_{12})f(r_{13})f(r_{23})$$

$$\times R^5dRdxd(y^2), \qquad (3.4)$$

where (see Fig. 4)

$$R=r_{12},\quad (x^2+y^2)R^2=r_{13}^2,\quad [(1-x)^2+y^2]R^2=r_{23}^2.$$

[4] T. Kihara, J. Phys. Soc. Japan, 3, 265 (1948); 6, 184 (1951).

First we carry out the integration with respect to R. Integrating by parts we have

$$-\int_0^\infty f(r_{12})f(r_{13})f(r_{23})R^5dR$$
$$=\tfrac{1}{6}\int_0^\infty\frac{\partial f(r_{12})f(r_{13})f(r_{23})}{\partial R}R^6dR. \qquad (3.5)$$

Here the product of f functions can be written as the sum

$$f(r_{12})f(r_{13})f(r_{23})=f^{(0)}-f^{(1)}-f^{(2)}-f^{(3)}$$
$$+f(r_{12})+f(r_{13})+f(r_{23}),$$

in which

$$f^{(0)}=\exp[-(kT)^{-1}\{U(r_{12})+U(r_{13})+U(r_{23})\}]-1,$$
$$f^{(1)}=\exp[-(kT)^{-1}\{U(r_{12})+U(r_{13})\}]-1,$$
$$f^{(2)}=\exp[-(kT)^{-1}\{U(r_{12})+U(r_{23})\}]-1,$$
$$f^{(3)}=\exp[-(kT)^{-1}\{U(r_{13})+U(r_{23})\}]-1.$$

For $m>6$, the integral of the sum of these seven terms can be evaluated by the sum of the seven integrals,

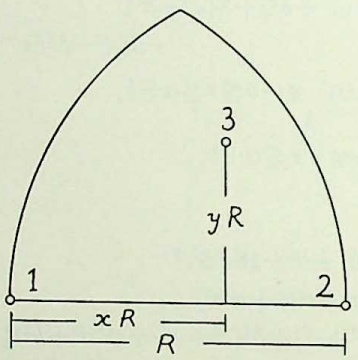


FIG. 4. The (x, y) domain of integration for (3.4).

each integral concerning each term. Therefore, in the same way as that of Lennard-Jones, we can expand (3.5) into

$$-\frac{1}{n}\left(\frac{\lambda}{kT}\right)^{6/n}\sum_{t=0}^{\infty}C_ty^t,$$

$$y=\frac{\mu}{kT}\left(\frac{kT}{\lambda}\right)^{m/n},$$

where

$$C_t=\frac{1}{t!}\Gamma\left(\frac{tm-6}{n}\right)\left[(1+\xi^n+\eta^n)^{6/n}\left\{\frac{1+\xi^m+\eta^m}{(1+\xi^n+\eta^n)^{m/n}}\right\}^t\right.$$
$$-(1+\xi^n)^{6/n}\left\{\frac{1+\xi^m}{(1+\xi^n)^{m/n}}\right\}^t$$
$$-(1+\eta^n)^{6/n}\left\{\frac{1+\eta^m}{(1+\eta^n)^{m/n}}\right\}^t$$
$$\left.-(\xi^n+\eta^n)^{6/n}\left\{\frac{\xi^m+\eta^m}{(\xi^n+\eta^n)^{m/n}}\right\}^t+1+\xi^6+\eta^6\right],$$

$$\xi=R/r_{13}=(x^2+y^2)^{-\frac{1}{2}},\quad \eta=R/r_{23}=[(1-x)^2+y^2]^{-\frac{1}{2}}.$$

CC-0. In Public Domain. Gurukul Kangri Collection, Haridwar

Digitized by Arya Samaj Foundation Chennai and eGangotri

Thus we obtain

$$C=-\frac{4\pi^2}{n}\left(\frac{\lambda}{kT}\right)^{6/n}\sum_{t=0}^{\infty}y^t\int_0^{\frac{1}{2}}\int_{1-(1-y^2)^{\frac{1}{2}}}^{(1-y^2)^{\frac{1}{2}}}C_t dx d(y^2). \quad (3.6)$$

In the case we need, $m=6$, C_1 becomes indefinite. We may, however, take the limit $m\to 6$, since in the original form this value is not any singular point:

$$\lim_{m\to 6} C_1=\ln\frac{(1+\xi^n)(1+\eta^n)}{1+\xi^n+\eta^n}+\xi^6\ln\frac{(1+\xi^n)(\xi^n+\eta^n)}{\xi^n(1+\xi^n+\eta^n)}+\eta^6\ln\frac{(1+\eta^n)(\xi^n+\eta^n)}{\eta^n(1+\xi^n+\eta^n)}.$$

Let us fix m equal to 6, and confine ourselves to the $(6, n)$ potential

$$U(r)=U_0\left[\frac{6}{n-6}\left(\frac{r_0}{r}\right)^n-\frac{n}{n-6}\left(\frac{r_0}{r}\right)^6\right] \quad (3.7)$$

hereafter.

TABLE III. Coefficients in the series expansion (3.8) of the third virial coefficient for Lennard-Jones (6.9) and (6.12) potentials.

t	$\gamma_t(9)$	$\gamma_t(12)$
0	+1.561	+1.383
1	−2.940	−2.562
2	+0.929	+1.215
3	0.716	0.766
4	0.503	0.343
5	0.291	0.047
6	0.105	−0.112
7	−0.04	−0.168
8	−0.14	−0.164
9	−0.20	−0.134
10	−0.23	−0.098
11	−0.23	−0.067

Our result (3.6) may be written as

$$C=10v_0\sum_{t=0}^{\infty}\gamma_t(n)\left(\frac{y}{2}\right)^t, \quad (3.8)$$

where

$$v_0=\frac{\pi}{6}\left(\frac{\lambda}{kT}\right)^{3/n}=\frac{\pi}{6}r_0^3\left(\frac{6}{n-6}\frac{U_0}{kT}\right)^{3/n},$$

$$\frac{y}{2}=\frac{1}{2}\frac{\mu}{kT}\left(\frac{kT}{\lambda}\right)^{6/n}=\frac{n}{12}\left(\frac{6}{n-6}\frac{U_0}{kT}\right)^{(n-6)/n}.$$

The values of $\gamma_t(n)$, which have been obtained by numerical calculation of the double integrals, are given in Table III.[5]

Comparison with observed values is shown in Fig. 5. Consulting the conclusions of the preceding section, we see that the bowl of the Lennard-Jones (6, 12) potential is not sufficiently wide for molecules of the rare gases.

[5] In the case of (6, 12) potential, a highly accurate table for C is given by Bird, Spotz, and Hirschfelder, J. Chem. Phys. 18, 1395 (1950).

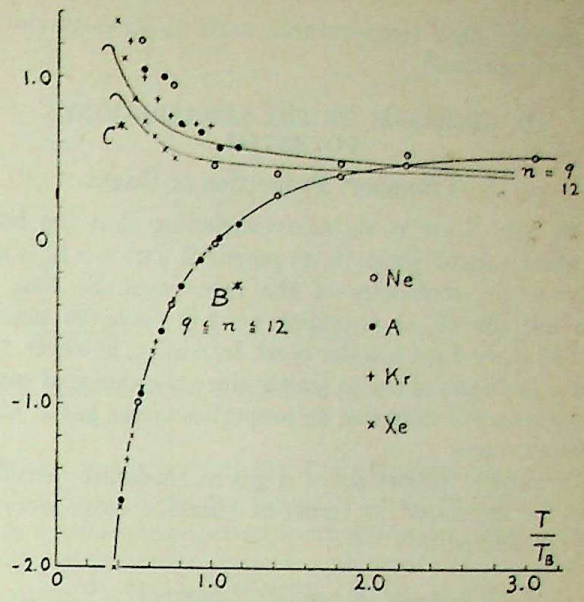


FIG. 5. Reduced virial coefficients compared with curves for Lennard-Jones $(6, n)$ potential.

4. Inverse-Power Repulsive Potential

When the attractive part of the intermolecular potential is negligible, the model

$$U(r)=\lambda r^{-n}, \quad \lambda>0, \quad n>3 \quad (4.1)$$

may be used. The exponent n may be seen as a measure of the hardness of the molecules.

In this case the $(\nu+1)$-th virial coefficient is written in the form $b_\nu(\lambda/kT)^{3\nu/n}$, b_ν being independent of the temperature. In particular, from (3.2), the second virial coefficient is

$$B=\frac{2\pi}{3}\Gamma\left(\frac{n-3}{n}\right)\left(\frac{\lambda}{kT}\right)^{3/n}, \quad (4.2)$$

and, from (3.8), the third virial coefficient is

$$C=\frac{5\pi^2}{18}\gamma_0(n)\left(\frac{\lambda}{kT}\right)^{6/n}. \quad (4.3)$$

The values of $\gamma_0(n)$ are given in Table IV.

This inverse-power repulsive potential, and therefore the results (4.2) and (4.3), can be applied to gases at

TABLE IV. Numerical factor in the third virial coefficient (4.3) for the inverse nth power potential.

n	$\gamma_0(n)$
6	2.032
9	1.561
12	1.383
15	1.291
18	1.233
∞	1.000

CC-0. In Public Domain. Gurukul Kangri Collection, Haridwar

Digitized by Arya Samaj Foundation Chennai and eGangotri

extremely high temperatures, such as gases produced by detonations.[6]

II. CRITICISM OF THE LENNARD-JONES POTENTIAL

5. Transport Properties of Gases

In Sec. 3 we came near concluding that the bowl of the Lennard-Jones $(6, n)$ potential with $n=12$ is too narrow for molecules of the rare gases. So long as we use the $(6, n)$ potential we will have to choose $n<12$ if we want a wider bowl. In reality, however, the state of affairs is not so simple since the choice of small n exerts some influence on properties of the gas at high temperatures.

Transport properties of a gas at moderate densities can be expressed in terms of effective cross sections $\Omega^{(l)}{}_{(r)}$ defined by[7]

$$\Omega^{(l)}{}_{(r)}=\pi^{\frac{1}{2}}\int_0^\infty \phi^{(l)}V^{2r+2}\exp(-V^2)dV,$$

$$\phi^{(l)}=\int_0^\infty (1-\cos^l\theta)gbdb, \tag{5.1}$$

$$l=1, 2, \cdots; \quad r=l, \quad l+1, \quad l+2, \cdots.$$

TABLE V. Functions defined by (5.2) for $(6, \infty)$ potential (5.3), ζ being given by (5.4).[a]

ζ	$F_1{}^1(\zeta)$	$F_2{}^2(\zeta)$	$F_2{}^1(\zeta)$	$F_3{}^2(\zeta)$
0.00	0.5000	1.5000	1.0000	4.0000
0.01	0.5017	1.5034	1.0036	4.0106
0.02	0.5036	1.5068	1.0074	4.0218
0.03	0.5056	1.5102	1.0116	4.0335
0.04	0.5077	1.5137	1.0159	4.0457
0.05	0.5099	1.5173	1.0205	4.0585
0.075	0.5159	1.5268	1.0330	4.0927
0.100	0.5225	1.5369	1.0468	4.1299
0.125	0.5296	1.5478	1.0617	4.1700
0.150	0.5369	1.5595	1.0774	4.2127
0.175	0.5444	1.5719	1.0939	4.2578
0.200	0.5521	1.5849	1.1115	4.3053
0.250	0.5674	1.6126	1.1464	4.4055
0.375	0.6048	1.6872	1.2376	4.6777
0.500	0.6401	1.7648	1.3264	4.9615
0.625	0.6733	1.8426	1.4090	5.2403
0.750	0.7045	1.9189	1.4846	5.5053
0.875	0.7338	1.9929	1.5537	5.7530
1.000	0.7614	2.0635	1.6167	5.9828
1.125	0.7874	2.1308	1.6753	6.1963
1.250	0.8119	2.1945	1.7294	6.3950
1.375	0.8351	2.2551	1.7800	6.5809
1.500	0.8571	2.3125	1.8275	6.7556
1.625	0.8780	2.3673	1.8725	6.9205
1.750	0.8981	2.4197	1.9153	7.0771
1.875	0.9172	2.4698	1.9560	7.2262
2.000	0.9357	2.5183	1.9950	7.3689

[a] The values are taken from M. Kotani, Proc. Phys. Math. Soc. Japan 24, 76 (1942).

[6] T. Kihara and T. Hikita, *Fourth Symposium on Combustion* (Williams & Wilkins Company, Baltimore, Maryland, 1953), p. 458.

[7] S. Chapman and T. G. Cowling, *The Mathematical Theory of Non-Uniform Gases* (Cambridge University Press, London, 1939).

Here g is the relative velocity, b the impact parameter, θ the deflection angle in the orbit of relative motion, and

$$V=(m^*/2kT)^{\frac{1}{2}}g, \quad m^*=\text{reduced mass}.$$

In particular, when the Lennard-Jones $(6, n)$ potential

$$U(r)=\lambda r^{-n}-\mu r^{-6}$$

is adopted, the $\Omega^{(l)}{}_{(r)}$ are given in the form

$$\Omega^{(l)}{}_{(r)}=\left(\frac{2\pi kT}{m^*}\right)^{\frac{1}{2}}\left(\frac{\lambda}{2kT}\right)^{2/n}F_r{}^l(\zeta), \tag{5.2}$$

in which

$$\zeta=\frac{1}{2kT}\left(\frac{\mu^n}{\lambda^6}\right)^{1/(n-6)}.$$

The functions $F_r{}^l(\zeta)$ have been calculated for $(6, \infty)$ potential,[8] i.e.,

$$U(r)=\begin{cases}-\mu r^{-6} & \text{for } r>a\\ \infty & \text{for } r<a,\end{cases} \tag{5.3}$$

$$\zeta=\frac{1}{2}\frac{\mu}{kTa^6}, \tag{5.4}$$

and for (6, 12) potential,[9,10] i.e.,

$$U(r)=\frac{\lambda}{r^{12}}-\frac{\mu}{r^6}=U_0\left[\left(\frac{r_0}{r}\right)^{12}-2\left(\frac{r_0}{r}\right)^6\right], \tag{5.5}$$

$$\zeta=\frac{1}{2kT}\frac{\mu^2}{\lambda}=\frac{2U_0}{kT}. \tag{5.6}$$

The results are given in Tables V and VI.

The viscosity, η, of a pure gas is given by

$$\eta=\frac{5kT}{8\Omega^{(2)}(2)}\left[1+\frac{3}{49}\left(\frac{\Omega^{(2)}(3)}{\Omega^{(2)}(2)}-\frac{7}{2}\right)^2\right] \tag{5.7}$$

(compare Appendix). Figure 6 shows calculat curves and observed values of the reduced viscosity

$$\eta(mkT)^{-\frac{1}{2}}v_B{}^3,$$

where m is the mass per molecule, and T_B and v_B a taken from Table I.

The isotopic thermal diffusion ratio k_T is given by (compare Appendix)

$$k_T=\frac{15}{8}\frac{n_1n_2}{(n_1+n_2)^2}\frac{m_1-m_2}{m_1+m_2}\frac{2\Omega^{(1)}(2)-5\Omega^{(1)}(1)}{\Omega^{(2)}(2)}, \tag{5.8}$$

where m_1/m_2 is the ratio of the masses of the two kinds of molecules $(m_1>m_2)$, and $n_1/(n_1+n_2)$ and $n_2/(n_1+n_2)$

[8] M. Kotani, Proc. Phys.-Math. Soc. Japan 24, 76 (1942).

[9] T. Kihara and M. Kotani, Proc. Phys.-Math. Soc. Japan 25, 602 (1953).

[10] Hirschfelder, Bird, and Spotz, J. Chem. Phys. 16, 968 (1948); 17, 1343 (1949).

CC-0. In Public Domain. Gurukul Kangri Collection, Haridwar

Digitized by Arya Samaj Foundation Chennai and eGangotri

TABLE VI. Functions defined by (5.2) for (6, 12) potential (5.5), ζ being given by (5.6).[a]

ζ	$F_1^{(1)}(\zeta)$	$F_2^{(1)}(\zeta)$	$F_2^{(2)}(\zeta)$	$F_3^{(2)}(\zeta)$
0.000	0.5063	1.4344	1.1564	4.433
0.025	0.4950	1.4073	1.1201	4.310
0.050	0.4912	1.3976	1.1070	4.264
0.075	0.4889	1.3909	1.0982	4.232
0.100	0.4873	1.3859	1.0916	4.207
0.150	0.4857	1.3789	1.0828	4.171
0.200	0.4853	1.3745	1.0779	4.146
0.250	0.4858	1.3720	1.0755	4.129
0.375	0.4897	1.3710	1.0779	4.111
0.500	0.4964	1.3756	1.0883	4.117
0.625	0.5050	1.3842	1.1046	4.141
0.750	0.5150	1.3960	1.1251	4.179
0.875	0.5259	1.4104	1.1486	4.228
1.000	0.5376	1.4270	1.1749	4.286
1.125	0.5499	1.4456	1.2028	4.353
1.250	0.5626	1.4657	1.2321	4.425
1.375	0.5756	1.4872	1.2622	4.503
1.500	0.5887	1.5099	1.2930	4.586
1.625	0.6019	1.5336	1.3240	4.672
1.750	0.6151	1.5581	1.3549	4.761
1.875	0.6283	1.5833	1.3857	4.852
2.000	0.6413	1.6092	1.4162	4.944

[a] The values are taken from T. Kihara and M. Kotani, Proc. Phys.-Math. Soc. Japan 25, 602 (1943).

are their mole fractions. The "reduced thermal diffusion ratio,"

$$k_T^* \equiv k_T\left[\frac{n_1 n_2}{(n_1+n_2)^2}\frac{m_1-m_2}{m_1+m_2}\right]^{-1} = \frac{15}{8}\frac{2\Omega^{(1)}(2)-5\Omega^{(1)}(1)}{\Omega^{(2)}(2)},$$

is shown in Fig. 7, together with Stier's[11] observations.

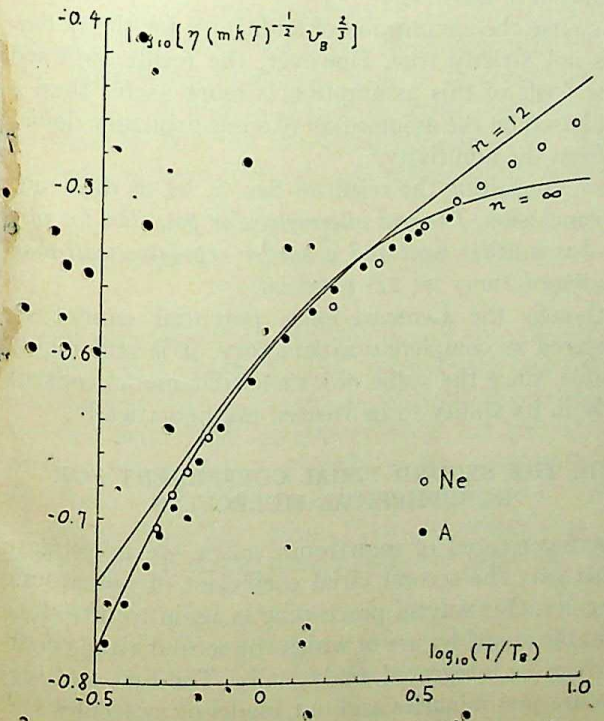


FIG. 6. Reduced viscosity compared with curves for Lennard-Jones $(6, n)$ potential.

[11] L. G. Stier, Phys. Rev. 62, 548 (1942).

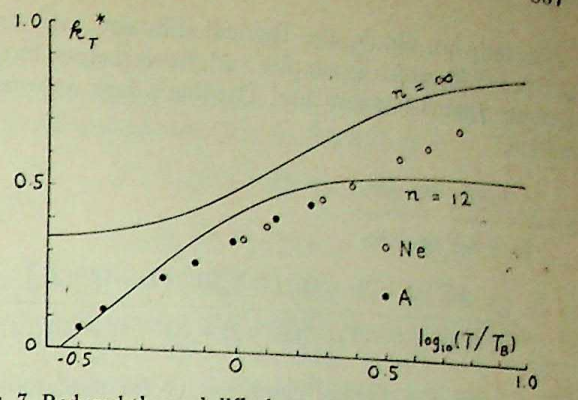


FIG. 7. Reduced thermal diffusion ratio compared with curves for Lennard-Jones $(6, n)$ potential.

From the discrepancies at high temperatures shown in Figs. 6 and 7, we may draw the following conclusion: In order to explain the transport properties of neon and argon (perhaps also krypton and xenon) at high temperatures it is necessary to choose $n>12$. In other words, the repulsive wall of the intermolecular potential for rare gases is harder than that of the (6, 12) potential.

Appendix to Section 5

The effective cross sections (5.1) depend, in general, on the temperature as

$$T\frac{d}{dT}\Omega^{(l)}(r) = \Omega^{(l)}(r+1) - (r+\tfrac{3}{2})\Omega^{(l)}(r).$$

In particular, if $\phi^{(l)}$ do not depend on the relative speed g, $\Omega^{(l)}(r)$ are independent of the temperature. Although the derivatives of $\Omega^{(l)}(r)$ do not necessarily vanish for real molecules, the absolute values for

$$\frac{T^t}{\Omega^{(1)}(1)}\frac{d^t\Omega^{(1)}(1)}{dT^t}, \quad \frac{T^t}{\Omega^{(2)}(2)}\frac{d^t\Omega^{(2)}(2)}{dT^t}, \quad \cdots, \quad t=1, 2, \cdots$$

are always small.

The expression (5.7) for the viscosity is an approximation which has been obtained by neglecting derivatives of the second and higher orders and also neglecting third and higher powers of the first derivative. This approximation is simpler and more accurate, and therefore more convenient for numerical calculations, than Chapman and Cowling's[7] second approximation

$$\eta = \frac{5kT}{2\Omega^{(2)}(2)}\left(1+\frac{b_{12}^2}{b_{11}b_{22}-b_{12}^2}\right),$$

where

$$b_{11} = 4\Omega^{(2)}(2),$$

$$b_{12} = 7\Omega^{(2)}(2) - 2\Omega^{(2)}(3),$$

$$b_{22} = \frac{301}{12}\Omega^{(2)}(2) - 7\Omega^{(2)}(3) + \Omega^{(2)}(4).$$ [12]

[12] The accuracies of these two approximations are quantitatively compared by E. A. Mason, J. Chem. Phys. (to be published).

CC-0. In Public Domain. Gurukul Kangri Collection, Haridwar

Digitized by Arya Samaj Foundation Chennai and eGangotri

Similarly we obtain the thermal diffusion ratio for isotopes (5.8), which is simpler and, nevertheless, more accurate than Chapman and Cowling's first approximation,

$$k_T=\frac{n_1n_2}{(n_1+n_2)^2}\frac{m_1-m_2}{m_1+m_2}\times\frac{15[2\Omega^{(1)}(2)-5\Omega^{(1)}(1)][5\Omega^{(1)}(1)+\Omega^{(2)}(2)]}{\Omega^{(2)}(2)[55\Omega^{(1)}(1)-20\Omega^{(1)}(2)+4\Omega^{(1)}(3)+8\Omega^{(2)}(2)]}.$$

As regards the thermal conductivity for monatomic gases, our approximation is

$$C_v\frac{25kT}{16\Omega^{(2)}(2)}\left[1+\frac{2}{21}\left(\frac{\Omega^{(2)}(3)}{\Omega^{(2)}(2)}-\frac{7}{2}\right)^2\right],$$

where C_v is the heat capacity at constant volume for the unit mass.

6. Stability of Crystal Structures

Before we draw our final conclusion, we want to examine another property of rare gases.

Neon, argon, krypton, and xenon crystallize at low temperatures in a lattice of *cubic* closest packing. For this lattice structure, the number of nearest neighbor molecules around one molecule is 12, the number of second nearest neighbors, which are $2^{\frac{1}{2}}$ times farther away from the original molecule, is 6; and the third nearest neighbors are $3^{\frac{1}{2}}$ times farther away. For hexagonal closest packing, on the other hand, the number of first nearest neighbors is also 12, that of the second nearest neighbors, which are $2^{\frac{1}{2}}$ times farther away, is also 6; but the third nearest neighbors are $(2+\frac{2}{3})^{\frac{1}{2}}$ times farther away, a little nearer than the third nearest neighbors in the cubic structure. In order to explain the stability of the cubic structure in comparison to the hexagonal one, we must therefore choose a potential with a more or less wide bowl, in so far as the additivity of the intermolecular potential is assumed.

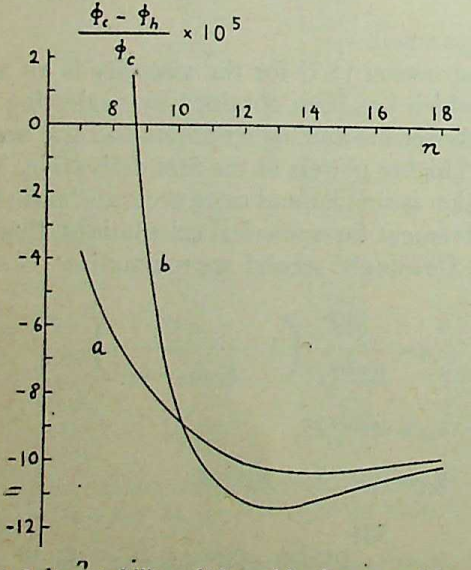


FIG. 8. Relative stability of the cubic closest packing structure to the hexagonal; Φ_h/Φ_c is the ratio of the crystallization energy of the hexagonal to the cubic. Curve "a" is for Lennard-Jones $(6, n)$ potential, curve "b" is for the potential (6.1).

Let us further assume, besides the assumption of the additivity, that the zero-point energy does not play any essential role regarding the stability of the cubic closest packing structure. (The solid helium seems to be hexagonal!) Then we can straightforwardly calculate the crystallization energies of these two lattice structures.[13] The comparison by means of the Lennard-Jones $(6, n)$ potential is shown in Fig. 8, from which it follows that the Lennard-Jones potential cannot explain the absolute stability of the cubic structure.

If we choose for another example

$$U(r)=U_0\left[\frac{6}{n-6}\exp\frac{n(r_0-r)}{r_0}-\frac{n}{n-6}\left(\frac{r_0}{r}\right)^6\right], \quad (6.1)$$

the cubic structure can become more stable than the hexagonal structure for $n<8.675$ (see Fig. 8). Two Lennard-Jones potentials, $n=9$, and 12, and the potential (6.1) with the critical value $n=8.675$ are compared in Fig. 9.

Thus we obtain the following result: In order to explain the stability of the cubic structure as compared to the hexagonal one, we have to choose a potential bowl wider than that of the Lennard-Jones (6, 12) potential in so far as the additivity of the intermolecular potential is assumed. This is in accordance with the conclusion reached in Sec. 3 which is also based on the assumption of additivity.

Of course the assumption of additivity for the potential is not strictly true. However, the result obtained on the basis of this assumption is more useful than a result based on the assumption of some arbitrary deviation from the additivity.

Now, consulting the result of Sec. 5, let us draw our final conclusion. *The real intermolecular potential for rare gases has a wider bowl and a harder repulsive wall than the Lennard-Jones* (6, 12) *potential.*

Although the Lennard-Jones potential cannot be considered as completely satisfactory, it is still highly valuable, since the value of a molecular model consists chiefly in its ability to be treated mathematically.

III. THE SECOND VIRIAL COEFFICIENT FOR NONSPHERICAL MOLECULES

Having treated of monatomic gases, we investigate in this part the second virial coefficient of polyatomic molecules. Our way of proceeding is again to introduce a suitable model by use of which the second virial coefficient can be integrated analytically. The first two sections are preliminaries and our model of molecules will be introduced in the last section.

[13] T. Kihara and S. Koba, J. Phys. Soc. Japan 7, 348 (1952).

CC-0. In Public Domain. Gurukul Kangri Collection, Haridwar

Digitized by Arya Samaj Foundation Chennai and eGangotri

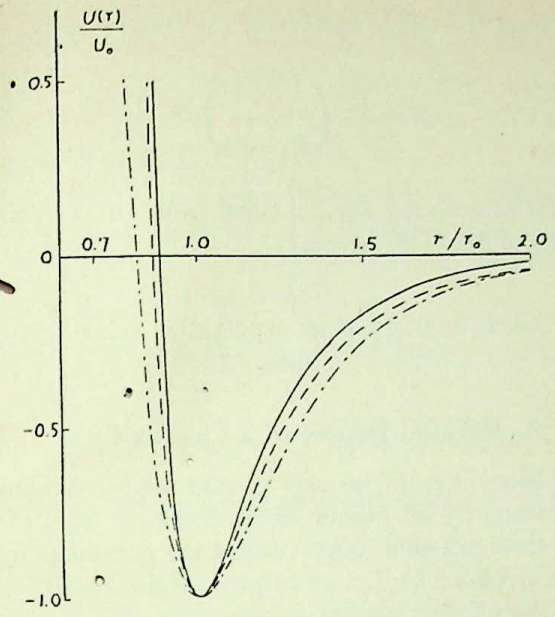


FIG. 9. Width of the bowl of intermolecular potentials. The full line is for Lennard-Jones (6, 12) potential, the broken line for Lennard-Jones (6, 9) potential, the chain line for the potential (6.1) with $n=8.675$.

7. Rigid Convex Body

A body is called convex if any line segment whose end points are inside lies entirely in that body.

Let us choose a coordinate origin O inside a (fixed) convex body and take coordinates of direction θ and φ ($0\leqq\theta\leqq\pi$, $0\leqq\varphi\leqq 2\pi$). For any direction (θ, φ), there is one and only one plane which is in contact with the convex body and whose normal from the origin is in the direction (θ, φ). This plane is named the supporting plane in the direction (θ, φ); the perpendicular distance from the origin to the supporting plane is called the supporting function, when it is considered as a function of θ and φ. The supporting function will be denoted by $H(\theta, \varphi)$. Let us further denote by $\langle H\rangle_{Av}$ the average value of $H(\theta, \varphi)$ with respect to all directions:

$$\langle H\rangle_{Av}\equiv\frac{1}{4\pi}\int_0^{2\pi}\int_0^{\pi} H(\theta, \varphi)\sin\theta d\theta d\varphi, \qquad (7.1)$$

which is independent of the choice of the origin O.

Let us first assume that the convex body has a smooth surface and that each supporting plane has a contact of the first order with the convex body. Let $\mathbf{r}(\theta, \varphi)$ be the radius vector from the origin to the contact point of the body with the supporting plane in the direction (θ, φ); compare Fig. 10(a). Then the surface area S and the volume V of the convex body are given by

$$S=\int_0^{2\pi}\int_0^{\pi}\left|\frac{\partial\mathbf{r}}{\partial\theta}\times\frac{\partial\mathbf{r}}{\partial\varphi}\right|d\theta d\varphi \qquad (7.2)$$

and

$$V=\tfrac{1}{3}\int_0^{2\pi}\int_0^{\pi}\mathbf{r}\cdot\left(\frac{\partial\mathbf{r}}{\partial\theta}\times\frac{\partial\mathbf{r}}{\partial\varphi}\right)d\theta d\varphi, \qquad (7.3)$$

respectively.

Now we consider two convex bodies labelled A and B and in each body choose a coordinate origin O_A and O_B. The supporting function, the $\mathbf{r}$ function, the volume, and the surface area will be denoted by

$$H_A(\theta, \varphi),\quad \mathbf{r}_A(\theta, \varphi),\quad V_A,\quad S_A,$$

and

$$H_B(\theta, \varphi),\quad \mathbf{r}_B(\theta, \varphi),\quad V_B,\quad S_B,$$

respectively. Keeping O_A and the orientation of A fixed, and keeping the orientation of B also fixed, let us move B around A keeping contact from outside. Then the locus of O_B forms the surface of another convex body, whose $\mathbf{r}$ function is

$$\mathbf{r}(\theta, \varphi)=\mathbf{r}_A(\theta, \varphi)+\mathbf{r}_B^*(\theta, \varphi),$$

where

$$\mathbf{r}_B^*(\theta, \varphi)=-\mathbf{r}_B(\pi-\theta, -\varphi),$$

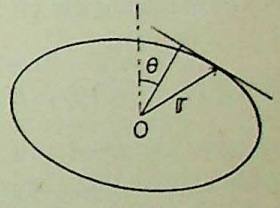
see Fig. 10(b). The volume of this third convex body,

$$V_{AB}=\tfrac{1}{3}\int\int(\mathbf{r}_A+\mathbf{r}_B^*)\left[\left(\frac{\partial\mathbf{r}_A}{\partial\theta}+\frac{\partial\mathbf{r}_B^*}{\partial\theta}\right)\times\left(\frac{\partial\mathbf{r}_A}{\partial\varphi}+\frac{\partial\mathbf{r}_B^*}{\partial\varphi}\right)\right]d\theta d\varphi,$$

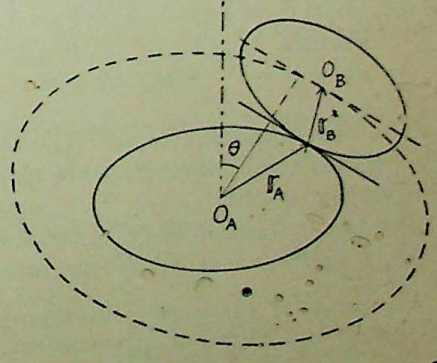
must be first evaluated.

Considering the identity

$$\frac{\partial}{\partial\theta}\left[\mathbf{r}_B^*\cdot\left(\mathbf{r}_A\times\frac{\partial\mathbf{r}_A}{\partial\varphi}\right)\right]+\frac{\partial}{\partial\varphi}\left[\mathbf{r}_B^*\cdot\left(\frac{\partial\mathbf{r}_A}{\partial\theta}\times\mathbf{r}_A\right)\right]$$
$$=2\mathbf{r}_B^*\cdot\left(\frac{\partial\mathbf{r}_A}{\partial\theta}\times\frac{\partial\mathbf{r}_A}{\partial\varphi}\right)-\mathbf{r}_A\cdot\left(\frac{\partial\mathbf{r}_B^*}{\partial\theta}\times\frac{\partial\mathbf{r}_A}{\partial\varphi}\right)$$
$$-\mathbf{r}_A\cdot\left(\frac{\partial\mathbf{r}_A}{\partial\theta}\times\frac{\partial\mathbf{r}_B^*}{\partial\varphi}\right),$$



(a)



(b)

FIG. 10. Convex bodies and their supporting planes.

CC-0. In Public Domain. Gurukul Kangri Collection, Haridwar

Digitized by Arya Samaj Foundation Chennai and eGangotri

we have

$$\int\int\left[\mathbf{r}_A\cdot\left(\frac{\partial\mathbf{r}_B^*}{\partial\theta}\times\frac{\partial\mathbf{r}_A}{\partial\varphi}\right)+\mathbf{r}_A\cdot\left(\frac{\partial\mathbf{r}_A}{\partial\theta}\times\frac{\partial\mathbf{r}_B^*}{\partial\varphi}\right)\right]d\theta d\varphi$$
$$=2\int\int\mathbf{r}_B^*\cdot\left(\frac{\partial\mathbf{r}_A}{\partial\theta}\times\frac{\partial\mathbf{r}_A}{\partial\varphi}\right)d\theta d\varphi,$$

since the integral of the divergence expression vanishes. Making use of this relation and the other similar one, we obtain

$$V_{AB}=V_A+V_B+\int\int\mathbf{r}_B^*\cdot\left(\frac{\partial\mathbf{r}_A}{\partial\theta}\times\frac{\partial\mathbf{r}_A}{\partial\varphi}\right)d\theta d\varphi$$
$$+\int\int\mathbf{r}_A\cdot\left(\frac{\partial\mathbf{r}_B^*}{\partial\theta}\times\frac{\partial\mathbf{r}_B^*}{\partial\varphi}\right)d\theta d\varphi,$$

or, in terms of the supporting functions

$$V_{AB}=V_A+V_B$$
$$+\int\int H_B(\pi-\theta,\varphi)\left|\frac{\partial\mathbf{r}_A}{\partial\theta}\times\frac{\partial\mathbf{r}_A}{\partial\varphi}\right|d\theta d\varphi$$
$$+\int\int H_A(\theta,\varphi)\left|\frac{\partial\mathbf{r}_B^*}{\partial\theta}\times\frac{\partial\mathbf{r}_B^*}{\partial\varphi}\right|d\theta d\varphi.$$

Up to this point the orientation of the convex body B has been kept fixed. The next step is to take the average with respect to all orientations of the body B. When H_B in the third term on the right-hand side is averaged with respect to orientations of the body B, the value no longer depends on θ and φ and is equal to $\langle H_B\rangle_{Av}$. The average value of the third term, therefore, is $\langle H_B\rangle_{Av}S_A$; the fourth term is similarly $\langle H_A\rangle_{Av}S_B$. Hence the average value of V_{AB} becomes

$$\langle V_{AB}\rangle_{Av}=V_A+V_B+\langle H_B\rangle_{Av}S_A+\langle H_A\rangle_{Av}S_B. \quad (7.4)$$

After we have obtained this relation it is no longer necessary to assume that the convex body has a smooth surface and that each supporting plane has a contact of the first order with the convex body.

If the two convex bodies A and B are of the same shape, i.e., if $V_A=V_B=V, S_A=S_B=S$ and $H_A=H_B=H$, (7.4) becomes

$$2(V+\langle H\rangle_{Av}S). \quad (7.5)$$

The neat formula (7.4) or (7.5) was recently found by Isihara;[14] the improved proof given above is partly due to Minkowski.[15]

For the evaluation of $\langle H\rangle_{Av}$ the following theorem is useful: $4\pi\langle H\rangle_{Av}$ is equal to the mean curvature integrated over the whole surface of the convex body,

$$M\equiv\int\frac{1}{2}\left(\frac{1}{R_1}+\frac{1}{R_2}\right)dS, \quad (7.6)$$

where R_1 and R_2 are the principal radii of curvature.[16] In terms of M, (7.5) becomes

$$2\left(V+\frac{1}{4\pi}MS\right). \quad (7.7)$$

8. Parallel Bodies of a Convex Core

Definition: Let C be any convex body. A convex body formed by all points whose distances from C are smaller than or equal to $\frac{1}{2}\rho$ is called the parallel body of C in the distance $\frac{1}{2}\rho$. Let us call the original body C the core of the parallel bodies.

We first consider as the core a convex polyhedron. Let the length of each edge be $l_1, l_2, \cdots, l_N$ (N being the number of edges of the polyhedron) and the angle of the ith edge be α_i ($i=1, 2, \cdots N$).

A parallel body of this polyhedron in the distance $\frac{1}{2}\rho$ is composed of several parts of a sphere of diameter ρ, several parts of a circular cylinder of diameter ρ, and several parts of a plane. The surface integral of the mean curvature, M, of this parallel body is therefore given by

$$M=\frac{2}{\rho}\times(\text{surface area of all spherical parts})$$
$$+\frac{1}{\rho}\times(\text{surface area of all cylindrical parts}).$$

Since the spherical parts, when they are gathered together, form a complete sphere, we have

$$M=\frac{2}{\rho}\times(\text{surface area of a sphere of diameter }\rho)$$
$$+\frac{1}{\rho}\times\sum_{i=1}^{N}(\pi-\alpha_i)\frac{\rho}{2}l_i=2\pi\rho+M_0. \quad (8.1)$$

Here

$$M_0=\tfrac{1}{2}\sum_{i=1}^{N}(\pi-\alpha_i)l_i \quad (8.2)$$

is the surface integral of the mean curvature for the core. Similarly, the surface area S of the parallel body is

$$S=\pi\rho^2+M_0\rho+S_0, \quad (8.3)$$

where S_0 is the surface area of the core; and the volume

[14] A. Isihara, J. Chem. Phys. 18, 1446 (1950); A. Isihara and T. Hayashida, J. Phys. Soc. Japan 6, 40 and 46 (1951); T. Kihara, J. Phys. Soc. Japan 8, 686 (1953).

[15] H. Minkowski, Math. Ann. 57, 447 (1903).

[16] As regards the proof, compare for example, T. Bonnesen and W. Fenchel, *Theorie der konvexen Koerper* (Ergebnisse der Mathematik und ihrer Grenzgebeite, Bd. 3, Heft 1, Julius Springer, Berlin, 1934).

CC-0. In Public Domain. Gurukul Kangri Collection, Haridwar

Digitized by Arya Samaj Foundation Chennai and eGangotri

V is

$$V=\frac{\pi}{6}\rho^3+\tfrac{1}{4}M_0\rho^2+\tfrac{1}{2}S_0\rho+V_0, \qquad (8.4)$$

V_0 being the volume of the core.

Although we have been considering a polyhedron as the core, (8.1), (8.3), and (8.4) hold for parallel bodies of any convex core, since any convex body can be represented as a limit of polyhedrons.

In particular, when the core is a perpendicular prism of height l, area of the base f, and circumference of the base c, we have

$$V_0=fl, \quad S_0=2f+cl, \quad M_0=\pi l+(\pi/2)c. \qquad (8.5)$$

From (8.5), taking the appropriate limit, we obtain

$$V_0=0, \quad S_0=2f, \quad M_0=(\pi/2)c, \qquad (8.6)$$

TABLE VII. Volume V_0 surface area S_0 and surface integral of the mean curvature M_0 of convex cores.

Core	V_0	S_0	M_0
Sphere (radius a)	$3^{-1}4\pi a^3$	$4\pi a^2$	$4\pi a$
Rectangular parallelopiped (length of each edge l_1, l_2, l_3)	$l_1l_2l_3$	$2(l_1l_2+l_1l_3+l_2l_3)$	$\pi(l_1+l_2+l_3)$
Regular tetrahedron (length of one edge l)	$6^{-1}2^{-\frac{1}{2}}l^3$	$3^{\frac{1}{2}}l^2$	$6l\tan^{-1}(2^{\frac{1}{2}})$
Regular octahedron (length of one edge l)	$3^{-1}2^{\frac{1}{2}}l^3$	$3^{\frac{1}{2}}2l^2$	$12l\cot^{-1}(2^{\frac{1}{2}})$
Circular cylinder (length l, radius a)	πa^2l	$2\pi a(a+l)$	$\pi(\pi a+l)$
Circular disk (radius a)	0	$2\pi a^2$	π^2a
Rectangle (length of each side l_1, l_2)	0	$2l_1l_2$	$\pi(l_1+l_2)$
Regular triangle (length of one side l)	0	$2^{-1}3^{\frac{1}{2}}l^2$	$2^{-1}3\pi l$
Regular hexagon (length of one side l)	0	$3^{\frac{1}{2}}3l^2$	$3\pi l$
Thin rod (length l)	0	0	πl

for a thin plate ($l=0$), and

$$V_0=0, \quad S_0=0, \quad M_0=\pi l, \qquad (8.7)$$

for a thin rod ($f=0$, $c=0$).

The values of V_0, S_0, and M_0 for several typical shapes are given in Table VII.

9. Core Model

We assume an appropriate convex core inside each molecule and define the intermolecular distance ρ as the shortest distance between two cores. The intermolecular potential U is assumed to be a function of ρ only, $U=U(\rho)$, for which $U(0)=\infty$.

In order to determine the core of a molecule, it is necessary to have information about the interatomic distances (and bond angles if any) of the molecule. We prepare, therefore, Table VIII. Consulting this table we fix our cores as in Table IX; The volume V_0, the surface area S_0, and the surface integral of the mean curvature M_0 of the core are also tabulated.

TABLE VIII. Interatomic distances.[a]

Molecule	Bond	Distance in A
H_2	H−H	0.74
N_2	N−N	1.094
CO_2	C−O	1.15
CH_4	C−H	1.093
CF_4	C−F	1.42
C_2H_4	C−C	1.33
	C−H	1.087
(Angle H−C−H is $2\tan^{-1}(2^{\frac{1}{2}})=109°30'$.)		
C_6H_6	C−C	1.39
	C−H	1.08

[a] The values are taken from L. Pauling, *The Nature of the Chemical Bond* (Cornell University Press, Ithaca, New York, 1948), pp. 167–172 and p. 196.

For spherically symmetrical molecules the second virial coefficient B can be written in the form

$$B=\int_{r=0}^{r=\infty}\left[1-\exp\frac{-U(r)}{kT}\right]db_0(r),$$

where $b_0(r)$ is the second virial coefficient for a rigid sphere with diameter r: $b_0(r)=2\pi r^3/3$. Similarly, for our core model B is given by

$$B=\int_{\rho=0}^{\rho=\infty}\left[1-\exp\frac{-U(\rho)}{kT}\right]db(\rho)+b(0). \qquad (9.1)$$

In this expression $b(\rho)$ is the second virial coefficient for the rigid parallel body of our molecular core in the distance $\frac{1}{2}\rho$.

By consulting the statistical mechanical procedure of deriving (1.2), it is clear that $b(\rho)$ is equal to one-half of (7.7),

$$b(\rho)=V+\frac{1}{4\pi}MS,$$

TABLE IX. The cores of molecules.

Hydrogen H_2: thin rod connecting 2 H's (length 0.74A)
$V_0=0$, $S_0=0$, $M_0=2.32$A.

Nitrogen N_2: thin rod connecting 2 N's (length 1.094A)
$V_0=0$, $S_0=0$, $M_0=3.44$A.

Carbon dioxide CO_2: thin rod connecting 2 O's (length 2.30A)
$V_0=0$, $S_0=0$, $M_0=7.23$A.

Methane CH_4: regular tetrahedron connecting 4 H's (length of one edge 1.785A)
$V_0=0.670$A^3, $S_0=5.52$A^2, $M_0=10.23$A.

Carbon tetrafluoride CF_4: regular tetrahedron connecting 4 F's (length of one edge 2.32A)
$V_0=1.47$A^3, $S_0=9.32$A^2, $M_0=13.30$A.

Ethylene C_2H_4: rectangle connecting the mid-point of each C−H bond (length of each side 0.89A and 1.95A)
$V_0=0$, $S_0=3.47$A^2, $M_0=8.92$A.

Benzene C_6H_6: regular hexagon connecting the mid-point of each C−H bond (length of one side 1.93A)
$V_0=0$, $S_0=19.4$A^2, $M_0=18.2$A.

CC-0. In Public Domain. Gurukul Kangri Collection, Haridwar

Digitized by Arya Samaj Foundation Chennai and eGangotri

where M, S, and V are given by (8.1), (8.3), and (8.4), respectively. We have, therefore,

$$b(\rho)=\frac{2\pi}{3}\rho^3+M_0\rho^2+\left(S_0+\frac{1}{4\pi}M_0^2\right)\rho+\left(V_0+\frac{1}{4\pi}M_0S_0\right). \quad (9.2)$$

If we assume, furthermore, the Lennard-Jones function for $U(\rho)$

$$U(\rho)=U_0\left[\frac{m}{n-m}\left(\frac{\rho_0}{\rho}\right)^n-\frac{n}{n-m}\left(\frac{\rho_0}{\rho}\right)^m\right], \quad n>m>3,$$

we obtain

$$B=\frac{2\pi}{3}\rho_0^3F_3\left(\frac{U_0}{kT}\right)+M_0\rho_0^2F_2\left(\frac{U_0}{kT}\right)+\left(S_0+\frac{1}{4\pi}M_0^2\right)\rho_0F_1\left(\frac{U_0}{kT}\right)+\left(V_0+\frac{1}{4\pi}M_0S_0\right), \quad (9.3)$$

TABLE X. Functions in the second virial coefficient (9.3) for the core model (9.4).[a]

$-\log_{10}z$	$F_3(z)$	$F_2(z)$	$F_1(z)$
−0.4	−9.859	−5.211	−1.784
−0.3	−6.138	−3.008	−0.7761
−0.2	−4.003	−1.776	−0.2221
−0.1	−2.673	−1.027	0.1091
0.0	−1.795	−0.5424	0.3198
0.1	−1.189	−0.2151	0.4600
0.2	−0.7587	0.0132	0.5562
0.3	−0.4465	0.1758	0.6234
0.4	−0.2170	0.2930	0.6710
0.5	−0.0469	0.3779	0.7045
0.6	0.0794	0.4392	0.7279
0.7	0.1729	0.4829	0.7436
0.8	0.2415	0.5134	0.7536
0.9	0.2911	0.5336	0.7591
1.0	0.3259	0.5459	0.7611
1.1	0.3493	0.5521	0.7603
1.2	0.3638	0.5534	0.7575
1.3	0.3715	0.5510	0.7528
1.4	0.3737	0.5457	0.7468
1.5	0.3718	0.5381	0.7396
1.6	0.3668	0.5287	0.7320
1.7	0.3594	0.5179	0.7228
1.8	0.3501	0.5062	0.7135
1.9	0.3396	0.4937	0.7038
2.0	0.3281	0.4806	0.6937

[a] The values are taken from T. Kihara, Nippon Buturigakukaisi 2, 11 (1947). The functions

$$G_s(z)=\frac{d}{dz}[zF_s(z)], \quad s=1, 2, 3,$$

which are necessary for investigation of the Joule-Thomson effect, are also tabulated in the same paper.

TABLE XI. The second virial coefficient for nonspherical molecules.

	T°K	B A^3	Reference
H_2	65.1	−30.3	a
	90.0	−9.2	
	123	4.9	
	173	15.1	
	223	20.0	
	273	23.2	
	323	25.1	
	373	25.7	
	473	26.0	
N_2	143	−132	a
	173	−86.0	
	223	−43.8	
	273	−17.2	
	323	−0.4	
	373	10.2	
	423	19.1	
	473	25.5	
	573	34.3	
	673	39.0	
CO_2	273	−241	b
	323	−170	
	373	−119	
	423	−84.0	
	473	−56.6	
	573	−22.5	
	673	−2.6	
	773	10.0	
	873	20.1	
CH_4	273	−89.6	c
	298	−72.1	
	323	−57.6	
	348	−46.1	
	373	−35.9	
	398	−27.2	
	423	−19.3	
CF_4	273	−184	d
	323	−117	
	373	−71.6	
	423	−43.2	
	523	−2.1	
	573	15.4	
	673	38.2	
C_2H_4	273	−280	e
	298	−234	
	323	−197	
	348	−166	
	373	−142	
	398	−121	
	423	−104	
C_6H_6	316	−2160	f
	331	−1890	
	353	−1610	
	372	−1520	
	398	−1220	

[a] The data are due to Holborn and Otto; the values are taken from Fowler and Guggenheim, *Statistical Thermodynamics* (Cambridge University Press, Cambridge, 1939), p. 283.
[b] K. E. MacCormack and W. G. Schneider, J. Chem. Phys. 18, 1269 (1950).
[c] A. Michels and G. W. Nederbragt, Physica 3, 569 (1936).
[d] K. E. MacCormack and W. G. Schneider, J. Chem. Phys. 19, 845, 849 (1951).
[e] A. Michels and M. Geldermans, Physica 9, 967 (1942).
[f] Francis, McGlasham, Hamann, and McManamey, J. Chem. Phys. 20, 1341 (1952).

CC-0. In Public Domain. Gurukul Kangri Collection, Haridwar

Digitized by Arya Samaj Foundation Chennai and eGangotri

where

$$F_s(z)=\int_0^\infty\left[1-\exp\left(-\frac{m}{n-m}\frac{z}{\xi^n}+\frac{n}{n-m}\frac{z}{\xi^m}\right)\right]d(\xi^s)$$

$$=-\frac{s}{n}\sum_{t=0}^{\infty}\frac{1}{t!}\Gamma\left(\frac{tm-s}{n}\right)$$

$$\times\left(\frac{n}{m}\right)^t\left(\frac{m}{n-m}z\right)^{[(n-m)t+s]/n}.$$

For the case $m=6$, $n=12$, namely

$$U(\rho)=U_0\left[\left(\frac{\rho_0}{\rho}\right)^{12}-2\left(\frac{\rho_0}{\rho}\right)^{6}\right], \qquad (9.4)$$

the values of $F_3(z)$, $F_2(z)$, and $F_1(z)$ are given in Table X.

Making use of this table and observed values of the second virial coefficient given in Table XI, we can determine ρ_0 and U_0/k; the results are given in Table XII. Figure 11 shows the parallel body of the core in the distance of $\frac{1}{2}\rho_0$, which represents the shape and the size of each molecule.

TABLE XII. The constants in the model (9.4) when the core is chosen as in Table IX.

	ρ_0 A	U_0/k°K
H_2	2.81	39.4
N_2	3.47	124
CO_2	3.36	309
CH_4	1.92	378
CF_4	2.48	372
C_2H_4	2.5	470
C_6H_6	3.4[a]	830

[a] This value of ρ_0 is taken from the lattice constant of graphite, since observed values for benzene are not sufficient to determine both ρ_0 and U_0.

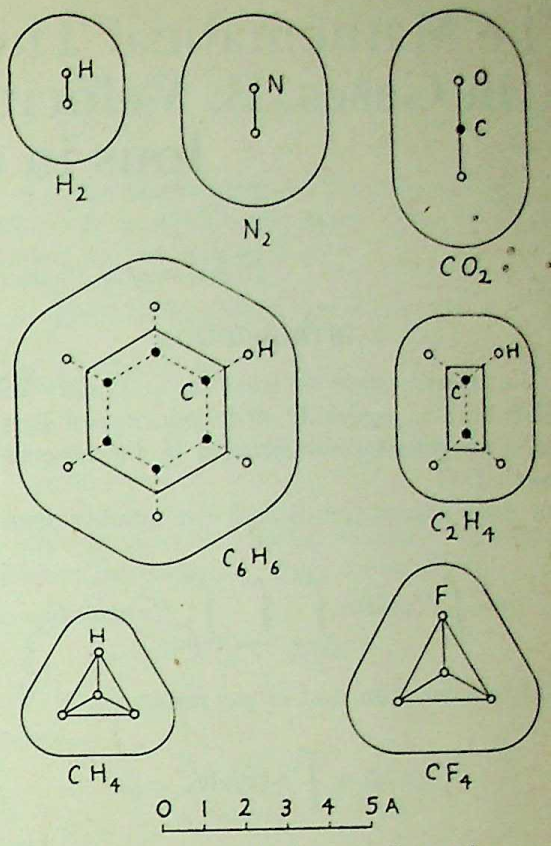


FIG. 11. Shape and size of molecules according to the core model.

ACKNOWLEDGMENT

The author wishes to thank Professor J. O. Hirschfelder, Professor C. F. Curtiss, Dr. E. A. Mason, and other members of the Department of Chemistry at the University of Wisconsin for their useful discussions and linguistic help.

CC-0. In Public Domain. Gurukul Kangri Collection, Haridwar

Digitized by Arya Samaj Foundation Chennai and eGangotri

REVIEWS OF MODERN PHYSICS VOLUME 25, NUMBER 4 OCTOBER, 1953

The Mathematical Theory of Electrical Discharges in Gases. B. Velocity-Distribution of Positive Ions in a Static Field*†

TARO KIHARA

Department of Physics, University of Tokyo, Tokyo, Japan

1. INTRODUCTION

IN the present paper we treat the stationary velocity distribution, especially drift velocity, of ions in a static, homogeneous electric field in the absence of a magnetic field.

Our main assumption is that the number-density of ions,

$$n=\int f(\mathbf{c})d\mathbf{c}\equiv\int_{-\infty}^{\infty}\int_{-\infty}^{\infty}\int_{-\infty}^{\infty}f(\mathbf{c})dudvdw, \quad (1.1)$$

is much smaller than that of gas molecules,

$$N=\int f_1(\mathbf{c}_1)d\mathbf{c}_1. \quad (1.2)$$

Here $\mathbf{c}(u, v, w)$ and $f(\mathbf{c})$ are the velocity and the velocity-distribution function of the ions; $\mathbf{c}_1(u_1, v_1, w_1)$ and $f_1(\mathbf{c}_1)$ are those of the gas molecules.

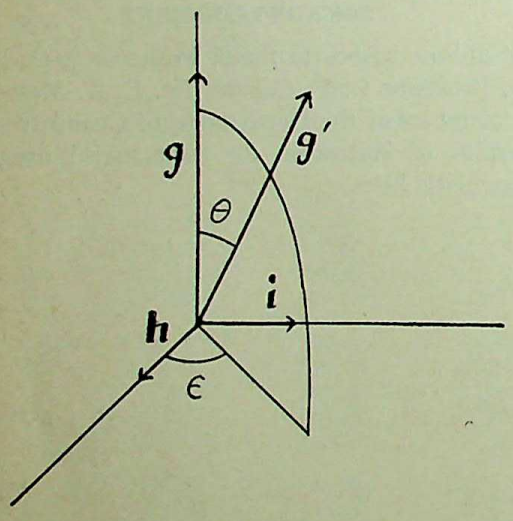


FIG. 1. Vector representation of relative velocity.

Under this assumption, f_1 takes the Maxwellian distribution,

$$f_1=N\left(\frac{m_1}{2\pi kT}\right)^{\frac{3}{2}}\exp\left(-\frac{m_1c_1^2}{2kT}\right), \quad c_1=|\mathbf{c}_1|, \quad (1.3)$$

which remains unchanged by the electric field. Here m_1 is the mass of a gas molecule; k and T are the Boltzmann constant and the absolute temperature, respectively. Moreover, the Boltzmann equation becomes linear with respect to f:

$$\frac{eE}{m}\frac{\partial f}{\partial w}=\int\int\int(f'f_1'-ff_1)gI(g,\theta)\sin\theta d\theta d\epsilon d\mathbf{c}_1, \qquad E=|\mathbf{E}|,$$

when the z axis is taken in the direction of the electric field $\mathbf{E}$. Here e and m denote the charge and the mass of the ion, respectively; $f'f_1'-ff_1$ is the abbreviation for $f(\mathbf{c}')f_1(\mathbf{c}_1')-f(\mathbf{c})f_1(\mathbf{c}_1)$, $\mathbf{c}'$ and $\mathbf{c}_1'$ are the final velocities of the ion and the gas molecule encountering with initial velocities $\mathbf{c}$ and $\mathbf{c}_1$ with diffraction angle θ for the orbit of relative motion; $I(g,\theta)\sin\theta d\theta d\epsilon$ indicates the differential cross section for scattering into the solid angle $\sin\theta d\theta d\epsilon$ for the relative speed $g=|\mathbf{c}-\mathbf{c}_1|=|\mathbf{c}'-\mathbf{c}_1'|$ (see Fig. 1).

In terms of the function

$$f^{(0)}\equiv n\left(\frac{m}{2\pi kT}\right)^{\frac{3}{2}}\exp\left(-\frac{mc^2}{2kT}\right), \quad c=|\mathbf{c}|, \quad (1.4)$$

to which f would reduce in case of no electric field, let

$$f=f^{(0)}(1+\Phi). \quad (1.5)$$

Then the Boltzmann equation can be expressed as

$$\frac{eE}{m}\frac{\partial f}{\partial w}=-Nf^{(0)}\mathrm{J}\Phi. \quad (1.6)$$

Here J is a linear operator operating on any function $\phi(\mathbf{c})$ of the velocity of ions,

$$\mathrm{J}\phi=\frac{1}{N}\int\int\int f_1(\phi-\phi')gI(g,\theta)\sin\theta d\theta d\epsilon d\mathbf{c}_1, \quad (1.7)$$

$\phi-\phi'$ being the abbreviation for $\phi(\mathbf{c})-\phi(\mathbf{c}')$.

* This work was carried out at the University of Wisconsin U. S. Naval Research Laboratory, Madison, Wisconsin.

† In my previous article of the same title (T. Kihara, Revs. Modern Phys. 24, 45 (1952)), hereafter referred to as A, I quoted several passages from my book *Imperfect Gases*. This book was originally written in Japanese and published in 1949. Although the whole text was translated into English in the United States (by U. S. Air Force in U. S. Air Force Technical Reports), the distribution of the translation is unfortunately limited. Therefore, I want to publish a revised version of the parts to which the previous article is related. In consequence, references in footnotes 2, 3, and 5 of Part A are to be rewritten as Eq. (3.1), Eq. (2.8), and Section 2 of Part B, respectively.

CC-0. In Public Domain. Gurukul Kangri Collection, Haridwar

Digitized by Arya Samaj Foundation Chennai and eGangotri

When we define the inner product of two functions, $\phi(\mathbf{c})$ and $\psi(\mathbf{c})$, by

$$(\phi, \psi)=\frac{1}{n}\int f^{(0)}\phi\psi d\mathbf{c}, \tag{1.8}$$

the operator J is symmetric,

$$(\psi, J\phi)=(\phi, J\psi), \tag{1.9}$$

and positive-definite,

$$(\phi, J\phi)\geqq 0. \tag{1.10}$$

Multiplying both sides of (1.6) by $-\phi(\mathbf{c})d\mathbf{c}$ and integrating, we have

$$-\frac{eE}{m}\int\frac{\partial f}{\partial w}\phi d\mathbf{c}=N\int f^{(0)}\phi J\Phi d\mathbf{c}.$$

Integrating by parts on the left side and using the relation $J(1+\Phi)=J\Phi$ and the symmetric property of J on the right side, we obtain

$$\frac{eE}{m}\int f\frac{\partial\phi}{\partial w}d\mathbf{c}=N\int fJ\phi d\mathbf{c}.$$

With average value symbols defined by

$$\langle\psi\rangle_{Av}=\frac{1}{n}\int f\psi d\mathbf{c},$$

this relation becomes

$$\frac{eE}{m}\left(\frac{\partial\phi}{\partial w}\right)_{Av}=N\langle J\phi\rangle_{Av}. \tag{1.11}$$

In particular, when w is taken for ϕ, we have

$$eE/m=N\langle Jw\rangle_{Av}. \tag{1.12}$$

2. HEAVY IONS IN A LIGHT GAS

First,

$$J\mathbf{c}=\frac{1}{N}\int\int\int f_1(\mathbf{c}-\mathbf{c}')gI(g,\theta)\sin\theta d\theta d\epsilon d\mathbf{c}_1 \tag{2.1}$$

will be transformed generally.

In terms of the velocity of the center of mass and the relative velocity before encounter,

$$\mathbf{G}=\frac{m_1}{m_1+m}\mathbf{c}_1+\frac{m}{m_1+m}\mathbf{c},\quad \mathbf{g}=\mathbf{c}-\mathbf{c}_1, \tag{2.2}$$

we have

$$\mathbf{c}=\mathbf{G}+\frac{m_1}{m_1+m}\mathbf{g},$$

and, since G remains unchanged by the collision,

$$J\mathbf{c}=\frac{1}{N}\frac{m_1}{m_1+m}\int\int\int f_1(\mathbf{g}-\mathbf{g}')gI(g,\theta)\sin\theta d\theta d\epsilon d\mathbf{c}_1,$$

where $\mathbf{g}'$ is the relative velocity after encounter.

Taking two unit vectors perpendicular to $\mathbf{g}$ and to each other, we can express $\mathbf{g}'$ as

$$\mathbf{g}'=\mathbf{g}\cos\theta+g\mathbf{h}\sin\theta\cos\epsilon+g\mathbf{i}\sin\theta\sin\epsilon$$

(see Fig. 1). Therefore,

$$J\mathbf{c}=\frac{2\pi}{N}\frac{m_1}{m_1+m}\int\int f_1\mathbf{g}(1-\cos\theta)gI(g,\theta)\sin\theta d\theta d\mathbf{c}_1.$$

In terms of effective collision cross sections between the ion and the molecule, which are defined by

$$\phi^{(l)}=\int_0^\pi(1-\cos^l\theta)gI(g,\theta)\sin\theta d\theta,\quad l=1,2,\cdots, \tag{2.3}$$

we have

$$J\mathbf{c}=\frac{2\pi}{N}\frac{m_1}{m_1+m}\int f_1\mathbf{g}\phi^{(1)}d\mathbf{c}_1,$$

namely

$$J\mathbf{c}=\frac{2\pi}{N}\frac{m_1}{m_1+m}\int f_1(\mathbf{c}-\mathbf{c}_1)\phi^{(1)}d\mathbf{c}_1, \tag{2.4}$$

or, in terms of the z component,

$$Jw=\frac{2\pi}{N}\frac{m_1}{m_1+m}\int f_1(w-w_1)\phi^{(1)}d\mathbf{c}_1. \tag{2.5}$$

Up to this point no approximations have been made in the calculations.

Now, we treat the special case where the mass of an ion is sufficiently large in comparison with that of a gas molecule, i.e., $m\gg m_1$. Let us consider the problem on the condition that the drift velocity of the ions is much smaller than the thermal velocity of the gas molecules; i.e.,

$$(\langle w\rangle_{Av})^2\ll kT/m_1. \tag{2.6}$$

The effective cross section $\phi^{(1)}$ is a function of the reduced mass $m_1m/(m_1+m)$ and the relative speed g. In the present case the former can be put equal to m_1, and the latter is

$$g=(c_1^2-2\mathbf{c}_1\cdot\mathbf{c}+c^2)^{\frac{1}{2}}\fallingdotseq c_1-\mathbf{c}_1\cdot\mathbf{c}/c_1.$$

Hence the cross section becomes

$$\phi^{(1)}(g)=\phi^{(1)}(c_1)-\frac{\mathbf{c}\cdot\mathbf{c}_1}{c_1}\frac{\partial\phi^{(1)}}{\partial c_1}.$$

Inserting this in (2.5) and denoting $\phi^{(1)}(c_1)$ by $\phi^{(1)}$

CC-0. In Public Domain. Gurukul Kangri Collection, Haridwar

Digitized by Arya Samaj Foundation Chennai and eGangotri

anew, we obtain

$$\frac{N}{2\pi}\frac{m_1+m}{m_1}\mathrm{J}w=w\int f_1\phi^{(1)}d\mathbf{c}_1+w\int f_1\frac{\partial\phi^{(1)}}{\partial c_1}\frac{w_1^2}{c_1}d\mathbf{c}_1,$$

the integrals of odd functions of $\mathbf{c}_1$ vanishing. The first term on the right-hand side is equal to

$$4\pi w\int_0^\infty f_1\phi^{(1)}c_1^2dc_1,$$

and the second term is

$$\frac{1}{3}w\int f_1\frac{\partial\phi^{(1)}}{\partial c_1}c_1d\mathbf{c}_1=\frac{4\pi}{3}w\int_0^\infty f_1\frac{\partial\phi^{(1)}}{\partial c_1}c_1^3dc_1$$

$$=-4\pi w\int_0^\infty f_1\phi^{(1)}c_1^2dc_1+\frac{4\pi}{3}w\frac{m_1}{kT}\int_0^\infty f_1\phi^{(1)}c_1^4dc_1.$$

We have, therefore,

$$\mathrm{J}w=\frac{2\pi}{N}\frac{m_1}{m_1+m}\frac{4\pi}{3}w\frac{m_1}{kT}\int_0^\infty f_1\phi^{(1)}c_1^4dc_1$$

$$=\frac{16}{3}\frac{m_1}{m_1+m}w\pi^{\frac{1}{2}}\int_0^\infty\exp(-V^2)V^4\phi^{(1)}dV,$$

$$V=(m_1/2kT)^{\frac{1}{2}}c_1.$$

In terms of weighted mean values of the effective cross sections, defined as

$$\Omega^{(l)}(r)=\pi^{\frac{1}{2}}\int_0^\infty\phi^{(l)}V^{2r+2}\exp(-V^2)dV,\qquad r=l,\,l+1,\,\cdots,$$

$$V=\left(\frac{m_1m}{m_1+m}\frac{1}{2kT}\right)^{\frac{1}{2}}g,\tag{2.7}$$

we obtain finally

$$\mathrm{J}w=\lambda w,\quad\lambda=\frac{16}{3}\frac{m_1}{m_1+m}\Omega^{(1)}(1).\tag{2.8}$$

Inserting (2.8) into (1.12), we have

$$\langle w\rangle_{\mathrm{Av}}=\frac{eE}{mN\lambda}=\frac{3}{16}\frac{m_1+m}{m_1m}\frac{eE}{N\Omega^{(1)}(1)}.\tag{2.9}$$

The mobility of heavy ions in a light gas is independent of the field strength, so long as our condition (2.6) holds.

Let us find the velocity distribution function. First,

$$\mathrm{J}(w^p)=\frac{1}{N}\int\int\int f_1(w^p-w'^p)gI(g,\theta)d\theta d\epsilon d\mathbf{c}_1$$

will be evaluated for any positive integer p. Considering

$$w^p-w'^p=\left(G_z+\frac{m_1}{m_1+m}g_z\right)^p-\left(G_z+\frac{m_1}{m_1+m}g_z'\right)^p$$

$$\doteqdot p\frac{m_1}{m_1+m}(g_z-g_z')G_z^{p-1},$$

we have, after a procedure similar to that used in obtaining (2.5),

$$\mathrm{J}(w^p)=\frac{2\pi}{N}\frac{m_1}{m_1+m}p\int f_1g_zG_z^{p-1}\phi^{(1)}d\mathbf{c}_1$$

$$=\frac{2\pi}{N}\frac{m_1}{m_1+m}p\int f_1(w-w_1)\times\left(w+\frac{m_1}{m_1+m}w_1\right)^{p-1}\phi^{(1)}d\mathbf{c}_1.$$

Bearing in mind that mw^2 and $m_1w_1^2$ are of the same order of magnitude, we can carry out calculations similar to the above and obtain

$$\mathrm{J}(w^p)=\lambda\left[pw^p-p(p-1)w^{p-2}\frac{kT}{m}\right],\tag{2.10}$$

where λ is the same as in (2.8), which is a special case of (2.10). When this is rewritten as

$$\mathrm{J}(w^p)=\lambda\left[w\frac{d(w^p)}{dw}-\frac{kT}{m}\frac{d^2(w^p)}{dw^2}\right],$$

it is easy to see that the relation

$$\mathrm{J}\Phi=\lambda\left(w\frac{d\Phi}{dw}-\frac{kT}{m}\frac{d^2\Phi}{dw^2}\right)\tag{2.11}$$

holds for any function Φ which is expressed by a power series in w and does not depend on the other components of $\mathbf{c}$.

Anticipating that Φ in (1.5) and (1.6) is an analytic function of w only, and does not depend on the other components, u and v, we make use of (2.11). After some manipulation, we have

$$\frac{eE}{m}\frac{\partial f}{\partial w}=N\lambda\left(\frac{kT}{m}\frac{\partial^2f}{\partial w^2}+w\frac{\partial f}{\partial w}+f\right),$$

or, in terms of $\langle w\rangle_{\mathrm{Av}}$,

$$\frac{kT}{m}\frac{\partial^2f}{\partial w^2}+(w-\langle w\rangle_{\mathrm{Av}})\frac{\partial f}{\partial w}+f=0.$$

From this differential equation it is evident that f can be obtained by replacing w in $f^{(0)}$ by $w-\langle w\rangle_{\mathrm{Av}}$. Namely,

CC-0. In Public Domain. Gurukul Kangri Collection, Haridwar

Digitized by Arya Samaj Foundation Chennai and eGangotri

we obtain

$$f=n\left(\frac{m}{2\pi kT}\right)^{\frac{3}{2}}\exp\left[-\frac{m}{2kT}\{u^2+v^2+(w-\langle w\rangle_{Av})^2\}\right], \quad (2.12)$$

in accordance with our anticipation. *The velocity distribution of heavy ions in a light gas is Maxwellian around the drift velocity*, so long as (2.6) holds.

3. MAXWELLIAN MODEL OF COLLISION CROSS SECTIONS

The Maxwellian model is defined by the idealization that the scattering coefficient $I(g,\theta)$ is inversely proportional to the relative speed g. For this model each $\phi^{(l)}$ becomes independent of g, and the mathematical handling is simple without any assumption as regards the ratio of the mass of an ion to that of a molecule.

In this case, (2.5) is reduced to

$$\mathrm{J}w=2\pi\phi^{(1)}\frac{m_1}{m_1+m}w. \quad (3.1)$$

Hence we have, by use of (1.12),

$$\langle w\rangle_{Av}=\frac{eE}{2\pi\phi^{(1)}N}\frac{m_1+m}{m_1m}. \quad (3.2)$$

For the Maxwellian model, the mobility times gas density, $N\langle w\rangle_{Av}/E$, is independent of the field strength and the temperature.

When $\phi^{(1)}$ does not depend on the relative speed, $\Omega^{(1)}(1)$ is equal to $3\pi\phi^{(1)}/8$, and Eq. (3.2) can be rewritten as

$$\langle w\rangle_{Av}=\frac{3}{16}\frac{m_1+m}{m_1m}\frac{eE}{N\Omega^{(1)}(1)}, \quad (3.3)$$

which is identical with (2.9). This formula, which is valid in these two idealized cases, is the first approximation to a more detailed expression to be derived in the next section.

Equation (3.1) indicates that w is one of the eigenfunctions of the symmetric linear operator J, and the corresponding eigenvalue is $2\pi\phi^{(1)}m_1/(m_1+m)$. Let us make a little preparation to investigate other eigenfunctions and eigenvalues.

Sonine polynomials $S_m^{(n)}(x)$ are defined by the expression

$$(1-s)^{-m-1}\exp\left(-\frac{xs}{1-s}\right)=\sum_{n=0}^{\infty}S_m^{(n)}(x)s^n, \quad (3.4)$$

where $0<s<1$, and x and m are real. In particular,

$$S_m^{(0)}=1, \quad S_m^{(1)}(x)=m+1-x. \quad (3.5)$$

Since

$$(1-s)^{-m-1}(1-t)^{-m-1}\times\int_0^{\infty}\exp\left[-x\left(1+\frac{s}{1-s}+\frac{t}{1-t}\right)\right]x^m dx$$
$$=(1-s)^{-m-1}(1-t)^{-m-1}\int_0^{\infty}\exp\left[-\frac{x(1-st)}{(1-s)(1-t)}\right]x^m dx$$
$$=(1-st)^{-m-1}\Gamma(m+1),$$

we obtain, by equating coefficients of s^pt^q, the orthogonality relation,

$$\int_0^{\infty}e^{-x}S_m^{(p)}(x)S_m^{(q)}(x)x^m dx=\frac{\Gamma(m+p+1)}{p!}\delta_{pq}, \quad (3.6)$$

where δ_{pq} is unity for $p=q$ and zero for $p\neq q$. Differentiating each side of (3.4) with respect to x, we have

$$\frac{d}{dx}S_m^{(n)}(x)=-S_{m+1}^{(n-1)}(x). \quad (3.7)$$

Multiplying each side of (3.4) by $1-s$, we have a recursion formula,

$$S_{m-1}^{(n)}=S_m^{(n)}-S_m^{(n-1)}. \quad (3.8)$$

By differentiating (3.4) with respect to s and replacing m by $m-1$, and n by $n-1$, we have another relation

$$mS_m^{(n-1)}(x)-xS_{m+1}^{(n-1)}(x)=nS_{m-1}^{(n)}(x). \quad (3.9)$$

Finally, by combining (3.8) and (3.9), we have

$$mS_m^{(n)}(x)-xS_{m+1}^{(n-1)}(x)=(m+n)S_{m-1}^{(n)}(x). \quad (3.10)$$

In terms of these Sonine polynomials, we define functions of $\mathbf{c}$ by

$$\psi_l^{(r)}=\left(\frac{mc^2}{2kT}\right)^{l/2}P_l\left(\frac{w}{c}\right)S_{l+\frac{1}{2}}^{(r)}\left(\frac{mc^2}{2kT}\right), \quad (3.11)$$
$$l, r=0, 1, 2, \cdots,$$

P_l being Legendre polynomials. Then each $\psi_l^{(r)}$ is a polynomial of degree $l+2r$ in the components of $\mathbf{c}$; and the orthogonality relation is given by

$$(\psi_l^{(r)},\psi_{l'}^{(r')})=\frac{1}{n}\int f^{(0)}\psi_l^{(r)}\psi_{l'}^{(r')}d\mathbf{c}$$
$$=\frac{2}{2l+1}\frac{1}{\pi^{\frac{1}{2}}}\frac{1}{r!}\Gamma(l+r+\tfrac{3}{2})\delta_{ll'}\delta_{rr'}. \quad (3.12)$$

Let us specialize ϕ in (1.11) to $\psi_l^{(r)}$. Since, by use of (3.7) and (3.10) and similar relations for the Legendre

CC-0. In Public Domain. Gurukul Kangri Collection, Haridwar

Digitized by Arya Samaj Foundation Chennai and eGangotri

polynomials, the relation

$$(l+\tfrac{1}{2})\left(\frac{2kT}{m}\right)^{\frac{1}{2}}\frac{\partial\psi_l^{(r)}}{\partial w}=l(l+\tfrac{1}{2}+r)\psi_{l-1}^{(r)}-(l+1)\psi_{l+1}^{(r-1)}$$

($\psi_{l+1}^{(-1)}\equiv 0$) can be derived, we obtain generally

$$(l+\tfrac{1}{2})\langle \mathrm{J}\psi_l^{(r)}\rangle_{\mathrm{Av}}=\mathcal{E}[l(l+\tfrac{1}{2}+r)\langle\psi_{l-1}^{(r)}\rangle_{\mathrm{Av}} -(l+1)\langle\psi_{l+1}^{(r-1)}\rangle_{\mathrm{Av}}], \quad (3.13)$$

where

$$\mathcal{E}\equiv(eE/mN)(m/2kT)^{\frac{1}{2}}. \quad (3.14)$$

In particular, for the Maxwellian model each $\psi_l^{(r)}$ is an eigenfunction of the operator J:

$$\mathrm{J}\psi_l^{(r)}=\lambda_r(l)\psi_l^{(r)}. \quad (3.15)$$

This can be directly ascertained for $l+2r$ small; in terms of

$$W\equiv\left(\frac{m}{2kT}\right)^{\frac{1}{2}}w, \quad C^2\equiv\frac{mc^2}{2kT},$$

and

$$M_1\equiv\frac{m_1}{m_1+m}, \quad M_2\equiv\frac{m}{m_1+m}, \quad (3.16)$$

the eigenfunctions and eigenvalues for $l+2r\leqq 3$ are as follows:

$$\psi_0^{(0)}=1, \qquad \lambda_0(0)=0;$$
$$\psi_1^{(0)}=W, \qquad \lambda_0(1)=2\pi M_1\phi^{(1)};$$
$$\psi_0^{(1)}=\tfrac{3}{2}-C^2, \qquad \lambda_1(0)=4\pi M_1M_2\phi^{(1)};$$
$$\psi_2^{(0)}=\tfrac{3}{2}W^2-\tfrac{1}{2}C^2,$$
$$\lambda_0(2)=\pi M_1(4M_2\phi^{(1)}+3M_1\phi^{(2)});$$
$$\psi_1^{(1)}=W[(5/2)-C^2],$$
$$\lambda_1(1)=2\pi M_1(M_1^2\phi^{(1)}+3M_2^2\phi^{(1)}+2M_1M_2\phi^{(2)});$$
$$\psi_3^{(0)}=(5/2)W^3-\tfrac{3}{2}WC^2,$$
$$\lambda_0(3)=\pi M_1(-3M_1^2\phi^{(1)}+6M_2^2\phi^{(1)} +9M_1M_2\phi^{(2)}+5M_1^2\phi^{(3)}).$$

In general,

$$\lambda_r(l)>0 \quad \text{for} \quad l+2r>0.$$

Inserting (3.15) into (3.13), we have

$$(l+\tfrac{1}{2})\lambda_r(l)\langle\psi_l^{(r)}\rangle_{\mathrm{Av}}=\mathcal{E}[l(l+\tfrac{1}{2}+r)\langle\psi_{l-1}^{(r)}\rangle_{\mathrm{Av}} -(l+1)\langle\psi_{l+1}^{(r-1)}\rangle_{\mathrm{Av}}], \quad (3.17)$$

from which it is evident that $(-1)^r\langle\psi_l^{(r)}\rangle_{\mathrm{Av}}$ is positive and proportional to E^{l+2r}.

By this system of equations each $\langle\psi_l^{(r)}\rangle_{\mathrm{Av}}$ can be expressed in terms of the $\lambda_r(l)$:

$$\langle\psi_l^{(0)}\rangle_{\mathrm{Av}}=l!\mathcal{E}^l/\lambda_0(1)\lambda_0(2)\cdots\lambda_0(l), \quad l=1, 2, \cdots,$$
$$\langle\psi_0^{(1)}\rangle_{\mathrm{Av}}=-2\mathcal{E}^2/\lambda_0(1)\lambda_1(0),$$
$$\langle\psi_1^{(1)}\rangle_{\mathrm{Av}}=-\frac{2}{3}\frac{\mathcal{E}^3}{\lambda_0(1)\lambda_1(1)}\left[\frac{4}{\lambda_0(2)}+\frac{5}{\lambda_1(0)}\right],$$

etc. Since

$$\frac{m}{2kT}\langle u^2\rangle_{\mathrm{Av}}-\tfrac{1}{2}=\frac{m}{2kT}\langle v^2\rangle_{\mathrm{Av}}-\tfrac{1}{2}$$
$$=-\tfrac{1}{3}(\langle\psi_0^{(1)}\rangle_{\mathrm{Av}}+\langle\psi_2^{(0)}\rangle_{\mathrm{Av}})$$
$$=\frac{2}{3}\frac{\mathcal{E}^2}{\lambda_0(1)}\left[\frac{1}{\lambda_1(0)}-\frac{1}{\lambda_0(2)}\right]$$
$$=2\pi\phi^{(2)}\mathcal{E}^2M_1^2/\lambda_0(1)\lambda_1(0)\lambda_0(2)>0,$$

and

$$\frac{m}{2kT}\langle(w-\langle w\rangle_{\mathrm{Av}})^2\rangle_{\mathrm{Av}}-\tfrac{1}{2}$$
$$=\tfrac{1}{3}(2\langle\psi_2^{(0)}\rangle_{\mathrm{Av}}-\langle\psi_0^{(1)}\rangle_{\mathrm{Av}}-3\langle\psi_1^{(0)}\rangle_{\mathrm{Av}}^2)$$
$$=\frac{1}{3}\frac{\mathcal{E}^2}{\lambda_0(1)}\left[\frac{4}{\lambda_0(2)}+\frac{2}{\lambda_1(0)}-\frac{3}{\lambda_0(1)}\right]$$
$$=\frac{2\pi M_1^2\mathcal{E}^2}{\lambda_0(1)\lambda_1(0)\lambda_0(2)}[M_1\phi^{(2)}+2M_2(2\phi^{(1)}-\phi^{(2)})]>0,$$

it follows that *the velocity distribution is less sharp than the Maxwellian distribution corresponding to the same temperature.*

In order to argue more in detail, let us assume between an ion and a gas molecule an attractive potential, inversely proportional to the fourth power of the distance. For this type of Maxwellian model we have the following numerical values:[1]

$$\phi^{(2)}/\phi^{(1)}=0.70, \quad \phi^{(3)}/\phi^{(1)}=1.2.$$

By use of these it can be shown that

$$\langle(w-\langle w\rangle_{\mathrm{Av}})^2\rangle_{\mathrm{Av}}-\langle u^2\rangle_{\mathrm{Av}}>0,$$

and

$$\langle(w-\langle w\rangle_{\mathrm{Av}})^3\rangle_{\mathrm{Av}}>0.$$

These inequalities provide information concerning the deviations from spherical symmetry and plane symmetry of the velocity distribution: *the distribution of the z component of ion velocities is less sharp than that of the other components; its rate of decrease in the rear is steeper than that in the front, the maximum taking place at a negative z component of the velocity.*

4. GENERAL THEORY OF MOBILITY

In the two preceding sections we have treated special cases; the general case will be dealt with in this section.

Except for the Maxwellian model, the $\psi_l^{(r)}$ defined by (3.11) are not necessarily eigenfunctions of the linear operator J. However, since J is spherically symmetric, we can let

$$\mathrm{J}\psi_l^{(r)}=\sum_s a_{rs}(l)\psi_l^{(s)}, \quad (4.1)$$

[1] The first value is taken from H. R. Hassé, Phil. Mag. **1**, 139 (1926); H. R. Hassé and W. R. Cook, Phil. Mag. **3**, 977 (1927).

CC-0. In Public Domain. Gurukul Kangri Collection, Haridwar

Digitized by Arya Samaj Foundation Chennai and eGangotri

with

$$a_{rs}(l)=(\psi_l^{(s)}, J\psi_l^{(r)})/(\psi_l^{(s)}, \psi_l^{(s)}). \quad (4.2)$$

In particular, $a_{rr}(l)\geqq 0$, since J is positive-definite.

Inserting (4.1) into (3.13), we have

$$(l+\tfrac{1}{2})\sum_s a_{rs}(l)\langle\psi_l^{(s)}\rangle_{Av}=\mathcal{E}[l(l+\tfrac{1}{2}+r)\langle\psi_{l-1}^{(r)}\rangle_{Av} - (l+1)\langle\psi_{l+1}^{(r-1)}\rangle_{Av}] \quad (4.3)$$

$(\psi_{l+1}^{(-1)}\equiv 0)$, from which it is evident that $\langle\psi_l^{(r)}\rangle_{Av}$ is an even function of E for l even and an odd function of E for l odd. Hence the drift velocity and the mobility are odd and even, respectively. Equation (4.3) can be solved by means of successive approximations as follows:

The nondiagonal coefficients, $a_{rs}(l)$ for $r\neq s$, are considered to be small, since they vanish in the case of the Maxwellian model. Therefore, we can determine the first approximation, which will be referred to as $\langle\psi_l^{(r)}\rangle_{AvI}$, from

$$(l+\tfrac{1}{2})a_{rr}(l)\langle\psi_l^{(r)}\rangle_{AvI}=\mathcal{E}[l(l+\tfrac{1}{2}+r)\langle\psi_{l-1}^{(r)}\rangle_{AvI} - (l+1)\langle\psi_{l+1}^{(r-1)}\rangle_{AvI}]. \quad (4.4)$$

It is evident that $(-1)^r\langle\psi_l^{(r)}\rangle_{AvI}$ is positive and proportional to the $(l+2r)$th power of the field strength.

In particular,

$$a_{00}(1)\langle\psi_1^{(0)}\rangle_{AvI}=\mathcal{E},$$

or

$$\langle w\rangle_{AvI}=\frac{eE}{Nm}\frac{1}{a_{00}(1)}. \quad (4.5)$$

The second approximation can be determined from the equation to which (4.3) reduces when the first approximations are inserted into terms with nondiagonal coefficients. That is,

$$\langle\psi_1^{(0)}\rangle_{AvII}[a_{00}(1)+a_{01}(1)\langle\psi_1^{(1)}\rangle_{AvI}/\langle\psi_1^{(0)}\rangle_{AvI}+\cdots]=\mathcal{E},$$

or

$$\langle w\rangle_{AvII}=\frac{eE}{Nm}\left[\sum_{r=0}^{\infty}a_{0r}(1)\frac{\langle\psi_1^{(r)}\rangle_{AvI}}{\langle\psi_1^{(0)}\rangle_{AvI}}\right]^{-1}. \quad (4.6)$$

Now we must evaluate

$$a_{0r}(1)=(\psi_1^{(r)}, J\psi_1^{(0)})/(\psi_1^{(r)}, \psi_1^{(r)}) =\frac{3}{2}\frac{\pi^{\frac{1}{2}}r!}{\Gamma[r+(5/2)]}(\psi_1^{(r)}, J\psi_1^{(0)}). \quad (4.7)$$

By the definition of the Sonine polynomials, $(\psi_1^{(r)}, J\psi_1^{(0)})$ is the coefficient of s^r in the expansion of

$$\frac{m}{2kT}\frac{1}{n}(1-s)^{-(5/2)}\int f^{(0)}\exp\left(-\frac{s}{1-s}\frac{mc^2}{2kT}\right)wJwd\mathbf{c}, \quad (4.8)$$

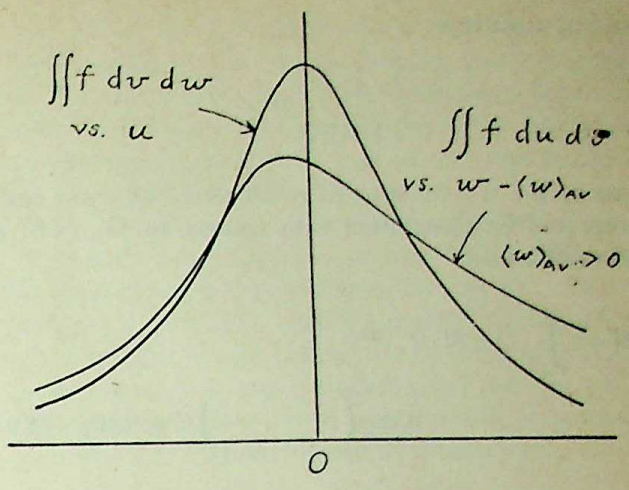


FIG. 2. Asymmetry of the velocity distribution of ions with a positive drift velocity.

which is equal to, by virtue of (2.5), (1.3), and (1.4),

$$\frac{\pi}{kT}\frac{m_1m}{m_1+m}\frac{(m_1m)^{\frac{3}{2}}}{(2\pi kT)^3}(1-s)^{-(5/2)} \times\int\int\exp(-A)w(w-w_1)\phi^{(1)}d\mathbf{c}d\mathbf{c}_1,$$

where

$$A\equiv\frac{m_1c_1^2}{2kT}+\frac{1}{1-s}\frac{mc^2}{2kT}.$$

In terms of the velocity of the center of mass, $\mathbf{G}$, and the relative velocity, $\mathbf{g}$, given by (2.2), we have

$$A=\frac{1}{1-s}\frac{m_1+m}{2kT}[(1-M_1s)G^2+M_1M_2(1-M_2s)g^2 +2M_1M_2s\mathbf{G}\cdot\mathbf{g}]$$

$(G=|\mathbf{G}|, g=|\mathbf{g}|)$, where M_1 and M_2 are given by (3.16). By use of a new variable

$$\mathbf{G}'=\mathbf{G}+\frac{M_1M_2s}{1-s}\mathbf{g}, \quad G'=|\mathbf{G}'|,$$

this can be transformed into a quadratic form:

$$A=\frac{1-M_1s}{1-s}\frac{m_1+m}{2kT}G'^2+\frac{1}{1-M_1s}\frac{1}{2kT}\frac{m_1m}{m_1+m}g^2.$$

Since

$$\frac{\partial(\mathbf{G},\mathbf{g})}{\partial(\mathbf{c},\mathbf{c}_1)}=\frac{\partial(\mathbf{G}',\mathbf{g})}{\partial(\mathbf{G},\mathbf{g})}=1,$$

we can substitute $d\mathbf{G}'d\mathbf{g}$ for $d\mathbf{c}d\mathbf{c}_1$. Furthermore, for

$$w(w-w_1)=(G_z+M_1g_z)g_z =\left(G_z'+\frac{1-s}{1-M_1s}M_1g_z\right)g_z$$

CC-0. In Public Domain. Gurukul Kangri Collection, Haridwar

Digitized by Arya Samaj Foundation Chennai and eGangotri

we can substitute

$$\frac{1}{3}\frac{1-s}{1-M_1 s}M_1 g^2,$$

because $\phi^{(1)}$ is a function of g. By use of all these realtions, and by integration with respect to G', (4.8) is transformed into

$$\frac{8}{3}M_1\pi^{\frac{1}{2}}\int_0^\infty (1-M_1 s)^{-(5/2)} \times\exp\left(-\frac{V^2}{1-M_1 s}\right)V^4\phi^{(1)}dV, \quad (4.9)$$

$$V=\left(\frac{m_1 m}{m_1+m}\frac{1}{2kT}\right)^{\frac{1}{2}}g.$$

Consulting the definition of $\Omega^{(1)}(1)$, (2.7), we see that (4.9) divided by $8M_1/3$ is equal to $\Omega^{(1)}(1)$ in which T is replaced by $T(1-M_1 s)$. (4.9) is, therefore, equal to

$$\frac{8}{3}M_1\sum_{r=0}^{\infty}\frac{(-1)^r}{r!}(M_1 sT)^r\frac{d^r}{dT^r}\Omega^{(1)}(1).$$

Hence it follows that

$$(\psi_1^{(r)}, J\psi_1^{(0)})=\frac{8}{3}M_1\frac{(-1)^r}{r!}(M_1 T)^r\frac{d^r}{dT^r}\Omega^{(1)}(1). \quad (4.10)$$

(Making use of the relation

$$T\frac{d}{dT}\Omega^{(l)}(r)=\Omega^{(l)}(r+1)-(r+\tfrac{3}{2})\Omega^{(l)}(r),$$

or from (4.9) directly, we can express (4.10) in terms of $\Omega^{(1)}(1)$, $\Omega^{(1)}(2)$, $\cdots$, $\Omega^{(1)}(r+1)$. We prefer, however, not to rewrite for the present purpose.)

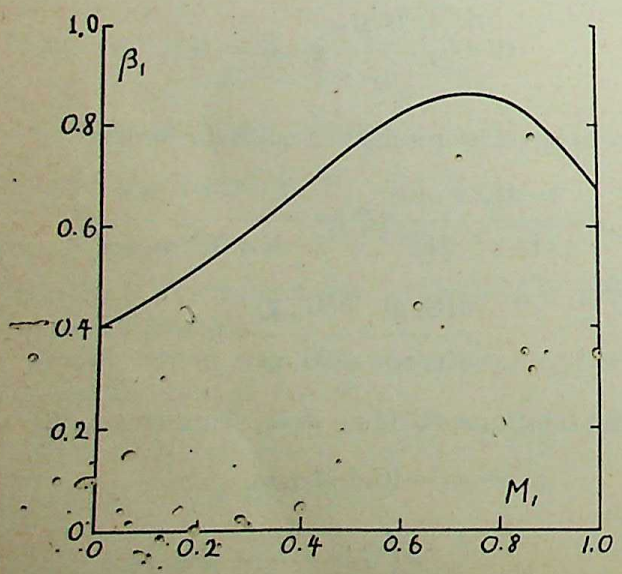


FIG. 3. Values of the factor β_1 in the coefficient b_1.

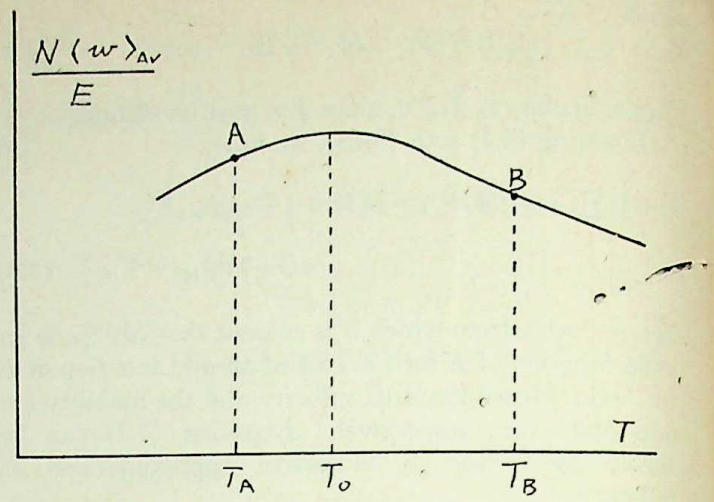


FIG. 4. Mobility times gas density for infinitesimal field strength as a function of temperature. Points A and B correspond to A and B in Fig. 5, respectively.

Inserting (4.10) into (4.7), and consulting (4.5) and (4.6), we obtain finally

$$\langle w\rangle_{AvI}=\frac{3}{16}\frac{m_1+m}{m_1 m}\frac{eE}{N\Omega^{(1)}(1)}, \quad (4.11)$$

$$\langle w\rangle_{AvII}=\frac{3}{16}\frac{m_1+m}{m_1 m}\frac{eE}{N}\left[\sum_{r=0}^{\infty}\frac{(b_r T)^r}{r!}\frac{d^r}{dT^r}\Omega^{(1)}(1)\right]^{-1}, \quad (4.12)$$

where

$$(b_r)^r=\frac{3}{4}\frac{\pi^{\frac{1}{2}}r!}{\Gamma[r+(5/2)]}\frac{(-1)^r\langle\psi_1^{(r)}\rangle_{AvI}}{\langle\psi_1^{(0)}\rangle_{AvI}}(M_1)^r. \quad (4.13)$$

The b_r are positive and proportional to E^{2r}, except that $b_0=1$.

In the case of the Maxwellian model, for which $\Omega^{(l)}(r)$ is independent of T, our first and second approximations coincide with each other. For heavy ions also, subject to the condition (2.6), the second approximation becomes identical with the first, because $b_1, b_2, \cdots$, which can be expressed in the form

$$b_r=\frac{m_1}{2kT}(\langle w\rangle_{Av})^2\beta_r, \quad r=1, 2, \cdots,$$

with β_r remaining finite for the limit $M_1\to 0$, vanish. In these two cases the first approximation is exact, as we already know.

In general cases let us content ourselves with the second approximation. The mobility is then given by the right-hand side of (4.12) divided by E. The relationship shows that an increase of E^2 and an increase of T have a somewhat similar effect on the mobility. The weaker the field is, the more accurately holds the similarity. *For a sufficiently weak field, mobility times density is a function of one variable,* $T(1+b_1)$.

CC-0. In Public Domain. Gurukul Kangri Collection, Haridwar

Digitized by Arya Samaj Foundation Chennai and eGangotri

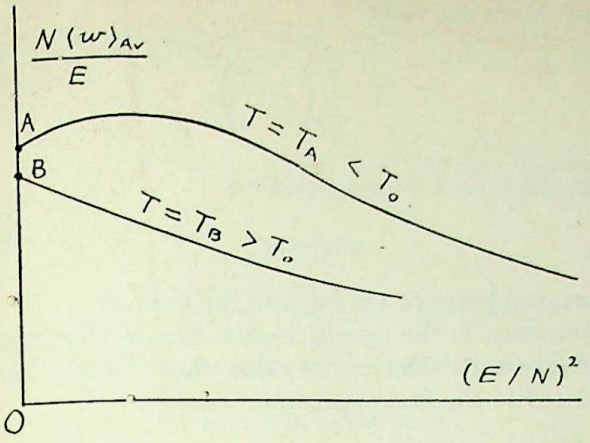


FIG. 5. Mobility times gas density as functions of $(E/N)^2$, E and N being the field strength and the number-density of gas molecules, respectively (see Fig. 4).

As regards

$$b_1=\frac{m_1}{2kT}(\langle w\rangle_{Av})^2\beta_1, \tag{4.14}$$

we obtain

$$\beta_1=\frac{4}{15}M_2\left[\frac{a_{00}(1)}{a_{11}(1)}\left(4\frac{a_{00}(1)}{a_{00}(2)}+5\frac{a_{00}(1)}{a_{11}(0)}\right)\right],$$

which can be approximated by the value for the Maxwellian model

$$\beta_1=\frac{4}{15}M_2\left[\frac{\lambda_0(1)}{\lambda_1(1)}\left(4\frac{\lambda_0(1)}{\lambda_0(2)}+5\frac{\lambda_0(1)}{\lambda_1(0)}\right)\right]$$
$$=\tfrac{2}{5}(12M_2+3M_1\phi^{(2)}/\phi^{(1)})$$
$$\times(4M_2+3M_1\phi^{(2)}/\phi^{(1)})^{-1}$$
$$\times(M_1^2+3M_2^2+2M_1M_2\phi^{(2)}/\phi^{(1)})^{-1}.$$

Figure 3 shows β_1 for $\phi^{(2)}/\phi^{(1)}=0.70$.

According to experimental results, the temperature variation of the mobility times gas density for infinitesimal field strength has a maximum at a certain temperature, T_0, as shown in Fig. 4, indicating that $\Omega^{(1)}(1)$ has a minimum at that temperature. Consulting this fact, our theory can predict the following field variation of the mobility.

For temperatures a little lower than T_0, the mobility first increases with the field strength, then takes a maximum and finally decreases; for temperatures higher than T_0, the mobility decreases from the beginning (see Fig. 5).

The temperatures T_0 are such as are given in Table I. Since T_0 is usually higher than room temperatures, the mobility usually must first increase with the field strength. In fact, measurements by Mitchell and Ridler[2] on the mobility of Li^+, Na^+, K^+, Rb^+, Cs^+, NH_3^+, $Na^+(NH_3)$, and N_2^+ in N_2 as well as those by Hershey[3] on the mobility of K^+ in H_2, He, Ne, and A correspond to the case $T<T_0$. It is regrettable that many recent measurements made at the Bell Telephone Laboratory[4] are lacking in weak field regions and cannot be used for the present purpose.

Recently Wannier[5] at the Bell Telephone Laboratory tackled the same problem as the present article. After he treated some special cases, such as the case of an extremely high field and the case of the Maxwellian cross section, he concluded: "It is to be hoped that a more satisfactory way of proceeding can be found." The present author hopes that the way of proceeding developed in this section will be satisfactory.

5. MOBILITY IN A WEAK FIELD

When the electric field is infinitesimal, both the first and the second approximations of the drift velocity are given by the right-hand side of (4.11). The aim of this section is to derive a more accurate formula in this case, chiefly in order to have some information about the accuracy of our formula (4.12). (We can use the experimental results of the mobility in a weak field for the purpose of determining the force between an ion and a molecule. An accurate expression is desirable for this purpose, too.)

When the electric field is sufficiently weak, Eq. (4.3) reduces to

$$\sum_s a_{rs}(l)\langle\psi_l^{(s)}\rangle_{Av}=\mathcal{E}\delta_{r0}\delta_{l0},$$

or

$$\langle\psi_l^{(r)}\rangle_{Av}=0 \quad \text{for} \quad l\neq 1 \tag{5.1}$$

and for $l=1$,

$$\sum_s a_{rs}\langle\psi_1^{(s)}\rangle_{Av}=\mathcal{E}\delta_{r0}, \tag{5.2}$$

where

$$a_{rs}\equiv a_{rs}(1).$$

Let the first approximation, $\langle\psi_1^{(r)}\rangle_{AvI}$, be determined by

$$a_{rr}\langle\psi_1^{(r)}\rangle_{AvI}=\mathcal{E}\delta_{r0},$$

and the nth approximation, $\langle\psi_1^{(r)}\rangle_{Avn}$, be determined by

$$a_{rr}\langle\psi_1^{(r)}\rangle_{Avn}+\sum_s(1-\delta_{rs})a_{rs}\langle\psi_1^{(s)}\rangle_{Avn-1}=\mathcal{E}\delta_{r0}$$

TABLE I. The temperatures corresponding to the minimum of $\Omega^{(1)}(1)$.

	T_0	Reference
He^+ in He	*ca* 300°K	a
N_2^+ in N_2	*ca* 700	a
Cs^+ in He	210	b
Na^+ in He	*ca* 600	b
Li^+ in He	*ca* 700	c
K^+ in A	400	d

[a] A. M. Tyndall and A. F. Pearce, Proc. Roy. Soc. (London) A149, 426 (1935).
[b] A. F. Pearce, Proc. Roy. Soc. (London) A155, 490 (1936).
[c] K. Hoselitz, Proc. Roy. Soc. (London) A177, 200 (1941).

[2] J. H. Mitchell and K. E. W. Ridler, Proc. Roy. Soc. (London) A146, 911 (1934).

[3] A. V. Hershey, Phys. Rev. 56, 908 (1939).
[4] J. A. Hornbeck, Phys. Rev. 84, 615 (1951); R. N. Varney, Phys. Rev. 88, 362 (1952); 89, 708 (1953).
[5] G. H. Wannier, Phys. Rev. 83, 281 (1951); 87, 795 (1952).

CC-0. In Public Domain. Gurukul Kangri Collection, Haridwar

Digitized by Arya Samaj Foundation Chennai and eGangotri

($n=$II, III, $\cdots$). Then we obtain, for instance,

$$\langle\psi_1^{(r)}\rangle_{\text{AvIII}}=\frac{\mathcal{E}}{a_{rr}}\left[\delta_{r0}-(1-\delta_{r0})\frac{a_{r0}}{a_{00}}+\sum_s(1-\delta_{rs})(1-\delta_{s0})\frac{a_{rs}a_{s0}}{a_{ss}a_{00}}\right].$$

In particular, for $r=0$

$$\langle w\rangle_{\text{AvIII}}=\langle w\rangle_{\text{AvI}}\left[1+\sum_{s=1}^{\infty}\frac{a_{0s}a_{s0}}{a_{ss}a_{00}}\right]. \tag{5.3}$$

Let us adopt

$$\langle w\rangle_{\text{AvI}}(1+a_{01}a_{10}/a_{11}a_{00})$$

as an approximation to $\langle w\rangle_{\text{Av}}$. Since we have

$$\frac{a_{01}a_{10}}{a_{11}a_{00}}=\frac{a_{00}}{a_{11}}\cdot\frac{a_{01}}{a_{00}}\frac{a_{10}}{a_{00}}=\frac{2}{5}\frac{a_{00}}{a_{11}}M_1^2\left(\frac{T}{\Omega^{(1)}(1)}\frac{d\Omega^{(1)}(1)}{dT}\right)^2,$$

and a_{00}/a_{11} can be approximated by the value for the Maxwellian model,

$$\frac{\lambda_0(1)}{\lambda_1(1)}=(M_1^2+3M_2^2+2M_1M_2\phi^{(2)}/\phi^{(1)})^{-1},$$

we obtain

$$\langle w\rangle_{\text{Av}}\doteqdot\langle w\rangle_{\text{AvI}}(1+\Delta), \tag{5.4}$$

where

$$\Delta=\tfrac{2}{5}(M_1^2+3M_2^2+2M_1M_2\phi^{(2)}/\phi^{(1)})^{-1}\times\left(M_1\frac{d\ln\Omega^{(1)}(1)}{d\ln T}\right)^2, \tag{5.5}$$

in which 0.7 can be substituted for $\phi^{(2)}/\phi^{(1)}$.

The Δ is large when $M_2=1-M_1$ is small. For M_2 sufficiently small, we have

$$\Delta=\frac{2}{5}\left(\frac{d\ln\Omega^{(1)}(1)}{d\ln T}\right)^2,$$

which takes the value

$$\Delta=\frac{1}{10}\left(1-\frac{4}{s}\right)^2, \tag{5.6}$$

when the inverse power potential

$$u(r)=\lambda r^{-s} \tag{5.7}$$

is assumed between the ion and the molecule.

Moreover, in the case of $M_2\ll1$, the problem can be treated exactly.[6] The precise value when (5.7) is adopted is related to the first approximation as

$$\frac{\langle w\rangle_{\text{Av}}}{\langle w\rangle_{\text{AvI}}}=\frac{16}{9\pi}\Gamma\left(3-\frac{2}{s}\right)\Gamma\left(2+\frac{2}{s}\right). \tag{5.8}$$

The numerical values of (5.8) and $1+\Delta$, obtainable from (5.6), are as follows:

s	∞	12	4	2
$1+\Delta$	1.100	1.044	1	1.100
(5.8)	1.132	1.056	1	1.132

Since the actual case corresponds to such values of s as $4\lesssim s\lesssim12$, the accuracy of (5.4) is satisfactory, and Eq. (4.12) is accurate within the error of $6M_1^2$ percent, at least for weak fields.

ERRATA FOR PART A

In the second term on the left-hand side of (2.2), change $\partial\mathbf{c}$ to $\partial\mathbf{r}$.

Four lines above Eq. (A.1), change $\langle\mathbf{c}^2\rangle_{\text{Av}}$ to $|\langle\mathbf{c}\rangle_{\text{Av}}|^2$.

Five lines above Eq. (A.2), change $1-\cos l\theta$ to $1-\cos^l\theta$.

First column of Table II, change He, IIe, $\cdots$ to He, Ne, $\cdots$.

Eqs. (10.1) and (10.5), take out the absolute value symbols.

[6] S. Chapman and T. G. Cowling, *The Mathematical Theory of Non-Uniform Gases* (Cambridge University Press, London, 1939), p. 187.

CC-0. In Public Domain. Gurukul Kangri Collection, Haridwar

Digitized by Arya Samaj Foundation Chennai and eGangotri

REVIEWS OF MODERN PHYSICS VOLUME 25, NUMBER 4 OCTOBER, 1953

Interpretation of the Virtual Level of the Deuteron

S. T. MA*

Division of Physics, National Research Council, Ottawa, Canada

I. Introduction
II. Definitions of the Virtual Level
  A. Approximate Definition
  B. Exact Definitions for the Square-Well Potential
  C. The Theory of Effective Range
III. The Virtual Level according to the Theory of the S Matrix
  A. The Functions S and f
  B. Bound, Virtual and Decaying States
  C. Examples
  D. The Effective-Range Theory in Factorized Form
IV. The Virtual Level according to the Theory of Resonance Levels
  A. The Functions R and Q
  B. One-Level Formulas

I. INTRODUCTION

FROM the measurements of the cross section of low-energy neutron-proton scattering, it became evident to physicists[1,2,3] in the early days that the interaction of the neutron and the proton is spin-dependent. According to these authors, there is a ^1S state that plays a role in the theoretical formula for the ^1S scattering similar to that played by the ground state of the deuteron for the ^3S scattering. Experiments on the scattering of neutrons by *ortho-* and *para*-hydrogen have led to the conclusion that the ^1S state is a virtual state having a negative binding energy.

While the bound state is a familiar concept in quantum mechanics, the true nature of the virtual state has been a subject of much discussion during the subsequent years, and various definitions of the virtual level of the deuteron have appeared in the literature. In view of the interest this subject has received, it is desirable to clarify the theoretical background of the definitions that have been proposed.

The object of this article is not to give a comprehensive exposition of the motives that led to the various definitions of the virtual level, but rather to elucidate some of the definitions from the viewpoint of the theory of S matrix (scattering matrix)[4] and the theory of R (derivative) and Q matrices.[5] After a brief general review in Part II, we shall confine our attention to the following definitions: (1) definitions which are based on the analogy of the ^1S virtual state with the ^3S bound state, and which fit in a simple way into the theory of the S matrix; (2) a definition that identifies the ^1S virtual level with the lowest ^1S resonance level according to the theory of the R matrix. From a general formula connecting the S and R matrices, one can derive a simple connection between the two kinds of definitions. There have been scattered remarks on this subject in the literature. It is our purpose to give a connected account. It should be mentioned that the term "virtual level" has been given different meanings in the literature. In this article we use it only for the energy levels that form the basis of one-level representations of the low-energy neutron-proton ^1S scattering cross section. As usual, we use the term "resonance level" for the energy levels that occur in resonance scattering and resonance reactions. It is beyond the scope of the present article to discuss in detail the theory of resonance, and we shall merely mention briefly the definitions of the resonance level that have been given in terms of the S, R, and Q matrices.

In dealing with the neutron-proton system we shall confine our attention to the central-force approximation and the S states. The matrix elements of the S, R, and Q matrices that concern us are simply functions of the momentum or energy of the relative motion of the two nucleons.

II. DEFINITIONS OF THE VIRTUAL LEVEL

A. Approximate Definition

The wave equation for the S states of the neutron-proton system is, for the center-of-mass frame of reference,

$$[-(d/dr)^2+V(r)]u(r)=Eu(r). \quad (1)$$

Here r is the distance between the nucleons, E and $V(r)$ are the total energy and the potential energy, divided by the factor $\hbar^2/2m$, m being the reduced mass of the nucleons.[5a] For the scattering problem, there is a continuous spectrum of energies $E_k=k^2$, extending from $k=0$ to $k=\infty$, and the wave Eq. (1) corresponding to an energy E_k is of the form

$$[(d/dr)^2+k^2]u_k(r)=V(r)u_k(r). \quad (2)$$

The wave function $u_k(r)$ vanishes at $r=0$ and has the asymptotic expression

$$u_k(r)=\text{const}\sin[kr+\delta(k)]. \quad (3)$$

* Now at School of Physics, University of Sydney, Sydney, Australia.

[1] The idea suggested by E. P. Wigner was developed by H. A. Bethe and R. F. Bacher, Revs. Modern Phys. 8, 82 (1936); See also H. A. Bethe, *Elementary Nuclear Theory* (John Wiley and Sons, Inc., New York, 1947).

[2] E. Fermi, Phys. Rev. 48, 570 (1935); Ricerca sci. 7, No. II, 13 (1936); E. Amaldi and E. Fermi, Phys. Rev. 50, 899 (1936).

[3] J. Schwinger and E. Teller, Phys. Rev. 52, 286 (1937).

[4] J. A. Wheeler, Phys. Rev. 52, 1107 (1937); W. Heisenberg, Z. Physik 120, 513, 673 (1943); Z. Naturforsch. 1, 608 (1946); C. Møller, Kgl. Danske Videnenskab Selskab. Mat-fys. Medd. 23, No. 1 (1945); 22, No. 19 (1946).

[5] E. P. Wigner and L. Eisenbud, Phys. Rev. 72, 29 (1947); T. Teichmann and E. P. Wigner, Phys. Rev. 87, 123 (1952).

[5a] The quantity E will be referred to as energy for brevity.

CC-0. In Public Domain. Gurukul Kangri Collection, Haridwar

Digitized by Arya Samaj Foundation Chennai and eGangotri

for large r, $\delta(k)$ being the phase shift. The scattering cross section is given by

$$\sigma(k)=4\pi \sin^2[\delta(k)]/k^2 \tag{4}$$

or

$$\sigma(k)=4\pi/k^2\{1+\cot^2[\delta(k)]\}. \tag{5}$$

At low energies we have approximately

$$\cot[\delta(k)]=-\alpha/k, \tag{6}$$

where

$$\alpha=-\lim_{k\to 0} k\cot[\delta(k)], \tag{7}$$

and therefore

$$\sigma(k)=4\pi/(k^2+\alpha^2). \tag{8}$$

The quantity α is the reciprocal of Fermi's scattering length.

The connection between the scattering cross section and the bound and virtual states arises from the following situation. It is known theoretically that the existence of a bound state for the deuteron depends on the sign of the scattering length. If $\alpha>0$, there is a bound state whose energy is approximately $E_\alpha=-\alpha^2$. On the other hand, there is no bound state if $\alpha<0$. These conclusions have been drawn from the mathematical scheme of wave mechanics.[1,6] A simple derivation of these conclusions provided by the theory of the S matrix will be given in Sec. IIIB. The first of the above two possibilities holds for ^3S. In this case the scattering cross section can be expressed in terms of the binding energy of the ground state of the deuteron according to the approximate formula

$$\sigma(k)=4\pi/(E_k+|E_\alpha|). \tag{9}$$

In the case of ^1S, the second possibility holds and there is no bound state. However, Eq. (9) is still valid if one introduces a virtual state whose energy is numerically equal to α^2. It is customary to speak of a positive binding energy if the state is real, a negative binding energy if it is virtual.

B. Exact Definitions for the Square-Well Potential

The definition of the virtual level given above is approximate. Exact definitions have been given, without reference to the scattering formula, for the case of a nuclear potential having the shape of a square well,

$$V(r)=\begin{cases}-V_0 & (r<a)\\ 0 & (r>a).\end{cases} \tag{10}$$

As a preparation for our later general discussions we shall discuss some of these definitions that are better known.[7]

In the case of ^3S, there is a bound state of energy $E_\gamma=-\gamma^2$. Its wave function for $r\geqslant a$ is

$$u(r)=\text{const}\exp(-\gamma r) \tag{11}$$

with $\gamma>0$. The continuity of $u(r)$ and its derivative at $r=a$ requires

$$(V_0-\gamma^2)^{\frac{1}{2}}\cot[(V_0-\gamma^2)^{\frac{1}{2}}a]=-\gamma. \tag{12}$$

The solutions of this equation have been discussed by Schiff[8] and by Mott and Massey.[9] There is only one solution of Eq. (12) for the deuteron because V_0 is only slightly larger than the critical value $(\pi/2a)^2$. Breit and his collaborators[10,11] have expressed the scattering cross section in terms of k and γ. Their result is

$$\sigma(k)=[4\pi/(k^2+\gamma^2)][1+(\gamma a)+G_2(\gamma a)^2+G_3(\gamma a)^3+\cdots], \tag{13}$$

where the coefficients G_n are even functions of k and γ.

In the case of ^1S, the value of V_0 is slightly smaller than $(\pi/2a)^2$. The value of γ that satisfies Eq. (12) is now negative and the wave function given by Eq. (11) is no longer permissible. It now becomes necessary to introduce a virtual level. The choice of reference 10 amounts to using Eq. (12) also for ^1S, with the understanding that γ is negative, and the magnitude of the energy of the virtual level is defined to be γ^2. This choice for the virtual level was designed to make the expansion expressed by Eq. (13) valid also for ^1S. It appears natural from the viewpoint of the theory of the S matrix, as will be seen in Sec. IIIB.

A slightly different choice[12] is to define the energy of the virtual level as the positive energy $k^2=\gamma^2$ for which

$$(d/dr)u_k(r)/u_k(r)=k \quad (r=a). \tag{14}$$

This leads to the condition

$$(V_0+\gamma^2)^{\frac{1}{2}}\cot[(V_0+\gamma^2)^{\frac{1}{2}}a]=\gamma \quad (\gamma>0) \tag{15}$$

for the virtual level.

According to a general definition given by Hulthén,[11,13] the virtual state is the positive-energy state k such that

$$\int_0^\infty [u_k(r)]^2|V(r)|dr=\text{maximum}, \tag{16}$$

$u_k(r)$ being normalized in the energy scale. For the square-well potential, Eq. (16) reduces to

$$\int_0^a [u_k(r)]^2dr=\text{maximum}. \tag{17}$$

[6] J. M. Blatt and V. F. Weisskopf, *Theoretical Nuclear Physics*, (John Wiley and Sons, New York, 1952).

[7] There is an extensive collection of definitions of the virtual level for the square-well potential in a recent article by O. Bergmann, Acta Phys. Austriaca **5**, 240 (1951).

[8] L. I. Schiff, *Quantum Mechanics*, (McGraw-Hill Book Company, Inc., New York, 1949).

[9] N. F. Mott and H. S. W. Massey, *Theory of Atomic Collisions* (Oxford University Press, Oxford, 1949).

[10] Breit, Thaxton, and Eisenbud, Phys. Rev. **55**, 1018 (1939); C. Kittel and G. Breit, Phys. Rev. **56**, 744 (1939).

[11] L. Rosenfeld, *Nuclear Physics* (Interscience Publishers, New York, 1949), Chap. 5.

[12] M. S. Plesset and F. W. Brown, Proc. Natl. Acad. Sci. U. S. **25**, 600 (1939).

[13] L. Hulthén, Arkiv. Mat. Astron. Fysik. **29**, No. 1 (1942).

CC-0. In Public Domain. Gurukul Kangri Collection, Haridwar

Digitized by Arya Samaj Foundation Chennai and eGangotri

Flügge, Hückel,[14] Wu, and Foley[15] have shown that it is possible to take the lowest energy λ^2 satisfying the equation

$$\cot[(V_0+\lambda^2)^{\frac{1}{2}}a]=0 \tag{18}$$

to be the virtual level. Equation (18) is the condition for the derivative of $u_k(r)$ to vanish at $r=a$, $k=\lambda$. Treating k and λ as small quantities, these authors obtained the following formulas:

$$\sigma(k)=4\pi(1-\lambda^2a^2)/[k^2+(k^2-\lambda^2)^2a^2/4], \tag{19}$$

$$\sigma(k)=4\pi/[k^2+(k^2+\lambda^2)^2a^2/4]. \tag{20}$$

Equation (19) is the result of reference 14, including the correction factor $(1-\lambda^2a^2)$ given in their later publications. Equation (20) is the result of reference 15. These results are consistent with each other, as can be seen by transferring the factor $1-\lambda^2a^2$ in Eq. (19) from the numerator to the denominator and retaining only the first two terms in the expansion in powers of k^2 and λ^2. The cross sections given by Eqs. (19) and (20) decrease monotonically with energy, but the ratio of $\sigma(k)$ to $4\pi/E_k$ has a maximum at $k=\lambda$ according to both formulas. For $k\ll\lambda$, Eq. (20) may be replaced by[15a]

$$\sigma(k)=4\pi/[k^2+(a\lambda^2/2)^2]. \tag{21}$$

As will be seen in Sec. IVA, Eq. (18) is the condition for resonance levels adopted by many authors. Eisenbud[16] has discussed the formula of Flügge and Hückel from this point of view. Eisenbud's energy of resonance includes, besides λ^2, the level shift.

A similar formula has been derived by Schiff.[8] For low energies Schiff's result reduces to

$$\sigma(k)=4\pi/[k^2+V_0\cot^2(V_0a^2)^{\frac{1}{2}}]. \tag{22}$$

This is the same as Eq. (21), since

$$\begin{aligned}(V_0a^2)^{\frac{1}{2}}&\cot(V_0a^2)^{\frac{1}{2}}\\ &=[(\pi/2)^2-\lambda^2a^2]^{\frac{1}{2}}\cot[(\pi/2)^2-\lambda^2a^2]^{\frac{1}{2}}\\ &\doteq\tfrac{1}{2}\lambda^2a^2\end{aligned} \tag{23}$$

for small λ. The case of resonance at zero energy occurs when $V_0=(\pi/2a)^2$ and $\lambda=0$. The use of Eq. (18) for the virtual level has also been discussed in reference 12 and by Bohm.[17]

The condition for resonance levels expressed by Eq. (18) may also be written in the more general form

$$\cot[ka+\delta(k)]=0 \quad (k=\lambda). \tag{24}$$

A different condition for the resonance levels has been adopted by Sexl[18] and Bergmann,[7] namely

$$\cot[\delta(k)]=0. \tag{25}$$

This condition will be discussed in Sec. IVA.

For the same square-well potential, the condition for the decaying states is

$$(V_0+k_c^2)^{\frac{1}{2}}\cot[(V_0+k_c^2)^{\frac{1}{2}}a]=ik_c, \tag{26}$$

where k_c is a complex number. The general condition corresponding to Eq. (26) will be given in Sec. IIIB.

C. The Theory of Effective Range

The theory of effective range developed by Schwinger,[19] Blatt and Jackson,[20] and Bethe and Longmire[21] is an improvement on the approximate treatment of Sec. IIA. In the shape-independent approximation for low-energy ^3S scattering, the phase shift is given by

$$k\cot[\delta(k)]=-\alpha+\tfrac{1}{2}r_0k^2 \tag{27}$$

or

$$k\cot[\delta(k)]=-\gamma+\tfrac{1}{2}r_0(\gamma^2+k^2). \tag{28}$$

Here α is the reciprocal of the scattering length, r_0 is a constant known as the effective range, γ is connected with the binding energy and wave function of the bound state according to the relations $E_\gamma=-\gamma^2$ and $u(r)=\text{const}\exp(-\gamma r)$ for large r. The relation between α and γ is given by the equations

$$\gamma(1-\tfrac{1}{2}\gamma r_0)=\alpha, \tag{29}$$

$$\gamma=[1-(1-2\alpha r_0)^{\frac{1}{2}}]/r_0. \tag{30}$$

The observed values of α, γ, r_0 and $1-2\alpha r_0$ are all positive. Substitution of Eqs. (27) and (28) into Eq. (5) gives

$$\sigma(k)=4\pi/[k^2+(-\alpha+\tfrac{1}{2}r_0k^2)^2], \tag{31}$$

$$\sigma(k)=4\pi/(k^2+\gamma^2)[1-\gamma r_0+(k^2+\gamma^2)r_0^2/4], \tag{32}$$

respectively. Equation (32) gives the connection between σ and the binding energy γ^2.

In the case of the ^1S scattering, Eqs. (27) and (31) hold with the appropriate values for α and r_0. The numbers r_0 and $1-2\alpha r_0$ are still positive, but α is now negative and so, by Eq. (30), γ is also negative. Hence there is no bound state. However, Eqs. (28), (29), (30), and (32) remain mathematically valid. As pointed out in references 20, 21, one can introduce a virtual level whose energy is numerically equal to γ^2. Equation (32) gives now the connection between σ and the virtual state instead of the bound state. Blatt and Jackson have discussed this question from the viewpoint of the theory of the S matrix. We shall give a more detailed discussion in Sec. IIID.

---

[14] S. Flügge and E. Hückel, Phys. Rev. 73, 520 (1948); E. Hückel, Z. Naturforsch. 3, 134, 308 (1948).

[15] T. Y. Wu and H. M. Foley, Phys. Rev. 73, 1117 (1948).

[15a] Comparison of Eq. (21) with the lowest approximation for Eq. (13) gives

$$\gamma^2=(a\lambda^2/2)^2, \tag{21a}$$

which is a special case of a formula to be given in Sec. IVB. Since $(a\lambda)^2$ is of the order 0.2, the ratio γ^2/λ^2 is of the order 1/20. Numerical values given in the literature are about 0.06 Mev for the energy γ^2 and 0.9–1.9 Mev for the energy λ^2.

[16] L. Eisenbud, Phys. Rev. 73, 1407 (1948).

[17] D. Bohm, *Quantum Theory* (Prentice Hall, Inc., New York, 1951), p. 262.

[18] T. Sexl, Z. Physik. 115, 571 (1940).

[19] J. Schwinger, *Lecture Notes on Nuclear Physics* (Harvard, Cambridge, 1947).

[20] J. M. Blatt and J. D. Jackson, Phys. Rev. 76, 18 (1949).

[21] H. A. Bethe, Phys. Rev. 76, 38 (1949); H. A. Bethe and C. Longmire, Phys. Rev. 77, 647 (1950).

CC-0. In Public Domain. Gurukul Kangri Collection, Haridwar

Digitized by Arya Samaj Foundation Chennai and eGangotri

III. THE VIRTUAL LEVEL ACCORDING TO THE THEORY OF THE S MATRIX

A. The Functions S and f

The matrix elements of the S matrix for the S states having a particular value of spin are represented by the function

$$S(k)=\exp[2i\delta(k)]. \tag{33}$$

From Eq. (33) we obtain

$$S(k)=\{\cot[\delta(k)]+i\}/\{\cot[\delta(k)]-i\}, \tag{34}$$

and

$$\cot[\delta(k)]=i[S(k)+1]/[S(k)-1]. \tag{35}$$

Because of Eq. (33), Eq. (4) may be written as

$$\sigma(k)=(\pi/k^2)|S(k)-1|^2. \tag{36}$$

The function $S(k)$ can be expressed in terms of the functions $f(\pm k)$.[22–24] These functions are the values of $f(\pm k, r)$ at $r=0$, where $f(\pm k, r)$ are two linearly independent solutions of Eq. (2) specified by the asymptotic behavior

$$\lim_{r\to\infty} f(\pm k, r)\exp(\pm ikr)=1. \tag{37}$$

The solutions $f(\pm k, r)$ are complex conjugate of each other, and satisfy the relation

$$f(k,r)(d/dr)f(-k,r)-f(-k,r)(d/dr)f(k,r)=2ik. \tag{38}$$

Hence for $k\neq 0$ there is no solution $f(\pm k, r)$ that vanishes at $r=0$. The solution of Eq. (2) that satisfies the requirement for a wave function at $r=0$ must be a linear combination of the form

$$u_k(r)=\text{const}[f(k)f(-k,r)-f(-k)f(k,r)]. \tag{39}$$

Comparing Eq. (3) with the asymptotic expression of $u_k(r)$ given by Eq. (39), we find

$$S(k)=f(k)/f(-k). \tag{40}$$

On account of the relation

$$f(k)^*=f(-k), \tag{41}$$

one can write

$$\delta(k)=\arg[f(k)]. \tag{42}$$

It can be shown that $f(\infty)=1$. Hence one can set $\delta(\infty)=0$.

The functions $f(\pm k)$ and $S(k)$ are defined above for $0\leq k<\infty$, but may be extended by analytic continuation to the complex plane. It has been shown by Jost and Bargmann that, if

$$\int_0^\infty r|V(r)|dr<\infty, \tag{43}$$

then $f(k)$ is regular in the region Im $k<0$ and continuous on the real axis. In the region Im $k\geq 0$, the analytic continuation of $f(k)$ exists in the problems we shall be concerned with, but it has, in general, singularities. The generalization of Eq. (41) for complex values of k is

$$f(k^*)^*=f(-k). \tag{41}^*$$

If the potential energy satisfies the equation

$$\int_0^\infty \exp(2\kappa r)|V(r)|dr<\infty \quad (\kappa>0), \tag{44}$$

then the function $f(k)$ is regular in region Im $k<\kappa$.

Levinson[25] has shown that, for potentials satisfying the condition

$$\int_0^\infty r^2|V(r)|dr<\infty, \tag{45}$$

the phase shift at $k=+0$ is connected with the number of bound states m by the relation

$$\left.\begin{aligned}\delta(+0)&=m\pi \quad \text{if} \quad f(0)\neq 0,\\ \delta(+0)&=(m+\tfrac{1}{2})\pi \quad \text{if} \quad f(0)=0.\end{aligned}\right\} \tag{46}$$

Hence $S(0)=\pm 1$ for the two cases.

B. Bound, Virtual, and Decaying States

While the function $f(k)$ does not vanish for any real nonvanishing k, it may have imaginary zeros. Corresponding to any real number γ that satisfies the equation

$$f(-i\gamma)=0 \tag{47}$$

there is a solution $f(-i\gamma, r)$ of Eq. (1) that vanishes at $r=0$ and varies as $\exp(-\gamma r)$ for large r, with $E=-\gamma^2$. If γ is positive, the function $f(-i\gamma, r)$ satisfies the requirements for the wave function of a bound state. On the other hand, a negative γ does not correspond to a bound state.

As a result of Eq. (40), any γ that satisfies Eq. (47) often satisfies also the equations

$$S(-i\gamma)=0, \tag{48}$$

$$S(i\gamma)=\infty, \tag{49}$$

and vice versa. The connection between the bound states and the zeros and poles of $S(k)$ was first observed by Kramers.[4] Subsequent investigations have shown that there are exceptions.[22,23] For Eq. (47) does not necessarily imply Eqs. (48), (49) if

$$f(i\gamma)=0, \tag{50}$$

while Eqs. (48), (49) do not necessarily imply Eq. (47) if

$$f(i\gamma)=\infty. \tag{51}$$

Thus Kramers' relation should be more precisely stated as follows: Eq. (47) is equivalent to Eqs. (48), (49) if

[22] R. Jost, Helv. Phys. Acta 20, 256 (1947); R. Jost and W. Kohn, Phys. Rev. 87, 977 (1952); Kgl. Danske Videnskab Selskab Mat-fys. Medd. 27, No. 9 (1953).

[23] V. Bargmann, Phys. Rev. 75, 301 (1949); Revs. Modern Phys. 21, 488 (1949).

[24] J. Meixner, Z. Naturfursh, 3, 75 (1948).

[25] N. Levinson, Kgl. Danske Videnskab Selskab Math-fys. Medd. 25, No. 9 (1949).

CC-0. In Public Domain. Gurukul Kangri Collection, Haridwar

Digitized by Arya Samaj Foundation Chennai and eGangotri

$f(i\gamma)$ is neither zero nor infinite. Otherwise there may be zeros of f and S that do not coincide.

A negative imaginary zero of $S(k)$ that is not a zero of $f(k)$ has been referred to as redundant or false zero in the literature. Since $f(k)$ is regular in the region Im $k<0$, a number γ that satisfies Eq. (51) must be positive. If Eq. (44) holds, there is no solution of Eq. (51) for $\gamma<\kappa$ and therefore no redundant zero in the region $-\kappa<\text{Im } k<0$. An example of $f(k)$ that satisfies both Eq. (47) and Eq. (50), but not Eqs. (48), (49), has recently been given by Jost and Kohn.

The connection between the existence of a bound state and the sign of the scattering length mentioned in Sec. IIA follows immediately if $f(k)$ is regular and has one and only one simple zero $-i\gamma$ near the origin, so that

$$f(k)=\text{const}\ (k+i\gamma) \tag{52}$$

in this neighborhood. For we have then, on account of Eqs. (40) and (35),

$$S(k)=(i\gamma+k)/(i\gamma-k), \tag{53}$$

and

$$\cot[\delta(k)]=-\gamma/k. \tag{54}$$

The quantity γ here takes the place of the quantity α of Sec. IIA. As before, the scattering cross section is approximately given by

$$\sigma(k)=4\pi/(k^2+\gamma^2). \tag{55}$$

If $\gamma>0$ there is a bound state having the energy $E_\gamma=-\gamma^2$ and we can express $\sigma(k)$ in the form

$$\sigma(k)=4\pi/(E_k+|E_\gamma|). \tag{56}$$

If $\gamma<0$ there is no bound state, but one can retain Eq. (56) by introducing a virtual state whose energy is numerically equal to γ^2.

This situation is the same as in Sec. IIA. However, our discussion suggests the following *exact* definition of the virtual state. A real number γ satisfying Eq. (47) corresponds to a bound or virtual state according as γ is positive or negative. If the magnitude of the potential energy is varied so that γ decreases from a positive value to a negative value, a bound state disappears and is replaced by a virtual state. Interpretation of the virtual state along this line has been proposed by several authors. The definition of virtual state expressed by Eq. (12) and that mentioned in Sec. IIC are consistent with this interpretation.

It should be noted that the validity of the preceding considerations depends on the assumption expressed by Eq. (52). This is true of the special problems in which the question of virtual state has arisen.

Besides zeros and poles on the imaginary axis, there are complex zeros and poles that are of physical interest. They are related to what are usually called the decaying or radioactive states.[4,6,26] Without entering into a detailed discussion, we shall merely mention the analogs of Eqs. (47), (48), and (49) for the decaying states, namely

$$f(-k_c)=0, \tag{57}$$

$$S(-k_c)=0, \tag{58}$$

$$S(k_c)=\infty, \tag{59}$$

$$f(k_c^*)=0, \tag{57}^*$$

$$S(k_c^*)=0, \tag{58}^*$$

$$S(-k_c^*)=\infty. \tag{59}^*$$

In these equations k_c stands for a complex number. The complex energies $E_c=k_c^2$ have played an important part in the theory of α decay[27] and the theory of resonance scattering and reactions.[28]

C. Examples

The following potentials provide simple illustrations for the bound states and their passage into virtual states according to the discussion of the preceding section.

(i) The square-well potential: In this case

$$f(k,r)=\exp(-ikr) \quad (r\geqslant a) \tag{60}$$

and

$$f(k,r)=\{(k'-k)\exp[ik'(r-a)]+(k'+k)\times\exp[-ik'(r-a)]\}\exp(-ika)/2k' \quad (r\leqslant a) \tag{61}$$

with $k'=(V_0+k^2)^{\frac{1}{2}}$. Hence

$$f(k)=[\cos(k'a)+ik\sin(k'a)/k']\exp(-ika), \tag{62}$$

so that the general conditions expressed by Eqs. (47) and (57) reduce to Eqs. (12) and (26), respectively.

(ii) The attractive exponential potential

$$V(r)=-V_0\exp(-r/a) \quad (V_0>0): \tag{63}$$

In this case

$$f(k)=(z/2)^{-\nu}\Gamma(1+\nu)J_\nu(z), \tag{64}$$

with $\nu=2iak$, and $z=2aV_0^{\frac{1}{2}}$. The function $f(k)$ is singular at $\nu=-n$ $(n=1, 2, \cdots)$ or $k=in/2a$. For $\nu\neq-n$, Eq. (64) may be written as[29]

$$f(k)=\prod_{n=1}^{\infty}[1-(z/j_{\nu,n})^2], \tag{65}$$

where the $j_{\nu,n}$ are zeros of $z^{-\nu}J_\nu(z)$. For $z\geqslant 0$, ν real, the equation[1]

$$J_\nu(z)=0 \tag{66}$$

gives an infinite number of curves starting from the points $\nu=-n$ on the ν axis with z increasing mono-

[26] W. Heitler and N. Hu, Nature 159, 776 (1947).

[27] G. Gamow and C. L. Critchfield, *Theory of Atomic Nucleus and Nuclear Energy Sources* (Oxford University Press, Oxford, 1949).

[28] J. Humblet, Mem. soc. roy. scien. Liège 12, No. 4 (1952); N. G. Van Kampen, Phys. Rev. 89, 1072 (1953). See also the previous papers mentioned in these publications.

[29] W. Magnus and F. Oberhettinger, *Special Functions of Math. Physics* (Chelsea Publishing Company, New York, 1949), p. 25.

CC-0. In Public Domain. Gurukul Kangri Collection, Haridwar

Digitized by Arya Samaj Foundation Chennai and eGangotri

11 2446

tonically with k. These curves cross the z axis at the points $z_1=2.40$, $z_2=5.52$, etc. A bound state disappears at every critical point $V_0=(z_n/2a)^2$.

(iii) Hulthén's potential[22,30]

$$V(r)=-V_0\exp(-r/a)/[1-\exp(-r/a)] \qquad (-\infty<V_0<\infty): \quad (67)$$

Here

$$f(k)=\prod_{n=1}^{\infty}(k+i\gamma_n)/(k-i\gamma_n'), \quad (68)$$

with

$$\left.\begin{aligned}\gamma_n&=(V_0a^2-n^2)/2an,\\ \gamma_n'&=n/2a.\end{aligned}\right\} \quad (69)$$

A bound state disappears at every critical point $V_0=(n/a)^2$.

(iv) An Eckart potential[22,23]

$$V(r)=-V_0\exp(-r/a)/[1+(V_0a^2/2)\exp(-r/a)]^2 \qquad (V_0a^2>-2): \quad (70)$$

Here

$$f(k)=(k+i\gamma_1)/(k-i\gamma_1'), \quad (71)$$

with

$$\left.\begin{aligned}\gamma_1&=(1/2a)(V_0a^2-2)/(V_0a^2+2),\\ \gamma_1'&=1/2a.\end{aligned}\right\} \quad (72)$$

There is a bound state when $V_0a^2>2$.

In examples (iii) and (iv) the function $f(k)$ is of the form

$$f(k)=\prod_{n=1}^{N}(k+i\gamma_n)/(k-i\gamma_n'), \quad (73)$$

where N may be finite or infinite. Hence

$$S(k)=\prod_{n=1}^{N}\sigma_n\sigma_n', \quad (74)$$

where

$$\sigma_n=(k+i\gamma_n)/(k-i\gamma_n), \quad (75)$$

and σ_n' is given by Eq. (75) with γ_n' instead of γ_n. The zero $-i\gamma_n$ of the factor σ_n corresponds to a bound or virtual state according as $\gamma_n>$ or <0. The zero $-i\gamma_n'$ of σ_n' is a redundant zero and γ_n' is always positive. If we take the argument of each factor σ_n or σ_n' to be zero when $k\to+\infty$, then, as $k\to+0$, the argument of σ_n becomes $\pm\pi$ or 0 according as $\gamma_n\gtrless$ or $=0$, and the argument of σ_n' becomes π. Thus the validity of Levinson's theorem expressed by Eq. (46) is obvious for the class of problem specified by Eqs. (73)–(75). Special examples of this general theorem can also be found in the books of Bethe[1] and Mott and Massey.[9]

[30] L. Hulthén, Ark. Mat. Astron. Fysik. 28A, No. 5 (1942).

D. The Effective-Range Theory in Factorized Form

To see the connection of the bound and virtual states of Sec. IIC with the function $S(k)$, we write

$$k\cot[\delta(k)]\pm ik=(r_0/2)(k\pm i\gamma)(k\pm i\gamma'). \quad (76)$$

Comparison of Eqs. (27) and (76) gives

$$\gamma+\gamma'=2/r_0, \quad (77)$$

$$\gamma\gamma'=2\alpha/r_0. \quad (78)$$

It follows from these equations that γ and γ' both satisfy the quadratic equation (29). The numerically smaller root is given by Eq. (30). The other root is

$$\gamma'=[1+(1-2\alpha r_0)^{\frac{1}{2}}]/r_0. \quad (79)$$

Substituting Eq. (76) into Eq. (34) we obtain

$$S(k)=(k+i\gamma)(k+i\gamma')/(k-i\gamma)(k-i\gamma'), \quad (80)$$

showing that $S(k)$ has two pairs of zeros and poles $\pm i\gamma$, $\pm i\gamma'$.

The connection between $\pm i\gamma$ and the bound and virtual states of Sec. IIC is consistent with the general definition suggested by the theory of the S matrix. As has been mentioned in Sec. IIIB, there may be zeros and poles of $S(k)$ that have no connection with any bound or virtual state. This is the case with $\pm i\gamma'$. Jost and Kohn have shown the function $f(k)$ for the deuteron is of the form

$$f(k)=(k+i\gamma)/(k-i\gamma'), \quad (81)$$

which shows that $-i\gamma'$ is a zero of $S(k)$ but not a zero of $f(k)$.

Using Eq. (76) or Eq. (80) we obtain the factorized form

$$\sigma(k)=4\pi(\gamma+\gamma')^2/(k^2+\gamma^2)(k^2+\gamma'^2) \quad (82)$$

for the scattering cross section. This formula is identical with Eq. (32), though it looks somewhat simpler. Factorization of $S(k)$ and $\sigma(k)$ is possible also for the higher approximation in the expansion of $k\cot[\delta(k)]$,

$$k\cot[\delta(k)]=-\alpha+\tfrac{1}{2}r_0k^2-Tk^4. \quad (83)$$

The equation

$$k\cot[\delta(k)]\pm ik=-T\prod_{n=1}^{4}(k\pm i\gamma^{(n)}) \quad (84)$$

determines four numbers $\gamma^{(n)}$. The functions S and σ can be factorized as follows:

$$S(k)=\prod_{n=1}^{4}(k+i\gamma^{(n)})/(k-i\gamma^{(n)}), \quad (85)$$

$$\sigma(k)=(4\pi/T^2)\prod_{n=1}^{4}(k^2+\gamma^{(n)2})^{-1}. \quad (86)$$

CC-0. In Public Domain. Gurukul Kangri Collection, Haridwar

Digitized by Arya Samaj Foundation Chennai and eGangotri

IV. THE VIRTUAL LEVEL ACCORDING TO THE THEORY OF RESONANCE LEVELS

A. The Functions R and Q

The R matrix of Wigner and Eisenbud reduces in the present problem to the derivative function $R(E)$.[31] For real nonnegative E, the function $R(E)$ is defined by

$$R(E)=[u_k(r)/(d/dr)u_k(r)]_{r=a}, \tag{87}$$

where $E=E_k=k^2$ and a is the range of the short-range interaction. The variable E is, in general, a complex number. The function R is the reciprocal of the logarithmic derivative of $u_k(r)$ at $r=a$, which we shall denote by $L(E)$. The connection of the latter with the resonance levels has been investigated by Feshbach, Peaslee, and Weisskopf.[6,32]

We shall confine our attention to the function R for those problems in which $V(r)$ vanishes for $r>a$ but is arbitrary otherwise. We have then

$$R(E)=(1/k)\tan[ka+\delta(k)], \tag{88}$$

and so

$$\cot[\delta(k)]=[kR(E)\sin(ka)+\cos(ka)]/[kR(E)\cos(ka)-\sin(ka)], \tag{89}$$

$$\sin^2[\delta(k)]=[kR(E)\cos(ka)-\sin(ka)]^2/[k^2R(E)^2+1]. \tag{90}$$

It follows from Eqs. (33) and (88) that the functions R and S are connected by the following formulas:

$$R(E)=(1/ik)[S(k)\exp(2ika)-1]/[S(k)\exp(2ika)+1], \tag{91}$$

$$S(k)=\exp(-2ika)[1+ikR(E)]/[1-ikR(E)]. \tag{92}$$

The function $R(E)$ admits of an expansion of the form

$$R(E)=\sum_\lambda \omega_\lambda/(E_\lambda-E), \tag{93}$$

where ω_λ and E_λ are real numbers, $\omega_\lambda>0$. This is a special case of a general result of references 5, 31. It shows that R is a meromorphic function of E whose poles E_ρ are all on the real axis. When $E_k=E_\lambda$, the derivative of $u_k(r)$ vanishes at $r=a$. The energies E_λ are often referred to as the resonance energies because of their relation to observed resonance levels. The condition for such resonance energies may be put in the form[32a]

$$R(E_\lambda)=\infty. \tag{94}$$

Wigner and Teichmann have considered a Q matrix[33] that shows resonance features like the R matrix. The Q matrix is connected with the S matrix by the general relation

$$S=(1+iQ)/(1-iQ). \tag{95}$$

The function

$$Q(E)=\tan[\delta(k)] \tag{96}$$

is related to the Q matrix in the same way as the functions $R(E)$ and $S(k)$ are related to the R and S matrices. It follows from Eqs. (5) and (96) that

$$\sigma(k)=4\pi/k^2\{1+[1/Q(k)]^2\}. \tag{97}$$

The condition for resonance expressed by Eq. (25) may be written in the form[33a]

$$Q(E_\rho)=\infty. \tag{98}$$

B. One-Level Formulas

It is the object of this section to discuss representation of the low-energy scattering cross section by means of a low-energy resonance level E_λ or E_ρ.

Equation (27) of the effective-range theory may be rewritten as

$$Q(E)=(2k/r_0)/(E-E_\rho), \tag{99}$$

where

$$E_\rho=2\alpha/r_0 \tag{100}$$

is a resonance energy according to Eq. (98). Equation (100) shows that E_ρ is positive for ^3S and negative for ^1S. Substituting Eq. (99) into Eq. (97) we find

$$\sigma(k)=4\pi/[E+(E-E_\rho)^2r_0^2/4]. \tag{101}$$

This is just Eq. (31) written in a slightly different form.

In the neighborhood of a resonance level E_λ, $R(E)$ is approximately given by

$$R(E)=\omega_\lambda/(E_\lambda-E). \tag{102}$$

Using this one-level formula, we see that, for small E and E_λ, Eq. (89) may be approximately written in the form of Eq. (27) with

$$\alpha=-E_\lambda/\omega_\lambda, \tag{103}$$

$$r_0=2(\omega_\lambda a-1)/\omega_\lambda. \tag{104}$$

Conversely, given Eq. (27) we obtain Eq. (102) by using Eq. (88). Owing to the approximations we have made, the values of α and r_0 given by Eqs. (103) and (104) are only nearly the same as the values of these constants in the effective-range theory. The correspondence between the resonance levels E_λ and E_ρ is given by the relation

$$E_\rho=E_\lambda/(1-\omega_\lambda a). \tag{105}$$

---

[31] E. P. Wigner, Ann. Math. 53, 36 (1951); Proc. Camb. Phil. Soc. 47, 790 (1951); Revista Mexicana de Fisica 1, 91 (1952); Am. Math. Mon. 59, 669 (1952); W. Schützer and J. Tiomno, Phys. Rev. 83, 249 (1951).

[32] Feshbach, Peaslee, and Weisskopf, Phys. Rev. 71, 145 (1947).

[32a] For positive values $E_\lambda=\lambda^2$. Eq. (94) is equivalent to Eq. (24). There may also be negative values E_λ and E_ρ that satisfy Eq. (94) and Eq. (98) below.

[33] As mentioned by these authors, the Q matrix is equal to Heitler's K matrix multiplied by a numerical factor.

[33a] As has been mentioned in Sec. IIIB, a further condition for resonance levels expressed in terms of the function S exists in the literature.

CC-0. In Public Domain. Gurukul Kangri Collection, Haridwar

Digitized by Arya Samaj Foundation Chennai and eGangotri

We have seen in Sec. IIID that Eqs. (27) and (80) are equivalent. There is therefore a simple connection between E_λ and the energy E_γ of the S matrix theory.[33b] Using Eq. (103) we obtain approximately

$$|E_\gamma| = |E_a| = (E_\lambda/\omega_\lambda)^2. \tag{106}$$

The scattering cross section can be given in terms of E_λ as follows. From Eqs. (4) and (90) we obtain, expanding in powers of E and E_λ and retaining only the first two terms in the numerator and denominator,

$$\sigma(k) = 4\pi\{1-(a/\omega_\lambda)[E(a\omega_\lambda-2)+2E_\lambda]\}/ [E+(E-E_\lambda)^2/\omega_\lambda{}^2]. \tag{107}$$

Similarly, from Eqs. (5) and (89),

$$\sigma(k) = 4\pi/\{E+[E_\lambda+(\omega_\lambda a-1)E]^2/\omega_\lambda{}^2\}. \tag{108}$$

These formulas are generalizations of Eqs. (19) and (20), respectively. Eq. (108) is identical with Eq. (101). For $E \ll |E_\lambda|$, $|E_\rho|$ the denominators of Eqs. (101) and (108) are approximately equal to $E+(E_\rho r_0/2)^2$ and $E+(E_\lambda/\omega_\lambda)^2$, respectively. These are the same as the denominator $E+|E_a|$ in Eq. (9).

In the case of the square-well potential the function $R(E)$ is given by

$$R(E) = \tan[(V_0+E)^{\frac{1}{2}}a]/(V_0+E)^{\frac{1}{2}}. \tag{109}$$

It can therefore be expanded in the form[34]

$$R(E) = (2/a)\sum_{n=0}^{\infty}[(n+\tfrac{1}{2})^2(\pi/a)^2 - V_0 - E]^{-1}. \tag{110}$$

Hence

$$\omega_\lambda = 2/a, \tag{111}$$

and

$$E_\lambda = (\pi/2a)^2 - V_0 \tag{112}$$

for the lowest E_λ. From Eq. (112) it follows that E_λ is positive for ^1S and negative for ^3S. By Eq. (105),

$$E_\rho = -E_\lambda, \tag{113}$$

showing that E_λ and E_ρ are opposite in sign.

The condition for the bound states and the various definitions for the virtual level can also be stated simply in terms of the logarithmic derivative $L(E)$. The Eqs. (12), (15), and (18) for the square-well potential determine the zeros of the functions $L(-x^2)+x$, $L(x^2)-x$, and $L(x^2)$, respectively. Given any suitable function of $L(\pm x^2)$, there is a one-level representation for a low-energy scattering formula.

The writer wishes to thank Dr. T. Y. Wu for valuable discussions.

[33b] Eqs. (103)–(106) are valid for small E_λ. For $E_\lambda \gg \omega_\lambda{}^2/4$ we find from Eqs. (92) and (102) that $S(k)$ has zeros near $k = \pm E_\lambda{}^{\frac{1}{2}} + i\omega_\lambda/2$ and poles near $k = \pm E_\lambda{}^{\frac{1}{2}} - i\omega_\lambda/2$.

[34] E. C. Titchmarsh, *Theory of Functions* (Oxford University Press, Oxford, 1939), p. 113.



CC-0. In Public Domain. Gurukul Kangri Collection, Haridwar

Digitized by Arya Samaj Foundation Chennai and eGangotri

CC-0. In Public Domain. Gurukul Kangri Collection, Haridwar

Digitized by Arya Samaj Foundation Chennai and eGangotri

R
530.5
AM3R
V.25

पुस्तकालय
गुरुकुल कांगड़ी विश्वविद्यालय, हरिद्वार

पुस्तक-वितरण की तिथि नीचे अंकित है। इस तिथि सहित १५ वें दिन तक यह पुस्तक पुस्तकालय में वापिस आ जानी चाहिये। अन्यथा ५ पैसे प्रतिदिन के हिसाब से विलम्ब दण्ड लगेगा।

3900

Compiled
1999-2000

यह पुस्तक वितरित न की जाय
NOT TO BE ISSUED

CC-0. In Public Domain. Gurukul Kangri Collection, Haridwar

Digitized by Arya Samaj Foundation Chennai and eGangotri

पुस्तकालय, गुरुकुल कांगड़ी विश्वविद्यालय,
हरिद्वार।

CC-0. In Public Domain. Gurukul Kangri Collection, Haridwar

Digitized by Arya Samaj Foundation Chennai and eGangotri